สัญญาเลขที่ BRG5780016





รายงานวิจัยฉบับสมบูรณ์

"ผลของฮอร์โมนเพศชายต่อสมองในหนูอ้วนและการรักษา"

"Neurological Effects of Testosterone in Obese Rats And the Therapeutic Interventions"

โดย

ศาสตราจารย์ ดร. ทันตแพทย์หญิงสิริพร ฉัตรทิพากร
ภาควิชาชีววิทยาช่องปากและวิทยาการวินิจฉัยโรคช่องปาก
คณะทันตแพทยศาสตร์ มหาวิทยาลัยเชียงใหม่
(หัวหน้าโครงการวิจัยผู้รับทุน)

กรกฎาคม 2560

สัญญาเลขที่ BRG5780016

รายงานวิจัยฉบับสมบูรณ์

"ผลของฮอร์โมนเพศชายต่อสมองในหนูอ้วนและการรักษา"

"Neurological effects of testosterone in obese rats and the therapeutic interventions"

คณะผู้วิจัย	สังกัด
ศ. ดร. ทพญ. สิริพร ฉัตรทิพากร	ภาควิชาชีววิทยาช่องปากและวิทยาการวินิจฉัยโรคช่องปาก คณะทันตแพทยศาสตร์ มหาวิทยาลัยเชียงใหม่, ศูนย์วิจัยและฝึกอบรมสาขาโรคทางไฟฟ้าของหัวใจ (Cardiac Electrophysiology Research & Training Center (CERT)) คณะแพทยศาสตร์ มหาวิทยาลัยเชียงใหม่
ดร. หิรัญญา ปินตานา	ศูนย์วิจัยและฝึกอบรมสาขาโรคทางไฟฟ้าของหัวใจ (Cardiac Electrophysiology Research & Training Center (CERT)) คณะแพทยศาสตร์ มหาวิทยาลัยเชียงใหม่
ศ. (เชี่ยวชาญ) ดร. นพ. นิพนธ์ ฉัตรทิพากร	ศูนย์วิจัยและฝึกอบรมสาขาโรคทางไฟฟ้าของหัวใจ (Cardiac Electrophysiology Research & Training Center (CERT)) คณะแพทยศาสตร์ มหาวิทยาลัยเชียงใหม่

สนับสนุนโดยสำนักงานคณะกรรมการการอุดมศึกษา
และสำนักงานกองทุนสนับสนุนการวิจัย

(ความเห็นในรายงานนี้เป็นของผู้วิจัย สกอ. และสกว. ไม่จำเป็นต้องเห็นด้วยเสมอไป)

คำนำ

ผู้วิจัยขอขอบคุณ ดร. หริญญา ปินตานา, ผศ.ดร. วาสนา ปรัชญาสกุล, ดร. วันพิทักษ์ ป้องกัน, ดร. ณัฐยาภรณ์ อภัยใจ, นางรจนา ทาวัน ในฐานะผู้ช่วยวิจัยที่ช่วยดำเนินการทดลองและให้ความช่วยเหลือในทุกทางตลอดโครงการ นอกจากนี้ ขอขอบคุณศูนย์วิจัยและฝึกอบรมสาขาโรคทางไฟฟ้าของหัวใจ (CERT CENTER) ภายใต้การดูแลของ ศาสตราจารย์ (เชี่ยวชาญพิเศษ) ดร. นายแพทย์ นิพนธ์ ฉัตรทิพากร ผู้อำนวยการศูนย์วิจัยและฝึกอบรมสาขาโรคทางไฟฟ้าของหัวใจ คณะแพทยศาสตร์ มหาวิทยาลัยเชียงใหม่ ที่ให้ความอนุเคราะห์ในการใช้เครื่องมือสำหรับงานวิจัยครั้งนี้ การศึกษานี้ได้รับการสนับสนุนจากกองทุนวิจัยจาก ทุนวิจัยองค์ความรู้ใหม่ที่เป็นพื้นฐานต่อการพัฒนา (วุฒิเมธีวิจัย สกว.) (BRG5780016)

สิริพร ฉัตรทิพากร

กรกฎาคม 2560

สารบัญ

	หน้า
คำนำ	3
สารบัญ	4
สารบัญรูปภาพ	5
สารบัญตาราง	6
บทคัดย่อภาษาไทย	7
บทคัดย่อภาษาอังกฤษ	9
Exclusive Summary	11
Chapter I:	21
Chapter II:	47
Chapter III:	73
Chapter IV:	99
กิตติกรรมประกาศ	125
Output	127
ภาคผนวก	139
บทความสำหรับเผยแพร่	149
เอกสารแนบ	150

สารบัญรูปภาพ

		หน้า
Chapter II:	Figure 1	64
	Figure 2	65
	Figure 3	66
	Figure 4	67
	Figure 5	68
Chapter III:	Figure 1	93
	Figure 2	94
	Figure 3	95
	Figure 4	96
	Figure 5	97
Chapter IV:	Figure 1	119
	Figure 2	120
	Figure 3	121
	Figure 4	122
	Figure 5	123
	Figure 6	124

สารบัญตาราง

		หน้า
Chapter II:	Table 1	60
	Table 2	61
	Table 3	62
	Table 4	63
Chapter III:	Table 1	91
	Table 2	92
Chapter IV:	Table 1	117
	Table 2	118

บทคัดย่อภาษาไทย

ภาวะอ้วนมีความสัมพันธ์ต่อการลดลงของฮอร์โมนเทสโทสเตอร์โรนตามอายุที่เพิ่มขึ้นในเพศชาย หลายๆการศึกษาที่ผ่านมาทั้งในสัตว์ทดลองและผู้ชาย รายงานถึงการขาดฮอร์โมนเทสโทสเตอร์โรนหรือการมีภาวะอ้วนมีความสัมพันธ์ต่อการลดลงของการเรียนรู้ และความจำ จากหลักฐานข้างต้นอาจกล่าวได้ว่าฮอร์โมนเทสโทสเตอร์โรนมีความสำคัญในการควบคุมระบบเมตาบอลิค, การเรียนรู้ และความจำ แต่อย่างไรก็ตามการศึกษาถึงผลของการมีภาวะอ้วนร่วมกับการขาดฮอร์โมนเทสโทสเตอร์โรนต่อระบบเมตาบอลิค การเรียนรู้ และความจำยังไม่มีรายงานการศึกษามาก่อนจึงเป็นที่มาของการศึกษาในครั้งนี้ โดยเราจะทำการศึกษาทั้งหมด 4 การศึกษาใหญ่ คือ

การศึกษาที่ 1 ทำการศึกษาถึงผลของการมีภาวะอ้วนจากการรับประทานอาหารไขมันสูงร่วมกับการขาดฮอร์โมนเทสโทสเตอร์โรนต่อระบบเมตาบอลิค, การเรียนรู้ และความจำในหนูเพศผู้ จากนั้นใน**การศึกษาที่ 2** ทำการศึกษาถึงผลต่อระบบเมตาบอลิคของการให้ยาวิลดากลิปทินซึ่งเป็นยารักษาเบาหวานต่อภาวะอ้วนร่วมกับการขาดฮอร์โมนเทสโทสเตอร์โรนดังกล่าว ใน**การศึกษาที่ 3** จึงทำการศึกษาถึงผลของการให้ยาวิลดากลิปทินต่อ การเรียนรู้ และความจำในภาวะดังกล่าวข้างต้น นอกจากนี้จากการศึกษาที่ผ่านหลายการศึกษายังพบว่าการรับประทานอาหารไขมันสูงเป็นระยะเวลานานก่อให้เกิดภาวะดื้อต่ออินซูลินของเนื้อเยื่อส่วนปลายและในสมอง ทั้งยังส่งผลต่อการเรียนการเรียนรู้ และความจำที่ลดลง ปัจจุบันเป็นที่น่าสนใจว่าการจำกัดปริมาณแคลอรี่ในอาหารที่รับประทานสามารถช่วยฟื้นฟูการทำงานระบบเมตาบอลิคของร่างกายในสัตว์ทดลองที่มีภาวะอ้วนหรือภาวะสูงอายุ แต่อย่างไรก็ตามการศึกษาถึงผลของการจำกัดปริมาณแคลอรี่ในอาหารที่รับประทานต่อระบบเมตาบอลิค, การเรียนรู้ และความจำ ในภาวะอ้วนและดื้อต่ออินซูลินจากการรับประทานอาหารไขมันสูงยังไม่มีรายงานการศึกษามาก่อน ดังนั้นใน**การศึกษาที่ 4** จึงทำการศึกษาถึงผลของการจำกัดปริมาณแคลอรี่ในอาหาร รวมทั้งการจำกัดปริมาณแคลอรี่ในอาหารร่วมกับการให้ยาวิลดากลิปทินต่อระบบเมตาบอลิค, การเรียนรู้ และความจำในหนูอ้วนเพศผู้ที่มีภาวะดื้อต่ออินซูลิน

จากการศึกษานี้สรุปได้ว่าการขาดฮอร์โมนเทสโทสเตอร์โรนจะเร่งการเกิดความบกพร่องของการทำงานของจุดประสานประสาทของสมอง และความบกพร่องของการเรียนรู้ ความจำ แต่ไม่ส่งผลต่อการเกิดภาวะดื้อต่ออินซูลินในเนื้อเยื่อส่วนปลายและในสมอง รวมถึงไม่ส่งผลต่อการทำงานของไมโตคอนเดรียในสมองของหนูที่ได้รับการทำหมันโดยการตัดลูกอัณฑะ โดยการรับประทานอาหารไขมันสูงที่ก่อให้เกิดภาวะอ้วนเป็นตัวการสำคัญในการเกิดภาวะดื้อต่ออินซูลิน

มากกว่าผลของการขาดฮอร์โมนเทสโทสเตอร์โรน การให้ยาวิลดากลิปทินช่วยฟื้นฟูภาวะดื้อต่ออินซูลินของเนื้อเยื่อส่วนปลายในหนูที่มีภาวะอ้วนเพียงอย่างเดียวและในกลุ่มที่มีภาวะอ้วนร่วมกับการขาดฮอร์โมนเทสโทสเตอร์โรน นอกจากนี้การให้ยาวิลดากลิปทินที่ช่วยฟื้นฟูภาวะดื้อต่ออินซูลินของสมองในหนูกลุ่มที่มีภาวะอ้วนร่วมกับการขาดฮอร์โมนเทสโทสเตอร์โรน โดยไม่ช่วยในการฟื้นฟูการเรียนรู้และความจำเลย การศึกษานี้ยังพบว่าทั้งการจำกัดปริมาณแคลอรี่ในอาหารเพียงอย่างเดียว หรือการจำกัดปริมาณแคลอรี่ในอาหารร่วมกับการให้ยาวิลดากลิปทินมีผลเท่าเทียมกันในการช่วยภาวะดื้อต่ออินซูลินในเนื้อเยื่อส่วนปลาย แต่การจำกัดปริมาณแคลอรี่ในอาหารร่วมกับการให้ยาวิลดากลิปทินเท่านั้นที่ช่วยฟื้นฟูภาวะดื้อต่ออินซูลินของสมอง และช่วยฟื้นฟูความบกพร่องของการเรียนรู้ ความจำในหนูอ้วนเพศผู้ที่มีภาวะดื้อต่ออินซูลิน

Keywords: ฮอร์โมน, เทสโทสเตอร์โรน, อ้วน, การเรียนรู้, แคลอรี่, สมอง

ABSTRACT

Obesity has been shown to be associated with the reduction of testosterone levels alongin aging population. Moreover, several studies reported the correlation between cognitive decline and either testosterone deprivation or obesity in both human and animal models. All of those findings suggested that testosterone is an important hormone involved with metabolic control and cognitive function. However, the effect of the combination of obesity along with testosterone deprivation on metabolic effects and cognitive function had never been investigated. Vildagliptin (dipeptidyl peptidase-4 inhibitor) is an anti-diabetic drug, which exerts beneficial effects in diabetic and insulin resistant models. Nevertheless, the effect of vildagliptin on metabolic effects and cognitive function in testosterone deprived with or without obesity had never been investigated. Regarding several studies have been shown that high-fat diet (HFD)-induced obesity contributed to the impairment of peripheral insulin resistance, brain insulin resistance, as well as cognitive dysfunction. Interestingly, several evidence also demonstrated that calories restriction (CR) in obesity and aged models, significantly improved the metabolic impairment. However, the effect of calories restriction on metabolic parameters and coginiton in obese-insulin resistant condition has never been investigated. Therefore, the hypotheses of the present study are that; 1) testosterone deprivation alone causes the impairment of peripheral insulin sensitivity, brain insulin sensitivity, brain mitochondrial function, brain synaptic plasticity as well as learning and memory; 2) the combination of obesity induced by HFD consumption along with testosterone deprivation aggravates these impairments; 3) vildagliptin treatment attenuates the impairments of peripheral insulin sensitivity, brain insulin sensitivity, brain mitochondrial function, brain synaptic plasticity as well as learning and memory in either testosterone deprivation alone or combination of HFD-induced obesity with testosterone deprivation; and 4) the combination of calorie restriction and vildagliptin have a higher efficacy on the improvement of peripheral insulin sensitivity, brain insulin sensitivity, brain mitochondrial function, brain synaptic plasticity as well as on learning and memory in an obese-insulin resistant condition, when compared to calorie restriction alone.

Our findings suggest that testosterone deprivation early initiating an impairment of hippocampal synaptic plasticity and cognitive dysfunction, but it does not cause peripheral and brain insulin resistance as well as brain mitochondrial dysfunction in testosterone-derpived condition. Rather HFD-induced obesity than estosterone deprivation dominates the development of the insulin resistance. Vildagliptin therapy attenuates peripheral insulin sensitivity in both obese-insulin resistant condition with and without testosterone deprivation. Vildagliptin improves brain insulin resistance in testosterone-deprived with obese condition. The present study also demonstrates that both calorie restriction and calorie restriction with vildagliptin therapy equally improve peripheral insulin sensitivity, however only calorie restriction with vildagliptin therapy attenuates brain insulin resistance and cognitive function in obese-insulin resistant male rats.

Keywords: Hormone, Testonstorone, Obese, meomory, Calorie, Brain

EXECUTIVE SUMMARY

ชื่อโครงการ: "ผลของฮอร์โมนเพศชายต่อสมองในหนูอ้วนและการรักษา"

"Neurological effects of testosterone in obese rats and the therapeutic interventions"

ชื่อหัวหน้าโครงการ หน่วยงานที่สังกัด ที่อยู่ หมายเลขโทรศัพท์ โทรสาร และ e-mail

ศาสตราจารย์ ดร. ทันตแพทยหญิง สิริพร ฉัตรทิพากร

ภาควิชาชีววิทยาช่องปากและวิทยาการวินิจฉัยโรคช่องปาก

คณะทันตแพทยศาสตร์ มหาวิทยาลัยเชียงใหม่

ต. สุเทพ อ.เมือง จ. เชียงใหม่ 50200

โทร: 053 94 4451 Fax: 053 93 5368

E-mail: scchattipakorn@gmail.com

สาขาวิชาที่ทำการวิจัย: Neurophysiology

งบประมาณรวมทั้งโครงการ: 2,000,000.00 บาท

ระยะเวลาดำเนินงาน: 3 ปี

Insulin resistance is the hallmark of the metabolic syndrome, leading to the development of several complications including type 2 diabetes mellitus (T2DM), cardiovascular diseases, and neurodegenerative disorder (1-3) It has been known that obesity is the major cause for the development of insulin resistance (4) Recently, we have shown that 15-week of high-fat diet (HFD) consumption leads to obesity, peripheral and brain insulin resistance, brain mitochondrial dysfunction and the impairment of learning and memory (5; 6) Our findings suggest the roles of obesity with peripheral insulin resistance on the impairment of brain insulin signaling, brain mitochondria and cognitive function.

Testosterone is an androgenic sex steroid hormone. Under the physiological condition, testosterone plays important roles in maintaining the physiological function of

several peripheral organs, including reproductive system for promoting secondary sexual characteristics, and involved in bone growth as well as the modulation of normal brain functions, including brain development and cognition (7; 8) Several studies demonstrated that testosterone deficiency is associated with many pathological conditions including erectile dysfunction(9), cardiovascular disease(10), cognitive impairment(7), type 2 diabetes mellitus and metabolic syndrome.(11) In the brain, it has been shown that testosterone acts as neuroprotective agents (8) Previous studies reported that peripheral insulin resistance and obesity have been associated with the condition of testosterone deficiency (12; 13) Moreover, several studies demonstrated that animals with testosterone deficiency had increased risk of developing Alzheimer's disease, memory decline and decreased synaptic plasticity in the hippocampal area (14; 15). However, the effects of testosterone deprivation alone or obesity with peripheral insulin resistance together with testosterone deprivation on brain insulin receptor function, brain mitochondrial function, synaptic plasticity and cognition, have not yet been investigated.

Glucagon-like-peptide 1 (GLP-1) is an incretin hormone, secreted by enteroendocrine cells in the jejunum during ingestion of nutrients.(16; 17) GLP-1 plays an important role in insulinotropy and to improve glycemic control via binding to GLP-1 receptors.(17; 18) GLP-1 receptors are not only expressed in peripheral tissues, but also expressed in the brain, particularly in the hippocampus.(19) GLP-1 has a very short half-life (< two minutes) since it is rapidly degraded by a dipeptidyl peptidase IV (DPP-4) enzyme in the circulation.(18; 20; 21) Vildagliptin is one of DPP-4 inhibitor which has been shown to increase insulin biogenesis and secretion, to improve glycemic control, and to reduce HbA1c in both Zucker diabetic fatty (ZDF) rats and diabetic patients in clinical studies.(22; 23) Vildagliptin has been shown to effectively attenuate the impairment of brain activity in type-2 diabetes milletus (T2DM) models.(24; 25) Our recent study demonstrated that vildagliptin has beneficial effects to improve not only peripheral insulin resistance, but also brain insulin resistance on insulin resistant obese rats.(6) Therefore, DPP-4 inhibitors could provide beneficial effects on insulin receptor signaling which leads to improved learning and memory impaired by HFD consumption.(6; 26) However, the effects of DPP-4 inhibitor on brain insulin receptor function, brain mitochondrial function

and cognitive behavior in insulin resistant rats induced by HFD under the condition of testosterone deprivation have not been investigated.

It has been shown that high-fat feeding resulted in severely compromised obesity and peripheral insulin resistance as well as brain insulin resistance.(27; 28) Interestingly, several studies demonstrated that dietary intervention by reversal of high-fat feeding or the reversal of obesity significantly improved insulin sensitivity in human studies and animal studies.(29) Despite these reports, there is only one study which investigated and reported that dietary intervention by reversal of high-fat feeding significantly improved the hippocampal synaptic plasticity in animal models.(30) However, the effects of dietary intervention by reversal of high-fat feeding on brain insulin receptor function, brain mitochondrial function and cognitive behavior in insulin resistant rats induced by HFD with or without testosterone deprivation have not yet been investigated.

According to the above limitations on knowledge regarding the associations and effects among obesity, insulin resistance and testosterone on the brain, we hypothesize that testosterone deprivation can worsen the brain insulin resistance, the impairment of learning and memory, the decline of synaptic plasticity, and brain mitochondrial dysfunction in obese-insulin resistant rats. It has been known that testosterone supplement in testosterone deprivation is controversy and has many side effects. Therefore, pharmacological intervention or diet reversal could be potential therapies if they provide benefits against impairment in the brain under obese insulin resistant with or without testosterone deprivation. Therefore, we aim to test the other hypothesis that pharmacological intervention with the DDP-IV inhibitor as well as the dietary intervention can restore those impairments in obese-insulin resistant rats with or without testosterone deprivation.

Therefore, in the present study, we hypothesize that 1) the conditions of testosterone deprivation alone can cause peripheral insulin resistance, brain insulin resistance, brain mitochondrial dysfunction, impaired synaptic plasticity as well as cognitive decline; 2) obesity leads to worsen those conditions of testosterone deprivation and 3) either DDP-IV inhibitor or the dietary intervention restores those defects in obese rats with or without testosterone deprivation

วัตถุประสงค์

Specific Aim 1: To determine whether testosterone deprivation alone causes 1) brain insulin resistance by decreased neuronal insulin receptor function (insulin-induced LTD) and brain insulin signaling, 2) the impairment of synaptic plasticity by decreased hippocampal long-term potentiation (LTP), 3) the impairment of brain mitochondrial function, 4) decreased in hippocampal dendritic spines and 5) the cognitive decline.

Specific Aim 2: To investigate whether the combination of obesity induced by HFD consumption and the loss of testosterone accelerates brain insulin resistance, the impairment of synaptic plasticity, the impairment of brain mitochondrial function, decreased hippocampal dendritic spines, and cognitive decline, compared to those with obesity alone or those with testosterone deprivation alone.

Specific Aim 3: To investigate the effects of anti-diabetic drug DPP-4 inhibitor on brain insulin resistance, hippocampal synaptic plasticity, hippocampal dendritic spine formation, brain mitochondrial function and cognition in obese male rats induced by HFD consumption with or without testosterone deprivation.

Specific Aim 4: To investigate the effects of dietary intervention on brain insulin resistance including brain insulin receptor function and brain insulin signaling, hippocampal synaptic plasticity, hippocampal dendritic spine formation, brain mitochondrial function and cognition in obese male rats induced by HFD consumption with or without testosterone deprivation.

ระเบียบวิธีวิจัย

Experimental Design for specific aims 1and 2 in the protocol I:

Study Protocol I: One week after acclimatization, rats will be divided into 2 groups (n = 48/group): sham operated group or bilateral orchiectomy (ORX) group. After 1 week of surgery, rats in each group will be divided into 2 groups (n =24/group) to receive a normal diet (ND) or a high fat diet (HFD) for 4, 8 or 12 weeks (n=8/sub-groups). Animals in the ND group will be fed with standard laboratory chow for 4, 8 or 12 weeks (Mouse Feed Food No. 082, C.P. Company, Bangkok, Thailand), which has energy content of 4.02 kcal/g and 19.77% of total energy (%E from fat). Animals in the HFD group will be fed by

HFD for 4, 8 or 12 weeks, which has energy content of 5.35 kcal/g and 59.28 (% E from fat). All animals will be given free access to the diet and drinking water. Body weight and food intake will be recorded daily, blood samples will be collected from the tail vein at baseline and at each time course (4, 8 and 12 weeks) after fasting for 5-6 hours. Blood samples will be centrifuged at 6,000 rpm, 4°C for 5 minutes and the plasma will be kept at -80°C for further determination of glucose, cholesterol, and insulin levels.

All rats will be tested for their locomotor activities by the open-field test (OFT), and their learning and memory by the Morris water maze (MWM) test before be sacrificed. At the end of each time course, rats will be sacrificed by decapitation after which the brain will be removed and used to determine brain mitochondrial function, dendritic spine density, the synaptic plasticity, electrical induced long-term potentiation (LTP), insulin induced long-term depression (LTD) and brain insulin signaling.

Protocol II for specific aim 3: One week after acclimatization, rats will be divided into 2 groups (n = 40/group): sham operated group or bilateral orchiectomy (ORX) group. After 1 week of surgery, rats in each group will be divided into 2 groups (n =20/subgroup) to receive a normal diet (ND) or a high fat diet (HFD) for 12 weeks. Animals in the ND group will be fed with standard laboratory chow for 12 weeks (Mouse Feed Food No. 082, C.P. Company, Bangkok, Thailand), which has energy content of 4.02 kcal/g and 19.77% of total energy (%E from fat). Animals in the HFD group will be fed by HFD for 12 weeks, which has energy content of 5.35 kcal/g and 59.28 (% E from fat). The end of the 12th week of each dietary feeding, animal in each subgroup will be further divided into 2 treatment groups: vehicle and vildagliptin.

All animals will be given free access to the diet and drinking water. Body weight and food intake will be recorded daily, blood samples will be collected from the tail vein at baseline and at the end of protocol after fasting for 5-6 hours. Blood samples will be centrifuged at 6,000 rpm, 4°C for 5 minutes and the plasma will be kept at -80°C for further determination of glucose, cholesterol, and insulin levels.

All rats will be tested for their locomotor activities by the open-field test (OFT), and their learning and memory by the Morris water maze (MWM) test before being sacrificed. At the end of the protocol, rats will be sacrificed by decapitation after which the brain will be

removed and used to determine brain mitochondrial function, dendritic spine density, the synaptic plasticity, electrical induced long-term potentiation (LTP), insulin induced long-term depression (LTD) and brain insulin signaling.

Experimental Design for specific aim 4 in protocol III: One week after acclimatization, rats will be divided into 2 groups (n = 30/group): sham operated group or bilateral orchiectomy (ORX) group. After 1 week of surgery, rats in each group will be received a high fat diet (HFD), which has energy content of 5.35 kcal/g and 59.28 (% E from fat) for 12 weeks. The end of the 12th week of animals in each group will be fed with standard laboratory chow for 4, 8 and 12 weeks (n=10 per subgroup) (Mouse Feed Food No. 082, C.P. Company, Bangkok, Thailand), which has energy content of 4.02 kcal/g and 19.77% of total energy (%E from fat).

All animals will be given free access to the diet and drinking water. Body weight and food intake will be recorded daily, blood samples will be collected from the tail vein at baseline and at the end of protocol after fasting for 5-6 hours. Blood samples will be centrifuged at 6,000 rpm, 4°C for 5 minutes and the plasma will be kept at -80°C for further determination of glucose, cholesterol, and insulin levels.

All rats will be tested for their locomotor activities by the open-field test (OFT), and their learning and memory by the Morris water maze (MWM) test before being sacrificed. At the end of the protocol, rats will be sacrificed by decapitation after which the brain will be removed and used to determine brain mitochondrial function, dendritic spine density, the synaptic plasticity, electrical induced long-term potentiation (LTP), insulin induced long-term depression (LTD) and brain insulin signaling.

We found that peripheral insulin resistance was developed at week 8 in HFD with sham operation rats (HFS) and HFD with orchiectomized rats (HFO) but not ND with sham operation rats (NDO) as indicated by increased plasma insulin levels with normal plasma blood glucose and increased HOMA index. Brain insulin resistance was developed at week 12 in HFS and HFO rats indicated by impaired insulin-induced long term depression (LTD) and impaired brain insulin signaling. Brain mitochondrial dysfunction was also observed in HFS and HFO rats at week 12, as indicated by increased brain mitochondrial ROS production, increased brain mitochondrial membrane depolarization, and brain

mitochondrial swelling. Furthermore, NDO and HFO occurred early initiating hippocampal synaptic dysfunction and impaired of cognition at week 8, whereas HFS rat was occurred the impairment at week 12. Testosterone replacement improved peripheral insulin sensitivity, and reduced brain mitochondrial ROS production in HFOTes rats. However, testosterone failed to restore brain insulin resistance, hippocampal synaptic dysfunction and cognitive function in HFOTes rats. In contrast, testosterone replacement attenuated brain mitochondrial ROS production, hippocampal synaptic dysfunction as well as cognitive dysfunction in NDOTes rats. Moreover, vildagliptin treatment improved insulin sensitivity and reduced brain mitochondrial ROS production as well as restored brain insulin resistance in HFOVil rats. However, vildagliptin did not restore hippocampal synaptic dysfunction and cognitive dysfunction in both NDOVil and HFOVil rats. In the last study, CR and CR plus Vil treatment equally improved peripheral insulin resistance in HFRV and HFRVil rats. However, only CR plus Vil restored brain insulin resistance, brain mitochondrial dysfunction, hippocampal synaptic plasticity dysfunction and cognitive dysfunction in HFV rats.

Our findings suggest that testosterone deprivation early initiating an impairment of hippocampal synaptic plasticity and cognitive dysfunction, but it does not cause peripheral and brain insulin resistance as well as brain mitochondrial dysfunction in orchiectomized male rats. HFD-induced obesity dominates the development of the insulin resistance more than the effect of testosterone deprivation. Testosterone replacement and vildagliptin attenuated peripheral insulin sensitivity in both obese-insulin resistance with or without testosterone deprivation male rats. Only Testosterone replacement improves cognitive dysfunction in testosterone-deprived without obesity, whereas only vildagliptin improves brain insulin resistance in testosterone-deprived with obesity male rats. This study also demonstrate that even both CR and CR plus vildagliptin equally improve peripheral insulin resistance, but only CR plus vildagliptin attenuate brain insulin resistance and cognitive function in obese-insulin resistant male rats.

References:

1. Biessels GJ, Kappelle LJ: Increased risk of Alzheimer's disease in Type II diabetes: insulin resistance of the brain or insulin-induced amyloid pathology? Biochem Soc Trans 33:1041-1044, 2005

2. Reusch JE: Current concepts in insulin resistance, type 2 diabetes mellitus, and the metabolic syndrome. Am J Cardiol 90:19G-26G, 2002

3. Umegaki H: Pathophysiology of cognitive dysfunction in older people with type 2 diabetes: vascular changes or neurodegeneration? Age Ageing 39:8-10, 2010

4. Steinberg GR: Inflammation in obesity is the common link between defects in fatty acid metabolism and insulin resistance. Cell Cycle 6:888-894, 2007

5. Pintana H, Apaijai N, Pratchayasakul W, Chattipakorn N, Chattipakorn SC: Effects of metformin on learning and memory behaviors and brain mitochondrial functions in high fat diet induced insulin resistant rats. Life Sci, 2012

6. Pipatpiboon N, Pintana H, Pratchayasakul W, Chattipakorn N, Chattipakorn SC: DPP4-inhibitor improves neuronal insulin receptor function, brain mitochondrial function and cognitive function in rats with insulin resistance induced by high-fat diet consumption. Eur J Neurosci, 2012

7. Janowsky JS: Thinking with your gonads: testosterone and cognition. Trends Cogn Sci 10:77-82, 2006

8. Meydan S, Kus I, Tas U, Ogeturk M, Sancakdar E, Dabak DO, Zararsiz I, Sarsilmaz M: Effects of testosterone on orchiectomy-induced oxidative damage in the rat hippocampus. J Chem Neuroanat 40:281-285, 2010

9. Traish AM, Goldstein I, Kim NN: Testosterone and erectile function: from basic research to a new clinical paradigm for managing men with androgen insufficiency and erectile dysfunction. Eur Urol 52:54-70, 2007

10. Traish AM, Saad F, Feeley RJ, Guay A: The dark side of testosterone deficiency: III. Cardiovascular disease. J Androl 30:477-494, 2009

11. Traish AM, Saad F, Guay A: The dark side of testosterone deficiency: II. Type 2 diabetes and insulin resistance. J Androl 30:23-32, 2009

12. Grossmann M, Thomas MC, Panagiotopoulos S, Sharpe K, Macisaac RJ, Clarke S, Zajac JD, Jerums G: Low testosterone levels are common and associated with insulin resistance in men with diabetes. J Clin Endocrinol Metab 93:1834-1840, 2008

13. Haffner SM, Karhapaa P, Mykkanen L, Laakso M: Insulin resistance, body fat distribution, and sex hormones in men. Diabetes 43:212-219, 1994

14. Hogervorst E, Williams J, Budge M, Barnetson L, Combrinck M, Smith AD: Serum total testosterone is lower in men with Alzheimer's disease. Neuro Endocrinol Lett 22:163-168, 2001

15. Romeo RD, Staub D, Jasnow AM, Karatsoreos IN, Thornton JE, McEwen BS: Dihydrotestosterone increases hippocampal N-methyl-D-aspartate binding but does not affect choline acetyltransferase cell number in the forebrain or choline transporter levels in the CA1 region of adult male rats. Endocrinology 146:2091-2097, 2005

16. Pratley RE, Salsali A: Inhibition of DPP-4: a new therapeutic approach for the treatment of type 2 diabetes. Curr Med Res Opin 23:919-931, 2007

17. Verspohl EJ: Novel therapeutics for type 2 diabetes: incretin hormone mimetics (glucagon-like peptide-1 receptor agonists) and dipeptidyl peptidase-4 inhibitors. Pharmacol Ther 124:113-138, 2009

18. Drucker DJ, Nauck MA: The incretin system: glucagon-like peptide-1 receptor agonists and dipeptidyl peptidase-4 inhibitors in type 2 diabetes. Lancet 368:1696-1705, 2006

19. Dunphy JL, Taylor RG, Fuller PJ: Tissue distribution of rat glucagon receptor and GLP-1 receptor gene expression. Mol Cell Endocrinol 141:179-186, 1998

20. Akarte AS, Srinivasan BP, Gandhi S: A novel long acting DPP-IV inhibitor PKF-275-055 stimulates beta-cell proliferation resulting in improved glucose homeostasis in diabetic rats. Biochem Pharmacol 83:241-252, 2011

21. Ranganath LR: Incretins: pathophysiological and therapeutic implications of glucose-dependent insulinotropic polypeptide and glucagon-like peptide-1. J Clin Pathol 61:401-409, 2008

22. Doupis J, Veves A: DPP4 inhibitors: a new approach in diabetes treatment. Adv Ther 25:627-643, 2008

23. Nauck MA, Meier JJ: Glucagon-like peptide 1 and its derivatives in the treatment of diabetes. Regul Pept 128:135-148, 2005

24. Gault VA, Holscher C: GLP-1 agonists facilitate hippocampal LTP and reverse the impairment of LTP induced by beta-amyloid. Eur J Pharmacol 587:112-117, 2008

25. McClean PL, Gault VA, Harriott P, Holscher C: Glucagon-like peptide-1 analogues enhance synaptic plasticity in the brain: a link between diabetes and Alzheimer's disease. Eur J Pharmacol 630:158-162, 2010

26. Pintana H, Apaijai N, Chattipakorn N, Chattipakorn SC: DPP-4 inhibitors improve cognition and brain mitochondrial function of insulin resistant rats. J Endocrinol, 2013

27. Clegg DJ, Gotoh K, Kemp C, Wortman MD, Benoit SC, Brown LM, D'Alessio D, Tso P, Seeley RJ, Woods SC: Consumption of a high-fat diet induces central insulin resistance independent of adiposity. Physiol Behav 103:10-16, 2011

28. Pratchayasakul W, Kerdphoo S, Petsophonsakul P, Pongchaidecha A, Chattipakorn N, Chattipakorn SC: Effects of high-fat diet on insulin receptor function in rat hippocampus and the level of neuronal corticosterone. Life Sci 88:619-627, 2011

29. Ferland A, Eckel RH: Does sustained weight loss reverse the metabolic syndrome? Curr Hypertens Rep 13:456-464, 2011

30. Porter DW, Irwin N, Flatt PR, Holscher C, Gault VA: Prolonged GIP receptor activation improves cognitive function, hippocampal synaptic plasticity and glucose homeostasis in high-fat fed mice. Eur J Pharmacol 650:688-693, 2011

Chapter I

สัญญาเลขที่ BRG5780016

CHAPTER I

Introduction: Testosterone deficiency, obesity and cognition

Testosterone is an androgenic sex steroid hormone, synthesized from the endoplasmic reticulum of Leydig cells in testis and from the adrenal gland (1, 2). The secretion of testosterone is controlled by the hypothalamic-pituitary-testes axis (HPT axis) (3-5). There are three different forms of circulating testosterone, including free testosterone (2-3%), albumin-bound testosterone (20-40%), and sex hormone-binding globulin (SHBG) bound testosterone (60-80%) (6, 7). Free testosterone, an active form of testosterone, is metabolized to be 5α-dihydrotestosterone (DHT) via 5α-reductase enzyme (8, 9). Free testosterone and DHT directly exert their effects via binding androgen receptors (ARs) in various parts of the body, including reproductive organs, liver, kidney, muscles, bone, heart and brain (9-12). Under physiological condition, testosterone plays important roles in the development of secondary male sexual characteristics (13), the regulation of glucose and lipid metabolism (14, 15), bone growth as well as the modulation of normal brain function, including cognition (9, 16, 17). However, testosterone can be converted to be estradiol via the aromatase enzyme. Therefore, it implies that testosterone can also activate estrogen receptors (ERs) (9, 16, 18).

Testosterone deficiency is a low testosterone condition with serum total testosterone levels < 3.2 ng/ml and free testosterone levels < 64 pg/ml in middle aged and elderly men (19). The serum testosterone concentration gradually reduces in the aging process and it declines about 1.6% per year after 40 years of age (20). Testosterone deficiency has been associated with an increased risk of several systemic changes in male, particularly obesity (21-23) and cognitive decline (24-26). Although previous studies in men showed a positive correlation between insulin-resistant obesity and testosterone deficiency (27, 28), several studies in animal models demonstrated inconsistent findings (29-31). In addition, it has been shown that either insulin-resistant obesity alone (32-34) or testosterone deficiency alone (9, 16, 17) is involved in the development of the cognitive

impairment. Although most previous studies demonstrated the beneficial effects of testosterone on cognition, a recent systematic review demonstrated that the association between testosterone and cognitive function was not significantly different in both genders (35).

Obesity and testosterone deficiency

Obesity is a public health problem which has increased dramatically in many countries around the world (36). Obesity causes serious medical complications, including atherosclerosis (37, 38), cardiovascular diseases (39) and cognitive decline (32, 34, 40-42). The possible causes of obesity are due to genetic inheritance (43, 44), physical inactivity (45) and high calorie diet consumption (46). Previous studies reported that obesity due to high calorie intake is a major cause of insulin resistance, Type 2 diabetes mellitus (T2DM) and metabolic syndrome (47, 48).

Interestingly, both preclinical studies and clinical reports demonstrated that obesity is associated with low serum testosterone levels or testosterone deficiency. These reports are summarized in Table 1. In preclinical studies, obese male animals induced by long-term high-calories diet consumption developed peripheral insulin resistance by impaired lipid profile, increased plasma insulin levels and increased adipose tissue accumulation as well as decreased plasma testosterone levels (49-55). In this regard, obesity induced testosterone deficiency has been proposed to occur through obese-induced insulin resistance since insulin-resistant obesity has been shown to increase inflammatory process (54, 56, 57), and aromatase enzyme production (58). The studies in male rabbit models demonstrated that obesity leads to the increase of several pro-inflammatory substrates such as TNF-α, IL-8, IL-6, and IL1$\alpha\beta$, which have been shown to trigger the development of peripheral insulin resistance (54). Increased TNF-α has been shown to decrease hypothalamic-pituitary axis activity, resulting in a decrease in testosterone secretion (56, 57). Another study in high-fat diet (HFD) induced male obese rabbits also showed that obesity leads to increased inflammation and decreased plasma testosterone levels via decreased gonadotropin-releasing hormone (GnRH), luteinizing hormone (LH), and follicle-stimulating hormone (FSH) signals (50). Moreover, it has been shown that

increased adipose tissues in obese male rats were found to cause increased aromatase enzyme production, in which this enzyme could convert testosterone to estradiol thus resulting in a decrease in plasma testosterone levels (55). The increased adipose tissue has also been shown to increase the secretion of adipokines such as plasma leptin (51, 55, 59). Several studies showed that increased leptin levels and estradiol levels could inhibit the HPT axis by inhibiting Kisspeptin, which has been shown to play a role in the regulation of GnRH secretion in the hypothalamus in order to produce normal testosterone levels (60-62). The inhibition of Kisspeptin also leads to a decrease in LH pulse to testis and further reduced testosterone secretion (60, 61, 63). In addition, a study in HFD-induced obesity rats showed the reduction of AR expression and decreased Akt protein expression in the ventral prostate (53). All of these findings suggest that obese-insulin resistant condition is closely associated with the decreased testosterone secretion and reduced testosterone activity. In addition, complications following obesity are not only insulin resistance, but also hypertension (64, 65). Both complications lead to increased circulating oxidative stress, possibly causing decreased testosterone levels in obesity.

Consistent with preclinical studies, studies in men also demonstrated that increased body weight or body mass index (BMI) together with insulin resistance, as indicated by increased HOMA-IR index, is associated with low plasma testosterone and SHBG levels (28, 66-71). Furthermore, a study in men with insulin-resistant obesity demonstrated the impairment of insulin receptor function in Leydig cells and decreased testosterone secretion (67). The findings of testosterone deficiency in obese men may occur due to the combination of aging and other systemic abnormalities including increased oxidative stress following insulin-resistant obesity.

In contrast, some studies demonstrated that body weight loss correlated with a low testosterone level, particularly in amateur wrestlers and weight lifters (72-74). Those studies suggest that weight loss with decreased testosterone levels could be due to the limitation of food intake and high levels of cortisol during their training.

From these reports, it can be concluded that obesity by itself could lead to a gradual decrease of testosterone levels in both animals and men by increased inflammatory

substrates, increased aromatase enzymes that convert testosterone to estradiol, as well as suppressed HPT axis.

Does testosterone deficiency lead to insulin-resistant obesity?

The relationship between testosterone deficiency and insulin-resistant obesity is still unclear. Previous studies suggest that not only obesity could induce hopogonadism, but also hypogonadism could lead to obesity (60, 61, 75). Studies of male castrated animals showed increased body weight, increased visceral fat deposition, increased BMI, increased plasma insulin level and plasma leptin levels as well as impaired lipid profiles (15, 76, 77). Consistent with those studies, it has been demonstrated that testosterone is involved in lipolysis and lipid homeostasis, because testosterone deficiency impaired lipid homeostasis, and resulted in increased adipogenesis (61, 78). Furthermore, another study showed that orchiectomized animals had decreased insulin responsiveness and insulin sensitivity (76). Studies in cultured adipocytes and skeletal muscle cells found that testosterone increased glucose transporter-4 (GLUT-4) expression and increased insulin receptor substrates-1 (IRS-1) phosphorylation (79). These findings suggest that testosterone is involved in glucose metabolism and insulin signaling. Therefore, a state of testosterone deficiency could impair glucose homeostasis and impair insulin signaling, leading to the development of obesity, insulin resistance and T2DM.

In clinical studies, the longitudinal studies in middle-aged men followed for more than five years demonstrated that low levels of testosterone and SHBG can lead to obesity, increased body mass index (BMI), increased waist hip ratio (WHR), and the development of the metabolic syndrome or T2DM (21, 80, 81).

Despite those reports, several studies in castrated rats showed the reduction of body weight and decreased muscle mass following testosterone deficiency (29-31, 82-85). The data suggested that the reduction of body weight in orchiectomized rats was caused by the reduction of daily food intake (29, 85) and muscle atrophy (29, 82, 84). It has been proposed that rats with testosterone deficiency had decreased neuropeptide-Y in the hypothalamus (86), resulting in a decreased appetite. However, Barat and colleagues demonstrated gonadectomy in obese male Zucker rats did not consistently alter weight gain (87). All findings in animal models indicate that the testosterone deficiency in rats

showed weight reduction whereas in larger animal models such as cats and rabbits increased weight was shown. The findings in the latter groups were consistent with the clinical reports. All of these findings emphasized the different effects of testosterone deficiency in different species. The differences in those findings could depend on strain, age of animals or length of gonadectomy. A summary of those reports was shown in part of preclinical study of Table 2. However, the underlying mechanisms of the differences need to be further investigated.

From these reports, it can be concluded that testosterone deficiency could lead to obesity via increased fat accumulation, impaired lipid and glucose metabolism in both men and larger animals such as rabbits and cats. However, the negative obese development following testosterone deficiency in rats might be due to the strong effect of testosterone on appetite in the rat model.

Testosterone acts as a neuroprotective agent in the brain.

The beneficial effects of testosterone are not only on the peripheral tissues, but also represent in the brain (88). Under the physiological condition, testosterone exerts its effects on brain development, behavior controls, and provides neuroprotection (9, 16). Previous studies demonstrated that testosterone and its metabolite, DHT, can pass the blood-brain barrier (BBB) to exert their effects in the brain via androgen receptors (ARs) (89). ARs are widely distributed in various parts of the brain, including the prefrontal cortex, amygdala, and hippocampus (9).

The studies of the primary cerebellar granule cell cultures demonstrated that testosterone and its metabolite, DHT, increased cell viability, deceased cell apoptosis and cell death following the induction with either the aggregation of Aβ peptides (90) or H2O2 induced apoptosis cell death (91). Furthermore, a previous study showed that testosterone increased anti-oxidant enzyme, catalase, in H2O2 induced apoptosis of cerebellar granule cells death (91). The study in neuroblastoma (N2a) cells transfected with βAPP695 and in primary neuronal cell cultures also found that testosterone treatment decreased the amyloid-β precursor protein (92).

Consistent with in vitro studies, castration in male rats caused an increased neuronal apoptosis, decreased anti-oxidant enzymes in hippocampal regions and

increased Aβ accumulation in the brain (17, 93). These adverse effects following castration could be reversed by testosterone treatment (17, 93, 94). In addition, a previous study showed that testosterone treatment after castration in rats could decrease Aβ accumulation in the brain via the activation of ARs (93). This finding agrees with a previous study in mice showing that decreased AR expression in brain of castrated mice could be restored by testosterone treatment (94). All of these findings suggest that testosterone and its metabolites could act as a neuroprotective agent in the brain.

Although most studies demonstrated the beneficial effects of testosterone as a neuroprotective agent in the brain, several in vitro and in vivo studies demonstrated that testosterone can cause adverse effects in the pathological brain or neuronal cells. For example, 1) the administration of testosterone at 10 μM increased the percentage of cells killed in the model of glutamate-induced neuronal cell death (95). 2) The administration of testosterone and DHT at 100 nM increased the percentage of apoptotic cells and caused mitochondrial dysfunction via either increased peroxide levels or decreased thiols levels as well as activated the PKC apoptotic pathway in the model of dopaminergic cell lines (N27 cells) (96). 3) The administration of testosterone in micromoles (1μM and 10 μM) increased cell apoptosis via alters inositol 1,4,5-trisphosphate receptor(InsP3R)-mediated Ca2+ release and resulting the prolong Ca2+ signals lead to apoptotic cell death in human neuroblastoma cell line (97). 4) A single dose of testosterone propionate (5 μg) administered to adult male CD-1 mice before induced neurotoxicity with methamphetamine caused severe neurotoxicity by decreased vesicular monoamine transporter-2 (VMAT-2) protein expression as well as decreased striatal dopamine levels (98).

A summary of these reports are shown in Table 3. All of these findings suggest that the adverse effects of testosterone may occur in models of a brain with pathology, whereas the beneficial effects or neutral effect of testosterone can be found in normal brain models with testosterone deficiency.

From these reports, it can be concluded that testosterone provides neuroprotective effects such as deceased cell apoptosis and cell death, increased anti-oxidant enzymes, prevented the aggregation of Aβ precursor protein in both in vitro and in vivo studies.

However, some evidence also demonstrated that testosterone can cause adverse effects in the brain when administrated with high doses during a pathological condition. Therefore, the testosterone supplement in human needs to be of concern regarding dosage, duration and any pathological conditions before the administration.

Testosterone deficiency and cognitive function

Synaptic plasticity is the underlying mechanism for modulating the learning and memory formation in the brain (99). Testosterone has been shown to be involved in the synaptic plasticity formation by modulating the normal synaptic formation in the brain (100). Previous studies demonstrated the positive correlation between memory decline and low plasma testosterone levels in the model of Alzheimer's disease (101-104), indicating that testosterone could be involved in the cognitive function.

Romeo and colleagues reported that testosterone plays a role in the synaptic plasticity and cognitive function in the brain by mediating neurotransmitter release, such as glutamate, acetylcholine and also involving in N-methyl-D-aspartate (NMDA) receptors insertion at the post-synaptic sites in adult male rats (105). It is known that the modulation of the synaptic plasticity in the brain is crucial for learning and memory. In orchiectomized rodents, the impairment of learning and memory in those animals has been demonstrated (106-109). In addition, the reduction of the number of dendritic spines and changes in dendritic spine morphology in hippocampal CA1 regions have been found in male orchiectomized rodents (110), which could be restored by testosterone or DHT replacement (110-112). Consistent with preclinical reports, the preliminary and pilot clinical studies in older men demonstrated that low testosterone levels were correlated with learning and memory decline (24, 25), and that testosterone treatment could improve verbal memory test and spatial learning and memory in hypogonadal men and men with Alzheimer's disease (113-115). However, other co-morbid pathologies should be of concern in the older male population, because those co-morbid pathologies could influence testosterone action and lead to cognitive impairment.

Although most of the previous studies demonstrated beneficial effects of testosterone on cognition, the recent systematic review from Boss and colleagues demonstrated non-significant findings in humans for testosterone and cognitive function, in

which Boss suggested that those findings may have been influenced by methodological differences from others, including research designs, sufficiently consistent cognitive measurements, and clear descriptions of handling and storage of biological specimens (35). Furthermore, the recent study of Cunningham and colleagues showed that normal testosterone levels in an oxidative stress condition were associated with cognitive impairment in Caucasian men, whereas not associated in an obese Mexican American population (116). This finding suggests that ethnic differences could affect the relationship between testosterone and cognition. Therefore, the complex multifactorial relationship between testosterone and cognition in clinical studies must consider factors including age, dose of testosterone, pathological conditions in the brain as well as ethnicity.

In addition, the effects of testosterone replacement in hypogonadal conditions of both animal models (117-120) and humans (102, 104, 121-123) are still controversial, particularly regarding the learning and memory, since several studies demonstrated that testosterone replacement in a hypogonadal condition had either no effect or adverse effect on cognition, a summary of those reports is shown in Table 4. Controversial findings in animal studies could be due to differences in animal models, doses of testosterone, duration of treatment and routes of testosterone administration. Adverse effects of testosterone on cognitive function were also found when testosterone was directly injected into the hippocampal region (108, 109, 117, 118). However, the controversial reports in the clinical studies may involve the differences in ages and degree of memory loss in each clinical study. Therefore, the effects of testosterone replacement should be further investigated by focusing on the effective doses, routes of administration, and duration of treatment to clarify the certain effects of testosterone replacement on cognition.

Furthermore, previous studies suggest that SHBG levels and other hormones such as thyroid stimulating hormone (TSH) were related to the incidence of Alzheimer's disease (AD) (124, 125). For example, it has been shown that either increased SHBG levels or decreased thyroid stimulating hormone in elderly men was associated with a high incidence of AD (124). Muller and colleagues also found that higher levels of SHBG increased the risk for AD and overall dementia in elderly men and women (126). In addition, a previous study in elderly men also demonstrated that men with AD were

correlated with low level of insulin-like growth factors (IGF-1) (127). It has been shown that IGF-1 exerts a protective effect against Aβ toxicity and inhibits tau phosphorylation (128), suggesting that decreased IGF-1 levels could be associated with the increased incidence of AD in elderly men. These findings suggest that in addition to testosterone, SHBG, TSH and IGF-1 could be potential predictors of cognitive impairment.

From these reports, it can be concluded that testosterone has bidirectional effects on cognitive function in both animals and men. The positive or negative effects of testosterone on cognition in animal studies could be due to differences in animal models, doses of testosterone, duration of treatment and routes of testosterone administration. However, the positive or negative effects of testosterone on cognition in the clinical studies may involve the differences in ages and degree of memory loss in each clinical study. Therefore, the effects of testosterone replacement on cognition should be further investigated by focusing on the effective doses, routes of administration, and duration of treatment. In addition to testosterone, SHBG or TSH as well as IGF-1 could be a predictor of cognitive impairment.

Insulin-resistant obesity and cognitive function

Obesity is known to lead to cognitive declines in animal models and humans (129). Our previous studies demonstrated that obese rats induced by HFD impaired peripheral insulin sensitivity, impaired brain insulin receptor function, increased brain oxidative stress, leading to impaired learning and memory (130-132). Several in vivo studies suggest that obesity associated with the impairment of cognition could be related to an insulin resistant condition (32-34). In addition, several studies in HFD-induced obese rodents demonstrated that obesity with insulin resistance caused Aβ plaques and Aβ accumulation in the hippocampal area (133, 134) as well as increased TNF-α and IL-6 in the brain (135). These conditions had been shown to cause the reduction in learning and memory in those animal models. Consistent with preclinical studies, several clinical studies in men demonstrated that insulin-resistant obesity is associated with a high risk of memory decline and Alzheimer's disease (34, 136-138).

From these reports, it can be concluded that insulin-resistant obesity could lead to cognitive impairment. The underlying mechanism may be that obesity leads to the

development of insulin resistance, increased brain oxidative stress, impaired brain insulin signaling, as well as increased Aβ accumulation, resulting cognitive impairment in both animals and men.

Evidence on the association among testosterone deficiency, insulin-resistant obesity, and memory decline

Several studies demonstrated that insulin-resistant obesity is associated with testosterone deficiency or vice versa (29-31, 51-54). Furthermore, either obese-insulin resistance or testosterone deficiency has been shown to cause brain dysfunction, leading to memory decline and the development of Alzheimer's disease (101).

The impairment of learning and memory occurring following decreased testosterone levels (60, 61, 75), may result from either the direct effect of testosterone deficiency onto the brain function or testosterone deficiency caused fat accumulation, insulin resistance and brain dysfunction. Testosterone deficiency caused direct adverse effects in the brain, including increased Aβ protein accumulation (93), increased oxidative stress (17), decreased AR expression (93, 94), decreased synaptic plasticity (106), decreased neurotransmitter release (105), and decreased dendritic spine density (110-112). Furthermore, it has been shown that a long-term effect of a high calorie diet (34, 52, 53) and testosterone deficiency (61, 78) could cause increased adipose tissue deposition, leading to the development of insulin resistance via lipotoxicity (139), increased inflammatory substrates (47), increased oxidative stress(32, 33), decreased anti-oxidant agents, impaired insulin sensitivity (130, 132), impaired lipid profiles (34, 140) and impaired brain insulin receptor function (130-132), resulting in the impairment of learning and memory. In addition, an increase of fat accumulation could cause an increased inflammatory substrates (50), increased leptin, and increased aromatase enzyme, resulting in the inhibition of the HPT axis, thus leading to the decrease in GnRH and decreased LH pulse (51, 55, 58). These proposed mechanisms explain the possible roles of insulin-resistant obesity together with testosterone deficiency in promoting a decline in cognitive function. In conclusion, cognitive impairment may result from either the direct effect of testosterone deficiency on the brain function or testosterone deficiency associated with obesity that caused fat accumulation, insulin resistance and finally cognitive impairment.

In addition to testosterone, future studies are needed to verify other hormones such as SHBG, TSH or IGF-1 as possible predictors of cognitive impairment.

All of previous findings led to several research questions. 1) What were the effects of testosterone deprivation together with obesity on the synaptic plasticity or dendritic spine density? Our recent study demonstrated that vildagliptin effectively restored brain insulin receptor function and prevented brain mitochondrial dysfunction, thus attenuating the impaired cognitive function caused by HFD. 2) Could DDP-IV inhibitor restore those impairments in obese-insulin resistant rats with testosterone deprivation? In addition, the effect of dietary intervention involved simply switching from HFD to regular chow in obese insulin resistant rats with or without testosterone deprivation on brain insulin resistance, synaptic plasticity, brain mitochondrial function and cognition has not yet been investigated. 3) Could dietary intervention involved simply switching from HFD to regular chow in obese insulin resistant rats with or without testosterone deprivation improve brain insulin resistance, synaptic plasticity, brain mitochondrial function and cognition?

Therefore, in the present study hypothesized that 1) **Testosterone deprivation alone** caused the peripheral insulin resistance, brain insulin resistance, the impairment of synaptic plasticity, the impairment of brain mitochondrial function, decreased in hippocampal dendritic spine formation and the cognitive decline.; 2) The combination of obesity induced by HFD consumption and loss of testosterone **accelerated** peripheral insulin resistance, brain insulin resistance, the impairment of synaptic plasticity, the impairment of brain mitochondrial function, decreased hippocampal dendritic spine formation, and the cognitive decline, compared to those with obesity alone or those with testosterone deprivation alone; and 3) **either DDP-IV inhibitor or the dietary intervention** improved brain insulin resistance, synaptic plasticity, increased dendritic spine formation, increased brain mitochondrial function and cognition in obese-insulin resistant rats with or without testosterone deprivation.

Objectives of study

Specific Aim 1: To determine whether testosterone deprivation alone causes 1) brain insulin resistance by decreased neuronal insulin receptor function (insulin-induced LTD) and brain insulin signaling, 2) the impairment of synaptic plasticity by decreased

hippocampal long-term potentiation (LTP), 3) the impairment of brain mitochondrial function, 4) decreased in hippocampal dendritic spines and 5) the cognitive decline.

Specific Aim 2: To investigate whether the combination of obesity induced by HFD consumption and the loss of testosterone **accelerates** brain insulin resistance, the impairment of synaptic plasticity, the impairment of brain mitochondrial function, decreased hippocampal dendritic spines, and cognitive decline, compared to those with obesity alone or those with testosterone deprivation alone.

Specific Aim 3: To investigate the effects of anti-diabetic drug DPP-4 inhibitor on brain insulin resistance, hippocampal synaptic plasticity, hippocampal dendritic spine formation, brain mitochondrial function and cognition in obese male rats induced by HFD consumption with or without testosterone deprivation.

Specific Aim 4: To investigate the effects of dietary intervention on brain insulin resistance including brain insulin receptor function and brain insulin signaling, hippocampal synaptic plasticity, hippocampal dendritic spine formation, brain mitochondrial function and cognition in obese male rats induced by HFD consumption with or without testosterone deprivation.

References

1. Ewing LL, Wing TY, Cochran RC, Kromann N, Zirkin BR. Effect of luteinizing hormone on Leydig cell structure and testosterone secretion. Endocrinology. 1983 May;112(5):1763-9.

2. Vinson GP, Bell JB, Whitehouse BJ. Production of testosterone and corticosteroids by the rat adrenal gland incubated in vitro and the effects of stimulation with ACTH, LH and FSH. J Steroid Biochem. 1976 May;7(5):407-11.

3. Emanuele MA, Emanuele N. Alcohol and the male reproductive system. Alcohol Res Health. 2001;25(4):282-7.

4. Franchimont P, Chari S, Demoulin A. Hypothalamus-pituitary-testis interaction. J Reprod Fertil. 1975 Aug;44(2):335-50.

5. Nunemaker CS, Satin LS. Episodic hormone secretion: a comparison of the basis of pulsatile secretion of insulin and GnRH. Endocrine. 2014 Mar 8.

6. Kapoor D, Malkin CJ, Channer KS, Jones TH. Androgens, insulin resistance and vascular disease in men. Clin Endocrinol (Oxf). 2005 Sep;63(3):239-50.

7. Betancourt-Albrecht M, Cunningham GR. Hypogonadism and diabetes. Int J Impot Res. 2003 Aug;15 Suppl 4:S14-20.

8. Li J, Al-Azzawi F. Mechanism of androgen receptor action. Maturitas. 2009 Jun 20;63(2):142-8.

9. Janowsky JS. Thinking with your gonads: testosterone and cognition. Trends Cogn Sci. 2006 Feb;10(2):77-82.

10. Pelletier G, Labrie C, Labrie F. Localization of oestrogen receptor alpha, oestrogen receptor beta and androgen receptors in the rat reproductive organs. J Endocrinol. 2000 May;165(2):359-70.

11. Takeda H, Chodak G, Mutchnik S, Nakamoto T, Chang C. Immunohistochemical localization of androgen receptors with mono- and polyclonal antibodies to androgen receptor. J Endocrinol. 1990 Jul;126(1):17-25.

12. Volterrani M, Rosano G, Iellamo F. Testosterone and heart failure. Endocrine. 2012 Oct;42(2):272-7.

13. Schiavi RC, White D. Androgens and male sexual function: a review of human studies. J Sex Marital Ther. 1976 Fall;2(3):214-28.

14. Aydilek N, Aksakal M. Effects of testosterone on lipid peroxidation, lipid profiles and some coagulation parameters in rabbits. J Vet Med A Physiol Pathol Clin Med. 2005 Nov;52(9):436-9.

15. Christoffersen BO, Gade LP, Golozoubova V, Svendsen O, Raun K. Influence of castration-induced testosterone and estradiol deficiency on obesity and glucose metabolism in male Gottingen minipigs. Steroids. 2010 Oct;75(10):676-84.

16. Filova B, Ostatnikova D, Celec P, Hodosy J. The effect of testosterone on the formation of brain structures. Cells Tissues Organs. 2013;197(3):169-77.

17. Meydan S, Kus I, Tas U, Ogeturk M, Sancakdar E, Dabak DO, et al. Effects of testosterone on orchiectomy-induced oxidative damage in the rat hippocampus. J Chem Neuroanat. 2010 Dec;40(4):281-5.

18. Ogawa S, Lubahn DB, Korach KS, Pfaff DW. Behavioral effects of estrogen receptor gene disruption in male mice. Proc Natl Acad Sci U S A. 1997 Feb 18;94(4):1476-81.

19. Wu FC, Tajar A, Beynon JM, Pye SR, Silman AJ, Finn JD, et al. Identification of late-onset hypogonadism in middle-aged and elderly men. N Engl J Med. 2010 Jul 8;363(2):123-35.

20. Tsujimura A. The Relationship between Testosterone Deficiency and Men's Health. World J Mens Health. 2013 Aug;31(2):126-35.

21. Shi Z, Araujo AB, Martin S, O'Loughlin P, Wittert GA. Longitudinal changes in testosterone over five years in community-dwelling men. J Clin Endocrinol Metab. 2013 Aug;98(8):3289-97.

22. Stellato RK, Feldman HA, Hamdy O, Horton ES, McKinlay JB. Testosterone, sex hormone-binding globulin, and the development of type 2 diabetes in middle-aged men: prospective results from the Massachusetts male aging study. Diabetes Care. 2000 Apr;23(4):490-4.

23. Montalcini T, Migliaccio V, Ferro Y, Gazzaruso C, Pujia A. Androgens for postmenopausal women's health? Endocrine. 2012 Dec;42(3):514-20.

24. Janowsky JS, Oviatt SK, Orwoll ES. Testosterone influences spatial cognition in older men. Behav Neurosci. 1994 Apr;108(2):325-32.

25. Morley JE, Perry HM, 3rd. Androgen deficiency in aging men. Med Clin North Am. 1999 Sep;83(5):1279-89, vii.

26. Trolle C, Hjerrild B, Cleemann L, Mortensen KH, Gravholt CH. Sex hormone replacement in Turner syndrome. Endocrine. 2012 Apr;41(2):200-19.

27. Grossmann M, Thomas MC, Panagiotopoulos S, Sharpe K, Macisaac RJ, Clarke S, et al. Low testosterone levels are common and associated with insulin resistance in men with diabetes. J Clin Endocrinol Metab. 2008 May;93(5):1834-40.

28. Haffner SM, Karhapaa P, Mykkanen L, Laakso M. Insulin resistance, body fat distribution, and sex hormones in men. Diabetes. 1994 Feb;43(2):212-9.

29. Borst SE, Conover CF. Orchiectomized Fischer 344 male rat models body composition in hypogonadal state. Life Sci. 2006 Jun 20;79(4):411-5.

30. Erben RG, Eberle J, Stahr K, Goldberg M. Androgen deficiency induces high turnover osteopenia in aged male rats: a sequential histomorphometric study. J Bone Miner Res. 2000 Jun;15(6):1085-98.

31. Kakolewski JW, Cox VC, Valenstein ES. Sex differences in body-weight change following gonadectomy of rats. Psychol Rep. 1968 Apr;22(2):547-54.

32. Pintana H, Apaijai N, Chattipakorn N, Chattipakorn SC. DPP-4 inhibitors improve cognition and brain mitochondrial function of insulin resistant rats. J Endocrinol. 2013 Apr 16.

33. Pintana H, Apaijai N, Pratchayasakul W, Chattipakorn N, Chattipakorn SC. Effects of metformin on learning and memory behaviors and brain mitochondrial functions in high fat diet induced insulin resistant rats. Life Sci. 2012 Aug 20.

34. Stranahan AM, Norman ED, Lee K, Cutler RG, Telljohann RS, Egan JM, et al. Diet-induced insulin resistance impairs hippocampal synaptic plasticity and cognition in middle-aged rats. Hippocampus. 2008;18(11):1085-8.

35. Boss L, Kang DH, Marcus M, Bergstrom N. Endogenous sex hormones and cognitive function in older adults: a systematic review. West J Nurs Res. 2014 Mar;36(3):388-426.

36. Kitzinger H, Karle B. The epidemiology of obesity. Eur Surg. 2013;45(2):80-2.

37. Semenkovich CF. Insulin resistance and atherosclerosis. J Clin Invest. 2006 Jul;116(7):1813-22.

38. Kohara K. Sarcopenic obesity in aging population: current status and future directions for research. Endocrine. 2014 Feb;45(1):15-25.

39. Abbasi F, Brown BW, Jr., Lamendola C, McLaughlin T, Reaven GM. Relationship between obesity, insulin resistance, and coronary heart disease risk. J Am Coll Cardiol. 2002 Sep 4;40(5):937-43.

40. Greenwood CE, Winocur G. Glucose treatment reduces memory deficits in young adult rats fed high-fat diets. Neurobiol Learn Mem. 2001 Mar;75(2):179-89.

41. Winocur G, Greenwood CE, Piroli GG, Grillo CA, Reznikov LR, Reagan LP, et al. Memory impairment in obese Zucker rats: an investigation of cognitive function in an animal model of insulin resistance and obesity. Behav Neurosci. 2005 Oct;119(5):1389-95.

42. Reusch JE. Current concepts in insulin resistance, type 2 diabetes mellitus, and the metabolic syndrome. Am J Cardiol. 2002 Sep 5;90(5A):19G-26G.

43. Fawcett KA, Barroso I. The genetics of obesity: FTO leads the way. Trends Genet. 2010 Jun;26(6):266-74.

44. Park EJ, Lee JH, Yu GY, He G, Ali SR, Holzer RG, et al. Dietary and genetic obesity promote liver inflammation and tumorigenesis by enhancing IL-6 and TNF expression. Cell. 2010 Jan 22;140(2):197-208.

45. Eckardt K, Taube A, Eckel J. Obesity-associated insulin resistance in skeletal muscle: role of lipid accumulation and physical inactivity. Rev Endocr Metab Disord. 2011 Sep;12(3):163-72.

46. Clegg DJ, Gotoh K, Kemp C, Wortman MD, Benoit SC, Brown LM, et al. Consumption of a high-fat diet induces central insulin resistance independent of adiposity. Physiol Behav. 2011 Apr 18;103(1):10-6.

47. Kahn BB, Flier JS. Obesity and insulin resistance. J Clin Invest. 2000 Aug;106(4):473-81.

48. Pandolfi C, Pellegrini L, Sbalzarini G, Mercantini F. [Obesity and insulin resistance]. Minerva Med. 1994 Apr;85(4):167-71.

49. Erdemir F, Atilgan D, Markoc F, Boztepe O, Suha-Parlaktas B, Sahin S. [The effect of diet induced obesity on testicular tissue and serum oxidative stress parameters]. Actas Urol Esp. 2012 Mar;36(3):153-9.

50. Filippi S, Vignozzi L, Morelli A, Chavalmane AK, Sarchielli E, Fibbi B, et al. Testosterone partially ameliorates metabolic profile and erectile responsiveness to PDE5 inhibitors in an animal model of male metabolic syndrome. J Sex Med. 2009 Dec;6(12):3274-88.

51. Olivares A, Mendez JP, Zambrano E, Cardenas M, Tovar A, Perera-Marin G, et al. Reproductive axis function and gonadotropin microheterogeneity in a male rat model of diet-induced obesity. Gen Comp Endocrinol. 2009 Apr 1;166(2):356-64.

52. Ribeiro DL, Pinto ME, Maeda SY, Taboga SR, Goes RM. High fat-induced obesity associated with insulin-resistance increases FGF-2 content and causes stromal hyperplasia in rat ventral prostate. Cell Tissue Res. 2012 Aug;349(2):577-88.

53. Ribeiro DL, Pinto ME, Rafacho A, Bosqueiro JR, Maeda SY, Anselmo-Franci JA, et al. High-Fat Diet Obesity Associated with Insulin Resistance Increases Cell Proliferation, Estrogen Receptor, and PI3K Proteins in Rat Ventral Prostate. J Androl. 2012 Apr 5.

54. Vignozzi L, Morelli A, Sarchielli E, Comeglio P, Filippi S, Cellai I, et al. Testosterone protects from metabolic syndrome-associated prostate inflammation: an experimental study in rabbit. J Endocrinol. 2012 Jan;212(1):71-84.

55. Vigueras-Villasenor RM, Rojas-Castaneda JC, Chavez-Saldana M, Gutierrez-Perez O, Garcia-Cruz ME, Cuevas-Alpuche O, et al. Alterations in the spermatic function generated by obesity in rats. Acta Histochem. 2011 Feb;113(2):214-20.

56. Jones TH. Testosterone deficiency: a risk factor for cardiovascular disease? Trends Endocrinol Metab. 2010 Aug;21(8):496-503.

57. Jones TH. Effects of testosterone on Type 2 diabetes and components of the metabolic syndrome. J Diabetes. 2010 Sep;2(3):146-56.

58. Cohen PG. Aromatase, adiposity, aging and disease. The hypogonadal-metabolic-atherogenic-disease and aging connection. Med Hypotheses. 2001 Jun;56(6):702-8.

59. Martin LJ. Implications of adiponectin in linking metabolism to testicular function. Endocrine. 2014 May;46(1):16-28.

60. Cohen PG. The hypogonadal-obesity cycle: role of aromatase in modulating the testosterone-estradiol shunt--a major factor in the genesis of morbid obesity. Med Hypotheses. 1999 Jan;52(1):49-51.

61. Kelly DM, Jones TH. Testosterone: a metabolic hormone in health and disease. J Endocrinol. 2013 Jun;217(3):R25-45.

62. Okamura H, Tsukamura H, Ohkura S, Uenoyama Y, Wakabayashi Y, Maeda K. Kisspeptin and GnRH pulse generation. Adv Exp Med Biol. 2013;784:297-323.

63. Smith JT, Dungan HM, Stoll EA, Gottsch ML, Braun RE, Eacker SM, et al. Differential regulation of KiSS-1 mRNA expression by sex steroids in the brain of the male mouse. Endocrinology. 2005 Jul;146(7):2976-84.

64. Fogari R, Zoppi A, Preti P, Rinaldi A, Marasi G, Vanasia A, et al. Sexual activity and plasma testosterone levels in hypertensive males. Am J Hypertens. 2002 Mar;15(3):217-21.

65. Torkler S, Wallaschofski H, Baumeister SE, Volzke H, Dorr M, Felix S, et al. Inverse association between total testosterone concentrations, incident hypertension and blood pressure. Aging Male. 2011 Sep;14(3):176-82.

66. Ho CH, Yu HJ, Wang CY, Jaw FS, Hsieh JT, Liao WC, et al. Prediabetes is associated with an increased risk of testosterone deficiency, independent of obesity and metabolic syndrome. PLoS One. 2013;8(9):e74173.

67. Pitteloud N, Hardin M, Dwyer AA, Valassi E, Yialamas M, Elahi D, et al. Increasing insulin resistance is associated with a decrease in Leydig cell testosterone secretion in men. J Clin Endocrinol Metab. 2005 May;90(5):2636-41.

68. Tsai EC, Matsumoto AM, Fujimoto WY, Boyko EJ. Association of bioavailable, free, and total testosterone with insulin resistance: influence of sex hormone-binding globulin and body fat. Diabetes Care. 2004 Apr;27(4):861-8.

69. Tylinska M, Broncel M. [The relationship between testosterone deficiency and metabolic syndrome in obese men]. Pol Merkur Lekarski. 2013 Jan;34(199):24-8.

70. Yeap BB, Chubb SA, Hyde Z, Jamrozik K, Hankey GJ, Flicker L, et al. Lower serum testosterone is independently associated with insulin resistance in non-diabetic older men: the Health In Men Study. Eur J Endocrinol. 2009 Oct;161(4):591-8.

71. Zhang J, Huang X, Liao M, Gao Y, Tan A, Yang X, et al. Both total testosterone and sex hormone-binding globulin are independent risk factors for metabolic syndrome: results from Fangchenggang Area Male Health and Examination Survey in China. Diabetes Metab Res Rev. 2013 Jul;29(5):391-7.

72. Roemmich JN, Sinning WE. Weight loss and wrestling training: effects on growth-related hormones. J Appl Physiol (1985). 1997 Jun;82(6):1760-4.

73. Strauss RH, Lanese RR, Malarkey WB. Weight loss in amateur wrestlers and its effect on serum testosterone levels. JAMA. 1985 Dec 20;254(23):3337-8.

74. Di Luigi L, Romanelli F, Sgro P, Lenzi A. Andrological aspects of physical exercise and sport medicine. Endocrine. 2012 Oct;42(2):278-84.

75. Muraleedharan V, Jones TH. Testosterone and the metabolic syndrome. Ther Adv Endocrinol Metab. 2010 Oct;1(5):207-23.

76. Georgiev IP, Georgieva TM, Ivanov V, Dimitrova S, Kanelov I, Vlaykova T, et al. Effects of castration-induced visceral obesity and antioxidant treatment on lipid profile and insulin sensitivity in New Zealand white rabbits. Res Vet Sci. 2011 Apr;90(2):196-204.

77. Kanchuk ML, Backus RC, Calvert CC, Morris JG, Rogers QR. Weight gain in gonadectomized normal and lipoprotein lipase-deficient male domestic cats results from increased food intake and not decreased energy expenditure. J Nutr. 2003 Jun;133(6):1866-74.

78. Santosa S, Jensen MD. Effects of male hypogonadism on regional adipose tissue fatty acid storage and lipogenic proteins. PLoS One. 2012;7(2):e31473.

79. Chen X, Li X, Huang HY, Lin JF. [Effects of testosterone on insulin receptor substrate-1 and glucose transporter 4 expression in cells sensitive to insulin]. Zhonghua Yi Xue Za Zhi. 2006 Jun 6;86(21):1474-7.

80. Haffner SM, Shaten J, Stern MP, Smith GD, Kuller L. Low levels of sex hormone-binding globulin and testosterone predict the development of non-insulin-dependent diabetes mellitus in men. MRFIT Research Group. Multiple Risk Factor Intervention Trial. Am J Epidemiol. 1996 May 1;143(9):889-97.

81. Laaksonen DE, Niskanen L, Punnonen K, Nyyssonen K, Tuomainen TP, Valkonen VP, et al. Testosterone and sex hormone-binding globulin predict the metabolic syndrome and diabetes in middle-aged men. Diabetes Care. 2004 May;27(5):1036-41.

82. Axell AM, MacLean HE, Plant DR, Harcourt LJ, Davis JA, Jimenez M, et al. Continuous testosterone administration prevents skeletal muscle atrophy and enhances resistance to fatigue in orchidectomized male mice. Am J Physiol Endocrinol Metab. 2006 Sep;291(3):E506-16.

83. Chai JK, Blaha V, Meguid MM, Laviano A, Yang ZJ, Varma M. Use of orchiectomy and testosterone replacement to explore meal number-to-meal size relationship in male rats. Am J Physiol. 1999 May;276(5 Pt 2):R1366-73.

84. Gao W, Reiser PJ, Coss CC, Phelps MA, Kearbey JD, Miller DD, et al. Selective androgen receptor modulator treatment improves muscle strength and body composition and prevents bone loss in orchidectomized rats. Endocrinology. 2005 Nov;146(11):4887-97.

85. Gentry RT, Wade GN. Androgenic control of food intake and body weight in male rats. J Comp Physiol Psychol. 1976 Jan;90(1):18-25.

86. Sahu A, Kalra SP, Crowley WR, Kalra PS. Testosterone raises neuropeptide-Y concentration in selected hypothalamic sites and in vitro release from the medial basal hypothalamus of castrated male rats. Endocrinology. 1989 Jan;124(1):410-4.

87. Barat P, Livingstone DE, Elferink CM, McDonnell CR, Walker BR, Andrew R. Effects of gonadectomy on glucocorticoid metabolism in obese Zucker rats. Endocrinology. 2007 Oct;148(10):4836-43.

88. Durdiakova J, Ostatnikova D, Celec P. Testosterone and its metabolites--modulators of brain functions. Acta Neurobiol Exp (Wars). 2011;71(4):434-54.

89. Pardridge WM, Mietus LJ. Transport of steroid hormones through the rat blood-brain barrier. Primary role of albumin-bound hormone. J Clin Invest. 1979 Jul;64(1):145-54.

90. Pike CJ. Testosterone attenuates beta-amyloid toxicity in cultured hippocampal neurons. Brain Res. 2001 Nov 16;919(1):160-5.

91. Ahlbom E, Prins GS, Ceccatelli S. Testosterone protects cerebellar granule cells from oxidative stress-induced cell death through a receptor mediated mechanism. Brain Res. 2001 Feb 23;892(2):255-62.

92. Gouras GK, Xu H, Gross RS, Greenfield JP, Hai B, Wang R, et al. Testosterone reduces neuronal secretion of Alzheimer's beta-amyloid peptides. Proc Natl Acad Sci U S A. 2000 Feb 1;97(3):1202-5.

93. Ramsden M, Nyborg AC, Murphy MP, Chang L, Stanczyk FZ, Golde TE, et al. Androgens modulate beta-amyloid levels in male rat brain. J Neurochem. 2003 Nov;87(4):1052-5.

94. Apostolinas S, Rajendren G, Dobrjansky A, Gibson MJ. Androgen receptor immunoreactivity in specific neural regions in normal and hypogonadal male mice: effect of androgens. Brain Res. 1999 Jan 30;817(1-2):19-24.

95. Yang SH, Perez E, Cutright J, Liu R, He Z, Day AL, et al. Testosterone increases neurotoxicity of glutamate in vitro and ischemia-reperfusion injury in an animal model. J Appl Physiol (1985). 2002 Jan;92(1):195-201.

96. Cunningham RL, Giuffrida A, Roberts JL. Androgens induce dopaminergic neurotoxicity via caspase-3-dependent activation of protein kinase Cdelta. Endocrinology. 2009 Dec;150(12):5539-48.

97. Estrada M, Varshney A, Ehrlich BE. Elevated testosterone induces apoptosis in neuronal cells. J Biol Chem. 2006 Sep 1;281(35):25492-501.

98. Buletko AB, Dluzen DE, McDermott JL, Darvesh AS, Geldenhuys WJ. Markers associated with testosterone enhancement of methamphetamine-induced striatal dopaminergic neurotoxicity. Neurotoxicol Teratol. 2012 May-Jun;34(3):338-43.

99. Martin SJ, Grimwood PD, Morris RG. Synaptic plasticity and memory: an evaluation of the hypothesis. Annu Rev Neurosci. 2000;23:649-711.

100. MacLusky NJ, Hajszan T, Prange-Kiel J, Leranth C. Androgen modulation of hippocampal synaptic plasticity. Neuroscience. 2006;138(3):957-65.

101. Hogervorst E, Williams J, Budge M, Barnetson L, Combrinck M, Smith AD. Serum total testosterone is lower in men with Alzheimer's disease. Neuro Endocrinol Lett. 2001 Jun;22(3):163-8.

102. Lu PH, Masterman DA, Mulnard R, Cotman C, Miller B, Yaffe K, et al. Effects of testosterone on cognition and mood in male patients with mild Alzheimer disease and healthy elderly men. Arch Neurol. 2006 Feb;63(2):177-85.

103. Okun MS, DeLong MR, Hanfelt J, Gearing M, Levey A. Plasma testosterone levels in Alzheimer and Parkinson diseases. Neurology. 2004 Feb 10;62(3):411-3.

104. Kenny AM, Fabregas G, Song C, Biskup B, Bellantonio S. Effects of testosterone on behavior, depression, and cognitive function in older men with mild cognitive loss. J Gerontol A Biol Sci Med Sci. 2004 Jan;59(1):75-8.

105. Romeo RD, Staub D, Jasnow AM, Karatsoreos IN, Thornton JE, McEwen BS. Dihydrotestosterone increases hippocampal N-methyl-D-aspartate binding but does not affect choline acetyltransferase cell number in the forebrain or choline transporter levels in the CA1 region of adult male rats. Endocrinology. 2005 Apr;146(4):2091-7.

106. Sakata K, Tokue A, Kawai N. Altered synaptic transmission in the hippocampus of the castrated male mouse is reversed by testosterone replacement. J Urol. 2000 Apr;163(4):1333-8.

107. Sandstrom NJ, Kim JH, Wasserman MA. Testosterone modulates performance on a spatial working memory task in male rats. Horm Behav. 2006 Jun;50(1):18-26.

108. Spritzer MD, Daviau ED, Coneeny MK, Engelman SM, Prince WT, Rodriguez-Wisdom KN. Effects of testosterone on spatial learning and memory in adult male rats. Horm Behav. 2011 Apr;59(4):484-96.

109. Naghdi N, Majlessi N, Bozorgmehr T. The effect of intrahippocampal injection of testosterone enanthate (an androgen receptor agonist) and anisomycin (protein synthesis inhibitor) on spatial learning and memory in adult, male rats. Behav Brain Res. 2005 Jan 30;156(2):263-8.

110. Leranth C, Petnehazy O, MacLusky NJ. Gonadal hormones affect spine synaptic density in the CA1 hippocampal subfield of male rats. J Neurosci. 2003 Mar 1;23(5):1588-92.

111. Danzer SC, McMullen NT, Rance NE. Testosterone modulates the dendritic architecture of arcuate neuroendocrine neurons in adult male rats. Brain Res. 2001 Jan 26;890(1):78-85.

112. Li M, Masugi-Tokita M, Takanami K, Yamada S, Kawata M. Testosterone has sublayer-specific effects on dendritic spine maturation mediated by BDNF and PSD-95 in pyramidal neurons in the hippocampus CA1 area. Brain Res. 2012 Nov 12;1484:76-84.

113. Cherrier MM, Craft S, Matsumoto AH. Cognitive changes associated with supplementation of testosterone or dihydrotestosterone in mildly hypogonadal men: a preliminary report. J Androl. 2003 Jul-Aug;24(4):568-76.

114. Cherrier MM, Matsumoto AM, Amory JK, Ahmed S, Bremner W, Peskind ER, et al. The role of aromatization in testosterone supplementation: effects on cognition in older men. Neurology. 2005 Jan 25;64(2):290-6.

115. Tan RS, Pu SJ. A pilot study on the effects of testosterone in hypogonadal aging male patients with Alzheimer's disease. Aging Male. 2003 Mar;6(1):13-7.

116. Cunningham RL, Singh M, O'Bryant SE, Hall JR, Barber RC. Oxidative stress, testosterone, and cognition among Caucasian and Mexican-American men with and without Alzheimer's disease. J Alzheimers Dis. 2014;40(3):563-73.

117. Emamian S, Naghdi N, Sepehri H, Jahanshahi M, Sadeghi Y, Choopani S. Learning impairment caused by intra-CA1 microinjection of testosterone increases the number of astrocytes. Behav Brain Res. 2010 Mar 17;208(1):30-7.

118. Harooni HE, Naghdi N, Sepehri H, Rohani AH. Intra hippocampal injection of testosterone impaired acquisition, consolidation and retrieval of inhibitory avoidance learning and memory in adult male rats. Behav Brain Res. 2008 Mar 17;188(1):71-7.

119. Khorshidahmad T, Tabrizian K, Vakilzadeh G, Nikbin P, Moradi S, Hosseini-Sharifabad A, et al. Interactive effects of a protein kinase AII inhibitor and testosterone on spatial learning in the Morris water maze. Behav Brain Res. 2012 Mar 17;228(2):432-9.

120. Naghdi N, Asadollahi A. Genomic and nongenomic effects of intrahippocampal microinjection of testosterone on long-term memory in male adult rats. Behav Brain Res. 2004 Aug 12;153(1):1-6.

121. Maki PM, Ernst M, London ED, Mordecai KL, Perschler P, Durso SC, et al. Intramuscular testosterone treatment in elderly men: evidence of memory decline and altered brain function. J Clin Endocrinol Metab. 2007 Nov;92(11):4107-14.

122. Vaughan C, Goldstein FC, Tenover JL. Exogenous testosterone alone or with finasteride does not improve measurements of cognition in healthy older men with low serum testosterone. J Androl. 2007 Nov-Dec;28(6):875-82.

123. Wolf OT, Preut R, Hellhammer DH, Kudielka BM, Schurmeyer TH, Kirschbaum C. Testosterone and cognition in elderly men: a single testosterone injection blocks the practice effect in verbal fluency, but has no effect on spatial or verbal memory. Biol Psychiatry. 2000 Apr 1;47(7):650-4.

124. Holland J, Bandelow S, Hogervorst E. Testosterone levels and cognition in elderly men: a review. Maturitas. 2011 Aug;69(4):322-37.

125. Hogervorst E, Matthews FE, Brayne C. Are optimal levels of testosterone associated with better cognitive function in healthy older women and men? Biochim Biophys Acta. 2010 Oct;1800(10):1145-52.

126. Muller M, Schupf N, Manly JJ, Mayeux R, Luchsinger JA. Sex hormone binding globulin and incident Alzheimer's disease in elderly men and women. Neurobiol Aging. 2010 Oct;31(10):1758-65.

127. Duron E, Funalot B, Brunel N, Coste J, Quinquis L, Viollet C, et al. Insulin-like growth factor-I and insulin-like growth factor binding protein-3 in Alzheimer's disease. J Clin Endocrinol Metab. 2012 Dec;97(12):4673-81.

128. Carro E, Trejo JL, Gomez-Isla T, LeRoith D, Torres-Aleman I. Serum insulin-like growth factor I regulates brain amyloid-beta levels. Nat Med. 2002 Dec;8(12):1390-7.

129. Greenwood CE, Winocur G. High-fat diets, insulin resistance and declining cognitive function. Neurobiol Aging. 2005 Dec;26 Suppl 1:42-5.

130. Pipatpiboon N, Pintana H, Pratchayasakul W, Chattipakorn N, Chattipakorn SC. DPP4-inhibitor improves neuronal insulin receptor function, brain mitochondrial function and cognitive function in rats with insulin resistance induced by high-fat diet consumption. Eur J Neurosci. 2013 Dec 12.

131. Pipatpiboon N, Pratchayasakul W, Chattipakorn N, Chattipakorn SC. PPARgamma agonist improves neuronal insulin receptor function in hippocampus and brain mitochondria function in rats with insulin resistance induced by long term high-fat diets. Endocrinology. 2012 Jan;153(1):329-38.

132. Pratchayasakul W, Kerdphoo S, Petsophonsakul P, Pongchaidecha A, Chattipakorn N, Chattipakorn SC. Effects of high-fat diet on insulin receptor function in rat hippocampus and the level of neuronal corticosterone. Life Sci. 2011 Mar 28;88(13-14):619-27.

133. Barron AM, Rosario ER, Elteriefi R, Pike CJ. Sex-Specific Effects of High Fat Diet on Indices of Metabolic Syndrome in 3xTg-AD Mice: Implications for Alzheimer's Disease. PLoS One. 2013;8(10):e78554.

134. Maesako M, Uemura K, Kubota M, Kuzuya A, Sasaki K, Hayashida N, et al. Exercise is more effective than diet control in preventing high fat diet-induced beta-amyloid deposition and memory deficit in amyloid precursor protein transgenic mice. J Biol Chem. 2012 Jun 29;287(27):23024-33.

135. Pistell PJ, Morrison CD, Gupta S, Knight AG, Keller JN, Ingram DK, et al. Cognitive impairment following high fat diet consumption is associated with brain inflammation. J Neuroimmunol. 2010 Feb 26;219(1-2):25-32.

136. de la Monte SM. Insulin resistance and Alzheimer's disease. BMB Rep. 2009 Aug 31;42(8):475-81.

137. Hiltunen M, Khandelwal VK, Yaluri N, Tiilikainen T, Tusa M, Koivisto H, et al. Contribution of genetic and dietary insulin resistance to Alzheimer phenotype in APP/PS1 transgenic mice. J Cell Mol Med. 2012 Jun;16(6):1206-22.

138. Thambisetty M, Jeffrey Metter E, Yang A, Dolan H, Marano C, Zonderman AB, et al. Glucose intolerance, insulin resistance, and pathological features of Alzheimer disease in the Baltimore longitudinal study of aging. JAMA Neurol. 2013 Sep 1;70(9):1167-72.

139. Summers SA. Ceramides in insulin resistance and lipotoxicity. Prog Lipid Res. 2006 Jan;45(1):42-72.

140. Ros Perez M, Medina-Gomez G. [Obesity, adipogenesis and insulin resistance]. Endocrinol Nutr. 2011 Aug-Sep;58(7):360-9.

141. Hammond J, Le Q, Goodyer C, Gelfand M, Trifiro M, LeBlanc A. Testosterone-mediated neuroprotection through the androgen receptor in human primary neurons. J Neurochem. 2001 Jun;77(5):1319-26.

142. Matsumoto A. Androgen stimulates neuronal plasticity in the perineal motoneurons of aged male rats. J Comp Neurol. 2001 Feb 12;430(3):389-95.

143. McConnell SE, Alla J, Wheat E, Romeo RD, McEwen B, Thornton JE. The role of testicular hormones and luteinizing hormone in spatial memory in adult male rats. Horm Behav. 2012 Apr;61(4):479-86.

144. Valladolid-Acebes I, Stucchi P, Cano V, Fernandez-Alfonso MS, Merino B, Gil-Ortega M, et al. High-fat diets impair spatial learning in the radial-arm maze in mice. Neurobiol Learn Mem. 2011 Jan;95(1):80-5.

145. Whitmer RA, Gunderson EP, Barrett-Connor E, Quesenberry CP, Jr., Yaffe K. Obesity in middle age and future risk of dementia: a 27 year longitudinal population based study. BMJ. 2005 Jun 11;330(7504):1360.

146. Elias MF, Elias PK, Sullivan LM, Wolf PA, D'Agostino RB. Lower cognitive function in the presence of obesity and hypertension: the Framingham heart study. Int J Obes Relat Metab Disord. 2003 Feb;27(2):260-8.

147. van den Berg E, Biessels GJ, de Craen AJ, Gussekloo J, Westendorp RG. The metabolic syndrome is associated with decelerated cognitive decline in the oldest old. Neurology. 2007 Sep 4;69(10):979-85.

148. Dahl A, Hassing LB, Fransson E, Berg S, Gatz M, Reynolds CA, et al. Being overweight in midlife is associated with lower cognitive ability and steeper cognitive decline in late life. J Gerontol A Biol Sci Med Sci. 2010 Jan;65(1):57-62.

149. Wolf PA, Beiser A, Elias MF, Au R, Vasan RS, Seshadri S. Relation of obesity to cognitive function: importance of central obesity and synergistic influence of concomitant hypertension. The Framingham Heart Study. Curr Alzheimer Res. 2007 Apr;4(2):111-6.

Chapter II

Chapeter II

Specific Aim 1 and 2: Testosterone deprivation without obesity does not cause brain insulin resistance and brain mitochondrial dysfunction in orchiectomized rats.

Insulin resistance is a hallmark of the metabolic syndrome, which can lead to Type 2 diabetes mellitus (T2DM) (1). It has been known that a long-term high-calorie diet caused insulin resistance and T2DM in the animal model (2; 3). Consistent with our previous study, 12 to 15 weeks of a high-fat diet (HFD) consumption in male rats lead not only to peripheral insulin resistance but also neuronal insulin resistance, indicated by an impairment in insulin induced long-term depression (LTD) and impaired insulin signaling in the brain, as well as brain mitochondrial dysfunction (4-6). Furthermore, androgenic sex steroid hormone such as testosterone is a significant factor in physiological function including the reproductive system for promoting secondary sexual characteristics (7), metabolic effects to regulate glucose and lipid metabolism (8; 9), as well as modulation of normal brain functions (10; 11). In addition, a previous study suggested that testosterone was involved in glucose metabolism and insulin signaling (12). Thus, testosterone deficiency impaired both glucose homeostasis and insulin signaling. Consequently, previous studies reported that insulin resistance and obesity are also associated with testosterone deficiency in obese animals, (9; 13) and obese men (14; 15). Furthermore, controversy has developed among several studies in castrated male rats demonstrating that testosterone deprivation does not induce obesity (16-19).

However, the effects of testosterone deprivation with or without obesity on brain insulin receptor function, brain insulin signaling and brain mitochondrial function at different time periods had not yet been investigated which lead to this study. Therefore, we hypothesized that obesity with testosterone deprivation accelerated an impairment of brain insulin receptor function, brain insulin signaling and brain mitochondrial dysfunction in the brain.

METERIALS AND METHODS

Animal Models and experimental protocols

Seventy-two male Wistar Rats, weighing 180-200 g (aged ~ 6 weeks), from the National Animal Center, Salaya Campus, Mahidol University, Bangkok, Thailand were used for this study. All experiments were conducted in accordance with approved protocol from the Faculty of Medicine, Chiang Mai University Institutional Animal Care and Use Committee, in compliance with NIH guidelines. All animals were housed in environmentally controlled conditions (25 ± 0.5 °C, 12 hour light/dark cycle) and allowed to acclimate for one week. Rats were then divided into two groups (n = 36/group) as either sham-operated (Sham;S) or orchiectomized (ORX;O). One week after the surgery, each group was fed either the normal diet (ND; 19.77% E fat) or the high-fat diet (HFD; 59.28% E fat) for either 4,8 or 12 weeks, in which animals were divided into four subgroups in each time period such as NDS, NDO, HFS and HFO (NDS; sham-operated rats fed with normal diet, NDO; orchiectomized rats fed with normal diet, HFS; sham-operated rats fed with high-fat diet and HFO; orchiectomized rats fed with high-fat diet). Animals in the ND group were fed with standard laboratory pelleted diet (Mouse Feed Food No. 082, C.P. Company, Bangkok, Thailand), containing 19.77% total energy from fat, whereas animals in the HFD group were fed a diet containing 59.28% total energy from fat, as described in our previous study (6). All animals were given free access to drink water and their respective diets.

The body weight of all animals was recorded weekly. Blood samples were collected from a tail vein at week zero (before dietary feeding) and at the end of each time period (4, 8 and 12 weeks) for further plasma analysis. Oral glucose tolerance test (OGTT) was determined at the end of week 4, 8 and 12; method described previously (5; 6). At the end of each time period, animals were deeply anesthetized with isoflurane and sacrificed via decapitation. Each brain was rapidly removed to brain slices preparation for extracellular recording, immunoblot, brain oxidative stress levels and brain mitochondrial study.

Orchiectomized Procedure (20)

Rats were anesthetized and maintained by Isoflurane 2-3 % in a dorsal recumbent position and the skin of scrotal area was scrubbed utilizing sterile technique. A small incision was made at the tip of the scrotum. The tunica ulbuginea was incised and the testis, vas deferens and the spermatic blood vessels were exposed. Then, the blood vessels and vas deferens were ligated with 4-0 absorbable suture followed by the removal of the testis with open technique. When the bleeding stopped, the remaining tissue was returned into the sac and the procedure was repeated on the opposite testis. The skin incision was closed with a 4-0 silk (non-absorbable suture). The rats were monitored carefully to prevent chewing sutures and other complications. Analgesic (Tolfenamic acid) drugs and antibiotic (Marbofloxacin) drugs were injected (subcutaneous injection) after the surgery and continued for three days.

Plasma analysis

Plasma glucose and cholesterol levels were determined via the colorimetric assay (Biotech, Bangkok, Thailand). Plasma HDL and LDL levels were determined via a commercial colorimetric assay kit (Biovision, California, USA). Plasma insulin levels were determined via the Sandwich ELISA kit (LINCO Research, MO, USA). Peripheral insulin resistance was assessed via the Homeostasis Model Assessment (HOMA) as described in previous studies (21; 22). Serum malondialdehyde (MDA) was determined using high performance liquid chromatography (HPLC)-based assay (23). Plasma testosterone levels were measured using an enzyme immunoassay kit (Cayman chemical, Ann Arbor, Michigan, USA).

Brain slice preparation (4-6)

At the end of 4, 8 and 12 weeks animals were anesthetized with isoflurane and decapitated. The brain was rapidly removed, then immersed in ice-cold "high sucrose" artificial cerebrospinal fluid (aCSF), containing (mM): NaCl 85; KCl 2.5; MgSO4 4; CaCl2 0.5; NaH2PO4 1.25; NaHCO3 25; glucose 25; sucrose 75; kynurenic acid 2; ascorbate 0.5, saturated with 95%O2/5%CO2 (pH 7.4). The hippocampal slices were cut by using a vibratome (Vibratome Company, MO, USA). Following a 30-minute post-slice incubation in high sucrose aCSF, the slices were transferred to a standard aCSF solution containing

(mM): NaCl 119; KCl 2.5; CaCl2 2.5; MgSO4 1.3; NaH2PO4 1; NaHCO3 26; and glucose 10, saturated with 95% O2, 5%CO2 (pH 7.4) for an additional 30 minutes at room temperature (22-24 oC).

Extracellular recordings of hippocampal slices for insulin-induced long-term depression (LTD) (4-6)

The hippocampal slices were transferred to a submersion recording chamber and continuously perfused at 3 to 4 ml/minute with standard aCSF warmed to 25-28°C. Field excitatory postsynaptic potentials (fEPSPs) were evoked by stimulating the Schaffer collateral-commissural pathway with a bipolar tungsten electrode, while recordings were taken from the stratum radiatum of the hippocampal CA1 region with micropipettes (3 Mohm) filled with 2M NaCl. Stimulus frequency was 0.033 Hz. The stimulus intensity of fEPSPs was adjusted to 0.8-1.0 mV in amplitude. Hippocampal slices were perfused with aCSF (as baseline condition) for ten minutes, and then perfused with aCSF plus 500 nM insulin (as insulin-induced LTD) for additional 10 minutes. After that, the slices were perfused with aCSF again for a further 50 minutes and recorded. Data will was filtered at 3 kHz, digitized at 10 kHz, and stored in a computer using pClamp 9.2 software (Axon Instruments, CA, USA). The initial slope of the fEPSP were measured and plotted against time (4; 6).

Preparation of brain mitochondria

Brain mitochondria were isolated as described in our previous study (24). Briefly after decapitation, the brain was removed and placed in 5 ml ice-cold MSE solution, transferred to 10 ml ice-cold MSE-nagarse solution (0.05% nagarse in MSE solution), and homogenized at 600 rpm using a homogenizer. Then, brain homogenate was centrifuged at 2,000 g for 4 minutes. The supernatant was collected and further centrifuged at 12,000 g for eleven minutes. Mitochondrial pellets were collected and resuspended in 10-ml ice-cold MSE-digitonin solution (0.02% digitonin in MSE solution). Finally, the mitochondrial pellets were resuspended in respiration buffer (150 mM KCl, 5 mM HEPES, 5 mM $K_2HPO_4.3H_2O$, 2 mM L-glutamate, 5 mM pyruvate sodium salt). Mitochondrial protein concentration was measured via the BCA assay (5; 25).

Brain mitochondrial reactive oxygen species (ROS) assay

Brain mitochondrial reactive oxygen species (ROS) were measured via the use of dichloro-hydrofluoresceindiacetate (DCFHDA). Brain mitochondria (0.4 mg/ml) were incubated with 2-μM DCFHDA at 25°C for 20 minutes. The fluorescence was determined using a fluorescent microplate reader at the excitation wavelength of 485 nm and emission wavelength of 530 nm (24; 25).

Brain mitochondrial membrane potential ($\Delta\Psi m$) assay

The change in mitochondrial membrane potential ($\Delta\Psi m$) within isolated brain mitochondria was measured via the fluorescent dye 5, 5′, 6, 6′-tetrachloro-1, 1′, 3, 3′-tetraethyl benzimidazolcarbocyanine iodide (JC-1). JC-1 monomer form (green) fluorescence was excited at a wavelength of 485 nm and detected at the emission wavelength of 590 nm. JC-1 aggregate form (red) fluorescence was excited at a wavelength of 485 nm and detected at the emission wavelength of 530 nm. Brain mitochondria (0.4 mg/ml) were incubated with JC-1 dye at 37 °C for 15 minutes. Mitochondrial membrane potential was determined by fluorescent intensity via a fluorescent microplate reader. The change in mitochondrial membrane potential was calculated as the ratio of red to green fluorescent intensity (24; 25).

Brain mitochondria swelling assay

Brain mitochondrial swelling was determined by measuring the change in the absorbance of the brain mitochondrial suspension. Brain mitochondria (0.4 mg/ml) were incubated in 2 ml respiration buffer. The suspension was read at 540 nm via the use of a microplate reader. Mitochondrial swelling was indicated by a decrease in the absorbance (24; 25).

Determination of serum and brain malondialdehyde (MDA) levels

The HPLC method was used to evaluate concentrations of serum and brain melondialdehyde (MDA) which acts as an indicator of oxidative stress (26). To briefly summarize, the brain tissue was homogenized in a phosphate buffer (pH 2.8). The serum or brain homogenate was mixed with 10% trichloroacetic acid (TCA) containing butylated hydroxytoluene (BHT), incubated at 90 °C for 30 min, and centrifuged at 6,000 rpm for 10

min. The supernatant was mixed with H_3PO_4 and thiobabituric acid solution (TBA) and incubated at 90°C for 30 min to produce thiobarbituric acid reactive substances (TBARS). TBARS levels were measured via the absorbance which was read at 532 nm by the HPLC system. Absorbance was determined directly from the standard curve and reported as the equivalent concentration of MDA.

Immunoblotting for neuronal insulin signaling (4-6)

To investigate the expression of p-IR, IR, Akt/PKB, and insulinmediated Akt Ser473 phosphorylation, homogenated brain slices from each subgroup were boiled at 95 C, for 5 minutes. Then, proteins were separated by electrophoresis on 10% polyacrylamide gels (SDS-PAGE) (Bio-Rad Laboratories, Inc., Hercules,CA), and transferred into polyvinylidene difluoride membranes. After blocking with 5% nonfat milk/TBST, immunoblot was conducted with IR, Akt, Akt Ser473 antibody, and β-actin (rabbit polyclonals, 1:4000 in TBST; Santa Cruz Biotechnology, Inc.,Santa Cruz, CA) overnight. Membranes were incubated with a secondary goat anti rabbit antibody, conjugated with horseradish peroxidase (1:8000 in TBST, Bio-Rad Laboratories), and the protein bands were visualized on Amersham hyperfilm ECL using the Amersham ECL Western blotting detection reagents system (GE Healthcare, Buckinghamshire, UK). Band intensity was quantified by the Scion Image program (Scion Corp., Frederick, MD), and the results were shown as average signal intensity (arbitrary units).

Statistical analysis

Data were expressed as mean ± SE. For all comparisons, the significance of the difference in peripheral biochemical parameters was calculated by Mann-Whitney U test. Comparison percentage of insulin-induced LTD and brain mitochondrial function between groups was performed using the two-way ANOVA test followed by the Fisher's test as the post hoc analysis. $P < 0.05$ was considered statistically significant.

RESULTS

Metabolic parameters, circulating oxidative stress levels and brain oxidative stress levels in different time course (4, 8 and 12 weeks)

At baseline levels (before orchiectomy) the body weight, plasma insulin, plasma glucose, plasma testosterone, plasma total cholesterol, and HOMA index did not differ between sham-operated rats and orchiectomized-operated rats (Table 1).

At week 4, NDO significantly decreased body weight, food intake, visceral fat, seminal vesicle ratio and plasma testosterone in comparison with NDS (Table 2). HFS rats had significantly increased body weight, visceral fat in comparison with NDS rats, whereas HFO had significantly decreased in seminal vesicle ratio and plasma testosterone levels in comparison with NDS rats (Table 2). Both of orchiectomized-operated rats, NDO and HFO had significantly decreased body weight, food intake, visceral fat, seminal vesicle ratio and plasma testosterone levels in comparison with HFS (Table 2). HFO significantly increased body weight, food intake, and visceral fat in comparison with NDO (Table 2). However, there were no differences in plasma insulin, plasma glucose, HOMA index, plasma total cholesterol, LDL cholesterol, plasma triglyceride, plasma AUCg, serum and brain MDA levels among all groups (Table 2).

At week 8, NDO significantly decreased body weight, food intake, visceral fat, seminal vesicle ratio and plasma testosterone in comparison with NDS (Table 3). HFS had significantly increased body weight, visceral fat, plasma insulin, HOMA index, plasma total cholesterol, and plasma AUCg in comparison with NDS rats (Table 3), whereas HFS significantly decreased HDL cholesterol in comparison with NDS rats (Table 3). HFO had significantly increased plasma insulin, HOMA index, plasma total cholesterol, and plasma AUCg in comparison with NDS rats (Table 3), whereas HFO significantly decreased seminal vesicle ratio, plasma testosterone and HDL cholesterol in comparison with NDS rats (Table 3). Both of orchiectomized-operated rats, NDO and HFO had significantly decreased body weight, food intake, visceral fat, seminal vesicle ratio and plasma testosterone levels in comparison with HFS (Table 3). HFO significantly increased body weight, food intake, and visceral fat, plasma insulin, HOMA index, plasma total cholesterol, and plasma glucose AUCg in comparison with NDO (Table 3), whereas HFO significantly

decreased HDL cholesterol in comparison with NDO (Table 3). However, there were no differences in plasma glucose, LDL cholesterol, plasma triglyceride, and serum as well as brain MDA levels among all groups (Table 3). These findings suggested that obesity alone but not testosterone deprivation caused peripheral insulin resistance at week 8, and the combination of obesity and testosterone deprivation not accelerated that impairment, in which characterized by increased plasma insulin levels and HOMA index without an increase in plasma glucose levels.

At week 12, NDO significantly decreased body weight, food intake, visceral fat, seminal vesicle ratio and plasma testosterone in comparison with NDS (Table 4). HFS had significantly increased body weight, visceral fat, plasma insulin, HOMA index, plasma total cholesterol, LDL/VLDL cholesterol and plasma AUCg in comparison with NDS rats (Table 4), whereas HFS significantly decreased seminal vesicle ratio, plasma testosterone, and HDL cholesterol in comparison with NDS rats (Table 4). HFO had significantly increased plasma insulin, HOMA index, plasma total cholesterol, LDL cholesterol and plasma AUCg in comparison with NDS rats (Table 3), whereas HFO significantly decreased seminal vesicle ratio, plasma testosterone and HDL cholesterol in comparison with NDS rats (Table 4). Both of orchiectomized-operated rats, NDO and HFO had significantly decreased body weight, food intake, visceral fat, seminal vesicle ratio and plasma testosterone levels in comparison with HFS (Table 4). HFO significantly increased body weight, food intake, and visceral fat, plasma insulin, HOMA index, plasma total cholesterol, LDL cholesterol and plasma glucose AUCg in comparison with NDO (Table 4), whereas HFO significantly decreased HDL cholesterol in comparison with NDO (Table 4). However, there were no differences in plasma glucose and plasma triglyceride among all groups (Table 4). These findings indicated that both of high-fat fed rats, HFS and HFO also represented peripheral insulin resistance at week 12, and the combination of obesity and testosterone deprivation not accelerated that impairment, in which characterized by increased plasma insulin levels and HOMA index without an increase in plasma glucose levels. Furthermore, we also found that both of high-fat fed rats, HFS and HFO significantly increased serum and brain MDA levels at week 12 (Table 4). These findings

suggest that both of the high-fat fed rat groups, HFS and HFO induced not only peripheral insulin resistance, but also lead to increased oxidative stress in the circulating and brain.

Obesity and testosterone deprivation not accelerated the impairment of brain insulin receptor function in different time course (4, 8 and 12 weeks)

The brain insulin receptor function or insulin-induced LTD was determined by extracellular recording of hippocampal slices at CA-1 region. At week 4, the results showed that 500 nM insulin applications to hippocampal slices reduced the size of the fEPSP responses in among all groups (Fig 1A). At 30-minute post-insulin stimulation, the percentage reduction of the normalized fEPSP slope from NDS, NDO, HFS and HFO rats were 90.35±22.77%, 89.66±16.20%, 98.06±13.60% and 98.21±12.64%, respectively. The degree of insulin-mediated LTD were not significantly different among all groups (n=2-3 independent slices/subgroup, n=6 animals/subgroup, Fig 1A).

At week e8, the results also showed that 500 nM insulin applications to hippocampal slices reduced the size of the fEPSP responses in among all groups (Fig 1B). At 30-minute post-insulin stimulation, the percentage reduction of the normalized fEPSP slope from NDS, NDO, HFS and HFO rats were 77.18±7.95%, 82.29±7.92%, 64.69±13.19% and 58.53±20.10%, respectively. The degree of insulin-mediated LTD was not significantly different among all groups (n=2-3 independent slices/subgroup, n=6 animals/subgroup, Fig 1B).

At week 12, the degree of insulin-mediated LTD observed from slices of NDS and NDO groups were not significantly different between groups (Fig. 1C). However, the degree of insulin-induced LTD was significantly reduced in both of HFS and HFO compared with NDS (n=2-3 independent slices/subgroup, n=6 animals/subgroup, Fig. 1C). At 30-minute after application 500 nM insulin, the percentage reduction of the normalized fEPSP slope from NDS, NDO, HFS and HFO rats were 83.32±11.01%, 66.59±13.48%, 28.09±17.72% and 19.83±14.13%, respectively (Fig. 1C). These findings suggested that obesity alone but not testosterone deprivation caused the impairment of brain insulin receptor function, and the combination of obesity and testosterone deprivation not accelerated that impairment.

Obesity and testosterone deprivation not accelerated the impairment of brain insulin signaling pathway in different time course (4, 8 and 12 weeks)

To investigate mechanisms of obesity alone or testosterone deprivation alone as well as the combination of obesity and testosterone deprivation on brain insulin receptor function, we determined brain insulin signaling, particularly IR, Akt/PKB signaling in the brain. The results show that in 4, 8 and 12 weeks, the level of IR and Akt/PKB protein was not different among groups (Fig. 2B, 2D, 2F and Fig. 3B,3D,3F). The phosphorylation of IR and Akt/PKB at the serine 473 site was not significantly difference among groups in the 4 and 8 week (Fig. 2A, 2C and Fig. 3A, 3C). In the 12-week period the phosphorylation of IR and Akt/PKB at the serine 473 site significantly decreased in both of high-fat fed rats, HFS and HFO in comparison with NDS (Fig. 2E and Fig. 3E). However, there was no difference between NDS and NDO (Fig. 2E and Fig. 3E). These findings suggested that obesity alone but not testosterone deprivation caused the impairment of brain insulin signaling possibly via decreased IR and Akt/PKB phosphorylation at the serine 473 site in the 12-week period, and the combination of obesity and testosterone deprivation did not accelerate that impairment.

Obesity and testosterone deprivation did not accelerate the impairment of brain mitochondrial dysfunction in different time periods (4, 8 and 12 weeks)

To assess brain mitochondrial function, we measured the changes in brain mitochondria ROS production after H_2O_2 stimulation, $\Delta\Psi m$ after H_2O_2 stimulation, and brain mitochondrial swelling. We found that at week 4 and 8, there was no significant difference between groups of brain mitochondrial function in all experiment protocols (Fig 4A-F). At week 12, the results show that both of HFS and HFO caused brain mitochondrial dysfunction as indicated by increased brain mitochondrial ROS production, brain mitochondrial membrane depolarization, and brain mitochondrial swelling in comparison with the NDS (Fig. 4G-I). The brain mitochondrial morphology from an electron microscope are shown in Fig. 5. Electron microscopic images revealed that at 4 and 8 week apparent folded cristae of brain mitochondrial morphology occurred among all groups (Fig. 5A-H). At week 12, there was brain mitochondrial swelling observed as indicated by unfolded cristae in both HFS and HFO (Fig. 5K-L). All of these findings

suggest that obesity alone but not testosterone deprivation caused the impairment of brain mitochondrial dysfunction only at 12-week period, and testosterone deprivation did not accelerate that impairment.

DISCUSSION

Major findings from this study demonstrated that (1) peripheral insulin resistance was initially observed in both groups of high-fat fed rats, HFS and HFO at week 8, (2) circulating and brain oxidative stress levels were increased in both groups of high-fat fed rats, HFS and HFO at week 12, (3) the impairment of brain insulin receptor function (insulin-induced LTD), brain insulin signaling and brain mitochondrial dysfunction occurred in both groups of high-fat fed rats, HFS and HFO at week 12.

This study demonstrated that orchiectomized–operated rats had decreased body weight compared with sham-opearated rats in both the ND and HFD consumption groups. This consistency with previous studies found the reduction in body weight gain in orchiectomized rats via reduced food intake (28-30), in which consistent with present study also found that both groups of orchiectomized-operated rats (NDO and HFO) decreased their food intake in comparison with the sham-operated rats (NDS and HFS). Supporting these previous studies, testosterone deprivation rats had decreased neuropeptide-Y in the hypothalamus, resulting in a decreased appetite (27). In addition, in this study we also found that peripheral insulin resistance initial developed at week 8 in both groups of HFS and HFO, which was consistent with our previous study that also found that in the 8 week of HFD in male rats caused peripheral insulin resistance via increased body weight, increased visceral fat, increased plasma insulin and increased in HOMA index (6). Furthermore, previous studies confirmed that long-term HFD in rats caused peripheral insulin resistance represented by euglycemia, increased plasma insulin, increased HOMA index, impaired insulin sensitivity via oral glucose tolerance test (OGTT) and impaired lipid profile (2; 4; 28; 29). Interestingly, the results also show that peripheral insulin resistance developed in HFO in the 8 and 12 weeks, though body weight and visceral are not different from NDS. This mechanism may be due to orchiectomy with HFD consumption caused and impaired lipid profile such as increased cholesterol, decreased plasma HDL, increased plasma LDL and impaired insulin sensitivity. This finding suggested that high-fat

diet alone lead to the development of peripheral insulin resistance, whereas testosterone deprivation did not accelerate those impairments.

In addition, previous studies demonstrated that long-term intake of a high fat diet not only caused of peripheral insulin resistance but also initiated neuronal insulin resistance (6; 30). In this present study we found that both groups of HFD rats (HFS and HFO) showed a reduction of insulin induced-LTD at week 12. This study supports our previous study that suggested that neuronal insulin resistance developed in 12-15 weeks and impaired brain insulin receptor function indicated by impaired insulin induced-LTD (4-6). The proposed mechanism may be that neuronal insulin resistance caused an impairment of insulin signaling pathway in the brain. We are also demonstrated that HFD fed rats showed an impairment of insulin receptor (IR) phosphorylation and Akt/PKB serine-473, which relates to insulin signaling downstream. Consistent with a previous study of cultured neurons in insulin receptor knockout mice (NIRKO mice) showed reduction of PKB/Akt phosphorylation (31).

Furthermore, it has been know that to produced synaptic long term depression is involved with Ca2+ regulation (32-34). Brain mitochondria are organelle which produced ATP synthesis and regulate Ca2+ balance in the brain(35). Furthermore, previous studies suggest that long term high-fat diet consumption lead to brain mitochondrial dysfunction and development of insulin resistance and T2DM (36). Some of evidence also demonstrated that impaired brain mitochondrial function could trigger impairment of synaptic plasticity(35). In this study we are also found that HFD rats contributes to brain mitochondrial dysfunction via increased ROS production, brain mitochondrial depolarization and resulted in brain mitochondrial swelling, as show in Figures 4 and 5. Consistent with our previous studies HFD caused brain mitochondrial dysfunction (4; 5; 29; 37). Furthermore, it has been know that increasing of oxidative stress caused development of insulin resistance and T2DM via the oxidative stress pathway (38; 39), which was supported by this study that found an increased circulation and brain oxidative stress indicated by increased serum and brain MDA levels in both groups of HFS and HFO. All of these finding suggest that HFD caused neuronal insulin resistance via impaired brain mitochondrial dysfunction, impaired insulin signaling and resulted in impaired insulin

induced-LTD. Interestingly, from this study orchiectomy did not accelerate impairment of of peripheral or neuronal insulin resistance. This finding was supported by a previous study that determined that orchiectomy rats did not demonstrate characteristics of insulin resistance. These may imply that testosterone deprivation does not affect peripheral and neuronal insulin resistance, nor impair brain insulin receptor function and brain insulin signaling.

Conclusions for aim 1 and 2

This study suggests that long-term HFD caused neuronal insulin resistance via impaired brain mitochondrial dysfunction, impaired insulin signaling and resulted in impaired insulin induced-LTD. In addition, testosterone deprivation does not trigger or accelerate either peripheral or neuronal insulin resistance.

Table 1 Metabolic parameters and oxidative stress levels of sham-operated rats (Sham) and bilateral orchiectomy rats (ORX) at baseline (before orchiectomized)

Metabolic parameters	Sham	ORX
Body weight (g)	265±1.95	267.5±2.18
Plasma insulin (ng/ml)	1.12±1.04	1.04±0.44
Plasma testosterone (ng/dl)	1.75±0.75	2.05±1.06
Plasma glucose (mg/dl)	109.89±4.27	108.26±3.14
HOMA index	10.21±1.24	9.70±1.11
Plasma total cholesterol (mg/dl)	44.03±1.41	42.03±1.49

Table 2 Metabolic parameters and oxidative stress levels of sham-operated with normal diet fed rats (NDS), orchiectomized-operated with normal diet fed rats (NDO), sham-operated with high-fat diet fed rats (HFS) and orchiectomized-operated with high-fat diet fed rats (HFO) at week 4

Metabolic parameters	Week 4			
	NDS	NDO	HFS	HFO
Body weight (g)	392.50±8.27	356.9±5.11*,†	431.82±9.23*	400.91±5.47†,‡
Food intake (g)	23.22±0.57	20.73±0.60*,†	24.38±0.16	22.5±0.57†,‡
Visceral fat (g)	17.09±1.37	9.12±0.57*,†	31.13±2.79*	15.67±0.97†,‡
Seminal vesicle ratio ($x10^{-3}$)	2.84±0.42	0.27±0.05*,†	2.40±0.36	0.27±0.07*,†
Plasma testosterone (ng/dl)	1.53±0.45	0.08±0.01*,†	1.03±0.29	0.11±0.01*,†
Plasma insulin (ng/ml)	2.32±0.23	2.22±0.36	2.37±0.34	2.21±0.42
Plasma glucose (mg/dl)	136.68±8.67	147.48±6.86	140.75±7.34	138.32±6.42
HOMA index	19.08±2.29	19.81±2.02	21.71±3.19	17.89±3.87
Plasma total cholesterol (mg/dl)	42.12±1.71	41.90±2.64	35.03±0.74	38.02±2.82
HDL cholesterol (mg/dl)	4.87±1.14	4.84±1.10	3.37±0.36	3.47±0.34
LDL cholesterol (mg/dl)	31.47±3.83	36.43±3.05	28.08±1.26	30.86±2.30
Plasma triglyceride (mg/dl)	43.33±1.67	37.13±4.34	38.73±5.04	38.32±5.00
Plasma glucose AUC (AUCg) (mg/dlxminx10^4)	3.78±0.18	4.01±0.23	4.19±0.29	4.37±0.18
Serum MDA (µmol/ml)	1.53±0.16	1.69±0.10	1.62±0.23	1.72±0.16
Brain MDA (µmol/mg protein)	0.51±0.03	0.73±0.17	0.83±0.06	0.69±0.07

* $p < 0.05$ compared to NDS

† $p<0.05$ compared to HFS

‡ $p<0.05$ compared to NDO

Table 3 Metabolic parameters and oxidative stress levels of sham-operated with normal diet fed rats (NDS), orchiectomized-operated with normal diet fed rats (NDO), sham-operated with high-fat diet fed rats (HFS) and orchiectomized-operated with high-fat diet fed rats (HFO) at week 8

Metabolic parameters	Week 8			
	NDS	NDO	HFS	HFO
Body weight (g)	435.46±11.71	383.85±7.03*,†	498.46±9.66*	420.83±12.40†,‡
Food intake (g)	22.05±0.45	19.00±0.67*,†	23.11±0.34	21.06±0.67†,‡
Visceral fat (g)	21.49±1.73	12.75±1.40*,†	40.45±2.40*	20.68±2.39†,‡
Seminal vesicle ratio ($x10^{-3}$)	2.52±0.21	0.15±0.03*,†	2.66±0.04	0.18±0.04*,†
Plasma testosterone (ng/dl)	2.19±0.71	0.04±0.01*,†	1.20±0.31	0.08±0.01*,†
Plasma insulin (ng/ml)	1.93±0.21	2.04±0.17	3.00±0.34*	3.19±0.64*,‡
Plasma glucose (mg/dl)	137.83±6.47	129.93±4.46	141.04±6.59	134.77±7.96
HOMA index	14.42±1.34	15.16±1.17	27.98±4.43*	27.54±5.50*,‡
Plasma total cholesterol (mg/dl)	39.26±3.78	48.52±2.75	52.44±5.08*	54.93±4.94*,‡
HDL cholesterol (mg/dl)	4.94±0.35	5.25±0.23	3.80±0.26*	4.00±0.19*,‡
LDL cholesterol (mg/dl)	37.82±3.51	39.28±5.16	42.09±4.45	46.90±5.36
Plasma triglyceride (mg/dl)	30.15±6.84	31.04±8.00	31.60±3.02	29.87±3.03
Plasma glucose AUC (AUCg) (mg/dlxminx10^4)	3.71±0.12	3.90±0.21	4.35±0.16*	4.48±0.31*,‡
Serum MDA (µmol/ml)	1.39±0.03	1.47±0.06	1.45±0.02	1.42±0.02
Brain MDA (µmol/mg protein)	0.5±0.05	0.59±0.13	0.60±0.11	0.83±0.19

* $p < 0.05$ compared to NDS

† $p<0.05$ compared to HFS

‡ $p<0.05$ compared to NDO

Table 4 Metabolic parameters and oxidative stress levels of sham-operated with normal diet fed rats (NDS), orchiectomized-operated with normal diet fed rats (NDO), sham-operated with high-fat diet fed rats (HFS) and orchiectomized-operated with high-fat diet fed rats (HFO) at week 12

Metabolic parameters	Week 12			
	NDS	NDO	HFS	HFO
Body weight (g)	485.71±8.30	425.00±8.20*,†	554.17±10.83*	480.83±9.33†,‡
Food intake (g)	22.06±0.46	18.73±0.80*,†	23.02±0.43	21.00±0.53†,‡
Visceral fat (g)	28.02±1.4	14.92±1.8*,†	51.53±2.68*	26.51±.75†,‡
Seminal vesicle ratio ($x10^{-3}$)	3.75±0.33	0.14±0.02*,†	2.83±0.36*	0.19±0.03*,†
Plasma testosterone (ng/dl)	1.28±0.49	0.07±0.01*,†	0.44±0.05*	0.15±0.06*,†
Plasma insulin (ng/ml)	1.75±0.15	2.16±0.20	3.26±0.25*	3.40±0.63*,‡
Plasma glucose (mg/dl)	148.815.04	150.01±6.80	152.15±5.00	151.73±6.44
HOMA index	16.08±1.72	18.88±1.81	30.92±2.52*	29.80±7.50*,‡
Plasma total cholesterol (mg/dl)	43.04±3.40	48.94±4.95	60.07±3.63*	61.72±6.13*,‡
HDL cholesterol (mg/dl)	5.25±0.27	5.93±0.66	4.17±0.22*	3.91±0.42*,‡
LDL cholesterol (mg/dl)	39.87±3.97	47.57±7.33	59.65±3.22*	68.99±7.20*,‡
Plasma triglyceride (mg/dl)	36.28±3.62	35.52±5.44	37.16±2.76	35.79±3.14
Plasma glucose AUC (AUCg) (mg/dlxminx10^4)	3.94±0.12	4.08±0.27	4.92±0.10*	4.78±0.39*,‡
Serum MDA (µmol/ml)	1.27±0.05	1.36±0.07	1.69±0.15*	1.73±0.12*,‡
Brain MDA (µmol/mg protein)	1.39±0.14	1.48±0.30	2.59±0.41*	2.55±0.51*,‡

* $p < 0.05$ compared to NDS

† $p<0.05$ compared to HFS

‡ $p<0.05$ compared to NDO

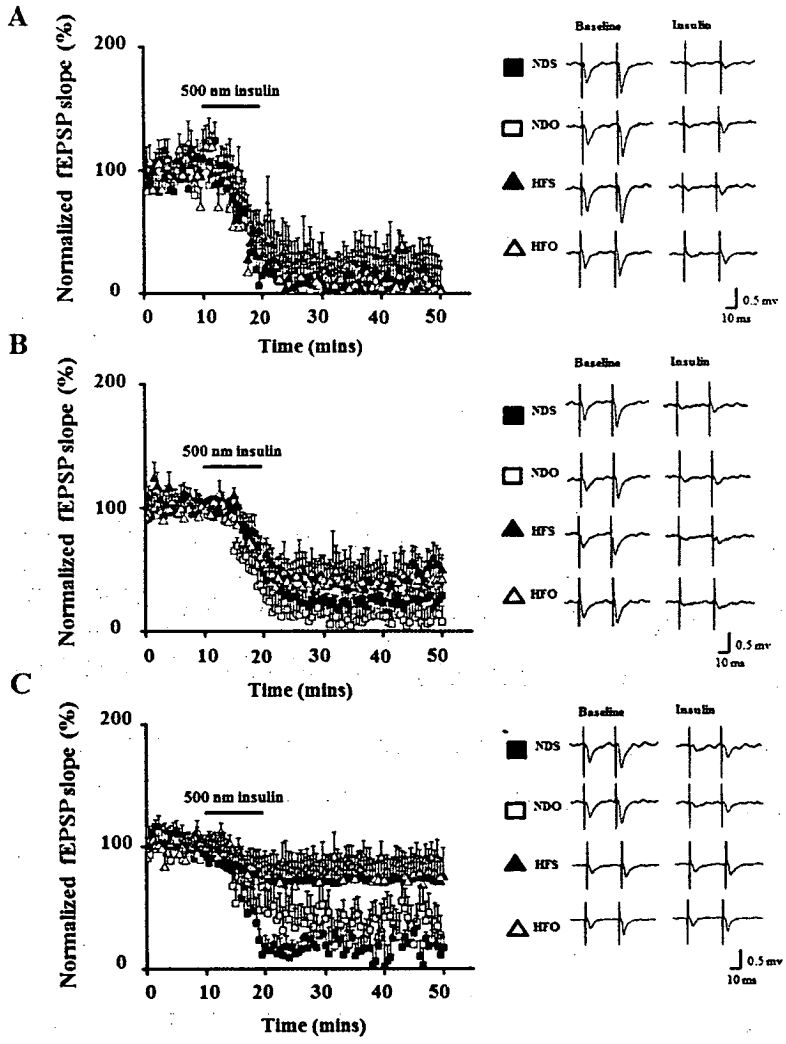


Figure 1: The effect of obesity with testosterone deprivation on brain insulin receptor function (insulin-induced LTD) in different time course. At week 4 and week 8, there was no effect on the ability of insulin-mediated long-term depression (LTD) among all groups (A-B). At week 12, the ability of insulin-mediated LTD was diminished in HFS and HFO rats (C). NDS; sham-operated with normal diet fed rats, NDO; orchiectomized-operated with normal diet fed rats, HFS; sham-operated with high-fat diet fed rats and HFO; orchiectomized-operated with high-fat diet fed rats.

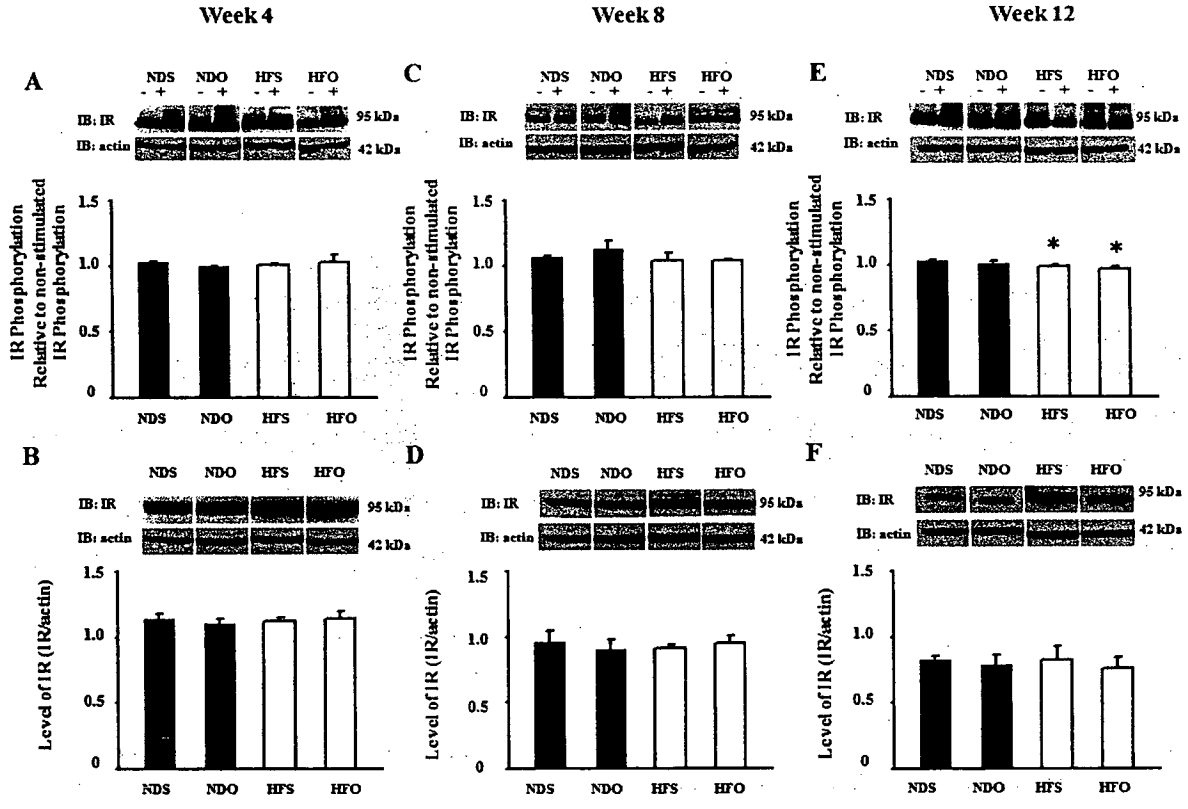


Figure 2: The effect of obesity with testosterone deprivation on the protein expression of insulin receptor phosphorylation (p-IR) and insulin receptor (IR) signaling of homogenate brain slices in different time periods. At week 4 and week 8, there was no different between protein expression of p-IR and IR protein expression among all groups (A-D). At week 12, HFS and HFO decreased phosphorylation of p-IR (E) but not different between IR protein expression among all groups (F). NDS; sham-operated with normal diet fed rats, NDO; orchiectomized-operated with normal diet fed rats, HFS; sham-operated with high-fat diet fed rats and HFO; orchiectomized-operated with high-fat diet fed rats. *$p<0.05$ vs NDS in same time period.

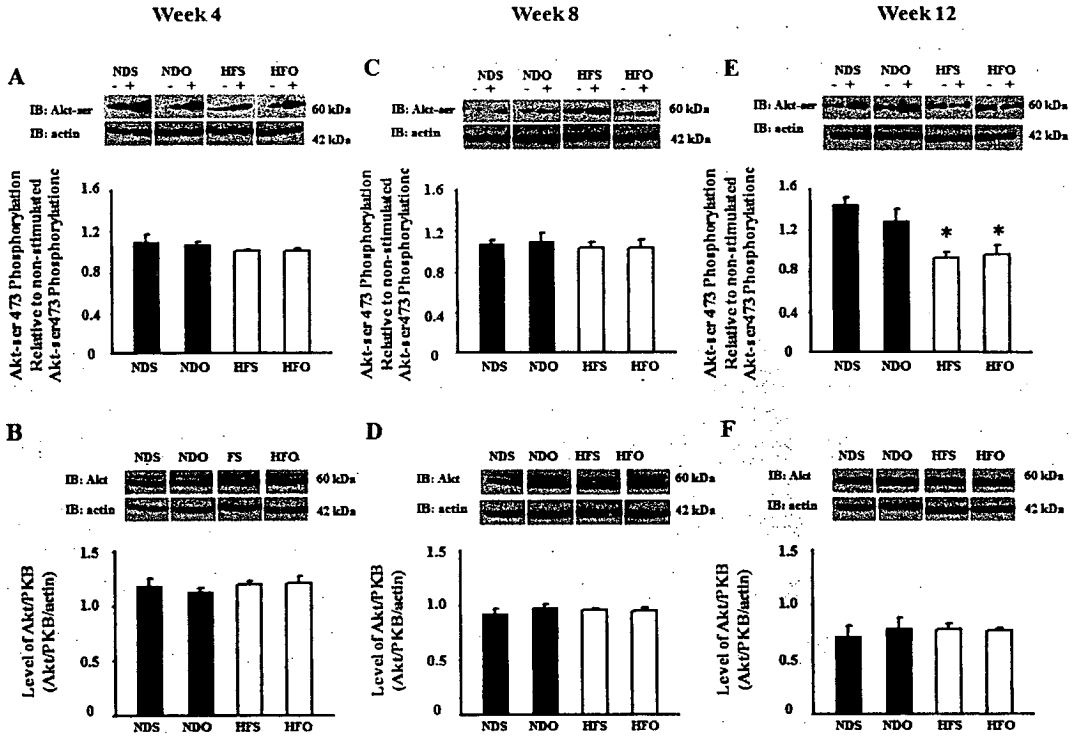


Figure 3: The effect of obesity with testosterone deprivation on the protein expression of Akt-Ser 483 and Akt/PKB of homogenate brain slices in different time course. At week 4 and week 8, there was no differences between protein expression of Akt-Ser 483 and Akt/PKB protein expression among all groups (A-D). At week 12, HFS and HFO decreased Akt-Ser 483 (E) but no difference of Akt/PKB protein expression among all groups (F). NDS; sham-operated with normal diet fed rats, NDO; orchiectomized-operated with normal diet fed rats, HFS; sham-operated with high-fat diet fed rats and HFO; orchiectomized-operated with high-fat diet fed rats. * $p<0.05$ vs NDS in same time course.

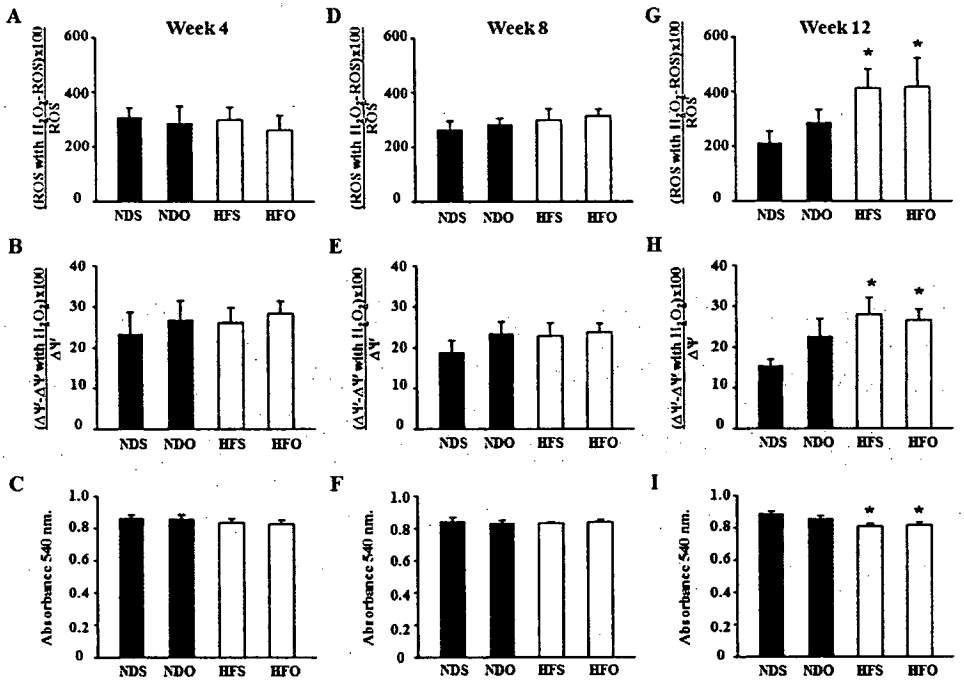


Figure 4: The effect of obesity with testosterone deprivation on brain mitochondrial function in different time course. At week 4 and week 8, there were no differences between brain mitochondrial function among all groups (A-F). At week 12, There was mitochondrial dysfunction present in both groups of HFS and HFO indicated by increased brain mitochondrial ROS production following H2O2 application (G), increased brain mitochondrial membrane potential change following H2O2 application (H) and decreased absorbance values at ten minutes, indicating the reduction of brain mitochondrial swelling (I). NDS; sham-operated with normal diet fed rats, NDO; orchiectomized-operated with normal diet fed rats, HFS; sham-operated with high-fat diet fed rats and HFO; orchiectomized-operated with high-fat diet fed rats. * $p<0.05$ vs NDS in same time course.

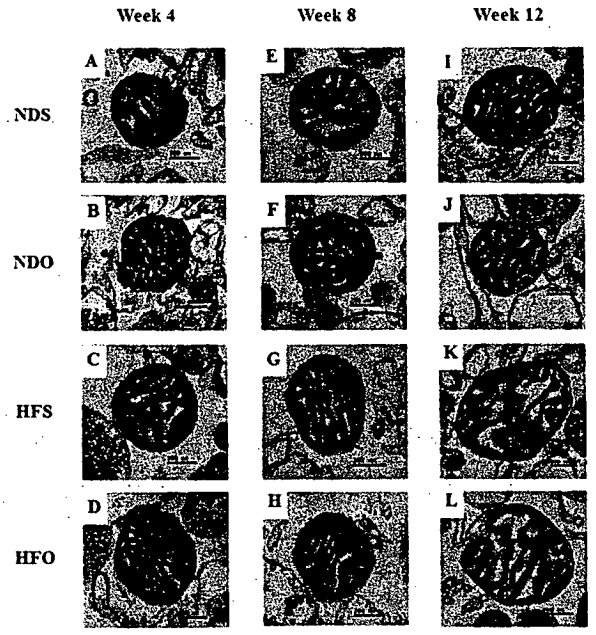


Figure 5: Representative pictures of brain mitochondrial ultrastructure morphology by transmission electron microscopy (original magnification, x15,000) in different time periods. At week 4 and week 8, there was shown apparent folded cristae of brain mitochondrial morphology among all groups (A-H). At week 12, NDS and NDO also demonstrated apparent folded cristae (I-J), but there was observed brain mitochondrial swelling as indicated by unfolded cristae in both the HFS and HFO groups (K-L). NDS; sham-operated with normal diet fed rats, NDO; orchiectomized-operated with normal diet fed rats, HFS; sham-operated with high-fat diet fed rats and HFO; orchiectomized-operated with high-fat diet fed rats.

References

1. Goldstein BJ: Insulin resistance as the core defect in type 2 diabetes mellitus. *Am J Cardiol* 90:3G-10G, 2002

2. Akiyama T, Tachibana I, Shirohara H, Watanabe N, Otsuki M: High-fat hypercaloric diet induces obesity, glucose intolerance and hyperlipidemia in normal adult male Wistar rat. *Diabetes Res Clin Pract* 31:27-35, 1996

3. Kraegen EW, Clark PW, Jenkins AB, Daley EA, Chisholm DJ, Storlien LH: Development of muscle insulin resistance after liver insulin resistance in high-fat-fed rats. *Diabetes* 40:1397-1403, 1991

4. Pipatpiboon N, Pintana H, Pratchayasakul W, Chattipakorn N, Chattipakorn SC: DPP4-inhibitor improves neuronal insulin receptor function, brain mitochondrial function and cognitive function in rats with insulin resistance induced by high-fat diet consumption. *Eur J Neurosci*, 2013

5. Pipatpiboon N, Pratchayasakul W, Chattipakorn N, Chattipakorn SC: PPARgamma agonist improves neuronal insulin receptor function in hippocampus and brain mitochondria function in rats with insulin resistance induced by long term high-fat diets. *Endocrinology* 153:329-338, 2012

6. Pratchayasakul W, Kerdphoo S, Petsophonsakul P, Pongchaidecha A, Chattipakorn N, Chattipakorn SC: Effects of high-fat diet on insulin receptor function in rat hippocampus and the level of neuronal corticosterone. *Life Sci* 88:619-627, 2011

7. Schiavi RC, White D: Androgens and male sexual function: a review of human studies. *J Sex Marital Ther* 2:214-228, 1976

8. Aydilek N, Aksakal M: Effects of testosterone on lipid peroxidation, lipid profiles and some coagulation parameters in rabbits. *J Vet Med A Physiol Pathol Clin Med* 52:436-439, 2005

9. Christoffersen BO, Gade LP, Golozoubova V, Svendsen O, Raun K: Influence of castration-induced testosterone and estradiol deficiency on obesity and glucose metabolism in male Gottingen minipigs. *Steroids* 75:676-684, 2010

10. Filova B, Ostatnikova D, Celec P, Hodosy J: The effect of testosterone on the formation of brain structures. *Cells Tissues Organs* 197:169-177, 2013

11. Janowsky JS: Thinking with your gonads: testosterone and cognition. *Trends Cogn Sci* 10:77-82, 2006

12. Chen X, Li X, Huang HY, Lin JF: [Effects of testosterone on insulin receptor substrate-1 and glucose transporter 4 expression in cells sensitive to insulin]. *Zhonghua Yi Xue Za Zhi* 86:1474-1477, 2006

13. Georgiev IP, Georgieva TM, Ivanov V, Dimitrova S, Kanelov I, Vlaykova T, Tanev S, Zaprianova D, Dichlianova E, Penchev G, Lazarov L, Vachkova E, Roussenov A: Effects of castration-induced visceral obesity and antioxidant treatment on lipid profile and insulin sensitivity in New Zealand white rabbits. *Res Vet Sci* 90:196-204, 2011

14. Shi Z, Araujo AB, Martin S, O'Loughlin P, Wittert GA: Longitudinal changes in testosterone over five years in community-dwelling men. *J Clin Endocrinol Metab* 98:3289-3297, 2013

15. Haffner SM, Shaten J, Stern MP, Smith GD, Kuller L: Low levels of sex hormone-binding globulin and testosterone predict the development of non-insulin-dependent diabetes mellitus in men. MRFIT Research Group. Multiple Risk Factor Intervention Trial. *Am J Epidemiol* 143:889-897, 1996

16. Borst SE, Conover CF: Orchiectomized Fischer 344 male rat models body composition in hypogonadal state. *Life Sci* 79:411-415, 2006

17. Erben RG, Eberle J, Stahr K, Goldberg M: Androgen deficiency induces high turnover osteopenia in aged male rats: a sequential histomorphometric study. *J Bone Miner Res* 15:1085-1098, 2000

18. Kakolewski JW, Cox VC, Valenstein ES: Sex differences in body-weight change following gonadectomy of rats. *Psychol Rep* 22:547-554, 1968

19. Gentry RT, Wade GN: Androgenic control of food intake and body weight in male rats. *J Comp Physiol Psychol* 90:18-25, 1976

20. Dulisch ML: A Castration Procedure for the Rabbit, Rat, Hamster, and Guinea Pig. *The Journal of Zoo Animal Medicine* 7:8-11, 1976

21. Appleton DJ, Rand JS, Sunvold GD: Basal plasma insulin and homeostasis model assessment (HOMA) are indicators of insulin sensitivity in cats. *J Feline Med Surg* 7:183-193, 2005

22. Haffner SM, Miettinen H, Stern MP: The homeostasis model in the San Antonio Heart Study. *Diabetes Care* 20:1087-1092, 1997

23. Grotto D, Santa Maria LD, Boeira S, Valentini J, Charao MF, Moro AM, Nascimento PC, Pomblum VJ, Garcia SC: Rapid quantification of malondialdehyde in plasma by high performance liquid chromatography-visible detection. *J Pharm Biomed Anal* 43:619-624, 2007

24. Pipatpiboon N, Pratchayasakul W, Chattipakorn N, Chattipakorn SC: PPARgamma Agonist Improves Neuronal Insulin Receptor Function in Hippocampus and Brain Mitochondria Function in Rats with Insulin Resistance Induced by Long Term High-Fat Diets. *Endocrinology*, 2012

25. Thummasorn S, Kumfu S, Chattipakorn S, Chattipakorn N: Granulocyte-colony stimulating factor attenuates mitochondrial dysfunction induced by oxidative stress in cardiac mitochondria. *Mitochondrion* 11:457-466, 2011

26. Candan N, Tuzmen N: Very rapid quantification of malondialdehyde (MDA) in rat brain exposed to lead, aluminium and phenolic antioxidants by high-performance liquid chromatography-fluorescence detection. *Neurotoxicology* 29:708-713, 2008

27. Sahu A, Kalra SP, Crowley WR, Kalra PS: Testosterone raises neuropeptide-Y concentration in selected hypothalamic sites and in vitro release from the medial basal hypothalamus of castrated male rats. *Endocrinology* 124:410-414, 1989

28. Matsuzawa-Nagata N, Takamura T, Ando H, Nakamura S, Kurita S, Misu H, Ota T, Yokoyama M, Honda M, Miyamoto K, Kaneko S: Increased oxidative stress precedes the onset of high-fat diet-induced insulin resistance and obesity. *Metabolism* 57:1071-1077, 2008

29. Pintana H, Apaijai N, Chattipakorn N, Chattipakorn SC: DPP-4 inhibitors improve cognition and brain mitochondrial function of insulin resistant rats. *J Endocrinol*, 2013

30. Clegg DJ, Gotoh K, Kemp C, Wortman MD, Benoit SC, Brown LM, D'Alessio D, Tso P, Seeley RJ, Woods SC: Consumption of a high-fat diet induces central insulin resistance independent of adiposity. *Physiol Behav* 103:10-16, 2011

31. Schubert M, Gautam D, Surjo D, Ueki K, Baudler S, Schubert D, Kondo T, Alber J, Galldiks N, Kustermann E, Arndt S, Jacobs AH, Krone W, Kahn CR, Bruning JC: Role for neuronal insulin resistance in neurodegenerative diseases. *Proc Natl Acad Sci U S A* 101:3100-3105, 2004

32. Artola A, Singer W: Long-term depression of excitatory synaptic transmission and its relationship to long-term potentiation. *Trends Neurosci* 16:480-487, 1993

33. Huang CC, Lee CC, Hsu KS: The role of insulin receptor signaling in synaptic plasticity and cognitive function. *Chang Gung Med J* 33:115-125, 2010

34. Huang CC, You JL, Lee CC, Hsu KS: Insulin induces a novel form of postsynaptic mossy fiber long-term depression in the hippocampus. *Mol Cell Neurosci* 24:831-841, 2003

35. Levy M, Faas GC, Saggau P, Craigen WJ, Sweatt JD: Mitochondrial regulation of synaptic plasticity in the hippocampus. *J Biol Chem* 278:17727-17734, 2003

36. Johannsen DL, Ravussin E: The role of mitochondria in health and disease. *Curr Opin Pharmacol* 9:780-786, 2009

37. Pintana H, Apaijai N, Pratchayasakul W, Chattipakorn N, Chattipakorn SC: Effects of metformin on learning and memory behaviors and brain mitochondrial functions in high fat diet induced insulin resistant rats. *Life Sci*, 2012

38. Rains JL, Jain SK: Oxidative stress, insulin signaling, and diabetes. *Free Radic Biol Med* 50:567-575, 2011

39. Henriksen EJ, Diamond-Stanic MK, Marchionne EM: Oxidative stress and the etiology of insulin resistance and type 2 diabetes. *Free Radic Biol Med* 51:993-999, 2011

Chapter III

Chapeter III

Specific Aim 3: DPP-4 Inhibitor improves brain insulin sensitivity, but fails to prevent dementia in ORX obese rats

Long-term high-calorie diets cause obesity, leading to the development of insulin resistance, metabolic syndrome and Type 2 diabetes mellitus (T2DM) (Kahn and Flier 2000; Pandolfi, et al. 1994). Moreover, several studies demonstrated that insulin resistance was also associated with cognitive decline (Craft 2005; Greenwood and Winocur 2005; Stranahan, et al. 2008). Our studies also showed that 12-weeks of a high-fat diet (HFD) consumption in male rats induced not only obese-insulin resistance, but also impaired brain insulin sensitivity, brain mitochondrial dysfunction and cognitive decline (Pintana, et al. 2013; Pintana, et al. 2012; Pipatpiboon, et al. 2013).

Testosterone is an androgenic steroid hormone, which plays an important role in the regulation of male reproduction and behaviors, as well as in the maintenance of glucose and lipid metabolism (Aydilek and Aksakal 2005; Christoffersen, et al. 2010). Several studies have shown that testosterone replacement exerted beneficial effects on brain function, including the prevention of neuronal cell death, the balancing of brain oxidative stress and antioxidant activity, improvement of synaptic plasticity and the involvement of cognitive formation in animal models (Filova, et al. 2013; Janowsky 2006; Meydan, et al. 2010). Interestingly, growing evidence demonstrated that testosterone deficiency is associated with obese insulin-resistance in men (Grossmann, et al. 2008; Haffner, et al. 1994; Shi, et al. 2013; Stellato, et al. 2000). All of those findings indicate that testosterone-deprivation can lead to obesity and cognitive decline. Therefore, it is possible that testosterone deprivation combined with obesity could lead to the worsening of cognitive decline.

The dipeptidyl peptidase-4 (DDP-IV) inhibitor, vildagliptin, is an anti-diabetic drug, which exerts beneficial effects in diabetic and insulin resistant models, such as the regulation of blood glucose levels without hypoglycemic incidence (Burkey, et al. 2005),

restoring pancreatic β-cells as well as preserving pancreatic function and improving insulin sensitivity (Ahren, et al. 2004). Our previous study demonstrated that vildagliptin improved not only peripheral insulin sensitivity, but also increased brain insulin sensitivity in obese-insulin resistant rats, as indicated by improvement in brain insulin receptor function (Pipatpiboon et al. 2013). In addition, vildagliptin have been shown to enhance hippocampal neurogenesis, leading to improved learning and memory in HFD-fed rodents (Gault, et al. 2015; Pintana et al. 2013; Pipatpiboon et al. 2013). All of these findings indicate the beneficial effects of vildagliptin on peripheral insulin sensitivity, brain insulin signaling and cognitive function in obese-insulin resistant conditions. However, the effects of vildagliptin on brain insulin sensitivity, brain mitochondrial function, hippocampal synaptic plasticity and cognitive function in testosterone-deprived obese rats have never been investigated. We tested the hypothesis that testosterone-deprived rats with or without obesity have impaired brain insulin receptor function, decreased brain insulin signaling, impaired brain mitochondrial function, and impaired hippocampal synaptic plasticity, thus leading to cognitive decline. We also hypothesized that vildagliptin could restore these impairments in testosterone-deprived conditions with or without obesity.

Materials and Methods

Animal models and experimental protocols

Thirty male Wistar Rats, weighing 180-200 g (aged ~ 5-6 weeks old) obtained from the National Animal Center, Salaya Campus, Mahidol University, Bangkok, Thailand were used. All experiments were conducted in accordance with the approved protocol from the Faculty of Medicine, Chiang Mai University Institutional Animal Care and Use Committee, in compliance with NIH guidelines. All animals were housed in environmentally controlled conditions (25 ± 0.5 °C and a 12 hour light/dark cycle) and allowed to acclimate for one week. Rats were then divided into two groups as either control sham-operated (S) (n=6) or bilateral orchiectomized (O) (n=24) rats as described previously (Dulisch 1976). Rats in the sham-operated group were fed with a ND for 12 weeks this was the control group (NDS), after that rats received vehicle until the end of experiment. Rats in orchiectomized group were randomized and fed with either a normal diet (ND: 19.77% E fat, NDO) or a high-fat diet (HFD: 59.28% E fat, HFO) for 12 weeks (Pratchayasakul, et al. 2011). At the end of 12 week, the rats in each group were divided into 2 subgroups (n=6/subgroup) and received either the vehicle (normal saline solution; 2 ml/kg/day) (NDOV and HFOV) or vildagliptin (Gulvus, Novartis, Bangkok, Thailand; 3 mg/kg/day) (NDOVil and HFOVil), via gavage feeding for 4 weeks (Burkey et al. 2005; Pintana et al. 2013). The cognitive function was subsequently determined by the Morris Water Maze (MWM) Test. Blood samples were collected from a tail vein at week 12, and week 15 for further plasma analysis. At the end of the experimental period, rats were deeply anesthetized with isoflurane and killed by decapitation. The brain of each rat was removed as quickly as possible after death and carefully sliced in preparation for extracellular recording (insulin-induced LTD and hippocampal synaptic LTP), immunoblot and brain mitochondrial functions. The study protocol is shown in Figure 1.

Blood sample assays

Plasma glucose and cholesterol levels were determined via colorimetric assay (Biotech, Bangkok, Thailand). Plasma HDL and LDL levels were determined using a

commercial colorimetric assay kit (Biovision, California, USA). Plasma insulin levels were determined using the Sandwich ELISA kit (LINCO Research, MO, USA). Peripheral insulin resistance was assessed using the Homeostasis Model Assessment (HOMA) as described in previous studies (Appleton, et al. 2005; Haffner, et al. 1997). Plasma testosterone levels were measured using the electrochemiluminescence immunoassay "ECLIA" technique (Roche Diagnostic, Indianapolis, Indiana, USA).

Oral glucose tolerance test (OGTT)

OGTT was performed as described previously (Pipatpiboon et al. 2013). Briefly, rats were starved overnight before the test and received 2 g/kg glucose solution via oral gavage. Blood samples were collected from the tail vein at 0, 15, 30, 60, 90 and 120 min after glucose administration. Areas under the curves (AUC) were calculated to evaluate glucose tolerance.

Brain slice preparation

At the end of experiment, animals were anesthetized with isoflurane and decapitated. The brain slice preparation was performed as described previously (Pipatpiboon et al. 2013; Pipatpiboon, et al. 2012; Pratchayasakul et al. 2011).

Extracellular recordings of hippocampal slices for insulin-induced long-term depression (LTD)

An extracellular recording of hippocampal slices for insulin-induced LTD was performed as described in our previous studies (Pipatpiboon et al. 2013; Pipatpiboon et al. 2012; Pratchayasakul et al. 2011). Field excitatory postsynaptic potentials (fEPSPs) were evoked by stimulating the Schaffer collateral-commissural pathway with a bipolar tungsten electrode, while recordings were taken from the stratum radiatum of the hippocampal CA1 region with micropipettes (3 Mohm) filled with 2M NaCl. Stimulus frequency was 0.033 Hz. The stimulus intensity of fEPSPs was adjusted to 0.8-1.0 mV in amplitude. Hippocampal slices were perfused with aCSF (as baseline condition) for ten minutes, and then perfused with aCSF plus 500 nM insulin (as insulin-induced LTD) for an additional ten minutes. Afterward, the slices were perfused with aCSF for an additional 50 minutes and readings recorded. Data was filtered at three kHz, digitized at ten kHz, and stored in a

computer using pClamp 9.2 software (Axon Instruments, CA, USA). The initial slope of the fEPSP was measured and plotted against time.

Extracellular recordings of hippocampal slices for synaptic long-term potentiation (LTP)

The examination of electrical-induced hippocampal synaptic long term potentiation (LTP) was performed as described in our previous study (Sripetchwandee, et al. 2014). Field excitatory postsynaptic potentials (fEPSPs) were evoked by stimulating the Schaffer collateral-commissural pathway with a bipolar tungsten electrode, while the fEPSPs recordings were taken from the stratum radiatum of the hippocampal CA1 region with micropipettes (3 Mohm) filled with 2M NaCl. LTP was induced by delivering high-frequency stimulation (HFS; four trains at 100 Hz; 0.5 s duration; 20 s interval). Experiments were performed for at least 40 minutes after HFS. The amount of potentiation was calculated at 40 minutes after tetanus. All data were filtered at three kHz, digitized at ten kHz, and stored in a computer using pClamp9.2 software (Axon Instruments, CA, USA). The initial slopes of the fEPSPs were measured and plotted against time.

Immunoblotting for brain insulin signaling

To investigate the expression of insulin receptor phosphorylation (p-IR) and insulin receptors (IR), homogenate brain slices from each subgroup were used as described in our previous study (Pipatpiboon et al. 2013; Pipatpiboon et al. 2012; Pratchayasakul et al. 2011). IR tyrosine phosphorylation were electrophoresed and immunoblotted with rabbit antibodies for IR at tyrosine, respectively. Examination of the level of IR protein expression was conducted with homogenates prepared from another set of four whole brain slices. These proteins were resolved by an immunoblot assay conducted with rabbit anti-IR at tyrosine phosphorylation (1:1000; sc-25103-R; Santa Cruz Biotechnology, CA, USA), IR (1:1000; sc-711; Santa Cruz Biotechnology, CA, USA). For a loading control, immunoblotting for each membrane was incubated with anti-β-actin (1:4000; #4967; Cell Signaling Technology, MA, USA). All membranes for visualizing the phosphorylation and the protein levels of IR expression were incubated with secondary goat anti-rabbit antibody conjugated with horseradish peroxidase (1:2000; #7074; Cell Signaling Technology, MA,

USA). The protein bands were visualized on Amersham hyperfilm ECL (GE Healthcare, Buckinghamshire, UK) using Amersham ECL Western blot detection reagents (GE, Healthcare). Band intensities were quantified by Scion Image and the results were shown as average signal intensity (arbitrary) units.

Preparation of brain mitochondria

Brain mitochondria were isolated using the method described previously (Pipatpiboon et al. 2013). Mitochondrial protein concentration was measured using BCA assay (Pipatpiboon et al. 2013), and brain mitochondrial functions including brain mitochondrial reactive oxygen species (ROS), mitochondrial membrane potential change ($\Delta\Psi$m) and mitochondrial swelling were determined.

Brain mitochondrial ROS assay

Brain mitochondrial reactive oxygen species (ROS) were measured using dichloro-hydrofluoresceindiacetate (DCFHDA) fluorescent dye. Brain mitochondria (0.4 mg/ml) were incubated with 2-μM DCFHDA at 25°C for 20 minutes. The fluorescence was determined using a fluorescent microplate reader at the excitation wavelength of 485 nm and emission wavelength of 530 nm (Pipatpiboon et al. 2013). Increased fluorescence intensity indicates increased ROS production.

Brain mitochondrial membrane potential ($\Delta\Psi$m) assay

The change in mitochondrial membrane potential ($\Delta\Psi$m) was measured using the fluorescent dye 5, 5′, 6, 6′-tetrachloro-1, 1′, 3, 3′-tetraethyl benzimidazolcarbocyanine iodide (JC-1). The JC-1 monomer form (green fluorescence) was excited at a wavelength of 485 nm and detected at the emission wavelength of 590 nm. JC-1 aggregate form (red fluorescence) was excited at a wavelength of 485 nm and detected at the emission wavelength of 530 nm. Brain mitochondria (0.4 mg/ml) were incubated with JC-1 dye at 37 °C for 15 minutes. Mitochondrial membrane potential changes were determined by measuring the fluorescence intensity using a fluorescent microplate reader. The change in mitochondrial membrane potential was calculated as the ratio of red to green fluorescent intensity (Pipatpiboon et al. 2013). Decreased red/green fluorescence intensity ratio indicates mitochondrial depolarization.

Brain mitochondrial swelling assay

Brain mitochondrial swelling was determined by measuring the change in the absorbance of brain mitochondrial suspension. Brain mitochondria (0.4 mg/ml) were incubated in 2 ml of respiration buffer. The suspension was read at 540 nm using a microplate reader. Mitochondrial swelling was indicated by a decrease in the absorbance (Pipatpiboon et al. 2013).

Cognitive function test

The open-field test (OFT) was used to screen locomotor activity via counting the number of lines that the rats crossed during the test, as described in previous studies (Arakawa 2005; Pintana et al. 2013). The assessment of cognitive function was performed by using Morris Water Maze (MWM) with two assessments including the acquisition test which was carried out for five consecutive days, and the probe test which was performed on day six (Pintana et al. 2013; Vorhees and Williams 2006). Data analysis of MWM test was done manually from video tape recordings by the investigators, who were blinded to experimental groups.

Statistical analysis

Data were expressed as mean ± SE. For all comparisons, the significance of the differences in peripheral biochemical parameters was calculated using the Mann-Whitney U test. The comparisons in the percentage of insulin-induced LTD, the percentage of LTP, brain mitochondrial function, immunoblot, the OFT tests and the MWM tests for the probe test among groups were performed using the one-way ANOVA test, followed by post-hoc LSD analysis. Comparisons among groups in MWM tests for the acquisition test were performed using a two-way ANOVA, followed by post-hoc LSD analysis. $P < 0.05$ was considered statistically significant.

Results

Obesity, but not testosterone deprivation, caused peripheral insulin resistance, which was attenuated by vildagliptin treatment

At the baseline levels (before orchiectomy), the metabolic parameters were not significantly different between the sham-operated group and the orchiectomized group (Table 1). After 12-weeks of diet regimens, orchiectomized HFD-fed rats (HFO) had

significantly increased plasma insulin, HOMA index and total cholesterol levels, when compared with sham-operated ND-fed rats (NDS) and orchiectomized ND-fed rats (NDO). Plasma glucose levels were not significantly different among groups. However, the body weight of NDO had significantly decreased, when compared with NDS (Table 1). These findings suggested that long-term HFD consumption caused peripheral insulin resistance as indicated by hyperinsulinemia with euglycemia and increased HOMA index. However, testosterone deprivation alone did not impair peripheral insulin sensitivity.

After four weeks of vildagliptin treatment, testosterone deprivation by orchiectomy was confirmed by reduced plasma testosterone levels in all orchiectomized rats. NDO rats treated with vehicle (NDOV) and NDO rats treated with vildagliptin (NDOVil) had significantly decreased body weight and visceral fat, without any significant alteration in plasma insulin, HOMA index, plasma glucose area under the curve of oral glucose tolerance test (AUCg), total cholesterol, plasma LDL cholesterol levels as well as plasma HDL cholesterol levels, when compared with those of NDS rats (Table 2). These findings indicated that peripheral insulin resistance was not observed in the NDOV and NDOVil rats. In contrast, HFO rats treated with vehicle (HFOV) showed the characteristics of peripheral insulin resistance, including increased plasma insulin, HOMA index, plasma AUCg, total cholesterol, plasma LDL cholesterol levels as well as decreased plasma HDL cholesterol levels, when compared with those of NDS rats. However, plasma glucose and plasma triglyceride levels showed no significant difference among all groups. Interestingly, HFO rats treated with vildagliptin (HFOVil) had significantly decreased plasma insulin, HOMA index, plasma AUCg and plasma LDL cholesterol levels as well as increased plasma HDL cholesterol levels, when compared with those of HFOV rats. All of these findings suggested that vildagliptin attenuated peripheral insulin resistance via increased peripheral insulin sensitivity and improved lipid profiles in testosterone-deprived obese rats.

Obesity, but not testosterone deprivation, caused the impairment of brain insulin receptor function, which was attenuated by vildagliptin treatment.

Brain insulin receptor function was tested by measuring insulin-induced long-term depression (insulin-induced LTD) and brain insulin signaling. For the insulin-induced LTD study, the degrees of insulin-mediated LTD in ND-fed rats (NDS, NDOV and NDOVil) were

not significantly different among groups (n=2-3 independent slices/animal, n=6 animals/group Fig. 2A). However, the degree of insulin-induced LTD was significantly reduced in HFOV rats, when compared with that of NDS rats (n=2-3 independent slices/animal, n=6 animals/group, Fig. 2A). After 4 weeks of vildagliptin administration, the degrees of insulin-induced LTD in HFOVil was significantly increased compared with that of HFOV rats (n=2-3 independent slices/animal, n=6 animals/group, Fig. 2A).

For the brain insulin signaling study, the expression of insulin receptors (IR) in all groups showed no significant different among them (Fig. 2C). The phosphorylation of insulin receptors (p-IR) was not significantly different among groups of ND-fed rats (NDS, NDOV and NDOVil) (Fig. 2B). However, levels of p-IR of HFOV rats were significantly decreased, when compared with those of NDS rats (Fig. 2B). Furthermore, vildagliptin treatment significantly increased p-IR levels in HFO rats (Fig. 2B). All of these findings suggested that the obese insulin-resistant condition, but not testosterone deprivation, caused the impairment of brain insulin receptor function and brain insulin signaling. In addition, vildagliptin restored the impairment of brain insulin receptor function as well as brain insulin signaling in the testosterone-deprived obese condition.

Obesity, but not testosterone deprivation, caused brain mitochondrial dysfunction and vildagliptin attenuated that impairment.

Brain mitochondrial function was determined by assessing changes in brain mitochondrial ROS production and brain mitochondrial membrane potential change ($\Delta\Psi m$) after H_2O_2 stimulation, and brain mitochondrial swelling. The results demonstrated that brain mitochondrial function, including brain mitochondrial ROS level, brain mitochondrial membrane potential changes, and brain mitochondrial swelling, was not significantly different among groups of ND-fed rats (NDS, NDOV and NDOVil) (Fig. 3A, 3B and 3C). These findings suggested that testosterone deprivation did not impair brain mitochondrial function. Furthermore, HFOV rats had significantly increased brain mitochondrial ROS production, brain mitochondrial depolarization, and brain mitochondrial swelling, when compared with those of NDS rats (Fig. 3A, 3B and 3C). In addition, vildagliptin treatment significantly decreased brain ROS production in HFOVil rats, when compared with that of HFOV rats (Fig. 3A). However, vildagliptin did not attenuate brain

mitochondrial depolarization and brain mitochondrial swelling in HFO rats (Fig. 3B and 3C). The morphological changes of brain mitochondria from all groups were shown in Fig. 4. Intact brain mitochondrial morphology with apparent folded cristae was observed in all ND-fed rats (Fig. 4A, 4B and 4C). Brain mitochondrial swelling was observed in both the HFOV and HFOVil groups as indicated by markedly unfolded cristae (Fig. 4D and 4E). All of these findings suggested that the obese insulin-resistant condition, but not testosterone deprivation, caused the impairment of brain mitochondrial function. In addition, vildagliptin attenuated brain mitochondrial dysfunction by reducing brain ROS production in the testosterone-deprived obese condition.

Testosterone deprivation with or without obesity caused impaired hippocampal synaptic plasticity and cognitive decline, and vildagliptin failed to restore those impairments.

To study hippocampal synaptic plasticity, electrical-induced long-term potentiation (LTP) was determined. The results demonstrated that the degrees of electrical-induced LTP significantly decreased in both NDOV and HFOV rats, when compared with that of NDS rats. The reduction of electrical–induced LTP in both NDOV and HFOV rats (n=2-3 independent slices/animal, n=6 animals/group Fig. 5A) was not significantly different. In addition, vildagliptin administration did not improve the degree of electrical-induced LTP in both NDO and HFO rats. These findings indicated that testosterone deprivation with or without obesity caused the impairment of hippocampal synaptic plasticity. However, vildagliptin treatment could not attenuate that impairment.

Furthermore, the open-field test (OFT) was used to screen locomotor activity. The results showed that it was not significantly different among all groups, indicating that the locomotor activity did not differ in all groups. In addition, the present study determined cognitive function by using the Morris water maze (MWM) test. For the acquisition test, the time to reach the platform was not significantly different among ND-fed rats (NDS, NDOV and NDOVil rats) (Fig. 5B). However, we found that HFOV and HFOVil rats took a longer time to reach the platform, when compared with that of NDS rats (Fig. 5B). For the probe test, the results showed that time spent in the target quadrant of the NDOV, NDOVil, HFOV and HFOVil rats was significantly decreased compared to NDS rats (Fig.

5C). These findings suggested that testosterone deprivation with or without obesity caused cognitive decline, and vildagliptin failed to restore cognitive function in the testosterone-deprived rats.

Discussion

The major findings of this study are as follows: [1] the condition of obesity in testosterone-deprived rats leads to the development of peripheral insulin resistance, impairment of brain insulin sensitivity, brain mitochondrial dysfunction and impaired hippocampal synaptic plasticity, resulting in cognitive decline; [2] testosterone deprivation alone does not cause peripheral insulin resistance, brain insulin resistance and brain mitochondrial dysfunction, but caused the impairment of hippocampal synaptic and cognitive decline, [3] Vildagliptin improves peripheral insulin sensitivity, brain insulin sensitivity and brain mitochondrial function in testosterone-deprived obese rats; and [4] Vildagliptin fails to restore hippocampal synaptic plasticity and cognitive function in testosterone deprived rats.

The present study demonstrates that peripheral insulin resistance, as indicated by increased HOMA index and impaired oral glucose tolerance test (OGTT) as well as impaired lipid profiles, developed in testosterone-deprived rats with obesity. Consistent with these findings, previous studies demonstrated that HFD-induced obesity caused the development of peripheral insulin resistance in male rats (Akiyama, et al. 1996; Pintana et al. 2013; Pipatpiboon et al. 2013; Stranahan et al. 2008). The development of peripheral insulin resistance in the present study depended on HFD-induced obesity, but not testosterone-deprivation, as confirmed by no change in insulin sensitivity in NDOV rats. The results of the previous study by Christofferson and colleagues also confirmed the present findings (Christoffersen, et al. 2006). However, some previous studies demonstrated that testosterone deprivation alone via ORX in male rodents caused the impairment of insulin sensitivity (Jayaraman, et al. 2014; Xia, et al. 2013). For example, Xia and colleagues (2013) found that ORX-induced testosterone deficiency increased fasting blood glucose in mature adult (10 weeks old) Sprague–Dawley male rats. Jayaraman and colleagues (2014) demonstrated that ORX adult mice (3 months of age)

had impaired insulin sensitivity. Since young adult male Wistar rats were used and were orchiectomized at 5-6 weeks of age in the present study, the differences in species and age of starting ORX procedure might cause the differences in these findings.

Interestingly, we found that HFOV rats, but not NDOV rats, developed brain insulin resistance as indicated by a reduction of insulin induced-LTD and decreased insulin receptor (IR) phosphorylation, as well as brain mitochondrial dysfunction through increased brain ROS production, brain mitochondrial depolarization and brain mitochondrial swelling. These findings and other previous studies indicated that obesity caused impaired brain mitochondrial function, resulting in brain insulin resistance (Pipatpiboon et al. 2013; Pipatpiboon et al. 2012).

Growing evidence demonstrated that testosterone deprivation is associated with cognitive decline in both men and animal models (Hogervorst, et al. 2004; Hogervorst, et al. 2001; Sakata, et al. 2000; Spritzer, et al. 2011). We also found that testosterone-deprived rats impaired cognition and impaired hippocampal synaptic plasticity, but HFD-induced obesity did not aggravate those impairments in the testosterone-deprived condition. The present findings and other previous studies (Naghdi, et al. 2005; Sakata et al. 2000; Sandstrom, et al. 2006; Spritzer et al. 2011) indicated that testosterone plays an important role in cognitive function. Since brain mitochondrial function and brain insulin sensitivity were intact in NDO rats, these results indicate that they were not mainly contributed to impaired synaptic plasticity and cognitive decline in testosterone-deprived model.

In the present study, vildagliptin treatment improved peripheral insulin resistance, attenuated brain insulin resistance and improved brain mitochondrial function in testosterone-deprived obese rats. The possible underlying mechanisms of vildagliptin, which improve both peripheral and brain insulin sensitivity, could be due to its ability to 1) inhibit the DPP-4 activity, resulting in an increase in plasma active GLP-1 levels, leading to improve insulin sensitivity, and 2) act as an anti-oxidant agent. Although the level of GLP-1 was not measured in the present study, our previous study already demonstrated that vildagliptin increased plasma and brain active GLP-1 levels, leading to increased peripheral and brain insulin sensitivity in obese male rats (Pipatpiboon et al. 2013). In

addition, an anti-oxidant effect of vildagliptin was already demonstrated via reduced MDA levels in the circulation and the brain in our previous report (Pintana et al. 2013). Although vildagliptin increased brain insulin sensitivity and decreased brain mitochondrial dysfunction, it could not restore hippocampal synaptic plasticity and cognitive function in testosterone-deprived rats with or without obesity. These findings also indicate that the impairment of synaptic plasticity that leads to cognitive decline in testosterone-deprived model was not mainly influenced by brain insulin resistance.

Conclusion for specific aim 3

Testosterone deprivation can lead to cognitive decline via impaired hippocampal synaptic plasticity. However, testosterone-deprived obese condition leads to not only the development of cognitive decline and impaired hippocampal synaptic plasticity, but also brain insulin resistance and brain mitochondrial dysfunction. These findings suggest that testosterone-deprivation with obese insulin-resistant condition causes severe brain dysfunction. Although DDP-IV inhibitor, vildagliptin, improves peripheral and brain insulin sensitivity as well as decreases brain mitochondrial ROS production, it fails to restore hippocampal synaptic plasticity and cognitive function. Therefore, vildagliptin does not provide benefits on preventing cognitive decline in subjects under testosterone-deprived obese condition.

References

Ahren B, Landin-Olsson M, Jansson PA, Svensson M, Holmes D & Schweizer A 2004 Inhibition of dipeptidyl peptidase-4 reduces glycemia, sustains insulin levels, and reduces glucagon levels in type 2 diabetes. *J Clin Endocrinol Metab* **89** 2078-2084.

Akiyama T, Tachibana I, Shirohara H, Watanabe N & Otsuki M 1996 High-fat hypercaloric diet induces obesity, glucose intolerance and hyperlipidemia in normal adult male Wistar rat. *Diabetes Res Clin Pract* **31** 27-35.

Appleton DJ, Rand JS & Sunvold GD 2005 Basal plasma insulin and homeostasis model assessment (HOMA) are indicators of insulin sensitivity in cats. *J Feline Med Surg* **7** 183-193.

Arakawa H 2005 Age dependent effects of space limitation and social tension on open-field behavior in male rats. *Physiol Behav* **84** 429-436.

Aydilek N & Aksakal M 2005 Effects of testosterone on lipid peroxidation, lipid profiles and some coagulation parameters in rabbits. *J Vet Med A Physiol Pathol Clin Med* **52** 436-439.

Burkey BF, Li X, Bolognese L, Balkan B, Mone M, Russell M, Hughes TE & Wang PR 2005 Acute and chronic effects of the incretin enhancer vildagliptin in insulin-resistant rats. *J Pharmacol Exp Ther* **315** 688-695.

Christoffersen B, Raun K, Svendsen O, Fledelius C & Golozoubova V 2006 Evalution of the castrated male Sprague-Dawley rat as a model of the metabolic syndrome and type 2 diabetes. *Int J Obes (Lond)* **30** 1288-1297.

Christoffersen BO, Gade LP, Golozoubova V, Svendsen O & Raun K 2010 Influence of castration-induced testosterone and estradiol deficiency on obesity and glucose metabolism in male Gottingen minipigs. *Steroids* **75** 676-684.

Craft S 2005 Insulin resistance syndrome and Alzheimer's disease: age- and obesity-related effects on memory, amyloid, and inflammation. *Neurobiol Aging* **26 Suppl 1** 65-69.

Dulisch ML 1976 A Castration Procedure for the Rabbit, Rat, Hamster, and Guinea Pig. *The Journal of Zoo Animal Medicine* **7** 8-11.

Evans JL, Maddux BA & Goldfine ID 2005 The molecular basis for oxidative stress-induced insulin resistance. *Antioxid Redox Signal* **7** 1040-1052.

Filova B, Ostatnikova D, Celec P & Hodosy J 2013 The effect of testosterone on the formation of brain structures. *Cells Tissues Organs* **197** 169-177.

Gault VA, Lennox R & Flatt PR 2015 Sitagliptin, a dipeptidyl peptidase-4 inhibitor, improves recognition memory, oxidative stress and hippocampal neurogenesis and upregulates key genes involved in cognitive decline. *Diabetes Obes Metab.*

Greenwood CE & Winocur G 2005 High-fat diets, insulin resistance and declining cognitive function. *Neurobiol Aging* **26 Suppl 1** 42-45.

Grossmann M, Thomas MC, Panagiotopoulos S, Sharpe K, Macisaac RJ, Clarke S, Zajac JD & Jerums G 2008 Low testosterone levels are common and associated with insulin resistance in men with diabetes. *J Clin Endocrinol Metab* **93** 1834-1840.

Haffner SM, Karhapaa P, Mykkanen L & Laakso M 1994 Insulin resistance, body fat distribution, and sex hormones in men. *Diabetes* **43** 212-219.

Haffner SM, Miettinen H & Stern MP 1997 The homeostasis model in the San Antonio Heart Study. *Diabetes Care* **20** 1087-1092.

Hogervorst E, Bandelow S, Combrinck M & Smith AD 2004 Low free testosterone is an independent risk factor for Alzheimer's disease. *Exp Gerontol* **39** 1633-1639.

Hogervorst E, Williams J, Budge M, Barnetson L, Combrinck M & Smith AD 2001 Serum total testosterone is lower in men with Alzheimer's disease. *Neuro Endocrinol Lett* **22** 163-168.

Janowsky JS 2006 Thinking with your gonads: testosterone and cognition. *Trends Cogn Sci* **10** 77-82.

Jayaraman A, Lent-Schochet D & Pike CJ 2014 Diet-induced obesity and low testosterone increase neuroinflammation and impair neural function. *J Neuroinflammation* **11** 162.

Kahn BB & Flier JS 2000 Obesity and insulin resistance. *J Clin Invest* **106** 473-481.

Kenny AM, Fabregas G, Song C, Biskup B & Bellantonio S 2004 Effects of testosterone on behavior, depression, and cognitive function in older men with mild cognitive loss. *J Gerontol A Biol Sci Med Sci* **59** 75-78.

Lu PH, Masterman DA, Mulnard R, Cotman C, Miller B, Yaffe K, Reback E, Porter V, Swerdloff R & Cummings JL 2006 Effects of testosterone on cognition and mood in male patients with mild Alzheimer disease and healthy elderly men. *Arch Neurol* **63** 177-185.

Matsuzawa-Nagata N, Takamura T, Ando H, Nakamura S, Kurita S, Misu H, Ota T, Yokoyama M, Honda M, Miyamoto K, et al. 2008 Increased oxidative stress precedes the onset of high-fat diet-induced insulin resistance and obesity. *Metabolism* **57** 1071-1077.

Meydan S, Kus I, Tas U, Ogeturk M, Sancakdar E, Dabak DO, Zararsiz I & Sarsilmaz M 2010 Effects of testosterone on orchiectomy-induced oxidative damage in the rat hippocampus. *J Chem Neuroanat* **40** 281-285.

Naghdi N, Majlessi N & Bozorgmehr T 2005 The effect of intrahippocampal injection of testosterone enanthate (an androgen receptor agonist) and anisomycin (protein synthesis inhibitor) on spatial learning and memory in adult, male rats. *Behav Brain Res* **156** 263-268.

Okun MS, DeLong MR, Hanfelt J, Gearing M & Levey A 2004 Plasma testosterone levels in Alzheimer and Parkinson diseases. *Neurology* **62** 411-413.

Pandolfi C, Pellegrini L, Sbalzarini G & Mercantini F 1994 [Obesity and insulin resistance]. *Minerva Med* **85** 167-171.

Pintana H, Apaijai N, Chattipakorn N & Chattipakorn SC 2013 DPP-4 inhibitors improve cognition and brain mitochondrial function of insulin resistant rats. *J Endocrinol* **218** 1-11.

Pintana H, Apaijai N, Pratchayasakul W, Chattipakorn N & Chattipakorn SC 2012 Effects of metformin on learning and memory behaviors and brain mitochondrial functions in high fat diet induced insulin resistant rats. *Life Sci* **91** 409-414.

Pipatpiboon N, Pintana H, Pratchayasakul W, Chattipakorn N & Chattipakorn SC 2013 DPP4-inhibitor improves neuronal insulin receptor function, brain mitochondrial function and cognitive function in rats with insulin resistance induced by high-fat diet consumption. *Eur J Neurosci* **37** 839-849.

Pipatpiboon N, Pratchayasakul W, Chattipakorn N & Chattipakorn SC 2012 PPARgamma agonist improves neuronal insulin receptor function in hippocampus and brain mitochondria function in rats with insulin resistance induced by long term high-fat diets. *Endocrinology* **153** 329-338.

Pratchayasakul W, Kerdphoo S, Petsophonsakul P, Pongchaidecha A, Chattipakorn N & Chattipakorn SC 2011 Effects of high-fat diet on insulin receptor function in rat hippocampus and the level of neuronal corticosterone. *Life Sci* **88** 619-627.

Sakata K, Tokue A & Kawai N 2000 Altered synaptic transmission in the hippocampus of the castrated male mouse is reversed by testosterone replacement. *J Urol* **163** 1333-1338.

Sandstrom NJ, Kim JH & Wasserman MA 2006 Testosterone modulates performance on a spatial working memory task in male rats. *Horm Behav* **50** 18-26.

Shi Z, Araujo AB, Martin S, O'Loughlin P & Wittert GA 2013 Longitudinal changes in testosterone over five years in community-dwelling men. *J Clin Endocrinol Metab* **98** 3289-3297.

Spritzer MD, Daviau ED, Coneeny MK, Engelman SM, Prince WT & Rodriguez-Wisdom KN 2011 Effects of testosterone on spatial learning and memory in adult male rats. *Horm Behav* **59** 484-496.

Sripetchwandee J, Pipatpiboon N, Chattipakorn N & Chattipakorn S 2014 Combined therapy of iron chelator and antioxidant completely restores brain dysfunction induced by iron toxicity. *PLoS One* **9** e85115.

Stellato RK, Feldman HA, Hamdy O, Horton ES & McKinlay JB 2000 Testosterone, sex hormone-binding globulin, and the development of type 2 diabetes in middle-aged men: prospective results from the Massachusetts male aging study. *Diabetes Care* **23** 490-494.

Stranahan AM, Norman ED, Lee K, Cutler RG, Telljohann RS, Egan JM & Mattson MP 2008 Diet-induced insulin resistance impairs hippocampal synaptic plasticity and cognition in middle-aged rats. *Hippocampus* **18** 1085-1088.

Vorhees CV & Williams MT 2006 Morris water maze: procedures for assessing spatial and related forms of learning and memory. *Nat Protoc* **1** 848-858.

Xia F, Xu X, Zhai H, Meng Y, Zhang H, Du S, Xu H, Wu H & Lu Y 2013 Castration-induced testosterone deficiency increases fasting glucose associated with hepatic and extra-hepatic insulin resistance in adult male rats. *Reprod Biol Endocrinol* **11** 106.

Table 1: Metabolic parameters at baseline and the end of week 12 (before treatment)

Metabolic parameters	Baseline		Week 12		
	Sham	ORX	NDS	NDO	HFO
Body weight (g)	192.5±3.7	197.5±3.7	466.6±4.9	409.2±14.1*,†	472.0±8.4
Plasma glucose (mg/dl)	106.8±4.5	111.8±4.3	133.8±4.9	140.0±5.5	139.9±7.1
Plasma insulin (ng/ml)	2.1±0.3	2.2±0.4	2.0±0.2	2.1±0.2†	3.7±0.3*
HOMA index	13.4±1.2	14.0±2.2	15.3±2.0	17.7±2.1†	27.6±3.4*
Plasma total cholesterol (mg/dl)	45.5±2.2	47.7±1.7	48.5±2.7	52.1±2.0†	75.0±6.6*

* compared to NDS
† compared to HFO

Table 2: Metabolic parameters after vildagliptin treatment for 4 weeks

Metabolic parameters	Groups				
	NDS	NDOV	NDOVil	HFOV	HFOVII
Body weight (g)	496.5±10.7	423.3±8.4*,†	417.2±17.6*,†	506.6±17.8	496.6±16.4
Visceral fat (g)	26.8±1.6	16.0±1.9*,†	15.7±1.4*,†	31.3±3.4	30.3±3.3
Plasma glucose (mg/dl)	131.5±10.6	129.0±13.1	137.3±3.1	134.1±8.9	131.7±6.3
Plasma insulin (ng/ml)	2.53±0.34	2.78±0.18	2.71±0.36	5.07±1.16*	2.37±0.37†
HOMA index	21.3±2.9	24.4±2.8	21.5±3.4	44.7±13.8*	20.6±3.8†
Plasma glucose AUC (AUCg) ($mg/dl \times min \times 10^4$)	4.47±0.20	5.01±0.33	4.48±0.23	5.92±0.25*	4.97±0.26†
Plasma total cholesterol (mg/dl)	68.0±5.5	63.8±2.6	73.3±5.8	110.8±14.9*	101.7±8.7*
Plasma triglyceride (mg/dl)	51.9±2.2	55.3±9.9	57.4±6.1	49.8±4.1	50.2±7.5
HDL cholesterol (mg/dl)	6.7±0.4	7.2±0.3	7.5±0.4	4.9±0.6*	6.9±0.4†
LDL cholesterol (mg/dl)	60.6±7.5	52.9±3.6	56.9±4.0	116.4±15.7*	81.5±8.1†

* compared to NDS
† compared to HFOV

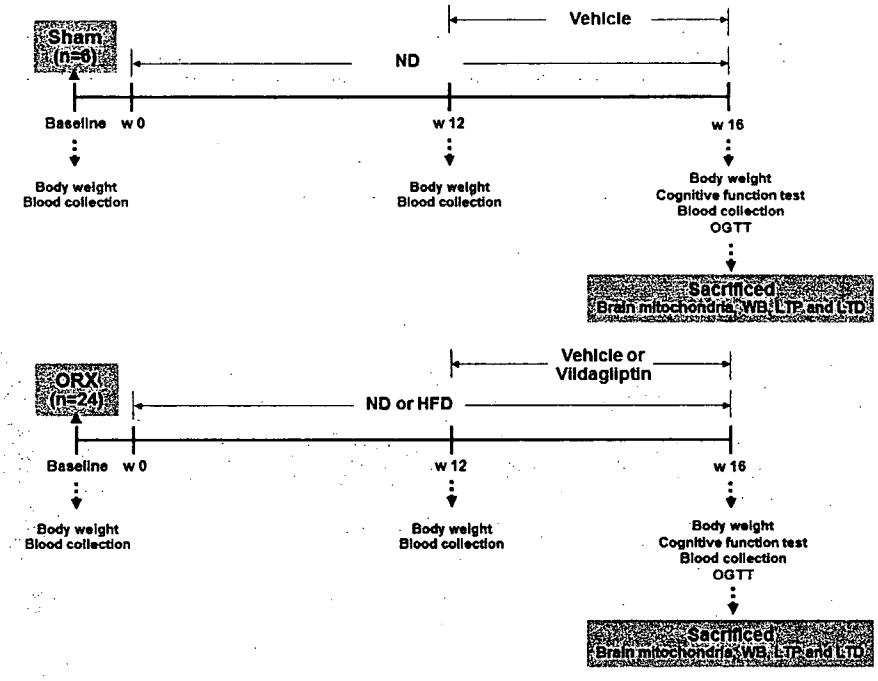


Figure 1: The experimental protocol of the present study

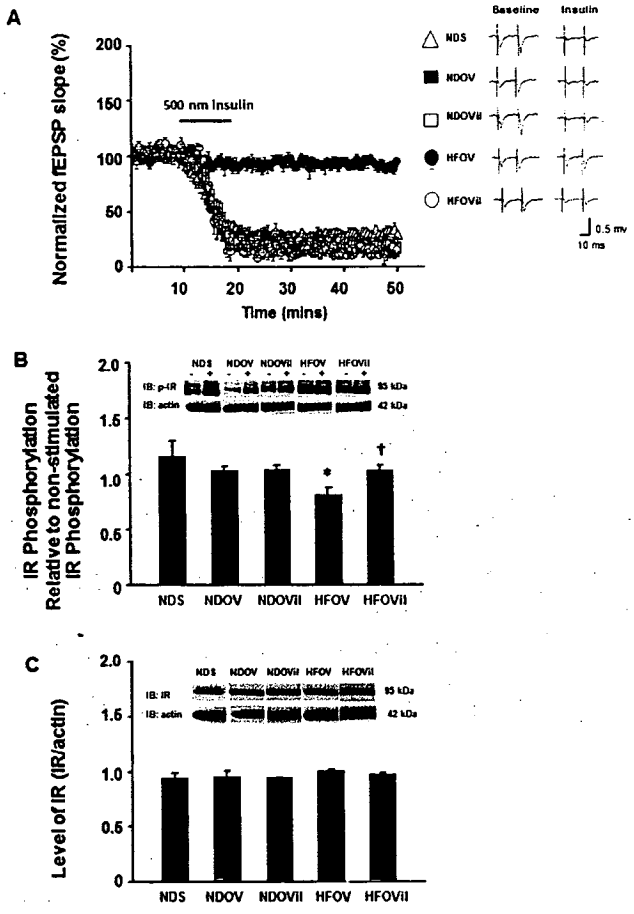


Figure 2: The effects of vildagliptin on brain insulin receptor function, including insulin-induced LTD, the phosphorylation of insulin receptor (p-IR) and the expression of insulin receptors (IR) in testosterone-deprived rats with or without obesity. Insulin-induced LTD in the CA1 hippocampus and the phosphorylation of IR significantly decreased in HFOV rats, when compared with that of NDS rats (A-B). The administration of vildagliptin for 4 weeks significantly improved the ability of insulin-induced LTD and the phosphorylation of IR in HFOVil rats, when compared with that of HFOV rats (A-B):. No differences in the expression of IR among all groups were found (C). NDS; sham-operated rats with normal diet feeding, NDOV; orchiectomized-operated rats with normal diet feeding and treated with vehicle, NDOVil; orchiectomized-operated rats with normal diet feeding and treated with vildagliptin, HFOV; orchiectomized-operated rats with high-fat diet feeding and treated with vehicle, and HFOVil; orchiectomized-operated rats fed with a high-fat diet and treated with vildagliptin, *$p<0.05$ vs NDS and † $p<0.05$ vs HFOV

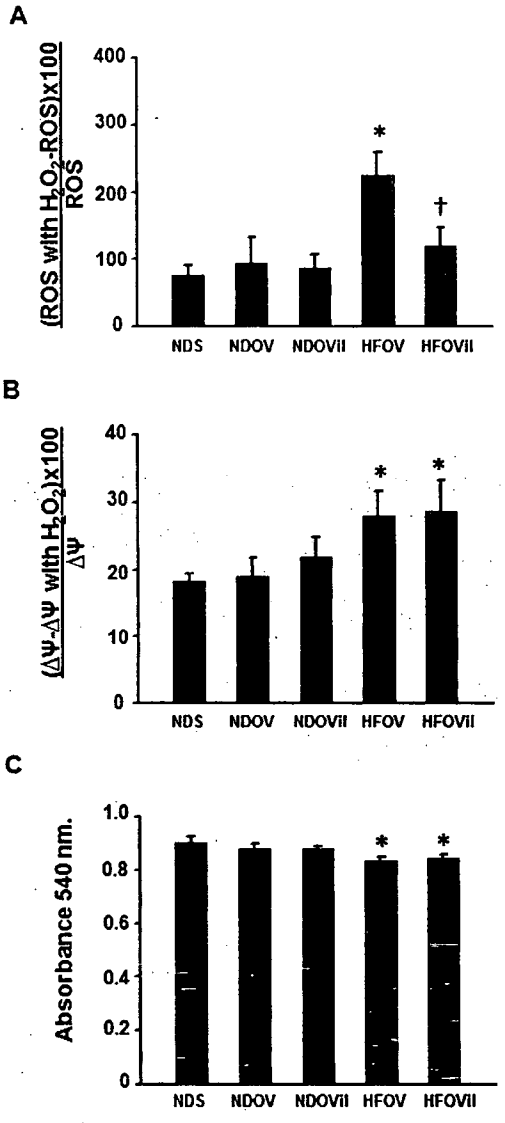

A
(ROS with H2O2-ROS)x100
ROS
400
300
200
100
0
*
†
NDS
NDOV
NDOVil
HFOV
HFOVil
B
(ΔΨ-ΔΨ with H2O2)x100
ΔΨ
40
30
20
10
0
*
*
NDS
NDOV
NDOVil
HFOV
HFOVil
C
Absorbance 540 nm.
1.0
0.8
0.6
0.4
0.2
0
*
*
NDS
NDOV
NDOVil
HFOV
HFOVil

Figure 3: The effects of vildagliptin on brain mitochondrial function in testosterone deprived rats with or without obesity. HFOV rats demonstrated brain mitochondrial dysfunction, as indicated by increased brain mitochondrial ROS production following H_2O_2 application (A), increased brain mitochondrial membrane potential change following H_2O_2 application (B) and decreased absorbance values, indicating brain mitochondrial swelling (C). The administration of vildagliptin for 4 weeks significantly decreased brain mitochondrial ROS production in HFOVil rats, when compared with that of NDS rats (A). However, vildagliptin did not improve brain mitochondrial membrane potential change and brain mitochondrial swelling in HFOVil rats (B and C). NDS; sham-operated rats with normal diet feeding, NDOV; orchiectomized-operated rats with normal diet feeding and treated with vehicle, NDOVil; orchiectomized-operated rats with normal diet feeding and treated with vildagliptin, HFOV; orchiectomized-operated rats with high-fat diet feeding and treated with vehicle, and HFOVil; orchiectomized-operated rats with high-fat diet feeding and treated with vildagliptin, *$p<0.05$ vs NDS and † $p<0.05$ vs HFOV

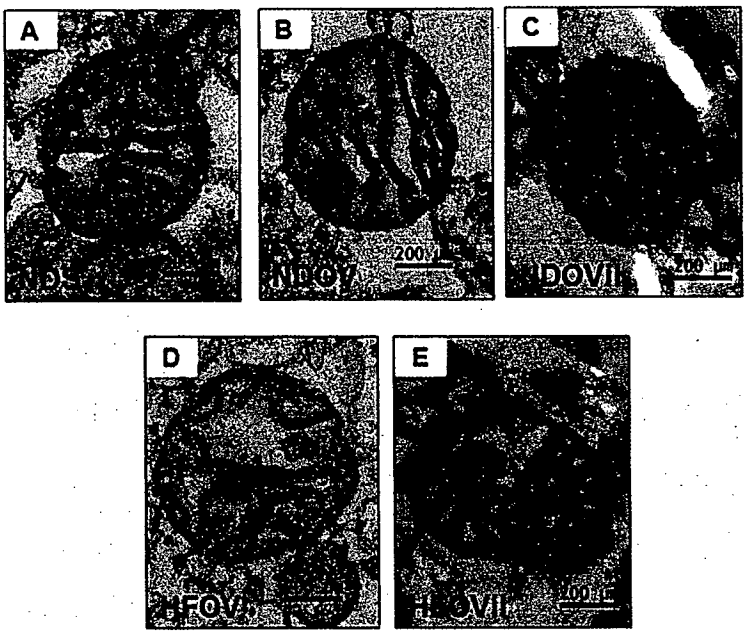


Figure 4: Representative images of brain mitochondrial morphology by transmission electron microscopy (original magnification x 15,000) after 4 weeks of vildagliptin treatment. Normal folding of cristae in brain mitochondrial morphology was shown among all ND-fed rats (A, B and C). However, brain mitochondrial swelling, as indicated by unfolded cristae, of both HFOV and HFOVil groups was observed (D and E). NDS; sham-operated rats with normal diet feeding, NDOV; orchiectomized-operated rats with normal diet feeding and treated with vehicle, NDOVil; orchiectomized-operated rats with normal diet feeding and treated with vildagliptin, HFOV; orchiectomized-operated rats with high-fat diet feeding and treated with vehicle, and HFOVil; orchiectomized-operated rats with high-fat diet feeding and treated with vildagliptin

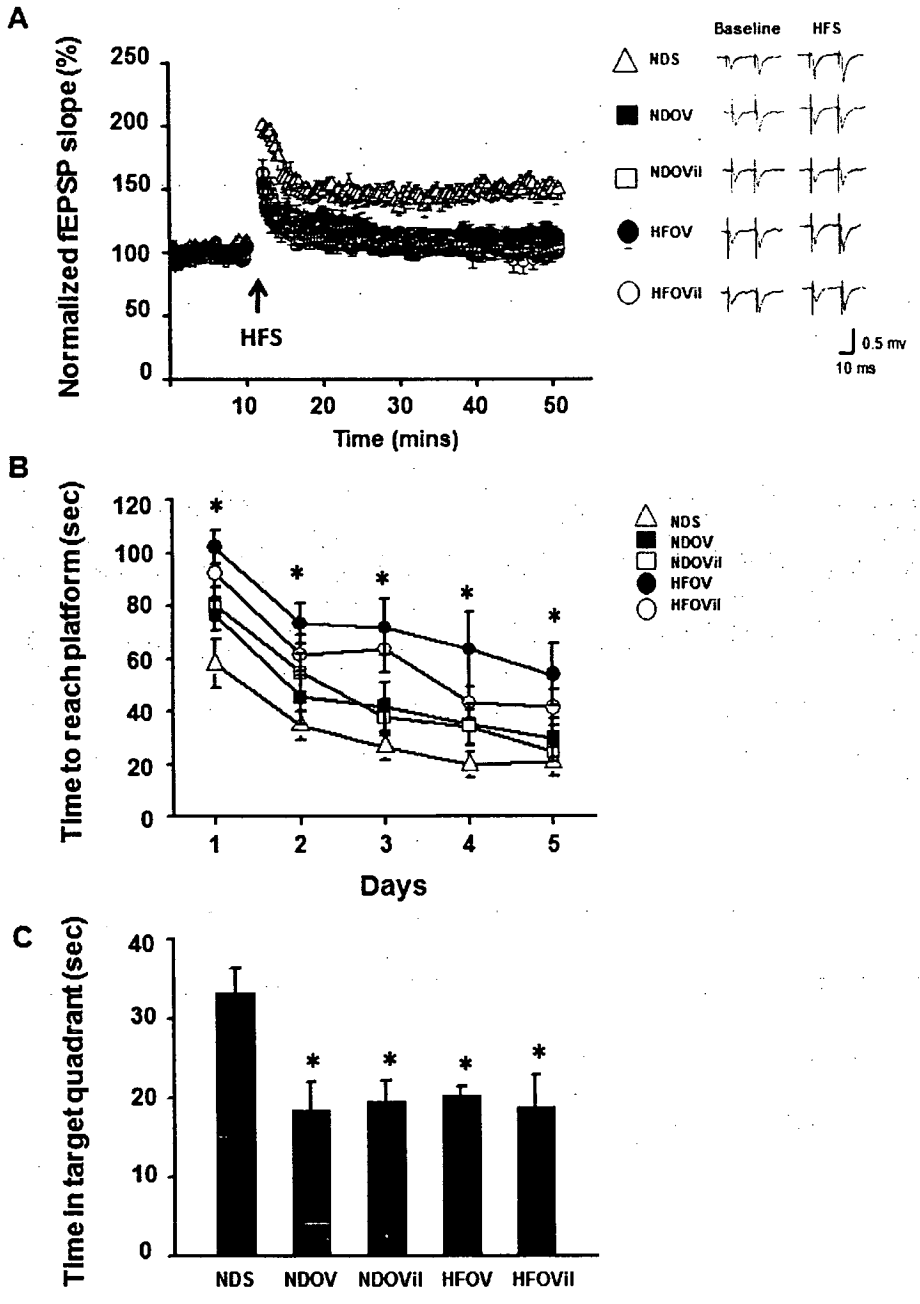


Figure 5: The effects of vildagliptin on hippocampal synaptic long-term potentiation (LTP) and the cognitive function determined by Morris water maze (MWM) test in testosterone-deprived rats with or without obesity. Both orchiectomized-operated groups (NDOV and HFOV rats) significantly reduced the percentage of normalized fEPSPs, when compared with that of NDS rats (A). The administration of vildagliptin for 4 weeks did not improve the percentage of normalized fEPSPs in both orchiectomized-operated groups (NDOVil and HFOVil),

when compared with that of HFOV rats (A). HFOV rats and HFOVil rats significantly increased time to reach the platform in the acquisition test as well as had a decreased time spent in target quadrant in the probe test, when compared with that of NDS rats (B and C). NDOV rats had a significantly decreased time spent in the target quadrant in the probe test, but there was no changed in time to reach the platform in the acquisition test (B and C). The administration of vildagliptin for 4 weeks did not restore the time taken to reach the platform in HFOVil rats, and the time spent in the target quadrant in both NDOVil and HFOVil rats (B and C). NDS; sham-operated rats with normal diet feeding, NDOV; orchiectomized-operated rats with normal diet feeding and treated with vehicle, NDOVil; orchiectomized-operated rats with normal diet feeding and treated with vildagliptin, HFOV; orchiectomized-operated rats with high-fat diet feeding and treated with vehicle, and HFOVil; orchiectomized-operated rats with high-fat diet feeding and treated with vildagliptin, HFS; high frequency stimulation. *$p<0.05$ vs NDS

Chapter IV

Chapter IV

Specific aim 4: Dipeptidyl peptidase-4 (DPP-4) inhibitor exerts better neuroprotection than calories restriction by attenuating mitochondrial dysfunction impaired by obese-insulin resistance in rats

Obesity is a hallmark of insulin resistance and metabolic syndrome, which has significantly increased in many countries (Kitzinger and Karle 2013). Previous studies demonstrated that high calorie diet-induced obesity led to develop insulin resistance and cognitive decline in animal model (Pistell, et al. 2010; Stranahan, et al. 2008). In addition, our previous studies showed that the development of peripheral insulin resistance, brain insulin resistance, brain mitochondrial dysfunction, as well as cognitive decline occurred in high-fat diet induced obese male rats (Pipatpiboon, et al. 2013; Pipatpiboon, et al. 2012).

Lifestyle modification, including calories restriction and dug intervention has been used for treatment of obese subjects and patients with type-2 diabetes mellitus. DDP-IV inhibitor, vildagliptin, is widely used for T2DM treatment, since it regulates blood glucose level without causing hypoglycemic effect (Burkey, et al. 2005). In addition, our previous studies reported that vildagliptin improved not only the peripheral insulin resistance, but also brain insulin resistance, as indicated by improving in brain insulin receptor function in obese-insulin resistant rats (Pipatpiboon et al. 2013). Furthermore, the enhancement of hippocampal neurogenesis and improvement of cognitive decline were found in high-fat fed rodents treated with vildagliptin (Gault, et al. 2015; Pintana, et al. 2013; Pipatpiboon et al. 2013). All of those findings suggest that vildagliptin exert beneficial effects on metabolic controls and the cognitive function.

Although drug therapy has been prescribed to treat obese-insulin resistance or diabetic condition, but several side effects have been concerned. Therefore, lifestyle modification including calories restriction is the other alternative treatment to reduce the cost and side effects from drug therapy. A previous review study showed that calorie restriction in aged animals improved the metabolic parameters and extended lifespan (Speakman and Mitchell 2011). Moderate calorie restriction (CR; ~60%) has been well-

known to have beneficial impacts on metabolic parameters, and improved insulin sensitivity in vitro and in vivo studies (Dean, et al. 1998; McCurdy, et al. 2005; Sharma, et al. 2012; Wilsey and Scarpace 2004). In addition, a previous study reported that the CR not only exerts the effects on metabolic control, but also improved brain function (Yamaoka and Tango 2012). Several studies demonstrated that CR increased an endogenous apoptosis inhibitor in the neuronal cells (Hiona and Leeuwenburgh 2004), decreased the rate of mitochondrial H_2O_2 production via reduced ROS production in aged rat brain (Sanz, et al. 2005). Furthermore, Adams and colleagues showed that CR preserved cognitive function in aged male rats (Adams, et al. 2008). All of those findings suggest that calorie restriction has beneficial effects in neuroprotection and preserving the cognitive function.

However, the effects of either calories restriction or the combination of calories restriction plus vildagliptin on brain function, including brain insulin sensitivity, brain mitochondrial function, hippocampal synaptic plasticity and cognitive function in obese-insulin resistant rats have never been investigated. The present study tested the hypothesis that the combination of calories restriction plus vildagliptin has better beneficial effects in the brain function of obese-insulin resistant rats than calories restriction alone.

Materials and Methods

Animal models and experimental protocols

Twenty-four male Wistar Rats, weighing 180-200 g (aged ~ 5-6 weeks old) obtained from the National Animal Center, Salaya Campus, Mahidol University, Bangkok, Thailand were used. All experiments were conducted in accordance with the approved protocol from the Faculty of Medicine, Chiang Mai University Institutional Animal Care and Use Committee, in compliance with NIH guidelines. All animals were housed in environmentally controlled conditions (25 ± 0.5 °C and a 12 hour light/dark cycle) and allowed to acclimate for one week. Rats were randomized and fed with either a normal diet (ND: 19.77% E fat, n=6) or a high-fat diet (HFD: 59.28% E fat, n=18) for 12 weeks (Pratchayasakul, et al. 2011). At the end of 12 week, rats in ND group was received NSS via intra-gastric gavage, as indicated a control group (NDV), and rats in HFD group were

subdivided to 3 subgroups; 1) 12-week HFD-fed rats were continued with HFD and together given NSS via intra-gastric gavage for 4 weeks (HFV), 2) 12-week HFD-fed rats were switched to restricted diet (ND containing only 60 % calorie intake, compared to calorie intake of HFD, as described in a previous study (Wilsey and Scarpace 2004)) and together given NSS via intragastric gavage for 4 weeks (HFRV) and 3) 12-week HFD-fed rats were switched to restricted diet and together given with 3 mg/kg/day vildagliptin (Novartis, Thailand) via intra-gastric gavage for 4 weeks (Burkey et al. 2005; Pintana et al. 2013). The cognitive function was subsequently determined by the Morris Water Maze (MWM) test. Blood samples were collected from a tail vein at week 0, 12 and week 16 for further plasma analysis. At the end of the experimental period, rats were deeply anesthetized with isoflurane and killed by decapitation. The brain of each rat was removed as quickly as possible after death and carefully sliced in preparation for extracellular recording (insulin-induced LTD and hippocampal synaptic LTP), immunoblot and brain mitochondrial functions. The experimental protocol was shown in Figure 1.

Blood sample assays

Plasma glucose and cholesterol levels were determined via colorimetric assay (Biotech, Bangkok, Thailand). Plasma HDL and LDL levels were determined using a commercial colorimetric assay kit (Biovision, California, USA). Plasma insulin levels were determined using the Sandwich ELISA kit (Millipore, MI, USA). Peripheral insulin resistance was assessed using the Homeostasis Model Assessment (HOMA), as previously described (Pipatpiboon et al. 2012).

Oral glucose tolerance test (OGTT)

OGTT was performed as described previously (Pintana et al. 2013; Pipatpiboon et al. 2013). Briefly, rats were starved overnight before the test and received 2 g/kg glucose solution via oral gavage. Blood samples were collected from the tail vein at 0, 15, 30, 60, 90 and 120 min after glucose administration. Areas under the curves (AUC) were calculated to evaluate glucose tolerance.

Brain slice preparation

At the end of experiment, animals were anesthetized with isoflurane and decapitated. The brain slice preparation was performed as described previously (Pipatpiboon et al. 2013; Pipatpiboon et al. 2012; Pratchayasakul et al. 2011).

Extracellular recordings of hippocampal slices for insulin-induced long-term depression (LTD)

An extracellular recording of hippocampal slices for insulin-induced LTD was performed as described in our previous studies (Pipatpiboon et al. 2013; Pipatpiboon et al. 2012; Pratchayasakul et al. 2011). Field excitatory postsynaptic potentials (fEPSPs) were evoked by stimulating the Schaffer collateral-commissural pathway with a bipolar tungsten electrode, while recordings were taken from the stratum radiatum of the hippocampal CA1 region with micropipettes (3 Mohm) filled with 2M NaCl. Stimulus frequency was 0.033 Hz. The stimulus intensity of fEPSPs was adjusted to 0.8-1.0 mV in amplitude. Hippocampal slices were perfused with aCSF (as baseline condition) for ten minutes, and then perfused with aCSF plus 500 nM insulin (as insulin-induced LTD) for an additional ten minutes. Afterward, the slices were perfused with aCSF for an additional 50 minutes and readings recorded. Data was filtered at three kHz, digitized at ten kHz, and stored in a computer using pClamp 9.2 software (Axon Instruments, CA, USA). The initial slope of the fEPSP was measured and plotted against time.

Extracellular recordings of hippocampal slices for synaptic long-term potentiation (LTP)

The examination of electrical-induced hippocampal synaptic long term potentiation (LTP) was performed as described in our previous study (Sripetchwandee, et al. 2014a). Field excitatory postsynaptic potentials (fEPSPs) were evoked by stimulating the Schaffer collateral-commissural pathway with a bipolar tungsten electrode, while the fEPSPs recordings were taken from the stratum radiatum of the hippocampal CA1 region with micropipettes (3 Mohm) filled with 2M NaCl. LTP was induced by delivering high-frequency stimulation (HFS; four trains at 100 Hz; 0.5 s duration; 20 s interval). Experiments were performed for at least 40 minutes after HFS. The amount of potentiation was calculated at 40 minutes after tetanus. All data were filtered at three kHz,

digitized at ten kHz, and stored in a computer using pClamp9.2 software (Axon Instruments, CA, USA). The initial slopes of the fEPSPs were measured and plotted against time.

Immunoblotting for brain insulin signaling

To investigate the expression of insulin receptor phosphorylation (p-IR), insulin receptors (IR), Akt/PKB, and insulin mediated Akt Ser473 phosphorylation, homogenate brain slices from each subgroup were used as described in our previous study (Pipatpiboon et al. 2013; Pipatpiboon et al. 2012; Pratchayasakul et al. 2011). IR tyrosine phosphorylation and Akt/PKB at serine 473 kinases phosphorylation were electrophoresed and immunoblotted with rabbit antibodies for IR at tyrosine and Akt/PKB at serine 473, respectively. Examination of the level of IR protein and Akt/PKB protein expression were conducted with homogenates prepared from another set of four whole brain slices. These proteins were resolved by an immunoblot assay conducted with rabbit anti-IR at tyrosine phosphorylation (p-IR$^{tyr1162/1163}$) (1:1000; sc-25103-R; Santa Cruz Biotechnology, CA, USA), IR (1:1000; sc-711; Santa Cruz Biotechnology, CA, USA), Akt/PKB at serine 473 kinases phosphorylation (1:1000; #9271; Cell Signaling Technology, MA, USA) and Akt/PKB (1:1000; #9272; Cell Signaling Technology, MA, USA). For a loading control, immunoblotting for each membrane was incubated with anti-β-actin (1:4000; #4967; Cell Signaling Technology, MA, USA). All membranes for visualizing the phosphorylation and the protein levels of IR and Akt/PKB expression were incubated with secondary goat anti-rabbit antibody conjugated with horseradish peroxidase (1:2000; #7074; Cell Signaling Technology, MA, USA). The protein bands were visualized on Amersham hyperfilm ECL (GE Healthcare, Buckinghamshire, UK) using Amersham ECL Western blot detection reagents (GE, Healthcare). Band densities of phosphorylated IR or Akt/PKB at serine 473 kinases phosphorylation were represented as a ratio of insulin stimulation (+) to no insulin stimulation (-) and were normalized to total IR or Akt/PKB. In addition, band intensities were quantified by Scion Image and the results were shown as average signal intensity (arbitrary) units.

Serum and brain malondialdehyde (MDA) levels

The high performance liquid chromatography (HPLC) method was used to evaluate concentrations of serum and brain malondialdehyde (MDA) as described previously (Candan and Tuzmen 2008; Mateos, et al. 2005; Pintana et al. 2013; Pintana, et al. 2014).

Brain mitochondrial function study

Brain mitochondria were isolated using the method described previously (Pipatpiboon et al. 2013). Mitochondrial protein concentration was measured using BCA assay (Pipatpiboon et al. 2013), and brain mitochondrial function including brain mitochondrial reactive oxygen species (ROS), mitochondrial membrane potential change ($\Delta\Psi m$) and mitochondrial swelling were determined. Brain mitochondrial reactive oxygen species (ROS) were measured using dichloro-hydrofluoresceindiacetate (DCFHDA) fluorescent dye. The change in mitochondrial membrane potential ($\Delta\Psi m$) was measured using the fluorescent dye 5, 5′, 6, 6′-tetrachloro-1, 1′, 3, 3′-tetraethyl benzimidazolcarbocyanine iodide (JC-1) and brain mitochondrial swelling was determined by measuring the change in the absorbance of brain mitochondrial suspension at 540 nm. All were determined by following the methods described previously (Pintana et al. 2013; Pipatpiboon et al. 2013) .

Cognitive function test

The open-field test (OFT) was used to screen locomotor activity by counting the number of lines that the rats crossed during the test, as described in previous studies (Arakawa 2005; Pintana et al. 2013). The assessment of cognitive function was performed by using the Morris Water Maze (MWM) with two assessments including the acquisition test which was carried out for five consecutive days, and the probe test which was performed on day six (Pintana et al. 2013; Vorhees and Williams 2006). Data analysis of MWM test was done manually from video tape recordings by the investigators, who were blinded to experimental groups.

Golgi staining and morphological analysis of dendritic spines

Golgi staining and morphological analysis using the method described previously (Sripetchwandee, et al. 2014b). After decapitation, brains were removed and rinsed with

double distilled water, and was processed for Golgi staining using a commercially available kit (FD Neurotechnologies kit, PK 401, Ellicott City, U.S.A.). For analysis of dendritic spine density, the secondary and tertiary dendrites of three neurons at CA1 hippocampus area were counted. Dendritic segments were viewed through an inverted microscope (IX-81, Olympus, Tokyo, Japan).

Statistical analysis

Data were expressed as mean ± SEM. For all comparisons, the significance of the differences in peripheral biochemical parameters was calculated using the Mann-Whitney U test. The comparisons in the percentage of insulin-induced LTD, the percentage of LTP, brain mitochondrial function, immunoblot, the OFT tests and the MWM tests for the probe test among groups were performed using the one-way ANOVA test, followed by post-hoc LSD analysis. Comparisons among groups in MWM tests for the acquisition test were performed using a two-way ANOVA, followed by post-hoc LSD analysis. $P < 0.05$ was considered statistically significant.

Results

Calories restriction as well as the combination of calories restriction plus vildagliptin treatment in obese-insulin resistance rats equally restored peripheral insulin sensitivity.

At the baseline levels (week 0), the metabolic parameters were not significantly different between the normal-diet fed rats (ND) and the high-fat diet fed rats (HFD) (Table 1). After 12 weeks of diet regimens, HFD group had significantly increased bodyweight, plasma insulin, HOMA index, total cholesterol levels and LDL cholesterol levels, when compared with ND group (Table 1). However, plasma glucose levels were not significantly different between groups (Table 1). These findings suggested that long-term HFD consumption caused peripheral insulin resistance as indicated by hyperinsulinemia with euglycemia and increased HOMA index.

After four weeks of treatment regimens, HFD-fed rats treated with vehicle (HFV) had significantly increased body weight, i visceral fat, plasma insulin levels, HOMA index, plasma glucose area under the curve of oral glucose tolerance test (AUCg), total

cholesterol, plasma LDL cholesterol levels , but decreased plasma HDL cholesterol levels, when compared with ND-fed rats treated with vehicle (NDV) (Table 2). These findings indicated that peripheral insulin resistance was still observed in HFV rats after 16 weeks. Interestingly, HFD-fed rats with restricted diet and vehicle (HFRV) and HFD-fed rats with restricted diet and vildaglptin (HFRVil) had significantly decreased body weight, visceral fat, plasma insulin, HOMA index, plasma glucose area under the curve of oral glucose tolerance test (AUCg), total plasma cholesterol, LDL cholesterol levels , but increased plasma HDL cholesterol levels, when compared with HFV rats (Table 2). However, plasma glucose and plasma triglyceride levels showed no significant difference among all groups (Table 2). All of these findings indicated that both calories restriction and the combination of calories restriction plus vildagliptin equally restored peripheral insulin sensitivity and improved lipid profiles in obese-insulin resistant rats.

Obesity caused the impairment of brain insulin receptor function, which was restored by only the combination of calories restriction plus vildagliptin treatment.

Brain insulin receptor function was tested by measuring insulin-induced long-term depression (insulin-induced LTD) and brain insulin signaling. After four weeks of treatment regimens, the degree of insulin-induced LTD of HFV rats significantly reduced, when compared with that of NDV rats (n=2-3 independent slices/animal, n=6 animals/group, Fig. 2A). Interestingly, insulin-induced LTD of only HFRVil rats significantly increased, when compared with that of HFV rats (n=2-3 independent slices/animal, n=6 animals/group, Fig. 2A). For brain insulin signaling, the levels of IR and Akt/PKB proteins expression were not different among groups (Fig. 2D and 2E). The phosphorylation of insulin receptors (p-IR) and Akt/PKB at the serine 473 site in both HFV and HFRV rats significantly decreased, when compared with NDV rats (Fig. 2B and 2C). However, the p-IR levels and Akt/PKB at the serine 473 site of only HFRVil rats significantly increased when compared with those of HFV rats (Fig. 2B and 2C).

All of these findings suggested that the obese insulin-resistant condition caused the impairment of brain insulin receptor function and brain insulin signaling. In addition, only the combination of calories restriction plus vildagiptin restored those impairments in obese-insulin resistant rats.

Obesity caused brain mitochondrial dysfunction, which was restored by only the combination of calories restriction plus vildagliptin treatment

Brain mitochondrial function was determined by assessing changes in brain mitochondrial ROS production and brain mitochondrial membrane potential change ($\Delta\Psi m$) after H_2O_2 stimulation, as well as brain mitochondrial swelling. After four weeks of treatment regimens, the results demonstrated that both HFV and HFRV rats had a significant increase in brain mitochondrial ROS production, brain mitochondrial depolarization, and brain mitochondrial swelling, when compared with NDV rats (Fig. 3A, 3B and 3C). Interestingly, only HFRVil rats significantly decreased brain ROS production, improved brain mitochondrial depolarization and improved brain mitochondrial swelling, when compared with HFV rats (Fig. 3A, 3B and 3C).

Furthermore, the morphological changes of brain mitochondria from all groups were showed in Fig. 3D. The brain mitochondrial swelling was observed in both the HFV and HFRV rats as indicated by markedly unfolded cristae (Fig. 3D). Interestingly, intact brain mitochondrial morphology with apparent folded cristae was observed in only HFRVil rats (Fig. 3D). All of these findings suggested that the obese insulin-resistant condition caused the impairment of brain mitochondrial function. In addition, only the combination of calories restriction plus vildagliptin restored the impairment of brain mitochondrial dysfunction in obese-insulin resistant rats.

Obesity caused increase circulation and brain oxidative stress levels, which was attenuated by calories restriction as well as the combination of calories restriction plus vildagliptin treatment

Circulation and brain oxidative stress were determined by assessing serum MDA and brain MDA levels. After four weeks of treatment regimens, the results demonstrated that both circulating MDA and brain MDA levels significantly increased in HFV rats compared to NDV rats (Fig. 4A and 4B). HFRV rats showed significantly decreased only in circulating MDA, when compared with HFV rats (Fig. 4A). Interestingly, HFRVil rats showed significantly decreased both circulating MDA and brain MDA levels, when compared with HFV rats (Fig. 4A and 4B).

All of these findings suggested that obese-insulin resistant condition increased both circulating and brain oxidative stress levels. In addition, calories restriction alone decreased only circulating oxidative stress and only the combination of calories restriction plus vildagliptin decreased both circulating and brain oxidative stress levels in obese-insulin resistant condition.

Obesity caused impaired hippocampal synaptic plasticity and cognitive decline, which was restored by only the combination of calories restriction plus vildagliptin treatment

To study hippocampal synaptic plasticity, electrical-induced long-term potentiation (LTP) was determined. After four weeks of treatment regimen, the results demonstrated that the degrees of electrical-induced LTP significantly decreased in both HFV and HFRV rats, when compared with NDV rats (n=2-3 independent slices/animal, n=6 animals/group Fig. 5A). The reduction of electrical–induced LTP in both HFV and HFRV rats was not significantly different (n=2-3 independent slices/animal, n=6 animals/group Fig. 5A). However, the degree of electrical-induced LTP of HFRVil rats significantly increased, when compared with that of HFV rats (n=2-3 independent slices/animal, n=6 animals/group Fig. 5A).

The density of hippocampal dendritic spines was determined at the secondary and tertiary dendrites in the apical dendrite of CA1 hippocampus to investigate the underlying mechanism of memory function. We found that dendritic spines density of HFV and HFRV rats significantly decreased, when compared with that of NDV rats (Fig. 5B). After treatment regimens, dendritic spines density of both HFRV and HFRVil rats significantly increased, when compared with that of HFV rats (Fig. 5B). However, dendritic spines density of HFRVil rats was significantly greater than that of HFRV rats (Fig. 5B).

All of these findings suggested that the obese insulin-resistant condition caused the impairment of hippocampal synaptic plasticity, including impaired electrical–induced LTP and reduced dendritic spine density. In addition, only the combination of calories restriction plus vildagiptin reversed the impairment of hippocampal synaptic plasticity in obese-insulin resistant rats.

Furthermore, the open-field test (OFT) was used to screen locomotor activity. The results showed that it was not significantly different among all groups, indicating that the locomotor activity did not differ in all groups. In addition, the present study determined cognitive function by using the Morris water maze (MWM) test after four weeks of treatment regimens. For the acquisition test, we found that both HFV and HFRV rats significantly increased time to reach the platform, when compared with NDV rats (Fig. 6A). However, HFRVil rats significantly decreased time to reach the platform, when compared with HFV rats (Fig. 6A). For the probe test, both HFV and HFRV rats significantly decreased time spent in the target quadrant, when compared to NDV rats (Fig. 6B). In constrast, HFRVil rats significantly increased time spent in the target quadrant, when compared with HFV rats (Fig. 6B).

All of these findings suggested that the obese insulin-resistant condition caused cognitive decline, both calories restriction and calories restriction plus vildagiptin could improve dendritic spines density. However, only the combination of calories restriction plus vildagiptin restored cognitive function in obese-insulin resistant rats.

Discussion

The major findings of the present study are as follows: [1] obese rats leads to the development of peripheral insulin resistance, impairment of brain insulin sensitivity, brain mitochondrial dysfunction, impaired hippocampal synaptic plasticity and decreased dendritic spine density, as well as cognitive decline; [2] both calories restriction and the combination of calories restriction plus vildagliptin equally improved peripheral insulin sensitivity and lipid profiles; [3] calories restriction alone decreased circulating oxidative stress, whereas the combination of calories restriction plus vildagliptin decreased both circulating and brain oxidative stress levels; and [4] only the combination of calories restriction plus vildagliptin restored brain insulin sensitivity, brain mitochondrial function , hippocampal synaptic plasticity and cognitive function in obese-insulin resistant rats.

Our present study demonstrated that diet-induced obesity developed the peripheral insulin resistance via impaired peripheral insulin sensitivity, impaired lipid profiles and increased both circulating as well as brain oxidative stress. These findings confirms other and our previous studies that diet induced obesity not only caused peripheral insulin resistance but also brain insulin resistance (Greenwood and Winocur 2005; Pratchayasakul et al. 2011). In addition, the impairment of brain insulin sensitivity, increased brain oxidative stress, and impaired brain mitochondrial dysfunction were found in our present study. These findings indicated that obesity caused increased oxidative stress and impaired brain mitochondrial function resulting in brain insulin resistance, in which could contribute to cognitive decline, as similar with previous studies (Pipatpiboon et al. 2013; Pipatpiboon et al. 2012).

In the present study, we demonstrated that calories restriction restored peripheral insulin sensitivity and improved lipid profile in obese-insulin resistant rats. This finding was supported by several previous studies, in which demonstrated that calories restriction (Dean et al. 1998; McCurdy et al. 2005; Sharma et al. 2012) improved metabolic effects in animal model. The possible explanation could be due to decreased in visceral fat and dyslipidemia following calorie restriction in our model. Decreased fat has been shown to reduce systemic inflammation (REFs) as well as circulating oxidative stress as shown in the present study and other previous studies (REFS). It has been known that impaired

peripheral insulin sensitivity was caused by inflammation and too much oxidative stress (REFS).

Although calorie restriction restored peripheral insulin sensitivity and decreased circulating oxidative stress, calories restriction alone failed to improve brain insulin sensitivity, brain mitochondrial dysfunction as well as failed to restore hippocampal synaptic plasticity and cognitive decline in obese-insulin resistant rats. In contrast to several previous studies, those studies showed that calorie restriction could have a beneficial effect as neuroprotection and preserved cognition. For example: 1) A previous study demonstrated that 40% of CR for 24 months reduced the rate of mitochondrial H_2O_2 production via reduced brain ROS production in aged rats (Sanz et al. 2005). 2) The study of 40% CR for 22-29 months also reported that CR prevented aged related deficit synaptic LTP and preserved NR1-subunit of NMDA receptor in aged Fisher 344 rats (Eckles-Smith, et al. 2000). 3) The study of 60% CR for 4 weeks in male rats demonstrated that CR stabilized synaptophysin expression and preserved cognitive function (Adams et al. 2008). 4) A recent study demonstrated that 70% CR for 28 days improved metabolic effects and cognitive decline via up-regulation of brain-derived neurotropic factor and decrease hippocampus oxidative stress in moderated high-fat diet (35% energy from fat) induced obese-metabolic syndrome male rats (Kishi, et al. 2015). The possible explanation in our findings could be that calorie restriction may not be enough to protect brain function in obese condition, because calorie restriction alone could not decrease brain MDA level in obese-insulin resistant rats (Figure XX). The other possible explanations of different findings between previous studies and our study could depend on the percentage of high-fat diet feeding, percentage and duration of food restriction, as well as differences in animal model. Nevertheless, further investigations are required to elucidate about the effect of calories restriction in obese-insulin resistant condition.

Interestingly, calories restriction combined with vildagliptin restored peripheral insulin sensitivity, brain insulin sensitivity, brain mitochondrial function, cognitive function, synaptic plasticity and decreased brain oxidative stress in obese-insulin resistant rats. These findings suggest that the beneficial effect of brain function should be due to the

action of vildagliptin, however the improvement of peripheral insulin sensitivity could be due to both calorie restriction and vildagliptin. The proposed underlying mechanism of vildagliptin, which improved brain insulin sensitivity, could be due to its ability to increase in plasma active GLP-1 levels via inhibiting DPP-4 action (Akarte, et al. 2012), leading to improve insulin sensitivity (Figure 2A), improve brain insulin signaling (Figure 2B and 2C), and reduced both circulating and brain oxidative stress (Figure 4). Although the level of GLP-1 was not measured in the present study, our previous study already demonstrated that vildagliptin increased plasma and brain active GLP-1 levels, leading to increased peripheral and brain insulin sensitivity in obese male rats (Pipatpiboon et al. 2013). Because calories restriction plus vildagliptin improved brain insulin sensitivity and brain mitochondrial function (Fig. 3), it could restore hippocampal synaptic plasticity (Fig.5A), resulting to improve cognitive decline (Fig.6) in obese-insulin resistance rats. Although, the effects of calories restriction alone could improve peripheral insulin resistance but fail to improve brain insulin sensitivity and brain mitochondrial dysfunction, may be due to it could not decreased enough brain oxidative stress levels (Fig.4B). Therefore, it fails to restore hippocampal synaptic plasticity (Fig.5A) and cognitive decline (Fig.6) in obese-insulin resistance rats.

Conclusion

The present study indicates that calories restriction or calories restriction plus vildagliptin equally restores peripheral insulin sensitivity and decreases circulating oxidative stress levels. However only calories restriction plus vildagliptin decreases brain oxidative stress levels and restores brain insulin sensitivity, brain mitochondrial function, hippocampal synaptic plasticity, and finally improved cognitive function in obese-insulin resistant rats.

References

Adams MM, Shi L, Linville MC, Forbes ME, Long AB, Bennett C, Newton IG, Carter CS, Sonntag WE, Riddle DR, et al. 2008 Caloric restriction and age affect synaptic proteins in hippocampal CA3 and spatial learning ability. *Exp Neurol* **211** 141-149.

Akarte AS, Srinivasan BP & Gandhi S 2012 Vildagliptin selectively ameliorates GLP-1, GLUT4, SREBP-1c mRNA levels and stimulates beta-cell proliferation resulting in improved glucose homeostasis in rats with streptozotocin-induced diabetes. *J Diabetes Complications* **26** 266-274.

Arakawa H 2005 Age dependent effects of space limitation and social tension on open-field behavior in male rats. *Physiol Behav* **84** 429-436.

Burkey BF, Li X, Bolognese L, Balkan B, Mone M, Russell M, Hughes TE & Wang PR 2005 Acute and chronic effects of the incretin enhancer vildagliptin in insulin-resistant rats. *J Pharmacol Exp Ther* **315** 688-695.

Candan N & Tuzmen N 2008 Very rapid quantification of malondialdehyde (MDA) in rat brain exposed to lead, aluminium and phenolic antioxidants by high-performance liquid chromatography-fluorescence detection. *Neurotoxicology* **29** 708-713.

Dean DJ, Brozinick JT, Jr., Cushman SW & Cartee GD 1998 Calorie restriction increases cell surface GLUT-4 in insulin-stimulated skeletal muscle. *Am J Physiol* **275** E957-964.

Eckles-Smith K, Clayton D, Bickford P & Browning MD 2000 Caloric restriction prevents age-related deficits in LTP and in NMDA receptor expression. *Brain Res Mol Brain Res* **78** 154-162.

Gault VA, Lennox R & Flatt PR 2015 Sitagliptin, a dipeptidyl peptidase-4 inhibitor, improves recognition memory, oxidative stress and hippocampal neurogenesis and upregulates key genes involved in cognitive decline. *Diabetes Obes Metab* **17** 403-413.

Greenwood CE & Winocur G 2005 High-fat diets, insulin resistance and declining cognitive function. *Neurobiol Aging* **26 Suppl 1** 42-45.

Hiona A & Leeuwenburgh C 2004 Effects of age and caloric restriction on brain neuronal cell death/survival. *Ann N Y Acad Sci* **1019** 96-105.

Kishi T, Hirooka Y, Nagayama T, Isegawa K, Katsuki M, Takesue K & Sunagawa K 2015 Calorie restriction improves cognitive decline via up-regulation of brain-derived neurotrophic factor: tropomyosin-related kinase B in hippocampus ofobesity-induced hypertensive rats. *Int Heart J* **56** 110-115.

Kitzinger H & Karle B 2013 The epidemiology of obesity. *Eur Surg* **45** 80-82.

Mateos R, Lecumberri E, Ramos S, Goya L & Bravo L 2005 Determination of malondialdehyde (MDA) by high-performance liquid chromatography in serum and liver as a biomarker for oxidative stress. Application to a rat model for hypercholesterolemia and evaluation of the effect of diets rich in phenolic antioxidants from fruits. *J Chromatogr B Analyt Technol Biomed Life Sci* **827** 76-82.

McCurdy CE, Davidson RT & Cartee GD 2005 Calorie restriction increases the ratio of phosphatidylinositol 3-kinase catalytic to regulatory subunits in rat skeletal muscle. *Am J Physiol Endocrinol Metab* **288** E996-E1001.

Morrison CD, Pistell PJ, Ingram DK, Johnson WD, Liu Y, Fernandez-Kim SO, White CL, Purpera MN, Uranga RM, Bruce-Keller AJ, et al. 2010 High fat diet increases hippocampal oxidative stress and cognitive impairment in aged mice: implications for decreased Nrf2 signaling. *J Neurochem* **114** 1581-1589.

Pintana H, Apaijai N, Chattipakorn N & Chattipakorn SC 2013 DPP-4 inhibitors improve cognition and brain mitochondrial function of insulin resistant rats. *J Endocrinol* **218** 1-11.

Pintana H, Sripetchwandee J, Supakul L, Apaijai N, Chattipakorn N & Chattipakorn S 2014 Garlic extract attenuates brain mitochondrial dysfunction and cognitive deficit in obese-insulin resistant rats. *Appl Physiol Nutr Metab* **39** 1373-1379.

Pipatpiboon N, Pintana H, Pratchayasakul W, Chattipakorn N & Chattipakorn SC 2013 DPP4-inhibitor improves neuronal insulin receptor function, brain mitochondrial function and cognitive function in rats with insulin resistance induced by high-fat diet consumption. *Eur J Neurosci* **37** 839-849.

Pipatpiboon N, Pratchayasakul W, Chattipakorn N & Chattipakorn SC 2012 PPARgamma agonist improves neuronal insulin receptor function in hippocampus and

brain mitochondria function in rats with insulin resistance induced by long term high-fat diets. *Endocrinology* **153** 329-338.

Pistell PJ, Morrison CD, Gupta S, Knight AG, Keller JN, Ingram DK & Bruce-Keller AJ 2010 Cognitive impairment following high fat diet consumption is associated with brain inflammation. *J Neuroimmunol* **219** 25-32.

Pratchayasakul W, Kerdphoo S, Petsophonsakul P, Pongchaidecha A, Chattipakorn N & Chattipakorn SC 2011 Effects of high-fat diet on insulin receptor function in rat hippocampus and the level of neuronal corticosterone. *Life Sci* **88** 619-627.

Sanz A, Caro P, Ibanez J, Gomez J, Gredilla R & Barja G 2005 Dietary restriction at old age lowers mitochondrial oxygen radical production and leak at complex I and oxidative DNA damage in rat brain. *J Bioenerg Biomembr* **37** 83-90.

Sharma N, Castorena CM & Cartee GD 2012 Greater insulin sensitivity in calorie restricted rats occurs with unaltered circulating levels of several important myokines and cytokines. *Nutr Metab (Lond)* **9** 90.

Speakman JR & Mitchell SE 2011 Caloric restriction. *Mol Aspects Med* **32** 159-221.
Sripetchwandee J, Pipatpiboon N, Chattipakorn N & Chattipakorn S 2014a Combined therapy of iron chelator and antioxidant completely restores brain dysfunction induced by iron toxicity. *PLoS One* **9** e85115.

Sripetchwandee J, Pipatpiboon N, Pratchayasakul W, Chattipakorn N & Chattipakorn SC 2014b DPP-4 inhibitor and PPARgamma agonist restore the loss of CA1 dendritic spines in obese insulin-resistant rats. *Arch Med Res* **45** 547-552.

Stranahan AM, Norman ED, Lee K, Cutler RG, Telljohann RS, Egan JM & Mattson MP 2008 Diet-induced insulin resistance impairs hippocampal synaptic plasticity and cognition in middle-aged rats. *Hippocampus* **18** 1085-1088.

Vorhees CV & Williams MT 2006 Morris water maze: procedures for assessing spatial and related forms of learning and memory. *Nat Protoc* **1** 848-858.
Wilsey J & Scarpace PJ 2004 Caloric restriction reverses the deficits in leptin receptor protein and leptin signaling capacity associated with diet-induced obesity: role of leptin in

the regulation of hypothalamic long-form leptin receptor expression. *J Endocrinol* **181** 297-306.

Yamaoka K & Tango T 2012 Effects of lifestyle modification on metabolic syndrome: a systematic review and meta-analysis. *BMC Med* **10** 138.

Table 1: Metabolic parameters at baseline and the end of week 12 (before treatment)

Metabolic parameters	Baseline		Week 12	
	ND	HFD	ND	HFD
Body weight (g)	199.6±2.7	206.9±2.4	476.3±6.0	560.8±12.5 *
Plasma glucose (mg/dl)	139.0±5.4	130.5±4.5	144.6±5.1	143.3±9.0
Plasma insulin (ng/ml)	2.4±0.6	2.4±0.5	2.9±0.4	4.7±0.6*
HOMA index	12.0±2.8	10.9±2.5	24.5±3.9	38.6±3.9*
Plasma total cholesterol (mg/dl)	68.0±3.4	67.8±3.8	66.9±3.9	81.5±4.2*
Plasma triglyceride (mg/dl)	51.9±3.7	48.1±4.5	60.2±7.6	62.0±8.7
HDL cholesterol (mg/dl)	32.5±1.5	29.7±1.3	30.1±1.6	28.0±3.3
LDL cholesterol (mg/dl)	23.6±3.5	28.9±4.0	23.7±2.7	39.9±3.0*

* compared to ND at same time course

Table 2: Metabolic parameters after calorie restriction and calories restriction plus vildagliptin treatment

Metabolic parameters	Groups			
	NDV	HFV	HFRV	HFRV il
Body weight (g)	490.7±9.4	597.9±15*	19.1±10.1†	511.3±10.5†
Visceral fat (g)	24.6±1.3	52.7±2.9*	30.0±1.3†	28.5±2.3†
Plasma glucose (mg/dl)	153.5±16.8	163.2±7.1	152.7±3.2	157.5±5.6
Plasma insulin (ng/ml)	4.2±0.2	6.4±0.8*	3.6±0.5†	4.0±0.6†
HOMA index	34.6±5.3	59.2±8.8*	32.7±4.4†	34.5±6.1†
Plasma glucose AUC (AUCg) (mg/dlxminx10^4)	4.8±0.2	6.0±0.3*	4.8±0.3†	4.9±0.2†
Plasma total cholesterol (mg/dl)	70.5±4.2	97.3±6.0*	76.5±2.4†	75.4±3.8†
Plasma triglyceride (mg/dl)	52.1±7.2	54.7±5.0	51.8±5.3	53.3±7.2
HDL cholesterol (mg/dl)	33.9±1.9	24.5±1.9*	35.9±2.2†	34.7±2.0†
LDL cholesterol (mg/dl)	26.9±3.1	52.8±6.0*	31.8±6.5†	28.3±4.3†

* compared to NDV

† compared to HFV

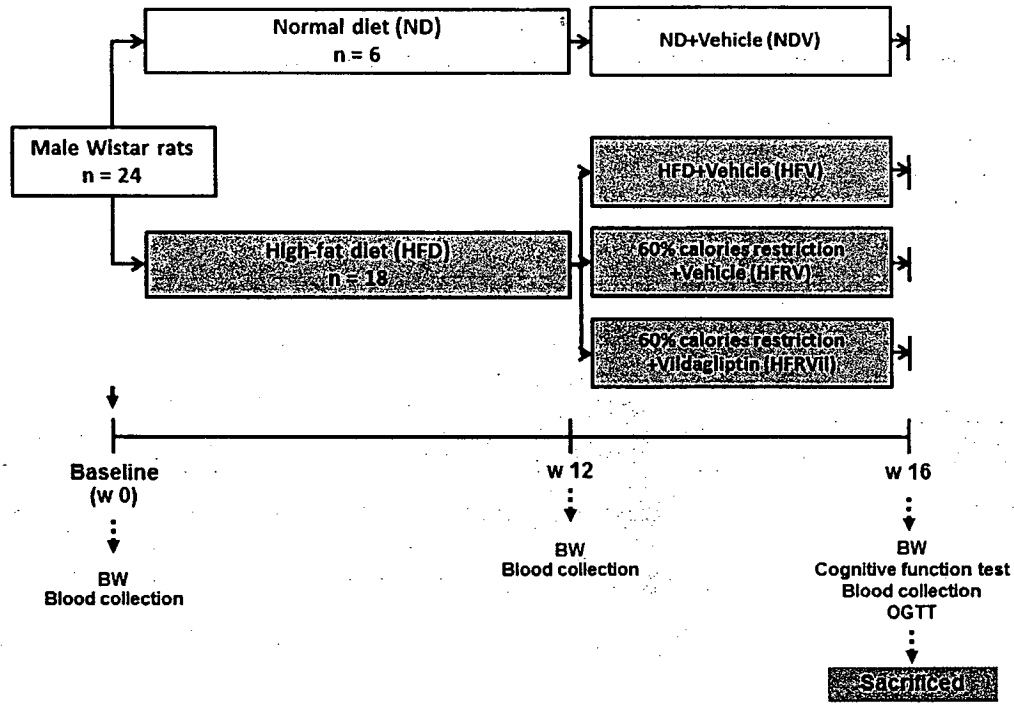


Figure 1: The experimental protocol of the study

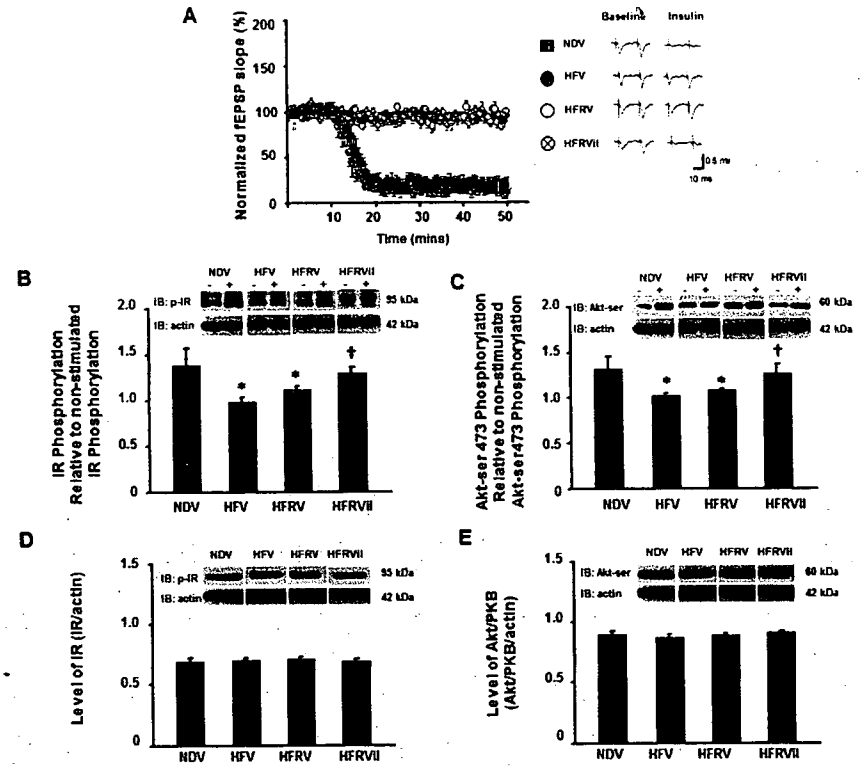


Figure 2: The effects of calories restriction and the combination of calories restriction plus vildagliptin on brain insulin receptor function (insulin-induced long term depression, LTD) and brain insulin signaling, including the phosphorylation of insulin receptor (p-IR), Akt-Ser 473, insulin receptors (IR) and Akt/PKB protein expression in obese-insulin resistant rats. The combination of calories restriction plus vildagliptin improves the ability of insulin-induced LTD in HFRVil rats, when compared with HFV rats (A). After four weeks of treatment, HFV and HFRV significantly decreased both p-IR and Akt-Ser 473 expression compared to NDV rats (B and C). The combination of calories restriction plus vildagliptin significantly increased both p-IR and Akt-Ser 473 expression compared to HFV rats (B and C). However, IR and Akt/PKB protein expression were not different among all groups (D and D). NDV: normal-diet fed rats treated with vehicle, HFV: high-fat diet fed rats treated with vehicle, HFRV: high-fat diet fed rats reversed food to normal diet with 60% calories restriction treated with vehicle and HFRVil: high-fat diet fed rats reversed food to normal diet with 60% calories restriction treated with vildagliptin. *$p<0.05$ vs NDV and † $p<0.05$ vs HFV

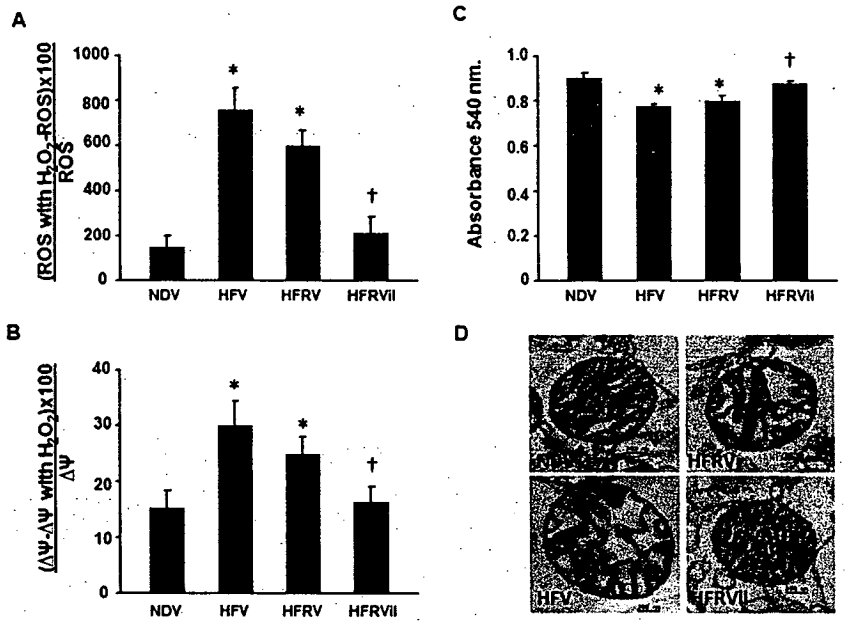


Figure 3: The effects of calories restriction and the combination of calories restriction plus vildagliptin on brain mitochondrial function and representative images of brain mitochondrial morphology by transmission electron microscopy (JEM-2200FS field emission electron microscope, original magnification x 20,000) in obese-insulin resistant rats. HFV and HFRV rats demonstrated brain mitochondrial dysfunction compared to NDV rats, as indicated by increased brain mitochondrial ROS production following H_2O_2 application (A), increased brain mitochondrial membrane potential change following H_2O_2 application (B) and decreased absorbance values, indicating brain mitochondrial swelling (C). The combination of calories restriction plus vildagliptin in HFRVil rats improved brain mitochondrial function compared with HFV rats, as indicated by significantly decreased brain mitochondrial ROS production (A), decreased brain mitochondrial membrane potential change (B) and increased absorbance values (C). Furthermore, normal folding of cristae in brain mitochondrial morphology was shown in both NDV and HFRVil rats (D). However, brain mitochondrial swelling, as indicated by unfolded cristae in both HFV and HFRV rats were observed (D). NDV: normal-diet fed rats treated with vehicle, HFV: high-fat diet fed rats treated with vehicle, HFRV: high-fat diet fed rats reversed food to normal diet with 60% calories restriction treated with vehicle and HFRVil: high-fat diet fed rats reversed food to normal diet with 60% calories restriction treated with vildagliptin, *$p<0.05$ vs NDV and † $p<0.05$ vs HFV

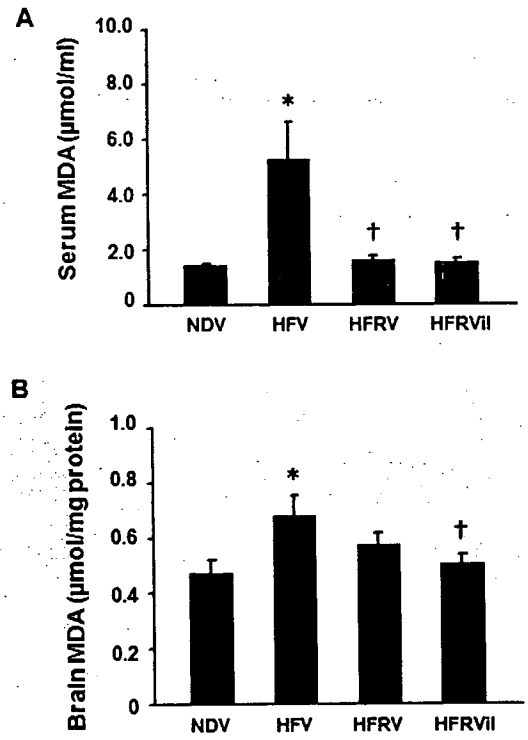


Figure 4: The effects of calories restriction and the combination of calories restriction plus vildagliptin on serum and brain malondialdehyde (MDA) levels in obese-insulin resistant rats. In addition, HFV significantly increased serum and brain MDA levels compared with NDV rats (A and B). HFRV rats significantly decreased only serum MDA levels compared with HFV rats (A). However, HFRVil rats significantly decreased both serum and brain MDA levels compared with HFV rats (A and B). NDV: normal-diet fed rats treated with vehicle, HFV: high-fat diet fed rats treated with vehicle, HFRV: high-fat diet fed rats reversed food to normal diet with 60% calories restriction treated with vehicle and HFRVil: high-fat diet fed rats reversed food to normal diet with 60% calories restriction treated with vildagliptin, *$p<0.05$ vs NDV and † $p<0.05$ vs HFV

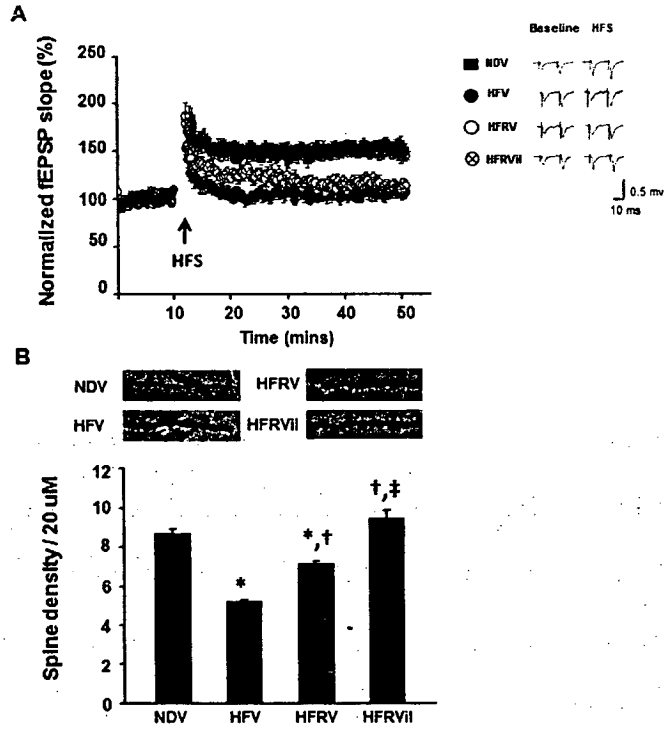


Figure 5: The effects of calories restriction and the combination of calories restriction plus vildagliptin on hippocampal synaptic long-term potentiation (LTP) and the number of dendritic spines on tertiary dendrites in apical dendrite in obese-insulin resistant rats. Both HFV and HFRV rats showed significantly a reduced percentage of normalized fEPSPs, when compared with NDV rats (A). The combination of calories restriction plus vildagliptin improves the percentage of normalized fEPSPs in only rats i in HFRVil rats, when compared with HFV rats (A). The number of dendritic spines on secondary or tertiary dendrites in hippocampal apical dendrite was decreased in HFV rats (B). Both HFRV and HFRVil rats showed significantly increase the number of dendritic spines after treatment regimen (B). NDV: normal-diet fed rats treated with vehicle, HFV: high-fat diet fed rats treated with vehicle, HFRV: high-fat diet fed rats reversed food to normal diet with 60% calories restriction treated with vehicle, HFRVil: high-fat diet fed rats reversed food to normal diet with 60% calories restriction treated with vildagliptin and HFS; high frequency stimulation. *$p<0.05$ vs NDV, † $p<0.05$ vs HFV and ‡ $p<0.05$ vs HFRV

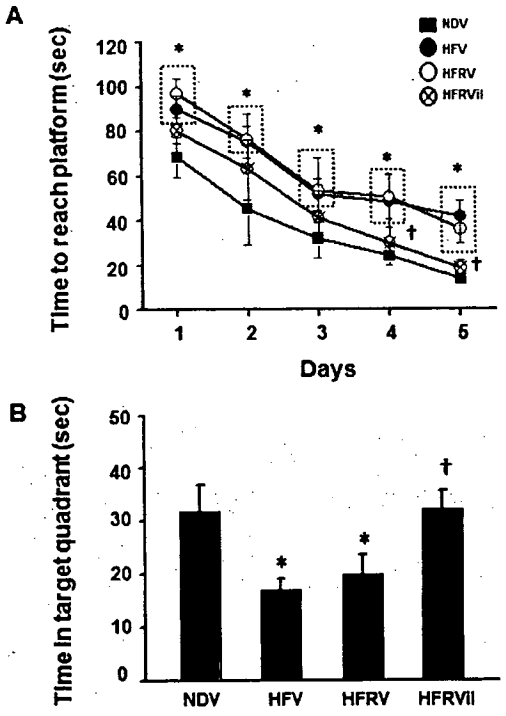


Figure 6: The effects of calories restriction and the combination of calories restriction plus vildagliptin on cognitive function determined by the Morris water maze (MWM) test in obese-insulin resistant rats. HFV and HFRV rats showed a significantly increased time to reach the platform in the acquisition test as well as having a decreased time spent in target quadrant in the probe test, when compared with NDV rats (A and B). HFRVil rats showed a significantly decreased time to reach the platform in the acquisition test as well as increased time spent in target quadrant in the probe test, when compared with HFV rats (A and B). NDV: normal-diet fed rats treated with vehicle, HFV: high-fat diet fed rats treated with vehicle, HFRV: high-fat diet fed rats reversed food to normal diet with 60% calories restriction treated with vehicle and HFRVil: high-fat diet fed rats reversed food to normal diet with 60% calories restriction treated with vildagliptin, *$p<0.05$ vs NDV, † $p<0.05$ vs HFV and ‡ $p<0.05$ vs HFRV

Chapter V

Chapert V

Conclusion

The present study was the study to report that obesity dominated testosterone deprivation in terms of causing the development of peripheral and brain insulin resistance. In addition, testosterone deprivation early initated an impairment of hippocampal synaptic plasticity and cognitive decline. However, testosterone deprivation did not cause peripheral and brain insulin resistance, as well as brain mitochondrial dysfunction. Obesity did not aggravate these brain impairments in testosterone-deprived condition. Vildagliptin therapy improved peripheral insulin sensitivity in both obese-insulin resistant condition with and without testosterone deprivation. Vildagliptin therapy exertedthe beneficial effects in improving brain insulin resistance in the condition of testosterone-deprivation with obesity. However, vildagliptin treatment could not restored coginitive decline in testosterone-deprived obese rats.

The present study also demonstrated that both calorie restriction and calorie restriction plus vildagliptin equally improved peripheral insulin sensitivity. Only calorie restriction plus vildagliptin markedly improved brain insulin sensitivity and cognitive function in obese-insulin resistant condition.

สัญญาเลขที่ BRG5780016

กิตติกรรมประกาศ

This work is supported by Thailand Research Fund: BGR5780016 (SC)

Output

OUTPUT

1. การเสนอผลงานในงานประชุมทางวิชาการต่าง ๆ

1. Tanajak P, Sa-nguanmoo P, Sivasinprasasn S, Thummasorn S, Intachai K, Siri-Angkul N, **Chattipakorn SC**, Chattipakorn N. Dipeptidyl peptidase-4 inhibitor markedly enhances the cardioprotective efficacy of sodium-glucose cotransporter-2 inhibitor in pre-diabetic rats with cardiac ischemia-reperfusion injury. *Cardiovasc Res* 2017;98:1(suppl):XXX. (in press) (Impact Factor = 5.465)
2. Chattipakorn N, Tunapong W, Yasom S, Wanchai K, Chunchai T, Tanajak P, Apaijai N, Thiennimitr P, Sirilun S, Chaiyasut C, Pongchaidecha A, Lungkapin A, Pratchayasakul W, **Chattipakorn SC**. Combined prebiotics and probiotics treatment is not superior to single regimen for cardioprotection in obese-insulin resistant rats. *J Am Col Cardiol* 2017 (in press) (Impact Factor=14.086)
3. Pattanakuhar S, Phrommintikul A, Tantiworawit A, Konginn S, Srichairattanakool S, Chattipakorn SC, **Chattipakorn** N. Decreased heart rate variability is associated with increased cardiac iron deposit determined by cardiac t2 *mri and decreased left ventricular function in transfusion dependent thalassemia patients. *J Am Col Cardiol* 2017 (in press) (Impact Factor=14.086)
4. Pongkan W, Xu L, Takatori O, Nagata N, Ni Y, Nakayama M, **Chattipakorn SC**, Usui S, Ota T, Chattipakorn N. Beta-cryptoxanthin exerts better cardioprotection against cardiac ischemia-reperfusion injury than astaxanthin via protecting mitochondrial dysfunction in mice. *J Am Col Cardiol* 2017 (in press) (Impact Factor=14.086)
5. Shinlapawittayatorn K, Nuntaphum W, Tanajak P, Thummasorn S, Khamseekaew J, Wongjaikam S, **Chattipakorn SC**, Chattipakorn N. Vagus nerve stimulation requires both ipsi- and contralateral vagal activition to fully exert its cardioprotection against cardiac ischemia/reperfusion injury. *J Am Col Cardiol* 2017 (in press) (Impact Factor=14.086)

6. Thummasorn S, Shinlapawittayatorn K, **Chattipakorn SC**, Chattipakorn N. High-dose humanin analogue applied during ischemia provides cardioprotection against ischemia-reperfusion injury through attenuating mitochondrial dysfunction. *J Am Col Cardiol* 2017 (in press) (Impact Factor=14.086)
7. Palee S, Minta W, Mantor D, Sutham W, Pratchayasakul W, **Chattipakorn SC**, Chattipakorn N. Estrogen deprivation aggravates cardiometabolic dysfunction and intracellular calcium dyshomeostasis in obese-insulin resistance rats. *J Am Col Cardiol* 2017 (in press) (Impact Factor=14.086)
8. Apaijai N, Palee S, Chunchai T, Jaiwongkam T, **Chattipakorn SC**, Chattipakorn N. Lack of testosterone in obese-insulin resistant condition aggravates cardiometabolic dysfunction through the impairment of cardiac mitochondrial function. *J Am Col Cardiol* 2017 (in press) (Impact Factor=14.086)
9. Sripetchwandee J, Wongjaikam S, Krintratun W, Chattipakorn N, **Chattipakorn SC**. Combined iron chelator and antioxidant therapy effectively diminishes the dendritic loss, Alzheimer's pathology and brain mitochondrial dynamic disruption in rats with chronic iron overload. *Alzheimers Dement* 2016:P4-021. (Impact Factor = 17.472)
10. Sripetchwandee N, Sa-nguanmoo P, Sripetchwandee J, Phrommintikul A, Chattipakorn N, **Chattipakorn SC**. Neutrophil-Lymphocyte Ratio (NLR) is a possible prognostic marker of poor cognitive performance in mets patients. *Alzheimers Dement* 2016:P2-160. (Impact Factor = 17.472)
11. Pratchayasakul W, Sivasinprasasn S, Sa-nguanmoo P, Proctor C, Kerdphoo S, Chattipakorn N, **Chattipakorn SC**. Estrogen and DPP-4 inhibitor reduced brain oxidative stress and increased dendritic spine density in ovariectomized obese and non-obese rats with cardiac ischemia-reperfusion injury. *Endocr Rev* 2016 (in press) (Impact Factor = 21.059)
12. Pintana H, Tanajak P, Pratchayasakul W, Sa-nguanmoo P, Chunchai T, Satjaritanun P, Leelarphat L, Chattipakorn N, **Chattipakorn SC**. Dipeptidyl peptidase-4 (DPP-4) inhibitor exerts better neuroprotection than calories restriction

by attenuating mitochondrial dysfunction impaired by obese-insulin resistance in rats. *Endocr Rev* 2016 (in press) (Impact Factor = 21.059)

13. Sa-nguanmoo P, Tanajak P, Kerdphoo S, Satjaritanun P, Wang X, Liang G, Li X, Jiang C, Pratchayasakul W, Chattipakorn N, **Chattipakorn SC**. FGF21 therapy improves cognitive function impaired by obese-insulin resistant condition via restoring synaptic plasticity and brain mitochondrial function. *Endocr Rev* 2016 (in press) (Impact Factor = 21.059)
14. Tanajak P, Pintana H, Siri-Angkul N, **Chattipakorn SC**, Chattipakorn N. DPP-4 inhibitor exerts better cardioprotection than caloric restriction by attenuating cardiac mitochondrial dysfunction and improving FGF21 sensitivity in obese-insulin resistant rats. *Endocr Rev* 2016 (in press) (Impact Factor = 21.059)
15. Apaijai N, Charoenphandhu N, Ittichaichareon J, Suntornsaratoon P, Krishnamra N, Aeimlapa R, **Chattipakorn SC**, Chattipakorn N. Estrogen deprivation aggravates adverse left ventricular remodeling in type 2 diabetic rats. *Endocr Rev* 2016 (in press) (Impact Factor = 21.059)
16. Pongkan W, Pintana H, Kumfu S, Sa-nguanmoo P, Jaiwongkam T, Sivasinprasan S, **Chattipakorn SC**, Chattipakorn N. Testosterone replacement protects the heart against ischemic-reperfusion injury and preserves cardiac performance in testosterone-deprived male rats with obese-insulin resistance. *Endocr Rev* 2016 (in press) (Impact Factor = 21.059)
17. Sivasinprasasn S, Tanajak P, Pongkan W, Pratchayasakul W, **Chattipakorn S**, Chattipakorn N. DPP-4 Inhibitor and Estrogen Attenuate Metabolic Dysfunction and Mitochondrial Impairment from Cardiac Ischemic-Reperfusion Injury in Obese-Insulin Resistant and Estrogen-Deprived Rats. *Endocr Rev* 2016 (in press) (Impact Factor = 21.059)
18. Apaijai N, Lekawanvijit S, **Chattipakorn SC**, Chattipakorn N. Dipeptidyl peptidase-4 inhibitor exerts better cardioprotection than enalapril against late-phase left ventricular remodeling after myocardial infarction in obese-insulin resistant rats. *Eur Heart J* 2015;36(suppl 1):P3781. (Impact Factor = 14.723)

19. Pongkan W, Pintana H, Sivasinprasasn S, Apaijai N, Kumfu S, Jaiwongkam T, Chattipakorn SC, **Chattipakorn N**. Testosterone deprivation accelerates cardiac dysfunction and cardiac mitochondrial impairments in obese-insulin resistant rats. *Eur Heart J* 2015;36(suppl 1): P5539. (Impact Factor = 14.723)
20. WongJaikam S, Kumfu S, Chattipakorn SC, Fucharoen S, **Chattipakorn N**. Head to head comparisons of therapeutic efficacy among three iron chelators on cardiac function in iron-overloaded rats. *Eur Heart J* 2015;36(suppl 1): P3786. (Impact Factor = 14.723)
21. Samniang B, Chanchai T, Shinlapawittayatorn K, Chattipakorn SC, **Chattipakorn N**. Chronic vagus nerve stimulation exerts glycemic control and cardioprotection via preventing cardiac mitochondrial dysfunction in obese-insulin resistant rats. *Eur Heart J* 2015;36(suppl 1):P4538. (Impact Factor = 14.723)
22. **Chattipakorn SC**, Pintana H, Pratchayasakul W, Sa-nguanmoo P, Pongkan W, Tawinvisan R, Chattipakorn N. Testosterone Deprivation Accelerates Cognitive Impairment in Obese-Insulin Resistant Rats. *Alzheimers Dement* 2015;P3-044. (Impact Factor = 17.472)
23. Chunchai T, Samniang B, Sripetchwandee J, Silapawitatorn K, KenKnight BH, Chattipakorn N, **Chattipakorn SC**. Vagus Nerve Stimulation Restores Cognitive Function Impaired By Chronic Obese-Insulin Resistant Rats. *Alzheimers Dement* 2015;P2-044. (Impact Factor = 17.472)
24. Sripetchwandee J, Semaming Y, Sa-nguanmoo P, Pintana H, Pannangpetch P, Chattipakorn N, **Chattipakorn SC**. Protocatechuic acid attenuates brain oxidative stress and brain mitochondrial dysfunction in insulin-dependent diabetic rats. *Alzheimers Dement* 2015;P4-175. (Impact Factor = 17.472)
25. Pintana H, Pongkan W, Pratchayasakul W, Chattipakorn N, **Chattipakorn SC**. DPP-4 inhibitor improves brain insulin sensitivity, but fail to restore hippocampal synaptic plasticity and cognitive function in testosterone-deprived obese rats. *Alzheimers Dement* 2015;P2-030. (Impact Factor = 17.472)

26. Kumfu S, **Chattipakorn S,** Fucharoen S, Chattipakorn N. T-type calcium channel blocker exerts similar efficacy as iron chelators in attenuating cardiovascular and mitochondrial dysfunction in iron-overload thalassemic mice. J Am Col Cardiol 2015;65(10S):A901. (Impact Factor=14.086)
27. Chattipakorn N, Inthachai T, Lekawanvijit S, **Chattipakorn SC**. Dipeptidyl peptidase-4 inhibitor attenuates cardiac dysfunction and adverse remodeling after myocardial infarction. J Am Col Cardiol 2015;65(10S):A905. (Impact Factor=14.086)
28. Sivasinprasasn S, Sa-nguanmoo P, Pratchayasakul W, Shinlapawittayatorn K, **Chattipakorn S**, Chattipakorn N. DPP-4 inhibitor and estrogen, but not metformin, exert cardioprotection via attenuating cardiac mitochondrial dysfunction in obese-insulin resistant and estrogen-deprived rats. J Am Col Cardiol 2015;65(10S):A799. (Impact Factor=14.086)

2. กิจกรรมที่เกี่ยวข้องกับการนำผลจากโครงการไปใช้ประโยชน์

2.1 การแต่งหนังสือ

1. Shinlapawittayatorn K, **Chattipakorn SC**, Chattipakorn N. Vagus Nerve Stimulation: A Promis-ing Cardioprotective Strategy Against Ischemia-Reperfusion Injury. In: *Coronary Artery Disease - Research and Practice.* iConcept Press Ltd. (ISBN 978-1-922227-98-0) (Year 2016)
2. Sripetchwandee J, Chattipakorn N, **Chattipakorn SC**. Cross-link of brain iron overload, brain calcium channels and underlying mechanisms regarding the cognitive impairment In. *Learning and Memory: Processes, Influences and Performance* Eula Townsend Nova Publishers (ISBN 978-1-63485-325-5) (Year 2016)
3. Pratchayasakul W, Chattipakorn N, **Chattipakorn SC**. Impact of malondialdehyde on cognitive dysfunction in obesity. In: Campbell J, ed. *Malondialdehyde (MDA): Structure, Biochemistry and Role in Disease.* Nova Publishers (ISBN 978-1-63482-793-5) (Year 2015)

4. **สิริพร ฉัตรทิพากร.** ภาวะอ้วน ภาวะดื้อต่ออินซูลินในสมองและสมองุเสื่อม ใน สิริพร ฉัตรทิพากร บรรณาธิการ .เชียงใหม่: บริษัท ทรีโอ แอดเวอร์ไทซิ่ง แอนด์ มีเดีย จำกัด; 2556:1-172. (ISBN 978-974-672-783-9) (Year 2013)

2.2 นักศึกษาภายใต้สังกัดได้รับรางวัล

1. **ดร. หิรัญญา ปินตานา นักศึกษาระดับปริญญาเอก**
ผลงานวิจัยยอดเยี่ยมชนิด Outstanding Oral Research Presentation Award
ในสาขาวิทยาศาสตร์การแพทย์
หน่วยงานที่มอบรางวัล โครงการปริญญาเอกกาญจนภิเษก (คปก.)
จากงานประชุมวิชาการโครงการปริญญาเอกกาญจนภิเษก ครั้งที่ 17 (RGJ-PhD. Congress 17)
ในวันที่ 8-11 มิถุนายน พ.ศ. 2559 ณ โรงแรมจอมเทียน ปาล์ม บีช จ.ชลบุรี
(โดยมี ศ. ดร. ทพญ. สิริพร ฉัตรทิพากร เป็นอาจารย์ที่ปรึกษาหลักวิทยานิพนธ์)

2. **ดร. ณัฐยาภรณ์ อภัยใจ นักศึกษาระดับปริญญาเอก**
ผลงานวิจัยยอดเยี่ยมชนิด Outstanding Oral Research Presentation Award
ในสาขาวิทยาศาสตร์การแพทย์
หน่วยงานที่มอบรางวัล โครงการปริญญาเอกกาญจนภิเษก (คปก.)
จากงานประชุมวิชาการโครงการปริญญาเอกกาญจนภิเษก ครั้งที่ 17 (RGJ-PhD. Congress17)
ในวันที่ 8-11 มิถุนายน พ.ศ. 2559 ณ โรงแรมจอมเทียน ปาล์ม บีช จ.ชลบุรี
(โดยมี ศ. ดร. ทพญ. สิริพร ฉัตรทิพากร เป็นอาจารย์ที่ปรึกษาร่วมวิทยานิพนธ์)
(โดยมี ศ. ดร. ทพญ. สิริพร ฉัตรทิพากร เป็นอาจารย์ที่ปรึกษาร่วมวิทยานิพนธ์)

3. **ดร. นสพ. เกริกเกียรติ จินดา นักศึกษาระดับปริญญาเอก**
ได้รับรางวัลวิทยานิพนธ์ดีเด่นระดับปริญญาเอก สาขาวิทยาศาสตร์สุขภาพ
หน่วยงานที่มอบรางวัล บัณฑิตวิทยาลัย มหาวิทยาลัยเชียงใหม่
ในวันที่ 22 มกราคม 2559 ณ บัณฑิตวิทยาลัย มหาวิทยาลัยเชียงใหม่
(โดยมี ศ. ดร. ทพญ. สิริพร ฉัตรทิพากร เป็นอาจารย์ที่ปรึกษาร่วมวิทยานิพนธ์)

4. **น.ส. ธารวิมล อินทรชัย นักศึกษาระดับปริญญาโท**

ได้รับรางวัลวิทยานิพนธ์ดีเด่นระดับปริญญาโท สาขาวิทยาศาสตร์สุขภาพ

หน่วยงานที่มอบรางวัล บัณฑิตวิทยาลัย มหาวิทยาลัยเชียงใหม่

ในวันที่ 22 มกราคม 2559 ณ บัณฑิตวิทยาลัย มหาวิทยาลัยเชียงใหม่

(โดยมี ศ. ดร. ทพญ. สิริพร ฉัตรทิพากร เป็นอาจารย์ที่ปรึกษาร่วมวิทยานิพนธ์)

5. **อ. ดร. ภก. จิรภาส ศรีเพชรวรรณดี**

ได้รับเกียรติบัตร รางวัล Young Scientist Award Winner for Oral Presentation

ผลงานวิจัยที่ทำให้ได้รับรางวัล เรื่อง Sripetchwandee J, Wongjaikam S, Krintratun W, Chattipakorn N, Chattipakorn SC.Therapeutic comparisons of three iron chelators in thebrain of iron-overload rats.

จากงานประชุมวิชาการนานาชาติ 8th FAOPS congress

หน่วยงานที่มอบรางวัล Physiological Society of Thailand (PST) Federation of The Asian and Oceanian Physiological Societies ในวันที่ 25 พฤศจิกายน 2558

(โดยมี ศ. ดร. ทพญ. สิริพร ฉัตรทิพากร เป็นอาจารย์ที่ปรึกษาหลักวิทยานิพนธ์)

6. **น.ส. สุวคนธ์ วงศ์ใจคำ นักศึกษาระดับปริญญาเอก**

ได้รับเกียรติบัตร รางวัล Young Scientist Award Winner for Oral Presentation

ผลงานวิจัยที่ทำให้ได้รับรางวัล เรื่อง Wongjaikam S, Kumfu S, Chattipakorn SC, Fucharoen S, Chattipakorn N. Combined therapy of iron chelator and antioxidant completely restores left ventricular dysfunction in iron-overloaded rats.

จากงานประชุมวิชาการนานาชาติ 8th FAOPS congress

หน่วยงานที่มอบรางวัล Physiological Society of Thailand (PST) Federation of The Asian and Oceanian Physiological ในวันที่ 25 พฤศจิกายน 2558

(โดยมี ศ. ดร. ทพญ. สิริพร ฉัตรทิพากร เป็นอาจารย์ที่ปรึกษาร่วมวิทยานิพนธ์)

7. **น.ส. ณัฐยาภรณ์ อภัยใจ นักศึกษาระดับปริญญาเอก**

ได้รับเกียรติบัตร รางวัล Young Scientist Award Winner for Oral Presentation

ผลงานวิจัยที่ทำให้ได้รับรางวัล เรื่อง Apaijai N, Lekawanvijit S, Chattipakorn SC,

Chattipakorn N. Dipeptidyl peptidase 4 inhibitor prevents left ventricular remodeling after chronic infarction in obese-insulin resistant rats.
จากงานประชุมวิชาการนานาชาติ 8th FAOPS congress
หน่วยงานที่มอบรางวัล Physiological Society of Thailand (PST) Federation of The Asian and Oceanian Physiological ในวันที่ 25 พฤศจิกายน 2558
(โดยมี ศ. ดร. ทพญ. สิริพร ฉัตรทิพากร เป็นอาจารย์ที่ปรึกษาร่วมวิทยานิพนธ์)

8. **นางสาวิตรี ชารุนันท์กร นักศึกษาระดับปริญญาเอก**
ได้รับเกียรติบัตร รางวัล Young Scientist Award Winner for Oral Presentation
ผลงานวิจัยที่ทำให้ได้รับรางวัล เรื่อง Charununtakorn ST, Apaijai N, Kerdphoo S, Shinlapawittayatorn K, Chattipakorn SC, Chattipakorn N. Humanin exerts cardioprotection against cardiac ischemia-reperfusion injury via attenuating cardiac mitochondrial dysfunction.
จากงานประชุมวิชาการนานาชาติ 8th FAOPS congress
หน่วยงานที่มอบรางวัล Physiological Society of Thailand (PST) Federation of The Asian and Oceanian Physiological ในวันที่ 25 พฤศจิกายน 2558
(โดยมี ศ. ดร. ทพญ. สิริพร ฉัตรทิพากร เป็นอาจารย์ที่ปรึกษาร่วมวิทยานิพนธ์)

9. **นายพงษ์พันธ์ ธนะจักร นักศึกษาระดับปริญญาเอก**
ได้รับเกียรติบัตร รางวัล Young Scientist Award Winner for Oral Presentation
ผลงานวิจัยที่ทำให้ได้รับรางวัล Tanajak P, Sa-nguanmoo P, Chattipakorn SC, Chattipakorn N. Fibroblast growth factor 21 improved cardiac function and cardiac autonomic regulation by attenuates metabolic disturbance, inflammation, and oxidative stress in obese insulin resistance rats.
จากงานประชุมวิชาการนานาชาติ 8th FAOPS congress
หน่วยงานที่มอบรางวัล Physiological Society of Thailand (PST) Federation of The Asian and Oceanian Physiological Societies ในวันที่ 25 พฤศจิกายน 2558
(โดยมี ศ. ดร. ทพญ. สิริพร ฉัตรทิพากร เป็นอาจารย์ที่ปรึกษาร่วมวิทยานิพนธ์)

10. **น.ส. เพียงขวัญ สงวนหมู่ นักศึกษาระดับปริญญาเอก**

ได้รับเกียรติบัตร รางวัล Young Scientist Award Winner for Poster Presentation

ผลงานวิจัยที่ทำให้ได้รับรางวัล เรื่อง Sa-nguanmoo P, Tanajak P, Pratchayasakul W, Chattipakorn N, Chattipakorn SC. Fibroblast growth factor 21 (FGF21) improved cognitive impairment in obese-insulin resistant rats.

จากงานประชุมวิชาการนานาชาติ 8th FAOPS congress

หน่วยงานที่มอบรางวัล Physiological Society of Thailand (PST) Federation of The Asian and Oceanian Physiological Societies ในวันที่ 25 พฤศจิกายน 2558

(โดยมี ศ. ดร. ทพญ. สิริพร ฉัตรทิพากร เป็นอาจารย์ที่ปรึกษาหลักวิทยานิพนธ์)

11. **นายฐิติกร จันทร์ไชย นักศึกษาระดับปริญญาโท**

ได้รับเกียรติบัตร รางวัล Young Scientist Award Winner for Oral Presentation

ผลงานวิจัยที่ทำให้ได้รับรางวัล Chunchai T, Thunapong W, Yasom S, Wanchai K, Thiennimitr P, Chaiyasut C, Chattipakorn N, Chattipakorn SC. The probiotic therapy with Lactobacillus paracasei increased cognitive function in obese-insulin resistance rats.

จากงานประชุมวิชาการนานาชาติ 8th FAOPS congress

หน่วยงานที่มอบรางวัล Physiological Society of Thailand (PST) Federation of The Asian and Oceanian Physiological Societies ในวันที่ 25 พฤศจิกายน 2558

(โดยมี ศ. ดร. ทพญ. สิริพร ฉัตรทิพากร เป็นอาจารย์ที่ปรึกษาหลักวิทยานิพนธ์)

12. **น.ส. เบญจรุนันท์ สำเนียง นักศึกษาระดับปริญญาโท**

ได้รับเกียรติบัตร รางวัลการ นำเสนอผลงานทางวิชาการของนักศึกษายอดเยี่ยม ผลงานวิจัยที่ทำให้ได้รับรางวัล เรื่อง Effects of chronic vagus nerve stimulation on cardiac function in obese-insulin resistant rats.

จากงานประชุมวิชาการ The 34th National Graduate research conference

หน่วยงานที่มอบรางวัล Graduate school, Khon Kaen University ในวันที่ 27 มีนาคม 2558

(โดยมี ศ. ดร. ทพญ. สิริพร ฉัตรทิพากร เป็นอาจารย์ที่ปรึกษาร่วมวิทยานิพนธ์)

13. **นายฐิติกร จันทร์ไชย นักศึกษาระดับปริญญาโท**

ได้รับเกียรติบัตร รางวัลการ นำเสนอผลงานทางวิชาการของนักศึกษายอดเยี่ยม ผลงานวิจัยที่ทำให้ได้รับรางวัล เรื่อง Effects of chronic vagus nerve stimulation on brain function in metabolic syndrome rats จากงานประชุมวิชาการ The 34th National Graduate research conference

หน่วยงานที่มอบรางวัล Graduate school, Khon Kaen University ในวันที่ 27 มีนาคม 2558

(โดยมี ศ. ดร. ทพญ. สิริพร ฉัตรทิพากร เป็นอาจารย์ที่ปรึกษาหลักวิทยานิพนธ์)

14. **นายฐิติกร จันทร์ไชย นักศึกษาระดับปริญญาโท**

ได้รับเกียรติบัตร รางวัล Travel Fellowship Award

ผลงานวิจัยที่ทำให้ได้รับรางวัล เรื่อง Chunchai T, Samniang B, Sripetchwandee J, Silapawitatorn K, KenKnight BH, Chattipakorn N, Chattipakorn SC. Vagus Nerve Stimulation Restores Cognitive Function Impaired By Chronic Obese-Insulin Resistant Rats. Alzheimers Dement 2015;P2-044. (Impact Factor = 17.472)

จากงานประชุมวิชาการนานาชาติ The Alzheimer's Association International Conference (AAIC)

ณ เมือง วอชิงตัน ดีซี (Washington DC) ประเทศ สหรัฐอเมริกา (USA)

ในวันที่ 22 กรกฎาคม 2558

(โดยมี ศ. ดร. ทพญ. สิริพร ฉัตรทิพากร เป็นอาจารย์ที่ปรึกษาหลักวิทยานิพนธ์)

15. **น.ส. เพียงขวัญ สงวนหมู่ นักศึกษาระดับปริญญาเอก**

ได้รับรางวัล Travel Grant Award

หน่วยงานที่มอบรางวัล IBRO-APRC School of Neuroscience

โดยจะเดินในวันที่ 1-30 พฤศจิกายน 2559 ณ ประเทศมาเลเซีย

จากงานประชุม 3rd international brain research organization (IBRO-APRC) advanced school of neuroscience

(โดยมี ศ. ดร. ทพญ. สิริพร ฉัตรทิพากร เป็นอาจารย์ที่ปรึกษาหลักวิทยานิพนธ์)

16. **นายฐิติกร จันทร์ไชย นักศึกษาระดับปริญญาเอก**

ได้รับรางวัล Travel Grant Award

หน่วยงานที่มอบรางวัล IBRO-APRC School of Neuroscience

โดยจะเดินทางในวันที่ 1-30 พฤศจิกายน 2559 ณ ประเทศมาเลเซีย

จากงานประชุม 3rd international brain research organization (IBRO- APRC) advanced school of neuroscience

(โดยมี ศ. ดร. ทพญ. สิริพร ฉัตรทิพากร เป็นอาจารย์ที่ปรึกษาหลักวิทยานิพนธ์)

17. **น.ส. จุฑามาศ คำสีแก้ว นักศึกษาระดับปริญญาเอก**

ผลงานจากงานวิจัยได้รับการคัดเลือกให้ขึ้นบนหน้าปกวารสาร Canadian Journal of Cardiology ซึ่งมี Impact Factor = 3.94

ผลงานวิจัยเรื่อง Khamseekaew J, Kumfu S, Chattipakorn SC, Chattipakorn N. Effects of iron overload on cardiac calcium regulation: translational insights into mechanisms and management of a global epidemic. Can J Cardiol 2016;32:1009-1016.

(โดยมี ศ. ดร. ทพญ. สิริพร ฉัตรทิพากร เป็นอาจารย์ที่ปรึกษาร่วมวิทยานิพนธ์)

2.3 การเชื่อมโยงกับต่างประเทศ

1. **Associate Professor Dr. Lai-Hua Xie**

   Department of Cell Biology and Molecular Medicine Rutgers University/ New Jersey Medical School

2. **Association Professor Dr. Morten Schak Nielsen**

   Chairman of the Danish Cardiovascular Research Academy (DaCRA) Section of Heart and Circulatory Research, Department of Biomedical Sciences, University of Copenhagen, Copenhagen, Denmark

3. **Professor Dr. Susanne Klaus**

   Research Group physiology of energy metabolism (EST)

   German Institute of Human Nutrition Potsdam-Rehbruecke, Brandenburg Germany

4. **Dr. Claire Rampon**

Senior Research Associate, CNRS, team co-head

Université de Toulouse (UPS) Centre de Recherches sur la Cognition Animale, Toulouse, France ; Centre National de la Recherche Scientifique (CNRS) Centre de Recherches sur la Cognition Animale, Toulouse, France

5. **Associate Professor Dr. Bruno Guiard**

Université de Toulouse (UPS) Centre de Recherches sur la Cognition Animale, Toulouse, France ; Centre National de la Recherche Scientifique (CNRS) Centre de Recherches sur la Cognition Animale, Toulouse, France; Faculté de Pharmacie, Université Paris Sud XI, Châtenay-Malabry, Cedex, France

2.4. รางวัลที่ได้รับ

1. รางวัลนักวิจัยดีเด่นแห่งชาติ ประจำปี 2559
   จาก สำนักงานคณะกรรมการวิจัยแห่งชาติ (วช.)
2. รางวัล 2017 TRF-OHEC-Thomson Reuters Research Excellence Awards จาก สำนักงานกองทุนสนับสนุนการวิจัย (สกว.)
3. รางวัลผลงานวิจัยเด่น สกว. ประจำปี 2558
   เรื่อง "ผลของยาต้านเบาหวานและเอสโตรเจนต่อการเรียนรู้ และความจำของสมองในภาวะอ้วนและขาดฮอร์โมนเพศหญิง"
   จาก สำนักงานกองทุนสนับสนุนการวิจัย (สกว.)
4. ทุนโครงการปริญญาเอกกาญจนภิเษก (คปก.) รุ่นที่ 18 จำนวน 2 ทุน พ.ศ. 2558
5. รางวัล "ช้างทองคำนักวิจัยดีเด่นสาขาวิทยาศาสตร์การแพทย์" ประจำปี 2557
   จาก มหาวิทยาลัยเชียงใหม่

ภาคผนวก

ภาคผนวก

ผลงานทางวิชาการ (Articles) จำนวน 66 เรื่อง

1. Kumfu S, Fucharoen S, **Chattipakorn SC**, Chattipakorn N. Cardiac complications in beta-thalassemia :From mice to men. *Exp Biol Med* 2017 (in press) (Impact Factor = 2.542) **(เอกสารแนบหมายเลข 1)**
2. Pratchayasakul W, Sivasinprasasn S, Sa-nguanmoo P, Proctor C, Kerdphoo S, Chattipakorn N, **Chattipakorn SC**. Estrogen and DPP-4 inhibitor share similar efficacy in reducing brain pathology caused by cardiac ischemia-reperfusion injury in both lean and obese estrogen-deprived rats. *Menopause* 2017 (in press) (Impact Factor = 3.361) **(เอกสารแนบหมายเลข 2)**
3. Ittichaicharoen J, Apaijai N, Tanajak P, Sa-nguanmoo P, Chattipakorn N, **Chattipakorn SC**. Impaired mitochondria and intracellular calcium transients in the salivary glands of obese rats. *Appl Physiol Nutr Me* 2017 Apr;42(4):420-429. (Impact Factor = 2.34) **(เอกสารแนบหมายเลข 3)**
4. Eaimworawuthikul S, Thiennimitr P, Chattipakorn N, **Chattipakorn SC**. Diet-induced obesity, gut microbiota and bone, including alveolar bone loss. *Arch Oral Biol* Feb 2017;78:65-81. (Impact Factor = 1.733) **(เอกสารแนบหมายเลข 4)**
5. Wongjaikam S, Kumfu S, Khamseekaew J, **Chattipakorn SC**, Chattipakorn N. Restoring the impaired cardiac calcium homeostasis and cardiac function in iron overload rats by the combined deferiprone and N-acetyl cysteine. *Sci Rep* 2017;7:44460. (Impact Factor = 5.228) **(เอกสารแนบหมายเลข 5)**
6. Khamseekaew J, Kumfu S, Wongjaikam S, Kerdphoo S, Jaiwongkam T, Srichairatanakool S, Fucharoen S, **Chattipakorn SC**, Chattipakorn N. Effects of iron overload, an iron chelator and a T-Type calcium channel blocker on cardiac mitochondrial biogenesis and mitochondrial dynamics in thalassemic mice. Eur J Pharmacol 2017;799:118-127. (Impact Factor = 2.730) **(เอกสารแนบหมายเลข 6)**

7. Charoenphandhu N, Suntornsaratoon P, Krishnamra N, Sa-nguanmoo P, Tanajak P, Wang X, Liang G, Li X, Jiang C, Chattipakorn N, **Chattipakorn SC**. Fibroblast growth factor-21 restores insulin sensitivity but induces aberrant bone microstructure in obese insulin-resistant rats. J Bone Miner Metab 2017;35(2):142-149. (Impact factor = 2.46) **(เอกสารแนบหมายเลข 7)**
8. Sawaddiruk P, Paiboonworachat S, Chattipakorn N, **Chattipakorn SC**. Alterations of brain activity in fibromyalgia patients. J Clin Neurosci 2017;38:13-22. (Impact Factor = 1.378) **(เอกสารแนบหมายเลข 8)**
9. Tanajak P, Pintana H, Siri-Angkul N, Khamseekaew J, Apaijai N, **Chattipakorn SC**, Chattipakorn N. Vildagliptin exerts better cardioprotection than caloric restriction by improving mitochondrial function in obese-insulin resistant rats. *J Endocrinol* 2017;232(2):189-204. (Impact Factor = 4.498)
(เอกสารแนบหมายเลข 9)
10. Procter C, Thiennimitr P, Chattipakorn N, **Chattipakorn SC**. Diet, gut microbiota and cognition. *Metab Brain Dis* 2017;32(1):1-17 . (Impact Factor = 2.638)
(เอกสารแนบหมายเลข 10)
11. Pintana H, Tanajak P, Pratchayasakul W, Sa-nguanmoo P, Chunchai T, Satjaritanun P, Leelarphat L, Chattipakorn N, **Chattipakorn SC**. Calorie restriction combined with DDP-IV inhibitor exerts neuroprotection in obese male rats. *Brit J Nutr* 2016;116-1700-1708. (Impact Factor = 3.411) **(เอกสารแนบหมายเลข 11)**
12. Chattipakorn N, Apaijai N, **Chattipakorn SC**. Dipeptidyl peptidase-4 inhibitors and the ischemic heart: Additional benefits beyond glycemic control. Int J Cardiol. 2016;202:415-6 (Impact Factor = 4.036) **(เอกสารแนบหมายเลข 12)**
13. Sarasamkan J, Scheunemann M, Apaijai N, Palee S, Parichatikanond W, Arunrungvichian K, Fischer S, **Chattipakorn SC**, Deuther-Conrad W, Schüürmann G, Brust P, Vajragupta O. Varying Chirality Across Nicotinic Acetylcholine Receptor Subtypes: Selective Binding of Quinuclidine Triazole Compounds. ACS Med Chem Lett. 2016 7(10):890-895. (Impact Factor = 3.355)
(เอกสารแนบหมายเลข 13)

14. Charununtakorn ST, Apaijai N, Kerdphoo S, Shinlapawittayatorn K, **Chattipakorn SC**, Chattipakorn N. Humanin exerts cardioprotection against cardiac ischemia-reperfusion injury through attenuation of mitochondrial dysfunction. Cardiovasc Ther 2016;34:404-414. (Impact Factor = 2.243) **(เอกสารแนบหมายเลข 14)**

15. Wongjaikam S, Kumfu S, Khamseekaew J, Sripetchwandee J, Srichairatanakool S, Fucharoen S, **Chattipakorn SC**, Chattipakorn N. Combined iron chelator and antioxidant exerted greater efficacy on cardioprotection than monotherapy in iron-overloaded rats. Plos One 2016 Jul 18;11(7):e0159414 (Impact Factor = 3.234) **(เอกสารแนบหมายเลข 15)**

16. Pongkan W, Pintana H, Jaiwongkam T, Kredphoo S, Sivasinprasasn S, **Chattipakorn SC**, Chattipakorn N. Vildagliptin reduces cardiac ischemic-reperfusion injury in obese-orchiectomized rats. *J Endocrinol* 2016;231(1):81-95. (Impact Factor = 4.498) **(เอกสารแนบหมายเลข 16)**

17. Sa-nguanmoo P, Tanajak P, Kerdphoo S, Satjaritanun P, Wang X, Liang G, Li X, Jiang C, Pratchayasakul W, Chattipakorn N, **Chattipakorn SC**. FGF21 Improves Cognition by Restored Synaptic Plasticity, Dendritic Spine Density, Brain Mitochondrial Function and Cell Apoptosis in Obese-Insulin Resistant Male Rats. *Horm Behav* 2016;85:86-95. (Impact Factor = 3.340) **(เอกสารแนบหมายเลข 17)**

18. Sripetchwandee J, Wongjaikam S, Krintratun W, Chattipakorn N, **Chattipakorn SC**. A combination of an iron chelator with an antioxidant effectively diminishes the dendritic loss, tau-hyperphosphorylation, amyloids-β accumulation and brain mitochondrial dynamic disruption in rats with chronic iron overload. *Neuroscience* 2016;332:191-202. (Impact Factor = 3.327) **(เอกสารแนบหมายเลข 18)**

19. Sivasinprasasn S, Sa-nguanmoo P, Pongkan W, Pratchayasakul W, **Chattipakorn SC**, Chattipakorn N. Estrogen and DPP-4 inhibitor, but not metformin, exert cardioprotection via attenuating cardiac mitochondrial dysfunction in obese- insulin resistant and estrogen-deprived female rats. Menopause 2016 ;23(8):894- 902 (Impact Factor = 3.361) **(เอกสารแนบหมายเลข 19)**

20. Tanajak P, Sa-Nguanmoo P, Wang X, Liang G, Li X, Jiang C, **Chattipakorn SC**, Chattipakorn N. FGF21 therapy attenuates left ventricular dysfunction and metabolic disturbance by improving FGF21 sensitivity, cardiac mitochondrial redox homeostasis and structural changes in pre-diabetic rats. Acta Physiol 2016;217(4):287-299. (Impact Factor = 4.382) **(เอกสารแนบหมายเลข 20)**

21. Apaijai N, Inthachai T, Lekawanvijit S, **Chattipakorn SC**, Chattipakorn N. Effects of dipeptidyl peptidase-4 inhibitor in insulin resistant rats with myocardial infarction. J Endocrinol 2016;229(3):245-58. (Impact Factor =4.498) **(เอกสารแนบหมายเลข 21)**

22. Pongkan W, Pintana H, Sivasinprasan S, Jaiwongkam T, **Chattipakorn SC**, Chattipakorn N. Testosterone deprivation accelerates cardiac dysfunction and cardiac mitochondrial impairment in obese male rats. J Endocrinol 2016;229(3):209-20. (Impact Factor = 4.498) **(เอกสารแนบหมายเลข 22)**

23. Khamseekaew J, Kumfu S, **Chattipakorn SC**, Chattipakorn N. Effects of iron overload on cardiac calcium regulation: translational insights into mechanisms and management of a global epidemic. *Can J Cardiol* 2016;32:1009-1016. (Impact Factor = 3.71) **(เอกสารแนบหมายเลข 23)**

24. Chunchai T, Samniang B, Sripetchwandee J, Pintana H, Pongkan W, Kumfu S, Shinlapawittayatorn K, KenKnight BH, Chattipakorn N, **Chattipakorn SC**. Vagus Nerve Stimulation Exerts the Neuroprotective Effects in Obese-Insulin Resistant Rats, Leading to the Improvement of Cognitive Function. *Sci Rep* 2016;6:26866 (Impact Factor = 5.578) **(เอกสารแนบหมายเลข 24)**

25. Kumfu S, Charunnuntakorn ST, Jaiwongkam T, Chattipakorn N, **Chattipakorn SC.** Humanin prevents brain mitochondrial dysfunction in a cardiac I/R injury model. *Exp Physiol* 2016;101(6):697-707. (Impact Factor=2.66) **(เอกสารแนบหมายเลข 25)**

26. Palee S, Apaijai N, Shinlapawittayatorn K, **Chattipakorn SC**, Chattipakorn N. Acetylcholine attenuates hydrogen peroxide-induced intracellular calcium dyshomeostasis through both muscarinic and nicotinic receptors in cardiomyocytes. *Cell Physiol Biochem* 2016;39:341-349. (Impact Factor = 2.875)
(เอกสารแนบหมายเลข 26)

27. Sivasinprasasn S, Sa-nguanmoo P, Pongkan W, Pratchayasakul W, **Chattipakorn SC**, Chattipakorn N. Estrogen and DPP-4 inhibitor, but not metformin, exert cardioprotection via attenuating cardiac mitochondrial dysfunction in obese- insulin resistant and estrogen-deprived female rats. Menopause 2016 ;23(8):894-902 (Impact Factor = 3.361) **(เอกสารแนบหมายเลข 27)**

28. Cole AR, Wijarnpreecha K, **Chattipakorn SC**, Chattipakorn N. Effects Tai Chi on heart rate variability. Complement Ther Clin Pract 2016;23:59-63. (Impact Factor = N/A) **(เอกสารแนบหมายเลข 28)**

29. Kumfu S, **Chattipakorn SC**, Fucharoen S, Chattipakorn N. Dual T-type and L-type calcium channel blocker exerts beneficial effects in attenuating cardiovascular dysfunction in iron-overload thalassemic mice. Exp Physiol 2016;101(4):521-39. (Impact Factor = 2.66) **(เอกสารแนบหมายเลข 29)**

30. Charununtakorn ST, Shinlapawittayatorn K, **Chattipakorn SC**, Chattipakorn N. Potential roles of humanin on apoptosis in the heart. *Cardiovasc Ther* 2016;34(2):107-114. (Impact Factor = 2.536) **(เอกสารแนบหมายเลข 30)**

31. Samniang B, Shinlapawittayatorn K, Chunchai T, Pongkan W, Kumfu S,**Chattipakorn SC**, KenKnight BH, Chattipakorn N. Vagus nerve stimulation improves cardiac function by preventing mitochondrial dysfunction in obese- insulin resistant rats. *Sci Rep 2016;6:19749.* (Impact Factor = 5.578) **(เอกสารแนบหมายเลข 31)**

32. Ittichaicharoen J, Chattipakorn N, **Chattipakorn SC**. Is Salivary Gland Function Altered in Noninsulin-Dependent Diabetes Mellitus and Obese-Insulin Resistance? *Arch Oral Biol* 2016;64:61-71. (Impact factor = 1.88) **(เอกสารแนบหมายเลข 32)**

33. Sa-nguanmoo P, Chattipakorn N, **Chattipakorn SC**. Potential roles of fibroblast growth factor 21 in the brain. *Metab Brain Dis* 2016;31(2):239-48. (Impact Factor = 2.398) **(เอกสารแนบหมายเลข 33)**

34. Kumfu S, **Chattipakorn SC**, Fucharoen S, Chattipakorn N. Effects of iron overload condition on liver toxicity and hepcidin/ferroportin expression in thalassemic mice. *Life Sciences* 2016;150:15-23. (Impact Factor = 2.702) **(เอกสารแนบหมายเลข 34)**

35. Potikanond S, Rattanachote P, Pintana H, Suntornsaratoon P, Charoenphandhu N, Chattipakorn N, **Chattipakorn SC**. Obesity does not aggravate osteoporosis or osteoblastic insulin resistance in orchiectomized rats. *J Endocrinol* 2015;228(2):85-95. (Impact Factor = 3.718) **(เอกสารแนบหมายเลข 35)**

36. Pintana H, Pratchayasakul W, Sa-nguanmoo P, Pongkan W, Tawinvisan R, Chattipakorn N, **Chattipakorn SC**. Testosterone deprivation has neither additive nor synergistic effects on the cognitive impairment in orchiectomized-obese male rats. *Metabolism* 2016;65:54-67. (Impact Factor = 3.89) **(เอกสารแนบหมายเลข 36)**

37. Nanegrungsunk D, Apaijai N, Yarana C, Limpastan K, Watcharasaksilp W, Vaniyapong T, Chattipakorn N, **Chattipakorn SC** Bevacizumab is superior to Temozolomide in causing mitochondrial dysfunction in human brain tumors. Neurol Res 2016 13:1-9 (Impact factor = 1.449) **(เอกสารแนบหมายเลข 37)**

38. Pongkan W, **Chattipakorn SC**, Chattipakorn N. Roles of testosterone replacement in cardiac ischemia-reperfusion injury. *J Cardiovasc Pharm Ther* 2016;21(1):27-43. (Impact Factor = 3.072) **(เอกสารแนบหมายเลข 38)**

39. Tanajak P, **Chattipakorn SC**, Chattipakorn N. Effects of fibroblast growth factor 21 on the heart. *J Endocrinol* 2015;227(2):R13-30. (Impact Factor = 3.718) **(เอกสารแนบหมายเลข 39)**

40. Pintana H, Pongkan W, Pratchayasakul W, Chattipakorn N, **Chattipakorn SC**. Testosterone replacement attenuates cognitive decline in testosterone-deprived lean rats, but not in obese rats, by mitigating brain oxidative stress. *AGE* 2015;37(5):84. (Impact Factor = 3.390) **(เอกสารแนบหมายเลข 40)**

41. Wongjaikam S, Kumfu S, **Chattipakorn SC**, Fucharoen S, Chattipakorn N. Current and future treatment strategies for iron overload cardiomyopathy. Eur J Pharmacol 2015;18:765:86-93. (Impact Factor = 2.684) **(เอกสารแนบหมายเลข 41)**

42. Pipatpiboon N, Sripetchwandee J, **Chattipakorn SC**, Chattipakorn N. Effects of PPARγ agonist on heart rate variability and cardiac mitochondrial function in obese-insulin resistant rats. Int J Cardiol 2015;201:121-122. (Impact Factor = 4.036) **(เอกสารแนบหมายเลข 42)**

43. Semaming Y, Sripetchwandee J, Sa-nguanmoo P, Pintana P, Pannangpetch P, Chattipakorn N, **Chattipakorn SC**. Protocatechuic acid protects brain mitochondrial function in streptozotocin-induced diabetic rats. Appl Physiol Nutr Me 2015;40(10):1078-1081. (Impact Factor = 2.34) **(เอกสารแนบหมายเลข 43)**

44. Pintana H, Pongkan W, Pratchayasakul W, Chattipakorn N, **Chattipakorn SC**. Dipeptidyl peptidase-4 inhibitor improves brain insulin sensitivity, but fails to prevent dementia in orchiectomy obese rats. J Endocrinol 2015;226(2):M1-M11. (Impact Factor = 3.586) **(เอกสารแนบหมายเลข 44)**

45. Pintana H, Chattipakorn N, **Chattipakorn SC**. Testosterone deficiency, insulin-resistant obesity and cognitive function. Metab Brain Dis 2015;30:853-876. (Impact Factor = 2.33) **(เอกสารแนบหมายเลข 45)**

46. Pratchayasakul W, Sa-nguanmoo P, Sivasinprasarn S, Pintana H, Tawinvisan R, Sripetchwandee J, Kumfu S, Chattipakorn N, **Chattipakorn SC**. Obesity accelerates cognitive decline by aggravating mitochondrial dysfunction, insulin resistance and synaptic dysfunction under estrogen-deprived condition. Horm Behav 2015;72:68-77. (Impact factor = 4.511) **(เอกสารแนบหมายเลข 46)**

47. Wijarnpreecha K, Siri-Angkul N, Shinlapawittayatorn K, Charoenkwan P, Silvilairat S, Siwasomboon C, Visarutratna P, Srichairatanakool S, Tantiworawit A, Phrommintikul A, **Chattipakorn SC**, Chattipakorn N. Heart rate variability as an alternative indicator for identifying cardiac iron status in non-transfusion dependent thalassemia patients. PLoS One 2015;10(6):e0130837. (Impact Factor = 3.534) **(เอกสารแนบหมายเลข 47)**

48. Inthachai T, Lekawanvijit S, Kumfu S, Apaijai N, Pongkan W, **Chattipakorn SC**, Chattipakorn N. Dipeptidyl peptidase-4 inhibitor improves cardiac function via attenuating adverse cardiac remodeling in rats with chronic myocardial infarction. Exp Physiol 2015;100(6):667-679. (Impact factor = 2.871) **(เอกสารแนบหมายเลข 48)**

49. Sivasinprasasn S, Sa-nguanmoo P, Pratchayasakul W, **Chattipakorn SC**, Chattipakorn N. Obese-insulin resistance accelerates and aggravates the

development of cardiometabolic disorder and cardiac mitochondrial dysfunction in estrogen-deprived female rats. AGE 2015;37(2):28. (Impact factor = 3.445) **(เอกสารแนบหมายเลข 49)**

50. Pongkan W, **Chattipakorn SC**, Chattipakorn N. Chronic testosterone replacement exerts cardioprotection against cardiac ischemia-reperfusion injury by attenuating mitochondrial dysfunction in testosterone-deprived rats. PLoS One 2015;10(3):e0122503. (Impact Factor = 3.534) **(เอกสารแนบหมายเลข 50)**
51. Wijarnpreecha K, Kumfu S, **Chattipakorn SC**, Chattipakorn N. Cardiomyopathy associated with iron overload: How does iron enter myocytes and what are the implications for pharmacological therapy? Hemoglobin 2015;39(1):9-17. (Impact factor = 0.955) **(เอกสารแนบหมายเลข 51)**
52. Nanegrungsunk D, Onchan W, Chattipakorn N, **Chattipakorn SC**. Current Evidence of Temozolomide and Bevacizumab in Treatment of Gliomas. Neurol Res 2015;37(2):167-183. (Impact Factor = 1.449) **(เอกสารแนบหมายเลข 52)**
53. Semaming Y, Pannengpetch P, **Chattipakorn SC**, Chattipakorn N. Pharmacological properties of protocatechuic acid and its potential roles as complementary medicine. Evid Based Complement Alternat Med. 2015;2015:593902 (Impact factor = 2.14) **(เอกสารแนบหมายเลข 53)**
54. Kumphune S, Surinkaew S, **Chattipakorn SC**, Chattipakorn N. Inhibition of p38 MAPK activation protects cardiac mitochondria from ischemia/reperfusion injury. Pharm Biol. 2015 Apr 16:1-11 (Impact factor = 1.23) **(เอกสารแนบหมายเลข 54)**
55. Apaijai N, **Chattipakorn SC**, Chattipakorn N. Roles of obese-insulin resistance and anti-diabetic drugs on the heart with ischemia-reperfusion injury. Cardiovasc Drugs Ther. 2014 Dec;28(6):549-62 (in press) (Impact Factor = 2.673) **(เอกสารแนบหมายเลข 55)**
56. Pintana H, Sripetchwandee J, Supakul L, Apaijai N, Chattipakorn N, **Chattipakorn SC**. Garlic extract attenuates brain mitochondrial dysfunction and cognitive deficit in obese-insulin resistant rats. Appl Physiol Nutr Metab. 2014 Dec;39(12):1373-9 (Impact factor = 2.01) **(เอกสารแนบหมายเลข 56)**

57. Sripetchwandee J, Pipatpiboon N, Chattipakorn N, **Chattipakorn SC**. DPP-4 inhibitor and PPARγ agonist restore the loss of CA1 dendritic spines in obese insulin resistant rats. Arch Med Res 2014;45:547-552. (Impact factor = 2.406) **(เอกสารแนบหมายเลข 59)**

58. **Chattipakorn SC**, Thummasorn S, Sanit J, Chattipakorn N. Phosphodiesterase-3 inhibitor (Cilostazol) attenuates oxidative stress-induced mitochondrial dysfunction in the heart. J Geriatr Cardiol 2014;11:151-157.8/3/20146/1/2017(Impact factor = 1.39) **(เอกสารแนบหมายเลข 58)**

59. Shinlapawittayatorn K, Chinda K, Palee S, Surinkaew S, Kumfu S, Kumphune S, **Chattipakorn S**, KenKnight BH, Chattipakorn N. Vagus nerve stimulation initiated late during ischemia, but not reperfusion, exerts cardioprotection via amelioration of cardiac mitochondrial dysfunction. Heart Rhythm. 2014 Dec;11(12):2278-87) (Impact Factor = 5.045) **(เอกสารแนบหมายเลข 55)**

60. Thunsiri K, Shinlapawittayatorn K, Chinda K, Palee S, Surinkaew S, **Chattipakorn S**, H. KenKnight B, Chattipakorn N. Vagus Nerve Stimulation Applied at the Onset of Ventricular Fibrillation Until Post-shock Period Decreases Defibrillation Threshold in Swine. Int J Cardiol. 2014 Oct 20;176(3):1030-2. (Impact Factor = 6.175) **(เอกสารแนบหมายเลข 60)**

61. Semaming Y, Kumfu S, Pannangpetch P, **Chattipakorn SC**, Chattipakorn N. Protocatechuic acid exerts cardioprotective effect in type-1 diabetic rats. J Endocrinol. 2014;223(1):13-23 (Impact Factor = 3.781) **(เอกสารแนบหมายเลข 61)**

62. Apaijai N, Chinda K, Palee S, **Chattipakorn S,** Chattipakorn N. Combined vildagliptin and metformin exert better cardioprotection than monotherapy against ischemia-reperfusion injury in obese-insulin resistant rats. PLOS ONE 2014;9(7):e102374. (Impact Factor = 3.534) **(เอกสารแนบหมายเลข 62)**

63. Wijarnpreecha K, Kumfu S, **Chattipakorn SC**, Chattipakorn N. Cardiomyopathy Associated with Iron Overload: How Does Iron Enter Myocytes and What are the Implications for Pharmacological Therapy? Hemoglobin 2015;39(1):9-17. (Impact factor = 0.894) **(เอกสารแนบหมายเลข 63)**

64. Pratchayasakul W, Chattipakorn N, **Chattipakorn SC**. Estrogen restores brain insulin sensitivity in ovariectomized non-obese rats, but not in ovariectomized obese rats. Metabolism. 2014 Jun;63(6):851-9. (Impact Factor = 3.894) **(เอกสารแนบหมายเลข 64)**
65. Pramojanee SN, Phimphilai M, Chattipakorn N, **Chattipakorn SC**. Possible roles of insulin signaling in osteoblasts Endocr Res. 2014;39(4):144-51. (Impact Factor = 1.278) **(เอกสารแนบหมายเลข 65)**
66. Sripetchwandee, Pipatpiboon N, Chattipakorn N, **Chattipakorn SC**. Combined therapy of iron chelator and antioxidant completely restores brain dysfunction induced by iron toxicity. PLOS ONE 2014 Jan 6;9(1):e85115 (Impact Factor = 3.534) **(เอกสารแนบหมายเลข 66)**

บทความสำหรับเผยแพร่

เรื่อง ภัยเงียบในสมองเมื่อมีภาวะอ้วนลงพุงของชายวัยทอง

เป็นที่ทราบกันดีว่าโรคอ้วนลงพุงกำลังคุกคามโลกมนุษย์ของเราอย่างหนัก งานวิจัยที่ทีมของเรา ได้ทำอยู่นั้น เป็นการศึกษาถึงผลกระทบของภาวะอ้วนลงพุง ต่อการเปลี่ยนแปลงการทำงานในสมอง โดยเราได้ทำการวิจัยศึกษา ตั้งแต่ในระดับของไมโตรคอนเดรียของเซลล์ประสาท ไปจนถึงการศึกษาพฤติกรรมการเรียนรู้และความจำในสัตว์ทดลอง และต่อยอดด้วยการนำความรู้ที่ได้ดังกล่าวจากในเซลล์และในสัตว์ทดลอง ไปใช้ในการศึกษาถึงการเรียนรู้และความจำในผู้ป่วยที่มีภาวะอ้วนลงพุง โดยผลจากงานวิจัยของเราที่ทำในสัตว์ทดลองพบว่า ยิ่งอ้วนลงพุงมากเท่าไร ยิ่งทำให้เกิดการเสื่อมของสมองมากเท่านั้น โดยการเสียการทำงานของสมองจากภาวะอ้วนนี้ จะเกิดตั้งแต่ในระดับ ไมโตรคอนเดีย และส่งผลให้เกิดการสูญเสียต่อพฤติกรรมการเรียนรู้ และความจำหรือ กล่าวสั้นๆ ว่า ยิ่งอ้วน ยิ่งมีการเรียนรู้และความจำที่แย่ลง ผลการทดลองนี้ได้รับการยืนยันในคนอ้วน โดยเราพบว่า คนที่มีขนาดเส้นรอบเอวที่มากขึ้น จะมีการเรียนรู้และความจำที่แย่ลง

นอกจากนี้เรายังได้ศึกษาพบว่า เมื่อมีภาวะอ้วนเกิดขึ้นร่วมกับการมีภาวะสมองเสื่อมไปแล้ว ถ้ามีการพยายามลดความอ้วนด้วยการจำกัดอาหารที่กินเข้าไปนั้น แม้ว่าจะสามารถช่วยลดพุงลงได้ แต่กลับไม่สามารถช่วยฟื้นฟูให้ สมองกลับมาทำงานเป็นปกติได้ แต่ที่น่าสนใจคือการศึกษาของเราพบว่า ภาวะสมองเสื่อมจากภาวะอ้วนลงพุงนั้น สามารถจะถูกฟื้นฟูให้กลับมาดีขึ้นได้ โดยการใช้ยาต้านเบาหวานบางตัว

นอกจากเรื่องอ้วนลงพุงแล้ว ทีมวิจัยของเรายังได้ศึกษาถึง ภัยต่อสมองในคนวัยทองที่มีภาวะอ้วนลงพุง ในเพศชาย

โดยผลการวิจัยของเราพบว่า เมื่อเข้าสู่วัยทองและมีการพร่องของฮอร์โมนเพศชาย การทำงานของสมองจะแย่ลง แต่ที่สำคัญกว่านั้นก็คือ เมื่อมีภาวะอ้วนร่วมเข้าไปด้วย จะทำให้สมองด้านการเรียนรู้และความจำเสื่อมลงไปมากขึ้น ทั้งนี้เราพบว่า ภาวะสมองเสื่อมที่เกิดในวัยทองร่วมกับอ้วนลงพุงนั้น สามารถที่จะไม่สามาถฟื้นฟูให้ดีขึ้นได้ โดยการใช้ ยาต้านเบาหวาน ดังนั้น จะเห็นได้ว่า ภาวะอ้วนลงพุงจัดเป็นภัยเงียบที่ทำร้าย สมองอย่างค่อยเป็นค่อยไป โดยเฉพาะอย่างยิ่งในคนสูงอายุ ซึ่งเมื่อเกิดภาวะสมองเสื่อมแล้วยากแก่การรักษาให้กลับมาเป็นปกติได้ สรุปก็คือ **การไร้พุง นอกจากจะดีกับสุขภาพกายแล้ว ยังส่งผลดีต่อสุขภาพสมอง** อีกด้วย

เอกสารแนบ

เอกสารแนบหมายเลข 1

Cardiac complications in beta-thalassemia: From mice to men

Sirinart Kumfu[1,2,3], Suthat Fucharoen[4], Siriporn C. Chattipakorn[1,3,5] and Nipon Chattipakorn[1,2,3]

[1]Faculty of Medicine, Cardiac Electrophysiology Research and Training Center, Chiang Mai University, Chiang Mai 50200, Thailand; [2]Faculty of Medicine, Department of Physiology, Cardiac Electrophysiology Unit, Chiang Mai University, Chiang Mai 50200, Thailand; [3]Center of Excellence in Cardiac Electrophysiology Research, Chiang Mai University, Chiang Mai 50200, Thailand; [4]Thalassemia Research Center, Institute of Molecular Biosciences, Mahidol University, Nakhon Pathom 73170, Thailand; [5]Faculty of Dentistry, Department of Oral Biology and Diagnostic Sciences, Chiang Mai University, Chiang Mai 50200, Thailand
Corresponding author: Nipon Chattipakorn. Email: nchattip@gmail.com

Impact statement

Iron overload cardiomyopathy is a major cause of morbidity and mortality in patients with thalassemia. Since investigation of iron overload cardiomyopathy in thalassemia patients has many limitations, a search for an animal model for this condition has been ongoing for decades. In the past decades, there is no doubt that the use of β-thalassemic mice as a study model to investigate the pathophysiology of iron overload cardiomyopathy and the role of various pharmacological interventions, has shed some light in understanding this serious complication and in improving the associated cardiac dysfunction. In this review, the effects of iron overload on the hearts of β-thalassemic mice under conditions of iron overload as well as the efficacy of pharmacological interventions to combat these adverse effects on the heart are reviewed and discussed.

Abstract

Beta-thalassemia is an inherited hemoglobin disorder caused by reduced or absent synthesis of the beta globin chains of hemoglobin. This results in variable outcomes ranging from clinically asymptomatic to severe anemia, which then typically requires regular blood transfusion. These regular blood transfusions can result in an iron overload condition. The iron overload condition can lead to iron accumulation in various organs, especially in the heart, leading to iron overload cardiomyopathy, which is the major cause of mortality in patients with thalassemia. In the past decades, there is no doubt that the use of β-thalassemic mice as a study model to investigate the pathophysiology of iron overload cardiomyopathy and the role of various pharmacological interventions, has shed some light in understanding this serious complication and in improving the associated cardiac dysfunction. In this review, the effects that iron overload has on the hearts of β-thalassemic mice under conditions of iron overload as well as the efficacy of pharmacological interventions to combat these adverse effects on the heart are reviewed and discussed. The in-depth understanding of biomolecular alterations in the heart of these iron overload thalassemic mice will help give guidance for more effective therapeutic approaches in the near future.

Keywords: Beta-thalassemic mice, heart, iron overload cardiomyopathy, cardiomyocytes, thalassemia, pathophysiology

***Experimental Biology and Medicine* 2017; 242: 1126–1135. DOI: 10.1177/1535370217708977**

Introduction

Thalassemia in humans is a group of inherited disorders of hemoglobin synthesis which are characterized by the absence or reduction in amounts of one or more of the globin chains of hemoglobin.[1–3] The absence or reduction of globin chain synthesis could generate an imbalance between the subunits of hemoglobin.[1,4] Hemoglobin is mainly composed of α- and β-globin polypeptide chains which are encoded by multigene clusters which have been conserved throughout mammalian evolution.[4–6] Beta-thalassemia caused by reduced (β^+) or absent (β^0) synthesis of the beta globin chains of hemoglobin results in variable outcomes ranging from severe anemia to clinically asymptomatic individuals.[1–3] These disorders can be divided into three major groups, β-thalassemia major, intermedia and minor (carrier or trait), based on the quantity of β-globin produced and symptomatic features.[1,3] β-thalassemia patients with severe anemia often require regular blood transfusions which can result in an iron overload state.[1,7] This iron overload condition can lead to iron accumulation in various organs, especially in the heart where it leads to iron overload cardiomyopathy. This is the major cause of mortality in patients with β-thalassemia.[7,8] Since investigation of iron overload cardiomyopathy in thalassemia patients has many limitations, a search for an animal model for this condition has been ongoing for decades.

In animals, although no naturally occurring β^0-thalassemia has been observed in mice, a mouse model with β^+-thalassemia exists. The mouse β-globin gene cluster is located on chromosome 7 and has four functional β-globin

Copyright © 2017 by the Society for Experimental Biology and Medicine

genes: *βh1* and *εy*, embryonic globin genes; and two adult globin genes, β^{major} and β^{minor}.[5,6,9] The β^{major} gene encodes for 80% and β^{minor} gene for 20% of β-globin production in adult mice.[10] Three mouse models of β-thalassemia have been developed relatively recently. First, a DNA deletion in the β-globin locus was developed which includes the whole β^{major} gene and its subsequent upstream sequences.[11,12] Mice homozygous for the deletion (Hbb^{th-1}/Hbb^{th-1}) have a survival to adulthood rate of 60%.[11,12] The heterozygous mice exhibit a mild phenotype which is related to the thalassemia trait in humans.[11,12] Second, the mouse model for β-thalassemia was created by targeted gene disruption of the mouse β^{major} gene.[12] Mice homozygous for an insertional disruption of the β^{major} gene (Hbb^{th-2}/Hbb^{th-2}) had severe anemia and did not survive after birth.[12] Finally, a mouse model for homozygous deletion of both β^{major} and β^{minor} genes (Hbb^{th-3}/Hbb^{th-3}) was developed which results in a severe form of β^0-thalassemia and the mice die perinatally. This is similar to the most severe form of Cooley anemia (β-thalassemia major) in humans.[13] The heterozygous animals with this deletion show a pathophysiology comparable to that of patients with human β-thalassemia intermedia.[13]

These β-thalassemic mouse models have been used in investigations to understand the pathophysiology of iron-overload cardiomyopathy found in patients. Currently, the model mostly used to study the heart in this condition is the heterozygous (Hbb^{th-3}/Hbb^{+}) β-thalassemic genotype.[14–19] Mice heterozygous for the deletion (Hbb^{th-3}/Hbb^{+}) showed characteristics typical of severe thalassemia such as: a significant decrease in hematocrit (Hct), hemoglobin (Hb), red blood cell (RBC) counts, mean corpuscular volume (MCV), mean corpuscular hemoglobin (MCH) and mean corpuscular hemoglobin concentration (MCHC), and increased reticulocyte counts, serum bilirubin concentrations, and red cell distribution width (RDW).[13] Heterozygous animals also exhibit bone deformities and splenic enlargement due to increased hematopoiesis which is a typical picture of β-thalassemia, and a spontaneous iron overload in the spleen, liver, and kidneys in this mouse model has been found.[13]

Although TI patients did not need blood transfusions to sustain levels of anemia, several other pathogenic mechanisms remained in play.[20] Ineffective erythropoiesis results in the suppression of hepcidin levels, leading to increased intestinal iron absorption and increased release of recycled iron from macrophages within the reticuloendothelial system, resulting in hepatocyte iron loading.[21,22] Although iron accumulation in patients with TI occurs more slowly than in TM patients who have received regular blood transfusions, it can reach levels much higher than the normal threshold, especially in aged patients.[22,23] Moreover, it has been found upon autopsy that some small subgroups of older TI patients had developed myocardial siderosis.[24–26] Damage to cardiac tissues may have resulted from exposure to NTBI, without the accumulation of toxic iron species within myocytes.[27,28] This suggests that even without evidence of cardiac siderosis, TI patients may still be at risk of iron-related cardiac dysfunction. Although homozygous β-thalassemic mice with blood transfusion is the model that is related to TM patients, these mice had severe anemia and did not survive after birth. Furthermore, giving mice a blood transfusion is a very difficult process. Therefore, the heterozygous β-thalassemic mice, which were similar to TI patients, were frequently used in this research field. However, to mimic the iron overload condition as observed in thalassemia major, iron loading either orally or intraperitoneally was commonly applied to these mice.[14,29–31] This also resulted in iron overload condition (indicated by the increased plasma NTBI), followed by mitochondrial dysfunction in those mice.[29] Therefore, heterozygous β-thalassemic mice with iron overload induced by iron injection or iron feeding is a suitable model for representing an iron overload condition and their pathophysiology was similar to that in thalassemia patients with blood transfusion.

The hearts of β-thalassemic mice

In *in vitro* studies, cultured cardiomyocytes of heterozygous (Hbb^{th-3}/Hbb^{+}) β-thalassemic mice showed increased intracellular accumulation of both Fe^{2+} and Fe^{3+},[17,18] whereas the cardiac mitochondrial function and morphology were still intact.[16] A summary of reports regarding the iron accumulation and mitochondrial function in the heart of β-thalassemic mice (*in vitro* models) is shown in Table 1.

In *in vivo* models, Gelderman and colleagues demonstrated that the hearts of heterozygous (Hbb^{th-3}/Hbb^{+}) β-thalassemic mice showed increased cardiac iron accumulation at 12 months of age,[32] a state consistent with reports from *in vitro* models. However, the hearts of 5-, 6- and 7–10-month-old β-thalassemic mice did not show any changes in cardiac iron accumulation, compared with normal mice.[14,19,30,33] These findings suggest that the level of iron deposition in cardiac tissue is associated with age in thalassemic mice. In addition, the older β-thalassemic mice (7–10 months old[14,19]) showed increased heart weight when compared with normal mice, but the heart weight of

Table 1 A summary of the reports on iron accumulation and mitochondrial function in the hearts of β-thalassemic mice (*in vitro* models) under basal conditions

Mouse models	Age	Cardiac iron	Cardiac mitochondria function and morphology	Ref.
Hbb^{th-3}/Hbb^{+} (Isolated cardiac mitochondria)	3–6 months		Function & morphology; normal	16
Hbb^{th-3}/Hbb^{+} (Cultured cardiomyocytes)	9–12 months	↑ Fe^{2+} accumulation		18
Hbb^{th-3}/Hbb^{+} (Cultured cardiomyocytes)	9–12 months	↑ Fe^{3+} accumulation		17

younger β-thalassemic mice (7 weeks old[13]) did not differ from normal mice.

The blood parameters from most studies of heterozygous (Hbb^{th-3}/Hbb^{+}) β-thalassemic mice showed decreased levels of RBC, Hb, and a decreased Hct, increased levels of ROS and serum iron, but non-altered levels of plasma NTBI and MDA levels.[13–15,19,30,32] Only one study[33] has shown increased levels of plasma NTBI in heterozygous (Hbb^{th-3}/Hbb^{+}) β-thalassemic 5-month old mice, which was inconsistent with three other studies.[14,19,30] This inconsistency might be due to the different techniques used for NTBI detection. For example, Gelderman *et al.* were detecting plasma NTBI levels at nanogram levels, whereas the other studies were limited to microgram levels.

The heart is known to be tightly controlled by the sympathetic and parasympathetic nerves of the cardiac autonomic nervous system. It has been shown that β-thalassemic mice have impaired cardiac autonomic function which is indicated by depressed heart rate variability (i.e. increased LF/HF ratio), increased stroke volume (SV) and cardiac output (CO) when compared with normal mice.[14,15,19] This indicates a high-output state in β-thalassemic mice, which is similar to that found in patients with thalassemia.[7] High-output state, as shown by increased stroke volume (SV) and cardiac output (CO), develops as a consequence of prolonged tissue hypoxia, resulting from chronic anemia in beta-thalassemia patients[34,35] and animal models.[14,29] Although thalassemia patients have high SV and CO, they still have cardiac dysfunctions such as decreased fractional shortening (FS) and ejection fraction (EF), when compared with a normal physiological state.[35,36] Moreover, when iron overload occurs in the heart, it can aggravate cardiac dysfunction, as shown by decreased SV, CO, FS and EF.[14,29,36] However, cardiac mitochondrial function and morphology in heterozygous (Hbb^{th-3}/Hbb^{+}) β-thalassemic mice has been found to be normal at this basal condition, these results being consistent with an *in vitro* study.[19]

The other models of β-thalassemic mice, homozygous (Hbb^{th1}/Hbb^{th1}), ($Hbb^{d3(th)}/Hbb^{d3(th)}$) and heterozygous $\beta^{IVSII-654}$, display a greater severity of the condition than the heterozygous (Hbb^{th-3}/Hbb^{+}) model does.[37–39] These mice showed decreased levels of RBC, Hb, Hct and impaired cardiac function indicated by decreased SV, EF, and FS.[37–39] Also, these mice also had increased heart weight and cardiac iron levels even at the basal condition when compared with normal mice.[37,39] However, the study by Stoyanova *et al.* was the only one not to observe increased cardiac iron accumulation in homozygous ($Hbb^{d3(th)}/Hbb^{d3(th)}$) β-thalassemic mice.[38] This discrepancy could be due to the fact that Stoyanova *et al.* used only Prussian blue staining to determine cardiac iron accumulation, which is a less sensitive method than the atomic absorption and colorimetric methods used by other studies. Consistent with a report concerning the heterozygous (Hbb^{th-3}/Hbb^{+}) β-thalassemic mice,[19] the cardiac mitochondrial morphology in the heterozygous $\beta^{IVSII-654}$ β-thalassemic mice was still normal under basal conditions.[37]

Both *in vitro* and *in vivo* studies indicated that heterozygous (Hbb^{th-3}/Hbb^{+}) β-thalassemic mice were anemic, had increased heart weight and cardiac iron accumulation when getting old, and had measurable cardiac dysfunction.[13–19,30,32,33,37–40] Moreover, the homozygous (Hbb^{th1}/Hbb^{th1}), ($Hbb^{d3(th)}/Hbb^{d3(th)}$) and heterozygous $\beta^{IVSII-654}$ β-thalassemic mice showed a greater severity of anemia and had higher levels of cardiac iron accumulation than the heterozygous (Hbb^{th-3}/Hbb^{+}) β-thalassemic mice did, even though the mice were still young.[37–39] A summary of reports regarding cardiac iron accumulation, cardiac function, and mitochondrial function in β-thalassemic mice (*in vivo* models) is shown in Table 2. Regarding the age influence on cardiac function, in Table 2, there are two studies on Hbb^{th-3}/Hbb^{+} which showed the same results of SV and CO, because the mice were the same age in these studies.[14,19] However, in the other two studies on $Hbb^{d3(th)}/Hbb^{d3(th)}$, cardiac function could not be compared since different parameters were determined.[38,40]

The hearts of β-thalassemic mice under an iron overload condition

Under conditions of iron overload, both Fe^{2+} and Fe^{3+} iron uptake was increased in cultured cardiomyocytes from heterozygous (Hbb^{th-3}/Hbb^{+}) β-thalassemic mice.[17,18] Moreover, the iron overload condition leads to increased cardiac mitochondrial ROS production, mitochondrial depolarization, and mitochondrial swelling in isolated cardiac mitochondria from the hearts of heterozygous (Hbb^{th-3}/Hbb^{+}) β-thalassemic mice.[16] These findings suggest that the iron overload condition leads to increased iron uptake and accumulation in cardiomyocytes which then leads to mitochondrial dysfunction in these mice. Available *in vitro* reports regarding the effects of iron overload on iron uptake and mitochondrial function in the hearts of β-thalassemic mice models are summarized in Table 3.

In the *in vivo* studies, conditions of iron overload led to increased plasma NTBI and MDA levels, and increased cardiac iron accumulation without altering the heart weight in heterozygous (Hbb^{th-3}/Hbb^{+}) β-thalassemic mice.[14,19,30,31,33] Also, iron overload impaired cardiac autonomic regulation as indicated by an increased LF/HF ratio, and impaired cardiac function by decreasing SV, CO, ESP, Pmax and dP/dtmax in these mice.[14,19,30] Cardiac mitochondrial dysfunction was demonstrated by increased cardiac mitochondrial ROS production, mitochondrial depolarization and swelling in the hearts of heterozygous (Hbb^{th-3}/Hbb^{+}) β-thalassemic mice under iron overload conditions.[19] All *in vivo* findings were consistent and suggested that iron overload can lead to increased cardiac iron accumulation and cardiac mitochondrial dysfunction, leading to left ventricular dysfunction in heterozygous (Hbb^{th-3}/Hbb^{+}) β-thalassemic mice.[14,19,30,31,33] Available *in vivo* reports regarding the effects of iron overload on cardiac iron accumulation, cardiac function and mitochondrial function of β-thalassemic mice are summarized in Table 4. In Table 4, the two studies on Hbb^{th-3}/Hbb^{+} did not show a difference in results on cardiac function, even though there was a difference in the time of iron expose between the two studies. However, these two studies showed that there was

Table 2 A summary of the reports on cardiac iron accumulation, cardiac function and mitochondrial function of β-thalassemic mice (*in vivo* models) under basal conditions

Mouse models	Age	Blood parameter	Heart weight	Cardiac iron	Cardiac autonomic regulation	Cardiac function	Cardiac mitochondria function and morphology	Ref.
Hbb^{th-3}/Hbb^{+}	7 weeks	↓ RBC, Hb, Hct	↔					13
Hbb^{th-3}/Hbb^{+}	3–5 months	↓ Hb ↑ ROS, SI			↑ LF/HF ratio			15
Hbb^{th-3}/Hbb^{+}	5 months	↑ Plasma iron, NTBI ↓ RBC, Hb, Hct		↔				33
Hbb^{th-3}/Hbb^{+}	6 months	↓ Hb ↔ Plasma NTBI, MDA		↔				30
Hbb^{th-3}/Hbb^{+}	7–10 months	↔ Plasma NTBI, MDA	↑	↔	↑ LF/HF ratio	↑ SV, CO		14
Hbb^{th-3}/Hbb^{+}	7–10 months	↔ Plasma NTBI, MDA	↑	↔	↑ LF/HF ratio	↑ SV, CO	Function & morphology; normal	19
Hbb^{th-3}/Hbb^{+}	12 months	↓ Hb		↑				32
Hbb^{th1}/Hbb^{th1}	15–35 weeks	↑ Plasma iron	↑	↑				39
Heterozygous $\beta^{IVSII-654}$	–	↓ Hb, Hct ↑ ROS		↑			Morphology; normal	37
$Hbb^{d3(th)}/Hbb^{d3(th)}$	14 weeks					↓ SV ↔ CO		38
$Hbb^{d3(th)}/Hbb^{d3(th)}$	15 months	↓ RBC, Hb, Hct	↑	↔		↓ EF, FS		40

RBC: red blood cell; Hb: hemoglobin; Hct: hematocrit; ROS: reactive oxygen species; SI: serum iron; NTBI: non-transferrin bound iron; MDA: malondialdehyde; LF/HF: low frequency/high frequency; SV: stroke volume; CO: cardiac output; EF: ejection fraction; FS: fractional shortening.

Table 3 A summary of the reports on the effects of iron overload on iron uptake and mitochondrial function in the hearts of β-thalassemic mice (*in vitro* models)

Mouse models	Age	Iron overload	Cardiac iron	Cardiac mitochondria function and morphology	Ref.
Hbb^{th-3}/Hbb^{+} (Isolated cardiac mitochondria)	3–6 months	FAC 0-5 μg/ml + 1 mM AA (Fe^{2+}), 5 min		↑ ROS & Swelling Mitochondrial depolarization Morphology; swelling	16
Hbb^{th-3}/Hbb^{+} (Cultured cardiomyocytes)	9–12 months	FAC 20 μg/ml + 1 mM AA (Fe^{2+}), 48 h	↑ Fe^{2+} uptake		18
Hbb^{th-3}/Hbb^{+} (Cultured cardiomyocytes)	9–12 months	FAC 20 μg/ml (Fe^{3+}), 48 h	↑ Fe^{3+} uptake		17

FAC: ferric ammonium citrate; AA: ascorbic acid; ROS: reactive oxygen species.

a progression in cardiac iron accumulation which correlated to the increased time of iron exposure.

The effects of pharmacological interventions on the hearts of β-thalassemic mice under iron overload conditions

Recently, several studies have investigated novel ways of treating iron overload cardiomyopathy besides the currently used iron chelator therapy in β-thalassemic mice models. Studies on cultured cardiomyocytes of heterozygous (Hbb^{th-3}/Hbb^{+}) β-thalassemic mice showed that treatment with a T-type calcium channel (TTCC) blocker and an iron chelator could prevent Fe^{2+} uptake into cardiomyocytes, whereas blockers of transferrin receptor1 (TfR1), divalent metal transporter1 (DMT1) and L-type calcium channel (LTCC) could not.[18] However, blockers of TfR1, DMT1, LTCC and TTCC could not prevent Fe^{3+} uptake into these cells.[17] These findings suggest that TTCC is an important pathway for Fe^{2+} uptake in a cultured thalassemic cardiomyocyte model. Reports also demonstrated other alternative pathways which could play a major role in Fe^{3+} uptake in thalassemic cardiomyocytes. Normally, mitochondrial calcium uniporter (MCU) mediates calcium uptake into the mitochondria. However, in the isolated cardiac mitochondria of heterozygous (Hbb^{th-3}/Hbb^{+})

Table 4 A summary of the reports on the effects of iron overload on cardiac iron accumulation, cardiac function and mitochondrial function of β-thalassemic mice (*in vivo* models)

Mouse models	Age	Iron overload	Blood parameter	Heart weight	Cardiac iron	Cardiac autonomic regulation	Cardiac function	Cardiac mitochondria function and morphology	Ref.
Hbb^{th-3}/Hbb^{+}	7 weeks	Iron dextran i.p. injection (20 mg/day), 2 weeks		↔	↑				31
Hbb^{th-3}/Hbb^{+}	2 months	Feeding with iron diet (0.2% ferrocene), 2 months	↑ Plasma NTBI & MDA		↑	↑ LF/HF ratio			30
Hbb^{th-3}/Hbb^{+}	3 months	0.2 ml packed RBCs transfused every 3 days (five transfusions) 15 days	↑ Plasma iron & NTBI ↑ RBC,Hb, Hct		↑				33
Hbb^{th-3}/Hbb^{+}	3–6 months	Feeding with iron diet (0.2% ferrocene), 3 months	↑ Plasma NTBI & MDA	↔	↑	↑ LF/HF ratio	↓ SV, CO, ESP, Pmax, dP/dtmax		14
Hbb^{th-3}/Hbb^{+}	3–6 months	Feeding with iron diet (0.2% w/w) ferrocene, 4 months	↑ Plasma NTBI & MDA	↔	↑	↑ LF/HF ratio	↓ SV, CO, ESP, Pmax, dP/dtmax	↓ Mitochondria function Morphology; swelling	19

RBC: red blood cell; Hb: hemoglobin; Hct: hematocrit; NTBI: non-transferrin bound iron; MDA: malondialdehyde; LF/HF: low frequency/high frequency; SV: stroke volume; CO: cardiac output; ESP: end systolic pressure; Pmax: maximum pressure; dP/dtmax: maximum dP/dt; i.p.: intra-peritoneal.

β-thalassemic mice, it was shown that MCU acts as a major portal for Fe^{2+} entry into cardiac mitochondria.[16] By using the MCU blocker, ROS production and mitochondrial depolarization could be effectively prevented, and mitochondrial swelling caused by Fe^{2+} overload attenuated.[16] Future clinical studies are needed to warrant the clinical usefulness of MCU blockers in thalassemia patients. Available *in vitro* reports regarding the effects of pharmacological intervention on iron uptake and mitochondrial function in the hearts of β-thalassemic mice (models) under iron overload conditions are summarized in Table 5.

Several *in vivo* studies showed that treatment with either LTCC blockers (verapamil, nifedipine, amlodipine), a TTCC blocker (efonidipine), a DMT1 blocker (ebselen) or an antioxidant (curcuminoid) effectively reduced plasma NTBI levels and cardiac iron deposition, and improved cardiac autonomic regulation and left ventricular function in heterozygous (Hbb^{th-3}/Hbb^{+}) β-thalassemic mice under conditions of iron overload with the same efficacy as commercial iron chelators (deferoxamine, deferasirox or deferiprone).[14,19,30] No treatments had any effect on the heart weights of heterozygous (Hbb^{th-3}/Hbb^{+}) β-thalassemic mice under iron overload conditions.[14,19,31,33] Moreover, treatment with either an LTCC blocker (amlodipine) or a TTCC blocker (efonidipine) led to improved mitochondrial function in heterozygous (Hbb^{th-3}/Hbb^{+}) β-thalassemic mice under iron overload conditions to the same degree as three commercial iron chelators (deferoxamine, deferasirox or deferiprone).[19] Treatment with apo-transferrin also decreased plasma iron levels, plasma NTBI levels, and cardiac iron deposition in heterozygous (Hbb^{th-3}/Hbb^{+}) β-thalassemic mice even though they were under a basal condition.[33] All findings in the *in vivo* studies suggested that a TTCC blocker, a LTCC blocker, a DMT1 blocker, an antioxidant and apo-transferrin could be beneficial for treatment of an iron overloaded state, especially for iron overload cardiomyopathy in β-thalassemia models. Available *in vivo* reports regarding the effects of pharmacological intervention on cardiac iron accumulation, cardiac function and mitochondrial function of β-thalassemic mice under iron overload conditions are summarized in Table 6.

Cardiac complications in beta-thalassemia patients

Thalassemic cardiomyopathy and arrhythmia, caused by cardiac iron overload, are the most important complications of iron overload in beta-thalassemia patients and are responsible for 71% of deaths, globally, in these patients.[41] In the early stages, patients are usually asymptomatic and symptoms are related to the degree of ventricular impairment.[42] Cardiac arrhythmias, including premature ventricular contraction, ST-T changes, QT prolongation, and second- and third-degree atrioventricular block have been reported in iron overload beta-thalassemia patients.[43–46] In view of cardiac complications, serum ferritin concentrations have been shown to correlate poorly with all stages of cardiac dysfunction.[35,47] Non-transferrin-bound iron (NTBI) seems to be the most accurate parameter among serum iron markers; however, it is commonly used only

Table 5 A summary of the reports on the effects of pharmacological interventions on iron uptake and mitochondrial function in the heart of β-thalassemic mice (*in vitro* models) under conditions of iron overload

Mouse models	Age	Iron overload	Intervention	Cardiac iron	Cardiac mitochondria function and morphology	Ref.
Hbb^{th-3}/Hbb^{+} (Isolated cardiac mitochondria)	3–6 months	FAC 0-5 μg/ml + 1 mM AA (Fe^{2+}), 5 min	MCU blocker (Ru360) 10 μM		↓↓ ROS & Swelling Restoration mitochondrial depolarization Morphology; normal	16
			mPTP blocker [Cyclosporin A (CsA)] 5 μM		↓ ROS ↔ Swelling Mitochondrial depolarization Morphology; swelling	
Hbb^{th-3}/Hbb^{+} (Cultured cardiomyocytes)	9–12 months	FAC 20 μg/ml + 1 mM AA (Fe^{2+}), 48 h	Efonidipine 0–20 μM, DFO 0–20 μg/ml	↓ Fe^{2+} uptake		18
			Anti-TfR 0–10 μg/ml, Ebselen 0–25 μM, Verapamil 0–80 μM	↔ Fe^{2+} uptake		
Hbb^{th-3}/Hbb^{+} (Cultured cardiomyocytes)	9–12 months	FAC 20 μg/ml (Fe^{3+}), 48 h	DFO 0–20 μg/ml	↓ Fe^{3+} uptake		17
			Efonidipine 0–20 μM, Anti-TfR 0–10 μg/ml, Ebselen 0–25 μM, Verapamil 0–80 μM	↔ Fe^{3+} uptake		

FAC: ferric ammonium citrate; AA: ascorbic acid; ROS: reactive oxygen species; DFO: deferoxamine; TfR: transferrin receptor; MCU: mitochondrial calcium uniporter; mPTP: mitochondrial permeability transition pore.

in research studies.[48–53] Accurate assessments of cardiac dysfunction and/or cardiac iron status are currently based on imaging techniques. The T2-star magnetic resonance imaging (MRI-T2*) has been demonstrated as evaluating cardiac iron status accurately and allows the early detection of global ventricular dysfunction.[47] In addition, it can be used for monitoring myocardial iron levels during iron chelation therapy.[54,55] In beta-thalassemia major patients with normal myocardial T2* (>20 ms), the right ventricular (RV) and left ventricular (LV) ejection fraction (EF) was found to be within the normal range.[47,56] It has been shown that lower myocardial T2* values (<20 ms) are associated with an increase in RV and LV dysfunction,[47,56] whereas an improvement in myocardial T2* results in improvement in LV and RV EF in beta-thalassemia major patients.[54,55] There was a linear relationship between RV and LV EF.[56] Clinical findings were consistent with *in vivo* reports in β-thalassemic mice, suggesting that iron overload can lead to increased cardiac iron accumulation and cardiac dysfunction in β-thalassemic mice.[14,19,30,31,33]

An altered sympathovagal balance, as shown by depressed heart rate variability, was found in thalassemia major patients.[51,57–59] Heart rate variability parameters were reduced even in β-thalassemia major patients without evident cardiac siderosis (T2* >20 ms)[57] and preclinical stages of heart disease.[58] The studies show that reduction in heart rate variability may start before cardiac iron loading and preclinical stages of cardiac disease in β-thalassemia major and non-transfusion-dependent thalassemia patients.[50–53,57,58] β-thalassemic mice had impaired cardiac autonomic function which was indicated by depressed heart rate variability.[14,15,19] This was consistent with and showed a correlation with the results that were found in β-thalassemia patients. These findings suggest that cardiac autonomic dysregulation may precede clinical signs of iron overload cardiomyopathy.

Iron chelation is the main therapy available to treat conditions of iron overload. The therapy uses the parenteral iron chelator deferoxamine (DFO), and the oral iron chelators deferiprone (DFP) and deferasirox (DFX). Many studies have shown that DFO, DFP and DFX can cause a reduction in myocardial iron and improve cardiac function in β-thalassemia patients.[55,60–65] However, it has been suggested that combined chelation therapy be used in some iron overload β-thalassemia patients who have shown no improvement when treated with a single iron chelator, due to its increased efficacy.[62–65] At this time, new evidence indicates a greater efficacy for iron chelation when an iron chelator was combined with an antioxidant such as vitamin E and N-acetylcysteine (NAC).[66,67] Combined iron chelator plus NAC shows greater efficacy than vitamin E in reducing DNA damage in children β-thalassemia patients.[66] Currently, only the LTCC blocker has supporting evidence from clinical studies showing the improved cardiac function and decreased cardiac iron level in β-thalassemia patients; however, the study was only carried out using a small population.[68] Fernandes *et al.* showed that amlodipine reduces cardiac iron overload patients with

Table 6 A summary of the reports on the effects of pharmacological interventions on cardiac iron accumulation, cardiac function, and mitochondrial function of β-thalassemic mice (*in vivo* models) under iron overload conditions

Mouse models	Age	Iron overload	Intervention	Blood parameter	Heart weight	Cardiac iron	Cardiac autonomic regulation	Cardiac function	Cardiac mitochondria function and morphology	Ref.
Hbb^{th-3}/*Hbb*$^{+}$	7 weeks	Iron dextran i.p. injection (20 mg/day), 2 weeks	DFO (125 μg/g BW), 7 days		↔	↔				31
			Deferiprone (80 μg/g BW), 7 days		↔	↓				
Hbb^{th-3}/*Hbb*$^{+}$	2 months	Feeding with iron diet 0.2% ferrocene, 2 months	Curcuminoid (Cur; 200 mg/kg/day), 2 months	↓ Plasma NTBI & MDA		↓	↓ LF/HF ratio			30
			Deferiprone (DFP; 50 mg/kg/day), 2 months	↓ Plasma NTBI, ↔ MDA		↓	↓ LF/HF ratio			
Hbb^{th-3}/*Hbb*$^{+}$	3 months	–	300 mg/kg/d (i.p.) Apo-transferrin, 60 days	↓ Plasma iron & NTBI ↑ RBC,Hb, Hct		↓				33
Hbb^{th-3}/*Hbb*$^{+}$	3–6 months	Feeding with iron diet 0.2% ferrocene, 3 months	DFO (42 mg/kg/day) Verapamil (10 mg/kg/day) Nifedipine (5 mg/kg/day) Efonidipine (4 mg/kg/day) Ebselen (5 mg/kg/day), 1 month	↓ Plasma NTBI ↓ Plasma MDA (except Ver & Nife)	↔	↓	↓ LF/HF ratio	↑ SV, CO, ESP, Pmax, dP/dtmax		14
Hbb^{th-3}/*Hbb*$^{+}$	3–6 months	Feeding with iron diet 0.2% ferrocene, 4 months	DFO (42 mg/kg/day) Deferiprone (75 mg/kg/day) Deferasirox (30 mg/kg/day) Efonidipine (4 mg/kg/day) Amlodipine (5 mg/kg/day), 1 month	↓ Plasma NTBI ↓ Plasma MDA (except amlodipine)	↔	↓	↓ LF/HF ratio	↑ SV, CO, ESP, Pmax, dP/dtmax	↑Mitochondria function Morphology; normal	19

RBC: red blood cell; Hb: hemoglobin; Hct: hematocrit; NTBI: non-transferrin bound iron; MDA: malondialdehyde; LF/HF: low frequency/high frequency; SV: stroke volume; CO: cardiac output; ESP: end systolic pressure; Pmax: maximum pressure; dP/dtmax: maximum dP/dt; i.p.: intra-peritoneal; DFO: deferoxamine.

β-thalassemia major; however, again only a small sample size was included in the study.[69] Only one case report showed that treatment with verapamil plus DFO improved cardiac function in an early stage of iron overload cardiomyopathy.[68] Larger and longer cohort studies are needed to verify these findings. Although treatment with LTCC blockers, TTCC blockers, DMT1 blockers or antioxidants were successful in animal models, large cohort clinical studies are needed to warrant their use in patients. The proposed mechanism responsible for these benefits could be due to the fact that iron chelators are effective in removing excess iron accumulation in cells and calcium channel blockers are expected to be particularly effective early on in iron overload by reducing tissue iron uptake and preventing oxidative stress occurring during the disease progression.

Conclusions

Information obtained from studies into the pathophysiologic mechanisms of iron overload on the heart in thalassemia mice have led us to better understand the clinical pictures of iron overload cardiomyopathy. In addition to the traditional pathways of iron uptake into cardiomyocytes, these studies using thalassemia mouse models have allowed us to discover novel pathways which could potentially cause iron overload cardiomyopathy, and ultimately may lead to the development of new strategies and drugs to prevent this lethal complication in thalassemia.

Authors' contributions: SK and NC collected experimental data and reviewed all articles cited in the paper; SK and NC wrote the main text; SK, SF, SCC, and NC revised the paper. All authors read and approved the final manuscript.

ACKNOWLEDGEMENTS

This work is supported by grants from the Thailand Research Fund MRG5980222 (SK) and RTA (SCC), the NSTDA Research Chair Grant from the National Science and Technology Development Agency Thailand (NC), and Chiang Mai University Center of Excellence Award (NC).

DECLARATION OF CONFLICTING INTERESTS

The author(s) declared no potential conflicts of interest with respect to the research, authorship, and/or publication of this article.

REFERENCES

1. Rund D, Rachmilewitz E. Beta-thalassemia. *N Engl J Med* 2005;353:1135–46
2. Clegg JB, Weatherall DJ. Molecular basis of thalassaemia. *Br Med Bull* 1976;32:262–9
3. Cao A, Galanello R. Beta-thalassemia. *Genet Med* 2010;12:61–76
4. Weatherall DJ, Clegg JB. Molecular genetics of human hemoglobin. *Annu Rev Genet* 1976;10:157–78
5. Jahn CL, Hutchison CA 3rd, Phillips SJ, Weaver S, Haigwood NL, Voliva CF, Edgell MH. DNA sequence organization of the beta-globin complex in the BALB/c mouse. *Cell* 1980;21:159–68
6. Whitelaw E, Tsai SF, Hogben P, Orkin SH. Regulated expression of globin chains and the erythroid transcription factor GATA-1 during erythropoiesis in the developing mouse. *Mol Cell Biol* 1990;10:6596–606
7. Kremastinos DT, Farmakis D, Aessopos A, Hahalis G, Hamodraka E, Tsiapras D, Keren A. Beta-thalassemia cardiomyopathy: history, present considerations, and future perspectives. *Circ Heart Fail* 2010;3:451–8
8. Lekawanvijit S, Chattipakorn N. Iron overload thalassemic cardiomyopathy: iron status assessment and mechanisms of mechanical and electrical disturbance due to iron toxicity. *Can J Cardiol* 2009;25:213–8
9. Li Q, Peterson KR, Fang X, Stamatoyannopoulos G. Locus control regions. *Blood* 2002;100:3077–86
10. Russell ES. Hereditary anemias of the mouse: a review for geneticists. *Adv Genet* 1979;20:357–459
11. Skow LC, Burkhart BA, Johnson FM, Popp RA, Popp DM, Goldberg SZ, Anderson WF, Barnett LB, Lewis SE. A mouse model for beta-thalassemia. *Cell* 1983;34:1043–52
12. Shehee WR, Oliver P, Smithies O. Lethal thalassemia after insertional disruption of the mouse major adult beta-globin gene. *Proc Natl Acad Sci U S A* 1993;90:3177–81
13. Yang B, Kirby S, Lewis J, Detloff PJ, Maeda N, Smithies O. A mouse model for beta 0-thalassemia. *Proc Natl Acad Sci U S A* 1995;92:11608–12
14. Kumfu S, Chattipakorn S, Chinda K, Fucharoen S, Chattipakorn N. T-type calcium channel blockade improves survival and cardiovascular function in thalassemic mice. *Eur J Haematol* 2012;88:535–48
15. Incharoen T, Thephinlap C, Srichairatanakool S, Chattipakorn S, Winichagoon P, Fucharoen S, Vadolas J, Chattipakorn N. Heart rate variability in beta-thalassemic mice. *Int J Cardiol* 2007;121:203–4
16. Kumfu S, Chattipakorn S, Fucharoen S, Chattipakorn N. Mitochondrial calcium uniporter blocker prevents cardiac mitochondrial dysfunction induced by iron overload in thalassemic mice. *Biometals* 2012;25:1167–75
17. Kumfu S, Chattipakorn S, Fucharoen S, Chattipakorn N. Ferric iron uptake into cardiomyocytes of beta-thalassemic mice is not through calcium channels. *Drug Chem Toxicol* 2013;36:329–34
18. Kumfu S, Chattipakorn S, Srichairatanakool S, Settakorn J, Fucharoen S, Chattipakorn N. T-type calcium channel as a portal of iron uptake into cardiomyocytes of beta-thalassemic mice. *Eur J Haematol* 2011;86:156–66
19. Kumfu S, Chattipakorn SC, Fucharoen S, Chattipakorn N. Dual T-type and L-type calcium channel blocker exerts beneficial effects in attenuating cardiovascular dysfunction in iron-overloaded thalassaemic mice. *Exp Physiol* 2016;101:521–39
20. Musallam KM, Taher AT, Rachmilewitz EA. beta-thalassemia intermedia: a clinical perspective. *Cold Spring Harb Perspect Med* 2012;2:a013482
21. Origa R, Galanello R, Ganz T, Giagu N, Maccioni L, Faa G, Nemeth E. Liver iron concentrations and urinary hepcidin in beta-thalassemia. *Haematologica* 2007;92:583–8
22. Taher A, El Rassi F, Isma'eel H, Koussa S, Inati A, Cappellini MD. Correlation of liver iron concentration determined by R2 magnetic resonance imaging with serum ferritin in patients with thalassemia intermedia. *Haematologica* 2008;93:1584–6
23. Taher AT, Musallam KM, El-Beshlawy A, Karimi M, Daar S, Belhoul K, Saned MS, Graziadei G, Cappellini MD. Age-related complications in treatment-naive patients with thalassaemia intermedia. *Br J Haematol* 2010;150:486–9
24. Voskaridou E, Douskou M, Terpos E, Papassotiriou I, Stamoulakatou A, Ourailidis A, Loutradi A, Loukopoulos D. Magnetic resonance imaging in the evaluation of iron overload in patients with beta thalassaemia and sickle cell disease. *Br J Haematol* 2004;126:736–42
25. Lombardo T, Tamburino C, Bartoloni G, Morrone ML, Frontini V, Italia F, Cordaro S, Privitera A, Calvi V. Cardiac iron overload in thalassemic patients: an endomyocardial biopsy study. *Ann Hematol* 1995;71:135–41
26. Au WY, Lam WW, Chu WW, Tam S, Wong WK, Lau J, Yeung YM, Liu HS, Liang R. Organ-specific hemosiderosis and functional correlation in Chinese patients with thalassemia intermedia and hemoglobin H disease. *Ann Hematol* 2009;88:947–50
27. Glickstein H, El RB, Link G, Breuer W, Konijn AM, Hershko C, Nick H, Cabantchik ZI. Action of chelators in iron-loaded cardiac cells: accessibility to intracellular labile iron and functional consequences. *Blood* 2006;108:3195–203
28. Taher AT, Musallam KM, Wood JC, Cappellini MD. Magnetic resonance evaluation of hepatic and myocardial iron deposition in

transfusion-independent thalassemia intermedia compared to regularly transfused thalassemia major patients. *Am J Hematol* 2010;85:288–90
29. Kumfu S, Chattipakorn SC, Fucharoen S, Chattipakorn N. Effects of iron overload condition on liver toxicity and hepcidin/ferroportin expression in thalassemic mice. *Life Sci* 2016;150:15–23
30. Thephinlap C, Phisalaphong C, Lailerd N, Chattipakorn N, Winichagoon P, Vadolas J, Fucharoen S, Porter JB, Srichairatanakool S. Reversal of cardiac iron loading and dysfunction in thalassemic mice by curcuminoids. *Med Chem* 2011;7:62–9
31. Yatmark P, Morales NP, Chaisri U, Wichaiyo S, Hemstapat W, Srichairatanakool S, Svasti S, Fucharoen S. Iron distribution and histopathological characterization of the liver and heart of beta-thalassemic mice with parenteral iron overload: Effects of deferoxamine and deferiprone. *Exp Toxicol Pathol* 2014;66:333–43
32. Gardenghi S, Marongiu MF, Ramos P, Guy E, Breda L, Chadburn A, Liu Y, Amariglio N, Rechavi G, Rachmilewitz EA, Breuer W, Cabantchik ZI, Wrighting DM, Andrews NC, de Sousa M, Giardina PJ, Grady RW, Rivella S. Ineffective erythropoiesis in beta-thalassemia is characterized by increased iron absorption mediated by down-regulation of hepcidin and up-regulation of ferroportin. *Blood* 2007;109:5027–35
33. Gelderman MP, Baek JH, Yalamanoglu A, Puglia M, Vallelian F, Burla B, Vostal J, Schaer DJ, Buehler PW. Reversal of hemochromatosis by apotransferrin in non-transfused and transfused Hbbth3/+ (heterozygous B1/B2 globin gene deletion) mice. *Haematologica* 2015;100:611–22
34. Wood JC. Cardiac complications in thalassemia major. *Hemoglobin* 2009;33:S81–6
35. Aessopos A, Farmakis D, Hatziliami A, Fragodimitri C, Karabatsos F, Joussef J, Mitilineou E, Diamanti-Kandaraki E, Meletis J, Karagiorga M. Cardiac status in well-treated patients with thalassemia major. *Eur J Haematol* 2004;73:359–66
36. Marsella M, Borgna-Pignatti C, Meloni A, Caldarelli V, Dell'Amico MC, Spasiano A, Pitrolo L, Cracolici E, Valeri G, Positano V, Lombardi M, Pepe A. Cardiac iron and cardiac disease in males and females with transfusion-dependent thalassemia major: a T2* magnetic resonance imaging study. *Haematologica* 2011;96:515–20
37. Sanyear C, Butthep P, Nithipongvanich R, Sirankapracha P, Winichagoon P, Fucharoen S, Svasti S. Cardiomyocyte ultrastructural damage in beta-thalassaemic mice. *Int J Exp Pathol* 2013;94:336–42
38. Stoyanova E, Trudel M, Felfly H, Garcia D, Cloutier G. Characterization of circulatory disorders in beta-thalassemic mice by noninvasive ultrasound biomicroscopy. *Physiol Genomics* 2007;29:84–90
39. Van Wyck DB, Tancer ME, Popp RA. Iron homeostasis in beta-thalassemic mice. *Blood* 1987;70:1462–5
40. Stoyanova E, Cloutier G, Felfly H, Lemsaddek W, Ah-Son N, Trudel M. Evidence for a novel mechanism independent of myocardial iron in beta-thalassemia cardiac pathogenesis. *PLoS One* 2012;7:e52128
41. Borgna-Pignatti C, Cappellini MD, De Stefano P, Del Vecchio GC, Forni GL, Gamberini MR, Ghilardi R, Origa R, Piga A, Romeo MA, Zhao H, Cnaan A. Survival and complications in thalassemia. *Ann N Y Acad Sci* 2005;1054:40–7
42. Carpenter JP, He T, Kirk P, Roughton M, Anderson LJ, de Noronha SV, Sheppard MN, Porter JB, Walker JM, Wood JC, Galanello R, Forni G, Catani G, Matta G, Fucharoen S, Fleming A, House MJ, Black G, Firmin DN, St Pierre TG, Pennell DJ. On T2* magnetic resonance and cardiac iron. *Circulation* 2011;123:1519–28
43. Kaye SB, Owen M. Cardiac arrhythmias in thalassaemia major: evaluation of chelation treatment using ambulatory monitoring. *Br Med J* 1978;1:342
44. Engle MA, Erlandson M, Smith CH. Late cardiac complications of chronic, severe, refractory anemia with hemochromatosis. *Circulation* 1964;30:698–705
45. Detterich J, Noetzli L, Dorey F, Bar-Cohen Y, Harmatz P, Coates T, Wood J. Electrocardiographic consequences of cardiac iron overload in thalassemia major. *Am J Hematol* 2012;87:139–44
46. Russo V, Rago A, Papa AA, Nigro G. Electrocardiographic presentation, cardiac arrhythmias, and their management in beta-thalassemia major patients. *Ann Noninvasive Electrocardiol* 2016;21:335–42
47. Anderson LJ, Holden S, Davis B, Prescott E, Charrier CC, Bunce NH, Firmin DN, Wonke B, Porter J, Walker JM, Pennell DJ. Cardiovascular T2-star (T2*) magnetic resonance for the early diagnosis of myocardial iron overload. *Eur Heart J* 2001;22:2171–9
48. Breuer W, Ermers MJ, Pootrakul P, Abramov A, Hershko C, Cabantchik ZI. Desferrioxamine-chelatable iron, a component of serum non-transferrin-bound iron, used for assessing chelation therapy. *Blood* 2001;97:792–8
49. Jakeman A, Thompson T, McHattie J, Lehotay DC. Sensitive method for nontransferrin-bound iron quantification by graphite furnace atomic absorption spectrometry. *Clin Biochem* 2001;34:43–7
50. Koonrungsesomboon N, Tantiworawit A, Phrommintikul A, Saekho S, Srichairattanakool S, Chattipakorn N. Heart rate variability for early detection of iron overload cardiomyopathy in beta-thalassemia patients. *Hemoglobin* 2015;39:281–6
51. Rutjanaprom W, Kanlop N, Charoenkwan P, Sittiwangkul R, Srichairatanakool S, Tantiworawit A, Phrommintikul A, Chattipakorn S, Fucharoen S, Chattipakorn N. Heart rate variability in beta-thalassemia patients. *Eur J Haematol* 2009;83:483–9
52. Silvilairat S, Charoenkwan P, Saekho S, Tantiworawit A, Phrommintikul A, Srichairatanakool S, Chattipakorn N. Heart rate variability for early detection of cardiac iron deposition in patients with transfusion-dependent thalassemia. *PLoS One* 2016;11:e0164300
53. Wijarnpreecha K, Siri-Angkul N, Shinlapawittayatorn K, Charoenkwan P, Silvilairat S, Siwasomboon C, Visarutratna P, Srichairatanakool S, Tantiworawit A, Phrommintikul A, Chattipakorn SC, Chattipakorn N. Heart rate variability as an alternative indicator for identifying cardiac iron status in non-transfusion dependent thalassemia patients. *PLoS One* 2015;10:e0130837
54. Anderson LJ, Westwood MA, Holden S, Davis B, Prescott E, Wonke B, Porter JB, Walker JM, Pennell DJ. Myocardial iron clearance during reversal of siderotic cardiomyopathy with intravenous desferrioxamine: a prospective study using T2* cardiovascular magnetic resonance. *Br J Haematol* 2004;127:348–55
55. Smith GC, Alpendurada F, Carpenter JP, Alam MH, Berdoukas V, Karagiorga M, Ladis V, Piga A, Aessopos A, Gotsis ED, Tanner MA, Westwood MA, Galanello R, Roughton M, Pennell DJ. Effect of deferiprone or deferoxamine on right ventricular function in thalassemia major patients with myocardial iron overload. *J Cardiovasc Magn Reson* 2011;13:34
56. Alpendurada F, Carpenter JP, Deac M, Kirk P, Walker JM, Porter JB, Banya W, He T, Smith GC, Pennell DJ. Relation of myocardial T2* to right ventricular function in thalassaemia major. *Eur Heart J* 2010;31:1648–54
57. Alp A, Ozdogan O, Guloglu CC, Turker M, Atabay B. Heart rate variability in beta-thalassaemia major with or without cardiac siderosis. *Cardiol Young* 2014;24:263–7
58. Gurses D, Ulger Z, Levent E, Aydinok Y, Ozyurek AR. Time domain heart rate variability analysis in patients with thalassaemia major. *Acta Cardiol* 2005;60:477–81
59. Kardelen F, Tezcan G, Akcurin G, Ertug H, Yesilipek A. Heart rate variability in patients with thalassemia major. *Pediatr Cardiol* 2008;29:935–9
60. Pennell DJ, Porter JB, Cappellini MD, Chan LL, El-Beshlawy A, Aydinok Y, Ibrahim H, Li CK, Viprakasit V, Elalfy MS, Kattamis A, Smith G, Habr D, Domokos G, Roubert B, Taher A. Deferasirox for up to 3 years leads to continued improvement of myocardial T2* in patients with beta-thalassemia major. *Haematologica* 2012;97:842–8
61. Pennell DJ, Berdoukas V, Karagiorga M, Ladis V, Piga A, Aessopos A, Gotsis ED, Tanner MA, Smith GC, Westwood MA, Wonke B, Galanello R. Randomized controlled trial of deferiprone or deferoxamine in beta-thalassemia major patients with asymptomatic myocardial siderosis. *Blood* 2006;107:3738–44
62. Pennell DJ, Carpenter JP, Roughton M, Cabantchik Z. On improvement in ejection fraction with iron chelation in thalassemia major and the risk of future heart failure. *J Cardiovasc Magn Reson* 2011;13:45
63. Pepe A, Meloni A, Rossi G, Cuccia L, D'Ascola GD, Santodirocco M, Cianciulli P, Caruso V, Romeo MA, Filosa A, Pitrolo L, Putti MC, Peluso A, Campisi S, Missere M, Midiri M, Gulino L, Positano V,

Lombardi M, Ricchi P. Cardiac and hepatic iron and ejection fraction in thalassemia major: multicentre prospective comparison of combined deferiprone and deferoxamine therapy against deferiprone or deferoxamine monotherapy. *J Cardiovasc Magn Reson* 2013;**15**:1

64. Lai ME, Grady RW, Vacquer S, Pepe A, Carta MP, Bina P, Sau F, Cianciulli P, Maggio A, Galanello R, Farci P. Increased survival and reversion of iron-induced cardiac disease in patients with thalassemia major receiving intensive combined chelation therapy as compared to desferoxamine alone. *Blood Cells Mol Dis* 2010;**45**:136–9
65. Wongjaikam S, Kumfu S, Chattipakorn SC, Fucharoen S, Chattipakorn N. Current and future treatment strategies for iron overload cardiomyopathy. *Eur J Pharmacol* 2015;**765**:86–93
66. Ozdemir ZC, Koc A, Aycicek A, Kocyigit A. N-acetylcysteine supplementation reduces oxidative stress and DNA damage in children with β-thalassemia. *Hemoglobin* 2014;**15**:1–6
67. Rachmilewitz EA, Weizer-Stern O, Adamsky K, Amariglio N, Rechavi G, Breda L, Rivella S, Cabantchik ZI. Role of iron in inducing oxidative stress in thalassemia: can it be prevented by inhibition of absorption and by antioxidants? *Ann N Y Acad Sci* 2005;**1054**:118–123
68. Sugishita K, Asakawa M, Usui S, Takahashi T. A case of iron overload cardiomyopathy: beneficial effects of iron chelating agent and calcium channel blocker on left ventricular dysfunction. *Int Heart J* 2009;**50**:829–38
69. Fernandes JL, Sampaio EF, Fertrin K, Coelho OR, Loggetto S, Piga A, Verissimo M, Saad ST. Amlodipine reduces cardiac iron overload in patients with thalassemia major: a pilot trial. *Am J Med* 2013;**126**:834–7

เอกสารแนบหมายเลข 2

Menopause: The Journal of The North American Menopause Society
Vol. 24, No. 7, pp. 000-000
DOI: 10.1097/GME.0000000000000838
© 2017 by The North American Menopause Society

Estrogen and DPP-4 inhibitor share similar efficacy in reducing brain pathology caused by cardiac ischemia-reperfusion injury in both lean and obese estrogen-deprived rats

Wasana Pratchayasakul, PhD,[1,2] Sivaporn Sivasinprasasn, PhD,[1,3] Piangkwan Sa-Nguanmoo, MSc,[1,2] Cicely Proctor, BSc,[4] Sasiwan Kerdphoo, MSc,[1] Nipon Chattipakorn, MD, PhD,[1,2] and Siriporn C. Chattipakorn, DDS, PhD[1,5]

Abstract

Objective: Cardiac ischemia-reperfusion injury (I/R) caused an oxidative burst, increased beta-amyloid production, and decreased dendritic spine density in the brain. However, the effect of cardiac I/R in the brain of estrogen-deprived rats who were or were not obese have not been investigated. Moreover, the benefits of estrogen or dipeptidyl peptidase-4 (DDP-4) inhibitor therapies in those conditions have never been determined. We hypothesized that cardiac I/R aggravates brain pathology in estrogen-deprived obese rats, to a greater extent when compared with estrogen-deprived lean rats, and treatment with either estrogen or a DPP-4 inhibitor attenuates those adverse effects.

Methods: In protocol 1, rats were divided into sham operation (n = 12) or ovariectomy (n = 24). Sham-operated rats were fed with normal diet (ND) and ovariectomized rats were fed with either ND or high-fat diet (HF) for 12 weeks. Then, rats were subdivided to sham operation or cardiac I/R injury. In protocol 2, ovariectomized rats were given either ND (n = 18) or HF (n = 18). At week 13, ovariectomized rats were subdivided to receive vehicle, estradiol, or DPP-4 inhibitor for 4 weeks. Then, all rats were subjected to cardiac I/R.

Results: Cardiac I/R injury aggravated brain oxidative stress, beta-amyloid production, and decreased dendritic spine density in either sham-operated or ovariectomized ND-fed rats, but not in ovariectomized HF-fed rats. Either estrogen or DPP-4 inhibitor therapies reduced those conditions in all rats with cardiac I/R.

Conclusions: Cardiac I/R aggravates brain toxicity in estrogen-deprived lean rats, but not in the estrogen-deprived obese rats. Estrogen and DPP-4 inhibitor treatments attenuate those effects in all groups.

Key Words: DPP-4 inhibitor – Brain – Cardiac ischemia-reperfusion injury – Estrogen – Obesity – Ovariectomy.

Cardiac ischemia-reperfusion (cardiac I/R) injury can lead to not only myocardial damage but also increased brain pathology. Previous studies have shown that cardiac I/R injury induced an oxidative burst in many organs, including the brain.[1,2] In addition, the deleterious effects of cardiac I/R injury have been demonstrated in the brain of lean male rats as indicated by blood-brain barrier (BBB) breakdown, increased brain oxidative stress, increased brain mitochondrial dysfunction, and an increased susceptibility to brain apoptosis.[3] Furthermore, it has been shown that increased brain oxidative stress could cause Alzheimer's disease via increasing beta-amyloid (Aβ) production and reduced dendritic spine density.[4-6] In addition, recent studies have demonstrated that both obesity and estrogen deprivation significantly aggravated the severity of oxidative stress and myocardial damage in animal models of cardiac I/R injury. This increase in severity was indicated by increased cardiac malondialdehyde (MDA) level, increased cardiac mitochondrial dysfunction and cardiac calcium dysregulation, and impaired left ventricle (LV) function.[7-9] These findings suggest an influential role of female hormones and obesity on the adverse effects of the heart caused by I/R injury. Despite these findings on the heart, the effects of cardiac I/R injury on brain oxidative stress, Aβ production, and dendritic spine density in estrogen-deprived lean or obese rats have never been investigated.

Received October 20, 2016; revised and accepted December 13, 2016.
From the [1]Neurophysiology Unit, Cardiac Electrophysiology Research and Training Center, and [2]Department of Physiology, Faculty of Medicine, Chiang Mai University, Chiang Mai, Thailand; [3]School of Health Science, Mae Fah Luang University, Chiang Rai, Thailand; [4]Faculty of Life Sciences, The University of Manchester, Manchester, UK; and [5]Department of Oral Biology and Diagnostic Sciences, Faculty of Dentistry, Chiang Mai University, Chiang Mai, Thailand.
Funding/support: This work was supported by the Thailand Research Fund BRG5780016 (S.C.C.) and MRG5980198 (W.P.), a NSTDA Research Chair Grant from the National Science and Technology Development Agency Thailand (N.C.), and a Chiang Mai University Center of Excellence Award (N.C.).

Financial disclosure/conflicts of interest: None reported.
Address correspondence to: Siriporn C. Chattipakorn, DDS, PhD, Department of Oral Biology and Diagnostic Sciences, Faculty of Dentistry, Chiang Mai University, Chiang Mai 50200, Thailand. E-mail: scchattipakorn@gmail.com; siriporn.c@cmu.ac.th

Copyright © 2017 The North American Menopause Society. Unauthorized reproduction of this article is prohibited.

Several studies have shown that estrogen has beneficial effects on cardiac I/R injury as indicated by reduced myocardial infarction and improved postischemic recovery after estrogen administration in in vitro, in vivo, and clinical studies.[8,10,11] Furthermore, our previous study found that an antidiabetic drug dipeptidyl peptidase-4 (DPP-4) inhibitor (Vildagliptin) attenuated the adverse effects of cardiac I/R injury in obese male rats, as indicated by decreased cardiac oxidative stress levels and improved cardiac mitochondrial function.[9] However, the potential benefits of either estrogen or DPP-4 inhibitor on brain oxidative stress levels, Aβ production, and dendritic spine density in a cardiac I/R injury model of lean or obese rats with an estrogen-deprived condition have never been determined. In this study, our hypothesis was that incidence of cardiac I/R injury aggravates brain oxidative stress level, increases Aβ production, and decreases dendritic spine density in both lean and obese rats with estrogen deprivation, and that administration of estrogen or DPP-4 inhibitor leads to an attenuation of these adverse effects in the brain.

METHODS

Animal models and experimental protocols

All experiments were conducted in accordance with the approved protocol from the Faculty of Medicine, Chiang Mai University Institutional Animal Care and Use Committee, in compliance with NIH guidelines. Seventy-two female Wistar rats weighing 200 to 220 g (aged ~6 weeks old) were obtained from the National Animal Center, Salaya Campus, Mahidol University, Thailand. At baseline, there was no significant difference in weight between all groups. The mean body weights for normal diet (ND)-fed rats and high-fat diet (HF)-fed rats at baseline (week 0) were 213.50 ± 2.98 g and 210.00 ± 3.09 g, respectively. All animals were individually housed in a temperature-controlled environment with a 12:12 light-dark cycle. The experimental protocols were divided into two protocols.

In protocol 1 (Fig. 1A), 36 rats were randomly assigned to either the sham-operated group (S; n = 12) or the ovariectomized group (O; n = 24). One week after the surgery, the sham-operated group was fed with a normal diet (ND; NDS) for 12 weeks, whereas the ovariectomized group was further subdivided into two subgroups. Each of these subgroups received either a ND (NDO; n = 12) or a HF (HFO; n = 12) for 12 weeks. Animals in the HF group were fed a diet containing 59.3% total energy from fat, with the major component being saturated fatty acids from lard, as described in our previous study.[12] The animals were given ad libitum access to food and water. Body weight and food intake were

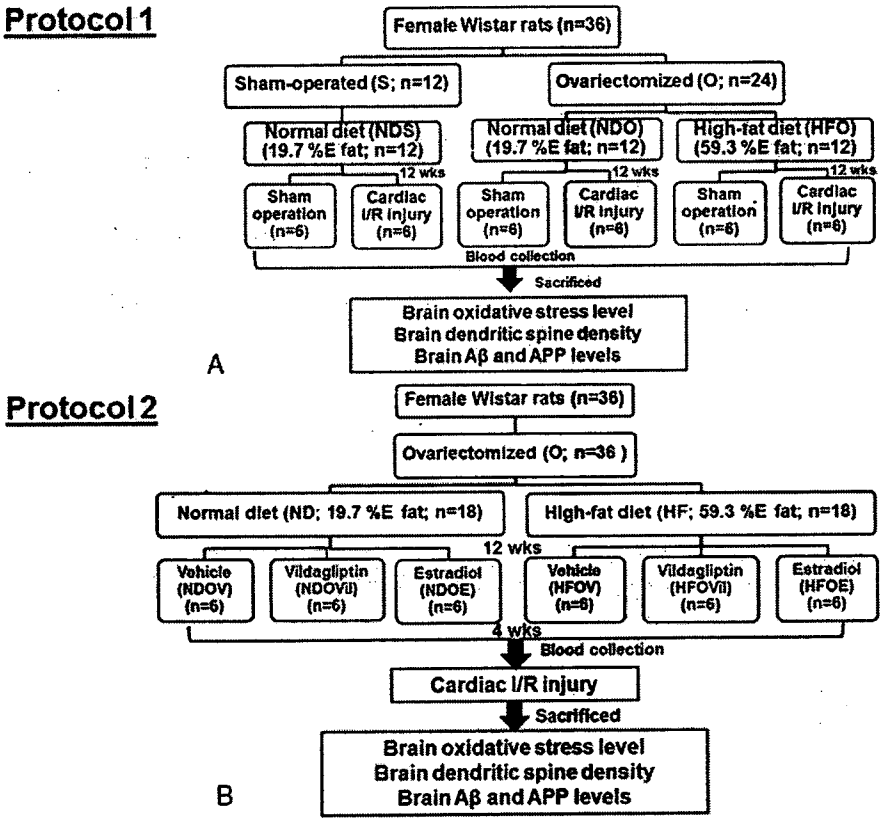


FIG. 1. Experimental protocol 1 (**A**) and protocol 2 (**B**) of the study. Aβ, beta-amyloid; APP, amyloid precursor protein; cardiac I/R, cardiac ischemia-reperfusion injury; HF, high-fat diet; HFO, ovariectomized HF-fed rats; HFOE, ovariectomized HF-fed rats with estradiol administration; HFOV, ovariectomized HF-fed rats with vehicle treatment; HFOVil, ovariectomized HF-fed rats with vildagliptin administration; ND, normal diet; NDO, ovariectomized ND-fed rats; NDOE, ovariectomized ND-fed rats with estradiol administration; NDOV, ovariectomized ND-fed rats with vehicle administration; NDOVil, ovariectomized ND-fed rats with vildagliptin administration; NDS, sham ND-fed rats; O, ovariectomy; S, sham-operated.

© 2017 The North American Menopause Society

Copyright © 2017 The North American Menopause Society. Unauthorized reproduction of this article is prohibited.

recorded daily. At the end of the dietary period, the animals were put into deep anesthesia using isoflurane after fasting for at least 5 hours. Blood samples were collected for determining metabolic parameters (glucose, total cholesterol, triglycerides, high-density lipoprotein [HDL], low-density lipoprotein [LDL], insulin), estrogen, and MDA levels. Finally, rats in each dietary group were further subdivided and either received a sham operation or had cardiac I/R injury (n = 6/subgroup) instigated by left anterior descending (LAD) artery occlusion for 30 minutes, followed by 120-minute reperfusion. At the end of the protocol, animals were sacrificed by decapitation. Their brains were rapidly removed, and all brain tissues from all of the animals in this study were included in the various analyses. The left hemisphere of the brain was used to determine dendritic spine density by using Golgi staining method. The right hemisphere of the brain was used to determine the levels of brain oxidative stress by measuring MDA levels and Aβ protein by using western blot analysis. Total visceral fat, including peritoneal, periovarian, and perirenal fat pads, were removed and weighed.

In protocol 2 (Fig. 1B), 36 ovariectomized (O) rats were subdivided and were given either a ND (NDO; n = 18) or a HF (HFO; n = 18) for 12 weeks. At the end of week 13, the ovariectomized rats in each dietary group were further divided into three subgroups to receive one of the following daily: a vehicle (sesame oil in equal volume with estradiol [E_2]) via subcutaneous injection (V; NDOV and HFOV; n = 6/subgroup); 50 μg/kg E_2 via subcutaneous injection (NDOE and HFOE; n = 6/subgroup); or 3 mg/kg DPP-4 inhibitor (Vildagliptin) via intragastric gavage (NDOVil and HFOVil; n = 6/subgroup) for 4 weeks. We chose these doses because previous studies have already demonstrated the beneficial effects of these doses on the improvement of peripheral insulin sensitivity,[13,14] brain insulin sensitivity,[15,16] and cardiac function[14,17] in both obese insulin-resistant model and ovariectomized model. In addition, previous studies found that only the highest dose of estrogen, which produced plasma E_2 levels above 250 pg/mL, could enhance dendritic spine density and cognitive function.[18,19] At the end of the experimental period (week 16), the animals were deeply anesthetized with isoflurane after fasting for at least 5 hours. Blood samples were collected to allow the determination of metabolic parameters (glucose, total cholesterol, triglycerides, HDL, LDL, insulin), estrogen and MDA levels. Finally, all of the rats were subjected to cardiac I/R injury by LAD artery occlusion for 30 minutes, followed by 120-minute reperfusion. At the end of the protocol, animals were sacrificed by decapitation. Their brains were rapidly removed, and all brain tissues from all of the animals in this study were included in the various analyses. The left hemisphere of the brain was used to determine dendritic spine density by using Golgi staining method. The right hemisphere of the brain was used to determine the levels of brain oxidative stress by measuring MDA levels and Aβ protein by using western blot analysis. Total visceral fat, including peritoneal, periovarian, and perirenal fat pads, were removed and weighed.

Ovariectomy procedure

The details of the ovariectomy procedure have been described previously.[15,20] Briefly, female rats were anesthetized by intramuscular injection with Xylazine (0.15 mg/kg; LaboratoriosCalier, Barcelona, Spain) and Zoletil (50 mg/kg; Virbac Laboratories, Carros, France). After that, the bilateral ovariectomy was performed using double dorso-lateral skin incisions.

Cardiac ischemia-reperfusion injury protocol

The details of the cardiac I/R injury protocol have been described previously.[9] Briefly, female rats were anesthetized by intramuscular injection with Xylazine (0.15 mg/kg; Laboratorios Calier, Barcelona, Spain) and Zoletil (50 mg/kg; Virbac Laboratories, Carros, France). The LAD coronary artery was ligated using a 5-0 silk suture underneath the LAD, near its origin at the aorta (approximately 2 mm distal to its origin). The end of a ligature was passed through a small vinyl tube, which is used to occlude the LAD by pulling the thread. Ischemia was confirmed by ST elevation. The heart was subjected to ischemia for 30 minutes, followed by 120-min reperfusion.

Chemical analysis for assessment of insulin, glucose, triglyceride, cholesterol, LDL, HDL, and estrogen levels

Fasting plasma insulin levels were measured using a commercial sandwich ELISA kit (LINCO Research, MO). Fasting plasma glucose, triglyceride, cholesterol, LDL, and HDL concentrations were measured using commercially available colorimetric assay kits (ERBA diagnostic; Mannheim, Germany). Serum estrogen levels were determined using an enzyme immunoassay kit (Cayman chemical, Ann Arbor, MI). All chemical analyses used to identify metabolic parameters were performed in duplicate in the same assay. The coefficient of variation for the intra and inter assays were 6.67% and 12.54% for insulin; 5.31% and 4.54% for glucose; 8.43% and 11.55% for triglycerides; 4.84% and 8.48% for cholesterol; 7.66% and 10.80% for LDL; 3.45% and 5.30% for HDL; and 6.51% and 12.92% for estrogen, respectively.

Determination of insulin resistance

The Homeostasis Model Assessment (HOMA) index was calculated from fasting plasma insulin and fasting plasma glucose concentrations.[21] A higher HOMA index indicates a higher degree of insulin resistance.

Determination of malondialdehyde levels

Malondialdehyde levels were measured using a high-performance liquid chromatography (HPLC) method.[22] Briefly, serum and brain fractions were prepared by trichloroacetic acid (TCA) protein precipitation. The supernatant was mixed with thiobarbituric acid solution (TBA). MDA levels were measured using an HPLC system at 532 nm.

Immunoblotting

The details of the subsequent brain homogenates for immunoblotting have been described previously.[12] The whole brain

Copyright © 2017 The North American Menopause Society. Unauthorized reproduction of this article is prohibited.

in each conditioned group was homogenized. After that, the cytosol fractions were separated and used for further immunoblotting of the Aβ and amyloid precursor protein (APP) expression. Immunoblotting was conducted with rabbit antibodies for Aβ (1:1000; Santa Cruz Biotechnology, Santa Cruz, CA) and APP (1:1000; Merck Millipore Corporation, Darmstadt, Germany). The primary antibody was detected by horseradish peroxidase (HRP) conjugated antirabbit antibody (1:2000; Cell Signaling Technology, Beverly, MA) to measure Aβ expression, and HRP-conjugated antimouse antibody (1:2000; Cell Signaling Technology, MA) to measure APP expression. The protein bands were visualized on Amersham Hyperfilm Enhanced Chemiluminescence (GE Healthcare, Buckinghamshire, UK).

Golgi impregnation and analysis

The details of dendritic spine density analysis have been described previously.[23] After decapitation, the brains were processed for Golgi staining using a commercially available kit (FD Neurotechnologies kit, PK 401, Ellicott City, MD). For the dendritic spine density analysis, three segments from a pyramidal cell in the CA1 area of the hippocampus (three slices/animal, n = 6 animals/group) were randomly measured using the Xcellence imaging software (Olympus, Tokyo, Japan).

Statistical analysis

Data were presented as mean ± SEM. All statistical analyses were performed using the program SPSS (version 16; SPSS, Chicago, IL). In protocol 1, the two-way analysis of variance (ANOVA) (diet × surgery) and post-hoc analysis with Fisher's tests were used to test significant differences for all comparisons. Independent Student's test was used to test between sham operation and cardiac I/R injury condition in the same diet and surgery groups. In protocol 2, a two-way ANOVA (diet × treatment) and post-hoc analysis with Fisher's tests were used to test significant differences for all comparisons. P value less than 0.05 was statistically significant.

RESULTS

Obesity aggravated the peripheral insulin resistance and dyslipidemia in ovariectomized rats, and both vildagliptin and estradiol administrations attenuated these metabolic impairments

Ovariectomized ND-fed rats displayed peripheral insulin resistance as demonstrated by significantly increased fasting plasma insulin levels, fasting plasma glucose levels, and HOMA index when compared with the sham-operated ND-fed rats (Table 1). In addition, HF consumption increased the severity of peripheral insulin resistance and dyslipidemia in the ovariectomized group, as shown by significantly increased fasting plasma glucose levels, HOMA index, body weight, visceral fat, fasting plasma cholesterol, and LDL levels, when compared with ovariectomized ND-fed rats (Table 1). Interestingly, the administration of either vildagliptin or E_2 led to a significant decrease in the severity of peripheral insulin resistance and dyslipidemia in ovariectomized ND-fed rats and ovariectomized HF-fed rats (Table 1). The uterine weight and serum estrogen levels significantly decreased in all ovariectomized rats, confirming the effectiveness of estrogen deprivation via bilateral ovariectomy (Table 1).

The effects of cardiac I/R injury on brain pathological conditions in both ovariectomized ND-fed rats and HF-fed rats

We found that estrogen deprivation by ovariectomy increased serum and brain oxidative stress levels in the ND-fed rats, as indicated by increased serum and brain MDA levels. In addition, HF-induced obesity showed a correlation with an increase in the severity of serum and brain oxidative stress levels in the ovariectomized group (Table 1, Fig. 2A). Interestingly, we found that cardiac I/R

TABLE 1. *Metabolic parameters after vildagliptin and estradiol treatment*

	Normal diet				High-fat diet		
Parameters	NDS	NDOV	NDOVil	NDOE	HFOV	HFOVil	HFOE
Body weight, g	290 ± 13	342 ± 7[a]	340 ± 11[a]	302 ± 9[b]	398 ± 11[a,b]	401 ± 5[a,b]	346 ± 4[a,c]
Visceral fat, g	16 ± 1	16 ± 2	13 ± 1	12 ± 2	31 ± 2[a,b]	31 ± 3[a,b]	19 ± 2[c]
Uterine mass, g	0.40 ± 0.02	0.08 ± 0.0[a]	0.07 ± 0.0[a]	0.41 ± 0.02[b]	0.06 ± 0.0[a]	0.06 ± 0.0[a]	0.38 ± 0.02[c]
Plasma estrogen, pg/mL	121 ± 10	59 ± 7[a]	60 ± 7[a]	252 ± 32[b]	65 ± 12[a]	53 ± 11[a]	249 ± 38[c]
Glucose, mg%	132.61 ± 2.73	185.77 ± 3.61[a]	134.04 ± 3.97[b]	134.43 ± 3.92[b]	239.89 ± 5.81[a,b]	151.66 ± 5.31[c]	158.32 ± 6.47[c]
Insulin, ng/mL	1.13 ± 0.08	2.97 ± 0.35[a]	1.12 ± 0.06[b]	1.17 ± 0.06[b]	3.15 ± 0.39[a]	1.13 ± 0.10[c]	1.30 ± 0.04[c]
HOMA index	9.32 ± 0.83	32.27 ± 3.76[a]	8.97 ± 0.62[b]	9.13 ± 0.51[b]	43.96 ± 4.90[a,b]	10.04 ± 0.79[c]	12.15 ± 0.66[c]
Triglyceride, mg%	56.01 ± 4.97	54.62 ± 6.05	54.80 ± 5.18	51.20 ± 5.52	56.94 ± 4.95	52.11 ± 6.77	52.37 ± 4.00
Cholesterol, mg%	72.95 ± 3.71	97.98 ± 4.16[a]	81.96 ± 5.58	83.96 ± 5.17	154.75 ± 6.97[a,b]	145.11 ± 12.67	140.98 ± 8.51
LDL, mg/dL	29.17 ± 2.13	55.61 ± 3.75[a]	30.59 ± 5.95[b]	30.96 ± 6.93[b]	118.27 ± 5.65[a,b]	90.01 ± 15.37[c]	91.38 ± 7.31[c]
HDL, mg/dL	41.79 ± 2.78	32.36 ± 1.74[a]	42.04 ± 1.94[b]	39.98 ± 1.94[b]	29.16 ± 2.53[a]	43.78 ± 3.97[c]	39.128 ± 3.45[c]
Serum MDA, μM	5.64 ± 0.27	6.41 ± 0.16[a]	5.43 ± 0.27[b]	5.94 ± 0.26[b]	7.13 ± 0.25[a,b]	5.73 ± 0.23[c]	5.42 ± 0.44[c]

HDL, high-density lipoprotein; HF, high-fat diet; HFOE, ovariectomized HF-fed rats with estradiol administration; HFOV, ovariectomized HF-fed rats with vehicle treatment; HFOVil, ovariectomized HF-fed rats with vildagliptin administration; HOMA, Homeostasis Model Assessment; LDL, low-density lipoprotein; MDA; malondialdehyde; ND, normal diet; NDOE, ovariectomized ND-fed rats with estradiol administration; NDOV, ovariectomized ND-fed rats with vehicle administration; NDOVil, ovariectomized ND-fed rats with vildagliptin administration; NDS, sham ND-fed rats.
[a] $P < 0.05$ from NDS.
[b] $P < 0.05$ from NDOV.
[c] $P < 0.05$ from HFOV (n = 6/group).

© 2017 The North American Menopause Society

Copyright © 2017 The North American Menopause Society. Unauthorized reproduction of this article is prohibited.

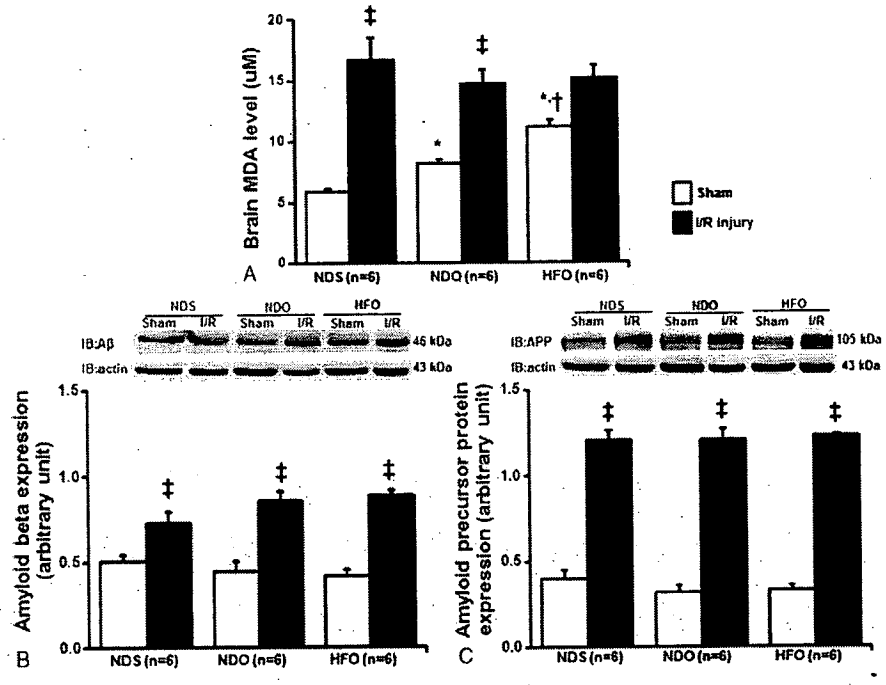


FIG. 2. The effects of cardiac I/R injury on malondialdehyde (MDA) levels (**A**), beta-amyloid (Aβ) levels (**B**), and amyloid precursor protein (APP) levels (**C**) in brains harvested from the NDS, NDO, and HFO rats with sham or cardiac I/R injury. $^{*}P < 0.05$ compared with NDS; $^{\dagger}P < 0.05$ compared with NDO; $^{\ddagger}P < 0.05$ compared with sham; n = 6/group. HF, high-fat diet; HFO, ovariectomized HF-fed rats; I/R injury, ischemia-reperfusion injury; ND, normal diet; NDO, ovariectomized ND-fed rats; NDS, sham ND-fed rats; Sham, sham operation.

injury alone led to increased brain oxidative stress levels in the ND-fed rats, when compared with ND-fed rats with noncardiac I/R injury (Fig. 2A). Under conditions of estrogen-deprivation, cardiac I/R injury aggravated brain oxidative stress levels in the ND-fed rats, but not in the HF-fed rats, when compared with the sham group ($P < 0.05$; Fig. 2A).

In addition, we found that estrogen-deprivation in both ND-fed rats and HF-fed rats did not cause the accumulation of Aβ and APP levels in the brains of noncardiac I/R injury (Fig. 2B and C). However, an increase in the Aβ and APP protein expression in the brains of all groups occurred to a similar degree after cardiac I/R injury (Fig. 2B and C), indicating that cardiac I/R injury caused the accumulation of Aβ and APP in

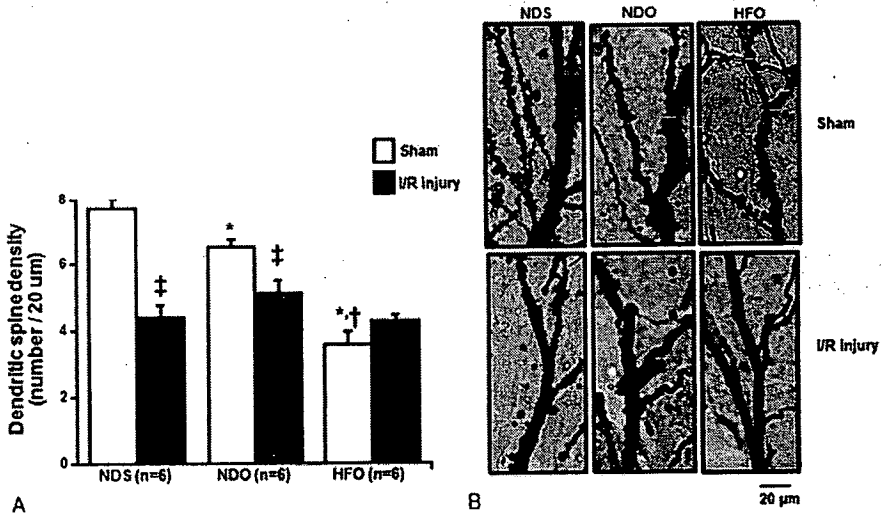


FIG. 3. The effects of cardiac I/R injury on (**A**) the number of dendritic spines on tertiary apical dendrites in brains harvested from the NDS, NDO, and HFO rats with sham or cardiac I/R injury; (**B**) a picture of a representative dendritic spines from the NDS, NDO, and HFO rats with sham or cardiac I/R injury. $^{*}P < 0.05$ compared with NDS; $^{\dagger}P < 0.05$ compared with NDO; $^{\ddagger}P < 0.05$ compared with sham; n = 6/group. HF, high-fat diet; HFO, ovariectomized HF-fed rats; I/R injury, ischemia-reperfusion injury; ND, normal diet; NDO, ovariectomized ND-fed rats; NDS, sham ND-fed rats; Sham, sham operation.

Copyright © 2017 The North American Menopause Society. Unauthorized reproduction of this article is prohibited.

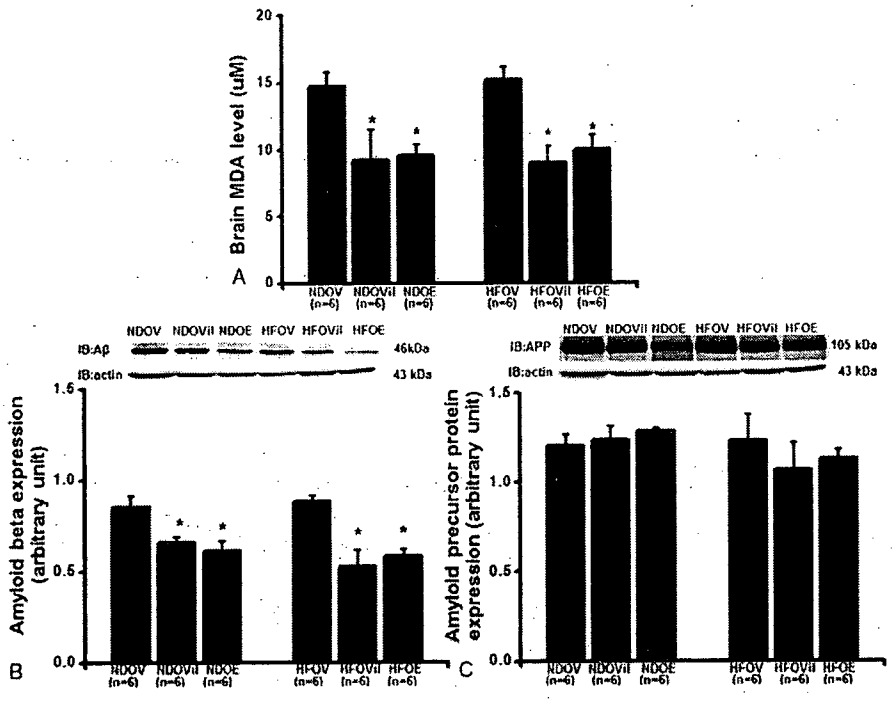


FIG. 4. The effects of vildagliptin and estrogen administration on malondialdehyde (MDA) levels (**A**), the beta-amyloid (Aβ) levels (**B**), and amyloid precursor protein (APP) levels (**C**) in brains harvested from the NDOV, NDOVil, NDOE, HFOV, HFOVil, and HFOE rats. $^{*}P < 0.05$ compared with vehicle group; n = 6/group. HF, high-fat diet; HFOE, ovariectomized HF-fed rats with estradiol administration; HFOV, ovariectomized HF-fed rats with vehicle treatment; HFOVil, ovariectomized HF-fed rats with vildagliptin administration; ND, normal diet; NDOE, ovariectomized ND-fed rats with estradiol administration; NDOV, ovariectomized ND-fed rats with vehicle administration; NDOVil, ovariectomized ND-fed rats with vildagliptin administration.

the sham-operated ND-fed rats, ovariectomized ND-fed rats, and ovariectomized HF-fed rats.

Results also showed that estrogen deprivation decreased the density of dendritic spines in the CA1 area of the hippocampus in the sham-operated ND-fed rats (Fig. 3A and B). In addition, obesity significantly aggravated the reduction of dendritic spine density in the sham-operated ovariectomized group (Fig. 3A and B). Interestingly, we found that cardiac I/R injury alone caused the reduction of dendritic spine density in the ND-fed rats. In the estrogen-deprived condition, cardiac I/R injury aggravated the reduction of dendritic spine density in the ND-fed rats, but not in the HF-fed rats ($P < 0.05$; Fig. 3A and B).

The effect of either vildagliptin or estradiol administration on brain oxidative stress, Aβ, and APP expression in both ovariectomized ND-fed rats and HF-fed rats with cardiac I/R injury

Either vildagliptin or E_2 administrations led to an equally reduced brain MDA level in both the ovariectomized ND-fed rats and ovariectomized HF-fed rats with cardiac I/R injury ($P < 0.05$; Fig. 4A), indicating that either vildagliptin or E_2 led to reduced brain oxidative stress levels in both the ovariectomized ND-fed rats and the ovariectomized HF-fed rats with cardiac I/R injury.

Either vildagliptin or E_2 administration showed a correlation with equally reduced Aβ protein expression in the brains harvested from both ovariectomized ND-fed rats and the ovariectomized HF-fed rats with cardiac I/R injury ($P < 0.05$; Fig. 4B), indicating that either vildagliptin or E_2 reduced Aβ production in both the ovariectomized ND-fed rats and the ovariectomized HF-fed rats with cardiac I/R injury. However, neither treatment reduced APP expression in both the ovariectomized ND-fed rats and the ovariectomized HFD-fed rats with cardiac I/R injury (Fig. 4C).

The effects of either vildagliptin or estradiol administration on dendritic spine density in both ovariectomized ND-fed rats and HF-fed rats with cardiac I/R injury

Either vildagliptin or E_2 administration led to an equal increase in the number of dendritic spines in the CA1 area of the hippocampus of both ovariectomized ND-fed rats and the ovariectomized HF-fed rats with cardiac I/R injury ($P < 0.05$; Fig. 5A and B), indicating that either vildagliptin or E_2 treatment led to improved dendritic spine density in both the ovariectomized ND-fed rats and the ovariectomized HF-fed rats with cardiac I/R injury.

DISCUSSION

The major findings of the present study are as follows: (1) estrogen deprivation caused the reduction in dendritic spine density and increased brain oxidative stress levels; (2) obesity aggravated the reduction in dendritic spine density and increased brain oxidative stress levels in estrogen-deprived rats; (3) cardiac I/R injury alone caused the reduction of dendritic spines and increased brain oxidative stress levels in sham-operated ND-fed rats; (4) in the estrogen-deprived condition, cardiac I/R injury aggravated dendritic spine loss

© 2017 The North American Menopause Society

Copyright © 2017 The North American Menopause Society. Unauthorized reproduction of this article is prohibited.

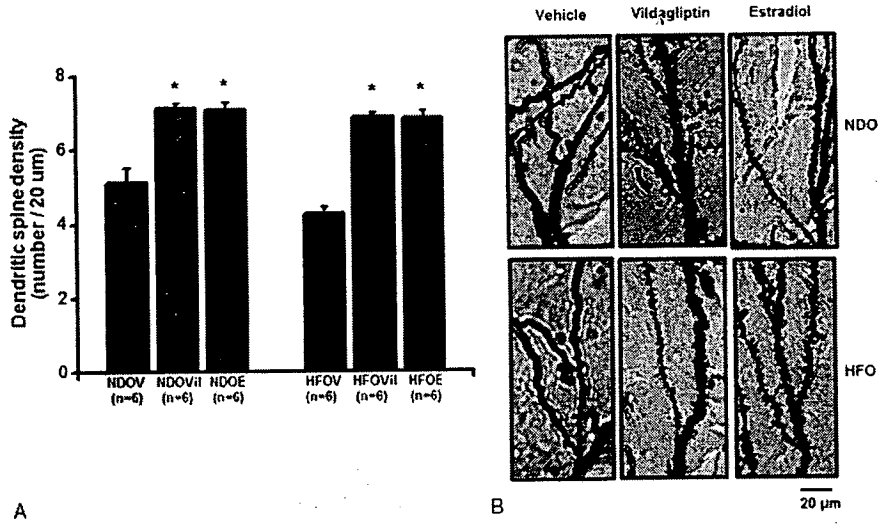


FIG. 5. The effects of vildagliptin and estrogen administration on (**A**) the number of dendritic spines on tertiary apical dendrites in brains harvested from the NDOV, NDOVil, NDOE, HFOV, HFOVil, and HFOE rats; (**B**) a picture of a representative dendritic spines from the NDOV, NDOVil, NDOE, HFOV, HFOVil, and HFOE rats. $^{*}P < 0.05$ compared with the vehicle group; n = 6/group. HF, high-fat diet; HFOE, ovariectomized HF-fed rats with estradiol administration; HFOV, ovariectomized HF-fed rats with vehicle treatment; HFOVil, ovariectomized HF-fed rats with vildagliptin administration; ND, normal diet; NDOE, ovariectomized ND-fed rats with estradiol administration; NDOV, ovariectomized ND-fed rats with vehicle administration; NDOVil, ovariectomized ND-fed rats with vildagliptin administration; NDO, ovariectomized ND-fed rats; HFO, ovariectomized HF-fed rats.

and the rise in brain oxidative stress levels in ND-fed rats, but not in HF-fed rats; (5) neither obesity or estrogen deprivation without cardiac I/R injury increased Aβ or APP levels; (6) cardiac I/R injury caused the accumulation of Aβ and APP in all groups; (7) and estrogen and DPP-4 inhibitor treatments equally attenuated brain oxidative stress levels, decreased Aβ production, and increased dendritic spine density in the ovariectomized ND-fed rats and the ovariectomized HF-fed rats with cardiac I/R injury.

Our findings showed that ovariectomy increased peripheral insulin resistance, brain oxidative stress levels, and dendritic spine loss, and obesity aggravated these impairments in ovariectomized rats. Previous studies have demonstrated that peripheral insulin resistance and oxidative stress are known to play an important role in the impairment of dendritic spine density via the reduction of brain-derived neurotrophic factor (BDNF) level and excessive synaptic depression.[5,24] As a result, the highest levels of peripheral insulin resistance and brain oxidative stress found in ovariectomized HF-fed rats in this study could lead to a marked increase in dendritic spine loss, when compared with the sham-operated ND-fed rats and the ovariectomized ND-fed rats.

This is also the first study to demonstrate that cardiac I/R injury aggravated brain oxidative stress, increased Aβ protein expression, increased APP protein expression, and decreased dendritic spine density as observed in the sham-operated ND-fed rats (Figs. 2 and 3). It has been demonstrated that excessive brain oxidative stress levels cause cognitive decline via increased Aβ production, which leads to decreased dendritic spine density in Alzheimer's diseases.[4-6] As a result, cardiac I/R injury by itself, in sham-operated ND-fed rats, could cause increased brain oxidative stress levels, leading to increased Aβ and APP production, and decreased dendritic spine density, as found in this study. Under conditions of estrogen deprivation, our results showed that cardiac I/R injury aggravates this brain toxicity only in ND-fed rats, but not in HF-fed rats. The possible explanation could be due to the severity of brain toxicity in ovariectomized HF-fed rats, which may have already reached maximum levels, before cardiac I/R injury occurred. This is supported by the findings that the levels of oxidative stress was more severe in ovariectomized HF-fed rats, compared with ovariectomized ND-fed rats, even before cardiac I/R injury.

Interestingly, under conditions of cardiac I/R injury, we found that E_2 and vildagliptin treatments significantly reduced brain oxidative stress, Aβ production, and increased dendritic spine density in both ovariectomized ND-fed rats and HF-fed rats (Figs. 4 and 5). Both E_2 and vildagliptin have been shown to exert antioxidant effects in several models including conditions of obesity, ovariectomy, and cardiac I/R injury.[25-27] Therefore, E_2 and vildagliptin could have acted as antioxidant agents, thus decreasing brain oxidative stress levels in ovariectomized ND-fed rats and HF-fed rats with cardiac I/R injury. This decrement caused the reduction in Aβ production in the brain, which ultimately leads to the prevention of dendritic spine loss.

Potential clinical value

The objective of this animal model was to understand brain pathology (brain oxidative stress, Aβ production, and dendritic spine loss) caused by cardiac I/R injury in both lean and obese estrogen-deprived models. Cardiac I/R injury is a common pathological state that occurs in postmenopausal women. This study demonstrated that it can lead to not only myocardial damage but also increased brain pathology. In

Copyright © 2017 The North American Menopause Society. Unauthorized reproduction of this article is prohibited.

addition, the severity of brain pathology after cardiac I/R injury is associated with obesity, and also estrogen deprivation. This study is the first to report that pharmacological interventions by either estrogen or DPP-4 inhibitor share a similar efficacy in reducing brain pathology caused by cardiac I/R injury in both lean and obese estrogen-deprived model.

Limitations

The limitation of the present study was the lack of investigation into the effects of aged rats on brain pathology caused by cardiac I/R injury in both lean and obese estrogen-deprived model. It is known that ageing affected brain function.[28,29] However, since the main purpose of the present study was to determine the effect of cardiac I/R injury on brain functions in models of estrogen deprivation with or without obesity, we therefore did not use aged rats, so that the ageing-related confounding factors other than estrogen deprivation could be limited. Another limitation of the present study was the lack of investigation into cognitive function. However, previous studies from our group and others already reported the cognitive decline in obesity, and also estrogen-deprived models.[19,20,30]

Furthermore, the phytoestrogen-free chow was not used in this study. However, this small amount of phytoestrogen in our rat chow did not affect serum estrogen levels, which was indicated by a decrease in uterine weight and serum estrogen levels in ovariectomized ND-fed rats. In addition, the HF used in our study also contained similar small amount of phytoestrogen as in the normal-diet chow.

CONCLUSIONS

Our findings demonstrate that cardiac I/R injury itself could cause an increase in brain oxidative burst and a reduction in dendritic spines. In conditions of estrogen deprivation, cardiac I/R injury aggravates brain oxidative stress and increases dendritic spine loss. However, estrogen deprivation with obese-insulin resistance already causes the severest brain toxicity, and therefore is no further affected by the cardiac I/R injury. Since estrogen and DPP-4 inhibitor treatments share similar efficacy on brain protection affected by cardiac I/R injury, DPP-4 inhibitor may be considered as an alternative drug to estrogen replacement in those who have contraindications to the use of estrogen.

REFERENCES

1. Nour M, Scalzo F, Liebeskind DS. Ischemia-reperfusion injury in stroke. *Interv Neurol* 2013;1:185-199.
2. Kalogeris T, Baines CP, Krenz M, Korthuis RJ. Cell biology of ischemia/reperfusion injury. *Int Rev Cell Mol Biol* 2012;298:229-317.
3. Kumfu S, Charununtakorn ST, Jaiwongkam T, Chattipakorn N, Chattipakorn SC. Humanin prevents brain mitochondrial dysfunction in a cardiac ischaemia-reperfusion injury model. *Exp Physiol* 2016;101:697-707.
4. Texel SJ, Mattson MP. Impaired adaptive cellular responses to oxidative stress and the pathogenesis of Alzheimer's disease. *Antioxid Redox Signal* 2011;14:1519-1534.
5. Yu W, Lu B. Synapses and dendritic spines as pathogenic targets in Alzheimer's disease. *Neural Plast* 2012;2012:247150.
6. Butterfield DA, Reed T, Newman SF, Sultana R. Roles of amyloid beta-peptide-associated oxidative stress and brain protein modifications in the pathogenesis of Alzheimer's disease and mild cognitive impairment. *Free Radic Biol Med* 2007;43:658-677.
7. Ross JL, Howlett SE. Age and ovariectomy abolish beneficial effects of female sex on rat ventricular myocytes exposed to simulated ischemia and reperfusion. *PloS One* 2012;7:e38425.
8. Sivasinprasasn S, Shinlapawittayatorn K, Chattipakorn SC, Chattipakorn N. Estrogenic impact on cardiac ischemic/reperfusion injury. *J Cardiovasc Transl Res* 2016;9:23-39.
9. Apaijai N, Chinda K, Palee S, Chattipakorn S, Chattipakorn N. Combined vildagliptin and metformin exert better cardioprotection than monotherapy against ischemia-reperfusion injury in obese-insulin resistant rats. *PloS One* 2014;9:e102374.
10. Wang Y, Wang Q, Zhao Y, et al. Protective effects of estrogen against reperfusion arrhythmias following severe myocardial ischemia in rats. *Circ J* 2010;74:634-643.
11. Li WL, Xiang W, Ping Y. Activation of novel estrogen receptor GPER results in inhibition of cardiocyte apoptosis and cardioprotection. *Mol Med Rep* 2015;12:2425-2430.
12. Pratchayasakul W, Kerdphoo S, Petsophonsakul P, Pongchaidecha A, Chattipakorn N, Chattipakorn SC. Effects of high-fat diet on insulin receptor function in rat hippocampus and the level of neuronal corticosterone. *Life Sci* 2011;88:619-627.
13. Bryzgalova G, Lundholm L, Portwood N, et al. Mechanisms of antidiabetogenic and body weight-lowering effects of estrogen in high-fat diet-fed mice. *Am J Physiol Endocrinol Metab* 2008;295:E904-E912.
14. Apaijai N, Inthachai T, Lekawanvijit S, Chattipakorn SC, Chattipakorn N. Effects of dipeptidyl peptidase-4 inhibitor in insulin-resistant rats with myocardial infarction. *J Endocrinol* 2016;229:245-258.
15. Pratchayasakul W, Chattipakorn N, Chattipakorn SC. Estrogen restores brain insulin sensitivity in ovariectomized non-obese rats, but not in ovariectomized obese rats. *Metabolism* 2014;63:851-859.
16. Pintana H, Pongkan W, Pratchayasakul W, Chattipakorn N, Chattipakorn SC. Dipeptidyl peptidase 4 inhibitor improves brain insulin sensitivity, but fails to prevent cognitive impairment in orchiectomy obese rats. *J Endocrinol* 2015;226:M1-M11.
17. Sivasinprasasn S, Sa-Nguanmoo P, Pongkan W, Pratchayasakul W, Chattipakorn SC, Chattipakorn N. Estrogen and DPP4 inhibitor, but not metformin, exert cardioprotection via attenuating cardiac mitochondrial dysfunction in obese insulin-resistant and estrogen-deprived female rats. *Menopause* 2016;23:894-902.
18. Gould E, Woolley CS, Frankfurt M, McEwen BS. Gonadal steroids regulate dendritic spine density in hippocampal pyramidal cells in adulthood. *J Neurosci* 1990;10:1286-1291.
19. Leuner B, Mendolia-Loffredo S, Shors TJ. High levels of estrogen enhance associative memory formation in ovariectomized females. *Psychoneuroendocrinology* 2004;29:883-890.
20. Pratchayasakul W, Sa-Nguanmoo P, Sivasinprasasn S, et al. Obesity accelerates cognitive decline by aggravating mitochondrial dysfunction, insulin resistance and synaptic dysfunction under estrogen-deprived conditions. *Horm Behav* 2015;72:68-77.
21. Matthews DR, Hosker JP, Rudenski AS, Naylor BA, Treacher DF, Turner RC. Homeostasis model assessment: insulin resistance and beta-cell function from fasting plasma glucose and insulin concentrations in man. *Diabetologia* 1985;28:412-419.
22. Candan N, Tuzmen N. Very rapid quantification of malondialdehyde (MDA) in rat brain exposed to lead, aluminium and phenolic antioxidants by high-performance liquid chromatography-fluorescence detection. *Neurotoxicology* 2008;29:708-713.
23. Sripetchwandee J, Pipatpiboon N, Pratchayasakul W, Chattipakorn N, Chattipakorn SC. DPP-4 inhibitor and PPARgamma agonist restore the loss of CA1 dendritic spines in obese insulin-resistant rats. *Arch Med Res* 2014;45:547-552.
24. Stranahan AM, Norman ED, Lee K, et al. Diet-induced insulin resistance impairs hippocampal synaptic plasticity and cognition in middle-aged rats. *Hippocampus* 2008;18:1085-1088.
25. Moosmann B, Behl C. The antioxidant neuroprotective effects of estrogens and phenolic compounds are independent from their estrogenic properties. *Proc Natl Acad Sci U S A* 1999;96:8867-8872.
26. Abdelsalam RM, Safar MM. Neuroprotective effects of vildagliptin in rat rotenone Parkinson's disease model: role of RAGE-NFkappaB and Nrf2-antioxidant signaling pathways. *J Neurochem* 2015;133:700-707.

© 2017 The North American Menopause Society

Copyright © 2017 The North American Menopause Society. Unauthorized reproduction of this article is prohibited.

27. El Batsh MM, El Batch MM, Shafik NM, Younos IH. Favorable effects of vildagliptin on metabolic and cognitive dysfunctions in streptozotocin-induced diabetic rats. *Eur J Pharmacol* 2015;769:297-305.
28. Smith CC, Vedder LC, Nelson AR, Bredemann TM, McMahon LL. Duration of estrogen deprivation, not chronological age, prevents estrogen's ability to enhance hippocampal synaptic physiology. *Proc Natl Acad Sci U S A* 2010;107:19543-19548.
29. Lagunas N, Calmarza-Font I, Diz-Chaves Y, Garcia-Segura LM. Long-term ovariectomy enhances anxiety and depressive-like behaviors in mice submitted to chronic unpredictable stress. *Horm Behav* 2010;58:786-791.
30. Pintana H, Apaijai N, Pratchayasakul W, Chattipakorn N, Chattipakorn SC. Effects of metformin on learning and memory behaviors and brain mitochondrial functions in high fat diet induced insulin resistant rats. *Life Sci* 2012;91:409-414.

Copyright © 2017 The North American Menopause Society. Unauthorized reproduction of this article is prohibited.

เอกสารแนบหมายเลข 3

NRC Research Press

ARTICLE

Impaired mitochondria and intracellular calcium transients in the salivary glands of obese rats

Jitjiroj Ittichaicharoen, Nattayaporn Apaijai, Pongpan Tanajak, Piangkwan Sa-nguanmoo, Nipon Chattipakorn, and Siriporn C. Chattipakorn

Appl. Physiol. Nutr. Metab. Downloaded from www.nrcresearchpress.com by 110.171.135.216 on 03/17/17
For personal use only.

Abstract: Long-term consumption of a high-fat diet (HFD) causes not only obese-insulin resistance, but is also associated with mitochondrial dysfunction in several organs. However, the effect of obese-insulin resistance on salivary glands has not been investigated. We hypothesized that obese-insulin resistance induced by HFD impaired salivary gland function by reducing salivation, increasing inflammation, and fibrosis, as well as impairing mitochondrial function and calcium transient signaling. Male Wistar rats (200–220 g) were fed either a ND or an HFD (n = 8/group) for 16 weeks. At the end of week 16, salivary flow rates, metabolic parameters, and plasma oxidative stress were determined. Rats were then sacrificed and submandibular glands were removed to determine inflammation, fibrosis, apoptosis, mitochondrial function and dynamics, and intracellular calcium transient signaling. Long-term consumption of an HFD caused obese-insulin resistance and increased oxidative stress, fibrosis, inflammation, and apoptosis in the salivary glands. In addition, impaired mitochondrial function, as indicated by increased mitochondrial reactive oxygen species, mitochondrial membrane depolarization, and mitochondrial swelling in salivary glands and impaired intracellular calcium regulation, as indicated by a reduced intracellular calcium transient rising rate, decay rates, and amplitude of salivary acinar cells, were observed in HFD-fed rats. However, salivary flow rate and level of aquaporin 5 protein were not different between both groups. Although HFD consumption did not affect salivation, it caused obese-insulin resistance, leading to pathophysiological alteration of salivary glands, including impaired intracellular calcium transients, increased oxidative stress and inflammation, and salivary mitochondrial dysfunction.

Key words: insulin, obesity, metabolic syndrome, salivary gland function, mitochondria.

Résumé : La consommation à long terme d'aliments riches en gras (« HFD ») n'entraîne pas seulement l'insulinorésistance liée à l'obésité, mais est aussi associée au dysfonctionnement mitochondrial dans plusieurs organes. Toutefois, il n'y a pas d'études à propos de l'insulinorésistance liée à l'obésité et les glandes salivaires. Nous posons l'hypothèse selon laquelle l'insulinorésistance liée à l'obésité et causée par un HFD entrave le fonctionnement de la glande salivaire en diminuant la salivation, augmentant l'inflammation et la fibrose et en altérant la fonction mitochondriale et la signalisation du calcium transitoire. On soumet des rats mâles Wistar (200–220 g) à un régime normal ou HFD (n = 8/groupe) durant 16 semaines. À la fin de la 16e semaine, on mesure le débit de salive, des variables métaboliques et le stress oxydatif dans le plasma, puis on sacrifie les rats et on prélève les glandes sous-maxillaires pour la détermination de l'inflammation, de la fibrose, de l'apoptose, de la fonction et de la dynamique mitochondriale de même que de la signalisation du calcium transitoire intracellulaire. La consommation à long terme de HFD entraîne l'insulinorésistance liée à l'obésité, l'augmentation du stress oxydatif, la fibrose, l'inflammation et l'apoptose dans les glandes salivaires. De plus, on observe chez les rats à l'alimentation HFD une altération de la fonction mitochondriale comme le révèlent l'augmentation des espèces réactives de l'oxygène dans la mitochondrie, la dépolarisation de la membrane mitochondriale et un œdème mitochondrial dans les glandes salivaires; on observe aussi un trouble de la régulation du calcium intracellulaire comme le révèlent la diminution du taux d'augmentation du calcium transitoire, du taux de décroissance et de la grosseur des cellules acineuses. Le taux d'écoulement salivaire et la concentration de la protéine aquaporine 5 ne diffèrent pas d'un groupe à l'autre. Même si la consommation de HFD ne modifie pas la salivation, elle entraîne l'insulinorésistance liée à l'obésité d'où découle une altération pathophysiologique des glandes salivaires : dérèglement du calcium transitoire intracellulaire, augmentation du stress oxydatif et de l'inflammation et dysfonctionnement mitochondrial de la salive. [Traduit par la Rédaction]

Mots-clés : insuline, obésité, syndrome métabolique, fonction des glandes salivaires, mitochondrie.

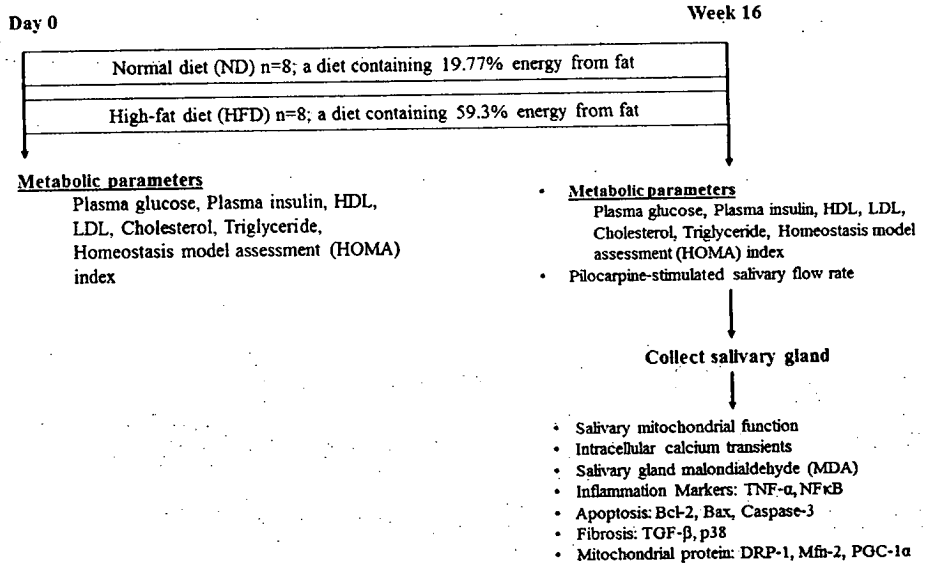
Introduction

Obesity is rapidly becoming a prevalent condition in many countries around the world (Kitzinger and Karle 2013). Several studies have demonstrated that obesity leads to insulin resistance, which contributes to the development of metabolic syndrome, type 2 diabetes mellitus (T2DM), various cardiovascular diseases, and some neurodegenerative disorders (Pereira et al. 2009; Tremblay et al. 2011). Furthermore, a study by Goldman and Julian showed

Received 30 September 2016. Accepted 14 December 2016.

J. Ittichaicharoen and S.C. Chattipakorn. Department of Oral Biology and Diagnostic Sciences, Faculty of Dentistry, Neurophysiology Unit, Cardiac Electrophysiology Research and Training Center, Faculty of Medicine, Center of Excellence in Cardiac Electrophysiology Research, Chiang Mai University, Chiang Mai, 50200, Thailand.
N. Apaijai. Neurophysiology Unit, Cardiac Electrophysiology Research and Training Center, Faculty of Medicine, Center of Excellence in Cardiac Electrophysiology Research, Chiang Mai University, Chiang Mai, 50200, Thailand.
P. Tanajak, P. Sa-nguanmoo, and N. Chattipakorn. Neurophysiology Unit, Cardiac Electrophysiology Research and Training Center, Faculty of Medicine, Department of Physiology, Faculty of Medicine, Center of Excellence in Cardiac Electrophysiology Research, Chiang Mai University, Chiang Mai, 50200, Thailand.
Corresponding author: Siriporn C. Chattipakorn (email: scchattipakorn@gmail.com).
Copyright remains with the author(s) or their institution(s). Permission for reuse (free in most cases) can be obtained from RightsLink.

Fig. 1. The experimental protocol of the present study. HDL, high-density lipoprotein; LDL, low-density lipoprotein; NFκB, nuclear factor kappa B; TGF-β, transforming growth factor beta; TNF-α, tumor necrosis factor alpha.



that pseudo-Sjögren's syndrome, which is characterized by persistent dry mouth and eyes, has developed in obese subjects (Goldman and Julian 1977). The pathogenesis of Sjögren's syndrome is chronic inflammation, leading to the destruction of exocrine glands including the salivary glands (Gannot et al. 2000). Our previous studies demonstrated that 12–16 weeks of consumption of a high-fat diet (HFD) caused obesity and the development of peripheral insulin resistance, leading to increased oxidative stress and impaired mitochondrial function in several vital organs such as the heart and the brain (Apaijai et al. 2013; Pintana et al. 2013; Pipatpiboon et al. 2013). In addition, a previous study demonstrated that after 5 weeks on an HFD, rats developed peripheral insulin resistance and increased levels of oxidative stress in their submandibular glands (Zalewska et al. 2013). A high level of oxidative stress caused intracellular calcium transient impairment in isolated salivary gland epithelial cells (Al-Rawi 2011). Since intracellular calcium transient regulation is important in controlling salivary secretion, an impairment of intracellular calcium transients could be associated with the development of salivary gland dysfunction (Ambudkar 2014; Proctor and Carpenter 2014).

In most cells, mitochondria are the major source of the reliable investigative measurement of oxidative stress by recording reactive oxygen species (ROS) (Rabøl et al. 2006; Park et al. 2011). As they control cell survival and death, which they do in response to the changes of environment through the mitochondrial fission and fusion process, mitochondria are vital dynamic organelles (Ni et al. 2015). Also since they are the powerhouses of the cells, impairment of mitochondrial function could ultimately lead to organ dysfunction including that of salivary glands. To date, however, the effect of obese-insulin resistance on salivary gland function, including salivary flow rate, intracellular calcium transient signaling, inflammation, oxidative stress, fibrosis, mitochondrial function and dynamics, and apoptosis has never been investigated. Therefore, the present study aims to investigate the effect of obese-insulin resistance induced by HFD consumption on those parameters in the salivary glands. The hypothesis is that long-term HFD consumption impairs salivary gland function by reducing salivary flow rate, increases inflammation, oxidative stress, fibrosis, apoptosis, and impairs mitochondrial function and dynamics, as well as reducing intracellular calcium transient signaling.

Materials and methods

All experimental protocols were approved by the Faculty of Medicine, Chiang Mai University Institutional Animal Care and Use Committee (permit no. 32/2557), in compliance with ethical standards for research involving animals in accordance with National Institutes of Health and ARRIVE guidelines for reporting experiments involving animals. Sixteen male Wistar rats weighing 200–220 g were purchased from the National Animal Center, Salaya Campus, Mahidol University, Thailand. The rats were housed in a temperature-controlled environment under a 12-h light/12-h dark cycle. After acclimatization, rats were randomly divided into 2 dietary groups (n = 8 per group) and for 16 weeks were given either a normal-diet (ND; 19.77% energy from fat), or an HFD (59.28% energy from fat) (Pratchayasakul et al. 2011). The ND was a standard laboratory chow (Mouse Feed Food No. 082, C.P. Company, Bangkok, Thailand), while the HFD consisted of the standard rat diet, casein (250 g/kg food), lard (310 g/kg food), cholesterol (10 g/kg food), vitamins (60 g/kg food), DL-methionine (3 g/kg food), yeast powder (1 g/kg food), and sodium chloride (1 g/kg food). Therefore, the major source of fat in the present study was saturated fatty acids, derived from lard (Pratchayasakul et al. 2011; Pipatpiboon et al. 2012). Body weight and food intake were recorded weekly. Blood samples were collected from the tail vein at week 0 (to give baseline data) and week 16 to determine metabolic parameters. The visceral fat, including mesenteric fat, perirenal fat, retroperitoneal fat, and epididymal fat were removed after the animal was sacrificed. Then, the total visceral fat was determined using a high-precision balance (Pratchayasakul et al. 2011; Pipatpiboon et al. 2012). The experimental protocol is shown in Fig. 1.

Salivary flow rate determination

At the end of week 16, rats were anesthetized using a combination of 50 mg/kg of Zoletil (Virbac Laboratories, Carros, France) and 0.15 mg/kg of Xylazine (Laboratorios Calier, Barcelona, Spain) via intraperitoneal injection. To determine stimulated salivary flow rate, saliva was collected at 10 min after pilocarpine (Alcon Laboratories, Tex., USA) administration (2 mg/kg, intraperitoneal injection) (Fedirko et al. 2006).

Appl. Physiol. Nutr. Metab. Downloaded from www.nrcresearchpress.com by 110.171.135.216 on 03/11/17
For personal use only.

Appl. Physiol. Nutr. Metab. Downloaded from www.nrcresearchpress.com by 110.171.135.216 on 03/17/17
For personal use only.

Chemical analysis of metabolic parameters

At baseline (week 0) and at week 16 of HFD consumption, blood samples were drawn from the tail vein, and plasma samples were collected for chemical analysis of metabolic parameters. Fasting plasma glucose, cholesterol, and triglyceride levels were determined using a colorimetric assay kit (ERBA diagnostic, Mannheim, Germany). Fasting plasma high-density lipoprotein (HDL) levels were determined using a commercial colorimetric assay kit (Biovision, Calif., USA). Plasma low-density lipoprotein (LDL) levels were calculated using Friedewald's equation (Martin et al. 2013). Fasting plasma insulin levels were evaluated using a commercial sandwich enzyme-linked immunosorbent assay (ELISA) kit (Millipore, Mich., USA). The severity of peripheral insulin resistance was assessed using the homeostatic model assessment (HOMA) index as described previously (Pratchayasakul et al. 2011; Pipatpiboon et al. 2012). An oral glucose tolerance test (OGTT) was performed, and the area under the curves (AUCs) were calculated to determine insulin sensitivity (Pipatpiboon et al. 2013).

Preparation of isolated salivary acinar cells for the measurement of calcium transients

Rat salivary acinar cells were isolated from the submandibular gland as described in a previous study (Pringle et al. 2011). To investigate salivary acinar cell calcium transients, cells were incubated with 25 μmol/L Fura-2/AM (Sigma–Aldrich, Mass., USA) in 37 °C for 30 min. Fura-2 was excited at the wavelengths of 340 nm and 387 nm, and emitted at a wavelength of 500 nm. The ratio of fluorescent intensity from Fura-2 was recorded as the index of intracellular calcium transients (Cell R, Olympus, Tokyo, Japan). The intracellular calcium transient parameters, including the Ca^{2+} transient amplitude, the Ca^{2+} transient rising rate, the maximum Ca^{2+} transient decay rates (maximum slope of Ca^{2+} transient decay), the average Ca^{2+} transient decay rates (the slope of Ca^{2+} transient decay measured from the peak to the end of each Ca^{2+} transient cycle), and the diastolic Ca^{2+} level, were measured.

Salivary mitochondrial isolation and mitochondrial function determination

To determine mitochondrial function of the salivary glands, we evaluated mitochondrial ROS production, mitochondrial membrane potential ($\Delta\Psi m$), and mitochondrial swelling as described previously (Apaijai et al. 2013). Briefly, a submandibular gland was homogenized with 10 mL of the isolating buffer, comprising 300 mmol/L sucrose, 5 mmol/L *N*-[tris(hydroxymethyl)-methyl]-2-aminoethanesulfonic sodium salt, and 0.2 mmol/L ethylene glycol tetraacetic acid. The homogenized sample then was centrifuged at 800*g* for 5 min. The supernatant was collected and centrifuged at 8800*g* for 5 min. The pellet was resuspended in a respiration buffer containing 50 mmol/L sucrose, 100 mmol/L KCl, 10 mmol/L HEPES, and 5 mmol/L KH_2PO_4. This isolated solution was ready for further mitochondrial function investigation.

Salivary mitochondrial ROS production was investigated by adding 2 mmol/L 2′7′-dichlorfluorescein-diacetate dye into the isolated salivary mitochondrial solution and being incubated at 25 °C for 20 min. The ROS production was detected at λ_{ex} 485 nm and detected at λ_{em} 530 nm using a fluorescent microplate reader (BioTek Instruments, Winooski, Vt., USA).

The salivary mitochondrial membrane potential change was determined by incubating the isolated salivary mitochondrial solution with 5 mmol/L 5,5′,6,6′-tetrachloro-1,1′,3,3′-tetra ethylbenzimidazolcarbocyanine iodide (JC-1) dye at 37 °C for 30 min, and then the fluorescence intensity was detected by using a fluorescent microplate reader. The decrease in the red/green fluorescence intensity ratio was considered to be an indicator of salivary mitochondrial membrane depolarization.

The salivary mitochondrial swelling was determined by measuring the absorbance every minute for 30 min using a spectrophotometer. The isolated salivary mitochondria (0.4 mg/mL) were incubated in 1.5 mL of respiration buffer (containing 100 mmol/L KCl, 50 mmol/L sucrose, 10 mmol/L HEPES, 5 mmol/L KH_2PO_4, pH 7.4) at room temperature. The absorbance of mitochondrial suspension was used to determine salivary mitochondrial swelling using a spectrophotometer for 30 min at 540 nm. The mitochondrial absorbance at 30 min was normalized with the absorbance at the first minute. The decrease in $absorbance_{30min}/absorbance_{0min}$ demonstrated the increase of mitochondrial swelling (Yarana et al. 2012; Apaijai et al. 2013; Sripetchwandee et al. 2014). Mitochondrial morphology was determined using transmission electron microscopy.

Measurement of tumor necrosis factor alpha (TNF-α) levels in the salivary glands

The TNF-α levels in the submandibular glands were measured using monoclonal mouse anti-rat TNF-α monoclonal antibodies from a commercial immunoassay kit (Biosource International, Calif., USA) (Ben-Ari et al. 2002).

Determination of submandibular gland malondialdehyde (MDA) levels

Submandibular gland MDA was measured using an HPLC-based assay kit (Thermo Scientific, Bangkok, Thailand). Homogenized submandibular glands were added to H_3PO_4 and thiobarbituric acid (TBA) to produce TBA reactive substances (TBARS). Then the submandibular gland TBARS concentration was determined in accordance with standard curve (Apaijai et al. 2013).

Western blot analysis

Fifty to 80 μg of the total protein isolated from the submandibular glands were mixed with a loading buffer (5% betamercaptoethanol, 0.05% bromophenol blue, 75 mmol/L Tris-HCl (pH 6.8), 2% sodium dodecyl sulfate (SDS) and 10% glycerol), and loaded onto 10% SDS-acrylamide gels. Then, the proteins were separated by electrophoresis and transferred on to nitrocellulose membranes as previously described (Pratchayasakul et al. 2011). Immunoblotting was conducted with mouse polyclonal anti-rat nuclear factor kappa B (NFκB) p65 (no. 8242), phosphorylated NFκB (p-NFκB) $p65^{ser536}$ (no. 3031), transforming growth factor beta (TGF-β) (no. 3711), total p-38 (no. 9212), p-$p38^{Thr180/Tyr182}$ (no. 9211), Bcl-2 (no. 2876), Mfn-2 (no. 9482), DRP-1 (no. 8570), pro-caspase 3 (no. 9662), cleaved-caspase 3^{asp175} (no. 9661) (1:1 000 dilution; Cell Signaling Technology, Mass., USA), Bax (no. sc-493; 1:1 000 dilution), proliferator-activated receptor gamma coactivator 1 alpha (PGC-1α) (no. sc13067; 1:200 dilution), β-actin (no. sc.47778; 1:2 000 dilution) (Santa Cruz Biotechnology, Calif., USA), and polyclonal anti-rabbit Aquaporin 5 (AQP5) (no. ab78486; 1:500 dilution) (Abcam, Cambridge, Mass., USA). Horseradish peroxidase conjugated with anti-rabbit IgG (no. 7074, 7076; 1:2 000 dilution, Cell Signaling Technology) was used to detect the bound antibodies. The membranes were exposed to enhanced chemiluminescence Western blotting substrate (Bio-Rad Laboratories, Calif., USA) and the densitometric analysis was performed using the ChemiDoc Touch Imaging system (Bio-Rad Laboratories).

Fibrosis analysis

At the end of experiment, the salivary glands were fixed in 4% paraformaldehyde, embedded in paraffin, and then sliced into 10-μm thick slices. The slices were stained with picrosirius red (Aperio, Calif., USA) to enable the amount of collagen in the salivary gland tissue to be quantified. An increase in collagen deposits in the salivary gland tissue indicates a proportional increase in the severity of fibrosis. Then the histopathological pictures were analyzed using Image J program (Lekawanvijit et al. 2012; Inthachai et al. 2015; Apaijai et al. 2016).

Statistical analysis

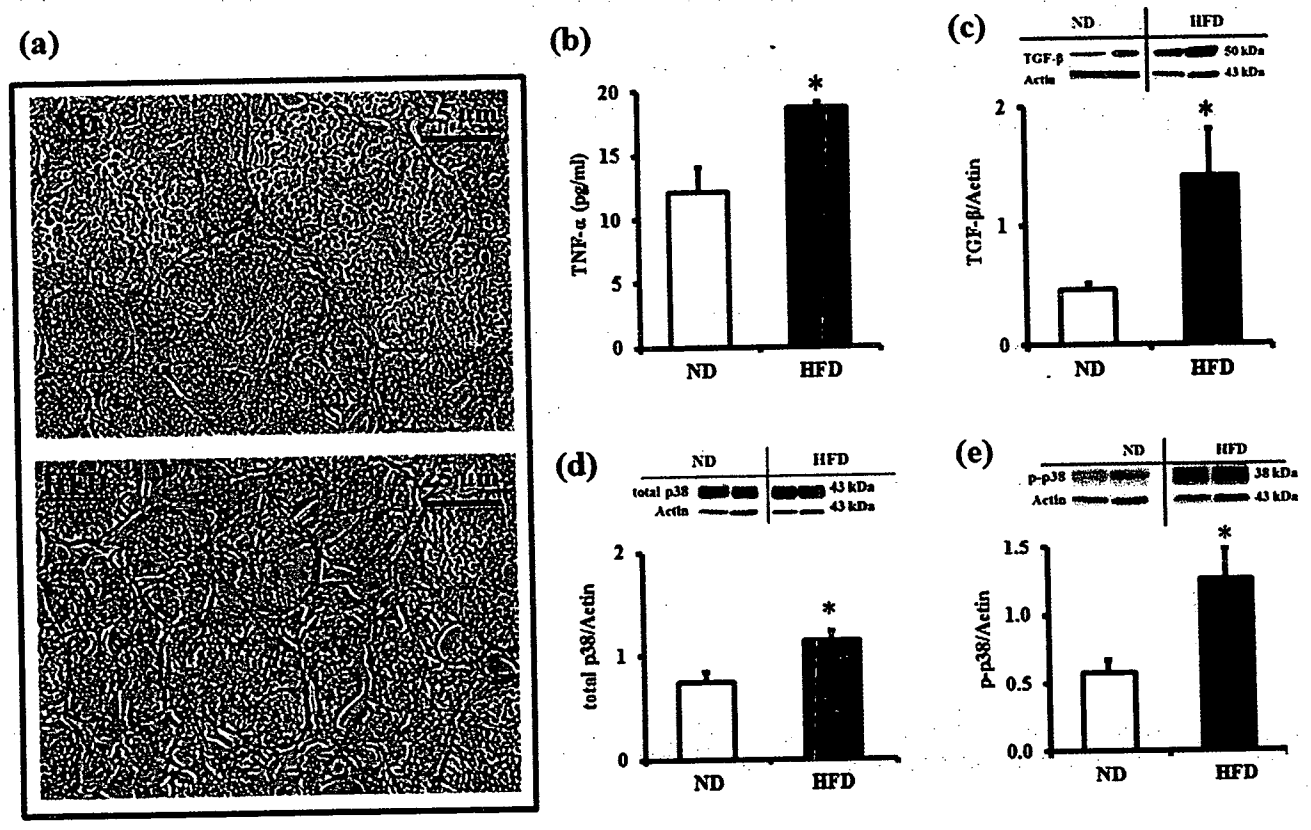
Data were expressed as means ± SE. Independent *t* tests were used to test the statistical differences between the groups. $p < 0.05$ was accepted as a measure of confidence limits between groups.

Table 1. The effects of HFD consumption on peripheral insulin sensitivity parameters, MDA level, and salivary flow rate in rats fed an ND or a HFD for 16 weeks.

	Baseline		Week 16	
Parameters	ND	HFD	ND	HFD
Body weight (g)	200±3	220±3	371.43±13.05	607.50±12.50*
Plasma insulin (ng/mL)	2.59±0.45	2.42±0.39	1.96±0.51	5.38±3.15*
Plasma glucose (mg/dL)	138.01±3.90	135.86±4.48	116.36±10.19	118.81±21.46
OGTT ($mg \cdot dL^{-1} \cdot min^{-1} \cdot 10^{-4}$)	—	—	4.6±0.2	6.7±0.3*
HOMA index	13.57±1.98	12.17±2.47	10.35±3.46	26.04±10.80*
Plasma total cholesterol (mg/dL)	67±3	65±3	81.39±6.31	112.74±19.78*
HDL cholesterol (mg/dL)	31.1±1	29.94±0.7	35.39±1.44	28.42±1.99*
LDL cholesterol (mg/dL)	31.26±7	33.9±7	52.78±4.42	75.44±5.34*
Plasma triglyceride (mg/dL)	47.45±3.70	47.17±4.53	56.54±10.37	56.15±5.05
Visceral fat weight (g)	—	—	8.18±4.58	48.91±5.19*
Salivary gland MDA levels (mmol/mL)	—	—	1.28±0.34	5.57±3.19*
Stimulated salivary flow rate (mL/min)	—	—	0.06±0.004	0.04±0.003

Note: HDL, high-density lipoprotein; HFD, high-fat diet; HOMA, homeostatic model assessment; LDL, low-density lipoprotein; MDA, malondialdehyde; ND, normal diet; OGTT, oral glucose tolerance test. *, $p < 0.05$ vs. ND group.

Fig. 2. The effects of 16-week HFD consumption on inflammation and fibrosis in salivary glands. (*a*) Picrosirius red staining to determine submandibular gland fibrosis, (*b*) TNF-α, (*c*) TGF-β, (*d*) total p38 and (*e*) p-p38 (*, $p < 0.05$ vs. ND group). HFD, high-fat diet; ND, normal diet; TGF-β, transforming growth factor beta; TNF-α, tumor necrosis factor alpha. [Color online.]



Results

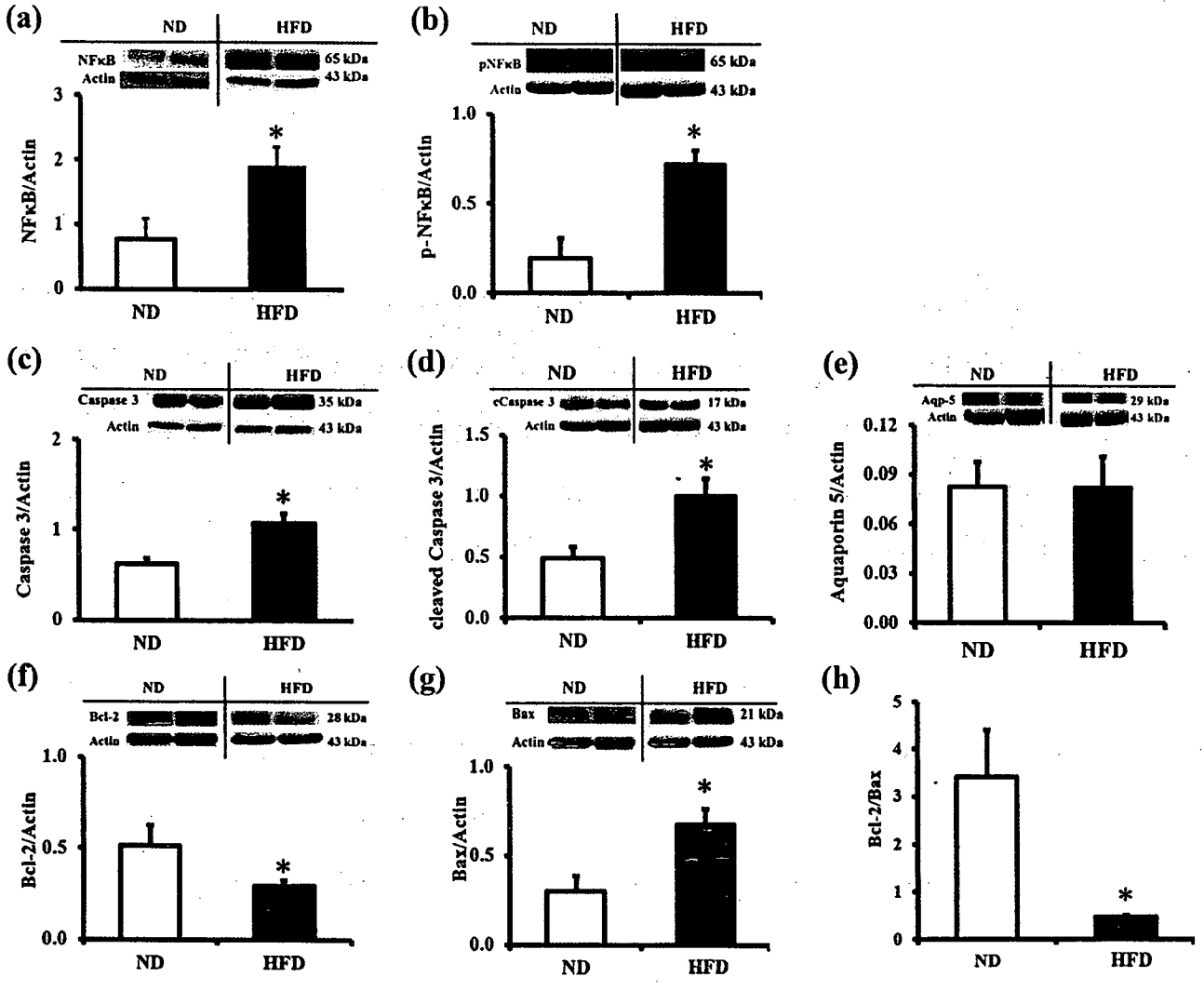
Chronic HFD consumption caused not only obese-insulin resistance, but also increased submandibular gland oxidative stress without alteration of the salivary flow rate

At the baseline levels (week 0), there were no differences in all metabolic parameters between ND and HFD groups (Table 1). After 16 weeks of the dietary regimen, the HFD-fed rats had significantly increased body weight, visceral fat, total plasma cholesterol levels, plasma LDL levels, plasma insulin levels, plasma glucose AUC during OGTT and HOMA index, compared with the rats fed an ND. Plasma HDL levels were lower in HFD-fed rats compared with ND-fed rats ($p < 0.05$, Table 1). However, plasma glucose level was no different between the groups (Table 1). This condition of hyperinsulinemia with euglycemia indicated an insulin-resistant status. Although HFD rats had altered metabolic parameters, their salivary flow rates were not significantly different from those observed in ND-fed rats (Table 1). However, the submandibular gland MDA was increased in HFD-fed rats. These findings indicate that 16-weeks of HFD consumption caused obese-insulin resistance and increased oxidative stress in the salivary glands without any changes in salivary flow rate.

Appl. Physiol. Nutr. Metab. Downloaded from www.nrcresearchpress.com by 110.171.135.216 on 03/11/11
For personal use only.

Appl. Physiol. Nutr. Metab. Downloaded from www.nrcresearchpress.com by 110.171.135.216 on 03/17/17
For personal use only.

Fig. 3. The effects of 16 weeks of high-fat diet (HFD) consumption on inflammation and apoptosis in salivary glands. (*a*) Nuclear factor kappa B (NFκB), (*b*) phosphorylated NFκB (p-NFκB), (*c*) pro-caspase 3, (*d*) cleaved-caspase 3, (*e*) aquaporin 5 (Aqp-5), (*f*) Bcl-2, (*g*) Bax, and (*h*) Bcl-2/Bax ratio (*, $p < 0.05$ vs. normal-diet (ND) group).



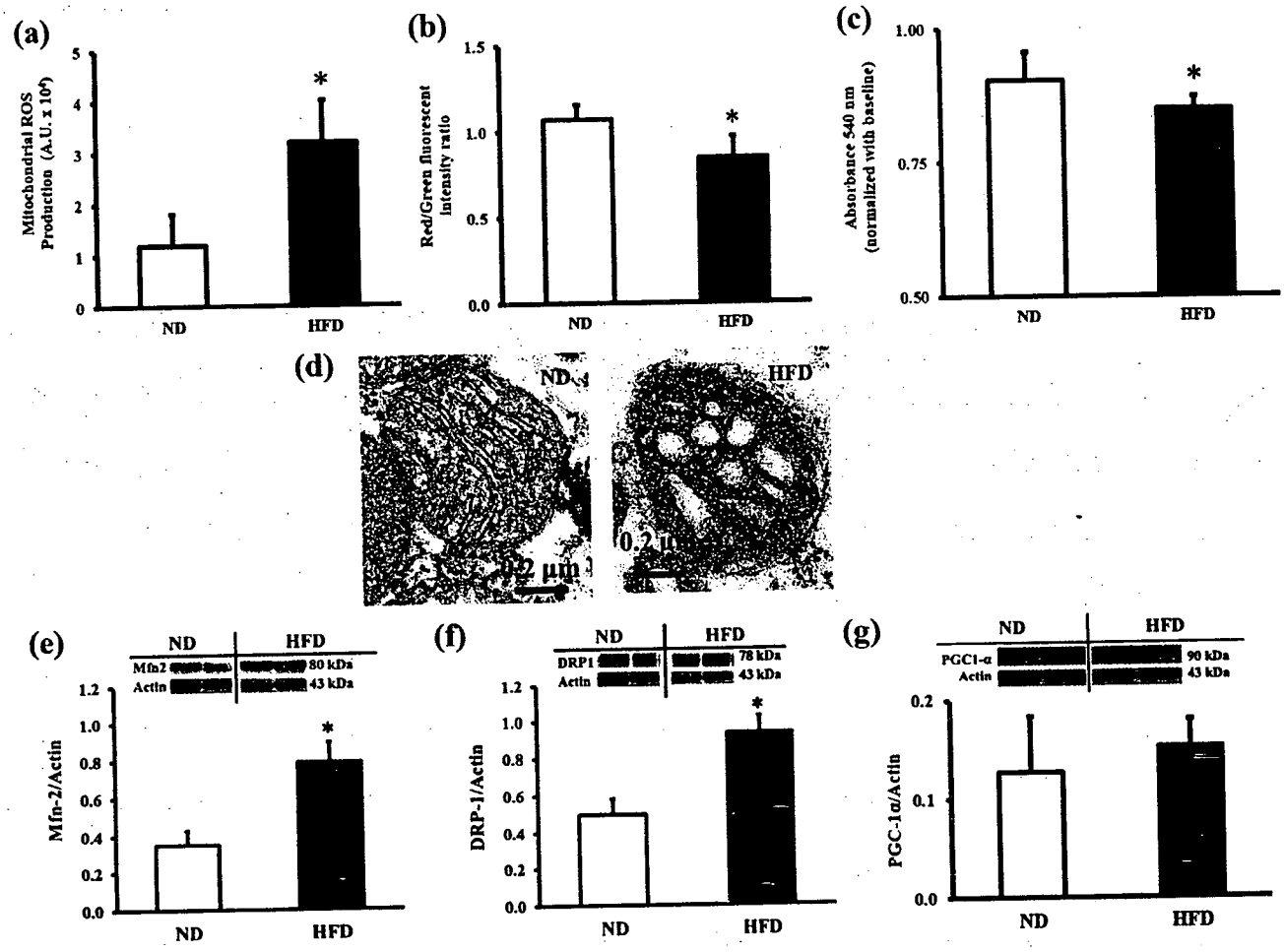
Chronic HFD consumption increased inflammation, fibrosis, and apoptosis, but did not change the expression of AQP5 in the salivary glands

Although the pathological analysis of submandibular fibrosis was not observed in both HFD-fed rats and ND-fed rats (Fig. 2*a*), there were structural changes at the molecular level in the submandibular glands. An increase in systemic inflammation, as indicated by increased plasma TNF-α levels, was observed in HFD-fed rats when compared with ND-fed rats ($p < 0.05$, Fig. 2*b*). In addition, the expression of TGF-β, which is a fibrosis marker, was increased in the submandibular glands of HFD-fed rats when compared with the ND-fed rats ($p < 0.05$, Fig. 2*c*). The present study also determined the downstream signaling of TGF-β, including p-38 as a cellular stress kinases marker and NFκB as a cellular inflammatory marker. Our data demonstrated that both p-p38$^{Thr180/Tyr182}$ (Fig. 2*e*) and p-NFκB^{ser536} (Fig. 3*b*) were increased in HFD-fed rats, when compared with ND-fed rats. The expression of pro-apoptotic markers including caspase 3 and Bax, and an anti-apoptosis marker, Bcl-2, in the submandibular glands were also determined. The results showed that the expression of cleaved-caspase 3 was increased in HFD-fed rats compared with ND-fed rats, suggesting that the apoptotic process occurred in the salivary glands of HFD-fed rats (Fig. 3*d*). Although the expression of Bcl-2 was no different between the groups (Fig. 3*f*), the Bax expression of HFD-fed rats was significantly increased when compared with that of ND-fed rats (Fig. 3*g*). In addition, the Bcl-2 to Bax ratio was significantly reduced in HFD-fed rats compared with ND-fed rats (Fig. 3*h*). These findings suggested that long-term HFD consumption increased inflammation, fibrosis, and apoptosis in salivary glands. To confirm there was no change in salivation between the groups, the expression of AQP5 in salivary glands from both groups was determined. We found that the expression of AQP5 in the salivary glands between ND-fed rats and HFD-fed rats was not different, suggesting similar salivation between both groups (Fig. 3*e*).

Impaired mitochondrial function occurs in the salivary glands of obese-insulin-resistant rats

Submandibular glands of HFD-fed rats showed an increase in mitochondrial ROS production, mitochondrial membrane potential change (i.e., depolarization), and mitochondrial swelling when compared with ND-fed rats ($p < 0.05$, Figs. 4*a*–4*c*). We also found that unfolded cristae were observed in the mitochondria in the submandibular glands of HFD-fed rats compared with those in

Fig. 4. The effects of 16 weeks of high-fat diet (HFD) consumption on salivary gland mitochondrial function and dynamics. (*a*) Salivary reactive oxygen species (ROS) production, (*b*) mitochondrial membrane depolarization, (*c*) mitochondrial swelling, (*d*) mitochondrial morphology, (*e*) Mfn-2 expression, (*f*) DRP-1 expression, and (*g*) proliferator-activated receptor gamma coactivator 1 alpha (PGC-1α) expression (*, $p < 0.05$ vs. normal-diet (ND) group).



ND-fed rats (Fig. 4*d*). Our findings suggest that the HFD-fed rats had salivary gland mitochondrial dysfunction.

In addition, the mitochondrial dynamics of submandibular glands were also determined by measuring a mitochondrial biogenesis marker, PGC-1α, a mitochondrial fission protein, DRP-1, and a mitochondrial fusion protein, Mfn-2. Both Mfn-2 and DRP-1 expression were higher in HFD-fed rats when compared with those of ND-fed rats (Figs. 4*e* and 4*f*), whereas PGC-1α protein expression showed no alteration (Fig. 4*g*). These findings suggest that although impaired mitochondrial function of salivary glands in the obese-insulin–resistant rats' condition occurred, those cells may have a compensatory mechanism in preserving the remaining mitochondria via balancing the mitochondrial fission/fusion process.

A decrease in intracellular calcium transients in salivary acinar cells found in obese-insulin–resistant rats

A decrease in intracellular calcium transients in the salivary acinar cells of HFD-fed rats occurred when compared with ND-fed rats. The calcium transient amplitude, the calcium transient rising rate, and the maximum calcium transient decay rates were decreased in HFD-fed rats levels (Figs. 5*a*–5*c*, 5*e*). However, there were no statistically significant differences in the diastolic calcium levels (Fig. 5*d*). These findings indicate an impairment of intracellular calcium transients in the salivary acinar cells in HFD-fed rats. It has been shown that intracellular calcium transients are required for salivary secretion (Ambudkar 2000; Proctor and Carpenter 2014). However, since the salivation was not altered in this study, it may be possible that the level of severity of intracellular calcium transient dysregulation was not sufficient to cause salivary flow dysfunction in these HFD-fed rats, as indicated by no change in the diastolic calcium levels.

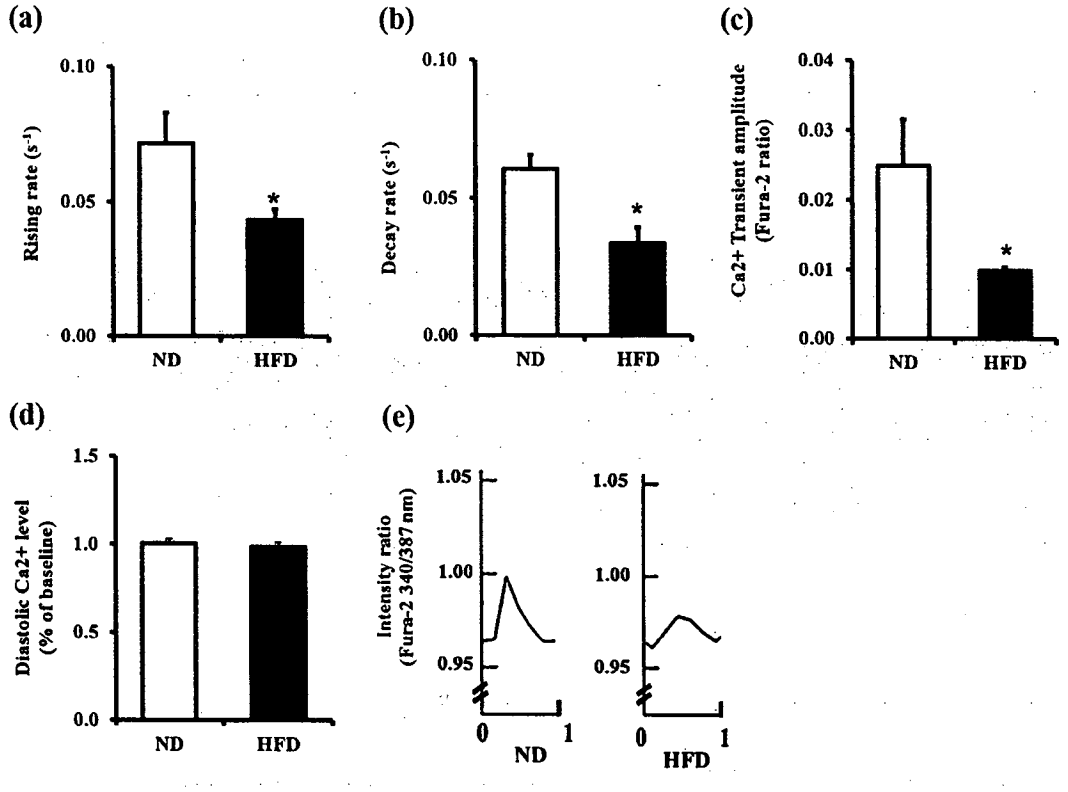
Discussion

The major findings of this study indicate that long-term HFD consumption in Wistar rats could lead to (*i*) obese-insulin resistance; (*ii*) increased oxidative stress, fibrosis, inflammation, and apoptosis in salivary glands; (*iii*) impaired mitochondrial function and mitochondrial dynamics in salivary glands; and (*iv*) impaired intracellular calcium transients in salivary acinar cells; but (*v*) have no effect on salivary flow rate or salivation.

In the present study, rats who were subjected to 16 weeks of HFD consumption developed obese-insulin resistance, as shown by body weight gain along with the characteristics of insulin resistance such as hyperinsulinemia, euglycemia, and higher HOMA index, as well as dyslipidemia. These findings are consistent with our previous studies, demonstrating obese-insulin resistance with cardiac and brain dysfunction following 16 weeks of HFD consumption (Pratchayasakul et al. 2011; Pintana et al. 2013; Sivasinprasasn

Appl. Physiol. Nutr. Metab. Downloaded from www.nrcresearchpress.com by 110.171.133.210 on 05/11/11
For personal use only.

Fig. 5. The effects of 16 weeks of high-fat diet (HFD) consumption on transient calcium signaling in isolated acinar cells from submandibular glands (n = 30 cells per group). (*a*) The rising rate, (*b*) the average Ca^{2+} transient decay rates, (*c*) the Ca^{2+} transient amplitude, (*d*) the diastolic Ca^{2+} level, and (*e*) the characteristic of calcium transient tracing enabling calcium transient parameter determination (*, $p < 0.05$ vs. normal-diet (ND) group).



et al. 2015). Although salivation was not impaired in obese-insulin–resistant rats, deterioration at the molecular level of salivary glands was observed. Our findings showed increased TGF-β, which is a fibrosis marker (Imai et al. 1997; Yamachika et al. 2000; Hall et al. 2010), in the salivary glands of obese-insulin–resistant rats. When TGF-β is activated, it then binds with TGF-β receptors and activates its downstream signaling cascades, including p38 and NFκB (Marber et al. 2011), which were expressed at high rates in the salivary glands of HFD-fed rats. Although the expression of TGF-β and its downstream signaling pathways were upregulated in the salivary glands of HFD-fed rats, the histological features of fibrosis were not exhibited. These findings suggest that in the prediabetic state (i.e., obese-insulin resistance), the severity of metabolic impairment was not sufficient to increase the TGF-β level to the point where it could activate the extracellular matrix deposition in the submandibular glands of obese-insulin–resistant rats. This is supported by previous reports in diabetic models with fibrosis in salivary glands, in which the level of TGF-β was higher than that found in this study (Leask and Abraham 2004; Hall et al. 2010).

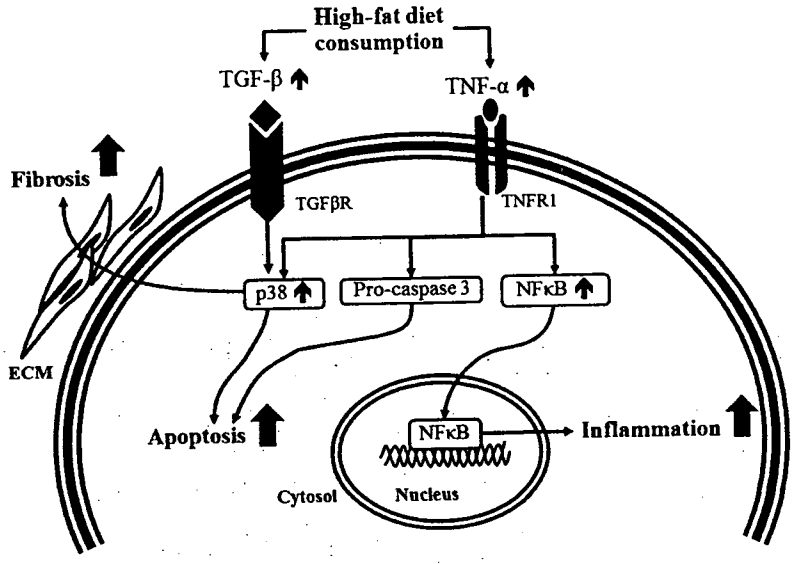
Several studies demonstrated that chronic inflammation in salivary glands, such as Sjögren's syndrome, could activate the p-38 mitogen-activated protein kinaseand NFκB (Kawakami et al. 2007; Ping et al. 2012). Also, there is an in vitro study showing that p38 and NFκB were upregulated in HSY human parotid gland epithelial cell lines treated with saturated fatty acids (Shikama et al. 2013). In addition, it has been shown that NFκB expression increased in response to cellular inflammation (Wellen and Hotamisligil 2005; Esser et al. 2014). Previous studies have shown that NFκB translocated into the nucleus caused an increase in inflammatory gene transcription including TNF-α. This study also confirms those findings, specifically that obese-insulin resistance induced by HFD consumption, led to an increase in inflammation and fibrosis inside salivary glands, as shown by increased TNF-α and NFκB levels (Figs. 2*b* and 3*a*).

It has been shown that both stress and inflammation could initiate cellular apoptosis via increased p38 (Marber et al. 2011). Our results showed that salivary glands of obese-insulin–resistant rats had increased p38 levels as well as increased Bax and caspase 3 expression. These findings indicate that 16 weeks of HFD consumption induced not only insulin resistance, but also systemic inflammation and cellular stress, leading to the activation of the fibrosis-apoptosis pathway in salivary glands through TGF-β and its signaling cascade (as shown in Fig. 6).

Since apoptosis and energy production are regulated by mitochondria (Frank et al. 2001; Maria et al. 2013), we also determined mitochondrial function and dynamics. Our data demonstrated that the mitochondrial function of salivary glands in obese-insulin–resistant rats was impaired, as indicated by increased mitochondrial oxidative stress, increased mitochondrial membrane depolarization, and finally, disrupted mitochondrial structure. Although mitochondrial function was impaired in the salivary glands of obese-insulin–resistant rats, mitochondrial dynamics were not affected in those rats. One possible explanation could be that the mitochondria in salivary glands exhibited compensatory mechanisms via the balance of mitochondrial fission/fusion following mitochondrial dysfunction. The balance of mitochondrial fusion/fission is necessary to maintain ATP production (Ni et al. 2015). Although there was an increased fission process, fusion process was also increased, thus maintaining the balance of fission/fusion in these salivary glands of obese-insulin–resistant rats. These findings suggest that during the early prediabetic state mitochondrial function was impaired without disrupting mitochondrial dynamics in salivary glands. Since the mitochondrial dynamic

Appl. Physiol. Nutr. Metab. Downloaded from www.nrcresearchpress.com by 110.171.135.216 on 03/17/17
For personal use only.

Fig. 6. The possible mechanism of the pathological changes at molecular level of the salivary glands induced by high-fat diet consumption. Long-term high-fat diet consumption caused increased inflammation through the TNF-α signaling pathway and increased NFκB expression. An increase in TNF-α levels could lead to increased caspase 3 expression, which leads to apoptosis of acinar cells. In addition, increased TGF-β expression following long-term high-fat diet consumption could upregulate p38 MAPK expression and finally may lead to increased apoptosis of the acinar cells and fibrosis of the ECM. ECM, extracellular matrix; NFκB, nuclear factor kappa B; p38 MAPK, p38 mitogen-activated protein kinases; TGF-β, transforming growth factor beta; TGFβR, TGF-β receptor; TNF-α, tumor necrosis factor alpha; TNFR1, TNF-α receptor 1.



balance was still intact, ATP production should be sufficient to maintain normal salivary flow rate in obese-insulin–resistant rats. However, further studies are needed to test this hypothesis.

Since the salivary flow is regulated by the calcium concentration within the acinar cells (Melvin et al. 2005; Ambudkar 2014), we determined intracellular calcium regulation by measuring intracellular calcium transients. Although salivary flow rates showed no change in our study, intracellular calcium dyshomeostasis was observed. The findings from the present study were unexpected as HFD impaired intracellular calcium transients and mitochondrial function in salivary glands without affecting salivation. However, since there was no change in the level of intracellular calcium between HFD-fed and ND-fed rats, this suggested that acinar cells in both groups could secrete saliva at similar flow rates. Previous studies showed that AQP5 played a major role in salivation (Ma et al. 1999; Asari et al. 2009; Lee et al. 2012; Matsuzaki et al. 2012). The unchanged AQP5 protein expression in HFD-fed rats, when compared with ND-fed rats, indicated that salivation was not impaired in HFD-fed rats. Since impaired intracellular calcium transients and mitochondrial function occurred without the alteration of the salivation in this study, the possible compensatory mechanisms that could contribute to these findings could be as follows: (*i*) the level of severity of intracellular calcium transient dysregulation was not sufficient to cause the impairment of salivation; and (*ii*) the mitochondrial dynamic balance was still intact.

In addition, data pertinent to salivary flow rates from patients with type 2 diabetes (hyperinsulinemia with hyperglycemia) were controversial. Two earlier studies show that salivary flow rates are reduced in diabetic patients (Lasisi and Fasanmade 2012; Lopez-Pintor et al. 2016), whereas 3 other studies show that salivary flow rates are unchanged in diabetic patients when compared with nondiabetic patients. (Dodds and Dodds 1997; Meurman et al. 1998; Prathibha et al. 2013). In the animal model of type 1 diabetes (hyperglycemia), a decrease in salivary flow rate has been found (Jonsson et al. 2006). However, our study is the first study that determined salivary gland function, salivation, and mechanistic insight in a prediabetic model (hyperinsulinemia with euglycemia), and we found that the salivary flow rates were unchanged during the prediabetic state. Therefore, previous results and ours suggest that plasma glucose levels may play an important role in the severity of functional outcome of the salivary gland.

The limitation of the present study is that the time-course effects of HFD consumption on the molecular changes of the salivary gland were not investigated. Future study is needed to study whether these changes occur at an earlier stage of HFD consumption.

Conclusion

Although an obese-insulin–resistant condition did not alter salivation, there was salivary gland dysfunction at the molecular level indicated by impaired intracellular calcium transients, increased oxidative stress and inflammation, and salivary mitochondrial dysfunction. The obese-insulin–resistant condition (i.e., prediabetic state) in the present study could be insufficiently severe to damage the structure of salivary glands, thus allowing the salivary glands to compensate their function via altering mitochondrial dynamics, resulting in the maintenance of intact salivary acinar cell function. These findings provide an important clinical insight in which obese-insulin resistance can already cause salivary gland dysfunction at the molecular level, and that early pharmacological intervention in the obese-insulin–resistant condition may protect salivary glands against dysfunction and deterioration.

Conflict of interest statement

The authors declare that there are no conflicts of interest.

Acknowledgements

This work was supported by Thailand Research Fund grant: TRF-BRG 5780016 (S.C.C.); the National Research Council of Thailand (S.C.C.); a CMU 50th Anniversary grant by Chiang Mai University (PHD/021/2556; J.I. and S.C.C.); a NSTDA Research Chair Grant from the National Science and Technology Development Agency Thailand (N.C.), and a Chiang Mai University Center of Excellence Award (N.C.). The authors would like to thank Ms. Cicely Proctor for her editorial assistance.

Appl. Physiol. Nutr. Metab. Downloaded from www.nrcresearchpress.com by 110.1/1.133.210 on 05/11/17
For personal use only.

Appl. Physiol. Nutr. Metab. Downloaded from www.nrcresearchpress.com by 110.171.135.216 on 03/17/17
For personal use only.

References

Al-Rawi, N.H. 2011. Oxidative stress, antioxidant status and lipid profile in the saliva of type 2 diabetics. Diabetes Vasc. Dis. Res. 8: 22–28. doi:10.1177/1479164110390243. PMID:21262867.

Ambudkar, I.S. 2000. Regulation of Calcium in Salivary Gland Secretion. Crit. Rev. Oral Biol. Med. 11: 4–25. doi:10.1177/10454411000110010301. PMID: 10682899.

Ambudkar, I.S. 2014. Ca^{2+} signaling and regulation of fluid secretion in salivary gland acinar cells. Cell Calcium, 55: 297–305. doi:10.1016/j.ceca.2014.02.009. PMID:24646566.

Apaijai, N., Pintana, H., Chattipakorn, S.C., and Chattipakorn, N. 2013. Effects of vildagliptin versus sitagliptin, on cardiac function, heart rate variability and mitochondrial function in obese insulin-resistant rats. Br. J. Pharmacol. 169: 1048–1057. doi:10.1111/bph.12176. PMID:23488656.

Apaijai, N., Inthachai, T., Lekawanvijit, S., Chattipakorn, S.C., and Chattipakorn, N. 2016. Effects of dipeptidyl peptidase-4 inhibitor in insulin-resistant rats with myocardial infarction. J. Endocrinol. 229: 245–258. doi:10.1530/joe-16-0096. PMID:27044778.

Asari, T., Maruyama, K., and Kusama, H. 2009. Salivation triggered by pilocarpine involves aquaporin-5 in normal rats but not in irradiated rats. Clin. Exp. Pharmacol. Physiol. 36(5–6): 531–538. doi:10.1111/j.1440-1681.2008.05104.x. PMID:19673936.

Ben-Ari, Z., Hochhauser, E., Burstein, I., Papo, O., Kaganovsky, E., Krasnov, T., et al. 2002. Role of anti-tumor necrosis factor-alpha in ischemia/reperfusion injury in isolated rat liver in a blood-free environment. Transplantation, 73: 1875–80. doi:10.1097/00007890-200206270-00004. PMID:12131680.

Dodds, M.W., and Dodds, A.P. 1997. Effects of glycemic control on saliva flow rates and protein composition in non-insulin-dependent diabetes mellitus. Oral Surg. Oral Med. Oral Pathol. Oral Radiol. Endodont. 83: 465–470. doi:10.1016/S1079-2104(97)90147-5. PMID:9127379.

Esser, N., Legrand-Poels, S., Piette, J., Scheen, A.J., and Paquot, N. 2014. Inflammation as a link between obesity, metabolic syndrome and type 2 diabetes. Diabetes Res. Clin. Pract. 105: 141–150. doi:10.1016/j.diabres.2014.04.006. PMID:24798950.

Fedirko, N.V., Kruglikov, I.A., Kopach, O.V., Vats, J.A., Kostyuk, P.G., and Voitenko, N.V. 2006. Changes in functioning of rat submandibular salivary gland under streptozotocin-induced diabetes are associated with alterations of Ca2+ signaling and Ca2+ transporting pumps. Biochim. Biophys. Acta, 1762: 294–303. doi:10.1016/j.bbadis.2005.12.002. PMID:16443349.

Frank, S., Gaume, B., Bergmann-Leitner, E.S., Leitner, W.W., Robert, E.G., Catez, F., et al. 2001. The role of dynamin-related protein 1, a mediator of mitochondrial fission, in apoptosis. Dev. Cell 1: 515–525. PMID:11703942.

Gannot, G., Lancaster, H.E., and Fox, P.C. 2000. Clinical course of primary Sjogren's syndrome: salivary, oral, and serologic aspects. J. Rheumatol. 27: 1905–1909. PMID:10955331.

Goldman, J.A., and Julian, E.H. 1977. Pseudo-Sjogren syndrome with hyperlipoproteinemia. JAMA, 237: 1582–1584. doi:10.1001/jama.1977.03270420050015. PMID:576655.

Hall, B.E., Zheng, C., Swaim, W.D., Cho, A., Nagineni, C.N., Eckhaus, M.A., et al. 2010. Conditional overexpression of TGF-beta1 disrupts mouse salivary gland development and function. Lab. Invest. 90: 543–555. doi:10.1038/labinvest.2010.5. PMID:20142803.

Imai, K., Hiramatsu, A., Fukushima, D., Pierschbacher, M.D., and Okada, Y. 1997. Degradation of decorin by matrix metalloproteinases: identification of the cleavage sites, kinetic analyses and transforming growth factor-beta1 release. Biochem. J. 322(3): 809–814. doi:10.1042/bj3220809. PMID:9148753.

Inthachai, T., Lekawanvijit, S., Kumfu, S., Apaijai, N., Pongkan, W., Chattipakorn, S.C., and Chattipakorn, N. 2015. Dipeptidyl peptidase-4 inhibitor improves cardiac function by attenuating adverse cardiac remodelling in rats with chronic myocardial infarction. Exp. Physiol. 100: 667–679. doi:10.1113/ep085108. PMID:25823534.

Jonsson, M.V., Delaleu, N., Brokstad, K.A., Berggreen, E., and Skarstein, K. 2006. Impaired salivary gland function in NOD mice: association with changes in cytokine profile but not with histopathologic changes in the salivary gland. Arthritis Rheum. 54: 2300–2305. doi:10.1002/art.21945. PMID:16802370.

Kawakami, A., Nakashima, K., Tamai, M., Nakamura, H., Iwanaga, N., Fujikawa, K., et al. 2007. Toll-like receptor in salivary glands from patients with Sjogren's syndrome: functional analysis by human salivary gland cell line. J. Rheumatol. 34: 1019–1026. PMID:17407216.

Kitzinger, H.B., and Karle, B. 2013. The epidemiology of obesity. Eur. Surg. 45: 80–82. doi:10.1007/s10353-013-0196-x.

Lasisi, T.J., and Fasanmade, A.A. 2012. Salivary flow and composition in diabetic and non-diabetic subjects. Niger. J. Physiol. Sci. 27: 79–82. PMID:23235312.

Leask, A., and Abraham, D.J. 2004. TGF-beta signaling and the fibrotic response. FASEB J. 18: 816–827. doi:10.1096/fj.03-1273rev. PMID:15117886.

Lee, M.G., Ohana, E., Park, H.W., Yang, D., and Muallem, S. 2012. Molecular mechanism of pancreatic and salivary gland fluid and HCO_3^- secretion. Physiol. Rev. 92(1): 39–74. doi:10.1152/physrev.00011.2011. PMID:22298651.

Lekawanvijit, S., Kompa, A.R., Manabe, M., Wang, B.H., Langham, R.G., Nishijima, F., et al. 2012. Chronic kidney disease-induced cardiac fibrosis is ameliorated by reducing circulating levels of a non-dialysable uremic toxin, indoxyl sulfate. PLoS One, 7: e41281. doi:10.1371/journal.pone.0041281. PMID: 22829936.

Lopez-Pintor, R.M., Casanas, E., Gonzalez-Serrano, J., Serrano, J., Ramirez, L., de Arriba, L., and Hernandez, G. 2016. Xerostomia, Hyposalivation, and Salivary Flow in Diabetes Patients. J. Diabetes Res. 2016: 4372852. doi:10.1155/2016/4372852. PMID:4958434.

Marber, M.S., Rose, B., and Wang, Y. 2011. The p38 mitogen-activated protein kinase pathway – A potential target for intervention in infarction, hypertrophy, and heart failure. J. Mol. Cell Cardiol. 51: 485–490. doi:10.1016/j.yjmcc.2010.10.021. PMID:21062627.

Ma, T., Song, Y., Gillespie, A., Carlson, E.J., Epstein, C.J., and Verkman, A.S. 1999. Defective secretion of saliva in transgenic mice lacking aquaporin-5 water channels. J. Biol. Chem. 274(29): 20071–20074. PMID:10400615.

Maria, D.A., de Souza, J.G., Morais, K.L., Berra, C.M., Zampolli Hde, C., Demasi, M., et al. 2013. A novel proteasome inhibitor acting in mitochondrial dysfunction, ER stress and ROS production. Invest. New Drugs, 31: 493–505. doi:10.1007/s10637-012-9871-1. PMID:22975862.

Martin, S.S., Blaha, M.J., Elshazly, M.B., Brinton, E.A., Toth, P.P., McEvoy, J.W., et al. 2013. Friedewald-estimated versus directly measured low-density lipoprotein cholesterol and treatment implications. J. Am. Coll. Cardiol. 62: 732–739. doi:10.1016/j.jacc.2013.01.079. PMID:23524048.

Matsuzaki, T., Susa, T., Shimizu, K., Sawai, N., Suzuki, T., Aoki, T., et al. 2012. Function of the membrane water channel aquaporin-5 in the salivary gland. Acta Histochem. Cytochem. 45(5): 251–259. doi:10.1267/ahc.12018. PMID: 23209334.

Melvin, J.E., Yule, D., Shuttleworth, T., and Begenisich, T. 2005. Regulation of fluid and electrolyte secretion in salivary gland acinar cells. Annu. Rev. Physiol. 67: 445–469. doi:10.1146/annurev.physiol.67.041703.084745. PMID: 15709965.

Meurman, J.H., Collin, H.L., Niskanen, L., Töyry, J., Alakuijala, P., Keinänen, S., and Uusitupa, M. 1998. Saliva in non-insulin-dependent diabetic patients and control subjects: The role of the autonomic nervous system. Oral Surg. Oral Med. Oral Pathol. Oral Radiol. Endod. 86: 69–76. doi:10.1016/S1079-2104(98)90152-4. PMID:9690248.

Ni, H.-M., Williams, J.A., and Ding, W.-X. 2015. Mitochondrial dynamics and mitochondrial quality control. Redox Biol. 4: 6–13. doi:10.1016/j.redox.2014.11.006. PMID:25479550.

Park, J., Lee, J., and Choi, C. 2011. Mitochondrial network determines intracellular ROS dynamics and sensitivity to oxidative stress through switching inter-mitochondrial messengers. PLoS One, 6: e23211. doi:10.1371/journal.pone.0023211. PMID:21829717.

Pereira, R.M.R., de Carvalho, J.F., and Bonfá, E. 2009. Metabolic syndrome in rheumatological diseases. Autoimmun. Rev. 8: 415–419. doi:10.1016/j.autrev.2009.01.001. PMID:19168158.

Ping, L., Ogawa, N., Zhang, Y., Sugai, S., Masaki, Y., and Weiguo, X. 2012. p38 mitogen-activated protein kinase and nuclear factor-kappaB facilitate CD40-mediated salivary epithelial cell death. J. Rheumatol. 39: 1256–1264. doi:10.3899/jrheum.110097. PMID:22505709.

Pintana, H., Apaijai, N., Chattipakorn, N., and Chattipakorn, S.C. 2013. DPP-4 inhibitors improve cognition and brain mitochondrial function of insulin-resistant rats. J. Endocrinol. 218: 1–11. doi:10.1530/joe-12-0521. PMID:23591914.

Pipatpiboon, N., Pratchayasakul, W., Chattipakorn, N., and Chattipakorn, S.C. 2012. PPARgamma agonist improves neuronal insulin receptor function in hippocampus and brain mitochondria function in rats with insulin resistance induced by long term high-fat diets. Endocrinology, 153: 329–338. doi:10.1210/en.2011-1502. PMID:22109891.

Pipatpiboon, N., Pintana, H., Pratchayasakul, W., Chattipakorn, N., and Chattipakorn, S.C. 2013. DPP4-inhibitor improves neuronal insulin receptor function, brain mitochondrial function and cognitive function in rats with insulin resistance induced by high-fat diet consumption. Eur. J. Neurosci. 37: 839–849. doi:10.1111/ejn.12088. PMID:23240760.

Pratchayasakul, W., Kerdphoo, S., Petsophonsakul, P., Pongchaidecha, A., Chattipakorn, N., and Chattipakorn, S.C. 2011. Effects of high-fat diet on insulin receptor function in rat hippocampus and the level of neuronal corticosterone. Life Sci. 88: 619–627. doi:10.1016/j.lfs.2011.02.003. PMID:21315737.

Prathibha, K.M., Johnson, P., Ganesh, M., and Subhashini, A.S. 2013. Evaluation of Salivary Profile among Adult Type 2 Diabetes Mellitus Patients in South India. J Clin Diagn Res 7: 1592–1595. doi:10.7860/JCDR/2013/5749.3232. PMID: 3782905.

Pringle, S., Nanduri, L.S., van der Zwaag, M., van Os, R., and Coppes, R.P. 2011. Isolation of mouse salivary gland stem cells. J. Vis. Exp. doi:10.3791/2484. PMID:21339725.

Proctor, G.B., and Carpenter, G.H. 2014. Salivary secretion: mechanism and neural regulation. Monogr. Oral Sci. 24: 14–29. doi:10.1159/000358781. PMID: 24862591.

Rabøl, R., Boushel, R., and Dela, F. 2006. Mitochondrial oxidative function and type 2 diabetes. Appl. Physiol. Nutr. Metab. 31: 675–683. doi:10.1139/h06-071. PMID:17213881.

Shikama, Y., Ishimaru, N., Kudo, Y., Bando, Y., Aki, N., Hayashi, Y., and Funaki, M. 2013. Effects of free fatty acids on human salivary gland epithelial cells. J. Dent. Res. 92: 540–546. doi:10.1177/0022034513487378. PMID:23603335.

Sivasinprasasn, S., Sa-Nguanmoo, P., Pratchayasakul, W., Kumfu, S., Chattipakorn, S.C., and Chattipakorn, N. 2015. Obese-insulin resistance accelerates and aggravates cardiometabolic disorders and cardiac mitochon-

Pagination not final (cite DOI) / Pagination provisoire (citer le DOI)

drial dysfunction in estrogen-deprived female rats. Age (Dordr), 37: 28. doi: 10.1007/s11357-015-9766-0. PMID:25791519.

Sripetchwandee, J., Pipatpiboon, N., Pratchayasakul, W., Chattipakorn, N., and Chattipakorn, S.C. 2014. DPP-4 Inhibitor and PPARγ Agonist Restore the Loss of CA1 Dendritic Spines in Obese Insulin-resistant Rats. Arch. Med. Res. 45: 547–552. doi:10.1016/j.arcmed.2014.09.002. PMID:25281415.

Tremblay, M., Gaudet, D., and Brisson, D. 2011. Metabolic syndrome and oral markers of cardiometabolic risk. J. Can. Dent. Assoc. 77: b125. PMID: 21975074.

Wellen, K.E., and Hotamisligil, G.S. 2005. Inflammation, stress, and diabetes. J. Clin. Invest. 115: 1111–1119. doi:10.1172/jci25102. PMID:15864338.

Yamachika, S., Brayer, J., Oxford, G.E., Peck, A.B., and Humphreys-Beher, M.G. 2000. Aberrant proteolytic digestion of biglycan and decorin by saliva and exocrine gland lysates from the NOD mouse model for autoimmune exocrinopathy. Clin. Exp. Rheumatol. 18: 233–240. PMID:10812497.

Yarana, C., Sanit, J., Chattipakorn, N., and Chattipakorn, S. 2012. Synaptic and nonsynaptic mitochondria demonstrate a different degree of calcium-induced mitochondrial dysfunction. Life Sci. 90: 808–814. doi:10.1016/j.lfs.2012.04.004. PMID:22525373.

Zalewska, A., Knaś, M., Niczyporuk, M., Razak, H.H., Waszkiewicz, N., Przystupa, A.W., et al. 2013. Salivary lysosomal exoglycosidases profiles in patients with insulin-dependent and noninsulin-dependent diabetes mellitus. Adv. Clin. Exp. Med. 22: 659–666. PMID:24285450.

Appl. Physiol. Nutr. Metab. Downloaded from www.nrcresearchpress.com by 110.171.135.216 on 05/11/11
For personal use only.

เอกสารแนบหมายเลข 4

Archives of Oral Biology 78 (2017) 65–81

Contents lists available at ScienceDirect

Archives of Oral Biology

journal homepage: www.elsevier.com/locate/aob

Diet-induced obesity, gut microbiota and bone, including alveolar bone loss

Sathima Eaimworawuthikul[a,b], Parameth Thiennimitr[c], Nipon Chattipakorn[b], Siriporn C. Chattipakorn[a,b,*]

[a] Neurophysiology Unit, Cardiac Electrophysiology Research and Training Center Faculty of Medicine, Chiang Mai University, Chiang Mai, 50200, Thailand
[b] Department of Oral Biology and Diagnostic Sciences, Faculty of Dentistry, Chiang Mai University, Chiang Mai, 5020, Thailand
[c] Department of Microbiology, Faculty of Medicine, Chiang Mai University, Chiang Mai, 50200, Thailand

ARTICLE INFO

Article history:
Received 27 October 2016
Received in revised form 9 January 2017
Accepted 6 February 2017

Keywords:
Obesity
Insulin resistance
Jaw bone
Gut microbiota

ABSTRACT

Obesity is a major risk factor for several pathologies, including jaw bone resorption. The underlying mechanisms involved in pathological conditions resulting from obesity include chronic systemic inflammation and the development of insulin resistance. Although numerous studies have indicated the importance of the role of gut microbiota in the pathogenesis of inflammation and insulin resistance in obesity, only a few studies have established a relationship between obesity, gut microbiota and status of the jaw bone. This review aims to summarize current findings relating to these issues, focusing on the role of obesity and gut microbiota on jaw bone health, including possible mechanisms which can explain this link.

© 2017 Elsevier Ltd. All rights reserved.

Contents

1. Introduction 65
2. Bone metabolism in obesity 66
3. Obese-insulin resistance and alveolar bone loss 67
4. Alterations of gut microbiota in high-fat diet-induced obesity from animal studies 67
5. Probiotics and prebiotics as potential ways to manipulate gut microbiota and protect the immune system 69
6. Bone health, gut microbiota and the immune system 72
7. Connection between obesity, bone and gut microbiota 74
8. Conclusion 78
Conflict of interest 79
Acknowledgements 79
References 79

1. Introduction

Obesity has increased remarkably worldwide and to date is one of the major public health concerns (Correction Naghavi et al., 2015). Obesity, itself, can lead to the development of several pathological conditions, including insulin resistance, type II diabetes mellitus (T2DM), atherosclerosis, cardiovascular disorders, neurodegeneration, arthritis and osteoporosis (Abou-Raya & Abou-Raya, 2006; Compston, 2015; Eckel et al., 2011; Spielman, Little, & Klegeris, 2014). Previous studies have shown that chronic systemic inflammation due to the accumulation of macrophages in white adipose tissues in individuals exhibiting the obese condition, plays a key role in the pathogenesis of obesity-induced insulin resistance (Kawasaki, Asada, Saito, Kanemoto, & Imaizumi, 2012; Lee & Lee, 2014; Xu et al., 2003). Insulin resistance is a pathological

* Corresponding author at: Neurophysiology Unit, Cardiac Electrophysiology Research and Training Center, Faculty of Medicine, Chiang Mai University, Department of Oral Biology and Diagnostic Sciences, Faculty of Dentistry Chiang Mai University, Chiang Mai, 50200, Thailand.
E-mail addresses: scchattipakorn@gmail.com, siriporn.c@cmu.ac.th (S.C. Chattipakorn).

http://dx.doi.org/10.1016/j.archoralbio.2017.02.009
0003-9969/© 2017 Elsevier Ltd. All rights reserved.

condition, as indicated by impaired insulin signaling at the target tissues. It can be characterized by hyperglycemia with euglycemia (de Luca & Olefsky, 2008). The long-term consumption of a high-fat or a high-fat with high-carbohydrate diet has been associated with the pathogenesis of obesity, insulin resistance, systemic inflammation, and metabolic bone disorders, including osteoporosis (Cao, 2011; Jin & Flavell, 2013). In addition, our previous studies demonstrated that the rats who had been on a high-fat diet for 12-weeks developed obese-insulin resistance with osteoporosis in both tibias and the jaw bone (Potikanond et al., 2016; Pramojanee, Phimphilai, Kumphune, Chattipakorn, & Chattipakorn, 2013).

The effects of obese-insulin resistance on bones have been reported as having both beneficial and detrimental effects (Berg et al., 2015; Caffarelli, Alessi, Nuti, & Gonnelli, 2014; Cao, 2011; Dimitri, Bishop, Walsh, & Eastell, 2012; Gourlay, Hammett-Stabler, Renner, & Rubin, 2014; Mosca et al., 2014; Yang, Nguyen, Center, Eisman, & Nguyen, 2013). The reported beneficial effects of obesity on bone, using data from several human studies, are that obesity exerts a protective effect against osteoporosis due to obesity-increased bone mineral density (BMD). High body weight in the obese condition directly reinforces mechanical loading on the long bones (Crepaldi, Romanato, Tonin, & Maggi, 2007; De Laet et al., 2005; Evans, Paggiosi, Eastell, & Walsh, 2015). Nevertheless, several studies in both human and animals showed that the metabolic complications of obesity including T2DM and insulin resistance had a negative impact on bone structure through impairing bone turnover and diminishing bone quality, despite an increase in BMD (Lecka-Czernik, Stechschulte, Czernik, & Dowling, 2015; Rubin & Patsch, 2016; Sellmeyer et al., 2016). Compared to studies on long bones, there are only a few reports which have investigated the role of high-fat diet-induced obesity and insulin resistance on jaw bones and the findings from these studies are controversial.

In recent years, the role of gut microbiota, a group of trillions of beneficial microbes living inside the host intestinal tract, has been extensively studied regarding their involvement in numerous diseases including obesity-related pathologies (Gérard, 2016). The beneficial effects of gut microbiota to the health of the host include: (i) stimulating the proper development of an immune system; (ii) providing the host with extra energy sources, and (iii) protecting the host against invading pathogens (Belkaid & Hand, 2014; Flint, Scott, Louis, & Duncan, 2012; Tamburini, Shen, Wu, & Clemente, 2016). However, findings of studies into the role of gut microbiota on the host bone health remain inconclusive. Some reports showed that gut microbiota could affect the host bone mass metabolism through the manipulation of the host immune system (Ohlsson & Sjogren, 2015; Sjogren et al., 2012). For example: 1) by using germ-free (GF) mice, Sjogren and colleagues demonstrated that gut microbiota could stimulate osteoclast-mediated bone resorption, resulting in decreased bone mass (Sjogren et al., 2012). 2) An imbalance in gut microbiota, termed "gut dysbiosis", has been associated with several human diseases, including obesity, T2DM, metabolic syndrome (MetS), non-alcoholic fatty acid syndrome (Ojeda, Bobe, Dolan, Leone, & Martinez, 2016), and osteoporosis (Ejtahed, Soroush, Angoorani, Larijani, & Hasani-Ranjbar, 2016; Ohlsson & Sjogren, 2015). Thus, targeting gut microbiota as a therapeutic approach for metabolic disorders such as obesity has been recently reviewed (Ejtahed et al., 2016). Consumption of beneficial microorganisms called probiotics, and non-digestible fibers termed prebiotics, is believed to be an effective therapeutic intervention used for gut microbiota manipulation (Tamburini et al., 2016). The beneficial effects of probiotic and prebiotic consumption on the health of long bones have also been reported in gut dysbiotic individuals (Britton et al., 2014; Parvaneh et al., 2015; Weaver et al., 2011). However, there are only a few studies which link obesity, gut microbiota, and jaw bone density. In this review, we have summarized the beneficial and adverse effects of obesity on bone health, including alveolar bone and the possible role of gut microbiota on jaw bone health, using current findings of both human studies and animal research. The possible underlying mechanisms for the effects of obesity and gut microbiota on bone health are also discussed below.

2. Bone metabolism in obesity

In the obese condition, excessive fat results in the accumulation of macrophages in white adipose tissue, leading to a low-grade chronic systemic inflammation (Kawasaki et al., 2012; Lee & Lee, 2014; Xu et al., 2003). Recent studies have supported the detrimental effects of obesity-derived systemic inflammation on bone metabolism (Amar, Zhou, Shaik-Dasthagirisaheb, & Leeman, 2007; Lecka-Czernik et al., 2015). For example, Potikanond and colleagues postulated that trabecular bone density was decreased in high-fat diet-induced obese rats (Potikanond et al., 2016). Other studies claimed that bone inflammation observed in obese-induced insulin-resistant rats seems to show a direct correlation with chronic systemic inflammation (Blasco-Baque et al., 2012; Cavagni et al., 2015; Li, Lu et al., 2015; Muluke et al., 2015). Several findings suggested that systemic inflammation, an increased inflammatory tone in blood circulation, could be a key factor in bone inflammation as well as bone loss in obesity. Increased levels of pro-inflammatory cytokines such as tumor necrosis factor (TNF)-α, interleukin (IL)-1β and IL-6 in blood circulation exacerbated osteoclastogenesis, the process of stem cell differentiation into osteoclasts, resulting in increased bone resorption (Amar et al., 2007; Blasco-Baque et al., 2012; Li, Lu et al., 2015; Weitzmann, 2013). Increased osteoclastogenesis following the systemic inflammation possibly occurs through the up-regulation of macrophage colony stimulating factor (M-CSF), the receptor activator of nuclear factor (NF)-κB ligand (RANKL), and finally an increase in all downstream cytokines, which directly activate osteoclastogenesis in the osteoclast precursor cells (Kim, Yoon, Kim, & Yoon, 2014; Lacey et al., 1998; Takeshita, Kaji, & Kudo, 2000; Yamashita et al., 2015).

Both osteoblasts and adipocytes are derived from mesenchymal stem cells and their differentiation is altered by the long-term consumption of a high-fat diet (Luo et al., 2015; Shu et al., 2015). Increased shift from the osteoblasts to adipocytes has been observed in cases of obesity (Luo et al., 2015). In contrast to Luo's study, Shu and colleagues found that, along with high adipogenesis, osteoblast activity increased in cases of obesity (Shu et al., 2015). The increase in osteoblast activities in Shu's study might be in part due to a compensatory effect of increased osteoclastogenesis at the time-point they analyzed. In addition, obesity is found to be associated with the impaired osteoblastic insulin signaling, the reduction of osteoblast cell survival, and decreased bone formation rate (Potikanond et al., 2016; Pramojanee et al., 2013). All of those findings suggest that obesity could affect bone metabolism by enhancing bone resorption and reducing bone formation.

Furthermore, obesity is associated with the change in the levels of substances termed "adipokines" released from the adipose tissues. Also increased leptin and decreased adiponectin levels have been found in the obese individual (Leal & Mafra, 2013). These two major adipokines, including leptin and adiponectin, play direct and indirect roles in both metabolic disorders and bone metabolism (Ducy et al., 2000; Elefteriou et al., 2004; Holloway et al., 2002; Oshima et al., 2005). Leptin has roles in reducing appetite, increasing energy expenditure and inducing inflammation in adipose tissues (Leal & Mafra, 2013). However, the precise effect of leptin on bone metabolism is still poorly understood. It has been shown that the previous leptin levels of each individual played a

role in the various outcomes of leptin on bone metabolism (Cao, 2011). In the non-obese condition, the physiological leptin level is thought to be responsible for directly enhancing bone mass density by decreasing osteoclastogenesis and increasing osteoblastogenesis (Cornish et al., 2002; Holloway et al., 2002). Nonetheless, hyperleptinemia in diet-induced obesity has been reported to increase systemic inflammatory responses (Loffreda et al., 1998) and then indirectly reduce bone mass density (Fujita, Watanabe, & Maki, 2012; Shu et al., 2015). High leptin levels also increased pro-inflammatory cytokine production and alveolar bone inflammation in the periodontitic experiments in which beagle dogs were fed with a normal diet (Li, Huang, Liu, Hou, & Meng, 2015). Adiponectin plays a role in an anti-inflammatory process (Leal & Mafra, 2013) and indirectly increases bone mass via the inhibition of osteoclastogenesis (Oshima et al., 2005). Several studies exhibited the direct effects of adiponectin on bone mass in various conditions (Pu et al., 2016; Yamaguchi et al., 2007; Zhang et al., 2014). An example of this is found when Yamaguchi and colleagues demonstrated that adiponectin resulted from the activation of periodontogenic bacterial lipopolysaccharides (*Actinobacillus actinomycetemcomitans*) which could inhibit osteoclastogenesis in the mouse cell lines by suppressing the transcription factor NF-κB, essential for osteoclast formation (Yamaguchi et al., 2007). Adiponectin promotes osteoblastogenesis in human jaw bone marrow mesenchymal stem cells (Pu et al., 2016). Moreover, adiponectin could ameliorate alveolar bone loss by reducing an inflammatory process and osteoclastogenesis in the diet-induced obese mouse (Zhang et al., 2014). Taken together, alterations in levels of adipokines, including increased leptin and decreased adiponectin, in high-fat diet-induced obesity may play a crucial role in bone metabolism and bone loss.

3. Obese-insulin resistance and alveolar bone loss

Several animal studies showed that jaw bone density loss, as indicated by decreased alveolar bone height or decreased bone mechanical properties, including bone mineral density (BMD), bone strength, and bone histomorphometry, could be affected by diet-induced obesity with or without insulin resistance in both mature and growing animals (Amar et al., 2007; Blasco-Baque et al., 2012; Cavagni et al., 2013; Cavagni et al., 2015; Fujita & Maki, 2015; Li, Lu et al., 2015; Muluke et al., 2015; Pramojanee et al., 2013; do Nascimento et al., 2013). Furthermore, the systematic review and meta-analysis by Moura-Grec and colleagues in 2014 reported that periodontitis, chronic inflammation of the tissue surrounding the teeth causing alveolar bone loss, was associated with obesity (in 25 out of 31 studies), through an unknown mechanism (Moura-Grec, Marsicano, Carvalho, & Sales-Peres, 2014). Animal studies also showed that an increase in body weight could exacerbate the severity of periodontitis (Cavagni et al., 2015; Muluke et al., 2015; Verzeletti, Gaio, Linhares, & Rosing, 2012). Diet-induced obese female Wistar rats exhibited greater alveolar bone loss at their palatal sides than their lean counterparts (Verzeletti et al., 2012). Muluke and colleagues found that increased plasma fatty acid levels together with increased body weight enhanced alveolar bone loss after *Porphyromonas gingivalis* infection (Muluke et al., 2015). Obesity and hyperlipidemia from long-term cafeteria (high-fat/high-carbohydrate) diet consumption could exacerbate the severity of ligature-induced periodontitis in the Wistar rat (Cavagni et al., 2015). All of those findings suggest that high-fat diet-induced obesity can trigger alveolar bone loss and aggravate the severity of periodontitis.

However, there are two controversial reports regarding the contribution of obesity to alveolar bone loss. First, Priesnitz and colleagues in 2008 showed that 4 months of consumption of a cafeteria style-diet did not promote the progression of alveolar bone loss in female Wistar rats with ligature-induced periodontitis (Priesnitz Simch, José Gaio, & Kuchenbecker Rösing, 2008). Although that study showed there were differences in body weight between the control and experimental groups, they were only 13% different, which was relatively small and not statistically significant. Moreover, the insulin levels were not shown in the results. Thus, those animals may not have developed insulin resistance. These findings could also suggest that the combination of obesity and insulin resistance might be needed to exacerbate alveolar bone loss. Secondly, Cavagni and colleagues in 2013 (Cavagni et al., 2013) demonstrated the effect of a cafeteria-diet on spontaneous periodontal disease without any mechanical or bacterial induction. That study showed that obesity alone increased the incidence of periodontal tissue breakdown without bone loss, when compared to lean rats. Therefore, it is possible that the obesity-derived tissue inflammation occurred prior to bone loss. Table 1 is a summary of those findings.

4. Alterations of gut microbiota in high-fat diet-induced obesity from animal studies

The gut microbiota population in humans and rodents share similar bacterial profiles. The two predominant phyla in the population are Bacteroidetes and Firmicutes. Other minority bacteria phyla represented include Actinobacteria, Proteobacteria, and Verrucomicrobia (Consortium, 2012; Donaldson, Lee, & Mazmanian, 2016). Several factors can influence the composition of gut microbiota and the gut immune system. Shifting the balance of a gut microbiota population which is within normal limits to an imbalanced population is termed "gut dysbiosis" which is associated with several diseases including obesity (Alard et al., 2015; Bron, van Baarlen, & Kleerebezem, 2012; Cani et al., 2007; Chang et al., 2015; Ding et al., 2010; Kim, Gu, Lee, Joh, & Kim, 2012; Moya-Perez, Neef, & Sanz, 2015; Naito et al., 2011; Park, Cho, Lee, & Lim, 2015; Rajpal et al., 2015; Roberfroid et al., 2010; Tanida et al., 2008; Tojo et al., 2014; Woting et al., 2015; Woting, Pfeiffer, Loh, Klaus, & Blaut, 2014; Zhang et al., 2015).

The studies in mice with no gut microbiota, termed germ free, exhibit the crucial role of gut microbiota in the induction of obesity instigated by a high-fat diet (Ding et al., 2010; Woting et al., 2014; Woting et al., 2015). The consumption of a high-fat diet did not result in either the development of obesity, inflammation or insulin resistance in the mice without normal gut microbiota (Ding et al., 2010). Furthermore, when the gut microbiota from the high-fat diet-induced obese-insulin resistant mice was colonized in recipient germ free mice, the inflammatory process occurred at the same level as the donor's (Ding et al., 2010). In addition, Woting and colleagues presented that the specific bacteria *Clostridium ramosum* was essential in the diet-induced obesity (Woting et al., 2014; Woting et al., 2015).

Long term consumption of a high-fat diet resulted in gut dysbiosis in which the Firmicutes/Bacteroidetes (F/B) ratio was increased, enhancing the proliferation of the facultative anaerobic and lipopolysaccharide (LPS)-bearing bacteria which belong to the phylum Proteobacteria (e.g. family Enterobacteriaceae), and decreasing the mucosal-protective bacteria of the phylum Actinobacteria (especially in family Bifidobacteriaceae) (Kim et al., 2012; de La Serre et al., 2010). Interestingly, one feature of high-fat-induced obesity, leading to gut dysbiosis, is an increase in Proteobacteria levels (Brown, DeCoffe, Molcan, & Gibson, 2012). Bacteria belonging to the phylum Proteobacteria are mainly LPS-bearing Gram-negative bacteria. LPS is a major component of the outer membrane of Gram negative bacteria and it is recognized by the host's innate immune sensor Toll-like receptor (TLR)- 4 (Alexander & Rietschel, 2001). The binding of bacterial LPS and host TLR-4 found on gut epithelia and several immune cells results

Table 1
The effects of obesity-insulin resistance on jaw bone.

Model	Age	Duration of diet consumption	Major findings	Interpretation	References
Male wistar rats induced obesity by high fat diet (59.28% fat)	Adulthood	12 weeks	↑ Body weight ↑ Visceral fat ↑ Plasma cholesterol ↑ Plasma insulin ↑ HOMA index ↓ Trabecular bone mass ↓ Plasma osteocalcin ↓ Bone formation rate ↓ Osteoblast proliferation ↑ Osteoblast apoptosis ↓ Osteoblastic insulin signaling pathway biomolecules (p-IR,p-IRS, p-Akt)	Obesity-insulin resistance induced jaw bone loss via impaired osteoblastic insulin signaling.	Pramojanee et al. (2013)
C57BL6/J male mice induced obesity by high fat diet (72% fat)	Adulthood	4 weeks	↑ Body weight ↑ Plasma insulin ↑ Glucose-tolerance test ↑ Pro-inflammatory cytokines mRNA (TNF-α,IL-1β,IL-6) in periodontal tissue ↑ Alveolar bone loss	Obesity-insulin resistance induced alveolar bone loss, leading to periodontitis.	Blasco-Baque et al. (2012)
Male wistar rats with periodontitis induced obesity and hyperlipidemia by cafeteria diet (55% CHO and 20% fat)	Adulthood	17 weeks	↑ Body weight ↑ Lee index ↔ Serum pro-inflammatory cytokines (TNF-α, IL-1β) ↑ Alveolar bone loss	Obesity and hyperlipidemia promoted alveolar bone loss and the progression of periodontitis via modulating host-immune response to challenge.	Cavagni et al. (2015)
Female wistar rats with periodontitis induced obesity by cafeteria diet diet (68% CHO and 18% fat)	Adulthood	16 weeks	↑ Body weight ↑ Alveolar bone loss	Obesity promoted alveolar bone loss, leading to the progression in periodontitis.	Verzeletti et al. (2012)
Male mice with periodontitis induced obesity by high fat diet (particularly palmitic acid-enriched)	Adulthood	16 weeks	↑ Pro-inflammatory cytokines and gene expression in osteoclast cell culture (TNF-α, IL-6, TLR4, TLR2) ↓ Serum CTX ↓ Serum osteocalcin, PINP(N-terminal propeptide) ↑ Alveolar bone loss	Specific fatty acid profile-induced obesity promoted alveolar bone loss progression in periodontitis	Muluke et al. (2015)
Male mice with periodontitis induced MetS by high fat diet (% fat not mentioned)	Adulthood	16 weeks	↑ Body weight ↑ Plasma lipids (TG,Cholesterol, FFA) ↑ Plasma insulin ↑ Alveolar bone loss ↑ Osteoclast cell and osteoclastogenic gene expression (IL-6, RANKL, MCP-1, M-CSF) in periodontal tissue	HFD-induced MetS promoted the progression of alveolar bone loss in periodontitis by increasing osteoclastogenesis	Li, Lu et al. (2015)
Male wistar rats with periodontitis induced obesity by cafeteria diet (38.5% CHO and 46.5% fat)	Adulthood	24 weeks	↑ Body weight ↑ Lee index ↑ Retroperitoneal and peri-ependymal fats ↑ Alveolar bone loss	Obesity promoted the progression of alveolar bone loss in periodontitis.	do Nascimento et al. (2013)
Male C57BL/6 mice with periodontitis induced obesity by high fat diet (60% fat)	Adulthood	16 weeks	↑ Body weight ↓ Serum pro-inflammatory cytokines (TNF-α, IL-6) ↑ Bacterial count and delayed bacterial clearance in periodontium ↑ Alveolar bone loss	Obesity promoted the progression of alveolar bone loss in periodontitis by altering immune responses to bacteria.	Amar et al. (2007)
Male C57BL6/J mice induced obesity by high fat diet(62% fat)	Childhood	4/8/12 weeks	↑ Body weight ↑ Serum total cholesterol, LDL, HDL ↓ Serum triglycerides ↑ Serum leptin ↓ Trabecular bone mass in mandible after 4 weeks of treatment ↓ Cortical bone mass in mandible after 12 weeks of treatment	Obesity triggered alveolar bone loss and spontaneous periodontal disease in growing mice.	Fujita and Maki (2015)

Table 1 (*Continued*)

Model	Age	Duration of diet consumption	Major findings	Interpretation	References
			↕ Cortical bone growth of mandible (Ct.Th + Ct.CSA) after 4 weeks of treatment Disrupt periodontal ligament to loss their orientation		
Male wistar rats induced obesity by cafeteria diet(48% CHO and 20% fat)	Adulthood	17 weeks	↑ Body weight ↑ Lee index ↔ Alveolar bone loss ↑ Occurrence of periodontal diseases	Obesity may promote periodontal disease without causing alveolar bone loss.	Cavagni et al. (2013)
Female wistar rats with periodontitis induced obesity by cafeteria diet (68% CHO and 18% fat)	Adulthood	120 days	↑ Body weight ↔ Fasting blood glucose ↔ Alveolar bone loss	Obesity did not promote the progression of alveolar bone loss in periodontitis	Priesnitz Simch et al. (2008)

Abbreviation: p-phosphorylation IR-insulin receptor IRS-insulin receptor substrate TNF-tumor necrotic factor IL-interleukin CHO-carbohydrate TLR-toll-like receptor CTX-C-terminal telopeptide MetS-metabolic syndrome TG-triglyceride FFA-free fatty acid RANKL-receptor activator of nuclear factor ligand MCP-monocyte chemoattractant protein M-CSF-macrophage colony stimulating factor LDL-low density lipoprotein HDL-high density lipoprotein Ct.Th-cortical thickness Ct.CSA-cortical cross-sectional area.

in an increase in the production of pro-inflammatory cytokines and hence increases the inflammatory response (Rakoff-Nahoum, Paglino, Eslami-Varzaneh, Edberg, & Medzhitov, 2004; Thaiss, Levy, Suez, & Elinav, 2014). In terms of adipokine alteration, LPS can inhibit adiponectin and leptin secretion in vitro and may contribute to the development of obesity-related metabolic disorders (Taira et al., 2015). In addition, gut dysbiosis shows a correlation with serum leptin levels in rodents (Queipo-Ortuno et al., 2013; Rajala et al., 2014). This is exemplified in a study by Queipo-Ortuno and colleagues who found a significant positive correlation between the quantity of Bifidobacterium and Lactobacillus and serum leptin levels (Queipo-Ortuno et al., 2013) whereas Rajala and colleagues demonstrated that leptin could directly modulate gut microbial composition (Rajala et al., 2014). However, it is difficult to conclude whether adipokine alteration in diet-induced obesity is the cause or consequence of gut dysbiosis and further studies are still required.

Obesity can also affect the gut barrier. Using the high-fat diet-induced obese mouse model, Kim and colleagues showed that prolonged consumption of a high -fat diet impaired the integrity of the gut mucosal barrier by decreasing the expression of tight junction proteins (Kim et al., 2012). High-fat diet fed mice developed insulin resistance accompanied by TLR-4 dependent colitis, increased serum LPS levels and increased viable numbers of LPS-containing Enterobacteriaceae were also detected in mouse fecal samples (Kim et al., 2012). Metabolic endotoxemia is a condition where levels of serum LPS are consistently high during the day and night after consumption of a high-fat diet. This was first described by Cani and colleagues (Cani et al., 2007). These authors found that feeding mice on a high-fat diet (containing 72% fat from corn oil and lard) for 4 weeks resulted in the loss of daily fluctuating serum LPS levels (physiologic endotoxemia), a phenomenon which occurs prior to the development of insulin resistance in obese mice (Cani et al., 2007). Taken together, these findings suggested that the alteration of host immune responses both locally (gut) and systemically (blood circulation) following a high-fat diet consumption might provide a link between obesity and insulin resistance, possibly via gut dysbiosis. The summary of these findings is in Table 2.

5. Probiotics and prebiotics as potential ways to manipulate gut microbiota and protect the immune system

The world health organization (WHO) defined probiotics as "*live microorganisms which when administered in adequate amounts confer a health benefit to the consumer*"(Morelli & Capurso, 2012). Whereas, a dietary prebiotic is "*a selectively fermented ingredient that results in specific changes in the composition and/or activity of the gastrointestinal microbiota, thus conferring benefit(s) to the hosts health*" (Roberfroid et al., 2010). In the past decade, several studies have supported the beneficial health claims of using probiotics, prebiotics and synbiotics (a combination of probiotics and prebiotics) in several human diseases including metabolic disorders such as obesity (Alard et al., 2015; Chang et al., 2015; Moya-Perez et al., 2015; Naito et al., 2011; Park et al., 2015; Rajpal et al., 2015; Tanida et al., 2008; Woting et al., 2015).

Table 3 is a summary of the effects of probiotic and prebiotic treatments in high-fat diet-induced obese animals. However, the use of probiotic bacteria is among the most well-studied of the gut microbiota modulating approaches compared with the use of prebiotics and synbiotics, as reviewed by Bron and colleagues (Bron et al., 2012). Probiotic bacteria could benefit human health through at least three major proposed mechanisms (Bron et al., 2012). First, gut-colonized probiotic bacteria can protect the host from invading pathogens by developing resistance by directly competing for available nutrient sources and space. Secondly, several probiotic bacteria can strengthen the gut mucosal barrier integrity by increasing mucus production, antimicrobial peptide secretion or tight junction protein expression within the gut epithelium. Thirdly, probiotic bacteria can modulate the host's immune system, in particular via the gut immune system. In the host's gastrointestinal tract, there are several mechanisms which allow gut microbiota to mount an appropriate host immune response to fight the invading pathogens without the excessive induction of a deleterious immune response to the host's body as reviewed recently (Baumler & Sperandio, 2016; Pamer, 2016). Several studies also showed that manipulation of the host's immune system by probiotic bacteria provided a benefit to diet-induced obesity (Alard et al., 2015; Moya-Perez et al., 2015; Naito

Table 2
Alterations of gut microbiota in high-fat diet induced obesity from animal studies.

Model	Age	Duration	Major findings	Interpretation	References
Studies in germ-free/gnotobiotic models					
Male CONV but specific pathogen free C57BL/6 mice induced obesity by high fat diet (45% fat)	Adulthood	16 weeks	↑ Body weight since week 6th ↑ Fat mass since week 6th ↑ Plasma insulin ↑ HOMA index ↑ Pro-inflammatory cytokine mRNA in ileum (TNF-α) since week 6th ↑ Intestinal pro-inflammatory transcription factor (NF-κB)	Gut microbiota plays a crucial role to induce obesity and insulin resistance by HFD consumption via pro-inflammatory changes.	Ding et al. (2010)
Male germ-free C57BL/6 mice induced obesity by high fat diet (45% fat)	Adulthood	16 weeks	↔ Body weight ↔ Fat mass ↔ Intestinal pro-inflammatory cytokine mRNA (TNF-α) When colonization of HFD-CONV feces: ↑ Intestinal pro-inflammatory transcription factor (NF-κB)		
Male CONV and gnotobiotic SIHUMI C3H/HeOu mice induced obesity by high fat diet (44.7% fat)	Adulthood	5 weeks	↑ Body weight ↑ Glucose tolerance ↑ Fat mass	Gut microbiota plays a crucial role inducing obesity by HFD consumption.	Woting et al. (2015)
Male gnotobiotic SIHUMI C3H/HeOu mice induced obesity by high fat diet (44.7% fat)	Adulthood	4 weeks	↑ Body weight ↑ Body fat ↑ Food efficiency (Glut2,fatty acid translocase in gut)	Gut microbiota especially *Clostridium ramosum* plays a crucial role in the induced obesity by HFD consumption.	Woting et al. (2014)
Male gnotobiotic SIHUMI **without** *Clostridium ramosum* C3H/HeOu mice induced obesity by high fat diet(44.7% fat)	Adulthood	4 weeks	↔ Body weight ↔ Body fat ↔ Food efficiency (Glut2,fatty acid translocase in gut)		
Male gnotobiotic **with** *Clostridium ramosum* **only** C3H/HeOu mice induced obesity by high fat diet(44.7% fat)	Adulthood	4 weeks	↑ Body weight ↑ Body fat ↑ Food efficiency (Glut2,fatty acid translocase in gut)		
Studies in wild type models					
Male Sprague-Dawley rats induced obesity by high fat diet (45% fat)	Adulthood	12 weeks	↑ Body weight since week 8th ↑ Adiposity index since week 8th ↑ Energy intake since week 8th ↑ Inflammation in ileum (↑MPO,↑LPS, ↑TLR4,↓IAP) ↑ Gut permeability ↑ Bacterodoidales since week 8th ↑ Clostridiales since week 8th ↑ Enterobacteriales since week 8th	HFD-induced obesity is associated with gut microbiota alteration and gut inflammation.	de La Serre et al. (2010)
Male C57BL/6 mice induced obesity by high fat diet (60% fat)	–	8 weeks	↑ Body weight ↑ Epididymal fat ↑ Plasma cholesterol ↑ Plasma triglyceride ↑ Plasma insulin ↑ Fasting blood glucose ↑ Circulating pro-inflammatory cytokines (TNF-α, IL-1β, IL-6) ↑ Pro-inflammatory mRNA (TNF-α, IL-1β, IL-6) in adipose tissue ↑ Adipogenic mRNA (PPARγ, C/EBP, FAS, aFABP) in adipose tissue ↑ Macrophage mRNA (CD68, F4/80) in adipose tissue ↑ Endotoxin levels (LPS) in plasma and feces ↑ Intestinal inflammation (MPO, iNOS, TLR4, p-IKKβ, p-p65, COX2) ↑ Gut permeability (↓ tight junction) ↑ Oxidative stress (p-Akt, p-FOXO3a, p-mTOR) ↑ Firmicutes: Bacteroides ratio ↑ Enterobacteria ↓ Bifidobacteria	HFD-induced obesity and metabolic disturbance are associated with gut microbiota alteration, leading to inflammation via TLR4 signaling pathway.	Kim et al. (2012)
Male TLR4 deficient C57BL/10ScNJ mice induced obesity by high fat diet (60% fat)	–	8 weeks	↑ Body weight ↑ Epididymal fat ↔ Metabolic parameters		

Table 2 (*Continued*)

Model	Age	Duration	Major findings	Interpretation	References
			↔ Circulating pro-inflammatory cytokines ↔ Endotoxin levels ↔ Intestinal inflammation ↔ Oxidative stress		
Male C57BL/6NCrlBltw mice induced obesity by high fat diet(60% fat)	Adulthood	16 weeks	↑ Body weight ↑ Epididymal and subcutaneous fat ↑ Adipocyte size and numbers ↑ Insulin resistance (p-IRS-1) ↑ Pro-inflammatory mRNA (TNF-α, IL-1β, IL-6) and macrophages in liver and adipose tissue ↓ Anti-inflammatory mRNA level (IL-10) and regulatory T-cells in liver and adipose tissue ↑ Serum endotoxin levels (LPS) ↑ TLR-4 signaling pathway (TLR-4, P-JNK) ↑ Gut permeability (↓ tight junction) ↑ Firmicutes: Bacteroides ratio	HFD-induced obesity with insulin resistance is associated with gut microbiota alteration, leading to inflammation via TLR4 signaling pathway.	Chang et al. (2015)
Male C57BL/6J mice induced obesity by high fat diet(34.3% fat)	Adulthood	6 weeks	↑ Adipocyte size ↑ Firmicutes: Bacteroides ratio ↓ Lactobacillaceae	HFD-induced obesity is associated with gut microbiota alteration.	Park et al. (2015)
C57BL/6J mice induced obesity by high fat diet(58% fat)	Adulthood	32 weeks	↑ Body weight ↑ Plasma triglyceride ↑ Plasma cholesterol ↑ Insulin resistance ↑ Plasma insulin ↑ Fasting blood glucose ↓ Microbial diversity ↑ Firmicutes: Bacteroides ratio ↑ Proteobacteria	HFD-induced obesity and metabolic disturbance are associated with gut microbiota alteration.	Zheng et al. (2016)
Male C57BL/6J mice induced obesity by high fat diet(45% fat)	Adulthood	14 weeks	↑ Body weight ↑ Body fat ↑ Plasma triglyceride ↑ Plasma cholesterol ↓ Plasma adinopectin ↑ Plasma glucose ↑ Plasma insulin ↑ Insulin resistance (HOMA index) ↑ Pro-inflammatory cytokines (TNF-α, IL-1β, IL-6) in plasma and liver ↓ Anti-inflammatory cytokines (IL-10) in plasma and liver ↑ Firmicutes: Bacteroidetes ratio ↑ Firmicutes ↓ Bacteroidetes (Especially Akkermansia)	HFD-induced obesity and metabolic disturbance are associated with gut microbiota alteration and systemic inflammation.	Song et al. (2015)
Male C57BL/6J mice induced obesity by high fat diet(60% fat)	Adulthood	16 weeks	↑ Body weight since week 8th ↑ White adipose tissue mass ↑ Plasma cholesterol ↑ Plasma glucose ↑ Plasma insulin ↑ Insulin resistance (HOMA index) ↑ Hepatic stenosis ↑ Monocyte/macrophage markers ↓ Regulatory T-cell (Foxp3/PPARγ gene expression) ↑ Pro-inflammatory cytokines (TNF-α, IL-1, IL-6,IL-17) in liver ↓ Anti-inflammatory cytokines (IL-10) in liver ↑ Firmicutes: Bacteroidetes ratio ↑ Firmicutes (Especially Lactobacillaceae) ↓ Bacteroidetes (Especially	HFD-induced obesity and metabolic disturbance are associated with gut microbiota alteration and systemic inflammation.	Alard et al. (2015)

Table 2 (*Continued*)

Model	Age	Duration	Major findings	Interpretation	References
			Akkermansia and Rikenellaceae) ↓ SCFA		
Male specific pathogen-free wistar rats induced obesity by high fat diet (60% fat)	Adulthood	10 weeks	↑ Body weight ↑ Fat mass ↓ SCFA-producing bacteria	HFD-induced obesity is associated with gut microbiota alteration.	Zhang et al. (2015)
Male C57BL/6J mice induced obesity by high fat diet(60% fat)	Adulthood	14 weeks	↑ Body weight gain ↑ Plasma triglyceride ↑ Plasma cholesterol ↑ Plasma glucose ↑ Plasma insulin ↓ Glucose tolerance ↑ Insulin resistance (HOMA index) ↓ Regulatory T-cell in plasma and adipose tissue ↑ Pro-inflammatory cytokines (TNF-α, IL-1, IL-6,IL-17) in plasma, adipose tissue, gut and liver ↑ Plasma LPS ↑ Firmicutes (Especially Lactobacillaceae) ↑ Proteobacteria	HFD-induced obesity and metabolic disturbance are associated with gut microbiota alteration and systemic inflammation.	Moya-Perez et al. (2015)
Male Sprague-Dawley rats induced obesity by high fat diet (43% fat)	Adulthood	16 weeks	↑ Body weight ↑ Body fat ↑ plasma triglyceride ↑ plasma leptin ↑ Glucose tolerance ↑ SCFA producing bacteria	Changes in gut microbiota correlate with obesity-related metabolic parameters.	Lecomte et al. (2015)

Abbreviation: CONV-conventional TNF-tumor necrotic factor NF-nuclear factor HFD-high fat diet MPO-myeloperoxidase LPS-lipopolysaccharides TLR-toll -like receptor IAP-intestinal alkaline phosphatase IL-interleukin PPAR-peroxisome proliferation activator receptor iNOS-inducible nitric oxide synthase p -phosphorylation COX-cyclooxygenase IRS-insulin receptor substrate SCFA-short chain fatty acid.

et al., 2011; Park et al., 2015; Woting et al., 2015; Zhang et al., 2015). Nonetheless, gut microbiota manipulation by probiotics, prebiotics and synbiotics, on jaw bone health is still poorly understood, particularly in obesity-induced jaw bone loss.

6. Bone health, gut microbiota and the immune system

Interestingly, recent studies found that gut microbiota can regulate bone mass in mice (Sjogren et al., 2012). The authors of this study showed that the germ free mice have greater bone mass when compared to normal mice, which it can be assumed is associated with decreased pro-inflammatory cytokine levels followed by decreased osteoclast levels, cells which play a major role in bone resorption. This study also demonstrated that gut microbiota regulated host bone density by allowing mice to properly develop a specific immune cell (helper or $CD4^+$ T cell) and the osteoclast precursor cells ($CD11b^+$/GR1) in their bone marrow. These findings suggested that gut microbiota manipulate host immune responses in a way that activates physiological bone resorption by promoting bone marrow-derived osteoclast function and also contributing to normal bone homeostasis. The manipulation of gut microbiota and host immune responses may be a potential therapeutic target for alveolar bone loss in the obese condition.

In recent studies, the manipulation of gut microbiota was often used as a new therapeutic strategy for treatment of bone diseases. Both probiotics and prebiotics, as well as synbiotics, have been given to rodents to explore the effects on bone, mainly in long bones, in various conditions. Particularly, regarding the model of estrogen deficiency-induced osteoporosis via an ovariectomy, the studies found that the administration of either probiotics or prebiotics can attenuate bone loss (Britton et al., 2014; Ohlsson et al., 2014; Parvaneh et al., 2015; Yang, Wu, Lu, & Lin, 2013). For example: 1) probiotic *Lactobacillus reuteri* significantly protected menopausal ovariectomized mice from bone loss by modifying gut microbiota communities and host immune cells followed by decreasing levels of osteoclast bone resorption markers and activators (tartrate-resistant acid phosphatase, Trap5, and RANKL) (Britton et al., 2014); 2) The osteoblast bone formation markers were also increased after treatment with probiotic *Bifidobacterium longum* in ovariectomized female mice (Parvaneh et al., 2015); 3) An aqueous extract of prebiotic *Anoectochilus formosanus* also prevented bone loss in the ovariectomized female Wistar rats (Yang, Wu et al., 2013). The administration of *A. formosanus* extract enhanced numbers of gut mucosal-protective *Bifidobacterium* spp., acidity levels, calcium absorption and retention in the rat's intestinal tract (cecum).

The role of prebiotics on long bone health in growing animals has also been reported (Bryk et al., 2015; Weaver et al., 2011). For instance, prebiotic galacto-oligosaccharide (GOS) treatment in growing rats increased numbers of *Bifidobacterium* spp. and modified the gut microenvironment which enhanced calcium and magnesium utilization and reduced the number of osteoclast cells, resulting in improved bone mechanical properties (Weaver et al., 2011). Furthermore, intake of the synbiotic Yacon flour with *B.longum* led to an increase in the concentration of minerals in the long bones of normal male mice even though the bone properties were no different (Rodrigues et al., 2012).

There have been a few studies which demonstrated the role of probiotics and prebiotics in promoting jaw bone health. Most of

Table 3
Effects of probiotic and prebiotic treatments in HFD-induced obese animal models.

Model	Duration of HFD (30–60%)	Pro/Prebiotics	Duration	Major findings	Interpretation	References
Probiotic treatment						
Male wistar rats	8 weeks	*L. paracasei* (1×10^9CFU/day)	+8 weeks	↓ Body weight ↓ Final abdominal fat ↑ Lipolysis (plasma free fatty acid levels) ↑ Sympathetic nerve activity in brown adipose tissue ↓ Hepatic vagal nerve activity	*L. paracasei* affected autonomic activities, enhanced lipolysis, leading to reduce body weight.	Tanida et al. (2008)
Male C57BL/6 mice	11 weeks	*L.casei* (0.05%w/w)	+5 weeks	↔ Body weight, fat mass ↓ Total fat, triglyceride and cholesterol in liver ↓ Insulin resistance (insulin tolerance test, OGTT) ↔ plasma insulin ↓ Plasme endotoxemia (Lipopolysaccharide binding protein, LBP)	*L.casei* improved insulin resistance and glucose intolerance without body weight loss by reducing endotoxemia.	Naito et al. (2011)
Male C57BL/6J mice	6 weeks	*L. plantarum* FH185 (1×10^9CFU/day)	6 weeks	↓ Adipocyte size ↓ Firmicutes: Bacteroides ratio ↑ Lactobacillaceae	*L. plantarum* FH185 improved obesity by altering gut microbiota.	Park et al. (2015)
Male C57BL/6J mice	16 weeks	Mixture of *L. salivarius, L. rhamnosus* and *B. animalis* (1×10^9CFU/day)	17 weeks	↓ Body weight since week 8th ↓ White adipose tissue mass ↓ Plasma cholesterol ↓ Plasma glucose ↓ Plasma insulin ↓ Insulin resistance (HOMA index) ↓ Hepatic stenosis ↓ Monocyte/macrophage markers ↑ Regulatory T-cell (Foxp3/ PPARγ gene expression) ↓ Pro-inflammatory cytokines (TNF-α, IL-1, IL-6,IL-17) in liver ↑ Anti-inflammatory cytokines (IL-10) in liver ↓ Firmicutes: Bacteroidetes ratio ↓ Firmicutes (Especially Lactobacillaceae) ↑ Bacteroidetes (Especially Akkermansia and Rikenellaceae) ↑ SCFA	Probiotic treatment improved obesity and metabolic disturbance by altering gut microbiota and reducing inflammation.	Alard et al. (2015)
Male C57BL/6J mice	14 weeks	*B. pseudocatenulatum* CECT7765 (1×10^9CFU/day)	14 weeks	↓ Body weight gain ↓ Plasma triglyceride ↓ Plasma cholesterol ↓ Plasma glucose ↓ Plasma insulin ↑ Glucose tolerance ↓ Insulin resistance (HOMA index) ↑ Regulatory T-cell in plasma and adipose tissue ↓ Pro-inflammatory cytokines (TNF-α, IL-1, IL-6,IL-17) in plasma, adipose tissue, gut and liver ↓ Plasma LPS ↓ Firmicutes (Especially Lactobacillaceae) ↓ Proteobacteria	*Bifidobacterium pseudocatenulatum* CECT 7765 reduced obesity-associated inflammation by restoring the lymphocyte-macrophage balance and gut microbiota structure in high-fat diet-fed mice.	Moya-Perez et al. (2015)
Prebiotic treatment						
Male C57BL/6 mice	2 weeks	Fructo-oligosaccharides (10%)	2 weeks	↓ Body weight ↓ Body fat ↔Plasma triglyceride ↔Plasma glucose ↔Plasma insulin ↑ Bacteroidetes	Prebiotic treatment reduced body weight and body fat without changes in metabolic profiles by altering gut microbiota.	Rajpal et al. (2015)

Table 3 (*Continued*)

Model	Duration of HFD (30–60%)	Pro/Prebiotics	Duration	Major findings	Interpretation	References
Male C57BL/6NCrlBltw mice	16 weeks	Water-extracted *Ganoderma lucidum* (2–8%)	+8 weeks	↓ Body weight ↓ Epididymal and subcutaneous fat ↓ Adipocyte size and numbers ↓ Insulin resistance (p-IRS-1) ↓ Pro-inflammatory mRNA (TNF-α, IL-1β, IL-6) and macrophages in liver and adipose tissue ↑ Anti-inflammatory mRNA (IL-10) and regulatory T-cells in liver and adipose tissue ↓ Serum endotoxin (LPS) ↓ TLR-4 signaling pathway (TLR-4, P-JNK) ↓ Gut permeability (↑ tight junction) ↓ Firmicutes: Bacteroides ratio	Prebiotic treatment reduced obesity by modulating the composition of the gut microbiota and providing anti-inflammation.	Chang et al. (2015)
Male conventional C3H/HeOu male mice	5 weeks	Fructo-oligosaccharides (10%)	5 weeks	↔ Body weight ↔ Glucose tolerance	Oligofructose reduced obesity and improved glucose tolerance independently of presence of *Bifidobacterium longum*.	Woting et al. (2015)
Male gnotobiotic SIHUMI C3H/HeOu mice	5 weeks	Fructo-oligosaccharides	5 weeks	↓ Body weight ↓ Fat mass ↑ Glucose tolerance		
Male gnotobiotic SIHUMI without *B. longum* C3H/HeOu mice	5 weeks	Fructo-oligosaccharides	5 weeks	↓ Body weight ↓ Fat mass ↑ Glucose tolerance		

Abbreviation: HFD-high fat diet OGTT-oral glucose tolerance test PPAR-peroxisome proliferation activator receptor TNF-tumor necrotic factor IL-interleukin SCFA-short chain fatty acid LPS-lipopolysaccharides p-phosphorylation IRS-insulin receptor substrate TLR-toll-like receptor JNK-Jun-amino terminal kinase.

those studies specifically determined the local effects of probiotics on alveolar bone loss in rats with periodontitis (Garcia et al., 2016; Maekawa & Hajishengallis, 2014). The topical application of probiotic *Lactobacillus brevis* CD2 onto the gingiva resulted in significantly decreased bone loss and the level of pro-inflammatory cytokines, including interleukin (IL)-1β, IL-6, IL-17A and tumor necrosis factor (TNF) in ligature-induced periodontitis (Maekawa & Hajishengallis, 2014). These effects could be due to the release of arginine deiminase from the viable *L. brevis* CD2 cells. Arginine deiminase is an enzyme which can inhibit the production of nitric oxide and demonstrates a role in damping inflammation (Maekawa & Hajishengallis, 2014). Besides probiotic bacteria, a brewer's yeast, *Saccharomyces cerevisiae*, has been successfully used as a potential topical probiotic to improve the gingival tissue repairing process in ligature-induced periodontitis in rats (Garcia et al., 2016). Local irrigation of probiotic *S. cerevisiae* led to decreased pro-inflammatory cytokines TNF-α and IL-1β and increased immunosuppressive cytokine IL-10 staining in the first molar tissues of the rats with ligature-induced periodontitis (Garcia et al., 2016). These findings suggested that some probiotic organisms could be of benefit to host jaw bone health via the local regulation of the host immune response. However, the roles of probiotic, prebiotic and synbiotic consumption in maintaining jaw bone health are still poorly understood.

Increasing bone mineral content depends on the body's mineral absorption and retention, this is particularly evident during 'growth spurts', as can be seen iduring puberty. Randomized controlled trials have been carried out on the effects of prebiotics on bone health in puberty (Abrams et al., 2005; Whisner et al., 2013; Whisner et al., 2014). Calcium and magnesium were absorbed and retained more in the body when prebiotics were administered. Long-term (one year) daily consumption of prebiotic inulin-type fructans led to increased calcium absorption and bone mineral density in pubertal adolescents aged between 9 and 13 years old(Abrams et al., 2005). Whisner and colleagues also found that consumption of the prebiotic GOS for a three-week period increases numbers of *Bifidobacterium* spp (determined by quantitative polymerase chain reaction; qPCR) and calcium absorption (determined by urinary calcium excretion) in healthy adolescent girls aged between 10 and 13 years old (Whisner et al., 2013). The evidence regarding the relationship between bone and gut microbiota, including the effects of probiotics, prebiotics and synbiotics on bone are summarized in Table 4.

7. Connection between obesity, bone and gut microbiota

There are some studies which link obesity, bone and gut microbiota (Cho et al., 2012; Collins et al., 2015; Luo et al., 2015). Cho and colleagues showed that altering gut microbiota composition by sub-therapeutic antibiotic treatment (STAT), in a murine model, affected host metabolism including bone metabolism (Cho et al., 2012). The authors demonstrated that the STAT group showed increased bone mineral density only in the early weeks after STAT administration, when compared to the control group. The authors claimed that STAT can alter gut microbiota composition (increased F/B ratio), resulting in the differentiation of pluripotent stem cells into osteoblasts during the dynamic phase of bone growth. This finding suggested there is a role of gut microbiota in regulating bone health. The authors also showed that STAT could increase adiposity (increased fat mass without a

Table 4
Evidence in relationship between bone and gut microbiota.

Model	Age	Intervention	Duration	Major findings	Interpretation	References
Studies in germ-free model						
Female germ-free mice	Adulthood	–	–	↑ Trabecular bone mass ↓ TNF-α, IL-6 mRNA in bone ↓ TNF-α mRNA in bone marrow ↓ TNF-α mRNA in colon ↓ Osteoclast cells in bone ↓ $CD4^+$T cells ↓ Osteoclast precursors in bone marrow	The gut microbiota could regulate bone mass in mice via the mechanism involving altered immune status in bone and decreased osteoclast-mediated bone resorption.	Sjogren et al. (2012)
		Colonization GM to GF-mice	–	↓ Trabecular bone mass ↓ BMD ↑ Osteoclast cells in bone ↑ $CD4^+$T cells ↑ Osteoclast precursors in bone marrow		
Probiotic treatment and its effects on bone						
Female mice induced bone loss by ovariectomy	Adulthood	*L.paracasei, L. plantarum, L.mix (1×10^8CFU/ml in drinking water)*	6 weeks	↑ Cortical BMC ↑ OPG in bone ↓ RANKL:OPG ratio in bone ↑ TGFβ1 in bone marrow ↓ Pro-inflammatory cytokines (TNF-α, IL-1β) in bone ↓ Fractional calcium excretion	Probiotic treatment altered the immune status in bone resulting in attenuated bone resorption in ovariectomized animal.	Ohlsson et al. (2014)
Female mice induced bone loss by ovariectomy	Adulthood	*L.reuteri (1×10^9CFU/ml oral gavage with 1.5×10^8CFU/ml drinking water)*	4 weeks	↑ Trabecular bone mass ↓ Osteoclast cells in bone marrow culture ↓ RANKL in bone marrow ↔ Bone formation rate ↓ $CD4^+$T cells in bone marrow ↑ $CD8^+$T cells in bone marrow ↓ Bacteriodales in colon ↑ Clostridiales in colon	Probiotic treatment suppressed bone resorption in estrogen deprived models by modifying microbial communities in the gut.	Britton et al. (2014)
Female Sprague-Dawley rats induced bone loss by ovariectomy	Adulthood	*Bifidobacterium longum (10^9–10^8 CFU/day)*	16 weeks	↑ Trabecular bone mass ↑ BMD ↑ Bone bending strength ↓ Osteoclast cells in bone ↓ Serum CTX ↑ Serum osteocalcin ↑ Osteoblast cells in bone ↑ Osteoblastogenic gene expression (BMP2) in bone ↑ Calcification (Sparc gene expression) ↑ Bifidobacteria in feces	Probiotic treatment reduced bone loss in ovariectomized rats by decreasing bone resorption and increasing bone formation.	Parvaneh et al. (2015)
Male wistar rats induced alveolar bone loss by periodontitis-induced by gingival ligation	Adulthood	*Saccharomyces cerevisiae (topical injection)*	7/15/30 days	↓ Alveolar bone loss on day 15th when combined with mechanical treatment	Probiotic treatment reduced bone loss in periodontitis by decreasing inflammation when combined with mechanical therapy.	Garcia et al. (2016)

Table 4 (*Continued*)

Model	Age	Intervention	Duration	Major findings	Interpretation	References
				↑ Tissue-repair process accompanied with mechanical treatment ↓ TNF-α and IL-1β immunostaining of periodontal tissue ↑ IL-10 immunostaining of periodontal tissue		
Male C57BL/6 mice induced alveolar bone loss by ligature-induced periodontitis	Childhood	topical *Lactobacillus brevis* CD2 (8×10^5CFU)	5 days	↓ Alveolar bone loss ↓ Pro-inflammatory mRNA (TNF-α, IL-1β, IL-6 and IL-17A) in gingiva ↓ Anaerobic bacteria in periodontal microbiota ↑ Aerobic bacteria in periodontal microbiota	Probiotic treatment decreased bone loss in periodontitis by modulating periodontal microbiota and reducing inflammation.	Maekawa and Hajishengallis (2014)
Prebiotic treatment and its effects on bone						
Female wistar rats induced bone loss by ovariectomy	Adulthood	Standardized aqueous extract of *Anoectochilus formosanus* (SAEAF) (200–400 mg/kg)	12 weeks	↑ Trabecular bone mass ↑ BMC, BMD ↑ Bone strength ↑ Bone stiffness ↑ Elastic modulus of bone ↓ Bone turnover (serum OCN) ↓ Bone resorption (urinary-GT) ↑ Calcium absorption and retention ↓ Cecum pH ↑ Cecum weight ↑ Calcium binding protein mRNA in cecum ↑ Free-Ca concentration in cecum ↑ SCFA ↑ Fecal Bifidobacteria	SAEAF reduced bone loss and improved mechanical bone properties in ovariectomized rats by altering gut microbiota.	Yang, Wu et al. (2013)
Male rats	Childhood	Galacto-oligosaccharides (2–8%)	9 weeks	↑ Bone bending strength ↓ Osteoclast cells in bone ↑ Calcium absorption and retention ↑ Magnesium absorption and retention ↓ Cecum pH ↑ Bifidobacteria in feces	Prebiotic treatment improves bone mechanical properties in young rats by increasing calcium and magnesium utilization, resulting from gut microbiota alteration.	Weaver et al. (2011)
Male wistar rats	Childhood	Mixtures of fructo-oligosaccharides and galacto-oligosaccharides (5.3%)	50 days	↑ Trabecular bone volume ↑ Trabecular BMD ↑ Tibia length ↑ Bone stiffness ↑ Elastic modulus of bone ↑ Osteoblast surface ↑ Bone mineral content (Ca, P) ↓ Fecal Ca, Mg, P ↑ Ca, Mg, P absorption ↑ Cecum weight ↓ Cecum pH ↑ Lactobacillus	Supplementing diets with GOS/FOS mixture improves bone mechanical properties in young rats by increasing calcium and magnesium utilization, resulting from gut microbiota alteration	Bryk et al. (2015)

Table 4 (*Continued*)

Model	Age	Intervention	Duration	Major findings	Interpretation	References
Synbiotic treatment and its effects on bone						
Male wistar rats	Adulthood	Yacon flour (Fructo-oligosaccharides) (15.6%) and *B. Longum* (1×10^8 *CFU/day*)	4 weeks	↔ bone thickness, length, strength ↑ bone mineral content (Ca,P,Mg) ↑ SCFA ↑ Cecum weight ↑ Anaerobic bacteria	–Yacon flour in combination with B.longum helped increase the concentration of minerals in bones. – Modulation of gut microbiota by synbiotic treatment improves bone mineral content but not bone properties.	Rodrigues et al. (2012)
Clinical studies						
100 puberty human RCT	9–13 years old	Inulin-type fructans	8 g/d for 8 weeks and 12 months	↑ BMD and BMC ↑ Calcium absorption in Fok1 genotype FF (VitD receptor)	Prebiotic treatment improves BMD and BMC in adolescents by increasing calcium absorption and modulating genetic factors (vitamin D receptor gene polymorphisms).	Abrams et al. (2005)
26 young girls Double-blind cross-over RCT	10–13 years old	Galacto-oligosaccharides	5 g/d for 3 weeks	↑ Fractional calcium absorption in 48 h ↑ Bifidobacteria in feces	Modulation of gut microbiota by prebiotic treatment increased calcium absorption in adolescents.	Whisner et al. (2013)
15 boys + 9 girls Double-blind RCT	12–15 years old	Soluble maze fibre	12 g/d for 3 weeks	↑ Calcium absorption ↔ Calcium retention ↓ Firmecutes ↑ Bacteroidetes	Consumption of soluble maize fibre affected short-term calcium absorption in adolescent boys and girl.	Whisner et al. (2014)

Abbreviation: GM-gut microbiota GF-germ free TNF-tumor necrosis factor IL-interleukin BMD-bone mineral density BMC-bone mineral content OPG-osteoprotegerin RANKL-receptor activator of nuclear factor TGF-transforming growth factor CTX-C-terminal telopeptide BMP-bone morphogenetic protein OCN-osteocalcin SCFA-short chain fatty acid.

Table 5
Evidence in relationship among obesity, bone and gut microbiota.

Model	Age	Duration	Major findings	Interpretation	References
Male C57BL/6 mice induced obesity by high fat diet	Adulthood	6 weeks	↑ Body weight and BMI ↑ Mesenchymal stem cells in bone marrow ↑ Adipocytes and adipogenic gene expression (PPARγ) in bone marrow ↑ Adipocytes in bone ↓ Osteoblast in bone marrow ↓ Osteoblast in bone ↓ Bone formation gene expression (OPN) in bone marrow ↑ Hematopoeitic stem cells in bone marrow ↑ Multipotent stem cells and Myeloid progenitors in bone marrow ↓ Lymphoid progenitors and B-cells in bone marrow ↑ Firmicutes: Bacteroides ratio	Obesity-mediated gut microbiota induced alteration in stem cell differentiation, resulting in decreased osteoblastic bone formation and increased osteoclastic bone resorption.	Luo et al. (2015)
Male C57BL/6J mice altered GM by sub-therapeutic antibiotic treatment (STAT)	Childhood	7 weeks	↔ Body weight ↑ Fat mass, body fat ↑ Hepatic lipogenesis ↑ BMD at week 3 ↑ Firmicutes:Bacteroides ratio	Gut microbiota altered by antibiotics caused increased adiposity and higher BMD during growth.	Cho et al. (2012)
Male Sprague-Dawley rats induced obesity by high fat diet	adulthood	28 week	↑ Body mass and body fat ↑ Leptin in synovial fluid and serum ↑ Osteoarthritis development (modified Mankin Score in joints) ↑ Pro-inflammatory cytokines in synovial fluid and serum ↑ Serum LPS ↑ Enterobactericeae ↑ Firmicutes: Bacteroides ratio	HFD-induced obesity was associated with the development of osteoarthritis and gut microbiota alterations.	Collins et al. (2015)

Abbreviation: BMI-body mass index PPAR-peroxisome proliferation activator receptor OPN-osteopontin BMD-bone mineral density LPS-lipopolysaccharide.

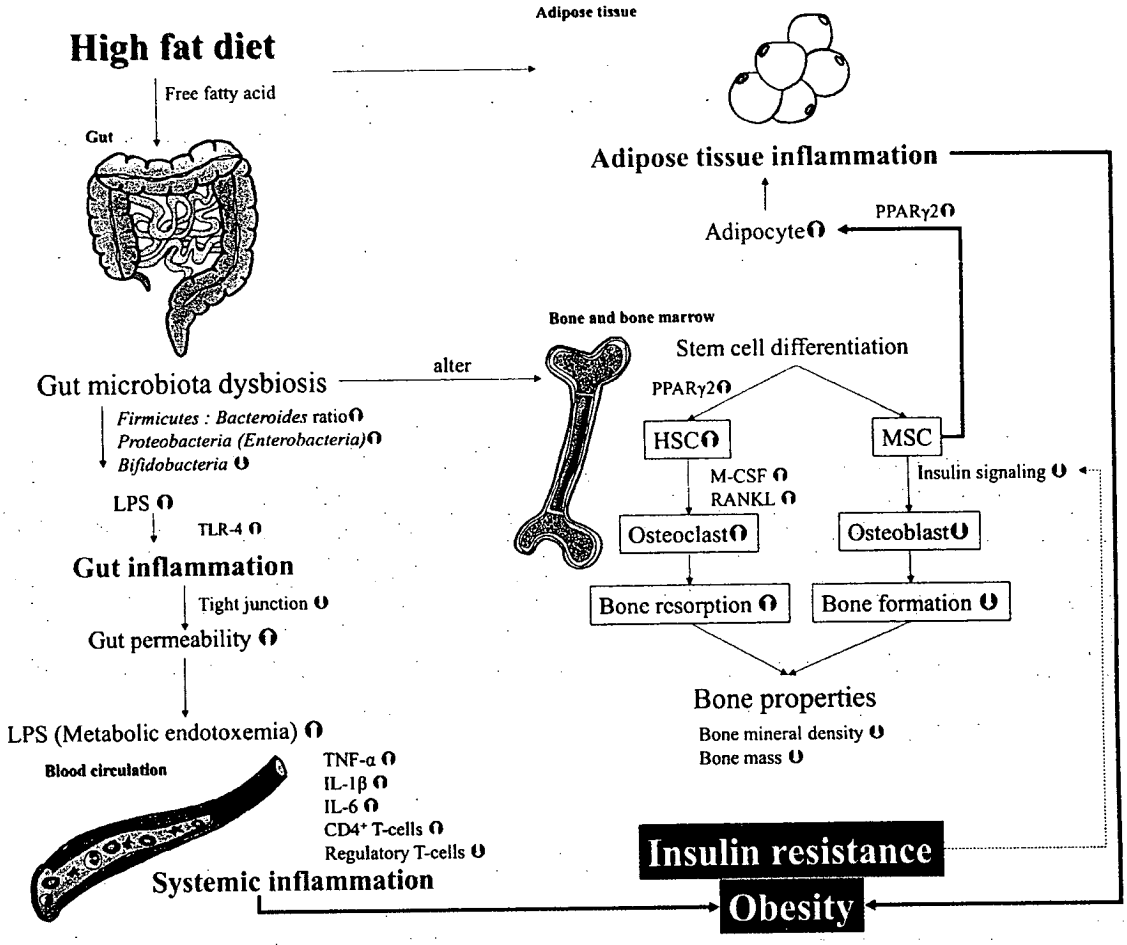


Fig. 1. Proposed relationship among diet-induced obesity, gut microbiota and bone structure. High free fatty acid levels as a result of high-fat diet consumption can lead to the development of obese-insulin resistance and the reduction of bone density via these two possible mechanisms: 1) Too high a level of free fatty acids initiates gut microbiota dysbiosis as seen by an increased Firmicutes/Bacteroides ratio, increased Proteobacteria and decreased Bifidobacteria, leading to increased lipopolysaccharide (LPS) levels. A high LPS activates the innate immune system via the toll-like receptor (TLR)-4, resulting in gut inflammation, an impaired gut tight junction, increased gut permeability, and the leakage of LPS into the bloodstream (Metabolic endotoxemia). Metabolic endotoxemia stimulates chronic systemic inflammation by producing pro-inflammatory cytokines such as tumor necrosis factor (TNF)-α, interleukin (IL)-1β and IL-6, together with enhancing CD4+ T-cells and inhibiting regulatory T-cells. These phenomena contribute to obese-insulin resistance. The obese-insulin resistant condition also leads to a deterioration in osteoblastic signaling, resulting in decreased bone formation. 2) Gut dysbiosis which alters stem cell differentiation in the bone marrow via peroxisome proliferator-activated receptors (PPAR-γ2). The bone marrow niche changes the population from mesenchymal stem cells (MSCs) to adipocytes, causing adipose tissue inflammation, and leads to increased numbers of hematopoietic stem cells (HSCs). Osteoclasts are further differentiated from HSCs via the induction of a macrophage colony stimulating factor (M-CSF) and receptor activator of nuclear factor-κB ligands (RANKL). These incidences may result in increased bone resorption and decreased bone formation.

significant change in body weight) in mice. Alterations of gut microbiota by antibiotics seem to affect not only gut microbiota, but also host metabolism.

In addition, Collins and colleagues reported that diet-induced obese rats developed greater metabolic endotoxemia, gut dysbiosis and osteoarthritis compared to their lean counterparts (Collins et al., 2015). Luo and colleagues recently investigated the effect of high-fat diet-induced obesity on the hematopoietic stem cell compartment and bone-derived niche. The authors found that high-fat diet consumption resulted in gut dysbiosis (identified by an increased F/B ratio) and initiated a shift in hematopoietic stem cell differentiation from lymphoid to myeloid lineage which could be partially rescued by antibiotic treatment and fecal transplantation (Luo et al., 2015). Consumption of a high-fat diet can strongly activate peroxisome proliferator-activated receptor gamma (PPAR-γ) 2 in bone marrow, resulting in decreased osteoblastic bone formation and increased osteoclastic bone resorption. This study suggested that the metabolic stress of a high-fat diet and resulting dysbiotic gut microbiota might together play a role in changes in the bone marrow niche for bone formation These findings are summarized in Table 5.

For the improvement of bone health through gut microbiota manipulation, however, more well-designed studies are required to elucidate the connection between gut microbiota, bone metabolism and obesity. Here, we propose the possible underlying mechanistic explanations of the relationship between gut microbiota and the host immune response in the bone health of rats with obesity, the summary is shown in Fig. 1.

8. Conclusion

Recent data suggest that diet-induced obesity has a negative impact on bone health possibly via the alteration of gut microbiota and host immune status. Gut dysbiosis, an imbalance of the resident gut microbiota population, instigated by a long-term high-fat and high-sugar diet consumption results in an increased inflammatory tone both locally and systemically. These chronic inflammatory conditions have been proposed as pivotal factors for

the subsequent bone loss found in the obese model. The diminished bone mass following a chronic high-fat and high-sugar diet consumption is caused by an increased osteoclastogenesis and decreased osteoblastogenesis. The other plausible explanations are altered serum adipokines, increased leptin and decreased adiponectin levels which could both directly and indirectly affect bone metabolism in cases of obesity.

In this study, we have reviewed the role of host-friendly probiotic bacteria, prebiotics and synbiotics in association with alveolar bone health. Several studies have already supported the beneficial use of probiotics in the case of several human diseases including obesity and metabolic disorders. Major modes of action of probiotics in human health are proposed as manipulators of both gut microbiota and the host immune response. However, the practically use of probiotics, prebiotics or synbiotics to prevent or improve the loss of jaw bone density caused by chronic systemic inflammation in conditions of obesity should be carefully considered. Due to a lack of available supportive data, new well-designed experiments and/or randomized control clinical trial data would definitely benefit this field. Understanding more of the underlying mechanisms of how gut microbiota plays a role in cafeteria diet (high-fat/high carbohydrate diet)-induced obesity and its related pathology, including jaw bone density loss, is essential for the field of dental research. This review has gathered the available up-to-date published findings, which are mainly from animal studies, and summarized this evidence which exhibits an association between obesity, gut microbiota and jaw bone density.

Conflict of interest

The authors declare that there is no conflict of interest.

Acknowledgements

This work was supported by Thailand Research Fund grants: TRF-BRG 5780016 (SC) and TRG5880041 (PT); a CMU^{50th} Anniversary grant by Chiang Mai University (PHD/014/2557 SE&SC); the National Research Council of Thailand (SC); a NSTDA Research Chair Grant from the National Science and Technology Development Agency Thailand (NC) and a Chiang Mai University Center of Excellence Award (NC). The authors would like to thank Ms. Maria Love for her editorial assistance.

References

Abou-Raya, A., & Abou-Raya, S. (2006). Inflammation: A pivotal link between autoimmune diseases and atherosclerosis. *Autoimmunity Reviews, 5*(5), 331–337.

Abrams, S. A., Griffin, I. J., Hawthorne, K. M., Liang, L., Gunn, S. K., Darlington, G., & Ellis, K. J. (2005). A combination of prebiotic short- and long-chain inulin-type fructans enhances calcium absorption and bone mineralization in young adolescents. *The American Journal of Clinical Nutrition, 82*(2), 471–476.

Alard, J., Lehrter, V., Rhimi, M., Mangin, I., Peucelle, V., Abraham, A. L., ... Grangette, C. (2015). Beneficial metabolic effects of selected probiotics on diet-induced obesity and insulin resistance in mice are associated with improvement of dysbiotic gut microbiota. *Environmental Microbiology Reports, 18*(5), 1484–1497.

Alexander, C., & Rietschel, E. T. (2001). Bacterial lipopolysaccharides and innate immunity. *Journal of Endotoxin Research, 7*(3), 167–202.

Amar, S., Zhou, Q., Shaik-Dasthagirisaheb, Y., & Leeman, S. (2007). Diet-induced obesity in mice causes changes in immune responses and bone loss manifested by bacterial challenge. *Proceedings of the National Academy of Sciences of the United States of America, 104*(51), 20466–20471.

Baumler, A. J., & Sperandio, V. (2016). Interactions between the microbiota and pathogenic bacteria in the gut. *Nature, 535*(7610), 85–93.

Belkaid, Y., & Hand, T. W. (2014). Role of the microbiota in immunity and inflammation. *Cell, 157*(1), 121–141.

Berg, R. M., Wallaschofski, H., Nauck, M., Rettig, R., Markus, M. R., Laqua, R., ... Hannemann, A. (2015). Positive association between adipose tissue and bone stiffness. *Calcified Tissue International, 97*(1), 40–49.

Blasco-Baque, V., Serino, M., Vergnes, J. N., Riant, E., Loubieres, P., Arnal, J. F., ... Kemoun, P. (2012). High-fat diet induces periodontitis in mice through lipopolysaccharides (LPS) receptor signaling: Protective action of estrogens. *PLoS One, 7*(11), e48220.

Britton, R. A., Irwin, R., Quach, D., Schaefer, L., Zhang, J., Lee, T., ... McCabe, L. (2014). Probiotic L. reuteri treatment prevents bone loss in a menopausal ovariectomized mouse model. *Journal of Cellular Physiology, 229*(11), 1822–1830.

Bron, P. A., van Baarlen, P., & Kleerebezem, M. (2012). Emerging molecular insights into the interaction between probiotics and the host intestinal mucosa. *Nature Reviews Microbiology, 10*(1), 66–78.

Brown, K., DeCoffe, D., Molcan, E., & Gibson, D. L. (2012). Diet-induced dysbiosis of the intestinal microbiota and the effects on immunity and disease. *Nutrients, 4*(8), 1095–1119.

Bryk, G., Coronel, M. Z., Pellegrini, G., Mandalunis, P., Rio, M. E., de Portela, M. L., & Zeni, S. N. (2015). Effect of a combination GOS/FOS(R) prebiotic mixture and interaction with calcium intake on mineral absorption and bone parameters in growing rats? *European Journal of Nutrition, 54*(6), 913–923.

Caffarelli, C., Alessi, C., Nuti, R., & Gonnelli, S. (2014). Divergent effects of obesity on fragility fractures. *Clinical Interventions in Aging, 9*, 1629–1636.

Cani, P. D., Amar, J., Iglesias, M. A., Poggi, M., Knauf, C., Bastelica, D., ... Burcelin, R. (2007). Metabolic endotoxemia initiates obesity and insulin resistance. *Diabetes, 56*(7), 1761–1772.

Cao, J. J. (2011). Effects of obesity on bone metabolism. *Journal of Orthopaedic Surgery and Research, 6*, 30.

Cavagni, J., Wagner, T. P., Gaio, E. J., Rego, R. O., Torres, I. L., & Rosing, C. K. (2013). Obesity may increase the occurrence of spontaneous periodontal disease in Wistar rats. *Archives of Oral Biology, 58*(8), 1034–1039.

Cavagni, J., de Macedo, I. C., Gaio, E. J., Souza, A., de Molon, R. S., Cirelli, J. A., ... Rosing, C. K. (2015). Obesity and hyperlipidemia modulate alveolar bone loss in wistar rats. *Journal of Periodontology*1–15.

Chang, C. J., Lin, C. S., Lu, C. C., Martel, J., Ko, Y. F., Ojcius, D. M., ... Lai, H. C. (2015). Ganoderma lucidum reduces obesity in mice by modulating the composition of the gut microbiota. *Nature Communications, 6*, 7489.

Cho, I., Yamanishi, S., Cox, L., Methe, B. A., Zavadil, J., Li, K., ... Blaser, M. J. (2012). Antibiotics in early life alter the murine colonic microbiome and adiposity. *Nature, 488*(7413), 621–626.

Collins, K. H., Paul, H. A., Reimer, R. A., Seerattan, R. A., Hart, D. A., & Herzog, W. (2015). Relationship between inflammation the gut microbiota, and metabolic osteoarthritis development: Studies in a rat model. *Osteoarthritis and Cartilage, 23*(11), 1989–1998.

Compston, J. (2015). Obesity and fractures in postmenopausal women? *Current Opinion in Rheumatology, 27*(4), 414–419.

Consortium, T. H. M. P. (2012). Structure, function and diversity of the healthy human microbiome. *Nature, 486*(7402), 207–214.

Cornish, J., Callon, K. E., Bava, U., Lin, C., Naot, D., Hill, B. L., ... Reid, I. R. (2002). Leptin directly regulates bone cell function in vitro and reduces bone fragility in vivo. *The Journal of Endocrinology, 175*(2), 405–415.

Correction Naghavi, M., Wang, H., Lozano, R., Davis, A., Liang, X., Zhou, M., ... Abd-Allah, F. (2015). Global, regional, and national age-sex specific all-cause and cause-specific mortality for 240 causes of death, 1990–2013. *The Lancet, 385*(9963), 117–171.

Crepaldi, G., Romanato, G., Tonin, P., & Maggi, S. (2007). Osteoporosis and body composition. *Journal of Endocrinological Investigation, 30*(Suppl. 6), 42–47.

de La Serre, C. B., Ellis, C. L., Lee, J., Hartman, A. L., Rutledge, J. C., & Raybould, H. E. (2010). Propensity to high-fat diet-induced obesity in rats is associated with changes in the gut microbiota and gut inflammation? *American Journal of Physiology Gastrointestinal and Liver Physiology, 299*(2), G440–448.

De Laet, C., Kanis, J. A., Oden, A., Johanson, H., Johnell, O., Delmas, P., ... Tenenhouse, A. (2005). Body mass index as a predictor of fracture risk: A meta-analysis. *Osteoporosis International, 16*(11), 1330–1338.

de Luca, C., & Olefsky, J. M. (2008). Inflammation and insulin resistance. *FEBS Letters, 582*(1), 97–105.

do Nascimento, C. M., Cassol, T., da Silva, F. S., Bonfleur, M. L., Nassar, C. A., & Nassar, P. O. (2013). Radiographic evaluation of the effect of obesity on alveolar bone in rats with ligature-induced periodontal disease. *Diabetes Metabolic Syndrome and Obesity, 6*, 365–370.

Dimitri, P., Bishop, N., Walsh, J. S., & Eastell, R. (2012). Obesity is a risk factor for fracture in children but is protective against fracture in adults: A paradox? *Bone, 50*(2), 457–466.

Ding, S., Chi, M. M., Scull, B. P., Rigby, R., Schwerbrock, N. M., Magness, S., ... Lund, P. K. (2010). High-fat diet: Bacteria interactions promote intestinal inflammation which precedes and correlates with obesity and insulin resistance in mouse. *PLoS One, 5*(8), e12191.

Donaldson, G. P., Lee, S. M., & Mazmanian, S. K. (2016). Gut biogeography of the bacterial microbiota. *Nature Reviews Microbiology, 14*(1), 20–32.

Ducy, P., Amling, M., Takeda, S., Priemel, M., Schilling, A. F., Beil, F. T., ... Karsenty, G. (2000). Leptin inhibits bone formation through a hypothalamic relay: A central control of bone mass. *Cell, 100*(2), 197–207.

Eckel, R. H., Kahn, S. E., Ferrannini, E., Goldfine, A. B., Nathan, D. M., Schwartz, M. W., ... Smith, S. R. (2011). Obesity and type 2 diabetes: What can be unified and what needs to be individualized? *The Journal of Clinical Endocrinology & Metabolism, 96*(6), 1654–1663.

Ejtahed, H. S., Soroush, A. R., Angoorani, P., Larijani, B., & Hasani-Ranjbar, S. (2016). Gut microbiota as a target in the pathogenesis of metabolic disorders: A new approach to novel therapeutic agents. *Hormone and Metabolic Research, 48*(06), 349–358.

Elefteriou, F., Takeda, S., Ebihara, K., Magre, J., Patano, N., Kim, C. A., ... Karsenty, G. (2004). Serum leptin level is a regulator of bone mass. *Proceedings of the National Academy of Sciences of the United States of America, 101*(9), 3258–3263.

Evans, A. L., Paggiosi, M. A., Eastell, R., & Walsh, J. S. (2015). Bone density: Microstructure and strength in obese and normal weight men and women in younger and older adulthood. *Journal of Bone and Mineral Research, 30*(5), 920–928.

Flint, H. J., Scott, K. P., Louis, P., & Duncan, S. H. (2012). The role of the gut microbiota in nutrition and health. *Nature Reviews Gastroenterology & Hepatology, 9*(10), 577–589.

Fujita, Y., & Maki, K. (2015). High-fat diet-induced obesity triggers alveolar bone loss and spontaneous periodontal disease in growing mice. *BMC Obesity, 3*, 1.

Fujita, Y., Watanabe, K., & Maki, K. (2012). Serum leptin levels negatively correlate with trabecular bone mineral density in high-fat diet-induced obesity mice. *Journal of Musculoskeletal & Neuronal Interactions, 12*(2), 84–94.

Gérard, P. (2016). Gut microbiota and obesity. *Cellular and Molecular Life Sciences, 73*(1), 147–162.

Garcia, V. G., Knoll, L. R., Longo, M., Novaes, V. C., Assem, N. Z., Ervolino, E., ... Theodoro, L. H. (2016). Effect of the probiotic Saccharomyces cerevisiae on ligature-induced periodontitis in rats. *Journal of Periodontal Research, 51*(1), 26–37.

Gourlay, M. L., Hammett-Stabler, C. A., Renner, J. B., & Rubin, J. E. (2014). Associations between body composition, hormonal and lifestyle factors, bone turnover, and BMD. *Journal of Bone Metabolism, 21*(1), 61–68.

Holloway, W. R., Collier, F. M., Aitken, C. J., Myers, D. E., Hodge, J. M., Malakellis, M., ... Nicholson, G. C. (2002). Leptin inhibits osteoclast generation. *Journal of Bone and Mineral Research, 17*(2), 200–209.

Jin, C., & Flavell, R. A. (2013). Innate sensors of pathogen and stress: Linking inflammation to obesity. *The Journal of Allergy and Clinical Immunology, 132*(2), 287–294.

Kawasaki, N., Asada, R., Saito, A., Kanemoto, S., & Imaizumi, K. (2012). Obesity-induced endoplasmic reticulum stress causes chronic inflammation in adipose tissue. *Scientific Reports, 2*, 799.

Kim, K. A., Gu, W., Lee, I. A., Joh, E. H., & Kim, D. H. (2012). High fat diet-induced gut microbiota exacerbates inflammation and obesity in mice via the TLR4 signaling pathway. *PLoS One, 7*(10), e47713.

Kim, H. J., Yoon, H. J., Kim, S. Y., & Yoon, Y. R. (2014). A medium-chain fatty acid, capric acid, inhibits RANKL-induced osteoclast differentiation via the suppression of NF-kappaB signaling and blocks cytoskeletal organization and survival in mature osteoclasts. *Molecules and Cells, 37*(8), 598–604.

Lacey, D. L., Timms, E., Tan, H. L., Kelley, M. J., Dunstan, C. R., Burgess, T., ... Boyle, W. J. (1998). Osteoprotegerin ligand is a cytokine that regulates osteoclast differentiation and activation. *Cell, 93*(2), 165–176.

Leal, V. D. O., & Mafra, D. (2013). Adipokines in obesity. *Clinica Chimica Acta, 419*, 87–94.

Lecka-Czernik, B., Stechschulte, L. A., Czernik, P. J., & Dowling, A. R. (2015). High bone mass in adult mice with diet-induced obesity results from a combination of initial increase in bone mass followed by attenuation in bone formation; Implications for high bone mass and decreased bone quality in obesity. *Molecular and Cellular Endocrinology, 410*, 35–41.

Lee, B. C., & Lee, J. (2014). Cellular and molecular players in adipose tissue inflammation in the development of obesity-induced insulin resistance. *Biochimica et Biophysica Acta, 1842*(3), 446–462.

Lecomte, V., Kaakoush, N. O., Maloney, C. A., Raipuria, M., Huinao, K. D., Mitchell, H. M., & Morris, M. J. (2015). Changes in gut microbiota in rats fed a high fat diet correlate with obesity-associated metabolic parameters. *PLoS One, 10*(5), e0126931.

Li, W., Huang, B., Liu, K., Hou, J., & Meng, H. (2015). Upregulated leptin in periodontitis promotes inflammatory cytokine expression in periodontal ligament cells. *Journal of Periodontology, 86*(7), 917–926.

Li, Y., Lu, Z., Zhang, X., Yu, H., Kirkwood, K. L., Lopes-Virella, M. F., & Huang, Y. (2015). Metabolic syndrome exacerbates inflammation and bone loss in periodontitis? *Journal of Dental Research, 94*(2), 362–370.

Loffreda, S., Yang, S. Q., Lin, H. Z., Karp, C. L., Brengman, M. L., Wang, D. J., ... Diehl, A. M. (1998). Leptin regulates proinflammatory immune responses. *FASEB Journal, 12*(1), 57–65.

Luo, Y., Chen, G. L., Hannemann, N., Ipseiz, N., Kronke, G., Bauerle, T., & Bozec (2015). Microbiota from obese mice regulate hematopoietic stem cell differentiation by altering the bone niche. *Cell Metabolism, 22*(5), 886–894.

Maekawa, T., & Hajishengallis, G. (2014). Topical treatment with probiotic Lactobacillus brevis CD2 inhibits experimental periodontal inflammation and bone loss. *Journal of Periodontal Research, 49*(6), 785–791.

Morelli, L., & Capurso, L. (2012). FAO/WHO guidelines on probiotics: 10 years later. *Journal of Clinical Gastroenterology, 46*(Suppl), S1–S2.

Mosca, L. N., Goldberg, T. B., da Silva, V. N., da Silva, C. C., Kurokawa, C. S., Bisi Rizzo, A. C., & Corrente, J. E. (2014). Excess body fat negatively affects bone mass in adolescents? *Nutrition, 30*(7–8), 847–852.

Moura-Grec, P. G., Marsicano, J. A., Carvalho, C. A., & Sales-Peres, S. H. (2014). Obesity and periodontitis: Systematic review and meta-analysis. *Ciencia & Saude Coletiva, 19*(6), 1763–1772.

Moya-Perez, A., Neef, A., & Sanz, Y. (2015). Bifidobacterium pseudocatenulatum CECT 7765 reduces obesity-associated inflammation by restoring the lymphocyte-macrophage balance and gut microbiota structure in high-fat diet-fed mice. *PLoS One, 10*(7), e0126976.

Muluke, M., Gold, T., Kiefhaber, K., Al-Sahli, A., Celenti, R., Jiang, H., ... Spate, U. (2015). Diet-Induced obesity and its differential impact on periodontal bone loss. *Journal of Dental Research, 95*(2), 223–229.

Naito, E., Yoshida, Y., Makino, K., Kounoshi, Y., Kunihiro, S., Takahashi, R., ... Ishikawa, F. (2011). Beneficial effect of oral administration of Lactobacillus casei strain Shirota on insulin resistance in diet-induced obesity mice. *Journal of Applied Microbiology, 110*(3), 650–657.

Ohlsson, C., & Sjogren, K. (2015). Effects of the gut microbiota on bone mass. *Trends in Endocrinology and Metabolism, 26*(2), 69–74.

Ohlsson, C., Engdahl, C., Fak, F., Andersson, A., Windahl, S. H., Farman, H. H., ... Sjogren, K. (2014). Probiotics protect mice from ovariectomy-induced cortical bone loss. *PLoS One, 9*(3), e92368.

Ojeda, P., Bobe, A., Dolan, K., Leone, V., & Martinez, K. (2016). Nutritional modulation of gut microbiota - The impact on metabolic disease pathophysiology. *The Journal of Nutritional Biochemistry, 28*, 191–200.

Oshima, K., Nampei, A., Matsuda, M., Iwaki, M., Fukuhara, A., Hashimoto, J., ... Shimomura, I. (2005). Adiponectin increases bone mass by suppressing osteoclast and activating osteoblast. *Biochemical and Biophysical Research Communications, 331*(2), 520–526.

Pamer, E. G. (2016). Resurrecting the intestinal microbiota to combat antibiotic-resistant pathogens? *Science, 352*(6285), 535–538.

Park, S. Y., Cho, S. A., Lee, M. K., & Lim, S. D. (2015). Effect of Lactobacillus plantarum FH185 on the reduction of adipocyte size and gut microbial changes in mice with diet-induced obesity. *Korean Journal for Food Science of Animal Resources, 35*(2), 171–178.

Parvaneh, K., Ebrahimi, M., Sabran, M. R., Karimi, G., Hwei, A. N., Abdul-Majeed, S., ... Jamaluddin, R. (2015). Probiotics (Bifidobacterium longum) increase bone mass density and upregulate sparc and bmp-2 genes in rats with bone loss resulting from ovariectomy. *BioMed Research International, 2015*, 897639.

Potikanond, S., Rattanachote, P., Pintana, H., Suntornsaratoon, P., Charoenphandhu, N., Chattipakorn, N., & Chattipakorn, S. (2016). Obesity does not aggravate osteoporosis or osteoblastic insulin resistance in orchiectomized rats. *The Journal of Endocrinology, 228*(2), 85–95.

Pramojanee, S. N., Phimphilai, M., Kumphune, S., Chattipakorn, N., & Chattipakorn, S. C. (2013). Decreased jaw bone density and osteoblastic insulin signaling in a model of obesity? *Journal of Dental Research, 92*(6), 560–565.

Priesnitz Simch, R., José Gaio, E., & Kuchenbecker Rösing, C. (2008). Effect of body weight in the pathogenesis of ligature-induced periodontal disease in Wistar rats. *Acta Odontologica Scandinavica, 66*(3), 130–134.

Pu, Y., Wu, H., Lu, S., Hu, H., Li, D., Wu, Y., & Tang, Z. (2016). Adiponectin promotes human jaw bone marrow stem cell osteogenesis. *Journal of Dental Research, 95*(7), 769–775.

Queipo-Ortuno, M. I., Seoane, L. M., Murri, M., Pardo, M., Gomez-Zumaquero, J. M., Cardona, F., ... Tinahones, F. J. (2013). Gut microbiota composition in male rat models under different nutritional status and physical activity and its association with serum leptin and ghrelin levels. *PLoS One, 8*(5), e65465.

Rajala, M. W., Patterson, C. M., Opp, J. S., Foltin, S. K., Young, V. B., & Myers, M. G. Jr. (2014). Leptin acts independently of food intake to modulate gut microbial composition in male mice? *Endocrinology, 155*(3), 748–757.

Rajpal, D. K., Klein, J. L., Mayhew, D., Boucheron, J., Spivak, A. T., Kumar, V., ... Brown, J. R. (2015). Selective spectrum antibiotic modulation of the gut microbiome in obesity and diabetes rodent models. *PLoS One, 10*(12), e0145499.

Rakoff-Nahoum, S., Paglino, J., Eslami-Varzaneh, F., Edberg, S., & Medzhitov, R. (2004). Recognition of commensal microflora by toll-like receptors is required for intestinal homeostasis. *Cell, 118*(2), 229–241.

Roberfroid, M., Gibson, G. R., Hoyles, L., McCartney, A. L., Rastall, R., Rowland, I., ... Meheust, A. (2010). Prebiotic effects: Metabolic and health benefits. *The British Journal of Nutrition, 104*(Suppl. 2), S1–63.

Rodrigues, F. C., Castro, A. S., Rodrigues, V. C., Fernandes, S. A., Fontes, E. A., de Oliveira, T. T., ... de Luces Fortes Ferreira, C. L. (2012). Yacon flour and Bifidobacterium longum modulate bone health in rats. *Journal of Medicinal Food, 15*(7), 664–670.

Rubin, M. R., & Patsch, J. M. (2016). Assessment of bone turnover and bone quality in type 2 diabetic bone disease: Current concepts and future directions. *Bone Research, 4*, 16001.

Sellmeyer, D. E., Civitelli, R., Hofbauer, L. C., Khosla, S., Lecka-Czernik, B., & Schwartz, A. V. (2016). Skeletal metabolism, fracture risk, and fracture outcomes in type 1 and type 2 diabetes. *Diabetes, 65*(7), 1757–1766.

Shu, L., Beier, E., Sheu, T., Zhang, H., Zuscik, M. J., Puzas, E. J., ... Xing, L. (2015). High-fat diet causes bone loss in young mice by promoting osteoclastogenesis through alteration of the bone marrow environment. *Calcified Tissue International, 96*(4), 313–323.

Sjogren, K., Engdahl, C., Henning, P., Lerner, U. H., Tremaroli, V., Lagerquist, M. K., ... Ohlsson, C. (2012). The gut microbiota regulates bone mass in mice. *Journal of Bone and Mineral Research, 27*(6), 1357–1367.

Song, H., Chu, Q., Yan, F., Yang, Y., Han, W., & Zheng, X. (2015). Red pitaya betacyanins protects from diet-induced obesity, liver steatosis and insulin resistance in association with modulation of gut microbiota in mice. *Journal of Gastroenterology and Hepatology, 31*(8), 1462–1469.

Spielman, L. J., Little, J. P., & Klegeris, A. (2014). Inflammation and insulin/IGF-1 resistance as the possible link between obesity and neurodegeneration. *Journal of Neuroimmunology, 273*(1–2), 8–21.

Taira, R., Yamaguchi, S., Shimizu, K., Nakamura, K., Ayabe, T., & Taira, T. (2015). Bacterial cell wall components regulate adipokine secretion from visceral adipocytes. *Journal of Clinical Biochemistry and Nutrition, 56*(2), 149–154.

Takeshita, S., Kaji, K., & Kudo, A. (2000). Identification and characterization of the new osteoclast progenitor with macrophage phenotypes being able to differentiate into mature osteoclasts? *Journal of Bone and Mineral Research, 15*(8), 1477–1488.

Tamburini, S., Shen, N., Wu, H. C., & Clemente, J. C. (2016). The microbiome in early life: Implications for health outcomes. *Nature Medicine*, *22*(7), 713–722.

Tanida, M., Shen, J., Maeda, K., Horii, Y., Yamano, T., Fukushima, Y., & Nagai, K. (2008). High-fat diet-induced obesity is attenuated by probiotic strain Lactobacillus paracasei ST11 (NCC2461) in rats. *Obesity Research & Clinical Practice*, *2*(3), I–ii.

Thaiss, C. A., Levy, M., Suez, J., & Elinav, E. (2014). The interplay between the innate immune system and the microbiota. *Current Opinion in Immunology*, *26*, 41–48.

Tojo, R., Suarez, A., Clemente, M. G., de los Reyes-Gavilan, C. G., Margolles, A., Gueimonde, M., & Ruas-Madiedo, P. (2014). Intestinal microbiota in health and disease: Role of bifidobacteria in gut homeostasis? *World Journal of Gastroenterology*, *20*(41), 15163–15176.

Verzeletti, G. N., Gaio, E. J., Linhares, D. S., & Rosing, C. K. (2012). Effect of obesity on alveolar bone loss in experimental periodontitis in Wistar rats. *Journal of Applied Oral Science*, *20*(2), 218–221.

Weaver, C. M., Martin, B. R., Nakatsu, C. H., Armstrong, A. P., Clavijo, A., McCabe, L. D., ... van den Heuvel, E. G. (2011). Galactooligosaccharides improve mineral absorption and bone properties in growing rats through gut fermentation. *Journal of Agricultural and Food Chemistry*, *59*(12), 6501–6510.

Weitzmann, M. N. (2013). The role of inflammatory cytokines, the RANKL/OPG axis, and the immunoskeletal interface in physiological bone turnover and osteoporosis. *Scientifica*, *2013*, 29.

Whisner, C. M., Martin, B. R., Schoterman, M. H., Nakatsu, C. H., McCabe, L. D., McCabe, G. P., ... Weaver, C. M. (2013). Galacto-oligosaccharides increase calcium absorption and gut bifidobacteria in young girls: A double-blind cross-over trial. *The British Journal of Nutrition*, *110*(7), 1292–1303.

Whisner, C. M., Martin, B. R., Nakatsu, C. H., McCabe, G. P., McCabe, L. D., Peacock, M., & Weaver, C. M. (2014). Soluble maize fibre affects short-term calcium absorption in adolescent boys and girls: A randomised controlled trial using dual stable isotopic tracers. *The British Journal of Nutrition*, *112*(3), 446–456.

Woting, A., Pfeiffer, N., Loh, G., Klaus, S., & Blaut, M. (2014). Clostridium ramosum promotes high-fat diet-induced obesity in gnotobiotic mouse models. *MBio*, *5*(5), e01530–01514.

Woting, A., Pfeiffer, N., Hanske, L., Loh, G., Klaus, S., & Blaut, M. (2015). Alleviation of high fat diet-induced obesity by oligofructose in gnotobiotic mice is independent of presence of Bifidobacterium longum? *Molecular Nutrition & Food Research*, *59*(11), 2267–2278.

Xu, H., Barnes, G. T., Yang, Q., Tan, G., Yang, D., Chou, C. J., ... Chen, H. (2003). Chronic inflammation in fat plays a crucial role in the development of obesity-related insulin resistance. *The Journal of Clinical Investigation*, *112*(12), 1821–1830.

Yamaguchi, N., Kukita, T., Li, Y. J., Martinez Argueta, J. G., Saito, T., Hanazawa, S., & Yamashita, Y. (2007). Adiponectin inhibits osteoclast formation stimulated by lipopolysaccharide from Actinobacillus actinomycetemcomitans. *FEMS Immunology and Medical Microbiology*, *49*(1), 28–34.

Yamashita, Y., Ukai, T., Nakamura, H., Yoshinaga, Y., Kobayashi, H., Takamori, Y., ... Hara, Y. (2015). RANKL pretreatment plays an important role in the differentiation of pit-forming osteoclasts induced by TNF-alpha on murine bone marrow macrophages. *Archives of Oral Biology*, *60*(9), 1273–1282.

Yang, S., Nguyen, N. D., Center, J. R., Eisman, J. A., & Nguyen, T. V. (2013). Association between abdominal obesity and fracture risk: A prospective study. *The Journal of Clinical Endocrinology & Metabolism*, *98*(6), 2478–2483.

Yang, L. C., Wu, J. B., Lu, T. J., & Lin, W. C. (2013). The prebiotic effect of Anoectochilus formosanus and its consequences on bone health. *The British Journal of Nutrition*, *109*(10), 1779–1788.

Zhang, L., Meng, S., Tu, Q., Yu, L., Tang, Y., Dard, M. M., ... Chen, J. (2014). Adiponectin ameliorates experimental periodontitis in diet-induced obesity mice. *PLoS One*, *9*(5), e97824.

Zhang, X., Zhao, Y., Xu, J., Xue, Z., Zhang, M., Pang, X., ... Zhao, L. (2015). Modulation of gut microbiota by berberine and metformin during the treatment of high-fat diet-induced obesity in rats. *Scientific Reports*, *5*, 14405.

Zheng, J., Xiao, X., Zhang, Q., Yu, M., Xu, J., Qi, C., & Wang, T. (2016). The programming effects of nutrition-induced catch-up growth on gut microbiota and metabolic diseases in adult mice. *MicrobiologyOpen*, *5*(2), 296–306.

เอกสารแนบหมายเลข 5

SCIENTIFIC REPORTS

OPEN

Received: 28 November 2016
Accepted: 08 February 2017
Published: 13 March 2017

Restoring the impaired cardiac calcium homeostasis and cardiac function in iron overload rats by the combined deferiprone and N-acetyl cysteine

Suwakon Wongjaikam[1,2,3], Sirinart Kumfu[1,2,3], Juthamas Khamseekaew[1,2,3], Siriporn C. Chattipakorn[1,3,4] & Nipon Chattipakorn[1,2,3]

Intracellular calcium $[Ca^{2+}]_i$ dysregulation plays an important role in the pathophysiology of iron overload cardiomyopathy. Although either iron chelators or antioxidants provide cardioprotection, a comparison of the efficacy of deferoxamine (DFO), deferiprone (DFP), deferasirox (DFX), N-acetyl cysteine (NAC) or a combination of DFP plus NAC on cardiac $[Ca^{2+}]_i$ homeostasis in chronic iron overload has never been investigated. Male Wistar rats were fed with either a normal diet or a high iron (HFe) diet for 4 months. At 2 months, HFe rats were divided into 6 groups and treated with either a vehicle, DFO (25 mg/kg/day), DFP (75 mg/kg/day), DFX (20 mg/kg/day), NAC (100 mg/kg/day), or combined DFP plus NAC. At 4 months, the number of cardiac T-type calcium channels was increased, whereas cardiac sarcoplasmic-endoplasmic reticulum Ca^{2+} ATPase (SERCA) was decreased, leading to cardiac iron overload and impaired cardiac $[Ca^{2+}]i$ homeostasis. All pharmacological interventions restored SERCA levels. Although DFO, DFP, DFX or NAC alone shared similar efficacy in improving cardiac $[Ca^{2+}]i$ homeostasis, only DFP + NAC restored cardiac $[Ca^{2+}]i$ homeostasis, leading to restoring left ventricular function in the HFe-fed rats. Thus, the combined DFP + NAC was more effective than any monotherapy in restoring cardiac $[Ca^{2+}]_i$ homeostasis, leading to restored myocardial contractility in iron-overloaded rats.

Iron overload cardiomyopathy is the primary cause of death in hereditary hemochromatosis[1,2] and transfusion dependent thalassemia (TDT) patients[3,4]. Non-transferrin bound iron (NTBI) occurs when transferrin becomes saturated and can therefore no longer bind free iron[5,6]. NTBI is represented in the plasma of iron-overloaded patients when transferrin saturation is more than 70% and which two conditions are associated with iron overload cardiomyopathy in thalassemic patients[7,8]. In addition, labile plasma iron (LPI) is a redox active, and a labile-chelatable component of NTBI, which is presented in the plasma of TDT and non-transfusion dependent thalassemia (NTDT) patients[7,9–11]. Excess plasma NTBI and LPI leads to iron overload, both systemically and within tissues, resulting in increased reactive oxygen species (ROS) via Haber-Weiss and Fenton's reactions[6,7]. Increased ROS is a major cause of tissue and organ damage, particularly in the heart[6,12]. Plasma NTBI and LPI can rapidly enter cardiomyocytes, resulting in increased free iron or labile cellular iron, which causes increased cardiac oxidative stress and iron overload cardiomyopathy[7]. L-type calcium (Ca^{2+}) channels (LTCC) and T-type Ca^{2+} channels (TTCC) are voltage-gated ion channels which are abundantly expressed in the heart, and play an important role in the excitation–contraction coupling of cardiomyocytes[13,14]. Previous studies found that LTCC and TTCC are major portals for iron entry into the heart in iron overload cardiomyopathy[15–19]. In addition, TTCC

[1]Cardiac Electrophysiology Research and Training Center, Faculty of Medicine, Chiang Mai University, Chiang Mai, Thailand. [2]Cardiac Electrophysiology Unit, Department of Physiology, Faculty of Medicine, Chiang Mai University, Chiang Mai, Thailand. [3]Center of Excellence in Cardiac Electrophysiology Research, Chiang Mai University, Chiang Mai, Thailand. [4]Department of Oral Biology and Diagnostic Sciences, Faculty of Dentistry, Chiang Mai University, Chiang Mai, Thailand. Correspondence and requests for materials should be addressed to N.C. (email: nchattip@gmail.com)

exist and contribute to cardiac electrical activity during the early embryonic state[20] and disappear shortly after birth so they cannot be found in adult ventricular cardiomyocytes under physiological conditions[21,22]. However, TTCC reappear in ventricular myocytes under some pathological conditions such as ventricular hypertrophy[23], post myocardial infarction[22], and iron overload[18,19]. Previous studies have demonstrated that an increase in cardiac iron concentration depended on Fe^{2+} influx through either LTCC or TTCC, leading to abnormal cardiac contractility and cardiac dysfunction under conditions of iron overload[15,16,18,19]. Increased ROS production mediated by iron overload can directly affect key regulators of excitation-contraction coupling, in particular sarcoplasmic-endoplasmic reticulum Ca^{2+} ATPase (SERCA) and/or sodium- Ca^{2+} exchangers (NCXs), which leads to impaired cardiac intracellular Ca^{2+} $[Ca^{2+}]i$ transients causing diminished cardiac contractility and heart failure[2,24]. Additionally, SERCA is very sensitive to oxidative stress leading to protein damage and dysfunction which can be a major cause of increased diastolic Ca^{2+} level and prolonged Ca^{2+} decay rate leading to cardiac dysfunction and heart failure under the conditions of iron overload[2,25].

There are several iron regulatory proteins which monitor iron metabolism in the heart. Divalent metal transporter 1 (DMT1) has an important role in the uptake of iron into the heart[26]. However, studies on the function of DMT1 in the iron-overloaded heart have inconsistent findings. A study found that iron overload could suppress the level of cardiac DMT1 protein but it had no significant effect on DMT1 mRNA expression in the heart of the rats[27]. On the contrary, a few studies found that the level of DMT1 protein did not alter in the hearts of rats[26] and thalassemic mice[17] under conditions of iron overload. Zrt- and Irt-like protein 14 (Zip14) are abundantly expressed in the liver, pancreas and heart[26,28]. A previous study found that Zip14 mediated the uptake of zinc and NTBI into the liver[29] and it may also mediate the uptake of NTBI into the heart. In addition, hepcidin and ferroportin are iron regulatory proteins which play an important role in iron homeostasis. Previous studies demonstrated that hepcidin and ferroportin are presented in the heart[17,30]. Ferroportin functions to export iron when iron is too abundant in the heart[17,30]. On the other hand, hepcidin is a negative regulator of iron metabolism by promoting ferroportin internalization and degradation[31,32] leading to reduced cardiomyocyte iron efflux[30]. Additionally, hepcidin functions in a decreased dietary iron absorption form duodenal enterocyte under iron overload conditions leading to iron homeostasis[33,34].

At the present time, three frequently used iron chelators; subcutaneous deferoxamine (DFO), oral deferiprone (DFP) and oral deferasirox (DFX), are used to treat patients with iron overload cardiomyopathy[35–37]. Nevertheless, a head to head comparison of the comparative therapeutic effects between DFO, DFP or DFX on cardiac $[Ca^{2+}]i$ homeostasis as well as calcium cycling and iron regulatory proteins in iron-overloaded rats has never been investigated. In addition, growing evidence indicates that N-acetyl cysteine (NAC) has an iron chelating property[38], and is a potent antioxidant which is used to treat children with β-thalassemia[39]. Moreover, our recent study also found that combined DFP plus NAC had synergistic beneficial effects in restoring function to the brain[40,41] and heart[42] in iron-overloaded rats. However, the effects of combining an oral iron chelator DFP and an antioxidant NAC on cardiac $[Ca^{2+}]i$ homeostasis as well as the impact of this treatment on calcium cycling and iron regulatory proteins in iron-overloaded rats have never been investigated. The aim of this study was to investigate the hypothesis that DFO, DFP, DFX or NAC alone can improve cardiac $[Ca^{2+}]i$ homeostasis and left ventricular (LV) function in iron-overloaded rats, as well as whether the combined DFP plus NAC treatment can synergistically provide beneficial effects for these conditions.

Results

Effects of the pharmacological interventions on plasma NTBI and MDA levels, and cardiac iron and MDA concentrations. Plasma NTBI level was significantly increased in the HFeV rats when compared with the NDV rats, indicating that an iron overload condition occurred in the HFe-fed rats (Supplementary Table 1). On the other hand, plasma NTBI level was significantly decreased in iron-overloaded rats treated with DFO, DFP, DFX, NAC and combined DFP plus NAC treatment for 2 months (Supplementary Table 1). In consistency with plasma NTBI level, plasma MDA level was significantly increased in the HFeV rats, when compared with the NDV rats, indicating that plasma oxidative stress occurred in the HFe-fed rats (Supplementary Table 1). All pharmacological interventions significantly decreased plasma MDA level in iron-overloaded rats after 2 months of treatment. In addition, the cardiac iron status showed that cardiac iron concentration was significantly increased in the HFeV rats when compared with the NDV rats (Supplementary Table 1). DFO, DFP or DFX alone decreased cardiac iron concentration, and NAC exerted iron chelating properties as it also lowered cardiac iron concentration in iron-overloaded rats (Supplementary Table 1). However, only combined DFP plus NAC significantly decreased cardiac iron concentration to a normal level as shown in the NDV rats (Supplementary Table 1). Also, cardiac MDA concentration was significantly increased in the HFeV rats when compared with the NDV rats (Supplementary Table 1). Although monotherapy alone could reduce cardiac MDA concentration, combined DFP plus NAC reduced cardiac MDA concentration to a normal level as shown in the NDV rats (Supplementary Table 1). These results suggest that a combination therapy of DFP and NAC can effectively restore cardiac iron concentration and oxidative stress in iron-overloaded rats.

Effects of the pharmacological interventions on cardiac function. Chronic iron overload led to cardiac dysfunction in iron-overloaded rats. The percentage of LV ejection fraction (%LVEF) decreased markedly in the HFeV rats at 3 months (Fig. 1a), and 4 months (Fig. 1b) when compared with the NDV rats at 3 and 4 months, respectively. At 3 months (after 1 month of treatment with all pharmacological interventions), DFO, DFP, DFX or NAC monotherapy significantly increased %LVEF in the HFe-fed rats, while only the combination therapy of DFP and NAC led to significant increases in %LVEF, attaining a normal level similar to the NDV rats (Fig. 1a). Consistently, %LVEF was similar after 2 months of treatment (at the end of the experiment) with all pharmacological interventions in iron-overloaded rats (Fig. 1b). The results suggest that combined DFP plus

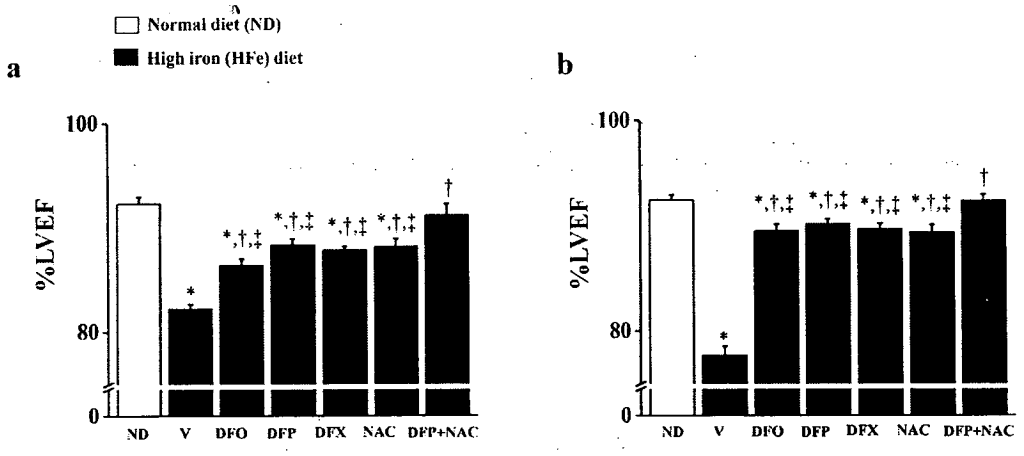


Figure 1. Combined DFP + NAC restores left ventricular (LV) function in iron-overloaded rats. The effects of the pharmacological interventions on percentage of LV ejection fraction (%LVEF) at 3 months (a) and 4 months (b), respectively in iron-overloaded rats. $^{*}P < 0.05$ vs. ND control, $^{\dagger}P < 0.05$ vs. HFeV, $^{\ddagger}P < 0.05$ vs. HFeDFP + NAC.

NAC can effectively restore cardiac function in iron-overloaded rats which exerts greater cardioprotective effects than either DFO, DFP, DFX or NAC monotherapy after 1 month of treatment.

Effects of the pharmacological interventions on cardiac $[Ca^{2+}]i$ homeostasis. An impaired level of cardiac $[Ca^{2+}]i$ transients occurred in iron-overloaded rats when compared with the NDV rats (Fig. 2a–e). The results found that cardiac $[Ca^{2+}]i$ transient amplitude, rising rate and decay rate were all significantly decreased, whilst diastolic Ca^{2+} levels were significantly increased in the HFeV rats, indicating cardiac $[Ca^{2+}]i$ dyshomeostasis, when compared with the NDV rats (Fig. 2a–e). After 2 months of treatment, DFO, DFP, DFX or NAC alone caused improved $[Ca^{2+}]i$ transient amplitude and rising rate, while only combined DFP plus NAC led to restored normal $[Ca^{2+}]i$ transient amplitude and rising rate in iron-overloaded rats (Fig. 2a,b). On the other hand, all of the pharmacological intervention treatments led to restored $[Ca^{2+}]i$ transient decay rates and diastolic Ca^{2+} levels in iron-overloaded rats to normal levels similar to those in the NDV rats (Fig. 2c,d). The results suggest that only combined DFP plus NAC effectively restores all parameters of Ca^{2+} homeostasis in iron-overloaded rats.

Effects of the pharmacological interventions on cardiac Ca^{2+} cycling protein. The levels of TTCC were significantly increased and the level of SERCA was significantly decreased in the HFeV rats when compared with the NDV rats, while the levels of LTCC and NCX did not differ between the NDV rats and iron loading groups (Fig. 3a–d). After 2 months of treatment, all pharmacological interventions led to the restoration of SERCA protein expression to a normal level in the HFe-fed rats. On the other hand, the levels of LTCC, TTCC or NCX did not alter in the HFe-fed rats after treatment with either DFO, DFP, DFX, NAC or combined DFP plus NAC for 2 months (Fig. 3a,b,d).

Effects of the pharmacological interventions on cardiac iron transporter and regulatory proteins. In iron-overloaded heart, the levels of cardiac iron transporter protein, including DMT1 and Zip14 as well as the levels of cardiac iron regulatory protein including ferroportin and hepcidin, did not differ in all groups of iron-overloaded rats when compared with the NDV rats (Fig. 4a–d). Similarly, all protein levels did not alter in the HFe-fed rats after 2 months of treatment with either DFO, DFP, DFX, NAC or combined DFP plus NAC when compared with the HFeV rats (Fig. 4a–d).

Discussion

The main conclusions which could be drawn from this study were as following: (1) chronic iron overload led to increased levels of TTCC, decreased level of SERCA, and impaired cardiac $[Ca^{2+}]i$ homeostasis, including decreased $[Ca^{2+}]i$ transient amplitude, rising rate, and decay rate as well as increased diastolic Ca^{2+} levels leading to LV dysfunction; (2) DFO, DFP, DFX or NAC monotherapy could lead to the restoration of the level of SERCA protein, improvement in cardiac $[Ca^{2+}]i$ transient amplitude, rising rate as well as restoring $[Ca^{2+}]i$ transient decay rate and diastolic Ca^{2+} level leading to improved LV function in iron-overloaded rats; (3) only a combination of DFP plus NAC resulted in a restoration of all parameters of Ca^{2+} homeostasis leading to restored normal LV function in iron-overloaded rats; (4) chronic iron overload and all pharmacological interventions had no effect on the levels of DMT1, ZIP14, hepcidin, ferroportin, LTCC and NCX in iron-overloaded rats. The summary of major findings of this study is shown in Table 1.

This is the first study to demonstrate the cardioprotective effects of DFO, DFP, DFX, NAC or combined DFP plus NAC treatment on iron overload-induced cardiac $[Ca^{2+}]i$ dysregulation in rats. It is also significant that our results show that combined DFP plus NAC exerted synergistically beneficial effects on cardiac $[Ca^{2+}]i$ transients, and the combination therapy was more effective than monotherapy in iron-overloaded rats. Ca^{2+} function as secondary messengers and play an important role in many signaling pathways in all cell types[43–45]. In

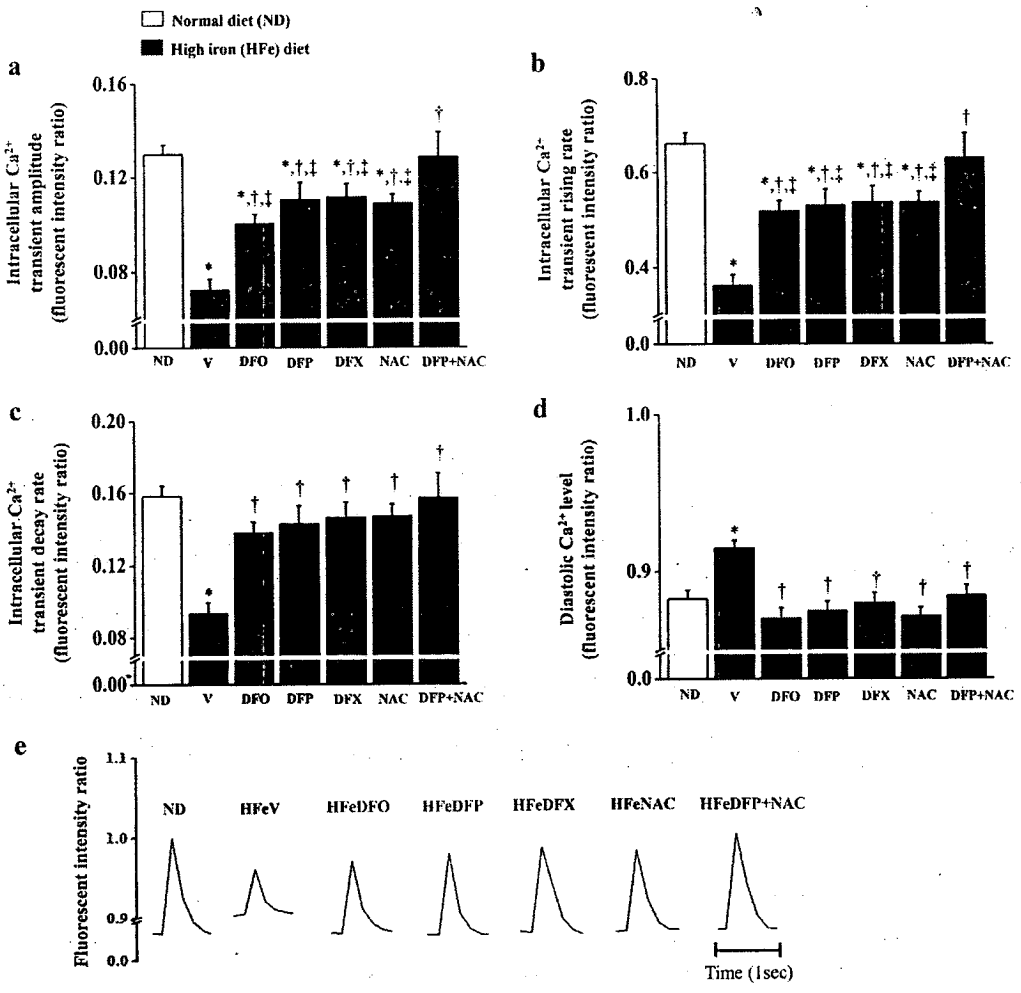


Figure 2. Combined DFP + NAC restores calcium homeostasis in iron-overloaded rats. The effects of the pharmacological interventions on cardiac intracellular calcium transients: (**a**) intracellular Ca^{2+} transient amplitude; (**b**) intracellular Ca^{2+} transient rising rate; (**c**) intracellular Ca^{2+} transient decay rate; (**d**) diastolic Ca^{2+} level, and (**e**) calcium tracing in iron-overloaded rats. $^{*}P < 0.05$ vs. ND control, $^{\dagger}P < 0.05$ vs. HFeV, $^{\ddagger}P < 0.05$ vs. HFeDFP + NAC.

cardiomyocytes, $[Ca^{2+}]i$ regulate electrical signals which play a role in cardiac rhythm and excitation–contraction coupling leading to cardiac contraction and relaxation[43]. During cardiac action potentials, LTCCs are activated and then an influx of Ca^{2+} triggers Ca^{2+} release from the sarcoplasmic reticulum through ryanodine receptor2 (RyR2), which is called Ca^{2+} -induced Ca^{2+} release leading to directly activated cardiomyocyte contraction[43,46]. During cardiac relaxation, Ca^{2+} is removed from the cytosol by four types of Ca^{2+} transporters: (1) Ca^{2+} is taken up into the sarcoplasmic reticulum by SERCA; (2) Ca^{2+} is removed from cytosol by NCX, and (3) sarcolemmal Ca^{2+}-ATPase; (4) Ca^{2+} is taken up into mitochondria by mitochondrial Ca^{2+} uniporters[46]. Under conditions of iron overload, LTCC and TTCC are the major pathways for iron entry into the heart leading to disturbance in cardiac contractility and iron overload cardiomyopathy[15,16,18,19]. Previous studies found that at a high concentration of ferrous iron (Fe^{2+}), Ca^{2+} current could decrease, indicating that Fe^{2+} might compete with Ca^{2+} influx into the heart through LTCC which may contribute to systolic dysfunction in cases of iron overload cardiomyopathy[47,48]. Additionally, we found that the decay of the Ca^{2+} current was slower when Fe^{2+} concentration was increased in isolated ventricular cardiomyocytes of rats, which might possibly contribute to impaired diastolic function[47,48]. However, the mechanism of extracellular Fe^{2+} entry into the cardiomyocytes through TTCC in iron overload conditions may be similar to LTCC. As expected, a previous study found that $Ca_V3.1$ TTCC was a significant portal for Fe^{2+} entry into cells leading to an iron overload condition[49]. Consistent with a recent study indicated that at a high concentration of free Fe^{2+} may compete with a Ca^{2+} influx into the myocardium through Ca^{2+} channels by both LTCC and TTCC[50]. Our previous study also found that TTCC is an important pathway for Fe^{2+} entry into the heart of thalassemic mice under iron overload conditions[17–19]. Hence, elevated TTCC expression in this study indicates that it may be an important portal for iron uptake into the cardiomyocytes and causes an increased cardiac iron concentration in rats suffering from iron-overload. Although iron overload did not alter the level of cardiac LTCC protein in this study, LTCC activity might be altered in the hearts of the HFe-fed rats

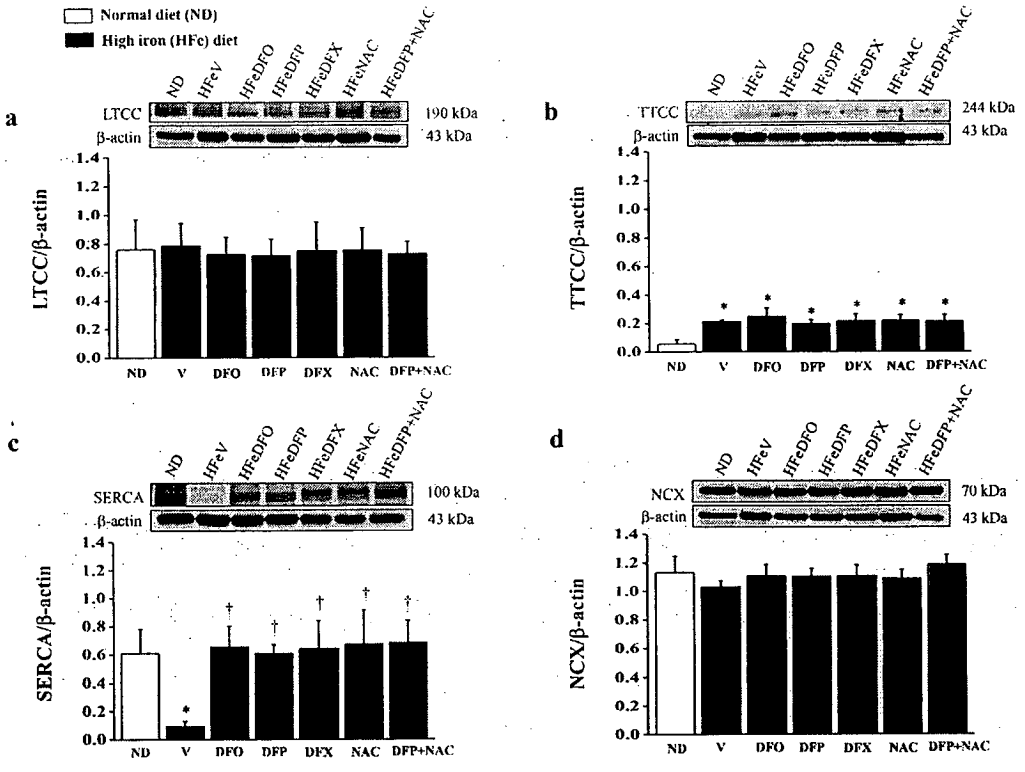


Figure 3. Combined DFP + NAC restores the levels of SERCA protein in iron-overloaded rats. The effects of the pharmacological interventions on the levels of calcium cycling proteins: (**a**) L-type Ca^{2+} channels (LTCC); (**b**) T-type Ca^{2+} channels (TTCC); (**c**) sarcoplasmic-endoplasmic reticulum Ca^{2+} ATPase (SERCA), and (**d**) sodium- Ca^{2+} exchangers (NCX) in iron-overloaded rats. $^{*}P < 0.05$ vs. ND control, $^{\dagger}P < 0.05$ vs. HFeV. The full-length blots are presented in Supplementary Figures 1, 2 and 3.

and this needs to be investigated further. In addition, our previous study found that rats with iron-overload for 4 months had both increased systemic iron (plasma NTBI) and cardiac iron concentrations[42] which were consistent with an increase in TTCC protein expression in this study. Plasma NTBI levels were used to determine an iron status in iron-overloaded patients including hereditary hemochromatosis, β-thalassemia, myelodysplastic syndrome and sickle cell disease[51]. However, the mere presence of NTBI in plasma of patients with iron overload might not be sufficient for causing heart iron overload as found in hypertransfused sickle cell anemia[52], and in most cases of myelodysplastic syndrome[53]. A previous study found that heart disease was not present in patients with thalassemia major and intermedia who showed negative plasma NTBI and had a plasma transferrin saturation of less than 70%[8]. On the other hand, all thalassemic patients with heart disease found that they were plasma NTBI positive and had a plasma transferrin saturation above 70%[8]. However, several previous studies noted that LPI is found in iron-overloaded patients, which is used as a marker of iron toxicity[7,9–11]. An increase in LPI leads to increased labile cellular iron in the heart, resulting in increased cardiac oxidative stress and cardiomyopathy[7]. In addition, glutathione (GSH) system is an endogenous antioxidant that plays an important role in scavenging cellular oxidative stress, particularly in an iron overload condition[54]. Oxidative stress can occur in systemic iron overload, caused by a decrease in the levels of antioxidants, such as GSH and glutathione peroxidase (GPX), and an increase in highly toxic free radicals such as hydroxyl radical and superoxide anion[7,54]. Therefore, LPI and those of GSH levels should be further determined to warrant the levels of free iron and antioxidant as well as oxidative stress in plasma and heart tissues in our iron-overloaded animals.

Iron-catalyzed Haber-Weiss and Fenton's reactions led to increased ROS production in iron overloaded rat's plasma and heart tissue[42]. Iron overloading mediated oxidative stress and altered cardiac excitation-contraction coupling which contributed to decreased systolic and increased diastolic Ca^{2+} levels, which resulted in inhibited systolic and diastolic functions; a characteristic of iron overload cardiomyopathy[2,48]. Defects of calcium cycling protein including LTCC, RyR2, SERCA2a and NCX were the result of impaired calcium signaling and led to heart failure[43]. Importantly, a previous study indicated that chronic iron overload led to reduced levels of SERCA2a in both its mRNA and protein form, resulting in abnormal Ca^{2+} cycling and decreased cardiac function[2]. Consistent with this line of reasoning the level of cardiac SERCA protein was significantly decreased in iron-overloaded rats which could have led to the resulting impaired cardiac $[Ca^{2+}]i$ transients and cardiac contractility in the present study. Impaired cardiac SERCA function could prolong $[Ca^{2+}]i$ transient decay rates, leading to reduced Ca^{2+} reuptake into the sarcoplasmic reticulum and resulting in increased diastolic Ca^{2+} level in the present study. In addition, a previous study found that Fe^{2+} could directly inhibit the binding of [3H] ryanodine to its high affinity sites on RyR2 which led to reduced sensitivity of cardiac ryanodine receptors towards activation by Ca^{2+} [55].

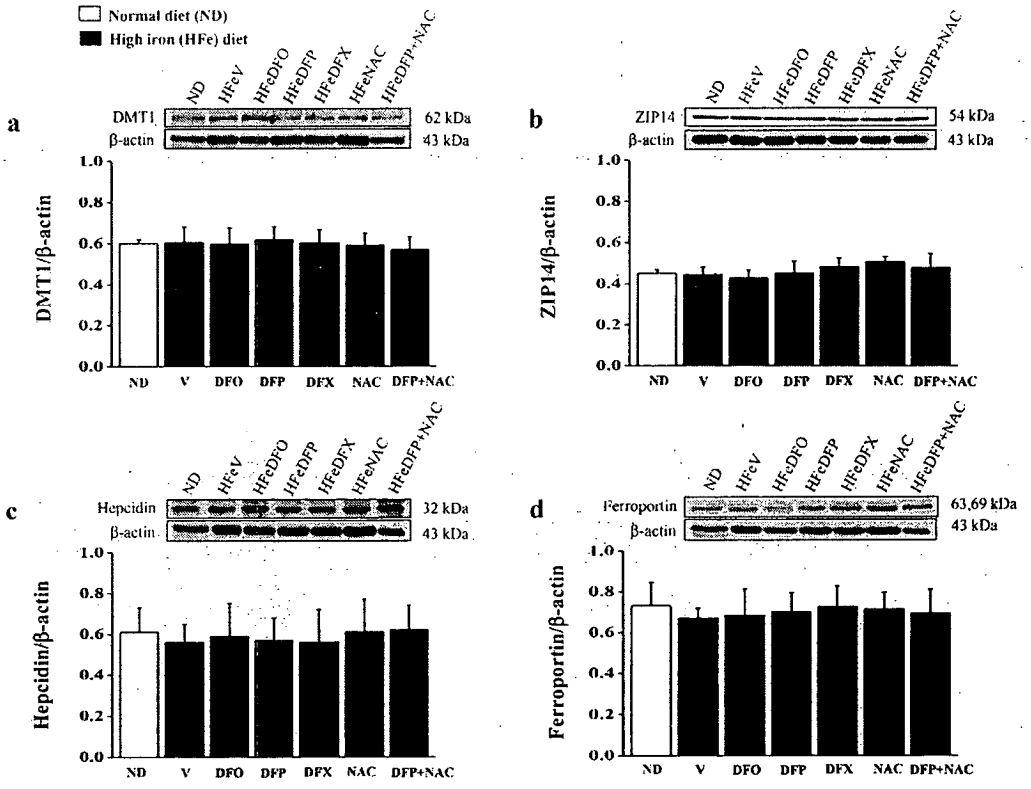


Figure 4. All treatments has no effect on the levels of iron transporter and regulatory proteins. The effects of the pharmacological interventions on the levels of iron transporter protein: (**a**) divalent metal transporter 1 (DMT1); (**b**) ZRT/IRT-like protein 14 (ZIP14); the levels of iron regulatory protein (**c**) hepcidin, and (**d**) ferroportin in iron-overloaded rats. The full-length blots are presented in Supplementary Figures 1, 2 and 3.

This same study indicated that Fe^{2+} competed with Ca^{2+} at the activating sites on RyR2 leading to decreased Ca^{2+}-induced Ca^{2+} release in rat hearts which might contribute to impaired cardiac $[Ca^{2+}]i$ homeostasis, and cardiac dysfunction under conditions of iron overload[55]. Therefore, iron overload might subsequently result in reduced Ca^{2+} release by the sarcoplasmic reticulum leading to decreased $[Ca^{2+}]i$ transient amplitude and rising rate, and caused impaired cardiac contractility in the present study. Finally, %LVEF was significantly decreased in the HFe-fed rats leading to LV dysfunction in our study. In addition, our previous study and others demonstrated that an increase in cardiac iron store led to increased cardiac oxidative stress which caused increased mitochondrial dysfunction, resulting in cardiac dysfunction and iron overload cardiomyopathy[7,42]. In consistency, a previous study found that iron overload-evoked production of cardiac oxidative stress contributed to damage to mitochondrial DNA, reduced complex I (NADH dehydrogenase) and complex IV (cytochrome c oxidase) activities, and decreased cardiac mitochondrial respiration, leading to mitochondrial and cardiac dysfunctions in iron-overloaded mice[56]. Hence, cardiac mitochondrial dysfunction evoked by chronic iron overload might cause reduced ATP production in cardiomyocytes[7]. In addition, SERCA uses the free energy of ATP to transport Ca^{2+} into the sarcoplasmic reticulum through a concentration gradient which leads to intracellular Ca^{2+} homeostasis[57]. This may lead to a decrease in ATP levels in cardiac iron overload and cause reduced SERCA function and/or activity, which results in impaired Ca^{2+} homeostasis as shown in our present study. Therefore, the restoration of Ca^{2+} homeostasis in iron-overloaded heart could be an indicator of functional restoration, which might have resulted from improved ATP production and respiration, due to both iron detoxification and an improved reductive capacity by either iron chelators or antioxidant(s). Nevertheless, the effects of iron chelators and/or antioxidant(s) on cardiac mitochondrial ATP production and respiration in iron-overloaded rats should be further investigated.

However, in our present study the levels of DMT1 and ZIP14 did not alter in the HFe-fed rats when compared with the NDV rats. The results support the findings in previous studies which demonstrated that DMT1 and ZIP14 were not the common pathways for iron entry into the heart under iron overload conditions[18,26]. In addition, the levels of cardiac ferroportin and hepcidin also did not alter in the HFe-fed rats when compared with the NDV rats. This result was consistent with our previous study in which cardiac ferroportin and hepcidin did not alter in the wild type mice after 4 months of iron loading when compared with the ND control groups[17]. However, previous studies demonstrated that hepcidin is primarily produced and secreted by the liver leading to the regulation of iron exporter ferroportin, all of which play a major role in controlling systemic iron concentrations in conditions of iron overload[58,59]. Hence, ferroportin and hepcidin may not play an important role in the heart in the iron overload conditions induced in this present study.

Cardiac parameters	ND	HFeV	HFeDFO	HFeDFP	HFeDFX	HFeNAC	HFeDFP + NAC
Echocardiography							
- % LVEF	+++	+	++	++	++	++	+++
Intracellular Ca^{2+} transients							
- Amplitude	+++	+	++	++	++	++	+++
- Rising rate	+++	+	++	++	++	++	+++
- Decay rate	+++	+	+++	+++	+++	+++	+++
- Diastolic Ca^{2+} level	+++	++ ++	+++	+++	+++	+++	+++
The levels of Ca^{2+} cycling protein							
- LTCC	+++	+++	+++	+++	+++	+++	+++
- TTCC	+	++	++	++	++	++	++
- SERCA	+++	+	+++	+++	+++	+++	+++
- NCX	+++	+++	+++	+++	+++	+++	+++
The levels of iron transporter and regulatory proteins							
- DMT1	+++	+++	+++	+++	+++	+++	+++
- ZIP14	+++	+++	+++	+++	+++	+++	+++
- Hepcidin	+++	+++	+++	+++	+++	+++	+++
- Ferroportin	+++	+++	+++	+++	+++	+++	+++

Table 1. Summary the effects of all pharmacological interventions in each cardiac parameter.

Interestingly, our recent studies found that the combination of an oral iron chelator DFP and an antioxidant NAC could improve and restore normal brain and heart function effectively and provided more robust results than either DFO, DFP, DFX or NAC alone in the iron-overloaded rat model[40,42]. Consistently in the present study, a combination of DFP plus NAC provided more effective results than either DFO, DFP, DFX, or NAC alone in restoring cardiac $[Ca^{2+}]i$ homeostasis leading to restored normal cardiac contractility and LV function by increased %LVEF to a normal condition in iron-overloaded rats. Although previous studies reported that neither DFO nor DFX have shown to be efficient in improving %LVEF in thalassemia major or TDT patients[60,61], DFP has effectively improved % LVEF in these patients[60]. On the other hand, a recent study found that although % LVEF was not altered, cardiac iron concentration was continuously reduced, and end-diastolic and end-systolic left ventricular volume were significantly diminished, leading to improved cardiac function in TDT patients after 5 years of treatment with DFX[62]. In an animal study, it has been shown that %LVEF was improved by chronic treatment with DFO, leading to improve cardiac function in iron-overloaded gerbils[63]. In consistency, our present study found that long-term treatment with DFO or DFX for 2 months could ameliorate cardiac function by increasing %LVEF, as well as improve hemodynamic parameters, including left ventricular end-systolic pressure, maximum pressure, cardiac output and stroke volume, contributing to improved cardiac function in iron-overloaded rats as shown in our previous study[42]. However, the dose and duration of treatment with DFX or DFO in TDT patients and iron-overloaded gerbils were different from our present study. Consequently, the present study indicate that chronic and continuous treatments with DFO or DFX might help to ameliorate cardiac function in patients with iron overload cardiomyopathy. The mechanisms regarding the combination of DFP and NAC in restoring cardiac $[Ca^{2+}]i$ transients could be clarified by the following reasons. First, DFP has the lowest molecule weight of iron chelators when compared with DFO and DFX, and has a high lipophilicity which means it can rapidly penetrate into cells[64] leading to DFP chelating intracellularly effectively free irons from heart tissue[42], and may contribute to attenuating impaired cardiac $[Ca^{2+}]i$ homeostasis. Second, NAC is an antioxidant that can decrease ROS levels, increase SERCA2a activity as well as enhance cytosolic Ca^{2+} removal[65]. In addition, NAC provides an iron chelating activity[38] as it can remove excessive free irons out of the heart[42] which may lead to a decrease in iron-mediated cardiac $[Ca^{2+}]i$ dysregulation in this study. Moreover, NAC has been considered and used as a promoter of GSH synthesis and thereby cell reductive power[66]. As such, it could have facilitated iron removal from iron-overloaded cells or tissues by chelators, by rendering the accumulated iron more accessible (indirectly via its reduction). Therefore, these two conditions have shown the synergistic effects of combined DFP plus NAC on cardiac $[Ca^{2+}]i$ homeostasis in the present study. The effects of all pharmacological interventions on cardiac $[Ca^{2+}]i$ homeostasis and LV function in iron-overloaded rats are summarized in Fig. 5. However, the usefulness of combined DFP plus NAC needs clinical trials to warrant its cardioprotective effects in human patients with iron overload cardiomyopathy. In conclusion, all pharmacological interventions had no effect on the levels of DMT1, ZIP14, hepcidin, ferroportin, LTCC, TTCC or NCX in the heart. However, only cardiac SERCA levels were restored by all pharmacological intervention treatments in rats with iron-overload. In addition, DFO, DFP, DFX or NAC alone exerted similar effects in improving $[Ca^{2+}]i$ homeostasis leading to improved LV function. Although these monotherapy treatments showed similar efficacy to combined DFP plus NAC in restoring $[Ca^{2+}]i$ transient decay rate and diastolic Ca^{2+} level, only combined DFP plus NAC could restore all parameters of $[Ca^{2+}]i$ transients, including $[Ca^{2+}]i$ transient amplitude, rising rate, decay rate as well as diastolic Ca^{2+} levels. These factors led to a restored normal LV function in rats with iron-overload. For this reason, combined DFP plus NAC therapy may provide these similar cardioprotective results in patients with iron overload and so may be used as a future therapeutic strategy for treatment of iron overload cardiomyopathy particularly in hemochromatosis and TDT patients.

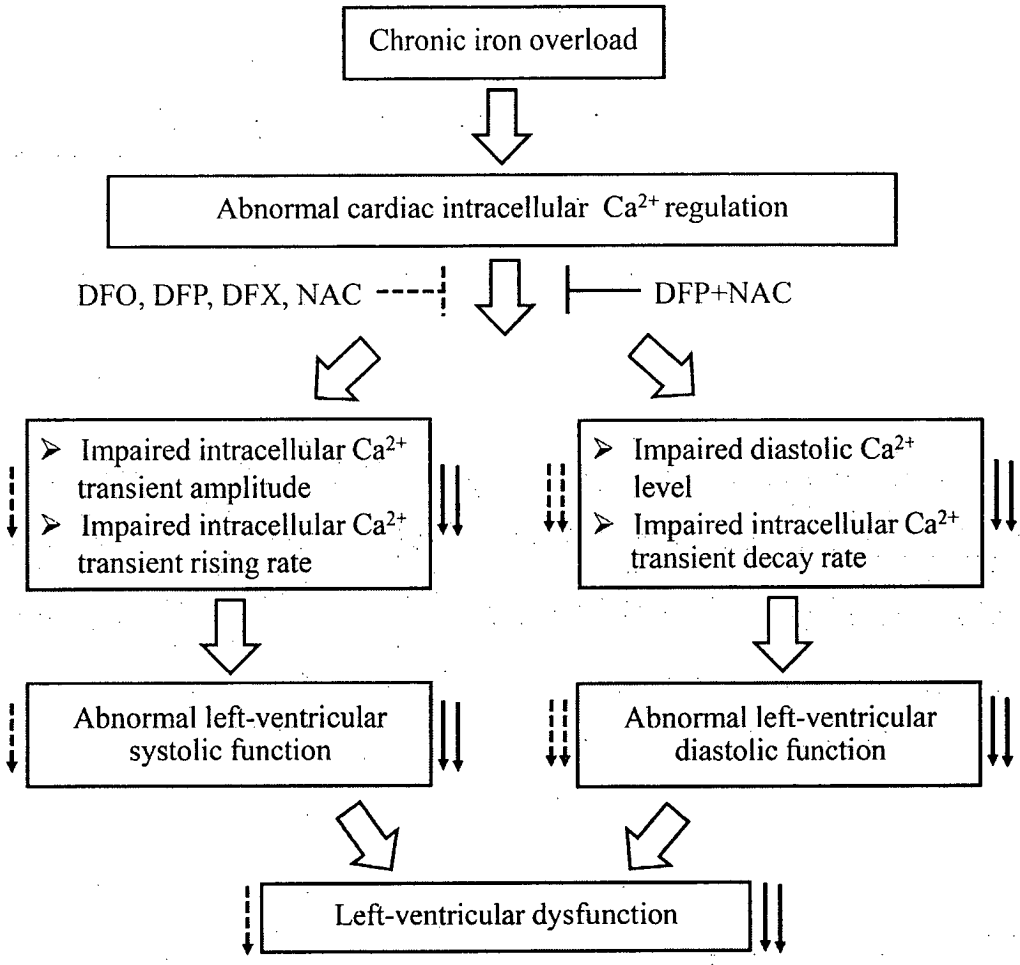


Figure 5. The effects of the pharmacological interventions on calcium homeostasis in iron-overloaded rats. Diagram demonstrating the suggested mechanisms of chronic iron overload on cardiac intracellular Ca^{2+} homeostasis, and left ventricular function as well as the effects of the pharmacological interventions on cardiac intracellular Ca^{2+} homeostasis, and left ventricular dysfunction mediated by chronic iron overload. Dashed arrows indicate the effects of either DFO, DFP, DFX or NAC treatment; solid arrows indicate the effects of combined DFP plus NAC treatment. Ca^{2+} = calcium; DFO = deferoxamine; DFP = deferiprone; DFX = deferasirox; NAC = N-acetyl cysteine.

Methods

Animal preparation. The Institutional Animal Care and Use Committee (IACUC) at the Faculty of Medicine, Chiang Mai University authorized the animal study protocols (Permit number: 21/2557), in compliance with NIH guidelines, and in accordance with the ARRIVE guidelines for reporting experiments involving animals[67]. The National Laboratory Animal Center, Mahidol University, Bangkok, Thailand supplied all adult male Wistar rats which had a body weight of 180–200 g An animal holding room was used to house all rats in a controlled environment of 23 ± 2 °C, 50 ± 10% humidity and 12 h light/dark cycles. Throughout the entire experiment all rats were given drinking water *ad libitum* and were acclimatized for 7 days prior to the experimental protocols.

Experimental protocols. A standard laboratory rat diet containing 0.2% of ferrocene ($C_{10}H_{10}Fe$; Sigma-Aldrich, Co., St. Louis, USA) (w/w) was prepared as previously outlined[42]. Adult male Wistar rats were divided into 2 groups and were given either a normal diet (a chow diet, ND) (n = 12), or a high iron diet (0.2% ferrocene w/w, HFe) (n = 72) for 4 months. At 2 months, ND-fed rats had a vehicle (normal saline solution, NSS) (NDV or ND control group) administered once a day via either subcutaneous injection (n = 6) or gavage feeding (n = 6) and a normal chow diet was maintained for 2 months. The HFe-fed rats were divided into 6 groups (n = 12/group) and were given: (1) NSS (HFeV) once a day via either subcutaneous injection (n = 6) or gavage feeding (n = 6), (2) deferoxamine (DFO; Desferal®, Novartis Pharma Stein AG, Stein, Switzerland), (HFeDFO) 25 mg/kg/ day via subcutaneous injection, (3) deferiprone (DFP; Ferriprox®, Apotex Inc., Toronto, Ontario, Canada), (HFeDFP) 75 mg/kg/day, (4) deferasirox (DFX; Exjade®, ICL670, Novartis Pharma Stein AG, Stein, Switzerland), (HFeDFX) 20 mg/kg/day, (5) N-acetyl cysteine (NAC, Sigma-Aldrich, Co., St. Louis, USA),

(HFeNAC) 100 mg/kg/day, or (6) combined DFP 75 mg/kg/day plus NAC 100 mg/kg/day (HFeDFP + NAC) through gavage feeding for 2 months, and all iron loading groups were regularly fed with the high iron diet. Since DFO is a parenteral iron chelator, it may cause suffering in patients with cardiac iron overload who are continuously treated with this drug. Previous studies have shown that DFP was significantly more potent than DFO in diminishing cardiac iron overload in TDT patients[35,60]. Although DFP and DFX are oral iron chelators, the cost of DFX is more expensive than DFP. Additionally, DFP was found to exert greater efficacy than DFX in reducing severe cardiac iron and improving cardiac function in TDT patients[35,68]. DFX also failed to reduce cardiac iron concentration in TDT patients with severe hepatic iron loading[69]. Hence, DFP was chosen in combination with NAC in this study for determining its effects on chronic iron-mediated the impairment of cardiac $[Ca^{2+}]i$ homeostasis. Dosage of all iron chelators are the lowest therapeutic range that can be used to treat patients with iron overload[36]. At the end of 3 and 4 months of the experiment, all rat groups had their cardiac function determined by echocardiography. After 4 months of the experimental period, half of the rats in each group (n = 6/group) were deeply anesthetized by intraperitoneal injections of Zolitil (ZolazepamTiletamine) 50 mg/kg combined with Xylazine 3 mg/kg[70], then the hearts were rapidly removed. The heart tissues were frozen in liquid nitrogen immediately, and stored at −80 °C in preparation for western blot analysis. In addition, the other half of the rats from each group (n = 6/group) were deeply anesthetized with thiopental (0.5 mg/kg; Research institute of antibiotics and biotransformations, Roztoky, Czech Republic), and then the hearts of the rats were rapidly removed for single ventricular myocyte isolation[71]. Cardiomyocyte cells were isolated by using an enzymatic technique[71,72]. In brief, rats were injected intraperitoneally with 0.2 mL heparin for 10 minutes. After the initiation of deep anesthesia using 100 mg/kg thiopental, the heart was excised and the aorta was cannulated rapidly to enable cardiomyocyte isolation. Then, isolated cardiomyocytes from the hearts of the rats in each group (n = 5–8 cells/rat) were used for the measurement of $[Ca^{2+}]i$ transients.

Echocardiographic studies. Cardiac function was determined using echocardiography (GE Vivid I)[42]. Echocardiographic study was performed using a method described previously[42]. The parameters from the echocardiography including LV end-systolic volume (LVESV), and end-diastolic volume (LVEDV) were determined. The percentage of ejection fraction was calculated by using the following formula: %EF (Teich) = (LVEDV-LVESV) × 100/ LVEDV[42,73].

Experimental protocol for studying cardiac $[Ca^{2+}]i$ transients. The Ca^{2+} transient level in rat ventricular myocytes was measured using a fluorimetric ratio technique[71,72]. The fluorescent Ca^{2+} indicator Fura-2 was loaded by incubating the cardiomyocytes at room temperature for 30 minutes with 25 μM of Fura-2-AM (Sigma Chemical, St. Louis, MO, USA). Ultraviolet light wavelengths of 340 and 387 nm were used for the excitation of the Fura-2 from a xenon arc lamp controlled by a microfluorometry system (Cell^R, MT 20, Olympus Soft Imaging Solutions GmbH, Germany) and the excitation light beam was directed into an inverted microscope (IX-81, Olympus Tokyo, Japan). The ratio of emitted fluorescence signals from the Fura-2/AM loaded cardiomyocytes at 510 nm was recorded. The Ca^{2+} transient parameters including the $[Ca^{2+}]i$ transient amplitude, rising rate, and decay rate, as well as the diastolic Ca^{2+} level were recorded during electrical pacing (1 hertz field-stimulation, 10 millisecond duration and 15 volts). The ratio of the emission wavelengths is directly related to the amount of cardiac $[Ca^{2+}]i$[74]. The fluorescence ratio data was processed and stored in a computer using Xcellence imaging software (Olympus, Tokyo, Japan)[71,72].

Western blot analysis. The heart tissues were extracted in a homogenizer in a lysis buffer (20 mM Tris–HCl, 1 mM Na_3VO_4, 5 mM NaF, and 1% proteinase inhibitor) at 4 °C, and subsequently centrifuged at 13,500 rpm for 10 minutes. The total protein of 40 mg was mixed with the loading buffer (1 mg/mL), boiled for 10 minutes and loaded onto 10% gradient sodium dodecyl sulfate (SDS)-polyacrylamide gels. Proteins were transferred to a nitrocellulose blotting membrane (GE Healthcare Life Sciences, Freiburg, Germany). Immunoblots were blocked with either 5% of bovine serum albumin or 5% of skimmed milk in Tris-buffered saline (pH 7.4) containing 0.1% Tween 20 (TBST) for 1 hour at room temperature. Then, immunoblots were exposed to the primary antibodies including the iron transporter protein DMT1 (ab55812; Abcam, Cambridge, MA, USA) and Zip14 (ab106568; Abcam, Cambridge, MA, USA), iron regulatory protein ferroportin (ab85370; Abcam, Cambridge, MA, USA) and hepcidin (ab75883; Abcam, Cambridge, MA, USA), Ca^{2+} cycling protein LTCC (C1603; Sigma-Aldrich Co. LLC., Saint Louis, MO, USA.), TTCC (sc25691; Santa Cruz Biotechnology Inc., Dallas, Texas, USA), SERCA (sc30110; Santa Cruz Biotechnology Inc., Dallas, Texas, USA) and NCX (sc32881; Santa Cruz Biotechnology Inc., Dallas, Texas, USA), and β-actin (sc47778; Santa Cruz Biotechnology Inc., Dallas, Texas, USA) for a loading control at 4 °C overnight. After that, the membrane was washed five times with TBST and then incubated with the horseradish peroxidase-conjugated secondary antibody at room temperature for 1 hour. After washing the membrane again five times with TBST, the blots were visualized with an enhanced chemiluminescence (ECL) reagent and exposed by using ChemiDoc™ Touch Imaging System (Life science AP, Bio-Rad, CA, USA). The images of the western blots were analysed using the ImageJ (NIHimage) analysis software[17,75].

Statistical analysis. Data were expressed as mean ± standard error of mean (SEM). The data were processed using SPSS (Statistical Package for Social Sciences, Chicago, IL, USA) release 22.0 for Windows. Differences between groups were tested for via One-way ANOVA analyses. Significant difference between groups was assumed if P values < 0.05.

References

1. von Herbay, A. *et al.* -Cardiomyopathy as the cause of death in genetic hemochromatosis. *Z Gastroenterol* **34,** 178–182 (1996).
2. Das, S. K. *et al.* Iron-overload injury and cardiomyopathy in acquired and genetic models is attenuated by resveratrol therapy. *Sci Rep* **5,** 18132 (2015).
3. Zurlo, M. G. *et al.* Survival and causes of death in thalassaemia major. *Lancet* **2,** 27–30 (1989).
4. Kremastinos, D. T. *et al.* Beta-thalassemia cardiomyopathy: history, present considerations, and future perspectives. *Circ Heart Fail* **3,** 451–458 (2010).
5. Hider, R. C., Silva, A. M., Podinovskaia, M. & Ma, Y. Monitoring the efficiency of iron chelation therapy: the potential of nontransferrin-bound iron. *Ann N Y Acad Sci* **1202,** 94–99 (2010).
6. Hershko, C. Pathogenesis and management of iron toxicity in thalassemia. *Ann NY Acad Sci* **1202,** 1–9 (2010).
7. Berdoukas, V., Coates, T. D. & Cabantchik, Z. I. Iron and oxidative stress in cardiomyopathy in thalassemia. *Free Radic Biol Med* **88,** 3–9 (2015).
8. Piga, A. *et al.* High nontransferrin bound iron levels and heart disease in thalassemia major. *Am J Hematol* **84,** 29–33 (2009).
9. Le Lan, C. *et al.* Redox active plasma iron in C282Y/C282Y hemochromatosis. *Blood* **105,** 4527–4531 (2005).
10. Pootrakul, P. *et al.* Labile plasma iron (LPI) as an indicator of chelatable plasma redox activity in iron-overloaded beta-thalassemia/HbE patients treated with an oral chelator. *Blood* **104,** 1504–1510 (2004).
11. Lal, A. *et al.* Combined chelation therapy with deferasirox and deferoxamine in thalassemia. *Blood Cells Mol Dis* **50,** 99–104 (2013).
12. Wongjaikam, S., Kumfu, S., Chattipakorn, S. C., Fucharoen, S. & Chattipakorn, N. Current and future treatment strategies for iron overload cardiomyopathy. *Eur J Pharmacol* **765,** 86–93 (2015).
13. Das, S. K. & Oudit, G. Y. Voltage-gated Ca2+ channels as key mediators of iron-transport and iron-overload cardiomyopathy: L-type vs. T-type Ca+ channels. *Eur J Haematol* **88,** 476–477 (2012).
14. Catterall, W. A. Structure and regulation of voltage-gated Ca2+ channels. *Annu Rev Cell Dev Biol* **16,** 521–555 (2000).
15. Oudit, G. Y., Trivieri, M. G., Khaper, N., Liu, P. P. & Backx, P. H. Role of L-type Ca2+ channels in iron transport and iron-overload cardiomyopathy. *J Mol Med (Berl)* **84,** 349–364 (2006).
16. Oudit, G. Y. *et al.* L-type Ca2+ channels provide a major pathway for iron entry into cardiomyocytes in iron-overload cardiomyopathy. *Nat Med* **9,** 1187–1194 (2003).
17. Kumfu, S., Chattipakorn, S. C., Fucharoen, S. & Chattipakorn, N. Dual T-type and L-type calcium channel blocker exerts beneficial effects in attenuating cardiovascular dysfunction in iron-overloaded thalassaemic mice. *Exp Physiol* **101,** 521–539 (2016).
18. Kumfu, S. *et al.* T-type calcium channel as a portal of iron uptake into cardiomyocytes of beta-thalassemic mice. *Eur J Haematol* **86,** 156–166 (2011).
19. Kumfu, S., Chattipakorn, S., Chinda, K., Fucharoen, S. & Chattipakorn, N. T-type calcium channel blockade improves survival and cardiovascular function in thalassemic mice. *Eur J Haematol* **88,** 535–548 (2012).
20. Niwa, N. *et al.* Cav3.2 subunit underlies the functional T-type Ca2+ channel in murine hearts during the embryonic period. *Am J Physiol Heart Circ Physiol* **286,** H2257–2263 (2004).
21. Yasui, K. *et al.* Pathophysiological significance of T-type Ca2+ channels: expression of T-type Ca2+ channels in fetal and diseased heart. *J Pharmacol Sci* **99,** 205–210 (2005).
22. Huang, B., Qin, D., Deng, L., Boutjdir, M. & Nabil, El-Sherif Reexpression of T-type Ca2+ channel gene and current in post-infarction remodeled rat left ventricle. *Cardiovasc Res* **46,** 442–449 (2000).
23. Martinez, M. L., Heredia, M. P. & Delgado, C. Expression of T-type Ca(2+) channels in ventricular cells from hypertrophied rat hearts. *J Mol Cell Cardiol* **31,** 1617–1625 (1999).
24. Xie, L. H., Doye, A. A., Conley, E. & Gwathmey, J. K. Sickle cell anemia: the impact of discovery, politics, and business. *J Health Care Poor Underserved* **24,** 147–158 (2013).
25. Li, X., Li, W., Gao, Z. & Li, H. Association of cardiac injury with iron-increased oxidative and nitrative modifications of the SERCA2a isoform of sarcoplasmic reticulum Ca(2+)-ATPase in diabetic rats. *Biochimie* **127,** 144–152 (2016).
26. Nam, H. *et al.* ZIP14 and DMT1 in the liver, pancreas, and heart are differentially regulated by iron deficiency and overload: implications for tissue iron uptake in iron-related disorders. *Haematologica* **98,** 1049–1057 (2013).
27. Ke, Y. *et al.* Post-transcriptional expression of DMT1 in the heart of rat. *J Cell Physiol* **196,** 124–130 (2003).
28. Taylor, K. M., Morgan, H. E., Johnson, A. & Nicholson, R. I. Structure-function analysis of a novel member of the LIV-1 subfamily of zinc transporters, ZIP14. *FEBS Lett* **579,** 427–432 (2005).
29. Liuzzi, J. P., Aydemir, F., Nam, H., Knutson, M. D. & Cousins, R. J. Zip14 (Slc39a14) mediates non-transferrin-bound iron uptake into cells. *Proc Natl Acad Sci USA* **103,** 13612–13617 (2006).
30. Lakhal-Littleton, S. *et al.* Cardiac ferroportin regulates cellular iron homeostasis and is important for cardiac function. *Proc Natl Acad Sci USA* **112,** 3164–3169 (2015).
31. Qiao, B. *et al.* Hepcidin-induced endocytosis of ferroportin is dependent on ferroportin ubiquitination. *Cell Metab* **15,** 918–924 (2012).
32. Nemeth, E. *et al.* Hepcidin regulates cellular iron efflux by binding to ferroportin and inducing its internalization. *Science* **306,** 2090–2093 (2004).
33. Hansen, S. L. *et al.* High dietary iron reduces transporters involved in iron and manganese metabolism and increases intestinal permeability in calves. *J Dairy Sci* **93,** 656–665 (2010).
34. Brasse-Lagnel, C. *et al.* Intestinal DMT1 cotransporter is down-regulated by hepcidin via proteasome internalization and degradation. *Gastroenterology* **140,** 1261–1271 e1261 (2011).
35. Pepe, A. *et al.* Deferasirox, deferiprone and desferrioxamine treatment in thalassemia major patients: cardiac iron and function comparison determined by quantitative magnetic resonance imaging. *Haematologica* **96,** 41–47 (2011).
36. Kwiatkowski, J. L. Management of transfusional iron overload - differential properties and efficacy of iron chelating agents. *J Blood Med* **2,** 135–149 (2011).
37. Hoffbrand, A. V., Taher, A. & Cappellini, M. D. How I treat transfusional iron overload. *Blood* **120,** 3657–3669 (2012).
38. Hjortso, E., Fomsgaard, J. S. & Fogh-Andersen, N. Does N-acetylcysteine increase the excretion of trace metals (calcium, magnesium, iron, zinc and copper) when given orally? *Eur J Clin Pharmacol* **39,** 29–31 (1990).
39. Ozdemir, Z. C., Koc, A., Aycicek, A. & Kocyigit, A. N-Acetylcysteine supplementation reduces oxidative stress and DNA damage in children with beta-thalassemia. *Hemoglobin* **38,** 359–364 (2014).
40. Sripetchwandee, J., Wongjaikam, S., Krintratun, W., Chattipakorn, N. & Chattipakorn, S. C. A combination of an iron chelator with an antioxidant effectively diminishes the dendritic loss, tau-hyperphosphorylation, amyloids-beta accumulation and brain mitochondrial dynamic disruption in rats with chronic iron-overload. *Neuroscience* **332,** 191–202 (2016).
41. Sripetchwandee, J., Pipatpiboon, N., Chattipakorn, N. & Chattipakorn, S. Combined therapy of iron chelator and antioxidant completely restores brain dysfunction induced by iron toxicity. *PLoS One* **9,** e85115 (2014).
42. Wongjaikam, S. *et al.* Combined iron chelator and antioxidant exerted greater efficacy on cardioprotection than monotherapy in iron-overloaded rats. *PLoS One* **11,** e0159414 (2016).
43. Kho, C., Lee, A. & Hajjar, R. J. Altered sarcoplasmic reticulum calcium cycling–targets for heart failure therapy. *Nat Rev Cardiol* **9,** 717–733 (2012).
44. Clapham, D. E. Calcium signaling. *Cell* **80,** 259–268 (1995).

45. Berridge, M. J., Lipp, P. & Bootman, M. D. The versatility and universality of calcium signalling. *Nat Rev Mol Cell Biol* **1**, 11–21 (2000).
46. Bers, D. M. Calcium fluxes involved in control of cardiac myocyte contraction. *Circ Res* **87**, 275–281 (2000).
47. Tsushima, R. G. *et al.* Modulation of iron uptake in heart by L-type Ca2+ channel modifiers: possible implications in iron overload. *Circ Res* **84**, 1302–1309 (1999).
48. Murphy, C. J. & Oudit, G. Y. Iron-overload cardiomyopathy: pathophysiology, diagnosis, and treatment. *J Card Fail* **16**, 888–900 (2010).
49. Lopin, K. V., Gray, I. P., Obejero-Paz, C. A., Thevenod, F. & Jones, S. W. Fe(2)(+) block and permeation of CaV3.1 (alpha1G) T-type calcium channels: candidate mechanism for non-transferrin-mediated Fe(2)(+) influx. *Mol Pharmacol* **82**, 1194–1204 (2012).
50. Avila, R. A. *et al.* Mechanisms involved in the *in vitro* contractile dysfunction induced by different concentrations of ferrous iron in the rat myocardium. *Toxicol In Vitro* **36**, 38–45 (2016).
51. Maas, R. P., Voets, P. J., de Swart, L. & Swinkels, D. W. [Non-transferrin-bound iron: a promising biomarker in iron overload disorders]. *Ned Tijdschr Geneeskd* **157**, A6258 (2013).
52. Koren, A., Fink, D., Admoni, O., Tennenbaum-Rakover, Y. & Levin, C. Non-transferrin-bound labile plasma iron and iron overload in sickle-cell disease: a comparative study between sickle-cell disease and beta-thalassemic patients. *Eur J Haematol* **84**, 72–78 (2010).
53. Konen, E. *et al.* No evidence for myocardial iron overload in multitransfused patients with myelodysplastic syndrome using cardiac magnetic resonance T2 technique. *Am J Hematol* **82**, 1013–1016 (2007).
54. Kalpravidh, R. W. *et al.* Glutathione redox system in beta -thalassemia/Hb E patients. *ScientificWorldJournal* **2013**, 543973 (2013).
55. Kim, E., Giri, S. N. & Pessah, I. N. Iron(II) is a modulator of ryanodine-sensitive calcium channels of cardiac muscle sarcoplasmic reticulum. *Toxicol Appl Pharmacol* **130**, 57–66 (1995).
56. Gao, X. *et al.* Mitochondrial dysfunction may explain the cardiomyopathy of chronic iron overload. *Free Radic Biol Med* **49**, 401–407 (2010).
57. Horakova, L., Strosova, M. K., Spickett, C. M. & Blaskovic, D. Impairment of calcium ATPases by high glucose and potential pharmacological protection. *Free Radic Res* **47** Suppl 1, 81–92 (2013).
58. Gardenghi, S. *et al.* Ineffective erythropoiesis in beta-thalassemia is characterized by increased iron absorption mediated by down-regulation of hepcidin and up-regulation of ferroportin. *Blood* **109**, 5027–5035 (2007).
59. Ganz, T. & Nemeth, E. Hepcidin and disorders of iron metabolism. *Annu Rev Med* **62**, 347–360 (2011).
60. Pennell, D. J. *et al.* Randomized controlled trial of deferiprone or deferoxamine in beta-thalassemia major patients with asymptomatic myocardial siderosis. *Blood* **107**, 3738–3744 (2006).
61. Pennell, D. J. *et al.* A 1-year randomized controlled trial of deferasirox vs deferoxamine for myocardial iron removal in beta-thalassemia major (CORDELIA). *Blood* **123**, 1447–1454 (2014).
62. Cassinerio, E. *et al.* A 5-year follow-up in deferasirox treatment: improvement of cardiac and hepatic iron overload and amelioration in cardiac function in thalassemia major patients. *Ann Hematol* **94**, 939–945 (2015).
63. Walker, E. M. Jr. *et al.* Acetaminophen combinations protect against iron-induced cardiac damage in gerbils. *Ann Clin Lab Sci* **39**, 378–385 (2009).
64. Glickstein, H., El, R. B., Shvartsman, M. & Cabantchik, Z. I. Intracellular labile iron pools as direct targets of iron chelators: a fluorescence study of chelator action in living cells. *Blood* **106**, 3242–3250 (2005).
65. Balderas-Villalobos, J. *et al.* Oxidative stress in cardiomyocytes contributes to decreased SERCA2a activity in rats with metabolic syndrome. *Am J Physiol Heart Circ Physiol* **305**, H1344–1353 (2013).
66. Arakawa, M. & Ito, Y. N-acetylcysteine and neurodegenerative diseases: basic and clinical pharmacology. *Cerebellum* **6**, 308–314 (2007).
67. Kilkenny, C., Browne, W., Cuthill, I. C., Emerson, M. & Altman, D. G. Animal research: reporting *in vivo* experiments–the ARRIVE guidelines. *J Cereb Blood Flow Metab* **31**, 991–993 (2011).
68. Berdoukas, V. *et al.* The efficacy of iron chelator regimes in reducing cardiac and hepatic iron in patients with thalassaemia major: a clinical observational study. *J Cardiovasc Magn Reson* **11**, 20 (2009).
69. Wood, J. C. *et al.* The effect of deferasirox on cardiac iron in thalassemia major: impact of total body iron stores. *Blood* **116**, 537–543 (2010).
70. Chinda, K., Sanit, J., Chattipakorn, S. & Chattipakorn, N. Dipeptidyl peptidase-4 inhibitor reduces infarct size and preserves cardiac function via mitochondrial protection in ischaemia-reperfusion rat heart. *Diab Vasc Dis Res* **11**, 75–83 (2014).
71. Palee, S., Apaijai, N., Shinlapawittayatorn, K., Chattipakorn, S. C. & Chattipakorn, N. Acetylcholine Attenuates Hydrogen Peroxide-Induced Intracellular Calcium Dyshomeostasis Through Both Muscarinic and Nicotinic Receptors in Cardiomyocytes. *Cell Physiol Biochem* **39**, 341–349 (2016).
72. Weerateerangkul, P., Palee, S., Chinda, K., Chattipakorn, S. C. & Chattipakorn, N. Effects of Kaempferia parviflora Wall. Ex. Baker and sildenafil citrate on cGMP level, cardiac function, and intracellular Ca2+ regulation in rat hearts. *J Cardiovasc Pharmacol* **60**, 299–309 (2012).
73. Pongkan, W., Chattipakorn, S. C. & Chattipakorn, N. Chronic testosterone replacement exerts cardioprotection against cardiac ischemia-reperfusion injury by attenuating mitochondrial dysfunction in testosterone-deprived rats. *PLoS One* **10**, e0122503 (2015).
74. Grynkiewicz, G., Poenie, M. & Tsien, R. Y. A new generation of Ca2+ indicators with greatly improved fluorescence properties. *J Biol Chem* **260**, 3440–3450 (1985).
75. Tanajak, P. *et al.* Fibroblast growth factor 21 (FGF21) therapy attenuates left ventricular dysfunction and metabolic disturbance by improving FGF21 sensitivity, cardiac mitochondrial redox homoeostasis and structural changes in pre-diabetic rats. *Acta Physiol (Oxf)* **217**, 287–299 (2016).

Acknowledgements

We would like to thank Miss Maria Love for her editorial assistance, and Miss Sasiwan Kerdphoo and Miss Thidarat Jaiwongkam for their technical assistance. This work was supported by the NSTDA Research Chair Grant from the National Science and Technology Development Agency Thailand (NC) and grants from the Thailand Research Fund BRG5780016 (SC), MRG5980222 (SK), the Royal Golden Jubilee program (SC and SW), Chiang Mai University Center of Excellence Award (NC), and the Faculty of Medicine Chiang Mai University Fund (SW and NC).

Author Contributions

S.W. and J.K. performed the research; N.C. and S.C. designed research study; N.C. and S.C. contributed essential materials and reagents; S.W., S.K. and J.K. analysed the data; S.W., S.K., S.C. and N.C. wrote and revised the manuscript; S.C. and N.C. critically reviewed and approved of the submitted and the final version.

Additional Information

Suppiementary information accompanies this paper at http://www.nature.com/srep

Competing Interests: The authors declare no competing financial interests.

How to cite this article: Wongjaikam, S. *et al.* Restoring the impaired cardiac calcium homeostasis and cardiac function in iron overload rats by the combined deferiprone and N-acetyl cysteine. *Sci. Rep.* 7, 44460; doi: 10.1038/srep44460 (2017).

Publisher's note: Springer Nature remains neutral with regard to jurisdictional claims in published maps and institutional affiliations.

This work is licensed under a Creative Commons Attribution 4.0 International License. The images or other third party material in this article are included in the article's Creative Commons license, unless indicated otherwise in the credit line; if the material is not included under the Creative Commons license, users will need to obtain permission from the license holder to reproduce the material. To view a copy of this license, visit http://creativecommons.org/licenses/by/4.0/

© The Author(s) 2017

เอกสารแนบหมายเลข 6

European Journal of Pharmacology 799 (2017) 118–127

Contents lists available at ScienceDirect

European Journal of Pharmacology

journal homepage: www.elsevier.com/locate/ejphar

Cardiovascular pharmacology

Effects of iron overload, an iron chelator and a T-Type calcium channel blocker on cardiac mitochondrial biogenesis and mitochondrial dynamics in thalassemic mice

Juthamas Khamseekaew[a,b,c], Sirinart Kumfu[a,b,c], Suwakon Wongjaikam[a,b,c], Sasiwan Kerdphoo[a,c], Thidarat Jaiwongkam[a,c], Somdet Srichairatanakool[e], Suthat Fucharoen[f], Siriporn C. Chattipakorn[a,c,d], Nipon Chattipakorn[a,b,c,*]

[a] Cardiac Electrophysiology Research and Training Center, Faculty of Medicine, Chiang Mai University, Chiang Mai, Thailand
[b] Cardiac Electrophysiology Unit, Department of Physiology, Faculty of Medicine, Chiang Mai University, Chiang Mai, Thailand
[c] Center of Excellence in Cardiac Electrophysiology Research, Chiang Mai University, Chiang Mai, Thailand
[d] Department of Oral Biology and Diagnostic Sciences, Faculty of Dentistry, Chiang Mai University, Chiang Mai, Thailand
[e] Department of Biochemistry, Faculty of Medicine, Chiang Mai University, Chiang Mai, Thailand
[f] Thalassemia Research Center, Institute of Molecular Biosciences, Mahidol University, Nakhon Pathom, Thailand

ARTICLE INFO

Chemical compounds studied in this article:
Deferiprone (PubChem CID: 2972)
Efonidipine (PubChem CID: 163838)

Keywords:
Cardiomyopathy
Iron overload
Mitochondrial dynamics
Oxidative phosphorylation
Thalassemic mice

ABSTRACT

Although cardiac mitochondrial dysfunction is involved in the pathophysiology of iron-overload cardiomyopathy, the precise mechanisms of iron-induced mitochondrial dysfunction, and the roles of the iron chelator deferiprone and the T-type calcium channel blocker efonidipine on cardiac mitochondrial biogenesis in thalassemic mice are still unknown. β-thalassemic (HT) mice were fed with a normal diet (ND) or a high iron-diet (FE) for 90 days. Then, the FE-fed mice were treated with deferiprone (75 mg/kg/day) or efonidipine (4 mg/kg/day) for 30 days. The hearts were used to determine cardiac mitochondrial function, biogenesis, mitochondrial dynamics and protein expressions for oxidative phosphorylation (OXPHOS) and apoptosis. ND-fed HT mice had impaired heart rate variability (HRV), increased mitochondrial dynamic proteins and caspase-3, compared with ND-fed wild-type mice. Iron overload led to increased plasma non-transferrin bound iron, oxidative stress, and the impairments of HRV and left ventricular function, cardiac mitochondrial function and mitochondrial dynamics, and decreased complex IV in thalassemic mice. Our results suggested that deferiprone and efonidipine treatment showed similar benefit in attenuating cardiac iron deposit and oxidative stress, and improved cardiac mitochondrial function, leading to improved left ventricular function, without altering the cardiac mitochondrial biogenesis, and apoptosis proteins in iron-overload thalassemic mice.

1. Introduction

Iron-overload cardiomyopathy is a serious complication in transfusion-dependent thalassemic patients (Breuer et al., 2000). Iron overload leads to existence of plasma non-transferrin bound iron (NTBI) (Anderson and Shah, 2013), and leads to increased reactive oxygen species, resulting in oxidative stress which can damage cells and mitochondria (Bartfay and Bartfay, 2000). Although cardiac mitochondrial dysfunction has been shown to involve in the pathogenesis of iron-overload cardiomyopathy (Kumfu et al., 2016), the mechanisms of iron overload-induced mitochondrial dysfunction are still unclear.

Mitochondria are regarded as energy generators that produced ATP for the cells through oxidative phosphorylation (OXPHOS) (Gao et al., 2008). Iron overload causes cardiac mitochondrial dysfunction which is characterized by increased mitochondrial reactive oxygen species production, mitochondrial membrane depolarization and mitochondrial swelling (Kumfu et al., 2012b). Mitochondrial dysfunction leads to mitochondrial-cytochrome c released and contributes to the activation of the caspase pathway, resulting in apoptosis (Kumfu et al., 2016). Previous study showed that iron overload decreased the respiratory chain components activity including complex I and IV (Gao et al., 2009). However, the mechanism of iron overload-induced apoptosis and altered OXPHOS expression in thalassemic mice heart has never been investigated.

Mitochondrial morphology is regulated by the balance between fusion and fission, called mitochondrial dynamics, which are important

* Corresponding author at: Cardiac Electrophysiology Research and Training Center, Faculty of Medicine, Chiang Mai University, Chiang Mai 50200, Thailand.
E-mail address: nchattip@gmail.com (N. Chattipakorn).

http://dx.doi.org/10.1016/j.ejphar.2017.02.015
Received 28 October 2016; Received in revised form 7 February 2017; Accepted 9 February 2017
Available online 10 February 2017
0014-2999/ © 2017 Elsevier B.V. All rights reserved.

in cellular processes (Chen et al., 2011; Ishihara et al., 2015; Lee et al., 2004). Mitochondrial fusion is regulated by mitofusin-1 and -2 (Mfn-1, Mfn-2) (Legros et al., 2002) while fission is regulated by dynamin-related protein-1 (Drp-1) (Smirnova et al., 1998). Furthermore, peroxisome proliferator-activated receptor gamma coactivator-1α (PGC-1α), an inducer of mitochondrial biogenesis, is a proven mediator for the stimulation of Mfn-2 expression to increase mitochondrial fusion and metabolism (Soriano et al., 2006). Previous studies demonstrated that mitochondrial dynamics imbalance is involved in pathological processes including ischemic-reperfusion injury (Ong et al., 2010). Therefore, mitochondrial dynamics may well be affected by iron overload conditions which could contribute to mitochondrial dysfunction. However, the expression of mitochondrial dynamic and biogenesis markers in the heart of iron-overloaded thalassemic mice has never been investigated.

T-type calcium channel (TTCC) is re-expressed in thalassemic mice hearts and can mediate iron entry in the heart (Kumfu et al., 2011). Treatment with efonidipine, the TTCC blocker (Tanaka and Shigenobu, 2002), can prevent Fe^{2+} uptake into the thalassemic cardiomyocytes (Kumfu et al., 2011), and provides broad beneficial effects similar to the iron chelator, deferiprone (DFP), in iron-overloaded thalassemic mice model (Kumfu et al., 2016). Although DFP has been shown to prevent iron-overload induced cardiac dysfunction in thalassemic patients, and had high efficacy in cardiac iron removal (Olivieri et al., 1995), the effects of DFP or efonidipine on the cardiac mitochondrial dynamics and OXPHOS in the heart of iron-overloaded thalassemic mice have never been investigated.

In this study, we determined effects of cardiac iron overload and the roles of DFP and efonidipine on cardiac mitochondrial biogenesis, dynamics, OXPHOS and cardiac apoptosis in iron-overloaded thalassemic mice. We hypothesized that DFP and efonidipine attenuate cardiac mitochondrial dynamics imbalance and apoptosis, and improve OXPHOS expression in iron-overloaded thalassemic mice.

2. Materials and methods

2.1. Animal models

Two types of adult male C57BL/6 mice aged 3–6 months old (weighing 20–25 g.), including wild-type (mu$\beta^{+/+}$, WT) and heterozygous β^{KO} type (mu$\beta^{th-3/+}$, HT) were used. These mice were obtained from the Thalassemia Research Center, Institute of Molecular Biosciences, Mahidol University, Nakhon Pathom, Thailand. All animal studies were approved by the Institutional Animal Care and Use Committee (IAGUG) at the Faculty of Medicine, Chiang Mai University (Permit number: 11/2558) and conformed to the *Guide for the Care and Use of Laboratory Animals* published by the US National Institutes of Health (NIH guide, 8th edition, 2011). The mice were housed in a room maintained under constant environmental conditions (temperature 22–25 °C and a constant 12-h light/dark cycle) and were given *ad libitum* access to food and water.

2.2. Iron treatment and pharmacological intervention

WT and HT mice in the control group (ND group) were fed on a standard chow diet, whereas the iron overloaded group (FE group) in both types of mice were fed on iron-diet (0.2% Ferrocene/kg of diet) for 90 days (Kumfu et al., 2012a). The ND group received a vehicle including 0.5% DMSO (via s.c. injection, daily, *n=3* each) or normal saline solution (NSS; via oral gavage feeding, twice a day, *n=3* each) as a control group. Mice in the FE group were randomly divided into 3 subgroups (*n*=6 each), including: 1) FE mice treated with either 0.5% DMSO (*n=3* each) or NSS (*n=3* each) (FE group); 2) FE mice treated with DFP (FE-DFP group), and 3) FE mice treated with efonidipine (FE-EFO group). FE-DFP subgroups received 75 mg/kg/day of DFP (Government Pharmaceutical Organization, Bangkok, Thailand; dissolved in NSS), via oral gavage feeding, twice a day. FE-EFO subgroups received 4 mg/kg/day of efonidipine (Sigma-Aldrich, St. Louis, MO, USA; dissolved in 0.5% DMSO), via s.c. injection, daily. Each subgroup received the assigned treatment for 30 consecutive days. At the end of the experiments (i.e. 4 months after the start of iron loading and treatment), blood pressure (BP), HRV, cardiac function, cardiac iron deposition, malondialdehyde (MDA) levels, cardiac mitochondrial function, and mitochondrial dynamics, biogenesis and OXPHOS as well as apoptotic protein expression were evaluated in all mice.

2.3. Measurement of blood pressure (BP)

Mice were preheated under an infrared warming pad for at least five min to dilate the tail vein and acclimate to the holder. An occlusion cuff and volume pressure recording were attached to the tail. Blood pressure measurement was performed by using a CODA2 channel non-invasive blood pressure system (Kent Scientific Corporation, Wyoming, USA). A mean blood pressure value was achieved by taking an average of 20 consecutive measurements at a steady state (Samniang et al., 2016; Tanajak et al., 2016).

2.4. Measurement of heart rate variability (HRV)

Cardiac autonomic nervous activity was evaluated by spectral analysis of the RR interval variability. Lead II electrocardiogram (ECG) was recorded continuously in conscious mice using a signal transducer (PowerLab 4/25T, ADInstrument) and operated through the Chart 5.0 program as described previously (Kumfu et al., 2012a). The ECG data were analyzed using the frequency-domain method of the MATLAB program (Kumfu et al., 2012a). The cardiac autonomic balance was reported as the LF/HF ratio. An increased LF/HF ratio indicates depressed HRV or cardiac autonomic imbalance (Kumfu et al., 2012a).

2.5. Measurement of echocardiogram

Cardiac function was assessed by echocardiography (Vivid i, GE Medical Systems, Aurora, OH, USA). Mice were lightly inducted and maintained with 0.8–1% isoflurane with oxygen (1 L/min) inhalation (Das et al., 2015). Signals from M-mode images were recorded at the papillary muscle level to determine %left ventricle fractional shortening (%LVFS) and %LV ejection fraction (%LVEF) (Das et al., 2015). Then, the %LVFS and %LVEF were determined using the LV function mode. A decrease in %LVFS and %LVEF were considered to be an indicator of decreased LV function (Das et al., 2015; Tanajak et al., 2016).

2.6. Quantification of plasma non-transferrin bound iron (NTBI)

Plasma NTBI concentration was measured using the nitrilotriacetic acid disodium salt (NTA) chelation/flow cytometry method established by Ma et al. (2014). Plasma samples were incubated with 80-mM NTA solution, pH 7.0 for 30 min at room temperature to produce an Fe^{3+}-$(NTA)_2$ complex. Afterwards, the Fe^{3+}-$(NTA)_2$ was separated from plasma proteins by spinning the plasma mixture through a membrane filter (NanoSep®, 30-kDa cut off, polysulfone type; Pall Life Sciences, Ann Arbor, MI, USA). The Fe^{3+}-$(NTA)_2$ concentration representing NTBI in the ultrafitrate was determined using chelatable fluorescent beads based on flow cytometry (Guava EasyCyte HT, Merck Millipore, Germany). Plasma NTBI concentration was calculated from a standard curve using GraphPad Prism software.

2.7. Cardiac iron content and iron deposition determination

Cardiac iron determination was established using a method as described previously (Kumfu et al., 2012a). The homogenate heart was precipitated in precipitation solution and was heated at 95 °C for one h,

and allowed to cool at room temperature for two min. Then, the mixed sample was centrifuged at 8200*g* for ten min. The supernatant was mixed with chromogen solution (1:1) and was incubated for 30 min at room temperature. Absorbance of the sample was determined using a microplate reader at 562 nm. The cardiac iron concentration was compared to the standard iron curve. Regarding the cardiac iron content assay, this method was designed specifically to facilitate the measurement of non-heme iron in animal tissue (Kumfu et al., 2012a; Rebouche et al., 2004). Moreover, the blood was washed out from the heart tissue before it was used in this assay. Therefore, circulating iron contents and plasma NTBI were not detected by this method. Cardiac iron deposition was determined by staining with a Prussian blue dye solution. The tissue slides were examined under a light microscope and recorded with a digital camera (Kumfu et al., 2012a).

2.8. Determination of cardiac malondialdehyde (MDA) concentration

To determine the lipid peroxidation marker, cardiac MDA concentrations were measured by using a HPLC method as described previously (Kumfu et al., 2012a). Briefly, the supernatant of homogenate heart was mixed with H_3PO_4 and thiobarbituric acid (TBA) solution, and then incubated at 90°C for 30 min to produce thiobarbituric acid reactive substances (TBARS). The cardiac TBARS concentrations were calculated directly from a standard curve and reported as MDA equivalent concentrations.

2.9. Cardiac mitochondrial function study

Cardiac mitochondria were isolated using the method described previously (Kumfu et al., 2012b). Briefly, the minced ventricular tissue was homogenized in ice cold mitochondrial isolation buffer (MIB). The homogenates were used to isolate mitochondria by differential centrifugation (Thummasorn et al., 2011). After that, 5 μg/ml of ferric ammonium citrate co-administered with 1 mM ascorbic acid, serving to represent the ascorbate-reduced form of iron (Fe^{2+}), was applied to the isolated cardiac mitochondria for five min (Kumfu et al., 2016). Finally, assessment of mitochondrial reactive oxygen species production, mitochondrial membrane potential change and mitochondrial swelling was performed according to the experimental protocols.

The cardiac mitochondrial reactive oxygen species production was determined by using fluorescent dye dichlorohydrofluorescein diacetate (DCFDA). After Fe^{2+} loading, cardiac mitochondria were incubated at 25 °C with DCFDA for 20 min. The reactive oxygen species level was assessed at an excitation/emission wavelength at 485/530 nm using a fluorescent microplate reader (Bio Tek Instruments, Inc., Winooski, Vermont, USA). The increased fluorescent intensity indicates increased mitochondrial reactive oxygen species production (Kumfu et al., 2016; Thummasorn et al., 2011).

The cardiac mitochondrial membrane potential was determined by using the dye 5,5′,6,6′-tetrachloro-1,1′,3,3′-tetraethylbenzimidazolcarbocyanine iodide (JC-1). After Fe^{2+} loading, mitochondrial proteins were stained with JC-1 at 37 °C for 30 min and then mitochondrial membrane potential was determined as fluorescence intensity by using a fluorescent microplate reader. JC-1 monomer (green fluorescence) and aggregate (red fluorescence) form was excited/emitted at a wavelength of 485/530 nm and 485/590 nm, respectively. A decrease in the red/green fluorescence intensity ratio indicated mitochondrial depolarization (Thummasorn et al., 2011).

The cardiac mitochondrial swelling was determined using a microplate reader to measure the change in the absorbance at 540 nm for 30 min. A decreased absorbance indicated increased cardiac mitochondrial swelling (Thummasorn et al., 2011). The cardiac mitochondrial morphology was identified by using transmission electron microscopy (TEM) (Thummasorn et al., 2011).

2.10. Western blot analysis

The heart homogenate and cardiac mitochondrial fraction were lysed with an extraction buffer and a protease inhibitor (Palee et al., 2013). The heart homogenate was used to study Mfn-2, Drp-1, PGC-1α, Bax, Bcl-2, and caspase-3 expression. The mitochondrial fraction was used to study total OXPHOS expression. Total protein concentration was determined using a Bio-Rad protein assay kit (Bio-Rad Laboratories Ltd., Hercules, California, USA). The total protein sample was mixed with a loading buffer and boiled for five min at 95 °C and subsequently separated by electrophoresis on a 10% TGX Stain-Free™ FastCast™ Acrylamide Kit (Bio-Rad Laboratories Ltd.). The total protein stained was scanned using the ChemiDoc™ Touch Gel Imaging System (Bio-Rad Laboratories Ltd.). Proteins were then transferred onto a nitrocellulose membrane in a glycine/methanol-transfer buffer (Palee et al., 2013) in a Wet/Tank blotting system. Membranes were blocked for one h with 5% nonfat dry milk in TBST. They were probed overnight at 4 °C with the primary antibodies which recognize Bax, PGC-1α (Santa Cruz, Biotechnology Inc., Dallas, Texas, USA), Bcl-2, Caspase 3, Mfn2, Drp1(Cell signaling technology, Inc., Danvers, MA, USA), and OXPHOS (Abcam, Cambridge, MA, USA). The membranes were subsequently incubated with secondary antibody for one h, and were visualized using Clarity™ Western ECL Blotting Substrate (Bio-Rad Laboratories Ltd.) and were scanned using ChemiDoc™ Touch Gel Imaging System. The western blot images were analyzed using Image J (NIH image) analysis software.

2.11. Statistical analysis

All data were reported as a mean ± standard error of mean (S.E.M.) and were processed using IBM SPSS software (release 21.0 for Windows; IBM Statistical Package for Social Sciences, Armonk, NY, USA). One-way ANOVA followed by LSD post-hoc test analysis were performed for group comparisons, and paired comparisons were performed by Student's *t*-tests. P-value < 0.05 was considered statistically significant.

3. Results

3.1. Effects of DFP and efonidipine on plasma NTBI level

FE groups in both WT and HT mice had an iron overload condition as indicated by increased plasma NTBI level, whereas plasma NTBI levels in the ND groups (both WT and HT) were not detected. Both DFP and efonidipine led to effectively decreased plasma NTBI levels in both types of mice compared with the FE groups, and there was no significant difference between groups of treatments (Fig. 1A).

3.2. Effects of DFP and efonidipine on blood pressure

In the ND groups, mean arterial pressure (MAP) was not different between the WT and HT mice. The FE groups in both WT and HT mice demonstrated significantly increased MAP, compared with their ND groups. Both DFP and efonidipine treatment led to no significant improvement of MAP in the iron-overloaded mice (Fig. 1B).

3.3. Effects of DFP and efonidipine on HRV and cardiac function

In the ND groups, HT mice had a higher LF/HF ratio than WT mice, indicating cardiac sympathovagal imbalance in HT mice even without an iron overload condition (Fig. 1C). The FE groups in both WT and HT mice had an increased LF/HF ratio, compared with their ND groups, suggesting that iron overload impaired cardiac autonomic balance in both types of mice. Both DFP and efonidipine treatment significantly decreased the LF/HF ratio, indicating an improved cardiac autonomic balance in both WT and HT mice (Fig. 1C). Moreover, iron

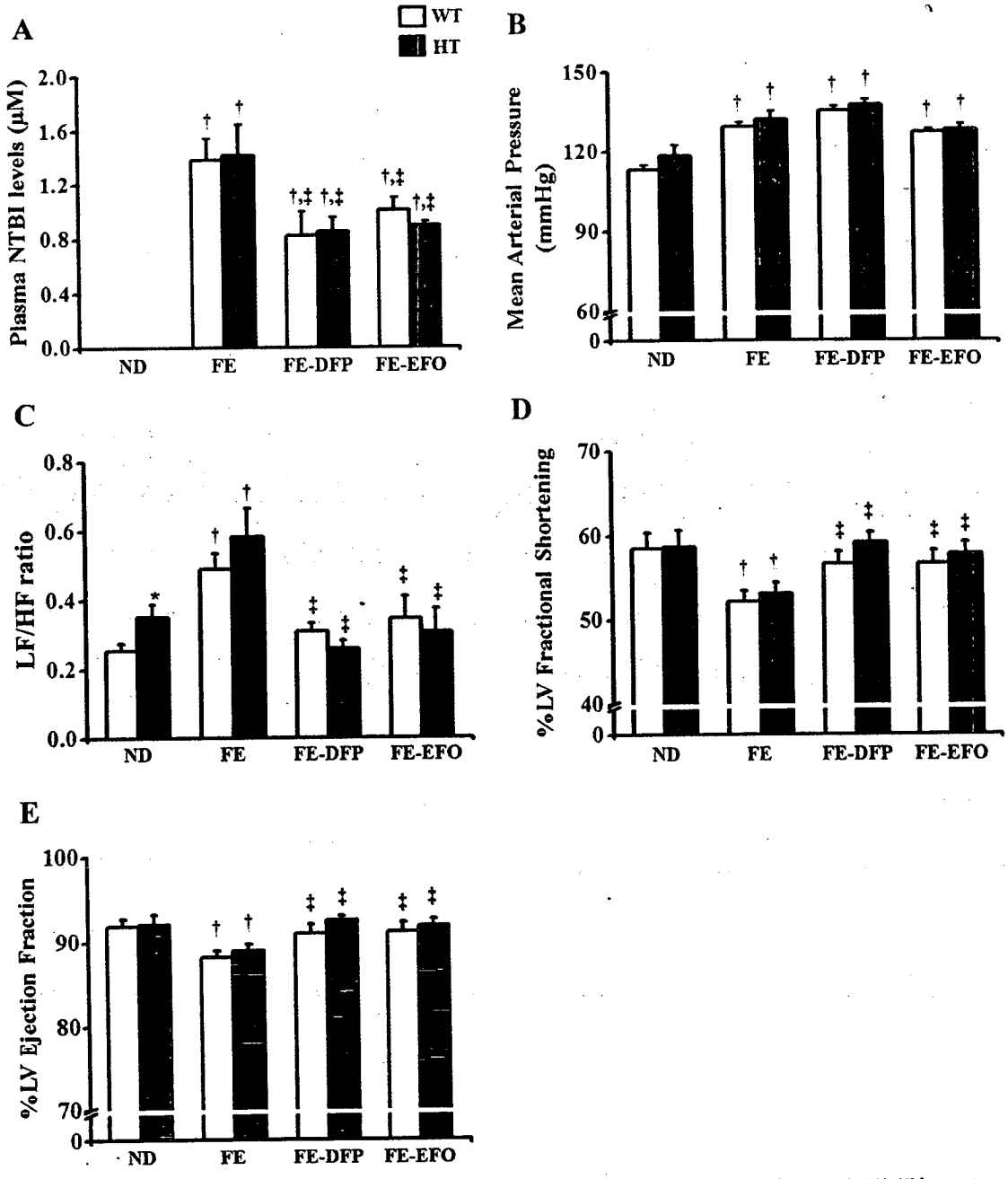


Fig. 1. Effects of deferiprone (DFP) and efonidipine (EFO) on (A) plasma non-transferrin bound iron (NTBI) level, (B) mean arterial pressure (MAP), (C) heart rate variability, (D) %LV fraction shortening (%LVFS) and (E) %LV ejection fraction (%LVEF), in iron-overloaded WT and HT mice. DFP and EFO reduced plasma NTBI levels and LF/HF ratio, and also improved %LVFS and %LVEF, but did not reduce MAP in both WT and HT mice under an iron overload condition. Data are expressed as mean ± S.E.M., $^{*}P < 0.05$ vs. WT-ND, $^{\dagger}P < 0.05$ vs. ND, $^{\ddagger}P < 0.05$ vs. FE, n=6/group.

overload caused impaired left ventricular function as shown by echocardiographic assessment (Fig. 1D-E). The FE groups in both WT and HT mice had a decreased %LVFS and %LVEF, compared with their ND groups. Both DFP and efonidipine treatment led to significantly increased %LVFS and %LVEF, indicating an improvement in left ventricular function in both types of mice (Fig. 1D-E).

3.4. Effects of DFP and efonidipine on cardiac iron concentration and MDA level

In the ND groups, cardiac iron concentration was no different between WT and HT mice. The FE groups in both WT and HT mice demonstrated significantly increased cardiac iron concentration, compared with their ND groups. Both DFP and efonidipine treatment led to significantly reduced cardiac iron concentration in both types of iron-overloaded mice (Fig. 2A). The location of iron deposits within the heart was revealed via Prussian blue staining (Fig. 2C). For the cardiac MDA level, the FE groups in both WT and HT mice had increased cardiac MDA levels, compared with their ND groups. Both DFP and efonidipine treatment led to restoration of the MDA level back to the normal level in both types of mice (Fig. 2B).

3.5. Effects of DFP and efonidipine on cardiac mitochondrial function and morphology

The FE groups in both WT and HT mice had increased cardiac

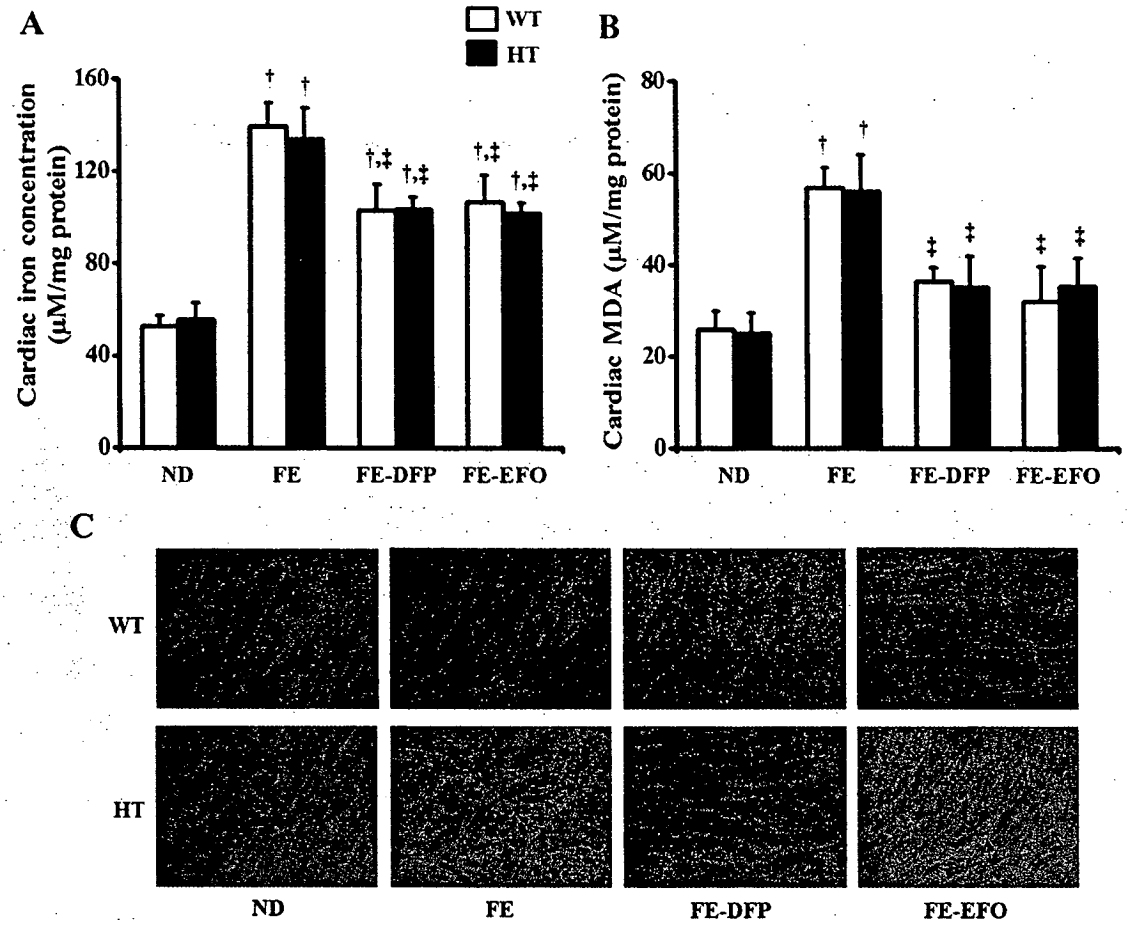


Fig. 2. Effects of deferiprone (DFP) and efonidipine on (EFO) (A) cardiac iron concentration, (B) cardiac malondialdehyde (MDA) levels and (C) Prussian blue iron staining of heart tissues (40× magnification objective lens, Arrow indicated iron staining in blue color.) from iron-overloaded WT and HT mice. DFP and EFO reduced cardiac iron contents and cardiac MDA levels in both WT and HT mice under an iron overload condition. Data are expressed as mean ± S.E.M., †$P < 0.05$ vs. ND, ‡$P < 0.05$ vs. FE, n=6/group. (For interpretation of the references to color in this figure legend, the reader is referred to the web version of this article).

mitochondrial reactive oxygen species production, decreased red/green fluorescent intensity ratio which indicated cardiac mitochondrial membrane depolarization, and decreased absorbance which indicated cardiac mitochondrial swelling, compared with their ND groups (Fig. 3A-C). Both DFP and efonidipine treatment led to significantly decreased cardiac mitochondrial reactive oxygen species production and attenuated cardiac mitochondrial membrane depolarization and cardiac mitochondrial swelling in both iron-overloaded WT and HT mice (Fig. 3A-C). The representative electron micrographs of cardiac mitochondrial morphology from all groups are shown in Fig. 3D. The unfolded cristae were mostly detected in the FE groups in both types of mice. Interestingly, treatment with either DFP or efonidipine effectively attenuated cardiac mitochondrial swelling as shown by preserved cristae in both iron-overloaded WT and HT mice (Fig. 3D).

3.6. Effects of DFP and efonidipine on cardiac mitochondrial dynamics and biogenesis

The expression of mitochondrial fission Drp-1 (Fig. 4A) and mitochondrial fusion Mfn-2 (Fig. 4B) was not significantly different among groups in the WT mice. However, the expression of Drp-1 and Mfn-2 proteins was significantly increased in the control HT mice compared with the control WT mice. Drp-1 and Mfn-2 expression were significantly decreased in the FE group in the HT mice, compared with the control HT mice (Fig. 4A-B). Treatment with either DFP or efonidipine did not change the expression of Drp-1 and Mfn-2 proteins in iron-overloaded HT mice. The FE group and the pharmacologically treated groups in WT mice, as well as all groups of HT mice had significantly increased Drp-1/Mfn-1 ratio, compared with the control WT mice (Fig. 4C). These findings indicated that the mice in these groups had imbalanced mitochondrial dynamics and exhibited higher levels of the fission process. Moreover, the protein levels of mitochondrial biogenesis marker PGC-1α was not significantly different between groups in the WT mice. However, the FE group in HT mice had significantly increased PGC-1α expression, compared with the control WT mice (Fig. 4D). These findings indicate that the iron overload condition might increase mitochondrial biogenesis in HT mice.

3.7. Effects of DFP and efonidipine on total oxidative phosphorylation (OXPHOS) in the heart

The protein levels of OXPHOS or several respiratory chain subunits (NDUFB8 in complex I, SDHB in complex II, UQCRC2 in complex III, COX1 in complex IV, and ATP-alpha subunit in complex V) in the cardiac mitochondrial fraction were not significantly different between WT and HT mice in ND groups (Fig. 5A-F). In the FE groups, WT and HT mice had significantly decreased complex IV protein expression, and treatment with either DFP or efonidipine did not change this protein expression in iron-overloaded WT and HT mice (Fig. 5E). Moreover, the FE group in HT mice had significantly decreased complex V, compared with the control HT mice, and treatment with either DFP or efonidipine did not change complex V protein expression (Fig. 5F).

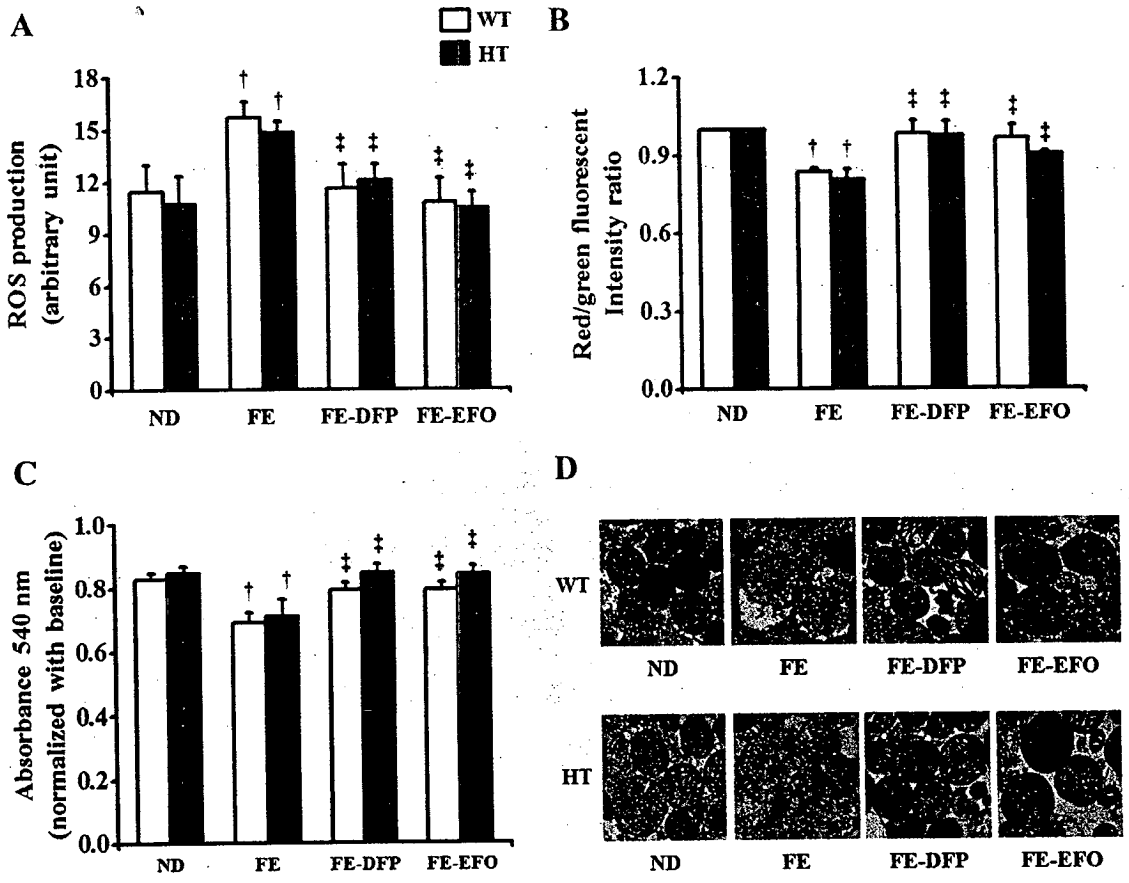


Fig. 3. Effects of deferiprone (DFP) and efonidipine (EFO) on cardiac mitochondrial function, including (A) cardiac mitochondrial reactive oxygen species production, (B) mitochondrial membrane potential change, (C) mitochondrial swelling and (D) cardiac mitochondrial morphological change, in iron-overloaded WT and HT mice. DFP and EFO decreased cardiac mitochondrial reactive oxygen species production, mitochondrial membrane potential change, mitochondrial swelling and mitochondrial morphological change in both WT and HT mice under an iron overload condition. Data are expressed as mean ± S.E.M., †$P < 0.05$ vs. ND, ‡$P < 0.05$ vs. FE, n=6/group.

3.8. Effects of DFP and efonidipine on cardiac apoptotic signaling

The protein levels of pro-apoptotic Bax and anti-apoptotic Bcl-2 and the Bax/Bcl-2 ratio were not significantly different between groups in both types of mice (Fig. 6A-C). In the ND groups, the expressions of cleaved-caspase 3/total-caspase 3 ratio were significantly increased in HT mice compared with WT mice. Iron-overloaded WT and HT mice had significantly increased caspase 3 activity, compared with their ND groups (Fig. 6D). These findings indicate that iron overload and thalassemic conditions could increase cardiac apoptosis through activation of the caspase 3 cascade. Treatment with either DFP or efonidipine did not change the level of caspase 3 activity under the condition of iron overload in both types of mice.

4. Discussion

The major findings of the present study are as follows. Firstly, long-term high iron diet consumption caused iron overload both in WT and HT mice, indicated by increasing plasma NTBI level. Secondly, iron overload led to increased cardiac iron concentrations, cardiac iron deposition, cardiac MDA level, MAP and LF/HF ratio and impaired LV function, identified by decreased %LVFS and %LVEF, impaired cardiac mitochondrial function as indicated by increased mitochondrial reactive oxygen species production, mitochondrial depolarization and mitochondrial swelling, and treatment with either DFP or efonidipine shared similar efficacy in reversing these effects, except for MAP, both in WT and HT mice. Thirdly, iron overload caused an increase in the Drp-1/Mfn-2 ratio in only WT mice, decreased Drp-1 and Mfn-2 and increased PGC-1α expression in only HT mice and also increased caspase-3 activity in both WT and HT mice. Treatment with either DFP or efonidipine did not alter Drp-1 and Mfn-2 expression, Drp-1/Mfn-2 ratio, PGC-1α expression and caspase-3 activity in the iron-overloaded mice. Fourthly, iron overload led to decreased OXPHOS expression such as complex IV in WT mice, and complexes IV and V in HT mice, and treatment with either DFP or efonidipine did not change the expression of OXPHOS proteins.

In our study, the iron-overloaded mice were in the early development stage of cardiomyopathy, as they displayed decreased LV function by decreased %LVFS and %LVEF. Moreover, a previous study from our team showed that after inducing an iron overload condition for 4 months in mice, they had impaired LV function indicated by decreased end systolic pressure (ESP), $Pressure_{max}$, dP/dt_{max} values, stroke volume and cardiac output, which were studied using Pressure-Volume loop analysis (Kumfu et al., 2016). However, cardiac hypertrophy did not develop in these iron-overloaded mice since the heart weight/body weight ratio was not changed in iron-overloaded mice compared to their ND groups (Kumfu et al., 2016).

Regarding the WT and HT mice, they both responded similarly to iron overload, which could possibly be due to the fact that high iron overload condition was induced in both groups of mice for a long time, causing severe iron overload at a similar level in both WT and HT mice. Moreover, we measured all parameters at the end of the experiment (i.e. 4 months after iron overload began to be induced). Therefore, the different responses to iron overload might not have been observed in both types of mice. However, our results demonstrated that some of the mitochondrial markers in HT mice were different from WT mice. Since the HT mice have mild anemia and a higher-cardiac output (CO) state than WT mice, in order to compensate for low hemoglobin levels in the

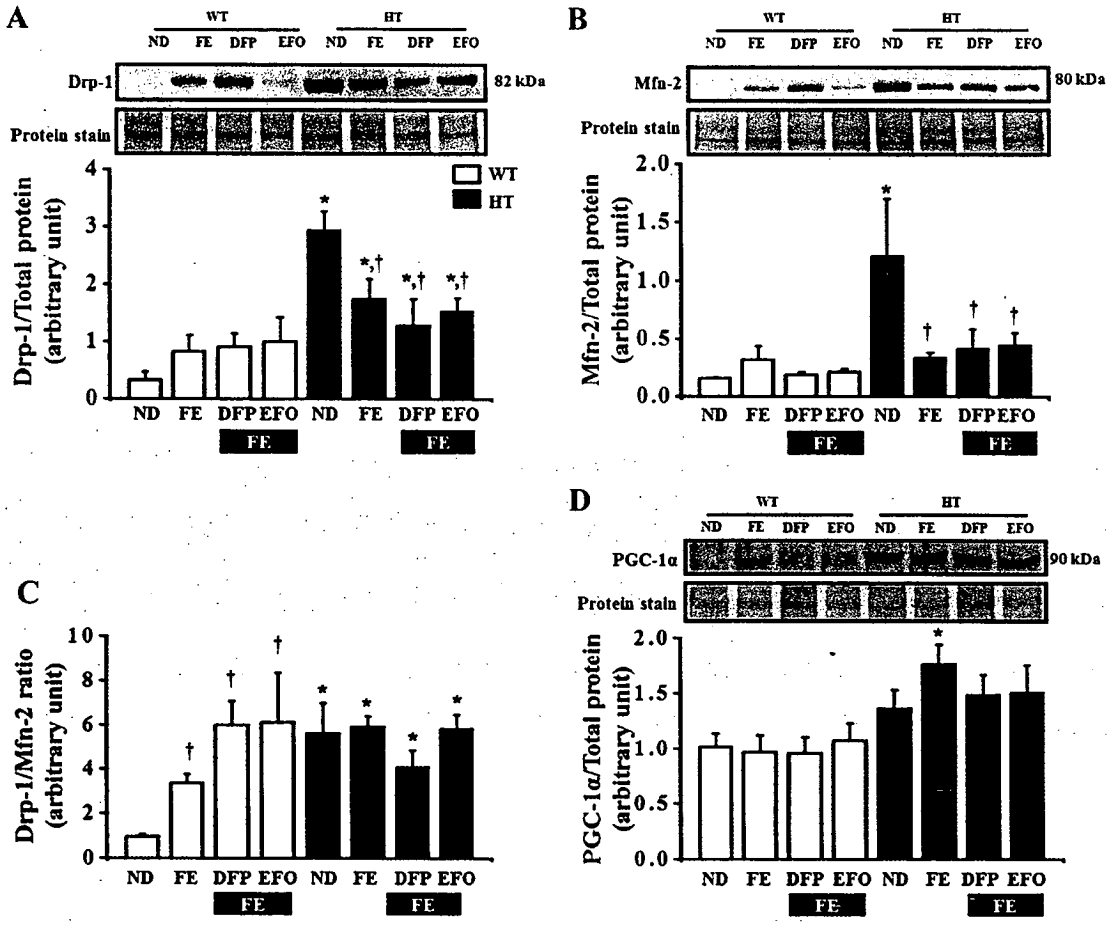


Fig. 4. Effects of deferiprone (DFP) and efonidipine (EFO) on mitochondrial dynamics and mitochondrial biogenesis measured in the whole heart homogenates of iron-overloaded WT and HT mice. (A-D) Western blot of mitochondrial fission protein dynamin-related protein-1 (Drp-1), mitochondrial fusion protein mitofusin-2 (Mfn-2), Drp-1/Mfn-2 ratio and cardiac mitochondrial biogenesis marker PGC-1α, respectively. DFP and EFO did not change the expression of Drp-1, Mfn-2 and PGC-1α in iron-overloaded HT mice and Drp-1/Mfn-2 ratio in both WT and HT mice under an iron overload condition. Data are expressed as mean ± S.E.M., $^{*}P < 0.05$ vs. WT-ND, $^{\dagger}P < 0.05$ vs. ND, n=6/group.

body (Kumfu et al., 2016; Wood et al., 2005), the heart might require higher energy levels or ATP production to support its contractile function. In our present study, HT mice had high levels of mitochondrial dynamics (fission and fusion events), which might be a defense mechanism to preserve ATP levels for the cells. However, a limitation in our study was that the level of ATP in the cardiomyocytes was not measured.

In this study, chronic iron overload led to increased plasma NTBI and also increased cardiac iron deposition. NTBI is known as a highly toxic form of iron, which can increase reactive oxygen species production via Fenton and Haber-Weiss reactions (Breuer et al., 2000). The iron overload-induced reactive oxygen species production has been shown to cause cellular lipid peroxidation and also increase cytotoxic aldehyde products such as MDA (Link et al., 1989). In this study, iron-overloaded mice also had increased cardiac MDA levels. Moreover, the iron overload-induced reactive oxygen species production can damage cardiac mitochondria, and lead to cardiac mitochondrial dysfunction as indicated by increased cardiac mitochondrial reactive oxygen species production, mitochondrial depolarization, and mitochondrial swelling and also induced mitochondrial morphological change which has also been previously reported (Kumfu et al., 2012b, 2016; Sripetchwandee et al., 2014). Cardiac mitochondrial dysfunction has been shown to be associated with cardiac autonomic imbalance and cardiac dysfunction in iron-overloaded mice (Gao et al., 2009, 2010). Moreover, previous studies demonstrated that an increased iron overload can decrease vascular endothelial function and increase systolic blood pressure, as observed in a thalassemic patient (Wood et al., 2005). Consistent with these findings, our study demonstrated an increase in MAP in iron-overloaded mice. Efonidipine showed similar efficacy to DFP in decreasing plasma NTBI, cardiac iron concentration and cardiac MDA, and also led to improvement in cardiac mitochondrial function and cardiac autonomic balance as well as improved cardiac function, which are consistent with our previously reported findings (Kumfu et al., 2012a, 2016). These findings also confirm that TTCC could play important roles in cardiac iron uptake under iron overload conditions. Treatment with the TTCC blocker efonidipine provided beneficial effects similar to the iron chelator DFP.

Other studies have reported that mitochondrial dysfunction has been shown to cause cellular apoptosis (Chen et al., 2014; Wang et al., 2011). In this study, iron-overload led to increase cellular damage and cardiac mitochondrial dysfunction, as well as increased expression of cleaved caspase-3 in iron-overloaded WT mice and all groups of HT mice. These findings demonstrated that iron overload can induce cardiomyocytes apoptosis, and that HT mice were more vulnerable to cardiac apoptosis than WT mice. However, treatment with either DFP or efonidipine did not change these deleterious effects. These findings contradict results from a recent study that used a HL-1 cardiomyocyte loaded with iron, which found treatment with DFP, but not efonidipine, caused decreased iron-induced cardiomyocyte apoptosis (Chen et al., 2014). The discrepancy in the findings could be due to the use of different models (*in vitro vs. in vivo*), the nature of cardiomyocytes and dose of iron administration examined. Since cardiac apoptosis in these models were not through the Bax and Bcl-2 dependent pathway, induced iron overload may induce cardiomyocyte apoptosis via another

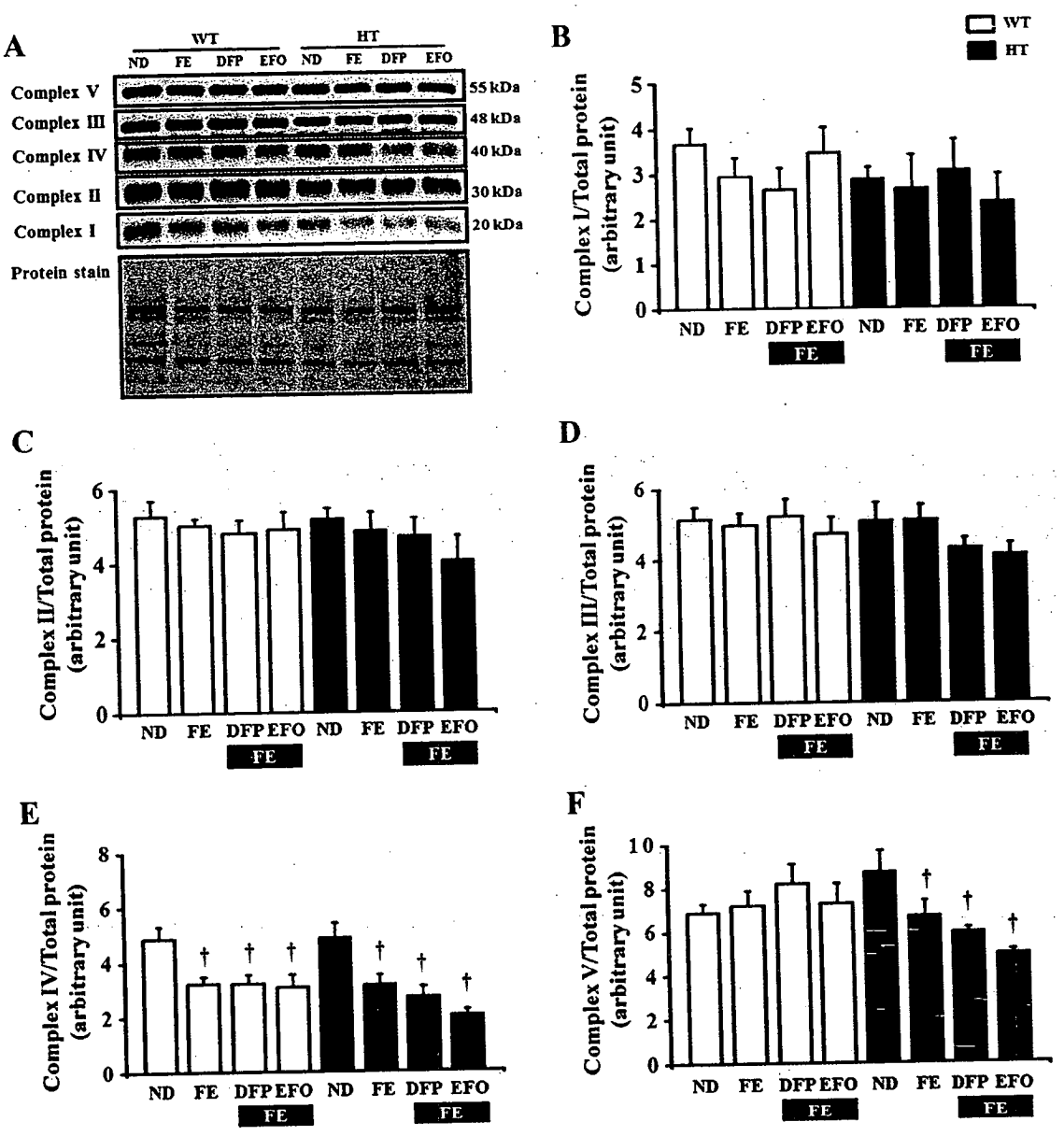


Fig. 5. Effects of deferiprone (DFP) and efonidipine (EFO) on total oxidative phosphorylation (OXPHOS) measured in the cardiac mitochondrial fraction of whole heart homogenates of iron-overloaded WT and HT mice. (A) Representative western blotting band of total OXPHOS. (B-F) Western blotting protein levels of total OXPHOS complexes I-V, respectively. DFP and EFO did not change complex IV expression in iron-overloaded WT mice and complex IV and V expression in iron-overload HT mice. Data are expressed as mean ± S.E.M., †$P < 0.05$ vs. ND, n=6/group.

mechanism such as an imbalance of mitochondrial dynamics (Arnoult, 2007).

An imbalance of mitochondrial dynamics has been reported during apoptosis and a proposal has been made that mitochondrial fragmentation is an additional, alternative or complementary mechanism in the mitochondrial-dependent apoptosis pathway (Arnoult, 2007; Bossy-Wetzel et al., 2003; Karbowski and Youle, 2003). In the present study, our results demonstrated for the first time that mitochondrial fission and fusion protein expression was higher in control HT mice than control WT mice. These finding suggest that HT mice had high mitochondrial dynamics of fission and fusion events which is a defense mechanism to preserve the ATP production in the cells. Moreover, our results showed that iron overload decreased the expression of fission and fusion proteins in only HT mice suggesting that the defense mechanism was impaired, and treatment with either DFP or efonidipine did not change the expression of these proteins. However, the Drp-1/Mfn-2 ratio was reduced in iron-overloaded WT mice and all groups of HT mice compared with control WT mice, indicating that the mice in these groups had imbalanced mitochondrial dynamics by increased mitochondrial fission. These findings are consistent with increased cleaved caspase-3 protein expression in these models. An increase in mitochondrial fission can cause mitochondrial fragmentation, loss of membrane potential and facilitate the cytochrome c release from mitochondria which contributes to caspase cascade activation, resulting in cardiac apoptosis (Arnoult, 2007; Karbowski and Youle, 2003). The present study found that PGC-1alpha expression was increased in only iron-overloaded HT mice. These findings suggest that there might be a compensatory process for cell apoptosis by increasing mitochondrial biogenesis in these mice. Although a previous study indicated that PGC-1alpha can stimulate Mfn-2 expression to increase mitochondrial fusion in rat myotube cell lines (Soriano et al., 2006), our *in vivo* study demonstrated a decreased Mfn-2 in iron-overloaded heart in HT mice.

The effects of iron overload and therapeutic treatment on OXPHOS

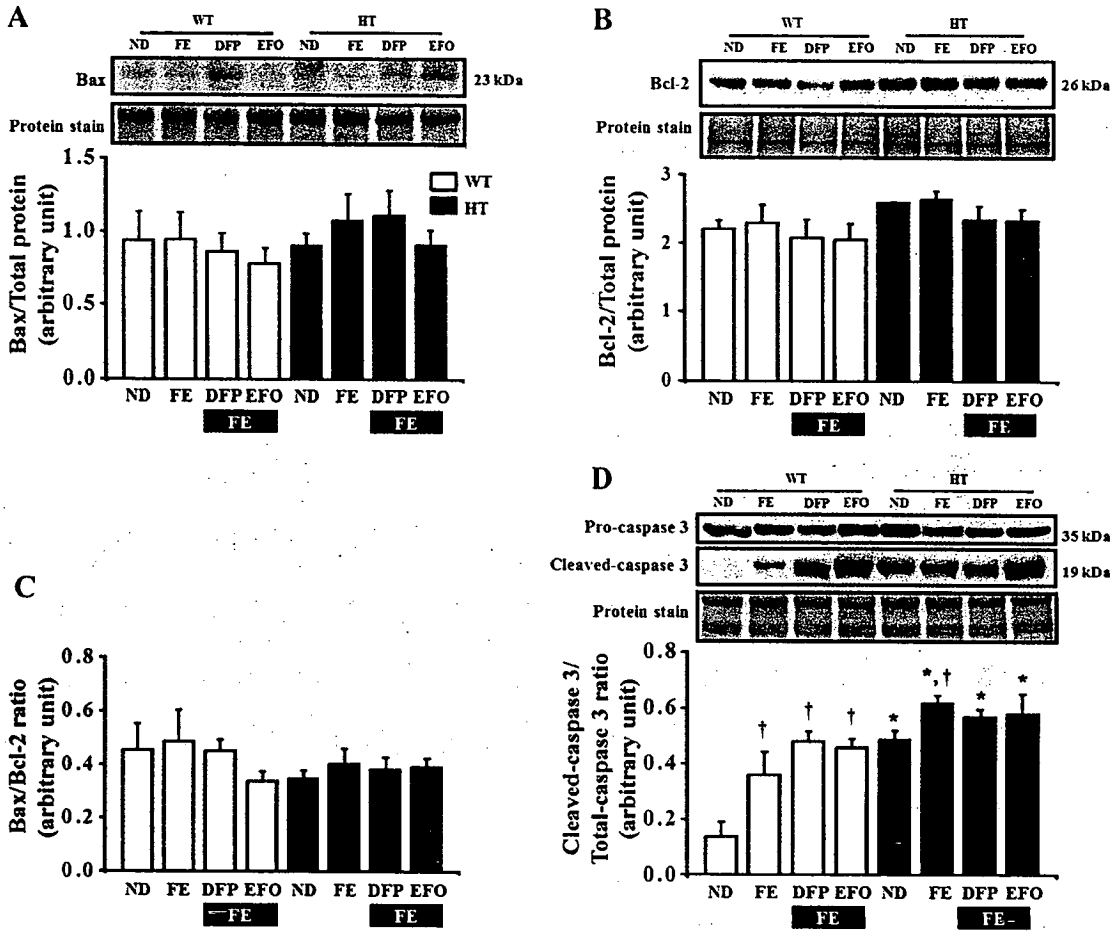


Fig. 6. Effects of deferiprone (DFP) and efonidipine (EFO) on cardiac apoptotic protein expression measured in the whole heart homogenates of iron-overloaded WT and HT mice. (A-D) Western blot of pro-apoptotic Bax, anti-apoptotic Bcl-2, Bax/Bcl-2 ratio and cleaved-caspase 3/total-caspase 3 ratio, respectively. DFP and EFO did not change caspase 3 activity in both WT and HT mice under an iron overload condition. Data are expressed as mean ± S.E.M., $^{*}P < 0.05$ vs. WT-ND, $^{\dagger}P < 0.05$ vs. ND, n=6/group.

protein expression were investigated in this study. Our results showed that the expression of complex IV was decreased in iron-overloaded WT and HT mice. Treatment with either DFP or efonidipine did not affect these changes. These findings suggest that iron overload alters the expression of complex IV and may lead to respiratory dysfunction and impaired ATP synthesis. This was consistent with a previous study of iron-overloaded H9c2 cardiomyocytes, which found iron overload caused mitochondrial DNA (mtDNA) damage and decreased levels of mRNA expression of mitochondrial respiratory chain subunits encoded by mitochondrial DNA, including complex I and complex IV, eventually leading to respiratory dysfunction and results in decreased ATP content (Gao et al., 2009, 2010). Consistent with previous studies, our study indicated complex IV might be a prior protein which was impaired by iron overload because it was decreased in both WT and HT mice. In addition, previous studies showed that the intramitochondrial iron accumulation could damage the mtDNA and the mitochondrial encoded genes such as the ATP synthase subunit 6 and 8 mRNA in several organs in sideroblastic anemic patients (Matthes et al., 2006) and β^{o}-thalassemia/Hb E patients (Khungwanmaythawee et al., 2016). This might result in decreased complex V expression and ATP content. Consistently, our study obviously demonstrated that the level of ATP-alpha subunit protein expression in complex V was decreased in only iron-overloaded HT mice. Interestingly, this is the first study to demonstrate that iron toxicity mediated the reduction of complex V leading to complex V dysfunction under chronic iron overload in the heart of HT mice. All of these findings indicate that the mitochondrial dysfunction and altered mitochondrial respiration chain subunits play an important role in the mechanisms of iron-overload cardiomyopathy, particularly in the thalassemic condition.

In conclusion, chronic iron overload induced cardiac dysfunction via an elevation of cardiac iron concentration, lipid peroxidation and cardiac mitochondrial dysfunction, alteration of mitochondrial biogenesis and dynamics, and increased apoptosis. DFP and efonidipine had a similar efficacy for cardioprotection through a reduction of plasma NTBI, cardiac iron concentration, lipid peroxidation and mitochondrial reactive oxygen species production, and treatment also led to improved cardiac mitochondrial function. However, these interventions did not attenuate the imbalance of mitochondrial dynamics and apoptotic protein expression in the heart of iron-overloaded mice. Further studies are needed to investigate the roles of increasing dose and administration duration and their effects on mitochondrial dynamics in the iron overloaded heart. Moreover, the iron-diet might contain too high a concentration of iron which caused high severity iron overload at a similar level, in both WT and HT mice, thus resulting in no difference between WT and HT mice. Future study is needed using lower iron concentrations in the iron-diet to see whether there are any different effects of iron overload between WT and HT mice.

Acknowledgments

We would like to thank Bencharunan Samniang from the Cardiac Electrophysiology Research and Training Center, Faculty of Medicine, Chiang Mai University, for her technical assistance. This work was supported by an NSTDA Research Chair Grant from the National

Science and Technology Development Agency Thailand (N.C.); the Thailand Research Funds BRG5780016 (S.C.) and MRG5980222 (S.K.); the TRF Royal Golden Jubilee Program (N.C. and J.K.); the Faculty of Medicine Endowment Fund, Faculty of Medicine, Chiang Mai University (S.K.); the office of the Higher Education Commission and Mahidol University under the National Research Universities Initiative (S.F.) and a Chiang Mai University Center of Excellence Award (N.C).

References

Anderson, E.R., Shah, Y.M., 2013. Iron homeostasis in the liver. Compr. Physiol. 3, 315–330. http://dx.doi.org/10.1002/cphy.c120016.

Arnoult, D., 2007. Mitochondrial fragmentation in apoptosis. Trends Cell. Biol. 17, 6–12. http://dx.doi.org/10.1016/j.tcb.2006.11.001.

Bartfay, W.J., Bartfay, E., 2000. Iron-overload cardiomyopathy: evidence for a free radical–mediated mechanism of injury and dysfunction in a murine model. Biol. Res. Nurs. 2, 49–59. http://dx.doi.org/10.1177/109980040000200106.

Bossy-Wetzel, E., Barsoum, M.J., Godzik, A., Schwarzenbacher, R., Lipton, S.A., 2003. Mitochondrial fission in apoptosis, neurodegeneration and aging. Curr. Opin. Cell. Biol. 15, 706–716. http://dx.doi.org/10.1016/j.ceb.2003.10.015.

Breuer, W., Hershko, C., Cabantchik, Z.I., 2000. The importance of non-transferrin bound iron in disorders of iron metabolism. Transfus. Sci. 23, 185–192. http://dx.doi.org/10.1016/S0955-3886(00)00087-4.

Chen, M.P., Cabantchik, Z.I., Chan, S., Chan, G.C., Cheung, Y.F., 2014. Iron overload and apoptosis of HL-1 cardiomyocytes: effects of calcium channel blockade. PLoS. One 9, e112915. http://dx.doi.org/10.1371/journal.pone.0112915.

Chen, Y., Liu, Y., Dorn, G.W., 2nd, 2011. Mitochondrial fusion is essential for organelle function and cardiac homeostasis. Circ. Res. 109, 1327–1331. http://dx.doi.org/10.1161/CIRCRESAHA.111.258723.

Das, S.K., Wang, W., Zhabyeyev, P., Basu, R., McLean, B., Fan, D., Parajuli, N., DesAulniers, J., Patel, V.B., Hajjar, R.J., Dyck, J.R., Kassiri, Z., Oudit, G.Y., 2015. Iron-overload injury and cardiomyopathy in acquired and genetic models is attenuated by resveratrol therapy. Sci. Rep. 5, 18132. http://dx.doi.org/10.1038/srep18132.

Gao, L., Laude, K., Cai, H., 2008. Mitochondrial pathophysiology, reactive oxygen species, and cardiovascular diseases. Vet. Clin. North. Am. Small. Anim. Pract. 38, 137–155. http://dx.doi.org/10.1016/j.cvsm.2007.10.004.

Gao, X., Campian, J.L., Qian, M., Sun, X.F., Eaton, J.W., 2009. Mitochondrial DNA damage in iron overload. J. Biol. Chem. 284, 4767–4775. http://dx.doi.org/10.1074/jbc.M806235200.

Gao, X., Qian, M., Campian, J.L., Marshall, J., Zhou, Z., Roberts, A.M., Kang, Y.J., Prabhu, S.D., Sun, X.F., Eaton, J.W., 2010. Mitochondrial dysfunction may explain the cardiomyopathy of chronic iron overload. Free. Radic. Biol. Med. 49, 401–407. http://dx.doi.org/10.1016/j.freeradbiomed.2010.04.033.

Ishihara, T., Ban-Ishihara, R., Maeda, M., Matsunaga, Y., Ichimura, A., Kyogoku, S., Aoki, H., Katada, S., Nakada, K., Nomura, M., Mizushima, N., Mihara, K., Ishihara, N., 2015. Dynamics of mitochondrial DNA nucleoids regulated by mitochondrial fission is essential for maintenance of homogeneously active mitochondria during neonatal heart development. Mol. Cell. Biol. 35, 211–223. http://dx.doi.org/10.1128/MCB.01054-14.

Karbowski, M., Youle, R.J., 2003. Dynamics of mitochondrial morphology in healthy cells and during apoptosis. Cell. Death Differ. 10, 870–880. http://dx.doi.org/10.1038/sj.cdd.4401260.

Khungwanmaythawee, K., Sornjai, W., Paemanee, A., Jaratsittisin, J., Fucharoen, S., Svasti, S., Lithanatudom, P., Roytrakul, S., Smith, D.R., 2016. Mitochondrial changes in beta0-thalassemia/Hb E disease. PLoS. One 11, e0153831. http://dx.doi.org/10.1371/journal.pone.0153831.

Kumfu, S., Chattipakorn, S., Chinda, K., Fucharoen, S., Chattipakorn, N., 2012a. T-type calcium channel blockade improves survival and cardiovascular function in thalassemic mice. Eur. J. Haematol. 88, 535–548. http://dx.doi.org/10.1111/j.1600-0609.2012.01779.x.

Kumfu, S., Chattipakorn, S., Fucharoen, S., Chattipakorn, N., 2012b. Mitochondrial calcium uniporter blocker prevents cardiac mitochondrial dysfunction induced by iron overload in thalassemic mice. Biometals 25, 1167–1175. http://dx.doi.org/10.1007/s10534-012-9579-x.

Kumfu, S., Chattipakorn, S., Srichairatanakool, S., Settakorn, J., Fucharoen, S., Chattipakorn, N., 2011. T-type calcium channel as a portal of iron uptake into cardiomyocytes of beta-thalassemic mice. Eur. J. Haematol. 86, 156–166. http://dx.doi.org/10.1111/j.1600-0609.2010.01549.x.

Kumfu, S., Chattipakorn, S.C., Fucharoen, S., Chattipakorn, N., 2016. Dual T-type and L-type calcium channel blocker exerts beneficial effects in attenuating cardiovascular dysfunction in iron-overloaded thalassaemic mice. Exp. Physiol. 101, 521–539. http://dx.doi.org/10.1113/EP085517.

Lee, Y.J., Jeong, S.Y., Karbowski, M., Smith, C.L., Youle, R.J., 2004. Roles of the mammalian mitochondrial fission and fusion mediators Fis1, Drp1, and Opa1 in apoptosis. Mol. Biol. Cell. 15, 5001–5011. http://dx.doi.org/10.1091/mbc.E04-04-0294.

Legros, F., Lombes, A., Frachon, P., Rojo, M., 2002. Mitochondrial fusion in human cells is efficient, requires the inner membrane potential, and is mediated by mitofusins. Mol. Biol. Cell. 13, 4343–4354. http://dx.doi.org/10.1091/mbc.E02-06-0330.

Link, G., Pinson, A., Kahane, I., Hershko, C., 1989. Iron loading modifies the fatty acid composition of cultured rat myocardial cells and liposomal vesicles: effect of ascorbate and alpha-tocopherol on myocardial lipid peroxidation. J. Lab. Clin. Med. 114, 243–249 http://www.ncbi.nlm.nih.gov/pubmed/2769018.

Ma, Y., Podinovskaia, M., Evans, P.J., Emma, G., Schaible, U.E., Porter, J., Hider, R.C., 2014. A novel method for non-transferrin-bound iron quantification by chelatable fluorescent beads based on flow cytometry. Biochem. J. 463, 351–362. http://dx.doi.org/10.1042/BJ20140795.

Matthes, T., Rustin, P., Trachsel, H., Darbellay, R., Costaridou, S., Xaidara, A., Rideau, A., Beris, P., 2006. Different pathophysiological mechanisms of intramitochondrial iron accumulation in acquired and congenital sideroblastic anemia caused by mitochondrial DNA deletion. Eur. J. Haematol. 77, 169–174. http://dx.doi.org/10.1111/j.1600-0609.2006.00674.x.

Olivieri, N.F., Brittenham, G.M., Matsui, D., Berkovitch, M., Blendis, L.M., Cameron, R.G., McClelland, R.A., Liu, P.P., Templeton, D.M., Koren, G., 1995. Iron-chelation therapy with oral deferipronein patients with thalassemia major. N. Engl. J. Med. 332, 918–922. http://dx.doi.org/10.1056/NEJM199504063321404.

Ong, S.B., Subrayan, S., Lim, S.Y., Yellon, D.M., Davidson, S.M., Hausenloy, D.J., 2010. Inhibiting mitochondrial fission protects the heart against ischemia/reperfusion injury. Circulation 121, 2012–2022. http://dx.doi.org/10.1161/CIRCULATIONAHA.109.906610.

Palee, S., Weerateerangkul, P., Chinda, K., Chattipakorn, S.C., Chattipakorn, N., 2013. Mechanisms responsible for beneficial and adverse effects of rosiglitazone in a rat model of acute cardiac ischaemia-reperfusion. Exp. Physiol. 98, 1028–1037. http://dx.doi.org/10.1113/expphysiol.2012.070433.

Rebouche, C.J., Wilcox, C.L., Widness, J.A., 2004. Microanalysis of non-heme iron in animal tissues. J. Biochem Biophys. Methods 58, 239–251. http://dx.doi.org/10.1016/j.jbbm.2003.11.003.

Samniang, B., Shinlapawittayatorn, K., Chunchai, T., Pongkan, W., Kumfu, S., Chattipakorn, S.C., KenKnight, B.H., Chattipakorn, N., 2016. Vagus nerve stimulation improves cardiac function by preventing mitochondrial dysfunction in obese-insulin resistant rats. Sci. Rep. 6, 19749. http://dx.doi.org/10.1038/srep19749.

Smirnova, E., Shurland, D.L., Ryazantsev, S.N., van der Bliek, A.M., 1998. A human dynamin-related protein controls the distribution of mitochondria. J. Cell. Biol. 143, 351–358. http://dx.doi.org/10.1083/jcb.143.2.351.

Soriano, F.X., Liesa, M., Bach, D., Chan, D.C., Palacin, M., Zorzano, A., 2006. Evidence for a mitochondrial regulatory pathway defined by peroxisome proliferator-activated receptor-gamma coactivator-1 alpha, estrogen-related receptor-alpha, and mitofusin 2. Diabetes 55, 1783–1791. http://dx.doi.org/10.2337/db05-0509.

Sripetchwandee, J., KenKnight, S.B., Sanit, J., Chattipakorn, S., Chattipakorn, N., 2014. Blockade of mitochondrial calcium uniporter prevents cardiac mitochondrial dysfunction caused by iron overload. Acta Physiol. 210, 330–341. http://dx.doi.org/10.1111/apha.12162.

Tanajak, P., Sa-Nguanmoo, P., Wang, X., Liang, G., Li, X., Jiang, C., Chattipakorn, S.C., Chattipakorn, N., 2016. Fibroblast growth factor 21 (FGF21) therapy attenuates left ventricular dysfunction and metabolic disturbance by improving FGF21 sensitivity, cardiac mitochondrial redox homoeostasis and structural changes in pre-diabetic rats. Acta Physiol. 217, 287–299. http://dx.doi.org/10.1111/apha.12698.

Tanaka, H., Shigenobu, K., 2002. Efonidipine hydrochloride: a dual blocker of L- and T-type ca(2+) channels. Cardiovasc. Drug. Rev. 20, 81–92. http://dx.doi.org/10.1111/j.1527-3466.2002.tb00084.x.

Thummasorn, S., Kumfu, S., Chattipakorn, S., Chattipakorn, N., 2011. Granulocyte-colony stimulating factor attenuates mitochondrial dysfunction induced by oxidative stress in cardiac mitochondria. Mitochondrion 11, 457–466. http://dx.doi.org/10.1016/j.mito.2011.01.008.

Wang, Y., Wu, M., Al-Rousan, R., Liu, H., Fannin, J., Paturi, S., Arvapalli, R.K., Katta, A., Kakarla, S.K., Rice, K.M., Triest, W.E., Blough, E.R., 2011. Iron-induced cardiac damage: role of apoptosis and deferasirox intervention. J. Pharmacol. Exp. Ther. 336, 56–63. http://dx.doi.org/10.1124/jpet.110.172668.

Wood, J.C., Enriquez, C., Ghugre, N., Otto-Duessel, M., Aguilar, M., Nelson, M.D., Moats, R., Coates, T.D., 2005. Physiology and pathophysiology of iron cardiomyopathy in thalassemia. Ann. N. Y. Acad. Sci. 1054, 386–395. http://dx.doi.org/10.1196/annals.1345.047.

เอกสารแนบหมายเลข 7

J Bone Miner Metab (2017) 35:142–149
DOI 10.1007/s00774-016-0745-z

ORIGINAL ARTICLE

Fibroblast growth factor-21 restores insulin sensitivity but induces aberrant bone microstructure in obese insulin-resistant rats

Narattaphol Charoenphandhu[1,2] · Panan Suntornsaratoon[2] · Nateetip Krishnamra[1,2] · Piangkwan Sa-nguanmoo[3,4] · Pongpun Tanajak[3,4] · Xiaojie Wang[5] · Guang Liang[5] · Xiaokun Li[5] · Chao Jiang[5] · Nipon Chattipakorn[3,4] · Siriporn Chattipakorn[3,6]

Received: 9 November 2015 / Accepted: 15 February 2016 / Published online: 29 March 2016
© The Japanese Society for Bone and Mineral Research and Springer Japan 2016

Abstract Fibroblast growth factor (FGF)-21 is a potent endocrine factor that improves insulin resistance and obesity-associated metabolic disorders. However, concomitant activation of peroxisome proliferator-activated receptor-γ by FGF-21 makes bone susceptible to osteopenia and fragility fracture. Since an increase in body weight often induced adaptive change in bone by making it resistant to fracture, it was unclear whether FGF-21 would still induce bone defects in overweight rats. Therefore, the present study aimed to investigate bone microstructure and its mechanical properties in high fat diet (HF)-fed rats treated with 0.1 mg/kg/day FGF-21. Eighteen male rats were divided into two groups to receive either a normal diet or HF for 12 weeks. HF rats were then divided into two subgroups to receive either vehicle or FGF-21 for 4 weeks. The results showed that HF led to obesity, dyslipidemia and insulin resistance, as indicated by hyperinsulinemia with euglycemia. In HF rats, there was an increase in tibial yield displacement (an indicator of ability to be deformed without losing toughness, as determined by 3-point bending) without changes in tibial trabecular volumetric bone mineral density (vBMD) or cortical bone parameters, e.g., cortical thickness and bone area. FGF-21 treatment strongly improved the metabolic parameters and increased insulin sensitivity in HF rats. However, FGF-21-treated HF rats showed lower yield displacement, trabecular vBMD, trabecular bone volume, trabecular thickness, and osteoblast surface compared with vehicle-treated HF rats. These findings suggest that, despite being a potent antagonist of insulin resistance and visceral fat accumulation, FGF-21 is associated with bone defects in HF rats.

Keywords Fibroblast growth factor (FGF)-21 · High fat diet (HF) · Insulin sensitivity · Osteopenia · Peroxisome proliferator-activated receptor (PPAR)-γ

Electronic supplementary material The online version of this article (doi:10.1007/s00774-016-0745-z) contains supplementary material, which is available to authorized users.

✉ Siriporn Chattipakorn
siriporn.c@cmu.ac.th; scchattipakorn@gmail.com

1 Department of Physiology, Faculty of Science, Mahidol University, Bangkok, Thailand

2 Center of Calcium and Bone Research (COCAB), Faculty of Science, Mahidol University, Bangkok, Thailand

3 Neurophysiology Unit, Faculty of Medicine, Cardiac Electrophysiology Research and Training Center, Chiang Mai University, Chiang Mai, Thailand

4 Department of Physiology, Faculty of Medicine, Chiang Mai University, Chiang Mai, Thailand

5 School of Pharmaceutical Sciences, Wenzhou Medical University, University-town, Wenzhou, Zhejiang, China

6 Department of Oral Biology and Diagnostic Science, Faculty of Dentistry, Chiang Mai University, Chiang Mai 50200, Thailand

Introduction

As a major cause of metabolic disturbance with high global prevalence, long-term consumption of a high-fat diet (HF) is detrimental to the body, leading to obesity, insulin resistance, and metabolic disease. Besides insulin, other endocrine factors such as adipokines and certain members of fibroblast growth factor (FGF), play a role in protecting against abnormal fat metabolism. FGF-21 in particular could be a major anti-diabetic agent since it potently enhances adipocyte glucose uptake, decreases circulating

glucose and triglyceride levels, and improves insulin sensitivity in obese and diabetic animals [1, 2]. Since mesenchymal stem cells, osteoblast precursor cells, and osteoblasts themselves also abundantly express several subtypes of FGF receptors (FGFRs), e.g., FGFR1 and FGFR2, it is possible that systemic FGF-21 is capable of altering bone microstructure, bone mineral density (BMD), and bone mechanical properties in rodents.

Most members of the FGF family exert their functions locally because they have a strong interaction with extracellular matrix. On the other hand, FGF21 is generally recognized as a member of the endocrine family of FGF as it lacks the heparin-binding domain, which is required for binding most FGFs to the extracellular matrix of their target tissue [3, 4]. Several tissues, such as liver, pancreas, and adipose tissue itself, are the most important sources of circulating FGF21 in rodents [5–7]. After being released into the circulation, FGF21 binds to certain subtypes of FGFRs, especially FGFR1 and FGFR2, together with a co-receptor called β-klotho before activating various intracellular signaling pathways, e.g., ERK1/2, AMPK, and peroxisome proliferator-activated receptor (PPAR)-γ [8]. At the systemic level, FGF21 is considered a starvation hormone that increases energy expenditure and fat utilization [8].

High circulating levels of FGF-21 induced by high-dose injections (1 mg/kg/day) or gain-of-function mutation have previously been shown to induce bone loss and skeletal fragility [9]. FGF-21 has also been reported to strongly induce the sumoylation of PPAR-γ, thereby prolonging the action of this transcription factor which is known to modulate not only the function of adipocytes but also osteoblasts and osteoclasts causing bone loss and fracture through inhibition of osteoblast function [10]. Hence, FGF-21-induced bone loss could be due to its activation of PPAR-γ. Interestingly, bone is a dynamic tissue and long bone was found to be slightly more resistant to fracture with increased body weight. Therefore, it was unclear whether obese rats treated with FGF-21 as part of early treatment for insulin resistance or diabetes might, on the other hand, exhibit bone loss with impaired bone mechanical properties.

In the present study, obesity with insulin resistance was induced by treating rats with HF, as reported previously [11, 12]. FGF-21 was administered to demonstrate whether FGF-21 could restore metabolic parameters in obese insulin-resistant rats. The principal objective of this study was to evaluate bone mechanical property and bone microstructure in HF-fed rats treated with low-dose FGF-21 (0.1 mg/kg/day), which appeared to effectively alleviate insulin resistance.

Materials and methods

Animals

Six-week old male Wistar rats were obtained from the National Laboratory Animal Center, Mahidol University, Thailand. Rats were individually housed in a temperature- and humidity-controlled room with a 12-h light/12-h dark cycle. This study was approved by the Institutional Animal Care and Use Committee, Faculty of Medicine, Chiang Mai University, Thailand.

Experimental design

Rats were randomly divided into 3 groups (n = 4–6/group)—vehicle (normal saline)-treated normal diet (ND)-fed rats, vehicle-treated HF-fed rats, and FGF-21-treated HF-fed rats. The ND and HF contained 19.77 and 59.28 % energy from fat, respectively. The rats were fed ND or HF for 12 weeks prior to FGF-21 administration. Recombinant FGF-21 (kindly provided by School of Pharmaceutical Sciences, Wenzhou Medical University, Wenzhou, Zhejiang, China) was injected subcutaneously (s.c.) once daily at 0.1 mg/kg of body weight for 4 weeks. Body weight and food intake were recorded weekly throughout the experiment. After 16 weeks of HF and/or FGF-21 treatments, all the rats were killed by isoflurane, and bone, visceral fat, and plasma samples were collected. Bone specimens were evaluated for microstructural defect and mechanical properties, while plasma samples were used to determine levels of glucose, cholesterol, triglyceride, insulin, homeostatic model assessment (HOMA; an index of insulin resistance), and the area under the curve of plasma glucose (AUCg). Serum levels of FGF-21 were determined using a commercial enzyme immunoassay kit (MF 2100; R&D Systems, Minneapolis, MN, USA). The experimental protocol is depicted in Fig. 1a.

Analysis of bone mechanical properties using the 3-point bending test

The right tibiae were dissected, cleaned of adhering tissue, and kept moist until analysis using 3-point bending apparatus (model 5943; Instron, Norwood, MA, USA). After measuring the anteroposterior midshaft diameter of the tibiae, each tibia was placed with anterior part facing down on two rounded supporting bars with a distance of 18 mm. A preload of 2 N was applied at the midshaft with a displacement rate of 2 mm/min until failure. From the force–displacement curve, the mechanical parameters were determined using Bluehill 3 software. The measured parameters

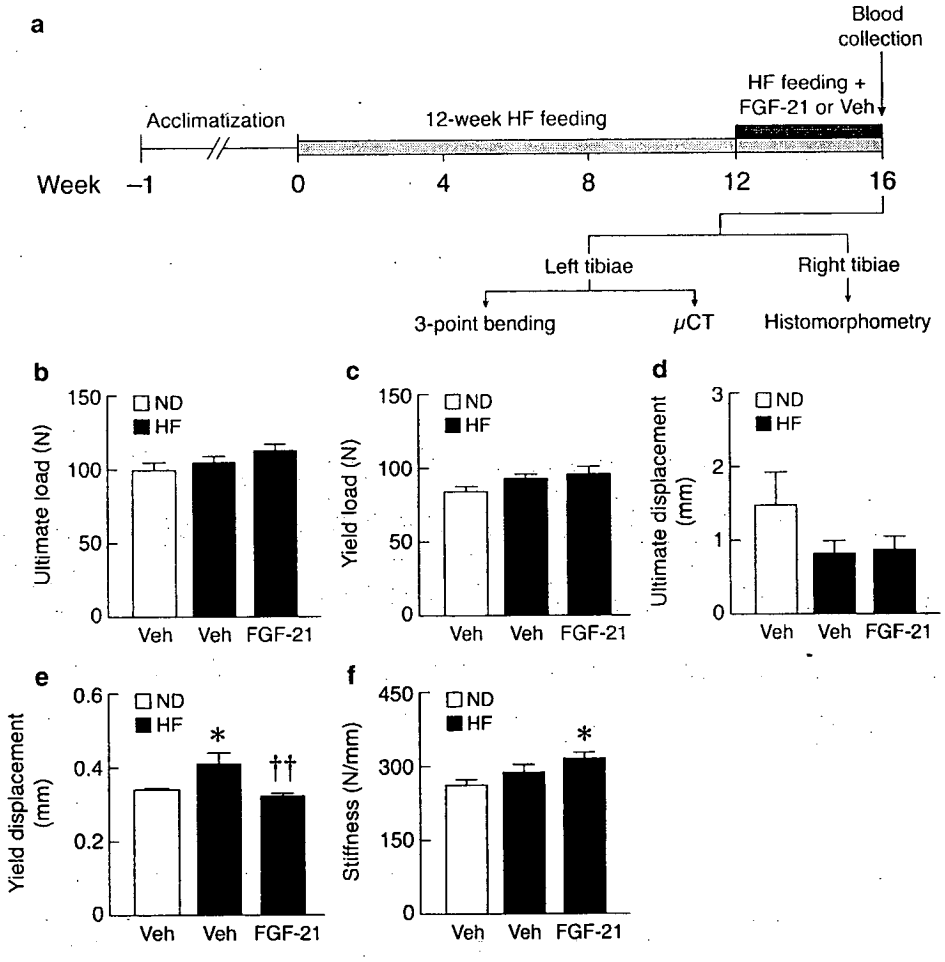


Fig. 1 **a** Timeline of the present experiment. **b–f** Mechanical properties of tibial midshaft in rats fed high-fat diet (HF) or normal diet (ND). Twelve rats were fed HF for 12 weeks prior to 4-week FGF-21 administration (0.1 mg/kg body weight, s.c.) or vehicle (Veh). Total duration for ND or HF treatment was 16 weeks. Values are mean ± standard error (n = 4–6 per group). *$P < 0.05$ compared with vehicle-treated ND rats; ††$P < 0.01$ compared with vehicle-treated HF rats

included ultimate load, yield load, ultimate displacement, yield displacement, and stiffness.

Analysis of bone microstructure using microcomputed tomography (μCT)

The right tibiae were dissected and wrapped in moist gauze to prevent tissue drying during scanning, and placed in a horizontal position on a polystyrene supporter. Images were acquired by a μCT (model Skyscan 1178; Bruker MicroCT, Kontich, Belgium) at 65 kV, 615 μA with rotation angle of 0.54°, and voxel resolution of 85 μm. Thereafter, images were reconstructed by NRecon software (version 1.6.4.8) with a ring artifact and hardening correction of 10 and 30 %, respectively. CTAn software (version 1.14.4) was used to analyze volumetric BMD (vBMD) and cortical microstructure. Trabecular vBMD and cortical vBMD were analyzed at 1.360–5.610 and 14.110–18.360 mm, respectively, distal to the proximal growth plate. Microstructural indices of cortex included cortical thickness (mm), cortical area (mm^2), periosteal perimeter (mm), endosteal perimeter (mm), moment of inertia (MMI; mm^4) in x- and y-axes, and polar MMI.

Bone histomorphometric analysis of bone trabecular structure

The proximal part of each left tibia (approximately 1.5 mm long) was cleaned of connective tissue, dehydrated in graded ethanol (i.e., 70, 95 % and absolute ethanol for 3, 3 and 2 days, respectively), and embedded in methyl methacrylate resin. As described previously [13], embedded bone samples were sliced to obtain frontal sections of 7-μm thickness using a semi-automated rotary microtome (model RM2255; Leica, Nussloch, Germany). Each section was mounted on a standard microscopic slide. After

drying, bone sections were stained with Goldner's trichrome. Microstructural analyses of cancellous bone were obtained under a light microscope (model eclipse Ni-U; Nikon) using the OsteoMeasure system version 4.10 (OsteoMetrics, Atlanta, GA, USA). Trabecular microstructure was analyzed at a location 1 mm distal to the epiphyseal plate (i.e., secondary spongiosa). Microstructural parameters included trabecular bone volume normalized by tissue volume (also known as bone volume fraction, %), trabecular thickness (μm), trabecular separation (μm), trabecular number (mm^{-1}), osteoblast surface normalized by bone surface (%), osteoclast surface (%), and adipocyte number normalized by tissue area (mm^{-2}).

Biochemical analyses of blood compositions and HOMA index

Plasma glucose and cholesterol levels were determined by colorimetric assay (Biotech, Bangkok, Thailand). Plasma insulin levels were determined using a sandwich ELISA kit (Linco Research, St. Charles, MO, USA). Peripheral insulin resistance was assessed using HOMA, as described in previous studies [14, 15].

Oral glucose tolerance test (OGTT) and AUCg

OGTT was performed as described previously [16]. Briefly, rats were starved overnight before the test and received 2 g/kg body weight of glucose solution via oral gavage. Blood samples were collected from the tail vein at 0, 15, 30, 60, 90 and 120 min after glucose administration. AUCg was then calculated to evaluate glucose tolerance.

Statistical analysis

Two groups of data were analyzed by unpaired Student's *t* test, while multiple groups of data were compared by one-way analysis of variance (ANOVA). All statistical tests were performed by GraphPad Prism 6 for Mac OS X. The level of significance was $P < 0.05$.

Results

The effects of FGF-21 on body weight, visceral fat, and biochemical parameters in plasma are shown in Table 1. The vehicle-treated HF-fed rats had a significantly increased body weight, visceral fat, plasma cholesterol level, plasma insulin level, and HOMA index compared to the vehicle-treated ND-fed rats ($P < 0.05$). FGF-21 significantly decreased plasma cholesterol level, plasma insulin level and HOMA index in HF-fed rats ($P < 0.05$). Regarding the glucose tolerance test, the AUCg of the vehicle-treated HF group was significantly greater than that of the vehicle-treated ND group (Table 1). The administration of FGF-21 also decreased the AUCg in HF-fed rats ($P < 0.05$). Meanwhile, HF also elevated the plasma FGF-21 levels by ~2.5-fold, suggesting the presence of FGF-21 resistance in obese rats, whereas exogenous FGF-21 administration markedly increased FGF-21 levels by approximately eight-fold (Table 1).

The 3-point bending test revealed that tibiae of HF rats increased the yield displacement, which was used as an indicator of ability to be deformed without losing toughness (Fig. 1; values are presented in Supplemental Table S1). Other mechanical properties, i.e., ultimate load, yield

Table 1 Effects of high-fat diet and FGF-21 administration on the body weight, visceral fat, food intake, metabolic parameters, and plasma FGF-21 levels

Parameters	NDV	HFV	HFF
Body weight (kg)	500.83 ± 9.17	640.00 ± 18.44*	570.00 ± 30.87*†
Visceral fat (g)	23.79 ± 1.71	61.68 ± 3.65*	51.62 ± 1.95*†
Food intake (g/day)	20.88 ± 0.76	22.54 ± 1.00	20.30 ± 1.47
Plasma glucose (mg/dL)	128.62 ± 1.65	130.49 ± 6.54	130.35 ± 3.87
Cholesterol (mg/dL)	79.31 ± 4.18	112.23 ± 4.32*	88.47 ± 3.59†
Triglyceride (mg/dL)	55.53 ± 3.92	55.68 ± 1.95	56.02 ± 2.20
Insulin (ng/mL)	2.65 ± 0.20	4.43 ± 0.46*	2.80 ± 0.29†
HOMA index	17.50 ± 1.49	32.47 ± 5.23*	17.32 ± 1.77†
AUCg (mg/dL × min × 10^4)	5.20 ± 0.33	6.89 ± 0.68*	5.38 ± 0.32†
Plasma FGF-21 (pg/mL)	96.73 ± 27.95	244.00 ± 52.41*	743.09 ± 117.99*†

Values are mean ± standard error, $n = 6$/group. Rats were treated with normal diet (ND) or high-fat diet (HF) for 16 weeks. At week 13, HF rats were injected s.c. with FGF-21 (HFF) or vehicle (HFV) for 4 weeks. Vehicle-treated ND rats (NDV)

HOMA homeostatic model assessment for insulin resistance, *AUCg* area under the curve of plasma glucose

* $P < 0.05$ compared with vehicle-treated ND rats, † $P < 0.05$ compared with vehicle-treated HF rats

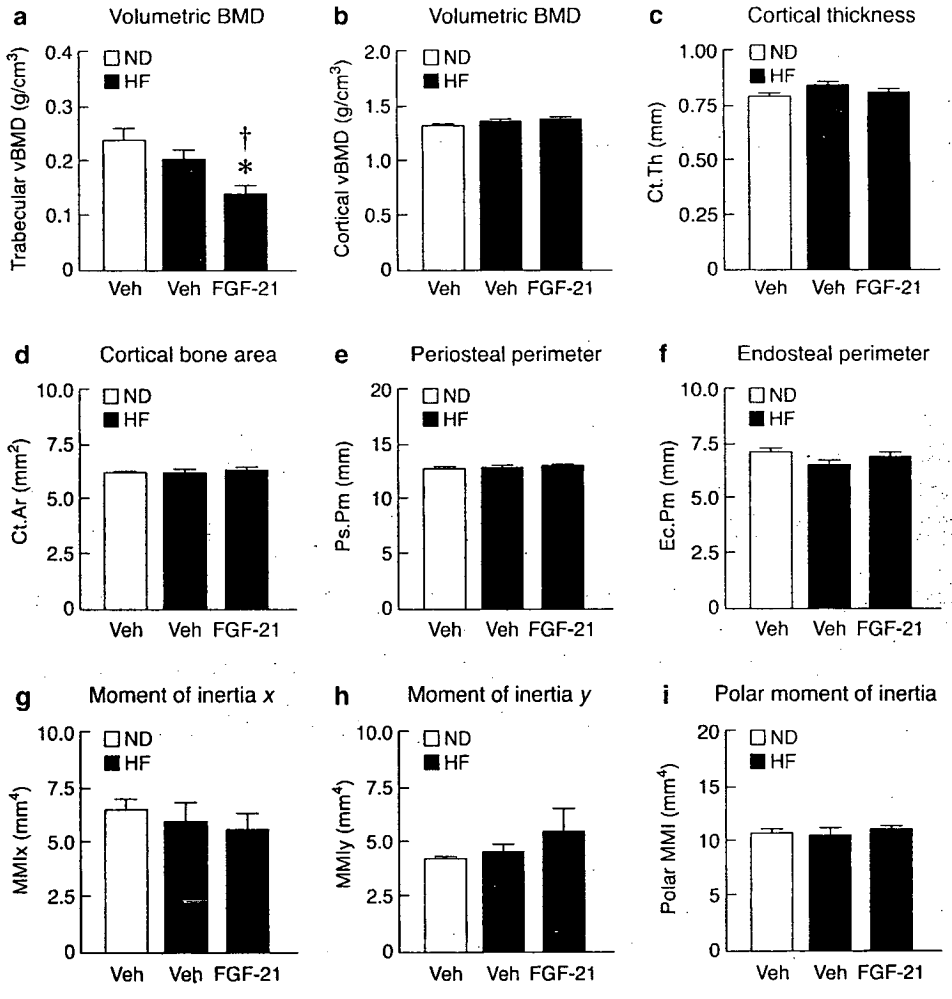


Fig. 2 Three-dimensional analyses of tibial microstructure by μCT in rats fed high-fat diet (HF) or normal diet (ND). During treatment, HF rats were subcutaneously injected once daily with 0.1 mg/kg FGF-21 or vehicle (Veh). The measured parameters are trabecular **a** and cortical **b** volumetric bone mineral density (vBMD), cortical thickness (Ct.Th; **c**), cortical bone area (Ct.Ar; **d**), periosteal perimeter (Ps.Pm; **e**), endosteal perimeter (Ec.Pm; **f**), moment of inertia in *x*- and *y*-axes (MMIx and MMIy; **g**, **h**), and polar moment of inertia (polar MMI; **i**). Values are mean ± standard error ($n = 4$ per group). $^{*}P < 0.05$ compared with vehicle-treated ND rats. $^{\dagger}P < 0.05$ compared with vehicle-treated HF rats

load, ultimate displacement, and stiffness, were not altered by HF treatment (Fig. 1). In addition, 16-week HF treatment did not alter vBMD, cortical thickness, cortical bone area, periosteal perimeter, endosteal perimeter, or moment of inertia (Fig. 2).

However, FGF-21 attenuated the HF-associated increase in yield displacement (Fig. 1e), and increased bone stiffness compared to ND-fed rats (Fig. 1f). Although μCT analysis of tibiae from FGF-21-treated HF-fed rats (Fig. 2) did not show changes in cortical parameters compared to vehicle-treated HF-fed rats, trabecular vBMD was significantly lower in the FGF-21-treated HF-fed rats than vehicle-treated HF-fed rats (Fig. 2a). Mineralized tissues (green color in Goldner's trichrome-stained section; Fig. 3a) were apparently diminished after FGF-21 treatment, while marrow fats (white spots in bone marrow, as indicated by arrow heads; Fig. 3a) were conspicuously increased, consistent with the hypothesis that FGF-21 can direct mesenchymal stem cells toward adipocytes rather than osteoblasts [8]. Further bone histomorphometric study thus demonstrated that HF-fed rats treated with FGF-21 had less trabecular bone volume, trabecular thickness, and osteoblast surface with no changes in trabecular separation, trabecular number, or osteoclast surface when compared with those treated with vehicle (Figs. 3b–e, 4a, b). Adipocyte number was also greater in FGF-21-treated HF rats than vehicle-treated HF rats (Fig. 4c).

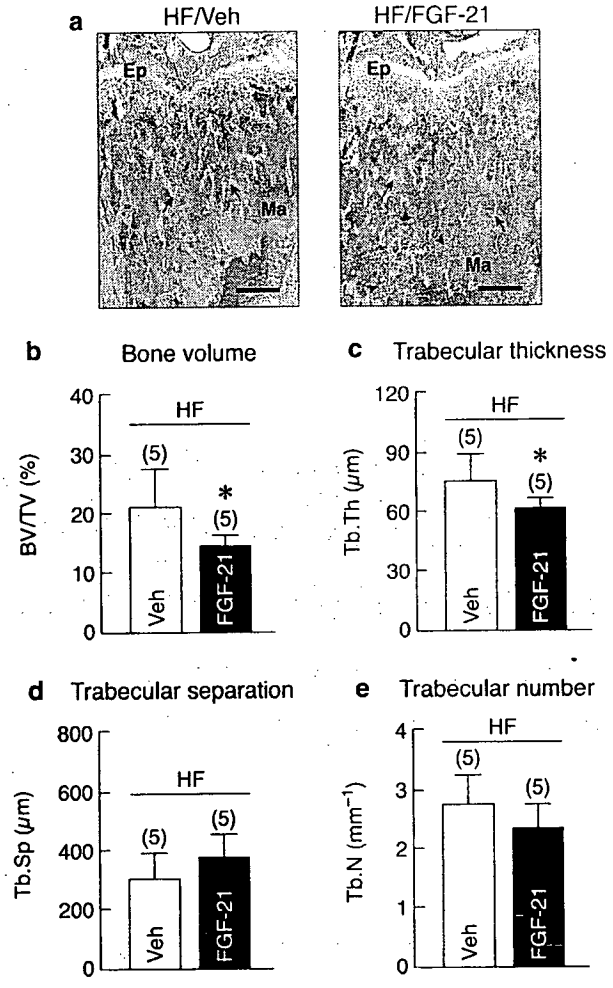


Fig. 3 Microstructural analyses of proximal tibial metaphyses by bone histomorphometry. **a** Representative Goldner's trichrome-stained photomicrographs of the tibial metaphyses. *Scale bars* 1,000 μm; Ep, epiphyseal plate; Ma, bone marrow. *Arrows* and *arrow heads* indicate bone trabeculae (*green*) and marrow fat (i.e., *white spots* in bone marrow), respectively. Quantitative parameters are bone volume fraction (BV/TV; **b**), trabecular thickness (Tb.Th; **c**), trabecular separation (Tb.Sp; **d**), and trabecular number (Tb.N; **e**). Rats were fed high fat diet (HF) for 16 weeks and were injected s.c. once daily with 0.1 mg/kg FGF-21 or vehicle (Veh) for 4 weeks. Results are mean ± standard deviation ($n = 5$ per group). $^*P < 0.05$ compared with vehicle-treated rats

Discussion

Long-term HF consumption is detrimental to body metabolism, leading to visceral fat accumulation, dyslipidemia, and insulin resistance [16, 17]. FGF-21 administration has been proposed as an efficient therapeutic approach to correct these metabolic disorders, especially at their early stages, e.g., insulin resistance with euglycemia and prediabetes [1, 18]. In the present study, FGF-21 clearly mitigated metabolic disturbance in HF-fed rats by reducing body weight, visceral fat, blood cholesterol, and insulin resistance compared to control HF-fed rats. Furthermore, we elaborated that a relatively low dose of FGF-21 (i.e., 0.1 mg/kg/day), which appeared to effectively alleviate insulin resistance, could eventually induce bone loss in obese rats. This led us to draw a conclusion that FGF-21 was indeed very useful for alleviation of insulin resistance and perhaps prediabetes. However, bone health should be regularly evaluated during FGF-21 treatment since this low-dose FGF-21 administration was able to impair bone microstructure and its mechanical properties.

FGF-21 has been reported to act via a number of mechanisms to reduce body weight and insulin resistance. For example, Xu et al. [19] provided evidence that FGF-21 increased whole-body energy expenditure and physical activity, in part, by inducing the mRNA expression of uncoupling protein-1 and -2 in brown adipocytes. Moreover, it also enhanced the expression of glucose transporter-1 for glucose uptake in adipose tissue as well as the insulin-induced suppression of hepatic glucose output and insulin sensitivity in the heart and skeletal muscle [19, 20]. Glucose uptake in adipocytes was markedly stimulated by FGF-21 [1]. Under certain conditions, such as during cold exposure, FGF-21 was also capable of promoting the browning of white fat for thermogenesis [8].

Although FGF-21 showed several positive effects on metabolic parameters, its administration led to deterioration of bone mechanical property and microstructure. Specifically, HF was associated with an increase in yield displacement (Fig. 1), making bone more ductile, which could be an adaptive change in response to overweight. This higher yield displacement therefore indicated more work required to make a permanent damage to the bone structure under HF conditions. After FGF-21 treatment, bone became more susceptible to permanent damage (plastic deformation) as the FGF-21-treated HF rats with inappropriately reduced yield displacement still had greater body weight than ND rats. In other words, FGF-21-treated HF rats should maintain yield displacement above the level of ND rats to accommodate ~70 g extra body weight (body weights of vehicle-treated ND rats and FGF-21-treated HF rats were ~500 and 570, respectively). Furthermore, although stiffness often represented how much force to elastically deform bone, an increase in stiffness was not necessary a protective factor against bone deformation. Rigid or highly mineralized bone with increased stiffness was apparently brittle and sometimes required less-than-normal energy to fracture. Taken together, after FGF-21 treatment, the HF-associated increase in yield displacement completely disappeared and inappropriate bone stiffness was observed which, in turn, might make bone more susceptible to fracture. Indeed, these signs of impaired mechanical properties occurred despite no change in cortical parameter, e.g.,

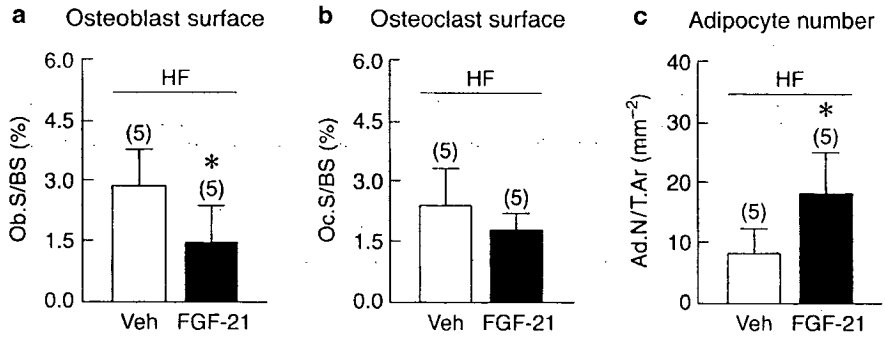


Fig. 4 Osteoblast surface normalized by bone surface (Ob.S/BS; **a**), osteoclast surface (Oc.S/BS; **b**), and adipocyte number normalized by tissue area (Ad.N/T.Ar; **c**) as determined by static bone histomorphometry. Rats were fed high fat diet (HF) for 16 weeks and were injected s.c. once daily with 0.1 mg/kg FGF-21 or vehicle (Veh) for 4 weeks. Results are mean ± standard deviation ($n = 5$ per group). *$P < 0.05$ compared with vehicle-treated rats

cortical thickness, cortical bone area, or moment of inertia, as evaluated by μCT.

Meanwhile, the trabecular portion of long bone was apparently more vulnerable to FGF-21 administration. Results showed that the tibial trabecular vBMD was significantly decreased by FGF-21 compared to vehicle-treated HF-fed rats. Further investigation of the tibial secondary spongiosum, a trabecula-rich area of the long bone, consistently revealed decreases in bone volume and trabecular thickness without change in trabecular separation or number. The observed negative effects of FGF-21 on bone of HF-fed rats could be explained based on the previous finding that FGF-21 was a potent stimulator of PPAR-γ activity [9]. This transcription factor plays its salient role in deciding whether mesenchymal stem cells will differentiate into adipocytes or osteoblast [21]. Therefore, its upregulation could lead to inhibition of osteoblastogenesis from mesenchymal stem cells, thereby suppressing bone formation [9]. Other activators of PPAR-γ known as thiazolidinediones, e.g., the anti-diabetic drug rosiglitazone, also induced bone loss by a similar mechanism [10, 22]. Hence, an increase in adipocyte number and a decrease in osteoblast surface well confirmed the aforementioned PPAR-γ hypothesis. Nevertheless, since mature osteoblasts abundantly expressed FGFRs [23], it was tempting to postulate that FGF-21 could also directly suppress osteoblast function. In addition to suppression of bone formation, the FGF-21-induced decreases in trabecular bone volume and thickness might have resulted from PPAR-γ-mediated osteoclastogenesis [24, 25]. Wan et al. [24] clearly showed that activation of PPAR-γ promoted osteoclast differentiation through the c-Fos-dependent pathway, leading to osteoclast-mediated bone resorption and osteoporosis. However, osteoclast surface was not altered in the present study, perhaps due to the use of low-dose FGF-21 administration; however, more investigations are required to directly determine osteoclast activity and circulating levels of osteoclastogenic markers, such as receptor activator of nuclear factor κB ligand (RANKL).

In conclusion, FGF-21 altered bone mechanical properties and reduced trabecular vBMD as well as trabecular bone volume and thickness in the tibial metaphysis of HF-fed rats. Although further experiments are required to demonstrate the underlying cellular and molecular mechanisms of FGF-21, related bone biomarkers (e.g., osteocalcin, osterix, RANKL, and osteoprotegerin), and contributions of other obesity-related osteoregulatory endocrine factors (particularly leptin) [26] in obese animals, FGF-21 can be used to improve metabolic disturbance and insulin resistance caused by HF consumption. However, bone change should be closely monitored during long-term administration.

Acknowledgments This work was supported by grants from the Cluster and Program Management Office (CPMO), National Science and Technology Development Agency (P-13-00100 to N. Charoenphandhu), the Thailand Research Fund (TRF)–Mahidol University through the TRF Senior Research Scholar Grant (RTA5780001 to N. Charoenphandhu), Government Budget, Mahidol University (N. Charoenphandhu), Thailand Research Fund Grants: TRF-BRG 5780016 (S. Chattipakorn), a NSTDA Research Chair Grant from the National Science and Technology Development Agency (N. Chattipakorn), and a Chiang Mai University Center of Excellence Award (N. Chattipakorn).

Compliance with ethical standards

Conflict of interest The authors declare that there is no conflict of interest.

References

1. Kharitonenkov A, Shiyanova TL, Koester A, Ford AM, Micanovic R, Galbreath EJ, Sandusky GE, Hammond LJ,

Moyers JS, Owens RA, Gromada J, Brozinick JT, Hawkins ED, Wroblewski VJ, Li DS, Mehrbod F, Jaskunas SR, Shanafelt AB (2005) FGF-21 as a novel metabolic regulator. J Clin Invest 115:1627–1635
2. Kharitonenkov A, Wroblewski VJ, Koester A, Chen YF, Clutinger CK, Tigno XT, Hansen BC, Shanafelt AB, Etgen GJ (2007) The metabolic state of diabetic monkeys is regulated by fibroblast growth factor-21. Endocrinology 148:774–781
3. Goetz R, Beenken A, Ibrahimi OA, Kalinina J, Olsen SK et al (2007) Molecular insights into the klotho-dependent, endocrine mode of action of fibroblast growth factor 19 subfamily members. Mol Cell Biol 27:3417–3428
4. Zhang X, Ibrahimi OA, Olsen SK, Umemori H, Mohammadi M, Ornitz DM (2006) Receptor specificity of the fibroblast growth factor family. The complete mammalian FGF family. J Biol Chem 281:15694–15700
5. Nishimura T, Nakatake Y, Konishi M, Itoh N (2000) Identification of a novel FGF, FGF-21, preferentially expressed in the liver. Biochim Biophys Acta 1492:203–206
6. Wente W, Efanov AM, Brenner M, Kharitonenkov A, Koster A, Sandusky GE, Sewing S, Treinies I, Zitzer H, Gromada J (2006) Fibroblast growth factor-21 improves pancreatic β-cell function and survival by activation of extracellular signal-regulated kinase 1/2 and Akt signaling pathways. Diabetes 55:2470–2478
7. Muise ES, Azzolina B, Kuo DW, El-Sherbeini M, Tan Y, Yuan X, Mu J, Thompson JR, Berger JP, Wong KK (2008) Adipose fibroblast growth factor 21 is up-regulated by peroxisome proliferator-activated receptor γ and altered metabolic states. Mol Pharmacol 74:403–412
8. Cantó C, Auwerx J (2012) Cell biology. FGF21 takes a fat bite. Science 336:675–676
9. Wei W, Dutchak PA, Wang X, Ding X, Wang X, Bookout AL, Goetz R, Mohammadi M, Gerard RD, Dechow PC, Mangelsdorf DJ, Kliewer SA, Wan Y (2012) Fibroblast growth factor 21 promotes bone loss by potentiating the effects of peroxisome proliferator-activated receptor gamma. Proc Natl Acad Sci USA 109:3143–3148
10. Ali AA, Weinstein RS, Stewart SA, Parfitt AM, Manolagas SC, Jilka RL (2005) Rosiglitazone causes bone loss in mice by suppressing osteoblast differentiation and bone formation. Endocrinology 146:1226–1235
11. Apaijai N, Pintana H, Chattipakorn SC, Chattipakorn N (2012) Cardioprotective effects of metformin and vildagliptin in adult rats with insulin resistance induced by a high-fat diet. Endocrinology 153:3878–3885
12. Pintana H, Apaijai N, Pratchayasakul W, Chattipakorn N, Chattipakorn SC (2012) Effects of metformin on learning and memory behaviors and brain mitochondrial functions in high fat diet induced insulin resistant rats. Life Sci 91:409–414
13. Suntornsaratoon P, Krishnamra N, Charoenphandhu N (2015) Positive long-term outcomes from presuckling calcium supplementation in lactating rats and the offspring. Am J Physiol Endocrinol Metab 308:E1010–E1022
14. Appleton DJ, Rand JS, Sunvold GD (2005) Basal plasma insulin and homeostasis model assessment (HOMA) are indicators of insulin sensitivity in cats. J Feline Med Surg 7:183–193
15. Haffner SM, Miettinen H, Stern MP (1997) The homeostasis model in the San Antonio Heart Study. Diabetes Care 20:1087–1092
16. Pipatpiboon N, Pintana H, Pratchayasakul W, Chattipakorn N, Chattipakorn SC (2013) DPP4-inhibitor improves neuronal insulin receptor function, brain mitochondrial function and cognitive function in rats with insulin resistance induced by high-fat diet consumption. Eur J Neurosci 37:839–849
17. Pipatpiboon N, Pratchayasakul W, Chattipakorn N, Chattipakorn SC (2012) PPARγ agonist improves neuronal insulin receptor function in hippocampus and brain mitochondria function in rats with insulin resistance induced by long term high-fat diets. Endocrinology 153:329–338
18. Huang J, Ishino T, Chen G, Rolzin P, Osothprarop TF, Retting K, Li L, Jin P, Matin MJ, Huyghe B, Talukdar S, Bradshaw CW, Palanki M, Violand BN, Woodnutt G, Lappe RW, Ogilvie K, Levin N (2013) Development of a novel long-acting antidiabetic FGF21 mimetic by targeted conjugation to a scaffold antibody. J Pharmacol Exp Ther 346:270–280
19. Xu J, Lloyd DJ, Hale C, Stanislaus S, Chen M, Sivits G, Vonderfecht S, Hecht R, Li YS, Lindberg RA, Chen JL, Jung DY, Zhang Z, Ko HJ, Kim JK, Veniant MM (2009) Fibroblast growth factor 21 reverses hepatic steatosis, increases energy expenditure, and improves insulin sensitivity in diet-induced obese mice. Diabetes 58:250–259
20. Berglund ED, Li CY, Bina HA, Lynes SE, Michael MD, Shanafelt AB, Kharitonenkov A, Wasserman DH (2009) Fibroblast growth factor 21 controls glycemia via regulation of hepatic glucose flux and insulin sensitivity. Endocrinology 150:4084–4093
21. Lecka-Czernik B, Moerman EJ, Grant DF, Lehmann JM, Manolagas SC, Jilka RL (2002) Divergent effects of selective peroxisome proliferator-activated receptor-γ 2 ligands on adipocyte versus osteoblast differentiation. Endocrinology 143:2376–2384
22. Rzonca SO, Suva LJ, Gaddy D, Montague DC, Lecka-Czernik B (2004) Bone is a target for the antidiabetic compound rosiglitazone. Endocrinology 145:401–406
23. Caverzasio J, Thouverey C (2011) Activation of FGF receptors is a new mechanism by which strontium ranelate induces osteoblastic cell growth. Cell Physiol Biochem 27:243–250
24. Wan Y, Chong LW, Evans RM (2007) PPAR-γ regulates osteoclastogenesis in mice. Nat Med 13:1496–1503
25. Wan Y (2013) Bone marrow mesenchymal stem cells: fat on and blast off by FGF21. Int J Biochem Cell Biol 45:546–549
26. Chen XX, Yang T (2015) Roles of leptin in bone metabolism and bone diseases. J Bone Miner Metab 33:474–485

เอกสารแนบหมายเลข 8

Journal of Clinical Neuroscience 38 (2017) 13–22

Contents lists available at ScienceDirect

Journal of Clinical Neuroscience

journal homepage: www.elsevier.com/locate/jocn

Review article

Alterations of brain activity in fibromyalgia patients

Passakorn Sawaddiruk [a,c], Sahattaya Paiboonworachat [a,c], Nipon Chattipakorn [a,b], Siriporn C. Chattipakorn [a,d,*]

[a] Neurophysiology Unit, Cardiac Electrophysiology Research and Training Center, Faculty of Medicine, Chiang Mai University, Chiang Mai, Thailand
[b] Department of Physiology, Faculty of Medicine, Chiang Mai University, Chiang Mai, Thailand
[c] Department of Anesthesiology, Faculty of Medicine, Chiang Mai University, Chiang Mai, Thailand
[d] Department of Oral Biology and Diagnostic Sciences, Faculty of Dentistry, Chiang Mai University, Chiang Mai, Thailand

ARTICLE INFO

Article history:
Received 25 September 2016
Accepted 26 December 2016

Keywords:
Fibromyalgia
Brain activity
Brain morphology
Functional Magnetic Resonance Imaging
Anterior cingulate cortex
Insula

ABSTRACT

Fibromyalgia is a chronic pain syndrome, characterized by widespread musculoskeletal pain with diffuse tenderness at multiple tender points. Despite intense investigations, the pathophysiology of fibromyalgia remains elusive. Evidence shows that it could be due to changes in either the peripheral or central nervous system (CNS). For the CNS changes, alterations in the high brain area of fibromyalgia patients have been investigated but the definite mechanisms are still unclear. Magnetic Resonance Imaging (MRI) and Functional Magnetic Resonance (fMRI) have been used to gather evidence regarding the changes of brain morphologies and activities in fibromyalgia patients. Nevertheless, due to few studies, limited knowledge for alterations in brain activities in fibromyalgia is currently available. In this review, the changes in brain activity in various brain areas obtained from reports in fibromyalgia patients are comprehensively summarized. Changes of the grey matter in multiple regions such as the superior temporal gyrus, posterior thalamus, amygdala, basal ganglia, cerebellum, cingulate cortex, SII, caudate and putamen from the MRI as well as the increase of brain activities in the cerebellum, prefrontal cortex, anterior cingulate cortex, thalamus, somatosensory cortex, insula in fMRI studies are presented and discussed. Moreover, evidence from pharmacological interventions offering benefits for fibromyalgia patients by reducing brain activity is presented. Because of limited knowledge regarding the roles of brain activity alterations in fibromyalgia, this summarized review will encourage more future studies to elucidate the underlying mechanisms involved in the brains of these patients.

© 2017 Elsevier Ltd. All rights reserved.

1. Introduction

Fibromyalgia syndrome (FMS) is chronic widespread musculoskeletal pain, with diffuse tenderness at multiple tender points [1]. FMS is a common pain disorder which affects 2–4% of the population, with 80% of those suffering being women [2]. Patients with fibromyalgia reported a lower pain threshold and higher pain rating in response to noxious or non-noxious stimuli, when compared with healthy controls [3–5]. The pathophysiology of fibromyalgia remains elusive. Several studies demonstrated that the peripheral sensitization together with changes in the central nervous system may play an important role in fibromyalgia development and progression [6–9]. For example, impaired anti-nociception and altered central processing of nociceptive input, such as pathological wind-up mechanisms [9], have been proposed as the potential neurobiological basis [10] of the chronic pain experienced in fibromyalgia. Moreover, vanilloid receptor, purino-receptors, and acid-sensing ion channel receptors, which are important nociceptive systems in the muscles and skin, seem to have some changes in fibromyalgia patients through unknown mechanisms [11]. Furthermore, the mediators of inflammation and nerve growth factors have been shown to stimulate these receptors and cause alterations in pain sensitivity, without any inflammatory lesions [11]. These findings suggest that the underlying mechanisms of fibromyalgia could be due to changes in the central nervous system without peripheral causes. The possible underlying mechanisms have been proposed including an impaired mechanism for descending pain inhibition, and the inhibition and diminished activation of the rostral anterior cingulate cortex and the brainstem, known as brain regions for pain modulation [2,12].

Despite these potential roles of the central nervous system (CNS) in fibromyalgia, limited knowledge is available at this time.

* Corresponding author at: Neurophysiology Unit, Cardiac Electrophysiology Research and Training Center, Faculty of Medicine, Chiang Mai University, Chiang Mai 50200, Thailand. Fax: +011 66 53 935 329.
E-mail addresses: scchattipakorn@gmail.com, siriporn.c@cmu.ac.th (S.C. Chattipakorn).

http://dx.doi.org/10.1016/j.jocn.2016.12.014
0967-5868/© 2017 Elsevier Ltd. All rights reserved.

In this review, the changes in brain activity in various brain areas obtained from reports in fibromyalgia patients are comprehensively summarized. Evidence from the Magnetic Resonance Imaging (MRI) as well as the Functional Magnetic Resonance Imaging (fMRI) studies in fibromyalgia patients are presented and discussed. Moreover, evidence from non-pharmacological and pharmacological interventions offering benefits for fibromyalgia patients by reducing brain activities is presented. By using fMRI, those findings observed the correlation of elicited changes on the behavioral level and brain physiology [13–19]. In addition, fMRI during experimental pain of fibromyalgia patients showed an increase in pain sensitivity together with enhancement of brain activation, when compared with that of healthy controls [20]. Although peripheral nervous changes were widely investigated in *in vitro* and *in vivo* studies, several studies found the alterations of CNS, including the spinal cord and brainstem of fibromyalgia patients [2,9,12,13,16–20]. These findings emphasize the important roles of the high brain in the pathogenesis of fibromyalgia. However, the alterations of brain morphology and brain activity in fibromyalgia patients remain unclear. Therefore, the aim of the present review was to summarize possible alterations of brain morphology and brain activity in fibromyalgia patients and to provide the potential brain regions, which could play an important role in maintaining pain of fibromyalgia patients.

2. Evidence of the morphological changes in brain of fibromyalgia patients

Fibromyalgia has been proposed as one of the central nervous system disorders with an abnormal level of augmented sensory processing and an inability to modulate pain effectively [21]. Previous reports have used MRI and fMRI to investigate changes in the brain activity of fibromyalgia patients [2,21–23]. Changes have been found in both brain morphology and activity [23]. For brain morphology, changes in both white and grey matter have been found in fibromyalgia patients.

The white matter of the brain is composed of nerve fibers and myelin which are responsible for insulation and acceleration of impulse conduction [21]. White matter of the anterior cingulate cortex appears to be a functionally and morphologically conspicuous site in fibromyalgia patients [12,21,23]. Jensen and colleagues found a significantly lower volume of cortical white matter (the left rostral anterior cingulate cortex and the left lateral orbitofrontal cortex) of fibromyalgia patients, compared to healthy controls [23]. When the white matter reduces the conduction of impulses along nerve fibers slows down or completely fails, leading to impair brain function. These findings suggest that decreased white matter in those brain regions could be linked to a dysregulation of the inhibitory pain mechanism in fibromyalgia patients.

Grey matter consists of cell bodies and many synapses. Several studies showed a decrease in grey matters of some brain areas, but an increase in grey matter in other brain regions in fibromyalgia patients [14–16]. Increasing grey matter was found in the orbitofrontal cortex, cerebellum, basal ganglia, cingulate cortex, insula, SII and caudate, whereas the superior temporal gyrus, thalamus, amygdala, periaqueductal grey, insula and putamen were found to have a reduction in grey matter [21–24]. The orbitofrontal cortex (OFC) plays a role in the antinociceptive system, particularly to cognitive modulation of pain whereas the cerebellum shows an activation in response to nociceptive stimuli and is thus regarded as part of the pain processing network [25]. Activation in the cerebellum of fibromyalgia patients was highly

Table 1
Evidence of the brain morphological changes in the brain of fibromyalgia patients.

Study model	Sample size	Modality	Changes in brain morphology			References
			White matter	Grey matter		
			↓	↑	↓	
Case Controlled Study	20 FM Patients22 Healthy Controls	MRI, Voxel-Based Morphometry		• Lt. Orbitofrontal Cortex • Lt. Cerebellum • Bilat. Striatum	• Rt. Superior Temporal Gyrus • Lt. Posterior Thalamus	[21]
Cross Sectional Study	29 FM patients with affective disorders (AD), 29 FM patients without AD and 29 healthy controls	MRI, Voxel-Based Morphometry			• Lt. anterior insula (FM patients with AD)	[24]
Cross Sectional Study	9 FM Patients11 Healthy Controls	MRI		• Anterior Cingulate Cortex • Insula • Basal Ganglia • SII • Caudate	• Amygdala • Thalamus • Periaqueductal Grey • Putamen	[22]
Cross Sectional Study	26 FM Patients13 Healthy Controls	MRI	• Cortical White Matter • Lt. Rostral Anterior Cingulate Cortex • Lt. Lateral Orbitofrontal Cortex		• Cortical Grey Matter • Subcortical Grey Matter • Rostral Anterior Cingulate Cortex • Lt. Lateral Orbitofrontal Cortex	[23]
Observational Study	46 Premenopausal Women (23 FM Patients, 23 Age-Matched Healthy Controls)	MRI, Voxel-Based Morphometry		• Superior Frontal-Gyrus • Cerebellum • Medial • Orbitofrontal Cortex • Frontal Superior Medial Cortex	• Medial Orbitofrontal Cortex	[26]

FM = fibromyalgia; MRI = magnetic resonance imaging; Lt = left; Bilat = bilateral; SII = secondary somatosensory cortex.

Table 2
Evidence of the pathophysiological changes in the brain activities of fibromyalgia patients.

Study model	Sample size	Modality	Changes in brain activities		References
			↑	↓	
Case Control Study	29 FM Patients	fMRI	• Ipsilateral Claustrum • Cerebellum • Dorsolateral Prefrontal Cortex • Parietal Cortex • Contralateral Dorsal Anterior Cingulate Gyrus • Dorsolateral Prefrontal Cortex • Medial Frontal Cortex • Lentiform Nuclei		[25]
Case Control Study	13 FM Patients11 Healthy Control	fMRI	• Ipsilateral and Contralateral Thalamus • Medial Thalamus • SI • Bilateral SII • Mid and Posterior Insula • Rostral and Mid Anterior Cingulate Cortex		[9]
Case Control Study	16 Female FM Patients16 Age-Matched Healthy Controls	fMRI	• Bilat. Insula • Cerebellum • Thalamus	• Rostral Anterior Cingulate Cortex • Brainstem	[12]
Case Control Study	18 Female FM Patients19 Healthy Female Controls	fMRI	• Fronto-Cingulate Cortex • Thalamus		[20]
Case Control Study	18 FM Patients18 Age-Matched Healthy Controls	fMRI	• Insula • SII		[27]
Case Control Study	17 FM Patients, 16 Rheumatoid Arthritis17 Healthy Controls	fMRI	• Frontal Cortex • Motor Cortex • Cingulate Cortex		[28]
Cross Sectional Study	14 Healthy28 Age-Matched FM Patients	fMRI	• Rostral Anterior Cingulate Cortex • Thalamus		[2]
Cross Sectional Study	19 FM Patients20 Age MatchedHealthy Female Control Subjects	Resting-State fMRI (rs-fMRI)	• SI • Dorsolateral prefrontal cortex • Amygdala		[29]
Cross Sectional Study	26 FM Patients 13 Age- And Gender-Matched Healthy Controls	fMRI		• Rostral Anterior Cingulate Cortex • Medial Prefrontal Cortex	[23]

FM = fibromyalgia; fMRI = functional magnetic resonance imaging; Bilat = bilateral; SI = primary somatosensory cortex; SII = secondary somatosensory cortex.

correlated with catastrophizing scores [25]. Therefore, the cerebellum could play a role in pain expectancy and assessment mechanisms [21]. Moreover, striatal grey matter was increased in patients suffering from fibromyalgia [21]. That study suggested that brain morphological alterations in fibromyalgia patients could be due to neuroplastic changes via increased nociceptive inputs or that alteration in the area of chronic pain genesis, striatum. Interestingly, a key region for modulation of pain, rostral Anterior Cingulate Cortex (rACC) and anterior insula had the significant reduction of brain volume, regional functional connectivity and cortical thickness in fibromyalgia patients [23,24]. Diaz P and colleagues found that larger psychological distress was associated with local decrements of grey matter volume (GMV) in the medial orbitofrontal cortex [26]. However, an increase of a specific GMV area was positively related to the specific characteristics of fibromyalgia patients [26]. For example, (1) increased pain scores were associated with increased GMC at the superior frontal gyrus; (2) psychological distress was positively associated with GMV at the cerebellum; (3) anxiety was positively related to augmented GMV of the medial orbitofrontal cortex; and (4) sleepiness was positively correlated with increased GMV of the frontal superior medial cortex. The clinical characteristics of fibromyalgia patients were also associated with deformations in the subcortical structures and volumes changes [26]. Another interesting study by Hsu and colleagues revealed a significant difference in left anterior insula GMV in fibromyalgia patients with affective disorders whereas FM patients without the affective disorders did not differ significantly from healthy controls [24]. These findings suggested that brain morphologies of fibromyalgia patients were altered by their pain sensation and their specific characteristics.

In addition, an increase in grey matter of fibromyalgia patients was found in the left orbitofrontal cortex, left cerebellum and bilateral basal ganglia [21], whereas a decrease in grey matter was found at the right superior temporal gyrus, left rostral anterior cingulate cortex and left posterior thalamus [23]. Cifre and colleagues also found an increase of grey matter in the anterior cingulate cortex, insula, basal ganglia, SII and caudate and decrease of grey matter in amygdala, thalamus, periaqueductal grey and putamen [22]. Those findings supported that the significant changes in brain morphologies of fibromyalgia patients occurred. The comprehensive summary of those findings is shown in Table 1.

3. Evidence of the activities changes in brain of fibromyalgia patients

To assess the brain activity in fibromyalgia patients, fMRI has been used. Changes in brain activities were found in all studies of fibromyalgia patients. Insula and cortex were found as common areas which had an increase in brain activity [2,9,12,20,25,27–29]. The thalamus, cerebellum and amygdala were areas which had an increase in brain activity in fibromyalgia patients [12]. These findings support the hypothesis that pain catastrophizing appears to be associated with increased activation in brain areas involved in anticipation of pain (cerebellum and medial frontal cortex),

Table 3
Evidence of the pathophysiological changes in the brain activities of fibromyalgia patients following sensory testing.

Study model	Sample size	Modality	Stimuli/treatment	Major findings	Interpretation	References
Case Control Study	9 FM Patients9 Healthy Controls	fMRI	Heat Pain	• Sensitivity to heat pain: FM > controls • greater activity in prefrontal, insular, and anterior cingulate cortices (non-painful stimuli): FM > control • greater activity in the contralateral insular cortex (painful stimuli): FM > Control	FM patients exhibited greater activity than controls over multiple brain regions in response to both non-painful and painful stimuli	[13]
RCT	16 FM Patients18 Control	fMRI	Painful Heat Stimuli	• Positive Relationships Between brain responses and physical Activity to Pain in posterior cingulate cortex, posterior insula, and dorsolateral prefrontal cortexin FM Patients	There is an association between the central nervous system's processing of pain and measures of physical activity	[14]
Cross Sectional Study	13 FM Patients11 Healthy Controls	fMRI	Repetitive Heat Pulses at 0.33 Hz to The Right Foot	• Significantly lower stimulus intensities required in FM patients	Interactions in brain regions associated with temporal summation of "Second Pain" (TSSP)	[15]
Case Control Study	11 Women FM Patients	fMRI	Painful Heat Stimuli	• Pain was related to brain responses including the dorsolateral prefrontal cortex, the dorsal posterior cingulate and the periaqueductal grey	Sedentary behaviors and physical activity are related to the central nervous System's (ACC, PAG and Posterior Thalamus) regulation of pain in FM	[16]
Case Control Study	19 Fm Patients14 Age- and Sex-Matched Healthy Controls	Proton Magnetic Resonance Spectroscopy (H-MRS)	Pressure Pain Testing	• Levels of glutamate and combined glutamate and glutamine within the right posterior insula: FM > control	Enhanced glutamatergic neurotransmission in the posterior insula may be related to the pathophysiology of FM	[17]
Cross Sectional Study	83 FM Patients	fMRI	Computer-Controlled Pressure Stimulator	• Depressive symptoms, anxiety, or catastrophizing scores did not correlate with sensitivity to pressure pain or clinical pain.	Negative mood does not influence performance on assessments of clinical and experimental pain in FM Patients.	[18]
Cross Sectional Study	31 FM14 Controls	fMRI	Cuff Pressure Pain Stimuli on the Leg	• Less robust activation at ventral tegmental area during both anticipation of pain and relief • Activity in the ventral tegmental area during periods of pain was reduced	FM patients exhibit disrupted brain responses towards rewards and punishments	[19]

RCT = randomized controlled trial; FM = fibromyalgia; fMRI = functional magnetic resonance imaging; PA = physical activity; ACC = anterior cingulate cortex; PAG = periaqueductal grey.

emotion aspects of pain (closely connected to amygdala and claustrum), attention to pain (dorsolateral prefrontal cortex and dorsal anterior cingulate cortex) and motor control. It influences pain perception through its effect on attentional responses to pain. Interestingly, Jensen and colleagues found decreased levels of brain activities of fibromyalgia patients in the anterior cingulate cortex, medial prefrontal cortex and brainstem, suggesting an impaired mechanism for descending pain inhibition in the central pain regulatory system in fibromyalgia patients [23]. The comprehensive summary of these findings is shown in Table 2.

Magnetic resonance spectroscopy (MRS) has also been used to evaluate the brain metabolite patterns in fibromyalgia patients. A significant increase of glutamate and glutamine levels were found in the posterior cingulate cortex in the fibromyalgia patients, suggesting that glutamate could be involved in the molecular processes in fibromyalgia [30]. Proton magnetic resonance spectroscopy (H-MRS) suggested that reducing glutamatergic activity by using pharmacological treatment could improve the symptoms of patients with fibromyalgia [30].

4. Evidence of the pathophysiological changes in the brain activities of fibromyalgia patients following sensory testing

After stimulation with heat, fibromyalgia patients exhibited greater brain activity and required lower stimulus intensities than controls over multiple brain regions such as the posterior insula, posterior cingulate cortex and dorsolateral prefrontal cortex [13–16]. Craggs and colleagues found that fibromyalgia patients required significantly lower stimulus intensities when compared to healthy controls due to the interactions in brain regions, including the thalamus, posterior insula, SI, SII and the anterior midcingulate cortex. Those brain areas have been shown to be associated with the summation of dorsal horn neurons evoked responses of C-fiber or "windup" [15].

In pressure pain testing, Harris and colleagues using Proton magnetic resonance spectroscopy (H-MRS) reported that levels of glutamate and glutamine within the right posterior insula were higher in fibromyalgia patients than in healthy control patients [17]. Loggia and colleagues found a less robust activation at ventral tegmental area (areas of rewards and punishments) of fibromyalgia patients during both anticipation of pain and pain relief [19]. That finding suggested that fibromyalgia patients exhibited a disrupted brain response towards rewards and punishments [19]. From Table 3, after sensory testing by heat pain and pressure pain of fibromyalgia patients, multiple brain regions in response to both non-painful and painful stimuli were increased. The comprehensive summary of those findings is shown in Table 3.

5. Pharmacological treatment in fibromyalgia patients caused changes in brain activity

Pharmacologic treatments of fibromyalgia have been extensively investigated to achieve the pain relief in fibromyalgia patients. Staud and colleagues found that dextromethorphan could be clinically effective for fibromyalgia patients [31]. Harris and colleagues investigated the efficacy of opiates in fibromyalgia patients and found reduced efficacy of exogenous opiates in fibromyalgia patients due to a reduction in the binding potential in several brain regions including the nucleus accumbens, amygdala and the dorsal cingulate cortex [32]. Harris and colleagues found that pregabalin exerted good efficacy in reducing chronic pain intensity of fibromyalgia patients as well as the reduction of glutamatergic and neuronal activity within the posterior insula [33]. They suggested that pregabalin reduced pain in fibromyalgia patients

Table 4
Effects of pharmacological therapies on the brain activities of fibromyalgia (FM) patients.

Study model	Sample size	Therapy	Dose/time	Major findings	Interpretation	References
RCT	14 Female FM Patients10 Female Healthy Controls	Dextromethorphan	0, 60, and 90 mg × 1 Dose	• Thermal and mechanical stimulus intensity were required less than controls to achieve maximal windup of second pain in FM patients • Oral doses of dextromethorphan attenuated thermal and mechanical similarly in FM patients and controls	FM patients do not have altered NMDA receptor mechanisms	[31]
Cross-Sectional Study	17 FM Patients17 Age- and Sex-Matched Healthy Controls	Carfentanil	10–15 Mcl (370–555 MBq)	• Reduction of MOR binding potential (BP) within several regions including the amygdala, the dorsal cingulate and nucleus accumbens in FM patients	Exogenous opiates reduced efficacy in FM	[32]
RCT	17 FM Patients	Pregabalin	Escalating Dose up to 450 mg/day × 14 days	• Pregabalin decreases combined glutamate and glutamine levels within the posterior insula	Pregabalin reduced pain in fibromyalgia patients by reducing insular glutamatergic activity, in which that reduction caused a decrease in the functional connectivity between brain regions during chronic pain states.	[33]
RCT	77 patients	Milnacipran	100, 150, 200 mg/day × 7 weeks	• Milnacipran is a dose-dependent analgesic	Milnacipran had predominantly supraspinal analgesic effect	[53]
RCT	21 female FM patients11 age- and gender-matched healthy controls	Pregabalin	Routine clinical treatment using pregabalin	• 5 of 6 clinical tests (BDI, BFI, FIQ, SSS, WPI) after treatment was associated with reduced clinical scores Post treatment Brain activation was significantly lower in 13 regions of the brain than that pre-treatment	Pregabalin changes the neuronal activity during the pain state, reduced pain and other core symptoms of FM	[34]

RCT = randomized controlled trial; FM = fibromyalgia; mg = milligram; mCi = millicurie; MBq = megabecquerel; FIQ = Fibromyalgia Impact Questionnaire; BFI = brief fatigue inventory; BDI = Beck Depression Inventory; WPI = Widespread Pain Index; SSS = symptom severity scale score; NMDA = N-methyl-D-aspartate.

Table 5
Effects of non-pharmacological therapies on the brain activities of fibromyalgia patients

Study model	Sample size	Modality	Stimuli/treatment	Major findings	Interpretation	References
Case control study	12 female FM subjects 11 female healthy controls	Isometric exercise	90 s	• Isometric exercise resulted in increased mechanical thresholds and substantially increased thermal pain ratings in FM patients	Exercise effects result from abnormal descending inhibition or excessive activation of muscle nociceptive afferents in FM patients	[10]
RCT	32 FM patients	Transcranial Direct Current Stimulation (tDCS)	2 mA 20 min × 5 days	• Anodal tDCS of the primary motor cortex induced significantly greater pain improvement.	Transcranial direct current stimulation is useful in FM	[43]
Case control study	12 FM patients	Non-pharmacological treatment program (Educational sessions about fibromyalgia, physical exercise, and cognitive-behavioral therapy)	3 weeks	• The number of positive tender points, present pain, pain area and CES-D score were significantly reduced after the treatment	Improvement of HPA axis function maybe one of the active mechanisms.	[54]
RCT	15 female FM patients15 healthy women	Somatosensory stimulation	2 randomized interstimulus intervals of 550 ms (±50 ms), separated by a fixed intertrain interval of 12 s	• Event-related potentials (ERPs) amplitudes elicited by the somatosensory and auditory SII stimuli were significantly reduced	Lack of inhibitory control to repetitive non-painful somatosensory information during cognitive evaluation and stimulus coding may be a cause of FM	[55]
RCT	32 FM patients	Transcranial Direct Current Stimulation (tDCS)	2 mA, 20 min × 5 days	• Primary motor cortex treatment increased sleep efficiency and decreased arousals	The therapeutic effects of tDCS in FM is via sleep modulation that is specific to modulation of primary motor cortex activity	[44]
RCT	30 FM patients	Unilateral repetitive transcranial magnetic stimulation (rTMS)	10 daily sessions	• Active rTMS significantly reduced pain and improved several aspects of quality of life	Unilateral rTMS of the motor cortex caused a decrease in chronic widespread pain	[45]
Case control study	12 FM female patients aged 18–60	Breathing exercise	10 weekly sessions	• Clinically significant decreases in depression and pain and improvement in functioning after breathing exercise	Breathing exercise may be a useful treatment for FM	[56]
Case Control Study	10 FM patients	Proton magnetic resonance spectroscopy and fMRI	Acupuncture	• Raito of pre- to post-treatment in Glu/Cr levels did not correlate with the experimental pain thresholds, but was correlated with changes in clinical pain • Changes in the fMRI correlated with changes in Glu/Cr levels within the contralateral insula	Changes in multiple pain domains in FM patients were related with changes in Glu levels within the insula	[35]
RCT	24 FM female patients	Meditation	2 months	• The meditation based stress-reduction treatment significantly reduced basal electrodermal activity and SCL activity during meditation	Basal sympathetic activity was reduced following mediation-based stress-reduction treatment	[42]
Case Control Study	19 FM patients14 age- and sex-matched healthy controls	Acupuncture	4 weeks	• Significantly higher levels of combined glutamate and glutamine and Glu within the right posterior insula	higher concentrations of Glu within the posterior insula results in Enhanced glutamatergic neurotransmission may related to the pathophysiology of FM	[17]
Case Control Study	20 FM patients	fMRI	Virtual reality exposure therapy (VRET)	• Pain catastrophizing was releated to triggered brain areas after exposure to visuals of various exercise activities in FM patients	Decrease exercise-related pain catastrophizing in FM patients was possibly related to repeated exposure to visuals of te exercise activities using a VRET program. This occurred in the SII, contralateral insula, SI, contralateral anterior ACC, inferior parietal lobule and thalamus, the contralateral and ipsilateral lentiform, anterior and posterior cerebellum, superior and inferior frontal gyrus, and posterior cingulate gyrus	[36]
RCT	20 FM patients	Left Prefrontal rTMS	4000 pulses at 10 Hz TMS x 10 sessions over 2 weeks	• 29% reduction in pain symptoms in comparison to their baseline pain in patients who received active TMS	rTMS trial stimulating lead to reductions in fibromyalgia pain	[46]

Table 5 (*continued*)

Study model	Sample size	Modality	Stimuli/treatment	Major findings	Interpretation	References
RCT	40 FM patients	Transcranial magnetic stimulation	15 series of 10 s pulses with a frequency of 10 Hz and an interval of 50 s between each train, giving a total of 1500 pulses per session	• Active rTMS significantly reduced pain intensity	TMS may be a valuable and safe new therapeutic option in patients with fibromyalgia	[47]
RCT	16 FM patients18 healthy controls	Physical Activity	7 days	• Positive relationships between brain responses and physical activity were observed in the posterior cingulate cortex, dorsolateral prefrontal cortex, posterior insula,, regions implicated in pain regulation	There is an association between the central nervous system's processing of pain and measures of physical activity	[14]
RCT	23 muscular dystrophy patients, 16 FM patients23 healthy controls	Hand grip exercise	Repeating a hand grip with 50% of maximum voluntary strength at a frequency of 1–2/s until the patient can no longer attain this force level	• Intracortical inhibition was already reduced pre-exercise in muscular dystrophy and FM patients	Reduced intracortical inhibition may be an indicator of primary central inhibitory mechanism in FM and muscular dystrophy	[41]
Case Control Study	10 FM patients	fMRI	Painful mechanical stimuli applied to the second phalanx of the left second digit	• Behavioral treatment reduced interference from pain significantly in the FM patients • Insula Activation shifted bilaterally (from a more anterior site to a more posterior location)	There is a relationship between higher activation and successful behavioral treatment in the posterior insula bilaterally and in the primary somatosensory cortex contralaterally.	[37]
Case Control Study	17 FM patients	fMRI	Acupuncture x 4 weeks	• Clinical pain was reduced following therapy • Reductions in pain correlated with reduced intrinsic default mode network (DMN) connectivity to the insula	Intrinsic brain connectivity may be used as an objective marker in FM	[38]
RCT	11 FM patients	Exercise	48 h	• Physical activity was positively related to brain responses in regions implicated in pain modulation including the dorsal posterior cingulate cortex, periaqueductal grey, and dorsolateral prefrontal cortex (DLPFC) during distraction from pain	Central nervous system's regulation of pain was related to physical activity and sedentary behaviors in FM patients	[16]
RCT	16 FM patients16 healthy controls	Multi-coil repetitive transcranial magnetic stimulation (rTMS)	30 min consisting of 1800 pulses	• rTMS coil produced a significant pain inhibition	Multi-coil rTMS may be a safe and effective treatment in acute and chronic pain	[48]
RCT	57 FM patients	Cranial Electrical Stimulation (CES)	60 min/day x 8 weeks	• Active CES device results in a greater decrease in average pain in FM patientsDecrease in activation in the pain processing regions of the brain was found in FM patients using an active CES device compared to those using a sham device	A CES device can reduce pain in FM	[49]
Case–control study	25 FM patients23 healthy controls	Isometric muscle exhaustion task	As long as possible with the elbow extended and the hand pronated	• Shorter average time to exhaustion was found in participants with FM than in healthy control	Shorter exhaustion times and fewer objective signs of muscle fatigue were found in women with FM during an exhausting isometric shoulder abduction	[40]
RCT	38 FM patients	Repetitive transcranial magnetic stimulation of the motor cortex	10 Hz at 80% of rest motor threshold x 11 weeks	• No significant difference in neuropsychological performance when compared to baseline	Unilateral rTMS of the motor cortex over a three-month period could not change cognitive functions in chronic pain patients	[50]
RCT	20 FM patients	Delta-embedded music program	4 weeks	• FIQ median score improved	Delta-embedded music may benefits for FM patients	[57]
RCT	15 FM patients	Pain test	2 min	• Patients who had an increase in motor evoked potentials during the pain test had an increase in pain after exercise	There is a change in corticomotor excitability during the application of a noxious stimulus	[58]

RCT = randomized controlled trial; FM = fibromyalgia; fMRI = functional magnetic resonance imaging; rTMS = repetitive transcranial magnetic stimulation; mA = milliamps; msec = millisecond; Hz = hertz; s = second; CES-D = Center for Epidemiologic Studies Depression Scale; SII = secondary somatosensory cortex; Glu = glutamate; Cr = creatinine; SCL = skin conductance level; FIQ = Fibromyalgia Impact Questionnaire; HPA = hypothalamic–pituitary–adrenal; ACC = anterior cingulate cortex.

by reducing insular glutamatergic activity, in which that reduction caused a decrease in the functional connectivity between brain regions during chronic pain states. Kim and colleagues also found that pregabalin reduced brain activation in multiple brain regions, in which those regions have been activated during pain state [34]. The comprehensive summary of those findings is shown in Table 4.

6. Evidence of the alterations in the brain activities of fibromyalgia patients following different non-pharmacological therapies

Various non-pharmacological therapies such as exercise, acupuncture, meditation and virtual reality exposure therapy, have been used to treat pain of fibromyalgia patients [35–38]. Non-pharmacological therapies revealed benefits for fibromyalgia patients by reduction of pain. The possible mechanisms of pain reliefs could be due to a decrease in brain activities following those therapies [36,38]. For example, Martin D and colleagues found that non-pharmacological treatment (pain behavioral treatment) in fibromyalgia could reduce pain severity and bilateral activation in pain-evoked activity in the posterior insula and the primary somatosensory cortex [37]. That finding suggested that that behavioral treatment to relieve pain was associated with higher activation bilaterally in the posterior insula and in the contralateral primary somatosensory cortex [37].

Exercise has been used as one of the alternative treatments for fibromyalgia [10,14,16,39–41]. Exercise has been shown to reduce pain intensity by improving the descending pain inhibition and decreasing the activation of pain afferents [10,16]. Ellingson and colleagues found a positive correlation between exercise and brain responses including in the dorsolateral prefrontal cortex, dorsal posterior cingulate cortex and the periaqueductal grey in fibromyalgia patients [16]. McLoughlin and colleagues reported a positive correlation between physical activity and brain response to pain at the posterior insula, posterior cingulate cortex, and dorsolateral prefrontal cortex, posterior cingulate cortex, and the posterior insula. Those studies indicated that those brain regions play role in pain regulation [14,16]. In addition, Schwenkreis and colleagues found that intracortical inhibition was reduced pre-exercise in fibromyalgia, suggesting that the intracortical inhibitory activities should have some roles in the primary central inhibitory mechanism in fibromyalgia [41].

Meditation was beneficial for fibromyalgia patients [42]. It has been known that increased sympathetic activity is correlated with increased pain [42]. Lush and colleagues found that the meditation-based stress-reduction therapy significantly reduced basal sympathetic activity following meditation [42].

Transcranial direct current stimulation has been reported to provide benefits in relieving pain of fibromyalgia patients [43–50]. The possible explanation of the pain relief following transcranial direct current stimulation was that the injection of a weak DC current into the brain for several minutes resulted in a polarity-dependent modulation of brain activity, particularly stimulating at the motor cortex [43] and changes motor cortex excitability resulted in a decrease of chronic widespread pain [43]. Previous studies demonstrated that subjects with transcranial direct current stimulation onto the primary motor cortex led to significant increased sleep efficiency, greater pain improvement and improved several aspects of life quality [43–50].

Harris and colleagues used proton magnetic resonance spectroscopy to assess the effect of acupuncture on the changes in the brain activity of fibromyalgia patients [35]. They found that changes in glutamine levels within the insula were associated with alterations of multiple pain domains in fibromyalgia patients. Moreover, changes in the fMRI were correlated with changes in Glu/Cr levels within the contralateral insula [35]. After virtual reality exposure therapy, decreased brain activities were found in the SI, SII, contralateral insula, inferior parietal lobule and thalamus, contralateral anterior cingulate cortex, cerebellum and cingulate gyrus [36]. Diers and colleagues found activation in the contralateral primary somatosensory cortex and this shifted bilaterally from a more anterior site to more posterior location in insula after the non-pharmacologic intervention [37]. Those findings suggested that non-pharmacological therapies such as acupuncture, virtual reality exposure therapy can result in clinical pain reduction after therapy by reduction of brain activities in multiple brain regions, particularly areas for the activation of pain afferents and increased in brain activities in the descending pain. The comprehensive summary of those findings is shown in Table 5.

7. Evidence of changes in the brain activities of fibromyalgia patients with combined pharmacological therapy and non-pharmacological intervention

By combining pharmacological and non-pharmacological treatment, Walitt and colleagues found that clinical symptoms of fibromyalgia patients were improved after medication treatment with cognitive behavioral therapy, physical therapy, and weekly physician phone calls [51]. Jones and colleagues found that exercise and pyridostigmine improved the symptoms of fibromyalgia (sleep, anxiety and quality of life) by improving vagal tone [52]. The comprehensive summary of those findings is shown in Table 6.

Table 6
Effects of combined pharmacological therapy and non-pharmacological intervention on the brain activities of fibromyalgia patients.

Study model	Sample size	Therapy	Dose/time	Major findings	Interpretation	References
Case control study	9 FM patients	Comprehensive treatment program (medications, cognitive behavioral therapy, physical therapy, and weekly physician phone calls)	8 weeks	• Clinical symptoms improved with treatment • Increases in brain metabolism were noted in various components of the limbic system	Limbic system attenuates FM symptoms	[51]
RCT	165 FM patients	Exercise and Pyridostigmine (PYD)	2 months each, PYD was titrated over the following 11 days to the full dosage of 180 mg/day	• Significant improvement in quality of life, sleep and anxiety in PYD group	PYD and exercise yielded an improvement in most FM symptoms	[52]

RCT = randomized controlled trial; FM = fibromyalgia.

8. Conclusion

Fibromyalgia is a chronic pain disease with unclear pathophysiology. Lower pain thresholds and higher pain rating score were reported in all fibromyalgia patients. Changes in both brain morphologies and activities also occurred in fibromyalgia patients. Non-pharmacological therapies reduced brain activity in insula which led to a reduction in pain. For pharmacological treatment, drugs which had an effect on glutamatergic activity were found to be beneficial in pain relief in fibromyalgia patients. Transcranial direct current stimulation acts by modulating primary motor cortex activity and results in decreasing of chronic widespread pain. Decreased brain activity at the insula and pain relief were found following non-pharmacological and pharmacological therapies, indicating that activity of insula plays an important role in pathophysiological changes in fibromyalgia patients.

Conflict of interest

There is no conflict of interest to report.

Acknowledgements

This work was supported by the Thailand Research Fund under Grant BRG5780016 (SC); a NSTDA Research Chair Grant from the National Science and Technology Development Agency (NC) and a Chiang Mai University Center of Excellence Award (NC).

References

[1] Wolfe F, Smythe HA, Yunus MB, et al. The American College of Rheumatology 1990 criteria for the classification of fibromyalgia. Report of the multicenter criteria committee. Arthritis Rheum 1990;33:160–72.
[2] Jensen KB, Loitoile R, Kosek E, et al. Patients with fibromyalgia display less functional connectivity in the brain's pain inhibitory network. Mol Pain 2012;8:32.
[3] Granges G, Littlejohn G. Pressure pain threshold in pain-free subjects, in patients with chronic regional pain syndromes, and in patients with fibromyalgia syndrome. Arthritis Rheum 1993;36:642–6.
[4] Desmeules JA, Cedraschi C, Rapiti E, et al. Neurophysiologic evidence for a central sensitization in patients with fibromyalgia. Arthritis Rheum 2003;48:1420–9.
[5] Petzke F, Clauw DJ, Ambrose K, et al. Increased pain sensitivity in fibromyalgia: effects of stimulus type and mode of presentation. Pain 2003;105:403–13.
[6] Littlejohn GO, Weinstein C, Helme RD. Increased neurogenic inflammation in fibrositis syndrome. J Rheumatol 1987;14:1022–5.
[7] Clauw DJ. Fibromyalgia: update on mechanisms and management. J Clin Rheumatol 2007;13:102–9.
[8] Yunus MB. Fibromyalgia and overlapping disorders: the unifying concept of central sensitivity syndromes. Semin Arthritis Rheum 2007;36:339–56.
[9] Staud R, Craggs JG, Perlstein WM, et al. Brain activity associated with slow temporal summation of C-fiber evoked pain in fibromyalgia patients and healthy controls. Eur J Pain 2008;12:1078–89.
[10] Staud R, Robinson ME, Price DD. Isometric exercise has opposite effects on central pain mechanisms in fibromyalgia patients compared to normal controls. Pain 2005;118:176–84.
[11] Staud R, Smitherman ML. Peripheral and central sensitization in fibromyalgia: pathogenetic role. Curr Pain Headache Rep 2002;6:259–66.
[12] Jensen KB, Kosek E, Petzke F, et al. Evidence of dysfunctional pain inhibition in Fibromyalgia reflected in rACC during provoked pain. Pain 2009;144:95–100.
[13] Cook DB, Lange G, Ciccone DS, et al. Functional imaging of pain in patients with primary fibromyalgia. J Rheumatol 2004;31:364–78.
[14] McLoughlin MJ, Stegner AJ, Cook DB. The relationship between physical activity and brain responses to pain in fibromyalgia. J Pain 2011;12:640–51.
[15] Craggs JG, Staud R, Robinson ME, et al. Effective connectivity among brain regions associated with slow temporal summation of C-fiber-evoked pain in fibromyalgia patients and healthy controls. J Pain 2012;13:390–400.
[16] Ellingson LD, Shields MR, Stegner AJ, et al. Physical activity, sustained sedentary behavior, and pain modulation in women with fibromyalgia. J Pain 2012;13:195–206.
[17] Harris RE, Sundgren PC, Craig AD, et al. Elevated insular glutamate in fibromyalgia is associated with experimental pain. Arthritis Rheum 2009;60:3146–52.
[18] Jensen KB, Petzke F, Carville S, et al. Anxiety and depressive symptoms in fibromyalgia are related to poor perception of health but not to pain sensitivity or cerebral processing of pain. Arthritis Rheum 2010;62:3488–95.
[19] Loggia ML, Berna C, Kim J, et al. Disrupted brain circuitry for pain-related reward/punishment in fibromyalgia. Arthritis Rheumatol 2014;66:203–12.
[20] Burgmer M, Pogatzki-Zahn E, Gaubitz M, et al. Altered brain activity during pain processing in fibromyalgia. Neuroimage 2009;44:502–8.
[21] Schmidt-Wilcke T, Luerding R, Weigand T, et al. Striatal grey matter increase in patients suffering from fibromyalgia–a voxel-based morphometry study. Pain 2007;132(Suppl 1):S109–16.
[22] Cifre I, Sitges C, Fraiman D, et al. Disrupted functional connectivity of the pain network in fibromyalgia. Psychosom Med 2012;74:55–62.
[23] Jensen KB, Srinivasan P, Spaeth R, et al. Overlapping structural and functional brain changes in patients with long-term exposure to fibromyalgia pain. Arthritis Rheum 2013;65:3293–303.
[24] Hsu MC, Harris RE, Sundgren PC, et al. No consistent difference in gray matter volume between individuals with fibromyalgia and age-matched healthy subjects when controlling for affective disorder. Pain 2009;143:262–7.
[25] Gracely RH, Geisser ME, Giesecke T, et al. Pain catastrophizing and neural responses to pain among persons with fibromyalgia. Brain 2004;127:835–43.
[26] Diaz-Piedra C, Guzman MA, Buela-Casal G, et al. The impact of fibromyalgia symptoms on brain morphometry. Brain Imag Behav 2015.
[27] Napadow V, LaCount L, Park K, et al. Intrinsic brain connectivity in fibromyalgia is associated with chronic pain intensity. Arthritis Rheum 2010;62:2545–55.
[28] Burgmer M, Pogatzki-Zahn E, Gaubitz M, et al. Fibromyalgia unique temporal brain activation during experimental pain: a controlled fMRI Study. J Neural Trans 2010;117:123–31.
[29] Kim JY, Kim SH, Seo J, et al. Increased power spectral density in resting-state pain-related brain networks in fibromyalgia. Pain 2013;154:1792–7.
[30] Fayed N, Andres E, Rojas G, et al. Brain dysfunction in fibromyalgia and somatization disorder using proton magnetic resonance spectroscopy: a controlled study. Acta Psychiatr Scand 2012;126:115–25.
[31] Staud R, Vierck CJ, Robinson ME, et al. Effects of the N-methyl-D-aspartate receptor antagonist dextromethorphan on temporal summation of pain are similar in fibromyalgia patients and normal control subjects. J Pain 2005;6:323–32.
[32] Harris RE, Clauw DJ, Scott DJ, et al. Decreased central mu-opioid receptor availability in fibromyalgia. J Neurosci 2007;27:10000–6.
[33] Harris RE, Napadow V, Huggins JP, et al. Pregabalin rectifies aberrant brain chemistry, connectivity, and functional response in chronic pain patients. Anesthesiology 2013;119:1453–64.
[34] Kim SH, Lee Y, Lee S, et al. Evaluation of the effectiveness of pregabalin in alleviating pain associated with fibromyalgia: using functional magnetic resonance imaging study. PLoS ONE 2013;8:e74099.
[35] Harris RE, Sundgren PC, Pang Y, et al. Dynamic levels of glutamate within the insula are associated with improvements in multiple pain domains in fibromyalgia. Arthritis Rheum 2008;58:903–7.
[36] Morris LD, Grimmer-Somers KA, Spottiswoode B, et al. Virtual reality exposure therapy as treatment for pain catastrophizing in fibromyalgia patients: proof-of-concept study (Study Protocol). BMC Musculoskelet Disord 2011;12:85.
[37] Diers M, Yilmaz P, Rance M, et al. Treatment-related changes in brain activation in patients with fibromyalgia syndrome. Exp Brain Res 2012;218:619–28.
[38] Napadow V, Kim J, Clauw DJ, et al. Decreased intrinsic brain connectivity is associated with reduced clinical pain in fibromyalgia. Arthritis Rheum 2012;64:2398–403.
[39] Bote ME, García JJ, Hinchado MD, et al. An exploratory study of the effect of regular aquatic exercise on the function of neutrophils from women with fibromyalgia: role of IL-8 and noradrenaline. Brain Behav Immun 2014;39:107–12.
[40] Bandak E, Amris K, Bliddal H, et al. Muscle fatigue in fibromyalgia is in the brain, not in the muscles: a case-control study of perceived versus objective muscle fatigue. Ann Rheum Dis 2013;72:963–6.
[41] Schwenkreis P, Voigt M, Hasenbring M, et al. Central mechanisms during fatiguing muscle exercise in muscular dystrophy and fibromyalgia syndrome: a study with transcranial magnetic stimulation. Muscle Nerve 2011;43:479–84.
[42] Lush E, Salmon P, Floyd A, et al. Mindfulness meditation for symptom reduction in fibromyalgia: psychophysiological correlates. J Clin Psychol Med Settings 2009;16:200–7.
[43] Fregni F, Gimenes R, Valle AC, et al. A randomized, sham-controlled, proof of principle study of transcranial direct current stimulation for the treatment of pain in fibromyalgia. Arthritis Rheum 2006;54:3988–98.
[44] Roizenblatt S, Fregni F, Gimenez R, et al. Site-specific effects of transcranial direct current stimulation on sleep and pain in fibromyalgia: a randomized, sham-controlled study. Pain Pract 2007;7:297–306.
[45] Passard A, Attal N, Benadhira R, et al. Effects of unilateral repetitive transcranial magnetic stimulation of the motor cortex on chronic widespread pain in fibromyalgia. Brain 2007;130:2661–70.
[46] Short EB, Borckardt JJ, Anderson BS, et al. Ten sessions of adjunctive left prefrontal rTMS significantly reduces fibromyalgia pain: a randomized, controlled pilot study. Pain 2011;152:2477–84.
[47] Mhalla A, Baudic S, Ciampi de Andrade D, et al. Long-term maintenance of the analgesic effects of transcranial magnetic stimulation in fibromyalgia. Pain 2011;152:1478–85.
[48] Tzabazis A, Aparici CM, Rowbotham MC, et al. Shaped magnetic field pulses by multi-coil repetitive transcranial magnetic stimulation (rTMS) differentially modulate anterior cingulate cortex responses and pain in volunteers and fibromyalgia patients. Mol Pain 2013;9:33.

[49] Taylor AG, Anderson JG, Riedel SL, et al. A randomized, controlled, double-blind pilot study of the effects of cranial electrical stimulation on activity in brain pain processing regions in individuals with fibromyalgia. Explore (NY). 2013;9:32–40.
[50] Baudic S, Attal N, Mhalla A, et al. Unilateral repetitive transcranial magnetic stimulation of the motor cortex does not affect cognition in patients with fibromyalgia. J Psychiatr Res 2013;47:72–7.
[51] Walitt B, Roebuck-Spencer T, Esposito G, et al. The effects of multidisciplinary therapy on positron emission tomography of the brain in fibromyalgia: a pilot study. Rheumatol Int 2007;27:1019–24.
[52] Jones KD, Burckhardt CS, Deodhar AA, et al. A six-month randomized controlled trial of exercise and pyridostigmine in the treatment of fibromyalgia. Arthritis Rheum 2008;58:612–22.
[53] Matthey A, Cedraschi C, Piguet V, et al. Dual reuptake inhibitor milnacipran and spinal pain pathways in fibromyalgia patients: a randomized, double-blind, placebo-controlled trial. Pain Physician 2013;16:E553–62.
[54] Bonifazi M, Suman AL, Cambiaggi C, et al. Changes in salivary cortisol and corticosteroid receptor-alpha mRNA expression following a 3-week multidisciplinary treatment program in patients with fibromyalgia. Psychoneuroendocrinology 2006;31:1076–86.
[55] Montoya P, Sitges C, García-Herrera M, et al. Reduced brain habituation to somatosensory stimulation in patients with fibromyalgia. Arthritis Rheum 2006;54:1995–2003.
[56] Hassett AL, Radvanski DC, Vaschillo EG, et al. A pilot study of the efficacy of heart rate variability (HRV) biofeedback in patients with fibromyalgia. Appl Psychophysiol Biofeedback 2007;32:1–10.
[57] Picard LM, Bartel LR, Gordon AS, et al. Music as a sleep aid in fibromyalgia. Pain Res Manag 2014;19:97–101.
[58] Hoeger Bement MK, Weyer AD, Yoon T, et al. Corticomotor excitability during a noxious stimulus before and after exercise in women with fibromyalgia. J Clin Neurophysiol 2014;31:94–8.

เอกสารแนบหมายเลข 9

Vildagliptin and caloric restriction for cardioprotection in pre-diabetic rats

Pongpan Tanajak[1,2,3], Hiranya Pintana[1,2,3], Natthaphat Siri-Angkul[1,2,3], Juthamas Khamseekaew[1,2,3], Nattayaporn Apaijai[1,2,3], Siriporn C Chattipakorn[1,3,4] and Nipon Chattipakorn[1,2,3]

[1]Cardiac Electrophysiology Research and Training Center, Faculty of Medicine, Chiang Mai University, Chiang Mai, Thailand
[2]Cardiac Electrophysiology Unit, Department of Physiology, Faculty of Medicine, Chiang Mai University, Chiang Mai, Thailand
[3]Center of Excellence in Cardiac Electrophysiology Research, Chiang Mai University, Chiang Mai, Thailand
[4]Department of Oral Biology and Diagnostic Sciences, Faculty of Dentistry, Chiang Mai University, Chiang Mai, Thailand

Correspondence should be addressed to N Chattipakorn
Email
nchattip@gmail.com

Abstract

Long-term high-fat diet (HFD) consumption causes cardiac dysfunction. Although calorie restriction (CR) has been shown to be useful in obesity, we hypothesized that combined CR with dipeptidyl peptidase-4 (DPP-4) inhibitor provides greater efficacy than monotherapy in attenuating cardiac dysfunction and metabolic impairment in HFD-induced obese-insulin resistant rats. Thirty male Wistar rats were divided into 2 groups to be fed on either a normal diet (ND, $n=6$) or a HFD ($n=24$) for 12 weeks. Then, HFD rats were divided into 4 subgroups ($n=6$/subgroup) to receive just the vehicle, CR diet (60% of mean energy intake and changed to ND), vildagliptin (3 mg/kg/day) or combined CR and vildagliptin for 4 weeks. Metabolic parameters, heart rate variability (HRV), cardiac mitochondrial function, left ventricular (LV) and fibroblast growth factor (FGF) 21 signaling pathway were determined. Rats on a HFD developed insulin and FGF21 resistance, oxidative stress, cardiac mitochondrial dysfunction and impaired LV function. Rats on CR alone showed both decreased body weight and visceral fat accumulation, whereas vildagliptin did not alter these parameters. Rats in CR, vildagliptin and CR plus vildagliptin subgroups had improved insulin sensitivity and oxidative stress. However, vildagliptin improved heart rate variability (HRV), cardiac mitochondrial function and LV function better than the CR. Chronic HFD consumption leads to obese-insulin resistance and FGF21 resistance. Although CR is effective in improving metabolic regulation, vildagliptin provides greater efficacy in preventing cardiac dysfunction by improving anti-apoptosis and FGF21 signaling pathways and attenuating cardiac mitochondrial dysfunction in obese-insulin-resistant rats.

Key Words
- caloric restriction
- obesity
- insulin resistance
- mitochondria
- FGF21 sensitivity
- apoptosis
- fatty acid β-oxidation
- cardiac function
- DPP-4 inhibitor

Journal of Endocrinology (2017) **232**, 189–204

Journal of Endocrinology

Introduction

Long-term consumption of high-fat diet (HFD) can lead to obese-insulin resistance (Pratchayasakul *et al.* 2011, Pipatpiboon *et al.* 2012), which is characterized by body weight gain, hyperinsulinemia and euglycemia and is also associated with metabolic dysregulation and dyslipidemia (Pratchayasakul *et al.* 2011, Pipatpiboon *et al.* 2013,

http://joe.endocrinology-journals.org
DOI: 10.1530/JOE-16-0406
© 2017 Society for Endocrinology
Printed in Great Britain
Published by Bioscientifica Ltd.

Apaijai *et al.* 2014). Obese-insulin resistance impairs not only the metabolic parameters but also damages the cardiovascular system including an increased blood pressure and cardiac dysfunction in various models (Fontana *et al.* 2004, Dolinsky *et al.* 2010). In past decades, cardiac mitochondrial dysfunction had been proposed as a crucial mechanism of cardiac dysfunction in high-fat diet-induced obese-insulin-resistant models (Chinda *et al.* 2013, Apaijai *et al.* 2014). Therefore, the therapeutic approaches that can attenuate metabolic complications and cardiac mitochondrial dysfunction caused by obese-insulin resistance may lead to improved cardiac function.

Currently, lifestyle modification, including caloric restriction (CR), is the first therapeutic approach for diabetic management. CR combined with anti-diabetic drugs has been shown to be effective for metabolic regulation and glycemic control in diabetes (Inzucchi *et al.* 2015). Clinical studies showed that CR, with or without exercise, improved glycemic control, metabolic function, increased life spans and also reduced cardiovascular disease (CVD) risk factors in Type 2 diabetes mellitus (T2DM) patients (Wycherley *et al.* 2008). Furthermore, in animal studies, CR also reduced body weight, core temperature, heart rate and motor activity in normal rats (Aydin & Gordon 2013). However, the role of CR on the heart in obese-insulin-resistant rats by switching from HFD to normal diet (ND) form is still unknown.

Fibroblast growth factor 21 (FGF21) is the most recent candidate FGF and plays a major role in metabolic regulation and lipid and energy homeostasis in a pathological state (Kharitonenkov 2009, Chau *et al.* 2010, Itoh & Ornitz 2011). The FGF21 signaling pathways have a protective role in several organs including the liver (Yu *et al.* 2015) and pancreas (Wente *et al.* 2006), and it can also have a direct effect on the heart by activating the receptor complex FGFR1c/β-Klotho (Planavila *et al.* 2013, 2014, Patel *et al.* 2014, Zhang *et al.* 2015). Previous studies demonstrated that FGF21 plays a cardioprotective role in arteriosclerosis (Lu *et al.* 2010, Wu *et al.* 2014), diabetes cardiomyopathy (DCM) (Yan *et al.* 2015, Zhang *et al.* 2015), cardiac ischemia–reperfusion (I/R) injury (Cong *et al.* 2013, Liu *et al.* 2013), myocardial infarction (MI) (Liu *et al.* 2012, 2013, Joki *et al.* 2015) and cardiac hypertrophy (Planavila *et al.* 2013, 2014). Interestingly, an increase in FGF21 levels is associated with future cardiovascular risk in T2DM patients (Shen *et al.* 2013, Ong *et al.* 2015). The 'FGF21 resistance' concept in obesity (Fisher *et al.* 2010, Tan *et al.* 2011) and in the heart (Patel *et al.* 2014) has been proposed. In addition, therapeutic strategies that overcome this condition also need to be investigated, and these therapies are expected to improve FGF21 sensitivity contributing to the potential cardioprotection role (Tanajak *et al.* 2015). Interestingly, a clinical study in obese children demonstrated that a low-carbohydrate diet and a low-fat diet consumption for 2 months improved the metabolic profile and decreased the serum FGF21 levels, suggesting that this CR could improve FGF21 sensitivity (Wycherley *et al.* 2008).

Vildagliptin is an oral anti-diabetic drug that has been used to treat T2DM patients (Inzucchi *et al.* 2015). Previous studies demonstrated that vildagliptin exerted cardioprotective effects in addition to its glycemic control in obese-insulin-resistant (Apaijai *et al.* 2012, 2013), MI (Inthachai *et al.* 2015) and I/R injury rat models (Apaijai *et al.* 2014). Although both CR and vildagliptin exert cardioprotective effects, the effects of long-term CR, vildagliptin and the combined therapy on metabolic regulation, heart rate variability (HRV), cardiac function, cardiac mitochondrial function and FGF21 signaling pathways in HFD-induced obese-insulin-resistant rats have not been investigated.

In this study, we hypothesized that long-term CR and vildagliptin increase insulin sensitivity, attenuate FGF21 resistance, improve cardiac mitochondrial fatty acid oxidation (FAO) and reduce cardiac apoptosis and cardiac mitochondrial dysfunction, leading to improved cardiac function in HFD-induced obese-insulin resistant rats and that combined therapy exerts greater cardioprotection than a single regimen.

Material and methods

Ethical approval

All experiments in this study were approved by the Faculty of Medicine, Chiang Mai University Institutional Animal Care and Use Committee (Permit No. 31/2557), in compliance with NIH guidelines and in accordance with the ARRIVE guidelines for reporting experiments involving animals (Kilkenny *et al.* 2010).

Animals and diet

Thirty adult male Wistar rats weighing 180–200 g were obtained from the National Animal Center, Salaya Campus, Mahidol University, Bangkok, Thailand. All rats were housed in an environment with controlled temperature and humidity and a light–darkness (12:12 h) cycle. Rats were fed on either a ND or HFD. The ND is a standard laboratory pelleted diet (Mouse Feed Food

http://joe.endocrinology-journals.org
DOI: 10.1530/JOE-16-0406
© 2017 Society for Endocrinology
Printed in Great Britain
Published by Bioscientifica Ltd.

No. 082, C.P. Company, Bangkok, Thailand) containing 19.77% energy from fat and gives a total energy of 4.02 kcal/g. The HFD contains 59.28% energy from fat and consists of standard rat diet (Mouse Feed Food No. 082, C.P. Company, Bangkok, Thailand, 365 g/kg food), casein (250 g/kg food), lard (310 g/kg food), cholesterol (10 g/kg food), vitamins (60 g/kg food), DL-Methionine (3 g/kg food), yeast powder (1 g/kg food) and sodium chloride (1 g/kg food) giving a total energy of 5.35 kcal/g (Pratchayasakul *et al.* 2011). The CR was achieved in rats by switching from HFD to ND and also by decreasing the energy intake, after the 12-week average food intake, to 60% energy intake in ND form and feeding for 30 days (Wilsey & Scarpace 2004).

Drugs and vehicle

The DDP-4 inhibitor vildagliptin (3 mg/kg/day) (Galvus, Novartis, Bangkok, Thailand) was used in this study. It was dissolved into 0.9% normal saline solution (0.9% NSS) (Burkey *et al.* 2005, Apaijai *et al.* 2012, 2013). The 0.9% NSS in an equal volume was used as a vehicle (Apaijai *et al.* 2012, 2014). Rats were fed vildagliptin or the vehicle via oral gavage feeding once a day for 30 days.

The experiments and study protocol

After the acclimatization week, rats were divided into 2 groups and were given either ND ($n=6$) or HFD ($n=24$) for 12 weeks. At week 12, ND rats were continuously fed with ND and vehicle (NDV) for 30 days. For HFD rats, at week 12, they were divided into 4 subgroups ($n=6$/group) and each group received one of the following: (1) vehicle (HFV); (2) CR diet and vehicle (HFCR); (3) vildagliptin (HFVil) and (4) CR diet plus vildagliptin (HFCRVil). All treatments were continued for 30 days. On week 12 and at the end of the experiments, rats in all groups were examined. The data collected were body weight, food intake, heart rate variability (HRV), cardiac function by echocardiography and tail blood pressure (BP) measurement using a tail cuff. In addition, the rats were fasted for 6 h, and then blood was collected from the tail vein to determine the plasma metabolic parameters (fasting blood glucose (FPG), insulin, homeostasis model assessment (HOMA), total cholesterol (TC), triglyceride (TG), high-density lipoprotein cholesterol (HDL-C) and low-density lipoprotein cholesterol (LDL-C)) and plasma FGF21 by ELISA kit (R&D Systems), and serum malondialdehyde (MDA) levels by high-performance liquid chromatography (HPLC) base assay. In addition, rats were fasted overnight to determine the insulin sensitivity using the oral glucose tolerance test (OGTT) (Apaijai *et al.* 2012, 2013). In addition, rats were fasted overnight to determine the insulin sensitivity using the oral glucose tolerance test (OGTT). An OGTT was carried out consisting of 2 g/kg body weight glucose fed through a gavage (Apaijai *et al.* 2012, 2013). Blood was centrifuged at 3300 ***g***, 4°C for 5 min for plasma collection and 825 ***g***, 4°C for 5 min for serum collection, then plasma and serum were kept at −80°C until required (Thummasorn *et al.* 2011, Apaijai *et al.* 2012, 2013, Pipatpiboon *et al.* 2012, 2013, Surinkaew *et al.* 2013, Chinda *et al.* 2014). At the end of the experiments, rats had their left ventricular (LV) function determined by pressure–volume (P–V) loop measurement, and they were then killed to allow the following to be studied: cardiac mitochondrial function, cardiac mitochondrial morphology by transmission electron microscopy (TEM), cardiac tissue MDA levels by HPLC base assay and cardiac FGF21 signaling cascade protein expression by Western blot analysis. Moreover, the visceral fat was weighed on removal from the rats after killing. The experimental protocol of this study is shown in Fig. 1.

Metabolic parameters assessments

A commercial colorimetric assay kit (Erba Diagnostics Mannheim GmbH, Mannheim, Germany) was purchased for the determination of FPG, TC and TG levels (Pratchayasakul *et al.* 2011, Apaijai *et al.* 2014). A second commercial colorimetric assay kit (Biovision) was purchased for determining the plasma HDL-C level (Apaijai *et al.* 2013). After that the Friedewald equation was used to calculate the plasma LDL-C levels (Friedewald *et al.* 1972, Apaijai *et al.* 2014). The commercial sandwich ELISA kit (LINCO Research) was purchased to determine the plasma insulin levels (Apaijai *et al.* 2013, 2014). The degree of insulin sensitivity was determined by using the HOMA index, an increase in the HOMA index indicates a higher degree of insulin resistance (Pipatpiboon *et al.* 2012).

Plasma FGF21 assessment

Plasma FGF21 levels were determined using a quantitative sandwich enzyme immunoassay technique by using a mouse/Rat FGF21 ELISA kit (R&D Systems) (Yan *et al.* 2015).

http://joe.endocrinology-journals.org
DOI: 10.1530/JOE-16-0406
© 2017 Society for Endocrinology
Printed in Great Britain
Published by Bioscientifica Ltd.

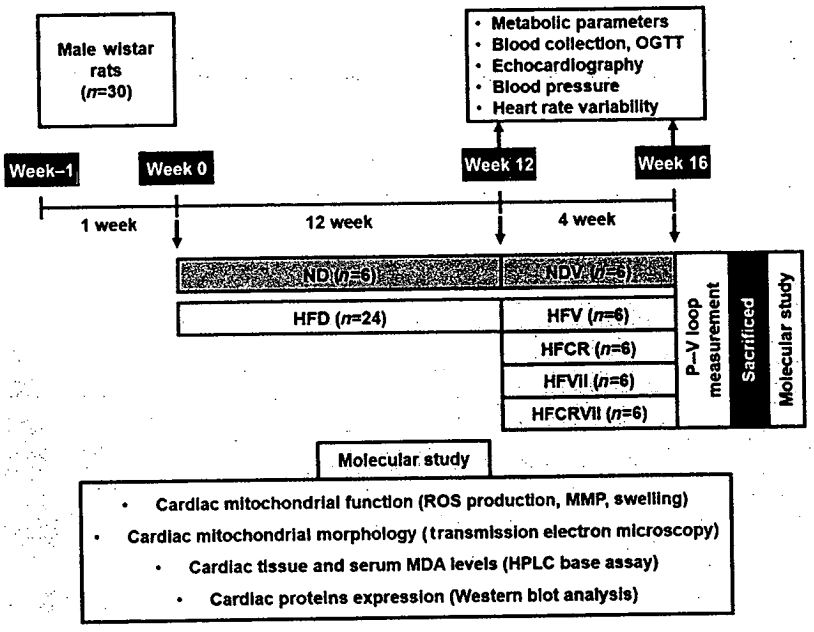


Figure 1
The experimental protocol of the study. HFCR, high-fat diet treated with CR diet; HFCRVil, high-fat diet treated with CR diet and vildagliptin; HFD, high-fat diet; HFV, high-fat diet treated with vehicle; HFVil, high-fat diet treated with vildagliptin; HPLC, high-performance liquid chromatography; MDA, Malondialdehyde; MMP, mitochondrial membrane potential; ND, normal diet; NDV, normal diet treated with vehicle; OGTT, oral glucose tolerance test; P–V loop, pressure–volume loop; ROS, reactive oxygen species.

Heart rate variability (HRV) determination

Electrocardiography was performed by immobilizing the limbs of rats in a prone position under 2.5% isoflurane inhalation anesthesia. Needle electrodes were inserted subcutaneously into the positions of lead II electrocardiogram (ECG). Rats were allowed to gain full consciousness prior to ECG recording. During ECG recording, rats were kept restrained and prohibited from movement. HRV was determined from lead II ECG by using PowerLab (AD Instruments, Colorado Springs, CO, USA) equipped with the Chart 5.0 program for 20 min. A stable ECG was used to determine the relationship between the RR interval and the beat numbers (Tachogram) using a MATLAB program (Chattipakorn *et al.* 2007, Pratchayasakul *et al.* 2011, Apaijai *et al.* 2013). Power spectra of RR interval variability were obtained using the fast Fourier transform (FFT) algorithm. The high frequency (HF; 0.6–3 Hz) band, low frequency (LF; 0.2–0.6 Hz) band and very low frequency (VLF; below 0.2 Hz) band were detected. Each spectral component was calculated as intervals under the respective part of the power spectral density function and was presented in absolute units (ms^2) (Chattipakorn *et al.* 2007). To minimize the effect of changes in total power on the LF and HF bands, LF and HF were expressed as normalized units by dividing the reading by the total power minus VLF (Chattipakorn *et al.* 2007). The increase of the LF/HF ratio indicates an increase in sympathetic activity or depressed HRV (Pongchaidecha *et al.* 2009, Apaijai *et al.* 2013).

Tail cuff blood pressure measurement

Blood pressure was measured by using the non-invasive CODA 2 on the volume–pressure recording (VPR) tail-cuff method (Kent Scientific Corporation, Torrington, CT, USA) (Feng *et al.* 2008). Rat tails were attached to an occlusion cuff proximally (O-Cuff) and VPR distally and acclimatized in the holder on the infrared warming platform 32–35°C using levels for this temperature control for at least 5 min. The first five cycles were acclimatization cycles and were not included in the data analysis. The mean blood pressure was calculated from the next 20 consecutive cycles.

LV function study for echocardiography

Rats were anesthetized by inhaling isoflurane and oxygen supplementation at 3 liters per minute for 3–5 min. During anesthesia, the LV function was determined using a Vivid i echocardiograph (GE Medical Systems). The image by echocardiography was produced by M-mode and collected in the parasternal short axis of the heart at the papillary muscle levels and % fractional shortening (%FS) was determined. Increased %FS indicated increased LV contractile function (Apaijai *et al.* 2012, 2013).

http://joe.endocrinology-journals.org
DOI: 10.1530/JOE-16-0406
© 2017 Society for Endocrinology
Printed in Great Britain
Published by Bioscientifica Ltd.

LV function using a P–V loop

Rats were anesthetized by intramuscular injection with Zoletil (50 mg/kg, Vibbac Laboratories, Carros, France) plus Xylazine (0.15 mg/kg, Laboratories Calier, S.A., Barcelona, Spain). After that an incision was made on the midline of the anterior cervical area and then a tracheostomy tube was inserted into the trachea. Subsequently, the right common carotid artery (CCA) was identified and the P–V loop catheter (Scisense, Ontorio, Cannada) was inserted into the right CCA and placed into the ascending aorta allowing the recording of systolic blood pressure (SBP) and diastolic blood pressure (DBP). Then, the catheter was advanced into the LV chamber for determining the LV function including heart rate (HR), end-systolic pressure (ESP), end-diastolic pressure (EDP), dP/dt_{max}, dP/dt_{min} and stroke volume (SV). Data from the P–V loop measurement were recorded using an analytical software program (Labscribe2, Dover, New Hampshire, USA) (Apaijai *et al.* 2013, Chinda *et al.* 2014). At the end of this protocol, the rats were decapitated, and the hearts were removed rapidly for further cardiac tissue protocols described below.

Determination of cardiac mitochondrial function and morphology

The rats hearts were perfused with 10 mL of 0.9% NSS and removed rapidly. The cardiac mitochondrial isolation protocols were performed as previously described (Thummasorn *et al.* 2011, Apaijai *et al.* 2012, 2013). The cardiac mitochondria reactive oxygen species (ROS) production was determined by incubating the mitochondria with 2 M DCFH-DA dye at 25°C for 20 min, and the fluorescent intensity of the solution was detected by a fluorescent microplate reader with excitation wavelength at 485 nm and emission wavelength at 530 nm (BioTek Instruments). An increase in the fluorescent intensity indicated an increased mitochondrial ROS production (Thummasorn *et al.* 2011, Chinda *et al.* 2013).

The cardiac mitochondrial membrane potential change ($\Delta\Psi$) was determined using 5-μM JC-1 dye and incubating the mitochondria with JC-1 at 37°C for 30 min (Thummasorn *et al.* 2011, Apaijai *et al.* 2014). The cardiac mitochondrial membrane potential changes were detected using a fluorescent microplate reader. The JC-1 monomer form concentration is represented by the green fluorescence and is excited by a wavelength of 485 nm and the emission is detected at 590 nm. The aggregate form of JC-1 is represented by the red fluorescence and is excited at a wavelength of 485 nm and the emission is detected at 530 nm. A decrease in the red/green fluorescent intensity ratio indicates an increase in cardiac mitochondrial membrane depolarization (Thummasorn *et al.* 2011, Chinda *et al.* 2013).

The cardiac mitochondrial swelling was determined by incubating cardiac mitochondria with 1.5-mM respiration buffer. The absorbance was determined using a spectrophotometer. A decreased absorbance indicated increased cardiac mitochondrial swelling (Thummasorn *et al.* 2011, Apaijai *et al.* 2013).

The cardiac mitochondria were collected during the cardiac mitochondrial function assessment and fixed by 2.5% glutaraldehyde in a 0.1-M phosphate buffer overnight. After that, they were fixed in a 1% cacodylate-buffer osmium tetroxide for 2 h and a graded series of ethanol were used to dehydrate them. A diamond knife was used to cut the cardiac mitochondria embedded in Epon-Araldite and stained with uranyl acetate. Finally, the cardiac mitochondria's morphology was observed using a transmission electron microscope (TEM) at 15,000× by JEM-2200FS field emission electron microscope (Thummasorn *et al.* 2011, Apaijai *et al.* 2014).

Determination of MDA concentration

The cardiac tissue and plasma MDA concentrations were determined using a HPLC-based assay (Thermo Scientific) (Apaijai *et al.* 2012, 2013). Plasma and cardiac MDA were mixed with H_3PO_4 and thiobarbituric acid (TBA) to produce TBA-reactive substances (TBARS). The plasma and cardiac TBARS concentration were determined directly from a standard curve and reported as equivalent to the MDA concentration (Apaijai *et al.* 2012, 2013).

Cardiac protein expression by Western blot analysis

Cardiac tissues for determining the protein expressions were obtained from the fresh hearts at the LV apex. Myocardial protein extracts were prepared by homogenization of nitrogen-frozen myocardial tissues in a 300-μL extraction buffer containing 20-mM Tris–HCl (pH 6.8), 1-mM sodium orthovanadate, 5-mM sodium fluoride and protease inhibitor. Total protein concentration was determined using a Bio-Rad protein assay kit (Bio-Rad Laboratories). Total protein was mixed with loading buffer (5% beta mercaptoethanol, 0.05% bromophenol blue, 75 mM Tris–HCl (pH 6.8), 2% SDS

http://joe.endocrinology-journals.org
DOI: 10.1530/JOE-16-0406
© 2017 Society for Endocrinology
Printed in Great Britain
Published by Bioscientifica Ltd.

Table 1 The effects of calorie restriction, vildagliptin and calorie restriction plus vildagliptin on metabolic parameters in HFD rats after treatment for 4 weeks. Body weight and visceral fat were recorded at the end of experiment. Moreover, the rats were fasted for 6 h then blood was collected from the tail vein to determine the plasma metabolic parameters (fasting plasma glucose FBS, insulin, Homeostasis Model Assessment (HOMA)-index, total cholesterol (TC), triglyceride (TG), high density lipoprotein-cholesterol (HDL-C), and low-density lipoprotein-cholesterol (LDL-C), serum maladehyde (MDA) levels and cardiac tissue MDA by high liquid chromatography (HPL)C base assay. In addition, rats were fasted overnight to determine the insulin sensitivity using the area under the curve (AUCg) by oral glucose tolerance test (OGTT).

	Groups				
Parameters	NDV	HFV	HFCR	HFVil	HFCRVil
Body weight (g)	519±24	627±21*	523±23†	625±38*,‡	518±14†,#
Visceral fat (g)	32±3	54±4*	36±4†	58±5*,‡	30±2†,#
Plasma glucose (mM)	8.1±1.0	8.4±0.2	8.5±0.1	8.5±0.3	8.6±0.3
Plasma TC (mM)	3.9±0.3	5.4±0.2*	4.2±0.1†	4.3±0.5†	4.2±0.3†
Plasma TG (mM)	2.9±0.5	3.1±0.3	2.8±0.3	2.7±0.2	2.8±0.4
Plasma HDL-C (mM)	1.9±0.1	1.4±0.1*	2.1±0.1†	1.9±0.1†	2.0±0.1†
Plasma LDL-C (mM)	1.3±0.1	3.0±0.4*	1.6±0.4†	1.4±0.2†	1.4±0.2†
Plasma insulin (ng/mL)	4.3±0.3	6.7±0.8*	4.1±0.5†	3.8±0.5†	4.6±0.6†
HOMA index	33.2±6.1	61.5±10.0*	33.6±5.1†	29.8±3.8†	33.8±7.2†
Serum MDA (μmol/mL)	1.5±0.1	6.0±1.4*	1.7±0.1†	1.2±0.1†	1.5±0.1†
Tissue MDA (μmol/mg protein)	0.80±0.08	2.91±0.54*	0.71±0.08†	0.64±0.07†	0.72±0.06†
AUCg (mM×min×10^5)	9.23±0.25	12.6±0.70*	8.87±0.57†	9.81±0.27†	9.08±0.32†

*$P<0.05$ vs NDV, †$P<0.05$ vs HFV, ‡$P<0.05$ vs HFCR.
HFCR, high-fat diet treated with CR diet; HFCRVil, high-fat diet treated with CR diet and vildagliptin; HFD, high-fat diet; HFV, high-fat diet treated with vehicle; HFVil, high-fat diet treated with vildagliptin; ND, normal diet; NDV, normal diet treated with vehicle.

and 10% glycerol) and boiled at 95°C for 10 min. Forty micrograms of total proteins from each group were loaded in each well (total volume was 20 μL/well). The samples were loaded onto the 10% SDS-polyacrylamide gels (Apaijai *et al.* 2014, Pongkan *et al.* 2016). Then, proteins were transferred to nitrocellulose membranes in a glycine/methanol transfer buffer in a wet/tank blotting system (Bio-Rad Laboratories). Membranes were blocked in either 5% skim milk or 5% bovine serum albumin in Tris-buffered saline and Tween (TBST) buffer. The FGF21 signaling proteins including fibroblast growth factor receptor (FGFR) 1 and phospho-FGFR1 (p-FGFR1) (1:200 dilution, Sigma-Aldrich), β-Klotho (1:200 dilution), extracellular signal-regulated kinase (ERK1/2), phosphor-ERK1/2 (p-ERK1/2) (1:1000 dilution, Santa Cruz technologies), Akt and p-Akt (1:500 dilution, Cell Signaling Technology) were determined. Moreover, Bax (1:1000 dilution), cleaved caspase-3 (1:1000 dilution), proliferator-activated receptor gamma coactivator 1-alpha (PGC-1α) (1:200 dilution), carnitine palmitoyltransferase 1 (CPT1) (1:200 dilution), β-actin (1:2000 dilution, Santa Cruz Biotechnology) and B-cell lymphoma 2 (Bcl2) (1:1000 dilution, Cell Signaling Technology) were determined. Bound antibody for β-actin (Surinkaew *et al.* 2013) was detected by horse anti-mouse IgG-conjugated horseradish peroxidase (HRP)-linked antibody (1:2000 dilution, Cell Signaling Technology). Bound antibody for β-Klotho was detected using a rabbit anti-goat IgG-conjugated HRP-linked antibody (1:2000 dilution, Santa Cruz Biotechnology). Bound antibodies for FGFR1, p-FGFR1, ERK1/2, p-ERK1/2, Akt, p-Akt, Bax, Bcl-2, cleaved caspase-3, PGC-1α and CPT-1 were detected using a goat anti-rabbit IgG-conjugated HRP-linked antibody (1:2000 dilution, Cell Signaling Technology). Enhanced chemiluminescence (ECL) detection reagents were used to visualize peroxidase reaction products (Clarity ECL Western blotting substrate, Bio-Rad) (Pongkan *et al.* 2016). However, due to our protocol, we used invisible markers BLUeye Prestained Protein Ladder (Cat. No. PM007-0500; GeneDireX, Inc. Miaoli County 350, Taiwan, R.O.C.). The WesternSure Pen (Li-cor biotechnology, Lincoln, Nebraska, USA) was used to annotate visible protein ladders prior to detecting chemiluminescent intensity from Western blot using the ChemiDoc system. The membranes were developed in the ChemiDoc touch imaging system (Bio-Rad Laboratories) by placing a membrane on the chemi/UV/strain-free tray. Then, the image was adjusted to an appropriate size, and the blot

http://joe.endocrinology-journals.org
DOI: 10.1530/JOE-16-0406
© 2017 Society for Endocrinology
Printed in Great Britain
Published by Bioscientifica Ltd.

Table 2 The effects of calorie restriction, vildagliptin, and calorie restriction plus vildagliptin on heart rate and blood pressure in HFD rats after treatment for 4 weeks. At the end of experiment, systolic blood pressure (SBP), diastolic blood pressure (DBP), mean arterial pressure (MAP), and heart rate (HR) were was measured by using the non-invasive CODA 2 on the volume–pressure recording (VPR) tail-cuff method.

	Groups				
Parameters	NDV	HFV	HFCR	HFVil	HFCRVil
SBP (mmHg)	132±5	156±3*	152±8*	134±4†,‡	129±5†,‡
DBP (mmHg)	87±7	88±3	87±6	82±5	87±6
MAP (mmHg)	104±4	117±2*	118±3*	103±3†,‡	100±3†,‡
HR (bpm)	401±6	436±10*	429±10*	383±21†,‡	392±12†,‡

*$P<0.05$ vs NDV, †$P<0.05$ vs HFV, ‡$P<0.05$ vs HFCR.
HFCR, high-fat diet treated with CR diet; HFCRVil, high-fat diet treated with CR diet and vildagliptin; HFD, high-fat diet; HFV, high-fat diet treated with vehicle; HFVil, high-fat diet treated with vildagliptin; ND, normal diet; NDV, normal diet treated with vehicle.

chemiluminescence category was chosen for exposure and to take a Western blot image. The densitometric analysis was done by the ImageJ program (Chinda *et al.* 2014). Each protein expression was normalized with β-actin expression.

Statistical analysis

Data were expressed as mean±S.E.M. One-way analysis of variance (ANOVA) by least significant difference (LSD) *post hoc* test was used to test the difference between the groups. $P<0.05$ was considered statistically significant.

Results

CR, vildagliptin and combined therapy restored metabolic disturbance in obese-insulin-resistant rats

At 16 weeks after HFD feeding, HFV rats had significantly increased BW and visceral fat, compared with the NDV group (Table 1). The dietary intervention HFCR group had significantly decreased BW and visceral fat, compared with the HFV group. However, no differences in the BW and visceral fat were found in the HFVil rats, compared with the HFV group. Nevertheless, the combined therapy HFCRVil rats had significantly decreased BW and visceral fat, compared with the HFV and HFVil groups (Table 1).

The plasma TC, plasma LDL-C, plasma insulin, HOMA index, serum MDA, cardiac MDA, AUCg and the HOMA index were increased, whereas the plasma HDL-C was decreased in the HFV rats, compared with the NDV group (Table 1). These parameters were improved in the HFCR, HFVil and HFCRVil rats, when compared with the HFV group. However, plasma glucose and plasma TG showed no difference between the groups ($P>0.05$, Table 1). Moreover, the HFV rats had significantly increased HR, SBP and MAP, compared with the NDV group. Only rats in the vildagliptin-treated groups (HFVil and HFCRVil) had significantly decreased HR, SBP and MAP, compared with the HFV group (Table 2).

Vildagliptin increased cardiac autonomic regulation and LV function in obese-insulin-resistant rats more extensively than CR

Regarding HRV, the results showed that HFD results showed a significant increase in the LF/HF ratio since week 12 in the HFD rats, compared with the ND group (Fig. 2A). In the same way, it was found that the %FS was significantly decreased at week 12 in the HFD group, compared with the ND group (Fig. 2B). After 16 weeks of HFD feeding, there was still a significant increase in the LF/HF ratio and decreased %FS in the HFV rats, compared with the NDV group. In addition, the LF/HF ratio was significantly decreased in the HFCR group (Fig. 2C), when compared with the HFV group. Moreover, the LF/HF ratio was also significantly decreased in the HFVil and HFCRVil groups (Fig. 2C), when compared with the HFV and HFCR groups. Furthermore, the %FS was significantly increased in the HFCR group (Fig. 2D), when compared with the HFV group. Moreover, the %FS was also significantly increased in the HFVil and HFCRVil groups (Fig. 2D), when compared with the HFV and HFCR groups.

At 16 weeks after HFD feeding, the P–V loop showed that the HFV rats had significantly increased SBP and MAP and also had impaired cardiac function identified by increased HR and EDP, and decreased ESP, $\pm dP/dt$

http://joe.endocrinology-journals.org
DOI: 10.1530/JOE-16-0406
© 2017 Society for Endocrinology
Printed in Great Britain
Published by Bioscientifica Ltd.

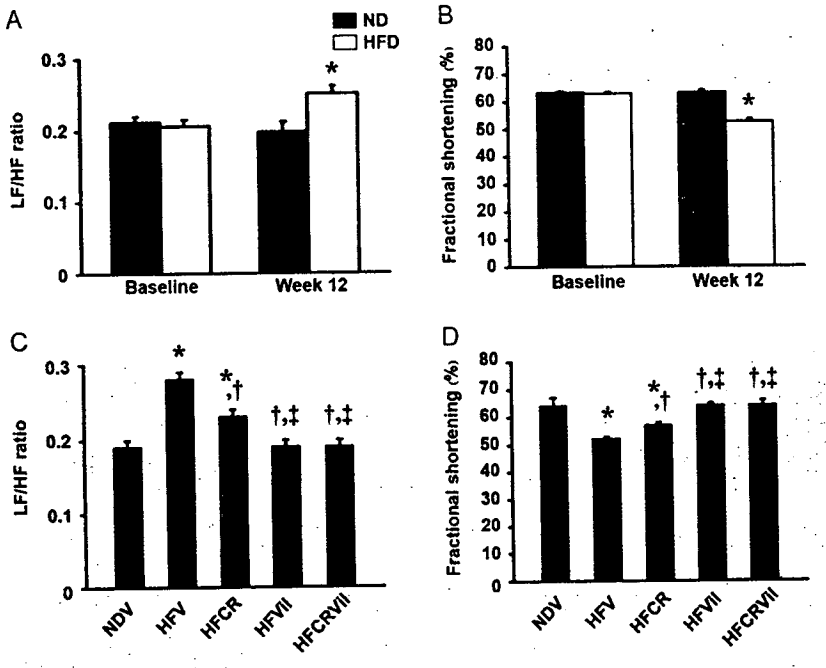


Figure 2
The effects of HFD consumption, HFCR, vildagliptin, and combined HFCR and vildagliptin on HRV and echocardiographic parameters. (A) HRV and (B) % fractional shortening (%FS) in ND and HFD rats at baseline and week 12. *$P<0.05$ vs ND (independent sample *t*-test, $n=6$ for ND group and $n=12$ for HFD group). (C) HRV and (D) %FS in ND and HFD rats treated with vehicle, calorie restriction (CR), vildagliptin and CR combined vildagliptin. *$P<0.05$ vs NDV, †$P<0.05$ vs HFV, ‡$P<0.05$ vs HFCR, #$P<0.05$ vs HFCR (1-WAY ANOVA, LSD *post hoc* test, $n=6$ per subgroups). HFCR, high-fat diet treated with CR diet; HFCRVil, high-fat diet treated with CR diet and vildagliptin; HFD, high-fat diet; HF, high frequency; HFV, high-fat diet treated with vehicle; HFVil, high-fat diet treated with vildagliptin; HRV, heart rate variability; LF, low frequency; ND, normal diet; NDV, normal diet treated with vehicle.

and SV, when compared with the NDV group (Table 3). However, only rats in the vildagliptin-treated groups (HFVil and HFCRVil) had improved blood pressure indicated by decreased SBP and MAP, when compared with the HFV group. The HFCR group had improved cardiac function shown by increased ESP, $\pm dP/dt$ and SV and also decreased HR and EDP, when compared with the HFV group (Table 3). Moreover, vildagliptin-treated groups (HFVil and HFCRVil) also had improved cardiac function illustrated by increased ESP, $\pm dP/dt$ and SV, and also decreased HR and EDP, when compared with the HFV and HFCR groups (Table 3).

Vildagliptin restored FGF21 sensitivity and activated anti-apoptotic pathways in the heart more effectively than CR

The levels of plasma FGF21 were significantly higher in the HFV group, compared to the ND rats at week 12 of HFD feeding (Fig. 3A). Plasma FGF21 levels at week 16 were also

Table 3 Effects of calorie restriction, vildagliptin, and calorie restriction plus vildagliptin on cardiac function in HFD rats after treatment for 4 weeks. At the end of experiment left ventricular (LV) function was measured by using the pressure–volume (P–V) loop. P–V loop catheter (Scisense, Ontorio, Cannada) was inserted into the right common carotid artery (CCA) and placed into the ascending aorta allowing the recording of systolic blood pressure (SBP) and diastolic blood pressure (DBP). Then the catheter was advanced into the LV chamber for the determining of LV function including heart rate (HR), end-systolic pressure (ESP), end-diastolic pressure (EDP), dP/dt_{max}, dP/dt_{min}, and stroke volume (SV).

	Groups				
Parameters	NDV	HFV	HFCR	HFVil	HFCRVil
HR (bpm)	303±26	383±6*	370±2*	326±11†,‡	324±2†,‡
SBP (mmHg)	127±1	135±1*	133±1*	125±2†,‡	125±1†,‡
DBP (mmHg)	84±1	84±1	85±1	84±1	84±1
ESP (mmHg)	127±1	106±1*	116±2*,†	125±3†,‡	124±1†,‡
EDP (mmHg)	19±1	36±1*	26±1*,†	19±1†,‡	19±1†,‡
+*dP/dt* (mmHg/s)	8360±29	6268±89*	7567±99*,†	8298±165†,‡	8341±50†,‡
−*dP/dt* (mmHg/s)	5681±188	3852±100*	5273±65*,†	5595±39†,‡	5646±57†,‡
SV (mL/g·BW)	1.06±0.02	0.75±0.02*	0.93±0.05*,†	1.08±0.03†,‡	1.14±0.05†,‡

*$P<0.05$ vs NDV, †$P<0.05$ vs HFV, ‡$P<0.05$ vs HFCR.
HFCR, high-fat diet treated with CR diet; HFCRVil, high-fat diet treated with CR diet and vildagliptin; HFD, high-fat diet; HFV, high-fat diet treated with vehicle; HFVil, high-fat diet treated with vildagliptin; ND, normal diet; NDV, normal diet treated with vehicle.

http://joe.endocrinology-journals.org
DOI: 10.1530/JOE-16-0406
© 2017 Society for Endocrinology
Printed in Great Britain
Published by Bioscientifica Ltd.

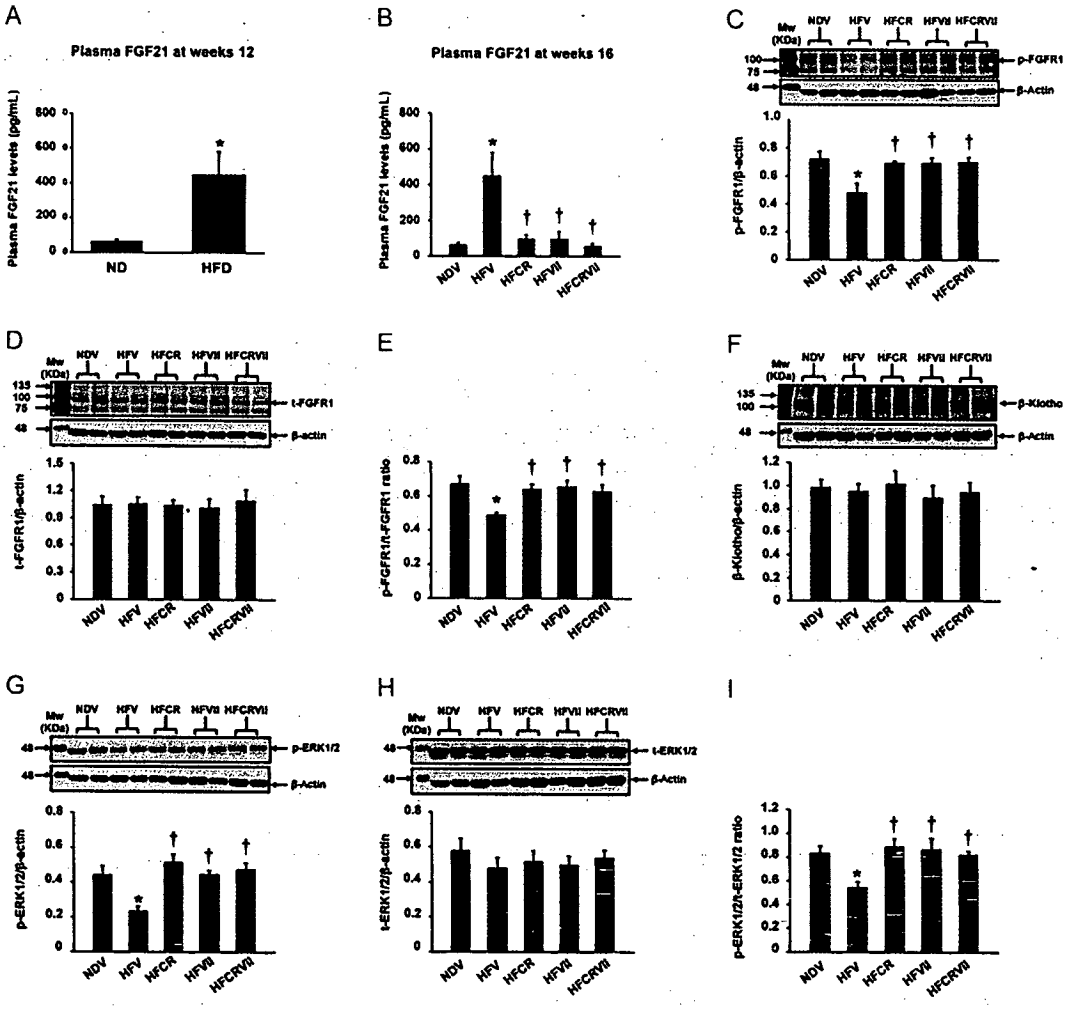


Figure 3

The effects of HFCR, vildagliptin and combined HFCR and vildagliptin on plasma FGF21 levels, FGFR1/β-Klotho receptors complex and intracellular Erk1/2 expression and phosphorylation. (A) Plasma FGF21 levels at weeks 12, (B) plasma FGF21 levels post treatment, (C) p-FGFR1, (D) t-FGFR1, (E) p-FGFR1/t-FGFR1, (F) β-Klotho, (G) p-Erk1/2, (H) t-Erk1/2, and (I) p-Erk1/2/t-Erk1/2 ratio in ND and HFD rats treated with vehicle, Calorie restriction (CR), vildagliptin, and CR combined with vildagliptin. *$P<0.05$ vs NDV, †$P<0.05$ vs HFV, ‡$P<0.05$ vs HFCR (1-WAY ANOVA, LSD *post hoc* test, $n=4$–6 per subgroups). Erk1/2, extracellular signal-regulated protein kinases 1 and 2; FGFR1, fibroblast growth factor receptors 1; HFCR, high-fat diet treated with CR diet; HFCRVil, high-fat diet treated with CR diet and vildagliptin; HFD, high-fat diet; HFV, high-fat diet treated with vehicle; HFVil, high-fat diet treated with vildagliptin; ND, normal diet; NDV, normal diet treated with vehicle; p-FGFR1, phospho FGFR1; p-ERK1/2, phospho ERK1/2; t-ERK1/2, total ERK1/2.

significantly increased in the HFV group, compared with the NDV group (Fig. 3B). However, the plasma FGF21 levels were significantly decreased in the HFCR, HFVil and HFCRVil groups (Fig. 3B). The FGF21 receptor complex and signaling cascade protein expression and phosphorylation by Western blot analysis demonstrated that the HFV group had decreased p-FGFR1 (Fig. 3C) and also a p-FGFR1/t-FGFR1 ratio (Fig. 3E) when compared with the NDV group. HFCR, HFVil and HFCRVil groups had restored p-FGFR1 (Fig. 3C) and p-FGFR1/t-FGFR1 ratios when compared with the HFV group (Fig. 3E). However, no alteration of t-FGFR1 (Fig. 3D) and β-Klotho (Fig. 3F) expression were found in all groups. Regarding downstream signaling, the HFV rats had decreased p-ERK1/2 (Fig. 3G) and also p-ERK1/2/t-ERK1/2 ratio (Fig. 3I), whereas all treatments increased p-ERK1/2 (Fig. 3G) and p-ERK1/2/t-ERK1/2 ratios (Fig. 3I). However, no alteration of t-ERK1/2 (Fig. 3H) expression was found in all groups. In addition, the p-Akt/t-Akt ratio was not significantly different between groups (0.57 ± 0.05, 0.49 ± 0.06, 0.55 ± 0.12, 0.47 ± 0.07 and 0.51 ± 0.10 unit for NDV, HFV, HFCR, HFVil and HFCRVil, respectively).

In regard to anti-apoptotic signaling pathways, rats in the HFV group had significantly increased apoptotic protein expression including Bax (Fig. 4A), Bax/BCL-2

© 2017 Society for Endocrinology
Printed in Great Britain
Published by Bioscientifica Ltd.

Journal of Endocrinology

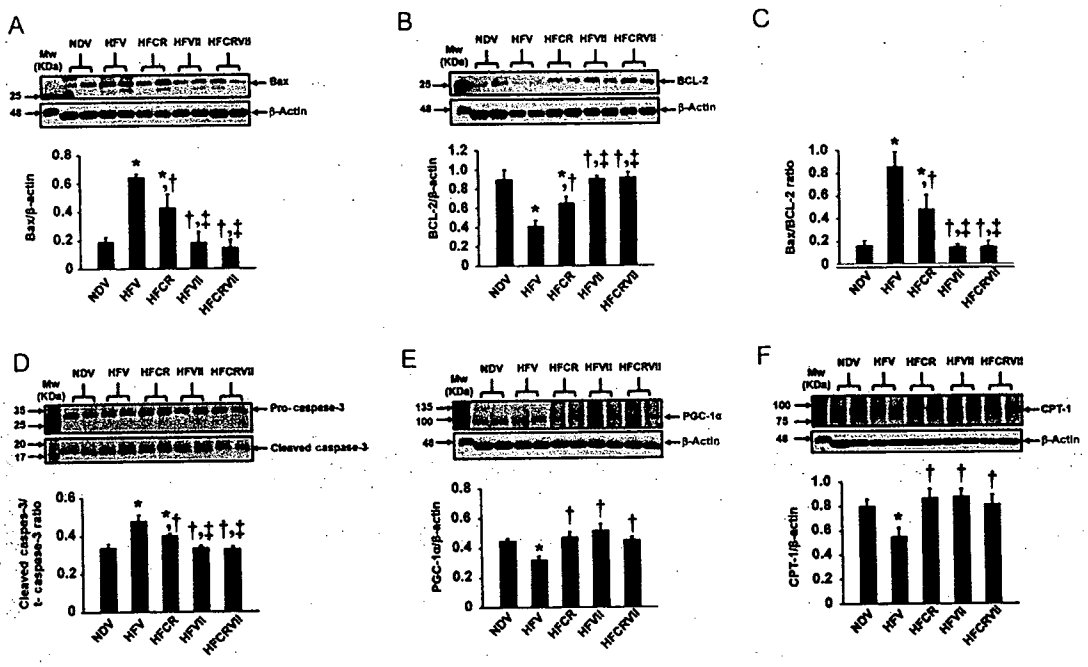


Figure 4

Effects of HFCR, vildagliptin and combined HFCR and vildagliptin on intracellular FGF21 signaling pathways including anti-apoptosis and fatty acid oxidation pathways. (A) Bax, (B) BCL-2, (C) Bax/BCL-2 ratio, (D) Cleaved Caspase-3/t-Caspase-3 ratio, (E) PGC-1α, and (F) CPT-1 in ND and HFD rats treated with vehicle, Caloric restriction (CR), vildagliptin, and CR combined vildagliptin. *$P<0.05$ vs NDV, †$P<0.05$ vs HFV, ‡$P<0.05$ vs HFCR (1-WAY ANOVA, LSD *post hoc* test, $n=4$–6 per subgroups). CPT1, carnitine palmitoyltransferase 1; HFCR, high-fat diet treated with CR diet; HFCRVil, high-fat diet treated with CR diet and vildagliptin; HFD, high-fat diet; HFV, high-fat diet treated with vehicle; HFVil, high-fat diet treated with vildagliptin; ND, normal diet; NDV, normal diet treated with vehicle; PGC-1α, proliferator-activated receptor gamma coactivator 1-alpha.

ratio (Fig. 4C) and cleaved caspase-3 (Fig. 4D), when compared with the NDV group. Moreover, the HFV group also had significantly decreased anti-apoptotic signaling molecules as shown by decreased BCL-2 (Fig. 4B), when compared with the NDV group. Our results showed that HFCR rats had significantly decreased Bax (Fig. 4A), Bax/BCL-2 ratio (Fig. 4C) and cleaved caspase-3 (Fig. 4D), when compared with the HFV group. Moreover, the HFCR group had significantly increased levels of BCL-2 (Fig. 4B), when compared with the HFV group. Interestingly, we found that vildagliptin-treated groups (HFVil and HFCRVil) had a greater reduction in Bax (Fig. 4A), Bax/BCL-2 ratio (Fig. 4C) and cleaved caspase-3 (Fig. 4D), when compared with the HFV and HFCR groups. Vildagliptin-treated groups (HFVil and HFCRVil) also had greater increased levels of BCL-2 (Fig. 4B), when compared with HFV and HFCR groups.

CR and vildagliptin restored fatty acid β-oxidation (FAO) pathway protein expression in the heart

At the end of 16 weeks of feeding on a HFD, the results in mitochondrial FAO pathways protein expression demonstrated that HFV rats had significantly decreased PGC-1α (Fig. 4E) and CPT-1 (Fig. 4F) protein expression when compared with the NDV group. All treatments in HFCR, HFVil, and HFCRVil groups had led to significantly increased PGC-1α (Fig. 4E) and CPT-1 (Fig. 4F) protein expression when compared with the HFV group.

Vildagliptin exerted more effective cardiac mitochondrial protection than CR in obese-insulin-resistant rats

At the end of 16 weeks of feeding on a HFD, the results regarding cardiac mitochondrial function demonstrated that HFD consumption significantly increased cardiac mitochondrial ROS production (Fig. 5A), decreased cardiac mitochondrial membrane potential changes verified by an attenuated red/green fluorescent intensity ratio ($\Delta\Psi$; Fig. 5B) and also increased cardiac mitochondrial swelling (Fig. 5C), when compared with the NDV group. HFCR, HFVil and HFCRVil groups had significantly decreased cardiac mitochondrial ROS production when compared with the HFV group (Fig. 5A). Moreover, the HFCR group had improved cardiac mitochondrial function identified by increased cardiac mitochondrial membrane potential changes ($\Delta\Psi$; Fig. 5B) and mitochondrial absorbance (Fig. 5C), when compared with the HFV groups.

http://joe.endocrinology-journals.org
DOI: 10.1530/JOE-16-0406
© 2017 Society for Endocrinology
Printed in Great Britain
Published by Bioscientifica Ltd.

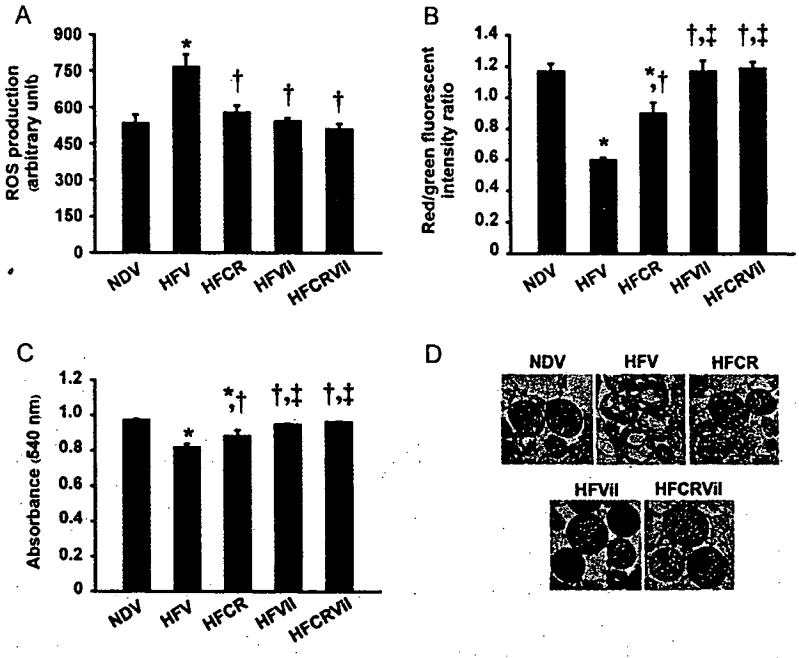


Figure 5
Effects of HFCR, vildagliptin and combined HFCR and vildagliptin on cardiac mitochondrial function and cardiac mitochondria morphology. (A) Cardiac mitochondrial ROS production, (B) red/green fluorescent intensity ratio, (C) Cardiac mitochondrial swelling, and (D) Cardiac mitochondria morphology by transmission electron microscope (TEM) in ND and HFD treated with vehicle, CR, vildagliptin, and CR combined with vildagliptin. $^{*}P<0.05$ vs NDV, $^{\dagger}P<0.05$ vs HFV, $^{\ddagger}P<0.05$ vs HFCR (1-WAY ANOVA, LSD *post hoc* test, $n=6$ per subgroups). HFCR, high-fat diet treated with CR diet; HFCRVil, high-fat diet treated with CR diet and vildagliptin; HFD, high-fat diet; HFV, high-fat diet treated with vehicle; HFVil, high-fat diet treated with vildagliptin; ND, normal diet; NDV, normal diet treated with vehicle; ROS, reactive oxygen species.

However, vildagliptin-treated groups (HFVil and HFCRVil) provided greater efficacy in improving cardiac mitochondrial function by restoring the cardiac mitochondrial membrane potential changes ($\Delta\Psi$; Fig. 5B) and mitochondrial absorbance (Fig. 5C), when compared with the HFV and HFCR groups. Moreover, the cardiac mitochondrial morphology viewed by transmission electron microscope (TEM) demonstrated unfolded cristae in the mitochondria in the HFV group, indicating cardiac mitochondrial swelling in the HFV group. Although the cardiac mitochondrial morphology had improved in the HFCR group, when compared with the HFV group, this parameter had been restored to normal levels in vildagliptin-treated groups (HFVil and HFCRVil), when compared with HFV and HFCR groups (Fig. 5D).

Discussion

The major findings of this study are as follows: long-term HFD consumption led to obesity, insulin resistance, FGF21 resistance and increased oxidative stress levels. Moreover, high systolic blood pressure, cardiac mitochondrial dysfunction and cardiac sympathovagal imbalance were observed, and all of these factors contributed to LV dysfunction in obese-insulin-resistant rats. The three interventions in this study, including caloric restriction (CR), vildagliptin and combined CR and vildagliptin, had similar efficacy in improving insulin resistance, FGF21 resistance, metabolic disturbance, cardiac and serum MDA levels and mitochondrial ROS production. Interestingly, vildagliptin exerted greater cardioprotection than CR as vildagliptin appeared to reduce cardiac apoptosis, preserve cardiac mitochondrial membrane potential and attenuate cardiac mitochondrial swelling more effectively than CR. From all of these beneficial effects, vildagliptin effectively reduced blood pressure, improved cardiac sympathovagal imbalance and cardiac dysfunction in obese-insulin-resistant rats.

In previous reports, 12–16 weeks of HFD consumption did not affect plasma triglyceride levels (Pratchayasakul *et al.* 2011, 2014). However, the excessive fat intake usually does lead to an accumulation of triglyceride (TG) in the liver and adipose tissues. This is due to the fact that it might take time to release (TG) from the liver and adipose tissue into the blood stream. Therefore, a longer duration of HFD feeding may be needed to increase plasma triglyceride levels as shown in previous reports (Manco *et al.* 2004, Gauthier *et al.* 2006, Hwang *et al.* 2010, Pratchayasakul *et al.* 2011, 2014).

In our obese-insulin-resistant rats, plasma glucose and triglyceride levels were not altered, compared to their baseline levels. This suggested that our obese-insulin-resistant rats had hyperinsulinemia with euglycemia and normotriglyceridemia. Treatment with vildagliptin and caloric restriction did not affect plasma glucose and triglyceride levels. However, these interventions reduced plasma cholesterol and low-density lipoprotein (LDL) levels in obese-insulin-resistant rats. As the plasma levels

http://joe.endocrinology-journals.org
DOI: 10.1530/JOE-16-0406
© 2017 Society for Endocrinology
Printed in Great Britain
Published by Bioscientifica Ltd.

of glucose and TG were not increased, both interventions did not interrupt the metabolism of glucose and TG at their physiological levels. Consistent with our previous reports in the obese-insulin-resistant model, our high-fat fed rats were considered as pre-diabetic state rats (Pratchayasakul *et al.* 2011, Pongkan *et al.* 2016).

Regarding the effect of DDP4-inhibitor vildagliptin on FBG, reports from our group and others demonstrated that vildagliptin acted as a glycemic control agent without having a hypoglycemic effect (Yin *et al.* 2011, Maeda *et al.* 2012, Apaijai *et al.* 2014). This is due to the fact that vildagliptin reduced glucagon levels during hyperglycemia and at the same time did not inhibit any counter-regulatory glucagon response during hypoglycemia (Farngren *et al.* 2012). Moreover, vildagliptin also enhanced glucose sensitivity in alpha-cells by promoting the direct effect of low blood glucose levels to stimulate glucagon secretion (Ahren *et al.* 2011, Farngren *et al.* 2012). In addition, the increase of glucose-dependent insulinotropic polypeptide (GIP) was observed by vildagliptin therapy (Ahren *et al.* 2004, Mari *et al.* 2005, Farngren *et al.* 2012), thus stimulating glucagon secretion during low blood glucose levels (Meier *et al.* 2003, Christensen *et al.* 2011). Consistent with previous studies, our results showed that vildagliptin improved insulin sensitivity leading to reduced plasma insulin without affecting plasma glucose levels in obese-insulin-resistant rats (Apaijai *et al.* 2014, Pongkan *et al.* 2016).

Our previous studies have shown that long-term HFD consumption led to obese-insulin resistance with impaired cardiac sympathovagal balance and cardiac dysfunction (Apaijai *et al.* 2013, 2014). Previously, we proposed various mechanisms as being responsible for these impairments, such as metabolic disturbance, oxidative stress and cardiac mitochondrial dysfunction. In this study, we demonstrated that the HFD-fed rats had FGF21 resistance and impaired cardiac metabolism. FGF21 resistance was observed in our obese-insulin-resistant rats and is associated with a reduction in FGF receptor function, as FGF receptor expression and β-Klotho expression were unaffected in our model. However, there are several discrepancies regarding the mechanism responsible for FGF21 resistance. Fisher and coworkers reported that mice fed with a high-fat/high-sucrose diet for 22 weeks had FGF21 resistance and found that FGF21 receptor mRNA expression was reduced, whereas β-Klotho mRNA expression was unchanged in the liver of obese mice, compared to lean mice. However unlike in the liver, both FGF21 receptor and β-Klotho mRNA expression were reduced in white adipose tissue of obese mice, compared to lean mice (Fisher *et al.* 2010). In addition, our study on the HFD-induced obese-insulin-resistant rat model demonstrated that HFD consumption did not alter FGF21 receptor protein expression in the heart (Tanajak *et al.* 2016). These findings suggest that the mechanism of FGF21 resistance is specific to the organ. However, Patel and coworkers reported that 12 weeks of HFD consumption reduced β-Klotho protein expression in the heart (Patel *et al.* 2014). Although they found that β-Klotho protein expression in the heart was decreased, the p-FGFR1 protein expression had not been investigated. Therefore, the role of HFD consumption of FGF21 receptors complex expression and function in the heart are still controversial. Future studies are needed to investigate the role of HFD consumption in FGF21 resistance, particularly with the changes of FGF21 receptor complex expression (β-Klotho, FGFR1 and p-FGFR1) on the heart at different time points. In this model, however, the expression of β-klotho, the FGFR1 co-receptor, was unchanged. The decrease in FGF21 receptor complex function could lead to the impairment of the downstream signaling molecules, such as reduced ERK1/2 phosphorylation. Furthermore, we also found that the utilization of fatty acids was reduced in the HFD-fed rats as indicated by a reduction in PGC-1α and CPT1 expression. Therefore, the FGF21 resistance and the alteration of cardiac metabolism could also contribute to cardiac dysfunction in our obese-insulin-resistant rats.

Besides ERK1/2, FGF21 receptor activation also regulates Akt, AMPK and adiponectin, which are known to determine cardiac metabolism. However, the definite mechanisms are still controversy. In cardiac ischemia–reperfusion injury model, it has been shown that FGF21 administration exerted cardioprotection via the activation of Akt and AMPK (Patel *et al.* 2014). However, Xu and coworkers demonstrated that FGF21 therapy did not alter Akt in the insulin-resistant C57BL6 mice heart (Xu *et al.* 2009). However, our results showed that there was no difference in the p-Akt/t-Akt ratio between all groups. This could be due to the use of different models and drugs in these studies. Regarding adiponectin, Joki and coworkers demonstrated that activation of FGF21 receptors increased plasma adiponectin, which contributed to reduced cardiac inflammation and exerted cardioprotection against cardiac remodeling in the myocardial infarction mice model (Joki *et al.* 2015).

http://joe.endocrinology-journals.org
DOI: 10.1530/JOE-16-0406
© 2017 Society for Endocrinology
Printed in Great Britain
Published by Bioscientifica Ltd.

Future studies are needed to investigate the roles of FGF21 receptor activation on AMPK and adiponectin in obese-insulin-resistant condition.

In this study, although all interventions effectively reduced insulin resistance, only CR led to reduced body weight gain in obese-insulin-resistant rats. This is due to a reduction of caloric intake, which led to reduced visceral fat deposition. Our findings are consistent with previous studies, which also showed that CR reduced body weight gain in various animal models (Wilsey & Scarpace 2004, Park *et al.* 2006, Niemann *et al.* 2010, Takatsu *et al.* 2013), whereas vildagliptin improved insulin resistance without any changes in body weight (Pipatpiboon *et al.* 2013, Apaijai *et al.* 2014). In addition, there is growing evidence that cardiac mitochondrial dysfunction impairs cardiac function and cardiac autonomic function. It has been reported that there is a relationship between cardiac mitochondrial dysfunction, cardiac dysfunction and cardiac autonomic imbalance in diabetic patients (Momiyama *et al.* 2002). In this study, vildagliptin led to greater improvement in cardiac mitochondrial function than CR in obese-insulin-resistant rats. Although both vildagliptin and CR have similar effects on oxidative stress, including on levels of MDA and mitochondrial ROS, vildagliptin attenuated cardiac mitochondrial membrane depolarization and mitochondrial swelling more effectively than CR. These findings indicate that vildagliptin exerted greater cardioprotection by protecting mitochondrial dysfunction more effectively than CR in obese-insulin-resistant rats.

Moreover, it has been shown that mitochondria could regulate the apoptotic process. In this study, we found that vildagliptin appeared to reduce cardiac apoptosis more effectively than CR in the obese-insulin-resistant model as shown by greater reduction of Bax and cleaved caspase-3 expression and higher BCL-2 expression. This in turn would have then caused reduced Bax translocation to the mitochondrial outer membrane. Previous reports have shown that Bax translocation after stress stimuli caused mitochondrial membrane depolarization (Smaili *et al.* 2001). Furthermore, Bax binds with voltage-dependent anion channels (VDAC), which is followed by conformational change of the mitochondrial permeability transition pores (mPTP). This process allows proton and water influx across the mitochondrial membrane into the mitochondrial matrix, leading to mitochondrial swelling. These mechanisms could be responsible for the superior effects of vildagliptin to CR on cardiac function and cardiac autonomic function in obese-insulin-resistant rats.

In this study, we also demonstrated that chronic HFD consumption is related to FGF21 resistance. FGF21 has been shown to regulate cardiac function in various models (Cong *et al.* 2013, Planavila *et al.* 2013, 2014, Tanajak *et al.* 2015, Yan *et al.* 2015). Our results showed that both CR and vildagliptin improved FGF21 resistance by improving FGF21 receptor function and its downstream signaling. These beneficial effects could also contribute to improved LV function in obese-insulin-resistant rats observed in this study. Although the vildagliptin-treated group demonstrated greater efficacy than caloric restriction in improving anti-apoptotic pathways and attenuating cardiac mitochondrial dysfunction, the combination of vildagliptin and caloric restriction did not provide an additional effect. It is possible that vildagliptin therapy already had a superior effect to caloric restriction as our results showed that vildagliptin could reverse the metabolic and cardiac adverse effects caused by long-term HFD consumption back to the normal physiological levels, whereas this restoration was not observed in the caloric restriction group.

In conclusion, chronic HFD consumption leads to obese-insulin resistance and FGF21 resistance. Although CR is effective in improving metabolic regulation and FGF21 sensitivity, vildagliptin provides greater efficacy in preventing cardiac dysfunction by improving anti-apoptotic pathways and attenuating cardiac mitochondrial dysfunction in obese-insulin-resistant rats.

Declaration of interest

The authors declare that there is no conflict of interest that could be perceived as prejudicing the impartiality of the research reported.

Funding

This work was supported by a NSTDA Research Chair Grant from the National Science and Technology Development Agency Thailand (NC), the Thailand Research Fund Royal Golden Jubilee Program (PHD/0078/2557 PT&SC), BRG5780016 (SC) and Chiang Mai University Center of Excellence Award (NC).

Author contribution statement

S C and N C conceived and designed the experiments. P T and H P conducted the experiments. P T, H P, N S, J K, N A, S C and N C analyzed the data. P T, N A, S C and N C wrote the manuscript.

Acknowledgements

The authors would like to thank Piangkwan Sa-nguanmoo for her technical assistance on metabolic parameter assessment and Cicely Proctor for her editorial assistance of this paper.

http://joe.endocrinology-journals.org
DOI: 10.1530/JOE-16-0406

© 2017 Society for Endocrinology
Printed in Great Britain

Published by Bioscientifica Ltd.

References

Ahren B, Landin-Olsson M, Jansson PA, Svensson M, Holmes D & Schweizer A 2004 Inhibition of dipeptidyl peptidase-4 reduces glycemia, sustains insulin levels, and reduces glucagon levels in type 2 diabetes. *Journal of Clinical Endocrinology and Metabolism* **89** 2078–2084. (doi:10.1210/jc.2003-031907)

Ahren B, Schweizer A, Dejager S, Villhauer EB, Dunning BE & Foley JE 2011 Mechanisms of action of the dipeptidyl peptidase-4 inhibitor vildagliptin in humans. *Diabetes, Obesity and Metabolism* **13** 775–783. (doi:10.1111/j.1463-1326.2011.01414.x)

Apaijai N, Pintana H, Chattipakorn SC & Chattipakorn N 2012 Cardioprotective effects of metformin and vildagliptin in adult rats with insulin resistance induced by a high-fat diet. *Endocrinology* **153** 3878–3885. (doi:10.1210/en.2012-1262)

Apaijai N, Pintana H, Chattipakorn SC & Chattipakorn N 2013 Effects of vildagliptin versus sitagliptin, on cardiac function, heart rate variability and mitochondrial function in obese insulin-resistant rats. *British Journal of Pharmacology* **169** 1048–1057. (doi:10.1111/bph.12176)

Apaijai N, Chinda K, Palee S, Chattipakorn S & Chattipakorn N 2014 Combined vildagliptin and metformin exert better cardioprotection than monotherapy against ischemia-reperfusion injury in obese-insulin resistant rats. *PLoS ONE* **9** e102374. (doi:10.1371/journal.pone.0102374)

Aydin C & Gordon CJ 2013 Thermoregulatory, cardiovascular, and metabolic responses to mild caloric restriction in the Brown Norway rat. *Physiological Reports* **1** e00016. (doi:10.1002/phy2.16)

Burkey BF, Li X, Bolognese L, Balkan B, Mone M, Russell M, Hughes TE & Wang PR 2005 Acute and chronic effects of the incretin enhancer vildagliptin in insulin-resistant rats. *Journal of Pharmacology and Experimental Therapeutics* **315** 688–695. (doi:10.1124/jpet.105.087064)

Chattipakorn N, Incharoen T, Kanlop N & Chattipakorn S 2007 Heart rate variability in myocardial infarction and heart failure. *International Journal of Cardiology* **120** 289–296. (doi:10.1016/j.ijcard.2006.11.221)

Chau MD, Gao J, Yang Q, Wu Z & Gromada J 2010 Fibroblast growth factor 21 regulates energy metabolism by activating the AMPK-SIRT1-PGC-1alpha pathway. *PNAS* **107** 12553–12558. (doi:10.1073/pnas.1006962107)

Chinda K, Palee S, Surinkaew S, Phornphutkul M, Chattipakorn S & Chattipakorn N 2013 Cardioprotective effect of dipeptidyl peptidase-4 inhibitor during ischemia-reperfusion injury. *International Journal of Cardiology* **167** 451–457. (doi:10.1016/j.ijcard.2012.01.011)

Chinda K, Sanit J, Chattipakorn S & Chattipakorn N 2014 Dipeptidyl peptidase-4 inhibitor reduces infarct size and preserves cardiac function via mitochondrial protection in ischaemia-reperfusion rat heart. *Diabetes and Vascular Disease Research* **11** 75–83. (doi:10.1177/1479164113516134)

Christensen M, Vedtofte L, Holst JJ, Vilsboll T & Knop FK 2011 Glucose-dependent insulinotropic polypeptide: a bifunctional glucose-dependent regulator of glucagon and insulin secretion in humans. *Diabetes* **60** 3103–3109. (doi:10.2337/db11-0979)

Cong WT, Ling J, Tian HS, Ling R, Wang Y, Huang BB, Zhao T, Duan YM, Jin LT & Li XK 2013 Proteomic study on the protective mechanism of fibroblast growth factor 21 to ischemia-reperfusion injury. *Canadian Journal of Physiology and Pharmacology* **91** 973–984. (doi:10.1139/cjpp-2012-0441)

Dolinsky VW, Morton JS, Oka T, Robillard-Frayne I, Bagdan M, Lopaschuk GD, Des Rosiers C, Walsh K, Davidge ST & Dyck JR 2010 Calorie restriction prevents hypertension and cardiac hypertrophy in the spontaneously hypertensive rat. *Hypertension* **56** 412–421. (doi:10.1161/HYPERTENSIONAHA.110.154732)

Farngren J, Persson M, Schweizer A, Foley JE & Ahren B 2012 Vildagliptin reduces glucagon during hyperglycemia and sustains glucagon counterregulation during hypoglycemia in type 1 diabetes. *Journal of Clinical Endocrinology and Metabolism* **97** 3799–3806. (doi:10.1210/jc.2012-2332)

Feng M, Whitesall S, Zhang Y, Beibel M, D'Alecy L & DiPetrillo K 2008 Validation of volume-pressure recording tail-cuff blood pressure measurements. *American Journal of Hypertension* **21** 1288–1291. (doi:10.1038/ajh.2008.301)

Fisher FM, Chui PC, Antonellis PJ, Bina HA, Kharitonenkov A, Flier JS & Maratos-Flier E 2010 Obesity is a fibroblast growth factor 21 (FGF21)-resistant state. *Diabetes* **59** 2781–2789. (doi:10.2337/db10-0193)

Fontana L, Meyer TE, Klein S & Holloszy JO 2004 Long-term calorie restriction is highly effective in reducing the risk for atherosclerosis in humans. *PNAS* **101** 6659–6663. (doi:10.1073/pnas.0308291101)

Friedewald WT, Levy RI & Fredrickson DS 1972 Estimation of the concentration of low-density lipoprotein cholesterol in plasma, without use of the preparative ultracentrifuge. *Clinical Chemistry* **18** 499–502.

Gauthier MS, Favier R & Lavoie JM 2006 Time course of the development of non-alcoholic hepatic steatosis in response to high-fat diet-induced obesity in rats. *British Journal of Nutrition* **95** 273–281. (doi:10.1079/BJN20051635)

Hwang LL, Wang CH, Li TL, Chang SD, Lin LC, Chen CP, Chen CT, Liang KC, Ho IK, Yang WS, *et al.* 2010 Sex differences in high-fat diet-induced obesity, metabolic alterations and learning, and synaptic plasticity deficits in mice. *Obesity* **18** 463–469. (doi:10.1038/oby.2009.273)

Inthachai T, Lekawanvijit S, Kumfu S, Apaijai N, Pongkan W, Chattipakorn SC & Chattipakorn N 2015 Dipeptidyl peptidase-4 inhibitor improves cardiac function by attenuating adverse cardiac remodelling in rats with chronic myocardial infarction. *Experimental Physiology* **100** 667–679. (doi:10.1113/EP085108)

Inzucchi SE, Bergenstal RM, Buse JB, Diamant M, Ferrannini E, Nauck M, Peters AL, Tsapas A, Wender R & Matthews DR 2015 Management of hyperglycemia in type 2 diabetes, 2015: a patient-centered approach: update to a position statement of the American Diabetes Association and the European Association for the Study of Diabetes. *Diabetes Care* **38** 140–149. (doi:10.2337/dc14-2441)

Itoh N & Ornitz DM 2011 Fibroblast growth factors: from molecular evolution to roles in development, metabolism and disease. *Journal of Biochemistry* **149** 121–130. (doi:10.1093/jb/mvq121)

Joki Y, Ohashi K, Yuasa D, Shibata R, Ito M, Matsuo K, Kambara T, Uemura Y, Hayakawa S, Hiramatsu-Ito M, *et al.* 2015 FGF21 attenuates pathological myocardial remodeling following myocardial infarction through the adiponectin-dependent mechanism. *Biochemical and Biophysical Research Communications* **459** 124–130. (doi:10.1016/j.bbrc.2015.02.081)

Kharitonenkov A 2009 FGFs and metabolism. *Current Opinion in Pharmacology* **9** 805–810. (doi:10.1016/j.coph.2009.07.001)

Kilkenny C, Browne W, Cuthill IC, Emerson M, Altman DG & NC3Rs Reporting Guidelines Working Group 2010 Animal research: reporting in vivo experiments: the ARRIVE guidelines. *British Journal of Pharmacology* **160** 1577–1579. (doi:10.1111/j.1476-5381.2010.00872.x)

Liu SQ, Tefft BJ, Roberts DT, Zhang LQ, Ren Y, Li YC, Huang Y, Zhang D, Phillips HR & Wu YH 2012 Cardioprotective proteins upregulated in the liver in response to experimental myocardial ischemia. *American Journal of Physiology: Heart and Circulatory Physiology* **303** H1446–H1458. (doi:10.1152/ajpheart.00362.2012)

Liu SQ, Roberts D, Kharitonenkov A, Zhang B, Hanson SM, Li YC, Zhang LQ & Wu YH 2013 Endocrine protection of ischemic myocardium by FGF21 from the liver and adipose tissue. *Scientific Reports* **3** 2767. (doi:10.1038/srep02767)

Lu Y, Liu JH, Zhang LK, Du J, Zeng XJ, Hao G, Huang J, Zhao DH, Wang GZ & Zhang YC 2010 Fibroblast growth factor 21 as a possible endogenous factor inhibits apoptosis in cardiac endothelial cells. *Chinese Medical Journal* **123** 3417–3421. (doi:10.3760/cma.j.issn.0366-6999.2010.23.008)

Maeda S, Matsui T & Yamagishi S 2012 Vildagliptin inhibits oxidative stress and vascular damage in streptozotocin-induced diabetic rats.

http://joe.endocrinology-journals.org
DOI: 10.1530/JOE-16-0406

© 2017 Society for Endocrinology
Printed in Great Britain

Published by Bioscientifica Ltd.

International Journal of Cardiology **158** 171–173. (doi:10.1016/j.ijcard.2012.04.087)

Manco M, Calvani M & Mingrone G 2004 Effects of dietary fatty acids on insulin sensitivity and secretion. *Diabetes, Obesity and Metabolism* **6** 402–413. (doi:10.1111/j.1462-8902.2004.00356.x)

Mari A, Sallas WM, He YL, Watson C, Ligueros-Saylan M, Dunning BE, Deacon CF, Holst JJ & Foley JE 2005 Vildagliptin, a dipeptidyl peptidase-IV inhibitor, improves model-assessed beta-cell function in patients with type 2 diabetes. *Journal of Clinical Endocrinology and Metabolism* **90** 4888–4894. (doi:10.1210/jc.2004-2460)

Meier JJ, Gallwitz B, Siepmann N, Holst JJ, Deacon CF, Schmidt WE & Nauck MA 2003 Gastric inhibitory polypeptide (GIP) dose-dependently stimulates glucagon secretion in healthy human subjects at euglycaemia. *Diabetologia* **46** 798–801. (doi:10.1007/s00125-003-1103-y)

Momiyama Y, Suzuki Y, Ohtomo M, Atsumi Y, Matsuoka K, Ohsuzu F & Kimura M 2002 Cardiac autonomic nervous dysfunction in diabetic patients with a mitochondrial DNA mutation: assessment by heart rate variability. *Diabetes Care* **25** 2308–2313. (doi:10.2337/diacare.25.12.2308)

Niemann B, Chen Y, Issa H, Silber RE & Rohrbach S 2010 Caloric restriction delays cardiac ageing in rats: role of mitochondria. *Cardiovascular Research* **88** 267–276. (doi:10.1093/cvr/cvq273)

Ong KL, Januszewski AS, O'Connell R, Jenkins AJ, Xu A, Sullivan DR, Barter PJ, Hung WT, Scott RS, Taskinen MR, *et al.* 2015 The relationship of fibroblast growth factor 21 with cardiovascular outcome events in the Fenofibrate Intervention and Event Lowering in Diabetes study. *Diabetologia* **58** 464–473. (doi:10.1007/s00125-014-3458-7)

Park S, Komatsu T, Hayashi H, Yamaza H, Chiba T, Higami Y, Kuramoto K & Shimokawa I 2006 Calorie restriction initiated at middle age improved glucose tolerance without affecting age-related impairments of insulin signaling in rat skeletal muscle. *Experimental Gerontology* **41** 837–845. (doi:10.1016/j.exger.2006.06.055)

Patel V, Adya R, Chen J, Ramanjaneya M, Bari MF, Bhudia SK, Hillhouse EW, Tan BK & Randeva HS 2014 Novel insights into the cardio-protective effects of FGF21 in lean and obese rat hearts. *PLoS ONE* **9** e87102. (doi:10.1371/journal.pone.0087102)

Pipatpiboon N, Pratchayasakul W, Chattipakorn N & Chattipakorn SC 2012 PPARgamma agonist improves neuronal insulin receptor function in hippocampus and brain mitochondria function in rats with insulin resistance induced by long term high-fat diets. *Endocrinology* **153** 329–338. (doi:10.1210/en.2011-1502)

Pipatpiboon N, Pintana H, Pratchayasakul W, Chattipakorn N & Chattipakorn SC 2013 DPP4-inhibitor improves neuronal insulin receptor function, brain mitochondrial function and cognitive function in rats with insulin resistance induced by high-fat diet consumption. *European Journal of Neuroscience* **37** 839–849. (doi:10.1111/ejn.12088)

Planavila A, Redondo I, Hondares E, Vinciguerra M, Munts C, Iglesias R, Gabrielli LA, Sitges M, Giralt M, van Bilsen M, *et al.* 2013 Fibroblast growth factor 21 protects against cardiac hypertrophy in mice. *Nature Communications* **4** 2019. (doi:10.1038/ncomms3019)

Planavila A, Redondo-Angulo I, Ribas F, Garrabou G, Casademont J, Giralt M & Villarroya F 2014 Fibroblast growth factor 21 protects the heart from oxidative stress. *Cardiovascular Research* **106** 19–31. (doi:10.1093/cvr/cvu263)

Pongchaidecha A, Lailerd N, Boonprasert W & Chattipakorn N 2009 Effects of curcuminoid supplement on cardiac autonomic status in high-fat-induced obese rats. *Nutrition* **25** 870–878. (doi:10.1016/j.nut.2009.02.001)

Pongkan W, Pintana H, Jaiwongkam T, Kredphoo S, Sivasinprasasn S, Chattipakorn SC & Chattipakorn N 2016 Vildagliptin reduces cardiac ischemic-reperfusion injury in obese orchiectomized rats. *Journal of Endocrinology* **231** 81–95. (doi:10.1530/JOE-16-0232)

Pratchayasakul W, Kerdphoo S, Petsophonsakul P, Pongchaidecha A, Chattipakorn N & Chattipakorn SC 2011 Effects of high-fat diet on insulin receptor function in rat hippocampus and the level of neuronal corticosterone. *Life Science* **88** 619–627. (doi:10.1016/j.lfs.2011.02.003)

Pratchayasakul W, Chattipakorn N & Chattipakorn SC 2014 Estrogen restores brain insulin sensitivity in ovariectomized non-obese rats, but not in ovariectomized obese rats. *Metabolism* **63** 851–859. (doi:10.1016/j.metabol.2014.03.009)

Shen Y, Ma X, Zhou J, Pan X, Hao Y, Zhou M, Lu Z, Gao M, Bao Y & Jia W 2013 Additive relationship between serum fibroblast growth factor 21 level and coronary artery disease. *Cardiovascular Diabetology* **12** 124. (doi:10.1186/1475-2840-12-124)

Smaili SS, Hsu YT, Sanders KM, Russell JT & Youle RJ 2001 Bax translocation to mitochondria subsequent to a rapid loss of mitochondrial membrane potential. *Cell Death and Differentiation* **8** 909–920. (doi:10.1038/sj.cdd.4400889)

Surinkaew S, Kumphune S, Chattipakorn S & Chattipakorn N 2013 Inhibition of p38 MAPK during ischemia, but not reperfusion, effectively attenuates fatal arrhythmia in ischemia/reperfusion heart. *Journal of Cardiovascular Pharmacology* **61** 133–141. (doi:10.1097/FJC.0b013e318279b7b1)

Takatsu M, Nakashima C, Takahashi K, Murase T, Hattori T, Ito H, Murohara T & Nagata K 2013 Calorie restriction attenuates cardiac remodeling and diastolic dysfunction in a rat model of metabolic syndrome. *Hypertension* **62** 957–965. (doi:10.1161/HYPERTENSIONAHA.113.02093)

Tan BK, Hallschmid M, Adya R, Kern W, Lehnert H & Randeva HS 2011 Fibroblast growth factor 21 (FGF21) in human cerebrospinal fluid: relationship with plasma FGF21 and body adiposity. *Diabetes* **60** 2758–2762. (doi:10.2337/db11-0672)

Tanajak P, Chattipakorn SC & Chattipakorn N 2015 Effects of fibroblast growth factor 21 on the heart. *Journal of Endocrinology* **227** R13–R30. (doi:10.1530/JOE-15-0289)

Tanajak P, Sa-Nguanmoo P, Wang X, Liang G, Li X, Jiang C, Chattipakorn SC & Chattipakorn N 2016 Fibroblast growth factor 21 (FGF21) therapy attenuates left ventricular dysfunction and metabolic disturbance by improving FGF21 sensitivity, cardiac mitochondrial redox homoeostasis and structural changes in pre-diabetic rats. *Acta Physiologica* **217** 287–299. (doi:10.1111/apha.12698)

Thummasorn S, Kumfu S, Chattipakorn S & Chattipakorn N 2011 Granulocyte-colony stimulating factor attenuates mitochondrial dysfunction induced by oxidative stress in cardiac mitochondria. *Mitochondrion* **11** 457–466. (doi:10.1016/j.mito.2011.01.008)

Wente W, Efanov AM, Brenner M, Kharitonenkov A, Koster A, Sandusky GE, Sewing S, Treinies I, Zitzer H & Gromada J 2006 Fibroblast growth factor-21 improves pancreatic beta-cell function and survival by activation of extracellular signal-regulated kinase 1/2 and Akt signaling pathways. *Diabetes* **55** 2470–2478. (doi:10.2337/db05-1435)

Wilsey J & Scarpace PJ 2004 Caloric restriction reverses the deficits in leptin receptor protein and leptin signaling capacity associated with diet-induced obesity: role of leptin in the regulation of hypothalamic long-form leptin receptor expression. *Journal of Endocrinology* **181** 297–306. (doi:10.1677/joe.0.1810297)

Wu X, Qi YF, Chang JR, Lu WW, Zhang JS, Wang SP, Cheng SJ, Zhang M, Fan Q, Lv Y, *et al.* 2014 Possible role of fibroblast growth factor 21 on atherosclerosis via amelioration of endoplasmic reticulum stress-mediated apoptosis in apoE mice. *Heart and Vessels* **30** 657–668. (doi:10.1007/s00380-014-0557-9)

Wycherley TP, Brinkworth GD, Noakes M, Buckley JD & Clifton PM 2008 Effect of caloric restriction with and without exercise training on oxidative stress and endothelial function in obese subjects with type 2 diabetes. *Diabetes, Obesity and Metabolism* **10** 1062–1073. (doi:10.1111/j.1463-1326.2008.00863.x)

http://joe.endocrinology-journals.org
DOI: 10.1530/JOE-16-0406

© 2017 Society for Endocrinology
Printed in Great Britain

Published by Bioscientifica Ltd.

Xu J, Stanislaus S, Chinookoswong N, Lau YY, Hager T, Patel J, Ge H, Weiszmann J, Lu SC, Graham M, *et al.* 2009 Acute glucose-lowering and insulin-sensitizing action of FGF21 in insulin-resistant mouse models – association with liver and adipose tissue effects. *American Journal of Physiology: Endocrinology and Metabolism* **297** E1105–E1114. (doi:10.1152/ajpendo.00348.2009)

Yan X, Chen J, Zhang C, Zhou S, Zhang Z, Chen J, Feng W, Li X & Tan Y 2015 FGF21 deletion exacerbates diabetic cardiomyopathy by aggravating cardiac lipid accumulation. *Journal of Cellular and Molecular Medicine* **19** 1557–1568. (doi:10.1111/jcmm.12530)

Yin M, Sillje HH, Meissner M, van Gilst WH & de Boer RA 2011 Early and late effects of the DPP-4 inhibitor vildagliptin in a rat model of post-myocardial infarction heart failure. *Cardiovascular Diabetology* **10** 85. (doi:10.1186/1475-2840-10-85)

Yu Y, Bai F, Liu Y, Yang Y, Yuan Q, Zou D, Qu S, Tian G, Song L, Zhang T, *et al.* 2015 Fibroblast growth factor (FGF21) protects mouse liver against D-galactose-induced oxidative stress and apoptosis via activating Nrf2 and PI3K/Akt pathways. *Molecular and Cellular Biochemistry* **403** 287–299. (doi:10.1007/s11010-015-2358-6)

Zhang C, Huang Z, Gu J, Yan X, Lu X, Zhou S, Wang S, Shao M, Zhang F, Cheng P, *et al.* 2015 Fibroblast growth factor 21 protects the heart from apoptosis in a diabetic mouse model via extracellular signal-regulated kinase 1/2-dependent signalling pathway. *Diabetologia* **58** 1937–1948. (doi:10.1007/s00125-015-3630-8)

Received in final form 19 October 2016
Accepted 13 November 2016
Accepted Preprint published online 14 November 2016

http://joe.endocrinology-journals.org
DOI: 10.1530/JOE-16-0406

© 2017 Society for Endocrinology
Printed in Great Britain

Published by Bioscientifica Ltd.

เอกสารแนบหมายเลข 10

Metab Brain Dis (2017) 32:1–17
DOI 10.1007/s11011-016-9917-8

REVIEW ARTICLE

Diet, gut microbiota and cognition

Cicely Proctor[1,2,3,4] · **Parameth Thiennimitr**[5] · **Nipon Chattipakorn**[2,3,4] · **Siriporn C Chattipakorn**[2,3,6]

Received: 17 March 2016 / Accepted: 23 September 2016 / Published online: 5 October 2016
© Springer Science+Business Media New York 2016

Abstract The consumption of a diet high in fat and sugar can lead to the development of obesity, type 2 diabetes mellitus (T2DM), cardiovascular disease and cognitive decline. In the human gut, the trillions of harmless microorganisms harboured in the host's gastrointestinal tract are called the 'gut microbiota'. Consumption of a diet high in fat and sugar changes the healthy microbiota composition which leads to an imbalanced microbial population in the gut, a phenomenon known as "gut dysbiosis". It has been shown that certain types of gut microbiota are linked to the pathogenesis of obesity. In addition, long-term consumption of a high fat diet is associated with cognitive decline. It has recently been proposed that the gut microbiota is part of a mechanistic link between the consumption of a high fat diet and the impaired cognition of an individual, termed "microbiota-gut-brain axis". In this complex relationship between the gut, the brain and the gut microbiota, there are several types of gut microbiota and host mechanisms involved. Most of these mechanisms are still poorly understood. Therefore, this review comprehensively summarizes the current evidence from mainly in vivo (rodent and human) studies of the relationship between diet, gut microbiota and cognition. The possible mechanisms that the diet and the gut microbiota have on cognition are also presented and discussed.

Keywords Obesity · A high fat/high sugar diet · Cognition · Gut microbiota

Cicely Proctor and Parameth Thiennimitr equally contributed to this work

✉ Siriporn C Chattipakorn
scchattipakorn@gmail.com; siriporn.c@cmu.ac.th

[1] Faculty of Life Sciences, The University of Manchester, Manchester, UK

[2] Neurophysiology Unit, Cardiac Electrophysiology Research and Training Center, Faculty of Medicine, Chiang Mai University, Chiang Mai, Thailand

[3] Cardiac Electrophysiology Unit, Department of Physiology, Faculty of Medicine, Chiang Mai University, Chiang Mai, Thailand

[4] Center of Excellence in Cardiac Electrophysiology Research, Chiang Mai University, Chiang Mai, Thailand

[5] Department of Microbiology, Faculty of Medicine, Chiang Mai University, Chiang Mai, Thailand

[6] Department of Oral Biology and Diagnostic Sciences, Faculty of Dentistry, Chiang Mai University, Chiang Mai 50200, Thailand

Introduction

Obesity is one of the major health issues encountered in the world today. In 2014, 600 million adults (13 % of the world's population) were classified as obese (WHO 2015) (body mass index ≥30 kg/m^2) (Cox et al. 2015). In addition, 42 million children under the age of 5 were classified as obese by WHO in the same year (WHO 2015). Obesity increases the risk for developing several diseases, including: type 2 diabetes mellitus (T2DM), metabolic syndrome (MetS), various cancers, cardiovascular disease (CVD) and cognitive defects, such as Alzheimer's disease (Haslam and James 2005; Walker and Harrison 2015). Obesity is caused by a complex interaction between genetic, behavioural and environmental factors. The common cause of obesity is long-term consumption of high-fat and high-sugar diets or poor diets. A poor diet is known to cause obesity and has then been linked to a change in the microbiota's composition. The human gut microbiota has been believed to contain at least 10 times more cells than the human body in which make up about 1–3 % of total body mass (MacDougall 2012). However, this ratio has been recently revised (Sender et al. 2016). By considering the gradient of

bacterial concentration along the gastrointestinal tract (from ileum to feces), the actual colonic bacteria concentration should be lesser than the previously thought. The new ratio of bacteria to human cells should be closer to 1:1 (3.8×10^{13} to 3.0×10^{13} for total number of bacteria and human cells, respectively) (Sender et al. 2016). Several studies suggest that a mammalian host establishes their core microbiota at birth. However, an individual's microbiota composition could be influenced by their maternal genetics and environmental factors (Org et al. 2015). The beneficial roles of the gut microbiota to a mammalian host include: stimulating the proper development of host immune system, providing the host with extra energy sources and protecting the host against invading pathogens (Belkaid et al. 2014). A decline in gut microbiota homeostasis, termed "gut dysbiosis", has been associated with several human diseases, including the following diet-generated diseases: obesity, T2DM, MetS and non-alcoholic fatty acid syndrome (Ojeda et al. 2015).

Diet has a large role in the determination of the composition of the gut microbiota (Ley et al. 2006; Flint et al. 2012). A previous study showed that a diet with high in fat and sugar appeared to have detrimental effects on cognition, both throughout childhood and during adulthood (Khan et al. 2014). Several studies also suggested that an imbalance in gut microbiota (gut dysbiosis) might be a crucial factor for influencing the impaired cognition found in diet-induced obesity (Bercik 2011; Desbonnet et al. 2014; Logan 2015). In this review, we summarize and discuss the recent published evidence derived from different studied models including animals (both germ-free and wild type) and humans. Due to the limitations of the existence in each model, it is important to compare the study outcomes from different studied models. This review demonstrates the relationship between the brain, the gut and its microbiota, which is termed *'the microbiota-gut-brain axis'*, and its possible role in the mechanisms involved in how diet-induced gut dysbiosis could result in the impairment of cognitive function.

How diet shapes the Host's gut microbiota

The gut microbiota is composed of two dominant phyla, which make up over 99 % of the diversity in the distal gut and faecal bacteria: Firmicutes and Bacteroidetes. Both of these phyla are made up of anaerobic bacteria and play a role in aiding the digestion of the host's food (Gill et al. 2006; Ojeda et al. 2015; Ussar et al. 2015). In healthy adults the ratio of Firmicutes to Bacteriodetes was reported as 10.9/1 (Mariat et al. 2009). Many studies have linked a prolonged consumption of a high-fat diet to gut microbiota changes or gut dysbiosis (Fava et al. 2013; Kim et al. 2012; Ussar et al. 2015). A change in diet has been shown to have an impact on the composition of the gut microbiota within 24 h of the diet change (Ley et al. 2006). For example, 1) Long term consumption of a high-fat diet increases the ratio of Firmicutes to Bacteroidetes (Org et al. 2015; Shi et al. 2015; Ussar et al. 2015). This shift has been linked to obesity (Ley et al. 2006). However, Mariat and colleagues demonstrated that this ratio can be changed at different stages of life in people with unrestricted Western-type diet (Mariat et al. 2009). That study showed an increase in the ratio of Firmicutes to Bacteroidetes in the adults, but a decrease in the elderly, suggesting that the reduced ratio might be related to the decline in cognition seen in the elderly. 2) The effects of different types of dietary fat and carbohydrate on the gut microbiota composition has recently been reported by Fava and colleagues, who showed a reduction in the overall gut microbiota diversity in the people at risk for MetS and who were fed a high fat diet. In addition, the consumption of a diet high in carbohydrate but low in fat resulted in a marked increase in the faecal *Bifidobacterium* spp. numbers. High carbohydrate together with a high glycemic index diet showed a correlation with an increase in faecal Bacteroidetes, whilst a high carbohydrate but low glycemic diet led to an enhanced growth of *Faecalibacterium prausnitzii* (Fava et al. 2013). The increase of Bacteroidetes seen in the high carbohydrate diet in Fava's study contrasts with the documented high fat diet induced decrease in Bacteroidetes seen in other recent studies (Org et al. 2015; Shi et al. 2015; Ussar et al. 2015). It is well known that Bacteroidetes are involved in the fermentation of complex non-digestible dietary carbohydrates and host-derived glycans in the host's gut; this could be due to an extensive part of the genome of Bacteroidetes containing a large part of genes encoding proteins involved in carbohydrate metabolism. (Flint et al. 2012). The differences in these observations suggest that each specific change in bacterial population due to different diets can alter the gut microbiota in different ways, thus resulting in the variation of individual gut microbiota profiles.

There is, also, one study which illustrates the connection between the gut microbiota and whether the individual's diet is plant or animal-based (David et al. 2014). The short-term consumption of a diet composed entirely of animal or plant products alters the gut microbial gene expression rapidly. Animal-based diet consumption led to increased bile-tolerant microbiota (*Alistipes* spp., *Bilophila* spp. and *Bacteroidetes* spp.) and decreased dietary plant polysaccharide fermenters, i.e. Firmicutes (*Roseburia* spp., *Eubacterium rectale* and *Ruminococcus bromii*) in the gut. Moreover, an increase in the gut presence of *Bilophila wadsworthia*, the commensal, Gram negative, anaerobic, asaccharolytic (unable to breakdown carbohydrate), bile resistant rod bacterium was shown to be associated with host gut inflammatory conditions including acute appendicitis and inflammatory bowel disease (IBD) (David et al. 2014; Finegold et al. 1992). These studies suggest that an animal-based diet could result in diseases linked with an inflamed gut by promoting the growth of a microbiota

population which specializes in protein degradation. Therefore, all findings suggest that diet plays a crucial role in shaping the host's gut microbiota.

Metabolic syndrome and gut microbiota

Metabolic syndrome (MetS) is a combination of pathogenic phenotypes, including: abdominal obesity, hypertension, irregular glucose homeostasis (impaired fasting glucose and glucose tolerance, insulin resistance and T2DM and dyslipidaemia (high triglyceride (TG) levels and low high density lipoprotein (HDL) cholesterol levels) (Kim and Je 2015). It is estimated that over 34 % of Americans over the age of 20 have metabolic syndrome (Yates et al. 2012). The consumption of a diet high in fat and sugar, together with a sedentary lifestyle, has long been known to be a major risk factor of MetS. As this diet is known to alter the gut microbiota composition, many studies have linked the microbiota alterations to specific MetS parameters.

A study which focused on 110 genetically different mouse strains fed with a high fat/high sugar (HF/HS) diet found that *Roseburia* spp. and *Ruminococcus gnavus* numbers showed a positive correlation with insulin levels, HOMA index by increasing the expression of an interleukin-1 receptor-associated kinase 4 (*Irak4*) gene, a gene involved in the innate immune response, and decreasing the expression of oxysterol binding protein (*Osbp*) gene, a gene in adipose tissue, respectively (Org et al. 2015). Conversely, the same study linked increased *Akkermansia muciniphila* numbers with improved glucose and insulin regulation as indicated by increasing the expression of insulin-like growth factor 1 receptor (*Igf1r*), nuclear receptor subfamily 2 group F member 2 (*Nr2f2*) and catenin-beta-like 1 (*Ctnnbl1*) genes, genes involved in glucose, insulin regulation and obesity. However, the abundance of *A. muciniphila* also associated with expression of lipopolysaccharide binding protein (*Lbp*) gene, which was positively correlated with body fat and insulin levels. Those findings suggested that different gut microbiota species could have different effects on host insulin sensitivity. Moreover, the same species of gut microbiota might affect differently on the host metabolic genes involved in insulin sensitivity (Org et al. 2015). In addition, a study in obese-resistant mice and obese-prone high-fat diet fed mice found that *A. muciniphila*, *Anaerotruncus colihominis*, *Mucispirillum schaedleri* and *Lactobacillus reuteri* showed positive correlations with an increase in body weight, and that *Lactobacillus* spp. and *A. muciniphila* were linked with systemic inflammation, thus perhaps having a role in MetS pathology (Ussar et al. 2015).

In germ free mice, *B. thetaiotaomicron* was shown to be linked to an increase in body fat (Bäckhed et al. 2004). Semova and colleagues found that numbers of Firmicutes accompanied an increase in lipid droplet density in germ-free zebrafish (Semova et al. 2012), which could explain why a higher proportion of the Firmicutes is seen in the gut of obese individuals. Also, Gram negative bacterium's lipopolysaccharides (LPS) were shown to be linked with an increase in inflammation in high-fat diet fed rats (de La Serre et al. 2010); LPS are a major part of Gram negative bacterial cell outer membranes and which strongly activates the host innate immune response (Alexander and Rietschel 2001). Insulin resistance is defined as an inefficient response of tissue to normal plasma insulin levels and can be characterized by hyperinsulinemia with euglycemia. Several studies have shown that obesity is positively correlated with the development of insulin resistance, as indicated by increased plasma insulin levels (Clegg et al. 2011; Khan et al. 2014; Pratchayasakul et al. 2011). In obese human studies, Bacteriodetes were shown to have a negative correlation with body weight (Ley et al. 2006); also the higher numbers in butyrate-producing, and more diverse gut microbiota population was shown to improve insulin resistance (Vrieze et al. 2012). In addition, *Bifidobacterium* spp. showed a negative correlation with insulin levels (Vrieze et al. 2012), therefore it is reasonable to assume that a decrease in Bacteriodetes and a decrease in Bifidobacterium numbers could be linked to insulin resistance. Table 1 is a summary of those findings.

Nonetheless, there are two main limitations of the studies summarised in Table 1. One is that some of the studies are conducted on rodents, and whilst rodents and humans have a similar microbiota composition to humans, they are not exactly identical (Nguyen et al. 2015). Thus, applying the interpretations from the data produced from the animal studies (rodents and zebra fish) to humans should be challenged. Another limitation is that the most of the studies analysed gut microbiota from faecal samples, probably due to the practicality of collecting the samples, especially in the human studies. However, there are differences in the microhabitats along the gastrointestinal tract such as the gut lumen, mucus layer and luminal crypt. The heterogeneity of the microbial niches in the host's gut affects the distribution of gut microbiota, as reviewed by (Donaldson et al. 2015). Therefore, the gut microbiota data obtained from the faecal samples cannot represent the spatial heterogeneity of the gut microbiota in the host gastrointestinal tract, due to faecal samples containing microbes from all environments above the anus (Savage 1977).

However, it is still poorly understood whether a high fat diet itself causes the disrupted gut microbial communities prior to MetS development or whether the MetS parameters are caused by high-fat diet induced gut dysbiosis. Further studies will be required to investigate this point.

Can the gut microbiota alone cause obesity?

Since diet clearly has an effect on gut microbiota, and it is known that obese individuals have been shown to have a specific gut microbiota profile, termed *'obese microbiota'*,

Table 1 A summary of the correlations between metabolic parameters and members of the gut/faecal microbial communities. Human models are shown below the thick line, whilst all other models are shown above. *Abbreviations BF* = Body fat , *CD68* = Cluster of differentiation 68, *Ctnnbl1* = Catenin-beta-like 1 gene, *HFD* = High fat diet, *HOMA* = Homeostatic model assessment, *IL-6* = Interleukin-6, *IR* = Insulin resistance, *Igf1r* = insulin-like growth factor 1 receptor gene, *Irak4* = interleukin-1 receptor-associated kinase 4 gene, LPS = lipopolysaccharides, *Lpb* = lipopolysaccharide binding protein gene, MetS = metabolic syndrome, ND = normal diet, *Nr2f2* = nuclear receptor subfamily 2 group F member 2 gene, *Osbp* = oxysterol binding protein gene, *PAI-1* = plasminogen activator inhibitor-1, *TLR4* = Toll-like receptor 4, *TNF-α* = tumor necrosis factor alpha, *spp.* = Several species of the same genus, and *OGTT-AUC* = Oral glucose tolerance test-the area under the curve. + = positively correlated or associated with and - = negatively correlated or associated with

Model	Bacteria	Correlation between bacteria species and MetS	The metabolic profiles gene expression	Interpretations	Ref
Sequenced Mice −110 strains. Fed with a high fat and high sugar diet for 8 weeks.	Roseburia spp.	+ +	BF, insulin levels, HOMA index Irak4 gene (Linked to IR)	Roseburia spp. may be involved in the development of insulin resistance.	(Org et al. 2015)
	Ruminococcus gnavus	+ −	BF, insulin levels, HOMA index Osbp gene (Linked to adipose fat metabolism)	A rise in the numbers of Ruminococcus gnavus is seen with an increase in insulin resistance and an altered adipose fat metabolism state.	
	Akkermansia muciniphila	− + +	BF and insulin levels Igf1r, Nr2f2, Ctnnbl1 genes (Linked to glucose and insulin regulation and obesity) Lpb genes (Linked to BF increase and insulin levels)	A. muciniphila is linked with decreased BF and improved insulin resistance possibly via upregulating Igf1r , Nr2f2 and Ctnnbl1 genes. However, A. muciniphila is also linked to increased Lpb genes expression which associated with BF increase and insulin levels.	
Obese resistant and obese prone mice fed with a high fat diet (60 % fat) for 22 weeks.	M. schaedleri	+	Body weight	M. schaedleri, R. intestinalis and L. reuteri modulate body weight.	(Ussar et al. 2015)
	L. reuteri	+ +	Body weight FGF21 levels	Lactobacillus spp. and A. muciniphila are linked with inflammatory markers, therefore may be linked to cognition or MetS as both are affected by inflammation.	
	Clostridium spp.	−	Body weight		
	R. intestinalis	−	Body weight		
	Lactobacillus spp.	+	Inflammatory markers (IL-6, TNF-α, PAI-1)		
	L. gasseri	− +	Serum free fatty acid levels Insulin levels		
	A. muciniphila	+	CD68, IL-6 and TNF-α		
	Anaerotruncus colihominis	+	OGTT AUC		
Germ free mice.	B. thetaiotaomicron	+	Body fat	B. thetaiotaomicron is linked with an increase in body fat.	(Bäckhed et al. 2004)
Gnotobiotic zebrafish.	Firmicutes	+	Lipid droplet density	Firmicutes correlates with an increase in lipid droplet density (i.e. fat storage).	(Semova et al. 2012)
Rats fed with a HFD (45 % fat) or ND (10 % fat) for 8 and 12 weeks.	Gram negative species	+	(Inflammation and insulin resistance due to LPS weakening gut epithelium via TLR4 and activating macrophages, which then invade adipose tissue.)	The presence of Gram negative bacteria in the gut is linked with an increase in inflammation and insulin resistance.	(de La Serre et al. 2010)

Table 1 (continued)

Model	Bacteria	Correlation between bacteria species and MetS	The metabolic profiles gene expression	Interpretations	Ref
Obese humans, a proportion on diet interventions.	Bacteroidetes	–	Body weight	A decrease in body weight is seen when the number of Bacteriodetes increase.	(Ley et al. 2006)
Obese and lean male humans.	Butyrate producers	–	Insulin resistance	Butyrate producers and a higher level of phylogenetic diversity in the gut microbiome improve insulin resistance.	(Vrieze et al. 2012)
	More diversity alone	–	Insulin resistance		
Human patients with a minimum of two MetS parameters.	Bifidobacterium spp.	–	Insulin levels	Increased Bifidobacterium spp. numbers correlates with a decrease in insulin levels – indicating a link between the bacteria and insulin resistance.	(Fava et al. 2013)

many studies have hypothesized that this profile alone is sufficient to cause obesity. The main method used to demonstrate the direct role of gut microbiota in obesity pathogenesis has been to transfer, by faecal transplantation, 'obese type microbiota' from obese animals or 'lean type microbiota' from lean animals into germ-free (GF, no microbiota) animals (Bäckhed et al. 2004; Fava et al. 2013; Org et al. 2015; Shi et al. 2015; Ussar et al. 2015).

Bäckhed and colleagues found that germ-free mice who had faecal content (gut microbiota) transplanted from the normal conventionally raised mice, showed an increase in their body fat percentage, serum triglyceride levels and insulin resistance. To our knowledge, this is the first evidence that illustrates the direct role of gut microbiota in obesity (Bäckhed et al. 2004). This study suggested that the presence of gut microbiota allowed the host to extract more energy from their diet. The proposed mechanism for this is that gut microbiota can breakdown the complex molecules of non-digestible polysaccharides into smaller metabolites such as short chain fatty acids enabling the host to utilize these metabolites as an extra energy source. This study indicated that the presence of gut microbiota alone, regardless of if it is from lean or obese models, is enough to cause weight gain. Several other studies also support the finding that transmissible gut microbiota can cause obesity (Ley et al. 2006; Ridaura et al. 2013; Turnbaugh et al. 2006). Moreover, a lean phenotype in mice can be induced by faecal transplantation of 'lean-type gut microbiota'. Liou et al. demonstrated this by transferring faecal microbiota from a gastric bypass (Roux-en-Y) mouse model (this surgery being implemented to cause weight loss) into non-operated GF mice; a significant decrease in body fat and a significant increase in weight loss were seen. In terms of the microbiota, an increase in the numbers of *Escherichia* spp. and *Akkermansia* spp. were seen (Liou et al. 2013). These studies support the hypothesis that gut microbiota alone can cause obesity.

To further illustrate the role of host genetics and environment (diet) on the individual's gut microbiota composition, Org and colleagues analysed gut microbiota profiles using a 16 s rRNA gene sequencing method in a mouse neonatal cross-fostered model (Org et al. 2015). New-borns of an obese-resistant mouse strain (SWR) were fostered by an obese-prone mouse strain (AxB19). They found that the gut microbiota composition of the fostered SWR mice resembled the obese prone (AxB19) mice rather than the SWR mice. In one series of experiments the fostered SWR mice were fed with a HF/HS diet at 4 weeks old. Both male and female cross-fostered pups showed increased weight gain when compared to the SWR mice. Interestingly, only the male cross-fostered mice gained weight and showed an increased body fat composition after being fed on the HF/HS diet for 8 weeks. Male cross-fostered mice also exhibited increased plasma triglyceride levels when compared to the SWR mice. However,

after 8 weeks of being fed on the HF/HS diet, the gut microbiota of the cross-fostered mice reverted back to resemble their 'original' maternal SWR strain's gut microbiota. Therefore, this study showed that not only does diet affect the gut microbiota community, but there are also the host genotypes partly contribute to the variation in the individual's gut microbiota profile.

All of these findings suggest that the presence of an 'obese type' gut microbiota alone can be sufficient to cause obesity, the opposite being true for a 'lean type' gut microbiota which can help to reverse the obese phenotype if transferred into an obese subject. Thus, the differing microbiota profiles of obese and lean populations can combat the weight phenotype, whether it is induced by genotype or other environmental factors. These conclusions also provide insight into whether faecal transplants could, one day, be used to prevent/treat obesity.

Diet and cognition

Diet induced cognition deficits

It has been highly documented that a diet with high in fat and sugar has a detrimental effect on cognition. This abnormality could be due to the disturbance of the physiology of gut-brain axis. Reported cognitive disturbances due to a poor diet include depression, memory impairment, decreased planning and problem solving abilities, decreased mental flexibility and altered inhibitory processes. Such disturbances indicate changes in the hippocampus and the frontal lobe in obese human models (Castanon et al. 2014). Many studies have related this to a decrease in brain derived neurotrophic factor (BDNF) levels in the hippocampus (Molteni et al. 2002). This nerve growth factor is a key survival signal for striatal neurones in the brain and is released by cortical neurones. It is thought that the protein plays a role in stress regulation and mood disorders, since it has low expression in individuals with Alzheimer's and Huntington's disease (NCBI 2015). BDNF uses synapsin 1 and CREB (cyclic AMP-response element binding protein) to modulate the synapse. This modulation is linked to synaptic plasticity, so these proteins therefore drive learning and memory (Wu et al. 2004). BDNF, synapsin 1, CREB and mRNA for a protein important for neurite growth (growth associated protein 43) have all been found to have decreased levels after continued consumption of a high-fat diet (Molteni et al. 2002; Wu et al. 2004). Brain reactive oxygen species (ROS) have also been shown to be increased after consumption of a high-fat diet (Molteni et al. 2004; Pipatpiboon et al. 2012), which could be the cause of the decrease in the four aforementioned factors. These mechanisms result in a decrease in spatial learning capacity (measured by the Morris water maze test in rodents), reduced dendritic spine density (mainly in the hippocampus, perirhinal cortex and the prefrontal cortex), and reduced long term potentiation (LTP) in CA1 synapses (Bocarsly et al. 2015; Pintana et al. 2013; Sripetchwandee et al. 2014; Stranahan et al. 2008). Another cognitive deficit caused by long term consumption of a high-fat diet is a reduction in neurogenesis. The mechanism for this is most likely due to an increase in malondialdehyde (MDA) levels caused by the high-fat diet consumption. MDA is toxic to neural progenitor cells, and therefore inhibits neurogenesis (Park et al. 2010). A high-fat diet is also thought to decrease cognition levels by impairing the blood brain barrier (BBB); this impairment has been linked to the development of Alzheimer's disease. It has been shown that a high-fat diet increases the BBB's permeability and reduces the rate of leptin and ghrelin's active transport across the BBB (Cordner and Tamashiro 2015). It is known that obese individuals are resistant to leptin (an anorexigenic hormone) (Klok et al. 2007), thus BBB dysfunction could be a contributor to leptin resistance and not a direct link to a decrease in cognition.

Molteni and colleagues found that exercise reversed these high-fat diet induced cognition deficits. Exercise increased levels of BDNF, synapsin 1 and CREB, as well as increasing the activation of synapsin 1 and CREB. It also decreased levels of ROS in the hippocampus and increased performance in the Morris water maze, indicating an improvement in cognition. The Morris water maze has been linked to hippocampal NMDA receptor activity and hippocampal long term potentiation (LTP) (Cordner and Tamashiro 2015). This information shows that exercise can combat the cognitive deficit caused by high-fat diet using the same mechanisms that caused the deficits, specifically in the hippocampal region (Molteni et al. 2004). These findings are summarised in Fig. 1.

Another diet induced cognitive effect was seen, when Bocarsley and colleagues demonstrated that rats fed with a high-fat diet for 8 weeks resulted in changes in microglia morphology in areas of synaptic loss in the prefrontal cortex. They inferred that these changes in the microglia caused excessive pruning of synapses which resulted in the seen synaptic loss. They also found decreased levels of corticosterone in the obese rats, which has been linked to reduced dendritic spine density in the prefrontal cortex (Bocarsly et al. 2015).

In human studies, obesity has been shown to have an effect on cognition throughout childhood development, as reviewed in (Yates et al. 2012). One study investigated P300 auditory event-related potentials in pre-pubescent children and those potentials reflected the amplitude of the response of brain waves to an auditory stimulus as well as level of cognition (Medvidovic et al. 2013). They found that there was a decrease in both the amplitude and prolonged latency of the P300 wav in obese children, suggesting that they had a decreased level of cognition. In addition, insulin-resistant condition seemed to worsen the cognitive deficit in the children (Tascilar et al. 2011). Body mass index (BMI) also found to have a negative correlation with prefrontal inhibitory control, general mental ability and visuospatial organisation in

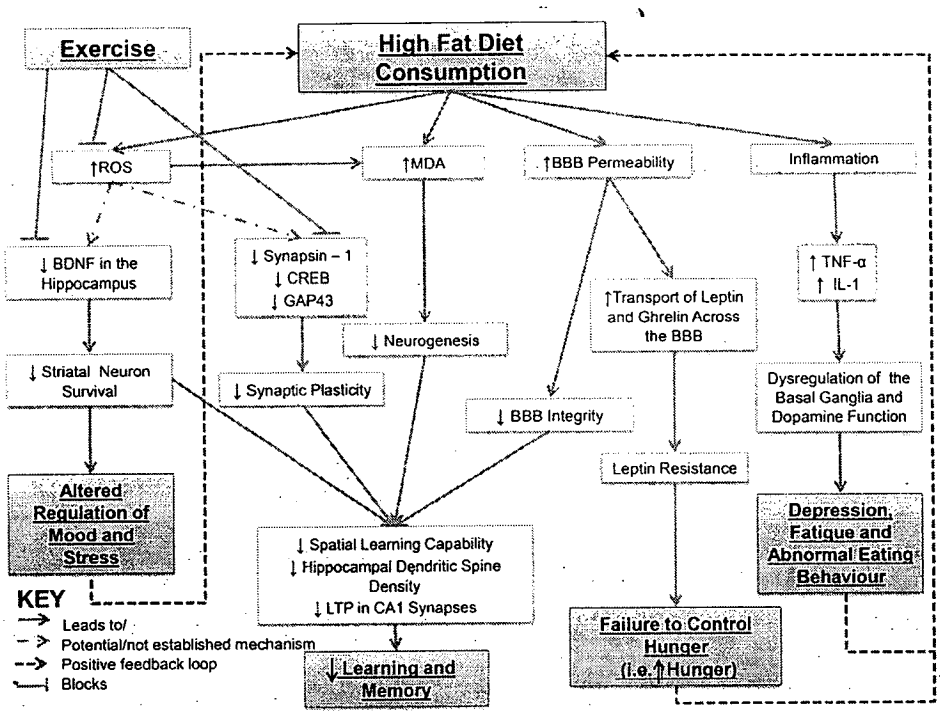


Fig. 1 The possible mechanisms linking the consumption of a high fat diet and cognition defects and how exercise could reverse these possible mechanisms. In addition, the positive feedback loop between the resulting behaviours causing a continued consumption of an unhealthy diet is illustrated. ROS – reactive oxygen species, MDA – malondialdehyde, BBB – blood brain barrier, BDNF – brain derived neurotrophic factor, CREB – cAMP response binding element protein, GAP43 – growth associated protein 43, TNF-α – tumour necrosis factor alpha, IL-1 – interleukin 1, LTP – long term potentiation, CA1 – region 1 of hippocampus proper

children. Khan and colleagues showed that performance in academic test scores has been negatively linked to body weight in many studies (Khan et al. 2014). Khan and colleagues hypothesized that decreased cognition could affect obesity, but not vice versa. They showed that poor prefrontal inhibitory control at 2 years old was seen as a predictor of obesity at 5.5 years old. In addition, a higher level of cognition at 4 years old was linked with a healthy weight when the individual reached 6 years of age. Those findings indicate that poorly developed cognition and self-regulation may be a factor in the likelihood of becoming obese during childhood (Khan et al. 2014). It has also been shown that an increased body weight is linked to higher levels of impulsivity in children (Pauli-Pott et al. 2010); this impulsivity could lead to irregular feeding behaviour which could be the cause of the obese phenotype seen in the study group. An explanation for this poor inhibitory control seen in obese children is that frontal lobes are still developing in adolescence, so they might be more vulnerable to obesity- induced changes (Yates et al. 2012). In contrast with those findings, one study by LeBlanc and colleagues found that adiposity did not show a correlation with test scores in children (LeBlanc et al. 2012).

Regarding the adulthood, similar conclusions have been made. Obese individuals were shown to have significantly lower performance in executive functioning tests which infers poor planning, problem solving and mental flexibility (Boeka and Lokken 2008). It has also been reported that obese young adults are more likely to be highly impulsive (Chamberlain et al. 2015), which again could be the cause for the poor feeding decisions or could be as a result of the poor diet consumption. However, one study found that impulsivity was only associated with food related cognition and not directly with binge eating (Mason and Lewis 2015). As it was with children, this has been linked to poor cognitive inhibition. Zhang and colleagues found, through fMRI scans, that obese men showed less inhibitory control during a fasting state and suggested that this was due to a faulty reward system between the frontal cortex and the striatum (Zhang et al. 2015). This impaired frontal cortex inhibitory control in male adults led to increase hunger and poor feeding habits (Wang et al. 2009).

It has also been shown that obesity has a correlation with decreased brain volume, notably in the hippocampus, anterior cingulate and prefrontal cortex (Bocarsly et al. 2015), areas of the brain which have been linked to impulsivity (Liu et al. 2012). This could be another reason for the obesity induced impulsive behaviours described above.

Taken together, these studies in both children and adults demonstrate the bi-directionality of the relationship between obesity and cognition. In other words, poor cognition can lead to poor diet choices and therefore obesity, through the mechanism of poor frontal cortex inhibitory control; and that also obesity, though a high-fat diet, can affect cognition levels.

Obesity-induced inflammation is linked to impairment in cognition

The consumption of a high-fat diet leads to an increase in obesity, insulin resistance and chronic-low grade systemic inflammation (Wellen and Hotamisligil 2005; Xu et al. 2003).

Obesity-induced inflammation has also been linked to altered cognition (Castanon et al. 2014). In the obese state, the brain, liver, adipose tissue and pancreas are all exposed to higher levels of pro-inflammatory cytokines than normal condition. Pro-inflammatory cytokines, such as tumour necrosis factor-α (TNF-α), interleukin-6 (IL-6), interleukin-1β (IL-1β) and monocyte chemoattractant protein-1 (MCP-1 or also known as chemokine (C-C motif) ligand 2 or CCL2), are secreted by adipocytes and activated macrophages in the white adipose tissue (WAT) (Shoelson et al. 2007). Moreover, other metabolic-related molecules secreted by adipocytes in the WAT, including resistin, visfatin, retinol-binding protein-4 (RBP-4), plasminogen activator inhibitor-1 (PAI-1) and serum amyloid A (SAA) can affect the immune response (Gregor and Hotamisligil 2011; Tilg and Moschen 2006). Resistin is known to induce insulin resistance (Trayhurn and Beattie 2001). Therefore having more WAT (due to a high-fat diet consumption) raises inflammation levels via the release of pro-inflammatory cytokines. In addition, the WAT of the obese individuals has increased macrophage infiltration. These macrophages are termed "adipose tissue macrophages" (ATMs) and have a distinct phenotype when compared to the classical activated macrophage (Kratz et al. 2014). ATMs are a major source of pro-inflammatory cytokines in obese subjects (Subramanian and Ferrante 2009; Xu et al. 2003). ATMs can be "metabolically activated" by certain factors such as glucose, insulin and palmitate and all of these markers have increased levels in individuals with obesity and MetS (Kratz et al. 2014). IL-1β (a pro-inflammatory cytokine produced by ATMs) causes insulin resistance by disrupting insulin signalling in peripheral tissues or inducing the dysfunction of beta-cells, thus resulting in decreased insulin levels (Esser et al. 2014). Another proposed mechanism of pro-inflammatory cytokines causing insulin resistance is through the endoplasmic reticulum stress signalling pathway (Boden et al. 2014). The state of chronic low-grade inflammation found in obesity can also be termed "*metaflammation*" (Gregor and Hotamisligil 2011). The possible underlying mechanisms of obesity-induced insulin resistance are summarised in Fig. 2. One study of over 3000 participants found a link between T2DM and reduced cognition (poor memory and slower processing speed), but not between MetS and reduced cognition (Tournoy et al. 2010). This indicates that insulin resistance rather than the other components of MetS is the main driving component of obesity induced cognitive defects.

A possible consequence of consumption of a high-fat diet which may cause systemic inflammation could be an increase in the numbers of Gram-negative bacteria seen in an obese gut (Kim et al. 2012). Long-term high-fat diet consumption enhances the growth of gram negative bacteria from the Proteobacteria phylum, whose outer membranes are composed of lipopolysaccharides (LPS). Bacterial LPS is a ligand of a human innate immune receptor - the Toll-like receptor 4 (TLR4), which is found on gut epithelia and immune cells. Recognition of bacterial LPS by TLR4 results in increased levels of pro-inflammatory cytokine secretion. High-fat diet consumption can increase gut inflammatory tone and can also disrupt gut epithelium integrity (by decreasing tight junction protein expression); thus allowing more gut luminal LPS to diffuse into the gut tissue vasculature and therefore cause systemic inflammation and insulin resistance (Cani et al. 2007; de La Serre et al. 2010; Kim et al. 2012).

An excess of pro-inflammatory cytokines, which are increased during insulin resistance, such as TNF-α and IL-1 are known to have an effect on dopamine function in the subcortical brain structures, especially in the basal ganglia (Felger and Miller 2012). The basal ganglia plays a major role in motivation and motor activity regulation which is modulated by dopamine. Dysregulation of the basal ganglia and dopamine function can lead to depression, fatigue, anxiety and psychomotor symptoms (i.e. abnormal eating behaviour) (Capuron et al. 2007; Capuron et al. 2012; Haroon et al. 2012; Liu and Hong 2003). Thus, obesity-induced inflammation due to gut dysbiosis via increased numbers of LPS-containing bacterial species, may be a crucial risk factor in the causes of altered cognition states such as depression and abnormal eating patterns and those two states are often found in MetS subjects (Koponen et al. 2008).

Gut microbiota and cognition

The composition of gut microbiota affects cognition

Although the role of chronic systemic inflammation (excess pro-inflammatory cytokine production) in the alteration of the function of the CNS is quite well-studied, the contribution of gut microbiota composition is still poorly understood. In this review several studies are included which illustrate the link between gut microbiota composition and altered cognitive function. The details of this are shown in Table 2. Several aspects of cognition have been found to be linked with changes in the gut microbiota composition, such as visceral hypersensitivity, anxiety, learning and memory, development of Schizophrenia and autism-like behaviours (Castro-Nallar et al. 2015; Desbonnet et al. 2014; O'Mahony et al. 2014; Savignac et al. 2015). O'Mahony and colleagues showed that neonatal mice treated with an antibiotic of vancomycin developed visceral hypersensitivity together with a shift in their gut microbiota profile. The early-life vancomycin exposure resulted in an overall decrease in gut microbial diversity, but an increase in the numbers of bacteria in the Proteobacteria phylum. That disruption of bacterial colonisation had only one significant change in cognition which was long lasting visceral hypersensitivity in the male rats, but there were no

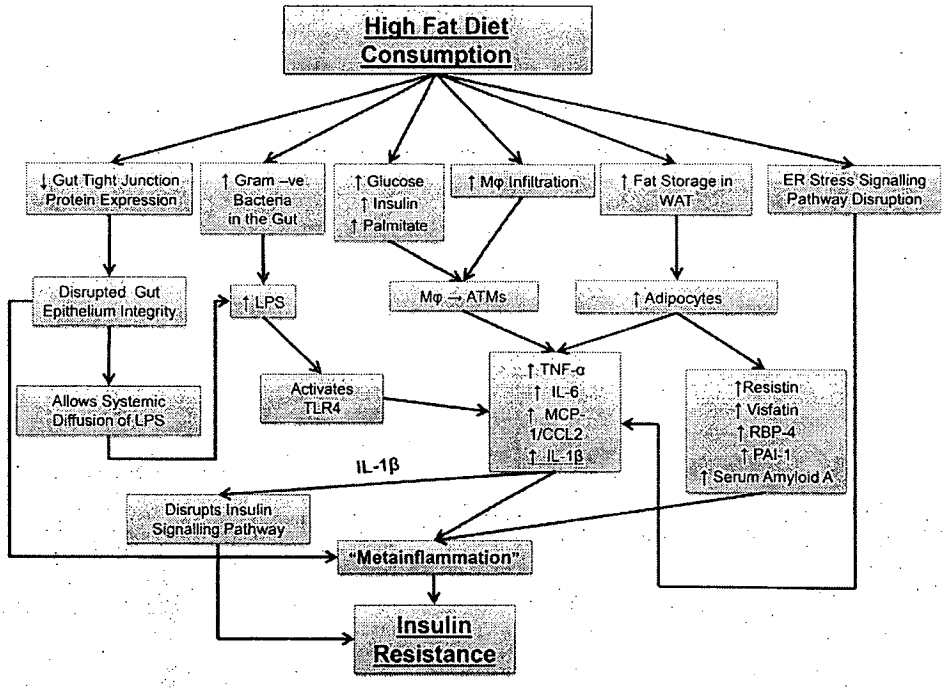


Fig. 2 The consumption of a high fat diet could lead to insulin resistance via "metainflammation" -ve – negative, Mφ – macrophage, WAT – white adipose tissue, ER – endoplasmic reticulum, LPS – lipopolysaccharide, ATMs – adipose tissue macrophages, TLR4 – Toll like receptor 4, TNF-α – tumour necrosis factor alpha, IL-6 – interleukin 6, MCP-1/CCL2 - monocyte chemoattractant protein-1 or also known as chemokine (C-C motif) ligand 2, IL-1β – interleukin 1 beta, RBP-4 – retinol binding protein, PAI-1 – plasminogen activator inhibitor 1, WAT – white adipose tissue

significant differences in anxiety or cognitive performance in the Morris Water Maze test seen in both genders. However, that study found that this early-life antibiotic exposure had no effect on systemic cytokine levels, stress hormone levels or body weight in the rats (O'Mahony et al. 2014). Thus there was no change in the inflammatory state, so that antibiotic exposure could not have altered cognition through the inflammatory pathway seen in Fig. 1, nor could it combat insulin resistance through the mechanisms described in Fig. 2. In another study, when mice were fed *Bifidobacterium longum* 1714 as a probiotic, there was an observed improvement in learning and memory, demonstrated by increased performance in an object recognition test and a Barnes maze test. In the same experiment, *Bifidobacterium breve* 1205, as a probiotic, failed to show a positive impact on mouse cognition (Savignac et al. 2015). These findings support the role of specific bacteria in cognition and also that probiotics have strain-specific effects. One possible mechanistic link between gut microbiota and cognition, reported by Yuan et al., is that the gut microbiota-derived metabolite 'urolithins' can prevent beta-amyloid fibrillation in a nematode model of Alzheimer's disease (Yuan et al. 2015). Urolithins are gut microbial fermentation by-products derived from ellagitannins (found in pomegranate extract and juice). However, species of gut microbiota being responsible for urolithin production in mammalian hosts is still unknown.

Another study, by Gareau and colleagues, has demonstrated how mice with no gut microbiota (germ-free mice) showed memory dysfunction when compared with their conventional counterpart. However, treatment with probiotics prevented this memory dysfunction. That study, with evidence from an object recognition test and a T-maze, showed that germ-free mice had reduced dorsal hippocampal function (Gareau et al. 2011). These findings suggest that gut microbiota have a crucial role in hippocampus-dependent memory development.

Gut microbiota has been linked to several other diseases including psychiatric disorders such as a depression. Gut microbiota has an influence on the hypothalamus-pituitary-adrenal (HPA) axis (Gareau 2014) and that hyperactivity of this axis is related to depression (Pariante and Lightman 2008). It was shown that germ-free mice exhibited increased HPA axis activation, indicating a susceptibility to depression (Gareau 2014). It has also been reported that insulin resistant adolescents had poor HPA axis integrity (Ursache et al. 2012), which demonstrates that IR could be the potential link between the microbiota and HPA axis function.

Moreover, an alteration in gut microbiota composition has been associated with several immunologically-based neurological disorders (Catanzaro et al. 2015; Maranduba et al. 2015). The pathogenesis of autoimmune diseases involving the central nervous system (e.g. multiple sclerosis) is still poorly understood. The breakthrough study of Berer and colleagues, showed that commensal gut bacteria and an endogenous autoantigen, myelin oligodendrocyte glycoprotein, can trigger the activation of myelin-specific helper T-cells and autoantibody-producing B-cells in a mouse model of experimental autoimmune encephalomyelitis (Berer et al. 2011). Some Japanese MS patients also developed gut dysbiosis, which was characterized by increased levels of obligate anaerobic bacteria which belonged to the Clostridia clusters XIVa

Table 2 A summary of the evidence linking microbiota components to several aspects of cognition. Rodents are summarised above the thick line with human models below. *Abbreviations ASD* = Autism spectrum disorder, *BBB* = Blood brain barrier, *BDNF* = Brain-derived neutrophic factor, *BW* = Body weight, *HFD* = High fat diet, *ND* = Normal diet, *spp.* = Several species of the same genus, *SFCA* = Short chain fatty acids, + = positively correlated or associated with and -The = negatively correlated or associated with

Model	Methods	Bacteria Species/Phyla or Bacterial Product	Bacterial Species Correlation with Cognition	Additional Information	Interpretations	Ref
HFD (60 % fat) and ND (10 % fat) mice for 8 weeks.	Light dark exploration test.	Lachnospiraceae Streptococcaceae Ruminococcaceae *Butyricicoccus* spp.	- Anxiety +Anxiety + Anxiety + Anxiety	+ BW + BW + BW	Several bacterial species are linked to an increase in anxiety and body weight, suggesting that there might be a link between all three. However, the presence of Lachnospiraceae in the gut microbiota is beneficial in reducing anxiety.	(Kang et al. 2014)
Chemically induced colitis mouse model.	Treated with an oral probiotic.	*Bifidobacterium longum NCC3001*	- Anxiety	Normalized BDNF levels	Suggests a possible use for a probiotic to combat anxiety, perhaps via the vagal pathway and increased striatal neuron survival (raised BDNF levels).	(Bercik 2011)
Asymptomatic, 8 week old mice infected with an enteropathogen.	Tested on elevated plus maze.	*Campylobacter jejuni*	+ Anxiety		Implies communication between the gut and the brain (most likely via the vagal nerve) during GI tract infection.	(Lyte et al. 1998)
Rats, 4–13 days old.	Fed Vancomycin – (early life microbiota disruption) and tested on open field tests.	Reduced diversity	+ Visceral hyper sensitivity (in males)	+ BW	Reduced bacterial diversity in the gut of rats may modulate their perception of pain.	(O'Mahony et al. 2014)
BALB/c male mice.	Fed *B. longum* or *B. breve* for 11 weeks before measuring cognition levels with object recognition, Barnes maze and fear conditioning.	*Bifidobacterium longum and breve*	+ Learning and memory No effect on stress parameters		These probiotics may affect hippocampal processes, as learning and memory was improved.	(Savignac et al. 2015)
Germ free mice.	Three chambered sociability and food preference tests.	Germ free	Low investigation and social skills, also high self-grooming.	These behaviours are linked with autism and other neurodevelopmental disorders.	Not having a microbiota may cause the development of autism and other disorders.	(Desbonnet et al. 2014)
Mice, 21 days old.	One group treated with antibiotic cocktail. BDNF levels were tested. Food preference test. Novel object recognition Light/ dark box test.	Reduced faecal bacteria load by 400 fold. (– Firmicutes and Bacteriodetes, + Cyanobacteria and Proteobacteria)	Increased anxiety. Reduced BDNF, oxytocin and vasopressin levels. Altered tryptophan pathway.	Oxytocin and vasopressin impact on social behaviour. Tryptophan is a precursor to serotonin, so decreased microbiota means less serotonin produced.	Reduced bacterial numbers in the microbiota is linked to increased anxiety, altered social behaviour and altered mood levels (due to the depletion of serotonin).	(Desbonnet et al. 2015)
Hepatic encephalopathy patients	Review of several studies linking microbiota to hepatic encephalopathy symptoms.	Enterobacteriaceae	- Cognition		Several phyla of bacteria are linked with a decrease in cognition.	(Bajaj 2014)
		Alcaligenaceae Porphyromonadaceae *Prevotella* spp.	- Cognition - Cognition + Cognition	- Inflammation	Bacteria may alter cognition through affecting inflammation levels.	

Table 2 (continued)

Model	Methods	Bacteria Species/Phyla or Bacterial Product	Bacterial Species Correlation with Cognition	Additional Information	Interpretations	Ref
		Enterococcus spp.	- Cognition	+ Inflammation		
Chronic fatigue syndrome patients.	Faecal microbial analysis.	*Enterococcus* spp. *Streptococcus* spp.	- Cognition - Neurological impairment	Both of these phyla are D-lactate producers.	D-lactate may negatively affect cognition and may be linked to chronic fatigue syndrome. D-lactate in this model has also been found to be linked to an impaired gut barrier.	(Maes et al. 2007; Sheedy et al. 2009)
Control and Schizophrenic patients – both genders and aged 18–65.	Shotgun metagenomic analysis of oropharyngeal microbiota.	*Lactobacillus* spp. *Bifidobacterium* spp. *Eubacterium hallii* *Candida* spp. *Capnocytophaga* spp. *Neisseria* spp. *Haemophilus* spp.	+ Schizophrenia + Schizophrenia + Schizophrenia + Schizophrenia - Schizophrenia - Schizophrenia - Schizophrenia		These bacteria may be linked to dysfunction in the prefrontal basal ganglia or to hyperactivity in the substantia nigra, as these areas are linked with schizophrenia.	(Castro-Nallar et al. 2015) (Yoon et al. 2013)
Adult rats.	Intraventricular administration of proprionate.	Propionate (a SCFA)	+ Austism like behaviours	+ Innate neuro-inflammation + Oxidative stress	The presence of bacterial species which produce propionate in the gut microbiota is positively correlated to the development of autism in a rat model. Inflammation could be the link between this SCFA and the seen behaviours.	(MacFabe 2012)
Children with ASD $n = 23$, age matched healthy control $n = 31$.	Faecal samples were measured for SFCAs, phenols and ammonia concentrations.	Acetic acid (Iso)Butyric acid (Iso)Valeric acid	+ ASD in children		These faecal SFCAs, and thus bacteria that produce them, are linked with autism in children. This demonstrates a connection between the gut and the brain via the microbiota.	(Skowronska and Albrecht 2012; Wang et al. 2012)
		Ammonia	+ ASD in children		Ammonia producing bacteria may cause autism in children. Perhaps via impaired BBB and abnormal neurotransmitter production.	

and IV and the Bacteroidetes phyla (Miyake et al. 2015). Moreover, a human study by Farrokhi et al. found that the levels of a gastrointestinal and oral microbiota-derived lipopeptide, lipid 654, the ligand of innate immune receptor Toll-like receptor 2 (TLR2), in MS patients are significantly lower than in healthy individuals. This finding suggests that the presence of serum levels of microbiota-derived molecules such as lipid 654 may play an essential role in MS pathogenesis.

Mechanisms and pathways for the microbiota affecting cognition

There are several mechanisms proposed for how bidirectional communication between gut microbiota and the brain occurs including neuronal, immunological, biochemical and endocrine pathways (Dinan et al. 2015; Galland 2014; Montiel-Castro et al. 2013; Tillisch 2014). Firstly, communication between the brain and gut microbiota has been shown via the vagus nerve. The vagus nerve (cranial nerve X) contains both afferent and efferent branches, which play a vital role in signalling between the brain and the gut. Asymptomatic mice which had no overt immune response, were infected with the enteropathogen, *Campylobacter jejuni*, and were found to be more anxious than non-infected control mice (Lyte et al. 1998). This study demonstrates the role of the nervous system, probably via the vagal pathway, in the communication between the gut and the brain during gastrointestinal tract infection. Administration of probiotic bacteria, *Bifidobacterium longum* NCC3001, in a chemically-induced colitis mouse model showed a vagal pathway-dependent anxiolytic (reduction in anxiety) effect and normalized brain derived neurotrophic factor (BDNF) levels (Bercik et al. 2011). This probiotic could, therefore, be used as therapy for patients who experience anxiety.

Secondly, the immune system plays a vital role in the bidirectional communication between the gut and the brain. Systemic inflammation is represented by increased levels of serum pro-inflammatory cytokines - such as IL-1, IL-6, and TNF-α which are associated with depression and sickness symptoms in patients (Kelley et al. 2003; Myers 2008). IL-1 and IL-6 stimulate the release of corticotrophin releasing hormone (CRH), the regulator of the HPA, which as stated earlier can be linked to depression. Thus, inflammation can be directly linked to depression. Recognition of the gut microbe's structural components, such as LPS, by the host's innate immune receptors results in the production of pro-inflammatory cytokines (Duerkop et al. 2009), therefore showing how the gut microbiota can cause cognition deficits via inflammation.

Chronic gut immune activation is associated with impaired gut barrier integrity and increased systemic inflammation (Kim et al. 2012). Administration of some probiotic strains was shown to improve gut barrier integrity by increasing tight junction protein expression levels (Han et al. 2015; Shi et al. 2014; Ulluwishewa et al. 2011). Treatment with *Lactobacillus plantarum* as a probiotic attenuated colonic epithelial barrier dysfunction in a spontaneous mouse colitis model (Chen et al. 2010; Han et al. 2015). In addition, several studies found that the incidence of certain bacteria was a potential link between cognition and inflammation (see in Table 2) (Bajaj 2014; Castro-Nallar et al. 2015; Desbonnet et al. 2014; Desbonnet et al. 2015; Kang et al. 2014; O'Mahony et al. 2014; Savignac et al. 2015). These findings may provide the information that gut microbiota were one of the central mediators between obese-induced inflammation and cognition. As systemic inflammation is known to be a major risk factor for obesity and insulin resistance in MetS, it suggests that gut microbiota alteration might be a link between systemic inflammation, obesity and impaired CNS function. Kang et al. showed that an increase in anxiety levels and declined cognitive levels are positively correlated with increased bacterial numbers in the phyla Firmicutes, Bacteroidetes and Proteobacteria, while bacteria in the family of Lachnospiraceae are associated with a reduced anxiety phenotype. High-fat diet fed obese mice also exhibited higher levels of anxiety when compared to control mice (Kang et al. 2014). These findings support the connection of the gut to the brain via the immune response.

In addition, gut microbiota produce many types of metabolites which have an effect on the CNS, specifically D-lactate, ammonia and short-chain fatty acids (SCFA) (Galland 2014). In chronic fatigue syndrome (CFS) patients with cognitive dysfunction and neurological impairment, increased levels of D-lactate producing bacteria such as *Enterococcus* spp. and *Streptococcus* spp. were found in their stools, indicating that D-lactate might have a modulatory role on cognition (Galland 2014; Sheedy et al. 2009). The impaired gut barrier state found in CFS patients has been linked to increased levels of serum D-lactate (Maes et al. 2007). Taken together, these studies suggest that increased levels of D-lactate producing bacteria and an impaired gut barrier can result in impairment of brain function. Some strains of *Lactobacillus* spp. (bacteria which can produce D-lactate) (Ewaschuk et al. 2005) when used as a probiotic, can cause impaired CNS functions especially in patients with short bowel syndrome; therefore the presence of these bacteria in the gut microbiota may have a detrimental effect on cognition. Munakata et al. reported that a 5-year old girl developed D-lactic acidosis after treatment with the probiotic Lactomin, a commercial probiotic product (Munakata et al. 2010). Recurrent D-lactic acidosis in a 14-year-old boy with short bowel syndrome without ingestion of the probiotic supplementation was also reported (Puwanant et al. 2005). These findings support the possible neurotoxicity effect of lactic acid produced by gut microbiota.

Ammonia (NH_3) is a well-known neurotoxic molecule. Bacterial urease converts urea to ammonia and carbon

Table 3 Taxonomical classification of gut microbiota reviewed in this article according to the five dominant bacterial phyla

Phylum Bacteroidetes	
Alistipes spp.	Porphyromonadaceae
Bacteroides spp.	*Prevotella* spp.
Capnocytophaga spp.	
Phylum Firmicutes	
Anaerotruncus colihominis	*Lactobacillus* spp.
Butyricicoccus spp.	*Mucispirillum schaedleri*
Enterococcus spp.	*Roseburia* spp.
Eubacterium hallii	*Ruminococcus* spp.
Faecalibacterium prausnitzii	*Streptococcus* spp.
Lacnospiraceae	
Phylum Proteobacteria	
Alcaligenaceae	Enterobacteriaceae
Bilophila wadsworthia	*Haemophilus* spp.
Campylobacter jejuni	*Neisseria* spp.
Phylum Actinobacteria	
Bifidobacterium spp.	
Phylum Verrucomicrobia	
Akkermansia muciniphila	

dioxide. Hyperammonemia, the state of increased levels of NH_3 in the blood leads to: impaired blood-brain barrier integrity, intracerebral productions of the neurotransmitters serotonin and dopamine and the production of abnormal neurotransmitters octopamine and phenylethylamine (Skowronska and Albrecht 2012). Therefore, the presence of species which produce bacterial urease in the gut microbiota may cause these detrimental effects in the CNS.

Short-chain fatty acids (SCFAs) such as acetate, propionate and butyrate, are bacterial fermentation products that play a crucial role in the development of the host's gut immune homeostasis. Propionate promotes regulatory T cells (Treg), which have anti-inflammatory effects and can prevent excess inflammation in the gut mucosal tissue (Furusawa et al. 2013; Smith et al. 2013). However, MacFabe and colleagues proposed that propionate has been linked to autism-like behaviours. An intraventricular administration of this SFCA in adult rats caused impaired behaviour, such as abnormal motor movements, cognitive deficits, repetitive interests and impaired social interactions. These behaviours were also linked to neuroinflammation (MacFabe 2012), suggesting that inflammation was the central mediator between the SFCAs and the outcome. Certain faecal SCFAs (acetic, butyric, isobutyric, valeric, and isovaleric) are significantly increased in children who suffer from autism spectrum disorder (ASD) when compared to control groups (Wang et al. 2012). This evidence supports the role of gut microbial products as a communication pathway connecting the gut and the brain.

Another possible explanation is that some bacterial strains have been found to produce neurotransmitters such as gamma-amino butyrate (GABA), serotonin, 5-hydroxytryptamine, (5-HT), dopamine (DA), epinephrine, norepinephrine (NE) and histamine which can access the CNS via the enteric nervous system (Tillisch 2014). These gut microbe-derived neurotransmitters can affect CNS functions with both positive and negative outcomes.

Recently, the gut microbiome, the collective term for the gut microbial genes, has been proposed to have a large influence in the *'gut -brain axis,'* even though the epigenetic

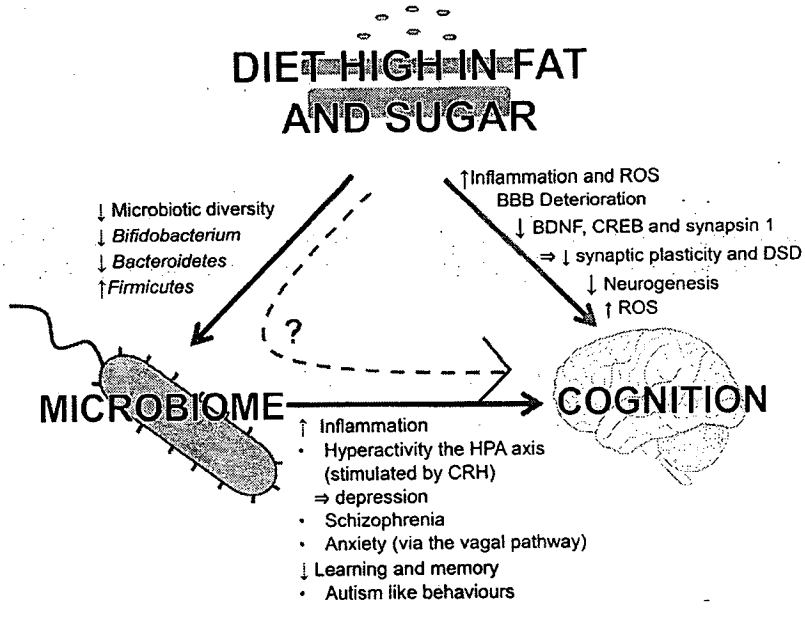


Fig. 3 The proposed mechanisms behind the detrimental relationships between a diet high in fat and sugar, cognition and the microbiome. The dashed arrow indicates the hypothesis that the microbiome may be a central mediator between a poor diet and cognition deficits. DPD – dendritic spine density, HPA axis – the hypothalamic-pituitary-adrenal axis, CRH – corticotropin-releasing hormone, BBB – blood brain barrier, BDNF – brain derived neurotrophic factor, CREB – cAMP response binding element protein, ROS – reactive oxygen species

regulation by the gut microbiome in CNS disorders is still poorly defined. Stillling and colleagues hypothesised that the gut microbiome could act as an epigenetic factor to the host's genome and cause alterations of the host chromatin's plasticity in neurons which would lead to altered neuronal transcription (Stilling et al. 2014). It is also clear that the convergence of the fields of neuroscience, microbiology and molecular biology are necessary to decipher the gut-microbiome-brain interaction in health and disease. All gut microbes and their taxonomic classifications regarding to the five bacterial dominant phyla that contribute to "the microbiota-gut-brain axis" in this review is summarized in Table 3.

Conclusion

A poor diet, leading to obesity and MetS, is known to have vast detrimental effects on cognition. The mechanisms linked to this relationship include inflammation, insulin resistance and impairment of the BBB. Also, a poor diet in childhood has been shown to cause issues concerning behaviour and intelligence in later life. A poor diet is responsible for various changes in the constitution and condition of the microbiota, which is also related to certain MetS symptoms and a marked increase in systemic as well as cerebral inflammation. It is clear that the composition of the microbiota can modulate level of cognition. Recently, it has been speculated that changes in the gut microbiota population (gut dysbiosis) may be one of the major factors in the pathogenesis of schizophrenia, depression, anxiety, autism and multiple sclerosis. Several mechanisms have been demonstrated to link the CNS and the gut microbiota, including BBB impairment, inflammation and the abnormal production of neurotransmitters, possibly via the microbiota's production of certain SCFAs, urease and D- lactate. All of those findings suggest that not just one factor or the single mechanism, is responsible for the relationship among obesity, gut microbiota and the cognition, but the combination of several factors should be involved. .

The possible mechanism that the gut microbiota plays the mediating role between consumption of a diet with high in fat and sugar and the cognitive deficits is summarized in Fig. 3. Therefore, it is possible that the clinical administration of probiotics or prebiotics may be able to modulate this and provide beneficial effects for MetS patients or for sufferers of various psychological disorders. Further investigations are required to confirm the directionality of the relationship between poor diet, gut microbiota and cognition.

Acknowledgments This work was supported by Thailand Research Fund grants: TRF-BRG 5780016 (SC) and TRG5880041 (PT); the National Research Council of Thailand (SC); a NSTDA Research Chair Grant from the National Science and Technology Development Agency Thailand (NC) and the Chiang Mai University Center of Excellence Award (NC).

Compliance with ethical standards

Conflict of interest The authors declare that they have no conflict of interest.

References

Alexander C, Rietschel ET (2001) Bacterial lipopolysaccharides and innate immunity. J Endotoxin Res 7:167–202

Bäckhed F et al (2004) The gut microbiota as an environmental factor that regulates fat storage. Proc Natl Acad Sci U S A 101:15718–15723. doi:10.1073/pnas.0407076101

Bajaj JS (2014) The role of microbiota in hepatic encephalopathy. Gut Microbes 5:397–403. doi:10.4161/gmic.28684

Belkaid Y, Hand TW (2014) Role of the microbioa in immunity and inflammation. Cell 157:121–141

Bercik P (2011) The microbiota-gut-brain axis: learning from intestinal bacteria? Gut 60:288–289. doi:10.1136/gut.2010.22904710.1136/gut.2010.226779

Bercik P et al (2011) The anxiolytic effect of Bifidobacterium longum NCC3001 involves vagal pathways for gut-brain communication. Neurogastroenterol Motil 23:1132–1139. doi:10.1111/j.1365-2982.2011.01796.x

Berer K et al (2011) Commensal microbiota and myelin autoantigen cooperate to trigger autoimmune demyelination. Nature 479:538–541. doi:10.1038/nature10554

Bocarsly ME et al (2015) Obesity diminishes synaptic markers, alters microglial morphology, and impairs cognitive function. Proc Natl Acad Sci U S A 112:15731–15736. doi:10.1073/pnas.1511593112

Boden G, Cheung P, Kresge K, Homko C, Powers B, Ferrer L (2014) Insulin resistance is associated with diminished endoplasmic reticulum stress responses in adipose tissue of healthy and diabetic subjects. Diabetes 63:2977–2983. doi:10.2337/db14-0055

Boeka AG, Lokken KL (2008) Neuropsychological performance of a clinical sample of extremely obese individuals. Archives of Clinical Neuropsychology : The Official Journal of the National Academy of Neuropsychologists 23:467–474. doi:10.1016/j.acn.2008.03.003

Cani PD et al (2007) Metabolic endotoxemia initiates obesity and insulin resistance. Diabetes 56:1761–1772. doi:10.2337/db06-1491

Capuron L et al (2007) Basal ganglia hypermetabolism and symptoms of fatigue during interferon-alpha therapy. Neuropsychopharmacology 32:2384–2392. doi:10.1038/sj.npp.1301362

Capuron L et al (2012) Dopaminergic mechanisms of reduced basal ganglia responses to hedonic reward during interferon alfa administration. Arch Gen Psychiatry 69:1044–1053. doi:10.1001/archgenpsychiatry.2011.2094

Castanon N, Lasselin J, Capuron L (2014) Neuropsychiatric comorbidity in obesity: role of inflammatory processes. Front Endocrinol:5–74. doi:10.3389/fendo.2014.00074

Castro-Nallar E et al (2015) Composition, taxonomy and functional diversity of the oropharynx microbiome in individuals with schizophrenia and controls. Peer J 3:e1140. doi:10.7717/peerj.1140

Catanzaro R et al (2015) The gut microbiota and its correlations with the central nervous system disorders. Panminerva Med 57:127–143

Chamberlain SR, Derbyshire KL, Leppink E, Grant JE (2015) Obesity and dissociable forms of impulsivity in young adults. CNS spectrums 20:500–507. doi:10.1017/s1092852914000625

Chen HQ et al (2010) Lactobacillus plantarum ameliorates colonic epithelial barrier dysfunction by modulating the apical junctional complex and PepT1 in IL-10 knockout mice. Am J Physiol Gastrointest Liver Physiol 299:G1287–G1297. doi:10.1152/ajpgi.00196.2010

Clegg DJ et al (2011) Consumption of a high-fat diet induces central insulin resistance independent of adiposity. Physiol Behav 103:10–16. doi:10.1016/j.physbeh.2011.01.010

Cordner ZA, Tamashiro KL (2015) Effects of high-fat diet exposure on learning & memory. Physiol Behav. doi:10.1016/j.physbeh.2015.06.008

Cox AJ, West NP, Cripps AW (2015) Obesity, inflammation, and the gut microbiota. Lancet Diabetes Endocrinol 3:207–215. doi:10.1016/S2213-8587(14)70134-2

David LA et al (2014) Diet rapidly and reproducibly alters the human gut microbiome. Nature 505:559–563. doi:10.1038/nature12820

de La Serre CB, Ellis CL, Lee J, Hartman AL, Rutledge JC, Raybould HE (2010) Propensity to high-fat diet-induced obesity in rats is associated with changes in the gut microbiota and gut inflammation. American journal of physiology - gastrointestinal and liver. Physiology 299:G440–G448. doi:10.1152/ajpgi.00098.2010

Desbonnet L, Clarke G, Shanahan F, Dinan TG, Cryan JF (2014) Microbiota is essential for social development in the mouse. Mol Psychiatry 19:146–148. doi:10.1038/mp.2013.65

Desbonnet L et al (2015) Gut microbiota depletion from early adolescence in mice: Implications for brain and behaviour. Brain Behav Immun 48:165–173. doi:10.1016/j.bbi.2015.04.004

Dinan TG, Stilling RM, Stanton C, Cryan JF (2015) Collective unconscious: how gut microbes shape human behavior. J Psychiatr Res 63:1–9. doi:10.1016/j.jpsychires.2015.02.021

Donaldson GP, Lee SM, Mazmanian SK (2015) Gut biogeography of the bacterial microbiota. Nat Rev Microbiol 14:20–32. doi:10.1038/nrmicro3552

Duerkop BA, Vaishnava S, Hooper LV (2009) Immune responses to the microbiota at the intestinal mucosal surface. Immunity 31:368–376. doi:10.1016/j.immuni.2009.08.009

Esser N, Legrand-Poels S, Piette J, Scheen AJ, Paquot N (2014) Inflammation as a link between obesity, metabolic syndrome and type 2 diabetes. Diabetes Res Clin Pract 105:141–150. doi:10.1016/j.diabres.2014.04.006

Ewaschuk JB, Naylor JM, Zello GA (2005) D-lactate in human and ruminant metabolism. J Nutr 135:1619–1625

Fava F, Gitau R, Griffin BA, Gibson GR, Tuohy KM, Lovegrove JA (2013) The type and quantity of dietary fat and carbohydrate alter faecal microbiome and short-chain fatty acid excretion in a metabolic syndrome 'at-risk' population. Int J Obes 37:216–223. doi:10.1038/ijo.2012.33

Felger JC, Miller AH (2012) Cytokine effects on the basal ganglia and dopamine function: the subcortical source of inflammatory malaise. Front Neuroendocrinol 33:315–327. doi:10.1016/j.yfrne.2012.09.003

Finegold S, Summanen P, Hunt Gerardo S, Baron E (1992) Clinical importance of Bilophila wadsworthia European journal of clinical microbiology & infectious diseases : official publication of the European Society of Clinical Microbiology 11:1058–1063

Flint HJ, Scott KP, Duncan SH, Louis P, Forano E (2012) Microbial degradation of complex carbohydrates in the gut. Gut Microbes 3:289–306. doi:10.4161/gmic.19897

Furusawa Y et al (2013) Commensal microbe-derived butyrate induces the differentiation of colonic regulatory. T Cells Nature 504:446–450. doi:10.1038/nature12721

Galland L (2014) The gut microbiome and the brain. J Med Food 17:1261–1272. doi:10.1089/jmf.2014.7000

Gareau MG (2014) Microbiota-gut-brain axis and cognitive function. Adv Exp Med Biol 817:357–371. doi:10.1007/978-1-4939-0897-4_16

Gareau MG et al (2011) Bacterial infection causes stress-induced memory dysfunction in mice. Gut 60:307–317. doi:10.1136/gut.2009.202515

Gill SR et al (2006) Metagenomic analysis of the human distal gut microbiome. Science 312:1355–1359. doi:10.1126/science.1124234

Gregor MF, Hotamisligil GS (2011) Inflammatory mechanisms in obesity. Annu Rev Immunol 29:415–445. doi:10.1146/annurev-immunol-031210-101322

Han HZ, Zhao YJ, Shi CZ, Liang Y, Yang J (2015) Effect of lactobacillus plantarum on intestinal infection in multiple drug-resistant bacteria mice. Surg Infect 16:762–768. doi:10.1089/sur.2014.222

Haroon E, Raison CL, Miller AH (2012) Psychoneuroimmunology meets neuropsychopharmacology: translational implications of the impact of inflammation on behavior. Neuropsychopharmacology 37:137–162. doi:10.1038/npp.2011.205

Haslam DW, James WPT (2005) Obesity. Lancet 366:1197–1209. doi:10.1016/S0140-6736(05)67483-1

Kang SS et al. (2014) Diet and exercise orthogonally alter the gut microbiome and reveal independent associations with anxiety and cognition. Mol Neurodegener, 9:36 doi:10.1186/1750-1326-9-36

Kelley KW, Bluthe RM, Dantzer R, Zhou JH, Shen WH, Johnson RW, Broussard SR (2003) Cytokine-induced sickness behavior. Brain Behav Immun 17(Suppl 1):S112–S118

Khan NA, Raine LB, Donovan SM, Hillman CH (2014) IV The cognitive implications of obesity and nutrition in childhood. Monogr Soc Res Child Dev 79:51–71

Kim Y, Je Y (2015) Dairy consumption and risk of metabolic syndrome: a meta-analysis. Diabet Med. doi:10.1111/dme.12970

Kim KA, Gu W, Lee IA, Joh EH, Kim DH (2012) High fat diet-induced gut microbiota exacerbates inflammation and obesity in mice via the TLR4 signaling pathway. PLoS One 7:e47713. doi:10.1371/journal.pone.0047713

Klok MD, Jakobsdottir S, Drent ML (2007) The role of leptin and ghrelin in the regulation of food intake and body weight in humans: a review. Obes Rev 8:21–34. doi:10.1111/j.1467-789X.2006.00270.x

Koponen H, Jokelainen J, Keinanen-Kiukaanniemi S, Kumpusalo E, Vanhala M (2008) Metabolic syndrome predisposes to depressive symptoms: a population-based 7-year follow-up study. J Clinic Psych 69:178–182

Kratz M et al (2014) Metabolic dysfunction drives a mechanistically distinct proinflammatory phenotype in adipose tissue macrophages. Cell Metab 20:614–625. doi:10.1016/j.cmet.2014.08.010

LeBlanc MM et al (2012) Adiposity and physical activity are not related to academic achievement in school-aged children. J Develop Behav Pediatrics JDBP 33:486–494. doi:10.1097/DBP.0b013e31825b849e

Ley RE, Turnbaugh PJ, Klein S, Gordon JI (2006) Microbial ecology: human gut microbes associated with obesity. Nature 444:1022–1023

Liou AP, Paziuk M, Luevano J-M, Machineni S, Turnbaugh PJ, Kaplan LM (2013) Conserved shifts in the gut microbiota due to gastric bypass reduce host weight and adiposity. Sci Transl Med 5:178ra141. doi:10.1126/scitranslmed.3005687

Liu B, Hong JS (2003) Role of microglia in inflammation-mediated neurodegenerative diseases: mechanisms and strategies for therapeutic intervention. J Pharmacol Exp Ther 304:1–7. doi:10.1124/jpet.102.035048

Liu J, Zubieta J-K, Heitzeg M (2012) Sex differences in anterior cingulate cortex activation during impulse inhibition and behavioral correlates. Psychiatry Res 201:54–62. doi:10.1016/j.pscychresns.2011.05.008

Logan AC (2015) Dysbiotic drift: mental health, environmental grey space, and microbiota. J Physiol Anthropol 34:23. doi:10.1186/s40101-015-0061-7

Lyte M, Varcoe JJ, Bailey MT (1998) Anxiogenic effect of subclinical bacterial infection in mice in the absence of overt immune activation. Physiol Behav 65:63–68

MacDougall R (2012) NIH Human Microbiomes Project defines normal bacterial makeup of body. National Institues of Health

MacFabe DF (2012) Short-chain fatty acid fermentation products of the gut microbiome: implications in autism spectrum disorders. Microb Ecol Health Dis 23:10.3402/mehd.v3423i3400.19260. doi:10.3402/mehd.v23i0.19260

Maes M, Mihaylova I, Leunis JC (2007) Increased serum IgA and IgM against LPS of enterobacteria in chronic fatigue syndrome (CFS): indication for the involvement of gram-negative enterobacteria in the etiology of CFS and for the presence of an increased gut-intestinal permeability. J Affect Disord 99:237–240. doi:10.1016/j.jad.2006.08.021

Maranduba CM et al (2015) Intestinal microbiota as modulators of the immune system and neuroimmune system: impact on the host health and homeostasis. J Immunol Res 2015:931574. doi:10.1155/2015/931574

Mariat D et al (2009) The Firmicutes/Bacteroidetes ratio of the human microbiota changes with age. BMC Microbiol 9:1–6. doi:10.1186/1471-2180-9-123

Mason TB, Lewis RJ (2015) Assessing the roles of impulsivity, food-related cognitions, BMI, and demographics in the dual pathway model of binge eating among men and women. Eat Behav 18:151–155. doi:10.1016/j.eatbeh.2015.05.015

Medvidovic S, Titlic M, Maras-Simunic M (2013) P300 evoked potential in patients with mild cognitive impairment. Acta Informatica Medica 21:89–92. doi:10.5455/aim.2013.21.89-92

Miyake S et al (2015) Dysbiosis in the gut microbiota of patients with multiple sclerosis, with a striking depletion of species belonging to clostridia XIVa and IV clusters. PLoS One 10:e0137429. doi:10.1371/journal.pone.0137429

Molteni R, Barnard RJ, Ying Z, Roberts CK, Gómez-Pinilla F (2002) A high-fat, refined sugar diet reduces hippocampal brain-derived neurotrophic factor, neuronal plasticity, and learning. Neuroscience 112:803–814. doi:10.1016/S0306-4522(02)00123-9

Molteni R, Wu A, Vaynman S, Ying Z, Barnard RJ, Gómez-Pinilla F (2004) Exercise reverses the harmful effects of consumption of a high-fat diet on synaptic and behavioral plasticity associated to the action of brain-derived neurotrophic factor. Neuroscience 123:429–440. doi:10.1016/j.neuroscience.2003.09.020

Montiel-Castro AJ, Gonzalez-Cervantes RM, Bravo-Ruiseco G, Pacheco-Lopez G (2013) The microbiota-gut-brain axis: neurobehavioral correlates, health and sociality. Front Integr Neurosci 7. doi:10.3389/fnint.2013.00070

Munakata S, Arakawa C, Kohira R, Fujita Y, Fuchigami T, Mugishima H (2010) A case of D-lactic acid encephalopathy associated with use of probiotics. Brain Dev 32:691–694. doi:10.1016/j.braindev.2009.09.024

Myers JS (2008) Proinflammatory cytokines and sickness behavior: implications for depression and cancer-related symptoms. Oncol Nurs Forum 35:802–807. doi:10.1188/08.ONF.802-807

NCBI (2015) BDNF brain derived neurotrophic facto [*Homo sapiens* (human)]. Gene

Nguyen TLA, Vieira-Silva S, Liston A, Raes J (2015) How informative is the mouse for human gut microbiota research? Disease Models Mechanisms 8:1–16. doi:10.1242/dmm.017400

O'Mahony SM et al (2014) Disturbance of the gut microbiota in early-life selectively affects visceral pain in adulthood without impacting cognitive or anxiety-related behaviors in male rats. Neuroscience 277:885–901. doi:10.1016/j.neuroscience.2014.07.054

Ojeda P, Bobe A, Dolan K, Leone V, Martinez K (2015) Nutritional modulation of gut microbiota - the impact on metabolic disease pathophysiology. J Nutr Biochem. doi:10.1016/j.jnutbio.2015.08.013

Org E et al (2015) Genetic and environmental control of host-gut microbiota interactions. Genome Res 25:1558–1569. doi:10.1101/gr.194118.115

Pariante CM, Lightman SL (2008) The HPA axis in major depression: classical theories and new developments. Trends Neurosci 31:464–468. doi:10.1016/j.tins.2008.06.006

Park HR, Park M, Choi J, Park K-Y, Chung HY, Lee J (2010) A high-fat diet impairs neurogenesis: involvement of lipid peroxidation and brain-derived neurotrophic factor. Neurosci Lett 482:235–239. doi:10.1016/j.neulet.2010.07.046

Pauli-Pott U, Albayrak O, Hebebrand J, Pott W (2010) Association between inhibitory control capacity and body weight in overweight and obese children and adolescents: dependence on age and inhibitory control component. Child Neuropsychology : a Journal on Normal and Abnormal Development in Childhood and Adolescence 16:592–603. doi:10.1080/09297049.2010.485980

Pintana H, Apaijai N, Chattipakorn N, Chattipakorn SC (2013) DPP-4 inhibitors improve cognition and brain mitochondrial function of insulin-resistant rats. J Endocrinol 218:1–11. doi:10.1530/joe-12-0521

Pipatpiboon N, Pratchayasakul W, Chattipakorn N, Chattipakorn SC (2012) PPARgamma agonist improves neuronal insulin receptor function in hippocampus and brain mitochondria function in rats with insulin resistance induced by long term high-fat diets. Endocrinology 153:329–338. doi:10.1210/en.2011-1502

Pratchayasakul W, Kerdphoo S, Petsophonsakul P, Pongchaidecha A, Chattipakorn N, Chattipakorn SC (2011) Effects of high-fat diet on insulin receptor function in rat hippocampus and the level of neuronal corticosterone. Life Sci 88:619–627. doi:10.1016/j.lfs.2011.02.003

Puwanant M, Mo-Suwan L, Patrapinyokul S (2005) Recurrent D-lactic acidosis in a child with short bowel syndrome. Asia Pac J Clin Nutr 14:195–198

Ridaura VK et al (2013) Gut microbiota from twins discordant for obesity modulate metabolism in mice. Science 341. doi:10.1126/science.1241214

Savage DC (1997) Microbial ecology of the gastrointestinal tract. Annu Rev Microbiol 31:107–133

Savignac HM, Tramullas M, Kiely B, Dinan TG, Cryan JF (2015) Bifidobacteria modulate cognitive processes in an anxious mouse strain. Behav Brain Res 287:59–72. doi:10.1016/j.bbr.2015.02.044

Semova I, Carten Juliana D, Stombaugh J, Mackey Lantz C, Knight R, Farber Steven A, Rawls John F (2012) Microbiota Regulate Intestinal Absorption and Metabolism of Fatty Acids in the Zebrafish. Cell Host Microbe 12:277–288. doi:10.1016/j.chom.2012.08.003

Sender R, Fuchs S, Milo R (2016) Are we really vastly outnumbered? Revisiting the ratio of bacterial to host cells in humans. Cell 164:337–340. doi:10.1016/j.cell.2016.01.013

Sheedy JR et al (2009) Increased d-lactic acid intestinal bacteria in patients with chronic fatigue syndrome. In Vivo 23:621–628

Shi CZ et al (2014) Combined probiotic bacteria promotes intestinal epithelial barrier function in interleukin-10-gene-deficient mice. World J Gastroenterol 20:4636–4647. doi:10.3748/wjg.v20.i16.4636

Shi LL, Li Y, Wang Y, Feng Y (2015) MDG-1, an Ophiopogon polysaccharide, regulate gut microbiota in high-fat diet-induced obese C57BL/6 mice. Int J Biol Macromol 81:576–583. doi:10.1016/j.ijbiomac.2015.08.057

Shoelson SE, Herrero L, Naaz A (2007) Obesity, inflammation, and insulin resistance. Gastroenterology 132:2169–2180. doi:10.1053/j.gastro.2007.03.059

Skowronska M, Albrecht J (2012) Alterations of blood brain barrier function in hyperammonemia: an overview. Neurotox Res 21:236–244. doi:10.1007/s12640-011-9269-4

Smith PM et al (2013) The microbial metabolites, short-chain fatty acids, regulate colonic Treg cell homeostasis. Science 341:569–573. doi:10.1126/science.1241165

Sripetchwandee J, Pipatpiboon N, Pratchayasakul W, Chattipakorn N, Chattipakorn SC (2014) DPP-4 inhibitor and PPARγ agonist restore the loss of CA1 dendritic spines in obese insulin-resistant rats. Arch Med Res 45:547–552. doi:10.1016/j.arcmed.2014.09.002

Stilling RM, Dinan TG, Cryan JF (2014) Microbial genes, brain & behaviour - epigenetic regulation of the gut-brain axis. Genes Brain Behav 13:69–86. doi:10.1111/gbb.12109

Stranahan AM, Norman ED, Lee K, Cutler RG, Telljohann RS, Egan JM, Mattson MP (2008) Diet-induced insulin resistance impairs hippocampal synaptic plasticity and cognition in middle-aged rats. Hippocampus 18:1085–1088. doi:10.1002/hipo.20470

Subramanian V, Ferrante AW Jr (2009) Obesity, inflammation, and macrophages. Nestle Nutrition Workshop Series Paediatric Programme 63:151–159 . doi:10.1159/000209979discussion 159–162, 259–168

Tascilar ME et al (2011) P300 auditory event-related potentials in children with obesity: is childhood obesity related to impairment in cognitive functions? Pediatr Diabetes 12:589–595. doi:10.1111/j.1399-5448.2010.00748.x

Tilg H, Moschen AR (2006) Adipocytokines: mediators linking adipose tissue, inflammation and immunity. Nat Rev Immunol 6:772–783

Tillisch K (2014) The effects of gut microbiota on CNS function in humans. Gut Microbes 5:404–410. doi:10.4161/gmic.29232

Tournoy J et al (2010) Association of cognitive performance with the metabolic syndrome and with glycaemia in middle-aged and older European men: the European Male Ageing Study. Diabetes Metab Res Rev 26:668–676. doi:10.1002/dmrr.1144

Trayhurn P, Beattie JH (2001) Physiological role of adipose tissue: white adipose tissue as an endocrine and secretory organ. The Proceedings of the Nutrition Society 60:329–339

Turnbaugh PJ, Ley RE, Mahowald MA, Magrini V, Mardis ER, Gordon JI (2006) An obesity-associated gut microbiome with increased capacity for energy harvest. Nature 444:1027–1031. doi:10.1038/nature05414

Ulluwishewa D, Anderson RC, McNabb WC, Moughan PJ, Wells JM, Roy NC (2011) Regulation of tight junction permeability by intestinal bacteria and dietary components. J Nutr 141:769–776. doi:10.3945/jn.110.135657

Ursache A, Wedin W, Tirsi A, Convit A (2012) Preliminary evidence for obesity and elevations in fasting insulin mediating associations between cortisol awakening response and hippocampal volumes and frontal atrophy. Psychoneuroendocrinology 37:1270–1276. doi:10.1016/j.psyneuen.2011.12.020

Ussar S et al (2015) Interactions between Gut Microbiota, Host Genetics and Diet Modulate the Predisposition to Obesity and Metabolic Syndrome. Cell Metab 22:516–530. doi:10.1016/j.cmet.2015.07.007

Vrieze A et al (2012) Transfer of intestinal microbiota from lean donors increases insulin sensitivity in individuals with metabolic syndrome. Gastroenterology 143:913–916.e917

Walker JM, Harrison FE (2015) Shared neuropathological characteristics of obesity, type 2 diabetes and Alzheimer's disease: impacts on cognitive decline. Nutrients 7:7332–7357. doi:10.3390/nu7095341

Wang GJ et al (2009) Evidence of gender differences in the ability to inhibit brain activation elicited by food stimulation. Proc Natl Acad Sci U S A 106:1249–1254. doi:10.1073/pnas.0807423106

Wang L, Christophersen CT, Sorich MJ, Gerber JP, Angley MT, Conlon MA (2012) Elevated fecal short chain fatty acid and ammonia concentrations in children with autism spectrum disorder. Dig Dis Sci 57:2096–2102. doi:10.1007/s10620-012-2167-7

Wellen KE, Hotamisligil GS (2005) Inflammation, stress, and diabetes. J Clin Investig 115:1111–1119. doi:10.1172/JCI200525102

WHO (2015) Obesity and overweight WHO Media Centre Fact Sheet

Wu A, Ying Z, Gomez-Pinilla F (2004) The interplay between oxidative stress and brain-derived neurotrophic factor modulates the outcome of a saturated fat diet on synaptic plasticity and cognition. Eur J Neurosci 19:1699–1707. doi:10.1111/j.1460-9568.2004.03246.x

Xu H et al (2003) Chronic inflammation in fat plays a crucial role in the development of obesity-related insulin resistance. J Clin Invest 112:1821–1830. doi:10.1172/JCI19451

Yates KF, Sweat V, Yau PL, Turchiano MM, Convit A (2012) Impact of metabolic syndrome on cognition and brain: a selected review of the literature. Arterioscler Thromb Vasc Biol 32:2060–2067. doi:10.1161/atvbaha.112.252759

Yoon JH, Minzenberg MJ, Raouf S, D'Esposito M, Carter CS (2013) Impaired prefrontal-basal ganglia functional connectivity and substantia nigra hyperactivity in schizophrenia. Biol Psychiatry 74:122–129. doi:10.1016/j.biopsych.2012.11.018

Yuan T et al (2015) Pomegranate's Neuroprotective Effects against Alzheimer's Disease Are Mediated by Urolithins, Its Ellagitannin-Gut Microbial Derived Metabolites. ACS Chem Neurosci. doi:10.1021/acschemneuro.5b00260

Zhang B et al (2015) Altered baseline brain activities before food intake in obese men: a resting state fMRI study. Neurosci Lett 584:156–161. doi:10.1016/j.neulet.2014.10.020

เอกสารแนบหมายเลข 11

British Journal of Nutrition (2016), **116**, 1700–1708
doi:10.1017/S0007114516003871
© The Authors 2016

Energy restriction combined with dipeptidyl peptidase-4 inhibitor exerts neuroprotection in obese male rats

Hiranya Pintana[1,2], Pongpan Tanajak[1,2], Wasana Pratchayasakul[1,2], Piangkwan Sa-nguanmoo[1,2], Titikorn Chunchai[1,2], Pattarapong Satjaritanun[1,2], Linlada Leelarphat[1,2], Nipon Chattipakorn[1,2] and Siripom C. Chattipakorn[1,3]*

[1]*Neurophysiology Unit, Cardiac Electrophysiology Research and Training Center, Faculty of Medicine, Chiang Mai University, Chiang Mai 50200, Thailand*
[2]*Department of Physiology, Faculty of Medicine, Chiang Mai University, Chiang Mai 50200, Thailand*
[3]*Department of Oral Biology and Diagnostic Science, Faculty of Dentistry, Chiang Mai University, Chiang Mai 50200, Thailand*

(Submitted 25 May 2016 – Final revision received 19 August 2016 – Accepted 10 October 2016 – First published online 17 November 2016)

Abstract

Dipeptidyl peptidase-4 (DDP-4) inhibitors and energy restriction (ER) are widely used to treat insulin resistance and type 2 diabetes mellitus. However, the effects of ER or the combination with vildagliptin on brain insulin sensitivity, brain mitochondrial function, hippocampal synaptic plasticity and cognitive function in obese insulin-resistant rats have never been investigated. We hypothesised that ER with DDP-4 inhibitor exerts better efficacy than ER alone in improving cognition in obese insulin-resistant male rats by restoring brain insulin sensitivity, brain mitochondrial function and hippocampal synaptic plasticity. A total of twenty-four male Wistar rats were divided into two groups and fed either a normal diet or a high-fat diet (HFD) for 12 weeks. At week 13, the HFD rats were divided into three subgroups (n 6/subgroup) to receive one of the following treatments: vehicle, ER (60 % of energy received during the previous 12 weeks) or ER plus vildagliptin (3 mg/kg per d, p.o.) for 4 weeks. At the end of the treatment, cognitive function, metabolic parameters, brain insulin sensitivity, hippocampal synaptic plasticity and brain mitochondrial function were determined. We found that HFD-fed rats demonstrated weight gain with peripheral insulin resistance, dyslipidaemia, oxidative stress, brain insulin resistance, impaired brain mitochondrial function and cognitive dysfunction. Although HFD-fed rats treated with ER and ER plus vildagliptin showed restored peripheral insulin sensitivity and improved lipid profiles, only ER plus vildagliptin rats had restored brain insulin sensitivity, brain mitochondrial function, hippocampal synaptic plasticity and cognitive function. These findings suggest that only a combination of ER with DPP-4 inhibitor provides neuroprotective effects in obese insulin-resistant male rats.

Key words: Energy restriction: Vildagliptin: Obese insulin-resistant rats: Brain mitochondrial functions: Hippocampal synaptic plasticity: Cognitive functions

Obesity is a hallmark of insulin resistance and the metabolic syndrome, which has significantly increased worldwide[1]. Previous studies demonstrated that high-energy-diet-induced obesity led to the development of insulin resistance and cognitive decline in animal models[2,3]. In addition, our previous studies showed that the development of peripheral insulin resistance, brain insulin resistance, brain mitochondrial dysfunction, as well as cognitive decline, occurred in high-fat-diet (HFD)-induced obese male rats[4,5]. The dipeptidyl peptidase-4 inhibitor, vildagliptin, is widely used in the treatment of type 2 diabetes mellitus (T2DM) because of its beneficial effects on the regulation of the blood glucose level without causing any hypoglycaemic effects[6]. In addition, our previous studies reported that vildagliptin improved not only peripheral insulin resistance but also brain insulin resistance, as indicated by improved brain insulin receptor function in obese insulin-resistant rats[4]. Furthermore, the enhancement of hippocampal neurogenesis and improvement in cognition were found in HFD-fed rodents treated with vildagliptin[4,7,8]. All of those findings suggest that vildagliptin exerts beneficial effects on metabolic control and cognitive function.

Although several types of medication have been prescribed for the treatment of T2DM or the obese insulin-resistant condition, several side effects of medication have been observed. Therefore, a lifestyle modification, including energy restriction

Abbreviations: aCSF, artificial cerebrospinal fluid; Akt/PKB, serine/threonine-specific protein kinase B; ER, energy restriction; HFD, high-fat diet; HFRV, HFD-fed rats on a restricted diet and vehicle; HFRVil, HFD-fed rats on a restricted diet and vildaglptin; HFV, HFD-fed rats treated with the vehicle; IR, insulin receptor; LTD, long-term depression; LTP, long-term potentiation; MDA, malondialdehyde; MWM, Morris Water Maze; ND, normal diet; NDV, ND-fed rats treated with vehicle; ROS, reactive oxygen species.

* **Corresponding author:** S. C. Chattipakorn, fax +011 66 53 222 844, email scchattipakorn@gmail.com

Downloaded from https://www.cambridge.org/core. Chiang Mai University Library, on 06 Jun 2017 at 03:10:15, subject to the Cambridge Core terms of use, available at https://www.cambridge.org/core/terms. https://doi.org/10.1017/S0007114516003871

(ER), has been used as an alternative therapy in the obese insulin-resistant condition and T2DM. A previous study showed that ER in older animals led to improved metabolic parameters and also an extended lifespan[9]. Although adverse effects of ER such as promoting bone loss[10] and decreasing wound healing rate[11], in rats have been reported, several studies have shown that ER mimetics conferred the benefits of ER without its side effects[12,13]. Moderate ER had a beneficial impact on metabolic parameters, and improved insulin sensitivity in *in vitro* and *in vivo* studies[14–17]. In addition, a previous study reported that ER not only exerts a positive effect on metabolic control but also leads to improved brain function[18,19]. Several studies demonstrated that ER caused an increase in an endogenous apoptosis inhibitor in the neuronal cells[20], induced neuroprotection[21], decreased mitochondrial reactive oxygen species (ROS) production in aged rat brains[22] and preserved cognitive function in aged male rats[23]. All of those findings suggest that ER has beneficial effects in neuroprotection and the preservation of cognitive function.

However, the effects of either ER or the combination of ER plus vildagliptin on brain function, including brain insulin sensitivity, brain mitochondrial function, hippocampal synaptic plasticity and cognitive function in obese insulin-resistant rats have never been investigated. This study tests the hypothesis that the combination of ER plus vildagliptin has greater beneficial effects on the brain function of obese insulin-resistant rats than ER alone.

Methods

Animal models and experimental protocols

In total, twenty-four male Wistar rats weighing 180–200 g (approximately aged 5–6 weeks old), obtained from the National Animal Center, Salaya Campus, Mahidol University, Bangkok, Thailand, were used. All experiments were conducted in accordance with the approved protocol from the Faculty of Medicine, Chiang Mai University's Institutional Animal Care and Use Committee, in compliance with NIH guidelines (protocol number: 31/2557). All animals were housed in environmentally controlled conditions (25 ± 0·5°C and a 12 h light–12 h dark cycle) and were allowed to acclimate for 1 week. Rats were randomly divided into two groups and fed on either a normal diet (ND: 19·77 % energy (%E) from fat, n 6) or a HFD (59·28 %E from fat, n 18) for 12 weeks[24]. At the end of the 12th week, rats in the ND group received normal saline solution (NSS) via intra-gastric gavage, as indicated, and were designated the control group (ND-fed rats treated with the vehicle (NDV)), and rats in the HFD group were subdivided into three subgroups: (1) 12-week HFD-fed rats continued with HFD and in addition were given NSS via intra-gastric gavage for 4 weeks (HFD-fed rats treated with the vehicle (HFV)); (2) 12-week HFD-fed rats were switched to a restricted diet (ND, containing only 60 % energy intake compared with the energy intake of HFD), as described in a previous study[17], and were also given NSS via intra-gastric gavage for 4 weeks (HFD-fed rats on a restricted diet and vehicle (HFRV)); and (3) 12-week HFD-fed rats were switched to a restricted diet and in addition were given 3 mg/kg per d vildagliptin (Novartis, Thailand) via intra-gastric gavage for 4 weeks[6,8]. The rats' cognitive function was subsequently determined by the Morris Water Maze (MWM) test. Blood samples were collected from a tail vein at weeks 0, 12 and 16 for further plasma analysis. At the end of the experimental period, rats were deeply anesthetised with 2–3 % isoflurane and killed by decapitation. The brain of each rat was rapidly removed after death and carefully sliced in preparation for extracellular recording (insulin-induced long-term depression (LTD) and hippocampal synaptic long-term potentiation (LTP)), immunoblot and brain mitochondrial functions. The experimental protocol is shown in Fig. 1.

Blood sample assays

Plasma glucose and cholesterol levels were determined via colorimetric assay (Biotech). Plasma HDL and LDL levels were determined using a commercial colorimetric assay kit (Biovision). Plasma insulin levels were determined using the Sandwich ELISA kit (Millipore). Peripheral insulin resistance was assessed using the homoeostasis model assessment (HOMA), as previously described[5].

Oral glucose tolerance test

Oral glucose tolerance test (OGTT) was performed as described previously[4,8]. In brief, rats were starved overnight before the test and received 2 g/kg glucose solution via oral gavage, and then blood samples were collected at different time points. AUC were calculated to evaluate glucose tolerance.

Brain-slice preparation

The brain-slice preparation was performed as described previously[4,5,24]. In brief, the whole brain was rapidly removed after decapitation and then immersed in ice-cold high-sucrose artificial cerebrospinal fluid (aCSF). The hippocampal slices were cut using a vibratome (Vibratome Company). Following a 30-min post-slice incubation in high-sucrose aCSF, the slices were transferred to a standard aCSF for an additional 30 min at room temperature (22–24°C).

Extracellular recordings of hippocampal slices for insulin-induced long-term depression

An extracellular recording of hippocampal slices for insulin-induced LTD was performed as described in previous studies[4,5,24]. Hippocampal slices were perfused with aCSF (as a baseline condition) for 10 min, and then perfused with aCSF plus 500 nM-insulin (as an insulin-induced LTD) for an additional 10 min. After this, the slices were perfused with aCSF for an additional 50 min and readings recorded.

Extracellular recordings of hippocampal slices for synaptic long-term potentiation

The examination of electrical-induced hippocampal synaptic LTP was performed as described in a previous study[25]. In brief, LTP was induced by delivering high-frequency

Downloaded from https://www.cambridge.org/core. Chiang Mai University Library, on 06 Jun 2017 at 03:10:15, subject to the Cambridge Core terms of use, available at https://www.cambridge.org/core/terms. https://doi.org/10.1017/S0007114516003871

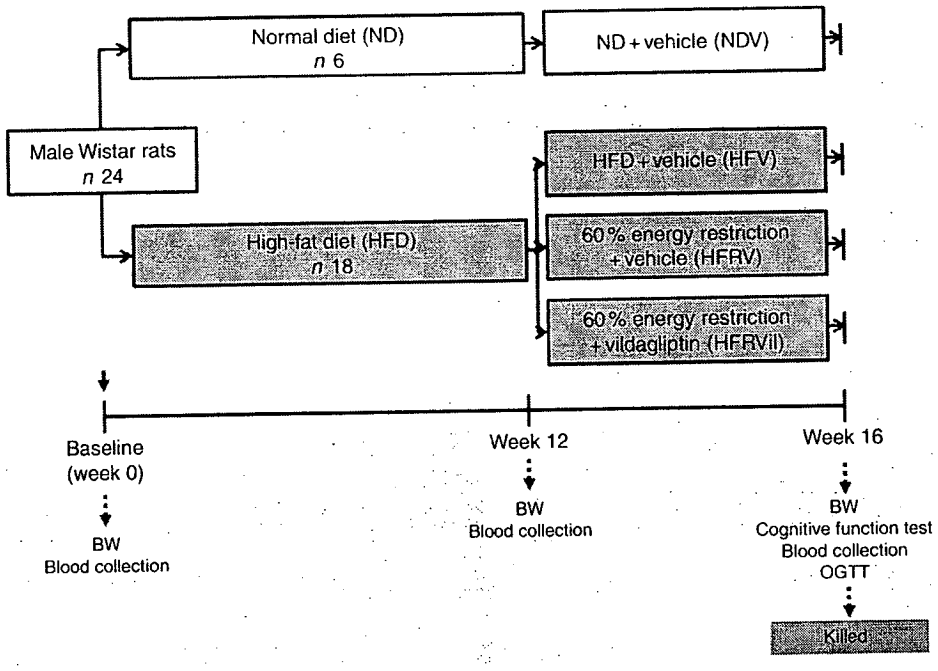


Fig. 1. The experimental protocol of the study. OGTT, oral glucose tolerance test.

stimulation (HFS; four trains at 100 Hz; 0·5-s duration; 20-s interval). Experiments were performed for 40 min after HFS.

Immunoblotting for brain insulin signalling

To investigate the expression of insulin receptor phosphorylation (p-IR), insulin receptors (IR), serine/threonine-specific protein kinase B (Akt/PKB) and insulin-mediated Akt Ser473 phosphorylation, homogenated brain slices from each subgroup were used as described in our previous study[4,5,24]. The p-IR, IR, Akt/PKB at serine 473 kinase phosphorylation and Akt/PKB were electrophoresed and immunoblotted with rabbit anti-IR at tyrosine phosphorylation (p-IR$^{tyr1162/1163}$) (1:1000, sc-25103-R; Santa Cruz Biotechnology), IR (1:1000, sc-711; Santa Cruz Biotechnology), Akt/PKB at serine 473 kinase phosphorylation (1:1000, no. 9271; Cell Signaling Technology) and Akt/PKB (1:1000, no. 9272; Cell Signaling Technology). For a loading control, the immunoblot for each membrane was incubated with anti-β-actin (1:4000, no. 4967; Cell Signaling Technology). All membranes enabling the visualisation of the phosphorylation and the protein levels of IR and Akt/PKB expression were incubated with secondary goat anti-rabbit antibody conjugated with horseradish peroxidase (1:2000, no. 7074; Cell Signaling Technology). Band densities of phosphorylated IR or Akt/PKB at serine 473 kinase phosphorylation were represented as a ratio of insulin stimulation (+):no insulin stimulation (–) and were normalised to total IR or Akt/PKB. Band intensities were quantified using Scion Imaging, and the results were shown as average signal intensity (arbitrary) units.

Serum and brain malondialdehyde levels

HPLC method was used to evaluate the concentrations of serum and brain malondialdehyde (MDA), as described previously[8,26–28].

Brain mitochondrial function study

Brain mitochondria were isolated using the method described previously[4]. Brain mitochondrial function including brain mitochondrial ROS, mitochondrial membrane potential change ($\Delta\Psi$m) and mitochondrial swelling were determined. Brain mitochondrial ROS were measured using dichloro-hydrofluorescein diacetate fluorescent dye. The change in mitochondrial membrane potential ($\Delta\Psi$m) was measured using the fluorescent dye 5, 52, 6, 62-tetrachloro-1, 12, 3, 32-tetraethyl benzimidazol carbocyanine iodide (JC-1) and brain mitochondrial swelling was determined by measuring the change in the absorbance of brain mitochondrial suspension at 540 nm. All were determined by following the methods described previously[4,8].

Cognitive function test

The open-field test (OFT) was used to screen locomotor activity, as described in previous studies[8,29]. The assessment of cognitive function was performed using the MWM test with two assessments including the acquisition test, which was carried out for 5 consecutive days, and the probe test, which was performed on day 6[8,30]. Data analysis of the MWM test was done manually from video tape recordings by the investigators, who were blinded to experimental groups.

Golgi staining and morphological analysis of dendritic spines

Golgi staining and morphological analysis were carried out using the method described previously[31]. After decapitation, brains were removed and rinsed with double-distilled water and were processed for Golgi staining using a commercially

Downloaded from https://www.cambridge.org/core. Chiang Mai University Library, on 06 Jun 2017 at 03:10:15, subject to the Cambridge Core terms of use, available at https://www.cambridge.org/core/terms. https://doi.org/10.1017/S0007114516003871

British Journal of Nutrition

available kit (FD Rapid GolgiStain™ Kit #PK401; FD Neurotechnologies, Inc.). For analysis of dendritic spine density, the secondary and tertiary dendrites of three neurons in the CA1 hippocampus area were counted. Dendritic segments were viewed through an inverted microscope (IX-81; Olympus).

Statistical analysis

Data were expressed as mean values with their standard errors. For all comparisons, the significance of the differences in peripheral biochemical parameters was calculated using the Mann–Whitney *U* test. The comparisons in the percentage of insulin-induced LTD, the percentage of LTP, brain mitochondrial function, immunoblot, the OFT tests and the MWM tests for the probe test between groups were performed using the one-way ANOVA test, followed by *post hoc* Fisher's least significant difference (LSD) analysis. As the acquisition phase of the MWM test has two independent factors (treatment and time), we used the two-way ANOVA followed by *post hoc* Fisher's LSD analysis to analyse the data. $P<0{\cdot}05$ was considered as a measure of statistical significance.

Results

Energy restriction and the combination of energy restriction plus vildagliptin in obese insulin-resistant rats equally restored peripheral insulin sensitivity

At baseline levels (week 0), the metabolic parameters were not significantly different between the ND-fed rats and the HFD-fed rats (Table 1). After 12 weeks of diet regimens, the HFD group had significantly increased body weight, plasma insulin, HOMA index, total cholesterol levels and LDL-cholesterol levels, when compared with the ND group (Table 1). However, plasma glucose levels were not significantly different between the groups (Table 1).

After 4 weeks of the treatment, HFV had significantly increased body weight, visceral fat, plasma insulin levels, HOMA index, plasma glucose AUC of OGTT (AUCg), total cholesterol and plasma LDL-cholesterol levels, but had decreased plasma HDL-cholesterol levels, when compared with NDV (Table 2). These findings indicated that peripheral insulin resistance was still observed in HFV rats after 16 weeks. Interestingly, HFRV and HFD-fed rats on a restricted diet and vildaglptin (HFRVil) had significantly decreased body weight, visceral fat, plasma insulin, HOMA index, plasma glucose AUCg, total plasma cholesterol and LDL-cholesterol levels, but increased plasma HDL-cholesterol levels, when compared with HFV rats (Table 2). However, there was no significant difference in plasma glucose and plasma TAG levels between all groups (Table 2).

Obesity caused the impairment of brain insulin receptor function, which was only restored by the combination of energy restriction plus vildagliptin

After 4 weeks of the treatment, the degree of insulin-induced LTD in HFV rats was significantly reduced, when compared with that in NDV rats (n 2–3 independent slices/animal, n 6 animals/group, Fig. 2(a)). Interestingly, the degree of insulin-induced LTD in only HFRVil rats showed a significant increase, when compared with that of HFV rats and HFR rats (n 2–3 independent slices/animal, n 6 animals/group, Fig. 2(a)). Regarding brain insulin signalling, the levels of IR and Akt/PKB proteins expression showed no difference between the groups (Fig. 2(d) and (e)). The p-IR and Akt/PKB at the serine 473 site in both HFV and HFRV rats showed a significant decrease, when compared with that of NDV rats (Fig. 2(b) and (c)). However, the p-IR levels and Akt/PKB at the serine 473 site of only HFRVil rats showed a significant increase when compared with those of HFV rats (Fig. 2(b) and (c)).

Obesity led to brain mitochondrial dysfunction, which improved following treatment with the combination of energy restriction plus vildagliptin

After 4 weeks of treatment, brain mitochondrial dysfunction was observed in HFV rats as indicated by increased brain mitochondrial ROS production, brain mitochondrial membrane depolarisation and brain mitochondrial swelling (Fig. 3(a), (b) and (c)). HFRV rats also had a significant increase in brain mitochondrial ROS production, brain mitochondrial depolarisation

Table 1. Metabolic parameters at week 0 (baseline) and the end of week 12 (before treatment) (Mean values with their standard errors)

	Baseline				Week 12			
	ND		HFD		ND		HFD	
Metabolic parameters	Mean	SEM	Mean	SEM	Mean	SEM	Mean	SEM
Body weight (g)	199·6	2·7	206·9	2·4	476·3	6·0	560·8	12·5*
Plasma glucose (mg/dl)	139·0	5·4	130·5	4·5	144·6	5·1	143·3	9·0
Plasma insulin (ng/ml)	2·4	0·6	2·4	0·5	2·9	0·4	4·7	0·6*
HOMA index	12·0	2·8	10·9	2·5	24·5	3·9	38·6	3·9*
Plasma total cholesterol (mg/dl)	68·0	3·4	67·8	3·8	66·9	3·9	81·5	4·2*
Plasma TAG (mg/dl)	51·9	3·7	48·1	4·5	60·2	7·6	62·0	8·7
HDL-cholesterol (mg/dl)	32·5	1·5	29·7	1·3	30·1	1·6	28·0	3·3
LDL-cholesterol (mg/dl)	23·6	3·5	28·9	4·0	23·7	2·7	39·9	3·0*

ND, normal-diet-fed rats; HFD, high-fat-diet-fed rats; HOMA, homoeostasis model assessment.
* Compared with ND at the same time interval.

Downloaded from https://www.cambridge.org/core. Chiang Mai University Library, on 06 Jun 2017 at 03:10:15, subject to the Cambridge Core terms of use, available at https://www.cambridge.org/core/terms. https://doi.org/10.1017/S0007114516003871

Table 2. Metabolic parameters after energy restriction and energy restriction plus vildagliptin treatment (Mean values with their standard errors)

	Groups							
	NDV		HFV		HFRV		HFRVil	
Metabolic parameters	Mean	SEM	Mean	SEM	Mean	SEM	Mean	SEM
Body weight (g)	490·7	9·4	597·9	15*	519·1	10·1†	511·3	10·5†
Visceral fat (g)	24·6	1·3	52·7	2·9*	30·0	1·3†	28·5	2·3†
Plasma glucose (mg/dl)	153·5	16·8	163·2	7·1	152·7	3·2	157·5	5·6
Plasma insulin (ng/ml)	4·2	0·2	6·4	0·8*	3·6	0·5†	4·0	0·6†
HOMA index	34·6	5·3	59·2	8·8*	32·7	4·4†	34·5	6·1†
Plasma glucose AUC (AUCg) (mg/dlxminx10^4)	4·8	0·2	6·0	0·3*	4·8	0·3†	4·9	0·2†
Plasma total cholesterol (mg/dl)	70·5	4·2	97·3	6·0*	76·5	2·4†	75·4	3·8†
Plasma TAG (mg/dl)	52·1	7·2	54·7	5·0	51·8	5·3	53·3	7·2
HDL-cholesterol (mg/dl)	33·9	1·9	24·5	1·9*	35·9	2·2†	34·7	2·0†
LDL-cholesterol (mg/dl)	26·9	3·1	52·8	6·0*	31·8	6·5†	28·3	4·3†
Serum MDA (μmol/ml)	1·42	0·05	5·30	1·33*	1·63	0·12†	1·54	0·11†
Brain MDA (μmol/mg protein)	0·47	0·05	0·68	0·07*	0·57	0·04	0·50	0·02†

NDV, normal-diet-fed rats treated with vehicle; HFV, high-fat-diet-fed rats treated with vehicle; HFRV, high-fat-diet-fed rats reversed to normal diet with 60% energy restriction treated with vehicle; HFRVil, high-fat-diet-fed rats reversed to normal diet with 60% energy restriction treated with vildagliptin; HOMA, homoeostasis model assessment; MDA, malondialdehyde.
* Compared with NDV.
† Compared with HFV.

and brain mitochondrial swelling, when compared with NDV rats (Fig. 3(a), (b) and (c)). Interestingly, only HFRVil rats showed a significant decrease in brain ROS production, and improvement in brain mitochondrial depolarisation and brain mitochondrial swelling, when compared with HFV rats (Fig. 3(a), (b) and (c)).

Furthermore, there were morphological changes in brain mitochondria; representatives from all groups are shown in Fig. 3(d). Brain mitochondrial swelling was observed in both the HFV and HFRV rats, as indicated by markedly unfolded cristae (Fig. 3(d)). Interestingly, brain mitochondrial morphology with apparent folded cristae was observed in only HFRVil rats (Fig. 3(d)).

Obesity led to increased brain oxidative stress levels, which was attenuated by the combination of energy restriction plus vildagliptin

After 4 weeks of treatment, both circulating MDA and brain MDA levels significantly increased in HFV rats compared with NDV rats (Table 2). HFRV rats only showed a significant decrease in circulating MDA, when compared with HFV rats (Table 2). Interestingly, HFRVil rats showed a significant decrease in both circulating MDA and brain MDA levels, when compared with HFV rats (Table 2).

Obesity caused impaired hippocampal synaptic plasticity and cognitive decline, which only showed restoration with the combination of energy restriction plus vildagliptin

After 4 weeks of treatment, the results demonstrated that the degrees of electrical-induced LTP significantly decreased in both HFV and HFRV rats, when compared with NDV rats (n 2–3 independent slices/animal, n 6 animals/group, Fig. 4(a)). The reduction of electrical-induced LTP in both HFV and HFRV rats was not significantly different (n 2–3 independent slices/animal, n 6 animals/group, Fig. 4(a)). However, the degree of electrical-induced LTP of HFRVil rats significantly increased, when compared with that of HFV rats (n 2–3 independent slices/animal, n 6 animals/group, Fig. 4(a)).

The density of hippocampal dendritic spines was determined at the secondary and tertiary dendrites in the apical dendrite of the CA1 hippocampus to investigate the underlying mechanism of memory function. It was found that the dendritic spine density of HFV and HFRV rats decreased significantly, when compared with that of NDV rats (Fig. 4(b)). After treatment regimens, the dendritic spine density of both HFRV and HFRVil rats showed a significant increase, when compared with that of HFV rats (Fig. 4(b)). However, dendritic spine density of HFRVil rats was significantly greater than that of HFRV rats (Fig. 4(b)).

The OFT was used to screen locomotor activity. The results showed that there was no significant difference between all groups, indicating that the locomotor activity did not differ in all groups. In addition, the study determined cognitive function by using the MWM test after 4 weeks of the treatment regimens. For the acquisition test, it was found that both HFV and HFRV rats showed a significantly increased time to reach the platform, when compared with NDV rats (Fig. 4(c)). However, HFRVil rats showed a significantly decreased time to reach the platform, when compared with HFV rats (Fig. 4(c)). For the probe test, both HFV and HFRV rats had a significantly decreased time spent in the target quadrant, when compared with NDV rats (Fig. 4(d)). In contrast, HFRVil rats had a significantly increased time spent in the target quadrant, when compared with HFV rats (Fig. 4(d)).

Discussion

The major findings of this study are as follows: (1) obesity induced by HFD consumption leads to the development of peripheral insulin resistance, impairment of brain insulin sensitivity, brain mitochondrial dysfunction, impaired hippocampal synaptic

Downloaded from https://www.cambridge.org/core. Chiang Mai University Library, on 06 Jun 2017 at 03:10:15, subject to the Cambridge Core terms of use, available at https://www.cambridge.org/core/terms. https://doi.org/10.1017/S0007114516003871

British Journal of Nutrition

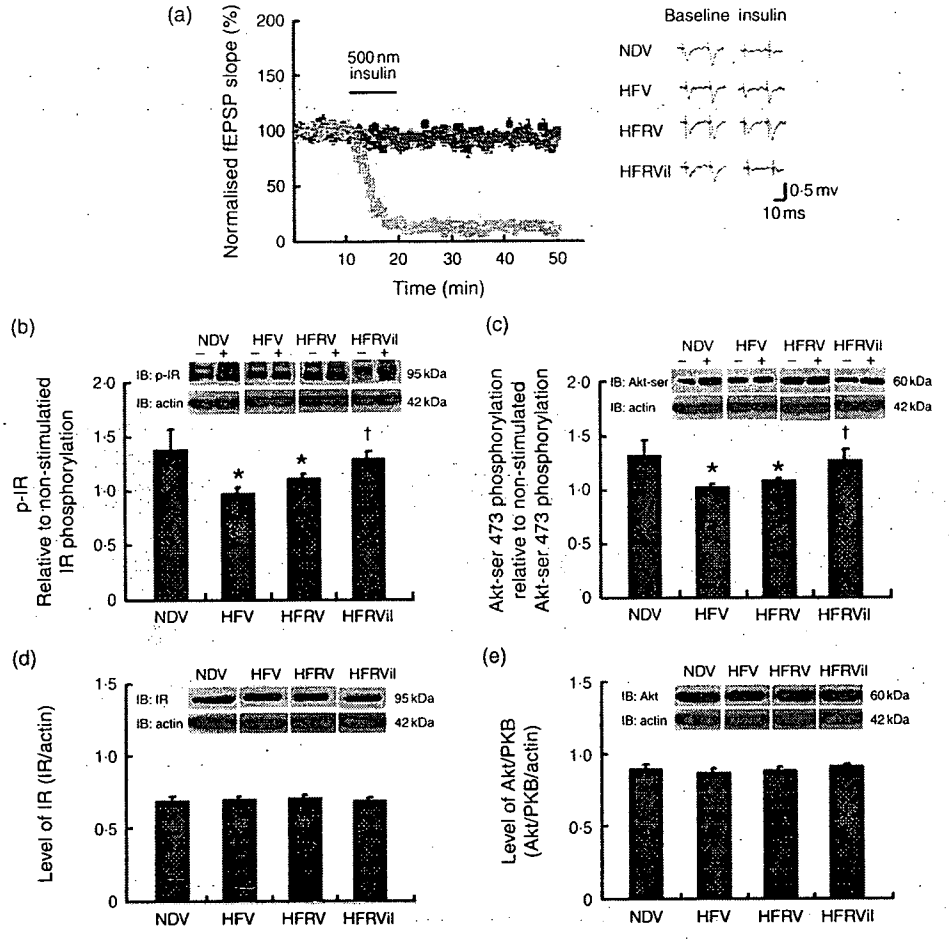


Fig. 2. The effects of energy restriction (ER) and the combination of ER plus vildagliptin on brain insulin receptor function (insulin-induced long-term depression (LTD)) and brain insulin signalling, including the phosphorylation of insulin receptors (p-IR), Akt-Ser 473, insulin receptors (IR) and serine/threonine-specific protein kinase B (Akt/PKB) protein expression in obese insulin-resistant rats. The combination of ER plus vildagliptin improves the ability of insulin-induced LTD in high-fat-diet-fed rats reversed to normal diet with 60 % ER treated with vildagliptin (HFRVil), when compared with high-fat-diet-fed rats treated with vehicle (HFV) (a). After 4 weeks of treatment, both p-IR and Akt-Ser 473 expression levels were significantly decreased in HFV and high-fat-diet-fed rats reversed to normal diet with 60 % ER treated with vehicle (HFRV) when compared with normal-diet-fed rats treated with vehicle (NDV) ((b) and (c)). Both p-IR and Akt-Ser 473 expression increased significantly after the combination of ER plus vildagliptin when compared with HFV rats ((b) and (c)). However, there was no difference in IR and Akt/PKB protein expression between all groups ((d) and (e)). *$P<0{\cdot}05$ *v.* NDV and † $P<0{\cdot}05$ *v.* HFV. ▨, NDV; ▩, HFV; ■, HFRV; ▦, HFRVil. fEPSP, field excitatory postsynaptic potential.

plasticity, decreased dendritic spine density and cognitive decline; (2) both ER and the combination of ER plus vildagliptin showed equally improved peripheral insulin sensitivity and lipid profiles; (3) ER alone showed a decrease only in circulating oxidative stress, whereas the combination of ER plus vildagliptin showed a decrease in both circulating and brain oxidative stress levels; and (4) only the combination of ER plus vildagliptin showed a correlation with restored brain insulin sensitivity, brain mitochondrial function, hippocampal synaptic plasticity and cognitive function in obese insulin-resistant rats.

This study has demonstrated that diet-induced obesity led to the development of the peripheral insulin resistance via impaired peripheral insulin sensitivity, impaired lipid profiles and an increase in both circulating and brain oxidative stress. These findings confirmed other studies and our previous studies that diet-induced obesity not only caused peripheral insulin resistance but also brain insulin resistance[24,32]. The present findings indicated that obesity increased oxidative stress and impaired brain mitochondrial function, resulting in brain insulin resistance and cognitive decline.

This study demonstrates that ER enhanced peripheral insulin sensitivity and improved lipid profiles in obese insulin-resistant rats. A possible explanation of these findings may be that ER decreased visceral fat and dyslipidaemia. Decreased fat has been shown to reduce systemic inflammation[33], as well as oxidative stress, as shown in Table 2 and in a previous study[34]. An increase in inflammation and oxidative stress led to the impairment of peripheral insulin sensitivity[35,36]. Therefore, ER in the present study led to improved peripheral insulin sensitivity, possibly via the reduction of oxidative stress.

Although ER led to the restoration of peripheral insulin sensitivity and decreased circulating oxidative stress, ER alone failed to cause improvement in brain insulin sensitivity and brain mitochondrial dysfunction, as well as failed to restore hippocampal synaptic plasticity and cognitive decline in obese insulin-resistant rats. This may be because of our finding that ER

Downloaded from https://www.cambridge.org/core. Chiang Mai University Library, on 06 Jun 2017 at 03:10:15, subject to the Cambridge Core terms of use, available at https://www.cambridge.org/core/terms. https://doi.org/10.1017/S0007114516003871

British Journal of Nutrition

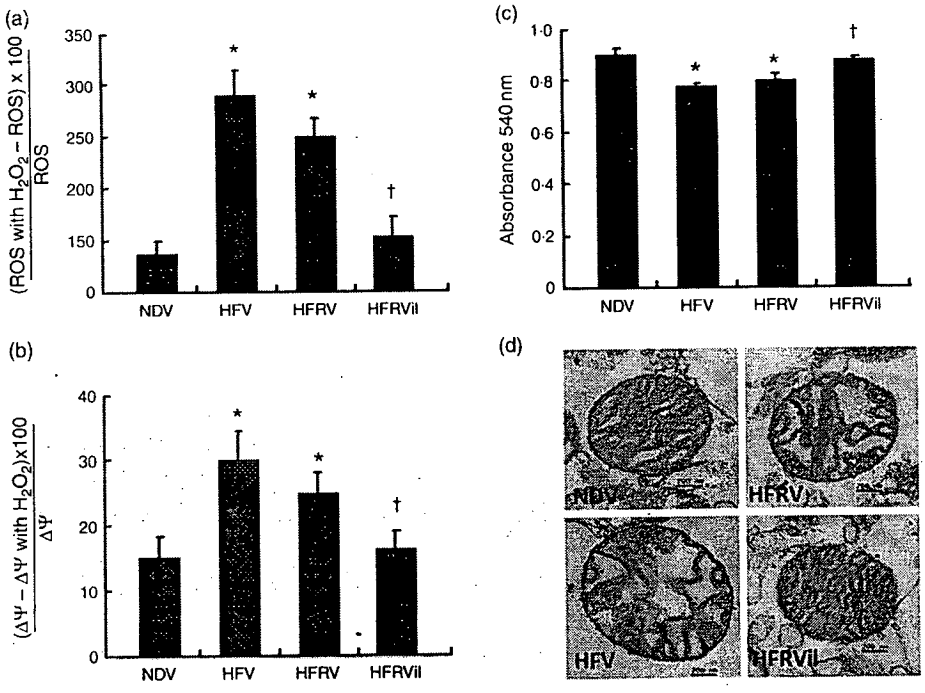


Fig. 3. The effects of energy restriction (ER) and the combination of ER plus vildagliptin on brain mitochondrial function and representative images of brain mitochondrial morphology by transmission electron microscopy (JEM-2200FS field emission electron microscope, original magnification 20 000 ×) in obese insulin-resistant rats. High-fat-diet-fed rats treated with vehicle (HFV) and high-fat-diet-fed rats reversed to normal diet with 60 % ER treated with vehicle (HFRV) demonstrated brain mitochondrial dysfunction when compared with normal-diet-fed rats treated with vehicle (NDV), as indicated by increased brain mitochondrial reactive oxygen species (ROS) production following H_2O_2 application (a), increased brain mitochondrial membrane potential change following H_2O_2 application (b) and decreased absorbance values, indicating brain mitochondrial swelling (c). The combination of ER plus vildagliptin in high-fat-diet-fed rats reversed to normal diet with 60 % ER treated with vildagliptin (HFRVil) showed improved brain mitochondrial function when compared with HFV rats, as indicated by significantly decreased brain mitochondrial ROS production (a), decreased brain mitochondrial membrane potential change (b) and increased absorbance values (c). Furthermore, normal folding of cristae in brain mitochondrial morphology was shown in both NDV and HFRVil rats (d). However, brain mitochondrial swelling, as indicated by unfolded cristae in both HFV and HFRV rats, was observed (d). *$P < 0{\cdot}05$ *v.* NDV and † $P < 0{\cdot}05$ *v.* HFV.

alone could neither decrease brain oxidative stress levels nor brain mitochondrial dysfunction, whereas treatment with combined ER and vildagliptin effectively improved both parameters in obese insulin-resistant rats (Table 2).

Unlike this study, previous studies showed that ER had beneficial effects on neuroprotection and preservation of cognition. For example, (1) a previous study demonstrated that 40 % of ER for 24 months reduced the rate of mitochondrial H_2O_2 production via reduced brain ROS production in aged rats[22]. (2) The study involving 40 % ER for 22–29 months also reported that ER prevented age-related deficit synaptic LTP and the preservation of the NR1-subunit of *N*-methyl-D-aspartate (NMDA) receptors in aged Fisher 344 rats[37]. (3) The study of 60 % ER for 4 weeks in male rats demonstrated that ER stabilised synaptophysin expression and preserved cognitive function[23]. (4) A recent study demonstrated that 70 % ER for 28 d improved metabolic effects and cognitive decline via up-regulation of brain-derived neurotrophic factor and decreased hippocampal oxidative stress in the obese-metabolic syndrome male rats induced by a moderated HFD (35 %E from fat)[19]. The different findings between previous studies and the present study could be dependent on the percentage of HFD feeding and the duration of ER. Future studies are needed to verify this issue.

One important finding from this study is that ER combined with vildagliptin restored peripheral insulin sensitivity, brain insulin sensitivity, brain mitochondrial function, synaptic plasticity and cognitive function in obese insulin-resistant rats. This means of intervention provided better efficacy than ER alone in this model. These findings suggest that the beneficial effects on brain function in this group could be because of the action of vildagliptin. This is consistent with our previous studies, which showed that vildagliptin led to the restoration of cognitive function in the obese model, via improved brain insulin sensitivity and reduced brain oxidative stress[4,8]. As demonstrated in this study, the combined ER with vildagliptin improved/restored both brain insulin resistance and brain oxidative stress better than ER alone. These findings indicated that ER in combination with the vildagliptin treatment provided more beneficial effects than ER alone in our study model. However, other ER feeding regimens and delivery could have given similar or different results as observed in the present study and require further investigation.

Limitations of the study

The two-factorial design study was not conducted in the present study; therefore, the effects of ER or its combination with vildagliptin in ND-fed rats (lean rats) were not known. However, our previous studies showed that the administration of vildagliptin in ND-fed rats has no effect on the metabolic parameters or brain function, when compared with vehicle-treated ND-fed rats[4,8].

Downloaded from https://www.cambridge.org/core. Chiang Mai University Library, on 06 Jun 2017 at 03:10:15, subject to the Cambridge Core terms of use, available at https://www.cambridge.org/core/terms. https://doi.org/10.1017/S0007114516003871

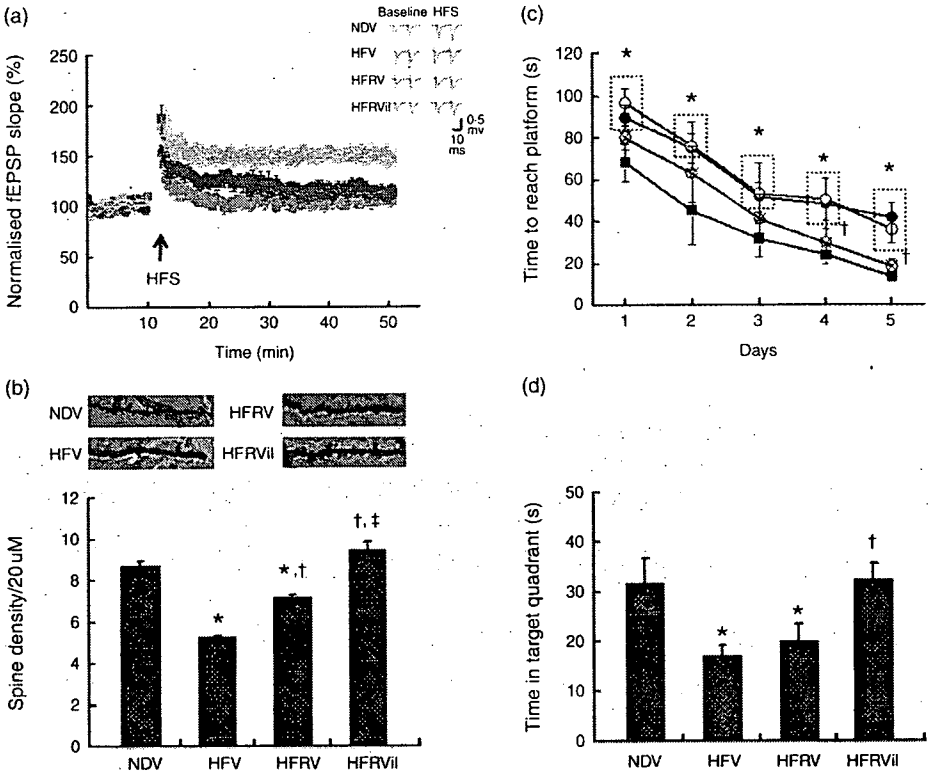


Fig. 4. The effects of energy restriction (ER) and the combination of ER plus vildagliptin on hippocampal synaptic long-term potentiation (LTP) and the number of dendritic spines on tertiary dendrites on apical dendrites, as well as cognitive function, in obese insulin-resistant rats. Both high-fat-diet-fed rats treated with vehicle (HFV) and high-fat-diet-fed rats reversed to normal diet with 60 % ER treated with vehicle (HFRV) showed a significantly reduced degree of LTP, when compared with normal-diet-fed rats treated with vehicle (NDV) (a). The degree of LTP showed improvement after a combination of ER plus vildagliptin when compared with HFV rats (a). The number of dendritic spines on secondary or tertiary dendrites in hippocampal apical dendrites was decreased in HFV rats (b). Both HFRV and high-fat-diet-fed rats reversed to normal diet with 60 % ER treated with vildagliptin (HFRVil) showed significantly increased numbers of dendritic spines after the treatment regimen (b). HFV and HFRV rats showed a significantly increased time to reach the platform in the acquisition test, as well as having a decreased time spent in the target quadrant in the probe test, when compared with NDV rats ((c) and (d)). HFRVil rats showed a significantly decreased time to reach the platform in the acquisition test, as well as an increased time spent in the target quadrant in the probe test, when compared with HFV rats ((c) and (d)). HFS, high-frequency stimulation. *$P<0·05$ *v.* NDV, † $P<0·05$ *v.* HFV and ‡ $P<0·05$ *v.* HFRV. (a) ▨, NDV; ▨, HFV; ▨, HFRV; ▨, HFRVil; (c) ■, NDV; ●, HFV; ○, HFRV; ⊗, HFRVil. fEPSP, field excitatory postsynaptic potential.

In addition, ER had been shown to exert benefits in attenuating cognitive decline via an up-regulation of the brain-derived neurotrophic factor and tropomyosin-related kinase B in obese, hypertensive rats[19]; these markers were not investigated in this study.

Conclusion

This study indicates that although ER restored peripheral insulin sensitivity and decreased circulating oxidative stress levels regardless of the addition of vildagliptin, only ER plus vildagliptin exerted the best efficacy in effectively decreasing brain oxidative stress levels, as well as the restoration of brain insulin sensitivity, brain mitochondrial function, hippocampal synaptic plasticity and cognition. All of these findings suggest that the addition of vildagliptin to ER provides greater therapeutic benefits on brain function than ER alone in obesity.

Acknowledgements

This work was supported by grants from the Thailand Research Fund (TRF-BRG5780016 (SC), TRF-MRG5980198 (WP)), the Royal Golden Jubilee PhD programme (PHD/0025/2555 HP&SC), National Research Council of Thailand (SC), a NSTDA Research Chair Grant from the National Science and Technology Development Agency (NC) and Chiang Mai University Excellent Center Award (NC).

H. P., N. C., S. C. C. performed the experiments, analysed the data and wrote the manuscript. P. T., W. P., P. Sa-nguanmoo, T. C. performed the experiments and analysed the data. P. Satjaritanun, L. L. analysed the data.

The authors have no conflicts of interest to disclose.

References

1. Kitzinger H & Karle B (2013) The epidemiology of obesity. *Eur Surg* **45**, 80–82.
2. Stranahan AM, Norman ED, Lee K, *et al.* (2008) Diet-induced insulin resistance impairs hippocampal synaptic plasticity and cognition in middle-aged rats. *Hippocampus* **18**, 1085–1088.
3. Pistell PJ, Morrison CD, Gupta S, *et al.* (2010) Cognitive impairment following high fat diet consumption is associated with brain inflammation. *J Neuroimmunol* **219**, 25–32.

Downloaded from https://www.cambridge.org/core. Chiang Mai University Library, on 06 Jun 2017 at 03:10:15, subject to the Cambridge Core terms of use, available at https://www.cambridge.org/core/terms. https://doi.org/10.1017/S0007114516003871

4. Pipatpiboon N, Pintana H, Pratchayasakul W, *et al.* (2013) DPP4-inhibitor improves neuronal insulin receptor function, brain mitochondrial function and cognitive function in rats with insulin resistance induced by high-fat diet consumption. *Eur J Neurosci* **37**, 839–849.
5. Pipatpiboon N, Pratchayasakul W, Chattipakorn N, *et al.* (2012) PPARgamma agonist improves neuronal insulin receptor function in hippocampus and brain mitochondria function in rats with insulin resistance induced by long term high-fat diets. *Endocrinology* **153**, 329–338.
6. Burkey BF, Li X, Bolognese L, *et al.* (2005) Acute and chronic effects of the incretin enhancer vildagliptin in insulin-resistant rats. *J Pharmacol Exp Ther* **315**, 688–695.
7. Gault VA, Lennox R & Flatt PR (2015) Sitagliptin, a dipeptidyl peptidase-4 inhibitor, improves recognition memory, oxidative stress and hippocampal neurogenesis and upregulates key genes involved in cognitive decline. *Diabetes Obes Metab* **17**, 403–413.
8. Pintana H, Apaijai N, Chattipakorn N, *et al.* (2013) DPP-4 inhibitors improve cognition and brain mitochondrial function of insulin resistant rats. *J Endocrinol* **218**, 1–11.
9. Speakman JR & Mitchell SE (2011) Caloric restriction. *Mol Aspects Med* **32**, 159–221.
10. Baek K, Barlow AA, Allen MR, *et al.* (2008) Food restriction and simulated microgravity: effects on bone and serum leptin. *J Appl Physiol* **104**, 1086–1093.
11. Reiser K, McGee C, Rucker R, *et al.* (1995) Effects of aging and caloric restriction on extracellular matrix biosynthesis in a model of injury repair in rats. *J Gerontol A Biol Sci Med Sci* **50A**, B40–B47.
12. de Magalhaes JP, Wuttke D, Wood SH, *et al.* (2012) Genome-environment interactions that modulate aging: powerful targets for drug discovery. *Pharmacol Rev* **64**, 88–101.
13. Ingram DK, Zhu M, Mamczarz J, *et al.* (2006) Calorie restriction mimetics: an emerging research field. *Aging cell* **5**, 97–108.
14. McCurdy CE, Davidson RT & Cartee GD (2005) Calorie restriction increases the ratio of phosphatidylinositol 3-kinase catalytic to regulatory subunits in rat skeletal muscle. *Am J Physiol Endocrinol Metab* **288**, E996–E1001.
15. Dean DJ, Brozinick JT Jr, Cushman SW, *et al.* (1998) Calorie restriction increases cell surface GLUT-4 in insulin-stimulated skeletal muscle. *Am J Physiol* **275**, E957–E964.
16. Sharma N, Castorena CM & Cartee GD (2012) Greater insulin sensitivity in calorie restricted rats occurs with unaltered circulating levels of several important myokines and cytokines. *Nutr Metab (Lond)* **9**, 90.
17. Wilsey J & Scarpace PJ (2004) Caloric restriction reverses the deficits in leptin receptor protein and leptin signaling capacity associated with diet-induced obesity: role of leptin in the regulation of hypothalamic long-form leptin receptor expression. *J Endocrinol* **181**, 297–306.
18. Yamaoka K & Tango T (2012) Effects of lifestyle modification on metabolic syndrome: a systematic review and meta-analysis. *BMC Med* **10**, 138.
19. Kishi T, Hirooka Y, Nagayama T, *et al.* (2015) Calorie restriction improves cognitive decline via up-regulation of brain-derived neurotrophic factor: tropomyosin-related kinase B in hippocampus of obesity-induced hypertensive rats. *Int Heart J* **56**, 110–115.
20. Hiona A & Leeuwenburgh C (2004) Effects of age and caloric restriction on brain neuronal cell death/survival. *Ann N Y Acad Sci* **1019**, 96–105.
21. Wood SH, van Dam S, Craig T, *et al.* (2015) Transcriptome analysis in calorie-restricted rats implicates epigenetic and post-translational mechanisms in neuroprotection and aging. *Genome Biol* **16**, 285.
22. Sanz A, Caro P, Ibanez J, *et al.* (2005) Dietary restriction at old age lowers mitochondrial oxygen radical production and leak at complex I and oxidative DNA damage in rat brain. *J Bioenerg Biomembr* **37**, 83–90.
23. Adams MM, Shi L, Linville MC, *et al.* (2008) Caloric restriction and age affect synaptic proteins in hippocampal CA3 and spatial learning ability. *Exp Neurol* **211**, 141–149.
24. Pratchayasakul W, Kerdphoo S, Petsophonsakul P, *et al.* (2011) Effects of high-fat diet on insulin receptor function in rat hippocampus and the level of neuronal corticosterone. *Life Sci* **88**, 619–627.
25. Sripetchwandee J, Pipatpiboon N, Chattipakorn N, *et al.* (2014) Combined therapy of iron chelator and antioxidant completely restores brain dysfunction induced by iron toxicity. *PLOS ONE* **9**, e85115.
26. Candan N & Tuzmen N (2008) Very rapid quantification of malondialdehyde (MDA) in rat brain exposed to lead, aluminium and phenolic antioxidants by high-performance liquid chromatography-fluorescence detection. *Neurotoxicology* **29**, 708–713.
27. Mateos R, Lecumberri E, Ramos S, *et al.* (2005) Determination of malondialdehyde (MDA) by high-performance liquid chromatography in serum and liver as a biomarker for oxidative stress. Application to a rat model for hypercholesterolemia and evaluation of the effect of diets rich in phenolic antioxidants from fruits. *J Chromatogr B Analyt Technol Biomed Life Sci* **827**, 76–82.
28. Pintana H, Sripetchwandee J, Supakul L, *et al.* (2014) Garlic extract attenuates brain mitochondrial dysfunction and cognitive deficit in obese-insulin resistant rats. *Appl Physiol Nutr Metab* **39**, 1373–1379.
29. Arakawa H (2005) Age dependent effects of space limitation and social tension on open-field behavior in male rats. *Physiol Behav* **84**, 429–436.
30. Vorhees CV & Williams MT (2006) Morris water maze: procedures for assessing spatial and related forms of learning and memory. *Nat Protoc* **1**, 848–858.
31. Sripetchwandee J, Pipatpiboon N, Pratchayasakul W, *et al.* (2014) DPP-4 inhibitor and PPARgamma agonist restore the loss of CA1 dendritic spines in obese insulin-resistant rats. *Arch Med Res* **45**, 547–552.
32. Greenwood CE & Winocur G (2005) High-fat diets, insulin resistance and declining cognitive function. *Neurobiol Aging* **26**, Suppl. 1, 42–45.
33. Hatori M, Vollmers C, Zarrinpar A, *et al.* (2012) Time-restricted feeding without reducing caloric intake prevents metabolic diseases in mice fed a high-fat diet. *Cell Metab* **15**, 848–860.
34. Jeon BT, Jeong EA, Shin HJ, *et al.* (2012) Resveratrol attenuates obesity-associated peripheral and central inflammation and improves memory deficit in mice fed a high-fat diet. *Diabetes* **61**, 1444–1454.
35. Rains JL & Jain SK (2011) Oxidative stress, insulin signaling, and diabetes. *Free Radic Biol Med* **50**, 567–575.
36. Glass CK & Olefsky JM (2012) Inflammation and lipid signaling in the etiology of insulin resistance. *Cell Metab* **15**, 635–645.
37. Eckles-Smith K, Clayton D, Bickford P, *et al.* (2000) Caloric restriction prevents age-related deficits in LTP and in NMDA receptor expression. *Brain Res Mol Brain Res* **78**, 154–162.

British Journal of Nutrition

Downloaded from https://www.cambridge.org/core. Chiang Mai University Library, on 06 Jun 2017 at 03:10:15, subject to the Cambridge Core terms of use, available at https://www.cambridge.org/core/terms. https://doi.org/10.1017/S0007114516003871

เอกสารแนบหมายเลข 12

International Journal of Cardiology 202 (2016) 415–416

Contents lists available at ScienceDirect

International Journal of Cardiology

journal homepage: www.elsevier.com/locate/ijcard

Correspondence

Dipeptidyl peptidase-4 inhibitors and the ischemic heart: Additional benefits beyond glycemic control☆

Nipon Chattipakorn [a,b,c,*], Nattayaporn Apaijai [a,b,c], Siriporn C. Chattipakorn [a,c,d]

[a] Cardiac Electrophysiology Research and Training Center, Faculty of Medicine, Chiang Mai University, Chiang Mai, Thailand
[b] Cardiac Electrophysiology Unit, Department of Physiology, Faculty of Medicine, Chiang Mai University, Chiang Mai, Thailand
[c] Center of Excellence in Cardiac Electrophysiology Research, Chiang Mai University, Chiang Mai, Thailand
[d] Department of Oral Biology and Diagnostic Science, Faculty of Dentistry, Chiang Mai University, Chiang Mai, Thailand

ARTICLE INFO

Article history:
Received 26 August 2015
Accepted 19 September 2015
Available online 21 September 2015

Keywords:
DPP-4 inhibitor
Ischemia–reperfusion
Obesity
Insulin resistance

ABSTRACT

Obese-insulin resistance and type 2 diabetes mellitus (T2DM) have become global health problems, and they are both associated with a higher risk of ischemic heart disease. Although reperfusion therapy is the treatment to increase blood supply to the ischemic myocardium, this intervention potentially causes cardiac tissue damage and instigates arrhythmias, processes known as reperfusion injury. Dipeptidyl peptidase 4 (DPP-4) inhibitors are glycemic control drugs commonly used in T2DM patients. Growing evidence from basic and clinical studies demonstrates that a DPP-4 inhibitor could exert cardioprotection and improve left ventricular function by reducing oxidative stress, apoptosis, and increasing reperfusion injury salvage kinase (RISK) activity. However, recent reports also showed potentially adverse cardiac events due to the use of a DPP-4 inhibitor. To investigate this disparity, future large clinical trials are essential in verifying whether DPP-4 inhibitors are beneficial beyond their glycemic control particularly for the ischemic heart in obese-insulin resistant subjects and T2DM patients.
© 2015 Elsevier Ireland Ltd. All rights reserved.

Cardiovascular diseases have been a global health burden for many decades. With increasing unhealthy food consumption and poor daily lifestyle, the prevalence of obesity and type-2 diabetes mellitus (T2DM) have also dramatically increased [1]. Reports have shown that the incidence of ischemic heart disease has increased in obese and T2DM patients, mainly due to blockage of the coronary artery [1]. Although myocardial salvage by opening the clogged coronary artery, i.e., reperfusion therapy, could increase the blood supply to the ischemic myocardium, it can also cause damage to myocardial tissue and instigates arrhythmias due to an elevation of oxidative stress. This is known as reperfusion injury [2]. In addition to ischemia/reperfusion (I/R) injury, oxidative stress also plays an important role in obese-insulin resistance and T2DM [3]. Obese-insulin resistance has been shown to significantly aggravate dysfunction of the left ventricle (LV) by increased oxidative stress and impaired cardiac mitochondrial function [3].

Obese-insulin resistance has become a global concern with increasing cardiovascular risks in those subjects. In the animal model, under conditions of I/R, it has been shown that obese-insulin resistant rats had a higher mortality rate than lean rats [3]. Since reperfusion injury causes myocardial tissue damage, increases arrhythmia incidence and is worsened by obese-insulin resistance, pharmacological intervention to reduce these adverse effects and improve LV function have been of interest for some time. There is an increasing body of evidence which suggests that several oral anti-diabetic drugs exert cardioprotection against I/R injury [4]. The dipeptidyl peptidase-4 (DPP-4) inhibitors, a class of oral anti-diabetic drugs, have been extensively studied and evidence shows that they may exert beneficial effects beyond their glycemic control.

There are six forms of DPP-4 inhibitor which are commercially available, including vildagliptin, sitagliptin, saxagliptin, alogliptin and linagliptin. These drugs can prolong GLP-1 half-life, thus allowing it to stimulate insulin secretion in a glucose-dependent manner and improve insulin sensitivity in patients with T2DM [4]. Additionally, DPP-4 inhibitors also improved insulin function and reduced blood glucose without hypoglycemia [4]. Moreover, DPP-4 inhibitors did not only help to improve insulin resistance but they were also found to exert cardioprotection in non-DM animals with I/R injury [5]. In this issue of *Int J Cardiol*, Yang and colleagues have summarized the potential benefits of DPP-4 inhibitors where they could be a feasible therapeutic pharmacological intervention for I/R [6]. Indeed, it has been proposed that DPP-4 inhibitors exert beneficial effects beyond their glycemic control including cardioprotection [4]. In addition to the potential benefits in I/R hearts as discussed in Yang et al. report [6], the cardioprotective

☆ Funding Sources: The NSTDA Research Chair Grant from the National Science and Technology Development Agency Thailand (NC), the Thailand Research Fund grants BRG5780016 (SC), the TRF Golden Jubilee PhD Program (NA and NC) and Chiang Mai University Center of Excellence Award (NC).

* Corresponding author at: Cardiac Electrophysiology Research and Training Center, Faculty of Medicine, Chiang Mai University, Chiang Mai 50200, Thailand.
E-mail address: nchattip@gmail.com (N. Chattipakorn).

http://dx.doi.org/10.1016/j.ijcard.2015.09.044
0167-5273/© 2015 Elsevier Ireland Ltd. All rights reserved.

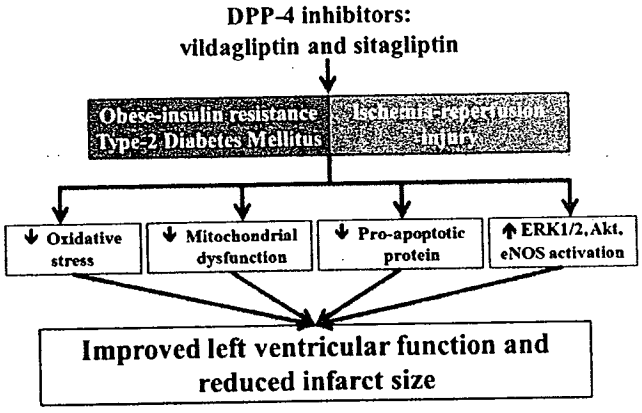


Fig. 1. The possible mechanisms responsible for the cardioprotective effects of DPP-4 inhibitors in obese-insulin resistance and T2DM with ischemia/reperfusion injury.

effects of DPP-4 inhibitors have been demonstrated in other animal models including those with induced obese-insulin resistance, with and without cardiac I/R injury.

Previous studies demonstrated that obese-insulin resistance significantly impaired left ventricular function in rats through increased oxidative stress and inflammation and impaired cardiac mitochondrial function [2,3]. Moreover, under conditions of I/R, obese-insulin resistant rats have been more severely affected by I/R, compared to lean rats [3]. Mitochondria are recognized as the major site of energy production and, at the same time, the source of oxidative stress production [2]. Cardiac mitochondrial function has been shown to be markedly impaired by the I/R itself as well as being impaired under obese-insulin resistant conditions [2,3]. Cardiac mitochondrial dysfunction, including increased ROS production, mitochondrial depolarization and mitochondrial swelling, has been proposed as the mechanism responsible for LV dysfunction in conditions both of cardiac I/R and obese-insulin resistance [3, 5]. For these reasons, pharmacological intervention that effectively preserves cardiac mitochondrial function could provide significant benefits especially in terms of cardioprotection.

Over the past 10 years there is a growing body of evidence to show that DPP-4 inhibitors exert cardioprotective action, in addition to their glycemic control, via various molecular mechanisms against I/R injury, leading to improved LV function and decreased infarct size [5]. Evidence shows that oxidative stress is a common mediator of cardiac injury [3], and a greater level of oxidative stress has been observed in a setting of obese-insulin resistance with I/R. Interestingly, it has been demonstrated that DPP-4 inhibitors are capable of exerting an anti-oxidant effect along with their anti-hyperglycemic property [3]. It has been shown that treatment with vildagliptin reduces oxidative stress as well as attenuating cardiac mitochondrial damage [3]. In addition to its ability to preserve cardiac mitochondrial function, DPP-4 inhibitor have also been shown to reduce apoptotic Bax expression under I/R conditions, leading to a reduced infarct size [3]. Treatment with DPP-4 inhibitors also activated the reperfusion injury salvage kinase (RISK) pathway including the extracellular signal-regulated kinases (ERK 1/2), Akt, and e-NOS in type-2 diabetic animals [7,8]. All of these effects could be the potential mechanisms conferring cardioprotective benefits of DPP-4 inhibitors (Fig. 1). Despite the fact that several DPP-4 inhibitors including vildagliptin and sitagliptin have been shown to exert cardioprotection against I/R injury in various animal models with obese-insulin resistance and T2DM, the effects of others DPP-4 inhibitors are still unclear.

Although evidence exists regarding the undesirable effects of DPP-4 inhibitors in clinical outcomes, for example the increased duration of hospitalization due to the use of saxagliptin [9], several studies involving the use of other DPP-4 inhibitors reported otherwise. For example, the use of vildagliptin showed no correlation with an increased risk of heart failure [10], and vildagliptin, sitagliptin and alogliptin showed no association with major adverse cardiovascular events in T2DM patients [10–12]. Despite the effect of DPP-4 inhibitors on the heart failure incidence still being unclear, there are three studies aimed at determining LV function in T2DM patients who were prescribed DPP-4 inhibitors after acute myocardial infarction. One of these studies reported that DPP-4 inhibitors improved E/e' and e'/a' ratio, and it was suggested that the DPP-4 inhibitor improved LV diastolic function when compared to other anti-diabetic drugs [10]. Another study investigated dobutamine stress echocardiography at baseline and after 4 weeks of sitagliptin treatment [11]. The results indicated that sitagliptin improved the LV ejection fraction when compared to the baseline. White and colleagues also reported that alogliptin did not increase the risk of major cardiovascular events [12].

In summary, in the case of obese-insulin resistance and T2DM with I/R, DPP-4 inhibitors, vildagliptin, sitagliptin, and alogliptin exert cardioprotective effects, in addition to their glycemic control effects, by improving LV function and decreasing infarct size potentially via their anti-oxidative stress and cardiac mitochondrial protection.

References

[1] M. Laakso, Cardiovascular disease in type 2 diabetes from population to man to mechanisms: the Kelly West Award Lecture 2008, Diabetes Care 33 (2010) 442–449.
[2] T. Kalogeris, Y. Bao, R.J. Korthuis, Mitochondrial reactive oxygen species: a double edged sword in ischemia/reperfusion vs preconditioning, Redox Biol. 2 (2014) 702–714.
[3] N. Apaijai, K. Chinda, S. Palee, S. Chattipakorn, N. Chattipakorn, Combined vildagliptin and metformin exert better cardioprotection than monotherapy against ischemia–reperfusion injury in obese-insulin resistant rats, PLoS One 9 (2014) e102374.
[4] M. Yin, B.D. Westenbrink, M. Meissner, W.H. van Gilst, R.A. de Boer, Variable effects of anti-diabetic drugs in animal models of myocardial ischemia and remodeling: a translational perspective for the cardiologist, Int. J. Cardiol. 169 (2013) 385–393.
[5] K. Chinda, S. Palee, S. Surinkaew, M. Phornphutkul, S. Chattipakorn, N. Chattipakorn, Cardioprotective effect of dipeptidyl peptidase-4 inhibitor during ischemia–reperfusion injury, Int. J. Cardiol. 167 (2013) 451–457.
[6] C. Yang, J. Yang, J. Yang, Z.X. Fan, DPP-4 inhibitors: Promising feasible therapeutic approach for myocardial ischemia–reperfusion injury, Int. J. Cardiol. 201 (2015) 253–254.
[7] N. Hamdani, A.S. Hervent, L. Vandekerckhove, V. Matheeussen, M. Demolder, L. Baerts, et al., Left ventricular diastolic dysfunction and myocardial stiffness in diabetic mice is attenuated by inhibition of dipeptidyl peptidase 4, Cardiovasc. Res. 104 (2014) 423–431.
[8] M. Sauve, K. Ban, M.A. Momen, Y.Q. Zhou, R.M. Henkelman, M. Husain, et al., Genetic deletion or pharmacological inhibition of dipeptidyl peptidase-4 improves cardiovascular outcomes after myocardial infarction in mice, Diabetes 59 (2010) 1063–1073.
[9] B.M. Scirica, D.L. Bhatt, E. Braunwald, P.G. Steg, J. Davidson, B. Hirshberg, et al., Saxagliptin and cardiovascular outcomes in patients with type 2 diabetes mellitus, N. Engl. J. Med. 369 (2013) 1317–1326.
[10] L.M. McCormick, A.C. Kydd, P.A. Read, L.S. Ring, S.J. Bond, S.P. Hoole, et al., Chronic dipeptidyl peptidase-4 inhibition with sitagliptin is associated with sustained protection against ischemic left ventricular dysfunction in a pilot study of patients with type 2 diabetes mellitus and coronary artery disease, Circ. Cardiovasc. Imaging 7 (2014) 274–281.
[11] P.A. Read, F.Z. Khan, P.M. Heck, S.P. Hoole, D.P. Dutka, DPP-4 inhibition by sitagliptin improves the myocardial response to dobutamine stress and mitigates stunning in a pilot study of patients with coronary artery disease, Circ. Cardiovasc. Imaging 3 (2010) 195–201.
[12] W.B. White, C.P. Cannon, S.R. Heller, S.E. Nissen, R.M. Bergenstal, G.L. Bakris, et al., Alogliptin after acute coronary syndrome in patients with type 2 diabetes, N. Engl. J. Med. 369 (2013) 1327–1335.

เอกสารแนบหมายเลข 13

ACS Medicinal Chemistry Letters

Letter

pubs.acs.org/acsmedchemlett

Varying Chirality Across Nicotinic Acetylcholine Receptor Subtypes: Selective Binding of Quinuclidine Triazole Compounds

Jiradanai Sarasamkan,[†,‡,§] Matthias Scheunemann,[‡] Nattayaporn Apaijai,[∥] Siripong Palee,[∥] Warisara Parichatikanond,[⊥] Kuntarat Arunrungvichian,[†] Steffen Fischer,[‡] Siriporn Chattipakorn,[∥] Winnie Deuther-Conrad,[‡] Gerrit Schüürmann,[▽,#] Peter Brust,[‡] and Opa Vajragupta*[,†]

[†]Center of Excellence for Innovation in Drug Design and Discovery, Faculty of Pharmacy, Mahidol University, 447 Sri-Ayutthaya Road, Bangkok 10400, Thailand

[‡]Department of Neuroradiopharmaceuticals, Institute of Radiopharmaceutical Cancer Research, Helmholtz-Zentrum Dresden-Rossendorf, Permoserstraße15, 04318 Leipzig, Germany

[§]National Cyclotron and PET Centre, Chulabhorn Hospital, 54 Kamphaengphet 6 Road, Bangkok 10210, Thailand

[∥]Neurophysiology Unit, Cardiac Electrophysiology Research and Training Center, Faculty of Medicine, Chiang Mai University, Chiang Mai 50200, Thailand

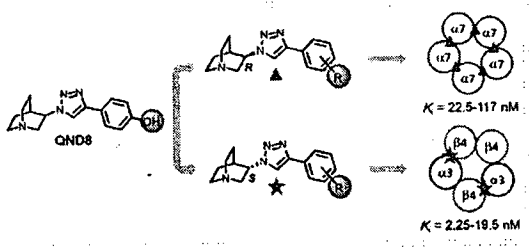
[⊥]Department of Pharmacology, Faculty of Pharmacy, Mahidol University, 447 Sri-Ayutthaya Road, Bangkok 10400, Thailand

[▽]Department of Ecological Chemistry, Helmholtz Centre for Environmental Research−UFZ, Permoserstraße15, 04318 Leipzig, Germany

[#]Institute for Organic Chemistry, Technical University Bergakademie Freiberg, Leipziger Straße29, 09596 Freiberg, Germany

Supporting Information

ABSTRACT: The novel quinuclidine *anti*-1,2,3-triazole derivatives **T1**−**T6** were designed based on the structure of **QND8**. The binding studies revealed that the stereochemistry at the C3 position of the quinuclidine scaffold plays an important role in the nAChR subtype selectivity. Whereas the (*R*)-enantiomers are selective to $\alpha7$ over $\alpha4\beta2$ (by factors of 44−225) and to a smaller degree over $\alpha3\beta4$ (3−33), their (*S*)-counterparts prefer $\alpha3\beta4$ over $\alpha4\beta2$ (62−237) as well as over $\alpha7$ (5−294). The (*R*)-derivatives were highly selective to $\alpha7$ over $\alpha3\beta4$ subtypes compared to (*RS*)- and (*R*)-**QND8**. The (*S*)-enantiomers are 5−10 times more selective to $\alpha4\beta2$ than their (*R*) forms. The overall strongest affinity is observed for the (*S*)-enantiomer binding to $\alpha3\beta4$ (K_i, 2.25−19.5 nM) followed by their (*R*)-counterpart binding to $\alpha7$ (K_i, 22.5−117 nM), with a significantly weaker (*S*)-enantiomer binding to $\alpha4\beta2$ (K_i, 414−1980 nM) still above the very weak respective (*R*)-analogue affinity (K_i, 5059−10436 nM).



KEYWORDS: *Nicotinic acetylcholine receptor, positron emission tomography, quinuclidine anti-1,2,3-triazole, click chemistry*

Nicotinic acetylcholine receptors (nAChRs) are members of the Cys-loop receptor superfamily of ligand-gated ion channels that mediate fast synaptic transmission in the central (CNS) and peripheral (PNS) nervous systems.[1−4] They are pentameric structures of homomeric or heteromeric subunits symmetrically arranged around a central ion channel. There are 16 homologous mammalian nAChR subunits encoded by this multigene family. These subunits combine to form many different nAChR subtypes with various expression patterns, diverse functional properties, and different pharmacological characteristics.[1] Currently, there are at least 12 known nAChR subunits ($\alpha2-\alpha10$ and $\beta2-\beta4$) expressed in the brain.[4] The most predominant nAChRs found in the brain, associated with cognition, memory formation, and behavior, are the $\alpha4\beta2$ and $\alpha7$ subtypes.[3] The $\alpha4\beta2$ nAChR in mammalian brain accounts for the majority of the high affinity sites for nicotine[4] and is mainly found in the thalamus, cortical regions, striatum, and colliculi, whereas the distribution pattern of the $\alpha7$ nAChR with high affinity for α-bungarotoxin is rather diffuse with focally high density in thalamus and rather low expression in the cerebellum.[3] A further important receptor subtype in the central nervous system (CNS) is the $\alpha3\beta4$ nAChR because of its involvement in drug addiction and depression pathways.[5] In contrast to $\alpha4\beta2$ and $\alpha7$, this subtype is mainly expressed in the autonomic ganglia and only in selected brain regions (subsets of neurons in the medial habenula, nucleus interpeduncularis, dorsal medulla, pineal gland, and retina).[4] The nAChRs are well recognized as key receptors involved not only in a variety of neuropsychiatric and neurodegenerative disorders, including Parkinson's disease (PD), attention deficit hyperactivity

Received: April 7, 2016
Accepted: August 9, 2016
Published: August 9, 2016

ACS Publications © 2016 American Chemical Society

DOI: 10.1021/acsmedchemlett.6b00146
ACS Med. Chem. Lett. 2016, 7, 890−895

disorder (ADHD), schizophrenia, Alzheimer's disease (AD), depression, epilepsy, and nicotine and drug addiction[6−12] but also in cancer.[13,14] The multiplicity of nAChR subtypes, their localization in the CNS, and periphery along with their pharmacological, physiological, and kinetic properties afford the opportunities to develop novel subtype-specific nAChR ligands for treatment of these diseases.[14,15]

Several compounds have been designed and synthesized based on known nAChR ligand recognition components covering the protonated amine that triggers the cation−π interaction, the hydrogen bond acceptor, and the hydrophobic stabilization. The availability of aromatic moieties in this hydrophobic part may participate in favorable electron−π interactions, which can be either electrostatic or dispersive. The tertiary quinuclidine amine is one of the most promising core structures used for the design and development of α7 nAChR ligands (Figure 1A). Besides the core structure, the effective

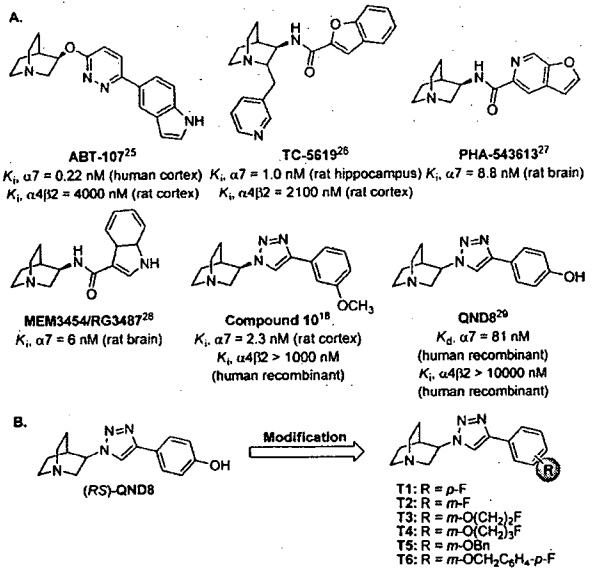


Figure 1. Structure of some nAChR ligands containing quinuclidine scaffold (A)[18,25−29] and design strategy (B).

pharmacophore linkers at position 3 of the quinuclidine scaffold are ether, carbamate, urea, amide, sulfonamide, oxazole, oxadiazole, and triazole.[16,17] Another approach in the design of α7 ligands was the synthesis of conformational restricted analogues such as oxazolidinone AR-R17779.[16] Among them, the compounds containing the quinuclidine *anti*-1,2,3-triazole skeleton bind with high affinity and selectivity to the α7 nAChR.[18] This hydrophobic motif in particular plays an important role in receptor subtype recognition through the interaction with amino acid residues of the complementary face, which has been demonstrated as an essential part for ligand selectivity among various nAChR subtypes.[19−21] We recently reported three series of novel potent and selective α7 nAChR agonists featuring the quinuclidine *anti*-1,2,3-triazole containing molecules (IND8 and QND8) that demonstrated cognitive enhancement in mice.[22] There is not only the pharmacological benefit of using the *anti*-1,2,3-triazole as the linker, but the triazole moiety itself is stable and largely resistant to metabolic degradation.[23,24]

In the present design, four different approaches were applied to the lead compound, (*RS*)-QND8 (Figure 1B) to improve the potency and selectivity profiles at the most important neuronal nAChR subtypes (α7, $\alpha3\beta4$, $\alpha4\beta2$). First, the chirality at position 3 of the quinuclidine scaffold was investigated by individual analysis of the two enantiomers of the racemic compounds. Quinuclidine-containing compounds are well recognized for nAChR interaction and the selectivity of their (*R*)-enantiomers for α7 nAChR. However, detailed information with regard to their (*S*)-enantiomers was missing at the beginning of this study.[18,29] Thus, both enantiomers were prepared to investigate the influence of chirality on the selectivity as well as the affinity for nAChR. Second, the orientation of the hydrophobic aromatic ring was explored by altering the substitution from *para* to *meta*. With regard to α7 nAChR, the binding affinity of quinuclidine derivatives was found to prefer the *meta*-phenyl substitution, compared to the *para*-position.[18] The *m*-phenyl substitution was included to verify this notion. Third, the hydrophobic side chains were extended to enhance the binding affinity and selectivity, based on the increase in size as well as the lipophilicity for receptor binding. The expansion of the structure was conducted via an ether linkage (R in Figure 1B), where the phenol of QND8 resides. Finally, the fluorine atoms were introduced into the structure for further development as potential positron emission tomography (PET) radioligands for imaging the nAChR in the brain.

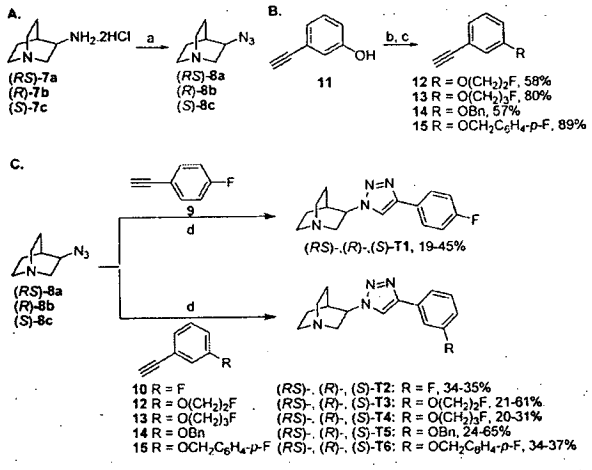
Herein we report the synthesis and the binding affinity of quinuclidine derivatives T1−T6 (*RS*, *R*, *S*) at neuronal α7, $\alpha3\beta4$, and $\alpha4\beta2$ nAChR subtypes. Promising compounds of high $\alpha3\beta4$ binding affinity and good selectivity toward other nAChRs were further screened in functional assays using HEK cells expressing human nAChR subtypes.

The general procedure for the preparation of the designed compounds started with the synthesis of the azide building block by a diazo transfer reaction and synthesis of terminal alkynes through the Sonogashira cross-coupling reaction, followed by the copper-catalyzed azide−alkyne cycloaddition (CuAAC) reaction resulting in the formation of the final *anti*-1,2,3-triazole-containing ligands (Scheme 1). The diazo transfer reaction for the preparation of azidoquinuclidine compounds (*RS*)-8a, (*R*)-8b, and (*S*)-8c were achieved, respectively, by using 3-aminoquinuclidine dihydrochloride (*RS*)-7a, (*R*)-7b, and (*S*)-7c interacted with freshly prepared trifluoromethanesulfonyl azide (TfN_3). The 3-ethynylphenol 11 was used as a starting material for the Williamson etherification with 1-fluoro-2-iodoethane, 1-fluoro-3-iodopropane, benzyl chloride, and 4-fluorobenzyl chloride to afford the 3-ethynyl-phenylethers 12, 13, 14, and 15, respectively. The final compounds (*RS*)-T1, (*R*)-T1, and (*S*)-T1 were synthesized by the reaction of the respective azidoquinuclidines (*RS*)-8a, (*R*)-8b, and (*S*)-8c with 4-fluoro-phenylacetylene 9 under CuAAC conditions. Cycloaddition of these azidoquinuclidines with 3-fluorophenylacetylene 10 yielded the final compounds (*RS*)-T2, (*R*)-T2, and (*S*)-T2. CuAAC or click reactions between 8a−c and terminal alkyne 12 resulted in the formation of its corresponding T3 compounds. The remaining quinuclidine *anti*-1,2,3-triazoles T4−T6 were prepared by the same synthetic route as described above.

The blood−brain barrier (BBB) penetration of CNS drugs depends on several physicochemical properties including molecular weight (MW), pK_a, hydrophobicity (log P and log D), and topological polar surface area (TPSA). These

DOI: 10.1021/acsmedchemlett.6b00146
ACS Med. Chem. Lett. 2016, 7, 890−895

Scheme 1. Synthesis of Azide (A), Terminal Alkynes (B), and the Quinuclidine *anti*-1,2,3-Triazole Containing Molecules (C)[a]



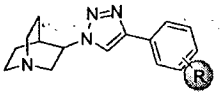
[a]Reagents and conditions: (a) TfN_3, K_2CO_3, $CuSO_4{\cdot}5H_2O$, CH_3OH, H_2O, rt, overnight; (b) 1-fluoro-2-iodoethane for **12** and 1-fluoro-3-iodopropane for **13**, K_2CO_3, CH_3CN, 70 °C, 10 h; (c) benzyl chloride for **14** and 4-fluorobenzyl chloride for **15**, K_2CO_3, CH_3CN, 80 °C, 6 h; (d) 5 mol % $CuSO_4{\cdot}5H_2O$, 10 mol % sodium ascorbate, *t*-BuOH, H_2O, rt, overnight.

parameters were calculated for all synthesized compounds using the ACD/ADME Suite software, and the predicted values fall within the ranges of CNS drug-like properties. Calculated log BB values of ≥ -1.0 indicate sufficient BBB permeation of all compounds[30] (Supplemental Table S1). Additional support for a good BBB penetration of the compounds is provided by calculated pK_a values in the range of 7.5−10.5, which furthermore suggest sufficient protonation of the compounds in the CNS for cation−π or other electrostatic interactions with conserved amino acid residues or residues comprising electron-rich aromatic moieties in the binding sites of nAChRs.

The *in vitro* binding affinities of all modified compounds for the nicotinic receptor subtypes were examined in competitive radioligand displacement studies using [^{3}H]methyllycaconitine and [^{3}H]epibatidine as selective radioligands for human $\alpha7$ nAChR as well as human $\alpha4\beta2$ and $\alpha3\beta4$ nAChRs, respectively (Supporting Information). The binding affinities of the compounds tested are presented in Table 1. The racemic compounds showed K_i values at $\alpha7$ nAChR in the range of 73−133 nM. In addition, all of them bound with higher affinity toward $\alpha3\beta4$ nAChR. Replacement of the hydroxyl group of the lead compound **QND8** by a fluorine atom decreases the binding affinity on $\alpha7$ as the K_i value of (*RS*)-**T1** at $\alpha7$ nAChR is 7 times higher than that of (*RS*)-**QND8** (73 vs 10 nM). However, this modified compound showed better selectivity at $\alpha7$ over $\alpha3\beta4$.

The most important finding was the significant dependence of the nAChR subtype affinity on the handedness of the

Table 1. *In Vitro* Binding Affinities of 21 Quinuclidine *anti*-1,2,3-Triazole Derivatives Towards nAChRs[a]

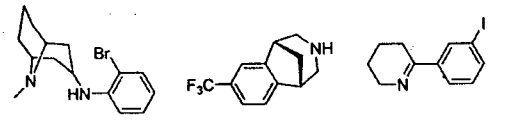


R	compd	inhibition constant K_i in nM; mean ± SD			selectivity[b] (inverse of respective K_i ratio)		
		$\alpha7$[c]	$\alpha3\beta4$[d]	$\alpha4\beta2$[d]	$\alpha7$ vs $\alpha3\beta4$	$\alpha7$ vs $\alpha4\beta2$	$\alpha3\beta4$ vs $\alpha4\beta2$
p-F	(*RS*)-T1	72.8 ± 13	8.50 ± 0.50	449 ± 127	1/8.6	6.2	53
	(*R*)-T1	73.0 ± 15	1010 ± 162	10436 ± 1943	14	143	10
	(*S*)-T1	174.5 ± 66	3.09 ± 0.10	515 ± 64	1/56	3.0	167
m-F	(*RS*)-T2	133 ± 40	5.24 ± 0.35	748 ± 114	1/25	5.6	143
	(*R*)-T2	117 ± 4	362 ± 27	5201 ± 412	3.1	44	14
	(*S*)-T2	660.5 ± 139	2.25 ± 0.42	519 ± 20	1/294	1/1.3	231
m-$O(CH_2)_2F$	(*RS*)-T3	98.7 ± 39	20.9 ± 0.7	1962 ± 228	1/4.7	20	94
	(*R*)-T3	38.8 ± 8	558 ± 34	7050 ± 200	14	182	13
	(*S*)-T3	74.9 ± 20	11.8 ± 0.3	1262 ± 187	1/6.3	17	107
m-$O(CH_2)_3F$	(*RS*)-T4	74.6 ± 14	44.4 ± 8.0	3894 ± 252	1/1.7	52	88
	(*R*)-T4	62.3 ± 10	1628 ± 11	9010 ± 5,034	26	145	5.5
	(*S*)-T4	96.9 ± 17	19.5 ± 0.4	1980 ± 117	1/5.0	20	102
m-OBn	(*RS*)-T5	91.3 ± 9	7.57 ± 2.9	668 ± 7	1/12	7.3	88
	(*R*)-T5	22.5 ± 9	631 ± 206	5059 ± 374	28	225	8.0
	(*S*)-T5	279 ± 31	6.67 ± 0.7	414 ± 59	1/42	1.5	62
m-$OCH_2C_6H_4F$	(*RS*)-T6	127 ± 5	13.9 ± 2.8	1,013 ± 107	1/9.1	8.0	73
	(*R*)-T6	33.2 ± 7	1090 ± 163	6392 ± 230	33	193	5.9
	(*S*)-T6	149 ± 42	7.17 ± 1.2	537 ± 11	1/21	3.6	75
p-OH	(*RS*)-QND8	9.61 ± 1.47	3.44 ± 0.04	627 ± 52	1/2.8	65	182
	(*R*)-QND8	10.9 ± 1.42	138 ± 0	7389 ± 42	12.7	678	54
	(*S*)-QND8	29.3 ± 0.18	2.48 ± 0.04	461 ± 89	1/11.8	16	186

[a]Binding affinities are represented by the inhibition constant K_i determined for individual compounds in two separate experiments each performed as triplicate. [b]Selectivity is reported in terms of the reciprocal of the ratio of the respective K_i values. [c]Human $\alpha7$ nAChR in stably transfected SH-SY5Y cells, with radiotracer [^{3}H]methyllycaconitine (0.5−1 nM); K_d = 2.0 nM. [d]Human $\alpha4\beta2$ and $\alpha3\beta4$ nAChR in stably transfected HEK-293 cells, with radiotracer [^{3}H]epibatidine (0.5−1 nM); K_d = 0.025 nM for h$\alpha4\beta2$ nAChR; K_d = 0.117 nM for h$\alpha3\beta4$ nAChR.

DOI: 10.1021/acsmedchemlett.6b00146
ACS Med. Chem. Lett. 2016, 7, 890−895

ligands. The chirality of the binding sites of the different nAChR subtypes offers a rationale for the enantioselective affinity profiles of chiral ligands for $\alpha7$, $\alpha4\beta2$, and $\alpha3\beta4$ nAChRs. More specifically, the experimentally determined affinities (Table 1) reveal the following pattern: first, all (*R*)-enantiomers showed a significant selectivity for $\alpha7$ over $\alpha4\beta2$ and to a lesser degree also over $\alpha3\beta4$. They bind with low nanomolar affinity at $\alpha7$, with high nanomolar affinity at $\alpha3\beta4$, and with micromolar affinities at $\alpha4\beta2$. The resulting selectivity values in the range of 3.1−33 and 44−225 for $\alpha7$ vs $\alpha3\beta4$ and $\alpha4\beta2$, respectively, indicate preference for the $\alpha7$ nAChR binding site. Atypically, (*R*)-**T2** provides only weak preference for $\alpha7$ over $\alpha3\beta4$ (selectivity of 3.1). Second, all (*S*)-enantiomers are highly selective for $\alpha3\beta4$ over $\alpha4\beta2$ and mostly to a lesser degree also over $\alpha7$. They bind with low nanomolar affinity at $\alpha3\beta4$ and with high nanomolar to micromolar affinities at $\alpha7$ and $\alpha4\beta2$. The selectivity values of $\alpha3\beta4$ vs $\alpha7$ and $\alpha4\beta2$ were estimated in the range of 5−294 and 62−231 and indicate preference of the (*S*)-enantiomers of quinuclidine-*anti*-1,2,3-triazole containing nAChR ligands for the binding site of $\alpha3\beta4$ nAChR. Compound **T2** plays again a special role, with its (*S*)-enantiomer showing the overall highest selectivity (294) for $\alpha3\beta4$ over $\alpha7$. Notably **AT-1001** previously reported as a high affinity and selective $\alpha3\beta4$ nAChR antagonist[31] also falls into this category, although with slightly lower affinity and selectivity than **T2**. However, two other recently reported ligands for the $\alpha3\beta4$ nAChR, **CP-601932**[32] and an anabaseine analogue,[33] showed modest selectivity of binding to $\alpha3\beta4$ over $\alpha4\beta2$ and $\alpha3\beta4$ over $\alpha7$, respectively (Figure 2). Third, the preference of the (*S*)-



AT-1001[31]	CP-601932[32]	anabaseine analogue[33]
K_i, α3β4 = 2.64 nM	K_i, α3β4 = 21 nM	K_i, α3β4 = 4.7 nM
K_i, α4β2 = 476 nM	K_i, α4β2 = 21 nM	K_i, α4β2 = 3790 nM
K_i, α7 = 221 nM	K_i, α7 > 300 nM	K_i, α7 = 11.3 nM

Figure 2. Structures of selected $\alpha3\beta4$ nAChR ligands.

enantiomers for $\alpha3\beta4$ over $\alpha4\beta2$ (selectivity 62−231) is more pronounced than the preference of the (*R*)-enantiomers for $\alpha7$ over $\alpha3\beta4$ (selectivity 3−33). Fourthly, the overall highest binding affinities for the herein assessed nAChR subtypes were observed for binding of the (*S*)-enantiomers to $\alpha3\beta4$ (K_i = 2.25−19.5 nM) followed by the binding of the (*R*)-enantiomers to $\alpha7$ (K_i= 22.5−117 nM). Concerning binding to $\alpha4\beta2$, the affinity of the (*S*)-enantiomers is higher than of the (*R*)-enantiomers (414−1980 vs 5059−10436 nM).

By more detailed investigation of the interaction of the herein presented ligands with $\alpha7$ nAChR, the fluorine-substituted enantiomers (*R*)-**T1** and(*R*)-**T2**, bearing F, at *p*- and *m*-position of the phenyl ring, respectively, showed binding profiles comparable to their racemic mixture with (*R*)-**T1** being 3-fold more selective for $\alpha7$ over $\alpha4\beta2$ than (*R*)-**T2** (factors 143 vs 44). The binding affinity increases about 2-fold when replacing the (*R*)-**T4** phenyl substituent *m*-$O(CH_2)_3F$ (K_i = 62.3 nM) by the smaller and less hydrophobic *m*-$O(CH_2)_2F$ group ((*R*)-**T3**, K_i = 38.8 nM) as well as by the larger and more hydrophobic groups *m*-OBn ((*R*)-**T5**, K_i = 22.5 nM) and *m*-$OCH_2C_6H_4F$ ((*R*)-**T6**, K_i = 33.2 nM). A possible explanation would be that the respective variation in K_i might be triggered by the presence or absence of a spatially suitable electron donor functionality of the ligand (e.g., as H-bond acceptor), either through its F lone pair electrons (**T4**) or through the benzylic π-electrons (**T5**, **T6**).

For the corresponding (*S*)-enantiomers, (*S*)-**T2** shows a 5-fold higher selectivity for $\alpha3\beta4$ over $\alpha7$ in comparison to (*S*)-**T1**. Regarding further substituents, the following pattern is observed for the affinity of the (*S*)-enantiomers to $\alpha3\beta4$ nAChR. Here, *m*-$O(CH_2)_2F$ ((*S*)-**T3** with an K_i of 11.8 nM) is again ~2-fold more potent than *m*-$O(CH_2)_3F$ ((*S*)-**T4**, Ki = 19.5 nM), but now the two phenyl-containing (*S*)-**T5** (K_i = 6.67 nM) and (*S*)-**T6** (K_i = 7.17 nM) yield a further ~2-fold increase in binding affinity. These results support the suggestion that a ligand π-electron donor capability at a site distant from the quinuclidine triazole moiety may contribute to stabilizing the ligand−receptor complex. Interestingly, (*S*)-**T2** and (*S*)-**T1** as the two most promising $\alpha3\beta4$ ligands (K_i = 2.25 vs 3.09 nM) are the only derivatives with an F-substituted phenyl ring, where *m*-F (*S*)-**T2** yields the overall highest $\alpha3\beta4$ selectivity over both $\alpha7$ and $\alpha4\beta2$ as discussed above. The significant difference in the selectivity profiles of the F-substituted isomers (*S*)-**T1** and (*S*)-**T2** suggests the following tentative explanation. In (*S*)-**T1**, the electronegative F is in *p*-position to the electron-rich triazole, the latter of which may partly compensate the electron shift from the benzene ring to F. By contrast, the respective conjugative substitution pattern is missing in (*S*)-**T2**, thus probably resulting in a stronger loss of π-electron density through inductive charge transfer to *m*-F. From this viewpoint it is likely that an electron-poor character of the benzylic moiety in compound (*S*)-**T2** triggers for a strong $\alpha3\beta4$ selectivity, with K_i-based selectivity of 294 (over $\alpha7$) and 231 (over $\alpha4\beta2$), respectively. Interestingly, it was apparent that (*S*)-enantiomers were more selective to $\alpha3\beta4$ (47−326 times) and $\alpha4\beta2$ nAChR (4.5−20 times) than their corresponding (*R*)-counterparts. Up until now, the selective binding of (*S*)-quinuclidine based compounds on $\alpha3\beta4$ and $\alpha4\beta2$ subtypes have never been reported before.

Four compounds with good affinity (K_i < 10 nM), which are (*S*)-enantiomers of **T1**, **T2**, **T5**, and **T6**, were evaluated for the binding at related receptors, these four compounds had no significant effect on N-muscle type nAChR (2−12% inhibition at 1 μM). For the 5-HT_3 receptor, (*S*)-enantiomers of **T1**, **T2**, **T5**, and **T6** were tested at 100 nM, all except (*S*)-**T6** showed no significant binding at the 5-HT_3 receptor.

To see whether the designed compounds are agonist as **QND8** or antagonist as **AT-1001**, the functional assays of the potential compounds **T1** and **T2** in both (*R*) and (*S*) forms were performed using SH-SY5Y cells stably expressing human $\alpha7$ nAChR and HEK 293 cells stably expressing human $\alpha3\beta4$ nAChR. The screening results indicated that (*R*)-**T1**, (*R*)-**T2**, (*S*)-**T1**, and (*S*)-**T2** are $\alpha7$ nAChR agonists (Supplemental Figure S1). Compounds (*R*)-**T2** and (*S*)-**T1** are $\alpha3\beta4$ nAChR agonists, whereas (*R*)-**T1** and (*S*)-**T2** are $\alpha3\beta4$ nAChR antagonists (Supplemental Figure S2). However, the selectivity cannot be concluded due to the high testing concentration (10 μM) in the screening assay for functional effects.

Overall, according to the binding data of all novel analogues presented herein, the stereocenter at C3 position of the quinuclidine motif has significant impact on the selectivity of modified compounds to nAChR subtypes. (*R*)-Enantiomers bind preferably toward $\alpha7$, while (*S*)-enantiomers were more selective for the $\alpha3\beta4$ nAChR. Among all, (*R*)-**T5** was the most

DOI: 10.1021/acsmedchemlett.6b00146
ACS Med. Chem. Lett. 2016, 7, 890−895

favorable ligand for the $\alpha7$ nAChR, (*S*)-**T2** and (*S*)-**T1** for the $\alpha3\beta4$ nAChR with almost equal affinities, and (although significantly less strong) (*S*)-**T5** was the most promising $\alpha4\beta2$ nAChR ligand.

In conclusion, we have successfully designed two potent compounds (*S*)-**T1** and (*S*)-**T2** that bind selectively to $\alpha3\beta4$ nAChR over $\alpha7$ nAChR. Among the (*R*)- and (*S*)-enantiomers of the quinuclidine-based compounds, the binding affinities of (*S*)-enantiomers are higher compared to their (*R*) counterparts. This finding may have implications for the treatment of several brain diseases such as drug addiction and dependence. Compounds (*R*)-**QND8** and (*R*)-**T6**, which displayed higher affinity for the $\alpha7$ nAChR and higher selectivity toward the $\alpha3\beta4$ nAChR than its parent (*RS*)-**QND8** might be useful candidate molecules in further drug development for the treatment of cognitive disorders. In addition, the introduction of a fluorine substituent in the structure makes it possible to develop the designed compounds as PET radioligands for brain imaging to localize the $\alpha3\beta4$ and $\alpha7$ nAChR subtypes in the brain and monitor drug efficacy.

■ ASSOCIATED CONTENT

Supporting Information

The Supporting Information is available free of charge on the ACS Publications website at DOI: 10.1021/acsmedchemlett.6b00146.

Experimental procedures and analytical data (PDF)

■ AUTHOR INFORMATION

Corresponding Author

*Phone: +66-2-644-8695. E-mail: opa.vaj@mahidol.ac.th.

Funding

This work was supported by Thailand Research Fund (TRF) through the Royal Golden Jubilee Ph.D. Program (Grant No.PHD/0272/2552) to J.S. and O.V., BRG 5780016 to S.C., the Office of the High Education Commission, Thailand; Thailand Research Fund (TRF) and Faculty of Pharmacy, Mahidol University (IRG578007) to O.V.

Notes

The authors declare no competing financial interest.

■ ABBREVIATIONS

nAChR, nicotinic acetylcholine receptor; PET, positron emission tomography; CuAAC, copper-catalyzed azide−alkyne cycloaddition; PD, Parkinson's disease; ADHD, attention deficit hyperactivity disorder; AD, Alzheimer's disease

■ REFERENCES

(1) Dani, J. A. Neuronal nicotinic acetylcholine receptor structure and function and response to nicotine. *Int. Rev. Neurobiol.* **2015**, *124*, 3−19.

(2) Dineley, K. T.; Pandya, A. A.; Yakel, J. L. Nicotinic ACh receptors as therapeutic targets in CNS disorders. *Trends Pharmacol. Sci.* **2015**, *36*, 96−108.

(3) Brust, P.; Deuther-Conrad, W.; Donat, C. K.; Barthel, H.; Riss, P.; Paterson, L.; Hoepping, A.; Sabri, O.; Cumming, P. Preclinical aspects of nicotinic acetylcholine receptor imaging. In *PET and SPECT of Neurobiological Systems*; Dierckx, R. A. J. O., Ed.; Springer: Berlin Heidelberg, 2014; pp 465−512.

(4) Gotti, C.; Clementi, F.; Fornari, A.; Gaimarri, A.; Guiducci, S.; Manfredi, I.; Moretti, M.; Pedrazzi, P.; Pucci, L.; Zoli, M. Structural and functional diversity of native brain neuronal nicotinic receptors. *Biochem. Pharmacol.* **2009**, *78*, 703−711.

(5) Rahman, S.; Engleman, E. A.; Bell, R. L. Nicotinic receptor modulation to treat alcohol and drug dependence. *Front. Neurosci.* **2015**, *8*, 426.

(6) Posadas, I.; Lopez-Hernandez, B.; Cena, V. Nicotinic receptors in neurodegeneration. *Curr. Neuropharmacol.* **2013**, *11*, 298−314.

(7) Toyohara, J.; Hashimoto, K. $\alpha7$ Nicotinic receptor agonists: potential therapeutic drugs for treatment of cognitive impairments in Schizophrenia and Alzheimer's Disease. *Open Med. Chem. J.* **2010**, *4*, 37−56.

(8) Dani, J. A.; Bertrand, D. Nicotinic acetylcholine receptors and nicotinic cholinergic mechanisms of the central nervous system. *Annu. Rev. Pharmacol. Toxicol.* **2007**, *47*, 699−729.

(9) Wilens, T. E.; Decker, M. W. Neuronal nicotinic receptor agonists for the treatment of attention-deficit/hyperactivity disorder: focus on cognition. *Biochem. Pharmacol.* **2007**, *74*, 1212−1223.

(10) Glick, S. D.; Maisonneuve, I. M.; Kitchen, B. A.; Fleck, M. W. Antagonism of a3b4 nicotinic receptors as a strategy to reduce opioid and stimulant self-administration. *Eur. J. Pharmacol.* **2002**, *438*, 99−105.

(11) Haydar, S. N.; Dunlop, J. Neuronal nicotinic acetylcholine receptors - targets for the development of drugs to treat cognitive impairment associated with schizophrenia and Alzheimer's disease. *Curr. Top. Med. Chem.* **2010**, *10*, 144−152.

(12) Taraschenko, O. D.; Panchal, V.; Maisonneuve, I. M.; Glick, S. D. Is antagonism of a3b4 nicotinic receptors a strategy to reduce morphine dependence? *Eur. J. Pharmacol.* **2005**, *513*, 207−218.

(13) Zhao, Y. The oncogenic functions of nicotinic acetylcholine receptors. *J. Oncol.* **2016**, *2016*, 1.

(14) Mucchietto, V.; Crespi, A.; Fasoli, F.; Clementi, F.; Gotti, C. Neuronal acetylcholine nicotinic receptors as new targets for lung cancer treatment. *Curr. Pharm. Des.* **2016**, *22*, 2160−2169.

(15) Gotti, C.; Zoli, M.; Clementi, F. Brain nicotinic acetylcholine receptors: native subtypes and their relevance. *Trends Pharmacol. Sci.* **2006**, *27*, 482−491.

(16) Pin, F.; Vercouillie, J.; Ouach, A.; Mavel, S.; Gulhan, Z.; Chicheri, G.; Jarry, C.; Massip, S.; Deloye, J. B.; Guilloteau, D.; Suzenet, F.; Chalon, S.; Routier, S. Design of a7 nicotinic acetylcholine receptor ligands in quinuclidine, tropane and quinazoline series. Chemistry, molecular modeling, radiochemistry, in vitro and in rats evaluations of a [^{18}F] quinuclidine derivative. *Eur. J. Med. Chem.* **2014**, *82*, 214−224.

(17) Mazurov, A. A.; Speake, J. D.; Yohannes, D. Discovery and development of a7 nicotinic acetylcholine receptor modulators. *J. Med. Chem.* **2011**, *54*, 7943−7961.

(18) Ouach, A.; Pin, F.; Bertrand, E.; Vercouillie, J.; Gulhan, Z.; Mothes, C.; Deloye, J. B.; Guilloteau, D.; Suzenet, F.; Chalon, S.; Routier, S. Design of a7 nicotinic acetylcholine receptor ligands using the (het)Aryl-1,2,3-triazole core: Synthesis, in vitro evaluation and SAR studies. *Eur. J. Med. Chem.* **2016**, *107*, 153−164.

(19) Cohen, B. N.; Figl, A.; Quick, M. W.; Labarca, C.; Davidson, N.; Lester, H. A. Regions of b2 and b4 responsible for differences between the steady state dose-response relationships of the a3b2 and a3b4 neuronal nicotinic receptors. *J. Gen. Physiol.* **1995**, *105*, 745−764.

(20) Parker, M. J.; Beck, A.; Luetje, C. W. Neuronal nicotinic receptor b2 and b4 subunits confer large differences in agonist binding affinity. *Mol. Pharmacol.* **1998**, *54*, 1132−1139.

(21) Luetje, C. W.; Patrick, J. Both a- and b-subunits contribute to the agonist sensitivity of neuronal nicotinic acetylcholine receptors. *J. Neurosci.* **1991**, *11*, 837−845.

(22) Arunrungvichian, K.; Boonyarat, C.; Fokin, V. V.; Taylor, P.; Vajragupta, O. Cognitive improvements in a mouse model with substituted 1,2,3-triazole agonists for nicotinic acetylcholine receptors. *ACS Chem. Neurosci.* **2015**, *6*, 1331−1340.

(23) Keck, T. M.; Banala, A. K.; Slack, R. D.; Burzynski, C.; Bonifazi, A.; Okunola-Bakare, O. M.; Moore, M.; Deschamps, J. R.; Rais, R.; Slusher, B. S. Using click chemistry toward novel 1, 2, 3-triazole-linked dopamine D3 receptor ligands. *Bioorg. Med. Chem.* **2015**, *23*, 4000−4012.

DOI: 10.1021/acsmedchemlett.6b00146
ACS Med. Chem. Lett. 2016, 7, 890−895

(24) Beltramo, M.; Robert, V.; Galibert, M.; Madinier, J.-B.; Marceau, P.; Dardente, H.; Decourt, C.; De Roux, N.; Lomet, D.; Delmas, A. F. Rational design of triazololipopeptides analogs of kisspeptin inducing a long-lasting increase of gonadotropins. *J. Med. Chem.* **2015**, *58*, 3459−3470.

(25) Malysz, J.; Anderson, D. J.; Gronlien, J. H.; Ji, J.; Bunnelle, W. H.; Haakerud, M.; Thorin-Hagene, K.; Ween, H.; Helfrich, R.; Hu, M.; Gubbins, E.; Gopalakrishnan, S.; Puttfarcken, P. S.; Briggs, C.; Li, J.; Meyer, M. D.; Dyhring, T.; Ahring, P. K.; Nielsen, E. O.; Peters, D.; Timmermann, D. B.; Gopalakrishnan, M. In vitro pharmacological characterization of a novel selective a7 neuronal nicotinic acetylcholine receptor agonist ABT-107. *J. Pharmacol. Exp. Ther.* **2010**, *334*, 863−874.

(26) Hauser, T. A.; Kucinski, A.; Jordan, K. G.; Gatto, G. J.; Wersinger, S. R.; Hesse, R. A.; Stachowiak, E. K.; Stachowiak, M. K.; Papke, R. L.; Lippiello, P. M.; Bencherif, M. TC-5619: an alpha7 neuronal nicotinic receptor-selective agonist that demonstrates efficacy in animal models of the positive and negative symptoms and cognitive dysfunction of schizophrenia. *Biochem. Pharmacol.* **2009**, *78*, 803−812.

(27) Wishka, D. G.; Walker, D. P.; Yates, K. M.; Reitz, S. C.; Jia, S.; Myers, J. K.; Olson, K. L.; Jacobsen, E. J.; Wolfe, M. L.; Groppi, V. E.; Hanchar, A. J.; Thornburgh, B. A.; Cortes-Burgos, L. A.; Wong, E. H.; Staton, B. A.; Raub, T. J.; Higdon, N. R.; Wall, T. M.; Hurst, R. S.; Walters, R. R.; Hoffmann, W. E.; Hajos, M.; Franklin, S.; Carey, G.; Gold, L. H.; Cook, K. K.; Sands, S. B.; Zhao, S. X.; Soglia, J. R.; Kalgutkar, A. S.; Arneric, S. P.; Rogers, B. N. Discovery of *N*-[(3R)-1-azabicyclo[2.2.2]oct-3-yl]furo[2,3-c]pyridine-5-carboxamide, an agonist of the a7 nicotinic acetylcholine receptor, for the potential treatment of cognitive deficits in schizophrenia: synthesis and structure−activity relationship. *J. Med. Chem.* **2006**, *49*, 4425−4436.

(28) Wallace, T. L.; Callahan, P. M.; Tehim, A.; Bertrand, D.; Tombaugh, G.; Wang, S.; Xie, W.; Rowe, W. B.; Ong, V.; Graham, E.; Terry, A. V., Jr.; Rodefer, J. S.; Herbert, B.; Murray, M.; Porter, R.; Santarelli, L.; Lowe, D. A. RG3487, a novel nicotinic a7 receptor partial agonist, improves cognition and sensorimotor gating in rodents. *J. Pharmacol. Exp. Ther.* **2011**, *336*, 242−253.

(29) Arunrungvichian, K.; Fokin, V. V.; Vajragupta, O.; Taylor, P. Selectivity optimization of substituted 1,2,3-triazoles as a7 nicotinic acetylcholine receptor agonists. *ACS Chem. Neurosci.* **2015**, *6*, 1317−1330.

(30) Ghose, A. K.; Herbertz, T.; Hudkins, R. L.; Dorsey, B. D.; Mallamo, J. P. Knowledge-based, central nervous system (CNS) lead selection and lead optimization for CNS drug discovery. *ACS Chem. Neurosci.* **2012**, *3*, 50−68.

(31) Toll, L.; Zaveri, N. T.; Polgar, W. E.; Jiang, F.; Khroyan, T. V.; Zhou, W.; Xie, X. S.; Stauber, G. B.; Costello, M. R.; Leslie, F. M. AT-1001: a high affinity and selective a3b4 nicotinic acetylcholine receptor antagonist blocks nicotine self-administration in rats. *Neuropsychopharmacology* **2012**, *37*, 1367−1376.

(32) Chatterjee, S.; Steensland, P.; Simms, J. A.; Holgate, J.; Coe, J. W.; Hurst, R. S.; Shaffer, C. L.; Lowe, J.; Rollema, H.; Bartlett, S. E. Partial agonists of the a3b4* neuronal nicotinic acetylcholine receptor reduce ethanol consumption and seeking in rats. *Neuropsychopharmacology* **2011**, *36*, 603−615.

(33) Matera, C.; Quadri, M.; Sciaccaluga, M.; Pome, D. Y.; Fasoli, F.; De Amici, M.; Fucile, S.; Gotti, C.; Dallanoce, C.; Grazioso, G. Modification of the anabaseine pyridine nucleus allows achieving binding and functional selectivity for the a3b4 nicotinic acetylcholine receptor subtype. *Eur. J. Med. Chem.* **2016**, *108*, 392−405.

DOI: 10.1021/acsmedchemlett.6b00146
ACS Med. Chem. Lett. 2016, 7, 890−895

เอกสารแนบหมายเลข 14

DOI: 10.1111/1755-5922.12210

WILEY Cardiovascular Therapeutics

ORIGINAL RESEARCH ARTICLE

Humanin exerts cardioprotection against cardiac ischemia/reperfusion injury through attenuation of mitochondrial dysfunction

Savitree Thummasorn[1,2,3] | Nattayaporn Apaijai[1,2,3] | Sasiwan Kerdphoo[1] | Krekwit Shinlapawittayatorn[1,2,3] | Siriporn C. Chattipakorn[1,2,3,4] | Nipon Chattipakorn[1,2,3]

[1]Cardiac Electrophysiology Research and Training Center, Faculty of Medicine, Chiang Mai University, Chiang Mai, Thailand

[2]Cardiac Electrophysiology Unit, Department of Physiology, Faculty of Medicine, Chiang Mai University, Chiang Mai, Thailand

[3]Center of Excellence in Cardiac Electrophysiology, Chiang Mai University, Chiang Mai, Thailand

[4]Department of Oral Biology and Diagnostic Sciences, Faculty of Dentistry, Chiang Mai University, Chiang Mai, Thailand

Correspondence
Nipon Chattipakorn, M.D., Ph.D., Cardiac Electrophysiology Research and Training Center, Faculty of Medicine, Chiang Mai University, Chiang Mai, Thailand.
Email: nchattip@gmail.com

Summary

Aim: Myocardial reperfusion via the re-canalization of occluded coronary arteries is gold standard for the treatment of acute myocardial infarction. However, reperfusion itself can cause myocardial damage due to increased reactive oxygen species (ROS) production, a process known as ischemia/reperfusion (I/R) injury. Cardiac mitochondria are the major organelle of ROS production in the heart. Cardiac mitochondrial dysfunction caused by an increased ROS production can increase cardiac arrhythmia incidence, myocardial infarct size, and cardiac dysfunction. Thus, preservation of cardiac mitochondrial function is a promising pharmacological approach to reduce cardiac I/R injury. Humanin (HN), a newly discovered 24-amino acid polypeptide, has been shown to exert antioxidative stress and antiapoptotic effects. Although the cardioprotective effects of HN against I/R injury has been reported, the effect of HN on cardiac mitochondrial function has not yet been investigated. Thus, we tested the hypothesis that HN exerts its cardioprotective effects against I/R injury through the attenuation of cardiac mitochondrial dysfunction.

Methods: I/R protocol was carried out using a 30-minutes occlusion of a left anterior descending coronary artery followed by a 120-minutes of reperfusion. The plasma HN level, infarct size, arrhythmia incidence, left ventricular function, and cardiac mitochondrial function were determined.

Results: Endogenous HN level before I/R injury showed no difference between groups, but was markedly decreased after I/R injury. HN analogue pretreatment decreased arrhythmia incidence and infarct size, improved cardiac mitochondrial function, and attenuated cardiac dysfunction.

Conclusions: Humanin analogue pretreatment exerted cardioprotective effects against I/R injury through the attenuation of cardiac mitochondrial dysfunction.

KEYWORDS
Apoptosis, Heart, Humanin, Ischemia/reperfusion injury, Mitochondrial dysfunction, Oxidative stress

1 | INTRODUCTION

Acute myocardial infarction remains a leading cause of morbidity and mortality worldwide. Although myocardial reperfusion therapy is essential, reperfusion itself can induce myocardial damage and increase infarct size due to an increase in reactive oxygen species (ROS) production in the ischemic myocardium.[1,2] It is known that cardiac mitochondria are involved in the heart, including ATP synthesis, energy metabolism, apoptotic regulation as well as Ca^{2+} homeostasis.[3,4] Studies reported that these events were disturbed and lead

to myocardial damage during myocardial ischemia/reperfusion (I/R) injury.[3–5] In addition, I/R injury can markedly increase ROS levels in cardiomyocytes.[6] It is known that cardiac mitochondria are the major organelle of ROS production in the heart.[6] In a myocardial I/R injury model, ROS levels in cardiomyocytes were increased via the increased activity of complexes I and III of the electron transport chain in cardiac mitochondria.[6] This increase in mitochondrial ROS level can activate apoptosis pathways and lead to cardiomyocyte death.[1,2] Additionally, studies demonstrated that an increase in mitochondrial ROS production caused by I/R injury could activate cardiac mitochondrial dysfunction through increasing cardiac mitochondrial depolarization and cardiac mitochondrial swelling.[7,8] Furthermore, cardiac mitochondrial dysfunction has been shown to increase cardiac arrhythmias and cardiac dysfunction during I/R injury.[7,9] Thus, the preservation of cardiac mitochondrial function via decreasing mitochondrial ROS level is a promising pharmacological approach to reduce myocardial I/R injury.

Recently, humanin (HN), a newly discovered 24-amino acid polypeptide, has been shown to exert several beneficial effects including a decrease in both cellular apoptosis and oxidative stress.[10–14] Under certain physiological conditions, the endogenous HN is produced by several tissues in the body such as heart, brain, kidney, skeletal muscle, and liver.[10,15–18] The endogenous HN is secreted into the blood circulation and transported to several targeted tissues which express HN receptors including the heart.[19,20] A growing number of studies have demonstrated that HN exerts cardioprotective benefits through an antioxidative stress mechanism in cultured cardiomyocytes and a cultured endothelial cell model.[11,21] Moreover, HN has been shown to prevent apoptosis through the attenuation of oxidative stress in aortic endothelial cells.[21] Oxidative stress is an imbalance between the ROS production and the ROS scavenging in cardiac cells.[1] Thus, HN may exert cardioprotective effects against myocardial I/R injury via the attenuation of oxidative stress.

Recently, HN has been shown to exert cardioprotection against I/R injury by reducing myocardial infarct size and attenuating cardiac dysfunction through the activation of AMPK–eNOS signaling.[10] Although the cardioprotective effect of HN against I/R injury has been reported in Muzumdar's study, the effects of HN on cardiac mitochondrial function have never been investigated. Moreover, as timing of the drug administration is an important determinant of therapeutic efficacy against I/R injury,[22] the effects of HN administered against myocardial I/R injury at the designated different time points (preischemia, during ischemia, and onset of reperfusion) are also crucial for its therapeutic application in a clinical setting. Furthermore, the effects of HN on cardiac mitochondria when administered at different time points during cardiac I/R have never been tested.

In this study, we sought to investigate the effects of HN administered on cardiac arrhythmia, myocardial infarct size, cardiac mitochondrial function, left ventricular function, and the underlying mechanisms against myocardial I/R injury. We tested the hypothesis that HN administered at the designated different time points (preischemia, during ischemia, and onset of reperfusion) can exert its cardioprotection against cardiac I/R injury through attenuation of cardiac mitochondrial dysfunction.

2 | MATERIALS AND METHODS

2.1 | Animal preparation

All experiments in this study were approved by the Faculty of Medicine, Chiang Mai University Institutional Animal Care and Use Committee (Permit No. 12/2558), and were conducted in accordance with the internationally accepted principles (NIH guidelines) for laboratory animal use and care.[23] Male Wistar rats weighing 300–350 g were obtained from the National Laboratory Animal Center, Mahidol University, Bangkok, Thailand. Rats were housed in a room maintained under the constant environmental conditions (temperature 22–25°C and a constant 12-h light/dark cycle). All animals were given a standard pelted rat diet and water ad libitum.

2.2 | Surgical preparation of myocardial I/R model in rats

Rats were anesthetized using an intramuscular injection of zoletil (50 mg/kg) and xylazine (3 mL/kg).[7,22] Then, a tracheotomy was performed via a ventral midline incision. Rats were ventilated via the tracheotomy with room air from the ventilator to control respiration.[7,22] An electrocardiogram (ECG) was recorded throughout the experiment.[7,22] Following this, a left-side thoracotomy was performed, and the heart was exposed. The left anterior descending coronary artery (LAD) was ligated at approximately 2 mm distal to its origin for the coronary artery occlusion. Myocardial I/R injury was induced by ischemia for 30 minutes, followed by reperfusion for 120 minutes.[7,22] Ischemia was confirmed by the observation of ST elevation on the ECG and by the change in color of myocardial tissue in the ischemic area.[7,22]

2.3 | Experimental design

Male rats were randomly divided into seven groups (n=6/group) as follows (Figure 1). Group 1 was a sham group (surgery was performed without LAD occlusion). Groups 2 and 3 were myocardial I/R groups with vehicle (0.5 mL normal saline solution) or humanin analogue (HNG, 84 μg/kg) administration via intravenous injection (IV) at 15 minutes before I/R, respectively. Groups 4 and 5 were myocardial I/R groups with vehicle or HNG administration at 15 minutes after LAD occlusion (during ischemia). Groups 6 and 7 were myocardial I/R groups with vehicle or HNG administration at the onset of reperfusion. In this study, the dosage of HNG was used based on a previously reported effective dose for the protection of acute ischemic stroke.[24] The left femoral vein was cannulated for the administration of HNG or vehicle. Blood was collected from the tail vein to determine plasma HN levels at different designated time points as shown in Figure 1.

2.4 | Plasma HN level measurement

Plasma HN levels were measured using a commercial Humanin ELISA kit (BlueGene Biotech CO., LTD., Putuo District, Shanghai, China). Blood was collected using EDTA or heparin as an anticoagulant and centrifuged

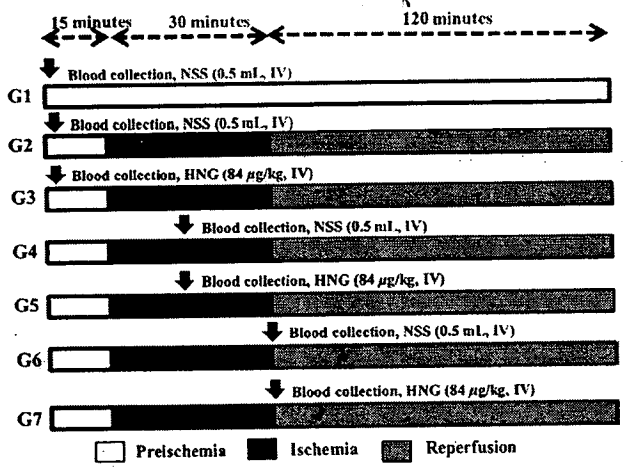


FIGURE 1 Schematic representation of the study protocol (n=6/group). HNG, humanin analogue; NSS, normal saline solution; IV, intravenous

for 15 minutes at 1000 *g* (or 3000 rpm). After this, plasma was collected and aliquoted and stored at −20°C or −80°C. To facilitate the detection of plasma HN levels, plasma (100 μL) was added to a microtiter plate. The conjugate (50 μL) was added to each well and incubated at 37°C for 60 minutes. After incubation, microtiter plates were washed using a wash solution. Substrate A (50 μL) and substrate B (50 μL) were added to each well and incubated for 15 minutes at 37°C. Stop solution was added to each well. Finally, optical density (OD) at 450 nm was used to determine the HN level by using a microplate reader.

2.5 | Arrhythmia determination

The ECG lead II was recorded using Power Lab 4/25T (AD Instruments, Inc., Colorado Springs, CO, USA) throughout the experiment to determine the arrhythmia scores, time to the first ventricular tachycardia/ventricular fibrillation (VT/VF) onset and mortality rate. The occurrence of arrhythmia was characterized using the Lambeth Conventions, and arrhythmia score was determined based on the criteria of Curtis and Walker.[25]

2.6 | Left ventricular function measurement

During I/R, the rats were operated on to expose the right common carotid artery, and a pressure–volume (PV) catheter (Transonic Scisense Inc., London, ON, Canada) was inserted into the left ventricle, for determination of the PV relationship. Left ventricular function such as stroke volume (SV), end-systolic volume, end-diastolic volume, end-systolic pressure (ESP), end-diastolic pressure (EDP), ejection fraction, maximum +dP/dt, and maximum −dP/dt was measured by using an analytical software program (Labscribe, Dover, NH, USA).[26]

2.7 | Infarct size measurement

At the end of the study, the heart was rapidly removed for infarct size determination. The LAD was occluded again at the same occlusion sites during I/R, and Evan's blue dye was perfused via the aorta to determine left ventricular areas at risk (AAR).[7] Next, the heart was sectioned horizontally from the apex to the occlusion site into 7–9 slices.[7] Then, 2, 3, 5-triphenyltetrazolium chloride (TTC) was added to each slice for 15 minutes, and the area with viable tissue was seen in red. Infarct size was determined via the area that was not stained with Evan's blue and TTC.[27] The infarct size and AAR were determined using the image tool software version 3.0 and were calculated according to Reiss et al.'s formula.[27]

2.8 | Isolated cardiac mitochondria preparation

At the end of I/R, cardiac mitochondria were isolated from the nonischemic (remote area) and ischemic areas of the ventricles as previously described.[28,29] Protein concentration was determined according to a bicinchoninic acid assay.[30] After the cardiac mitochondrial concentration was determined, cardiac mitochondria in each group were studied to examine mitochondrial morphology and function.

Regarding mitochondrial morphology, a transmission electron microscope (TEM) was used to identify cardiac mitochondrial swelling.[29] Isolated cardiac mitochondria were fixed in 2.5% glutaraldehyde overnight and postfixed in a 1% cacodylate buffer–osmium tetroxide for 2 hours.[29] Next, isolated cardiac mitochondria were dehydrated in a series of ethanol and embedded in Epon–Araldite. Ultrathin sections were cut with a diamond knife and observed with a TEM.[29]

For the mitochondrial function protocol, the parameters that were measured were as follows: mitochondrial swelling, mitochondrial membrane potential (MMP) change, and ROS production in isolated cardiac mitochondria. Mitochondrial swelling was assessed by measuring the change in the absorbance of the suspension at 540 nm using a microplate reader (Synergy HT; BioTek, Winooski, VT, USA). The decrease in the absorbance in cardiac mitochondrial suspension was used as a measure of cardiac mitochondrial swelling.[29,31] The change in MMP of isolated cardiac mitochondria was investigated using the 5,5′,6,6′-tetrachloro-1,1′,3,3′-tetraethylbenzimidazolcarbocyanine iodide (JC-1) dye. After incubation of cardiac mitochondria with JC-1 dye, the intensity of fluorescence was determined using a fluorescent microplate reader. The JC-1 monomer (green fluorescent) and aggregate (red fluorescent) forms were excited at the same wavelength of 485 nm, whereas the emission of the JC-1 monomer and aggregate forms was detected at wavelength 590 and 530 nm, respectively. Mitochondrial depolarization was indicated by a decrease in the red/green fluorescent ratio.[29,32,33]

In this study, cardiac mitochondrial ROS production was measured using a fluorescent microplate reader with dichlorohydro-fluorescein diacetate (DCFDA).[34] It is known that DCFDA is oxidized in the presence of ROS to dichlorohydro-fluorescent (DCF). Fluorescence of DCF is excited at 485 nm, and the emission is detected at 528 nm. Mitochondrial ROS level was determined as the intensity of fluorescence.[29,34]

2.9 | Western blot analysis

Myocardial protein extracts were divided into ischemic and nonischemic (remote) areas. The ischemic myocardium was obtained from

the left ventricular apex, and the nonischemic (remote) area was obtained from the right ventricle. After that, cardiac proteins from these areas were added to a lysis buffer.[7] Protein concentration from the heart tissue was determined using a Bio-Rad protein assay kit (Bio-Rad Laboratories, Hercules, CA, USA). Protein (50–80 μg) was added to the loading buffer.[7] After that, proteins were transferred to polyvinylidenedifluoride (PVDF) membranes in the presence of a transfer buffer.[7] PVDF membranes were blocked with 5% skimmed milk for 1 hour at room temperature. Next, the membranes were exposed overnight to anti-Bax, anti-Bcl2, anti-caspase-3, anti-connexin-43 (Cx43), and anti-connexin-43 phosphorylated at Ser368 (Cell Signaling Technology, Danvers, MA, USA). Subsequently, the membranes were washed and incubated with horseradish peroxidase conjugated with anti-rabbit IgG (Cell Signaling Technology). Finally, bands were detected and used for the analysis of protein expression.[7]

2.10 | Isolated mitochondrial studies

Isolated cardiac mitochondria were investigated for the direct effects of HNG on ROS overload-induced mitochondrial dysfunction. In this study, ROS overload was induced by 2 mM H_2O_2 application for 5 minutes in isolated cardiac mitochondria.[29] Briefly, cardiac mitochondria were isolated from male Wistar rats (300–350 g) as described previously [29] through differential centrifugation. After that, isolated cardiac mitochondria were randomly divided into three groups: H_2O_2 (2 mM),[29] H_2O_2 (2 mM) pretreated with HNG (2 μM), and vehicle-treated mitochondria as a control group (n=4/group). At the end of experiment, mitochondrial ROS levels were investigated in isolated cardiac mitochondria as described previously.[29]

2.11 | Data analysis

All data are presented as mean±SEM. A one-way ANOVA followed by a post hoc Fisher's test was used to test the differences between the groups. Mortality rate and VT/VF incidence were analyzed using a chi-squared test. A P value <.05 was considered as statistically significant.

3 | RESULTS

3.1 | Plasma HN level before and after HNG administration

The endogenous HN levels without HNG application are shown in Figure 2A. At baseline, the endogenous HN level before I/R showed no difference when compared with the sham group. However, at the end of I/R, the endogenous HN level was significantly decreased when compared with the sham and before I/R groups (Figure 2A). Total HN level (endogenous HN+HNG) after HNG or vehicle was administrated at different time points (preischemia, during ischemia, at the reperfusion) as shown in Figure 2B. At the end of I/R, total HN level in the HNG-treated groups applied during ischemia and at the onset of reperfusion was significantly increased when compared with the vehicle group. Interestingly, for HNG application prior to I/R, the total HN level at the end of reperfusion showed no difference when compared with the vehicle group (Figure 2B).

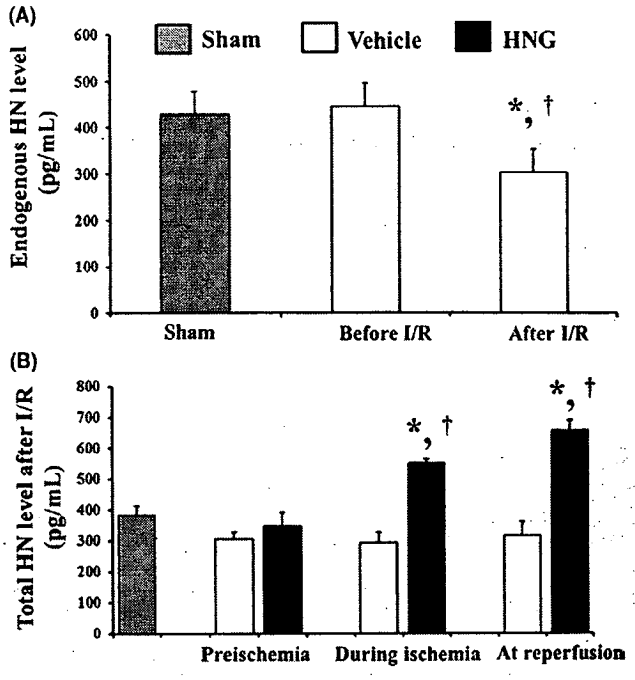


FIGURE 2 (A) Endogenous humanin (HN) levels showed no significant difference between the sham and before I/R group. However, after I/R, the endogenous HN level was decreased, when compared with baseline and before I/R (n=6/group). *P<.05 vs sham, †P<.05 vs before I/R group. (B) At the end of I/R, total HN level (endogenous HN+HNG) in each group was investigated. When HNG was administrated during ischemia and at the reperfusion, total HN levels were significantly higher, compared to the vehicle group. Interestingly, the application of HNG prior to I/R resulted in no difference in the total HN level at the end of experiment when compared with the vehicle group (n=6/group). *P<.05 vs vehicle within group; †P<.05 vs HNG-preischemia group. HNG, humanin analogue

3.2 | HNG reduced cardiac arrhythmias during I/R

The arrhythmia score in the HNG-pretreated I/R group was significantly lower when compared with the vehicle group, whereas the arrhythmia score in HNG-treated I/R groups at the other time points showed no difference when compared with the vehicle group (Figure 3A). During I/R, the time to first VT/VF onset showed no difference among all groups (Figure 3B). The mortality rate in the HNG-pretreated group was significantly lower when compared with the vehicle group, whereas the mortality rate in HNG-treated I/R groups at the other time points was not different when compared with the vehicle group (Figure 3C). Additionally, the level of Cx43 phosphorylation (p-Cx43) in cardiac tissues was determined. The Cx43 phosphorylation was significantly higher in the HNG-pretreated group compared with the vehicle group, whereas the phosphorylation of Cx43 at the other time points was not different when compared with the vehicle-treated group (Figure 3D).

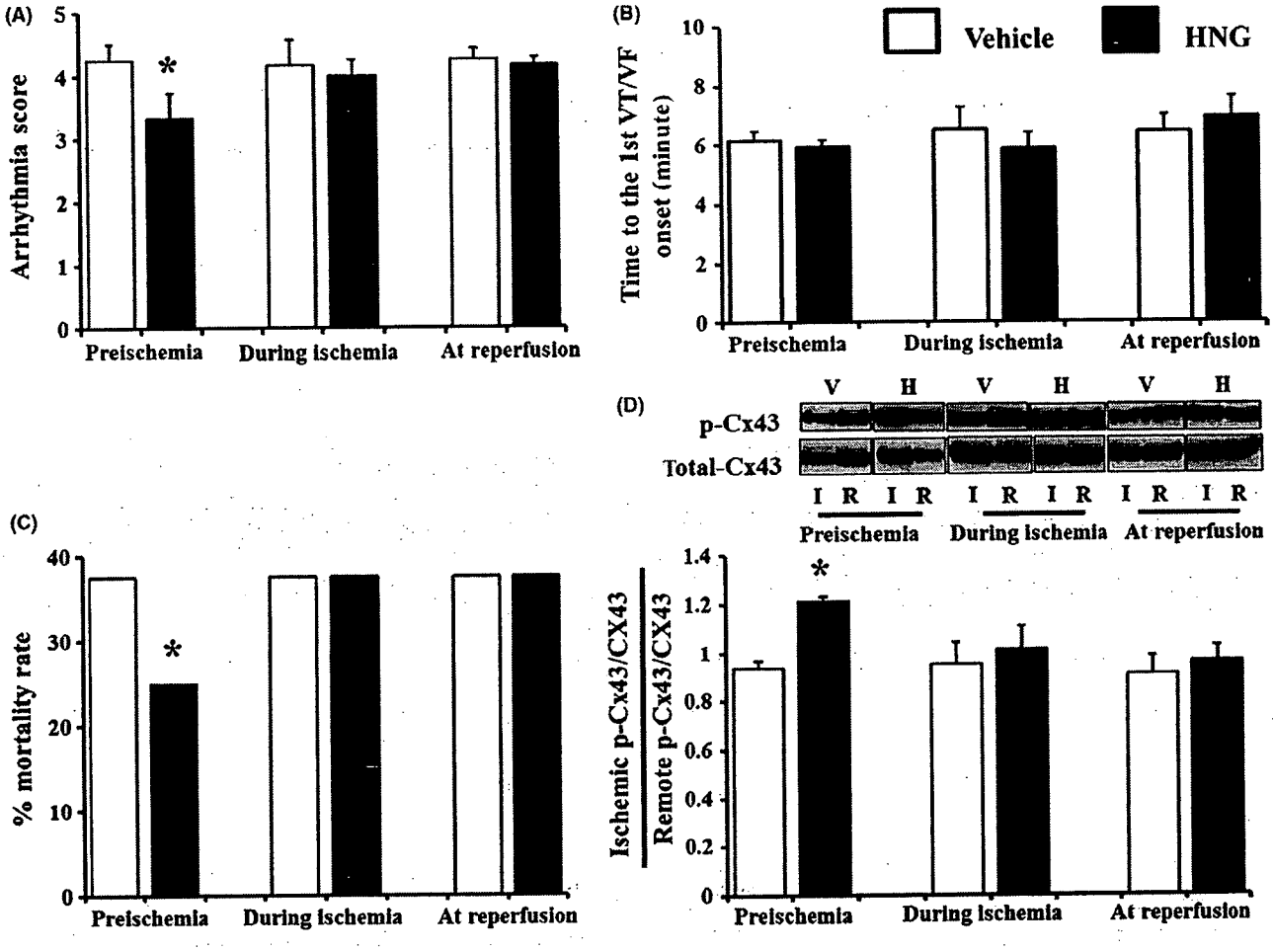


FIGURE 3 Humanin analogue (HNG) pretreatment could reduce arrhythmia score (A) but not time to ventricular tachycardia/ventricular fibrillation (VT/VF) onset (B) and decreased mortality rate (C) against I/R. HNG pretreatment increased the expression of Cx43 phosphorylation compared with the vehicle group (D, n=6/group in each experiment). *P<.05 vs vehicle within group. Cx43, connexin-43; p-Cx43, phosphorylation of connexin-43; I, ischemic area; R, remote area; V, vehicle; H, humanin analogue

3.3 | HNG decreased the infarct size during I/R

The AAR was not different in all groups (vehicle-pretreated group [33 ± 0.9%], HNG-pretreated group [31 ± 0.9%], vehicle-treated group during ischemic period [31 ± 1.4%], HNG-treated group during ischemic period [30 ± 1.3%], vehicle-treated group at reperfusion [33 ± 0.6%], and the HNG-treated group at reperfusion [32 ± 1.1%]). However, the infarct size in the HNG-pretreated group was markedly smaller than the vehicle-treated group, whereas the infarct size in the HNG-treated groups at other time points showed no difference when compared with the vehicle-treated group (Figure 4A,B). The Bax, Bcl2, and pro-caspase-3 expression are shown in Figure 4C–E. Our results showed that the application of HNG prior to ischemia had a significant correlation with the reduction in Bax expression when compared with the vehicle-treated group (Figure 4C). Although there was no significant difference in Bcl2 expression between the vehicle- and HNG-treated groups (Figure 4D), HNG given prior to ischemia also significantly decreased the expression of pro-caspase-3 protein, compared with the vehicle-treated group (Figure 4E).

3.4 | HNG improved cardiac mitochondrial function

In the HNG-pretreated group, cardiac mitochondrial ROS level was significantly decreased when compared with the vehicle-pretreated group (Figure 5A). Moreover, the mitochondrial depolarization and mitochondrial swelling showed a significant decrease in the HNG pretreatment compared with the vehicle-pretreated group (Figure 5B,C). Our results also showed that the ROS level in the HNG-treated group during the ischemic period was significantly decreased when compared with the vehicle-treated group, whereas the mitochondrial depolarization and mitochondrial swelling showed no significant different between the vehicle- and HNG-treated groups during the ischemic period (Figure 5A–C). However, the ROS level in the HNG-treated group during ischemic period was still significantly higher than that in the HNG-pretreated group (Figure 5A). Regarding HNG treatment at the onset of reperfusion, there was no significant difference in the mitochondrial ROS level, mitochondrial depolarization as well as mitochondrial swelling between the vehicle- and HNG-treated groups (Figure 5A–C).

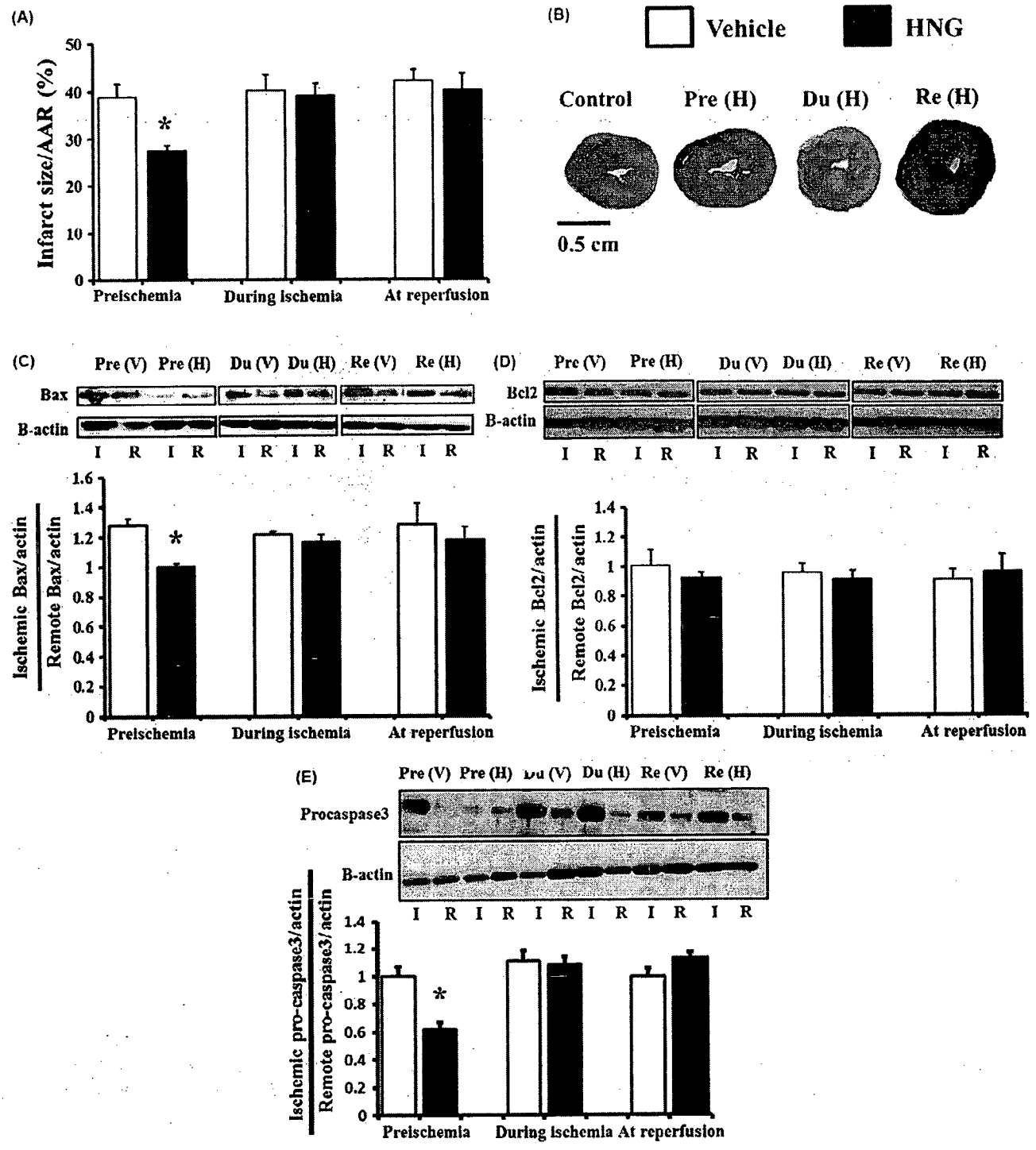


FIGURE 4 Humanin analogue (HNG) pretreatment decreased infarct size compared to the vehicle group (A). The representative of the infarcted heart in each group is represented in (B). HNG pretreatment attenuated apoptotic process as indicated by decreased Bax expression (C) but not Bcl2 expression (D), compared to the vehicle within the group. HNG given prior to ischemia also significantly decreased the expression of pro-caspase-3 protein, compared with the vehicle-treated group (E) (n=6/group in each experiment). *$P<.05$ vs vehicle within group. I, ischemic area; R, remote area; V, vehicle; H, humanin analogue

The representative electron micrographs of cardiac mitochondria are shown in Figure 5D. Cardiac mitochondria in vehicle-treated I/R groups at the different time points showed mitochondrial swelling as indicated by markedly unfolded cristae. Cardiac mitochondria in the HNG-pretreated I/R group showed more normal folded cristae compared with the vehicle-treated group, indicating less mitochondrial swelling. Cardiac mitochondria in the HNG-treated groups at other time points showed markedly

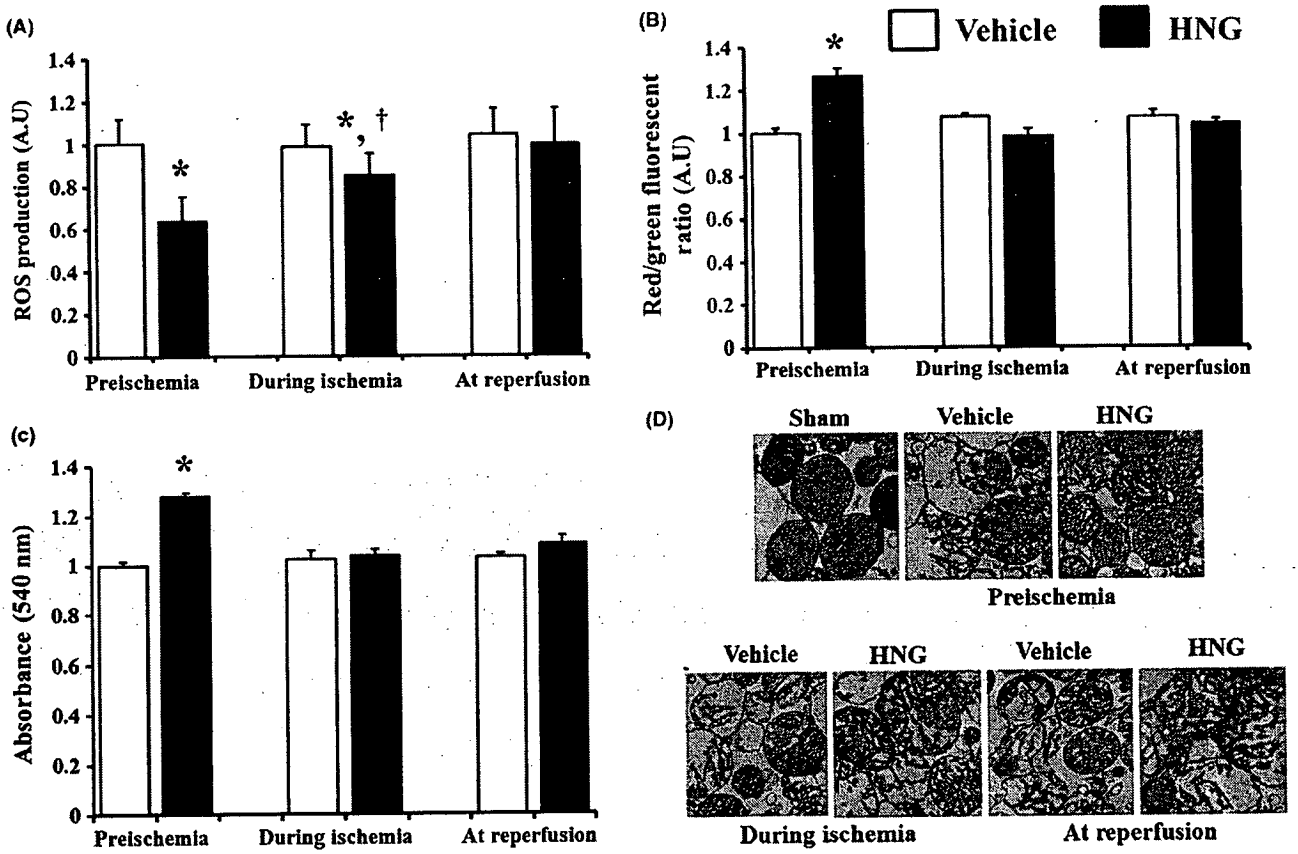


FIGURE 5 Humanin analogue (HNG) pretreatment improved cardiac mitochondrial function by showing reduced reactive oxygen species (ROS) levels (A), attenuated mitochondrial membrane depolarization (B), and decreased mitochondrial swelling in ischemic area (C). HNG pretreatment also improved the deterioration of cardiac mitochondrial morphology (D). An HNG supplement during the ischemic period had no effect on the attenuation of mitochondrial swelling and mitochondrial depolarization, and even the ROS level was significantly decreased compared with the vehicle group (n=6/group in each experiment). *P<.05 vs vehicle within group, †P<.05 vs HNG-preischemia group

unfolded cristae similar to those observed in the vehicle-treated group (Figure 5D).

3.5 | HNG attenuated left ventricular dysfunction caused by I/R injury

Changes in left ventricular function at different time points are summarized in Tables 1–3. At the baseline, there was no significant difference in left ventricular parameters among groups (Table 1). After LAD occlusion, left ventricular function during the ischemic period is shown in Table 2. The results showed that HNG pretreatment improved left ventricular end-systolic pressure (LVESP), left ventricular end-diastolic pressure (LVEDP), and maximum +dP/dt during the ischemic period (Table 2). However, at the reperfusion period, only LVESP and maximum +dP/dt in the HNG-pretreated group showed an improvement against I/R injury (Table 3).

3.6 | HNG decreased the mitochondrial ROS level in isolated cardiac mitochondria

After H_2O_2 application in isolated cardiac mitochondria, the level of ROS was significantly increased when compared with the vehicle-treated group (Figure 6). However, after HNG pretreatment, the mitochondrial ROS level in the 2 μM HNG-treated group was significantly decreased when compared with H_2O_2-treated group (Figure 6).

4 | DISCUSSION

In this study, the cardioprotective effects of HN against myocardial I/R injury via attenuating cardiac mitochondrial dysfunction were demonstrated. The endogenous HN level showed a marked decreased after I/R injury. Interestingly, HNG pretreatment exerted the beneficial effects against I/R as indicated by the following: (1) attenuating cardiac mitochondrial dysfunction as indicated by reducing ROS production, mitochondrial membrane depolarization, and mitochondrial swelling; (2) decreasing the incidence of fatal cardiac arrhythmias and increased Cx43 phosphorylation; (3) decreasing infarct size and Bax expression; and (4) attenuating left ventricular dysfunction.

In this study, the endogenous HN level showed a marked decrease after I/R injury. This is consistent with the results of a previous study, which showed that plasma endogenous humanin levels in patients with acute coronary syndromes were significantly decreased when

TABLE 1 Left ventricular function parameters at baseline

	Treatments					
	Preischemia		During ischemia		At reperfusion	
Parameters	Vehicle	HNG	Vehicle	HNG	Vehicle	HNG
Heart rate	274 ± −3.8	281 ± 5.3	277 ± 9.0	289 ± 19.1	286 ± 9.8	285 ± 14.9
LVESP (mm Hg)	107 ± 1.8	106 ± 0.6	107 ± 1.3	101 ± 5.4	107 ± 1.7	105 ± 2.9
LVEDP (mm Hg)	22 ± 1.1	22 ± 0.7	22 ± 0.5	21 ± 0.6	23 ± 1.9	22 ± 1.1
+dP/dt (mm Hg/s)	8670 ± 75	8725 ± 555	8844 ± 541	8354 ± 467	8643 ± 301	9539 ± 355
−dP/dt (mm Hg/s)	−4850 ± 80	−4710 ± 52	−4812 ± 161	−4793 ± 72	−4912 ± 287	−4927 ± 194
SV (μL)	339 ± 10	332 ± 9	345 ± 16	350 ± 13	345 ± 10	336 ± 15

HNG, humanin analogue; LVESP, left ventricular end-systolic pressure; LVEDP, left ventricular end-diastolic pressure; +dP/dt, maximal slope of the systolic pressure increment; −dP/dt, minimal slope of the diastolic pressure decrement; SV, stoke volume, N=6/group.

TABLE 2 Left ventricular function parameters during the ischemic period

	Treatments					
	Preischemia		During ischemia		At reperfusion	
Parameters	Vehicle	HNG	Vehicle	HNG	Vehicle	HNG
Heart rate	312 ± 8	313 ± 6	298 ± 5	328 ± 14	316 ± 10	302 ± 9
LVESP (mm Hg)	98 ± 2	104 ± 2*	84 ± 5	89 ± 5	85 ± 6	91 ± 8
LVEDP (mm Hg)	29 ± 1	22 ± 3*	28 ± 2	26 ± 1	29 ± 1	25 ± 2
+dP/dt (mm Hg/s)	6547 ± 603	8119 ± 240*	7254 ± 588	8214 ± 352	7758 ± 209	7994 ± 954
−dP/dt (mm Hg/s)	−4094 ± 104	−4179 ± 297	−4099 ± 357	−4164 ± 208	−4125 ± 70	−4425 ± 128
SV (μL)	240 ± 11	267 ± 6	233 ± 6	241 ± 7	233 ± 7	237 ± 4

HNG, humanin analogue; LVESP, left ventricular end-systolic pressure; LVEDP, left ventricular end-diastolic pressure; +dP/dt, maximal slope of the systolic pressure increment; −dP/dt, minimal slope of the diastolic pressure decrement; SV, stoke volume.
*$P<.05$ vs vehicle within group, N=6/group.

TABLE 3 Left ventricular function parameters during the reperfusion period

	Treatments					
	Preischemia		During ischemia		At reperfusion	
Parameters	Vehicle	HNG	Vehicle	HNG	Vehicle	HNG
Heart rate	286 ± 9	280 ± 8	289 ± 13	287 ± 9	289 ± 12	288 ± 12
LVESP (mm Hg)	96 ± 4	107 ± 1*	100 ± 4	101 ± 5	103 ± 4	104 ± 1
LVEDP (mm Hg)	24 ± 2	25 ± 2	24 ± 1	24 ± 2	23 ± 5	26 ± 5
+dP/dt (mm Hg/s)	7421 ± 267	8624 ± 431*	8017 ± 576	7515 ± 774	8224 ± 290	7971 ± 703
−dP/dt (mm Hg/s)	−4695 ± 89	−4340 ± 74	−4004 ± 173	−4134 ± 399	−4393 ± 422	−4383 ± 220
SV (μL)	266 ± 6	287 ± 10	244 ± 14	257 ± 9	252 ± 12	258 ± 14

HNG, humanin analogue; LVESP, left ventricular end-systolic pressure; LVEDP, left ventricular end-diastolic pressure; +dP/dt, maximal slope of the systolic pressure increment; −dP/dt, minimal slope of the diastolic pressure decrement; SV, stoke volume.
*$P<.05$ vs vehicle within group, N=6/group.

compared with healthy subjects.[35] This could be due to the defense mechanisms against myocardial damage in the early stages of I/R injury in which the endogenous HN was recruited from the blood circulation into the ischemic myocardium. This is also supported by the report that the endogenous HN levels in the heart were higher after I/R compared to those before I/R.[10] Although the endogenous HN is produced from several tissues in the body including the heart tissue,[10,15,20] it may not be sufficient to prevent the myocardial damage caused by myocardial I/R injury. Therefore, an HNG supplement may help to augment the cardioprotective effects of endogenous HN against myocardial I/R.

In this study, cardiac mitochondrial dysfunction, as indicated by increased cardiac mitochondrial ROS production, cardiac mitochondrial

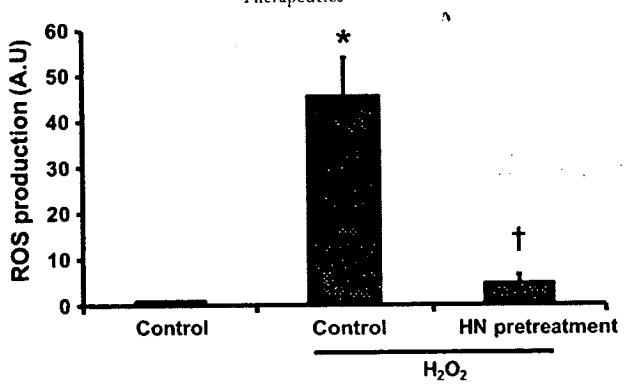


FIGURE 6 After H_2O_2 application in isolated cardiac mitochondria, the level of reactive oxygen species (ROS) was significantly increased when compared with the vehicle-treated group. However, after humanin analogue (HNG) pretreatment in isolated cardiac mitochondria, the mitochondrial ROS level in the 2 μM HNG-treated group was significantly decreased when compared with H_2O_2-treated group. *P<.05 vs vehicle group, †P<.05 vs H_2O_2-treated group

depolarization, and cardiac mitochondrial swelling, was observed in the ischemic myocardium. It is known that myocardial I/R can cause an increase in cardiac mitochondrial ROS production and lead to oxidative stress.[6,36] When the increased ROS level reaches a critical threshold level,[8] it triggers the opening of the mitochondrial permeability transition pores (mPTP) or the inner membrane anion channels (IMAC), resulting in the release of anions such as O_2^- across the cardiac mitochondrial membrane.[8,29,37,38] Following this, the decrease in the MMP (mitochondrial depolarization) is initiated. Moreover, prolonged mPTP opening by an increased ROS level can induce mitochondrial swelling and rupture in cardiac cells.[39,40] In this study, HNG pretreatment could attenuate mitochondrial damage through a decrease in cardiac mitochondrial ROS levels. This finding is consistent with a previous study which demonstrates that HN exerts cardioprotective effects via decreasing ROS level in the cultured H9c2 cells.[11] In this study, a reduction in cardiac mitochondrial ROS level may lead to the attenuation of cardiac mitochondrial depolarization and cardiac mitochondrial swelling. Interestingly, the ROS level in the HNG-treated group during the ischemic period was significantly decreased when compared with the vehicle-treated group, whereas the mitochondrial depolarization and mitochondrial swelling were not different when the vehicle- and HNG-treated groups were compared during the ischemic period. A possible explanation of this finding could be due to the extent of ROS reduction. The ROS level in the HNG-treated group during the ischemic period might not sufficiently decrease to the level which is lower than the critical threshold level[8]; thus, no decrease in mitochondrial depolarization and mitochondrial swelling was observed in these groups. However, this study investigated the effect of HN with only one concentration. Whether higher concentrations of HN given during ischemia or reperfusion can improve cardiac function will need further evaluation in the future studies.

Recently, the molecular mechanism of cardiac arrhythmias has been shown that cardiac mitochondrial depolarization caused by an increase in mitochondrial ROS level was associated with an increase in cardiac arrhythmia incidence.[9] In this study, HN pretreatment effectively decreases cardiac mitochondrial depolarization against I/R injury. Thus, antiarrhythmic effect of HN has been demonstrated in this study through its ability to reduce cardiac mitochondrial depolarization caused by I/R injury. Additionally, the antiarrhythmic effect of HN could be due to its effect on Cx43. Cx43 is a cardiac gap junction protein, which facilitates cell-to-cell communication via the electrical current flow.[41] The previous study demonstrated that phosphorylation of Cx43 at serine 368 increased the trafficking of Cx43 to the plasma membrane, leading to the formation of a gap junction.[41] This finding is also consistent with another study reporting that an increased phosphorylation of Cx43 at serine 368 attenuated cardiac arrhythmia in the heart subject to ischemia.[42] Therefore, the increased Cx43 phosphorylation by HNG pretreatment could be a mechanism responsible for the arrhythmia reduction found in this study.

In this study, HNG pretreatment decreased the infarct size caused by I/R injury by 30% when compared with the vehicle-treated group. Although our findings were consistent with Muzumdar's study reporting that HNG pretreatment significantly reduced the infarct size in mice which had undergone I/R injury,[10] we further demonstrated the novel findings that a reduction in infarct size by HNG pretreatment was due to its ability to attenuate cardiac mitochondrial dysfunction in the ischemic myocardium Previous studies showed that I/R injury increased apoptosis via increasing the expression of pro-caspase-3 protein in cardiac tissues.[43,44] Our study demonstrated that myocardial infarct size was increased through the increase in pro-caspase-3 expression after myocardial I/R injury. This finding was consistent with results from our previous study demonstrating that the thalassemic mice were more vulnerable to cardiac apoptosis than normal mice as shown by the increased level of pro-caspase-3 protein.[45] In this study, the levels of pro-caspase-3 expression in the group of HNG given prior to ischemia were significantly decreased when compared with the vehicle-treated group. These findings suggested that HNG decreased myocardial infarct size via decreasing the expressions of Bax and pro-caspase-3 proteins. It is well established that an increase in cardiac ROS level induced by I/R injury increases the translocation of Bax to the cardiac mitochondria leading to the activation of the apoptotic cascade.[1,2,7,8] Previously, we reported that decreasing cardiac mitochondrial ROS level by pharmacological intervention can attenuate cardiac mitochondrial dysfunction and apoptosis.[7] Thus, a reduction in the myocardial infarct size observed in the HNG pretreatment group might be due to its ability to decrease the cardiac mitochondrial ROS level in the ischemic myocardium, which ultimately results in the improvement of the left ventricular function.

In addition to the effects of HNG against myocardial I/R injury through attenuation of mitochondrial dysfunction in an in vivo study, our study also showed that HNG pretreatment could directly decrease the mitochondrial ROS level in isolated cardiac mitochondria against oxidative stress induced by ROS overload, suggesting the direct effects of HN on cardiac mitochondria. As we did not investigate the roles of HN on the mPTP and IMAC, future studies are needed to investigate the mechanisms of HN on the mPTP and IMAC on cardiac mitochondria.

5 | CONCLUSION

These findings demonstrate that HNG pretreatment exerted cardioprotective effects against myocardial I/R by causing a decrease in cardiac arrhythmia, a reduction in infarct size, and hence improving left ventricular function. The mechanisms responsible for these beneficial effects of HNG supplement could be due to its ability to attenuate cardiac mitochondrial dysfunction. It is important to note that the cardioprotective effects of HNG in this study were seen only when it was applied prior to I/R injury. Moreover, a single dose of HNG was investigated. In the clinical setting, patients can only receive treatment after the onset of symptoms. Therefore, the efficacy of higher doses of HNG applied during ischemia will require further investigation.

ACKNOWLEDGMENTS

This work was supported by the Thailand Research Fund Royal Golden Jubilee PhD program (STC and NC); a NSTDA Research Chair Grant from the National Science and Technology Development Agency Thailand (NC); the Thailand Research Fund RSA5880015 (KS), BRG5780016 (SCC), and the Chiang Mai University Center of Excellence Award (NC).

CONFLICT OF INTEREST

The authors declare no conflict of interest.

AUTHORS' CONTRIBUTIONS

Savitree Thummasorn designed the study, performed the laboratory investigations, and wrote the manuscript. Nattayaporn Apaijai and Sasiwan Kerdphoo performed laboratory analyses and in vivo investigations. Krekwit Shinlapawittayatorn designed the study, performed critical manuscript review, and approved the article. Siriporn C. Chattipakorn designed the study, performed critical manuscript review, and approved the article. Nipon Chattipakorn designed the study, performed critical manuscript review, and approved the article.

REFERENCES

1. Elahi MM, Kong YX, Matata BM. Oxidative stress as a mediator of cardiovascular disease. *Oxid Med Cell Longev*. 2009;2:259-269.
2. Yang CH, Sheu JJ, Tsai TH, et al. Effect of tacrolimus on myocardial infarction is associated with inflammation, ROS, MAP kinase and Akt pathways in mini-pigs. *J Atheroscler Thromb*. 2013;20:9-22.
3. Sucher R, Gehwolf P, Kaier T, et al. Intracellular signaling pathways control mitochondrial events associated with the development of ischemia/reperfusion-associated damage. *Transpl Int*. 2009;22:922-930.
4. Sommer S, Leistner M, Aleksic I, et al. Impact of levosimendan and ischaemia-reperfusion injury on myocardial subsarcolemmal mitochondrial respiratory chain, mitochondrial membrane potential, Ca^{2+} cycling and ATP synthesis. *Eur J Cardiothorac Surg*. 2016;49:e54-e62; discussion e62.
5. Sloan RC, Moukdar F, Frasier CR, et al. Mitochondrial permeability transition in the diabetic heart: contributions of thiol redox state and mitochondrial calcium to augmented reperfusion injury. *J Mol Cell Cardiol*. 2012;52:1009-1018.
6. Granger DN, Kvietys PR. Reperfusion injury and reactive oxygen species: the evolution of a concept. *Redox Biol*. 2015;6:524-551.
7. Apaijai N, Chinda K, Palee S, Chattipakorn S, Chattipakorn N. Combined vildagliptin and metformin exert better cardioprotection than monotherapy against ischemia-reperfusion injury in obese-insulin resistant rats. *PLoS One*. 2014;9:e102374.
8. Aon MA, Cortassa S, Marban E, O'Rourke B. Synchronized whole cell oscillations in mitochondrial metabolism triggered by a local release of reactive oxygen species in cardiac myocytes. *J Biol Chem*. 2003;278:44735-44744.
9. O'Rourke B, Cortassa S, Aon MA. Mitochondrial ion channels: gatekeepers of life and death. *Physiology (Bethesda)*. 2005;20:303-315.
10. Muzumdar RH, Huffman DM, Calvert JW, et al. Acute humanin therapy attenuates myocardial ischemia and reperfusion injury in mice. *Arterioscler Thromb Vasc Biol*. 2010;30:1940-1948.
11. Klein LE, Cui L, Gong Z, Su K, Muzumdar R. A humanin analog decreases oxidative stress and preserves mitochondrial integrity in cardiac myoblasts. *Biochem Biophys Res Commun*. 2013;440:197-203.
12. Zhai D, Luciano F, Zhu X, Guo B, Satterthwait AC, Reed JC. Humanin binds and nullifies Bid activity by blocking its activation of Bax and Bak. *J Biol Chem*. 2005;280:15815-15824.
13. Guo B, Zhai D, Cabezas E, et al. Humanin peptide suppresses apoptosis by interfering with Bax activation. *Nature*. 2003;423:456-461.
14. Luciano F, Zhai D, Zhu X, et al. Cytoprotective peptide humanin binds and inhibits proapoptotic Bcl-2/Bax family protein BimEL. *J Biol Chem*. 2005;280:15825-15835.
15. Hashimoto Y, Ito Y, Niikura T, et al. Mechanisms of neuroprotection by a novel rescue factor humanin from Swedish mutant amyloid precursor protein. *Biochem Biophys Res Commun*. 2001;283:460-468.
16. Jia Y, Lue YH, Swerdloff R, et al. The cytoprotective peptide humanin is induced and neutralizes Bax after pro-apoptotic stress in the rat testis. *Andrology*. 2013;1:651-659.
17. Chin YP, Keni J, Wan J, et al. Pharmacokinetics and tissue distribution of humanin and its analogues in male rodents. *Endocrinology*. 2013;154:3739-3744.
18. Kin T, Sugie K, Hirano M, Goto Y, Nishino I, Ueno S. Humanin expression in skeletal muscles of patients with chronic progressive external ophthalmoplegia. *J Hum Genet*. 2006;51:555-558.
19. Yamagishi Y, Hashimoto Y, Niikura T, Nishimoto I. Identification of essential amino acids in Humanin, a neuroprotective factor against Alzheimer's disease-relevant insults. *Peptides*. 2003;24:585-595.
20. Hashimoto Y, Niikura T, Tajima H, et al. A rescue factor abolishing neuronal cell death by a wide spectrum of familial Alzheimer's disease genes and Abeta. *Proc Natl Acad Sci USA*. 2001;98:6336-6341.
21. Bachar AR, Scheffer L, Schroeder AS, et al. Humanin is expressed in human vascular walls and has a cytoprotective effect against oxidized LDL-induced oxidative stress. *Cardiovasc Res*. 2010;88:360-366.
22. Surinkaew S, Kumphune S, Chattipakorn S, Chattipakorn N. Inhibition of p38 MAPK during ischemia, but not reperfusion, effectively attenuates fatal arrhythmia in ischemia/reperfusion heart. *J Cardiovasc Pharmacol*. 2013;61:133-141.
23. Kilkenny C, Browne W, Cuthill IC, Emerson M, Altman DG, Group NCRRGW. Animal research: reporting in vivo experiments: the ARRIVE guidelines. *Br J Pharmacol*. 2010;160:1577-1579.
24. Wang T, Huang Y, Zhang M, et al. [Gly14]-Humanin offers neuroprotection through glycogen synthase kinase-3beta inhibition in a mouse model of intracerebral hemorrhage. *Behav Brain Res*. 2013;247:132-139.
25. Curtis MJ, Hancox JC, Farkas A, et al. The Lambeth Conventions (II): guidelines for the study of animal and human ventricular and supraventricular arrhythmias. *Pharmacol Ther*. 2013;139:213-248.
26. Chinda K, Sanit J, Chattipakorn S, Chattipakorn N. Dipeptidyl peptidase-4 inhibitor reduces infarct size and preserves cardiac function

via mitochondrial protection in ischaemia-reperfusion rat heart. *Diab Vasc Dis Res*. 2014;11:75–83.
27. Riess ML, Rhodes SS, Stowe DF, Aldakkak M, Camara AK. Comparison of cumulative planimetry versus manual dissection to assess experimental infarct size in isolated hearts. *J Pharmacol Toxicol Methods*. 2009;60:275–280.
28. Larche J, Lancel S, Hassoun SM, et al. Inhibition of mitochondrial permeability transition prevents sepsis-induced myocardial dysfunction and mortality. *J Am Coll Cardiol*. 2006;48:377–385.
29. Thummasorn S, Kumfu S, Chattipakorn S, Chattipakorn N. Granulocyte-colony stimulating factor attenuates mitochondrial dysfunction induced by oxidative stress in cardiac mitochondria. *Mitochondrion*. 2011;11:457–466.
30. Walker JM. The bicinchoninic acid (BCA) assay for protein quantitation. *Methods Mol Biol*. 1994;32:5–8.
31. Ruiz-Meana M, Garcia-Dorado D, Miro-Casas E, Abellan A, Soler-Soler J. Mitochondrial Ca^{2+} uptake during simulated ischemia does not affect permeability transition pore opening upon simulated reperfusion. *Cardiovasc Res*. 2006;71:715–724.
32. Tong V, Teng XW, Chang TK, Abbott FS. Valproic acid II: effects on oxidative stress, mitochondrial membrane potential, and cytotoxicity in glutathione-depleted rat hepatocytes. *Toxicol Sci*. 2005;86:436–443.
33. Di Lisa F, Blank PS, Colonna R, et al. Mitochondrial membrane potential in single living adult rat cardiac myocytes exposed to anoxia or metabolic inhibition. *J Physiol*. 1995;486(Pt 1):1–13.
34. Novalija E, Kevin LG, Eells JT, Henry MM, Stowe DF. Anesthetic preconditioning improves adenosine triphosphate synthesis and reduces reactive oxygen species formation in mitochondria after ischemia by a redox dependent mechanism. *Anesthesiology*. 2003;98:1155–1163.
35. Widmer RJ, Flammer AJ, Herrmann J, et al. Circulating humanin levels are associated with preserved coronary endothelial function. *Am J Physiol Heart Circ Physiol*. 2013;304:H393–H397.
36. Tompkins AJ, Burwell LS, Digerness SB, Zaragoza C, Holman WL, Brookes PS. Mitochondrial dysfunction in cardiac ischemia-reperfusion injury: ROS from complex I, without inhibition. *Biochim Biophys Acta*. 2006;1762:223–231.
37. Brady NR, Hamacher-Brady A, Westerhoff HV, Gottlieb RA. A wave of reactive oxygen species (ROS)-induced ROS release in a sea of excitable mitochondria. *Antioxid Redox Signal*. 2006;8:1651–1665.
38. Cortassa S, Aon MA, Winslow RL, O'Rourke B. A mitochondrial oscillator dependent on reactive oxygen species. *Biophys J*. 2004;87:2060–2073.
39. Kroemer G, Dallaporta B, Resche-Rigon M. The mitochondrial death/life regulator in apoptosis and necrosis. *Annu Rev Physiol*. 1998;60:619–642.
40. Griffiths EJ, Halestrap AP. Mitochondrial non-specific pores remain closed during cardiac ischaemia, but open upon reperfusion. *Biochem J*. 1995;307(Pt 1):93–98.
41. Lampe PD, TenBroek EM, Burt JM, Kurata WE, Johnson RG, Lau AF. Phosphorylation of connexin43 on serine368 by protein kinase C regulates gap junctional communication. *J Cell Biol*. 2000;149:1503–1512.
42. Miura T, Yano T, Naitoh K, et al. Delta-opioid receptor activation before ischemia reduces gap junction permeability in ischemic myocardium by PKC-epsilon-mediated phosphorylation of connexin 43. *Am J Physiol Heart Circ Physiol*. 2007;293:H1425–H1431.
43. Xing K, Fu X, Jiang L, et al. Cardioprotective effect of anisodamine against myocardial ischemia injury and its influence on cardiomyocytes apoptosis. *Cell Biochem Biophys*. 2015;73:707–716.
44. Song CL, Liu B, Diao HY, et al. Down-regulation of microRNA-320 suppresses cardiomyocyte apoptosis and protects against myocardial ischemia and reperfusion injury by targeting IGF-1. *Oncotarget*. 2016;7:39740–39757.
45. Kumfu S, Chattipakorn SC, Fucharoen S, Chattipakorn N. Dual T-type and L-type calcium channel blocker exerts beneficial effects in attenuating cardiovascular dysfunction in iron-overloaded thalassaemic mice. *Exp Physiol*. 2016;101:521–539.

เอกสารแนบหมายเลข 15

PLOS | ONE

RESEARCH ARTICLE

Combined Iron Chelator and Antioxidant Exerted Greater Efficacy on Cardioprotection Than Monotherapy in Iron-Overloaded Rats

Suwakon Wongjaikam[1,2,3], Sirinart Kumfu[1,2,3], Juthamas Khamseekaew[1,2,3], Jirapas Sripetchwandee[1,2,3], Somdet Srichairatanakool[5], Suthat Fucharoen[6], Siriporn C. Chattipakorn[1,2,4], Nipon Chattipakorn[1,2,3]*

1 Cardiac Electrophysiology Research and Training Center, Faculty of Medicine, Chiang Mai University, Chiang Mai, Thailand, **2** Cardiac Electrophysiology Unit, Department of Physiology, Faculty of Medicine, Chiang Mai University, Chiang Mai, Thailand, **3** Center of Excellence in Cardiac Electrophysiology Research, Chiang Mai University, Chiang Mai, Thailand, **4** Department of Oral Biology and Diagnostic Sciences, Faculty of Dentistry, Chiang Mai University, Chiang Mai, Thailand, **5** Department of Biochemistry, Faculty of Medicine, Chiang Mai University, Chiang Mai, Thailand, **6** Thalassemia Research Center, Institute of Molecular Bioscience, Mahidol University, Nakhon Pathom, Thailand

* nchattip@gmail.com

CrossMark
click for updates

OPEN ACCESS

Citation: Wongjaikam S, Kumfu S, Khamseekaew J, Sripetchwandee J, Srichairatanakool S, Fucharoen S, et al. (2016) Combined Iron Chelator and Antioxidant Exerted Greater Efficacy on Cardioprotection Than Monotherapy in Iron-Overloaded Rats. PLoS ONE 11 (7): e0159414. doi:10.1371/journal.pone.0159414

Editor: Michael Bader, Max-Delbrück Center for Molecular Medicine (MDC), GERMANY

Received: May 12, 2016

Accepted: July 2, 2016

Published: July 18, 2016

Copyright: © 2016 Wongjaikam et al. This is an open access article distributed under the terms of the Creative Commons Attribution License, which permits unrestricted use, distribution, and reproduction in any medium, provided the original author and source are credited.

Data Availability Statement: All relevant data are within the paper and its Supporting Information files.

Funding: This work was supported by the NSTDA Research Chair Grant from the National Science and Technology Development Agency Thailand (NC) and grants from the Thailand Research Fund BRG5780016 (SC), MRG5980222 (SK), TRG5880045 (JS), the Royal Golden Jubilee PhD program (SC and SW), Chiang Mai University Center of Excellence Award (NC), and the Faculty of Medicine Chiang Mai University Fund (SW and NC). The funders had no role in study design, data

Abstract

Background

Iron chelators are used to treat iron overload cardiomyopathy patients. However, a direct comparison of the benefits of three common iron chelators (deferoxamine (DFO), deferiprone (DFP) and deferasirox (DFX)) or an antioxidant (N-acetyl cysteine (NAC)) with a combined DFP and NAC treatments on left ventricular (LV) function with iron overload has not been investigated.

Methods and Findings

Male Wistar rats were fed with either a normal diet or a high iron diet (HFe group) for 4 months. After 2 months, the HFe-fed rats were divided into 6 groups to receive either: a vehicle, DFO (25 mg/kg/day), DFP (75 mg/kg/day), DFX (20 mg/kg/day), NAC (100 mg/kg/day) or the combined DFP and NAC for 2 months. Our results demonstrated that HFe rats had increased plasma non-transferrin bound iron (NTBI), malondialdehyde (MDA), cardiac iron and MDA levels and cardiac mitochondrial dysfunction, leading to LV dysfunction. Although DFO, DFP, DFX or NAC improved these parameters, leading to improved LV function, the combined DFP and NAC therapy caused greater improvement, leading to more extensively improved LV function.

Conclusions

The combined DFP and NAC treatment had greater efficacy than monotherapy in cardioprotection through the reduction of cardiac iron deposition and improved cardiac mitochondrial function in iron-overloaded rats.

collection and analysis, decision to publish, or preparation of the manuscript.

Competing Interests: The authors have declared that no competing interests exist.

Introduction

The iron overload condition is often seen in transfusion dependent thalassemia (TDT) patients due to repeated blood transfusions, and also in hereditary hemochromatosis patients due to increased dietary iron absorption into the duodenal enterocytes [1–5]. Iron overload leads to increased free iron (labile iron) in the plasma which is called non-transferrin bound iron (NTBI) [6, 7]. The accumulation of excess plasma NTBI leads to an increase in the entry of free iron into cells and this accumulation causes the dysfunction of many cellular organelles and also to direct tissue damage, especially in the heart [6–8]. Excess cardiac iron accumulation can cause iron overload cardiomyopathy which is a common cause of death in these patients [1–5]. It has been shown that free iron enters into the heart mainly through L-type calcium channels (LTCC) [9, 10], and T-type calcium channels (TTCC) [11, 12] under conditions of iron overload. Cardiac iron toxicity occurs when there is too much labile iron in the cell and this free iron reacts with superoxide (O_2•-) and hydrogen peroxide (H_2O_2) via Haber-Weiss and Fenton's reactions to produce the highly toxic hydroxyl radical (•OH). The production of this free radical leads to an increase in the levels of reactive oxygen species (ROS) [13, 14] and cardiac oxidative stress, leading to damages of cardiac cells which results in cardiac dysfunction and heart failure [14, 15]. Moreover, increase ROS production under iron overload condition led to plasma membrane lipid peroxidation which resulted in the increase of cytotoxic aldehydes, especially malondialdehyde (MDA) via Haber-Weiss and Fenton's reactions [16]. MDA is very toxic to cells and highly increased in cardiac iron overload, leading to cardiac dysfunction in a murine model [16]. Previous studies also found that MDA was increased both in plasma and tissue of iron-overloaded rats [17–19].

The production of O_2•- and H_2O_2 is derived largely from mitochondrial activity particularly in the heart [20, 21]. Iron interacts with O_2•- and H_2O_2, which are supplied by the mitochondrial electron transport [22]. Iron-catalyzed oxidants cause mitochondrial DNA damage and mitochondrial dysfunction, leading to a loss of respiratory capacity and cardiac dysfunction [23]. Further evidence of this is documented in a previous study which demonstrated that iron overload caused increased cardiac ROS production which led to cardiac mitochondrial depolarization and swelling in isolated cardiac mitochondria of wild type and β-thalassemic mice [24].

Currently, three common iron chelators including deferoxamine (DFO), deferiprone (DFP) and deferasirox (DFX) are used to treat and prevent cardiac iron deposition and cardiac dysfunction in iron overload cardiomyopathy [25–33]. Nonetheless, direct comparisons between the therapeutic effects of DFO, DFP and DFX on the heart under conditions of iron overload have not yet been investigated. Moreover, growing evidence showed that N-acetyl cysteine (NAC) is a potent antioxidant and a precursor of an antioxidant glutathione [34] which can scavenge free radicals such as H_2O_2 and •OH in cells [35]. Under an iron overloaded condition, NAC provided protective effects on brain dysfunction in iron-overloaded rats [18], and it may also reduce ROS levels and DNA damage in β-thalassemia patients [36]. Interestingly, combined DFP plus NAC therapy has been shown to provide synergistically therapeutic benefits in improving and restoring brain function which was impaired by iron toxicity [18]. However, the protective effects of NAC alone or combined DFP plus NAC on cardiac dysfunction caused by the iron overload condition have not yet been investigated. This study aimed to test the hypothesis that pharmacological interventions with DFO, DFP, DFX, NAC or combined DFP plus NAC can attenuate cardiac iron concentration, diminish cardiac oxidative stress, and improve left ventricular (LV) function and cardiac mitochondrial function in iron-overloaded rats, and that a combination of a chelator with NAC therapy can synergistically provide beneficial effects for these conditions.

Materials and Methods

Animal preparation

All animal studies were approved by the Institutional Animal Care and Use Committee (IACUC) at the Faculty of Medicine, Chiang Mai University (Permit number: 21/2557). Forty-two adult male Wistar rats, body weight 180–200 g, were obtained from the National Laboratory Animal Center, Mahidol University, Bangkok, Thailand. Animals were housed in an animal holding room under controlled conditions at 23 ± 2°C, 50 ± 10% humidity and 12 h light/dark cycles. The animals were acclimatized for a week prior to the experiment and received drinking water *ad libitum* throughout the entire experiment.

High iron diet preparation

A chow diet containing 0.2% of ferrocene ($C_{10}H_{10}Fe$; Sigma-Aldrich, Co., St. Louis, USA) (w/w) was prepared as described previously [18]. In brief, one kilogram of a chow diet was grinded and 2 g of ferrocene were added with mixing well. Then, 1.2 L of deionized water was added in the iron-loading diet and mixed well again. After that, iron loading diet was molded and baked at 80°C for 24 hours in a hot air oven.

Experimental protocols

Adult male Wistar rats (180–200 g) were divided into 2 groups to receive either a normal diet (a chow diet, ND) (n = 6), or high iron diet (0.2% ferrocene w/w, HFe) (n = 36) for 4 months. Two months into this protocol, ND-fed rats received a vehicle (normal saline solution, NSS) (control group) once a day via either subcutaneous injection (n = 3) or gavage feeding (n = 3) and continued with their normal diet for 2 months. HFe-fed rats were divided into 6 groups (n = 6/group) including 1) HFe given NSS (HFeV) once a day via either subcutaneous injection (n = 3) or gavage feeding (n = 3), 2) deferoxamine (DFO; Desferal®, Novartis Pharma Stein AG, Stein, Switzerland), (HFeDFO) 25 mg/kg/ day via subcutaneous injection, 3) deferiprone (DFP; Ferriprox®, Apotex Inc.,Toronto, Ontario, Canada), (HFeDFP) 75 mg/kg/day, 4) deferasirox (DFX; Exjade®, ICL670, Novartis Pharma Stein AG, Stein, Switzerland), (HFeDFX) 20 mg/kg/day, 5) N-acetyl cysteine (NAC, Sigma-Aldrich, Co., St. Louis, USA), (HFeNAC) 100 mg/kg/day, or 6) combined DFP 75 mg/kg/day plus NAC 100 mg/kg/day (HFeDFP+NAC) via gavage feeding for 2 months, and all of these groups were continuously fed with the high iron diet. Although DFO could remove cardiac iron in patients with cardiac iron loading, the route of DFO administration is a subcutaneous or an intravenous injection which causes sufferring in patients who are treated with this iron chelator. In addition, DFP showed to be more effective than DFO in removing excess cardiac iron store in TDT patients [27, 37]. DFX is an expensive oral iron chelator compared to the cost of DFP. Moreover, previous studies demonstrated that DFP was more effective than DFX in reducing severe cardiac iron loading in TDT patients [37, 38]. Therefore, DFP was chosen to combine with NAC in this study. At the end of the experiment (4 months after the start of the diets) heart rate variability (HRV), echocardiography and left ventricular pressure-volume (P-V) loop analysis were determined in all groups. Rats were deeply anesthetized by intraperitoneal injections of Zolitil (ZolazepamTiletamine) 50 mg/kg combined with Xylazine 3 mg/kg [39], and then P-V loop analysis was performed for 20 minutes. After P-V loop analysis, the blood was collected to measure plasma non-transferrin bound iron (NTBI) and plasma malondialdehyde (MDA) levels. Then, the deeply anesthetized rats were sacrificed by rapidly removal of the heart. The heart was used to determine cardiac iron concentration, cardiac MDA content and the study of cardiac mitochondria in all groups. The summary of the experimental protocol is shown in Fig 1.

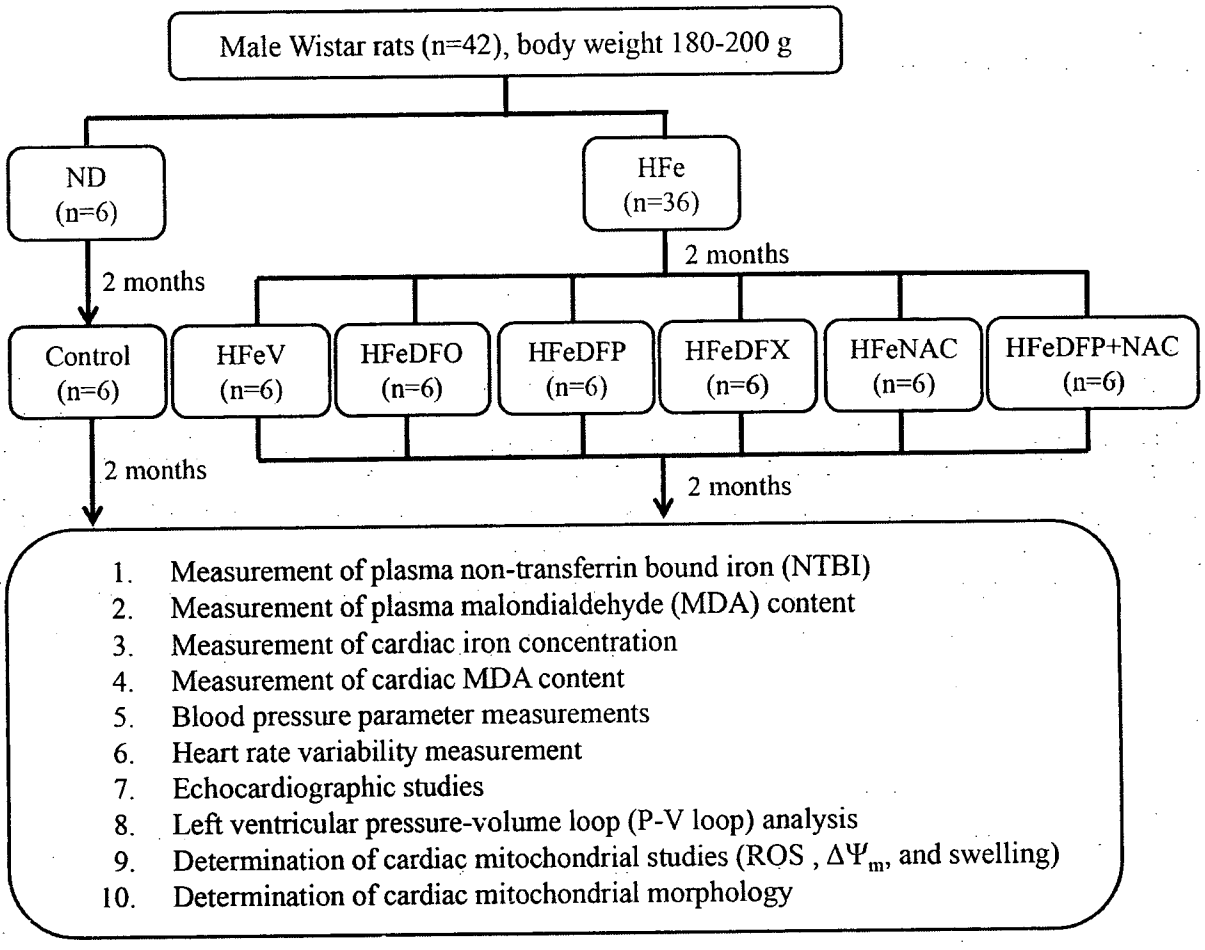


Fig 1. The summary of the experimental protocol. ND = normal diet group; HFe = high iron diet group; V = vehicle; DFO = deferoxamine; DFP = deferiprone; DFX = deferasirox; NAC = N-acetyl cysteine; NTBI = non-transferrin bound iron; MDA = malondialdehyde; ROS = reactive oxygen species; $\Delta\Psi_m$ = membrane potential change.

doi:10.1371/journal.pone.0159414.g001

Measurement of plasma non-transferrin bound iron (NTBI) concentration

To determine the presence of an iron overload condition, plasma NTBI level was measured using nitrilotriacetic acid disodium salt (NTA) chelation/flow cytometry [40, 41] with some modifications. Plasma was incubated with NTA solution (at a final concentration of 80 mM) pH 7.0 for 30 minutes at room temperature to allow Fe^{3+}-$(NTA)_2$ complexes to form. Then, the Fe^{3+}-$(NTA)_2$ complexes were separated from the plasma proteins by spinning the plasma mixture through a membrane filter (NanoSep® 30-kDa cut off, polysulfone type; Pall Life Sciences, Ann Arbor, MI, USA). The concentration of Fe^{3+}-$(NTA)_2$ complexes represented NTBI in the ultrafiltrate. Ferric nitrate was used as a standard and was prepared at a final concentration of 0–10 μM. Standard or Plasma- Fe^{3+}-$(NTA)_2$ was added with chelatable fluorescent beads ($5X10^6$ beads/mL) (1:1), followed by 180 μL of 50 mM MOPS buffer pH 7.0 and inserted into a 96 well microplate. Then, it was mixed and shaken in the dark for 2 hours. The NTBI (via Fe^{3+}-$(NTA)_2$ complexes) concentrations were measured by flow cytometry (Guava EasyCyte HT, Merck Millipore, Germany) and were calculated from a standard curve using GraphPad Prism software.

Measurement of malondialdehyde (MDA) concentration

To determine plasma and cardiac MDA concentrations to assess the oxidative stress state of the heart samples were measured using the high-performance liquid chromatography (HPLC) method [42]. Heart tissues were homogenized in a phosphate buffer solution (pH 2.8), containing with butylated hydroxytoluene (BHT) which is an antioxidant in the homogenized buffer, 1:10 (w /v) on ice. Homogenated heart tissue or plasma was mixed with 10% trichloroacetic acid containing BHT (50 ppm), heated at 90°C for 30 minutes, and then cooled for 2 minutes, followed by centrifugation at 6,000 rpm for 10 minutes. After that, the supernatant was mixed with 0.44M H_3PO_4 and 0.6% thiobarbituric acid solutions and then incubated at 90°C for 30 minutes. Plasma or cardiac MDA content was determined by absorbance detected at 532 nm by the HPLC system, and was calculated directly from the standard curve.

Measurement of cardiac iron concentration

Cardiac iron concentration was determined by using a colorimetric assay for measuring a non-heme iron concentration in heart tissues [11, 43]. Heart tissues were homogenized in deionized water 1:10 (w /v) on ice. Homogenated heart tissue was precipitated in protein precipitated solution (1:1) and heated at 95°C for 1 hour. After that, the tubes were cooled for 2 minutes, vortex mixed, and then centrifuged at 8,200 g for 10 minutes. The supernatant was mixed in a ferrozine solution (1:1) and was incubated at room temperature for 30 minutes. After incubation, the absorbance was measured at 562 nm, and the cardiac iron concentration was calculated directly from the iron standard curve.

Blood pressure parameter measurements

Blood pressure measurements from the tail vein of animals were performed by using a non-invasive blood pressure system (Kent Scientific Corporation, Wyoming, USA) [44, 45]. Animals were preheated under an infrared warming pad for at least 5 minutes to dilate their tail veins and acclimatize to the holder. Then, volume pressure recording and occlusion cuffs were attached to the tail. The blood pressure parameters, including systolic pressure, diastolic pressure and mean arterial pressure were recorded by taking an average of 20 consecutive measurements at a steady state.

Heart rate variability (HRV) measurement

Cardiac autonomic nervous activity was evaluated using spectral analysis of R-R interval variability. The electrocardiogram (ECG) was recorded for 15 minutes in each rat using the Power Lab system (Power Lab 4/25T, AD instrument) with chart 5.0 software. Data from the ECG recording was analyzed by using the MATLAB program [46]. A power spectrum of R-R interval variability was obtained by use of the Fast Fourier Transform (FFT) algorithm. Three major oscillatory components are detectable using this system: 1) the high frequency component (HF; about 0.6–3 Hz which varies with respiration), which is associated with parasympathetic activity, 2) the low frequency component (LF; about 0.2–0.6 Hz) which is associated with sympathetic and parasympathetic activity, and 3) the very low frequency component (VLF; the power below 0.2 Hz). To minimize the effect of changes in total power on the LF and HF components, LF and HF were expressed as normalized units (LFnu and HFnu) by dividing it by the total power minus VLF. The LF/HF ratio is considered an index of cardiac sympathetic/parasympathetic tone balance [47, 48]. An increase in LF/HF ratio indicates a cardiac sympathovagal imbalance [49, 50].

Echocardiographic studies

Left ventricular function was determined using an echocardiography (GE Vivid I) [50]. Rats were lightly inducted and maintained with 2% isoflurane with oxygen (2 L/min) inhalation. Their chest areas were shaved and the rats were stabilized for 1–2 minutes in the supine position prior to starting the protocol. The probe was gently placed on the chest and moved to enable the collection of data along the short and long axes of the heart. Signals from M-mode echocardiography at the level of the papillary muscles were recorded. Parameters from the echocardiograph, including left ventricular internal diameter end systole (LVIDs) and end diastole (LVIDd), were recorded. Fractional shortening was calculated by using the following formula: %FS = (LVIDd–LVIDs) x 100 /LVIDd [50].

Left ventricular pressure-volume (P-V) loop analysis

Left ventricular P-V loop analysis was carried out to assess left ventricular function using a pressure-volume conductance catheter system [39, 51]. Rats were anesthetized by intraperitoneal injections of Zolitil (ZolazepamTiletamine) 50 mg/kg combined with Xylazine 3 mg/kg [39]. Then, the neck was opened with a ventral midline incision and ventilated with room air from a positive pressure ventilator by a Harvard rodent ventilator model 683 (Harvard Apparatus, Massachusetts, USA). It was started immediately with room air using a volume of 200–250 μL and ventilator rate of 70–110 breaths/min to maintain PCO_2, PO_2, and pH parameters of the physiological condition. The right carotid artery was canulated with a pressure-conductance catheter (Scisense, Ontario, Canada) [39, 51] which was used for measuring left ventricular pressure and volume for 20 minutes. Heart rate, left ventricular end-systolic pressure (LVESP) and end-diastolic pressure (LVEDP), maximum and minimum pressures (Pmax and Pmin), cardiac output and stroke volume were measured in each rat.

Cardiac mitochondrial isolation

After P-V loop analysis, heart tissues were rapidly removed, minced and then homogenized in mitochondrial isolation buffer (MIB), pH 7.2 on ice. Then, homogenated heart tissue was centrifuged at 800 g, 4°C for 5 minutes. The supernatant was collected and centrifuged at 8,800 g, 4°C for 5 minutes. Then, mitochondrial pellets were re-suspended in MIB and centrifuged at 8,800 g, 4°C for 5 minutes. Finally, the mitochondrial pellet was re-suspended in a respiration buffer [52]. Protein concentration was determined using the Bicinchoninic Acid assay [53].

Determination of cardiac mitochondrial reactive oxygen species (ROS) production

The fluorescent dye dichlorohydro-fluorescein diacetate (DCFDA) was used to determine the level of ROS production in cardiac mitochondria [39, 52]. Cardiac mitochondria (0.4 mg/ mL) were incubated at 25°C with DCFDA for 20 minutes. DCFDA can pass through the mitochondrial membrane, and is oxidized by ROS in the mitochondria into DCF (a fluorescent form) [39, 52]. Fluorescence was excited at 485 nm and the emission fluorescence was recorded at 530 nm using a fluorescence microplate reader (Bio-Tek Instruments, Inc. Winooski, Vermont USA). The ROS level was expressed as arbitrary units of fluorescence intensity of DCF.

Determination of cardiac mitochondrial membrane potential change ($\Delta\Psi_m$)

Mitochondrial membrane potential change was determined by using the dye 5,50,6,60-tetrachloro-1,10,3,30-tetraethylbenzimidazolcarbocyanine iodide (JC-1) and was determined as

fluorescence intensity using a fluorescent microplate reader [39, 52]. JC-1 is characterized as a cation and remains in the mitochondrial matrix in a monomeric (green fluorescence) form. In addition, it can interact with anions in the mitochondrial matrix to form an aggregate (red fluorescence) form [39, 52]. JC-1 monomer and aggregate fluorescence were excited at the same wavelength of 485 nm. The emission fluorescence of JC-1 monomer and aggregate was detected at 530 and 590 nm, respectively. Cardiac mitochondrial depolarization was assessed by a decrease in the red/green fluorescence intensity ratio.

Determination of cardiac mitochondrial swelling

Mitochondrial swelling was studied by using the isolated-mitochondrial suspension [39, 52]. The change in the absorbance of the mitochondrial suspension was measured at 540 nm using a microplate reader (Synergy HT, Bio Tek, Winooski, Vermont, USA). Cardiac mitochondrial swelling was evaluated by a decrease in the absorbance of the mitochondrial suspension.

Cardiac mitochondrial morphology was also determined by using transmission electron microscopy [39, 52]. Cardiac mitochondrial isolations were fixed overnight in 2.5% glutaraldehyde in 0.1 M cacodylate buffer, pH 7.4 at 4°C. Then, they were post-fixed with 1% cacodylate-buffered osmium tetroxide at room temperature for 2 hours. After that, the pellets were dehydrated in a graded series of ethanols and embedded in Epon-Araldite. Ultrathin sections were cut using a diamond knife and placed on copper grids. Finally, they were stained with uranyl acetate and lead citrate, and cardiac mitochondrial morphology was observed using a transmission electron microscope.

Statistical analysis

Data in each experiment were expressed as mean ± standard error of mean (SEM). The data were processed using SPSS (Statistical Package for Social Sciences, Chicago, IL, USA) release 17.0 for Windows. Student's *t* test and One-way ANOVA analyses were performed to test for differences between groups. NTBI concentrations were analyzed using a non-parametric Kruskal-Wallis H, followed by a Mann-Whitney U test. *P* values <0.05 were considered as indicating a statistically significant difference between groups.

Results

The effects of the pharmacological interventions on plasma NTBI and plasma MDA levels

Plasma NTBI was significantly increased in the HFe-fed rats, while levels of plasma NTBI could not be detected in the control group (Fig 2A), indicating that an iron overload condition occurred in the HFe-fed rats. After 2 months of treatment with DFO, DFP, DFX, NAC and combined DFP plus NAC, plasma NTBI level was significantly reduced in the HFe-fed rats (Fig 2A). Plasma MDA level was significantly increased in the HFe-fed rats when compared with the control group (Fig 2B). All of the pharmacological interventions showed a correlation with a significantly decreased plasma MDA level in the HFe-fed rats (Fig 2B). This finding suggests that iron overload increased oxidative stress as shown by increased levels of a lipid peroxidation product (MDA) in the plasma of HFe-fed rats. Moreover, these pharmacological interventions also provided similar efficacy in lowering plasma NTBI and MDA levels.

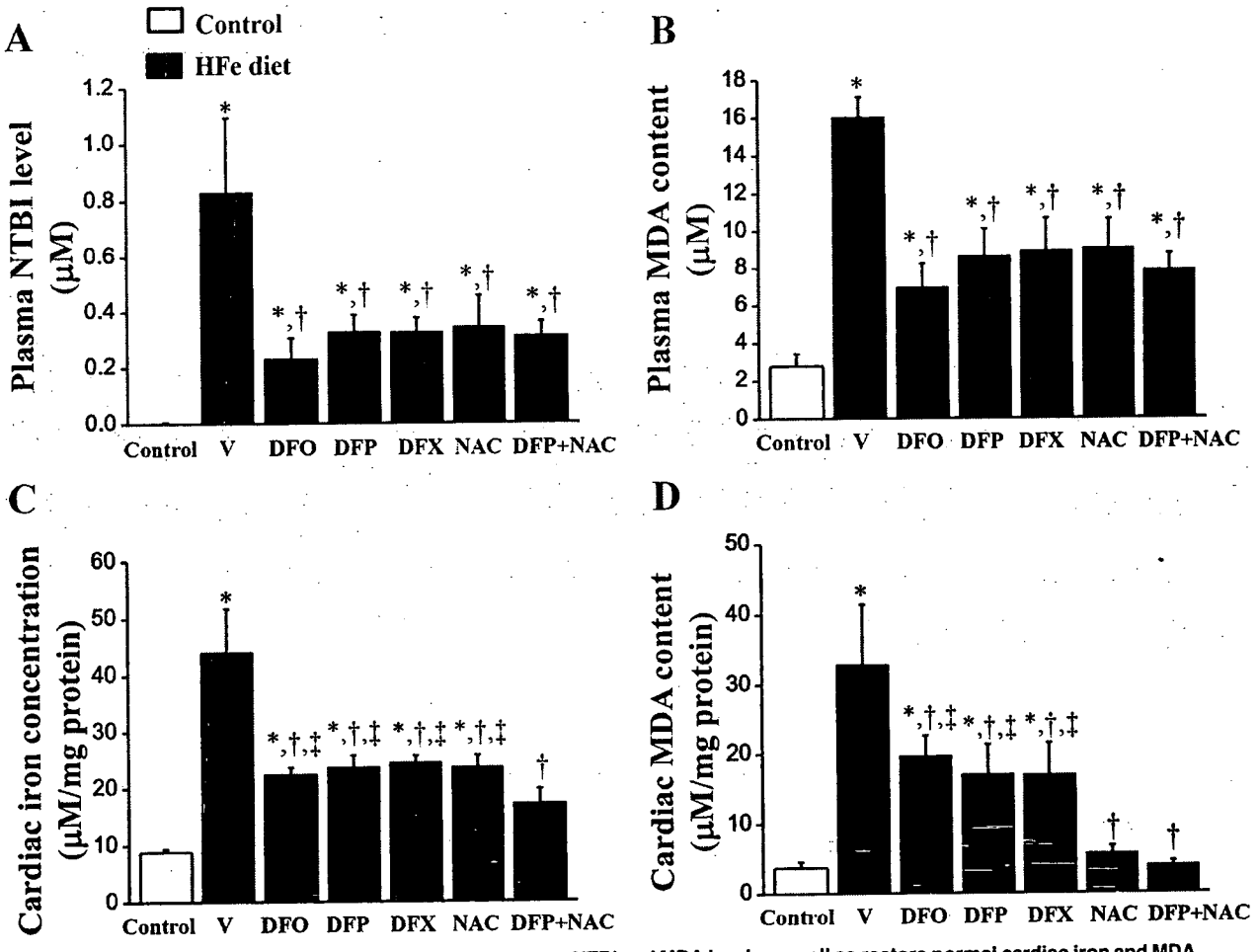


Fig 2. Combined DFP+NAC treatment could decrease plasma NTBI and MDA levels as well as restore normal cardiac iron and MDA content in iron-overloaded rats. The effects of the pharmacological interventions on: (A) plasma non-transferrin bound iron (NTBI) level; (B) plasma malondialdehyde (MDA) content; (C) cardiac iron concentration and (D) cardiac MDA content in iron-overloaded rats. *$P < 0.05$ vs. control, †$P < 0.05$ vs. HFe, ‡$P < 0.05$ vs. HFeDFP+NAC.

doi:10.1371/journal.pone.0159414.g002

The effects of the pharmacological interventions on cardiac iron concentration and cardiac MDA content

Iron concentration was significantly increased in the heart tissue of the HFe-fed rats when compared with the control group (Fig 2C), whereas DFO, DFP, DFX or NAC treatment showed similar efficacy in attenuating cardiac iron concentration. However, only combined DFP plus NAC decreased cardiac iron concentration to a normal level (i.e. the same as the control group) (Fig 2C). Consistently, cardiac MDA content was significantly increased in the HFe-fed rats when compared with the control group (Fig 2D). DFO, DFP and DFX showed the same efficacy in reducing cardiac MDA content, while NAC and combined DFP plus NAC decreased cardiac MDA content to a normal level the same as the control group (Fig 2D). These results suggest that the combination of DFP and NAC treatment led to the restoration of both cardiac iron concentration and cardiac MDA content in iron-overloaded rats.

Table 1. The effects of the pharmacological interventions on blood pressure parameters in iron-overloaded rats.

Groups	Systolic Pressure(mmHg)	Diastolic Pressure(mmHg)	Mean Arterial Pressure(mmHg)
Control	129±3	88±3	101±3
HFeV	125±5	93±4	103±4
HFeDFO	126±4	92±5	103±4
HFeDFP	127±2	92±4	103±3
HFeDFX	127±5	85±5	99±5
HFeNAC	125±1	87±2	100±1
HFeDFP+NAC	128±1	90±5	102±3

Data are shown as mean ±SE. HFe; high iron diet, V; vehicle, DFO; deferoxamine, DFP; deferiprone, DFX; deferasirox, NAC; N-acetyl cysteine, SE; standard error.

doi:10.1371/journal.pone.0159414.t001

The effects of the pharmacological interventions on blood pressure parameters

There was no significant difference in the blood pressure parameters including systolic pressure, diastolic pressure, and mean arterial pressure between the HFe-fed rats and the control group (Table 1). Similarly, systolic pressure, diastolic pressure and mean arterial pressure were not significantly different in any of the pharmacological intervention groups when compared with vehicle-treated HFe-fed rats (Table 1).

The effects of the iron overload condition and the pharmacological interventions on heart rate variability (HRV)

At baseline, the LF/HF ratio did not differ between HFe-fed rats and the control group (Fig 3A). After iron was administered for 2, 3 and 4 months, the LF/HF ratio was significantly increased in the HFe-fed rats in a time-dependent manner when compared with the control group. These findings indicate a cardiac sympathovagal imbalance in the rats with iron-

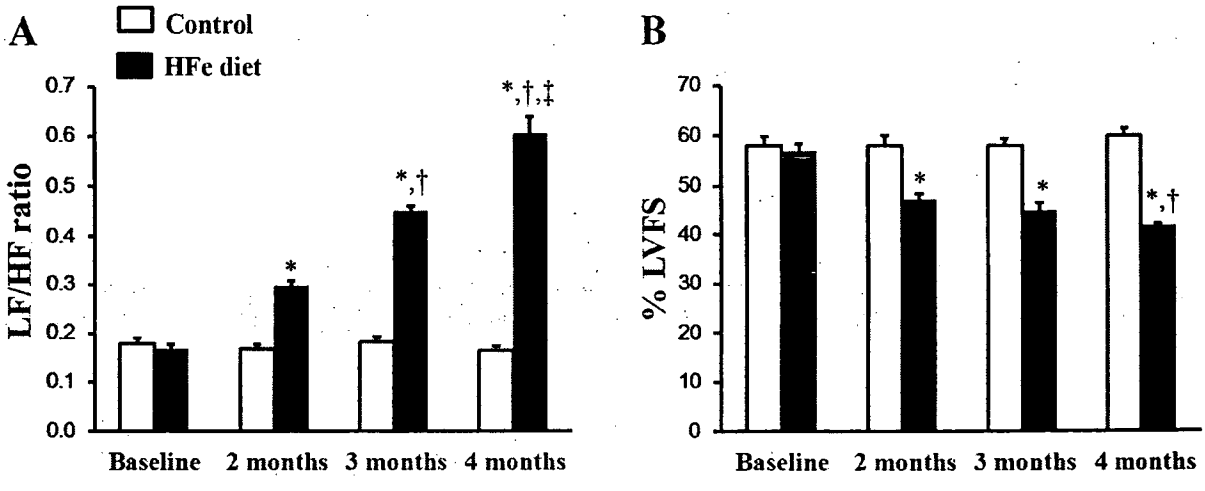


Fig 3. Chronic iron overloaded impaired heart rate variability and decreased cardiac function in iron-overloaded rats. The effects of the iron overload condition on: (A) heart rate variability at baseline, 2, 3 and 4 months, and (B) the percentage of left ventricular fractional shortening (%LVFS) measured using echocardiography at baseline, 2, 3 and 4 months in iron-overloaded rats. *$P < 0.05$ vs. control, †$P < 0.05$ vs. HFe diet for 2 months, ‡$P < 0.05$ vs. HFe diet for 3 months.

doi:10.1371/journal.pone.0159414.g003

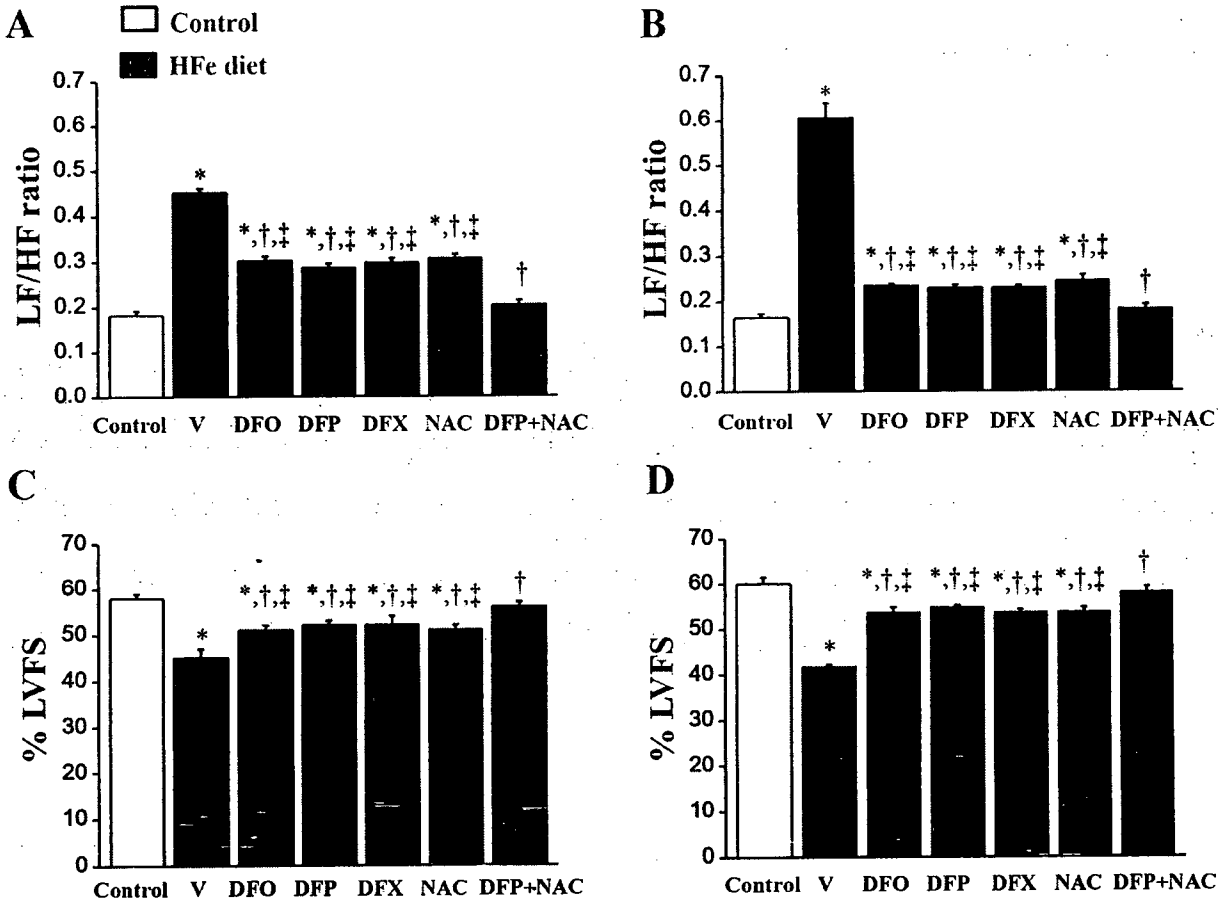


Fig 4. Combined DFP+NAC treatment could restore heart rate variability and cardiac function in iron-overloaded rats. The effects of the pharmacological interventions on heart rate variability at 3 months (A), and 4 months (B), and the percentage of left ventricular fractional shortening (%LVFS) measured using echocardiography at 3 months (C), and 4 months (D) in iron-overloaded rats. *$P < 0.05$ vs. control, †$P < 0.05$ vs. HFe, ‡$P < 0.05$ vs. HFeDFP+NAC.

doi:10.1371/journal.pone.0159414.g004

overload after 2 months of HFe feeding, and it increased successively at 3 months and 4 months, respectively (Fig 3A). DFO, DFP, DFX or NAC treatments had similar effects in attenuating the LF/HF ratio in the HFe-fed rats thus indicating improved cardiac sympathovagal balance after 1 month (at 3 months) and 2 months (at 4 months) of treatment, respectively (Fig 4A and 4B). However, only the combined DFP plus NAC treatment led to significant attenuation of the LF/HF ratio in the iron-overloaded rats to a control value after 1 month of treatment (Fig 4A), and continued to restore HRV after treatment with the combination of an iron chelator and an antioxidant for 2 months (Fig 4B). This result suggests that the combination of DFP and NAC treatment can significantly improve and restore the HRV in rats with iron-overload rats.

The effects of the iron overload condition and the pharmacological interventions on cardiac function

From echocardiographic data, the percentage of left ventricular fractional shortening (%LVFS) did not differ at baseline between the HFe-fed rats and the control group (Fig 3B). However,

Table 2. The effects of the pharmacological interventions on hemodynamic parameters in iron-overloaded rats.

Hemodynamic parameters	Control	HFeV	HFeDFO	HFeDFP	HFeDFX	HFeNAC	HFeDFP+NAC
Heart rate (beats / min)	253±2	233±9	240±11	237±7	255±18	235±17	253±12
LVESP (mmHg)	141±5	110±5*	126±4*,†	124±5*,†	124±6*,†	125±3*,†	132±1†
LVEDP (mmHg)	24±1	20±3	23±2	25±2	22±3	26±3	25±2
Pmax (mmHg)	144±4	115±4*	129±5*,†	128±5*,†	129±6*,†	128±3*,†	135±2†
Pmin (mmHg)	20±0.2	15±3	17±2	21±2	18±3	21±3	21±1
Cardiac output (mL/min)	132±4	91±4*	111±3*,†	111±6*,†	112±8*,†	110±5*,†	118±8†
Stroke volume (μL)	517±13	396±10*	434±9*,†	447±12*,†	434±13*,†	436±4*,†	459±7*,†

LVESP, LVEDP, left-ventricular end-systolic and end-diastolic pressure; Pmax, Pmin, maximum and minimum pressure.

*$P < 0.05$ vs. control,

†$P < 0.05$ vs. HFe.

doi:10.1371/journal.pone.0159414.t002

beginning at 2 months after HFe feeding, %LVFS was significantly decreased in the HFe-fed rats when compared with the control group, indicating left ventricular dysfunction in the iron-overloaded rats, and it continued to decrease at 3 and 4 months after HFe feeding (Fig 3B). DFO, DFP, DFX or NAC therapy could improve %LVEF after 1 month of treatment (Fig 4C), and these treatments did continue to improve cardiac function after 2 months of treatment (Fig 4D). Although DFO, DFP, DFX or NAC monotherapy significantly increased %LVFS, only the combination of DFP plus NAC increased %LVFS in the HFe-fed rats to the same level as shown in the control group after 1 month of treatment (Fig 4C). These results remained the same at 2 months of treatment (Fig 4D). These findings suggest that the combination of DFP and NAC treatment can significantly improve and restore LV function in iron-overloaded rats, and provide more robust effects than monotherapy with either an iron chelator or an antioxidant alone.

The P-V loop data demonstrated that HFe-fed rats had significantly decreased LVESP, Pmax, cardiac output and stroke volume when compared with the control group, indicating left ventricular dysfunction in these rats (Table 2). Treatments with DFO, DFP, DFX and NAC significantly improved LVESP, Pmax, cardiac output as well as stroke volume in the HFe-fed rats (Table 2). Only the combined DFP plus NAC treatment led to the restoration of LVESP, Pmax and cardiac output in iron-overloaded rats (Table 2). These results suggest that combined DFP plus NAC treatment exerted greater efficacy than monotherapy in improving LV function in iron-overloaded rats.

The effects of the pharmacological interventions on cardiac mitochondrial function in rats with iron- overload

ROS production was significantly increased in the HFe-fed rats when compared with the control group (Fig 5A). Although DFO, DFP, DFX and NAC treatments significantly reduced ROS production, only the combined DFP plus NAC treatment attenuated the ROS level to the same level as that observed in the control group (Fig 5A). Cardiac mitochondrial depolarization was observed as indicated by decreased red/green fluorescent intensity ratio in the HFe-fed rats when compared with the control group (Fig 5B). Although DFO, DFP, DFX and NAC monotherapy significantly reduced cardiac mitochondrial depolarization, only the combined DFP plus NAC led to the restoration of cardiac mitochondrial depolarization (Fig 5B). Consistently, cardiac mitochondrial swelling was significantly increased in the HFe-fed rats when compared with the control group (Fig 5C). All of the pharmacological interventions led to significant restoration of cardiac mitochondrial swelling in the iron-overloaded rats (Fig 5C). The

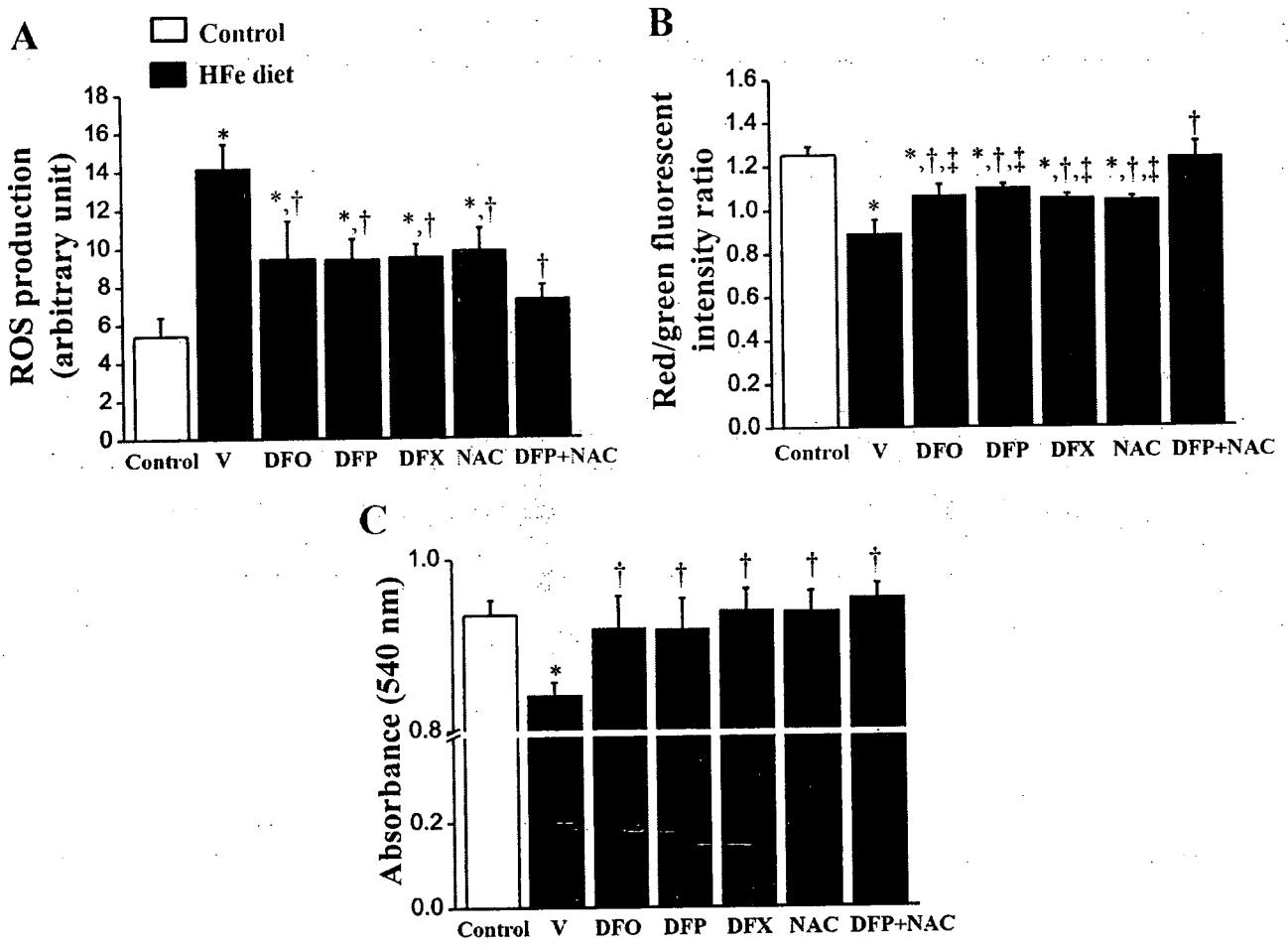


Fig 5. Combined DFP+NAC treatment could restore cardiac mitochondrial function in iron-overloaded rats. The effects of the pharmacological interventions on: (A) cardiac mitochondrial reactive oxygen species (ROS) production; (B) cardiac mitochondrial membrane potential change and (C) cardiac mitochondrial swelling in iron-overloaded rats. *$P < 0.05$ vs. control, †$P < 0.05$ vs. HFe, ‡$P < 0.05$ vs. HFeDFP +NAC.

doi:10.1371/journal.pone.0159414.g005

representative electron micrographs demonstrated that the HFe-fed rats had unfolded cristae and irregularly shaped mitochondria, indicating mitochondrial swelling (Fig 6). Cardiac mitochondrial structure was effectively restored by all pharmacological interventions in the iron-overloaded rats (Fig 6).

Discussion

The major findings of this study are as follows: 1) chronic iron loading for 4 months led to an iron overload condition developing in the rats, shown by an increase in the following: plasma NTBI and MDA, cardiac iron concentration, cardiac oxidative stress, cardiac mitochondrial dysfunction, cardiac sympathovagal imbalance and left ventricular dysfunction; 2) interventions by using DFO, DFP, DFX and NAC provided similar beneficial effects in reducing systemic and cardiac iron overload as well as lowering plasma and cardiac oxidative stress levels, leading to improved cardiac mitochondrial function, cardiac sympathovagal balance and left ventricular function; 3) combined DFP plus NAC treatment showed synergistic effects which

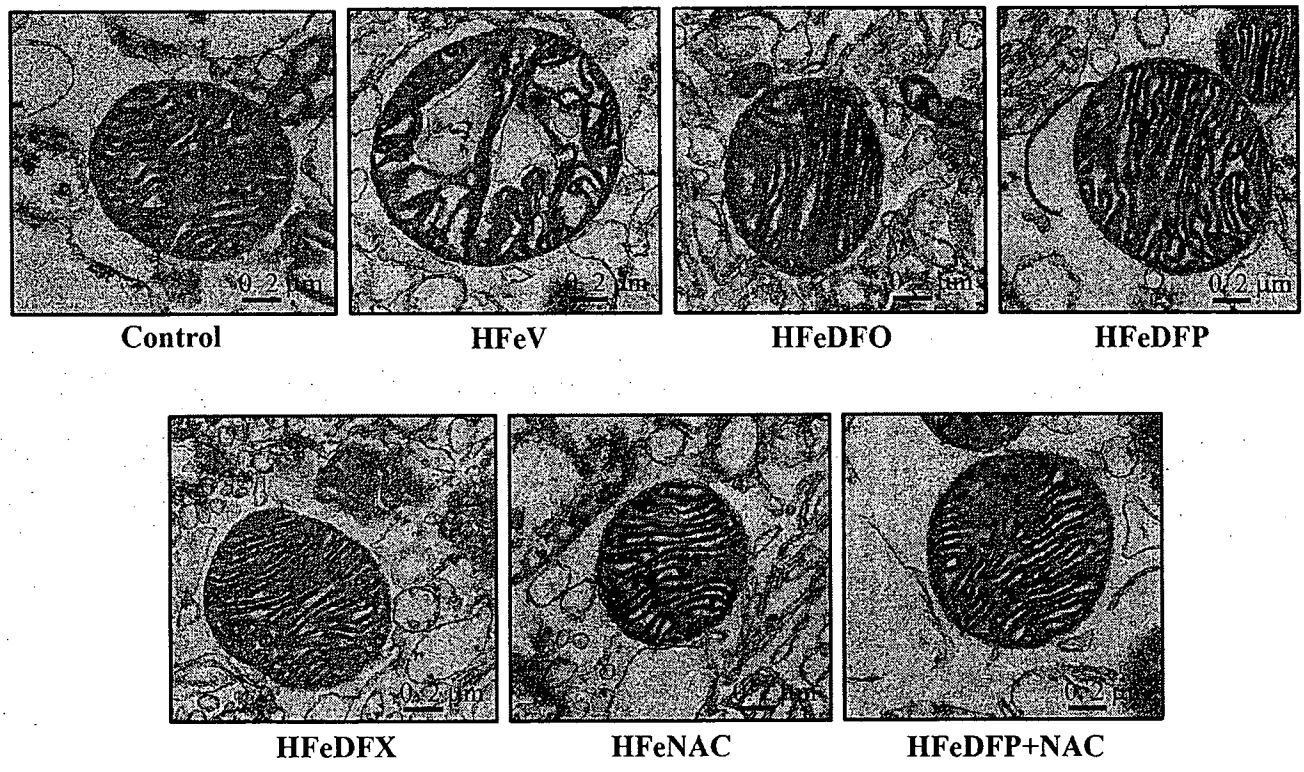


Fig 6. Electron micrographs of cardiac mitochondria from control, HFeV, HFeDFO, HFeDFP, HFeDFX, HFeNAC and HFeDFP+NAC groups. Iron-overloaded rats led to dysmorphic morphology and swelling of cardiac mitochondria compared to the control group. All of the pharmacological interventions could restore cardiac mitochondrial morphology which was obtained by using a transmission electron microscope in iron-overloaded rats.

doi:10.1371/journal.pone.0159414.g006

were more marked than the results monotherapy gave in the heart tissue by attenuating and restoring cardiac iron concentration and cardiac MDA level, and restoring cardiac mitochondrial function, cardiac sympathovagal balance and left ventricular function; 4) this is the first study to demonstrate the protective effects of a combination of DFP and NAC treatment against iron overload induced-cardiac dysfunction and that this combination therapy significantly improved and restored cardiac function in iron-overloaded rats.

Under conditions of iron overload, plasma NTBI or free iron accumulation is caused by saturated-transferrin bound iron [6, 7]. Increased plasma NTBI leads to an increase in the entry of free iron into heart tissues through both LTCCs [9, 10] and TTCCs [11, 12]. Excess free iron in cardiac cells causes increased oxidative stress via Haber-Weiss and Fenton's reactions [13, 14]. In this study, plasma NTBI and cardiac iron concentrations in the HFe-fed group were increased, indicating an iron overload condition in this animal model. Iron overload causes the production of ROS leading to the lipid-peroxidation of cellular membranes as well as damage to cellular proteins, nucleic acids and organelles [13, 14]. MDA is the end product of lipid peroxidation and is used as an indicator of oxidative stress and cell injury [54, 55]. This study showed that MDA levels were increased in both the plasma and the heart tissues of the rats with iron-overload, thus demonstrating an increase in systemic and intracardiac oxidative stress levels. In addition, cardiac mitochondria were also damaged by increased oxidative stress and mitochondrial depolarization, also mitochondrial swelling occurred in the iron-overloaded rats. Since mitochondria are vital organelles and function as the power houses of cells [56], iron-mediated oxidative stress caused cardiac mitochondrial damage and dysfunction, leading

to impaired LV function as observed in this study. Moreover, since oxidative stress has a strong influence on the changes in the HRV [4, 11, 57], increased oxidative stress in iron overloaded rats could lead to impaired HRV as shown in this study. These mechanisms could help explain and support the findings that iron-overloaded rats had impaired LV function as shown by decreased %LVEF together with decreased LVESP, Pmax, cardiac output and stroke volume. This impairment was similar to that observed in TDT patients who often exhibit LV dysfunction [58, 59]. In the present study, although DFO, DFP, DFX or NAC treatment could improve LVESP, Pmax, cardiac output and stroke volume in the HFe-fed rats, only a combination of DFP plus NAC facilitated the restoration of LVESP, Pmax and cardiac output to a normal level, thus demonstrating that the combined therapy exerted better protection on cardiac mitochondrial function than monotherapy, leading to restoration of the LV function in iron-overloaded rats.

Currently, iron chelation is the main therapy used to treat patients with conditions of iron overload. DFO, DFP and DFX (three common iron chelators) have been shown to attenuate myocardial iron deposition, which led to improved cardiac function in TDT patients [26–29, 32, 33]. A previous study showed that NAC (a potent antioxidant) [34] has the ability to diminish oxidative stress and DNA damage due to iron-induced toxicity in β-thalassemia patients [36]. This current study demonstrated that despite plasma NTBI and MDA levels being attenuated by all treatments, these two parameters did not reach the normal levels as shown by the results from the control group. This result suggests that all of the pharmacological interventions had similar efficacy in reducing systemic NTBI and MDA levels. In reference to cardiac iron overload, the present study found that DFO, DFP, DFX and NAC demonstrated protective effects on cardiac dysfunction by reducing cardiac iron deposition, lowering oxidative stress, and improving cardiac mitochondrial function as well as improving the HRV and LV function in iron-overloaded rats. However, their protective effects did not sufficiently restore the LV function to reach the normal levels shown in the normal diet/control group. Although the present study and other [60] demonstrated that two oral iron chelators DFP and DFX had a similar efficacy in reducing cardiac iron and improving cardiac function in iron-overloaded rats, inconsistent findings exist regarding the effects of DFP and DFX. It has been reported that DFP was more effective than DFX in reducing cardiac iron and improving systolic ventricular function in TDT patients [37, 38]. In addition, DFX was shown to fail to remove cardiac iron in TDT patients with severe liver iron store [33]. Nevertheless, a large clinical study found that DFX was more effective than DFP in reducing liver iron content in TDT patients [38]. Additionally, although NAC did not cause any reduction in cardiac iron concentration to a normal level, it could decrease cardiac MDA content in the HFe-fed rats to a normal level (that found in the control group). This benefit might result from its anti-oxidative effects [34, 36].

Interestingly, a previous study showed that a combination of DFP plus NAC therapy exerted greater efficacy than monotherapy in attenuating brain oxidative stress and restoring brain function impaired by conditions of iron overload found in iron-overloaded rats [18]. In the present study, it was demonstrated that a combination of DFP plus NAC provides better cardioprotective effects than a monotherapy and could effectively reduce cardiac iron concentration and oxidative stress as well as being able to diminish mitochondrial ROS levels, mitochondrial depolarization and swelling to the extent of reaching normal levels as shown by the control group. Finally, cardiac sympathovagal balance was also effectively restored by the combined therapy, followed by improved and restored LV function in iron-overloaded rats.

The combination of an iron chelator and an antioxidant may provide these effectively protective effects on iron overload-induced cardiac dysfunction by several mechanisms. Firstly, DFP can chelate free iron in the cell [61] which leads to decreased cardiac iron concentration, and therefore results in a decrease in oxidative stress caused by Haber-Weiss and Fenton's

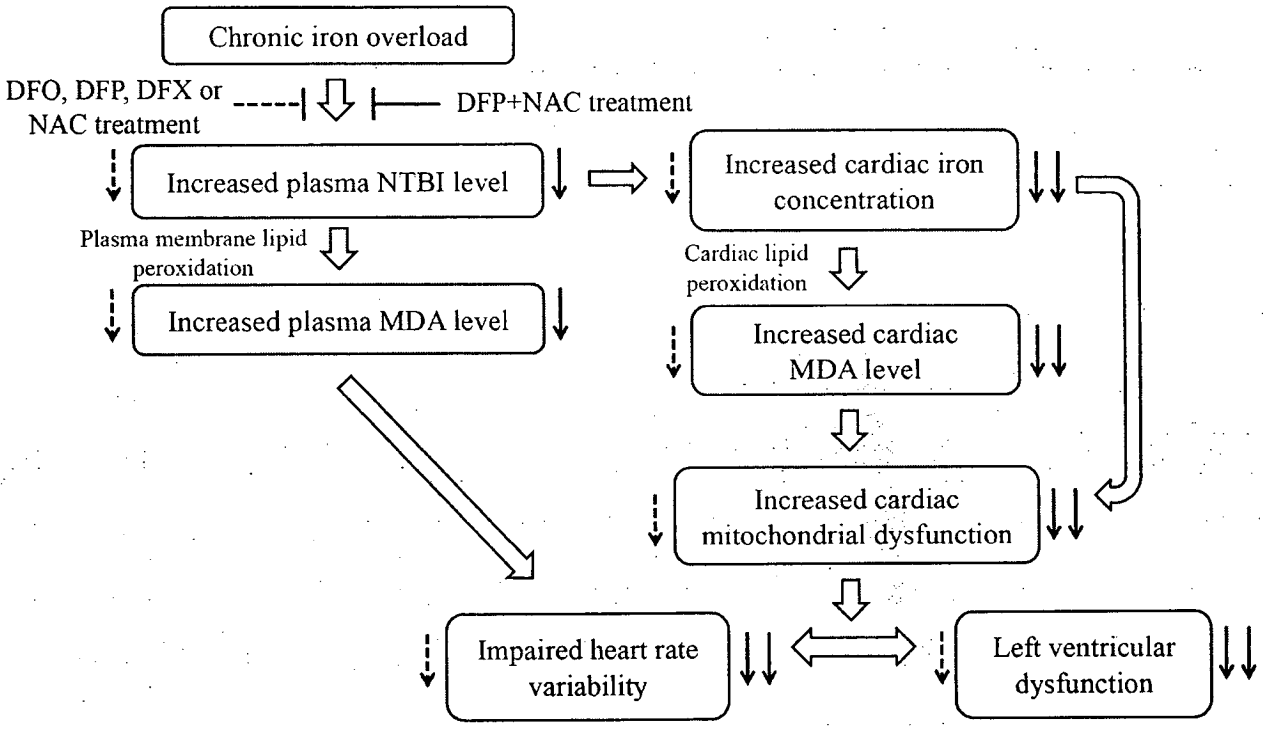


Fig 7. Diagram illustrating the proposed mechanisms of chronic iron overload on cardiac dysfunction and the effects of all pharmacological interventions on cardiac dysfunctions caused by chronic iron overload. Dashed arrows indicate the effects of either DFO, DFP, DFX or NAC treatment; solid arrows indicate the effects of combined DFP plus NAC treatment. DFO = deferoxamine; DFP = deferiprone; DFX = deferasirox; NAC = N-acetyl cysteine; NTBI = non-transferrin bound iron; MDA = malondialdehyde.

doi:10.1371/journal.pone.0159414.g007

reactions. Secondly, NAC can scavenge free radicals [34] and it is also known to have metal-chelating properties [62] including iron [63] which leads to decreased levels of both ROS and cardiac iron concentration. NAC might also complex with NTBI in the plasma and excreted by the kidney via glomerular infiltration [63]. Therefore, in this study a combination of DFP plus NAC provided synergistic cardioprotective effects and thus significantly improved and restored cardiac function in iron-overloaded rats. The mechanisms of chronic iron overload on cardiac dysfunction and the effects of all pharmacological interventions on cardiac dysfunction in iron-overloaded rats are summarized in Fig 7. These findings identify the need for future clinical trials to determine and warrant the clinical usefulness of combined iron chelator and NAC therapy in patients with iron overload cardiomyopathy.

Conclusions

DFO, DFP, DFX and NAC monotherapy had similar efficacy in improving cardiac function in iron-overloaded rats. Interestingly, combined DFP plus NAC had synergistically therapeutic benefits and exerted more robust beneficial results than monotherapy in its cardioprotective effects. This was shown by restored cardiac iron concentration, oxidative stress, and cardiac mitochondrial function which led to restored cardiac sympathovagal balance and LV function to a normal physiological condition in iron-overloaded rats. This study may provide extensive insights into future therapeutic strategies for better treatment of iron overload cardiomyopathy.

Limitations

A previous study indicated that DFO and BHT were added into the homogenized buffer to prevent iron-catalyzed, *ex vivo* MDA formation for determining MDA content in tissues [64]. Since DFO was not added in this study, it might be possible that the exogenous MDA was included in the measured MDA level. Also, MDA was used for oxidative stress status in the present study. Previous studies reported that 8-isoprostane is a prostaglandin (PG)-F_2-like compound belonging to the F_2 isoprostane class which is produced by the free radical-catalyzed peroxidation of arachidonic acid [65, 66]. 8-isoprostane is an accurate marker of lipid peroxidation and has been used to determine oxidative stress in *in vivo* [66, 67], especially in iron-overloaded rat model [68], which could be more specific to oxidative stress than MDA.

Acknowledgments

We would like to thank Cicely Proctor for her editorial assistance.

Author Contributions

Conceived and designed the experiments: NC SF SC. Performed the experiments: SW JK JS. Analyzed the data: SW SK JS SC NC. Contributed reagents/materials/analysis tools: NC SC SS SF. Wrote the paper: SW SK SC NC.

References

1. Abetz L, Baladi JF, Jones P, Rofail D. The impact of iron overload and its treatment on quality of life: results from a literature review. Health Qual Life Outcomes. 2006; 4:73. PMID: 17007645
2. Burke W, Reyes M, Imperatore G. Hereditary haemochromatosis: a realistic approach to prevention of iron overload disease in the population. Best Pract Res Clin Haematol. 2002; 15:315–28. PMID: 12401310
3. Kremastinos DT, Farmakis D,.Aessopos A, Hahalis G, Hamodraka E, Tsiapras D, et al. Beta-thalassemia cardiomyopathy: history, present considerations, and future perspectives. Circ Heart Fail. 2010; 3:451–8. doi: 10.1161/CIRCHEARTFAILURE.109.913863 PMID: 20484195
4. Wijampreecha K, Siri-Angkul N, Shinlapawittayatorn K, Charoenkwan P, Silvilairat S, Siwasomboon C, et al. Heart Rate Variability as an Alternative Indicator for Identifying Cardiac Iron Status in Non-Transfusion Dependent Thalassemia Patients. PLoS One. 2015; 10(6):e0130837. doi: 10.1371/journal.pone.0130837 PMID: 26083259
5. Zurlo MG, De Stefano P, Borgna-Pignatti C, Di Palma A, Piga A, Melevendi C. Survival and causes of death in thalassaemia major. Lancet. 1989; 2:27–30. PMID: 2567801
6. Hershko C. Pathogenesis and management of iron toxicity in thalassemia. Ann NY Acad Sci. 2010; 1202:1–9. doi: 10.1111/j.1749-6632.2010.05544.x PMID: 20712765
7. Hider RC, Silva AM, Podinovskaia M, Ma Y. Monitoring the efficiency of iron chelation therapy: the potential of nontransferrin-bound iron. Ann NY Acad Sci. 2010; 1202:94–9. doi: 10.1111/j.1749-6632.2010.05573.x PMID: 20712779
8. Wongjaikam S, Kumfu S, Chattipakorn SC, Fucharoen S, Chattipakorn N. Current and future treatment strategies for iron overload cardiomyopathy. Eur J Pharmacol. 2015; 765:86–93. doi: 10.1016/j.ejphar.2015.08.017 PMID: 26291660
9. Oudit GY, Sun H, Trivieri MG. L-type Ca(2+) channels provide a major pathway for iron entry into cardiomyocytes in iron-overload cardiomyopathy. Nat Med. 2003; 9:1187–94. PMID: 12937413
10. Oudit GY, Trivieri MG, Khaper N, Liu PP, Backx PH. Role of L-type Ca^{2+} channels in iron transport and iron-overload cardiomyopathy. J Mol Med (Berl). 2006; 84(5):349–64.
11. Kumfu S, Chattipakorn S, Chinda K, Fucharoen S, Chattipakorn N. T-type calcium channel blockade improves survival and cardiovascular function in thalassemic mice. Eur J Haematol. 2012; 88 535–48. doi: 10.1111/j.1600-0609.2012.01779.x PMID: 22404220
12. Kumfu S, Chattipakorn S, Srichairatanakool S, Settakorn J, Fucharoen S, Chattipakorn N. T-type calcium channel as a portal of iron uptake into cardiomyocytes of beta-thalassemic mice. Eur J Haematol. 2011; 86:156–66. doi: 10.1111/j.1600-0609.2010.01549.x PMID: 21059103

13. Fibach E, Rachmilewitz EA. The role of antioxidants and iron chelators in the treatment of oxidative stress in thalassemia. Ann NY Acad Sci. 2010; 1202:10–6. doi: 10.1111/j.1749-6632.2010.05577.x PMID: 20712766

14. Kremastinos DT, Farmakis D. Iron overload cardiomyopathy in clinical practice. Circulation. 2011; 124:2253–63. doi: 10.1161/CIRCULATIONAHA.111.050773 PMID: 22083147

15. Murphy CJ, Oudit GY. Iron-overload cardiomyopathy: pathophysiology, diagnosis, and treatment. J Card Fail. 2010; 16:888–900. doi: 10.1016/j.cardfail.2010.05.009 PMID: 21055653

16. Bartfay WJ, Dawood F, Wen WH, Lehotay DC, Hou D, Bartfay E, et al. Cardiac function and cytotoxic aldehyde production in a murine model of chronic iron-overload. Cardiovasc Res. 1999; 43(4):892–900. PMID: 10615416

17. Houglum K, Filip M, Witztum JL, Chojkier M. Malondialdehyde and 4-hydroxynonenal protein adducts in plasma and liver of rats with iron overload. J Clin Invest. 1990; 86(6):1991–8. PMID: 2123889

18. Sripetchwandee J, Pipatpiboon N, Chattipakorn N, Chattipakorn S. Combined therapy of iron chelator and antioxidant completely restores brain dysfunction induced by iron toxicity. PLoS ONE. 2014; 9(1): e85115. doi: 10.1371/journal.pone.0085115 PMID: 24400127

19. Aziza SA, Azab M-S, El-Shall SK. Ameliorating role of rutin on oxidative stress induced by iron overload in hepatic tissue of rats. Pak J Biol Sci. 2014; 17(8):964–77. PMID: 26031015

20. Chance B, Sies H, Boveris A. Hydroperoxide metabolism in mammalian organs. Physiol Rev. 1979; 59:527–605. PMID: 37532

21. Harman D. Free radical theory of aging: consequences of mitochondrial aging. Age. 1983; 6:86–94.

22. Gao X, Campian JL, Qian M, Sun X, Eaton JW. Mitochondrial DNA damage in iron overload. Journal of Biological Chemistry. 2009; 284(8):4767–75. doi: 10.1074/jbc.M806235200 PMID: 19095657

23. Gao X, Qian M, Campian JL. Mitochondrial dysfunction may explain the cardiomyopathy of chronic iron overload. Free Radical Bio Med. 2010; 49:401–7.

24. Kumfu S, Chattipakorn S, Fucharoen S, Chattipakorn N. Mitochondrial calcium uniporter blocker prevents cardiac mitochondrial dysfunction induced by iron overload in thalassemic mice. Biometals 2012; 25(6):1167–75. doi: 10.1007/s10534-012-9579-x PMID: 22910858

25. Hershko C. Oral iron chelators: new opportunities and new dilemmas. Haematologica. 2006; 91 (10):1307–12. PMID: 17018378

26. Maggio A, D'Amico G, Morabito A, Caprà M, Ciaccio C, Cianciulli P, et al. Deferiprone versus deferoxamine in patients with thalassemia major: a randomized clinical trial. Blood Cells Mol Dis. 2002; 28 (2):196–208. PMID: 12064916

27. Pennell DJ, Berdoukas V, Karagiorga M, Ladis V, Piga A, Aessopos A, et al. Randomized controlled trial of deferiprone or deferoxamine in beta-thalassemia major patients with asymptomatic myocardial siderosis. Blood. 2006; 107(9):3738–44. PMID: 16352815

28. Pennell DJ, Porter JB, Cappellini MD, Chan LL, El-Beshlawy A, Aydinok Y, et al. Deferasirox for up to 3 years leads to continued improvement of myocardial T2* in patients with β-thalassemia major. Haematologica. 2012; 97(6):842–8. doi: 10.3324/haematol.2011.049957 PMID: 22271905

29. Pepe A, Lombardi M, Positano V, Cracolici E, Capra M, Malizia R, et al. Evaluation of the efficacy of oral deferiprone in beta-thalassemia major by multislice multiecho T2*. Eur J Haematol. 2006; 76 (3):183–92. PMID: 16451393

30. Piga A, Roggero S, Salussolia I, Massano D, Serra M, Longo F. Deferiprone. Ann NY Acad Sci. 2010; 1202:75–8. doi: 10.1111/j.1749-6632.2010.05586.x PMID: 20712776

31. Porter JB. Deferasirox—current knowledge and future challenges. Ann NY Acad Sci 2010; 1202:87–93. doi: 10.1111/j.1749-6632.2010.05582.x PMID: 20712778

32. Tanner MA, Galanello R, Dessi C. A randomized, placebo-controlled, double-blind trial of the effect of combined therapy with deferoxamine and deferiprone on myocardial iron in thalassemia major using cardiovascular magnetic resonance. Circulation. 2007; 115 1876–84. PMID: 17372174

33. Wood JC, Kang BP, Thompson A, Giardina P, Harmatz P, Glynos T, et al. The effect of deferasirox on cardiac iron in thalassemia major: impact of total body iron stores. Blood. 2010; 116(4):537–43. doi: 10.1182/blood-2009-11-250308 PMID: 20421452

34. Bavarsad Shahripour R, Harrigan MR, Alexandrov AV. N-acetylcysteine (NAC) in neurological disorders:mechanisms of action and therapeutic opportunities. Brain Behav. 2014; 4(2):108–22. doi: 10.1002/brb3.208 PMID: 24683506

35. Aruoma OI, Halliwell B, Hoey BM, Butler J. The antioxidant action of N-acetylcysteine: its reaction with hydrogen peroxide, hydroxyl radical, superoxide, and hypochlorous acid. Free Radical Biol Med. 1989; 6:593–7.

36. Ozdemir ZC, Koc A, Aycicek A, Kocyigit A. N-acetylcysteine supplementation reduces oxidative stress and DNA damage in children with β-thalassemia. Hemoglobin. 2014; 15:1–6.

37. Pepe A, Meloni A, Capra M, Cianciulli P, Prossomariti L, Malaventura C, et al. Deferasirox, deferiprone and desferrioxamine treatment in thalassemia major patients: cardiac iron and function comparison determined by quantitative magnetic resonance imaging. Haematologica. 2011; 96(1):41–7. doi: 10.3324/haematol.2009.019042 PMID: 20884710

38. Berdoukas V, Chouliaras G, Moraitis P, Zannikos K, Berdoussi E, Ladis V. The efficacy of iron chelator regimes in reducing cardiac and hepatic iron in patients with thalassaemia major: a clinical observational study. J Cardiovasc Magn Reson. 2009; 11(20).

39. Chinda K, Sanit J, Chattipakorn S, Chattipakorn N. Dipeptidyl peptidase-4 inhibitor reduces infarct size and preserves cardiac function via mitochondrial protection in ischaemia-reperfusion rat heart. Diab Vasc Dis Res. 2014; 11(2):75–83. doi: 10.1177/1479164113516134 PMID: 24357666

40. Singh S, Hider RC, Porter JB. A direct method for quantification of non-transferrin-bound iron. Anal Biochem. 1990; 186:320–3. PMID: 2363505

41. MA Y, Podinovskaia M, Evans PJ, Emma G, Schaible UE, Porter J, et al. A novel method for non-transferrin-bound iron quantification by chelatable fluorescent beads based on flow cytometry. Biochem J. 2014; 463:351–62. doi: 10.1042/BJ20140795 PMID: 25093426

42. Grotto D, Santa Maria LD, Boeira S, Valentini J, Charao MF, Moro AM, et al. Rapid quantification of malondialdehyde in plasma by high performance liquid chromatography-visible detection. J Pharm Biomed Anal. 2007; 43:619–24. PMID: 16949242

43. Rebouche CJ, Wilcox CL, Widness JA. Microanalysis of non-heme iron in animal tissues. J Biochem Biophys Methods. 2004; 58:239–51. PMID: 15026210

44. Lekawanvijit S, Kompa AR, Manabe M, Wang BH, Langham RG, Nishijima F, et al. Chronic kidney disease-induced cardiac fibrosis is ameliorated by reducing circulating levels of a non-dialysable uremic toxin, indoxyl sulfate. PLoS ONE. 2012; 7(7):e41281. doi: 10.1371/journal.pone.0041281 PMID: 22829936

45. Samniang B, Shinlapawittayatorn K, Chunchai T, Pongkan W, Kumfu S, Chattipakorn SC, et al. Vagus nerve stimulation improves cardiac function by preventing mitochondrial dysfunction in obese-insulin resistant rats. Sci Rep. 2016; 1(6):19749.

46. Glos M, Romberg D, Fietze I, Penzel T. Heart rate and systolic blood pressure variability before and during obstructive sleep apnea episodes. ConfProc IEEE Eng Med Biol Soc. 2007; 2007:263–6.

47. Lima AH, Forjaz CL, Silva GQ, Meneses AL, Silva AJ, Ritti-Dias RM. Acute effect of resistance exercise intensity in cardiac autonomic modulation after exercise. Arq Bras Cardiol. 2011; 96(6):498–503. PMID: 21503389

48. Latchman PL, Mathur M, Bartels MN, Axtell RS, De Meersman RE. Impaired autonomic function in normotensive obese children. Clin Auton Res. 2011; 21(5):319–23. doi: 10.1007/s10286-011-0116-8 PMID: 21318460

49. Apaijai N, Chinda K, Palee S, Chattipakorn S, Chattipakorn N. Combined vildagliptin and metformin exert better cardioprotection than monotherapy against ischemia-reperfusion injury in obese-insulin resistant rats. PLoS ONE. 2014; 9(7):e102374. doi: 10.1371/journal.pone.0102374 PMID: 25036861

50. Pongkan W, Chattipakorn SC, Chattipakorn N. Chronic testosterone replacement exerts cardioprotection against cardiac ischemia- reperfusion injury by attenuating mitochondrial dysfunction in testosterone-deprived rats. PLoS ONE. 2015; 10(3):e0122503. doi: 10.1371/journal.pone.0122503 PMID: 25822979

51. Surinkaew S, Kumphune S, Chattipakorn S, Chattipakorn N. Inhibition of p38 MAPK during ischemia, but not reperfusion, effectively attenuates fatal arrhythmia in ischemia/reperfusion heart. J Cardiovasc Pharmacol. 2013; 61(2):133–41. doi: 10.1097/FJC.0b013e318279b7b1 PMID: 23107875

52. Thummasorn S, Kumfu S, Chattipakorn S, Chattipakorn N. Granulocyte-colony stimulating factor attenuates mitochondrial dysfunction induced by oxidative stress in cardiac mitochondria. Mitochondrion. 2011; 11:457–66. doi: 10.1016/j.mito.2011.01.008 PMID: 21292035

53. Walker JM. The bicinchoninic acid (BCA) assay for protein quantitation. Methods Mol Biol. 1994; 32:5–8. PMID: 7951748

54. Asif M, Manzoor Z, Farooq Muhammad Shehzad, Munawar SH, Aziz A, Khan IA. Status of oxidant, antioxidantand serum enzymes in thalassaemic children receiving multiple blood transfusions. J Pak Med Assoc. 2015; 65(8):838–43. PMID: 26228327

55. Zannos-Mariolea L, Tzortzatou F, Dendaki-Svolaki K, Katerellos C, Kavallari M, Matsaniotwas N. Serum vitamin E levels with beta-thalassemia major: preliminary report. Br J Haematol. 2008; 26:193–9.

56. Darley-Usmar V. The powerhouse takes control of the cell; the role of mitochondria in signal transduction. Free Radic Biol Med. 2004; 37:753–4. PMID: 15304251

57. Ziegler D, Buchholz S, Sohr C, Nourooz-Zadeh J, Roden M. Oxidative stress predicts progression of peripheral and cardiac autonomic nerve dysfunction over 6 years in diabetic patients. Acta Diabetol. 2015; 52(1):65–72. doi: 10.1007/s00592-014-0601-3 PMID: 24898524

58. Tabatabaie M, Hooman N, Arjmandi-Rafsanjani K, Isa-Tafreshi R. Ambulatory blood pressure monitoring for children with β–thalassemia major. Iran J Kidney Dis. 2013; 7:299–303. PMID: 23880807

59. Hui L, Leung MP, Ha SY, Chau AK, Cheung YF. Early detection of left ventricular dysfunction in patients with beta thalassaemia major by dobutamine stress echocardiography. Heart. 2003; 89:669–70. PMID: 12748234

60. Wood JC, Otto-Duessel M, Gonzalez I, Aguilar MI, Shimada H, Nick H, et al. Deferasirox and deferiprone remove cardiac iron in the iron-overloaded gerbil. Transl Res. 2006; 148(5):272–80. PMID: 17145573

61. Glickstein H, El RB, Shvartsman M, Cabantchik ZI. Intracellular labile iron pools as direct targets of iron chelators: a fluorescence study of chelator action in living cells. Blood. 2005; 106(9):3242–50. PMID: 16020512

62. Banner WJ, Koch M, Capin DM, Hopf SB, Chang S, Tong TG. Experimental chelation therapy in chromium, lead, and boron intoxication with N-acetylcysteine and other compounds. Toxicol Appl Pharmacol. 1986; 83(1):142–7. PMID: 3952743

63. Hjortsø E, Fomsgaard JS, Fogh-Andersen N. Does N-acetylcysteine increase the excretion of trace metals (calcium, magnesium, iron, zinc and copper) when given orally? Eur J Clin Pharmacol. 1990; 39 (1):29–31. PMID: 2276385

64. Knutson MD, Walter PB, Ames BN, Viteri FE. Both iron deficiency and daily iron supplements increase lipid peroxidation in rats. J Nutr. 2000; 130(3):621–8. PMID: 10702595

65. Montuschi P, Corradi M, Ciabattoni G, Nightingale J, Kharitonov SA, Barnes PJ. Increased 8-isoprostane, a marker of oxidative stress, in exhaled condensate of asthma patients. Am J Respir Crit Care Med. 1999; 160(1):216–20. PMID: 10390403

66. Morrow JD, Roberts LJn. The isoprostanes. Current knowledge and directions for future research. Biochem Pharmacol. 1996; 51(1):1–9. PMID: 8534261

67. Morrow JD, Hill KE, Burk RF, Nammour TM, Badr KF, Roberts LJn. A series of prostaglandin F2-like compounds are produced in vivo in humans by a non-cyclooxygenase, free radical-catalyzed mechanism. Proc Natl Acad Sci. 1990; 87(23):9383–7. PMID: 2123555

68. Kramer JH, Spurney CF, Iantorno M, Tziros C, Chmielinska JJ, Mak IT, et al. d-Propranolol protects against oxidative stress and progressive cardiac dysfunction in iron overloaded rats. Can J Physiol Pharmacol. 2012; 90(9):1257–68. doi: 10.1139/y2012-091 PMID: 22913465

เอกสารแนบหมายเลข 16

Vildagliptin reduces cardiac ischemic-reperfusion injury in obese orchiectomized rats

Wanpitak Pongkan[1,2,3], Hiranya Pintana[1,2], Thidarat Jaiwongkam[1,2,3], Sasiwan Kredphoo[1,2,3], Sivaporn Sivasinprasasn[1,2,3], Siriporn C Chattipakorn[1,2,4] and Nipon Chattipakorn[1,2,3]

[1]Cardiac Electrophysiology Research and Training Center, Faculty of Medicine, Chiang Mai University, Chiang Mai, Thailand
[2]Cardiac Electrophysiology Unit, Department of Physiology, Faculty of Medicine, Chiang Mai University, Chiang Mai, Thailand
[3]Center of Excellence in Cardiac Electrophysiology Research, Chiang Mai University, Chiang Mai, Thailand
[4]Department of Oral Biology and Diagnostic Science, Faculty of Dentistry, Chiang Mai University, Chiang Mai, Thailand

Correspondence should be addressed to N Chattipakorn
Email
nchattip@gmail.com

Abstract

Obesity and testosterone deprivation are associated with coronary artery disease. Testosterone and vildagliptin (dipeptidyl peptidase-4 inhibitors) exert cardioprotection during ischemic-reperfusion (I/R) injury. However, the effect of these drugs on I/R heart in a testosterone-deprived, obese, insulin-resistant model is unclear. This study investigated the effects of testosterone and vildagliptin on cardiac function, arrhythmias and the infarct size in I/R heart of testosterone-deprived rats with obese insulin resistance. Orchiectomized (O) or sham operated (S) male Wistar rats were divided into 2 groups to receive normal diet (ND) or high-fat diet (HFD) for 12 weeks. Orchiectomized rats in each diet were divided to receive testosterone (2 mg/kg), vildagliptin (3 mg/kg) or the vehicle daily for 4 weeks. Then, I/R was performed by a 30-min left anterior descending coronary artery ligation, followed by a 120-min reperfusion. LV function, arrhythmia scores, infarct size and cardiac mitochondrial function were determined. HFD groups developed insulin resistance at week 12. At week 16, cardiac function was impaired in NDO, HFO and HFS rats, but was restored in all testosterone- and vildagliptin-treated rats. During I/R injury, arrhythmia scores, infarct size and cardiac mitochondrial dysfunction were prominently increased in NDO, HFO and HFS rats, compared with those in NDS rats. Treatment with either testosterone or vildagliptin similarly attenuated these impairments during I/R injury. These finding suggest that both testosterone replacement and vildagliptin share similar efficacy for cardioprotection during I/R injury by decreasing the infarct size and attenuating cardiac mitochondrial dysfunction caused by I/R injury in testosterone-deprived rats with obese insulin resistance.

Key Words
- obese testosterone deprivation
- dipeptidyl peptidase-4 inhibitors
- ischemia–reperfusion
- cardiac mitochondrial function

Journal of Endocrinology (2016) **231**, 81–95

http://joe.endocrinology-journals.org
DOI: 10.1530/JOE-16-0232

© 2016 Society for Endocrinology
Printed in Great Britain

Published by Bioscientifica Ltd.

Introduction

Androgen deficiency occurs commonly in middle-aged to older men and also sometimes in younger men with underlying hypothalamopituitary or testicular disorders (Handelsman & Zajac 2004). It is a primary risk factor for many disorders including obesity, metabolic syndrome, dyslipidemia, and especially coronary artery diseases (CAD) (Traish & Kypreos 2011). Low testosterone levels have been shown to be related to CAD (Cornoldi *et al.* 2009) in which lower testosterone levels were associated with a higher prevalence of CAD (Wu & von Eckardstein 2003).

Similar to increased aging population, the prevalence of obesity has increased dramatically over the past decades (Ogden *et al.* 2015). Long-term consumption of a high-fat diet (HFD) has been shown to cause not only obesity but also insulin resistance, a state in which the insulin receptors do not respond to insulin properly leading to impaired glycemic control (Pratchayasakul *et al.* 2011). The main causes of this impairment begins at an intracellular level, in which overproduction of reactive oxygen species (ROS) leads to increased oxidative stress and impaired insulin signaling cascade (Valle *et al.* 2011). This impairment can cause energy insufficiency in the heart, leading to serious progressive impairments including coronary artery disease (Espinola-Klein *et al.* 2011), acute myocardial infarction (Ducimetiere *et al.* 1980) and chronic heart failure (Krishnamoorthy *et al.* 2016). As a large number of aging men are found to be obese (Flegal *et al.* 2012), the adverse effect on the heart could be cumulative from both obese insulin resistance and testosterone deprivation.

In this study, the cardioprotective effects of testosterone and vildagliptin (dipeptidyl peptidase-4 inhibitors) were investigated in testosterone-deprived and obese insulin-resistant model during ischemic and reperfusion (I/R) injury. The rational for the use of vildagliptin in orchiectomized rats in this study was due to the fact that previous studies demonstrated that testosterone deprivation is associated with the development of several disorders including obesity, insulin resistance and metabolic syndrome (Traish *et al.* 2009) as well as induced cardiovascular diseases and ischemic heart diseases (Kelly & Jones 2013). Regarding the treatment, recent studies have demonstrated the beneficial effects of testosterone replacement and DPP4 inhibitor (vildagliptin) on insulin resistance and metabolic profile (Apaijai *et al.* 2014, Pintana *et al.* 2015) and on ischemic insults of the heart (Chinda *et al.* 2014, Pongkan *et al.* 2015). However, the effect of testosterone replacement and vildagliptin in the heart subjected with I/R injury with testosterone deprivation combined with obese insulin resistance has never been investigated. Therefore, if vildagliptin exerts cardioprotection in testosterone-deprived subjects similar to testosterone replacement, it would be a great benefit and provide a new alternative treatment for the heart especially in elderly men who suffer from testosterone deprivation and metabolic syndrome, whereas testosterone replacement could not ameliorate peripheral insulin resistance (Garrido *et al.* 2014) and may cause undesirable effects (Reckelhoff *et al.* 2005). In this study, we tested the hypothesis that during cardiac I/R injury in obese insulin-resistant rats with testosterone deprivation, both testosterone and vildagliptin share similar efficacy in improving LV function and decreasing the incidence of arrhythmias and myocardial infarction size by attenuating cardiac mitochondrial dysfunction and apoptosis.

Materials and methods

Animal preparation

All experiments were approved by the Institutional Animal Care and Use Committee of the Faculty of Medicine, Chiang Mai University, Chiang Mai, Thailand. Male Wistar rats weighing ~200 g were obtained from the National Laboratory Animal Center, Mahidol University, Bangkok, Thailand and were used for this study. Food and water were given *ad libitum*. The experimental protocol is illustrated in Fig. 1. For orchiectomy procedure, rats were anesthetized using isoflurane 2–3%, and the orchiectomy was performed using the scrotal approach technique (Foley 2005). Rats vital signs were monitored throughout the operative time and observed for any other complications. Analgesic drugs and antibiotics were injected subcutaneously for 3 days after the operation.

Surgical procedure of myocardial I/R

Rats were anesthetized by intramuscular injection of Zoletil (zolazepam and tiletamine) 50 mg/kg combined with xylazine 3 mg/kg, and the rats were ventilated with air via a tracheotomy by Harvard Rodent Ventilator Model 683 (Harvard Apparatus, Holliston, MA, USA) (Pongkan *et al.* 2015). Lead II electrocardiogram (ECG) (PowerLab 4/25 T, AD Instrument) was recorded throughout the

http://joe.endocrinology-journals.org
DOI: 10.1530/JOE-16-0232
© 2016 Society for Endocrinology
Printed in Great Britain
Published by Bioscientifica Ltd.

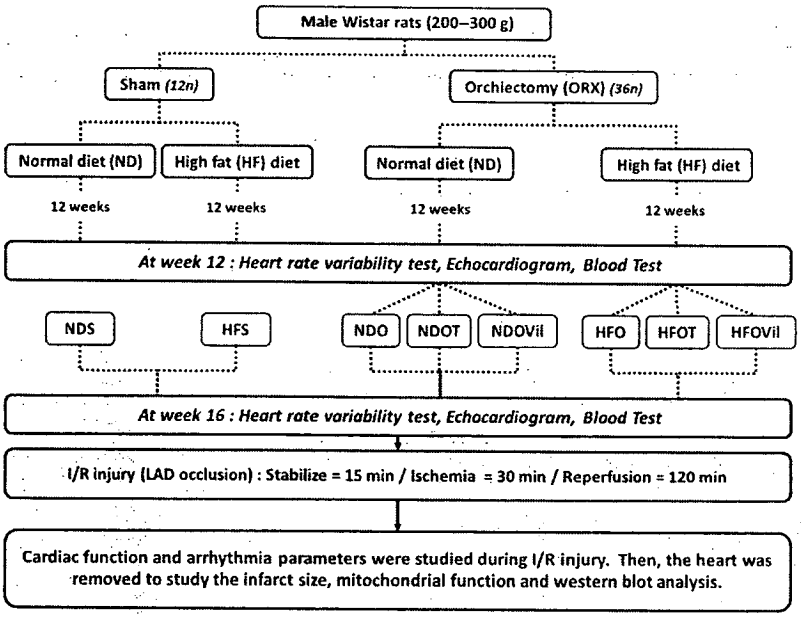


Figure 1
Schematic representation of the study protocol. Orchiectomized or sham operated rats were divided to receive normal diet (ND) or high-fat diet (HFD) for 12 weeks. Then, orchiectomized rats in ND or HFD were divided to receive vehicle (castor oil; subcutaneously (s.c.)), testosterone 2 mg/kg BW (s.c. daily for 4 weeks) or vildagliptin (Galvas, Novartis) 3 mg/kg BW (intragastric gavage daily for 4 weeks), daily for 4 weeks. The cardiac function and HRV were determined at 12th and 16th week. I/R was performed by 30-min LAD ligation, followed by 120-min reperfusion. HFO, high fat + orchiectomy; HFOT, high fat + orchiectomy + testosterone; HFOVil, high fat + orchiectomy + testosterone; HFS, high fat + sham; NDO, normal diet + orchiectomy; NDOT, normal diet + orchiectomy + testosterone; NDOVil, normal diet + orchiectomy + vildagliptin; NDS, normal diet + sham; Sc., subcutaneous injection.

study. The right carotid artery was cannulated with a pressure–volume (P-V) conductance catheter. The heart was exposed as described by previous study (Chinda *et al.* 2014). Ischemia was confirmed by an ST elevation on the ECG and regional pallor of myocardial tissues of the ischemic area. I/R injury was instigated by 30-min ischemia, followed by 120-min reperfusion.

Normal diet and high-fat diet preparation

Standard laboratory chow (Mouse Feed Food No.082, C.P. Company, Bangkok, Thailand), considered as a normal diet (19.77% of energy fat), was fed to the control rats. The high-fat diet (57.60% of energy fat) consisted of the following ingredients: standard rat diet, casein, lard, cholesterol, vitamins, DL-methionine, yeast powder and sodium chloride (Pratchayasakul *et al.* 2011). All the ingredients were mixed and molded into a spherical shape. Rats were fed on these two diets for 12 weeks.

Heart rate variability determination

HRV is a noninvasive assessment of cardiac autonomic function, which is used to determine cardiac sympathovagal balance (Chattipakorn *et al.* 2007). In this experiment, HRV was analyzed at the 12th and 16th weeks of the study. An electrocardiogram (ECG) was conducted on each rat using PowerLab (PowerLab 4/25T, AD instrument, Bella Vista, NSW, Australia) with chart 5.0 continuously for 20 min while the animals were still conscious. Data from the ECG recording were analyzed using the MATLAB program and analyzed as described previously (Pongkan *et al.* 2015). An increased LF/HF ratio is indicative of cardiac sympathovagal imbalance (Chattipakorn *et al.* 2007).

LV function determination

LV function was determined using an echocardiograph (Vivid-i, GE) and was analyzed at the 12th and 16th weeks of the study. Rats were anesthetized and maintained with 2% isoflurane with oxygen (2 L mL^{-1}) inhalation. Signals from an M-mode echocardiogram at the level of the papillary muscles were recorded. Parameters obtained included right ventricular dimension during diastole, interventricular septum dimension during systole and diastole, LV internal dimension during systole (LVIDs) and diastole (LVIDd), and LV posterior wall thickness during systole and diastole. Fractional shortening (FS) was calculated using the formula: %FS = (LVIDd − LVIDs) × 100/LVIDd (Rottman *et al.* 2007).

At the end of the experiment (week 16), LV function during I/R injury was evaluated using a P-V catheter (Scisense Instrument, Ontario, Canada). The right carotid artery was cannulated, and the pressure–volume relationship in the LV chamber was recorded using a LabScribe2 program (iWorx Systems Inc, Dover, NH, USA) (Chinda *et al.* 2014). Heart rate (HR), LV end-systolic pressure (LVESP) and LV end-diastolic pressure (LVEDP), P_{max}, P_{min}, positive dp/dt, negative dp/dt and stroke volume (SV) were assessed at the

http://joe.endocrinology-journals.org
DOI: 10.1530/JOE-16-0232
© 2016 Society for Endocrinology
Printed in Great Britain
Published by Bioscientifica Ltd.

baseline, end of the ischemic period and at the end of the reperfusion period.

Arrhythmia determination during I/R period

ECG (Lead II) was monitored throughout the I/R period using a PowerLab 4/25 (AD Instruments, Inc, Colorado Springs, CO, USA). The occurrence of arrhythmia was characterized using Lambeth Conventions (Curtis *et al.* 2013), and arrhythmia scores were determined based on the following criteria as described previously (Pongkan *et al.* 2015).

Infarct size determination

At the end of the experiment, the heart was removed and the LAD was re-occluded. The heart was perfused by cold normal saline (Pongkan *et al.* 2015). Evans blue (0.5%) was retrogradely infused through the aortic root. Nonstained area by Evans blue was defined as the area at risk (AAR). The heart was cut horizontally to 7–8 slices (Chinda *et al.* 2014), and then immersed and incubated in 37°C triphenyl tetrazolium chloride (TTC) for 12–15 min to differentiate the infarct tissues (white area) from the viable myocardium (red area). The red and white areas were defined as the remote area, whereas only the white area was defined as the infarct area. The area measurements were calculated using the ImageTool software, version 3.0 (Chinda *et al.* 2014).

Cardiac mitochondrial function study

At the end of the experiment, cardiac mitochondria were isolated from nonischemic (remote area, R) and ischemic areas (I). The heart tissues were homogenized in a homogenizer as described previously (Pongkan *et al.* 2015). Cardiac mitochondrial functions were determined as mitochondrial reactive oxygen species (ROS) production, mitochondrial membrane potential change ($\Delta\Psi m$) and mitochondrial swelling. Transmission electron microscopy (TEM) was also used to determine the morphology of the isolated cardiac mitochondria (Pongkan *et al.* 2015).

Metabolic parameters, insulin resistance and testosterone level determination

Fasting plasma glucose, total cholesterol and triglyceride concentrations were determined by an enzymatic colorimetric assay from a detection kit (Biotech, Bangkok, Thailand). Fasting plasma HDL was determined using colorimetric and fluorometric assays from a detection kit (BioVision), whereas plasma LDL was determined using Friedewald's equation using the fasting plasma HDL values (Friedewald *et al.* 1972). Fasting plasma insulin levels were determined using a sandwich ELISA (Millipore). Insulin resistance was assessed using the Homeostasis Model Assessment (HOMA) (Appleton *et al.* 2005). A higher HOMA index indicates a higher degree of insulin resistance (Pratchayasakul *et al.* 2011). Total plasma testosterone (ng/mL) was analyzed by ELISA at the Central Laboratory Service of Maharaj Nakorn Chiang Mai Hospital, Faculty of Medicine, Chiang Mai University.

Western blot analysis

Myocardial protein extract was prepared by homogenization of the frozen heart tissues in a lysis buffer (containing 1% Nonidet P-40 (Calbiochem, Merck Millipore), 0.5% sodium deoxycholate, 0.1% sodium dodecyl sulfate (SDS) in 1×PBS). The total protein was mixed with a loading buffer and boiled at 95°C for 10 min. Then, it was loaded into 10% gradient SDS-polyacrylamide gel and transferred to polyvinylidene difluoride (PVDF) membranes using transfer system (Bio-Rad). PVDF membranes were blocked with 5% nonfat skimmed milk in TBST for 1 h (Pongkan *et al.* 2015). The membranes were exposed, overnight (at 4°C), to anti-β-actin, anti-Bax (Santa Cruz Biotechnology), anti-Bcl-2, anti-caspase3, anti-total Cx43 and anti-Cx43 phosphorylated at S368 (Cell Signaling Technology) for 12 h. On the next day, bound antibody was detected by horseradish peroxidase–conjugated with anti-mouse IgG. Enhanced chemiluminescence (ECL) detection reagents were used to visualize peroxidase reaction products. The band density was analyzed using ImageJ 1.47V analysis (NIH image).

Statistical analysis

Data are expressed as mean ± S.E.M. Biochemical parameters were compared using the Mann–Whitney *U* test. VT/VF incidence was compared among groups using $\chi 2$ test. Statistical comparisons between groups were analyzed using Student's *t*-tests and one-way ANOVAs with post hoc LSD tests using SPSS, version 10.0. A *P* value less than 0.05 was considered statistically significant.

http://joe.endocrinology-journals.org
DOI: 10.1530/JOE-16-0232

© 2016 Society for Endocrinology
Printed in Great Britain

Published by Bioscientifica Ltd.

Results

Obesity, but not testosterone deficiency, caused peripheral insulin resistance, which was attenuated by vildagliptin and testosterone treatment

Testosterone deprivation was confirmed by decreased plasma testosterone levels as well as the ratio of seminal vesicle to body weight (seminal vesicle ratio). Orchiectomized rats without/with obese insulin resistance in both dietary groups (NDO and HFO) had significantly decreased plasma testosterone levels and seminal vesicle ratios, when compared with the sham group (NDS and HFS). Testosterone replacement significantly increased plasma testosterone levels in orchiectomized rats (NDOT and HFOT) compared with those in the NDO and HFO groups, but was not different from the NDS group. However, the testosterone level in rats treated with vildagliptin (NDOVil and HFOVil) was still in the same level as that in the NDO and HFO groups (Table 1).

HFD rats showed a significant increase in body weight, compared with the ND group. Orchiectomized rats had significantly decreased body weight and visceral fat, compared with the sham rats in the same dietary groups. Interestingly, testosterone replacement significantly increased only the body weight in NDOT and HFOT rats, but not visceral fat, compared with that in NDO and HFO groups, whereas vildagliptin treatment did not show any beneficial effects on body weight or visceral fat in NDOVil and HFOVil groups (Table 1). Moreover, peripheral insulin resistance developed only in the HFD groups (HFS and HFO), as shown by both increased plasma insulin levels and HOMA index, whereas total cholesterol levels and plasma LDL cholesterol levels were increased and plasma HDL cholesterol levels were decreased, compared with those of the NDS group (Table 1). No additive adverse effect in these parameters was found in the HFO group, compared with those in the HFS group, except in the case of plasma total cholesterol. Unlike rats in the HFD groups, NDO group did not have any significant alteration in these metabolic parameters, compared with the NDS group. These findings suggest that peripheral insulin resistance did not develop in the NDO rats.

Interestingly, testosterone replacement attenuated the severity of peripheral insulin resistance in the HFOT group, by decreasing plasma insulin levels and HOMA index, decreasing total cholesterol levels and decreasing plasma LDL cholesterol levels, whereas vildagliptin demonstrated the same beneficial effects in these parameters as well as increasing plasma HDL cholesterol levels in the HFOVil group, compared with the HFO group (Table 1). These findings suggest that testosterone replacement and vildagliptin treatment could attenuate

Table 1 Effects of testosterone and vildagliptin on metabolic parameters in testosterone-deprived rats at the end of week 16 (n=4–6/group).

	Normal diet				High-fat diet			
Parameters	NDS	NDO	NDOT	NDOVil	HFS	HFO	HFOT	HFOVil
Body weight (g)	517±11	456±11[a]	494±2[b]	452±14[a]	605±16[a]	526±18[b,c]	572±17[a,d,e]	522±17[c,f]
Visceral fat (g)	36.3±3.4	21.4±1.7[a]	24±1.8[a]	19.9±2.5[a]	64.5±2.0[a]	41.6±1.5[b,c]	43.4±2.5[a,c,e]	41.5±2.0[c,f]
Plasma testosterone (ng/mL)	2.9±0.5	<0.025[a]	3.4±0.5[b]	<0.025[a]	0.5±0.1[a]	<0.025[c]	3.9±0.7[c,d]	<0.025[c]
Seminal vesicle ratio (×10³)	4.10±0.02	0.23±0.02[a]	4.06±0.1	0.23±0.02[a]	2.75±0.14[a]	0.14±0.01[a,c]	4.20±0.4	0.4±0.2[a,c]
Plasma insulin (ng/mL)	2.15±0.2	2.2±0.3	2.02±0.34	1.93±0.36	3.70±0.42[a]	3.58±0.77[a]	1.94±0.40[c,d]	1.98±0.3[c,d]
Plasma glucose (mg/dL)	184.2±17.6	173±7.1	174±19.8	179.4±8.7	163.5±12.4	184.7±8.8	178.7±9.0	179.6±11.3
HOMA index	18.7±2.5	19.8±3.2	19.1±3.5	19.9±1.8	32.25±3.7[a]	35.5±9.9[a]	16.1±2.1[c,d]	18.6±1.9[c,d]
Plasma total cholesterol (mg/dL)	59.2±1.6	62.7±2.3	57.1±3.9	59.3±4.1	87.5±4.5[a]	101.2±4.8[a,c]	75.1±6.3[a,d]	80.8±6.6[a,d]
Plasma triglyceride (mg/dL)	84.1±6.5	83.3±14.0	82.8±4.7	80.1±5.7	91.1±13.8	81.6±6.2	86.6±11.2	83.2±5.2
Plasma HDL (mg/dL)	33.3± 1.6	36.4±1.4	31.4±2.1	34±1.3	23.8±2.5[a]	25.7±2.0[a]	25.3±2.1[a]	33.7±2.4[c,d]
Plasma LDL (mg/dL)	8.4±2.3	9.5±2.7	8.5±1.0	10.1±3.0	33.5±5.7[a]	54.4±5.6[a]	37.3±4.3[a,d]	37.7±4[a,d]

HFO, high-fat diet+orchiectomy; HFOT, high-fat diet+orchiectomy+testosterone; HFOVil, high-fat diet+orchiectomy+vildagliptin; HFS, high-fat diet+sham surgery; HOMA, Homeostasis Model Assessment; MDA, malondialdehyde; NDO, normal diet+orchiectomy; NDOT, normal diet+orchiectomy+testosterone; NDOVil, normal diet+orchiectomy+vildagliptin; NDS, normal diet+sham surgery.
[a]P<0.05 vs NDS, [b]P<0.05 vs NDO, [c]P<0.05 vs HFS, [d]P<0.05 vs HFO, [e]P<0.05 vs NDOT, [f]P<0.05 vs NDOVil.

http://joe.endocrinology-journals.org
DOI: 10.1530/JOE-16-0232
© 2016 Society for Endocrinology
Printed in Great Britain
Published by Bioscientifica Ltd.

peripheral insulin resistance in testosterone-deprived rats with obese insulin resistance by improving both insulin sensitivity and lipid profiles.

Testosterone and vildagliptin preserved both LV function and HRV in testosterone-deprived rats with obese insulin resistance before I/R injury

At week 12, LV dysfunction and sympathovagal imbalance were found in the NDO, HFS and HFO groups as indicated by decreased %fractional shortening (Fig. 2A) and increased LF/HF ratio (Fig. 2C), compared with the NDS group. At week 16, impaired LV function and cardiac sympathovagal imbalance were found in NDO, HFS and HFO groups, and these parameters were not different between groups (Fig. 2B and D). Moreover, our results demonstrated that both testosterone replacement and vildagliptin treatment could preserve LV function and HRV by increased %fractional shortening and decreased the LF/HF ratio in NDOT and NDOVil groups and HFOT and HFOVil groups, compared with that in NDO and HFO groups, respectively. No significant differences in

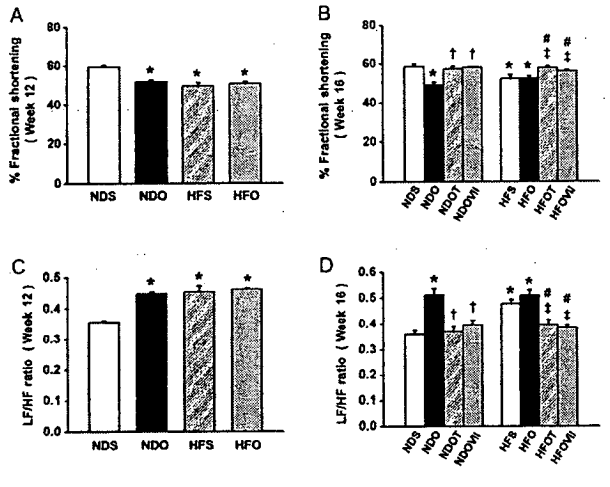


Figure 2
Effects of obese insulin resistance induced by long-term high-fat diet (HFD) consumption and testosterone deprivation at 12 weeks followed by testosterone and vildagliptin replacement on fractional shortening (FS) and heart rate variability (represented as low frequency/high frequency ratio: LF/HF ratio) before I/R injury. (A and B) Testosterone and vildagliptin restored the FS after treatment for 4 weeks, compared with the NDO and HFO groups. (C and D) Testosterone and vildagliptin reduced LF/HF ratio after treatment for 4 weeks, compared with the NDO or HFO groups. (*$P<0.05$ vs NDS, †$P<0.05$ vs NDO, ‡$P<0.05$ vs HFS, #$P<0.05$ vs HFO). HFO, high fat + orchiectomy; HFOT, high fat + orchiectomy + testosterone; HFOVil, high fat + orchiectomy + testosterone; HFS, high fat + sham; NDO, normal diet + orchiectomy; NDOT, normal diet + orchiectomy + testosterone; NDOVil, normal diet + orchiectomy + vildagliptin; NDS, normal diet + sham.

Table 2 Effects of testosterone and vildagliptin on cardiac function (at baseline) during I/R injury ($n=4$–6/group).

	Normal diet				High-fat diet			
Cardiac function parameters	NDS	NDO	NDOT	NDOVil	HFS	HFO	HFOT	HFOVil
Heart rate (bpm)	266 ± 9	229 ± 17	241 ± 4	262 ± 9	248 ± 18	266 ± 8	265 ± 20	267 ± 8
LVESP (mmHg)	96 ± 5	92 ± 4	95 ± 11	95 ± 8	95 ± 11	90 ± 9	87 ± 3	98 ± 7
LVEDP (mmHg)	9.8 ± 2	13 ± 1	12 ± 2	11.9 ± 2	14.5 ± 5	14.6 ± 3	10.9 ± 3	13.4 ± 1
Pmax (mmHg)	103 ± 4	97 ± 6	96 ± 9	103 ± 7	108 ± 9	104 ± 7	94 ± 4	129 ± 10
Pmin (mmHg)	6.3 ± 4	7.6 ± 1	11 ± 5	10.8 ± 4	8.3 ± 6	9.7 ± 3	7.3 ± 3	10.1 ± 2
dP/dtmax (mmHg/s)	224,872 ± 5629	203,491 ± 3578	181,951 ± 9509	227,987 ± 7890	233,037 ± 7611	223,466 ± 8889	235,131 ± 8404	235,582 ± 9330
dP/dtmin (mmHg/s)	−4649 ± 939	−5073 ± 319	−4461 ± 746	−5474 ± 676	−4630 ± 703	−4619 ± 670	−4724 ± 432	−4679 ± 1356
Stroke volume (μL)	542 ± 39	533 ± 15	501 ± 32	528 ± 19	511 ± 15	510 ± 6	530 ± 6	522 ± 5

BP, blood pressure; HFO, high-fat diet + orchiectomy; HFOT, high-fat diet + orchiectomy + testosterone; HFOVil, high-fat diet + orchiectomy + vildagliptin; HFS, high-fat diet + sham surgery; LVEDP, left ventricular end-diastolic pressure; LVESP, left ventricular end-systolic pressure; NDO, normal diet + orchiectomy; NDOT, normal diet + orchiectomy + testosterone; NDOVil, normal diet + orchiectomy + vildagliptin; NDS, normal diet + sham surgery.
[a]$P<0.05$ vs NDS, [b]$P<0.05$ vs NDO, [c]$P<0.05$ vs HFS, [d]$P<0.05$ vs HFO.

http://joe.endocrinology-journals.org
DOI: 10.1530/JOE-16-0232
© 2016 Society for Endocrinology
Printed in Great Britain
Published by Bioscientifica Ltd.

http://joe.endocrinology-journals.org
DOI: 10.1530/JOE-16-0232

© 2016 Society for Endocrinology
Printed in Great Britain

Published by Bioscientifica Ltd.

Table 3 Effects of testosterone and vildagliptin on cardiac function (during the ischemic period) in I/R injury (n=4–6/group).

Cardiac function parameters	Normal diet				High-fat diet			
	NDS	NDO	NDOT	NDOVil	HFS	HFO	HFOT	HFOVil
Heart rate (bpm)	235±10	224±10	219±10	235±6	276±30	252±13	227±23	268±31
LVESP (mmHg)	85±2	83±7	76±3	88±12	93±12	94.8±4	84±8	103±18
LVEDP (mmHg)	11.8±1	21.5±1[a]	15±1[b]	14±4[b]	17.5±1[a]	22.9±2[a,c]	15.8±2[d]	14.5±0.3[c,d]
Pmax (mmHg)	96±5	104±6	92±8	96±11	86±13	84±14	89±6	93±21
Pmin (mmHg)	8.7±0.5	15.5±1	9.8±2	8.4±5	14±2	15.5±2	14.1±2	13.2±1
dP/dtmax (mmHg/s)	219,674±10,070	210,125±25,306	230,472±12,896	227,641±11,834	250,833±7793	231,060±9081	245,777±11,270	229,512±13,480
dP/dtmin (mmHg/s)	−4321±18	−3124±233[a]	−4067±310[b]	−4851±352[b]	−3455±465	−3014±624	−3664±683	−4197±1237
Stroke volume (μL)	436±65	319±12[a]	467±49[b]	363±12[b]	327±10[a]	257±10[a,c]	341±18[d]	344±41[d]

BP, blood pressure; HFO, high-fat diet+orchiectomy; HFOT, high-fat diet+orchiectomy+testosterone; HFOVil, high-fat diet+orchiectomy+vildagliptin; HFS, high-fat diet+sham surgery; LVEDP, left ventricular end-diastolic pressure; LVESP, left ventricular end-systolic pressure; NDO, normal diet+orchiectomy; NDOT, normal diet+orchiectomy+testosterone; NDOVil, normal diet+orchiectomy+vildagliptin; NDS, normal diet+sham surgery.
[a]P<0.05 vs NDS, [b]P<0.05 vs NDO, [c]P<0.05 vs HFS, [d]P<0.05 vs HFO.

Table 4 Effects of testosterone and vildagliptin on cardiac function (during reperfusion period) in I/R injury (n=4–6/group).

Cardiac function parameters	Normal diet				High-fat diet			
	NDS	NDO	NDOT	NDOVil	HFS	HFO	HFOT	HFOVil
Heart rate (bpm)	244±9	202±4	208±15	210±23	200±20	215±8	210±22	212±16
LVESP (mmHg)	82±6	90±4	92±4	100±7	104±1	94±3[c]	96±4	95±9
LVEDP (mmHg)	11±4	21.1±2[a]	15.5±1[b]	15.3±1[b]	19±2[a]	20.7±2[a]	11.1±2[c,d]	13.8±1[c,d]
Pmax (mmHg)	97±9	97±4	98±3	105±4	107±1	100±5	106±4	97±9
Pmin (mmHg)	7.3±4	15±2	10.3±1	13±3	14.8±2	16.7±1	9.8±4	13±1
dP/dtmax (mmHg/s)	225,758±12,862	241,918±8443	187,639±43,417	229,454±11,118	246,268±13,276	233,425±9741	250,021±11,877	225,561±12,186
dP/dt min (mmHg/s)	−4270±313	−2933±141[a]	−4040±77[b]	−3584±139[b]	−2051±345[a]	−1821±601[a]	−3647±352[c,d]	−3147±452[c,d]
Stroke volume (μL)	312±46	207±19[a]	368±8[b]	426±73[b]	193±39[a]	191±30[a]	319±24[c,d]	335±48[c,d]

BP, blood pressure; HFO, high-fat diet+orchiectomy; HFOT, high-fat diet+orchiectomy+testosterone; HFOVil, high-fat diet+orchiectomy+vildagliptin; HFS, high-fat diet+sham surgery; LVEDP, left ventricular end-diastolic pressure; LVESP, left ventricular end-systolic pressure; NDO, normal diet+orchiectomy; NDOT, normal diet+orchiectomy+testosterone; NDOVil, normal diet+orchiectomy+vildagliptin; NDS, normal diet+sham surgery.
[a]P<0.05 vs NDS, [b]P<0.05 vs NDO, [c]P<0.05 vs HFS, [d]P<0.05 vs HFO.

%fractional shortening and LF/HF ratio were found with testosterone and vildagliptin treatment in all groups (Fig. 2B and D). These findings suggest that testosterone replacement and vildagliptin treatment could preserve LV function and HRV by increasing %fractional shortening and decreasing the LF/HF ratio in testosterone-deprived rats with obese insulin resistance.

Testosterone and vildagliptin preserved LV function during I/R injury in testosterone-deprived rats with obese insulin resistance

The changes in LV function parameters during I/R injury are shown in Tables 2,3 and 4. At the baseline, LV functions were not different between any groups (Table 2). During I/R injury (at the end of ischemia), the NDO group had increased LVEDP and dP/dtmin as well as decreased stroke volume, compared with the NDS group. Interestingly, testosterone and vildagliptin treatment in the ND group significantly decreased LVEDP, dP/dtmin and increased stroke volume, compared with the NDO group. In addition, the HFD group (HFS and HFO group) had increased LVEDP and deceased stroke volume compared with the NDS group. However, the HFO group demonstrated greater severity in these parameters than the HFS group. Both testosterone and vildagliptin treatment in the HFD group could attenuate LV dysfunction by significantly decreasing LVEDP and increasing stroke volume, compared with that in the HFO group (Table 3). At the end of reperfusion, most parameters remained similar to those during the ischemic period except that rats in the HFO group had decreased LVESP, compared with those in the HFS group, suggesting that testosterone and vildagliptin treatment in the HFD group could attenuate LV dysfunction by significantly decreasing LVEDP, dp/dtmin and increasing stroke volume, when compared with the HFO group (Table 4). These findings suggest that testosterone replacement and vildagliptin treatment could attenuate LV dysfunction by decreasing diastolic dysfunction and increasing stroke volume in testosterone-deprived rats with obese insulin resistance.

Testosterone replacement and vildagliptin decreased the occurrence of cardiac arrhythmias in testosterone-deprived rats with obese insulin resistance during I/R injury

The VT/VF incidence during I/R injury was not different between groups (Fig. 3A). However, in the NDO group,

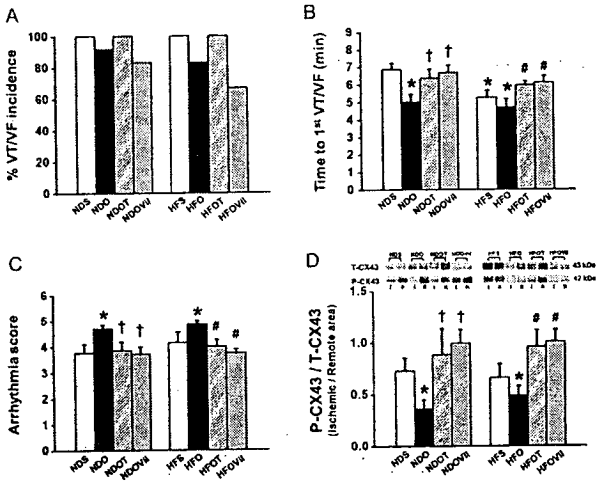


Figure 3
Effects of testosterone and vildagliptin on the occurrence of cardiac arrhythmia during the ischemic-reperfusion period in a normal diet-fed, obese insulin-resistant with testosterone deprivation model. Testosterone and vildagliptin did not reduce: (A) VT/VF incidence in normal diet and obese insulin-resistant and testosterone-deprived rats but reduced cardiac arrhythmia by increasing (B) time to 1st VT/VF incidence and decreased (C) arrhythmia score, when compared with the NDO or HFO groups. (D) Testosterone and vildagliptin increased P-Cx43/T-Cx43 ratio when compared with the NDO and HFO groups. (*$P<0.05$ vs NDS, †$P<0.05$ vs NDO, #$P<0.05$ vs HFO). HFO, high fat + orchiectomy; HFOT, high fat + orchiectomy + testosterone; HFOVil, high fat + orchiectomy + testosterone; HFS, high fat + sham; I, ischemic area; NDO, normal diet + orchiectomy; NDOT, normal diet + orchiectomy + testosterone; NDOVil, normal diet + orchiectomy + vildagliptin; NDS, normal diet + sham; R, remote area; VF, ventricular fibrillation; VT, ventricular tachycardia.

the time to first VT/VF onset was significantly decreased, whereas the arrhythmia score was significantly greater, compared with the NDS group. Interestingly, testosterone replacement and vildagliptin treatment significantly reduced cardiac arrhythmia by increasing the time to 1st VT/VF (Fig. 3B) and reducing the arrhythmia score during I/R injury (Fig. 3C), when compared with the NDO group. The HFS group demonstrated a decreased time to 1st VT/VF and showed no difference in arrhythmia score, compared with the NDS group, whereas the HFO group demonstrated a decreased time to the 1st VT/VF and increased arrhythmia during I/R injury, compared with the NDS group. However, time to 1st VT/VF and arrhythmia score in the HFS and HFO group showed no difference. Interestingly, testosterone replacement and vildagliptin could increase the time to 1st VT/VF (Fig. 3B) and reduce arrhythmia score during I/R injury (Fig. 3C), compared with the HFO group.

Our study demonstrated that the phosphorylated Cx43 per total Cx43 ratio (P-Cx43/T-Cx43 ratio) of the ischemic-to-remote areas was significantly decreased

http://joe.endocrinology-journals.org
DOI: 10.1530/JOE-16-0232
© 2016 Society for Endocrinology
Printed in Great Britain
Published by Bioscientifica Ltd.

in NDO and HFO groups, whereas all treatment groups (NDOT, HFOT, NDOVil and HFOVil) had a significantly increased P-Cx43/T-Cx43 ratio, compared with sham rats being fed with the same diets (Fig. 3D). These findings suggest that both testosterone replacement and vildagliptin treatment can attenuate cardiac arrhythmia during I/R injury in testosterone-deprived rats with obese insulin resistance.

Testosterone replacement and vildagliptin treatment reduced the infarct size in the I/R heart of testosterone-deprived rats with obese insulin resistance

The area at risk (AAR) was not different between all groups. However, the infarct size of NDO, HFO and HFS groups were significantly greater compared with the NDS group. Interestingly, testosterone and vildagliptin reduced the infarct size by 35.7 and 44.1%, respectively, when compared with that in the NDO group and also a reduced infarct size by 55.4 and 49.5%, respectively, compared with that in the HFO group (Fig. 4A). Representative images of the infarct size are shown in Fig. 4B.

Western blot analysis demonstrated that the expression of pro-apoptotic/anti-apoptotic protein (Bax/Bcl-2 ratio) was markedly increased in NDO and HFO groups (Fig. 4C), whereas the expression of pro-caspase3 was not significantly different in the NDO and HFO groups (Fig. 4D), when compared with the NDS group. Interestingly, testosterone replacement and vildagliptin in ND and HFD decreased Bax/Bcl-2 ratio and increased pro-caspase3 expression, compared with the NDO and HFO groups, respectively (Fig. 4C and D). These findings suggest that testosterone replacement and vildagliptin treatment effectively reduced the infarct size by attenuating apoptotic processes in testosterone-deprived rats with obese insulin resistance.

Testosterone replacement and vildagliptin treatment attenuated mitochondrial dysfunction in the I/R heart of testosterone-deprived rats with obese insulin resistance

There were no differences among groups in ROS production levels, mitochondrial depolarization or mitochondrial swelling of cardiac mitochondria taken from the nonischemic myocardium. Cardiac mitochondria taken from the ischemic areas of the NDO, HFS and HFO groups had significantly increased mitochondrial ROS (Fig. 5A), increased mitochondrial depolarization indicated by a decrease in the red/green fluorescent intensity ratio (Fig. 5B), and increased mitochondrial swelling indicated by a decrease in absorbance at 540 nm (Fig. 5C), when compared with that from the NDS group.

Testosterone replacement and vildagliptin treatment in both ND and HFD groups attenuated mitochondrial dysfunction in the ischemic myocardium of all ORX groups as indicated by reduced ROS production (Fig. 5A), attenuated mitochondrial depolarization (Fig. 5B) and

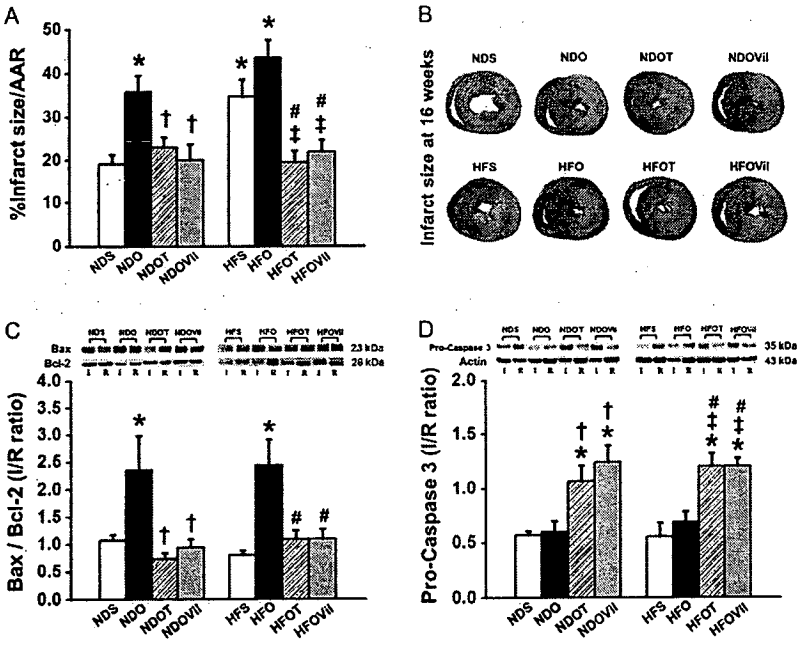


Figure 4
Effects of testosterone and vildagliptin on the infarct size, anti-apoptotic and pro-apoptotic proteins after ischemic-reperfusion period in a normal diet-fed, obese-insulin resistant with testosterone deprivation model. The area at risk (AAR) was not different between all groups. (A and B) Testosterone and vildagliptin reduced the infarct size by 35.7 and 44.1%, respectively, compared with those in the NDO group and reduced the infarct size by 55.4 and 49.5%, respectively, compared with those in the HFO group. Testosterone and vildagliptin attenuated apoptotic process (C) by decreasing pro-apoptotic/anti-apoptotic ratio (Bax/Bcl-2 ratio) and (D) increasing pro-caspase3 expression, compared with the NDO and HFO groups (*$P<0.05$ vs NDS, †$P<0.05$ vs NDO, ‡$P<0.05$ vs HFS, #$P<0.05$ vs HFO). HFO, high fat + orchiectomy; HFOT, high fat + orchiectomy + testosterone; HFOVil, high fat + orchiectomy + testosterone; HFS, high fat + sham; I, ischemic area; NDO, normal diet + orchiectomy; NDOT, normal diet + orchiectomy + testosterone; NDOVil, normal diet + orchiectomy + vildagliptin; NDS, normal diet + sham; R, remote area.

http://joe.endocrinology-journals.org
DOI: 10.1530/JOE-16-0232
© 2016 Society for Endocrinology
Printed in Great Britain
Published by Bioscientifica Ltd.

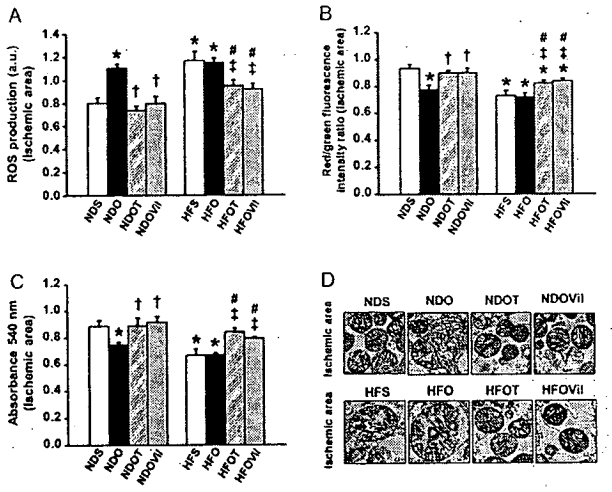


Figure 5
Effects of testosterone and vildagliptin on cardiac mitochondria after ischemic-reperfusion period in a normal diet-fed, obese insulin-resistant with testosterone deprivation model. Testosterone and vildagliptin improved cardiac mitochondrial function by (A) reducing reactive oxygen species (ROS) production, (B) attenuating mitochondrial membrane depolarization and (C) attenuating mitochondrial swelling in ischemic areas. (D) Testosterone and vildagliptin also attenuated the deterioration of cardiac mitochondrial morphology (*$P<0.05$ vs NDS, †$P<0.05$ vs NDO, ‡$P<0.05$ vs HFS, #$P<0.05$ vs HFO). HFO, high fat + orchiectomy; HFOT, high fat + orchiectomy + testosterone; HFOVil, high fat + orchiectomy + testosterone; HFS, high fat + sham; NDO, normal diet + orchiectomy; NDOT, normal diet + orchiectomy + testosterone; NDOVil, normal diet + orchiectomy + vildagliptin; NDS, normal diet + sham; ROS, reactive oxygen species.

reduced mitochondrial swelling (Fig. 5C), compared with the ORX group of the same diet regimen. Representative transmission electron microscope (TEM) pictures of cardiac mitochondria in the ischemic myocardium demonstrated that NDO, HFO and HFS groups had more severe mitochondrial swelling, which was indicated by abnormal morphology together with the loss of cristae in the cardiac mitochondrion, than the NDS and ORX group on testosterone or vildagliptin treatment (Fig. 5D). These findings suggest that testosterone replacement and vildagliptin treatment shared similar efficacy in attenuating the cardiac mitochondrial dysfunction by reducing cardiac mitochondrial ROS production, mitochondrial depolarization and mitochondrial swelling in the I/R hearts of testosterone-deprived rats with obese insulin resistance.

Discussion and conclusions

This study has demonstrated the potential cardioprotective effects of testosterone replacement and DPP-4 inhibitor on the I/R hearts of testosterone-deprived rats with obese insulin resistance. The major findings of this study are as follows. First, high-fat diet, but not testosterone deprivation, induced obese insulin resistance, whereas testosterone replacement and DPP-4 inhibitor (vildagliptin) treatment improved insulin sensitivity and metabolic parameters in testosterone-deprived rats with obese insulin resistance. Secondly, LV function and the HRV were impaired with testosterone deprivation in both obese and nonobese insulin resistance models. Thirdly, testosterone and vildagliptin provided cardioprotective effects in cases of testosterone deprivation alone and in a testosterone-deprived rat with obese insulin resistance model. Fourthly, during the I/R period, testosterone and vildagliptin exerted cardioprotective effects in a testosterone deprivation model and in a testosterone deprivation with obese insulin resistance model, identified by improving LV pressure and stroke volume, reducing cardiac arrhythmias, decreasing the infarct size and attenuating cardiac mitochondrial dysfunction caused by I/R injury.

This study demonstrated that testosterone deprivation alone (NDO group) neither induced insulin resistance nor had adverse effects on metabolic parameters. On the other hand, HFS and HFO groups developed insulin resistance, which is consistent with previous studies which reported that long-term consumption of a HFD caused obese insulin resistance, which is indicated both by increased plasma insulin levels and HOMA index (Pratchayasakul *et al.* 2011, Pintana *et al.* 2015, Pongkan *et al.* 2016). As the severity of insulin resistance at 16 weeks was not significantly different between the HFS and HFO group, this finding suggests that these two conditions were not additive in terms of insulin resistance. Therefore, this finding suggests that these two conditions were not additive in terms of insulin resistance. In this study, our results further demonstrated that testosterone deprivation also did not aggravate the severity of the cardiac impairments such as LV dysfunction and cardiac sympathovagal imbalance in the obese insulin resistant model.

In addition, low testosterone levels and obese insulin resistance are known as risk factors of cardiac dysfunction (Culic & Busic 2015) due mainly to increased oxidative stress (Hwang *et al.* 2011) in the heart, and leading to depressed HRV (Brook *et al.* 2010). Moreover, previous studies found the association of low testosterone and the increase in the reactive oxygen species (ROS) level (Pongkan *et al.* 2015, 2016). Lateef and coworkers demonstrated that low testosterone increased the

http://joe.endocrinology-journals.org
DOI: 10.1530/JOE-16-0232
© 2016 Society for Endocrinology
Printed in Great Britain
Published by Bioscientifica Ltd.

synthesis of nitric oxide (NO), which could upregulate urokinase plasminogen activation receptor (uPAR) expression, resulting in plasmin formation, which activates matrix metalloproteinase 9 (MMP-9), leading to extracellular matrix degradation resulting in increased ROS, especially in the mitochondria (Lateef *et al.* 2013). Moreover, they found that ROS production from extracellular matrix disruption also induced lipid peroxidation and caused the reduction of antioxidant levels such as glutathione reductase, catalase and glutathione-dependent enzyme (Lateef *et al.* 2013). When the accumulation of ROS in mitochondria reach a critical threshold level, it triggers the opening of the mitochondrial permeability transition pores (mPTP), resulting in induced mitochondrial membrane depolarization (Hausenloy *et al.* 2003). Moreover, the prolonged opening of mPTP could lead to an increase in the matrix osmotic pressure, resulting in mitochondrial swelling and/or mitochondrial membrane rupture. This will cause the release of pro-apoptotic cytochrome C and other pro-apoptotic proteins, leading to apoptotic cell death (Halestrap & Pasdois 2009). The increase in apoptotic cells induces the enlargement of myocardial infarct size and, as myocardial infarction plays an essential role in cardiac dysfunction, reduction in the infarct size would be of great benefit regarding contractility. This study is consistent with previous studies, demonstrating that NDO, HFS and HFO groups exhibit cardiac dysfunction and depressed HRV in both 12 and 16 weeks.

Regarding therapeutic outcomes, after treatment with a physiological dose of testosterone for 4 weeks, the level of plasma testosterone in the NDOT and HFOT groups was restored back to the same level as the NDS group, whereas plasma testosterone levels in the HFS was significantly lower than those in the NDS and testosterone-treated groups. In NDOVil and HFOVil groups, the level of testosterone was not altered. Interestingly, our study demonstrated that testosterone replacement and vildagliptin treatment in ORX rats with obese insulin resistance (HFO) improved insulin resistance by decreasing plasma insulin levels, HOMA index, total cholesterol levels and plasma LDL cholesterol levels. This is consistent with our previous studies (Apaijai *et al.* 2012, Pintana *et al.* 2015) as well as others (Traish *et al.* 2014, Bayram *et al.* 2016), which demonstrated that testosterone replacement and vildagliptin treatment could attenuate insulin resistance with testosterone deprivation with obese insulin resistance model. These findings suggest that vildagliptin gives beneficial effects similar to testosterone replacement by improving insulin resistance and other metabolic parameters in testosterone-deprived rats with obese insulin resistance. Moreover, decreasing insulin resistance in several anti-diabetic drugs of different classes such as metformin, liraglutide and vildagliptin demonstrated the cardioprotective effect (Apaijai *et al.* 2012, 2014, Barreto-Vianna *et al.* 2016). However, DPP-4 inhibitor itself might exert direct beneficial effects on the cardiomyocyte, for example, promote the endothelial cell function and upregulate protein expression resulting in cardioprotection (Giannocco *et al.* 2013, Ishii *et al.* 2014).

In addition to the benefits on metabolic parameters, testosterone replacement and vildagliptin treatment also exhibited similar beneficial effects on cardiac function and HRV in ORX rats with/without obese insulin resistance (HFO and NDO groups) by increasing %fractional shortening and decreasing the LF/HF ratios, respectively, when compared with the ORX group. Although previous studies demonstrated that either testosterone or vildagliptin exerted beneficial effects on cardiac function in HFO and NDO groups in a testosterone-deprived model (Pongkan *et al.* 2015), obese-insulin resistance model (Apaijai *et al.* 2012, 2014) and testosterone-deprived with obese-insulin resistance model (Francomano *et al.* 2014), our study is the first to compare the efficacy of testosterone replacement and vildagliptin for their cardioprotection. Regarding the effects of testosterone replacement and vildagliptin on the suppression of mitochondrial ROS production and apoptosis, previous studies demonstrated that either testosterone (Hwang *et al.* 2011, Zhang *et al.* 2013, Pintana *et al.* 2015) or vildagliptin (Avila Dde *et al.* 2013, Apaijai *et al.* 2014, Chinda *et al.* 2014) could effectively reduce ROS generation and suppressed oxidative stress. In addition, Alessandro and coworkers reported that testosterone decreased ROS production by binding to cytoplasmic androgen receptor (AR) and promoting its translocation to the nucleus, resulting in enhanced extracellular matrix (ECM) production via the transcription-inducing complex c-FOS/c-JUN (Bertolo *et al.* 2014). Moreover, previous studies demonstrated that both testosterone (Mancini *et al.* 2008, Zhang *et al.* 2013) and vildagliptin (Avila Dde *et al.* 2013, El-Sherbeeny & Nader 2016) could decrease oxidative stress by increasing the antioxidative substance such as catalase (CAT), superoxide dismutase (SOD) and glutathione peroxidase (GPx). This hypothesis is supported by the findings in this study that HFO and NDO groups had increased cardiac mitochondrial ROS production and that both testosterone and vildagliptin effectively attenuated cardiac mitochondrial ROS levels and reduced mitochondrial dysfunction (Chinda *et al.* 2014, Pongkan *et al.* 2015). Therefore, it is possible

http://joe.endocrinology-journals.org
DOI: 10.1530/JOE-16-0232
© 2016 Society for Endocrinology
Printed in Great Britain
Published by Bioscientifica Ltd.

that the enhancement of the antioxidant defense system and reduction in the levels of oxidative stress of testosterone and vildagliptin could be responsible for their cardioprotection. As both testosterone replacement and vildagliptin share similar efficacy in cardioprotection, these findings could provide an implication for future clinical treatment options in those patients who cannot be treated with testosterone.

During the I/R injury, the results clearly demonstrated that the HFS, HFO and NDO groups demonstrated an impairment of LV function, whereas either testosterone or vildagliptin exerted similar efficacy in cardioprotection in this case. This could be due to their similar efficacy in reducing the infarct size and improving cardiac mitochondrial function, which was impaired during I/R injury. Moreover, as myocardial infarct size has been shown to be associated with the severity of left ventricular dysfunction (Chinda *et al.* 2014), reduction in the infarct size would be of great benefit regarding improved LV function. In this study, HFS, HFO and NDO groups demonstrated a larger infarct size/area at risk than NDS group. Interestingly, either testosterone or vildagliptin exerted similar efficacy in reducing the infarct size in this case. Previous studies on myocardial apoptosis attenuation demonstrated that testosterone replacement could reduce the myocardial infarct size and the potential mechanism could be due to reduced apoptosis and the reduction of cardiac mitochondrial dysfunction, which was demonstrated that testosterone attenuated myocardial apoptosis by increasing anti-apoptotic (Bcl-2) proteins and reducing pro-apoptotic (Bax) proteins (Pongkan *et al.* 2015). Moreover, Huang and coworkers demonstrated that chronic exogenous testosterone replacement improved cardiac function via Akt/PKB signaling pathway resulting in decreased pro-apoptotic (Bax, Fas-L protein) and increased anti-apoptotic proteins (Bcl-2, p-Bad, p-FOXO3a) in isolated heart investigation (Huang *et al.* 2010). For vildagliptin, it has been shown that this drug reduced the infarct size by attenuating myocardial apoptosis via increased anti-apoptotic (Bcl-2) proteins (Apaijai *et al.* 2014, Chinda *et al.* 2014), increased pro-caspase 3 (Chinda *et al.* 2014) and decreased pro-apoptotic (Bax) proteins (Apaijai *et al.* 2014) in I/R injury model as well as renal ischemia–reperfusion injury model (Glorie *et al.* 2012). Moreover, treatment with DPP4 inhibitor in obese, prediabetic (DIO) rats for 4 weeks has been shown to reduce myocardial infarct size after I/R via an increase of the phosphorylation of Akt/PKB signaling proteins, which involved in the RISK (reperfusion-induced salvage kinase) pathway (Huisamen *et al.* 2011). Consistent with previous studies, our results demonstrated that testosterone and vildagliptin attenuated cardiac mitochondrial dysfunction, which is indicated by decreased mitochondrial ROS production, mitochondrial depolarization and mitochondrial swelling as well as attenuated myocardial apoptosis by decreased Bax/Bcl-2 ratio and increased pro-caspase3 expression. This study also showed that I/R injury induced apoptosis by decreasing pro-caspase3, which is consistent with previous reports in models of I/R injury and obesity (Lu *et al.* 2007, 2016). Increased pro-caspase3 has been shown to play a beneficial role to the cell and acts as the critical point of apoptotic process because pro-caspase3 is an inactive form until it is converted to cleaved caspase3, which is an active form that induced apoptosis (Earnshaw *et al.* 1999, Peterson *et al.* 2009, Walters *et al.* 2009). Mitochondria are the organelles, which play an essential role in cell survival as well as regulation of cell death, especially in cardiomyocytes and increasing intracellular oxidative stress during I/R injury could lead to cardiomyocyte swelling and death (Pongkan *et al.* 2015). In this study, we are reporting for the first time similar beneficial effects of testosterone replacement and vildagliptin during I/R injury in an HFO model, and our findings demonstrate that vildagliptin exhibited similar beneficial effects on the infarct size reduction and improved cardiac mitochondrial function during I/R injury as did testosterone replacement in the HFO and NDO models.

Regarding cardiac arrhythmias, as cardiac mitochondrial depolarization and decreased phosphorylation of Cx43 have been shown to facilitate cardiac arrhythmias (Aon *et al.* 2009, Chinda *et al.* 2014), interventions that prevent these two events could attenuate the arrhythmia incidence (Maruyama *et al.* 2016). Our previous studies (Apaijai *et al.* 2014, Pongkan *et al.* 2015) also demonstrated that both testosterone and vildagliptin could attenuate mitochondrial depolarization and increased phosphorylation of Cx43. Our results in this study demonstrated that the ORX groups were more susceptible to arrhythmias as indicated by decreased time to 1st VT/VF onset and increased arrhythmia scores compared with the sham group of its own diet assignment. As treated groups (NDOT, NDOVil, HFOT and HFOVil) had longer times to 1st VT/VF onset and lower arrhythmia scores, compared with the ORX group, these findings indicated that testosterone and vildagliptin exerted similar antiarrhythmic effects in NDO and HFO groups during I/R injury.

http://joe.endocrinology-journals.org
DOI: 10.1530/JOE-16-0232
© 2016 Society for Endocrinology
Printed in Great Britain
Published by Bioscientifica Ltd.

Journal of Endocrinology

In conclusion, before I/R injury, vildagliptin treatment exhibits similar cardioprotective efficacy as testosterone replacement in testosterone-deprived rats with obese insulin resistance caused by long-term consumption of a HFD, by improving cardiac sympathovagal balance and LV function. During I/R injury, vildagliptin treatment and testosterone replacement also exerted similar cardioprotective effects by ameliorating left ventricular dysfunction and reducing the infarct size and cardiac arrhythmias caused by I/R injury under testosterone deprivation with obese insulin-resistant conditions. These beneficial effects of both testosterone and vildagliptin were due to their ability to increase Cx43 phosphorylation and attenuate cardiac mitochondrial dysfunction and cardiomyocyte apoptosis. These findings suggest that vildagliptin may be used as an alternative to testosterone in testosterone-deprived subjects with or without obese insulin resistance. Whether the combined treatment of vildagliptin and testosterone replacement would provide the synergistic effects needs to be investigated in the future.

Declaration of interest

The authors declare that there is no conflict of interest that could be perceived as prejudicing the impartiality of the research reported.

Funding

This work was supported by the NSTDA Research Chair Grant from the National Science and Technology Development Agency Thailand (N C) and grants from the Thailand Research Fund BRG5780016 (S C), the Royal Golden Jubilee PhD Program (N C and W P), the National Research Council Thailand (N C) and the Chiang Mai University Center of Excellence Center Award (N C).

References

Aon MA, Cortassa S, Akar FG, Brown DA, Zhou L & O'Rourke B 2009 From mitochondrial dynamics to arrhythmias. *International Journal of Biochemistry and Cell Biology* **41** 1940–1948. (doi:10.1016/j.biocel.2009.02.016)

Apaijai N, Pintana H, Chattipakorn SC & Chattipakorn N 2012 Cardioprotective effects of metformin and vildagliptin in adult rats with insulin resistance induced by a high-fat diet. *Endocrinology* **153** 3878–3885. (doi:10.1210/en.2012-1262)

Apaijai N, Chinda K, Palee S, Chattipakorn S & Chattipakorn N 2014 Combined vildagliptin and metformin exert better cardioprotection than monotherapy against ischemia-reperfusion injury in obese-insulin resistant rats. *PLoS ONE* **9** e102374. (doi:10.1371/journal.pone.0102374)

Appleton DJ, Rand JS & Sunvold GD 2005 Basal plasma insulin and homeostasis model assessment (HOMA) are indicators of insulin sensitivity in cats. *Journal of Feline Medicine and Surgery* **7** 183–193. (doi:10.1016/j.jfms.2004.12.002)

Avila Dde L, Araujo GR, Silva M, Miranda PH, Diniz MF, Pedrosa ML, Silva ME, de Lima WG & Costa DC 2013 Vildagliptin ameliorates oxidative stress and pancreatic beta cell destruction in type 1 diabetic rats. *Archives of Medical Research* **44** 194–202. (doi:10.1016/j.arcmed.2013.03.004)

Barreto-Vianna AR, Aguila MB & Mandarim-de-Lacerda CA 2016 Effects of liraglutide in hypothalamic arcuate nucleus of obese mice. *Obesity* **24** 626–633. (doi:10.1002/oby.21387)

Bayram F, Elbuken G, Korkmaz C, Aydogdu A, Karaca Z & Cakir I 2016 The effects of gonadotropin replacement therapy on metabolic parameters and body composition in men with idiopathic hypogonadotropic hypogonadism. *Hormone and Metabolic Research* **48** 112–117. (doi:10.1055/s-0035-1564252)

Bertolo A, Baur M, Aebli N, Ferguson SJ & Stoyanov J 2014 Physiological testosterone levels enhance chondrogenic extracellular matrix synthesis by male intervertebral disc cells in vitro, but not by mesenchymal stem cells. *Spine Journal* **14** 455–468. (doi:10.1016/j.spinee.2013.10.018)

Brook RD, Rajagopalan S, Pope CA 3rd, Brook JR, Bhatnagar A, Diez-Roux AV, Holguin F, Hong Y, Luepker RV, Mittleman MA *et al.* 2010 Particulate matter air pollution and cardiovascular disease: an update to the scientific statement from the American Heart Association. *Circulation* **121** 2331–2378. (doi:10.1161/CIR.0b013e3181dbece1)

Chattipakorn N, Incharoen T, Kanlop N & Chattipakorn S 2007 Heart rate variability in myocardial infarction and heart failure. *International Journal of Cardiology* **120** 289–296. (doi:10.1016/j.ijcard.2006.11.221)

Chinda K, Sanit J, Chattipakorn S & Chattipakorn N 2014 Dipeptidyl peptidase-4 inhibitor reduces infarct size and preserves cardiac function via mitochondrial protection in ischaemia-reperfusion rat heart. *Diabetes & Vascular Disease Research* **11** 75–83. (doi:10.1177/1479164113516134)

Cornoldi A, Caminiti G, Marazzi G, Vitale C, Patrizi R, Volterrani M, Miceli M, Fini M, Spera G & Rosano G 2009 Effects of chronic testosterone administration on myocardial ischemia, lipid metabolism and insulin resistance in elderly male diabetic patients with coronary artery disease. *International Journal of Cardiology* **142** 50–55. (doi:10.1016/j.ijcard.2008.12.107)

Culic V & Busic Z 2015 Testosterone may influence left ventricular diastolic function depending on previous myocardial infarction and smoking. *International Journal of Cardiology* **186** 67–71. (doi:10.1016/j.ijcard.2015.03.238)

Curtis MJ, Hancox JC, Farkas A, Wainwright CL, Stables CL, Saint DA, Clements-Jewery H, Lambiase PD, Billman GE, Janse MJ *et al.* 2013 The Lambeth Conventions (II): guidelines for the study of animal and human ventricular and supraventricular arrhythmias. *Pharmacology & Therapeutics* **139** 213–248. (doi:10.1016/j.pharmthera.2013.04.008)

Ducimetiere P, Eschwege E, Papoz L, Richard J, Claude J & Rosselin G 1980 Relationship of plasma insulin levels to the incidence of myocardial infarction and coronary heart disease mortality in a middle-aged population. *Diabetologia* **19** 205–210.

Earnshaw WC, Martins LM & Kaufmann SH 1999 Mammalian caspases: structure, activation, substrates, and functions during apoptosis. *Annual Review of Biochemistry* **68** 383–424. (doi:10.1146/annurev.biochem.68.1.383)

El-Sherbeeny NA & Nader MA 2016 The protective effect of vildagliptin in chronic experimental cyclosporine A-induced hepatotoxicity. *Canadian Journal of Physiology and Pharmacology* **94** 251–256. (doi:10.1139/cjpp-2015-0336)

Espinola-Klein C, Gori T, Blankenberg S & Munzel T 2011 Inflammatory markers and cardiovascular risk in the metabolic syndrome. *Frontiers in Biosciences* **16** 1663–1774. (doi:10.2741/3812)

Flegal KM, Carroll MD, Kit BK & Ogden CL 2012 Prevalence of obesity and trends in the distribution of body mass index among US adults, 1999–2010. *JAMA* **307** 491–497. (doi:10.1001/jama.2012.39)

Foley PL 2005 Common surgical procedures in rodents. In *Laboratory Animal Medicine and Management*. Eds JD Reuter & MA Suckow.

© 2016 Society for Endocrinology
Printed in Great Britain
Published by Bioscientifica Ltd.

Office of Animal Research Education and Compliance. University of Virginia, Charlottesville, VA, USA: International Veterinary Information Service, Ithaca, NY, USA. (www.ivis.org)

Francomano D, Bruzziches R, Barbaro G, Lenzi A & Aversa A 2014 Effects of testosterone undecanoate replacement and withdrawal on cardio-metabolic, hormonal and body composition outcomes in severely obese hypogonadal men: a pilot study. *Journal of Endocrinological Investigation* **37** 401–411. (doi:10.1007/s40618-014-0066-9)

Friedewald WT, Levy RI & Fredrickson DS 1972 Estimation of the concentration of low-density lipoprotein cholesterol in plasma, without use of the preparative ultracentrifuge. *Clinical Chemistry* **18** 499–502.

Garrido P, Salehzadeh F, Duque-Guimaraes DE & Al-Khalili L 2014 Negative regulation of glucose metabolism in human myotubes by supraphysiological doses of 17beta-estradiol or testosterone. *Metabolism* **63** 1178–1187. (doi:10.1016/j.metabol.2014.06.003)

Giannocco G, Oliveira KC, Crajoinas RO, Venturini G, Salles TA, Fonseca-Alaniz MH, Maciel RM & Girardi AC 2013 Dipeptidyl peptidase IV inhibition upregulates GLUT4 translocation and expression in heart and skeletal muscle of spontaneously hypertensive rats. *European Journal of Pharmacology* **698** 74–86. (doi:10.1016/j.ejphar.2012.09.043)

Glorie LL, Verhulst A, Matheeussen V, Baerts L, Magielse J, Hermans N, D'Haese PC, De Meester I & De Beuf A 2012 DPP4 inhibition improves functional outcome after renal ischemia-reperfusion injury. *American Journal of Physiology: Renal Physiology* **303** F681–F688. (doi:10.1152/ajprenal.00075.2012)

Halestrap AP & Pasdois P 2009 The role of the mitochondrial permeability transition pore in heart disease. *Biochimica et Biophysica Acta* **1787** 1402–1415. (doi:10.1016/j.bbabio.2008.12.017)

Handelsman DJ & Zajac JD 2004 Androgen deficiency and replacement therapy in men. *Medical Journal of Australia* **180** 529–535.

Hausenloy DJ, Duchen MR & Yellon DM 2003 Inhibiting mitochondrial permeability transition pore opening at reperfusion protects against ischaemia-reperfusion injury. *Cardiovascular Research* **60** 617–625. (doi:10.1016/j.cardiores.2003.09.025)

Huang C, Gu H, Zhang W, Herrmann JL & Wang M 2010 Testosterone-down-regulated Akt pathway during cardiac ischemia/reperfusion: a mechanism involving BAD, Bcl-2 and FOXO3a. *Journal of Surgical Research* **164** e1–e11. (doi:10.1016/j.jss.2010.07.041)

Huisamen B, Genis A, Marais E & Lochner A 2011 Pre-treatment with a DPP-4 inhibitor is infarct sparing in hearts from obese, pre-diabetic rats. *Cardiovascular Drugs Therapy* **25** 13–20. (doi:10.1007/s10557-010-6271-7)

Hwang TI, Liao TL, Lin JF, Lin YC, Lee SY, Lai YC & Kao SH 2011 Low-dose testosterone treatment decreases oxidative damage in TM3 Leydig cells. *Asian Journal of Andrology* **13** 432–437. (doi:10.1038/aja.2010.159)

Ishii M, Shibata R, Kondo K, Kambara T, Shimizu Y, Tanigawa T, Bando YK, Nishimura M, Ouchi N & Murohara T 2014 Vildagliptin stimulates endothelial cell network formation and ischemia-induced revascularization via an endothelial nitric-oxide synthase-dependent mechanism. *Journal of Biological Chemistry* **289** 27235–27245. (doi:10.1074/jbc.M114.557835)

Kelly DM & Jones TH 2013 Testosterone: a vascular hormone in health and disease. *Journal of Endocrinology* **217** R47–R71. (doi:10.1530/joe-12-0582)

Krishnamoorthy A, Greiner MA, Bertoni AG, Eapen ZJ, O'Brien EC, Curtis LH, Hernandez AF & Mentz RJ 2016 The obesity and heart failure epidemics among African Americans: insights from the Jackson Heart Study. *Journal of Cardiac Failure* **22** 589–597. (doi:10.1016/j.cardfail.2016.03.004)

Lateef A, Khan AQ, Tahir M, Khan R, Rehman MU, Ali F, Hamiza OO & Sultana S 2013 Androgen deprivation by flutamide modulates uPAR, MMP-9 expressions, lipid profile, and oxidative stress: amelioration by daidzein. *Molecular and Cellular Biochemistry* **374** 49–59. (doi:10.1007/s11010-012-1504-7)

Lu MC, Tzang BS, Kuo WW, Wu FL, Chen YS, Tsai CH, Huang CY & Lee SD 2007 More activated cardiac mitochondrial-dependent apoptotic pathway in obese Zucker rats. *Obesity* **15** 2634–2642. (doi:10.1038/oby.2007.315)

Lu SF, Huang Y, Wang N, Shen WX, Fu SP, Li Q, Yu ML, Liu WX, Chen X, Jing XY *et al.* 2016 Cardioprotective effect of electroacupuncture pretreatment on myocardial ischemia/reperfusion injury via antiapoptotic signaling. *Evidence-Based Complementary and Alternative Medicine* **2016** 4609784. (doi:10.1155/2016/4609784)

Mancini A, Leone E, Festa R, Grande G, Silvestrini A, de Marinis L, Pontecorvi A, Maira G, Littarru GP & Meucci E 2008 Effects of testosterone on antioxidant systems in male secondary hypogonadism. *Journal of Andrology* **29** 622–629. (doi:10.2164/jandrol.107.004838)

Maruyama D, Hirata N, Tokinaga Y, Kawaguchi R & Yamakage M 2016 Nitrite reduces ischemia-induced ventricular arrhythmias by attenuating connexin 43 dephosphorylation in rats. *Anesthesia and Analgesia* **122** 410–417. (doi:10.1213/ANE.0000000000001063)

Ogden CL, Carroll MD, Fryar CD & Flegal KM 2015 Prevalence of obesity among adults and youth: United States, 2011–2014. *NCHS Data Brief* 1–8.

Peterson QP, Hsu DC, Goode DR, Novotny CJ, Totten RK & Hergenrother PJ 2009 Procaspase-3 activation as an anti-cancer strategy: structure-activity relationship of procaspase-activating compound 1 (PAC-1) and its cellular co-localization with caspase-3. *Journal of Medicinal Chemistry* **52** 5721–5731. (doi:10.1021/jm900722z)

Pintana H, Pongkan W, Pratchayasakul W, Chattipakorn N & Chattipakorn SC 2015 Testosterone replacement attenuates cognitive decline in testosterone-deprived lean rats, but not in obese rats, by mitigating brain oxidative stress. *Age* **37** 84. (doi:10.1007/s11357-015-9827-4)

Pongkan W, Chattipakorn SC & Chattipakorn N 2015 Chronic testosterone replacement exerts cardioprotection against cardiac ischemia-reperfusion injury by attenuating mitochondrial dysfunction in testosterone-deprived rats. *PLoS ONE* **10** e0122503. (doi:10.1371/journal.pone.0122503)

Pongkan W, Pintana H, Sivasinprasan S, Jaiwongkam T, Chattipakorn N & Chattipakorn SC 2016 Testosterone deprivation accelerates cardiac dysfunction in obese male rats. *Journal of Endocrinology* **229** 209–220. (doi:10.1530/JOE-16-0002)

Pratchayasakul W, Kerdphoo S, Petsophonsakul P, Pongchaidecha A, Chattipakorn N & Chattipakorn SC 2011 Effects of high-fat diet on insulin receptor function in rat hippocampus and the level of neuronal corticosterone. *Life Science* **88** 619–627. (doi:10.1016/j.lfs.2011.02.003)

Reckelhoff JF, Yanes LL, Iliescu R, Fortepiani LA & Granger JP 2005 Testosterone supplementation in aging men and women: possible impact on cardiovascular-renal disease. *American Journal of Physiology: Renal Physiology* **289** F941–F948. (doi:10.1152/ajprenal.00034.2005)

Rottman JN, Ni G & Brown M 2007 Echocardiographic evaluation of ventricular function in mice. *Echocardiography* **24** 83–89. (doi:10.1111/j.1540-8175.2006.00356.x)

Traish AM & Kypreos KE 2011 Testosterone and cardiovascular disease: an old idea with modern clinical implications. *Atherosclerosis* **214** 244–248. (doi:10.1016/j.atherosclerosis.2010.08.078)

Traish AM, Saad F & Guay A 2009 The dark side of testosterone deficiency: II. Type 2 diabetes and insulin resistance. *Journal of Andrology* **30** 23–32. (doi:10.2164/jandrol.108.005751)

Traish AM, Haider A, Doros G & Saad F 2014 Long-term testosterone therapy in hypogonadal men ameliorates elements of the metabolic

http://joe.endocrinology-journals.org
DOI: 10.1530/JOE-16-0232

© 2016 Society for Endocrinology
Printed in Great Britain

Published by Bioscientifica Ltd.

syndrome: an observational, long-term registry study. *International Journal of Clinical Practice* **68** 314–329. (doi:10.1111/ijcp.12319)

Valle MM, Graciano MF, Lopes de Oliveira ER, Camporez JP, Akamine EH, Carvalho CR, Curi R & Carpinelli AR 2011 Alterations of NADPH oxidase activity in rat pancreatic islets induced by a high-fat diet. *Pancreas* **40** 390–395. (doi:10.1097/MPA.0b013e31820569d0)

Walters J, Pop C, Scott FL, Drag M, Swartz P, Mattos C, Salvesen GS & Clark AC 2009 A constitutively active and uninhibitable caspase-3 zymogen efficiently induces apoptosis. *Biochemical Journal* **424** 335–345. (doi:10.1042/BJ20090825)

Wu FC & von Eckardstein A 2003 Androgens and coronary artery disease. *Endocrine Reviews* **24** 183–217. (doi:10.1210/er.2001-0025)

Zhang L, Lei D, Zhu GP, Hong L & Wu SZ 2013 Physiological testosterone retards cardiomyocyte aging in Tfm mice via androgen receptor-independent pathway. *Chinese Medical Sciences Journal* **28** 88–94. (doi:10.1016/S1001-9294(13)60028-0)

Received in final form 16 August 2016
Accepted 19 August 2016
Accepted Preprint published online 19 August 2016

http://joe.endocrinology-journals.org
DOI: 10.1530/JOE-16-0232

© 2016 Society for Endocrinology
Printed in Great Britain

Published by Bioscientifica Ltd.

เอกสารแนบหมายเลข 17

Hormones and Behavior 85 (2016) 86–95

Contents lists available at ScienceDirect

Hormones and Behavior

journal homepage: www.elsevier.com/locate/yhbeh

FGF21 improves cognition by restored synaptic plasticity, dendritic spine density, brain mitochondrial function and cell apoptosis in obese-insulin resistant male rats

Piangkwan Sa-nguanmoo [a,b], Pongpan Tanajak [a,b], Sasiwan Kerdphoo [a,b], Pattarapong Satjaritanun [a,b], Xiaojie Wang [c], Guang Liang [c], Xiaokun Li [c], Chao Jiang [c], Wasana Pratchayasakul [a,b], Nipon Chattipakorn [a,b], Siriporn C. Chattipakorn [a,d,*]

[a] Neurophysiology Unit, Cardiac Electrophysiology Research and Training Center Faculty of Medicine, Chiang Mai University, Chiang Mai, Thailand
[b] Department of Physiology, Faculty of Medicine, Chiang Mai University, Chiang Mai, Thailand
[c] School of Pharmaceutical Sciences, Wenzhou Medical University, University-Town, Wenzhou, Zhejiang, China
[d] Department of Oral Biology and Diagnostic Science, Faculty of Dentistry, Chiang Mai University, Chiang Mai, Thailand

ARTICLE INFO

Article history:
Received 11 March 2016
Revised 13 August 2016
Accepted 19 August 2016
Available online 24 August 2016

Keywords:
FGF21
Obese
Insulin resistance
Cognition
Brain mitochondria

ABSTRACT

Fibroblast growth factor 21 (FGF21) is an endocrine hormone which exerts beneficial effects on metabolic regulation in obese and diabetic models. However, the effect of FGF21 on cognition in obese-insulin resistant rats has not been investigated. We hypothesized that FGF21 prevented cognitive decline in obese-insulin resistant rats by improving hippocampal synaptic plasticity, dendritic spine density, brain mitochondrial function and brain FGF21 signaling as well as decreasing brain cell apoptosis. Eighteen male Wistar rats were divided into two groups, and received either a normal diet (ND) ($n = 6$) or a high fat diet (HFD) ($n = 12$) for 12 weeks. At week 13, the HFD-fed rats were subdivided into two subgroups (n = 6/subgroup) to receive either vehicle or recombinant human FGF21 (0.1 mg/kg/day) for four weeks. ND-fed rats were given vehicle for four weeks. At the end of the treatment, cognitive function, metabolic parameters, pro-inflammatory markers, brain mitochondrial function, cell apoptosis, hippocampal synaptic plasticity, dendritic spine density and brain FGF21 signaling were determined. The results showed that vehicle-treated HFD-fed rats developed obese-insulin resistance and cognitive decline with impaired hippocampal synaptic plasticity, decreased dendritic spine density, brain mitochondrial dysfunction and increased brain cell apoptosis. Impaired brain FGF 21 signaling was found in these obese-insulin resistant rats. FGF21-treated obese-insulin resistant rats had improved peripheral insulin sensitivity, increased hippocampal synaptic plasticity, increased dendritic spine density, restored brain mitochondrial function, attenuated brain cells apoptosis and increased brain FGF21 signaling, leading to a prevention of cognitive decline. These findings suggest that FGF21 treatment exerts neuroprotection in obese-insulin resistant rats.
© 2016 Elsevier Inc. All rights reserved.

1. Introduction

Long term consumption of a high fat diet (HFD) has been shown to result in obesity, which then causes insulin resistance (Fung et al., 2001; Riccardi et al., 2004). We previously found that male rats fed with a 12-week HFD not only developed peripheral insulin resistance, but also brain insulin resistance indicated by the impairment of brain insulin signaling and insulin-induced long-term depression (LTD) (Pipatpiboon et al., 2012; Pratchayasakul et al., 2011). In addition, we found that those rats had increased brain oxidative stress, brain mitochondrial dysfunction, decreased synaptic plasticity as well as dendritic spine density in the CA1 region of the hippocampus (Pintana et al., 2013, 2012; Pratchayasakul et al., 2015), which is the region of the brain that involves the learning and memory process. The dysfunction of hippocampal neurons has been shown to cause a loss of learning and memory (Winocur et al., 2005). Furthermore, other previous studies also demonstrated that long-term HFD consumption significantly increased brain damage, leading to impaired long-term potentiation (LTP), decreased dendritic spine at apical CA1 hippocampus region and resulting in impaired learning and memory (Beilharz et al., 2015; Stranahan et al., 2008).

Several clinical studies demonstrated that overweight or higher body mass index (BMI) is correlated with poor cognition and learning

* Corresponding author at: Neurophysiology Unit, Cardiac Electrophysiology Research and Training Center, Faculty of Medicine, Chiang Mai University, Department of Oral Biology and Diagnostic Sciences, Faculty of Dentistry Chiang Mai University, Chiang Mai 50200, Thailand.
E-mail addresses: scchattipakorn@gmail.com, siriporn.c@cmu.ac.th (S.C. Chattipakorn).

http://dx.doi.org/10.1016/j.yhbeh.2016.08.006
0018-506X/© 2016 Elsevier Inc. All rights reserved.

and memory deficits including impaired executive function performance in middle aged adults (Cournot et al., 2006; Elias et al., 2003; Sabia et al., 2009). In addition, longitudinal studies have shown that higher body composition and central obesity are related with cognitive decline, particularly in global cognitive function, executive function, and memory over time (Gunstad et al., 2010). Raji and colleagues also demonstrated that a higher BMI can cause brain atrophy in various regions including the frontal lobe, anterior cingulate gyrus, hippocampus and thalamus, when compared with people with normal BMI (Raji et al., 2010). Furthermore, the impaired memory and executive functioning has been reported in patients with type 1 and type 2 diabetes (Munshi et al., 2006; Northam et al., 2001; Reaven et al., 1990). In addition, Den and colleagues demonstrated that subjects with type 2 diabetes also had hippocampal and amygdala atrophy when compared with control subjects (den Heijer et al., 2003). All of these findings from clinical studies suggest that the implication of hippocampus occur following obese-insulin resistant condition.

Fibroblast growth factor 21 (FGF21) is an endocrine hormone and is mainly expressed in the liver, adipose tissues and pancreas (Kharitonenkov and Shanafelt, 2009; Nishimura et al., 2000). Previous studies found that FGF21 exerts beneficial effects on metabolic regulation such as the controlling of glucose levels and lipid homeostasis (Kharitonenkov et al., 2007; Kim et al., 2013; Lin et al., 2013; Xu et al., 2009a, 2009b). FGF21 activity is mediated by the fibroblast growth factor receptor (FGFR) and β-klotho (KLB), which is an essential co-receptor for FGF21 activity; therefore the cells lacking β-Klotho are unable to respond to FGF21 (Adams et al., 2012; Ogawa et al., 2007). When FGF21 binds with those receptors, it causes the activation of downstream targets, including the phosphorylation of fibroblast growth factor receptor substrate 2 (FRS2) and extracellular-signal-regulated kinases (ERK1/2). Previous studies found that administration of FGF21 into ob/ob mice, db/db mice, diet-induced obese (DIO) mice and diabetic monkeys led to improved metabolic parameters such as weight loss promotion, improved insulin sensitivity and lipid profile, reduced blood glucose without hypoglycemia and decreased insulin levels (Kharitonenkov et al., 2007; Kim et al., 2013; Lin et al., 2013; Xu et al., 2009a, 2009b). It has been shown that FGF21 levels were also increased under several pathological conditions including obesity, metabolic syndrome and diabetes (Bobbert et al., 2013; Mashili et al., 2011; Novotny et al., 2014; Zhang et al., 2008). A recent study investigated the effect of LY2405319, an FGF21 analog, in obese humans with type 2 diabetic subjects, and found that FGF21 could improve dyslipidemia, reduce body weight gain, reduce fasting plasma insulin levels and increase adiponectin levels (Gaich et al., 2013).

FGF21 is expressed in the brain and can be produced by glia cells and neurons (Johanna Mäkelä et al., 2014). In addition, FGF21 can cross the blood brain barrier following exogenous application and it has been detected in human cerebrospinal fluid (Hsuchou et al., 2007; Tan et al., 2011). FGF21 exerted neuroprotective effects, which were mediated by an increase in the levels of peroxisome proliferator activated receptor γ coactivator 1α (PGC1-α) and its activity (Johanna Mäkelä et al., 2014). Those events subsequently increased the levels of mitochondrial antioxidant enzymes and improved mitochondrial biogenesis and cell viability (Johanna Mäkelä et al., 2014). Moreover, FGF21 has been shown to preserve cognitive function in D-galactose-induced aging mice (Yu et al., 2015). Despite these beneficial effects of FGF21 on improving metabolic function in obese and diabetic animal models, little is known about its effect on brain function under an obese-insulin resistant condition.

However, the effects of FGF21 on cognitive function, which associated with brain oxidative stress, brain mitochondrial function, brain apoptosis, hippocampal synaptic plasticity and dendritic spine density in obese-insulin resistant male rats have not been investigated. Therefore, in this study, we hypothesized that the prevention of cognitive decline by FGF 21 in the obese-insulin resistant male rats is associated with its ability to improve peripheral insulin sensitivity, reduce systemic inflammation, restore brain mitochondrial function, decrease brain oxidative stress, decrease brain cell apoptosis and restore hippocampal synaptic plasticity.

2. Materials and methods

2.1. Animal models and experimental protocols

All experimental protocols were approved by the Faculty of Medicine, Chiang Mai University Institutional Animal Care and Use Committee, in compliance with NIH guidelines. Eighteen male Wistar rats weighing 200–220 g were purchased from the National Animal Center, Salaya Campus, Mahidol University, Thailand. All animals were housed individually in a temperature-controlled environment under a light-dark cycle of 12:12 h. After the rats were acclimatized for one week, they were divided into two groups, one to receive a normal diet (ND; 19.77% E fat), which was a standard laboratory pellet diet (Mouse Feed Food No. 082, C.P. Company, Bangkok, Thailand) ($n = 6$), or a high fat diet (HFD; 59.28% E fat) group ($n = 12$). The HFD contained 59.3% total energy from fat with the major composition of fat being saturated fatty acid from lard as described in our previous study (Pratchayasakul et al., 2011). These diets were given for 12 weeks. At week 13, the HFD-fed rats were subdivided into two subgroups to receive either 0.9% normal saline solution (0.9% NSS; 0.1 mg/kg/day; i.p) as a vehicle (HFV) ($n = 6$) or recombinant human FGF21 (FGF21, 0.1 mg/kg/day; i.p) (HFF) ($n = 6$) for four weeks. We used 0.1 mg/kg/day of FGF 21 in the present study because this dose has been shown to improve peripheral insulin sensitivity in previous studies (Coskun et al., 2008; Zhang et al., 2013). Recombinant human FGF21 (rhFGF21) was obtained from Prof. Dr. Xiaokun Li, Zhejiang Provincial Key Laboratory of Biopharmaceuticals, Wenzhou Medical College, Wenzhou, Zhejiang 325,035, P.R. China. Recombinant human FGF21 (rhFGF21) was produced using *Escherichia coli* and purified to be endotoxin free (Wang et al., 2010). All animals were given ad libitum access to food and water. At the end of protocol, the locomotor activity of each rat was tested by an open field test (OFT). After that, the spatial learning and memory was determined by the Morris water maze (MWM) test. An oral glucose tolerance test (OGTT) was also carried out before the animals were sacrificed by decapitation. Blood samples were collected for determining metabolic parameters. The brain was rapidly removed for electrophysiological and biochemical analysis. For the sample size, we used $n = 6$/group for investigation of metabolic parameters, open field test, Morris water maze test, brain mitochondrial function, LTP and western blot analysis. We also used the separated animals

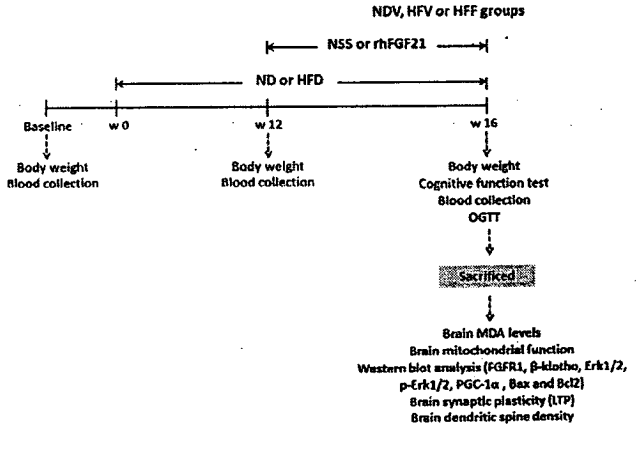


Fig. 1. The experimental protocol of the study. NDV; vehicle-treated normal diet fed rats, HFV; vehicle-treated high fat diet fed rats, HFF; FGF21-treated high fat diet fed rats, w; week, OGTT; oral glucose tolerance test, MDA; malondyaldehyde, FGFR1; fibroblast growth factor receptor 1, Erk1/2; extracellular-signal-regulated kinases, PCG-1α; peroxisome proliferator activated receptor γ coactivator 1α, LTP; Long-term potentiation.

(n = 6/group) for investigation of the dendritic spine density. The experimental protocol is shown in Fig. 1.

2.2. Chemical analysis for metabolic parameters

Fasting plasma glucose, cholesterol and triglyceride levels were determined by a colorimetric assay (ERBA diagnostic, Mannheim, Germany). Fasting plasma high-density lipoprotein (HDL) levels were determined by a commercial colorimetric assay kit (Biovision, CA, USA). The plasma low-density lipoproteins (LDL) levels were estimated from Friedewald's equation (Friedewald et al., 1972). Previous studies demonstrated that both HDL and LDL levels affected spatial learning and memory in several models such as rats fed with saturated fat, high fat, high cholesterol diet and obese-insulin resistant rats (Granholm et al., 2008; Pratchayasakul et al., 2015; Thirumangalakudi et al., 2008) by increased brain oxidative stress, activated brain microglia and proinflammatory cytokine as well as increased amyloid precursor protein (APP) processing enzyme. Therefore, the present study investigated the effect of a FGF21 on HDL and LDL in obese insulin resistant condition. Fasting plasma insulin levels were evaluated using a sandwich enzyme-linked immunosorbent assay (ELISA) kit (Millipore, MI, USA). The severity of peripheral insulin resistance was assessed by the homeostasis model assessment (HOMA) as described previously (Matthews et al., 1985). An oral glucose tolerance test (OGTT) was performed as described previously (Pratchayasakul et al., 2015). Areas under the curves (AUCs) were calculated to evaluate glucose tolerance.

2.3. Serum TNF-α, adiponectin and plasma FGF21 levels

Serum tumor necrosis factor alpha (TNF-α) levels were determined by a rat TNF-α enzyme-linked immunosorbent assay (ELISA) kit (GE Healthcare, UK). Serum adiponectin levels were determined by a rat adiponectin enzyme-linked immunosorbent assay (ELISA) (Invitrogen, life technologies, Carlsbad, CA, USA). Plasma FGF21 levels were determined by a Mouse/Rat FGF21 enzyme-linked immunosorbent assay (ELISA) kit (R&D systems Inc., Minneapolis, MN, USA).

2.4. Serum and brain malondyaldehylde (MDA) levels

Serum and brain MDA levels are markers of lipid peroxidation levels (Gulbahar et al., 2009). The levels of MDA were determined by high-performance liquid chromatography (HPLC) as described previously (Pintana et al., 2013).

2.5. Cognitive tests

In this study, the open-field test (OFT) was used to evaluate the locomotor activity of the.

rats. This method was modified from a previous study (Arakawa, 2005). The apparatus consisted of a square-based box opened from above (75 × 75 cm base, 40 cm height). The base was divided into 25 equal squares, each of them sized 15 × 15 cm. Lighting in the testing room was bright (1155 lx). Briefly, the rat was placed into a box, which consisted of white lines, and was observed for 2 min. The numbers of lines that the animals crossed was interpreted as activity (Pintana et al., 2013). To evaluate cognitive function, the protocol of the Morris Water Maze test was used as described previously (Pintana et al., 2012). The MWM set up was a round water pool (diameter 170 cm and height 60 cm) which was assigned with four cardinal points (N = north, S = south, E = east and W = west) and separated into four quadrants (NE = north east, NW = north west, SW = south west and SE = south east). Rats were given four different starting points per day. The round platform (diameter 10 cm) was located in the middle of one of the four quadrants (target quadrant). This protocol evaluated spatial learning and memory ability by two assessments: an acquisition test (hidden platform) and a probe test (removal of the platform from the water pool). Different shaped makers were pasted in the middle of each four quadrants higher than the edge of the pool by about 10 cm. For the acquisition test, rats were tested for five executive days at the same time on each day. The animals rested in the testing room 30 min before the experiment. After 30 min, the animals were placed in the water at one of the randomized starting points, and their time taken to reach the platform was recorded. The rats were left on the platform for 15 s after finding it. After that, the rats were removed from the water and allowed to rest for 15 s before being placed at the other three starting points. In the probe test, at day six, the hidden platform was removed and time spent in the target quadrant was recorded. Data analysis of the MWM test was performed using Smart 3.0 software (Panlab, Harvard Apparatus, Barcelona, Spain).

2.6. Extracellular recordings of hippocampal slices for electrical-induced long-term potentiation (LTP)

At the end of the experiment, animals were anesthetized and decapitated. The hippocampal slices were prepared as previously described (Chattipakorn and McMahon, 2002). Briefly, field excitatory postsynaptic potentials (fEPSPs) were evoked by stimulating the Schaffer collateral-commissural pathway with a bipolar tungsten electrode, whereas fEPSPs recordings were taken from the stratum radiatum of the hippocampal CA1 region with micropipettes (3 MΩ) filled with 2 M NaCl. The LTP protocol is described in a previous study (Sripetchwandee et al., 2014a). Data were filtered at 3 kHz, digitized at 10 kHz, and stored in a computer using pClamp9.2 software (Axon Instruments, CA, USA). The initial slope of the fEPSPs were measured and plotted against time.

2.7. Golgi impregnation and analysis

Previous studies reported that dendritic spine density was related to synaptic plasticity, LTP (Pratchayasakul et al., 2015), therefore we investigated the dendritic spine density in this experimental protocol. After sacrifice by decapitation, brains were removed and rinsed with double distilled water. After that, brain tissue was processed for Golgi staining using a commercially available kit (FD Neurotechnologies kit, PK 401, Ellicott City, USA) as described previously (Pratchayasakul et al., 2015; Sripetchwandee et al., 2016). Briefly, the area of the hippocampus and two segments of pyramidal cell in the CA1 region were randomly examined. Both segments were located on the tertiary apical dendrites. The dendritic spines were viewed through an inverted microscope (IX-81, Olympus, Tokyo, Japan). For the dendritic spine density analysis, two segments from pyramidal cells in the CA1 hippocampus area were randomly measured with 100–200 μm apart from soma and 20 μm in dendritic length. Three neuronal cells per brain slices were chosen for quantitative analysis (3 slices/animals, n = 6 animals/group). Therefore, nine neurons from each animal were analyzed. The number of spines was counted using a hand counter, and the dendritic lengths were measured using Xcellence imaging software (Olympus, Tokyo, Japan).

2.8. Immunoblotting

To investigate the expression of fibroblast growth factor receptor 1 (FGFR1), β-klotho, ERK1/2, ERK1/2 phosphorylation (p-Erk1/2), PGC-1α, and brain cells apoptosis markers; Bax and Bcl2, homogenated brain tissues from each subgroup were boiled at 95 °C for 5 min. Then, the proteins were separated by electrophoresis and transferred onto nitrocellulose membranes as previously described (Pipatpiboon et al., 2013). Immunoblotting was conducted with FGFR1, β-klotho, PGC-1α (1:200, Santa Cruz Biotechnology, Inc., Texas, USA), Erk1/2, p-Erk1/2, BAX (1: 1000, Santa Cruz Biotechnology, Inc., Texas, USA) and BCL-2 (1:1000, Cell Signaling Technology, Danvers, Massachusetts, USA) overnight. The primary antibody was detected by horse anti-mouse IgG conjugate HRP-linked antibody (1:2000 dilution, Cell Signaling Technology, Danvers, Massachusetts, USA) for β-Actin. Moreover, β-klotho was

detected by rabbit anti goat IgG conjugate HRP-linked antibody (1:2000 Santa Cruz Biotechnology, Inc., Texas, USA). FGFR1, Erk1/2, p-Erk1/2, PGC1-α, Bax and BCL-2 was detected by goat anti-rabbit IgG conjugate HRP-linked antibody (1:2000, Cell Signaling Technology, Danvers, Massachusetts, USA). The protein bands were visualized on Amersham hyperfilm ECL using the Amersham ECL western blotting detection reagents system (GE Healthcare, Buckinghamshire, UK). The membranes were developed using the ChemiDoc touch imaging system (Bio-Rad Laboratories, Hercules, California, USA) on chemiluminescence mode and the densitometric analysis was determined by using an image J program. The results are shown as average signal intensity (arbitrary units).

2.9. Brain mitochondrial function

Isolated mitochondria were prepared by using the same method as described in our previous studies (Pintana et al., 2012; Pipatpiboon et al., 2013). To determine brain mitochondrial function, we evaluated brain mitochondrial reactive oxygen species (ROS) production, brain mitochondrial membrane potential (ΔΨm) and brain mitochondrial swelling. The mitochondrial function was determined by following the method in our previous studies (Pintana et al., 2012; Pipatpiboon et al., 2013).

2.10. Brain mitochondrial ROS assay

Brain mitochondrial reactive oxygen species (ROS) were determined using dichloro-hydrofluoresceindiacetate (DCFHDA) fluorescent dye. Brain mitochondria (0.4 mg/ml) were incubated with 2-μM DCFHDA at 25 °C for 20 min. The fluorescence was determined using a fluorescent microplate reader at the excitation wavelength of 485 nm and emission wavelength of 530 nm (Pipatpiboon et al., 2012). Increased fluorescent intensity indicates increased ROS production.

2.11. Brain mitochondrial membrane potential (ΔΨm) assay

Mitochondrial membrane potential changes (ΔΨm) were determined using the fluorescent dye 5,5′,6,6′-tetrachloro-1,1′,3,3′-tetraethyl benzimidazolcarbocyanine iodide (JC-1). JC-1 monomer form, green fluorescence, was excited at a wavelength of 485 nm and detected at the emission wavelength of 590 nm. JC-1 aggregate form, red fluorescence, was excited at a wavelength of 485 nm and detected at the emission wavelength of 530 nm. Brain mitochondria (0.4 mg/ml) were incubated with JC-1 dye at 37 °C for 15 min. Mitochondrial membrane potential changes were determined by measuring the fluorescent intensity using a fluorescent microplate reader. The change in mitochondrial membrane potential was calculated as the ratio of red to green fluorescent intensity (Pipatpiboon et al., 2012). Decreased red/green fluorescent intensity ratio indicates mitochondrial depolarization.

2.12. Brain mitochondria swelling assay

Brain mitochondrial swelling was determined by measuring the change in the absorbance of the brain mitochondrial suspension. Brain mitochondria (0.4 mg/ml) were incubated in 2-ml respiration buffer. The suspension was read at 540 nm using a microplate reader. Decreased absorbance indicates mitochondria swelling (Pipatpiboon et al., 2012).

2.13. Statistical analysis

Data was expressed as mean ± SEM. Statistical analysis was assessed by using SPSS program (version17; SPSS, Chicago, Ill., USA). The significance of the differences in all parameters was calculated using one-way ANOVA followed by Tukey's post-hoc test. For the MWM acquisition test, a two-way ANOVA followed by Tukey's post-hoc test was used. For all comparisons, $p < 0.05$ was considered as statistically significant.

3. Results

3.1. Twelve weeks of high-fat diet (HFD) consumption caused obesity and peripheral insulin resistance

After 12 weeks of HFD consumption, 12-week HFD-fed rats had significantly increased body mass, plasma total cholesterol level, plasma LDL level, plasma insulin level, HOMA index and increased plasma glucose area under the curve (AUCg) with no change in plasma glucose level, when compared with 12-week ND-fed rats (for body mass: $F(1,10) = 28.592$, $p < 0.001$, $\eta^2 = 0.74$; for plasma total cholesterol level: $F(1,10) = 40.902$, $p < 0.001$, $\eta^2 = 0.804$; for plasma LDL level: $F(1,10) = 8.621$, $p = 0.015$, $\eta^2 = 0.463$; for plasma insulin level: $F(1,10) = 5.953$, $p = 0.035$, $\eta^2 = 0.373$; for HOMA index: $F(1,8) = 25.261$, $p = 0.001$, $\eta^2 = 0.759$; for plasma AUCg: $F(1,8) = 9.405$, $p = 0.015$, $\eta^2 = 0.540$; Table 1). These findings indicated that 12 weeks of HFD consumption caused obesity and peripheral insulin resistance.

3.2. FGF21 treatment attenuated peripheral insulin resistance, oxidative stress and pro-inflammatory cytokine caused by obesity

After 28 days of vehicle treatment, these HFD-fed rats (HFV) had significantly increased body mass, visceral fat, plasma total cholesterol levels, plasma LDL levels, plasma insulin levels, HOMA index and plasma glucose AUCg without hyperglycemia when compared with vehicle treated ND-fed rats (NDV) (for body mass: $F(2,15) = 61.725$, $p < 0.001$, $\eta^2 = 0.892$; for visceral fat: $F(2,15) = 93.733$, $p < 0.001$, $\eta^2 = 0.926$; for plasma total cholesterol level: $F(2,15) = 16.639$, $p < 0.01$ $\eta^2 = 0.689$; for plasma LDL level: $F(2,15) = 7.857$, $p = 0.005$, $\eta^2 = 0.512$; for plasma insulin level: $F(2,15) = 4.653$, $p = 0.027$, $\eta^2 = 0.383$; for HOMA index: $F(2,15) = 3.224$, $p = 0.05$, $\eta^2 = 0.301$; for plasma AUCg: $F(2,22) = 3.684$, $p = 0.042$, $\eta^2 = 0.251$; Table 2). Moreover, these HFV rats also had significantly increased serum MDA levels when compared with NDV rats ($F(2,15) = 5.379$, $p = 0.017$, $\eta^2 = 0.418$; Table 2). Additionally, HFV rats significantly increased TNF-α level with decreased serum adiponectin level when compared with NDV rats ($F(2,15) = 5.374$, $p = 0.017$, $\eta^2 = 0.417$; Table 2). These findings indicated that the long-term HFD consumption caused peripheral insulin resistance and the occurrence of peripheral insulin resistance was accompanied by an increase in the oxidative stress and pro-inflammatory cytokine in HFV.

After treatment with FGF21 for 28 days, FGF21 treated HFD-fed rats (HFF) showed significantly decreased body mass, visceral fat, plasma total cholesterol levels, plasma LDL levels, decreased plasma insulin levels, HOMA index, plasma glucose AUCg with increased plasma HDL levels when compared with the vehicle treated HFD-fed rats (HFV). Moreover, the HFF rats had significantly decreased serum MDA levels, decreased serum TNF-α and increased adiponectin levels when compared with HFV rats ($p < 0.05$, Table 2). Malondialdehyde (MDA) is the end product of lipid peroxidation levels and is widely used as a

Table 1
Metabolic parameters in rats fed with normal or high fat diet for 12 weeks.

Parameters	ND	HFD
Body mass (kg)	468.33 ± 8.33	580.00 ± 19.15*
Food intake (g/day)	24.36 ± 4.45	26.56 ± 8.44
Plasma glucose (mg%)	128.48 ± 4.01	130.10 ± 6.65
Plasma total cholesterol (mg/dl)	67.16 ± 2.55	88.00 ± 2.17*
Plasma triglyceride (mg/dl)	55.63 ± 6.20	59.44 ± 7.09
Plasma HDL (mg/dl)	29.79 ± 2.02	30.40 ± 3.90
Plasma LDL (mg/dl)	47.95 ± 3.98	62.83 ± 3.14*
Plasma insulin (ng/ml)	2.87 ± 0.61	4.99 ± 0.62*
HOMA index	17.24 ± 1.90	36.31 ± 3.73*
Plasma Glucose AUC (AUCg) (mg/dl × min × 10^4)	4.63 ± 0.71	6.18 ± 0.40*

ND; normal diet fed rats, HFD; high fat diet fed rats.
* $p < 0.05$ vs ND.

Table 2
Effects of FGF21 administration on peripheral insulin sensitivity parameters and MDA levels in HFD-fed rats.

Parameters	NDV	HFV	HFF
Body mass (kg)	520.83 ± 10.83	678.33 ± 11.38*	556.67 ± 9.19*,†
Visceral fat (g)	23.87 ± 1.94	63.94 ± 1.42*	50.51 ± 2.74*,†
Food intake (g/day)	23.87 ± 1.94	25.78 ± 3.56	23.97 ± 2.95
Plasma glucose (mg%)	127.62 ± 4.05	130.49 ± 6.54	130.03 ± 3.67
Plasma total cholesterol (mg/dl)	77.34 ± 2.25	114.51 ± 7.55*	81.51 ± 3.57†
Plasma triglyceride (mg/dl)	59.15 ± 4.60	54.62 ± 2.40	56.65 ± 2.58
Plasma HDL (mg/dl)	32.82 ± 1.94	24.52 ± 1.99*	31.10 ± 1.71†
Plasma LDL (mg/dl)	51.38 ± 2.99	74.39 ± 5.85*	55.59 ± 3.75†
Plasma insulin (ng/ml)	2.69 ± 0.86	4.96 ± 1.00*	2.82 ± 1.98†
HOMA index	16.13 ± 1.22	32.82 ± 8.73*	17.29 ± 1.76†
Plasma glucose AUC (AUCg) (mg/dl × min × 10^4)	5.29 ± 0.29	7.23 ± 0.65*	5.50 ± 0.36†
Plasma adiponectin (ng/ml)	23.00 ± 3.38	14.67 ± 2.94*	24.50 ± 1.69†
Plasma TNF-α (pg/ml)	1.11 ± 0.16	3.05 ± 0.67*	1.58 ± 3.07†
Serum MDA (μmol/ml)	1.14 ± 0.17	2.99 ± 0.76*	1.13 ± 0.18†
Brain MDA (μmol/mg protein)	0.67 ± 1.25	1.68 ± 0.22*	0.96 ± 0.22†
Plasma FGF21 levels (pg/ml)	47.94 ± 8.43	265.69 ± 30.74*	573.70 ± 131.10*,†

NDV; vehicle-treated normal diet fed rats, HFV; vehicle-treated high fat diet fed rats, HFF; FGF21-treated high fat diet fed rats.
* $p < 0.05$ vs NDV.
† $p < 0.05$ vs HFV.

biomarker of oxidative stress (Yagi, 1998). Previous studies demonstrated that the increased brain lipid peroxidation caused cell degeneration and cell death. This lead to impaired cognitive function in several models such as patients with amnestic mild cognitive impairment (MCI) (Markesbery et al., 2005) and obese-insulin resistant rats (Pintana et al., 2013). Therefore, the present study investigated the effect of a FGF21 on MDA in rats under an obese-insulin resistant condition. These findings suggested that FGF21 increased peripheral insulin sensitivity, decreased oxidative stress levels as well as reduced systemic inflammation.

3.3. Obesity caused impaired cognitive function, and FGF21 prevented cognitive decline in obese-insulin resistant rats

The open field test was used to determine the locomotor activity of each rat before the MWM test. The number of lines that the rats crossed

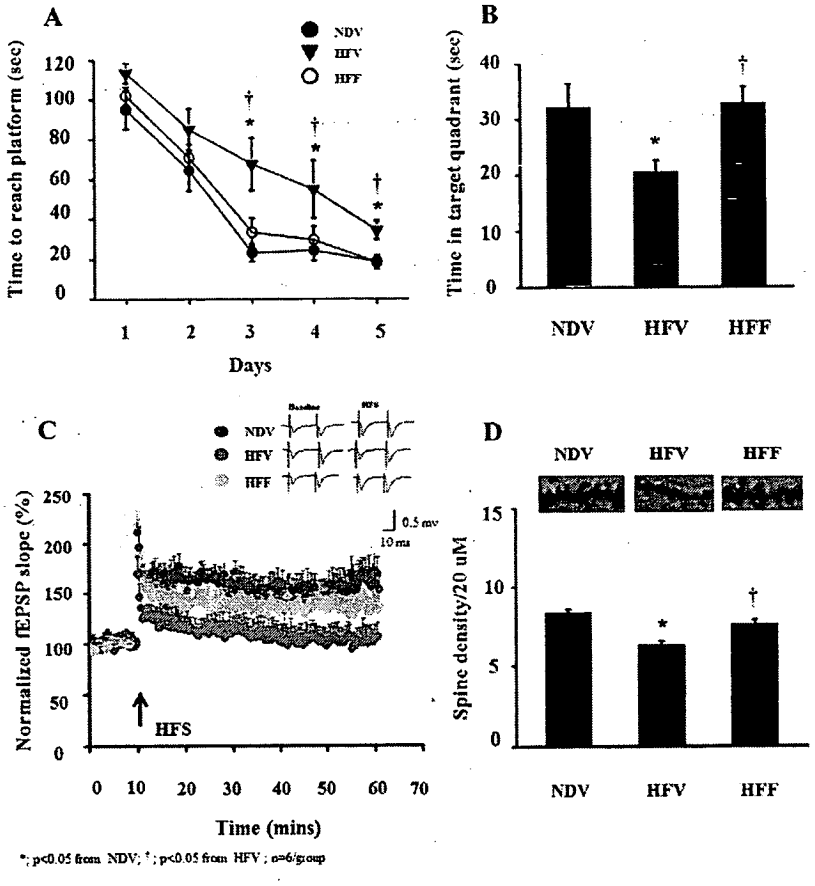


Fig. 2. Effects of FGF21 administration on Morris water maze test and hippocampal synaptic plasticity in obese-insulin resistant rats (A) Time to reach the platform in acquisition test and (B) time spent in target quadrant in probe test. (C) The degree of electrical-mediated LTP observed from hippocampal slices and (D) number of dendritic spines on tertiary dendrites in apical dendrite. NDV; vehicle-treated normal diet fed rats, HFV; vehicle-treated high fat diet fed rats, HFF; FGF21-treated high fat diet fed rats. *$p < 0.05$ vs. NDV, †$p < 0.05$ vs. HFV.

during the test was not significantly different between groups, indicating that the locomotor activity of all rats after treatment with either the vehicle or FGF21 was similar.

In the MWM test, the time to reach the platform during the acquisition test (day 3 to day 5) in HFV rats was significantly increased, when compared with that of NDV rats ($F(4,22) = 57.719$, $\eta^2 = 0.340$; Fig. 2A). Moreover, the mean time spent in the target quadrant during the probe test (day 6) in HFV rats was significantly decreased, when compared with that of NDV rats ($F(2,21) = 5.404$, $p = 0.013$, $\eta^2 = 0.340$; Fig. 2B). These results suggested that obese-insulin resistant rats exhibited cognitive decline. After treatment with FGF21 for 28 days, HFF rats had a decreased time to reach the platform during the acquisition test (day 3 to day 5) ($F(4,22) = 57.719$, $\eta^2 = 0.340$; Fig. 2A) and an increased mean time spent in the target quadrant during the probe test (day 6) when compared with HFV rats ($F(2,21) = 5.404$, $p = 0.013$, $\eta^2 = 0.340$; Fig. 2B). Moreover, we also found the swim speeds were not significantly different between groups (26.33 ± 3.86, 26.73 ± 3.82 and 30.85 ± 2.63 cm/s, in NDV, HFV and HFF, respectively). Meanwhile, the distance to reach the hidden platform in HFV rats was significantly increased when compared with that of the NDV rats ($F(2,13) = 10.42$, $p = 0.002$, $\eta^2 = 0.616$). Moreover, HFF rats had decreased the distance to reach the hidden platform when compared with that of HFV rats ($F(2,13) = 10.42$, $p = 0.002$, $\eta^2 = 0.616$) (349.40 ± 87.00, 1102.00 ± 226.60 and 347.50 ± 85.51 cm, in NDV, HFV and HFF, respectively). These findings confirmed that the impairment of cognitive function in HFD rats was due to spatial memory deficit, not because of movement related deficits following obesity, and FGF21 attenuated the cognitive impairment.

3.4. Obesity caused the impairment of hippocampal synaptic plasticity, and FGF21 restored this impairment in obese-insulin resistant rats

The degree of electrical-induced LTP of HFV rats significantly decreased when compared with that of NDV rats ($F(2,23) = 3.033$, $p = 0.05$, $\eta^2 = 0.209$; Fig. 2B). In addition, the number of dendritic spines in the CA1 hippocampus of HFV rats was significantly less than that of NDV rats ($F(2,13) = 15.901$, $p < 0.001$, $\eta^2 = 0.710$; Fig. 2D). These findings suggested that obese-insulin resistant rats had impaired hippocampal synaptic plasticity.

After FGF21 treatment for 28 days, HFF rats had an increase in the degree of electrical-induced LTP when compared with HFV rats ($F(2,23) = 3.033$, $p = 0.05$, $\eta^2 = 0.209$; Fig. 2B).

In addition, the dendritic spine density in CA1 hippocampus of HFF rats significantly increased when compared with that of HFV rats ($F(2,13) = 15.901$, $p < 0.001$, $\eta^2 = 0.710$; Fig. 2D). These findings suggested that FGF21 treatment restored hippocampal synaptic plasticity in obese-insulin resistant rats.

3.5. Obesity caused increased plasma FGF21 levels and impaired brain FGF21 signaling

The present study investigated the circulating FGF21 level, the expression of brain FGF21 receptors, including FGFR1 and β-klotho, and brain FGF21 signaling such as Erk1/2, phosphorylated-Erk1/2 (p-Erk1/2) and PGC-1α protein expression. We found that the HFV rats had higher circulating FGF21 levels when compared with NDV rats ($F(2,16) = 12.029$, $p = 0.001$, $\eta^2 = 0.601$; Table 2). The expression of β-klotho and FGFR1 in brain of HFV rats was not significantly different to that of NDV rats (Fig. 3A, B). Interestingly, the level of phosphorylated-FGFR1 (p-FGFR1) expression significantly reduced in HFV rats when compared with NDV rats ($F(2,7) = 18.658$, $p = 0.002$, $\eta^2 = 0.842$; Fig. 3C). Although the expression of total Erk1/2 (t-Erk1/2) expression did not differ between all groups (Fig. 3D) and p-Erk1/2 of HFV rats significantly decreased when compared with those of NDV rats ($F(2,19) = 4.127$, $p = 0.032$, $\eta^2 = 0.303$; Fig. 3E). Moreover, PGC1-α protein expression of HFV was significantly less than that of NDV rats ($F(2,11) = 7.354$, $p = 0.009$, $\eta^2 = 0.512$; Fig. 3F). These findings suggested that the impairment of brain FGF21 signaling occurred in obese-insulin resistant rats.

After FGF21 treatment for 28 days, the highest circulating levels of FGF21 levels were observed in HFF rats when compared with NDV and HFV rats ($F(2,16) = 12.029$, $p = 0.001$, $\eta^2 = 0.601$; Table 2). We did not find a statistically significant difference in β-klotho and FGFR1 expression among all groups (Fig. 3A, B). Moreover, HFF rats had an increase in the expression of p-FGFR1, and p-Erk1/2 protein expression when compared with those of HFV rats (for p-FGFR1: $F(2,7) = 18.658$, $p = 0.002$, $\eta^2 = 0.842$; for p-Erk1/2: $F(2,19) = 4.127$, $p = 0.032$, $\eta^2 = 0.303$; Fig. 3C, E). FGF21-treated HFD-fed rats also showed a significant increase in brain PGC-1α expression when compared with NDV and HFV rats ($F(2,11) = 7.354$, $p = 0.009$, $\eta^2 = 0.512$; Fig. 3F). These findings suggested that FGF21 treatment enhanced FGF21 mediated signaling indicated by the increased p-FGFR1, p-ERK1/2 and PGC1-α levels in obese-insulin resistant rats.

3.6. Obesity caused impaired brain mitochondrial function and increased brain oxidative stress which were attenuated by FGF21 treatment

HFV rats had an increase in brain mitochondrial ROS production, brain mitochondrial membrane potential change (i.e. depolarization) as well as brain mitochondrial swelling when compared with NDV rats (for brain mitochondrial ROS production: $F(2,17) = 3.611$, $p = 0.049$, $\eta^2 = 0.298$; for brain mitochondrial membrane potential change: $F(2,20) = 3.308$, $p = 0.05$, $\eta^2 = 0.249$; for brain mitochondrial swelling: $F(2,17) = 5.419$, $p = 0.015$, $\eta^2 = 0.389$; Fig. 4A, B, C).

We also found that the brain MDA level of HFV rats significantly increased when compared with that of NDV rats ($F(2,15) = 7.159$, $p = 0.007$, $\eta^2 = 0.488$; Table 2). These findings suggested that obese-insulin resistant rats had brain mitochondrial dysfunction with an increase in brain lipid peroxidation levels.

After FGF21 treatment for 28 days, brain mitochondrial ROS production, brain mitochondrial membrane potential change and brain mitochondrial swelling significantly decreased in HFF rats when compared with HFV rats (for brain mitochondrial ROS production: $F(2,17) = 3.611$, $p = 0.049$, $\eta^2 = 0.298$; for brain mitochondrial membrane potential change: $F(2,20) = 3.308$, $p = 0.05$, $\eta^2 = 0.249$; for brain mitochondrial swelling: $F(2,17) = 5.419$, $p = 0.015$, $\eta^2 = 0.389$; Fig. 4A, B, C). Moreover, brain MDA level of HFF rats was lower than that of HFV rats ($F(2,15) = 7.159$, $p = 0.007$, $\eta^2 = 0.488$; Table 2). In addition, the morphological changes of brain mitochondria were demonstrated by transmission electron microscopy (TEM), and were shown in Fig. 4C. Brain mitochondrial swelling was observed in HFV rats indicated by remarkably unfolded cristae. Brain mitochondrial morphology showed obvious folded cristae in NDV and HFF rats. These findings suggested that FGF21 treatment restored brain mitochondrial function and decreased brain oxidative stress levels in obese-insulin resistant rats.

3.7. Obesity caused brain cell apoptosis and FGF21 prevented it

Cells apoptosis in the brain was determined by the expression of Bcl-2 and Bax. The results demonstrated that HFV rats had an increase in the expression of a pro-apoptotic marker (Bax), decreased anti-apoptotic marker (Bcl2) and an increase in Bax/Bcl2 ratio when compared with those of NDV rats (for Bax: $F(2,17) = 13.022$, $p < 0.001$, $\eta^2 = 0.605$; for Bcl2: $F(2,12) = 7.610$, $p = 0.007$, $\eta^2 = 0.559$; for Bax/Bcl2: $F(2,16) = 36.571$, $p < 0.001$, $\eta^2 = 0.821$; Fig. 4D, E, F). These findings suggested that increased brain cell apoptosis was observed in obese-insulin resistant rats.

After FGF21 treatment for 28 days, the reduction in Bax protein expression, increased Bcl2 protein expression and a decrease in Bax/Bcl2 ratio were observed in HFF rats when compared with HFV rats (for Bax: $F(2,17) = 13.022$, $p < 0.001$, $\eta^2 = 0.605$; for Bcl2: $F(2,12) = 7.610$, $p = 0.007$, $\eta^2 = 0.559$; for Bax/Bcl2: $F(2,16) = 36.571$,

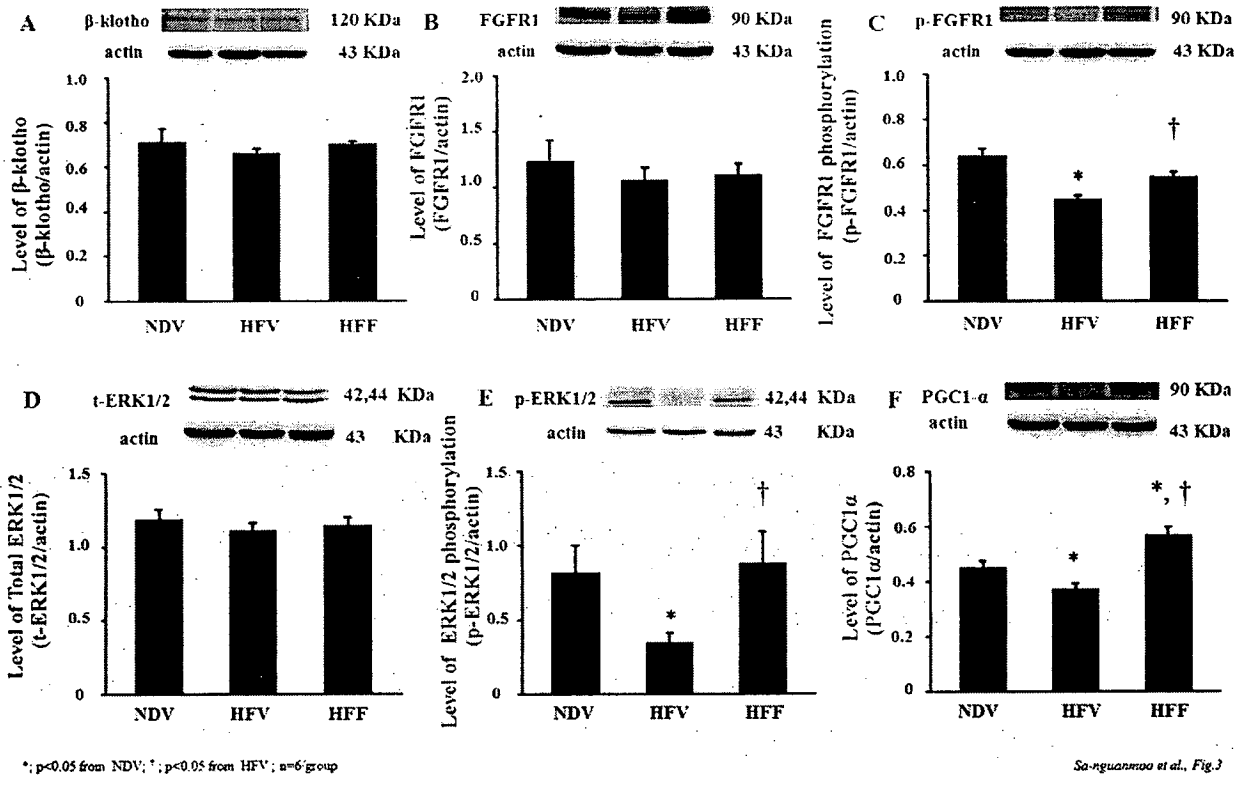


Fig. 3. Effects of FGF21 administration on FGF21 receptor, co-receptor and FGF21 signaling in the brain of obese-insulin resistant rats (A) β-klotho (B) FGFR1 (C) p-FGFR1 (D) t-Erk12 (E) p-Erk1/2 and (D) PGC-1α. NDV; vehicle-treated normal diet fed rats, HFV; vehicle-treated high fat diet fed rats, HFF; FGF21-treated high fat diet fed rats. *p < 0.05 vs. NDV, †p < 0.05 vs. HFV.

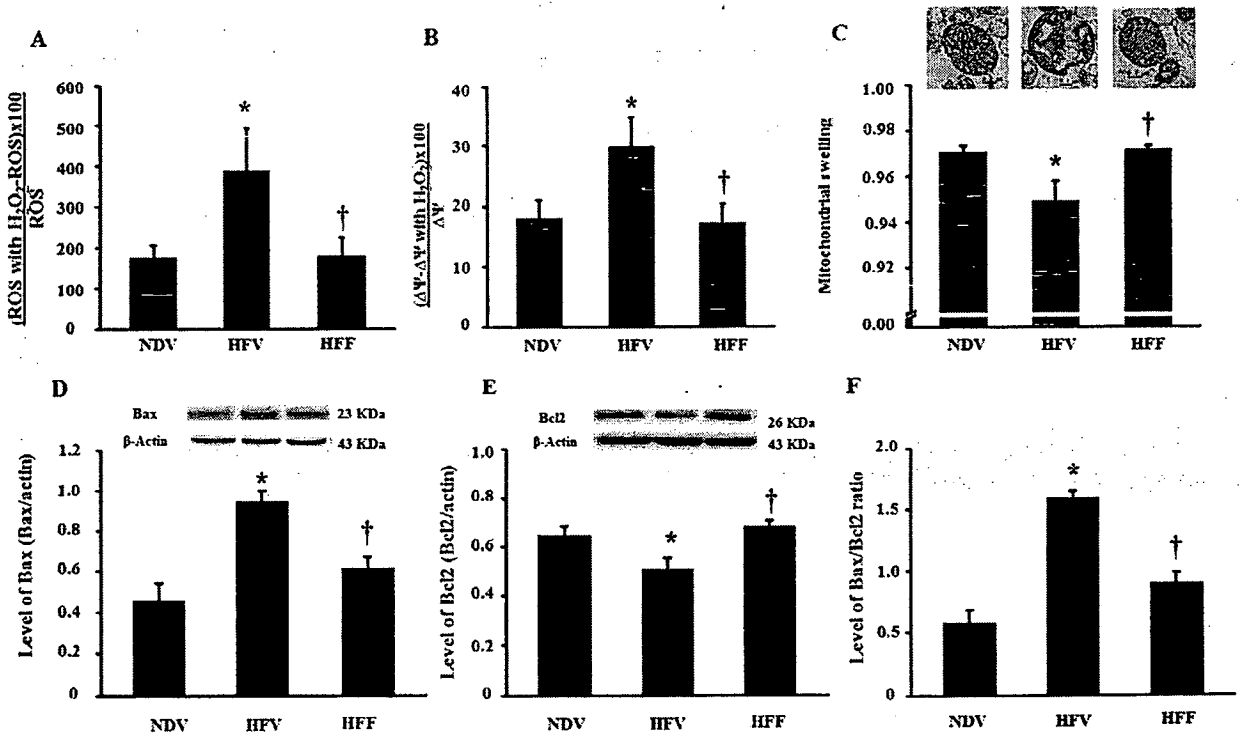


Fig. 4. Effects of FGF21 administration on brain mitochondrial function and cell apoptosis in obese-insulin resistant rats (A) Brain mitochondrial ROS production, (B) brain mitochondrial membrane potential change and (C) brain mitochondrial swelling and transmission electron microscopy (original magnification × 25,000), (D) Bax, (E) Bcl2 and (F) Bax/Bcl2 ratio. NDV; vehicle-treated normal diet fed rats, HFV; vehicle-treated high fat diet fed rats, HFF; FGF21-treated high fat diet fed rats. *p < 0.05 vs. NDV, †p < 0.05 vs. HFV.

$p < 0.001, \eta^2 = 0.821$; Fig. 4D, E, F). These findings indicated that FGF21 reduced brain cell apoptosis in obese-insulin resistant rats.

4. Discussion

The major findings of the present study demonstrated that FGF21 treated obese-insulin resistant male rats 1) improved metabolic parameters, decreased circulating pro-inflammatory cytokine and serum oxidative stress levels; 2) prevented cognitive decline; 3) restored hippocampal synaptic plasticity; 4) enhanced brain FGF21-mediated signaling; and 5) restored brain mitochondrial function, decreased brain oxidative stress levels as well as brain cell apoptosis.

In this present study, we demonstrated that obesity induced by HFD consumption caused the development of peripheral insulin resistance, which was indicated by increased body mass, plasma insulin levels, HOMA index, total area under the curve (TAUCg) and euglycemia (Table 1). These findings on metabolic parameters are consistent with our previous reports for this model (Pintana et al., 2013; Pipatpiboon et al., 2013; Pratchayasakul et al., 2011). Moreover, the present study demonstrated that long-term HFD consumption increased systemic inflammation indicated by increased pro-inflammatory cytokine level (TNF-α) and decreased adipokine level (adiponectin). Previous studies reported that obesity and adipocyte hypertrophy led to an increased level of pro-inflammatory cytokines and impaired the expression and secretion of adiponectin (Ouchi et al., 2011). Hypo-adiponectinemia can cause insulin resistance and diabetes (Kim et al., 2013; Lin et al., 2013). In addition, previous studies reported that low levels of adiponectin found in obesity and the administration of adiponectin in an animal model of obesity improved peripheral insulin sensitivity (Berg et al., 2001; Diez and Iglesias, 2010). All of those findings and our present findings indicated that HFD consumption led to not only obesity, but also systemic inflammation and hypo-adiponectinemia, in which finally resulted the impairment of peripheral insulin sensitivity.

We previously found that the obese-insulin resistant condition led to impaired brain functions (Pintana et al., 2013; Pratchayasakul et al., 2015; Sripetchwandee et al., 2014b). Those findings were confirmed in this study, where we found that long-term HFD consumption caused increased brain oxidative stress, brain mitochondrial dysfunction, impaired hippocampal synaptic plasticity, decreased dendritic spine density as well as impaired cognitive function. Moreover, we found that male rats with long-term HFD consumption had increased brain cell apoptosis which was indicated by an increase in Bax levels, decreased Bcl2 levels and an increased Bax/Bcl2 ratio. An increase in apoptotic markers together with increased mitochondrial dysfunction in the brain of obese-insulin resistant male rats could lead to impaired cognition found in this study.

Our results also showed that obese-insulin resistant male rats had increased serum FGF21 levels. Serum FGF21 levels have been shown to increase in several pathological conditions such as obesity, metabolic syndrome and diabetes (Bobbert et al., 2013; Mashili et al., 2011; Novotny et al., 2014; Zhang et al., 2008), and that this increased level of FGF21 in the obese model cannot restore or improve metabolic function. It has been suggested that when a state of high endogenous level of a metabolic regulator does not have any effects on the physiological function, but can lead to an improvement of metabolic function if under a high pharmacological level, this suggests a state of hormone resistance (Yang et al., 2012). In addition, the study by Fisher and colleagues demonstrated that diet-induced obese (DIO) mice fed with a high fat/high sucrose diet showed increased serum FGF21, decreased FGFR1 mRNA expression in both the liver and white adipose tissue (WAT), decreased β-klotho mRNA expression in the WAT but not in the liver (Fisher et al., 2010). These findings suggested that obese-insulin resistance may lead to FGF21 resistance and may alter the FGF21 receptor expression in liver and WAT.

This present study is the first study that has investigated the FGFR1 phosphorylation and β-klotho level in the brain of obese-insulin resistant male rats. Our results showed that, although there was no change in the protein expression of the receptor, the FGFR1 function was impaired in the brain of obese-insulin resistant male rats. All of the findings from our study suggested that obese-insulin resistant male rats had impaired brain FGF21 signaling.

In this study, FGF21 treatment in obese-insulin resistant male rats improved peripheral insulin sensitivity and decreased systemic inflammation which is possibly due to decreased body mass gain and decreased visceral fat. FGF21 reduced body mass gain in obese-insulin resistant male rats without the reduction of food intake. The possible explanations of this observation may be that 1) FGF21 level could induce an increase in the sympathetic activity as shown in a previous study (Douris et al., 2015; Owen et al., 2014) and 2) FGF21 could up regulate thermogenesis gene (UCP-1) in adipocytes as demonstrated in a previous study (Douris et al., 2015; Owen et al., 2014). These two possible explanations could increase energy expenditure, which caused body weight loss (Douris et al., 2015; Owen et al., 2014). Moreover, the effect of FGF21 on the improvement of peripheral insulin resistance could be due to the following mechanisms 1) increased rate of glucose uptake in adipocytes, increased insulin synthesis and reduced hepatic gluconeogenesis (Kharitonenkov et al., 2008; Kong et al., 2013; Kralisch et al., 2013; Liu et al., 2012; Xu et al., 2009b) and 2) reduced levels of pro-inflammatory cytokines such as TNF-α, MCP-1 and PAI-1, and 3) increased adiponectin biosynthesis in adipocytes, as shown in Table 2 and other previous studies (Kim et al., 2013; Lin et al., 2013).

Moreover, FGF21 treatment also improved brain FGF21 signaling, as indicated by an increased p-Erk1/2 level and subsequently to increased PGC-1α expression in obese-insulin resistant male rats (Fig. 3). FGF21 has been shown to improve mitochondrial function in human dopaminergic neurons, by increasing mitochondrial anti-oxidant levels and enhancing mitochondrial respiratory capacity, mediated by sirtuin-1 (SIRT1) and PGC-1α which leads to improved mitochondrial biogenesis and cell viability (Houten and Auwerx, 2004; Johanna Mäkelä et al., 2014; Lin et al., 2005; Wu et al., 1999). Moreover, increasing the activity of PGC-1α has been shown to protect oxidative stress-induced cell death and prevent neurodegeneration in Parkinson's disease (Pacelli et al., 2011; St-Pierre et al., 2006). It is known that oxidative stress caused increased neuronal apoptosis and impaired hippocampal synaptic plasticity as indicated by a decrease in the LTP amplitude and the reduction in dendritic spine density (Avila-Costa et al., 1999; Rivas-Arancibia et al., 2010). Additionally, a recent study found that FGF21 treatment improved behavioral performance in the MWM test and in the step-down test by reducing brain cell damage in the hippocampus and suppressing brain oxidative stress in D-galatactose-induced aging model (Yu et al., 2015). The present study showed for the first time that FGF21 treatment in obese-insulin resistant male rats could restore brain mitochondrial function by reducing ROS production, brain oxidative stress levels and these events led to reduced brain cell apoptosis, restored hippocampal synaptic plasticity, restored dendritic spine density as well as prevented cognitive decline.

In conclusion, the present study demonstrated that the effects of FGF21 on the prevention of cognitive decline in obese-insulin resistant condition is associated with its ability to improve peripheral insulin sensitivity, reduce systemic inflammation, restore brain mitochondrial function, decrease brain oxidative stress, decreased brain cell apoptosis and restore hippocampal synaptic plasticity. These beneficial effects of FGF21 in the brain were mediated by the FGF21 signaling pathway.

Limitation of the study

Although our results showed that FGF21 treatment for 4 weeks effectively improved cognitive function, it is not known whether a 4-week treatment of FGF21 is the optimal duration to see its beneficial effects. The sample size was also small in the present study. Future studies with larger sample size are needed to investigate the time course effects of FGF21 on the cognition in obese-insulin resistant rats.

Conflict of interest

The authors declare that there is no conflict of interest.

Acknowledgements

This work was supported by Thailand Research Fund grants: TRF-BRG 5780016 (SC) and MRG5980198 (WP), a CMU 50th Anniversary grant by Chiang Mai University (PHD/023/2556 PS&NC), a NSTDA Research Chair Grant from the National Science and Technology Development Agency Thailand (NC) and Chiang Mai University Center of Excellence Award (NC). The authors would like to thank Ms. Cicely Proctor and Ms. Gabrielle Metzler for their editorial assistance.

References

Adams, A.C., Cheng, C.C., Coskun, T., Kharitonenkov, A., 2012. FGF21 requires betaklotho to act in vivo. PLoS One 7, e49977.
Arakawa, H., 2005. Age dependent effects of space limitation and social tension on open-fieldbehavior in male rats. Physiol. Behav. 84, 429–436.
Avila-Costa, M.R., Colin-Barenque, L., Fortoul, T.I., Machado-Salas, P., Espinosa-Villanueva, J., Rugerio-Vargas, C., Rivas-Arancibia, S., 1999. Memory deterioration in an oxidative stress model and its correlation with cytological changes on rat hippocampus CA1. Neurosci. Lett. 270, 107–109.
Beilharz, J.E., Maniam, J., Morris, M.J., 2015. Diet-induced cognitive deficits: the role of fat and sugar, potential mechanisms and nutritional interventions. Nutrients 7, 6719–6738.
Berg, A.H., Combs, T.P., Du, X., Brownlee, M., Scherer, P.E., 2001. The adipocyte-secreted protein Acrp30 enhances hepatic insulin action. Nat. Med. 7, 947–953.
Bobbert, T., Schwarz, F., Fischer-Rosinsky, A., Pfeiffer, A.F., Mohlig, M., Mai, K., Spranger, J., 2013. Fibroblast growth factor 21 predicts the metabolic syndrome and type 2 diabetes in Caucasians. Diabetes Care 36, 145–149.
Chattipakorn, S.C., McMahon, L.L., 2002. Pharmacological characterization of glycine-gated chloride currents recorded in rat hippocampal slices. J. Neurophysiol. 87, 1515–1525.
Coskun, T., Bina, H.A., Schneider, M.A., Dunbar, J.D., Hu, C.C., Chen, Y., Moller, D.E., Kharitonenkov, A., 2008. Fibroblast growth factor 21 corrects obesity in mice. Endocrinology 149, 6018–6027.
Cournot, M., Marquie, J.C., Ansiau, D., Martinaud, C., Fonds, H., Ferrieres, J., Ruidavets, J.B., 2006. Relation between body mass index and cognitive function in healthy middle-aged men and women. Neurology 67, 1208–1214.
den Heijer, T., Vermeer, S.E., van Dijk, E.J., Prins, N.D., Koudstaal, P.J., Hofman, A., Breteler, M.M., 2003. Type 2 diabetes and atrophy of medial temporal lobe structures on brain MRI. Diabetologia 46, 1604–1610.
Diez, J.J., Iglesias, P., 2010. The role of the novel adipocyte-derived protein adiponectin in human disease: an update. Mini-Rev. Med. Chem. 10, 856–869.
Douris, N., Stevanovic, D.M., Fisher, F.M., Cisu, T.I., Chee, M.J., Nguyen, N.L., Zarebidaki, E., Adams, A.C., Kharitonenkov, A., Flier, J.S., Bartness, T.J., Maratos-Flier, E., 2015. Central fibroblast growth factor 21 browns white fat via sympathetic action in male mice. Endocrinology 156, 2470–2481.
Elias, M.F., Elias, P.K., Sullivan, L.M., Wolf, P.A., D'Agostino, R.B., 2003. Lower cognitive function in the presence of obesity and hypertension: the Framingham heart study. Int. J. Obes. Relat. Metab. Disord. 27, 260–268.
Fisher, F.M., Chui, P.C., Antonellis, P.J., Bina, H.A., Kharitonenkov, A., Flier, J.S., Maratos-Flier, E., 2010. Obesity is a fibroblast growth factor 21 (FGF21)-resistant state. Diabetes 59, 2781–2789.
Friedewald, W.T., Levy, R.I., Fredrickson, D.S., 1972. Estimation of the concentration of low-density lipoprotein cholesterol in plasma, without use of the preparative ultracentrifuge. Clin. Chem. 18, 499–502.
Fung, T.T., Rimm, E.B., Spiegelman, D., Rifai, N., Tofler, G.H., Willett, W.C., Hu, F.B., 2001. Association between dietary patterns and plasma biomarkers of obesity and cardiovascular disease risk. Am. J. Clin. Nutr. 73, 61–67.
Gaich, G., Chien, J.Y., Fu, H., Glass, L.C., Deeg, M.A., Holland, W.L., Kharitonenkov, A., Bumol, T., Schilske, H.K., Moller, D.E., 2013. The effects of LY2405319, an FGF21 analog, in obese human subjects with type 2 diabetes. Cell Metab. 18, 333–340.
Granholm, A.C., Bimonte-Nelson, H.A., Moore, A.B., Nelson, M.E., Freeman, L.R., Sambamurti, K., 2008. Effects of a saturated fat and high cholesterol diet on memory and hippocampal morphology in the middle-aged rat. J. Alzheimers Dis. 14, 133–145.
Gulbahar, O., Aricioglu, A., Akmansu, M., Turkozer, Z., 2009. Effects of radiation on protein oxidation and lipid peroxidation in the brain tissue. Transplant. Proc. 41, 4394–4396.
Gunstad, J., Lhotsky, A., Wendell, C.R., Ferrucci, L., Zonderman, A.B., 2010. Longitudinal examination of obesity and cognitive function: results from the Baltimore longitudinal study of aging. Neuroepidemiology 34, 222–229.
Houten, S.M., Auwerx, J., 2004. PGC-1alpha: turbocharging mitochondria. Cell 119, 5–7.
Hsuchou, H., Pan, W., Kastin, A.J., 2007. The fasting polypeptide FGF21 can enter brain from blood. Peptides 28, 2382–2386.
Johanna Mäkelä, T.V.T., Maiorana, F., Eriksson, O., Do, H.T., Mudò, G., Korhonen, L.T., Belluardo3, N., Lindholm, D., 2014. Fibroblast growth factor-21 enhances mitochondrial functions and increases the activity of PGC-1α in human dopaminergic neurons via Sirtuin-1. SpringerPlus 3, 1–12.
Kharitonenkov, A., Shanafelt, A.B., 2009. FGF21: a novel prospect for the treatment of metabolic diseases. Curr. Opin. Investig. Drugs 10, 359–364.
Kharitonenkov, A., Dunbar, J.D., Bina, H.A., Bright, S., Moyers, J.S., Zhang, C., Ding, L., Micanovic, R., Mehrbod, S.F., Knierman, M.D., Hale, J.E., Coskun, T., Shanafelt, A.B., 2008. FGF-21/FGF-21 receptor interaction and activation is determined by betaKlotho. J. Cell. Physiol. 215, 1–7.
Kharitonenkov, A., Wroblewski, V.J., Koester, A., Chen, Y.F., Clutinger, C.K., Tigno, X.T., Hansen, B.C., Shanafelt, A.B., Etgen, G.J., 2007. The metabolic state of diabetic monkeys is regulated by fibroblast growth factor-21. Endocrinology 148, 774–781.
Kim, H.W., Lee, J.E., Cha, J.J., Hyun, Y.Y., Kim, J.E., Lee, M.H., Song, H.K., Nam, D.H., Han, J.Y., Han, S.Y., Han, K.H., Kang, Y.S., Cha, D.R., 2013. Fibroblast growth factor 21 improves insulin resistance and ameliorates renal injury in db/db mice. Endocrinology 154, 3366–3376.
Kong, L.J., Feng, W., Wright, M., Chen, Y., Dallas-yang, Q., Zhou, Y.P., Berger, J.P., 2013. FGF21suppresses hepatic glucose production through the activation of atypical protein kinase Ciota/lambda. Eur. J. Pharmacol. 702, 302–308.
Kralisch, S., Tonjes, A., Krause, K., Richter, J., Lossner, U., Kovacs, P., Ebert, T., Bluher, M., Stumvoll, M., Fasshauer, M., 2013. Fibroblast growth factor-21 serum concentrations are associated with metabolic and hepatic markers in humans. J. Endocrinol. 216, 135–143.
Lin, J., Handschin, C., Spiegelman, B.M., 2005. Metabolic control through the PGC-1 family of transcription coactivators. Cell Metab. 1, 361–370.
Lin, Z., Tian, H., Lam, K.S., Lin, S., Hoo, R.C., Konishi, M., Itoh, N., Wang, Y., Bornstein, S.R., Xu, A., Li, X., 2013. Adiponectin mediates the metabolic effects of FGF21 on glucose homeostasis and insulin sensitivity in mice. Cell Metab. 17, 779–789.
Liu, M.Y., Wang, W.F., Hou, Y.T., Yu, Y.X., Ren, G.P., Kern, T.S., Sun, G.P., Li, D.S., 2012. Fibroblast growth factor (FGF)-21 regulates glucose uptake through GLUT1 translocation. Afr. J. Microbiol. Res. 6, 2504–2511.
Markesbery, W.R., Kryscio, R.J., Lovell, M.A., Morrow, J.D., 2005. Lipid peroxidation is an early event in the brain in amnestic mild cognitive impairment. Ann. Neurol. 58, 730–735.
Mashili, F.L., Austin, R.L., Deshmukh, A.S., Fritz, T., Caidahl, K., Bergdahl, K., Zierath, J.R., Chibalin, A.V., Moller, D.E., Kharitonenkov, A., Krook, A., 2011. Direct effects of FGF21 on glucose uptake in human skeletal muscle: implications for type 2 diabetes and obesity. Diabetes Metab. Res. Rev. 27, 286–297.
Matthews, D.R., Hosker, J.P., Rudenski, A.S., Naylor, B.A., Treacher, D.F., Turner, R.C., 1985. Homeostasis model assessment: insulin resistance and beta-cell function from fasting plasma glucose and insulin concentrations in man. Diabetologia 28, 412–419.
Munshi, M., Grande, L., Hayes, M., Ayres, D., Suhl, E., Capelson, R., Lin, S., Milberg, W., Weinger, K., 2006. Cognitive dysfunction is associated with poor diabetes control in older adults. Diabetes Care 29, 1794–1799.
Nishimura, T., Nakatake, Y., Konishi, M., Itoh, N., 2000. Identification of a novel FGF, FGF-21 preferentially expressed in the liver. Biochim. Biophys. Acta 1492, 203–206.
Northam, E.A., Anderson, P.J., Jacobs, R., Hughes, M., Warne, G.L., Werther, G.A., 2001. Neuropsychological profiles of children with type 1 diabetes 6 years after disease onset. Diabetes Care 24, 1541–1546.
Novotny, D., Vaverkova, H., Karasek, D., Lukes, J., Slavik, L., Malina, P., Orsag, J., 2014. Evaluation of total adiponectin, adipocyte fatty acid binding protein and fibroblast growth factor 21 levels in individuals with metabolic syndrome. Physiol. Res. 63, 219–228.
Ogawa, Y., Kurosu, H., Yamamoto, M., Nandi, A., Rosenblatt, K.P., Goetz, R., Eliseenkova, A.V., Mohammadi, M., Kuro-o, M., 2007. BetaKlotho is required for metabolic activity of fibroblast growth factor 21. Proc. Natl. Acad. Sci. U. S. A. 104, 7432–7437.
Ouchi, N., Parker, J.L., Lugus, J.J., Walsh, K., 2011. Adipokines in inflammation and metabolic disease. Nat. Rev. Immunol. 11, 85–97.
Owen, B.M., Ding, X., Morgan, D.A., Coate, K.C., Bookout, A.L., Rahmouni, K., Kliewer, S.A., Mangelsdorf, D.J., 2014. FGF21 acts centrally to induce sympathetic nerve activity, energy expenditure, and weight loss. Cell Metab. 20, 670–677.
Pacelli, C., De Rasmo, D., Signorile, A., Grattagliano, I., di Tullio, G., D'Orazio, A., Nico, B., Comi, G.P., Ronchi, D., Ferranini, E., Pirolo, D., Seibel, P., Schubert, S., Gaballo, A., Villani, G., Cocco, T., 2011. Mitochondrial defect and PGC-1alpha dysfunction in parkin-associated familial Parkinson's disease. Biochim. Biophys. Acta 1812, 1041–1053.
Pintana, H., Apaijai, N., Pratchayasakul, W., Chattipakorn, N., Chattipakorn, S.C., 2012. Effects of metformin on learning and memory behaviors and brain mitochondrial functions in high fat diet induced insulin resistant rats. Life Sci. 91, 409–414.
Pintana, H., Apaijai, N., Chattipakorn, N., Chattipakorn, S.C., 2013. DPP-4 inhibitors improve cognition and brain mitochondrial function of insulin-resistant rats. J. Endocrinol. 218, 1–11.
Pipatpiboon, N., Pratchayasakul, W., Chattipakorn, N., Chattipakorn, S.C., 2012. PPARgamma agonist improves neuronal insulin receptor function in hippocampus and brain mitochondria function in rats with insulin resistance induced by long term high-fat diets. Endocrinology 153, 329–338.
Pipatpiboon, N., Pintana, H., Pratchayasakul, W., Chattipakorn, N., Chattipakorn, S.C., 2013. DPP4-inhibitor improves neuronal insulin receptor function, brain mitochondrial function and cognitive function in rats with insulin resistance induced by high-fat diet consumption. Eur. J. Neurosci. 37, 839–849.
Pratchayasakul, W., Kerdphoo, S., Petsophonsakul, P., Pongchaidecha, A., Chattipakorn, N., Chattipakorn, S.C., 2011. Effects of high-fat diet on insulin receptor function in rat hippocampus and the level of neuronal corticosterone. Life Sci. 88, 619–627.
Pratchayasakul, W., Sa-Nguanmoo, P., Sivasinprasasn, S., Pintana, H., Tawinvisan, R., Sripetchwandee, J., Kumfu, S., Chattipakorn, N., Chattipakorn, S.C., 2015. Obesity accelerates cognitive decline by aggravating mitochondrial dysfunction, insulin resistance and synaptic dysfunction under estrogen-deprived conditions. Horm. Behav. 72, 68–77.

Raji, C.A., Ho, A.J., Parikshak, N.N., Becker, J.T., Lopez, O.L., Kuller, L.H., Hua, X., Leow, A.D., Toga, A.W., Thompson, P.M., 2010. Brain structure and obesity. Hum. Brain Mapp. 31, 353–364.

Reaven, G.M., Thompson, L.W., Nahum, D., Haskins, E., 1990. Relationship between hyperglycemia and cognitive function in older NIDDM patients. Diabetes Care 13, 16–21.

Riccardi, G., Giacco, R., Rivellese, A.A., 2004. Dietary fat, insulin sensitivity and the metabolic syndrome. Clin. Nutr. 23, 447–456.

Rivas-Arancibia, S., Guevara-Guzman, R., Lopez-Vidal, Y., Rodriguez-Martinez, E., Zanardo-Gomes, M., Angoa-Perez, M., Raisman-Vozari, R., 2010. Oxidative stress caused by ozone exposure induces loss of brain repair in the hippocampus of adult rats. Toxicol. Sci. 113, 187–197.

Sabia, S., Kivimaki, M., Shipley, M.J., Marmot, M.G., Singh-Manoux, A., 2009. Body mass index over the adult life course and cognition in late midlife: the Whitehall II Cohort Study. Am. J. Clin. Nutr. 89, 601–607.

Sripetchwandee, J., Pipatpiboon, N., Chattipakorn, N., Chattipakorn, S., 2014a. Combined therapy of iron chelator and antioxidant completely restores brain dysfunction induced by iron toxicity. PLoS One 9, e85115.

Sripetchwandee, J., Pipatpiboon, N., Pratchayasakul, W., Chattipakorn, N., Chattipakorn, S.C., 2014b. DPP-4 inhibitor and PPARgamma agonist restore the loss of CA1 dendritic spines in obese insulin-resistant rats. Arch. Med. Res. 45, 547–552.

Sripetchwandee, J., Wongjaikam, S., Krintratun, W., Chattipakorn, N., Chattipakorn, S.C., 2016. A combination of an iron chelator with an antioxidant effectively diminishes the dendritic loss, tau-hyperphosphorylation, amyloids-beta accumulation and brain mitochondrial dynamic disruption in rats with chronic iron-overload. Neuroscience 332, 191–202.

St-Pierre, J., Drori, S., Uldry, M., Silvaggi, J.M., Rhee, J., Jager, S., Handschin, C., Zheng, K., Lin, J., Yang, W., Simon, D.K., Bachoo, R., Spiegelman, B.M., 2006. Suppression of reactive oxygen species and neurodegeneration by the PGC-1 transcriptional coactivators. Cell 127, 397–408.

Stranahan, A.M., Norman, E.D., Lee, K., Cutler, R.G., Telljohann, R.S., Egan, J.M., Mattson, M.P., 2008. Diet-induced insulin resistance impairs hippocampal synaptic plasticity and cognition in middle-aged rats. Hippocampus 18, 1085–1088.

Tan, B.K., Hallschmid, M., Adya, R., Kern, W., Lehnert, H., Randeva, H.S., 2011. Fibroblast growth factor 21 (FGF21) in human cerebrospinal fluid: relationship with plasma FGF21 and body adiposity. Diabetes 60, 2758–2762.

Thirumangalakudi, L., Prakasam, A., Zhang, R., Bimonte-Nelson, H., Sambamurti, K., Kindy, M.S., Bhat, N.R., 2008. High cholesterol-induced neuroinflammation and amyloid precursor protein processing correlate with loss of working memory in mice. J. Neurochem. 106, 475–485.

Wang, H., Xiao, Y., Fu, L., Zhao, H., Zhang, Y., Wan, X., Qin, Y., Huang, Y., Gao, H., Li, X., 2010. High-level expression and purification of soluble recombinant FGF21 protein by SUMO fusion in *Escherichia coli*. BMC Biotechnol. 10, 14.

Winocur, G., Greenwood, C.E., Piroli, G.G., Grillo, C.A., Reznikov, L.R., Reagan, L.P., McEwen, B.S., 2005. Memory impairment in obese Zucker rats: an investigation of cognitive function in an animal model of insulin resistance and obesity. Behav. Neurosci. 119, 1389–1395.

Wu, Z., Puigserver, P., Andersson, U., Zhang, C., Adelmant, G., Mootha, V., Troy, A., Cinti, S., Lowell, B., Scarpulla, R.C., Spiegelman, B.M., 1999. Mechanisms controlling mitochondrial biogenesis and respiration through the thermogenic coactivator PGC-1. Cell 98, 115–124.

Xu, J., Lloyd, D.J., Hale, C., Stanislaus, S., Chen, M., Sivits, G., Vonderfecht, S., Hecht, R., Li, Y.S., Lindberg, R.A., Chen, J.L., Jung, D.Y., Zhang, Z., Ko, H.J., Kim, J.K., Veniant, M.M., 2009a. Fibroblast growth factor 21 reverses hepatic steatosis, increases energy expenditure, and improves insulin sensitivity in diet-induced obese mice. Diabetes 58, 250–259.

Xu, J., Stanislaus, S., Chinookoswong, N., Lau, Y.Y., Hager, T., Patel, J., Ge, H., Weiszmann, J., Lu, S.C., Graham, M., Busby, J., Hecht, R., Li, Y.S., Li, Y., Lindberg, R., Veniant, M.M., 2009b. Acute glucose-lowering and insulin-sensitizing action of FGF21 in insulin-resistant mouse models–association with liver and adipose tissue effects. Am. J. Physiol. Endocrinol. Metab. 297, E1105–E1114.

Yagi, K., 1998. Simple assay for the level of total lipid peroxides in serum or plasma. Methods Mol. Biol. 108, 101–106.

Yang, M., Zhang, L., Wang, C., Liu, H., Boden, G., Yang, G., Li, L., 2012. Liraglutide increases FGF-21 activity and insulin sensitivity in high fat diet and adiponectin knockdown induced insulin resistance. PLoS One 7, e48392.

Yu, Y., Bai, F., Wang, W., Liu, Y., Yuan, Q., Qu, S., Zhang, T., Tian, G., Li, S., Li, D., Ren, G., 2015. Fibroblast growth factor 21 protects mouse brain against d-galactose induced aging via suppression of oxidative stress response and advanced glycation end products formation. Pharmacol. Biochem. Behav. 133, 122–131.

Zhang, X., Yeung, D.C., Karpisek, M., Stejskal, D., Zhou, Z.G., Liu, F., Wong, R.L., Chow, W.S., Tso, A.W., Lam, K.S., Xu, A., 2008. Serum FGF21 levels are increased in obesity and are independently associated with the metabolic syndrome in humans. Diabetes 57, 1246–1253.

Zhang, C., Shao, M., Yang, H., Chen, L., Yu, L., Cong, W., Tian, H., Zhang, F., Cheng, P., Jin, L., Tan, Y., Li, X., Cai, L., Lu, X., 2013. Attenuation of hyperlipidemia- and diabetes-induced early-stage apoptosis and late-stage renal dysfunction via administration of fibroblast growth factor-21 is associated with suppression of renal inflammation. PLoS One 8, e82275.

เอกสารแนบหมายเลข 18

Neuroscience 332 (2016) 191–202

A COMBINATION OF AN IRON CHELATOR WITH AN ANTIOXIDANT EFFECTIVELY DIMINISHES THE DENDRITIC LOSS, TAU-HYPERPHOSPHORYLATION, AMYLOIDS-β ACCUMULATION AND BRAIN MITOCHONDRIAL DYNAMIC DISRUPTION IN RATS WITH CHRONIC IRON-OVERLOAD

JIRAPAS SRIPETCHWANDEE,[a,b†] SUWAKON WONGJAIKAM,[a,b†] WARUNSORN KRINTRATUN,[a,b] NIPON CHATTIPAKORN[a,b] AND SIRIPORN C. CHATTIPAKORN[a,c*]

[a] *Neurophysiology Unit, Cardiac Electrophysiology Research and Training Center, Faculty of Medicine, Chiang Mai University, Chiang Mai 50200, Thailand*

[b] *Department of Physiology, Faculty of Medicine, Chiang Mai University, Chiang Mai 50200, Thailand*

[c] *Department of Oral Biology and Diagnostic Sciences, Faculty of Dentistry, Chiang Mai University, Chiang Mai 50200, Thailand*

Abstract—Iron-overload can cause cognitive impairment due to blood–brain barrier (BBB) breakdown and brain mitochondrial dysfunction. Although deferiprone (DFP) has been shown to exert neuroprotection, the head-to-head comparison among iron chelators used clinically on brain iron-overload has not been investigated. Moreover, since antioxidant has been shown to be beneficial in iron-overload condition, its combined effect with iron chelator has not been tested. Therefore, the hypothesis is that all chelators provide neuroprotection under iron-overload condition, and that a combination of an iron chelator with an antioxidant has greater efficacy than monotherapy. Male Wistar rats ($n = 42$) were assigned to receive a normal diet (ND) or a high-iron diet (HFe) for 4 months. At the 2nd month, HFe-fed rats were treated with a vehicle, deferoxamine (DFO), DFP, deferasirox (DFX), n-acetyl cysteine (NAC) or a combination of DFP with NAC, while ND-fed rats received vehicle. At the end of the experiment, rats were decapitated and brains were removed to determine brain iron level and deposition, brain mitochondrial function, BBB protein expression, brain mitochondrial dynamic, brain apoptosis, tau-hyperphosphorylation, amyloid-β (Aβ) accumulation and dendritic spine density. The results showed that iron-overload induced BBB breakdown, brain iron accumulation, brain mitochondrial dysfunction, impaired brain mitochondrial dynamics, tau-hyperphosphorylation, Aβ accumulation and dendritic spine reduction. All treatments, except DFX, attenuated these impairments. Moreover, combined therapy provided a greater efficacy than monotherapy. These findings suggested that iron-overload induced brain iron toxicity and a combination of an iron chelator with an antioxidant provided a greatest efficacy for neuroprotection than monotherapy. **© 2016 IBRO. Published by Elsevier Ltd. All rights reserved.**

Key words: iron-overload, iron chelator, combined therapy, dendritic spine, mitochondrial dynamic.

INTRODUCTION

Iron-overload condition has commonly known to induce cellular toxicity by damaging the cellular compartments, such as DNA and mitochondria, as well as cause the membrane lipid peroxidation (Eaton and Qian, 2002). Moreover, the excessive amounts of iron in the brain have been shown to be associated with neurodegeneration (McNeill and Chinnery, 2011). A previous study demonstrated that the cognitive impairment following chronic iron-overload condition occurred by causing the breakdown of blood–brain barrier (BBB), impairing brain mitochondrial function leading to brain apoptosis (Sripetchwandee et al., 2014a). However, other possible underlying mechanisms regarding the cognitive decline under this condition including loss of dendritic spine density and impaired mitochondrial dynamics have not been investigated.

Dendritic spine density plays a fundamental role in the communication between neurons via synaptic transmissions of both electrical and chemical synapses and is responsible for cognitive function (Smrt and Zhao, 2010). A reduction in dendritic spine density has been shown to be associated with cognitive decline (Sripetchwandee et al., 2014b). Although it has been proposed that dendritic spines play a role in cognitive function, the effect of the iron-overload condition on dendritic spine density has not been investigated.

*Correspondence to: S. C. Chattipakorn, Neurophysiology Unit, Cardiac Electrophysiology Research and Training Center, Faculty of Medicine, Chiang Mai University, Chiang Mai 50200, Thailand. Fax: +66-53-222-844.
E-mail addresses: scchattipakorn@gmail.com, siriporn.c@cmu.ac.th (S. C. Chattipakorn).

† Equal contribution.

Abbreviations: AD, Alzheimer's disease; APP, amyloid precursor protein; Aβ, amyloid-β; BBB, blood–brain barrier; DFO, deferoxamine; DFP, deferiprone; DFX, deferasirox; Drp1, dynamin-related protein 1; HFe, high-iron diet; Mfn2, mitofusin2; NAC, n-acetyl cysteine; ND, normal diet; NTBI, non-transferrin bound iron; ROS, reactive oxygen species.

http://dx.doi.org/10.1016/j.neuroscience.2016.07.003
0306-4522/© 2016 IBRO. Published by Elsevier Ltd. All rights reserved.

The development of Alzheimer's disease (AD)-like pathological changes including the amyloid-β (Aβ) accumulation and tau-hyperphosphorylation are positively associated with cognitive impairment (Colijn and Grossberg, 2015). An Aβ aggregation has been related with brain oxidative stress (Misonou et al., 2000; Butterfield and Boyd-Kimball, 2004; Bartley et al., 2012) and its accumulation of Aβ impaired the mitochondrial electron transport chain via the induction of free radical generation, leading to the loss of ATP production, increased oxidative stress, promoted neurofibrillary tangles (NFTs) formation, and further caused the neuronal death (Yao et al., 2005; Dumont et al., 2011). Excessive amounts of iron caused generation of reactive oxygen species (ROS) and subsequently massively increased the level of oxidative stress (Koppenol, 2001). Although the involvement of iron accumulation in AD models has been observed (Leskovjan et al., 2011), alterations of AD pathology under conditions of iron-overload have not been studied.

An abnormality in mitochondria, including increased mitochondrial fragmentation, is an important factor that related with the dysfunction of mitochondria as well as cell death in aging and neurodegenerative diseases (Navarro and Boveris, 2010). It has been shown that a balance of mitochondrial dynamics, including mitochondrial fusion and fission, reflected in both of mitochondrial morphology and number (Westermann, 2010), and that this process plays an important role in cell life and death (Perfettini et al., 2005). Normally, the balance of mitochondrial fusion and fission is needed to maintain the mitochondrial shape, distribution and connectivity as well as their functions. Mitochondrial fusion is required for the expansion of the mitochondrial networks in cells which are an important factor in several processes such as a calcium signaling in cells and in certain developmental processes (Chen et al., 2003; Szabadkai et al., 2006). In contrast, mitochondrial fission is important to produce various in both morphological and functional of mitochondria (Ishihara et al., 2009). Although a recent study has shown that the exposure of iron treatment in rats during neonatal period resulted in changes in the expression of both protein and mRNA which are involved with mitochondrial fusion and fission mechanisms in the brain (da Silva et al., 2014), the effects of chronic iron-overload condition induced by long-term high-iron diet (HFe) consumption on brain mitochondrial dynamics in adult rats have not yet been investigated.

Iron chelation therapy has been used in practice to prevent tissue iron toxicity (Poggiali et al., 2012). The currently available iron chelators are deferoxamine (DFO), deferiprone (DFP) and deferasirox (DFX). These iron chelators provide therapeutic protective effects against cellular iron damage by reducing plasma non-transferrin bound iron (NTBI), cellular iron accumulation, and cell death in association with the improvement of cell survival and the maintenance of iron stores (Borgna-Pignatti and Marsella, 2015). However, the comparative efficacy of these iron chelators in the brain under iron-overload conditions has not yet been investigated. Our recent study also indicated that either DFP or an antioxidant, n-acetyl cysteine (NAC) attenuated brain iron toxicity under conditions of iron-overload. In addition, combined DFP + NAC therapy has been shown to restore brain mitochondrial function and cognitive function after impairment caused by iron-overload conditions (Sripetchwandee et al., 2014a). However, the effects of these iron chelators, NAC and a combination of an iron chelator with NAC on dendritic spine density, AD pathology and brain mitochondrial dynamics under conditions of iron-overload have not been demonstrated.

In this study the following hypotheses were tested: (1) An iron-overloaded condition decreases the dendritic spine density, increases AD pathology and induces an imbalance of brain mitochondrial dynamics; (2) pharmacological intervention with iron chelators: DFO, DFP, DFX as well as an antioxidant: NAC exerts equally protective effects on the brain under conditions of iron-overload and (3) combined therapy with an iron chelator and NAC in an iron-overloaded condition provides greater efficacy than monotherapy in preservation of dendritic spine density, prevention of the occurrence of AD pathology and restoration of the brain mitochondrial dynamic.

EXPERIMENTAL PROCEDURES

Experimental protocols

All animal studies were approved by the Institutional Animal Care and Use Committee (IACUC) at the Faculty of Medicine, Chiang Mai University. Young adult male Wistar rats weighing 180–200 g ($n = 42$) were obtained from the National Laboratory Animal Center, Salaya Campus, Mahidol University, Thailand. All rats were housed in an animal holding room under controlled conditions (20–22 °C, 50 ± 10% humidity) and lighting (12-hour day/night cycle) with free access to drinking water. After acclimatization for 1 week, then young adult rats were divided to receive either a normal diet (ND) or a HFe to induce an iron-overload condition (0.2% ferrocene/kg of diet) for 4 months with *ad libitum*. Moreover, body weight and food intake from all rats were record weekly. At 2 months into the experiment, ND-treated rats were given with a 0.9% of normal saline solution (NSS) 2 ml/kg/day as a vehicle via intragastric feeding (NDV, $n = 6$) while HFe-treated rats were randomly subdivided into six groups ($n = 6$/subgroup) to receive the assigned treatments including: 0.9% NSS 2 ml/kg/day (HFeV) and the pharmacological intervention of intraperitoneal injections of 25-mg/kg/day DFO (HFeDFO, IP), intragastric feeding of 75-mg/kg/day DFP (HFeDFP), 20-mg/kg/day DFX (HFeDFX), 100-mg/kg/day N-acetyl cysteine (HFeNAC) and a combination of 75-mg/kg/day DFP and 100-mg/kg/d NAC (HFeDFP + NAC). HFeDFO rats were injected intraperitoneally with DFO whereas the other HFe-treated rats were given their assigned treatment orally. All rats were given the assigned treatments continuously receiving their assigned diets for a further 2 months.

At the end of the experiment, rats were deeply anesthetized using 3% isoflurane and an intraperitoneal injection of 80 mg/kg thiopental and then decapitated.

Brain was rapidly removed in each case apart from the cerebellum, and separated into two halves. The first half was used for brain dendritic spine determination. The second half was used for either brain mitochondrial isolation or stored at −80 °C for further analysis. Blood samples were drawn from the tail vein at the end of experiment and collected in sodium heparin tubes. Plasma was obtained by centrifuging the blood at 3000 rpm, 4 °C for 15 min and then was kept frozen at −80 °C until required for plasma NTBI determination. Summarized experimental protocol is shown in Fig. 1.

Plasma NTBI measurement

Plasma NTBI concentration was measured by nitrilotriacetic acid disodium salt (NTA) chelation/flow cytometry as modified from a previous study (Ma et al., 2014). In brief, plasma was incubated in the NTA solution for 30 min to allow the formation of the Fe^{3+}-$(NTA)_2$ complex. A spinning technique of the plasma mixture through a membrane filter (NanoSep®, 30-kDa cut off, polysulfone type; Pall Life Sciences, Ann Arbor, MI, USA) was used for separated this complex from plasma proteins. The concentration of this Fe^{3+}-$(NTA)_2$ complex demonstrated the NTBI in the ultrafiltrate. A standard solution of ferric nitrate was used as with the final concentrations ranging from 0 to 10 μM. Plasma NTBI concentration was determined using a flow cytometry (Guava EasyCyte HT, Merck Millipore, Germany) and then was calculated from a standard curve using GraphPad Prism® software (GraphPad Software, Inc., La Jolla, CA, USA).

Brain iron level assay

The determination of brain iron was performed using a method modified from a previous study (Rebouche et al., 2004). Homogenized brain was precipitated in a protein precipitated solution (as a ratio of 1:1). Mixed solution was further heated for 1 h at 95 °C, cooled down to the room temperature and then centrifuged for 10 min at 8200*g*. Supernatant was mixed as a ratio of 1:1 with a chromagen solution, containing 0.508 mm ferrozine, 1.5 M sodium acetate and 0.1% thioglycolic acid, and was incubated for 30 min at room temperature. Absorbance of samples was determined using a microplate reader at 562 nm and brain iron concentration was compared with the standard curve (Sripetchwandee et al., 2014a).

Brain iron deposition assay

Brain iron deposition was determined using the Perl's Prussian blue staining techniques as modified from a previous study (Kumfu et al., 2012). Brain tissues were fixed in 10% neutral-buffer formalin, embedded in paraffin boxes, cut with a sliding microtome (5-μm thick sections) and stained with Perl's super vital dye solution. The Perl's stained tissue slides were examined under a light microscope (Olympus Corporation, Philadelphia USA) using a 60× magnification objective lens and images recorded with a digital camera (Sony, Japan).

Brain mitochondrial isolation

Brain mitochondria were isolated as previously described (Sripetchwandee et al., 2013). After decapitation the brain sections were removed into 5 ml ice-cold MSE solution. Then the brain sections were transferred to 10 ml of ice-cold MSE solution with 0.05% of nagarse, homogenized and centrifuged at 2000*g* for 4 min. Supernatant was collected and then centrifuged at 12,000*g* for 9 min. Mitochondrial pellets were collected and re-suspended in 10-ml ice-cold MSE solution with 0.02% of digitonin and further centrifuged at 12,000*g* for 11 min. Finally, mitochondrial pellets were resuspended in a mitochondrial respiration buffer (Sripetchwandee et al., 2013). Brain mitochondrial protein concentration were determined by BCA assay (Sripetchwandee et al., 2013).

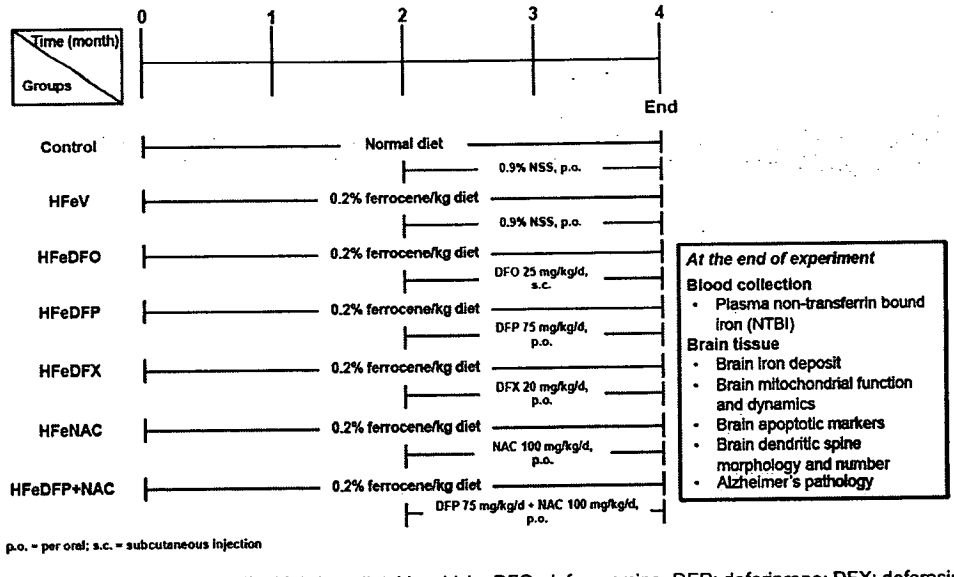


Fig. 1. Summarized experimental protocol. HFe: high-iron diet, V: vehicle, DFO: deferoxamine, DFP: deferiprone; DFX: deferasirox; NAC: n-acetyl cysteine.

Brain mitochondrial swelling assay

Brain mitochondrial swelling was determined by measuring the changes in the absorbance of the mitochondrial suspensions at 540 nm using a microplate reader (Bio-Tek Instruments, Inc. Winooski, Vermont USA) (Sripetchwandee et al., 2013). Mitochondria (0.4 mg/ml) were incubated in 2-ml respiration buffer. Brain mitochondrial swelling was represented as a decrease in absorbance value (Sripetchwandee et al., 2013).

Brain mitochondrial membrane potential ($\Delta\Psi_m$) change assay

Brain mitochondria membrane potential ($\Delta\psi_m$) change was measured using JC-1 dye (Sripetchwandee et al., 2013). Mitochondria (0.4 mg/ml) were stained with JC-1 (5 μM) at 37 °C for 15 min and determined a fluorescence intensity by use of a fluorescent microplate reader (Bio-Tek Instruments, Inc. Winooski, Vermont USA). JC-1 monomer-form (green fluorescence) was excited at 485 nm and detected the emission at 590 nm while JC-1 aggregated-form (red fluorescence) was excited at 485 nm and detected the emission at 530 nm. An alteration in mitochondrial membrane potential was calculated as the ratio of red to green fluorescence and a reduction of the red to green fluorescent intensity ratio was represented as brain mitochondrial depolarization (Sripetchwandee et al., 2013).

Brain Mitochondrial ROS production assay

Brain mitochondrial ROS level was measured using a DCFDA fluorescent dye (Sripetchwandee et al., 2013). Brain mitochondria (0.4 mg/ml) were incubated with 2 μM DCFDA at 25 °C for 20 min. ROS level was measured with a fluorescent microplate reader (Bio-Tek Instruments, Inc., Winooski, Vermont, USA) at a wavelength of 485 nm and an emission wavelength at 530 nm. An increase in fluorescent intensity represented an increase of brain mitochondrial ROS production (Sripetchwandee et al., 2013).

Western blot analysis

Brain protein extraction was prepared by homogenization of nitrogen-frozen brain tissues in an extraction buffer containing 1-mM EDTA, 1-mM EGTA, 1% NP-40, 1% Triton X-100 and protease inhibitor (Sripetchwandee et al., 2014a). Total protein concentration was determined using a Bio-Rad protein assay kit (Bio-Rad Laboratories, Hercules, California, USA). A 50- to 80-μg of total protein was mixed with a loading buffer (5% β-mercaptoethanol, 0.05% bromophenol blue, 75 mM Tris-HCl (pH 6.8), 2% SDS and 10% glycerol), and loaded onto the 10%–12.5% SDS-Acrylamide gels. After this, proteins were further transferred to polyvinylidene difluoride (PVDF) membranes in a Wet/Tank blotting system (Bio-Rad Laboratories, Hercules, California, USA). Membranes were blocked with 5% non-fat dry milk in Tris-Buffered Saline and Tween (TBST) buffer for 1 h at room temperature. Then, membranes were exposed overnight at 4 °C to primary antibodies including occludin (SC-5562, Santa Cruz Biotechnology, Santa Cruz, CA, USA), Bcl-2 (#2876, Cell Signaling Technology, Danvers, MA, USA), Bax (SC-493, Santa Cruz Biotechnology, Santa Cruz, CA, USA), mitofusins-2 (Mfn2) (#9482, Cell Signaling Technology, Danvers, MA, USA), dynamin-related protein 1 (Drp1) (#5391, Cell Signaling Technology, Danvers, MA, USA), tau (#4019, Cell Signaling Technology, Danvers, MA, USA) and its phosphorylated form (p-tau) (#12885, Cell Signaling Technology, Danvers, MA, USA), Aβ (SC-28395, Santa Cruz Biotechnology, Santa Cruz, CA, USA), amyloid precursor protein (APP) (07-667, Millipore, Temecula, CA, USA) and β-actin (SC-47778, Santa Cruz Biotechnology, Santa Cruz, CA, USA). All membranes were incubated with a secondary goat anti-rabbit antibody, conjugated with horseradish peroxidase. Protein bands were visualized using ECL western blotting detection reagent. Total results were represented as the average signal intensity.

Protein quantitation by the Bicinchoninic Acid (BCA) Assay

Brain protein concentration was determined according to the Bicinchoninic Acid (BCA) Assay. Reagent A was composed of sodium bicinchoninate (0.1 g), $Na_2CO_3{\cdot}H_2O$ (2.0 g), sodium tartrate (dihydrate) 0.16 g, NaOH (0.4 g), and $NaHCO_3$ (0.95 g), with the volume being made up to 100 ml. The pH was adjusted to 11.25 with NaOH if necessary. Reagent B was composed of $CuSO_4{\cdot}5H_2O$ (0.4 g) in 10 ml of water and the standard working reagent (SWR) is a mix of 100 ml of reagent A, with 2 ml of reagent B. The solution is apple green in color and is stable at room temperature for 1 week. SWR (1 ml) was added to brain mitochondrial protein (50 μl) and incubated at 60 °C for 30 min. The sample was cooled to room temperature and then the absorbance was measured at 562 nm using a spectrophotometer. A calibration curve was constructed using dilutions of a stock 1 mg/ml solution of bovine serum albumin (BSA) (Sripetchwandee et al., 2014a).

Golgi impregnation for dendritic spine density

Golgi impregnation was performed as previously described (Frankfurt et al., 2011; Sripetchwandee et al., 2014b). After decapitation, each half of rat's brain was rapidly removed, further rinsed with double-distilled water, and placed in the solutions provided in the Rapid Golgi Stain Kit (FD Neurotechnologies kit, PK 401, Ellicott City, MD, USA). In the hippocampal CA1 region, two segments from the pyramidal cells were randomly determined at the sections of 100–200 μm apart from the soma with the dendritic length ranging from 20- to 30-μm. First segment was addressed at the secondary basal dendrites whereas the another segment was addressed on the tertiary branch of apical dendrites. Dendritic spines were demonstrated using an inverted microscope through a 60× oil-immersion objective lens (IX-81, Olympus, Tokyo, Japan). Spine numbers were determined using a hand counter, and the dendritic length was analyzed using Xcellence® imaging software (Olympus, Tokyo, Japan).

Density of spine was represented as the number of spines/20-μm of dendritic length.

Data analysis

The data are presented as mean ± standard error of mean. The data were processed using SPSS release 17.0 for Windows (Statistical Package for Social Sciences, Chicago, IL, USA). The significance of the difference between the mean was calculated using a One-way ANOVA, followed by Fisher's least significant difference (LSD) post hoc analysis. The data from plasma NTBI were analyzed using non-parametric Kruskal-Wallis H followed by the Mann-Whitney U test. $p < 0.05$ was considered statistically significant.

RESULTS

Long-term high-iron diet (HFe) consumption caused an iron-overloaded condition and all pharmacological interventions, except DFX, attenuated brain iron-overload

Iron-overload condition by long-term HFe consumption significantly decreased the body weight (414 ± 11 g), when compared with ND-fed rats (518 ± 11 g) ($F = 44.454$, $p < 0.01$). In addition, ND-fed rats showed no plasma NTBI with a low level of brain iron (Fig. 2A). However, HFe-fed rats developed an iron-overloaded condition, as shown by significantly increased plasma NTBI as well as increased brain iron level, when compared with the ND-fed rats (Fig. 2A). All pharmacological interventions significantly decreased plasma NTBI, when compared with the control HFe-fed rats treated with vehicle (Fig. 2A). In the brain, all therapeutic interventions, except DFX, significantly ameliorated brain iron levels ($F = 6.979$, $p < 0.01$, Fig. 2B), and brain iron deposition was decreased as shown in the Perl's staining in the brain of HFe-fed rats (Fig. 2C).

Long-term HFe consumption disrupted the BBB and increased the Alzheimer's pathology, and all pharmacological interventions, except DFX, attenuated these adverse effects in the brain

The iron-overloaded condition induced the BBB disruption as indicated by a decreased expression of occludin which is a tight junction protein in the BBB ($F = 7.789$, $p < 0.01$, Fig. 3A). AD-like pathological changes were also observed, identified by the increased Aβ level ($F = 9.457$, $p < 0.01$) and amyloid-precursor protein (APP) level ($F = 8.942$, $p < 0.01$) in association with the increased phosphorylation-tau/total-tau ratio indicating hyper-phosphorylation, in the vehicle-treated HFe-fed rats ($F = 3.290$, $p = 0.023$), when compared with the ND-fed rats (Fig. 3B–D). All the pharmacological intervention treatments, except DFX, prevented these adverse events caused by iron-overload by protecting the brain against BBB breakdown and showing restorative effects in these AD-like proteins back to the normal level, compared with the vehicle-treated HFe-fed rats (Fig. 3).

Long-term HFe consumption impaired brain mitochondrial function, and all pharmacological interventions, except DFX, attenuated this adverse effect in the brain

Iron-overloaded condition induced brain mitochondrial dysfunction as indicated by the increased brain mitochondrial ROS production ($F = 4.479$, $p < 0.01$), increased brain mitochondrial membrane potential changes ($F = 12.006$, $p < 0.01$), decreased brain mitochondrial absorbance which represented brain mitochondrial swelling ($F = 10.169$, $p < 0.01$) (Fig. 4A–C). The treatment with DFO, DFP, NAC and combined therapy, but not DFX, in iron-overloaded rats attenuated brain mitochondrial dysfunction (Fig. 4).

Long-term HFe consumption induced brain apoptosis and impaired brain mitochondrial dynamic, and these were prevented by all pharmacological interventions, except DFX

Iron-overloaded rats demonstrated brain apoptosis as indicated by the increased Bax expression ($F = 4.186$, $p < 0.01$) and decreased Bcl-2 expression ($F = 5.314$, $p < 0.01$), when compared with the ND-fed rats (Fig. 5A and B). In addition, the iron-overloaded condition decreased the expression of a mitochondrial fusion protein: Mfn2 ($F = 3.628$, $p = 0.017$), as well as increasing the expression of a mitochondrial fission protein: Drp1 ($F = 9.755$, $p < 0.01$), suggesting an imbalance in brain mitochondrial dynamics in HFe-fed rats (Fig. 5C and D). Therapeutic administrations, including DFO, DFP, NAC and the combination therapy protected the brain against apoptosis and the imbalance of mitochondrial dynamics caused by an iron-overloaded condition. In contrast, the DFX treatment failed to provide these protective effects (Fig. 5).

Loss of the dendritic spine density in iron-overloaded rats could be attenuated by all pharmacological interventions, except DFX

The condition caused by iron-overload significantly reduced the dendritic spine density and morphology on the secondary and tertiary branches of the apical dendrites, when compared with those of ND-fed rats ($F = 8.819$, $p < 0.01$, Fig. 6). However, all pharmacological interventions, except DFX, prevented this effect. In addition, the combination therapy of DFP and NAC in HFe-fed rats stimulated the restoration of the spine density to the same levels of ND-fed rats (Fig. 6).

DISCUSSION

The major findings of this study are as follows: (1) HFe-fed rats demonstrated an iron-overload condition, as indicated by an increased plasma NTBI and the presence of brain iron toxicity. This was indicated by the BBB breakdown, brain iron-overload, brain mitochondrial dysfunction, brain mitochondrial dynamic imbalance, an AD-like pathology in the brain, and the loss of dendritic spines. (2) Pharmacological intervention with iron

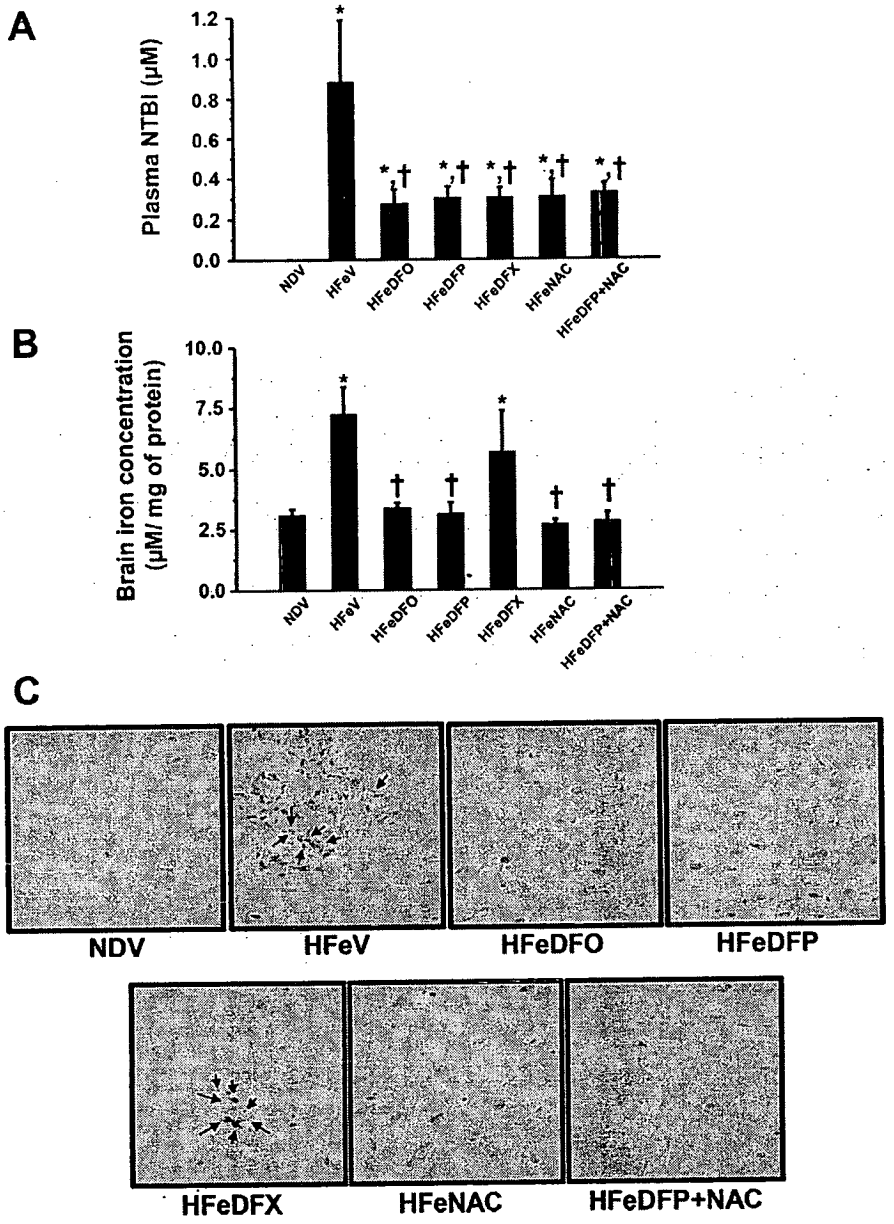


Fig. 2. The effects of a high-iron diet and the experimental pharmacological interventions on plasma non-transferrin bound iron (NTBI) (A), brain iron level (B) and the Prussian blue iron staining in brain tissues (400× total magnification). The arrows indicate brain iron staining in blue color. Values are mean ± SEM. ND: normal diet fed group; HFe: high-iron diet fed group, V: vehicle, DFO: deferoxamine, DFP: deferiprone; DFX: deferasirox; NAC: n-acetyl cysteine. $^{*}p < 0.05$ vs. ND treated with vehicle (NDV); $^{\dagger}p < 0.05$ vs. HFe treated with vehicle (HFeV). (For interpretation of the references to colour in this figure legend, the reader is referred to the web version of this article.)

chelators: DFO and DFP, but not DFX, significantly attenuated these adverse effects due to brain iron toxicity. (3) An antioxidant: NAC also ameliorated brain toxicity following iron-overload, and (4) a combination of DFP and NAC exerted greater efficacy than any monotherapy in neuroprotective effects against the iron-overloaded condition.

The iron-overloaded condition has been commonly known to contribute to tissue damage, including tissues in the heart and the brain (Lekawanvijit and Chattipakorn, 2009; Sripetchwandee et al., 2014a). It has been known that iron-overload condition can generate excessive free-radicals through Fenton's reaction resulting in the induction of severe oxidative stress (Crichton et al., 2002). This iron-toxicity damages several cellular compartment including the mitochondria, nucleus, DNA, ribosome etc. In addition, iron-induced oxidative stress also attacks the cell membrane, resulting in the production of cytotoxic aldehyde products including malondialdehyde (MDA) and 4-hydroxylnonenal (HNE) (Braughler et al., 1986). This phenomenon is called lipid peroxidation. Normally, the BBB acts as a defensive structure against pathogens in the brain. It consists of vascular endothelial cells and astrocytic end-feet

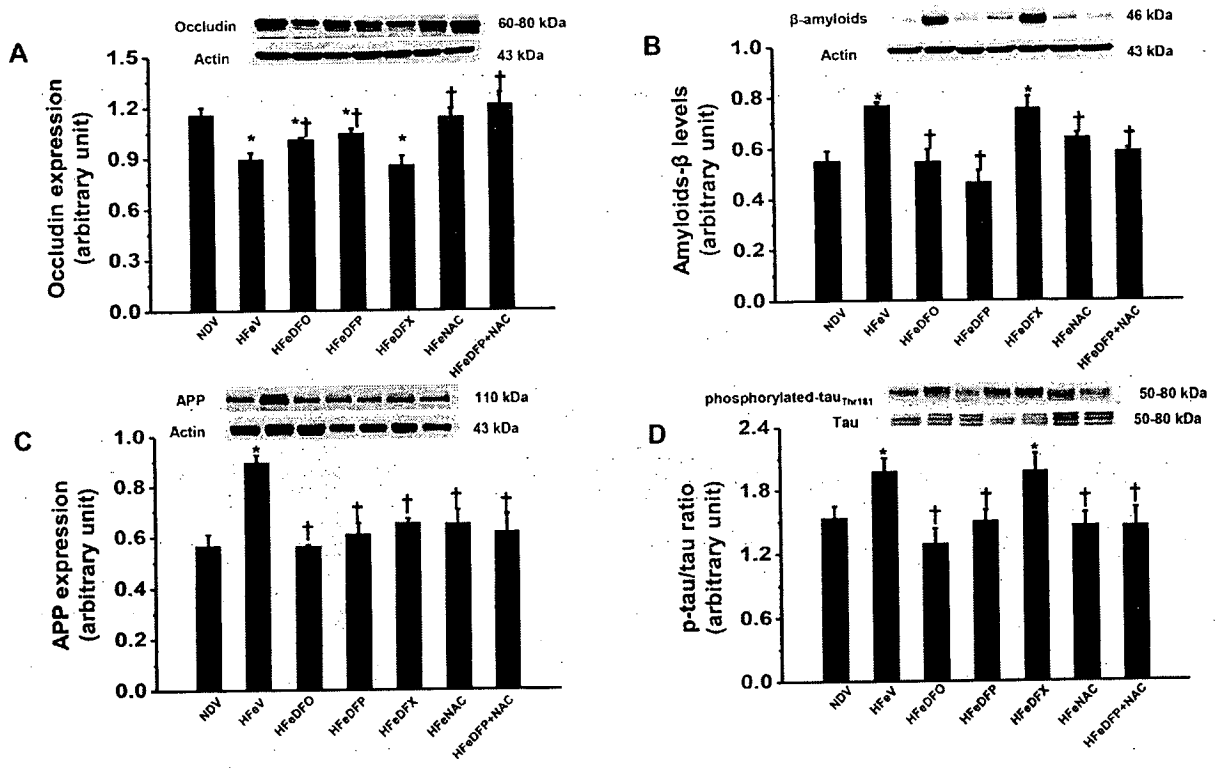


Fig. 3. The effect of iron-overloaded condition and the experimental pharmacological interventions on the blood–brain barrier and the Alzheimer's-like change. Each panel represented the expression of tight-protein; occludin (A) and the Alzheimer's-like change including amyloid-β (Aβ) (B), amyloid precursor protein (APP) (C) and phosphorylated-tau/total-tau ratio (D). Values are mean ± SEM. ND: normal diet fed group; HFe: high-iron diet fed group, V: vehicle, DFO: deferoxamine, DFP: deferiprone; DFX: deferasirox; NAC: n-acetyl cysteine. $^{*}p < 0.05$ vs. ND treated with vehicle (NDV); $^{\dagger}p < 0.05$ vs. HFe treated with vehicle (HFeV).

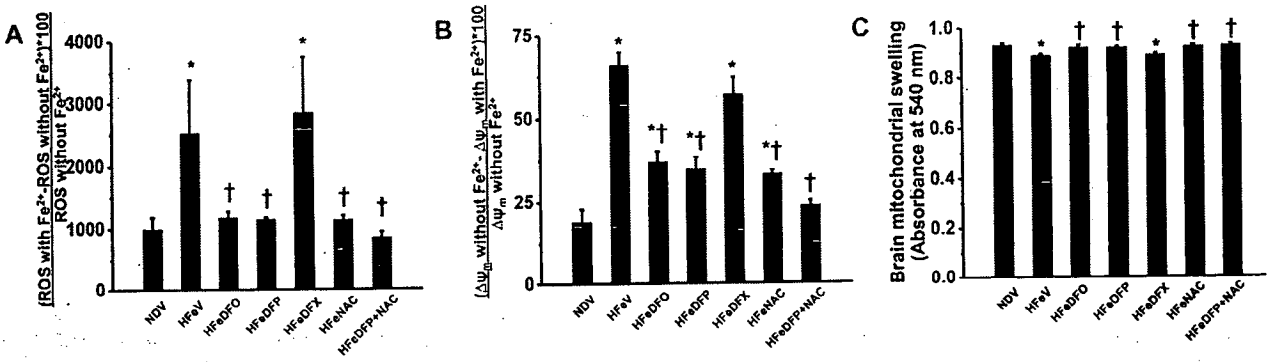


Fig. 4. The effects of an iron-overload condition and the experimental pharmacological interventions on the brain mitochondrial ROS production (A), brain mitochondrial membrane potential changes (B) and brain mitochondrial swelling as indicated by a decreased absorbance (C). Values are mean ± SEM. $^{*}p < 0.05$ vs. ND treated with vehicle (NDV); $^{\dagger}p < 0.05$ vs. HFe treated with vehicle (HFeV).

(Persidsky et al., 2006). Under the physiological condition, plasma iron cannot easily pass through the BBB into the brain. However, during the iron-overloaded condition, excessive free radicals produced by iron can damage this structure by inducing lipid peroxidation, which disrupts the BBB integrity and consequently causes the uptake of plasma iron into the brain (Sripetchwandee et al., 2014a). A recent study has shown the cognitive impairment of the brain in rats with an iron-overload condition which could be due to the disruption of the BBB in association with brain mitochondrial dysfunction (Sripetchwandee et al., 2014a). However, this study demonstrated that iron-overload not only induced breakdown of the BBB and brain mitochondrial dysfunction, but also caused brain mitochondrial dynamic imbalance, an AD-like pathology in the brain, and the loss of dendritic spine density. All of these findings support the hypothesis that the iron-overload condition leads to brain damage.

A recent study reported that the mitochondrial morphology and number depends on the balancing of mitochondrial activities in both mitochondrial fusion and fission, known as mitochondrial dynamics (Westermann,

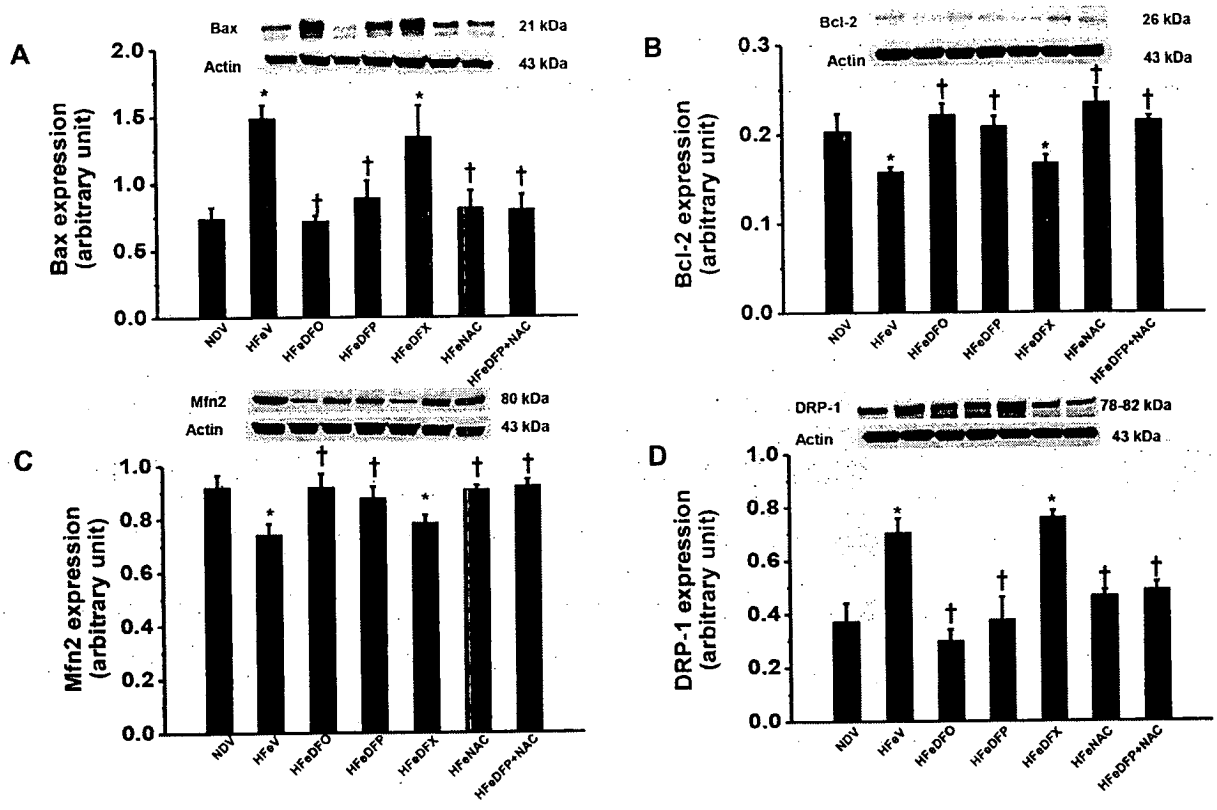


Fig. 5. The effect of an iron-overload condition and the experimental pharmacological interventions on the brain apoptosis and brain mitochondrial dynamics. Each panel represented the expression of apoptotic protein; Bax (A), anti-apoptotic protein; Bcl-2 (B), mitochondrial fusion protein; mitofusin2 (Mfn2) (C) and mitochondrial fission protein; dynamin-related protein 1 (Drp1) (D). Values are mean ± SEM. ND: normal diet fed group; HFe: high-iron diet fed group, V: vehicle, DFO: deferoxamine, DFP: deferiprone; DFX: deferasirox; NAC: n-acetyl cysteine. $^{*}p < 0.05$ vs. ND treated with vehicle (NDV); $^{\dagger}p < 0.05$ vs. HFe treated with vehicle (HFeV).

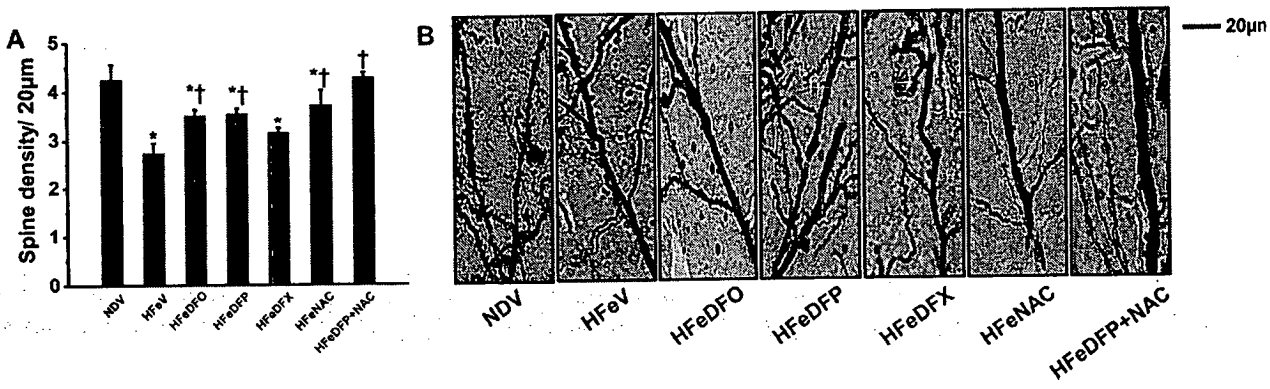


Fig. 6. The effects of an iron-overload condition and the experimental pharmacological interventions on the dendritic spine morphology and number Values are mean ± SEM. ND: normal diet fed group; HFe: high-iron diet fed group, V: vehicle, DFO: deferoxamine, DFP: deferiprone; DFX: deferasirox; NAC: n-acetyl cysteine. $^{*}p < 0.05$ vs. ND treated with vehicle (NDV); $^{\dagger}p < 0.05$ vs. HFe treated with vehicle (HFeV).

2010). Mitochondrial fusion and fission also play a role in cell survival and cell death (Perfettini et al., 2005). In the brain, it has been reported that the changes in mitochondrial dynamics have been associated with neurodegeneration (Knott and Bossy-Wetzel, 2008). Mitochondrial fusion is required for the extension of interconnected mitochondrial networks in cells as well as its protective effect against mtDNA mutations in the cells (Ono et al., 2001). In this regard, Mitofusin (Mfn), a mitochondrial protein which is divided into two homologs including Mfn1 and Mfn2, is known to be a core component protein in mitochondrial fusion in mammals (Chen et al., 2003). Several pathological conditions, such as the hypoxic condition and lipotoxicity, have been shown to have a reduction in the expression of Mfn2 protein (Diaz et al., 2015; Peng et al., 2015). On the other hand, mitochondrial fission is important in producing numerous morphological and functional mitochondria (Chan,

2006). Dynamin-related protein 1 (Drp1 or Dnm1), one of the core components needed for mammalian mitochondrial fission (Smirnova, 2001), was found in both the cytosol and the mitochondrial compartment. Previous studies indicated that an increase in either Drp1 activity or its protein expression was found under several pathological conditions, such as brain ischemia and diabetes (Chen et al., 2015; Huang et al., 2015). In addition, alterations in the mitochondrial dynamics as well as excessive brain iron accumulation have been reported to be responsible for the pathogenesis of neurodegeneration (Shirendeb et al., 2011). The results from the present study demonstrated that iron-overload condition induced by long-term HFe consumption could impair the brain mitochondrial dynamics as indicated by increased levels of brain mitochondrial fission protein; DRP-1 in association with a decreased brain mitochondrial fusion; Mfn2. However, this finding was different from a recent study by da Silva et al, which reported that the exposure of iron treatment in rats during neonatal period decreased the levels of both mitochondrial fission and fusion proteins in the hippocampal area, whereas the brain mitochondrial fusion protein expression did not change in the cortex area (da Silva et al., 2014). This inconsistent finding could be due to the different models of iron-overload condition between the two studies. In the present study, the whole brain was used for this analysis and the marker for brain mitochondrial fusion in our study (Mfn2) was different from da Silva et al. study (OPA1) (da Silva et al., 2014). These differences could be responsible for the different findings between these two studies. In addition, mitochondrial dynamics have been shown to play an important role in cellular apoptosis (Suen et al., 2008). Moreover, mitochondrial function was also regulated by the mitochondrial dynamics (Chen and Chan, 2009). All of these previous findings and the results of this study suggest that brain mitochondrial dynamic imbalance could lead to the development of mitochondrial dysfunction and subsequently induced brain apoptosis.

Many studies indicated that an increase in AD-like proteins including Aβ and tau-phosphorylation was associated with conditions of oxidative stress (Bartley et al., 2012). The aggregation of Aβ also appeared to impair mitochondrial function by increasing superoxide anion ($O_2^{\cdot}$) generation, leading to decreased ATP production. Moreover, Aβ aggregation can lead to the lipid production, resulting in the production of highly cytotoxic aldehyde products including 4-hydroxynonenal (4-HNE) and malondialdehyde (MDA). In addition, a recent study showed that 4-HNE promoted tau aggregation, leading to the formation of neurofibrillary tangles (NFTs) (Egana et al., 2003). The present study found that chronic iron-overload condition could increase the protein expression of APP in the brain. This finding was consistent with a previous study by Becerril et al., who have shown iron-induced KPI-APP overexpression in neurons (this is a pro-amyloidogenic form of APP) (Becerril-Ortega et al., 2014). Furthermore, the increased APP caused by the iron exposure occurs through the NMDA receptor (NMDAR) signaling pathway, since they showed that MK-801, an NMDAR blocker, inhibited this condition. Supporting this mechanism, a recent study reported that neuronal iron uptake was increased after NMDAR activation and blocked by MK-801 (Pelizzoni et al., 2011). These findings suggest that NMDARs exert a pivotal role in neuronal iron metabolism and might be one of the underlying mechanisms regarding cognitive impairment caused by iron-overload condition. Despite the Aβ aggregation and increased APP protein expression, iron also caused the AD progression by the induction of tau hyper-phosphorylation, resulting in neuronal death (Xie et al., 2012). In the present study, we have shown that hyperphosphorylation of tau protein at Thr 181 is associated with increased expression of Aβ and APP proteins. Although it has been known that tau is phosphorylated at various sites and hyperphosphorylation of tau is related to the development of neurodegeneration (Johnson and Stoothoff, 2004), several studies have reported that tau-hyperphosphorylation at thr181-amino acid could be a specific biomarker for brain pathological conditions including mild cognitive impairment, AD, frontotemporal dementia (Rosso et al., 2003; Thomann et al., 2009; Saman et al., 2012). These findings suggest that the iron-overload condition induces AD-like pathology and consequently can lead to the development of neurodegeneration. Furthermore, several studies have also reported that dendritic spine degeneration was associated with the progression of AD-like pathology (Aoki et al., 2007). The results of this study were consistent with those previous findings since the data showed that the iron-overload condition caused increased AD-like pathological changes and the loss of dendritic spines. The possible underlying mechanisms of brain iron toxicity could be due to iron-overload impaired brain mitochondrial balance and increased brain oxidative stress, resulting in the loss of dendritic spines that cause brain apoptosis and eventually increase in AD-like pathological changes.

The therapeutic effects of the three commercially available iron chelators were compared in this study. It was found that all iron chelators effectively reduced plasma iron levels. Moreover, DFO and DFP provided protective effects in the brain following an iron-overloaded condition by attenuating BBB breakdown, brain iron accumulation, brain mitochondrial dysfunction, brain mitochondrial dynamic disturbance, brain apoptosis and loss of dendritic spine density. These neuroprotective effects of DFO and DFP were due to their plasma iron chelating properties and their ability to cross the BBB and act as iron chelators in the brain (Fredenburg et al., 1996; Hua et al., 2008). Although the results demonstrated that both drugs had equally therapeutic effects in the brain, DFP has a greater advantage than DFO since it could be orally administered.

Surprisingly, DFX therapy failed to ameliorate the toxicity of the iron in the brain. This might be due to the fact that DFX has a limitation of being less able to penetrate the BBB (Finkenstedt et al., 2010; Kamalinia et al., 2013), and that a higher dose of DFX might be required. Since this study investigated only a single dose of DFX, it is possible that an insufficient dose of DFX was delivered. Also, the iron-binding affinities of DFO, DFP and DFX are significantly different, in which the

iron-binding ratio of the chelators: iron of DFO, DFP and DFX being 1:1, 1:2 and 1:3, respectively (Neufeld, 2010), and the dose of these three chelators were selected as being the effective therapeutic dosage of each drug as shown in a previous study (Kwiatkowski, 2011). Hence the DFX dose used in this study could have been insufficient to chelate iron to prevent brain iron toxicity, when compared with DFO and DFP. Future studies are needed to test this hypothesis.

In this study, it was found that NAC also provided beneficial therapeutic effects in the brain similar to those of the iron chelators DFO and DFP under conditions of iron-overload. These findings suggest that an antioxidant could be an alternative treatment in the case of the individuals who experience adverse effects to iron chelators. Most importantly, the results demonstrated that the combined therapy of DFP with NAC exerted greater therapeutic efficacy in protecting the brain from the iron-overload condition by restoring the dendritic spine density and preserving the BBB, when compared with the other interventions. These findings indicate the additive benefits of NAC to the iron chelators for neuroprotection in conditions of iron-overload.

CONCLUSION

This study provides a new insight into the mechanisms of brain iron toxicity, including the reduction of dendritic spine density, alteration of AD-like pathology and brain mitochondrial dynamic disruption, all caused by an iron-overloaded condition. The therapeutic approaches with several iron chelators: DFO and DFP and an antioxidant: NAC effectively attenuated brain iron toxicity. Most importantly, the combined therapy of DFP with NAC exerted the greatest efficacy in brain protection from an iron-overloaded induced brain toxicity, suggesting that this combined therapy could provide the best therapeutic approach for treatment of neurodegeneration caused by iron-overload.

Study limitations

Iron can normally be uptaken into the brain through iron-transferrin pathways (Mills et al., 2010). In contrast, under iron-overload condition, it has been shown that iron could enter the brain by disrupting the BBB in rat brain with iron-overload as indicated by the reduction of tight junction proteins expression at BBB (Won et al., 2011; Sripetchwandee et al., 2014a). However, the study of other BBB markers, such as zona occluden-1 (ZO-1), claudin-5 etc., as well as using an experimental method for determining the BBB integrity such as Evans Blue extravasation are needed to support the findings in this present study.

The present study showed that chronic iron-overload condition induced brain mitochondrial dysfunction and brain apoptosis. However, the effect of this pathological condition on the neuronal loss by directly determining cell viability or cell number in the brain will need to be further investigated.

CONFLICT OF INTEREST

There is no conflict of interest to report.

Acknowledgements—This work was supported by the Thailand Research Fund, Thailand BRG5780016 (S.C.), TRG5880045 (J.S.), The Royal Golden Jubilee program, Thailand (PHD/0222/2557: S.C. and S.W.), a NSTDA Research Chair Grant from the National Science and Technology Development Agency, Thailand (N.C.) and a Chiang Mai University Center of Excellence Award, Thailand (N.C.).

REFERENCES

Aoki C, Mahadomrongkul V, Fujisawa S, Habersat R, Shirao T (2007) Chemical and morphological alterations of spines within the hippocampus and entorhinal cortex precede the onset of Alzheimer's disease pathology in double knock-in mice. J Comp Neurol 505:352–362.

Bartley MG, Marquardt K, Kirchhof D, Wilkins HM, Patterson D, Linseman DA (2012) Overexpression of amyloid-beta protein precursor induces mitochondrial oxidative stress and activates the intrinsic apoptotic cascade. J Alzheimers Dis 28:855–868.

Becerril-Ortega J, Bordji K, Freret T, Rush T, Buisson A (2014) Iron overload accelerates neuronal amyloid-beta production and cognitive impairment in transgenic mice model of Alzheimer's disease. Neurobiol Aging 35:2288–2301.

Borgna-Pignatti C, Marsella M (2015) Iron chelation in thalassemia major. Clin Ther 37:2866–2877.

Braughler JM, Duncan LA, Chase RL (1986) The involvement of iron in lipid peroxidation. Importance of ferric to ferrous ratios in initiation. J Biol Chem 261:10282–10289.

Butterfield DA, Boyd-Kimball D (2004) Amyloid beta-peptide(1–42) contributes to the oxidative stress and neurodegeneration found in Alzheimer disease brain. Brain Pathol 14:426–432.

Chan DC (2006) Mitochondrial fusion and fission in mammals. Annu Rev Cell Dev Biol 22:79–99.

Chen H, Chan DC (2009) Mitochondrial dynamics–fusion, fission, movement, and mitophagy – in neurodegenerative diseases. Hum Mol Genet 18:R169–176.

Chen H, Detmer SA, Ewald AJ, Griffin EE, Fraser SE, Chan DC (2003) Mitofusins Mfn1 and Mfn2 coordinately regulate mitochondrial fusion and are essential for embryonic development. J Cell Biol 160:189–200.

Chen SD, Lin TK, Yang DI, Lee SY, Shaw FZ, Liou CW, Chuang YC (2015) Roles of PTEN-induced putative kinase 1 and dynamin-related protein 1 in transient global ischemia-induced hippocampal neuronal injury. Biochem Biophys Res Commun 460:397–403.

Colijn MA, Grossberg GT (2015) Amyloid and tau biomarkers in subjective cognitive impairment. J Alzheimers Dis 47:1–8.

Crichton RR, Wilmet S, Legssyer R, Ward RJ (2002) Molecular and cellular mechanisms of iron homeostasis and toxicity in mammalian cells. J Inorg Biochem 91:9–18.

da Silva VK, de Freitas BS, da Silva Dornelles A, Nery LR, Falavigna L, Ferreira RD, Bogo MR, Hallak JE, Zuardi AW, Crippa JA, Schroder N (2014) Cannabidiol normalizes caspase 3, synaptophysin, and mitochondrial fission protein DNM1L expression levels in rats with brain iron overload: implications for neuroprotection. Mol Neurobiol 49:222–233.

Diaz B, Fuentes-Mera L, Tovar A, Montiel T, Massieu L, Martinez-Rodriguez HG, Camacho A (2015) Saturated lipids decrease mitofusin 2 leading to endoplasmic reticulum stress activation and insulin resistance in hypothalamic cells. Brain Res 1627:80–89.

Dumont M, Stack C, Elipenahli C, Jainuddin S, Gerges M, Starkova NN, Yang L, Starkov AA, Beal F (2011) Behavioral deficit, oxidative stress, and mitochondrial dysfunction precede tau pathology in P301S transgenic mice. FASEB J 25:4063–4072.

Eaton JW, Qian M (2002) Molecular bases of cellular iron toxicity. Free Radical Biol Med 32:833–840.

Egana JT, Zambrano C, Nunez MT, Gonzalez-Billault C, Maccioni RB (2003) Iron-induced oxidative stress modify tau phosphorylation patterns in hippocampal cell cultures. Biometals 16:215–223.

Finkenstedt A, Wolf E, Hofner E, Gasser BI, Bosch S, Bakry R, Creus M, Kremser C, Schocke M, Theurl M, Moser P, Schranz M, Bonn G, Poewe W, Vogel W, Janecke AR, Zoller H (2010) Hepatic but not brain iron is rapidly chelated by deferasirox in aceruloplasminemia due to a novel gene mutation. J Hepatol 53:1101–1107.

Frankfurt M, Salas-Ramirez K, Friedman E, Luine V (2011) Cocaine alters dendritic spine density in cortical and subcortical brain regions of the postpartum and virgin female rat. Synapse 65:955–961.

Fredenburg AM, Sethi RK, Allen DD, Yokel RA (1996) The pharmacokinetics and blood–brain barrier permeation of the chelators 1,2 dimethly-, 1,2 diethyl-, and 1-[ethan-1'ol]-2-methyl-3-hydroxypyridin-4-one in the rat. Toxicology 108:191–199.

Hua Y, Keep RF, Hoff JT, Xi G (2008) Deferoxamine therapy for intracerebral hemorrhage. Acta Neurochir Suppl 105:3–6.

Huang S, Wang Y, Gan X, Fang D, Zhong C, Wu L, Hu G, Sosunov AA, McKhann GM, Yu H, Yan SS (2015) Drp1-mediated mitochondrial abnormalities link to synaptic injury in diabetes model. Diabetes 64:1728–1742.

Ishihara N, Nomura M, Jofuku A, Kato H, Suzuki SO, Masuda K, Otera H, Nakanishi Y, Nonaka I, Goto Y, Taguchi N, Morinaga H, Maeda M, Takayanagi R, Yokota S, Mihara K (2009) Mitochondrial fission factor Drp1 is essential for embryonic development and synapse formation in mice. Nat Cell Biol 11:958–966.

Johnson GV, Stoothoff WH (2004) Tau phosphorylation in neuronal cell function and dysfunction. J Cell Sci 117:5721–5729.

Kamalinia G, Khodagholi F, Atyabi F, Amini M, Shaerzadeh F, Sharifzadeh M, Dinarvand R (2013) Enhanced brain delivery of deferasirox-lactoferrin conjugates for iron chelation therapy in neurodegenerative disorders: in vitro and in vivo studies. Mol Pharm 10:4418–4431.

Knott AB, Bossy-Wetzel E (2008) Impairing the mitochondrial fission and fusion balance: a new mechanism of neurodegeneration. Ann N Y Acad Sci 1147:283–292.

Koppenol WH (2001) The Haber-Weiss cycle–70 years later. Redox Rep 6:229–234.

Kumfu S, Chattipakorn S, Chinda K, Fucharoen S, Chattipakorn N (2012) T-type calcium channel blockade improves survival and cardiovascular function in thalassemic mice. Eur J Haematol 88:535–548.

Kwiatkowski JL (2011) Management of transfusional iron overload – differential properties and efficacy of iron chelating agents. J Blood Med 2:135–149.

Lekawanvijit S, Chattipakorn N (2009) Iron overload thalassemic cardiomyopathy: iron status assessment and mechanisms of mechanical and electrical disturbance due to iron toxicity. Can J Cardiol 25:213–218.

Leskovjan AC, Kretlow A, Lanzirotti A, Barrea R, Vogt S, Miller LM (2011) Increased brain iron coincides with early plaque formation in a mouse model of Alzheimer's disease. NeuroImage 55:32–38.

Ma Y, Podinovskaia M, Evans PJ, Emma G, Schaible UE, Porter J, Hider RC (2014) A novel method for non-transferrin-bound iron quantification by chelatable fluorescent beads based on flow cytometry. Biochem J 463:351–362.

McNeill A, Chinnery PF (2011) Neurodegeneration with brain iron accumulation. Handb Clin Neurol 100:161–172.

Mills E, Dong XP, Wang F, Xu H (2010) Mechanisms of brain iron transport: insight into neurodegeneration and CNS disorders. Future Med Chem 2:51–64.

Misonou H, Morishima-Kawashima M, Ihara Y (2000) Oxidative stress induces intracellular accumulation of amyloid beta-protein (Abeta) in human neuroblastoma cells. Biochemistry 39:6951–6959.

Navarro A, Boveris A (2010) Brain mitochondrial dysfunction in aging, neurodegeneration, and Parkinson's disease. Front Aging Neurosci 2.

Neufeld EJ (2010) Update on iron chelators in thalassemia. Hematology Am Soc Hematol Educ Program 2010:451–455.

Ono T, Isobe K, Nakada K, Hayashi J (2001) Human cells are protected from mitochondrial dysfunction by complementation of DNA products in fused mitochondria. Nat Genet 28:272–275.

Pelizzoni I, Macco R, Morini MF, Zacchetti D, Grohovaz F, Codazzi F (2011) Iron handling in hippocampal neurons: activity-dependent iron entry and mitochondria-mediated neurotoxicity. Aging Cell 10:172–183.

Peng C, Rao W, Zhang L, Wang K, Hui H, Wang L, Su N, Luo P, Hao YL, Tu Y, Zhang S, Fei Z (2015) Mitofusin 2 ameliorates hypoxia-induced apoptosis via mitochondrial function and signaling pathways. Int J Biochem Cell Biol 69:29–40.

Perfettini JL, Roumier T, Kroemer G (2005) Mitochondrial fusion and fission in the control of apoptosis. Trends Cell Biol 15:179–183.

Persidsky Y, Ramirez SH, Haorah J, Kanmogne GD (2006) Blood–brain barrier: structural components and function under physiologic and pathologic conditions. J Neuroimmune Pharmacol 1:223–236.

Poggiali E, Cassinerio E, Zanaboni L, Cappellini MD (2012) An update on iron chelation therapy. Blood Transfus 10:411–422.

Rebouche CJ, Wilcox CL, Widness JA (2004) Microanalysis of non-heme iron in animal tissues. J Biochem Biophys Methods 58:239–251.

Rosso SM, van Herpen E, Pijnenburg YA, Schoonenboom NS, Scheltens P, Heutink P, van Swieten JC (2003) Total tau and phosphorylated tau 181 levels in the cerebrospinal fluid of patients with frontotemporal dementia due to P301L and G272V tau mutations. Arch Neurol 60:1209–1213.

Saman S, Kim W, Raya M, Visnick Y, Miro S, Saman S, Jackson B, McKee AC, Alvarez VE, Lee NC, Hall GF (2012) Exosome-associated tau is secreted in tauopathy models and is selectively phosphorylated in cerebrospinal fluid in early Alzheimer disease. J Biol Chem 287:3842–3849.

Shirendeb U, Reddy AP, Manczak M, Calkins MJ, Mao P, Tagle DA, Reddy PH (2011) Abnormal mitochondrial dynamics, mitochondrial loss and mutant huntingtin oligomers in Huntington's disease: implications for selective neuronal damage. Hum Mol Genet 20:1438–1455.

Smirnova E (2001) Dynamin-related protein Drp1 is required for mitochondrial division in mammalian cells. Mol Biol Cell 12:2245–2256.

Smrt RD, Zhao X (2010) Epigenetic regulation of neuronal dendrite and dendritic spine development. Front Biol 5:304–323.

Sripetchwandee J, Pipatpiboon N, Chattipakorn N, Chattipakorn S (2014a) Combined therapy of iron chelator and antioxidant completely restores brain dysfunction induced by iron toxicity. PLoS ONE 9:e85115.

Sripetchwandee J, Pipatpiboon N, Pratchayasakul W, Chattipakorn N, Chattipakorn SC (2014b) DPP-4 inhibitor and PPARgamma agonist restore the loss of CA1 dendritic spines in obese insulin-resistant rats. Arch Med Res 45:547–552.

Sripetchwandee J, Sanit J, Chattipakorn N, Chattipakorn SC (2013) Mitochondrial calcium uniporter blocker effectively prevents brain mitochondrial dysfunction caused by iron overload. Life Sci 92:298–304.

Suen DF, Norris KL, Youle RJ (2008) Mitochondrial dynamics and apoptosis. Genes Dev 22:1577–1590.

Szabadkai G, Simoni AM, Bianchi K, De Stefani D, Leo S, Wieckowski MR, Rizzuto R (2006) Mitochondrial dynamics and Ca^{2+} signaling. Biochim Biophys Acta 1763:442–449.

Thomann PA, Kaiser E, Schonknecht P, Pantel J, Essig M, Schroder J (2009) Association of total tau and phosphorylated tau 181 protein levels in cerebrospinal fluid with cerebral atrophy in mild cognitive impairment and Alzheimer disease. J Psychiatry Neurosci 34:136–142.

Westermann B (2010) Mitochondrial fusion and fission in cell life and death. Nat Rev Mol Cell Biol 11:872–884.

Won SM, Lee JH, Park UJ, Gwag J, Gwag BJ, Lee YB (2011) Iron mediates endothelial cell damage and blood–brain barrier opening in the hippocampus after transient forebrain ischemia in rats. Exp Mol Med 43:121–128.

Xie L, Zheng W, Xin N, Xie JW, Wang T, Wang ZY (2012) Ebselen inhibits iron-induced tau phosphorylation by attenuating DMT1 up-regulation and cellular iron uptake. Neurochem Int 61:334–340.

Yao M, Nguyen TV, Pike CJ (2005) Beta-amyloid-induced neuronal apoptosis involves c-Jun N-terminal kinase-dependent downregulation of Bcl-w. J Neurosci 25:1149–1158.

(Accepted 2 July 2016)
(Available online 09 July 2016)

เอกสารแนบหมายเลข 19

Menopause: The Journal of The North American Menopause Society
Vol. 23, No. 8, pp. 894-902
DOI: 10.1097/GME.0000000000000640
© 2016 by The North American Menopause Society

Estrogen and DPP4 inhibitor, but not metformin, exert cardioprotection via attenuating cardiac mitochondrial dysfunction in obese insulin-resistant and estrogen-deprived female rats

Sivaporn Sivasinprasasn, PhD,[1,2,4,5] *Piangkwan Sa-nguanmoo, MSc,*[1,2,4] *Wanpitak Pongkan, DVM,*[1,2,4] *Wasana Pratchayasakul, PhD,*[1,2,4] *Siriporn C. Chattipakorn, DDS, PhD,*[1,3,4] *and Nipon Chattipakorn, MD, PhD*[1,2,4]

Abstract

Objective: Cardiac function was markedly compromised in obese insulin-resistant and estrogen-deprived rats. Metformin and dipeptidyl peptidase-4 inhibitor (vildagliptin) were reported to improve cardiac function in insulin-resistant rats. Their effects on the heart under estrogen-deprived conditions are, however, unknown. Therefore, the effects of metformin, vildagliptin, and estrogen on the cardiac function in estrogen-deprived insulin-resistant female rats were investigated.

Methods: Bilateral ovariectomized female rats (n = 48) were divided to be fed with either a normal diet (ND) or a high-fat diet (HFD) for 12 weeks. Then, both ND- and HFD-fed groups were subdivided to receive a vehicle, estrogen (50 μg/kg), metformin (30 mg/kg), or vildagliptin (3 mg/kg) for 4 weeks (n = 6/group). Heart rate variability, echocardiography, metabolic and biochemical parameters, cardiac function, and mitochondrial function were determined. Sham-operated female rats (n = 6) were used as a control.

Results: Both ND- and HFD-fed ovariectomized rats developed insulin resistance, depressed heart rate variability, and decreased cardiac contractility. Although treatment with metformin, vildagliptin, and estrogen improved metabolic status and cardiac function, only estrogen and vildagliptin improved diastolic blood pressure and left ventricular ±dP/dt, and also reduced mitochondrial impairment, apoptosis, and oxidative stress in HD-fed ovariectomized rats.

Conclusions: Treatment with estrogen and vildagliptin provided more beneficial effects in the inhibition of oxidative stress, apoptosis, and cardiac mitochondrial dysfunction, and preserved cardiac contractile performance in estrogen-deprived insulin-resistant female rats.

Key Words: Cardiac function – DPP4 inhibitor – Estrogen – Insulin resistance – Metformin – Mitochondria.

Cardiovascular diseases (CVDs) are the leading cause of mortality and morbidity, accounting for 30% of all global deaths.[1,2] Metabolic disorders such as obesity, dyslipidemia, and diabetes are known to be the major risk factors of CVD.[2] Gender is also considered a CVD risk factor, as the prevalence of CVD is higher in men than in women.[3,4] The risk of CVD in women has, however, been found to increase after endogenous estrogen deprivation, by both bilateral ovariectomy (OVX) and natural menopause.[5,6] Owing to the cardiometabolic protective effects of estrogen, estrogen withdrawal has been shown to induce both cardiac and metabolic dysfunction, such as hypertension and impaired glucose tolerance, therefore resulting in an increased risk of developing CVD.[7] Estrogen hormone therapy has been shown to decrease fat accumulation, increase energy expenditure, suppress gluconeogenesis and lipogenesis, and enhance muscular insulin sensitivity, therefore resulting in improved metabolic syndrome conditions in OVX rats.[8,9] Moreover, estrogen helped in improving cardiac autonomic balance in the OVX model through the reduction of oxidative stress.[10,11] Oxidative stress is also considered as a factor responsible for the development of insulin resistance and cardiac dysfunction.[12,13] A recent study confirmed the positive effect of

Received November 10, 2015; revised and accepted January 25, 2016.

From the [1]Cardiac Electrophysiology Research and Training Center, [2]Cardiac Electrophysiology Unit, Department of Physiology, Faculty of Medicine, [3]Department of Oral Biology and Diagnostic Science, Faculty of Dentistry, and [4]Center of Excellence in Cardiac Electrophysiology Research, Chiang Mai University, Chiang Mai, Thailand; and [5]School of Medicine, Mae Fah Luang University, Chiang Rai, Thailand.

Funding/support: This work was supported by an NSTDA Research Chair Grant from the National Science and Technology Development Agency (NC), the Thailand Research Fund, BRG5780016 (SCC), TRG (WPr), and the Chiang Mai University Center of Excellence Award (NC).

Financial disclosure/conflicts of interest: None reported.

Supplemental digital content is available for this article. Direct URL citations appear in the printed text and are provided in the HTML and PDF versions of this article on the journal's Website (www.menopause.org).

Address correspondence to: Nipon Chattipakorn, MD, PhD, Cardiac Electrophysiology Research and Training Center, Faculty of Medicine, Chiang Mai University, Chiang Mai 50200, Thailand.
E-mail: nchattip@gmail.com

Copyright @ 2016 The North American Menopause Society. Unauthorized reproduction of this article is prohibited.

estrogen on antioxidative stress, due to the finding that cardiac reactive oxygen species (ROS) production was inhibited in OVX rats after receiving an estrogen supplement, resulting in an improved mitochondrial function.[14] The effect of the estrogen supplement on the cardiac mitochondrial function in estrogen-deprived rats with an obese insulin-resistant condition has, however, not yet been identified.

Metformin and dipeptidyl peptidase-4 (DPP4) inhibitor (vildagliptin) have been used for the treatment of type 2 diabetes mellitus. Metformin is an antihyperglycemic drug which has been shown to reduce hepatic glucose and lipid production, improve hepatic beta-cell function, and improve insulin sensitivity.[15] Vildagliptin exerts its antidiabetic action by inhibiting the DPP4 enzyme, resulting in increased insulin secretion and lower blood glucose levels.[16] In addition to the therapeutic effects on metabolic disorders, both metformin and vildagliptin were reported to be beneficial to the heart in both diabetic and nondiabetic rats.[17,18] Metformin and vildagliptin enhanced heart rate variability (HRV), and increased mitochondrial and myocardial function in an obese insulin-resistant rat model.[17] Their effects as therapeutic agents in obese insulin-resistant rats with estrogen deprivation have, however, not yet been investigated. Owing to the increasing prevalence of metabolic syndrome and CVD in postmenopausal women, together with the increased use of metformin and vildagliptin, we aimed to investigate the roles of these drugs on metabolic status and cardiac function. In addition, this study aimed to investigate the underlying mechanisms acting in estrogen-deprived, obese insulin-resistant rats. We hypothesized that estradiol, metformin, and vildagliptin improve the metabolic function, cardiac performance, and mitochondrial function in estrogen-deprived, obese insulin-resistant rats.

METHODS

Animals and ethical approval

A total of 54 female Wistar rats (weighing 200-220 g) were obtained from the National animal center (Salaya Campus, Mahidol University, Bangkok, Thailand). The rats were given time to acclimatize, and were housed in a temperature-controlled room (25°C) with a 12-hour dark/light cycle setting. All experimental procedures were approved by the Institutional Animal Care and Use Committee at the Faculty of Medicine, Chiang Mai University, in compliance with National Institutes of Health (NIH) guidelines.

Experimental protocol

Rats were randomly assigned to receive either a sham operation (S; n = 6) or a bilateral OVX (O; n = 48), and then allowed to recover for 1 week. Sham rats were fed a normal diet (ND: containing 19.77% energy from fat), whereas ovariectomized rats were further subdivided to be fed with either a ND or a high-fat diet (HFD: containing 59.28% energy from fat) for 12 weeks. At the end of the 12th week, HRV and echocardiography were examined and recorded as the pretreatment data. Rats in both the ND-fed ovariectomized (NDO) and the HFD-fed ovariectomized (HFO) groups were randomly subcategorized to be treated with either estradiol (E: 50 μg/kg body weight [BW] via subcutaneous injection, once daily [17β-estradiol; Sigma-Aldrich, St. Louis, MO]), metformin (M: 15 mg/kg BW, b.i.d., via gavage feeding [Glucophage; Merck Serono, Bangkok, Thailand]), vildagliptin (Vil: 3 mg/kg BW, daily, via gavage feeding [Galvus; Novartis, Bangkok, Thailand]), or vehicle (Ve: sesame oil, via subcutaneous injection in equal volumes with the estrogen treatment) for 4 weeks (n = 6/group; see supplement figure, Supplemental Digital Content 1, http://links.lww.com/MENO/A164). After 4 weeks of treatment, HRV and echocardiography were examined again as the posttreatment data. Blood samples were collected to investigate metabolic parameters. Left ventricular (LV) function was determined using an intraventricular pressure recording system. At the end, rats were terminated by decapitation, and the heart was removed to study cardiac mitochondrial function and biochemical activities.

Surgical procedure of OVX

The bilateral OVX was performed according to the protocol which has been previously described.[19] Rats were anesthetized with zoletil (50 mg/kg) and xylazine (1 mg/kg), and ventilated with room air.[19] The abdominal-pelvic cavity was accessed through a skin incision between the inferior crest of the rib cage and superior base. After the uterine tube and ovary were identified, both ovaries were excised and uterine horns were returned into the pelvic cavity. The abdominal wall and the skin incision were closed and cleaned. After the operation, rats were observed for respiratory status and the recovery, and then individually housed in a clear box for 1 week before being fed with ND or HFD diets.

Metabolic function and estrogen-level determination

Metabolic parameters were investigated from blood samples (n = 6/group), which were collected at pre- and posttreatment time points. Fasting plasma glucose, cholesterol, and triglyceride levels were determined by colorimetric assay using a commercial kit (Biotech, Bangkok, Thailand). Fasting plasma insulin levels were measured using a sandwich enzyme-linked immunosorbent assay (ELISA) kit (Millipore, Ann Arbor, MI). Homeostasis Model Assessment (HOMA) was calculated to evaluate the degree of insulin resistance.[19] Serum estradiol levels were determined using a competitive enzyme immunoassay kit (Cayman Chemical Company, Ann Arbor, MI).

Echocardiography

Echocardiography was performed to evaluate the LV function before and after treatment. This test was performed while the animal was unconscious (lightly anesthetized with 2% isoflurane with oxygen [2 L/min] via inhalation) by using an echocardiograph (SONOS4500; Agilent Technologies, Santa Clara, CA).[20] Data from M-mode echocardiography were recorded to determine LV internal diameter at the end of diastole and LV internal diameter at the end of systole.

Copyright @ 2016 The North American Menopause Society. Unauthorized reproduction of this article is prohibited.

Fractional shortening (%FS) and the ejection fraction (%EF) were calculated to estimate the contractile function (n = 6/group).[21]

HRV test

HRV measures were derived from electrocardiograms (lead II), which were recorded using a signal transducer (PowerLab 4/25T; ADInstruments, New South Wales, Australia) operated through the Chart 5.0 program for 20 minutes (n = 6/group). The frequency-domain method in the MATLAB program was used for electrocardiogram analysis.[22] The high-frequency (HF) component (ranging between 0.15 and 0.40 Hz) is considered to be a marker of parasympathetic tone, whereas the low-frequency (LF) component (ranging between 0.04 and 0.15 Hz) is considered to be a marker of parasympathetic and sympathetic tone.[23] The LF/HF ratio is considered to be an index of the cardiac sympathetic/parasympathetic balance. An increased LF/HF ratio indicates a suppressed HRV and cardiac sympathovagal imbalance.[20,23]

LV pressure determination

Rats were anesthetized by intramuscular injections with zoletil (50 mg/kg) and xylazine (0.15 mg/kg),[17] and were then ventilated with room air via a tracheostomy tube. A pressure catheter (Scisence, Ontario, Canada) was inserted into the right carotid artery, and the catheter tip was directed into the LV chamber. After a 5-minute stabilization period, the signaling data from the catheter were recorded for 20 minutes. Then, rats were terminated and their hearts were removed for further mitochondrial and biochemical studies (n = 6/group). LV end-systolic pressure, LV end-diastolic pressure, maximum and minimum dP/dt (+dP/dt and −dP/dt), and heart rate were recorded. All parameters were analyzed using Labscribe analytical software (Labscribe, Dover, NH).

Cardiac mitochondrial function study

The methods for studying cardiac mitochondrial function, that is the mitochondrial ROS production, mitochondrial membrane potential changes, and mitochondrial swelling, have previously been described.[20,24] The removed heart was cut into small sections, and then homogenized and centrifuged to isolate the cardiac mitochondria. Dichlorohydrofluorescein diacetate dye was used to stain the isolated cardiac mitochondria, and then the ROS level was measured using a fluorescent microplate reader (BioTek, Winooski, VT), set at an excitation wavelength of 485 nm and an emission wavelength of 530 nm.[20,24] Mitochondrial membrane potential change was detected by using the dye 5,5′,6,6′-tetrachloro-1,1′,3,3′-tetraethylbenzimidazolcarbocyanine iodide (JC-1). The monomer form of JC-1 was excited at the wavelength of 485 nm and the emission detected at 590 nm (green fluorescence), whereas the JC-1 aggregate form was excited at the wavelength of 485 nm and the emission detected at 530 nm (red fluorescence).[24] Depolarization of the mitochondrial membrane was indicated by a decreased red/green fluorescence intensity ratio.[24] Cardiac mitochondrial swelling was detected using a spectrophotometer at 540 nm, continuously for 30 minutes, swelling being indicated by a decrease in the absorbance of a mitochondrial suspension. A transmission electron microscope (JEM-1200 EX II; JEOL Ltd, Tokyo, Japan) was also used to observe the mitochondrial morphology, according to the previously described procedure.[18]

Determination of oxidative stress

Oxidative stress levels were indicated by the increased malondialdehyde (MDA) concentrations, which were measured by a high-performance liquid chromatography system (Thermo Scientific, Bangkok, Thailand), as previously described.[17] Serum and protein from cardiac tissues were mixed with 10% trichloroacetic acid. The mixture was centrifuged, and the supernatant was mixed with 0.44 M H_3PO_4 and 0.6% thiobabituric acid solution to generate thiobarbituric acid reactive substances, which were further measured by the high-performance liquid chromatography system with BDS software (BarSpec Ltd, Rehovot, Israel). The concentration of thiobarbituric acid reactive substances was determined directly from a standard curve and reported as an MDA equivalent concentration.[17]

Cardiac expression of Bax and Bcl-2

The expressions of Bax and Bcl-2 were determined by western blot analysis. Briefly, myocardial tissues were homogenized in a lysis buffer (containing 1% Nonidet P-40, 0.5% sodium deoxycholate, 0.1% sodium dodecyl sulfate [SDS] in 1 × phosphate buffered saline) and were then centrifuged at 13,000 rpm for 10 minutes. Myocardial protein was mixed with the loading buffer (consisting of 5% mercaptoethanol, 0.05% bromophenol blue, 75 nM Tris-HCl, 2% SDS, and 10% glycerol with pH 6.8) at 1 mg/mL concentration and boiled for 5 minutes. The protein was loaded into a 10% gradient SDS-polyacrylamide gel, and then transferred to a polyvinyldene difluoride membrane in a transfer system (Bio-Rad, Hercules, CA). The protein-contained membranes were incubated in 5% skimmed milk in 1 × Tris-buffered saline and Tween 20 solution-T buffer for 1 hour, and then exposed to anti-Bax, anti-Bcl-2 (Cell Signaling Technology, Danvers, MA) and anti-actin (Sigma-Aldrich). Horseradish peroxidase conjugated with antirabbit or antimouse IgG (Santa Cruz Biotechnology, Inc, Dallas, TX) was administered to produce a peroxidase reaction, which further developed the signal by enhanced chemiluminescence detection reagents. Finally, autoradiography was performed, and the immune-blotted films were investigated to examine the protein band density using the ImageJ program (NIH image).[18]

Chemicals and antibodies

Estradiol and sesame oil were obtained from Sigma-Aldrich. Metformin was from Merck Serono, and vildagliptin was from Novartis. Colorimetric assay kits for the determination of plasma glucose, cholesterol, and triglyceride were from Biotech. ELISA kit for the measurement of plasma

© 2016 The North American Menopause Society

Copyright @ 2016 The North American Menopause Society. Unauthorized reproduction of this article is prohibited.

insulin level was from Millipore. Enzyme immunoassay kit for serum estradiol-level detection was from Cayman Chemical Company. The antibodies against Bax and Bcl-2 were from Cell Signaling Technology and antiactin was from Sigma-Aldrich. The horseradish peroxidase conjugated with antirabbit and antimouse IgG were from Santa Cruz Biotechnology.

Statistical analysis

Data were derived from all rats in each experimental group (n = 6/group) in all experiments. All data were included in the statistical analysis and was presented as mean ± standard error of mean. A one-way analysis of variance followed by post-hoc least significant difference test, which was carried out using the SPSS program (SPSS version 16; SPSS Inc, Chicago, IL), was used to determine the differences between the means. $P < 0.05$ was considered statistically significant.

RESULTS

Effects of estrogen, metformin, and vildagliptin on metabolic function in obese insulin-resistant and estrogen-deprived rats

Metabolic parameters measured after 4 weeks of treatment are shown in Table 1. Both NDOVe and HFOVe rats exhibited metabolic disorders, shown by an increased BW, increased plasma cholesterol, and decreased plasma high-density lipoprotein level. NDOVe and HFOVe rats also had increased plasma insulin and glucose levels and a higher HOMA index, indicating insulin resistance. All interventions except the vehicle could reverse the insulin-resistant status in both NDO and HFO rats, as indicated by the decreased HOMA index and decreased plasma insulin and glucose levels, to the same level as those of ND-fed sham-operated (NDS) rats. BW was reduced in NDO and HFO rats that were treated with E and M, but not Vil, when compared with those who received the vehicle. HFO rats had a greater visceral fat mass when compared with NDS rats, and only E significantly reduced both BW and visceral fat accumulation. None of the treatments could decrease plasma cholesterol levels in HFO rats.

Effects of estrogen, metformin, and vildagliptin on cardiac function and autonomic regulation in estrogen-deprived, obese insulin-resistant rats

Before treatment, echocardiography data showed that both the %FS and %EF had declined, and HRV was suppressed in both NDO and HFO rats when compared with NDS rats (Fig. 1A–C). This indicated that NDO and HFO rats had cardiac contractile dysfunction and autonomic imbalance. All treatment groups except those in the vehicle-only group showed improvements in %FS (Fig. 2A) and corrections in the %EF (Fig. 2B) and LF/HF ratio (Fig. 2C), bringing them back to normal levels.

Heart rate was increased in both NDOVe and HFOVe rats compared with NDS rats, but this increase in heart rate was not seen in all drug-treated groups (Table 2). NDOVe and HFOVe rats had increased systolic and diastolic blood pressures (Table 2). Treatment with E, M, and Vil reduced systolic blood pressure in both NDO and HFO rats. Diastolic blood pressure was improved only in HFOE and HFOVil rats, not in HFOM rats. There were no differences in diastolic blood pressure among treated NDO rats. In HFO rats, there was a reduction in ±dP/dt in HFOVe and HFOM compared with NDS rats, but ±dP/dt was maintained in HFOE and HFOVil rats (Table 2). Moreover, LVESP was markedly decreased in HFOVe, HFOM, and HFOVil rats, but it was preserved only in HFOE rats (Table 2), suggesting that only estrogen and vildagliptin improved LV function to a greater extent compared with the other treatments in HFD-fed rats.

TABLE 1. *Metabolic parameters after 4 weeks of treatment*

		NDO				HFO			
Parameters	NDS	Ve	E	M	Vil	Ve	E	M	Vil
Body weight, g	294.2 ± 3	356.0 ± 8[a]	308.3 ± 9[b]	321.6 ± 7[b]	331.6 ± 11[a]	414.0 ± 17[a]	340.0 ± 13[a,c]	377.5 ± 6[a,c]	396.6 ± 17[a]
Visceral fat, g	14.9 ± 1.4	15.9 ± 1.6	13.3 ± 1.6	11.6 ± 1.3	14.9 ± 1.1	32.3 ± 3.2[a]	18.2 ± 1.3[c]	30.8 ± 2.1[a]	31.6 ± 4.6[a]
Uterus weight, g	0.50 ± 0.1	0.08 ± 0.0[a]	0.39 ± 0.0[b]	0.07 ± 0.0[a]	0.07 ± 0.0[a]	0.08 ± 0.0[a]	0.47 ± 0.0[c]	0.08 ± 0.0[a]	0.08 ± 0.0[a]
Glucose, mg%	125.8 ± 7.0	150.3 ± 8.8[a]	120.48 ± 7.2[b]	111.7 ± 2.7[b]	126.1 ± 9.2[b]	170.6 ± 11.0[a]	142.1 ± 8.6[c]	139.8 ± 11.3[c]	136.4 ± 7.8[c]
Cholesterol, mg%	71.3 ± 1.9	104.3 ± 1.5[a]	87.6 ± 8.4	78.8 ± 3.2[b]	88.3 ± 4.0	125.0 ± 5.7[a]	122.0 ± 10.6[a]	120.9 ± 1.9[a]	120.1 ± 5.43[a]
HDL, μg/μL	0.34 ± 0.0	0.30 ± 0.0[a]	0.31 ± 0.0	0.33 ± 0.0	0.33 ± 0.0	0.28 ± 0.0[a]	0.33 ± 0.0[c]	0.37 ± 0.0[c]	0.37 ± 0.0[c]
Triglyceride, mg%	30.5 ± 2.46	33.9 ± 1.5	32.3 ± 5.1	32.3 ± 4.5	32.5 ± 3.77	37.3 ± 1.9	32.0 ± 5.0	31.4 ± 1.5	33.4 ± 4.2
Insulin, ng/mL	0.92 ± 0.1	1.75 ± 0.1[a]	0.81 ± 0.1[b]	0.90 ± 0.4[b]	1.10 ± 0.1[b]	1.93 ± 0.1[a]	1.03 ± 0.0[c]	0.90 ± 0.0[c]	1.23 ± 0.3[c]
HOMA index	6.90 ± 1.4	16.28 ± 1.2[a]	5.72 ± 1.1[b]	6.13 ± 2.8[b]	8.99 ± 1.2[b]	20.43 ± 1.6[a]	8.11 ± 0.9[c]	7.70 ± 0.4[c]	7.08 ± 1.7[c]
Estradiol level, pg/mL	174.5 ± 24.4	78.6 ± 11.3[a]	195.7 ± 51.1[b]	88.6 ± 6.2[a]	71.1 ± 8.0[a]	80.3 ± 18.9[a]	224.9 ± 27.5[c]	97.6 ± 21.1[a]	77.7 ± 19.0[a]
Serum MDA, μmol/mL	2.02 ± 0.0	3.06 ± 0.1[a]	2.40 ± 0.1[b]	2.69 ± 0.0[a,b]	2.38 ± 0.0[b]	3.48 ± 0.1[a]	2.37 ± 0.0[c]	3.15 ± 0.0[a]	2.33 ± 0.0[c]
Tissue MDA, μmol/mL	1.72 ± 0.2	4.31 ± 0.5[a]	2.53 ± 0.2[b]	3.46 ± 0.2[a]	2.52 ± 0.2[b]	4.16 ± 0.4[a]	2.16 ± 0.4[c]	3.23 ± 0.3[a]	2.38 ± 0.0[c]
Food intake, g/d	12.5 ± 0.7	14.1 ± 1.8	12.8 ± 0.5	13.7 ± 0.4	12.9 ± 0.6	18.6 ± 0.0[a]	18.3 ± 0.5[a]	18.5 ± 0.5[a]	20.5 ± 1.2[a]

Values are mean ± SEM for six rats per group.
E, estradiol; HDL, high-density lipoprotein; HFO, high-fat diet-fed ovariectomized rats; HOMA, Homeostasis Model Assessment; M, metformin; MDA, malondialdehyde; NDO, normal diet-fed ovariectomized rats; NDS, normal diet-fed sham-operated rats; Ve, vehicle; Vil, vildagliptin.
[a] $P < 0.05$ versus NDS.
[b] $P < 0.05$ versus NDOVe.
[c] $P < 0.05$ versus HFOVe.

Copyright @ 2016 The North American Menopause Society. Unauthorized reproduction of this article is prohibited.

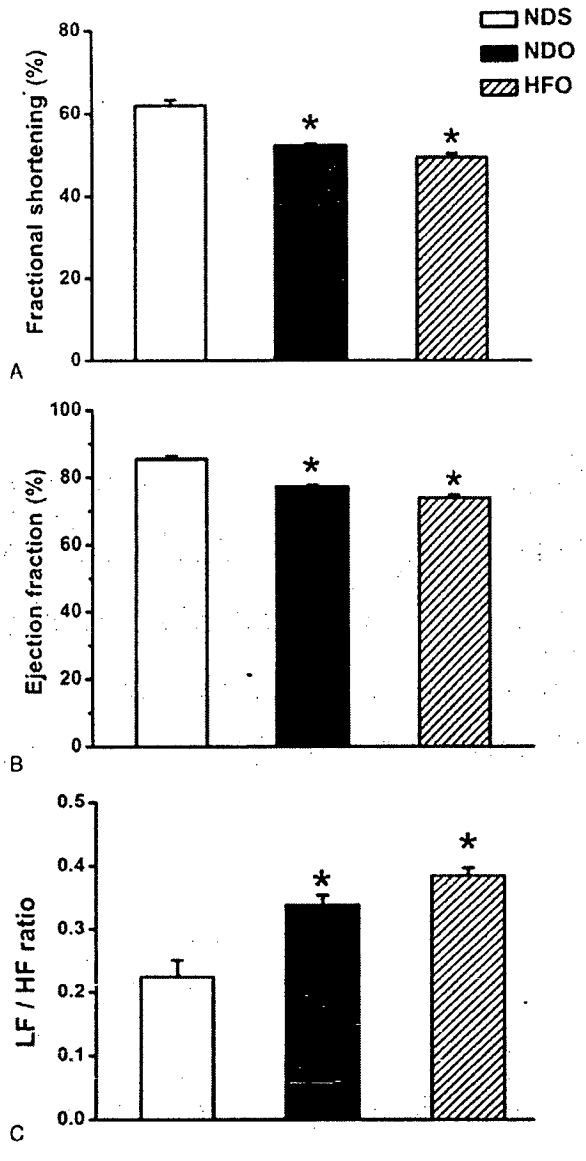


FIG. 1. Effects of estrogen deprivation and obese insulin resistance on left ventricular function and heart rate variability. At week 12 after ovariectomy, both estrogen-deprived rats who fed with NDO and those who fed with HFO had reduced fractional shortening (A), ejection fraction (B), and increased LF/HF ratio (C) when compared with NDS rats. Values are mean ± SEM (n = 6 rats/group). *$P < 0.05$ versus NDS. HF, high frequency; HFO, high-fat diet-fed ovariectomized rats; LF, low frequency; NDO, normal diet-fed ovariectomized rats; NDS, normal diet-fed sham-operated rats; SEM, standard error of mean.

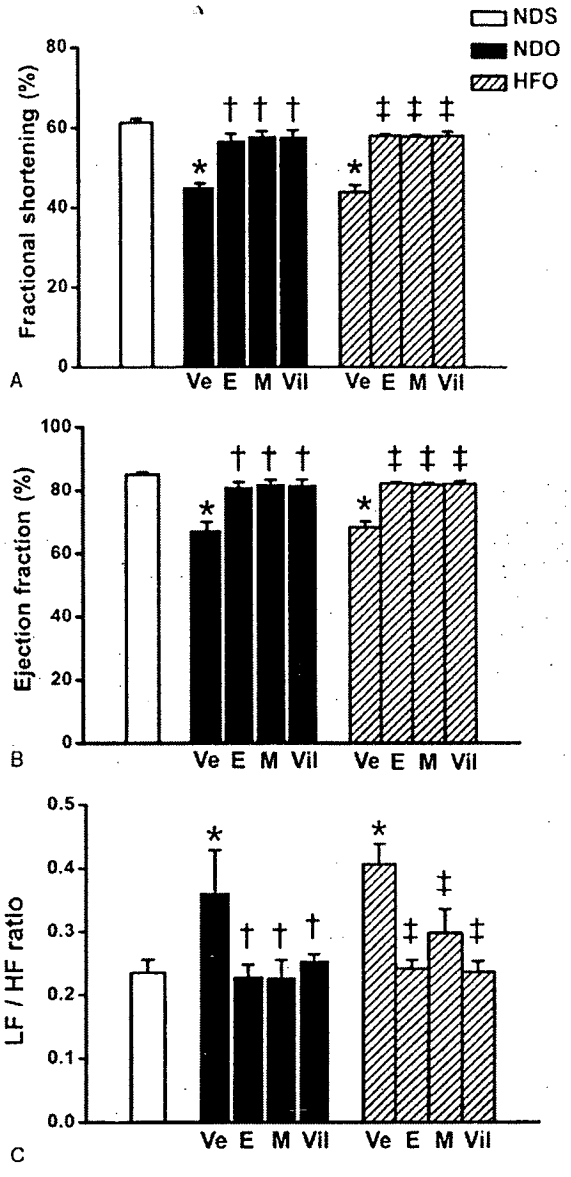


FIG. 2. Effects of E, M, and Vil on left ventricular function and heart rate variability of estrogen-deprived rats. After 4 weeks of treatment, fractional shortening (A) and ejection fraction (B) were improved, and LF/HF ratio (C) was restored in estrogen (E)-, metformin (M)-, and vildagliptin (Vil)-treated groups when compared with vehicle-treated NDO or HFO rats. Values are mean ± SEM (n = 6 rats/group). *$P < 0.05$ versus NDS; †$P < 0.05$ versus NDOVe; and ‡$P < 0.05$ versus HFOVe. E, estradiol; HF, high frequency; HFO, high-fat diet-fed ovariectomized rats; LF, low frequency; M, metformin; NDO, normal diet-fed ovariectomized rats; NDS, normal diet-fed sham-operated rats; SEM, standard error of mean; Ve, vehicle; Vil, vildagliptin.

Effects of estrogen, metformin, and vildagliptin on cardiac expression of Bax and Bcl-2 in estrogen-deprived, obese insulin-resistant rats

There were significant increases in the expression of the apoptotic protein Bax in NDOVe, HFOVe, and HFOM groups (Fig. 3A). The expression of the antiapoptotic protein Bcl-2 was significantly decreased in HFOVe and HFOM rats (Fig. 3B). The ratio of cardiac Bax/Bcl-2 was significantly higher in NDOVe, HFOVe, and HFOM rats compared with the NDS rats (Fig. 3C), whereas this ratio was lower in the HFOE and HFOVil groups, suggesting that only estrogen and vildagliptin could attenuate apoptosis in an obese insulin-resistant and estrogen-deprived rat model. A significant change in Bax and Bcl-2 expression was not observed in any NDO rats.

© 2016 The North American Menopause Society

Copyright @ 2016 The North American Menopause Society. Unauthorized reproduction of this article is prohibited.

TABLE 2. *Cardiac function after 4 weeks of treatment*

Parameters	NDS	NDO				HFO			
		Ve	E	M	Vil	Ve	E	M	Vil
Heart rate, bpm	238 ± 18	306 ± 5[a]	266 ± 8	275 ± 19	266 ± 9	307 ± 21[a]	273 ± 24	285 ± 28	286 ± 11
Systolic BP, mm Hg	118.5 ± 4	139.7 ± 10[a]	117.6 ± 5[b]	112.3 ± 5[b]	113.3 ± 3[b]	140.7 ± 6[a]	112.9 ± 3[c]	111.5 ± 6[c]	112.3 ± 5[c]
Diastolic BP, mm Hg	86.7 ± 4	108.9 ± 10[a]	89.1 ± 5	93.5 ± 7	93.8 ± 5	107.7 ± 5[a]	77.9 ± 7[c]	91.8 ± 6	87.1 ± 6[c]
LVESP, mm Hg	127.3 ± 7	99.7 ± 5[a]	113.7 ± 4	115.1 ± 4	111.9 ± 4	100.7 ± 2[a]	116.5 ± 3	111.6 ± 7[a]	108.9 ± 5[a]
LVEDP, mm Hg	12.0 ± 2	19.9 ± 2	15.2 ± 1	15.8 ± 4	15.5 ± 2	18.8 ± 2	16.2 ± 2	14.2 ± 1	13.7 ± 1
+dP/dt, mm Hg/s	11,339 ± 1,228	5,877 ± 458[a]	10,758 ± 4,949	10,427 ± 2,948	10,048 ± 3,858	5,894 ± 341[a]	6,555 ± 1,440	5,872 ± 286[a]	7,227 ± 932
−dP/dt, mm Hg/s	−7,677 ± 847	−4,397 ± 707[a]	−5,886 ± 1,005	−5,914 ± 997	−5,797 ± 1,284	−4,839 ± 623[a]	−5,626 ± 423	−4,706 ± 179[a]	−6,079 ± 1,218

Values are mean ± SEM (n = 6 per group).
BP, blood pressure; bpm, beats per minute; +dP/dt, maximal slope of the systolic pressure increment; −dP/dt, maximal slope of the diastolic pressure decrement; E, estradiol; HFO, high-fat diet-fed ovariectomized rats; LVEDP, left ventricular end-diastolic pressure; LVESP, left ventricular end-systolic pressure; M, metformin; NDO, normal diet-fed ovariectomized rats; NDS, normal diet-fed sham-operated rats; Ve, vehicle; Vil, vildagliptin.
[a] $P < 0.05$ versus NDS.
[b] $P < 0.05$ versus NDOVe.
[c] $P < 0.05$ versus HFOVe.

Effects of estrogen, metformin, and vildagliptin on cardiac mitochondrial function and oxidative stress in estrogen-deprived, obese insulin-resistant rats

Both NDOVe and HFOVe rats exhibited cardiac mitochondrial impairment, which was identified by the increased mitochondrial ROS level, decreased $\Delta\Psi$ indicating mitochondrial depolarization, and decreased absorbance intensity indicating mitochondrial swelling (Fig. 4A–D, respectively). In NDO rats, treatment with E completely halted mitochondrial dysfunction by markedly reducing ROS production, increasing $\Delta\Psi$, and attenuating mitochondrial swelling to normal levels. In HFOE rats, all mitochondrial parameters showed significant improvement, especially ROS production and $\Delta\Psi$, which were reversed to normal levels. Treatment with Vil also improved all mitochondrial parameters in both NDOVil and HFOVil when compared with vehicle-treated groups; however, it did not bring parameters back to normal levels (Fig. 4). Treatment with M could improve all mitochondrial parameters in NDOM rats; however, it failed to enhance any mitochondrial parameters in HFOM rats when compared with NDOVe rats.

DISCUSSION

The major findings from this study are as follows: (1) estrogen, metformin, and vildagliptin can attenuate insulin resistance in both ND- and HFD-fed estrogen-deprived rats; (2) although estrogen, metformin, and vildagliptin similarly attenuated cardiac autonomic dysfunction, estrogen and vildagliptin provided superior advantages through their ability to restore blood pressure and cardiac contractile performance in estrogen-deprived insulin-resistant rats; and (3) oxidative stress, apoptosis, and cardiac mitochondrial dysfunction were effectively decreased by estrogen and vildagliptin, but not by metformin.

Although the impairments of LV function in obese insulin-resistant rats and the benefits from the results may be subtle, these impairments as well as the efficacy of treatments by estrogen, metformin, or vildagliptin were demonstrated to be consistent and significant throughout the experiments. This subtle difference could also be due to the fact that we used the obese insulin-resistant model which was a prediabetic state model in which the severity is not high. Investigation in a model of type 2 diabetes with estrogen deprivation may reveal even larger benefits. Future studies are needed to evaluate this issue. Nevertheless, we believe that our findings indicated potential therapeutic efficacy of these antidiabetic drugs in menopause with obese insulin-resistant condition.

All therapeutic agents in this study, that is estrogen, vildagliptin, and metformin, clearly ameliorated insulin resistance, as indicated by the decreased levels of fasting insulin and glucose, and thus resulting in a reduced HOMA index. These results are consistent with a previous study which similarly showed that metformin and vildagliptin decreased insulin levels and the HOMA index in HFD-fed rats.[17] Estrogen supplements also exhibited similar beneficial effects, consistent with the results from a previous study, in

Copyright @ 2016 The North American Menopause Society. Unauthorized reproduction of this article is prohibited.

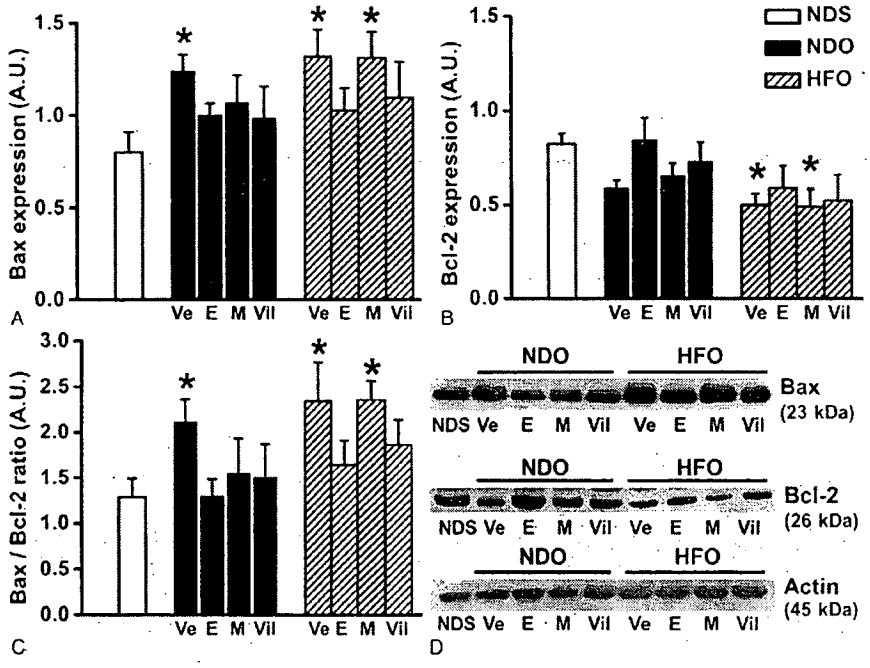


FIG. 3. Cardiac expression of apoptotic and antiapoptotic proteins after treatment with E, M, or Vil for 4 weeks. Expression levels of the apoptotic protein Bax (**A**) were significantly increased, whereas the expression levels of antiapoptotic protein, Bcl-2 (**B**), were reduced in HFOVe and HFOM rats. The Bax/Bcl-2 ratio (**C**) was significantly increased in NDOVe, HFOVe, and HFOM rats when compared with NDS rats. The represented protein expressions are in panel **D**. Values are mean ± SEM (n = 6 rats per group). $^{*}P < 0.05$ versus NDS. E, estradiol; HFO, high-fat diet-fed ovariectomized rats; M, metformin; NDO, normal diet-fed ovariectomized rats; NDS, normal diet-fed sham-operated rats; SEM, standard error of mean; Ve, vehicle; Vil, vildagliptin.

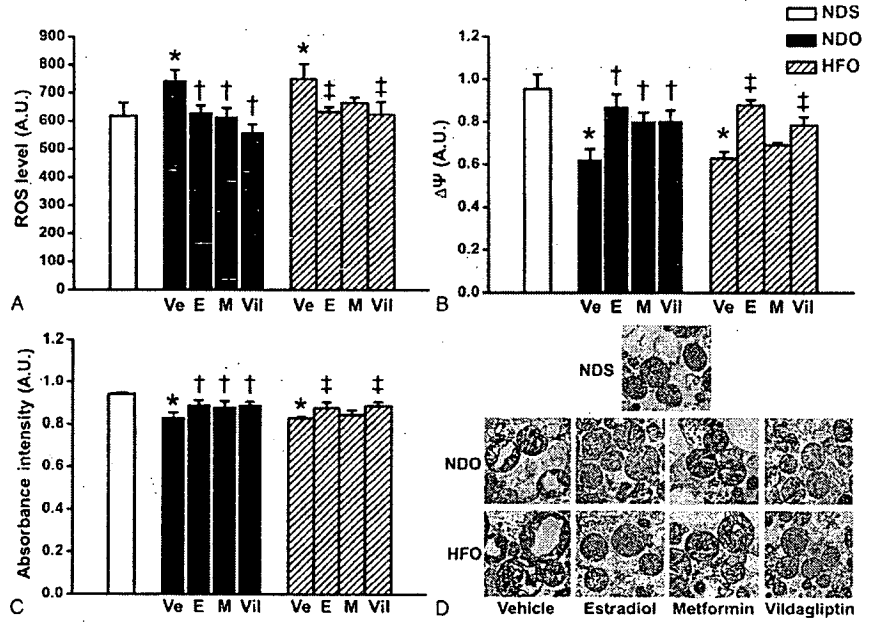


FIG. 4. Cardiac mitochondrial function in estrogen-deprived rats after treatment with E, M, or Vil for 4 weeks. Mitochondrial ROS level (**A**) was increased, whereas ΔΨ (**B**) and absorbance intensity (**C**) were decreased in NDOVe and HFOVe rats. Transmission electron micrographs (**D**) illustrate cardiac mitochondria morphology from rats in each group. Treatments with E and Vil improved all parameters of cardiac mitochondrial function in both NDO and HFO rats. Treatment with M, however, showed effective effects on mitochondrial function only in NDO, not in HFO rats. Values are mean ± SEM (n = 6 rats per group). $^{*}P < 0.05$ versus NDS; $^{\dagger}P < 0.05$ versus NDOVe; and $^{\ddagger}P < 0.05$ versus HFOVe. E, estradiol; HFO, high-fat diet-fed ovariectomized rats; M, metformin; NDO, normal diet-fed ovariectomized rats; NDS, normal diet-fed sham-operated rats; ROS, reactive oxygen species; SEM, standard error of mean; Ve, vehicle; Vil, vildagliptin.

© 2016 The North American Menopause Society

Copyright @ 2016 The North American Menopause Society. Unauthorized reproduction of this article is prohibited.

which insulin resistance was reversed after just 1 month of estrogen treatment.[19] Estrogen and metformin also efficiently inhibited BW gain in both ND- and HFD-fed rats. Estrogen had been previously reported to protect female mice from adipocyte hypertrophy, body fat accumulation, and weight gain, and the results of this study are consistent with these findings.[25] Likewise, metformin has previously been reported to increase fatty acid oxidation and decrease weight gain.[26] The ability of metformin to increase fatty acid oxidation, however, could be responsible for the high level of cytotoxicity and oxidative stress in metformin-treated rats, which was indicated by the elevated MDA levels and mitochondrial impairment. Metformin had been shown to decrease cholesterol synthesis and content; however, it has also been shown to increase ROS production in a macrophage cell line.[27] These results are similar to the findings in this study, in which cholesterol levels were reduced, whereas mitochondrial ROS levels were enhanced in metformin-treated rats.

In the present study, estrogen and vildagliptin had measurably enhanced effects on oxidative stress reduction, as they completely attenuated mitochondrial ROS production, decreased mitochondrial depolarization, decreased mitochondrial swelling, and restored serum and tissue MDA levels. Although metformin was able to reverse hyperglycemia, which is a condition linked to increased oxidative stress and inflammation,[28] it failed to improve mitochondrial function and decrease MDA concentrations, therefore could not effectively protect the heart from oxidative stress. This increased oxidative stress could subsequently induce cellular apoptosis,[29] which was indicated by the reduced Bcl-2 level and the upregulated levels of the Bax and Bax/Bcl-2 ratio in the myocardium of metformin-treated rats. Cardiomyocyte apoptosis is known to be associated with the pathogenesis of heart disease and heart failure.[30,31] This oxidative stress-induced cardiomyocyte apoptosis may contribute to decreased myocardium performance as observed in the metformin-treatment group. Moreover, a higher level of ROS, which was found in metformin-treated obese rats, is also harmful to endothelial membranes and nitric oxide function,[32] thus resulting in increased diastolic blood pressure. Estrogen has been reported to inhibit ROS production, decrease lipid peroxidation, and reduce oxidative stress in several cell types such as cardiomyocytes, fibroblasts, and hepatocytes.[33-35] Vildagliptin is also effective in the reduction of oxidative stress and mitochondrial dysfunction.[36] The antioxidant and antiapoptotic effects of estrogen and vildagliptin may play an important role in the attenuation of cardiometabolic disorders in obese insulin-resistant and estrogen-deprived rats.

Moreover, previous studies reported the similar effects of estrogen and vildagliptin regarding the reduction of oxidative stress and inflammatory markers.[37,38] Vildagliptin was also reported to enhance endothelial cell function and blood flow, through the upregulation of Akt and eNOS phosphorylation.[39] The activation of Akt and eNOS pathway had been demonstrated as the common mechanisms underlying estrogen cardioprotection[40,41]; therefore, the benefits of vildagliptin may share a similar pathway, and thus provide a similar effect as estrogen treatment, as observed in this study.

Potential clinical value

Previous studies from both basic and clinical reports demonstrated the adverse effects of estrogen therapy such as increased atrial fibrillation incidence, increased QT interval and dispersion.[42,43] The use of estrogen supplement has been contraindicated in individuals with the conditions of thromboembolism and migraine.[44,45] Moreover, estrogen supplement was reported to increase risks of glioma, meningioma, and all tumors of the central nervous system.[46] The findings in the present study, which demonstrated that the cardioprotective effects and efficacy of vildagliptin and metformin are similar to estrogen supplement in ovariectomized rats under normal and obese insulin-resistant conditions, provided important information for future clinical use of these drugs in obese insulin resistance particularly under menopause condition.

CONCLUSIONS

In summary, this study demonstrated that although metformin exerted similar effects to estrogen and vildagliptin on metabolic regulation, estrogen and vildagliptin offer greater advantage in terms of cardiac mitochondrial protection and LV performance, in obese insulin-resistant and estrogen-deprived rats. This study is the first to report the comparative efficacy of estrogen, metformin, and vildagliptin on the cardiometabolic and cardiac mitochondrial function in obese insulin-resistant ovariectomized rats. Treatment with vildagliptin and estrogen therapy similarly provided the cardioprotective benefits in obese insulin-resistant ovariectomized rats. Because estrogen supplement was reported to associate with increased venous thromboembolism and cancer risks, vildagliptin could be considered as an alternative therapy for those who have contraindication for female sex hormone therapy. Vildagliptin was reported as the medication that did not affect the cardiac conduction system and repolarization, and also exerted beneficial effect on ischemic heart.[18,47] The cardioprotective effects under myocardial ischemia of vildagliptin treatment in estrogen-deprived and insulin-resistant conditions still need to be investigated.

REFERENCES

1. Mendis S, Thygesen K, Kuulasmaa K, et al. World Health Organization definition of myocardial infarction: 2008-09 revision. *Int J Epidemiol* 2011;40:139-146.
2. Mendis S. The contribution of the Framingham Heart Study to the prevention of cardiovascular disease: a global perspective. *Prog Cardiovasc Dis* 2010;53:10-14.
3. Penno G, Solini A, Bonora E, et al. Gender differences in cardiovascular disease risk factors, treatments and complications in patients with type 2 diabetes: the RIACE Italian multicentre study. *J Intern Med* 2013;274:176-191.
4. Mendis S, Puska P, Norrving B. *Global Atlas on Cardiovascular Disease Prevention and Control*. Geneva, Switzerland: World Health Organization; 2011.
5. Giardina EG. Heart disease in women. *Int J Fertil Womens Med* 2000;45:350-357.

Copyright @ 2016 The North American Menopause Society. Unauthorized reproduction of this article is prohibited.

6. Stampfer MJ, Colditz GA, Willett WC. Menopause and heart disease. A review. *Ann N Y Acad Sci* 1990;592:193-203.
7. Rosano GM, Vitale C, Marazzi G, Volterrani M. Menopause and cardiovascular disease: the evidence. *Climacteric* 2007;10(suppl 1):19-24.
8. Jelenik T, Roden M. How estrogens prevent from lipid-induced insulin resistance. *Endocrinology* 2013;154:989-992.
9. Xu J, Xiang Q, Lin G, et al. Estrogen improved metabolic syndrome through down-regulation of VEGF and HIF-1alpha to inhibit hypoxia of periaortic and intra-abdominal fat in ovariectomized female rats. *Mol Biol Rep* 2012;39:8177-8185.
10. Campos C, Casali KR, Baraldi D, et al. Efficacy of a low dose of estrogen on antioxidant defenses and heart rate variability. *Oxid Med Cell Longev* 2014;2014:218749; Available at: http://www.hindawi.com/journals/omcl/2014/218749/. Accessed May 15, 2016.
11. Hernandez I, Delgado JL, Diaz J, et al. 17beta-estradiol prevents oxidative stress and decreases blood pressure in ovariectomized rats. *Am J Physiol Regul Integr Comp Physiol* 2000;279:R1599-R1605.
12. Brownlee M. Biochemistry and molecular cell biology of diabetic complications. *Nature* 2001;414:813-820.
13. Dhalla NS, Temsah RM, Netticadan T. Role of oxidative stress in cardiovascular diseases. *J Hypertens* 2000;18:655-673.
14. Rattanasopa C, Phungphong S, Wattanapermpool J, Bupha-Intr T. Significant role of estrogen in maintaining cardiac mitochondrial functions. *J Steroid Biochem Mol Biol* 2014;147C:1-9.
15. Bi Y, Tong GY, Yang HJ, et al. The beneficial effect of metformin on beta-cell function in non-obese Chinese subjects with newly diagnosed type 2 diabetes. *Diabetes Metab Res Rev* 2013;29:664-672.
16. Banerjee M, Younis N, Soran H. Vildagliptin in clinical practice: a review of literature. *Expert Opin Pharmacother* 2009;10:2745-2757.
17. Apaijai N, Pintana H, Chattipakorn SC, Chattipakorn N. Cardioprotective effects of metformin and vildagliptin in adult rats with insulin resistance induced by a high-fat diet. *Endocrinology* 2012;153:3878-3885.
18. Chinda K, Sanit J, Chattipakorn S, Chattipakorn N. Dipeptidyl peptidase-4 inhibitor reduces infarct size and preserves cardiac function via mitochondrial protection in ischaemia-reperfusion rat heart. *Diab Vasc Dis Res* 2014;11:75-83.
19. Pratchayasakul W, Chattipakorn N, Chattipakorn SC. Estrogen restores brain insulin sensitivity in ovariectomized non-obese rats, but not in ovariectomized obese rats. *Metabolism* 2014;63:851-859.
20. Semaming Y, Kumfu S, Pannangpetch P, Chattipakorn SC, Chattipakorn N. Protocatechuic acid exerts a cardioprotective effect in type 1 diabetic rats. *J Endocrinol* 2014;223:13-23.
21. Morgan EE, Faulx MD, McElfresh TA, et al. Validation of echocardiographic methods for assessing left ventricular dysfunction in rats with myocardial infarction. *Am J Physiol Heart Circ Physiol* 2004;287:H2049-H2053.
22. Apaijai N, Pintana H, Chattipakorn SC, Chattipakorn N. Effects of vildagliptin versus sitagliptin, on cardiac function, heart rate variability and mitochondrial function in obese insulin-resistant rats. *Br J Pharmacol* 2013;169:1048-1057.
23. Incharoen T, Thephinlap C, Srichairatanakool S, et al. Heart rate variability in beta-thalassemic mice. *Int J Cardiol* 2007;121:203-204.
24. Thummasorn S, Kumfu S, Chattipakorn S, Chattipakorn N. Granulocyte-colony stimulating factor attenuates mitochondrial dysfunction induced by oxidative stress in cardiac mitochondria. *Mitochondrion* 2011;11:457-466.
25. Stubbins RE, Najjar K, Holcomb VB, Hong J, Nunez NP. Oestrogen alters adipocyte biology and protects female mice from adipocyte inflammation and insulin resistance. *Diabetes Obes Metab* 2012;14:58-66.
26. Wang C, Liu F, Yuan Y, et al. Metformin suppresses lipid accumulation in skeletal muscle by promoting fatty acid oxidation. *Clin Lab* 2014;60:887-896.
27. Koren-Gluzer M, Aviram M, Hayek T. Metformin inhibits macrophage cholesterol biosynthesis rate: possible role for metformin-induced oxidative stress. *Biochem Biophys Res Commun* 2013;439:396-400.
28. Esposito K, Nappo F, Marfella R, et al. Inflammatory cytokine concentrations are acutely increased by hyperglycemia in humans: role of oxidative stress. *Circulation* 2002;106:2067-2072.
29. Cook SA, Sugden PH, Clerk A. Regulation of bcl-2 family proteins during development and in response to oxidative stress in cardiac myocytes: association with changes in mitochondrial membrane potential. *Circ Res* 1999;85:940-949.
30. Gill C, Mestril R, Samali A. Losing heart: the role of apoptosis in heart disease-a novel therapeutic target? *FASEB J* 2002;16:135-146.
31. Takemura G, Kanoh M, Minatoguchi S, Fujiwara H. Cardiomyocyte apoptosis in the failing heart-a critical review from definition and classification of cell death. *Int J Cardiol* 2013;167:2373-2386.
32. Annuk M, Zilmer M, Fellstrom B. Endothelium-dependent vasodilation and oxidative stress in chronic renal failure: impact on cardiovascular disease. *Kidney Int Suppl* 2003;84:S50-S53.
33. Hamden K, Carreau S, Ellouz F, Masmoudi H, El FA. Protective effect of 17beta-estradiol on oxidative stress and liver dysfunction in aged male rats. *J Physiol Biochem* 2007;63:195-201.
34. Richardson TE, Yu AE, Wen Y, Yang SH, Simpkins JW. Estrogen prevents oxidative damage to the mitochondria in Friedreich's ataxia skin fibroblasts. *PLoS One* 2012;7:e34600.
35. Urata Y, Ihara Y, Murata H, et al. 17Beta-estradiol protects against oxidative stress-induced cell death through the glutathione/glutaredoxin-dependent redox regulation of Akt in myocardiac H9c2 cells. *J Biol Chem* 2006;281:13092-13102.
36. Scheen AJ. Cardiovascular effects of gliptins. *Nat Rev Cardiol* 2013;10:73-84.
37. Lamas AZ, Caliman IF, Dalpiaz PL, et al. Comparative effects of estrogen, raloxifene and tamoxifen on endothelial dysfunction, inflammatory markers and oxidative stress in ovariectomized rats. *Life Sci* 2015;124:101-109.
38. Rizzo MR, Barbieri M, Marfella R, Paolisso G. Reduction of oxidative stress and inflammation by blunting daily acute glucose fluctuations in patients with type 2 diabetes: role of dipeptidyl peptidase-IV inhibition. *Diabetes Care* 2012;35:2076-2082.
39. Ishii M, Shibata R, Kondo K, et al. Vildagliptin stimulates endothelial cell network formation and ischemia-induced revascularization via an endothelial nitric-oxide synthase-dependent mechanism. *J Biol Chem* 2014;289:27235-27245.
40. Kim KH, Bender JR. Membrane-initiated actions of estrogen on the endothelium. *Mol Cell Endocrinol* 2009;308:3-8.
41. Murphy E, Steenbergen C. Cardioprotection in females: a role for nitric oxide and altered gene expression. *Heart Fail Rev* 2007;12:293-300.
42. Gokce M, Karahan B, Yilmaz R, Orem C, Erdol C, Ozdemir S. Long term effects of hormone replacement therapy on heart rate variability, QT interval, QT dispersion and frequencies of arrhythmia. *Int J Cardiol* 2005;99:373-379.
43. Perez MV, Wang PJ, Larson JC, et al. Effects of postmenopausal hormone therapy on incident atrial fibrillation: the Women's Health Initiative randomized controlled trials. *Circ Arrhythm Electrophysiol* 2012;5:1108-1116.
44. Tremollieres F, Brincat M, Erel CT, et al. EMAS position statement: managing menopausal women with a personal or family history of VTE. *Maturitas* 2011;69:195-198.
45. Vermeer LM, Gregory E, Winter MK, McCarson KE, Berman NE. Behavioral effects and mechanisms of migraine pathogenesis following estradiol exposure in a multibehavioral model of migraine in rat. *Exp Neurol* 2015;263:8-16.
46. Benson VS, Kirichek O, Beral V, Green J. Menopausal hormone therapy and central nervous system tumor risk: large UK prospective study and meta-analysis. *Int J Cancer* 2015;136:2369-2377.
47. He YL, Zhang Y, Serra D, Wang Y, Ligueros-Saylan M, Dole WP. Thorough QT study of the effects of vildagliptin, a dipeptidyl peptidase IV inhibitor, on cardiac repolarization and conduction in healthy volunteers. *Curr Med Res Opin* 2011;27:1453-1463.

© 2016 The North American Menopause Society

Copyright @ 2016 The North American Menopause Society. Unauthorized reproduction of this article is prohibited.

เอกสารแนบหมายเลข 20

ACTA PHYSIOLOGICA
Acta Physiol 2016, 217, 287–299

Fibroblast growth factor 21 (FGF21) therapy attenuates left ventricular dysfunction and metabolic disturbance by improving FGF21 sensitivity, cardiac mitochondrial redox homoeostasis and structural changes in pre-diabetic rats

P. Tanajak,[1,2,3] P. Sa-nguanmoo,[1,2,3] X. Wang,[4] G. Liang,[4] X. Li,[4] C. Jiang,[4] S. C. Chattipakorn[1,3,5] and N. Chattipakorn[1,2,3]

1 Cardiac Electrophysiology Research and Training Center, Faculty of Medicine, Chiang Mai University, Chiang Mai, Thailand
2 Cardiac Electrophysiology Unit, Department of Physiology, Faculty of Medicine, Chiang Mai University, Chiang Mai, Thailand
3 Center of Excellence in Cardiac Electrophysiology Research, Chiang Mai University, Chiang Mai, Thailand
4 School of Pharmaceutical Sciences, Wenzhou Medical University, University-Town, Wenzhou, Zhejiang, China
5 Department of Oral Biology and Diagnostic Sciences, Faculty of Dentistry, Chiang Mai University, Chiang Mai, Thailand

Received 9 January 2016,
revision requested 4 February 2016,
revision received 19 April 2016,
accepted 22 April 2016
Correspondence:
N. Chattipakorn, MD, PhD,
Cardiac Electrophysiology Research and Training Center,
Faculty of Medicine, Chiang Mai University, Chiang Mai 50200, Thailand.
E-mail: nchattip@gmail.com

Abstract

Aims: Fibroblast growth factor 21 (FGF21) acts as a metabolic regulator and exerts cardioprotective effects. However, the effects of long-term FGF21 administration on the heart under the FGF21-resistant condition in obese, insulin-resistant rats have not been investigated. We hypothesized that long-term FGF21 administration reduces FGF21 resistance and insulin resistance and attenuates cardiac dysfunction in obese, insulin-resistant rats.

Methods: Eighteen rats were fed on either a normal diet ($n = 6$) or a high-fat diet (HFD; $n = 12$) for 12 weeks. Then, rats in the HFD group were divided into two subgroups ($n = 6$ per subgroup) and received either the vehicle (HFV) or recombinant human FGF21 (rhFGF21, 0.1 mg kg^{-1} day^{-1}; HFF) injected intraperitoneally for 28 days. The metabolic parameters, inflammation, malondialdehyde (MDA), heart rate variability (HRV), left ventricular (LV) function, cardiac mitochondrial redox homoeostasis, cardiac mitochondrial fatty acid β-oxidation (FAO) and anti-apoptotic signalling pathways were determined.

Results: HFV rats had increased dyslipidaemia, insulin resistance, plasma FGF21 levels, TNF-α, adiponectin and MDA, depressed HRV, and impaired LV and mitochondrial function. HFV rats also had decreased cardiac Bcl-2, cardiac PGC-1α and CPT-1 protein expression. However, FGF21 restored metabolic parameters, decreased TNF-α and MDA, increased serum adiponectin, and improved HRV, cardiac mitochondrial and LV function in HFF rats. Moreover, HFF rats had increased cardiac Bcl-2, cardiac PGC-1α and CPT-1 protein expression.

Conclusion: Long-term FGF21 therapy attenuates FGF21 resistance and insulin resistance and exerts cardioprotection by improving cardiometabolic regulation via activating anti-apoptotic and cardiac mitochondrial FAO signalling pathways in obese, insulin-resistant rats.

Keywords cardiac function, fatty acid β-oxidation, fibroblast growth factor 21 (FGF21), FGF21 resistance, mitochondria, obesity–insulin resistance.

© 2016 Scandinavian Physiological Society. Published by John Wiley & Sons Ltd, doi: 10.1111/apha.12698

Long-term consumption of a high-fat diet (HFD) causes obesity–insulin resistance (Pratchayasakul *et al.* 2011, Pipatpiboon *et al.* 2012) and fibroblast growth factor 21 (FGF21) resistance (Fisher *et al.* 2010, Hale *et al.* 2012, Patel *et al.* 2014), leading to metabolic disturbance (Pratchayasakul *et al.* 2011, Pipatpiboon *et al.* 2012, Pintana *et al.* 2014), impaired cardiac autonomic regulation and left ventricular (LV) dysfunction (Ouwens *et al.* 2005, Apaijai *et al.* 2012, 2013, 2014). Growing evidence demonstrates that FGF21 plays an important role in the regulation of energy metabolism (Chau *et al.* 2010, Planavila *et al.* 2013) and may exert cardioprotection (Patel *et al.* 2014, Joki *et al.* 2015, Yan *et al.* 2015) in several pathological states such as cardiac ischaemia (Patel *et al.* 2014) and cardiac hypertrophy (Planavila *et al.* 2013). These benefits of FGF21 have been demonstrated to occur via its activation of the β-Klotho/FGFR1c receptor complex on the cell surface membrane (Cong *et al.* 2013, Planavila *et al.* 2013, 2014, Patel *et al.* 2014, Joki *et al.* 2015, Tanajak *et al.* 2015, Yan *et al.* 2015, Yu *et al.* 2015, Zhang *et al.* 2015). FGF21 resistance was reported for the first time in 2010 by Fisher *et al.*. They found that HFD-induced obesity led to significantly increased FGF21 levels, and the heart responded poorly to the endogenous FGF21 levels and exogenous FGF21 administration in acute therapy, thus giving rise to the term 'FGF21 resistance' (Fisher *et al.* 2010). Recently, Patel *et al.* (2014) demonstrated that short-term pre-treatment with FGF21 following cardiac ischaemia–reperfusion (I/R) injury in diet-induced obese rats responds poorly to exogenous FGF21 administration, indicating FGF21 resistance in the heart. Although short-term administration has been shown to be ineffective in cardioprotection (Fisher *et al.* 2010, Patel *et al.* 2014), the potential long-term FGF21 therapeutic benefits on FGF21 sensitivity, cardiac autonomic regulation, cardiac mitochondrial redox homoeostasis and structural changes and LV function in obesity–insulin resistance have not been investigated.

In this study, we tested the hypothesis that long-term FGF21 administration improves FGF21 sensitivity by increasing cardiac mitochondrial fatty acid β-oxidation (FAO) and cardiac anti-apoptotic signalling pathways and attenuating cardiac mitochondrial redox dyshomoeostasis and structural changes, leading to the improvement of cardiometabolic regulation and LV function in HFD-induced obese, insulin-resistant rats.

Materials and methods

Ethical approval

All experiments in this study were approved by the Faculty of Medicine, Chiang Mai University Institutional Animal Care and Use Committee (Permit No. 16/2558), were in compliance with NIH guidelines and were in accordance with the ARRIVE guidelines for reporting experiments involving animals (Kilkenny *et al.* 2010).

Animals and diet

Eighteen adult male Wistar rats weighing 180–200 g were purchased from the National Animal Center, Salaya Campus, Mahidol University, Bangkok, Thailand. All rats were housed in a temperature- and humidity-controlled housing unit with a light–dark cycle of 12 : 12 h with controlled temperature (25 °C). Rats were divided into two groups and received either a normal diet (ND) that contained 19.77% energy from fat or a HFD that contained 59.28% energy from fat for 12 weeks (Pratchayasakul *et al.* 2011).

Drugs and vehicle

Recombinant human FGF21 (rhFGF21) was produced using *Escherichia coli* and purified to be endotoxin-free (Wang *et al.* 2010). The rhFGF21 was obtained from Prof. Dr. Xiao Kun Li, Zhejiang Provincial Key Laboratory of Biopharmaceuticals, Wenzhou Medical College, Wenzhou, Zhejiang 325035, China. One vial (3.84 mg $vial^{-1}$; powder) was diluted in 10 mL 0.9% normal saline solution (NSS) to give a final concentration of 0.384 mg mL^{-1}. For a vehicle, 0.9% NSS was used in an equal volume to rhFGF21 (Apaijai *et al.* 2012, 2014). Rats were injected intraperitoneally with vehicle or rhFGF21 (0.1 mg kg^{-1}) once a day for 28 days.

Experiment protocol

After acclimatization for 1 week, all rats were divided into two groups and received either a ND (n = 6) or a HFD (n = 12) for 12 weeks. Then, rats in the ND group continued to receive ND food, whereas rats in the HFD group were divided into two subgroups and receive one of the following treatments: vehicle (HFV; n = 6) or rhFGF21 (HFF; n = 6) for another 4 weeks. The body weight, food intake, heart rate variability (HRV), blood pressure (BP) and echocardiography were recorded at week 12 and at the end of the experiments. Metabolic parameter measurements including plasma glucose, insulin, high-density lipoprotein cholesterol (HDL-C), low-density lipoprotein cholesterol (LDL-C), total cholesterol (TC) and triglyceride (TG) were determined at week 12 and at the end of the experiments. Blood chemistry parameters including serum adiponectin, serum TNF-α and plasma FGF21 levels were also determined. To determine the insulin sensitivity, an oral glucose tolerance test

 © 2016 Scandinavian Physiological Society. Published by John Wiley & Sons Ltd, doi: 10.1111/apha.12698

(OGTT) was also carried out. At the end of the treatment protocol, the pressure–volume (P-V) loop was used to determine the LV function. Finally, the hearts were removed and used to determine the cardiac mitochondrial redox homoeostasis and structural changes, serum and cardiac tissue malondialdehyde (MDA) levels and cardiac FGF21 signalling cascade protein expression including β-Klotho, FGFR1, p-FGFR1, ERK1/2, p-ERK1/2, Bax, Bcl-2, cleaved caspase-3, PGC-1α and CPT-1 using Western blot analysis.

Metabolic parameter assessments

The plasma HDL-C level was determined using a commercial colorimetric assay kit (BioVision, Milpitas, CA, USA) (Apaijai *et al.* 2013). The plasma glucose, TC and TG levels were determined using a colorimetric assay kit (ERBA Mannheim, Mannheim, Germany) (Pratchayasakul *et al.* 2011, Apaijai *et al.* 2014). The Friedewald equation was used to determine the plasma LDL-C level after plasma HDL-C, TC and TG were determined (Friedewald *et al.* 1972, Apaijai *et al.* 2014). The plasma insulin levels were determined using a commercial sandwich ELISA kit (LINCO Research, St. Charles, MO, USA) (Apaijai *et al.* 2013, 2014). Finally, the homoeostasis model assessment (HOMA) index was calculated using the following formula: HOMA index = [Fasting plasma insulin (μU mL^{-1})] × [fasting plasma glucose (mmol L^{-1})/22.5]. Increased HOMA index indicates a higher degree of insulin resistance (Pipatpiboon *et al.* 2012).

Serum TNF-α, adiponectin and plasma FGF21 assessments

Serum TNF-α level and serum adiponectin level were determined using an ELISA kit (Invitrogen, Life Technologies, Carlsbad, CA, USA). Plasma FGF21 levels were determined using the quantitative sandwich enzyme immunoassay technique for mouse/rat FGF21, the ELISA kit (R&D Systems, Minneapolis, MN, USA; Yan *et al.* 2015).

Tail-cuff BP measurement

Non-invasive BP was determined using the volume–pressure recording (VPR) tail-cuff method CODA 2 (Kent Scientific Corporation, Torrington, CT, USA; Feng *et al.* 2008). The BP was recorded at week 12 and at the end of the study. The animal warming platform was set at a controlled temperature of 32–35 °C. The rats were placed into the holder, and the thumb nut was tightened to allow the tail of the animal to extend out of the rear of the holder. The cuff was attached onto the rat's tail using the occlusion cuff, placing it near the base, while the VPR cuff was placed at the distal end. An average of the BP was taken from 20 cycles of measurement.

Heart rate variability

Heart rate variability was determined from lead II ECG using PowerLab (ADInstruments, Colorado Springs, CO, USA) equipped with the CHART 5.0 program for 20 min. The stable ECG that was displayed was used to determine the relationship between the RR interval and the beat numbers (tachogram) using a MATLAB program (Pratchayasakul *et al.* 2011, Apaijai *et al.* 2012, 2013). Power spectra of RR interval variability were obtained using the fast Fourier transform algorithm. The high-frequency (HF; 0.6–3 Hz) band, low-frequency (LF; 0.2–0.6 Hz) band and very low-frequency (VLF; below 0.2 Hz) band were detected. Each spectral component was calculated as integrals under the respective part of the power spectral density function and was presented in absolute units (ms^2) (Chattipakorn *et al.* 2007). To minimize the effect of changes in total power on the LF and HF bands, LF and HF were expressed as normalized units by dividing the reading by the total power minus VLF (Chattipakorn *et al.* 2007). The increase in the LF/HF ratio indicates an increase in sympathetic activity or depressed of HRV (Pongchaidecha *et al.* 2009, Apaijai *et al.* 2012, 2013).

Echocardiography for LV function assessment

The M-mode of echocardiography (Vivid i; GE Medical Systems, Aurora, OH, USA) was used to determine % fractional shortening (%FS) and was performed at the papillary muscle levels. The papillary muscle level was used as the positional landmark and the probe was adjusted to give the best image view. Then, the %FS was determined using the LV function mode. An increase in %FS was considered to be an indicator of increased LV function (Apaijai *et al.* 2012, 2013).

P-V loop assessment

Rats were anaesthetized with Zoletil (50 mg kg^{-1} BW) and xylazine (0.15 mg kg^{-1} BW) via intramuscular injection before starting the P-V loop protocol. The right common carotid artery was identified, and a P-V loop catheter (Sciences, London, ON, Canada) was inserted into it. After that, the systolic BP (SBP) and diastolic BP were determined with the catheter staying in the ascending aorta. LV function including heart rate (HR), end-systolic pressure (ESP), end-diastolic pressure (EDP), dP/dt_{max}, dP/dt_{min} and stroke volume (SV), was determined when the catheter was advanced into the LV chamber. P-V loop data analysis

© 2016 Scandinavian Physiological Society. Published by John Wiley & Sons Ltd, doi: 10.1111/apha.12698

was carried out using an analytical software program (LAB-SCRIBE2; iWorx System, Dover, NH, USA) (Apaijai *et al.* 2013, Chinda *et al.* 2014).

Measurements of cardiac mitochondrial redox homoeostasis and structural changes

The rats hearts were perfused with 10 mL of 0.9% NSS and removed rapidly. The hearts were then homogenized in ice-cold 7.2-pH buffer which contained 300 mM sucrose, 0.2 mM EGTA and 5 mM TES in 8 mL. The homogenates were centrifuged at 800 *g*, 4 °C for 5 min, and after that, the supernatant was kept and centrifuged at 8800 *g*, 4 °C for 5 min. The mitochondrial pellet was resuspended in 8 ml of isolation buffer and centrifuged at 8800 *g*, 4 °C for 5 min. The mitochondrial pellet from the last method was collected and resuspended in the respiration buffer in 2 mL per each buffer, and the protein concentration was determined using the UV-Vis spectrophotometer (UV-1700 series; BioSurplus, San Diego, CA, USA).

The cardiac mitochondrial reactive oxygen species (ROS) production was determined by incubating the mitochondria with 2 M DCFH-DA dye at 25 °C for 20 min, and the fluorescent intensity of the solution was detected by a fluorescent microplate reader with excitation wavelength at 485 nm and emission wavelength at 530 nm (BioTek Instruments, Winooski, VT, USA). An increase in the fluorescent intensity indicated an increased mitochondrial ROS production (Thummasorn *et al.* 2011, Apaijai *et al.* 2012, 2013, Chinda *et al.* 2013).

The cardiac mitochondrial membrane potential change ($\Delta\Psi$) was determined using 5 μM JC-1 dye and incubating the mitochondria with JC-1 at 37 °C for 30 min (Thummasorn *et al.* 2011, Apaijai *et al.* 2013, 2014). The changes in cardiac mitochondrial membrane potential were detected using a fluorescent microplate reader. The JC-1 monomer form concentration is represented by the green fluorescence and is excited by a wavelength of 485 nm, and the emission is detected at 590 nm. The aggregate form of JC-1 is represented by the red fluorescence and is excited at a wavelength of 485 nm, and the emission is detected at 530 nm. A decrease in the red/green fluorescent intensity ratio indicates an increase in cardiac mitochondrial membrane depolarization (Thummasorn *et al.* 2011, Apaijai *et al.* 2012, 2013, Chinda *et al.* 2013).

The cardiac mitochondrial swelling was determined by incubating cardiac mitochondria with 1.5 mM respiration buffer. The absorbance was determined using a spectrophotometer. A decreased absorbance indicated increased cardiac mitochondrial swelling (Thummasorn *et al.* 2011, Apaijai *et al.* 2012, 2013, Chinda *et al.* 2013).

The cardiac mitochondria were collected during the cardiac mitochondrial redox homoeostasis assessment and fixed by 2.5% glutaraldehyde in a 0.1 M phosphate buffer overnight. After that, they were fixed in a 1% cacodylate buffer–osmium tetroxide for 2 h, and a graded series of ethanols were used to dehydrate them. A diamond knife was used to cut the cardiac mitochondria embedded in Epon–Araldite and stained with uranyl acetate. Finally, the cardiac mitochondrial morphology was observed using a transmission electron microscope (Thummasorn *et al.* 2011, Apaijai *et al.* 2014).

Plasma and cardiac MDA by HPLC assay

The fresh cardiac tissues and serum were used to determine the MDA concentration levels by HPLC-based assay (Thermo Scientific, Bangkok, Thailand). Plasma and cardiac MDA levels were mixed with H_3PO_4 and thiobarbituric acid (TBA) to produce TBA-reactive substances (TBARS). The plasma and cardiac TBARS concentrations were determined directly from a standard curve and reported as equivalent to the MDA concentration (Apaijai *et al.* 2012, 2013).

Western blot analysis

Fresh heart tissues from the LV apex were obtained for the determination of the FGF21 signalling pathways at the end of experiments, as described in the previous studies (Palee *et al.* 2013, Surinkaew *et al.* 2013). The FGF21 signalling protein expression and phosphorylation were determined, including FGFR1 and p-FGFR1 as a dilution of 1 : 200 (Sigma-Aldrich, Singapore, Singapore), β-Klotho, PGC-1α, and CPT-1 as a 1 : 200 dilution (Santa Cruz Biotechnology, Dallas, TX, USA), ERK1/2, p-ERK1/2, Bax, cleaved caspase-3 as a 1 : 1000 dilution (Santa Cruz Biotechnology, Dallas, TX, USA), β-actin as a 1 : 2000 dilution (Santa Cruz Biotechnology, Dallas, TX, USA) and Bcl-2 as a 1 : 1000 dilution (Cell Signaling Technology, Danvers, MA, USA).

The horse anti-mouse IgG conjugate HRP-linked antibody in a 1:2,000 dilution (Cell Signaling Technology, Danvers, MA, USA) was used to detect the β-actin (Surinkaew *et al.* 2013); the rabbit anti-goat IgG conjugate HRP-linked antibody in a 1 : 2000 dilution (Santa Cruz Biotechnology, Dallas, TX, USA) was used to detect the for β-Klotho; and goat anti-rabbit IgG conjugate HRP-linked antibody in a 1 : 2000 dilution (Cell Signaling Technology, Danvers, MA, USA) was used to detect the following proteins: FGFR1, p-FGFR1, ERK1/2, p-ERK1/2, Bax, Bcl-2, cleaved caspase-3, PGC-1α and CPT-1. The ChemiDoc

 © 2016 Scandinavian Physiological Society. Published by John Wiley & Sons Ltd, doi: 10.1111/apha.12698

touch imaging system (Bio-Rad Laboratories, Hercules, CA, USA) was used to expose the membrane using the Chemiluminescence mode (Besic *et al.* 2015, Kmiecik *et al.* 2015, Liu *et al.* 2015, Tor *et al.* 2015). Finally, the ImageJ program was used to determine the densitometry which was normalized with β-actin (Chinda *et al.* 2014).

Statistical analysis

Data were expressed as mean ± SEM. A one-way ANOVA followed by LSD *post hoc* test was used to test the difference between the groups. $P < 0.05$ was considered statistically significant.

Results

FGF21 restores the metabolic disturbance, lipid peroxidation and blood chemistry

At 16 weeks after HFD feeding, the results showed that the body weight, visceral fat, plasma insulin, plasma TC, plasma LDL-C, serum MDA levels, serum TNF-α, the area under the curve (AUCg) by OGTT and HOMA index were increased in the HFD rats, compared with the NDV group (Table 1). Our results showed that the heart weight was not different between groups. However, the heart weight/body weight ratio was lower in the HFV rats, whereas this parameter was increased in the HFF rats (Table 1). This is due to the fact that the body weight was markedly increased in the HFV group, whereas the body weight was significantly decreased in the HFF rats. Moreover, serum adiponectin and plasma HDL-C were decreased in the HFD group, compared with the NDV group. The FGF21 therapy significantly decreased the body weight, visceral fat, plasma insulin, plasma TC, plasma HDL-C, serum and tissue MDA levels, serum TNF-α, AUCg and HOMA index, compared with the HFV group. Moreover, serum adiponectin and plasma HDL-C were increased in the HFF group, compared with the HFV group (Table 1).

FGF21 restores the BP and LV function impaired by HFD

At 16 weeks after HFD feeding, the results showed that the HFD significantly increased SBP, mean arterial pressure (MAP) and HR, compared with the NDV. However, rats in the HFF group had significantly decreased SBP, MAP and HR, compared with the HFV group (Table 2). Regarding LV function, the P-V loop results showed that there was a significant increase in EDP, and a decrease in ESP, $\pm dP/dt$ and SV in the HFV group, compared with the NDV group (Table 2). In the HFF group, there was a significant decrease in EDP, and an increase in ESP, $\pm dP/dt$ and SV, compared with the HFV group (Table 2).

Table 1 Effects of FGF21 treatment on metabolic parameters in HFD-induced obese, insulin-resistant rats

	Groups		
Parameters	NDV	HFV	HFF
Body weight (g)	440 ± 22	672 ± 15*	595 ± 20*,†
Visceral fat (g)	19 ± 2	66 ± 1*	56 ± 3*,†
Heart weight (g)	1.23 ± 0.02	1.25 ± 0.02	1.25 ± 0.01
HW/BW ratio (g kg^{-1})	2.69 ± 0.09	1.86 ± 0.06*	2.10 ± 0.07*,†
Food intake (g day^{-1})	28 ± 1	30 ± 1	29 ± 1
Plasma glucose (mg dL^{-1})	124 ± 3	137 ± 6	132 ± 4
Plasma TC (mg dL^{-1})	78 ± 3	113 ± 8*	86 ± 1†
Plasma TG (mg dL^{-1})	62 ± 6	55 ± 2	55 ± 2
Plasma LDL-C (mg dL^{-1})	38 ± 3	64 ± 7*	41 ± 5†
Plasma HDL-C (mg dL^{-1})	35 ± 1	25 ± 2*	36 ± 2†
Serum adiponectin (μg mL^{-1})	24.2 ± 3.7	8.7 ± 2.9*	25.7 ± 2.8†
Serum TNF-α (pg mL^{-1})	0.6 ± 0.1	2.6 ± 0.5*	1.6 ± 0.3†
Plasma insulin (ng mL^{-1})	2.5 ± 0.1	4.6 ± 0.6*	2.9 ± 0.3†
HOMA index	15.2 ± 0.9	33.2 ± 8.6*	17.7 ± 1.9†
Serum MDA (μmol mL^{-1})	1.36 ± 0.03	3.36 ± 1.05*	1.15 ± 0.17†
AUCg (mg dL^{-1} × min × 10^4)	49 252 ± 2330	67 362 ± 4643*	53 578 ± 3050†

HFD, high-fat diet; NDV, normal diet treated with vehicle; HFV, high-fat diet treated with vehicle; HFF, high-fat diet treated with FGF21; TC, total cholesterol; TG, triglyceride; LDL-C, low-density lipoprotein cholesterol; HDL-C, high-density lipoprotein cholesterol; TNF-α, tumour necrosis factor-alpha; HOMA, homoeostasis model assessment; MDA, malondialdehyde; AUCg, area under the curve.
*$P < 0.05$ vs. NDV, †$P < 0.05$ vs. HFV.

© 2016 Scandinavian Physiological Society. Published by John Wiley & Sons Ltd, doi: 10.1111/apha.12698

Table 2 Effects of FGF21 treatment on blood pressure and left ventricular function in high-fat diet-induced obese, insulin-resistant rats

Parameters	Groups		
	NDV	HFV	HFF
SBP (mmHg)	129 ± 5	153 ± 2*	139 ± 3†
DBP (mmHg)	85 ± 3	85 ± 3	86 ± 5
MAP (mmHg)	100 ± 4	115 ± 1*	102 ± 5†
HR (beats min^{-1})	393 ± 6	416 ± 6*	398 ± 5†
ESP (mmHg)	132 ± 5	116 ± 1*	126 ± 1†
EDP (mmHg)	19 ± 1	35 ± 1*	21 ± 1†
$+dP/dt$ (mmHg s^{-1})	8290 ± 36	6029 ± 184*	8816 ± 294†
$-dP/dt$ (mmHg s^{-1})	−5627 ± 198	−4040 ± 165*	−5813 ± 246†
SV (mL g^{-1} BW)	1.02 ± 0.04	0.74 ± 0.08*	1.05 ± 0.03†

SBP, systolic blood pressure; DBP, diastolic blood pressure; MAP, mean arterial pressure; HR, heart rate; ESP, end-systolic pressure; EDP, end-diastolic pressure; SV, stroke volume.
*$P < 0.05$ vs. NDV, †$P < 0.05$ vs. HFV.

FGF21 restores the HRV impaired by HFD

For the HRV, the results showed that HFD significantly increased the LF/HF ratio since week 12 in the HFD rats, compared with the ND (Fig. 1a). In the same way, it was found that %FS was significantly decreased at week 12 in the HFD group, compared with the ND group (Fig. 1b). After 16 weeks of HFD feeding, there was still a significant increase in the LF/HF ratio in the HFV rats, compared with the NDV group. However, the LF/HF ratio was significantly decreased after FGF21 administration in the HFF group, compared with the HFV group (Fig. 1c). Moreover, %FS also significantly decreased in the HFV group, compared with the NDV group. The % FS also significantly increased after FGF21 treatment in the HFF rats, compared with the HFV group (Fig. 1d).

FGF21 restores the FGF21 sensitivity by increased FGFR1 phosphorylation in the heart

The levels of plasma FGF21 were significantly higher in the HFD group, compared to the ND rats at week 12 of HFD feeding (Fig. 2a). Plasma FGF21 levels at week 16 were also significantly increased in the HFV group, compared with the NDV group (Fig. 2b). However, the plasma FGF21 levels were significantly increased in the HFF (894.9 ± 64.1 pg mL^{-1}) group, compared with the HFV and NDV groups (Fig. 2b).

The FGF21 receptor complex in the heart was significantly altered after HFD feeding. At 16 weeks

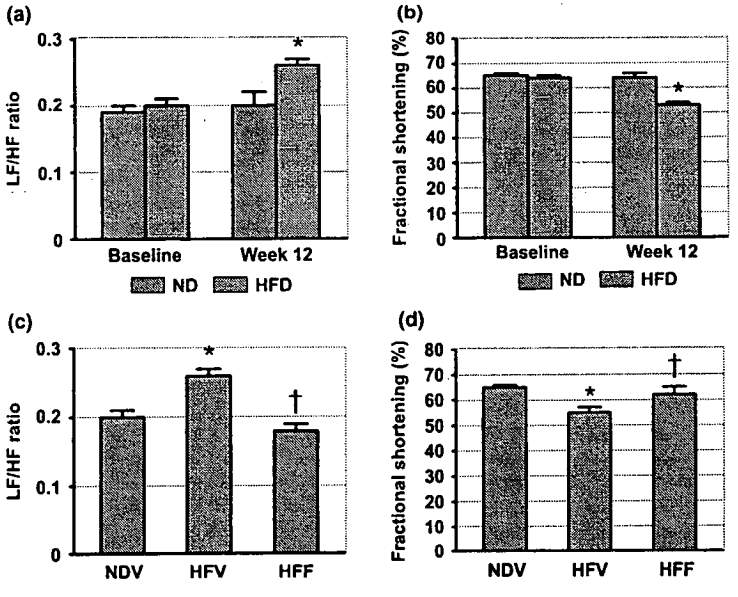


Figure 1 Effects of HFD consumption and FGF21 treatment on HRV and echocardiographic parameters. (a) HRV and (b) % fractional shortening (%FS) in ND and HFD rats at baseline and week 12. *$P < 0.05$ vs. ND. (c) HRV and (d) % FS in ND and HFD rats treated with vehicle and FGF21. *$P < 0.05$ vs. NDV, †$P < 0.05$ vs. HFV. HRV, heart rate variability; HFD, high-fat diet; ND, normal diet; NDV, normal diet treated with vehicle; HFV, high-fat diet treated with vehicle; HFF, high-fat diet treated with FGF21.

© 2016 Scandinavian Physiological Society. Published by John Wiley & Sons Ltd, doi: 10.1111/apha.12698

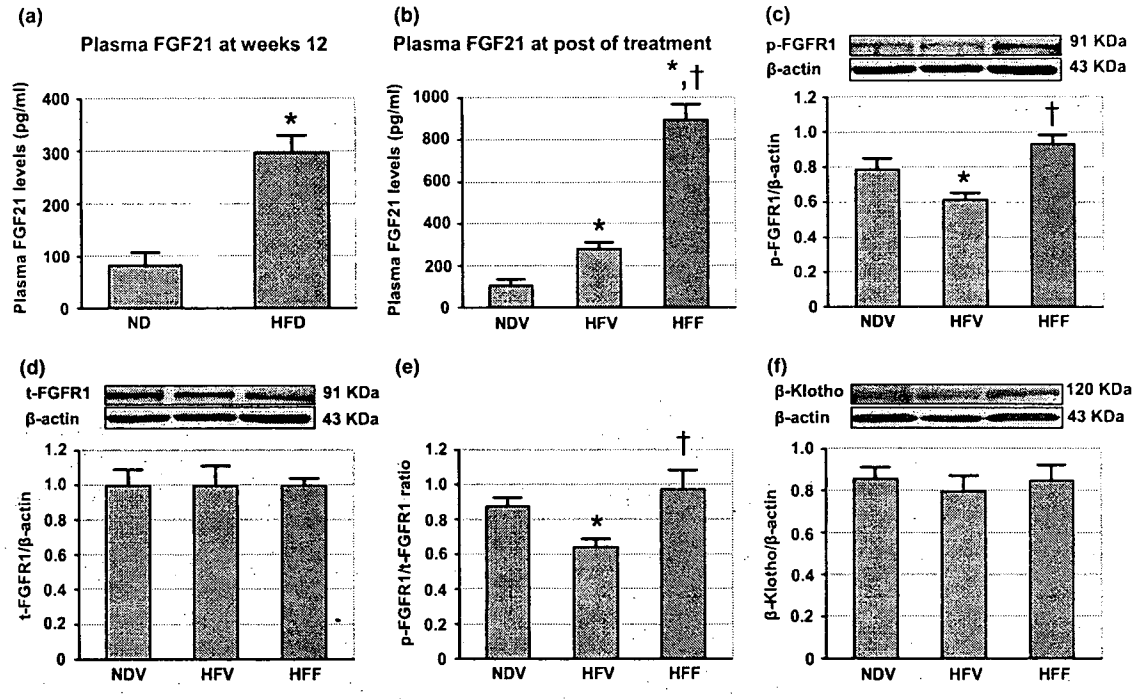


Figure 2 Effects of HFD consumption and FGF21 treatment on plasma FGF21 levels and FGFR1/β-Klotho receptors complex. (a) Plasma FGF21 levels at week 12, (b) plasma FGF21 levels post-treatment, (c) p-FGFR1, (d) t-FGFR1, (e) p-FGFR1/t-FGFR1 and (f) β-Klotho in ND and HFD rats treated with vehicle and FGF21. *$P < 0.05$ vs. NDV, †$P < 0.05$ vs. HFV. HFD, high-fat diet; ND, normal diet; NDV, normal diet treated with vehicle; HFV, high-fat diet treated with vehicle; HFF, high-fat diet treated with FGF21; FGFR1, fibroblast growth factor receptor 1.

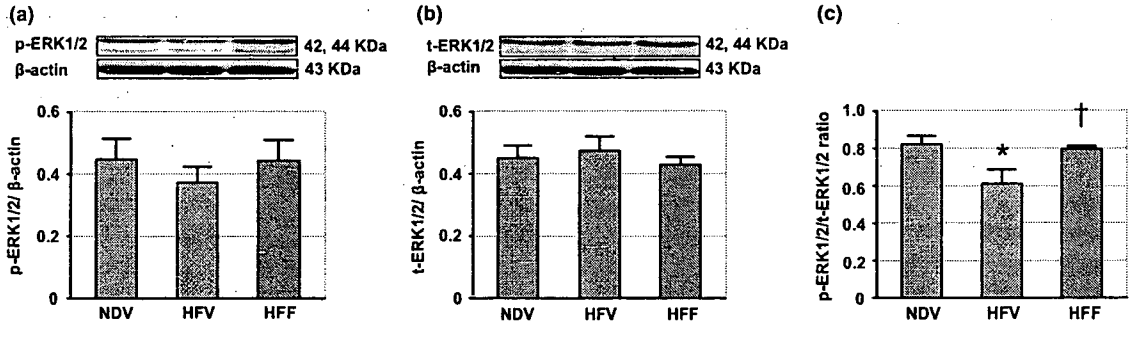


Figure 3 Effects of HFD consumption and FGF21 treatment on the ERK1/2 expression and phosphorylation. (a) p-ERK1/2, (b) t-ERK1/2 and (c) p-ERK1/2/t-ERK1/2 ratio in ND and HFD rats treated with vehicle and FGF21. *$P < 0.05$ vs. NDV, †$P < 0.05$ vs. HFV. HFD, high-fat diet; ND, normal diet; NDV, normal diet treated with vehicle; HFV, high-fat diet treated with vehicle; HFF, high-fat diet treated with FGF21; ERK1/2, extracellular signal regulated protein kinases 1 and 2.

after HFD feeding, there were significantly decreased levels of FGFR1 phosphorylation (p-FGFR1) (Fig. 2c) and the p-FGFR1/t-FGFR1 ratio (Fig. 2e) in the HFV rats, compared with the NDV group. FGF21 treatment significantly increased the levels of p-FGFR1/β-actin (Fig. 2c) and the p-FGFR1/t-FGFR1 ratio (Fig. 2e) in the HFF rats, compared with the HFV group. However, no difference was found in total FGFR1 (t-FGFR1) (Fig. 2d) and β-Klotho levels (Fig. 2f) between groups.

FGF21 restores the secondary messenger ERK1/2, anti-apoptotic and mitochondrial FAO signalling pathways in the heart

Our results showed that there was no significant difference in the levels of p-ERK1/2 (Fig. 3a) and t-ERK1/2 (Fig. 3b) between the NDV, HFV and HFF rats. However, a significant decrease in the p-ERK1/2/t-ERK1/2 ratio was observed in the HFV rats (Fig. 3c), compared with the NDV group. Moreover,

© 2016 Scandinavian Physiological Society. Published by John Wiley & Sons Ltd, doi: 10.1111/apha.12698

a significant increase in the p-ERK1/2/t-ERK1/2 ratio (Fig. 3c) was also observed in the HFF rats, compared with the HFV group.

Regarding apoptosis, a significant increase in Bax level (Fig. 4a), Bax/Bcl-2 ratio (Fig. 4c) and the cleaved caspase-3/t-caspase-3 ratio (Fig. 4d) was found in the HFV rats, compared with the NDV group. In addition, a significant increase in Bcl-2 (Fig. 4b), PGC-1α (Fig. 4e) and CPT-1 (Fig. 4f) was found in the HFV rats, compared with the NDV group. However, no significant difference in the levels of t-caspase-3 was found between all groups (Fig. 4d).

In the HFF rats, a significant decrease in the levels of Bax (Fig. 4a), Bax/Bcl-2 ratio (Fig. 4c) and the cleaved caspase-3/t-caspase-3 ratio was observed (Fig. 4d), compared with the HFV group. Moreover, a significant increase in the levels of Bcl-2 (Fig. 4b), PGC-1α (Fig. 4e) and CPT-1 was found (Fig. 4f) in the HFF rats, when compared to the HFV group.

FGF21 restores cardiac mitochondrial redox homoeostasis, structural changes and lipid peroxidation

In the HFV rats, there was a significant increase in cardiac mitochondrial ROS production (Fig. 5a), cardiac mitochondrial depolarization (Fig. 5b) and cardiac mitochondrial swelling (Fig. 5c), compared with the NDV group. However, after FGF21 treatment, the cardiac mitochondrial ROS production (Fig. 5a) was significantly decreased in the HFF rats, compared with the HFV group. In addition, cardiac mitochondrial depolarization (Fig. 5b), cardiac mitochondrial swelling (Fig. 5c) and cardiac lipid peroxidation (Fig. 5e) were significantly decreased in the HFF rats, compared with the HFV group. The representative electron micrographs illustrate the cardiac mitochondrial morphology with unfolded cristae in the heart of the HFV rat indicating mitochondrial swelling, and the FGF21 treatment attenuated the swelling as indicated by increased folded cristae in the mitochondria (Fig. 5d).

Discussion

The major findings of this study are as follows. First, long-term HFD consumption causes metabolic disturbance, progressive insulin resistance, activation of the systemic and cardiac oxidative stress processes, activation of the pro-inflammatory cytokines, increased BP, cardiac mitochondrial redox dyshomoeostasis and structural changes, progressive FGF21 resistance and decreased HRV; all of these lead to LV dysfunction.

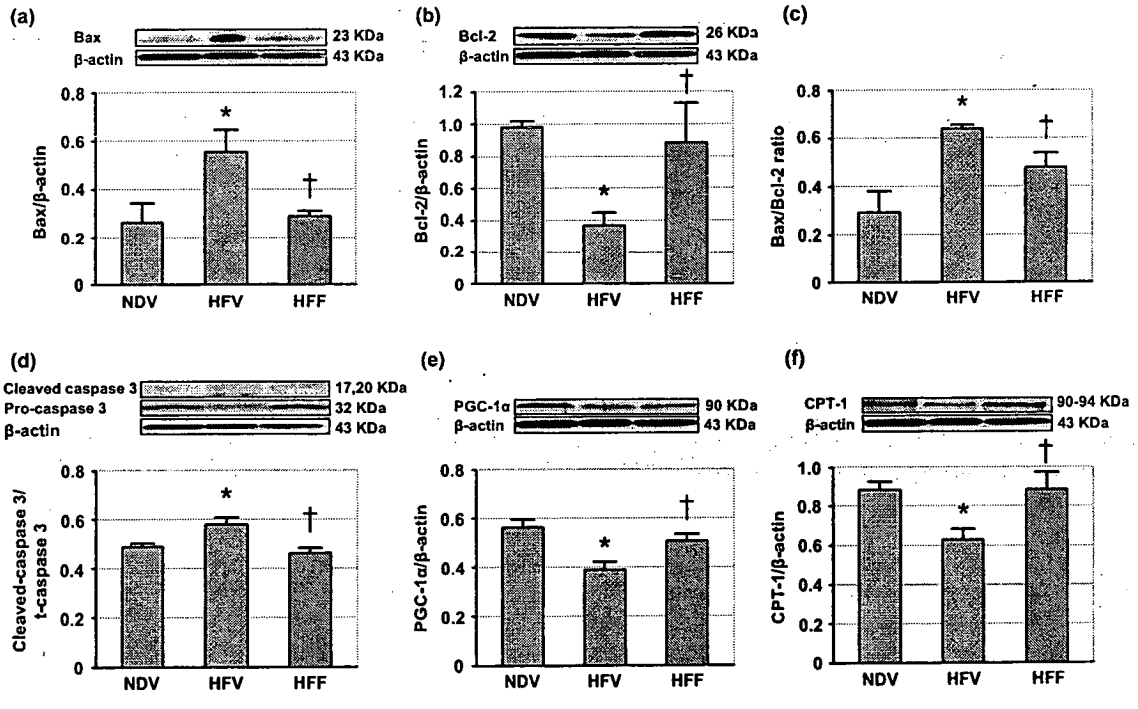


Figure 4 Effects of HFD consumption and FGF21 treatment on cardiac FGF21 signalling pathways. (a) Bax, (b) Bcl-2, (c) Bax/Bcl-2 ratio, (d) cleaved caspase-3/t-caspase-3 ratio, (e) PGC-1α and (f) CPT-1 in ND and HFD rats treated with vehicle and FGF21. *$P < 0.05$ vs. NDV, †$P < 0.05$ vs. HFV. HFD, high-fat diet, ND, normal diet; NDV, normal diet treated with vehicle; HFV, high-fat diet treated with vehicle; HFF, high-fat diet treated with FGF21.

 © 2016 Scandinavian Physiological Society. Published by John Wiley & Sons Ltd, doi: 10.1111/apha.12698

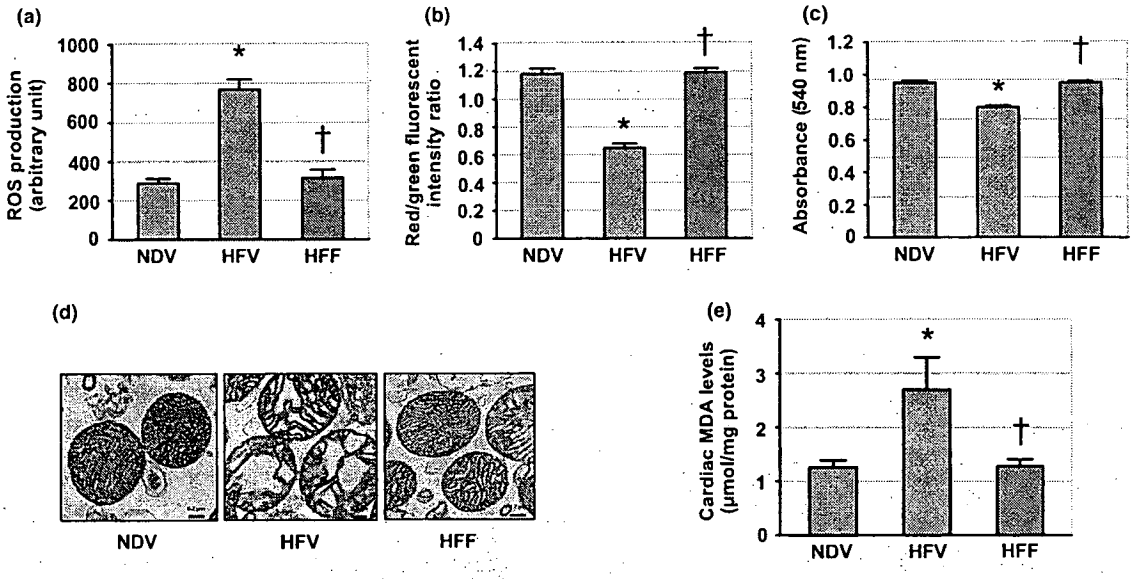


Figure 5 Effects of HFD consumption and FGF21 treatment on cardiac mitochondrial redox homoeostasis, structural changes and lipid peroxidation. (a) Cardiac mitochondrial ROS production, (b) red/green fluorescent intensity ratio, (c) cardiac mitochondrial swelling and (d) cardiac mitochondrial morphology by transmission electron microscope (TEM) and (e) cardiac lipid peroxidation in ND and HFD rats treated with vehicle and FGF21. *$P < 0.05$ vs. NDV, †$P < 0.05$ vs. HFV. HFD, high-fat diet; ND, normal diet; NDV, normal diet treated with vehicle; HFV, high-fat diet treated with vehicle; HFF, high-fat diet treated with FGF21.

Secondly, long-term FGF21 administration can reverse the adverse effects of HFD consumption by decreasing metabolic disturbance, systemic and cardiac oxidative stress and cardiac mitochondrial redox dyshomoeostasis and structural changes. It also leads to decreased pro-inflammatory cytokines, reduced BP and increased HRV, thus attenuating FGF21 resistance in the heart, and finally leading to restoration of LV function. However, the high levels of plasma FGF21 observed in the HFF group were due to the exogenous FGF21 administration that we continuously performed in those rats. Moreover, the exogenous FGF21 administration has been shown to cause an upregulation of the FGF21 synthesis, which might even lead to a further increase in the FGF21 levels (Planavila *et al.* 2013, Tanajak *et al.* 2015).

Obesity–insulin resistance due to consumption of a HFD has been shown to cause metabolic disturbance, leading to cardiac mitochondrial redox dyshomoeostasis and structural changes and impaired LV function (Apaijai *et al.* 2012, 2013, 2014). Our results also demonstrated that HFD consumption increased the serum levels of pro-inflammatory cytokine TNF-α and decreased serum adiponectin levels. TNF-α plays an important role in the inflammation process and has been shown to contribute to both heart and vascular damage (Kubota *et al.* 2000). In this study, long-term HFD consumption increased plasma TNF-α and cardiac mitochondrial ROS production, indicating an increase in inflammation and oxidative stress respectively. Increasing inflammation and oxidative stress are known to cause the impairment of endothelial nitric oxide synthesis and activity, leading to endothelial dysfunction and increased BP (Rees *et al.* 1989, Cai & Harrison 2000).

FGF21 resistance has been shown to affect metabolic regulation and cardiac function (Hale *et al.* 2012, Patel *et al.* 2014). In the obese, insulin-resistant rats, obesity being caused by long-term HFD consumption, increased plasma FGF21 levels were observed. Moreover, abnormal FGF21 signalling was also found in the heart of these rats despite the increased plasma FGF21 level. This was shown by decreased FGFR1 phosphorylation and decreased response of its downstream signalling pathways in the heart including p-ERK1/2/t-ERK1/2 ratio, Bcl-2, PGC-1α and CPT-1, while there were increases in Bax, Bax/Bcl-2 ratio and cleaved caspase-3 expression. These findings indicated FGF21 resistance in the heart of these obese, insulin-resistant rats. The decrease in FGF21 signalling cascades has been shown to interrupt the cardioprotective effects of FGF21 by reducing its anti-apoptosis (Cong *et al.* 2013, Zhang *et al.* 2015), antioxidative stress (Planavila *et al.* 2014), antihypertrophy and remodelling effects (Planavila *et al.* 2013, Joki *et al.* 2015), and also acceleration of

© 2016 Scandinavian Physiological Society. Published by John Wiley & Sons Ltd, doi: 10.1111/apha.12698

the development of diabetic cardiomyopathy (Yan *et al.* 2015, Zhang *et al.* 2015). From these findings, the FGF21-resistant state has been suggested as a limitation to FGF21 treatment to take action on the cells and leads to low efficiency or ineffective short-term FGF21 therapy. This is supported by the findings that acute FGF21 treatment by giving FGF21 for 10 min prior to I/R injury failed to decrease myocardial infarct size and was unable to improve cardiac function in diet-induced obesity models with FGF21 resistance as indicated by no improvement of a reduced response of the FGF21 receptor complex and FGF21 signalling cascade (Patel *et al.* 2014).

The FGF21-resistant state could be represented by a decrease in both primary receptors (FGFR1c and FGFR2c) and the coreceptor β-Klotho (Fisher *et al.* 2010), or a decrease in the β-Klotho expression without an alteration in the FGFR1c expression (Patel *et al.* 2014). In this study, FGF21 resistance was characterized by increased plasma FGF21 levels and decreased p-FGFR1 and p-FGFR1/t-FGFR1 ratio, whereas β-Klotho expression remained unaltered. However, the downstream signalling cascades including p-ERK1/2/t-ERK1/2 ratio were also decreased. Moreover, FGF21 resistance found in this study could contribute to a decreased cardiac mitochondrial FAO as indicated by decreased levels of PGC-1α and CPT-1 expression in the heart of obese, insulin-resistant rats.

Long-term FGF21 administration can reverse the adverse effects of long-term HFD consumption on inflammation as shown by the effective decrease in the serum TNF-α levels, suggesting it has the ability to decrease inflammation (Planavila *et al.* 2013). FGF21 also increased serum adiponectin levels, an adipokine secreted from adipocytes regulating glucose and lipid metabolism (Kadowaki *et al.* 2006). In the cardiovascular system, adiponectin has been shown to play an important role in improving endothelial dysfunction

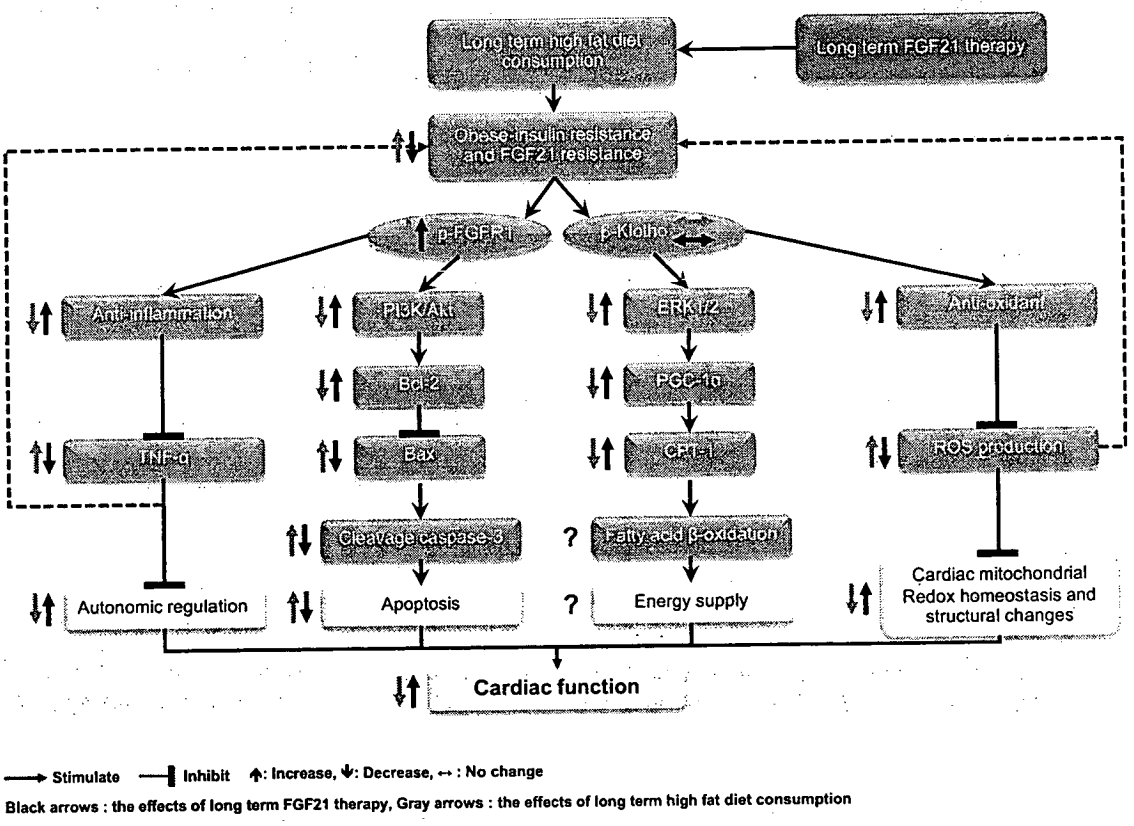


Figure 6 Effects of short-term and long-term FGF21 therapy on cardiac function in high-fat diet (HFD)-induced obese, insulin-resistant rats. Long-term consumption of a HFD decreases response of p-FGFR1 which contributes to inflammation, oxidative stress, apoptosis and impaired cardiac mitochondrial fatty acid β-oxidation (FAO). It also leads to impaired cardiac autonomic regulation, cardiac mitochondrial redox homoeostasis and structural changes and affected cardiac function. FGF21, fibroblast growth factor 21; p-FGFR1, fibroblast growth factor receptor 1 phosphorylation; TNF-α, tumour necrosis factor-alpha; PI3K, phosphatidylinositol-3-kinase; Akt, protein kinase B (PKB); ERK1/2, extracellular signal regulated protein kinases 1 and 2; PGC-1α, peroxisome proliferator-activated receptor gamma coactivator 1-alpha; CPT-1, carnitine palmitoyltransferase I; ?, unclear effects/association with the FAO and cardiac function.

 © 2016 Scandinavian Physiological Society. Published by John Wiley & Sons Ltd, doi: 10.1111/apha.12698

(Wang *et al.* 2009), atherosclerosis (Ewart *et al.* 2008) and hypertension (Yamawaki *et al.* 2011). The improved BP found in this study could be due to the protective effect of adiponectin. Moreover, the exogenous FGF21 has been shown to increase the expression of the antioxidant genes, leading to a decrease in the ROS production in neonatal cardiac myocytes (Planavila *et al.* 2014). Our study demonstrated that long-term exogenous FGF21 therapy effectively decreased ROS production in cardiac mitochondria, leading to improved cardiac mitochondrial redox homoeostasis and structural changes. In addition, this study also demonstrated that long-term FGF21 therapy could increase the anti-apoptosis signalling pathways by increasing Bcl-2 expression and also decreased Bax and cleaved caspase-3 expression.

As FGF21 played an important role in regulating the mitochondrial FAO metabolism, where the majority of ATP is generated in the heart (Neely *et al.* 1972, Neely & Morgan 1974), long-term FGF21 therapy in our study could effectively increase the PGC-1α and CPT-1 expression, hence promoting increased FAO and ATP synthesis in the heart. Although most studies regarding HFD-induced obesity and/or insulin resistance demonstrated the increased fatty acid oxidation (FAO) in the heart (Aasum *et al.* 2003, Mazumder *et al.* 2004, Alrob *et al.* 2014), inconsistent findings exist (Young *et al.* 2002, Atkinson *et al.* 2003, Gupte *et al.* 2013, Neves *et al.* 2014). It has been shown that FAO was not altered in insulin-resistant model (Atkinson *et al.* 2003) and HFD-induced obesity model (Gupte *et al.* 2013). Moreover, decreased FAO in HFD-induced obesity model (Neves *et al.* 2014) and obese model (Young *et al.* 2002) has been demonstrated. These findings indicate a complicate relationship between these two parameters. In the present study, the changes in PGC-1α and CPT-1 protein expression could be influenced by multiple factors which may explain these results. Firstly, FGF21 has been shown to regulate PGC-1α and CPT-1 mRNA and protein expression in the heart (Planavila *et al.* 2013). Additionally, several studies reported that long-term HFD consumption could induce FGF21 resistance, which could impair FGF21 receptor function (Fisher *et al.* 2010, Patel *et al.* 2014). An impairment of FGF21 receptor function could reduce FGF21's downstream signalling cascades including PGC-1α and CPT-1 (Planavila *et al.* 2013). These findings suggest that FGF21 induced by long-term HFD consumption could lead to reduced PGC-1α and CPT-1 levels as observed in our study. Secondly, the effect of obesity–insulin resistance and diabetes on the relationship between FAO and CPT-1 is still unclear. Although it has been shown that FAO levels were increased in obese, insulin-resistant rats and this was associated with an increase in CPT-1 expression (Neves *et al.* 2014), several studies reported that FAO and CPT-1 levels were unchanged in obese, insulin-resistant animals, when compared to healthy controls (Atkinson *et al.* 2003). Moreover, a previous study has reported a decrease in FAO in obese Zucker rats' hearts (Young *et al.* 2002). These findings suggest that changes (either decrease or increase) in PGC-1α and CPT-1 protein expression do not always reflect changes in the FAO in the heart. A summary of the cardioprotective effects of long-term FGF21 therapy in HFD-induced obese, insulin-resistant rats is shown in Figure 6.

Conclusions

Long-term FGF21 therapy attenuates FGF21 resistance by increasing FGF21 sensitivity and also improves insulin resistance by increasing insulin sensitivity in this model. Long-term FGF21 therapy not only activates anti-apoptotic pathways and improves cardiac mitochondrial redox homoeostasis and structural changes, but also activates mitochondrial FAO pathways in the heart, leading to improved cardiac function in obese, insulin-resistant rats with FGF21 resistance.

Conflict of interest

The authors declare no conflicts of interest.

The authors would like to thank Ms. Cicely Proctor for her editorial assistance. This work was supported by a NSTDA Research Chair Grant from the National Science and Technology Development Agency Thailand (NC), the Thailand Research Fund Royal Golden Jubilee Program (SC and PT), BRG5780016 (SC) and Chiang Mai University Center of Excellence Award (NC).

References

Aasum, E., Hafstad, A.D., Severson, D.L. & Larsen, T.S. 2003. Age-dependent changes in metabolism, contractile function, and ischemic sensitivity in hearts from db/db mice. *Diabetes* 52, 434–441.

Alrob, O.A., Sankaralingam, S., Ma, C., Wagg, C.S., Fillmore, N., Jaswal, J.S., Sack, M.N., Lehner, R., Gupta, M.P., Michelakis, E.D., Padwal, R.S., Johnstone, D.E., Sharma, A.M. & Lopaschuk, G.D. 2014. Obesity-induced lysine acetylation increases cardiac fatty acid oxidation and impairs insulin signalling. *Cardiovasc Res* 103, 485–497.

Apaijai, N., Pintana, H., Chattipakorn, S.C. & Chattipakorn, N. 2012. Cardioprotective effects of metformin and vildagliptin in adult rats with insulin resistance induced by a high-fat diet. *Endocrinology* 153, 3878–3885.

Apaijai, N., Pintana, H., Chattipakorn, S.C. & Chattipakorn, N. 2013. Effects of vildagliptin versus sitagliptin, on

© 2016 Scandinavian Physiological Society. Published by John Wiley & Sons Ltd, doi: 10.1111/apha.12698

cardiac function, heart rate variability and mitochondrial function in obese insulin-resistant rats. *Br J Pharmacol* 169, 1048–1057.

Apaijai, N., Chinda, K., Palee, S., Chattipakorn, S. & Chattipakorn, N. 2014. Combined vildagliptin and metformin exert better cardioprotection than monotherapy against ischemia-reperfusion injury in obese-insulin resistant rats. *PLoS ONE* 9, e102374.

Atkinson, L.L., Kozak, R., Kelly, S.E., Onay Besikci, A., Russell, J.C. & Lopaschuk, G.D. 2003. Potential mechanisms and consequences of cardiac triacylglycerol accumulation in insulin-resistant rats. *Am J Physiol Endocrinol Metab* 284, E923–E930.

Besic, V., Shi, H., Stubbs, R.S. & Hayes, M.T. 2015. Aberrant liver insulin receptor isoform a expression normalises with remission of type 2 diabetes after gastric bypass surgery. *PLoS ONE* 10, e0119270.

Cai, H. & Harrison, D.G. 2000. Endothelial dysfunction in cardiovascular diseases: the role of oxidant stress. *Circ Res* 87, 840–844.

Chattipakorn, N., Incharoen, T., Kanlop, N. & Chattipakorn, S. 2007. Heart rate variability in myocardial infarction and heart failure. *Int J Cardiol* 120, 289–296.

Chau, M.D., Gao, J., Yang, Q., Wu, Z. & Gromada, J. 2010. Fibroblast growth factor 21 regulates energy metabolism by activating the AMPK-SIRT1-PGC-1alpha pathway. *Proc Natl Acad Sci USA* 107, 12553–12558.

Chinda, K., Palee, S., Surinkaew, S., Phornphutkul, M., Chattipakorn, S. & Chattipakorn, N. 2013. Cardioprotective effect of dipeptidyl peptidase-4 inhibitor during ischemia-reperfusion injury. *Int J Cardiol* 167, 451–457.

Chinda, K., Sanit, J., Chattipakorn, S. & Chattipakorn, N. 2014. Dipeptidyl peptidase-4 inhibitor reduces infarct size and preserves cardiac function via mitochondrial protection in ischaemia-reperfusion rat heart. *Diab Vasc Dis Res* 11, 75–83.

Cong, W.T., Ling, J., Tian, H.S., Ling, R., Wang, Y., Huang, B.B., Zhao, T., Duan, Y.M., Jin, L.T. & Li, X.K. 2013. Proteomic study on the protective mechanism of fibroblast growth factor 21 to ischemia-reperfusion injury. *Can J Physiol Pharmacol* 91, 973–984.

Ewart, M.A., Kohlhaas, C.F. & Salt, I.P. 2008. Inhibition of tumor necrosis factor alpha-stimulated monocyte adhesion to human aortic endothelial cells by AMP-activated protein kinase. *Arterioscler Thromb Vasc Biol* 28, 2255–2257.

Feng, M., Whitesall, S., Zhang, Y., Beibel, M., D'Alecy, L. & DiPetrillo, K. 2008. Validation of volume-pressure recording tail-cuff blood pressure measurements. *Am J Hypertens* 21, 1288–1291.

Fisher, F.M., Chui, P.C., Antonellis, P.J., Bina, H.A., Kharitonenkov, A., Flier, J.S. & Maratos-Flier, E. 2010. Obesity is a fibroblast growth factor 21 (FGF21)-resistant state. *Diabetes* 59, 2781–2789.

Friedewald, W.T., Levy, R.I. & Fredrickson, D.S. 1972. Estimation of the concentration of low-density lipoprotein cholesterol in plasma, without use of the preparative ultracentrifuge. *Clin Chem* 18, 499–502.

Gupte, A.A., Minze, L.J., Reyes, M., Ren, Y., Wang, X., Brunner, G., Ghosn, M., Cordero-Reyes, A.M., Ding, K., Pratico, D., Morrisett, J., Shi, Z.Z., Hamilton, D.J., Lyon, C.J. & Hsueh, W.A. 2013. High-fat feeding-induced hyperinsulinemia increases cardiac glucose uptake and mitochondrial function despite peripheral insulin resistance. *Endocrinology* 154, 2650–2662.

Hale, C., Chen, M.M., Stanislaus, S., Chinookoswong, N., Hager, T., Wang, M., Veniant, M.M. & Xu, J. 2012. Lack of overt FGF21 resistance in two mouse models of obesity and insulin resistance. *Endocrinology* 153, 69–80.

Joki, Y., Ohashi, K., Yuasa, D., Shibata, R., Ito, M., Matsuo, K., Kambara, T., Uemura, Y., Hayakawa, S., Hiramatsu-Ito, M., Kanemura, N., Ogawa, H., Daida, H., Murohara, T. & Ouchi, N. 2015. FGF21 attenuates pathological myocardial remodeling following myocardial infarction through the adiponectin-dependent mechanism. *Biochem Biophys Res Commun* 459, 124–130.

Kadowaki, T., Yamauchi, T., Kubota, N., Hara, K., Ueki, K. & Tobe, K. 2006. Adiponectin and adiponectin receptors in insulin resistance, diabetes, and the metabolic syndrome. *J Clin Invest* 116, 1784–1792.

Kilkenny, C., Browne, W., Cuthill, I.C., Emerson, M., Altman, D.G. & Group, N.C.R.R.G.W. 2010. Animal research: reporting in vivo experiments: the ARRIVE guidelines. *Br J Pharmacol* 160, 1577–1579.

Kmiecik, A.M., Pula, B., Suchanski, J., Olbromski, M., Gomulkiewicz, A., Owczarek, T., Kruczak, A., Ambicka, A., Rys, J., Ugorski, M., Podhorska-Okolow, M. & Dziegiel, P. 2015. Metallothionein-3 increases triple-negative breast cancer cell invasiveness via induction of metalloproteinase expression. *PLoS ONE* 10, e0124865.

Kubota, T., Bounoutas, G.S., Miyagishima, M., Kadokami, T., Sanders, V.J., Bruton, C., Robbins, P.D., McTiernan, C.F. & Feldman, A.M. 2000. Soluble tumor necrosis factor receptor abrogates myocardial inflammation but not hypertrophy in cytokine-induced cardiomyopathy. *Circulation* 101, 2518–2525.

Liu, S., Niger, C., Koh, E.Y. & Stains, J.P. 2015. Connexin43 mediated delivery of ADAMTS5 targeting siRNAs from mesenchymal stem cells to synovial fibroblasts. *PLoS ONE* 10, e0129999.

Mazumder, P.K., O'Neill, B.T., Roberts, M.W., Buchanan, J., Yun, U.J., Cooksey, R.C., Boudina, S. & Abel, E.D. 2004. Impaired cardiac efficiency and increased fatty acid oxidation in insulin-resistant ob/ob mouse hearts. *Diabetes* 53, 2366–2374.

Neely, J.R. & Morgan, H.E. 1974. Relationship between carbohydrate and lipid metabolism and the energy balance of heart muscle. *Annu Rev Physiol* 36, 413–459.

Neely, J.R., Rovetto, M.J. & Oram, J.F. 1972. Myocardial utilization of carbohydrate and lipids. *Prog Cardiovasc Dis* 15, 289–329.

Neves, F.A., Cortez, E., Bernardo, A.F., Mattos, A.B., Vieira, A.K., Malafaia Tde, O., Thole, A.A., Rodrigues-Cunha, A.C., Garcia-Souza, E.P., Sichieri, R. & Moura, A.S. 2014. Heart energy metabolism impairment in Western-diet induced obese mice. *J Nutr Biochem* 25, 50–57.

Ouwens, D.M., Boer, C., Fodor, M., de Galan, P., Heine, R.J., Maassen, J.A. & Diamant, M. 2005. Cardiac dysfunction induced by high-fat diet is associated with altered

 © 2016 Scandinavian Physiological Society. Published by John Wiley & Sons Ltd, doi: 10.1111/apha.12698

myocardial insulin signalling in rats. *Diabetologia* 48, 1229–1237.

Palee, S., Weerateerangkul, P., Chinda, K., Chattipakorn, S.C. & Chattipakorn, N. 2013. Mechanisms responsible for beneficial and adverse effects of rosiglitazone in a rat model of acute cardiac ischaemia-reperfusion. *Exp Physiol* 98, 1028–1037.

Patel, V., Adya, R., Chen, J., Ramanjaneya, M., Bari, M.F., Bhudia, S.K., Hillhouse, E.W., Tan, B.K. & Randeva, H.S. 2014. Novel insights into the cardio-protective effects of FGF21 in lean and obese rat hearts. *PLoS ONE* 9, e87102.

Pintana, H., Sripetchwandee, J., Supakul, L., Apaijai, N., Chattipakorn, N. & Chattipakorn, S. 2014. Garlic extract attenuates brain mitochondrial dysfunction and cognitive deficit in obese-insulin resistant rats. *Appl Physiol Nutr Metab* 39, 1373–1379.

Pipatpiboon, N., Pratchayasakul, W., Chattipakorn, N. & Chattipakorn, S.C. 2012. PPARgamma agonist improves neuronal insulin receptor function in hippocampus and brain mitochondria function in rats with insulin resistance induced by long term high-fat diets. *Endocrinology* 153, 329–338.

Planavila, A., Redondo, I., Hondares, E., Vinciguerra, M., Munts, C., Iglesias, R., Gabrielli, L.A., Sitges, M., Giralt, M., van Bilsen, M. & Villarroya, F. 2013. Fibroblast growth factor 21 protects against cardiac hypertrophy in mice. *Nat Commun* 4, 2019.

Planavila, A., Redondo-Angulo, I., Ribas, F., Garrabou, G., Casademont, J., Giralt, M. & Villarroya, F. 2014. Fibroblast growth factor 21 protects the heart from oxidative stress. *Cardiovasc Res* 106, 19–31.

Pongchaidecha, A., Lailerd, N., Boonprasert, W. & Chattipakorn, N. 2009. Effects of curcuminoid supplement on cardiac autonomic status in high-fat-induced obese rats. *Nutrition* 25, 870–878.

Pratchayasakul, W., Kerdphoo, S., Petsophonsakul, P., Pongchaidecha, A., Chattipakorn, N. & Chattipakorn, S.C. 2011. Effects of high-fat diet on insulin receptor function in rat hippocampus and the level of neuronal corticosterone. *Life Sci* 88, 619–627.

Rees, D.D., Palmer, R.M. & Moncada, S. 1989. Role of endothelium-derived nitric oxide in the regulation of blood pressure. *Proc Natl Acad Sci USA* 86, 3375–3378.

Surinkaew, S., Kumphune, S., Chattipakorn, S. & Chattipakorn, N. 2013. Inhibition of p38 MAPK during ischemia, but not reperfusion, effectively attenuates fatal arrhythmia in ischemia/reperfusion heart. *J Cardiovasc Pharmacol* 61, 133–141.

Tanajak, P., Chattipakorn, S. & Chattipakorn, N. 2015. Effects of fibroblast growth factor 21 on the heart. *J Endocrinol* 227, R13–R30.

Thummasorn, S., Kumfu, S., Chattipakorn, S. & Chattipakorn, N. 2011. Granulocyte-colony stimulating factor attenuates mitochondrial dysfunction induced by oxidative stress in cardiac mitochondria. *Mitochondrion* 11, 457–466.

Tor, Y.S., Yazan, L.S., Foo, J.B., Wibowo, A., Ismail, N., Cheah, Y.K., Abdullah, R., Ismail, M., Ismail, I.S. & Yeap, S.K. 2015. Induction of apoptosis in MCF-7 cells via oxidative stress generation, mitochondria-dependent and caspase-independent pathway by ethyl acetate extract of *Dillenia suffruticosa* and its chemical profile. *PLoS ONE* 10, e0127441.

Wang, P., Xu, T.Y., Guan, Y.F., Su, D.F., Fan, G.R. & Miao, C.Y. 2009. Perivascular adipose tissue-derived visfatin is a vascular smooth muscle cell growth factor: role of nicotinamide mononucleotide. *Cardiovasc Res* 81, 370–380.

Wang, H., Xiao, Y., Fu, L., Zhao, H., Zhang, Y., Wan, X., Qin, Y., Huang, Y., Gao, H. & Li, X. 2010. High-level expression and purification of soluble recombinant FGF21 protein by SUMO fusion in *Escherichia coli*. *BMC Biotechnol* 10, 14.

Yamawaki, H., Kuramoto, J., Kameshima, S., Usui, T., Okada, M. & Hara, Y. 2011. Omentin, a novel adipocytokine inhibits TNF-induced vascular inflammation in human endothelial cells. *Biochem Biophys Res Commun* 408, 339–343.

Yan, X., Chen, J., Zhang, C., Zhou, S., Zhang, Z., Chen, J., Feng, W., Li, X. & Tan, Y. 2015. FGF21 deletion exacerbates diabetic cardiomyopathy by aggravating cardiac lipid accumulation. *J Cell Mol Med* 19, 1557–1568.

Young, M.E., Guthrie, P.H., Razeghi, P., Leighton, B., Abbasi, S., Patil, S., Youker, K.A. & Taegtmeyer, H. 2002. Impaired long-chain fatty acid oxidation and contractile dysfunction in the obese Zucker rat heart. *Diabetes* 51, 2587–2595.

Yu, Y., Bai, F., Liu, Y., Yang, Y., Yuan, Q., Zou, D., Qu, S., Tian, G., Song, L., Zhang, T., Li, S., Liu, Y., Wang, W., Ren, G. & Li, D. 2015. Fibroblast growth factor (FGF21) protects mouse liver against D-galactose-induced oxidative stress and apoptosis via activating Nrf2 and PI3K/Akt pathways. *Mol Cell Biochem* 403, 287–299.

Zhang, C., Huang, Z., Gu, J., Yan, X., Lu, X., Zhou, S., Wang, S., Shao, M., Zhang, F., Cheng, P., Feng, W., Tan, Y. & Li, X. 2015. Fibroblast growth factor 21 protects the heart from apoptosis in a diabetic mouse model via extracellular signal-regulated kinase 1/2-dependent signalling pathway. *Diabetologia* 58, 1937–1948.

© 2016 Scandinavian Physiological Society. Published by John Wiley & Sons Ltd, doi: 10.1111/apha.12698

เอกสารแนบหมายเลข 21

Research

229:3 245–258

Effects of dipeptidyl peptidase-4 inhibitor in insulin-resistant rats with myocardial infarction

Nattayaporn Apaijai[1,2,3], Tharnwimol Inthachai[1], Suree Lekawanvijit[1,4], Siriporn C Chattipakorn[1,3,5] and Nipon Chattipakorn[1,2,3]

[1]Cardiac Electrophysiology Research and Training Center, Faculty of Medicine, Chiang Mai University, Chiang Mai, Thailand
[2]Cardiac Electrophysiology Unit, Department of Physiology, Faculty of Medicine, Chiang Mai University, Chiang Mai, Thailand
[3]Center of Excellence in Cardiac Electrophysiology Research, Chiang Mai University, Chiang Mai, Thailand
[4]Department of Pathology, Faculty of Medicine, Chiang Mai University, Chiang Mai, Thailand
[5]Department of Oral Biology and Diagnostic Sciences, Faculty of Dentistry, Chiang Mai University, Chiang Mai, Thailand

Correspondence should be addressed to N Chattipakorn
Email
nchattip@gmail.com

Abstract

Adverse cardiac remodeling after myocardial infarction (MI) leads to progressive heart failure. Obese-insulin resistance increases risks of MI and heart failure. Although dipeptidyl peptidase-4 (DPP4) inhibitor is known to exert cardioprotection, its effects on adverse remodeling after MI in obese-insulin-resistant rats are unclear. We hypothesized that DPP4 inhibitor reduces adverse left ventricular (LV) remodeling and LV dysfunction in obese-insulin-resistant rats with MI. Rats were fed either normal diet (ND) or high-fat diet (HFD) for 12 weeks to induce obese-insulin resistance, followed by left anterior descending coronary artery ligation to induce MI. Then, rats in each dietary group were divided into five subgroups to receive vehicle, enalapril (10 mg/kg/day), metformin (30 mg/kg/day), DPP4 inhibitor vildagliptin (3 mg/kg/day), or combined metformin and vildagliptin for 8 weeks. Heart rate variability (HRV), LV function, pathological and biochemical studies for LV remodeling, and cardiomyocyte apoptosis were determined. Obese-insulin-resistant rats had severe insulin resistance and LV dysfunction. HFD rats had a higher mortality rate than ND rats, and all treatments reduced the mortality rate in obese-insulin-resistant rats. Although all drugs improved insulin resistance, HRV, LV function as well as reduced cardiac hypertrophy and fibrosis, vildagliptin effectively reduced cardiomyocyte cross-sectional areas more than enalapril and was related to markedly decreased ERK1/2 phosphorylation. In ND rats with MI, metformin neither improved LV ejection fraction nor reduced cardiac fibrosis. The infarct size and transforming growth factor-β expression were not different among groups. In obese-insulin-resistant rats with chronic MI, DPP4 inhibitor vildagliptin exerts better cardioprotection than enalapril in attenuating adverse LV remodeling.

Key Words
- myocardial infarction
- vildagliptin
- metformin
- obese-insulin-resistant rats

Journal of Endocrinology (2016) **229**, 245–258

http://joe.endocrinology-journals.org
DOI: 10.1530/JOE-16-0096

© 2016 Society for Endocrinology
Printed in Great Britain

Published by Bioscientifica Ltd.

Introduction

Heart failure is a major health problem that can be found in over 23 million people worldwide (Bui *et al.* 2011). A common cause of heart failure is coronary artery disease. Following myocardial ischemia due to coronary artery occlusion, left ventricular (LV) remodeling is known to occur. Postmyocardial infarction (MI) remodeling has been divided into early-phase (within 72 h post MI) and late-phase LV remodeling (beyond 72 h) (Sutton & Sharpe 2000). During the late-phase LV remodeling, LV architecture is changed, including the distortion of LV shape, LV dilation, cardiomyocyte hypertrophy, scar formation, and increased wall stress, all of which could lead to LV dysfunction (Sutton & Sharpe 2000).

It has been shown that long-term high-fat diet (HFD) consumption could induce obese-insulin resistance (Apaijai *et al.* 2012) and is related to an increased risk of MI (Oh *et al.* 2005), promotion of arrhythmic death, and worsening of LV dysfunction in a myocardial ischemia/reperfusion (I/R) injury model (Apaijai *et al.* 2014, Liu *et al.* 2014). However, the roles of obese-insulin resistance in LV remodeling after MI are unclear. Furthermore, previous studies have shown that several oral antidiabetic drugs, including metformin and vildagliptin, exert cardioprotective effects against MI as well as heart failure in various animal models (Gundewar *et al.* 2009, Apaijai *et al.* 2014, Chinda *et al.* 2014).

Vildagliptin (a dipeptidyl peptidase-4 inhibitor) is an oral antidiabetic drug that could reduce hyperglycemia in type 2 diabetes (Mari *et al.* 2005) and improve insulin sensitivity and cardiac sympathovagal balance in obese-insulin-resistant rats (Apaijai *et al.* 2012, Pipatpiboon *et al.* 2013). In the heart, vildagliptin has been shown to exert beneficial effects in various models (Apaijai *et al.* 2013, Chinda *et al.* 2014, Miyoshi *et al.* 2014). It has been shown to preserve LV function and reduce the infarct size in cardiac I/R injury (Chinda *et al.* 2013, 2014, Apaijai *et al.* 2014). Moreover, vildagliptin reduced myocyte hypertrophy and perivascular and cardiac fibrosis in isoproterenol (Miyoshi *et al.* 2014), and transverse aortic constriction-induced heart failure (Takahashi *et al.* 2013). However, inconsistent findings exist as reported by Yin and colleagues who found that vildagliptin did not reverse LV remodeling in post-MI-induced heart failure rats (Yin *et al.* 2011). Moreover, the effects of vildagliptin, metformin, and combined vildagliptin and metformin on the heart with late-phase LV remodeling following MI in subjects with obese-insulin-resistant condition have not been investigated.

In this study, we investigated the effects of vildagliptin, metformin, and combined vildagliptin and metformin on cardiac sympathovagal balance, LV function, LV remodeling, including cardiomyocyte hypertrophy, cardiac fibrosis, and the molecular mechanisms responsible for these effects in rats with obese-insulin resistance. We hypothesized that combined vildagliptin and metformin exert superior cardioprotection against late-phase LV remodeling following MI in obese-insulin-resistant rats compared with monotherapy.

Materials and methods

All experiments in this study were approved by the Institutional Animal Care and Use Committee of the Faculty of Medicine, Chiang Mai University, Chiang Mai, Thailand (permit no. 28/2557), in compliance with NIH and ARRIVE guidelines. Male Wistar rats weighing 180–200 g were obtained from the National Laboratory Animal Center, Salaya Campus, Mahidol University, Bangkok, Thailand. Rats were acclimatized for 7 days and housed in 12 h light:12 h darkness cycle with controlled temperature (25°C). Then, rats were divided into two dietary groups to receive either a normal diet (ND; a diet containing 19.8% energy from fat) or an HFD (a diet containing 59.3% energy from fat) for 12 weeks. At the 12th week, rats were subjected to permanent left anterior descending coronary artery (LAD) ligation to induce MI. Rats were allowed to acclimatize after surgery for 7 days when the inflammatory process of infarction was over and the scar formation was almost complete (Richer *et al.* 1999). After that, rats in each dietary group were subdivided into five subgroups ($n = 6$ per group) to receive one of the following treatments: vehicle (V; 0.9% normal saline solution in an equal volume), DPP4 inhibitor vildagliptin (Vil; 3 mg/kg/day, LAF 237, Novartis), metformin (M; 30 mg/kg/day, Glucophage, Merck Serono), combined vildagliptin and metformin (C), and enalapril (E; 10 mg/kg/day, served as positive control, Berlin, Bangkok, Thailand). Rats were treated with one of these drugs for 8 weeks via gavage feeding. These doses were selected based on our previous studies; our previous study showed that 3 mg/kg/day of vildagliptin, 30 mg/kg/day of metformin, and 10 mg/kg/day of enalapril exerted cardioprotection in various models, including obese-insulin-resistant rats (Apaijai *et al.* 2013), an I/R injury model (Apaijai *et al.* 2014), and normal rats with chronic MI (Inthachai *et al.* 2015).

http://joe.endocrinology-journals.org
DOI: 10.1530/JOE-16-0096
© 2016 Society for Endocrinology
Printed in Great Britain
Published by Bioscientifica Ltd.

Journal of Endocrinology

Chronic MI model

Rats were anesthetized using Zoletil (0.3 mL/kg, Virbac Laboratories, Carros, France) and Xylazine (0.075 mL/kg, Laboratorios Calier, S.A., Barcelona, Spain) via intramuscular injection. Surgery was performed under aseptic conditions, and thoracotomy was performed through the fourth intercostal space. The pericardium membrane was torn open, and the LAD was identified and ligated at 3 mm below its origin with 5-0 silk suture as previously described (Inthachai *et al.* 2015).

Determination of metabolic parameters

Body weight and food intake were recorded weekly. Blood samples were collected from the tail vein at baseline, week 12, and the end of treatment. Plasma glucose, total cholesterol, and triglyceride levels were determined using a commercial colorimetric assay kit (Erba Diagnostics Mannheim GmbH, Mannheim, Germany) (Apaijai *et al.* 2014). Plasma high-density lipoprotein (HDL) level was determined using a colorimetric assay kit (BioVision) (Apaijai *et al.* 2014). Plasma low-density lipoprotein (LDL) level was calculated using Friedewald equation (Apaijai *et al.* 2014). Plasma insulin levels were determined using a commercial ELISA kit (LINCO Research) (Pratchayasakul *et al.* 2011). The homeostatics model assessment (HOMA) index was used to assess insulin resistance, and the increased HOMA index indicates a higher degree of insulin resistance (Pratchayasakul *et al.* 2011). Plasma and cardiac 8-isoprostane levels were used as an oxidative stress marker and were determined using a commercial ELISA kit (OxiSelect, Cell Biolabs, Inc., San Diego, CA, USA) (Madian *et al.* 2011).

Heart rate variability determination

Heart rate variability (HRV) was used as an indicator of cardiac autonomic balance and was measured at baseline, week 4, week 8, week 12, and at the end of treatment. A lead II electrocardiogram was recorded for 20 min in conscious rats using PowerLab (ADInstruments, Sydney, Australia) with Chart 5.0 program (Apaijai *et al.* 2013). Power spectra of R–R interval variability were obtained using fast Fourier transform algorithm. A high-frequency band (HF; 0.6–3 Hz), a low-frequency band (LF; 0.2–0.6 Hz), and a very-low-frequency band (below 0.2 Hz) were analyzed using an analytical software program (Apaijai *et al.* 2013). Regarding the frequency domain analysis, the efferent vagal activity is a major contributor to the HF component, and the LF component represents both sympathetic and parasympathetic activities (Chattipakorn *et al.* 2007). The increased LF/HF ratio is considered as an index of cardiac sympathovagal imbalance (Chattipakorn *et al.* 2007).

LV function determination

Echocardiographic study Echocardiographic study was performed at baseline, week 4, week 8, week 12, and the end of treatment. M-mode echocardiography was performed at the level of papillary muscles using Vivid-i (GE) under light anesthesia (2% isoflurane with 98% oxygen, Forane, Kent, UK). The percentage of fractional shortening (%FS) and the percentage of LV ejection fraction (%LVEF) were determined (Apaijai *et al.* 2014).

Pressure–volume loop study This procedure was performed at the end of treatment. Rats were anesthetized using a combination of Zoletil (50 mg/kg) and Xylazine (3 mg/kg) via intramuscular injection. The right carotid artery was identified and the pressure–volume catheter (Scisense, London, Ontario, Canada) was inserted and advanced into the LV. End-systolic pressure, end-diastolic pressure (EDP), maximum and minimum dP/dt, and stroke volume to body weight ratio (SV/BW) were determined using an analytical software program (LabScribe, Dover, NH, USA) as previously described (Apaijai *et al.* 2013).

Blood pressure determination Blood pressure was measured at the end of treatment. A volume–pressure recording cuff and occlusion cuff were attached to the tail. Blood pressure measurement was performed using a CODA2 channel noninvasive blood pressure system (Kent Scientific Corporation, Torrington, CT, USA). Blood pressure values, including systolic and diastolic pressures, were achieved by taking an average of 20 consecutive measurements at a steady state (Lekawanvijit *et al.* 2012).

Histological studies

Infarct size and fibrosis determination Mid-LV cross sections were stained with picrosirius red and scanned (Aperio, Aperio Technologies Inc., San Diego, CA, USA) for infarct and fibrosis analysis. Infarct size was reported as the average of the proportions of endocardial and epicardial circumference by the infarct (Inthachai *et al.* 2015). Rats with nontransmural

http://joe.endocrinology-journals.org
DOI: 10.1530/JOE-16-0096
© 2016 Society for Endocrinology
Printed in Great Britain
Published by Bioscientifica Ltd.

Journal of Endocrinology

infarction were excluded from the study. Furthermore, picrosirius red-stained collagen matrix deposition from the whole LV myocardium was selected for its intensity, and the proportional area was calculated using a preset algorithm for picrosirius red stain intensity (Inthachai *et al.* 2015).

Cardiomyocyte cross-sectional area determination Cardiomyocyte cross-sectional area was determined using hematoxylin and eosin (H&E) staining. Fifty LV cardiomyocytes with equal-sized nuclei were randomly selected for analysis of cross-sectional area from prescanned images. Cell surface areas were calculated by measuring the circumferential length of the myocyte using Aperio ScanScope (Aperio, Aperio Technologies Inc., San Diego, CA, USA) (Inthachai *et al.* 2015).

Western blot analysis The myocardial tissues for western blot study were obtained from the fresh heart at the end of the treatment period following chronic MI. Myocardial protein extracts were prepared by the homogenization of nitrogen-frozen myocardial tissues in a 300 μL extraction buffer containing 20 mM Tris–HCl (pH 6.8), 1 mM sodium orthovanadate, 5 mM sodium fluoride, and a protease inhibitor. Total protein concentrations were determined using a Bio-Rad protein assay kit (Bio-Rad Laboratories). Sixty micrograms of total protein were mixed with the loading buffer (5% betamercaptoethanol, 0.05% bromophenol blue, 75 mM Tris–HCl (pH 6.8), 2% SDS, and 10% glycerol) and loaded onto 10% SDS–acrylamide gels. Proteins were transferred to nitrocellulose membranes in a glycine/methanol-transferred buffer in a wet/tank blotting system (Bio-Rad Laboratories). Membranes were blocked in 5% skim milk in Tris-buffered saline and Tween buffer. Membranes were exposed to mouse polyclonal anti-rat BCL2, total connexin 43, p-connexin 43^{ser368}, total p38 mitogen-activated protein kinase (MAPK), p-p38 $MAPK^{Thr180/Tyr182}$, total NF-κB, p-NF-$κB^{ser536}$, transforming growth factor (TGF)-β (1:1000 dilution, Cell Signaling Technology), BAX, total ERK1/2, p-$ERK1/2^{Thr202/Tyr204}$, and β-actin (1:1000 dilution, Santa Cruz Biotechnology). Bound antibodies were detected using horseradish peroxidase conjugated with anti-rabbit IgG (1:2000 dilution, Cell Signaling Technology). The membranes were developed using the Clarity ECL Western Blotting Substrate (Bio-Rad) and densitometric analyses were carried out (Apaijai *et al.* 2014, Chinda *et al.* 2014).

Statistical analysis

Data were expressed as mean ± S.E.M. One-way ANOVA followed by Tukey's *post hoc* test was used to determine the differences among groups. Time-course values of echocardiographic parameters and HRV were determined using two-way repeated measures ANOVA. Mortality rate was determined using χ^2-test. A P-value of <0.05 was considered as statistically significance.

Results

Effects of enalapril, vildagliptin, metformin, and combined drugs on metabolic parameters

At baseline (week 0 before HFD consumption), there were no differences in body weight, food intake, plasma glucose, insulin, total cholesterol, LDL, HDL, triglyceride levels, and HOMA index between the ND- and HFD-fed rats (Table 1). After 12-week HFD consumption, data showed that body weight, plasma insulin, total cholesterol, LDL levels, and HOMA index were increased in HFD-fed rats. However, there were no differences in food intake, plasma triglyceride, and HDL levels between the ND- and HFD-fed rats. Our data suggest that rats developed obese-insulin resistance after 12-week HFD consumption (Table 1).

Seven days after MI, rats received their assigned drugs for 8 weeks. At the end of treatment, we found that body weight was not changed in the ND and HFD groups, whereas LV/heart weight (HW) was increased in HFD-fed rats treated with vehicle (HFDV). All treatments reduced the LV/HW ratio in both MI rats; however, metformin did not reduce the LV/HW ratio in ND-fed rats (Table 2). Furthermore, we found that plasma glucose, insulin, and total cholesterol levels, and HOMA index were increased in HFDV compared with ND-fed rats treated with vehicle (NDV). Vildagliptin, metformin, and combined drugs reduced the levels of these parameters (Table 2).

Effects of enalapril, vildagliptin, metformin, and combined drugs on oxidative stress levels

We found that plasma and cardiac 8-isoprostane levels were higher in HFDV, compared with NDV. In ND-fed rats, treatment with enalapril, vildagliptin, and the combined drugs, but not metformin, reduced cardiac 8-isoprostane levels, whereas plasma 8-isoprostane level was not different among groups. In HFD-fed

© 2016 Society for Endocrinology
Printed in Great Britain
Published by Bioscientifica Ltd.

Table 1 Effects of HFD consumption on metabolic parameters at baseline and 12 weeks after HFD consumption.

	Baseline		Week 12	
Metabolic parameters	ND	HFD	ND	HFD
Body weight (g)	178±5	181±3	446±12	533±10*
Food intake (g/day)	15±2	18±2	19±2	21±2
Plasma glucose (mg/dL)	128±4	138±9	122±10	130±5
Plasma insulin (ng/dL)	2.4±0.4	2.3±0.5	2.6±0.3	4.2±0.3*
HOMA index	13±0.6	14±0.1	14±0.7	24±0.2*
Plasma total cholesterol (mg/dL)	54±6	54±4	53±6	74±3*
Plasma triglyceride (mg/dL)	123±5	118±4	119±1	118±2
Plasma HDL (mg/dL)	20±5	23±6	24±4	22±3
Plasma LDL (mg/dL)	9±6	8±8	7±2	28±2*

ND, normal diet-fed rats; HFD, high-fat diet-fed rats; HOMA, homeostatic model assessment; HDL, high-density lipoprotein; LDL, low-density lipoprotein.
*$P<0.05$ vs ND.

rats, all treatments could reduce plasma and cardiac 8-isoprostane levels (Table 2).

Effects of enalapril, vildagliptin, metformin, and combined drug on HRV

At baseline, there was no difference in the LF/HF ratio between ND- and HFD-fed rats. The LF/HF ratio was increased after 8 weeks of HFD consumption, indicating the development of cardiac sympathovagal imbalance (Fig. 1A). After MI, HFDV rats had higher LF/HF ratio than NDV rats (Fig. 1B). In ND-fed rats, enalapril, vildagliptin, and combined drugs, but not metformin, reduced the LF/HF ratio, whereas all treatments could reduce the LF/HF ratio in HFD-fed rats (Fig. 1B).

Effects of enalapril, vildagliptin, metformin, and combined drug on LV function

Echocardiographic parameters At baseline, there were no differences in the %FS and %LVEF between ND- and HFD-fed rats. We found that %FS and %LVEF were decreased after 12-week HFD consumption (Fig. 2A and B). Furthermore, after treatment, HFDV demonstrated a worsened %LVEF compared with NDV, whereas the %FS did not differ between HFDV and NDV rats (Fig. 2C and D). All treatments improved %FS and %LVEF in HFD-fed rats. However, metformin did not improve %FS and %LVEF in ND-fed rats compared with NDV rats (Fig. 2C and D).

Hemodynamic parameters At the end of treatment, only enalapril could reduce the systolic pressure in ND- and HFD-fed rats compared with NDV and HFDV rats (Table 3). Moreover, our data showed that HFDV rats had higher heart rate, higher EDP, and lower dP/dt_{min} compared with NDV rats. All treatments reduced EDP, and treatment with vildagliptin and combined drug increased dP/dt_{max} and dP/dt_{min} in HFD-fed rats. In ND-fed rats, treatment with vildagliptin and combined drug reduced EDP and increased dP/dt_{min}, and enalapril could reduce only EDP. Metformin did not improve any hemodynamic parameters in ND-fed rats (Table 3). Our data indicated that HFDV rats had worsened LV dysfunction than NDV rats, and all treatments improved LV function after MI in obese-insulin-resistant rats, whereas metformin did not improve any LV function parameters in ND-fed rats (Table 3).

Effects of enalapril, vildagliptin, metformin, and combined drug on mortality rate and LV remodeling For the perioperative mortality in the rats undergoing MI, the mortality rate was 27% in normal rats and 48% in obese-insulin-resistant rats during surgery. During 8 weeks of treatment period, we found that HFDV rats had a higher mortality rate after MI, and all treatments could reduce the mortality rate in HFD-fed rats (Fig. 3A). Our data also showed that connexin 43 (CX43) phosphorylation was lower in HFDV rats, and all treatment increased CX43 phosphorylation (Fig. 3B).

Infarct size, cardiac fibrosis, and cardiomyocyte cross-sectional area After MI, the infarct size did not differ between groups (Fig. 3C). We also determined an apoptotic (BAX) and antiapoptotic protein (BCL2) ratio, and found that BAX/BCL2 ratio was not different among groups (Fig. 3D).

In this study, we determined cardiomyocyte cross-sectional areas from H&E stained heart tissues, and

© 2016 Society for Endocrinology
Printed in Great Britain
Published by Bioscientifica Ltd.

Table 2 Effects of enalapril, vildagliptin, metformin, and combination of vildagliptin and metformin on metabolic parameters in ND- and HFD-fed rats with chronic MI.

Parameters	NDV	NDE	NDVil	NDM	NDC	HFDV	HFDE	HFDVil	HFDM	HFDC
Body weight (g)	545±3	525±5	475±8	490±6	520±4	635±9*	620±5*	655±4*	610±8*	640±9*
LV/HW	1.1±0.1	0.7±0.2*	0.8±0.1*	1.1±0.1	0.8±0.1*	1.2±0.1*	0.9±0.1†	0.8±0.1†	0.9±0.1†	0.8±0.1†
Visceral fat weight (g)	35±4	41±5	42±5	44±7	36±3	68±4*	62±5*	66±3*	65±9*	68±7*
Food intake (g/day)	17±1	16±1	17±1	19±1	15±1	17±1	14±1	14±1	15±1	16±1
Plasma glucose (mg/dL)	130±4	129±1	123±5	128±5	125±5	167±5*	155±7	142±5†	145±5†	143±6†
Plasma insulin (ng/dL)	3.0±0.2	3.0±0.7	2.8±0.4	3.1±0.4	3.1±0.4	4.3±0.1*	3.9±0.2	3.1±0.3†	2.7±0.2†	3.3±0.3†
HOMA index	17±0.5	17±0.2	15±0.7	18±0.7	17±0.7	32±0.9*	29±1	22±0.7†	20±0.6†	20±0.8†
Plasma total cholesterol (mg/dL)	60±9	65±6	68±3	68±5	61±3	151±13*	115±6†	117±6†	114±3†	113±2†
Plasma triglyceride (mg/dL)	120±5	121±9	135±6	118±7	133±10	123±10	124±10	119±5	122±6	129±5
Plasma HDL (mg/dL)	24±2	28±1	27±1	28±2	28±2	24±1	25±2	26±2	25±3	24±1
Plasma LDL (mg/dL)	12±4	13±6	14±2	16±3	16±3	102±5*	65±3†	67±2†	64±3†	63±3†
Plasma 8-isoprostane (ng/mL)	2.8±0.2	2±0.2	2.1±0.1	2.7±0.2	2.0±0.1	3.4±0.3*	2.3±0.1†	2.2±0.2†	2.5±0.1†	2.3±0.1†
Cardiac 8-iso-prostane (ng/mg)	3.4±0.1	2.9±0.1*	2.7±0.1*	3.4±0.3	2.4±0.1*	3.9±0.1*	3.1±0.2†	3.1±0.2†	3.1±0.1†	2.9±0.1†

LV/HW, left-ventricular weight/heart weight; HOMA, homeostatic model assessment; HDL, high-density lipoprotein; LDL, low-density lipoprotein; NDV, normal diet rats treated with vehicle; NDE, normal diet rats treated with enalapril; NDVil, normal diet rats treated with vildagliptin; NDM, normal diet rats treated with metformin; NDC, normal diet rats treated with combined drugs; HFDV, high-fat-fed rats treated with vehicle; HFDE, high-fat-fed rats treated with enalapril; HFDVil, high-fat-fed rats treated with vildagliptin; HFDM, high-fat-fed rats treated with metformin; HFDC, high-fat-fed rats treated with combined drugs.
*$P<0.05$ vs NDV, †$P<0.05$ vs HFDV.

cardiac fibrosis from picrosirius-stained heart tissues (Fig. 4A, B, C and D). Our results showed that cardiac fibrosis and cardiomyocyte cross-sectional areas were increased in HFDV rats, and all treatments reduced cardiomyocyte cross-sectional areas in HFD-fed rats (Fig. 4A, B, C and D). However, only metformin did not reduce cardiomyocyte cross-sectional areas in ND-fed rats. Interestingly, vildagliptin and combined drug treatment markedly reduced cardiomyocyte cross-sectional areas compared with enalapril in both ND- and HFD-fed rats (Fig. 4B). Furthermore, all treatments decreased cardiac fibrosis in HFD-fed rats, whereas metformin did not reduce cardiac fibrosis in ND-fed rats (Fig. 4A, B, C and D).

Our results showed that all treatments could reduce p38 phosphorylation in HFD-fed rats (Fig. 5A). In ND-fed rats, only metformin did not reduce p38 phosphorylation (Fig. 5A). ERK1/2 phosphorylation tended to increase in HFDV rats, and only vildagliptin reduced ERK1/2 phosphorylation in both ND- and HFD-fed rats (Fig. 5B). Furthermore, we found that all treatments decreased NF-κB phosphorylation in HFD-fed rats but not in ND-fed rats (Fig. 5C). TGF-β expression was not different among groups (Fig. 5D).

Discussion

The major findings of this study are as follows: vildagliptin, metformin, and combined metformin and vildagliptin effectively attenuated the insulin-resistant condition in obese-insulin-resistant rats. Furthermore, vildagliptin, metformin, combined drugs, and enalapril reduced plasma and cardiac oxidative stress, improved HRV, and attenuated LV dysfunction and LV remodeling in obese-insulin-resistant rats. However, vildagliptin reduced cardiac hypertrophy better than other regimens in this model. In ND-fed rats, both vildagliptin and enalapril exerted cardioprotection against adverse LV remodeling. However, metformin exerted no benefit on late-phase LV remodeling after MI in ND-fed rats.

© 2016 Society for Endocrinology
Printed in Great Britain
Published by Bioscientifica Ltd.
Journal of Endocrinology

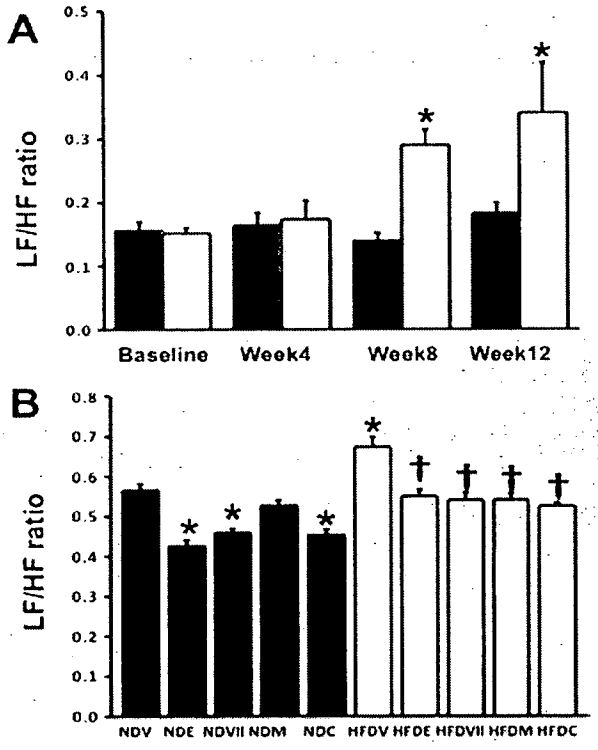


Figure 1
Effects of enalapril, vildagliptin, metformin, and combined drugs on HRV in normal and obese-insulin-resistant rats after chronic MI. The LF/HF ratio was increased after 8 weeks of HFD consumption. (A) $^{*}P<0.05$ vs ND. Enalapril, vildagliptin, metformin, and combined vildagliptin and metformin improved HRV in obese-insulin-resistant rats. In ND rats, enalapril, vildagliptin, and combined vildagliptin and metformin but not metformin reduced the LF/HF ratio. (B) $^{*}P<0.05$ vs NDV, $^{\dagger}P<0.05$ vs HFDV. ND, normal diet-fed rats; HFD, high-fat diet fed rats; LF, low-frequency; HF, high-frequency; NDV, normal diet rats treated with vehicle; NDE, normal diet rats treated with enalapril; NDVil, normal diet rats treated with vildagliptin; NDM, normal diet rats treated with metformin; NDC, normal diet rats treated with combined drugs; HFDV, high-fat-fed rats treated with vehicle; HFDE, high-fat-fed rats treated with enalapril; HFDVil, high-fat-fed rats treated with vildagliptin; HFDM, high-fat-fed rats treated with metformin; HFDC, high-fat-fed rats treated with combined drugs.

After chronic MI, obese-insulin-resistant rats exhibited severe insulin resistance by increased HOMA index and plasma glucose level. Our data demonstrated that vildagliptin, metformin, and combined drugs improved insulin resistance without hypoglycemia. This finding is consistent with previous studies, in which these drugs improved insulin resistance in patients with type 2 diabetes mellitus (T2DM) and in animal models of insulin resistance without MI (Bailey 2005, Apaijai *et al.* 2013, Pintana *et al.* 2013, Derosa *et al.* 2014). Furthermore, our data suggested that vildagliptin and metformin also effectively improved metabolic parameters in an animal model of obese-insulin resistance with chronic MI (Fig. 6).

In this study, only enalapril, an angiotensin-converting enzyme (ACE) inhibitor reduced systolic blood pressure and associated with reduced LDL cholesterol levels in obese-insulin-resistant rats. Clinical trials reported that enalapril reduced blood pressure by reduced angiotensin II level (Ocaranza *et al.* 2006) and LDL cholesterol level (Rachmani *et al.* 2000). Furthermore, the lower level of angiotensin II in addition to lower LDL cholesterol level could induce vasodilation (Kiliszek *et al.* 2007) and reduce systolic blood pressure. However, vildagliptin, metformin, and combined metformin and vildagliptin also reduced LDL cholesterol level without any changes in blood pressure. This finding consistent with previous reports in the heart failure model in which vildagliptin did not change blood pressure in rats with cardiac hypertrophy (Miyoshi *et al.* 2014), and metformin did not affect blood pressure and flow-mediated vasodilation in insulin-resistant patients with chronic HF (Wong *et al.* 2012). These data suggest that a reduction of LDL cholesterol level along with lower angiotensin II is necessary to reduce blood pressure in obese-insulin-resistant rats with chronic MI.

HRV is an indicator of cardiac sympathovagal balance as well as a predictor of sudden cardiac death after MI (Zuanetti *et al.* 1996, Chattipakorn *et al.* 2007), and depressed HRV is commonly found in MI patients (Chattipakorn *et al.* 2007). In our study, a depressed HRV was worsening in obese-insulin-resistant rats with chronic MI than in ND rats. Vildagliptin, metformin, combined vildagliptin and metformin, and enalapril improved HRV in obese-insulin-resistant rats. Vildagliptin, combined drugs, and enalapril, but not metformin, also improved HRV in ND rats. This finding was correlated with the reduction of oxidative stress level. Our data were consistent with several studies which reported that an increased oxidative stress level has a positive correlation with a degree of cardiac sympathovagal imbalance in insulin-resistant patients and in animal models (Manzella *et al.* 2001, Pavithran *et al.* 2008, Apaijai *et al.* 2013). This could be the explanation why vildagliptin and enalapril, but not metformin, improved HRV in ND-fed rats with MI because metformin did not reduce oxidative stress in this group (Fig. 6).

LV remodeling, including LV hypertrophy and cardiac fibrosis, is a common phenomenon that occurs following MI (Sutton & Sharpe 2000). In this study, vildagliptin, metformin, combined drugs, and enalapril reduced LV remodeling in obese-insulin-resistant rats. It is interesting that vildagliptin exerted better effect on LV remodeling because it could reduce cardiomyocyte hypertrophy

© 2016 Society for Endocrinology
Printed in Great Britain
Published by Bioscientifica Ltd.

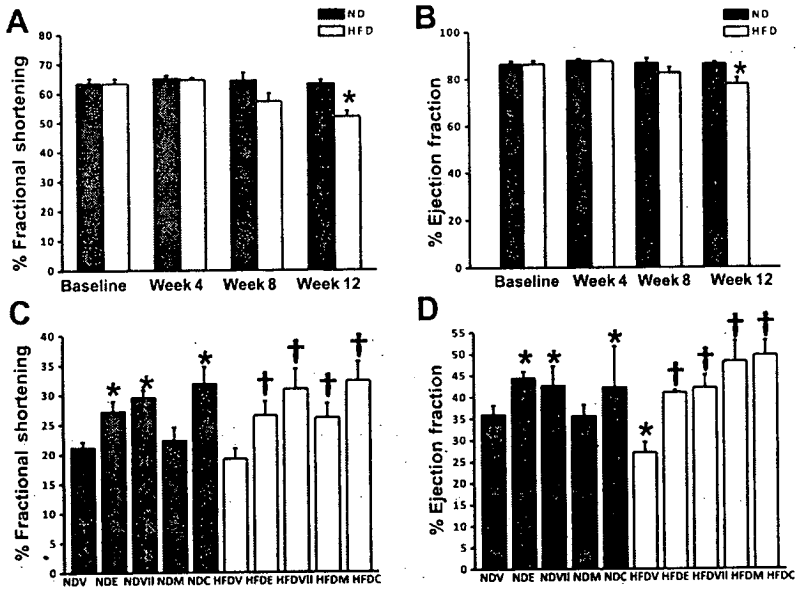


Figure 2
Effects of enalapril, vildagliptin, metformin, and combined drugs on %FS and %LVEF in normal and obese-insulin-resistant rats after chronic MI. %FS and %LVEF were decreased after 12-week of HFD consumption (A and B), $^{*}P<0.05$ vs ND. Enalapril, vildagliptin, metformin, and combined vildagliptin and metformin increased %FS and %LVEF in obese-insulin-resistant rats. In ND rats, enalapril, vildagliptin, and combined vildagliptin and metformin but not metformin increased %FS and %LVEF (C and D), $^{*}P<0.05$ vs NDV, $^{\dagger}P<0.05$ vs HFDV. ND, normal diet-fed rats; HFD, high-fat-diet fed rats; NDV, normal diet rats treated with vehicle; NDE, normal diet rats treated with enalapril; NDVil, normal diet rats treated with vildagliptin; NDM, normal diet rats treated with metformin; NDC, normal diet rats treated with combined drugs; HFDV, high-fat-fed rats treated with vehicle; HFDE, high-fat-fed rats treated with enalapril; HFDVil, high-fat-fed rats treated with vildagliptin; HFDM, high-fat-fed rats treated with metformin; HFDC, high-fat-fed rats treated with combined drugs.

greater than other regimens. Unlike our findings in obese-insulin-resistant rats, a previous study in normal rats with MI reported otherwise. Yin and colleagues reported that vildagliptin reduced neither cardiomyocyte size nor LV dysfunction when given at 3 weeks after MI (Yin *et al.* 2011), whereas our data suggested that vildagliptin exerted cardioprotection when given 7 days after MI in both normal and obese-insulin-resistant rats. This disparity in results could be influenced by the timing of drug administration and the models used in those studies. In this study, the mechanism responsible for the reduction of cardiomyocyte hypertrophy by vildagliptin was related to decrease ERK and p38 MAPK phosphorylation. ERK and p38 MAPK are the members of MAPK, which are activated by oxidative stress, and both ERK and p38 MAPK also regulate cardiomyocyte hypertrophy during LV remodeling. Yeh and colleagues reported that ERK phosphorylation was increased in mice after 4-week post MI and related with cardiac hypertrophy (Yeh *et al.* 2010). Vildagliptin and combined vildagliptin and metformin reduced ERK phosphorylation, thus attenuating cardiomyocyte hypertrophy in our rat model of obese-insulin-resistant and normal rats with chronic MI (Fig. 6).

Cardiac fibrosis has been identified as the developing process of heart failure after MI (Wang *et al.* 2012) and has been involved in p38 MAPK activation (Clerk & Sugden 2006). Our data demonstrated that all pharmacological interventions reduced p38 MAPK phosphorylation, whereas TGF-β, a fibrosis inducer, was unchanged. This finding was supported by a previous study which reported that p38 activation could mediate renal fibrosis in a TGF-β independent manner (Stambe *et al.* 2004). Therefore, vildagliptin, metformin, and enalapril given during late-phase LV remodeling in this study could reduce cardiac fibrosis through p38 MAPK signaling in a TGF-β independent manner. In addition, NF-κB, a transcription factor that regulates stress and inflammatory response, has been shown to be involved in LV remodeling process (Hamid *et al.* 2011). It has been shown that an activation of NF-κB is related with inflammation and postinfarcted LV remodeling after MI (Hamid *et al.* 2011). In our study, all treatments reduced NF-κB activity, suggesting that these drugs reduced inflammation and led to reduce LV remodeling in obese-insulin-resistant rats with chronic MI (Fig. 6).

Growing evidence demonstrates that LV dysfunction is markedly increased in late-phase LV remodeling (Pfeffer *et al.* 1991, Sutton & Sharpe 2000). Our results showed that cardiomyocyte hypertrophy and cardiac fibrosis and inflammation are the major contributors of LV dysfunction in our model. Vildagliptin, metformin, and enalapril reduced LV remodeling through several signaling pathways, including reduced ERK1/2, p38 MAPK, and NF-κB. Moreover, these drugs also reduced oxidative stress and improved cardiac sympathovagal balance. These beneficial effects could be responsible for improved LV function in both ND-fed and obese-insulin-resistant rats with chronic MI (Fig. 6).

It has been shown that an increase of mortality rate after MI is associated with hyperglycemia and cardiac

© 2016 Society for Endocrinology
Printed in Great Britain
Published by Bioscientifica Ltd.

229:3 253

Table 3 Effects of enalapril, vildagliptin, metformin, and combination of vildagliptin and metformin on blood pressure and LV function in ND- and HFD-fed rats with chronic MI.

Parameters	NDV	NDE	NDVil	NDM	NDC	HFDV	HFDE	HFDVil	HFDM	HFDC
SBP (mmHg)	145 ± 8	113 ± 4*	147 ± 2	144 ± 6	137 ± 3	154 ± 7	123 ± 3†	155 ± 3	153 ± 1	155 ± 1
DBP (mmHg)	105 ± 9	105 ± 1	102 ± 6	104 ± 7	111 ± 2	111 ± 7	106 ± 1	114 ± 1	119 ± 2	119 ± 2
HR (bpm)	251 ± 8	256 ± 5	277 ± 17	265 ± 13	245 ± 13	320 ± 17*	281 ± 10	287 ± 6	290 ± 4	297 ± 28
ESP (mmHg)	97 ± 4	101 ± 6	104 ± 7	99 ± 5	98 ± 3	79 ± 3	94 ± 2	95 ± 1	93 ± 3	101 ± 3
EDP (mmHg)	9 ± 2	5 ± 0.9*	4 ± 0.1*	9 ± 0.8	5 ± 0.7*	13 ± 0.8*	10 ± 0.2†	8 ± 0.6†	10 ± 0.6†	8 ± 0.7†
dP/dt_{max} (mmHg/s)	8763 ± 1304	9140 ± 2126	9321 ± 854	9342 ± 115	9361 ± 1591	6576 ± 1759	7633 ± 992	9478 ± 294†	7472 ± 382	10,131 ± 990†
dP/dt_{min} (mmHg/s)	4330 ± 486	4599 ± 444	5499 ± 272*	4203 ± 102	5615 ± 233*	3664 ± 487*	4286 ± 205	6615 ± 738†	3887 ± 244	6841 ± 687†
SV/BW (μL/g)	0.82 ± 0.14	0.84 ± 0.21	0.83 ± 0.21	0.83 ± 0.11	0.82 ± 0.20	0.79 ± 0.21	0.81 ± 0.22	0.80 ± 0.25	0.79 ± 0.18	0.81 ± 0.16

SBP, systolic blood pressure; DBP, diastolic blood pressure; HR, heart rate; bpm, beats per minute; ESP, end-systolic pressure; EDP, end-diastolic blood pressure; SV/BW, stroke volume/body weight; NDV, normal diet rats treated with vehicle; NDE, normal diet rats treated with enalapril; NDVil, normal diet rats treated with vildagliptin; NDM, normal diet rats treated with metformin; NDC, normal diet rats treated with combined drugs; HFDV, high-fat-fed rats treated with vehicle; HFDE, high-fat-fed rats treated with enalapril; HFDVil, high-fat-fed rats treated with vildagliptin; HFDM, high-fat-fed rats treated with metformin; HFDC, high-fat-fed rats treated with combined drugs.

*$P < 0.05$ vs NDV, †$P < 0.05$ vs HFD.

sympathovagal imbalance (Chattipakorn *et al.* 2007, Luo *et al.* 2014). In this study, the mortality rate was significantly increased in obese-insulin-resistant rats. This finding is also consistent with our previous report in the rat model of ischemia–reperfusion injury (Apaijai *et al.* 2014). Fatal arrhythmia has been shown to commonly develop and could be responsible for increased mortality in post-MI (Goncalves 1995). CX43 is a gap junction protein that influenced the development of cardiac arrhythmias after MI (Roell *et al.* 2007). It has been shown that increased CX43 phosphorylation was associated with reduced cardiac arrhythmias (Roell *et al.* 2007). In this study, all pharmacological interventions reduced hyperglycemia, improved cardiac sympathovagal balance, and increased CX43 phosphorylation, thus leading to decreased mortality in this study (Fig. 6).

In our model, LV remodeling has occurred following MI, leading to LV dysfunction, and the remodeling has developed through these following pathways: (i) fibrosis, (ii) apoptosis, (iii) MAPK pathway that is responsible for cell growth and proliferation, (iv) oxidative stress, and (v) inflammation (Sutton & Sharpe 2000, Kwak *et al.* 2006, Hori & Nishida 2009). In this study, important markers of each pathway were determined to represent the effects of vildagliptin and metformin on LV remodeling such as (i) TGF-β as a fibrosis marker, (ii) BAX and BCL2 as apoptosis markers, (iii) p38 and ERK1/2 as markers of cell growth and proliferation, (iv) 8-isoprostane as an oxidative stress marker, and (v) NF-κB as an inflammatory marker. Enalapril is known to reduce LV remodeling by directly inhibiting the ACE. However, the obese-insulin-resistant rats in this study had metabolic disturbances along with LV remodeling after chronic MI. In this study, we demonstrated that although enalapril, vildagliptin, and metformin effectively reduced LV remodeling via those pathways, only vildagliptin and metformin could attenuate the metabolic disturbances in these obese-insulin-resistant rats. These findings suggested that improvement of metabolic regulation could effectively attenuate adverse LV remodeling in obese-insulin-resistant rats with chronic MI.

Apart from the attenuation of insulin resistance, our data also demonstrated that vildagliptin exerted better cardioprotection than metformin through two pathways. First, vildagliptin exerted antioxidant effects in normal rats with chronic MI, whereas metformin could not. Second, vildagliptin reduced cell growth via a reduction of ERK1/2 phosphorylation in normal rats with chronic MI, whereas metformin could not. Therefore, our data suggest that vildagliptin exerted beneficial effects via a reduction

http://joe.endocrinology-journals.org
DOI: 10.1530/JOE-16-0096

© 2016 Society for Endocrinology
Printed in Great Britain

Published by Bioscientifica Ltd.

Journal of Endocrinology

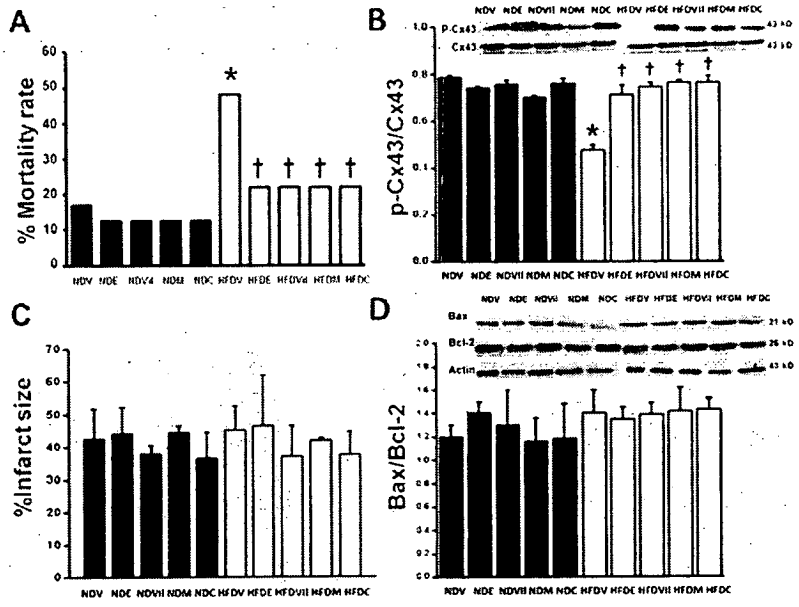


Figure 3
Effects of enalapril, vildagliptin, metformin, and combined drugs on mortality rate, CX43 phosphorylation, infarct size, and BAX/BCL2 ratio in normal and obese-insulin-resistant rats after chronic MI. Mortality rate was higher in HFDV, whereas enalapril, vildagliptin, metformin, and combined vildagliptin and metformin reduced mortality rate (A) and CX43 phosphorylation in obese-insulin-resistant rats after chronic MI (B). *$P<0.05$ vs NDV, †$P<0.05$ vs HFDV. Infarct size (C) and BAX/BCL2 ratio (D) were not different among groups. NDV, normal diet rats treated with vehicle; NDE, normal diet rats treated with enalapril; NDVil, normal diet rats treated with vildagliptin; NDM, normal diet rats treated with metformin; NDC, normal diet rats treated with combined drugs; HFDV, high-fat-fed rats treated with vehicle; HFDE, high-fat-fed rats treated with enalapril; HFDVil, high-fat-fed rats treated with vildagliptin; HFDM, high-fat-fed rats treated with metformin; HFDC, high-fat-fed rats treated with combined drugs.

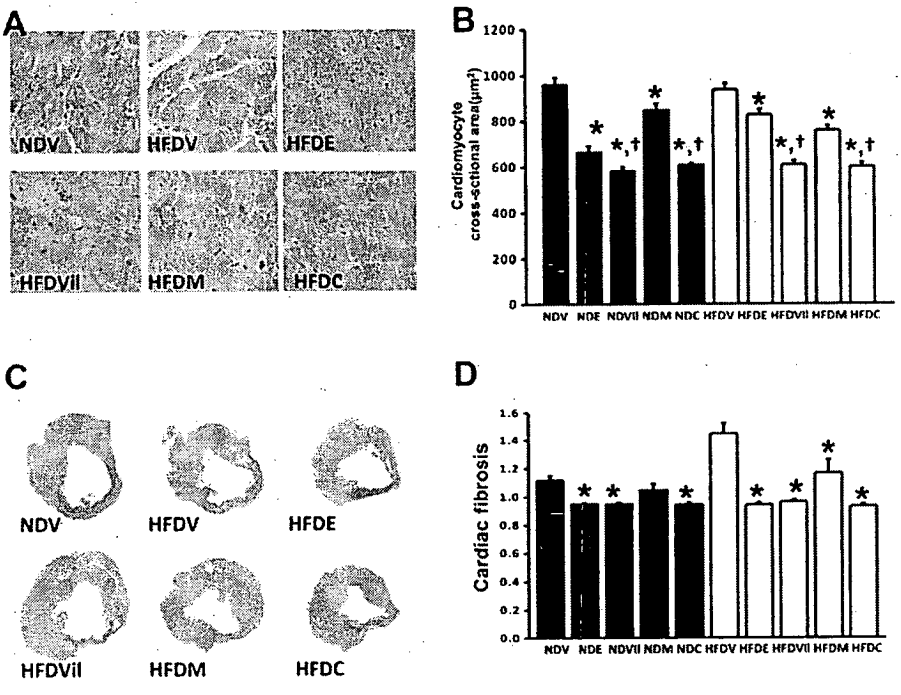


Figure 4
Effects of enalapril, vildagliptin, metformin, and combined drugs on cardiomyocyte cross-sectional area and cardiac fibrosis in normal and obese-insulin-resistant rats after chronic MI. Representative picture of cardiomyocyte cross-sectional area from H&E and picrosirius-stained heart tissue (A and C). Enalapril, vildagliptin, metformin, and combined vildagliptin and metformin decreased cardiomyocyte cross-sectional area in obese-insulin-resistant rats. In ND rats, enalapril, vildagliptin, and combined vildagliptin and metformin but not metformin decreased cardiomyocyte cross-sectional area. However, vildagliptin and combined drugs reduced cardiomyocytes cross-sectional area better than enalapril (B), *$P<0.05$ vs their dietary control, †$P<0.05$ vs enalapril-treated rats within group. Enalapril, vildagliptin, metformin, and combined vildagliptin and metformin reduced cardiac fibrosis in obese-insulin-resistant rats. In ND rats, enalapril, vildagliptin, and combined vildagliptin and metformin but not metformin reduced cardiac fibrosis (D), *$P<0.05$ vs their dietary control. NDV, normal diet rats treated with vehicle; NDE, normal diet rats treated with enalapril; NDVil, normal diet rats treated with vildagliptin; NDM, normal diet rats treated with metformin; NDC, normal diet rats treated with combined drugs; HFDV, high-fat-fed rats treated with vehicle; HFDE, high-fat-fed rats treated with enalapril; HFDVil, high-fat-fed rats treated with vildagliptin; HFDM, high-fat-fed rats treated with metformin; HFDC, high-fat-fed rats treated with combined drugs.

http://joe.endocrinology-journals.org
DOI: 10.1530/JOE-16-0096
© 2016 Society for Endocrinology
Printed in Great Britain
Published by Bioscientifica Ltd.

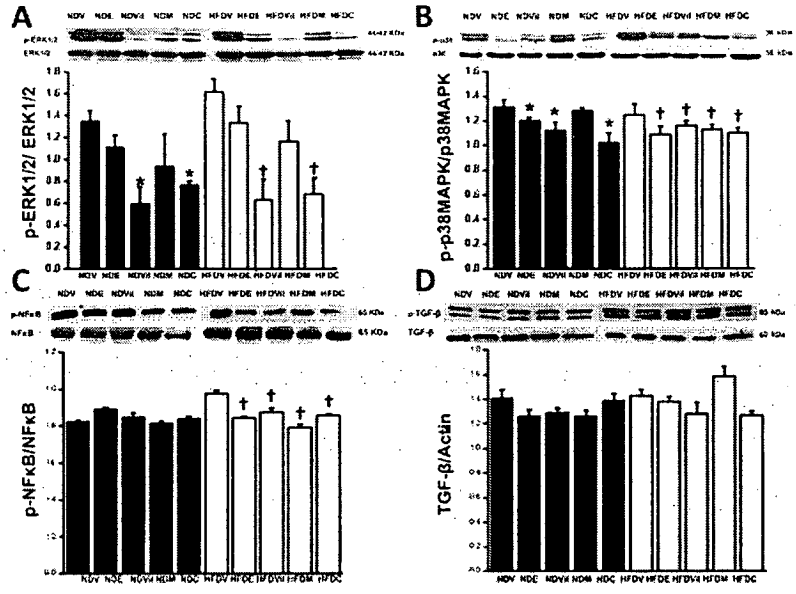


Figure 5
Effects of enalapril, vildagliptin, metformin, and combined drugs on p38MAPK phosphorylation, ERK1/2 phosphorylation, NF-κB phosphorylation, and TGF-β expression in normal and obese-insulin-resistant rats after chronic MI. Vildagliptin and combined vildagliptin and metformin reduced ERK phosphorylation in ND and obese-insulin-resistant rats (A). Enalapril, vildagliptin, metformin, and combined vildagliptin and metformin reduced p38 MAPK phosphorylation in obese-insulin-resistant rats. In ND rats, enalapril, vildagliptin, and combined vildagliptin and metformin but not metformin decreased reduced p38 MAPK phosphorylation (B). Enalapril, vildagliptin, metformin, and combined vildagliptin and metformin reduced NF-κB phosphorylation in obese-insulin-resistant rats (C). TGF-β expression was not different among groups (D), $^{*}P<0.05$ vs NDV, $^{\dagger}P<0.05$ vs HFDV. NDV, normal diet rats treated with vehicle; NDE, normal diet rats treated with enalapril; NDVil, normal diet rats treated with vildagliptin; NDM, normal diet rats treated with metformin; NDC, normal diet rats treated with combined drugs; HFDV, high-fat-fed rats treated with vehicle; HFDE, high-fat-fed rats treated with enalapril; HFDVil, high-fat-fed rats treated with vildagliptin; HFDM, high-fat-fed rats treated with metformin; HFDC, high-fat-fed rats treated with combined drugs.

in oxidative stress levels and ERK1/2 phosphorylation in normal rats with chronic MI.

Even though our data indicated that DPP4 inhibitor vildagliptin attenuated adverse LV remodeling in obese-insulin-resistant rats, the effects of DPP4 inhibitors on HF in the clinical setting are still unclear. At this time, there are five available commercial DPP4 inhibitors: alogliptin, sitagliptin, vildagliptin, saxagliptin, and linagliptin. A report from the EXAMINE trial showed that alogliptin did not increase the risk of a heart failure outcome in T2DM patients (White *et al.* 2013). For vildagliptin and sitagliptin, the reports from clinical trials still have conflicting data. Some studies reported that sitagliptin and vildagliptin increased neither the risk of adverse

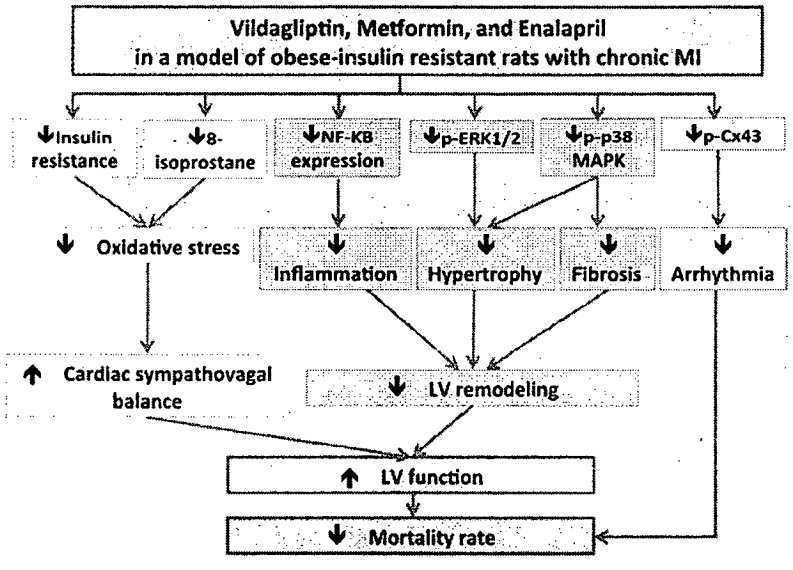


Figure 6
A diagram summarized the effects of vildagliptin, metformin, combined drugs, and enalapil in the obese-insulin-resistant rats with chronic MI. All treatment reduced insulin resistance, reduced oxidative stress, improved cardiac sympathovagal balance, reduced LV remodeling, and increased gap function protein function, leading to improved LV function and reduced mortality rate. CX43, connexin 43; LV, left ventricle. A full colour version of this figure is available at http://dx.doi.org/10.1530/JOE-16-0096.

© 2016 Society for Endocrinology
Printed in Great Britain
Published by Bioscientifica Ltd.

Journal of Endocrinology

cardiovascular events nor the rate of hospitalization for HF (McInnes *et al.* 2015, Wang *et al.* 2015, Fu *et al.* 2016). However, Suh and colleagues reported otherwise, as they showed that sitagliptin and vildagliptin increased the hospitalization rate for HF after 30 days of medication (Suh *et al.* 2015). For saxagliptin, the SAVOR-TIMI53 trial demonstrated that saxagliptin increased the rate of hospitalization for heart failure (Scirica *et al.* 2013). Because these drugs have different forms and different affinities to DPP4, the effect of these DPP4 inhibitors on HF could depend on the type of the drug used in that trial, and this point will need further investigation.

Unlike vildagliptin and enalapril, metformin exerted cardioprotection against MI only in obese-insulin-resistant rats. Previous clinical study reported that metformin did not improve LVEF in ST-elevated MI (STEMI) nondiabetic patients (Lexis *et al.* 2014*a*). However, metformin improved clinical outcomes in metabolic syndrome patients undergoing percutaneous coronary intervention (Li *et al.* 2014) and reduced MI size in diabetic patients with STEMI (Lexis *et al.* 2014*b*). Furthermore, metformin has been shown to improve cardiac function in normal rats with chronic MI (Soraya *et al.* 2012, 2014). All of these findings suggested that metformin exerts cardioprotection in obese-insulin-resistant rats but fails to protect the heart against MI in normal rats. Our findings are consistent with these reports because metformin did not attenuate cardiac autonomic imbalance, LV dysfunction, and LV remodeling in normal rats after MI, whereas it exhibited the beneficial effects in obese-insulin-resistant rats mainly by reducing insulin resistance and exerted cardioprotection after MI in obese-insulin-resistant rats. Data from this study indicated that oxidative stress influenced LV remodeling after MI; metformin did not exert direct antioxidative stress property because metformin did not exert cardioprotection against MI in normal rats. However, vildagliptin exhibited a direct antioxidative stress property in normal rats with MI.

Conclusions

Vildagliptin, metformin and enalapril attenuated insulin resistance and cardiac sympathovagal imbalance, improved LV function, decreased cardiac fibrosis, and reduced the mortality rate in obese-insulin-resistant rats with MI. However, vildagliptin exerted better efficacy in reducing cardiomyocytes hypertrophy than metformin and enalapril. Moreover, vildagliptin, but not metformin, also provided benefits in improving cardiac sympathovagal balance, reducing cardiomyocyte hypertrophy and cardiac fibrosis, and improving LV function in nonobese-insulin-resistant rats with MI.

Declaration of interest
The authors declare that there is no conflict of interest that could be perceived as prejudicing the impartiality of the research reported.

Funding
This work was supported by an NSTDA Research Chair Grant from the National Science and Technology Development Agency (N C), the Thailand Research Fund BRG 5780016 (S C C), the Royal Golden Jubilee program (N C and N A), and a Chiang Mai University Center of Excellence Award (N C).

Acknowledgments
The authors thank Dr Thanapat Sastraruji for his statistical assistance.

References

Apaijai N, Pintana H, Chattipakorn SC & Chattipakorn N 2012 Cardioprotective effects of metformin and vildagliptin in adult rats with insulin resistance induced by a high-fat diet. *Endocrinology* **153** 3878–3885. (doi:10.1210/en.2012-1262)

Apaijai N, Pintana H, Chattipakorn SC & Chattipakorn N 2013 Effects of vildagliptin versus sitagliptin, on cardiac function, heart rate variability and mitochondrial function in obese insulin-resistant rats. *British Journal of Pharmacology* **169** 1048–1057. (doi:10.1111/bph.12176)

Apaijai N, Chinda K, Palee S, Chattipakorn S & Chattipakorn N 2014 Combined vildagliptin and metformin exert better cardioprotection than monotherapy against ischemia-reperfusion injury in obese-insulin resistant rats. *PLoS ONE* **9** e102374. (doi:10.1371/journal.pone.0102374)

Bailey CJ 2005 Treating insulin resistance in type 2 diabetes with metformin and thiazolidinediones. *Diabetes, Obesity and Metabolism* **7** 675–691. (doi:10.1111/j.1463-1326.2005.00497.x)

Bui AL, Horwich TB & Fonarow GC 2011 Epidemiology and risk profile of heart failure. *Nature Reviews Cardiology* **8** 30–41. (doi:10.1038/nrcardio.2010.165)

Chattipakorn N, Incharoen T, Kanlop N & Chattipakorn S 2007 Heart rate variability in myocardial infarction and heart failure. *International Journal of Cardiology* **120** 289–296. (doi:10.1016/j.ijcard.2006.11.221)

Chinda K, Palee S, Surinkaew S, Phornphutkul M, Chattipakorn S & Chattipakorn N 2013 Cardioprotective effect of dipeptidyl peptidase-4 inhibitor during ischemia-reperfusion injury. *International Journal of Cardiology* **167** 451–457. (doi:10.1016/j.ijcard.2012.01.011)

Chinda K, Sanit J, Chattipakorn S & Chattipakorn N 2014 Dipeptidyl peptidase-4 inhibitor reduces infarct size and preserves cardiac function via mitochondrial protection in ischaemia-reperfusion rat heart. *Diabetes and Vascular Disease Research* **11** 75–83. (doi:10.1177/1479164113516134)

Clerk A & Sugden PH 2006 Inflame my heart (by p38-MAPK). *Circulation Research* **99** 455–458. (doi:10.1161/01.RES.0000241053.89089.c3)

Derosa G, Bonaventura A, Bianchi L, Romano D, Fogari E, D'Angelo A & Maffioli P 2014 Vildagliptin compared to glimepiride on post-

© 2016 Society for Endocrinology
Printed in Great Britain
Published by Bioscientifica Ltd.

Journal of Endocrinology

prandial lipemia and on insulin resistance in type 2 diabetic patients. *Metabolism* **63** 957–967. (doi:10.1016/j.metabol.2014.04.008)

Fu AZ, Johnston SS, Ghannam A, Tsai K, Cappell K, Fowler R, Riehle E, Cole AL, Kalsekar I & Sheehan J 2016 Association between hospitalization for heart failure and dipeptidyl peptidase-4 inhibitors in patients with type 2 diabetes: an observational study. *Diabetes Care* [in press]. (doi:10.2337/dc15-0764)

Goncalves L 1995 Risk stratification after myocardial infarction. Clinical evaluation before discharge. *Review Port Cardiology* **14** 475–482, 448.

Gundewar S, Calvert JW, Jha S, Toedt-Pingel I, Ji SY, Nunez D, Ramachandran A, Anaya-Cisneros M, Tian R & Lefer DJ 2009 Activation of AMP-activated protein kinase by metformin improves left ventricular function and survival in heart failure. *Circulation Research* **104** 403–411. (doi:10.1161/CIRCRESAHA.108.190918)

Hamid T, Guo SZ, Kingery JR, Xiang X, Dawn B & Prabhu SD 2011 Cardiomyocyte NF-kappaB p65 promotes adverse remodelling, apoptosis, and endoplasmic reticulum stress in heart failure. *Cardiovascular Research* **89** 129–138. (doi:10.1093/cvr/cvq274)

Hori M & Nishida K 2009 Oxidative stress and left ventricular remodeling after myocardial infarction. *Cardiovascular Research* **81** 457–464. (doi:10.1093/cvr/cvn335)

Inthachai T, Lekawanvijit S, Kumfu S, Apaijai N, Pongkan W, Chattipakorn SC & Chattipakorn N 2015 Dipeptidyl peptidase-4 inhibitor improves cardiac function by attenuating adverse cardiac remodelling in rats with chronic myocardial infarction. *Experimental Physiology* **100** 667–679. (doi:10.1113/ep085108)

Kiliszek M, Maczewski M, Styczynski G, Duda M, Opolski G & Beresewicz A 2007 Low-density lipoprotein reduction by simvastatin is accompanied by angiotensin II type 1 receptor downregulation, reduced oxidative stress, and improved endothelial function in patients with stable coronary artery disease. *Coronary Artery Disease* **18** 201–209. (doi:10.1097/MCA.0b013e32802c7cb0)

Kwak HB, Song W & Lawler JM 2006 Exercise training attenuates age-induced elevation in Bax/Bcl-2 ratio, apoptosis, and remodeling in the rat heart. *FASEB Journal* **20** 791–793.

Lekawanvijit S, Kompa AR, Zhang Y, Wang BH, Kelly DJ & Krum H 2012 Myocardial infarction impairs renal function, induces renal interstitial fibrosis, and increases renal KIM-1 expression: implications for cardiorenal syndrome. *American Journal of Physiology: Heart and Circulatory Physiology* **302** H1884–H1893.

Lexis CP, van der Horst IC, Lipsic E, Wieringa WG, de Boer RA, van den Heuvel AF, van der Werf HW, Schurer RA, Pundziute G, Tan ES, *et al.* 2014*a* Effect of metformin on left ventricular function after acute myocardial infarction in patients without diabetes: the GIPS-III randomized clinical trial. *JAMA* **311** 1526–1535.

Lexis CP, Wieringa WG, Hiemstra B, van Deursen VM, Lipsic E, van der Harst P, van Veldhuisen DJ & van der Horst IC 2014*b* Chronic metformin treatment is associated with reduced myocardial infarct size in diabetic patients with ST-segment elevation myocardial infarction. *Cardiovascular Drugs and Therapy* **28** 163–171.

Li J, Xu JP, Zhao XZ, Sun XJ, Xu ZW & Song SJ 2014 Protective effect of metformin on myocardial injury in metabolic syndrome patients following percutaneous coronary intervention. *Cardiology* **127** 133–139.

Liu J, Wang P, Zou L, Qu J, Litovsky S, Umeda P, Zhou L, Chatham J, Marsh SA, Dell'Italia LJ, *et al.* 2014 High-fat, low-carbohydrate diet promotes arrhythmic death and increases myocardial ischemia-reperfusion injury in rats. *American Journal of Physiology: Heart and Circulatory Physiology* **307** H598–H608.

Luo G, Liu H, Luo S, Li F, Su M & Lu H 2014 Fasting hyperglycemia increases in-hospital mortality risk in nondiabetic female patients with acute myocardial infarction: a retrospective study. *International Journal of Endocrinology* **2014** 745093.

Madian AG, Diaz-Maldonado N, Gao Q & Regnier FE 2011 Oxidative stress induced carbonylation in human plasma. *Journal of Proteomics* **74** 2395–2416. (doi:10.1016/j.jprot.2011.07.014)

Manzella D, Barbieri M, Ragno E & Paolisso G 2001 Chronic administration of pharmacologic doses of vitamin E improves the cardiac autonomic nervous system in patients with type 2 diabetes. *American Journal of Clinical Nutrition* **73** 1052–1057.

Mari A, Sallas WM, He YL, Watson C, Ligueros-Saylan M, Dunning BE, Deacon CF, Holst JJ & Foley JE 2005 Vildagliptin, a dipeptidyl peptidase-IV inhibitor, improves model-assessed beta-cell function in patients with type 2 diabetes. *Journal of Clinical Endocrinology and Metabolism* **90** 4888–4894.

McInnes G, Evans M, Del Prato S, Stumvoll M, Schweizer A, Lukashevich V, Shao Q & Kothny W 2015 Cardiovascular and heart failure safety profile of vildagliptin: a meta-analysis of 17 000 patients. *Diabetes, Obesity and Metabolism* **17** 1085–1092. (doi:10.1111/dom.12548)

Miyoshi T, Nakamura K, Yoshida M, Miura D, Oe H, Akagi S, Sugiyama H, Akazawa K, Yonezawa T, Wada J, *et al.* 2014 Effect of vildagliptin, a dipeptidyl peptidase 4 inhibitor, on cardiac hypertrophy induced by chronic beta-adrenergic stimulation in rats. *Cardiovascular Diabetology* **13** 43.

Ocaranza MP, Godoy I, Jalil JE, Varas M, Collantes P, Pinto M, Roman M, Ramirez C, Copaja M, Diaz-Araya G, *et al.* 2006 Enalapril attenuates downregulation of Angiotensin-converting enzyme 2 in the late phase of ventricular dysfunction in myocardial infarcted rat. *Hypertension* **48** 572–578. (doi:10.1161/01.HYP.0000237862.94083.45)

Oh K, Hu FB, Manson JE, Stampfer MJ & Willett WC 2005 Dietary fat intake and risk of coronary heart disease in women: 20 years of follow-up of the nurses' health study. *American Journal of Epidemiology* **161** 672–679. (doi:10.1093/aje/kwi085)

Pavithran P, Nandeesha H, Sathiyapriya V, Bobby Z & Madanmohan T 2008 Short-term heart variability and oxidative stress in newly diagnosed essential hypertension. *Clinical and Experimental Hypertension* **30** 486–496. (doi:10.1080/10641960802251875)

Pfeffer JM, Pfeffer MA, Fletcher PJ & Braunwald E 1991 Progressive ventricular remodeling in rat with myocardial infarction. *American Journal of Physiology* **260** H1406–H1414.

Pintana H, Apaijai N, Chattipakorn N & Chattipakorn SC 2013 DPP-4 inhibitors improve cognition and brain mitochondrial function of insulin-resistant rats. *Journal of Endocrinology* **218** 1–11. (doi:10.1530/JOE-12-0521)

Pipatpiboon N, Pintana H, Pratchayasakul W, Chattipakorn N & Chattipakorn SC 2013 DPP4-inhibitor improves neuronal insulin receptor function, brain mitochondrial function and cognitive function in rats with insulin resistance induced by high-fat diet consumption. *European Journal of Neuroscience* **37** 839–849. (doi:10.1111/ejn.12088)

Pratchayasakul W, Kerdphoo S, Petsophonsakul P, Pongchaidecha A, Chattipakorn N & Chattipakorn SC 2011 Effects of high-fat diet on insulin receptor function in rat hippocampus and the level of neuronal corticosterone. *Life Sciences* **88** 619–627. (doi:10.1016/j.lfs.2011.02.003)

Rachmani R, Lidar M, Brosh D, Levi Z & Ravid M 2000 Oxidation of low-density lipoprotein in normotensive type 2 diabetic patients. Comparative effects of enalapril versus nifedipine: a randomized cross-over over study. *Diabetes Research and Clinical Practice* **48** 139–145. (doi:10.1016/S0168-8227(99)00149-7)

Richer C, Fornes P, Cazaubon C, Domergue V, Nisato D & Giudicelli JF 1999 Effects of long-term angiotensin II AT1 receptor blockade on survival, hemodynamics and cardiac remodeling in chronic heart failure in rats. *Cardiovascular Research* **41** 100–108. (doi:10.1016/S0008-6363(98)00227-2)

© 2016 Society for Endocrinology
Printed in Great Britain
Published by Bioscientifica Ltd.

Journal of Endocrinology

Roell W, Lewalter T, Sasse P, Tallini YN, Choi BR, Breitbach M, Doran R, Becher UM, Hwang SM, Bostani T, *et al.* 2007 Engraftment of connexin 43-expressing cells prevents post-infarct arrhythmia. *Nature* **450** 819–824. (doi:10.1038/nature06321)

Scirica BM, Bhatt DL, Braunwald E, Steg PG, Davidson J, Hirshberg B, Ohman P, Frederich R, Wiviott SD, Hoffman EB, *et al.* 2013 Saxagliptin and cardiovascular outcomes in patients with type 2 diabetes mellitus. *New England Journal of Medicine* **369** 1373–1379. (doi:10.1056/NEJMcibr1308953)

Soraya H, Khorrami A, Garjani A, Maleki-Dizaji N & Garjani A 2012 Acute treatment with metformin improves cardiac function following isoproterenol induced myocardial infarction in rats. *Pharmacological Reports* **64** 1476–1484. (doi:10.1016/S1734-1140(12)70945-3)

Soraya H, Clanachan AS, Rameshrad M, Maleki-Dizaji N, Ghazi-Khansari M & Garjani A 2014 Chronic treatment with metformin suppresses toll-like receptor 4 signaling and attenuates left ventricular dysfunction following myocardial infarction. *European Journal of Pharmacology* **737** 77–84. (doi:10.1016/j.ejphar.2014.05.003)

Stambe C, Atkins RC, Tesch GH, Masaki T, Schreiner GF & Nikolic-Paterson DJ 2004 The role of p38alpha mitogen-activated protein kinase activation in renal fibrosis. *Journal of the American Society of Nephrology* **15** 370–379. (doi:10.1097/01.ASN.0000109669.23650.56)

Suh S, Seo GH, Jung CH, Kim MK, Jin SM, Hwang YC, Lee BW & Kim JH 2015 Increased risk of hospitalization for heart failure with newly prescribed dipeptidyl peptidase-4 inhibitors and pioglitazone using the korean health insurance claims database. *Diabetes Metabolism Journal* **39** 247–252. (doi:10.4093/dmj.2015.39.3.247)

Sutton MG & Sharpe N 2000 Left ventricular remodeling after myocardial infarction: pathophysiology and therapy. *Circulation* **101** 2981–2988. (doi:10.1161/01.CIR.101.25.2981)

Takahashi A, Asakura M, Ito S, Min KD, Shindo K, Yan Y, Liao Y, Yamazaki S, Sanada S, Asano Y, *et al.* 2013 Dipeptidyl-peptidase IV inhibition improves pathophysiology of heart failure and increases survival rate in pressure-overloaded mice. *American Journal of Physiology: Heart and Circulatory Physiology* **304** H1361–H1369.

Wang J, Huang W, Xu R, Nie Y, Cao X, Meng J, Xu X, Hu S & Zheng Z 2012 MicroRNA-24 regulates cardiac fibrosis after myocardial infarction. *Journal of Cellular and Molecular Medicine* **16** 2150–2160. (doi:10.1111/j.1582-4934.2012.01523.x)

Wang SH, Chen DY, Lin YS, Mao CT, Tsai ML, Hsieh MJ, Chou CC, Wen MS, Wang CC, Hsieh IC, *et al.* 2015 Cardiovascular outcomes of sitagliptin in type 2 diabetic patients with acute myocardial infarction, a population-based cohort study in taiwan. *PLoS ONE* **10** e0131122.

White WB, Cannon CP, Heller SR, Nissen SE, Bergenstal RM, Bakris GL, Perez AT, Fleck PR, Mehta CR, Kupfer S, *et al.* 2013 Alogliptin after acute coronary syndrome in patients with type 2 diabers. *New England Journal of Medicine* **369** 1327–1335. (doi:10.1056/NEJMoa1305889)

Wong AK, Symon R, AlZadjali MA, Ang DS, Ogston S, Choy A, Petrie JR, Struthers AD & Lang CC 2012 The effect of metformin on insulin resistance and exercise parameters in patients with heart failure. *European Journal of Heart Failure* **14** 1303–1310. (doi:10.1093/eurjhf/hfs106)

Yeh CC, Li H, Malhotra D, Turcato S, Nicholas S, Tu R, Zhu BQ, Cha J, Swigart PM, Myagmar BE, *et al.* 2010 Distinctive ERK and p38 signaling in remote and infarcted myocardium during post-MI remodeling in the mouse. *Journal of Cellular Biochemistry* **109** 1185–1191.

Yin M, Sillje HH, Meissner M, van Gilst WH & de Boer RA 2011 Early and late effects of the DPP-4 inhibitor vildagliptin in a rat model of post-myocardial infarction heart failure. *Cardiovascular Diabetology* **10** 85. (doi:10.1186/1475-2840-10-85)

Zuanetti G, Neilson JM, Latini R, Santoro E, Maggioni AP & Ewing DJ 1996 Prognostic significance of heart rate variability in post-myocardial infarction patients in the fibrinolytic era. The GISSI-2 results. Gruppo Italiano per lo Studio della Sopravvivenza nell' Infarto Miocardico. *Circulation* **94** 432–436. (doi:10.1161/01.CIR.94.3.432)

Received in final form 29 March 2016
Accepted 30 March 2016
Accepted Preprint published online 4 April 2016

http://joe.endocrinology-journals.org
DOI: 10.1530/JOE-16-0096

© 2016 Society for Endocrinology
Printed in Great Britain

Published by Bioscientifica Ltd.

เอกสารแนบหมายเลข 22

Research

229:3 209–220

Testosterone deprivation accelerates cardiac dysfunction in obese male rats

Wanpitak Pongkan[1,2,3], Hiranya Pintana[1,2,3], Sivaporn Sivasinprasasn[1,2,3], Thidarat Jaiwongkam[1,2,3], Siriporn C Chattipakorn[1,2,4] and Nipon Chattipakorn[1,2,3]

[1]Cardiac Electrophysiology Research and Training Center, Faculty of Medicine, Chiang Mai University, Chiang Mai, Thailand
[2]Cardiac Electrophysiology Unit, Department of Physiology, Faculty of Medicine, Chiang Mai University, Chiang Mai, Thailand
[3]Center of Excellence in Cardiac Electrophysiology Research, Chiang Mai University, Chiang Mai, Thailand
[4]Department of Oral Biology and Diagnostic Science, Faculty of Dentistry, Chiang Mai University, Chiang Mai, Thailand

Correspondence should be addressed to N Chattipakorn
Email
nchattip@gmail.com

Abstract

Low testosterone level is associated with increased risks of cardiovascular diseases. As obese-insulin-resistant condition could impair cardiac function and that the incidence of obesity is increased in aging men, a condition of testosterone deprivation could aggravate the cardiac dysfunction in obese-insulin-resistant subjects. However, the mechanism underlying this adverse effect is unclear. This study investigated the effects of obesity on metabolic parameters, heart rate variability (HRV), left ventricular (LV) function, and cardiac mitochondrial function in testosterone-deprived rats. Orchiectomized or sham-operated male Wistar rats ($n=36$ per group) were randomly divided into groups and were given either a normal diet (ND, 19.77% of energy fat) or a high-fat diet (HFD, 57.60% of energy fat) for 12 weeks. Metabolic parameters, HRV, LV function, and cardiac mitochondrial function were determined at 4, 8, and 12 weeks after starting each feeding program. We found that insulin resistance was observed after 8 weeks of the consumption of a HFD in both sham (HFS) and orchiectomized (HFO) rats. Neither the ND sham (NDS) group nor ND orchiectomized (NDO) rats developed insulin resistance. The development of depressed HRV, LV contractile dysfunction, and increased cardiac mitochondrial reactive oxygen species production was observed earlier in orchiectomized (NDO and HFO) rats at week 4, whereas HFS rats exhibited these impairments later at week 8. These findings suggest that testosterone deprivation accelerates the impairment of cardiac autonomic regulation and LV function via increased oxidative stress and impaired cardiac mitochondrial function in obese-orchiectomized male rats.

Key Words
- testosterone deprivation
- obese-insulin resistance
- cardiac function
- cardiac mitochondrial function

Journal of Endocrinology (2016) **229**, 209–220

Journal of Endocrinology

Introduction

Testosterone deprivation is a condition in which the oncentration of testosterone is lower than the normal physiological level (Handelsman & Zajac 2004). This state can be found in aging male individuals. The prevalence of testosterone deficiency increases substantially with age (Araujo *et al.* 2007) and is associated with the development of several disorders including obesity, dyslipidemia, insulin resistance, metabolic syndrome,

http://joe.endocrinology-journals.org
DOI: 10.1530/JOE-16-0002
© 2016 Society for Endocrinology
Printed in Great Britain
Published by Bioscientifica Ltd.

and cardiovascular disease (Grossmann *et al.* 2008, Oskui *et al.* 2013). Moreover, testosterone deprivation alone significantly induces left ventricular (LV) contractile dysfunction and cardiac sympathovagal imbalance in orchiectomized rats (Pongkan *et al.* 2015).

Obesity is one of the most important risk factors contributing to the overall burden of disease worldwide, and is known as the initial main sign of metabolic syndrome, which can manifest itself as many diseases, such as cardiovascular disease, type 2 diabetes mellitus, and several types of cancer (McMillen *et al.* 2009, WHO 2011). In men, there has been a significant increase in clinical obesity, rising from 31.8 to 37.1% in the past decade (Flegal *et al.* 2010). In animal studies, it has been shown that rats fed on a HFD for at least 8 weeks developed obese-insulin resistance (Pratchayasakul *et al.* 2011), leading to cardiac sympathovagal imbalance, LV contractile dysfunction, increased oxidative stress, and cardiac mitochondrial dysfunction (Apaijai *et al.* 2014). Although either testosterone deprivation or obese-insulin resistance affected cardiac function, the temporal effects of combined obese-insulin resistance and the loss of testosterone on metabolic parameters, cardiac function, heart rate variability (HRV), and cardiac mitochondrial function have never been investigated. We tested the hypothesis that testosterone deprivation in rats, together with obese-insulin resistance, accelerates and aggravates the impairment of metabolic parameters, cardiac function, HRV, and cardiac mitochondrial function.

Materials and methods

Animal preparation

All experiments were approved by the Institutional Animal Care and Use Committee of the Faculty of Medicine, Chiang Mai University, Chiang Mai, Thailand. Male Wistar rats weighing ~200 g (aged 5–6 weeks) were obtained from the National Laboratory Animal Center, Mahidol University, Bangkok, Thailand. All animals were housed in a climate-controlled room (22–25°C, with a ratio of 12 h light:12 h darkness cycle) and fed with standard laboratory chow (normal diet (ND)) or a high-fat diet (HFD) and water. Both food and water were given *ad libitum*.

Orchiectomy procedure

Rats were anesthetized and maintained using isoflurane 2–3% and the scrotal area was shaved and scrubbed using a sterile technique. The orchiectomy was performed using the scrotal approach technique (Foley 2005). The blood vessels and vas deferens were ligated with an absorbable suture. Then, both testes and epididymal fat pads were removed. The skin incision was closed using a nonabsorbable suture. Rats were monitored carefully to prevent them from chewing of sutures and also any other complications. Analgesic drugs and antibiotics were injected subcutaneously for 3 days after the operation.

ND and HFD preparation

Standard laboratory chow (Mouse Feed Food No. 082, C.P. Company, Bangkok, Thailand) was used as a ND (19.77% of energy fat) and fed to control rats. In addition, the HFD (57.60% of energy fat) was mixed with the following ingredients: standard rat diet, casein, lard, cholesterol, vitamins, DL-methionine, yeast powder, and sodium chloride (Pratchayasakul *et al.* 2011). All ingredients were mixed and molded into a spherical shape. Rats were fed with these diets for 12 weeks.

Experimental protocol

Rats were randomly divided into two groups: a sham-operated group and an orchiectomized (ORX) group. One week after surgery, rats in each group were divided into two subgroups and were given either a ND or a HFD for 4, 8, and 12 weeks ($n=6$ per group for each duration in each dietary group). Animals in the ND group were fed on standard laboratory chow (Mouse Feed Food No. 082, C.P. Company, Bangkok, Thailand), which had an energy content of 4.02 kcal/g and 19.77% of total energy (%E from fat). Animals in the HFD group were fed a HFD, which had an energy content of 5.35 kcal/g and 59.60% E from fat. Body weight and food intake were recorded daily, and blood samples were collected at baseline and then at 4th, 8th, and 12th week after fasting for 5–6 h. Plasma of blood samples were kept at −80°C and used for the determination of metabolic parameters. At the end of the study, the heart was removed and used to study cardiac mitochondrial function.

HRV determination

HRV is a noninvasive assessment of cardiac autonomic function, which is used to determine cardiac sympathovagal balance (Chattipakorn *et al.* 2007). HRV was analyzed before the operation and then at 4th, 8th, and 12th week after being fed a ND or HFD. An ECG was

© 2016 Society for Endocrinology
Printed in Great Britain
Published by Bioscientifica Ltd.
Journal of Endocrinology

conducted on each rat using PowerLab (PowerLab 4/25T, AD Instruments, Bella Vista, NSW, Australia) with chart 5.0 continuously for 20 min, while the animals were still conscious. Data from the ECG recording was analyzed using MATLAB program (Glos *et al.* 2007). A high frequency (HF, 0.6–0.3 Hz) was taken as parasympathetic activity, while a low frequency (LF, 0.2–0.6 Hz) was taken as a combination of sympathetic and parasympathetic activities (Chattipakorn *et al.* 2007). The LF/HF ratio was used as an index of cardiac sympathovagal balance (Latchman *et al.* 2011). An increased LF/HF ratio is indicative of cardiac sympathovagal imbalance (Apaijai *et al.* 2014).

Cardiac function determination

LV function was determined using an ECG (SONOS4500, Philips) and analyzed before the operation and then at 4-, 8-, and 12-week feeding program. Rats were stabilized in a supine position, and the probe was gently placed on the chest and moved to collect data along the short and long axes of the heart. Signals from an M-mode ECG at the level of the papillary muscles were recorded. Parameters obtained included right ventricular dimension during diastole, interventricular septum during systole and diastole, LV internal dimension during systole (LVIDs) and diastole (LVIDd), and LV posterior wall thickness during systole and diastole. Fractional shortening (FS) was calculated using the formula: %FS = (LVIDd–LVIDs) × 100/LVIDd.

At the end of the experiment (week 12), LV pressure was evaluated using a pressure catheter cannulated via the right carotid artery into the LV chamber. The LV pressure was recorded using LabScribe2 program (iWorx Systems Inc., Dover, NH, USA) (Chinda *et al.* 2014). Systolic and diastolic blood pressure, heart rate (HR), LV end-systolic pressure, and LV end-diastolic pressure (LVEDP) were assessed.

Cardiac mitochondrial function study

At the end of the experiment, cardiac mitochondria were isolated from the whole heart in each rat. Rats were deeply anesthetized and the hearts were removed and homogenized in ice-cold buffer. The tissues were homogenized by the homogenizer and then the homogenate was centrifuged at 800 ***g*** for 5 min. The supernatant was collected and centrifuged at 8800 ***g*** for 5 min. Mitochondrial pellets were resuspended in an ice-cold buffer and centrifuged one more time at 8800 ***g*** for 5 min. Protein concentration was determined by bicinchoninic acid assay as described previously (Thummasorn *et al.* 2011). Cardiac mitochondrial function was determined by measuring mitochondrial reactive oxygen species (ROS) production, mitochondrial membrane potential change ($\Delta\Psi m$), and mitochondrial swelling. Transmission electron microscopy (TEM) was also used to determine the morphology of the isolated cardiac mitochondria (Chinda *et al.* 2014).

Measurement of cardiac mitochondrial ROS production Mitochondrial ROS production was determined by using dichlorodihydrofluorescein diacetate dye (DCFDA) (Thummasorn *et al.* 2011). Cardiac mitochondrial proteins (0.4 mg/mL) were incubated at 25°C with 2 μM DCFDA for 20 min. The DCFDA diffuses through the mitochondrial membrane and is deacetylated by intracellular esterases to a nonfluorescent compound, which is later oxidized by ROS into dichlorofluorescein (DCF). DCF is a highly fluorescent compound, which can be detected by fluorescence spectroscopy with maximum excitation. An increase in DCF intensity indicates an increase in ROS production (Chinda *et al.* 2014). Fluorescent intensity of the DCF was measured at excitation wavelength (λ_{ex}) 485 nm (bandwidth 5 nm) and emission wavelength (λ_{em}) 530 nm (bandwidth 10 nm), using a fluorescent microplate reader, and represented as arbitrary units of fluorescent intensity.

Measurement of cardiac mitochondrial membrane potential change ($\Delta\Psi m$) Mitochondrial membrane potential change was determined using the dye 5,5′,6,6′-tetrachloro-1,1′,3,3′-tetraethylbenzimid azolcarbocyanine iodide (JC-1). The isolated cardiac mitochondria (0.4 mg/mL) were stained with JC-1 at 37°C for 30 min. The fluorescence intensity was determined by using a fluorescent microplate reader (Thummasorn *et al.* 2011).

In the mitochondrial membrane interaction, JC-1 could be changed to either a monomer form or an aggregate form, which have different fluorescent properties. The monomer form of JC-1 was a cation and caused a display of green fluorescence, whereas the aggregate form of JC-1 was a reaction between JC-1 (cation) and O_2^- (anion) within a mitochondrial matrix resulting in a display of red fluorescence. Inside unhealthy mitochondria, the levels of anions are lower, which leads to the reduction in the red (due to JC-1 (cation)/green (due to O_2^- (anion)) fluorescence ratio in the mitochondrial matrix; this represents mitochondrial depolarization. JC-1 monomer and aggregate form were excited at wavelengths 485 and 585 nm, whereas the emission of JC-1 monomer

http://joe.endocrinology-journals.org
DOI: 10.1530/JOE-16-0002
© 2016 Society for Endocrinology
Printed in Great Britain
Published by Bioscientifica Ltd.

Journal of Endocrinology

and aggregate form was detected at wavelengths 530 and 590 nm, respectively. The change in the mitochondrial membrane potential was calculated from the ratio of the intensity of red to green fluorescence. A decrease in the red/green fluorescence intensity ratio indicates mitochondrial membrane depolarization (Chinda *et al.* 2014).

Measurement of cardiac mitochondrial swelling The isolated mitochondrial suspension was prepared for the determination of the level of mitochondrial swelling. Mitochondria (0.4 mg/mL) were incubated in respiration buffer as described previously (Thummasorn *et al.* 2011). Mitochondrial swelling was determined by measuring the change in the absorbance of the suspension at 540 nm (A540) using a microplate reader (Synergy HT, BioTek). Cardiac mitochondrial swelling was indicated by a decrease in the absorbance by the mitochondrial suspension (Chinda *et al.* 2014). TEM was also used to determine the morphology of the isolated cardiac mitochondria (Chinda *et al.* 2014).

Metabolic parameters, insulin resistance, and testosterone level determination

Fasting plasma glucose, total cholesterol, and triglyceride concentrations were determined by an enzymatic colorimetric assay from a commercially available kit (Biotech, Bangkok, Thailand). Fasting plasma HDL was determined using a sensitive, colorimetric and fluorometric assay from a commercially available kit (BioVision), whereas plasma LDL was determined using Friedewald's equation (Friedewald *et al.* 1972). Fasting plasma insulin level was determined by Sandwich ELISA (Millipore).

Insulin resistance was assessed using the homeostasis model assessment (HOMA) (Appleton *et al.* 2005), which was calculated from fasting plasma insulin and fasting plasma glucose concentrations. A higher HOMA index indicates a higher degree of insulin resistance (Pratchayasakul *et al.* 2011). Total plasma testosterone (ng/dL) was analyzed by ELISA technique at the Central Laboratory Service of Maharaj Nakorn Chiang Mai Hospital, Faculty of Medicine, Chiang Mai University.

Determination of malondialdehyde in plasma and cardiac tissues

Plasma and tissue malondialdehyde (MDA) levels were measured using a HPLC system (Thermo Scientific) (Apaijai *et al.* 2012). Plasma or tissue MDA was mixed with 0.44 M H_3PO_4 and 0.6% thiobabituric acid solution, resulting in the generation of pink-colored products called thiobarbituric acid reactive substances (TBARS). Plasma or tissue TBARS concentrations were determined directly from a standard curve, and reported as an MDA equivalent concentration using an HPLC-based assay (Mateos *et al.* 2005).

Western blot analysis

Heart tissue was frozen in liquid nitrogen and stored at −80°C until use (Chinda *et al.* 2014). Myocardial protein extract was prepared by homogenization of the nitrogen-frozen heart tissues in a lysis buffer (containing 1% Nonidet P-40 (Merck Millipore), 0.5% sodium deoxycholate, 0.1% SDS in 1×PBS), and subsequently homogenized at 4°C. The homogenate was then centrifuged at 16,707 ***g*** for 15 min. The total protein from tissue pellets was mixed with a loading buffer (10% mercaptoethanol, 0.05% bromophenol blue, 75 mM Tris–HCl, pH 6.8, 2% SDS, and 10% glycerol) and heated at 95°C for 10 min. The protein samples were then subjected to 10 or 15% SDS–PAGE, and transferred to polyvinylidene difluoride membranes using a semi-dry transfer system (Trans-Blot SD; Bio-Rad). The membranes were blocked with 5% nonfat skimmed milk in TBST (20 mM Tris–HCl, pH 7.6, 137 mM NaCl, and 0.1% Tween 20) for 1 h. The membranes were subsequently exposed to anti-BAX (Santa Cruz Biotechnology), anti-BCL2 (Cell Signaling Technology), or β-actin (Santa Cruz Biotechnology) overnight at 4°C. On the following day, the membranes were washed and incubated with horseradish peroxidase-conjugated secondary antibody (Cell Signaling Technology) for 1 h at room temperature. The signals were developed by incubating with an enhanced chemiluminescense reagent and subjected to autoradiography. The immunoblot films were scanned, and the band density was analyzed using ImageJ software (NIH, Bethesda, MD, USA).

Statistical analysis

Data were expressed as mean ± S.E.M. Statistical comparisons at the different time points in the feeding program for HRV, cardiac function, and cardiac mitochondrial function were analyzed using a one-way ANOVA, followed by *post hoc* least significant difference analysis. Statistical comparisons of the biochemical parameters were calculated using the Mann–Whitney U test. All statistical analyses were performed using SPSS (version 16; SPSS). The statistical significance was accepted at a P value <0.05.

http://joe.endocrinology-journals.org
DOI: 10.1530/JOE-16-0002
© 2016 Society for Endocrinology
Printed in Great Britain
Published by Bioscientifica Ltd.

Results

Obesity, but not testosterone deficiency, led to insulin resistance

At week 4, testosterone deprivation was confirmed by decreased plasma testosterone levels and the ratio of seminal vesicle per body weight (seminal vesicle ratio). Orchiectomized rats in both dietary groups (NDO and HFO) had significantly decreased plasma testosterone levels and seminal vesicle ratio, when compared with sham rats at the same time points. Animals fed on a HFD for 4 weeks had significantly increased body weight compared with ND rats. In addition, orchiectomized rats in both dietary groups (NDO and HFO) had decreased body weight, food intake, and visceral fat when compared with sham rats in the same dietary groups. However, there was no significant difference in the metabolic parameters (the level of plasma insulin, plasma glucose, HOMA index, plasma total cholesterol, plasma triglyceride, plasma HDL and LDL in the blood) among the dietary groups at 4 weeks (Table 1).

At week 8, the body weight, food intake, and visceral fat mass were similar to the results at week 4. Peripheral insulin resistance developed only in the HFD groups (HFS and HFO) at 8 weeks, as shown by both an increased insulin level and HOMA index. The metabolic parameters did not differ between HFS and HFO, but they were significantly higher than those in ND rats (NDS and NDO) (Table 2).

At week 12, HF rats (HFS and HFO) still demonstrated consistent impairments in metabolic parameters, as shown by increased levels of all metabolic parameters, except triglyceride level, compared with NDS and NDO rats (Table 3). Moreover, HFS rats still showed a significant increase in body weight compared with NDS rats, whereas orchiectomized rats from both dietary groups (NDO and HFO) had decreased body weight, food intake, and visceral fat mass compared with the sham rats in the same dietary groups (Table 3).

Testosterone deprivation led to oxidative stress earlier than high-fat-induced obesity

Orchiectomized rats (NDO and HFO) had increased plasma MDA from week 4 onward, when compared with sham rats in the same dietary groups, whereas cardiac tissue MDA was increased only in the HFO group (Table 1). Plasma and cardiac tissue levels of MDA in orchiectomized rats (NDO and HFO) continued to show an increase at week 8 and 12. Plasma and cardiac tissue levels of MDA in the HFS group in week 8 (Table 2) and 12 (Table 3) were also elevated, showing the same levels of plasma MDA observed in the NDO and HFO groups, and was significantly different when compared with the NDS group.

Testosterone deprivation led to cardiac dysfunction and HRV impairment earlier than obesity

In ORX rats fed on either a normal diet (NDO) or a high-fat diet (HFO), both FS and ejection fraction (EF) showed a significant decrease at week 4, and continued to decrease by week 8 and 12, when compared with sham rats in the

Table 1 Effect of obese-insulin resistance in testosterone-deprived rats on metabolic parameters investigated at 4 weeks ($n=6$ per group).

	Normal diet		High-fat diet	
Parameters	**NDS**	**NDO**	**HFS**	**HFO**
Body weight (g)	448±12	420±9*	493±15*,†	460±10†,‡
Food intake (g/day)	20.7±0.2	18.8±0.4*,‡	21.1±0.1	20.4±0.3†,‡
Visceral fat (g)	22.8±2.07	15.8±2.16*,‡	35.2±2.22*	29±0.6*,†,‡
Plasma testosterone (ng/dL)	1.5±0.4	0.1±0.01*,‡	1.0±0.01	0.1±0.01*,‡
Seminal vesicle ratio ($\times 10^3$)	3.3±0.26	0.37±0.1*,‡	3.4±0.41	0.3±0.12*,‡
Plasma insulin (ng/mL)	2.1±0.2	2.0±0.2	2.2±0.3	2.2±0.3
Plasma glucose (mg/dL)	116±11	127±7	125±8	125±7
HOMA index	11±2	11.2±1	12.2±1	12.5±2
Plasma total cholesterol (mg/dL)	90±3	91±5	95±4	102±7
Plasma triglyceride (mg/dL)	134±12	139±8	138±16	142±7
Plasma HDL (mg/dL)	32±1	31±3	29±2	28±2
Plasma LDL (mg/dL)	62±3	68±3	67±5	69±8
Plasma MDA (mmol/mL)	4.7±0.08	5.6±0.19*,‡	5.0±0.06	5.5±0.17*,‡
Cardiac MDA (μmol/mL)	1.53±0.26	3.7±0.76	1.57±0.15	5.2±0.79*

*$P<0.05$ vs NDS; †$P<0.05$ vs NDO; ‡$P<0.05$ vs HFS.

© 2016 Society for Endocrinology
Printed in Great Britain
Published by Bioscientifica Ltd.

Journal of Endocrinology

Table 2 Effect of obese insulin resistance in testosterone-deprived rats on metabolic parameters investigated at 8 weeks ($n=6$ per group).

Parameters	Normal diet		High-fat diet	
	NDS	NDO	HFS	HFO
Body weight (g)	460±10	443±8*,‡	535±15*	497±10*,†,‡
Food intake (g/day)	19.2±0.7	17.7±0.6*,‡	21.9±0.1	19.8±0.3†,‡
Visceral fat (g)	30.3±0.8	18.3±1.8*,‡	48.5±3.1*	37.2±2.38*,†,‡
Plasma testosterone (ng/dL)	2.1±0.7	0.03±0.01*,‡	1.2±0.31*	0.08±0.01*,‡
Seminal vesicle ratio (×10³)	3.8±0.22	0.21±0.01*,‡	3.1±0.1*	0.34±0.04*,‡
Plasma insulin (ng/mL)	1.95±0.1	2.0±0.1	2.9±0.3*,†	2.8±0.3*,†
Plasma glucose (mg/dL)	123±7	133±7	128±4	130±9
HOMA index	11.0±1	11.2±1	16.6±1*,†	16.7±3*,†
Plasma total cholesterol (mg/dL)	91±4	93±4	108±6*,†	111±5*,†
Plasma triglyceride (mg/dL)	129±10	130±14	124±17	123±24
Plasma HDL (mg/dL)	31±2	33±2	23±2*,†	21±3*,†
Plasma LDL (mg/dL)	61±4	68±5	83±6*	89±5*,†
Plasma MDA (mmol/mL)	5.1±0.06	5.7±0.13*	5.9±0.1*	5.6±0.12*
Cardiac MDA (µmol/mL)	1.98±0.26	4.7±1.02*	4.39±0.79*	4.53±0.71*

*$P<0.05$ vs NDS; †$P<0.05$ vs NDO; ‡$P<0.05$ vs HFS.

same dietary groups (NDS and HFS). Unlike ORX rats, HFS rats exhibited a significant reduction in both %FS and %EF later at week 8 and 12 of the study, when compared with rats in the NDS group (Fig. 1A and B).

Consistent with the %FS and %EF data, ORX rats (NDO and HFO) were the first groups to present as having impaired sympathovagal balance. The LF/HF ratio in ORX rats showed a significant increase from week 4 onward, and still showed this impairment at week 8 and 12, when compared with the NDS group. The HFS group exhibited sympathovagal imbalance later, by week 8 and 12 (Fig. 1C). No significant difference in the LF/HF ratio was found in the NDO, HFS, and HFO groups at weeks 8 and 12.

The changes in the LV pressure at week 12 in all groups are given in Table 4. Rats in the NDO, HFS, and HFO groups had increased systolic and diastolic blood pressure when compared with rats in the NDS group. Moreover, these groups exhibited diastolic dysfunction at week 12, as shown by increased LVEDP, when compared with the NDS group.

Testosterone deprivation led to cardiac mitochondrial dysfunction earlier than obesity

In ORX rats (NDO and HFO), cardiac mitochondrial dysfunction had developed by week 4 and dysfunction

Table 3 Effect of obese-insulin resistance in testosterone-deprived rats on metabolic parameters investigated at 12 weeks ($n=6$ per group).

Parameters	Normal diet		High-fat diet	
	NDS	NDO	HFS	HFO
Body weight (g)	485±15	447±16*,‡	575±21*	508±17†,‡
Food intake (g/day)	20.7±0.2	16.4±1*,‡	20.3±0.4	18.4±0.3†,‡
Visceral fat (g)	30.2±2.6	21.8±0.6*,‡	51±4.6*	28.5±3.4†,‡
Plasma testosterone (ng/dL)	1.2±0.4	0.07±0.01*,‡	0.5±0.06*	0.1±0.06*,‡
Seminal vesicle ratio (×10³)	3.82±0.28	0.51±0.33*,‡	3.1±0.07*	0.18±0.02*,‡
Plasma insulin (ng/mL)	1.9±0.2	2.2±0.3	3.3±0.2*,†	3.0±0.3*,†
Plasma glucose (mg/dL)	140±5	136±4	132±4	136±6
HOMA index	13.5±1	12.5±1	20.1±1*,†	19.8±2*,†
Plasma total cholesterol (mg/dL)	89±5	100±2	109±6*,†	130±7*,†,‡
Plasma triglyceride (mg/dL)	133±32	135±10	146±9	133±4
Plasma HDL (mg/dL)	33±2	35±2	25±2*,†	25±3*,†
Plasma LDL (mg/dL)	63±5	73±4	82±8*	95±8*,†
Plasma MDA (mmol/mL)	4.04±0.4	5.6±0.27*	5.8±0.5*	5.4±0.15*
Cardiac MDA (µmol/mL)	2.48±0.63	6.08±0.75*	6.37±1.30*	7.07±0.67*

*$P<0.05$ vs NDS; †$P<0.05$ vs NDO; ‡$P<0.05$ vs HFS.

http://joe.endocrinology-journals.org
DOI: 10.1530/JOE-16-0002
© 2016 Society for Endocrinology
Printed in Great Britain
Published by Bioscientifica Ltd.

Journal of Endocrinology

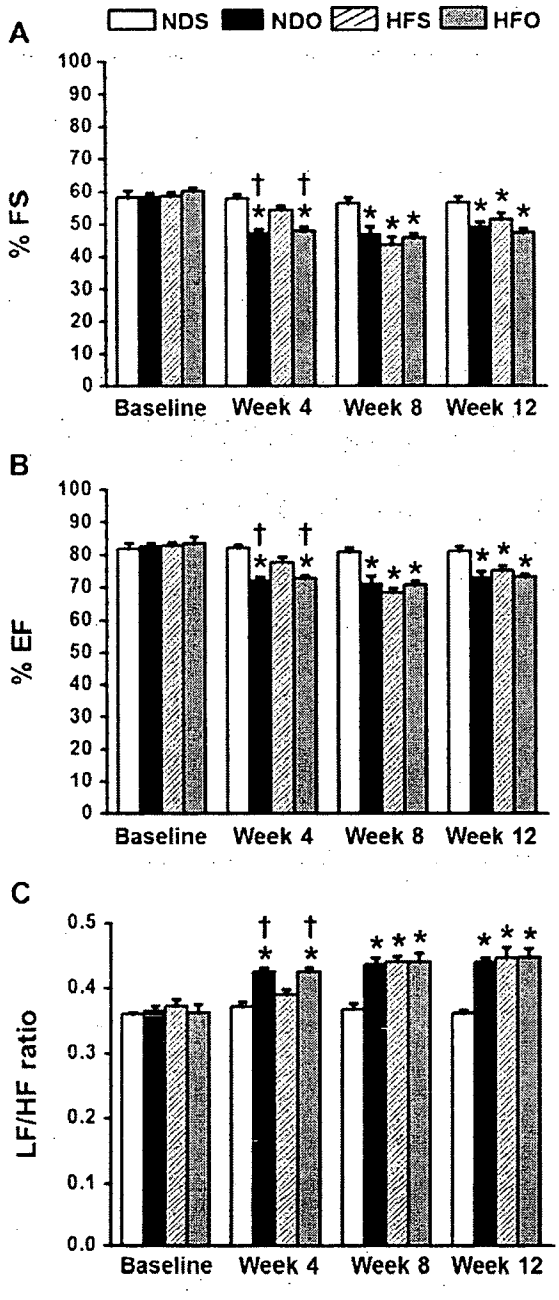


Figure 1
The effect of obese-insulin resistance in testosterone-deprived rats on FS, EF, and HRV (represented as LF/HF ratio) at different time courses (4, 8, and 12 weeks). (A) %FS and (B) %EF were decreased in NDO and HFO groups at any time following week 4, whereas %FS in the HFS group was decreased at week 8 and onward, compared with the NDS group. (C) LF/HF ratio was significantly increased in NDO and HFO groups from week 4, whereas the LF/HF ratio in the HFS group was increased at week 8, compared with the NDS group. *$P<0.05$ vs NDS, †$P<0.05$ vs HFS, $n=5$–6 per group. NDS, normal diet + sham surgery; NDO, normal diet + orchiectomy; HFS, high-fat diet + sham surgery; HFO, high-fat diet + orchiectomy.

continued to week 8 and 12, as indicated by increased mitochondrial ROS production (Fig. 2A), mitochondrial depolarization as indicated by a decrease in the red/green fluorescent intensity ratio (Fig. 2B) and mitochondrial swelling as indicated by a decrease in the absorbance at 540 nm (Fig. 2C) when compared with sham rats at the same point in time. In HFS rats, it was not until week 8 that cardiac mitochondrial dysfunction developed (Fig. 2). No significant difference in these cardiac mitochondrial parameters was found between NDO, HFS, and HFO groups at week 8 and 12. Representative TEM pictures of cardiac mitochondria are shown in Fig. 2D. Cardiac mitochondrial swelling could be observed in ORX rats (NDO and HFO) at week 4, 8, and 12, whereas in the HFS group was observed later, at week 8 and 12.

Increased cardiac apoptotic protein expression in testosterone-deprived rats with and without obese-insulin resistance

In the heart, the expression of BAX and BCL2 showed no significant difference between all groups at week 4. At week 8, when compared with the NDS group, the pro-apoptotic (BAX) level was increased in NDO, HFS, and HFO groups (Fig. 3A,D), whereas the anti-apoptotic (BCL2) levels showed no significant difference between the groups (Fig. 3B,D). At week 12, the BAX level in NDO, HFS, and HFO groups was continuously increasing (Fig. 3A,D), whereas the BCL2 level in NDO, HFS, and HFO groups was lower at this time point, compared with the NDS group (Fig. 3B,D). The BAX/BCL2 ratio increased earlier in the HFO group (week 4), whereas this ratio increased later (week 8) in the NDO and HFS groups (Fig. 3C).

Discussion

This study has demonstrated the adverse effects of testosterone deprivation and obese-insulin resistance on the heart. The major findings of this study are as follows. First, testosterone deprivation alone does not cause insulin resistance, but leads to earlier development of LV dysfunction, cardiac sympathovagal imbalance, cardiac mitochondrial dysfunction, and increased circulating oxidative stress. Secondly, long-term HFD consumption alone enhances the development of obese-insulin resistance, LV dysfunction, cardiac sympathovagal imbalance, cardiac mitochondrial dysfunction, and increased circulating and cardiac tissue oxidative stress. These adverse effects, however, developed later than

http://joe.endocrinology-journals.org
DOI: 10.1530/JOE-16-0002
© 2016 Society for Endocrinology
Printed in Great Britain
Published by Bioscientifica Ltd.

Table 4 Effect of obese insulin resistance in testosterone-deprived rats on cardiac function at 12 weeks ($n=6$ per group).

Cardiac function parameters	Normal diet		High-fat diet	
	NDS	NDO	HFS	HFO
Heart rate (bpm)	285±5	284±15	276±11	284±15
Systolic BP (mmHg)	109±2	128±7*	127±6*	129±6*
Diastolic BP (mmHg)	86±1	106±7*	99±7*	103±5*
LVESP (mmHg)	103±6	96±5	109±2	101±4
LVEDP (mmHg)	5±1	9±1*	10±1*	10±1*
P_{max} (mmHg)	106±6	104±6	115±3	106±4
P_{min} (mmHg)	3±1	6±3	7±1	8±1
dP/dt_{max} (mmHg/s)	7056±522	6757±410	7057±502	6264±286
dP/dt_{min} (mmHg/s)	−5458±461	−4433±449	−6463±662†	−5950±1001

BP, blood pressure; LVESP, left ventricular end-systolic pressure. *$P<0.05$ vs NDS; †$P<0.05$ vs NDO.

those observed in the testosterone-deprived rats. Thirdly, although obese-insulin resistance does not aggravate these adverse effects of testosterone deprivation, it accelerates the apoptotic process in the heart of testosterone-deprived rats. A summary of these findings is given in Table 5.

In this study, testosterone deprivation did not have adverse effects on metabolic parameters, except for weight loss, at all measured time points. The weight loss found in NDO rats could be due to decreased food intake. This finding is consistent with previous studies, which reported that an orchiectomy could cause permanent hypophagia (Gentry & Wade 1976), an increase in oxidative stress (Pongkan *et al.* 2015), and an increase in leptin (Baumgartner *et al.* 1999). The possible mechanism for this could be due to the induction of proinflammatory cytokines (via nuclear factor-κ-B signaling molecules) causing oxidative stress (Vlantis & Pasparakis 2010). This may result in an increased concentration of circulating leptin via activation of the leptin gene through the p38-MAPK pathway (Finck & Johnson 2002) and lead to decreased food intake and a resulting drop in body weight (Aoyama *et al.* 2015). Although testosterone deprivation did not appear to have any measurable effects on metabolic parameters, it caused LV dysfunction and cardiac autonomic imbalance as observed from week 4 onward. Cardiac autonomic control has been shown to be mainly influenced by oxidative stress (Brook *et al.* 2010). It has been shown that increased oxidative stress is associated with cardiac autonomic imbalance (Sivasinprasasn *et al.* 2015). Moreover, cardiac mitochondrial function has been

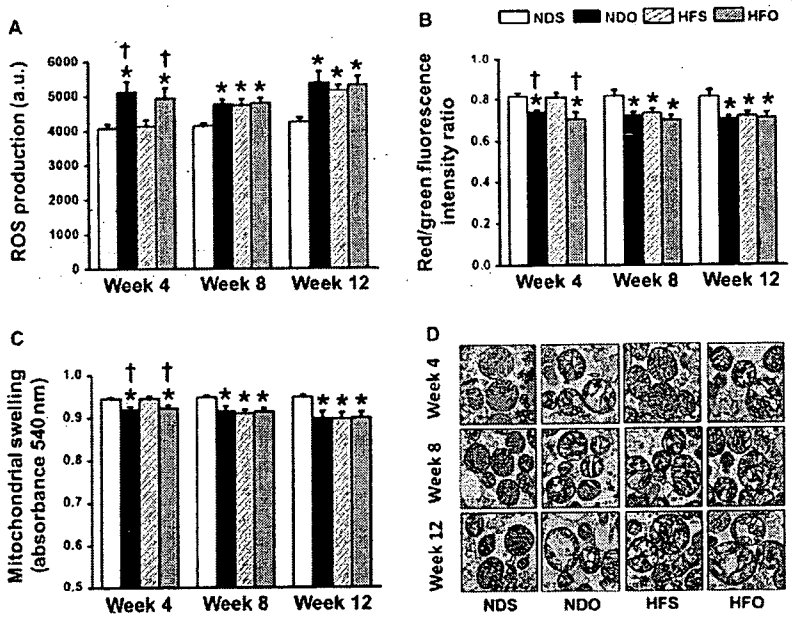


Figure 2
The effect of obese-insulin resistance in testosterone-deprived rats on cardiac mitochondrial function at different points in the feeding program (4, 8, and 12 weeks). (A) Mitochondrial ROS production; (B) mitochondrial membrane depolarization; and (C) mitochondrial swelling were all increased in NDO and HFO groups from week 4 onward, whereas the HFS group showed an increase in these parameters beginning at week 8. (D) Representative electron micrographs showed that obese-insulin resistance and testosterone deprivation caused cardiac mitochondrial swelling. *$P<0.05$ vs NDS, †$P<0.05$ vs HFS, $n=5$–6 per group. a.u., arbitrary units; NDS, normal diet + sham surgery; NDO, normal diet + orchiectomy; HFS, high-fat diet + sham surgery; HFO, high-fat diet + orchiectomy.

© 2016 Society for Endocrinology
Printed in Great Britain
Published by Bioscientifica Ltd.

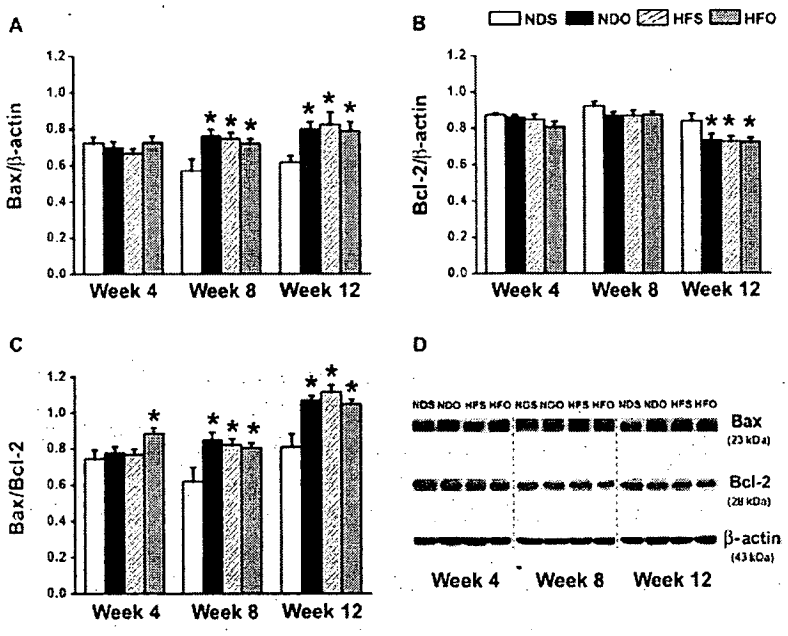


Figure 3
The effects of obese-insulin resistance in testosterone-deprived rats on myocardial apoptosis at different time courses (4, 8, and 12 weeks). Anti-apoptotic (BCL2) expression (A), pro-apoptotic (BAX) expression (B), BAX/BCL2 ratio (C), and representative bands from western blot analysis (D). BCL2 expression was reduced in NDO, HFS, and HFO groups at week 12, whereas BAX expression was increased in NDO, HFS, and HFO groups at week 8 and 12. BAX/BCL2 ratio showed an increase earlier in the HFO group (week 4), whereas this ratio increased later (week 8) in NDO, HFS, and HFO groups, compared with the NDS group at the same point in the feeding program. *$P<0.05$ vs NDS at the same point in the feeding program, $n=5$–6 per group. NDS, normal diet + sham surgery; NDO, normal diet + orchiectomy; HFS, high-fat diet + sham surgery; HFO, high-fat diet + orchiectomy.

shown to play an important role on cardiac contractile function (Marchini *et al.* 2013). Therefore, the adverse effects observed in testosterone-deprived rats could be due to the increased oxidative stress and impaired cardiac mitochondrial function, thus resulting in cardiac autonomic imbalance and LV dysfunction, respectively.

Long-term consumption of a HFD has been shown to cause obese-insulin resistance (Pratchayasakul *et al.* 2011), which is characterized by increased plasma insulin, HOMA index, and plasma total cholesterol levels (Pratchayasakul *et al.* 2011). Although body weight, food intake, and visceral fat were decreased in obese-testosterone deficiency (HFO) rats, the insulin resistance index (HOMA index) was not improved in this study. Since a previous report showed that the reduction of food intake and body weight could improve insulin sensitivity (Schenk *et al.* 2009), our finding emphasized the importance of testosterone deficiency condition, which might aggravate insulin resistance as observed in this study. Supporting this hypothesis is due to the fact that testosterone deficiency has been shown to cause insulin resistance (Dubois *et al.* 2015, Pintana *et al.* 2015*a*).

In this study, insulin resistance was not observed until after 8 weeks of consumption of a HFD, despite the fact that weight gain had been observed in these rats since week 4. However, the levels of metabolic impairment, LV dysfunction, and cardiac autonomic imbalance in HFS and HFO rats at weeks 8 and 12 were no different, suggesting that the obese-insulin-resistant condition did not aggravate these adverse effects caused by testosterone deprivation as observed in NDO rats. This is also supported by the findings that both HFO and HFS rats had similar levels of oxidative stress and cardiac mitochondrial dysfunction. However, these findings indicate that testosterone deprivation accelerated the development of cardiac autonomic disturbance and LV dysfunction as HFO rats had already developed these impairments by week 4, whereas HFS rats showed no signs of this at this period.

Table 5 A summary of the cardiometabolic impairment of the experimental groups at different points in the feeding program (4, 8, and 12 weeks).

	4 week				8 week				12 week			
Impairment	**NDS**	**NDO**	**HFS**	**HFO**	**NDS**	**NDO**	**HFS**	**HFO**	**NDS**	**NDO**	**HFS**	**HFO**
Metabolic disturbance							✓	✓			✓	✓
LV dysfunction		✓		✓		✓	✓	✓		✓	✓	✓
Cardiac autonomic imbalance		✓		✓		✓	✓	✓		✓	✓	✓
Oxidative stress		✓		✓		✓	✓	✓		✓	✓	✓
Mitochondrial impairment		✓		✓		✓	✓	✓		✓	✓	✓

http://joe.endocrinology-journals.org
DOI: 10.1530/JOE-16-0002
© 2016 Society for Endocrinology
Printed in Great Britain
Published by Bioscientifica Ltd.

Therefore, the dysfunctions in week 4 could be due to the influence of testosterone deprivation alone. Moreover, HFO rats at week 8 have testosterone deprivation combined with obese-insulin resistance and did not show any additive adverse effect, compared with the same group at 4 weeks. In addition, these abnormalities were similar between 8 and 12 weeks. These findings suggest an unclear relationship between the effects produced by testosterone deprivation on cardiac function and those caused by obesity and insulin resistance since no additive adverse effect of these two abnormal conditions was observed. This is consistent with the previous study demonstrating the effects of testosterone deprivation on the cognitive function (Pintana *et al.* 2016). However, whether additive adverse effects from these two conditions can be observed at a longer duration of obese-insulin-resistant condition are not known and need further investigation in the future. Nevertheless, at this point our study demonstrated that testosterone deprivation did not aggravate these impairments, but accelerated the development of these impairments in obese-insulin-resistant rats.

Regarding apoptotic markers, the HFO rats demonstrated an increased ratio of BAX/BCL2 from week 4, which was earlier than that observed in the HFS rats. The possible mechanism could be due to the increasing level of plasma and cardiac MDA, and increased cardiac mitochondrial ROS production in HFO rats. The increase in the level of oxidative stress in the heart may have aggravated an apoptotic pathway (Zorov *et al.* 2006) and led to a decrease in anti-apoptotic (BCL2) levels, and an increase in pro-apoptotic protein (BAX) levels (Pongkan *et al.* 2015), therefore, leading to cardiomyocyte apoptosis and finally LV dysfunction (Aon *et al.* 2009).

Our findings are consistent with previous clinical studies. The cohort clinical study demonstrated that the prevalence of cardiovascular morbidity and mortality increased in patients suffering from prostate cancer (PCa) who have undergone to androgen deprivation therapy (ADT), suggesting that testosterone deficiency was the risk factor of cardiovascular diseases (Gandaglia *et al.* 2015). Moreover, diastolic dysfunction was found in patients with type 2 diabetes with low testosterone level compared with similar patients with normal testosterone levels (Tinetti *et al.* 2015). Furthermore, patients suffering from congestive heart failure (Jankowska *et al.* 2006) and coronary artery disease (Li *et al.* 2012) have been shown to have lower levels of testosterone compared with healthy men, and the severity of these conditions had a strong correlation with the degree of testosterone deficiency (Li *et al.* 2012, Oskui *et al.* 2013). Recent clinical studies demonstrated that testosterone replacement could improve insulin sensitivity, increase lean mass, and decrease subcutaneous fat (Dhindsa *et al.* 2016) and also improve cardiometabolic parameters in type 2 diabetes men with testosterone deprivation (Hackett *et al.* 2014) and in hypogonadal men with metabolic syndrome (Saad *et al.* 2016).

Although low testosterone level may be a risk factor for diabetes or insulin resistance (Muraleedharan & Jones 2010), the effects of testosterone replacement on insulin resistance and metabolic parameters may depend on its dose. Physiological level of testosterone exhibited the beneficial effect on insulin resistance and metabolic parameters (Pintana *et al.* 2015*b*). However, supraphysiological level of testosterone had been shown to provide adverse effect on insulin resistance (Yasui *et al.* 2012, Garrido *et al.* 2014). In healthy and menopausal women, supraphysiological level of testosterone could induce the development of breast cancer, heart disease, and insulin resistance (Polderman *et al.* 1994, Yasui *et al.* 2012). Moreover, high-dose testosterone significantly decreased plasma HDL, increased LDL cholesterol in healthy men and postmenopausal women (Taggart *et al.* 1982, Hurley *et al.* 1984, Thompson *et al.* 1989), and induced insulin resistance in a rat model (Holmang & Bjorntorp 1992). High-dose testosterone also increased oxidative stress levels by decreasing the expression of endothelial nitric oxide synthase and consequently the formation of NO, resulting in endothelial dysfunction (Skogastierna *et al.* 2014). Moreover, in an ischemia and reperfusion (I/R) injury rabbit model, supraphysiological level of testosterone increased fibrosis and oxidative stress and exacerbated such detrimental effects of I/R (Chuang *et al.* 2013), whereas testosterone replacement at the physiological level exerted antioxidative effects by reducing mitochondrial oxidative stress (Pongkan *et al.* 2015; Pintana *et al.* 2015*b*) and serum MDA levels (Pintana *et al.* 2015*b*).

In conclusion, testosterone deprivation did not cause metabolic disturbance, but caused cardiac autonomic imbalance and LV dysfunction due to increased oxidative stress and impaired cardiac mitochondrial function. Obese-insulin resistance caused by long-term consumption of a HFD could lead to metabolic disorders, cardiac autonomic imbalance, and LV dysfunction due to increased oxidative stress and impaired cardiac mitochondrial function. Despite these similar adverse effects on the heart, the findings of this study demonstrated that testosterone deprivation did not aggravate these impairments, but accelerated the development of these impairments in

http://joe.endocrinology-journals.org
DOI: 10.1530/JOE-16-0002
© 2016 Society for Endocrinology
Printed in Great Britain
Published by Bioscientifica Ltd.

Journal of Endocrinology

obese-insulin-resistant rats, the obesity and resulting insulin resistance being caused by consumption of a HFD. These findings may suggest the necessity for early testosterone replacement to ensure cardioprotection in obese-insulin-resistant conditions linked with testosterone deprivation. Further studies are needed to investigate the roles of testosterone replacement therapy under these conditions.

Declaration of interest

The authors declare that there is no conflict of interest that could be perceived as prejudicing the impartiality of the research reported.

Funding

This work was supported by the National Science and Technology Development Agency (NSTDA) Research Chair Grant, Thailand (N C) and grants from the Thailand Research Fund BRG5780016 (S C), the Royal Golden Jubilee Program (N C and W P), the National Research Council Thailand (N C), and the Chiang Mai University Excellent Center Award (N C).

Acknowledgments

The authors thank Aimee Cole, Cicely Proctor, Drs Sirinart Kumfu, and Nattayaporn Apaijai for their editorial and technical assistance.

References

Aon MA, Cortassa S, Akar FG, Brown DA, Zhou L & O'Rourke B 2009 From mitochondrial dynamics to arrhythmias. *International Journal of Biochemistry and Cell Biology* **41** 1940–1948. (doi:10.1016/j.biocel.2009.02.016)

Aoyama N, Asano S, Shingu M, Ueno K, Miyashita M, Hamada H, Aikata H & Kataoka T 2015 Changes in appetite, nutrition, and oxidative stress reaction of cancer patients during chemotherapy. *Gan To Kagaku Ryoho* **42** 961–965.

Apaijai N, Pintana H, Chattipakorn SC & Chattipakorn N 2012 Cardioprotective effects of metformin and vildagliptin in adult rats with insulin resistance induced by a high-fat diet. *Endocrinology* **153** 3878–3885. (doi:10.1210/en.2012-1262)

Apaijai N, Chinda K, Palee S, Chattipakorn S & Chattipakorn N 2014 Combined vildagliptin and metformin exert better cardioprotection than monotherapy against ischemia-reperfusion injury in obese-insulin resistant rats. *PLoS ONE* **9** e102374. (doi:10.1371/journal.pone.0102374)

Appleton DJ, Rand JS & Sunvold GD 2005 Basal plasma insulin and homeostasis model assessment (HOMA) are indicators of insulin sensitivity in cats. *Journal of Feline Medicine and Surgery* **7** 183–193. (doi:10.1016/j.jfms.2004.12.002)

Araujo AB, Esche GR, Kupelian V, O'Donnell AB, Travison TG, Williams RE, Clark RV & McKinlay JB 2007 Prevalence of symptomatic androgen deficiency in men. *Journal of Clinical Endocrinology and Metabolism* **92** 4241–4247. (doi:10.1210/jc.2007-1245)

Baumgartner RN, Waters DL, Morley JE, Patrick P, Montoya GD & Garry PJ 1999 Age-related changes in sex hormones affect the sex difference in serum leptin independently of changes in body fat. *Metabolism* **48** 378–384. (doi:10.1016/S0026-0495(99)90089-6)

Brook RD, Rajagopalan S, Pope CA III, Brook JR, Bhatnagar A, Diez-Roux AV, Holguin F, Hong Y, Luepker RV, Mittleman MA, *et al.* 2010 Particulate matter air pollution and cardiovascular disease: an update to the scientific statement from the American Heart Association. *Circulation* **121** 2331–2378. (doi:10.1161/CIR.0b013e3181dbece1)

Chattipakorn N, Incharoen T, Kanlop N & Chattipakorn S 2007 Heart rate variability in myocardial infarction and heart failure. *International Journal of Cardiology* **120** 289–296. (doi:10.1016/j.ijcard.2006.11.221)

Chinda K, Sanit J, Chattipakorn S & Chattipakorn N 2014 Dipeptidyl peptidase-4 inhibitor reduces infarct size and preserves cardiac function via mitochondrial protection in ischaemia-reperfusion rat heart. *Diabetes & Vascular Disease Research* **11** 75–83. (doi:10.1177/1479164113516134)

Chuang SM, Liu KM, Lee YC, Lin RJ, Chang CY, Wu WJ, Chang WC, Levin RM & Juan YS 2013 Effects of supraphysiological testosterone treatment and orchiectomy on ischemia/reperfusion-induced bladder dysfunction in male rabbits. *Journal of Sexual Medicine* **10** 1278–1290. (doi:10.1111/jsm.12104)

Dhindsa S, Ghanim H, Batra M, Kuhadiya ND, Abuaysheh S, Sandhu S, Green K, Makdissi A, Hejna J, Chaudhuri A, *et al.* 2016 Insulin resistance and inflammation in hypogonadotropic hypogonadism and their reduction after testosterone replacement in men with type 2 diabetes. *Diabetes Care* **39** 82–91. (doi:10.2337/dc15-1518)

Dubois V, Laurent MR, Jardi F, Antonio L, Lemaire K, Goyvaerts L, Deldicque L, Carmeliet G, Decallonne B, Vanderschueren D, *et al.* 2015 Androgen deficiency exacerbates high fat diet-induced metabolic alterations in male mice. *Endocrinology* **157** 648–665. (doi:10.1210/en.2015-1713)

Finck BN & Johnson RW 2002 Anti-inflammatory agents inhibit the induction of leptin by tumor necrosis factor-alpha. *American Journal of Physiology: Regulatory, Integrative and Comparative Physiology* **282** R1429–R1435. (doi:10.1152/ajpregu.00569.2001)

Flegal KM, Carroll MD, Ogden CL & Curtin LR 2010 Prevalence and trends in obesity among US adults, 1999–2008. *JAMA* **303** 235–241. (doi:10.1001/jama.2009.2014)

Foley PL 2005 Common surgical procedures in rodents. In *Laboratory Animal Medicine and Management*. Eds JD Reuter & MA Suckow. Office of Animal Research Education and Compliance, University of Virginia, Charlottesville, VA, USA. Ithaca, NY, USA: International Veterinary Information Service. (available at: www.ivis.org)

Friedewald WT, Levy RI & Fredrickson DS 1972 Estimation of the concentration of low-density lipoprotein cholesterol in plasma, without use of the preparative ultracentrifuge. *Clinical Chemistry* **18** 499–502.

Gandaglia G, Sun M, Popa I, Schiffmann J, Trudeau V, Shariat SF, Trinh QD, Graefen M, Widmer H, Saad F, *et al.* 2015 Cardiovascular mortality in patients with metastatic prostate cancer exposed to androgen deprivation therapy: a population-based study. *Clinical Genitourinary Cancer* **13** e123–e130. (doi:10.1016/j.clgc.2014.12.003)

Garrido P, Salehzadeh F, Duque-Guimaraes DE & Al-Khalili L 2014 Negative regulation of glucose metabolism in human myotubes by supraphysiological doses of 17beta-estradiol or testosterone. *Metabolism* **63** 1178–1187. (doi:10.1016/j.metabol.2014.06.003)

Gentry RT & Wade GN 1976 Androgenic control of food intake and body weight in male rats. *Journal of Comparative and Physiological Psychology* **90** 18–25. (doi:10.1037/h0077264)

Glos M, Romberg D, Fietze I & Penzel T 2007 Heart rate and systolic blood pressure variability before and during obstructive sleep apnea episodes. *Conference Proceedings of the IEEE Engineering in Medicine and Biology Society* 263–266. (doi:10.1109/iembs.2007.4352274)

Grossmann M, Thomas MC, Panagiotopoulos S, Sharpe K, Macisaac RJ, Clarke S, Zajac JD & Jerums G 2008 Low testosterone levels are common and associated with insulin resistance in men with diabetes. *Journal of Clinical Endocrinology and Metabolism* **93** 1834–1840. (doi:10.1210/jc.2007-2177)

Hackett G, Cole N, Bhartia M, Kennedy D, Raju J & Wilkinson P 2014 Testosterone replacement therapy improves metabolic parameters

© 2016 Society for Endocrinology
Printed in Great Britain
Published by Bioscientifica Ltd.

Journal of Endocrinology

in hypogonadal men with type 2 diabetes but not in men with coexisting depression: the BLAST study. *Journal of Sexual Medicine* **11** 840–856. (doi:10.1111/jsm.12404)

Handelsman DJ & Zajac JD 2004 Androgen deficiency and replacement therapy in men. *Medical Journal of Australia* **180** 529–535.

Holmang A & Bjorntorp P 1992 The effects of testosterone on insulin sensitivity in male rats. *Acta Physiologica Scandinavica* **146** 505–510. (doi:10.1111/j.1748-1716.1992.tb09452.x)

Hurley BF, Seals DR, Hagberg JM, Goldberg AC, Ostrove SM, Holloszy JO, Wiest WG & Goldberg AP 1984 High-density-lipoprotein cholesterol in bodybuilders v powerlifters. Negative effects of androgen use. *JAMA* **252** 507–513. (doi:10.1001/jama.1984.03350040037019)

Jankowska EA, Biel B, Majda J, Szklarska A, Lopuszanska M, Medras M, Anker SD, Banasiak W, Poole-Wilson PA & Ponikowski P 2006 Anabolic deficiency in men with chronic heart failure: prevalence and detrimental impact on survival. *Circulation* **114** 1829–1837. (doi:10.1161/CIRCULATIONAHA.106.649426)

Latchman PL, Mathur M, Bartels MN, Axtell RS & De Meersman RE 2011 Impaired autonomic function in normotensive obese children. *Clinical Autonomic Research* **21** 319–323. (doi:10.1007/s10286-011-0116-8)

Li L, Guo CY, Jia EZ, Zhu TB, Wang LS, Cao KJ, Ma WZ & Yang ZJ 2012 Testosterone is negatively associated with the severity of coronary atherosclerosis in men. *Asian Journal of Andrology* **14** 875–878. (doi:10.1038/aja.2012.95)

Marchini T, Magnani N, D'Annunzio V, Tasat D, Gelpi RJ, Alvarez S & Evelson P 2013 Impaired cardiac mitochondrial function and contractile reserve following an acute exposure to environmental particulate matter. *Biochimica et Biophysica Acta* **1830** 2545–2552. (doi:10.1016/j.bbagen.2012.11.012)

Mateos R, Lecumberri E, Ramos S, Goya L & Bravo L 2005 Determination of malondialdehyde (MDA) by high-performance liquid chromatography in serum and liver as a biomarker for oxidative stress. Application to a rat model for hypercholesterolemia and evaluation of the effect of diets rich in phenolic antioxidants from fruits. *Journal of Chromatography B: Analytical Technologies in the Biomedical and Life Sciences* **827** 76–82. (doi:10.1016/j.jchromb.2005.06.035)

McMillen IC, Rattanatray L, Duffield JA, Morrison JL, MacLaughlin SM, Gentili S & Muhlhausler BS 2009 The early origins of later obesity: pathways and mechanisms. *Advances in Experimental Medicine and Biology* **646** 71–81. (doi:10.1007/978-1-4020-9173-5)

Muraleedharan V & Jones TH 2010 Testosterone and the metabolic syndrome. *Therapeutic Advances in Endocrinology and Metabolism* **1** 207–223. (doi:10.1177/2042018810390258)

Oskui PM, French WJ, Herring MJ, Mayeda GS, Burstein S & Kloner RA 2013 Testosterone and the cardiovascular system: a comprehensive review of the clinical literature. *Journal of the American Heart Association* **2** e000272. (doi:10.1161/JAHA.113.000272)

Pintana H, Chattipakorn N & Chattipakorn S 2015*a* Testosterone deficiency, insulin-resistant obesity and cognitive function. *Metabolic Brain Disease* **30** 853–876. (doi:10.1007/s11011-015-9655-3)

Pintana H, Pongkan W, Pratchayasakul W, Chattipakorn N & Chattipakorn SC 2015*b* Testosterone replacement attenuates cognitive decline in testosterone-deprived lean rats, but not in obese rats, by mitigating brain oxidative stress. *Age* **37** 84. (doi:10.1007/s11357-015-9827-4)

Pintana H, Pratchayasakul W, Sa-Nguanmoo P, Pongkan W, Tawinvisan R, Chattipakorn N & Chattipakorn SC 2016 Testosterone deprivation has neither additive nor synergistic effects with obesity on the cognitive impairment in orchiectomized and/or obese male rats. *Metabolism* **65** 54–67. (doi:10.1016/j.metabol.2015.10.015)

Polderman KH, Gooren LJ, Asscheman H, Bakker A & Heine RJ 1994 Induction of insulin resistance by androgens and estrogens. *Journal of Clinical Endocrinology and Metabolism* **79** 265–271. (doi:10.1210/jc.79.1.265)

Pongkan W, Chattipakorn SC & Chattipakorn N 2015 Chronic testosterone replacement exerts cardioprotection against cardiac ischemia-reperfusion injury by attenuating mitochondrial dysfunction in testosterone-deprived rats. *PLoS ONE* **10** e0122503. (doi:10.1371/journal.pone.0122503)

Pratchayasakul W, Kerdphoo S, Petsophonsakul P, Pongchaidecha A, Chattipakorn N & Chattipakorn SC 2011 Effects of high-fat diet on insulin receptor function in rat hippocampus and the level of neuronal corticosterone. *Life Sciences* **88** 619–627. (doi:10.1016/j.lfs.2011.02.003)

Saad F, Yassin A, Doros G & Haider A 2016 Effects of long-term treatment with testosterone on weight and waist size in 411 hypogonadal men with obesity classes I-III: observational data from two registry studies. *International Journal of Obesity* **40** 162–170. (doi:10.1038/ijo.2015.139)

Schenk S, Harber MP, Shrivastava CR, Burant CF & Horowitz JF 2009 Improved insulin sensitivity after weight loss and exercise training is mediated by a reduction in plasma fatty acid mobilization, not enhanced oxidative capacity. *Journal of Physiology* **587** 4949–4961. (doi:10.1113/jphysiol.2009.175489)

Sivasinprasasn S, Sa-Nguanmoo P, Pratchayasakul W, Kumfu S, Chattipakorn SC & Chattipakorn N 2015 Obese-insulin resistance accelerates and aggravates cardiometabolic disorders and cardiac mitochondrial dysfunction in estrogen-deprived female rats. *Age* **37** 28. (doi:10.1007/s11357-015-9766-0)

Skogastierna C, Hotzen M, Rane A & Ekstrom L 2014 A supraphysiological dose of testosterone induces nitric oxide production and oxidative stress. *European Journal of Preventive Cardiology* **21** 1049–1054. (doi:10.1177/2047487313481755)

Taggart HM, Applebaum-Bowden D, Haffner S, Warnick GR, Cheung MC, Albers JJ, Chestnut CH III & Hazzard WR 1982 Reduction in high density lipoproteins by anabolic steroid (stanozolol) therapy for postmenopausal osteoporosis. *Metabolism* **31** 1147–1152. (doi:10.1016/0026-0495(82)90166-4)

Thompson PD, Cullinane EM, Sady SP, Chenevert C, Saritelli AL, Sady MA & Herbert PN 1989 Contrasting effects of testosterone and stanozolol on serum lipoprotein levels. *JAMA* **261** 1165–1168. (doi:10.1001/jama.1989.03420080085036)

Thummasorn S, Kumfu S, Chattipakorn S & Chattipakorn N 2011 Granulocyte-colony stimulating factor attenuates mitochondrial dysfunction induced by oxidative stress in cardiac mitochondria. *Mitochondrion* **11** 457–466. (doi:10.1016/j.mito.2011.01.008)

Tinetti M, Gysel M, Farias J, Ferrer M, Lombardero M & Baranchuk A 2015 Left ventricular filling pressure in male patients with type 2 diabetes and normal versus low total testosterone levels. *Cardiology Journal* **22** 206–211. (doi:10.5603/CJ.a2014.0056)

Vlantis K & Pasparakis M 2010 Role of TNF in pathologies induced by nuclear factor kappaB deficiency. *Current Directions in Autoimmunity* **11** 80–93. (doi:10.1159/000289198)

WHO 2011 *Obesity and Overweight*. Fact sheet N°311. Geneva, Switzerland: World Health Organization. (available at: http://www.who.int/mediacentre/factsheets/fs311/en)

Yasui T, Matsui S, Tani A, Kunimi K, Yamamoto S & Irahara M 2012 Androgen in postmenopausal women. *Journal of Medical Investigation* **59** 12–27. (doi:10.2152/jmi.59.12)

Zorov DB, Juhaszova M & Sollott SJ 2006 Mitochondrial ROS-induced ROS release: an update and review. *Biochimica et Biophysica Acta* **1757** 509–517. (doi:10.1016/j.bbabio.2006.04.029)

Received in final form 23 February 2016
Accepted 17 March 2016
Accepted Preprint published online 21 March 2016

© 2016 Society for Endocrinology
Printed in Great Britain

Published by Bioscientifica Ltd.

Journal of Endocrinology

เอกสารแนบหมายเลข 23

ELSEVIER

Canadian Journal of Cardiology 32 (2016) 1009–1016

Review

Effects of Iron Overload on Cardiac Calcium Regulation: Translational Insights Into Mechanisms and Management of a Global Epidemic

Juthamas Khamseekaew, BSc,[a,b,c] Sirinart Kumfu, PhD,[a,b,c]
Siriporn C. Chattipakorn, DDS, PhD,[a,c,d] and Nipon Chattipakorn, MD, PhD[a,b,c]

[a] *Cardiac Electrophysiology Research and Training Center, Faculty of Medicine, Chiang Mai University, Chiang Mai, Thailand*

[b] *Cardiac Electrophysiology Unit, Department of Physiology, Faculty of Medicine, Chiang Mai University, Chiang Mai, Thailand*

[c] *Center of Excellence in Cardiac Electrophysiology Research, Chiang Mai University, Chiang Mai, Thailand*

[d] *Department of Oral Biology and Diagnostic Sciences, Faculty of Dentistry, Chiang Mai University, Chiang Mai, Thailand*

See editorial by Oudit and Backx, pages 938–940 of this issue.

ABSTRACT

Iron overload cardiomyopathy occurs in a rare primary form (ie, hemochromatosis) and a very common secondary form in a host of hemoglobinopathies (eg, thalassemia, sickle cell anemia) of substantial and growing global prevalence, which have transformed iron overload cardiomyopathy into a worldwide epidemic. Intracellular calcium ($[Ca^{2+}]_i$) is known to be a critical regulator of myocardial function, in which it plays a key role in maintaining cardiac excitation-contraction coupling. It has been proposed that a disturbance in cardiac calcium regulation is a major contributor to left ventricular dysfunction in iron overload cardiomyopathy. This review comprehensively summarizes reports concerned with the effects of iron overload on cardiac calcium regulation, including alteration in the intracellular calcium level, voltage-gated calcium channel function, and calcium cycling protein activity. Consistent reports, as well as inconsistent findings, from both *in vitro* and *in vivo* studies, are presented and discussed. The understanding of these mechanisms has provided important new pathophysiological insights and has led to the development of novel therapeutic and preventive strategies for patients with iron overload cardiomyopathy that are currently in clinical trials.

RÉSUMÉ

La cardiomyopathie par surcharge en fer se manifeste sous une forme primitive rare (c.-à-d. l'hémochromatose) et une forme secondaire très fréquente chez un porteur d'hémoglobinopathies (p. ex. la thalassémie, la dépranocytose) de prévalence substantielle et croissante à l'échelle mondiale, qui ont transformé la cardiomyopathie par surcharge en fer en une épidémie mondiale. Le calcium intracellulaire ($[Ca^{2+}]_i$) est connu comme étant un régulateur essentiel à la fonction du myocarde au sein duquel il joue un rôle clé dans le maintien du couplage de l'excitation et de la contraction du cœur. Il a été suggéré que la perturbation de la régulation des canaux calciques cardiaques contribue grandement à la dysfonction du ventricule gauche lors de cardiomyopathie par surcharge en fer. Cette revue résume de manière exhaustive les publications concernées par les effets de la surcharge en fer sur la régulation des canaux calciques cardiaques, y compris l'altération de la concentration en calcium intracellulaire, du fonctionnement d'un canal calcique sensible à la tension et de l'activité des protéines du cycle du calcium. Nous présentons et discutons des rapports concordants ainsi que des conclusions contradictoires des études *in vitro* et *in vivo*. La compréhension de ces mécanismes a fourni un nouvel aperçu important sur la physiopathologie et a mené au développement de nouvelles stratégies préventives et thérapeutiques pour les patients souffrant d'une cardiomyopathie par surcharge en fer qui font actuellement l'objet d'essais cliniques.

Iron overload is associated with primary hemochromatosis and secondary iron overload conditions, such as thalassemia and sickle cell anemia, and are among the most frequently inherited disorders worldwide.[1–8] The prevalence and global clinical burden of iron overload is increasing in epidemic proportions.[4,6,9] Iron overload cardiomyopathy is the most common cause of mortality in patients with secondary iron overload and is a major comorbidity in patients with primary hemochromatosis.[4,5,10–13] Primary iron overload is an inherited disorder in which there are mutations in several iron regulatory genes. It is characterized by inappropriately low levels of hepcidin, which results in increased gastrointestinal (GI) iron absorption, which eventually leads to iron overload.[14] Secondary iron overload occurs primarily in patients

Received for publication August 7, 2015. Accepted October 15, 2015.

Corresponding author: Dr Nipon Chattipakorn, Cardiac Electrophysiology Research and Training Center, Faculty of Medicine, Chiang Mai University, Chiang Mai, 50200, Thailand. Tel.: +66-53-945-329; fax: +66-53-945-368.

E-mail: nchattip@gmail.com

See page 1015 for disclosure information.

http://dx.doi.org/10.1016/j.cjca.2015.10.012

0828-282X/© 2016 Canadian Cardiovascular Society. Published by Elsevier Inc. All rights reserved.

with hereditary hemoglobinopathies, especially in cases of β-thalassemia,[15,16] which is a common genetic disease that is characterized by abnormalities in the synthesis of the β-globin chains of hemoglobin that results in ineffective erythropoiesis and severe hemolytic anemia.[15,16] Patients with β-thalassemia require regular blood transfusions because of this severe anemia.[16] Furthermore, ineffective erythropoiesis and tissue hypoxia in patients with β-thalassemia directly causes the downregulation of hepcidin expression, which leads to increased GI iron absorption.[17] The combination of regular blood transfusions, increased GI iron absorption, and the lack of effective iron excretory pathways subsequently leads to excessive iron accumulation and secondary iron overload.[15,16,18] Increased plasma iron levels can lead to iron deposition in many organs, including the heart, which may result in the condition known as iron overload cardiomyopathy.[19] This condition is an important cause of morbidity and mortality in patients with β-thalassemia because of the occurrence of left ventricular dysfunction, arrhythmia, and heart failure.[16,20,21] One mechanism that is believed to contribute to iron overload cardiomyopathy is a disturbance in cardiac calcium regulation.[22]

Cardiac excitation-contraction coupling is the essential process to maintain normal cardiac function. This process is a converting of electrical excitation into a contractile response of the heart, which is mediated by calcium (Ca^{2+}). Ca^{2+} entry into the cardiomyocyte through the L-type Ca^{2+} channels (LTCCs) at the sarcolemma initiates the release of Ca^{2+} from the sarcoplasmic reticulum (SR), causing a marked elevation of intracellular Ca^{2+} and leading to the contractile response of the myofilaments in the heart. Myocardial relaxation occurs through the separation of Ca^{2+} from myofilaments, when Ca^{2+} is taken up again into the SR and moved out into the extracellular space. Therefore, Ca^{2+} is crucial for maintaining cardiac contraction and relaxation in this process.[23,24] The regulation of cardiac calcium levels is closely associated with both the calcium current through voltage-gated L-type Ca^{2+} channels ($I_{Ca,L}$), and the activity of calcium cycling proteins.[25] The machinery of cardiac calcium regulation is displayed in Figure 1A. This mechanism is initiated by the depolarization of the cell membrane, which leads to the opening of voltage-gated LTCCs. When the LTCCs are opened, there is Ca^{2+} influx into the cytosol. Ca^{2+} then binds to ryanodine receptors (RyRs) in the SR, leading to Ca^{2+} release from the SR. This process is termed "Ca^{2+}-induced Ca^{2+} release," allowing a large amount of Ca^{2+} to be released, which leads to myofilament activation and contraction.

The force of cardiac contraction is mainly dependent on the kinetics and amplitude of the Ca^{2+} release, which is known as "the peak of Ca^{2+} transient." Ca^{2+} transient is the cytoplasmic Ca^{2+} accumulation that is measured during each cycle of the cardiac action potential.[24,25] During relaxation, Ca^{2+} is taken back up into the SR by the SR Ca^{2+} adenosine triphosphatase pump (SERCA) and moved out into the extracellular fluid, primarily by the sarcolemmal Na^{+}-Ca^{2+} exchanger (NCX). Moreover, small amounts of intracellular Ca^{2+} are extruded through the plasma membrane Ca^{2+}-adenosine triphosphatase (ATPase) pump and the mitochondrial calcium uniporter.[26] Abnormal alterations in the cardiac calcium regulation can lead to cardiac dysfunction.[25]

Under physiological conditions, iron binds to plasma transferrin, thus leaving no free form of iron (toxic form) in the circulation. Under iron overload conditions, transferrin becomes saturated, which leads to increased non–transferrin-bound iron (NTBI) levels in the circulation.[17,19] The effects of iron overload conditions on cardiac calcium regulation are illustrated in Figure 1B. It has been shown that ferrous iron (Fe^{2+}) can enter cardiomyocytes through the LTCCs.[22,27,28] Our previous studies demonstrated that T-type calcium channels (TTCCs) re-expressed in the cardiomyocytes of thalassemic mice played an important role in Fe^{2+} entry into cardiomyocytes under iron overload conditions.[29-31] Excess uptake of NTBI leads to the expansion of the labile intracellular iron pool as well as the formation of highly toxic reactive oxygen species (ROS), which are produced through the Fenton-catalyzed Haber-Weiss reaction and result in increased oxidative stress in the cells.[32] The oxidative stress can cause damage to lipids, cellular proteins, and nucleic acids,[33,34] which in turn can affect cardiac calcium regulation (Fig. 1B). However, data on the alteration of calcium regulation resulting from iron overload remain scarce and controversial. In this review, both *in vitro* and *in vivo* reports regarding the effects of iron overload on cardiac calcium levels, voltage-gated calcium channel function, and calcium cycling proteins are comprehensively summarized and discussed. Consistent findings, as well as controversial results, are presented, focusing on the effects of iron overload on the regulation of calcium in the heart.

Effects of Iron Overload on Intracellular Calcium Levels

A summary of the evidence pertinent to the effects of iron overload on cardiac contractile dysfunction resulting from the alteration of intracellular Ca^{2+} levels ($[Ca^{2+}]_i$) is shown in Table 1 (see Supplemental Table S1 for further details). Intracellular free iron has been shown to promote the formation of ROS,[32,39] which have been implicated as important factors in the pathogenesis of cellular injury, including $[Ca^{2+}]_i$ regulation in the heart under conditions of iron overload.[35,37] Nakamura et al.[35] reported that the reaction between H_2O_2 and intracellular iron increased $[Ca^{2+}]_i$ and impaired contractility in cultured fetal mice cardiomyocytes. This impairment in contractile function was aggravated by iron loading and attenuated by the impermeable iron chelator deferoxamine (DFO). Similarly, Horackova et al.[36] reported that the reaction between H_2O_2 and intracellular iron could alter the Ca^{2+} transient in a time-dependent manner and increase resting $[Ca^{2+}]_i$ in freshly isolated and cultured cardiomyocytes. These effects were reported to lead to a disturbance in contractile function and cause arrhythmia. After extended exposure to H_2O_2, the Ca^{2+} transient disappeared, whereas the diastolic $[Ca^{2+}]_i$ increased further, and the cells became inexcitable and finally stopped contracting.[36] These adverse effects were attenuated by DFO but completely suppressed by the permeable iron chelator salicylaldehyde isonicotinoyl hydrazone (SIH).[36] These findings suggested that intracellular free iron–mediated free radicals, generated after H_2O_2 exposure, could increase $[Ca^{2+}]_i$ and lead to contractile dysfunction and arrhythmia.[35,36]

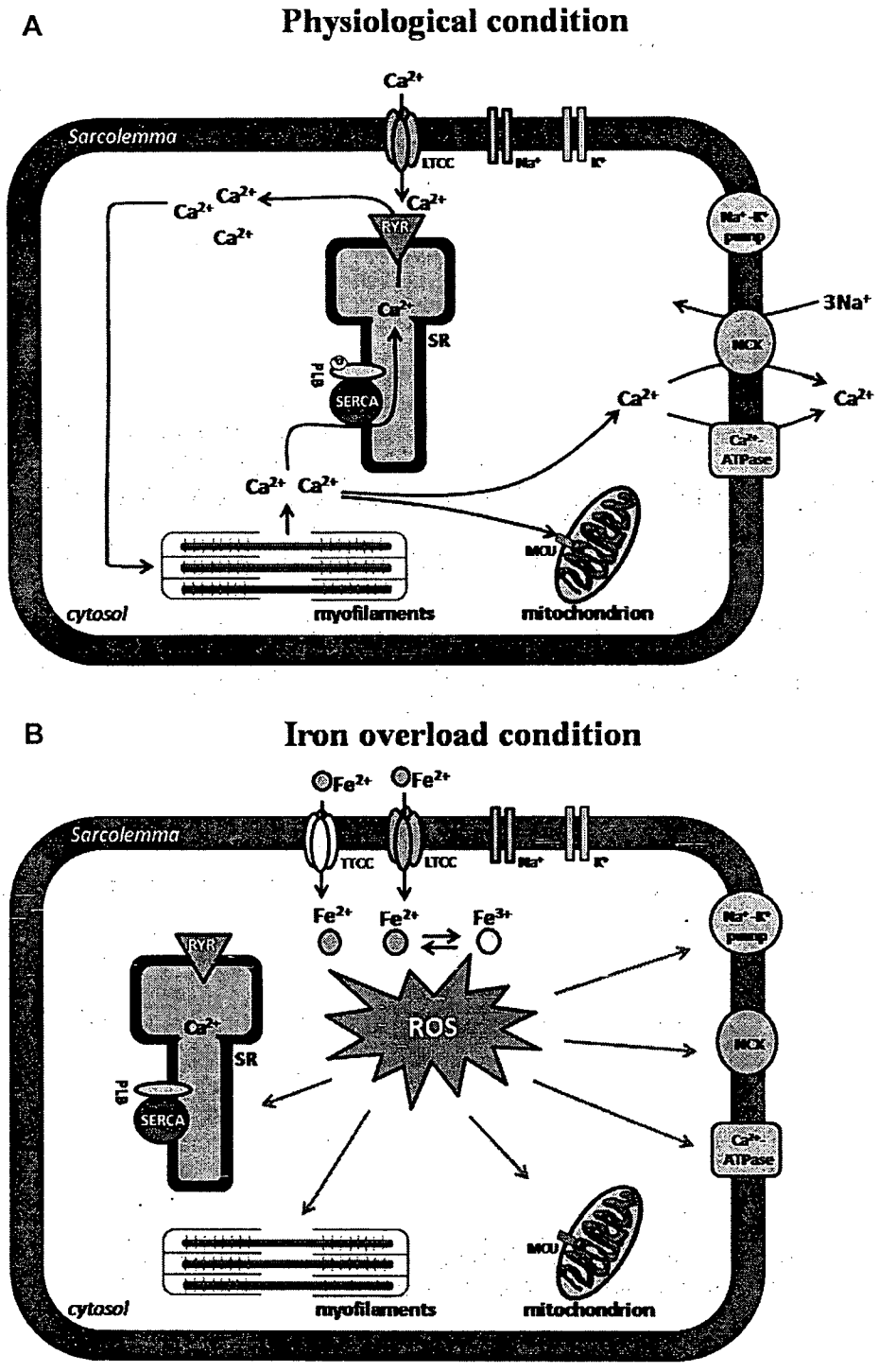


Figure 1. The proteins and mechanisms that are involved in the regulation of cardiac calcium. (**A**) Normal physiological conditions. (**B**) Iron overload conditions. K^+, potassium channel; LTCC, L-type calcium channel; MCU; mitochondrial calcium uniporter; Na^+, sodium channel; NCX, Na^+- Ca^{2+} exchanger; PLB, phospholamban; ROS, reactive oxygen species; RYR, ryanodine receptor; SERCA, sarcoplasmic reticulum Ca^{2+}-ATPase; TTCC, T-type calcium channel.

In Langendorff-perfused rabbit hearts, iron-mediated free radicals caused the inhibition of glycolysis and an increase in sugar phosphate accumulation, leading to partial depletion of adenosine triphosphate (ATP).[37] During the iron-mediated free radical infusion, Ca^{2+} transient and diastolic $[Ca^{2+}]_i$ were increased. These findings suggest that elevated diastolic $[Ca^{2+}]_i$ levels may result from the depletion of ATP.[37] In an iron-loading mice model, the elevation of cardiac iron

Table 1. Effects of iron overload on intracellular Ca^{2+} levels

Model	Intervention	Interpretation	Reference
Cultured fetal mouse cardiac myocytes	Cells were incubated with H_2O_2 and pretreated with DFO	Intracellular iron toxicity increased $[Ca^{2+}]_i$, leading to contractile dysfunction	Nakamura et al.[35]
Freshly isolated and cultured adult guinea pig ventricular cardiomyocytes	Cells were incubated with H_2O_2 and pretreated with SIH or DFO	Intracellular iron toxicity altered Ca^{2+} transient in a time-dependent manner and increased resting $[Ca^{2+}]_i$	Horackova et al.[36]
Isolated perfused Langendorff rabbit heart	Heart was perfused with iron and H_2O_2	Iron toxicity increased $[Ca^{2+}]_i$	Corretti et al.[37]
Hemojuvelin knockout mice	Iron-loaded mice were treated with verapamil	Cardiac iron accumulation showed a correlation with cardiac calcium concentration	Otto-Duesselet al.[38]

$[Ca^{2+}]_i$, intracellular Ca^{2+} level; DFO, deferoxamine; SIH, salicylaldehyde isonicotinoyl hydrazone.

concentration has been shown to have a positive correlation with cardiac calcium concentration.[38] Treatment with verapamil, a LTCC blocker, decreased both cardiac calcium and iron levels,[38] which may contribute to the improvement in cardiac function as observed in iron overload in verapamil-treated mice.[22] These findings indicate that intracellular iron-mediated free radicals could increase cardiac $[Ca^{2+}]_i$. The elevation of $[Ca^{2+}]_i$ causes impaired contractility, leading to cardiac dysfunction. These effects are illustrated in Figure 2.

Effects of Iron Overload on Cardiac Voltage-Gated Calcium Channel Function

Under conditions of iron overload, it has been shown that Fe^{2+} enters into the thalassemic cardiomyocytes through LTCCs and TTCCs,[22,27-30] which may affect their conductance. Available reports regarding the effects of iron overload on cardiac voltage-gated calcium channel function in cardiomyocytes are summarized in Table 2 (see Supplemental Table S2 for further details). It has been shown that low concentrations (250 μM) of Fe^{2+} slowed the rate of $I_{Ca,L}$ inactivation but did not alter the peak $I_{Ca,L}$.[28] However, at 500 μM of Fe^{2+}, the peak $I_{Ca,L}$ was increased. Higher concentrations of Fe^{2+} reduced the peak $I_{Ca,L}$ and slowed the current decay of $I_{Ca,L}$ in a dose-dependent manner.[28] Thus, the slowing of the inactivation of LTCCs might increase the net Ca^{2+} and Fe^{2+} influx, despite the reduction in the peak current.[28] It has been postulated that Fe^{2+}-induced slowing of LTCC inactivation, as well as the current decay, might result from the competition between Fe^{2+} and Ca^{2+} for the Ca^{2+} binding sites of Ca^{2+}-mediated inactivation of LTCCs, which has been observed in neurons.[43,44] These effects have been

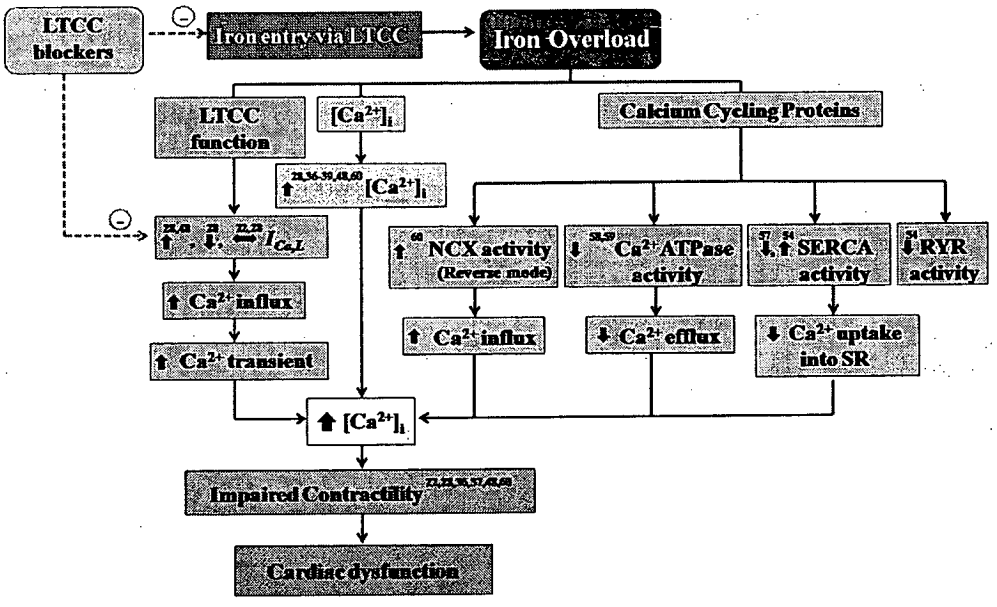


Figure 2. The effects of iron overload and LTCC blockers on cardiac calcium regulation under iron overload conditions. Iron overload affects the regulation of cardiac calcium, which alters LTCC function and calcium current through this channel, $[Ca^{2+}]_i$ and calcium cycling proteins, leading to cardiac dysfunction. LTCC blockers inhibit I_{Ca}, and iron entry into the cardiomyocytes, leading to a reduction of iron overload and potentially preserved cardiac calcium regulation under iron overload conditions. $[Ca^{2+}]_i$, intracellular calcium level; $I_{Ca,L}$, calcium current through voltage-gated L-type Ca^{2+} channels; LTCC, L-type calcium channel; NCX, Na^+-Ca^{2+} exchanger; RYR, ryanodine receptor; SERCA, sarcoplasmic reticulum Ca^{2+}-ATPase; SR; sarcoplasmic reticulum.

Table 2. Effects of iron overload on cardiac voltage-gated calcium channel function

Model	Intervention	Interpretation	Reference
Isolated male B6D2F1 mouse cardiomyocytes	Iron-loaded mice	Iron toxicity did not alter $I_{Ca,L}$	Oudit et al.[22]
Isolated Sprague-Dawley rat ventricular myocytes	Cells were incubated with iron	Fe^{2+} slowed $I_{Ca,L}$ inactivation, leading to $[Ca^{2+}]_i$ and Fe^{2+} overload	Tsushima et al.[23]
Isolated mouse SA node and right atrial myocytes	Iron-loaded mice	Iron toxicity reduced $I_{Ca,L}$ of SA node, leading to bradycardia	Rose et al.[40]
Isolated adult male Wistar rat ventricular myocytes	Cells were incubated with iron and H_2O_2, and pretreated with nitrendipine	Iron toxicity increased Ca^{2+} transient, leading to contractile dysfunction	Josephson et al.[41]
Cultured neonatal rat cardiomyocyte	Iron-loaded cells were incubated with iron	Extracellular Ca^{2+} increased Fe^{2+} uptake under iron overload conditions	Parkes et al.[42]

$I_{Ca,L}$, Ca^{2+} current through L-type calcium channel; $[Ca^{2+}]_i$, intracellular Ca^{2+} level; SA, sinoatrial.

shown to lead to an increase in Ca^{2+} and Fe^{2+} entry into the cardiomyocytes, resulting in calcium and iron overload, contributing to impaired diastolic function,[28,45] as observed during the early stages of iron overload.[46]

In contrast to *in vitro* studies, in iron-loaded mice with increased cardiac iron accumulation, it has been shown that the gating kinetic properties of LTCCs in these iron-loaded cardiomyocytes were not altered.[22] The application of verapamil reduced the peak $I_{Ca,L}$ and Ca^{2+} influx and also attenuated cardiac iron accumulation.[22] Indeed, a transferrin iron transport system is regulated in a negative-feedback manner by the iron-responsive element/iron-regulatory protein (IRE/IRP) system.[33,47] Iron transporter proteins, including divalent metal transporter 1 (DMT1) and transferrin receptor 1 (Tfr1), as well as the iron storage protein ferritin, contain IREs in their mRNA that are bound by IRPs. The IRE/IRP system is responsive to changes in cellular iron. When intracellular iron was increased, this system could downregulate the expression of DMT1 and Tfr1 and could upregulate ferritin. These processes can lead to a decrease in excess intracellular iron, returning it to normal levels. The study carried out by Oudit et al.[22] demonstrated that iron-mediated uptake through the LTCCs is not controlled by a negative feedback mechanism, which is consistent with the absence of IREs in LTCCs.[28] The LTCC subunit that is highly expressed in the sinoatrial node is the $Ca_V1.3$ subunit.[48] A previous study in iron-loaded mice showed that chronic iron overload could reduce $Ca_V1.3$ mRNA levels and $Ca_V1.3$-mediated $I_{Ca,L}$ density, resulting in bradycardia and a slowing of electrical conduction.[40] These findings were also observed in patients with β-thalassemia with iron overload cardiomyopathy.[49]

Iron-mediated free radicals also affect calcium regulation in the heart. It has been shown that these free radicals could increase the Ca^{2+} transient and intracellular systolic Ca^{2+} levels and could also increase diastolic Ca^{2+} levels, which may contribute to cardiac contractile dysfunction.[41] The calcium overload in this condition occurred without membrane leakage and ATP depletion, but occurred after increased Ca^{2+} influx through the LTCCs, which could be prevented by the sarcolemmal calcium channel blocker nitrendipine.[41] However, the early work of Parkes et al.[42] argued, based on cultured neonatal rat myocytes, that LTCCs are not major pathways for iron entry in conditions of high iron, yet subsequent animal studies showed otherwise.[22] It is possible that neonatal myocytes have much smaller LTCC currents compared with the adult myocardium with physiological function.[50,51] However, this hypothesis needs to be tested in the future.

Hypocalcemia has been reported as a late complication of iron overload in patients with β-thalassemia that occurs after iron-induced hypoparathyroidism.[49,52,53] It has been shown that hypocalcemia could cause reduced systolic and elevated diastolic function, leading to cardiac contractile dysfunction and heart failure.[16,20,54] However, it is still unclear at this time whether the mechanism of iron overload increases, decreases, or has no effect on the peak $I_{Ca,L}$ (Fig. 2). The disparity in these findings may result from differences in the models used and the concentration of iron exposure. Surprisingly, the results from these experiments consistently showed increased Ca^{2+} influx, despite no changes in the peak $I_{Ca,L}$. The elevation of Ca^{2+} influx leads to an increase in the Ca^{2+} transient and $[Ca^{2+}]_i$, which contributes to the impairment in the cardiac contractile function. This impairment can cause cardiac dysfunction, as observed in iron overload cardiomyopathy.

Effects of Iron Overload on Calcium Cycling Proteins

Under conditions of iron overload, iron toxicity is expected to have direct and indirect effects on cardiac calcium cycling proteins including RYRs, the SERCA, sarcolemmal Ca^{2+}-ATPase, and NCX function. A summary of these reports is shown in Table 3 (see Supplemental Table S3 for further details). Fe^{2+} can effectively compete with Ca^{2+} at the binding sites of RYRs, which are known as the ryanodine-sensitive Ca^{2+} channels.[55] However, the occupation of these high-affinity sites by Fe^{2+} fails to activate the RYRs and leads to a reduction in the Ca^{2+}-induced Ca^{2+}-release mechanism from the SR.[56] Moreover, Fe^{2+} increases the rate of active Ca^{2+} uptake into SR vesicles.[54] These effects may result in less calcium being available for cardiac excitation-contraction coupling and lead to impaired cardiac contractility.

Elevated oxidative stress in cardiac SR vesicles induced by isoproterenol or H_2O_2 has been shown to increase SR Ca^{2+} leakage through the RYRs.[59,60] Moreover, free radicals that were generated by conditions of iron overload had a direct effect on decreasing cardiac SERCA activity by directly

attacking the ATP binding site.[55] The occupation of the active site by ATP was found to protect against the loss of SERCA activity and SR Ca^{2+} transport.[55] Similarly, iron-mediated free radicals altered sarcolemmal sulfhydryl groups and led to a reduction in ATP-dependent Ca^{2+} accumulation and sarcolemmal Ca^{2+}-ATPase activity.[56,57] These effects caused a decrease in Ca^{2+} efflux through this channel, which may aggravate diastolic Ca^{2+} overload under iron overload conditions.

The NCX has been shown to be affected by iron-mediated free radicals.[58] The *in vitro* study by Zeitz et al.[58] demonstrated that myofilament alterations and increases in diastolic forces were observed after exposure to iron-mediated free radicals. It was also shown that KB-R7943, a selective inhibitor of the reverse mode of NCX, could prevent these effects. It was suggested that iron-mediated free radicals increased Ca^{2+} influx through the reverse mode of NCX and led to acute diastolic dysfunction. The elevation of the reverse mode of NCX can occur after alterations in sarcolemmal Na^+/K^+-ATPase activity in an iron-overloaded heart.[58,61] Because of impaired Na^+/K^+-ATPase activity, intracellular Na^+ was increased, which led to a shift in the Na^+ efflux through the NCX, resulting in Ca^{2+} influx through these channels. The Ca^{2+} influx may persist because of the impaired Ca^{2+} extrusion caused by the iron-inhibited sarcolemmal Ca^{2+} pump activity and may lead to cardiac dysfunction and arrhythmia.[56]

The effects of iron overload on the activity of calcium cycling proteins are summarized and illustrated in Figure 2. Iron can directly inhibit RYR activity and increase SERCA activity, leading to a decrease in $[Ca^{2+}]_i$. Conversely, iron-mediated free radicals also affect the activity of calcium cycling proteins by increasing the reverse mode of NCX activity, inhibiting Ca^{2+}-ATPase and SERCA activity, and increasing oxidative stress, resulting in increased Ca^{2+} leakage through the RYRs. This can lead to the elevation of $[Ca^{2+}]_i$ in cardiomyocytes. The contradictions in these findings may be the result of differences in the mechanisms of iron that affect the calcium cycling proteins, including the competition between iron and Ca^{2+} at the Ca^{2+}-binding site, the inhibition of ATPase activity by iron, and iron-mediated free radical production leading to lipid peroxidation and membrane destruction. Despite these contradictory results, the majority of reports show that disturbances in the activity of calcium cycling proteins, which play a role in the maintenance of the cardiac calcium regulation, can lead to an elevation of $[Ca^{2+}]_i$. These mechanisms could be responsible for the impairment in contractility and cardiac dysfunction as observed in iron overload cardiomyopathy.

Conclusions

Cardiac calcium regulation altered by conditions of iron overload plays an important role in impaired cardiac contractile function in iron overload cardiomyopathy. The effects of iron overload on cardiac calcium regulation occur through various pathways that cause the disturbance in $[Ca^{2+}]_i$, voltage-gated calcium channel function, and the activity of calcium cycling proteins, which ultimately lead to increases in $[Ca^{2+}]_i$. The elevation of $[Ca^{2+}]_i$ causes alterations in the contraction-relaxation cycle of the heart and leads to contractile dysfunction in iron overload cardiomyopathy.

Clinical Perspective

The beneficial effects of LTCC blockers that act to prevent iron toxicity in the heart have been investigated in several clinical trials. An early pilot trial showed that LTCC blockers (such as amlodipine) combined with standard chelation therapy effectively reduced iron accumulation in the heart as determined by cardiac T2* values.[62] A case report demonstrated that verapamil combined with standard chelation therapy improved left ventricular function in the early stage of iron overload cardiomyopathy.[63] Moreover, 3 ongoing trials investigating the effects of amlodipine combined with standard chelation therapy have progressed to phase II/III clinical trials, which are currently ongoing.[64-67] Findings from these trials will provide useful information regarding the clinical benefits of LTCC blockers in preventing iron overload cardiomyopathy. In addition, the LTCC blockers have been to shown to have protective effects on iron-induced neurotoxicity. Previous studies demonstrated that nicardipine could protect hippocampal and nigral neurons against neurotoxic effects of iron and that nifedipine could suppress iron-induced toxicity in dopaminergic neurons.[68,69] Because the heart is also regulated and modulated by neuronal activity, these protective effects of LTCC blockers on iron-induced neurotoxicity may also provide benefits of cardioprotection as well. Future studies are needed to investigate this relationship.

Table 3. Effects of iron overload on calcium cycling proteins

Model	Intervention	Interpretation	Reference
Rat cardiac SR vesicle	SR vesicles were incubated with iron	Fe^{2+} competed with Ca^{2+} on the RYR, leading to decrease in Ca^{2+} release	Kim et al.[54]
Rabbit cardiomyocytes SR vesicles	SR vesicles were incubated with iron and H_2O_2, and pretreated with ATP	Iron toxicity inhibited SERCA activity	Xu et al.[55]
Isolated rat heart sarcolemmal membranes	Sarcolemmal membranes were incubated with iron and H_2O_2	Iron toxicity depressed Ca^{2+}-ATPase activity	Kaneko et al.[56]
Isolated rat heart sarcolemmal membranes	Sarcolemmal membranes were incubated with iron and H_2O_2	Iron toxicity decreased Ca^{2+}-ATPase activity	Kaneko et al.[57]
Intact contracting Chinchilla bastard rabbits cardiac trabeculae	Cells were incubated with iron and H_2O_2 and treated with KB-R7943	Iron toxicity increased Ca^{2+} influx through the reverse mode of the Na^+-Ca^{2+} exchanger	Zeitz et al.[58]

ATP, adenosine triphosphate; ATPase, adenosine triphosphatase; KB-R7943, a selective inhibitor of the reverse mode of the sodium-calcium exchanger; RYR, ryanodine receptor; SERCA, sarcoplasmic reticulum Ca^{2+}-ATPase; SR, sarcoplasmic reticulum.

Funding Sources

This work was supported by grants from the NSTDA Research Chair Grant from the National Science and Technology Development Agency Thailand (N.C.), the Thailand Research Fund BRG5780016 (S.C.), TRG5780002 (S.K.), the TRF Royal Golden Jubilee PhD Program (N.C. and J.K.), and Chiang Mai University Center of Excellence Award (N.C.).

Disclosures

The authors have no conflicts of interest to disclose.

References

1. Barton JC, Bertoli LF. Hemochromatosis: the genetic disorder of the twenty-first century. Nat Med 1996;2:394-5.
2. Andrews NC. Disorders of iron metabolism. N Engl J Med 1999;341: 1986-95.
3. Fleming RE, Ponka P. Iron overload in human disease. N Engl J Med 2012;366:348-59.
4. Murphy CJ, Oudit GY. Iron-overload cardiomyopathy: pathophysiology, diagnosis, and treatment. J Card Fail 2010;16:888-900.
5. Pennell DJ, Udelson JE, Arai AE, et al. Cardiovascular function and treatment in beta-thalassemia major: a consensus statement from the American Heart Association. Circulation 2013;128:281-308.
6. Weatherall DJ, Clegg JB. Thalassemia—a global public health problem. Nat Med 1996;2:847-9.
7. Weatherall DJ, Clegg JB. Inherited haemoglobin disorders: an increasing global health problem. Bull WHO 2001;79:704-12.
8. Piel FB, Weatherall DJ. The alpha-thalassemias. N Engl J Med 2014;371:1908-16.
9. Felker GM, Thompson RE, Hare JM, et al. Underlying causes and long-term survival in patients with initially unexplained cardiomyopathy. N Engl J Med 2000;342:1077-84.
10. Olivieri NF, Nathan DG, MacMillan JH, et al. Survival in medically treated patients with homozygous beta-thalassemia. N Engl J Med 1994;331:574-8.
11. Allen KJ, Gurrin LC, Constantine CC, et al. Iron-overload-related disease in HFE hereditary hemochromatosis. N Engl J Med 2008;358: 221-30.
12. Olynyk JK, Cullen DJ, Aquilia S, et al. A population-based study of the clinical expression of the hemochromatosis gene. N Engl J Med 1999;341:718-24.
13. Brittenham GM, Griffith PM, Nienhuis AW, et al. Efficacy of deferoxamine in preventing complications of iron overload in patients with thalassemia major. N Engl J Med 1994;331:567-73.
14. Pietrangelo A. Hereditary hemochromatosis—a new look at an old disease. N Engl J Med 2004;350:2383-97.
15. Galanello R, Origa R. Beta-thalassemia. Orphanet J Rare Dis 2010;5:11.
16. Olivieri NF. The beta-thalassemias. N Engl J Med 1999;341:99-109.
17. Siddique A, Kowdley KV. Review article: the iron overload syndromes. Aliment Pharmacol Ther 2012;35:876-93.
18. Hershko C. Pathogenesis and management of iron toxicity in thalassemia. Ann NY Acad Sci 2010;1202:1-9.
19. Breuer W, Hershko C, Cabantchik ZI. The importance of non-transferrin bound iron in disorders of iron metabolism. Transfus Sci 2000;23:185-92.
20. Wood JC, Enriquez C, Ghugre N, et al. Physiology and pathophysiology of iron cardiomyopathy in thalassemia. Ann NY Acad Sci 2005;1054: 386-95.
21. Gujja P, Rosing DR, Tripodi DJ, et al. Iron overload cardiomyopathy: better understanding of an increasing disorder. J Am Coll Cardiol 2010;56:1001-12.
22. Oudit GY, Sun H, Trivieri MG, et al. L-type Ca2 + channels provide a major pathway for iron entry into cardiomyocytes in iron overload cardiomyopathy. Nat Med 2003;9:1187-94.
23. Richard S, Perrier E, Fauconnier J, et al. 'Ca(2+)-induced Ca(2+) entry' or how the L-type Ca(2+) channel remodels its own signalling pathway in cardiac cells. Prog Biophys Mol Biol 2006;90:118-35.
24. Bers DM. Cardiac excitation-contraction coupling. Nature 2002;415: 198-205.
25. Barry WH, Bridge JH. Intracellular calcium homeostasis in cardiac myocytes. Circulation 1993;87:1806-15.
26. Louch WE, Stokke MK, Sjaastad I, et al. No rest for the weary: diastolic calcium homeostasis in the normal and failing myocardium. Physiology 2012;27:308-23.
27. Oudit GY, Trivieri MG, Khaper N, et al. Role of L-type Ca2+ channels in iron transport and iron overload cardiomyopathy. J Mol Med 2006;84:349-64.
28. Tsushima RG, Wickenden AD, Bouchard RA, et al. Modulation of iron uptake in heart by L-type Ca2 + channel modifiers: possible implications in iron overload. Circ Res 1999;84:1302-9.
29. Kumfu S, Chattipakorn S, Srichairatanakool S, et al. T-type calcium channel as a portal of iron uptake into cardiomyocytes of beta-thalassemic mice. Eur J Haematol 2011;86:156-66.
30. Kumfu S, Chattipakorn S, Chinda K, et al. T-type calcium channel blockade improves survival and cardiovascular function in thalassemic mice. Eur J Haematol 2012;88:535-48.
31. Kumfu S, Chattipakorn S, Fucharoen S, et al. Ferric iron uptake into cardiomyocytes of beta-thalassemic mice is not through calcium channels. Drug Chem Toxicol 2013;36:329-34.
32. Eaton JW, Qian M. Molecular bases of cellular iron toxicity. Free Radic Biol Med 2002;32:833-40.
33. Hentze MW, Muckenthaler MU, Andrews NC. Balancing acts: molecular control of mammalian iron metabolism. Cell 2004;117:285-97.
34. Gutteridge JM, Rowley DA, Griffiths E, et al. Low-molecular-weight iron complexes and oxygen radical reactions in idiopathic haemochromatosis. Clin Sci 1985;68:463-7.
35. Nakamura TY, Goda K, Okamoto T, et al. Contractile and morphological impairment of cultured fetal mouse myocytes induced by oxygen radicals and oxidants. Correlation with intracellular Ca2+ concentration. Circ Res 1993;73:758-70.
36. Horackova M, Ponka P, Byczko Z. The antioxidant effects of a novel iron chelator salicylaldehyde isonicotinoyl hydrazone in the prevention of H(2)O(2) injury in adult cardiomyocytes. Cardiovasc Res 2000;47: 529-36.
37. Corretti MC, Koretsune Y, Kusuoka H, et al. Glycolytic inhibition and calcium overload as consequences of exogenously generated free radicals in rabbit hearts. J Clin Invest 1991;88:1014-25.

38. Otto-Duessel M, Brewer C, Wood JC. Interdependence of cardiac iron and calcium in a murine model of iron overload. Transl Res 2011;157: 92-9.

39. Thompson JA, Hess ML. The oxygen free radical system: a fundamental mechanism in the production of myocardial necrosis. Prog Cardiovasc Dis 1986;28:449-62.

40. Rose RA, Sellan M, Simpson JA, et al. Iron overload decreases CaV1.3-dependent L-type Ca2+ currents leading to bradycardia, altered electrical conduction, and atrial fibrillation. Circ Arrhythm electrophysiol 2011;4: 733-42.

41. Josephson RA, Silverman HS, Lakatta EG, et al. Study of the mechanisms of hydrogen peroxide and hydroxyl free radical-induced cellular injury and calcium overload in cardiac myocytes. J Biol Chem 1991;266: 2354-61.

42. Parkes JG, Olivieri NF, Templeton DM. Characterization of Fe2+ and Fe3+ transport by iron-loaded cardiac myocytes. Toxicology 1997;117: 141-51.

43. Imredy JP, Yue DT. Mechanism of Ca(2+)-sensitive inactivation of L-type Ca2+ channels. Neuron 1994;12:1301-18.

44. de Leon M, Wang Y, Jones L, et al. Essential Ca(2+)-binding motif for Ca(2+)-sensitive inactivation of L-type Ca2+ channels. Science 1995;270:1502-6.

45. Liu P, Olivieri N. Iron overload cardiomyopathies: new insights into an old disease. Cardiovasc Drug Ther 1994;8:101-10.

46. Olivieri NF, Brittenham GM, Matsui D, et al. Iron-chelation therapy with oral deferiprone in patients with thalassemia major. N Engl J Med 1995;332:918-22.

47. Pantopoulos K. Iron metabolism and the IRE/IRP regulatory system: an update. Ann NY Acad Sci 2004;1012:1-13.

48. Lipscombe D. L-type calcium channels: highs and new lows. Circ Res 2002;90:933-5.

49. De Sanctis V, Borsari G, Brachi S, et al. A rare cause of heart failure in iron overload thalassaemic patients-primary hypoparathyroidism. Georgian Med News 2008;111-3.

50. Liu L, O'Hara DS, Cala SE, et al. Developmental regulation of the L-type calcium channel alpha1C subunit expression in heart. Mol Cell Biochem 2000;205:101-9.

51. Takemura H, Yasui K, Opthof T, et al. Subtype switching of L-Type Ca 2+ channel from Cav1.3 to Cav1.2 in embryonic murine ventricle. Circ J 2005;69:1405-11.

52. Angelopoulos NG, Goula A, Rombopoulos G, et al. Hypoparathyroidism in transfusion-dependent patients with beta-thalassemia. J Bone Miner Metab 2006;24:158-45.

53. De Sanctis V, Vullo C, Bagni B, et al. Hypoparathyroidism in beta-thalassemia major. Clinical and laboratory observations in 24 patients. Acta Haematol 1992;88:105-8.

54. Kim E, Giri SN, Pessah IN. Iron(II) is a modulator of ryanodine-sensitive calcium channels of cardiac muscle sarcoplasmic reticulum. Toxicol Appl Pharmacol 1995;130:57-66.

55. Xu KY, Zweier JL, Becker LC. Hydroxyl radical inhibits sarcoplasmic reticulum Ca(2+)-ATPase function by direct attack on the ATP binding site. Circ Res 1997;80:76-81.

56. Kaneko M, Elimban V, Dhalla NS. Mechanism for depression of heart sarcolemmal Ca2+ pump by oxygen free radicals. Am J Physiol 1989;257:H804-11.

57. Kaneko M, Beamish RE, Dhalla NS. Depression of heart sarcolemmal Ca2+-pump activity by oxygen free radicals. Am J Physiol 1989;256: H1368-74.

58. Zeitz O, Maass AE, Van Nguyen P, et al. Hydroxyl radical-induced acute diastolic dysfunction is due to calcium overload via reverse-mode Na(+)-Ca(2+) exchange. Circ Res 2002;90:988-95.

59. Tokuhisa T, Yano M, Obayashi M, et al. AT1 receptor antagonist restores cardiac ryanodine receptor function, rendering isoproterenol-induced failing heart less susceptible to Ca2+ -leak induced by oxidative stress. Circ J 2006;70:777-86.

60. Kawakami M, Okabe E. Superoxide anion radical-triggered Ca2+ release from cardiac sarcoplasmic reticulum through ryanodine receptor Ca2+ channel. Mol Pharmacol 1998;53:497-503.

61. Link G, Pinson A, Hershko C. Ability of the orally effective iron chelators dimethyl- and diethyl-hydroxypyrid-4-one and of deferoxamine to restore sarcolemmal thiolic enzyme activity in iron-loaded heart cells. Blood 1994;83:2692-7.

62. Fernandes JL, Sampaio EF, Ferrrin K, et al. Amlodipine reduces cardiac iron overload in patients with thalassemia major: a pilot trial. Am J Med 2013;126:834-7.

63. Sugishita K, Asakawa M, Usui S, et al. A case of iron overload cardiomyopathy: beneficial effects of iron chelating agent and calcium channel blocker on left ventricular dysfunction. Int Heart J 2009;50:829-38.

64. Shahzor A, Zahoor M, Sadaf A, et al. Effect of L-type calcium channel blocker (amlodipine) on myocardial iron deposition in patients with thalassaemia with moderate-to-severe myocardial iron deposition: protocol for a randomised, controlled trial. BMJ Open 2014;4:e005360.

65. **Clinicaltrials.gov. Amlodipine as adjuvant treatment to iron chelation for prevention of cardiac iron overload in thalassemia patients. Available at:** www.clinicaltrials.gov/ct2/show/study/NCT02474420. **Accessed June 11, 2015.**

66. **Clinicaltrials.gov. Amlodipine use in the prevention and treatment of iron overload in patients with thalassemia major. Available at:** www.clinicaltrials.gov/ct2/show/NCT01125254. **Accessed May 13, 2010.**

67. **Clinicaltrials.gov. Amlodipine for myocardial iron in thalassemia. Available at:** www.clinicaltrials.gov/ct2/show/record/NCT02065492. **Accessed February 17, 2014.**

68. Bostanci MO, Bagirici F. Blocking of L-type calcium channels protects hippocampal and nigral neurons against iron neurotoxicity. The role of L-type calcium channels in iron-induced neurotoxicity. Int J Neurosci 2013;123:876-82.

69. Ma Z, Zhou Y, Xie J. Nifedipine prevents iron accumulation and reverses iron overload-induced dopamine neuron degeneration in the substantia nigra of rats. Neurotox Res 2012;22:274-9.

Supplementary Material

To access the supplementary material accompanying this article, visit the online version of the *Canadian Journal of Cardiology* at www.onlinecjc.ca and at http://dx.doi.org/10.1016/j.cjca.2015.10.012.

เอกสารแนบหมายเลข 24

SCIENTIFIC REPORTS

OPEN

Vagus Nerve Stimulation Exerts the Neuroprotective Effects in Obese-Insulin Resistant Rats, Leading to the Improvement of Cognitive Function

Received: 08 January 2016
Accepted: 11 April 2016
Published: 26 May 2016

Titikorn Chunchai[1,2], Bencharunan Samniang[1,2], Jirapas Sripetchwandee[1,2], Hiranya Pintana[1,2], Wanpitak Pongkan[1,2], Sirinart Kumfu[1,2], Krekwit Shinlapawittayatorn[1,2], Bruce H KenKnight[1,3], Nipon Chattipakorn[1,2] & Siriporn C. Chattipakorn[1,4]

Vagus nerve stimulation (VNS) therapy was shown to improve peripheral insulin sensitivity. However, the effects of chronic VNS therapy on brain insulin sensitivity, dendritic spine density, brain mitochondrial function, apoptosis and cognition in obese-insulin resistant subjects have never been investigated. Male Wistar rats (n = 24) were fed with either a normal diet (n = 8) or a HFD (n = 16) for 12 weeks. At week 13, HFD-fed rats were divided into 2 groups (n = 8/group). Each group was received either sham therapy or VNS therapy for an additional 12 weeks. At the end of treatment, cognitive function, metabolic parameters, brain insulin sensitivity, brain mitochondrial function, brain apoptosis, and dendritic spines were determined in each rat. The HFD-fed with Sham therapy developed brain insulin resistance, brain oxidative stress, brain inflammation, and brain apoptosis, resulting in the cognitive decline. The VNS group showed an improvement in peripheral and brain insulin sensitivity. VNS treatment attenuated brain mitochondrial dysfunction and cell apoptosis. In addition, VNS therapy increased dendritic spine density and improved cognitive function. These findings suggest that VNS attenuates cognitive decline in obese-insulin resistant rats by attenuating brain mitochondrial dysfunction, improving brain insulin sensitivity, decreasing cell apoptosis, and increasing dendritic spine density.

Obesity has reached epidemic proportions in many countries around the world[1]. Several studies have shown that obesity leads to the development of insulin resistance[2–4]. It has been shown that insulin resistance is associated with learning impairment and memory decline[5,6]. Previous studies from our group and others have demonstrated that obese rats, induced by high-fat diet (HFD) consumption, not only caused peripheral insulin resistance, but also brain insulin resistance, increased pro-inflammatory cytokines, increased brain oxidative stress, brain mitochondrial dysfunction, hippocampal synaptic dysfunction, decreased dendritic spine density, and instigated cognitive decline[2,6–11].

Vagus nerve stimulation (VNS) is commonly used to treat refractory epilepsy[12]. In addition to epileptic therapy, several studies demonstrated that VNS caused weight loss and reduced body fat in rodents[13,14]. Weight loss is a secondary outcome in individuals undergoing VNS for the treatment of refractory epilepsy[12] or depression[15]. The underlying mechanisms of VNS induced weight loss have been proposed to be due to the stimulation of vagal afferent fibers which provided the satiating effects via a gut-brain feedback mechanism, leading to lower food consumption and subsequent weight loss[16,17]. Furthermore, previous studies have shown that vagal nerve

[1]Neurophysiology Unit, Cardiac Electrophysiology Research and Training Center, Faculty of Medicine, Chiang Mai University, Chiang Mai, 50200, Thailand. [2]Cardiac Electrophysiology Research and Training Center, Department of Physiology, Faculty of Medicine, Chiang Mai University, Chiang Mai, 50200, Thailand. [3]Emerging Therapies, Cyberonics Inc, Houston, Texas, USA. [4]Department of Oral Biology and Diagnostic Sciences, Faculty of Dentistry, Chiang Mai University, Chiang Mai, 50200, Thailand. Correspondence and requests for materials should be addressed to S.C.C. (email: scchattipakorn@gmail.com or siriporn.c@cmu.ac.th)

Metabolic parameters	12-week ND	12-week HFD
Body weight (g)	475.55 ± 7.92	544.34 ± 5.83*
Food intake (g/day)	21.90 ± 1.30	21.15 ± 0.87
Plasma glucose (mg/dl)	131.25 ± 6.82	127.47 ± 5.04
Plasma insulin (ng/ml)	2.76 ± 0.34	5.87 ± 0.55*
HOMA index	23.76 ± 5.74	33.83 ± 4.53*

Table 1. The metabolic parameters after 12-week of ND or HFD consumption. *$p < 0.05$ in comparison with ND group.

Metabolic parameters	12 weeks post-treatment	
	Sham	VNS
Body weight (g)	613.34 ± 8.97	594.17 ± 10.83
Food intake (g/day)	19.28 ± 1.61	19.46 ± 1.22
Visceral fat (g)	61.01 ± 2.61	51.92 ± 3.53*
Plasma glucose (mg/dl)	131.47 ± 9.60	134.46 ± 3.98
Plasma insulin (ng/ml)	4.85 ± 1.36	3.04 ± 0.42*
HOMA index	30.93 ± 10.85	18.12 ± 2.37*
Plasma glucose AUC (AUCg) (mg/dl × min × 10^4)	5.58 ± 0.27	4.70 ± 0.23*
Plasma total cholesterol (mg/dl)	105.93 ± 6.34	81.42 ± 2.66*
Plasma total triglyceride (mg/dl)	28.73 ± 3.05	19.64 ± 1.60*
HDL cholesterol (mg/dl)	27.94 ± 1.67	27.39 ± 0.95
LDL/VLDL cholesterol (mg/dl)	70.17 ± 5.79	48.62 ± 1.63*

Table 2. The metabolic parameters after 12-week of VNS treatment in comparison with the sham group. *$p < 0.05$ in comparison with the sham group.

activity in the dorsal vagal complex plays important roles for the insulin secretion and glucose homeostasis[18,19]. However, the effect of VNS on peripheral and brain insulin sensitivity in an obese-insulin resistant model has not been investigated.

VNS has been shown to suppress inflammation and decrease oxidative stress *in vitro* studies[20,21]. Furthermore, VNS in model of depression increased neurogenesis and enhanced neural activity in many brain areas involving cognition[22,23]. Moreover, VNS in normal rats has been shown to modulate neuronal plasticity and increased dendritic complexity[24]. Those findings suggest that VNS could have the positive effect on the cognition in dementia condition. However, the effect of VNS on cognitive function in an obese-insulin resistant model has not yet been determined.

In the present study, the effects of chronic VNS on brain insulin sensitivity, synaptic plasticity and brain mitochondrial function, neuronal apoptosis and cognitive function were determined in obese-insulin resistant rats induced by HFD consumption. We tested the hypothesis that chronic VNS on the left vagus nerve in obese-insulin resistant rats induced by HFD improves cognitive function by restoring brain insulin sensitivity, attenuating brain mitochondrial dysfunction and enhancing dendritic spine density as well as attenuating neuronal apoptosis.

Results

Long-term HFD consumption caused peripheral insulin resistance but was improved by VNS.

After 12 weeks of HFD, the body weight, plasma insulin level and HOMA index of HFD-fed rats increased significantly when compared to ND-fed rats (Table 1). These findings suggested that 12-week HFD caused peripheral insulin resistance as indicated by hyperinsulinemia, increased HOMA index and the disruption in metabolic parameters.

After 12 weeks of VNS treatment, VNS-treated rats had a significant decrease in visceral fat, plasma insulin level, HOMA index, area under the curve of the oral glucose tolerance test (AUCg), plasma total cholesterol level, plasma total triglyceride and LDL/VLDL cholesterol level, when compared to the sham group (Table 2). All of these findings suggest that VNS attenuated peripheral insulin resistance via enhancing peripheral insulin sensitivity, and ameliorating the changes of lipid profiles in obese-insulin resistant rats.

VNS improved brain insulin signaling following long-term HFD consumption. The insulin-induced long-term depression (insulin-induced LTD) was measured to determine brain insulin receptor function. HFD-fed rats with sham therapy showed impaired insulin-induced LTD, whereas the VNS could reverse this impairment ($n = 2–3$ independent slices/animal, $n = 8$ animals/group Fig. 1A). In addition, the expression of insulin receptors (IR) with its phosphorylated form, and the expression of Akt protein with its phosphorylated form were measured to study brain insulin signaling. The phosphorylation of insulin receptors (p-IR) was significantly increased in VNS-treated rats when compared with sham group (Fig. 1B). Similarly, the

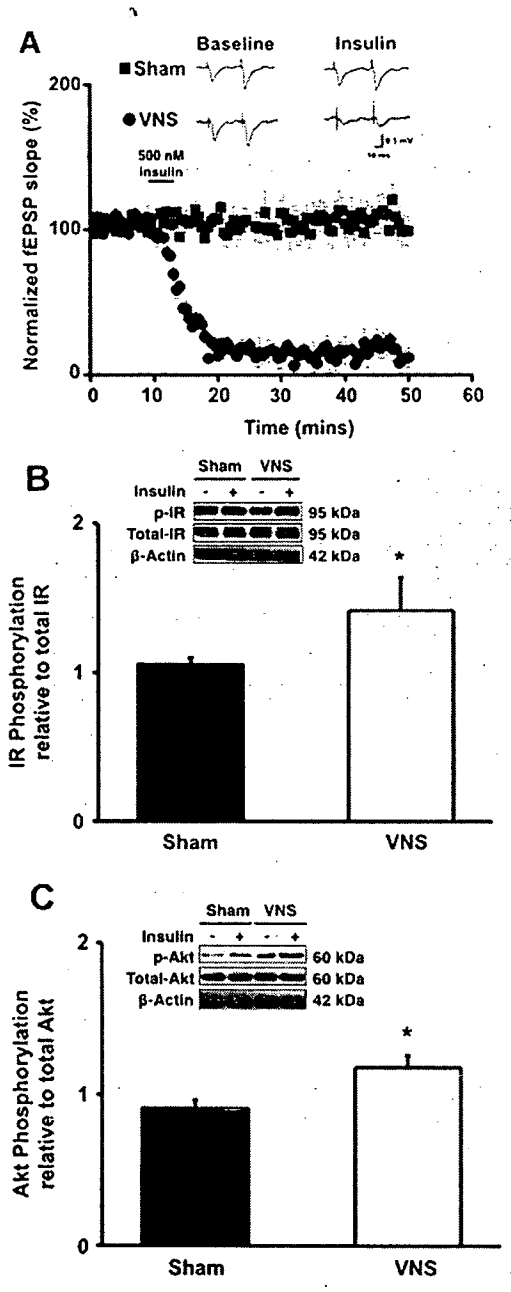


Figure 1. The effects of VNS on brain insulin receptor function, characterized by insulin-induced LTD (**A**), and its signaling, such as the phosphorylation levels of insulin receptor (**B**) and the phosphorylation levels of Akt protein (**C**) Sham: sham-operated HFD-fed rats; VNS: VNS-treated HFD-fed rats (N = 8 of each group) *$p < 0.05$ in comparison with the sham group.

VNS group had significantly increased phosphorylation of the Akt protein when compared with the sham group (Fig. 1C). All of these findings demonstrated that VNS restored insulin-induced LTD and improved brain insulin signaling that was previously impaired by long-term HFD consumption.

VNS attenuated brain mitochondrial dysfunction in obese-insulin resistant rats. Brain mitochondrial dysfunction was characterized by increased of brain mitochondrial ROS production, brain mitochondrial membrane potential depolarization and brain mitochondrial swelling[7–9]. Our results demonstrated that long-term HFD consumption induced brain mitochondrial dysfunction (Fig. 2A–C). In addition, the unfolding of cristae in the brain mitochondria from HFD-fed rats with sham therapy was observed, indicating brain mitochondrial swelling (Fig. 2D). In VNS-treated rats, there was a significant reduction in brain mitochondrial ROS production, brain mitochondrial membrane potential changes and brain mitochondrial swelling when compared

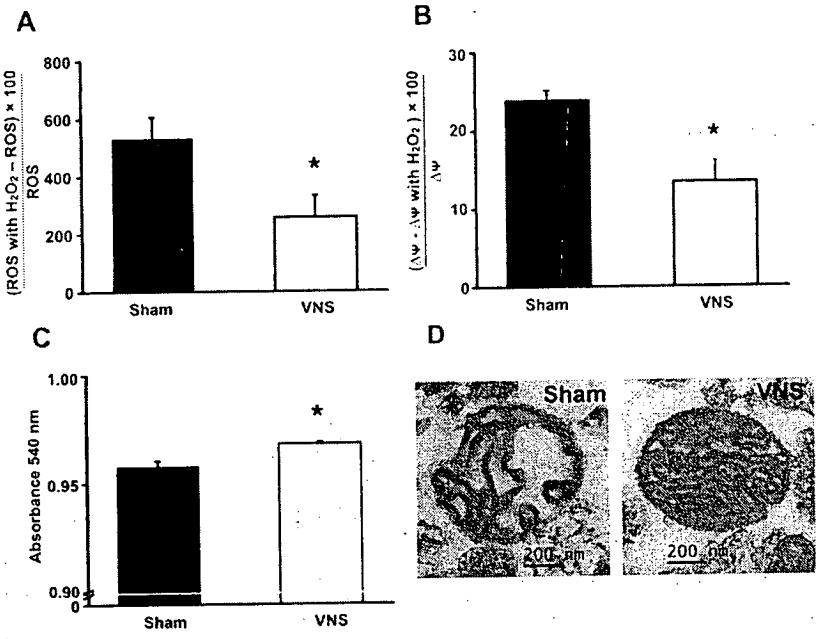


Figure 2. The effects of VNS on brain mitochondrial function in obese-insulin resistant rats, including brain mitochondrial ROS production (**A**), brain mitochondrial membrane potential changes (**B**) and brain mitochondrial swelling (**C**). Representative images demonstrate the morphology of brain mitochondria using transmission electron microscopy at the original magnification of 25,000x (**D**) Sham: sham-operated HFD-fed rats; VNS: VNS-treated HFD-fed rats (N = 8 of each group) *$p < 0.05$ in comparison with the sham group.

with the sham group (Fig. 2). All of these findings suggest that VNS attenuated brain mitochondrial dysfunction caused by long-term HFD consumption.

VNS attenuated inflammation, brain oxidative stress and cell apoptosis. To examine the anti-inflammatory effects of VNS, plasma and brain TNF-α level were determined. After 12 weeks of HFD consumption, the plasma TNF-α level was significantly increased when compared with baseline (5.03 ± 1.21 and 0.27 ± 0.15 pg/mg protein in 12-week HFD vs baseline, $p < 0.05$). After 12 weeks of VNS treatment, VNS-treated rats had significantly decreased TNF-α levels in both plasma (Fig. 3A) and brain (Fig. 3B) when compared with sham group. All of these findings suggest that VNS attenuated the systemic inflammation, as indicated by decreased plasma and brain TNF-α levels. Moreover, HFD-fed rats with sham therapy demonstrated brain oxidative stress as indicated by an increased brain MDA level (Fig. 3C). VNS treatment could ameliorate brain MDA levels, suggesting an anti-oxidant role of VNS.

The degree of cell apoptosis was also determined in the present study by measuring cell apoptotic markers, including the end product of the apoptotic marker Bax and the anti-apoptotic marker Bcl-2 levels. After 12 weeks of VNS, Bax expression significantly decreased when compared with the sham group. Although there were no significant difference in Bcl-2 levels between the groups, the Bax/Bcl-2 ratio of VNS-treated rats was significantly decreased when compared with sham group (Fig. 3D). All of these findings suggest that VNS also exerted anti-apoptotic effects.

VNS treatment improved dendritic spine density and cognitive function in obese-insulin resistant rats. There was a loss of dendritic spine density after HFD consumption in sham therapy (Fig. 4A–C). However, chronic stimulation of the vagus nerve increased dendritic spine density (Fig. 4D–F). The number of dendritic spines on the tertiary segment of the apical dendrites in VNS-treated rats was significantly increased when compared with the sham group (Fig. 4G), suggesting that VNS enhanced synaptic strength.

As previously demonstrated, long-term HFD consumption could lead to the induction of cognitive impairment in association with a reduction in dendritic spine density[10]. Consistent with a previous study, HFD consumption in the present study also caused memory impairment indicated by the increased time to reach the platform (Fig. 5A) and decreased time spent in the target quadrant in 12-week HFD-fed rats, compared to 12-week ND-fed rats (Fig. 5B). After VNS for 12 weeks in HFD-fed rats, the time to reach the platform in VNS-treated rats was significantly decreased when compared to sham group during the acquisition test (Fig. 5C). In addition, the time spent in the target quadrant during the probe test in VNS-treated rats was significantly higher than that of the sham group (Fig. 5D). All of these findings suggested that VNS effectively attenuates the impairment of learning and memory behaviors caused by long-term HFD consumption.

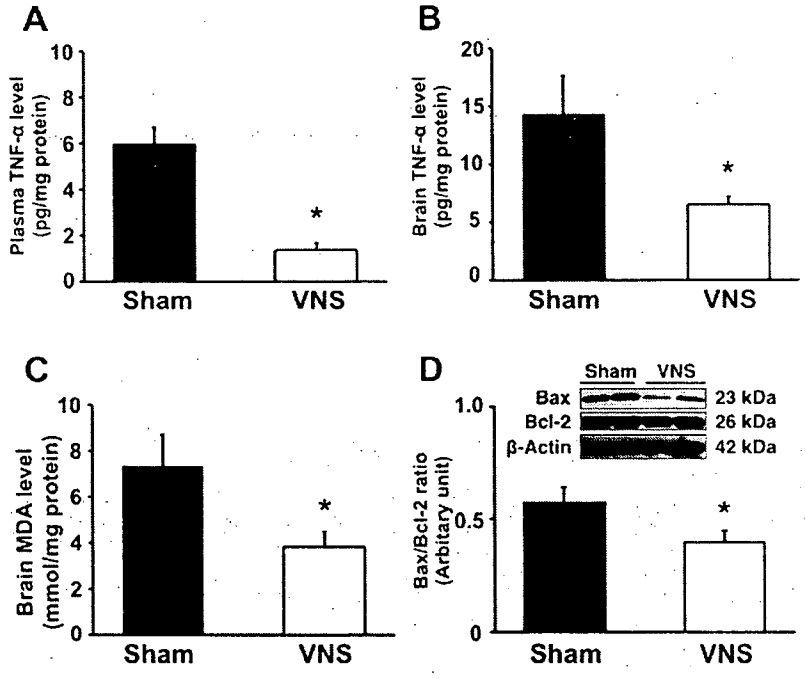


Figure 3. The effects of VNS on inflammation: plasma TNF-α level (**A**) and brain TNF-α level (**B**), brain MDA levels using HPLC system (**C**) and brain apoptosis including Bax/Bcl-2 ratio using western blot analysis (**D**) Sham: sham-operated HFD-fed rats; VNS: VNS-treated HFD-fed rats (N = 8 of each group) *$p < 0.05$ in comparison with the sham group.

Discussion

The major findings of the present study are as follows: 1) The obese condition following long-term HFD consumption led to the development of peripheral insulin resistance, brain insulin resistance, brain mitochondrial dysfunction and cognitive decline possibly through the induction of brain oxidative stress, brain inflammation, brain apoptosis and the reduction of dendritic spine density, and 2) VNS attenuated the undesirable effects of long-term HFD, leading to the improvement of cognitive function.

In the present study, the development of peripheral insulin resistance following long-term HFD consumption was clearly shown as indicated by an increase in the HOMA index, impaired oral glucose tolerance test (OGTT), and metabolic disturbances[7,9,25,26]. It is known that both oxidative stress and inflammation play an important role in the development of insulin resistance[27]. Consistent with this notion, the obese-insulin resistant rats in this study also had an increase in the pro-inflammatory cytokine TNF-α, and oxidative stress.

VNS is known to exert anti-inflammatory effect, and has been shown previously to decrease TNF-α in traumatic brain injury[21,28]. Our results demonstrated that VNS therapy provided the anti-inflammatory effect as evidenced by the decreased TNF-α level in obese-insulin resistant rats. Moreover, the present study also demonstrated that VNS therapy effectively decreased oxidative stress. These beneficial effects of VNS could contribute to the increased peripheral insulin sensitivity under this obese-insulin resistant condition. A clinical report in patients with impaired glucose tolerance demonstrated that VNS significantly reduce two-hour glucose tolerance in these patients[29], thus supporting our findings regarding the benefits of VNS on improved insulin sensitivity.

The present study also demonstrated that long-term HFD consumption not only caused peripheral insulin resistance, but also led to the development of brain insulin resistance, as indicated by the decreased insulin-induced LTD, the reduction of brain insulin signaling, the impaired brain mitochondrial function, and an increased apoptosis in the brain. These findings were consistent with our recent reports in which brain insulin resistance and brain mitochondrial dysfunction was developed after long-term HFD consumption[7,9,25]. It has been shown that obesity induced cell apoptosis by increased Bax level, decreased Bcl-2 level and impaired brain mitochondrial function[30]. Although previous studies demonstrated that VNS exerted protective effects on mitochondrial function in the heart[31,32], its effect on brain mitochondrial function has never been tested. In the present study, we demonstrated for the first time that VNS effectively attenuated brain insulin resistance, brain mitochondrial dysfunction, and brain apoptosis. Moreover, we found that VNS therapy also decreased brain MDA levels in these obese-insulin resistant rats, indicating that VNS could effectively decrease oxidative stress not only in the plasma, but also in the brain. Our findings suggested that a reduction of brain mitochondrial dysfunction and brain oxidative stress by VNS therapy could be mainly responsible for the neuroprotective effects of VNS in these obese-insulin resistant rats.

Growing evidence demonstrated the potential roles of VNS on cognition in the models of epilepsy and depression[33,34]. A recent study by Peña and colleagues demonstrated that VNS facilitated cognition through promoting

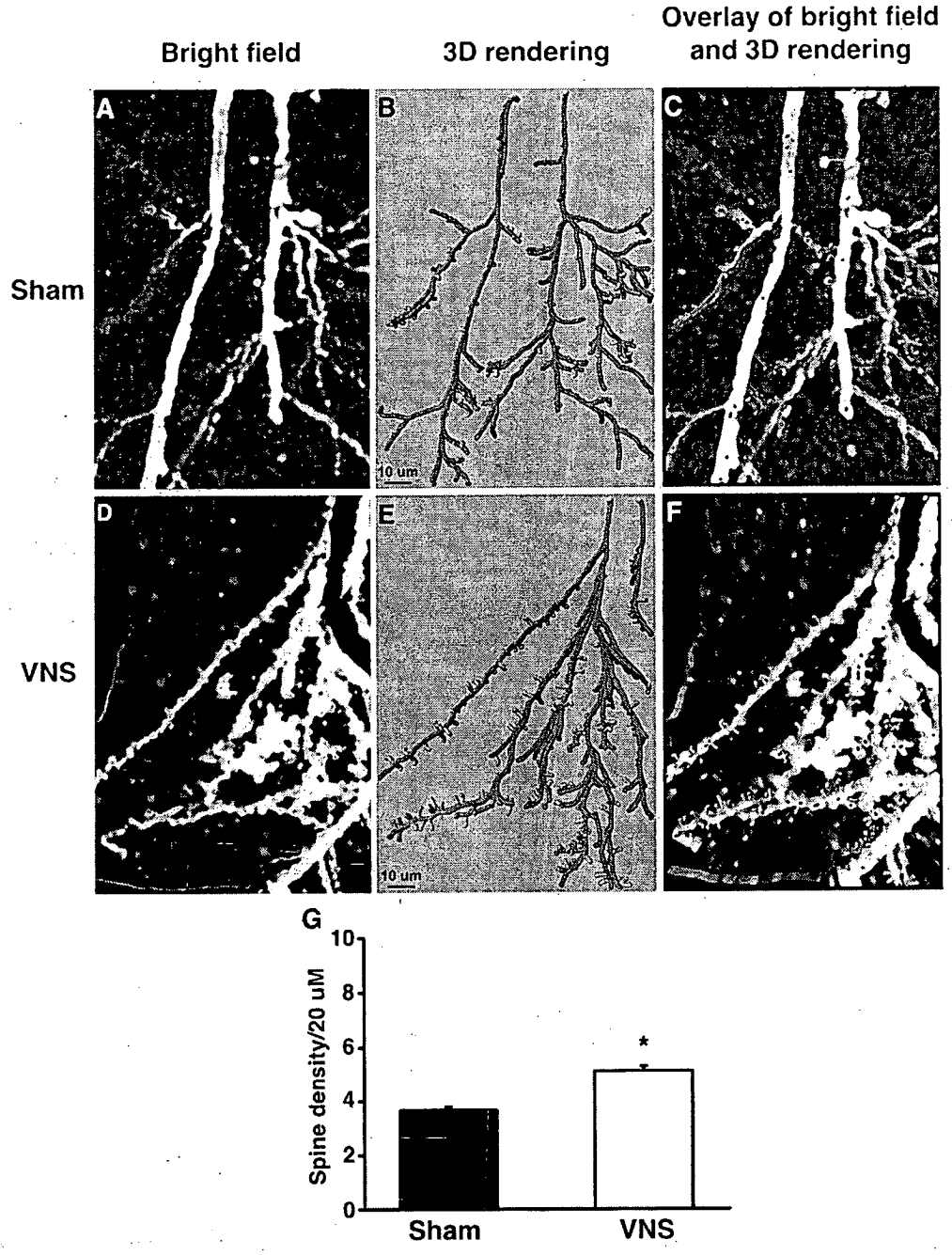


Figure 4. The effects of VNS on dendritic spine density. The representative images from invert bright field of dendritic spines (**A**,**D**) The representative 3D rendering of dendritic spine density was constructed using the Filament Tracer module of the Imaris Suite 7.0® software to generate spine reconstructions of the acquired invert bright field z-stack images (**B**,**E**) The representative overlay images from invert bright field of dendritic spines and 3D rendering (**C**,**F**) Upper panel (**A**–**C**) showed the representative dendritic spine density of sham group. Lower panel (**D**–**F**) showed the representative dendritic spine density of VNS group. (**G**) The effect of VNS or sham on the number of dendritic spines at CA1 region of hippocampus. Sham: sham-operated HFD-fed rats; VNS: VNS-treated HFD-fed rats (N = 8 of each group) *$p < 0.05$ in comparison with the sham group.

plasticity and preserving electrical-induced LTD in normal rats[35]. In the present study, we found that VNS could improve cognitive function and increase the dendritic spine density which were all impaired in obese-insulin resistant rats. The effects of VNS to decrease peripheral insulin resistance, brain inflammation, brain mitochondrial dysfunction, brain oxidative stress, brain apoptosis, and to increase brain insulin sensitivity could be responsible for the prevention of the dendritic spine density reduction, and thus leading to an improved cognition as observed in the obese-insulin resistant rats in the present study.

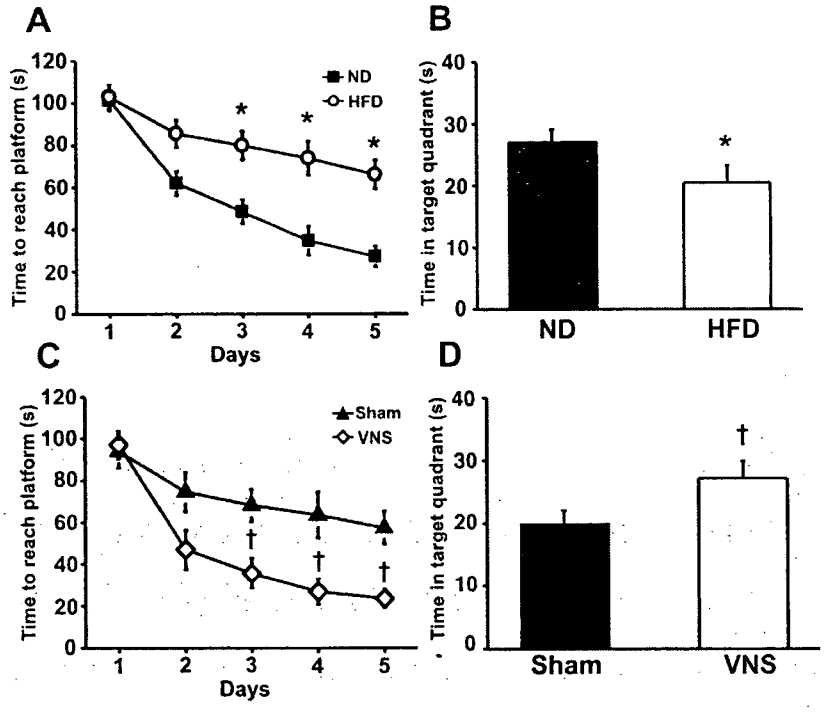


Figure 5. Learning and memory behavioral results from Morris Water Maze test. Chronic HFD consumption caused cognitive impairment as indicated by increased time required to reach the platform in the acquisition test (**A**) and decreased time spent in the target quadrant in the probe test (**B**). VNS treatment attenuated cognitive decline, as shown by decreased time required to reach the platform (**C**) and increased time spent in the target quadrant (**D**). ND: 12-week-normal diet-fed rats; HFD: 12-week high fat-fed rats; Sham: sham-operated HFD-fed rats; VNS: VNS-treated HFD-fed rats (N = 8 of each group) $^{*}p < 0.05$ in comparison with the ND-fed rats; $^{\dagger}p < 0.05$ in comparison with the sham group.

Conclusion

Obese-insulin resistant condition causes brain insulin resistance, brain oxidative stress and inflammation, and brain apoptosis, resulting in the cognitive decline. VNS exerts the neuroprotective effects in obese-insulin resistant rats via its anti-inflammation, anti-oxidation, anti-apoptosis, as well as its ability to act as an insulin sensitizer, leading to the improvement of cognitive function. This study also demonstrated that VNS is not only effective and safe therapeutic method, but also provides beneficial effects on cognition.

Methods

Animal models and experimental protocols. The methods were carried out in accordance with the approved guidelines. All experimental protocols were approved by the Institutional Animal Care and Use Committee (IACUC) of the Faculty of Medicine, Chiang Mai University (Permit number: 34/2557) and conformed to the Guide for the Care and Use of Laboratory Animals published by the US National Institutes of Health (NIH guide, 8th edition, 2011). Male Wistar rats (n = 24) were used in the present study, and obtained from the National Laboratory Animal Center, Salaya Campus, Mahidol University, Thailand. All rats were housed individually in a temperature-controlled environment (25 ± 0.5 °C) with a 12:12 hour light-dark cycle. After acclimatization for 1 week, rats were divided into two groups, those on a normal diet (ND; n = 8) and those on a high-fat diet (HFD; n = 16). In the ND group, rats were fed on a standard laboratory pelleted diet containing 19.77% fat, 51.99% carbohydrate and 28.24% protein (Mouse Feed Food No. 082, C.P. Company, Bangkok, Thailand) and the rats in the HFD group were fed on a diet consisting of 59.28% fat, 14.27% carbohydrate and 26.45% protein to create the obese-insulin resistant models[2]. After 12 weeks all rats were evaluated for cognitive function using the Morris Water Maze test. The HFD-fed rats were then randomly assigned to either the sham-operated group (Sham; n = 8) or the vagus nerve stimulation (VNS; n = 8) group. After a week of recovery, rats were continuously fed with a HFD for an additional 12 weeks. At week 25, the cognitive function and the oral glucose tolerance test (OGTT) of each rat were investigated. Blood samples were collected from a tail vein at week 12, and week 25 of the experimental protocol for plasma analysis. At the end of the experimental protocol, rats were deeply anesthetized with isoflurane and killed by decapitation. The brain of each rat was quickly removed and carefully sliced in preparation for investigation, including extracellular recording (insulin-induced LTD), immunoblot analysis, brain mitochondrial function and brain MDA measurement. The experimental protocol is summarized in Fig. 6.

Surgical procedure. Animals were randomized to receive either inactive VNS implantation, or active VNS implantation. All rats were anesthetized with xylazine (3 mg/kg, g, Laboratorios Calier, Barcelona, Spain) and

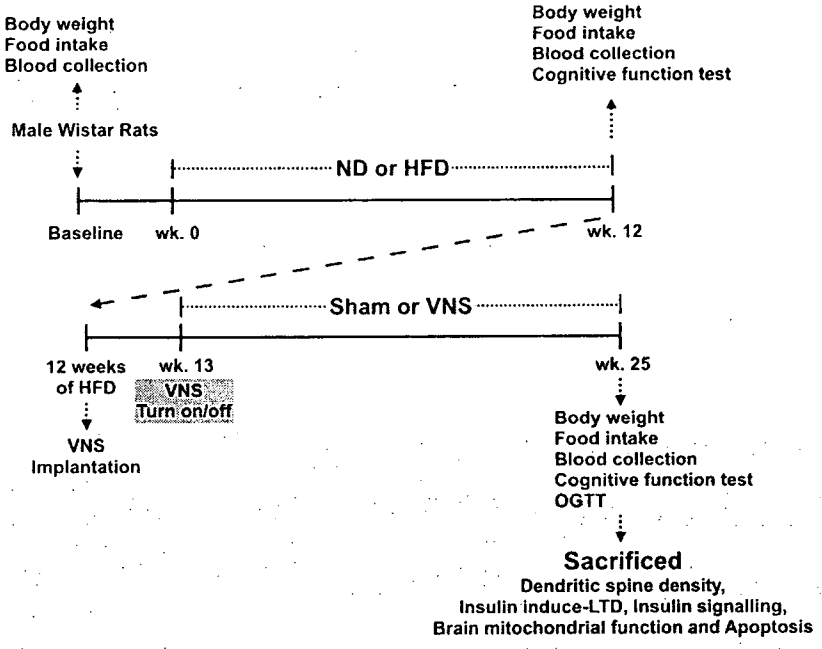


Figure 6. The experimental protocol of the present study.

zolitil (50 mg/kg, Virbac Laboratories, Carros, France)[36]. The hair was shaved and skin was cleaned on each rat before the bipolar cuff electrode was implanted around the left cervical vagus nerve and connected to a VNS Demipulse™ (Cyberonic, Inc., Houston, Texas). Animals were closely monitored and subcutaneously injected with both 10 mg/kg of marboflxacine and 16 mg/kg of tolfenamic acid[36]. Surgical wounds were bathed with povidine solution as necessary. The VNS group experienced a continuous 14 s delivery of stimulation at a frequency of 20 Hz, pulse width of 500 μs and a current of 0.5–0.75 mA followed by a 48 s rest. The same procedures, without stimulation, were performed in the sham group. For the 10 minutes preceding data collection, VNS therapy was turned off and remained off throughout the duration of the acquisition test and probe trial test.

Blood sample assays. Plasma glucose and cholesterol levels were determined via colorimetric assay (Biotech, Bangkok, Thailand). The commercial colorimetric assay kit (Biovision, California, USA) was used for determining plasma HDL and LDL levels. Plasma insulin levels were also determined using the Sandwich ELISA kit (LINCO Research, MO, USA). Homeostasis Model Assessment (HOMA) was used for assesse the peripheral insulin resistance as described in previous studies[37,38].

Oral glucose tolerance test (OGTT). OGTT was performed as described in Pintana *et al.*[7,9]. Briefly, rats were fasted overnight before the test and received 2 g/kg of glucose solution via oral gavage feeding. Blood samples were collected from the tail vein at 0, 15, 30, 60, 90 and 120 minutes after glucose administration. Areas under the curve (AUC) were calculated to evaluate glucose tolerance.

Brain slice preparation. At the end of experimental period, the rats were anesthetized with isoflurane and decapitated. As described previously[2,8,9], the brain tissue in each rat was removed and immersed in ice-cold artificial cerebrospinal fluid (aCSF) containing high sucrose for 30 minutes. Brain slices (400 μm) were cut on a vibratome (Vibratome Company, MO, USA). The slices were transferred to a room temperature (22–24 °C) CSF solution for an additional 30 minutes.

Extracellular recordings of hippocampal slices for insulin-induced long-term depression (LTD). Insulin-induce long-term depression (LTD) was examined using the method described in Pratchayasakul *et al.*[2] and Pipatpiboon *et al.*[2,8,9]. Briefly, the hippocampal slices were transferred to a recording chamber containing standard aCSF. Field excitatory postsynaptic potentials (fEPSPs) were evoked using a bipolar tungsten electrode to stimulate the Schaffer collateral-commissural pathway, while the fEPSPs recordings were taken by micropipettes (3 MΩ) filled with 2 M NaCl from the stratum radiatum in CA1 region of hippocampus. Frequency of the stimulation was 0.033 Hz and the stimulus intensity was adjusted to produce <50% of maximal monophasic responses with 0.8–1.0 mV in amplitude. The brain slices were perfused with aCSF (as the baseline condition) for 10 minutes, followed by perfusion with 500 nM insulin in aCSF (as insulin-induced LTD) for an additional 10 minutes. Thereafter, the slices were perfused with aCSF again for a further 50 minutes. Data were digitized and recorded in a computer using pClamp9.2 software (Axon Instruments, CA, USA). The initial of the fEPSP slope was measured and plotted against time.

Golgi staining and Image analysis. To examine dendritic spine density, Golgi staining was performed following Sripetchwandee *et al.*[10]. Briefly, the brain was transferred to Golgi staining solution according to FD Rapid Golgistain™ Kits (FD Neuro Technologies, Baltimore, MD, USA) and cut at 60 μm of thickness using Cyostat (Leica CM1950, Leica Biosystem Nussloch GmbH, Nussloch, Germany). For analysis, the three segments, 100–200 μm apart from the soma and 20–30 μm in dendritic length were used to randomly measure dendritic spine density. Three neuronal cells per brain slice, and three brain slices per animal were chosen for quantitative analysis. The number of spines was counted by double-blind hand counter, and the dendritic length was measured using Xcellence imaging software (Olympus). The representative of dendritic spine density was constructed using the Filament Tracer module of the Imaris Suite 7.0® software (Bitplane, Oxford instruments, Concord, MA, USA).

Immunoblotting for brain insulin signaling and apoptosis. To investigate the brain insulin signaling, homogenate brain slices were used, as described in references[2,8,9]. IR tyrosine phosphorylation was electrophoresed and an immunoblot analysis was carried out with rabbit antibodies. Examination of the level of IR protein expression was conducted with homogenates prepared from another set of four whole brain slices. These proteins were separated and identified by an immunoblot assay conducted with rabbit anti-IR at tyrosine phosphorylation (1:1000; sc-25103-R; Santa Cruz Biotechnology, CA, USA), IR (1:1000; sc-711; Santa Cruz Biotechnology, CA, USA). Similarly, the Akt phosphorylation were electrophoresed and immunoblotted with rabbit antibodies for Akt (1:1000; 9272S; Cell Signaling Technology, MA, USA). For a loading control, immunoblotting for each membrane was incubated with anti-β-actin (1:4000; #4967; Cell Signaling Technology, MA, USA). All membranes for visualizing the phosphorylation and the protein levels of IR expression were incubated with a secondary goat anti-rabbit antibody conjugated with horseradish peroxidase (1:2000; #7074; Cell Signaling Technology, MA, USA). The protein bands were visualized on Amersham hyperfilm ECL (GE Healthcare, Buckinghamshire, UK) using Amersham ECL Western blot detection reagents (GE, Healthcare). The band intensity was measured by Scion Image, and the results were represented as average signal intensity (arbitrary) units.

Brain malondialdehyde (MDA) level. To examine the brain oxidative stress, brain malondialdehyde (MDA) level was determined by high performance liquid chromatography (HPLC), as described in the previous studies[7,25].

Brain mitochondrial function. Brain mitochondria were isolated as described in Pipatpiboon *et al.*[8]. Mitochondrial protein was determined by the BCA assay as described previously[7], and brain mitochondrial function including brain mitochondrial reactive oxygen species (ROS), mitochondrial membrane potential change ($\Delta\Psi m$) and mitochondrial swelling were determined[7–9]. Brain mitochondrial reactive oxygen species (ROS) were measured using dichloro-hydrofluoresceindiacetate (DCFHDA) fluorescent dye. The change in mitochondrial membrane potential ($\Delta\Psi m$) was measured using the fluorescent dye 5, 5′, 6, 6′-tetrachloro-1, 1′, 3, 3′-tetraethyl benzimidazolcarbocyanine iodide (JC-1) and brain mitochondrial swelling was determined by measuring the change in the absorbance of brain mitochondrial suspension at 540 nm. All were determined by following the methods described previously[8,25].

Cognitive function test. The Morris Water Maze (MWM) test was performed determining cognitive function with two assessments, including five consecutive days of the acquisition test, and the probe test on day sixth. Time to find the platform was recorded in the acquisition test and the time spent in the target quadrant was also recorded in the probe test[25,39]. Data analysis of the MWM test was done manually from video tape recordings by the investigators, who were blinded to experimental groups.

Statistical analysis. Data from each experiment were expressed as mean ± S.E.M. For all comparisons, the significance of the difference in peripheral biochemical parameters, the percentage of insulin-induced LTD, brain mitochondrial function, immunoblot and probe test in the MWM tests were calculated using an independent t-test. Comparisons between the groups of the MWM tests for the acquisition test were performed using a two-way ANOVA, followed by post-hoc LSD analysis. A $P < 0.05$ was considered as statistically significant.

References

1. James, P. T. Obesity: the worldwide epidemic. *Clin Dermatol.* **22,** 276–280 (2004).
2. Pratchayasakul, W. *et al.* Effects of high-fat diet on insulin receptor function in rat hippocampus and the level of neuronal corticosterone. *Life Sci.* **88,** 619–627 (2011).
3. Clegg, D. J. *et al.* Consumption of a high-fat diet induces central insulin resistance independent of adiposity. *Physiol Behav.* **103,** 10–16 (2011).
4. Kahn, S. E., Hull, R. L. & Utzschneider, K. M. Mechanisms linking obesity to insulin resistance and type 2 diabetes. *Nature.* **444,** 840–846 (2006).
5. Greenwood, C. E. & Winocur, G. High-fat diets, insulin resistance and declining cognitive function. *Neurobiol Aging.* **26,** 42–45 (2005).
6. Stranahan, A. M. *et al.* Diet-induced insulin resistance impairs hippocampal synaptic plasticity and cognition in middle-aged rats. *Hippocampus.* **18,** 1085–1088 (2008).
7. Pintana, H., Apaijai, N., Pratchayasakul, W., Chattipakorn, N. & Chattipakorn, S. C. Effects of metformin on learning and memory behaviors and brain mitochondrial functions in high fat diet induced insulin resistant rats. *Life Sci.* **91,** 409–414 (2012).
8. Pipatpiboon, N., Pratchayasakul, W., Chattipakorn, N. & Chattipakorn, S. C. PPARgamma agonist improves neuronal insulin receptor function in hippocampus and brain mitochondria function in rats with insulin resistance induced by long term high-fat diets. *Endocrinology.* **153,** 329–338 (2012).
9. Pipatpiboon, N., Pintana, H., Pratchayasakul, W., Chattipakorn, N. & Chattipakorn, S. C. DPP4-inhibitor improves neuronal insulin receptor function, brain mitochondrial function and cognitive function in rats with insulin resistance induced by high-fat diet consumption. *Eur J Neurosci.* **37,** 839–849 (2013).

10. Sripetchwandee, J., Pipatpiboon, N., Pratchayasakul, W., Chattipakorn, N. & Chattipakorn, S. C. DPP-4 inhibitor and PPARgamma agonist restore the loss of CA1 dendritic spines in obese insulin-resistant rats. *Arch Med Res.* **45,** 547–552 (2014).
11. Pratchayasakul, W. *et al.* Obesity accelerates cognitive decline by aggravating mitochondrial dysfunction, insulin resistance and synaptic dysfunction under estrogen-deprived conditions. *Horm Behav.* **72,** 68–77 (2015).
12. Burneo, J. G., Faught, E., Knowlton, R., Morawetz, R. & Kuzniecky, R. Weight loss associated with vagus nerve stimulation. *Neurology.* **59,** 463–464 (2002).
13. Bugajski, A. J. *et al.* Effect of long-term vagal stimulation on food intake and body weight during diet induced obesity in rats. *J Physiol Pharmacol.* **58,** 5–12 (2007).
14. Krolczyk, G. *et al.* The effects of baclofen on the feeding behaviour and body weight of vagally stimulated rats. *J Physiol Pharmacol.* **56,** 121–131 (2005).
15. Bodenlos, J. S. *et al.* Vagus nerve stimulation and emotional responses to food among depressed patients. *J Diabetes Sci Technol.* **1,** 771–779 (2007).
16. Bray, G. A. Afferent signals regulating food intake. *Proc Nutr Soc.* **59,** 373–384 (2000).
17. Ritter, R. C., Ritter, S., Ewart, W. R. &,Wingate, D. L. Capsaicin attenuates hindbrain neuron responses to circulating cholecystokinin. *Am J Physiol.* **257,** R1162–1168 (1989).
18. Huang, L. *et al.* Influence of fasting, insulin and glucose on ghrelin in the dorsal vagal complex in rats. *J Endocrinol.* **211,** 257–262 (2011).
19. Huang, C. C., Lee, C. C. & Hsu, K. S. The role of insulin receptor signaling in synaptic plasticity and cognitive function. *Chang Gung Med J.* **33,** 115–125 (2010).
20. Shi, F. D. *et al.* Nicotinic attenuation of central nervous system inflammation and autoimmunity. *J Immunol.* **182,** 1730–1739 (2009).
21. Zhou, L. *et al.* Neuroprotective effects of vagus nerve stimulation on traumatic brain injury. *Neural Regen Res.* **9,** 1585–1591 (2014).
22. Gebhardt, N. *et al.* Vagus nerve stimulation ameliorated deficits in one-way active avoidance learning and stimulated hippocampal neurogenesis in bulbectomized rats. *Brain Stimul.* **6,** 78–83 (2013).
23. Furmaga, H., Sadhu, M. & Frazer, A. Comparison of DeltaFosB immunoreactivity induced by vagal nerve stimulation with that caused by pharmacologically diverse antidepressants. *J Pharmacol Exp Ther.* **341,** 317–325 (2012).
24. Biggio, F. *et al.* Chronic vagus nerve stimulation induces neuronal plasticity in the rat hippocampus. *Int J Neuropsychopharmacol.* **12,** 1209–1221 (2009).
25. Pintana, H., Apaijai, N., Chattipakorn, N. & Chattipakorn, S. C. DPP-4 inhibitors improve cognition and brain mitochondrial function of insulin resistant rats. *J Endocrinol.* **218,** 1–11 (2013).
26. Pintana, H. *et al.* Garlic extract attenuates brain mitochondrial dysfunction and cognitive deficit in obese-insulin resistant rats. *Appl Physiol Nutr Metab.* **39,** 1373–1379 (2014).
27. Sivaraman, K., Senthilkumar, G. P., Sankar, P. & Bobby, Z. Attenuation of oxidative stress, inflammation and insulin resistance by allium sativum in fructose-fed male rats. *J Clin Diagn Res.* **7,** 1860–1862 (2013).
28. Bansal, V. *et al.* Vagal stimulation modulates inflammation through a ghrelin mediated mechanism in traumatic brain injury. *Inflammation.* **35,** 214–220 (2012).
29. Huang, F. *et al.* Effect of transcutaneous auricular vagus nerve stimulation on impaired glucose tolerance: a pilot randomized study. *BMC Complement Altern Med.* **14,** 203 (2014).
30. Sinha-Hikim, I. *et al.* A novel cystine based antioxidant attenuates oxidative stress and hepatic steatosis in diet-induced obese mice. *Exp Mol Pathol.* **91,** 419–428 (2011).
31. Shinlapawittayatorn, K. *et al.* Vagus nerve stimulation initiated late during ischemia, but not reperfusion, exerts cardioprotection via amelioration of cardiac mitochondrial dysfunction. *Heart Rhythm.* **11,** 2278–2287 (2014).
32. Shinlapawittayatorn, K. *et al.* Low-amplitude, left vagus nerve stimulation significantly attenuates ventricular dysfunction and infarct size through prevention of mitochondrial dysfunction during acute ischemia-reperfusion injury. *Heart Rhythm.* **10,** 1700–1707 (2013).
33. Vonck, K. *et al.* Vagus nerve stimulation...25 years later! What do we know about the effects on cognition? *Neurosci Biobehav Rev.* **45,** 63–71 (2014).
34. Ogbonnaya, S. & Kaliaperumal, C. Vagal nerve stimulator: Evolving trends. *J Nat Sci Biol Med.* **4,** 8–13 (2013).
35. Pena, D. F. *et al.* Vagus nerve stimulation enhances extinction of conditioned fear and modulates plasticity in the pathway from the ventromedial prefrontal cortex to the amygdala. *Front Behav Neurosci.* **8,** 327 (2014).
36. Pongkan, W., Chattipakorn, S. C. & Chattipakorn, N. Chronic Testosterone Replacement Exerts Cardioprotection against Cardiac Ischemia-Reperfusion Injury by Attenuating Mitochondrial Dysfunction in Testosterone-Deprived Rats. *Plos One.* **10,** e0122503 (2015).
37. Appleton, D. J., Rand, J. S. & Sunvold, G. D. Basal plasma insulin and homeostasis model assessment (HOMA) are indicators of insulin sensitivity in cats. *J Feline Med Surg.* **7,** 183–193 (2005).
38. Haffner, S. M., Miettinen, H. & Stern, M. P. The homeostasis model in the San Antonio Heart Study. *Diabetes Care.* **20,** 1087–1092 (1997).
39. Vorhees, C. V. & Williams, M. T. Morris water maze: procedures for assessing spatial and related forms of learning and memory. *Nat Protoc.* **1,** 848–858 (2006).

Acknowledgements

This work was supported by Thailand Research Fund TRF-BRG5780016 (SC), TRG-5880045 (JS), RSA-5880015 (KS), TRG-5780002 (SK), the National Research Council of Thailand (SC), a NSTDA Research Chair Grant from the National Science and Technology Development Agency Thailand (NC) and Chiang Mai University Excellent Center Award (NC). The authors would like to thank Ms. Thidarat Jaiwongkum and Ms. Sasiwan Kerdpoo for their technical assistance in this project.

Author Contributions

T.C., B.S., J.S., H.P., W.P., S.K. and K.S. performed the experiments and analyzed the data. T.C. and J.S. wrote the manuscript. B.H.K. participated in data analysis and critically revised the manuscript. N.C. designed study, analyzed the data, and wrote the manuscript. S.C.C. designed study, analyzed the data, wrote the manuscript and had final approval of the submitted and published versions. All authors reviewed the manuscript.

Additional Information

Competing financial interests: The authors declare no competing financial interests.

How to cite this article: Chunchai, T. *et al.* Vagus Nerve Stimulation Exerts the Neuroprotective Effects in Obese-Insulin Resistant Rats, Leading to the Improvement of Cognitive Function. *Sci. Rep.* **6**, 26866; doi: 10.1038/srep26866 (2016).

This work is licensed under a Creative Commons Attribution 4.0 International License. The images or other third party material in this article are included in the article's Creative Commons license, unless indicated otherwise in the credit line; if the material is not included under the Creative Commons license, users will need to obtain permission from the license holder to reproduce the material. To view a copy of this license, visit http://creativecommons.org/licenses/by/4.0/

เอกสารแนบหมายเลข 25

Exp Physiol 101.6 (2016) pp 697–707

Research Paper

Humanin prevents brain mitochondrial dysfunction in a cardiac ischaemia–reperfusion injury model

Sirinart Kumfu[1,2,3], Savitree T. Charununtakorn[1,2,3], Thidarat Jaiwongkam[1,2,3], Nipon Chattipakorn[1,2,3] and Siriporn C. Chattipakorn[1,3,4]

[1]*Neurophysiology Unit, Cardiac Electrophysiology Research and Training Center, Faculty of Medicine, Chiang Mai University, Chiang Mai, Thailand*
[2]*Cardiac Electrophysiology Unit, Department of Physiology, Faculty of Medicine, Chiang Mai University, Chiang Mai, Thailand*
[3]*Center of Excellence in Cardiac Electrophysiology Research, Chiang Mai University, Chiang Mai, Thailand*
[4]*Department of Oral Biology and Diagnostic Sciences, Faculty of Dentistry, Chiang Mai University, Chiang Mai, Thailand*

New Findings

- **What is the central question of this study?**
  Myocardial ischaemia–reperfusion (I/R) injury causes interference in the systemic circulation and damages not only the heart but also several vital organs, including the brain. Recently, a novel peptide called humanin has been shown to exert potent neuroprotective effects. However, the effect of humanin on the brain during cardiac I/R injury has not yet been investigated.
- **What is the main finding and its importance?**
  The I/R injury caused blood–brain barrier breakdown, increased brain oxidative stress and resulted in mitochondrial dysfunction. Only the humanin treatment before ischaemia attenuated brain mitochondrial dysfunction, but it did not prevent blood–brain barrier breakdown or brain oxidative stress. Humanin treatment during ischaemia and in the reperfusion period provided no neuroprotection. These findings indicate that humanin exerted neuroprotection during cardiac I/R injury via improved brain mitochondrial function.

Myocardial ischaemia–reperfusion (I/R) injury causes interference in the systemic circulation and damages not only the heart but also several vital organs, including the brain. Nevertheless, limited information is available regarding the effect of cardiac I/R injury on the brain, including blood–brain barrier (BBB) breakdown, brain oxidative stress and mitochondrial function. Recently, a novel peptide called humanin has been shown to exert potent neuroprotective effects. However, the effect of humanin on the brain during cardiac I/R injury has not yet been investigated. Forty-two male Wistar rats were divided into the following two groups: an I/R group, which was subjected to a 30 min left anterior descending coronary artery occlusion followed by 120 min reperfusion (I/R group; $n = 36$); and a sham group ($n = 6$). The I/R group was divided into six subgroups. Each subgroup was given either vehicle or humanin analogue (84 μg kg^{-1}, I.V.) at three different time points, namely before ischaemia, during ischaemia or at the onset of reperfusion. At the end of the experimental protocol, animals were killed and the brains removed for determination of mitochondrial function, oxidative stress and Western blot analyses. The I/R injury caused BBB breakdown, increased brain oxidative stress and resulted in mitochondrial dysfunction. Only the humanin treatment before ischaemia attenuated brain mitochondrial dysfunction, but it did not prevent BBB breakdown or brain

Experimental Physiology

© 2016 The Authors. Experimental Physiology © 2016 The Physiological Society

DOI: 10.1113/EP085749

oxidative stress. Humanin treatment during ischaemia and in the reperfusion period provided no neuroprotection. These findings indicate that humanin exerted neuroprotection during cardiac I/R injury via improved brain mitochondrial function.

(Received 9 February 2016; accepted after revision 31 March 2016; first published online 5 April 2016)
Corresponding author S. C. Chattipakorn: Neurophysiology Unit, Cardiac Electrophysiology Research and Training Center, Faculty of Medicine, Chiang Mai University, Chiang Mai 50200, Thailand. Email: scchattipakorn@gmail.com and siriporn.c@cmu.ac.th

Introduction

Acute myocardial infarction is a major cause of death worldwide (Hausenloy & Yellon, 2013; Okwuosa *et al.* 2016). In patients with acute myocardial infarction, the treatment of choice for reducing acute myocardial ischaemic injury and limiting the infarct size is myocardial reperfusion (Honda *et al.* 2014; Horvat & Vincelj, 2015). However, myocardial reperfusion itself is known to cause deleterious effects to the ischaemic myocardium, a process known as reperfusion injury (Buja, 2005; Hausenloy & Yellon, 2013). The major mediators of reperfusion injury are free radicals, calcium loading and neutrophil infiltration, which cause massively increased oxidative stress levels in the heart (Zweier *et al.* 1987; Miyamae *et al.* 1996; Hausenloy & Yellon, 2013). Compromised circulation as a result of acute myocardial infarction and reperfusion injury also causes interference in the systemic blood flow (Iwakura *et al.* 1996; Buja, 2005). Therefore, when myocardial ischaemia–reperfusion (I/R) injury occurs, several vital organs, including the brain, are also affected (Hausenloy & Yellon, 2013; Sanderson *et al.* 2013). Similar to the heart, I/R injury could occur in the brain during myocardial I/R injury, resulting in a burst of oxidative stress in the brain that leads to blood–brain barrier (BBB) breakdown, oxidative stress, mitochondrial swelling, brain apoptosis and brain death (Nour *et al.* 2013; Sanderson *et al.* 2013). The integrity of the BBB is vital because it controls and maintains cerebral homeostasis (Alves, 2014). Disruption of the BBB leads to increased membrane lipid peroxidation and oxidative cell damage and contributes to further damage by increasing vascular permeability (Mertsch *et al.* 2001; Donkin *et al.* 2009). All of these events after BBB breakdown can lead to brain edema (Donkin *et al.* 2009; Bektas *et al.* 2010; Katada *et al.* 2012).

Mitochondria play a critical role in the pathogenesis of cerebral I/R injury (Silachev *et al.* 2015; Novgorodov *et al.* 2016). Mitochondrial dynamics, including mitochondrial fusion and fission, regulate the mitochondrial function, shape control and communication (Detmer & Chan, 2007; Chen & Chan, 2009). At least four proteins have been shown to be associated with mitochondrial fusion and fission. Three mammalian proteins, including Mfn1, Mfn2 and OPA, are required for mitochondrial fusion (Song *et al.* 2009), whereas dynamin-like protein (DRP1) is recruited to mitochondria during fission (Otera *et al.* 2010). Disruption of mitochondrial dynamics has been found in several major neurodegenerative diseases, including Parkinson's, Alzheimer's and Huntington's diseases (Detmer & Chan, 2007; Chen & Chan, 2009). Currently, the molecular events in the brain, including BBB breakdown and the disruption of mitochondrial dynamics, in conditions of myocardial I/R injury have rarely been investigated.

Humanin is a protein normally encoded by mitochondrial DNA and with some known/suspected normal physiological role(s). It has been shown that humanin protects cells from oxidative stress, serum starvation, hypoxia and other insults *in vitro* and also improves cardiovascular disease and Alzheimer's disease *in vivo* (Klein *et al.* 2013; Yen *et al.* 2013). Humanin is a novel neuroprotective and cytoprotective peptide that has anti-apoptotic, antioxidant and anti-inflammatory properties (Klein *et al.* 2013). Moreover, humanin suppressed the neuronal cell death induced by proteins related to Alzheimer's disease and amyloid-β accumulation (Hashimoto *et al.* 2001). Humanin is also found to bind selectively to the pro-apoptotic protein Bax and prevent Bax translocation from the cytoplasm to the mitochondria, resulting in suppression of cell apoptosis (Luciano *et al.* 2005). Moreover, a humanin analogue has been found to decrease oxidative stress and preserve mitochondrial integrity in cardiac myoblasts (Klein *et al.* 2013). Humanin has been shown previously to exert neuroprotection in the brain with I/R injury (Xu *et al.* 2006). Also, humanin has been shown to provide cardioprotection during cardiac injury (Muzumdar *et al.* 2010). However, the effect of cardiac I/R insult on the brain mitochondrial function and whether humanin exerts protective effects on the brain mitochondrial function impaired by cardiac I/R injury has not previously been investigated.

In this study, we investigated whether myocardial I/R injury could lead to BBB breakdown, increased brain oxidative stress, brain mitochondrial dysfunction, brain mitochondrial dynamic imbalance and susceptibility of the brain to apoptosis. In addition, we determined the temporal effect of administration of the humanin analogue on the brain in response to myocardial I/R injury.

© 2016 The Authors. Experimental Physiology © 2016 The Physiological Society

Methods

Ethical approval

All animal studies were approved by the Institutional Animal Care and Use Committee of the Faculty of Medicine, Chiang Mai University (permit number: 31/2558), and conformed to the *Guide for the Care and Use of Laboratory Animals* published by the US National Institutes of Health (NIH guide, 8th edition, 2011). We understand the ethical principles under which the journal operates, and our work complies with the animal ethics checklist. Adult male Wistar rats (300–350 g, $n = 42$) were obtained from the National Laboratory Animal Center, Mahidol University, Bangkok, Thailand. All animals were given *ad libitum* access to food and water. All animals were housed in rooms with controlled temperature and humidity and with 12 h–12 h light–dark cycles.

Experimental design

Male Wistar rats were subjected to a myocardial I/R injury protocol. Rats were randomly divided into seven groups ($n = 6$ per group) as follows: (i) sham group; (ii) myocardial I/R group with normal saline (NSS) administration 15 min before I/R; (iii) myocardial I/R group with humanin analogue (HNG) administration (84 μg kg^{-1}, I.V.; Wang *et al.* 2013) 15 min before I/R; (iv) myocardial I/R group with NSS administration 15 min after occlusion; (v) myocardial I/R group with HNG administration (84 μg kg^{-1}, I.V.; Wang *et al.* 2013) 15 min after occlusion; (vi) myocardial I/R group with NSS administration at the onset of reperfusion; and (vii) myocardial I/R group with HNG administration (84 μg kg^{-1}, I.V.; Wang *et al.* 2013) at the onset of reperfusion. The animals were killed by an overdose injection of Zoletil (Zoletil contain Tiletamine 50 mg and Zolazepam 50 mg, Virbac Corporation, Fort Worth, TX, USA) (100 mg kg^{-1}), I.M. prior to organ removal. One half of the brain was rapidly removed for mitochondrial isolation and the other half was used for Western blot and malondialdehyde (MDA) analysis. Isolated brain mitochondria were used to investigate mitochondrial function. The experimental protocol is shown in Fig. 1.

Myocardial I/R injury protocol

Rats were anaesthetized using an I.M. injection of Zoletil (50 mg kg^{-1}) and xylazine X-LAZINE (Xylazine 20 mg, L.B.S. laboratory Ltd., Bangkok, Thailand) (0.15 ml kg^{-1}). The depth of anesthesia was checked by testing the absence of the eyelid reflex, the pedal withdrawal reflex and the tail pinch reflex. If rats retained the reflex, they were given another Zoletil and xylazine injection at the same dose as before to induce deep anaesthesia. A tracheostomy was performed, and rats were ventilated with room air using a rodent ventilator at a volume of 200–250 μl, with the ventilation rate at 70–110 breaths min^{-1} to maintain the P_{CO_2}, P_{O_2} and pH within the normal physiological ranges (Palee *et al.* 2013; Surinkaew *et al.* 2013). A left-sided thoracotomy was performed at the fourth intercostal space, and the pericardium was incised to expose the heart (Palee *et al.* 2013; Surinkaew *et al.* 2013). The left anterior descending coronary artery was identified and

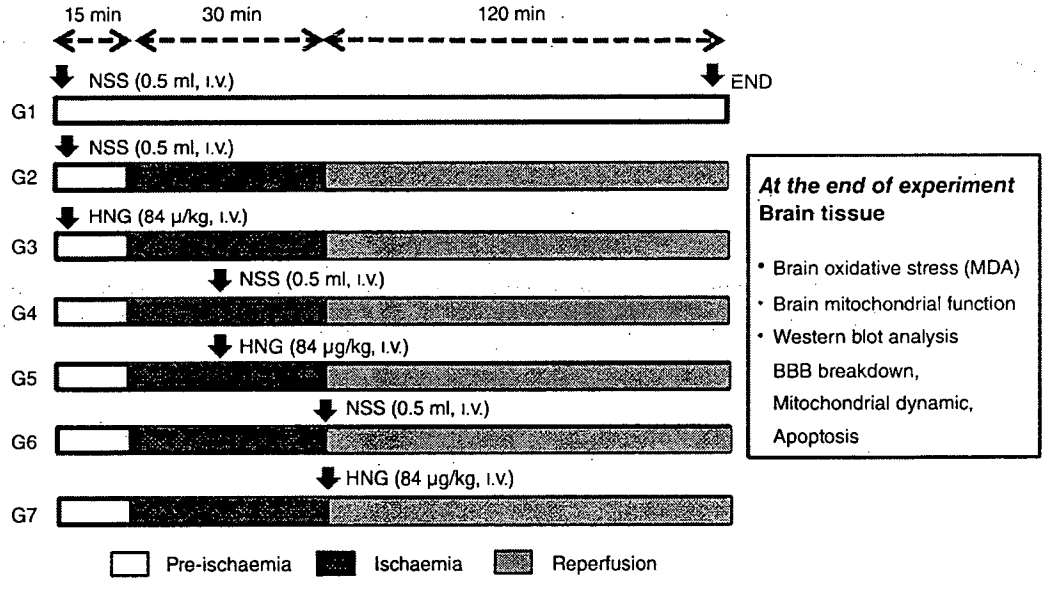


Figure 1. Study protocol for experimental groups (G1–G7) and timing of humanin analogue (HNG) or normal saline solution (NSS) administration

© 2016 The Authors. Experimental Physiology © 2016 The Physiological Society

ligated ~2 mm distal to its origin. The end of a ligature was passed through a small vinyl tube, and was used to occlude the coronary artery by pulling the thread. The lead II ECG was recorded throughout the experiment, and ST elevation was used to confirm ischaemia. The heart was subjected to ischaemia for 30 min, after which the ligature was loosened for the ischaemic myocardium to be reperfused for 120 min (Palee *et al.* 2013; Surinkaew *et al.* 2013).

Determination of brain oxidative stress by measuring malondialdehyde concentration

The brain MDA concentration measured by using the HPLC method as previously described (Sripetchwandee *et al.* 2014). The brain tissues were homogenized in a phosphate buffer, and brain homogenate was mixed with 10% (w/v) trichloroacetic acid, heated to 90°C for 30 min and cooled down to room temperature. The mixture was centrifuged at 3300 g for 10 min to achieve a clear supernatant. The supernatant was mixed with 0.44 M H_3PO_4 and 0.6% (w/v) thiobarbituric acid solution and incubated at 90°C for 30 min to produce pink products called thiobarbituric acid-reactive substances (TBARS). The solution was passed through a syringe filter (polysulfone type membrane, pore size 0.45 μm) and analysed with the HPLC system at 532 nm. Data were collected and analysed using the BDS software (BarSpec Ltd., Rehovot, Israel). Tissue TBARS concentrations were determined directly from a standard curve and reported as the MDA equivalent concentration in micromolar per milligram of protein.

Isolation of brain mitochondria

Brain mitochondria were isolated using the differential centrifugation method (Sripetchwandee *et al.* 2014). The rat brains were quickly removed into ice-cold MSE solution (225 mM mannitol, 75 mM sucrose, 1 mM EGTA, 5 mM Hepes and 1 mg ml^{-1} bovine serum albumin, pH 7.4) to flush the blood out rapidly. Each brain was transferred into 5 ml of cold MSE–nagarse solution (0.05% nagarse enzyme (protease) in MSE solution). The brain tissue was finely minced and homogenized by the homogenizer at 600 r.p.m. The homogenate was then centrifuged at 2000*g* for 4 min, and the supernatants were collected and centrifuged at 12,000*g* for 9 min. Mitochondrial pellets were resuspended in cold MSE–digitonin solution and centrifuged once more at 12,000*g* for 11 min. Mitochondrial pellets were collected and dissolved in cold respiration (RES) buffer (containing 150 mM KCl, 5 mM Hepes, 5 mM $K_2HPO_4.3H_2O$, 2 mM L-glutamate and 5 mM pyruvate sodium salt). The protein concentration was determined according to the bicinchoninic acid assay as previously described (Sripetchwandee *et al.* 2014).

Determination of brain mitochondrial reactive oxygen species (ROS) production

Brain mitochondrial ROS production was determined using the dichlorohydro-fluorescein diacetate (DCFDA) dye (Novalija *et al.* 2003). Brain mitochondria were incubated with 2 μM DCFDA at 25°C for 20 min. The ROS levels were determined via a fluorescent microplate reader at an excitation wavelength of 485 nm and an emission wavelength of 530 nm. The ROS level was represented as arbitrary units of fluorescence intensity of dichlorohydro-fluorescein (DCF).

Determination of brain mitochondrial membrane potential changes ($\Delta\Psi$m)

Brain mitochondrial membrane potential changes were measured using the dye 5,5′,6,6′-tetrachloro-1,1′,3,3′-tetraethylbenzimidazolcarbocyanine iodide (JC-1; Tong *et al.* 2005). Brain mitochondria were stained with JC-1 (310 nM) at 37°C for 15 min. The fluorescence intensity was determined using a fluorescence microplate reader. The fluorescence of JC-1 monomer form (green) was excited at 488 nm, and the emission was detected at 530 nm. JC-1 aggregate (red) fluorescence was excited at 488 nm, and emission fluorescence was detected at 590 nm. Mitochondrial depolarization was indicated by a decreased red/green fluorescent intensity ratio ($\Delta\Psi$m).

Determination of brain mitochondrial swelling

Brain mitochondrial swelling was determined by the changes in the absorbance of the mitochondrial suspensions at 540 nm using a microplate reader (Ruiz-Meana *et al.* 2006). Mitochondria were incubated in RES buffer. A decrease in absorbance represented brain mitochondrial swelling.

Identification of brain mitochondria using electron microscopy

A transmission electron microscope was used to study brain mitochondrial morphology (Sripetchwandee *et al.* 2014). Isolated brain mitochondria were fixed overnight in 2.5% glutaraldehyde in 0.1 M cacodylate buffer, pH 7.4 at 4°C. After that, brain mitochondria were postfixed with 1% cacodylate-buffered osmium tetroxide for 2 h at room temperature. The brain mitochondrial pellets were subsequently dehydrated in a graded series of ethanol and embedded in Epon-Araldite. Ultrathin sections were cut with a diamond knife, placed on copper grids, stained with uranyl acetate and lead citrate, and observed with a transmission electron microscope.

© 2016 The Authors. Experimental Physiology © 2016 The Physiological Society

Western blot analysis

At the end of experiment, the brain tissues were collected, quickly frozen in liquid nitrogen, and stored at −80°C for further analysis. Whole brain tissues were lysed with extraction buffer (20 mmol l^{-1} Tris–HCl, 1 mmol l^{-1} Na_3VO_4 and 5 mmol l^{-1} NaF) and separated by electrophoresis on a 10% SDS–polyacrylamide gel and then transferred onto nitrocellulose membranes (Sripetchwandee *et al.* 2014). Immunoblots were blocked for 1 h with 5% non-fat dry milk in Tris-buffered saline (pH 7.4) containing 0.1% Tween 20. They were then probed overnight at 4°C with the primary antibodies (1:1000 dilution; Cell Signaling Technology, Danvers, MA, USA and Santa Cruz Biotechnology, Inc., Dallas, TX, USA) that recognized the tight junction protein [occludin (H-279)], pro-apoptotic protein [Bax (D3R2M)], anti-apoptotic protein [Bcl-2, code 2876], mitochondrial fusion protein [Mfn2 (D2D10)], mitochondrial fission protein [DRP1 (D8H5)] and a loading control (β-actin). This process was followed by 1 h of incubation at room temperature with a horseradish peroxidase-conjugated secondary antibody. The blots were then visualized with an enhanced chemiluminescence (ECL) reagent. The film images of the Western blots were scanned and subsequently analysed using ImageJ (NIH image) analysis software.

Statistical analysis

All data were presented as means ± SEM and processed using SPSS (Statistical Package for Social Sciences release 16.0; SPSS Inc., Chicago, IL, USA). A one-way ANOVA followed by Tukey's HSD *post hoc* test was performed for the comparison among all cardiac I/R groups. Student's unpaired *t* test was performed for the comparison between the sham and the cardiac I/R groups. A P value of <0.05 was considered statistically significant.

Results

Effects of myocardial I/R injury on the brain

Myocardial I/R injury led to an increase in BBB breakdown as shown by a decrease in the expression of occludin, when compared with the sham group (Fig. 2*A*). In addition, increased brain MDA levels were observed in the I/R group, when compared with the sham group (Fig. 2*B*). These findings suggested that myocardial I/R injury leads to BBB breakdown and increased brain oxidative stress. In the I/R group, brain mitochondrial ROS production (Fig. 3*A*), brain mitochondrial depolarization (Fig. 3*B*) and brain mitochondrial swelling (Fig. 3*C* and *D*) were significantly greater than those of the sham group. These findings suggested that myocardial I/R injury led to increased brain mitochondrial dysfunction.

Rats in the I/R group showed a decrease in brain Mfn2 protein expression (Fig. 4*A*), whereas the expression of DRP1 was not altered in both the sham and the I/R groups (Fig. 4*B*). The Mfn2/DRP1 ratio was also decreased in the brain of rats with myocardial I/R injury (Fig. 4*C*), suggesting that the I/R led to brain mitochondrial dynamic imbalance. Moreover, myocardial I/R injury led to an increase in brain pro-apoptotic (Bax) protein expression (Fig. 5*A*), but had no effect on anti-apoptotic (Bcl-2) protein expression (Fig. 5*B*). The Bax/Bcl-2 ratio was also increased in the brain of I/R rats (Fig. 5*C*), suggesting that rats in the I/R group were susceptible to brain apoptosis.

Effects of HNG treatment on BBB breakdown and brain MDA levels in rats with myocardial I/R injury

Treatment with HNG before ischaemia, during ischaemia and at the onset of reperfusion did not increase occludin

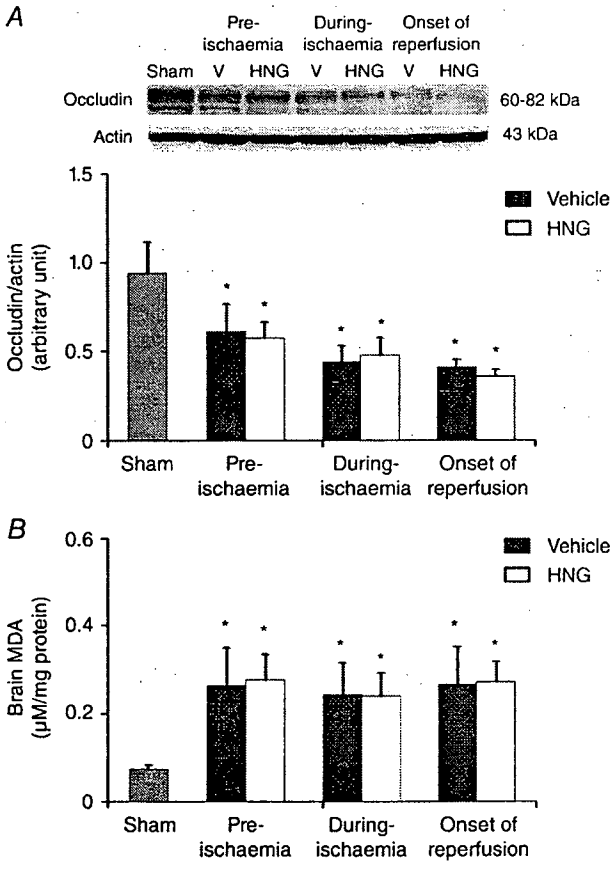


Figure 2. The effects of HNG treatment on blood–brain barrier breakdown (*A*) and brain malondialdehyde (MDA) level (*B*)
Abbreviations: HNG, humanin analogue; Sham, surgery without ischaemia–reperfusion; Vehicle, vehicle group with myocardial ischaemia–reperfusion injury; and V, vehicle.
*$P < 0.01$ *versus* sham group.

© 2016 The Authors. Experimental Physiology © 2016 The Physiological Society

expression (Fig. 2*A*), suggesting that HNG treatment did not prevent BBB breakdown in I/R rats. In addition, in all periods of treatment with HNG, brain MDA levels did not decrease (Fig. 2*B*), indicating that HNG treatment did not reduce brain oxidative stress in the I/R group.

Effects of HNG treatment on brain mitochondrial function

Only treatment with HNG before ischaemia restored brain mitochondrial function, as shown by decreased brain mitochondrial ROS levels (Fig. 3*A*), decreased brain mitochondrial depolarization (Fig. 3*B*), reduced brain mitochondrial swelling (Fig. 3*C*) and preserved brain mitochondrial morphology (Fig. 3*D*). However, treatment with HNG during ischaemia and at the onset of reperfusion did not improve brain mitochondrial function in these myocardial I/R rats (Fig. 3*A–D*).

Effects of HNG treatment on brain mitochondrial fusion and fission

Treatment with HNG before ischaemia, during ischaemia and at the onset of reperfusion altered neither the expression of Mfn2 and DRP1 nor the Mfn2/DRP1 ratio in myocardial I/R rats, when compared with vehicle-treated I/R rats (Fig. 4*A–D*). These findings suggested that HNG did not improve the brain mitochondrial dynamic balance in rats experiencing myocardial I/R.

Effects of HNG treatment on susceptibility of the brain to apoptosis

Only treatment with HNG before ischaemia effectively reduced Bax protein expression (Fig. 5*A* and *D*) and decreased the Bax/Bcl2 ratio (Fig. 5*C*) in these myocardial I/R rats. However, treatment with HNG during ischaemia and at the onset of reperfusion did not decrease Bax

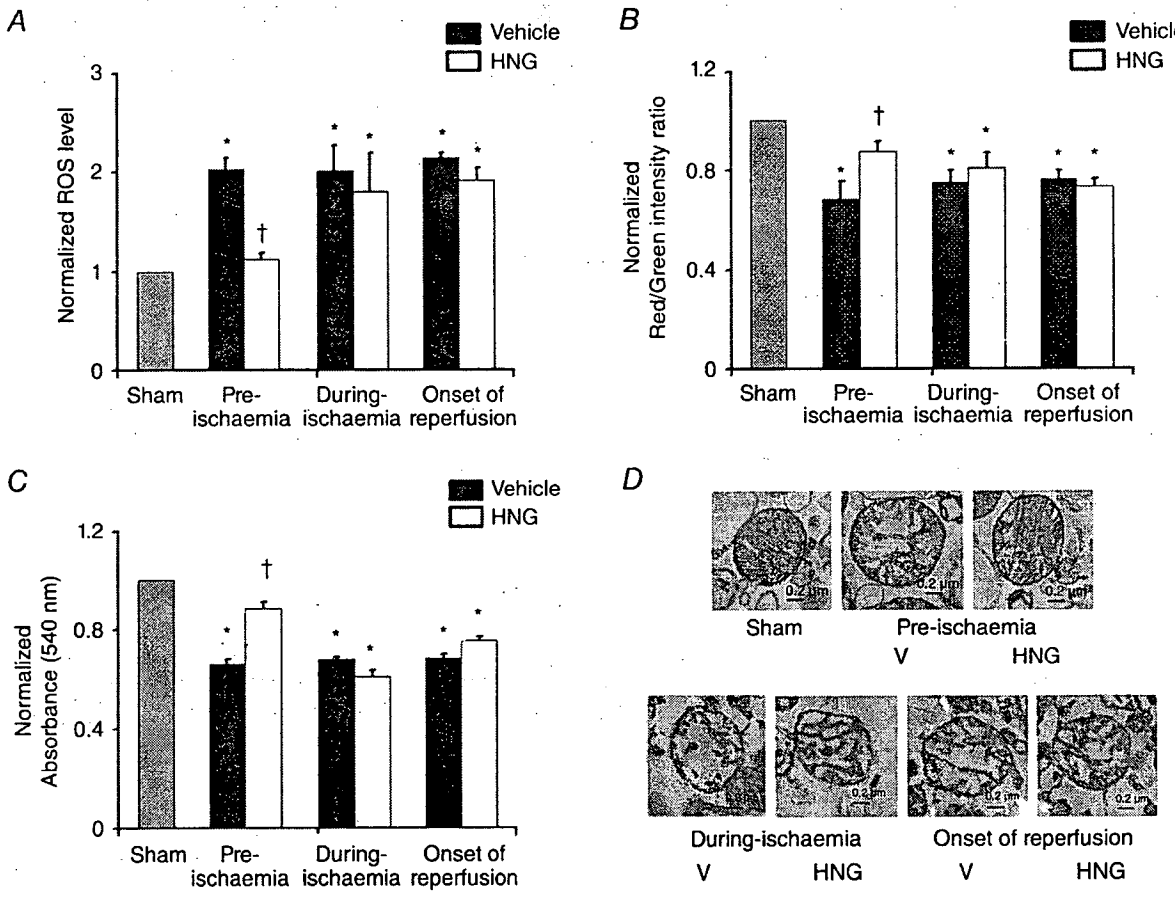


Figure 3. The effects of HNG treatment on mitochondrial function
A, brain mitochondrial reactive oxygen species (ROS) production. *B*, brain mitochondrial depolarization. *C*, brain mitochondrial swelling. *D*, brain mitochondrial morphology. Abbreviations: HNG, humanin analogue; and V, vehicle. $^{*}P < 0.05$ *versus* sham group. $^{\dagger}P < 0.05$ *versus* vehicle group with myocardial ischaemia–reperfusion injury.

© 2016 The Authors. Experimental Physiology © 2016 The Physiological Society

protein expression (Fig. 5*A* and *D*) or the Bax/Bcl2 ratio (Fig. 5*C*). None of the treatments altered Bcl2 protein expression (Fig. 5*B*). These findings suggested that only treatment with HNG before ischaemia could effectively reduce the susceptibility of the brain to apoptosis as a result of myocardial I/R injury.

Discussion

The major findings of the present study are as follows. First, myocardial I/R injury caused BBB breakdown, leading to an increase in brain oxidative stress. Second, myocardial I/R injury caused increased brain mitochondrial ROS production, brain mitochondrial depolarization and brain mitochondrial swelling, resulting in brain mitochondrial dysfunction. Third, myocardial I/R injury also caused brain mitochondrial dynamic imbalance and increased the susceptibility of the brain to apoptosis. Fourth, treatment with humanin before myocardial I/R injury attenuated brain mitochondrial dysfunction and reduced the susceptibility of the brain to apoptosis, but had no effect on BBB breakdown, brain oxidative stress and mitochondrial dynamics. Fifth, treatment with humanin during ischaemia or in the reperfusion period did not improve any of the studied brain parameters in rats undergoing myocardial I/R injury.

Previous studies have shown that myocardial I/R injury can lead to I/R injury in other organs or tissues, particularly in the brain (Hausenloy & Yellon, 2013; Sanderson *et al.* 2013). It has been shown that during brain I/R injury a burst of oxidative stress is observed in the brain, leading to BBB breakdown, mitochondrial swelling, brain apoptosis and brain death (Nour *et al.* 2013; Sanderson *et al.* 2013). The increase in ROS is known to increase permeability of the BBB in a time- and concentration-dependent manner (Lee *et al.* 2004; Haorah *et al.* 2007). In the present study, we demonstrated that I/R injury in the heart, not in the brain, also caused BBB breakdown as shown by a decrease in brain occludin protein expression, leading to increased brain oxidative

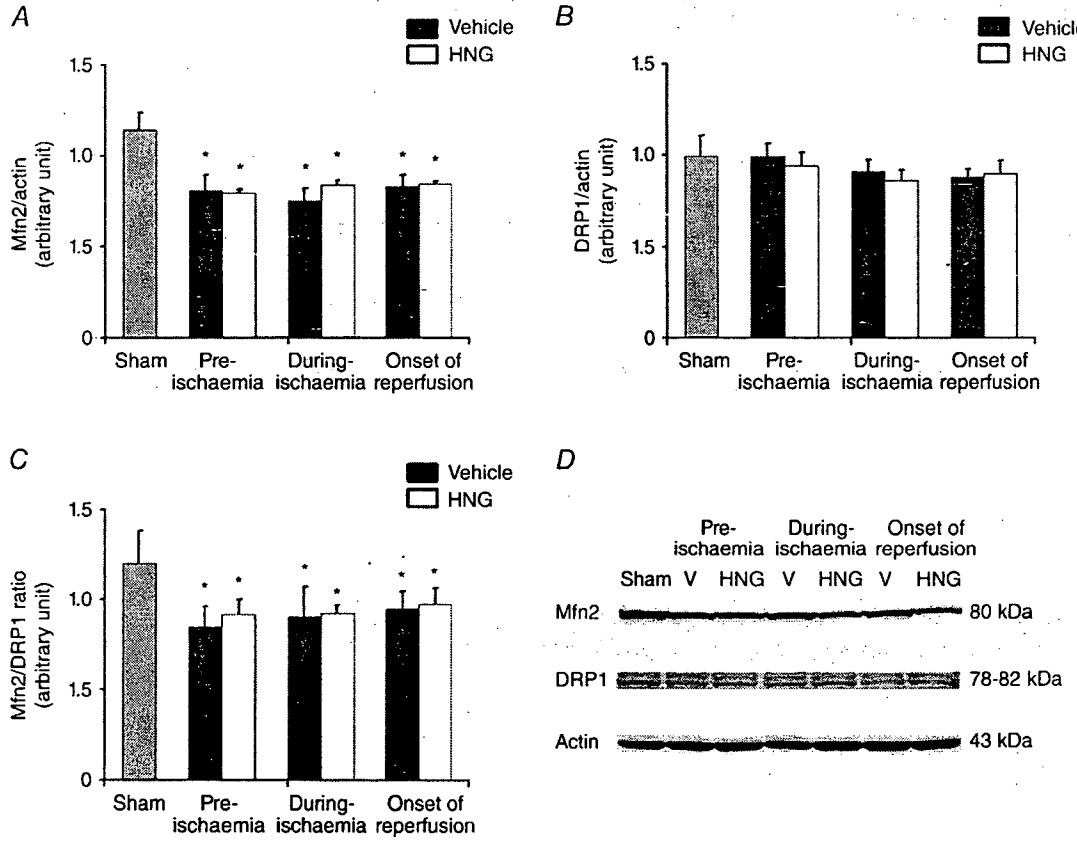


Figure 4. The effects of HNG treatment on mitochondrial dynamic balance
A, mitochondrial fusion (Mfn2) protein expression. *B*, mitochondrial fission (DRP1) protein expression. *C*, Mfn2/DRP1 ratio. *D*, Western blot band. Abbreviations: HNG, humanin analogue; and V, vehicle. $^{*}P < 0.05$ *versus* sham group.

© 2016 The Authors. Experimental Physiology © 2016 The Physiological Society

stress, as shown by markedly increased brain MDA levels. Moreover, increased brain oxidative stress, caused by myocardial I/R injury, could lead to brain mitochondrial dysfunction, as shown by increased brain mitochondrial ROS production, brain mitochondrial depolarization and brain mitochondrial swelling.

It has been shown that the ratio of fusion/fission proteins is important for the maintenance of neuronal mitochondrial morphology and viability (Uo *et al.* 2009; Wang *et al.* 2009). Moreover, a study in a mouse model of heart failure demonstrated that an imbalance of fusion/fission proteins occurred (Givvimani *et al.* 2012). Therefore, the balance of mitochondrial dynamics, as indicated by the ratio of Mfn2/DRP1 in our study, plays a critical role in cell growth, cell signaling mechanisms and cell death. An imbalance of mitochondrial dynamics, resulting in abnormal mitochondrial function and cell apoptosis, has been found in several neurodegenerative diseases and cardiovascular diseases (Detmer & Chan, 2007; Chen & Chan, 2009; Givvimani *et al.* 2014). We demonstrated in the present study that brain stress induced by myocardial I/R injury also caused brain mitochondrial dynamic imbalance and increased the susceptibility of the brain to apoptosis, as indicated by the decreased Mfn2/DRP1 ratio and increased Bax/Bcl2 ratio, respectively. All of these findings suggest that myocardial I/R injury can lead to brain death by causing BBB breakdown, brain mitochondrial dysfunction and increased susceptibility of the brain to apoptosis.

Humanin is a newly discovered 21- or 24-amino-acid peptide, depending on mitochondrial or cytoplasmic translation, respectively (Zapała *et al.* 2010; Yen *et al.* 2013). Humanin has been shown to exert neuroprotective and cytoprotective effects, with anti-apoptotic, antioxidant and anti-inflammatory properties (Klein *et al.* 2013). In the present study, myocardial I/R injury caused a decrease in occludin and increased brain MDA, thus indicating BBB breakdown and increased brain oxidative stress. However, our results showed that treatment with HNG before ischaemia, during ischaemia and at the onset of reperfusion did not increase occludin expression and decreased brain MDA levels, indicating that it did not

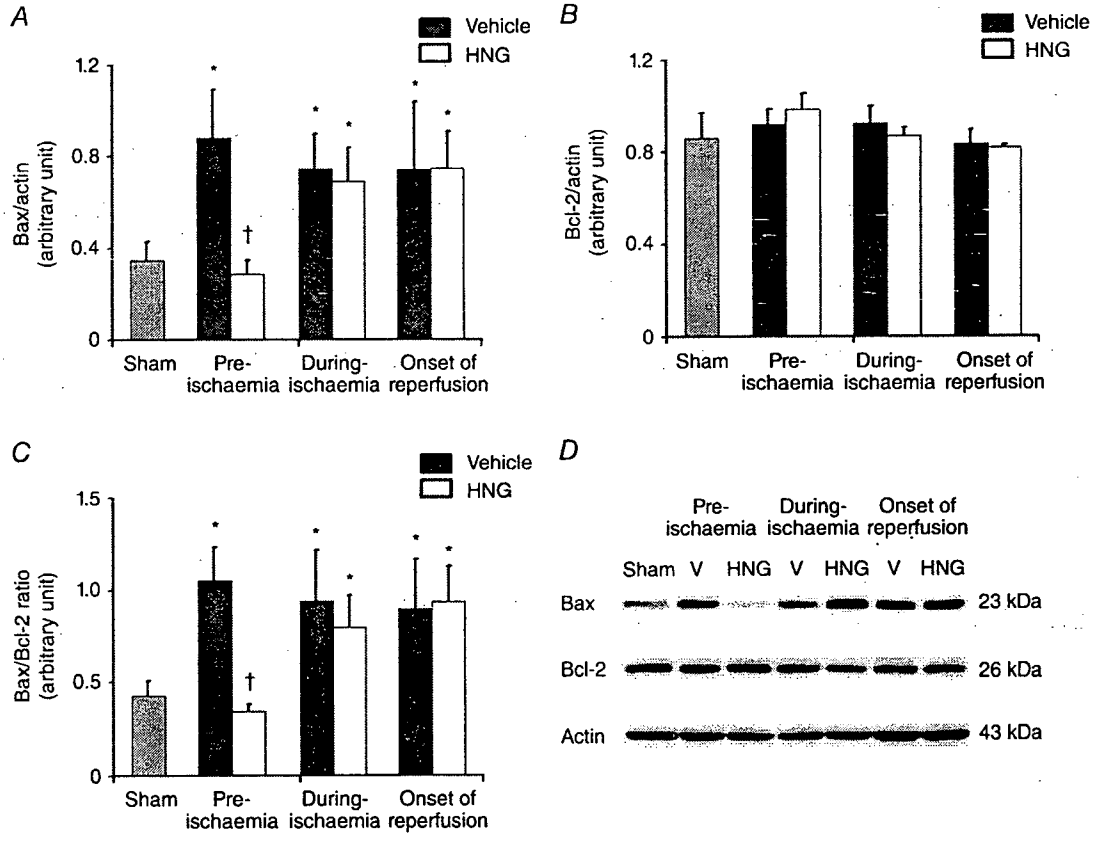


Figure 5. The effects of HNG treatment on susceptibility of the brain to apoptosis
A, pro-apoptotic Bax protein expression. *B*, anti-apoptotic Bcl-2 protein expression. *C*, Bax/Bcl-2 ratio. *D*, Western blot band. Abbreviations: HNG, humanin analogue; and V, vehicle. *$P < 0.05$ *versus* sham group. †$P < 0.05$ *versus* vehicle group with myocardial ischaemia–reperfusion injury.

© 2016 The Authors. Experimental Physiology © 2016 The Physiological Society

attenuate BBB breakdown or oxidative stress in the brain after myocardial I/R injury. Although previous *in vitro* studies demonstrated that humanin can protect cells from oxidative stress induced by hydrogen peroxide, oxidized low-density lipoprotein and I/R injury in endothelial cells (Bachar *et al.* 2010), cardiac myoblasts (Klein *et al.* 2013), cortical neuronal culture (Zhao *et al.* 2012) and in endothelial cells of ApoE-deficient mice (Oh *et al.* 2011), our findings from *in vivo* models indicated otherwise, suggesting the importance of study models for clinical application. However, the effective dose of humunin used in the ApoE-deficient mice was higher than the dose used in the present study (Oh *et al.* 2011). Therefore, it is also possible that the HNG concentration used in the present study might not be sufficient to reduce oxidative stress in the brain after myocardial I/R injury.

In this study, myocardial I/R injury was found to cause brain mitochondrial stress, including brain mitochondrial dysfunction, brain mitochondrial dynamic imbalance and an increase in the susceptibility of the brain to apoptosis. Only treatment with HNG before ischaemia decreased brain mitochondrial ROS levels, suggesting that HNG exerted antioxidant properties. In the present study, treatment with HNG before ischaemia effectively reduced Bax protein expression and decreased the Bax/Bcl2 ratio in these rats undergoing myocardial I/R. Moreover, only humanin treatment before myocardial I/R injury attenuated brain mitochondrial dysfunction. These findings suggested that humanin exerted an anti-apoptotic effect, which is consistent with a previous study demonstrating that HNG prevents mitochondrial dysfunction in stressed conditions by selectively binding to Bax in the cytoplasm and preventing Bax translocation from the cytoplasm to the mitochondria, thus suppressing apoptosis (Guo *et al.* 2003; Jin *et al.* 2010; Klein *et al.* 2013). However, the mechanism by which humanin reduces Bax protein expression, as shown in the present study, is still unknown. It might be that humanin interacts with Bax and leads to a protein conformational change and may lead to degradation, then reduced susceptibility to apoptosis. However, treatment with humanin during ischaemia or at the onset of reperfusion period did not improve any of the parameters of brain dysfunction in rats undergoing myocardial I/R injury. This may be because these treatment periods are too late to improve brain stress and brain dysfunction in conditions of myocardial I/R injury. Moreover, future study is needed to investigate the dose-dependent effect of HNG administered during these periods.

Although there is currently no direct evidence that humanin could cross the BBB, several studies have demonstrated this possibility. For example, Krejcova *et al.* (2004) showed that administration of HNG (I.P.) in rats reversed the impairment of spatial memory induced by 3-quinuclidinyl benzilate, suggesting that HNG could cross the BBB in the absence of a disrupted BBB. Xu *et al.* (2006) showed that HNG administration I.P. reduced the infarct volume in mice with cerebral I/R injury, suggesting that the disruption of BBB endothelial cells by I/R injury facilitated the crossing of HNG through the BBB. Alternatively, it is possible that HNG can cross the BBB without disruptions in some conditions, such as ischaemic brain damage (Xu *et al.* 2006).

There are several limitations to the present study. First, there was no dose-dependent study performed to test an optimal dose for the maximal neuroprotective effects following cardiac I/R injury. Second, the data of protein analysis (Western blot) were from the whole brain cell lysate, not from the mitochondrial fraction; therefore, the change of total protein expression in whole cells could be different from that in the mitochondrial fraction. Moreover, although no direct evidence that humanin could cross the BBB is available, several studies have demonstrated this possibility (Krejcova *et al.* 2004; Xu *et al.* 2006). Future studies are needed to investigate this issue.

In conclusion, the present study demonstrates the deleterious effects of myocardial I/R injury in the brain as represented by BBB breakdown, brain oxidative stress, brain mitochondrial dysfunction and the increased susceptibility of the brain to apoptosis. Pretreatment with humanin attenuated mitochondrial dysfunction and reduced the susceptibility of the brain to apoptosis in response to myocardial I/R injury. These findings suggest that prophylactic therapy with humanin might be useful to preserve brain function after myocardial I/R injury. However, the suitable doses of HNG to protect the brain completely after acute myocardial infarction will require further study.

References

Alves JL (2014). Blood-brain barrier and traumatic brain injury. *J Neurosci Res* **92**, 141–147.

Bachar AR, Scheffer L, Schroeder AS, Nakamura HK, Cobb LJ, Oh YK, Lerman LO, Pagano RE, Cohen P & Lerman A (2010). Humanin is expressed in human vascular walls and has a cytoprotective effect against oxidized LDL-induced oxidative stress. *Cardiovasc Res* **88**, 360–366.

Bektas H, Wu TC, Kasam M, Harun N, Sitton CW, Grotta JC & Savitz SI (2010). Increased blood–brain barrier permeability on perfusion CT might predict malignant middle cerebral artery infarction. *Stroke* **41**, 2539–2544.

Buja LM (2005). Myocardial ischemia and reperfusion injury. *Cardiovasc Pathol* **14**, 170–175.

Chen H & Chan DC (2009). Mitochondrial dynamics–fusion, fission, movement, and mitophagy–in neurodegenerative diseases. *Hum Mol Genet* **18**, R169–R176.

Detmer SA & Chan DC (2007). Functions and dysfunctions of mitochondrial dynamics. *Nat Rev Mol Cell Biol* **8**, 870–879.

© 2016 The Authors. Experimental Physiology © 2016 The Physiological Society

Donkin JJ, Nimmo AJ, Cernak I, Blumbergs PC & Vink R (2009). Substance P is associated with the development of brain edema and functional deficits after traumatic brain injury. *J Cereb Blood Flow Metab* **29**, 1388–1398.

Givvimani S, Munjal C, Tyagi N, Sen U, Metreveli N & Tyagi SC (2012). Mitochondrial division/mitophagy inhibitor (Mdivi) ameliorates pressure overload induced heart failure. *PLoS ONE* **7**, e32388.

Givvimani S, Pushpakumar S, Veeranki S & Tyagi SC (2014). Dysregulation of Mfn2 and Drp-1 proteins in heart failure. *Can J Physiol Pharmacol* **92**, 583–591.

Guo B, Zhai D, Cabezas E, Welsh K, Nouraini S, Satterthwait AC & Reed JC (2003). Humanin peptide suppresses apoptosis by interfering with Bax activation. *Nature* **423**, 456–461.

Haorah J, Ramirez SH, Schall K, Smith D, Pandya R & Persidsky Y (2007). Oxidative stress activates protein tyrosine kinase and matrix metalloproteinases leading to blood–brain barrier dysfunction. *J Neurochem* **101**, 566–576.

Hashimoto Y, Niikura T, Tajima H, Yasukawa T, Sudo H, Ito Y, Kita Y, Kawasumi M, Kouyama K, Doyu M, Sobue G, Koide T, Tsuji S, Lang J, Kurokawa K & Nishimoto I (2001). A rescue factor abolishing neuronal cell death by a wide spectrum of familial Alzheimer's disease genes and Aβ. *Proc Natl Acad Sci USA* **98**, 6336–6341.

Hausenloy DJ & Yellon DM (2013). Myocardial ischemia-reperfusion injury: a neglected therapeutic target. *J Clin Invest* **123**, 92–100.

Honda S, Asaumi Y, Yamane T, Nagai T, Miyagi T, Noguchi T, Anzai T, Goto Y, Ishihara M, Nishimura K, Ogawa H, Ishibashi-Ueda H & Yasuda S (2014). Trends in the clinical and pathological characteristics of cardiac rupture in patients with acute myocardial infarction over 35 years. *J Am Heart Assoc* **3**, e000984.

Horvat D & Vincelj J (2015). Impact of reperfusion therapy and infarct localization on frequency of premature ventricular beats in acute myocardial infarction. *Med Glas (Zenica)* **12**, 139–143.

Iwakura K, Ito H, Takiuchi S, Taniyama Y, Nakatsuchi Y, Negoro S, Higashino Y, Okamura A, Masuyama T, Hori M, Fujii K & Minamino T (1996). Alternation in the coronary blood flow velocity pattern in patients with no reflow and reperfused acute myocardial infarction. *Circulation* **94**, 1269–1275.

Jin H, Liu T, Wang WX, Xu JH, Yang PB, Lu HX, Sun QR & Hu HT (2010). Protective effects of [Gly14]-Humanin on β-amyloid-induced PC12 cell death by preventing mitochondrial dysfunction. *Neurochem Int* **56**, 417–423.

Katada R, Nishitani Y, Honmou O, Mizuo K, Okazaki S, Tateda K, Watanabe S & Matsumoto H (2012). Expression of aquaporin-4 augments cytotoxic brain edema after traumatic brain injury during acute ethanol exposure. *Am J Pathol* **180**, 17–23.

Klein LE, Cui L, Gong Z, Su K & Muzumdar R (2013). A humanin analog decreases oxidative stress and preserves mitochondrial integrity in cardiac myoblasts. *Biochem Biophys Res Commun* **440**, 197–203.

Krejcova G, Patocka J & Slaninova J (2004). Effect of humanin analogues on experimentally induced impairment of spatial memory in rats. *J Pept Sci* **10**, 636–639.

Lee HS, Namkoong K, Kim DH, Kim KJ, Cheong YH, Kim SS, Lee WB & Kim KY (2004). Hydrogen peroxide-induced alterations of tight junction proteins in bovine brain microvascular endothelial cells. *Microvasc Res* **68**, 231–238.

Luciano F, Zhai D, Zhu X, Bailly-Maitre B, Ricci JE, Satterthwait AC & Reed JC (2005). Cytoprotective peptide humanin binds and inhibits proapoptotic Bcl-2/Bax family protein BimEL. *J Biol Chem* **280**, 15825–15835.

Mertsch K, Blasig I & Grune T (2001). 4-Hydroxynonenal impairs the permeability of an in vitro rat blood–brain barrier. *Neurosci Lett* **314**, 135–138.

Miyamae M, Camacho SA, Weiner MW & Figueredo VM (1996). Attenuation of postischemic reperfusion injury is related to prevention of $[Ca^{2+}]_m$ overload in rat hearts. *Am J Physiol Heart Circ Physiol* **271**, H2145–H2153.

Muzumdar RH, Huffman DM, Calvert JW, Jha S, Weinberg Y, Cui L, Nemkal A, Atzmon G, Klein L, Gundewar S, Ji SY, Lavu M, Predmore BL & Lefer DJ (2010). Acute humanin therapy attenuates myocardial ischemia and reperfusion injury in mice. *Arterioscler Thromb Vasc Biol* **30**, 1940–1948.

Nour M, Scalzo F & Liebeskind DS (2013). Ischemia-reperfusion injury in stroke. *Interv Neurol* **1**, 185–199.

Novalija E, Kevin LG, Eells JT, Henry MM & Stowe DF (2003). Anesthetic preconditioning improves adenosine triphosphate synthesis and reduces reactive oxygen species formation in mitochondria after ischemia by a redox dependent mechanism. *Anesthesiology* **98**, 1155–1163.

Novgorodov SA, Riley CL, Keffler JA, Yu J, Kindy MS, Macklin WB, Lombard DB & Gudz TI (2016). SIRT3 deacetylates ceramide synthases: implications for mitochondrial dysfunction and brain injury. *J Biol Chem* **291**, 1957–1973.

Oh YK, Bachar AR, Zacharias DG, Kim SG, Wan J, Cobb LJ, Lerman LO, Cohen P & Lerman A (2011). Humanin preserves endothelial function and prevents atherosclerotic plaque progression in hypercholesterolemic ApoE deficient mice. *Atherosclerosis* **219**, 65–73.

Okwuosa IS, Lewsey SC, Adesiyun T, Blumenthal RS & Yancy CW (2016). Worldwide disparities in cardiovascular disease: challenges and solutions. *Int J Cardiol* **202**, 433–440.

Otera H, Wang C, Cleland MM, Setoguchi K, Yokota S, Youle RJ & Mihara K (2010). Mff is an essential factor for mitochondrial recruitment of Drp1 during mitochondrial fission in mammalian cells. *J Cell Biol* **191**, 1141–1158.

Palee S, Weerateerangkul P, Chinda K, Chattipakorn SC & Chattipakorn N (2013). Mechanisms responsible for beneficial and adverse effects of rosiglitazone in a rat model of acute cardiac ischaemia–reperfusion. *Exp Physiol* **98**, 1028–1037.

Ruiz-Meana M, Garcia-Dorado D, Miró-Casas E, Abellán A & Soler-Soler J (2006). Mitochondrial Ca^{2+} uptake during simulated ischemia does not affect permeability transition pore opening upon simulated reperfusion. *Cardiovasc Res* **71**, 715–724.

© 2016 The Authors. Experimental Physiology © 2016 The Physiological Society

Sanderson TH, Reynolds CA, Kumar R, Przyklenk K & Hüttemann M (2013). Molecular mechanisms of ischemia–reperfusion injury in brain: pivotal role of the mitochondrial membrane potential in reactive oxygen species generation. *Mol Neurobiol* **47**, 9–23.

Silachev DN, Plotnikov EY, Zorova LD, Pevzner IB, Sumbatyan NV, Korshunova GA, Gulyaev MV, Pirogov YA, Skulachev VP & Zorov DB (2015). Neuroprotective effects of mitochondria-targeted plastoquinone and thymoquinone in a rat model of brain ischemia/reperfusion injury. *Molecules* **20**, 14487–14503.

Song Z, Ghochani M, McCaffery JM, Frey TG & Chan DC (2009). Mitofusins and OPA1 mediate sequential steps in mitochondrial membrane fusion. *Mol Biol Cell* **20**, 3525–3532.

Sripetchwandee J, Pipatpiboon N, Chattipakorn N & Chattipakorn S (2014). Combined therapy of iron chelator and antioxidant completely restores brain dysfunction induced by iron toxicity. *PLoS ONE* **9**, e85115.

Surinkaew S, Kumphune S, Chattipakorn S & Chattipakorn N (2013). Inhibition of p38 MAPK during ischemia, but not reperfusion, effectively attenuates fatal arrhythmia in ischemia/reperfusion heart. *J Cardiovasc Pharmacol* **61**, 133–141.

Tong V, Teng XW, Chang TK & Abbott FS (2005). Valproic acid II: effects on oxidative stress, mitochondrial membrane potential, and cytotoxicity in glutathione-depleted rat hepatocytes. *Toxicol Sci* **86**, 436–443.

Uo T, Dworzak J, Kinoshita C, Inman DM, Kinoshita Y, Horner PJ & Morrison RS (2009). Drp1 levels constitutively regulate mitochondrial dynamics and cell survival in cortical neurons. *Exp Neurol* **218**, 274–285.

Wang T, Huang Y, Zhang M, Wang L, Wang Y, Zhang L, Dong W, Chang P, Wang Z, Chen X & Tao L (2013). [Gly14]-Humanin offers neuroprotection through glycogen synthase kinase-3β inhibition in a mouse model of intracerebral hemorrhage. *Behav Brain Res* **247**, 132–139.

Wang X, Su B, Lee HG, Li X, Perry G, Smith MA & Zhu X (2009). Impaired balance of mitochondrial fission and fusion in Alzheimer's disease. *J Neurosci* **29**, 9090–9103.

Xu X, Chua CC, Gao J, Hamdy RC & Chua BH (2006). Humanin is a novel neuroprotective agent against stroke. *Stroke* **37**, 2613–2619.

Yen K, Lee C, Mehta H & Cohen P (2013). The emerging role of the mitochondrial-derived peptide humanin in stress resistance. *J Mol Endocrinol* **50**, R11–R19.

Zapała B, Kaczyński L, Kieć-Wilk B, Staszel T, Knapp A, Thoresen GH, Wybrańska I & Dembińska-Kieć A (2010). Humanins, the neuroprotective and cytoprotective peptides with antiapoptotic and anti-inflammatory properties. *Pharmacol Rep* **62**, 767–777.

Zhao ST, Huang XT, Zhang C & Ke Y (2012). Humanin protects cortical neurons from ischemia and reperfusion injury by the increased activity of superoxide dismutase. *Neurochem Res* **37**, 153–160.

Zweier JL, Flaherty JT & Weisfeldt ML (1987). Direct measurement of free radical generation following reperfusion of ischemic myocardium. *Proc Natl Acad Sci USA* **84**, 1404–1407.

Additional information

Competing interests

None declared.

Author contributions

Conception and design of the study: S.K., S.C.C. and N.C. Performed the experiments and analysed data: S.K., S.C.C., S.T.C. and T.J. Initial draft of manuscript: S.K. and S.C.C. Manuscript editing: S.K., S.C.C. and N.C. Final approval: S.K., S.C.C., S.T.C., T.J. and N.C. All authors agree to be accountable for all aspects of the work in ensuring that questions related to the accuracy or integrity of any part of the work are appropriately investigated and resolved. All persons designated as authors qualify for authorship, and all those who qualify for authorship are listed.

Funding

This work is supported by grants from the Thailand Research Fund TRG5780002 (S.K.) and BRG5780016 (S.C.C.), the Thailand Research Fund Royal Golden Jubilee PhD programme (S.T.C. and N.C.), the NSTDA Research Chair Grant from the National Science and Technology Development Agency Thailand (N.C.) and Chiang Mai University Center of Excellence Award (N.C.).

Acknowledgements

We are thankful to Cicely Proctor for editing this manuscript.

© 2016 The Authors. Experimental Physiology © 2016 The Physiological Society

เอกสารแนบหมายเลข 26

Cellular Physiology and Biochemistry

Cell Physiol Biochem 2016;39:341-349
DOI: 10.1159/000445628
Published online: June 29, 2016
Accepted: May 23, 2016

© 2016 The Author(s)
Published by S. Karger AG, Basel
1421-9778/16/0391-0341$39.50/0
www.karger.com/cpb

This article is licensed under the Creative Commons Attribution-NonCommercial-NoDerivatives 4.0 International License (CC BY-NC-ND) (http://www.karger.com/Services/OpenAccessLicense). Usage and distribution for commercial purposes as well as any distribution of modified material requires written permission.

Original Paper

Acetylcholine Attenuates Hydrogen Peroxide-Induced Intracellular Calcium Dyshomeostasis Through Both Muscarinic and Nicotinic Receptors in Cardiomyocytes

Siripong Palee[a,b,d] Nattayaporn Apaijai[b,c,d] Krekwit Shinlapawittayatorn[b,c,d]
Siriporn C. Chattipakorn[b,d,e] Nipon Chattipakorn[b,c,d]

[a]School of Medicine, Mae Fah Luang University, Chiang Rai, [b]Cardiac Electrophysiology Research and Training Center, Faculty of Medicine, Chiang Mai University, Chiang Mai, [c]Cardiac Electrophysiology Unit, Department of Physiology, Faculty of Medicine, Chiang Mai University, Chiang Mai, [d]Center of Excellence in Cardiac Electrophysiology, Chiang Mai University, Chiang Mai, [e]Department of Oral Biology and Diagnostic Science, Faculty of Dentistry, Chiang Mai University, Chiang Mai, Thailand

Key Words
Acetylcholine • Oxidative stress • Hydrogen peroxide • Calcium transient

Abstract
Background/Aims: Oxidative stress induced intracellular Ca^{2+} overload plays an important role in the pathophysiology of several heart diseases. Acetylcholine (ACh) has been shown to suppress reactive oxygen species generation during oxidative stress. However, there is little information regarding the effects of ACh on the intracellular Ca^{2+} regulation in the presence of oxidative stress. Therefore, we investigated the effects of ACh applied before or after hydrogen peroxide (H_2O_2) treatment on the intracellular Ca^{2+} regulation in isolated cardiomyocytes. ***Methods:*** Single ventricular myocytes were isolated from the male Wistar rats for the intracellular Ca^{2+} transient study by a fluorimetric ratio technique. ***Results:*** H_2O_2 significantly decreased both of intracellular Ca^{2+} transient amplitude and decay rate. ACh applied before, but not after, H_2O_2 treatment attenuated the reduction of intracellular Ca^{2+} transient amplitude and decay rate. Both atropine (a muscarinic acetylcholine receptor blocker) and mecamylamine (a nicotinic acetylcholine receptor blocker) significantly decreased the protective effects of acetylcholine on the intracellular Ca^{2+} regulation. Moreover, the combination of atropine and mecamylamine completely abolished the protective effects of acetylcholine on intracellular Ca^{2+} transient amplitude and decay rate. ***Conclusion:*** ACh pretreatment attenuates H_2O_2-induced intracellular Ca^{2+} dyshomeostasis through both muscarinic and nicotinic receptors.

© 2016 The Author(s)
Published by S. Karger AG, Basel

Nipon Chattipakorn, MD, PhD

Cardiac Electrophysiology Research and Training Center, Faculty of Medicine, Chiang Mai University, Chiang Mai, 50200, (Thailand)
Tel. +66-53-935329, Fax +66-53-935368, E-Mail nchattip@gmail.com

Introduction

Oxidative stress has been shown to play an important role in the pathophysiology of several pathological conditions including acute myocardial infarction (MI) [1-3]. In MI patients, timely myocardial reperfusion of coronary blood flow is necessary to resuscitate the ischemic or hypoxic myocardium [4, 5]. Reperfusion facilitates cardiac myocytes salvage and decreases cardiac morbidity and mortality. However, reperfusion of an ischemic myocardium may result in paradoxical cardiac dysfunction, a phenomenon known as "ischemia/reperfusion (I/R) injury" [5]. The hydrogen peroxide (H_2O_2) is one of the key mediators underlying cellular oxidative stress during I/R [5]. The formation of H_2O_2 during I/R injury results in intracellular Ca^{2+} overload due to increased lipid peroxidation and sulfhydryl group oxidation in the I/R heart [1]. Therefore, any therapeutic approach which can prevent intracellular Ca^{2+} overload and improves intracellular Ca^{2+} regulation would be beneficial for reperfused heart.

Acetylcholine (ACh) has been shown to suppress reactive oxygen species generation during oxidative stress [6, 7]. Moreover, previous studies reported that parasympathetic activation by vagus nerve stimulation (VNS)-induced ACh release exerted cardioprotective effects against I/R injury [8-11]. Moreover, our recent study demonstrated that VNS reduced the occurrence of ventricular fibrillation and decreases myocardial infarction size in I/R model [12, 13]. Furthermore, VNS could improve cardiac mitochondrial function which was impaired in I/R hearts [12]. Despite these beneficial effects, there is little information regarding the effects of ACh on the intracellular Ca^{2+} regulation in the presence of oxidative stress. In this study, we investigated the effects of ACh applied before or after H_2O_2 treatment on intracellular calcium regulation in isolated cardiomyocytes. We hypothesized that ACh can attenuate intracellular Ca^{2+} dyshomeostasis caused by H_2O_2 in cardiomyocytes.

Materials and Methods

Animal preparation and study protocol

This study was approved by the Institutional Animal Care and Use Committees of the Faculty of Medicine, Chiang Mai University. All the animals were fed with normal rat chow and water ad libitum before the study. Male Wistar rats (250-300 g) were used. The rats were deeply anesthesized with thiopental (0.5 mg/kg; Research institute of antibiotics and biotransformations, Roztoky, Czech Republic) after which the hearts were removed for single ventricular myocyte isolation [14]. The isolated cardiomyocytes were used in each study protocol for the measurement of intracellular Ca^{2+} transient. Data were compared between the experimental groups.

In the protocol 1, cardiomyocytes were divided into 5 groups (n = 8 cells/rat and 8 rats/group) as shown in Fig. 1A. Cardiomyocytes were divided into 5 groups. In groups I, cardiomyocytes were treated with normal saline solution (NSS) for 5 minutes as a control group. Group II was treated with ACh (10 μM) (Acetylcholine chloride, Sigma-Aldrich, St. Louis, MO, USA) for 5 minutes, and Group III was treated with NSS for 2 minutes followed by H_2O_2 (2 mM) for 3 minutes. Group IV was treated with a muscarinic receptor blocker, atropine (1 μM) for 5 minutes, and Group V was treated with a nicotinic receptor blocker mecamylamine (1 μM) (Sigma-Aldrich, St. Louis, MO, USA) for 5 minutes. The real-time Ca^{2+} transient measurement was performed at the beginning of the study (baseline) and at the end of treatment in each group.

In protocol 2, cardiomyocytes were divided into 5 groups (n = 8 cells/rat and 8 rats/group) as shown in Fig. 1B. Cardiomyocytes were divided into 5 groups. In groups I, they were treated with NSS for 10 minutes followed by H_2O_2 (2 mM) for 3 minutes and served as a control group. Group II was treated with NSS for 5 minutes followed by ACh (10 μM) for 5 minutes followed by H_2O_2 (2 mM) for 3 minutes. Group III was treated with atropine (1 μM) for 5 minutes followed by ACh (10 μM) for 5 minutes and then H_2O_2 (2 mM) for 3 minutes. Group IV was treated with a mecamylamine (1 μM) for 5 minutes followed by ACh (10 μM) for 5 minutes and then H_2O_2 (2 mM) for 3 minutes. Group V was treated with a mecamylamine (1 μM) and atropine (1 μM) for 5 minutes followed by ACh (10 μM) for 5 minutes and then H_2O_2 (2 mM) for 3

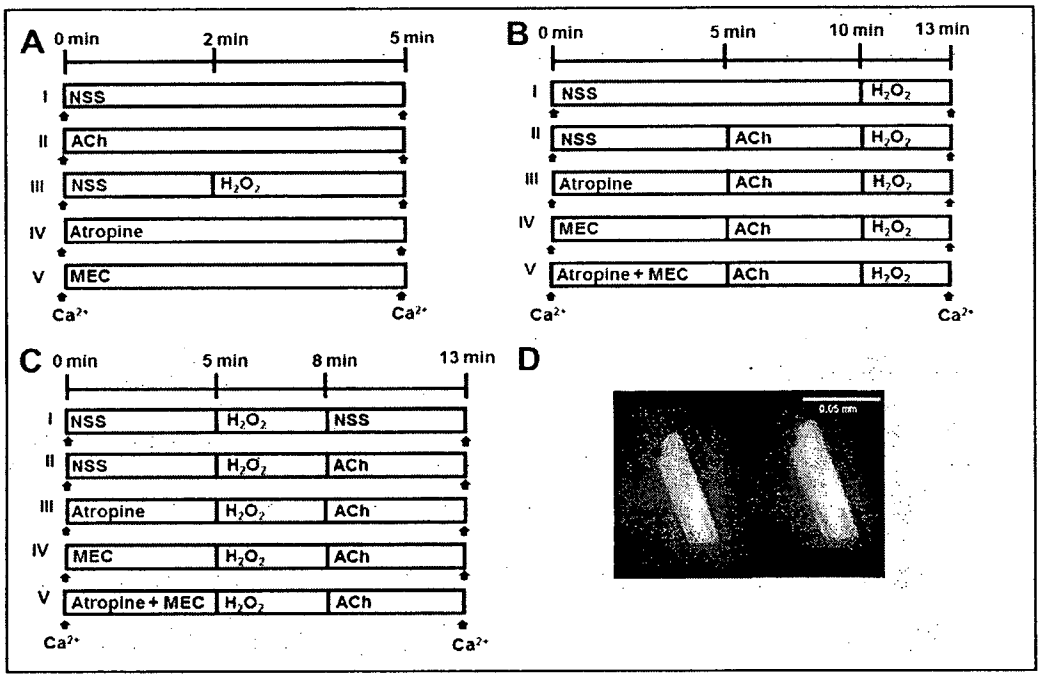


Fig. 1. Experimental groups and the treatment protocol of protocol 1 (A), protocol 2: pre-treatment groups (B), protocol 3: post-treatment groups (C), Cardiac myocytes loaded with fluorescent dye Fura-2/AM (D). NSS=normal saline solution, ACh=acetylcholine, MEC=mecamylamine, H_2O_2=hydrogen peroxide, Ca^{2+}=intracellular calcium measurement.

minutes. The real-time Ca^{2+} transient measurement was performed at the beginning of the study (baseline) and at the end of treatment in each group.

In protocol 3, cardiomyocytes were divided into 5 groups (n = 8 cells/rat and 8 rats/group) as shown in Fig. 1C. In this protocol, cardiomyocytes were divided into 5 groups. Cardiomyocytes in groups I were treated with NSS for 5 minutes followed by H_2O_2 (2 mM) for 3 minutes and then NSS for 5 minutes, and served as a control group. Group II was treated with NSS for 5 minutes followed by H_2O_2 (2 mM) for 3 minutes and then ACh (10 μM) for 5 minutes, and Group III was treated with atropine (1 μM) for 5 minutes followed by H_2O_2 (2 mM) for 3 minutes and then ACh (10 μM) for 5 minutes. Group IV was treated with a mecamylamine (1 μM) for 5 minutes followed by H_2O_2 (2 mM) for 3 minutes and then ACh (10 μM) for 5 minutes. Group V was treated with the combination of mecamylamine (1 μM) and atropine (1 μM) for 5 minutes followed by H_2O_2 (2 mM) for 3 minutes and then ACh (10 μM) for 5 minutes. The real-time Ca^{2+} measurement was performed at the beginning of the study and after the treatment in all groups.

Calcium transient measurement

Cardiomyocytes were isolated from the hearts of male Wistar rats using a method described previously [15]. In brief, under deep anesthesia, the heart was immediately removed and placed into a modified Langendroff apparatus. The hearts were perfused with modified Krebs solution (130 mM NaCl, 4.5 mM KCl, 1.4 mM $MgCl_2$, 0.4 mM NaH_2PO_4, 0.75 mM $CaCl_2$, 4.2 mM HEPES, 20 mM taurine, 10 mM creatine and 10 mM glucose, pH 7.3 at 37°C) for 5 minutes, followed by calcium-free solution (100 μM EGTA) for 4 minutes, Tyrode's solution with collagenase (0.1 mg/ml) for 10 minutes, and modified Krebs solution containing 100 μM $CaCl_2$ and 1 mg/ml type II collagenase for another 8 minutes. The ventricles were removed from the cannula, cut into small pieces and incubated in 10 ml of collagenase solution gassed with 100% O_2 for 7 minutes at 37°C, with regular triturating. The cardiomyocytes were separated from undigested ventricular tissues by filtering through cell strainer, and were settling into a loose pellet. Then, the supernatant was removed and replaced with modified Krebs solution containing 1% BSA and 500 μM $CaCl_2$. This process was repeated with modified Krebs solution containing 1 mM $CaCl_2$. After this procedure, the cardiomyocytes were ready for recording [15]. The isolated cardiomyocytes were placed in a modified

Krebs solution containing 1 mM $CaCl_2$. Intracellular Ca^{2+} transient were measured using the CELL^R imaging software (Olympus Soft Imaging Solutions GmbH, Germany). The isolated cardiomyocytes were loaded with Fura-2/AM at the final concentration of 5 μM [16] and fluorescent intensity was recorded during electrical pacing (1 Hz, 10 ms duration, 15 V) [17]. The ratio of the emissions wavelengths is directly related to the amount of intracellular Ca^{2+} [18]. When Ca^{2+} binds to a ratiometric indicator, it changes the optimum excitation or emission wavelength of the indicator. An elevation of Ca^{2+} concentration induces an increase in Fura-2 emission fluorescence when the indicator is excited at 340 nm, with a corresponding decrease in fluorescence at 380 nm excitation [19, 20]. The experiments were performed in the temperature controlled chamber system at 37°C. The H_2O_2 concentration at 2 mM is a stock solution. The final concentration in the recording chamber is 50 μM which is widely used to trigger oxidative stress-induced intracellular Ca^{2+} dyshomeostasis in cardiomyocytes [21, 22]. Intracellular Ca^{2+} transient decay rate which approximates the rate of Ca^{2+} uptake into the SR by sarco/endoplasmic reticulum Ca^{2+}-ATPase (SERCA), intracellular calcium transient amplitude which approximates the intracellular Ca^{2+} level during systolic period, and diastolic Ca^{2+} level which approximates the intracellular Ca^{2+} level during diastolic period were recorded before and after treatment.

Statistical analysis

Data were expressed as mean ± SD. Comparisons of variables were performed using the one-way ANOVA followed by LSD post-hoc test. $P < 0.05$ was considered statistically significant.

Results

ACh at the concentrations of 1, 10 and 100 μM did not alter the diastolic Ca^{2+} level compared to the baseline. However, all concentrations of ACh significantly decreased the intracellular Ca^{2+} transient amplitude (0.03 ± 0.015 in 1 μM, 0.02 ± 0.005 in 10 μM, and 0.03 ± 0.005 in 100 μM, compared to 0.06 ± 0.001 at baseline) and Ca^{2+} transient decay rate (0.09 ± 0.003 in 1 μM, 0.09 ± 0.004 in 10 μM, and 0.06 ± 0.002 in 100 μM, compared to 0.23 ± 0.02 at baseline). In the first protocol, the effects of H_2O_2, ACh, atropine and mecamylamine on the intracellular Ca^{2+} transient were investigated. H_2O_2 significantly decreased both of intracellular Ca^{2+} transient amplitude (Fig. 2A) and intracellular Ca^{2+} transient decay rate (Fig. 2B). The intracellular Ca^{2+} diastolic level was not altered (Fig. 2C) compared to the control group in response to all treatments. In addition, ACh at 10 μM significantly decreased the intracellular Ca^{2+} transient amplitude (Fig. 2A) and Ca^{2+} transient decay rate (Fig. 2B), but did not alter the level of intracellular diastolic Ca^{2+} level (Fig. 2C) compared to the control group. However, atropine and mecamylamine did not alter the intracellular Ca^{2+} transient amplitude, Ca^{2+} transient decay rate and the intracellular diastolic Ca^{2+} level. The effect of H_2O_2, ACh, atropine and mecamylamine on the intracellular Ca^{2+} transient tracing shape is shown in Fig. 2D.

In the second protocol, the effects of ACh administered prior to H_2O_2 application were investigated. The intracellular Ca^{2+} transient amplitude was significantly decreased in H_2O_2 treated group. However, pretreated with ACh significantly prevent the reduction of the intracellular Ca^{2+} transient amplitude compare to the H_2O_2 treated group, $p < 0.05$ (Fig. 3A). Furthermore, pretreated with ACh significantly increased the intracellular Ca^{2+} transient decay rate compared to the H_2O_2 treated group (Fig. 2B). However, in all experimental groups, ACh did not alter the level of intracellular diastolic calcium (Fig. 3C) compared to the H_2O_2 treated group. The protective effect of ACh was reduced when cardiomyocytes were exposed to the muscarinic receptor blocker (atropine) and nicotinic receptor blocker (mecamylamine) prior to ACh application (Fig. 3B, 3C). Moreover, co-incubation of atropine and mecamylamine completely abolished the cardioprotective effects of ACh on intracellular Ca^{2+} transient amplitude and decay rate. The effects of ACh on Ca^{2+} transient tracing shape is shown in Fig. 3D.

In the third protocol, we investigated the effects of ACh administered after H_2O_2 application on intracellular Ca^{2+} transient. Our results showed that in cardiomyocytes treated

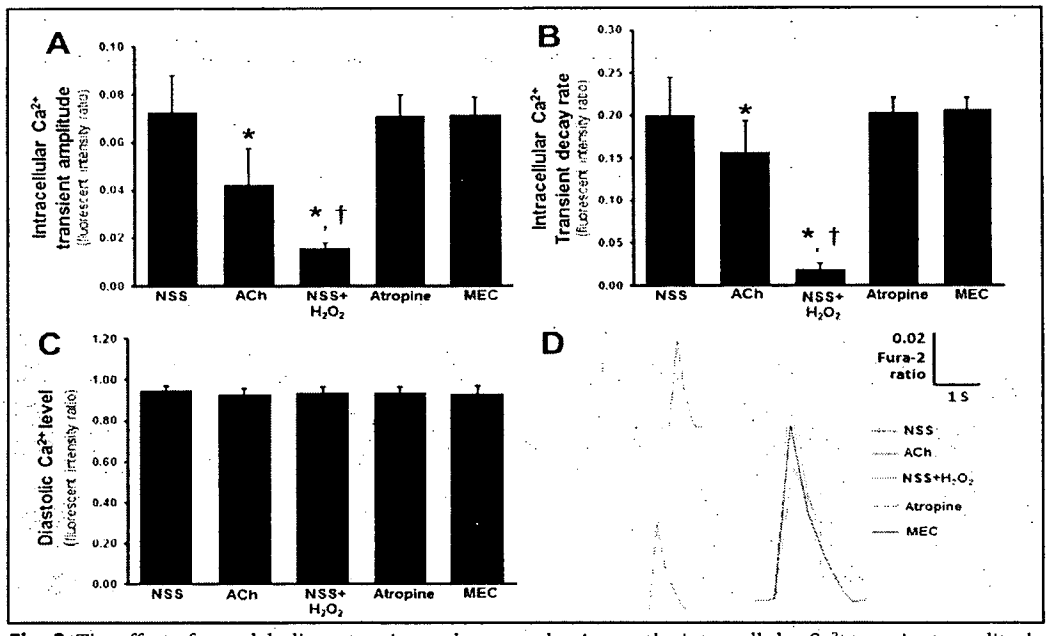


Fig. 2. The effect of acetylcholine, atropine and mecamylamine on the intracellular Ca^{2+} transient amplitude (A), and intracellular Ca^{2+} transient decay rate (B) and intracellular diastolic Ca^{2+} level (C). The effects of ACh on Ca^{2+} transient tracing shape (D). * $p < 0.05$ vs. NSS, † $p < 0.05$ vs. ACh. NSS=normal saline solution, ACh=acetylcholine, MEC= mecamylamine, H_2O_2= hydrogen peroxide, Ca^{2+}= intracellular calcium measurement.

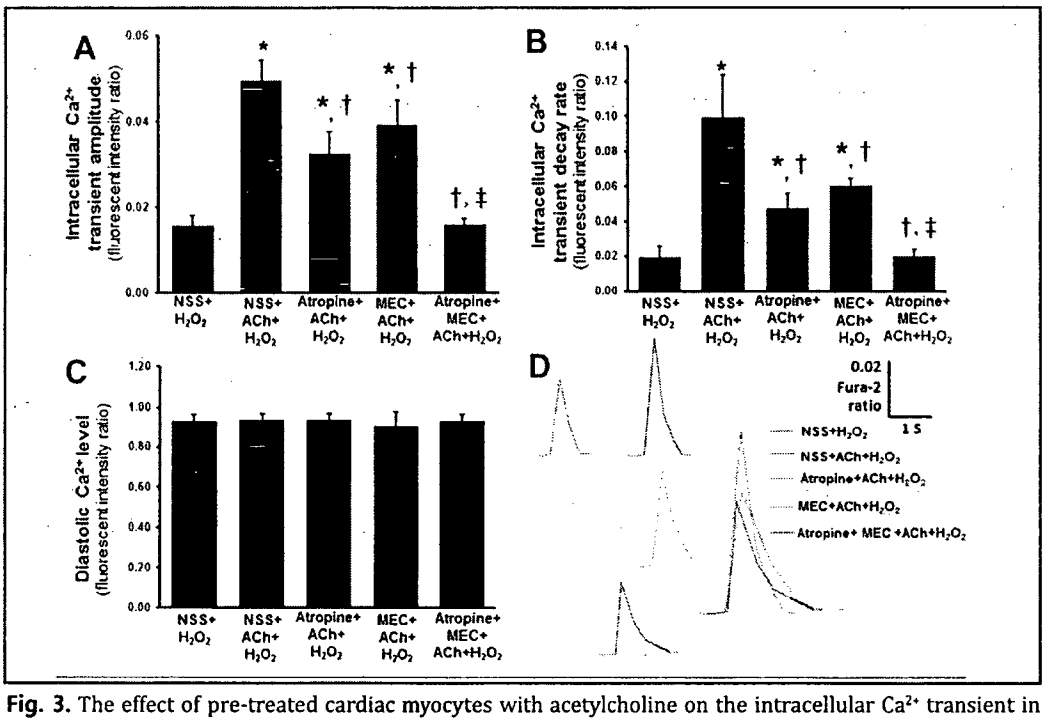


Fig. 3. The effect of pre-treated cardiac myocytes with acetylcholine on the intracellular Ca^{2+} transient in isolated cardiac myocytes under H_2O_2-induced oxidative stress. ACh significantly attenuated the reduction of intracellular Ca^{2+}transient amplitude (A) and increased intracellular Ca^{2+} transient decay rate (B) but did not alter intracellular diastolic calcium level (C) compared with H_2O_2 group. The protective effects of ACh were abolished by ACh receptor blocking agents. The effects of ACh on Ca^{2+} transient tracing shape (D). * $p < 0.05$ vs. NSS, † $p < 0.05$ vs. H_2O_2, ‡ $p < 0.05$ vs. ACh. NSS=normal saline solution, ACh= acetylcholine, MEC=-mecamylamine, H_2O_2= hydrogen peroxide, Ca^{2+}=intracellular calcium measurement.

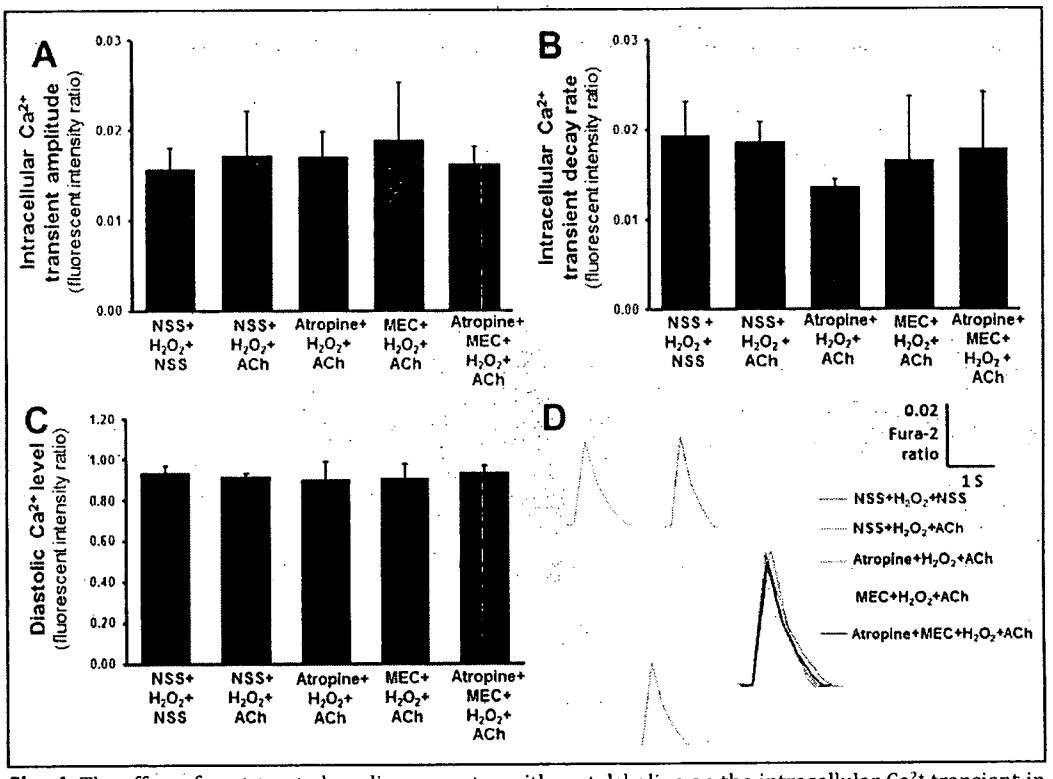


Fig. 4. The effect of post-treated cardiac myocytes with acetylcholine on the intracellular Ca^{2+} transient in isolated cardiac myocytes H_2O_2-induced oxidative stress. ACh did not improve intracellular Ca^{2+} transient amplitude (A), intracellular Ca^{2+} transient decay rate (B) and intracellular diastolic Ca^{2+} level (C) compared with H_2O_2 group. The effects of ACh on Ca^{2+} transient tracing shape (D). NSS= normal saline solution, ACh= acetylcholine, MEC= mecamylamine, H_2O_2= hydrogen peroxide, Ca^{2+}= intracellular calcium measurement.

with H_2O_2 followed by ACh, the intracellular Ca^{2+} transient amplitude (Fig. 4A), intracellular Ca^{2+} transient decay rate (Fig. 4B) and the intracellular Ca^{2+} diastolic level (Fig. 4C) did not alter, compared to cardiomyocyte treated with H_2O_2 followed by NSS. Furthermore, atropine and mecamylamine or co-incubation of atropine and mecamylamine did not alter the intracellular Ca^{2+} transient amplitude (Fig. 4A), intracellular Ca^{2+} transient decay rate (Fig. 4B) and intracellular Ca^{2+} diastolic level (Fig. 4C). The effects of Ach given after H_2O_2 application in cardiomyocytes on Ca^{2+} transient tracing shape is shown in Fig. 4D.

Discussion

The major findings of the present study are as follows. In cardiomyocytes under H_2O_2-induced oxidative stress, pre-treated cardiomyocytes with ACh (1) did not alter the intracellular diastolic Ca^{2+} level, (2) attenuated the reduction of intracellular Ca^{2+} transient amplitude and intracellular Ca^{2+} transient decay rate are caused by H_2O_2, (3) both atropine (a muscarinic acetylcholine receptor blocker) and mecamylamine (a nicotinic acetylcholine receptor blocker) significantly decreased the protective effects of ACh on the intracellular Ca^{2+} regulation, (4) the combination of muscarinic and nicotinic blockers completely abolished the protective effects of ACh on intracellular Ca^{2+} transient amplitude and decay rate. Finally, ACh given after H_2O_2 application did not improve intracellular Ca^{2+} regulation impaired by oxidative stress.

The present study demonstrated that H_2O_2 application impaired intracellular Ca^{2+} regulation in isolated cardiomyocytes. Both intracellular Ca^{2+} transient amplitude and

decay rate significantly reduced in H_2O_2 treated group. Our findings are consistent with the previous study in the rat ventricular myocyte which demonstrated that H_2O_2 significantly decreased both intracellular Ca^{2+} transient amplitude and the rate of systolic Ca^{2+} removal [23]. The reduction of intracellular Ca^{2+} removal due to the impaired SERCA activity was shown to lead to intracellular Ca^{2+} overload and cardiac dysfunction [23]. Previous study also demonstrated that ACh is required for the maintenance of the cardiac Ca^{2+} cycling proteins [24]. Specifically, lack of ACh significantly reduces intracellular Ca^{2+} transient amplitude and intracellular Ca^{2+} transient decay rate, suggesting that ACh is necessary for the maintenance of intracellular Ca^{2+} transient regulation [24].

The timing of ACh application was also crucial for its protective effect in our study in which early application of ACh prior to H_2O_2 application showed better benefit. This may explain the findings reported previously in a swine model of I/R injury that vagus nerve stimulation (VNS) applied early at the onset of the ischemic period exerts cardioprotection against I/R injury [12, 13]. However, VNS applied at the onset of reperfusion did not produce cardioprotection against I/R injury, suggesting that the timing of VNS application with respect to the onset of myocardial ischemia is an important determinant factor [13].

It has been shown previously that ACh significantly decreased both Ca^{2+} transient amplitude and decay rate by reducing cAMP-PKA-dependent phosphorylation of ryanodine receptors and phospholamban, leading to the reduced open probability of the ryanodine receptor, and slower SERCA-mediated intracellular Ca^{2+} re-uptake into the SR, respectively [25]. However, H_2O_2 has been shown to decrease SERCA and NCX activities [26, 27] by inhibiting PKC activities, leading to the alteration of the intracellular Ca^{2+} homeostasis. Thus, ACh and H_2O_2 mediate the intracellular Ca^{2+} homeostasis through different signaling pathways. Although the potential mechanism by which ACh prestimulation protects cardiomyocytes against H_2O_2-induced intracellular Ca^{2+} dyshomeostasis are unclear, it might be due to the ability of ACh to protect cardiomyocytes from oxidative stress-related damage and prevent cardiac mitochondrial dysfunction as shown by previous studies. In rat's cardiomyoblasts, ACh exerted cardioprotection against oxidative injury through FoxO3a/PGC-1α signaling pathway [28]. Moreover, in endothelial cells, activation of α7 nicotinic acetylcholine receptor protected against oxidant stress damage through reducing vascular peroxidase-1 in a JNK signaling-dependent manner [29]. These protective mechanisms of ACh could be responsible for improved intracellular calcium homeostasis observed in the present study.

The important roles of both muscarinic and nicotinic cholinergic receptors on the intracellular calcium handling have been demonstrated in this study. We found that while either atropine (a muscarinic acetylcholine receptor blocker) or mecamylamine (a nicotinic acetylcholine receptor blocker) significantly decreased the protective effects of ACh on intracellular Ca^{2+} regulation, the combination of atropine and mecamylamine completely abolished the protective effects of ACh on intracellular Ca^{2+} transient amplitude and decay rate. These findings emphasize that ACh exerts the beneficial effect on intracellular Ca^{2+} regulation through both muscarinic and nicotinic receptors.

Study Limitations: In the present study, we only measured the Ca^{2+} transient at the beginning and at the end of the study. Future study is needed to investigate the changes of calcium transient over times. Although we did not assess the sarcoplasmic reticulum calcium content, previous studies demonstrated that the sarcoplasmic reticulum Ca^{2+} content was directly proportionate to intracellular Ca^{2+} transient amplitude and intracellular Ca^{2+} transient decay rate [30, 31].

Conclusion

Acetylcholine protects cardiomyocytes against H_2O_2-induced intracellular Ca^{2+} dyshomeostasis through the activation of both muscarinic and nicotinic receptors. These findings provide the important information regarding the mechanism underlying the cardioprotective effect of ACh against intracellular Ca^{2+} dyshomeostasis under oxidative

stress. Moreover, these roles of ACh may explain the cardioprotective benefits of VNS during I/R injury observed in the preclinical studies.

Disclosure Statement

The authors declare no conflict of interest.

Acknowledgements

This work was supported by the Thailand Research Fund grants TRG5780007 (SP), RSA5880015 (KS) and BRG5780016 (SCC), the NSTDA Research Chair grant from the National Science and Technology Development Agency Thailand (NC), and the Chiang Mai University Center of Excellence Award (NC).

References

1 Dhalla NS, Golfman L, Takeda S, Takeda N, Nagano M: Evidence for the role of oxidative stress in acute ischemic heart disease: a brief review. Can J Cardiol 1999;15:587-593.
2 Ferrari R, Guardigli G, Mele D, Percoco GF, Ceconi C, Curello S: Oxidative stress during myocardial ischaemia and heart failure. Curr Pharm Des 2004;10:1699-1711.
3 Rodrigo R, Libuy M, Feliu F, Hasson D: Oxidative stress-related biomarkers in essential hypertension and ischemia-reperfusion myocardial damage. Dis Markers 2013;35:773-790.
4 Bopassa JC: Protection of the ischemic myocardium during the reperfusion: between hope and reality. Am J Cardiovasc Dis 2012;2:223-236.
5 Monassier JP: Reperfusion injury in acute myocardial infarction. From bench to cath lab. Part i: basic considerations. Arch Cardiovasc Dis 2008;101:491-500.
6 Hausenloy DJ, Yellon DM: Reperfusion injury salvage kinase signalling: taking a risk for cardioprotection. Heart Fail Rev 2007;12:217-234.
7 Kakinuma Y, Ando M, Kuwabara M, Katare RG, Okudela K, Kobayashi M, Sato T: Acetylcholine from vagal stimulation protects cardiomyocytes against ischemia and hypoxia involving additive non-hypoxic induction of HIF-1alpha. FEBS Lett 2005;579:2111-2118.
8 Calvillo L, Vanoli E, Andreoli E, Besana A, Omodeo E, Gnecchi M, Zerbi P, Vago G, Busca G, Schwartz PJ: Vagal stimulation, through its nicotinic action, limits infarct size and the inflammatory response to myocardial ischemia and reperfusion. J Cardiovasc Pharmacol 2011;58:500-507.
9 Katare RG, Ando M, Kakinuma Y, Arikawa M, Yamasaki F, Sato T: Differential regulation of tnf receptors by vagal nerve stimulation protects heart against acute ischemic injury. J Mol Cell Cardiol 2010;49:234-244.
10 Li W, Olshansky B: Inflammatory cytokines and nitric oxide in heart failure and potential modulation by vagus nerve stimulation. Heart Fail Rev 2011;16:137-145.
11 Uemura K, Zheng C, Li M, Kawada T, Sugimachi M: Early short-term vagal nerve stimulation attenuates cardiac remodeling after reperfused myocardial infarction. J Card Fail 2010;16:689-699.
12 Shinlapawittayatorn K, Chinda K, Palee S, Surinkaew S, Thunsiri K, Weerateerangkul P, Chattipakorn S, KenKnight BH, Chattipakorn N: Low-amplitude, left vagus nerve stimulation significantly attenuates ventricular dysfunction and infarct size through prevention of mitochondrial dysfunction during acute ischemia-reperfusion injury. Heart Rhythm 2013;10:1700-1707.
13 Shinlapawittayatorn K, Chinda K, Palee S, Surinkaew S, Kumfu S, Kumphune S, Chattipakorn S, KenKnight BH, Chattipakorn N: Vagus nerve stimulation initiated late during ischemia, but not reperfusion, exerts cardioprotection via amelioration of cardiac mitochondrial dysfunction. Heart Rhythm 2014;11:2278-2287.
14 Palee S, Weerateerangkul P, Chinda K, Chattipakorn SC, Chattipakorn N: Mechanisms responsible for beneficial and adverse effects of rosiglitazone in a rat model of acute cardiac ischaemia-reperfusion. Exp Physiol 2013;98:1028-1037.

15 Weerateerangkul P, Palee S, Chinda K, Chattipakorn SC, Chattipakorn N: Effects of kaempferia parviflora Wall. Ex. Baker and sildenafil citrate on cGMP level, cardiac function, and intracellular Ca2+ regulation in rat hearts. J Cardiovasc Pharmacol 2012;60:299-309.
16 Xu YJ, Shao Q, Dhalla NS: Fura-2 fluorescent technique for the assessment of Ca2+ homeostasis in cardiomyocytes. Mol Cell Biochem 1997;172:149-157.
17 Palee S, Weerateerangkul P, Surinkeaw S, Chattipakorn S, Chattipakorn N: Effect of rosiglitazone on cardiac electrophysiology, infarct size and mitochondrial function in ischaemia and reperfusion of swine and rat heart. Exp Physiol 2011;96:778-789.
18 Grynkiewicz G, Poenie M, Tsien RY: A new generation of Ca2+ indicators with greatly improved fluorescence properties. J Biol Chem 1985;260:3440-3450.
19 Waldeck-Weiermair M, Bischof H, Blass S, Deak AT, Klec C, Graier T, Roller C, Rost R, Eroglu E, Gottschalk B, Hofmann NA, Graier WF, Malli R: Generation of red-shifted cameleons for imaging Ca2+ dynamics of the endoplasmic reticulum. Sensors (Basel) 2015;15:13052-13068.
20 Bootman MD, Rietdorf K, Collins T, Walker S, Sanderson M: Ca2+-sensitive fluorescent dyes and intracellular Ca2+ imaging. Cold Spring Harb Protoc 2013;2013:83-99.
21 Kaminishi T, Matsuoka T, Yanagishita T, Kako KJ: Increase vs. Decrease of calcium uptake by isolated heart cells induced by H2O2 vs. HOCl. Am J Physiol Cell Physiol 1989;256:C598-607.
22 Josephson RA, Silverman HS, Lakatta EG, Stern MD, Zweier JL: Study of the mechanisms of hydrogen peroxide and hydroxyl free radical-induced cellular injury and calcium overload in cardiac myocytes. J Biol Chem 1991;266:2354-2361.
23 Greensmith DJ, Eisner DA, Nirmalan M: The effects of hydrogen peroxide on intracellular calcium handling and contractility in the rat ventricular myocyte. Cell Calcium 2010;48:341-351.
24 Roy A, Fields WC, Rocha-Resende C, Resende RR, Guatimosim S, Prado VF, Gros R, Prado MA: Cardiomyocyte-secreted acetylcholine is required for maintenance of homeostasis in the heart. FASEB J 2013;27:5072-5082.
25 van Borren MM, Verkerk AO, Wilders R, Hajji N, Zegers JG, Bourier J, Tan HL, Verheijck EE, Peters SL, Alewijnse AE, Ravesloot JH: Effects of muscarinic receptor stimulation on Ca2+ transient, camp production and pacemaker frequency of rabbit sinoatrial node cells. Basic Res Cardiol 2010;105:73-87.
26 Reeves JP, Bailey CA, Hale CC: Redox modification of sodium-calcium exchange activity in cardiac sarcolemmal vesicles. J Biol Chem 1986;261:4948-4955.
27 Goldhaber JI: Free radicals enhance Na+/Ca2+ exchange in ventricular myocytes. Am J Physiol 1996;271:H823-833.
28 Sun L, Zang WJ, Wang H, Zhao M, Yu XJ, He X, Miao Y, Zhou J: Acetylcholine promotes ROS detoxification against hypoxia/reoxygenation-induced oxidative stress through FoxO3a/PGC-1α dependent superoxide dismutase. Cell Physiol Biochem 2014;34:1614-1625.
29 Li DJ, Zhao T, Xin RJ, Wang YY, Fei YB, Shen FM: Activation of α7 nicotinic acetylcholine receptor protects against oxidant stress damage through reducing vascular peroxidase-1 in a JNK signaling-dependent manner in endothelial cells. Cell Physiol Biochem 2014;33:468-478.
30 Sankaranarayanan R, Li Y, Greensmith DJ, Eisner DA, Venetucci L: Biphasic decay of the Ca transient results from increased sarcoplasmic reticulum Ca leak. J Physiol 2016;594:611-623.
31 Feridooni HA, Dibb KM, Howlett SE: How cardiomyocyte excitation, calcium release and contraction become altered with age. J Mol Cell Cardiol 2015;83:62-72.

เอกสารแนบหมายเลข 27

Menopause: The Journal of The North American Menopause Society
Vol. 23, No. 8, pp. 894-902
DOI: 10.1097/GME.0000000000000640
© 2016 by The North American Menopause Society

Estrogen and DPP4 inhibitor, but not metformin, exert cardioprotection via attenuating cardiac mitochondrial dysfunction in obese insulin-resistant and estrogen-deprived female rats

Sivaporn Sivasinprasasn, PhD,[1,2,4,5] Piangkwan Sa-nguanmoo, MSc,[1,2,4] Wanpitak Pongkan, DVM,[1,2,4] Wasana Pratchayasakul, PhD,[1,2,4] Siriporn C. Chattipakorn, DDS, PhD,[1,3,4] and Nipon Chattipakorn, MD, PhD[1,2,4]

Abstract

Objective: Cardiac function was markedly compromised in obese insulin-resistant and estrogen-deprived rats. Metformin and dipeptidyl peptidase-4 inhibitor (vildagliptin) were reported to improve cardiac function in insulin-resistant rats. Their effects on the heart under estrogen-deprived conditions are, however, unknown. Therefore, the effects of metformin, vildagliptin, and estrogen on the cardiac function in estrogen-deprived insulin-resistant female rats were investigated.

Methods: Bilateral ovariectomized female rats (n = 48) were divided to be fed with either a normal diet (ND) or a high-fat diet (HFD) for 12 weeks. Then, both ND- and HFD-fed groups were subdivided to receive a vehicle, estrogen (50 μg/kg), metformin (30 mg/kg), or vildagliptin (3 mg/kg) for 4 weeks (n = 6/group). Heart rate variability, echocardiography, metabolic and biochemical parameters, cardiac function, and mitochondrial function were determined. Sham-operated female rats (n = 6) were used as a control.

Results: Both ND- and HFD-fed ovariectomized rats developed insulin resistance, depressed heart rate variability, and decreased cardiac contractility. Although treatment with metformin, vildagliptin, and estrogen improved metabolic status and cardiac function, only estrogen and vildagliptin improved diastolic blood pressure and left ventricular ±dP/dt, and also reduced mitochondrial impairment, apoptosis, and oxidative stress in HD-fed ovariectomized rats.

Conclusions: Treatment with estrogen and vildagliptin provided more beneficial effects in the inhibition of oxidative stress, apoptosis, and cardiac mitochondrial dysfunction, and preserved cardiac contractile performance in estrogen-deprived insulin-resistant female rats.

Key Words: Cardiac function – DPP4 inhibitor – Estrogen – Insulin resistance – Metformin – Mitochondria.

Cardiovascular diseases (CVDs) are the leading cause of mortality and morbidity, accounting for 30% of all global deaths.[1,2] Metabolic disorders such as obesity, dyslipidemia, and diabetes are known to be the major risk factors of CVD.[2] Gender is also considered a CVD risk factor, as the prevalence of CVD is higher in men than in women.[3,4] The risk of CVD in women has, however, been found to increase after endogenous estrogen deprivation, by both bilateral ovariectomy (OVX) and natural menopause.[5,6] Owing to the cardiometabolic protective effects of estrogen, estrogen withdrawal has been shown to induce both cardiac and metabolic dysfunction, such as hypertension and impaired glucose tolerance, therefore resulting in an increased risk of developing CVD.[7] Estrogen hormone therapy has been shown to decrease fat accumulation, increase energy expenditure, suppress gluconeogenesis and lipogenesis, and enhance muscular insulin sensitivity, therefore resulting in improved metabolic syndrome conditions in OVX rats.[8,9] Moreover, estrogen helped in improving cardiac autonomic balance in the OVX model through the reduction of oxidative stress.[10,11] Oxidative stress is also considered as a factor responsible for the development of insulin resistance and cardiac dysfunction.[12,13] A recent study confirmed the positive effect of

Received November 10, 2015; revised and accepted January 25, 2016.

From the [1]Cardiac Electrophysiology Research and Training Center, [2]Cardiac Electrophysiology Unit, Department of Physiology, Faculty of Medicine, [3]Department of Oral Biology and Diagnostic Science, Faculty of Dentistry, and [4]Center of Excellence in Cardiac Electrophysiology Research, Chiang Mai University, Chiang Mai, Thailand; and [5]School of Medicine, Mae Fah Luang University, Chiang Rai, Thailand.

Funding/support: This work was supported by an NSTDA Research Chair Grant from the National Science and Technology Development Agency (NC), the Thailand Research Fund, BRG5780016 (SCC), TRG (WPr), and the Chiang Mai University Center of Excellence Award (NC).

Financial disclosure/conflicts of interest: None reported.

Supplemental digital content is available for this article. Direct URL citations appear in the printed text and are provided in the HTML and PDF versions of this article on the journal's Website (www.menopause.org).

Address correspondence to: Nipon Chattipakorn, MD, PhD, Cardiac Electrophysiology Research and Training Center, Faculty of Medicine, Chiang Mai University, Chiang Mai 50200, Thailand.
E-mail: nchattip@gmail.com

Copyright @ 2016 The North American Menopause Society. Unauthorized reproduction of this article is prohibited.

estrogen on antioxidative stress, due to the finding that cardiac reactive oxygen species (ROS) production was inhibited in OVX rats after receiving an estrogen supplement, resulting in an improved mitochondrial function.[14] The effect of the estrogen supplement on the cardiac mitochondrial function in estrogen-deprived rats with an obese insulin-resistant condition has, however, not yet been identified.

Metformin and dipeptidyl peptidase-4 (DPP4) inhibitor (vildagliptin) have been used for the treatment of type 2 diabetes mellitus. Metformin is an antihyperglycemic drug which has been shown to reduce hepatic glucose and lipid production, improve hepatic beta-cell function, and improve insulin sensitivity.[15] Vildagliptin exerts its antidiabetic action by inhibiting the DPP4 enzyme, resulting in increased insulin secretion and lower blood glucose levels.[16] In addition to the therapeutic effects on metabolic disorders, both metformin and vildagliptin were reported to be beneficial to the heart in both diabetic and nondiabetic rats.[17,18] Metformin and vildagliptin enhanced heart rate variability (HRV), and increased mitochondrial and myocardial function in an obese insulin-resistant rat model.[17] Their effects as therapeutic agents in obese insulin-resistant rats with estrogen deprivation have, however, not yet been investigated. Owing to the increasing prevalence of metabolic syndrome and CVD in postmenopausal women, together with the increased use of metformin and vildagliptin, we aimed to investigate the roles of these drugs on metabolic status and cardiac function. In addition, this study aimed to investigate the underlying mechanisms acting in estrogen-deprived, obese insulin-resistant rats. We hypothesized that estradiol, metformin, and vildagliptin improve the metabolic function, cardiac performance, and mitochondrial function in estrogen-deprived, obese insulin-resistant rats.

METHODS

Animals and ethical approval

A total of 54 female Wistar rats (weighing 200-220 g) were obtained from the National animal center (Salaya Campus, Mahidol University, Bangkok, Thailand). The rats were given time to acclimatize, and were housed in a temperature-controlled room (25°C) with a 12-hour dark/light cycle setting. All experimental procedures were approved by the Institutional Animal Care and Use Committee at the Faculty of Medicine, Chiang Mai University, in compliance with National Institutes of Health (NIH) guidelines.

Experimental protocol

Rats were randomly assigned to receive either a sham operation (S; n = 6) or a bilateral OVX (O; n = 48), and then allowed to recover for 1 week. Sham rats were fed a normal diet (ND: containing 19.77% energy from fat), whereas ovariectomized rats were further subdivided to be fed with either a ND or a high-fat diet (HFD: containing 59.28% energy from fat) for 12 weeks. At the end of the 12th week, HRV and echocardiography were examined and recorded as the pretreatment data. Rats in both the ND-fed ovariectomized (NDO) and the HFD-fed ovariectomized (HFO) groups were randomly subcategorized to be treated with either estradiol (E: 50 μg/kg body weight [BW] via subcutaneous injection, once daily [17β-estradiol; Sigma-Aldrich, St. Louis, MO]), metformin (M: 15 mg/kg BW, b.i.d., via gavage feeding [Glucophage; Merck Serono, Bangkok, Thailand]), vildagliptin (Vil: 3 mg/kg BW, daily, via gavage feeding [Galvus; Novartis, Bangkok, Thailand]), or vehicle (Ve: sesame oil, via subcutaneous injection in equal volumes with the estrogen treatment) for 4 weeks (n = 6/group; see supplement figure, Supplemental Digital Content 1, http://links.lww.com/MENO/A164). After 4 weeks of treatment, HRV and echocardiography were examined again as the posttreatment data. Blood samples were collected to investigate metabolic parameters. Left ventricular (LV) function was determined using an intraventricular pressure recording system. At the end, rats were terminated by decapitation, and the heart was removed to study cardiac mitochondrial function and biochemical activities.

Surgical procedure of OVX

The bilateral OVX was performed according to the protocol which has been previously described.[19] Rats were anesthetized with zoletil (50 mg/kg) and xylazine (1 mg/kg), and ventilated with room air.[19] The abdominal-pelvic cavity was accessed through a skin incision between the inferior crest of the rib cage and superior base. After the uterine tube and ovary were identified, both ovaries were excised and uterine horns were returned into the pelvic cavity. The abdominal wall and the skin incision were closed and cleaned. After the operation, rats were observed for respiratory status and the recovery, and then individually housed in a clear box for 1 week before being fed with ND or HFD diets.

Metabolic function and estrogen-level determination

Metabolic parameters were investigated from blood samples (n = 6/group), which were collected at pre- and posttreatment time points. Fasting plasma glucose, cholesterol, and triglyceride levels were determined by colorimetric assay using a commercial kit (Biotech, Bangkok, Thailand). Fasting plasma insulin levels were measured using a sandwich enzyme-linked immunosorbent assay (ELISA) kit (Millipore, Ann Arbor, MI). Homeostasis Model Assessment (HOMA) was calculated to evaluate the degree of insulin resistance.[19] Serum estradiol levels were determined using a competitive enzyme immunoassay kit (Cayman Chemical Company, Ann Arbor, MI).

Echocardiography

Echocardiography was performed to evaluate the LV function before and after treatment. This test was performed while the animal was unconscious (lightly anesthetized with 2% isoflurane with oxygen [2 L/min] via inhalation) by using an echocardiograph (SONOS4500; Agilent Technologies, Santa Clara, CA).[20] Data from M-mode echocardiography were recorded to determine LV internal diameter at the end of diastole and LV internal diameter at the end of systole.

Copyright @ 2016 The North American Menopause Society. Unauthorized reproduction of this article is prohibited.

Fractional shortening (%FS) and the ejection fraction (%EF) were calculated to estimate the contractile function (n = 6/group).[21]

HRV test

HRV measures were derived from electrocardiograms (lead II), which were recorded using a signal transducer (PowerLab 4/25T; ADInstruments, New South Wales, Australia) operated through the Chart 5.0 program for 20 minutes (n = 6/group). The frequency-domain method in the MATLAB program was used for electrocardiogram analysis.[22] The high-frequency (HF) component (ranging between 0.15 and 0.40 Hz) is considered to be a marker of parasympathetic tone, whereas the low-frequency (LF) component (ranging between 0.04 and 0.15 Hz) is considered to be a marker of parasympathetic and sympathetic tone.[23] The LF/HF ratio is considered to be an index of the cardiac sympathetic/parasympathetic balance. An increased LF/HF ratio indicates a suppressed HRV and cardiac sympathovagal imbalance.[20,23]

LV pressure determination

Rats were anesthetized by intramuscular injections with zoletil (50 mg/kg) and xylazine (0.15 mg/kg),[17] and were then ventilated with room air via a tracheostomy tube. A pressure catheter (Scisence, Ontario, Canada) was inserted into the right carotid artery, and the catheter tip was directed into the LV chamber. After a 5-minute stabilization period, the signaling data from the catheter were recorded for 20 minutes. Then, rats were terminated and their hearts were removed for further mitochondrial and biochemical studies (n = 6/group). LV end-systolic pressure, LV end-diastolic pressure, maximum and minimum dP/dt (+dP/dt and −dP/dt), and heart rate were recorded. All parameters were analyzed using Labscribe analytical software (Labscribe, Dover, NH).

Cardiac mitochondrial function study

The methods for studying cardiac mitochondrial function, that is the mitochondrial ROS production, mitochondrial membrane potential changes, and mitochondrial swelling, have previously been described.[20,24] The removed heart was cut into small sections, and then homogenized and centrifuged to isolate the cardiac mitochondria. Dichlorohydrofluorescein diacetate dye was used to stain the isolated cardiac mitochondria, and then the ROS level was measured using a fluorescent microplate reader (BioTek, Winooski, VT), set at an excitation wavelength of 485 nm and an emission wavelength of 530 nm.[20,24] Mitochondrial membrane potential change was detected by using the dye 5,5′,6,6′-tetrachloro-1,1′,3,3′-tetraethylbenzimidazolcarbocyanine iodide (JC-1). The monomer form of JC-1 was excited at the wavelength of 485 nm and the emission detected at 590 nm (green fluorescence), whereas the JC-1 aggregate form was excited at the wavelength of 485 nm and the emission detected at 530 nm (red fluorescence).[24] Depolarization of the mitochondrial membrane was indicated by a decreased red/green fluorescence intensity ratio.[24] Cardiac mitochondrial swelling was detected using a spectrophotometer at 540 nm, continuously for 30 minutes, swelling being indicated by a decrease in the absorbance of a mitochondrial suspension. A transmission electron microscope (JEM-1200 EX II; JEOL Ltd, Tokyo, Japan) was also used to observe the mitochondrial morphology, according to the previously described procedure.[18]

Determination of oxidative stress

Oxidative stress levels were indicated by the increased malondialdehyde (MDA) concentrations, which were measured by a high-performance liquid chromatography system (Thermo Scientific, Bangkok, Thailand), as previously described.[17] Serum and protein from cardiac tissues were mixed with 10% trichloroacetic acid. The mixture was centrifuged, and the supernatant was mixed with 0.44 M H_3PO_4 and 0.6% thiobabituric acid solution to generate thiobarbituric acid reactive substances, which were further measured by the high-performance liquid chromatography system with BDS software (BarSpec Ltd, Rehovot, Israel). The concentration of thiobarbituric acid reactive substances was determined directly from a standard curve and reported as an MDA equivalent concentration.[17]

Cardiac expression of Bax and Bcl-2

The expressions of Bax and Bcl-2 were determined by western blot analysis. Briefly, myocardial tissues were homogenized in a lysis buffer (containing 1% Nonidet P-40, 0.5% sodium deoxycholate, 0.1% sodium dodecyl sulfate [SDS] in 1 × phosphate buffered saline) and were then centrifuged at 13,000 rpm for 10 minutes. Myocardial protein was mixed with the loading buffer (consisting of 5% mercaptoethanol, 0.05% bromophenol blue, 75 nM Tris-HCl, 2% SDS, and 10% glycerol with pH 6.8) at 1 mg/mL concentration and boiled for 5 minutes. The protein was loaded into a 10% gradient SDS-polyacrylamide gel, and then transferred to a polyvinyldene difluoride membrane in a transfer system (Bio-Rad, Hercules, CA). The protein-contained membranes were incubated in 5% skimmed milk in 1 × Tris-buffered saline and Tween 20 solution-T buffer for 1 hour, and then exposed to anti-Bax, anti-Bcl-2 (Cell Signaling Technology, Danvers, MA) and anti-actin (Sigma-Aldrich). Horseradish peroxidase conjugated with antirabbit or antimouse IgG (Santa Cruz Biotechnology, Inc, Dallas, TX) was administered to produce a peroxidase reaction, which further developed the signal by enhanced chemiluminescence detection reagents. Finally, autoradiography was performed, and the immune-blotted films were investigated to examine the protein band density using the ImageJ program (NIH image).[18]

Chemicals and antibodies

Estradiol and sesame oil were obtained from Sigma-Aldrich. Metformin was from Merck Serono, and vildagliptin was from Novartis. Colorimetric assay kits for the determination of plasma glucose, cholesterol, and triglyceride were from Biotech. ELISA kit for the measurement of plasma

© 2016 The North American Menopause Society

Copyright @ 2016 The North American Menopause Society. Unauthorized reproduction of this article is prohibited.

insulin level was from Millipore. Enzyme immunoassay kit for serum estradiol-level detection was from Cayman Chemical Company. The antibodies against Bax and Bcl-2 were from Cell Signaling Technology and antiactin was from Sigma-Aldrich. The horseradish peroxidase conjugated with antirabbit and antimouse IgG were from Santa Cruz Biotechnology.

Statistical analysis

Data were derived from all rats in each experimental group (n = 6/group) in all experiments. All data were included in the statistical analysis and was presented as mean ± standard error of mean. A one-way analysis of variance followed by post-hoc least significant difference test, which was carried out using the SPSS program (SPSS version 16; SPSS Inc, Chicago, IL), was used to determine the differences between the means. $P < 0.05$ was considered statistically significant.

RESULTS

Effects of estrogen, metformin, and vildagliptin on metabolic function in obese insulin-resistant and estrogen-deprived rats

Metabolic parameters measured after 4 weeks of treatment are shown in Table 1. Both NDOVe and HFOVe rats exhibited metabolic disorders, shown by an increased BW, increased plasma cholesterol, and decreased plasma high-density lipoprotein level. NDOVe and HFOVe rats also had increased plasma insulin and glucose levels and a higher HOMA index, indicating insulin resistance. All interventions except the vehicle could reverse the insulin-resistant status in both NDO and HFO rats, as indicated by the decreased HOMA index and decreased plasma insulin and glucose levels, to the same level as those of ND-fed sham-operated (NDS) rats. BW was reduced in NDO and HFO rats that were treated with E and M, but not Vil, when compared with those who received the vehicle. HFO rats had a greater visceral fat mass when compared with NDS rats, and only E significantly reduced both BW and visceral fat accumulation. None of the treatments could decrease plasma cholesterol levels in HFO rats.

Effects of estrogen, metformin, and vildagliptin on cardiac function and autonomic regulation in estrogen-deprived, obese insulin-resistant rats

Before treatment, echocardiography data showed that both the %FS and %EF had declined, and HRV was suppressed in both NDO and HFO rats when compared with NDS rats (Fig. 1A–C). This indicated that NDO and HFO rats had cardiac contractile dysfunction and autonomic imbalance. All treatment groups except those in the vehicle-only group showed improvements in %FS (Fig. 2A) and corrections in the %EF (Fig. 2B) and LF/HF ratio (Fig. 2C), bringing them back to normal levels.

Heart rate was increased in both NDOVe and HFOVe rats compared with NDS rats, but this increase in heart rate was not seen in all drug-treated groups (Table 2). NDOVe and HFOVe rats had increased systolic and diastolic blood pressures (Table 2). Treatment with E, M, and Vil reduced systolic blood pressure in both NDO and HFO rats. Diastolic blood pressure was improved only in HFOE and HFOVil rats, not in HFOM rats. There were no differences in diastolic blood pressure among treated NDO rats. In HFO rats, there was a reduction in ±dP/dt in HFOVe and HFOM compared with NDS rats, but ±dP/dt was maintained in HFOE and HFOVil rats (Table 2). Moreover, LVESP was markedly decreased in HFOVe, HFOM, and HFOVil rats, but it was preserved only in HFOE rats (Table 2), suggesting that only estrogen and vildagliptin improved LV function to a greater extent compared with the other treatments in HFD-fed rats.

TABLE 1. *Metabolic parameters after 4 weeks of treatment*

		NDO				HFO			
Parameters	NDS	Ve	E	M	Vil	Ve	E	M	Vil
Body weight, g	294.2 ± 3	356.0 ± 8[a]	308.3 ± 9[b]	321.6 ± 7[b]	331.6 ± 11[a]	414.0 ± 17[a]	340.0 ± 13[a,c]	377.5 ± 6[a,c]	396.6 ± 17[a]
Visceral fat, g	14.9 ± 1.4	15.9 ± 1.6	13.3 ± 1.6	11.6 ± 1.3	14.9 ± 1.1	32.3 ± 3.2[a]	18.2 ± 1.3[c]	30.8 ± 2.1[a]	31.6 ± 4.6[a]
Uterus weight, g	0.50 ± 0.1	0.08 ± 0.0[a]	0.39 ± 0.0[b]	0.07 ± 0.0[a]	0.07 ± 0.0[a]	0.08 ± 0.0[a]	0.47 ± 0.0[c]	0.08 ± 0.0[a]	0.08 ± 0.0[a]
Glucose, mg%	125.8 ± 7.0	150.3 ± 8.8[a]	120.48 ± 7.2[b]	111.7 ± 2.7[b]	126.1 ± 9.2[b]	170.6 ± 11.0[a]	142.1 ± 8.6[c]	139.8 ± 11.3[c]	136.4 ± 7.8[c]
Cholesterol, mg%	71.3 ± 1.9	104.3 ± 1.5[a]	87.6 ± 8.4	78.8 ± 3.2[b]	88.3 ± 4.0	125.0 ± 5.7[a]	122.0 ± 10.6[a]	120.9 ± 1.9[a]	120.1 ± 5.43[a]
HDL, μg/μL	0.34 ± 0.0	0.30 ± 0.0[a]	0.31 ± 0.0	0.33 ± 0.0	0.33 ± 0.0	0.28 ± 0.0[a]	0.33 ± 0.0[c]	0.37 ± 0.0[c]	0.37 ± 0.0[c]
Triglyceride, mg%	30.5 ± 2.46	33.9 ± 1.5	32.3 ± 5.1	32.3 ± 4.5	32.5 ± 3.77	37.3 ± 1.9	32.0 ± 5.0	31.4 ± 1.5	33.4 ± 4.2
Insulin, ng/mL	0.92 ± 0.1	1.75 ± 0.1[a]	0.81 ± 0.1[b]	0.90 ± 0.4[b]	1.10 ± 0.1[b]	1.93 ± 0.1[a]	1.03 ± 0.0[c]	0.90 ± 0.0[c]	1.23 ± 0.3[c]
HOMA index	6.90 ± 1.4	16.28 ± 1.2[a]	5.72 ± 1.1[b]	6.13 ± 2.8[b]	8.99 ± 1.2[b]	20.43 ± 1.6[a]	8.11 ± 0.9[c]	7.70 ± 0.4[c]	7.08 ± 1.7[c]
Estradiol level, pg/mL	174.5 ± 24.4	78.6 ± 11.3[a]	195.7 ± 51.1[b]	88.6 ± 6.2[a]	71.1 ± 8.0[a]	80.3 ± 18.9[a]	224.9 ± 27.5[c]	97.6 ± 21.1[a]	77.7 ± 19.0[a]
Serum MDA, μmol/mL	2.02 ± 0.0	3.06 ± 0.1[a]	2.40 ± 0.1[b]	2.69 ± 0.0[a,b]	2.38 ± 0.0[b]	3.48 ± 0.1[a]	2.37 ± 0.0[c]	3.15 ± 0.0[a]	2.33 ± 0.0[c]
Tissue MDA, μmol/mL	1.72 ± 0.2	4.31 ± 0.5[a]	2.53 ± 0.2[b]	3.46 ± 0.2[a]	2.52 ± 0.2[b]	4.16 ± 0.4[a]	2.16 ± 0.4[c]	3.23 ± 0.3[a]	2.38 ± 0.0[c]
Food intake, g/d	12.5 ± 0.7	14.1 ± 1.8	12.8 ± 0.5	13.7 ± 0.4	12.9 ± 0.6	18.6 ± 0.0[a]	18.3 ± 0.5[a]	18.5 ± 0.5[a]	20.5 ± 1.2[a]

Values are mean ± SEM for six rats per group.
E, estradiol; HDL, high-density lipoprotein; HFO, high-fat diet-fed ovariectomized rats; HOMA, Homeostasis Model Assessment; M, metformin; MDA, malondialdehyde; NDO, normal diet-fed ovariectomized rats; NDS, normal diet-fed sham-operated rats; Ve, vehicle; Vil, vildagliptin.
[a] $P < 0.05$ versus NDS.
[b] $P < 0.05$ versus NDOVe.
[c] $P < 0.05$ versus HFOVe.

Copyright @ 2016 The North American Menopause Society. Unauthorized reproduction of this article is prohibited.

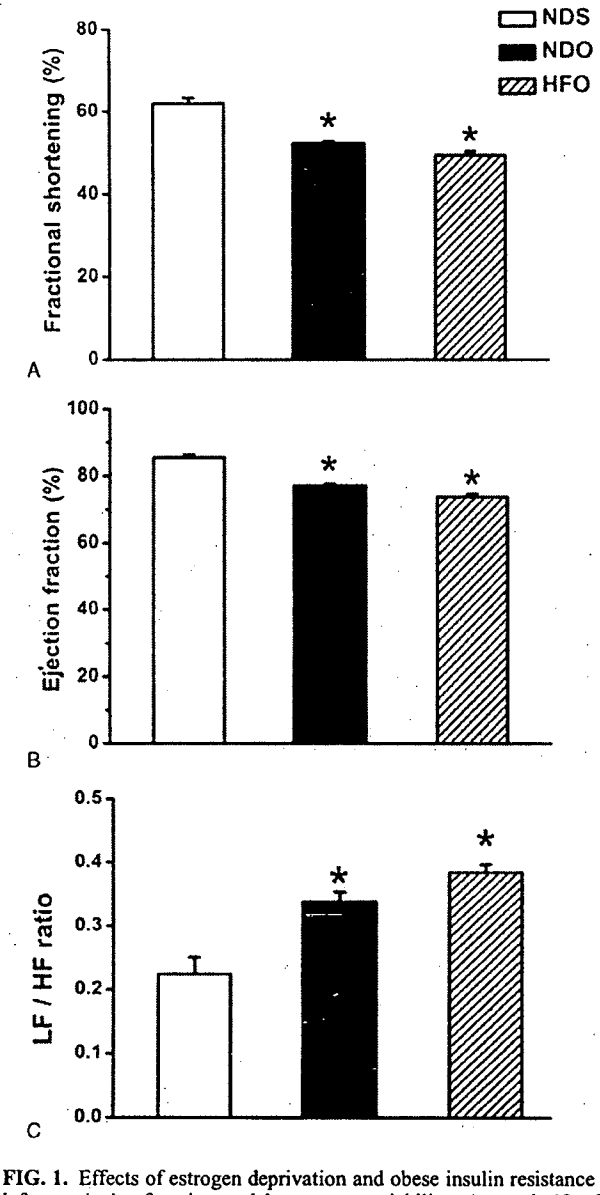


FIG. 1. Effects of estrogen deprivation and obese insulin resistance on left ventricular function and heart rate variability. At week 12 after ovariectomy, both estrogen-deprived rats who fed with NDO and those who fed with HFO had reduced fractional shortening (**A**), ejection fraction (**B**), and increased LF/HF ratio (**C**) when compared with NDS rats. Values are mean ± SEM (n = 6 rats/group). $^{*}P < 0.05$ versus NDS. HF, high frequency; HFO, high-fat diet-fed ovariectomized rats; LF, low frequency; NDO, normal diet-fed ovariectomized rats; NDS, normal diet-fed sham-operated rats; SEM, standard error of mean.

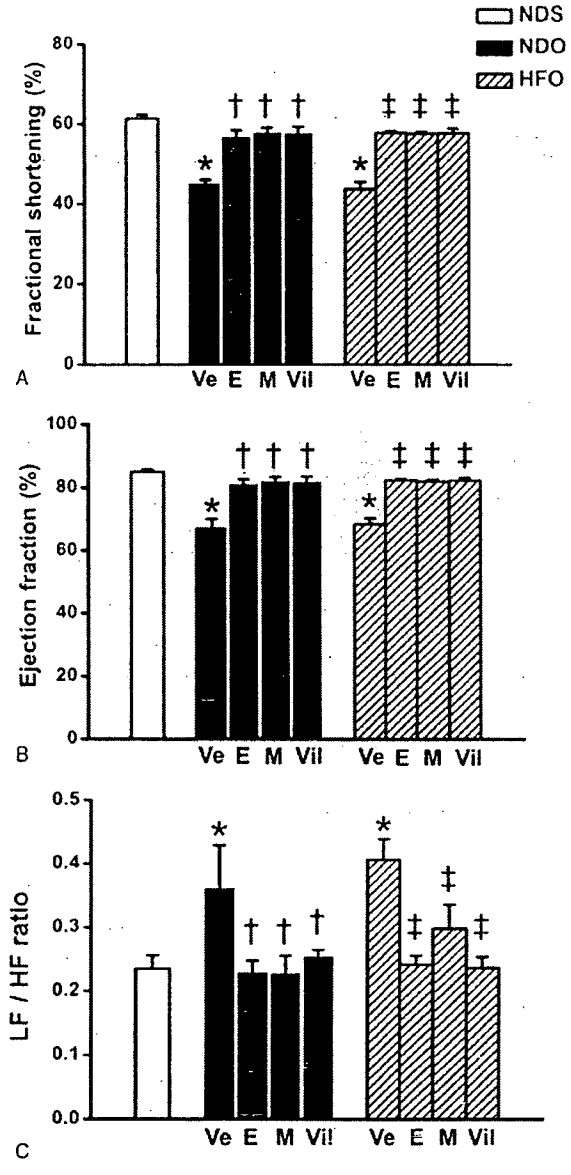


FIG. 2. Effects of E, M, and Vil on left ventricular function and heart rate variability of estrogen-deprived rats. After 4 weeks of treatment, fractional shortening (**A**) and ejection fraction (**B**) were improved, and LF/HF ratio (**C**) was restored in estrogen (E)-, metformin (M)-, and vildagliptin (Vil)-treated groups when compared with vehicle-treated NDO or HFO rats. Values are mean ± SEM (n = 6 rats/group). $^{*}P < 0.05$ versus NDS; $^{\dagger}P < 0.05$ versus NDOVe; and $^{\ddagger}P < 0.05$ versus HFOVe. E, estradiol; HF, high frequency; HFO, high-fat diet-fed ovariectomized rats; LF, low frequency; M, metformin; NDO, normal diet-fed ovariectomized rats; NDS, normal diet-fed sham-operated rats; SEM, standard error of mean; Ve, vehicle; Vil, vildagliptin.

Effects of estrogen, metformin, and vildagliptin on cardiac expression of Bax and Bcl-2 in estrogen-deprived, obese insulin-resistant rats

There were significant increases in the expression of the apoptotic protein Bax in NDOVe, HFOVe, and HFOM groups (Fig. 3A). The expression of the antiapoptotic protein Bcl-2 was significantly decreased in HFOVe and HFOM rats (Fig. 3B). The ratio of cardiac Bax/Bcl-2 was significantly higher in NDOVe, HFOVe, and HFOM rats compared with the NDS rats (Fig. 3C), whereas this ratio was lower in the HFOE and HFOVil groups, suggesting that only estrogen and vildagliptin could attenuate apoptosis in an obese insulin-resistant and estrogen-deprived rat model. A significant change in Bax and Bcl-2 expression was not observed in any NDO rats.

© 2016 The North American Menopause Society

Copyright @ 2016 The North American Menopause Society. Unauthorized reproduction of this article is prohibited.

TABLE 2. *Cardiac function after 4 weeks of treatment*

Parameters	NDS	NDO				HFO			
		Ve	E	M	Vil	Ve	E	M	Vil
Heart rate, bpm	238 ± 18	306 ± 5[a]	266 ± 8	275 ± 19	266 ± 9	307 ± 21[a]	273 ± 24	285 ± 28	286 ± 11
Systolic BP, mm Hg	118.5 ± 4	139.7 ± 10[a]	117.6 ± 5[b]	112.3 ± 5[b]	113.3 ± 3[b]	140.7 ± 6[a]	112.9 ± 3[c]	111.5 ± 6[c]	112.3 ± 5[c]
Diastolic BP, mm Hg	86.7 ± 4	108.9 ± 10[a]	89.1 ± 5	93.5 ± 7	93.8 ± 5	107.7 ± 5[a]	77.9 ± 7[c]	91.8 ± 6	87.1 ± 6[c]
LVESP, mm Hg	127.3 ± 7	99.7 ± 5[a]	113.7 ± 4	115.1 ± 4	111.9 ± 4	100.7 ± 2[a]	116.5 ± 3	111.6 ± 7[a]	108.9 ± 5[a]
LVEDP, mm Hg	12.0 ± 2	19.9 ± 2	15.2 ± 1	15.8 ± 4	15.5 ± 2	18.8 ± 2	16.2 ± 2	14.2 ± 1	13.7 ± 1
+dP/dt, mm Hg/s	11,339 ± 1,228	5,877 ± 458[a]	10,758 ± 4,949	10,427 ± 2,948	10,048 ± 3,858	5,894 ± 341[a]	6,555 ± 1,440	5,872 ± 286[a]	7,227 ± 932
−dP/dt, mm Hg/s	−7,677 ± 847	−4,397 ± 707[a]	−5,886 ± 1,005	−5,914 ± 997	−5,797 ± 1,284	−4,839 ± 623[a]	−5,626 ± 423	−4,706 ± 179[a]	−6,079 ± 1,218

Values are mean ± SEM (n = 6 per group).
BP, blood pressure; bpm, beats per minute; +dP/dt, maximal slope of the systolic pressure increment; −dP/dt, maximal slope of the diastolic pressure decrement; E, estradiol; HFO, high-fat diet-fed ovariectomized rats; LVEDP, left ventricular end-diastolic pressure; LVESP, left ventricular end-systolic pressure; M, metformin; NDO, normal diet-fed ovariectomized rats; NDS, normal diet-fed sham-operated rats; Ve, vehicle; Vil, vildagliptin.
[a] $P < 0.05$ versus NDS.
[b] $P < 0.05$ versus NDOVe.
[c] $P < 0.05$ versus HFOVe.

Effects of estrogen, metformin, and vildagliptin on cardiac mitochondrial function and oxidative stress in estrogen-deprived, obese insulin-resistant rats

Both NDOVe and HFOVe rats exhibited cardiac mitochondrial impairment, which was identified by the increased mitochondrial ROS level, decreased $\Delta\Psi$ indicating mitochondrial depolarization, and decreased absorbance intensity indicating mitochondrial swelling (Fig. 4A–D, respectively). In NDO rats, treatment with E completely halted mitochondrial dysfunction by markedly reducing ROS production, increasing $\Delta\Psi$, and attenuating mitochondrial swelling to normal levels. In HFOE rats, all mitochondrial parameters showed significant improvement, especially ROS production and $\Delta\Psi$, which were reversed to normal levels. Treatment with Vil also improved all mitochondrial parameters in both NDOVil and HFOVil when compared with vehicle-treated groups; however, it did not bring parameters back to normal levels (Fig. 4). Treatment with M could improve all mitochondrial parameters in NDOM rats; however, it failed to enhance any mitochondrial parameters in HFOM rats when compared with NDOVe rats.

DISCUSSION

The major findings from this study are as follows: (1) estrogen, metformin, and vildagliptin can attenuate insulin resistance in both ND- and HFD-fed estrogen-deprived rats; (2) although estrogen, metformin, and vildagliptin similarly attenuated cardiac autonomic dysfunction, estrogen and vildagliptin provided superior advantages through their ability to restore blood pressure and cardiac contractile performance in estrogen-deprived insulin-resistant rats; and (3) oxidative stress, apoptosis, and cardiac mitochondrial dysfunction were effectively decreased by estrogen and vildagliptin, but not by metformin.

Although the impairments of LV function in obese insulin-resistant rats and the benefits from the results may be subtle, these impairments as well as the efficacy of treatments by estrogen, metformin, or vildagliptin were demonstrated to be consistent and significant throughout the experiments. This subtle difference could also be due to the fact that we used the obese insulin-resistant model which was a prediabetic state model in which the severity is not high. Investigation in a model of type 2 diabetes with estrogen deprivation may reveal even larger benefits. Future studies are needed to evaluate this issue. Nevertheless, we believe that our findings indicated potential therapeutic efficacy of these antidiabetic drugs in menopause with obese insulin-resistant condition.

All therapeutic agents in this study, that is estrogen, vildagliptin, and metformin, clearly ameliorated insulin resistance, as indicated by the decreased levels of fasting insulin and glucose, and thus resulting in a reduced HOMA index. These results are consistent with a previous study which similarly showed that metformin and vildagliptin decreased insulin levels and the HOMA index in HFD-fed rats.[17] Estrogen supplements also exhibited similar beneficial effects, consistent with the results from a previous study, in

Copyright @ 2016 The North American Menopause Society. Unauthorized reproduction of this article is prohibited.

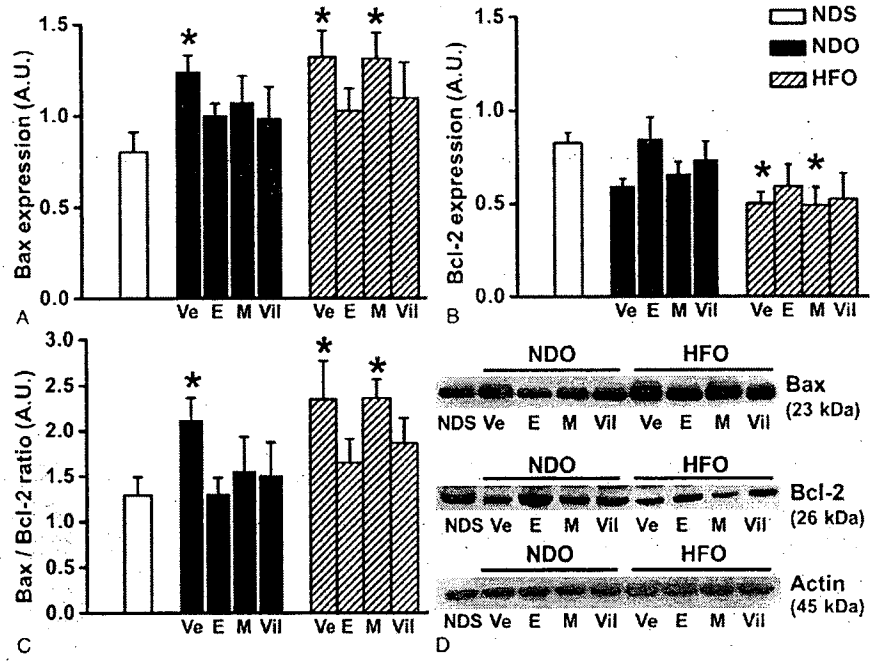


FIG. 3. Cardiac expression of apoptotic and antiapoptotic proteins after treatment with E, M, or Vil for 4 weeks. Expression levels of the apoptotic protein Bax (A) were significantly increased, whereas the expression levels of antiapoptotic protein, Bcl-2 (B), were reduced in HFOVe and HFOM rats. The Bax/Bcl-2 ratio (C) was significantly increased in NDOVe, HFOVe, and HFOM rats when compared with NDS rats. The represented protein expressions are in panel D. Values are mean ± SEM (n = 6 rats per group). $^{*}P < 0.05$ versus NDS. E, estradiol; HFO, high-fat diet-fed ovariectomized rats; M, metformin; NDO, normal diet-fed ovariectomized rats; NDS, normal diet-fed sham-operated rats; SEM, standard error of mean; Ve, vehicle; Vil, vildagliptin.

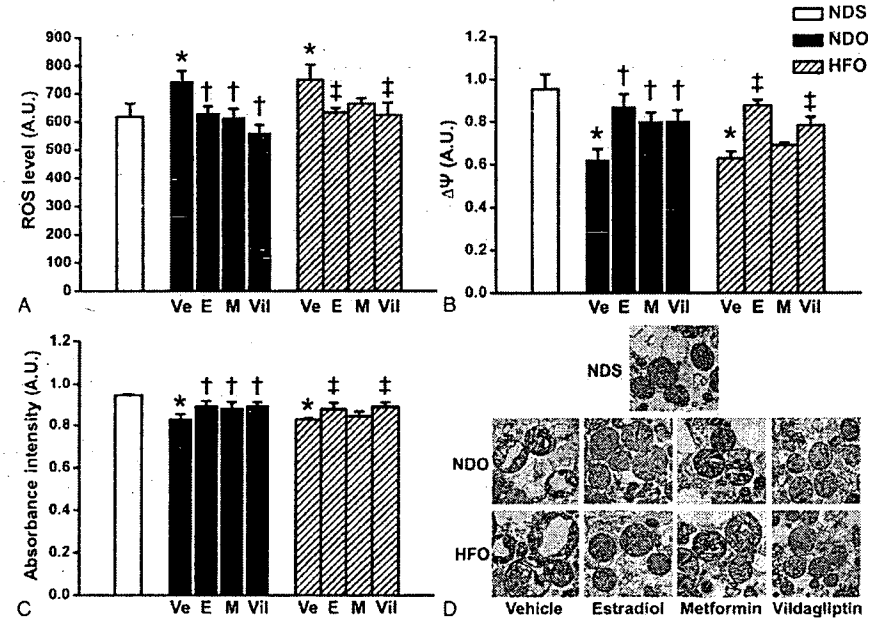


FIG. 4. Cardiac mitochondrial function in estrogen-deprived rats after treatment with E, M, or Vil for 4 weeks. Mitochondrial ROS level (A) was increased, whereas ΔΨ (B) and absorbance intensity (C) were decreased in NDOVe and HFOVe rats. Transmission electron micrographs (D) illustrate cardiac mitochondria morphology from rats in each group. Treatments with E and Vil improved all parameters of cardiac mitochondrial function in both NDO and HFO rats. Treatment with M, however, showed effective effects on mitochondrial function only in NDO, not in HFO rats. Values are mean ± SEM (n = 6 rats per group). $^{*}P < 0.05$ versus NDS; $^{\dagger}P < 0.05$ versus NDOVe; and $^{\ddagger}P < 0.05$ versus HFOVe. E, estradiol; HFO, high-fat diet-fed ovariectomized rats; M, metformin; NDO, normal diet-fed ovariectomized rats; NDS, normal diet-fed sham-operated rats; ROS, reactive oxygen species; SEM, standard error of mean; Ve, vehicle; Vil, vildagliptin.

© 2016 The North American Menopause Society

Copyright @ 2016 The North American Menopause Society. Unauthorized reproduction of this article is prohibited.

which insulin resistance was reversed after just 1 month of estrogen treatment.[19] Estrogen and metformin also efficiently inhibited BW gain in both ND- and HFD-fed rats. Estrogen had been previously reported to protect female mice from adipocyte hypertrophy, body fat accumulation, and weight gain, and the results of this study are consistent with these findings.[25] Likewise, metformin has previously been reported to increase fatty acid oxidation and decrease weight gain.[26] The ability of metformin to increase fatty acid oxidation, however, could be responsible for the high level of cytotoxicity and oxidative stress in metformin-treated rats, which was indicated by the elevated MDA levels and mitochondrial impairment. Metformin had been shown to decrease cholesterol synthesis and content; however, it has also been shown to increase ROS production in a macrophage cell line.[27] These results are similar to the findings in this study, in which cholesterol levels were reduced, whereas mitochondrial ROS levels were enhanced in metformin-treated rats.

In the present study, estrogen and vildagliptin had measurably enhanced effects on oxidative stress reduction, as they completely attenuated mitochondrial ROS production, decreased mitochondrial depolarization, decreased mitochondrial swelling, and restored serum and tissue MDA levels. Although metformin was able to reverse hyperglycemia, which is a condition linked to increased oxidative stress and inflammation,[28] it failed to improve mitochondrial function and decrease MDA concentrations, therefore could not effectively protect the heart from oxidative stress. This increased oxidative stress could subsequently induce cellular apoptosis,[29] which was indicated by the reduced Bcl-2 level and the upregulated levels of the Bax and Bax/Bcl-2 ratio in the myocardium of metformin-treated rats. Cardiomyocyte apoptosis is known to be associated with the pathogenesis of heart disease and heart failure.[30,31] This oxidative stress-induced cardiomyocyte apoptosis may contribute to decreased myocardium performance as observed in the metformin-treatment group. Moreover, a higher level of ROS, which was found in metformin-treated obese rats, is also harmful to endothelial membranes and nitric oxide function,[32] thus resulting in increased diastolic blood pressure. Estrogen has been reported to inhibit ROS production, decrease lipid peroxidation, and reduce oxidative stress in several cell types such as cardiomyocytes, fibroblasts, and hepatocytes.[33-35] Vildagliptin is also effective in the reduction of oxidative stress and mitochondrial dysfunction.[36] The antioxidant and antiapoptotic effects of estrogen and vildagliptin may play an important role in the attenuation of cardiometabolic disorders in obese insulin-resistant and estrogen-deprived rats.

Moreover, previous studies reported the similar effects of estrogen and vildagliptin regarding the reduction of oxidative stress and inflammatory markers.[37,38] Vildagliptin was also reported to enhance endothelial cell function and blood flow, through the upregulation of Akt and eNOS phosphorylation.[39] The activation of Akt and eNOS pathway had been demonstrated as the common mechanisms underlying estrogen cardioprotection[40,41]; therefore, the benefits of vildagliptin may share a similar pathway, and thus provide a similar effect as estrogen treatment, as observed in this study.

Potential clinical value

Previous studies from both basic and clinical reports demonstrated the adverse effects of estrogen therapy such as increased atrial fibrillation incidence, increased QT interval and dispersion.[42,43] The use of estrogen supplement has been contraindicated in individuals with the conditions of thromboembolism and migraine.[44,45] Moreover, estrogen supplement was reported to increase risks of glioma, meningioma, and all tumors of the central nervous system.[46] The findings in the present study, which demonstrated that the cardioprotective effects and efficacy of vildagliptin and metformin are similar to estrogen supplement in ovariectomized rats under normal and obese insulin-resistant conditions, provided important information for future clinical use of these drugs in obese insulin resistance particularly under menopause condition.

CONCLUSIONS

In summary, this study demonstrated that although metformin exerted similar effects to estrogen and vildagliptin on metabolic regulation, estrogen and vildagliptin offer greater advantage in terms of cardiac mitochondrial protection and LV performance, in obese insulin-resistant and estrogen-deprived rats. This study is the first to report the comparative efficacy of estrogen, metformin, and vildagliptin on the cardiometabolic and cardiac mitochondrial function in obese insulin-resistant ovariectomized rats. Treatment with vildagliptin and estrogen therapy similarly provided the cardioprotective benefits in obese insulin-resistant ovariectomized rats. Because estrogen supplement was reported to associate with increased venous thromboembolism and cancer risks, vildagliptin could be considered as an alternative therapy for those who have contraindication for female sex hormone therapy. Vildagliptin was reported as the medication that did not affect the cardiac conduction system and repolarization, and also exerted beneficial effect on ischemic heart.[18,47] The cardioprotective effects under myocardial ischemia of vildagliptin treatment in estrogen-deprived and insulin-resistant conditions still need to be investigated.

REFERENCES

1. Mendis S, Thygesen K, Kuulasmaa K, et al. World Health Organization definition of myocardial infarction: 2008-09 revision. *Int J Epidemiol* 2011;40:139-146.
2. Mendis S. The contribution of the Framingham Heart Study to the prevention of cardiovascular disease: a global perspective. *Prog Cardiovasc Dis* 2010;53:10-14.
3. Penno G, Solini A, Bonora E, et al. Gender differences in cardiovascular disease risk factors, treatments and complications in patients with type 2 diabetes: the RIACE Italian multicentre study. *J Intern Med* 2013;274: 176-191.
4. Mendis S, Puska P, Norrving B. *Global Atlas on Cardiovascular Disease Prevention and Control*. Geneva, Switzerland: World Health Organization; 2011.
5. Giardina EG. Heart disease in women. *Int J Fertil Womens Med* 2000;45: 350-357.

Copyright @ 2016 The North American Menopause Society. Unauthorized reproduction of this article is prohibited.

6. Stampfer MJ, Colditz GA, Willett WC. Menopause and heart disease. A review. *Ann N Y Acad Sci* 1990;592:193-203.
7. Rosano GM, Vitale C, Marazzi G, Volterrani M. Menopause and cardiovascular disease: the evidence. *Climacteric* 2007;10(suppl 1):19-24.
8. Jelenik T, Roden M. How estrogens prevent from lipid-induced insulin resistance. *Endocrinology* 2013;154:989-992.
9. Xu J, Xiang Q, Lin G, et al. Estrogen improved metabolic syndrome through down-regulation of VEGF and HIF-1alpha to inhibit hypoxia of periaortic and intra-abdominal fat in ovariectomized female rats. *Mol Biol Rep* 2012;39:8177-8185.
10. Campos C, Casali KR, Baraldi D, et al. Efficacy of a low dose of estrogen on antioxidant defenses and heart rate variability. *Oxid Med Cell Longev* 2014;2014:218749; Available at: http://www.hindawi.com/journals/omcl/2014/218749/. Accessed May 15, 2016.
11. Hernandez I, Delgado JL, Diaz J, et al. 17beta-estradiol prevents oxidative stress and decreases blood pressure in ovariectomized rats. *Am J Physiol Regul Integr Comp Physiol* 2000;279:R1599-R1605.
12. Brownlee M. Biochemistry and molecular cell biology of diabetic complications. *Nature* 2001;414:813-820.
13. Dhalla NS, Temsah RM, Netticadan T. Role of oxidative stress in cardiovascular diseases. *J Hypertens* 2000;18:655-673.
14. Rattanasopa C, Phungphong S, Wattanapermpool J, Bupha-Intr T. Significant role of estrogen in maintaining cardiac mitochondrial functions. *J Steroid Biochem Mol Biol* 2014;147C:1-9.
15. Bi Y, Tong GY, Yang HJ, et al. The beneficial effect of metformin on beta-cell function in non-obese Chinese subjects with newly diagnosed type 2 diabetes. *Diabetes Metab Res Rev* 2013;29:664-672.
16. Banerjee M, Younis N, Soran H. Vildagliptin in clinical practice: a review of literature. *Expert Opin Pharmacother* 2009;10:2745-2757.
17. Apaijai N, Pintana H, Chattipakorn SC, Chattipakorn N. Cardioprotective effects of metformin and vildagliptin in adult rats with insulin resistance induced by a high-fat diet. *Endocrinology* 2012;153:3878-3885.
18. Chinda K, Sanit J, Chattipakorn S, Chattipakorn N. Dipeptidyl peptidase-4 inhibitor reduces infarct size and preserves cardiac function via mitochondrial protection in ischaemia-reperfusion rat heart. *Diab Vasc Dis Res* 2014;11:75-83.
19. Pratchayasakul W, Chattipakorn N, Chattipakorn SC. Estrogen restores brain insulin sensitivity in ovariectomized non-obese rats, but not in ovariectomized obese rats. *Metabolism* 2014;63:851-859.
20. Semaming Y, Kumfu S, Pannangpetch P, Chattipakorn SC, Chattipakorn N. Protocatechuic acid exerts a cardioprotective effect in type 1 diabetic rats. *J Endocrinol* 2014;223:13-23.
21. Morgan EE, Faulx MD, McElfresh TA, et al. Validation of echocardiographic methods for assessing left ventricular dysfunction in rats with myocardial infarction. *Am J Physiol Heart Circ Physiol* 2004;287:H2049-H2053.
22. Apaijai N, Pintana H, Chattipakorn SC, Chattipakorn N. Effects of vildagliptin versus sitagliptin, on cardiac function, heart rate variability and mitochondrial function in obese insulin-resistant rats. *Br J Pharmacol* 2013;169:1048-1057.
23. Incharoen T, Thephinlap C, Srichairatanakool S, et al. Heart rate variability in beta-thalassemic mice. *Int J Cardiol* 2007;121:203-204.
24. Thummasorn S, Kumfu S, Chattipakorn S, Chattipakorn N. Granulocyte-colony stimulating factor attenuates mitochondrial dysfunction induced by oxidative stress in cardiac mitochondria. *Mitochondrion* 2011;11:457-466.
25. Stubbins RE, Najjar K, Holcomb VB, Hong J, Nunez NP. Oestrogen alters adipocyte biology and protects female mice from adipocyte inflammation and insulin resistance. *Diabetes Obes Metab* 2012;14:58-66.
26. Wang C, Liu F, Yuan Y, et al. Metformin suppresses lipid accumulation in skeletal muscle by promoting fatty acid oxidation. *Clin Lab* 2014;60:887-896.
27. Koren-Gluzer M, Aviram M, Hayek T. Metformin inhibits macrophage cholesterol biosynthesis rate: possible role for metformin-induced oxidative stress. *Biochem Biophys Res Commun* 2013;439:396-400.
28. Esposito K, Nappo F, Marfella R, et al. Inflammatory cytokine concentrations are acutely increased by hyperglycemia in humans: role of oxidative stress. *Circulation* 2002;106:2067-2072.
29. Cook SA, Sugden PH, Clerk A. Regulation of bcl-2 family proteins during development and in response to oxidative stress in cardiac myocytes: association with changes in mitochondrial membrane potential. *Circ Res* 1999;85:940-949.
30. Gill C, Mestril R, Samali A. Losing heart: the role of apoptosis in heart disease-a novel therapeutic target? *FASEB J* 2002;16:135-146.
31. Takemura G, Kanoh M, Minatoguchi S, Fujiwara H. Cardiomyocyte apoptosis in the failing heart-a critical review from definition and classification of cell death. *Int J Cardiol* 2013;167:2373-2386.
32. Annuk M, Zilmer M, Fellstrom B. Endothelium-dependent vasodilation and oxidative stress in chronic renal failure: impact on cardiovascular disease. *Kidney Int Suppl* 2003;84:S50-S53.
33. Hamden K, Carreau S, Ellouz F, Masmoudi H, El FA. Protective effect of 17beta-estradiol on oxidative stress and liver dysfunction in aged male rats. *J Physiol Biochem* 2007;63:195-201.
34. Richardson TE, Yu AE, Wen Y, Yang SH, Simpkins JW. Estrogen prevents oxidative damage to the mitochondria in Friedreich's ataxia skin fibroblasts. *PLoS One* 2012;7:e34600.
35. Urata Y, Jhara Y, Murata H, et al. 17Beta-estradiol protects against oxidative stress-induced cell death through the glutathione/glutaredoxin-dependent redox regulation of Akt in myocardiac H9c2 cells. *J Biol Chem* 2006;281:13092-13102.
36. Scheen AJ. Cardiovascular effects of gliptins. *Nat Rev Cardiol* 2013;10:73-84.
37. Lamas AZ, Caliman IF, Dalpiaz PL, et al. Comparative effects of estrogen, raloxifene and tamoxifen on endothelial dysfunction, inflammatory markers and oxidative stress in ovariectomized rats. *Life Sci* 2015;124:101-109.
38. Rizzo MR, Barbieri M, Marfella R, Paolisso G. Reduction of oxidative stress and inflammation by blunting daily acute glucose fluctuations in patients with type 2 diabetes: role of dipeptidyl peptidase-IV inhibition. *Diabetes Care* 2012;35:2076-2082.
39. Ishii M, Shibata R, Kondo K, et al. Vildagliptin stimulates endothelial cell network formation and ischemia-induced revascularization via an endothelial nitric-oxide synthase-dependent mechanism. *J Biol Chem* 2014;289:27235-27245.
40. Kim KH, Bender JR. Membrane-initiated actions of estrogen on the endothelium. *Mol Cell Endocrinol* 2009;308:3-8.
41. Murphy E, Steenbergen C. Cardioprotection in females: a role for nitric oxide and altered gene expression. *Heart Fail Rev* 2007;12:293-300.
42. Gokce M, Karahan B, Yilmaz R, Orem C, Erdol C, Ozdemir S. Long term effects of hormone replacement therapy on heart rate variability, QT interval, QT dispersion and frequencies of arrhythmia. *Int J Cardiol* 2005;99:373-379.
43. Perez MV, Wang PJ, Larson JC, et al. Effects of postmenopausal hormone therapy on incident atrial fibrillation: the Women's Health Initiative randomized controlled trials. *Circ Arrhythm Electrophysiol* 2012;5:1108-1116.
44. Tremollieres F, Brincat M, Erel CT, et al. EMAS position statement: managing menopausal women with a personal or family history of VTE. *Maturitas* 2011;69:195-198.
45. Vermeer LM, Gregory E, Winter MK, McCarson KE, Berman NE. Behavioral effects and mechanisms of migraine pathogenesis following estradiol exposure in a multibehavioral model of migraine in rat. *Exp Neurol* 2015;263:8-16.
46. Benson VS, Kirichek O, Beral V, Green J. Menopausal hormone therapy and central nervous system tumor risk: large UK prospective study and meta-analysis. *Int J Cancer* 2015;136:2369-2377.
47. He YL, Zhang Y, Serra D, Wang Y, Ligueros-Saylan M, Dole WP. Thorough QT study of the effects of vildagliptin, a dipeptidyl peptidase IV inhibitor, on cardiac repolarization and conduction in healthy volunteers. *Curr Med Res Opin* 2011;27:1453-1463.

© 2016 The North American Menopause Society

Copyright @ 2016 The North American Menopause Society. Unauthorized reproduction of this article is prohibited.

เอกสารแนบหมายเลข 28

Complementary Therapies in Clinical Practice 23 (2016) 59–63

Contents lists available at ScienceDirect

Complementary Therapies in Clinical Practice

journal homepage: www.elsevier.com/locate/ctcp

Effects of Tai Chi exercise on heart rate variability

Aimee R. Cole [a, b, c, e], Karn Wijarnpreecha [a, b, c], Siriporn C. Chattipakorn [a, c, d], Nipon Chattipakorn [a, b, c, *]

[a] Cardiac Electrophysiology Research and Training Center, Faculty of Medicine, Chiang Mai University, Chiang Mai, Thailand
[b] Cardiac Electrophysiology Unit, Department of Physiology, Faculty of Medicine, Chiang Mai University, Chiang Mai, Thailand
[c] Center of Excellence in Cardiac Electrophysiology, Chiang Mai University, Chiang Mai, Thailand
[d] Department of Oral Biology and Diagnostic Sciences, Faculty of Dentistry, Chiang Mai University, Chiang Mai 50200, Thailand
[e] Faculty of Life Sciences, The University of Manchester, Manchester, United Kingdom

ARTICLE INFO

Article history:
Received 17 January 2016
Accepted 23 March 2016

Keywords:
Heart rate variability
Heart
Holter monitoring
Autonomic nervous system
Tai Chi
Physical activity

ABSTRACT

Tai Chi is a callisthenic exercise form that incorporates aerobic exercise with diaphragmatic breathing. These two aspects alone have been shown to enhance the heart rate variability, warranting research into the effects of Tai Chi on autonomic nervous system modulation and heart rate variability. A low heart rate variability has been shown to be indicative of compromised health. Any methods to enhance the heart rate variability, in particular, non-pharmacological methods, are therefore seen as beneficial to health and are sought after. The aim of this review was to comprehensively summarize the currently published studies regarding the effects of Tai Chi on heart rate variability. Both consistent and inconsistent findings are presented and discussed, and an overall conclusion attained which could benefit future clinical studies.

© 2016 Elsevier Ltd. All rights reserved.

1. Introduction

Tai Chi (TC), also termed Tai Chi Chuan (TCC) [1] is a callisthenic exercise form, originating from China over 400 years ago [2–5]. It is a moderate [6] aerobic exercise form [7,8], which elicits a meditative effect [9,10], and incorporates slow [3] and deep breathing [1,2,11], with mental concentration [1,3,4,7] and slow [2–4,7,12], gentle circular movements [3,7]. The upper body moves whilst the lower body is kept in a semi squat position [2,3]. The movements called 'postures' are performed continuously one after the other to produce a "form" [2,3,7,12]. There are various styles of TC, namely Yang, Sun, Chen, and Wu [5]. Other forms/modifications include Taijiquan/Taichiquan (TCQ), and Tai Chi Chih (TCCh) [1]. The styles of TC can be modified to alter the number of postures to make the form easier to learn and perform [2,13]. The postures can also be altered to make them safer to perform [13]. Likewise, the postures can be modified, or certain postures selected in order to improve specific aspects of participants' fitness [2,13]. TC can therefore be made suitable for any age and health status. Hence, TC has been shown to be safe for not only patients with good health, but also those with prolonged illnesses [2,5].

TC is becoming increasingly popular worldwide, given its numerous health benefits [2,3]. It has been shown that TC has the ability to improve symptoms of several types of cancer [14], Parkinson's and cognitive impairment [15], reduce anxiety [16] and stress [15,17], enhance balance [17–19], augment flexibility [20], increase strength [17,18,20], improve cardiovascular risk factors, increase aerobic capacity [18], improve symptoms ensuing rheumatologic diseases [17], and reduce blood pressure [16]. Additional benefits of TC include its ability to be practised individually at home or as part of a group [2,12] since it can either incorporate exercise into busy lifestyles, or facilitate socialising [2]. Moreover, TC can be performed anywhere, does not require any equipment [2,12,21], is a cheap form of exercise [2,21], and is suitable for all [12] due to its ability to be adapted.

One of several objective measures to determine the effectiveness of TC includes its possible ability to alter the cardiac autonomic control, known as the heart rate variability (HRV). HRV is the variation in the period between consecutive R–R intervals on an electrocardiogram (ECG) [22]. HRV parameters can be used to infer the cardiac sympatho-vagal balance in our body, and the degree of parasympathetic to sympathetic modulation [23]. Although there are various markers of autonomic modulation [22,23], HRV is

* Corresponding author. Cardiac Electrophysiology Research and Training Center Faculty of Medicine, Chiang Mai University, Chiang Mai 50200, Thailand.
E-mail address: nchattip@gmail.com (N. Chattipakorn).

http://dx.doi.org/10.1016/j.ctcp.2016.03.007
1744-3881/© 2016 Elsevier Ltd. All rights reserved.

considered a superior option due to its low cost [23] and ease to record [22] since it can be measured automatically [22] and non-invasively [23].

Problems in cardiac autonomic modulation can be identified by a depressed HRV [24,25]. This decrease in the variation in beat-to-beat intervals is due to an imbalance in sympathetic to vagal modulation, more specifically, a deficiency in the parasympathetic influence [26], and markedly enhanced sympathetic activity [22,27]. Depressed HRV offers prognostic significance in a number of different circumstances. It can be used as a prognostic indicator following acute myocardial infarction [28–30], coronary heart disease (CHD) [24,31] and heart failure [24,32]. A depressed HRV can also have prognostic implications in the general population, and may be representative of poor health [27,33]. Any methods to increase HRV are therefore considered beneficial to health and are sought after. Slow and deep breathing [34–36] and aerobic exercise are two methods shown to enhance vagal modulation [37,38] and therefore increase the HRV. Since TC famously incorporates aerobic exercise [7,8] with "diaphragmatic breathing" [11], this justifies the assumption that TC has the possibility to enhance HRV [11].

It has been shown that the elderly [39–41] and those suffering with a cardiovascular disorder (CVD) are two major groups who often display depressed HRV [24,26]. Exercise is essential and integral in these populations, and it is particularly important for any exercise methods these patients attempt to be safe. TC could be a chosen exercise form [12], since it is suitable for participants who cannot cope with average intensity exercise [42], those with chronic disorders [42], and those with CVDs [43] or stroke [18]. This is because TC can be altered to make it appropriate for all fitness levels [2,13].

In this review, studies published on PubMed which have investigated the effects of TC on ANS modulation and therefore HRV are comprehensively summarized. Both consistent and inconsistent findings are presented and discussed. Since there were a limited number of relevant studies and only eleven articles were found which were deemed relevant and reliable to be included in this review, we have suggested further investigation regarding the roles of TC on HRV, to elucidate its possible clinical benefits in the future.

In order to have effectively presented and compared the results of each study, the meaning of the 'short term effects' of TC, in comparison to 'long term effects' had to be elucidated. With regards to the studies here, the short term or acute effects of TC were regarded as the change in HRV from pre to post TC exercise. This was either immediately after cessation of exercise, or after a certain period of time, usually 30 min. The 'long term effects' were regarded as a change in resting HRV over an extended period of time, a minimum of 3 months. The resting HRV was regarded as the HRV prior to any form of exercise. Only one study used 24 h HRV analysis [44], whereas the rest of the studies used short term measurements [3,4,9,12,21,25,45–48].

1.1. Beneficial acute effects of Tai Chi on heart rate variability

Five cross - sectional studies observed the change in HRV in TC/TCQ experienced practitioners from pre to post TC [3,12,21,25,47]. A summary of these studies is shown in Table 1. These studies demonstrated that TC could acutely enhance parasympathetic/vagal modulation [12,47], and reduce the sympathetic modulation [3,21,25], and hence increase the HRV. Väänänen et al. [12] showed that TCQ could acutely increase the HRV in both elderly TCQ experienced men, and young physical education male students [12]. The effects of TC on ANS modulation, irrespective of the breathing frequency was investigated by Lu and Kuo [47]. They found that the ability of TC to acutely enhance the vagal modulation was not solely due to the breathing frequency of the practitioners [47].

Similarly, Motivala et al. [4] also demonstrated that TC can acutely decrease the sympathetic modulation. In this study, the change in preejection period (PEP) was measured rather than HRV. PEP is inversely correlated with sympathetic activity [4,49], and was recorded throughout two 10-min periods, pre and post 20 min of either TCCh, passive rest, or slow moving exercise. This latter group was included to ensure any changes in PEP were due to the overall effects of TCCh rather than just the physical aspects. PEP significantly increased following the task period in the TCCh group only. These findings indicated that TCCh could acutely decrease sympathetic modulation [4].

Chang et al. [45] also investigated the acute effects of TC on HRV immediately following exercise every 3 months over a 9 month period (Table 1). They also concluded that TC can enhance the vagal modulation, and reduce the sympathetic modulation in the short term. In the study by Väänänen et al. [12], the HRV was acutely increased in the TC naïve participants' first TC experience. On the contrary, in the study by Chang et al. [45], it took over 6 months of practise by the TC naïve participants before these positive short term effects of TC on HRV frequency domain parameters (representing parasympathetic and sympathetic modulation) became significant [45] (Table 1). These findings suggest that a TC beginner may not benefit from any changes in ANS modulation following TC exercise until they are fluent in TC practise. Evidently, further studies are required to investigate the exact duration of TC practise a beginner requires before acute benefits on ANS modulation and HRV are seen following TC practise.

1.2. Beneficial effects of Tai Chi on resting heart rate variability

There are only two studies indicated beneficial effects of extended TC practise on resting HRV (Table 2). One of these was a cross sectional study, in which no TC was performed [46]. Instead, two groups of participants, one a TC naïve sedentary control group (SCG), and one a TC practitioner group, performed movements designed to imitate daily activities. Participants rested, then executed a sustained isometric contraction (SIC), and then stood. Firstly, greater parasympathetic modulation was displayed in the TC group compared to the SCG at rest. These findings indicated a potential benefit of long term TC practise. Since the parasympathetic modulation was higher at *rest* in the TC practitioners (before doing any exercise), this could indicate extended TC practise may lead to beneficial long term effects on resting HRV [46]. Likewise, significantly lesser sympathetic modulation, and greater parasympathetic modulation was demonstrated during the SIC in the TC group [46].

In addition, this study also presented indications of further possible benefits of extended TC practise. Practitioners in this study demonstrated natural breathing rates of 6–8 breaths per min. This slower-than normal breathing rate of the practitioners could suggest that they had adopted a slower breathing pattern in their everyday lives as a consequence of extended TC practise. Since slow and deep breathing alone can enhance HRV [34–36], the long term adoption of this breathing manner could be another possible benefit of extended TC practise.

The second study which found positive effects of TCC on resting HRV, was the 3 month longitudinal study by Audette et al. [9] (Table 2). They incorporated three groups, a brisk walking group, TC group, and a SCG, and compared the resting HRV parameters at baseline to those at 3 months. After three months, there was a significant enhancement in the nHFP, and decrement in nLFP when compared to baseline in the TCC group only, signifying enhanced parasympathetic modulation, and decreased sympathetic modulation [9].

Table 1
Summary of studies regarding acute positive effects of Tai Chi on heart rate variability.

Number of subjects	Age (mean ± SD)	Type of study	Exercise description	HRV findings		Interpretation	Ref
				Time	Frequency		
90 (30 TCC, 30 WTK, 30 CG)	TCC group: 53.0 WTK group: 58.5 CG: 56.5 (Median)	Cross - sectional	TCC: Tape led WTK: Instructor led CG: No task	- Increased SDNN - Decreased HR	- Increased LFP, HFP, nHFP - Decreased LF/HF	TCC acutely increases parasympathetic and decreases sympathetic modulation.	[3]
10 (TC)	54 ± 2.04 y (Mean ± SE)	Cross - sectional	TC in study: Yang/Sun style, no info about tape or physician led	- Increased SDNN - Decreased HR	- Increased nHFP - Decreased nLFP - Decreased LF/HF	TC acutely increases parasympathetic and decreases sympathetic modulation.	[35]
29 (15 elderly TCQ experienced, 14 young male PE students)	Elderly men: 63.6 ± 8.2 y PE group: 21.2 ± 0.8 y	Cross – sectional	TCQ in study Given personal teaching	- Increased SDNN in both groups - Increased HR in old group	- Increased TV in young group	TCQ acutely increases parasympathetic activity and HRV in young and old groups.	[12]
40 (20 TCC practitioners, 20 CG)	TCC group: 52.8 ± 7.5 y CG: 56.3 ± 8.5 y	Cross – sectional	TCC in study Tape led	No changes in time domain parameters	- Increased nHFP - Decreased LF/HF	TCC acutely enhances parasympathetic and decreases sympathetic modulation in older persons.	[21]
61 (22 TC, 39 CG) CAD patients	TC group: 58.2 ± 11.3 y CG: 66.3 ± 9.5 y	Longitudinal (9 months)	TC in study Video CD for home	- Decreased HR	- Decreased nLFP - Increased nHFP - Decreased LF/HF	Consistent TC practise acutely increases parasympathetic and decreases sympathetic modulation.	[45]
50 (25 TCC practitioners, 25 SCG)	TCC group: 56 y SCG: 59 y (Median)	Cross - sectional	TCC in study: Yang. Tape led	- Increased BF, HR*BF - Decreased MnRR/BF	- Increased nHFP, nHFP*BF - Decreased nLFP	TC acutely increases parasympathetic modulation irrespective of BF.	[47]

BF = breathing frequency, **CG** = control group, **HFP** = high frequency power, **HR** = heart rate, **HR*BF** = HR without effects of BF, **HRV** = heat rate variability, **LF/HF** = Ratio of LFP to HFP, **LFP** = low frequency power, **MnRR/BF** = mean RRI without effects of BF, **nHFP** = normalised high frequency power, **nHFP*BF** = nHFP without effects of BF, **nLFP** = normalised low frequency power, **PE** = physical education, **SCG** = sedentary control group, **SDNN** = Standard deviation of the NN interval [22], **TC** = Tai Chi, **TCC** = Tai Chi Chuan, **TCQ** = Taichiquan, **TV** = total variability, **WTK** = Wai Tan Kung.

Table 2
Summary of studies regarding positive effects of Tai Chi on resting heart rate variability.

Number of subjects	Age (mean ± SD)	Type of study	Exercise description	HRV findings		Interpretation	Ref
				Time	Frequency		
27 (11 TCC, 8 brisk walking group, 8 SCG)	TCC group: 71.5 ± 4.6 y Brisk walking group: 71.3 ± 4.4 y SCG: 73.5 ± 5.7 y	Longitudinal (3 months)	TCC in study: Modified Yang Brisk walking in study Physician led.	NA	- Increased nHFP - Decreased nLFP In TCC group only	TCC can lead to a "trend towards" improvement in ANS modulation. TCC increases parasympathetic modulation and decreases SNS modulation.	[9]
26 (13 TCC, 13 SCG)	TCC group: 42 ± 5 y SCG: 44 ± 5 y	Cross – sectional	No TCC performed. Participants rested (sat), performed SIC, and stood	No differences in HR between groups	- Higher nHFP, lower nLF and LF/HF during rest, and SIC in TCC practitioners	Long term TCC practise improves HRV.	[46]

ANS = autonomic nervous system, **HR** = heart rate, **LF/HF** = Ratio of LFP to HFP, **nHFP** = normalised high frequency power, **nLFP** = normalised low frequency power, **NA** = Not available, **SCG** = sedentary control group, **SIC** = sustained isometric contraction, **SNS** = sympathetic nervous system, **TCC** = Tai Chi Chuan.

1.3. Null effects of Tai Chi on resting heart rate variability

There are three reports that found null effects of Tai Chi on resting HRV (Table 3). These three remaining studies were longitudinal, and incorporated participants with either chronic heart failure (CHF) [44], coronary artery disease (CAD) [45], or CHD [48]. Two of these studies compared resting HRV parameters at baseline to those at the end of the study period [45,48]. Both found no significant differences in the changes in resting HRV parameters over the study period between the TC group and CG [45,48] (Table 3). Likewise, Yeh et al. found no significant changes in the 24-h HRV analysis from pre to post 3 months TC [44] (Table 3).

ANS modulation and HRV is often compromised in many cardiovascular disorders [24,26,31,32,40,50,51], therefore the presence or absence of a CVD could play an important role in the Tai Chi exercise. The longitudinal studies which demonstrated positive effects of TC on resting HRV used healthy participants [9,46], whereas the studies which investigated patients suffering from a CVD all found null effects of TC on resting HRV [44,45,48].

Despite the null effects seen in the three longitudinal studies, all three studies did still present a degree of positivity in terms of TC's effects on ANS modulation. For instance, Chang et al. [45] demonstrated TC has positive acute effects on HRV immediately after exercise [45]. Yeh et al. [44] presented possible enhancements in parasympathetic modulation, since their results demonstrated a movement towards enhanced short term HRV during sleep after three months of TC [44] (Table 3). Furthermore, despite no change in resting HRV parameters post 1 year TC, there was a significant

Table 3
Summary of studies which found null effects of Tai Chi on resting heart rate variability.

Number and type of subjects	Age (mean ± SD)	Type of study	Exercise description	HRV findings		Interpretation	Ref
				Time	Frequency		
18 CHF patients (8 TC, 10 CG)	TC group: 64.2 ± 16.2 y CG: 54.7 ± 11.8 y	Longitudinal (3 months)	TC in study: Yang, Physician led, plus TC video for home	- No changes in time domain 24 h HRV parameters within or between groups	No changes in frequency domain parameters within or between groups in 24 h HRV	TC has no long term effect on HRV in CHF patients.	[44]
61 CAD patients (22 TC, 39 CG)	TC group: 58.2 ± 11.3 y CG: 66.3 ± 9.5 y	Longitudinal (9 months)	TC in study: Yang, Physician led. Video CD for home	No changes in time domain HRV parameters	No changes in frequency domain HRV parameters	TC has no long term effect on HRV in CAD patients.	[45]
20 CHD patients (10 TC, 10 CG)	TC group: 68 ± 5 y CG: 68 ± 4 y	Longitudinal (1 year)	TC in study: Yang Style, physician led, plus 20 min TC video for home	NA	No different in HRV parameters between groups	TC has no effect on HRV in CHD patients.	[48]

ANS = autonomic nervous system, **CAD** = coronary artery disease, **CG** = control group, **CHD** = coronary heart disease, **CHF** = chronic heart failure, **HRV** = heat rate variability, **NA** = Not available, **pNN30** = Value after dividing NN30 by the total number of NN intervals [23], **TC** = Tai Chi.

increase in baroreflex sensitivity (BRS) in the study by Sato et al. [48]. Since BRS is an alternative marker of autonomic activity [48], it is possible that TC can enhance reflex parasympathetic modulation, but not tonic parasympathetic modulation [48].

Further evidence that could indicate a null long term effect of TC on resting HRV was the lack of correlation between years of experience TC and corresponding resting HRV parameters, observed in three of the studies (Table 3). Interestingly, no correlations were found between these two variables in all three studies [3,21,25]. This could suggest extended TC practise does not impact resting HRV. If it could, one would presume positive correlations between the resting HRV parameters and the degree of experience would be found. However, Lu and Kuo [21] suggested the lack of correlation could be due to the fact that differences in characteristics of the practitioners, such as overall health, dedication to TC, and complexity of their TC style may all contribute to the effects on resting HRV, rather than simply their years' experience of TC [21]. This could also be a possible reason for why contradictory results were attained in terms of the long term effects of extended TC practise on resting HRV. Future studies are needed to test this hypothesis.

2. Future studies into the effects of Tai Chi on heart rate variability

Given the small number and preliminary nature of relevant studies published on the effects of TC on HRV, it is clear such investigations are in their earliest stages. Many articles emphasised their studies were prospective [44] or pilot [9,25], and have therefore only produced preliminary results and conclusions [9,25,44]. Evidently a lot more studies are required but with improved methodologies. Future studies should use a physician led approach, with larger sample sizes [2,7,18], with participants randomized [2,18]. Moreover, previous findings suggested that studies should be at least 6 months, and each session should last at least 40 min in order for some consistency in the intensity of TC to be present for a considerable amount of time in the study [2]. Furthermore, more longitudinal studies are required, investigating the effects of TC on resting HRV [12,25,45]. At this time, the results of studies regarding the acute effects of TC on HRV are generally in agreement, whereas there is still ambiguity with regards to the long term effects of extended TC practise on resting HRV. Furthermore, the ability of TC to influence resting HRV from a long term perspective is of more clinical interest than its ability to enhance the HRV acutely. If one is able to reduce resting HRV, this would offer a significant positive impact on the prognosis of patients.

3. Conclusion

Although it is not justifiable to produce a firm conclusion on whether TC can enhance HRV based on these limited currently published articles, most of which being preliminary in nature, it was a reasonable assumption to believe that TC could enhance HRV or parasympathetic modulation, given its incorporation of diaphragmatic breathing, and aerobic exercise. In TC experienced practitioners, TC can acutely enhance vagal modulation, reduce the sympathetic modulation, and shift the sympatho-vagal balance towards enhanced parasympathetic dominance, thereby increasing the HRV. However, more studies are required to investigate the effects of extended TC practise on resting HRV to warrant its clinical usefulness. Future studies with larger sample sizes are also needed to gain a greater insight regarding the definite effects of TC on HRV.

Conflicts of interest

None.

Disclosures

All authors have approved the final article.

Acknowledgement

This work was supported by a Research Chair Grant from the National Science and Technology Development Agency Thailand (N.C.), the Thailand Research Fund BRG5780016 (S.C.), and the Chiang Mai University Center of Excellence Award (N.C.). None of the funders played any role in the study design, in the collection, analysis and interpretation of data; in the writing of the manuscript; and in the decision to submit the manuscript for publication.

References

[1] C.E. Rogers, L.K. Larkey, C. Keller, A review of clinical trials of tai chi and qigong in older adults, West J. Nurs. Res. 31 (2) (2009 Mar) 245–279, http://dx.doi.org/10.1177/0193945908327529.
[2] C. Lan, S.Y. Chen, J.S. Lai, A.M. Wong, Tai chi chuan in medicine and health promotion, Evid. Based Complement. Altern. Med. 2013 (2013) 502131, http://dx.doi.org/10.1155/2013/502131.
[3] W.A. Lu, C.D. Kuo, Comparison of the effects of Tai Chi Chuan and Wai Tan Kung exercises on autonomic nervous system modulation and on hemodynamics in elder adults, Am. J. Chin. Med. 34 (6) (2006) 959–968, http://dx.doi.org/10.1142/S0192415X06004430.
[4] S.J. Motivala, J. Sollers, J. Thayer, M.R. Irwin, Tai Chi Chih acutely decreases sympathetic nervous system activity in older adults, J. Gerontol. A Biol. Sci. Med. Sci. 61 (11) (2006 Nov) 1177–1180.
[5] C. Wang, J.P. Collet, J. Lau, The effect of Tai Chi on health outcomes in patients with chronic conditions: a systematic review, Arch. Intern Med. 164 (5) (2004

Mar 8) 493–501, http://dx.doi.org/10.1001/archinte.164.5.493.
[6] J.X. Li, Y. Hong, K.M. Chan, Tai chi: physiological characteristics and beneficial effects on health, Br. J. Sports Med. 35 (3) (2001 Jun) 148–156.
[7] T. Field, Tai Chi research review, Complement. Ther. Clin. Pract. 17 (3) (2011 Aug) 141–146, http://dx.doi.org/10.1016/j.ctcp.2010.10.002.
[8] C. Lan, S.Y. Chen, J.S. Lai, M.K. Wong, Heart rate responses and oxygen consumption during Tai Chi Chuan practice, Am. J. Chin. Med. 29 (3–4) (2001) 403–410, http://dx.doi.org/10.1142/S0192415X01000423.
[9] J.F. Audette, Y.S. Jin, R. Newcomer, L. Stein, G. Duncan, W.R. Frontera, Tai Chi versus brisk walking in elderly women, Age Ageing 35 (4) (2006 Jul) 388–393, http://dx.doi.org/10.1093/ageing/afl006.
[10] L. Larkey, R. Jahnke, J. Etnier, J. Gonzalez, Meditative movement as a category of exercise: implications for research, J. Phys. Act. Health 6 (2) (2009 Mar) 230–238.
[11] C. Lan, Tai chi improves natural harmony in autonomic function, N. Am. J. Med. Sci. 4 (6) (2012 Jun) 276–277.
[12] J. Vaananen, S. Xusheng, S. Wang, T. Laitinen, H. Pekkarinen, E. Lansimies, Taichiquan acutely increases heart rate variability, Clin. Physiol. Funct. Imaging 22 (1) (2002 Jan) 2–3.
[13] R. Jahnke, L. Larkey, C. Rogers, J. Etnier, F. Lin, A comprehensive review of health benefits of qigong and tai chi, Am. J. Health Promot 24 (6) (2010 Jul-Aug) e1–e25, http://dx.doi.org/10.4278/ajhp.081013-LIT-248.
[14] Y. Zeng, T. Luo, H. Xie, M. Huang, A.S. Cheng, Health benefits of qigong or tai chi for cancer patients: a systematic review and meta-analyses, Complement. Ther. Med. 22 (1) (2014 Feb) 173–186, http://dx.doi.org/10.1016/j.ctim.2013.11.010.
[15] R. Abbott, H. Lavretsky, Tai Chi and Qigong for the treatment and prevention of mental disorders, Psychiatr. Clin. North Am. 36 (1) (2013 Mar) 109–119, http://dx.doi.org/10.1016/j.psc.2013.01.011.
[16] J.C. Tsai, W.H. Wang, P. Chan, L.J. Lin, C.H. Wang, B. Tomlinson, et al., The beneficial effects of Tai Chi Chuan on blood pressure and lipid profile and anxiety status in a randomized controlled trial, J. Altern. Complement. Med. 9 (5) (2003 Oct) 747–754, http://dx.doi.org/10.1089/107555303322524599.
[17] C. Wang, Role of Tai Chi in the treatment of rheumatologic diseases, Curr. Rheumatol. Rep. 14 (6) (2012 Dec) 598–603, http://dx.doi.org/10.1007/s11926-012-0294-y.
[18] C. Lan, S.Y. Chen, M.K. Wong, J.S. Lai, Tai chi chuan exercise for patients with cardiovascular disease, Evid. Based Complement. Altern. Med. 2013 (2013) 983208, http://dx.doi.org/10.1155/2013/983208.
[19] L. Wolfson, R. Whipple, C. Derby, J. Judge, M. King, P. Amerman, et al., Balance and strength training in older adults: intervention gains and Tai Chi maintenance, J. Am. Geriatr. Soc. 44 (5) (1996 May) 498–506.
[20] C. Lan, J.S. Lai, S.Y. Chen, M.K. Wong, 12-month Tai Chi training in the elderly: its effect on health fitness, Med. Sci. Sports Exerc. 30 (3) (1998 Mar) 345–351.
[21] W.A. Lu, C.D. Kuo, The effect of Tai Chi Chuan on the autonomic nervous modulation in older persons, Med. Sci. Sports Exerc. 35 (12) (2003 Dec) 1972–1976, 10.1249/01.MSS.0000099242.10669.F7.
[22] Heart rate variability: standards of measurement, physiological interpretation and clinical use. Task force of the european society of cardiology and the North American society of pacing and electrophysiology, Circulation 93 (5) (1996 Mar 1) 1043–1065.
[23] M.K. Lahiri, P.J. Kannankeril, J.J. Goldberger, Assessment of autonomic function in cardiovascular disease: physiological basis and prognostic implications, J. Am. Coll. Cardiol. 51 (18) (2008 May 6) 1725–1733, http://dx.doi.org/10.1016/j.jacc.2008.01.038.
[24] K.H. Greiser, A. Kluttig, B. Schumann, J.A. Kors, C.A. Swenne, O. Kuss, et al., Cardiovascular disease, risk factors and heart rate variability in the elderly general population: design and objectives of the CARdiovascular disease, Living and Ageing in Halle (CARLA) Study, BMC Cardiovasc Disord. 5 (2005) 33, http://dx.doi.org/10.1186/1471-2261-5-33.
[25] P. Kalsaria, H. Li, G.N. Waite, M.M. Moga, D.J. Kingsley, R.W. Geib, Acute effects of tai chi exercise on cardiac autonomic function in healthy adults with tai chi experience, Biomed. Sci. Instrum. 48 (2012) 226–231.
[26] J.F. Thayer, S.S. Yamamoto, J.F. Brosschot, The relationship of autonomic imbalance, heart rate variability and cardiovascular disease risk factors, Int. J. Cardiol. 141 (2) (2010 May 28) 122–131, http://dx.doi.org/10.1016/j.ijcard.2009.09.543.
[27] J.M. Dekker, R.S. Crow, A.R. Folsom, P.J. Hannan, D. Liao, C.A. Swenne, et al., Low heart rate variability in a 2-minute rhythm strip predicts risk of coronary heart disease and mortality from several causes: the ARIC Study. Atherosclerosis Risk in Communities, Circulation 102 (11) (2000 Sep 12) 1239–1244.
[28] R.E. Kleiger, J.P. Miller, J.T. Bigger Jr., A.J. Moss, Decreased heart rate variability and its association with increased mortality after acute myocardial infarction, Am. J. Cardiol. 59 (4) (1987 Feb 1) 256–262.
[29] M.T. La Rovere, J.T. Bigger Jr., F.I. Marcus, A. Mortara, P.J. Schwartz, Baroreflex sensitivity and heart-rate variability in prediction of total cardiac mortality after myocardial infarction. ATRAMI (Autonomic tone and reflexes after myocardial infarction) investigators, Lancet 351 (9101) (1998 Feb 14) 478–484.
[30] S. Vaishnav, R. Stevenson, B. Marchant, K. Lagi, K. Ranjadayalan, A.D. Timmis, Relation between heart rate variability early after acute myocardial infarction and long-term mortality, Am. J. Cardiol. 73 (9) (1994 Apr 1) 653–657.
[31] I. Janszky, M. Ericson, M.A. Mittleman, S. Wamala, F. Al-Khalili, K. Schenck-Gustafsson, et al., Heart rate variability in long-term risk assessment in middle-aged women with coronary heart disease: the Stockholm female coronary risk study, J. Intern Med. 255 (1) (2004 Jan) 13–21.
[32] J. Nolan, P.D. Batin, R. Andrews, S.J. Lindsay, P. Brooksby, M. Mullen, et al., Prospective study of heart rate variability and mortality in chronic heart failure: results of the United Kingdom heart failure evaluation and assessment of risk trial (UK-heart), Circulation 98 (15) (1998 Oct 13) 1510–1516.
[33] J.M. Dekker, E.G. Schouten, P. Klootwijk, J. Pool, C.A. Swenne, D. Kromhout, Heart rate variability from short electrocardiographic recordings predicts mortality from all causes in middle-aged and elderly men. The Zutphen Study, Am. J. Epidemiol. 145 (10) (1997 May 15) 899–908.
[34] P. Chalaye, P. Goffaux, S. Lafrenaye, S. Marchand, Respiratory effects on experimental heat pain and cardiac activity, Pain Med. 10 (8) (2009 Nov) 1334–1340, http://dx.doi.org/10.1111/j.1526-4637.2009.00681.x.
[35] G.K. Pal, S. Velkumary, Madanmohan, Effect of short-term practice of breathing exercises on autonomic functions in normal human volunteers, Indian J. Med. Res. 120 (2) (2004 Aug) 115–121.
[36] R. Jerath, J.W. Edry, V.A. Barnes, V. Jerath, Physiology of long pranayamic breathing: neural respiratory elements may provide a mechanism that explains how slow deep breathing shifts the autonomic nervous system, Med. Hypotheses 67 (3) (2006) 566–571, http://dx.doi.org/10.1016/j.mehy.2006.02.042.
[37] R.E. De Meersman, Respiratory sinus arrhythmia alteration following training in endurance athletes, Eur. J. Appl. Physiol. Occup. Physiol. 64 (5) (1992) 434–436.
[38] R.P. Sloan, P.A. Shapiro, R.E. DeMeersman, E. Bagiella, E.N. Brondolo, P.S. McKinley, et al., The effect of aerobic training and cardiac autonomic regulation in young adults, Am. J. Public Health 99 (5) (2009 May) 921–928, http://dx.doi.org/10.2105/AJPH.2007.133165.
[39] D. Liao, R.W. Barnes, L.E. Chambless, R.J. Simpson Jr., P. Sorlie, G. Heiss, Age, race, and sex differences in autonomic cardiac function measured by spectral analysis of heart rate variability--the ARIC study. Atherosclerosis Risk in Communities, Am. J. Cardiol. 76 (12) (1995 Nov 1) 906–912.
[40] D. Liao, J. Cai, W.D. Rosamond, R.W. Barnes, R.G. Hutchinson, E.A. Whitsel, et al., Cardiac autonomic function and incident coronary heart disease: a population-based case-cohort study. The ARIC Study. Atherosclerosis Risk in Communities Study, Am. J. Epidemiol. 145 (8) (1997 Apr 15) 696–706.
[41] I.A. O'Brien, P. O'Hare, R.J. Corrall, Heart rate variability in healthy subjects: effect of age and the derivation of normal ranges for tests of autonomic function, Br. Heart J. 55 (4) (1986 Apr) 348–354.
[42] J.A. Fontana, C. Colella, B.R. Wilson, L. Baas, The energy costs of a modified form of T'ai Chi exercise, Nurs. Res. 49 (2) (2000 Mar-Apr) 91–96.
[43] D. Schneider, R. Leung, Metabolic and cardiorespiratory responses to the performance of Wing Chun and T'ai Chi Chuan exercise, Int. J. Sports Med. 12 (3) (1991 Jun) 319–323, http://dx.doi.org/10.1055/s-2007-1024689.
[44] G.Y. Yeh, P.M. Wayne, R.S. Phillips, T'ai Chi exercise in patients with chronic heart failure, Med. Sport Sci. 52 (2008) 195–208, http://dx.doi.org/10.1159/000134300.
[45] R.Y. Chang, M. Koo, Z.R. Yu, C.B. Kan, I.T. Chu, C.T. Hsu, et al., The effect of t'ai chi exercise on autonomic nervous function of patients with coronary artery disease, J. Altern. Complement. Med. 14 (9) (2008 Nov) 1107–1113, http://dx.doi.org/10.1089/acm.2008.0166.
[46] M.A. Figueroa, R.E. Demeersman, J. Manning, The autonomic and rate pressure product responses of tai chi practitioners, N. Am. J. Med. Sci. 4 (6) (2012 Jun) 270–275, http://dx.doi.org/10.4103/1947-2714.97208.
[47] W.A. Lu, C.D. Kuo, Breathing frequency-independent effect of Tai Chi Chuan on autonomic modulation, Clin. Auton. Res. 24 (2) (2014 Apr) 47–52, http://dx.doi.org/10.1007/s10286-014-0224-3.
[48] S. Sato, S. Makita, R. Uchida, S. Ishihara, M. Masuda, Effect of Tai Chi training on baroreflex sensitivity and heart rate variability in patients with coronary heart disease, Int. Heart J. 51 (4) (2010 Jul) 238–241.
[49] J.T. Cacioppo, G.G. Berntson, P.F. Binkley, K.S. Quigley, B.N. Uchino, A. Fieldstone, Autonomic cardiac control. II. Noninvasive indices and basal response as revealed by autonomic blockades, Psychophysiology 31 (6) (1994 Nov) 586–598.
[50] H. Tsuji, M.G. Larson, F.J. Venditti Jr., E.S. Manders, J.C. Evans, C.L. Feldman, et al., Impact of reduced heart rate variability on risk for cardiac events. The Framingham Heart Study, Circulation 94 (11) (1996 Dec 1) 2850–2855.
[51] H.V. Huikuri, V. Jokinen, M. Syvanne, M.S. Nieminen, K.E. Airaksinen, M.J. Ikaheimo, et al., Heart rate variability and progression of coronary atherosclerosis, Arterioscler. Thromb. Vasc. Biol. 19 (8) (1999 Aug) 1979–1985.

เอกสารแนบหมายเลข 29

Research Paper

Dual T-type and L-type calcium channel blocker exerts beneficial effects in attenuating cardiovascular dysfunction in iron-overloaded thalassaemic mice

Sirinart Kumfu[1,2,3], Siriporn C. Chattipakorn[1,3,4], Suthat Fucharoen[5] and Nipon Chattipakorn[1,2,3]

[1]Cardiac Electrophysiology Research and Training Center, Faculty of Medicine, Chiang Mai University, Chiang Mai, Thailand
[2]Cardiac Electrophysiology Unit, Department of Physiology, Faculty of Medicine, Chiang Mai University, Chiang Mai, Thailand
[3]Center of Excellence in Cardiac Electrophysiology Research, Chiang Mai University, Chiang Mai, Thailand
[4]Department of Oral Biology and Diagnostic Sciences, Faculty of Dentistry, Chiang Mai University, Chiang Mai, Thailand
[5]Thalassemia Research Center, Institute of Molecular Biosciences, Mahidol University, Nakhon Pathom, Thailand

New Findings

- **What is the central question of this study?**
  Head-to-head comparison of the therapeutic efficacy among commercial iron chelators and a dual T- (TTCC) and L-type calcium channel (LTCC) blocker on cardiac function, mitochondrial function and the protein expression of cardiac iron transporters in thalassaemic mice in iron-overloaded conditions has not been assessed.
- **What is the main finding and its importance?**
  The dual TTCC and LTCC blocker efonidipine could provide broad beneficial effects in the heart, liver, plasma and mitochondria in both wild-type and thalassaemic mice in iron-overloaded conditions. Its beneficial effects are of the same degree as the three commercial iron chelators currently used clinically. It is possible that efonidipine could be an alternative choice in patients unable to take iron chelators for the treatment of iron-overload conditions.

Iron chelation therapy is a standard treatment in thalassaemia patients; however, its poor cardioprotective efficacy and serious side-effects are a cause for concern. Previous studies have shown that treatment with L-type calcium channel (LTCC) blockers or dual T-type calcium channel (TTCC) and LTCC blockers decreases cardiac iron and improves cardiac dysfunction in an iron-overloaded rodent model. Currently, the head-to-head comparison of therapeutic efficacy among commercial iron chelators, a dual TTCC and LTCC blocker and an LTCC blocker on cardiac function, mitochondrial function and the protein expression of cardiac iron transporters in thalassaemic mice in an iron-overloaded state has never been investigated. An iron-overloaded state was induced in β-thalassaemic and wild-type mice. Cardiac iron overload was induced to a greater extent than in a previous study by feeding the mice with an iron-enriched diet for 4 months. Then, an LTCC blocker (amlodipine) or a dual TTCC and LTCC blocker (efonidipine) or one of the commercial iron chelators (deferoxamine, deferasirox or deferiprone) was administered for 1 month with continuous iron feeding. All treatments reduced cardiac iron deposition and improved mitochondrial and cardiac dysfunction in both types of mice. Only efonidipine and the iron chelators reduced liver iron accumulation, liver malondialdehyde and plasma malondialdehyde in these mice. Although all pharmacological interventions reduced cardiac iron deposition, they did not alter the protein expression levels of

© 2016 The Authors. Experimental Physiology © 2016 The Physiological Society
DOI: 10.1113/EP085517

Experimental Physiology

cardiac iron transporter. These findings indicated that efonidipine provided all benefits to the same degree as the three commercial iron chelators. These findings indicate that a dual TTCC and LTCC blocker could be beneficial for treatment of an iron-overloaded state.

(Received 8 September 2015; accepted after revision 27 January 2016; first published online 29 January 2016)
Corresponding author N. Chattipakorn: Cardiac Electrophysiology Research and Training Center, Faculty of Medicine, Chiang Mai University, Chiang Mai, 50200, Thailand. Email: nchattip@gmail.com

Introduction

In thalassaemic patients, iron-overload-induced cardiomyopathy leading to cardiac dysfunction is a major cause of morbidity and mortality (Zurlo *et al.* 1989; Wood *et al.* 2005; Lekawanvijit & Chattipakorn, 2009). Moreover, heart rate variability (HRV) was reduced both in thalassaemia patients (Kardelen *et al.* 2008; Rutjanaprom *et al.* 2009) and in a mouse model of β-thalassaemia (Incharoen *et al.* 2007; Kumfu *et al.* 2012*a*), indicating cardiac autonomic imbalance. Although iron chelation therapy is the standard treatment in these patients, its poor cardioprotective efficacy and serious side-effects are a cause for concern (Hershko *et al.* 2005; Brittenham, 2011; Poggiali *et al.* 2012). Therefore, understanding how iron enters cardiac cells is key for establishing the most effective treatments and prevention strategies for this fatal complication in thalassaemia.

The major cause of this fatal cardiac complication is proposed to be mainly a result of excess iron accumulating in the heart of these patients (Hahalis *et al.* 2001; Lekawanvijit & Chattipakorn, 2009). It has been shown that L-type calcium channels (LTCCs), T-type calcium channels (TTCCs) and divalent metal transporter1 (DMT1) play a role in iron uptake into the heart in a iron-overloaded conditions (Tsushima *et al.* 1999; Crowe & Bartfay, 2002; Oudit *et al.* 2003; Kumfu *et al.* 2011, 2012*a*; Lopin *et al.* 2012; Musumeci *et al.* 2013). Once iron is taken up into the cells, it is either stored as ferritin or transferred across the cell membrane into the blood circulation by the iron exporter ferroportin (Gunshin *et al.* 1997; Fleming *et al.* 1998; Abboud & Haile, 2000; Donovan *et al.* 2000). Ferroportin is negatively regulated by the iron-regulatory hormone hepcidin (Nemeth *et al.* 2006; Singh *et al.* 2011). Hepcidin controls iron levels by interacting directly with ferroportin, resulting in the internalization and degradation of ferroportin when iron levels are high (Nemeth *et al.* 2006; Singh *et al.* 2011). Recent studies reported the expression of Zip14 (Slc39a14; the ZIP family of metal ion transporters) in the heart in iron-overloaded conditions (Kumfu *et al.* 2012*a*; Nam *et al.* 2013). However, its expression in the heart of thalassaemic mice has never been studied.

In mitochondria, iron is necessary for the synthesis of heme and iron sulfur cluster-containing proteins involved in electron transport and oxidative phosphorylation (Levi & Rovida, 2009; Richardson *et al.* 2010). However, excess iron levels can lead to increased reactive oxygen species (ROS) production via the Haber–Weiss and Fenton reactions (Bartfay & Bartfay, 2000; Lekawanvijit & Chattipakorn, 2009). High ROS production can damage cellular lipids, proteins, DNA and mitochondria (Bartfay & Bartfay, 2000; Lekawanvijit & Chattipakorn, 2009). Previous studies suggested that mitochondrial dysfunction could be responsible for cardiac failure resulting from chronic iron overload (Gao *et al.* 2009, 2010). Furthermore, the increased ROS production can cause mitochondrial depolarization and mitochondrial swelling, leading to the release of cytochrome *c*, activation of caspase pathways and cell death by necrosis and/or apoptosis (Zorov *et al.* 2006; Thummasorn *et al.* 2011). A previous study demonstrated that iron-overloaded conditions can lead to increased cardiomyocyte apoptosis because of an increased ratio of the pro-apoptotic protein Bax to the anti-apoptotic protein Bcl-2, which subsequently increased caspase3 activity (Wang *et al.* 2011).

Several studies have shown the beneficial effects of iron chelators, a dual TTCC and LTCC blocker and an LTCC blocker on cardiac iron accumulation and cardiac function in iron-overloaded conditions (Tsushima *et al.* 1999; Crowe & Bartfay, 2002; Oudit *et al.* 2003; Kumfu *et al.* 2011, 2012*a*; Lopin *et al.* 2012; Musumeci *et al.* 2013). However, none of these studies has determined the comparative beneficial effects between the three commercial iron chelators, a dual TTCC and LTCC blocker and an LTCC blocker on cardiac iron accumulation, cardiac function, cardiac mitochondrial function, cardiac iron transporters (Zip14, DMT1, TTCC and LTCC), iron exporter (ferroportin), iron regulatory hormone (hepcidin) and apoptotic protein expression, in normal and thalassaemic mice in iron-overloaded conditions. In the present study, iron overload was induced to a greater degree of severity compared with a previous study (Kumfu *et al.* 2012*a*), by feeding mice with an iron-enriched diet for 120 days. We hypothesized that the three iron chelators, the dual TTCC and LTCC blocker and the LTCC blocker have equal cardioprotective efficacy in thalassaemic mice in an iron-overloaded state.

© 2016 The Authors. Experimental Physiology © 2016 The Physiological Society.

Methods

Ethical approval

All animal studies were approved by the Institutional Animal Care and Use Committee (IACUC) of the Faculty of Medicine, Chiang Mai University (permit no.: 09/2557) and conformed to the *Guide for the Care and Use of Laboratory Animals* published by the US National Institutes of Health (NIH guide, 8th edition, 2011). We understand the ethical principles under which the journal operates, and our work complies with the animal ethics checklist. All animals were given *ad libitum* access to food and water. All animals were housed in rooms with controlled temperature and humidity and with 12 h–12 h light–dark cycles.

Animal models

Two types of adult C57/BL6 male mice (3–6 months old), wild-type ($mu\beta^{+/+}$, WT, $n = 42$) and heterozygous β^{KO} type ($mu\beta^{th-3/+}$, HT, $n = 42$), weighing 20–25 g, were used in this study. Mice were obtained from the Thalassemia Research Center, Institute of Molecular Biosciences, Mahidol University, Nakhon Pathom, Thailand (Jamsai *et al.* 2005, 2006).

Iron treatment and pharmacological interventions

Iron overload was induced by feeding WT and HT mice with FE diet (0.2% ferrocene, w/w). An iron-overloaded state was induced to a greater degree compared with the previous study (Kumfu *et al.* 2012*a*) by feeding the mice with FE diet for 120 days (FE group). The WT and HT mice in the control group were fed with a normal diet for 120 days. Then, mice in the FE group were randomly divided into six subgroups ($n = 6$ each) and were treated with drugs whilst being fed with the FE diet for a further 30 days. Group I (FE) mice were injected s.c. with 0.5% DMSO daily. Group II (FE/DFO) mice were injected with deferoxamine (DFO, Novartis Pharma Stein AG, Stein, Switzerland; 42 mg kg^{-1} day^{-1}) in normal saline solution (NSS) s.c. daily (Kumfu *et al.* 2012*a*). Group III (FE/DFX) mice were fed with deferasirox (DFX, Novartis Pharma Stein AG, Stein, Switzerland; 30 mg kg^{-1} day^{-1}) in NSS via gavage feeding daily (Pennell *et al.* 2010). Group IV (FE/DFP) mice were fed with deferiprone (DFP, ApoPharma USA, Inc, Rockville, MD, USA; 75 mg kg^{-1} day^{-1}) in NSS via gavage feeding twice daily (Berdoukas *et al.* 2012). Group V (FE/Efo) mice were injected s.c. with the dual TTCC and LTCC blocker efonidipine (Sigma-Aldrich, St. Louis, MO, USA; 4 mg kg^{-1} day^{-1}) in 0.5% DMSO daily (Matsumura *et al.* 1995). Group VI (FE/Amlo) mice were fed with the LTCC blocker amlodipine (Berlin Pharmaceutical Industry Co., Ltd., Ratchathewi, Bangkok, Thailand; 5 mg kg^{-1} day^{-1}) in NSS via gavage feeding daily (Kumfu *et al.* 2012*a*). Mice in the control group were injected s.c. with 0.5% DMSO or gavage feeding with NSS daily and fed with a normal diet. Each group of mice were administered with the drug via injection or feeding at 18.00 h each day, except for the Fe/DFP group, which were gavage fed twice daily at 06.00 and 18.00 h each day. The routes for drug administration were based on their clinical administration in patients. Injectate volumes 40 μl were used for s.c. and i.p. (zoletil) injection. At the end of treatments (i.e. 5 months after the start of iron loading and treatment), the left ventricular (LV) function, HRV, cardiac and liver iron deposition, cardiac mitochondrial function and protein expressions of iron transporter were assessed in all mice.

Measurement of HRV

Cardiac autonomic nervous activity was evaluated by a spectral analysis of the R–R interval variability. All mice underwent measurement of HRV at the end of treatment as described previously (Incharoen *et al.* 2007). In brief, during animal preparation the mice were anaesthetized by inhalation of 1.5–2.5% isoflurane prior to needle insertion. The mice were allowed to recover and regained full consciousness before ECG recording. Lead II ECG was recorded using 27.5 gauge needle electrodes and recorded continuously using Power Lab with Chart 5.0 (Incharoen *et al.* 2007). The ECG data were analysed using the MATLAB program; the power spectra of R–R interval variability were obtained using a fast Fourier transform algorithm, and the high-frequency (HF, 0.6–3 Hz), low-frequency (LF, 0.2–0.6 Hz) and very low frequency (VLF, below 0.2 Hz) components were determined (Incharoen *et al.* 2007). To minimize the effect of changes in total power on the LF and HF components, LF and HF were expressed as normalized units (LFnu and HFnu) by dividing the LF and HF by the total power minus VLF (Incharoen *et al.* 2007; Rutjanaprom *et al.* 2009). The LF/HF ratio is considered to be an index of autonomic balance (Incharoen *et al.* 2007; Rutjanaprom *et al.* 2009). An increased LF/HF ratio indicates depressed HRV or cardiac autonomic imbalance.

After anaesthesia by inhalation of 1.5–2.5% isoflurane for HRV measurement, mice were continuously observed and monitored in a warm environment until they had fully recovered from anaesthesia and were then observed for 3–6 h postoperatively and again at 18–24 h postoperatively for signs of pain or infection.

Left ventricular pressure–volume (*P–V*) loop analysis

The WT and HT mice were anaesthetized and maintained in physiological conditions. General anaesthesia was

© 2016 The Authors. Experimental Physiology © 2016 The Physiological Society

induced with Zoletil (Zoletil contain Tiletamine 10 mg and Zolazepam 10 mg, Virbac Corporation, Fort Worth, TX, USA) [20 mg (kg body weight)$^{-1}$] injected I.P. (40 μl) (Lee *et al.* 2011). The mice were shown to have complete absence of the pedal withdrawal reflex, which reflected a good anaesthetic induction. However, if mice still had a pedal withdrawal reflex, they were given another zoletil injection at the same dose to induce deep anaesthesia. An endotracheal tube was inserted and respiration was maintained using a rodent ventilator, starting immediately with room air using a volume of 200–250 μl and a ventilator rate of 110–130 breaths min^{-1} to maintain partial pressures of CO_2 and O_2 and pH parameters (Pacher *et al.* 2008). The LV pressure and volume were measured using a pressure–volume conductance catheter (Transonic SciSense, London, ON, Canada; Pacher *et al.* 2008; Kumfu *et al.* 2012*a*). The abdomen was opened subcostally. The diaphragm was incised via a transverse substernal approach, leaving the pericardium intact. The left ventricle was entered through an apical stab with a 23.5 gauge needle, followed immediately by the pressure–volume conductance catheter for measurement of LV pressure and volume (Pacher *et al.* 2008; Kumfu *et al.* 2012*a*). The end-systolic pressure (ESP) and end-diastolic pressure (EDP), maximal pressure (P_{max}) and minimal pressure (P_{min}), maximal and minimal rates of change of pressure (dP/dt_{max} and dP/dt_{min}), stroke volume (SV), cardiac output (CO), stroke work (SW) and heart rate were measured using the *P–V* conductance catheter system (Lips *et al.* 2004; Pacher *et al.* 2008; Kumfu *et al.* 2012*a*). After *P–V* loop analysis had been performed under anaesthesia, mice were killed by injection with an overdose of Zoletil (Zoletil contain Tiletamine 50 mg and Zolazepam 50 mg, Virbac Corporation, Fort Worth, TX, USA) [100 mg (kg body weight)$^{-1}$] prior to organ removal. Blood was collected for further analysis.

Percentage organ weight index

The heart, liver, spleen and kidney were removed and weighed. The weight index was determined by using the equation: weight index (%) = (organ weight/body weight) × 100 (van Acker *et al.* 2001). All organs were frozen at −80°C for further analysis.

Determination of cardiac and liver iron

At the end of the *P–V* loop determination, the heart and liver were removed and homogenized in deionized water 1:10 (w/v). Next, 100 μl of heart or liver tissue homogenate was precipitated in precipitation solution (1 N HCl and 10% trichloroacetic acid) and heated at 95°C for 1 h. The tubes were cooled down at room temperature for 2 min, vortex mixed and then centrifuged at 8200*g* for 10 min. The supernatants (50 μl) were mixed with 50 μl of chromogen solution [0.508 mmol l^{-1} ferrozine, 1.5 mol l^{-1} sodium acetate and 0.1% or 1.5% (v/v) thioglycolic acid] and incubated at room temperature for 30 min. After incubation, the absorbance was measured at 562 nm, and the cardiac or liver iron concentration was compared with the iron standard curve (Rebouche *et al.* 2004).

Quantification of plasma non-transferrin-bound iron (NTBI)

The NTBI concentration was measured using the nitrilotriacetic acid (NTA) chelation/HPLC method established by Singh *et al.* (1990), with the aluminium blocking step. Plasma was incubated with NTA solution (a final concentration of 80 mM) pH 7.0 for 30 min at room temperature to produce an Fe^{3+}-$(NTA)_2$ complex, and subsequently spun through a membrane filter (NanoSep®, 30 kDa cut-off, polysulfone type; Pall Life Sciences, Ann Arbor, MI, USA). The concentration of the Fe^{3+}-$(NTA)_2$ representing NTBI in the ultrafiltrate was determined using a non-metallic HPLC system as described previously (Kumfu *et al.* 2012*a*). The NTBI concentration was calculated from a calibration curve made with different iron concentrations of Fe^{3+}-$(NTA)_2$ in 80 mM NTA, pH 7.0, ranging from 0 to 16 μM.

Determination of malondialdehyde (MDA) concentration

The heart, liver and plasma MDA concentrations were measured using the HPLC method as described previously (Grotto *et al.* 2007; Kumfu *et al.* 2012*a*). Briefly, the liver tissues (100 mg) or heart tissues (30 mg) were homogenized in phosphate buffer. The homogenate or plasma was mixed with 10% (w/v) trichloroacetic acid containing Butylated hydroxytoluene (BHT) (50 ppm), then heated at 90°C for 30 min and centrifuged at 3300 g for 10 min to achieve a clear supernatant. The supernatant was mixed with 0.44 M H_3PO_4 and 0.6% (w/v) thiobarbituric acid solution and incubated at 90°C for 30 min to produce pink product called thiobarbituric acid reactive substances. The solution was then passed through a syringe filter (polysulfone type membrane, pore size 0.45 μm; Whatman International, Maidstone, UK) and analysed with the HPLC system (Kumfu *et al.* 2012*a*). A standard curve was constructed from the peak height of standard 1,1,3,3-tetramethoxypropane (standard reagent for MDA) at different concentrations (0–100 μM). Tissues and plasma concentrations of thiobarbituric acid reactive substances were determined directly from the standard curve and are reported as MDA equivalent concentrations (Grotto *et al.* 2007). The MDA concentrations were expressed as micromolar per milligram of protein for heart and liver tissues and as micromolar for plasma samples.

© 2016 The Authors. Experimental Physiology © 2016 The Physiological Society

Preparation of cardiac mitochondria

After the mice had been sacrificed, the hearts were removed, finely minced and homogenized in ice-cold buffer containing (in mmol l^{-1}): sucrose 300, Tes 5 and EGTA 0.2, pH 7.2. The homogenates were used to isolate mitochondria by differential centrifugation as described previously (Kumfu *et al.* 2012*b*). Ferric ammonium citrate (5 μg ml^{-1}) co-administered with 1 mM ascorbic acid, serving to represent the ascorbate-reduced form of iron (Fe^{2+}), were applied to all groups of isolated cardiac mitochondria for 5 min. Next, assessments of ROS production, mitochondrial membrane potential change ($\Delta\Psi_m$) and mitochondrial swelling were performed according to the experimental protocols.

Identification of cardiac mitochondria with electron microscopy

Electron microscopy was used to identify isolated cardiac mitochondria (Chelli *et al.* 2001; Thummasorn *et al.* 2011). All groups of isolated cardiac mitochondria were fixed in 2.5% glutaraldehyde in 0.1 M cacodylate buffer, pH 7.4 at 4°C. After rinsing in cacodylate buffer, the mitochondrial pellets were fixed in 1% cacodylate-buffered osmium tetroxide for 2 h at room temperature, then dehydrated in a graded series of ethanol. The mitochondria were then embedded in Epon–Araldite. Ultrathin sections were cut with a diamond knife, placed on copper grids, stained with uranyl acetate and lead citrate, and observed with a transmission electron microscope.

Determination of cardiac mitochondrial ROS production

Production of ROS was measured with the dye dichlorohydrofluoresceindiacetate (DCFDA; Novalija *et al.* 2003; Thummasorn *et al.* 2011). After Fe^{2+} loading for 5 min, all groups of isolated cardiac mitochondria were incubated with 2 μM DCFDA at 25°C for 20 min. The ROS levels were determined via a fluorescent microplate reader at excitation wavelength 485 nm and and emission wavelength 530 nm.

Determination of cardiac mitochondrial membrane potential change

Mitochondrial membrane potential change ($\Delta\Psi_m$) was measured with the dye 5,5′,6,6′-tetrachloro-1,1′,3,3′-tetraethylbenzimidazolcarbocyanine iodide (JC-1; Di Lisa *et al.* 1995; Thummasorn *et al.* 2011). After Fe^{2+} loading for 5 min, all groups of isolated cardiac mitochondria were stained with JC-1 (310 nM) at 37°C for 30 min. Mitochondrial membrane potential was determined as fluorescence intensity via the use of a fluorescent microplate reader. JC-1 monomer (green) fluorescence was excited at the wavelength of 485 nm and the emission detected at 530 nm. JC-1 aggregate form (red) fluorescence was excited at 485 nm and the emission detected at 590 nm. The $\Delta\Psi_m$ was calculated as the ratio of red to green fluorescence. Mitochondrial depolarization was indicated by a decrease in the red/green fluorescence intensity ratio.

Determination of cardiac mitochondrial swelling

Isolated cardiac mitochondria from all groups were incubated in respiration buffer (containing 100 mM KCl, 50 mM sucrose, 10 mM Hepes and 5 mM KH_2PO_4, pH 7.4 at 37°C) with the addition of 10 mM pyruvate/malate. After Fe^{2+} loading for 5 min, cardiac mitochondrial swelling was detected as a decrease in the absorbance of the suspension at 540 nm using a spectrophotometer for 30 min (Ruiz-Meana *et al.* 2006; Thummasorn *et al.* 2011).

Western blot analysis

At the end of treatments, the heart tissues were collected, quickly frozen in liquid nitrogen, and stored at −80°C until analysis. Left ventricular tissues were lysed with extraction buffer (20 mmol l^{-1} Tris–HCl, 1 mmol l^{-1} Na_3VO_4 and 5 mmol l^{-1} NaF), separated by electrophoresis on 10% sodium dodecyl sulfate–polyacrylamide gel and transferred onto nitrocellulose membranes (Surinkaew *et al.* 2013). Immunoblots were blocked for 1 h with 5% non-fat dry milk in Tris-buffered saline (pH 7.4) containing 0.1% Tween 20. They were then probed overnight at 4°C with the primary antibodies that recognized iron transporters (TTCC, LTCC, DMT1 and Zip14), the iron exporter ferroportin, the iron regulatory hormone hepcidin, markers of apoptosis (Bax, Bcl-2 and caspase3), and a loading control (Actin). This was followed by 1 h of incubation at room temperature with the horseradish peroxidase–conjugated secondary antibody. The blots were then visualized with an enhanced chemiluminescence (ECL) reagent. The film images of the Western blots were scanned and subsequently analysed using ImageJ (NIH image) analysis software.

Statistical analysis

All data were presented as means ± SEM and processed using SPSS (Statistical Package for Social Sciences, Chicago, IL, USA) release 16.0 for Windows. Two-way ANOVA followed by a LSD *post hoc* test were performed for group comparisons. A value of $P < 0.05$ was considered statistically significant.

© 2016 The Authors. Experimental Physiology © 2016 The Physiological Society

Results

Effects of pharmacological interventions on organ weight index

The heart weight indexes of the HT mice were significantly larger than those for the WT mice in the control group (Fig. 1*A*). In the FE groups, the heart weight index in both types of mice (WT and HT) were not significantly different from those of the control group (Fig. 1*A*). In the control group, the liver weight index of the HT mice was significantly larger than that of the WT mice (Fig. 1*B*). In the FE groups, both types of mice demonstrated a significantly increased liver weight index. Pharmacological interventions did not prevent elevation of the liver weight index (Fig. 1*B*). The spleen weight index of the HT mice was significantly larger than that of the WT mice in the control group (Fig. 1*C*). In the FE groups, both WT and HT mice demonstrated a significantly increased spleen weight index, and none of the pharmacological interventions prevented or attenuated it (Fig. 1*C*). Kidney weight indexes were not different in both types of mice and in all groups throughout the experiment (Fig. 1*D*).

Effects of pharmacological interventions on cardiac iron concentration and cardiac MDA content

In the FE group, both WT and HT mice had significantly increased cardiac iron, compared with the control group (Fig. 2*A*). Deferoxamine, DFX, DFP, efonidipine or amlodipine decreased the cardiac iron concentration in

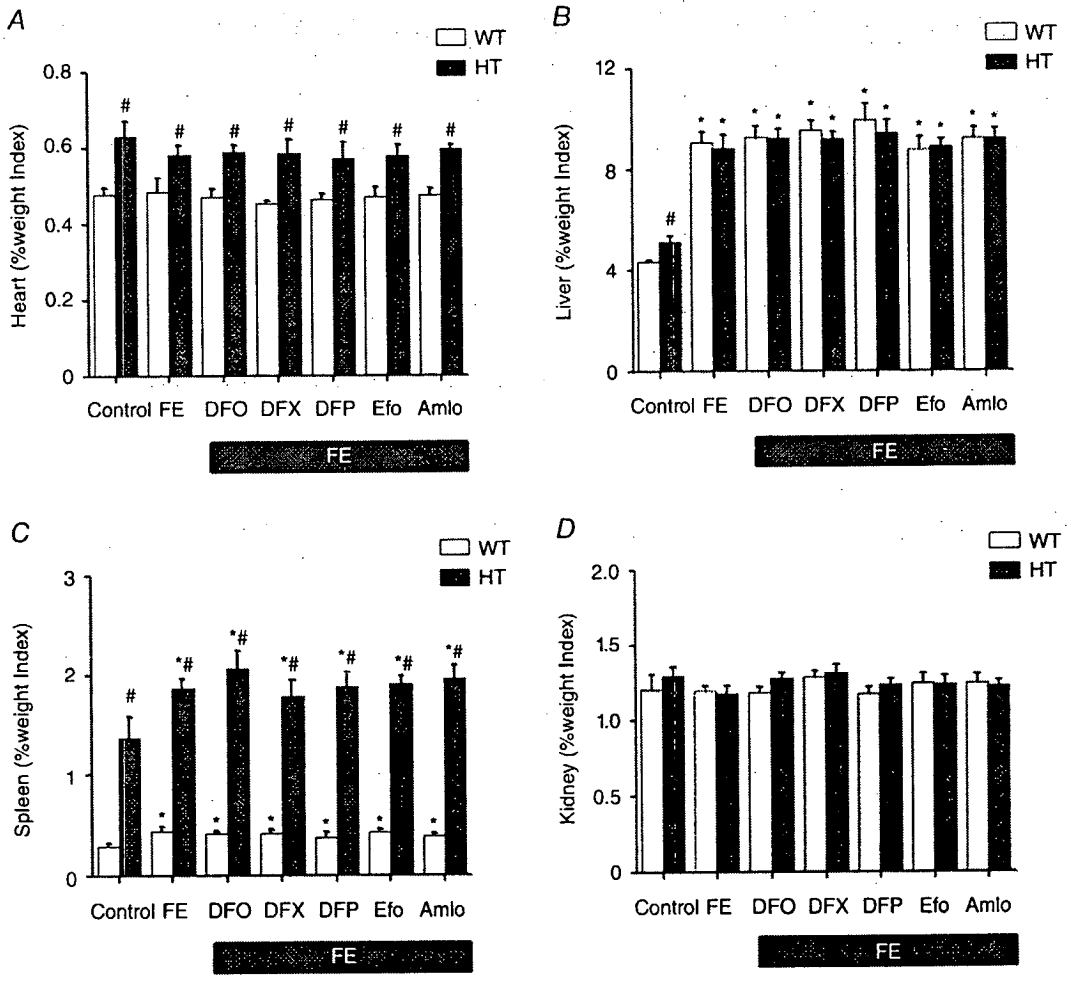


Figure 1. Effects of pharmacological interventions on percentage of organ weight index in the heart (*A*), liver (*B*), spleen (*C*) and kidney (*D*) in WT and HT mice
$n = 6$ per group. Abbreviations in this and subsequent figures: Amlo, amlodipine; DFO, deferoxamine; DFP, deferiprone; DFX, deferasirox; Efo, efonidipine; FE, iron overload; HT, thalassaemic; and WT, wild-type. $^{*}P < 0.01$ *versus* control and $^{\#}P < 0.01$ *versus* WT.

© 2016 The Authors. Experimental Physiology © 2016 The Physiological Society

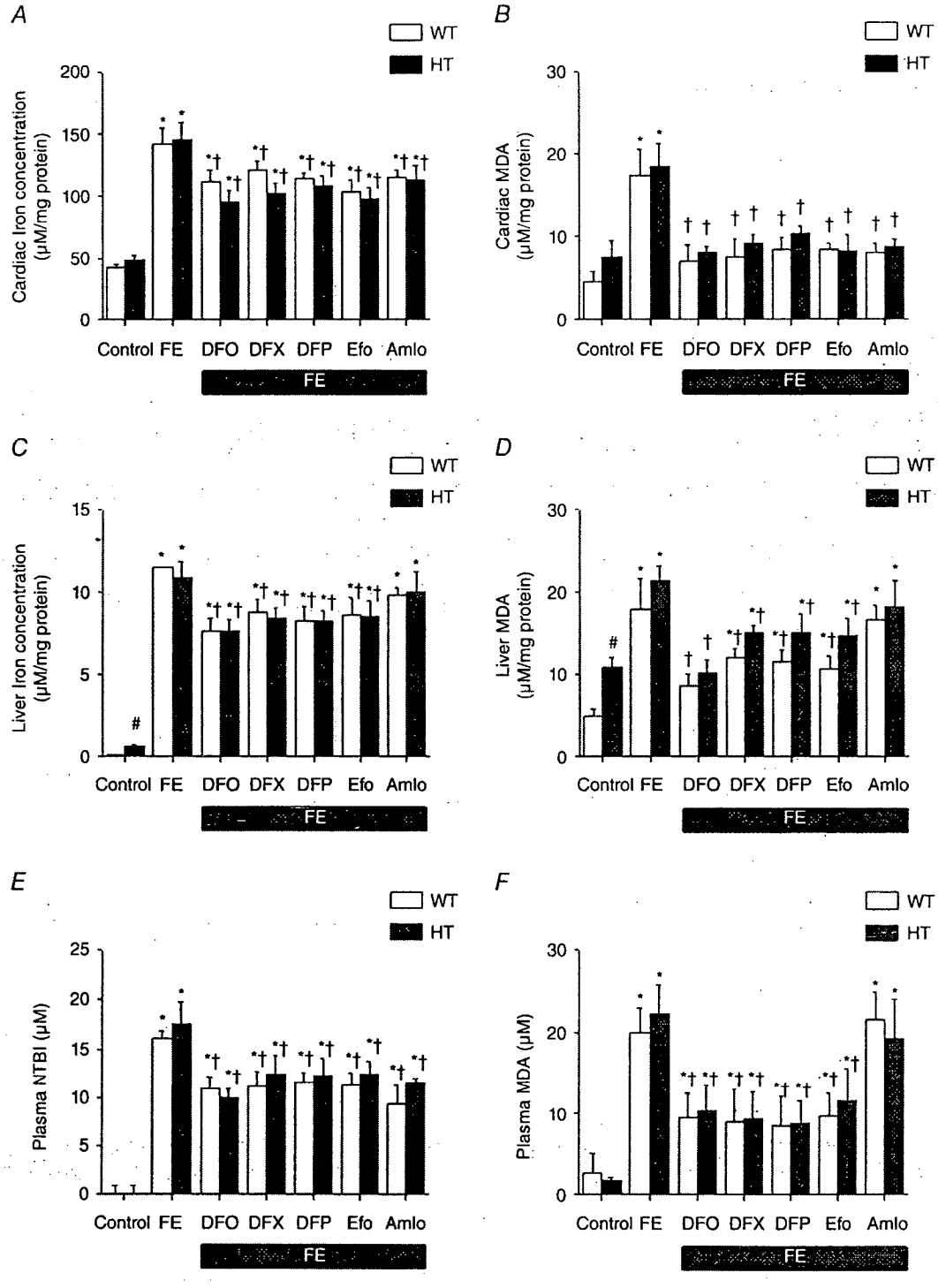


Figure 2. Effects of pharmacological interventions on cardiac iron concentration and cardiac malondialdehyde (MDA) content (*A* and *B*), liver iron concentration and liver MDA content (*C* and *D*), plasma non-transferrin bound iron (NTBI) level and plasma MDA content (*E* and *F*) in WT and HT mice $n = 6$ per group. $^{*}P < 0.05$ *versus* control, $^{\dagger}P < 0.05$ *versus* FE and $^{\#}P < 0.05$ *versus* WT.

© 2016 The Authors. Experimental Physiology © 2016 The Physiological Society

both types of mice, compared with the FE group, and there were no differences among groups of treatments (Fig. 2*A*). Similar results were found in cardiac MDA content, for which both types of mice (WT and HT) in the FE group had significantly increased cardiac MDA content, compared with the control group (Fig. 2*B*). Each of the pharmacological interventions effectively decreased the cardiac MDA concentration in both types of mice back to normal levels, compared with the FE group, and there were no differences among groups of treatments (Fig. 2*B*).

Effects of pharmacological interventions on liver iron concentration and liver MDA content

In the control group, liver iron [0.62 ± 0.13 *versus* 0.09 ± 0.06 μM (mg protein)$^{-1}$] and liver MDA levels [10.97 ± 1.11 *versus* 4.90 ± 0.94 μM (mg protein)$^{-1}$] of HT mice were significantly higher than those of WT mice, respectively ($P < 0.01$; Fig. 2*C* and *D*). In the FE group, both WT and HT mice had significantly increased liver iron, compared with the control group (Fig. 2*C*). Only DFO, DFX, DFP or efonidipine effectively decreased the liver iron concentration in both types of mice, compared with the FE group (Fig. 2*C*). Similar results were found for the liver MDA content, in that mice in the FE group (WT and HT) had significantly increased liver MDA content when compared with the control group (Fig. 2*D*). Only DFO, DFX, DFP or efonidipine decreased the liver MDA concentrations in both types of mice when compared with the FE group (Fig. 2*D*).

Effects of pharmacological interventions on plasma NTBI and plasma MDA level

In the control group, the levels of plasma NTBI were not detectable in both WT and thalassaemic mice (Fig. 2*E*). Both types of mice in the FE group (WT and HT) had significantly increased plasma NTBI, compared with the control group (Fig. 2*E*). Deferoxamine, DFX, DFP, efonidipine or amlodipine decreased plasma NTBI in both types of mice compared with the FE group, and there were no significant differences among groups of treatments (Fig. 2*E*). In the FE group, both WT and HT mice demonstrated increased plasma MDA, when compared with the control group (Fig. 2*F*), and only DFO, DFX, DFP or efonidipine effectively decreased the plasma MDA, compared with the FE group (Fig. 2*F*).

Effect of pharmacological interventions on HRV

In the control group, thalassaemic mice had a higher LFnu (Fig. 3*A*), lower HFnu (Fig. 3*B*) and higher LF/HF ratio (Fig. 3*C*) compared with WT mice. Both WT and HT mice in the FE groups had increased LF/HF ratios, increased LFnu values and decreased HFnu values, suggesting that iron overload impaired cardiac autonomic regulation when compared with the control group (Fig. 3*A–C*). In both WT and HT mice, DFO, DFX, DFP, efonidipine or amlodipine significantly decreased the LF/HF ratio and LFnu power, and increased the HFnu power back to normal levels (Fig. 3*A–C*). The heart rates in both types of mice after pharmacological interventions were not significantly different from the control group throughout the experiment (Fig. 3*D*). Examples of the power spectra from the WT and HT groups are shown in Fig. 3*E*.

Effect of pharmacological interventions on LV function

Both types of mice (WT and HT) in the FE groups demonstrated significantly decreased ESP, P_{max} and dP/dt_{max} values when compared with the control group (Fig. 4*A*, *C* and *E*). Treatment with DFO, DFX, DFP, efonidipine or amlodipine significantly increased ESP, P_{max} and dP/dt_{max} values, which returned back to the levels in the control group in both WT and HT mice (Fig. 4*A*, *C* and *E*). The EDP, P_{min} and dP/dt_{min} in both WT and HT mice after pharmacological interventions were not significantly different from the control group throughout the experiment (Fig. 4*B*, *D* and *F*).

The heart rates in both types of mice (WT and HT) after pharmacological interventions were not significantly different from the control group throughout the experiment (Fig. 5*A*). The SV, CO and SW in the control group in HT mice were higher than those in WT mice (Fig. 5*B–D*), indicating the high-output state in HT mice, which is similar to that found in thalassaemia patients (Kremastinos *et al.* 2010). Significantly decreased SV, CO and SW values were also demonstrated in the FE group of both WT and HT mice when compared with the control group (Fig. 5*B–D*). Treatment with DFO, DFX, DFP, efonidipine or amlodipine significantly increased SV, CO and SW, which were returned to the levels seen in the control group (Fig. 5*B–D*).

Effects of pharmacological interventions on cardiac mitochondrial function

After 5 months of iron administration, ROS levels in cardiac mitochondria from both types of mice (WT and HT) were significantly increased in the FE group, compared with the control group (Fig. 6*A*). Consistent results were also found in the $\Delta\Psi_m$ values. In the iron-overloaded state, in the FE group, cardiac mitochondrial depolarization was observed in both WT and HT mice, as indicated by a significant decrease in the Ψ_m (Fig. 6*B*). Moreover, iron overload resulted in significantly decreased absorbance in the mitochondria of the FE group (Fig. 6*C*), indicating that

© 2016 The Authors. Experimental Physiology © 2016 The Physiological Society

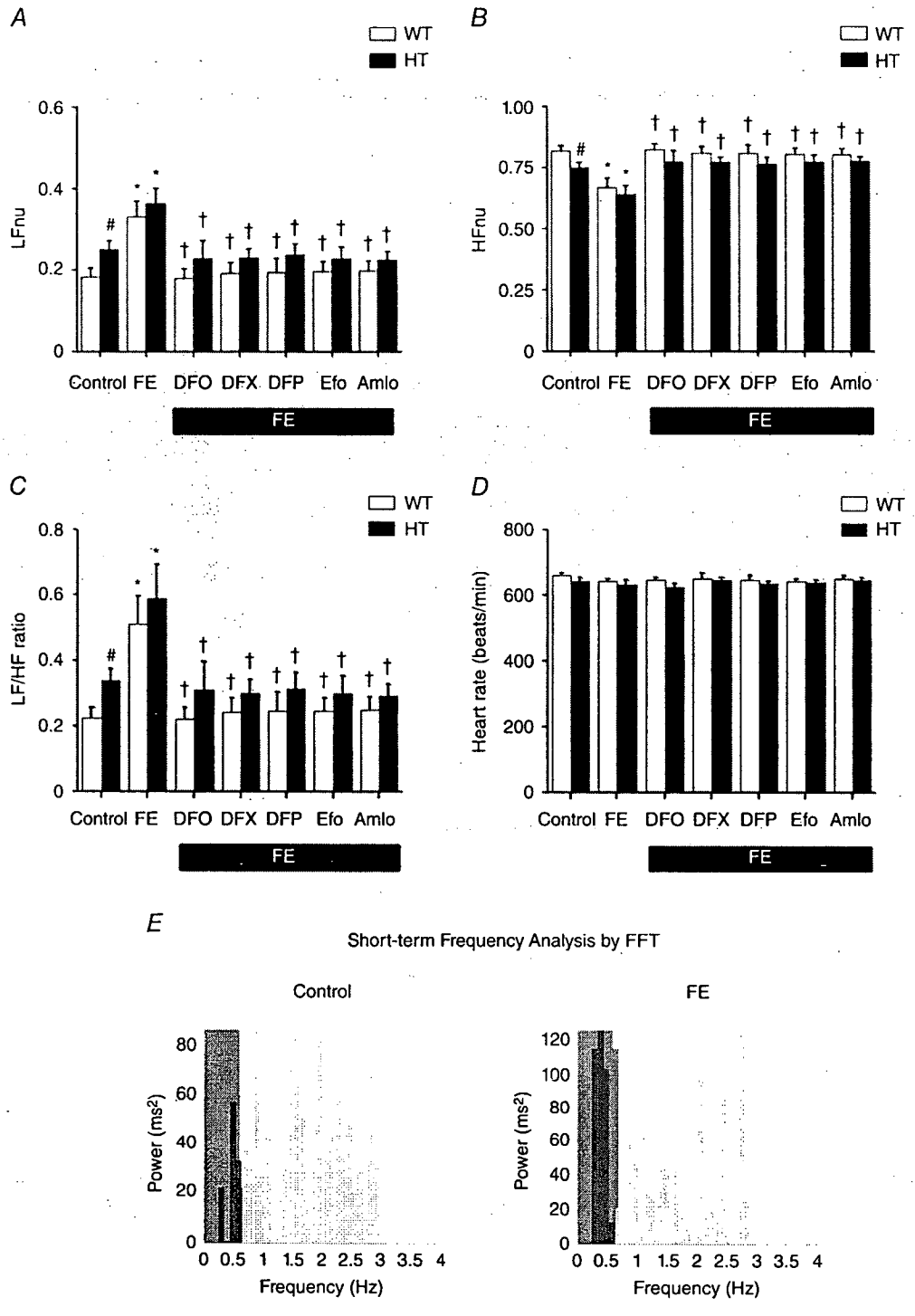


Figure 3. Effects of pharmacological interventions on heart rate variability (HRV) in WT and HT mice
$n = 6$ per group. Normalized low-frequency power (Lfnu; *A*), normalized high-frequency power (Hfnu; *B*), LF/HF ratio (*C*), heart rate (*D*) and power spectra of R–R interval variability (*E*). $^{*}P < 0.05$ *versus* control, $^{\dagger}P < 0.05$ *versus* FE and $^{\#}P < 0.05$ *versus* WT.

© 2016 The Authors. Experimental Physiology © 2016 The Physiological Society

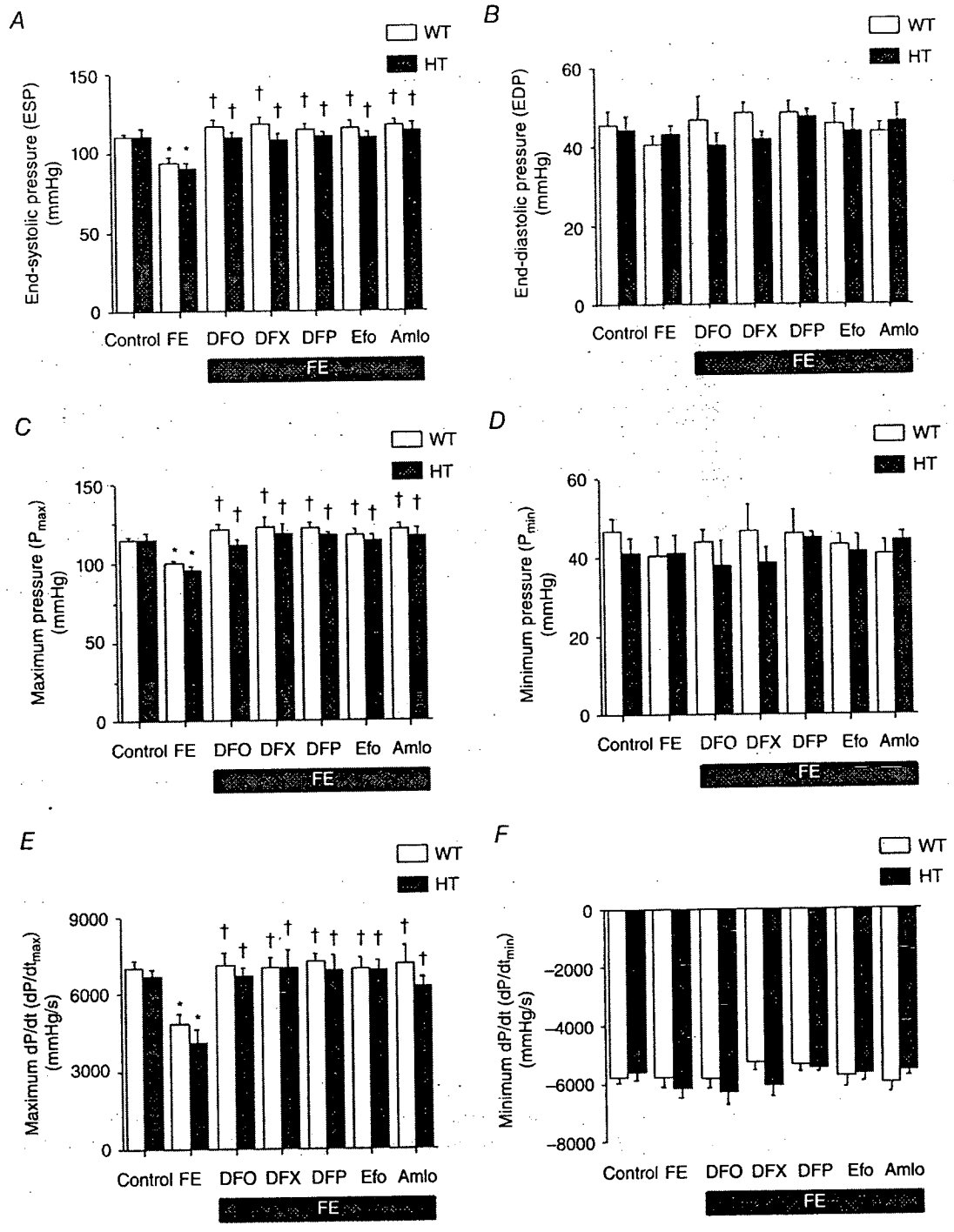


Figure 4. Effects of pharmacological interventions on left ventricular (LV) function in WT and HT mice
$n = 6$ per group. End-systolic pressure (ESP; *A*), end-diastolic pressure (EDP; *B*), maximal pressure (P_{max}; *C*), minimal pressure (P_{min}; *D*), maximal rate of change of pressure (dP/dt_{max}; *E*) and minimal rate of change of pressure (dP/dt_{min}; *F*). $^{*}P < 0.05$ *versus* control and $^{\dagger}P < 0.05$ *versus* FE.

© 2016 The Authors. Experimental Physiology © 2016 The Physiological Society

an iron-overloaded state significantly increased cardiac mitochondrial swelling in both types of mice.

Treatment with DFO, DFX, DFP, efonidipine or amlodipine caused a significant decrease in ROS production in cardiac mitochondria of WT and HT mice, compared with the control group (Fig. 6*A*). Furthermore, treatment with DFO, DFX, DFP, efonidipine or amlodipine significantly attenuated cardiac mitochondrial depolarization (Fig. 6*B*). Moreover, DFO, DFX, DFP, efonidipine or amlodipine also attenuated the reduction in absorbance, compared with the control group (Fig. 6*C*), indicating that each drug effectively attenuated cardiac mitochondrial swelling.

Identification of cardiac mitochondria by electron microscopy

A transmission electron microscope was used to identify the cardiac mitochondria. Both WT and HT cardiac mitochondria in the FE group demonstrated cardiac mitochondrial swelling as indicated by markedly unfolded cristae (Fig. 7*A* and *B*). When treated with DFO, DFX, DFP, efonidipine or amlodipine, the morphology of the cardiac mitochondria was well preserved in both types of mice (Fig. 7*A* and *B*). This indicated the effectiveness of the drugs in attenuating cardiac mitochondrial swelling in iron-overloaded mice.

Effects of pharmacological interventions on cardiac apoptotic signalling

The expression of Bax and Bcl-2 proteins and the Bax/Bcl-2 ratio were not significantly different among groups in both WT and HT mice (Fig. 8*A–C*). However, the expression of pro-caspase3 protein was significantly increased in HT mice compared with WT mice, even before iron feeding (Fig. 8*D*). After induction of the iron-overloaded state, pro-caspase3 expression was significantly increased in the FE group in HT mice, as well as in the pharmacologically treated groups, when compared with the control group

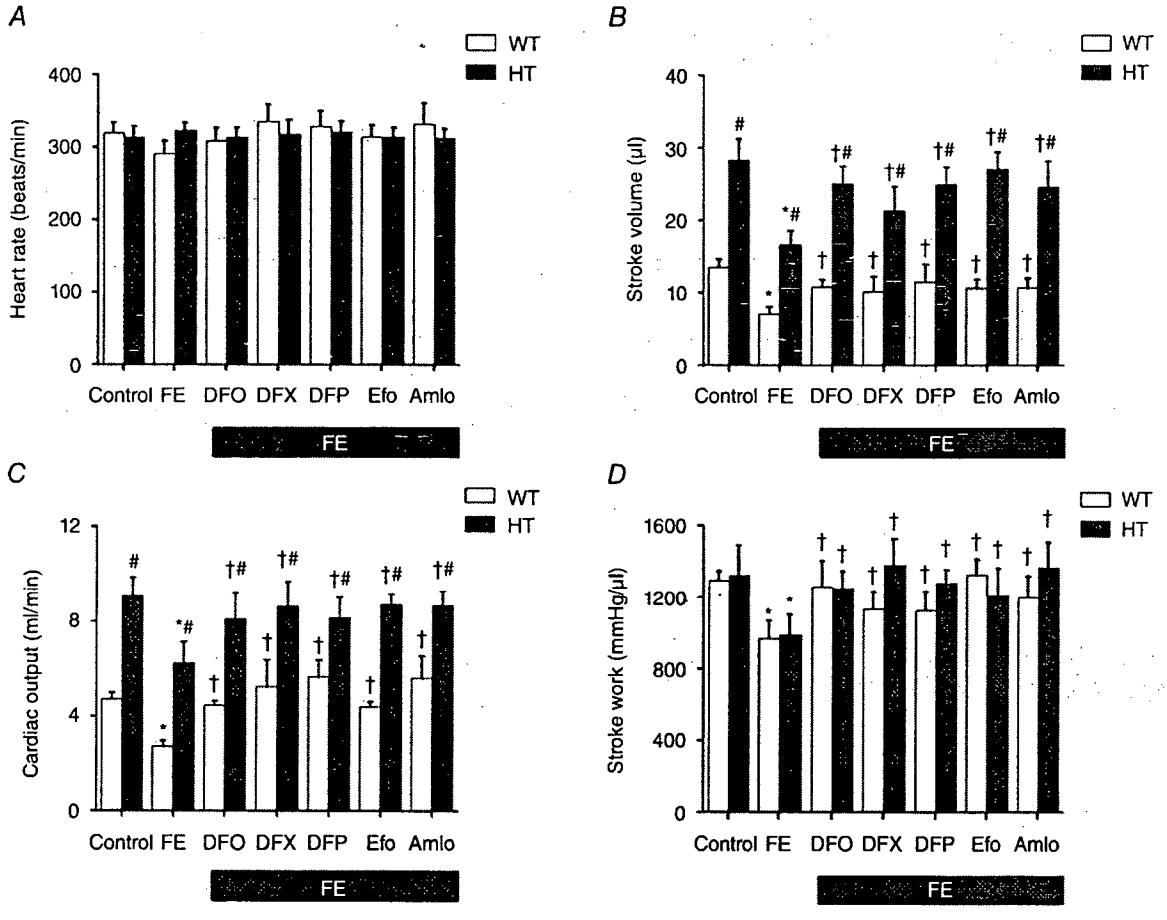


Figure 5. Effects of pharmacological interventions on LV function in WT and HT mice
$n = 6$ per group. Heart rate (*A*), stroke volume (SV; *B*), cardiac output (CO; *C*) and stroke work (SW; *D*). $^{*}P < 0.05$ *versus* control, $^{\dagger}P < 0.05$ *versus* FE and $^{\#}P < 0.05$ *versus* WT.

© 2016 The Authors. Experimental Physiology © 2016 The Physiological Society

(Fig. 8*D*). However, active-caspase3 protein was not found in either WT or HT mice (Fig. 8*D*).

Effects of pharmacological interventions on iron regulator protein expression

Levels of the iron exporter ferroportin and the iron regulatory hormone hepcidin were markedly higher in the HT mice than the WT mice, even before iron loading (Fig. 9*A* and *B*). After iron overloading, ferroportin and hepcidin expression were not significantly different among groups in the FE groups and in the pharmacologically treated groups, when compared with the control group in WT and HT mice (Fig. 9*A* and *B*).

Effects of pharmacological interventions on iron transporter protein expression

The expression of cardiac iron transporter proteins, including LTCC, DMT1 and Zip14, were not significantly different among groups in both types of mice (Fig. 10*A–C*). However, the expression of TTCC protein was not detected in the present study in either WT or HT mice.

Discussion

The major findings of the present study are as follows. First, iron overload led to increased cardiac and liver iron accumulation, cardiac and liver MDA, plasma NTBI, plasma MDA and LF/HF ratio, impaired

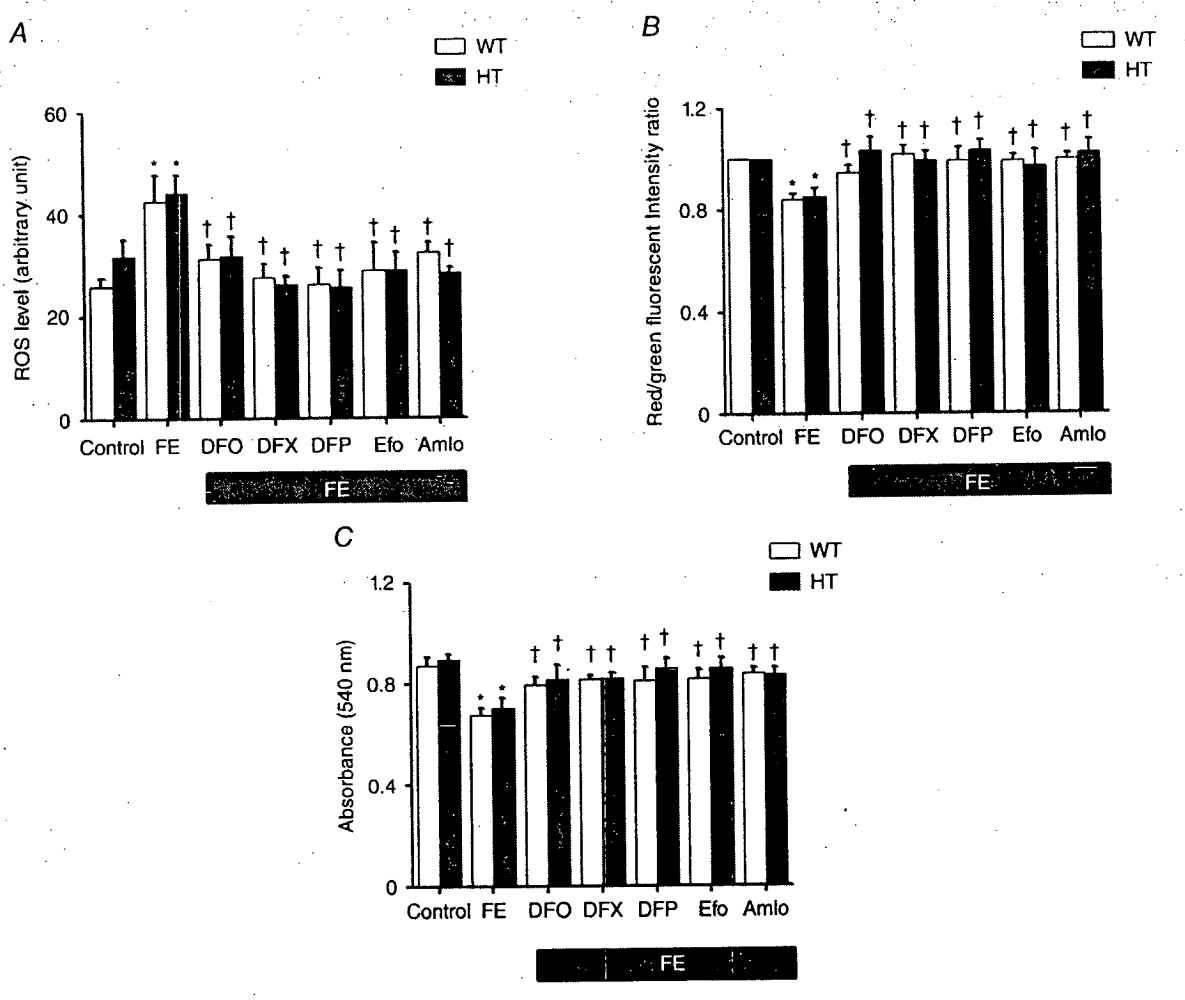


Figure 6. Effects of pharmacological interventions on cardiac mitochondrial reactive oxygen species (ROS) production (*A*), mitochondrial membrane potential change (*B*) and mitochondrial swelling (*C*) in WT and HT mice
$n = 6$ per group. For mitochondrial membrane potential change, the mitochondrial depolarization is indicated by a decrease in the red/green fluorescence intensity ratio. For mitochondrial swelling, a decrease in the absorbance of the isolated mitochondrial suspension indicates mitochondrial swelling. $^{*}P < 0.05$ *versus* control and $^{\dagger}P < 0.05$ *versus* FE.

© 2016 The Authors. Experimental Physiology © 2016 The Physiological Society

LV function and cardiac mitochondrial function and increased pro-caspase3 protein expression, but did not alter the protein expression of the iron transporters LTCC, DMT1 and Zip14. Second, treatment with amlodipine, efonidipine or three iron chelators shared similar efficacy in decreasing cardiac iron and MDA, plasma NTBI and the LF/HF ratio, and improving LV function and cardiac mitochondrial function, but did not alter iron transporter protein expression in either WT or HT mice. Third, only the efonidipine or the three iron chelators effectively decreased liver iron, liver MDA and plasma MDA in both WT and HT mice, whereas the LTCC blocker did not.

In the present study, the development of LV dysfunction and autonomic imbalance observed in iron-overloaded mice was indicated by decreased ESP, P_{max}, dP/dt_{max}, SV, CO and SW and increased LF/HF ratio. The LTCC blocker amlodipine and dual TTCC and LTCC blocker efonidipine decreased cardiac iron and MDA and improved cardiac function in both WT and HT mice. This was consistent with previous studies, in which the LTCC blocker and the dual TTCC and LTCC blocker decreased cardiac iron and attenuated cardiac dysfunction in iron-overloaded mice (Crowe & Bartfay, 2002; Oudit *et al.* 2003; Kumfu *et al.* 2012*a*; Musumeci *et al.* 2013). Moreover, our results demonstrated that the three iron chelators could also attenuate cardiac dysfunction caused by iron overload in both WT and HT mice to the same degree as the dual TTCC and LTCC blocker and the LTCC blocker. These findings suggest that both TTCC and LTCC could play important roles in cardiac iron uptake, and treatment with a dual TTCC and LTCC blocker or an LTCC blocker could provide beneficial effects similar to those of the three iron chelators currently used to treat cardiac iron-overloaded conditions.

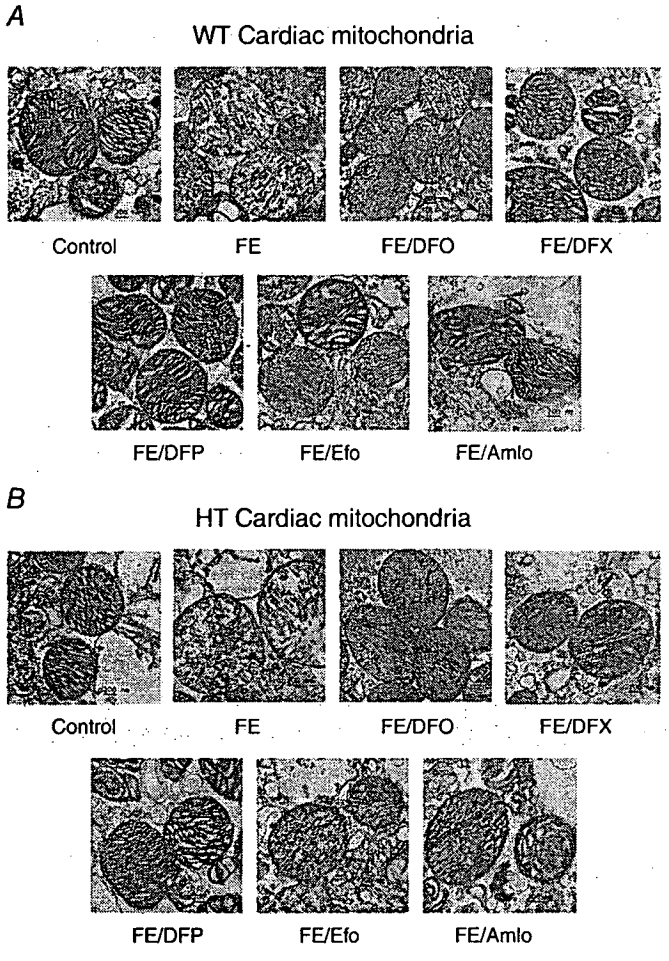


Figure 7. Effects of pharmacological interventions on cardiac mitochondrial morphology by using transmission electron microscopy
A, WT cardiac mitochondria. *B*, thalassaemic cardiac mitochondria.

© 2016 The Authors. Experimental Physiology © 2016 The Physiological Society

Our study demonstrated that the LTCC protein could be detected by the Western blot analysis at a very low level, whereas the TTCC protein could not be detected. This could be because the TTCC has much lower level than the LTCC in the heart (Qu & Boutjdir, 2001). This is supported by our previous reports, which demonstrated that TTCC re-expression in the heart of thalassaemic mice could be detected by real-time PCR and microarray (Kumfu *et al.* 2011, 2012*a*). Moreover, Lopin *et al.* (2012) demonstrated that Fe^{2+} inhibited Ca^{2+} currents and that Fe^{2+} could enter cardiomyocytes through the TTCC in iron-overloaded conditions. These findings suggest that the TTCC could play an important role in cardiac iron uptake in iron-overloaded conditions.

Chronic iron overload can lead to increased production of ROS via Haber–Weiss and Fenton reactions (Bartfay & Bartfay, 2000; Lekawanvijit & Chattipakorn, 2009). The excess of free radicals can damage cellular lipids, proteins, DNA and mitochondria (Bartfay & Bartfay, 2000; Lekawanvijit & Chattipakorn, 2009). Moreover, mitochondrial dysfunction could be responsible for the cardiac failure resulting from chronic iron overload (Gao *et al.* 2009, 2010). The increase in ROS production can cause mitochondrial depolarization and mitochondrial swelling, leading to the release of cytochrome *c* and resulting in apoptotic cell death (Zorov *et al.* 2006; Thummasorn *et al.* 2011). In the present study, the increased cardiac iron concentrations and MDA in both types of mice in iron-overloaded conditions were associated with increased cardiac mitochondrial dysfunction, indicating the cardiac cellular and mitochondrial damage caused by iron overload.

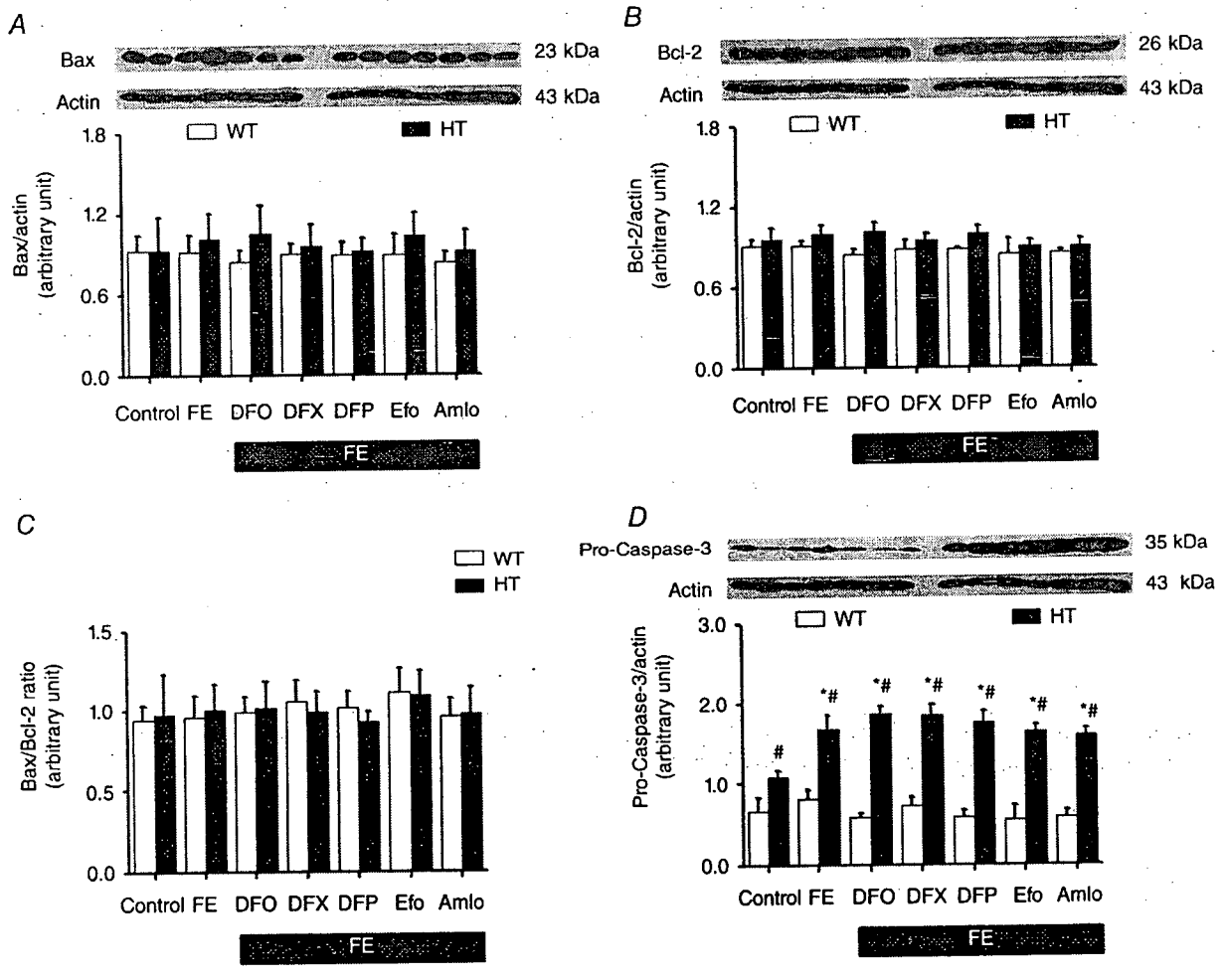


Figure 8. Effects of pharmacological interventions on cardiac apoptotic protein expression in WT and HT mice
$n = 6$ per group. Pro-apoptotic Bax (*A*), anti-apoptotic Bcl-2 (*B*), Bax/Bcl-2 ratio (*C*) and pro-caspase3 (*D*); actin was the loading control. $^{*}P < 0.05$ *versus* control and $^{\#}P < 0.05$ *versus* WT.

© 2016 The Authors. Experimental Physiology © 2016 The Physiological Society

Moreover, this is the first study to determine the effects of iron chelators and blockers of LTCC and TTCC on cardiac mitochondrial function in an iron-overloaded state. Each of the pharmacological interventions provided protective effects by preventing mitochondrial ROS production and mitochondrial depolarization. They also attenuated the mitochondrial swelling caused by the cardiac iron-overloaded conditions.

In the present study, cardiomyocyte apoptosis was not observed, because Bax and Bcl-2 protein expressions were not changed, and active-caspase3 protein was not detected in the iron-overloaded conditions. These finding contradicts results from a previous study that used an iron-overloaded gerbil model, in which iron overload was induced by iron dextran injection for 3 months, which found increased cardiac apoptosis indicated by increased Bax/Bcl-2 ratios and active-caspase3 (Wang *et al.* 2011). The discrepancy in findings may be because of a difference in the severity of the iron-overloaded conditions. However, our study showed that the level of pro-caspase3 protein in the HT mice was markedly higher than that in WT mice even before iron loading, suggesting that HT mice were more vulnerable to cardiac apoptosis than WT mice. This hypothesis is consistent with a previous study, which demonstrated that overexpression of pro-caspase3 in the heart of mice was associated with increased infarct size, depressed cardiac function and a pronounced susceptibility to mortality (Condorelli *et al.* 2001).

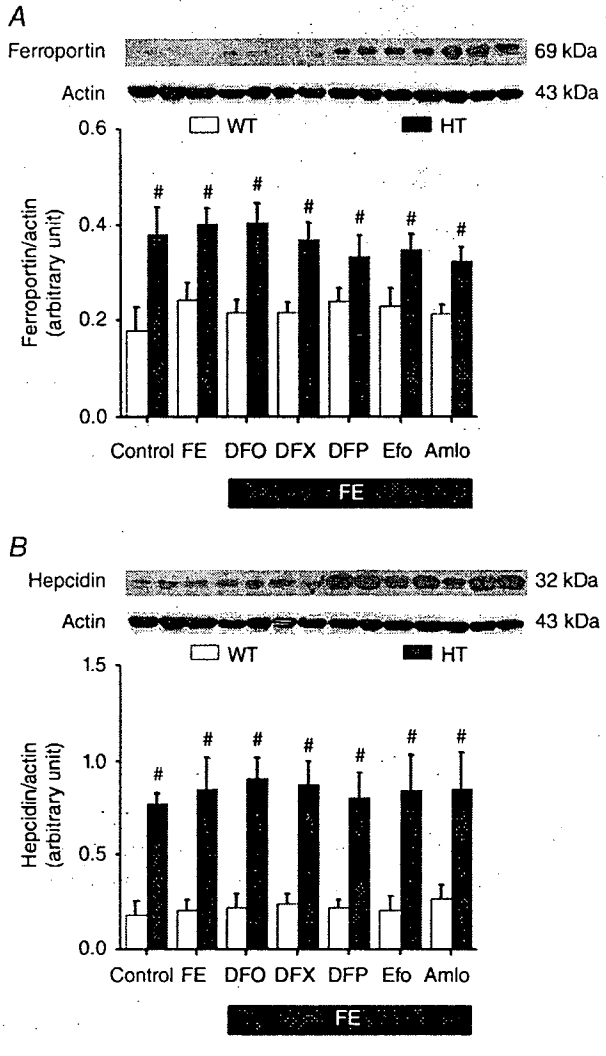


Figure 9. Effects of pharmacological interventions on protein expressions of the iron exporter ferroportin (*A*) and the iron regulatory hormone hepcidin (*B*) in WT and HT mice
n = 6 per group. Actin was the loading control.
$^{\#}P < 0.05$ *versus* WT.

In the present study, protein expressions of ferroportin and hepcidin in thalassaemic mice were significantly higher than in WT mice. The increase of the iron exporter ferroportin might be a defense mechanism in thalassaemic mice to reduce iron accumulation in cardiomyocytes, because iron accumulation in thalassaemic cardiomyocytes was greater than in WT cardiomyocytes (Kumfu *et al.* 2011). A previous study suggested that inflammation is a common complication in thalassaemia patients (Lekawanvijit & Chattipakorn, 2009; Murphy & Oudit, 2010). Iron accumulation and inflammation lead to increased hepcidin expression in order to limit iron release into the bloodstream (Gardenghi *et al.* 2010). The increase of hepcidin expression in thalassaemic hearts might be a response to iron overload and inflammation in thalassaemic mice. Given that neither iron chelators nor calcium channel blockers alter the increased expressions of ferroportin and hepcidin in thalassaemic mice as a response to iron overload, alternative therapeutic strategies may therefore be needed to increase cardiac iron elimination in thalassaemic hearts.

In the present study, iron overload was induced by feeding WT and HT mice with an FE diet for 120 days to induce cardiac iron overload to a greater extent than in the previous study (Kumfu *et al.* 2012*a*). The iron-overloaded WT and HT mice demonstrated an increase in cardiac iron accumulation and liver MDA compared with our previous study (Kumfu *et al.* 2012*a*). Moreover, after 5 months of iron administration, increased NTBI was demonstrated in the FE group (WT and HT mice), and the change in the NTBI increased in a time-dependent manner when compared with our previous study (Kumfu *et al.* 2012*a*). These findings suggest that feeding mice with an iron-enriched diet for 120 days induced cardiac, liver and systemic iron overload to a greater extent than in the previous study (Kumfu *et al.* 2012*a*).

© 2016 The Authors. Experimental Physiology © 2016 The Physiological Society

Although all pharmacological interventions in the present study could reduce the cardiac iron concentration and improve cardiac function to a similar extent in both types of mice, the effects of each pharmacological intervention on liver iron accumulation and the reduction in MDA in both plasma and liver were not the same. The dual TTCC and LTCC blocker and the three iron chelators could reduce the liver iron concentration, liver MDA and plasma MDA to a greater extent than the LTCC blocker in both WT and HT mice. These findings are consistent with previous studies, which showed that the LTCC blockers verapamil, amlodipine and nifedipine did not decrease liver iron in iron-overloaded mice, because hepatocytes had a very low expression of LTCC (Oudit *et al.* 2003; Kumfu *et al.* 2012*a*). Our findings indicated that the dual TTCC and LTCC blocker could provide systemic benefits to the same degree as the three commercial iron chelators, whereas the LTCC blocker could not. Although efonidipine is known to block both LTCC and TTCC, it has been shown that it could block TTCC more effectively than LTCC (Kinoshita *et al.* 2009). In a patch-clamp study, efonidipine reduced the amplitude of the T-type Ca^{2+} current by 57 ± 12% ($n = 4$), while reducing the amplitude of the L-type Ca^{2+} current by only 21 ± 4% ($n = 5$) in isolated cardiomyocytes (Kinoshita *et al.* 2009). This indicated that efonidipine selectively inhibited TTCC more than LTCC (Kinoshita *et al.* 2009). Moreover, we previously compared the effects of the LTCC blocker verapamil and the dual TTCC and LTCC blocker efonidipine and reported that their effects on iron overload in the heart were different, suggesting that the dual TTCC and LTCC blocker efonidipine acted on not only LTCC but

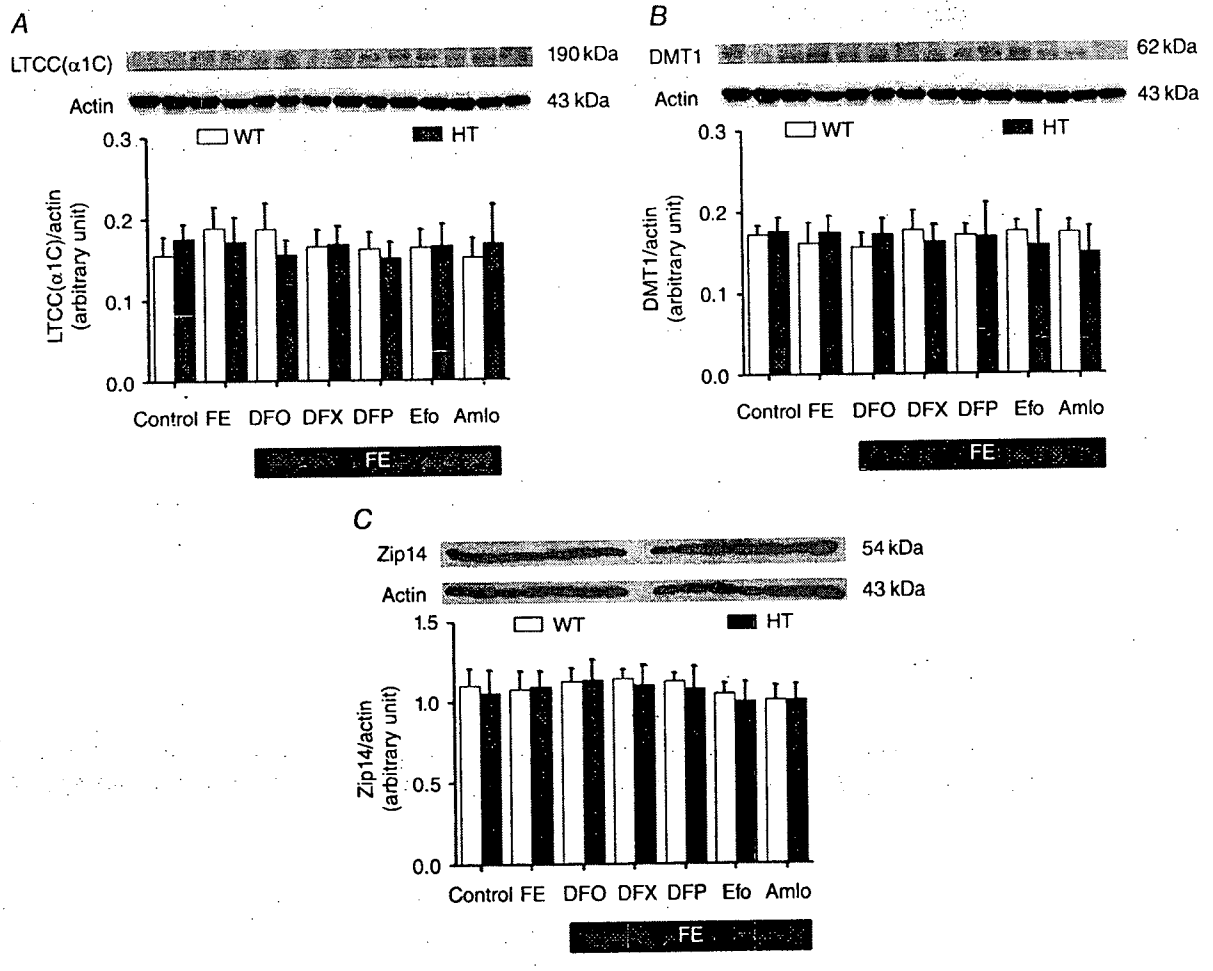


Figure 10. Effects of pharmacological interventions on iron transporter protein expressions in WT and HT mice
$n = 6$ per group. L-type calcium channel (LTCC; *A*), divalent metal transporter1 (DMT1; *B*) and Zip14 (*C*); actin was the loading control.

© 2016 The Authors. Experimental Physiology © 2016 The Physiological Society

also TTCC and provided additional benefits (Kumfu *et al.* 2011). The limitation of the present study is that we did not evaluate the effects of the drugs used on their own. Moreover, the body weight was used instead of the tibial length to normalize several parameters for comparisons in the present study.

In conclusion, given that the dual TTCC and LTCC blocker efonidipine could provide broad beneficial effects on the heart, liver, plasma and mitochondria in both WT and HT mice in an iron-overloaded state, it is possible that efonidipine could be another drug of choice for the treatment of iron-overloaded conditions. Unlike iron chelators that are effective in removing excess iron accumulation in cells, dual TTCC and LTCC blockers are expected to be particularly effective early in iron overload, by reducing tissue iron uptake and preventing disease progression. Moreover, combined therapy of iron chelators with efonidipine may provide additive benefits in preventing cardiac and systemic complications in iron-overloaded conditions. Future clinical studies are needed to validate the clinical significance for the use of efonidipine in iron-overloaded patients.

References

Abboud S & Haile DJ (2000). A novel mammalian iron-regulated protein involved in intracellular iron metabolism. *J Biol Chem* **275**, 19906–19912.

Bartfay WJ & Bartfay E (2000). Iron-overload cardiomyopathy: evidence for a free radical-mediated mechanism of injury and dysfunction in a murine model. *Biol Res Nurs* **2**, 49–59.

Berdoukas V, Farmaki K, Carson S, Wood J & Coates T (2012). Treating thalassemia major-related iron overload: the role of deferiprone. *J Blood Med* **3**, 119–129.

Brittenham GM (2011). Iron-chelating therapy for transfusional iron overload. *N Engl J Med* **364**, 146–156.

Chelli B, Falleni A, Salvetti F, Gremigni V, Lucacchini A & Martini C (2001). Peripheral-type benzodiazepine receptor ligands: mitochondrial permeability transition induction in rat cardiac tissue. *Biochem Pharmacol* **61**, 695–705.

Condorelli G, Roncarati R, Ross J Jr, Pisani A, Stassi G, Todaro M, Trocha S, Drusco A, Gu Y, Russo MA, Frati G, Jones SP, Lefer DJ, Napoli C & Croce CM (2001). Heart-targeted overexpression of *caspase3* in mice increases infarct size and depresses cardiac function. *Proc Natl Acad Sci USA* **98**, 9977–9982.

Crowe S & Bartfay WJ (2002). Amlodipine decreases iron uptake and oxygen free radical production in the heart of chronically iron overloaded mice. *Biol Res Nurs* **3**, 189–197.

Di Lisa F, Blank PS, Colonna R, Gambassi G, Silverman HS, Stern MD & Hansford RG (1995). Mitochondrial membrane potential in single living adult rat cardiac myocytes exposed to anoxia or metabolic inhibition. *J Physiol* **486**, 1–13.

Donovan A, Brownlie A, Zhou Y, Shepard J, Pratt SJ, Moynihan J, Paw BH, Drejer A, Barut B, Zapata A, Law TC, Brugnara C, Lux SE, Pinkus GS, Pinkus JL, Kingsley PD, Palis J, Fleming MD, Andrews NC & Zon LI (2000). Positional cloning of zebrafish *ferroportin1* identifies a conserved vertebrate iron exporter. *Nature* **403**, 776–781.

Fleming MD, Romano MA, Su MA, Garrick LM, Garrick MD & Andrews NC (1998). *Nramp2* is mutated in the anemic Belgrade (*b*) rat: evidence of a role for Nramp2 in endosomal iron transport. *Proc Natl Acad Sci USA* **95**, 1148–1153.

Gao X, Campian JL, Qian M, Sun XF & Eaton JW (2009). Mitochondrial DNA damage in iron overload. *J Biol Chem* **284**, 4767–4775.

Gao X, Qian M, Campian JL, Marshall J, Zhou Z, Roberts AM, Kang YJ, Prabhu SD, Sun XF & Eaton JW (2010). Mitochondrial dysfunction may explain the cardiomyopathy of chronic iron overload. *Free Radic Biol Med* **49**, 401–407.

Gardenghi S, Ramos P, Follenzi A, Rao N, Rachmilewitz EA, Giardina PJ, Grady RW & Rivella S (2010). Hepcidin and Hfe in iron overload in β-thalassemia. *Ann N Y Acad Sci* **1202**, 221–225.

Grotto D, Santa Maria LD, Boeira S, Valentini J, Charão MF, Moro AM, Nascimento PC, Pomblum VJ & Garcia SC (2007). Rapid quantification of malondialdehyde in plasma by high performance liquid chromatography–visible detection. *J Pharm Biomed Anal* **43**, 619–624.

Gunshin H, Mackenzie B, Berger UV, Gunshin Y, Romero MF, Boron WF, Nussberger S, Gollan JL & Hediger MA (1997). Cloning and characterization of a mammalian proton-coupled metal-ion transporter. *Nature* **388**, 482–488.

Hahalis G, Manolis AS, Gerasimidou I, Alexopoulos D, Sitafidis G, Kourakli A, Körfer R, Koerner MM, Vagenakis AG & Zoumbos NC (2001). Right ventricular diastolic function in β-thalassemia major: echocardiographic and clinical correlates. *Am Heart J* **141**, 428–434.

Hershko C, Link G, Konijn AM & Cabantchik ZI (2005). Objectives and mechanism of iron chelation therapy. *Ann N Y Acad Sci* **1054**, 124–135.

Incharoen T, Thephinlap C, Srichairatanakool S, Chattipakorn S, Winichagoon P, Fucharoen S, Vadolas J & Chattipakorn N (2007). Heart rate variability in β-thalassemic mice. *Int J Cardiol* **121**, 203–204.

Jamsai D, Zaibak F, Khongnium W, Vadolas J, Voullaire L, Fowler KJ, Gazeas S, Fucharoen S, Williamson R & Ioannou PA (2005). A humanized mouse model for a common β^0-thalassemia mutation. *Genomics* **85**, 453–461.

Jamsai D, Zaibak F, Vadolas J, Voullaire L, Fowler KJ, Gazeas S, Peters H, Fucharoen S, Williamson R & Ioannou PA (2006). A humanized BAC transgenic/knockout mouse model for HbE/β-thalassemia. *Genomics* **88**, 309–315.

Kardelen F, Tezcan G, Akcurin G, Ertug H & Yesilipek A (2008). Heart rate variability in patients with thalassemia major. *Pediatr Cardiol* **29**, 935–939.

Kinoshita H, Kuwahara K, Takano M, Arai Y, Kuwabara Y, Yasuno S, Nakagawa Y, Nakanishi M, Harada M, Fujiwara M, Murakami M, Ueshima K & Nakao K (2009). T-type Ca^{2+} channel blockade prevents sudden death in mice with heart failure. *Circulation* **120**, 743–752.

© 2016 The Authors. Experimental Physiology © 2016 The Physiological Society

Kremastinos DT, Farmakis D, Aessopos A, Hahalis G, Hamodraka E, Tsiapras D & Keren A (2010). β-Thalassemia cardiomyopathy: history, present considerations, and future perspectives. *Circ Heart Fail* **3**, 451–458.

Kumfu S, Chattipakorn S, Chinda K, Fucharoen S & Chattipakorn N (2012*a*). T-type calcium channel blockade improves survival and cardiovascular function in thalassemic mice. *Eur J Haematol* **88**, 535–548.

Kumfu S, Chattipakorn S, Fucharoen S & Chattipakorn N (2012*b*). Mitochondrial calcium uniporter blocker prevents cardiac mitochondrial dysfunction induced by iron overload in thalassemic mice. *Biometals* **25**, 1167–1175.

Kumfu S, Chattipakorn S, Srichairatanakool S, Settakorn J, Fucharoen S & Chattipakorn N (2011). T-type calcium channel as a portal of iron uptake into cardiomyocytes of beta-thalassemic mice. *Eur J Haematol* **86**, 156–166.

Lee DW, Lee TK, Cho IS, Park HE, Jin S, Cho HJ, Kim SH, Oh S & Kim HS (2011). Creation of myocardial fibrosis by transplantation of fibroblasts primed with survival factors. *Am J Physiol Heart Circ Physiol* **301**, H1004–H1014.

Lekawanvijit S & Chattipakorn N (2009). Iron overload thalassemic cardiomyopathy: iron status assessment and mechanisms of mechanical and electrical disturbance due to iron toxicity. *Can J Cardiol* **25**, 213–218.

Levi S & Rovida E (2009). The role of iron in mitochondrial function. *Biochim Biophys Acta* **1790**, 629–636.

Lips DJ, van der Nagel T, Steendijk P, Palmen M, Janssen BJ, van Dantzig JM, de Windt LJ & Doevendans PA (2004). Left ventricular pressure-volume measurements in mice: comparison of closed-chest versus open-chest approach. *Basic Res Cardiol* **99**, 351–359.

Lopin KV, Gray IP, Obejero-Paz CA, Thévenod F & Jones SW (2012). Fe^{2+} block and permeation of $Ca_V3.1$ (α1G) T-type calcium channels: candidate mechanism for non-transferrin-mediated Fe^{2+} influx. *Mol Pharmacol* **82**, 1194–1204.

Matsumura T, Furuichi H, Izumi J, Suda H, Ito S, Takei M, Nishi N, Mori T, Tanaka Y & Kurimoto T (1995). [Effect of efonidipine hydrochloride, a calcium channel blocker, on the experimental cerebral ischemia/anoxia]. *Nippon Yakurigaku Zasshi* **105**, 437–446.

Murphy CJ & Oudit GY (2010). Iron-overload cardiomyopathy: pathophysiology, diagnosis, and treatment. *J Card Fail* **16**, 888–900.

Musumeci M, Maccari S, Sestili P, Massimi A, Corritore E, Marano G & Catalano L (2013). The C57BL/6 genetic background confers cardioprotection in iron-overloaded mice. *Blood Transfus* **11**, 88–93.

Nam H, Wang CY, Zhang L, Zhang W, Hojyo S, Fukada T & Knutson MD (2013). ZIP14 and DMT1 in the liver, pancreas, and heart are differentially regulated by iron deficiency and overload: implications for tissue iron uptake in iron-related disorders. *Haematologica* **98**, 1049–1057.

Nemeth E, Preza GC, Jung CL, Kaplan J, Waring AJ & Ganz T (2006). The N-terminus of hepcidin is essential for its interaction with ferroportin: structure-function study. *Blood* **107**, 328–333.

Novalija E, Kevin LG, Eells JT, Henry MM & Stowe DF (2003). Anesthetic preconditioning improves adenosine triphosphate synthesis and reduces reactive oxygen species formation in mitochondria after ischemia by a redox dependent mechanism. *Anesthesiology* **98**, 1155–1163.

Oudit GY, Sun H, Trivieri MG, Koch SE, Dawood F, Ackerley C, Yazdanpanah M, Wilson GJ, Schwartz A, Liu PP & Backx PH (2003). L-type Ca^{2+} channels provide a major pathway for iron entry into cardiomyocytes in iron-overload cardiomyopathy. *Nat Med* **9**, 1187–1194.

Pacher P, Nagayama T, Mukhopadhyay P, Bátkai S & Kass DA (2008). Measurement of cardiac function using pressure–volume conductance catheter technique in mice and rats. *Nat Protoc* **3**, 1422–1434.

Pennell DJ, Porter JB, Cappellini MD, El-Beshlawy A, Chan LL, Aydinok Y, Elalfy MS, Sutcharitchan P, Li CK, Ibrahim H, Viprakasit V, Kattamis A, Smith G, Habr D, Domokos G, Roubert B & Taher A (2010). Efficacy of deferasirox in reducing and preventing cardiac iron overload in β-thalassemia. *Blood* **115**, 2364–2371.

Poggiali E, Cassinerio E, Zanaboni L & Cappellini MD (2012). An update on iron chelation therapy. *Blood Transfus* **10**, 411–422.

Qu Y & Boutjdir M (2001). Gene expression of SERCA2a and L- and T-type Ca channels during human heart development. *Pediatr Res* **50**, 569–574.

Rebouche CJ, Wilcox CL & Widness JA (2004). Microanalysis of non-heme iron in animal tissues. *J Biochem Biophys Methods* **58**, 239–251.

Richardson DR, Lane DJ, Becker EM, Huang ML, Whitnall M, Suryo Rahmanto Y, Sheftel AD & Ponka P (2010). Mitochondrial iron trafficking and the integration of iron metabolism between the mitochondrion and cytosol. *Proc Natl Acad Sci USA* **107**, 10775–10782.

Ruiz-Meana M, Garcia-Dorado D, Miró-Casas E, Abellán A & Soler-Soler J (2006). Mitochondrial Ca^{2+} uptake during simulated ischemia does not affect permeability transition pore opening upon simulated reperfusion. *Cardiovasc Res* **71**, 715–724.

Rutjanaprom W, Kanlop N, Charoenkwan P, Sittiwangkul R, Srichairatanakool S, Tantiworawit A, Phrommintikul A, Chattipakorn S, Fucharoen S & Chattipakorn N (2009). Heart rate variability in beta-thalassemia patients. *Eur J Haematol* **83**, 483–489.

Singh B, Arora S, Agrawal P & Gupta SK (2011). Hepcidin: a novel peptide hormone regulating iron metabolism. *Clin Chim Acta* **412**, 823–830.

Singh S, Hider RC & Porter JB (1990). A direct method for quantification of non-transferrin-bound iron. *Anal Biochem* **186**, 320–323.

Surinkaew S, Kumphune S, Chattipakorn S & Chattipakorn N (2013). Inhibition of p38 MAPK during ischemia, but not reperfusion, effectively attenuates fatal arrhythmia in ischemia/reperfusion heart. *J Cardiovasc Pharmacol* **61**, 133–141.

Thummasorn S, Kumfu S, Chattipakorn S & Chattipakorn N (2011). Granulocyte-colony stimulating factor attenuates mitochondrial dysfunction induced by oxidative stress in cardiac mitochondria. *Mitochondrion* **11**, 457–466.

© 2016 The Authors. Experimental Physiology © 2016 The Physiological Society

Tsushima RG, Wickenden AD, Bouchard RA, Oudit GY, Liu PP & Backx PH (1999). Modulation of iron uptake in heart by L-type Ca^{2+} channel modifiers: possible implications in iron overload. *Circ Res* **84**, 1302–1309.

van Acker FA, Boven E, Kramer K, Haenen GR, Bast A & van der Vijgh WJ (2001). Frederine, a new and promising protector against doxorubicin-induced cardiotoxicity. *Clin Cancer Res* **7**, 1378–1384.

Wang Y, Wu M, Al-Rousan R, Liu H, Fannin J, Paturi S, Arvapalli RK, Katta A, Kakarla SK, Rice KM, Triest WE & Blough ER (2011). Iron-induced cardiac damage: role of apoptosis and deferasirox intervention. *J Pharmacol Exp Ther* **336**, 56–63.

Wood JC, Enriquez C, Ghugre N, Otto-Duessel M, Aguilar M, Nelson MD, Moats R & Coates TD (2005). Physiology and pathophysiology of iron cardiomyopathy in thalassemia. *Ann N Y Acad Sci* **1054**, 386–395.

Zorov DB, Juhaszova M & Sollott SJ (2006). Mitochondrial ROS-induced ROS release: an update and review. *Biochim Biophys Acta* **1757**, 509–517.

Zurlo MG, De Stefano P, Borgna-Pignatti C, Di Palma A, Piga A, Melevendi C, Di Gregorio F, Burattini MG & Terzoli S (1989). Survival and causes of death in thalassaemia major. *Lancet* **2**, 27–30.

Additional information

Competing interests

None declared.

Author contributions

Conception and design of the study: S.K., S.C.C., S.F. and N.C. Performed the experiments, analysed data and wrote the initial draft of the manuscript: S.K. and N.C. Manuscript editing and final approval: S.K., S.C.C., S.F. and N.C.

Funding

This work was supported by grants from the Thailand Research Fund TRG5780002 (S.K.) and BRG5780016 (S.C.), the NSTDA Research Chair Grant from the National Science and Technology Development Agency Thailand (N.C.), The office of the Higher Education Commission and Mahidol University under the National Research Universities Initiative (S.F.), Chiang Mai University Center of Excellence Award (N.C.), the CMU Junior Research Fellowship Program, Chiang Mai University (S.K.) and the Faculty of Medicine Endowment Fund, Faculty of Medicine, Chiang Mai University (S.K.).

© 2016 The Authors. Experimental Physiology © 2016 The Physiological Society

เอกสารแนบหมายเลข 30

UNSOLICITED REVIEW

Cardiovascular Therapeutics

Potential Roles of Humanin on Apoptosis in the Heart

Savitree T. Charununtakorn,[1,2,3] Krekwit Shinlapawittayatorn,[1,2,3] Siriporn C. Chattipakorn[1,2,3,4] & Nipon Chattipakorn[1,2,3]

1 Cardiac Electrophysiology Research and Training Center, Faculty of Medicine, Chiang Mai University, Chiang Mai, Thailand
2 Cardiac Electrophysiology Unit, Department of Physiology, Faculty of Medicine, Chiang Mai University, Chiang Mai, Thailand
3 Center of Excellence in Cardiac Electrophysiology, Chiang Mai University, Chiang Mai, Thailand
4 Department of Oral Biology and Diagnostic Sciences, Faculty of Dentistry, Chiang Mai University, Chiang Mai, Thailand

Keywords
Apoptosis; Heart; Humanin; Oxidative stress.

Correspondence
Nipon Chattipakorn, M.D., Ph.D., Cardiac Electrophysiology Research and Training Center, Faculty of Medicine, Chiang Mai University, Chiang Mai 50200, Thailand.
Tel.: +66-53-935-329;
Fax: +66-53-935-368;
E-mail: nchattip@gmail.com

doi: 10.1111/1755-5922.12168

SUMMARY

The process of programmed cell death, or apoptosis, is known as a key player in the development and progression of cardiovascular disease. The proposed mechanism for apoptosis is the activation of two main apoptotic signaling pathways (the extrinsic and intrinsic pathways), which lead to cell death. As the rate and amount of cardiomyocyte loss is the most important determinant of patient morbidity and mortality, novel treatment strategies targeting apoptosis are crucial. Recently, Humanin has been shown to exert protective effects against cellular apoptosis in both experimental and clinical studies. The potential cardioprotective mechanisms of Humanin have been shown to involve both the extracellular and intracellular signaling pathways. In this review, the current knowledge and the mechanisms inhibiting cellular apoptosis by Humanin during cardiac injury are comprehensively summarized. In addition, both research and clinical findings regarding the effects of Humanin on the heart and vasculature are also presented and discussed. Currently available information suggests that Humanin may exert cardioprotective benefits and could potentially be used as a novel pharmacological intervention against cellular apoptosis during myocardial injury.

Introduction

Apoptosis is the process of programmed cell death occurring due to the activation of diverse signaling cascades, ultimately leading to cell death [1]. Under physiological conditions, apoptosis is a defense mechanism to destroy unnecessary cells. However, an excess of cellular apoptosis can cause pathological conditions in that organ and may result in a fatal outcome [1]. The morphological changes during the apoptotic process include cell shrinkage, chromatin condensation, and nuclear and DNA fragmentation [2,3]. Apoptosis plays an important role in various cardiovascular diseases including cardiac ischemia/reperfusion (I/R) injury [4]. I/R injury has been shown to induce myocardial damage and cause significant production of reactive oxygen species (ROS) [5]. This excessive production of ROS in turn activates the apoptotic signaling pathway, leading to cell death [6]. In the past decades, pharmacological intervention is one of several strategies that has been used to reduce the oxidative stress and apoptosis occurring during cardiac injury [7].

Humanin, a 24-amino acid polypeptide, was first discovered in 2001 by Hashimoto and his colleagues [8,9]. Growing evidence demonstrates that Humanin exerts protective effects against cellular apoptosis in several pathological conditions including cardiac injury, neurodegeneration, and diabetes mellitus [8–11]. It has been shown that Humanin, and its analogue, reduced apoptosis and cell death by binding to specific putative receptors such as formylpeptide receptor-like-1 (FPRL1) [12] and trimeric complex receptors (CNTFR, WSX-1 and gp130) [13]. Upon activation, each receptor initiates different downstream signaling cascades [12–15]. In addition to the direct activation of its receptors (extracellular pathway), Humanin has also been shown to prevent cellular apoptosis through the activation of the intracellular signaling pathway by inhibiting the translocation of pro-apoptotic proteins to the mitochondria [16,17]. Recently, two forms of Humanin with differing amino acid sequences (cytoplasmic form and mitochondrial form) have been clarified [9,18,19]. Evidence demonstrates that the cytoplasmic Humanin form is encoded in the nuclear genome and is translated within the cytoplasm [20], whereas the mitochondrial Humanin is encoded and translated within mitochondria [21]. When each type of Humanin is produced, they are secreted into the blood circulation and transported to several target cells which express Humanin receptors [9]. This process shows that Humanin acts like an endocrine signal. Interestingly, the mitochondrial Humanin cannot only act as an endocrine signal, but can also act like a paracrine signal via a retrograde signaling pathway [22]. Retrograde signaling is a novel concept of communication from the mitochondria to the cell that regulates intracellular activities such as energy production and apoptosis [23]. This finding was consistent with a previous study reported that Humanin prevented cellular apoptosis through the activation of an intracellular signaling pathway (an inactivation of pro-apoptotic proteins) [17]. Thus, the protective effect of Huma-

© 2015 John Wiley & Sons Ltd

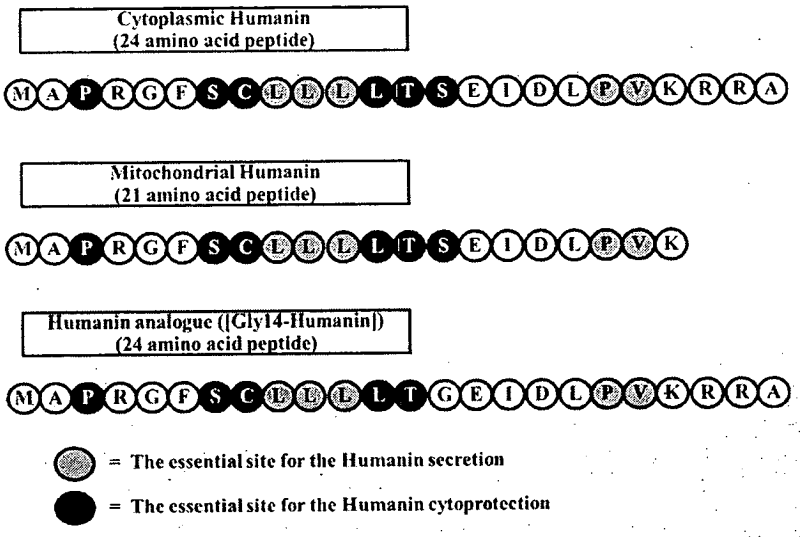


Figure 1 The amino acid sequence of human cytoplasmic Humanin, mitochondrial Humanin, and Humanin analogue. Although the amino acid sequence of Humanin differs slightly in the three forms of Humanin, they contain the same essential domains for Humanin secretion (gray amino acids) and cytoprotection (black amino acids). M, methionine; A, alanine; P, proline; R, arginine; G, glycine; F, phenylalanine; S, serine; C, cysteine; L, leucine; T, threonine; E, glutamic acid; I, isoleucine; D, aspartic acid; V, valine; K, lysine.

nin not only acts through an endocrine signal, but also acts similar to a paracrine signal, which regulates intracellular activity.

In the heart, growing evidence has demonstrated that Humanin exerts antioxidative effects, preserves cardiac mitochondrial function, and decreases apoptosis under several stressful conditions [11,24,25]. In this review, the currently available information regarding the potential effects of Humanin and its protective mechanisms against apoptosis during cardiac injury are comprehensively summarized and discussed.

Humanin, Humanin Receptors, and Apoptosis

In 2001, Hashimoto et al. discovered Humanin, a short-chain amino acid polypeptide, in the brain sections of a patient with Alzheimer's disease (AD) [8,9]. Under physiological conditions, endogenous Humanin is produced by tissues in several organs including the brain, heart, kidney, skeletal muscle, and liver [8,16,24,26,27]. Two forms of Humanin with differing amino acid sequences have been discovered. The cytoplasmic form is a 24-amino acid peptide [9,19], whereas the mitochondrial form is a 21-amino acid peptide [18]. Evidence demonstrates that the cytoplasmic Humanin form is encoded in the nuclear genome and is translated within the cytoplasm [20], whereas the mitochondrial Humanin is encoded and translated from an open reading frame (ORF) within the mitochondrial DNA which encodes for 16S RNA [21]. Although the sequence differs slightly between cytoplasmic and mitochondrial Humanin (Figure 1), they contain the same essential domains for Humanin secretion and cytoprotection [18,19,28]. When endogenous Humanin is produced by cells, it can be secreted into the blood circulation and transported to several target cells which express Humanin receptors [9]. As endogenous Humanin is naturally produced by several tissues in the body, this may allow Humanin to act in various cells with fewer side effects compared to other synthetic drugs. Recently, the Humanin analogue ([Gly14-Humanin]) was synthesized to elucidate the actions of endogenous Humanin in both *in vitro* and *in vivo* studies [12,14]. [Gly14-Humanin] is produced by an amino acid substitution at position 14 (Gly for Ser) [8]. Although the amino acid sequence of the Humanin analogue ([Gly14-Humanin]) differs slightly from the endogenous Humanin, they contain the same essential domains for Humanin secretion and cytoprotection (Figure 1) [18,19,28]. Previous studies have demonstrated that the effects of [Gly14-Humanin] were 1000-fold more potent than of the endogenous Humanin against AD-relevant insults [8,9]. The higher potency of [Gly14-Humanin] has been shown to be due to an augmentation in maintaining an active conformation of endogenous Humanin through D-isomerization [29].

One of the cytoprotective effects of Humanin is its anti-apoptotic effect. Several studies have shown that Humanin mediates its effects through the extracellular (Humanin receptors) [12,14,15] and/or intracellular pathways (a mitochondrial-mediated pathway) [20]. The Humanin extracellular pathway depends on specific receptors such as G protein-coupled formylpeptide receptor-like-1 (FPRL1) or trimeric complex receptors [12–15]. The Humanin receptors have patterns of expression that vary by tissue. It has been shown that FPRL1 and trimeric complex receptors are expressed in neuronal cells [12–15,30]. In contrast, only the expression of trimeric complex receptors was detected in cardiac cells [31].

Upon activation by Humanin, it has been shown that each receptor initiates different downstream signaling cascades [12–15]. Currently, at least five different pathways have been identified. For example, Ying et al. demonstrated that Humanin prevented A_β-induced cell death by competitively inhibiting the binding of A_β to FPRL1 [32]. They found that Humanin interacted

© 2015 John Wiley & Sons Ltd

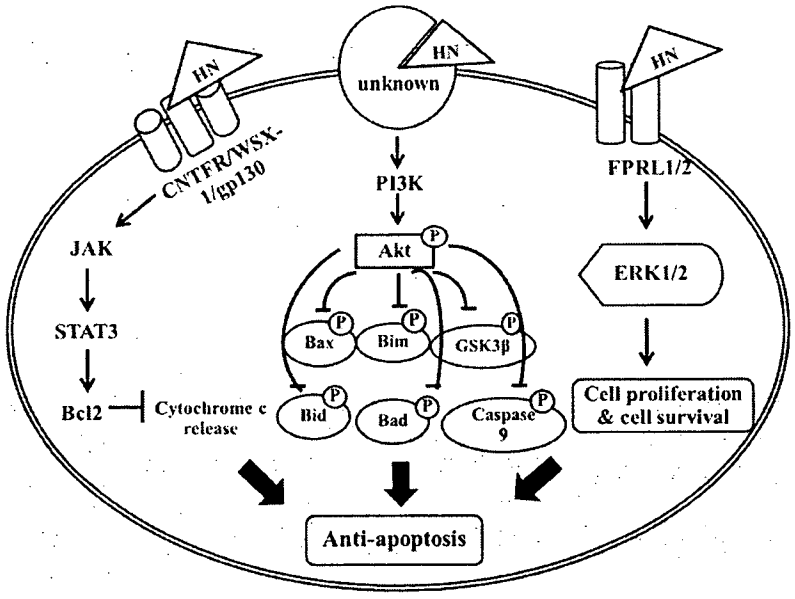


Figure 2 The anti-apoptotic effects of Humanin through the extracellular signaling pathways. During stress conditions, Humanin mediates its effects through the different receptors and its signaling pathways. Interaction of Humanin with FPRL1 activates the ERK1/2 signaling pathway and leads to cell proliferation. Moreover, Humanin can activate the PI3K/Akt pathway and lead to the inactivation of a pro-apoptotic protein. However, the receptor which is mediated by humanin and activates the PI3K/Akt pathway is unknown. Thus, the identity of this receptor must be discovered to aid the research into Humanin's cytoprotective effects. In addition to FPRL1, Humanin also activates the JAK and STAT3 signaling pathways through the trimeric complex receptors. Although the three pathways are different, they all have the same final result: initiating the anti-apoptotic effect. FPRL1, formyl peptide receptor-like1; CNTFR, WSX-1 and gp130, trimeric complex receptors; HN, Humanin.

with FPRL1 and activated the downstream signaling cascade through the ERK1/2 signaling pathway, leading to an anti-apoptotic effect and improved cell survival [32]. Furthermore, an *in vivo* study also showed that Humanin protected neuronal function and cell death via ERK signaling in mice with stroke, leading to cell proliferation and cell survival (Figure 2) [33].

In addition, the protective effect of Humanin showed that Humanin reduced neuronal cell death through the PI3K/Akt pathway [14]. In this study, Humanin activated PI3K and subsequently led to Akt activation [14]. As a downstream signaling pathway of Akt is the inactivation of pro-apoptotic proteins including Bad, Bax, Bim, Bid, and caspase9 [34,35], Humanin effect might improve cell survival through the activation of the PI3K/Akt pathway (Figure 2) [14]. Moreover, Humanin can also reduce apoptosis through the PI3K-Akt/GSK3β signaling pathway, which was seen in an intracerebral hemorrhage (ICH) model [30]. Humanin was shown to increase p-Akt and Bcl-2 level, and decrease p-GSK3β and caspase3 level, leading to improved cell survival in this condition [30] (Figure 2). However, the identity of the receptor which is mediated by Humanin and which activates the PI3K/Akt pathway is still unknown. Thus, the identity of this receptor must be discovered to aid the research into Humanin's cytoprotective effects (Figure 2). Although the effect of Humanin through the PI3K-Akt signaling pathway has been shown in neuronal cells [14,30], whether this holds true in the heart remains to be investigated.

The trimeric complex receptors (CNTFR, WSX-1, and gp130) are the novel Humanin receptors discovered by Hashimoto et al.[13]. In *in vitro* studies, the activation of the trimeric complex receptors by Humanin led to the activation of the JAK and STAT3 signaling pathways [13,36]. Similarly, an *in vivo* study also showed that the interaction of Humanin and its receptors (CNTFR, WSX-1, and gp130) could activate the STAT3 signaling pathway via an increase in STAT3 expression and consequently lead to the increase of beta cell survival in the pancreas [37]. The summary of the extracellular pathways of Humanin including the action of its receptors against apoptosis are shown in Figure 2.

In addition to the extracellular signaling pathways, the anti-apoptotic effects of Humanin can also mediate through the intracellular signaling pathway, known as the mitochondrial-mediated apoptotic pathway, in which pro-apoptotic proteins such as Bax, Bid, and Bim are inactivated [12,16,17,38]. An *in vitro* study has shown that Humanin can prevent apoptosis by inhibiting the translocation of Bax protein to the mitochondria [12]. As mitochondria play an important role in the apoptotic process, preserving mitochondrial function by inhibiting cytochrome c release from the mitochondria is an important mechanism in the prevention of apoptosis [39,40]. An *in vitro* study by Guo et al. demonstrated that a Humanin peptide suppressed apoptosis by interfering with Bax activation [20]. Similarly, an *in vivo* study showed that Humanin decreased apoptosis by decreasing Bax activity, which led to a decrease in Bax translocation [24]. Moreover, Luciano et al. have reported that Bim, a pro-apoptotic protein family, is an additional target protein for Humanin. In particular, Humanin could bind and inactivate the Bim protein and evoke the inhibition of BimEL-induced cytochrome c release

© 2015 John Wiley & Sons Ltd

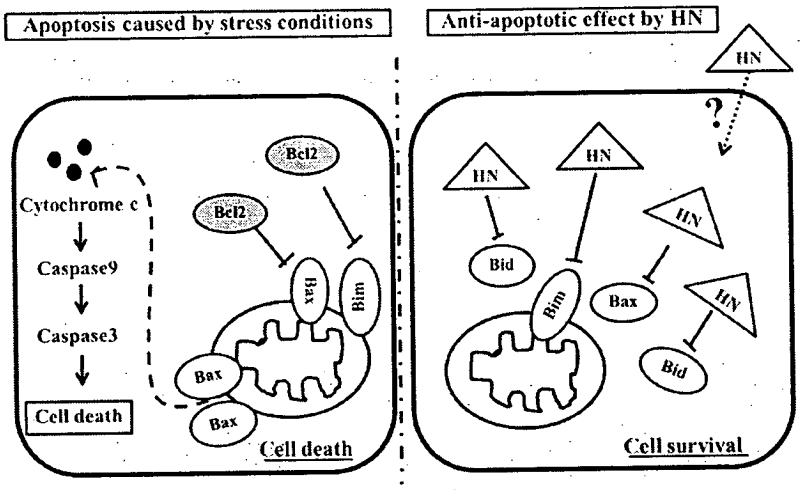


Figure 3 The anti-apoptotic effects of Humanin through the intracellular signaling pathway. During stress conditions, pro-apoptotic proteins such as Bax, Bim, and Bid are translocated from the cytoplasm to the mitochondrial membrane. Afterward, these pro-apoptotic proteins form a large pore where cytochrome c is released from the mitochondria into the cytoplasm. Finally, an apoptotic signaling cascade is initiated. When Humanin is administered, it can mediate the anti-apoptotic effect by causing the inactivation of several pro-apoptotic proteins. HN, Humanin.

from mitochondria [17]. However, it is still unclear whether the endogenous Humanin is transported from neighboring cells via direct penetration through the cell membrane, or produced within the cells. Thus, further studies are required to elucidate the mechanism of Humanin on the intracellular signaling pathways. The summary of the action of intracellular signaling pathways of Humanin against apoptosis is shown in Figure 3.

Effects of Humanin on Oxidative Stress and Apoptosis in the Heart: Bench Evidence

Endogenous Humanin levels have been shown to increase in cardiovascular disease [24]. Muzumdar et al. demonstrated that levels of plasma endogenous Humanin were increased after myocardial ischemia/reperfusion (I/R) injury [24]. It is known that myocardial I/R injury can cause myocardial damage due to a marked increase in mitochondrial ROS levels, and this can lead to severe oxidative stress [41]. It is possible that this marked increase in mitochondrial ROS levels may act to recruit Humanin from several tissues in the body to damaged areas such as the ischemic myocardium. Thus, the increased plasma Humanin levels could be the body response to a marked increase in mitochondrial ROS levels caused by myocardial I/R injury [24]. Evidence demonstrates that Humanin exerts an antioxidative stress action and this effect could help preserve cell survival [11]. In human aortic endothelial cells (HAECs), Humanin has been shown to prevent apoptosis by decreasing the ROS production [25]. In cultured H9c2 cell line, Humanin significantly decreased the oxidative stress induced by H_2O_2 application, preserved mitochondrial function, and attenuated cellular apoptosis via decreasing ROS level [11]. These effects could be responsible for the effects of Humanin in increasing H9c2 cell viability [11]. Currently, the precise mechanism underlying the effects of Humanin on cell viability in the heart, whether it occurs via the activation of survival pathways in the cells, or by a decrease in the degree of apoptosis, or both is still unclear. Further investigation is needed to elucidate this mechanism. A summary of currently available information regarding the effects of Humanin on oxidative stress and cellular apoptosis from *in vitro* studies is shown in Table 1.

In addition to *in vitro* reports, evidence from *in vivo* studies regarding the anti-apoptotic effects of Humanin also exists. In mice subjected to 45-min ischemia and 24-h reperfusion, Humanin administered prior to ischemia has been shown to reduce the infarct size in a dose-dependent manner, resulting in improved cardiac function [24]. It was found that Humanin significantly decreased apoptosis by increasing the expression of p-AMPK and p-eNOS, as well as attenuating Bax expression following I/R injury [24]. Moreover, p-STAT3 level was increased in the Humanin-treated group, when compared to the control group [24].

In the heart, Humanin mediates its action through an extracellular signaling pathway (which involves Humanin receptors) by interacting with the trimeric complex receptors (CNTFR, WSX-1, and gp130) [31]. Activation of one of these receptors (gp130) was shown to activate the JAK/STAT3 signaling pathway in cardiomyocytes [42]. Consequently, the AMPK/eNOS signaling pathway was activated as a result of the downstream signaling cascade of this interaction.[24,43] eNOS is known to inhibit the opening of mitochondrial permeability transition pores (mPTP), leading to the suppression of cytochrome c release [44]. These findings were consistent with the results seen in the thoracic aorta, when Oh et al. showed that Humanin reduced apoptosis by increasing the expression of eNOS [43]. Currently, only the anti-apoptosis effect of Humanin through the AMPK/eNOS signaling pathway was shown in the heart. Future studies are needed to investigate whether Humanin could act through other signaling pathways such as PI3K/Akt pathway and JAK/STAT3 pathway in the heart. In addition to the extracellular signaling pathway, Humanin may mediate its cardioprotective effects through the intracellular sig-

© 2015 John Wiley & Sons Ltd

Table 1 The effects of Humanin on oxidative stress and cellular apoptosis in the heart: the summary of *in vitro* studies

Study model	Study protocol	Drug/dose/route	Major findings	Interpretation	References
Aortic endothelial cells (HAECs)	Cell culture with Ox-LDL-induced apoptosis (100 mg/mL)	Humanin analogue (0.1 μM) pretreatment	Humanin analogue significantly 1) decreased Ox-LDL-induced ROS production 2) decreased Ox-LDL-induced apoptosis	Humanin analogue prevented Ox-LDL-induced oxidative stress and apoptosis.	[25]
H9c2 cell line	Cell culture with H_2O_2 – induced apoptosis	Co-incubation of Humanin analogue (10 nM) with H_2O_2 (100 μM) for 30 min	Humanin analogue significantly 1) decreased ROS production 2) decreased mitochondrial depolarization 3) increased ATP production 4) preserved mitochondrial integrity	Humanin analogue prevented H_2O_2-induced oxidative stress and apoptosis via restoring mitochondrial function.	[11]
H9c2 cell line	Cells with daunorubicin-induced apoptosis	Incubation of Humanin analogue (1 nM) prior to daunorubicin application	Humanin analogue increased cell survival and decreased apoptosis.	Humanin analogue decreased apoptosis and increased cell viability against daunorubicin-induced apoptosis.	[24]

Ox-LDL, Oxidized -low density lipoprotein; ROS, Reactive oxygen species.

naling pathway. It has been demonstrated that Humanin suppressed Bax activation by directly inactivating Bax proteins, and consequently leading to the decrease in the apoptotic process; however, this has only been shown in kidney and human colon cancer cell lines [17,20]. Further studies are needed to show whether this still applies in cardiomyocytes. The proposed mechanisms of Humanin action against apoptosis via the activation of both extracellular and intracellular pathways are summarized in Figure 4. The currently available information regarding the anti-apoptotic effects of Humanin on the heart in *in vivo* studies is also summarized in Table 2.

Clinical Evidence Regarding the Effects of Humanin on the Heart and Vasculature

Current clinical reports are in support of the basic studies regarding the anti-apoptotic and antioxidative stress effects of Humanin on the heart and vasculature [25,45,46]. One of the dominant causes of cardiovascular disease is atherosclerosis [47,48], and oxidative stress-induced apoptosis has been implicated in the pathogenesis of atherosclerosis [49]. The increased ROS level during the development of atherosclerosis has been shown to induce cellular apoptosis and activate several pro-inflammatory cytokines [49], leading to the formation of atherosclerotic plaque [49]. Inhibition of the ROS formation in the atherosclerotic plaque has been shown to decrease cellular apoptosis and the progression of atherosclerosis [49]. Interestingly, Bachar et al. demonstrated that the endogenous Humanin may exert protective effects against atherosclerosis by attenuating ROS formation and apoptosis in human endothelial coronary arteries [25]. Furthermore, in the *in vitro* study, exogenously added Humanin also exerted cytoprotective effects against ROS and apoptosis in Human Aortic Endothelial Cells (HAECs) [25]. These findings suggested that endogenous Humanin may play an important role as a defensive

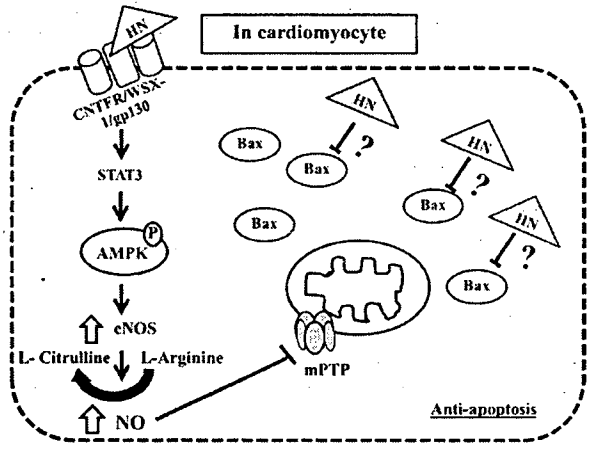


Figure 4 The anti-apoptotic effects of Humanin on the heart through the extracellular and intracellular signaling pathway. In the heart, Humanin mediates its beneficial effects through the extracellular signaling pathway (which involves Humanin receptors) by the interaction between Humanin and trimeric complex receptors (CNTFR, WSX-1, and gp130). Consequently, the AMPK/eNOS signaling pathway is activated in response to Humanin. However, the intracellular signaling pathway of Humanin action on the heart has not been studied. Thus, it is essential that its cardioprotective effect via the intracellular signaling pathway is studied in the future. STAT3, signal transduction and transcription; AMPK 5′, adenosine monophosphate-activated protein kinase; eNOS, endothelial nitric oxide synthase; NO, nitric oxide; mPTP, mitochondrial permeability transition pore; HN, Humanin.

anti-apoptotic mechanism in human endothelial coronary arteries during the pathogenesis of atherosclerosis [25]. Growing bodies of evidence also suggest that Humanin may be used as a potential cardiac biomarker for early detection of cardiac injury [25,45,46]. It is well known that the incidence of all forms of atherosclerosis

© 2015 John Wiley & Sons Ltd

Table 2 The effects of Humanin on oxidative stress and cellular apoptosis in the heart: the summary of *in vivo* studies

Study model	Study protocol	Drug/dose/route	Major findings	Interpretation	References
Mice/heart	Ischemia induced by left coronary artery ligation for 45 min, followed by 24-h reperfusion	Humanin analogue treatment (2 mg/kg, IP) given 1 h prior to ischemia	Humanin analogue significantly 1) reduced infarct size and improved cardiac function 2) attenuated Bax protein levels in heart tissues 3) increased phosphorylation of AMPK and eNOS in heart tissues	Humanin analogue decreased apoptosis and protected myocardial I/R injury through the activation of AMPK-eNOS signaling.	[24]
ApoE-deficient mice/endothelial cell	Atherosclerotic arteries induced by high cholesterol diet (HC, 0.15% cholesterol and 42% milk fat by weight) administration for 16 weeks	Humanin analogue (0.4 mg/kg/day) or vehicle administration, IP injection for 16 weeks	Humanin analogue treatment significantly 1) reduced apoptosis in the thoracic aorta 2) increased eNOS expression in the thoracic aorta	Humanin analogue protected endothelial function and cell viability via increasing eNOS expression under atherosclerotic conditions induced by hypercholesterolemia.	[43]

IP, Intraperitoneal; I/R, Ischemic reperfusion; ApoE, Apolipoprotein E.

Table 3 The effects of Humanin on the heart and vasculature: the summary of clinical reports

Types of patients	Study model	Major findings	Interpretation	References
Patients who died from an atherosclerotic coronary event (N = 25) Healthy volunteers (N = 32)	Samples were obtained from internal mammary arteries (n = 5), atherosclerotic coronary arteries (n = 17), and greater saphenous vein (n = 3). Blood samples were collected from 16 younger healthy volunteers (mean age = 39 ± 4) and 16 older healthy volunteers (mean age = 60 ± 6)	1) Endogenous Humanin was detected in the atherosclerotic human vasculature. 2) In vitro study, Humanin pretreatment attenuated ROS production and apoptosis in HAECs treated with Ox-LDL. Levels of endogenous Humanin in the plasma were decreased in older healthy volunteers, when compared with the younger healthy volunteers.	Endogenous Humanin exerted protective effects against atherosclerosis by attenuating ROS production and apoptosis. Level of endogenous Humanin in the plasma was associated with an increase in oxidative stress and atherosclerosis in aging.	[25]
Patients with coronary artery disease (n = 40)	Blood samples were collected from patients with early stages of coronary artery disease.	Level of endogenous Humanin was decreased in patients with coronary endothelial dysfunction compared to normal endothelial function.	Circulating Humanin levels were associated with preserved coronary endothelial function.	[45]
Patients with coronary artery disease (N = 34)	Plaque specimens (vessel tissues) were obtained from patients undergoing carotid endarterectomy.	1) Expression of endogenous Humanin was increased in the unstable plaques of symptomatic compared to asymptomatic patients. 2) The level of apoptotic markers in the plaques of symptomatic patients was higher compared to asymptomatic.	Endogenous Humanin levels were up regulated in plaque specimens of the patients with atherosclerosis as an endogenous response to the apoptotic process.	[46]

ROS, Reactive oxygen species; Ox-LDL, Oxidized-low density lipoprotein.

increases with age [50]. A recent study demonstrated that the level of plasma Humanin decreased significantly in older healthy volunteers compared with the younger healthy volunteers and therefore may be associated with the increased risk of atherosclerotic progression in elderly individuals. This finding suggests that the decrease in plasma Humanin level may be used as a biomarker for the early development of atherosclerosis [25]. This is consistent with the results of another clinical study, which showed that the levels of plasma Humanin were significantly decreased in patients with coronary endothelial dysfunction when compared to patients with normal endothelial function [45]. It is possible that the endogenous Humanin levels act to preserve coronary endothelial function and that its attenuation may lead to the development of atherosclerotic coronary disease [45]. However,

© 2015 John Wiley & Sons Ltd

Zacharias et al. demonstrated that the endogenous Humanin levels in plaque specimens were higher in symptomatic compared to asymptomatic patients [46]. In this study, plaque specimens (vessel tissues of patients) were obtained from patients with coronary artery disease (CAD), and it was found that the level of an apoptotic marker (DNA fragmentation by TUNEL assay) in the plaques of symptomatic patients was higher compared to the asymptomatic subjects [46]. A possible reason for this discrepancy might be due to the differences in the stage and severity of the disease. Specifically, a study by Widmer et al. recruited patients with early-stage coronary atherosclerosis [45]. The decrease in plasma Humanin levels may be due to an overuse of the Humanin by the affected tissues following the stressful conditions in the early stages of disease progression. In contrast, Zacharias et al. recruited patients with late-stage coronary atherosclerosis (symptomatic patients). During the late stages of atherosclerosis, the increased endogenous Humanin levels found could be a compensatory response to conditions of chronic stress. Further studies are needed to test this hypothesis. A comprehensive summary of clinical reports regarding the effects of Humanin on the heart and vasculature is shown in Table 3. As limited clinical information is available at this time regarding the effects of Humanin on the heart, further investigation is required to understand the effects of Humanin and its underlying protective mechanism against cardiac injury.

Conclusions and Prospects

During the progression of cardiovascular disease, the level of oxidative stress is dramatically increased, leading to cellular apoptosis. Evidence from *in vitro, in vivo,* and clinical studies suggests that Humanin may exert potential cardioprotective effects against oxidative stress and cellular apoptosis. Clinical reports also suggest that Humanin may be a potential biomarker for the early detection of cardiovascular injury. Currently, limited information on Humanin is available, therefore more studies are needed to investigate and substantiate its cardiovascular effects as well as to elucidate the underlying mechanism for the potential beneficial effects of Humanin.

Acknowledgments

This work was supported by the NSTDA Research Chair Grant from the National Science and Technology Development Agency Thailand (NC), the Thailand Research Fund Royal Golden Jubilee PhD program (STC and NC), the Thailand Research Fund RSA5880015 (KS), BRG5780016 (SCC), and the Chiang Mai University Center of Excellence Award (NC).

Conflict of Interest

The authors declare no conflict of interest.

Author Contributions

Savitree T. Charununtakorn involved in critical literature review, drafting of the article, and approval of the article. Krekwit Shinlapawittayatorn contributed in critical manuscript review, approval of the article. Siriporn C. Chattipakorn and Nipon Chattipakorn participated in critical literature review, critical manuscript review, approval of the article.

References

1. Orogo AM, Gustafsson AB. Cell death in the myocardium: my heart won't go on. *IUBMB Life* 2013;**65**:651–656.
2. Walker PR, Kokileva L, LeBlanc J, Sikorska M. Detection of the initial stages of DNA fragmentation in apoptosis. *Biotechniques* 1993;**15**:1032–1040.
3. Oberhammer F, Wilson JW, Dive C, et al. Apoptotic death in epithelial cells: cleavage of DNA to 300 and/or 50 kb fragments prior to or in the absence of internucleosomal fragmentation. *EMBO J* 1993;**12**:3679–3684.
4. Melberg T, Burman R, Dickstein K. The impact of the 2007 ESC-ACC-AHA-WHF Universal definition on the incidence and classification of acute myocardial infarction: a retrospective cohort study. *Int J Cardiol* 2010;**139**:228–233.
5. Elahi MM, Kong YX, Matata BM. Oxidative stress as a mediator of cardiovascular disease. *Oxid Med Cell Longev* 2009;**2**:259–269.
6. Becker LB. New concepts in reactive oxygen species and cardiovascular reperfusion physiology. *Cardiovasc Res* 2004;**61**:461–470.
7. Fischer U, Schulze-Osthoff K. New approaches and therapeutics targeting apoptosis in disease. *Pharmacol Rev* 2005;**57**:187–215.
8. Hashimoto Y, Ito Y, Niikura T, et al. Mechanisms of neuroprotection by a novel rescue factor humanin from Swedish mutant amyloid precursor protein. *Biochem Biophys Res Commun* 2001;**283**:460–468.
9. Hashimoto Y, Niikura T, Tajima H, et al. A rescue factor abolishing neuronal cell death by a wide spectrum of familial Alzheimer's disease genes and Abeta. *Proc Natl Acad Sci USA* 2001;**98**:6336–6341.
10. Muzumdar RH, Huffman DM, Atzmon G, et al. Humanin: a novel central regulator of peripheral insulin action. *PLoS One* 2009;**4**:e6334.
11. Klein LE, Cui L, Gong Z, Su K, Muzumdar R. A humanin analog decreases oxidative stress and preserves mitochondrial integrity in cardiac myoblasts. *Biochem Biophys Res Commun* 2013;**440**:197–203.
12. Harada M, Habata Y, Hosoya M, et al. N-Formylated humanin activates both formyl peptide receptor-like 1 and 2. *Biochem Biophys Res Commun* 2004;**324**:255–261.
13. Hashimoto Y, Kurita M, Aiso S, Nishimoto I, Matsuoka M. Humanin inhibits neuronal cell death by interacting with a cytokine receptor complex or complexes involving CNTF receptor alpha/WSX-1/gp130. *Mol Biol Cell* 2009;**20**:2864–2873.
14. Xu X, Chua CC, Gao J, et al. Neuroprotective effect of humanin on cerebral ischemia/reperfusion injury is mediated by a PI3K/Akt pathway. *Brain Res* 2008;**1227**:12–18.
15. Hashimoto Y, Suzuki H, Aiso S, Niikura T, Nishimoto I, Matsuoka M. Involvement of tyrosine kinases and STAT3 in Humanin-mediated neuroprotection. *Life Sci* 2005;**77**:3092–3104.
16. Jia Y, Lue YH, Swerdloff R, et al. The cytoprotective peptide humanin is induced and neutralizes Bax after pro-apoptotic stress in the rat testis. *Andrology* 2013;**1**:651–659.
17. Luciano F, Zhai D, Zhu X, et al. Cytoprotective peptide humanin binds and inhibits proapoptotic Bcl-2/Bax family protein BimEL. *J Biol Chem* 2005;**280**:15825–15835.
18. Maximov V, Martynenko A, Hunsmann G, Tarantul V. Mitochondrial 16S rRNA gene encodes a functional peptide, a potential drug for Alzheimer's disease and target for cancer therapy. *Med Hypotheses* 2002;**59**:670–673.
19. Yamagishi Y, Hashimoto Y, Niikura T, Nishimoto I. Identification of essential amino acids in Humanin, a neuroprotective factor against Alzheimer's disease-relevant insults. *Peptides* 2003;**24**:585–595.

© 2015 John Wiley & Sons Ltd

20. Guo B, Zhai D, Cabezas E, et al. Humanin peptide suppresses apoptosis by interfering with Bax activation. *Nature* 2003;**423**:456–461.
21. Paharkova V, Alvarez G, Nakamura H, Cohen P, Lee KW. Rat Humanin is encoded and translated in mitochondria and is localized to the mitochondrial compartment where it regulates ROS production. *Mol Cell Endocrinol* 2015;**413**:96–100.
22. Lee C, Yen K, Cohen P. Humanin: a harbinger of mitochondrial-derived peptides? *Trends Endocrinol Metab* 2013;**24**:222–228.
23. Verdin E, Hirschey MD, Finley LW, Haigis MC. Sirtuin regulation of mitochondria: energy production, apoptosis, and signaling. *Trends Biochem Sci* 2010;**35**:669–675.
24. Muzumdar RH, Huffman DM, Calvert JW, et al. Acute humanin therapy attenuates myocardial ischemia and reperfusion injury in mice. *Arterioscler Thromb Vasc Biol* 2010;**30**:1940–1948.
25. Bachar AR, Scheffer L, Schroeder AS, et al. Humanin is expressed in human vascular walls and has a cytoprotective effect against oxidized LDL-induced oxidative stress. *Cardiovasc Res* 2010;**88**:360–366.
26. Chin YP, Keni J, Wan J, et al. Pharmacokinetics and tissue distribution of humanin and its analogues in male rodents. *Endocrinology* 2013;**154**:3739–3744.
27. Kin T, Sugie K, Hirano M, Goto Y, Nishino I, Ueno S. Humanin expression in skeletal muscles of patients with chronic progressive external ophthalmoplegia. *J Hum Genet* 2006;**51**:555–558.
28. Anderson S, Bankier AT, Barrell BG, et al. Sequence and organization of the human mitochondrial genome. *Nature* 1981;**290**:457–465.
29. Terashita K, Hashimoto Y, Niikura T, et al. Two serine residues distinctly regulate the rescue function of Humanin, an inhibiting factor of Alzheimer's disease-related neurotoxicity: functional potentiation by isomerization and dimerization. *J Neurochem* 2003;**85**:1521–1538.
30. Wang T, Huang Y, Zhang M, et al. [Gly14]-Humanin offers neuroprotection through glycogen synthase kinase-3beta inhibition in a mouse model of intracerebral hemorrhage. *Behav Brain Res* 2013;**247**:132–139.
31. Fischer P, Hilfiker-Kleiner D. Role of gp130-mediated signalling pathways in the heart and its impact on potential therapeutic aspects. *Br J Pharmacol* 2008;**153**(Suppl 1):S414–S427.
32. Ying G, Iribarren P, Zhou Y, et al. Humanin, a newly identified neuroprotective factor, uses the G protein-coupled formylpeptide receptor-like-1 as a functional receptor. *J Immunol* 2004;**172**:7078–7085.
33. Xu X, Chua CC, Gao J, Hamdy RC, Chua BH. Humanin is a novel neuroprotective agent against stroke. *Stroke* 2006;**37**:2613–2619.
34. Kuwahara K, Saito Y, Kishimoto I, et al. Cardiotrophin-1 phosphorylates akt and BAD, and prolongs cell survival via a PI3K-dependent pathway in cardiac myocytes. *J Mol Cell Cardiol* 2000;**32**:1385–1394.
35. Pastukh V, Ricci C, Solodushko V, Mozaffari M, Schaffer SW. Contribution of the PI 3-kinase/Akt survival pathway toward osmotic preconditioning. *Mol Cell Biochem* 2005;**269**:59–67.
36. Takeshita Y, Hashimoto Y, Nawa M, Uchino H, Matsuoka M. SH3-binding protein 5 mediates the neuroprotective effect of the secreted bioactive peptide humanin by inhibiting c-Jun NH2-terminal kinase. *J Biol Chem* 2013;**288**:24691–24704.
37. Hoang PT, Park P, Cobb LJ, et al. The neurosurvival factor Humanin inhibits beta-cell apoptosis via signal transducer and activator of transcription 3 activation and delays and ameliorates diabetes in nonobese diabetic mice. *Metabolism* 2010;**59**:343–349.
38. Choi J, Zhai D, Zhou X, Satterthwait A, Reed JC, Marassi FM. Mapping the specific cytoprotective interaction of humanin with the pro-apoptotic protein bid. *Chem Biol Drug Des* 2007;**70**:383–392.
39. Chen Q, Lesnefsky EJ. Heart mitochondria and calpain 1: location, function, and targets. *Biochim Biophys Acta* 2015;**1852**:2372–2378.
40. Biala AK, Kirshenbaum LA. The interplay between cell death signaling pathways in the heart. *Trends Cardiovasc Med* 2014;**24**:325–331.
41. Ong SB, Gustafsson AB. New roles for mitochondria in cell death in the reperfused myocardium. *Cardiovasc Res* 2012;**94**:190–196.
42. Cittadini A, Monti MG, Iaccarino G, et al. SOCS1 gene transfer accelerates the transition to heart failure through the inhibition of the gp130/JAK/STAT pathway. *Cardiovasc Res* 2012;**96**:381–390.
43. Oh YK, Bachar AR, Zacharias DG, et al. Humanin preserves endothelial function and prevents atherosclerotic plaque progression in hypercholesterolemic ApoE deficient mice. *Atherosclerosis* 2011;**219**:65–73.
44. Fontaine E, Eriksson O, Ichas F, Bernardi P. Regulation of the permeability transition pore in skeletal muscle mitochondria. Modulation By electron flow through the respiratory chain complex i. *J Biol Chem* 1998;**273**:12662–12668.
45. Widmer RJ, Flammer AJ, Herrmann J, et al. Circulating humanin levels are associated with preserved coronary endothelial function. *Am J Physiol Heart Circ Physiol* 2013;**304**:H393–H397.
46. Zacharias DG, Kim SG, Massat AE, et al. Humanin, a cytoprotective peptide, is expressed in carotid atherosclerotic [corrected] plaques in humans. *PLoS One* 2012;**7**:e31065.
47. Diehl P, Bode C, Duerschmied D. Clinical potential of vorapaxar in cardiovascular risk reduction in patients with atherosclerosis. *Ther Clin Risk Manag* 2015;**11**:1133–1138.
48. Hansson GK. Atherosclerosis–an immune disease: the Anitschkov Lecture 2007. *Atherosclerosis* 2009;**202**:2–10.
49. Bluestone JA, Herold K, Eisenbarth G. Genetics, pathogenesis and clinical interventions in type 1 diabetes. *Nature* 2010;**464**:1293–1300.
50. Gong Z, Tas E, Muzumdar R. Humanin and age-related diseases: a new link? *Front Endocrinol (Lausanne)* 2014;**5**:210.

© 2015 John Wiley & Sons Ltd

เอกสารแนบหมายเลข 31

SCIENTIFIC REPORTS

OPEN

Vagus Nerve Stimulation Improves Cardiac Function by Preventing Mitochondrial Dysfunction in Obese-Insulin Resistant Rats

Received: 28 August 2015
Accepted: 17 December 2015
Published: 01 February 2016

Bencharunan Samniang[1,2,3,*], Krekwit Shinlapawittayatorn[1,2,3,*], Titikorn Chunchai[1,2,3], Wanpitak Pongkan[1,2,3], Sirinart Kumfu[1,2,3], Siriporn C. Chattipakorn[1,2,3,4], Bruce H. KenKnight[5] & Nipon Chattipakorn[1,2,3]

Long-term high-fat diet (HFD) consumption leads to not only obese-insulin resistance, but also impaired left ventricular (LV) function. Vagus nerve stimulation (VNS) has been shown to exert cardioprotection. However, its effects on the heart and metabolic parameters under obese-insulin resistant condition is not known. We determined the effects of VNS on metabolic parameters, heart rate variability (HRV) and LV function in obese-insulin resistant rats. Male Wistar rats were fed with HFD for 12 weeks, and were randomly divided into sham and VNS groups. VNS was applied for the next 12 weeks. Echocardiography, blood pressure and HRV were examined. Blood samples were collected for metabolic parameters. At the end, the heart was removed for determination of apoptosis, inflammation, oxidative stress, and cardiac mitochondrial function. VNS for 12 weeks significantly decreased plasma insulin, HOMA index, total cholesterol, triglyceride, LDL and visceral fat. Serum adiponectin was significantly increased in the VNS group. VNS also significantly decreased blood pressure, improved HRV and LV function, decreased cardiac MDA, TNF-α and Bax levels, and improved cardiac mitochondrial function. VNS improves metabolic and hemodynamic parameters, and the LV function via its ability against apoptosis, inflammation and oxidative stress, and preserved cardiac mitochondrial function in obese-insulin resistant rats.

Obesity rates have drastically increased across all age and socio-economic groups around the world[1]. Obesity is also an important factor that leads to the development of the metabolic syndrome which includes a constellation of risk factors for cardiovascular disease such as insulin resistance, dyslipidemia, hyperglycemia and hypertension[2], and contributes to increased morbidity and mortality in the affected patients[3]. Growing evidence also demonstrates that increased inflammation and oxidative stress play a key role in metabolic syndrome[4,5]. Moreover, abnormal production and secretion of adipokines has been observed in metabolic syndrome[6]. It has been shown that all of these parameters can cause a decreased parasympathetic activity and increased risk of cardiovascular disease[7].

Although pharmacological agents still play a vital role in both metabolic syndrome and cardiovascular disease treatments, they could cause serious adverse effects[8]. Growing evidence demonstrates that augmenting parasympathetic activity by vagus nerve stimulation (VNS) exerted a wide range of beneficial effects including cardioprotection and maintaining metabolic homeostasis[9–12]. Specifically, VNS has been shown to improve left ventricular (LV) function and prevent cardiac arrhythmia in a model of acute myocardial infarction through its anti-inflammatory and anti-apoptosis effects[11–14]. In addition to its cardioprotective effects, VNS has been shown to exert the beneficial effect in maintaining metabolic homeostasis by reducing the two-hour glucose tolerance in

[1]Cardiac Electrophysiology Research and Training Center, Faculty of Medicine, Chiang Mai University, Chiang Mai, 50200, Thailand. [2]Cardiac Electrophysiology Unit, Department of Physiology, Faculty of Medicine, Chiang Mai University, Chiang Mai, 50200, Thailand. [3]Center of Excellence in Cardiac Electrophysiology, Faculty of Medicine, Chiang Mai University, Chiang Mai, 50200, Thailand. [4]Department of Oral Biology and Diagnostic Sciences, Faculty of Dentistry, Chiang Mai University, Chiang Mai, 50200, Thailand. [5]Emerging Therapies, Cyberonics Inc, Houston, Texas, USA. *These authors contributed equally to this work. Correspondence and requests for materials should be addressed to N.C. (email: nchattip@gmail.com)

the impaired glucose tolerance patients[10]. Furthermore, chronic VNS has been shown to cause weight loss, as a result of its effect on eating behavior and appetite[15], and reduced food intake, body weight and mass cells through an increase in vagal afferent satiety signals in obese rats[16].

Although VNS treatment exerts cardioprotective and metabolic benefits, the effects of VNS on the heart in obese-insulin resistant condition have never been investigated. In the present study, we determined the effects of the long-term VNS treatment on the metabolic parameters and LV function in obese-insulin resistant rats. We tested the hypothesis that VNS improves insulin sensitivity and cardiac function by its ability to decrease oxidative stress, inflammation, apoptosis and cardiac mitochondrial dysfunction caused by obese-insulin resistance.

Results

Effects of obese-insulin resistance and VNS on blood pressure. At baseline, systolic blood pressure (SBP), diastolic blood pressure (DBP) and mean arterial pressure (MAP) were not different between sham and VNS groups (Fig. 1). SBP was significantly increased after 12 weeks of high-fat diet consumption, compared with baseline (Fig. 1A). DBP and MAP were significantly increased after 20 weeks of high-fat diet consumption (Fig. 1B,C). Interestingly, at 4 weeks after VNS treatment, there was a significant improvement of SBP, DBP and MAP in the VNS group (Fig. 1). Moreover, VNS significantly reduced SBP, DBP and MAP at weeks 4, 8 and 12 after VNS treatment (Fig. 1).

Effects of obese-insulin resistance and VNS on cardiac function and HRV. At baseline, %FS was not different between sham and VNS groups (Fig. 2A). After 12 weeks of high-fat diet consumption, %FS decreased significantly in both groups (Fig. 2A). In VNS group, %FS at weeks 8 and 12 after VNS treatment increased significantly (Fig. 2A). Although ESP and +dP/dt were not different among groups, VNS significantly reduced EDP and increased −dP/dt and SV, compared with the sham group (Table 1). Moreover, there was no difference in LV stroke work (SW) between the sham and the VNS groups.

For the HRV, the LF/HF ratio was not different between sham and VNS groups (Fig. 2B) at baseline. However, the LF/HF ratio significantly increased at week 12 after high-fat diet consumption (Fig. 2B), indicating cardiac sympathovagal imbalance. In the VNS group, the LF/HF ratio decreased significantly at weeks 4, 8 and 12 after VNS treatment (Fig. 2B), suggesting an improved cardiac sympathovagal balance by VNS.

Effects of obese-insulin resistance and VNS on metabolic parameters. At baseline, metabolic parameters were not different between Sham and VNS groups (Table 2). After 12 weeks of high-fat diet consumption, the body weight, plasma insulin, HOMA index, plasma total cholesterol and plasma LDL levels significantly increased in both groups (Table 2). Plasma insulin, HOMA index, plasma total cholesterol, plasma triglyceride and plasma LDL levels decreased significantly after 12 weeks of VNS. No differences in body weight and food intake between the sham and VNS groups (Table 2). Moreover, after 12 weeks of VNS, plasma glucose AUC and visceral fat decreased significantly (Fig. 3), whereas the serum adiponectin level significantly increased in the VNS group (Fig. 3C).

Effects of VNS on the oxidative stress, apoptosis and inflammation in obese-insulin resistance. After 12 weeks of VNS treatment, VNS significantly decreased Bax expression compared with the sham group (Fig. 4A,D), whereas the Bcl-2 expression was not different among groups (Fig. 4B,D). However, the Bax/Bcl-2 ratio decreased significantly in the VNS group (Fig. 4C) suggesting that VNS attenuated cardiac apoptosis in obese-insulin resistance. Cardiac MDA level decreased significantly after 12 weeks of VNS treatment in the VNS group (Fig. 5A). Moreover, after 12 weeks of VNS treatment, VNS significantly reduced both cardiac and serum TNF-α levels compared with the sham group (Fig. 5B,C), suggesting that VNS attenuated cardiac inflammation and oxidative stress in obese-insulin resistance.

Effects of VNS on cardiac mitochondrial function in obese-insulin resistance. After 12 weeks of VNS treatment, VNS significantly reduced mitochondrial ROS production compared with the sham group (Fig. 6A). For mitochondrial membrane potential change, VNS significantly increased the red/green fluorescent intensity ratio compared with the sham group (Fig. 6B), indicating a reduced mitochondrial depolarization. In addition, the absorbance increased significantly in the VNS group, suggesting an attenuated mitochondrial swelling (Fig. 6C). For cardiac mitochondrial ultrastructure, the unfolded cristae were mostly detected in the sham group (Fig. 6D, left). Interestingly, VNS effectively prevented mitochondrial swelling as shown by preserved cristae in obese-insulin resistance (Fig. 6D, right).

Discussion

In this study, we investigated the effects of VNS on metabolic parameters and cardiac function in obese-insulin resistant animal model. The major findings of this study are as follows: 1) VNS effectively improved insulin resistant condition by increased insulin sensitivity, and increased serum adiponectin level, 2) VNS improved LV function and HRV impaired by obese-insulin resistant condition, 3) VNS significantly decreased blood pressure and 4) VNS exerted anti-oxidant, anti-apoptosis and anti-inflammation properties. Our results provide novel evidence that chronic VNS applied later after the presence obese-insulin resistant condition provides effective cardioprotection and improved metabolic parameters in an obese-insulin resistant model.

In the present study, rats developed hypertension and insulin resistance after 12 weeks of HFD consumption. This finding is consistent with our previous studies in which long-term HFD consumption induces insulin resistance, as well as increases oxidative stress and induces cardiac mitochondrial dysfunction[17–19]. A previous study has shown the presence of an autonomic imbalance shifting toward augmented sympathetic tone during the development from normal glucose tolerance to impaired glucose tolerance and finally diabetes[20]. Metabolic syndrome also has been shown to have an inverse correlation with the vagal component of high-frequency

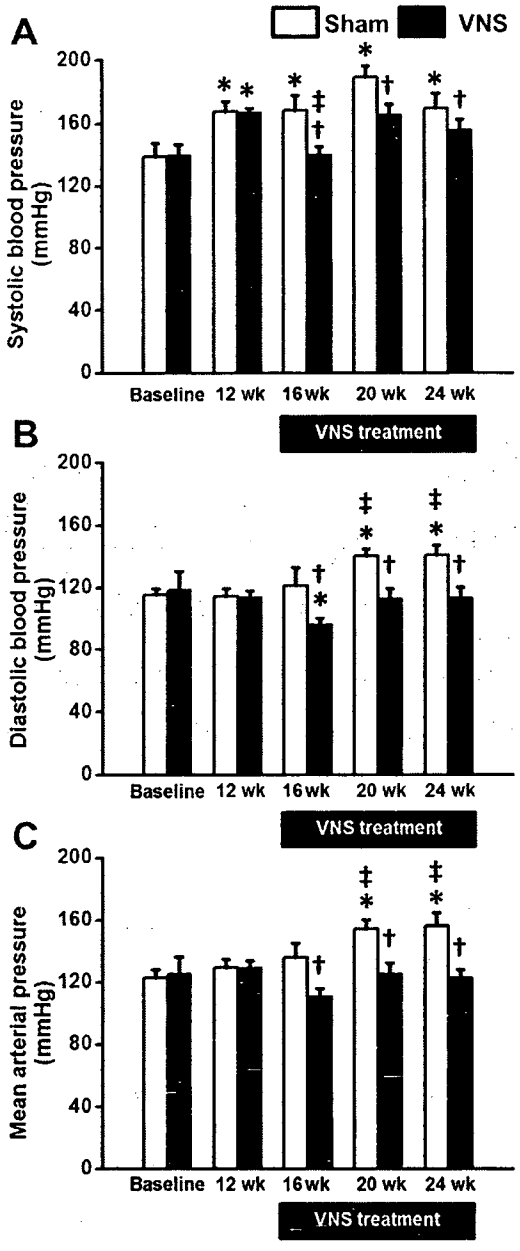


Figure 1. Effects of vagus nerve stimulation on blood pressure. (**A**) SBP increased significantly at week 12th of HFD consumption. VNS significantly decreased SBP at week 16th, week 20th and week 24th in obese-insulin resistance. (**B**) DBP increased significantly at week 20th of HFD consumption. VNS significantly decreased DBP at week 16th, week 20th and week 24th in obese-insulin resistance. (**C**) MAP increased significantly at week 20th of HFD consumption. VNS significantly decreased MAP at week 16th, week 20th and week 24th in obese-insulin resistance. Data were expressed as mean ± SEM. *$p < 0.05$ vs baseline, †$p < 0.05$ vs sham group, ‡$p < 0.05$ vs at 12 week after high-fat feeding of the same group, n = 8/group.

component of the HRV[21]. Thus, rebalancing the autonomic system by VNS may lead to the attenuation of the metabolic parameters in our study. Moreover, in the present study, VNS also significantly increased serum adiponectin and decreased visceral fat after 12 weeks of VNS treatment. Adiponectin is a bioactive adipokine that is expressed in adipose tissues and directly sensitizes the body to plasma insulin. In addition, adiponectin also regulates the energy homeostasis, glucose and lipid metabolism[22]. Previous studies have shown that plasma adiponectin level is lower in patients with diabetes, hypertension, and dyslipidemia[23–25]. Accumulating evidence indicates that adiponectin directly interacts with cardiovascular tissues and prevents cardiovascular pathology. Therefore, the beneficial effects of VNS on metabolic and hemodynamic parameters might be due to its ability to increase adiponectin in obese-insulin resistant condition.

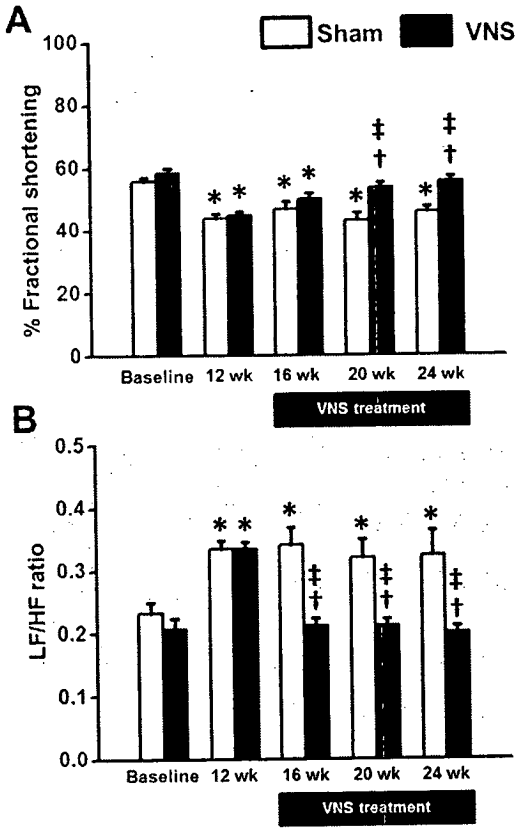


Figure 2. Effects of vagus nerve stimulation on left ventricular function. (**A**) %FS decreased significantly at week 12th of HFD consumption. VNS significantly increased %FS at week 20th and week 24th in obese-insulin resistance. (**B**) LF/HF ratio increased significantly at week 12th of HFD consumption. VNS significantly decreased LF/HF ratio at week 16th, week 20th and week 24th in obese-insulin resistance. Data were expressed as mean ± SEM. *$p < 0.05$ vs baseline, †$p < 0.05$ vs sham group, ‡$p < 0.05$ vs at 12 week after high-fat feeding of the same group, n = 8/group.

Cardiac function	Sham	VNS
Heart rate (bpm)	302.1 ± 26.4	279.9 ± 10.1
ESP (mmHg)	133.2 ± 4.6	103.6 ± 11.3
EDP (mmHg)	24.3 ± 3.5	8.4 ± 1.9*
+dP/dt (mmHg/s)	11846.9 ± 2130.81	9026.6 ± 1205.4
−dP/dt (mmHg/s)	−12129.3 ± 2638.9	−29903.1 ± 5629.3*
SV (μl)	486.1 ± 18	·619.8 ± 15*
SW (mmHg.μl)	57626.2 ± 1462.4	53635.9 ± 2847.9

Table 1. Effects of vagus nerve stimulation on cardiac function after 24 weeks of HFD consumption. Data were expressed as mean ± SEM. *$p < 0.05$ vs. sham group, n = 8/group. ESP, end-systolic pressure; EDP, end-diastolic pressure; +dP/dt, maximal slope of the systolic pressure increment; −dP/dt, maximal slope of the diastolic pressure decrement; SV, stroke volume and SW, stroke work.

Previous study has shown that central obesity causes an increase in sympathetic activity[26]. Furthermore, when patients have both metabolic syndrome and obesity, the level of sympathetic activity is even higher[27]. In the present study, we found that the insulin-resistant condition and obesity were developed at week 12 after HFD consumption. In addition, the LF/HF ratio increased significantly at week 12 following HFD consumption, indicating cardiac sympathovagal disturbance. Increased oxidative stress has been shown to strongly influence cardiac autonomic regulation[28]. The increased oxidative stress in our obese-insulin resistant rats could contribute to the impaired cardiac autonomic balance observed in this study.

A growing number of studies have also shown the strong correlation between metabolic syndrome and ROS production[29]. In a rat model, HFD induced obesity significantly increases the blood pressure and oxidative stress level[5]. Moreover, an increased ROS production can induce mitochondrial dysfunction, apoptosis and cell death[30].

Metabolic parameters	Baseline	After HF 12 weeks	Post VNS 12 weeks	
			Sham	VNS
Body weight (g)	261.1 ± 1.6	544.5 ± 6*	612.9 ± 9.6*	599.1 ± 10.6*
Food intake (g/day)	27.3 ± 0.5	20.8 ± 0.5*	20.4 ± 1.8*	20.2 ± 1.3*
Plasma glucose (mg/dl)	128.7 ± 6.7	127.9 ± 5.8	133.6 ± 4.3	133.7 ± 8.8
Plasma insulin (ng/ml)	1.7 ± 0.2	5.3 ± 0.3*	4.9 ± 1.4*	2.7 ± 0.2*,†,‡
HOMA index	9.2 ± 1.1	33.4 ± 5.5*	30.9 ± 10.8*	17.4 ± 2.9*,†,‡
Plasma total cholesterol (mg/dl)	61.8 ± 2	76.3 ± 2.7*	107.6 ± 7.5*,†	79.8 ± 2.7*,‡
Plasma triglyceride (mg/dl)	32.1 ± 2.1	30.6 ± 2.1	30.2 ± 3.3	21.4 ± 1.6*,†,‡
Plasma HDL (mg/dl)	23.5 ± 1.6	24.7 ± 1	25.3 ± 2.1	28.6 ± 1
Plasma LDL (mg/dl)	32.5 ± 2.2	46.1 ± 2.1*	66.4 ± 6*,†	48.6 ± 1.6*,‡

Table 2. Effects of vagus nerve stimulation on metabolic parameters. Data were expressed as mean ± SEM. *$p < 0.05$ vs. baseline, †$p < 0.05$ vs. after HF 12 weeks, ‡$p < 0.05$ vs. sham group, n = 8/group.

Cardiac mitochondria supply energy to produce the proper cardiac contraction and relaxation on a beat to beat basis. Previous study has shown that worsening of intrinsic myocardial contraction in the transition from obesity to diabetes mellitus is likely related to cardiac mitochondrial dysfunction[31]. Moreover, our previous studies have shown that long-term HFD consumption can cause LV dysfunction due to mitochondrial dysfunction, oxidative stress and inflammation[17,19]. Moreover, TNF-α increased significantly during the development of obesity and metabolic syndrome[4,32].

In the present study, we found that VNS significantly reduced cardiac and serum TNF-α levels after VNS application for 12 weeks. Previous study has shown that VNS inhibits the synthesis of TNF-α and decreases inflammatory responses via nicotinic receptor activation leading to the inhibition of other inflammatory cytokines release[33]. Furthermore, the cardiac MDA level also decreased significantly in the VNS group in our study. Moreover, VNS significantly improved cardiac mitochondrial function impaired by obese-insulin resistance. This beneficial effect of VNS could be exerted through inhibition of opening of mitochondrial permeability transition pore as shown in the previous study[34]. The results obtained from this study indicate the cardio-metabolic protective benefits of VNS in the obese-insulin resistant rats induced by long-term high-fat diet consumption. Moreover, its contribution on cardiac mitochondrial protection could be an important underlying mechanism of this protection on the heart. In addition, the influence of vascular bed alterations in obesity may also contribute to these effects. Since VNS improved cardiac mitochondrial function, decreased oxidative stress, reduced apoptosis and inflammation, this could be the responsible mechanisms for an improved LV function in obese-insulin resistant rats observed in the present study.

Long-term HFD consumption obviously induced obese-insulin resistance, LV dysfunction, increased oxidative stress, inflammation, and cardiac autonomic imbalance. Under obese-insulin resistance condition, chronic VNS improved LV contractile function, cardiac autonomic regulation and metabolic parameters via its ability against apoptosis, oxidative stress, inflammation, cardiac mitochondrial dysfunction, and increased serum adiponectin level. Moreover, VNS significantly reduced blood pressure by increase parasympathetic activity in obese-insulin resistant rats. These findings suggest that VNS may be beneficial as a novel adjuvant therapeutic approach in obese-insulin resistant patients.

Methods

Animals and diet. All experiments in this study were approved by the Faculty of Medicine, Chiang Mai University Institutional Animal Care and Use Committee, in compliance with NIH guidelines, and in accordance with the ARRIVE guidelines for reporting experiments involving animals[35]. In this study, male Wistar rats (180–200 g) were obtained from the National animal center, Salaya campus, Mahidol University, Bangkok, Thailand. Rats were fed with high-fat diet for 12 weeks then rats were randomly divided into 2 groups, sham group (n = 8) and VNS group (n = 8). After 12-week of long-term high-fat diet consumption, all rats (500–580 g) were subjected to VNS implantation. Rats were fully recovered at 3–5 days after surgery. After 1 week of recovery period, VNS will be stimulated for 12 weeks. At week 12th of high-fat diet feeding and weeks 4th, 8th, 12th of VNS treatment, blood samplings were collected for the investigations of glucose, total cholesterol, triglyceride, low density lipoprotein (LDL), high density lipoprotein (HDL), and insulin levels. Heart rate variability (HRV), blood pressure (BP) and echocardiography were also examined. At the end of the study, pressure-volume (P-V) loops were analyzed. Then, rats were sacrificed by decapitation and the heart were rapidly removed and homogenized for mitochondrial and biochemical studies including western blotting for Bax, Bcl-2, and actin.

Vagus nerve stimulation. Rats were anesthetized with xylazine (3 mg/kg) and zoletil (50 mg/kg). After hair shaving and skin cleaning, a bipolar cuff electrode were implanted around the left cervical vagus nerve and connected to an implantable pulse generator (Demipulse, Model 103, Cyberonics). A period of one week was allowed for recovery from the surgical implantation of the stimulation system. VNS was continuously delivered at 20 Hz, 500 μs pulse width, 0.5–0.75 mA, turn ON 14 s and turn OFF 48 s (23% duty cycle). These VNS parameters were sufficient to produce a 5% reduction in heart rate, and the effect of VNS was completely disappeared within 20 seconds after the cessation of VNS as evidenced by the decreased heart rate back to the pre-stimulation values. Prior to data collection, VNS was turned off for 5–10 min and remained off for duration of the hemodynamic

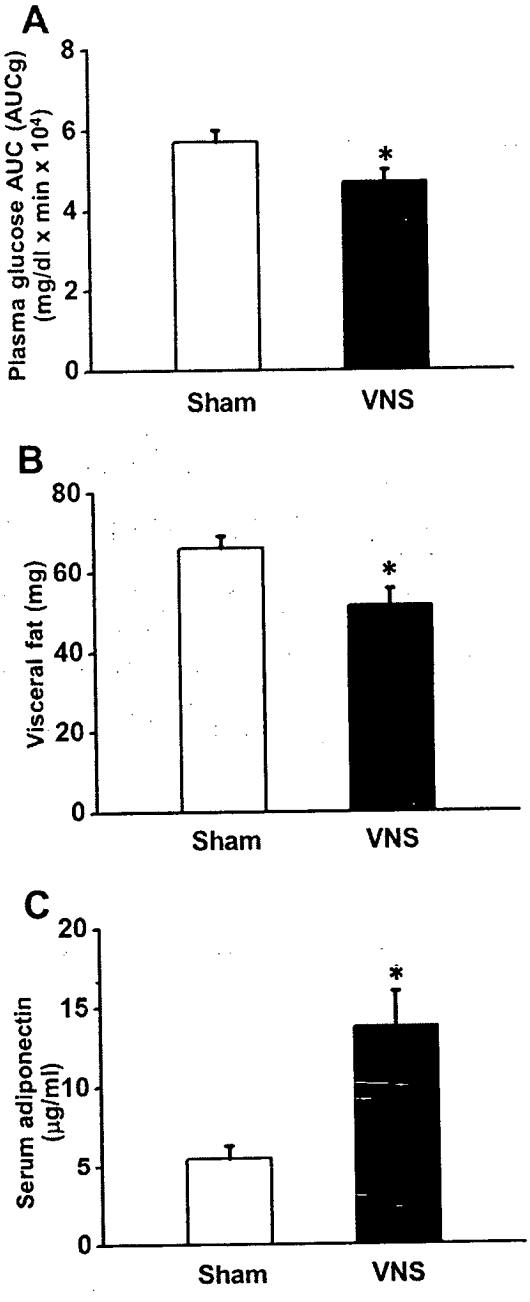


Figure 3. Effects of vagus nerve stimulation on plasma glucose, visceral fat and serum adiponectin after 24 weeks of HFD consumption. (A) VNS significantly decreased plasma glucose AUC in obese-insulin resistance. (B) VNS significantly decreased visceral fat in obese-insulin resistant. (C) VNS significantly increased serum adiponectin in obese-insulin resistance. Data were expressed as mean ± SEM. *$p < 0.05$ vs sham group, $n = 8$/group.

evaluations, echocardiographic, BP and HRV measurements. In the sham group, similar surgical procedure were done except that the programmed VNS was turn off.

Measurement of blood pressure (BP). Rats were preheated under infrared warming pad for at least 5 minutes to dilate the tail vein and acclimate to the holder. Blood pressure measurement was performed by using a CODA2 channel non-invasive blood pressure system (Kent Scientific Corporation, Wyoming, USA). A blood pressure value was achieved from taking an average of 20 consecutive measurements at a steady state[36]. Blood pressure was measured at baseline, 12, 16, 20 and 24 weeks.

Echocardiography. Animals were lightly anesthetized and placed in a supine position. An echocardiography probe (S12, Hewlett Packard) which was connected to an echocardiography machine (SONOS 4500, Philips)

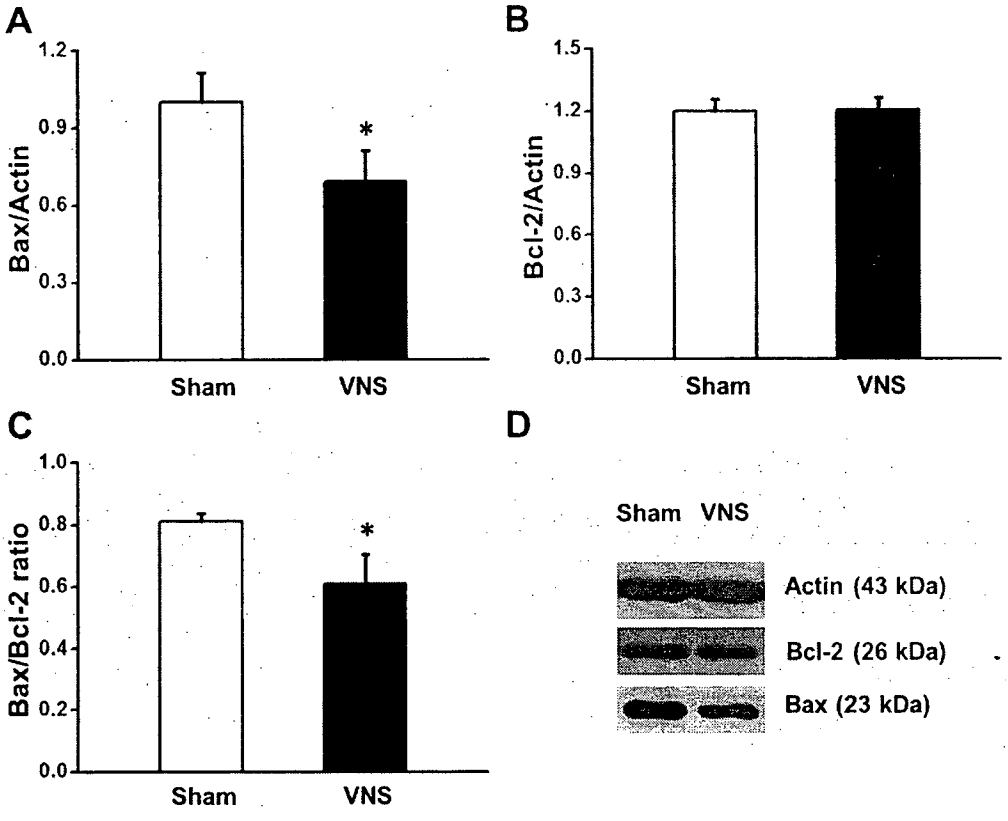


Figure 4. Effects of vagus nerve stimulation on Bax, and Bcl-2 expression after 24 weeks of HFD consumption. (A) VNS significantly decreased Bax expression in obese-insulin resistance. (B) VNS did not change the expression of Bcl-2 in obese-insulin resistance. (C) Bax/Bcl-2 ratio decreased significantly in VNS group in obese-insulin resistance. (D) Representative images showing band width of Bax, Bcl-2 and actin expression. Data were expressed as mean ± SEM. *$p < 0.05$ vs. sham group, n = 8/group. The full length blots are presented in supplementary Fig S1.

was gently placed on the chest and moved for collecting the data along short axis of the heart. Signals from M-mode echocardiography at the level of papillary muscles were recorded. Then, the percentage of the fractional shortening (%FS) was calculated[17]. Echocardiogram was recorded at baseline, 12, 16, 20 and 24 weeks.

Heart rate variability (HRV). Lead II Electrocardiograms (ECG) was recorded for 20 minutes in conscious animals using a signal transducer (PowerLab 4/25T, ADInstrument) and operated through Chart 5.0 program. ECG data was then analyzed using the frequency-domain method by the MATLAB program. High-frequency (HF) component was considered as a marker of parasympathetic tone while low-frequency (LF) component was considered as a marker of parasympathetic tone and sympathetic tone. The cardiac sympathetic/parasympathetic balance was reported as the LF/HF ratio. Increased LF/HF ratio indicates cardiac sympathovagal imbalance[37,38]. HRV was recorded at week 0 (baseline), 12, 16, 20 and 24.

Determination of metabolic parameters. Plasma insulin level was measured using a commercial sandwich ELISA kit (Millipore, MI, USA)[18,39]. Insulin resistance was assessed by Homeostasis Model Assessment (HOMA) which calculated from fasting plasma insulin and fasting plasma glucose concentration. Higher HOMA index shows a higher degree of insulin resistance[39]. Plasma glucose, total cholesterol, and triglyceride levels were determined using a commercial colorimetric assay kit (Biotech, Bangkok, Thailand)[18,39]. Plasma HDL level was determined using a commercial colorimetric assay kit (Biovision, California, USA)[17], and plasma LDL level was calculated using Friedewald equation[40]. Serum adiponectin level was determined using a commercial sandwich ELISA kit (Invitrogen, Frederick, USA)[41].

Left ventricular pressure-volume loops (P-V loops) analysis. At the end of the study, rats were anesthetized by intramuscular injection of the combination of zoletil (50 mg/kg) and xylazine (3 mg/kg)[42]. LV function was evaluated using a pressure-volume (P-V) conductance catheter (1.9F; Scisense Instrument, Ontario, Canada). The catheter was inserted into the right carotid artery and advanced into the LV chamber to record LV pressure and volume relationship. Heart rate (HR), left ventricular end-systolic pressure (LVESP), left ventricular end-diastolic pressure (LVEDP), maximal slope of the systolic pressure increment (+dP/dt), maximal slope of the diastolic pressure decrement (−dP/dt), stroke volume (SV) and stroke work (SW) were assessed[42,43].

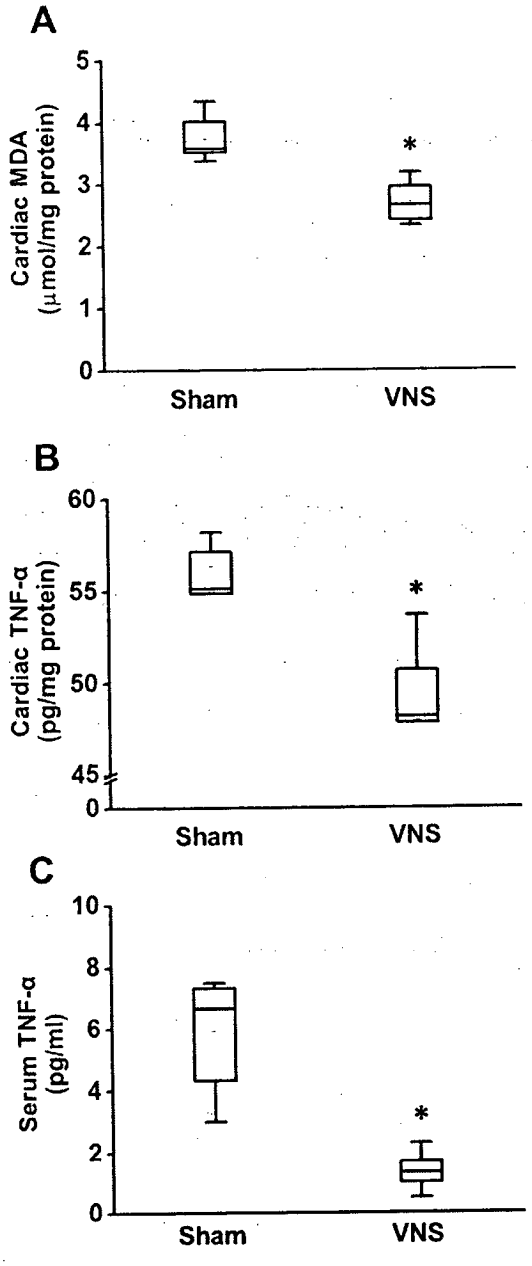


Figure 5. Box plots representing the effects of vagus nerve stimulation on cardiac MDA, cardiac TNF-α and serum TNF-α after 24 weeks of HFD consumption. (A) VNS significantly decreased cardiac MDA in obese-insulin resistance. (B) VNS significantly decreased cardiac TNF-α in obese-insulin resistance. (C) VNS significantly decreased serum TNF-α in obese-insulin resistance. *$p < 0.05$ vs. sham group, $n = 8$/group.

Determination of cardiac malondialdehyde (MDA) level. Malondialdehyde (MDA) concentration in cardiac tissue was measured by a HPLC system (Thermo scientific, Bangkok, Thailand)[44]. A sample was mixed with H_3PO_4 and thiobabituric acid (TBA) solution to generate thiobarbituric acid reactive substances (TBARS). Cardiac TBARS concentration was determined directly from standard curve and reported as MDA equivalent concentration[45].

Determination of cardiac mitochondrial function. At the end of the study, rats were deeply anesthesized by intramuscular injection of the combination of zoletil (50 mg/kg) and xylazine (3 mg/kg). Then, the heart was rapidly removed, and chopped into small pieces on iced-cold plate. Cardiac tissues were homogenized in ice-cold isolated heart buffer which contained (in mmol/l) sucrose 300, TES 5 and EGTA 0.2, pH 7.2 (4 °C). The homogenate was centrifuged at 800 *g* for 5 minutes, and the supernatant was collected and then centrifuged at 8,800 *g* for 5 minutes. The pellet was resuspended in ice-cold buffer and centrifuged at 8,800 *g* for 5 minutes. Isolated mitochondria were collected and the protein concentration were determined[46].

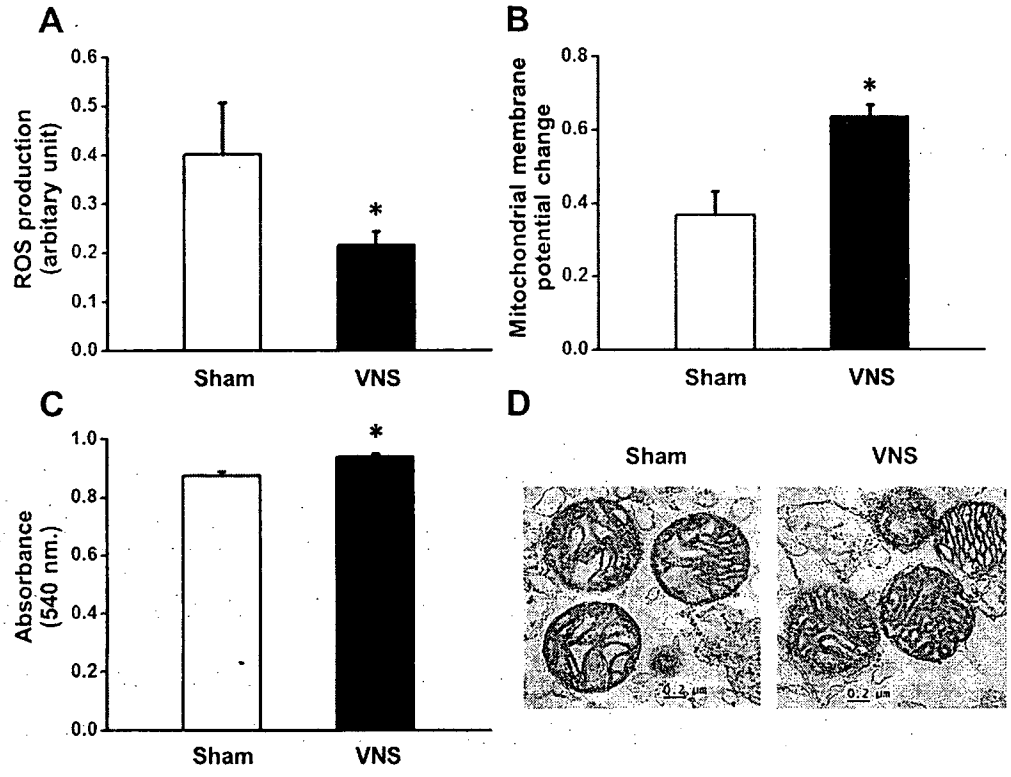


Figure 6. Effects of vagus nerve stimulation on cardiac mitochondrial function and morphology after 24 weeks of HFD consumption. **(A)** VNS significantly reduced mitochondrial ROS production in obese-insulin resistance. **(B)** VNS significantly increased mitochondrial membrane potential change in obese-insulin resistance. **(C)** VNS significantly increased cardiac mitochondrial absorbance in obese-insulin resistance. **(D)** Representative images showing VNS dramatically prevented mitochondrial swelling. Data were expressed as mean ± SEM. $^*p < 0.05$ vs. sham group, n = 8/group.

Cardiac mitochondrial ROS production. The production of reactive oxygen species (ROS) in cardiac mitochondria were measured by dichlorohydrofluorescein diacetate (DCFDA) dye staining. The mitochondria were incubated with 2 μM DCFDA for 25 minutes in 25 °C. The ROS level was assessed at the wavelength of 485 nm (bandwidth 5 nm) and emission wavelength at 530 nm (bandwidth 10 nm) using a fluorescent microplate reader (BioTek Instruments, Winooski, Vermont, USA). Increased fluorescent intensity indicates increased mitochondrial ROS production[46].

Cardiac mitochondrial membrane potential changes. Mitochondria membrane potential were measured by staining with the dye 5,5′,6,6′ tetrachloro-1,1′,3,3′-tetraethylbenzimidazolcarbocyanine iodide (JC-1). Isolated cardiac mitochondria were stained with JC-1 (5 μM) at 37 °C for 30 minutes, and then the membrane potential was determined as fluorescence intensity by using a fluorescent microplate reader. The change in mitochondrial membrane potential was calculated as the ratio of red to green fluorescence. Decreased red/green fluorescent ratio indicates mitochondrial depolarization[46].

Cardiac mitochondrial swelling. Isolated cardiac mitochondria were incubated in 1.5 ml of respiration buffer (constaining 100 mM KCl, 50 mM sucrose, 10 mM HEPES, 5 mM KH_2PO_4, pH 7.4 at 37 °C) with addition of 10 mM pyruvate/malate for 1 minute. Mitochondrial swelling were evaluated by measuring the change of absorbance, using spectrophotometer, for 30 minutes and detected by decreasing of absorbance of suspension at 540 nm[46].

Cardiac mitochondria morphology. Isolated cardiac mitochondria were fixed with 2.5% glutaraldehyde in a 0.1-M phosphate buffer overnight and post fixed in a 1% cacodylate-buffer osmium tetroxide, then dehydrated with graded series of ethanol. Cardiac mitochondria morphology was determined using a transmission electron microscope[46].

Western blot analysis. Myocardial tissues were homogenized in a lysis buffer (containing 1% Nonidet P-40, 0.5% sodium deoxycholate, 0.1% sodium dodecyl sulfate (SDS) in 1xPBS) in order to extract protein. Total protein were mixed with the loading buffer (consist of 5% mercaptoethanol, 0.05% bromophenol blue, 75 nM Tris-HCl, 2% SDS and 10% glycerol with pH 6.8) in 1 mg/ml proportion. The mixture were boiled for 5 minutes

and loaded into 10% gradient SDS-polyacrylamide gel. After that, proteins were transfer to a polyvinyldene difluoride (PVDF) membrane with the presence of glycine/methanol transfer buffer (containing 20 mM Tris base, 0.15 M glycine and 20% methanol) in a transfer system (Bio-Rad). PVDF membranes were incubated in 5% skim milk in 1xTBS-T buffer (containing 20 mM Tris-HCl (pH 7.6), 137 nM NaCl, 0.05% Tween-20) for 1 hour at room temperature[43]. The membrane were exposed to anti-Bax, anti-Bcl-2 (Cell Signaling Technology, Danvers, MA, USA) and anti-actin (Sigma-Aldrich, St. Louis, MO, USA) for 12 hours. Bound antibody was detected by horseradish peroxidase conjugated with anti-mouse IgG. Enhanced chemiluminescence (ECL) detection reagents were administrated to visualize peroxidase reaction products[42].

Inflammation analysis. TNF-α concentration in cardiac tissues and serum were measured by using an ELISA kit (Invitrogen, CA, USA). During the first incubation, the Rat TNF-α antigen binds to the immobilized antibody on one site. During the second incubation, this antibody binds to the immobilized Rat TNF-α captured during the first incubation. The intensity of this colored product is directly proportional to the concentration of Rat TNF-α present in the original specimen[47].

Statistical Analysis. Data were expressed as mean ± SEM. One-way ANOVA followed by Fisher's least significant difference post-hoc was used to test the different among groups. Mitochondrial function was analyzed using Kruskal-Wallis H followed by Mann-Whitney U test. $P < 0.05$ was considered statistical significant.

References

1. Sharma, A. M. The value of current interventions for obesity. *Nat Clin Pract Cardiovasc Med.* 5 Suppl 1, S3 (2008).
2. Reaven, G. M. Banting Lecture 1988. Role of insulin resistance in human disease. 1988. *Nutrition.* **13(1)**, 65; discussion 64 (1997).
3. Hall, J. E. *et al.* Obesity-induced hypertension: role of sympathetic nervous system, leptin, and melanocortins. *J Biol Chem.* **285(23)**, 17271 (2010).
4. Gregor, M. F. & Hotamisligil, G. S. Inflammatory mechanisms in obesity. *Annu Rev Immunol.* **29**, 415 (2011).
5. Dobrian, A. D., Davies, M. J., Schriver, S. D., Lauterio, T. J. & Prewitt, R. L. Oxidative stress in a rat model of obesity-induced hypertension. *Hypertension.* **37(2 Pt 2)**, 554 (2001).
6. Chaudhary, K., Buddineni, J. P., Nistala, R. & Whaley-Connell, A. Resistant hypertension in the high-risk metabolic patient. *Curr Diab Rep.* **11(1)**, 41 (2011).
7. Ford, E. S., Li, C., Zhao, G., Pearson, W. S. & Mokdad, A. H. Prevalence of the metabolic syndrome among U.S. adolescents using the definition from the International Diabetes Federation. *Diabetes Care.* **31(3)**, 587 (2008).
8. Barron, A. J. *et al.* Systematic review of genuine versus spurious side-effects of beta-blockers in heart failure using placebo control: recommendations for patient information. *Int J Cardiol.* **168(4)**, 3572 (2013).
9. De Ferrari, G. M. *et al.* Chronic vagus nerve stimulation: a new and promising therapeutic approach for chronic heart failure. *Eur Heart J.* **32(7)**, 847 (2011).
10. Huang, F. *et al.* Effect of transcutaneous auricular vagus nerve stimulation on impaired glucose tolerance: a pilot randomized study. *BMC Complement Altern Med.* **14**, 203 (2014).
11. Shinlapawittayatorn, K. *et al.* Vagus nerve stimulation initiated late during ischemia, but not reperfusion, exerts cardioprotection via amelioration of cardiac mitochondrial dysfunction. *Heart Rhythm.* **11(12)**, 2278 (2014).
12. Shinlapawittayatorn, K. *et al.* Low-amplitude, left vagus nerve stimulation significantly attenuates ventricular dysfunction and infarct size through prevention of mitochondrial dysfunction during acute ischemia-reperfusion injury. *Heart Rhythm.* **10(11)**, 1700 (2013).
13. Ando, M. *et al.* Efferent vagal nerve stimulation protects heart against ischemia-induced arrhythmias by preserving connexin43 protein. *Circulation.* **1122)**, 164 (2005).
14. Kong, S. S. *et al.* Optimizing the parameters of vagus nerve stimulation by uniform design in rats with acute myocardial infarction. *PLoS One.* **7(11)**, e42799 (2012).
15. Gil, K., Bugajski, A. & Thor, P. Electrical vagus nerve stimulation decreases food consumption and weight gain in rats fed a high-fat diet. *J Physiol Pharmacol.* **62(6)**, 637 (2011).
16. Ogbonnaya, S. & Kaliaperumal, C. Vagal nerve stimulator: Evolving trends. *J Nat Sci Biol Med.* **4(1)**, 8 (2013).
17. Apaijai, N., Pintana, H., Chattipakorn, S. C. & Chattipakorn, N. Effects of vildagliptin versus sitagliptin, on cardiac function, heart rate variability and mitochondrial function in obese insulin-resistant rats. *Br J Pharmacol.* **169(5)**, 1048 (2013).
18. Pratchayasakul, W. *et al.* Effects of high-fat diet on insulin receptor function in rat hippocampus and the level of neuronal corticosterone. *Life Sci.* **88(13–14)**, 619 (2011).
19. Supakul, L. *et al.* Protective effects of garlic extract on cardiac function, heart rate variability, and cardiac mitochondria in obese insulin-resistant rats. *Eur J Nutr.* **53(3)**, 919 (2014).
20. Wu, J. S. *et al.* Epidemiological evidence of altered cardiac autonomic function in subjects with impaired glucose tolerance but not isolated impaired fasting glucose. *J Clin Endocrinol Metab.* **92(10)**, 3885 (2007).
21. Licht, C. M. *et al.* Increased sympathetic and decreased parasympathetic activity rather than changes in hypothalamic-pituitary-adrenal axis activity is associated with metabolic abnormalities. *J Clin Endocrinol Metab.* **95(5)**, 2458 (2010).
22. Yamauchi, T. *et al.* Adiponectin stimulates glucose utilization and fatty-acid oxidation by activating AMP-activated protein kinase. *Nat Med.* **8(11)**, 1288 (2002).
23. Matsubara, M., Maruoka, S. & Katayose, S. Decreased plasma adiponectin concentrations in women with dyslipidemia. *J Clin Endocrinol Metab.* **87(6)**, 2764 (2002).
24. Hotta, K. *et al.* Circulating concentrations of the adipocyte protein adiponectin are decreased in parallel with reduced insulin sensitivity during the progression to type 2 diabetes in rhesus monkeys. *Diabetes.* **50(5)**, 1126 (2001).
25. Iwashima, Y. *et al.* Hypoadiponectinemia is an independent risk factor for hypertension. *Hypertension.* **43(6)**, 1318 (2004).
26. Alvarez, G. E., Ballard, T. P., Beske, S. D. & Davy, K. P. Subcutaneous obesity is not associated with sympathetic neural activation. *Am J Physiol Heart Circ Physiol.* **287(1)**, H414 (2004).
27. Grassi, G. Sympathetic overdrive and cardiovascular risk in the metabolic syndrome. *Hypertens Res.* **29(11)**, 839 (2006).
28. Hans, C. P. *et al.* Protective effects of PARP-1 knockout on dyslipidemia-induced autonomic and vascular dysfunction in ApoE mice: effects on eNOS and oxidative stress. *PLoS One.* **4(10)**, e7430 (2009).
29. Vincent, H. K. & Taylor, A. G. Biomarkers and potential mechanisms of obesity-induced oxidant stress in humans. *Int J Obes (Lond).* **30(3)**, 400 (2006).
30. Vial, G. *et al.* Effects of a high-fat diet on energy metabolism and ROS production in rat liver. *J Hepatol.* **54(2)**, 348 (2011).
31. Montaigne, D. *et al.* Myocardial contractile dysfunction is associated with impaired mitochondrial function and dynamics in type 2 diabetic but not in obese patients. *Circulation.* **130(7)**, 554 (2014).

32. Hotamisligil, G. S., Arner, P., Caro, J. F., Atkinson, R. L. & Spiegelman, B. M. Increased adipose tissue expression of tumor necrosis factor-alpha in human obesity and insulin resistance. *J Clin Invest.* **95(5)**, 2409 (1995).
33. Li, W. & Olshansky, B. Inflammatory cytokines and nitric oxide in heart failure and potential modulation by vagus nerve stimulation. *Heart Fail Rev.* **16(2)**, 137 (2011).
34. Katare, R. G. *et al.* Vagal nerve stimulation prevents reperfusion injury through inhibition of opening of mitochondrial permeability transition pore independent of the bradycardiac effect. *J Thorac Cardiovasc Surg.* **137(1)**, 223 (2009).
35. Kilkenny, C., Browne, W., Cuthill, I. C., Emerson, M. & Altman, D.G. Animal research: reporting *in vivo* experiments–the ARRIVE guidelines. *J Cereb Blood Flow Metab.* **31(4)**, 991 (2011).
36. Lekawanvijit, S. *et al.* Chronic kidney disease-induced cardiac fibrosis is ameliorated by reducing circulating levels of a non-dialysable uremic toxin, indoxyl sulfate. *PLoS One.* **7(7)**, e41281 (2012).
37. Lima, A. H. *et al.* Acute effect of resistance exercise intensity in cardiac autonomic modulation after exercise. *Arq Bras Cardiol.* **96(6)**, 498 (2011).
38. Latchman, P. L., Mathur, M., Bartels, M. N., Axtell, R. S. & De Meersman, R. E. Impaired autonomic function in normotensive obese children. *Clin Auton Res.* **21(5)**, 319 (2011).
39. Pipatpiboon, N., Pratchayasakul, W., Chattipakorn, N. & Chattipakorn, S. C. PPARgamma agonist improves neuronal insulin receptor function in hippocampus and brain mitochondria function in rats with insulin resistance induced by long term high-fat diets. *Endocrinology.* **153(1)**, 329 (2012).
40. Friedewald, W. T., Levy, R. I. & Fredrickson, D. S. Estimation of the concentration of low-density lipoprotein cholesterol in plasma, without use of the preparative ultracentrifuge. *Clin Chem.* **18(6)**, 499 (1972).
41. Yamauchi, T. *et al.* Globular adiponectin protected ob/ob mice from diabetes and ApoE-deficient mice from atherosclerosis. *J Biol Chem.* **278(4)**, 2461 (2003).
42. Surinkaew, S., Kumphune, S., Chattipakorn, S. & Chattipakorn, N. Inhibition of p38 MAPK during ischemia, but not reperfusion, effectively attenuates fatal arrhythmia in ischemia/reperfusion heart. *J Cardiovasc Pharmacol.* **61(2)**, 133 (2013).
43. Palee, S., Weerateerangkul, P., Chinda, K., Chattipakorn, S. C. & Chattipakorn, N. Mechanisms responsible for beneficial and adverse effects of rosiglitazone in a rat model of acute cardiac ischaemia-reperfusion. *Exp Physiol.* **98(5)**, 1028 (2013).
44. Thephinlap, C. *et al.* Reversal of cardiac iron loading and dysfunction in thalassemic mice by curcuminoids. *Med Chem.* **7(1)**, 62 (2011).
45. Mateos, R., Lecumberri, E., Ramos, S., Goya, L. & Bravo, L. Determination of malondialdehyde (MDA) by high-performance liquid chromatography in serum and liver as a biomarker for oxidative stress. Application to a rat model for hypercholesterolemia and evaluation of the effect of diets rich in phenolic antioxidants from fruits. *J Chromatogr B Analyt Technol Biomed Life Sci.* **827(1)**, 76 (2005).
46. Thummasorn, S., Kumfu, S., Chattipakorn, S. & Chattipakorn, N. Granulocyte-colony stimulating factor attenuates mitochondrial dysfunction induced by oxidative stress in cardiac mitochondria. *Mitochondrion.* **113)**, 457 (2011).
47. He, K. L. & Ting, A. T. A20 inhibits tumor necrosis factor (TNF) alpha-induced apoptosis by disrupting recruitment of TRADD and RIP to the TNF receptor 1 complex in Jurkat T cells. *Mol Cell Biol.* **22(17)**, 6034 (2002).

Acknowledgements

This work was supported by the NSTDA Research Chair Grant from the National Science and technology Development Agency Thailand (NC), the Thailand Research Fund [BRG5780016 (SC), RSA5880015 (KS), TRG5780002 (SK)], and the Chiang Mai University Center of Excellence Award (NC).

Author Contributions

N.C., S.C., B.H.K. and K.S. designed the study. B.S., T.C., W.P., S.K. performed experiments. N.C., S.C., K.S., B.S., T.C. performed data analysis and drafted the manuscript. N.C., S.C., B.H.K. and K.S. critically revised the manuscript. All authors reviewed the final manuscript.

Additional Information

Supplementary information accompanies this paper at http://www.nature.com/srep

Competing financial interests: B.H.K. is an employee of Cyberonics Inc, however the other authors declare no competing financial interests.

How to cite this article: Samniang, B. *et al.* Vagus Nerve Stimulation Improves Cardiac Function by Preventing Mitochondrial Dysfunction in Obese-Insulin Resistant Rats. *Sci. Rep.* **6**, 19749; doi: 10.1038/srep19749 (2016).

This work is licensed under a Creative Commons Attribution 4.0 International License. The images or other third party material in this article are included in the article's Creative Commons license, unless indicated otherwise in the credit line; if the material is not included under the Creative Commons license, users will need to obtain permission from the license holder to reproduce the material. To view a copy of this license, visit http://creativecommons.org/licenses/by/4.0/

เอกสารแนบหมายเลข 32

Archives of Oral Biology 64 (2016) 61–71

Contents lists available at ScienceDirect

Archives of Oral Biology

journal homepage: www.elsevier.com/locate/aob

Review

Is salivary gland function altered in noninsulin-dependent diabetes mellitus and obesity–insulin resistance?

Jitjiroj Ittichaicharoen[a,b], Nipon Chattipakorn[b,c], Siriporn C. Chattipakorn[a,b,*]

[a] Department of Oral Biology and Diagnostic Sciences, Faculty of Dentistry Chiang Mai University, Chiang Mai, Thailand
[b] Neurophysiology Unit, Cardiac Electrophysiology Research and Training Center, Faculty of Medicine, Chiang Mai University, Chiang Mai, Thailand
[c] Department of Physiology, Faculty of Medicine, Chiang Mai University, Chiang Mai, Thailand

ARTICLE INFO

Article history:
Received 6 October 2015
Received in revised form 23 December 2015
Accepted 5 January 2016

Keyword:
Insulin
Obesity
Diabetes
Salivary gland function

ABSTRACT

Salivary gland dysfunction in several systemic diseases has been shown to decrease the quality of life in patients. In non-insulin dependent diabetes mellitus (NIDDM), inadequate salivary gland function has been evidenced to closely associate with this abnormal glycemic control condition. Although several studies demonstrated that NIDDM has a positive correlation with impaired salivary gland function, including decreased salivary flow rate, some studies demonstrated contradictory findings. Moreover, the changes of the salivary gland function in pre-diabetic stage known as insulin resistance are still unclear. The aim of this review is to comprehensively summarize the current evidence from *in vitro*,*in vivo* and *clinical* studies regarding the relationship between NIDDM and salivary gland function, as well as the correlation between obesity and salivary gland function. Consistent findings as well as controversial reports and the mechanistic insights regarding the effect of NIDDM and obesity–insulin resistance on salivary gland function are also presented and discussed.

© 2016 Elsevier Ltd. All rights reserved.

Contents

1. Introduction 61
   1.1. Search strategy and selection criteria for this review 63
   1.2. Salivary flow rate in NIDDM from *clinical studies* 63
   1.3. Salivary secretion in NIDDM from *clinical studies* 67
   1.4. Possible mechanisms of salivary gland dysfunction in NIDDM and obesity–insulin resistance: lesson learned from *in vitro* and *in vivo* studies 69
2. Conclusion 70
   Conflict of interest 70
   Author contribution 70
   Acknowledgments 70
   References 70

1. Introduction

The salivary glands are important organs in the oral cavity and are responsible for the secretion of saliva into the oral and pharyngeal cavity. The main functions of saliva are to maintain oral mucosa integrity, prevent oral infection and to promote appetite (Hayward & Shea, 2009), resulting in a comfortable quality of life (Amerongen & Veerman, 2002). The acinar cells of the salivary glands are the secretory units that synthesize and secrete proteins, while water and electrolytes can be pass though the acinar cells *via* variety of mechanism (Proctor & Carpenter, 2007). Therefore, saliva is mainly composed of 99% water and only a small portion of 1% proteins. The activity of salivary glands is regulated by the sympathetic and parasympathetic innervations (Garrett & Kidd, 1993). The activation of parasympathetic innervations in the

* Corresponding author at: Neurophysiology Unit, Cardiac Electrophysiology Research and Training Center, Faculty of Medicine, Chiang Mai University Department of Oral Biology and Diagnostic Science, Faculty of Dentistry Chiang Mai University, Chiang Mai, 50200, Thailand.
Tel: +66 53 944 451; fax: +66 53 222 844.
E-mail addresses: scchattipakorn@gmail.com, siriporn.c@cmu.ac.th (S.C. Chattipakorn).

http://dx.doi.org/10.1016/j.archoralbio.2016.01.002
0003-9969/© 2016 Elsevier Ltd. All rights reserved.

Table 1
The evidence of salivary flow rate in NIDDM from *clinical studies*.

Model (all human)	Age	Method	Major findings	Interpretation	Ref.
• Obese with NIDDM • Female: 11 • Male: 9 • Non-obese with NIDDM • Female: 10 • Male: 10 • Healthy subject • Female: 12 • Male: 10	38–66 years	• Fasting and unstimulated saliva levels 5 min or 5 mL • No medication details of patients'	No change in salivary flow rate in all groups	NIDDM had no effect on the salivary flow rate	Aydin (2007)
• NIDDM[a] with hypoglycemic, anti-hypertensive and anti-cholesterol medication • Female: 12 • Male: 33 • Healthy subjects • Female: 23 • Male: 13	20–65 years	• Each patient attended an out-patient diabetes educational program • Fasting blood glucose (FBS) • Unstimulated whole saliva and citric acid-stimulated parotid saliva	• NIDDM: Fasting blood sugar (FBS) ↑ • No difference in unstimulated and stimulated salivary flow rate between all groups	• NIDDM without xerogenic medication had no influence on salivary output • Salivary flow rate was not changed following the change of FBS • The glycemic control program did not affect the salivary flow rate	Dodds and Dodds (1997)
Men • Study A • Impaired glucose tolerance (IGT): 10 • NIDDM: 10 • Control: 12 • Study B • NIDDM patients • Insulin treatment:15 • Anti-diabetic drugs: 9 • Control:12	59–77 years	• Citric acid-stimulated parotid saliva collection at 0, 15, 30, 45, 60 and 120 min (interval 0.5–1 min) • Patients in study A were not on any medication • OGTT was used to determine NIDDM and IGT in study A • HbA1C was used to determine treatment, either insulin or anti-diabetic drug treatment, for the patients in study B	• In study A, there was no change in salivary flow rate. • In study B, there was no change in salivary flow rate between insulin-treated NIDDM patients and medication-treated NIDDM patients	• NIDDM had no effect on stimulated salivary flow rates	(Borg Andersson et al., 1998)
• NIDDM: 45 • Female: 13 • HbA1C: 9.2 ± 2.2 • Male: 32 • HbA1C: 8.2 ± 1.9 • Control: 86 • Female: 45 • Male: 32	59–79 years	• The medication use in NIDDM and control subjects was recorded • Unstimulated saliva was collected at 1 h after meal for 5 min • Paraffin wax-stimulated whole saliva was collected for 5 min • Deep breathing test (expiratory to inspiratory (E/I) ratio), • E/I ≤ 1.10 indicates parasympathetic neuropathy • Orthostatic test (systolic blood pressure change) • SBP decreased more than 30 mmHg: indicates sympathetic neuropathy	• Parasympathetic and sympathetic neuropathies were significantly higher in NIDDM patients • No difference in unstimulated and stimulated salivary flow rate among groups • An increase in the number of drugs used daily resulted in a decrease in both resting and stimulated flow rate in the control subjects, but not in NIDDM patients	• The resting and stimulated saliva secretions were not different between the NIDDM patients and the control subjects • NIDDM did not seem to affect salivary flow	Meurman et al., (1998)
• Non-NIDDM: 38 • Female: 20 • Male: 18 • NIDDM:35 • Female: 17 • Male: 18	43–45 ± 13 years	• Unstimulated whole saliva for 10 min • Flow rate (mL/min) • Salivary resistin (ng/mL)	• No difference in salivary flow rate between groups	NIDDM had no effect on the salivary flow rate	Yin et al. (2012)
• Non-NIDDM • Female: 14 • Male: 9 • Well-controlled NIDDM • Female: 3 • Male: 8 • Poor-controlled NIDDM (HbA1C > 9%) • Female: 10 • Male: 8	54–90 years	• OGTT, HbA_{1c} • Unstimulated whole saliva collection • Unstimulated parotid saliva collection using Carlson-Crittenden cup • Stimulated parotid saliva collection • All current medication use were recorded	• No differences in salivary flow rate between well-controlled NIDDM and non-NIDDM. • Poor-controlled DM: • ↓ salivary flow rate • Taking xerostomia medication in well-controlled and poor-controlled NIDDM: ↓ salivary flow rate	• Poorly-controlled DM could be associated with salivary dysfunction • Xerogenic medication accelerated a decrease in salivary flow rate in NIDDM	Chavez et al., (2000)

Table 1 (*Continued*)

Model (all human)	Age	Method	Major findings	Interpretation	Ref.
• Healthy: 24 • Female: 13 • Male: 11 • NIDDM: 24 • Female: 13 • Male: 11	58.8–70.8 years	• Citric-acid stimulated salivary flow rate • Parotid gland (PS) • Submandibular and sublingual gland (SS) • Total protein • Parotid gland (PS) • Submandibular and sublingual gland (SS)	• Salivary flow rate (PS) • Parotid gland: no change • Submandibular and sublingual gland: ↓	• Diabetic patients showed a reduction in salivary gland production and secretion in specific salivary glands	Izumi et al. (2015)
• Group 1: NIDDM with xerostomia • Female: 13 • Male: 23 • Group 2: NIDDM without xerostomia • Female: 13 • Male: 23 • Control Group: no NIDDM • Female: 1 • Male:23	56 years	• Known xerogenic drugs were stopped 1 week before study. • Fasting salivary uptake (UR)—which represents the function of salivary production • Fasting salivary excretion ratio (ER), —which represents the function of salivary excretion • measured by scintigraphy	• Group 1 had significantly lower UR values and ER values at the 1st and 15th minute, when compared with controls and NIDDM patients without xerostomia	• Impaired salivary production and excretion were found in NIDDM patients with xerostomic symptoms	Lin et al. (2002)

[a] All NIDDM patients without xerogenic medication.

salivary glands through the muscarinic acetylcholine receptors, particularly M1 and M3 receptors causes fluid secretion (Nakamura et al., 2004). On the other hand, the sympathetic stimulation of salivary glands *via* β-adrenergic receptors leads to the release of salivary proteins (Proctor & Carpenter, 2007). It has been demonstrated that levels of alpha-amylase in saliva represents the sympathetic activity of salivary glands (Enberg, Alho, Loimaranta, & Lenander-Lumikari, 2001). The activation of parasympathetic nerves results in a high salivary flow rate with low salivary proteins. However, sympathetic activation leads to secretion of a high level of salivary proteins without the reduction in salivary flow rate (Carpenter, 2013). Therefore, salivary flow rate is the direct result of parasympathetic function.

Non-insulin dependent diabetes mellitus (NIDDM) (also known as Type 2 Diabetes Mellitus) is a chronic metabolic disorder, characterized by insulin resistance, hyperglycemia, as well as Langerhans islets beta-cells dysfunction (DeFronzo, 2004a, 2004b). NIDDM causes complications in several organs, including salivary glands (Al-Rawi, 2011; Desai & Mathews, 2014). Xerostomia is one of the most common complaints in NIDDM patients (Albert et al., 2012; Ali & Kunzel, 2011; Chomkhakhai, Thanakun, Khovidhunkit, Khovidhunkit, & Thaweboon, 2009; Collin, Niskanen, et al., 2000; Collin, Sorsa et al., 2000). Several clinical studies demonstrated that NIDDM subjects had a reduction in salivary flow rate (Chavez, Taylor, Borrell, & Ship, 2000; Izumi et al., 2015; Lin, Sun, Kao, & Lee, 2002). However, some studies showed contradictive findings (Aydin, 2007; Borg Andersson, Birkhed, Berntorp, Lindgarde, & Matsson, 1998; Hartman et al., 2015; Meurman et al., 1998; Yin, Gao, Yang, Xu, & Li, 2012). Currently, it is known that obesity is a risk factor of developing insulin resistance and NIDDM (Arner & Rydén, 2015; Esser, Legrand-Poels, Piette, Scheen, & Paquot, 2014; Guo, 2014; Hardy, Czech, & Corvera, 2012; Leahy, 2005; Vollenweider, von Eckardstein, & Widmann, 2015; Wellen & Hotamisligil, 2005). Excess free fatty acids (FFAs) from an obese condition has been shown to impair insulin signaling through both cell autonomous mechanisms and inflammatory process (Hardy, Czech, & Corvera, 2012). It has been shown that obesity–insulin resistance could cause the salivary gland dysfunction (Mozaffari et al., 2011; Zalewska et al., 2014).

Despite these previous reports, the relationships between NIDDM, obesity–insulin resistance, and salivary gland function are still not clearly understood. In this review, the current evidence of the available reports regarding the relationship between NIDDM, obesity–insulin resistance and the alterations of the salivary glands are comprehensively summarized. Controversial reports as well as the mechanistic insights regarding the roles of NIDDM and obesity on salivary gland function are also presented and discussed.

1.1. Search strategy and selection criteria for this review

Relevant publications in the PubMed database published before August, 2015 were identified by using search terms "NIDDM or type 2 diabetes and salivary gland" and "obesity–insulin resistance and salivary gland". Only articles published in English were reviewed.

1.2. Salivary flow rate in NIDDM from clinical studies

NIDDM has been shown to lead to the development of systemic inflammation and that this inflammation subsequently initiates micro-angiopathy, macro-angiopathy and neuropathy in several vital organs (Garcia et al., 2010; Lee et al., 2012; Rolo & Palmeira, 2006). The effects of NIDDM on the salivary gland function have been widely studied; however these findings are still controversial. The salivary gland function has been evaluated by several methods, including the measurement of salivary flow rate, alpha-amylase activity, salivary cortisol levels, salivary adipokine levels and other salivary inflammatory biomarkers (Desai & Mathews, 2014). However, the most common indicator for salivary gland function is to measure salivary flow rate.

In NIDMM subjects, it has been shown that the salivary flow rate in both adults and children was not significantly different from the normal subject group (Aydin, 2007; Borg Andersson et al., 1998; Chavez, Borrell, Taylor, & Ship, 2001; Dodds, & Dodds, 1997; Hartman et al., 2015; Meurman et al., 1998; Yin et al., 2012). These studies measured the salivary flow rate by performing either unstimulated saliva collection (Aydin, 2007; Borg Andersson et al., 1998; Chavez et al., 2001; Dodds, & Dodds, 1997; Hartman et al., 2015; Yin et al., 2012) or stimulated saliva collection (Borg Andersson et al., 1998; Dodds, & Dodds, 1997; Meurman et al., 1998). Since whole unstimulated salivary flow rate indicates the function of the submandibular and sublingual glands which

Table 2
Evidence of salivary secretions in NIDDM from *clinical studies*.

Model	Age	Method	Major findings	Interpretation	Ref.

• Obese with NIDDM (OD)
  • Female: 11
  • Male: 9
• Non-obese subjects with NIDDM (NOD)
  • Female: 10
  • Male: 10
• Healthy subjects
  • Female: 12
  • Male: 10
	38–66 years	• No medication
		• Plasma and saliva ghrelin levels were measured
		• Plasma glucose levels were measured
		• Total salivary protein was measured
		• Amylase activity was measured
			• OD and ND subjects
			  • Salivary glucose: ↑
			  • Total protein: ↑
			  • α-amylase activity: ↑
				• Glucose was released into saliva of T2DM subjects
				• Sympathetic stimulation was increased regarding to the increase of α-amylase activity
				• Parasympathetic stimulation did not change
					Aydin (2007)

• NIDDM[a] with hypoglycemic, anti-hypertensive and anti-cholesterol medication
  • Female: 12
  • Male: 33
• Healthy subjects
  • Female: 23
  • Male: 13
	20–65 years	• Each patient attended an out-patient diabetes educational program.
		• Fasting blood glucose (FBG)
		• Unstimulated whole saliva and citric acid-stimulated parotid saliva
		• Parotid salivary protein, including proline-rich proteins (PRPs), histatins, statherin and amylase
		• Amylase activity compared between
		  • DM and control
		  • DM with glycemic control and DM without glycemic control
			• NIDDM after glycemic control program
			  • Amylase activity: ↓
			• No differences in salivary proteins among all groups
				• Amylase activity showed a positive correlation with blood glucose level
				• The salivary proteins were not changed along with the glycemic condition
					Dodds & Dodds (1997)

Men
• Study A
  • Impaired glucose tolerance (IGT): 10
  • NIDDM: 10
  • Control: 12
• Study B
  • NIDDM patients
  • Insulin treatment: 15
  • Anti-diabetic drugs: 9
• Control: 12
	59–77 years	• Citric acid-stimulated parotid saliva collection at 0, 15, 30, 45, 60 and 120 min (interval 0.5–1 min)
		• Patients in study A were not on any medication
		• OGTT was used to determine NIDDM and IGT in study A
		• HbA1C was used to determine treatment, either insulin or anti-diabetic drug treatment, for the patients in study B
			• **Study A**:
			  • IGT and NIDDM: salivary glucose ↑ compared with control
			  • The salivary glucose between IGT and NIDDM were not significantly different
			• **Study B**:
			  • Both diabetic groups: salivary glucose ↑ compared with control
			  • The salivary glucose levels between IGT and NIDDM were not significantly different
			• **Both study A and study B**
			  • Blood glucose: NIDDM > IGT > Normal
			  • A positive correlation between salivary glucose and blood glucose concentration was found
				• Salivary glucose concentration was varied according to blood glucose concentration	Borg Andersson et al. (1998)

• Healthy: 24
  • Female: 13
  • Male: 11
• NIDDM: 24
  • Female: 13
  • Male: 11
	58.8–70.8 years	• Citric-acid stimulated salivary flow rate
		  • Parotid gland (PS)
		  • Submandibular and sublingual gland (SS)
		• Total protein
		  • Parotid gland (PS)
		  • Submandibular and sublingual gland (SS)
			• FBG of diabetic patient was significantly higher than control
			• Parotid gland
			  • Total protein: no change
			• Submandibular and sublingual gland
			  • Total protein: ↓
				• NIDDM patients showed a reduction in salivary gland production and secretion	Izumi et al. (2015)

• NIDDM: 45
  • Female: 13
  • Male: 32
• Control: 86
  • Female: 45
  • Male: 32
	59–79 years	• The history of medication use in NIDDM and control subject was record
		• Unstimulated saliva was collected at 1 h after meal for 5 min
		• Paraffin wax-stimulated whole saliva was collected for 5 min
		• Biochemical analyses:
		  • Lysozyme
		  • Amylase
		  • Total protein, albumin, Ig (G, M and A)
		  • Urea
			• Salivary composition showed no difference between groups.
			• There were no statistically significant differences in the concentrations of salivary secretion between well-glycemic controlled patients and poor- glycemic controlled patients (using the median of HbA1c values to classify)
				• The resting and stimulated saliva secretions were not different between the NIDDM patients and the control subjects
				• Stimulated salivary secretion can reflect the quality of parasympathetic and sympathetic activity
					Meurman et al. (1998)

Table 2 (*Continued*)

Model	Age	Method	Major findings	Interpretation	Ref.
• Control • Female: 30 • Male: 30 • NIDDM • Female: 30 • Male: 30	Adult	• Fasted for 2 h, unstimulated saliva collection, • colorimetric assay for • Salivary exoglycosidases: *N*-acetyl-β-glucosaminidase (HEX) activity, showing impaired epithelial membrane structure • β-D-glucuronidase activity (GLU), showing degradation of proteoglycans, representing salivary dysfunction	• NIDDM • HEX A: activity and output ↑ • HEX B: activity and output ↑ • GLU: activity and output ↑	• There were functional changes in the salivary gland of DM patients • There was a degeneration of the salivary glands of NIDDM patients • There was local inflammation in the salivary glands of DM patients	Zalewska et al. (2013)
• Non-NIDDM: 38 • Female: 20 • Male: 18 • NIDDM:35 • Female: 17 • Male: 18	43–45 ± 13 years	• Unstimulated whole saliva for 10 min • Flow rate (mL/min). • resistin (ng/mL) • Unstimulated whole saliva	• Salivary resistin: ↑ • Salivary and serum resistin were not affected by eating • There was a positive correlation between salivary and serum resistin	• Salivary resistin can reflect NIDDM condition	Yin et al. (2012)
Human parotid glands • NIDDM: 5 • Control:11	42–68 years	Immunocytochemistry: immunogold labeling human amylase and visualization with transmission electron microscope (TEM).	• NIDDM showed only the increase of secretory granules, but the deposition of anti α-amylase- labelled gold particle was not different when compared with the control • No significant difference in the number of lysosomes or lipid droplets	• Changes in salivary gland morphology were found in NIDDM • NIDDM showed only the increase of secretory granules, but the expression of α-amylase was not different when compared with the control	Piras et al. (2010)
NIDDM patients: • Controlled NIDDM: 27 • Uncontrolled NIDDM: 26 • Healthy group: 40	33–84 years	• Unstimulated whole saliva • Chemicals: glucose, protein and Uric acid (UA) assays • Salivary enzymatic antioxidants: catalase (CAT), superoxide dismutase (SOD) • Salivary non-enzymatic parameters: antioxidant activity (AOA), glutathione (GSH), UA, glucose and total protein	• NIDDM: • high UA, GSH and total protein • low AOA and CAT • Strong positive association between • salivary glucose and blood glucose • salivary glucose and GSH • salivary glucose and UA	• Saliva can be used for the diagnosis and the management of DM	Mussavira et al. (2015)

[a] All NIDDM patients without xerogenic medication.

maintain oral moisture during resting period (Falcao, da Mota, Pires, & Bezerra, 2013), and that the salivary flow rate during the resting period is commonly regulated by the parasympathetic nervous system (Carpenter, 2013; Proctor & Carpenter, 2007), those findings suggested that the parasympathetic activity in salivary glands of NIDDM patients has not been affected. This suggestion has been supported by the study of Meurman and colleagues who demonstrated that no significant difference in salivary flow rate or parasympathetic activity (measured by the expiratory to inspiratory (E/I) ratio) was seen between NIDDM and control groups (Meurman et al., 1998). In addition, the salivary flow rate of the NIDDM subjects had no correlation with fasting plasma glucose levels (Dodds & Dodds, 1997; Meurman et al., 1998). Although the salivary flow rate did not change in NIDDM patients, the amylase activity, which represents sympathetic activity in salivary glands, significantly increased (Aydin, 2007; Dodds & Dodds, 1997). These findings indicate that the diabetic condition alters the salivary gland activity, particularly sympathetic activity, without changes in salivary flow rate. Interestingly, these patients did not have any record of using xerogenic medications.

Despite those reports, inconsistent findings exist. Several clinical studies demonstrated the reduction of salivary flow rate in diabetes (Chavez et al., 2000; Izumi et al., 2015; Lin et al., 2002). For example, the study of Chavez and colleagues demonstrated that the poorly glycemic controlled NIDDM patients (HbA1C >9%) had lower unstimulated salivary flow rate, compared with well-controlled NIDDM patients and the control group. In addition, unstimulated salivary flow rate was significantly reduced in poor-controlled NIDDM patients and well-controlled NIDDM patients who were taking xerogenic medications, when compared with the non-NIDDM subjects (Chavez et al., 2000). Moreover, Izumi et al. (2015) showed that the stimulated salivary flow rate and total proteins produced by the parotid gland showed no rate of change between diabetic patients and healthy control subjects, whilst the stimulated salivary flow rate and total proteins collected from submandibular and sublingual glands of diabetic patients showed a significant decrease, when compared with that of healthy control subjects. Furthermore, Lin and colleagues demonstrated that impaired salivary function was found in NIDDM patients with xerostomia by the reduction of salivary secretory rate and excretory rate (Lin et al., 2002). The reduction of salivary flow rate in NIDDM patients from these previous studies (Chavez et al., 2000; Izumi et al., 2015; Lin et al., 2002) may be associated with the severity of NIDDM condition, the xerogenic medication, and the specific salivary gland where saliva was collected from. The comprehensive summary of reports on salivary flow rate in NIDDM patients is shown in Table 1.

Table 3
The evidence of salivary flow rate and salivary secretions in obesity–insulin resistance from *clinical* studies.

Model	Age	Method	Major findings	Interpretation	Ref.

Human
• Obese ($n = 369$)
• Healthy ($n = 60$)
	~50 years old	• Screening tests for Cushing's syndrome:
		  • Dexamethasone suppression test (DST)
		  • Measurements of 24-h urine creatinine and cortisol excretion (UFC)
		• Measurement of bedtime salivary cortisol
		  • Analyzed all metabolic parameters
			Salivary cortisol tended to rise as BMI increased and correlated with an increase in waist circumference	Obese people had an increase in salivary cortisol levels	Abraham, Rubino, Sinali, Ramsey and Nieman, (2013)

Children ($n = 213$ from total of 8319)
Body Mass Index (BMI) z-score was used to classified the subjects into
• Normal
• Underweight
• Overweight
• Obese
	11 years	• 3 mL Unstimulated whole saliva collection
		  • Flow rate (mL/h)
		  • Total protein (mg/dL)
			• No differences in salivary flow rate among groups
			• No differences in total salivary protein concentration among groups
				• BMI did not affect salivary flow rate and total salivary protein concentration	Goodson et al. (2014)

Children ($n = 8319$)
Body Mass Index (BMI) z-score was used to classified the subjects into
• Normal
• Underweight
• Overweight
• Obese
	11 years	• 3 mL Unstimulated whole saliva collection
		  • Insulin
		  • C-reactive protein (CRP)
		  • Adiponectin
		  • Leptin
			• Obese:
			  • Insulin ↑
			  • CRP ↑
			  • Adiponectin ↓
			  • Leptin ↑
				• Obese children tended to be metabolic syndrome	Goodson et al. (2014)

Children ($n = 744$ from total of 8319)
• Obese healthy group (OH): 186
• Obese with high insulin (OI): 186
• Obese with high CRP (OC): 186
• Non-Obese with high CRP (NC): 186
• Non-Obese with high insulin (NI):186
• Non-obese healthy group (NH): 186
	11 years	• Sjögren's syndrome related cytokines
		  • IL-4
		  • IL-10
		  • L12p70
		  • Ib-17A
		  • IFN-γ
		• NIDDM related cytokines
		  • Insulin
		  • Ghrelin
		  • Myeloperoxidase (MPO)
		  • Vascular endothelial growth factor (VEGF)
			• OC: ↑ CRP and IL-6, leptin
			• NC: ↑ CRP, IL-6, IL-10, IL-1β, MM-9 and resistin
			• OH: ↑ IL-10 and adiponectin
				• Many cytokines could be detected in saliva
				• Those cytokines could be used as screening or adjunctive tool
					Goodson et al. (2014)

Human • Normal weight: 30 • Underweight: 2 • Overweight: 12 • Obese: 21	10.6 ± 0.2 years	• Salivary flow rate • Salivary glucose: glucose oxidase method using fluorescent emission • Plasma glucose analysis	• Blood pressure and fasting plasma glucose showed no difference among groups • Salivary flow rate and salivary glucose showed no difference among groups • Salivary flow rate did not correlate with fasting plasma glucose levels • There was a significant association between plasma and salivary glucose levels	• Obesity had no effect on salivary flow rate • Salivary glucose level could be a useful marker as a diagnostic screening tool for high plasma glucose levels in children	Hartman et al. (2015)

Human • Metabolic syndrome • Female (5) • Male (7) • Healthy • Female (14) • Male (20)	20–70 years	• Blood pressure • Waist circumference • Fasting 12 h then collection of: • Blood glucose • Total cholesterol • Triglycerides • HDL, LDL, insulin • HOMA-IR • Unstimulated saliva collection (11–12 pm) • Salivary cortisol	Midnight salivary cortisol concentrations were significantly and positively correlated with abdominal circumference, fasting blood glucose and HOMA-IR	There was a positive correlation between midnight salivary cortisol and the metabolic syndrome (MetS)	Jang, Lee, Kim, Kim and Song, (2012)

1.3. *Salivary secretion in NIDDM from* clinical studies

The alterations of salivary secretion in NIDDM have been demonstrated. It has been shown that increased amylase activity was found in salivary glands of NIDDM patients (Aydin, 2007; Dodds & Dodds, 1997). In a report by Piras and colleagues, they found no significant difference in amylase expression of salivary gland isolated from NIDDM patients, when compared with that of the control group (Piras, Hand, Mednieks, & Piludu, 2010). However, amylase activity was not investigated in that study. NIDDM patients also showed higher levels of salivary and serum resistin (a peptide hormone) and pro-inflammatory cytokines which are produced by adipocytes and macrophages (Yin et al., 2012), than non-NIDDM patients. Moreover, it has been shown that there was an increase in salivary pro-inflammatory cytokines, including interleukins-1b, -6 and -8 (IL-1b, -6 and -8), tumor necrosis factor-α (TNF-α) and matrix metalloproteinases (MMP)-8 and -9 in NIDDM patients (Collin, Niskanen, et al., 2000; Collin, Sorsa et al., 2000; Rathnayake et al., 2013). The positive correlation of glucose levels between blood and saliva in impaired glucose tolerance subjects and NIDDM subjects suggested the potential role of plasma glucose on salivary gland function (Aydin, 2007; Borg Andersson et al., 1998; Garcia et al., 2010; Yin et al., 2012). In addition, Zalewska et al. (2013) showed that the salivary glands of NIDDM patients exhibited greater changes in function and morphology than those of control, by increasing salivary *N*-acetyl-β-glucosaminidase, representing impaired epithelial membrane structure, and salivary β-D-glucuronidase activity, representing the degradation of proteoglycans). All of these findings suggest that increased sympathetic activity, increased inflammation, impaired insulin signaling, and the degradation of extracellular matrix occurs in salivary glands of NIDDM subjects. The comprehensive summary of reports on salivary secretions in NIDDM patients is shown in Table 2.

All of these clinical studies indicate that NIDDM can lead to alterations in the salivary gland with or without a reduction in salivary flow rate. The factors influencing the salivary flow rate in NIDDM could be dependent on the severity of the diabetic condition, the use of xerogenic medication and the specific collected salivary gland.

Salivary flow rate and salivary secretions in obesity–insulin resistance or pre-diabetic condition from *clinical studies*

Evidence demonstrated that obesity–insulin resistance does not have an effect on salivary flow rate (Borg Andersson et al., 1998; Hartman et al., 2015). Impaired secretion of saliva is indicated using the unstimulated salivary flow rate ≤0.2 mL/min in men and ≤0.18 mL/min in women (Chavez et al., 2000). In subjects with impaired glucose tolerance (IGT or obesity–insulin resistance), it has been shown that the unstimulated salivary flow rates were not significantly different from the control group (Borg Andersson et al., 1998). Goodson and colleagues in 2014 evaluated twenty biomarkers in fasting saliva samples taken from 11-year old children who had been designated as underweight, normal healthy weight, overweight and obese subjects. The study found that salivary C-reactive protein (CRP), insulin and leptin levels of obese subjects significantly increased, when compared with those of normal healthy weight subjects. However, salivary adiponectin level in obese children significantly showed a decrease, when compared with levels in normal healthy weight subjects (Goodson et al., 2014). Alterations in those biomarkers in plasma could be the indicators of the development of the metabolic syndrome (MetS) (Oh et al., 2014). In addition, Goodson's study showed that neither total salivary protein level nor salivary flow rate were significantly different between body weight groups. The results of Goodson's study suggested that obesity did not affect salivary protein levels or salivary flow rate in this population, but the alteration of salivary

Table 4
The evidence of salivary gland alterations in the NIDDM and obesity–insulin resistance from *in vivo* studies.

Model	Age	Experimental period	Methods	Major findings	Interpretation	Ref.

Female mice (each group $n=6$)
• Normal
  • C57BL/6
  • BALB/c
• Non-obese diabetic mice (NOD mice):
  • NOD/Lt
  • NOD-*scid*
  • NOD.B10.H
Decorin and biglycan maintain ECM structure in the salivary gland and can be destroyed by MMP
	8–20 weeks	–	• Stimulated saliva collection for 10 min: stimulated by either pilocarpine (0.5 mg/100 g) or isoproterenol (0.2 mg/100 g)
			• Protein analysis in saliva and salivary glands by detecting MMP, proteoglycans and TGFβ1
			• Detection of salivary decorin and biglycan
				• TGFβ1 ↑ in NOD mice both in saliva and lysated salivary gland
				• MMP inhibitor can reduce the expression of TGFβ1
				• Decorin and biglycan were degraded in the saliva of diabetic mice
					• The salivary glands in diabetic mice were destroyed *via* increased proteolytic activities inside the salivary glands	Yamachika et al. (2000)

Male obese Zucker rats
• Lean (LZR) ($n=7$-9)
• Obese (OZR)
• OZR- fed Cr 5 mg/kg ($n=7$–9)
• OZR- fed Cr 10 mg/kg ($n=7$–9)
(Cr: Chromium picolinate for glycemic control)
	6 weeks	6 Months after chromium administration	○ Fasting plasma glucose
			○ Insulin sensitivity by QUICKI
			○ Western blot: NF-κB, phospho-NF-κB, VCAM-1 and ICAM-1 in salivary glands
				• OZR:
				  • ↑ Plasma insulin levels
				  • ↑ QUICKI
				  • ↑ Lipid droplet
				  • ↑ p-NF-κB/NF-κB ratio
				  • ↑ ICAM-1
				• OZR-fed Cr 10: showed a benign expansion of the secretory acinar units
				• Histological features of salivary glands: OZR similar to LZR
					Obesity led to an increase in the inflammation of the salivary glands without significant morphological changes	Mozaffari et al. (2011)

Male Wistar rats
• Normal diet (C): n = 9
• High fat diet (HFD): $n=9$
		5 Weeks of dietary program	• Blood analysis: insulin, glucose and fatty acid methyl esters
			• Antioxidant profile of parotid gland (PG) and submandibular glands (SG)
			  • Specific activity of salivary peroxidase
			  • Superoxide dismutase 2 (SOD2)
			  • CAT
			• Uric acid (UA)
			  • Total antioxidant salivary status (TAS)
				• HFD-fed rats developed the insulin resistant condition
				• HFD:
				  • ↓ SG peroxidase activity
				  • ↓ PG peroxidase activity
				  • ↓ total PG peroxidase
					• Obesity–insulin resistance led to the decrease of antioxidants in salivary glands
					• Parotid and submandibular glands responded differently to the insulin resistant conditions
					• The parotid glands seemed to be more affected following the insulin resistant condition
					• The main source of antioxidants was in the parotid glands
						Zalewska et al. (2014)

Lacrimal gland (LG) and submandibular gland (SG) of male Wistar rats
• Young: 2 months old
• Old: 20 months old
			• Insulin tolerance test after injection of 100 μL of 10 μM insulin
			• Tissue collection: 3 min after injection of 100 μL of 10 μM insulin into the inferior vena cava
			• Immunoblotting: IR, Shc and STAT-1
				• Old rats: euglycemia and hyperinsulinemia
				• Old rats LG:
				  • ↓ p-IR
				• Old rats SG:
				  • ↓ p-IR
				  • ↓ p-STAT-1
					• Aging induced a reduction in tyrosine phosphorylation of insulin receptors in the LG and SG, suggesting insulin resistance in the exocrine glands of aging rats	Rocha et al. (2003)

Female mice
• NOD: $n=9$
• BALB/c: $n=9$
	24 weeks	24 weeks	• Pilocarpine-stimulated salivary flow rate for 10 min
			• Evaluation of submandibular salivary gland inflammation by the number of mononuclear cells in H&E-stained slides and immunohistochemistry analysis (CD4+ T-cell).
			• Salivary cytokine levels
			• Serum cytokines levels
				• 24-week-old NOD mice
				  • Salivary flow rate ↓
				  • IL-4 ↑
				  • Granulocyte–macrophage colony-stimulating factor
				  • (GM-CSF) ↑
				  • TNF-α ↑
				  • IL-5 ↓
				  • IFN-γ: not detectable
					• The longer duration of insulin-resistant conditions led to a lower salivary flow rate and an increase in salivary gland inflammation	Jonsson, Delaleu, Brokstad, Berggreen and Skarstein. (2006)

biomarkers, including CRP, insulin, leptin and adiponectin, instead of plasma biomarkers, may be useful indicators of the occurrence of MetS in children (Goodson et al., 2014). In addition, Hartman and colleagues demonstrated that salivary glucose levels may be useful for the screening of high fasting plasma glucose levels in children (Hartman et al., 2015). The recent study also showed that significant alterations in salivary adipocytokines were observed in overweight and obese children, when compared with normal-weight children (Shi et al., 2015). All of these findings suggested that salivary biomarkers in obese subjects could be useful tools to predict the development or progression of MetS, particularly in children.

An increase in salivary cytokines, including IFN-γ, TNF-α, IL-1, IL-4, IL-10, IL-12, and IL-17, have been shown to be associated with oral dryness in primary and secondary Sjögren's syndrome (Furuzawa-Carballeda et al., 2014; Kang, Lee, Hyon, Yun, & Song, 2011; von Bültzingslöwen et al., 2007). These findings suggested that an increase in these particular salivary cytokines could be a predictor of oral dryness.

Despite the unaltered salivary flow rate in obesity–insulin resistance, both studies showed an increase in saliva glucose levels (Borg Andersson et al., 1998; Hartman et al., 2015). These findings suggest that impaired insulin signaling might occur in the salivary glands of obesity–insulin resistance.

In obese subjects, it has been demonstrated that saliva cortisol levels were significantly increased, compared to normal subjects (Abraham, Rubino, Sinaii, Ramsey, & Nieman, 2013; Jang, Lee, Kim, Kim, & Song, 2012). Several studies showed that there was an increased level of salivary pro-inflammatory cytokines in insulin-resistant obese patients, including tumor necrosis factor-alpha (TNF-α), interleukin-6 (IL-6), interferon gamma (IFN-γ), macrophage inflammatory protein-1 beta (MIP-1β) (Desai & Mathews, 2014) as well as an increased level of oxidative stress (Al-Rawi, 2011). These findings suggest that obesity–insulin resistance subjects developed impaired insulin sensitivity in the salivary gland, increased level of salivary oxidative stress, and increased level of inflammation, possibly leading to salivary gland dysfunction. The comprehensive summary of reports on salivary gland dysfunction in obesity–insulin resistance is shown in Table 3.

1.4. Possible mechanisms of salivary gland dysfunction in NIDDM and obesity–insulin resistance: lesson learned from in vitro *and* in vivo *studies*

Although alterations in salivary gland activity with or without a change in salivary flow rate in NIDDM and obesity–insulin resistance have been reported in clinical studies, the underlying mechanisms responsible for these alterations have been documented from basic studies. Findings from *in vivo* studies supported the clinical findings from NIDDM and obesity–insulin resistance for the occurrence of salivary gland dysfunction. NIDDM rats have been shown to develop the degradation of salivary glands through an increase in salivary decorin and biglycan levels (Yamachika, Brayer, Oxford, Peck, & Humphreys-Beher, 2000). Decorin and biglycan are parts of the extracellular matrix structure in the salivary gland, and degradation can be caused by matrix metalloproteinases (MMPs) (Yamachika et al., 1998). An increase in salivary decorin and biglycan represents the degradation of salivary glands (Yamachika et al., 2000). In addition, Masago and colleagues demonstrated the elevation of proapoptotic Bax

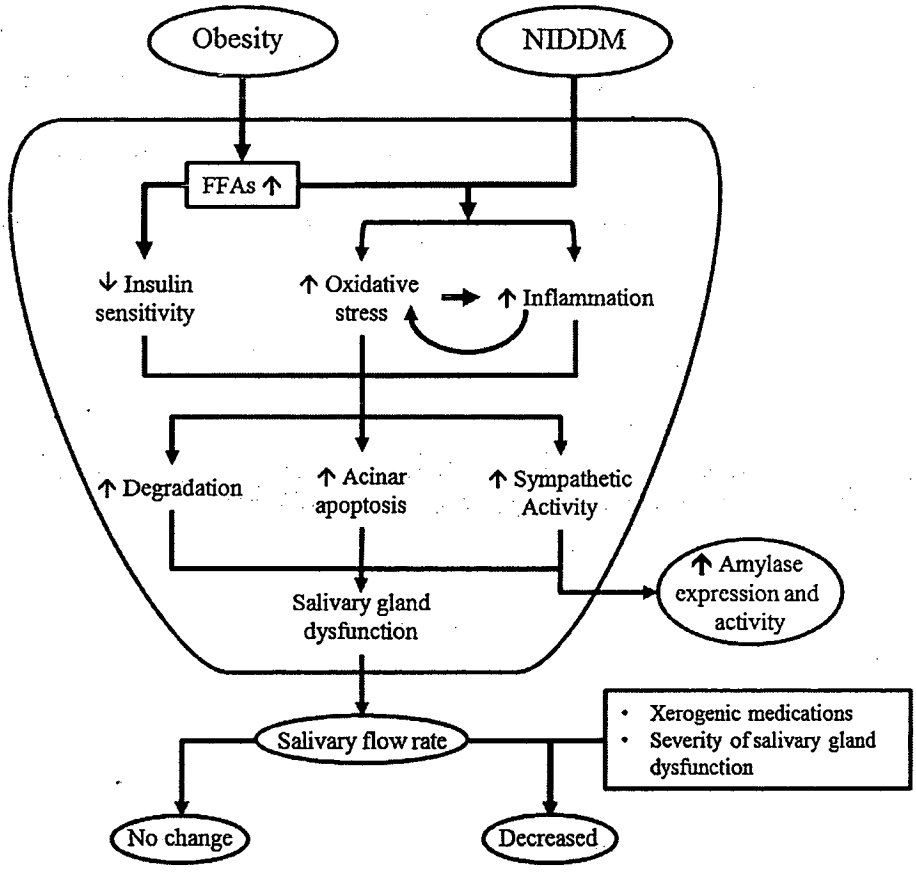


Fig. 1. The possible mechanisms of salivary gland dysfunction in NIDDM and obesity–insulin resistance.

and caspase 3 activation in glandular parenchyma of non-obese diabetic mice (Masago et al., 2001). Thus, the degradation of salivary gland in NIDDM and the obese-insulin resistant condition could be due to the role of apoptosis in glandular parenchyma. It has been shown that increased inflammation correlates with TGF-β1 expression (Imai, Hiramatsu, Fukushima, Pierschbacher, & Okada, 1997). In addition, decorin and biglycan are known as the reservoirs of TGF-β1 (Cs-Szabo, Roughley, Plaas, & Glant, 1995). These findings suggest that salivary gland inflammation as well as the degradation of the salivary gland develops in NIDDM. The excessive inflammation and degradation of salivary gland in NIDDM could be responsible for salivary gland dysfunction, resulting in the decrease of salivary flow rate. However, it is possible that less severe salivary gland dysfunction might not alter the salivary flow rate in NIDDM, as observed in several clinical studies (Aydin, 2007; Borg Andersson et al., 1998; Chavez et al., 2001; Dodds, & Dodds, 1997; Hartman et al., 2015; Meurman et al., 1998; Yin et al., 2012).

Increased free fatty acid levels in the plasma are commonly found in obesity–insulin resistance (DeFronzo, 2004a, 2004b). In human parotid/submandibular gland epithelial cell lines, the application of saturated fatty acids (SFAs) on them can lead to increased IL-6 secretion, cell apoptosis and the degradation of salivary gland cells (Shikama et al., 2013). These findings suggested that high levels of free fatty acid could cause salivary glands damage. In addition, several *in vivo* studies support these findings. Zalewska et al. (2014) found that there was a reduction in antioxidants levels, by measuring peroxidase activity, in both the submandibular and parotid glands in insulin-resistant obese rats induced by high-fat diet, when compared with the control group. Interestingly, the peroxidase enzyme activity in the submandibular gland was still higher than that in the parotid gland of the high-fat diet-fed rats. These findings suggest that obesity–insulin resistance could lead to increased oxidative stress in the parotid glands, rather the submandibular glands. In obese Zucker rats, an increase in inflammation, demonstrated by increased NFκB phosphorylation and ICAM-1 levels, was demonstrated in their salivary glands (Mozaffari et al., 2011). However, no histological changes in the salivary glands of these obese Zucker rats were found. A possible explanation for this could be that the level of inflammation in the salivary glands of obese Zucker rats might not be high enough to cause morphological changes. Rocha and colleagues also demonstrated that aged rats (20 months old) developed insulin resistance, characterized by hyperinsulinemia with euglycemia, and that the reduction of insulin receptor phosphorylation in salivary glands also developed in these aged rats (Rocha, Carvalho, Saad, & Velloso, 2003).

All of these findings suggest that obesity–insulin resistance leads to increased oxidative stress, inflammation and decreased insulin sensitivity in salivary gland, possibly leading to further degradation of salivary glands. The comprehensive summary of reports on salivary gland dysfunction in obesity–insulin resistance and NIDDM from basic research is shown in Table 4.

2. Conclusion

Although the alterations of salivary flow rate in NIDDM have been demonstrated previously (Chavez et al., 2000; Izumi et al., 2015; Lin et al., 2002), several studies showed contradictory findings (Aydin, 2007; Borg Andersson et al., 1998; Chavez et al., 2001; Dodds, & Dodds, 1997; Hartman et al., 2015; Meurman et al., 1998; Yin et al., 2012). These inconsistent findings could be due to the difference in the severity of the diabetic condition, the use of xerogenic medications and the different methods for saliva collection in those studies. Changes in salivary gland activity with or without an alteration in salivary flow rate can be found in NIDDM and obesity–insulin resistance. The underlying mechanisms of salivary gland dysfunction could be due to hyperglycemia, hyperinsulinemia and dyslipidemia following NIDDM and obesity–insulin resistance, resulting in increased oxidative stress, inflammation, increased sympathetic activity, and impaired insulin signaling in the salivary gland. High levels of oxidative stress, inflammation and insulin resistance in the salivary gland can lead to the degradation of the salivary gland. In addition, this degradation in NIDDM and obese patients can cause a reduction in salivary flow rate. These potential mechanisms responsible for salivary gland dysfunction in NIDDM and obesity–insulin resistance are summarized in Fig. 1. Since the development of salivary gland dysfunction could happen as early as the development of obesity–insulin resistance (*i.e.* before the occurrence of NIDDM), future studies are needed and a suggested focus is on the protection of salivary gland function in obesity–insulin resistance.

Conflict of interest

The authors declare that there is no conflict of interest.

Author contribution

JI co-designed the study, analyzed the data and wrote the manuscript. NC co-designed the study, and wrote the manuscript. SCC co-designed the study, analyzed the data and wrote the manuscript. All authors have read and approved the final article.

Acknowledgments

This work was supported by grants from the Thailand Research Fund TRF-BRG5780016 (SC), a CMU 50th Anniversary grant by Chiang Mai University (JI and SC), National Research Council of Thailand (SC), a NSTDA Research Chair Grant from the National Science and Technology Development Agency Thailand (NC), and the Chiang Mai University Excellent Center Award (NC).

References

Abraham, S. B., Rubino, D., Sinaii, N., Ramsey, S., & Nieman, L. K. (2013). Cortisol, obesity, and the metabolic syndrome: a cross-sectional study of obese subjects and review of the literature. *Obesity (Silver Spring, Md), 21*(1), E105–117.

Al-Rawi, N. H. (2011). Oxidative stress, antioxidant status and lipid profile in the saliva of type 2 diabetics. *Diabetes & Vascular Disease Research: Official Journal of the International Society of Diabetes and Vascular Disease, 8*(1), 22–28.

Albert, D. A., Ward, A., Allweiss, P., Graves, D. T., Knowler, W. C., Kunzel, C., et al. (2012). Diabetes and oral disease: implications for health professionals. *Annals of the New York Academy of Sciences, 1255*(1), 1–15.

Ali, D., & Kunzel, C. (2011). Diabetes mellitus: update and relevance for dentistry. *Dentistry Today, 30*(12) 45–46, 48–50; quiz 51.

Amerongen, A. V., & Veerman, E. C. (2002). Saliva—the defender of the oral cavity. *Oral Diseases, 8*(1), 12–22.

Arner, P., & Rydén, M. (2015). Fatty acids, obesity and insulin resistance. *Obesity Facts, 8*(2), 147–155.

Aydin, S. (2007). A comparison of ghrelin, glucose, alpha-amylase and protein levels in saliva from diabetics. *Journal of Biochemistry and Molecular Biology, 40*(1), 29–35.

Borg Andersson, A., Birkhed, D., Berntorp, K., Lindgarde, F., & Matsson, L. (1998). Glucose concentration in parotid saliva after glucose/food intake in individuals with glucose intolerance and diabetes mellitus. *European Journal of Oral Sciences, 106*(5), 931–937.

Carpenter, G. H. (2013). The secretion, components, and properties of saliva. *Annual Review of Food Science and Technology, 4*(1), 267–276.

Chavez, E. M., Borrell, L. N., Taylor, G. W., & Ship, J. A. (2001). A longitudinal analysis of salivary flow in control subjects and older adults with type 2 diabetes. *Oral Surgery, Oral Medicine, Oral Pathology, Oral Radiology, and Endodontics, 91*(2), 166–173.

Chavez, E. M., Taylor, G. W., Borrell, L. N., & Ship, J. A. (2000). Salivary function and glycemic control in older persons with diabetes. *Oral Surgery, Oral Medicine, Oral Pathology, Oral Radiology, and Endodontics, 89*(3), 305–311.

Chomkhakhai, U., Thanakun, S., Khovidhunkit, S.-o. P., Khovidhunkit, W., & Thaweboon, S. (2009). Oral health in Thai patients with metabolic syndrome. *Diabetes & Metabolic Syndrome: Clinical Research & Reviews, 3*(4), 192–197.

Collin, H. L., Niskanen, L., Uusitupa, M., Töyry, J., Collin, P., Koivisto, A.-M., et al. (2000). Oral symptoms and signs in elderly patients with type 2 diabetes mellitus: a focus on diabetic neuropathy. *Oral Surgery, Oral Medicine, Oral Pathology, Oral Radiology, and Endodontology, 90*(3), 299–305.

Collin, H. L., Sorsa, T., Meurman, J. H., Niskanen, L., Salo, T., Ronka, H., et al. (2000). Salivary matrix metalloproteinase (MMP-8) levels and gelatinase (MMP-9) activities in patients with type 2 diabetes mellitus. *Journal of Periodontal Research, 35*(5), 259–265.

Cs-Szabo, G., Roughley, P. J., Plaas, A. H., & Glant, T. T. (1995). Large and small proteoglycans of osteoarthritic and rheumatoid articular cartilage. *Arthritis & Rheumatology, 38*(5), 660–668.

DeFronzo, R. A. (2004a). Dysfunctional fat cells, lipotoxicity and type 2 diabetes. *International Journal Of Clinical Practice*(Suppl. (143)), 9–21.

DeFronzo, R. A. (2004b). Pathogenesis of type 2 diabetes mellitus. *Medical Clinics of North America, 88*(4), 787–835, ix.

Desai, G. S., & Mathews, S. T. (2014). Saliva as a non-invasive diagnostic tool for inflammation and insulin-resistance. *World Journal of Diabetes, 5*(6), 730–738.

Dodds, M. W., & Dodds, A. P. (1997). Effects of glycemic control on saliva flow rates and protein composition in non-insulin-dependent diabetes mellitus. *Oral Surgery, Oral Medicine, Oral Pathology, Oral Radiology, and Endodontics, 83*(4), 465–470.

Enberg, N., Alho, H., Loimaranta, V., & Lenander-Lumikari, M. (2001). Saliva flow rate, amylase activity, and protein and electrolyte concentrations in saliva after acute alcohol consumption. *Oral Surgery, Oral Medicine, Oral Pathology, Oral Radiology, and Endodontics, 92*(3), 292–298.

Esser, N., Legrand-Poels, S., Piette, J., Scheen, A. J., & Paquot, N. (2014). Inflammation as a link between obesity, metabolic syndrome and type 2 diabetes. *Diabetes Research and Clinical Practice, 105*(2), 141–150.

Falcao, D. P., da Mota, L. M., Pires, A. L., & Bezerra, A. C. (2013). Sialometry: aspects of clinical interest. *Revista Brasileira de Reumatologia, 53*(6), 525–531.

Furuzawa-Carballeda, J., Sanchez-Guerrero, J., Betanzos, J. L., Enriquez, A. B., Avila-Casado, C., Llorente, L., et al. (2014). Differential cytokine expression and regulatory cells in patients with primary and secondary Sjogren's syndrome. *Scandinavian Journal of Immunology, 80*(6), 432–440.

Garcia, C., Feve, B., Ferré, P., Halimi, S., Baizri, H., Bordier, L., et al. (2010). Diabetes and inflammation: Fundamental aspects and clinical implications. *Diabetes & Metabolism, 36*(5), 327–338.

Garrett, J. R., & Kidd, A. (1993). The innervation of salivary glands as revealed by morphological methods. *Microscopy Research and Technique, 26*(1), 75–91.

Goodson, J. M., Kantarci, A., Hartman, M. L., Denis, G. V., Stephens, D., Hasturk, H., et al. (2014). Metabolic disease risk in children by salivary biomarker analysis. *PLoS One, 9*(6), e98799.

Guo, S. (2014). Insulin signaling, resistance, and the metabolic syndrome: insights from mouse models into disease mechanisms. *The Journal of Endocrinology, 220*(2), T1–T23.

Hardy, O. T., Czech, M. P., & Corvera, S. (2012). What causes the insulin resistance underlying obesity? *Current Opinion in Endocrinology, Diabetes and Obesity, 19*(2), 81–87.

Hartman, M. L., Goodson, J. M., Barake, R., Alsmadi, O., Al-Mutawa, S., Ariga, J., et al. (2015). Salivary glucose concentration exhibits threshold kinetics in normal-weight, overweight, and obese children. *Diabetes, Metabolic Syndrome and Obesity: Targets and Therapy, 2015*(8), 9–15.

Hayward, M. C., & Shea, A. M. (2009). Nutritional needs of patients with malignancies of the head and neck. *Seminars in Oncology Nursing, 25*(3), 203–211.

Imai, K., Hiramatsu, A., Fukushima, D., Pierschbacher, M. D., & Okada, Y. (1997). Degradation of decorin by matrix metalloproteinases: identification of the cleavage sites, kinetic analyses and transforming growth factor-beta1 release. *The Biochemical Journal, 322*(Pt. 3), 809–814.

Izumi, M., Zhang, B. X., Dean, D. D., Lin, A. L., Saunders, M. J., Hazuda, H. P., et al. (2015). Secretion of salivary statherin is compromised in uncontrolled diabetic patients. *BBA Clinical, 3*, 135–140.

Jang, Y. M., Lee, E. J., Kim, D. L., Kim, S. K., & Song, K. H. (2012). The association between midnight salivary cortisol and metabolic syndrome in Korean adults. *Diabetes & Metabolism Journal, 36*(3), 245–250.

Jonsson, M. V., Delaleu, N., Brokstad, K. A., Berggreen, E., & Skarstein, K. (2006). Impaired salivary gland function in NOD mice: association with changes in cytokine profile but not with histopathologic changes in the salivary gland. *Arthritis & Rheumatology, 54*(7), 2300–2305.

Kang, E. H., Lee, Y. J., Hyon, J. Y., Yun, P. Y., & Song, Y. W. (2011). Salivary cytokine profiles in primary Sjogren's syndrome differ from those in non-Sjogren sicca in terms of TNF-alpha levels and Th-1/Th-2 ratios. *Clinical and Experimental Rheumatology, 29*(6), 970–976.

Leahy, J. L. (2005). Pathogenesis of Type 2 diabetes mellitus. *Archives of Medical Research, 36*(3), 197–209.

Lee, G. K., Lee, L. C., Chong, E., Lee, C. H., Teo, S. G., Chia, B. L., et al. (2012). The long-term predictive value of the neutrophil-to-lymphocyte ratio in Type 2 diabetic patients presenting with acute myocardial infarction. *QJM, 105*(11), 1075–1082.

Lin, C. C., Sun, S. S., Kao, A., & Lee, C. C. (2002). Impaired salivary function in patients with noninsulin-dependent diabetes mellitus with xerostomia. *J, 16*(2), 176–179.

Masago, R., Aiba-Masago, S., Talal, N., Zuluaga, F. J., Al-Hashimi, I., Moody, M., et al. (2001). Elevated proapoptotic Bax and caspase 3 activation in the NOD.scid model of Sjogren's syndrome. *Arthritis & Rheumatology, 44*(3), 693–702.

Meurman, J. H., Collin, H. L., Niskanen, L., Toyry, J., Alakuijala, P., Keinanen, S., et al. (1998). Saliva in non-insulin-dependent diabetic patients and control subjects: the role of the autonomic nervous system. *Oral Surgery, Oral Medicine, Oral Pathology, Oral Radiology, and Endodontics, 86*(1), 69–76.

Mozaffari, M. S., Abdelsayed, R., Zakhary, I., El-Salanty, M., Liu, J. Y., Wimborne, H., et al. (2011). Submandibular gland and caries susceptibility in the obese Zucker rat. *Journal of Oral Pathology & Medicine: Official Publication of the International Association of Oral Pathologists and the American Academy of Oral Pathology, 40*(2), 194–200.

Mussavira, S., Dharmalingam, M., & Omana Sukumaran, B. (2015). Salivary glucose and antioxidant defense markers in type II diabetes mellitus. *Turkish Journal of Medical Sciences, 45*(1), 141–147.

Nakamura, T., Matsui, M., Uchida, K., Futatsugi, A., Kusakawa, S., Matsumoto, N., et al. (2004). M(3) muscarinic acetylcholine receptor plays a critical role in parasympathetic control of salivation in mice. *The Journal of Physiology, 558*(Pt 2), 561–575.

Oh, S., Tanaka, K., Noh, J. W., So, R., Tsujimoto, T., Sasai, H., et al. (2014). Abdominal obesity: causal factor or simply a symptom of obesity-related health risk. *Diabetes, Metabolic Syndrome and Obesity: Targets and Therapy, 7*, 289–296.

Piras, M., Hand, A. R., Mednieks, M. I., & Piludu, M. (2010). Amylase and cyclic amp receptor protein expression in human diabetic parotid glands. *Journal of oral pathology & medicine: Official Publication of the International Association of Oral Pathologists and the American Academy of Oral Pathology, 39*(9), 715–721.

Proctor, G. B., & Carpenter, G. H. (2007). Regulation of salivary gland function by autonomic nerves. *Autonomic Neuroscience: Basic & Clinical, 133*(1), 3–18.

Rathnayake, N., Åkerman, S., Klinge, B., Lundegren, N., Jansson, H., Tryselius, Y., et al. (2013). Salivary biomarkers for detection of systemic diseases. *PLoS One, 8*(4), e61356.

Rocha, E. M., Carvalho, C. R., Saad, M. J., & Velloso, L. A. (2003). The influence of ageing on the insulin signalling system in rat lacrimal and salivary glands. *Acta Ophthalmologica Scandinavica, 81*(6), 639–645.

Rolo, A. P., & Palmeira, C. M. (2006). Diabetes and mitochondrial function: Role of hyperglycemia and oxidative stress. *Toxicology and Applied Pharmacology, 212*(2), 167–178.

Shi, P., Goodson, J. M., Hartman, M. L., Hasturk, H., Yaskell, T., Vargas, J., et al. (2015). Continuous metabolic syndrome scores for children using salivary biomarkers. *PLoS One, 10*(9), e0138979.

Shikama, Y., Ishimaru, N., Kudo, Y., Bando, Y., Aki, N., Hayashi, Y., et al. (2013). Effects of free fatty acids on human salivary gland epithelial cells. *Journal of Dental Research, 92*(6), 540–546.

von Bültzingslöwen, I., Sollecito, T. P., Fox, P. C., Daniels, T., Jonsson, R., Lockhart, P. B., et al. (2007). Salivary dysfunction associated with systemic diseases: systematic review and clinical management recommendations. *Oral Surgery, Oral Medicine, Oral Pathology, Oral Radiology, and Endodontology, 103*(Suppl. (0)) e51–S57.e15.

Vollenweider, P., von Eckardstein, A., & Widmann, C. (2015). HDLs, diabetes: and metabolic syndrome. *Handbook of Experimental Pharmacology, 224*, 405–421.

Wellen, K. E., & Hotamisligil, G. S. (2005). Inflammation, stress, and diabetes. *The Journal of Clinical Investigation, 115*(5), 1111–1119.

Yamachika, S., Brayer, J., Oxford, G. E., Peck, A. B., & Humphreys-Beher, M. G. (2000). Aberrant proteolytic digestion of biglycan and decorin by saliva and exocrine gland lysates from the NOD mouse model for autoimmune exocrinopathy. *Clinical and Experimental Rheumatology, 18*(2), 233–240.

Yamachika, S., Nanni, J. M., Nguyen, K. H., Garces, L., Lowry, J. M., Robinson, C. P., et al. (1998). Excessive synthesis of matrix metalloproteinases in exocrine tissues of NOD mouse models for Sjogren's syndrome. *The Journal of Rheumatology, 25*(12), 2371–2380.

Yin, J., Gao, H., Yang, J., Xu, L., & Li, M. (2012). Measurement of salivary resistin level in patients with type 2 diabetes. *I*2012.

Zalewska, A., Knas, M., Niczyporuk, M., Razak, H. H., Waszkiewicz, N., Przystupa, A. W., et al. (2013). Salivary lysosomal exoglycosidases profiles in patients with insulin-dependent and noninsulin-dependent diabetes mellitus. *Advances in Clinical and Experimental Medicine: Official Organ Wroclaw Medical University, 22*(5), 659–666.

Zalewska, A., Knas, M., Zendzian-Piotrowska, M., Waszkiewicz, N., Szulimowska, J., Prokopiuk, S., et al. (2014). Antioxidant profile of salivary glands in high fat diet-induced insulin resistance rats. *Oral Diseases, 20*(6), 560–566.

เอกสารแนบหมายเลข 33

Metab Brain Dis (2016) 31:239–248
DOI 10.1007/s11011-015-9789-3

REVIEW ARTICLE

Potential roles of fibroblast growth factor 21 in the brain

Piangkwan Sa-nguanmoo[1,2,3] · Nipon Chattipakorn[1,2,3] · Siriporn C. Chattipakorn[1,3,4]

Received: 5 September 2015 / Accepted: 28 December 2015 / Published online: 6 January 2016
© Springer Science+Business Media New York 2016

Abstract Fibroblast growth factor 21 (FGF21) is an endocrine hormone, playing an important role in the regulation of metabolism. FGF21 is primarily expressed by several tissues, including liver, pancreas, thymus, heart, muscle, adipose tissue, and brain. In addition to the effects of FGF21 in lowering glucose and lipid levels, increasing insulin sensitivity and regulating energy homeostasis in rodents and non-human primate models of diabetes and obesity, previous reports have demonstrated that FGF21 also plays an important role in the brain involving it in potential effects in metabolic regulation, neuroprotection and cognition. In this review, the current available evidence from both in vitro and in vivo investigations regarding the roles of FGF21 and its function in the brain are comprehensively summarized. In addition, the mechanistic insights regarding the roles of FGF21 in the brain and its potential neuroprotective benefits are also presented and discussed.

Keywords FGF21 · Hypothalamus · Cognition · Metabolism · Brain

✉ Siriporn C. Chattipakorn
scchattipakorn@gmail.com; siriporn.c@cmu.ac.th

[1] Neurophysiology Unit, Cardiac Electrophysiology Research and Training Center, Faculty of Medicine, Chiang Mai University, Chiang Mai 50200, Thailand

[2] Department of Physiology, Faculty of Medicine, Chiang Mai University, Chiang Mai, Thailand

[3] Cardiac Electrophysiology Research and Training Center, Faculty of Medicine, Chiang Mai University, Chiang Mai, Thailand

[4] Department of Oral Biology and Diagnostic Sciences, Faculty of Dentistry, Chiang Mai University, Chiang Mai, Thailand

Introduction

Fibroblast growth factor 21 (FGF21) is a polypeptide of 209 amino acids in the FGF family. It acts in a similar way to an endocrine hormone, and is preferentially expressed by adipose tissue and muscle and tissues in the liver, pancreas, testis, heart, thymus and brain (Brahma et al. 2014; Fon Tacer et al. 2010; Kharitonenkov and Shanafelt 2009; Nishimura et al. 2000). FGF21 activity occurs when FGF21 binds to the fibroblast growth factor receptor (FGFR), which is a tyrosine kinase receptor, and β-klotho (KLB), a single-pass transmembrane protein (Kharitonenkov 2009). FGFRs consist of seven major isoforms, including 1b, 1c, 2b, 2c, 3b, 3c and 4. Although FGF21 can bind with one of various FGFR isoforms, FGFR1c is the primary receptor of FGF21 in the mediation of its activity in in vivo studies (Ge et al. 2012; Tomiyama et al. 2010; Yang et al. 2012a). β-Klotho is an essential co-receptor for FGF21 activity, therefore cells without β-Klotho are unable to respond to FGF21 (Adams et al. 2012; Ogawa et al. 2007). When FGF21 binds to its receptor and co-receptor, it leads to the rapid phosphorylation of components of its downstream signaling mechanism, such as fibroblast growth factor receptor substrate 2 (FRS2). FRS2 phosphorylation activates other components of the downstream pathways, including RAS-RAF-mitogen-activation protein kinase (MAPK), phosphatidylinositol 3-kinase (PI3K)-serine-threonine protein kinase (AKT), signal transducer, the activator of transcription (STAT) and phosphoinositide phospholipase C (PLC) γ (Itoh and Ornitz 2011).

FGF21 is classified as a metabolic hormone which is stimulated to cause its physiological actions during starvation (Zhang et al. 2012). Circulating FGF21 levels were found to increase in mice fasting for 12 h (Inagaki et al. 2007), and in humans fasting for 7 days (Galman et al. 2008). FGF21

secretion was regulated by circadian rhythms in both mice and humans under fasting conditions (Yu et al. 2011). During fasting or starvation, the increased fatty acid levels activate peroxisome proliferator activated α (PPARα) in the liver, which in turn stimulate FGF21 expression via increased FGF21 transcription (Lundasen et al. 2007). Furthermore, during fasting, glucagon is also secreted from α-cells of the pancreas, which binds to the glucagon receptors in the liver, subsequently activating cAMP and downstream targets, such as protein kinase A (PKA) and exchange proteins activated by cAMP (EPAC). PKA and EPAC then activate p38MAPK and AMPK, which in turn lead to an increase in the level of FGF21 (Cyphert et al. 2014). In the liver, FGF21 increases gluconeogenesis and ketogenesis to raise glucose and ketone levels in the body, as glucose and ketone are the major sources of energy during prolonged fasting or starvation (Badman et al. 2007; Inagaki et al. 2007; Potthoff et al. 2009). Moreover, it has been shown that hyperglycemia can regulate FGF21 gene expression by activating protein phosphatase 2A (PP2A) and a carbohydrate-responsive element-binding protein (chREBP) in the liver (Uebanso et al. 2011). Therefore, FGF21 increases in line with the level of nutritional crisis, including starvation and overfeeding. A diagram illustrating the regulation of FGF21 during starvation is summarized in Fig. 1.

In a fed state under normal physiological conditions, FGF21 is found to be increased in white adipose tissue (WAT), but not in the liver, and does not pass into the circulation (Dutchak et al. 2012). FGF21 in WAT has an autocrine function through its activation of the peroxisome proliferator activated γ (PPARγ) in adipose tissue which regulates adipocyte function, by increasing lipolysis, glucose uptake, thermogenesis and fat browning (Hondares et al. 2011; Moyers et al. 2007). In addition, PPARα agonists such as fibrate drugs, a ketogenic diet (low carbohydrate, high protein), cold, amino acid deprivation, exercise and liraglutide can increase FGF21 levels (Badman et al. 2007; De Sousa-Coelho et al. 2012; Hondares et al. 2011; Kim et al. 2013; Yang et al. 2012b). FGF21 has a very short half-life (~30 min in mice, and ~2 h in monkeys), and is eliminated through renal clearance (Hindricks et al. 2014). The diagram of the regulation of FGF21 under the physiological conditions caused by overfeeding is shown in Fig. 1.

Obesity and FGF21

Obesity is becoming a major health problem worldwide. Obesity has been shown to cause insulin resistance in several

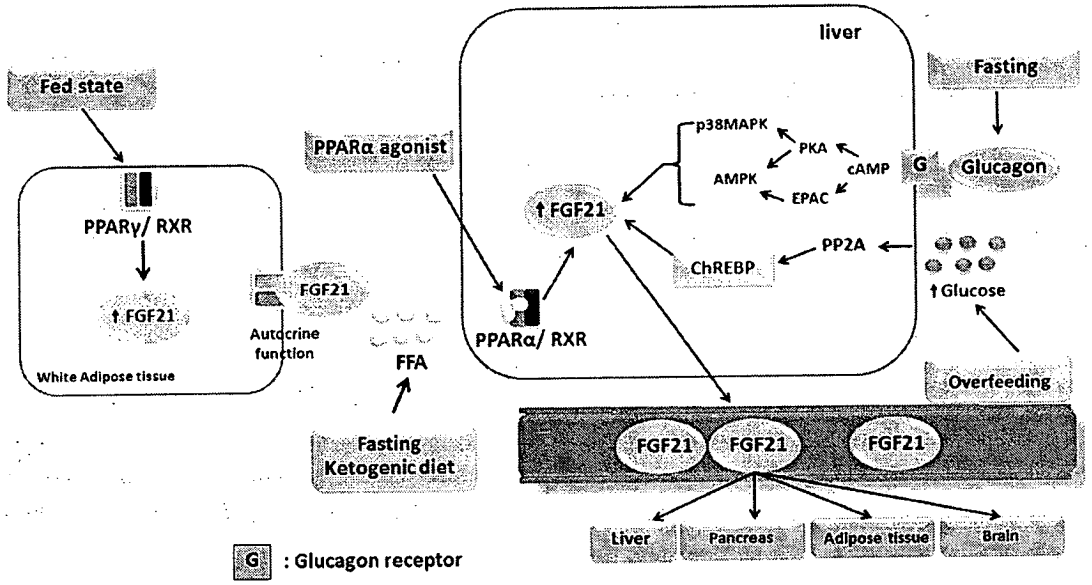


Fig. 1 Represents the mechanism of FGF21 secretion in both fed and fasting states. During the fed state, FGF21 levels are increased in white adipose tissue (WAT) due to the activation of peroxisome proliferator activated γ (PPARγ) and acts in an autocrine function via binding its receptors and co-receptor in WAT. During fasting or when fed with a ketogenic diet, the increased fatty acid levels activate peroxisome proliferator activated α (PPARα) in the liver and lead to increased FGF21 expression. Moreover, PPARα agonist can also activate directly through PPARα to increase FGF21 expression in the liver. Furthermore, during fasting, glucagon is also secreted, which binds to the glucagon receptors in the liver, subsequently activating cAMP and downstream targets, such as protein kinase A (PKA) and exchange proteins activated by cAMP (EPAC). PKA and EPAC then activate p38MAPK and AMPK, resulting to an increase in the level of FGF21. Moreover, overfeeding or hyperglycemia can regulate FGF21 gene expression by activating protein phosphatase 2A (PP2A) and a carbohydrate-responsive element-binding protein (chREBP) in the liver. Increased FGF21 expression from WAT or liver leads to augmented circulating FGF21 levels, resulting in the activation of FGF21 signaling in the target tissues, including the liver, pancreas, adipose tissue and brain

organs (Martyn et al. 2008; Shoelson et al. 2007), and can lead to the development of type 2 diabetes mellitus (T2DM) and other complications such as cardiovascular disease (Meshkani and Adeli 2009), metabolic syndrome (Mlinar et al. 2007), cognitive dysfunction (Greenwood and Winocur 2005; Umegaki 2010) and Alzheimer's disease (Biessels et al. 2005). Recent studies have demonstrated the protective effects of FGF21 and proposed that it could be a potential candidate for the treatment of those related metabolic diseases (Inagaki et al. 2005; Kharitonenkov et al. 2005; Wente et al. 2006; Zhang et al. 2006). For example: 1) loss of endogenous FGF21 in in vivo conditions led to increased insulin resistance and pancreatic islet beta cell dysfunction (So et al. 2015); 2) mice with an overexpression of FGF21 demonstrated resistance to diet-induced obesity (Kharitonenkov et al. 2005); and 3) the ability of FGF21 to increase glucose uptake in adipose tissues (Kharitonenkov et al. 2005). These findings suggest that FGF21 could act as one of the metabolic regulators. However, there have been reports in obese models in both animal and human clinical studies in which increased endogenous serum FGF21 levels were observed (An et al. 2012; Fisher et al. 2010; Hale et al. 2012; Tan et al. 2011). It has been proposed that the increased level of endogenous FGF21 is due to the bodies' response to impaired FGF21 receptor function, a condition known as "FGF21 resistance".

Although much evidence has been cited regarding the role of FGF21 in metabolic regulation, growing evidence demonstrates the potential roles of FGF21 in the brain (Bookout et al. 2013; Owen et al. 2014; Sarruf et al. 2010). Moreover, a recent study showed that FGF21 is also expressed in several areas of the brain, including the substantia nigra, striatum, hippocampus and cortex (Mäkelä et al. 2014). In addition, it has been shown that the administration of FGF21 in D-galactose induced aged mice improved cognitive function (Yu et al. 2015). Those findings indicate that FGF21 could play a role in normal physiological functions in the brain. Nevertheless, due to limited information regarding the FGF21 in the brain at this time, the relationship between FGF21 and its role in the brain are still not clearly understood. In this review, the current evidence of the relationship between FGF21 and its effects on the brain is comprehensively summarized. Consistent and controversial reports as well as the mechanistic insights regarding the roles of FGF21 in the brain is presented and discussed. The search strategy and selection criteria for this review identified the relevant publications by using search terms "FGF21 and brain" in the PubMed database published before August 2015. Only articles published in English were reviewed.

The expression of FGF 21 and its receptors in the brain

A recent study demonstrated that FGF21 is expressed in various regions of the brain, specifically regions of the midbrain, which involved dopaminergic neurons such as substantia nigra, striatum, hippocampus and cortex (Mäkelä et al. 2014). FGF21 is produced by glial cells, as evidenced by immunoblotting (Mäkelä et al. 2014). In addition to FGF21 produced in the brain itself, it has been shown that plasma FGF21 can cross the blood brain barrier by simple diffusion, and can be detected in human cerebrospinal fluid and brain tissues of rodents (Hsuchou et al. 2007; Tan et al. 2011). β-klotho is also present in several brain areas, including the

Table 1 Evidence of the roles of FGF 21 on the hypothalamic–pituitary–adrenal axis and hypothalamic-pituitary-gonadal axis

Model	Dose and durations	Major findings	Interpretation	Ref.
FGF21 knockout mice	Recombinant mouse FGF21 (0.02 μg/day; intracerebroventricular injection via cannula implanted)	↑ blood glucose levels ↑ hepatic PGC1-α, PEPCK and G6Pase expression ↑ corticotropin-releasing hormone (CRH) levels in hypothalamus ↑ adrenocorticotropic hormone (ACTH) ↑ serum corticosterone	FGF21 acts via the brain to induce corticosterone production and hepatic gluconeogenesis.	(Liang et al. 2014)
$Klb^{tm1(Camk2a)}$/Tg female mice (selectively eliminated klb expression in the SCN and DVC of Tg(fgf21) mice) compared with same aged Klb^{tm1}/Tg control mice	–	↑ vasopressin (Avp) mRNA levels in the SCN ↑ Kiss1 gene expression in AVPV nucleus	FGF21 causes female infertility in adult mice via β-klotho dependent FGF21 signaling in SCN in hypothalamus.	(Owen et al. 2013)
Klb^{tm1}/Tg control mice compared with $Klb^{tm1(Camk2a)}$ mice (selectively eliminated klb expression in the SCN and DVC)	Recombinant humanFGF21 (1.1 μg/h; subcutaneous osmotic minipumps) for 3, 7 days	↓ vasopressin (Avp) mRNA levels ↓ Kiss1 gene expression ↓ Kisspeptin levels ↓ luteinizing hormone (LH)	Fasting levels of FGF21 cause female infertility in adult mice via β-klotho dependent FGF21 signaling in SCN in hypothalamus.	(Owen et al. 2013)

suprachiasmatic nucleus (SCN); the dorsal vagal complex (DVC) of the hindbrain, in the area postrema (AP); the nucleus tractus solitarii (NTS); the nodose ganglia (Bookout et al. 2013) and the paraventricular nucleus (PVN) (Liang et al. 2014). Moreover, FGFRs have been found to be broadly expressed in the central nervous system (Fon Tacer et al. 2010). Interestingly, FGFR1c is also predominantly expressed in the brain and associated areas including the brain stem, cerebellum, cerebrum, corpus striatum, olfactory bulb, spinal cord, hypothalamus and pituitary gland (Fon Tacer et al. 2010). These findings of FGF21 expression and its receptor and co-receptor existence in the brain indicate the potential regulating roles of FGF21 in the central nervous system. Although several studies showed that that FGF21 and β-klotho might not be expressed in the same tissues (Bookout et al. 2013; Mäkelä et al. 2014; Liang et al. 2014), most of those studies demonstrated that the activation of FGF21 could not occur in the target tissue without β-klotho (Adams et al. 2012; Bookout et al. 2013; Ding et al. 2012; Owen et al. 2014). For example: 1) the study in 2012 by Ding and colleagues demonstrated that administration of FGF21 to mice lacking β-klotho in adipose tissues reduced the effect of FGF21 on reducing plasma glucose in an insulin tolerance test (Ding et al. 2012). This finding suggested that the insulin-sensitizing effect of FGF21 required β-klotho in adipose tissue. 2) The study in 2012 by Adams and colleagues demonstrated the effects of FGF21-induced normalization of glucose homeostasis, attenuation of dyslipidemia, elevation of energy expenditure and weight lost disappeared in β-klotho knockout mice (Adams et al. 2012). 3) Bookout and colleagues demonstrated that FGF21-transgenic (Tg) mice with disrupted β-klotho gene in the hypothalamus ($klb^{tml(camk2a)}$ ::Tg (Fgf21) mice), the effect of reduced plasma insulin level and body weight loss were disappeared (Bookout et al. 2013). 4) Owen and colleagues demonstrated that administration of FGF21 to mice with disrupted β-klotho gene in the hypothalamus when fed with high fat diet for 12-weeks (DIO klb^{camk2a} mice), the effect of FGF21 on reduced body weight, decreased percent

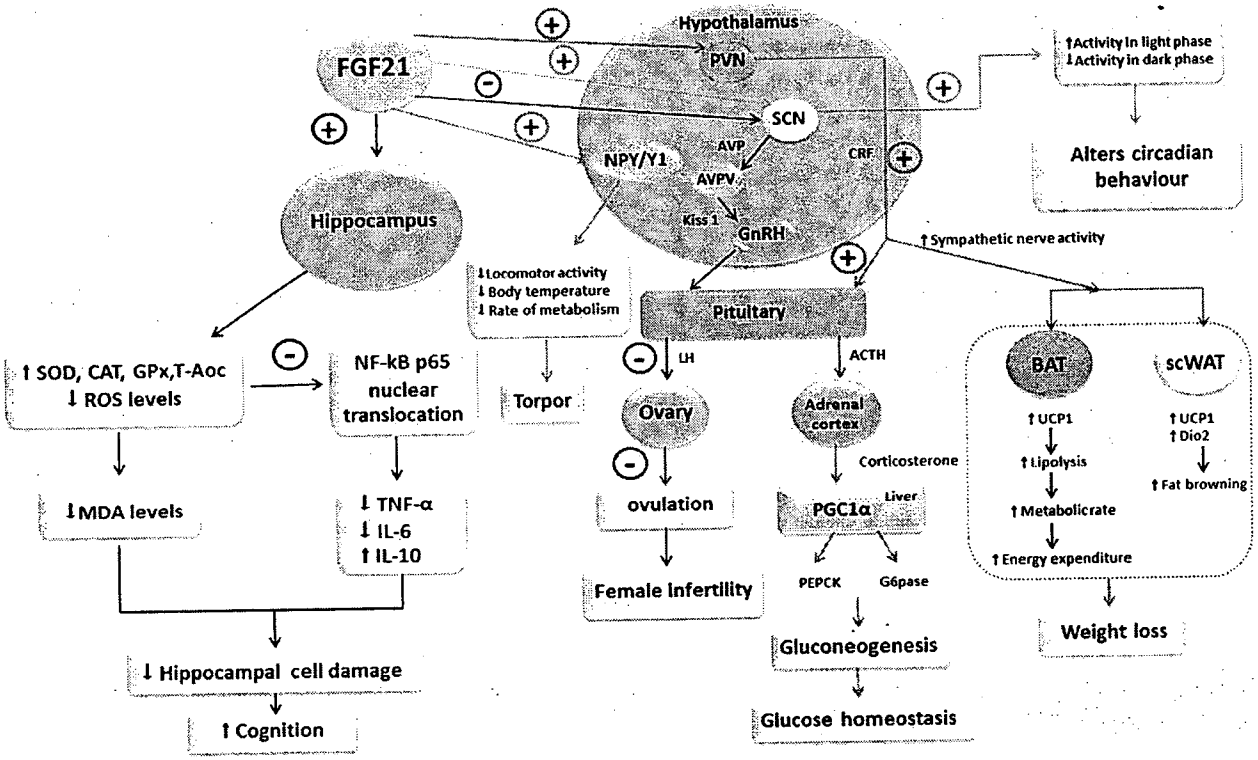


Fig. 2 Represents the effects of FGF21 on the brain. The *red arrow* suggests that the direct activation of FGF21 in the paraventricular nucleus (PVN) leads to increased levels of corticotrophin releasing factor (CRF) and increased sympathetic activity to brown and white adipose tissues, resulting to body weight loss. In addition, an increase in CRF activates the pituitary gland, leading to increase hepatic gluconeogenesis during prolonged fasting to prevent hypoglycemia. The *green arrow* suggests that the direct activation of FGF21 in the suprachiasmatic nucleus (SCN) subsequently alters circadian behavior. The *blue arrow* suggests that the direct inhibition of FGF21 in the SCN subsequently inhibits luteinizing hormone (LH) surge and ovulation, resulting in female infertility. The *orange arrow* suggests that the direct activation of FGF21 in the hypothalamus leads to increased neuropeptide Y (NPY) levels and NPY activates Y1 receptors in the hypothalamus resulting in torpor condition. The *black arrow* proposes the underlying mechanism of the effect of FGF21 on hippocampus possibly by increased anti-oxidant enzyme, decreased reactive oxygen species (ROS) levels and malondialdehyde (MDA) levels, inhibited nuclear factor kappa B (NF-κB) p65 translocation to the nucleus, decreased inflammatory markers and increased anti-inflammatory markers, which in turn decreases brain cell damage and improves cognition. +: activation; −: inhibition

Table 2 Evidence of the effects of FGF 21 on the brain involving metabolic regulation

Model	Dose and durations	Major findings	Interpretation	Ref.
Male wistar rats with obesity induced by 8-week 60 % high-fat diet compared with same aged-lean mice	Recombinant human FGF21 (0.04 μg/day; infused into lateral cerebral ventricle via osmotic minipump) for 2 weeks	↑ food intake ↑ energy expenditure ↑ glucose infusion rate ↑ G6Pase and Pepck mRNA expression ↑ peripheral and hepatic insulin sensitivity	FGF 21 action in the brain increases energy expenditure and insulin sensitivity in diet induced obese mice.	(Sarruf et al. 2010)
$Klb^{fl/fl}$ (control) mice with obesity induced by 12-week 60 % high-fat diet compared with same aged- Klb^{Camk2a} /Tg mice (selectively eliminated klb expression in the SCN and DVC of Tg(fgf21) mice)	Recombinant human FGF21 (0.8 mg/kg/day; osmotic minipumps) for 2 weeks	↓ body weight ↓ percent body fat ↓ plasma insulin levels ↓ plasma glucose levels ↓ plasma cholesterol levels ↓ plasma leptin levels ↑ UCP-1 expression in brown adipose tissue (BAT) and white adipose tissue (WAT)	β-klotho in the SCN is required for the pharmacological action of FGF21 in diet induced obese mice to reduce body weight and improve metabolic parameters.	(Owen et al. 2014)
$Klb^{fl/fl}$ (control) mice compared with Klb^{Camk2a} /Tg mice (selectively eliminated klb expression in the SCN and DVC of Tg(fgf21) mice)	Recombinant human FGF21 (1 μg; intracerebroventricular (i.c.v) injection) Recombinant human FGF21 (1 mg; Intraveneous injection). Recombinant human FGF21 (1 mg; intraperitoneal injection)	↑ brown adipose tissue (BAT) sympathetic nerve activity (SNA) ↑ brown adipose tissue (BAT) sympathetic nerve activity (SNA) but slower than i.c.v injection ↑ corticotropin releasing factor (CRF) mRNA levels in hypothalamus ↑ plasma adrenocorticotropic hormone (ACTH) levels	β-klotho in the CNS is required to enable effects of FGF21 on energy expenditure to induce CRF and to stimulate sympathetic nerve activity (SNA), subsequently inducing UCP1 and lipolysis in BAT leading to increased energy expenditure.	(Owen et al. 2014)
Male wild-type (WT) mice	Recombinant human FGF21 (0.4 μg/d; intracerebroventricular (i.c.v) infusion for 5 days	↑ UCP-1 and Dio2 in white adipose tissue (WAT) ↑ UCP-1 protein in brown adipose tissue (BAT) ↑ norepinephrine turnover in white and brown adipose tissue ↑ O_2 consumption	FGF21 acts directly through the brain, to stimulate sympathetic activity leading to increased thermogenesis and increased metabolic rate.	(Douris et al. 2015)

body fat, decreased plasma insulin, decreased plasma glucose, decreased plasma cholesterol, decreased plasma leptin and increased thermogenesis gene such as UCP-1 were absent (Owen et al. 2014). All of these findings suggest that the function of FGF21 requires β-klotho. However, only one study by Tomiyama et al. demonstrated that FGF21 signaling still occurred without the co-factor, β-klotho, in the adipose tissues (Tomiyama et al. 2010). This study reported that administration of FGF21 to β-klotho knockout (β-$kl^{-/-}$) mice led to activated FGF21 signaling, resulting in increased early growth response protein 1 (Egr-1) mRNA expression in white adipose tissue (WAT) and brown adipose tissue (BAT) (Tomiyama et al. 2010). This finding suggested that β-klotho was not essential for FGF21-mediated signaling in adipose tissue of β-klotho knockout (β-$kl^{-/-}$) mice. The contradictary findings between Tomiyama's study and other studies might be different in FGF21 mediated downstream signaling or function in each studies.

Roles of FGF 21 on the hypothalamic–pituitary–adrenal axis and hypothalamic-pituitary-gonadal axis

Growing evidence indicates that the expression of β-klotho and FGFR1c in the areas of the brain involved in the hypothalamic–pituitary–adrenal axis (HPA) and hypothalamic-pituitary-gonadal axis (HPG) include the hypothalamus, SCN, PVN and pituitary gland (Bookout et al. 2013; Fon Tacer et al. 2010; Liang et al. 2014). These findings suggest that FGF21 could play an important role in the HPA and HPG axis. A recent study found that FGF21 maintains glucose homeostasis via the cross talk between the liver and the brain,

which is mediated by the hypothalamic-pituitary-adrenal (HPA) axis during starvation (Liang et al. 2014). Liang and colleagues demonstrated that the over-expression of FGF21 in the liver during starving increased the circulating level of FGF21, leading to FGF21 crossing the blood brain barrier (Liang et al. 2014). This increased the FGF21 levels in the brain binding to the receptors in the hypothalamus, leading to the activation and phosphorylation of ERK1/2, resulting in the secretion of corticotrophin releasing hormone (CRH) from the hypothalamus (Liang et al. 2014). CRH then stimulates the pituitary gland to release adrenocorticotrophic hormone (ACTH), which in turn causes the release of adrenal corticosterone from the adrenal cortex. The adrenal corticosterone binds to its receptors in the liver, thus inducing PGC-1α expression. PGC-1α mediates the expression of gluconeogenic genes such as glucose 6 phosphatase (G6Pase) and phosphoenolpyruvate carboxykinase (PEPCK). These events have been shown to increase hepatic gluconeogenesis during prolonged fasting to prevent hypoglycemia, possibly via the activation of FGF 21 (Liang et al. 2014).

In addition, increased FGF 21 levels to the physiological FGF 21 levels at fasting state have been shown to influence the SCN in the hypothalamus of female mice, resulting in infertility. The underlying mechanism of FGF21 in inhibiting fertility is related to the hypothalamic-pituitary-gonadal axis (Owen et al. 2013). The mechanism of FGF21 action on infertility could be due to the fact that the SCN in the hypothalamus has an essential role in ovulation, by releasing vasopressin (Apv) to activate the anteroventral periventricular nuclei (AVPV) (Owen et al. 2013). This activation can lead to the expression of kisspeptin by the hypothalamus (Owen et al. 2013). Kisspeptin regulates the gonadotropin-releasing hormone (GnRH) secretion, and GnRH stimulates the anterior pituitary gland to release luteinizing hormone (LH). The release of LH normally leads to normal ovulation. However, the higher levels of FGF21 in Tg female mice disturbed the liver-neuroendocrine axis, by decreasing Apv and Kiss1 gene expression in the AVPV nucleus, resulting in the reduction of kisspeptin, thus leading to a reduction in the LH surge and abnormal ovulation (Owen et al. 2013). All of those findings suggest that FGF21 can regulate the HPA or HPG axis by acting at SCN in the hypothalamus and downstream targets in the hypothalamus as well as the pituitary gland. The effects of FGF21 on the HPA and HPG axis are summarized in detail in Table 1 and Fig. 2.

Roles of FGF21 on brain areas involved with metabolic regulation

Evidence shows that the effects of FGF21 on peripheral metabolic regulation can be mediated by the brain (Sarruf et al. 2010). The infusion of FGF21 to the lateral cerebral ventricle for 2 weeks in diet-induced obese rats resulted in increased food intake, increased energy expenditure, improved peripheral and hepatic insulin sensitivity and decreased hepatic glucose production (Sarruf et al. 2010). It has been proposed that a decrease in gluconeogenic genes in the liver, such as G6Pase and PEPCK, found following FGF21 administration into the brain in the obese model was responsible for these effects (Sarruf et al. 2010). Owen and colleagues demonstrated that the action of FGF21 in diet-induced obese mice was mediated by β-klotho in the nervous system (Owen et al. 2014). They showed that the administration of FGF21 (0.8 mg/kg/day) via subcutaneous pumps in diet-induced obese mice for 2 weeks resulted in reduced body weight, lower percentage of body fat, and improved metabolic parameters as indicated by a reduction in plasma insulin levels, plasma glucose levels, plasma cholesterol levels and plasma leptin levels. Moreover, they observed increased uncoupling protein 1 (UCP-1) expression, a thermogenic gene, which plays an important role in thermogenesis in white adipose tissue and brown adipose tissue. These effects of FGF21 disappeared in diet-induced obese Klb^{Camk2a} mice (mice lacking β-klotho in both areas of the hypothalamus, SCN and DVC) (Owen et al. 2014). All of these findings suggest that FGF21 effects on metabolic regulation in diet-induced obese mice were mediated via the activation of β-klotho in the hypothalamus.

A previous study found that administration of FGF21 (1 mg/kg) via intraperitoneal injection in normal mice led to increase in corticotrophin releasing factor (CRF) mRNA expression in the hypothalamus. This finding suggests that FGF21 can exert its beneficial effects by increasing corticotrophin releasing factor (CRF) mRNA expression in the PVN of the hypothalamus (Owen et al. 2014). It has been demonstrated that increased CRF in the hypothalamus could cause increased sympathetic nerve activity in brown adipose tissue (Owen et al. 2014), resulting in an upregulation of UCP-1 expression and increased lipolysis in brown adipose tissue (Owen et al. 2014), thus leading to increased energy expenditure and reduced weight gain in diet-induced obese mice model (Owen et al. 2014). The report by Owen and colleagues indicates that FGF21 mediated energy expenditure and body weight loss through the activation of hypothalamic neurons.

The role of FGF21 on the PVN has also recently been reported on by Douris and colleagues who demonstrated that FGF21 increased sympathetic activity and increased fat-browning via the activation of PVN (Douris et al. 2015). By infusing FGF21 (0.4 μg/day for 5 days) intracerebroventricularly in normal mice, they showed that FGF21 increased p-ERK in PVN and subsequently increased sympathetic outflow by increased norepinephrine turnover (NETO) in adipocytes. An increase in norepinephrine led to increased UCP-1 in white and brown adipocytes as well as deionase2 (Dio2) in white adipose tissues. Increased UCP-1 protein levels in brown adipose tissue led to enhanced thermogenesis and an increased metabolic rate (O_2

Table 3 Evidence of the effects of FGF 21 on behaviors and cognition

Model	Dose and durations	Major findings	Interpretation	Ref.
Transgenic overexpression of FGF21 (TgFgf21)	–	↓ total wheel running activity ↓ activity in dark phase	FGF21 acts on SCN to regulate circadian behavior.	(Bookout et al. 2013)
$Klb^{tm1(Camk2a)}$:Tg(fgf21) mice (selectively eliminated klb expression in the SCN and DVC of Tg(fgf21) mice)	–	↓ total wheel running activity ↑ activity in light phase		
Transgenic overexpression of FGF21 (TgFgf21) fasting for 24 h.	–	↓ locomotor activity ↓ body temperature	FGF21 affects the conservation of energy (Torpor) during starvation.	(Inagaki et al. 2007)
Human dopaminergic neuron	FGF21 (50 ng/ml) for 24 h.	↑ $Namp^+$ and NAD^+ ↑ sirtuin 1(SIRT1) ↑ deacetylation of PGC1-α ↑ cell viability ↑ SOD2 and Trx2 ↑ basal respiratory and higher maximal respiratory capacity	The neuroprotection effects of FGF21 were possible due to increased mitochondrial antioxidant behavior and improved mitochondrial function.	(Mäkelä et al. 2014)
Primary culture of cerebellar granule neuron of L1-/y mice (L1: The neural cell adhesion molecule L1) (age: 6–8 days)	FGF21 (0.5, 1, 2, 4 μg)	↑ neuritic outgrowth ↑ total length of neurites	FGF21 promotes neuritic outgrowth in the absence of L1. (L1 mediates outgrowth, adhesion, fasciculation and guidance of axons as well as neuronal migration and survival)	(Huang et al. 2013)
Aging male Kunming mice induced by D-galactose (age: 12-weeks)	FGF21 (1, 2, 5 mg/kg/day; subcutaneous injection) for 7 weeks	↑ spatial learning and memory in Morris water maze test and step down test ↓ hippocampal cell damage ↓ brain reactive oxygen species (ROS) and malondialdehyde (MDA) levels ↓ brain advanced glylation end products (AGEs) ↑ brain superoxide dismutase (SOD), glutathione peroxidase (Gpx), catalase (CAT) and total anti-oxidation capability (T-AOC) ↓ brain total choline esterase (TChE) activity ↓ NF-kB p65 nuclear translocation ↓ TNFα and IL-6 levels ↑ IL-10 levels	FGF21 protects mouse brain from D-galactose induced aging by decreasing hippocampal cell damage, oxidative stress, AGEs, TChE activity, pro-inflammatory cytokines and inhibiting the NF-kB pathway, resulting to improved spatial learning and memory.	(Yu et al. 2015)

consumption). These effects of FGF 21 disappeared in β-adreno-receptor ablation mice (Douris et al. 2015). The study by Douris and colleagues indicated that FGF21 acts directly through the PVN of hypothalamus, leading to increased norepinephrine levels, resulting in activation of β-adrenergic signaling, and finally increasing thermogenesis and metabolic rate in wild type (WT) mice (Douris et al. 2015). All of these findings suggest that the physiological effects of FGF21 on metabolic regulation such as enhanced metabolic parameters, increased energy expenditure, body weight loss and increased metabolic rate, happen in the brain. The possible explanation of the fact that FGF21 administration increased food intake, but reduced body weight, could be due to the activation of FGF21 at PVN. Previous studies showed that the activation of PVN led to increased sympathetic outflow to brown adipose tissue (BAT) and an increase in the expression of thermogenesis genes (e.g.

uncoupling protein 1 (UCP-1)), resulting in an increase in lipolysis, metabolic rate and energy expenditure (Owen et al. 2014). In addition, FGF21 increased thermogenesis genes such as UCP-1 and Dio-2 in WAT resulting in fat browning. Therefore, an increase in sympathetic outflow and thermogenesis following FGF21 administration could lead to a reduced body weight (Douris et al. 2015; Owen et al. 2014). The effects of FGF21 on metabolic regulation mediated by the brain are summarized in Table 2.

Physiological roles of FGF21 on behavior and cognition

Growing evidence indicates increasing roles of FGF21 on behavior and cognition. The transgenic overexpression of FGF21 (TgFgf21) mice resulted in an increased activity during the light phase, but decreased activity during the dark phase (Bookout et al. 2013). Bookout and colleague investigated the influence of FGF21 on this behavior alteration by using $Klb^{tm1(Camk2a)}$:Tg(fgf21) mice (which had selectively eliminated klb expression in the SCN and DVC in the brain of Tg(Fgf21) mice). The circadian behavior alterations did not occur in these mice. These effects of FGF21 were mediated by the SCN in the hypothalamus (Bookout et al. 2013). These findings suggest that FGF21 may potentially regulate the circadian behavior in the brain. Inagaki and colleagues demonstrated that mice with transgenically overexpressed FGF21 (TgFgf21), which had been fasting for 24-h, had reduced locomotor activity and a decreased body temperature (Inagaki et al. 2007). These findings suggest that FGF21 affects the conservation of energy (Torpor) during the fasting state. In addition, Pelz and Dark demonstrated that torpor-like hypothermia mechanisms were related to the increase in neuropeptide Y (NPY) mediated through Y1 receptors in the hypothalamus of Siberian hamsters (Pelz and Dark 2007). These findings suggest that FGF21 may have a torpor effect through regulating the expression of neuropeptide Y (NPY) and Y1 receptors in the hypothalamus (Ishida 2009).

Growing evidence also demonstrates that FGF21 has beneficial effects in the brain, including the neuroprotective effects and improved cognition. It has been shown that incubated FGF21 50 ng/ml in human dopaminergic neurons resulted in improved mitochondrial function, measured by increased mitochondrial anti-oxidant levels such as superoxide dismutase 2 (SOD2) and thioredoxin (Trx2), and enhanced mitochondrial respiratory capacity, indicated by increased sirtuin-1 (SIRT1), and peroxisome proliferator activated receptor γ coactivator 1α (PGC-1α), resulting in improved mitochondrial biogenesis and cell viability (Houten and Auwerx 2004; Mäkelä et al. 2014; Lin et al. 2005; Wu et al. 1999). In an in vitro study, FGF21 had been shown to promote neurite outgrowth in a primary culture of cerebellar granule neurons with or without L1, (the neural cell adhesion molecule) (Huang et al. 2013). Moreover, a recent study by Yu and colleagues reported that administration of FGF21 via subcutaneous injection for 7 weeks into D-galactose-induced aging mice resulted in preserved cognitive function, due to its ability to reduce neuronal damage in the hippocampus, by suppressing brain oxidative stress, increasing anti-oxidant activity in the brain, reducing total choline esterase (TAchE) activity, reducing TNF-α and IL-6 levels and increasing IL-10 (Yu et al. 2015). Since the expression of β-klotho in the hippocampus has not been demonstrated (Bookout et al. 2013; Fon Tacer et al. 2010), these neuroprotective effects of FGF21 in the hippocampus could be moderated via an FGF receptor-independent mechanism. All of these findings suggest that FGF21 improved cognition due to decreased oxidative stress and inflammation as well as increased anti-oxidants and anti-inflammation. The effects of FGF21 on physiological behavior and cognition are summarized in details of Table 3 and Fig. 2.

In conclusion, evidence strongly shows the important roles and potential benefits of FGF21 in the brain. FGF21 exerts beneficial effects on metabolic regulation, mediated by the SCN in the hypothalamus. FGF21 also has an influence on female infertility, mediated by the HPG axis. In addition, FGF 21 plays an important role on circadian behavior and the torpor condition. Interestingly, a growing amount of evidence has accrued to show the beneficial effects of FGF21 on neuroprotection and cognition. Nevertheless, the underlying mechanisms responsible for this benefit are still unclear. The way forward with this very important and relevant area of study should be further investigated in the mechanistic processes involved in the roles of FGF21 in the brain, particularly in the area of cognitive function.

Acknowledgments This work was supported by Thailand Research Fund grants: TRF-BRG 5780016 (SC), a CMU^{50th} Anniversary grant by Chiang Mai University (PHD/0023/2556 PS&NC), the National Research Council of Thailand (SC), a NSTDA Research Chair Grant from the National Science and Technology Development Agency Thailand (NC) and Chiang Mai University Center of Excellence Award (NC).

References

Adams AC, Cheng CC, Coskun T, Kharitonenkov A (2012) FGF21 requires betaklotho to act in vivo. PLoS One 7, e49977. doi:10.1371/journal.pone.0049977

An SY et al (2012) Serum fibroblast growth factor 21 was elevated in subjects with type 2 diabetes mellitus and was associated with the presence of carotid artery plaques. Diabetes Res Clin Pract 96:196–203. doi:10.1016/j.diabres.2012.01.004

Badman MK, Pissios P, Kennedy AR, Koukos G, Flier JS, Maratos-Flier E (2007) Hepatic fibroblast growth factor 21 is regulated by PPARalpha and is a key mediator of hepatic lipid metabolism in ketotic states. Cell Metab 5:426–437. doi:10.1016/j.cmet.2007.05.002

Biessels GJ, Kappelle LJ, Utrecht Diabetic Encephalopathy Study G (2005) Increased risk of Alzheimer's disease in Type II diabetes: insulin resistance of the brain or insulin-induced amyloid pathology? Biochem Soc Trans 33:1041–1044. doi:10.1042/BST20051041

Bookout AL et al (2013) FGF21 regulates metabolism and circadian behavior by acting on the nervous system. Nat Med 19:1147–1152. doi:10.1038/nm.3249

Brahma MK et al (2014) Fibroblast growth factor 21 is induced upon cardiac stress and alters cardiac lipid homeostasis. J Lipid Res 55:2229–2241. doi:10.1194/jlr.M044784

Cyphert HA, Alonge KM, Ippagunta SM, Hillgartner FB (2014) Glucagon stimulates hepatic FGF21 secretion through a PKA- and EPAC-dependent posttranscriptional mechanism. PLoS One 9, e94996. doi:10.1371/journal.pone.0094996

De Sousa-Coelho AL, Marrero PF, Haro D (2012) Activating transcription factor 4-dependent induction of FGF21 during amino acid deprivation. Biochem J 443:165–171. doi:10.1042/BJ20111748

Ding X, Boney-Montoya J, Owen BM, Bookout AL, Coate KC, Mangelsdorf DJ, Kliewer SA (2012) betaKlotho is required for fibroblast growth factor 21 effects on growth and metabolism. Cell Metab 16:387–393. doi:10.1016/j.cmet.2012.08.002

Douris N et al (2015) Central fibroblast growth factor 21 browns white fat via sympathetic action in male mice. Endocrinology 156:2470–2481. doi:10.1210/en.2014-2001

Dutchak PA, Katafuchi T, Bookout AL, Choi JH, Yu RT, Mangelsdorf DJ, Kliewer SA (2012) Fibroblast growth factor-21 regulates PPARgamma activity and the antidiabetic actions of thiazolidinediones. Cell 148:556–567. doi:10.1016/j.cell.2011.11.062

Fisher FM, Chui PC, Antonellis PJ, Bina HA, Kharitonenkov A, Flier JS, Maratos-Flier E (2010) Obesity is a fibroblast growth factor 21 (FGF21)-resistant state. Diabetes 59:2781–2789. doi:10.2337/db10-0193

Fon Tacer K et al (2010) Research resource: comprehensive expression atlas of the fibroblast growth factor system in adult mouse. Mol Endocrinol 24:2050–2064. doi:10.1210/me.2010-0142

Galman C et al (2008) The circulating metabolic regulator FGF21 is induced by prolonged fasting and PPARalpha activation in man. Cell Metab 8:169–174. doi:10.1016/j.cmet.2008.06.014

Ge H et al (2012) Characterization of a FGF19 variant with altered receptor specificity revealed a central role for FGFR1c in the regulation of glucose metabolism. PLoS One 7, e33603. doi:10.1371/journal.pone.0033603

Greenwood CE, Winocur G (2005) High-fat diets, insulin resistance and declining cognitive function. Neurobiol Aging 26(Suppl 1):42–45. doi:10.1016/j.neurobiolaging.2005.08.017

Hale C et al (2012) Lack of overt FGF21 resistance in two mouse models of obesity and insulin resistance. Endocrinology 153:69–80. doi:10.1210/en.2010-1262

Hindricks J et al (2014) Serum levels of fibroblast growth factor-21 are increased in chronic and acute renal dysfunction. Clin Endocrinol 80:918–924. doi:10.1111/cen.12380

Hondares E, Iglesias R, Giralt A, Gonzalez FJ, Giralt M, Mampel T, Villarroya F (2011) Thermogenic activation induces FGF21 expression and release in brown adipose tissue. J Biol Chem 286:12983–12990. doi:10.1074/jbc.M110.215889

Houten SM, Auwerx J (2004) PGC-1alpha: turbocharging mitochondria. Cell 119:5–7. doi:10.1016/j.cell.2004.09.016

Hsuchou H, Pan W, Kastin AJ (2007) The fasting polypeptide FGF21 can enter brain from blood. Peptides 28:2382–2386. doi:10.1016/j.peptides.2007.10.007

Huang X et al (2013) The cell adhesion molecule L1 regulates the expression of FGF21 and enhances neurite outgrowth. Brain Res 1530:13–21. doi:10.1016/j.brainres.2013.07.043

Inagaki T et al (2005) Fibroblast growth factor 15 functions as an enterohepatic signal to regulate bile acid homeostasis. Cell Metab 2:217–225. doi:10.1016/j.cmet.2005.09.001

Inagaki T et al (2007) Endocrine regulation of the fasting response by PPARalpha-mediated induction of fibroblast growth factor 21. Cell Metab 5:415–425. doi:10.1016/j.cmet.2007.05.003

Ishida N (2009) Role of PPARalpha in the control of torpor through FGF21-NPY pathway: from circadian clock to seasonal change in mammals. PPAR Res 2009:412949. doi:10.1155/2009/412949

Itoh N, Ornitz DM (2011) Fibroblast growth factors: from molecular evolution to roles in development, metabolism and disease. J Biochem 149:121–130. doi:10.1093/jb/mvq121

Kharitonenkov A (2009) FGFs and metabolism. Curr Opin Pharmacol 9:805–810. doi:10.1016/j.coph.2009.07.001

Kharitonenkov A, Shanafelt AB (2009) FGF21: a novel prospect for the treatment of metabolic diseases. Curr Opin Investig Drugs 10:359–364

Kharitonenkov A et al (2005) FGF-21 as a novel metabolic regulator. J Clin Invest 115:1627–1635. doi:10.1172/JCI23606

Kim KH, Kim SH, Min YK, Yang HM, Lee JB, Lee MS (2013) Acute exercise induces FGF21 expression in mice and in healthy humans. PLoS One 8, e63517. doi:10.1371/journal.pone.0063517

Liang Q et al (2014) FGF21 Maintains glucose homeostasis by mediating the cross talk between liver and brain during prolonged fasting. Diabetes 63:4064–4075. doi:10.2337/db14-0541

Lin J, Handschin C, Spiegelman BM (2005) Metabolic control through the PGC-1 family of transcription coactivators. Cell Metab 1:361–370. doi:10.1016/j.cmet.2005.05.004

Lundåsen T, Hunt MC, Nilsson LM, Sanyal S, Angelin B, Alexson SE, Rudling M (2007) PPARalpha is a key regulator of hepatic FGF21. Biochem Biophys Res Commun 360:437–440. doi:10.1016/j.bbrc.2007.06.068

Mäkelä J, Tselykh TV, Maiorana F, Eriksson O, Do HT, Mudò G, Korhonen LT, Belluardo N, Lindholm D (2014) Fibroblast growth factor-21 enhances mitochondrial functions and increases the activity of PGC-1α in human dopaminergic neurons via Sirtuin-1. SpringerPlus 3:1–12

Martyn JA, Kaneki M, Yasuhara S (2008) Obesity-induced insulin resistance and hyperglycemia: etiologic factors and molecular mechanisms. Anesthesiology 109:137–148. doi:10.1097/ALN.0b013e3181799d45

Meshkani R, Adeli K (2009) Hepatic insulin resistance, metabolic syndrome and cardiovascular disease. Clin Biochem 42:1331–1346. doi:10.1016/j.clinbiochem.2009.05.018

Mlinar B, Marc J, Janez A, Pfeifer M (2007) Molecular mechanisms of insulin resistance and associated diseases. Clin Chim Acta 375:20–35. doi:10.1016/j.cca.2006.07.005

Moyers JS et al (2007) Molecular determinants of FGF-21 activity-synergy and cross-talk with PPARgamma signaling. J Cell Physiol 210:1–6. doi:10.1002/jcp.20847

Nishimura T, Nakatake Y, Konishi M, Itoh N (2000) Identification of a novel FGF, FGF-21, preferentially expressed in the liver. Biochim Biophys Acta 1492:203–206

Ogawa Y et al (2007) BetaKlotho is required for metabolic activity of fibroblast growth factor 21. Proc Natl Acad Sci U S A 104:7432–7437. doi:10.1073/pnas.0701600104

Owen BM et al (2013) FGF21 contributes to neuroendocrine control of female reproduction. Nat Med 19:1153–1156. doi:10.1038/nm.3250

Owen BM et al (2014) FGF21 acts centrally to induce sympathetic nerve activity, energy expenditure, and weight loss. Cell Metab 20:670–677. doi:10.1016/j.cmet.2014.07.012

Pelz KM, Dark J (2007) ICV NPY Y1 receptor agonist but not Y5 agonist induces torpor-like hypothermia in cold-acclimated Siberian hamsters. Am J Physiol Regul Integr Comp Physiol 292:R2299–R2311. doi:10.1152/ajpregu.00790.2006

Potthoff MJ et al (2009) FGF21 induces PGC-1alpha and regulates carbohydrate and fatty acid metabolism during the adaptive starvation response. Proc Natl Acad Sci U S A 106:10853–10858. doi:10.1073/pnas.0904187106

Sarruf DA, Thaler JP, Morton GJ, German J, Fischer JD, Ogimoto K, Schwartz MW (2010) Fibroblast growth factor 21 action in the brain increases energy expenditure and insulin sensitivity in obese rats. Diabetes 59:1817–1824. doi:10.2337/db09-1878

Shoelson SE, Herrero L, Naaz A (2007) Obesity, inflammation, and insulin resistance. Gastroenterology 132:2169–2180. doi:10.1053/j.gastro.2007.03.059

So WY, Cheng Q, Xu A, Lam KS, Leung PS (2015) Loss of fibroblast growth factor 21 action induces insulin resistance, pancreatic islet hyperplasia and dysfunction in mice. Cell Death Dis 6, e1707. doi:10.1038/cddis.2015.80

Tan BK, Hallschmid M, Adya R, Kern W, Lehnert H, Randeva HS (2011) Fibroblast growth factor 21 (FGF21) in human cerebrospinal fluid: relationship with plasma FGF21 and body adiposity. Diabetes 60:2758–2762. doi:10.2337/db11-0672

Tomiyama K et al (2010) Relevant use of Klotho in FGF19 subfamily signaling system in vivo. Proc Natl Acad Sci U S A 107:1666–1671. doi:10.1073/pnas.0913986107

Uebanso T et al (2011) Paradoxical regulation of human FGF21 by both fasting and feeding signals: is FGF21 a nutritional adaptation factor? PLoS One 6, e22976. doi:10.1371/journal.pone.0022976

Umegaki H (2010) Pathophysiology of cognitive dysfunction in older people with type 2 diabetes: vascular changes or neurodegeneration? Age Ageing 39:8–10. doi:10.1093/ageing/afp211

Wente W et al (2006) Fibroblast growth factor-21 improves pancreatic beta-cell function and survival by activation of extracellular signal-regulated kinase 1/2 and Akt signaling pathways. Diabetes 55:2470–2478. doi:10.2337/db05-1435

Wu Z et al (1999) Mechanisms controlling mitochondrial biogenesis and respiration through the thermogenic coactivator PGC-1. Cell 98:115–124. doi:10.1016/S0092-8674(00)80611-X

Yang C, Jin C, Li X, Wang F, McKeehan WL, Luo Y (2012a) Differential specificity of endocrine FGF19 and FGF21 to FGFR1 and FGFR4 in complex with KLB. PLoS One 7, e33870. doi:10.1371/journal.pone.0033870

Yang M, Zhang L, Wang C, Liu H, Boden G, Yang G, Li L (2012b) Liraglutide increases FGF-21 activity and insulin sensitivity in high fat diet and adiponectin knockdown induced insulin resistance. PLoS One 7, e48392. doi:10.1371/journal.pone.0048392

Yu H et al (2011) Circadian rhythm of circulating fibroblast growth factor 21 is related to diurnal changes in fatty acids in humans. Clin Chem 57:691–700. doi:10.1373/clinchem.2010.155184

Yu Y et al (2015) Fibroblast growth factor 21 protects mouse brain against d-galactose induced aging via suppression of oxidative stress response and advanced glycation end products formation. Pharmacol Biochem Behav. doi:10.1016/j.pbb.2015.03.020

Zhang X, Ibrahimi OA, Olsen SK, Umemori H, Mohammadi M, Ornitz DM (2006) Receptor specificity of the fibroblast growth factor family. The complete mammalian FGF family. J Biol Chem 281:15694–15700. doi:10.1074/jbc.M601252200

Zhang Y et al (2012) The starvation hormone, fibroblast growth factor-21, extends lifespan in mice. eLife 1, e00065. doi:10.7554/eLife.00065

เอกสารแนบหมายเลข 34

Life Sciences 150 (2016) 15–23

Contents lists available at ScienceDirect

Life Sciences

journal homepage: www.elsevier.com/locate/lifescie

Effects of iron overload condition on liver toxicity and hepcidin/ferroportin expression in thalassemic mice

Sirinart Kumfu [a,b,c], Siriporn C. Chattipakorn [a,c,d], Suthat Fucharoen [e], Nipon Chattipakorn [a,b,c,*]

[a] Cardiac Electrophysiology Research and Training Center, Faculty of Medicine, Chiang Mai University, Chiang Mai, Thailand
[b] Cardiac Electrophysiology Unit, Department of Physiology, Faculty of Medicine, Chiang Mai University, Chiang Mai, Thailand
[c] Center of Excellence in Cardiac Electrophysiology Research, Chiang Mai University, Chiang Mai, Thailand
[d] Department of Oral Biology and Diagnostic Sciences, Faculty of Dentistry, Chiang Mai University, Chiang Mai, Thailand
[e] Thalassemia Research Center, Institute of Molecular Biosciences, Mahidol University, Nakhon Pathom, Thailand

ARTICLE INFO

Article history:
Received 17 October 2015
Received in revised form 23 December 2015
Accepted 23 February 2016
Available online 24 February 2016

Keywords:
Thalassemia
Hepcidin
Liver apoptosis
Iron-overload
Oxidative stress

ABSTRACT

Aims: Although iron-overload conditions can be found in β-thalassemic patients, resulting in cellular damage, particularly in the liver, the mechanism for this iron-mediated hepatic injury specifically in β-thalassemic (HT) mice is unclear. This study aimed to investigate the roles of L-type calcium channels (LTCC), T-type calcium channels (TTCC) and divalent metal transporter1 (DMT1) in iron-mediated hepatic injury in HT mice.
Main methods: Iron chelator deferoxamine (DFO), LTCC blocker, TTCC blocker and DMT1 blocker were used to determine the roles of these channels regarding liver iron accumulation, apoptosis and iron regulatory protein expression in HT mice.
Key findings: TTCC and DMT1 blockers and DFO decreased liver iron and malondialdehyde (MDA) in HT mice indicating their antioxidant effects, whereas LTCC blocker produced no decrease in liver iron or MDA. However, only DFO decreased liver apoptosis through the reduced Bax/Bcl-2 ratio in wild type (WT) mice. The levels of iron regulatory hormone hepcidin were markedly higher in HT mice even before iron loading while ferroportin levels did not alter. Each of the pharmacological interventions increased ferroportin protein back to normal levels only in WT while HT mice showed no difference.
Significance: Thalassemic mice have different hepcidin/ferroportin and apoptotic protein expression as a defense mechanism to iron-overload compared with those in WT mice. DFO was the most effective intervention in preventing liver apoptosis under iron-overload conditions in WT but did not have the same effect in HT mice.
© 2016 Elsevier Inc. All rights reserved.

1. Introduction

One of the most common complications found in thalassemia patients is iron-overload conditions that results in the accumulation of iron in many organs, particularly in the liver which is the main storage site for iron in body, leading to abnormal function in those organs [1–5]. Iron-overload conditions can lead to increased reactive oxygen species (ROS) production, which can damage cellular lipids, proteins, DNA and mitochondria [4–8]. Evidence has demonstrated that iron-overload is associated with an increased risk of liver complications including fibrosis, cirrhosis and hepatocellular carcinoma [4,7,8]. Previous studies demonstrated that hepatocyte apoptosis promotes liver fibrosis [9,10]. Several studies have demonstrated that caspase-3 plays a central role in cellular apoptosis [11,12]. Caspase-3 is activated by a group of signaling cascades, among which the interaction of anti-apoptotic Bcl-2 and pro-apoptotic Bax proteins play a critical role [12–14]. Previous studies have demonstrated that iron-overload conditions can lead to increased hepatocyte apoptosis due to an increased Bax/Bcl-2 ratio and caspase-3 activity [15,16]. However, the mechanism underlying hepatocyte apoptosis in thalassemic mice has never been investigated.

Previous studies demonstrated that the L-type calcium channels (LTCC), T-type calcium channels (TTCC) and divalent metal transporter1 (DMT1) were expressed in liver tissues [17–20]. Although DMT1 is known to be a common pathway for iron uptake in hepatocytes [18,21], under conditions of iron-overload the mRNA and subsequent protein expression of DMT1 in liver were suppressed [18,22]. Recently, previous study demonstrated that DMT1, LTCC, and TTCC played important roles regarding iron entry in thalassemic heart under iron-overload conditions [23]. However, the roles of TTCC, LTCC and DMT1 on iron uptake and apoptosis in hepatocytes under iron-overload conditions in thalassemic mice have never been investigated. Moreover, recent studies have demonstrated that Zinc transporter 14 (Zip14) could be a novel portal for cellular iron uptake in liver [24,25]. However, the expression of liver Zip14 protein in thalassemic mice is still unknown.

Hepcidin is a 25-amino acid peptide hormone which mainly synthesized in liver [26,27]. Under conditions of iron overload and

* Corresponding author at: Cardiac Electrophysiology Research and Training Center, Faculty of Medicine, Chiang Mai University, Chiang Mai 50200, Thailand.
E-mail address: nchattip@gmail.com (N. Chattipakorn).

http://dx.doi.org/10.1016/j.lfs.2016.02.082
0024-3205/© 2016 Elsevier Inc. All rights reserved.

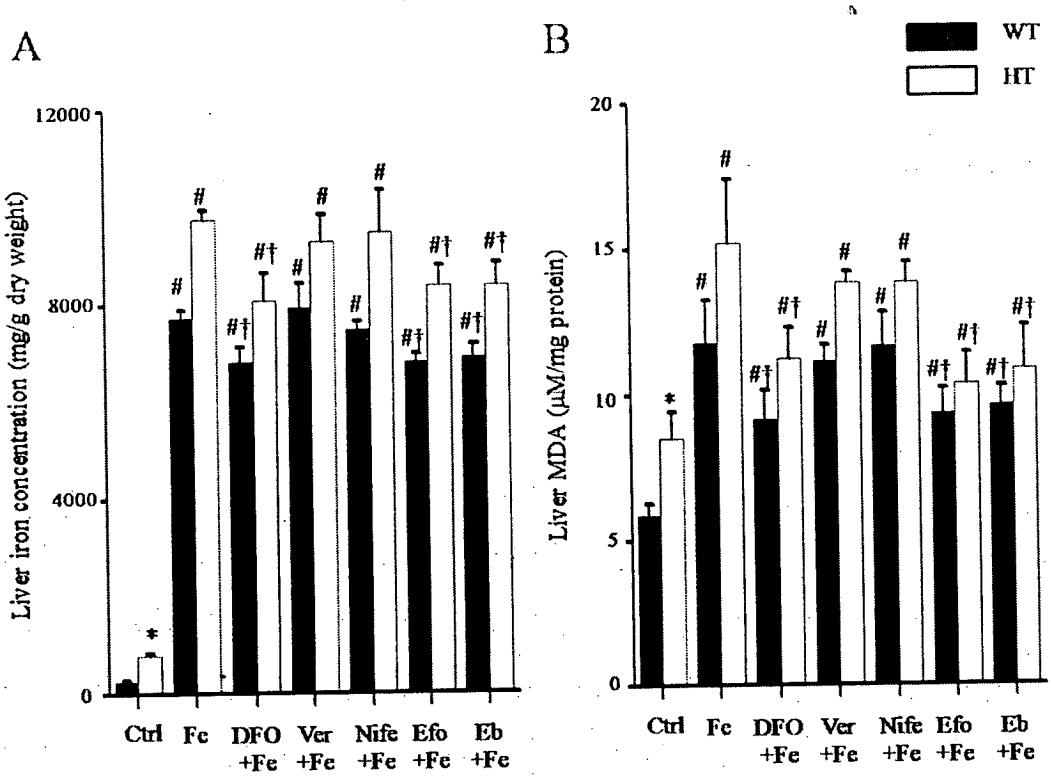


Fig. 1. Effects of pharmacological intervention on iron concentration in the liver (A) and liver malondialdehyde (B) in wild-type (WT) and thalassemic mice (HT) ($n = 6$/group). $^{\#}P < 0.05$ vs. WT, $^{*}P < 0.05$ vs. control, $^{\dagger}P < 0.05$ vs. FE.

inflammation, hepcidin level is high resulting in the reduction of serum iron due to iron being trapped within macrophages and liver cells, and also decreased gut iron absorption [26,27]. Hepcidin controls iron levels by interacting directly with iron exporter ferroportin (FPN), resulting in internalization and degradation of FPN when iron levels are high [26, 27]. However, the expression of liver hepcidin and ferroportin protein in thalassemic mice, as well as the alteration of these proteins under conditions of iron overload, are still unknown. Investigation into and clarification regarding these novel findings could lead to better treatment and prevention strategies for iron overload induced liver toxicity in thalassemia patients in very near future.

Therefore, in this study, the hypotheses tested are that: (1) thalassemic mice display more severe liver iron-overload, and altered expressions of Zip14, hepcidin and ferroportin, and (2) these alterations can be attenuated by administration of iron chelator and blockers of LTCC, TTCC and DMT1 in thalassemic mice.

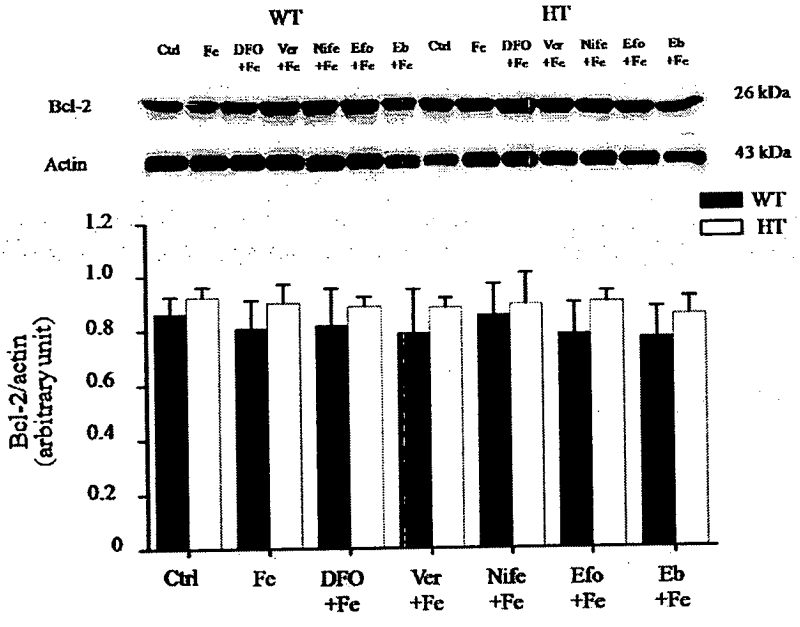


Fig. 2. Effects of pharmacological intervention on *anti*-apoptotic Bcl-2 protein expression in liver tissue in wild-type (WT) and thalassemic mice (HT) ($n = 6$/group). Loading control; actin.

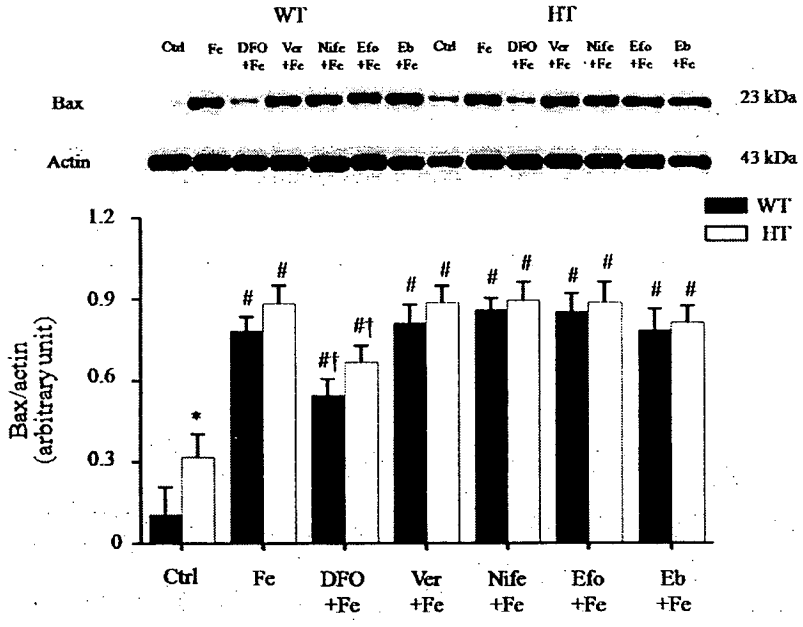


Fig. 3. Effects of pharmacological intervention on pro-apoptotic Bax protein expression in liver tissue in wild-type (WT) and thalassemic mice (HT) ($n = 6$/group). Loading control; actin. *$P < 0.05$ vs. WT, #$P < 0.05$ vs. control, †$P < 0.05$ vs. FE.

2. Materials and methods

2.1. Animal models

Two types of adult C57/BL6 mice (three to six months old), wild type (mu$\beta^{+/+}$, WT) and heterozygous β^{KO} type (mu$\beta^{th-3/+}$, HT), were used in this study [28,29]. HT mice have mild anemia as shown by a decreased hemoglobin level, increased serum iron and reactive oxygen species production, and depressed heart rate variability (HRV), all complications which are similar to thalassemia intermedia observed in humans [30]. All procedures were approved by the Institutional Animal Care and Use Committee (IACUC) of the Faculty of Medicine, Chiang Mai University, and conformed to the Guide for the Care and Use of Laboratory Animals published by the US National Institutes of Health (NIH Publication No. 85-23, revised 1996). All animals were housed in controlled temperature and humidity rooms with 12 h light–dark cycles.

2.2. Iron treatment and pharmacological interventions

Wild type and thalassemic mice were induced iron overload by feeding mice with an FE diet (0.2% ferrocene w/w; Sigma-Aldrich, St. Louis, MO, USA) (FE group) for 90 days. In the control group, WT and HT mice were fed with a normal diet for 90 days, followed by being injected with vehicle (0.5% DMSO) intraperitoneally (IP) daily and fed with normal diet for 30 days. Mice in the FE group were divided into six subgroups ($n = 6$/subgroup) and were treated with drugs with continuous FE diet feeding for 30 days. Group I (FE) mice were injected with vehicle IP daily. Group II (FE/DFO) mice were given IP injection with an iron chelator deferoxamine (Novartis, Basel, Switzerland) (DFO, 42 mg/kg) dissolved in vehicle IP daily [31]. Group III (FE/verapamil) mice were injected intraperitoneally with LTCC blocker verapamil (Sigma-Aldrich, St. Louis, MO, USA) (10 mg/kg) twice daily [32]. Group IV (FE/nifedipine) mice were given IP injection with the LTCC blocker, nifedipine, (Sigma-Aldrich, St. Louis, MO, USA) (5 mg/kg) daily [33]. Group V (FE/efonidipine) mice were given IP injection with the TTCC blocker, efonidipine, (Sigma-Aldrich, St. Louis, MO, USA) (4 mg/kg) daily [34]. Group VI (FE/ebselen) mice were given IP injection with the DMT1 blocker, ebselen, (Sigma-Aldrich, St. Louis, MO, USA) (5 mg/kg) dissolved in vehicle daily [35]. At the end of treatment, the effects of the pharmacological intervention were assessed by determining liver iron deposition and liver MDA in all mice. The western blot analysis of liver apoptosis proteins and iron regulatory proteins were also determined in all groups.

2.3. Hepatic iron content determination

The liver iron content was determined using a 2,4,6-tripyridyl-*s*-triazine (TPTZ) (Sigma-Aldrich, St. Louis, MO, USA) colorimetric technique as describe previously [36]. Briefly, the mixture of concentrated sulfuric acid and concentrated nitric acid (1:1, v/v) were used to digest dried liver tissue and adjusted volume with deionized water. The ferric ion in tissue hydrolysate was reduced to ferrous ion by incubated with hydroxylamine hydrochloride solution at room temperature for 10 min. The ferrous ion (Fe^{2+}) in the solution was reacted with a TPTZ solution and OD of violet-colored product was measured at

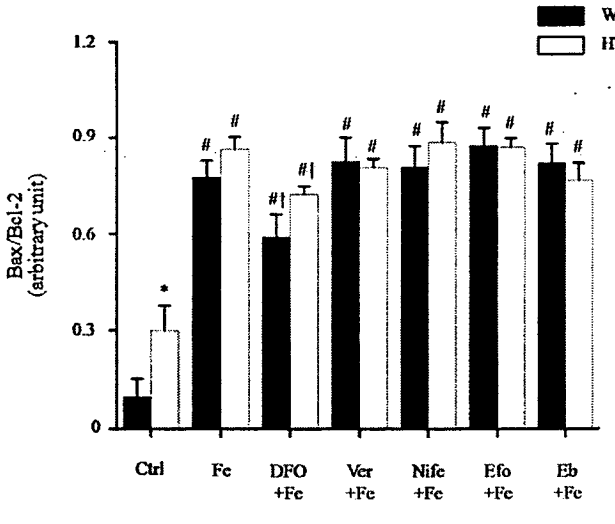


Fig. 4. Effects of pharmacological intervention on the Bax/Bcl-2 ratio in liver tissue in wild-type (WT) and thalassemic mice (HT) ($n = 6$/group). *$P < 0.05$ vs. WT, #$P < 0.05$ vs. control, †$P < 0.05$ vs. FE.

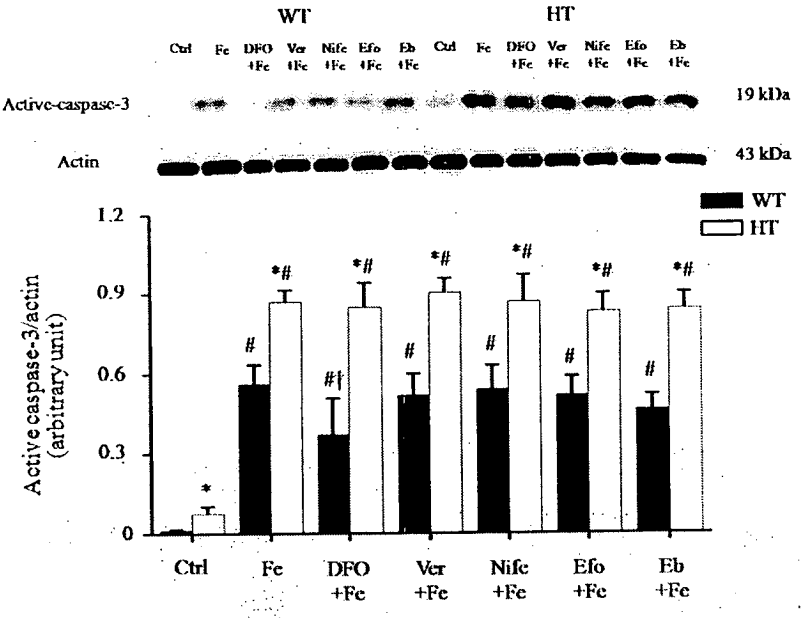


Fig. 5. Effects of pharmacological intervention on active caspase-3 protein expression in liver tissue in wild-type (WT) and thalassemic mice (HT) ($n = 6$/group). Loading control; actin. $^{*}P < 0.05$ vs. WT, $^{\#}P < 0.05$ vs. control, $^{\dagger}P < 0.05$ vs. FE.

593 nm. The ferrous ammonium sulfate was used to make standard curve at different concentrations (12.5–200 μM). Data of liver iron content was calculated from standard curve and expressed as mg/g dry weight.

2.4. Determination of liver malondialdehyde concentration

The liver malondialdehyde (MDA) concentrations were measured using the TBARS–HPLC method as describe previously [37]. The liver tissue was homogenized in the phosphate solution (50 mM phosphate buffer pH 2.8, methanol and 50 ppm butyratedhydroxytoluene (BHT)) in an ice bath. The homogenate was incubated with 10% (w/v) trichloroacetic acid (TCA) containing 50 ppm BHT and heated at 90 °C for 30 min. The mixture was centrifuged at 3300 *g* for 10 min. The supernatant was mixed with 0.44 M H_3PO_4 and 0.6% (w/v) thiobarbituric acid (TBA) (Sigma-Aldrich, St. Louis, MO, USA) solution and heated at 90 °C for 30 min to produce thiobarbituric acid-reactive substances (TBARS) as shown in pink-colored. The solution was passed through a syringe filter (polysulfone type membrane, pore size 0.45 μm; Whatman International, Maidstone, UK) and analyzed using the HPLC system. The adsorption column (Water Spherosorb ODS2 type, 250 × 4.3 mm, 5 μm) were used to fractionate TBARS and eluted with a mobile-phase solvent (50 mM KH_2PO_4: methanol (65:35 v/v)) and detected at 532 nm. Data were analyzed with the BDS software (BarSpec Ltd.). A 1,1,3,3-tetramethoxypropane (standard reagent for MDA) was used to make standard curve at different concentrations (0–100 μm). Liver MDA concentrations were calculated from the standard curve and the data of liver MDA were expressed as μM/mg protein [37].

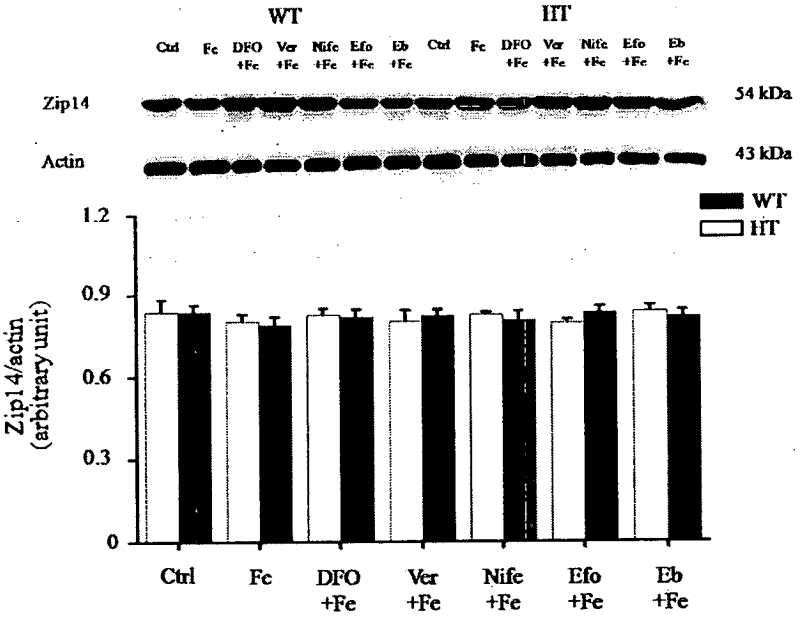


Fig. 6. Effects of pharmacological intervention on Zip14 protein expression in liver tissue in wild-type (WT) and thalassemic mice (HT) ($n = 6$/group). Loading control; actin.

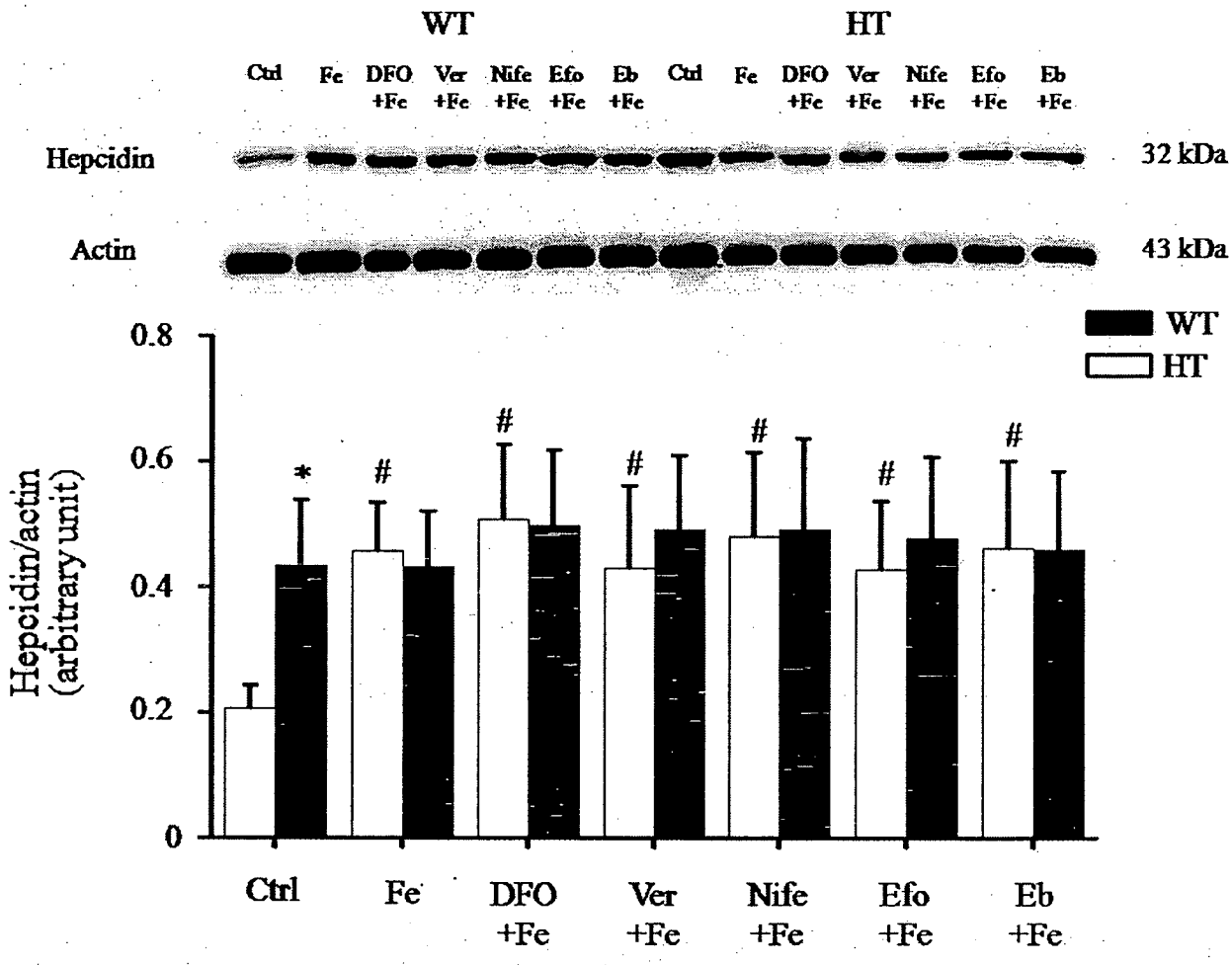


Fig. 7. Effects of pharmacological intervention on iron regulatory hormone hepcidin protein expression in liver tissue in wild-type (WT) and thalassemic mice (HT) ($n = 6$/group). Loading control: actin. $^{*}P < 0.05$ vs. WT, $^{\#}P < 0.05$ vs. control.

2.5. Western blot analysis

At the end of experiment, the liver tissues were quickly frozen in liquid nitrogen and stored at −80 °C until analysis. Liver tissues were lysed with extraction buffer (1 mmol/L Na_3VO_4, 20 mmol/L Tris–HCl, 5 mmol/L NaF). The liver protein samples were separated by electrophoresis on 10% sodium dodecyl sulfate–polyacrylamide gel and then were transferred onto nitrocellulose membranes [38]. After transferred, nitrocellulose membranes were blocked with 5% nonfat dry milk in Tris-buffer saline (pH 7.4) containing 0.1% Tween 20 for 1 h. Then, they were probed with the primary antibodies (Cell signaling technology, Inc., Danvers, MA, USA) that identify Bax, Bcl-2, caspase-3; a marker of apoptosis, and (Abcam, Cambridge, MA, USA) that identify Zip14, hepcidin, ferroportin; iron regulatory proteins, and β-actin; a loading control overnight at 4 °C, followed by incubation with the horseradish peroxidase–conjugated secondary antibody at room temperature for 1 h. The immunoblots were visualized by ECL reagent. The western blots film images were scanned and were analyzed using Image J (NIH image) analysis software.

2.6. Statistical analysis

Data was reported as the mean ± standard error of mean (SEM) and were processed using the SPSS (Statistical Package for Social Sciences, Chicago, IL, USA) release 16.0 for Windows. One-way ANOVA followed by LSD post-hoc test were performed for group comparisons. *P*-value < 0.05 was considered statistically significant.

3. Results

3.1. Effects of pharmacological intervention on liver iron concentration

In the control group, the liver iron of HT mice was significantly higher than that found in the WT mice ($P < 0.01$) (Fig. 1A). After four months of iron administration, mice in FE group (WT, HT) had significantly increased liver iron compared with the control group (Fig. 1A). Only DFO, efonidipine and ebselen caused a decrease in the liver iron concentration in both types of mice, compared with the FE group (Fig. 1A).

3.2. Effects of pharmacological intervention on liver MDA content

Iron-overload induced oxidative stress causing increased lipid peroxidation and leading to the increase in cytotoxic aldehyde products such as 4-hydroxynonenal (HNE) and MDA [5,6]. Consistent results of liver iron were found in the MDA content in the liver (Fig. 1B). Mice in the FE group (WT, HT) had a significantly increased liver MDA content, compared with the control group (Fig. 1B). These finding suggested that conditions of iron-overload can lead to increased liver oxidative stress. Only DFO, efonidipine and ebselen caused a decrease in the liver MDA concentration in both types of mice, compared with the FE group (Fig. 1B).

3.3. Effects of pharmacological intervention on liver Bax/Bcl-2 apoptotic signaling

The anti-apoptotic protein Bcl-2 and the pro-apoptotic protein Bax play key roles in the regulation of apoptosis [12–14]. The expression of an anti-apoptotic Bcl-2 protein was not different between groups in both types of mice (WT, HT) (Fig. 2). However, the expression of Bax protein, which is a pro-apoptotic protein, showed a significant increase in HT mice compared with the WT even before the high iron diet was started (Fig. 3). After iron-overload, Bax expression was significantly increased in the FE group in both types of mice compared with the control group (Fig. 3). The Bax/Bcl-2 ratio in HT mice was higher than the WT mice (Fig. 4). In the FE group, the Bax/Bcl-2 ratio showed a significant increase in both types of mice when compared with the control group (Fig. 4). After treatment, only the DFO caused a significant decrease in the Bax and Bax/Bcl-2 ratio in both types of mice under iron-overload conditions (Figs. 3 and 4).

3.4. Effects of pharmacological intervention on the activation of liver caspase-3

In the HT mice, the level of active caspase-3 (19-kDa fragments) was markedly higher than that seen in the WT mice even before iron loading (Fig. 5). Compared with the control, the level of active caspase-3 was significantly increased in the iron-overloaded liver (FE group) in both types of mice (Fig. 5). Only DFO treatment reduced active caspase-3 in

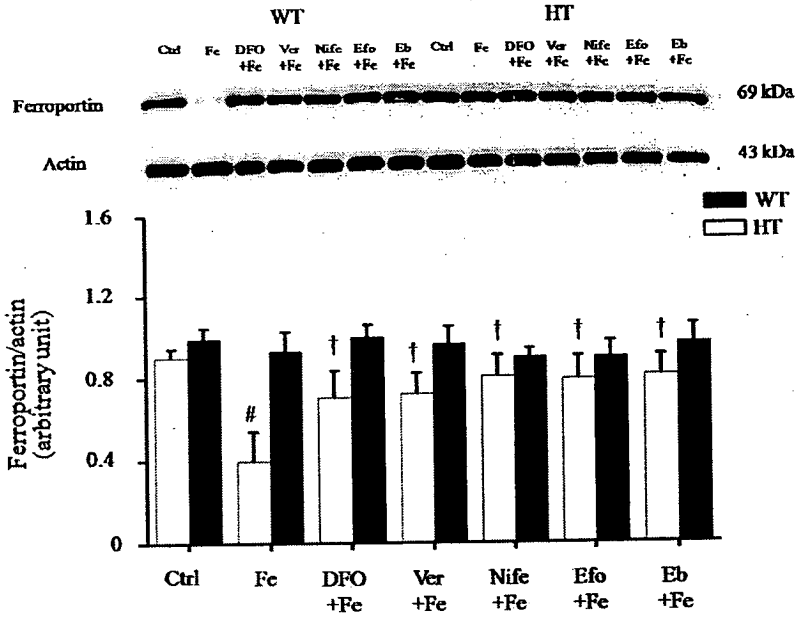


Fig. 8. Effects of pharmacological intervention on iron exporter ferroportin protein expression in liver tissue in wild-type (WT) and thalassemic mice (HT) ($n = 6$/group). Loading control: actin. *$P < 0.05$ vs. WT, †$P < 0.05$ vs. FE.

the WT mice (Fig. 5). Other pharmacological treatment could not reduce the active caspase-3 in the HT mice.

3.5. Effects of pharmacological intervention on liver Zip14 protein expression

There was no significant difference in the expression of Zip14 protein between groups in both types of mice (WT, HT) (Fig. 6).

3.6. Effects of pharmacological intervention on liver iron regulator protein expression

The levels of the iron regulatory hormone hepcidin were markedly higher in the HT mice compared to those seen in the WT mice, even before iron loading (Fig. 7). After iron-overload, hepcidin expression was significantly increased in the FE group of WT mice as well as in the pharmacologically treated groups when compared with the control group (Fig. 7). However, the expression of hepcidin protein showed no significant difference between the groups of HT mice (Fig. 7).

In the control group, the expression of the iron exporter ferroportin was not significantly different between the WT and HT mice (Fig. 8). After iron-overload, the ferroportin expression in the FE group as well as in the pharmacologically treated groups of HT mice was not significantly different between groups when compared with the control group (Fig. 8). However, the levels of the iron exporter ferroportin were significantly decreased in the FE group of WT mice when compared with the control group (Fig. 8). Each of the pharmacological interventions increased ferroportin protein levels back to within normal limits in the WT mice, and there were no differences among groups of treatment (Fig. 8).

4. Discussion

The major findings in this study are that: (i) In the HT mice, the level of liver iron, MDA, liver apoptosis, and liver hepcidin was markedly higher than those seen in the WT mice at the baseline condition; (ii) iron-overload condition caused increased liver iron, liver MDA, and liver apoptosis compared to the control group; (iii) treatment with a TTCC blocker, a DMT1 blocker and iron chelator (DFO) decreased the liver iron and MDA levels in both types of mice (WT, HT), compared to the FE group, whereas the LTCC blocker did not provide this benefit; (iv) In WT mice, only the iron chelator (DFO) decreased liver apoptosis through reducing the Bax/Bcl-2 ratio and decreasing the active caspase-3; (v) In HT mice, only the iron chelator (DFO) decreased Bax/Bcl-2, but did not decrease the active caspase-3; (vi) conditions of iron-overload increased liver hepcidin expression only in WT mice, and showed no difference between the FE group and pharmacologically treated groups; (vii) conditions of iron-overload decreased liver ferroportin expression only in WT mice, and each of the pharmacological interventions increased the level of ferroportin protein back to within normal levels.

The TTCC blocker and DMT1 blocker as well as the DFO reduced the liver iron concentration and liver MDA to a greater extent than the LTCC blockers did in both WT and HT mice. In this study, LTCC blockers did not decrease liver iron and liver MDA, suggesting that LTCC did not play an important role in iron uptake in the liver. The LTCC blockers did not decrease liver iron and apoptosis in conditions of iron-overload in mice since it has been shown that hepatocytes express a low level of LTCC [20].

Although DMT1 has been shown to be a route of iron entry into normal cells, previous studies showed that the mRNA and protein expressions of DMT1 in the liver were suppressed under conditions of iron-overload [18,22]. Furthermore, it has been shown in the DMT1 knockout mouse model ($Dmt1^{liv/liv}$) that DMT1 was not required for hepatic iron uptake under iron-overload conditions [18]. These reports suggested that DMT1 may not be necessary as a portal for iron entry into cells. However, in the present study demonstrated that the DMT1 blocker ebselen could decrease the liver iron level compared to the control group, and was supported by the decreased MDA level in the liver in thalassemic mice. Our findings suggested that DMT1 still played a role in the entry of iron into hepatocytes in thalassemic mice under conditions of iron overload. These findings were consistent with the previous report which demonstrated that DMT1 also played a role as a portal for iron entry into cardiomyocytes in the heart [23]. Furthermore, it has been shown previously that the DMT1 blocker ebselen also had antioxidative effects [39]. This could also be the mechanism responsible for the decreased MDA levels in the liver found in this study.

Regarding TTCC, although it was expressed in hepatocytes, the function of this channel in hepatocytes is still unclear [17]. Previous studies demonstrated that TTCC played an important role in iron entry into cardiomyocytes of thalassemic mice [23,40]. In the present study, the results showed that the TTCC blocker efonidipine could decrease liver iron levels as well as MDA levels, indicating that TTCC also played a role regarding iron entry in the liver. Furthermore, the finding that the level of MDA was reduced in the TTCC blocker-treated mice was consistent with a previous report that TTCC blocker could exert an antioxidant effect [41].

Despite the fact that both the TTCC blocker efonidipine and the DMT1 blocker ebselen could reduce the iron level in the liver as well as liver MDA levels, they did not decrease iron-overload induced liver apoptosis. Only the treatment with the iron chelator DFO reduced liver iron, liver MDA, Bax/Bcl-2 ratio, and caspase-3 in WT mice. These findings are consistent with previous reports that DFO reduced apoptosis in the liver under iron-overload conditions in normal animal models [42,43], suggesting that DFO is still the drug of choice for the treatment of liver iron-overload in iron-overloaded mice. Despite the beneficial effects of DFO on liver apoptosis, the effects of DFO in thalassemia have never been studied. Our findings demonstrated for the first time that DFO did not decrease hepatocyte apoptosis in these thalassemic mice since caspase-3 level was not decreased in the liver. In HT mice, the level of liver iron, MDA and liver apoptosis was markedly higher than those seen in WT mice at baseline conditions, suggesting that HT mice had a greater severity than WT mice. This may explain why DFO could not reduce liver apoptosis in HT mice compared with WT mice under conditions of iron-overload. Future investigations are needed to study the outcomes of varying doses and/or duration of DFO treatment which could possibly increase the treatment efficacy of DFO for iron-overload induced liver damage in thalassemic mice. Recent studies demonstrated that Zinc transporter 14 (Zip14) could be a new possible portal for cellular iron uptake in the liver [24,25]. In this study, liver Zip14 protein expression was not significantly different in wild type and thalassemic mice. These finding suggested that not play a role in iron uptake in the liver of thalassemic mice. Future investigations regarding the function of Zip14 in iron uptake in the liver of thalassemic mice should be carried out.

A previous study suggested that inflammation is a common complication in thalassemia patients [5,44]. Iron accumulation and inflammation led to increased hepcidin expression which limits iron release into the blood stream [45]. In the present study, the levels of the iron regulatory hormone hepcidin were markedly higher in the HT mice compared to the WT mice, even before iron loading. In addition, under conditions of iron overload, the level of liver hepcidin protein was significantly increased in the FE group of WT mice and none of the pharmacological interventions altered the level of its expression. The increase of hepcidin expression by the liver of iron overloaded WT mice and thalassemic mice might be a response to iron overload and inflammation in these mice.

In WT mice, the decrease of the iron exporter ferroportin in the FE group might be negatively regulated by the increase in hepcidin. Interestingly, each of the pharmacological interventions increased ferroportin protein to back to within normal levels. These findings suggested that all of treatments might increase iron export from the liver via ferroportin. Although LTCC blockers increased the iron exporter

ferroportin, these drugs did not block iron uptake into the liver. These results could be the reason why LTCC blocker did not decrease liver iron accumulation while the other drugs could. In HT mice, the liver ferroportin expression was not altered even after iron loading and all pharmacological intervention. The high level of the iron exporter ferroportin may be a defense mechanism in thalassemic mice to reduce iron accumulation in liver, since iron accumulation in thalassemic liver is higher than WT liver. Since neither iron chelators nor calcium channel blockers alter the expressions of ferroportin and hepcidin in HT mice in response to iron-overload, alternative therapeutic strategies may therefore be needed to increase liver iron elimination in a thalassemic liver. The limitation of this study is that PCR or immunohistochemistry techniques was not performed to confirm the findings from the western blot study.

5. Conclusion

DFO could decrease liver iron, liver MDA and hepatocyte apoptosis in WT mice under conditions of iron-overload, suggesting that DFO is still a drug of choice for the treatment of the iron-overload condition in WT. It is important to note that although DFO, a DMT1 blocker and a TTCC blocker could decrease liver iron and liver MDA (thus indicating their antioxidant effect) in thalassemic mice, none of them could cause a decrease in liver apoptosis and did not alter liver iron regulatory protein expression in these mice under iron-overload conditions. All of these novel findings suggested that thalassemic mice have different responses to iron overload induced liver toxicity mechanisms compared with WT mice. These findings suggest that other alternative pathways could play a role in liver iron uptake and apoptosis in thalassemic mice. Future studies are needed to further test this hypothesis in thalassemic mice under conditions of iron-overload to lead to better treatment and prevention strategies for iron overload induced liver toxicity in thalassemia patients in the very near future.

Conflict of interest

The authors declare that there are no conflicts of interest.

Acknowledgments

This work is supported by grants from the NSTDA Research Chair Grant from the National Science and technology Development Agency (NC), the Thailand Research Fund BRG5780016 (SC), TRG5780002 (SK), the office of the Higher Education Commission and Mahidol University under the National Research Universities Initiative (SF), and Chiang Mai University Center of Excellence Award (NC).

References

[1] D.J. Weatherall, J.B. Clegg, Inherited haemoglobin disorders: an increasing global health problem, Bull. World Health Organ. 79 (2001) 704–712.
[2] N.F. Olivieri, The beta-thalassemias, N. Engl. J. Med. 341 (1999) 99–109.
[3] D.T. Kremastinos, D. Farmakis, A. Aessopos, G. Hahalis, E. Hamodraka, D. Tsiapras, et al., Beta-thalassemia cardiomyopathy: history, present considerations, and future perspectives, Circ. Heart Fail. 3 (2013) 451–458.
[4] P. Brissot, M. Ropert, C. Le Lan, O. Loreal, Non-transferrin bound iron: a key role in iron overload and iron toxicity, Biochim. Biophys. Acta 1820 (2012) 403–410.
[5] S. Lekawanvijit, N. Chattipakorn, Iron overload thalassemic cardiomyopathy: iron status assessment and mechanisms of mechanical and electrical disturbance due to iron toxicity, Can. J. Cardiol. 25 (2009) 213–218.
[6] W.J. Bartfay, E. Bartfay, Iron-overload cardiomyopathy: evidence for a free radical-mediated mechanism of injury and dysfunction in a murine model, Biol. Res. Nurs. 2 (2000) 49–59.
[7] G. Poli, Pathogenesis of liver fibrosis: role of oxidative stress, Mol. Asp. Med. 21 (2000) 49–98.
[8] G.A. Ramm, R.G. Ruddell, Iron homeostasis, hepatocellular injury, and fibrogenesis in hemochromatosis: the role of inflammation in a noninflammatory liver disease, Semin. Liver Dis. 30 (2010) 271–287.
[9] S. Faouzi, B.E. Burckhardt, J.C. Hanson, C.B. Campe, L.W. Schrum, R.A. Rippe, et al., Anti-Fas induces hepatic chemokines and promotes inflammation by an NF-kappa B-independent, caspase-3-dependent pathway, J. Biol. Chem. 276 (2001) 49077–49082.
[10] H. Jaeschke, G.J. Gores, A.I. Cederbaum, J.A. Hinson, D. Pessayre, J.J. Lemasters, Mechanisms of hepatotoxicity, Toxicol. Sci. 65 (2002) 166–176.
[11] R.U. Janicke, P. Ng, M.L. Sprengart, A.G. Porter, Caspase-3 is required for alpha-fodrin cleavage but dispensable for cleavage of other death substrates in apoptosis, J. Biol. Chem. 273 (1998) 15540–15545.
[12] A. Gross, J. Jockel, M.C. Wei, S.J. Korsmeyer, Enforced dimerization of BAX results in its translocation, mitochondrial dysfunction and apoptosis, EMBO J. 17 (1998) 3878–3885.
[13] K.M. Murphy, V. Ranganathan, M.L. Farnsworth, M. Kavallaris, R.B. Lock, Bcl-2 inhibits Bax translocation from cytosol to mitochondria during drug-induced apoptosis of human tumor cells, Cell Death Differ. 7 (2000) 102–111.
[14] M. Narita, S. Shimizu, T. Ito, T. Chittenden, R.J. Lutz, H. Matsuda, et al., Bax interacts with the permeability transition pore to induce permeability transition and cytochrome c release in isolated mitochondria, Proc. Natl. Acad. Sci. U. S. A. 95 (1998) 14681–14686.
[15] Z. Yajun, C. Hongshan, S. Baoxi, Y. Dengbing, S. Jianhua, G. Xinshun, et al., Translocation of Bax in rat hepatocytes cultured with ferric nitrilotriacetate, Life Sci. 76 (2005) 2763–2772.
[16] H. Inoue, I. Shimizu, G. Lu, M. Itonaga, X. Cui, Y. Okamura, et al., Idoxifene and estradiol enhance antiapoptotic activity through estrogen receptor-beta in cultured rat hepatocytes, Dig. Dis. Sci. 48 (2003) 570–580.
[17] M.E. Williams, M.S. Washburn, M. Hans, A. Urrutia, P.F. Brust, P. Prodanovich, et al., Structure and functional characterization of a novel human low-voltage activated calcium channel, J. Neurochem. 72 (1999) 791–799.
[18] C.Y. Wang, M.D. Knutson, Hepatocyte divalent metal-ion transporter-1 is dispensable for hepatic iron accumulation and non-transferrin-bound iron uptake in mice, Hepatology 58 (2013) 788–798.
[19] L. Lacinova, N. Klugbauer, F. Hofmann, Low voltage activated calcium channels: from genes to function, Gen. Physiol. Biophys. 19 (2000) 121–136.
[20] E.M. Graf, M. Bock, J.F. Heubach, I. Zahanich, S. Boxberger, W. Richter, et al., Tissue distribution of a human Ca v 1.2 alpha1 subunit splice variant with a 75 bp insertion, Cell Calcium 38 (2005) 11–21.
[21] M.L. Wallander, E.A. Leibold, R.S. Eisenstein, Molecular control of vertebrate iron homeostasis by iron regulatory proteins, Biochim. Biophys. Acta 1763 (2006) 668–689.
[22] Y. Ke, Y.Y. Chen, Y.Z. Chang, X.L. Duan, K.P. Ho, D.H. Jiang, et al., Post-transcriptional expression of DMT1 in the heart of rat, J. Cell. Physiol. 196 (2003) 124–130.
[23] S. Kumfu, S. Chattipakorn, K. Chinda, S. Fucharoen, N. Chattipakorn, T-type calcium channel blockade improves survival and cardiovascular function in thalassemic mice, Eur. J. Haematol. 88 (2012) 535–548.
[24] J.P. Liuzzi, F. Aydemir, H. Nam, M.D. Knutson, R.J. Cousins, Zip14 (Slc39a14) mediates non-transferrin-bound iron uptake into cells, Proc. Natl. Acad. Sci. U. S. A. 103 (2006) 13612–13617.
[25] H. Nam, C.Y. Wang, L. Zhang, W. Zhang, S. Hojyo, T. Fukada, et al., ZIP14 and DMT1 in the liver, pancreas, and heart are differentially regulated by iron deficiency and overload: implications for tissue iron uptake in iron-related disorders, Haematologica 98 (2013) 1049–1057.
[26] B. Singh, S. Arora, P. Agrawal, S.K. Gupta, Hepcidin: a novel peptide hormone regulating iron metabolism, Clin. Chim. Acta 412 (2011) 823–830.
[27] E. Nemeth, G.C. Preza, C.L. Jung, J. Kaplan, A.J. Waring, T. Ganz, The N-terminus of hepcidin is essential for its interaction with ferroportin: structure-function study, Blood 107 (2006) 328–333.
[28] D. Jamsai, F. Zaibak, W. Khongnium, J. Vadolas, L. Voullaire, K.J. Fowler, et al., A humanized mouse model for a common beta0-thalassemia mutation, Genomics 85 (2005) 453–461.
[29] D. Jamsai, F. Zaibak, J. Vadolas, L. Voullaire, K.J. Fowler, S. Gazeas, et al., A humanized BAC transgenic/knockout mouse model for HbE/beta-thalassemia, Genomics 88 (2006) 309–315.
[30] T. Incharoen, C. Thephinlap, S. Srichairatanakool, S. Chattipakorn, P. Winichagoon, S. Fucharoen, et al., Heart rate variability in beta-thalassemic mice, Int. J. Cardiol. 121 (2007) 203–204.
[31] E.M. Walker Jr., R.G. Morrison, L. Dornon, J.P. Laurino, S.M. Walker, M. Studeny, et al., Acetaminophen combinations protect against iron-induced cardiac damage in gerbils, Ann. Clin. Lab. Sci. 39 (2009) 378–385.
[32] F. Paquette, G. Jasmin, L. Dumont, Cardioprotective efficacy of verapamil and mibefradil in young UM-X7.1 cardiomyopathic hamsters, Cardiovasc. Drugs Ther. 13 (1999) 525–530.
[33] S. Ludwiczek, I. Theurl, M.U. Muckenthaler, M. Jakab, S.M. Mair, M. Theurl, et al., Ca^{2+} channel blockers reverse iron overload by a new mechanism via divalent metal transporter-1, Nat. Med. 13 (2007) 448–454.
[34] T. Matsumura, H. Furuichi, J. Izumi, H. Suda, S. Ito, M. Takei, et al., [Effect of efonidipine hydrochloride, a calcium channel blocker, on the experimental cerebral ischemia/anoxia], Nippon Yakurigaku Zasshi 105 (1995) 437–446.
[35] R. Dhanarajan, P. Abraham, B. Isaac, Protective effect of ebselen, a selenoorganic drug, against gentamicin-induced renal damage in rats, Basic Clin Pharmacol. Toxicol. 99 (2006) 267–272.
[36] C.S. Cheng, T.D. Sullivan, P.K. Li, Iron toxicity screening, JACEP. 8 (1979) 238–240.
[37] D. Grotto, L.D. Santa Maria, S. Boeira, J. Valentini, M.F. Charao, A.M. Moro, et al., Rapid quantification of malondialdehyde in plasma by high performance liquid chromatography-visible detection, J. Pharm. Biomed. Anal. 43 (2007) 619–624.
[38] S. Surinkaew, S. Kumphune, S. Chattipakorn, N. Chattipakorn, Inhibition of p38 MAPK during ischemia, but not reperfusion, effectively attenuates fatal arrhythmia in ischemia/reperfusion heart, J. Cardiovasc. Pharmacol. 61 (2013) 133–141.
[39] M.T. Davis, W.J. Bartfay, Ebselen decreases oxygen free radical production and iron concentrations in the hearts of chronically iron-overloaded mice, Biol. Res. Nurs. 6 (2004) 37–45.

[40] S. Kumfu, S. Chattipakorn, S. Srichairatanakool, J. Settakorn, S. Fucharoen, N. Chattipakorn, T-type calcium channel as a portal of iron uptake into cardiomyocytes of beta-thalassemic mice, Eur. J. Haematol. 86 (2011) 156–166.
[41] T. Oshima, R. Ozono, Y. Yano, Y. Higashi, H. Teragawa, N. Miho, et al., Beneficial effect of T-type calcium channel blockers on endothelial function in patients with essential hypertension, Hypertens. Res. 28 (2005) 889–894.
[42] Y. Gao, N. Wang, Y. Zhang, Z. Ma, P. Guan, J. Ma, et al., Mechanism of protective effects of Danshen against iron overload-induced injury in mice, J. Ethnopharmacol. 145 (2013) 254–260.
[43] Y. Zhang, Y. Xie, Y. Gao, J. Ma, J. Yuan, J. Li, et al., Multitargeted inhibition of hepatic fibrosis in chronic iron-overloaded mice by Salvia miltiorrhiza, J. Ethnopharmacol. 148 (2013) 671–681.
[44] C.J. Murphy, G.Y. Oudit, Iron-overload cardiomyopathy: pathophysiology, diagnosis, and treatment, J. Card. Fail. 16 (2010) 888–900.
[45] S. Gardenghi, P. Ramos, A. Follenzi, N. Rao, E.A. Rachmilewitz, P.J. Giardina, et al., Hepcidin and Hfe in iron overload in beta-thalassemia, Ann. N. Y. Acad. Sci. 1202 (2010) 221–225.

เอกสารแนบหมายเลข 35

Research

228:2 85–95

Obesity does not aggravate osteoporosis or osteoblastic insulin resistance in orchiectomized rats

Saranyapin Potikanond[1,2], Pinyada Rattanachote[1], Hiranya Pintana[2], Panan Suntornsaratoon[3,4], Narattaphol Charoenphandhu[3,4], Nipon Chattipakorn[2,5,6] and Siriporn Chattipakorn[2,7]

[1]Department of Pharmacology, Faculty of Medicine, Chiang Mai University, Chiang Mai, Thailand
[2]Neurophysiology Unit, Cardiac Electrophysiology Research and Training Center, Faculty of Medicine, Chiang Mai University, Chiang Mai, Thailand
[3]Center of Calcium and Bone Research (COCAB), Faculty of Science, Mahidol University, Bangkok, Thailand
[4]Department of Physiology, Faculty of Science, Mahidol University, Bangkok, Thailand
[5]Cardiac Electrophysiology Unit, Department of Physiology, Faculty of Medicine, Chiang Mai University, Chiang Mai, Thailand
[6]Center of Excellence in Cardiac Electrophysiology Research, Chiang Mai University, Chiang Mai, Thailand
[7]Department of Oral Biology and Diagnostic Sciences, Faculty of Dentistry, Chiang Mai University, Chiang Mai, Thailand

Correspondence should be addressed to S C Chattipakorn
Email
scchattipakorn@gmail.com or siriporn.c@cmu.ac.th

Abstract

The present study aimed to test the hypothesis that testosterone deprivation impairs osteoblastic insulin signaling, decreases osteoblast survival, reduces bone density, and that obesity aggravates those deleterious effects in testosterone-deprived rats. Twenty four male Wistar rats underwent either a bilateral orchiectomy (O, $n=12$) or a sham operation (S, $n=12$). Then the rats in each group were further divided into two subgroups fed with either a normal diet (ND) or a high-fat diet (HF) for 12 weeks. At the end of the protocol, blood samples were collected to determine metabolic parameters and osteocalcin ratios. The tibiae were collected to determine bone mass using microcomputed tomography and for osteoblast isolation. The results showed that rats fed with HF (sham-operated HF-fed rats (HFS) and ORX HF-fed rats (HFO)) developed peripheral insulin resistance and had decreased trabecular bone density. In ND-fed rats, only the ORX ND-fed rats (NDO) group had decreased trabecular bone density. In addition, osteoblastic insulin resistance, as indicated by a decrease in tyrosine phosphorylation of the insulin receptor and Akt, were observed in all groups except the sham-operated ND-fed rats (NDS) rats. Those groups, again with the exception of the NDS rats, also had decreased osteoblastic survival. No differences in the levels of osteoblastic insulin resistance and osteoblastic survival were found among the NDO, HFS, and HFO groups. These findings suggest that either testosterone deprivation or obesity alone can impair osteoblastic insulin signaling and decrease osteoblastic survival leading to the development of osteoporosis. However, obesity does not aggravate those deleterious effects in the bone of testosterone-deprived rats.

Key Words
- osteoblastic insulin signaling
- testosterone deprivation
- high-fat diet induced obesity

Journal of Endocrinology (2016) 228, 85–95

http://joe.endocrinology-journals.org
DOI: 10.1530/JOE-15-0333

© 2016 Society for Endocrinology
Printed in Great Britain

Published by Bioscientifica Ltd.

Introduction

Insulin and insulin receptors play important roles in bone development and in promoting bone formation (Pun *et al.* 1989, Fulzele *et al.* 2010). Several studies have demonstrated that the downstream signaling molecules of insulin receptors, including IR, IRS1 and Akt, are required for osteoblastic proliferation and differentiation (Ogata *et al.* 2000, Kawamura *et al.* 2007). Our previous study demonstrated that obese-insulin resistant rats induced by a 12-week high-fat diet (HF) resulted in impairment of osteoblastic insulin signaling, decreased osteoblastic proliferation, increased osteoblastic apoptosis, and can lead to osteoporosis in the jaw bone (Pramojanee *et al.* 2013).

Preclinical and clinical studies have reported that obesity is associated with low serum testosterone levels or testosterone deficiency (Wang *et al.* 2011, Saboor Aftab *et al.* 2013). In addition, studies indicate that a state of testosterone deficiency could impair glucose homeostasis and insulin signaling, leading to the development of obesity, insulin resistance, and type 2 diabetes mellitus (Grossmann *et al.* 2009). Several studies have also demonstrated that a testosterone-deficient condition causes osteopenia and osteoporosis (Dupree & Dobs 2004, Tsujimura 2013). However, the effects of combined testosterone deprivation and obese insulin resistance on bone morphology, osteoblastic insulin signaling and cell survival have not yet been investigated. The present study aimed to determine the effect of combined testosterone deprivation plus an obese-insulin resistant condition on bone morphology, osteoblastic insulin signaling, and osteoblastic survival. The hypotheses of the present study are that i) either testosterone deprivation alone or an obese-insulin resistant condition alone causes impairment of osteoblastic insulin signaling, a decrease in osteoblastic survival and leads to osteoporosis, or ii) an obesity-induced insulin resistant condition aggravates those deleterious effects on bone under testosterone-deprived conditions.

Materials and methods

Animal preparation

All experiments were conducted in accordance with the approved protocol of the Faculty of Medicine, Chiang Mai University and the Institutional Animal Care Committee. Twenty-four male Wistar rats weighing 180–200 g were purchased from the National Animal Center, Salaya Campus, Mahidol University, Bangkok, Thailand.

Experimental protocol

The rats were divided into two groups ($n=12$/group), either the sham-operation (S) group or the bilateral orchiectomy (O) group. After 1 week following the orchiectomy, the rats in each group were further divided into two subgroups to receive either a normal diet (ND) or a HF for an additional 12 weeks ($n=6$/sub-group), following the procedure decribed in a study by Pramojanee *et al.* (2013). Blood samples were collected from the rats' tails for determination of glucose, cholesterol, insulin, testosterone, and osteocalcin levels at week 0 and week 12. At the end of the experiment, animals were deeply anesthetized and sacrificed. The tibiae were removed, cleaned, and kept with in normal saline at −80 °C before micro-computed tomography (micro-CT) and histomorphometry analysis. Also, total visceral fat, including peritoneal, periovarian, and perirenal fat pads were removed and weighed (Pratchayasakul *et al.* 2014). A summary of the experimental protocol is provided in Fig. 1.

Orchiectomy procedure

Orchiectomy was performed using the method described in previous studies (Dulisch 1976, Pongkan *et al.* 2015).

Plasma analysis

Plasma glucose and cholesterol levels were determined by a colorimetric assay (Biotech, Bangkok, Thailand). Plasma HDL and LDL levels were determined using a commercial colorimetric assay kit (Biovision, CA, USA). Plasma insulin levels were determined using a Sandwich ELISA kit (LINCO Research, St. Claire, MO, USA). Plasma testosterone levels were measured using the electrochemiluminescence immunoassay 'ECLIA' technique (Roche Diagnostic). Peripheral insulin resistance was assessed by the homeostasis model assessment (HOMA) (Haffner *et al.* 1997,

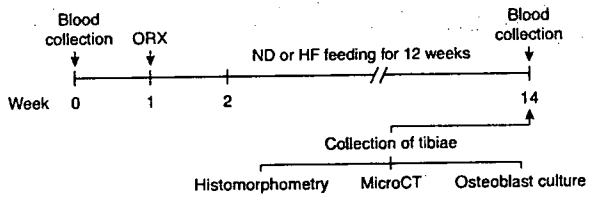


Figure 1
Experimental schematic. At the start of the first week, rats were divided into two groups: a sham-operation (S) group and a bilateral orchiectomy (ORX) group. One week after surgery, rats in each group were divided into two subgroups, receiving either a ND or a HF for 12 weeks.

http://joe.endocrinology-journals.org
DOI: 10.1530/JOE-15-0333
© 2016 Society for Endocrinology
Printed in Great Britain
Published by Bioscientifica Ltd.
Journal of Endocrinology

Appleton *et al.* 2005), a mathematical model describing the degree of insulin resistance, calculated from fasting plasma insulin and fasting plasma glucose concentration. A higher HOMA index indicates a higher degree of insulin resistance. The HOMA index was determined by the following equation: (fasting plasma insulin (μU/ml))× (fasting plasma glucose (mmol/l))/22.5 (Haffner *et al.* 1997, Appleton *et al.* 2005). The plasma Gla and Glu osteoclacin levels were measured by a rat Glu-Osteocalcin high sensitive EIA Kit (Takara Bio, Inc., Shiga, Japan) with 0.125 ng/ml minimum sensitivity of detection, 4.8% inter assay, and 6.3% intra assay.

Primary osteoblastic culture

Left tibiae were prepared in pieces for osteoblastic isolation using the serial enzymatic method (Pramojanee *et al.* 2013). Osteoblastic cells were identified with Alizarin red (Sigma–Aldrich) and alkaline phostphatase (Wako, Osaka, Japan), as described in a previous study (Pramojanee *et al.* 2013).

Cell proliferation and apoptosis assay

The osteoblastic cells were plated on glass coverslips in 96-well plates at a density of 1×10^4 cells/well and cultured for 24 h in DMEM which was supplemented with 10% FBS as previously described (Pramojanee *et al.* 2013). Cell proliferation and apoptosis assay was carried out by the following method: the osteoblasts isolated from all groups were plated in 96-well plates at the density of 1×10^4 cells/well and cultured in DMEM supplemented with 10% FBS for 24 h. Cells were starved by DMEM supplemented with 1% FBS for 24 h before stimulating with 10 nM insulin for 24 h. Cell proliferation levels were measured by a AlamarblueTM fluorometric cell viability assay (Biosource, California, USA). A TUNEL assay (Click-iT TUNEL Alexa Fluor imaging assays; Invitrogen) was used to determine cellular apoptosis levels, as described in a previous study: (Pramojanee *et al.* 2013). Cell proliferation/apoptosis was given as a percentage of the control (non-insulin stimulated cells). Three sections per sample were used in the TUNEL analysis.

Western blot analysis

The osteoblastic cells were lysed in a lysis buffer (20 mmol/l Tris–HCl, 1 mmol/l Na_3VO_4, 5 mmol/l NaF and phosphatase inhibitor) containing protease inhibitors. Protein analysis using western blot analysis was performed as previously decribed (Pramojanee *et al.* 2013). The protein preparations were separated by 10% w/v SDS–PAGE and transferred to PVDF membranes (Millipore, MA, USA). Primary antibodies at 1:1000 were used for phosphorylation of IR (Tyr 1162/1163), IRB-subunit and Cyclin D1 (Santa Cruz Biotechnology, Inc.). β-actin at 1:2000 (Santa Cruz Biotechnology, Inc.) was used as a loading control. pAkt (Ser 473), Akt and secondary at 1: 1000, anti-rabbit or anti-mouse HRP conjugated antibodies at 1:2000 were obtained from Cell Signaling Technology, Inc. (Danvers, MA, USA). The protein bands were visualized by ECL western blotting detection reagent and quantitated using ImageJ Software (NIH, Bethesda, MA, USA; http://imagej.nih.gov/ij/).

Micro-CT and trabecular microstructural analysis

Right tibiae were analyzed by a micro-CT system (model SkyScan 1178;SkyScan, Kontich, Belgium) followed by hisomorphomety for trabecular microstructural analysis as previously described (Suntornsaratoon *et al.* 2014). We analyzed the results by using a section in the mid-sagittal plane, and examined 25 areas within the tibial secondary spongiosa.

Statistical analysis

All data were expressed as mean ± S.E.M. One-way ANOVA with Dunnett's multiple comparison test was used for multiple sets of data. $P<0.05$ was considered statistically significant.

Results

HF consumption, but not testosterone deprivation, caused peripheral insulin resistance

At baseline levels (before orchiectomy), no metabolic parameters were significantly different between rats in the sham-operation (S) group and rats in the orchiectomized group (Table 1). The success of the orichectomy was

Table 1 Metabolic parameters at baseline (week 0) before operating on the sham-operated group (SHAM) and the orchiectomized group (ORX)

Metabolic parameters	SHAM	ORX
Body weight (g)	191.67±3.33	197.50±4.03
Plasma glucose (mg/dl)	105.64±6.49	109.18±4.54
Plasma insulin (ng/ml)	2.31±0.33	2.33±0.31
HOMA index	14.02±1.19	14.98±1.98
Plasma total cholesterol (mg/dl)	48.33±3.69	47.72±2.53

http://joe.endocrinology-journals.org
DOI: 10.1530/JOE-15-0333
© 2016 Society for Endocrinology
Printed in Great Britain
Published by Bioscientifica Ltd.

Journal of Endocrinology

Table 2 Metabolic parameters and plasma osteoclacin levels following either orchiectomy or sham operation

Metabolic parameters	NDS	NDO	HFS	HFO
Body weight (g)	475±8.5	425.8±10.8*,†	550±16.9*	510±14.1†
Visceral fat (g)	31.8±2.8	18.8±3.7*,†	46.0±4.5*	30.7±2.8†
Plasma insulin (ng/ml)	1.7±0.2	2.0±0.3	3.1±0.4*	2.9±0.3*
Plasma glucose (mg/dl)	145.2±6.0	143.2±12.5	147.4±6.5	146.3±7.3
HOMA index	14.6±1.7	17.2±3.2	26.6±3.0*	25.2±4.1*
Plasma total cholesterol (mg/dl)	49.4±3.7	50.0±5.7	70.7±3.3*	65.3±7.0*
Plasma testosterone (ng/dl)	0.75±0.2	0.07±0.01*,†	0.46±0.01*	0.15±0.06*,†
Gla osteoclacin (ng/ml)	150.3±11.6	171.9±13.1	171.7±14.0	163.8±30.0
Glu osteoclacin (ng/ml)	39.2±3.5	51.8±3.9*	55.4±5.6*	55.2±8.6*
Osteocalcin Gla/Glu ratio	4.5±0.4	3.3±0.2*	3.3±0.3*	3.8±0.3*

*$P<0.05$ vs NDS, †$P<0.05$ vs HFS.

confirmed by decreased plasma testosterone levels (Table 2). Interestingly, the testosterone levels of the sham-operated HF-fed rats (HFS) group also decreased significantly compared with that of the sham-operated ND-fed rats (NDS) group. After 12 weeks of the dietry protocol, both the HFS and the ORX HF-fed rats (HFO) rats presented characteristics of impaired peripheral insulin sensitivity as indicated by increased body weight, increased visceral fat, hyperinsulinemia with euglycemia, an increased HOMA index and increased plasma cholesterol levels when compared with the NDS group (Table 2). Although the body weight and quanity of visceral fat in the HFO group were significantly greater than in the NDS group, the HFO group had a lower body weight and less visceral fat than the HFS group (Table 2). In addition, the ORX ND-fed rats (NDO) rats had significantly decreased body weight and visceral fat compared with the NDS group. These findings suggest that a HF, but not testosterone deprivation, caused the obesity and the peripheral insulin resistance.

Decreased Gla/Glu osteocalcin ratio observed in both HF-fed rats and testosterone-deprived rats

The plasma Gla/Glu-osteocalcin ratio was used as a marker of bone formation. It was found that the Gla/Glu osteocalcin ratio was significantly decreased in the NDO, HFS, and HFO groups compared with that of the NDS group (Table 2). However, the ratios were not different among the NDO, HFS, and HFO rats. These findings suggest that either HF consumption or testosterone deprivation can cause a reduction in bone formation. Obesity, however, did not aggravate this deleterious effect in testosterone-deprived rats.

Trabecular bone microstructure deceased in HF-fed rats and in testosterone-deprived rats

The morphology of the tibial bones was analysed using a micro-CT. The cortical parameters, inclucing *x*-axis moment of inertia, *y*-axis moment of inertia, cortical thickness, cortical bone area, cortical periosteal perimeter, and cortical endosteal perimeter were not different among the groups (Fig. 2A, B, C, D, and F). Interestingly, trabecular bone mineral density was significantly decreased in the NDO, HFS, and HFO groups (Fig. 2G). This indicated thatosteoporosis occurred in this area. Bone histomorphometry was used to further investigate the bone microstructure. Goldner's trichrome-stained tibial sections indicated that testosterone deprivation and HF consumption led to a decrease in mineralized tissue (green) and bone volume (Fig. 3A and B). Testosterone deprivation in both ND and HF rats increased trabecular separation (Fig. 3D) and decreased trabecular number (Fig. 3E). The decrease in trabecular bone volume in HFS was probably the result of the decreased trabecular number rather than the decreased trabecular thickness (Fig. 3E).

Osteoblastic proliferation significantly decreased in HF-fed rats and testosterone-deprived rats

Cells isolated from tibiae and cultured in osteogenic medium were positively stained with Alizarin red (Fig. 4A, C, E, and G) and alkaline phosphatase (Fig. 4B, D, F, and H), to identify osteoblastic characteristics. AlamarBlue fluorometric cell viability assay was performed at 1, 2, 4, 6, 24, 48, and 72 h after initial culturing. The number of cells was significantly decreased in the NDO, HFS, and HFO groups at 48 and 72 h when compared with the NDS group (Fig. 4J).

http://joe.endocrinology-journals.org
DOI: 10.1530/JOE-15-0333
© 2016 Society for Endocrinology
Printed in Great Britain
Published by Bioscientifica Ltd.

Journal of Endocrinology

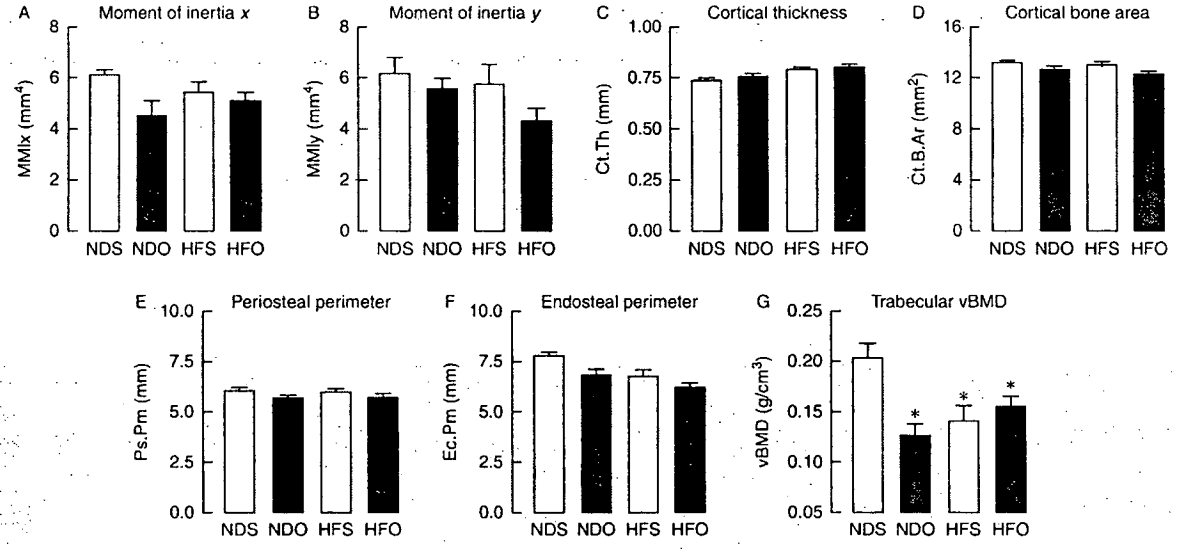


Figure 2
The tibial diaphysis of rats at 12 weeks post surgery was determined by micro-CT, *x*-axis moment of inertia (MMIx; A), *y*-axis moment of inertia (MMIy; B), cortical thickness (Ct.Th; C), cortical bone area (Ct.B.Ar; D), cortical periosteal perimeter (Ct.Pe.Pm; E), cortical endosteal perimeter (Ct.En.Pm; F), and tibial bone mineral density (T.BMD; G). $^{*}P<0.05$ vs NDS group.

A proliferation signal, Cyclin D1 protein, was decreased in the HF-fed rats and testosterone-deprived rats (Fig. 4L). No differences in these factors were found among the NDO, HFS, and HFO groups. These findings suggest that either testoterone deprivation alone or HF consumption alone can cause a reduction in osteoblastic proliferation, but that obesity induced by HF consumption does not aggravate this effect in testosterone-deprived rats.

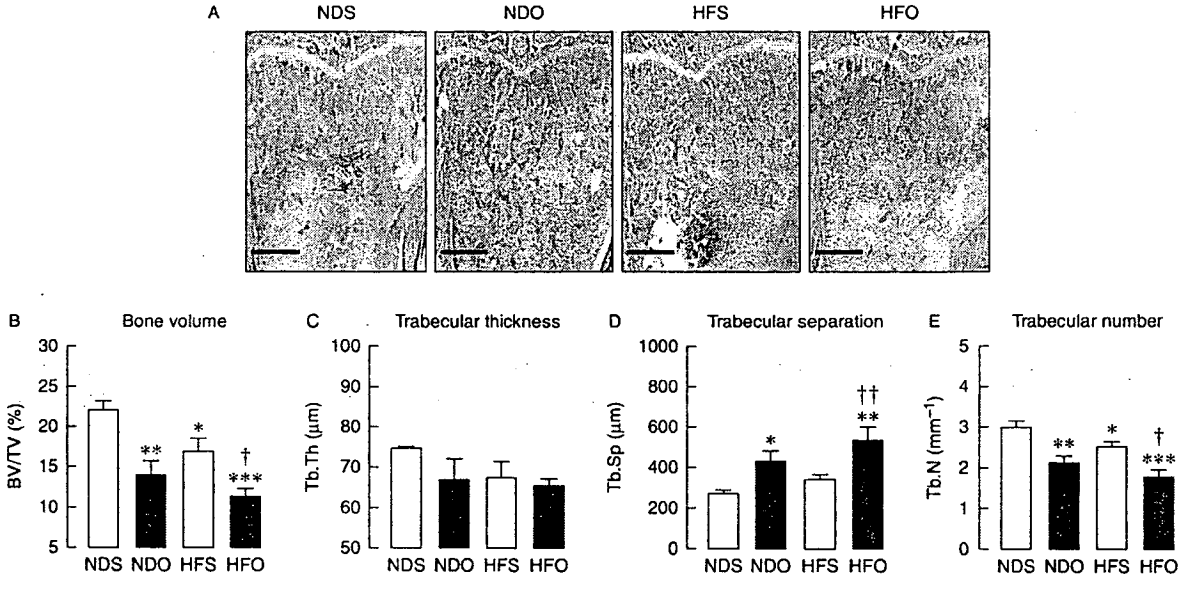


Figure 3
Micrographs of proximal tibial metaphyses (A). Scale bars = 1000 μm. Bar graphs represent bone volume fraction (BV/TV) (B), trabecular thickness (Tb.Th) (C), trabecular separation (Tb.Sp) (D), and trabecular number (Tb.N) (E). $^{*}P<0.05$ vs NDS group; $^{**}P<0.01$ vs NDS group; $^{***}P<0.001$ vs the NDS group; $^{\dagger}P<0.05$ vs the HFS group; $^{\dagger\dagger}P<0.01$ vs the HFS group. A full colour version of this figure is available at http://dx.doi.org/10.1530/JOE-15-0333.

© 2016 Society for Endocrinology
Printed in Great Britain
Published by Bioscientifica Ltd.

Journal of Endocrinology

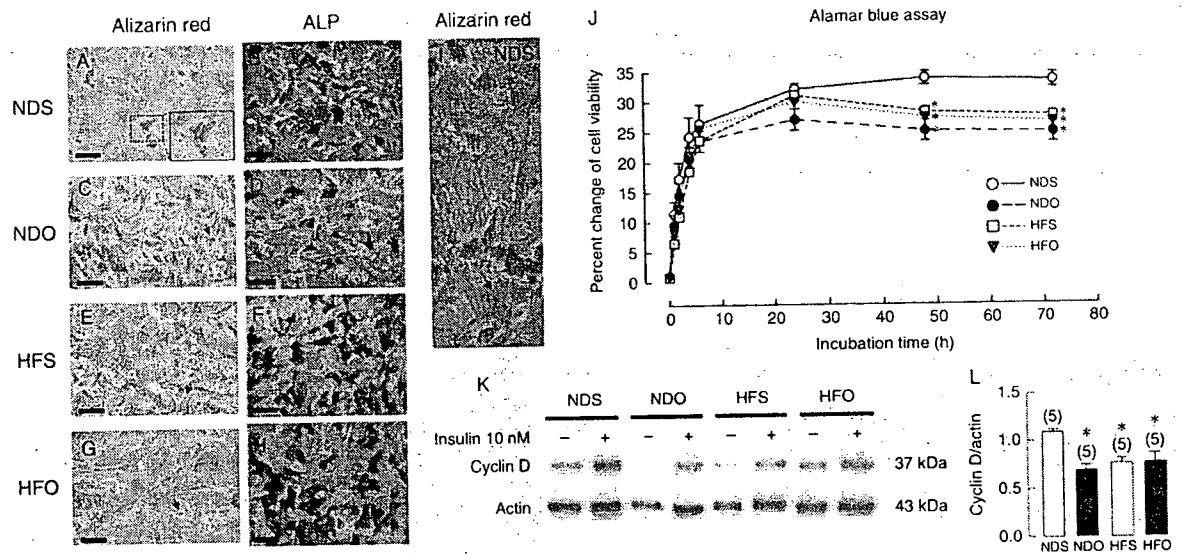


Figure 4
Alizarin red (A, C, E, and G) and alkaline phosphatase staining (B, D, F, and H) were performed to characterize osteoblasts. (I) Magnified image of cultured osteoblasts (stellate cell with nucleus; arrow) from NDS group. Alizarin-stained nodules (red) are scattered in matrix. The percentage change of cell viability using alamarBlue fluoremetric cell viability assay is shown in J. The representation of cyclinD protein expression with insulin stimulation (+) and without insulin stimulation (−) are shown in K. Bar graphs represent densitometric values of cyclin D calculating by the level of cyclin D without insulin stimulation normalizing with level of actin (L). *$P<0.05$ vs NDS group. A full colour version of this figure is available at http://dx.doi.org/10.1530/JOE-15-0333.

Osteoblastic apoptosis significantly increased in both HF-fed rats and testosterone-deprived rats

Apoptotic cell death, measured with TUNEL assay, significantly increased in the NDO, HFS, and HFO groups when compared with the NDS group (Fig. 5). No differences in apoptotic cell death were found among the NDO, HFS, and HFO groups. These findings suggest that either obesity alone or testosterone deprivation alone results in increased osteoblastic apoptosis. However, obesity induced by HF consumption did not aggravate apoptotic cell death in testosterone-deprived rats.

Osteoblastic insulin signaling impaired in both HF-fed rats and testosterone-deprived rats

The osteoblastic insulin signaling activity was determined by tyrosine phosphorylation of insulin receptors after stimulation with10 nM of insulin for 10 min. The phosphorylation of the insulin receptor was decreased in the NDO, HFS, and HFO groups compared with that of the NDS group (Fig. 6A and B). In addition, the phosphorylation of the downstream insulin signaling molecule, Akt, was significantly decreased in the NDO, HFS, and HFO groups when compared with that in the NDS group (Fig. 6A and C).

Discussion

Based on the findings of this study, it appears that HF consumption, not testosterone deprivation, causes obesity and peripheral insulin resistance. Furthermore, testosterone deprivation alone and HF-induced obsity alone lead to a decrease in serum osteocalcin, decreased osteoblastic proliferation, increased osteoblastic apoptosis, osteoblastic insulin resistance, and the impairment of bone microarchitectures. In addition, an obesity-induced insulin resistant condition does not aggravate those deleterious effects in the bones of testosterone-deprived rats.

The present findings and those of previous reports (Winzell & Ahren 2004, Pramojanee *et al.* 2013) demonstrate that obesity induced by 12-week HF consumption causes peripheral insulin resistance as indicated by increased body weight, increased visceral fat, hyperinsulinemia with euglycemia, and an increased HOMA index. The development of peripheral insulin resistance in the present study was dependent on HF-induced obesity, but not testosterone deprivation, as confirmed by the fact

© 2016 Society for Endocrinology
Printed in Great Britain
Published by Bioscientifica Ltd.

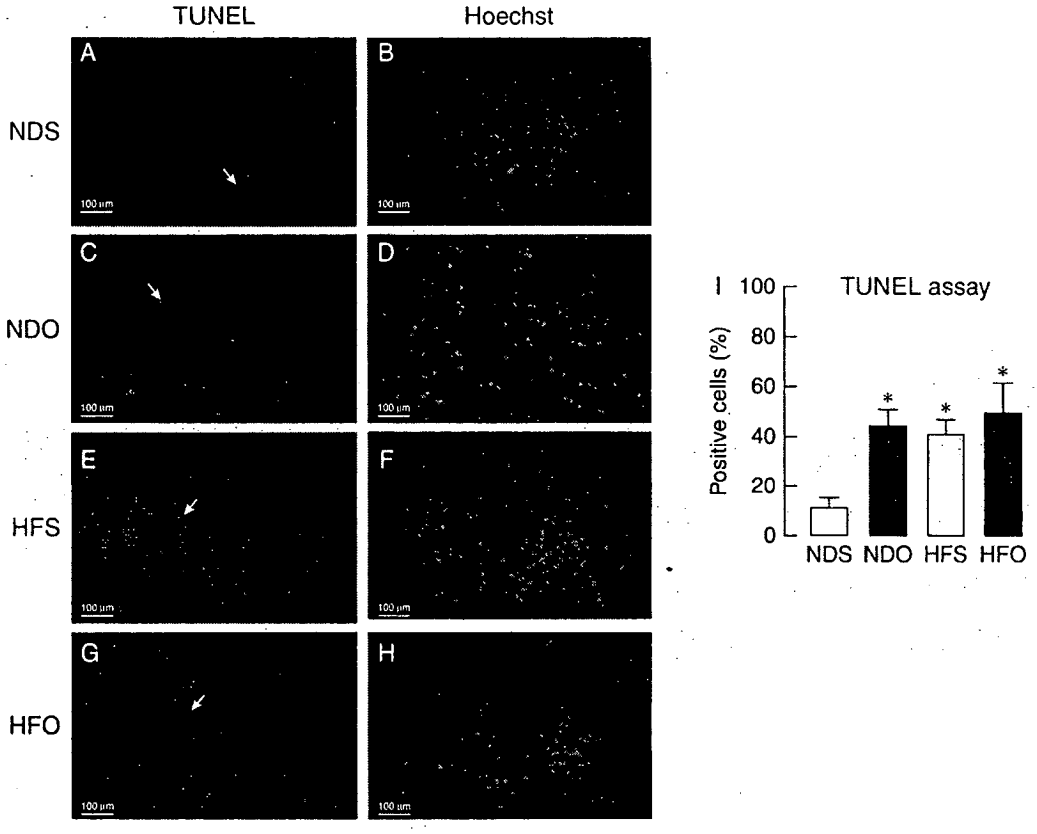


Figure 5
Measurement of apoptotic cell death was performed by TUNEL assay. Apoptotic cells were labeled with green fluorescent (A, C, E, and G) and are indicated by arrows. Nuclease labeling with Hoechst stain is shown in B, D, F, and H. Scale bars are 100 μm. The bar graph represents the percentage of positive TUNEL cells (I). *$P<0.05$ vs NDS group. A full colour version of this figure is available at http://dx.doi.org/10.1530/JOE-15-0333.

that there was no change in the HOMA index in the NDO rats. These findings are consistent with a report by Christoffersen *et al.* (2006). However, several previous studies have reported that testosterone deprivation alone via orchiectomy (ORX) in male rodents causes impairment of insulin sensitivity (Xia *et al.* 2013, Jayaraman *et al.* 2014*a*). For example, Xia *et al.* (2013) found that ORX-induced testosterone deficiency increased fasting blood glucose in mature adult (10 week old) male Sprague–Dawley rats. Jayaraman *et al.* (2014a b) demonstrated that ORX adult mice (3 months of age) had impaired insulin sensitivity. Differences in the breed and age at the start of the ORX procedure (this study used young adult male Wistar rats orchiectomized at 5–6 weeks of age rather than Sprague–Dawley rats) might be the cause of the differences in the results.

Previous studies reported the role of osteocalcin in increased insulin sensitivity in the target organs (Saleem *et al.* 2010, Xiao *et al.* 2014). The present study showed that the ratio of Gla/Glu ratio and Glu osteocalcin levels in NDO, HFS, and HFO groups significantly reduced, when compared with that of the NDS group. However, Gla osteocalcin levels among all four groups were not significantly different. These findings suggested that the reduction of Gla/Glu osteocalcin ratio in NDO, HFS, and HFO groups was due to increased Glu levels, implying that decreased insulin sensitivity could occur in NDO, HFS, and HFO groups. The present study, however, also demonstrated a reduction in the Gla/Glu osteovlacin ratio as well as the impairment of osteoblastic insulin signaling as indicated by decreased phosphorylation of the insulin receptor and its downstream signaling molecule, Akt protein, in either orchiectomy alone or HF-induced obesity alone. Our findings suggested that the osteoblastic insulin resistance in both testosterone-deprived rats and obese-insulin resistant rats could possibly occur via the

© 2016 Society for Endocrinology
Printed in Great Britain
Published by Bioscientifica Ltd.

Journal of Endocrinology

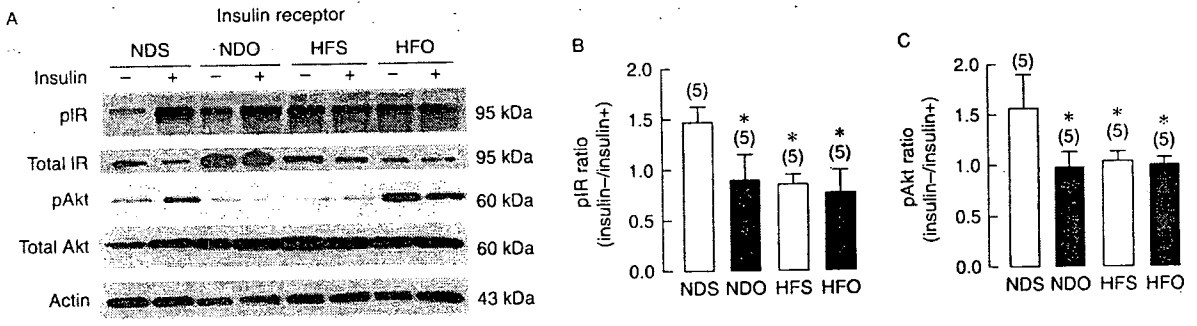


Figure 6
Effects of HFD and testosterone deprivation on insulin signaling. Cells were stimulated either with or without 10 nM of insulin for 10 min. Western blotting bands of pIR, total IR, pAkt, total Akt, and actin were shown in A. The bar graphs represent densitometric values of pIR (B) and pAkt (C) which are calculating by divided the insulin stimulation by without insulin stimulation (insulin+/insulin−), then normalizing with total protein expression. *$P<0.05$ vs NDS group.

effects of low osteocalcin levels as previously observed in pancreatic β cells and adipocytes (Ferron *et al.* 2008, Hwang *et al.* 2012).

The testosterone deprivation following orchiectomy was confirmed by the decreased testosterone level in the orchiectomized rats. However, the HFS rats also showed a decrease in plasma testosterone levels, a finding consistent with previous clinical reports which demonstrated that obesity in men is associated with low testosterone levels (Barrett-Connor 1992, Andersson *et al.* 1994, Grossmann 2013, Mogri *et al.* 2013). The reduction of testosterone levels in the HFS rats could be a factor in the decrease in the hypothalamo–pituitary–gonadal axis due to inflammation following obesity as decribed in previous studies (Cohen 1999, Gregor & Hotamisligil 2011, Mammi *et al.* 2012, Jayaraman *et al.* 2014b). Although it has been shown that obesity could increase the estrogen levels in female rats (Pratchayasakul *et al.* 2011), our previous study demonstrated that 12 weeks of high-fat diet feeding did not affect the circulating estrogen levels in male rats (Pratchayasakul *et al.* 2011). Moreover, a recent report also demonstrated that estradiol administration did not affect cardiac function in orchiectomized male rats (Ayaz *et al.* 2015). All of these findings indicated the important role of decreased testosterone levels rather than increased estrogen levels in obese male rats.

A previous study demonstrated that orchiectomy-induced trabecular bone degeneration was possibly caused by a decrease in the expressions of osteogenic genes (Chin & Ima-Nirwana 2015). Several studies have demonstrated that testosterone played an important role in osteoblastic proliferation by enhancing mitogenesis and differentiation in bone cells (Sömjen *et al.* 1989, Kasperk *et al.* 1990, Gray *et al.* 1992). In addition, testosterone has been shown to play a role in osteoblast apoptosis in which a lack of testosterone enhanced osteoblast apoptosis through an increased Bax/Bcl-2 ratio (Wiren *et al.* 2006, Chen *et al.* 2010). Our results showed that a reduction of the Gla/Glu osteocalcin ratio, decreased osteoblastic proliferation and increased osteoblastic apoptosis in testosterone-deprived rats was associated with microstructural changes in the tibial trabecular bones and a significant overall reduction in mineral density of those bones. Our findings and a previous report (Fulzele *et al.* 2010) demonstrated that the impairment of osteoblastic insulin receptors results in a decrease in osteoblast proliferation. All of these findings suggest that testosterone deprivation decreases osteoblastic activity and osteoblastic proliferation while increasing ostoblastic apoptosis, leading to osteoporosis.

The effects of obesity on bone density is still unclear. Several studies have shown that obesity could increase bone density (Harris *et al.* 1992, Albala *et al.* 1996, Vandewalle *et al.* 2013); however, other studies have found that obesity has either no effect on bone density (Greco *et al.* 2010) or increases bone porosity (Rosen & Bouxsein 2006, Zhao *et al.* 2008, Gómez *et al.* 2009). The present study, also, found that obese and insulin resistant rats had a decreased Gla/Glu-osteocalcin ratio, decreased osteoblastic proliferation, increased osteoblastic apoptosis, osteoblastic insulin resistance and increased bone porosity. These findings indicate the deleterious effects of obesity on bone quality. Interestingly, obesity did not aggravate those forms of deterioration in testosterone-deprived rats as indicated by the lack of differences in trabecular bone quality between the HFO and the NDO groups (Fig. 3B, D, and E). There are several possible explanations for these findings. First, the deleterious effects found in osteoblasts of testosterone-deprived rats

© 2016 Society for Endocrinology
Printed in Great Britain
Published by Bioscientifica Ltd.

could have been at their maximum level, thus obesity could not have had further additive effects on those osteoblastic cells. Secondly, it could be that the lack of testosterone, rather than obesity, that was the major aggressive factor causing the impairment of trabecular bone structures as this impairment was also observed in NDO rats. However, in the present study no significant differences in cortical bones were observed among the experimental groups. Two previous studies found that the cortical bone markers had markedly decreased 6 months after castration (Danielsen *et al.* 1992, Reim *et al.* 2008). It is possible that the 3-month period of castration in the present study might not have been long enough to observe cortical bone change. However, the hypothesis of this study is supported by the fact that the response of cortical bone mass to HF-induced obesity differs by age (Ionova-Martin *et al.* 2011). The Ionova-Martin group demonstrated that femur thickness does not change in young mice after 16 weeks of HF comsumption although those mice, as in the mice in the present study, had poor bone quality.

The limitation of the present study was that testosterone deprivation and obesity were not independently assessed as the cause of osteoporosis due to the fact that decreased testosterone levels was also observed in the obese-insulin resistant rats. However, it has been shown previously that testosterone deprivation alone could cause osteoporosis (Tuck & Francis 2009). Moreover, the recent study by Donner *et al.* (2015) demonstrated that diet-induced visceral obesity resulted in decreased bone mineral area and content and impaired femoral stiffness and strength without changes in testosterone levels. All of these findings indicated that either obesity or testosterone deprivation could lead to osteoporosis. In addition, the aim of the present study was to mainly investigate the synergistic effects of obesity and testosterone deprivation on osteoporosis. Findings from the present study clearly demonstrated that either obesity alone or testosterone deprivation alone led to osteoporosis, however no additive or synergistic effect of obesity and testosterone deprivation on osteoporosis could be found.

Lack of results pertaining to bone cellular activities is one of the limitations of the present study. However, neither serum bone biomarkers nor tissue samples for dynamic bone histomorphometry were collected from those rats. Therefore, it is not possible for us to quantify bone cellular activities in the present study. However, we believe that the available bone parameters provided in the present study provided sufficient evidence to confirm the detrimental effects of testosterone deprivation and insulin resistance on bone. The overall adiposity was not measured. However, the visceral fat was determined and used to represent the level of metabolic complications in this obese-insulin resistant model (Hansen *et al.* 1997, Morakinyo *et al.* 2015).

Conclusions

Either testosterone deprivation alone or HF-induced obesity alone can cause impairment of osteoblastic insulin signaling and reduction in osteoblastic survival, leading to osteoporosis. However, obesity does not augment the adverse effects on bone density under testosterone-deprived conditions.

Declaration of interest
The authors declare that there is no conflict of interest that could be perceived as prejudicing the impartiality of the research reported.

Funding
This study was supported by grants from the Thailand Research Fund (TRF-BRG5780016 to SC); TRF Senior Research Scholar (RTA5780001 to N Charoenphandhu), a NSTDA Research Chair Grant from the National Science and Technology Development Agency (NC) and a Chiang Mai University Excellent Center Award (NC) as well as the China Medical Board of New York; the Faculty of Medicine, Chiang Mai University (S P).

Author contribution statement
S P performed the experiments, analyzed the data, and wrote the manuscript. P R performed the experiments and analyzed the data. H P performed the animal experiments and analyzed the metabolic data. P S and Na C performed and analyzed the bone histomophometry. N C designed the study and wrote the manuscript. S C designed the study, analyzed the data, and wrote the manuscript.

Acknowledgements
The authors would also like to thank Dr G Lamar Robert for assistance in editing the manuscript.

References

Albala C, Yáñez M, Devoto E, Sostin C, Zeballos L & Santos JL 1996 Obesity as a protective factor for postmenopausal osteoporosis. *International Journal of Obesity and Related Metabolic Disorders* **20** 1027–1032.

Andersson B, Marin P, Lissner L, Vermeulen A & Bjorntorp P 1994 Testosterone concentrations in women and men with NIDDM. *Diabetes Care* **17** 405–411. (doi:10.2337/diacare.17.5.405)

Appleton DJ, Rand JS & Sunvold GD 2005 Basal plasma insulin and homeostasis model assessment (HOMA) are indicators of insulin sensitivity in cats. *Journal of Feline Medicine and Surgery* **7** 183–193. (doi:10.1016/j.jfms.2004.12.002)

© 2016 Society for Endocrinology
Printed in Great Britain
Published by Bioscientifica Ltd.

Journal of Endocrinology

Ayaz M, Akand M, Kucukbagriacik Y & Dursunoglu D 2015 The effects of estradiol on cardiac muscle electrophysiology in orchiectomized rat model: a new insight to side effects caused by castration. *European Review for Medical and Pharmacological Sciences* **19** 2866–2874.

Barrett-Connor E 1992 Lower endogenous androgen levels and dyslipidemia in men with non-insulin-dependent diabetes mellitus. *Annals of Internal Medicine* **117** 807–811. (doi:10.7326/0003-4819-117-10-807)

Chen X, Deng Y, Zhou Z, Tao Q, Zhu J, Li X, Chen J & Hou J 2010 17β-estradiol combined with testosterone promotes chicken osteoblast proliferation and differentiation by accelerating the cell cycle and inhibiting apoptosis *in vitro*. *Veterinary Research Communications* **34** 143–152. (doi:10.1007/s11259-010-9340-2)

Chin K-Y & Ima-Nirwana S 2015 The effects of orchidectomy and supraphysiological testosterone administration on trabecular bone structure and gene expression in rats. *Aging Male* **18** 60–66. (doi:10.3109/13685538.2014.954995)

Christoffersen B, Raun K, Svendsen O, Fledelius C & Golozoubova V 2006 Evalution of the castrated male Sprague-Dawley rat as a model of the metabolic syndrome and type 2 diabetes. *International Journal of Obesity* **30** 1288–1297. (doi:10.1038/sj.ijo.0803261)

Cohen PG 1999 The hypogonadal-obesity cycle: role of aromatase in modulating the testosterone-estradiol shunt–a major factor in the genesis of morbid obesity. *Medical Hypotheses* **52** 49–51. (doi:10.1054/mehy.1997.0624)

Danielsen CC, Mosekilde L & Andreassen TT 1992 Long-term effect of orchidectomy on cortical bone from rat femur: bone mass and mechanical properties. *Calcified Tissue International* **50** 169–174. (doi:10.1007/BF00298796)

Donner DG, Elliott GE, Beck BR, Forwood MR & Du-Toit EF 2015 The effects of visceral obesity and androgens on bone: trenbolone protects against loss of femoral bone mineral density and structural strength in viscerally obese and testosterone-deficient male rats. *Osteoporosis International* [in press]. (doi:10.1007/s00198-015-3345-1)

Dulisch ML 1976 A castration procedure for the rabbit, rat, hamster, and guinea pig. *Journal of Zoo Animal Medicine* **7** 8–11. (doi:10.2307/20094380)

Dupree K & Dobs A 2004 Osteopenia and male hypogonadism. *Reviews in Urology* **6** (Suppl 6) S30–S34.

Ferron M, Hinoi E, Karsenty G & Ducy P 2008 Osteocalcin differentially regulates β cell and adipocyte gene expression and affects the development of metabolic diseases in wild-type mice. *PNAS* **105** 5266–5270. (doi:10.1073/pnas.0711119105)

Fulzele K, Riddle RC, DiGirolamo DJ, Cao X, Wan C, Chen D, Faugere M-C, Aja S, Hussain MA, Brüning JC *et al.* 2010 Insulin receptor signaling in osteoblasts regulates postnatal bone acquisition and body composition. *Cell* **142** 309–319. (doi:10.1016/j.cell.2010.06.002)

Gómez JM, Vilarrasa N, Masdevall C, Pujol J, Solano E, Soler J, Elio I, Gallart L & Vendrell J 2009 Regulation of bone mineral density in morbidly obese women: a cross-sectional study in two cohorts before and after bypass surgery. *Obesity Surgery* **19** 345–350. (doi:10.1007/s11695-008-9529-4)

Gray C, Colston KW, Mackay AG, Taylor ML & Arnett TR 1992 Interaction of androgen and 1,25-dihydroxyvitamin D3: effects on normal rat bone cells. *Journal of Bone and Mineral Research* **7** 41–46. (doi:10.1002/jbmr.5650070107)

Greco EA, Fornari R, Rossi F, Santiemma V, Prossomariti G, Annoscia C, Aversa A, Brama M, Marini M, Donini LM *et al.* 2010 Is obesity protective for osteoporosis? Evaluation of bone mineral density in individuals with high body mass index *International Journal of Clinical Practice* **64** 817–820. (doi:10.1111/j.1742-1241.2009.02301.x)

Gregor MF & Hotamisligil GS 2011 Inflammatory mechanisms in obesity. *Annual Review of Immunology* **29** 415–445. (doi:10.1146/annurev-immunol-031210-101322)

Grossmann M. 2013 Low Testosterone in Men with Type 2 Diabetes: Significance and Treatment.

Grossmann M, Panagiotopolous S, Sharpe K, MacIsaac RJ, Clarke S, Zajac JD, Jerums G & Thomas MC 2009 Low testosterone and anaemia in men with type 2 diabetes. *Clinical Endocrinology* **70** 547–553. (doi:10.1111/j.1365-2265.2008.03357.x)

Haffner SM, Miettinen H & Stern MP 1997 The homeostasis model in the San Antonio heart study. *Diabetes Care* **20** 1087–1092. (doi:10.2337/diacare.20.7.1087)

Hansen PA, Han DH, Nolte LA, Chen M & Holloszy JO 1997 DHEA protects against visceral obesity and muscle insulin resistance in rats fed a high-fat diet. *American Journal of Physiology* **273** R1704–R1708.

Harris S, Dallal GE & Dawson-Hughes B 1992 Influence of body weight on rates of change in bone density of the spine, hip, and radius in postmenopausal women. *Calcified Tissue International* **50** 19–23. (doi:10.1007/BF00297292)

Hwang Y-C, Jeong I-K, Ahn K-J & Chung H-Y 2012 Circulating osteocalcin level is associated with improved glucose tolerance, insulin secretion and sensitivity independent of the plasma adiponectin level. *Osteoporosis International* **23** 1337–1342. (doi:10.1007/s00198-011-1679-x)

Ionova-Martin SS, Wade JM, Tang S, Shahnazari M, Ager JW, Lane NE, Yao W, Alliston T, Vaisse C & Ritchie RO 2011 Changes in cortical bone response to high-fat diet from adolescence to adulthood in mice. *Osteoporosis International* **22** 2283–2293. (doi:10.1007/s00198-010-1432-x)

Jayaraman A, Lent-Schochet D & Pike CJ 2014*a* Diet-induced obesity and low testosterone increase neuroinflammation and impair neural function. *Journal of Neuroinflammation* **11** 162. (doi:10.1186/s12974-014-0162-y)

Jayaraman A, Lent-Schochet D & Pike CJ 2014*b* Diet-induced obesity and low testosterone increase neuroinflammation and impair neural function. *Journal of Neuroinflammation* **11** 162. (doi:10.1186/s12974-014-0162-y)

Kasperk C, Fitzsimmons R, Strong D, Mohan S, Jennings J, Wergedal J & Baylink D 1990 Studies of the mechanism by which androgens enhance mitogenesis and differentiation in bone cells. *Journal of Clinical Endocrinology and Metabolism* **71** 1322–1329. (doi:10.1210/jcem-71-5-1322)

Kawamura N, Kugimiya F, Oshima Y, Ohba S, Ikeda T, Saito T, Shinoda Y, Kawasaki Y, Ogata N, Hoshi K *et al.* 2007 Akt1 in osteoblasts and osteoclasts controls bone remodeling. *PLoS ONE* **2** e1058. (doi:10.1371/journal.pone.0001058)

Mammi C, Calanchini M, Antelmi A, Cinti F, Rosano GM, Lenzi A, Caprio M & Fabbri A 2012 Androgens and adipose tissue in males: a complex and reciprocal interplay. *International Journal of Endocrinology* **2012** 789653. (doi:10.1155/2012/789653)

Mogri M, Dhindsa S, Quattrin T, Ghanim H & Dandona P 2013 Testosterone concentrations in young pubertal and post-pubertal obese males. *Clinical Endocrinology* **78** 593–599. (doi:10.1111/cen.12018)

Morakinyo AO, Samuel TA, Adekunbi DA & Adegoke OA 2015 Niacin improves adiponectin secretion, glucose tolerance and insulin sensitivity in diet-induced obese rats. *Egyptian Journal of Basic and Applied Sciences* **2** 261–267. (doi:10.1016/j.ejbas.2015.08.003)

Ogata N, Chikazu D, Kubota N, Terauchi Y, Tobe K, Azuma Y, Ohta T, Kadowaki T, Nakamura K & Kawaguchi H 2000 Insulin receptor substrate-1 in osteoblast is indispensable for maintaining bone turnover. *Journal of Clinical Investigation* **105** 935–943. (doi:10.1172/JCI9017)

Pongkan W, Chattipakorn SC & Chattipakorn N 2015 Chronic testosterone replacement exerts cardioprotection against cardiac ischemia–reperfusion injury by attenuating mitochondrial dysfunction in testosterone-deprived rats. *PLoS ONE* **10** e0122503. (doi:10.1371/journal.pone.0122503)

Pramojanee SN, Phimphilai M, Kumphune S, Chattipakorn N & Chattipakorn SC 2013 Decreased jaw bone density and osteoblastic insulin signaling in a model of obesity. *Journal of Dental Research* **92** 560–565. (doi:10.1177/0022034513485600)

Pratchayasakul W, Kerdphoo S, Petsophonsakul P, Pongchaidecha A, Chattipakorn N & Chattipakorn SC 2011 Effects of high-fat diet on insulin receptor function in rat hippocampus and the level of neuronal corticosterone. *Life Sciences* **88** 619–627. (doi:10.1016/j.lfs.2011.02.003)

© 2016 Society for Endocrinology
Printed in Great Britain

Published by Bioscientifica Ltd.

Journal of Endocrinology

Pratchayasakul W, Chattipakorn N & Chattipakorn SC 2014 Estrogen restores brain insulin sensitivity in ovariectomized non-obese rats, but not in ovariectomized obese rats. *Metabolism* **63** 851–859. (doi:10.1016/j.metabol.2014.03.009)

Pun KK, Lau P & Ho PW 1989 The characterization, regulation, and function of insulin receptors on osteoblast-like clonal osteosarcoma cell line. *Journal of Bone and Mineral Research* **4** 853–862. (doi:10.1002/jbmr.5650040610)

Reim NS, Breig B, Stahr K, Eberle J, Hoeflich A, Wolf E & Erben RG 2008 Cortical bone loss in androgen-deficient aged male rats is mainly caused by increased endocortical bone remodeling. *Journal of Bone and Mineral Research* **23** 694–704. (doi:10.1359/jbmr.080202)

Rosen CJ & Bouxsein ML 2006 Mechanisms of disease: is osteoporosis the obesity of bone? *Nature Clinical Practice. Rheumatology* **2** 35–43. (doi:10.1038/ncprheum0070)

Saboor Aftab SA, Kumar S & Barber TM 2013 The role of obesity and type 2 diabetes mellitus in the development of male obesity-associated secondary hypogonadism. *Clinical Endocrinology* **78** 330–337. (doi:10.1111/cen.12092)

Saleem U, Mosley TH & Kullo IJ 2010 Serum osteocalcin is associated with measures of insulin resistance, adipokine levels, and the presence of metabolic syndrome. *Arteriosclerosis, Thrombosis, and Vascular Biology* **30** 1474–1478. (doi:10.1161/ATVBAHA.110.204859)

Sömjen D, Weisman Y, Harell A, Berger E & Kaye AM 1989 Direct and sex-specific stimulation by sex steroids of creatine kinase activity and DNA synthesis in rat bone. *PNAS* **86** 3361–3365.

Suntornsaratoon P, Kraidith K, Teerapornpuntakit J, Dorkkam N, Wongdee K, Krishnamra N & Charoenphandhu N 2014 Pre-suckling calcium supplementation effectively prevents lactation-induced osteopenia in rats. *American Journal of Physiology. Endocrinology and Metabolism* **306** E177–E188. (doi:10.1152/ajpendo.00556.2013)

Tsujimura A 2013 The relationship between testosterone deficiency and men's health. *World Journal of Men's Health* **31** 126–135. (doi:10.5534/wjmh.2013.31.2.126)

Tuck SP & Francis RM 2009 Testosterone, bone and osteoporosis. *Frontiers of Hormone Research* **37** 123–132. (doi:10.1159/000176049)

Vandewalle S, Taes Y, Van Helvoirt M, Debode P, Herregods N, Ernst C, Roef G, Van-Caenegem E, Roggen I, Verhelle F *et al.* 2013 Bone size and bone strength are increased in obese male adolescents. *Journal of Clinical Endocrinology and Metabolism* **98** 3019–3028. (doi:10.1210/jc.2012-3914)

Wang C, Jackson G, Jones TH, Matsumoto AM, Nehra A, Perelman MA, Swerdloff RS, Traish A, Zitzmann M & Cunningham G 2011 Low testosterone associated with obesity and the metabolic syndrome contributes to sexual dysfunction and cardiovascular disease risk in men with type 2 diabetes. *Diabetes Care* **34** 1669–1675. (doi:10.2337/dc10-2339)

Winzell MS & Ahren B 2004 The high-fat diet-fed mouse: a model for studying mechanisms and treatment of impaired glucose tolerance and type 2 diabetes. *Diabetes* **53** S215–S219. (doi:10.2337/diabetes.53.suppl_3.S215)

Wiren KM, Toombs AR, Semirale AA & Zhang X 2006 Osteoblast and osteocyte apoptosis associated with androgen action in bone: requirement of increased Bax/Bcl-2 ratio. *Bone* **38** 637–651. (doi:10.1016/j.bone.2005.10.029)

Xia F, Xu X, Zhai H, Meng Y, Zhang H, Du S, Xu H, Wu H & Lu Y 2013 Castration-induced testosterone deficiency increases fasting glucose associated with hepatic and extra-hepatic insulin resistance in adult male rats. *Reproductive Biology and Endocrinology* **11** 106. (doi:10.1186/1477-7827-11-106)

Xiao L, Wang XM, Yang T, Xiong Y, Zhang ZG, Ding J, Xu C & Xiong CY 2014 Changes of serum osteocalcin, calcium, and potassium in a rat model of type 2 diabetes. *Cell Biochemistry and Biophysics* **71** 437–440. (doi:10.1007/s12013-014-0220-1)

Zhao L-J, Jiang H, Papasian CJ, Maulik D, Drees B, Hamilton J & Deng H-W 2008 Correlation of obesity and osteoporosis: effect of fat mass on the determination of osteoporosis. *Journal of Bone and Mineral Research* **23** 17–29. (doi:10.1359/jbmr.070813)

Received in final form 9 November 2015
Accepted 13 November 2015

Journal of Endocrinology

© 2016 Society for Endocrinology
Printed in Great Britain
Published by Bioscientifica Ltd.

เอกสารแนบหมายเลข 36

METABOLISM CLINICAL AND EXPERIMENTAL 65 (2016) 54–67

Available online at www.sciencedirect.com

Metabolism

www.metabolismjournal.com

Testosterone deprivation has neither additive nor synergistic effects with obesity on the cognitive impairment in orchiectomized and/or obese male rats

Hiranya Pintana[a,b], Wasana Pratchayasakul[a,b], Piangkwan Sa-nguanmoo[a,b], Wanpitak Pongkan[a,b], Rungroj Tawinvisan[a,b], Nipon Chattipakorn[a,b], Siriporn C. Chattipakorn[a,c,*]

[a] Neurophysiology Unit, Cardiac Electrophysiology Research and Training Center, Faculty of Medicine, Chiang Mai University, Chiang Mai, Thailand

[b] Department of Physiology, Faculty of Medicine, Chiang Mai University, Chiang Mai, Thailand

[c] Department of Oral Biology and Diagnostic Sciences, Faculty of Dentistry, Chiang Mai University, Chiang Mai, Thailand

ARTICLE INFO

Article history:
Received 8 July 2015
Accepted 5 October 2015

Keywords:
Obese-insulin resistance
Testosterone deprivation
Brain insulin sensitivity
Brain mitochondrial function
Hippocampal synaptic function

ABSTRACT

Objective. Previous studies demonstrated a correlation between cognitive decline and either testosterone deprivation or obesity. However, the effect of obesity combined with testosterone deprivation on cognitive function has not been investigated. This study investigated the effects of obesity on brain insulin sensitivity, brain mitochondrial function, hippocampal synaptic plasticity and cognitive function in testosterone-deprived male rats.

Materials/Methods. Male Wistar rats were divided into sham-operated (control) and bilateral orchiectomized (ORX) groups. Rats in each group were further divided into two subgroups to receive either a normal diet (ND) or a high fat diet (HFD) for 4, 8 or 12 weeks. Blood samples were collected to determine metabolic parameters. Cognitive function was tested using the Morris Water Maze Test. At the end of the study, brains were removed to investigate brain insulin sensitivity, brain mitochondrial function and hippocampal synaptic plasticity.

Results. Both control-obese and ORX-obese rats developed peripheral insulin resistance at week eight, and brain insulin resistance as well as brain mitochondrial dysfunction at week 12. However, the ORX-obese rats developed cognitive impairment and decreased hippocampal synaptic plasticity beginning at week eight, whereas the control-obese rats developed these impairments later at week 12. Although both peripheral and brain insulin

Abbreviations: S, sham-operated; O, bilateral orchiectomized; ND, normal diet; HFD, high fat diet; NDS, control-lean rats; NDO, ORX-lean rats; HFS, control-obese rats; HFO, ORX-obese rats; T2DM, type-2 diabetes mellitus; LTD, insulin-induced long-term depression; CA1, cornus ammonis 1; DHT, dihydrotestosterone; MWM, Morris water maze test; OGTT, oral glucose tolerance test; LTP, hippocampal synaptic long-term potentiation; HDL, high-density lipoprotein; LDL, low-density lipoprotein; HOMA, Homeostasis Model Assessment; MDA, malondialdehyde levels; ECLIA, the electrochemiluminescence immunoassay; fEPSPs, field excitatory postsynaptic potentials; aCSF, artificial cerebrospinal fluid; p-IR, insulin receptor phosphorylation; IR, insulin receptor; Akt/PKB, serine/threonine protein kinase/protein kinase B; BCA, bicinchoninic acid; ROS, reactive oxygen species, $\Delta\Psi m$, mitochondrial membrane potential change; DCFHDA, dichloro-hydrofluoresceindiacetate; JC-1, fluorescent dye 5,5′,6,6′-tetrachloro-1,1′,3,3′-tetraethyl benzimidazolcarbocyanine iodide; HPLC, high performance liquid chromatography; OFT, open-field test.

* *Corresponding author at:* Neurophysiology Unit, Cardiac Electrophysiology Research and Training Center, Faculty of Medicine, Department of Oral Biology and Diagnostic Science, Faculty of Dentistry, Chiang Mai University, Chiang Mai, 50200, Thailand. Tel.: +66 53 944 451; fax: +66 53 222 844.

E-mail addresses: scchattipakorn@gmail.com, siriporn.c@cmu.ac.th (S.C. Chattipakorn).

http://dx.doi.org/10.1016/j.metabol.2015.10.015
0026-0495/© 2015 Elsevier Inc. All rights reserved.

resistance were not observed in both the control-lean and ORX-lean rats, impaired cognition and decreased hippocampal synaptic plasticity were found in the ORX-lean rats beginning at week eight.

Conclusion. These findings suggest that testosterone deprivation has neither additive nor synergistic effects over obesity in the development of cognitive dysfunction in orchiectomized-obese male rats.

© 2015 Elsevier Inc. All rights reserved.

1. Introduction

Insulin resistance is a hallmark of metabolic syndrome, which can lead to the development of type-2 diabetes mellitus (T2DM) [1]. It has been shown that long-term high calorie diet consumption causes obesity, insulin resistance, and T2DM in animal models [2,3]. Our previous work has also demonstrated that male rats fed long-term on a high-fat diet (HFD) developed not only obesity and insulin resistance, but also brain insulin resistance, as indicated by an impairment in insulin-induced long-term depression (LTD), impaired insulin signaling in the brain and brain mitochondrial dysfunction as well as cognitive impairment [4–6]. Moreover, HFD also caused increased oxidative stress and finally decreased synaptic plasticity [7], and cognition [8,9].

In addition to obesity, the androgenic sex steroid hormone, testosterone, has been shown to play an important role in the regulation of glucose metabolism and insulin signaling [10], as well as the modulation of normal brain function, including improved synaptic plasticity, and is involved in cognitive formation [11,12]. In orchiectomized rodents, the impairment of learning and memory has been demonstrated, indicating that testosterone was involved in cognitive function [13–16]. Furthermore, the reduction of the number of dendritic spines and changes in dendritic spine morphology in hippocampal CA1 regions have been observed in male orchiectomized rodents [17], which were restored by testosterone or dihydrotestosterone (DHT) replacement [18,19]. Although obese-insulin resistant has been shown to be associated with testosterone deficiency in animal models [20,21] and human studies [22,23], several reports regarding castrated male rats demonstrated that testosterone deprivation did not induce obesity [24–27].

Despite some links reported among testosterone, obesity and cognition, the effects of testosterone deprivation with or without obesity on brain insulin receptor function, brain insulin signaling and brain mitochondrial functions have not been reported. In addition, the effects of testosterone deprivation with or without obesity on hippocampal synaptic plasticity as well as cognitive function have not been thoroughly determined In the present study, we hypothesized that testosterone deprivation alone can cause an impairment of brain insulin receptor function, decreased brain insulin signaling, impaired brain mitochondrial function, impaired hippocampal synaptic plasticity, resulting in cognitive dysfunction. We also hypothesized that obesity accelerates these impairments in the brain of testosterone-deprived male rats. Although several parameters have been determined in the present study, the first endpoint was recorded in line with the changes in cognitive function.

2. Materials and Methods

2.1. Animal Models and Experimental Protocols

Seventy-two male Wistar Rats, weighing 180–200 g (aged ~5–6 weeks old) obtained from the National Animal Center, Salaya Campus, Mahidol University, Bangkok, Thailand were used. All experiments were conducted in accordance with the approved protocol from the Faculty of Medicine, Chiang Mai University Institutional Animal Care and Use Committee, in compliance with NIH guidelines. All animals were housed in environmentally controlled conditions (25 ± 0.5 °C, 12 hour light/dark cycle) and allowed to acclimate for one week. Rats were then divided into two groups (n = 36/group) as either sham-operated (S) or orchiectomized (O) rats. One week after the surgery, each group was subdivided into two subgroups. Animals in each subgroup were fed either a normal diet (ND: 19.77% E fat) or a high-fat diet (HFD: 59.28% E fat) for 4, 8 or 12 weeks [6]. In each time period, animals were divided into four different treated groups, including NDS (control-lean rats), NDO (ORX-lean rats), HFS (control-obese rats) and HFO (ORX-obese rats). All animals were given free access to drinking water and their respective diets.

An open field test was performed to test locomotive function. The cognitive function was determined by the Morris Water Maze (MWM) Test. Both tests were determined at the end of each time period (4, 8 and 12 weeks). The body mass of each animal was recorded weekly. Blood samples were collected from a tail vein at week zero, (before dietary feeding) and at the end of each time period (4, 8 and 12 weeks) for further plasma analysis. The oral glucose tolerance test (OGTT) was performed at the end of weeks 4, 8 and 12, using the technique described previously [6,28]. At the end of each time period, animals were deeply anesthetized with isoflurane and sacrificed via decapitation. Each brain was rapidly removed and carefully sliced in preparation for extracellular recording (insulin-induced LTD and hippocampal synaptic LTP), immunoblot, brain oxidative stress and brain mitochondrial study as well as dendritic spine density determination.

2.2. Orchiectomized Procedure

Orchiectomy was performed using the method described previously [29]. Rats were anesthetized and maintained by 2–3% isoflurane in a dorsal recumbent position, and the skin of scrotal area was scrubbed utilizing sterile technique. A small incision was made at the tip of the scrotum. The tunica albuginea was incised and the testis, vas deferens and the spermatic blood vessels were exposed. Then, the blood vessels and vas deferens were ligated with 4–0 absorbable

suture followed by the removal of the testis. When the bleeding stopped, the remaining tissue was returned to the sac, and the procedure was repeated on the opposite testis. The skin incision was closed with a 4–0 silk thread (non-absorbable suture). The rats were carefully monitored to prevent them from chewing the sutures and other complications. The analgesic drug, Tolfedine 4 mg/kg, (VETOQUINOL S.A., Magny-Vernois, France) and antibiotic drug, Marbocyl 2 mg/kg (VETOQUINOL UK Limited, UK) were administrated subcutaneously after the surgery, and were continually administered for three days [30].

2.3. *Plasma Analysis*

Plasma glucose and cholesterol levels were determined via the colorimetric assay (Biotech, Bangkok, Thailand). Plasma HDL and LDL levels were determined via a commercial colorimetric assay kit (Biovision, CA, USA). Plasma insulin levels were determined via the Sandwich ELISA kit (LINCO Research, MO, USA). Peripheral insulin resistance was assessed via the Homeostasis Model Assessment (HOMA) as described in previous studies [31,32]. Serum malondialdehyde (MDA) was determined using high performance liquid chromatography (HPLC)-based assay [4,33]. Plasma testosterone levels were measured using the electrochemiluminescence immunoassay "ECLIA" technique (Roche Diagnostic, Indianapolis, IN, USA).

2.4. *Brain Slice Preparation*

An extracellular recording of hippocampal slices for insulin-induced LTD was performed as described in our previous studies [5,6,28].

2.5. *Extracellular Recordings of Hippocampal Slices for Insulin-Induced Long-Term Depression (LTD)*

An extracellular recording of hippocampal slices for insulin-induced LTD was performed as described in our previous studies [5,6,28]. At the end of 4, 8 and 12 weeks animals were anesthetized with isoflurane and decapitated. The brain was rapidly removed, then immersed in ice-cold "high sucrose" artificial cerebrospinal fluid (aCSF), containing (mM): NaCl 85; KCl 2.5; MgSO4 4; CaCl2 0.5; NaH2PO4 1.25; NaHCO3 25; glucose 25; sucrose 75; kynurenic acid 2; ascorbate 0.5, saturated with 95%O2/5%CO2 (pH 7.4). The hippocampal slices were cut by using a vibratome (Vibratome Company, MO, USA). Following a 30-minute post-slice incubation in high sucrose aCSF, the slices were transferred to a standard aCSF solution containing (mM): NaCl 119; KCl 2.5; CaCl2 2.5; MgSO4 1.3; NaH2PO4 1; NaHCO3 26; and glucose 10, saturated with 95% O2, 5%CO2 (pH 7.4) for an additional 30 minutes at room temperature (22–24 °C). Field excitatory postsynaptic potentials (fEPSPs) were evoked by stimulating the Schaffer collateral-commissural pathway with a bipolar tungsten electrode, while recordings were taken from the stratum radiatum of the hippocampal CA1 region with micropipettes (3 MΩ) filled with 2 M NaCl. Stimulus frequency was 0.033 Hz. The stimulus intensity of fEPSPs was adjusted to 0.8-1.0 mV in amplitude. Hippocampal slices were perfused with aCSF (as baseline condition) for ten minutes, and then perfused with aCSF plus 500 nM insulin (as insulin-induced LTD) for an additional ten minutes. Afterward, the slices were perfused with aCSF an additional 50 minutes and recorded. Data was filtered at three kHz, digitized at ten kHz, and stored in a computer using pClamp 9.2 software (Axon Instruments, CA, USA). The initial slope of the fEPSP was measured and plotted against time.

2.6. *Extracellular Recordings of Hippocampal Slices for Synaptic Long-Term Potentiation (LTP)*

To examine electrical-induced hippocampal synaptic long term potentiation (LTP) was performed as described in our previous study [34]. At the end of 4, 8 and 12 weeks animals were anesthetized with isoflurane and decapitated. The brain was rapidly removed, then immersed in ice-cold "high sucrose" artificial cerebrospinal fluid (aCSF), containing (mM): NaCl 85; KCl 2.5; MgSO4 4; CaCl2 0.5; NaH2PO4 1.25; NaHCO3 25; glucose 25; sucrose 75; kynurenic acid 2; ascorbate 0.5, saturated with 95%O2/5%CO2 (pH 7.4). The hippocampal slices were cut by using a vibratome (Vibratome Company, MO, USA). Following a 30-minute post-slice incubation in high sucrose aCSF, the slices were transferred to a standard aCSF solution containing (mM): NaCl 119; KCl 2.5; CaCl2 2.5; MgSO4 1.3; NaH2PO4 1; NaHCO3 26; and glucose 10, saturated with 95% O2, 5%CO2 (pH 7.4) for an additional 30 minutes at room temperature (22–24 °C). Field excitatory postsynaptic potentials (fEPSPs) were evoked by stimulating the Schaffer collateral-commissural pathway with a bipolar tungsten electrode, while the fEPSPs recordings were taken from the stratum radiatum of the hippocampal CA1 region with micropipettes (3 MΩ) filled with 2 M NaCl. LTP was induced by delivering high-frequency stimulation (HFS; four trains at 100 Hz; 0.5 s duration; 20 s interval). Experiments were performed for at least 40 minutes after HFS. The amount of potentiation was calculated at 40 minutes after tetanus. All data were filtered at three kHz, digitized at ten kHz, and stored in a computer using pClamp9.2 software (Axon Instruments, CA, USA). The initial slopes of the fEPSPs were measured and plotted against time.

2.7. *Immunoblotting for Brain Insulin Signaling*

To investigate the expression of insulin receptor phosphorylation (p-IR), insulin receptor (IR), Akt/PKB, and insulin mediated Akt Ser473 phosphorylation, homogenate brain slices from each subgroup were used as described in our previous study [5,6,28]. IR tyrosine phosphorylation and Akt/PKB at serine 473 kinases phosphorylation were electrophoresed and immunoblotted with rabbit antibodies for IR at tyrosine and Akt/PKB at serine 473, respectively. Examination of the level of IR and Akt/PKB protein expression were conducted with homogenates prepared from another set of four whole brain slices. These proteins were resolved by the immunoblot assay conducted with rabbit anti-IR at tyrosine phosphorylation (1:1000; sc-25103-R; Santa Cruz Biotechnology, Santa Cruz, CA, USA), IR (1:1000; sc-711; Santa Cruz Biotechnology, CA, USA), Akt/PKB at serine 473 kinases phosphorylation (1:1000; #9271; Cell Signaling Technology, MA, USA) and Akt/PKB (1:1000; #9272; Cell Signaling Technology, MA, USA). For loading control, immunoblotting for each membrane was incubated with anti-β-actin (1:4000; #4967;

Cell Signaling Technology, MA, USA). All membranes for visualizing the phosphorylation and the protein levels of IR and Akt/PKB expression were incubated with secondary goat anti-rabbit antibody conjugated with horseradish peroxidase (1:2000; #7074; Cell Signaling Technology, MA, USA). The protein bands were visualized on Amersham hyperfilm ECL (GE Healthcare, Buckinghamshire, UK) using Amersham ECL Western blot detection reagents (GE, Healthcare). Band intensities were quantified by Scion Image and the results were shown in average signal intensity (arbitrary) units.

2.8. Preparation of Brain Mitochondria

Brain mitochondria were isolated using the method described previously [5]. Mitochondrial protein concentration was measured via the BCA assay [5], and brain mitochondrial functions including brain mitochondrial reactive oxygen species (ROS), mitochondrial membrane potential change ($\Delta\Psi m$) and mitochondrial swelling were determined.

2.8.1. Brain Mitochondrial ROS Assay

Brain mitochondrial reactive oxygen species (ROS) were measured using dichloro-hydrofluoresceindiacetate (DCFHDA) fluorescent dye. Brain mitochondria (0.4 mg/ml) were incubated with 2-μM DCFHDA at 25 °C for 20 minutes. The fluorescence was determined using a fluorescent microplate reader at the excitation wavelength of 485 nm and emission wavelength of 530 nm [5]. Increased fluorescent intensity indicates increased ROS production.

2.8.2. Brain Mitochondrial Membrane Potential ($\Delta\Psi m$) Assay

The change in mitochondrial membrane potential ($\Delta\Psi m$) was measured using the fluorescent dye 5,5′,6,6′-tetrachloro-1,1′,3,3′-tetraethyl benzimidazolcarbocyanine iodide (JC-1). JC-1 monomer form (green fluorescence) was excited at a wavelength of 485 nm and detected at the emission wavelength of 590 nm. JC-1 aggregate form (red fluorescence) was excited at a wavelength of 485 nm and detected at the emission wavelength of 530 nm. Brain mitochondria (0.4 mg/ml) were incubated with JC-1 dye at 37 °C for 15 minutes. Mitochondrial membrane potential changes were determined by measuring the fluorescent intensity using a fluorescent microplate reader. The change in mitochondrial membrane potential was calculated as the ratio of red to green fluorescent intensity [5]. Decreased red/green fluorescent intensity ratio indicates mitochondrial depolarization.

2.8.3. Brain Mitochondria Swelling Assay

Brain mitochondrial swelling was determined by measuring the change in the absorbance of the brain mitochondrial suspension. Brain mitochondria (0.4 mg/ml) were incubated in 2-ml respiration buffer. The suspension was read at 540 nm using a microplate reader. Mitochondrial swelling was indicated by a decrease in the absorbance [5].

2.9. Determination of Serum and Brain Malondialdehyde (MDA) Levels

The high performance liquid chromatography (HPLC) method was used to evaluate concentrations of serum and brain malondialdehyde (MDA) as described previously [4,33,35].

2.10. Golgi Staining and Morphological Analysis of Dendritic Spines

After decapitation, brains were removed and rinsed with double distilled water, and was processed for Golgi staining using a commercially available kit (FD Neurotechnologies kit, PK 401, Ellicott City, U.S.A.). For analysis of dendritic spine density, the secondary and tertiary dendrites of three neurons at CA1 hippocampus area were counted. Dendritic segments were viewed through an inverted microscope (IX-81, Olympus, Tokyo, Japan).

2.11. Cognitive Function Test

The open-field test (OFT) was used to screen locomotor activity via counting the number of lines that the rats crossed during the test. The OFT was done as described in previous studies [4,36]. The assessment of cognitive function was performed by using Morris Water Maze (MWM) [4,37]. MWM test had two different assessments including the acquisition test which was done for five consecutive days, and the probe test which was performed on day six. Data analysis of MWM test was done manually from video tape recordings by the investigators, who were blinded to experimental groups.

2.12. Statistical Analysis

Data were expressed as mean ± SEM. For all comparisons, the significance of the differences in peripheral biochemical parameters was calculated using the Mann–Whitney U test. The comparisons in the percentage of insulin-induced LTD, the percentage of LTP, brain mitochondrial function, immunoblot, the OFT tests and the MWM tests for the probe test among groups were performed using the one-way ANOVA test, followed by post-hoc LSD analysis. Comparisons among groups in MWM tests for the acquisition test were performed using a two-way ANOVA, followed by post-hoc LSD analysis. $P < 0.05$ was considered statistically significant

3. Results

3.1. Obesity, but not Testosterone Deprivation, Caused Peripheral Insulin Resistance and Increased Circulating and Brain Oxidative Stress Levels

At the baseline levels (before orchiectomy), all metabolic parameters were not significantly different between rats in the sham-operated group (control) and rats in the orchiectomized group (ORX). Testosterone deprivation by orchiectomy was confirmed by decreased plasma testosterone levels. ORX rats in both dietary groups had significantly decreased seminal vesicle ratio and plasma testosterone levels ($p < 0.05$), when compared with the control group, indicating the testosterone deprivation. Interestingly, we found that the level of testosterone in the 12-week control-obese rats was significantly reduced in comparison with that of the 12-week control-lean rats group ($p < 0.05$, Table 1).

At week four, ORX-lean rats had a significant decrease in body mass, food intake and visceral fat in comparison with

control-lean rats ($p < 0.05$, Table 1). However, control-obese and ORX-obese rats had a significant increase in body mass and visceral fat in comparison with control-lean and ORX-lean rats, respectively ($p < 0.05$, Table 1). Plasma insulin level, plasma glucose level, HOMA index, plasma total cholesterol, LDL cholesterol, plasma triglyceride levels, serum and brain MDA levels, and the total area under the glucose curve (AUCg) from the OGTT were not significantly different among groups at this period (Table 1).

At weeks eight and twelve, ORX-lean rats had significantly decreased body mass, food intake and visceral fat ($p < 0.05$), without the alteration in plasma insulin, HOMA index, and cholesterol level in comparison with the control-lean rats (Table 1), indicating that no peripheral insulin resistance was developed in the ORX-lean and control-lean rats. In contrast, control-obese and ORX-obese rats developed the peripheral insulin resistance at the same time since week eight as indicated by increased plasma insulin level, HOMA index, plasma total cholesterol level, and plasma AUCg and decreased HDL cholesterol level ($p < 0.05$). At week eight, levels of serum MDA and brain MDA were not different among groups (Table 1). However, serum and brain MDA levels at week 12 of the control-obese and ORX-obese rats were significantly increased compared with the control-lean rats and ORX-lean rats, respectively ($p < 0.05$, Table 1).

3.2. *Obesity, but not Testosterone Deprivation, Caused the Impairment of Insulin-Induced Long-Term Depression (Insulin-Induced LTD)*

At weeks four and eight, the degree of insulin-mediated LTD was not significantly different among groups (n = 2-3 independent slices/animal, n = 6 animals/group, Fig. 1A–B). At week 12, the degree of insulin-mediated LTD observed from brain slices of the control-lean and ORX-lean rats were not significantly different between groups (Fig. 1C). However, the degree of insulin-induced LTD was significantly reduced in both the control-obese and ORX-obese rats ($p < 0.05$), compared with the control-lean rats (n = 2-3 independent slices/animal, n = 6 animals/group, Fig. 1C). No difference in the degree of insulin-mediated LTD between the control-obese and ORX-obese rats was found (Fig. 1C).

3.3. *Obesity, but not Testosterone Deprivation, Caused the Impairment of Brain Insulin Signaling*

Brain insulin signaling, particularly IR, and Akt/PKB signaling were determined in the present study. The results showed that at weeks 4, 8 and 12, the levels of IR and Akt/PKB proteins were not different among groups. The phosphorylation of IR/total IR and Akt/PKB at the serine 473 site/total Akt were not significantly different among groups at weeks 4 and 8 (Fig. 2A, B, C and D).

At week 12, the phosphorylation of IR/total IR and Akt/PKB at the serine 473 site/total Akt showed no difference between the control-lean rats and ORX-lean rats (Fig. 2E and F). However, the phosphorylation of IR/total IR and Akt/PKB at the serine 473 site/total Akt was significantly decreased in the control-obese rats and ORX-obese rats, compared with the control-lean rats and ORX-lean rats, respectively ($p < 0.05$, Fig. 2E and F). The phosphorylation of IR/total IR and Akt/PKB at the serine 473 site/total Akt were no different in the control-obese and ORX-obese rats (Fig. 2E and F).

3.4. *Obesity, but not Testosterone Deprivation, Caused Brain Mitochondrial Dysfunction*

At weeks 4 and 8, there were no significant differences among groups of brain mitochondrial function including brain mitochondrial ROS level, brain mitochondrial membrane potential changes, and brain mitochondrial swelling (Fig. 3A–F). At week 12, the results showed that the control-obese and ORX-obese rats had brain mitochondrial dysfunction as indicated by increased brain mitochondrial ROS production, brain mitochondrial membrane depolarization and brain mitochondrial swelling, compared with the control-lean and ORX-lean rats, respectively ($p < 0.05$, Fig. 3G–I). However, no differences in these parameters were found between the control-obese rats and ORX-obese rats. However, brain mitochondrial dysfunction was not detected in the control-lean and ORX-lean rats. Electron micrographs of brain mitochondria from different groups were shown in Fig. 3C, F and I. At weeks 4 and 8, intact brain mitochondrial morphology with apparent folded cristae was observed in all groups (Fig. 3C and F). At week 12, brain mitochondrial swelling was observed in both the control-obese and ORX-obese rats as indicated by markedly unfolded cristae (Fig. 3I). In contrast, brain mitochondrial morphology at week 12 in the control-lean and ORX-lean rats was similar to that at weeks 4 and 8.

3.5. *Testosterone Deprivation Accelerated the Development of Cognitive Impairment in Obese-Insulin Resistant Condition*

The locomotor activity determined by an open-field test at 4, 8 and 12 weeks demonstrated that there was not significantly different among groups, indicating that the locomotor activity did not differ among groups.

In the present study, Morris Water Maze (MWM) test was used to determine cognitive function. For the acquisition test, time to reach the platform at weeks 4 and 8 were not different among groups (Fig. 4A and C). At week 12, time to reach the platform was significantly increased at day four and day five in the control-obese and ORX-obese rats, compared with the control-lean rats ($p < 0.05$). However no differences were found between the control-obese and ORX-obese rats (Fig. 4E). For the probe test, time spent in the target quadrant at week four was not different among groups (Fig. 4B). However, at week eight, time spent in the target quadrant of the ORX-lean and ORX-obese rats was significantly decreased, compared with the control-lean rats ($p < 0.05$, Fig. 4D). However, no difference was found between the control-obese and control-lean rats (Fig. 4D). At week 12, time spent in target quadrant of the ORX-lean, ORX-obese and control-obese rats was significantly decreased, compared with that of the control-lean rats ($p < 0.05$, Fig. 4F). However, no difference was found among the ORX-lean, control-obese and ORX-obese rats (Fig. 4F).

3.6. *Testosterone Deprivation Accelerated the Impairment of Synaptic Plasticity in Obese-Insulin Resistant Condition*

Synaptic plasticity is the underlying mechanism for modulating the learning and memory formation in the brain [38]. To

Table 1 – Metabolic parameters and oxidative stress levels of control-lean rats (NDS), ORX-lean rats (NDO), control-obese rats (HFS) and ORX-obese rats (HFO) at weeks 4, 8 and 12.

Metabolic parameters	Week 4				Week 8				Week 12			
	NDS	NDO	HFS	HFO	NDS	NDO	HFS	HFO	NDS	NDO	HFS	HFO
Body mass (g)	392.5 ± 8.3	356.9 ± 5.1 *,†	431.8 ± 9.2 *	400.9 ± 5.5 †,‡	435.5 ± 11.7	383.8 ± 7.0 *,†	498.5 ± 9.7 *	420.8 ± 12.4 †,‡	485.7 ± 8.3	425.0 ± 8.2 *,†	554.2 ± 10.8 *	480.8 ± 9.3 †,‡
Food intake (g)	23.2 ± 0.6	20.7 ± 0.6 *,†	24.4 ± 0.2	22.5 ± 0.5 †,‡	22.05 ± 0.4	19.0 ± 0.7 *,†	23.1 ± 0.3	21.0 ± 0.6 †,‡	22.0 ± 0.4	18.7 ± 0.8 *,†	23.0 ± 0.3	21.0 ± 0.4 †,‡
Visceral fat (g)	17.1 ± 1.4	9.1 ± 0.6 *,†	31.1 ± 2.7 *	15.7 ± 1.0 †,‡	21.5 ± 1.7	12.8 ± 1.4 *,†	40.5 ± 2.4 *	20.7 ± 2.4 †,‡	28.0 ± 1.4	14.9 ± 1.8 *,†	51.5 ± 2.7 *	26.5 ± 1.8 †,‡
Plasma testosterone (ng/dl)	1.5 ± 0.5	0.08 ± 0.01 *,†	1.0 ± 0.3	0.1 ± 0.01 *,†	2.2 ± 0.7	0.04 ± 0.01 *,†	1.2 ± 0.3	0.08 ± 0.01 *,†	1.3 ± 0.5	0.07 ± 0.01 *,†	0.4 ± 0.05 *	0.15 ± 0.06 *,†
Plasma insulin (ng/ml)	2.3 ± 0.2	2.2 ± 0.4	2.4 ± 0.3	2.2 ± 0.4	1.9 ± 0.2	2.0 ± 0.2	3.0 ± 0.3 *	3.2 ± 0.6 *,‡	1.8 ± 0.2	2.2 ± 0.2	3.3 ± 0.3 *	3.4 ± 0.6 *,‡
Plasma glucose (mg/dl)	136.7 ± 8.7	147.5 ± 6.8	140.7 ± 7.3	138.3 ± 6.4	137.8 ± 6.4	129.9 ± 4.5	141.0 ± 6.5	134.8 ± 8.0	148.8 ± 5.0	150.0 ± 6.8	152.2 ± 5.0	151.7 ± 6.4
HOMA index	19.1 ± 2.3	19.8 ± 2.0	21.7 ± 3.2	17.89 ± 3.87	14.4 ± 1.3	15.2 ± 1.2	28.0 ± 4.4 *	27.5 ± 5.5 *,‡	16.1 ± 1.7	18.8 ± 1.8	30.9 ± 2.5 *	29.8 ± 7.5 *,‡
Plasma total cholesterol (mg/dl)	42.1 ± 1.7	41.9 ± 2.6	35.0 ± 0.7	38.0 ± 2.8	39.3 ± 3.8	48.5 ± 2.8	52.4 ± 5.0 *	54.9 ± 4.9 *,‡	43.0 ± 3.4	48.9 ± 4.9	60.1 ± 3.6 *	61.7 ± 6.1 *,‡
HDL cholesterol (mg/dl)	4.9 ± 1.1	4.8 ± 1.1	3.4 ± 0.4	3.5 ± 0.3	4.9 ± 0.3	5.2 ± 0.2	3.8 ± 0.2 *	4.0 ± 0.2 *,‡	5.2 ± 0.2	5.9 ± 0.6	4.1 ± 0.2 *	3.9 ± 0.4 *,‡
LDL cholesterol (mg/dl)	31.4 ± 3.8	36.4 ± 3.1	28.1 ± 1.3	30.9 ± 2.3	37.8 ± 3.5	39.28 ± 5.16	42.1 ± 4.5	46.9 ± 5.4	40.0 ± 4.0	47.6 ± 7.3	59.7 ± 3.2 *	68.9 ± 7.2 *,‡
Plasma triglyceride (mg/dl)	43.3 ± 1.6	37.1 ± 4.3	38.7 ± 5.0	38.3 ± 5.0	30.2 ± 6.8	31.0 ± 8.0	31.6 ± 3.0	30.0 ± 3.0	36.3 ± 3.6	35.5 ± 5.4	37.2 ± 2.8	35.8 ± 3.1
Plasma glucose AUC (AUCg) (mg/dlxminx10⁴)	3.8 ± 0.2	4.0 ± 0.2	4.2 ± 0.3	4.4 ± 0.2	3.7 ± 0.1	3.9 ± 0.2	4.4 ± 0.1 *	4.5 ± 0.3 *,‡	3.9 ± 0.1	4.0 ± 0.3	4.9 ± 0.1 *	4.8 ± 0.4 *,‡
Serum MDA (µmol/ml)	1.5 ± 0.2	1.6 ± 0.1	1.6 ± 0.2	1.7 ± 0.2	1.4 ± 0.03	1.5 ± 0.1	1.5 ± 0.02	1.4 ± 0.02	1.3 ± 0.1	1.4 ± 0.1	1.7 ± 0.2 *	1.7 ± 0.1 *,‡
Brain MDA (µmol/mg protein)	0.5 ± 0.03	0.7 ± 0.2	0.8 ± 0.1	0.6 ± 0.1	0.5 ± 0.1	0.6 ± 0.1	0.6 ± 0.1	0.8 ± 0.2	1.4 ± 0.1	1.5 ± 0.3	2.6 ± 0.4 *	2.6 ± 0.5 *,‡

* $p < 0.05$ compared to NDS.
† $p < 0.05$ compared to HFS.
‡ $p < 0.05$ compared to NDO.

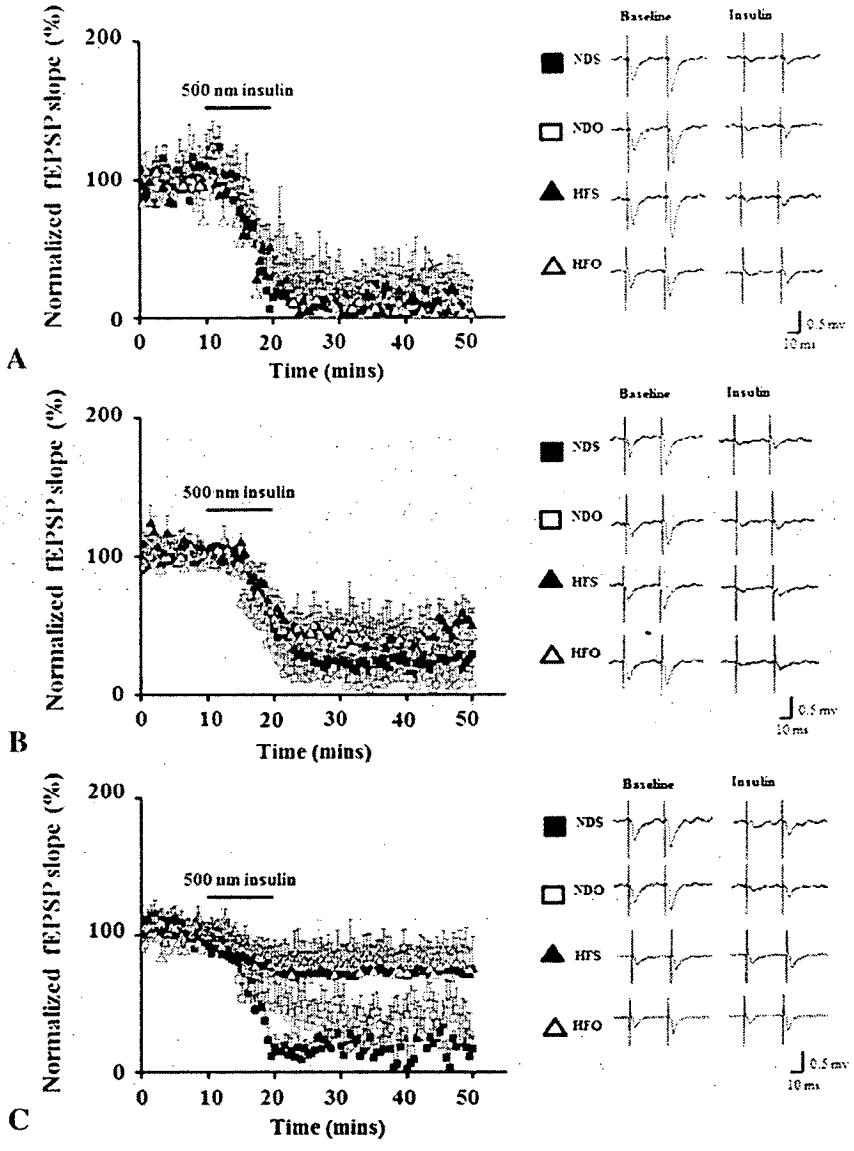


Fig. 1 – The effects of obesity with or without testosterone deprivation on brain insulin receptor function (insulin-induced LTD) in different time courses. At week 4 (A) and week 8 (B), there was no effect on the ability of insulin-mediated long-term depression (LTD) among groups. At week 12, the ability of insulin-mediated LTD was diminished in HFS and HFO rats (C). NDS, control-lean rats. NDO, ORX-lean rats; HFS, control-obese rats; and HFO, ORX-obese rats.

study synaptic plasticity, electrical-induced long-term potentiation (LTP) and dendritic spine density were determined.

At week four, the degree of electrical-induced LTP was not significantly different among groups (n = 2–3 independent slices/animal, n = 6 animals/group, Fig. 5A). At week eight, the percentages in electrical-induced LTP in the ORX-lean and ORX-obese rats were significantly decreased, compared with that of the control-lean and control-obese rats, respectively (n = 2–3 independent slices/animal, n = 6 animals/group, $p < 0.05$, Fig. 5B). However, no difference was found between the ORX-obese and ORX-lean rats as well as between the control-obese and control-lean rats. At week 12, the percentages in electrical-induced LTP in the ORX-lean, control-obese and ORX-obese rats were significantly decreased, compared with that of the control-lean rats (n = 2-3 independent slices/animal, n = 6 animals/group, $p < 0.05$, Fig. 5C). No significant difference was found among the ORX-lean, control-obese and ORX-obese rats.

In addition, the density of hippocampal dendritic spines was determined at the secondary and tertiary dendrites in the apical dendrite of CA1 hippocampus. At week four, we found that the density of dendritic spines was not significantly different among the groups (Fig. 6A). At week eight, the density of dendritic spines of both the ORX-lean and ORX-obese rats was significantly decreased, compared with that of the control-lean rats (Fig. 6B) ($p < 0.05$). However, no difference was found between the ORX-obese and ORX-lean rats as well as between the control-obese and control-lean rats (Fig. 6B). At week 12, the density of dendritic spines of the ORX-lean, control-obese and

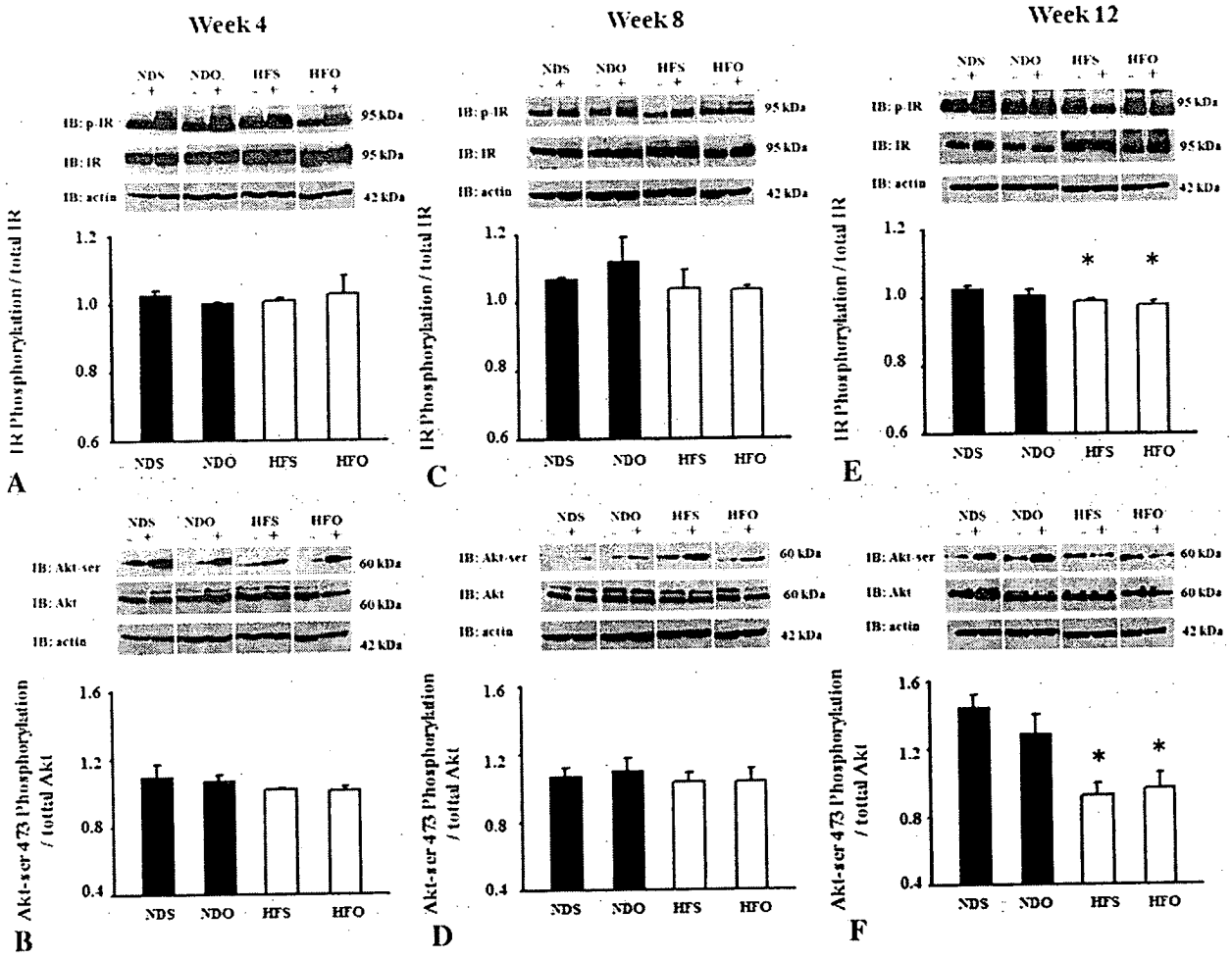


Fig. 2 – The effects of obesity with or without testosterone deprivation on the protein expression of insulin receptor phosphorylation (p-IR) and insulin receptor (IR) signaling of homogenate brain slices at different time periods. At week 4 and week 8, there was no difference between IR phosphorylation/IR protein expression and Akt-ser 473 phosphorylation/ Akt protein expression among groups (A–D). At week 12, HFS and HFO decreased IR phosphorylation/IR protein expression and Akt-ser 473 phosphorylation/ Akt protein expression, compared with NDS (E and F). NDS, control-lean rats; NDO, ORX-lean rats; HFS, control-obese rats; and HFO, ORX-obese rats. *p < 0.05 vs NDS in the same time period.

ORX-obese rats was significantly decreased, compared with that of the control-lean rats ($p < 0.05$, Fig. 6C). However, no difference was found among the ORX-lean, control-obese and ORX-obese rats (Fig. 6C).

4. Discussion

Major findings of the present study (as summarized in Table 2) are as followings. First, testosterone deprivation alone does not lead to peripheral insulin resistance, brain mitochondrial dysfunction and brain insulin resistance, but causes the hippocampal synaptic dysfunction and cognitive impairment. Second, obesity induced by HFD consumption alone leads to the development of the peripheral insulin resistance, increased brain oxidative stress, brain mitochondrial dysfunction, brain insulin resistance, hippocampal synaptic dysfunction and cognitive decline. Third, obesity does not accelerate cognitive dysfunction under testosterone-deprived condition. Fourth, testosterone deprivation has neither additive nor synergistic effects over obesity in the development of cognitive dysfunction in orchiectomized-obese male rats.

The present study found that testosterone deprivation alone did not impair peripheral insulin sensitivity, but the development of peripheral insulin resistance was initially found at week eight in both HFD-fed rats. These findings suggest that the development of peripheral insulin resistance is mainly dependent on the HFD consumption. This finding is supported by our previous study and other studies [2,3,5,6,39], demonstrating that the HFD-fed male rats developed peripheral insulin resistance via increased body mass, increased visceral fat, increased plasma insulin levels, increased HOMA index, impaired insulin sensitivity and impaired lipid profile.

Interestingly, the present study demonstrated for the first time that testosterone deprivation itself had no effects on

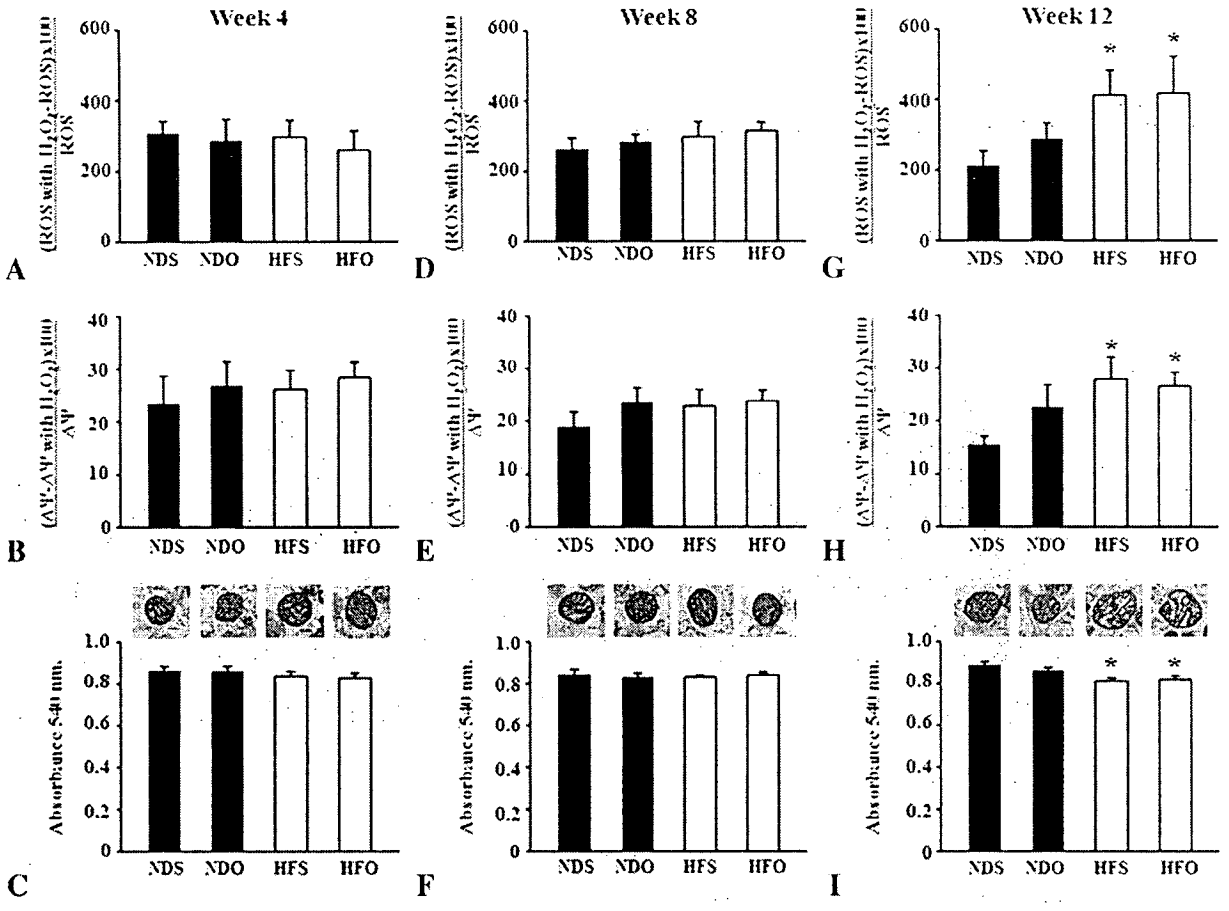


Fig. 3 – The effects of obesity with or without testosterone deprivation on brain mitochondrial function in different time courses. At week 4 and week 8, there were no differences between brain mitochondrial function among groups. (A–F) At week 12, HFS and HFO demonstrated brain mitochondrial dysfunction, as indicated by increased brain mitochondrial ROS production following H_2O_2 application (G), increased brain mitochondrial membrane potential change following H_2O_2 application (H) and decreased absorbance values at five minutes, indicating brain mitochondrial swelling. (I) In addition, representative pictures of brain mitochondrial ultrastructure morphology by transmission electron microscopy (original magnification ×15,000), normally folded cristae of brain mitochondrial morphology was shown in all groups at week 4 and week 8. (C and F) At week 12, NDS and NDO also demonstrated clearly folded cristae, but brain mitochondrial swelling, as indicated by unfolded cristae of both HFS and HFO groups was observed. (I) NDS, control-lean rats; NDO, ORX-lean rats; HFS, control-obese rats; and HFO, ORX-obese rats. * $p < 0.05$ vs NDS in same time course.

brain mitochondrial function, brain oxidative stress levels, and brain insulin sensitivity. In contrast, both groups of HFD-fed rats (control-obese rats and ORX-obese rats) had brain mitochondrial dysfunction, increased brain oxidative stress levels, and brain insulin resistance as indicated by a reduction of insulin induced-LTD and decreased insulin receptor (IR) phosphorylation and Akt/PKB serine-473 phosphorylation at week 12. These findings are consistent with our previous reports showing that brain insulin resistance developed following 12 weeks of HFD feeding [5,6,28]. Our findings indicate that it is the obesity induced by HFD consumption, not testosterone deprivation that causes the impairment of brain mitochondrial function and increased brain oxidative stress levels, resulting in brain insulin resistance. Furthermore, previous studies demonstrated that an increase in MDA levels and mitochondrial dysfunction are associated with cognitive decline, obesity and testosterone deficiency in animal models [40–44]. In addition, our previous studies demonstrated that brain mitochondrial dysfunction and increased plasma as well as brain MDA levels are associated with cognitive impairment in obese rats [4,45]. Those findings suggest that increased brain oxidative stress plays an important role in the development of the cognitive impairment in an obese model. This study, further demonstrated that obesity could lead to increased brain oxidative stress and brain mitochondrial dysfunction, resulting in a cognitive impairment. However, no additive or synergistic effects of obesity and testosterone deficiency on brain oxidative stress and brain mitochondrial function have been found.

A previous study demonstrated that obesity induced by HFD consumption caused the impairment of cognition and

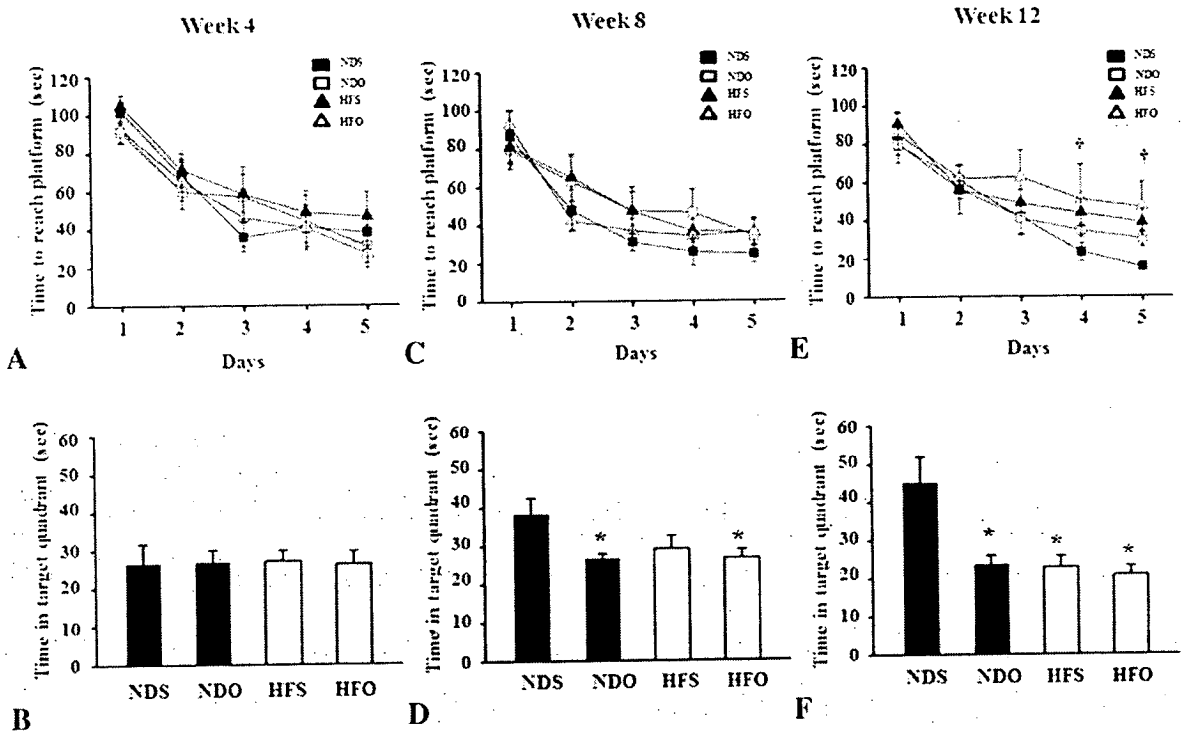


Fig. 4 – The effect of testosterone deprivation with or without obese-insulin resistant conditions on the cognitive function determined by Morris water maze (MWM) test at different time periods. At week 4, there were no differences among groups of time taken to reach the platform in the acquisition test and time spent in target quadrant in the probe test. (A–B) At week eight, there was no difference among groups of time to reach the platform in acquisition test (C), whereas NDO and HFO groups had a significantly decreased time spent in target quadrant in the probe test. (D) At week 12, HFS and HFO significantly increased time to reach the platform in acquisition test (E), whereas NDO, HFS and HFO significantly decreased time spent in target quadrant in the probe test. (F) * $p < 0.05$ compared to NDS, † $p < 0.05$ HFS and HFO compared to NDS. NDS, control-lean rats; NDO, ORX-lean rats; HFS, control-obese rats; and HFO, ORX-obese rats.

hippocampal synaptic plasticity [39]. In addition, several studies reported that testosterone deficiency is correlated with cognitive impairment [13–15]. Consistent with those reports, our results demonstrated that both ORX-obese and ORX-lean rats as well as the control-obese rats developed cognitive impairment. However, these impairments were found beginning at week eight in all orchiectomized rats, i.e. ORX-lean rats and ORX-obese rats, regardless of dietary regimens. Unlike orchiectomized rats, the cognitive impairments were found later at week 12 in the control-obese rats, suggesting that testosterone deprivation dominates obesity in the development of cognitive dysfunction in orchiectomized-obese male rats. The present study demonstrated that cognitive impairment occurred in control-obese rats following consumption of a HFD for 12 weeks. In addition, the level of testosterone in those rats was significantly reduced, when compared with that of control-lean rats. These findings suggest that the cognitive impairment could depend on testosterone levels. This is also supported by previous reports that decreased testosterone level could lead to cognitive impairment [14,46–48]. However, an increase in testosterone level following testosterone replacement could also lead to impaired cognition as shown by the results of the Morris water maze test in normal male rats [49,50]. All of these findings indicate that the physiological level of testosterone should be at its optimum to maintain intact cognition. Although it has been shown that obesity could increase the estrogen levels [51], our previous study demonstrated that 12 weeks of high fat feeding did not affect the circulating and brain estrogen levels in male rats [6]. Moreover, a recent report also demonstrated that estradiol administration did not affect cardiac electrophysiological function in orchiectomized male rats [52]. All of these findings indicate the important role of decreased testosterone rather than increased estrogen levels in male rats.

To study the underlying mechanism of cognitive dysfunction, the hippocampal synaptic long-term synaptic plasticity (LTP) and dendritic spine densities were determined in the present study. It has been shown that synaptic plasticity is a driving mechanism in modulating the learning and memory formation in the brain [38]. LTP is an activation of the excitatory synapse resulting in increased synaptic strength and enhanced synaptic transmission [53]. In the present study, the degree of electrical-induced LTP was significantly decreased in both orchiectomized groups (ORX-lean rats and ORX-obese rats) at week eight, which was at the same time period of the cognitive impairment. Our findings were consistent with previous reports which demonstrated that impaired LTP was associated with cognitive impairment [54,55]. Moreover, the reduction of the density of dendritic spines and dendritic spine morphology changes in CA1 hippocampus had

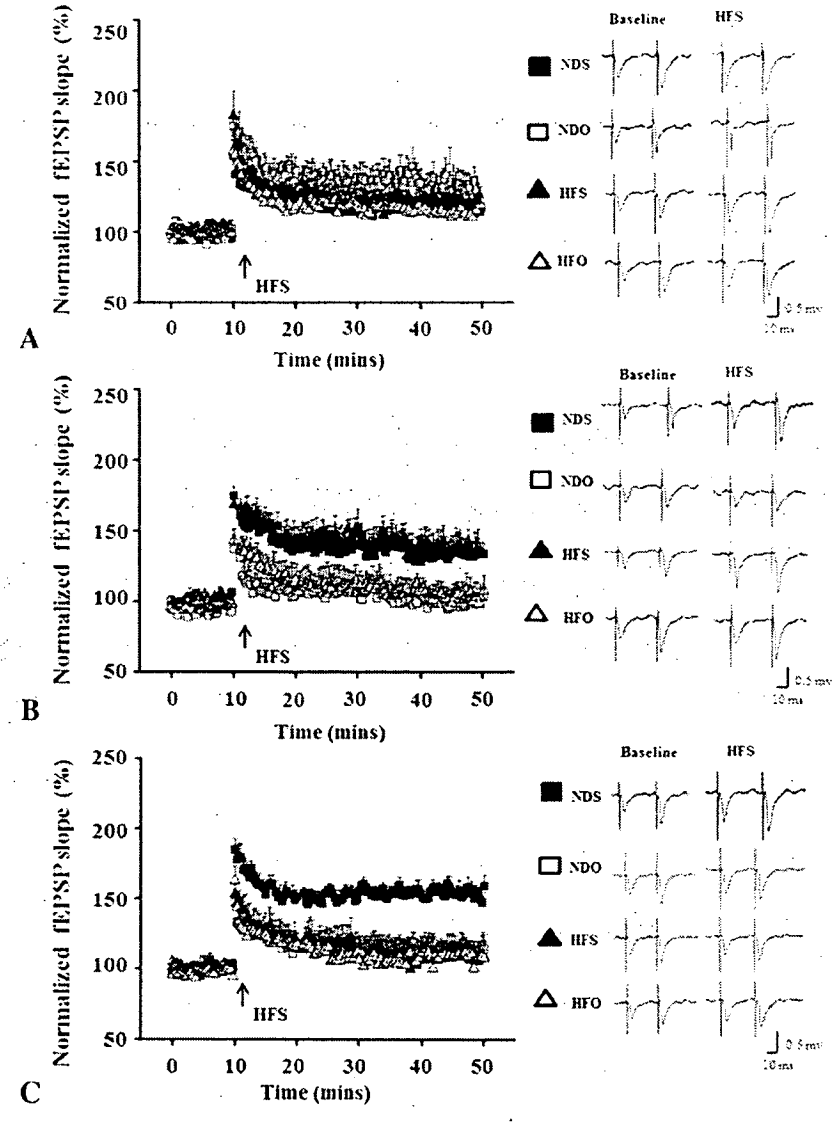


Fig. 5 – The effect of testosterone deprivation with or without obese-insulin resistant condition on hippocampal synaptic long-term potentiation (LTP) at different time periods. At week 4, there were no differences among groups of percentage normalized fEPSPs (fEPSPt/fEPSPo with fEPSPs being points at which fEPSP slopes stabilized). (A) At week 8, NDO and HFO had a significantly reduced percentage of normalized fEPSPs. (B) At week 12, NDO, HFS and HFO had significantly reduced percentages of normalized fEPSPs. (C) HF, high frequency stimulation; NDS, control-lean rats; NDO, ORX-lean rats; HFS, control-obese rats; and HFO, ORX-obese rats.

been demonstrated previously in orchiectomized rats [17]. In the present study, the density of hippocampal dendritic spines at CA1 hippocampus in both orchiectomized groups (ORX-lean rats and ORX-obese rats) was substantially reduced at week eight. All of these findings by ourselves and others suggest that testosterone deprivation may play an important role in cognitive impairment through impaired synaptic plasticity as well as decreased hippocampal dendritic spine density.

Despite the fact that previous studies demonstrated the effects of obesity on cognitive decline [56,57], there is a report demonstrating that diet-induced cognitive impairment could precede weight gain and obesity [58]. This study did not include an investigation into the effects of a fat-rich diet on brain function in non-obese rats. Whether the adverse effects observed were due to obesity or a fat-rich diet remains to be elucidated.

In summary, the obese-insulin resistant condition alone (control-obese rats) caused cognitive impairment and decreased synaptic plasticity at a later period (i.e. week 12), compared to the orchiectomized rats (i.e. ORX-lean and ORX-obese rats). Moreover, obesity did not accelerate these cognitive impairments in testosterone-deprived rats. These findings indicate that testosterone deprivation dominates obesity in the development of the impairment of cognitive function and the reduction of hippocampal synaptic plasticity in orchiectomized-obese male rats.

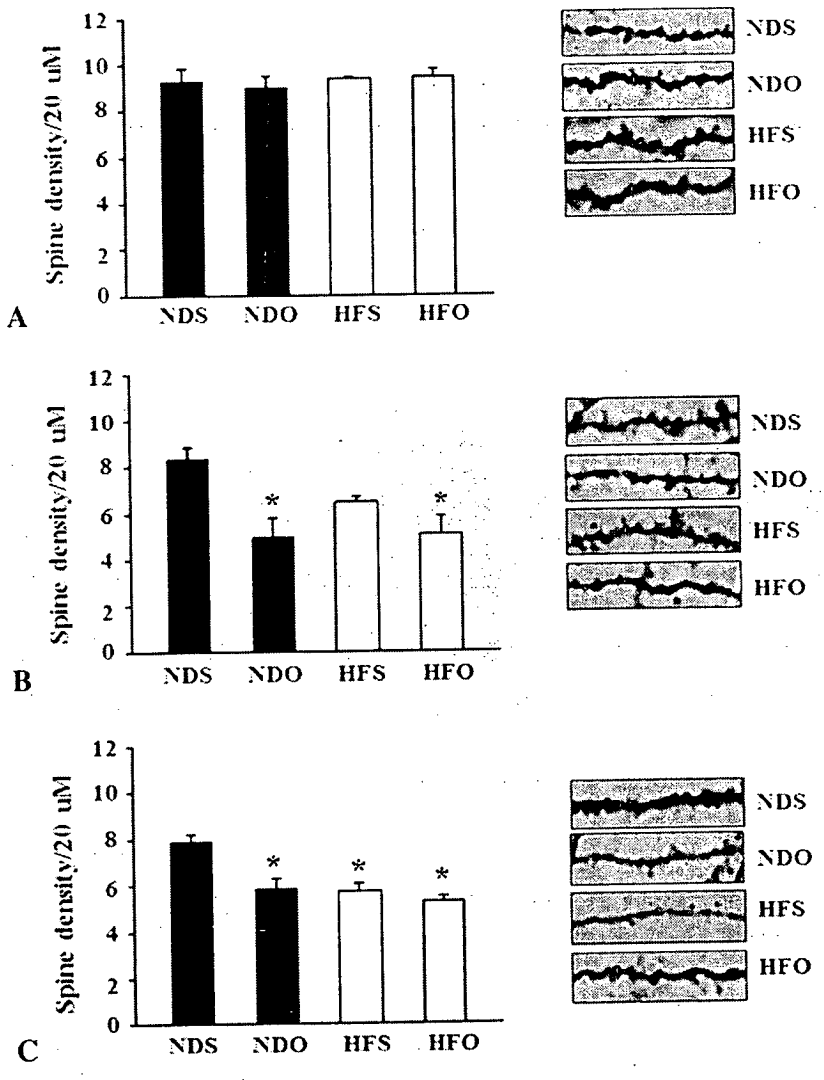


Fig. 6 – The effect of testosterone deprivation with or without obese-insulin resistant condition on the number of dendritic spines at CA1 region of hippocampal at different time periods. At week four, there was no difference in the number of dendritic spines among groups. (A) At week eight, NDO and HFO groups had a significantly reduced number of dendritic spines. (B) At week 12, NDO, HFS and HFO were significantly reduced number of dendritic spines. (C) * $p < 0.05$ compared to NDS in same time course. NDS, control-lean rats; NDO, ORX-lean rats; HFS, control-obese rats; and HFO, ORX-obese rats.

5. Conclusion

An obese-insulin resistant condition can cause brain insulin resistance via decreased peripheral insulin sensitivity, increased oxidative stress and impaired brain mitochondrial function, leading to impaired hippocampal synaptic plasticity and cognition. Unlike long term HFD consumption, testosterone deprivation alone does not impair peripheral insulin sensitivity, brain insulin sensitivity and brain mitochondrial function. However, testosterone deprivation can cause cognitive impairment via impaired hippocampal synaptic plasticity and reduced hippocampal

Table 2 – The summary of all findings in the present study.

Major findings	Testosterone deprivation	Obesity	Obesity + testosterone deprivation
Peripheral insulin resistance	×	√ (week 8,12)	√ (week 8,12)
Brain mitochondrial dysfunction	×	√ (week 12)	√ (week 12)
Increased brain oxidative stress	×	√ (week 12)	√ (week 12)
Brain insulin resistance	×	√ (week 12)	√ (week 12)
Synaptic dysfunction	√ (week 8,12)	√ (week 12)	√ (week 8,12)
Cognitive impairment	√ (week 8,12)	√ (week 12)	√ (week 8,12)

dendritic spine numbers. Moreover, an obese-insulin resistant condition does not accelerate or aggravate cognitive impairment in the testosterone deprived condition. These findings suggest that testosterone deprivation has neither additive nor synergistic effects over obesity in the development of cognitive dysfunction in orchiectomized-obese male rats.

Author Contribution

HP performed the experiments, analyzed the data and wrote the manuscript. WP, PS and WP performed the experiments and analyzed the data. RT analyzed the data. NC co-designed the study, analyzed the data and wrote the manuscript. SCC co-designed the study, performed the experiments, analyzed the data and wrote the manuscript.

Acknowledgments and Funding

The authors thank Sirinart Kumfu, PhD; Jirapas Sripecthwandee, PhD; Nattayaporn Apaijai, M.Sc. and Jantira Sanit, MSc for all technical support in the present study. This work was supported by Thailand Research Fund grants: TRF-BRG 5780016 (SC), TRF-TRG5680018 (WP), The Royal Golden Jubilee PhD Program (PHD/0025/2555 HP&SC), National Research Council of Thailand (SC), a NSTDA Research Chair Grant from the National Science and Technology Development Agency (NC) and a Chiang Mai University Excellence Center Award (NC).

Disclosure Statement

The authors declare no conflicts of interest.

REFERENCES

[1] Goldstein BJ. Insulin resistance as the core defect in type 2 diabetes mellitus. Am J Cardiol 2002;90:3G–10G.
[2] Akiyama T, Tachibana I, Shirohara H, Watanabe N, Otsuki M. High-fat hypercaloric diet induces obesity, glucose intolerance and hyperlipidemia in normal adult male Wistar rat. Diabetes Res Clin Pract 1996;31:27–35.
[3] Kraegen EW, Clark PW, Jenkins AB, Daley EA, Chisholm DJ, Storlien LH. Development of muscle insulin resistance after liver insulin resistance in high-fat-fed rats. Diabetes 1991;40:1397–403.
[4] Pintana H, Apaijai N, Chattipakorn N, Chattipakorn SC. DPP-4 inhibitors improve cognition and brain mitochondrial function of insulin resistant rats. J Endocrinol 2013;218:1–11.
[5] Pipatpiboon N, Pintana H, Pratchayasakul W, Chattipakorn N, Chattipakorn SC. DPP4-inhibitor improves neuronal insulin receptor function, brain mitochondrial function and cognitive function in rats with insulin resistance induced by high-fat diet consumption. Eur J Neurosci 2013;37:839–49.
[6] Pratchayasakul W, Kerdphoo S, Petsophonsakul P, Pongchaidecha A, Chattipakorn N, Chattipakorn SC. Effects of high-fat diet on insulin receptor function in rat hippocampus and the level of neuronal corticosterone. Life Sci 2011;88:619–27.
[7] Wu A, Ying Z, Gomez-Pinilla F. The interplay between oxidative stress and brain-derived neurotrophic factor modulates the outcome of a saturated fat diet on synaptic plasticity and cognition. Eur J Neurosci 2004;19:1699–707.
[8] Morrison CD, Pistell PJ, Ingram DK, Johnson WD, Liu Y, Fernandez-Kim SO, et al. High fat diet increases hippocampal oxidative stress and cognitive impairment in aged mice: implications for decreased Nrf2 signaling. J Neurochem 2010;114:1581–9.
[9] Pistell PJ, Morrison CD, Gupta S, Knight AG, Keller JN, Ingram DK, et al. Cognitive impairment following high fat diet consumption is associated with brain inflammation. J Neuroimmunol 2010;219:25–32.
[10] Chen X, Li X, Huang HY, Lin JF. Effects of testosterone on insulin receptor substrate-1 and glucose transporter 4 expression in cells sensitive to insulin. Zhonghua Yi Xue Za Zhi 2006;86:1474–7.
[11] Filova B, Ostatnikova D, Celec P, Hodosy J. The effect of testosterone on the formation of brain structures. Cells Tissues Organs 2013;197:169–77.
[12] Janowsky JS. Thinking with your gonads: testosterone and cognition. Trends Cogn Sci 2006;10:77–82.
[13] Sakata K, Tokue A, Kawai N. Altered synaptic transmission in the hippocampus of the castrated male mouse is reversed by testosterone replacement. J Urol 2000;163:1333–8.
[14] Sandstrom NJ, Kim JH, Wasserman MA. Testosterone modulates performance on a spatial working memory task in male rats. Horm Behav 2006;50:18–26.
[15] Spritzer MD, Daviau ED, Coneeny MK, Engelman SM, Prince WT, Rodriguez-Wisdom KN. Effects of testosterone on spatial learning and memory in adult male rats. Horm Behav 2011;59:484–96.
[16] Naghdi N, Majlessi N, Bozorgmehr T. The effect of intrahippocampal injection of testosterone enanthate (an androgen receptor agonist) and anisomycin (protein synthesis inhibitor) on spatial learning and memory in adult, male rats. Behav Brain Res 2005;156:263–8.
[17] Leranth C, Petnehazy O, MacLusky NJ. Gonadal hormones affect spine synaptic density in the CA1 hippocampal subfield of male rats. J Neurosci 2003;23:1588–92.
[18] Danzer SC, McMullen NT, Rance NE. Testosterone modulates the dendritic architecture of arcuate neuroendocrine neurons in adult male rats. Brain Res 2001;890:78–85.
[19] Li M, Masugi-Tokita M, Takanami K, Yamada S, Kawata M. Testosterone has sublayer-specific effects on dendritic spine maturation mediated by BDNF and PSD-95 in pyramidal neurons in the hippocampus CA1 area. Brain Res 2012;1484:76–84.
[20] Christoffersen BO, Gade LP, Golozoubova V, Svendsen O, Raun K. Influence of castration-induced testosterone and estradiol deficiency on obesity and glucose metabolism in male Gottingen minipigs. Steroids 2010;75:676–84.
[21] Georgiev IP, Georgieva TM, Ivanov V, Dimitrova S, Kanelov I, Vlaykova T, et al. Effects of castration-induced visceral obesity and antioxidant treatment on lipid profile and insulin sensitivity in New Zealand white rabbits. Res Vet Sci 2011;90:196–204.
[22] Shi Z, Araujo AB, Martin S, O'Loughlin P, Wittert GA. Longitudinal changes in testosterone over five years in community-dwelling men. J Clin Endocrinol Metab 2013;98:3289–97.
[23] Haffner SM, Shaten J, Stern MP, Smith GD, Kuller L. Low levels of sex hormone-binding globulin and testosterone predict the development of non-insulin-dependent diabetes mellitus in men. MRFIT Research Group. Multiple Risk Factor Intervention Trial. Am J Epidemiol 1996;143:889–97.
[24] Borst SE, Conover CF. Orchiectomized Fischer 344 male rat models body composition in hypogonadal state. Life Sci 2006;79:411–5.

[25] Erben RG, Eberle J, Stahr K, Goldberg M. Androgen deficiency induces high turnover osteopenia in aged male rats: a sequential histomorphometric study. J Bone Miner Res 2000; 15:1085–98.
[26] Kakolewski JW, Cox VC, Valenstein ES. Sex differences in body-weight change following gonadectomy of rats. Psychol Rep 1968;22:547–54.
[27] Gentry RT, Wade GN. Androgenic control of food intake and body weight in male rats. J Comp Physiol Psychol 1976;90: 18–25.
[28] Pipatpiboon N, Pratchayasakul W, Chattipakorn N, Chattipakorn SC. PPARgamma agonist improves neuronal insulin receptor function in hippocampus and brain mitochondria function in rats with insulin resistance induced by long term high-fat diets. Endocrinology 2012;153:329–38.
[29] Dulisch ML. A Castration Procedure for the Rabbit, Rat, Hamster, and Guinea Pig. J Zoo Anim Med 1976;7:8–11.
[30] Carpenter JW. Antimicrobial and antifungal agents used in rodents. In: Carpenter JW, editor. Exotic animal formulary. 3rd ed. Elsevier saunders; 2005. p. 376–82.
[31] Appleton DJ, Rand JS, Sunvold GD. Basal plasma insulin and homeostasis model assessment (HOMA) are indicators of insulin sensitivity in cats. J Feline Med Surg 2005;7:183–93.
[32] Haffner SM, Miettinen H, Stern MP. The homeostasis model in the San Antonio Heart Study. Diabetes Care 1997;20:1087–92.
[33] Mateos R, Lecumberri E, Ramos S, Goya L, Bravo L. Determination of malondialdehyde (MDA) by high-performance liquid chromatography in serum and liver as a biomarker for oxidative stress. Application to a rat model for hypercholesterolemia and evaluation of the effect of diets rich in phenolic antioxidants from fruits. J Chromatogr B Analyt Technol Biomed Life Sci 2005;827:76–82.
[34] Sripetchwandee J, Pipatpiboon N, Chattipakorn N, Chattipakorn S. Combined therapy of iron chelator and antioxidant completely restores brain dysfunction induced by iron toxicity. PLoS One 2014;9:e85115.
[35] Candan N, Tuzmen N. Very rapid quantification of malondialdehyde (MDA) in rat brain exposed to lead, aluminium and phenolic antioxidants by high-performance liquid chromatography-fluorescence detection. Neurotoxicology 2008;29:708–13.
[36] Arakawa H. Age dependent effects of space limitation and social tension on open-field behavior in male rats. Physiol Behav 2005;84:429–36.
[37] Vorhees CV, Williams MT. Morris water maze: procedures for assessing spatial and related forms of learning and memory. Nat Protoc 2006;1:848–58.
[38] Martin SJ, Grimwood PD, Morris RG. Synaptic plasticity and memory: an evaluation of the hypothesis. Annu Rev Neurosci 2000;23:649–711.
[39] Stranahan AM, Norman ED, Lee K, Cutler RG, Telljohann RS, Egan JM, et al. Diet-induced insulin resistance impairs hippocampal synaptic plasticity and cognition in middle-aged rats. Hippocampus 2008;18:1085–8.
[40] Liu J. The effects and mechanisms of mitochondrial nutrient alpha-lipoic acid on improving age-associated mitochondrial and cognitive dysfunction: an overview. Neurochem Res 2008;33:194–203.
[41] Cotman CW, Head E, Muggenburg BA, Zicker S, Milgram NW. Brain aging in the canine: a diet enriched in antioxidants reduces cognitive dysfunction. Neurobiol Aging 2002;23: 809–18.
[42] McManus MJ, Murphy MP, Franklin JL. The mitochondria-targeted antioxidant MitoQ prevents loss of spatial memory retention and early neuropathology in a transgenic mouse model of Alzheimer's disease. J Neurosci 2011;31:15703–15.
[43] Pintana H, Pongkan W, Pratchayasakul W, Chattipakorn N, Chattipakorn SC. Testosterone replacement attenuates cognitive decline in testosterone-deprived lean rats, but not in obese rats, by mitigating brain oxidative stress. Age 2015; 37:9827. http://dx.doi.org/10.1007/s11357-015-9827-4.
[44] Pintana H, Pongkan W, Pratchayasakul W, Chattipakorn N, Chattipakorn SC. Dipeptidyl peptidase 4 inhibitor improves brain insulin sensitivity, but fails to prevent cognitive impairment in orchiectomy obese rats. J Endocrinol 2015;226: M1–M11.
[45] Pintana H, Sripetchwandee J, Supakul L, Apaijai N, Chattipakorn N, Chattipakorn S. Garlic extract attenuates brain mitochondrial dysfunction and cognitive deficit in obese-insulin resistant rats. Appl Physiol Nutr Metab 2014;39: 1373–9.
[46] McConnell SE, Alla J, Wheat E, Romeo RD, McEwen B, Thornton JE. The role of testicular hormones and luteinizing hormone in spatial memory in adult male rats. Horm Behav 2012;61:479–86.
[47] Daniel JM, Winsauer PJ, Moerschbaecher JM. Castration in rats impairs performance during acquisition of a working memory task and exacerbates deficits in working memory produced by scopolamine and mecamylamine. Psychopharmacology 2003;170:294–300.
[48] Spritzer MD, Gill M, Weinberg A, Galea LA. Castration differentially affects spatial working and reference memory in male rats. Arch Sex Behav 2008;37:19–29.
[49] Emamian S, Naghdi N, Sepehri H, Jahanshahi M, Sadeghi Y, Choopani S. Learning impairment caused by intra-CA1 microinjection of testosterone increases the number of astrocytes. Behav Brain Res 2010;208:30–7.
[50] Khorshidahmad T, Tabrizian K, Vakilzadeh G, Nikbin P, Moradi S, Hosseini-Sharifabad A, et al. Interactive effects of a protein kinase AII inhibitor and testosterone on spatial learning in the Morris water maze. Behav Brain Res 2012;228: 432–9.
[51] Fernandez CD, Bellentani FF, Fernandes GS, Perobelli JE, Favareto AP, Nascimento AF, et al. Diet-induced obesity in rats leads to a decrease in sperm motility. Reprod Biol Endocrinol 2011;9:32. http://dx.doi.org/10.1186/1477-7827-9-32.
[52] Ayaz M, Akand M, Kucukbagriacik Y, Dursunoglu D. The effects of estradiol on cardiac muscle electrophysiology in orchiectomized rat model: a new insight to side effects caused by castration. Eur Rev Med Pharmacol Sci 2015;19: 2866–74.
[53] Maren S, Baudry M. Properties and mechanisms of long-term synaptic plasticity in the mammalian brain: relationships to learning and memory. Neurobiol Learn Mem 1995; 63:1–18.
[54] Dawson GR, Seabrook GR, Zheng H, Smith DW, Graham S, O'Dowd G, et al. Age-related cognitive deficits, impaired long-term potentiation and reduction in synaptic marker density in mice lacking the beta-amyloid precursor protein. Neuroscience 1999;90:1–13.
[55] Yang J, Hou C, Ma N, Liu J, Zhang Y, Zhou J, et al. Enriched environment treatment restores impaired hippocampal synaptic plasticity and cognitive deficits induced by prenatal chronic stress. Neurobiol Learn Mem 2007;87:257–63.
[56] Winocur G, Greenwood CE, Piroli GG, Grillo CA, Reznikov LR, Reagan LP, et al. Memory impairment in obese Zucker rats: an investigation of cognitive function in an animal model of insulin resistance and obesity. Behav Neurosci 2005;119: 1389–95.
[57] Gerges NZ, Aleisa AM, Alkadhi KA. Impaired long-term potentiation in obese zucker rats: possible involvement of presynaptic mechanism. Neuroscience 2003;120:535–9.
[58] Davidson TL, Hargrave SL, Swithers SE, Sample CH, Fu X, Kinzig KP, et al. Inter-relationships among diet, obesity and hippocampal-dependent cognitive function. Neuroscience 2013;253:110–22.

เอกสารแนบหมายเลข 37



Taylor & Francis

Neurological Research

A Journal of Progress in Neurosurgery, Neurology and Neuro Sciences

ISSN: 0161-6412 (Print) 1743-1328 (Online) Journal homepage: http://www.tandfonline.com/loi/yner20

Bevacizumab is superior to Temozolomide in causing mitochondrial dysfunction in human brain tumors

Danop Nanegrungsunk, Nattayaporn Apaijai, Chontida Yarana, Jirapas Sripetchwandee, Kriengsak Limpastan, Wanarak Watcharasaksilp, Tanat Vaniyapong, Nipon Chattipakorn & Siriporn C Chattipakorn

To cite this article: Danop Nanegrungsunk, Nattayaporn Apaijai, Chontida Yarana, Jirapas Sripetchwandee, Kriengsak Limpastan, Wanarak Watcharasaksilp, Tanat Vaniyapong, Nipon Chattipakorn & Siriporn C Chattipakorn (2016) Bevacizumab is superior to Temozolomide in causing mitochondrial dysfunction in human brain tumors, Neurological Research, 38:4, 285-293, DOI: 10.1080/01616412.2015.1114233

To link to this article: http://dx.doi.org/10.1080/01616412.2015.1114233

Published online: 13 Apr 2016.

Submit your article to this journal

Article views: 46

View related articles

View Crossmark data

Full Terms & Conditions of access and use can be found at
http://www.tandfonline.com/action/journalInformation?journalCode=yner20

Download by: [Chiang Mai University] **Date:** 27 May 2016, At: 01:52

Bevacizumab is superior to Temozolomide in causing mitochondrial dysfunction in human brain tumors

Danop Nanegrungsunk[1,2], Nattayaporn Apaijai[2], Chontida Yarana[2], Jirapas Sripetchwandee[2], Kriengsak Limpastan[3], Wanarak Watcharasaksilp[3], Tanat Vaniyapong[3], Nipon Chattipakorn[2], Siriporn C Chattipakorn[2,4]

[1]Department of Anesthesiology, Faculty of Medicine, Chiang Mai University, Chiang Mai, Thailand, [2]Neurophysiology Unit, Cardiac Electrophysiology Research and Training Center, Faculty of Medicine, Chiang Mai University, Chiang Mai, Thailand, [3]Neurosurgery Division, Department of Surgery, Faculty of Medicine, Chiang Mai University, Chiang Mai, Thailand, [4]Department of Oral Biology and Diagnostic Science, Faculty of Dentistry, Chiang Mai University, Chiang Mai, Thailand

Downloaded by [Chiang Mai University] at 01:52 27 May 2016

Objective: Current chemotherapy treatments available for treating high-grade brain tumors, Temozolomide (TMZ) or Bevacizumab (BEV), not only have specific anti-tumor mechanisms, but also have an effect on mitochondria. However, effects of both drugs on mitochondria isolated from human brain tumors have not been thoroughly investigated. This study determined the direct effects of TMZ and BEV as well as the neurotoxic condition (calcium overload), on the function of mitochondria and compared these effects on mitochondria isolated from low- and high-grade human brain tumors.

Methods: Mitochondria were isolated from either low- or high-grade human primary brain tumors. Calcium overload conditions (100 or 200 μM), TMZ (300 μM), and BEV (2 mg/mL) were applied to isolated mitochondria from low- and high-grade brain tumors. Following the treatment, mitochondrial function, including reactive oxygen species production, membrane potential changes, and swelling, were determined. The mitochondrial morphology was also examined.

Results: In calcium overload conditions, mitochondrial dysfunction was only found to have occurred in low-grade tumors. In TMZ and BEV treatment, BEV, rather than TMZ, caused greater membrane depolarization and mitochondrial swelling in both grades of brain tumors.

Conclusions: TMZ and BEV can directly cause the dysfunction of mitochondria isolated from human brain tumors. However, BEV has a greater ability to disturb mitochondrial function in mitochondria isolated from human brain tumors than either TMZ or calcium overload conditions.

Keywords: Human brain tumor, Mitochondria, Calcium overload, Temozolomide and bevacizumab

Introduction

Primary brain tumors are classified into four grades (Grade I–IV) according to the World Health Organization (WHO). Grade I and II tumors are clinically categorized as low-grade, whereas grades III and IV as high-grade tumors.[1] The two most common chemotherapy treatments for high-grade brain tumors are temozolomide (TMZ) and bevacizumab (BEV). TMZ is an alkylating agent that forms O^6 methylguanine (O^6MeG), which causes DNA changes and leads to cell cycle arrest in G2/M,[2] leading to cell apoptosis and/or autophagy as demonstrated in brain cancer cell lines.[3] BEV is a humanized monoclonal antibody against vascular endothelial growth factor-A (VEGF-A). It prevents VEGF receptor activation and subsequently inhibits tumor angiogenesis, leading to tumor cell death through hypoxia-induced autophagy or unspecific indirect effects on cancer cells.[3,4]

Mitochondria play an important role in cell apoptosis and tumor cell survival. Previous studies showed brain tumor resistance to TMZ could be due to mitochondrial adaptive response [5] along with remodeling of the electron transport chain secondary to increased mitochondrial coupling.[6] In addition, it has been shown that BEV-induced hypoxia leads to a decrease in mitochondrial number and an increase in infiltrating glioblastoma cells.[7]

In recent studies, TMZ and BEV have been shown to cause damage to mitochondria.[8,9] TMZ induces mitochondrial depolarization and causes the loss of mitochondria mass in the human glioblastoma cell line[8]; however, both these might be an indirect result of increased reactive

Correspondence to: Siriporn Chattipakorn Neurophysiology Unit, Cardiac Electrophysiology Research and Training Center, Faculty of Medicine, Department of Physiology, Chiang Mai University, Chiang Mai 50200, Thailand. Email: siriporn.c@cmu.ac.th

© 2016 Informa UK Limited, trading as Taylor & Francis Group
DOI 10.1080/01616412.2015.1114233

oxygen species (ROS). BEV has shown its dose-dependent effect in decreasing mitochondrial activity in human microvascular endothelial cells, a phenomenon detected by mitochondrial dehydrogenase activity.[9]

Normal brain mitochondria have been shown to deteriorate as a result of intracellular calcium overload, an intracellular neurotoxicity, which is responsible for increased ROS production, mitochondrial membrane depolarization, and mitochondrial swelling.[10,11]

However, the effects of TMZ, BEV, and calcium overload on mitochondria isolated from either low-grade or high-grade human brain tumors have not yet been determined. Therefore, this study has investigated the direct mitochondrial response to chemotherapeutic drugs and has identified the difference in response of mitochondria between low- and high-grade brain tumors under various conditions: calcium overload or treatment with TMZ and /or BEV. The hypothesis was that either TMZ, BEV, or calcium overload led to the dysfunction of mitochondria isolated from low-grade human brain tumors, but not those isolated from high-grade human brain tumors which display greater clinical and histological aggressiveness.[12,13]

Materials and methods

Tissue samples

All patients underwent neurosurgery with general anesthesia to remove brain tumors during the period of September 2011 to August 2013. Dissected human brain tumor samples were collected from 38 patients who had all completed consent forms. Tumor tissue samples were divided into two groups: low-grade tumors and high-grade tumors. All tumor samples were used in two experimental protocols. The first protocol was a calcium overload protocol. Fifteen samples were used in this protocol [low-grade tumors (n = 8) and high-grade tumors (n = 7)]. The second protocol was a chemotherapy protocol. Twenty-three samples were used in the second protocol. [Low-grade tumors (n = 15) and high-grade tumors (n = 8)]. In both protocols, low-grade tumors consisted of WHO grade I–II (i.e. pleomorphic xanthoastrocytoma, schwannoma, atypical meningioma, and meningioma), and high-grade brain tumors were those listed as WHO grades III–IV (i.e. glioblastoma multiforme and anaplastic astrocytoma).

Experimental protocols

Both calcium overload and chemotherapy protocols were conducted using isolated brain tumor mitochondria and performed in triplicate.

Calcium overload protocol

100 μM $CaCl_2$, 200 μM $CaCl_2$, or vehicle (control) was applied to isolated brain tumor mitochondria for 15 min before measuring mitochondrial function as described in a previous study.[11]

Chemotherapy protocol

Two agents: TMZ (300 μM) (Temodal™, Schering-Plough, Turku, Finland) and BEV (2 mg/mL) (Avastin®, Roche, Basel, Switzerland) were applied to elucidate their putative efficacy in causing deterioration of mitochondrial function. These concentrations have been shown to be effective in killing tumor cells.[6,14] Both TMZ and BEV were separately applied to isolated mitochondria either 15 or 30 min before measuring mitochondrial function.[11] Vehicle-treated mitochondria were used as a control group.

Mitochondrial function was determined by measuring ROS production, membrane potential changes, swelling, and morphological changes.

Isolation of mitochondria from human brain tumors

Tumor brain mitochondria were isolated according to the procedure described by Rosental *et al.* 1987.[15] Fresh human brain tumor tissues were transferred to cold MSE solution containing D-mannitol 225 mM, sucrose 75 mM, EGTA 1 mM, HEPES 5 mM, and BSA 1mg/ml, pH 7.4 (4 °C). The pH was adjusted with NaOH and HCl. Tissues were then chopped into small pieces, placed in MSE-nagarse solution (0.05% nagarse in MSE solution), and homogenized at 600 rpm/min. Next, the homogenate was centrifuged at 2,000× g for 4 min; the supernatant was collected and centrifuged at 12,000× g for 9 min. Then, mitochondrial pellets were suspended in 0.02% digitonin in MSE solution and centrifuged at 12,000× g for 11 min. The concentration of mitochondria in suspension was determined using the Bicinchoninic Acid (BCA) assay.

Mitochondrial protein concentration assay

The mitochondrial protein concentration was determined by the BCA assay described by Walker and colleagues.[16] In brief, 1 ml of a standard working reagent was added to 50 μl mitochondrial protein, after which the suspension was incubated at 60 °C for 30 min. Then, the sample was cooled to room temperature (25 °C) and its absorbance was measured at 562 nm using a spectrophotometer.

Measurement of mitochondrial ROS production

ROS production from mitochondria was measured using a fluorescent microplate reader with dichlorohydro-fluorescein diacetate (DCFH-DA). Brain mitochondria at a concentration of 0.4 mg/ml were incubated at 25 °C with 10 μM DCFDA for 15 min. DCFDA was oxidized in the presence of H_2O_2 to DCF. Fluorescence was determined at λ_{em} 530 nm (bandwidth 10 nm) and λ_{ex} 485 nm (bandwidth 3 nm), according to the spectral characteristics of DCF. The ROS formation was expressed as arbitrary units of fluorescence intensity of DCF.[17]

Downloaded by [Chiang Mai University] at 01:52 27 May 2016

Downloaded by [Chiang Mai University] at 01:52 27 May 2016

Measurement of mitochondrial membrane potential changes

Changes in mitochondrial membrane potential were monitored with the dye 5,5',6,6'-tetrachloro-1,1',3,3'-tetraethylbenzimidazolcarbocyanine iodide (JC-1).[18] JC-1 is a ratiometric dye that is internalized as a monomer dye (green fluorescence, emission wavelength (λ_{em}) at 530 nm) and is concentrated by respiring mitochondria with a negative inner membrane potential into J-aggregate dye (red fluorescence, emission wavelength (λ_{em}) at 590 nm). Consequently, mitochondrial depolarization is indicated by a decrease in the red/green fluorescence intensity ratio. The isolated mitochondria (0.4 mg/ml) were stained with JC-1 (3 μM) at 37 °C for 15 min[19]; then, the intensity of fluorescence was determined using a fluorescent microplate reader. The JC-1 aggregate (red) fluorescence was excited at 485 nm and detected at 590 nm, and the JC-1 monomer (green) fluorescence was excited at 485 nm and detected at 530 nm. The ratio of red to green fluorescence was calculated.[15,20]

Measurement of mitochondrial swelling

The level of mitochondrial swelling was measured by the change in the absorbance of the suspension at 540 nm using a microplate reader.[21] Mitochondria (0.4 mg/ml) were incubated for 1 min in 2 ml respiration buffer containing KCl 150 mM, HEPES 5 mM, $K_2HPO_4.3H_2O$ 2 mM, glutamate 5 mM, pyruvate 5 mM, pH 7.2 at 4 °C.[22] Mitochondrial swelling was detected when the absorbance of the suspension decreased.

Identification of morphological changes in mitochondria using electron microscopy

Transmission electron microscopy was used to identify morphological changes indicating mitochondrial damage. Isolated mitochondria were fixed overnight in 2.5% glutaraldehyde in 0.1 M cacodylate buffer, pH 7.4 at 4 °C, and then fixed with 1% cacodylate-buffered osmium tetroxide for 2 h at room temperature. Then, the pellets were dehydrated using a graded series of ethanols and embedded in Epon–Araldite.[23] After being cut with a diamond knife, ultrathin sections were placed on copper grids, stained with uranyl acetate and lead citrate, and observed using a transmission electron microscope.

Data analysis

Data were presented as mean ± SEM. All statistical analyses were performed using the program SPSS (version 17; SPSS, Chicago, Ill., USA). The significance of the difference in the calcium protocol was calculated using a two-way ANOVA (dose X tumor grade) followed by *post hoc* Fisher's protected least significant difference (LSD) test. The significance of the difference in the chemotherapy protocol was calculated using a two-way ANOVA (drugs X drug exposure time) at the same tumor grade for ROS production and a two-way ANOVA (drug exposure time X tumor grade) at each drug and followed by *post hoc* Fisher's protected LSD test.

Results

Calcium dominantly induced mitochondrial ROS production, mitochondrial membrane depolarization, and mitochondrial swelling in those isolated from low-grade brain tumors, but not in those isolated from high-grade brain tumors.

After applying 100 and 200 μM CaCl2, mitochondrial ROS production increased in low-grade brain tumors compared to the control group (Fig. 1(a)).

However, no significant difference in ROS production between doses of $CaCl_2$ treatment in the same tumor grade as well as between low-grade and high-grade brain tumors in the same dose of $CaCl_2$ treatment was found.

However, application of both 100 and 200 μM calcium caused significant mitochondrial membrane potential depolarization when compared to the control group. In addition, the degree of mitochondrial depolarization in mitochondria isolated from low-grade tumors was significantly greater than those isolated from high-grade tumors (Fig. 1(b)). However, no significant difference in the degree of mitochondrial membrane potential depolarization between doses of $CaCl_2$ treatment in the same tumor grade as well as between low-grade and high-grade brain tumors in the same dose of CaCl2 treatment was found.

Also, addition of 100 and 200 μM calcium caused swelling of mitochondria isolated from low-grade tumors (Fig. 1(c)). No significant difference in mitochondrial swelling between doses of $CaCl_2$ treatment in the same tumor grade as well as between low-grade and high-grade brain tumors in the same dose of $CaCl_2$ treatment was found.

These findings were consistent with morphological changes identified by an electron microscope (Fig. 2). In the control group of both low-grade and high-grade tumors, apparent folded cristae in the mitochondria were observed indicating intact brain mitochondrial morphology. Brain mitochondrial swelling was observed in the calcium treatment group of low-grade brain tumors as indicated by markedly unfolded cristae in the mitochondria. These findings indicated that mitochondrial structure from those extracted from low-grade tumors showed greater damage than those from high-grade tumors following calcium overload (Fig. 2).

Bevacizumab caused greater dysfunction than Temozolomide in mitochondria isolated from both low-grade and high-grade brain tumors.

Application of TMZ resulted in a significant increased ROS production in brain mitochondria from the low-grade brain tumors, when compared to the BEV treatment (Fig. 3(a)). No significant difference was found between the 15- and 30-min exposure of TMZ in the low-grade brain tumors. Both TMZ and BEV application caused no

Downloaded by [Chiang Mai University] at 01:52 27 May 2016

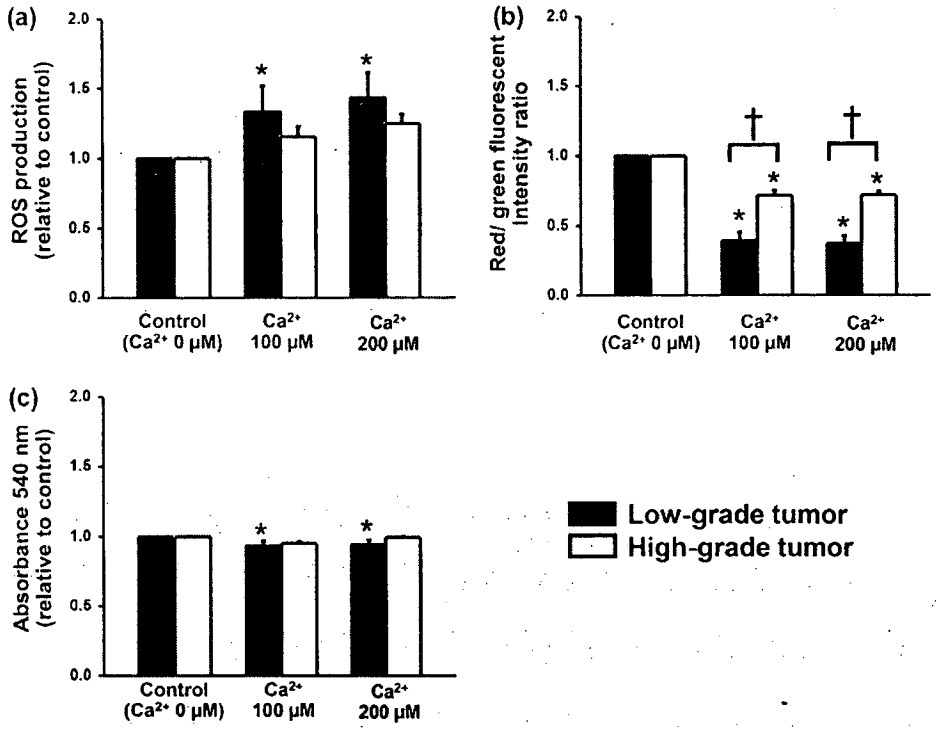


Figure 1 Determination of mitochondrial function after application with CaCl2 at concentration 100 and 200 µM for 15 min. (a) ROS production was estimated by spectrofluorometry using DCFDA in mitochondria from low-grade and high-grade brain tumors (b) Mitochondrial membrane potential changes were estimated by comparing the ratio of red to green fluorescein of JC-1 stained mitochondria of low- grade and high-grade brain tumors. Decreased red/green ratio represents mitochondrial membrane depolarization. (c) Mitochondrial swelling of low-grade and high-grade brain tumors was measured by absorbance at 540 nm wavelength. Data were represented by the absorbance relative to the control group. Decreased absorbance represents mitochondrial swelling *, $p < 0.05$ compared to the control group; †, $p < 0.05$ differences between high-grade tumor and low-grade tumor. Each data is expressed as mean ± SEM

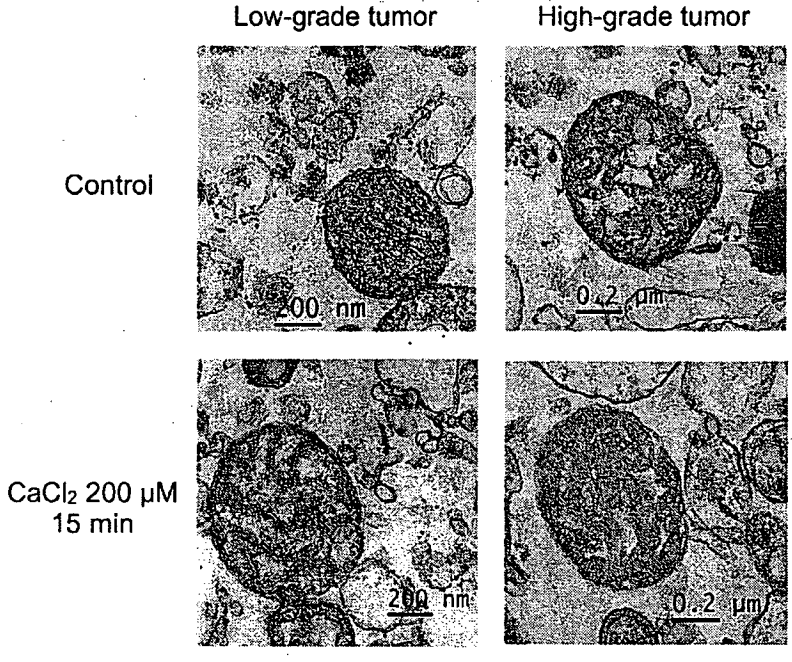


Figure 2 Morphologic structure of mitochondria isolated from either low- or high-grade brain tumors after application with $CaCl_2$ 200 µM for 15 min, magnification 1:15,000

difference in ROS production in mitochondria isolated from high-grade brain tumors. In the assay of mitochondrial membrane potential, we found that the percentage change in mitochondrial membrane potential (i.e. mitochondrial depolarization) following BEV application was significantly greater than those following TMZ application

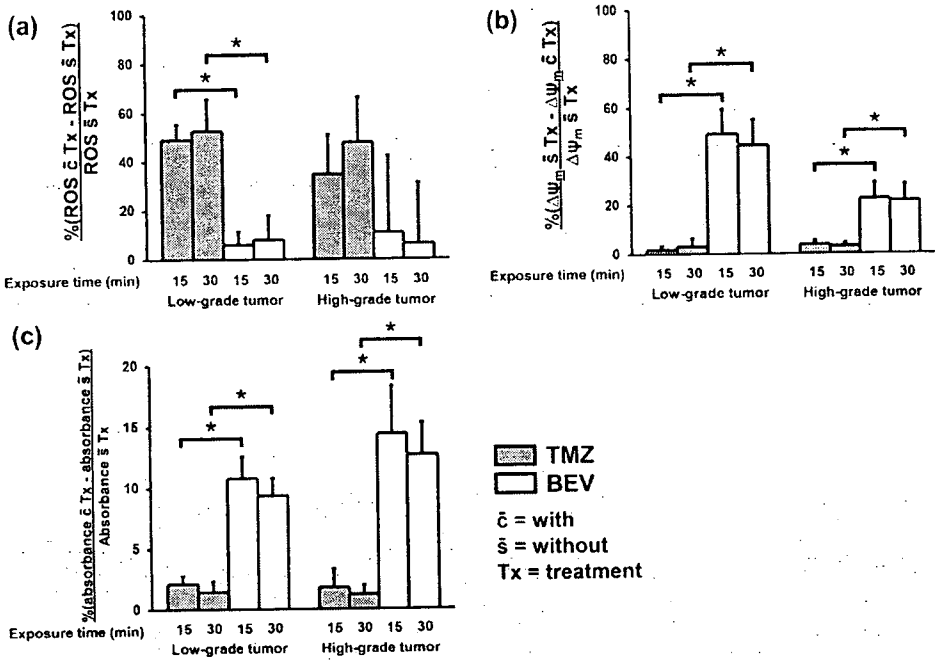


Figure 3 Determination of mitochondrial function after application with either 300 μM Temozolomide (TMZ) or 2 mg/mL Bevacizumab (BEV) for 15 or 30 min among isolated mitochondria of low- and high-grade brain tumors. (a) Percentage difference of ROS production [%(ROS with treatment-ROS without treatment)/ ROS without treatment]. (b) Percentage difference of mitochondrial membrane potential change [%(Δψm ROS without treatment-Δψm ROS with treatment)/Δψm ROS without treatment]. (c) Percentage difference of mitochondrial swelling [%(absorbance with treatment-absorbance without treatment)/ absorbance without treatment]. *, $p < 0.05$ compared between TMZ and BEV group

in mitochondria from both low-grade and high-grade brain tumors (Fig. 3(b)). No significant difference was found between the 15- and 30-min exposure of BEV at the same tumor grade. In addition, there was no significant difference in the percentage change in mitochondrial membrane potential between low-grade and high-grade brain tumors at either 15- or 30-min exposure of BEV. In the assay of the mitochondrial swelling, the percentage changes of the absorbance following BEV application were greater than those following TMZ application in the mitochondria from both low- and high-grade tumors (Fig. 3(c)). No significant difference was found between the 15- and 30-min exposure of BEV at the same tumor grade. In addition, there was no significant difference in the percentage change in mitochondrial swelling between low-grade and high-grade brain tumors at either 15- or 30-min exposure of BEV. Consistent with the swelling assay, the BEV-induced mitochondrial damage detected by electron microscopy was obvious in both low-grade and high-grade brain tumors, whereas no damaged mitochondria were observed following the application of TMZ (Fig. 4). Intact brain mitochondrial morphology with apparent folded cristae was observed in the control group of low-grade and high-grade brain tumors (Fig. 4). Brain mitochondrial swelling was observed in the BEV treatment group of low-grade and high-grade brain tumors as indicated by markedly unfolded cristae (Fig. 4).

Discussion

The major findings of this study are as follows: (1) calcium overload leads to mitochondrial dysfunction as indicated by increased membrane depolarization and mitochondrial swelling, dominantly in mitochondria isolated from low-grade brain tumors, and (2) BEV causes greater deterioration than TMZ in mitochondria, as shown by profound depolarization of membrane potential and mitochondrial swelling in mitochondria from both low and high-grade brain tumors.

Mitochondria are involved in several cellular processes, including regulation of cell death. Previous studies suggested that mitochondria played a pivotal role in shaping the oncogenic signaling cascade [24] and also that a variation of responses to external stimuli by mitochondria depended upon the types of mitochondria.[11] In addition to points 1 and 2 above, the present study also demonstrated that mitochondria isolated from high-grade brain tumors were less susceptible to external stimuli, i.e. calcium overload, than those from low-grade brain tumors, since calcium overload induced mitochondrial dysfunction only in low-grade tumors, but not in high-grade tumors. These findings were consistent with previous studies in demonstrating that high-grade brain tumors have greater clinical and histological aggressiveness.[12,13] These findings suggested that the mitochondrial properties in tumors might determine their aggression.

Several studies showed that calcium overload could induce an increase in mitochondrial ROS production in normal brain cells[11]; however, calcium overload did not cause a significant increase in mitochondrial ROS production in brain tumors in this study. It has been shown that an increase in baseline ROS generation of cancer cells itself

Downloaded by [Chiang Mai University] at 01:52 27 May 2016

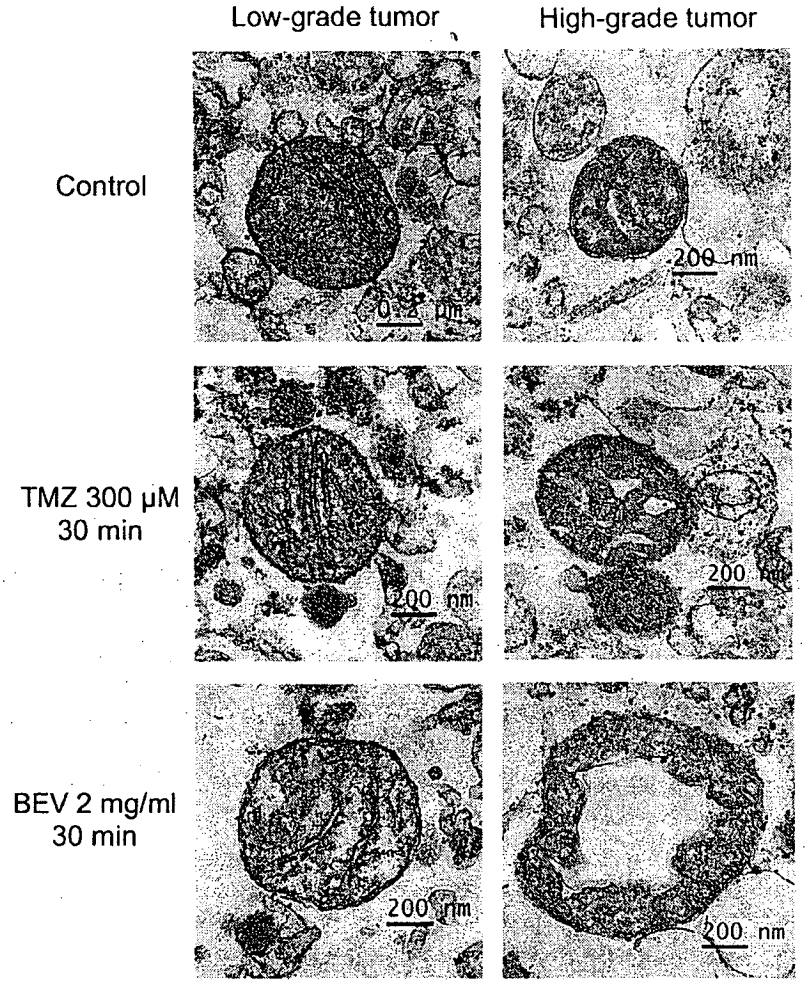


Figure 4 Morphologic structure of mitochondria isolated from either low- or high-grade brain tumors after application with either 300 μM Temozolomide (TMZ) or 2 mg/mL Bevacizumab (BEV) for 30 min, magnification: 1:15,000

Downloaded by [Chiang Mai University] at 01:52 27 May 2016

may disturb the redox adaptation response by an increase in anti-oxidant capacity and a shift in the ROS redox system (high generation and elimination) to maintain the free radical level below the toxic threshold to cause cancer cell death via apoptosis.[25-27] Using this postulated theory, the unchanged ROS level from calcium overload can be partially explained. However, this study demonstrated that calcium overload directly led to mitochondrial depolarization. The possible explanation of calcium-induced membrane depolarization is that calcium may directly open mitochondrial membrane transition pores (mPTP), and that calcium could therefore directly lead to mitochondrial membrane potential dissipation, cytochrome C release, and cell death in brain cells.[28]

Although TMZ, rather than BEV, is the first drug of choice to treat newly diagnosed high-grade brain tumors, the findings of this study demonstrated that BEV was more potent than TMZ in causing mitochondrial dysfunction in both low-grade and high-grade brain tumors. In addition, the present study showed for the first time that BEV had a direct perturbation effect in the mitochondria of primary brain tumors, as a mitochondrial membrane depolarizer. BEV-induced mitochondrial depolarization in this study should be independent from the ROS pathway since the application of BEV to brain tumor mitochondria did not increase ROS production. The possible explanation may be that BEV could directly open mPTP, subsequently depolarize the mitochondrial membrane and cause mitochondrial swelling as shown in Figs. 3 and 4. Although TMZ induced an increase in mitochondrial ROS production in low and high-grade primary brain tumors, it failed to cause mitochondrial depolarization and mitochondrial swelling as shown in Figs. 3 and 4. It is possible that increased ROS production following TMZ may not be high enough to reach the ROS threshold for activating the opening of mPTP. Therefore, TMZ would not appear to be harmful to mitochondria in both low-grade and high-grade brain tumors. These findings are supported by the clinical studies demonstrating that brain tumors are resistant to TMZ therapy.[29,30] Therefore, the possible explanation of the resistance of brain tumors to TMZ may occur through a mitochondrial adaptive response to TMZ. This possibility has been supported by a previous study demonstrating the mitochondrial adaptive response to TMZ during genotoxic stress.[6,31]

The combination of TMZ and BEV may give an insight into a solution to increase cancer cell death and to extend

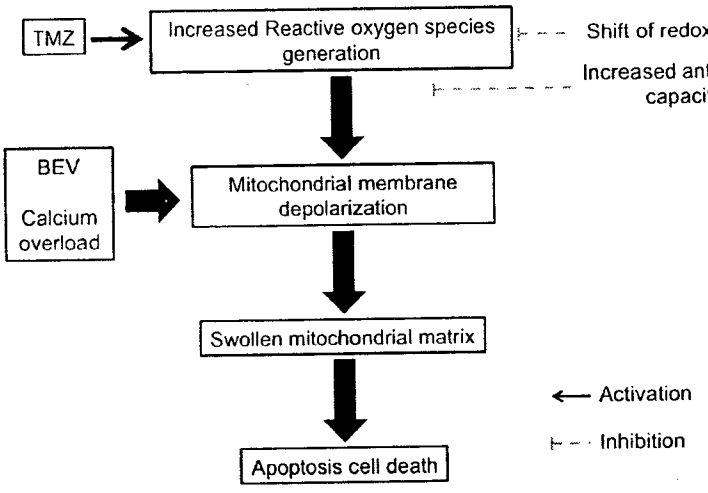


Figure 5 The plausible effects of calcium overload, Temozolomide (TMZ), and bevacizumab (BEV) onto isolated mitochondria from low-grade and high-grade primary brain tumors. The death of cells could occur through their sequences of mitochondrial dysfunction, including lowered coupling efficiency of electron transport and ATP production, increased electron leakage, increased reactive oxygen species (ROS) generation during respiration, mitochondrial membrane depolarization, swollen matrix, and subsequence in apoptosis cell death. However, in brain tumor model, ROS production might be inhibited or attenuated from some mechanisms as a shown diagram above. The shift of mitochondrial redox system in cancer cells alters the balance between ROS generation and elimination [30]; as a result, ROS level might not achieve the threshold to consequently trigger the depolarization process. An increase of antioxidant capacity might also attenuate the effect and level of ROS. TMZ can induce an increase of ROS generation; however, it could not induce mitochondrial membrane depolarization or swollen matrix probably due to TMZ-specific mitochondrial adaptive response. Bypassing the inhibiting mechanism, BEV and high calcium level can directly depolarize mitochondrial membrane potential leading to swollen matrix and cell death

Downloaded by [Chiang Mai University] at 01:52 27 May 2016

survival time of high-grade brain tumor patients. This study shows that TMZ and BEV may have different targets at the mitochondrial level (as summarized in Fig. 5). TMZ mainly increased the mitochondrial ROS production, while BEV induced mitochondrial membrane potential depolarization. By implication, the combination of both drugs, acting on different targets, might give additive mitochondrial perturbation effects, which is congruent with the *in vivo* report that combining BEV with TMZ increased the anti-tumor efficacy of TMZ in a human glioblastoma orthotopic xenograft model.[32] In addition, several clinical trials supported that the practice of combining both agents with radiotherapy enhanced the survival duration of glioma patients.[33–36]

Conclusion

This study established for the first time that conditions of calcium overload caused different mitochondrial perturbation outcomes in different grades of brain tumor. High-grade brain tumors resisted calcium overload but low-grade brain tumors were more susceptible to mitochondrial dysfunction from calcium overload. In all grades of brain tumor, BEV showed direct mitochondrial perturbation effects, specifically mitochondrial membrane depolarization and the induction of swollen matrices, both effects being superior to those caused by TMZ. This is the first study to demonstrate BEV as a mitochondrial membrane depolarizer. Therefore, it is reasonable to assume that the combination of BEV and TMZ might have a more beneficial effect in treating high-grade brain tumors and may lead to an increase in the survival time of high-grade brain tumor patients.

Disclaimer Statements

Notes on contributors

Danop Nanegrungsunk is a research fellow at University of Illinois at Chicago. His research interests include neuropathology. His recent publications appear in Brain Research.

Nattayaporn Apaijai is a postdoctoral fellow at Chiang Mai University. Her research interests include cardiac electrophysiology. Her recent publications appear in International Journal of Cardiology.

Chontida Yarana is a student at University of Kentucky. Her research interests include molecular biology, cell biology, and physiology. Her recent publications appear in Achrives Medical Research.

Jirapas Sripetchwandee is a junior instructor at Chiang Mai University. His research interests include neurophysiology, particularly in neurodegeneration. His recent publications appear in Applied Physiology Nutrition and Metabolism.

Kriengsak Limpastan is an associate professor at Chiang Mai University. His research interests include Traumatology, Neurosurgery, and Neurology. His recent publications appear in Journal of the Medical Association of Thailand.

Wanarak Watcharasaksilp is an instructor at Chiang Mai University. His research interests include Traumatology, Neurosurgery, and Neurology. His recent publications appear in Journal of the Medical Association of Thailand.

Wanarak Watcharasaksilp is an instructor at Chiang Mai University. His research interests include Traumatology, Neurosurgery, and Neurology. His recent publications appear in Journal of the Medical Association of Thailand.
Tanat Vaniyapong is an instructor at Chiang Mai University. His research interests include Neurosurgery and Clinical Trials. His recent publications appear in The Cochrane Database of Systematic Reviews.
Nipon Chattipakorn is a professor at Chiang Mai University. His research interests include cardiac electrophysiology. His recent publications appear in Scientific Reports.
Siriporn C Chattipakorn is a professor at Chiang Mai University. Her research interests include neurophysiology. Her recent publications appear in Scientific Reports.

Funding

This work was supported by the Thailand Research Fund [TRF-BRG5780016] (SC), [TRG 5880045] (JS); National Research Council of Thailand (SC); a NSTDA Research Chair Grant from the National Science and Technology Development Agency (NC); Chiang Mai University Excellent Center Award (NC).

Conflicts of Interest

The authors declare that there is no conflict of interest.

Ethical approval

The study was approved by The Research Ethics Committee, Faculty of Medicine, Chiang Mai University.

References

1 Thurnher MM. World Health Organization classification of tumours of the central nervous system. Cancer Imaging : The Official Publication of the International Cancer Imaging Society 2009. 2007;9 Spec No A:S1–3.
2 Hirst TC, Vesterinen HM, Sena ES, *et al.* Systematic review and meta-analysis of temozolomide in animal models of glioma: was clinical efficacy predicted? Br J Cancer. 2013;108:64–71.
3 Nanegrungsunk D, Onchan W, Chattipakorn N, *et al.* Current evidence of temozolomide and bevacizumab in treatment of gliomas. Neurol Res. 2015;37:167–183.
4 Narita Y. Drug review: safety and efficacy of bevacizumab for glioblastoma and other brain tumors. Jpn J Clin Oncol. 2013;43:587–595.
5 Adam-Vizi V, Starkov AA. Calcium and mitochondrial reactive oxygen species generation: how to read the facts. J Alzheimer's Dis : JAD. 2010;20(Suppl 2):S413–426.
6 Oliva CR, Moellering DR, Gillespie GY, *et al.* Acquisition of chemoresistance in gliomas is associated with increased mitochondrial coupling and decreased ROS production. PLoS ONE. 2011;6:e24665.
7 Keunen O, Johansson M, Oudin A, *et al.* Anti-VEGF treatment reduces blood supply and increases tumor cell invasion in glioblastoma. Proc Nat Acad Sci USA. 2011;108:3749–3754.
8 Lin CJ, Lee CC, Shih YL, *et al.* Inhibition of mitochondria- and endoplasmic reticulum stress-mediated autophagy augments temozolomide-induced apoptosis in glioma cells. PLoS ONE. 2012;7:e38706.
9 Luthra S, Sharma A, Dong J, *et al.* Effect of bevacizumab (Avastin (TM)) on mitochondrial function of *in vitro* retinal pigment epithelial, neurosensory retinal and microvascular endothelial cells. Indian J Ophthalmology. 2013;61:705–710.
10 Brookes PS, Yoon Y, Robotham JL, *et al.* Calcium, ATP, and ROS: a mitochondrial love-hate triangle. Am J Physiol Cell Physiol. 2004;287:C817–C833.
11 Yarana C, Sanit J, Chattipakorn N, *et al.* Synaptic and nonsynaptic mitochondria demonstrate a different degree of calcium-induced mitochondrial dysfunction. Life Sci. 2012;90:808–814.
12 Belda-Iniesta C, de Castro Carpeño J, Casado Saenz E, *et al.* Molecular biology of malignant gliomas. Clin Transl Oncol : Official Publ Fed Spanish Oncol Soc Nat Cancer Inst Mexico. 2006;8:635–641.
13 Miller CR, Perry A. Glioblastoma. Arch Pathol Lab Med. 2007;131:397–406.
14 Rusovici R, Sakhalkar M, Chalam kV. Evaluation of cytotoxicity of bevacizumab on VEGF-enriched corneal endothelial cells. Mol Vision. 2011;17:3339–3346.
15 Rosenthal RE, Hamud F, Fiskum G, *et al.* Cerebral ischemia and reperfusion: prevention of brain mitochondrial injury by lidoflazine. J Cereb Blood Flow Metab : Official J Int Soc Cereb Blood Flow Metab. 1987;7:752–758.
16 Walker JM. The bicinchoninic acid (BCA) assay for protein quantitation. Methods Mol Biol. 1994;32:5–8.
17 Maciel EN, Vercesi AE, Castilho RF. Oxidative stress in Ca(2+)-induced membrane permeability transition in brain mitochondria. J Neurochem. 2001;79:1237–1245.
18 Tong V, Teng XW, Chang TK, *et al.* Valproic acid II: effects on oxidative stress, mitochondrial membrane potential, and cytotoxicity in glutathione-depleted rat hepatocytes. Toxicol Sci. 2005;86:436–443.
19 Rodriguez-Pallares J, Parga JA, Joglar B, *et al.* The mitochondrial ATP-sensitive potassium channel blocker 5-hydroxydecanoate inhibits toxicity of 6-hydroxydopamine on dopaminergic neurons. Neurotox Res. 2009;15:82–95.
20 Dedov VN, Mandadi S, Armati PJ, *et al.* Capsaicin-induced depolarisation of mitochondria in dorsal root ganglion neurons is enhanced by vanilloid receptors. Neuroscience. 2001;103:219–226.
21 Ruiz-Meana M, Garcia-Dorado D, Miro-Casas E, *et al.* Mitochondrial Ca2+ uptake during simulated ischemia does not affect permeability transition pore opening upon simulated reperfusion. Cardiovasc Res. 2006;71:715–724.
22 Du H, Guo L, Zhang W, *et al.* Cyclophilin D deficiency improves mitochondrial function and learning/memory in aging Alzheimer disease mouse model. Neurobiol Aging. 2011;32:398–406.
23 Chelli B, Falleni A, Salvetti F, *et al.* Peripheral-type benzodiazepine receptor ligands: mitochondrial permeability transition induction in rat cardiac tissue. Biochem Pharmacol. 2001;61:695–705.
24 Frezza C. The role of mitochondria in the oncogenic signal transduction. Int J Biochem Cell biol. 2014;48:11–17.
25 Trachootham D, Alexandre J, Huang P. Targeting cancer cells by ROS-mediated mechanisms: a radical therapeutic approach? Nat Rev Drug Discovery. 2009;8:579–591.
26 Gupta SC, Hevia D, Patchva S, *et al.* Upsides and downsides of reactive oxygen species for cancer: the roles of reactive oxygen species in tumorigenesis, prevention, and therapy. Antioxid Redox Signal. 2012;16:1295–1322.
27 Schumacker PT. Reactive oxygen species in cancer cells: live by the sword, die by the sword. Cancer Cell. 2006;10:175–176.
28 Kobayashi T, Kuroda S, Tada M, *et al.* Calcium-induced mitochondrial swelling and cytochrome c release in the brain: its biochemical characteristics and implication in ischemic neuronal injury. Brain Res. 2003;960:62–70.
29 Ramirez YP, Weatherbee JL, Wheelhouse RT, *et al.* Glioblastoma multiforme therapy and mechanisms of resistance. Pharmaceuticals. 2013;6:1475–1506.
30 Minniti G, Muni R, Lanzetta G, *et al.* Chemotherapy for glioblastoma: current treatment and future perspectives for cytotoxic and targeted agents. Anticancer Res. 2009;29:5171–5184.
31 Oliva CR, Nozell SE, Diers A, *et al.* Acquisition of temozolomide chemoresistance in gliomas leads to remodeling of mitochondrial electron transport chain. J Biol Chem. 2010;285:39759–39767.
32 Mathieu V, De Nève N, Le Mercier M, *et al.* Combining bevacizumab with temozolomide increases the antitumor efficacy of temozolomide in a human glioblastoma orthotopic xenograft model. Neoplasia. 2008;10:1383–1392.
33 Lai A, Tran A, Nghiemphu PL, *et al.* Phase II study of bevacizumab plus temozolomide during and after radiation therapy for patients with newly diagnosed glioblastoma multiforme. J Clin Oncol : Official J Am Soc Clin Oncology. 2011;29:142–148.
34 Narayana A, Gruber D, Kunnakkat S, *et al.* A clinical trial of bevacizumab, temozolomide, and radiation for newly diagnosed glioblastoma. J Neurosurg. 2012;116:341–345.
35 Vredenburgh JJ, Desjardins A, Reardon DA, *et al.* The addition of bevacizumab to standard radiation therapy and temozolomide

Downloaded by [Chiang Mai University] at 01:52 27 May 2016

followed by bevacizumab, temozolomide, and irinotecan for newly diagnosed glioblastoma. Clin Cancer Res : An Official J Am Assoc Cancer Res. 2011;17:4119–4124.

36 Sampson JH, Heimberger AB, Archer GE, *et al.* Immunologic escape after prolonged progression-free survival with epidermal growth factor receptor variant III peptide vaccination in patients with newly diagnosed glioblastoma. J Clin Oncol : Official J Am Soc Clin Oncol. 2010;28:4722–4729.

Downloaded by [Chiang Mai University] at 01:52 27 May 2016

เอกสารแนบหมายเลข 38

Review

Journal of Cardiovascular Pharmacology and Therapeutics
1-17
© The Author(s) 2015
Reprints and permission:
sagepub.com/journalsPermissions.nav
DOI: 10.1177/1074248415587977
cpt.sagepub.com
SAGE

Roles of Testosterone Replacement in Cardiac Ischemia–Reperfusion Injury

Wanpitak Pongkan, DVM[1,2,3], Siriporn C. Chattipakorn, DDS, PhD[2,3,4], and Nipon Chattipakorn, MD, PhD[1,2,3]

Abstract

Testosterone is an anabolic steroid hormone, which is the major circulating androgen hormone in males. Testosterone levels decreasing below the normal physiological levels lead to a status known as androgen deficiency. Androgen deficiency has been shown to be a major risk factor in the development of several disorders, including obesity, metabolic syndrome, and ischemic heart disease. In the past decades, although several studies from animal models as well as clinical studies demonstrated that testosterone exerted cardioprotection, particularly during ischemia–reperfusion (I/R) injury, other preclinical and clinical studies have shown an inverse relationship between testosterone levels and cardioprotective effects. As a result, the effects of testosterone replacement on the heart remain controversial. In this review, reports regarding the roles of testosterone replacement in the heart following I/R injury are comprehensively summarized and discussed. At present, it may be concluded that chronic testosterone replacement at a physiological dose demonstrated cardioprotective effects, whereas acute testosterone replacement can cause adverse effects in the I/R heart.

Keywords

testosterone, ischemia–reperfusion injury, heart, aging

Introduction

Testosterone (or androgen) deficiency is a condition in which the concentration of testosterone hormone is lower than the normal physiological level.[1,2] The primary cause of testosterone deficiency is due to a testicular disorder or an abnormal function of the hypothalamus–pituitary axis, while a secondary cause or transient testosterone deficiency is caused by the effect of drugs; aging; acute or chronic diseases; or chronic comorbidities such as obesity, metabolic syndrome, dyslipidemia, and insulin resistance.[1,3-5]

The prevalence of symptomatic testosterone deficiency is approximately 481 000 new cases per year in US men aged between 40 and 69 years[2] and 5.6% in men aged 30 to 79 years.[6] Another study reported a higher prevalence of hypogonadism (38.7%) in men aged ≥45 years (mean age = 60 years) visiting primary care practices in the United States.[7] The prevalence of hypogonadism also increases substantially with age[6,8] in which the prevalence increased to 20% of men older than 60 years, 30% older than 70 years, and 50% older than 80 years.[9] Although this condition commonly occurs in middle- to older aged men, it can also be found in younger men.[1,2,6,8] In addition, lower levels of serum testosterone are associated with the development of several disorders including obesity, dyslipidemia, insulin resistance, metabolic syndrome, cardiovascular disease, and coronary artery disease (ischemic heart disease).[5,10-13]

Previous studies reported that men have a higher incidence, mortality, and risk of coronary artery disease than women[14-16] and the risk of coronary artery disease increases markedly with age.[16] In addition, patients with coronary artery disease[17-20] and congestive heart failure[21] have been shown to have lower levels of endogenous testosterone compared with healthy men, and the severity of both diseases shows a strong correlation with the degree of testosterone deficiency.[5,17,22] It has also been suggested that low serum testosterone levels could be used as a predictive marker for cardiovascular disease in men.[23]

[1] Faculty of Medicine, Cardiac Electrophysiology Research and Training Center, Chiang Mai University, Chiang Mai, Thailand
[2] Department of Physiology, Faculty of Medicine, Cardiac Electrophysiology Unit, Chiang Mai University, Chiang Mai, Thailand
[3] Center of Excellence in Cardiac Electrophysiology Research, Chiang Mai University, Chiang Mai, Thailand
[4] Department of Oral Biology and Diagnostic Sciences, Faculty of Dentistry, Chiang Mai University, Chiang Mai, Thailand

Manuscript submitted: March 3, 2015; **accepted:** April 20, 2015.

Corresponding Author:
Nipon Chattipakorn, Faculty of Medicine, Cardiac Electrophysiology Research and Training Center, Chiang Mai University, Chiang Mai 50200, Thailand.
Email: nchattip@gmail.com

Downloaded from cpt.sagepub.com by guest on May 27, 2015

Although there are many reports indicating that testosterone provided cardioprotective effects[24-26] such as antiarrhythmic properties,[27] reduced infarct size,[28] enhanced vasodilatation,[29] decreased atherosclerosis,[30] and improved metabolic parameters,[31] these findings are controversial at this time.[32-36] Moreover, when it comes to the role of testosterone in the ischemic heart or cardiac ischemia–reperfusion (I/R) injury, limited data are currently available. Despite limited data, inconsistent reports exist regarding the effects of testosterone in I/R hearts. In this review, the roles of testosterone in the heart following I/R injury are comprehensively summarized and discussed. The consistent findings, as well as controversial results, are also presented, focusing on the effects of testosterone on the heart during an I/R injury.

Physiological Roles of Testosterone in the Heart

The cardiac muscle is one target tissue of the testosterone hormone.[37,38] It is well known that the level of testosterone is associated with effects on the cardiomyocytes such as hypertrophy and cardiomyocyte apoptosis[39,40] and is also associated with the contractility of cardiac muscle.[38,41-43] Previous studies reported the beneficial effect of testosterone at physiological levels on cardiovascular function by inducing vasorelaxation of vascular smooth muscle.[39,44,45] Testosterone controlled cardiac relaxation by acting mainly through sarcoendoplasmic reticulum Ca^{2+}-ATPase (SERCA),[46] increasing or regulating cardiac contractility, and Ca^{2+} handling in the heart.[38,43,47] However, conflicting evidence was that chronic administration of a synthetic testosterone (nandrolone decanoate) decreased left ventricular myocardial function and thus overall cardiac performance without altering contractility in rats.[48]

The physiological effects of testosterone on cardiac electrophysiology have been reported. It has been shown that the Q-T interval was shorter in men than in women.[49-52] Moreover, both endogenous and exogenous testosterone could shorten or decrease the dispersion of the Q-T interval,[50,53,54] whereas a contrasting study found that the testosterone level and the Q-T interval on electrocardiogram did not have any relationship with each other.[55] Furthermore, beneficial effects of testosterone on the ST-segment and atrial fibrillation have been reported. Testosterone was shown to modulate the early phase of ventricular repolarization resulting in decreasing the ST-segment.[56,57] Other studies reported that aging men with decreased serum testosterone levels had a high incidence of atrial fibrillation.[58,59] These were consistent with the study using a rat model, which reported that deficiency of testosterone was arrhythmogenic in rat atria possibly through less binding of FK506-binding protein (FKBP12.6) to ryanodine receptor type 2 (RyR2), resulting in calcium leakage from the sarcoendoplasmic reticulum.[60] Testosterone also plays an essential role in the Ca^{2+} regulation in male hearts in both genomic and nongenomic pathways.[46,61-63] It has been shown that testosterone maintained or increased the expression of dihydropyridine receptor (α1c-subunit of L-type calcium channel) messenger RNA (mRNA) level and also increased the Na^+/Ca^{2+} exchanger mRNA level,[62,64,65] improved the cardiac L-type calcium current,[62,63] increased Ca^{2+} released via the ryanodine receptor,[61] maintained FK506-binding protein 12.6 in ryanodine receptor type 2,[60] maintained or increased SERCA and Na^+/Ca^{2+} exchanger activity,[46,61] and maintained phosphorylation of phospholamban Thr_{17},[46] thus resulting in faster Ca^{2+} removal out of the cytoplasm.

Testosterone and the Pathological Heart

Previous studies demonstrated that a reduction in plasma testosterone levels can be either the direct cause or the consequence of several cardiovascular diseases such as hypertension, diabetes, atherosclerosis, and heart failure.[23,66-73] There is also a correlation between low levels of testosterone and the severity of each of these diseases.[71-74] The incidence of chronic heart failure due to idiopathic dilated cardiomyopathy is associated with a significant decrease in testosterone concentrations,[74] in which androgen replacement therapy could improve heart failure symptoms.[75] Several lines of evidence indicate that testosterone may effectively provide protective effects in the cardiovascular system[76,77] and that decreased circulating testosterone may increase cardiovascular risk, atherosclerosis, and mortality in men.[76,77] Testosterone therapy has also been shown to improve the cardiac ischemic condition, comparable to the effects of existing antianginal drugs but has no beneficial effects in peripheral arterial and cerebrovascular diseases.[76] On the other hand, several conflicting studies have shown that testosterone replacement also increases the incidence of cardiovascular disease.[33,67,76,78] However, a recent review by Morgentaler et al clarified these controversial studies and concluded that low levels of total testosterone, bioavailable testosterone, and free testosterone are associated with an increased risk and severity of coronary artery disease, whereas high serum testosterone concentrations (endogenous or via testosterone therapy) markedly reduced cardiovascular disease and cardiovascular risk factors.[79] Furthermore, Morgentaler et al also revealed that testosterone therapy is associated with a reduction in obesity, fat mass, metabolic parameters, and inflammatory markers.[79]

Testosterone and Cardiac I/R Injury

Testosterone deficiency plays a role in the development of ischemic heart disease.[19,76,77] Men with heart disease or ischemic heart disease had lower levels of testosterone than men with normal coronary angiograms[18] and that testosterone improved ischemic tolerance and quality of life in hypogonadal men with angina.[80,81] However, inconsistent reports exist regarding the beneficial effects of testosterone in the heart,[32,33] and the questions remain whether it does truly provide cardioprotective benefits.[24,25] Currently, there are only a few studies investigating the roles of testosterone in the myocardial infarction model and in the I/R heart. In spite of limited data available, the effects of testosterone on several

Downloaded from cpt.sagepub.com by guest on May 27, 2015

Table 1. Summary of the Effect of Testosterone on the Infarct Size in I/R Heart.

Animal Species	Model	Drugs/Dose/Route	Major Findings	Interpretation	Ref
ORX rat	MI LAD ligation	Physiological dose testosterone propionate, 2 mg/kg, SC Pretreated for 1, 3, and 28 days	↓ Infarction size	Testosterone replacement decreasing the infarct size may be due to decrease in the number of apoptotic cells and testosterone-stimulating neovascularization by mobilization and homing of CD34+ cells into ischemic area. In addition, endogenous testosterone deprivations in rats impair angiogenesis following infarction.	25
Isolated rat heart (ORX rat)	I/R LAD ligation 30-Minute ischemia 120-Minute reperfusion	Physiological dose testosterone, 2 mg/kg, SC Pretreated for 8 weeks Noradrenaline 10^{-7} mol/L Pretreated during I/R	↓ Infarction size	The decreasing infarct size may be due to α1-adrenoceptor stimulation and reduction in myocardial apoptosis.	28
Isolated rat heart (ORX rat)	I/R LAD ligation 30-Minute ischemia 120-Minute reperfusion	Physiological dose testosterone, 2 mg/kg, SC Pretreated for 8 weeks Pretreated with U50-488H 10 mg/kg 24 hours before I/R	↓ Infarction size	Testosterone may decrease infarct size by enhanced stimulation of preconditioning by either metabolic inhibition or a κ-opioid receptor agonist resulting in increased heat shock protein 70 synthesis, which plays a role in cardioprotection.	82
ORX rat	I/R LAD ligation 60-Min ischemia 4-Hour reperfusion	Testosterone 0.02, 0.2, and 2.02 μg/kg Acute IV injection 15 minutes prior to reperfusion.	↓ Infarction size	Acute exogenous testosterone can reduce infarct size in ORX rats, the mechanism may be mediated by a nongenomic testosterone pathway.	83
ORX rat	MI LAD ligation	Testosterone undecanoate, 500 mg/kg Deep IM injection every 4 weeks for 8 weeks	No difference in myocardial infarct size analyzed by MRI	Chronic anabolic testosterone treatment had no detrimental effects following myocardial infarction.	84
Rabbits	I/R LAD ligation 30-Minute ischemia 3-Hours reperfusion	Supraphysiological dose of testosterone, 50 mg/kg, IM Pretreated for 1 weeks and 50 mg/kg, acute treated 5-10 minutes before I/R	No difference was found in myocardial infarct size	Supraphysiological dose of testosterone treatment had no detrimental effects on the infarct size.	85

Abbreviations: ORX rat, orchiectomized rat; MI, myocardial infarction; LAD, left anterior descending coronary artery; I/R, ischemic and reperfusion; IV, intravenous; MRI, magnetic resonance imaging; IM, intramuscular; SC, subcutaneous; IEI, infarct expansion index.

crucial parameters in the myocardial infarction as well as the I/R heart including infarct size, lactate dehydrogenase (LDH) release, myocyte viability, left ventricular contractile function, arrhythmias, and heart rate variability (HRV) have been reported with inconsistent findings. In this review, the effects of testosterone on each of these crucial parameters in the myocardial infarction and I/R heart are comprehensively summarized and discussed.

Effect of testosterone on the infarct size in I/R hearts. Testosterone has been shown to have an infarct limiting effect in ex vivo and in vivo models of orchiectomized (ORX) rats with I/R injury. These reports are summarized in Table 1. In the Langendorff isolated heart, a physiological dose of testosterone 2 mg/kg body weight has been shown to decrease the infarct size in I/R heart by either the reduction in myocardial apoptosis through α1-adrenoceptor stimulation[28] or the promotion of neovascularization of heart tissues in myocardial infarction model through increased synthesis of 70-kDa heat shock proteins (Hsp70s) [25] and activated κ-opioid receptor agonist.[82] Consistently, a recent in vivo model study in ORX rat's heart demonstrated that acute injection of testosterone prior to the reperfusion period could reduce the infarct size.[83] However, the supraphysiological dose of testosterone replacement (500 and 50 mg/kg) in the myocardial infarction and I/R models exerted neither adverse effect nor infarct size reduction benefits.[84,85]

It is of interest to note from these findings that physiological levels or low doses of testosterone may provide a cardioprotective effect against I/R injury. Most of the positive effects of testosterone on the infarct size in I/R models also occurred in the combination of testosterone supplement and conditional treatments, including I/R preconditioning and adrenergic receptor stimulation. The underlying mechanisms responsible for these findings need to be investigated in future studies.

Downloaded from cpt.sagepub.com by guest on May 27, 2015

Table 2. Summary of the Beneficial Effect of Testosterone on Cardiac Function in I/R Heart.

Animal Species	Model	Drugs/Dose/Route	Major Findings	Interpretation	Ref
Isolated rat heart (ORX rat)	I/R LAD ligation 30-Minute ischemia 120-Minute reperfusion	Physiological dose testosterone, 2 mg/kg, SC Pretreated for 8 weeks Noradrenaline 10^{-7} mol/L Pretreated during I/R	Improve contractile recovery during both I/R and sympathetic stimulation period	Testosterone may improve contractile function by enhancing the expression of α1a- and β1-adrenoceptors.	28
Isolated rat heart (ORX rat)	I/R LAD ligation 30-Minute ischemia 120-Minute reperfusion	Physiological dose testosterone, 2 mg/kg, SC Pretreated for 8 weeks Pretreated with U50-488H 10 mg/kg 24 h before I/R	Improve contractile recovery in reperfusion period by: – ↑ LVDP – ↓ LVEDP – Improve ± dp/dt max	Preconditioning requires testosterone to increase heat shock protein 70 synthesis, which plays a role in cardioprotection.	82
Isolated rat heart (ORX rat)	I/R 30-Minute global no flow ischemia 30-Minute reperfusion	Supraphysiological dose of testosterone undecanoate, 500 mg/kg, IM Pretreated for 2 weeks 5α-dihydrotestosterone (DHT), 75 mg/pellet, SC implantation, pretreated for 3 weeks	In testosterone treated group: – ↑ LVDP – ↓ LVEDP – ↓ Intracellular Ca^{2+} overload at end-ischemic and reperfusion period	Testosterone improves left ventricular contractile functions during I/R injury and attenuates reperfusion induced Ca^{2+} overload.	86
Isolated rat heart (ORX rat)	I/R 25-Minute global no flow ischemia 45-Minute reperfusion	Supraphysiological dose of testosterone, 1 mg/d (as pellet), SC implantation, pretreated for 3 weeks	↑ Aortic flow, cardiac output, cardiac work, LVDP, contractility (+dp/dt) in testosterone-treated group	Administration of high-dose testosterone confers cardioprotection via ARs by improved postischemic functional recovery.	24
ORX rat	MI LAD ligation	Physiological dose of testosterone propionate, 2 mg/kg, SC, pretreated for 1, 3, and 28 days	↑ % EF ↑ % FS ↓ LVEDP	Testosterone replacement therapy improved myocardial performance.	25

Abbreviations: ORX rat, orchiectomized rat; LAD, left anterior descending coronary artery; SC, subcutaneous; I/R, ischemic and reperfusion; IV, intravenous; IM, intramuscular; LVDP, left ventricular develop pressure; LVEDP, left ventricular end diastolic pressure; MI, myocardial infarction; ARs, androgen receptors; EF, ejection fraction; FS, fractional shortening.

Effect of testosterone on cardiac function in I/R hearts. Testosterone exerts a beneficial effect on cardiac function in ex vivo models of ORX rats with I/R injury and in vivo models of ORX rats with myocardial infarction (Table 2). The beneficial effects of testosterone in the ex vivo model using the Langendorff isolated heart preparation technique demonstrates that a physiological dose of testosterone (2 mg/kg) combined with I/R preconditioning,[82] and adrenergic receptor stimulation[28] improves contractile recovery during the I/R period. The postulated mechanism of this effect was through α1-adrenoceptor stimulation[28] and increased synthesis of Hsp70 via a κ-pioid receptor agonist.[82] Interestingly, supraphysiological doses of both testosterone and its metabolite (5α-dihydrotestosterone [DHT]) also exhibited a beneficial effect on cardiac function during I/R injury by attenuating intracellular Ca^{2+} overload during the reperfusion period,[24,86] whereas the supraphysiological dose of testosterone replacement (50 mg/kg) in another I/R model exerted neither adverse nor beneficial effect on cardiac function.[85] This suggests that testosterone plays a cardioprotective role by reducing intracellular acidification resulting in the maintenance of physiological cytosolic Ca^{2+} levels during ischemic stress.[86] In addition, echocardiographic study also demonstrated that testosterone replacement therapy (2 mg/kg) could improve myocardial performance in a myocardial infarction model.[25]

Inconsistent findings of the effect of testosterone on cardiac contractile function have been reported in ex vivo models of ORX rats with I/R injury. These reports are summarized in Table 3. The study using Langendorff isolated hearts reported that chronic exogenous testosterone (subcutaneous implantation of DHT 200 mg) neither improved nor worsened myocardial functional recovery after I/R injury.[87] Acute infusion of 17β-hydroxy-4-androsterone at a physiological level (10 ng/mL/min) in isolated hearts could depress the recovery of myocardial function during I/R injury[36] by inducing hypertrophic response in the heart via androgen receptors, resulting in an increase in ventricular stiffness.[36] There is a report that the androgen receptor blocker flutamide could improve cardiac contractile function during cardiac I/R injury.[88] However, this study was carried out in intact animals without testosterone deprivation. These findings suggest that endogenous testosterone may also act via other mechanisms instead of just the genomic effect on cardiac function during I/R injury.[38,89] This could be due to the nongenomic effects that are similar to other steroids,[89] which could bind to specific membrane binding sites and stimulate the secondary messenger signaling cascades,

Downloaded from cpt.sagepub.com by guest on May 27, 2015

Table 3. Summary of the Adverse or Neutral Effects of Testosterone on Cardiac Function in I/R Heart.

Animal Species	Model	Drugs/Dose/Route	Major Findings	Interpretation	Ref
Rabbits	I/R LAD ligation 30-Minute ischemia 3-Hour reperfusion	Supraphysiological dose of testosterone, 50 mg/kg, IM Pretreated for 1 weeks, and 50 mg/kg, acutely treated 5-10 minutes before I/R	No difference in left ventricular ejection fraction and left ventricular fractional shortening	Supraphysiological dose of testosterone treatment had no detrimental effects on cardiac function.	85
Isolated rat heart (ORX rat)	I/R 25-Minute global no flow ischemia, followed by 40-minute reperfusion	5α-Dihydrotestosterone (DHT), 200 mg (as pellet), SC implantation, pretreated for 3 weeks	No difference in postischemic recovery of LVDP between castrated male-treated and -untreated groups	Chronic exogenous testosterone neither improved nor had a detrimental effect on myocardial functional recovery following I/R injury.	87
Isolated rat heart (ORX rat)	I/R 25-Minute global no flow ischemia 40-minute reperfusion	Physiologic dose of 17β-hydroxy-4-androsterone, 10 ng/mL/min, acute infusion 5 minutes before ischemia	– ↓ LVDP – ↑ LVEDP – ↓ Contractility (+dp/dt) and ↓ relaxation (−dp/dt)	Acute exogenous testosterone depresses myocardial contractile functional recovery during I/R injury via nongenomic pathway.	36
Isolated rat heart (ORX rat)	I/R 25-Minute global no flow ischemia 40-minute reperfusion	Flutamide (testosterone receptor blocker) pellet, 10 mg SC implantation, pretreated for 3 weeks	Blocking of testosterone receptor: – ↑ LVDP – ↓ LVEDP – ↑ −dp/dt and +dp/dt	Lack of testosterone receptors depresses cardiac functional recovery during I/R injury.	88

Abbreviations: ORX rat, orchiectomized rat; MI, myocardial infarction; LAD, left anterior descending coronary artery; LV, left ventricular; I/R, ischemic and reperfusion; SC, subcutaneous; EF, ejection fraction; LVDP, left ventricular develop pressure; LVEDP, left ventricular end diastolic pressure.

protein kinases (A and C), mitogen-activated protein kinase (MAPK), adenylyl cyclase, and intracellular Ca^{2+}.[39,89-91] These alterations in the nongenomic effect could induce various cellular outcomes including a rapid rises in the intracellular Ca^{2+} concentration,[44,45,92] neuromuscular or junctional signal transduction,[39,44] and vasorelaxation[39,45] and could be responsible for cardioprotection.

The importance of endogenous testosterone is emphasized by many reports of androgen deprivation therapy in patients with prostate cancer, which demonstrated that androgen deprivation therapy could increase cardiovascular events such as increased risk of ischemic heart disease,[93,94] induction of metabolic syndrome,[93-96] increased fat mass and decreased lean mass,[97,98] and increased atherosclerosis in animal models.[30] However, there are a few clinical studies in patients with prostate cancer, demonstrating that androgen deprivation therapy did not have any correlation with cardiovascular disease and mortality.[99-102] The discrepancies in these clinical findings could be due to differences in study design and populations, selection bias in men treated with Androgen suppression therapy (AST), and confounding factors such as comorbidity or lifestyle. However, on the basis of the current data, lacking of endogenous testosterone or androgen suppression may be associated with increased risks of cardiovascular diseases.

The discrepancies in these findings regarding the role of testosterone in cardiac function during I/R could be due to differences in the experimental model, an addition of conditional treatments, and dosages of testosterone treatment (physiological or supraphysiological dosage). Moreover, it is interesting that most reports showing the positive effects of testosterone used similar durations of treatment (chronic treatment for 2-8 weeks), whereas acute treatment of testosterone (infusion 5 minutes before ischemia) in myocardial infarction model resulted in decreased cardiac function. Further studies are needed to elucidate the mechanisms responsible for these effects on cardiac function.

Effect of testosterone on LDH release in I/R hearts. Testosterone has been shown to exert beneficial effects in ex vivo models of ORX rats with I/R injury (Table 4). These studies using the Langendorff isolated hearts demonstrated that both a physiological dose (2 mg/kg) or supraphysiological dose of testosterone could decrease LDH release in the I/R heart,[24,28,82] and the proposed mechanisms could be via either α1-adrenoceptor stimulation[28] or increased synthesis of Hsp70s.[82]

Effect of testosterone on myocyte viability in I/R hearts. Testosterone has been shown to have beneficial effects on cell viability in ORX rats with I/R injury and ORX rats with the myocardial infarction model (Table 5). Recent in vitro studies using the isolated ventricular myocytes demonstrated that a physiological concentration of testosterone combined with I/R preconditioning[82] and adrenergic stimulation[28] could increase ventricular myocyte viability in the I/R model. Testosterone could work through the angiogenesis pathway[82] and α1-adrenoceptor stimulation, which are mediated by both androgen receptors and nongenomic actions.[28] A physiological dose of testosterone (2 mg/kg) has also been shown to decrease the apoptotic cells in the myocardial infarction model, and these beneficial effects are thought to occur through the nongenomic pathway.[25]

Downloaded from cpt.sagepub.com by guest on May 27, 2015

Table 4. Summary of the Effect of Testosterone on LDH Released in I/R Heart.

Animal Species	Model	Drugs/Dose/Route	Major Findings	Interpretation	Ref
Isolated rat heart (ORX rat)	I/R 25-Minute global no flow ischemia, followed by 45-minute reperfusion	Supraphysiological dose 1 mg/d (as pellet), SC implantation Pretreated for 3 weeks	Testosterone – ↓ LDH release during pre- and post-I/R – Prevented the reduction of LV catalase enzyme	Administration of high-dose testosterone confers cardioprotection via ARs by improving postischemic functional recovery.	24
Isolated rat heart (ORX rat)	I/R LAD ligation 30-Minute ischemia and 120-minute reperfusion	Physiological dose of testosterone 2 mg/kg, SC, pretreated for 8 weeks Noradrenaline 10^{-7} mol/L Pretreated during I/R	↓ LDH release during I/R	Testosterone decreases LDH release by enhancing the beneficial effect of α1-adrenoceptor resulting in reduced myocardial apoptosis.	28
Isolated rat heart (ORX rat)	I/R LAD ligation 30-Minute ischemia and 120-minute reperfusion	Physiological dose of testosterone 2 mg/kg, SC, pretreated for 8 weeks Pretreated with U50-488H, 10 mg/kg, 24 hours before I/R	↓ LDH release during I/R	Testosterone decreases LDH release by enhanced preconditioning or stimulation of a κ-opioid receptor agonist, resulting in increased synthesis of heat shock protein 70.	82

Abbreviations: ORX rat, orchiectomized rat; I/R, ischemic and reperfusion; SC, subcutaneous; LDH, lactate dehydrogenase; LV, left ventricular; ARs, androgen receptors; LAD, left anterior descending coronary artery.

Table 5. Summary of the Effect of Testosterone on Cardiomyocyte Viability in I/R Heart.

Animal Species	Model	Drugs/Dose/Route	Major Findings	Interpretation	Ref
ORX rat	MI LAD ligation	Physiological dose of testosterone propionate, 2 mg/kg, SC Pretreated for 1, 3, and 28 days Flutamide (testosterone receptor blocker), 30 mg/kg/d, SC, pretreated for 1, 3, and 28 days	Testosterone replacement, with and without testosterone receptor blocker, decreases the percentage of TUNEL-positive cells compare with castrated group.	Testosterone replacement decreases the number of apoptotic cells through nongenomic pathway mechanism.	25
Isolated rat ventricular myocytes (ORX rat)	I/R 10-Minute metabolic inhibition and anoxia 10-Minute reperfusion	Physiological dose of testosterone 2 mg/kg, SC, pretreated for 8 weeks Followed with 10^{-8} mol/L concentration of testosterone incubated for 24 hours before I/R Noradrenaline 10^{-7} mol/L Pretreated during I/R	– ↑ Expression of α1a- and β1-adrenoceptors. – ↑ Cell viability compared with the castrated group.	Testosterone reduces I/R injury by enhancing the beneficial effect of α1-adrenoceptor stimulation, which was greater than the adverse effect of β1-adrenoceptor stimulation through both androgen and nonandrogen receptors.	28
Isolated rat ventricular myocytes (ORX rat)	I/R 10-Minute metabolic inhibition and anoxia 10-Minute reperfusion	Physiological concentration Testosterone, 10^{-8} mol/L incubated for 24 hours before I/R pretreated with U50-488H 30 μmol/L 30 min before I/R	Testosterone combined with preconditioning restored the ventricular myocytes viability.	Testosterone is required for the cardioprotection of preconditioning. This effect is mediated by androgen receptors.	82

Abbreviations: ORX rat, orchiectomized rat; MI, myocardial infarction; LAD, left anterior descending coronary artery; TUNEL, terminal deoxynucleotidyl transferase dUTP nick end labeling; I/R, ischemic and reperfusion; SC, subcutaneous.

Downloaded from cpt.sagepub.com by guest on May 27, 2015

Effect of testosterone on molecular signaling in I/R hearts. Most of the molecular studies on testosterone replacement demonstrated adverse effects in an ex vivo model of ORX rats with I/R injury (Table 6). In Langendorff isolated hearts of ORX rats, acute exogenous testosterone replacement at a physiological level had damaging effects on the myocardium after I/R injury by the inhibition of signal transducers and activators of transcription 3 (STAT-3) and the suppression of the cytokine signaling 3 (SOCS-3) antiapoptotic pathway.[32] In addition, acute testosterone infusion to physiological level in an isolated heart also increased the activation of the p38 MAPK and c-Jun N-terminal kinase pathways. These molecular signalings were involved with myocardial inflammation,[36] increased apoptotic protein caspase 3,[36] decreased antiapoptotic protein Bcl-2,[36,103] and Forkhead box O3a phosphorylation (p-FOXO3a),[103] and downregulation of PI3K/Akt antiapoptotic pathways, resulting in reduced phosphorylation of Bcl-2-associated death promoter protein (Bad) and unable to inhibit Bax-triggered apoptosis.[103] Consistent with these results, blocking of androgen receptor in an I/R injury model using the Langendorff isolated heart resulted in decreased proinflammatory cytokine production, decreased p38-MAPK and caspase 1, decreasing the expression of apoptotic protein caspases 3 and 11, and increasing the antiapoptotic protein Bcl-2.[88]

In contrast to findings following acute testosterone administration, a study using chronic exogenous testosterone replacement demonstrated improved cardiac function and restored the activation of the myocardial PI3K/Akt pathway including decreased proapoptotic (Bax and Fas-L protein) and increased antiapoptotic proteins (Bcl-2, p-Bad, and p-FOXO3a) in this isolated heart investigation.[103] The beneficial effect of testosterone on molecular parameters has also been demonstrated in ORX rats with an myocardial infarction model. Testosterone administration at a physiological dose level (2 mg/kg) could promote angiogenesis after myocardial infarction by increasing hypoxia-inducible factor 1α (HIF-1α) and stromal cell-derived factor 1α (SDF-1α) signaling cytokines, which are generated at low oxygen concentration to promote neovascularization.[25] Moreover, testosterone could also increase the number of CD-34 progenitor stem cells that can differentiate into hematopoietic and endothelial progenitor cells in the ischemic myocardium.[25]

Regarding the effects of testosterone in an I/R model, it may be proposed that either acute exogenous testosterone replacement or endogenous testosterone could provide deleterious effects on the heart by accelerating the apoptotic signaling process after I/R injury. However, chronic exogenous testosterone replacement may exert a beneficial effect in both I/R and myocardial infarction models.

Effect of testosterone on cardiac arrhythmias in I/R hearts. In Langendorff perfused hearts, a physiological dose of testosterone (2 mg/kg) combined with adrenergic stimulation has been shown to reduce reperfusion arrhythmia during I/R injury by reducing the incidence of premature ventricular beats,[28] whereas the supraphysiological dose of testosterone replacement (50 mg/kg) demonstrated antiarrhythmic effect in I/R model.[85] The mechanism responsible for the protective effect of testosterone on arrhythmia reduction was thought to be through α1a-adrenoceptor stimulation[28] and shortened the QT interval.[85] Since this positive effect of testosterone on the cardiac arrhythmia during I/R occurred together with the use of adrenergic receptor stimulation (Table 7), it is still unclear whether testosterone alone could provide a similar benefit. This needs to be investigated further.

Effect of testosterone on HRV in myocardial infarction model. Currently, there is no basic study on the effects of testosterone on the HRV, and there is only 1 clinical study investigating the effect of testosterone on HRV in patients with coronary artery disease. This cross-sectional study in men with stable coronary artery disease (age 36-73 years, mean age: 56 years) reported that a high level of blood testosterone was associated with increased HRV (Table 7).[104] These findings suggested that testosterone might have a positive effect on cardiac autonomic regulation in men after myocardial infarction by promoting parasympathetic dominance. Future basic and clinical studies are needed to investigate the roles of testosterone in the cardiac autonomic balance in both I/R injury and myocardial infarction models.

The Relationship Between Testosterone Levels and Coronary Artery Disease in Clinical Studies

Clinical studies show that low levels of testosterone were linked to increased blood pressure, dyslipidemia, atherosclerosis, arrhythmia, thrombosis, and endothelial dysfunction, as well as to impaired left ventricular function.[105] Haring and colleagues demonstrated that serum testosterone levels were inversely related to mortality rate due to cardiovascular disease or cancer, whereas low serum testosterone was associated with an increased risk of all-cause mortality[23] and that plasma testosterone level could potentially be used as a predictive tool for mortality from cardiovascular disease.[106] Regarding the relationship between plasma testosterone levels and coronary artery disease, a previous clinical study has shown that the plasma level of total testosterone, free testosterone, and bioavailability testosterone was significantly lower in men with coronary artery disease than healthy men.[18] However, several reports found that only free testosterone was significantly lower in men with coronary artery disease.[107-110] It has also been shown that a low testosterone level was associated with atherosclerosis[111] and myocardial infarction[112] in men, supporting the previous findings that low levels of testosterone could increase the risk and contribute to a high prevalence of coronary artery disease in men.[22,110,113-116] In addition, the level of testosterone shows an inverse correlation with the severity of coronary artery stenosis.[17,107,108,117,118] These findings suggested that endogenous testosterone may play a preventive role in the development of coronary arteriosclerosis.[117,119] Despite these

Downloaded from cpt.sagepub.com by guest on May 27, 2015

Table 6. Summary of the effect of Testosterone on Molecular Parameters in I/R Heart.

Animal Species	Model	Drugs/Dose/Route	Major Findings	Interpretation	Ref
ORX rat	MI LAD ligation	Physiological dose of testosterone propionate, 2 mg/kg, SC Pretreated for 1, 3, and 28 days Flutamide (testosterone receptor blocker), 30 mg/kg/d, SC, pretreated for 1, 3, and 28 days	Testosterone – ↓ Levels of HIF-1α, SDF-1α, and VEGF mRNA expression. – ↑ The number of CD34+ cells Endogenous testosterone deprivation worsened cardiac function.	Exogenous testosterone replacement promotes neovascularization by the homing of CD34+ stem cells and increases the expression of cytokines HIF-1α, SDF-1α, and VEGF in the early stage of MI, resulting in an increased neovascularization in the MI heart.	25
Isolated rat heart (ORX rat)	I/R 25-Minute global no flow ischemia 40-Minute reperfusion	5α-Dihydrotestosterone (DHT) 100 mg (as pellet), SC implantation, pretreated for 3 weeks Physiologic dose of 17β-hydroxy-4-androsterone 10 ng/mL/min, acute infusion (AI) 5 minutes before ischemia	Depletion of endogenous testosterone – ↑ STAT-3 and SOCS-3 in male hearts Blockade of testosterone receptor – ↑ SOCS-3 levels in males Administration of exogenous testosterone to ORX male and female hearts – ↓ STAT-3 activity and SOCS-3 level	Testosterone downregulated antiapoptotic protein, STAT-3, and SOCS-3 expression in the myocardium after I/R injury.	32
Isolated rat heart (ORX rat)	I/R 25-Minute global no flow ischemia 40-Minute reperfusion	Physiologic dose of 17β-hydroxy-4-androsterone 10 ng/mL/min, acute infusion 5 minutes before ischemia	Testosterone – ↑ The activation of signaling enzymes of myocardial inflammation (p38 MAPK and JNK) – ↑ An expression of apoptotic protein (caspase-3) – ↓ Expression of antiapoptotic protein Bcl-2	Exogenous testosterone has detrimental effects on the myocardium after I/R injury.	36
Isolated rat heart (ORX rat)	I/R 25-Minute global no flow ischemia 40-Minute reperfusion	Flutamide (testosterone receptor blocker) pellet 10 mg, SC implantation, pretreated for 3 weeks	Blocking of testosterone receptor and castration – ↓ Proinflammatory cytokine production (TNF-α, IL-1β, and IL-6) – ↓ Expression of p38 MAPK – ↓ Expression of apoptotic protein (caspases 1, 3, and 11) – ↑ Expression of antiapoptotic protein (Bcl-2)	Decrease in androgen receptors causes an adverse effect on the I/R heart	88
Isolated rat heart (ORX rat)	I/R 25-Minute global no flow ischemia 40-Minute reperfusion	5α-Dihydrotestosterone (DHT) 100 mg (as pellet), SC implantation, pretreated for 3 weeks Physiologic dose of 17β-hydroxy-4-androsterone 10 ng/mL/min, acute infusion 5 minutes before ischemia	Castration or flutamide treatment – ↑ The activation of the myocardial Akt pathway, p-Bad, Bcl-2, and p-FOXO3a – ↓ Fas-L in male hearts – ↑ Bax Acute testosterone replacement reversed the effects of Akt signaling in castrated male hearts – ↓ p-Bad – ↓ Bcl-2/Bax ratio – ↓ Antiapoptotic protein p-FOXO3a Chronic testosterone replacement – ↓ Bax – ↑ Bcl-2/Bax ratio	Acute exogenous testosterone has damaging effects on myocardium after I/R injury through downregulation of the Akt pathway in male hearts following I/R. The chronic treatment of testosterone can provide cardioprotective effects.	103

Abbreviation: ORX rat, orchiectomized rat; MI, myocardial infarction; LAD, left anterior descending coronary artery; SC, subcutaneous; I/R, ischemic and reperfusion; HIF-1α, hypoxia-inducible factor 1-α; SDF-1α, stromal cell-derived factor 1α; VEGF, vascular endothelial growth factor; STAT-3, signal transducer and activator of transcription 3; SOCS-3, suppressor of cytokine signaling 3; mRNA, messenger RNA; p38 MAPK, p38 mitogen-activated protein kinase; JNK, c-Jun N-terminal kinases; Bcl-2, B-cell lymphoma 2; TNF-α, tumor necrosis factor α; IL-1β, interleukin 1β; IL-6, interleukin 6; Akt, protein kinase B; p-Bad, The Bcl-2-associated death promoter; FOXO3a, Forkhead box O3; Bax, bcl-2-like protein 4; Fas-L, Fas ligand.

Downloaded from cpt.sagepub.com by guest on May 27, 2015

Table 7. Summary of the Effect of Testosterone on Arrhythmia Parameters and Heart Rate Variability (HRV) in I/R Heart.

Animal Species	Model	Drugs/Dose/Route	Major Findings	Interpretation	Ref
Isolated rat heart (ORX rat)	I/R LAD ligation 30-Minute ischemia and 120-minute reperfusion	Physiological dose of testosterone 2 mg/kg, SC, pretreated for 8 weeks Noradrenaline 10^{-7} mol/L Pretreated during I/R	Testosterone restored the incidence of PVB to the sham control	Testosterone replacement, mediated by androgen receptors, reduces arrhythmia during I/R injury.	28
Rabbits	I/R LAD ligation 30-Minute ischemia 3-Hour reperfusion	Supraphysiological dose of testosterone, 50 mg/kg, IM Pretreated for 1 weeks and 50 mg/kg, acute treated 5-10 minute before I/R	Testosterone significantly shortened the QT interval by 9% compared with the control group	Supraphysiological dose of testosterone treatment may be anti-arrhythmic by shortening the QT interval.	85
Human aged 36-73 yr (cross-sectional study)	MI	88 Postinfarction men 24-Hour Holter monitoring Measure the levels of testosterone hormone	High level of blood testosterone associated with improved HRV by – ↑ SDNN – ↑ rMSSD – ↑ pNN50	Testosterone has a positive impact on cardiac autonomic regulation in men after MI by promoting parasympathetic dominance.	104

Abbreviations: ORX rat, orchiectomized rat; I/R, ischemic and reperfusion; LAD, left anterior descending coronary artery; SC, subcutaneous; PVB, premature ventricular beat; MI, myocardial infarction; SDNN, the standard deviation of NN intervals; rMSSD, root mean square of the successive differences; pNN50, the proportion of NN50; IM, intramuscular.

beneficial reports on testosterone, inconsistent findings exist. A recent clinical report demonstrated that both low and high levels of total testosterone were associated with an increased ischemic arterial disease risk ratio, suggesting that only an optimal range of plasma testosterone could provide cardiovascular protection.[120] A summary of clinical reports regarding the association between the plasma testosterone levels and coronary artery disease is shown in Table 8.

Effects of Testosterone Replacement on Myocardial Infarction and Heart Failure in Clinical Studies

Previous studies demonstrated that testosterone replacement therapy exerts protective effect against myocardial ischemia such as delayed time to ischemia,[80,81,121] reduced exercise-induced myocardial ischemia,[80,121] and decreased severity of coronary stenosis by increased coronary artery diameter and coronary blood flow.[122,123] This could be partly due to its effects of reducing cholesterol and triglycerides[81,122] and decreasing serum tumor necrotic factor α.[81] It has also been shown that testosterone therapy was associated with a reduced risk of myocardial infarction.[124] However, as discussed earlier, inconsistent findings from clinical reports exist. Several studies found that testosterone therapy could increase the risk of myocardial infarction, especially in older men.[33,67] Several complications have been reported with supraphysiologic doses of testosterone replacement in athletes including hypertension, cardiomyopathy, pulmonary embolism, cardiac arrhythmias, and myocardial infarction,[125] suggesting that unnecessary use of testosterone without medical supervision is likely to cause undesirable effects. A summary of clinical reports regarding the effects of testosterone replacement on myocardial infarction and heart failure is shown in Table 9.

Conclusion

The cardioprotective effects of chronic testosterone replacement to the physiological dose have been demonstrated in an I/R heart. This technique is seen to be effective by reducing the infarct size, improving contractile functions, decreasing LDH release, increasing ventricular myocytes viability, reducing arrhythmias, and improving autonomic regulation of the heart after I/R. These beneficial effects of testosterone are thought to occur via the stimulation and expression of α1a-adrenoceptor, increased synthesis of Hsp70, increased neovascularization of CD34+ stem cell and cytokines HIF-1α, SDF-1α, and vascular endothelial growth factor in the early stages of myocardial infarction. In addition, testosterone may play a beneficial role by maintaining intracellular Ca^{2+} homeostasis during ischemic stress (Figure 1). However, acute testosterone replacement might cause adverse effects in the I/R heart by reducing cardioprotective signaling proteins such as STAT-3 and SOCS-3 after I/R and also decreasing myocardial Akt activation, leading to reduced Bad phosphorylation and decreased Bcl-2 levels, which consequently results in worsened I/R-depressed myocardial function.

Downloaded from cpl.sagepub.com by guest on May 27, 2015

Table 8. Summary of Clinical Studies Reported on the Association Between Testosterone Levels and Coronary Artery Disease.

Model	n	Major Findings	Interpretation	Ref
Men with CAD	201	Plasma testosterone levels in patients with CAD were lower than in the healthy participants.	Low plasma testosterone level may be a risk factor for CAD.	113
Men with CAD	56	Men with coronary artery disease had lower TT levels, testosterone/estradiol ratio, and free androgen index than the control group.	Testosterone may be involved in the pathogenesis of coronary atherosclerosis.	115
Men with CAD	803	– Testosterone level was inversely associated with severity of coronary stenosis (Gensini coronary score). – The severity of CAD was lower in participants with high level of testosterone.	Lower testosterone levels are associated with greater coronary stenosis.	17
Men with CAD	191	– The level of FT and TT was lower in patients with CAD than in the control group. – Low TT was significantly correlated with CAD. – The severity of coronary stenosis (Gensini coronary score) was correlated with low TT and FT.	Low levels of testosterone are associated with premature coronary artery disease and its severity in young adults.	118
Men with CAD	201	– Testosterone level was inversely associated with the level of arteriosclerosis. – Lower concentrations of DHEA and testosterone were found in those men with more severe arteriosclerotic lesions.	• Testosterone may play a preventive role in the development of coronary arteriosclerosis. • Low levels of testosterone lead to greater severity of arteriosclerotic lesions.	117
Men with CAD	128	– TT levels were not different from control. – FT level in 3-vessel lesion group was lower than that in double-vessel lesion group and single-vessel lesion group.	FT levels are inversely associated with the severity of coronary artery lesions.	107
Men with CAD	69	– TT and FT levels in patients with CAD were lower than the control group. – Patients with FT levels below the cutoff value of 17.3 pg/mL had 3.3-fold risk of developing premature CAD compared to those with FT levels above the cutoff level.	Low levels of FT may be related to the development of premature CAD.	108
Men with CAD	129	– Patients with CAD had lower levels of TT and FT than controls. – Degree of CAD had an inverse relationship with plasma testosterone levels.	Low levels of plasma testosterone are associated with the increased risk of CAD in men.	22
Men with CAD	139	– TT, FT, SHBG, and AR levels in the CAD group were reduced compared with the control group. – TT and FT levels were negatively correlated with CAD.	Low levels of TT and SHBG could be risk factors for CAD in elderly men.	116
Men with CAD	105	Men with CAD had lower levels of FT than the control group.	Low levels of FT are associated with the development of CAD.	114
Men with CAD	237	– No differences in TT, SHBG, AR, and DHEA levels among groups. – Serum level of FT was lower in the CAD group than in the control group. – FT level was inversely correlated with CAD. – Age was negatively correlated with the levels of FT and AR	• Low levels of FT contribute to a high prevalence of CAD in elderly men. • The age-related reduction in FT and AR accelerates the progression of coronary atherosclerosis.	110
Men with CAD	100	Patients with CAD had lower values of FT	Low levels of FT may contribute to the development of premature coronary artery disease.	109
Men with MI	100	– Patients with STEMI and SA had low testosterone level – Hypotestosteronemia prevalence was higher among patients with STEMI compared with patients with SA – Hypotestosteronemia independently predicted both angio-MVO and ECG-MVO	Testosterone deficiency may contribute to the development of coronary instability and MVO pathogenesis.	112
Men with CAD	111	– Plasma testosterone level was inversely correlated with the degree of coronary stenosis. – Higher blood level of TT was associated with the lower number of stenosis in the coronary arteries.	Endogenous testosterone may provide protective effects on coronary arteries.	119
Men with CAD	3650	Lowest total testosterone had IAD risk ratio 2.23, whereas highest total testosterone had IAD risk ratio 3.61.	• High and low plasma testosterone levels are associated with an increased risk of IAD in elderly men. • An optimal range of plasma testosterone may confer cardiovascular protection.	120

Abbreviations: CAD, coronary artery disease; TT, total testosterone; FT, free testosterone; DHEA, dehydroepiandrosterone; SHBG, sex hormone binding globulin; AR, androgen receptor; MI, myocardial infarction; DHEA, dehydroepiandrosterone; MVO, microvascular obstruction; STEMI, ST-elevation myocardial infarction; SA, stable angina; ECG-MVO, electrocardiographic microvascular obstruction; angio-MVO, angiographic microvascular obstruction; IAD, ischemic arterial disease.

Downloaded from cpt.sagepub.com by guest on May 27, 2015

Table 9. Summary of Clinical Studies Reported on the Effect of Testosterone Replacement on Myocardial Infarction and Heart Failure.

Model	n	Treatment	Major Findings	Interpretation	Ref
Men with MI	46	5 mg testosterone daily by transdermal patch or matching placebo for 12 weeks.	Testosterone increased the time to 1-mm ST-segment depression.	Low-dose supplemental testosterone treatment in men with chronic stable angina reduces exercise-induced myocardial ischemia.	80
Men with MI	10	Testosterone injections (1 mL of 100 mg testosterone/mL) every 2 weeks for 1 month.	Testosterone therapy increased the time to 1-mm ST-segment depression and reduced total cholesterol and serum tumor necrosis factor α.	Testosterone replacement therapy in hypogonadal men delays time to ischemia and reduces the total cholesterol and inflammation.	81
Men with MI	15	Testosterone undecanoate, 250 mg/mL every 12 weeks for 12 months (intramuscular injection).	– Testosterone increased the time to 1-mm ST-segment depression and increased hemoglobin and hematocrit. – Testosterone decreased the CIMT, BMI, and serum triglycerides.	Testosterone exerts protective effects on myocardial ischemia.	122
Men with MI	6355	Eight-year follow-up of patients who treated with at least 1 intramuscular injection of testosterone enanthate, up to 1 mL; testosterone cypionate, up to 1 mL; testosterone cypionate, 100-200 mg; testosterone enanthate, 100-200 mg; testosterone suspension, up to 50 mg; testosterone propionate, up to 100 mg; and testosterone pellet, 75 mg	– Testosterone therapy was not associated with an increased risk of MI. – Testosterone therapy was associated with a reduced risk of MI.	Older men treated with intramuscular testosteroneinjections have no increased risk of MI. For men with high MI risk, testosterone use is modestly protective against MI.	124
Men with CAD	14	Testosterone (2.5 mg; intravenous in 5 minutes) before exercise tests.	Testosterone increased the time to 1-mm ST-segment depression and increased total exercise time.	Short-term administration of testosterone exerts a beneficial effect on exercise-induced myocardial ischemia in men with CAD. This benefit may be related to a direct coronary-relaxing effect.	121
Men with CAD	13	3-Minute intracoronary infusion of physiological concentrations testosterone (10^{-10} to 10^{-7} mol/L).	Testosterone increased coronary artery diameter and coronary blood flow.	Intracoronary infusion of testosterone induces coronary artery dilatation and increases coronary blood flow in men with CAD.	123
Men with MI (case report)	1	A recreational weight lifter was taking high-dose intramuscular testosterone for the previous 6 weeks and intermittently for 2 years.	Hematologic studies showed polycythemia and right coronary angiography revealed a total occlusion at the mid-portion of the vessel with intracoronary thrombus.	Association with and potential interplay between traditional cardiovascular risk factors, high-dose testosterone use, and possibly elevated plasma viscosity is proposed as possible contributors to this cardiovascular event.	125
Men with MI	46	Received two 2.5-mg self-adhesive active testosterone patches each night for 12 weeks.	There was no change in fibrinogen, tPA activity or PAI-1 activity, and hemoglobin concentration in the testosterone group.	Physiological testosterone replacement does not interfere with blood coagulation status.	126
Men with CAD	1223	– 13 Patients used testosterone gel (1% 5 g packets) – 436 Patients with testosterone injections (200 mg/mL) – 774 Patients used patches (2.5 mg/24-h patch) – (Average 531 days)	– Testosterone therapy was associated with increased risk of adverse outcomes including all-cause mortality, MI, and ischemic stroke. – No difference in the risk of adverse outcomes across the 3 testosterone formulations.	Testosterone therapy was associated with increased risk of adverse outcomes.	67

(continued)

Downloaded from cpt.sagepub.com by guest on May 27, 2015

Table 9. (continued)

Model	n	Treatment	Major Findings	Interpretation	Ref
Men with MI	55 593	Compared the incidence rate of MI (post/preprescription rate ratio [RR]) following initiation of testosterone therapy (TT) prescription.	– Younger men with a history of heart disease had a 2-3-fold increased risk of MI within 90 days after TT. – Men aged 65 years and older had a 2-fold increase in the risk of MI within 90 days after TT.	In older men and in younger men with preexisting diagnosed heart disease, the risk of MI following initiation of TT prescription is substantially increased.	33
Men with CHF	50	Testosterone enanthate (250mg/mL) 1 mL once every 4 weeks for 12 weeks (intramuscular injection).	Improved diastolic function and increased trend in 6-minute walk distance (6MWD) parameter.	Testosterone replacement exerts a beneficial role in improving functional capacity and quality of life in patients with heart failure.	127
Men with CHF	70	Testosterone undecanoate 1000 mg long-acting once every 6 weeks for 12 weeks (intramuscular injection)	Testosterone therapy improved oxygen consumption, quadriceps isometric strength, insulin sensitivity, and baroreflex.	Long-acting testosterone therapy improves exercise capacity, muscle strength, glucose metabolism, and baroreflex sensitivity in men with moderately severe CHF.	128
Men with CHF	76	Testosterone replacement therapy (5 mg Androderm) at physiological doses for 12 months	Improved exercise capacity, no adverse events.	Testosterone replacement therapy improves functional capacity and symptoms in men with moderately severe heart failure.	129

Abbreviations: MI, myocardial infarction; CIMT, carotid intima–media thickness; BMI, body mass index; CAD, coronary artery disease; PAI-1, plasminogen activator inhibitor 1; tPA, tissue plasminogen activator; CHF, congestive heart failure; TT, testosterone therapy; RR, post/preprescription rate ratio.

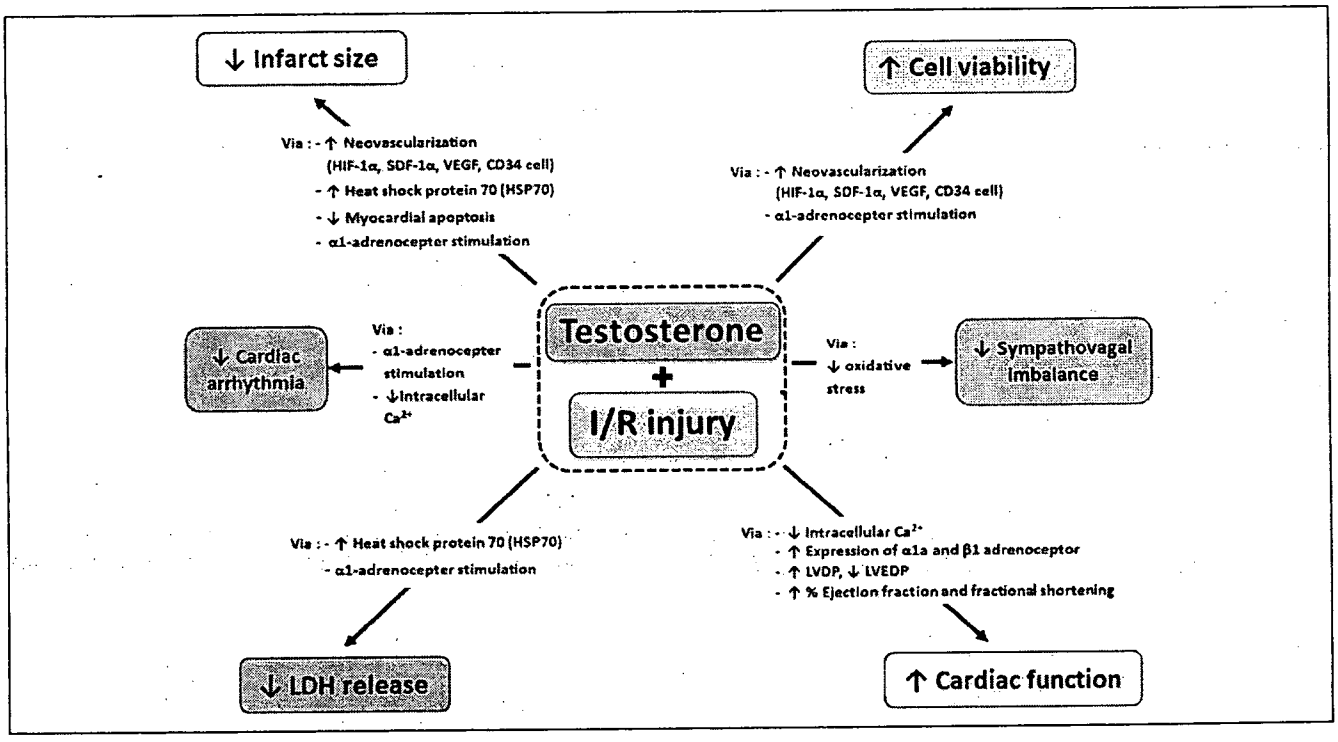


Figure 1. The potential roles of testosterone replacement in cardiac ischemia–reperfusion (I/R) and myocardial infarction models. During cardiac I/R, testosterone administration has been shown to reduce infarct size, decrease lactate dehydrogenase (LDH) release, and increase cell viability via increased neovascularization, increased heat shock protein 70 syntheses, α1a-adrenoceptor stimulation, and decreased myocardial apoptosis. The reduction in sympathovagal imbalance may occur due to decreased oxidative stress. The reduction in cardiac arrhythmia could occur due to decreased intracellular Ca^{2+} accumulation and α1a-adrenoceptor stimulation. Furthermore, testosterone could decrease intracellular Ca^{2+} accumulation, increase an expression of α1a- and β1-adrenoceptors, decrease LVEDP, increase LVDP, and ejection fraction, thus resulting in increased contractility and improved cardiac function. HIF-1α indicates hypoxia-inducible factor 1-α; SDF-1α, stromal cell-derived factor 1α; VEGF, vascular endothelial growth factor; CD34, hematopoietic progenitor cell antigen CD34; LVDP, left ventricular develop pressure; LVEDP, left ventricular end diastolic pressure.

Downloaded from cpt.sagepub.com by guest on May 27, 2015

Author Contribution

W. Pongkan and N. Chattipakorn contributed to conception and design; acquisition, analysis, and interpretation; drafted the article; critically revised the article; gave final approval, and agreed to be accountable for all aspects of work ensuring integrity and accuracy. S. Chattipakorn contributed to conception and design, analysis and interpretation, drafted the article, critically revised the article, gave final approval, and agreed to be accountable for all aspects of work ensuring integrity and accuracy.

Declaration of Conflicting Interests

The author(s) declared no potential conflicts of interest with respect to the research, authorship, and/or publication of this article.

Funding

The author(s) disclosed receipt of the following financial support for the research, authorship, and/or publication of this article: This work was supported by the Thailand Research Fund Royal Golden Jubilee PhD program (WP and NC), the Thailand Research Fund BRG5780016 (SC), a NSTDA Research Chair Grant from the National Science and Technology Development Agency Thailand (NC), and the Chiang Mai University Center of Excellence Award (NC).

References

1. Handelsman DJ, Zajac JD. Androgen deficiency and replacement therapy in men. *Med J Aust.* 2004;180(10):529-535.
2. Araujo AB, O'Donnell AB, Brambilla DJ, et al. Prevalence and incidence of androgen deficiency in middle-aged and older men: estimates from the Massachusetts Male Aging Study. *J Clin Endocrinol Metab.* 2004;89(12):5920-5926.
3. Spratt DI, Cox P, Orav J, Moloney J, Bigos T. Reproductive axis suppression in acute illness is related to disease severity. *J Clin Endocrinol Metab.* 1993;76(6):1548-1554.
4. Kalyani RR, Gavini S, Dobs AS. Male hypogonadism in systemic disease. *Endocrinol Metab Clin North Am.* 2007;36(2):333-48.
5. Oskui PM, French WJ, Herring MJ, Mayeda GS, Burstein S, Kloner RA. Testosterone and the cardiovascular system: a comprehensive review of the clinical literature. *J Am Heart Assoc.* 2013;2(6):e000272.
6. Araujo AB, Esche GR, Kupelian V, et al. Prevalence of symptomatic androgen deficiency in men. *J Clin Endocrinol Metab.* 2007;92(11):4241-7.
7. Mulligan T, Frick MF, Zuraw QC, Stemhagen A, McWhirter C. Prevalence of hypogonadism in males aged at least 45 years: the HIM study. *Int J Clin Pract.* 2006;60(7):762-769.
8. Kaufman JM, Vermeulen A. The decline of androgen levels in elderly men and its clinical and therapeutic implications. *Endocr Rev.* 2005;26(6):833-876.
9. Harman SM, Metter EJ, Tobin JD, Pearson J, Blackman MR; Baltimore Longitudinal Study of Aging. Longitudinal effects of aging on serum total and free testosterone levels in healthy men. Baltimore longitudinal study of aging. *J Clin Endocrinol Metab.* 2001;86(2):724-731.
10. Roubinian JR, Papoian R, Talal N. Androgenic hormones modulate autoantibody responses and improve survival in murine lupus. *J Clin Invest.* 1977;59(6):1066-1070.
11. Haffner SM, Karhapaa P, Mykkanen L, Laakso M. Insulin resistance, body fat distribution, and sex hormones in men. *Diabetes.* 1994;43(2):212-219.
12. Grossmann M, Thomas MC, Panagiotopoulos S, et al. Low testosterone levels are common and associated with insulin resistance in men with diabetes. *J Clin Endocrinol Metab.* 2008;93(5):1834-1840.
13. Ferdinandy P, Schulz R, Baxter GF. Interaction of cardiovascular risk factors with myocardial ischemia/reperfusion injury, preconditioning, and postconditioning. *Pharmacol Rev.* 2007;59(4):418-458.
14. Jousilahti P, Vartiainen E, Tuomilehto J, Puska P. Sex, age, cardiovascular risk factors, and coronary heart disease: a prospective follow-up study of 14 786 middle-aged men and women in Finland. *Circulation.* 1999;99(9):1165-1172.
15. Chrysohoou C, Panagiotakos DB, Pitsavos C, et al. Gender differences on the risk evaluation of acute coronary syndromes: the CARDIO2000 study. *Prev Cardiol.* 2003;6(2):71-77.
16. Mozaffarian D, Benjamin EJ, Go AS, et al. Heart disease and stroke statistics—2015 update: a report from the American Heart Association. *Circulation.* 2015;131(4):e29-e322.
17. Li L, Guo CY, Jia EZ, et al. Testosterone is negatively associated with the severity of coronary atherosclerosis in men. *Asian J Androl.* 2012;14(6):875-878.
18. English KM, Mandour O, Steeds RP, Diver MJ, Jones TH, Channer KS. Men with coronary artery disease have lower levels of androgens than men with normal coronary angiograms. *Eur Heart J.* 2000;21(11):890-894.
19. Wu FC, von Eckardstein A. Androgens and coronary artery disease. *Endocr Rev.* 2003;24(2):183-217.
20. Cornoldi A, Caminiti G, Marazzi G, et al. Effects of chronic testosterone administration on myocardial ischemia, lipid metabolism and insulin resistance in elderly male diabetic patients with coronary artery disease. *Int J Cardiol.* 2009;142(1):50-55.
21. Jankowska EA, Biel B, Majda J, et al. Anabolic deficiency in men with chronic heart failure: prevalence and detrimental impact on survival. *Circulation.* 2006;114(17):1829-1837.
22. Rosano GM, Sheiban I, Massaro R, et al. Low testosterone levels are associated with coronary artery disease in male patients with angina. *Int J Impot Res.* 2007;19(2):176-182.
23. Haring R, Volzke H, Steveling A, et al. Low serum testosterone levels are associated with increased risk of mortality in a population-based cohort of men aged 20-79. *Eur Heart J.* 2010;31(12):1494-1501.
24. Borst SE, Quindry JC, Yarrow JF, et al. Testosterone administration induces protection against global myocardial ischemia. *Horm Metab Res.* 2010;42(2):122-129.
25. Chen Y, Fu L, Han Y, et al. Testosterone replacement therapy promotes angiogenesis after acute myocardial infarction by enhancing expression of cytokines HIF-1a, SDF-1a and VEGF. *Eur J Pharmacol.* 2012;684(1-3):116-124.
26. Herring MJ, Oskui PM, Hale SL, Kloner RA. Testosterone and the cardiovascular system: a comprehensive review of the basic science literature. *J Am Heart Assoc.* 2013;2(4):e000271.
27. Brouillette J, Rivard K, Lizotte E, Fiset C. Sex and strain differences in adult mouse cardiac repolarization: importance of androgens. *Cardiovasc Res.* 2005;65(1):148-157.

Downloaded from cpt.sagepub.com by guest on May 27, 2015

28. Tsang S, Wu S, Liu J, Wong TM. Testosterone protects rat hearts against ischaemic insults by enhancing the effects of alpha(1)-adrenoceptor stimulation. *Br J Pharmacol.* 2008; 153(4):693-709.
29. O'Connor EK, Ivey JR, Bowles DK. Differential effects of androgens on coronary blood flow regulation and arteriolar diameter in intact and castrated swine. *Biol Sex Differ.* 2012;3(1):10.
30. Alexandersen P, Haarbo J, Byrjalsen I, et al. Natural androgens inhibit male atherosclerosis: a study in castrated, cholesterol-fed rabbits. *Circ Res.* 1999;84(7):813-819.
31. Filippi S, Vignozzi L, Morelli A, et al. Testosterone partially ameliorates metabolic profile and erectile responsiveness to PDE5 inhibitors in an animal model of male metabolic syndrome. *J Sex Med.* 2009;6(12):3274-3288.
32. Wang M, Wang Y, Abarbanell A, et al. Both endogenous and exogenous testosterone decrease myocardial STAT3 activation and SOCS3 expression after acute ischemia and reperfusion. *Surgery.* 2009;146(2):138-144.
33. Finkle WD, Greenland S, Ridgeway GK, et al. Increased risk of non-fatal myocardial infarction following testosterone therapy prescription in men. *PLoS One.* 2014;9(1):e85805.
34. Cavasin MA, Tao ZY, Yu AL, Yang XP. Testosterone enhances early cardiac remodeling after myocardial infarction, causing rupture and degrading cardiac function. *Am J Physiol Heart Circ Physiol.* 2006;290(5):H2043-H2050.
35. Ceballos G, Figueroa L, Rubio I, et al. Acute and nongenomic effects of testosterone on isolated and perfused rat heart. *J Cardiovasc Pharmacol.* 1999;33(5):691-697.
36. Crisostomo PR, Wang M, Wairiuko GM, Morrell ED, Meldrum DR. Brief exposure to exogenous testosterone increases death signaling and adversely affects myocardial function after ischemia. *Am J Physiol Regul Integr Comp Physiol.* 2006;290(5):R1168-R1174.
37. Marsh JD, Lehmann MH, Ritchie RH, Gwathmey JK, Green GE, Schiebinger RJ. Androgen receptors mediate hypertrophy in cardiac myocytes. *Circulation.* 1998;98(3):256-261.
38. Winters SJ. Androgen: endocrine physiology and pharmacology. In: Lin GC, Erinoff L, eds. *Anabolic Steroid Abuse.* Rockville, MD: National Institute on Drug Abuse; 1990:113-130.
39. Ling S, Komesaroff PA, Sudhir K. Cardiovascular physiology of androgens and androgen testosterone therapy in postmenopausal women. *Endocr Metab Immune Disord Drug Targets.* 2009; 9(1):29-37.
40. Papamitsou T, Barlagiannis D, Papaliagkas V, Kotanidou E, Dermentzopoulou-Theodoridou M. Testosterone-induced hypertrophy, fibrosis and apoptosis of cardiac cells—an ultrastructural and immunohistochemical study. *Med Sci Monit.* 2011;17(9): BR266-BR273.
41. Schaible TF, Malhotra A, Ciambrone G, Scheuer J. The effects of gonadectomy on left ventricular function and cardiac contractile proteins in male and female rats. *Circ Res.* 1984;54(1):38-49.
42. Scheuer J, Malhotra A, Schaible TF, Capasso J. Effects of gonadectomy and hormonal replacement on rat hearts. *Circ Res.* 1987; 61(1):12-19.
43. Golden KL, Marsh JD, Jiang Y, Moulden J. Acute actions of testosterone on contractile function of isolated rat ventricular myocytes. *Eur J Endocrinol.* 2005;152(3):479-483.
44. Heinlein CA, Chang C. The roles of androgen receptors and androgen-binding proteins in nongenomic androgen actions. *Mol Endocrinol.* 2002;16(10):2181-2187.
45. Perusquia M, Stallone JN. Do androgens play a beneficial role in the regulation of vascular tone? Nongenomic vascular effects of testosterone metabolites. *Am J Physiol Heart Circ Physiol.* 2010;298(5):H1301-H1307.
46. Witayavanitkul N, Woranush W, Bupha-Intr T, Wattanapermpool J. Testosterone regulates cardiac contractile activation by modulating SERCA but not NCX activity. *Am J Physiol Heart Circ Physiol.* 2013;304(3):H465-H472.
47. Curl CL, Delbridge LM, Canny BJ, Wendt IR. Testosterone modulates cardiomyocyte Ca(2+) handling and contractile function. *Physiol Res.* 2009;58(2):293-297.
48. Trifunovic B, Norton GR, Duffield MJ, Avraam P, Woodiwiss AJ. An androgenic steroid decreases left ventricular compliance in rats. *Am J Physiol.* 1995;268(3 pt 2):H1096-H1105.
49. Mayuga KA, Parker M, Sukthanker ND, et al. Effects of age and gender on the QT response to exercise. *Am J Cardiol.* 2001;87(2): 163-167.
50. Schwartz JB, Volterrani M, Caminiti G, et al. Effects of testosterone on the Q-T interval in older men and older women with chronic heart failure. *Int J Androl.* 2011;34(5 pt 2):e415-e421.
51. Charbit B, Christin-Maitre S, Demolis JL, Soustre E, Young J, Funck-Brentano C. Effects of testosterone on ventricular repolarization in hypogonadic men. *Am J Cardiol.* 2009;103(6): 887-890.
52. Jonsson MK, Vos MA, Duker G, Demolombe S, van Veen TA. Gender disparity in cardiac electrophysiology: implications for cardiac safety pharmacology. *Pharmacol Ther.* 2010;127(1): 9-18.
53. Sedlak T, Shufelt C, Iribarren C, Merz CN. Sex hormones and the QT interval: a review. *J Womens Health (Larchmt).* 2012;21(9): 933-941.
54. Malkin CJ, Morris PD, Pugh PJ, English KM, Channer KS. Effect of testosterone therapy on QT dispersion in men with heart failure. *Am J Cardiol.* 2003;92(10):1241-3.
55. van Noord C, Dorr M, Sturkenboom MC, et al. The association of serum testosterone levels and ventricular repolarization. *Eur J Epidemiol.* 2010;25(1):21-28.
56. Ezaki K, Nakagawa M, Taniguchi Y, et al. Gender differences in the ST segment: effect of androgen-deprivation therapy and possible role of testosterone. *Circ J.* 2010;74(11):2448-2454.
57. Jaffe MD. Effect of testosterone cypionate on postexercise ST segment depression. *Br Heart J.* 1977;39(11):1217-1222.
58. Tenover JS. Androgen administration to aging men. *Endocrinol Metab Clin North Am.* 1994;23(4):877-892.
59. Jeppesen LL, Jorgensen HS, Nakayama H, Raaschou HO, Olsen TS, Winther K. Decreased serum testosterone in men with acute ischemic stroke. *Arterioscler Thromb Vasc Biol.* 1996;16(6): 749-754.
60. Tsuneda T, Yamashita T, Kato T, et al. Deficiency of testosterone associates with the substrate of atrial fibrillation in the rat model. *J Cardiovasc Electrophysiol.* 2009;20(9):1055-1060.
61. Tsang S, Wong SS, Wu S, Kravtsov GM, Wong TM. Testosterone-augmented contractile responses to α1-and β1-adrenoceptor

Downloaded from cpt.sagepub.com by guest on May 27, 2015

stimulation are associated with increased activities of RyR, SERCA, and NCX in the heart. *Am J Physiol Cell Physiol.* 2009;296(4):C766-C782.
62. Er F, Gassanov N, Brandt MC, Madershahian N, Hoppe UC. Impact of dihydrotestosterone on L-type calcium channels in human ventricular cardiomyocytes. *Endocr Res.* 2009;34(3): 59-67.
63. Perrier E, Kerfant BG, Lalevee N, et al. Mineralocorticoid receptor antagonism prevents the electrical remodeling that precedes cellular hypertrophy after myocardial infarction. *Circulation.* 2004;110(7):776-783.
64. Golden KL, Marsh JD, Jiang Y, Brown T, Moulden J. Gonadectomy of adult male rats reduces contractility of isolated cardiac myocytes. *Am J Physiol Endocrinol Metab.* 2003;285(3): E449-E453.
65. Golden KL, Marsh JD, Jiang Y. Castration reduces mRNA levels for calcium regulatory proteins in rat heart. *Endocrine.* 2002; 19(3):339-344.
66. Chrysohoou C, Panagiotakos D, Pitsavos C, et al. Low total testosterone levels are associated with the metabolic syndrome in elderly men: the role of body weight, lipids, insulin resistance, and inflammation; the Ikaria study. *Rev Diabet Stud.* 2013; 10(1):27-38.
67. Vigen R, O'Donnell CI, Baron AE, et al. Association of testosterone therapy with mortality, myocardial infarction, and stroke in men with low testosterone levels. *JAMA.* 2013;310(17):1829-1836.
68. Kelly DM, Jones TH. Testosterone: a vascular hormone in health and disease. *J Endocrinol.* 2013;217(3):R47-R71.
69. Wang C, Jackson G, Jones TH, et al. Low testosterone associated with obesity and the metabolic syndrome contributes to sexual dysfunction and cardiovascular disease risk in men with type 2 diabetes. *Diabetes Care.* 2011;34(7):1669-1675.
70. Carrero JJ, Qureshi AR, Parini P, et al. Low serum testosterone increases mortality risk among male dialysis patients. *J Am Soc Nephrol.* 2009;20(3):613-620.
71. Hu X, Rui L, Zhu T, et al. Low testosterone level in middle-aged male patients with coronary artery disease. *Eur J Intern Med.* 2011;22(6):e133-e136.
72. Agarwal M, Naghi J, Philip K, et al. Growth hormone and testosterone in heart failure therapy. *Expert Opin Pharmacother.* 2010; 11(11):1835-1844.
73. Sarkar NN. Hormonal profiles behind the heart of a man. *Cardiol J.* 2009;16(4):300-306.
74. Kontoleon PE, Anastasiou-Nana MI, Papapetrou PD, et al. Hormonal profile in patients with congestive heart failure. *Int J Cardiol.* 2003;87(2-3):179-183.
75. Guder G, Allolio B, Angermann CE, Stork S. Androgen deficiency in heart failure. *Curr Heart Fail Rep.* 2011;8(2): 131-139.
76. Liu PY, Death AK, Handelsman DJ. Androgens and cardiovascular disease. *Endocr Rev.* 2003;24(3):313-340.
77. Yeap BB. Androgens and cardiovascular disease. *Curr Opin Endocrinol Diabetes Obes.* 2010;17(3):269-276.
78. Basaria S, Coviello AD, Travison TG, et al. Adverse events associated with testosterone administration. *N Engl J Med.* 2010; 363(2):109-122.
79. Morgentaler A, Miner MM, Caliber M, Guay AT, Khera M, Traish AM. Testosterone therapy and cardiovascular risk: advances and controversies. *Mayo Clin Proc.* 2015;90(2):224-251.
80. English KM, Steeds RP, Jones TH, et al. Low-dose transdermal testosterone therapy improves angina threshold in men with chronic stable angina: a randomized, double-blind, placebo-controlled study. *Circulation.* 2000;102(16):1906-1911.
81. Malkin CJ, Pugh PJ, Morris PD, et al. Testosterone replacement in hypogonadal men with angina improves ischaemic threshold and quality of life. *Heart.* 2004;90(8):871-876.
82. Liu J, Tsang S, Wong TM. Testosterone is required for delayed cardioprotection and enhanced heat shock protein 70 expression induced by preconditioning. *Endocrinology.* 2006;147(10): 4569-4577.
83. Rubio-Gayosso I, Ramirez-Sanchez I, Ita-Islas I, et al. Testosterone metabolites mediate its effects on myocardial damage induced by ischemia/reperfusion in male Wistar rats. *Steroids.* 2013;78(3):362-369.
84. Nahrendorf M, Frantz S, Hu K, et al. Effect of testosterone on post-myocardial infarction remodeling and function. *Cardiovasc Res.* 2003;57(2):370-378.
85. Herring M, Hale SL, Shi J, et al. Supraphysiological testosterone levels shorten the QT interval but do not alter total anatomic myocardial infarct size in rabbits with acute myocardial infarction. *Cardiol Pharmacol.* 2014;3(1):1000115.
86. Callies F, Stromer H, Schwinger RH, et al. Administration of testosterone is associated with a reduced susceptibility to myocardial ischemia. *Endocrinology.* 2003;144(10):4478-4483.
87. Nam UH, Wang M, Crisostomo PR, et al. The effect of chronic exogenous androgen on myocardial function following acute ischemia–reperfusion in hosts with different baseline levels of sex steroids. *J Surg Res.* 2007;142(1):113-118.
88. Wang M, Tsai BM, Kher A, et al. Role of endogenous testosterone in myocardial proinflammatory and proapoptotic signaling after acute ischemia–reperfusion. *Am J Physiol Heart Circ Physiol.* 2005;288(1):H221-H226.
89. Bennett NC, Gardiner RA, Hooper JD, et al. Molecular cell biology of androgen receptor signalling. *Int J Biochem Cell Biol.* 2010;42(6):813-827.
90. Klocker H, Gromoll J, Cato ACB. The androgen receptor: molecular biology. In: Nieshchlag E, Behre HM, eds. *Testosterone: Action, Deficiency, Substitution.* 3rd ed. United Kingdom: Cambridge University Press; 2004:39-92.
91. Michels G, Hoppe UC. Rapid actions of androgens. *Front Neuroendocrinol.* 2008;29(2):182-198.
92. Vicencio JM, Ibarra C, Estrada M, et al. Testosterone induces an intracellular calcium increase by a nongenomic mechanism in cultured rat cardiac myocytes. *Endocrinology.* 2006;147(3): 1386-1395.
93. Keating NL, O'Malley AJ, Smith MR. Diabetes and cardiovascular disease during androgen deprivation therapy for prostate cancer. *J Clin Oncol.* 2006;24(27):4448-4456.
94. Keating NL, O'Malley AJ, Freedland SJ, et al. Diabetes and cardiovascular disease during androgen deprivation therapy: observational study of veterans with prostate cancer. *J Natl Cancer Inst.* 2010;102(1):39-46.

Downloaded from cpt.sagepub.com by guest on May 27, 2015

95. Braga-Basaria M, Dobs AS, Muller DC, et al. Metabolic syndrome in men with prostate cancer undergoing long-term androgen-deprivation therapy. *J Clin Oncol.* 2006;24(24): 3979-3983.
96. Smith MR, Lee H, Nathan DM. Insulin sensitivity during combined androgen blockade for prostate cancer. *J Clin Endocrinol Metab.* 2006;91(4):1305-1308.
97. Smith MR, Finkelstein JS, McGovern FJ, et al. Changes in body composition during androgen deprivation therapy for prostate cancer. *J Clin Endocrinol Metab.* 2002;87(2):599-603.
98. Smith MR. Changes in fat and lean body mass during androgen-deprivation therapy for prostate cancer. *Urology.* 2004;63(4): 742-745.
99. D'Amico AV, Chen MH, Renshaw AA, Loffredo M, Kantoff PW. Causes of death in men undergoing androgen suppression therapy for newly diagnosed localized or recurrent prostate cancer. *Cancer.* 2008;113(12):3290-3297.
100. Nanda A, Chen MH, Braccioforte MH, Moran BJ, D'Amico AV. Hormonal therapy use for prostate cancer and mortality in men with coronary artery disease-induced congestive heart failure or myocardial infarction. *JAMA.* 2009;302(8):866-873.
101. Bolla M, de Reijke TM, Van Tienhoven G, et al. Duration of androgen suppression in the treatment of prostate cancer. *N Engl J Med.* 2009;360(24):2516-2527.
102. Alibhai SM, Duong-Hua M, Sutradhar R, et al. Impact of androgen deprivation therapy on cardiovascular disease and diabetes. *J Clin Oncol.* 2009;27(21):3452-3458.
103. Huang C, Gu H, Zhang W, Herrmann JL, Wang M. Testosterone-down-regulated Akt pathway during cardiac ischemia/reperfusion: a mechanism involving BAD, Bcl-2 and FOXO3a. *J Surg Res.* 2010;164(1):e1-e11.
104. Wranicz JK, Rosiak M, Cygankiewicz I, Kula P, Kula K, Zareba W. Sex steroids and heart rate variability in patients after myocardial infarction. *Ann Noninvasive Electrocardiol.* 2004;9(2):156-161.
105. Ruige JB, Ouwens DM, Kaufman JM. Beneficial and adverse effects of testosterone on the cardiovascular system in men. *J Clin Endocrinol Metab.* 2013;98(11):4300-4310.
106. Hyde Z, Norman PE, Flicker L, et al. Low free testosterone predicts mortality from cardiovascular disease but not other causes: the Health in Men Study. *J Clin Endocrinol Metab.* 2012;97(1): 179-189.
107. Gu HF, Yang YM, Xu ZR. Relationship between androgen levels and pathological changes of coronary atherosclerosis in elderly males [in Chinese]. *Zhejiang Da Xue Xue Bao Yi Xue Ban.* 2007;36(4):382-385.
108. Turhan S, Tulunay C, Gulec S, et al. The association between androgen levels and premature coronary artery disease in men. *Coronary Artery Dis.* 2007;18(3):159-162.
109. Helaly MA, Daoud E, El-Mashad N. Does the serum testosterone level have a relation to coronary artery disease in elderly men? *Curr Gerontol Geriatr Res.* 2011;2011:791765.
110. Zhang XJ, Li XY, Cao TT, Ye L. Correlation of endogenous androgen and androgen receptor level with coronary artery diseases in elderly males [in Chinese]. *Zhonghua yi xue za zhi.* 2011;91(14):984-986.
111. Svartberg J, von Muhlen D, Mathiesen E, Joakimsen O, Bønaa KH, Stensland-Bugge E. Low testosterone levels are associated with carotid atherosclerosis in men. *J Intern Med.* 2006;259(6): 576-582.
112. Niccoli G, Milardi D, D'Amario D, et al. Hypotestosteronemia is frequent in ST-elevation myocardial infarction patients and is associated with coronary microvascular obstruction [published online May 12, 2014]. *Eur J Prev Cardiol.* 2014.
113. Zhao SP, Li XP. The association of low plasma testosterone level with coronary artery disease in Chinese men. *Int J Cardiol.* 1998;63(2):161-164.
114. Sieminska L, Wojciechowska C, Swietochowska E, et al. Serum free testosterone in men with coronary artery atherosclerosis. *Med Sci Monit.* 2003;9(5):CR162-CR166.
115. Dunajska K, Milewicz A, Szymczak J, et al. Evaluation of sex hormone levels and some metabolic factors in men with coronary atherosclerosis. *Aging Male.* 2004;7(3):197-204.
116. Cao J, Zou H, Zhu BP, et al. Sex hormones and androgen receptor: risk factors of coronary heart disease in elderly men. *Chin Med Sci J.* 2010;25(1):44-49.
117. Adamkiewicz M, Zgliczyński S, Stowiliska-Srzednicka J, et al. The relationship between plasma androgens (dehydroepiandrosterone sulfate and testosterone) and coronary arteriosclerosis in men: the lower the androgens, the higher the coronary score of arteriosclerosis. *Aging Male.* 1999;2(1):22-32.
118. Alkamel A, Shafiee A, Jalali A, Boroumand M, Nozari Y. The association between premature coronary artery disease and level of testosterone in young adult males. *Arch Iran Med.* 2014;17(8): 545-550.
119. Wranicz JK, Cygankiewicz I, Kula P, et al. Endogenous estradiol and testosterone may predispose toward atherogenic lipid profile, but higher blood level of testosterone is associated with lower number of stenoses in the coronary arteries of men with coronary disease. *Int J Biomed Sci.* 2006;2(2):135-142.
120. Soisson V, Brailly-Tabard S, Helmer C, et al. A J-shaped association between plasma testosterone and risk of ischemic arterial event in elderly men: the French 3C cohort study. *Maturitas.* 2013;75(3):282-288.
121. Rosano GM, Leonardo F, Pagnotta P, et al. Acute anti-ischemic effect of testosterone in men with coronary artery disease. *Circulation.* 1999;99(13):1666-1670.
122. Mathur A, Malkin C, Saeed B, Muthusamy R, Jones TH, Channer K. Long-term benefits of testosterone replacement therapy on angina threshold and atheroma in men. *Eur J Endocrinol.* 2009;161(3):443-449.
123. Webb CM, McNeill JG, Hayward CS, de Zeigler D, Collins P. Effects of testosterone on coronary vasomotor regulation in men with coronary heart disease. *Circulation.* 1999;100(16): 1690-1696.
124. Baillargeon J, Urban RJ, Kuo YF, et al. Risk of myocardial infarction in older men receiving testosterone therapy. *Ann Pharmacother.* 2014;48(9):1138-1144.
125. Stergiopoulos K, Brennan JJ, Mathews R, Setaro JF, Kort S. Anabolic steroids, acute myocardial infarction and polycythemia: a case report and review of the literature. *Vasc Health Risk Manag.* 2008;4(6):1475-1480.

Downloaded from cpt.sagepub.com by guest on May 27, 2015

126. Smith AM, English KM, Malkin CJ, Jones RD, Jones TH, Channer KS. Testosterone does not adversely affect fibrinogen or tissue plasminogen activator (tPA) and plasminogen activator inhibitor-1 (PAI-1) levels in 46 men with chronic stable angina. *Eur J Endocrinol.* 2005;152(2):285-291.
127. Mirdamadi A, Garakyaraghi M, Pourmoghaddas A, Bahmani A, Mahmoudi H, Gharipour M. Beneficial effects of testosterone therapy on functional capacity, cardiovascular parameters, and quality of life in patients with congestive heart failure. *Biomed Res Int.* 2014;2014:392432.
128. Caminiti G, Volterrani M, Iellamo F, et al. Effect of long-acting testosterone treatment on functional exercise capacity, skeletal muscle performance, insulin resistance, and baroreflex sensitivity in elderly patients with chronic heart failure a double-blind, placebo-controlled, randomized study. *J Am Coll Cardiol.* 2009;54(10):919-927.
129. Malkin CJ, Pugh PJ, West JN, van Beek EJ, Jones TH, Channer KS. Testosterone therapy in men with moderate severity heart failure: a double-blind randomized placebo controlled trial. *Eur Heart J.* 2006;27(1):57-64.

Downloaded from cpt.sagepub.com by guest on May 27, 2015

เอกสารแนบหมายเลข 39

Review

227:2 R13–R30

Effects of fibroblast growth factor 21 on the heart

Pongpan Tanajak[1,2], Siriporn C Chattipakorn[1,3,4] and Nipon Chattipakorn[1,2,3]

[1]Cardiac Electrophysiology Research and Training Center, Faculty of Medicine, [2]Cardiac Electrophysiology Unit, Department of Physiology, Faculty of Medicine, [3]Center of Excellence in Cardiac Electrophysiology Research, and [4]Department of Oral Biology and Diagnostic Sciences, Faculty of Dentistry, Chiang Mai University, Chiang Mai 50200, Thailand

Correspondence should be addressed to N Chattipakorn
Email
ncchattip@gmail.com

Abstract

Fibroblast growth factor 21 (FGF21) is a novel polypeptide ligand that has been shown to be involved in several physiological and pathological processes including regulation of glucose and lipids as well as reduction of arteriosclerotic plaque formation in the great vessels. It has also been shown to exert cardioprotective effects in myocardial infarction, cardiac ischemia-reperfusion injury, cardiac hypertrophy and diabetic cardiomyopathy. Moreover, FGF21 protects the myocardium and great arteries by attenuating remodeling, inflammation, oxidative stress and also promoting the energy supply to the heart through fatty acid β-oxidation. This growing evidence emphasizes the important roles of FGF21 in cardioprotection. This review comprehensively summarizes and discusses the consistent and inconsistent findings regarding the beneficial effects of FGF21 on the heart available from both basic research and clinical reports. The details of the signaling, biological and pharmacological effects of FGF21 with regard to its protection of the heart are also presented and discussed in this review.

Key Words
- fibroblast growth factor 21
- myocardial injury
- cardiac metabolism
- oxidative stress

Journal of Endocrinology (2015) **227**, R13–R30

Journal of Endocrinology

Introduction

Fibroblast growth factors (FGFs) are polypeptide chains that have paracrine, autocrine or endocrine functions. The paracrine FGFs are further divided into five subfamilies, whereas the autocrine and endocrine FGFs are composed of one subfamily each (Itoh & Ornitz 2011, Itoh & Ohta 2013) (Fig. 1). FGFs act through cell surface FGF receptors (FGFRs), which are regulated by four types of genes including FGFR1, FGFR2, FGFR3 and FGFR4 (Mohammadi *et al.* 2005, Beenken & Mohammadi 2009, Goetz & Mohammadi 2013). Although FGFRs are essential for FGF action on the target cells, they cannot activate intracellular signaling without co-receptors (Kharitonenkov 2008). Previous studies show that heparan sulphate proteoglycans are essential co-receptors for paracrine and autocrine FGFs (Beenken & Mohammadi 2009, Goetz & Mohammadi 2013), whereas Klothos are essential co-receptors for endocrine FGFs to mediate their attachment to and activation of target FGFRs (Suzuki *et al.* 2008, Beenken & Mohammadi 2009, Goetz & Mohammadi 2013).

FGF21 is an endocrine FGF that consists of 209 amino acids. The FGF21 ligand is produced from several organs such as the liver and adipose tissue (Ito *et al.* 2000), skeletal muscle (Joki *et al.* 2015), and the heart (Nishimura *et al.* 2000, Kharitonenkov 2009, Planavila *et al.* 2013, Patel *et al.* 2014). To activate FGF21 signaling, FGF21 binds to FGFR1c with its C-terminus, and also with β-Klotho as its co-receptor with its N-terminus, to form the FGFR/β-Klotho complex (Kharitonenkov 2008, Suzuki *et al.* 2008, Yie *et al.* 2009, Ding *et al.* 2012, Hale *et al.* 2012).

http://joe.endocrinology-journals.org
DOI: 10.1530/JOE-15-0289

© 2015 Society for Endocrinology
Printed in Great Britain

Published by Bioscientifica Ltd.

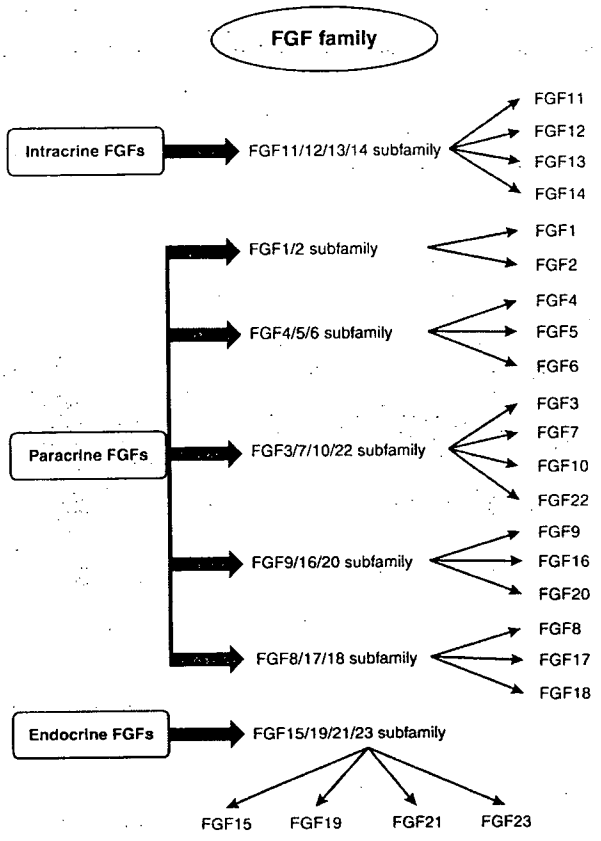


Figure 1
Fibroblast growth factors. FGFs have 22 members which can be divided into three classes and subdivided into seven subfamilies. Intracrine FGFs (11/12/13/14 subfamily); Paracrine FGFs (1/2 subfamily, 4/5/6 subfamily, 3/7/10/22 subfamily, 9/16/20 subfamily, and 8/17/18 subfamily); Endocrine FGFs (15/19/21/23 subfamily). Data from Itoh & Ohta (2013) and Itoh & Ornitz (2011).

The FGFR/β-Klotho complex then stimulates the autophosphorylation of the fibroblast receptor substrate 2 alpha (FRS2α), which is the first step in the downstream signaling of FGF21 (Kharitonenkov 2008, Suzuki *et al.* 2008). However, FGF21 is believed to have no action in physiological conditions since FGF21 knockout (FGF21-KO) mice were found to have normal development (Badman *et al.* 2009), and did not develop any pathological conditions such as insulin resistance (Hotta *et al.* 2009, Potthoff *et al.* 2009). Nevertheless, future studies are needed to evaluate this hypothesis.

FGF21 has been shown to play an important role in pathological processes, such as the regulation of plasma glucose level (Nishimura *et al.* 2000) and fatty acid β oxidation (FAO) which is the primary energy source for the myocardium (Vega *et al.* 2000, Planavila *et al.* 2013). Under stress conditions, FGF21 has been shown to reduce the apoptosis of Islet β cells (Wente *et al.* 2006), hepatocytes (Yu *et al.* 2015), vascular cells (Wu *et al.* 2014), cardiac endothelial cells (Lu *et al.* 2010) and cardiomyocytes (Cong *et al.* 2013, Liu *et al.* 2013). Interestingly, FGF21 also protects the heart from apoptosis and remodeling through the activation of adiponectin release to activate the adiponectin signaling pathways (Joki *et al.* 2015). Currently, the biological and pharmacological mechanism of FGF21 in cardioprotection is still to be elucidated. This review will focus on the effects of FGF21 and its roles in the heart. The consistent and inconsistent findings regarding the beneficial effects of FGF21 in the heart available from both basic research and clinical reports are comprehensively summarized and discussed. The details of the signaling, biological and pharmacological effects of FGF21 with regards to its protection of the heart are also presented and discussed in this review.

Effects of FGF21 on the heart

FGF21 is synthesized and expressed in the heart by cardiomyocytes (Planavila *et al.* 2013) and cardiac microvascular endothelial cells (CMECs) (Lu *et al.* 2010). A previous study demonstrated that cardiomyocytes secrete FGF21 into the media culture in basal conditions at a rate of ~0.05 ng/ml per 24 h (Planavila *et al.* 2013). In the heart, FGF21 ligands act via the FGFR1c (Suzuki *et al.* 2008, Liu *et al.* 2013, Planavila *et al.* 2013, Wu *et al.* 2014), and FGFR3 (Suzuki *et al.* 2008, Liu *et al.* 2013), utilizing β-Klotho as a co-receptor (Suzuki *et al.* 2008, Liu *et al.* 2013, Planavila *et al.* 2013). Endogenous and exogenous FGF21 plays an anti-apoptotic role in both *in vitro* and *in vivo* models, partially through the adiponectin signaling cascade (Joki *et al.* 2015). Recent studies found that FGF21 protects against isoproterenol (ISO) induced cardiac hypertrophy by activating anti-oxidative pathways (Planavila *et al.* 2013, 2014) and promoting FAO (Planavila *et al.* 2013). FGF21 also protects the heart from ischemic reperfusion (I/R) injury and myocardial infarction (MI) by activating several survival pathways (Cong *et al.* 2013, Liu *et al.* 2013, Patel *et al.* 2014). Moreover, FGF21 deficiency accelerated the development of diabetic cardiomyopathy (DCM) (Yan *et al.* 2015). In contrast, FGF21 administration also prevents lipotoxicity and diabetes induced cardiac apoptosis in DCM (Zhang *et al.* 2015a).

Interestingly, Liu and colleague demonstrated that the endogenous FGF21 which acted as endocrine protection in the ischemic myocardium was not from the heart but from the liver and adipose tissue (Liu *et al.* 2013),

http://joe.endocrinology-journals.org
DOI: 10.1530/JOE-15-0289
© 2015 Society for Endocrinology
Printed in Great Britain
Published by Bioscientifica Ltd.

Journal of Endocrinology

indicating that the major endogenous FGF21 proteins which preserve cardiac function are from the liver and adipose tissues. Although FGF21 from cardiomyocytes is not a major source, previous studies demonstrated that the autocrine action of FGF21 from cardiomyocytes is essential and could protect the heart from pathological conditions such as cardiomyocyte hypertrophy and I/R injury (Planavila *et al.* 2013, 2014).

Effects of FGF21 on myocyte apoptosis and myocardial infarction

Myocardial ischemia and I/R injury induce cell apoptosis and MI, leading to an impairment in cardiac function. Growing evidence from both *in vitro* and *in vivo* studies demonstrate that exogenous FGF21 protected the cardiomyocytes from apoptosis and MI, and improved cardiac function through activating the PI3K-Akt1-BAD pathway in FGF21-KO mice (Liu *et al.* 2013), and Akt-GSK3β-caspase 3 dependent pathways in H9c2 cell lines (Cong *et al.* 2013), resulting in the suppression of caspase 3 induced apoptosis. It was proposed that the activation of these pathways would lead to a decrease in the myocardial infarct area and increase cardiac function (Liu *et al.* 2013, Patel *et al.* 2014).

Evidence regarding the effects of FGF21 on inhibiting cardiovascular cell apoptosis in *in vitro* models is summarized in Table 1. FGF21 protects H9c2 cells from I/R injury in a dose dependent manner by promoting the energy supply, and reducing inflammation and apoptosis through the Akt-GSK3β pathway (Cong *et al.* 2013). On other hand, a previous study found peroxisome proliferator activated receptor alpha (PPARα) activation led to the synthesis and release of FGF21. FGF21 was released into the culture media, and protected the CMECs from lipotoxicity induced by Ox-LDL by decreasing DNA fragmentation in an autocrine manner (Lu *et al.* 2010). In an *ex vivo* model of global cardiac ischemia, it has been shown that recombinant rat FGF21 infusion 10 min prior to ischemia can protect the heart from I/R injury by decreasing MI and increasing the cardiac function through activation of the MAPK-PI3k-Akt signaling pathway (Patel *et al.* 2014). Moreover, FGF21 prevented oxidative stress (Cong *et al.* 2013, Planavila *et al.* 2014), and also increased the energy supply for cardiomyocytes in H9c2 cell lines under I/R injury conditions (Cong *et al.* 2013).

In addition to *in vitro* reports, evidence regarding the effects of FGF21 on cell apoptosis and myocardial infarction in *in vivo* models is summarized in Table 2. In FGF21-KO mice, FGF21 given intravenously at 50 ng/g per day for 3 days with the first dose being given immediately after I/R injury (I=30 min, R=1–30 days), had been shown to protect the heart from apoptosis, MI, and also increase cardiac function through activation of the FGFR1/β-Klotho-PI3K-Akt1-BAD signaling cascade (Liu *et al.* 2013). The acute MI in C57BL/6 mice showed that an i.v. injection of Recombinant mouse FGF21 10 ng/g in a single dose immediately post MI, which was caused by a left anterior descending coronary artery ligation, decreased the infarction area. It was also shown that these protective effects could be reversed by SiRNA-FGF21 intravenously injected 1 day prior to MI (Liu *et al.* 2012). Moreover, in chronic MI (2 weeks) C57BL6 and adiponectin-KO mice models it was demonstrated that FGF21 protein derived from skeletal muscles protected the heart from apoptosis through adiponectin signaling (Joki *et al.* 2015). In addition, FGF21 100 μg/kg per day s.c. injections for 4 weeks could protect the abdominal aorta from arteriosclerotic lesions through lipid regulation and ER stress induced vascular cell apoptosis in the ApoE-KO model (Wu *et al.* 2014).

All of these findings indicate that exogenous and endogenous FGF21 play an important role in protecting the heart from apoptosis via several pathways including PI3K-Akt1-BAD and Akt-GSK3β-caspase 3 dependent mechanisms, leading to decreased infarction and increased left ventricular function under I/R injury, lipotoxic and MI conditions.

Molecular basis of anti-apoptosis signaling cascades of FGF21

The anti-apoptotic signaling cascade of FGF21 from in *in vitro* and in *in vivo* models previously mentioned are summarized in Fig. 2. After FGF21 binding to FGFR1 and β-klotho via its N-terminus and C-terminus, respectively, the FGF21 ligand induces dimerization of receptors, and the autophosphorylation of tyrosine kinase recruits and phosphorylates FRS2α. In later steps, the anti-apoptotic signaling pathways in cardiomyocytes could be activated through 4 major survival pathways, including Erk1/2, RORα, PI3k-Akt and AMPK signaling pathways. Currently, the downstream signaling proteins involved in these processes are still unclear (Patel *et al.* 2014).

Previous studies demonstrated that the downstream signaling cascades of FGF21 begin with the autophosphorylation of the receptor after the binding of FGF21. This leads to the phosphorylation of FRS2α, and subsequent activation of PI3K (Liu *et al.* 2013, Patel *et al.* 2014, Yu *et al.* 2015) following its phosphorylation at Serin458

http://joe.endocrinology-journals.org
DOI: 10.1530/JOE-15-0289
© 2015 Society for Endocrinology
Printed in Great Britain
Published by Bioscientifica Ltd.

Journal of Endocrinology

http://joe.endocrinology-journals.org
DOI: 10.1530/JOE-15-0289

© 2015 Society for Endocrinology
Printed in Great Britain

Published by Bioscientifica Ltd.

Table 1 Effects of FGF21 on apoptosis in cardiomyocytes and endothelial cells

Model	Methods	Dose	Results	Interpretation	References
H9c2 cells (rat cardiomyocytes)	I/R injury ($I=3$ h, $R=1$, 3, 6 h)	FGF21 0.25, 0.5, 1, 1.5, 2, 4, 5, 6, 7, 8 μg/ml applied immediately at reperfusion	↑ Cell viability (dose-dependent) ↑ pAkt, GSK3β ↑ ATP synthase-α, Energy supply ↓ Apoptosis ↓ Cleaved caspase-3/pro-caspase 3 ratio ↓ TNFα, PAI1 ↓ H_2O_2 damaged cells	FGF21 protects H9c2 cells from I/R injury by promoting the energy supply, and reducing inflammation and apoptosis in cardiomyocytes through Akt-GSK3β pathway in a dose-dependent manner.	Cong *et al.* (2013)
CMECs	Lipotoxicity induced by Ox-LDL50 or 100 μg/ml 37 °C for 12 h	Bezafibrate (PPAR-α ligand) 50, 100, 200 μmol/l for 12 h, Transfected with shRNA-FGF21 vector	PPAR-α ligand 200 μmol/l ↑ Culture media FGF21 concentration ↓ DNA fragmentation shRNA-FGF21 transfection ↑ DNA fragmentation ↓ Culture media FGF21 concentration	PPAR-α activation increases FGF21 synthesis and release into culture media and protects the CMECs from lipotoxicity.	Lu *et al.* (2010)
Male wistar rats	I/R injury; *ex vivo* (I: 30 min, R: 120 min)	Rr FGF21 100 nM (in normal tyrodes solution) infusion 10 min prior to ischemia	↑ Rate pressure production ↑ ±dp/dt ↑ MAPK-PI3k-Akt signaling ↓ Total infarct size, LVDP	FGF21 increases cardiac function and decreases infarct size due to I/R injury through the activation of MAPK-PI3k-Akt signaling.	Patel *et al.* (2014)

I/R, ischemic reperfusion; GSK3β, glycogen synthase kinase 3β; TNF α, tumor necrosis factors alpha; PAI 1, plasminogen activator inhibitor 1; CMECs, Cultured cardiac micro vascular endothelial cells; OX-LDL, oxidized low density lipoprotein; PPARα, Peroxisome proliferator-activated receptor alpha; PGC1α, PPARγ coactivated 1 alpha; Rr, recombinant rats; LVDP, left ventricular diastolic pressure; MAPK, AMP-activated protein kinase; PI3K, phosphatidylinositol 3 kinase.

http://joe.endocrinology-journals.org
DOI: 10.1530/JOE-15-0289

© 2015 Society for Endocrinology
Printed in Great Britain

Published by Bioscientifica Ltd.

Table 2 Effects of FGF21 on myocardial infarction and apoptosis in *in vivo* models

Model	Methods	Dose	Results	Interpretation	References
FGF21-KO mice	I/R injury (I=30 min, R=1, 3, 5, 10, 20, 30 days)	FGF21 50 ng/g per day, i.v. immediately after myocardial injury, and for the next 3 days	↑ ± dp/dt, %FS ↑ FGF21 sensitivity ↓ Apoptosis, MI ↑ FGFR1/β-Klotho–PI3K–Akt1–BAD signaling	FGF21 decreases cellular apoptosis and increases cardiac function due to I/R injury through an activation of FGFR1/β-Klotho–PI3K–Akt1–BAD signaling.	Liu *et al.* (2013)
ApoE$^{-/-}$ mice	Abdominal aortic (AA) arteriosclerosis for 4 weeks	FGF21 100 μg/kg per day, s.c. injection for 4 weeks	↑ AA luminar diameter ↓ Arteriosclerotic lesion area ↓ TC, TG ↓ Cleaved caspase 12, CHOP, GRP94 ↓ Apoptotic rate	FGF21 protects the AA from arteriosclerotic lesion through lipid regulation and ER stress induced by vascular cell apoptosis.	Wu *et al.* (2014)
C57BL/6 mice	MI for 24 h	At MI, RmFGF21 10 ng/g, i.v. injection	↑ Infarct size by siRNA-FGF21 ↓ Infarct size by FGF211	FGF21 protects heart from acute MI by decreasing myocardial infarct area	Liu *et al.* (2012)
C57BL6, adiponectin-KO mice	Chronic MI (2 weeks)	Ad-FGF21 1×10^{-9} pfu/mouse, i.m. injection 3 days prior to MI	↑ Capillary density (CD31) ↑ Cardiac function ↓ TNFα, IL6 mRNA Reversed by adiponectin-KO	FGF21 protein was derived from skeletal muscle and protects the heart from apoptosis through adiponectin signaling.	Joki *et al.* (2015)

FGF21-KO, FGF21 knockout; ApoE$^{-/-}$, apolioprotein E knockout; I/R, ischemic reperfusion; MI, myocardial ischemia; Rm, Recombinant mouse; i.v., intravenous; PI3K, phosphatidylinositol 3 kinase; BAD, BCL2 antagonist of cell death; AA, Abdominal aortic; TC, total cholesterol; TG, triglyceride; CHOP, C/EBP homologous protein; GRP94, glucose-regulated proteins 94; ER, endoplasmic reticulum; LVDP, left ventricular diastolic pressure; MAPK, AMP-activated protein kinase.

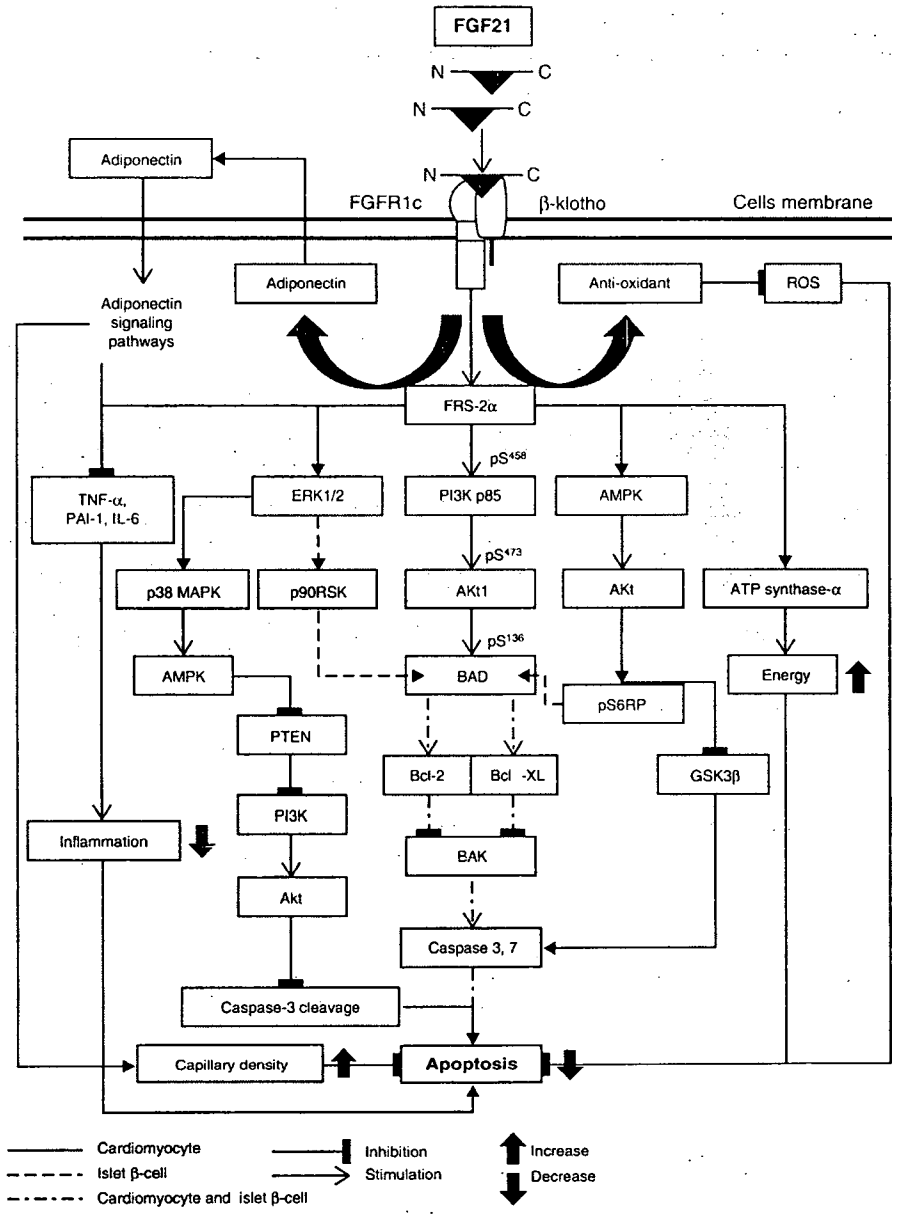


Figure 2
FGF21 signaling cascade in anti-apoptotic effects. FGF21 exerts anti-apoptotic effects in cardiomyocytes through decreased inflammation, improved FAO metabolism, increased capillary density and anti-oxidative stress. FGF21, Fibroblast growth factors 21; FGFR1c, Fibroblast growth factors receptors 1c; N, N-terminus residue of FGF21 or Amino acid terminal; C, C-terminus residue of FGF21 or Carboxylic terminal; FRS2α, Fibroblast growth factors substrate 2α; ROR, Retinoic acid receptor-related receptor; Erk1/2, Extracellular signal-regulated kinases 1/2; p90RSK, p90 ribosomal s6 kinase; pS6RP, pS6 ribosomal protein; AMPK, AMP dependent protein kinase; PI3K P85, Phosphatidylinositide-3 kinase P85; GSK3β, Glycogen synthase kinase-3b; BAD, BCL2 antagonist of cell death; BCL2, B cell lymphoma 2; BCL-XL, B cell lymphoma-extra-large; BAX, Bcl2 associated X protein; BAK, Bcl2 homologous antagonist killer; TNFα, tumor necrosis factors α; IL6, interleukin 6; PAI1, plasminogen activator inhibitor 1.

(pS^{458}). This leads to the recruitment and phosphorylation of a secondary messenger Akt1 by phosphorylation at Serine473 (pS^{473}). Akt1 in turn activates the BCL2 antagonist of cell death (BAD) by inducing the phosphorylation of BAD at Serine136 (pS^{136}). his causes BCL2 and BCL-XL to inhibit BAX and BAK induced caspase3/7 activity, which leads to decreased apoptosis in cardiomyocytes (Liu *et al.* 2013). In addition, FGF21 has

http://joe.endocrinology-journals.org
DOI: 10.1530/JOE-15-0289
© 2015 Society for Endocrinology
Printed in Great Britain
Published by Bioscientifica Ltd.

Journal of Endocrinology

been shown to inhibit apoptosis through another alternative pathway by activating Akt, thereby inhibiting GSK3β, thus leading to decreased caspase 3 activity (Akt-GSK3β-caspase 3 dependent pathways) (Cong *et al.* 2013) (Fig. 2). Moreover, FGF21 can protect the heart from apoptosis by activation of the Erk1/2-p38 MAPK-AMPK survival pathway (Zhang *et al.* 2015a). Evidence from these reports confirmed that FGF21 plays a critical role in myocardial protection and anti-apoptosis following myocardial injury (Patel *et al.* 2014, Joki *et al.* 2015, Zhang *et al.* 2015*a*).

Due to the potential cardioprotective benefits of FGF21, it is possible that FGF21 could be used to prevent and/or treat the myocardial apoptosis due to I/R injury or MI. However, evidence related to the roles of the time course of FGF21 administration and its beneficial effects to the pathological heart are still lacking.

Effects of FGF21 on cardiac hypertrophy and adverse cardiac remodeling

Myocardial ischemia resulting from coronary artery disease (CAD) is the primary cause of MI which could impair cardiac function by reducing the ejection fraction (EF), leading to insufficient oxygen supply to body tissues (Gheorghiade & Bonow 1998, Joki *et al.* 2015). This contributes to progression to cardiac hypertrophy and heart failure due to the compensatory mechanisms of the circulatory system to maintain the EF and carry oxygen to peripheral metabolic tissues, known as cardiac remodeling. This long-term maladaptive remodeling can cause increased ventricular hypertrophy, ventricular dilatation, interstitial growth and cardiac fibrosis (Neely *et al.* 1972).

Evidence regarding the effects of FGF21 on protection against adverse cardiac remodeling and hypertrophy in *in vitro* and *in vivo* models is summarized in Table 3. In a single *in vitro* study, pre-treatment with FGF21 protects neonatal cardiomyocytes (NCMs) from phenylephrine induced hypertrophy by promoting FAO gene expression, attenuating inflammation and oxidative stress through the activation of Sirt1 and Erk1/2-CREB signaling pathways (Planavila *et al.* 2013). This study also demonstrated that the Sirt1-PPARα pathway plays an important role in the control of FGF21 expression in the heart.

Evidence from *in vivo* studies demonstrate that continuous administration of ISO via s.c. infusion for 7 days in FGF21-KO mice induced cardiomyopathy and led to MI, impaired cardiac metabolism and loss of cardiac function in the rat heart (Heather *et al.* 2009, Planavila *et al.* 2013). Interestingly, the endocrine function of FGF21 derived from skeletal muscles attenuated cardiac hypertrophy, and reversed the adverse cardiac remodeling process, leading to improved left ventricular function in this chronic MI mice model (Joki *et al.* 2015). In FGF21-KO mice, it has been shown that FGF21 attenuated cardiac hypertrophy by decreasing hypertrophic markers including atrial natriuretic factor (ANF) and α skeletal actin (αSKA) (Planavila *et al.* 2013). Moreover, FGF21 decreased the heart weight/body weight ratio and cardiomyocytes area, and also improved cardiac function (Planavila *et al.* 2013, 2014).

In summary, the protective effects of FGF21 against cardiac hypertrophic damage have been evidenced. Conversely, FGF21 deficiency was found to enhance the induction of cardiac hypertrophy by promoting pro-inflammatory pathways, oxidative stress, cardiac fibrosis and impairing cardiac metabolism (Planavila *et al.* 2013, 2014). Results confirmed that cardiac FGF21 has an impact on activation of the autocrine loop and plays a protective role against cardiac hypertrophy and remodeling. However, further investigation and clinical studies are needed to warrant the usefulness of FGF21 against cardiac hypertrophy.

Molecular basis of anti-hypertrophic signaling cascades of FGF21

The FGF21 activates cells to autocrine function by binding to FGFR1 on the cell membrane, using β-Klotho as a co receptor. This event activates the dimerization of the receptor and causes autophosphorylation of tyrosine kinase. Tyrosine kinase then recruits and phosphorylates FRS2α. The FRS2α in turn affects four primary pathways, which in turn leads to the attenuation of cardiac hypertrophy. An illustrated diagram of the anti-hypertrophic effects of FGF21 in both the autocrine and endocrine manner by the loop autocrine function of FGF21 through the Sirt1/PPARα pathway is shown in Fig. 3.

The first of these four pathways is the activation of the Erk1/2-CREB-Sirt1-PGC1α signaling pathway as an autocrine function and autocrine loop regulation in FGF21-KO cardiomyocytes. This pathway leads to increased mitochondrial FAO enzyme genes expression including MCAD and mcpt1α, indicating increased cardiac mitochondrial FAO (Planavila *et al.* 2013). The second pathway involves the inhibition of the translocation of pro-inflammatory cytokines NFkβ into the nucleus to activate inflammatory cytokine expression including TNFα, IL6, and MCP1, resulting in a decrease in the

http://joe.endocrinology-journals.org
DOI: 10.1530/JOE-15-0289
© 2015 Society for Endocrinology
Printed in Great Britain
Published by Bioscientifica Ltd.

Journal of Endocrinology

http://joe.endocrinology-journals.org
DOI: 10.1530/JOE-15-0289

© 2015 Society for Endocrinology
Printed in Great Britain

Published by Bioscientifica Ltd.

Table 3 Effects of FGF21 on cardiac hypertrophy and remodeling

Model	Methods	Dose	Results	Interpretation	References
FGF21-KO mice	Cardiac hypertrophy induced by ISO 15 mg/kg per day for 7 days via s.c. Osmotic pump	FGF21 2.5 μg/kg per day, s.c. for 7 days	↓ HW/BW, cardiomyocyte area ↓ ANF, IL6 mRNA and protein ↓ αSKA mRNA ↑ PGC1α, MCAD, mcpt1α	FGF21 protects heart from ISO induced cardiac hypertrophy via promoting FAO gene expression, and reducing inflammation.	Planavila *et al.* (2013)
FGF21-KO mice	Cardiac hypertrophy induced by ISO	ISO 15 mg/kg per day, s.c. for 7 days	In FGF21-KO mice ↓ Antioxidant genes ↑ ROS production ↓ Aconitase activity ↑ Protein carbonyl	FGF21 protects heart from ISO induced cardiac hypertrophy through an anti-oxidative stress mechanism.	Planavila *et al.* (2014)
C57BL6 and adiponectin-KO mice	Chronic MI (2 weeks)	Ad-FGF21 1× 10^{-9} pfu/mouse i.m. injection 3 days prior MI	↑ Capillary density (CD31) ↑ Cardiac function ↓ Cardiac hypertrophy ↓ Apoptosis ↓ TNFα, IL6 mRNA – Reversed by adiponectin-KO	FGF21 protein was derived from skeletal muscle, it protects the heart by attenuating cardiac remodeling in chronic MI.	Joki *et al.* (2015)
NCMs	Cardiomyocyte hypertrophy induced by PE	FGF21 pre-treatment (5 nM) for 24 h	↑ PGC1α, mcpt1α genes ↑ pErk1/2, pCREB ↑ FGF21 mRNA and protein levels by Sirt1 overexpression ↓ ROS production ↓ NFKB activity, IL6 ↓ ANF, αSKA ↓ Cardiomyocyte area ↓ FGF21mRNA expression in PPARα-KO	FGF21 protects NCMs from PE induced hypertrophy by promoting FAO gene expression, attenuating inflammation and oxidative stress through the activation of Sirt1 and Erk1/2-CREP signaling pathways.	Planavila *et al.* (2013)

FGF21-KO, FGF21 knockout; ANF, atrial natriuretic factor; αSKA, alpha skeletal actin; IL6, interleukin 6; PGC1α, PPARγ coactivated 1 alpha; MCAD, medium chain acetyl CoA dehydrogenase; mcpt1α, mitochondrial carnitine palmitoyltransferase 1; ISO, isoproterenol; LPS, lipopolysaccharide; ROS, reactive oxygen species; pfu, plaque-forming units; i.m., intramuscular; TNFα, TNFα tumor necrosis factor alpha; NCMs, neonatal cardiomyocytes; ROS, reactive oxygen species; NFkB, nuclear factor kappa beta; IL6, interleukin 6; PE, phenylephrine; PPARα, Peroxisome proliferator-activated receptor alpha; FAO, fatty acid oxidation; Sirt1, Sirtuin 1; Erk1/2, Extracellular signal-regulated kinases 1/2; CREB, cAMP response element-binding protein.

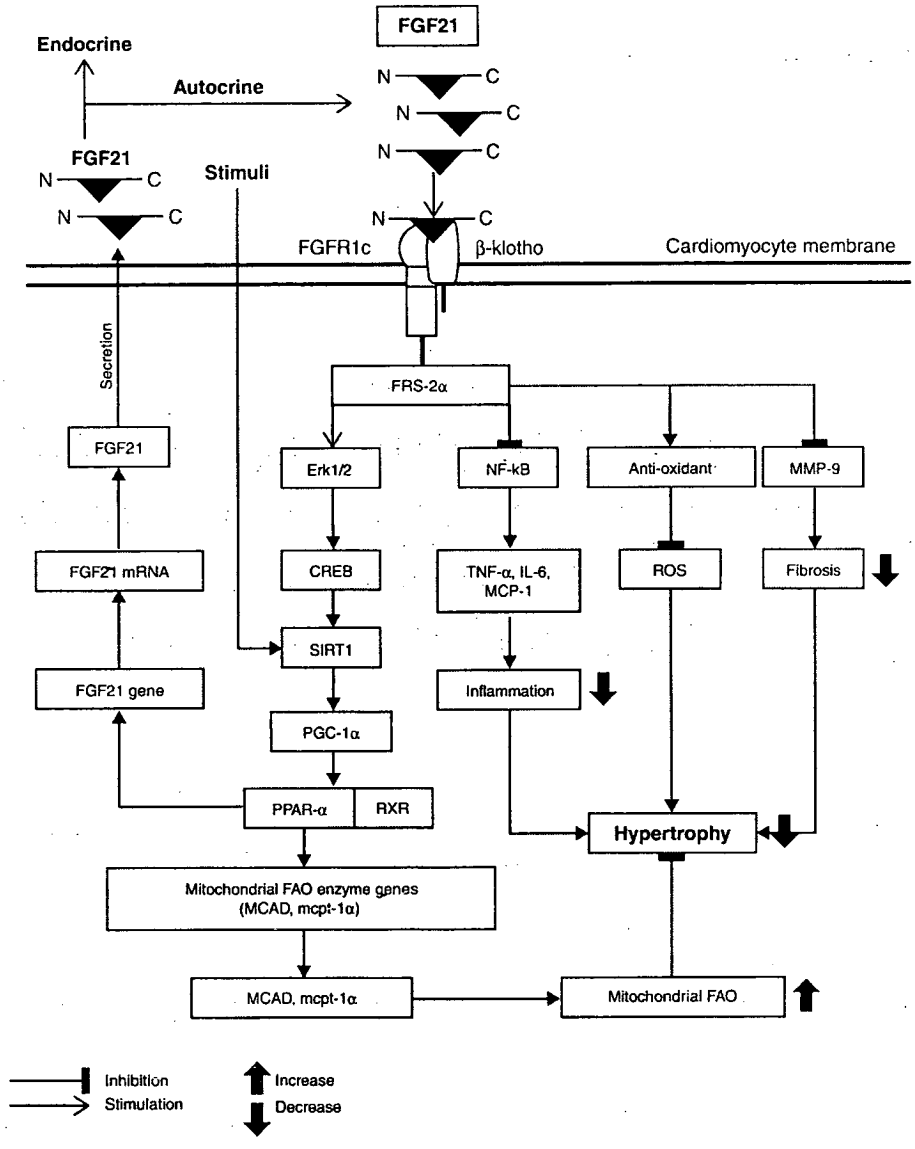


Figure 3
FGF21 signaling cascade in anti-hypertrophic effects of FGF21. FGF21 exerts anti-hypertrophic effects in autocrine and endocrine manners by loop autocrine function through the Sirt1/PPARα pathway. FAO, fatty acid β oxidation; PGC1α, peroxisome proliferator-activated receptor 1γ coactivator 1α; NFkB, nuclear factor Keppa B; SIRT1, sirtuin1; FGF21, fibroblast growth factors 21; FGFR1, fibroblast growth factors receptors 1; PPARα, peroxisome proliferator activated receptor α; MCAD, medium-chain acyl-CoA dehydrogenase; mcpt 1α, carnitine palmitoyltransferase Iα; Erk1/2, extracellular-signal-regulated kinases 1/2; CREB, cAMP response element-binding protein; RXR, retinoid X receptor; TNFα, tumour necrosis factors α; IL6, interleukin 6; MCP1, monocyte chemoattractant protein 1; MMP9, matrix metallopeptidase 9.

inflammatory processes (Planavila *et al.* 2013). The third pathway involves the inhibition of cardiac MMP9, which indicates a decrease in cardiac fibrotic formation following cardiac remodeling (Planavila *et al.* 2013). Finally, FGF21 activates the anti-oxidative pathway, resulting in the reduction of oxidative stress in the cells (Planavila *et al.* 2013, 2014).

FGF21 protects the heart from diabetes induced cardiomyopathy

Evidence regarding the protection of the heart from diabetes induced cardiomyopathy by FGF21 is summarized in Table 4. In FGF21 deficient mice, it has been shown that FGF21 is essential in the prevention of the

© 2015 Society for Endocrinology
Printed in Great Britain
Published by Bioscientifica Ltd.

Journal of Endocrinology

http://joe.endocrinology-journals.org
DOI: 10.1530/JOE-15-0289

© 2015 Society for Endocrinology
Printed in Great Britain

Published by Bioscientifica Ltd.

Table 4 Protective effects of FGF21 on the heart from diabetes induced cardiomyopathy

Model	Methods	Dose	Results	Interpretation	References
FGF21-KO mice	T1DM was induced by STZ 60 mg/kg once a day via i.p. injection for 6 days	–	↑ Blood glucose, TG ↑ Cardiac Nrf2 and CD36 ↑ Cardiac 3NT and 4HNE ↑ Cardiac TG ↑ Cardiac lipid accumulation ↑ Cardiac collagen accumulation ↑ Cardiac CTGF ↓ Cardiac PGC1α ↓ %EF, %FS	FGF21 deficiency up-regulation of Nrf2 driven CD36 expression exacerbates cardiac lipid uptake and accumulation, oxidative stress, impairs cardiac lipid and glucose utilization, leading to acceleration of the development of DCM.	Yan *et al.* (2015)
FGF21-KO and WT mice	NEFA 0.1 g/10 g, i.p. injection T1DM was induced by STZ	FGF21 100 μg/kg per day for 10 days, i.p. injection	↑ Cardiac function ↓ Blood glucose, plasma TAG ↓ Cleaved caspase 3 ↓ Apoptosis ↓ Collagen contents	FGF21 protects the heart from lipotoxicity and diabetes induced apoptosis through activation of the Erk1/2-p38MAPK-AMPK signaling pathway.	Zhang *et al.* (2015*a*,*b*)
H9C2 cells and cardiomyocytes	Pre-treated with pharmaceutical inhibitors or specific small interfering (si) RNAs against Erk1/2, p38MAPK, AMPK, PTEN and pPTEN	FGF21 50 ng/ml, followed palmitate treatment for 15 min	↑ Erk1/2-p38MAPK-AMPK signaling pathway ↓ tPTEN, pPTEN ↓ Apoptosis		

FGF21-KO, FGF21 knockout; T1DM, type 1 diabetes mellitus; STZ, streptozotocin; i.p., intraperitoneal; TG, triglyceride; Nrf2, nuclear factor (erythroid-derived 2)-like 2; 3NT, 3 nitrotyrosine; 4HNE, 4 hydroxynonenal; CTGF, connective tissue growth factor; PGC1α, peroxisome proliferator-activated receptor gamma co-activator 1α; %EF, percent ejection fraction; % FS, percent fractional shortening; DCM, diabetic cardiomyopathy; NEFA, non esterified fatty acid.

progression of T1DM induced cardiomyopathy (Yan *et al.* 2015). It has been proposed that four potential mechanisms are responsible for this adverse effect due to FGF21 deficiency. First, increased cardiac oxidative stress was observed, as shown by increased 3 nitrotyrosine (3NT) and 4 hydroxynonenal (4HNE). Second, increased nuclear factor (erythroid derived 2) like 2 (Nrf2) activated CD36 expression was seen, which led to increased plasma lipid uptake and accumulation into the cells. Third, decreased PGC1α protein expression was observed, which led to decreased FAO thus promoting lipid uptake and accumulation in cardiomyocytes via the CD36 receptor on the cell membranes. Fourth, increased myocardial collagen accumulation was observed as shown by increased connective tissue growth factor (CTGF). In contrast, FGF21 administration can protect the heart from lipotoxicity and diabetes induced cardiac apoptosis by the activating of the Erk1/2-p38 MAPK-AMPK survival pathway leading to decreased cardiac apoptosis and improved cardiac function (Zhang *et al.* 2015a). An illustrated diagram of these mechanisms is shown in Fig. 4. It has been proposed that these four potential mechanisms cause left ventricular dysfunction and accelerate the development and progression of DCM (Yan *et al.* 2015) and the effects can be reversed by FGF21 treatment (Zhang *et al.* 2015a).

FGF21 regulates energy supply in the heart

FAO is the major source of energy for cardiomyocytes, generating 50–70% of ATP in a normal adult heart, while only 20–30% of energy is released by glycolysis, and <5% from other sources (Neely *et al.* 1972, Neely & Morgan 1974). It has been shown that the transition from fetal glycolysis (fetal pattern) to FAO in the neonatal stage (Lockwood & Bailey 1970, Kelly *et al.* 1989) is brought about by increased PGC1α, PPARα, and FGF21 mRNA expression (Planavila *et al.* 2013). In contrast, the chicken ovalbumin upstream promoter transcription factor (COUP-TF) that regulates glycolysis is down regulated (Sack *et al.* 1997). PPARα is expressed at a high rate in mitochondrial FAO tissue, and is situated on the nuclear membrane with the retinoid X receptor (RXR). PGC1α binding to the PPARα/RXR on the nuclear membrane leads to the increased expression of FAO genes including MCAD and mcpt1α, hence promoting increased FAO and synthesis of the ATP supply for the heart in physiological conditions (Vega *et al.* 2000) (Fig. 5A).

Under pathological conditions such as cardiac hypertrophy, myocardium FAO enzyme genes are down regulated (Sack *et al.* 1997, Razeghi *et al.* 2001), while the COUP-TF is up regulated (Sack *et al.* 1997). This caused the switch of the energy source back to the fetal glycolysis pattern again (Fig. 5B). A recent study demonstrated that myocardium PGC1α, MCAD, and mcpt1α mRNA expression is regulated by FGF21 to promote FAO for the energy supply to the heart (Planavila *et al.* 2013). The deletion of FGF21 has been shown to increase CD36 and decrease PGC1α, leading to acceleration of DCM through aggravating cardiac lipid accumulation (Yan *et al.* 2015). Therefore, FGF21 might be beneficial as a pharmacological intervention under these conditions. Further studies are needed to give more evidence for the substantiation to this hypothesis.

Molecular basis of the antioxidant signaling cascade of FGF21 in cardiomyocytes

Previous studies demonstrated that following ISO induced cardiac hypertrophy by causing cardiac oxidative stress and inflammation, and that FGF21 was secreted from cardiomyocytes via Sirt1 activation. Sirt1 was found to stimulate FGF21mRNA and protein expression and secretion into the circulation, where FGF21 proceeded to act in a paracrine, autocrine and endocrine manner. n the autocrine loop function, FGF21 induces anti-oxidant gene expression through the Erk/Sirt1 pathway, including uncoupling protein 3 (UCP3), superoxide dismutase 2 (Sod 2), peroxiredoxin 5 (Prdx5), glutathione peroxidase 1 (GPX1), Catalase (CAT) and Sequestosome 1 (Sqstm1), resulting in a reduction in cardiac tissue injury (Planavila *et al.* 2014). Furthermore, FGF21 has been shown to activate the Nrf2 pathway in hepatocytes, which was found to lead to increased anti-oxidant gene expression, resulting in the reduction of liver tissue injury (Yu *et al.* 2015) (Fig. 6).

The stimulation of antioxidative pathways by FGF21 led to an increase in antioxidative gene and enzyme expression, and prevented oxidative stress by decreasing ROS production in cardiomocytes. Therefore, this protected the myocardium (Planavila *et al.* 2014) from oxidative stress and subsequent injury. Interestingly, a clinical study demonstrated that FGF21, UCP3, and Sod2 levels were increased in dilated cardiomyopathy patients in the final stages of heart failure (Planavila *et al.* 2014). This indicated that FGF21 could protect the cardiomyocytes or slow down the degree of damage following oxidative stress in a failing human heart.

http://joe.endocrinology-journals.org
DOI: 10.1530/JOE-15-0289
© 2015 Society for Endocrinology
Printed in Great Britain
Published by Bioscientifica Ltd.

Journal of Endocrinology

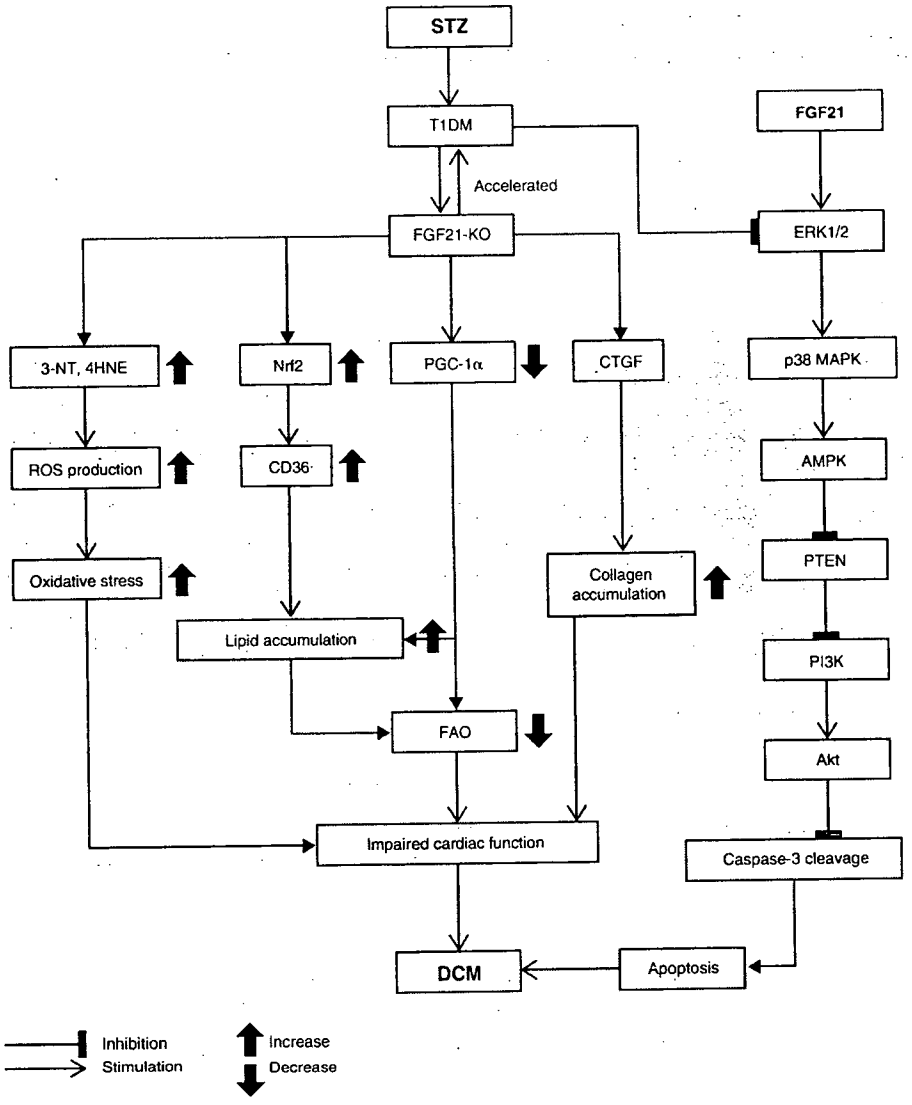


Figure 4
FGF21 protects the heart from diabetes induced cardiomyopathy. STZ, streptozotocin; T1DM, type 1 diabetes mellitus; FGF21-KO, FGF21 knock-out; Nrf2, nuclear factor (erythroid-derived 2)-like 2; 3NT, 3 nitrotyrosine; 4HNE, 4 hydroxynonenal; CTGF, connective tissue growth factor; PGC1α, peroxisome proliferator activated receptor gamma co-activator 1α; TG, triglyceride; FAO, fatty β acid oxidation; DCM, diabetic cardiomyopathy; Erk, extracellular signal-regulated kinase; p38 MAPK, mitogen-activated protein kinase 14; PTEN, phosphatase and tensin homologue; PI3K, phosphatidylinositol 3-kinase. Data from Yan *et al.* 2015, Zhang *et al.* 2015*a*.

It has been shown that these signaling pathways of FGF21 have the crosstalk at the secondary messenger levels such as ERK1/2 for anti-apoptosis (Zhang *et al.* 2015*a*), anti-hypertrophic (Planavila *et al.* 2013, 2014), and anti-oxidative stress (Yu *et al.* 2015) in the heart. Activation of FGFR/β-Klotho complex therefore could activate these effects of FGF21 simultaneously at this crosstalk. However, further studies are needed to investigate this issue.

Clinical evidence of the association between FGF21 and cardiovascular alteration

Evidence regarding the correlation of plasma FGF21 with cardiovascular alteration in clinical reports are summarized in Table 5. Serum FGF21 levels have been shown to have a strong correlation with waist circumference, systolic blood pressure, lower extremity arteriosclerotic disease (Zhang *et al.* 2015*b*) and carotid intima

http://joe.endocrinology-journals.org
DOI: 10.1530/JOE-15-0289
© 2015 Society for Endocrinology
Printed in Great Britain
Published by Bioscientifica Ltd.

Journal of Endocrinology

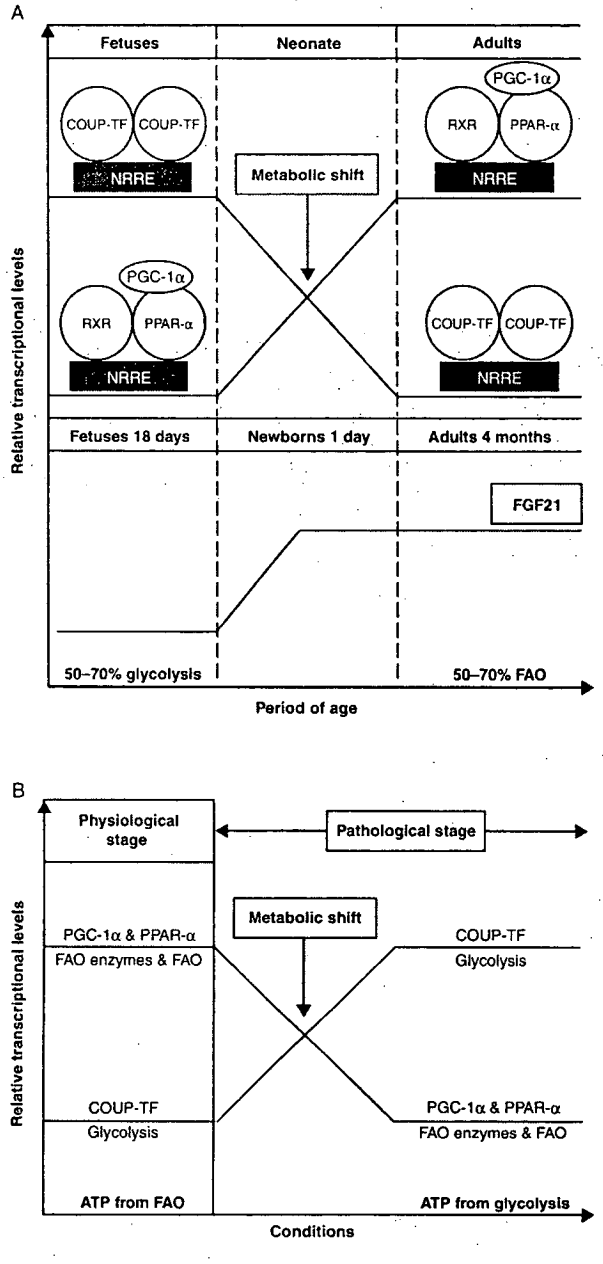


Figure 5
Relationship of FGF21 mRNA expression and FAO control in cardiomyocytes in different periods of age, and its alteration under physiological and pathological stages. (A) Relative transcriptional level of FGF21 mRNA and cardiac FAO enzyme gene regulator expression in different age brackets. (B) Relative transcriptional level of FGF21 mRNA and cardiac FAO enzyme gene regulator expression in physiological and pathological stages. PGC1α, peroxisome proliferator-activated receptor 1γ coactivator 1α; RXR, retinoid X receptor; PPARα, peroxisome proliferator activated receptor-α; COUP-TF, chicken ovalbumin upstream promoter transcription factor; NRRE, nuclear receptor response element; FAO, fatty acid β oxidation; ATP, Adenosine triphosphate.

media thickness (Chow *et al.* 2013) in T2DM (type 2 diabetes mellitus) patients. FGF21 level was also increased in atrial fibrillation (AF) patients and was shown to be an independent risk factor for AF (Han *et al.* 2015). In the cases of non-alcoholic fatty liver disease (NAFLD) and CAD, the serum FGF21 was associated with an adverse lipid profile and also showed a positive correlation with total cholesterol (TC) and triglycerides (TG) (Shen *et al.* 2013). Moreover, the CAD patient's serum FGF21 levels were also positively correlated with TG, fasting blood glucose, ApoB100, insulin, and HOMA-IR, and also have a negative correlation with HDL, and ApoA1 (Lin *et al.* 2010). Recent studies demonstrated that serum FGF21 levels correlate with metabolic status in patients. High serum FGF21 levels in several pathological conditions of the heart under metabolic dysregulation may be explained by FGF21 resistance conditions, which have been observed in *ex vivo* experiments with obese rat hearts (Patel *et al.* 2014) and *in vivo* experiments with DIO mice liver and white adipose tissue (Fisher *et al.* 2010). Therefore, serum FGF21 levels may be indicators of adverse metabolic dysregulation and prognosis for CVD.

The term 'FGF21 resistance' in the heart was first mentioned in chronic DIO rats by Patel and colleagues (Patel *et al.* 2014). They found that obese rat hearts had increased FGF21 mRNA, and FGF21 protein expression and secretion levels. Despite the high level of FGF21, disrupted FGF21-FGFR1-β-Klotho signaling and decreased ERK1/2, Akt and AMPK phosphorylation were observed under this condition (Patel *et al.* 2014). These findings indicate that obese condition caused the impairment of the FGF21 signaling cascades, and that the feedback mechanism allowed the increased production of FGF21 to overcome the FGF21 receptor signaling dysfunction. Unfortunately, the increased endogenous FGF21 level was not sufficient when the exogenous FGF21 administration comes into play a role for therapeutic strategy. The FGF21 resistance was also observed in clinical reports where serum FGF21 level was significantly increased in non-NAFLD (Shen *et al.* 2013), coronary heart disease (Lin *et al.* 2010, Shen *et al.* 2013), metabolic syndrome (Lee *et al.* 2014), and T2DM (Lenart-Lipinska *et al.* 2013). This condition is similar to what has been observed in subjects under 'insulin resistance' condition in which the impairment of insulin receptor and signaling cascades was found with increased plasma insulin level (Pratchayasakul *et al.* 2011, Pipatpiboon *et al.* 2012).

The cross sectional study in 15 male patients who underwent aorto-coronary bypass surgery showed that

http://joe.endocrinology-journals.org
DOI: 10.1530/JOE-15-0289
© 2015 Society for Endocrinology
Printed in Great Britain
Published by Bioscientifica Ltd.

Journal of Endocrinology

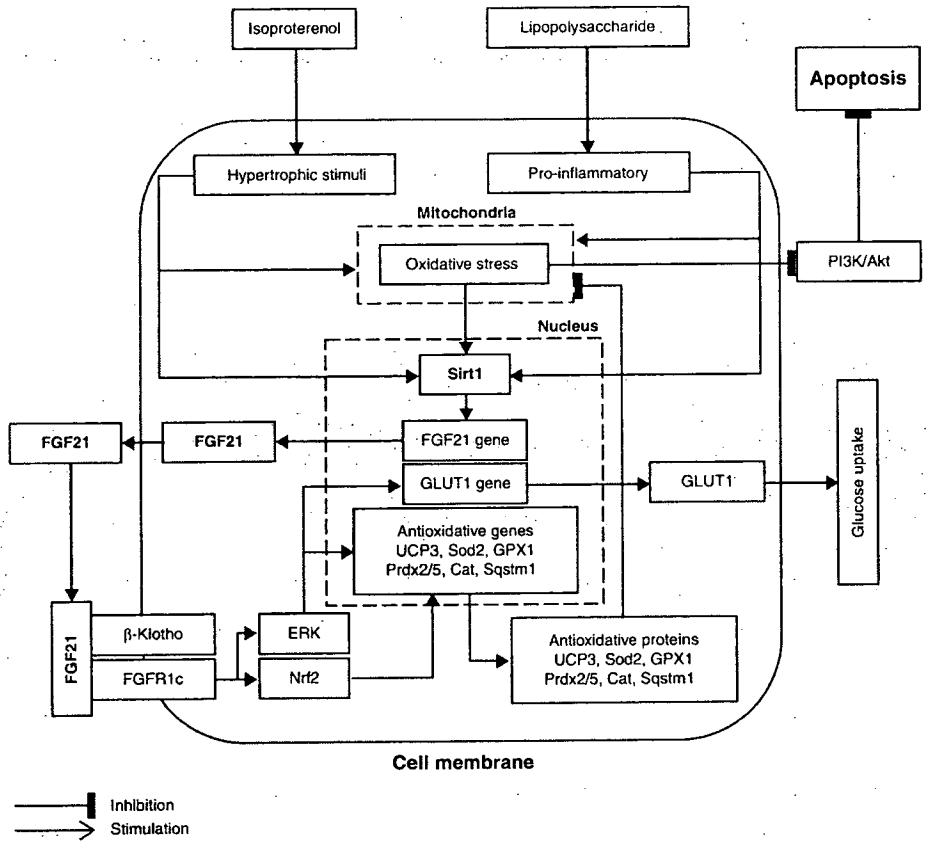


Figure 6
FGF21 mediates and plays a role in protecting against oxidative stress in cardiomyocytes. Sirt1, sirtuin 1; UCP3, uncoupling protein-3; Sod2, superoxide dismutase-2; Prdx2/5, peroxiredoxin-2/5; Cat, catalase; GPX1, glutathione peroxidase 1; Sqstm1, sequestosome 1; ROS, reactive oxygen species; Nrf2, Nuclear factor erythroid 2-related factor 2; PI3K, phosphatidylinositol 3-kinase. Data from Planavila *et al.* (2014) and Yu *et al.* (2015).

serum FGF21 levels increased to a peak at 6 h into surgery, and were associated with increased serum glucose, insulin, pro-inflammatory cytokines (TNFα, MCP1) and inflammatory cytokines (IL6, 8), but returned to baseline at 96 h after surgery (Kotulak *et al.* 2011). Moreover, epicardial fat and muscular FGF21 mRNA expression increased after surgery has reacted positively with blood glucose levels at the end of surgery (Kotulak *et al.* 2011) indicating that FGF21 mRNA expression and serum FGF21 levels regulated glucose homeostasis, increased the insulin sensitivity and attenuated the inflammatory process.

In a cross sectional study of 189 patients who underwent cardiac multidetector coronary computed tomography, it was found that serum FGF21 levels were associated with an adverse lipid profile and pericardial fat volume only in metabolic syndrome patients (Lee *et al.* 2014). Interestingly, cardiac tissue FGF21 mRNA and antioxidant genes (UCP3 and Sod2) are upregulated in six failing human hearts which may be mechanisms to preserve myocardial function in cases of heart failure (Planavila *et al.* 2014). All of these findings indicate that FGF21 plays an important role in metabolic regulation and attenuates cardiac oxidative stress in heart failure patients. The increased FGF21 level observed in heart failure patients was due to the FGF21 resistance as shown by a previous report (Planavila *et al.* 2014). Despite the increased endogenous FGF21 under this pathological condition, its level was still not sufficient to overcome the FGF21 resistance. Therefore, the role of exogenous FGF21 is considered as a potential therapeutic strategy to provide cardioprotective effects (Lu *et al.* 2010, Cong *et al.* 2013, Planavila *et al.* 2013, 2014, Zhang *et al.* 2015a). Previous reports at least from basic studies using exogenous FGF21 demonstrating the

© 2015 Society for Endocrinology
Printed in Great Britain
Published by Bioscientifica Ltd.

http://joe.endocrinology-journals.org
DOI: 10.1530/JOE-15-0289

© 2015 Society for Endocrinology
Printed in Great Britain

Published by Bioscientifica Ltd.

Table 5 The association between FGF21 level and cardiovascular alteration in clinical reports

Models	Type of study	N	Major findings	Interpretation	References
T2DM and CV risk factor prevalence study	Cohort study	670 (158: T2DM, 502: CV risk factor prevalence study)	– FGF21 shows a positive correlation with CIMT in women – FGF21 was an independent risk factor for ↑ CIMT, hsCRP ↑ dysglycemia ↑ dyslipidemia	Serum FGF21 levels are associated and independent established risk factor with carotid atherosclerosis.	Chow *et al.* (2013)
NAFLD, CAD, non NAFLD and CAD	Cohort study	253	↑ FGF21 in NAFLD vs non NAFLD ↑ FGF21 in CAD vs non CAD – Serum FGF21 levels showed a positive correlation with TC and TG	Serum FGF21 levels increased and were associated with adverse lipid profiles in NAFLD and CAD.	Shen *et al.* (2013)
DCMP and final stage HF	Cross-sectional study	6 HF 10 donor	↑ Cardiac tissue FGF21 mRNA ↑ Cardiac tissue antioxidant genes (UCP3 and Sod2 mRNA)	Serum FGF21 expression is up-regulated in the failing human heart	Planavila *et al.* (2014)
CAD	Cross-sectional study	135 patients	– Positively correlated with TG, FBG, Apo B100, insulin, and HOMA-IR – Negative correlation with HDL, Apo A1 – Independent association with TG and Apo A1	Serum FGF-21 level is associated with adverse lipid profiles in CAD patients	Lin *et al.* (2010)
IHD (Aorto-coronary bypass surgery)	Prospective	15 male patients	↑ Serum FGF21 levels during surgery, peak at 6 h ↑ Serum glucose, insulin, CRP, IL6, IL8, MCP1, and TNFα during surgery ↑ Epicardial fat FGF21 mRNA at after surgery – Muscles FGF21 mRNA are positively correlated with BG levels at the end of the surgery	FGF21 regulated glucose homeostasis, insulin sensitivity and attenuated inflammatory process.	Kotulak *et al.* (2011)
Patients had undergone 64 slice cardiac MDCT	Cross-sectional study	189 patients	↑ Serum FGF21 in MS, but not in diabetes or CAD – FGF21 showed a positive correlation with TG, LDL, insulin, HOMA-IR and PFV – Independent association with PFV	Serum FGF21 is associated with lipid profiles, insulin resistance, PFV and MS, but not altered in DM or CAD.	Lee *et al.* (2014)
T2DM	Prospective	9697	– Higher baseline plasma FGF21 levels had ↑ Total CV events – Finofibrate did not reduce CV events	High baseline plasma FGF21 levels in T2DM patients is associated with CV events.	Ong *et al.* (2015)
AF	Cross-sectional study	113 AF patients, 60 healthy volunteers	↑ FGF21 in permanent AF > persistent and paroxysmal AF – FGF21 was positively correlated with LA diameter	Serum FGF21 levels are increased in AF patients and are an independent risk factor for AF.	Han *et al.* (2015)

T2DM, type 2 diabetes mellitus; CV, cardiovascular; CIMT, carotid intima media thickening; hsCRP, high sensitivity C-reactive protein; FGF21, fibroblast growth factor 21; NAFLD, nonalcoholic fatty liver disease; CAD, coronary artery disease; TC, total cholesterol; TG, triglyceride; LDL, low density lipoprotein; DCMP, dilate cardiomyopathy; HF, heart failure; UCPs, uncoupling proteins; Sod, superoxide dismutase; FBG, fasting blood glucose; Apo, apolioprotein; HOMA-IR, homeostatic model assessment insulin resistance; HDL, high density lipoprotein; IHD, ischemic heart disease; IL, interleukin; MCP1, monocyte chemo attractant protein 1; TNFα, tumor necrosis factor alpha; cardiac MDCT, cardiac multidetector coronary computed tomography; MS, metabolic syndrome; PFV, pericardial fat volume; DM, diabetes mellitus; CVD, cardiovascular diseases; AF, atrial fibrillation; LA, left atrium.

improved cardiac function in cardiac I/R injury (Cong *et al.* 2013, Liu *et al.* 2013, Patel *et al.* 2014), cardiac hypertrophy (Planavila *et al.* 2013), and DCM (Zhang *et al.* 2015a) supported this hypothesis.

Although previous studies indicated that PPARα is the essential downstream signaling protein in regulating the expression of FGF21 mRNA in cardiomyocytes, and preserving the myocardial metabolism through regulating the FAO (Lu *et al.* 2010, Planavila *et al*), PPARα agonist (Finofibrate) has been shown to be unable to reduce cardiovascular events in T2DM patients after a 5-year follow-up (Ong *et al.* 2015). Moreover, the risk cardiovascular events in T2DM patients showed a correlation with baseline plasma FGF21 levels. Higher baseline plasma FGF21 levels correlated with an increased risk of cardiovascular events (Ong *et al.* 2015). This suggests that plasma FGF21 levels could be used as a biomarker of metabolic dysregulation, and increased plasma FGF21 levels may be indicative of a higher risk of cardiovascular events.

Despite the fact that FGF21 can preserve the heart in several pathological conditions, FGF21 resistance may be a limitation for the potential role of exogenous FGF21 administration. However, previous studies demonstrated that exogenous FGF21 exerted its effects in a dose-dependent manner (Cong *et al.* 2013, Planavila *et al.* 2014, Yu *et al.* 2015). Moreover, it is possible that FGF21 replacement during an early stage of FGF21 resistance may be more effective than late replacement. Future studies are needed to prove this hypothesis. Furthermore, long-term FGF21 treatment (Zhang *et al.* 2015a) may provide better outcome than the acute intervention (Patel *et al.* 2014). Lastly, combined therapy of FGF21 with specific drugs may provide better efficacy than FGF21 monotherapy. All of these hypothetical strategies still need to be verified in future studies.

Conclusion

Experimental studies of FGF21 in the heart have consistently demonstrated its beneficial effects in *in vitro, ex vivo* and *in vivo* models. Evidence has shown that FGF21 is crucial for cardioprotection in myocardial hypertrophy, ischemia, DCM and I/R injury. FGF21 provides its therapeutic benefits by attenuating apoptosis, oxidative stress and inflammation, and improving energy supply, and therefore could be used as an indicator of metabolic dysregulation. Moreover, FGF21 could be a potential therapeutic target for metabolic disorders and CVD in the future.

Declaration of interest
The authors declare that there is no conflict of interest that could be perceived as prejudicing the impartiality of this review.

Funding
This work was supported by a NSTDA Research Chair Grant from the National Science and Technology Development Agency Thailand (NC), the Thailand Research Fund Royal Golden Jubilee Program (SC and PT), BRG5780016 (SC), and Chiang Mai University Center of Excellence Award (NC).

References

Badman MK, Koester A, Flier JS, Kharitonenkov A & Maratos-Flier E 2009 Fibroblast growth factor 21-deficient mice demonstrate impaired adaptation to ketosis. *Endocrinology* **150** 4931–4940. (doi:10.1210/en.2009-0532)

Beenken A & Mohammadi M 2009 The FGF family: biology, pathophysiology and therapy. *Nature Reviews. Drug Discovery* **8** 235–253. (doi:10.1038/nrd2792)

Chow WS, Xu A, Woo YC, Tso AW, Cheung SC, Fong CH, Tse HF, Chau MT, Cheung BM & Lam KS 2013 Serum fibroblast growth factor-21 levels are associated with carotid atherosclerosis independent of established cardiovascular risk factors. *Arteriosclerosis, Thrombosis, and Vascular Biology* **33** 2454–2459. (doi:10.1161/ATVBAHA.113.301599)

Cong WT, Ling J, Tian HS, Ling R, Wang Y, Huang BB, Zhao T, Duan YM, Jin LT & Li XK 2013 Proteomic study on the protective mechanism of fibroblast growth factor 21 to ischemia-reperfusion injury. *Canadian Journal of Physiology and Pharmacology* **91** 973–984. (doi:10.1139/cjpp-2012-0441)

Ding X, Boney-Montoya J, Owen BM, Bookout AL, Coate KC, Mangelsdorf DJ & Kliewer SA 2012 βKlotho is required for fibroblast growth factor 21 effects on growth and metabolism. *Cell Metabolism* **16** 387–393. (doi:10.1016/j.cmet.2012.08.002)

Fisher FM, Chui PC, Antonellis PJ, Bina HA, Kharitonenkov A, Flier JS & Maratos-Flier E 2010 Obesity is a fibroblast growth factor 21 (FGF21)-resistant state. *Diabetes* **59** 2781–2789. (doi:10.2337/db10-0193)

Gheorghiade M & Bonow RO 1998 Chronic heart failure in the United States: a manifestation of coronary artery disease. *Circulation* **97** 282–289. (doi:10.1161/01.CIR.97.3.282)

Goetz R & Mohammadi M 2013 Exploring mechanisms of FGF signalling through the lens of structural biology. *Nature Reviews. Molecular Cell Biology* **14** 166–180. (doi:10.1038/nrm3528)

Hale C, Chen MM, Stanislaus S, Chinookoswong N, Hager T, Wang M, Veniant MM & Xu J 2012 Lack of overt FGF21 resistance in two mouse models of obesity and insulin resistance. *Endocrinology* **153** 69–80. (doi:10.1210/en.2010-1262)

Han X, Chen C, Cheng G, Xie C, Yang M, Shou X & Sun C 2015 Serum fibroblast growth factor 21 levels are increased in atrial fibrillation patients. *Cytokine* **73** 176–180. (doi:10.1016/j.cyto.2015.02.019)

Heather LC, Catchpole AF, Stuckey DJ, Cole MA, Carr CA & Clarke K 2009 Isoproterenol induces *in vivo* functional and metabolic abnormalities: similar to those found in the infarcted rat heart. *Journal of Physiology and Pharmacology* **60** 31–39.

Hotta Y, Nakamura H, Konishi M, Murata Y, Takagi H, Matsumura S, Inoue K, Fushiki T & Itoh N 2009 Fibroblast growth factor 21 regulates lipolysis in white adipose tissue but is not required for ketogenesis and triglyceride clearance in liver. *Endocrinology* **150** 4625–4633. (doi:10.1210/en.2009-0119)

Ito S, Kinoshita S, Shiraishi N, Nakagawa S, Sekine S, Fujimori T & Nabeshima YI 2000 Molecular cloning and expression analyses of mouse βklotho, which encodes a novel Klotho family protein.

© 2015 Society for Endocrinology
Printed in Great Britain
Published by Bioscientifica Ltd.

Journal of Endocrinology

Mechanisms of Development **98** 115–119. (doi:10.1016/S0925-4773(00)00439-1)

Itoh N & Ornitz DM 2011 Fibroblast growth factors: from molecular evolution to roles in development, metabolism and disease. *Journal of Biochemistry* **149** 121–130. (doi:10.1093/jb/mvq121)

Itoh N & Ohta H 2013 Pathophysiological roles of FGF signaling in the heart. *Frontiers in Physiology* **4** 247. (doi:10.3389/fphys.2013.00247)

Joki Y, Ohashi K, Yuasa D, Shibata R, Ito M, Matsuo K, Kambara T, Uemura Y, Hayakawa S & Hiramatsu-Ito M 2015 FGF21 attenuates pathological myocardial remodeling following myocardial infarction through the adiponectin-dependent mechanism. *Biochemical and Biophysical Research Communications* **459** 124–130. (doi:10.1016/j.bbrc.2015.02.081)

Kelly DP, Gordon JI, Alpers R & Strauss AW 1989 The tissue-specific expression and developmental regulation of two nuclear genes encoding rat mitochondrial proteins. Medium chain acyl-CoA dehydrogenase and mitochondrial malate dehydrogenase. *Journal of Biological Chemistry* **264** 18921–18925.

Kharitonenkov A 2008 FGF-21/FGF-21 receptor interaction and activation is determined by βKlotho. *Journal of Cellular Physiology* **215** 1–7. (doi:10.1002/jcp.21357)

Kharitonenkov A 2009 FGFs and metabolism. *Current Opinion in Pharmacology* **9** 805–810. (doi:10.1016/j.coph.2009.07.001)

Kotulak T, Drapalova J, Kopecky P, Lacinova Z, Kramar P, Riha H, Netuka I, Maly J, Housa D, Jaha J *et al.* 2011 Increased circulating and epicardial adipose tissue mRNA expression of fibroblast growth factor-21 after cardiac surgery: possible role in postoperative inflammatory response and insulin resistance. *Physiological Research* **60** 757–767.

Lee Y, Lim S, Hong ES, Kim JH, Moon MK, Chun EJ, Choi SI, Kim YB, Park YJ, Park KS *et al.* 2014 Serum FGF21 concentration is associated with hypertriglyceridaemia, hyperinsulinaemia and pericardial fat accumulation, independently of obesity, but not with current coronary artery status. *Clinical Endocrinology* **80** 57–64. (doi:10.1111/cen.12134)

Lenart-Lipinska M, Matyjaszek-Matuszek B, Gernand W, Nowakowski A & Solski J 2013 Serum fibroblast growth factor 21 is predictive of combined cardiovascular morbidity and mortality in patients with type 2 diabetes at a relatively short-term follow-up. *Diabetes Research and Clinical Practice* **101** 194–200. (doi:10.1016/j.diabres.2013.04.010)

Lin Z, Wu Z, Yin X, Liu Y, Yan X, Lin S, Xiao J, Wang X, Feng W & Li X 2010 Serum levels of FGF-21 are increased in coronary heart disease patients and are independently associated with adverse lipid profile. *PLoS ONE* **5** e15534. (doi:10.1371/journal.pone.0015534)

Liu SQ, Tefft BJ, Roberts DT, Zhang LQ, Ren Y, Li YC, Huang Y, Zhang D, Phillips HR & Wu YH 2012 Cardioprotective proteins upregulated in the liver in response to experimental myocardial ischemia. *American Journal of Physiology. Heart and Circulatory Physiology* **303** H1446–H1458. (doi:10.1152/ajpheart.00362.2012)

Liu SQ, Roberts D, Kharitonenkov A, Zhang B, Hanson SM, Li YC, Zhang LQ & Wu YH 2013 Endocrine protection of ischemic myocardium by FGF21 from the liver and adipose tissue. *Scientific Reports* **3** 2767. (doi:10.1038/srep02767)

Lockwood EA & Bailey E 1970 Fatty acid utilization during development of the rat. *Biochemical Journal* **120** 49–54. (doi:10.1042/bj1200049)

Lu Y, Liu JH, Zhang LK, Du J, Zeng XJ, Hao G, Huang J, Zhao DH, Wang GZ & Zhang YC 2010 Fibroblast growth factor 21 as a possible endogenous factor inhibits apoptosis in cardiac endothelial cells. *Chinese Medical Journal* **123** 3417–3421. (doi:10.3760/cma.j.issn.0366-6999.2010.23.008)

Mohammadi M, Olsen SK & Ibrahimi OA 2005 Structural basis for fibroblast growth factor receptor activation. *Cytokine & Growth Factor Reviews* **16** 107–137. (doi:10.1016/j.cytogfr.2005.01.008)

Neely JR & Morgan HE 1974 Relationship between carbohydrate and lipid metabolism and the energy balance of heart muscle. *Annual Review of Physiology* **36** 413–459. (doi:10.1146/annurev.ph.36.030174.002213)

Neely JR, Rovetto MJ & Oram JF 1972 Myocardial utilization of carbohydrate and lipids. *Progress in Cardiovascular Diseases* **15** 289–329. (doi:10.1016/0033-0620(72)90029-1)

Nishimura T, Nakatake Y, Konishi M & Itoh N 2000 Identification of a novel FGF, FGF-21, preferentially expressed in the liver. *Biochimica et Biophysica Acta* **1492** 203–206. (doi:10.1016/S0167-4781(00)00067-1)

Ong KL, Januszewski AS, O'Connell R, Jenkins AJ, Xu A, Sullivan DR, Barter PJ, Hung WT, Scott RS, Taskinen MR *et al.* 2015 The relationship of fibroblast growth factor 21 with cardiovascular outcome events in the Fenofibrate Intervention and Event Lowering in Diabetes study. *Diabetologia* **58** 464–473. (doi:10.1007/s00125-014-3458-7)

Patel V, Adya R, Chen J, Ramanjaneya M, Bari MF, Bhudia SK, Hillhouse EW, Tan BK & Randeva HS 2014 Novel insights into the cardio-protective effects of FGF21 in lean and obese rat hearts. *PLoS ONE* **9** e87102. (doi:10.1371/journal.pone.0087102)

Pipatpiboon N, Pratchayasakul W, Chattipakorn N & Chattipakorn SC 2012 PPARgamma agonist improves neuronal insulin receptor function in hippocampus and brain mitochondria function in rats with insulin resistance induced by long term high-fat diets. *Endocrinology* **153** 329–338. (doi:10.1210/en.2011-1502)

Planavila A, Redondo I, Hondares E, Vinciguerra M, Munts C, Iglesias R, Gabrielli LA, Sitges M, Giralt M, van Bilsen M *et al.* 2013 Fibroblast growth factor 21 protects against cardiac hypertrophy in mice. *Nature Communications* **4** 2019. (doi:10.1038/ncomms3019)

Planavila A, Redondo-Angulo I, Ribas F, Garrabou G, Casademont J, Giralt M & Villarroya F 2014 Fibroblast growth factor 21 protects the heart from oxidative stress. *Cardiovascular Research* **106** 19–31. (doi:10.1093/cvr/cvu263)

Potthoff MJ, Inagaki T, Satapati S, Ding X, He T, Goetz R, Mohammadi M, Finck BN, Mangelsdorf DJ, Kliewer SA *et al.* 2009 FGF21 induces PGC-1α and regulates carbohydrate and fatty acid metabolism during the adaptive starvation response. *PNAS* **106** 10853–10858. (doi:10.1073/pnas.0904187106)

Pratchayasakul W, Kerdphoo S, Petsophonsakul P, Pongchaidecha A, Chattipakorn N & Chattipakorn SC 2011 Effects of high-fat diet on insulin receptor function in rat hippocampus and the level of neuronal corticosterone. *Life Science* **88** 619–627. (doi:10.1016/j.lfs.2011.02.003)

Razeghi P, Young ME, Alcorn JL, Moravec CS, Frazier OH & Taegtmeyer H 2001 Metabolic gene expression in fetal and failing human heart. *Circulation* **104** 2923–2931. (doi:10.1161/hc4901.100526)

Sack MN, Disch DL, Rockman HA & Kelly DP 1997 A role for Sp and nuclear receptor transcription factors in a cardiac hypertrophic growth program. *PNAS* **94** 6438–6443. (doi:10.1073/pnas.94.12.6438)

Shen Y, Ma X, Zhou J, Pan X, Hao Y, Zhou M, Lu Z, Gao M, Bao Y & Jia W 2013 Additive relationship between serum fibroblast growth factor 21 level and coronary artery disease. *Cardiovascular Diabetology* **12** 124. (doi:10.1186/1475-2840-12-124)

Suzuki M, Uehara Y, Motomura-Matsuzaka K, Oki J, Koyama Y, Kimura M, Asada M, Komi-Kuramochi A, Oka S & Imamura T 2008 βKlotho is required for fibroblast growth factor (FGF) 21 signaling through FGF receptor (FGFR) 1c and FGFR3c. *Molecular Endocrinology* **22** 1006–1014. (doi:10.1210/me.2007-0313)

Vega RB, Huss JM & Kelly DP 2000 The coactivator PGC-1 cooperates with peroxisome proliferator-activated receptor α in transcriptional control of nuclear genes encoding mitochondrial fatty acid oxidation enzymes. *Molecular and Cellular Biology* **20** 1868–1876. (doi:10.1128/MCB.20.5.1868-1876.2000)

Wente W, Efanov AM, Brenner M, Kharitonenkov A, Koster A, Sandusky GE, Sewing S, Treinies I, Zitzer H & Gromada J 2006 Fibroblast growth factor-21 improves pancreatic β-cell function and survival by activation of extracellular signal-regulated kinase 1/2 and Akt signaling pathways. *Diabetes* **55** 2470–2478. (doi:10.2337/db05-1435)

Wu X, Qi YF, Chang JR, Lu WW, Zhang JS, Wang SP, Cheng SJ, Zhang M, Fan Q & Lv Y 2014 Possible role of fibroblast growth factor 21 on atherosclerosis via amelioration of endoplasmic reticulum

© 2015 Society for Endocrinology
Printed in Great Britain
Published by Bioscientifica Ltd.

Journal of Endocrinology

stress-mediated apoptosis in apoE mice. *Heart and Vessels* **30** 657–668. (doi:10.1007/s00380-014-0557-9)

Yan X, Chen J, Zhang C, Zhou S, Zhang Z, Chen J, Feng W, Li X & Tan Y 2015 FGF21 deletion exacerbates diabetic cardiomyopathy by aggravating cardiac lipid accumulation. *Journal of Cellular and Molecular Medicine* **19** 1157–1568. (doi:10.1111/jcmm.12530)

Yie J, Hecht R, Patel J, Stevens J, Wang W, Hawkins N, Steavenson S, Smith S, Winters D, Fisher S *et al.* 2009 FGF21 N- and C-termini play different roles in receptor interaction and activation. *FEBS Letters* **583** 19–24. (doi:10.1016/j.febslet.2008.11.023)

Yu Y, Bai F, Liu Y, Yang Y, Yuan Q, Zou D, Qu S, Tian G, Song L & Zhang T 2015 Fibroblast growth factor (FGF21) protects mouse liver against D-galactose-induced oxidative stress and apoptosis via activating Nrf2 and PI3K/Akt pathways. *Molecular and Cellular Biochemistry* **403** 287–299. (doi:10.1007/s11010-015-2358-6)

Zhang C, Huang Z, Gu J, Yan X, Lu X, Zhou S, Wang S, Shao M, Zhang F & Cheng P 2015*a* Fibroblast growth factor 21 protects the heart from apoptosis in a diabetic mouse model via extracellular signal-regulated kinase 1/2-dependent signalling pathway. *Diabetologia* **58** 1937–1948. (doi:10.1007/s00125-015-3630-8)

Zhang X, Hu Y, Zeng H, Li L, Zhao J, Zhao J, Liu F, Bao Y & Jia W 2015*b* Serum fibroblast growth factor 21 levels is associated with lower extremity atherosclerotic disease in Chinese female diabetic patients. *Cardiovascular Diabetology* **14** 190. (doi:10.1186/s12933-015-0190-7)

Received in final form 19 August 2015
Accepted 4 September 2015
Accepted Preprint published online 4 September 2015

Journal of Endocrinology

© 2015 Society for Endocrinology
Printed in Great Britain

Published by Bioscientifica Ltd.

เอกสารแนบหมายเลข 40

AGE (2015) 37: 84
DOI 10.1007/s11357-015-9827-4

Testosterone replacement attenuates cognitive decline in testosterone-deprived lean rats, but not in obese rats, by mitigating brain oxidative stress

Hiranya Pintana · Wanpitak Pongkan · Wasana Pratchayasakul · Nipon Chattipakorn · Siriporn C. Chattipakorn

Received: 28 May 2015 / Accepted: 7 August 2015 / Published online: 16 August 2015
© American Aging Association 2015

Abstract Testosterone replacement improves metabolic parameters and cognitive function in hypogonadism. However, the effects of testosterone therapy on cognition in obese condition with testosterone deprivation have not been investigated. We hypothesized that testosterone replacement improves cognitive function in testosterone-deprived obese rats by restoring brain insulin sensitivity, brain mitochondrial function, and hippocampal synaptic plasticity. Thirty male Wistar rats had either a bilateral orchiectomy (ORX: O, n=24) or a sham operation (S, n=6). ORX rats were further divided into two groups fed with either a normal diet (NDO) or a high-fat diet (HFO) for 12 weeks. Then, ORX rats in each dietary group were divided into two subgroups (n= 6/subgroup) and were given either castor oil or testosterone (2 mg/kg/day, s.c.) for 4 weeks. At the end of this protocol, cognitive function, metabolic parameters, brain insulin sensitivity, hippocampal synaptic plasticity, and brain mitochondrial function were determined. We found that testosterone replacement increased peripheral insulin sensitivity, decreased circulation and brain oxidative stress levels, and attenuated brain mitochondrial ROS production in HFO rats. However, testosterone failed to restore hippocampal synaptic plasticity and cognitive function in HFO rats. In contrast, in NDO rats, testosterone decreased circulation and brain oxidative stress levels, attenuated brain mitochondrial ROS production, and restored hippocampal synaptic plasticity as well as cognitive function. These findings suggest that testosterone replacement improved peripheral insulin sensitivity and decreased oxidative stress levels, but failed to restore hippocampal synaptic plasticity and cognitive function in testosterone-deprived obese rats. However, it provided beneficial effects in reversing cognitive impairment in testosterone-deprived non-obese rats.

Keywords Testosterone replacement · Obese insulin resistance · Testosterone deprivation · Brain mitochondrial function · Hippocampal synaptic plasticity · Cognitive function

H. Pintana · W. Pongkan · W. Pratchayasakul · N. Chattipakorn · S. C. Chattipakorn
Neurophysiology Unit, Cardiac Electrophysiology Research and Training Center, Faculty of Medicine, Chiang Mai University, Chiang Mai, Thailand

H. Pintana · W. Pongkan · W. Pratchayasakul · N. Chattipakorn
Department of Physiology, Faculty of Medicine, Chiang Mai University, Chiang Mai, Thailand

S. C. Chattipakorn (✉)
Department of Oral Biology and Diagnostic Science, Faculty of Dentistry, Chiang Mai University, Chiang Mai 50200, Thailand
e-mail: scchattipakorn@gmail.com

S. C. Chattipakorn
e-mail: siriporn.c@cmu.ac.th

Introduction

Testosterone plays a major role in reproductive function by promoting secondary sexual characteristics and emotions (Janowsky 2006). Previous studies demonstrated

that testosterone plays an important role in metabolic activities, including the regulation of glucose and lipid metabolism (Aydilek and Aksakal 2005; Christoffersen et al. 2010). Growing evidence has demonstrated that testosterone deficiency is associated with an increased incidence of obesity (Shi et al. 2013; Stellato et al. 2000). In addition, a positive correlation between obese-insulin resistance and testosterone deficiency has been reported (Grossmann et al. 2008; Haffner et al. 1994), but contradictory findings have been demonstrated in some animal models (Borst and Conover 2006; Erben et al. 2000; Kakolewski et al. 1968). In addition, our previous studies demonstrated that 15 weeks of a high-fat diet (HFD) consumption in male rats induced not only obese-related insulin resistance, but also impaired brain insulin sensitivity and brain mitochondrial dysfunction, leading to cognitive decline (Pintana et al. 2013; Pintana et al. 2012; Pipatpiboon et al. 2013). However, the effects of testosterone deprivation under obese insulin-resistant conditions on cognitive function have not been thoroughly investigated.

Although testosterone replacement has been prescribed to patients with hypogonadism to improve the quality of life and overall health, including the improvement of cognitive function in men (Donatucci et al. 2014) and animal models (Bassil and Morley 2010 ; Cunningham and Toma 2010; Margo and Winn 2006), several studies found that testosterone replacement in the hypogonadal condition has either no effect or adverse effects on cognition in animal models (Emamian et al. 2010; Harooni et al. 2008; Khorshidahmad et al. 2012; Naghdi and Asadollahi 2004) and humans (Kenny et al. 2004; Lu et al. 2006; Maki et al. 2007; Vaughan et al. 2007; Wolf et al. 2000). In addition, previous studies reported that a high dosage of testosterone could lead to increased cell apoptosis (Cunningham et al. 2009), neuronal toxicity (Buletko et al. 2012), and impaired learning and decreased memory capability in animal models (Emamian et al. 2010; Harooni et al. 2008; Naghdi et al. 2005; Spritzer et al. 2011).

At present, the effects of testosterone replacement on brain insulin receptor function, brain mitochondrial function, and cognitive function in either testosterone deprivation with or without obesity have not been investigated. The hypotheses of the present study are as follows:

1. Testosterone-deprived rats with or without obesity have impaired brain insulin receptor function, decreased brain insulin signaling, impaired brain mitochondrial function, and impaired hippocampal synaptic plasticity, thus leading to cognitive decline
2. Testosterone replacement restores these impairments in conditions of testosterone deprivation with or without obesity.

Materials and methods

Animal models and experimental protocols

All experiments were conducted in accordance with the approved protocol of the Faculty of Medicine, Chiang Mai University Institutional Animal Care and Use Committee, in compliance with NIH guidelines. Thirty male Wistar rats, weighing 180–200 g (aged ~5–6 weeks old) obtained from the National Animal Center, Salaya Campus, Mahidol University, Bangkok, Thailand, were used. All animals were housed in environmentally controlled conditions (25±0.5 °C and a 12-h light/dark cycle) and allowed to acclimate for 1 week. Rats were then divided into two groups, either control sham-operated rats (S) (n=6) or bilateral orchiectomized (O) rats (n=24), as described previously (Pongkan et al. 2015). Rats in the sham-operated group were fed with a normal diet (ND) for 16 weeks, and this group was the control group (NDS). Rats in the orchiectomized group were further divided into two dietary groups, where each group was fed on either a normal diet (ND 19.77 % E fat, NDO) or a high-fat diet (HFD 59.28 % E fat, HFO) for 12 weeks (Pratchayasakul et al. 2011). At the end of week 12, the rats in each dietary group were subdivided into two subgroups (n=6/subgroup). Each subgroup were given castor oil (NDOOil and HFOOil) or testosterone replacement 2 mg/kg/days (NDOTes and HFOTes), via subcutaneous injection for 4 weeks (Pongkan et al. 2015). The cognitive function was subsequently determined by the Morris water maze (MWM) test at the end of week 16 of the experimental protocol. Blood samples were collected from a tail vein at week 12, and week 16 of the experimental protocol for further plasma analysis. At the end of the experimental protocol, rats were deeply anesthetized with isoflurane and killed by decapitation. The brain of each rat was quickly removed and carefully sliced in preparation for investigation, including extracellular recording (insulin-induced long-term depression (LTD) and

hippocampal synaptic long-term potentiation (LTP)), immunoblot analysis, brain mitochondrial function and brain malondialdehyde (MDA) measurement. The experimental protocol is summarized in Fig. 1.

Blood sample assays

Plasma glucose and cholesterol levels were determined by colorimetric assay (Biotech, Bangkok, Thailand). Plasma HDL and LDL levels were determined using a commercial colorimetric assay kit (Biovision, CA, USA). Plasma insulin levels were determined using the sandwich enzyme-linked immunosorbent assay (ELISA) kit (Millipore, MI, USA). Peripheral insulin resistance was assessed using the homeostasis model assessment (HOMA) as described in previous studies (Pipatpiboon et al. 2013; Pratchayasakul et al. 2011). An oral glucose tolerance test (OGTT) was performed as described previously (Pipatpiboon et al. 2013). Areas under the curves (AUCs) were calculated to evaluate glucose tolerance. Plasma testosterone levels were determined as described previously (Pongkan et al. 2015).

Serum and brain MDA levels

The high-performance liquid chromatography (HPLC) method was used to evaluate concentrations of serum and brain MDA as described previously (Candan and Tuzmen 2008; Mateos et al. 2005; Pintana et al. 2013; Pintana et al. 2014).

Brain slice preparation

At the end of the experimental protocol, animals were anesthetized with isoflurane and decapitated. The hippocampal slices were prepared as described previously for extracellular recording to determine insulin-induced LTD and hippocampal synaptic LTP (Pipatpiboon et al. 2013; Pipatpiboon et al. 2012; Pratchayasakul et al. 2011).

Extracellular recordings from the hippocampal slices for insulin-induced LTD

An extracellular recording of hippocampal slices for insulin-induced LTD was performed as described in the previous studies (Pipatpiboon et al. 2013; Pipatpiboon et al. 2012; Pratchayasakul et al. 2011). Field excitatory postsynaptic potentials (fEPSPs) were evoked by stimulating the Schaffer collateral-commissural pathway with a bipolar tungsten electrode, while recordings were taken from the stratum radiatum of the hippocampal CA1 region with micropipettes (3 MΩ) filled with 2 M NaCl. Stimulus frequency was 0.033 Hz. The stimulus intensity of fEPSPs was adjusted to 0.8–1.0 mV in amplitude. Hippocampal slices were perfused with aCSF (as a baseline condition) for 10 min, and then perfused with aCSF plus 500 nM insulin (as insulin-induced LTD) for an additional 10 min. After this, the slices were perfused with aCSF for an additional 50 min and readings recorded. Data was filtered at 3 kHz, digitized at 10 kHz, and stored in a computer using pClamp 9.2 software (Axon Instruments, CA, USA). The initial slope of the fEPSP was measured and plotted against time.

Extracellular recordings from hippocampal slices for synaptic LTP

The examination of electrical-induced hippocampal synaptic LTP was performed as described in the previous study (Sripetchwandee et al. 2014). fEPSPs were evoked by stimulating the Schaffer collateral-commissural pathway with a bipolar tungsten electrode, while the fEPSP recordings were taken from the stratum radiatum of the hippocampal CA1 region with micropipettes (3 MΩ) filled with 2 M NaCl. LTP was induced by delivering high-frequency stimulation (HFS; four trains at 100 Hz; 0.5-s duration; 20-s interval). Experiments were performed for at least 40 min after HFS. The amount of potentiation was calculated at 40 min after tetanus. All data were filtered at 3 kHz, digitized at 10 kHz, and stored in a computer using pClamp9.2 software (Axon Instruments, CA, USA). The initial slopes of the fEPSPs were measured and plotted against time.

Immunoblotting for brain insulin signaling

To investigate the expression of insulin receptor phosphorylation (p-IR) and insulin receptors (IRs), homogenate brain slices from each subgroup were used as described in the previous study (Pipatpiboon et al. 2013; Pipatpiboon et al. 2012; Pratchayasakul et al. 2011). Electrophoresis and immunoblotting were carried out on IR tyrosine phosphorylation using rabbit antibodies for IR at tyrosine. The level of IR protein expression was assessed with homogenates prepared

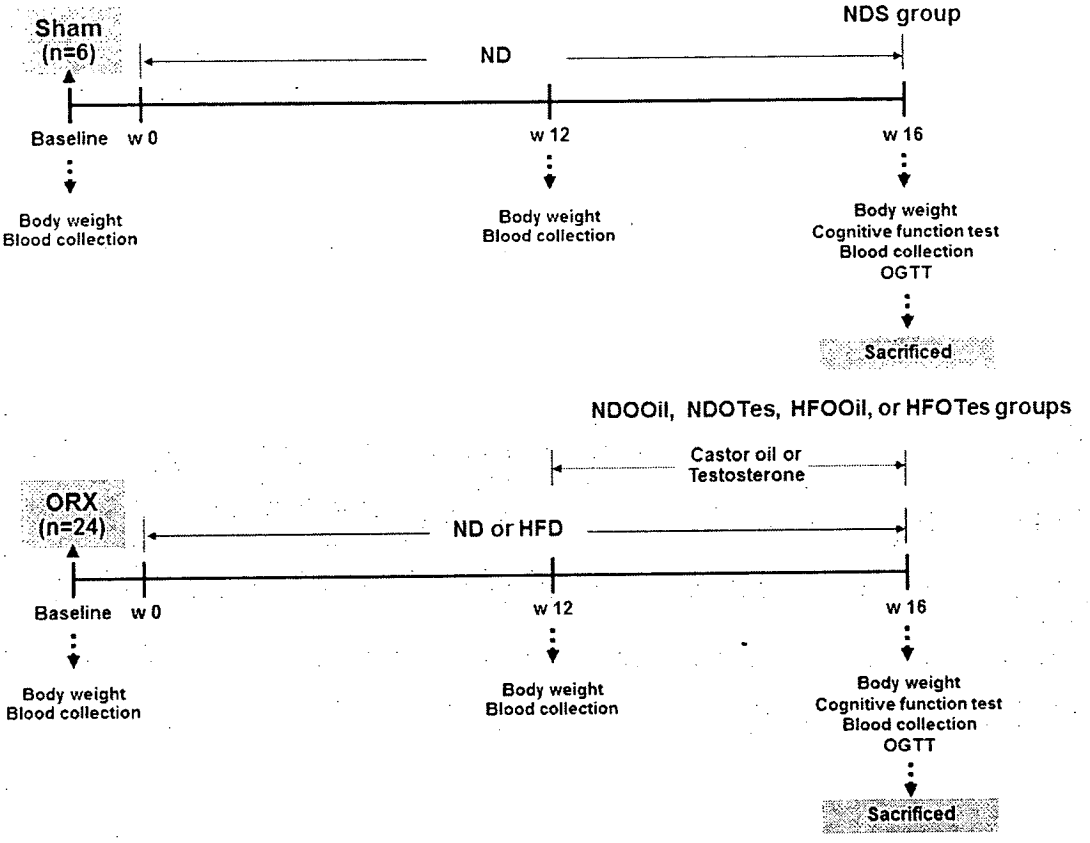


Fig. 1 The experimental protocol of the study. *ND* normal diet, *HFD* high-fat diet, *ORX* orchiectomy, *NDS* sham-operated rats with normal diet feeding, *NDOOil* orchiectomized-operated rats with normal diet feeding and treated with castor oil, *NDOTes* orchiectomized-operated rats with normal diet feeding and treated with testosterone, *HFOOil* orchiectomized-operated rats with high-fat diet feeding and treated with castor oil, *HFOTes* orchiectomized-operated rats fed with a high-fat diet and treated with testosterone, *w* week, *OGTT* oral glucose tolerance test

from another set of four whole brain slices. These proteins were resolved by an immunoblot assay conducted with rabbit anti-IR at tyrosine phosphorylation. These proteins were resolved by an immunoblot assay conducted with rabbit anti-IR at tyrosine phosphorylation (p-IR$^{tyr1162/1163}$) (1:1000; sc-25103-R; Santa Cruz Biotechnology, CA, USA), IR (1:1000; sc-711; Santa Cruz Biotechnology, CA, USA). For a loading control, an immunoblot for each membrane was incubated with anti-β-actin (1:4000; #4967; Cell Signaling Technology, MA, USA). All membranes for visualizing the phosphorylation and the protein levels of IR expression were incubated with secondary goat anti-rabbit antibody conjugated with horseradish peroxidase (1:2000; #7074; Cell Signaling Technology, MA, USA). The protein bands were visualized on Amersham hyperfilm ECL (GE Healthcare, Buckinghamshire, UK) using Amersham ECL Western blot detection reagents (GE, Healthcare). Band densities of phosphorylated IR were represented as a ratio of insulin stimulation (+) to no insulin stimulation (−) and were normalized to total IR. In addition, band intensities were quantified by Scion Imaging and the results were shown as average signal intensity (arbitrary) units.

Brain mitochondrial function study

Brain mitochondria were isolated using the method described previously (Pipatpiboon et al. 2013). Mitochondrial protein concentration was measured using BCA assay (Pipatpiboon et al. 2013), and brain mitochondrial function including brain mitochondrial reactive oxygen species (ROS), mitochondrial membrane potential change ($\Delta\Psi m$), and mitochondrial swelling were determined. Brain mitochondrial reactive oxygen species (ROS) were measured using dichlorohydrofluoresceindiacetate (DCFHDA) fluorescent dye. The change in $\Delta\Psi m$ was measured using the

fluorescent dye 5,5′,6, 6′-tetrachloro-1,1′,3,3′-tetraethyl benzimidazolcarbocyanine iodide (JC-1), and brain mitochondrial swelling was determined by measuring the change in the absorbance of brain mitochondrial suspension at 540 nm. All were determined by following the methods described previously (Pintana et al. 2013; Pipatpiboon et al. 2013).

Cognitive function test

The open-field test (OFT) was used to screen locomotor activity by counting the number of lines that the rats crossed during the test, as described in previous studies (Arakawa 2005; Pintana et al. 2013). The assessment of cognitive function was performed by using the MWM with two assessments including the acquisition test which was carried out for five consecutive days, and the probe test which was performed on day 6 (Pintana et al. 2013; Vorhees and Williams 2006). Data analysis of the MWM test was done manually from video tape recordings by the investigators, who were blinded to all experimental groups.

Statistical analysis

Data were expressed as mean±SEM. For all comparisons, the significance of the differences in peripheral biochemical parameters was calculated using the Mann–Whitney *U* test. The comparisons in the percentage of insulin-induced LTD, the percentage of LTP, brain mitochondrial function, immunoblot, the OFT tests and the MWM tests for the probe test between groups were performed using the one-way ANOVA test, followed by post hoc LSD analysis. Comparisons among groups in MWM tests for the acquisition test were performed using a two-way ANOVA, followed by post hoc LSD analysis. $P<0.05$ was considered statistically significant.

Results

Obesity, but not testosterone deprivation, caused peripheral insulin resistance

Testosterone deprivation by orchiectomy was confirmed by reduced plasma testosterone levels in NDO rats treated with castor oil (NDOOil) and HFO rats treated with castor oil (HFOOil) (Table 1). Testosterone replacement increased plasma testosterone levels in both NDO rats treated with testosterone (NDOTes) and HFO rats treated with testosterone (HFOTes), when compared to that of NDOOil and HFOOil rats (Table 1). NDOOil rats had significantly decreased body weight and less visceral fat, without any significant alteration in plasma insulin, HOMA index, plasma glucose area under the

Table 1 Metabolic parameters after 4 weeks of testosterone treatment

Metabolic parameters	Treatment group				
	NDS	NDOOil	NDOTes	HFOOil	HFOTes
Body weight (g)	506.8±10.4	423.7±13.8[a,b]	441.8±13.8[a,b]	508.3±18.6	515.7±9.7
Plasma testosterone levels (ng/ml)	0.79±0.05	<0.025	4.19±0.79[b,c]	<0.025	4.32±0.27[b,c]
Visceral fat (g)	28.3±1.0	15.6±1.1*[,b]	16.1±0.7[a,b]	28.5±1.7	29.5±1.9
Plasma glucose (mg/dl)	134.9±11.5	135.7±8.6	130.3±9.5	131.7±10.7	131.9±8.2
Plasma insulin (ng/ml)	2.73±0.31	3.30±0.52	2.88±0.33	5.45±1.01[a]	4.58±0.29[a]
HOMA index	22.7±2.9	26.1±4.9	24.8±3.7	45.9±10.0[a]	41.1±5[a]
Plasma glucose AUC (AUCg) (mg/dlxminx10^4)	4.6±0.18	4.8±0.5	4.7±0.1	6.0±0.4[a]	5.0±0.1[b]
Plasma total cholesterol (mg/dl)	75.9±6.4	76.4±6.2	73.6±3.9	115.3±7.6[a]	95.2±5.0[a,b]
Plasma triglyceride (mg/dl)	53.2±2.2	51.8±5.8	57.8±5.5	50.9±7.9	55.0±7.1
HDL cholesterol (mg/dl)	7.0±0.4	7.3±0.5	7.1±0.5	4.8±0.7[a]	6.0±0.2
LDL cholesterol (mg/dl)	56.2±7.4	56.6±6.6	56.2±6.1	105.2±6.9[a]	82.2±5.6[a,b]

[a] Compared to NDS

[b] Compared to HFOOil

[c] Compared to NDOOil

curve of oral glucose tolerance test (AUCg), total cholesterol, plasma LDL cholesterol levels as well as plasma HDL cholesterol levels, when compared with those of NDS rats. Furthermore, the body weight and visceral fat in NDOTes rats were significantly decreased, when compared with those in NDS rats and NDOOil rats. The plasma insulin, HOMA index, plasma glucose area under the curve of oral glucose tolerance test (AUCg), total cholesterol, plasma LDL cholesterol levels as well as plasma HDL cholesterol levels in NDOTes rats were not significantly different, when compared with those in NDS rats and NDOOil rats. These findings indicated that peripheral insulin resistance was not observed in the NDOOil and NDOTes rats.

HFOOil rats demonstrated the characteristics of peripheral insulin resistance, including increased plasma insulin, HOMA index, plasma AUCg, total cholesterol, plasma LDL cholesterol levels as well as decreased plasma HDL cholesterol levels, when compared with those of NDS rats. Interestingly, HFOTes rats had significantly decreased plasma AUCg, plasma total cholesterol and plasma LDL cholesterol levels, when compared with those of HFOOil rats (Table 1). However, plasma glucose and plasma triglyceride levels were not significantly different between all groups. All of these findings suggest that testosterone replacement attenuated peripheral insulin resistance in testosterone-deprived obese rats via improved peripheral insulin sensitivity as indicated by improved OGTT and reduced lipid profiles.

Obesity, but not testosterone deprivation, caused the impairment of brain insulin receptor function

Brain insulin receptor function was tested by measuring insulin-induced LTD and brain insulin signaling. For the insulin-induced LTD study, the degrees of insulin-mediated LTD in ND-fed rats (NDS, NDOOil, and NDOTes) were not significantly different between groups (n=2–3 independent slices/animal, n=6 animals/group Fig. 2a). However, the degree of insulin-induced LTD was significantly reduced in HFOOil rats, when compared with that of NDS, NDOOil, and NDOTes rats (n=2–3 independent slices/animal, n=6 animals/group, Fig. 2a). Testosterone replacement did not reverse that impairment in HFOTes rats (n=2–3 independent slices/animal, n=6 animals/rats, Fig. 2a).

As regards the brain insulin signaling study, the phosphorylation of insulin receptors (p-IR) showed no significant difference between rats in the groups of ND-fed rats (NDS, NDOOil, and NDOTes) (Fig. 2b). However, levels of p-IR of HFOOil rats were significantly decreased, when compared with those of ND-fed rats (Fig. 2b). In addition, the expression of insulin receptors (IR) in all groups showed no significant difference between all groups (Fig. 2c). Testosterone replacement did not reverse these impaired effects in HFOTes rats (Fig. 2b).

All of these findings suggest that the obese insulin-resistant condition, but not testosterone deprivation, caused the impairment of brain insulin receptor function and brain insulin signaling. Moreover, testosterone replacement failed to restore the impairment of brain insulin receptor function as well as brain insulin signaling in the testosterone-deprived obese condition.

Testosterone deprivation with obesity caused brain mitochondrial dysfunction and testosterone replacement reduced brain mitochondrial ROS production

Brain mitochondrial function was determined by assessing changes in brain mitochondrial ROS production and brain $\Delta\Psi m$ after H_2O_2 stimulation, and brain mitochondrial swelling. The results show that brain mitochondrial ROS production was significantly increased in NDOOil rats, when compared with NDS rats, whereas NDOTes rats had significantly decreased brain mitochondrial ROS production, when compared with NDOOil rats (Fig. 3a). However, brain mitochondrial membrane potential change and brain mitochondrial swelling were not significantly different between groups of ND-fed rats (NDS, NDOOil, and NDOTes) (Fig. 3b, c). Furthermore, HFOOil and HFOTes rats had significantly increased brain mitochondrial ROS production, brain mitochondrial depolarization, and brain mitochondrial swelling, when compared with those of NDS rats (Fig. 3a–c). Interestingly, the brain mitochondrial ROS production in the HFOOil group was significantly higher than that in NDOOil rats. This result suggests that the combination of high-fat diet and orchiectomy aggravates the severity of brain mitochondrial ROS production. In addition, testosterone replacement significantly decreased brain ROS production in HFOTes rats, when compared with that of HFOOil rats (Fig. 3a). However, testosterone replacement did not attenuate brain mitochondrial depolarization and brain mitochondrial swelling in HFOTes rats (Fig. 3b, c).

The morphological changes of brain mitochondria from all groups are shown in Fig. 4. Intact brain mitochondrial morphology with apparent folded cristae was

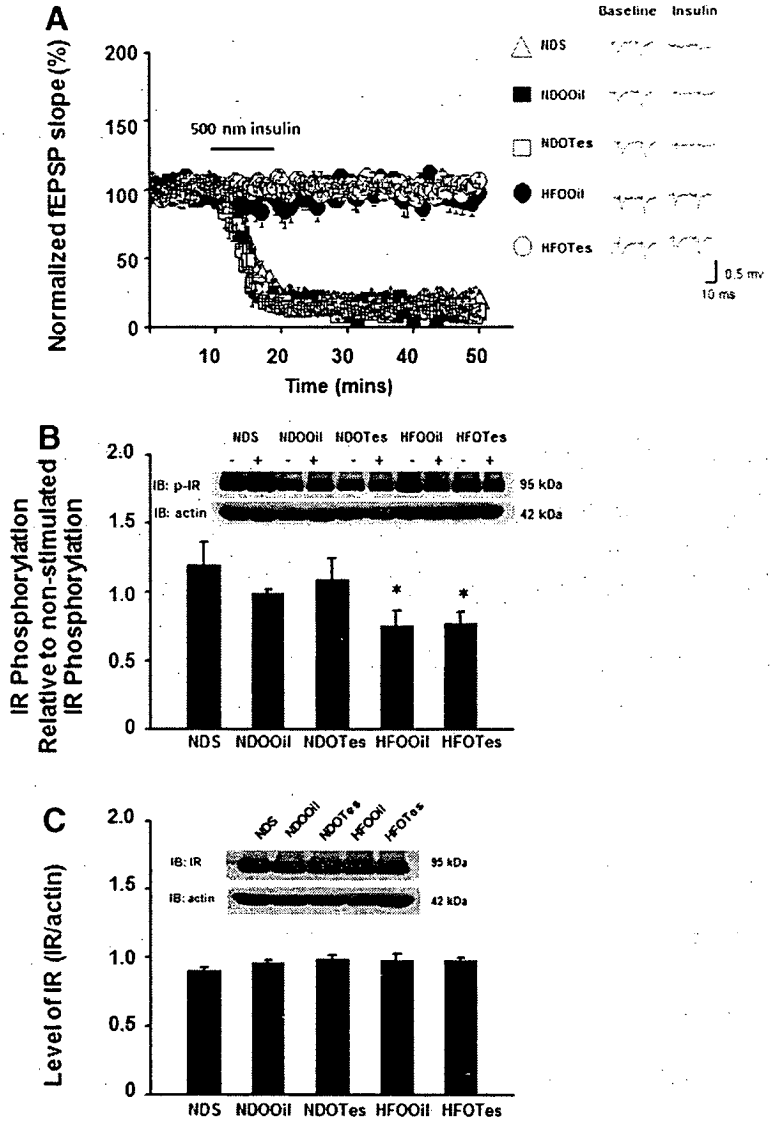
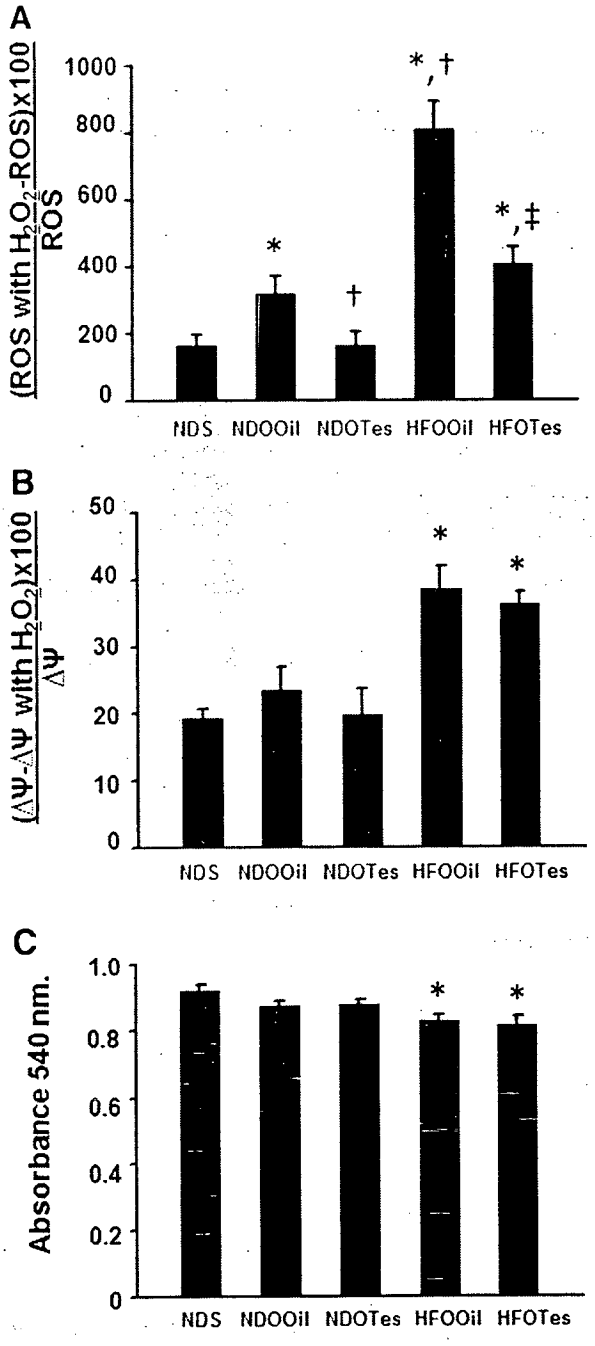


Fig. 2 The effects of testosterone replacement on brain insulin receptor function, including insulin-induced LTD, the phosphorylation of insulin receptor (p-IR), and the expression of insulin receptors (IR) in testosterone-deprived rats with or without obesity. Insulin-induced LTD in the CA1 hippocampus and the phosphorylation of IR are significantly decreased in rats in the HFOOil group, when compared with that of the NDS group (**a**, **b**). Testosterone replacement could not improve the ability of insulin-induced LTD and the phosphorylation of IR in rats in the HFOTes group, when compared with that of HFOOil rats (**a**, **b**). No differences in the expression of IR between all groups were found (**c**). *NDS* sham-operated rats with normal diet feeding, *NDOOil* orchiectomized-operated rats with normal diet feeding and treated with castor oil, *NDOTes* orchiectomized-operated rats with normal diet feeding and treated with testosterone, *HFOOil* orchiectomized-operated rats with high-fat diet feeding and treated with castor oil, *HFOTes* orchiectomized-operated rats fed with a high-fat diet and treated with testosterone; $*p<0.05$ vs NDS band densities of phosphorylated IR were represented as a ratio of insulin stimulation (+) and no insulin stimulation (−) and were normalized to total IR

observed in all ND-fed rats (NDS, NDOOil, and NDOTes) (Fig. 4a–c). Brain mitochondrial swelling was observed in both the HFOOil and HFOTes groups as indicated by markedly unfolded cristae (Fig. 4d, e). All of these findings suggest that testosterone deprivation, with or without obesity, caused an increase in brain mitochondrial ROS production. Obesity alone, but not testosterone deprivation, caused brain mitochondrial dysfunction via increased brain ROS production, brain mitochondrial depolarization and brain mitochondrial swelling. In addition, testosterone replacement reduced brain ROS production in the testosterone-deprived rats with or without obesity, but it did not restore other mitochondrial functions.



◀ **Fig. 3** The effects of testosterone replacement on brain mitochondrial function in testosterone-deprived rats with or without obesity. Rats in the NDOOil group show significantly increased brain mitochondrial ROS production following H_2O_2 application (**a**). Rats in the HFOOil group demonstrated brain mitochondrial dysfunction, as indicated by increased brain mitochondrial ROS production following H_2O_2 application (**a**), increased brain mitochondrial membrane potential change following H_2O_2 application (**b**), and decreased absorbance values, indicating brain mitochondrial swelling (**c**). Testosterone replacement significantly decreased brain mitochondrial ROS production in NDOTes and HFOTes rat groups (**a**). However, testosterone did not improve brain mitochondrial membrane potential change and brain mitochondrial swelling in rats in the HFOTes group (**b**, **c**). *NDS* sham-operated rats with normal diet feeding, *NDOOil* orchiectomized-operated rats with normal diet feeding and treated with castor oil, *NDOTes* orchiectomized-operated rats with normal diet feeding and treated with testosterone, *HFOOil* orchiectomized-operated rats with high-fat diet feeding and treated with castor oil, *HFOTes* orchiectomized-operated rats fed with a high-fat diet and treated with testosterone; $*p<0.05$ vs NDS, $\dagger p<0.05$ vs NDOOil, and $\ddagger p<0.05$ vs HFOOil

Testosterone deprivation with or without obesity caused an increase in brain lipid peroxidation, and testosterone replacement attenuated those impairments

Circulation and brain oxidative stress were determined by assessing serum MDA and brain MDA levels. The results demonstrated that both circulating MDA and brain MDA levels significantly increased in NDOOil, HFOOil, and HFOTes rats compared to NDS rats (Fig. 5a, b). Furthermore, rats in the HFOOil group showed both significantly increased circulating and brain MDA levels compared to NDOOil rats (Fig. 5a, b). Testosterone replacement significantly decreased both circulating MDA and brain MDA levels in NDOTes and HFOTes, but the levels of plasma and brain MDA in NDOTes rats were significantly lower than those in HFOTes rats.

These findings suggest that testosterone deprivation, with or without obesity, increased both circulating and brain lipid peroxidation levels, and testosterone replacement attenuated those impairments.

Testosterone deprivation causes cognitive impairment, and testosterone replacement restores this impairment in non-obese condition

To study hippocampal synaptic plasticity, electrical-induced LTP was determined. The results demonstrated that the degree of electrical-induced LTP was significantly decreased in both NDOOil and HFOOil rats, when compared with that of NDS rats. The reductions of electrical-induced LTP in both NDOOil and HFOOil rats (n=2–3 independent slices/animal, n=6 animals/group Fig. 6a) were not significantly different. In addition, testosterone replacement improved the degree of electrical-induced LTP in only NDOTes rats. These findings indicate that testosterone deprivation with or without obesity caused the impairment of hippocampal synaptic plasticity. However, testosterone replacement

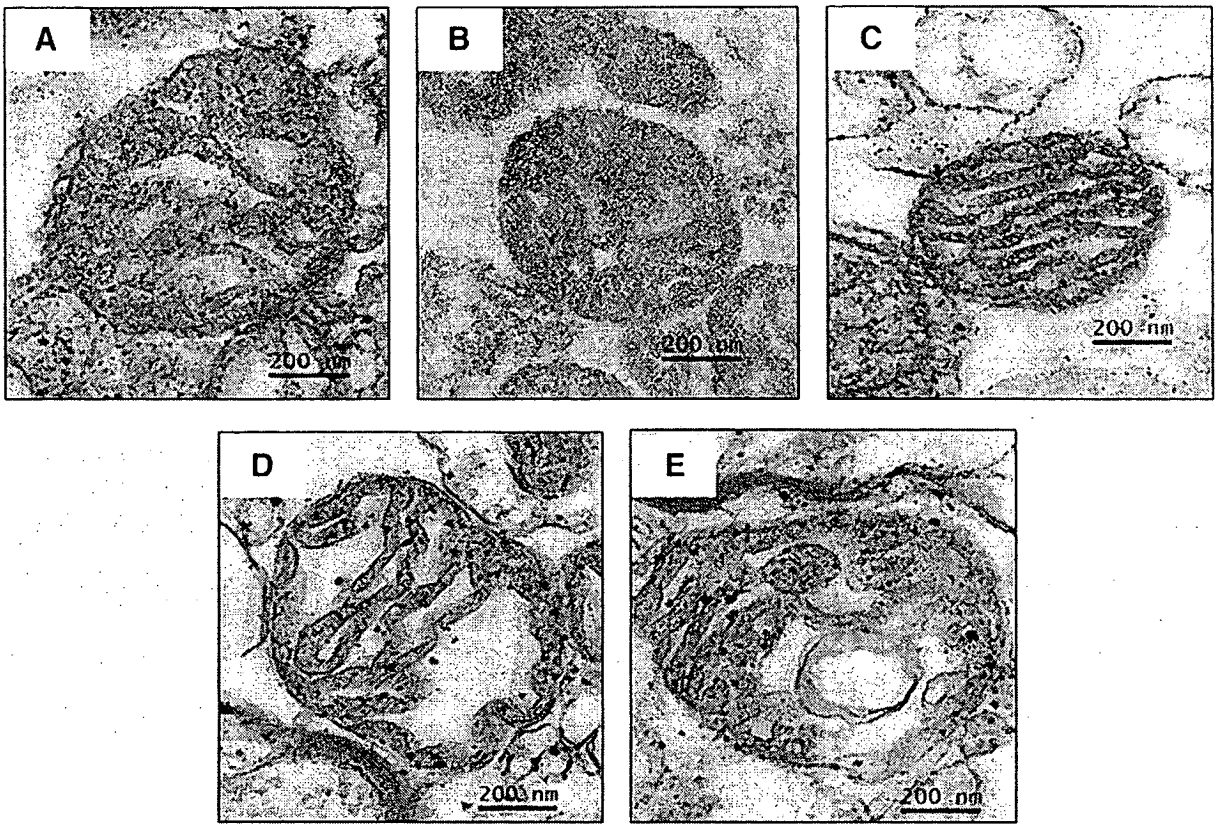


Fig. 4 Representative images of brain mitochondrial morphology by transmission electron microscopy (JEM-2200FS field emission electron microscope, original magnification ×20,000) after testosterone treatment. Normal folding of cristae in brain mitochondrial morphology was shown among all ND-fed rats (**a**–**c**). However, brain mitochondrial swelling, as indicated by unfolded cristae, of both HFOOil and HFOTes groups was observed (**d**, **e**). *NDS* sham-operated rats with normal diet feeding, *NDOOil* orchiectomized-operated rats with normal diet feeding and treated with castor oil, *NDOTes* orchiectomized-operated rats with normal diet feeding and treated with testosterone, *HFOOil* orchiectomized-operated rats with high-fat diet feeding and treated with castor oil, *HFOTes* orchiectomized-operated rats fed with a high-fat diet and treated with testosterone

restored that impairment in testosterone deprivation without obesity.

The OFT was used to screen locomotor activity. The results showed that there was no significant difference between all groups, indicating that the locomotor activity did not differ between the groups (data not shown). In addition, this study determined cognitive function by using the MWM test. For the acquisition test, the time to reach the platform of NDOOil and HFOOil rats was significantly longer than that of NDS rats (Fig. 6b). In addition, testosterone administration could not improve the time to reach the platform in these rats (Fig. 6b).

For the probe test, the time spent in the target quadrant of NDOOil and HFOOil rats was significantly decreased, when compared with that of NDS rats (Fig. 6c). However, no difference was found for this parameter between NDOOil and HFOOil rats (Fig. 6c). Testosterone replacement significantly increased the time spent in the target quadrant of NDOTes rats but not that of HFOTes rats (Fig. 6c).

These findings suggest that testosterone deprivation alone could cause cognitive decline, and testosterone replacement could help restore this impairment. However, testosterone failed to improve cognitive decline when testosterone deprivation was under obese condition. Table 2 summarizes all findings reported in the present study.

Discussion

The major findings of the present study are as follows: (1) testosterone deprivation alone causes the impairment of hippocampal synaptic plasticity and cognitive decline, without causing the impairment of peripheral insulin sensitivity and brain insulin sensitivity, and brain

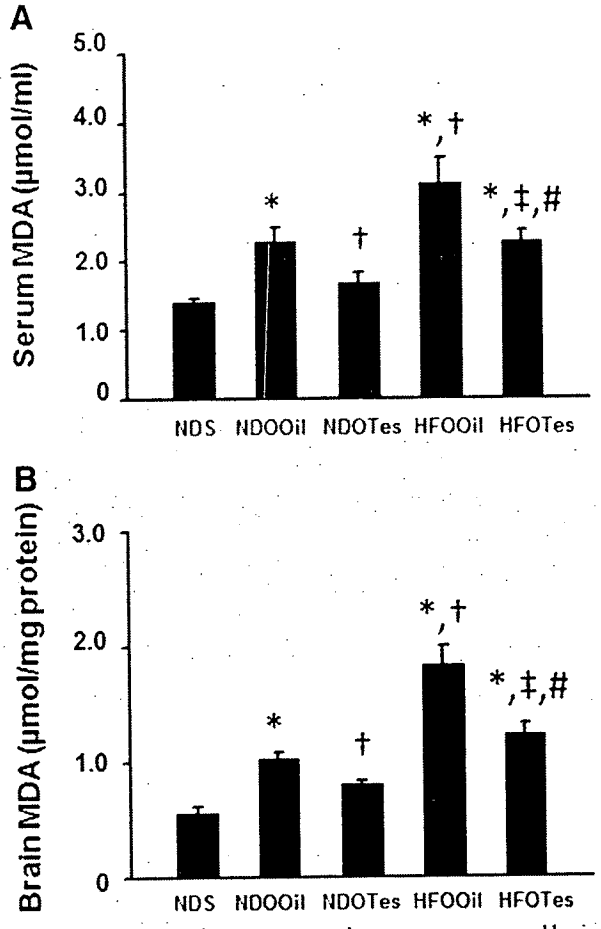


Fig. 5 The effects of testosterone replacement on serum and brain malondialdehyde (MDA) levels in testosterone deprived rats with or without obesity. Both NDOOil and HFOOil treatments significantly increased serum and brain MDA levels (**a**, **b**). Testosterone replacement significantly decreased both serum and brain MDA levels in rats in the NDOTes and HFOTes groups (**a**, **b**). *NDS* sham-operated rats with normal diet feeding, *NDOOil* orchiectomized-operated rats with normal diet feeding and treated with castor oil, *NDOTes* orchiectomized-operated rats with normal diet feeding and treated with testosterone, *HFOOil* orchiectomized-operated rats with high-fat diet feeding and treated with castor oil, *HFOTes* orchiectomized-operated rats fed with a high-fat diet and treated with testosterone; *$p<0.05$ vs NDS, †$p<0.05$ vs NDOOil, ‡$p<0.05$ vs HFOOil, and #$p<0.05$ vs NDOTes

mitochondrial function; (2) testosterone replacement effectively restores the hippocampal synaptic plasticity and cognitive function in these testosterone-deprived rats; (3) testosterone deprivation with obesity causes both peripheral and brain insulin sensitivity, brain mitochondrial dysfunction, and impaired hippocampal synaptic plasticity, resulting in cognitive decline; (4) testosterone replacement improves peripheral insulin sensitivity in these testosterone-deprived obese rats, but fails to restore brain insulin receptor function and cognitive function in testosterone-deprived obese rats; (5) regarding lipid peroxidation, testosterone deprivation increases circulating and brain lipid peroxidation, and obesity aggravates this condition in testosterone-deprived rats; and (6) testosterone replacement causes a decrease in both circulation and brain lipid peroxidation in both testosterone-deprived rats and testosterone-deprived obese rats, but at a greater degree in testosterone deprivation alone.

There is growing evidence that testosterone deprivation is associated with cognitive decline in both men and animal models (Hogervorst et al. 2004; Hogervorst et al. 2001; Sakata et al. 2000; Spritzer et al. 2011). A previous study demonstrated that testosterone deprivation in orchiectomized male rats caused increased oxidative damage and a reduction of antioxidants in the hippocampus (Meydan et al. 2010). In addition, several previous studies showed that testosterone plays an important role in cognitive function (Naghdi et al. 2005; Sakata et al. 2000; Sandstrom et al. 2006; Spritzer et al. 2011). The present study confirms previous findings that rats with testosterone deprivation alone developed cognitive decline, impaired hippocampal synaptic plasticity and showed an increase in brain lipid peroxidation. However, additional findings in this study further demonstrated that there were no alterations in brain insulin sensitivity and brain mitochondrial function in these testosterone-deprived rats. Since brain lipid peroxidation and brain mitochondrial function have been shown to play an important role in brain insulin sensitivity (Muriach et al. 2014; Pipatpiboon et al. 2013), the possible explanation of no alteration of brain insulin sensitivity and brain mitochondrial function in these rats could be due to the fact that the level of brain mitochondrial ROS production and brain lipid peroxidation in these testosterone-deprived rats was not sufficiently high to reach the critical threshold in order to cause brain mitochondrial dysfunction, thus no impaired brain insulin sensitivity was observed in these rats (Aon et al. 2006; Cortassa et al. 2004). Previous studies demonstrated that testosterone deficiency is associated with the impairment of insulin sensitivity (Christoffersen et al. 2010; Georgiev et al. 2011). Orchiectomized rats in that study had significant weight gain. However, in our study and others (Axell et al. 2006; Borst and Conover 2006; Chai et al. 1999; Erben et al. 2000; Gao et al. 2005; Gentry and Wade 1976; Kakolewski et al. 1968), no impairment of insulin

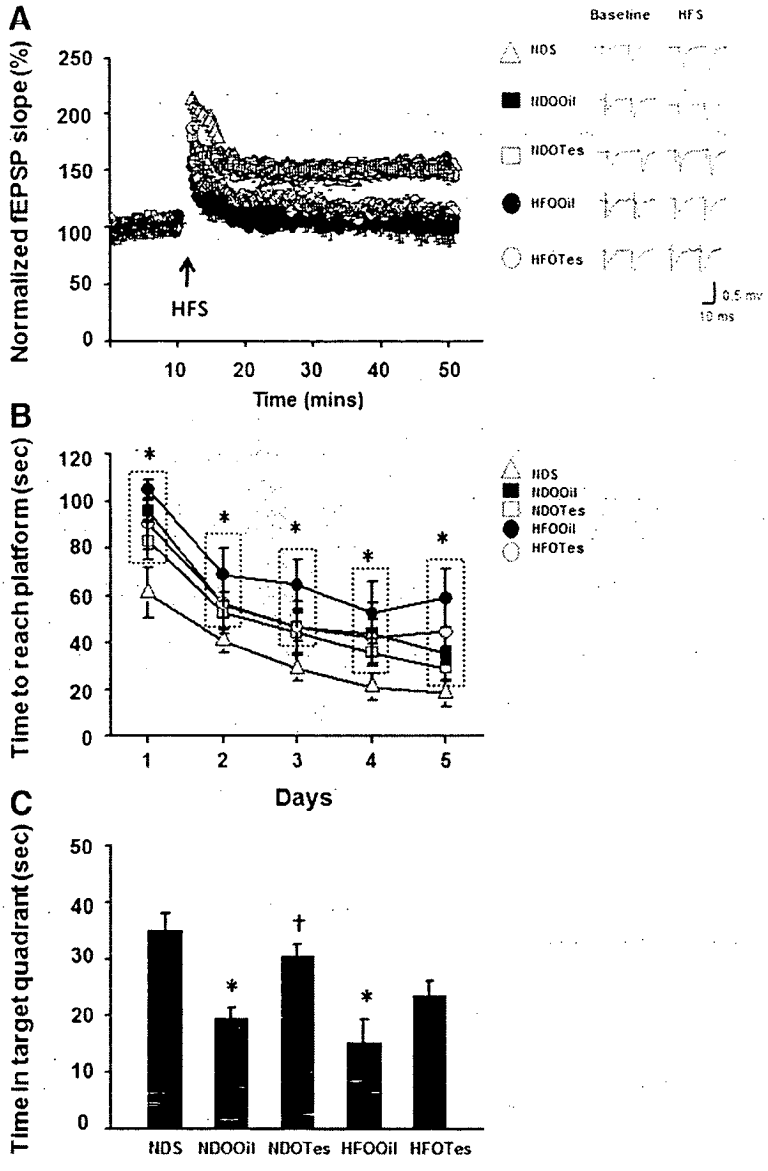


Fig. 6 The effects of testosterone replacement on hippocampal synaptic long-term potentiation (LTP) and cognitive function determined by the Morris water maze (MWM) test in testosterone-deprived rats with or without obesity. Both orchiectomized-operated groups (NDOOil and HFOOil rat groups) showed significantly a reduced percentage of normalized fEPSPs, when compared with that of NDS rats (**a**). Testosterone replacement improves the percentage of normalized fEPSPs in only rats in the NDOTes group, when compared with that of rats in the HFOOil group (**a**). The rats in the HFOOil group showed a significantly increased time to reach the platform in the acquisition test as well as having a decreased time spent in target quadrant in the probe test, when compared with that of the NDS rat group (**b**, **c**). Rats in the NDOOil group showed a significantly decreased time spent in the target quadrant in the probe test, but there was no change in the time taken to reach the platform in the acquisition test (**b**, **c**). Testosterone replacement restored the time spent in the target quadrant in NDOTes rats, but not in HFOTes rats (**c**). *NDS* sham-operated rats with normal diet feeding, *NDOOil* orchiectomized-operated rats with normal diet feeding and treated with castor oil, *NDOTes* orchiectomized-operated rats with normal diet feeding and treated with testosterone, *HFOOil* orchiectomized-operated rats fed on a high-fat diet and treated with castor oil, *HFOTes* orchiectomized-operated rats fed on a high-fat diet and treated with testosterone, *HFS* high-frequency stimulation. *$p<0.05$ vs NDS and †$p<0.05$ vs NDOOil

sensitivity was found. This could be due partly to the fact that no weight gain was observed in those orchiectomized rats.

Previous studies demonstrated that HFD-induced obesity caused the development of peripheral insulin resistance and brain insulin resistance in male rats (Akiyama

Table 2 Summary of findings in rats with and without testosterone treatment

Parameters	Treatment groups				
	NDS	NDOOil	NDOTes	HFOOil	HFOTes
Peripheral insulin sensitivity	Control	–	–	X	✓
Brain insulin sensitivity	Control	–	–	X	X
Brain mitochondrial function	Control	–	–	X	X
Circulation and brain oxidative stress	Control	X	✓	XX	✓
Hippocampal synaptic plasticity	Control	X	✓	X	X
Cognitive function	Control	X	✓	X	X

– no change compared with NDS group, *X* impairment compared with NDS and NDO groups, ✓ improvement when compared with the impaired group of the same diet type, *XX* greater impairment compared with NDO group

et al. 1996; Pratchayasakul et al. 2011; Stranahan et al. 2008). In addition, our previous studies suggest that brain mitochondrial dysfunction and increased brain oxidative stress caused the impairment of brain insulin sensitivity and cognitive decline in obese-insulin resistant rats (Pintana et al. 2013; Pipatpiboon et al. 2013; Pipatpiboon et al. 2012). The present study further demonstrated that it is the obese condition that caused peripheral insulin resistance, brain insulin resistance, and brain mitochondrial dysfunction in testosterone-deprived rats. Similarly to testosterone-deprived rats, these obese testosterone-deprived rats also had increased brain lipid peroxidation with impaired hippocampal synaptic plasticity and showed cognitive decline. All of these findings indicate that both testosterone and obesity play an important role in cognitive function.

Although several studies indicated that testosterone would be pro-oxidant (Siddiqui et al. 2005; Warner et al. 2004), our study showed that testosterone replacement exerted antioxidative effects, as indicated by a reduction in brain mitochondrial ROS level and MDA level in NDO and HFO rats. In the present study, testosterone replacement restored cognitive function, synaptic plasticity, and decreased lipid peroxidation in testosterone-deprived rats. However, testosterone replacement improved only peripheral insulin sensitivity but failed to improve brain insulin sensitivity, hippocampal synaptic plasticity, and cognition in testosterone-deprived obese rats. The beneficial effect of testosterone on metabolic parameters in obese condition was also supported by other previous reports (Isidori et al. 2005; Marin et al. 1992). For cognitive function, although testosterone replacement restored cognitive function possibly through the antioxidant effect in testosterone-deprived rats, we found that this treatment failed to restore cognition, hippocampal synaptic plasticity, and brain insulin sensitivity in testosterone-deprived obese rats. This could be due to the fact that testosterone replacement in the present study could reduce brain mitochondrial ROS production (Fig. 3a) and brain lipid peroxidation levels (Fig. 5b) to a lesser degree in testosterone-deprived obese rats when compared to rats with testosterone deprivation alone. These reductions were not sufficient to restore brain mitochondrial function, increase brain insulin sensitivity, and improve hippocampal synaptic plasticity and cognitive function in testosterone-deprived rats with obesity.

In conclusion, the present study indicates that in conditions of testosterone deprivation with obesity, testosterone replacement could only attenuate peripheral insulin sensitivity, improve lipid profiles, and decrease brain mitochondrial ROS production, as well as circulating and brain lipid peroxidation levels, without restoring hippocampal synaptic plasticity and improving cognitive function. In cases of testosterone deprivation alone, impaired hippocampal synaptic plasticity and cognitive function can be restored by testosterone replacement.

Funding This work was supported by grants from the Thailand Research Fund TRF-BRG5780016 (SC), TRF-TRG5680018 (WP), the Royal Golden Jubilee PhD program (PHD/0025/2555 HP&SC), National Research Council of Thailand (SC), a NSTDA Research Chair Grant from the National Science and Technology Development Agency Thailand (NC), and Chiang Mai University Excellent Center Award (NC).

Conflict of interest The authors declare that they have no conflict of interest.

References

Akiyama T, Tachibana I, Shirohara H, Watanabe N, Otsuki M (1996) High-fat hypercaloric diet induces obesity, glucose intolerance and hyperlipidemia in normal adult male Wistar rat. Diabetes Res Clin Pract 31:27–35

Aon MA, Cortassa S, Akar FG, O'Rourke B (2006) Mitochondrial criticality: a new concept at the turning point of life or death. Biochim Biophys Acta 1762:232–240. doi:10.1016/j.bbadis.2005.06.008

Arakawa H (2005) Age dependent effects of space limitation and social tension on open-field behavior in male rats. Physiol Behav 84:429–436. doi:10.1016/j.physbeh.2005.01.008

Axell AM et al (2006) Continuous testosterone administration prevents skeletal muscle atrophy and enhances resistance to fatigue in orchidectomized male mice. Am J Physiol Endocrinol Metab 291:E506–E516. doi:10.1152/ajpendo.00058.2006

Aydilek N, Aksakal M (2005) Effects of testosterone on lipid peroxidation, lipid profiles and some coagulation parameters in rabbits. J Vet Med A Physiol Pathol Clin Med 52:436–439. doi:10.1111/j.1439-0442.2005.00764.x

Bassil N, Morley JE (2010) Late-life onset hypogonadism: a review. Clin Geriatr Med 26:197–222. doi:10.1016/j.cger.2010.02.003

Borst SE, Conover CF (2006) Orchiectomized Fischer 344 male rat models body composition in hypogonadal state. Life Sci 79:411–415. doi:10.1016/j.lfs.2006.01.035

Buletko AB, Dluzen DE, McDermott JL, Darvesh AS, Geldenhuys WJ (2012) Markers associated with testosterone enhancement of methamphetamine-induced striatal dopaminergic neurotoxicity. Neurotoxicol Teratol 34:338–343. doi:10.1016/j.ntt.2012.03.003

Candan N, Tuzmen N (2008) Very rapid quantification of malondialdehyde (MDA) in rat brain exposed to lead, aluminium and phenolic antioxidants by high-performance liquid chromatography-fluorescence detection. Neurotoxicology 29:708–713. doi:10.1016/j.neuro.2008.04.012

Chai JK, Blaha V, Meguid MM, Laviano A, Yang ZJ, Varma M (1999) Use of orchiectomy and testosterone replacement to explore meal number-to-meal size relationship in male rats. Am J Physiol 276:R1366–R1373

Christoffersen BO, Gade LP, Golozoubova V, Svendsen O, Raun K (2010) Influence of castration-induced testosterone and estradiol deficiency on obesity and glucose metabolism in male Gottingen minipigs. Steroids 75:676–684. doi:10.1016/j.steroids.2010.04.004

Cortassa S, Aon MA, Winslow RL, O'Rourke B (2004) A mitochondrial oscillator dependent on reactive oxygen species. Biophys J 87:2060–2073. doi:10.1529/biophysj.104.041749

Cunningham GR, Toma SM (2010) Clinical review: why is androgen replacement in males controversial? J Clin Endocrinol Metab 96:38–52. doi:10.1210/jc.2010-0266

Cunningham RL, Giuffrida A, Roberts JL (2009) Androgens induce dopaminergic neurotoxicity via caspase-3-dependent activation of protein kinase Cdelta. Endocrinology 150:5539–5548. doi:10.1210/en.2009-0640

Donatucci C, Cui Z, Fang Y, Muram D (2014) Long-term treatment patterns of testosterone replacement medications. J Sex Med 11:2092–2099. doi:10.1111/jsm.12608

Emamian S, Naghdi N, Sepehri H, Jahanshahi M, Sadeghi Y, Choopani S (2010) Learning impairment caused by intra-CA1 microinjection of testosterone increases the number of astrocytes. Behav Brain Res 208:30–37. doi:10.1016/j.bbr.2009.11.004

Erben RG, Eberle J, Stahr K, Goldberg M (2000) Androgen deficiency induces high turnover osteopenia in aged male rats: a sequential histomorphometric study. J Bone Miner Res 15:1085–1098. doi:10.1359/jbmr.2000.15.6.1085

Gao W, Reiser PJ, Coss CC, Phelps MA, Kearbey JD, Miller DD, Dalton JT (2005) Selective androgen receptor modulator treatment improves muscle strength and body composition and prevents bone loss in orchidectomized rats. Endocrinology 146:4887–4897. doi:10.1210/en.2005-0572

Gentry RT, Wade GN (1976) Androgenic control of food intake and body weight in male rats. J Comp Physiol Psychol 90:18–25

Georgiev IP et al (2011) Effects of castration-induced visceral obesity and antioxidant treatment on lipid profile and insulin sensitivity in New Zealand white rabbits. Res Vet Sci 90:196–204. doi:10.1016/j.rvsc.2010.05.023

Grossmann M et al (2008) Low testosterone levels are common and associated with insulin resistance in men with diabetes. J Clin Endocrinol Metab 93:1834–1840. doi:10.1210/jc.2007-2177

Haffner SM, Karhapaa P, Mykkanen L, Laakso M (1994) Insulin resistance, body fat distribution, and sex hormones in men. Diabetes 43:212–219

Harooni HE, Naghdi N, Sepehri H, Rohani AH (2008) Intra hippocampal injection of testosterone impaired acquisition, consolidation and retrieval of inhibitory avoidance learning and memory in adult male rats. Behav Brain Res 188:71–77. doi:10.1016/j.bbr.2007.10.017

Hogervorst E, Williams J, Budge M, Barnetson L, Combrinck M, Smith AD (2001) Serum total testosterone is lower in men with Alzheimer's disease. Neuro Endocrinol Lett 22:163–168

Hogervorst E, Bandelow S, Combrinck M, Smith AD (2004) Low free testosterone is an independent risk factor for Alzheimer's disease. Exp Gerontol 39:1633–1639. doi:10.1016/j.exger.2004.06.019

Isidori AM et al (2005) Effects of testosterone on body composition, bone metabolism and serum lipid profile in middle-aged men: a meta-analysis. Clin Endocrinol (Oxf) 63:280–293. doi:10.1111/j.1365-2265.2005.02339.x

Janowsky JS (2006) Thinking with your gonads: testosterone and cognition. Trends Cogn Sci 10:77–82. doi:10.1016/j.tics.2005.12.010

Kakolewski JW, Cox VC, Valenstein ES (1968) Sex differences in body-weight change following gonadectomy of rats. Psychol Rep 22:547–554

Kenny AM, Fabregas G, Song C, Biskup B, Bellantonio S (2004) Effects of testosterone on behavior, depression, and cognitive function in older men with mild cognitive loss. J Gerontol A Biol Sci Med Sci 59:75–78

Khorshidahmad T et al (2012) Interactive effects of a protein kinase AII inhibitor and testosterone on spatial learning in the Morris water maze. Behav Brain Res 228:432–439. doi:10.1016/j.bbr.2011.12.028

Lu PH et al (2006) Effects of testosterone on cognition and mood in male patients with mild Alzheimer disease and healthy

elderly men. Arch Neurol 63:177–185. doi:10.1001/archneur.63.2.nct50002

Maki PM et al (2007) Intramuscular testosterone treatment in elderly men: evidence of memory decline and altered brain function. J Clin Endocrinol Metab 92:4107–4114. doi:10.1210/jc.2006-1805

Margo K, Winn R (2006) Testosterone treatments: why, when, and how? Am Fam Physician 73:1591–1598

Marin P et al (1992) The effects of testosterone treatment on body composition and metabolism in middle-aged obese men. Int J Obes Relat Metab Disord 16:991–997

Mateos R, Lecumberri E, Ramos S, Goya L, Bravo L (2005) Determination of malondialdehyde (MDA) by high-performance liquid chromatography in serum and liver as a biomarker for oxidative stress. Application to a rat model for hypercholesterolemia and evaluation of the effect of diets rich in phenolic antioxidants from. J Chromatogr B Analyt Technol Biomed Life Sci 827:76–82. doi:10.1016/j.jchromb.2005.06.035

Meydan S et al (2010) Effects of testosterone on orchiectomy-induced oxidative damage in the rat hippocampus. J Chem Neuroanat 40:281–285. doi:10.1016/j.jchemneu.2010.07.006

Muriach M, Flores-Bellver M, Romero FJ, Barcia JM (2014) Diabetes and the brain: oxidative stress, inflammation, and autophagy. Oxid Med Cell Longev 2014:102158. doi:10.1155/2014/102158

Naghdi N, Asadollahi A (2004) Genomic and nongenomic effects of intrahippocampal microinjection of testosterone on long-term memory in male adult rats. Behav Brain Res 153:1–6. doi:10.1016/j.bbr.2003.10.027

Naghdi N, Majlessi N, Bozorgmehr T (2005) The effect of intrahippocampal injection of testosterone enanthate (an androgen receptor agonist) and anisomycin (protein synthesis inhibitor) on spatial learning and memory in adult, male rats. Behav Brain Res 156:263–268. doi:10.1016/j.bbr.2004.05.032

Pintana H, Apaijai N, Pratchayasakul W, Chattipakorn N, Chattipakorn SC (2012) Effects of metformin on learning and memory behaviors and brain mitochondrial functions in high fat diet induced insulin resistant rats. Life Sci 91:409–414. doi:10.1016/j.lfs.2012.08.017

Pintana H, Apaijai N, Chattipakorn N, Chattipakorn SC (2013) DPP-4 inhibitors improve cognition and brain mitochondrial function of insulin resistant rats. J Endocrinol 218:1–11. doi:10.1530/JOE-12-0521

Pintana H, Sripetchwandee J, Supakul L, Apaijai N, Chattipakorn N, Chattipakorn S (2014) Garlic extract attenuates brain mitochondrial dysfunction and cognitive deficit in obese-insulin resistant rats. Appl Physiol Nutr Metab 39:1373–1379. doi:10.1139/apnm-2014-0255

Pipatpiboon N, Pratchayasakul W, Chattipakorn N, Chattipakorn SC (2012) PPARgamma agonist improves neuronal insulin receptor function in hippocampus and brain mitochondria function in rats with insulin resistance induced by long term high-fat diets. Endocrinology 153:329–338. doi:10.1210/en.2011-1502

Pipatpiboon N, Pintana H, Pratchayasakul W, Chattipakorn N, Chattipakorn SC (2013) DPP4-inhibitor improves neuronal insulin receptor function, brain mitochondrial function and cognitive function in rats with insulin resistance induced by high-fat diet consumption. Eur J Neurosci 37:839–849. doi:10.1111/ejn.12088

Pongkan W, Chattipakorn SC, Chattipakorn N (2015) Chronic testosterone replacement exerts cardioprotection against cardiac ischemia-reperfusion injury by attenuating mitochondrial dysfunction in testosterone-deprived rats. PLoS One 10, e0122503. doi:10.1371/journal.pone.0122503

Pratchayasakul W, Kerdphoo S, Petsophonsakul P, Pongchaidecha A, Chattipakorn N, Chattipakorn SC (2011) Effects of high-fat diet on insulin receptor function in rat hippocampus and the level of neuronal corticosterone. Life Sci 88:619–627. doi:10.1016/j.lfs.2011.02.003

Sakata K, Tokue A, Kawai N (2000) Altered synaptic transmission in the hippocampus of the castrated male mouse is reversed by testosterone replacement. J Urol 163:1333–1338

Sandstrom NJ, Kim JH, Wasserman MA (2006) Testosterone modulates performance on a spatial working memory task in male rats. Horm Behav 50:18–26. doi:10.1016/j.yhbeh.2005.09.008

Shi Z, Araujo AB, Martin S, O'Loughlin P, Wittert GA (2013) Longitudinal changes in testosterone over five years in community-dwelling men. J Clin Endocrinol Metab 98:3289–3297. doi:10.1210/jc.2012-3842

Siddiqui IA, Raisuddin S, Shukla Y (2005) Protective effects of black tea extract on testosterone induced oxidative damage in prostate. Cancer Lett 227:125–132. doi:10.1016/j.canlet.2004.10.046

Spritzer MD, Daviau ED, Coneeny MK, Engelman SM, Prince WT, Rodriguez-Wisdom KN (2011) Effects of testosterone on spatial learning and memory in adult male rats. Horm Behav 59:484–496. doi:10.1016/j.yhbeh.2011.01.009

Sripetchwandee J, Pipatpiboon N, Chattipakorn N, Chattipakorn S (2014) Combined therapy of iron chelator and antioxidant completely restores brain dysfunction induced by iron toxicity. PLoS One 9, e85115. doi:10.1371/journal.pone.0085115

Stellato RK, Feldman HA, Hamdy O, Horton ES, McKinlay JB (2000) Testosterone, sex hormone-binding globulin, and the development of type 2 diabetes in middle-aged men: prospective results from the Massachusetts male aging study. Diabetes Care 23:490–494

Stranahan AM, Norman ED, Lee K, Cutler RG, Telljohann RS, Egan JM, Mattson MP (2008) Diet-induced insulin resistance impairs hippocampal synaptic plasticity and cognition in middle-aged rats. Hippocampus 18:1085–1088. doi:10.1002/hipo.20470

Vaughan C, Goldstein FC, Tenover JL (2007) Exogenous testosterone alone or with finasteride does not improve measurements of cognition in healthy older men with low serum testosterone. J Androl 28:875–882. doi:10.2164/jandrol.107.002931

Vorhees CV, Williams MT (2006) Morris water maze: procedures for assessing spatial and related forms of learning and memory. Nat Protoc 1:848–858. doi:10.1038/nprot.2006.116

Warner DS, Sheng H, Batinic-Haberle I (2004) Oxidants, antioxidants and the ischemic brain. J Exp Biol 207:3221–3231. doi:10.1242/jeb.01022

Wolf OT, Preut R, Hellhammer DH, Kudielka BM, Schurmeyer TH, Kirschbaum C (2000) Testosterone and cognition in elderly men: a single testosterone injection blocks the practice effect in verbal fluency, but has no effect on spatial or verbal memory. Biol Psychiatry 47:650–654

เอกสารแนบหมายเลข 41

European Journal of Pharmacology 765 (2015) 86–93

Contents lists available at ScienceDirect

European Journal of Pharmacology

journal homepage: www.elsevier.com/locate/ejphar

Review

Current and future treatment strategies for iron overload cardiomyopathy

Suwakon Wongjaikam [a,b,c], Sirinart Kumfu [a,b,c], Siriporn C. Chattipakorn [a,c,d], Suthat Fucharoen [e], Nipon Chattipakorn [a,b,c,*]

[a] Cardiac Electrophysiology Research and Training Center, Faculty of Medicine, Chiang Mai University, Chiang Mai, Thailand
[b] Cardiac Electrophysiology Unit, Department of Physiology, Faculty of Medicine, Chiang Mai University, Chiang Mai, Thailand
[c] Center of Excellence in Cardiac Electrophysiology Research, Chiang Mai University, Chiang Mai, Thailand
[d] Department of Oral Biology and Diagnostic Sciences, Faculty of Dentistry, Chiang Mai University, Chiang Mai, Thailand
[e] Thalassemia Research Center, Institute of Molecular Bioscience, Mahidol University, Nakhon Pathom, Thailand

ARTICLE INFO

Article history:
Received 29 May 2015
Received in revised form
11 August 2015
Accepted 12 August 2015
Available online 18 August 2015

Keywords:
Iron overload cardiomyopathy
Iron chelator
Deferoxamine
Deferiprone
Deferasirox
Antioxidant

ABSTRACT

Iron overload cardiomyopathy is the major cause of death in transfusion-dependent thalassemia (TDT) patients. Growing evidence demonstrates that combined iron chelators, or the combination of an iron chelator with antioxidant(s) are effective in diminishing myocardial iron deposition and attenuating cardiac dysfunction. This review comprehensively summarizes basic and clinical reports on the therapeutic efficacy of combined iron chelators, or the combination of an iron chelator with antioxidant(s) on the heart. Promising benefits of these treatments in preventing cardiac dysfunction due to iron overload could provide extensive insight into future therapeutic strategies for better treatment and prevention of cardiomyopathy in TDT patients.

© 2015 Elsevier B.V. All rights reserved.

Contents

1. Iron overload cardiomyopathy and current therapy 86
2. Combined iron chelator therapy 87
   2.1. Effects of DFO+DFX 87
   2.2. Effects of DFO+DFP 89
   2.3. Effects of DFP+DFX 90
3. Combined iron chelator with antioxidant therapy 90
4. Possible roles of antioxidant therapy in iron overload cardiomyopathy 90
5. Conclusion 92
Acknowledgments 92
References 92

1. Iron overload cardiomyopathy and current therapy

Iron overload cardiomyopathy can progress to heart failure either as a result of excess dietary iron absorption in hereditary hemochromatosis, or from repeated blood transfusions in transfusion-dependent thalassemia (TDT) patients. Iron loading of cardiac tissue is often a late and dangerous complication of iron overload. Subsequent heart failure is the major cause of death (60%), greatly exceeding death from infection (13%) and liver disease (6%) in thalassemia patients (Borgna-Pignatti et al., 2004; Zurlo et al., 1989). Moreover, chronic iron overload can lead to several diseases in patients including cirrhosis, diabetes, neurodegenerative disease and endocrine disorders (Hershko, 2010; Wood et al., 2010).

* Corresponding author at: Cardiac Electrophysiology Research and Training Center, Faculty of Medicine, Chiang Mai University, Chiang Mai, Thailand. Fax: +66 53 945368.
E-mail address: nchattip@gmail.com (N. Chattipakorn).

http://dx.doi.org/10.1016/j.ejphar.2015.08.017
0014-2999/© 2015 Elsevier B.V. All rights reserved.

Under iron overload condition, non-transferrin bound iron (NTBI) can appear when the capacity of transferrin-bound iron becomes saturated, leading to increased free iron (labile iron) in plasma (Hershko, 2010; Hider et al., 2010). Excess plasma NTBI leads to increase in the entry of free iron into cells, leading to iron toxicity (Hershko, 2010; Hider et al., 2010). Growing evidence demonstrates that the calcium channels, both L-type calcium channel (LTCC) (Oudit et al., 2003, 2006) and T-type calcium channel (TTCC) (Kumfu et al., 2012, 2011), are potentially the main routes of iron uptake into the heart tissue under conditions of iron overload (Wijampreecha et al., 2015). In the heart, it has been shown that iron enters the myocardium through LTCC and TTCC, and is stored in the myocytes in the form of ferritin, hemosiderin and the labile cellular iron pool (Kremastinos and Farmakis, 2011). Labile iron leads to the formation of reactive oxygen species (ROS) via Fenton's reaction, in which ferrous iron reacts with hydrogen peroxide (H_2O_2) to generate highly toxic hydroxyl radicals (Fibach and Rachmilewitz, 2010; Kremastinos and Farmakis, 2011). Under conditions of iron overload, cellular antioxidant properties are exceeded, resulting in the peroxidation of membrane lipids, cellular proteins and nucleic acids (Fibach and Rachmilewitz, 2010; Hershko, 2010; Kremastinos and Farmakis, 2011). ROS damage many cellular organelles and lead to cardiac dysfunction and heart failure in patients, as shown in Fig. 1. Hence iron chelation treatment, which can reduce the storage of iron in the body and improve the long-term survival rate of iron overload cardiomyopathy patients, is considered a necessary adjuvant therapy.

Currently, iron chelation is the main therapy available to treat conditions of iron overload. The therapy uses the parenteral iron chelator deferoxamine (DFO), and the oral iron chelators deferiprone (DFP) and deferasirox (DFX). Many studies have shown that DFO, DFP and DFX can cause a reduction in myocardial iron with acceptable safety profiles (Hershko, 2006; Maggio et al., 2002; Pennell et al., 2006, 2012; Pepe et al., 2006; Piga et al., 2010; Porter, 2010; Tanner et al., 2007, 2008; Wood et al., 2010). However, some patients fail to respond adequately to monotherapy, whilst others often present with serious side effects which limit the use of the drugs (Otto-Duessel et al., 2008).

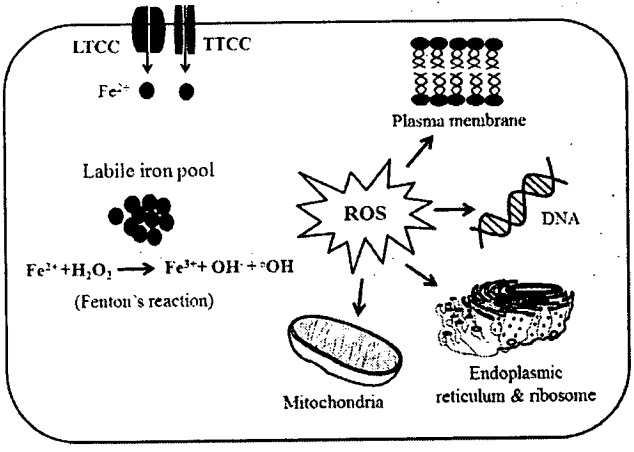


Fig. 1. The mechanism of iron overload cardiomyopathy. Although there are several portals for iron entry into the heart, L-type calcium channel (LTCC) and T-type calcium channel (TTCC) have been shown to play an important role in iron entry into cardiac cells. Ferrous iron (Fe^{2+}) is taken up into the heart through the main routes LTCC and TTCC under iron overload condition. Iron toxicity occurs when there is too much free iron or labile iron pool in the cells. Labile iron leads to the formation of reactive oxygen species (ROS) via Fenton's reaction, in which ferrous iron reacts with hydrogen peroxide (H_2O_2) to generate highly toxic hydroxyl radicals ($^{\bullet}OH$). ROS damages many cellular organelles including mitochondria, endoplasmic reticulum, ribosome, deoxyribonucleic acid (DNA) and plasma membrane which results in chronic cardiac dysfunction and heart failure.

DFO is the gold standard drug for treating transfusional iron overload, and is the chelator that has been in use for the longest (Hoffbrand et al., 2012). Although DFO efficiently removes cardiac iron, its efficacy is greater when administered continuously rather than intermittently (Aldouri et al., 1990; Lerner et al., 1990). It has been shown that DFO is effective for liver iron chelation but not for cardiac iron removal since some patients developed cardiac iron overload, arrhythmia and heart failure despite normal liver iron levels (Aldouri et al., 1990; Anderson et al., 2006; Lerner et al., 1990).

DFP has the lowest molecular weight of the 3 iron chelators and penetrates cells to chelate iron from intracellular organelles, such as lysosomes and mitochondria (Glickstein et al., 2005). DFP exerts superior beneficial effects compared to DFO in reducing cardiac iron levels (Anderson et al., 2002; Hershko, 2006; Piga et al., 2003, 2010), however a serious side effect following DFP administration is agranulocytosis (Hoffbrand et al., 2012; Piga et al., 2010). Agranulocytosis occurs in approximately 1% of patients in the first year of treatment, however it has also been reported in the second and later years, although more rarely (Hoffbrand et al., 2012). Although it may be reversible, this reaction can be fatal in some patients (Hoffbrand et al., 2012).

DFX is the most recently introduced iron chelator, and exerts its beneficial effects through removing iron from the heart tissue in patients (Cappellini et al., 2010; Pennell et al., 2011, 2010; Porter, 2010). DFX may cause renal and hepatic failure, and gastrointestinal hemorrhage which has led to death in some reported cases (Hoffbrand et al., 2012). However, these adverse effects of DFX are usually found in patients of advanced age, with high-risk myelodysplasia, and those with underlying renal or hepatic impairment or low platelet counts (Hoffbrand et al., 2012).

Currently, in patients in which treatment with a single iron chelator fails to lead to any therapeutic benefits, the intensity of chelation can be augmented by several options including increasing the duration of exposure to the chelator (Davis and Porter, 2000), raising the dose to the maximum tolerated level (Taher et al., 2009) or adding a second chelator (Tanner et al., 2007). Growing evidence has demonstrated that the combination of iron chelators, the combination of an iron chelator with antioxidant(s), or antioxidant(s) alone provide a high level of efficacy in reducing myocardial iron deposition and attenuating cardiac dysfunction. In this review, many reports have been comprehensively summarized to examine the efficacy of treatment using combined iron chelators, a combination of an iron chelator with an antioxidant, or an antioxidant alone on the heart using both animal models and TDT patients. The promising benefits of these treatments in preventing cardiac dysfunction due to iron overload could provide useful insight into future therapeutic strategies for better treatment and even enable prevention of symptoms in TDT patients.

2. Combined iron chelator therapy

Since conditions in some iron-overloaded patients showed no improvement when treated with a single iron chelator, a combined chelation therapy has been suggested as a better approach for patients with iron overload complications, due to its increased efficacy. Evidence supporting this notion is comprehensively summarized in Table 1 for DFO+DFX, Table 2 for DFO+DFP, and Table 3 for DFP+DFX.

2.1. Effects of DFO+DFX

Previous studies found that after 1 year of treatment with single iron chelator, DFO or DFX, serum ferritin decreased by 12–33% (Maggio et al., 2002; Pennell et al., 2006, 2014), and 30–33% (Merchant et al., 2012; Pennell et al., 2014), respectively. Magnetic

Table 1
Reports on the effects of combined DFO plus DFX in cases of iron overload cardiomyopathy.

Model	Iron overload induction	Intervention	Results		Interpretation	References
			Heart	Liver		
Female Mongolian gerbils	Iron dextran injection (200 mg/kg/day, s.c.)/10 weeks	DFO (200 mg/kg/day, s.c.)/DFX (100 mg/kg/day, p.o.)/combined DFO (200 mg/kg/day, s.c.)+DFX (100 mg/kg/day, p.o.)/4 weeks	Combined therapy exerted similar efficacy to monotherapy in promoting a decrease in cardiac iron concentration.	Only DFX caused a significant reduction in hepatic iron similar to combined therapy.	Combined DFO+DFX treatment produced no additional effects compared to monotherapy in either the liver or heart.	(Pitta-Dumrongdeesiri et al., 2008)
22 TM patients	Transfusion-dependent TM patients with either moderate iron overload (LIC ≤ 14 mg/g dry liver-weight) or severe iron overload (LIC > 14 mg/g dry liver-weight)	Combined DFO (35–50 mg/kg for 3–7 days/week, s.c.)+DFX (20–30 mg/kg/day, p.o.)/12 months	Combined therapy improved cardiac MRI T2*.	Combined therapy caused a significant decrease in liver iron concentration.	Combined DFO+DFX treatment caused a rapid decrease in liver and myocardial iron.	(Lai et al., 2013)
10 thalassemia patients	Transfusion-dependent thalassemia patients (ferritin level range 644–17,681 ng/ml)	Combined DFO (32 ± 4 mg/kg/day, for 3–4 days/week, s.c.)+DFX (20 ± 2 mg/kg/day, p.o.)/12 months	Combined therapy improved cardiac MRI T2*.	Combined therapy caused a significant decrease in liver iron concentration.	Combined DFO+DFX treatment was effective in reducing heart and liver iron concentrations.	(Cassinerio et al., 2014)

TM thalassemia major; **s.c.** subcutaneous injection; **p.o.** per oral; **DFO** deferoxamine; **DFX** deferasirox; **LIC** liver iron concentration; **MRI** magnetic resonance imaging.

Table 2
Reports on the effects of combined DFO plus DFP in cases of iron overload cardiomyopathy.

Model	Iron overload induction	Intervention	Results		Interpretation	References
			Heart	Liver		
79 TM patients	TM patients with severe iron overload (serum ferritin > 3000 ng/mL)	Combined DFO (40 ± 10 mg/kg for 2–6 days/week, s.c.)+ DFP (70–80 mg/kg/day, p.o.)/12–56 months	Combined therapy improved LVEF.	–	Combined DFO+DFP treatment was effective in improving heart function.	(Ortiga et al., 2005)
22 TM patients	TM patients with severe myocardial siderosis (T2* < 8 ms)	Combined DFO (38 ± 10.2 mg/kg for 5.3 days/week, s.c.)+DFP (73.9 ± 4.0 mg/kg/day, p.o.)/12 months	Combined therapy improved cardiac MRI T2* and LVEF.	Combined therapy improved liver MRI T2*.	Combined DFO+DFP treatment was effective in reducing myocardial iron and improving heart function.	(Tanner et al., 2008)
80 TM patients	TM patients with T2* 8–20 ms (mild-moderate iron loading) and T2* < 8 ms (severe iron loading)	Combined DFO (40.6 ± 13.2 mg/kg for 5 days/week, s.c.)+DFP (75 mg/kg/day, p.o.)/combined DFO (40.6 ± 13.2 mg/kg for 5 days/week, s.c.)+placebo (75 mg/kg/day, p.o.)/12 months	Combined therapy significantly increased RVEF and heart MRI T2*, and more effective than DFO alone.	–	Combined DFO+DFP treatment was more effective in improving right ventricular function and decreasing cardiac iron than DFO alone.	(Aipendurada et al., 2012)
164 TM patients	Transfusion-dependent TM patients	DFO (42.2 ± 6.7 mg/kg/day, s.c.)/DFP (79.2 ± 7.8 mg/kg/day, p.o.)/combined DFO (41.7 ± 6.5 mg/kg/day, s.c.)+DFP (65.2 ± 22.5 mg/kg/day, p.o.)/18 months	Combined therapy improved heart MRI T2* at a similar rate to DFP but at a greater rate than DFO, and exerted similar efficacy to monotherapy in improving biventricular function.	Combined therapy significantly decreased liver iron concentration and produced more effective than monotherapy.	Combined DFO+DFP treatment was more effective in removing cardiac iron than DFO alone, and was superior in clearing hepatic iron than monotherapy.	(Pepe et al., 2012)

TM thalassemia major; **s.c.** subcutaneous injection; **p.o.** per oral; **DFO** deferoxamine; **DFP** deferiprone; **MRI** magnetic resonance imaging; **LVEF** left ventricular ejection fraction; **RVEF** right ventricular ejection fraction.

Table 3
Reports on the effects of combined DFP plus DFX in cases of iron overload cardiomyopathy.

Model	Iron overload induction	Intervention	Results		Interpretation	Reference
			Heart	Liver		
One TM patient	A transfusion-dependent TM patient	Combined DFP (75 mg/kg/day, p.o.)+DFX (30 mg/kg/day, p.o.)/12 months	Combined therapy improved cardiac MRI T2*.	Combined therapy improved liver MRI T2*.	Combined DFP+DFX treatment was extremely effective in reducing heart and liver iron depositions.	(Voskaridou et al., 2011)
16 TM patients	Transfusion-dependent TM patients	Combined DFP (75–100 mg/kg/day, p.o.)+DFX (20–25 mg/kg/day, p.o.)/24 months	Combined therapy improved cardiac MRI T2* and LVEF in 2/4 patients.	Combined therapy significantly decreased liver iron concentration and improved liver MRI T2*.	Combined DFP+DFX treatment was effective and prevented associated symptoms of iron- overloaded liver and heart.	(Farmaki et al., 2011)
3 thalassemia patients	Patients with cardiac MRI T2* < 6 ms (severe iron loading)	Combined DFP (75 mg/kg/ day, p.o.)+DFX (20–40 mg/kg/day, p.o.)/7–28 months	Combined therapy decreased cardiac iron rapidly and improved cardiac MRI T2*.	Combined therapy decreased liver iron concentration in 1/3 patients.	Combined DFP+DFX treatment caused a significant decrease in cardiac iron and improved cardiac function.	(Berdoukas et al., 2010)

TM thalassemia major; **p.o.** per oral; **DFP** deferiprone; **DFX** deferasirox; **MRI** magnetic resonance imaging; **LVEF** left ventricular ejection fraction.

resonance imaging T2* (MRI T2*) is a non-invasive method for determining the level of iron accumulation in the heart/liver, and is currently considered as a very useful tool to predict cardiac/liver complication in thalassemia (Barzin et al., 2012; Hoffbrand et al., 2012). Cardiac T2* improved after 1 year of treatment with DFO by 7–13% (Pennell et al., 2006, 2014; Smith et al., 2011), and after 1 and 3 years of treatment with DFX by 12–29% (Merchant et al., 2012; Pennell et al., 2014) and 43% (Pennell et al., 2012), respectively. DFO improved LVEF by only 0.3–2% (Maggio et al., 2002; Pennell et al., 2006), and DFX did not alter LVEF (Merchant et al., 2012; Pennell et al., 2014) after 1 year of treatment.

Combined DFO plus DFX treatment has been shown to provide synergistic effects on iron excretion (Table 1). It can increase urine and stool iron excretion in TDT patients (Grady et al., 2013), and is more effective than single iron chelator therapy in reducing systemic, liver and myocardial iron concentrations, and improving cardiac T2* in TDT patients. (Cassinerio et al., 2014; Jetsrisuparb et al., 2010; Lal et al., 2013). This combined chelation treatment led to a decrease in serum ferritin by 24–40% after 1 year of treatment (Cassinerio et al., 2014; Lal et al., 2013) and 49% after more than 2 years of treatment (Jetsrisuparb et al., 2010). After 1 year of treatment with a combination of DFO plus DFX, cardiac T2* increased by 26–33% (Cassinerio et al., 2014; Lal et al., 2013) and left ventricular ejection fraction (LVEF) improved by 32% (Lal et al., 2013). Hence, therapy of a combination of DFO plus DFX gives a higher efficacy in reducing myocardial iron deposition and attenuating cardiac dysfunction in TDT patients, when compared with either DFO or DFX monotherapy. However, combined DFO plus DFX therapy had no additive effects in reducing liver and cardiac iron concentrations (Otto-Duessel et al., 2008). It is thought they might compete for the same iron pool, as observed in the gerbil model (Otto-Duessel et al., 2008).

2.2. Effects of DFO+DFP

Combined DFO plus DFP therapy also demonstrated a high efficacy in reducing liver and myocardial iron, and improving liver and cardiac T2* and heart function in TDT patients (Alpendurada et al., 2012; Origa et al., 2005; Pepe et al., 2013; Tanner et al., 2008) (Table 2). Combined DFO plus DFP treatment has been shown to produce superior results to DFO alone in reducing liver and cardiac iron accumulation, and improving cardiac T2* and right ventricular function (Alpendurada et al., 2012; Pepe et al., 2013). One study demonstrated that a combination therapy had a greater efficacy in reducing serum ferritin and liver iron than a monotherapy, but provided similar effects to DFP alone in reducing myocardial iron, improving cardiac T2* and heart function in TDT patients (Pepe et al., 2013). This study found that after more than 1–1.6 years of treatment with DFO plus DFP, serum ferritin decreased by 32% whereas treatment with DFO or DFP alone caused a decrease in serum ferritin by 10% and 8%, respectively (Pepe et al., 2013). Treatment with DFO plus DFP improved cardiac T2* by 44% compared with DFO or DFP alone, in which cardiac T2* was increased by 26% and 68% respectively (data showed no statistically significant difference between combined chelation and DFP alone) (Pepe et al., 2013). Furthermore, combined chelation therapy improved LVEF by 3–19% (Origa et al., 2005; Pepe et al., 2013) when compared with DFO or DFP alone, in which LVEF was improved by 3% and 9% respectively (Pepe et al., 2013). The right ventricular ejection fraction (RVEF) was improved by 5% compared with DFO or DFP alone, in which RVEF was improved by 0.3% and 12%, respectively (data showed no statistically significant difference between combined chelation and DFP alone) (Pepe et al., 2013). Mean urinary iron excretion was increased two fold in TDT patients after 1–5 years of treatment with DFO plus DFP therapy (Origa et al., 2005). However, it can be seen from previous studies

that this combination therapy is more efficacious than DFP treatment alone in decreasing serum ferritin, improving cardiac T2* and improving both LVEF and RVEF. For example, previous studies have shown that after 1 year of treatment with DFP, serum ferritin decreased by 10% (Maggio et al., 2002; Pennell et al., 2006), cardiac T2* improved by 27% (Pennell et al., 2006; Smith et al., 2011) and LVEF and RVEF improved by 3% (Pennell et al., 2006; Smith et al., 2011) and 4% (Smith et al., 2011), respectively. Therefore, combined DFO plus DFP therapy is effective in treating iron overload cardiomyopathy.

2.3. Effects of DFP+DFX

Evidence shows that combined treatment with two oral iron chelators, DFP and DFX, is efficacious and safe in patients (Berdoukas et al., 2010; Farmaki et al., 2011; Voskaridou et al., 2011). A summary of these reports is shown in Table 3. A combination of DFP plus DFX treatment was effective in reducing systemic iron concentrations (Voskaridou et al., 2011) and clearly caused a decrease in liver iron concentration and liver T2* (Farmaki et al., 2011; Voskaridou et al., 2011). There were three studies with a total of 20 patients who received this combination of chelators. In two of these studies, serum ferritin showed a large decrease, approximately 81% in 1 patient (Voskaridou et al., 2011) and 82% in 16 patients (Farmaki et al., 2011). In all three studies, there were a total of 6 patients who had symptoms of cardiac iron overload. They showed a reversal of cardiac dysfunction, in which cardiac T2* improved by 54–58% in 4 out of 6 patients (Berdoukas et al., 2010; Voskaridou et al., 2011) and by 8% in 2 out of 6 patients (Farmaki et al., 2011), and LVEF improved by 7% in 2 out of 6 patients (Farmaki et al., 2011), after 1–2 years of treatment with the combination of these two drugs. Hence, combined DFP plus DFX therapy can be said to exert protective effects on iron overload cardiomyopathy.

In summary, all of these studies demonstrate the high efficacy of combined chelation therapy in reducing myocardial iron concentration and improving cardiac dysfunction in conditions of iron overload cardiomyopathy. Firstly, a combination of DFO plus DFX exerts a higher efficacy compared to either DFO or DFX monotherapy. Secondly, combined DFO plus DFP also is more effective and a better treatment than either DFO or DFP monotherapy. Thirdly, a combination of DFP plus DFX is also more effective than either DFP or DFX monotherapy in decreasing systemic iron concentration.

Regarding the efficacy of these combined iron chelators, available data from reports in Tables 1–3 indicated that a combination of oral iron chelators DFP and DFX was shown to be the most effective in reducing cardiac iron deposition and improving cardiac T2*. This was followed by the combination of DFO plus DFP with finally the combination of DFO plus DFX having the least efficacy among these three combinations in this regard. However, combined DFO plus DFX may be superior in improving cardiac function, as shown by an increase in LVEF, when compared to combined DFO plus DFP and combined DFP plus DFX. Nevertheless, there are still a limited number of reports on the efficacy of combined DFP plus DFX therapy. Future long term studies using larger participant numbers are needed to substantiate the benefits of the combined iron chelator treatment in TDT patients.

3. Combined iron chelator with antioxidant therapy

Recent studies have demonstrated that the combination of iron chelators with antioxidants such as vitamin E and N-acetylcysteine (NAC) could be very effective in chelating iron (Ozdemir et al., 2014; Rachmilewitz et al., 2005). It is known that increased oxidative stress and DNA damage was obvious in β-thalassemia major patients (Ozdemir et al., 2014). A combination of DFP plus NAC therapy has been shown to significantly decrease oxidative stress and restore brain function which has been impaired by conditions of iron overload in iron-overloaded rats (Sripetchwandee et al., 2014). The beneficial effects of this treatment may also decrease oxidative stress in patients with iron overload. As expected, a recent study showed that the combination of an iron chelator DFX, DFP or combined DFO plus DFP with an antioxidant, such as either vitamin E or NAC, reduced oxidative stress in patients with iron overload (Ozdemir et al., 2014). In addition, the combined iron chelator plus NAC treatment showed higher efficacy than vitamin E alone in reducing DNA damage in pediatric β-thalassemia patients (Ozdemir et al., 2014). Also, there are reports that acetaminophen (paracetamol) is a potent antioxidant (Rice et al., 2012; Walker et al., 2009), and a combination of acetaminophen plus DFO treatment is effective in treating iron-overload associated cardiac complication at a rate superior to either acetaminophen or DFO alone in removing cardiac iron from iron-overloaded gerbils (Walker et al., 2009).

All of these findings suggest that the mechanisms of combination therapy in improving cardiac dysfunction induced by iron overload could be due to several beneficial effects provided by each agent. Combined therapy can decrease iron accumulation due to the actions of the iron chelator, and decrease iron-induced oxidative stress due to the actions of both the antioxidant and the iron chelator. As a result, the combined therapy can synergistically provide beneficial effects in both the plasma and directly in the heart. Since combining an iron chelator with an antioxidant exerts synergistic effects in treating iron overload cardiomyopathy, these effects might be superior to the combined treatment of 2 iron chelators. As expected, previous studies found that combined DFO plus acetaminophen were twice as effective as a combination of DFO plus DFX in reducing cardiac iron concentration of iron-overloaded gerbils (Otto-Duessel et al., 2008; Walker et al., 2009). However, the dose and duration of treatments in these two studies are different. Despite the concept that the combined treatment of an iron chelator with an antioxidant would be essential in treating iron overload condition, the effects of this combination on cardiac dysfunction and chronic iron overload in patients have been rarely investigated.

The combined treatment of an iron chelator with an antioxidant may provide enhanced therapeutic benefits by decreasing tissue iron levels and diminishing oxidative stress, and hence leading to the improvement in heart function in iron overload cardiomyopathy. Future studies are needed to investigate the effects of the combination of these two agents on iron overload cardiomyopathy both in animal and human models to explore its clinical usefulness.

4. Possible roles of antioxidant therapy in iron overload cardiomyopathy

Since iron is a pro-oxidant, the signaling pathways involved are associated with increased oxidative stress and inflammation (Cheng and Lian, 2013) which causes cell and organelle damage, particularly in the heart, as shown in Fig. 1. Many novel studies have shown that antioxidant compounds decrease cardiac oxidative stress (Zhang et al., 2013), increase cardiac antioxidant levels (Zhang et al., 2013), decrease cardiac iron deposition (Kramer et al., 2012; Lin et al., 2013; Thephinlap et al., 2011; Zhang et al., 2013) and improve cardiac dysfunction in iron-overload induced cardiomyopathy in animal models (Kramer et al., 2012; Lin et al., 2013; Thephinlap et al., 2011; Zhang et al., 2013).

Table 4 summarizes the therapeutic agents with antioxidative effect which have been shown to provide cardioprotection under iron overload condition. For example, Danshen is known to exert

Table 4
Report on the effects of antioxidant therapy in cases of iron overload cardiomyopathy.

Model	Iron overload induction	Intervention	Result	Interpretation	References
Male Kunming mice	Iron dextran injection (50 mg/kg/day, i.p.)/ 2 weeks	Low-dose Danshen (3 g/kg/day, i.p.)/high-dose Danshen (6 g/kg/day, i.p.)/ DFO (100 mg/kg/day, i.p.)/2 weeks	Low and high doses provided similar efficacy to DFO in a causing a decrease in cardiac iron content and cardiac malondialdehyde levels, as well as improving cardiac superoxide dismutase and glutathione peroxidase levels.	Danshen injections ameliorated iron overload-induced cardiac damage as effectively as DFO therapy.	(Zhang et al., 2013)
Male Sprague–Dawley rats	Iron dextran biweekly injection (2 mg/kg, i.p.)/ 3-5 weeks	*d*-propranolol (2, 4 and 8 mg/kg/day, i.p.)/3–5 weeks	1. At 3 weeks, a high dose (8 mg/kg/day) had the greatest effect on decreasing cardiac iron levels and restoring heart function. 2. At 5 weeks, a low dose (2 mg/kg/day) improved LVEF, LVFS and the mitral valve E/A ratio, at 4–8 mg/kg/day which also improved cardiac output and aortic pressure maximum, and at 8 mg/kg/day decreased cardiac inflammation.	*d*- propranolol is an antioxidant and preserves cardiac function during iron overload by reducing cardiac iron uptake as well as inflammation.	(Kramer et al., 2012)
Male C57/B6, H129 PPARα knockout and wild-type mice	Iron dextran injection (10 mg/25 g body weight on 5 days/week, i.p.)/4 weeks	Overexpression AAV-ADIPOQ (1×10^{12} viral particles in 50 ml of saline) via the tail vein (i.v.)/4 weeks.	Adiponectin ameliorated cardiac iron deposition, restored cardiac function and decreased inflammatory profiles.	Adiponectin acted as an anti-inflammatory and attenuated iron-induced cardiomyopathy.	(Lin et al., 2013)
Male C57BL/6 mice, wild-type (genotype $^{mu}\beta^{+/+}$), and heterozygous β-knockout (genotype $^{mu}\beta^{th-3/+}$)	Iron diet (normal chow diet plus ferrocene (0.2%w/w))/4 months	Curcuminoids (200 mg/kg/day, p.o.)/ DFP (50 mg/kg/day, p.o.)/2 months	Curcuminoids had similar efficacy to DFP in reducing cardiac iron accumulation and improving heart rate variability.	Curcuminoids treatment was effective in improving cardiac function in iron-loaded thalassemic mice.	(Thephinlap et al., 2011)

i.p. intraperitoneal injection; **i.v.** intravenous injection; **p.o.** per oral; **DFO** deferoxamine; **DFP** deferiprone; **LVEF** left ventricular ejection fraction; **LVFS** left ventricular fraction shortening; **AAV-ADIPOQ** associated virus with cardiac adiponectin gene.

potent antioxidative effects in treating diabetes and cardiovascular disease especially chronic heart failure (Cheng, 2007; Liu et al., 2015; Wang et al., 2006). Danshen injection has been shown to exert as effectively as DFO in reducing cardiac iron deposition, leading to the reduction of iron overload-induced cardiac damage in mice (Zhang et al., 2013). This benefit could be due partly to its antioxidative effects. *d*-propranolol is also an antioxidant which has been shown to reduce the entry of iron into cardiomyocytes (Kramer et al., 2006, 2012), and attenuate ROS levels and inflammation, leading to improved cardiac function in iron-overloaded rats (Kramer et al., 2012). Moreover, adiponectin which also exerted antioxidative and anti-inflammatory effects has been shown to reduce cardiac iron deposition, leading to improved cardiac function in iron-overloaded mice (Lin et al., 2013). Another potent antioxidant is curcuminoids (Thephinlap et al., 2011). In iron overloaded β-thalassemic mice, curcuminoids has been shown to act as effectively as DFP in reducing non-transferrin bound iron, lowering cardiac iron concentration and improving cardiac autonomic imbalance, leading to improved cardiac function (Thephinlap et al., 2011).

The possible mechanisms of the antioxidant therapies that enable them to improve heart dysfunction induced by conditions of iron overload are probably due to their antioxidative effects (Kramer et al., 2012; Lin et al., 2013; Thephinlap et al., 2011; Zhang et al., 2013) and ability to chelate free iron in cells, such as NAC (Banner et al., 1986; Flora, 2009) and curcumin (Nazari et al., 2013). However, further large clinical trials are needed to elucidate the protective effects of antioxidant therapy, particularly in patients with iron overload in heart tissue.

5. Conclusion

In summary, many reports suggest that the combination therapy of 2 iron chelators provides high efficacy in reducing cardiac iron deposition and improving cardiac dysfunction in TDT patients. In addition, the combination therapy of an iron chelator with an antioxidant exerts synergistic effects in attenuating iron concentration both in the plasma and the heart, leading to improved cardiac dysfunction in iron overload cardiomyopathy. Moreover, growing evidence also demonstrates that antioxidant compounds exert protective effects which can ameliorate heart injury and improve heart dysfunction caused by excessive free iron in the hearts of mice and rat models. Since some antioxidant supplements already demonstrate similar efficacy to a single iron chelator in treating iron-overloaded hearts of animals, the combined treatment of an iron chelator with an antioxidant, or an antioxidant alone (i.e. in TDT patients who fail to improve by iron chelation therapies or cannot take iron chelators) may be the future chosen therapy to treat patients with iron overload cardiomyopathy. More clinical trials are required to further investigate the potential effects of these therapies and warrant their clinical usefulness.

Acknowledgments

This work is supported by the NSTDA Research Chair Grant from the National Science and Technology Development Agency Thailand (NC) and grants from the Thailand Research Fund BRG5780016 (SC), TRG5780002 (SK), the Royal Golden Jubilee PhD program (NC and SW), Chiang Mai University Center of Excellence Award (NC), and the Faculty of Medicine Chiang Mai University Fund (SW and NC).

References

Aldouri, M.A., Wonke, B., Hoffbrand, A.V., Flynn, D.M., Ward, S.E., Agnew, J.E., Hilson, A.J., 1990. High incidence of cardiomyopathy in beta-thalassaemia patients receiving regular transfusion and iron chelation: reversal by intensified chelation. Acta Haematol. 84, 113–117.

Alpendurada, F., Smith, G.C., Carpenter, J.-P., Nair, S.V., Tanner, M.A., Banya, W., Dessi, C., Galanello, R., Walker, J.M., Pennell, D.J., 2012. Effects of combined deferiprone with deferoxamine on right ventricular function in thalassaemia major. J. Cardiovasc. Magn. Reson. 14, 1–10.

Anderson, L.J., Westwood, M.A., Prescott, E., Walker, J.M., Pennell, D.J., Wonke, B., 2006. Development of thalassaemic iron overload cardiomyopathy despite low liver iron levels and meticulous compliance to desferrioxamine. Acta Haematol. 115, 106–108.

Anderson, L.J., Wonke, B., Prescott, E., Holden, S., Walker, J.M., Pennell, D.J., 2002. Comparison of effects of oral deferiprone and subcutaneous desferrioxamine on myocardial iron levels and ventricular function in beta-thalassemia. Lancet 360, 516–520.

Banner, W.J., Koch, M., Capin, D.M., Hopt, S.B., Chang, S., Tong, T.G., 1986. Experimental chelation therapy in chromium, lead, and boron intoxication with N-acetylcysteine and other compounds. Toxicol. Appl. Pharmacol. 83, 142–147.

Barzin, M., Kowsarian, M., Akhlaghpoor, S., Jalalian, R., Taremi, M., 2012. Correlation of cardiac MRI T2* with echocardiography in thalassemia major. Eur. Rev. Med. Pharmacol. Sci. 16, 254–260.

Berdoukas, V., Carson, S., Nord, A., Dongelyan, A., Gavin, S., Hofstra, T.C., Wood, J.C., Coates, T., 2010. Combining two orally active iron chelators for thalassemia. Ann. Hematol. 89, 1177–1178.

Borgna-Pignatti, C., Rugolotto, S., De Stefano, P., Zhao, H., Cappellini, M.D., Del Vecchio, G.C., 2004. Survival and complications in patients with thalassemia major treated with transfusion and deferoxamine. Haematologica 89, 1187–1193.

Cappellini, M.D., Porter, J., El-Beshlawy, A., Li, C.K., Seymour, J.F., Elalfy, M., Gattermann, N., Giraudier, S., Lee, J.W., Chan, L.L., Lin, K.H., Rose, C., Taher, A., Thein, S.L., Viprakasit, V., Habr, D., Domokos, G., Roubert, B., Katramis, A., 2010. Tailoring iron chelation by iron intake and serum ferritin: the prospective EPIC study of deferasirox in1744 patients with transfusion-dependent anemias. Haematologica. 95, 557–566.

Cassinerio, E., Orofino, N., Roghi, A., Duca, L., Poggiali, E., Fraquelli, M., Zanaboni, L., Cappellini, M.D., 2014. Combination of deferasirox and deferoxamine in clinical practice: an alternative scheme of chelation in thalassemia major patients. Blood Cells Mol. Dis. 53, 164–167.

Cheng, C.F., Lian, W.S., 2013. Prooxidant mechanisms in iron overload cardiomyopathy. Biomed. Res. Int. 2013, 740573.

Cheng, T.O., 2007. Cardiovascular effects of Danshen. Int. J. Cardiol. 121, 9–22.

Davis, B.A., Porter, J.B., 2000. Long-term outcome of continuous 24-hour deferoxamine infusion via indwelling intravenous catheters in high-risk β-thalassemia. Blood 95, 1229–1236.

Farmaki, K., Tzoumari, I., Pappa, C., 2011. Oral chelators in transfusion-dependent thalassemia major patients may prevent or reverse iron overload complications. Blood Cells Mol. Dis. 47, 33–40.

Fibach, E., Rachmilewitz, E.A., 2010. The role of antioxidants and iron chelators in the treatment of oxidative stress in thalassemia. Ann. N.Y. Acad. Sci. 1202, 10–16.

Flora, S.J., 2009. Structural, chemical and biological aspects of antioxidants for strategies against metal and metalloid exposure. Oxid. Med. Cell. Longev. 2, 191–206.

Glickstein, H., El, R.B., Shvartsman, M., Cabantchik, Z.I., 2005. Intracellular labile iron pools as direct targets of iron chelators: a fluorescence study of chelator action in living cells. Blood 106, 3242–3250.

Grady, R.W., Galanello, R., Randolph, R.E., Kleinert, D.A., Dessi, C., Giardina, P.J., 2013. Toward optimizing the use of deferasirox: potential benefits of combined use with deferoxamine. Haematologica 98, 129–135.

Hershko, C., 2006. Oral iron chelators: new opportunities and new dilemmas. Haematologica 91, 1307–1312.

Hershko, C., 2010. Pathogenesis and management of iron toxicity in thalassemia. Ann. N.Y. Acad. Sci. 1202, 1–9.

Hider, R.C., Silva, A.M., Podinovskaia, M., Ma, Y., 2010. Monitoring the efficiency of iron chelation therapy: the potential of nontransferrin-bound iron. Ann. N.Y. Acad. Sci. 1202, 94–99.

Hoffbrand, A.V., Taher, A., Cappellini, M.D., 2012. How I treat transfusional iron overload. Blood 120, 3657–3669.

Jetsrisuparb, A., Komvilaisak, P., Wiangnon, S., Jetsrisuparb, C., 2010. Retrospective study on the combination of desferrioxamine and deferasirox for treatment of iron-overloaded thalassemic patients: first evidence of more than 2 years. J. Pediatr. Hematol. Oncol. 32, 400–403.

Kramer, J.H., Murthi, S.B., Wise, R.M., Mak, I.T., Weglicki, W.B., 2006. Antioxidant and lysosomotropic properties of acute d-propranolol underlies its cardioprotection of postischemic hearts from moderate iron-overloaded rats. Exp. Biol. Med. 231, 473–484.

Kramer, J.H., Spurney, C.F., Iantorno, M., Tziros, C., Chmielinska, J.J., Tong Mak, I., Weglicki, W.B., 2012. d-Propranolol protects against oxidative stress and progressive cardiac dysfunction in iron overloaded rats. Can. J. Physiol. Pharmacol. 90, 1257–1268.

Kremastinos, D.T., Farmakis, D., 2011. Iron overload cardiomyopathy in clinical practice. Circulation 124, 2253–2263.

Kumfu, S., Chattipakorn, S., Chinda, K., Fucharoen, S., Chattipakorn, N., 2012. T-type calcium channel blockade improves survival and cardiovascular function in thalassemic mice. Eur. J. Haematol. 88, 535–548.
Kumfu, S., Chattipakorn, S., Srichairatanakool, S., Settakorn, J., Fucharoen, S., Chattipakorn, N., 2011. T-type calcium channel as a portal of iron uptake into cardiomyocytes of beta-thalassemic mice. Eur. J. Haematol. 86, 156–166.
Lal, A., Porter, J., Sweeters, N., Ng, V., Evans, P., Neumayr, L., Kurio, G., Harmatz, P., Vichinsky, E., 2013. Combined chelation therapy with deferasirox and deferoxamine in Thalassemia. Blood. Cells. Mol. Dis 50, 99–104.
Lerner, N., Blei, F., Bierman, F., Johnson, L., Piomelli, S., 1990. Chelation therapy and cardiac status in older patients with thalassemia major. Am. J. Pediatr. Hematol. Oncol 12, 56–60.
Lin, H., Lian, W.-S., Chen, H.-H., Lai, P.-F., Cheng, C.-F., 2013. Adiponectin ameliorates iron-overload cardiomyopathy through the PPARα–PGC-1–dependent signaling pathway. Mol. Pharmacol. 84, 275–285.
Liu, Z., Xu, S., Huang, X., Wang, J., Gao, S., Li, H., Zhou, C., Ye, J., Chen, S., Jin, Z.G., Liu, P., 2015. Cryptotanshinone, an orally bioactive herbal compound from Danshen, attenuates atherosclerosis in apolipoprotein E-deficient mice: role of lectin-like oxidized LDL receptor-1 (LOX-1). Br. J. Pharmacol. 13068, 1–15.
Maggio, A., D'Amico, G., Morabito, A., Capra, M., Ciaccio, C., Cianciulli, P., Di Gregorio, F., Garozzo, G., Malizia, R., Magnano, C., Mangiagli, A., Quarta, G., Rizzo, M., D'Ascola, D.G., Rizzo, A., Midiri, M., 2002. Deferiprone versus deferoxamine in patients with thalassemia major: a randomized clinical trial. Blood. Cells. Mol. Dis. 28, 196–208.
Merchant, R., Ahmed, J., Krishnan, P., Jankharia, B., 2012. Efficacy and safety of deferasirox for reducing total body and cardiac iron in thalassemia. Indian Pediatr. 49, 281–285.
Nazari, Q.A., Kume, T., Izuo, N., Takada-Takatori, Y., Imaizumi, A., Hashimoto, T., Izumi, Y., Akaike, A., 2013. Neuroprotective effects of curcumin and highly bioavailable curcumin on oxidative stress induced by sodium nitroprusside in rat striatal cell culture. Biol. Pharm. Bull. 36, 1356–1362.
Origa, R., Bina, P., Agus, A., Crobu, G., Defraia, E., Dessi, C., Leoni, G.B., Muroni, F.P., Galanello, R., 2005. Combined therapy with deferiprone and desferrioxamine in thalassemia major. Haematologica 90, 1309–1314.
Otto-Duessel, M., Brewer, C., Gonzalez, I., Nick, H., Wood, J.C., 2008. Safety and efficacy of combined chelation therapy with deferasirox and deferoxamine in a gerbil model of iron overload. Acta. Haematol. 120, 123–128.
Oudit, G.Y., Sun, H., Trivieri, M.G., 2003. L-type Ca^{2+} channels provide a major pathway for iron entry into cardiomyocytes in iron-overload cardiomyopathy. Nat. Med. 9, 1187–1194.
Oudit, G.Y., Trivieri, M.G., Khaper, N., Liu, P.P., Backx, P.H., 2006. Role of L-type Ca^{2+} channels in iron transport and iron-overload cardiomyopathy. J. Mol. Med. (Berl) 84, 349–364.
Ozdemir, Z.C., Koc, A., Aycicek, A., Kocyigit, A., 2014. N-acetylcysteine supplementation reduces oxidative stress and DNA damage in children with β-thalassemia. Hemoglobin 15, 1–6.
Pennell, D.J., Berdoukas, V., Karagiorga, M., Ladis, V., Piga, A., Aessopos, A., Gotsis, E. D., Tanner, M.A., Smith, G.C., Westwood, M.A., Wonke, B., Galanello, R., 2006. Randomized controlled trial of deferiprone or deferoxamine in beta-thalassemia major patients with asymptomatic myocardial siderosis. Blood 107, 3738–3744.
Pennell, D.J., Porter, J.B., Cappellini, M.D., Chan, L.L., El-Beshlawy, A., Aydinok, Y., Ibrahim, H., Li, C.K., Viprakasit, V., Elalfy, M.S., Kattamis, A., Smith, G., Habr, D., Domokos, G., Roubert, B., Taher, A., 2011. Continued improvement in myocardial T2* over two years of deferasirox therapy in beta-thalassemia major patients with cardiac iron overload. Haematologica 96, 48–54.
Pennell, D.J., Porter, J.B., Cappellini, M.D., Chan, L.L., El-Beshlawy, A., Aydinok, Y., Ibrahim, H., Li, C.K., Viprakasit, V., Elalfy, M.S., Kattamis, A., Smith, G., Habr, D., Domokos, G., Roubert, B., Taher, A., 2012. Deferasirox for up to 3 years leads to continued improvement of myocardial T2* in patients with β-thalassemia major. Haematologica 97, 842–848.
Pennell, D.J., Porter, J.B., Cappellini, M.D., El-Beshlawy, A., Chan, L.L., Aydinok, Y., Elalfy, M.S., Sutcharitchan, P., Li, C.K., Ibrahim, H., Viprakasit, V., Kattamis, A., Smith, G., Habr, D., Domokos, G., Roubert, B., Taher, A., 2010. Efficacy of deferasirox in reducing and preventing cardiac iron overload in beta-thalassemia. Blood 115, 2364–2371.
Pennell, D.J., Porter, J.B., Piga, A., Lai, Y., El-Beshlawy, A., Belhoul, K.M., Elalfy, M., Yesilipek, A., Kilinç, Y., Lawniczek, T., Habr, D., Weisskopf, M., Zhang, Y., Aydinok, Y., 2014. A 1-year randomized controlled trial of deferasirox vs deferoxamine for myocardial iron removal in β-thalassemia major (CORDELIA). Blood 123, 1447–1454.
Pepe, A., Lombardi, M., Positano, V., Cracolici, E., Capra, M., Malizia, R., Prossomariti, L., De Marchi, D., Midiri, M., Maggio, A., 2006. Evaluation of the efficacy of oral deferiprone in beta-thalassemia major by multislice multiecho T2* Eur. J. Haematol. 76, 183–192.
Pepe, A., Meloni, A., Rossi, G., Cuccia, L., D'Ascola, G.D., Santodirocco, M., Cianciulli, P., Caruso, V., Romeo, M.A., Filosa, A., Pitrolo, L., Putti, M.C., Peluso, A., Campisi, S., Missere, M., Midiri, M., Gulino, L., Positano, V., Lombardi, M., Ricchi, P., 2013. Cardiac and hepatic iron and ejection fraction in thalassemia major: multicentre prospective comparison of combined deferiprone and deferoxamine therapy against deferiprone or deferoxamine monotherapy. J. Cardiovasc. Magn. Reson. 15, 1–11.
Piga, A., Caglioti, C., Fogliacco, E., Tricta, F., 2003. Comparative effects of deferiprone and deferoxamine on survival and cardiac disease in patients with thalassaemia major: a retrospective analysis. Haematologica 88, 489–496.
Piga, A., Roggero, S., Salusseglia, I. Massano, D., Serra, M., Longo, F., 2010. Deferiprone. Ann. N.Y. Acad. Sci. 1202, 75–78.
Porter, J.B., 2010. Deferasirox—current knowledge and future challenges. Ann. N.Y. Acad. Sci. 1202, 87–93.
Rachmilewitz, E.A., Weizer-Stern, O., Adamsky, K., Amariglio, N., Rechavi, G., Breda, L., Rivella, S., Cabantchik, Z.I., 2005. Role of iron in inducing oxidative stress in thalassemia: can it be prevented by inhibition of absorption and by antioxidants? Ann. N. Y. Acad. Sci 1054, 118–123.
Rice, 77, Meduru, S., Kakarla, Sb, Katta, A., Mupparaju, S.P., Kidd, B., Goebel, L.J., Blough, E.R., 2012. Chronic paracetamol treatment influences indices of reactive oxygen species accumulation in the aging Fischer 344 X Brown Norway rat aorta. Ann. Clin. Lab. Sci. 42, 152–161.
Smith, G.C., Alpendurada, F., Carpenter, J.P., Alam, M.H., Berdoukas, V., Karagiorga, M., Ladis, V., Piga, A., Aessopos, A., Gotsis, E.D., Tanner, M.A., Westwood, M.A., Galanello, R., Roughton, M., Pennell, D.J., 2011. Effect of deferiprone or desferoxamine on right ventricular function in thalassemia major patients with myocardial iron overload. J. Cardiovasc. Magn. Reson. 13, 1–7.
Sripetchwandee, J., Pipatpiboon, N., Chattipakorn, N., Chattipakorn, S., 2014. Combined therapy of iron chelator and antioxidant completely restores brain dysfunction induced by iron toxicity. PLOS ONE 9, e85115.
Taher, A., Cappellini, M.D., Vichinsky, E., Galanello, R., Piga, A., Lawniczek, T., Clark, J., Habr, D., Porter, J.B., 2009. Efficacy and safety of deferasirox doses of > 30 mg/kg per d in patients with transfusion-dependent anaemia and iron overload. Br. J. Haematol. 147, 752–759.
Tanner, M.A., Galanello, R., Dessi, C., 2007. A randomized, placebo-controlled, double- blind trial of the effect of combined therapy with deferoxamine and deferiprone on myocardial iron in thalassemia major using cardiovascular magnetic resonance. Circulation 115, 1876–1884.
Tanner, M.A., Galanello, R., Dessi, C., Smith, G.C., Westwood, M.A., Agus, A., Pibiri, M., Nair, S.V., Walker, J.M., Pennell, D.J., 2008. Combined chelation therapy in thalassemia major for the treatment of severe myocardial siderosis with left ventricular dysfunction. J. Cardiovasc. Magn. Reson. 10, 12.
Thephinlap, C., Phisalaphong, C., Lailerd, N., Chattipakorn, N., Winichagoon, P., Vadolas, J., Fucharoen, S., Porter, J.B., Srichairatanakool, S., 2011. Reversal of cardiac iron loading and dysfunction in thalassemic mice by curcuminoids. J. Med. Chem. 7, 62–69.
Voskaridou, E., Christoulas, D., Terpos, E., 2011. Successful chelation therapy with the combination of deferasirox and deferiprone in a patient with thalassaemia major and persisting severe iron overload after single-agent chelation therapies. Br. J. Haematol. 154, 654–665.
Walker, E.M.Jr, Morrison, R.G., Dornon, L., Laurino, J.P., Walker, S.M., Studeny, M., Wehner, P.S., Rice, K.M., Wu, M., Blough, E.R., 2009. Acetaminophen combinations protect against iron-induced cardiac damage in gerbils. Ann. Clin. Lab. Sci. 39, 378–385.
Wang, G., Wang, L., Xiong, Z.Y., Mao, B., Li, T.Q., 2006. Compound salvia pellet, a traditional Chinese medicine, for the treatment of chronic stable angina pectoris compared with nitrates: a meta-analysis. Med. Sci. Monit. 12, SR1–SR7.
Wijarnpreecha, K., Kumfu, S., Chattipakorn, S.C., Chattipakorn, N., 2015. Cardiomyopathy associated with iron overload: how does iron enter myocytes and what are the implications for pharmacological therapy? Hemoglobin 39, 9–17.
Wood, J.C., Kang, B.P., Thompson, A., Giardina, P., Harmatz, P., Glynos, T., Paley, C., Coates, T.D., 2010. The effect of deferasirox on cardiac iron in thalassemia major: impact of total body iron stores. Blood 116; , pp. 537–543.
Zhang, J.P., Zhang, Y.Y., Zhang, Y., Gao, Y.G., Ma, J.J., Wang, N., Wang, J.Y., Xie, Y., Zhang, F.H., Chu, L., 2013. Salvia miltiorrhiza (Danshen) injection ameliorates iron overload-induced cardiac damage in mice. Planta Med. 79, 744–752.
Zurlo, M.G., De Stefano, P., Borgna-Pignatti, C., Di Palma, A., Piga, A., Melevendi, C., 1989. Survival and causes of death in thalassaemia major. Lancet 2, 27–30.

เอกสารแนบหมายเลข 42

International Journal of Cardiology 201 (2015) 121–122

Contents lists available at ScienceDirect

International Journal of Cardiology

journal homepage: www.elsevier.com/locate/ijcard

Letter to the Editor

Effects of PPARγ agonist on heart rate variability and cardiac mitochondrial function in obese-insulin resistant rats☆

Noppamas Pipatpiboon [a,b,c], Jirapas Sripetchwandee [a,b,c], Siriporn C. Chattipakorn [a,c,d], Nipon Chattipakorn [a,b,c,*]

[a] Cardiac Electrophysiology Research and Training Center, Faculty of Medicine, Chiang Mai University, Chiang Mai, Thailand
[b] Cardiac Electrophysiology Unit, Department of Physiology, Faculty of Medicine, Chiang Mai University, Chiang Mai, Thailand
[c] Center of Excellence in Cardiac Electrophysiology Research, Chiang Mai University, Chiang Mai, Thailand
[d] Department of Oral Biology and Diagnostic Science, Faculty of Dentistry, Chiang Mai University, Chiang Mai, Thailand

ARTICLE INFO

Article history:
Received 20 June 2015
Accepted 29 July 2015
Available online 31 July 2015

Keywords:
Rosiglitazone
Cardiac mitochondria
High fat diet
Insulin resistance
Heart rate variability

Insulin resistance is the pathological condition in which target tissues cannot respond to plasma insulin at the optimal plasma insulin concentration [1]. We demonstrated previously that rats fed with high-fat diet (HFD) for 12 weeks developed insulin resistance as indicated by hyperinsulinemia and increased HOMA index with euglycemia [2]. Moreover, in the heart of obese-insulin resistant rats, cardiac autonomic imbalance and cardiac mitochondrial dysfunction including cardiac mitochondrial reactive oxygen species (ROS) production, cardiac mitochondrial depolarization and cardiac mitochondrial swelling can be found [3].

Peroxisome proliferator-activated receptor gamma (PPARγ) agonists such as rosiglitazone have been used for the treatment of type 2 diabetes and insulin resistance [1]. Rosiglitazone has been shown to attenuate oxidative stress induced by glucose [4], ischemia/reperfusion (I/R) injury [5], and hypoxia/reoxygenation [6]. However, the effects of rosiglitazone on the heart are still controversy [7]. Moreover, the roles of rosiglitazone on cardiac autonomic balance and cardiac mitochondrial function in obese-insulin resistant rats are still unclear. In the present study, we tested the hypothesis that rosiglitazone can reduce cardiac autonomic imbalance and attenuate cardiac mitochondrial dysfunction in obese-insulin resistant rats.

The study protocol was approved by the Institutional Animal Care and Use Committee (IACUC) of the Faculty of Medicine, Chiang Mai University. Male Wistar rats weighing 180–200 g were randomized into 2 groups, a normal diet (ND) group and a HFD group. Dietary regimen was the same as described previously [2]. After 12-week feeding, rats in each dietary group were divided into 2 subgroups (n = 5/subgroup) to received either rosiglitazone (5 mg/kg/day) or vehicle (normal saline) via gavage feeding for 14 days. Then, plasma glucose and insulin levels were determined [2]. Insulin resistance was assessed by Homeostasis Model Assessment (HOMA) [8,9]. A higher HOMA index indicates a higher degree of insulin resistance [2]. Heart rate variability (HRV) was used to represent cardiac sympathovagal activity as described previously [3]. In brief, the electrocardiogram (ECG) recording was done in each rat using Power Lab with chart 5.0 program [10]. R–R interval was determined using peaks of the QRS complex from the ECG and stored as an interval tachogram. The high frequency (HF, 0.6–3 Hz), low frequency (LF, 0.2–0.6 Hz), and very low frequency (VLF, 0.2 Hz) were determined using Fast Fourier Transform algorithm. The increased LF/HF ratio is considered an index of cardiac sympathovagal imbalance [3]. Cardiac mitochondrial function including mitochondrial

Table 1
Effects of rosiglitazone on body weight, visceral fat mass, plasma glucose, plasma insulin, HOMA index, and HRV.

Parameters	Normal diet		High fat diet	
	Vehicle	Rosiglitazone	Vehicle	Rosiglitazone
Body weight (g)	426.67 ± 8.82	459.17 ± 3.75*	584.33 ± 12.76*	613.33 ± 12.56*,†
Visceral fat (g)	23.67 ± 0.77	34.12 ± 1.42*	47.83 ± 2.78*	62.51 ± 4.29*,†
Glucose (mg%)	127.58 ± 5.69	101.86 ± 4.42*	137.25 ± 2.62	121.07 ± 2.35†
Insulin (ng/ml)	1.82 ± 0.15	1.78 ± 0.15	3.85 ± 0.18*	2.07 ± 0.08†
HOMA index	10.22 ± 0.57	8.39 ± 0.40	24.05 ± 0.90*	10.93 ± 0.50†
LFnu	0.13 ± 0.01	0.16 ± 0.01	0.20 ± 0.01*	0.23 ± 0.02*
HFnu	0.87 ± 0.01	0.83 ± 0.01	0.80 ± 0.01*	0.77 ± 0.02*
LF/HF ratio	0.15 ± 0.01	0.19 ± 0.02	0.25 ± 0.02*	0.30 ± 0.04*

* $P < 0.05$ vs. normal diet vehicle.
† $P < 0.05$ vs. high fat diet vehicle.

☆ Funding sources: the NSTDA Research Chair Grant from the National Science and Technology Development Agency Thailand (NC), the Thailand Research Fund grants BRG5780016 (SC) and TRG5880045 (JS), and Chiang Mai University Center of Excellence Award (NC).

* Corresponding author at: Cardiac Electrophysiology Research and Training Center Faculty of Medicine, Chiang Mai University, Chiang Mai 50200, Thailand.
E-mail address: nchattip@gmail.com (N. Chattipakorn).

http://dx.doi.org/10.1016/j.ijcard.2015.07.090
0167-5273/© 2015 Elsevier Ireland Ltd. All rights reserved.

ROS production, mitochondrial membrane potential change, and mitochondrial swelling was also determined as described previously [3]. Data were presented as mean ± SE. One-way ANOVA followed by post-hoc LSD test performed by the SPSS program (SPSS version 16, SPSS Inc.) was used to determine the differences between the means. A P-value less than 0.05 indicates statistical significant.

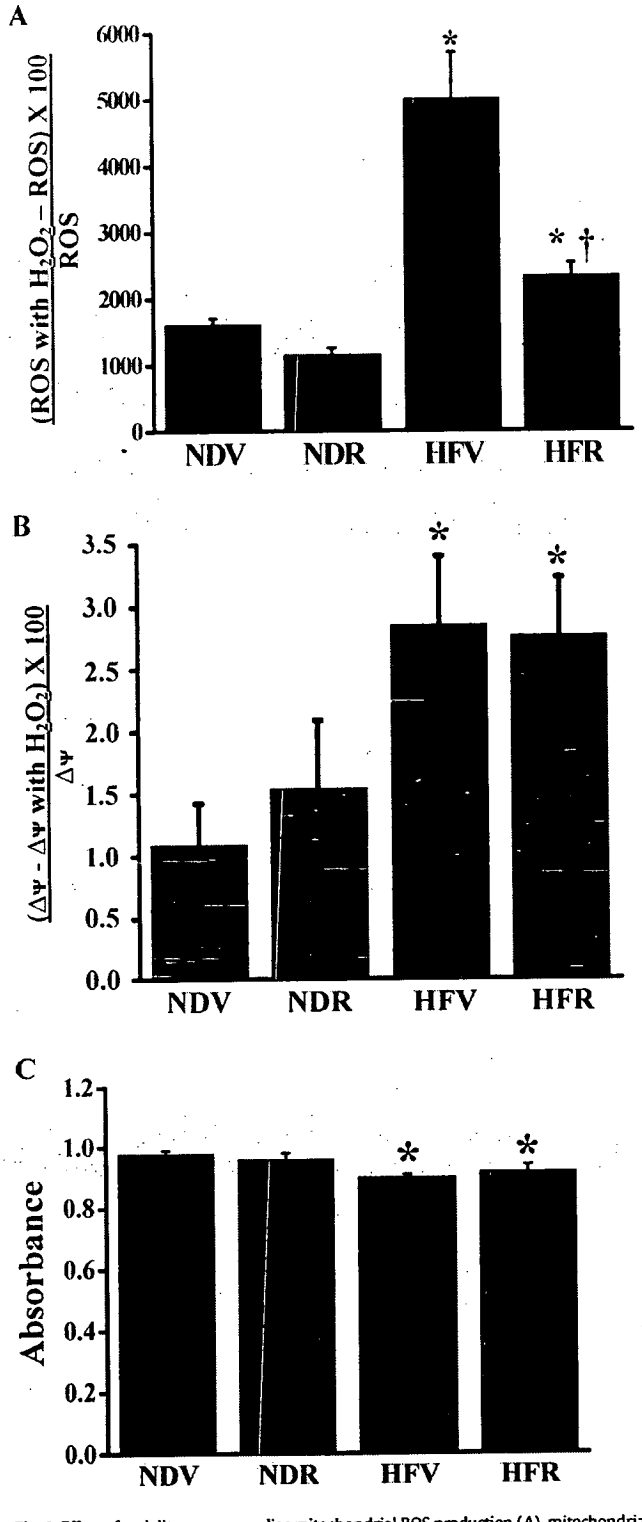


Fig. 1. Effect of rosiglitazone on cardiac mitochondrial ROS production (A), mitochondrial depolarization (B), and mitochondrial swelling (C), compared with ND rats. *P < 0.05 vs. NDV, †P < 0.05 vs. HFV.

The effects of rosiglitazone on body weight, visceral fat, and biochemical parameters are shown in Table 1. In HFD fed rats, the body weight, visceral fat, insulin, and HOMA index were significantly increased, compared with ND fed rats. Rosiglitazone treated rats in both ND group (NDR) and HF group (HFR) had significant increased body weight and visceral fat, compared to those treated with vehicle (NDV and HFV). However, HFR rats had significantly decreased plasma insulin level and HOMA index, compared to the HFV group. Rosiglitazone also decreased plasma glucose in rats of both dietary groups, compared to the vehicle treated rats.

HFV rats had increased LF/HF ratio, compared with the NDV group (Table 1). In HFR, the LF/HF ratio was also significantly increased, compared to the NDV rats. Moreover, the LF/HF ratio in HFR rats was not different from that in the HFV group, indicating no HRV improvement in rosiglitazone-treated rats.

For cardiac mitochondrial function, no differences were found between NDV and NDR rats for ROS level, mitochondrial membrane potential change and mitochondrial swelling (Fig. 1). In HFD rats, the mitochondrial ROS level was markedly increased in the HFV group, compared to the NDV group. HFR rats had lower ROS level than the HFV group (Fig. 1A). However, the ROS level in the HFR group was still significantly higher than that in the NDV group. Similar to ROS production, the cardiac mitochondrial depolarization was observed in the HFV group, compared to the NDV group. Rosiglitazone did not attenuate the mitochondrial depolarization caused by HFD (Fig. 1B). Moreover, cardiac mitochondrial swelling was observed as indicated by the decreased absorbance in HFV rats, and rosiglitazone did not attenuate this swelling in HFR rats (Fig. 1C).

Long-term high-fat diet consumption has been shown to cause obese-insulin resistant condition, depressed HRV, and cardiac mitochondrial dysfunction [3]. Consistent with previous studies, our rats demonstrated all of those abnormalities. Rosiglitazone treatment for 14 days in this study demonstrated its ability to decrease glucose, insulin, and HOMA index. However, it increased body weight, visceral fat, and caused the worsening of the HRV in obese-insulin resistant rats. Moreover, although rosiglitazone decreased ROS level, it attenuated neither cardiac mitochondrial depolarization nor mitochondrial swelling. These findings suggested that rosiglitazone increased cardiac sympathovagal imbalance and did not prevent cardiac mitochondrial dysfunction caused by obese-insulin resistant condition.

References

[1] L. Guo, R. Tabrizchi, Peroxisome proliferator-activated receptor gamma as a drug target in the pathogenesis of insulin resistance, Pharmacol. Ther. 111 (2006) 145–173.
[2] N. Pipatpiboon, W. Pratchayasakul, N. Chattipakorn, S.C. Chattipakorn, PPARgamma agonist improves neuronal insulin receptor function in hippocampus and brain mitochondria function in rats with insulin resistance induced by long term high-fat diets, Endocrinology 153 (2012) 329–338.
[3] N. Apaijai, H. Pintana, S.C. Chattipakorn, N. Chattipakorn, Effects of vildagliptin versus sitagliptin, on cardiac function, heart rate variability and mitochondrial function in obese insulin-resistant rats, Br. J. Pharmacol. 169 (2013) 1048–1057.
[4] G. Ceolotto, A. Gallo, I. Papparella, L. Franco, E. Murphy, E. Iori, et al., Rosiglitazone reduces glucose-induced oxidative stress mediated by NAD(P)H oxidase via AMPK-dependent mechanism, Arterioscler. Thromb. Vasc. Biol. 27 (2007) 2627–2633.
[5] J. Mersmann, N. Tran, P.A. Zacharowski, D. Grotemeyer, K. Zacharowski, Rosiglitazone is cardioprotective in a murine model of myocardial I/R, Shock 30 (2008) 64–68.
[6] Y.J. Yao, D.F. Geng, J.F. Wang, M.H. Yang, Y.L. Zhang, R.Q. Nie, et al., PPAR gamma agonist rosiglitazone alleviates hypoxia/reoxygenation-induced oxidative stress and apoptosis in rat cardiac myocytes, Nan Fang Yi Ke Da Xue Xue Bao 29 (2009) 689–693.
[7] S. Palee, S. Chattipakorn, A. Phrommintikul, N. Chattipakorn, PPARgamma activator, rosiglitazone: is it beneficial or harmful to the cardiovascular system? World J. Cardiol. 3 (2011) 144–152.
[8] S.M. Haffner, H. Miettinen, M.P. Stern, The homeostasis model in the San Antonio Heart Study, Diabetes Care 20 (1997) 1087–1092.
[9] D.J. Appleton, J.S. Rand, G.D. Sunvold, Basal plasma insulin and homeostasis model assessment (HOMA) are indicators of insulin sensitivity in cats, J. Feline Med. Surg. 7 (2005) 183–193.
[10] A. Pongchaidecha, N. Lailerd, W. Boonprasert, N. Chattipakorn, Effects of curcuminoid supplement on cardiac autonomic status in high-fat-induced obese rats, Nutrition 25 (2009) 870–878.

เอกสารแนบหมายเลข 43

NRC Research Press

BRIEF COMMUNICATION

Protocatechuic acid protects brain mitochondrial function in streptozotocin-induced diabetic rats

Yoswaris Semaming, Jirapas Sripetchwandee, Piangkwan Sa-nguanmoo, Hiranya Pintana, Patchareewan Pannangpetch, Nipon Chattipakorn, and Siriporn C. Chattipakorn

Abstract: Brain mitochondrial dysfunction has been demonstrated in diabetic animals with neurodegeneration. Protocatechuic acid (PCA), a major metabolite of anthocyanin, has been shown to exert glycemic control and oxidative stress reduction in the heart. However, its effects on oxidative stress and mitochondrial function in the brain under diabetic condition have never been investigated. We found that PCA exerted glycemic control, attenuates brain mitochondrial dysfunction, and contributes to the prevention of brain oxidative stress in diabetic rats.

Key words: insulin-dependent diabetes mellitus, oxidative stress, brain mitochondria protocatechuic acid.

Résumé : Le dysfonctionnement mitochondrial dans le cerveau a été démontré chez des animaux diabétiques présentant de la neurodégénérescence. L'acide protocatéchique (PCA), un important métabolite des anthocyanes, exerce, selon des études, un contrôle de la glycémie et diminue le stress oxydatif dans le cœur. Toutefois, il n'y a pas encore d'études sur les effets du PCA sur le stress oxydatif et la fonction mitochondriale dans le cerveau en présence de diabète. D'après nos observations, le PCA exerce un contrôle de la glycémie, atténue le dysfonctionnement mitochondrial dans le cerveau et contribue à la prévention du stress oxydatif dans le cerveau de rats diabétiques. [Traduit par la Rédaction]

Mots-clés : diabète sucré insulinodépendant, stress oxydatif, mitochondrie cérébrale, acide protocatéchique.

Introduction

Type 1 diabetes mellitus (T1DM) is a chronic disease caused by impaired insulin secretion, which affects both the central and peripheral nervous systems. T1DM causes the pathological changes in the brain, including cognitive decline, dementia, and Alzheimer's disease (AD) (Alvarez et al. 2009). A previous study in a mouse model of diabetic AD showed mitochondrial dysfunction in the brain (Wang et al. 2015). In addition to mitochondrial dysfunction, an increase in the levels of oxidative stress has been shown to play a key role in the pathogenesis of several organs of T1DM subjects (Cameron 2013).

Previous studies have demonstrated that protocatechuic acid (PCA; 3, 4-dihydroxy benzoic acid) exhibited various pharmacological properties, including antioxidant (Vari et al. 2011), anti-hyperglycemia (Lin et al. 2011), and anti-inflammation (Semaming et al. 2014). Recent study reported that PCA reduced cognitive impairment in aged AD mice through decreasing AD markers and reducing inflammation (Song et al. 2014). Despite these positive reports, the effect of PCA on oxidative stress and mitochondrial function in the brain of T1DM rats has not been investigated. The present study tested the hypothesis that PCA reduces brain oxidative stress by improving brain mitochondrial function in T1DM rats.

Materials and methods

Adult male Sprague–Dawley rats ($n = 36$) were acquired from the National Laboratory Animal Center, Mahidol University, Salaya, Nakornpathom. Rats ($n = 30$) were induced with T1DM by intraperitoneal injection of 50 mg/kg of streptozotocin (STZ), whereas other rats ($n = 6$) were injected with a citric buffer. Only diabetic rats with fasting blood glucose (FBG) over 300 mg/dL were included in the experiments (Semaming et al. 2014). All rats were assigned to receive 5 different treatments, including propylene glycol (vehicle), 4 U/kg insulin, 50 and 100 mg/kg PCA, and PCA combined with insulin, for 12 weeks. Propylene glycol and PCA were administrated orally by gavage feeding whereas insulin was subcutaneously injected. Body weight and food intake were recorded weekly. At the end of the 12-week treatment, blood was collected to measure plasma glucose, HbA_{1C}, insulin, and malondialdehyde (MDA) levels. At the end of the study protocol, all rats were deeply anesthetized, killed, and the brain was dissected out to determine brain mitochondrial function and brain MDA. FBG level was determined using a glucometer (Accu-Chek Advantage II;

Received 6 April 2015. Accepted 2 June 2015.

Y. Semaming.* Neurophysiology Unit, Cardiac Electrophysiology Research and Training Center, Faculty of Medicine, Chiang Mai University, Chiang Mai 50200, Thailand; Veterinary Technology Program, Faculty of Technology, Udon Thani Rajabhat University, Udon Thani 41000 Thailand.
J. Sripetchwandee,* P. Sa-nguanmoo, H. Pintana, and N. Chattipakorn. Neurophysiology Unit, Cardiac Electrophysiology Research and Training Center, Faculty of Medicine, Chiang Mai University, Chiang Mai 50200, Thailand; Department of Physiology, Faculty of Medicine, Chiang Mai University, Chiang Mai 50200, Thailand.
P. Pannangpetch. Neurophysiology Unit, Cardiac Electrophysiology Research and Training Center, Faculty of Medicine, Chiang Mai University, Chiang Mai 50200, Thailand; Department of Pharmacology, Faculty of Medicine, Khon Kaen University, Khon Kaen 40002, Thailand.
S.C. Chattipakorn. Neurophysiology Unit, Cardiac Electrophysiology Research and Training Center, Faculty of Medicine, Chiang Mai University, Chiang Mai 50200, Thailand; Department of Oral Biology and Diagnostic Sciences, Faculty of Dentistry, Chiang Mai University, Chiang Mai 50200, Thailand.

Corresponding author: Siriporn C. Chattipakorn (e-mails: scchattipakorn@gmail.com, siriporn.c@cmu.ac.th).
*These authors contributed equally in the manuscript.

Appl. Physiol. Nutr. Metab. Downloaded from www.nrcresearchpress.com by CONCORDIA UNIV on 10/06/15
For personal use only.

Appl. Physiol. Nutr. Metab. Downloaded from www.nrcresearchpress.com by CONCORDIA UNIV on 10/06/15
For personal use only.

Table 1. Effects of pharmacological interventions on metabolic parameters at the end of treatment.

Parameters	Normal rats: vehicle	Diabetic rats				
		Vehicle	Insulin	PCA 50 mg/kg	PCA 100 mg/kg	PCA 100 mg/kg + insulin 4 U/kg
Body weight (g)	453±62		354±21*,†	247±18*,†	251±20*,‡	348±15*,†
Food intake (g)	25±2	39±2*	32±1*,†	36±1*,‡	36±2*,‡	32±1*,†
FBG (mg/dL)	100±7	533±66*	175±24*,†	324±92*,†,‡	280±55*,†,‡	166±24*,†
Plasma insulin (ng/mL)	1.23±0.21	0.35±0.07*	1.22±0.78†	0.50±0.14*,‡	0.49±0.15*,‡	1.19±0.89†
Plasma HbA_{1c} (%)	4.48±0.81	9.50±0.11*	6.25±0.82†	7.63±0.38*,†	7.75±0.60*,†	5.28±0.35†
Plasma MDA (μmol/L)	2.13±0.03	2.26±0.04*	2.14±0.02†	2.18±0.02*,†	2.17±0.03*,†	2.12±0.01†
Brain MDA (μmol/mg protein)	0.71±0.09	1.81±0.37*	1.05±0.18†	1.10±0.19†	0.90±0.11†	0.80±0.09†

Note: Values are means ± SD. FBG, fasting blood glucose; MDA, malondialdehyde.
*$P < 0.05$ vs normal rats treated with vehicle.
†$P < 0.05$ vs diabetic rats treated with vehicle.
‡$P < 0.05$ vs diabetic rats treated with insulin.

Roche Diagnostics, Mannheim, Germany). Plasma insulin level was measured by Sandwich ELISA assay (LINCO Research, Mo., USA). HbA_{1C} was determined using a competitive turbidimetric inhibition immunoassay (Roche Diagnostics Ltd., Rotkreuz, Switzerland). Plasma and brain MDA levels were determined using a high-performance liquid chromatography-based assay (Sripetchwandee et al. 2014).

Brain mitochondrial function determination

Brain mitochondria were isolated according to the method described previously (Sripetchwandee et al. 2013). The measurement of brain mitochondrial function was made under the state IV respiration (Moore et al. 1991). Dichlorohydro-fluorescein diacetate dye was used for the determination of brain mitochondrial reactive oxygen species (ROS) production (Pipatpiboon et al. 2012; Sripetchwandee et al. 2013). The ROS level was indicated as the arbitrary units of fluorescence intensity of dichlorohydro-fluorescein.

Brain mitochondrial membrane potential was determined using a fluorescent JC-1 dye as previously described (Pipatpiboon et al. 2012; Sripetchwandee et al. 2013). Mitochondrial depolarization was indicated by a decreased red per green fluorescent intensity ratio ($\Delta\Psi m$).

Brain mitochondrial swelling assay was induced by 2 mmol/L of H_2O_2 for 5 min and measured by changes in the absorbance of the brain mitochondrial suspensions (Pipatpiboon et al. 2012; Sripetchwandee et al. 2013). A decrease in absorbance represented brain mitochondrial swelling. Brain mitochondrial morphology was identified using a transmission electron microscope as described previously (Sripetchwandee et al. 2013).

Statistical analysis

Metabolic parameter data was expressed as means ± SD; others were expressed as means ± SE. A 1-way ANOVA followed by a least significant difference post hoc test was used to test the differences among the group. $P < 0.05$ was considered to be statistically significant.

Ethics

All experiments were approved by the Institutional Animal Care and Use Committees of the Faculty of Medicine, Chiang Mai University, Chiang Mai, Thailand.

Results

Diabetic rats with vehicle were characterized by body weight loss, polyphagia, hyperglycemia, and insulin deficiency (Table 1). At the end of all treatments, diabetic rats treated with either insulin or combined 100 mg/kg PCA and insulin showed a significant increased body weight in association with a decreased food intake and FBG level, when compared with diabetic rats treated with vehicle (Table 1). Both insulin and combined PCA and insulin completely restored plasma insulin as well as plasma HbA_{1C}, when compared with diabetic control rats (Table 1). In diabetic rats treated with either 50 mg/kg or 100 mg/kg of PCA, the FBG and HbA_{1C} showed a significant decrease, when compared with diabetic rats treated with vehicle, whereas there was no alteration in body weight, food intake, and plasma insulin levels in these rats (Table 1).

At the end of all treatments, plasma and brain MDA levels were significantly increased in diabetic rats treated with vehicle, when compared with nondiabetic rats treated with vehicle (Table 1). Only insulin therapy and combined treatments, but not PCA treatment alone, reduced plasma MDA levels to normal level, when compared with diabetic rats treated with only the vehicle. In the brain, however, all treatments in diabetic rats significantly restored the brain MDA levels, when compared with diabetic rats treated with only the vehicle.

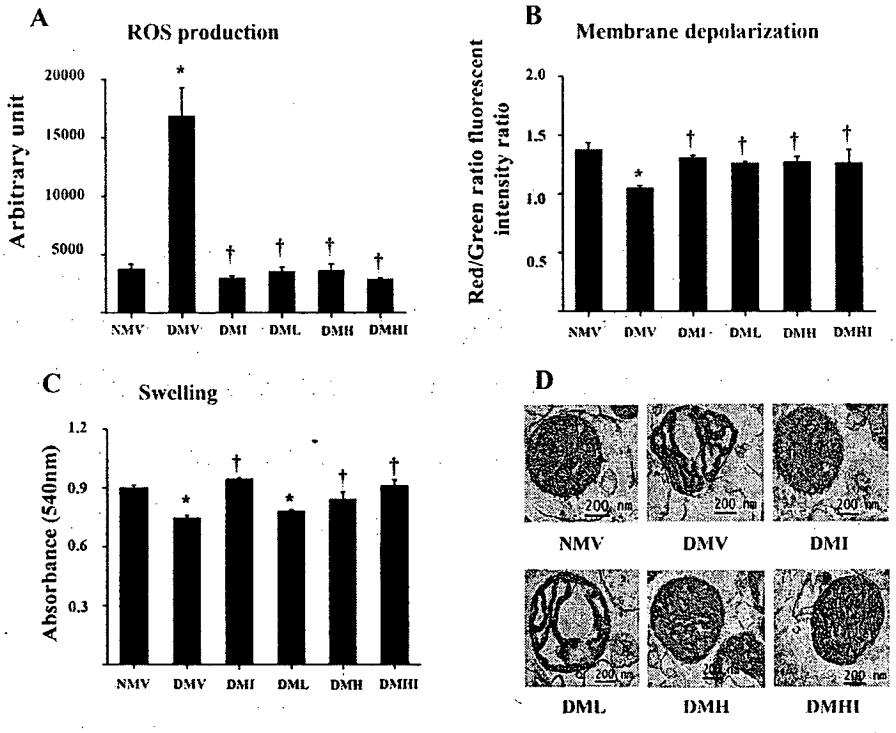
Diabetic rats showed brain mitochondrial dysfunction as indicated by increased ROS production, mitochondrial depolarization, and mitochondrial swelling (Fig. 1). The brain mitochondrial ROS production showed a significant increase in diabetic rats treated with vehicle, when compared with nondiabetic rats treated with the vehicle (Fig. 1A). All treatments in diabetic rats significantly restored the mitochondrial ROS levels, when compared with diabetic rats treated vehicle. Diabetic rats demonstrated a significantly decreased red/green fluorescence intensity ratio, when compared with nondiabetic rats, indicating brain mitochondrial depolarization. All treatments significantly attenuated mitochondrial depolarization, when compared with diabetic rats treated with vehicle (Fig. 1B).

In the assessment of brain mitochondrial swelling, the absorbance was significantly decreased in the diabetic rats, compared with nondiabetic rats, indicating brain mitochondrial swelling (Fig. 1C). Moreover, PCA at 100 mg/kg, insulin and combined insulin and PCA significantly attenuated mitochondrial swelling in diabetic rats, when compared with the diabetic rats treated vehicle (Fig. 1C). PCA at a lower dose did not attenuate brain mitochondrial swelling. The representative images of the transmission electron microscopy of the brain mitochondria from each group is shown in Fig. 1D. Compared with the intact brain mitochondria of the nondiabetic rat, the unfolded cristae were found mostly in diabetic rats, indicating brain mitochondrial swelling. Diabetic rats treated with 100 mg/kg PCA, insulin, or combined PCA and insulin attenuated swelling in brain mitochondrial, as indicated by a significant decrease in unfolded cristae.

Discussion

The lowering effects of PCA in plasma glucose, HbA_{1C}, and plasma insulin levels in diabetic rats has been previously demonstrated (Harini and Pugalendi 2010; Semaming et al. 2014), which is consistent with the present study. The possible explanation is that PCA normalized the activities of both gluconeogenic and

Fig. 1. Effects of pharmacological interventions on brain mitochondrial function and morphology (n = 6/group). (A) Brain mitochondrial reactive oxygen species (ROS) production (B) Brain membrane depolarization (C) Brain mitochondrial swelling (D) Representative transmission electron microscope images of mitochondrial morphology. Values are means ± SE. NMV, normal rats treated with vehicle; DMV, diabetic rats treated with vehicle; DMI, diabetic rats treated with insulin 4 U/kg; DML, diabetic rats treated with protocatechuic acid (PCA) 50 mg/kg; DMH, diabetic rats treated with PCA 100 mg/kg; DMHI, diabetic rats treated with PCA 100 mg/kg plus insulin 4 U/kg. *, $P < 0.05$ vs NMV; †, $P < 0.05$ vs DMV.



glycolytic enzymes in the liver (Harini and Pugalendi 2010) and exerted an insulin-like activity by increasing glucose uptake in adipose tissue (Scazzocchio et al. 2011). Those effects of PCA could be the underlying mechanisms responsible for the glycemic controls observed in the present study.

Both increased ROS generation and impaired antioxidant defenses were commonly known to be the contributing factors for causing oxidative stress in the diabetic condition (Giacco and Brownlee 2010). Most of ROS production in cells arise from mitochondria during the exposure to hyperglycemic condition (Nishikawa et al. 2000). Currently, reports on ROS generation in diabetic animals are still controversial. Several studies showed that the induction of hyperglycemia condition in the diabetic model led to changes in glutathione metabolism and mitochondrial respiratory functions, resulting in increased ROS overproduction in the brain as well as liver (Raza et al. 2015). However, there are studies demonstrating a decrease in ROS production in the heart, muscle, or kidney of diabetic animals (Herlein et al. 2009; Dugan et al. 2013). A decrease in ROS production under the diabetic condition in those studies has been shown to be due to an increased expression of antioxidant enzyme, including catalase in the heart and muscle of diabetic rats, and a reduction of mitochondrial function owing to an excessive calorie intake in diabetic models, thus resulting in less ROS production in the kidney. In the present study, we found that ROS generation was increased in the brain of streptozotocin-induced diabetic rats because of increased circulating oxidative stress induced by severe hyperglycemic condition in this model. It has been known that MDA is an index for oxidative damage (Nielsen et al. 1997). The present study shows that the diabetic rats treated with PCA had decreased oxidative damage in both the plasma and the brain. In addition, our results showed that PCA also attenuated brain mitochondrial ROS production in STZ-induced diabetic rats.

Overproduction of ROS in diabetes can affect mitochondrial function, resulting in the loss of mitochondrial membrane integrity (Boudina et al. 2005). In the heart, it has been shown that PCA prevented cardiac mitochondrial dysfunction and cardiac apoptosis in T1DM rats (Semaming et al. 2014). Our study demonstrates that these benefits of PCA also extended to the brain as it also improved brain mitochondrial function, which is seriously impaired in T1DM rats.

Although both insulin and PCA alone equally assist in the restoration of brain oxidative stress, our findings indicated that insulin could provide better efficacy for anti-oxidative effects since treatment with PCA alone could not decrease plasma MDA when compared with insulin therapy. In addition, although PCA and insulin could attenuate brain mitochondrial dysfunction to a similar degree, our findings also suggested that oxidative stress could be triggered through other mechanisms in addition to the mitochondria, such as nonenzymatic glycosylation, glucose oxidation, and hyperglycemia-induced lipid peroxidation (Wolff and Dean 1987). In addition, insulin therapy provides a greater efficacy in decreasing blood glucose levels and restoring HbA_{1C}, when compared with PCA alone, suggesting better efficacy in glycemic control. These findings supported that insulin treatment restores brain damage caused by oxidative stress through several mechanisms, including restoring glycemic control as well as improving brain mitochondrial function.

In summary, brain oxidative stress and brain mitochondrial dysfunction were developed in STZ-induced diabetic rats. The treatment with PCA alone, insulin alone, or combined PCA and insulin equally attenuated those adverse effects by attenuating

Appl. Physiol. Nutr. Metab. Downloaded from www.nrcresearchpress.com by CONCORDIA UNIV on 10/06/15
For personal use only.

hyperglycemia, brain oxidative damage, and brain mitochondrial dysfunction. These findings indicated for the first time that PCA exerts beneficial effects in the brain of T1DM, and may be used as a supplement to prevent diabetic-induced brain oxidative damage in diabetic patients.

Study limitation

Since there was no ADP in our respiratory buffer for mitochondrial study, it is possible that ROS production would be increased. However, since the same respiratory (RES) buffer was used in all groups of brain mitochondria, the changes in ROS production and mitochondrial potential changes observed in each group should represent the effects of diabetic condition and pharmacological interventions in this study.

Conflict of interest statement

The authors declare no conflict of interest.

Acknowledgements

This work was supported by the Thailand Research Fund BRG5780016 (S.C.), TRG5880045 (J.S.), a NSTDA Research Chair Grant from the National Science and Technology Development Agency (N.C.), Chiang Mai University Center of Excellence Award (N.C.), the Faculty of Medicine Endowment Fund, Chiang Mai University (N.C.), and Udon Thani Rajabhat University Fund (Y.S.).

References

Alvarez, E.O., Beauquis, J., Revsin, Y., Banzan, A.M., Roig, P., De Nicola, A.F., and Saravia, F. 2009. Cognitive dysfunction and hippocampal changes in experimental type 1 diabetes. Behav. Brain Res. **198**: 224–230. doi:10.1016/j.bbr.2008.11.001. PMID:19041902.

Boudina, S., Sena, S., O'Neill, B.T., Tathireddy, P., Young, M.E., and Abel, E.D. 2005. Reduced mitochondrial oxidative capacity and increased mitochondrial uncoupling impair myocardial energetics in obesity. Circulation, **112**: 2686–2695. doi:10.1161/CIRCULATIONAHA.105.554360. PMID:16246967.

Cameron, N.E. 2013. Role of endoplasmic reticulum stress in diabetic neuropathy. Diabetes, **62**: 696–697. doi:10.2337/db12-1469. PMID:23431013.

Dugan, L.L., You, Y.H., Ali, S.S., Diamond-Stanic, M., Miyamoto, S., DeCleves, A.E., et al. 2013. AMPK dysregulation promotes diabetes-related reduction of superoxide and mitochondrial function. J. Clin. Invest. **123**: 4888–4899. doi:10.1172/JCI66218. PMID:24135141.

Giacco, F., and Brownlee, M. 2010. Oxidative stress and diabetic complications. Circ. Res. **107**: 1058–1070. doi:10.1161/CIRCRESAHA.110.223545. PMID:21030723.

Harini, R., and Pugalendi, K.V. 2010. Antihyperglycemic effect of protocatechuic acid on streptozotocin-diabetic rats. J. Basic Clin. Physiol. Pharmacol. **21**: 79–91. PMID:20506690.

Herlein, J.A., Fink, B.D., O'Malley, Y., and Sivitz, W.I. 2009. Superoxide and respiratory coupling in mitochondria of insulin-deficient diabetic rats. Endocrinology, **150**: 46–55. doi:10.1210/en.2008-0404. PMID:18772240.

Lin, C.Y., Tsai, S.J., Huang, C.S., and Yin, M.C. 2011. Antiglycative effects of protocatechuic acid in the kidneys of diabetic mice. J. Agric. Food Chem. **59**: 5117–5124. doi:10.1021/jf200103f. PMID:21456600.

Moore, A.L., Dry, I.B., and Wiskich, J.T. 1991. Regulation of electron transport in plant mitochondria under state 4 conditions. Plant Physiol. **95**: 34–40. doi:10.1104/pp.95.1.34. PMID:16667977.

Nielsen, F., Mikkelsen, B.B., Nielsen, J.B., Andersen, H.R., and Grandjean, P. 1997. Plasma malondialdehyde as biomarker for oxidative stress: reference interval and effects of life-style factors. Clin. Chem. **43**: 1209–1214. PMID:9216458.

Nishikawa, T., Edelstein, D., Du, X.L., Yamagishi, S., Matsumura, T., Kaneda, Y., et al. 2000. Normalizing mitochondrial superoxide production blocks three pathways of hyperglycaemic damage. Nature, **404**: 787–790. doi:10.1038/35008121. PMID:10783895.

Pipatpiboon, N., Pratchayasakul, W., Chattipakorn, N., and Chattipakorn, S.C. 2012. PPARγ agonist improves neuronal insulin receptor function in hippocampus and brain mitochondria function in rats with insulin resistance induced by long term high-fat diets. Endocrinology, **153**: 329–338. doi:10.1210/en.2011-1502. PMID:22109891.

Raza, H., John, A., and Howarth, F.C. 2015. Increased oxidative stress and mitochondrial dysfunction in zucker diabetic rat liver and brain. Cell Physiol. Biochem. **35**: 1241–1251. doi:10.1159/000373947. PMID:25766534.

Scazzocchio, B., Vari, R., Filesi, C., D'Archivio, M., Santangelo, C., Giovannini, C., et al. 2011. Cyanidin-3-*O*-β-glucoside and protocatechuic acid exert insulin-like effects by upregulating PPARgamma activity in human omental adipocytes. Diabetes, **60**: 2234–2244. doi:10.2337/db10-1461. PMID:21788573.

Semaming, Y., Kumfu, S., Pannangpetch, P., Chattipakorn, S.C., and Chattipakorn, N. 2014. Protocatechuic acid exerts a cardioprotective effect in type 1 diabetic rats. J. Endocrinol. **223**: 13–23. doi:10.1530/JOE-14-0273. PMID:25074852.

Song, Y., Cui, T., Xie, N., Zhang, X., Qian, Z., and Liu, J. 2014. Protocatechuic acid improves cognitive deficits and attenuates amyloid deposits, inflammatory response in aged AβPP/PS1 double transgenic mice. Int. Immunopharmacol. **20**: 276–281. doi:10.1016/j.intimp.2014.03.006. PMID:24667368.

Sripetchwandee, J., Sanit, J., Chattipakorn, N., and Chattipakorn, S.C. 2013. Mitochondrial calcium uniporter blocker effectively prevents brain mitochondrial dysfunction caused by iron overload. Life Sci. **92**: 298–304. doi:10.1016/j.lfs.2013.01.004. PMID:23333832.

Sripetchwandee, J., Pipatpiboon, N., Chattipakorn, N., and Chattipakorn, S. 2014. Combined therapy of iron chelator and antioxidant completely restores brain dysfunction induced by iron toxicity. PLoS ONE, **9**: e85115. doi:10.1371/journal.pone.0085115. PMID:24400127.

Vari, R., D'Archivio, M., Filesi, C., Carotenuto, S., Scazzocchio, B., Santangelo, C., et al. 2011. Protocatechuic acid induces antioxidant/detoxifying enzyme expression through JNK-mediated Nrf2 activation in murine macrophages. J. Nutr. Biochem. **22**: 409–417. doi:10.1016/j.jnutbio.2010.03.008. PMID:20621462.

Wang, Y., Wu, L., Li, J., Fang, D., Zhong, C., Chen, J.X., and Yan, S.S. 2015. Synergistic exacerbation of mitochondrial and synaptic dysfunction and resultant learning and memory deficit in a mouse model of diabetic Alzheimer's disease. J. Alzheimers Dis. **43**: 451–463. PMID:25096625.

Wolff, S.P., and Dean, R.T. 1987. Glucose autoxidation and protein modification. The potential role of 'autoxidative glycosylation' in diabetes. Biochem. J. **245**: 243–250. PMID:3117042.

Appl. Physiol. Nutr. Metab. Downloaded from www.nrcresearchpress.com by CONCORDIA UNIV on 10/06/15
For personal use only.

เอกสารแนบหมายเลข 44

Thematic Research

226:2 M1–M11

Dipeptidyl peptidase 4 inhibitor improves brain insulin sensitivity, but fails to prevent cognitive impairment in orchiectomy obese rats

Hiranya Pintana[1,2], Wanpitak Pongkan[1,2], Wasana Pratchayasakul[1,2], Nipon Chattipakorn[1,2] and Siriporn C Chattipakorn[1,3]

[1]Neurophysiology Unit, Faculty of Medicine, Cardiac Electrophysiology Research and Training Center, [2]Department of Physiology, Faculty of Medicine, and [3]Department of Oral Biology and Diagnostic Science, Faculty of Dentistry, Chiang Mai University, Chiang Mai 50200, Thailand

Correspondence should be addressed to S C Chattipakorn
Email
scchattipakorn@gmail.com or siriporn.c@cmu.ac.th

Abstract

It is unclear whether the dipeptidyl peptidase 4 (DPP4) inhibitor can counteract brain insulin resistance, brain mitochondrial dysfunction, impairment of hippocampal synaptic plasticity and cognitive decline in testosterone-deprived obese rats. We hypothesized that DPP4 inhibitor vildagliptin improves cognitive function in testosterone-deprived obese rats by restoring brain insulin sensitivity, brain mitochondrial function and hippocampal synaptic plasticity. Thirty male Wistar rats received either a sham-operated (S, $n=6$) or bilateral orchiectomy (ORX, $n=24$). ORX rats were divided into two groups and fed with either a normal diet (ND (NDO)) or a high-fat diet (HFO) for 12 weeks. Then, ORX rats in each dietary group were divided into two subgroups ($n=6$/subgroup) to receive either a vehicle or vildagliptin (3 mg/kg per day, p.o.) for 4 weeks. After treatment, cognitive function, metabolic parameters, brain insulin sensitivity, hippocampal synaptic plasticity and brain mitochondrial function were determined in each rat. We found that HFO rats exhibited peripheral and brain insulin resistance, brain mitochondrial dysfunction, impaired hippocampal synaptic plasticity and cognitive decline. NDO rats did not develop peripheral and brain insulin resistance. However, impaired hippocampal synaptic plasticity and cognitive decline occurred. Vildagliptin significantly improved peripheral insulin sensitivity, restored brain insulin sensitivity and decreased brain mitochondrial reactive oxygen species production in HFO rats. However, vildagliptin did not restore hippocampal synaptic plasticity and cognitive function in both NDO and HFO rats. These findings suggest that vildagliptin could not counteract the impairment of hippocampal synaptic plasticity and cognitive decline in testosterone-deprived subjects, despite its effects on improved peripheral and brain insulin sensitivity as well as brain mitochondrial function.

Key Words
- vildagliptin
- obese-insulin resistance
- testosterone deprivation
- brain mitochondrial function
- hippocampal synaptic plasticity
- cognitive function

Journal of Endocrinology (2015) 226, M1–M11

http://joe.endocrinology-journals.org
DOI: 10.1530/JOE-15-0099

© 2015 Society for Endocrinology
Printed in Great Britain

Published by Bioscientifica Ltd.

Introduction

Long-term high-calorie diets cause obesity, leading to the development of insulin resistance, metabolic syndrome and type 2 diabetes mellitus (Pandolfi *et al.* 1994, Kahn & Flier 2000). Moreover, several studies demonstrated that insulin resistance was also associated with cognitive decline (Craft 2005, Greenwood & Winocur 2005, Stranahan *et al.* 2008). Our studies also showed that 12-weeks of a high-fat diet (HFD) consumption in male rats induced not only obese-insulin resistance, but also impaired brain insulin sensitivity, brain mitochondrial dysfunction and cognitive decline (Pintana *et al.* 2012, 2013, Pipatpiboon *et al.* 2013).

Testosterone is an androgenic steroid hormone, which plays an important role in the regulation of male reproduction and behaviors, as well as in the maintenance of glucose and lipid metabolism (Aydilek & Aksakal 2005, Christoffersen *et al.* 2010). Several studies have shown that testosterone replacement exerted beneficial effects on brain function, including the prevention of neuronal cell death, the balancing of brain oxidative stress and antioxidant activity, improvement of synaptic plasticity and the involvement of cognitive formation in animal models (Janowsky 2006, Meydan *et al.* 2010, Filova *et al.* 2013). Interestingly, growing evidence demonstrated that testosterone deficiency is associated with obese insulin-resistance in men (Haffner *et al.* 1994, Stellato *et al.* 2000, Grossmann *et al.* 2008, Shi *et al.* 2013). All of those findings indicate that testosterone-deprivation can lead to obesity and cognitive decline. Therefore, it is possible that testosterone deprivation combined with obesity could lead to the worsening of cognitive decline.

The dipeptidyl peptidase 4 (DPP4) inhibitor, vildagliptin, is an anti-diabetic drug, which exerts beneficial effects in diabetic and insulin resistant models, such as the regulation of blood glucose levels without hypoglycemic incidence (Burkey *et al.* 2005), restoring pancreatic β-cells as well as preserving pancreatic function and improving insulin sensitivity (Ahren *et al.* 2004). Our previous study demonstrated that vildagliptin improved not only peripheral insulin sensitivity, but also increased brain insulin sensitivity in obese-insulin resistant rats, as indicated by improvement in brain insulin receptor (IR) function (Pipatpiboon *et al.* 2013). In addition, vildagliptin have been shown to enhance hippocampal neurogenesis, leading to improved learning and memory in HFD-fed rodents (Pintana *et al.* 2013, Pipatpiboon *et al.* 2013, Gault *et al.* 2015). All of these findings indicate the beneficial effects of vildagliptin on peripheral insulin sensitivity, brain insulin signaling and cognitive function in obese-insulin resistant conditions. However, the effects of vildagliptin on brain insulin sensitivity, brain mitochondrial function, hippocampal synaptic plasticity and cognitive function in testosterone-deprived obese rats have never been investigated. We tested the hypothesis that testosterone-deprived rats with or without obesity have impaired brain IR function, decreased brain insulin signaling, impaired brain mitochondrial function and impaired hippocampal synaptic plasticity, thus leading to cognitive decline. We also hypothesized that vildagliptin could restore these impairments in testosterone-deprived conditions with or without obesity.

Materials and methods

Animal models and experimental protocols

Thirty male Wistar rats, weighing 180–200 g (aged ~5–6 weeks old) obtained from the National Animal Center, Salaya Campus, Mahidol University, Bangkok, Thailand were used. All experiments were conducted in accordance with the approved protocol from the Faculty of Medicine, Chiang Mai University Institutional Animal Care and Use Committee, in compliance with NIH guidelines. All animals were housed in environmentally controlled conditions (25±0.5 °C and a 12 h light:12 h darkness cycle) and allowed to acclimate for 1 week. Rats were then divided into two groups as either control sham-operated (S, $n=6$) or bilateral orchiectomized (ORX, $n=24$) rats as described previously (Dulisch 1976). Rats in the sham-operated group were fed with a ND for 12 weeks and were the control group (NDS); after that rats received vehicle until the end of experiment. Rats in ORX group were randomized and fed with either a normal diet (ND: 19.77% E fat, NDO) or a HFD (59.28% E fat, HFO) for 12 weeks (Pratchayasakul *et al.* 2011). At the end of 12 weeks, the rats in each group were divided into two subgroups ($n=6$/subgroup) and received either the vehicle (normal saline solution; 2 ml/kg per day) (NDO rats treated with vehicle (NDOV) and HFO rats treated with vehicle (HFOV)) or vildagliptin (Gulvus, Novartis, Bangkok, Thailand; 3 mg/kg per day) (NDO rats treated with vildagliptin (NDOVil) and HFO rats treated with vildagliptin (HFOVil)), via gavage feeding for 4 weeks (Burkey *et al.* 2005, Pintana *et al.* 2013). The cognitive function was subsequently determined by the Morris water maze (MWM) test. Blood samples were collected from a tail

http://joe.endocrinology-journals.org
DOI: 10.1530/JOE-15-0099
© 2015 Society for Endocrinology
Printed in Great Britain
Published by Bioscientifica Ltd.

Journal of Endocrinology

vein at week 12, and week 15 for further plasma analysis. At the end of the experimental period, rats were deeply anesthetized with isoflurane and killed by decapitation. The brain of each rat was removed as quickly as possible after death and carefully sliced in preparation for extracellular recording (insulin-induced long-term depression (LTD) and hippocampal synaptic long-term potentiation (LTP)), immunoblot and brain mitochondrial functions. The study protocol is shown in Fig. 1.

Blood sample assays

Plasma glucose and cholesterol levels were determined via colorimetric assay (Biotech, Bangkok, Thailand). Plasma HDL and LDL levels were determined using a commercial colorimetric assay kit (Biovision, CA, USA). Plasma insulin levels were determined using the Sandwich ELISA Kit (Linco Research, St Charles, MO, USA). Peripheral insulin resistance was assessed using the homeostasis model assessment (HOMA), which was calculated by the following formula: (fasting plasma insulin (μU/ml))× (fasting plasma glucose (mmol/l))/22.5 as previously described (Pipatpiboon *et al.* 2012). Plasma testosterone levels were measured using the electrochemiluminescence immunoassay (ECLIA) technique (Roche Diagnostics).

Oral glucose tolerance test

Oral glucose tolerance test (OGTT) was performed as described previously (Pipatpiboon *et al.* 2013). Briefly, rats were starved overnight before the test and received 2 g/kg glucose solution via oral gavage. Blood samples were collected from the tail vein at 0, 15, 30, 60, 90 and 120 min after glucose administration. Areas under the curves (AUC) were calculated to evaluate glucose tolerance.

Brain slice preparation

At the end of experiment, animals were anesthetized with isoflurane and decapitated. The brain slice preparation was

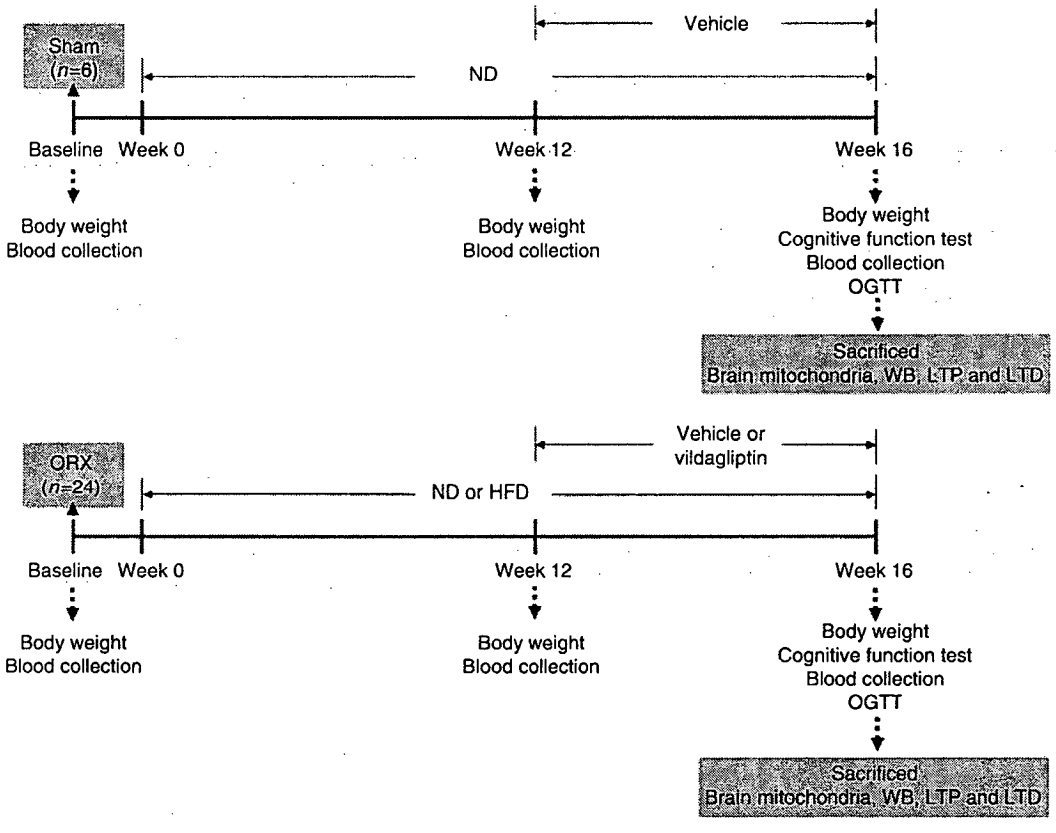


Figure 1
The experimental protocol of the present study.

© 2015 Society for Endocrinology
Printed in Great Britain
Published by Bioscientifica Ltd.

performed as described previously (Pratchayasakul *et al.* 2011, Pipatpiboon *et al.* 2012, 2013).

Extracellular recordings of hippocampal slices for insulin-induced LTD

An extracellular recording of hippocampal slices for insulin-induced LTD was performed as described in our previous studies (Pratchayasakul *et al.* 2011, Pipatpiboon *et al.* 2012, 2013). Field excitatory postsynaptic potentials (fEPSPs) were evoked by stimulating the Schaffer collateral–commissural pathway with a bipolar tungsten electrode, while recordings were taken from the stratum radiatum of the hippocampal CA1 region with micropipettes (3 Mohm) filled with 2 M NaCl. Stimulus frequency was 0.033 Hz. The stimulus intensity of fEPSPs was adjusted to 0.8–1.0 mV in amplitude. Hippocampal slices were perfused with aCSF (as baseline condition) for 10 min, and then perfused with aCSF plus 500 nM insulin (as insulin-induced LTD) for an additional 10 min. Afterward, the slices were perfused with aCSF for an additional 50 min and readings recorded. Data was filtered at 3 kHz, digitized at 10 kHz, and stored in a computer using pClamp 9.2 Software (Axon Instruments, Union City, CA, USA). The initial slope of the fEPSP was measured and plotted against time.

Extracellular recordings of hippocampal slices for synaptic LTP

The examination of electrical-induced hippocampal synaptic LTP was performed as described in our previous study (Sripetchwandee *et al.* 2014). fEPSPs were evoked by stimulating the Schaffer collateral–commissural pathway with a bipolar tungsten electrode, while the fEPSPs recordings were taken from the stratum radiatum of the hippocampal CA1 region with micropipettes (3 Mohm) filled with 2 M NaCl. LTP was induced by delivering high-frequency stimulation (HFS; four trains at 100 Hz; 0.5 s duration; 20 s interval). Experiments were performed for at least 40 min after HFS. The amount of potentiation was calculated at 40 min after tetanus. All data were filtered at 3 kHz, digitized at 10 kHz, and stored in a computer using pClamp9.2 Software (Axon Instruments). The initial slopes of the fEPSPs were measured and plotted against time.

Immunoblotting for brain insulin signaling

To investigate the expression of IR phosphorylation (p-IR) and IRs, homogenate brain slices from each subgroup were used as described in our previous study (Pratchayasakul *et al.* 2011, Pipatpiboon *et al.* 2012, 2013). IR tyrosine phosphorylation were electrophoresed and immunoblotted with rabbit antibodies for IR at tyrosine respectively. Examination of the level of IR protein expression was conducted with homogenates prepared from another set of four whole brain slices. These proteins were resolved by an immunoblot assay conducted with rabbit anti-IR at tyrosine phosphorylation (p-IR$^{Tyr1162/1163}$; 1:1000; sc-25103-R; Santa Cruz Biotechnology, Dallas, TX, USA), IR (1:1000; sc-711; Santa Cruz Biotechnology). For a loading control, immunoblotting for each membrane was incubated with anti-β-actin (1:4000; #4967; Cell Signaling Technology, Danvers, MA, USA). All membranes for visualizing the phosphorylation and the protein levels of IR expression were incubated with secondary goat anti-rabbit antibody conjugated with HRP (1:2000; #7074; Cell Signaling Technology). The protein bands were visualized on Amersham Hyperfilm ECL (GE Healthcare, Buckinghamshire, UK) using Amersham ECL Western Blot Detection Reagents (GE Healthcare). Band densities of phosphorylated IR were represented as a ratio of insulin stimulation (+) to no insulin stimulation (−) and were normalized to total IR. In addition, band intensities were quantified by Scion Image (Scion Corporation, National Institute of Health, Federick, MD, USA) and the results were shown as average signal intensity (arbitrary) units.

Preparation of brain mitochondria

Brain mitochondria were isolated using the method described previously (Pipatpiboon *et al.* 2013). Mitochondrial protein concentration was measured using BCA assay (Pipatpiboon *et al.* 2013). Brain mitochondrial functions including brain mitochondrial reactive oxygen species (ROS), mitochondrial membrane potential change ($\Delta\Psi m$) and mitochondrial swelling were also determined.

Brain mitochondrial ROS assay Brain mitochondrial ROS were measured using dichloro-hydrofluoresceindiacetate (DCFHDA) fluorescent dye. Brain mitochondria (0.4 mg/ml) were incubated with 2-μM DCFHDA at 25 °C for 20 min. The fluorescence was determined using a fluorescent microplate reader at the excitation wavelength of 485 nm and emission wavelength of 530 nm (Pipatpiboon *et al.* 2013). Increased fluorescence intensity indicates increased ROS production.

Brain $\Delta\Psi m$ assay The change in $\Delta\Psi m$ was measured using the fluorescent dye 5,5′,6,6′-tetrachloro-1,1′,3,3′-tetraethyl benzimidazolcarbocyanine iodide (JC-1).

© 2015 Society for Endocrinology
Printed in Great Britain
Published by Bioscientifica Ltd.

The JC-1 monomer form (green fluorescence) was excited at a wavelength of 485 nm and detected at the emission wavelength of 590 nm. JC-1 aggregate form (red fluorescence) was excited at a wavelength of 485 nm and detected at the emission wavelength of 530 nm. Brain mitochondria (0.4 mg/ml) were incubated with JC-1 dye at 37 °C for 15 min. $\Delta\Psi m$ changes were determined by measuring the fluorescence intensity using a fluorescent microplate reader. The change in $\Delta\Psi m$ was calculated as the ratio of red to green fluorescent intensity (Pipatpiboon *et al.* 2013). Decreased red/green fluorescence intensity ratio indicates mitochondrial depolarization.

Brain mitochondrial swelling assay Brain mitochondrial swelling was determined by measuring the change in the absorbance of brain mitochondrial suspension. Brain mitochondria (0.4 mg/ml) were incubated in 2 ml of respiration buffer. The suspension was read at 540 nm using a microplate reader. Mitochondrial swelling was indicated by a decrease in the absorbance (Pipatpiboon *et al.* 2013).

Cognitive function test

The open-field test (OFT) was used to screen locomotor activity via counting the number of lines that the rats crossed during the test, as described in previous studies (Arakawa 2005, Pintana *et al.* 2013). The assessment of cognitive function was performed by using MWM with two assessments including the acquisition test which was carried out for 5 consecutive days, and the probe test which was performed on day 6 (Vorhees & Williams 2006, Pintana *et al.* 2013). Data analysis of MWM test was done manually from video tape recordings by the investigators, who were blinded to experimental groups.

Statistical analysis

Data were expressed as mean ± S.E.M. For all comparisons, the significance of the differences in peripheral biochemical parameters was calculated using the Mann–Whitney *U* test. The comparisons in the percentage of insulin-induced LTD, the percentage of LTP, brain mitochondrial function, immunoblot, the OFTs and the MWM tests for the probe test among groups were performed using the one-way ANOVA test, followed by *post-hoc* Fisher's least significant difference (LSD) analysis. Comparisons among groups in MWM tests for the acquisition test were performed using a two-way ANOVA, followed by *post-hoc* LSD analysis. $P<0.05$ was considered statistically significant.

Results

Obesity, but not testosterone deprivation, caused peripheral insulin resistance, which was attenuated by vildagliptin treatment

At the baseline levels (before ORX), the metabolic parameters were not significantly different between the sham-operated group and the ORX group (Table 1). After 12 weeks of diet regimens, HFO rats had significantly increased plasma insulin, HOMA index and total cholesterol levels, when compared with NDS and NDO rats. Plasma glucose levels were not significantly different among groups. However, the body weight of NDO had significantly decreased, when compared with NDS (Table 1). These findings suggested that long-term HFD consumption caused peripheral insulin resistance as indicated by hyperinsulinemia with euglycemia and increased HOMA index. However, testosterone deprivation alone did not impair peripheral insulin sensitivity.

After 4 weeks of vildagliptin treatment, testosterone deprivation by ORX was confirmed by reduced plasma testosterone levels (<0.025 ng/ml) in all ORX groups (NDOV, NDOVil, HFOV and HFOVil) compared to NDS group (0.75 ± 0.06 ng/ml). NDOV and NDOVil had significantly decreased body weight and visceral fat, without any significant alteration in plasma insulin, HOMA index,

Table 1 Metabolic parameters at baseline and the end of week 12 (before treatment)

	Baseline		Week 12		
Metabolic parameters	Sham	ORX	NDS	NDO	HFO
Body weight (g)	192.5 ± 3.7	197.5 ± 3.7	466.6 ± 4.9	409.2 ± 14.1[a,b]	472.0 ± 8.4
Plasma glucose (mg/dl)	106.8 ± 4.5	111.8 ± 4.3	133.8 ± 4.9	140.0 ± 5.5	139.9 ± 7.1
Plasma insulin (ng/ml)	2.1 ± 0.3	2.2 ± 0.4	2.0 ± 0.2	2.1 ± 0.2[b]	3.7 ± 0.3[a]
HOMA index	13.4 ± 1.2	14.0 ± 2.2	15.3 ± 2.0	17.7 ± 2.1[b]	27.6 ± 3.4[a]
Plasma total cholesterol (mg/dl)	45.5 ± 2.2	47.7 ± 1.7	48.5 ± 2.7	52.1 ± 2.0[b]	75.0 ± 6.6[a]

[a]Compared to NDS.
[b]Compared to HFO.

© 2015 Society for Endocrinology
Printed in Great Britain
Published by Bioscientifica Ltd.

Journal of Endocrinology

Table 2 Metabolic parameters after vildagliptin treatment for 4 weeks

Metabolic parameters	Groups				
	NDS	NDOV	NDOVil	HFOV	HFOVil
Body weight (g)	496.5±10.7	423.3±8.4[a,b]	417.2±17.6[a,b]	506.6±17.8	496.6±16.4
Visceral fat (g)	26.8±1.6	16.0±1.9[a,b]	15.7±1.4[a,b]	31.3±3.4	30.3±3.3
Plasma glucose (mg/dl)	131.5±10.6	129.0±13.1	137.3±3.1	134.1±8.9	131.7±6.3
Plasma insulin (ng/ml)	2.53±0.34	2.78±0.18	2.71±0.36	5.07±1.16[a]	2.37±0.37[b]
HOMA index	21.3±2.9	24.4±2.8	21.5±3.4	44.7±13.8[a]	20.6±3.8[b]
Plasma glucose AUC (AUCg) (mg/dl×min×10^4)	4.47±0.20	5.01±0.33	4.48±0.23	5.92±0.25[a]	4.97±0.26[b]
Plasma total cholesterol (mg/dl)	68.0±5.5	63.8±2.6	73.3±5.8	110.8±14.9[a]	101.7±8.7[a]
Plasma triglyceride (mg/dl)	51.9±2.2	55.3±9.9	57.4±6.1	49.8±4.1	50.2±7.5
HDL cholesterol (mg/dl)	6.7±0.4	7.2±0.3	7.5±0.4	4.9±0.6[a]	6.9±0.4[b]
LDL cholesterol (mg/dl)	60.6±7.5	52.9±3.6	56.9±4.0	116.4±15.7[a]	81.5±8.1[b]

[a]Compared to NDS.
[b]Compared to HFOV.

plasma glucose AUC of OGTT (AUCg), total cholesterol, plasma LDL cholesterol levels as well as plasma HDL cholesterol levels, when compared with those of NDS rats (Table 2). These findings indicated that peripheral insulin resistance was not observed in the NDOV and NDOVil rats. In contrast, HFOV showed the characteristics of peripheral insulin resistance, including increased plasma insulin, HOMA index, plasma AUCg, total cholesterol, plasma LDL cholesterol levels as well as decreased plasma HDL cholesterol levels, when compared with those of NDS rats. However, plasma glucose and plasma triglyceride levels showed no significant difference among all groups. Interestingly, HFOVil had significantly decreased plasma insulin, HOMA index, plasma AUCg and plasma LDL cholesterol levels as well as increased plasma HDL cholesterol levels, when compared with those of HFOV rats. All of these findings suggested that vildagliptin attenuated peripheral insulin resistance via increased peripheral insulin sensitivity and improved lipid profiles in testosterone-deprived obese rats.

Obesity, but not testosterone deprivation, caused the impairment of brain IR function, which was attenuated by vildagliptin treatment

Brain IR function was tested by measuring insulin-induced LTD and brain insulin signaling. For the insulin-induced LTD study, the degrees of insulin-mediated LTD in ND-fed rats (NDS, NDOV and NDOVil) were not significantly different among groups (n=2–3 independent slices/animal, n=6 animals/group, Fig. 2A). However, the degree of insulin-induced LTD was significantly reduced in HFOV rats, when compared with that of NDS rats (n=2–3 independent slices/animal, n=6 animals/group, Fig. 2A). After 4 weeks of vildagliptin administration, the degrees of insulin-induced LTD in HFOVil was significantly increased compared with that of HFOV rats (n=2–3 independent slices/animal, n=6 animals/group, Fig. 2A).

For the brain insulin signaling study, the expression of IRs in all groups showed no significant different among them (Fig. 2C). The p-IRs at tyrosine site was not significantly different among groups of ND-fed rats (NDS, NDOV and NDOVil; Fig. 2B). However, levels of p-IR of HFOV rats were significantly decreased, when compared with those of NDOV rats (Fig. 2B). Furthermore, vildagliptin treatment significantly increased p-IR levels in HFO rats (Fig. 2B). All of these findings suggested that the obese insulin-resistant condition, but not testosterone deprivation, caused the impairment of brain IR function and brain insulin signaling. In addition, vildagliptin restored the impairment of brain IR function as well as brain insulin signaling in the testosterone-deprived obese condition.

Obesity, but not testosterone deprivation, caused brain mitochondrial dysfunction and vildagliptin attenuated that impairment

Brain mitochondrial function was determined by assessing changes in brain mitochondrial ROS production and brain $\Delta\Psi m$ change after H_2O_2 stimulation, and brain mitochondrial swelling. The results demonstrated that brain mitochondrial function, including brain mitochondrial ROS level, brain $\Delta\Psi m$ changes and brain mitochondrial swelling, was not significantly different among groups of ND-fed rats (NDS, NDOV and NDOVil; Fig. 3A, B and C). These findings suggested that testosterone deprivation did not impair brain mitochondrial function. Furthermore, HFOV rats had a significant increase in brain

© 2015 Society for Endocrinology
Printed in Great Britain
Published by Bioscientifica Ltd.

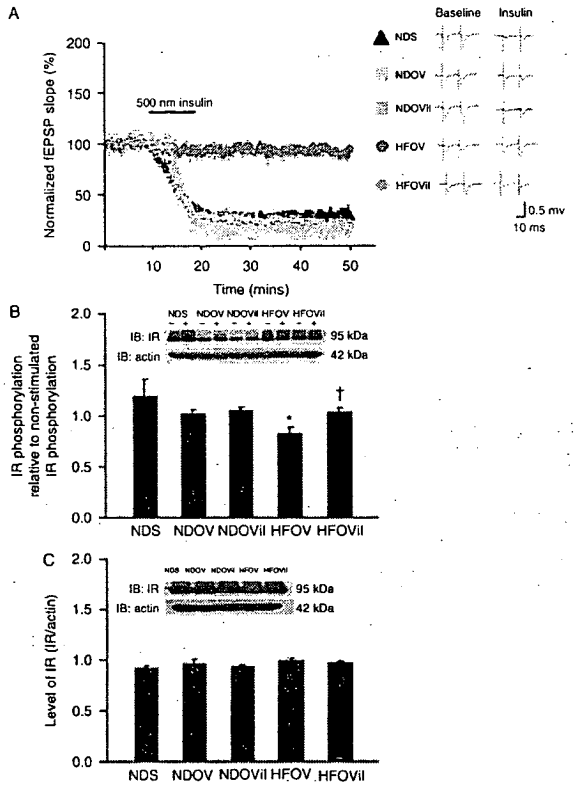


Figure 2
The effects of vildagliptin on brain insulin receptor (IR) function, including insulin-induced LTD, the phosphorylation of IR (p-IR) and the expression of IRs in testosterone-deprived rats with or without obesity. Insulin-induced LTD in the CA1 hippocampus and the p-IR significantly decreased in HFOV rats, when compared with that of NDS rats (A and B). The administration of vildagliptin for 4 weeks significantly improved the ability of insulin-induced LTD and the p-IR in HFOVil rats, when compared with that of HFOV rats (A and B). No differences in the expression of IR among all groups were found (C). NDS, sham-operated rats with normal diet feeding; NDOV, orchiectomized-operated rats with normal diet feeding and treated with vehicle; NDOVil, orchiectomized-operated rats with normal diet feeding and treated with vildagliptin; HFOV, orchiectomized-operated rats with high-fat diet feeding and treated with vehicle; HFOVil, orchiectomized-operated rats fed with a high-fat diet and treated with vildagliptin. *$P<0.05$ vs NDS and †$P<0.05$ vs HFOV. A full colour version of this figure is available at http://dx.doi.org/10.1530/JOE-15-0099.

mitochondrial ROS production, brain mitochondrial depolarization and brain mitochondrial swelling, when compared with those of NDOV rats (Fig. 3A, B and C). In addition, vildagliptin treatment significantly decreased brain ROS production in HFOVil rats, when compared with that of HFOV rats (Fig. 3A). However, vildagliptin did not attenuate brain mitochondrial depolarization and brain mitochondrial swelling in HFO rats (Fig. 3B and C). The morphological changes of brain mitochondria from all groups were shown in Fig. 4. Intact brain mitochondrial morphology with apparent folded cristae was observed in all ND-fed rats (Fig. 4A, B and C). Brain mitochondrial swelling was observed in both the HFOV and HFOVil groups as indicated by markedly unfolded cristae (Fig. 4D and E). All of these findings suggested that the obese

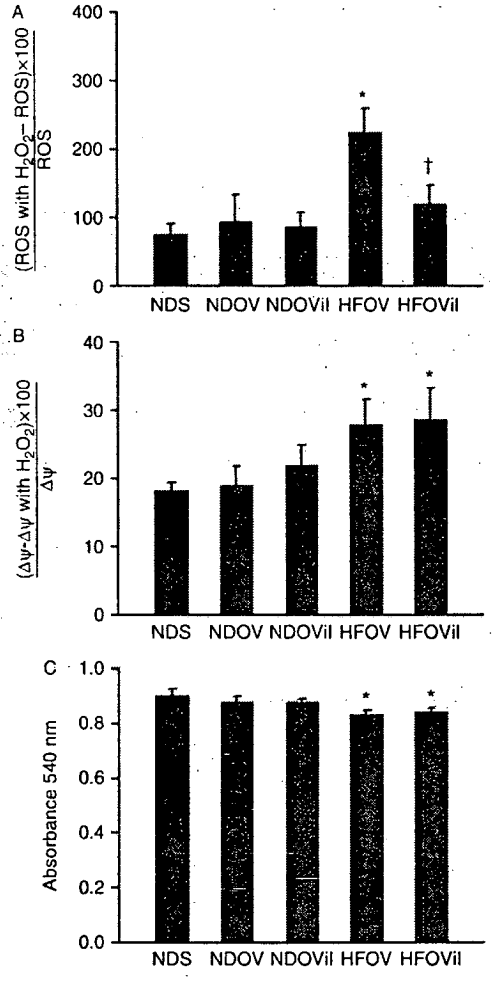


Figure 3
The effects of vildagliptin on brain mitochondrial function in testosterone deprived rats with or without obesity. HFOV rats demonstrated brain mitochondrial dysfunction, as indicated by increased brain mitochondrial ROS production following H_2O_2 application (A), increased brain mitochondrial membrane potential ($\Delta\Psi m$) change following H_2O_2 application (B) and decreased absorbance values, indicating brain mitochondrial swelling (C). The administration of vildagliptin for 4 weeks significantly decreased brain mitochondrial ROS production in HFOVil rats, when compared with that of HFOV rats (A). However, vildagliptin did not improve brain $\Delta\Psi m$ change and brain mitochondrial swelling in HFOVil rats (B and C). NDS, sham-operated rats with normal diet feeding; NDOV, orchiectomized-operated rats with normal diet feeding and treated with vehicle; NDOVil, orchiectomized-operated rats with normal diet feeding and treated with vildagliptin; HFOV, orchiectomized-operated rats with high-fat diet feeding and treated with vehicle; HFOVil, orchiectomized-operated rats with high-fat diet feeding and treated with vildagliptin. *$P<0.05$ vs NDOV and †$P<0.05$ vs HFOV.

© 2015 Society for Endocrinology
Printed in Great Britain
Published by Bioscientifica Ltd.
Journal of Endocrinology

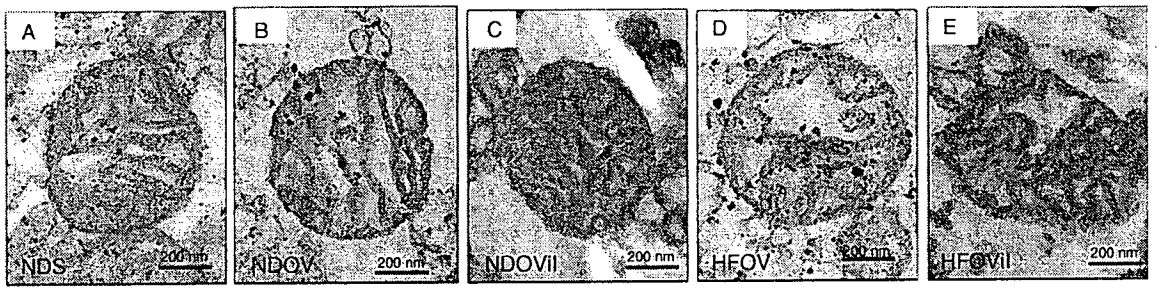


Figure 4
Representative images of brain mitochondrial morphology by transmission electron microscopy (JEM-2200FS field emission electron microscope, original magnification ×20 000) after 4 weeks of vildagliptin treatment. Normal folding of cristae in brain mitochondrial morphology was shown among all normal diet-fed rats (A, B and C). However, brain mitochondrial swelling, as indicated by unfolded cristae, of both HFOV and HFOVil groups was observed (D and E). NDS, sham-operated rats with normal diet feeding; NDOV, orchiectomized-operated rats with normal diet feeding and treated with vehicle; NDOVil, orchiectomized-operated rats with normal diet feeding and treated with vildagliptin; HFOV, orchiectomized-operated rats with high-fat diet feeding and treated with vehicle; HFOVil, orchiectomized-operated rats with high-fat diet feeding and treated with vildagliptin.

insulin-resistant condition, but not testosterone deprivation, caused the impairment of brain mitochondrial function. In addition, vildagliptin attenuated brain mitochondrial dysfunction by reducing brain ROS production in the testosterone-deprived obese condition.

Testosterone deprivation with or without obesity caused impaired hippocampal synaptic plasticity and cognitive decline, and vildagliptin failed to restore those impairments

To study hippocampal synaptic plasticity, electrical-induced LTP was determined. The results demonstrated that the degrees of electrical-induced LTP significantly decreased in both NDOV and HFOV rats, when compared with that of NDS rats. The reduction of electrical-induced LTP in both NDOV and HFOV rats ($n=2$–3 independent slices/animal, $n=6$ animals/group, Fig. 5A) was not significantly different. In addition, vildagliptin administration did not improve the degree of electrical-induced LTP in both NDO and HFO rats. These findings indicated that testosterone deprivation with or without obesity caused the impairment of hippocampal synaptic plasticity. However, vildagliptin treatment could not attenuate that impairment.

Furthermore, the OFT was used to screen locomotor activity. The results showed that it was not significantly different among all groups, indicating that the locomotor activity did not differ in all groups. In addition, the present study determined cognitive function by using the MWM test. For the acquisition test, the time to reach the platform was not significantly different among ND-fed rats (NDS, NDOV and NDOVil rats; Fig. 5B). However, we found that HFOV and HFOVil rats took a longer time to reach the platform, when compared with that of NDS rats (Fig. 5B). For the probe test, the results showed that time spent in the target quadrant of the NDOV, NDOVil, HFOV and HFOVil rats was significantly decreased compared to NDS rats (Fig. 5C). These findings suggested that testosterone deprivation with or without obesity caused cognitive decline, and vildagliptin failed to restore cognitive function in the testosterone-deprived rats.

Discussion

The major findings of the present study are as follows: i) the condition of obesity in testosterone-deprived rats leads to the development of peripheral insulin resistance, impairment of brain insulin sensitivity, brain mitochondrial dysfunction and impaired hippocampal synaptic plasticity, resulting in cognitive decline; ii) vildagliptin improves peripheral insulin sensitivity, brain insulin sensitivity and brain mitochondrial function in testosterone-deprived obese rats; and iii) vildagliptin fails to restore hippocampal synaptic plasticity and cognitive function in testosterone deprived rats.

The present study demonstrates that peripheral insulin resistance, as indicated by increased HOMA index and impaired OGTT as well as impaired lipid profiles, developed in testosterone-deprived rats with obesity. Consistent with these findings, previous studies demonstrated that HFD-induced obesity caused the development of peripheral insulin resistance in male rats (Akiyama *et al.* 1996, Stranahan *et al.* 2008, Pintana *et al.* 2013, Pipatpiboon *et al.* 2013). The development of peripheral insulin resistance in the present study

http://joe.endocrinology-journals.org
DOI: 10.1530/JOE-15-0099
© 2015 Society for Endocrinology
Printed in Great Britain
Published by Bioscientifica Ltd.

Journal of Endocrinology

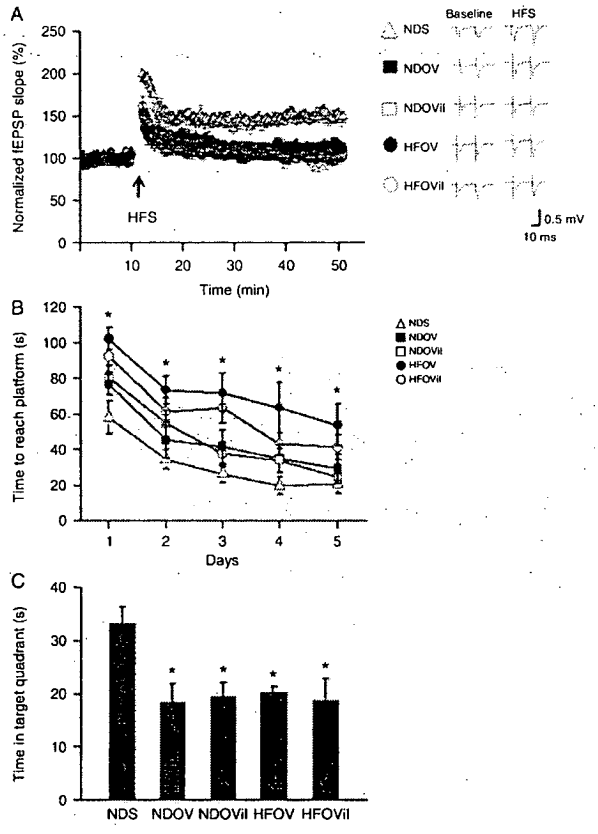


Figure 5

The effects of vildagliptin on hippocampal synaptic long-term potentiation (LTP) and the cognitive function determined by Morris water maze (MWM) test in testosterone-deprived rats with or without obesity. Both orchiectomized-operated groups (NDOV and HFOV rats) significantly reduced the percentage of normalized fEPSPs, when compared with that of NDS rats (A). The administration of vildagliptin for 4 weeks did not improve the percentage of normalized fEPSPs in both orchiectomized-operated groups (NDOVil and HFOVil), when compared with that of HFOV rats (A). HFOV rats and HFOVil rats significantly increased time to reach the platform in the acquisition test as well as had a decreased time spent in target quadrant in the probe test, when compared with that of NDS rats (B and C). NDOV rats had a significantly decreased time spent in the target quadrant in the probe test, but there was no changed in time to reach the platform in the acquisition test (B and C). The administration of vildagliptin for 4 weeks did not restore the time taken to reach the platform in HFOVil rats, and the time spent in the target quadrant in both NDOVil and HFOVil rats (B and C). NDS, sham-operated rats with normal diet feeding; NDOV, orchiectomized-operated rats with normal diet feeding and treated with vehicle; NDOVil, orchiectomized-operated rats with normal diet feeding and treated with vildagliptin; HFOV, orchiectomized-operated rats with high-fat diet feeding and treated with vehicle; HFOVil, orchiectomized-operated rats with high-fat diet feeding and treated with vildagliptin; HFS, high frequency stimulation. *$P<0.05$ vs NDS.

depended on HFD-induced obesity, but not testosterone-deprivation, as confirmed by no change in insulin sensitivity in NDOV rats. Our findings are also consistent with a previous report by Christoffersen *et al.* (2006). In addition, the present study demonstrated that ORX led to a loss of body weight. The reduction of daily food intake in the ORX group could be the explanation of weight loss in these rats. These findings are consistent with several previous studies, which showed that the reduction of body weight in ORX rats was caused by the reduction of daily food intake (Gentry & Wade 1976, Borst & Conover 2006) and muscle atrophy (Gao *et al.* 2005, Axell *et al.* 2006, Borst & Conover 2006). In contrast to our findings, the studies of Xia *et al.* (2013) found that ORX-induced testosterone deficiency increased the fasting blood glucose in mature adult (10 weeks old) Sprague–Dawley male rats. Jayaraman *et al.* (2014) demonstrated that ORX adult mice (3 months of age) had impaired insulin sensitivity. Since young adult male Wistar rats were used and were ORX at 5–6 weeks of age in the present study, the differences in species and age at the time of ORX procedure could be responsible for these inconsistent findings.

Interestingly, we found that HFOV rats, but not NDOV rats, developed brain insulin resistance as indicated by a reduction of insulin induced-LTD and decreased p-IR, as well as brain mitochondrial dysfunction through increased brain ROS production, brain mitochondrial depolarization and brain mitochondrial swelling. These findings and other previous studies indicated that obesity caused impaired brain mitochondrial function, resulting in brain insulin resistance (Pipatpiboon *et al.* 2012, 2013). Furthermore, our results demonstrated that testosterone deficiency alone had no effects on peripheral insulin resistance, brain insulin sensitivity as well as brain mitochondrial function. These findings suggest that testosterone deficiency is not required for the development of HFD-induced insulin resistance, and that factors contributing to peripheral and brain insulin resistance as well as brain mitochondrial dysfunction in this model could be mainly due to obesity.

Growing evidence demonstrated that testosterone deprivation is associated with cognitive decline in both men and animal models (Sakata *et al.* 2000, Hogervorst *et al.* 2001, 2004, Spritzer *et al.* 2011). We also found that testosterone-deprived rats impaired cognition and impaired hippocampal synaptic plasticity, but HFD-induced obesity did not aggravate those impairments in the testosterone-deprived condition. The present findings and other previous studies (Sakata *et al.* 2000, Naghdi *et al.* 2005, Sandstrom *et al.* 2006, Spritzer *et al.* 2011) indicated that testosterone plays an important role in cognitive function. Since brain mitochondrial function and brain insulin sensitivity were intact in NDO rats, these results indicate that they were not mainly contributed to

© 2015 Society for Endocrinology
Printed in Great Britain
Published by Bioscientifica Ltd.
Journal of Endocrinology

impaired synaptic plasticity and cognitive decline in testosterone-deprived model.

In the present study, vildagliptin treatment improved peripheral insulin resistance, attenuated brain insulin resistance and partially improved brain mitochondrial dysfunction in testosterone-deprived obese rats. The possible underlying mechanisms of vildagliptin, which improve both peripheral and brain insulin sensitivity, could be due to its ability to i) inhibit the DPP4 activity, resulting in an increase in plasma active GLP1 levels, leading to improve insulin sensitivity and ii) act as an anti-oxidant agent. Although the level of GLP1 was not measured in the present study, our previous study already demonstrated that vildagliptin increased plasma and brain active GLP1 levels, leading to increased peripheral and brain insulin sensitivity in obese male rats (Burkey *et al.* 2005, Pipatpiboon *et al.* 2013, Gault *et al.* 2015). In addition, an anti-oxidant effect of vildagliptin was already demonstrated via reduced malondialdehyde (MDA) levels in the circulation and the brain in our previous report (Pintana *et al.* 2013). Although vildagliptin increased brain insulin sensitivity and decreased brain mitochondrial dysfunction, it could not restore hippocampal synaptic plasticity and cognitive function in testosterone-deprived rats with or without obesity. Furthermore, findings from previous studies (Sandstrom *et al.* 2006, Spritzer *et al.* 2011, McConnell *et al.* 2012) and the present study (Fig. 5B and C) suggest that testosterone plays a critical role in maintaining the normal function of cognition. These findings also indicate that the impairment of synaptic plasticity that leads to cognitive decline in testosterone-deprived model was not mainly influenced by brain insulin resistance.

Conclusion

Testosterone deprivation can lead to cognitive decline via impaired hippocampal synaptic plasticity. However, testosterone-deprived obese condition leads to not only the development of cognitive decline and impaired hippocampal synaptic plasticity, but also brain insulin resistance and brain mitochondrial dysfunction. These findings suggest that testosterone-deprivation with obese insulin-resistant condition causes severe brain dysfunction. Although DPP4 inhibitor, vildagliptin, improves peripheral and brain insulin sensitivity as well as decreases brain mitochondrial ROS production, it fails to restore hippocampal synaptic plasticity and cognitive function. Therefore, vildagliptin does not provide benefits on preventing cognitive decline in subjects under testosterone-deprived obese condition.

Declaration of interest
The authors declare that there is no conflict of interest that could be perceived as prejudicing the impartiality of the research reported.

Funding
This work was supported by grants from the Thailand Research Fund TRF-BRG5780016 (S C C), the Royal Golden Jubilee PhD program (PHD/0025/2555, H P and S C C), National Research Council of Thailand (S C C), a NSTDA Research Chair Grant from the National Science and Technology Development Agency (N C) and Chiang Mai University Excellent Center Award (N C).

Author contribution statement
H P performed the experiments, analyzed the data and wrote the manuscript. W P performed the experiments and analyzed the data. W P performed the experiments and analyzed the data. N C designed the study, analyzed the data and wrote the manuscript. S C C designed the study, performed the experiments, analyzed the data and wrote the manuscript.

References

Ahren B, Landin-Olsson M, Jansson PA, Svensson M, Holmes D & Schweizer A 2004 Inhibition of dipeptidyl peptidase-4 reduces glycemia, sustains insulin levels, and reduces glucagon levels in type 2 diabetes. *Journal of Clinical Endocrinology and Metabolism* **89** 2078–2084. (doi:10.1210/jc.2003-031907)

Akiyama T, Tachibana I, Shirohara H, Watanabe N & Otsuki M 1996 High-fat hypercaloric diet induces obesity, glucose intolerance and hyperlipidemia in normal adult male Wistar rat. *Diabetes Research and Clinical Practice* **31** 27–35. (doi:10.1016/0168-8227(96)01205-3)

Arakawa H 2005 Age dependent effects of space limitation and social tension on open-field behavior in male rats. *Physiology & Behavior* **84** 429–436. (doi:10.1016/j.physbeh.2005.01.008)

Axell AM, MacLean HE, Plant DR, Harcourt LJ, Davis JA, Jimenez M, Handelsman DJ, Lynch GS & Zajac JD 2006 Continuous testosterone administration prevents skeletal muscle atrophy and enhances resistance to fatigue in orchidectomized male mice. *American Journal of Physiology. Endocrinology and Metabolism* **291** E506–E516. (doi:10.1152/ajpendo.00058.2006)

Aydilek N & Aksakal M 2005 Effects of testosterone on lipid peroxidation, lipid profiles and some coagulation parameters in rabbits. *Journal of Veterinary Medicine. A, Physiology, Pathology, Clinical Medicine* **52** 436–439. (doi:10.1111/j.1439-0442.2005.00764.x)

Borst SE & Conover CF 2006 Orchiectomized Fischer 344 male rat models body composition in hypogonadal state. *Life Sciences* **79** 411–415. (doi:10.1016/j.lfs.2006.01.035)

Burkey BF, Li X, Bolognese L, Balkan B, Mone M, Russell M, Hughes TE & Wang PR 2005 Acute and chronic effects of the incretin enhancer vildagliptin in insulin-resistant rats. *Journal of Pharmacology and Experimental Therapeutics* **315** 688–695. (doi:10.1124/jpet.105.087064)

Christoffersen B, Raun K, Svendsen O, Fledelius C & Golozoubova V 2006 Evalution of the castrated male Sprague–Dawley rat as a model of the metabolic syndrome and type 2 diabetes. *International Journal of Obesity* **30** 1288–1297. (doi:10.1038/sj.ijo.0803261)

Christoffersen BO, Gade LP, Golozoubova V, Svendsen O & Raun K 2010 Influence of castration-induced testosterone and estradiol deficiency on obesity and glucose metabolism in male Gottingen minipigs. *Steroids* **75** 676–684. (doi:10.1016/j.steroids.2010.04.004)

Craft S 2005 Insulin resistance syndrome and Alzheimer's disease: age- and obesity-related effects on memory, amyloid, and inflammation.

© 2015 Society for Endocrinology
Printed in Great Britain
Published by Bioscientifica Ltd.

Neurobiology of Aging **26**(Suppl 1) 65–69. (doi:10.1016/j.neurobiolaging.2005.08.021)

Dulisch ML 1976 A castration procedure for the rabbit, rat, hamster, and guinea pig. *Journal of Zoo Animal Medicine* **7** 8–11. (doi:10.2307/20094380)

Filova B, Ostatnikova D, Celec P & Hodosy J 2013 The effect of testosterone on the formation of brain structures. *Cells, Tissues, Organs* **197** 169–177. (doi:10.1159/000345567)

Gao W, Reiser PJ, Coss CC, Phelps MA, Kearbey JD, Miller DD & Dalton JT 2005 Selective androgen receptor modulator treatment improves muscle strength and body composition and prevents bone loss in orchidectomized rats. *Endocrinology* **146** 4887–4897. (doi:10.1210/en.2005-0572)

Gault VA, Lennox R & Flatt PR 2015 Sitagliptin, a dipeptidyl peptidase-4 inhibitor, improves recognition memory, oxidative stress and hippocampal neurogenesis and upregulates key genes involved in cognitive decline. *Diabetes, Obesity & Metabolism* **17** 403–413. (doi:10.1111/dom.12432)

Gentry RT & Wade GN 1976 Androgenic control of food intake and body weight in male rats. *Journal of Comparative and Physiological Psychology* **90** 18–25. (doi:10.1037/h0077264)

Greenwood CE & Winocur G 2005 High-fat diets, insulin resistance and declining cognitive function. *Neurobiology of Aging* **26**(Suppl 1) 42–45. (doi:10.1016/j.neurobiolaging.2005.08.017)

Grossmann M, Thomas MC, Panagiotopoulos S, Sharpe K, Macisaac RJ, Clarke S, Zajac JD & Jerums G 2008 Low testosterone levels are common and associated with insulin resistance in men with diabetes. *Journal of Clinical Endocrinology and Metabolism* **93** 1834–1840. (doi:10.1210/jc.2007-2177)

Haffner SM, Karhapaa P, Mykkanen L & Laakso M 1994 Insulin resistance, body fat distribution, and sex hormones in men. *Diabetes* **43** 212–219. (doi:10.2337/diab.43.2.212)

Hogervorst E, Williams J, Budge M, Barnetson L, Combrinck M & Smith AD 2001 Serum total testosterone is lower in men with Alzheimer's disease. *Neuro Endocrinology Letters* **22** 163–168.

Hogervorst E, Bandelow S, Combrinck M & Smith AD 2004 Low free testosterone is an independent risk factor for Alzheimer's disease. *Experimental Gerontology* **39** 1633–1639. (doi:10.1016/j.exger.2004.06.019)

Janowsky JS 2006 Thinking with your gonads: testosterone and cognition. *Trends in Cognitive Sciences* **10** 77–82. (doi:10.1016/j.tics.2005.12.010)

Jayaraman A, Lent-Schochet D & Pike CJ 2014 Diet-induced obesity and low testosterone increase neuroinflammation and impair neural function. *Journal of Neuroinflammation* **11** 162. (doi:10.1186/s12974-014-0162-y)

Kahn BB & Flier JS 2000 Obesity and insulin resistance. *Journal of Clinical Investigation* **106** 473–481. (doi:10.1172/JCI10842)

McConnell SE, Alla J, Wheat E, Romeo RD, McEwen B & Thornton JE 2012 The role of testicular hormones and luteinizing hormone in spatial memory in adult male rats. *Hormones and Behavior* **61** 479–486. (doi:10.1016/j.yhbeh.2012.01.003)

Meydan S, Kus I, Tas U, Ogeturk M, Sancakdar E, Dabak DO, Zararsiz I & Sarsilmaz M 2010 Effects of testosterone on orchiectomy-induced oxidative damage in the rat hippocampus. *Journal of Chemical Neuroanatomy* **40** 281–285. (doi:10.1016/j.jchemneu.2010.07.006)

Naghdi N, Majlessi N & Bozorgmehr T 2005 The effect of intrahippocampal injection of testosterone enanthate (an androgen receptor agonist) and anisomycin (protein synthesis inhibitor) on spatial learning and memory in adult, male rats. *Behavioural Brain Research* **156** 263–268. (doi:10.1016/j.bbr.2004.05.032)

Pandolfi C, Pellegrini L, Sbalzarini G & Mercantini F 1994 Obesity and insulin resistance. *Minerva Medica* **85** 167–171.

Pintana H, Apaijai N, Pratchayasakul W, Chattipakorn N & Chattipakorn SC 2012 Effects of metformin on learning and memory behaviors and brain mitochondrial functions in high fat diet induced insulin resistant rats. *Life Sciences* **91** 409–414. (doi:10.1016/j.lfs.2012.08.017)

Pintana H, Apaijai N, Chattipakorn N & Chattipakorn SC 2013 DPP-4 inhibitors improve cognition and brain mitochondrial function of insulin resistant rats. *Journal of Endocrinology* **218** 1–11. (doi:10.1530/JOE-12-0521)

Pipatpiboon N, Pratchayasakul W, Chattipakorn N & Chattipakorn SC 2012 PPARγ agonist improves neuronal insulin receptor function in hippocampus and brain mitochondria function in rats with insulin resistance induced by long term high-fat diets. *Endocrinology* **153** 329–338. (doi:10.1210/en.2011-1502)

Pipatpiboon N, Pintana H, Pratchayasakul W, Chattipakorn N & Chattipakorn SC 2013 DPP4-inhibitor improves neuronal insulin receptor function, brain mitochondrial function and cognitive function in rats with insulin resistance induced by high-fat diet consumption. *European Journal of Neuroscience* **37** 839–849. (doi:10.1111/ejn.12088)

Pratchayasakul W, Kerdphoo S, Petsophonsakul P, Pongchaidecha A, Chattipakorn N & Chattipakorn SC 2011 Effects of high-fat diet on insulin receptor function in rat hippocampus and the level of neuronal corticosterone. *Life Sciences* **88** 619–627. (doi:10.1016/j.lfs.2011.02.003)

Sakata K, Tokue A & Kawai N 2000 Altered synaptic transmission in the hippocampus of the castrated male mouse is reversed by testosterone replacement. *Journal of Urology* **163** 1333–1338. (doi:10.1016/S0022-5347(05)67773-7)

Sandstrom NJ, Kim JH & Wasserman MA 2006 Testosterone modulates performance on a spatial working memory task in male rats. *Hormones and Behavior* **50** 18–26. (doi:10.1016/j.yhbeh.2005.09.008)

Shi Z, Araujo AB, Martin S, O'Loughlin P & Wittert GA 2013 Longitudinal changes in testosterone over five years in community-dwelling men. *Journal of Clinical Endocrinology and Metabolism* **98** 3289–3297. (doi:10.1210/jc.2012-3842)

Spritzer MD, Daviau ED, Coneeny MK, Engelman SM, Prince WT & Rodriguez-Wisdom KN 2011 Effects of testosterone on spatial learning and memory in adult male rats. *Hormones and Behavior* **59** 484–496. (doi:10.1016/j.yhbeh.2011.01.009)

Sripetchwandee J, Pipatpiboon N, Chattipakorn N & Chattipakorn S 2014 Combined therapy of iron chelator and antioxidant completely restores brain dysfunction induced by iron toxicity. *PLoS ONE* **9** e85115. (doi:10.1371/journal.pone.0085115)

Stellato RK, Feldman HA, Hamdy O, Horton ES & McKinlay JB 2000 Testosterone, sex hormone-binding globulin, and the development of type 2 diabetes in middle-aged men: prospective results from the Massachusetts male aging study. *Diabetes Care* **23** 490–494. (doi:10.2337/diacare.23.4.490)

Stranahan AM, Norman ED, Lee K, Cutler RG, Telljohann RS, Egan JM & Mattson MP 2008 Diet-induced insulin resistance impairs hippocampal synaptic plasticity and cognition in middle-aged rats. *Hippocampus* **18** 1085–1088. (doi:10.1002/hipo.20470)

Vorhees CV & Williams MT 2006 Morris water maze: procedures for assessing spatial and related forms of learning and memory. *Nature Protocols* **1** 848–858. (doi:10.1038/nprot.2006.116)

Xia F, Xu X, Zhai H, Meng Y, Zhang H, Du S, Xu H, Wu H & Lu Y 2013 Castration-induced testosterone deficiency increases fasting glucose associated with hepatic and extra-hepatic insulin resistance in adult male rats. *Reproductive Biology and Endocrinology* **11** 106. (doi:10.1186/1477-7827-11-106)

Received in final form 17 May 2015
Accepted 26 May 2015
Accepted Preprint published online 27 May 2015

© 2015 Society for Endocrinology
Printed in Great Britain

Published by Bioscientifica Ltd.

เอกสารแนบหมายเลข 45

Metab Brain Dis (2015) 30:853–876
DOI 10.1007/s11011-015-9655-3

REVIEW ARTICLE

Testosterone deficiency, insulin-resistant obesity and cognitive function

Hiranya Pintana · Nipon Chattipakorn · Siriporn Chattipakorn

Received: 27 August 2014 / Accepted: 3 February 2015 / Published online: 24 February 2015
© Springer Science+Business Media New York 2015

Abstract Testosterone is an androgenic steroid hormone, which plays an important role in the regulation of male reproduction and behaviors, as well as in the maintenance of insulin sensitivity. Several studies showed that testosterone exerted beneficial effects in brain function, including preventing neuronal cell death, balancing brain oxidative stress and antioxidant activity, improving synaptic plasticity and involving cognitive formation. Although previous studies showed that testosterone deficiency is positively correlated with cognitive impairment and insulin-resistant obesity, several studies demonstrated contradictory findings. Thus, this review comprehensively summarizes the current evidence from in vitro, in vivo and clinical studies of the relationship between testosterone deficiency and insulin-resistant obesity as well as the correlation between either insulin-resistant obesity or testosterone deficiency and cognitive impairment. Controversial reports and the mechanistic insights regarding the roles of testosterone in insulin-resistant obesity and cognitive function are also presented and discussed.

Keywords Obesity · Insulin resistance · Testosterone deprivation · Neuroprotective effect · Cognitive function

H. Pintana · N. Chattipakorn · S. Chattipakorn (✉)
Neurophysiology Unit, Cardiac Electrophysiology Research and Training Center, Faculty of Medicine, Chiang Mai University, Chiang Mai, Thailand
e-mail: scchattipakorn@gmail.com

S. Chattipakorn
e-mail: siriporn.c@cmu.ac.th

H. Pintana · N. Chattipakorn
Department of Physiology, Faculty of Medicine, Chiang Mai University, Chiang Mai, Thailand

S. Chattipakorn
Department of Oral Biology and Diagnostic Sciences, Faculty of Dentistry, Chiang Mai University, Chiang Mai 50200, Thailand

Introduction

Testosterone is an androgenic sex steroid hormone, synthesized from the endoplasmic reticulum of Leydig cells in testis (95 %) and from the adrenal gland (5 %) (Ewing et al. 1983; Vinson et al. 1976). The synthesis and secretion of testosterone are mainly controlled by the hypothalamic-pituitary-testes axis (HPT axis) (Emanuele and Emanuele 2001; Franchimont et al. 1975; Nunemaker and Satin 2014). There are three different forms of circulating testosterone, including free testosterone (2–3 %), albumin-bound testosterone (20–40 %), and sex hormone-binding globulin (SHBG) bound testosterone (60–80 %) (Betancourt-Albrecht and Cunningham 2003; Kapoor et al. 2005). Free testosterone, an active form of testosterone, is metabolized to be 5α-dihydrotestosterone (DHT) via 5α-reductase enzyme (Janowsky 2006; Li and Al-Azzawi 2009). Free testosterone and DHT directly exert their effects via binding androgen receptors (ARs) in various parts of the body, including reproductive organs, liver, kidney, muscles, bone, heart and brain (Janowsky 2006; Pelletier et al. 2000; Takeda et al. 1990; Volterrani et al. 2012). Under physiological condition, testosterone plays important roles in the development of secondary male sexual characteristics (Schiavi and White 1976), the regulation of glucose and lipid metabolism (Aydilek and Aksakal 2005; Christoffersen et al. 2010), bone growth as well as the modulation of normal brain function, including cognition (Filova et al. 2013; Janowsky 2006; Meydan et al. 2010). However, testosterone can be converted to be estradiol via the aromatase enzyme. Therefore, it implies that testosterone can also activate estrogen receptors (ERs) (Filova et al. 2013; Janowsky 2006; Ogawa et al. 1997).

Testosterone deficiency is a low testosterone condition with serum total testosterone levels <3.2 ng/ml and free testosterone levels <64 pg./ml in middle aged and elderly men (Wu et al. 2010). The serum testosterone concentration gradually reduces in the aging process and it declines about 1.6 % per

year after 40 years of age (Tsujimura 2013). Testosterone deficiency has been associated with an increased risk of several systemic changes in male, particularly obesity (Montalcini et al. 2012; Shi et al. 2013; Stellato et al. 2000) and cognitive decline (Janowsky et al. 1994; Morley and Perry 1999; Trolle et al. 2012). Although previous studies in men showed a positive correlation between insulin-resistant obesity and testosterone deficiency (Grossmann et al. 2008; Haffner et al. 1994), several studies in animal models demonstrated inconsistent findings (Borst and Conover 2006; Erben et al. 2000; Kakolewski et al. 1968). In addition, it has been shown that either insulin-resistant obesity alone (Pintana et al. 2013; Pintana et al. 2012; Stranahan et al. 2008) or testosterone deficiency alone (Filova et al. 2013; Janowsky 2006; Meydan et al. 2010) is involved in the development of the cognitive impairment. Although most previous studies demonstrated the beneficial effects of testosterone on cognition, a recent systematic review demonstrated that the association between testosterone and cognitive function was not significantly different in both genders (Boss et al. 2014).

Despite these previous reports, the relationships among testosterone deficiency, insulin- resistant obesity, and cognition are still not clearly understood. In this review, the current evidence of the relationship between testosterone deficiency in the middle aged and older aged groups, and insulin-resistant obesity as well as the effects of either testosterone or insulin-resistant obesity on cognition are comprehensively summarized. Controversial reports as well as the mechanistic insights regarding the roles of testosterone in insulin-resistant obesity and cognition are also presented and discussed.

Search strategy and selection criteria for this review: Relevant publications in the PubMed database published before April, 2014 were identified by using search terms "testosterone deficiency and obesity", "testosterone deficiency and cognitive function", "obesity and cognitive function", "testosterone and brain function". Only articles published in English were reviewed.

Obesity and testosterone deficiency

Obesity is a public health problem which has increased dramatically in many countries around the world (Kitzinger and Karle 2013). Obesity causes serious medical complications, including atherosclerosis (Kohara 2014; Semenkovich 2006), cardiovascular diseases (Abbasi et al. 2002) and cognitive decline (Greenwood and Winocur 2001; Pintana et al. 2013; Reusch 2002; Stranahan et al. 2008; Winocur et al. 2005). The possible causes of obesity are due to genetic inheritance (Fawcett and Barroso 2010; Park et al. 2010), physical inactivity (Eckardt et al. 2011) and high calorie diet consumption (Clegg et al. 2011). Previous studies reported that obesity due to high calorie intake is a major cause of insulin resistance, Type 2 diabetes mellitus (T2DM) and metabolic syndrome (Kahn and Flier 2000; Pandolfi et al. 1994).

Interestingly, both preclinical studies and clinical reports demonstrated that obesity is associated with low serum testosterone levels or testosterone deficiency. These reports are summarized in Table 1. In preclinical studies, obese male animals induced by long-term high-calories diet consumption developed peripheral insulin resistance by impaired lipid profile, increased plasma insulin levels and increased adipose tissue accumulation as well as decreased plasma testosterone levels (Erdemir et al. 2012; Filippi et al. 2009; Olivares et al. 2009; Ribeiro et al. 2012a; Ribeiro et al. 2012b; Vignozzi et al. 2012; Vigueras-Villasenor et al. 2011). In this regard, obesity induced testosterone deficiency has been proposed to occur through obese-induced insulin resistance since insulin-resistant obesity has been shown to increase inflammatory process (Jones 2010a; Jones 2010b; Vignozzi et al. 2012), and aromatase enzyme production (Cohen 2001). The studies in male rabbit models demonstrated that obesity leads to the increase of several pro-inflammatory substrates such as TNF-α, IL-8, IL-6, and IL1β, which have been shown to trigger the development of peripheral insulin resistance (Vignozzi et al. 2012). Increased TNF-α has been shown to decrease hypothalamic-pituitary axis activity, resulting in a decrease in testosterone secretion (Jones 2010a; Jones 2010b). Another study in high-fat diet (HFD) induced male obese rabbits also showed that obesity leads to increased inflammation and decreased plasma testosterone levels via decreased gonadotropin-releasing hormone (GnRH), luteinizing hormone (LH), and follicle-stimulating hormone (FSH) signals (Filippi et al. 2009). Moreover, it has been shown that increased adipose tissues in obese male rats were found to cause increased aromatase enzyme production, in which this enzyme could convert testosterone to estradiol thus resulting in a decrease in plasma testosterone levels (Vigueras-Villasenor et al. 2011). The increased adipose tissue has also been shown to increase the secretion of adipokines such as plasma leptin (Martin 2014; Olivares et al. 2009; Vigueras-Villasenor et al. 2011). Several studies showed that increased leptin levels and estradiol levels could inhibit the HPT axis by inhibiting Kisspeptin, which has been shown to play a role in the regulation of GnRH secretion in the hypothalamus in order to produce normal testosterone levels (Cohen 1999; Kelly and Jones 2013; Okamura et al. 2013). The inhibition of Kisspeptin also leads to a decrease in LH pulse to testis and further reduced testosterone secretion (Cohen 1999; Kelly and Jones 2013; Smith et al. 2005). In addition, a study in HFD-induced obesity rats showed the reduction of AR expression and decreased Akt protein expression in the ventral prostate (Ribeiro et al. 2012b). All of these findings suggest that obese-insulin resistant condition is closely associated with the decreased testosterone secretion and reduced testosterone activity. In addition, complications following obesity are not only

Table 1 Evidence in obesity related to testosterone deficiency

Pre-clinical studies

Model	Duration	Age	Major finding	Interpretation	Ref
Adult Wistar rats induced obesity by high-fat diet (20 % saturated fat)	15 weeks	Adulthood	• ↑ body weight • ↑ insulin levels • ↓ plasma testosterone levels • ↑ epididymal and retroperitoneal fat • ↑ estrogen receptor beta (ERβ) of ventral prostate • ↓ plasma HDL levels • ↑ fibroblast growth factor-2 (FGF-2) of ventral prostate	• High-fat-diet induced obesity lead to insulin resistance condition related to decreased plasma testosterone levels	(Ribeiro et al. 2012a)
Male Wistar rats induced obesity by high-fat diet (20 % fat)	15 weeks	Adulthood	• ↑ body weight • ↑ insulin levels • ↓ plasma testosterone levels • ↓ androgen receptor (AR) of ventral prostate • ↓ Akt protein of ventral prostate	• High-fat-diet induced obesity and insulin resistance associate with testosterone deficiency decreased AR in rat prostate	(Ribeiro et al. 2012b)
Male Wistar rats induced obesity with saturated fat (20 % of total calories)	90 days and 180 days	Adulthood	• ↑ body weight • ↑ plasma insulin levels • ↓ plasma testosterone level • ↑ plasma triglyceride levels • ↑ plasma cholesterol levels • ↑ plasma leptin levels • ↓ plasma luteinizing hormone (LH)	• Obesity caused to reduce plasma testosterone levels, impair lipid profile and alter reproductive axis	(Olivares et al. 2009)
Male Wistar albino rats fed with high-fat diet	10 weeks	Adulthood	• ↑ body weight • ↓ plasma testosterone levels • ↑ plasma triglyceride levels • ↑ serum nitric oxide levels	• HFD induced obesity decreased testosterone levels and increased oxidative stress	(Erdemir et al. 2012)
Male rabbits fed a high-fat diet (HFD)			• ↑ visceral fat • ↓ plasma testosterone levels • ↓ follicular stimulating hormone (FSH) • ↓ luteinizing hormone (LH) • ↓ gonadotropin releasing hormone (GnRH) immunopositivity in hypothalamus • induced penile alterations	• HFD induced hypogonadotropic hypogonadism	(Filippi et al. 2009)
Male rabbits fed with high-fat diet (HFD; 0.5 % animal-derived cholesterol and 4 % peanut oil)	12 weeks	Adulthood	• ↑ visceral fat • ↓ plasma testosterone levels • ↑ plasma triglyceride levels • ↑ plasma cholesterol levels • Impaired oral glucose tolerance test • ↑ pro-inflammatory substrate (IL8, IL6, IL1b, and TNF-α mRNA expression) in prostate	• HFD caused the development of metabolic syndrome related to hypogonadism • HFD caused increased pro-inflammatory substrates in prostate.	(Vignozzi et al. 2012)
Sprague–Dawley male rats fed with high-fat die (20 % of lard)	90 days	Adulthood	• ↑ body mass index (BMI) • ↓ plasma testosterone levels • ↑ plasma estradiol levels • ↑ plasma leptin levels • ↑ lipid peroxidation in epididymal fat • ↓ spermatobioscopic parameters	• HFD induced obesity was related to decreased testosterone levels and increased estradiol levels.	(Vigueras-Villasenor et al. 2011)

Table 1 (continued)

Clinical studies Model	Study	Age	Major finding	Interpretation	Ref
21 normal men	Cross-sectional study	25–65 years	• ↑ BMI • ↑ homeostatic model assessment for insulin resistance (HOMA-IR) • ↓ plasma testosterone levels • ↓ insulin sensitivity (Hyperinsulinemic-euglycemic clamp)	• Insulin resistance was associated with decreased testosterone secretion in men	(Pitteloud et al. 2005)
211 non-diabetic men followed up for 3 years	Longitudinal cohort	45–65 years	• ↑ body weight • ↑ Abdominal fat • ↑ HOMA-IR • ↑ fasting plasma insulin levels • ↓ free testosterone and total testosterone	• Insulin resistance was related to decreased in testosterone levels	(Tsai et al. 2004)
87 men	Cross-sectional study		• ↑ BMI • ↑ waist-hip ratio (WHR) • ↑ fasting insulin • ↓ whole-body glucose disposal • ↓ total testosterone levels • ↓ SHBG levels	• Body weight and WHR were inversely correlated with testosterone levels and SHBG levels	(Haffner et al. 1994)
2361 metabolic syndrome men	Cross-sectional study	20–73 years	• ↑ body weight • ↑ HOMA index • ↓ total testosterone levels • ↓ bioavailable testosterone levels • ↓ free testosterone levels • ↓ SHBG levels	• Body weight and insulin resistance were inversely correlated with testosterone levels and SHBG levels	(Zhang et al. 2013)
77 males	Cross-sectional study	39–72 years	• ↑ body weight • ↑ waist circumference • ↓ total testosterone levels • ↓ SHBG levels • obese males aged more or equal to 39 frequency of testosterone deficiency is high (47 %)	• Metabolic syndrome associated with testosterone deficiency and decreased in SHBG levels	(Tylinska and Broncel 2013)
2470 non-diabetic men	Cross-sectional study	≥70 years	• ↑ body weight • ↑ waist circumference • ↑ HOMA2-IR • ↓ Total testosterone levels • ↓ free testosterone levels	• In older men, lower total testosterone is associated with insulin resistance independently of measures of central obesity	(Yeap et al. 2009)
1306 men	Cross-sectional study	Middle age	• ↑ BMI • ↑ waist circumference • ↓ total testosterone levels • ↓ free testosterone levels	• Pre-diabetes was associated with an increased risk of testosterone deficiency	(Ho et al. 2013)

insulin resistance, but also hypertension (Fogari et al. 2002; Torkler et al. 2011). Both complications lead to increased circulating oxidative stress, possibly causing decreased testosterone levels in obesity. Moreover, it has been shown that gonadectomy increased corticosterone in male rats and this was normalized by testosterone therapy (Seale et al. 2004). These findings suggest that the gonadal steroids, including testosterone, the end product of the hypothalamus-pituitary gland-gonadal (HPG) axis, actively modulates the function of the hypothalamic-pituitary-adrenal (HPA) axis. In addition, several studies showed that stress is accompanied by both an increase in the activity of the HPA axis, and a decrease in the reproductive functions of the HPG axis (Mastorakos et al. 2005; Rivier and Rivest 1991). All of these findings indicate a possible interaction between hormones of the HPA axis and those of the HPG axis. Previous studies also showed that an increase in cortisol and neuro-inflammatory cytokines, such as IL-1 and IL-10, were associated with decreased GnRH, LH, FSH and testosterone production (Hueston and Deak 2014; Smith et al. 1999). These results suggest that the HPG axis interacts with the HPA axis by modulating neuroinflammation, which may affect neurological performances. An increase in cortisol and neuroinflammation was also found to be associated with conditions such as testosterone deficiency (Hueston and Deak 2014; Smith et al. 1999), the development of insulin-resistant obesity (Hristova and Aloe 2006) and cognitive impairment (Lupien et al. 1994; Lupien et al. 1999; Ownby 2010). These findings suggest that the alteration of the HPG axis and the HPA axis in either testosterone deficiency or insulin-resistant obesity could lead to the cognitive decline, possibly via the regulation of neuroinflammation and corticosteroids.

Consistent with preclinical studies, studies in men also demonstrated that increased body weight or body mass index (BMI) together with insulin resistance, as indicated by increased HOMA-IR index, is associated with low plasma testosterone and SHBG levels (Haffner et al. 1994; Ho et al. 2013; Pitteloud et al. 2005; Tsai et al. 2004; Tylinska and Broncel 2013; Yeap et al. 2009; Zhang et al. 2013). Furthermore, a study in men with insulin-resistant obesity demonstrated the impairment of insulin receptor function in Leydig cells and decreased testosterone secretion (Pitteloud et al. 2005). The findings of testosterone deficiency in obese men may occur due to the combination of aging and other systemic abnormalities including increased oxidative stress following insulin-resistant obesity. A summary of these clinical reports is shown in Table 1. In contrast, some studies demonstrated that body weight loss correlated with a low testosterone level, particularly in amateur wrestlers and weight lifters (Di Luigi et al. 2012; Roemmich and Sinning 1997; Strauss et al. 1985). Those studies suggest that weight loss with decreased testosterone levels could be due to the limitation of food intake and high levels of cortisol during their training.

From these reports, it can be concluded that obesity could lead to a gradual decrease of testosterone levels in both animals and men by increased inflammatory substrates, increased aromatase enzymes that convert testosterone to estradiol, and suppressed HPT axis.

Does testosterone deficiency lead to insulin-resistant obesity?

The relationship between testosterone deficiency and insulin-resistant obesity is still unclear. Previous studies suggest that not only obesity could induce hopogonadism, but also hypogonadism could lead to obesity (Cohen 1999; Kelly and Jones 2013; Muraleedharan and Jones 2010). Studies of male castrated animals showed increased body weight, increased visceral fat deposition, increased BMI, increased plasma insulin level and plasma leptin levels as well as impaired lipid profiles (Christoffersen et al. 2010; Georgiev et al. 2011; Kanchuk et al. 2003). Consistent with those studies, it has been demonstrated that testosterone is involved in lipolysis and lipid homeostasis, because testosterone deficiency impaired lipid homeostasis, and resulted in increased adipogenesis (Kelly and Jones 2013; Santosa and Jensen 2012). Furthermore, another study showed that orchiectomized animals had decreased insulin responsiveness and insulin sensitivity (Georgiev et al. 2011). Studies in cultured adipocytes and skeletal muscle cells found that testosterone increased glucose transporter-4 (GLUT-4) expression and increased insulin receptor substrates-1 (IRS-1) phosphorylation (Chen et al. 2006). These findings suggest that testosterone is involved in glucose metabolism and insulin signaling. Therefore, a state of testosterone deficiency could impair glucose homeostasis and impair insulin signaling, leading to the development of obesity, insulin resistance and T2DM.

In clinical studies, the longitudinal studies in middle-aged men followed for more than five years demonstrated that low levels of testosterone and SHBG can lead to obesity, increased body mass index (BMI), increased waist hip ratio (WHR), and the development of the metabolic syndrome or T2DM (Haffner et al. 1996; Laaksonen et al. 2004; Shi et al. 2013). In addition, recent clinical studies demonstrated that obese patients with reduced testosterone levels can easily develop the metabolic syndrome as well as T2DM (Asare-Anane et al. 2014; Fui et al. 2014; Haring et al. 2010). A comprehensive summary of these reports is shown in Table 2.

Despite those reports, several studies in castrated rats showed the reduction of body weight and decreased muscle mass following testosterone deficiency (Axell et al. 2006; Borst and Conover 2006; Chai et al. 1999; Erben et al. 2000; Gao et al. 2005; Gentry and Wade 1976; Kakolewski et al. 1968). The data

Table 2 Evidence in testosterone deficiency leads to obesity

Pre-clinical studies

Testosterone deficiency induce obesity

Model	Duration	Age	Major finding	Interpretation	Ref
Six 12–13 months old male Göttingen minipigs with orchiectomy	10 days and 10 weeks	Adult	• ↑ body weight • ↓ plasma testosterone levels • ↑ plasma insulin • Impaired glucose tolerance • ↓ β-cell function	• Castration decreased plasma testosterone levels and induced obesity via disturbed glucose metabolism	(Christoffersen et al. 2010)
Male New Zealand white rabbits with orchiectomy	2 months	Adult	• ↑ body weight (BW) • ↓ plasma testosterone levels • ↑ body mass index (BMI) • ↑ visceral fat (VF) • ↑ VF/BW ratio • ↑ triglyceride levels • ↑ total cholesterol levels • ↑ area under the curve of glucose and insulin concentration in intra-venous glucose tolerance (IVGTT) test	• Castration-induced visceral obesity negatively affected the lipid profile and insulin sensitivity and/or responsiveness	(Georgiev et al. 2011)
Male domestic cats with orchiectomy	36 weeks	Adult	• ↑ body weight • ↓ plasma testosterone levels • ↑ plasma insulin levels • ↑ plasma leptin levels	• Gonadectomy-induced weight gain and increased plasma insulin levels and plasma leptin levels	(Kanchuk et al. 2003)

Testosterone deficiency without obesity

Model	Duration	Age	Major finding	Interpretation	Ref
Fischer 344 male rat, Brown Norway male rats and male Wistar rats with orchiectomy	56 days	Adulthood	• ↓ body weight gain • ↓ muscle mass weight • ↓ prostate weight • ↓ food intake • ↑ visceral fat moderately in Fischer 344 rat and substantially in Wistar rats	Castration decreased body weight gain in male rats via decreased food intake	(Borst and Conover 2006)
Sprague–Dawley rats with orchidectomy	1 month	Adulthood	• ↓ body weight gain • ↓ food intake	Castration decreased body weight gain in male rats via decreased food intake	(Gentry and Wade 1976)
Male Sprague Dawley rats with orchidectomy	12 weeks	Adulthood	• ↓ body weight gain • ↓ soleus muscle weight • No change of solcus/body weight ratio	Orchidectomy decreased body weight gain in male rats	(Gao et al. 2005)
Fischer 344 male rat with orchidectomy	9 month	Aged	• ↓ body weight gain • ↓ seminal vesicles weight	Orchidectomy decreased body weight gain in male rats	(Erben et al. 2000)
Adult C57Bl/6 J male mice with orchidectomy	10 weeks	Adulthood	• ↓ body weight gain • ↓ seminal vesicles weight • ↓ levator ani muscle mass	Orchidectomy reduced body weight gain and tissue atrophy	(Axell et al. 2006)
Fischer-344 rats with orchiectomy	24 days	Young adult	• ↓ body weight gain • No difference of food intake from sham-operated rats	Orchidectomy decreased body weight but no effect on food intake	(Chai et al. 1999)
Male albino rats with orchiectomy	70 days	Adulthood	• ↓ body weight gain	Orchidectomy decreased body weight gain in male rats	(Kakolewski et al. 1968)

Table 2 (continued)

Clinical studies Model	Study	Duration	Age	Major finding	Interpretation	Ref
702 normal men	Longitudinal cohort	11years	Middle aged	• 147 men had developed metabolic syndrome and 57 diabetic men • ↓ total testosterone levels • ↓ SHBG levels • ↑ fasting serum insulin level • ↑ BMI • ↑ WHR	• Low total testosterone and SHBG levels associated with metabolic syndrome and T2DM	(Laaksonen et al. 2004)
176 non-diabetic men	Longitudinal cohort	5years		• 176 men developed diabetes during 5years • ↓ bioavailable or free testosterone • ↓ SHBG levels • ↑ fasting insulin level	• Higher levels of fasting insulin and lower levels of total and free testosterone and SHBG were associated with development of diabetes	(Haffner et al. 1996)
1588 men	Longitudinal cohort	5years	Mean of age 54years	• ↓ plasma testosterone levels • ↑ BMI • ↑ waist circumference	• Age related to decline of testosterone levels associated with obesity	(Shi et al. 2013)
1709 normal men	Longitudinal cohort	7–10 years	40–70years	• ↓ total testosterone levels • ↓ free testosterone levels • ↓ SHBG levels • ↑ BMI	• Low levels of testosterone and SHBG play some role in the development obesity and T2DM	(Stellato et al. 2000)

suggested that the reduction of body weight in orchiectomized rats was caused by the reduction of daily food intake (Borst and Conover 2006; Gentry and Wade 1976) and muscle atrophy (Axell et al. 2006; Borst and Conover 2006; Gao et al. 2005). It has been proposed that rats with testosterone deficiency had decreased neuropeptide-Y in the hypothalamus (Sahu et al. 1989), resulting in a decreased appetite. However, Barat and colleagues demonstrated gonadectomy in obese male Zucker rats did not consistently alter weight gain (Barat et al. 2007). All findings in animal models indicate that the testosterone deficiency in rats showed weight reduction whereas in larger animal models such as cats and rabbits increased weight was shown. The findings in the latter groups were consistent with the clinical reports. All of these findings emphasized the different effects of testosterone deficiency in different species. The differences in those findings could depend on strain, age of animals or length of gonadectomy. A summary of those reports was shown in part of preclinical study of Table 2. However, the underlying mechanisms of the differences need to be further investigated.

From these reports, it can be concluded that testosterone deficiency could lead to obesity via increased fat accumulation, impaired lipid and glucose metabolism in both men and larger animals such as rabbits and cats. However, the negative obese development following testosterone deficiency in rats might be due to the strong effect of testosterone on appetite in the rat model.

Testosterone acts as a neuroprotective agent in the brain

The beneficial effects of testosterone are not only on the peripheral tissues, but also represent in the brain (Durdiakova et al. 2011). Under the physiological condition, testosterone exerts its effects on brain development, behavior controls, and provides neuroprotection (Filova et al. 2013; Janowsky 2006). Previous studies demonstrated that testosterone and its metabolite, DHT, can pass the blood–brain barrier (BBB) to exert their effects in the brain via androgen receptors (ARs) (Pardridge and Mietus 1979). ARs are widely distributed in various parts of the brain, including the prefrontal cortex, amygdala, and hippocampus (Janowsky 2006).

The studies of the primary cerebellar granule cell cultures demonstrated that testosterone and its metabolite, DHT, increased cell viability, deceased cell apoptosis and cell death following the induction with either the aggregation of Aβ peptides (Pike 2001) or H_2O_2 induced apoptosis cell death (Ahlbom et al. 2001). Furthermore, a previous study showed that testosterone increased anti-oxidant enzyme catalase in H_2O_2 induced apoptosis of cerebellar granule cells death (Ahlbom et al. 2001). The study in neuroblastoma (N2a) cells transfected with βAPP695 and in primary neuronal cell

cultures also found that testosterone treatment decreased the amyloid-β precursor protein (Gouras et al. 2000).

Consistent with in vitro studies, castration in male rats caused an increased neuronal apoptosis, decreased anti-oxidant enzymes in hippocampal regions and increased Aβ accumulation in the brain (Meydan et al. 2010; Ramsden et al. 2003). These adverse effects following castration could be reversed by testosterone treatment (Apostolinas et al. 1999; Meydan et al. 2010; Ramsden et al. 2003). In addition, a previous study showed that testosterone treatment after castration in rats could decrease Aβ accumulation in the brain via the activation of ARs (Ramsden et al. 2003). This finding agrees with a previous study in mice showing that decreased AR expression in brain of castrated mice could be restored by testosterone treatment (Apostolinas et al. 1999). All of these findings suggest that testosterone and its metabolites could act as a neuroprotective agent in the brain. A summary of these reports is shown in Table 3.

Although most studies demonstrated the beneficial effects of testosterone as a neuroprotective agent in the brain (Table 3), several in vitro and in vivo studies demonstrated that testosterone can cause adverse effects in the pathological brain or neuronal cells. For example, 1) the administration of testosterone at 10 μM increased the percentage of cells killed in the model of glutamate-induced neuronal cell death (Yang et al. 2002). 2) The administration of testosterone and DHT at 100 nM increased the percentage of apoptotic cells and caused mitochondrial dysfunction via either increased peroxide levels or decreased thiols levels as well as activated the PKC apoptotic pathway in the model of dopaminergic cell lines (N27 cells) (Cunningham et al. 2009). 3) The administration of testosterone in micromoles (1μM and 10 μM) increased cell apoptosis via alters inositol 1,4,5-trisphosphate receptor($InsP_3R$)-mediated Ca^{2+} release and resulting the prolong Ca^{2+} signals lead to apoptotic cell death in human neuroblastoma cell line (Estrada et al. 2006). 4) A single dose of testosterone propionate (5 μg) administered to adult male CD-1 mice before induced neurotoxicity with methamphetamine caused severe neurotoxicity by decreased vesicular monoamine transporter-2 (VMAT-2) protein expression as well as decreased striatal dopamine levels (Buletko et al. 2012).

A summary of these reports are shown in Table 3. All of these findings suggest that the adverse effects of testosterone may occur in models of a brain with pathology, whereas the beneficial effects or neutral effect of testosterone can be found in normal brain models with testosterone deficiency.

From these reports, it can be concluded that testosterone provides neuroprotective effects such as deceased cell apoptosis and cell death, increased anti-oxidant enzymes, prevented the aggregation of Aβ precursor protein in both in vitro and in vivo studies. However, some evidence also demonstrated that testosterone can cause adverse effects in the brain when administrated with high doses during a pathological condition. Therefore, the testosterone supplement in human needs to be of concern regarding dosage, duration and any pathological conditions before the administration.

Testosterone deficiency and cognitive function

Synaptic plasticity is the underlying mechanism for modulating the learning and memory formation in the brain (Martin et al. 2000). Testosterone has been shown to be involved in the synaptic plasticity formation by modulating the normal synaptic formation in the brain (MacLusky et al. 2006). Previous studies demonstrated the positive correlation between memory decline and low plasma testosterone levels in the model of Alzheimer's disease (Hogervorst et al. 2001; Kenny et al. 2004; Lu et al. 2006; Okun et al. 2004), indicating that testosterone could be involved in the cognitive function. This statement is supported by numerous reports from preclinical and clinical studies, as summarized in Table 4.

Romeo and colleagues reported that testosterone plays a role in the synaptic plasticity and cognitive function in the brain by mediating neurotransmitter release, such as glutamate, acetylcholine and also involving in N-methyl-D-aspartate (NMDA) receptors insertion at the post-synaptic sites in adult male rats (Romeo et al. 2005). It is known that the modulation of the synaptic plasticity in the brain is crucial for learning and memory. In orchiectomized rodents, the impairment of learning and memory in those animals has been demonstrated (Naghdi et al. 2005; Sakata et al. 2000; Sandstrom et al. 2006; Spritzer et al. 2011). In addition, the reduction of the number of dendritic spines and changes in dendritic spine morphology in hippocampal CA1 regions have been found in male orchiectomized rodents (Leranth et al. 2003), which could be restored by testosterone or DHT replacement (Danzer et al. 2001; Leranth et al. 2003; Li et al. 2012). Consistent with preclinical reports, the preliminary and pilot clinical studies in older men demonstrated that low testosterone levels were correlated with learning and memory decline (Janowsky et al. 1994; Morley and Perry 1999), and that testosterone treatment could improve verbal memory test and spatial learning and memory in hypogonadal men and men with Alzheimer's disease (Cherrier et al. 2003; Cherrier et al. 2005; Tan and Pu 2003). Alzheimer's disease (AD) is a progressive disease, and that several factors are contributed to its development and progression (Selkoe 2001). The cohort study from the Oxford Project to Investigate Memory and Ageing (OPTIMA) reported a decrease in testosterone level in elderly men with AD, but not in younger men with AD (Hogervorst et al. 2004). In addition, the study in aged men with prostate cancer who received androgen receptor blockers (flutamide and leuprolide) for 36 weeks demonstrated a marked decline of testosterone levels and an increase in plasma Aβ levels, which were negatively correlated with anxiety

Table 3 Evidence in testosterone and neuroprotective effect

Model	Study	Dose	Major finding	Interpretation	Ref
Beneficial effect					
The induction of primary cultures cell death with the aggregation of Aβ 1–40 peptides	In vitro	• Testosterone 1–100 nM • DHT 1–100 nM	• ↑ Cell viability	• Testosterone and DHT equally effective to improve cell viability in β-amyloid induced toxicity of hippocampal neurons	(Pike 2001)
Cerebellar granule cells (CGC) exposed to hydrogen peroxide (H_2O_2) undergo apoptosis condition	In vitro	• Testosterone 10 μM • Androgen receptor antagonist flutamide 10 μM	• ↓ apoptosis cells in hippocampus • ↑ antioxidant enzyme catalase • Flutamide abolished the neuroprotective effects of testosterone	• Testosterone potentiates the antioxidant effect on the brain via androgen rectors	(Ahlbom et al. 2001)
Human fetal brain tissue culture leading to apoptosis with serum deprivation	In vitro	• 2 nM 17-α-estradiol or 17-β-estradiol • 4 nM testosterone enanthate, epitestosterone or methyltestosterone	• Androgen (testosterone enanthate, epitestosterone or methyltestosterone) and estrogen (17-α-estradiol or 17-β-estradiol) decreased percentage of neuronal cell death	• Androgen and estrogen act as equally neuroprotective agents against serum-deprivation-medited apoptosis of human primary neurons • Androgen acts as the neuroprotective agents through the androgen receptor	(Hammond et al. 2001)
Neuroblastoma (N2a) Cells transfected with human wild type βAPP695 and primary neuronal cultures	In vitro	• Testosterone 200 nM for 10 days	• ↑ sβAPPα • ↓ Aβ release • ↓ 4-kDa Aβ1–40y42 peptides • ↓ 3-kDa Aβx-40/42 peptides	• Testosterone reduces secretion of amyloidogenic precursor protein in neuronal cell cultures • Testosterone can protect neurons against the development of Alzheimer's disease	(Gouras et al. 2000)
Wistar rats with orchiectomy	In vivo	• 0.5 mg/kg/day of testosterone propionate via subcutaneous injection for 30 days	• ↑ Superoxide dismutase (SOD) in hippocampus • ↑ Glutathione peroxidase (GSH-Px) in hippocampus • ↓ malondialdehyde (MDA) levels in hippocampus • ↓ apoptosis cells in hippocampus	• Testosterone reversed the effect of orchiectomy-induced oxidative damage and morphological change in hippocampal tissue	(Meydan et al. 2010)
Male mice with orchiectomy	In vivo	• Testosterone propionate releasing pellet to maintain plasma testosterone level 110 ng/ml for 1 week	• ↓ AR expression in medial preoptic area, the lateral ventral septum, the ventromedial hypothalamus, the bed nucleus of the stria terminalis and the medial amygdala region in the brain of male mice with castration • ↑ AR expression in hypothalamus and amygdala after testosterone treatment	• Testosterone increased AR expression in brain of castrated mice	(Apostolinas et al. 1999)
Male Sprague Dawley rats with orchiectomy	In vivo	• dihydrotestosterone (DHT) 12.5 mg or 0.72 mg 17β-estradiol slow release subcutaneous pellets for 21 days	• ↓ AR expression in brain tissue of ORX • ↑ β-amyloid protein (Aβ) in brain tissue of ORX • ↑ AR expression in brain tissue after treated with DHT • ↓ Aβ in brain tissue after treated with DHT	• Androgen depletion resulting increase of brain Aβ accumulation in the male rat brain • DHT decreased Aβ accumulation in male rat brain	(Ramsden et al. 2003)

Table 3 (continued)

Model	Study	Dose	Major finding	Interpretation	Ref
Adverse effect					
Glutamate-induced HT-22 cell-death	In vitro	• Testosterone 10 μM for 24 h	• ↑ percentage of cells killed (%kill)	• Testosterone increase the toxicity of glutamate-induced HT-22 cell-death Model	(Yang et al. 2002)
Dopaminergic cell line (N27 cells)	In vitro	• Testosterone and DHT 100 nM for 48 h	• ↑ % apoptotic cell • ↑ peroxide levels • ↑ Protein expression of peroxiredoxin-3 • ↑ cleavage of the full length PKCδ • ↓ Thiols	• Testosterone increases apoptosis cells • Testosterone increases mitochondrial dysfunction in N27 cells • Testosterone activates the PKC apoptotic pathway	(Cunningham et al. 2009)
Human neuroblastoma cell line	In vitro	• Testosterone 100 nM, 1μM and 10 μM	1μM and 10 μM • ↓ Cell viability • Sustained intracellular Ca^{2+} levels	• Micromolar testosterone increased cell apoptosis via alters InsP3R type 1-mediated intracellular Ca^{2+} signaling and that the prolonged Ca^{2+} signals lead to apoptotic cell death	(Estrada et al. 2006)
Adult male CD-1 mice received an injection of methamphetamine after 24 h treated with testosterone	In vivo	• Single dose of testosterone propionate 5 μg via subcutaneous injection	• ↓ Striatal dopamine levels • ↓ Vesicular monoamine transporter-2 (VMAT-2) protein expression	• Testosterone exacerbates the deleterious effects of methamphetamine indicated by decreased striatal dopamine levels and Vesicular monoamine transporter-2 (VMAT-2)	(Buletko et al. 2012)

and cognitive behaviors (Almeida et al. 2004). These findings suggest that testosterone deficiency in either short-term or long-term in elderly men was associated with AD in elderly men. However, testosterone deficiency in young men might not play a major role in the pathogenesis of AD. Furthermore, the study by Moffat and colleagues also demonstrated the age-related relationship between testosterone deficiency and cognitive functions (Moffat et al. 2002). A previous longitudinal study of 10-years, following normal aged men, reported that the gradual reduction of testosterone levels in aging was associated with a decrease in cognitive function (Moffat et al. 2002). These findings suggest that testosterone might have the neuroprotective effect for cognitive function under normal physiological conditions. However, the pathogenesis of cognitive impairment relating to testosterone deficiency does not seem to be a process with a simple on/off switch by testosterone levels. This is because not only testosterone, but also other factors, particularly inflammation, could play an important role in aged men regarding the cognitive function under pathological conditions, including obesity as demonstrated in previous studies (Craft 2005; Singh and Newman 2011).

The other co-morbid pathologies should be of concern in the older male population, because those co-morbid pathologies could influence testosterone action and lead to cognitive impairment. Furthermore, previous studies demonstrated that patients with genetic disorders, including Klinefelter syndrome (primary hypogonadism; the impairment of testes) and Kallmann syndrome (secondary hypogonadism; the impairment of GnRH producing neurons at the hypothalamus) have testosterone deficiency with the impairment of brain development, decreased brain volume and cognitive dysfunction (Groth et al. 2013; Kotan et al. 2014; Krams et al. 1999; Skakkebaek et al. 2014; Verhoeven et al. 2013). These findings suggest that testosterone plays an important role in cognitive function through regulating the normal brain development and normal brain volume.

Although most of the previous studies demonstrated beneficial effects of testosterone on cognition, the recent systematic review from Boss and colleagues demonstrated non-significant findings in humans for testosterone and cognitive function, in which Boss suggested that those findings may have been influenced by methodological differences from others, including research designs, sufficiently consistent cognitive measurements, and clear descriptions of handling and storage of biological specimens (Boss et al. 2014). Furthermore, the recent study of Cunningham and colleagues showed that normal testosterone levels in an oxidative stress condition were associated with cognitive impairment in Caucasian men, whereas not associated in an obese Mexican American population (Cunningham et al. 2014). This finding suggests that ethnic differences could affect the relationship between testosterone and cognition. Therefore, the complex multifactorial relationship between testosterone and cognition

Table 4 Evidence of testosterone and cognitive function

Beneficial effect of testosterone on cognition

Pre-clinical studies

Model	Age	Dose and duration	Major finding	Interpretation	Ref
Male Sprague Dawley rats with orchiectomy	Young adult	• Testosterone propionate 500 μg/day via subcutaneous injection for two days • Dihydrotestosterone (DHT) 500 μg/day via subcutaneous injection for two days	• ORX reduced the CA1 spine density ~50 % • Testosterone or DHT replacement restore spine intensity	• Testosterone and DHT increased spine synapse density in hippocampal CA1 region.	(Leranth et al. 2003)
24 months of age Wistar male rats with orchiectomy	Aged	• Testostorone subcutaneous releasing pellet (66 mg powder of testosterone) for one month	• ↑ size and density of synaptic density of the bulbocavernosus motoneurons • ↑ perimeter of somata of the bulbocavernosus motoneurons	• Testosterone increased size and synaptic density insomata of the bulbocavernosus motoneurons	(Matsumoto 2001)
Adult male Sprague–Dawley rats with orchiectomy	Young adult	• Subcutaneously implant of crystalline testosterone to produce physiological testosterone level for two months	• ↑ dendritic spine density of arcuate neuroendocrine neurons • ↓ dendritic length, volume and terminal branch number	• Testosterone increased dendritic spine but suppressed dendritic outgrowth in arcuate neuroendocrine neurons	(Danzer et al. 2001)
Nine-week-old mice with orchiectomy for two weeks	Adult	• Subcutaneous implant silastic capsules containing testosterone maintenance for 14 days	GDX • ↓ mushroom-type spine in CA1 region • ↑ stubby- and thin-type spines CA1 region • ↓ brain-derived neurotrophic factor (BDNF) and downstream target post-synaptic density protein 95 (PSD-95) Testosterone replacement • Recovered the changes in spine types to those found in controls in CA1 region • ↑ brain-derived neurotrophic factor (BDNF) and downstream target post-synaptic density protein 95 (PSD-95)	• Testosterone modulate the properties of dendritic spine maturation in the hippocampal CA1 area via the actions of BDNF and PSD-95	(Li et al. 2012)
Male Sprague Dawley rats with orchiectomy	Adult	• Testosterone (4-androsten-17β-ol-3-one) via subcutaneous injection	• Castrated male decreased in retention score at 60 min. but not at 10 min. of delayed matching-to-place MWM test • Testosterone replacement increased retention score at 60 min of delayed matching-to-place MWM test	• Testosterone restored an impairment of spatial working memory retention in castrated rat	(Sandstrom et al. 2006)
Male 12 weeks-old C57BL/6J mice with orchiectomy	Adulthood	• Testosterone propionate	• Castration did not alter long-term potentiation (LTP)	• Testosterone reversed PPF and evoked primed burst stimulation (PBS)	(Sakata et al. 2000)

Table 4 (continued)

			• Castration suppressed paired pulse facilitation (PPF) of the fEPSP • Castration with testosterone restore impaired paired pulse facilitation (PPF) of the fEPSP • Testosterone did not alter LTP in the hippocampal CA1 pyramidal cell layer but evoked by primed burst stimulation (PBS) restored potentiation to the control level		
Adult male Sprague–Dawley and Long-Evans rats with orchiectomy and measured learning and memory with MWM	Adult	• Testosterone propionate varies dose 0.0625–1.000 mg/0.1 ml of sesame oil via subcutaneous injection for seven days and 15 days	• ↑ time in target quadrant of 7 day (testosterone dose 0.250 and 1.000 mg) • ↓ path length of hidden platform of 15 days treatment (testosterone 0.0625–1.000 mg)	• Testosterone (0.250 and 1.000 mg) increased perseverative behavior in a reversal-learning task.	(Spritzer et al. 2011)
Adult male Sprague–Dawley rats with orchiectomy	Adult	• DHT replacement with subcutaneous implant capsule to produce physiological level of testosterone	• Gonadectomy decreased exploration time in moved object task of objective location memory test • DHT increased exploration time in moved object task of objective location memory test	• Gonadectomy impaired spatial memory • DHT restored an impairment of spatial memory	(McConnell et al. 2012)

Clinical studies

Model	Study	Age	Dose and duration	Major finding	Interpretation	Ref
21 hypogonadal men	Double blind RCT	34–70 years	• Testosterone in gel form (50 or 100 mg daily) 90 and 180 days • DHT in gel form (32 or 64 mg daily) 30 and 90 days	• Testosterone improve in story recall test at day 180 • DHT improve in route test (at day 30) and spatial array learning test (at day 90)	• Testosterone improved verbal memory • DHT improved spatial memory in mildly hypogonadal men	(Cherrier et al. 2003)
16 healthy men	Double blind RCT	50–90 years	• Testosterone enanthate 100 mg via intramuscular injection plus daily oral placebo pill • Testosterone enanthate 100 mg plus 1 mg daily of anastrozole, an aromatase inhibitor	• Testoesterone only and testosterone plus anastroazle groups improved in the spatial memory test • Testosterone plus anastroazle improves in verbal memory test	• Testosterone improve spatial memory with or without the effect of estradiol • Testosterone improves verbal memory depends on the aromatization of testosterone to estradiol	(Cherrier et al. 2005)
36 male patients with a diagnosis of Alzheimer's disease	Double blind RCT		• Testosterone enanthate 200 mg every two weeks for three, six, nine and 12 months	• Improve in Initial Alzheimer's Disease Assessment Scale cognitive subscale (ADAScog) • Improve in Mini Mental Status Examination (MMSE)	• Testosterone could improve cognition, including visual-spatial skills in mild to moderate Alzheimer's Disease	(Tan and Pu 2003)

Table 4 (continued)

No effect or adverse effect of testosterone on cognition					
Pre-clinical studies					
Model	Age	Dose and duration	Major finding	Interpretation	Ref
Male albino wistar rats	Adult	• Testosterone enanthate (80 μg/0.5 μl DMSO) and Anisomysin, protein synthesis inhibitor which prevent genomic effect, (2.5 μg/0.5 μl DMSO) via intrahippocampal injection	• Testosterone or anisomysin impaired spatial learning and memory in MWM test • Testosterone plus anisomysin improved latency and travel distance in spatial learning and memory in MWM test	• Testosterone alone impaired learning and memory • Testosterone plus anisomysin could improve learning and memory via non-genomic effect	(Naghdi et al. 2005)
Male albino Wistar rats	Adult	• Testosterone enanthate varies dose (10, 20, 40 or 80 μg/0.5 μl DMSO) • T-BSA to test non-genomic effects in varies dose (22.5, 35 or 55 μg/μl) via intrahippocampalinjection	• Testosterone enanthate 20 μg/0.5 μl DMSO and T-BSA 55 μg/μl reduce step-through latency duration in the passive avoidance task	• Testosterone impaired long-term memory in passive avoidance conditioning both via intracellular receptors and through nongenomic pathway	(Naghdi and Asadollahi 2004)
Male albino Wistar rats with orchiectomy	Adult	• Testosterone enanthate 80 μg/0.5 μl DMSO via intrahippocampal injection 30 min before measured with MWM	• ↑ escape latency and travel distance in training day • No different of time spent in target quadrant and percentage of target quadrant entries • ↑ astrocyte number in CA1 region	• Testosterone impaired spatial learning, memory • Testosterone increased astrocyte in hippocampal CA1 region	(Emamian et al. 2010)
Male Wistar rats with orchiectomy	Adult	• Testosterone enantate via intrahippocampal injection before training, immediately after training and 30 min. before retrieval in inhibitory avoidance task	• ORX did not influence performance on inhibitory avoidance • Testosterone injected before training, post-training and pre-retrieval intra CA1 decreased step-through latencies in inhibitory avoidance learning	• Testosterone impaired learning and memory acquisition, consolidation and retrieval in inhibitory avoidance test	(Harooni et al. 2008)
Three-month-old male Albino Wistar rats	Adult	• Testosterone varies dose (20, 40 and 80 μg/side) and H-89, selective protein PKAII inhibitor (5 and 10 μM/side) via intrahippocampal injection before 30–35 min of measured learning and memory	Testosterone dose 40 and 80 μg/side • ↑ escape latency and travel distance in training days and • ↓ time in target quadrant in probe test H-89 dose 10 μg/side • ↑escape latency and travel distance • ↓ time in target quadrant in probe test (dose 5 and 10 μg/side) Testosterone 20 μg/side plus H-89 5 μg/side • ↑ escape latency and travel distance in training days • ↓time in target quadrant in probe test	• PKAII inhibitor impaired spatial learning and memory • Testosterone did not improve these effects	(Khorshidahmad et al. 2012)
Clinical studies					

Table 4 (continued)

Model	Study	Age	Dose and duration	Major finding	Interpretation	Ref
69 elderly men	Double blind RCT	65–83 years	• Testosterone enanthate 200 mg via intramuscular injection every two weeks for 36 weeks	• Minimally differences were seen among in cognitive performance test	• Testosterone replacement for 36 months in healthy older men without cognitive impairment has no clinically significant effect on cognitive function test	(Vaughan et al. 2007)
16 male patients with Alzheimer disease	Double blind RCT	Elderly	• Testosterone in the form of hydroalcoholic gel (75 mg) applied daily to the skin for 24 weeks	• Testosterone had greater improvement in the scores on the caregiver version of the quality-of-life scale • Testosterone did not improve cognitive scores	• Testosterone replacement improved overall quality of life in Alzheimer disease patients, whereas minimal effects on cognition	(Lu et al. 2006)
11 men with early cognitive decline	Double blind RCT	73–87 years	• Testosterone enanthate (200 mg) via intramuscular injection every three weeks for 12 weeks	• Testosterone supplement no change in behaviors test, cognitive test, depression or activities of daily living	• Testosterone supplement did not alter cognitive and behavior test in early-to-moderate cognitive impairment	(Kenny et al. 2004)
15 cognitively normal men	Double blind RCT	66–86 year	• Testosterone enanthate 200 mg via intramuscular injection every other week for 90 days	• ↓ short-delay verbal memory test	• Supraphysiological doses of testosterone injection lead to declines in verbal memory	(Maki et al. 2007)
30 healthy men	Double blind RCT	Elderly	• Testosterone enanthate 250 mg via intramuscular injection for five days	• ↓ verbal fluency task • No effects of testosterone in the other verbal and spatial tasks	• Testosterone injection in healthy elderly men blocked the practice effect in verbal fluency without affecting other cognitive	(Wolf et al. 2000)

RCT randomized control trial

in clinical studies must consider factors including age, dose of testosterone, pathological conditions in the brain as well as ethnicity.

In addition, the effects of testosterone replacement in hypogonadal conditions of both animal models (Emamian et al. 2010; Harooni et al. 2008; Khorshidahmad et al. 2012; Naghdi and Asadollahi 2004) and humans (Kenny et al. 2004; Lu et al. 2006; Maki et al. 2007; Vaughan et al. 2007; Wolf et al. 2000) are still controversial, particularly regarding the learning and memory, since several studies demonstrated that testosterone replacement in a hypogonadal condition had either no effect or adverse effect on cognition, a summary of those reports is shown in Table 4. Controversial findings in animal studies could be due to differences in animal models, doses of testosterone, duration of treatment and routes of testosterone administration. Adverse effects of testosterone on cognitive function were also found when testosterone was directly injected into the hippocampal region (Emamian et al. 2010; Harooni et al. 2008; Naghdi et al. 2005; Spritzer et al. 2011). However, the controversial reports in the clinical studies may involve the differences in ages and degree of memory loss in each clinical study. Therefore, the effects of testosterone replacement should be further investigated by focusing on the effective doses, routes of administration, and duration of treatment to clarify the certain effects of testosterone replacement on cognition.

Furthermore, previous studies suggest that SHBG levels and other hormones such as thyroid stimulating hormone (TSH) were related to the incidence of Alzheimer's disease (AD) (Hogervorst et al. 2010; Holland et al. 2011). For example, it has been shown that either increased SHBG levels or decreased thyroid stimulating hormone in elderly men was associated with a high incidence of AD (Holland et al. 2011). Muller and colleagues also found that higher levels of SHBG increased the risk for AD and overall dementia in elderly men and women (Muller et al. 2010). In addition, a previous study in elderly men also demonstrated that men with AD were correlated with low level of insulin-like growth factors (IGF-1) (Duron et al. 2012). It has been shown that IGF-1 exerts a protective effect against Aβ toxicity and inhibits tau phosphorylation (Carro et al. 2002), suggesting that decreased IGF-1 levels could be associated with the increased incidence of AD in elderly men. Those previous studies have shown that Alzheimer's disease (AD) in the elderly was associated with testosterone deficiency (Kenny et al. 2004; Lu et al. 2006), decreased TSH levels (Holland et al. 2011) and decreased IGF-1 levels (Duron et al. 2012). This may be due to a decrease in hypothalamic neurons, and the resulting reduction of stimulating hormones secreted from the anterior pituitary gland (Goudsmit et al. 1990). In addition, the reduction of testosterone levels resulted in an increase in SHBG levels (Holland et al. 2011; Muller et al. 2010). All of these findings suggest that the alteration of not only testosterone, but also SHBG, TSH and IGF-1 play important roles in cognitive impairment.

From these reports, it can be concluded that testosterone has bidirectional effects on cognitive function in both animals and men. The positive or negative effects of testosterone on cognition in animal studies could be due to differences in animal models, doses of testosterone, duration of treatment and routes of testosterone administration. However, the positive or negative effects of testosterone on cognition in the clinical studies may involve the differences in ages and degree of memory loss in each clinical study. Therefore, the effects of testosterone replacement on cognition should be further investigated by focusing on the effective doses, routes of administration, and duration of treatment. In addition to testosterone, SHBG or TSH as well as IGF-1 could be a predictor of cognitive impairment.

Insulin-resistant obesity and cognitive function

Obesity is known to lead to cognitive declines in animal models and humans (Greenwood and Winocur 2005). A summary of reports regarding the association between obesity and cognition is shown in Table 5. Our previous studies demonstrated that obese rats induced by HFD impaired peripheral insulin sensitivity, impaired brain insulin receptor function, increased brain oxidative stress, leading to impaired learning and memory (Pipatpiboon et al. 2013; Pipatpiboon et al. 2012; Pratchayasakul et al. 2011). Several in vivo studies suggest that obesity associated with the impairment of cognition could be related to an insulin resistant condition (Pintana et al. 2013; Pintana et al. 2012; Stranahan et al. 2008). In addition, several studies in HFD-induced obese rodents demonstrated that obesity with insulin resistance caused Aβ plaques and Aβ accumulation in the hippocampal area (Barron et al. 2013; Maesako et al. 2012) as well as increased TNF-α and IL-6 in the brain (Pistell et al. 2010). These conditions had been shown to cause the reduction in learning and memory in those animal models. Consistent with preclinical studies, several clinical studies in men demonstrated that insulin-resistant obesity is associated with a high risk of memory decline and Alzheimer's disease (de la Monte 2009; Hiltunen et al. 2012; Stranahan et al. 2008; Thambisetty et al. 2013).

From these reports, it can be concluded that insulin-resistant obesity could lead to cognitive impairment. The underlying mechanism may be that obesity leads to the development of insulin resistance, increased brain oxidative stress, impaired brain insulin signaling, as well as increased Aβ accumulation, resulting cognitive impairment in both animals and men.

Table 5 Evidence in obesity and cognitive decline

Pre-clinical studies Model	Duration	Age	Major finding	Interpretation	Ref
Male rats induced obesity by high-fat, high-glucose diet supplemented with high-fructose corn syrup	8 months	Aged	• ↓ spatial learning and memory • ↓ hippocampal dendritic spines • ↓ brain-derived neurotrophic factor (BDNF) in the hippocampus • ↓ LTP in hippocampal in CA-1 region	• High-calorie diet induced obesity reduces hippocampal synaptic plasticity and impairs cognitive function, possibly through BDNF-mediated effects on dendritic spines	(Stranahan et al. 2008)
Male and female homozygous 3xTg-AD mice induced obesity by high-fat diet (60%kCal/fat)	4 months	Adulthood	• ↓ exploratory activity in Y-maze test in male mice • ↓ object recognition index in female mice • ↑ Aβ accumulation in the hippocampus of both sexes	• HFD induced obesity with insulin resistance condition caused of learning and memory decline in both sexes • HFD induced Aβ accumulation in hippocampal areas	(Barron et al. 2013)
Male Wistar rats induced obesity by high-fat diet (59.3 % E from lard)	12 weeks	Adulthood	• ↑ time to reach platform in acquisition test of Morris water maze test (MWM) • ↓ time spent in target quadrant in probe test of MWM • ↓ neuronal IR phosphorylation, IRS-1 phosphorylation and Akt/PKB-ser phosphorylation • Impaired insulin-induced long-term depression (LTD) • Impaired brain mitochondrial functions	• HFD induced obesity with insulin resistance condition caused learning and memory decline via impairment of brain mitochondrial function and impaired insulin receptor signaling	(Pipatpiboon et al. 2013)
Male Wistar rats induced obesity by high-fat diet (59.3 % E from lard)	12 weeks	Adulthood	• ↑ time to reach platform in acquisition test of Morris water maze test (MWM) • ↓ time spent in target quadrant in probe test of MWM • Impaired brain mitochondrial functions	• HFD induced obesity with insulin resistance condition caused learning and memory decline via impairment of brain mitochondrial function	(Pintana et al. 2013; Pintana et al. 2012)
C57BL/6 J mice induced obesity by high-fat diet (45 kcal% from fat)	8 weeks	Adulthood	• ↑ time spent in acquisition period of radial arm maze • ↑ time spent in retention test of radial arm maze • ↑ memory error and total error of radial arm maze	• Diet induced obesity in short term impairs spatial learning in male mice	(Valladolid-Acebes et al. 2011)
Amyloid precursor protein (APP)-overexpressing transgenicmice induced obesity by high-fat diet	20 weeks	Adulthood	• ↑ time to the platform quadrant in probe trial of MWM • ↓ number enter in the target quadrant in probe trial of MWM	• HFD-induced aggravation of cognitive decline in transgenic model mice of Alzheimer's disease	(Macsako et al. 2012)

Table 5 (continued)

(60 % fat)			• ↑ Aβ oligomer expression in the hippocampus • ↑ Aβ plaque accumulation in the hippocampus			
C57Bl/6 mice induced obesity by high-fat diet (60 % fat)	21 weeks	Adulthood	• ↑ acquisition errors in the Stone T-maze test • ↑ TNF-α, IL-6 and chemokine MCP-1 levels in the brain • ↓ BDNF levels in the brain	• HFD-induced obesity caused cognitive decline related with brain inflammation	(Pistell et al. 2010)	
Clinical studies						
Model	Study	Duration	Age	Major finding	Interpretation	Ref
10,276 men and women	Longitudinal cohort	27 years	40–45 year	• Obese people (body mass index ≥30) had a 74 % increased risk of dementia • overweight people (body mass index 25.0–29.9) had a 35 % risk of dementia	• Obesity in middle age increases the risk of future dementia	(Whitmer et al. 2005)
1423 men and women	Longitudinal cohort	6 years	55–88 years	• Obese men associated with poor cognitive performance and high risk of hypertension	• Obesity increases risk of cognitive decline and hypertension	(Elias et al. 2003)
599 men and women			≥ 85 years	• The metabolic syndrome was associated with a decelerated cognitive decline on the Mini-Mental State Examination, the Stroop Test and the Letter Digit Coding Test	• Metabolic syndrome associated with cognitive decline	(van den Berg et al. 2007)
781 men and women	Longitudinal cohort	16 years	25–63 years	• ↑ BMI • ↓ general cognitive ability	• Higher midlife BMI scores precede lower general cognitive ability and steeper cognitive decline in both men and women	(Dahl et al. 2010)
1814 men and women	Longitudinal cohort	12 years	40–69 years	• Central obesity and hypertension related to poorer performance on executive function & visual motor skills	• Mid-life elevated blood pressure and central obesity play a role in the reduced cognitive decline with age	(Wolf et al. 2007)

Evidence on the association among testosterone deficiency, insulin-resistant obesity, and memory decline

Several studies demonstrated that insulin-resistant obesity is associated with testosterone deficiency or vice versa (Borst and Conover 2006; Erben et al. 2000; Kakolewski et al. 1968; Olivares et al. 2009; Ribeiro et al. 2012a; Ribeiro et al. 2012b; Vignozzi et al. 2012). Furthermore, either obese-insulin resistance or testosterone deficiency has been shown to cause brain dysfunction, leading to memory decline and the development of Alzheimer's disease (Hogervorst et al. 2001). The proposed mechanism of the association between insulin-resistant obesity and testosterone deficiency to cognitive decline is illustrated in Fig. 1.

The impairment of learning and memory occurring following decreased testosterone levels (Cohen 1999; Kelly and Jones 2013; Muraleedharan and Jones 2010), may result from either the direct effect of testosterone deficiency onto the brain function or testosterone deficiency caused fat accumulation, insulin resistance and brain dysfunction. Testosterone deficiency caused direct adverse effects in the brain, including increased Aβ protein accumulation (Ramsden et al. 2003), increased oxidative stress (Meydan et al. 2010), decreased AR expression (Apostolinas et al. 1999; Ramsden et al. 2003), decreased synaptic plasticity (Sakata et al. 2000), decreased neurotransmitter release (Romeo et al. 2005), and decreased dendritic spine density (Danzer et al. 2001; Leranth et al. 2003; Li et al. 2012). Furthermore, it has been shown that a long-term effect of a high calorie diet (Ribeiro et al. 2012a; Ribeiro et al. 2012b; Stranahan et al. 2008) and testosterone deficiency (Kelly and Jones 2013; Santosa and Jensen 2012) could cause increased adipose tissue deposition, leading to the development of insulin resistance via lipotoxicity (Summers

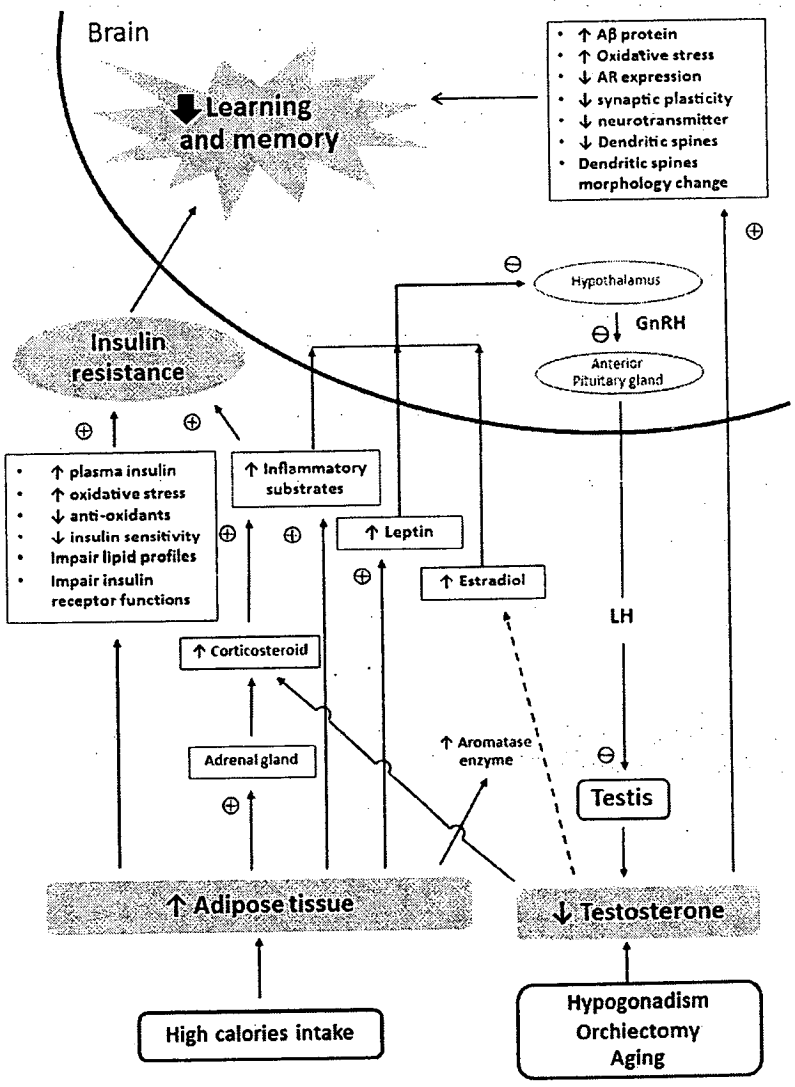


Fig. 1 The proposed mechanism of the association among testosterone deficiency, insulin resistant obesity, and memory decline + : enhancement; − : inhibition

2006), increased inflammatory substrates (Kahn and Flier 2000), increased oxidative stress (Pintana et al. 2013; Pintana et al. 2012), decreased anti-oxidant agents, impaired insulin sensitivity (Pipatpiboon et al. 2013; Pratchayasakul et al. 2011), impaired lipid profiles (Ros Perez and Medina-Gomez 2011; Stranahan et al. 2008) and impaired brain insulin receptor function (Pipatpiboon et al. 2013; Pipatpiboon et al. 2012; Pratchayasakul et al. 2011), resulting in the impairment of learning and memory. In addition, an increase of fat accumulation could cause an increased inflammatory substrates (Filippi et al. 2009), increased leptin, and increased aromatase enzyme, resulting in the inhibition of the HPT axis, thus leading to the decrease in GnRH and decreased LH pulse (Cohen 2001; Olivares et al. 2009; Vigueras-Villasenor et al. 2011). These proposed mechanisms explain the possible roles of insulin-resistant obesity together with testosterone deficiency in promoting a decline in cognitive function.

The current therapeutic approaches for treating testosterone deficiency is testosterone replacement therapy (TRT), starts with the screening and diagnosis of signs and symptoms of testosterone deficiency with low serum testosterone levels. The current guideline of testosterone deficiency therapy from The Endocrine Society 2013 can be as following: 1) testosterone enanthate or cypionate (75–100 mg/weeks or 150–200 mg every 2 weeks via intramuscular injection); 2) nongenital testosterone patch (5–10 mg testosterone over 24 h daily); 3) testosterone gel (various doses and regimens depending on the formulation); 4) testosterone bio-adhesive tablets twice daily; and 5) testosterone pellets 3–6 mg or 75–200 mg via subcutaneous implantation (Bhasin et al. 2010; Nieschlag 2014). Each regimen should be adjusted doses until levels of plasma testosterone are close to the physiological level (Bhasin et al. 2010; Morales et al. 2010). Although testosterone replacement therapy (TRT) has been prescribed to patients with hypogonadism to improve quality of life and overall health, including the improvement of cognitive function (Donatucci et al. 2014), several studies reported that TRT could lead to adverse effects, including prostate cancer, prostatic hypertrophy and heart failure (Bassil and Morley 2010; Bosland 2014; Cunningham and Toma 2011; Margo and Winn 2006). It has been proposed that testosterone replacement that maintains the physiological testosterone level may gain the benefit and could avoid the adverse effects (Nieschlag 2014). Further investigations on TRT are needed to warrant its clinical usefulness. Currently, it is still not clear what is the most critical and dominant player(s) in the mechanisms underlying the association among testosterone deficiency, insulin-resistant obesity and cognitive impairment. Several studies demonstrated that both testosterone deficiency (Mastorakos et al. 2005; Meydan et al. 2010; Rivier and Rivest 1991) and insulin-resistant obesity (Jayaraman et al. 2014; Pintana et al. 2013; Pistell et al. 2010; Purkayastha and Cai 2013) can lead to increased neuroinflammation and oxidative stress in the brain. In addition, neuroinflammation and oxidative stress are strongly associated with cognitive impairment (Agostinho et al. 2010; Pistell et al. 2010). Therefore, both inflammation and oxidative stress could be the most critical and dominant players underlying the pathophysiology of testosterone deficiency, insulin-resistant obesity and cognitive impairment.

In conclusion, this review summarizes the findings regarding testosterone deficiency in aging (by nature) as well as premature testosterone deficiency, and their association with obesity and cognitive impairment. Cognitive impairment may result from either the direct effect of testosterone deficiency on the brain function or testosterone deficiency associated with obesity that caused fat accumulation, insulin resistance and finally cognitive impairment. In addition to testosterone, future studies are needed to verify other hormones such as SHBG, TSH or IGF-1 as possible predictors of cognitive impairment.

Acknowledgments This work was supported by grants from the Thailand Research Fund TRF-BRG5780016 (SC), the Royal Golden Jubilee PhD program (PHD/0025/2555 HP&SC), National Research Council of Thailand (SC), a NSTDA Research Chair Grant from the National Science and Technology Development Agency (NC) and Chiang Mai University Excellent Center Award (NC).

References

Abbasi F, Brown BW, Jr., Lamendola C, McLaughlin T, Reaven GM (2002) Relationship between obesity, insulin resistance, and coronary heart disease risk J Am Coll Cardiol 40:937–943

Agostinho P, Cunha RA, Oliveira C (2010) Neuroinflammation, oxidative stress and the pathogenesis of Alzheimer's disease. Curr Pharm Des 16:2766–2778

Ahlbom E, Prins GS, Ceccatelli S (2001) Testosterone protects cerebellar granule cells from oxidative stress-induced cell death through a receptor mediated mechanism Brain Res 892:255–262

Almeida OP, Waterreus A, Spry N, Flicker L, Martins RN (2004) One year follow-up study of the association between chemical castration, sex hormones, beta-amyloid, memory and depression in men. Psychoneuroendocrinology 29:1071–1081. doi:10.1016/j.psyneuen.2003.11.002

Apostolinas S, Rajendren G, Dobrjansky A, Gibson MJ (1999) Androgen receptor immunoreactivity in specific neural regions in normal and hypogonadal male mice: effect of androgens Brain Res 817:19–24

Asare-Anane H et al. (2014) Obesity and testosterone levels in Ghanaian men with type 2 diabetes. Clin Diabetes 32:61–65. doi:10.2337/diaclin.32.2.61

Axell AM et al. (2006) Continuous testosterone administration prevents skeletal muscle atrophy and enhances resistance to fatigue in orchidectomized male mice. Am J Physiol Endocrinol Metab 291:E506–E516. doi:10.1152/ajpendo.00058.2006

Aydilek N, Aksakal M (2005) Effects of testosterone on lipid peroxidation, lipid profiles and some coagulation parameters in rabbits. J Vet Med A Physiol Pathol Clin Med 52:436–439. doi:10.1111/j.1439-0442.2005.00764.x

Barat P, Livingstone DE, Elferink CM, McDonnell CR, Walker BR, Andrew R (2007) Effects of gonadectomy on glucocorticoid

metabolism in obese Zucker rats. Endocrinology 148:4836–4843. doi:10.1210/en.2007-0597

Barron AM, Rosario ER, Elteriefi R, Pike CJ (2013) Sex-specific effects of high fat diet on indices of metabolic syndrome in 3xTg-AD mice: implications for alzheimer's disease. PLoS One 8:e78554. doi:10.1371/journal.pone.0078554

Bassil N, Morley JE (2010) Late-life onset hypogonadism: a review. Clin Geriatr Med 26:197–222. doi:10.1016/j.cger.2010.02.003

Betancourt-Albrecht M, Cunningham GR (2003) Hypogonadism and diabetes. Int J Impot Res 15(Suppl 4):S14–S20. doi:10.1038/sj.ijir.3901031

Bhasin S, Cunningham GR, Hayes FJ, Matsumoto AM, Snyder PJ, Swerdloff RS, Montori VM (2010) Testosterone therapy in men with androgen deficiency syndromes: an Endocrine Society clinical practice guideline. J Clin Endocrinol Metab 95:2536–2559. doi:10.1210/jc.2009-2354

Borst SE, Conover CF (2006) Orchiectomized Fischer 344 male rat models body composition in hypogonadal state. Life Sci 79:411–415. doi:10.1016/j.lfs.2006.01.035

Bosland MC (2014) Testosterone treatment is a potent tumor promoter for the rat prostate. Endocrinology. doi:10.1210/en.2014-1688

Boss L, Kang DH, Marcus M, Bergstrom N (2014) Endogenous sex hormones and cognitive function in older adults: a systematic review. West J Nurs Res 36:388–426. doi:10.1177/0193945913500566

Buletko AB, Dluzen DE, McDermott JL, Darvesh AS, Geldenhuys WJ (2012) Markers associated with testosterone enhancement of methamphetamine-induced striatal dopaminergic neurotoxicity. Neurotoxicol Teratol 34:338–343. doi:10.1016/j.ntt.2012.03.003

Carro E, Trejo JL, Gomez-Isla T, LeRoith D, Torres-Aleman I (2002) Serum insulin-like growth factor I regulates brain amyloid-beta levels. Nat Med 8:1390–1397. doi:10.1038/nm793nm793

Chai JK, Blaha V, Meguid MM, Laviano A, Yang ZJ, Varma M (1999) Use of orchiectomy and testosterone replacement to explore meal number-to-meal size relationship in male rats. Am J Physiol 276:R1366–R1373

Chen X, Li X, Huang HY, Lin JF (2006) [Effects of testosterone on insulin receptor substrate-1 and glucose transporter 4 expression in cells sensitive to insulin]. Zhonghua Yi Xue Za Zhi 86:1474–1477

Cherrier MM, Craft S, Matsumoto AH (2003) Cognitive changes associated with supplementation of testosterone or dihydrotestosterone in mildly hypogonadal men: a preliminary report. J Androl 24:568–576

Cherrier MM et al. (2005) The role of aromatization in testosterone supplementation: effects on cognition in older men. Neurology 64:290–296. doi:10.1212/01.WNL.0000149639.25136.CA

Christoffersen BO, Gade LP, Golozoubova V, Svendsen O, Raun K (2010) Influence of castration-induced testosterone and estradiol deficiency on obesity and glucose metabolism in male Gottingen minipigs. Steroids 75:676–684. doi:10.1016/j.steroids.2010.04.004

Clegg DJ et al. (2011) Consumption of a high-fat diet induces central insulin resistance independent of adiposity. Physiol Behav 103:10–16. doi:10.1016/j.physbeh.2011.01.010

Cohen PG (1999) The hypogonadal-obesity cycle: role of aromatase in modulating the testosterone-estradiol shunt–a major factor in the genesis of morbid obesity. Med Hypotheses 52:49–51. doi:10.1054/mehy.1997.0624

Cohen PG (2001) Aromatase, adiposity, aging and disease. The hypogonadal-metabolic-atherogenic-disease and aging connection Med Hypotheses 56:702–708. doi:10.1054/mehy.2000.1169

Craft S (2005) Insulin resistance syndrome and Alzheimer's disease: age- and obesity-related effects on memory, amyloid, and inflammation. Neurobiol Aging 26:65–69

Cunningham GR, Toma SM (2011) Clinical review: why is androgen replacement in males controversial? J Clin Endocrinol Metab 96:38–52. doi:10.1210/jc.2010-0266

Cunningham RL, Giuffrida A, Roberts JL (2009) Androgens induce dopaminergic neurotoxicity via caspase-3-dependent activation of protein kinase Cdelta. Endocrinology 150:5539–5548. doi:10.1210/en.2009-0640

Cunningham RL, Singh M, O'Bryant SE, Hall JR, Barber RC (2014) Oxidative stress, testosterone, and cognition among Caucasian and Mexican-American men with and without Alzheimer's disease. J Alzheimers Dis 40:563–573. doi:10.3233/JAD-131994

Dahl A, Hassing LB, Fransson E, Berg S, Gatz M, Reynolds CA, Pedersen NL (2010) Being overweight in midlife is associated with lower cognitive ability and steeper cognitive decline in late life. J Gerontol A Biol Sci Med Sci 65:57–62. doi:10.1093/gerona/glp035

Danzer SC, McMullen NT, Rance NE (2001) Testosterone modulates the dendritic architecture of arcuate neuroendocrine neurons in adult male rats. Brain Res 890:78–85

de la Monte SM (2009) Insulin resistance and Alzheimer's disease. BMB Rep 42:475–481

Di Luigi L, Romanelli F, Sgro P, Lenzi A (2012) Andrological aspects of physical exercise and sport medicine. Endocrine 42:278–284. doi:10.1007/s12020-012-9655-6

Donatucci C, Cui Z, Fang Y, Muram D (2014) Long-term treatment patterns of testosterone replacement medications. J Sex Med 11:2092–2099. doi:10.1111/jsm.12608

Durdiakova J, Ostatnikova D, Celec P (2011) Testosterone and its metabolites–modulators of brain functions. Acta Neurobiol Exp (Wars) 71:434–454

Duron E et al. (2012) Insulin-like growth factor-I and insulin-like growth factor binding protein-3 in Alzheimer's disease. J Clin Endocrinol Metab 97:4673–4681. doi:10.1210/jc.2012-2063

Eckardt K, Taube A, Eckel J (2011) Obesity-associated insulin resistance in skeletal muscle: role of lipid accumulation and physical inactivity. Rev Endocr Metab Disord 12:163–172. doi:10.1007/s11154-011-9168-2

Elias MF, Elias PK, Sullivan LM, Wolf PA, D'Agostino RB (2003) Lower cognitive function in the presence of obesity and hypertension: the Framingham heart study. Int J Obes Relat Metab Disord 27:260–268. doi:10.1038/sj.ijo.802225

Emamian S, Naghdi N, Sepehri H, Jahanshahi M, Sadeghi Y, Choopani S (2010) Learning impairment caused by intra-CA1 microinjection of testosterone increases the number of astrocytes. Behav Brain Res 208:30–37. doi:10.1016/j.bbr.2009.11.004

Emanuele MA, Emanuele N (2001) Alcohol and the male reproductive system Alcohol. Res Health 25:282–287

Erben RG, Eberle J, Stahr K, Goldberg M (2000) Androgen deficiency induces high turnover osteopenia in aged male rats: a sequential histomorphometric study. J Bone Miner Res 15:1085–1098. doi:10.1359/jbmr.2000.15.6.1085

Erdemir F, Atilgan D, Markoc F, Boztepe O, Suha-Parlaktas B, Sahin S (2012) The effect of diet induced obesity on testicular tissue and serum oxidative stress parameters. Actas Urol Esp 36:153–159. doi:10.1016/j.acuro.2011.06.019

Estrada M, Varshney A, Ehrlich BE (2006) Elevated testosterone induces apoptosis in neuronal cells. J Biol Chem 281:25492–25501. doi:10.1074/jbc.M603193200

Ewing LL, Wing TY, Cochran RC, Kromann N, Zirkin BR (1983) Effect of luteinizing hormone on Leydig cell structure and testosterone secretion. Endocrinology 112:1763–1769

Fawcett KA, Barroso I (2010) The genetics of obesity: FTO leads the way. Trends Genet 26:266–274. doi:10.1016/j.tig.2010.02.006

Filippi S et al. (2009) Testosterone partially ameliorates metabolic profile and erectile responsiveness to PDE5 inhibitors in an animal model of male metabolic syndrome. J Sex Med 6:3274–3288. doi:10.1111/j.1743-6109.2009.01467.x

Filova B, Ostatnikova D, Celec P, Hodosy J (2013) The effect of testosterone on the formation of brain structures. Cells Tissues Organs 197:169–177. doi:10.1159/000345567

Fogari R, Zoppi A, Preti P, Rinaldi A, Marasi G, Vanasia A, Mugellini A (2002) Sexual activity and plasma testosterone levels in hypertensive males. Am J Hypertens 15:217–221

Franchimont P, Chari S, Demoulin A (1975) Hypothalamus-pituitary-testis interaction. J Reprod Fertil 44:335–350

Fui MN, Dupuis P, Grossmann M (2014) Lowered testosterone in male obesity: mechanisms, morbidity and management. Asian J Androl 16:223–231. doi:10.4103/1008-682X.122365

Gao W, Reiser PJ, Coss CC, Phelps MA, Kearbey JD, Miller DD, Dalton JT (2005) Selective androgen receptor modulator treatment improves muscle strength and body composition and prevents bone loss in orchidectomized rats. Endocrinology 146:4887–4897 doi:10.1210/en.2005-0572

Gentry RT, Wade GN (1976) Androgenic control of food intake and body weight in male rats. J Comp Physiol Psychol 90:18–25

Georgiev IP et al. (2011) Effects of castration-induced visceral obesity and antioxidant treatment on lipid profile and insulin sensitivity in New Zealand white rabbits. Res Vet Sci 90:196–204. doi:10.1016/j.rvsc.2010.05.023

Goudsmit E, Hofman MA, Fliers E, Swaab DF (1990) The supraoptic and paraventricular nuclei of the human hypothalamus in relation to sex, age and Alzheimer's disease. Neurobiol Aging 11:529–536

Gouras GK, Xu H, Gross RS, Greenfield JP, Hai B, Wang R, Greengard P (2000) Testosterone reduces neuronal secretion of Alzheimer's beta-amyloid peptides. Proc Natl Acad Sci U S A 97:1202–1205

Greenwood CE, Winocur G (2001) Glucose treatment reduces memory deficits in young adult rats fed high-fat diets. Neurobiol Learn Mem 75:179–189. doi:10.1006/nlme.2000.3964

Greenwood CE, Winocur G (2005) High-fat diets, insulin resistance and declining cognitive function. Neurobiol Aging 26(Suppl 1):42–45. doi:10.1016/j.neurobiolaging.2005.08.017

Grossmann M et al. (2008) Low testosterone levels are common and associated with insulin resistance in men with diabetes. J Clin Endocrinol Metab 93:1834–1840. doi:10.1210/jc.2007-2177

Groth KA, Skakkebaek A, Host C, Gravholt CH, Bojesen A (2013) Clinical review: Klinefelter syndrome–a clinical update. J Clin Endocrinol Metab 98:20–30. doi:10.1210/jc.2012-2382

Haffner SM, Karhapaa P, Mykkanen L, Laakso M (1994) Insulin resistance, body fat distribution, and sex hormones in men. Diabetes 43:212–219

Haffner SM, Shaten J, Stern MP, Smith GD, Kuller L (1996) Low levels of sex hormone-binding globulin and testosterone predict the development of non-insulin-dependent diabetes mellitus in men. MRFIT research group. Multiple Risk Factor Intervention Trial. Am J Epidemiol 143:889–897

Hammond J, Le Q, Goodyer C, Gelfand M, Trifiro M, LeBlanc A (2001) Testosterone-mediated neuroprotection through the androgen receptor in human primary neurons. J Neurochem 77:1319–1326

Haring R et al. (2010) Prevalence, incidence and risk factors of testosterone deficiency in a population-based cohort of men: results from the study of health in Pomerania. Aging Male 13:247–257. doi:10.3109/13685538.2010.487553

Harooni HE, Naghdi N, Sepehri H, Rohani AH (2008) Intra hippocampal injection of testosterone impaired acquisition, consolidation and retrieval of inhibitory avoidance learning and memory in adult male rats. Behav Brain Res 188:71–77. doi:10.1016/j.bbr.2007.10.017

Hiltunen M et al. (2012) Contribution of genetic and dietary insulin resistance to Alzheimer phenotype in APP/PS1 transgenic mice. J Cell Mol Med 16:1206–1222. doi:10.1111/j.1582-4934.2011.01384.x

Ho CH et al. (2013) Prediabetes is associated with an increased risk of testosterone deficiency, independent of obesity and metabolic syndrome. PLoS One 8:e74173. doi:10.1371/journal.pone.0074173

Hogervorst E, Williams J, Budge M, Barnetson L, Combrinck M, Smith AD (2001) Serum total testosterone is lower in men with Alzheimer's disease. Neuro Endocrinol Lett 22:163–168

Hogervorst E, Bandelow S, Combrinck M, Smith AD (2004) Low free testosterone is an independent risk factor for Alzheimer's disease. Exp Gerontol 39:1633–1639. doi:10.1016/j.exger.2004.06.019

Hogervorst E, Matthews FE, Brayne C (2010) Are optimal levels of testosterone associated with better cognitive function in healthy older women and men? Biochim Biophys Acta 1800:1145–1152. doi:10.1016/j.bbagen.2009.12.009

Holland J, Bandelow S, Hogervorst E (2011) Testosterone levels and cognition in elderly men: a review. Maturitas 69:322–337. doi:10.1016/j.maturitas.2011.05.012

Hristova M, Aloe L (2006) Metabolic syndrome–neurotrophic hypothesis. Med Hypotheses 66:545–549 doi:10.1016/j.mehy.2005.08.055

Hueston CM, Deak T (2014) The inflamed axis: the interaction between stress, hormones, and the expression of inflammatory-related genes within key structures comprising the hypothalamic-pituitary-adrenal axis. Physiol Behav 124:77–91. doi:10.1016/j.physbeh.2013.10.035

Janowsky JS (2006) Thinking with your gonads: testosterone and cognition. Trends Cogn Sci 10:77–82. doi:10.1016/j.tics.2005.12.010

Janowsky JS, Oviatt SK, Orwoll ES (1994) Testosterone influences spatial cognition in older men. Behav Neurosci 108:325–332

Jayaraman A, Lent-Schochet D, Pike CJ (2014) Diet-induced obesity and low testosterone increase neuroinflammation and impair neural function. J Neuroinflammation 11:162. doi:10.1186/s12974-014-0162-y

Jones TH (2010a) Effects of testosterone on Type 2 diabetes and components of the metabolic syndrome. J Diabetes 2:146–156. doi:10.1111/j.1753-0407.2010.00085.x

Jones TH (2010b) Testosterone deficiency: a risk factor for cardiovascular disease? Trends Endocrinol Metab 21:496–503. doi:10.1016/j.tem.2010.03.002

Kahn BB, Flier JS (2000) Obesity and insulin resistance. J Clin Invest 106:473–481. doi:10.1172/JCI10842

Kakolewski JW, Cox VC, Valenstein ES (1968) Sex differences in body-weight change following gonadectomy of rats. Psychol Rep 22:547–554

Kanchuk ML, Backus RC, Calvert CC, Morris JG, Rogers QR (2003) Weight gain in gonadectomized normal and lipoprotein lipase-deficient male domestic cats results from increased food intake and not decreased energy expenditure. J Nutr 133:1866–1874

Kapoor D, Malkin CJ, Channer KS, Jones TH (2005) Androgens, insulin resistance and vascular disease in men. Clin Endocrinol (Oxf) 63:239–250. doi:10.1111/j.1365-2265.2005.02299.x

Kelly DM, Jones TH (2013) Testosterone: a metabolic hormone in health and disease. J Endocrinol 217:R25–R45. doi:10.1530/JOE-12-0455

Kenny AM, Fabregas G, Song C, Biskup B, Bellantonio S (2004) Effects of testosterone on behavior, depression, and cognitive function in older men with mild cognitive loss. J Gerontol A Biol Sci Med Sci 59:75–78

Khorshidahmad T et al. (2012) Interactive effects of a protein kinase AII inhibitor and testosterone on spatial learning in the Morris water maze. Behav Brain Res 228:432–439. doi:10.1016/j.bbr.2011.12.028

Kitzinger H, Karle B (2013) The epidemiology of obesity. Eur Surg 45:80–82. doi:10.1007/s10353-013-0196-x

Kohara K (2014) Sarcopenic obesity in aging population: current status and future directions for research. Endocrine 45:15–25. doi:10.1007/s12020-013-9992-0

Kotan LD et al. (2014) Mutations in FEZF1 cause Kallmann syndrome. Am J Hum Genet 95:326–331. doi:10.1016/j.ajhg.2014.08.006

Krams M, Quinton R, Ashburner J, Friston KJ, Frackowiak RS, Bouloux PM, Passingham RE (1999) Kallmann's syndrome: mirror movements associated with bilateral corticospinal tract hypertrophy. Neurology 52:816–822

Laaksonen DE et al. (2004) Testosterone and sex hormone-binding globulin predict the metabolic syndrome and diabetes in middle-aged men. Diabetes Care 27:1036–1041

Leranth C, Petnehazy O, MacLusky NJ (2003) Gonadal hormones affect spine synaptic density in the CA1 hippocampal subfield of male rats. J Neurosci 23:1588–1592

Li J, Al-Azzawi F (2009) Mechanism of androgen receptor action. Maturitas 63:142–148. doi:10.1016/j.maturitas.2009.03.008

Li M, Masugi-Tokita M, Takanami K, Yamada S, Kawata M (2012) Testosterone has sublayer-specific effects on dendritic spine maturation mediated by BDNF and PSD-95 in pyramidal neurons in the hippocampus CA1 area. Brain Res 1484:76–84. doi:10.1016/j.brainres.2012.09.028

Lu PH et al. (2006) Effects of testosterone on cognition and mood in male patients with mild Alzheimer disease and healthy elderly men. Arch Neurol 63:177–185. doi:10.1001/archneur.63.2.nct50002

Lupien S, Lecours AR, Lussier I, Schwartz G, Nair NP, Meaney MJ (1994) Basal cortisol levels and cognitive deficits in human aging. J Neurosci 14:2893–2903

Lupien SJ et al. (1999) Increased cortisol levels and impaired cognition in human aging: implication for depression and dementia in later life. Rev Neurosci 10:117–139

MacLusky NJ, Hajszan T, Prange-Kiel J, Leranth C (2006) Androgen modulation of hippocampal synaptic plasticity. Neuroscience 138: 957–965. doi:10.1016/j.neuroscience.2005.12.054

Maesako M et al. (2012) Exercise is more effective than diet control in preventing high fat diet-induced beta-amyloid deposition and memory deficit in amyloid precursor protein transgenic mice. J Biol Chem 287:23024–23033. doi:10.1074/jbc.M112.367011

Maki PM et al. (2007) Intramuscular testosterone treatment in elderly men: evidence of memory decline and altered brain function. J Clin Endocrinol Metab 92:4107–4114. doi:10.1210/jc.2006-1805

Margo K, Winn R (2006) Testosterone treatments: why, when, and how? Am Fam Physician 73:1591–1598

Martin LJ (2014) Implications of adiponectin in linking metabolism to testicular function. Endocrine 46:16–28. doi:10.1007/s12020-013-0102-0

Martin SJ, Grimwood PD, Morris RG (2000) Synaptic plasticity and memory: an evaluation of the hypothesis. Annu Rev Neurosci 23: 649–711. doi:10.1146/annurev.neuro.23.1.649

Mastorakos G, Pavlatou M, Diamanti-Kandarakis E, Chrousos GP (2005) Exercise and the stress system. Hormones (Athens) 4:73–89

Matsumoto A (2001) Androgen stimulates neuronal plasticity in the perineal motoneurons of aged male rats. J Comp Neurol 430:389–395 doi:1096-9861(2001/1096-9861(20010212)430:3<389::AID-CNE1038>3.0.CO;2-3

McConnell SE, Alla J, Wheat E, Romeo RD, McEwen B, Thornton JE (2012) The role of testicular hormones and luteinizing hormone in spatial memory in adult male rats. Horm Behav 61:479–486. doi:10.1016/j.yhbeh.2012.01.003

Meydan S et al. (2010) Effects of testosterone on orchiectomy-induced oxidative damage in the rat hippocampus. J Chem Neuroanat 40: 281–285. doi:10.1016/j.jchemneu.2010.07.006

Moffat SD, Zonderman AB, Metter EJ, Blackman MR, Harman SM, Resnick SM (2002) Longitudinal assessment of serum free testosterone concentration predicts memory performance and cognitive status in elderly men. J Clin Endocrinol Metab 87:5001–5007. doi:10.1210/jc.2002-020419

Montalcini T, Migliaccio V, Ferro Y, Gazzaruso C, Pujia A (2012) Androgens for postmenopausal women's health? Endocrine 42: 514–520. doi:10.1007/s12020-012-9692-1

Morales A et al. (2010) A practical guide to diagnosis, management and treatment of testosterone deficiency for Canadian physicians. Can Urol Assoc J 4:269–275

Morley JE, Perry HM, 3rd (1999) Androgen deficiency in aging men. Med Clin North Am 83:1279–1289, vii

Muller M, Schupf N, Manly JJ, Mayeux R, Luchsinger JA (2010) Sex hormone binding globulin and incident Alzheimer's disease in elderly men and women. Neurobiol Aging 31:1758–1765. doi:10.1016/j.neurobiolaging.2008.10.001

Muraleedharan V, Jones TH (2010) Testosterone and the metabolic syndrome. Ther Adv Endocrinol Metab 1:207–223. doi:10.1177/2042018810390258

Naghdi N, Asadollahi A (2004) Genomic and nongenomic effects of intrahippocampal microinjection of testosterone on long-term memory in male adult rats. Behav Brain Res 153:1–6. doi:10.1016/j.bbr.2003.10.027

Naghdi N, Majlessi N, Bozorgmehr T (2005) The effect of intrahippocampal injection of testosterone enanthate (an androgen receptor agonist) and anisomycin (protein synthesis inhibitor) on spatial learning and memory in adult, male rats. Behav Brain Res 156:263–268. doi:10.1016/j.bbr.2004.05.032

Nieschlag E (2014) Current topics in testosterone replacement of hypogonadal men. Best Practice & Research Clinical Endocrinology & Metabolism. doi:10.1016/j.beem.2014.09.008

Nunemaker CS, Satin LS (2014) Episodic hormone secretion: a comparison of the basis of pulsatile secretion of insulin and GnRH. Endocrine doi:10.1007/s12020-014-0212-3

Ogawa S, Lubahn DB, Korach KS, Pfaff DW (1997) Behavioral effects of estrogen receptor gene disruption in male mice. Proc Natl Acad Sci U S A 94:1476–1481

Okamura H, Tsukamura H, Ohkura S, Uenoyama Y, Wakabayashi Y, Maeda K (2013) Kisspeptin and GnRH pulse generation. Adv Exp Med Biol 784:297–323. doi:10.1007/978-1-4614-6199-9_14

Okun MS, DeLong MR, Hanfelt J, Gearing M, Levey A (2004) Plasma testosterone levels in Alzheimer and Parkinson diseases. Neurology 62:411–413

Olivares A, Mendez JP, Zambrano E, Cardenas M, Tovar A, Perera-Marin G, Ulloa-Aguirre A (2009) Reproductive axis function and gonadotropin microheterogeneity in a male rat model of diet-induced obesity. Gen Comp Endocrinol 166:356–364. doi:10.1016/j.ygcen.2009.12.007

Ownby RL (2010) Neuroinflammation and cognitive aging. Curr Psychiatry Rep 12:39–45. doi:10.1007/s11920-009-0082-1

Pandolfi C, Pellegrini L, Sbalzarini G, Mercantini F (1994) Obesity and insulin resistance. Minerva Med 85:167–171

Pardridge WM, Mietus LJ (1979) Transport of steroid hormones through the rat blood–brain barrier. Primary role of albumin-bound hormone. J Clin Invest 64:145–154. doi:10.1172/JCI109433

Park EJ et al. (2010) Dietary and genetic obesity promote liver inflammation and tumorigenesis by enhancing IL-6 and TNF expression. Cell 140:197–208. doi:10.1016/j.cell.2009.12.052

Pelletier G, Labrie C, Labrie F (2000) Localization of oestrogen receptor alpha, oestrogen receptor beta and androgen receptors in the rat reproductive organs. J Endocrinol 165:359–370

Pike CJ (2001) Testosterone attenuates beta-amyloid toxicity in cultured hippocampal neurons. Brain Res 919:160–165

Pintana H, Apaijai N, Pratchayasakul W, Chattipakorn N, Chattipakorn SC (2012) Effects of metformin on learning and memory behaviors and brain mitochondrial functions in high fat diet induced insulin resistant rats. Life Sci. doi:10.1016/j.lfs.2012.08.017

Pintana H, Apaijai N, Chattipakorn N, Chattipakorn SC (2013) DPP-4 inhibitors improve cognition and brain mitochondrial function of insulin resistant rats. J Endocrinol. doi:10.1530/JOE-12-0521

Pipatpiboon N, Pratchayasakul W, Chattipakorn N, Chattipakorn SC (2012) PPARgamma agonist improves neuronal insulin receptor function in hippocampus and brain mitochondria function in rats with insulin resistance induced by long term high-fat diets. Endocrinology 153:329–338. doi:10.1210/en.2011-1502

Pipatpiboon N, Pintana H, Pratchayasakul W, Chattipakorn N, Chattipakorn SC (2013) DPP4-inhibitor improves neuronal insulin receptor function, brain mitochondrial function and cognitive function in rats with insulin resistance induced by high-fat diet consumption. Eur J Neurosci. doi:10.1111/ejn.12088

Pistell PJ, Morrison CD, Gupta S, Knight AG, Keller JN, Ingram DK, Bruce-Keller AJ (2010) Cognitive impairment following high fat diet consumption is associated with brain inflammation. J Neuroimmunol 219:25–32. doi:10.1016/j.jneuroim.2009.11.010

Pitteloud N, Hardin M, Dwyer AA, Valassi E, Yialamas M, Elahi D, Hayes FJ (2005) Increasing insulin resistance is associated with a decrease in Leydig cell testosterone secretion in men. J Clin Endocrinol Metab 90:2636–2641 doi:10.1210/jc.2004-2190

Pratchayasakul W, Kerdphoo S, Petsophonsakul P, Pongchaidecha A, Chattipakorn N, Chattipakorn SC (2011) Effects of high-fat diet on insulin receptor function in rat hippocampus and the level of neuronal corticosterone. Life Sci 88:619–627. doi:10.1016/j.lfs.2011.02.003

Purkayastha S, Cai D (2013) Neuroinflammatory basis of metabolic syndrome. Mol Metab 2:356–363. doi:10.1016/j.molmet.2013.09.005

Ramsden M, Nyborg AC, Murphy MP, Chang L, Stanczyk FZ, Golde TE, Pike CJ (2003) Androgens modulate beta-amyloid levels in male rat brain. J Neurochem 87:1052–1055

Reusch JE (2002) Current concepts in insulin resistance, type 2 diabetes mellitus, and the metabolic syndrome. Am J Cardiol 90:19G–26G

Ribeiro DL, Pinto ME, Maeda SY, Taboga SR, Goes RM (2012a) High fat-induced obesity associated with insulin-resistance increases FGF-2 content and causes stromal hyperplasia in rat ventral prostate. Cell Tissue Res 349:577–588. doi:10.1007/s00441-012-1420-x

Ribeiro DL et al. (2012b) High-Fat Diet Obesity Associated with Insulin Resistance Increases Cell Proliferation, Estrogen Receptor, and PI3K Proteins in Rat Ventral Prostate. J Androl. doi:10.2164/jandrol.111.016089

Rivier C, Rivest S (1991) Effect of stress on the activity of the hypothalamic-pituitary-gonadal axis: peripheral and central mechanisms. Biol Reprod 45:523–532

Roemmich JN, Sinning WE (1997) Weight loss and wrestling training: effects on growth-related hormones. J Appl Physiol (1985) 82:1760–1764

Romeo RD, Staub D, Jasnow AM, Karatsoreos IN, Thornton JE, McEwen BS (2005) Dihydrotestosterone increases hippocampal N-methyl-D-aspartate binding but does not affect choline acetyltransferase cell number in the forebrain or choline transporter levels in the CA1 region of adult male rats. Endocrinology 146:2091–2097. doi:10.1210/en.2004-0886

Ros Perez M, Medina-Gomez G (2011) Obesity, adipogenesis and insulin resistance. Endocrinol Nutr 58:360–369. doi:10.1016/j.endonu.2011.05.008

Sahu A, Kalra SP, Crowley WR, Kalra PS (1989) Testosterone raises neuropeptide-Y concentration in selected hypothalamic sites and in vitro release from the medial basal hypothalamus of castrated male rats. Endocrinology 124:410–414

Sakata K, Tokue A, Kawai N (2000) Altered synaptic transmission in the hippocampus of the castrated male mouse is reversed by testosterone replacement. J Urol 163:1333–1338

Sandstrom NJ, Kim JH, Wasserman MA (2006) Testosterone modulates performance on a spatial working memory task in male rats. Horm Behav 50:18–26. doi:10.1016/j.yhbeh.2005.09.008

Santosa S, Jensen MD (2012) Effects of male hypogonadism on regional adipose tissue fatty acid storage and lipogenic proteins. PLoS One 7:e31473. doi:10.1371/journal.pone

Schiavi RC, White D (1976) Androgens and male sexual function: a review of human studies. J Sex Marital Ther 2:214–228. doi:10.1080/00926237608405324

Seale JV, Wood SA, Atkinson HC, Harbuz MS, Lightman SL (2004) Gonadal steroid replacement reverses gonadectomy-induced changes in the corticosterone pulse profile and stress-induced hypothalamic-pituitary-adrenal axis activity of male and female rats. J Neuroendocrinol 16:989–998. doi:10.1111/j.1365-2826.2004.01258.x

Selkoe DJ (2001) Alzheimer's disease: genes, proteins, and therapy. Physiol Rev 81:741–766

Semenkovich CF (2006) Insulin resistance and atherosclerosis. J Clin Invest 116:1813–1822. doi:10.1172/JCI29024

Shi Z, Araujo AB, Martin S, O'Loughlin P, Wittert GA (2013) Longitudinal changes in testosterone over five years in community-dwelling men. J Clin Endocrinol Metab 98:3289–3297. doi:10.1210/jc.2012-3842

Singh T, Newman AB (2011) Inflammatory markers in population studies of aging. Ageing research reviews 10:319–329

Skakkebaek A et al. (2014) Neuropsychology and brain morphology in Klinefelter syndrome - the impact of genetics. Andrology 2:632–640. doi:10.1111/j.2047-2927.2014.00229.x

Smith EM, Cadet P, Stefano GB, Opp MR, Hughes TK, Jr. (1999) IL-10 as a mediator in the HPA axis and brain J Neuroimmunol 100:140–148

Smith JT et al. (2005) Differential regulation of KiSS-1 mRNA expression by sex steroids in the brain of the male mouse. Endocrinology 146:2976–2984. doi:10.1210/en.2005-0323

Spritzer MD, Daviau ED, Coneeny MK, Engelman SM, Prince WT, Rodriguez-Wisdom KN (2011) Effects of testosterone on spatial learning and memory in adult male rats. Horm Behav 59:484–496. doi:10.1016/j.yhbeh.2011.01.009

Stellato RK, Feldman HA, Hamdy O, Horton ES, McKinlay JB (2000) Testosterone, sex hormone-binding globulin, and the development of type 2 diabetes in middle-aged men: prospective results from the Massachusetts male aging study. Diabetes Care 23:490–494

Stranahan AM, Norman ED, Lee K, Cutler RG, Telljohann RS, Egan JM, Mattson MP (2008) Diet-induced insulin resistance impairs hippocampal synaptic plasticity and cognition in middle-aged rats. Hippocampus 18:1085–1088. doi:10.1002/hipo.20470

Strauss RH, Lanese RR, Malarkey WB (1985) Weight loss in amateur wrestlers and its effect on serum testosterone levels. JAMA 254:3337–3338

Summers SA (2006) Ceramides in insulin resistance and lipotoxicity. Prog Lipid Res 45:42–72. doi:10.1016/j.plipres.2005.11.002

Takeda H, Chodak G, Mutchnik S, Nakamoto T, Chang C (1990) Immunohistochemical localization of androgen receptors with mono- and polyclonal antibodies to androgen receptor. J Endocrinol 126:17–25

Tan RS, Pu SJ (2003) A pilot study on the effects of testosterone in hypogonadal aging male patients with Alzheimer's disease. Aging Male 6:13–17

Thambisetty M et al. (2013) Glucose intolerance, insulin resistance, and pathological features of Alzheimer disease in the Baltimore longitudinal study of aging. JAMA Neurol 70:1167–1172. doi:10.1001/jamaneurol.2013.284

Torkler S et al. (2011) Inverse association between total testosterone concentrations, incident hypertension and blood pressure. Aging Male 14:176–182. doi:10.3109/13685538.2010.529194

Trolle C, Hjerrild B, Cleemann L, Mortensen KH, Gravholt CH (2012) Sex hormone replacement in Turner syndrome. Endocrine 41:200–219. doi:10.1007/s12020-011-9569-8

Tsai EC, Matsumoto AM, Fujimoto WY, Boyko EJ (2004) Association of bioavailable, free, and total testosterone with insulin resistance: influence of sex hormone-binding globulin and body fat. Diabetes Care 27:861–868

Tsujimura A (2013) The Relationship between Testosterone Deficiency and Men's Health World J Mens. Health 31:126–135. doi:10.5534/wjmh.2013.31.2.126

Tylinska M, Broncel M (2013) [The relationship between testosterone deficiency and metabolic syndrome in obese men]. Pol Merkur Lekarski 34:24–28

Valladolid-Acebes I et al. (2011) High-fat diets impair spatial learning in the radial-arm maze in mice. Neurobiol Learn Mem 95:80–85. doi:10.1016/j.nlm.2010.11.007

van den Berg E, Biessels GJ, de Craen AJ, Gussekloo J, Westendorp RG (2007) The metabolic syndrome is associated with decelerated cognitive decline in the oldest old. Neurology 69:979–985. doi:10.1212/01.wnl.0000271381.30143.75

Vaughan C, Goldstein FC, Tenover JL (2007) Exogenous testosterone alone or with finasteride does not improve measurements of cognition in healthy older men with low serum testosterone. J Androl 28:875–882. doi:10.2164/jandrol.107.002931

Verhoeven WM, Egger JI, Hovens JE, Hoefsloot L (2013) Kallmann syndrome and paranoid schizophrenia: a rare combination. BMJ Case Rep. doi:10.1136/bcr-2012-007387

Vignozzi L et al. (2012) Testosterone protects from metabolic syndrome-associated prostate inflammation: an experimental study in rabbit. J Endocrinol 212:71–84. doi:10.1530/JOE-11-0289

Vigueras-Villasenor RM et al. (2011) Alterations in the spermatic function generated by obesity in rats. Acta Histochem 113:214–220. doi:10.1016/j.acthis.2009.10.004

Vinson GP, Bell JB, Whitehouse BJ (1976) Production of testosterone and corticosteroids by the rat adrenal gland incubated in vitro and the effects of stimulation with ACTH, LH and FSH. J Steroid Biochem 7:407–411

Volterrani M, Rosano G, Iellamo F (2012) Testosterone and heart failure. Endocrine 42:272–277. doi:10.1007/s12020-012-9725-9

Whitmer RA, Gunderson EP, Barrett-Connor E, Quesenberry CP, Jr., Yaffe K (2005) Obesity in middle age and future risk of dementia: a 27 year longitudinal population based study. BMJ 330:1360 doi:10.1136/bmj.38446.466238.E0

Winocur G, Greenwood CE, Piroli GG, Grillo CA, Reznikov LR, Reagan LP, McEwen BS (2005) Memory impairment in obese Zucker rats: an investigation of cognitive function in an animal model of insulin resistance and obesity. Behav Neurosci 119:1389–1395. doi:10.1037/0735-7044.119.5.1389

Wolf OT, Preut R, Hellhammer DH, Kudielka BM, Schurmeyer TH, Kirschbaum C (2000) Testosterone and cognition in elderly men: a single testosterone injection blocks the practice effect in verbal fluency, but has no effect on spatial or verbal memory. Biol Psychiatry 47:650–654

Wolf PA, Beiser A, Elias MF, Au R, Vasan RS, Seshadri S (2007) Relation of obesity to cognitive function: importance of central obesity and synergistic influence of concomitant hypertension. The Framingham Heart Study Curr Alzheimer Res 4:111–116

Wu FC et al. (2010) Identification of late-onset hypogonadism in middle-aged and elderly men. N Engl J Med 363:123–135. doi:10.1056/NEJMoa0911101

Yang SH, Perez E, Cutright J, Liu R, He Z, Day AL, Simpkins JW (2002) Testosterone increases neurotoxicity of glutamate in vitro and ischemia-reperfusion injury in an animal model. J Appl Physiol (1985) 92:195–201

Yeap BB, Chubb SA, Hyde Z, Jamrozik K, Hankey GJ, Flicker L, Norman PE (2009) Lower serum testosterone is independently associated with insulin resistance in non-diabetic older men: the Health In Men Study. Eur J Endocrinol 161:591–598. doi:10.1530/EJE-09-0348

Zhang J et al. (2013) Both total testosterone and sex hormone-binding globulin are independent risk factors for metabolic syndrome: results from Fangchenggang Area Male Health and Examination Survey in China. Diabetes Metab Res Rev 29:391–397. doi:10.1002/dmrr.2405

เอกสารแนบหมายเลข 46

Hormones and Behavior 72 (2015) 68–77

Contents lists available at ScienceDirect

Hormones and Behavior

journal homepage: www.elsevier.com/locate/yhbeh

Obesity accelerates cognitive decline by aggravating mitochondrial dysfunction, insulin resistance and synaptic dysfunction under estrogen-deprived conditions

Wasana Pratchayasakul [a,b,1], Piangkwan Sa-nguanmoo [a,b,1], Sivaporn Sivasinprasasn [a,b], Hiranya Pintana [a,b], Rungroj Tawinvisan [a,b], Jirapas Sripetchwandee [a,b], Sirinart Kumfu [a,b], Nipon Chattipakorn [a,b], Siriporn C. Chattipakorn [a,c,*]

[a] Neurophysiology Unit, Cardiac Electrophysiology Research and Training Center, Faculty of Medicine, Chiang Mai University, Chiang Mai, Thailand
[b] Department of Physiology, Faculty of Medicine, Chiang Mai University, Chiang Mai, Thailand
[c] Department of Oral Biology and Diagnostic Science, Faculty of Dentistry, Chiang Mai University, Chiang Mai, Thailand

ARTICLE INFO

Article history:
Received 29 November 2014
Revised 22 April 2015
Accepted 29 April 2015
Available online 16 May 2015

Keywords:
High-fat diet
Estrogen deprivation
Brain insulin sensitivity
Mitochondrial function
Hippocampal synaptic function

ABSTRACT

Chronic consumption of a high-fat diet (HF) causes peripheral insulin resistance, brain insulin resistance, brain mitochondrial dysfunction and cognitive impairment. Estrogen deprivation has also been found to impair cognition. However, the combined effect of both conditions on the brain is unclear. We hypothesized that estrogen deprivation causes brain insulin resistance, brain mitochondrial dysfunction, hippocampal synaptic dysfunction and cognitive impairment, and that consumption of a HF accelerates these impairments in an estrogen-deprived condition. Seventy-two female rats were divided into sham (S) and ovariectomized (O) groups. Rats in each group were further divided into two subgroups to be fed with either a normal diet (ND) or HF for 4, 8 and 12 weeks. At the end of each period, the Morris water maze test was carried out, after which the blood and brain were collected for metabolic and brain function analysis. Obesity, peripheral insulin resistance, increased brain oxidative stress and hippocampal synaptic dysfunction were observed at the eighth week in the NDO, HFS and HFO rats. However, these impairments were worse in the HFO rats. Interestingly, brain insulin resistance, brain mitochondrial dysfunction and cognitive impairment developed earlier (week eight) in the HFO rats, whereas these conditions were observed later at week 12 in the NDO and HFS rats. Either estrogen deprivation or HF appears to cause peripheral insulin resistance, increased brain oxidative stress, hippocampal synaptic dysfunction, brain mitochondrial dysfunction and brain insulin resistance, which together can lead to cognitive impairment. A HF accelerates and aggravates these deleterious effects under estrogen-deprived conditions.
© 2015 Elsevier Inc. All rights reserved.

Introduction

Both estrogen and obesity have been shown to be involved in the functioning of insulin receptors and also in cognition. It has been shown in a previous study that either estrogen deprivation or obesity increased the oxidative stress level, and led to the development of insulin resistance and cognitive impairment (Evsen et al., 2013; Henderson, 2008; Matsuzawa-Nagata et al., 2008; Pintana et al., 2012). Our previous studies demonstrated that obesity induced by consumption of a high-fat diet (HF) increased brain oxidative stress, as indicated by an increased brain corticosterone level, brain malondialdehyde level and brain mitochondrial dysfunction which subsequently led to impaired brain insulin sensitivity, as indicated by the impairment of insulin-induced long-term depression (LTD) and impaired brain insulin signaling (Pintana et al., 2012; Pipatpiboon et al., 2012, 2013; Pratchayasakul et al., 2011b). Moreover, obesity has been shown to cause cognitive impairment as demonstrated by rats in the Morris water maze test (Pintana et al., 2012; Pipatpiboon et al., 2013) as well as impaired hippocampal synaptic function (Karimi et al., 2013; Stranahan et al., 2008).

Previous studies demonstrated that estrogen deprivation following a bilateral ovariectomy (OVX) caused impaired hippocampal synaptic function as indicated by decreased long-term potentiation (LTP) amplitude, dendritic spine density and synaptic proteins as well as cognitive impairment (Daniel et al., 1997; Luine et al., 1998). These impairments following OVX were alleviated by estrogen administration (Qu et al., 2013; Roseman et al., 2012; Sherwin, 2005). Although several studies demonstrated that either estrogen deprivation or obesity could impair

* Corresponding author at: Department of Oral Biology and Diagnostic Science, Faculty of Dentistry, Chiang Mai University; Neurophysiology Unit, Cardiac Electrophysiology Research and Training Center, Faculty of Medicine, Chiang Mai University, Chiang Mai 50200, Thailand. Fax: +66 11 66 53 222 844.
E-mail addresses: siriporn.c@cmu.ac.th, scchattipakorn@gmail.com (S.C. Chattipakorn).
[1] Co-first authors.

http://dx.doi.org/10.1016/j.yhbeh.2015.04.023
0018-506X/© 2015 Elsevier Inc. All rights reserved.

hippocampal synaptic function and cognitive function, it is still unclear how estrogen deprivation could affect brain insulin sensitivity and brain mitochondrial function. Moreover, whether obesity aggravates the impairment of and/or accelerates the development of peripheral and brain insulin sensitivity, oxidative stress, brain mitochondrial function, hippocampal synaptic function and cognitive behaviors under conditions of estrogen-deprivation have never been investigated. In the present study, the hypotheses tested were that: 1) estrogen deprivation alone causes the impairment of brain insulin sensitivity, brain mitochondrial function, hippocampal synaptic function and cognitive behaviors, and 2) obesity due to long-term HF consumption accelerates and aggravates those impairments in estrogen-deprived rats.

Materials and methods

Animal models and experimental protocols

All experimental protocols were approved by the Faculty of Medicine, Chiang Mai University Institutional Animal Care and Use Committee, in compliance with NIH guidelines. Female Wistar rats (200–220 g, n = 72) were obtained from the National Animal Center, Salaya Campus, Mahidol University, Thailand. All animals were housed individually in a temperature-controlled environment under a light–dark cycle of 12:12 h. One week after arrival, the rats were divided into sham-operated (S) and bilateral ovariectomized (O) groups. One week after surgery, rats were randomly assigned to either a normal diet (ND; 28.24% E protein, 51.99% E carbohydrates, 19.77% E fat) group, which received a standard laboratory pellet diet (CP 082; C.P. Company, Bangkok, Thailand) or a high-fat diet (HF; 26.45% E protein, 14.27% E carbohydrates, 59.28% E fat) group, which were fed a diet containing 59.28% total energy from fat as described in our previous study (Pratchayasakul et al., 2011b). All animals were given ad libitum access to food and water. At the end of weeks 4, 8 and 12, the locomotor activity test began 1 day prior to the first day of the spatial learning and memory behavior test. After that, the animals were allowed to rest for 1 day before an oral glucose tolerance test was performed. Then, animals were deeply anesthetized with isoflurane and killed by decapitation. Blood samples were collected for the determination of metabolic parameters. The brain was rapidly removed for electrophysiological study and biochemical analyses.

Ovariectomy procedure

Female rats were anesthetized using an intraperitoneal injection with xylazine (LBS Laboratories, Bangkok, Thailand; 0.15 ml/kg) and Zoletil (VirbacLabolatories, Carros, France; 50 mg/kg). The bilateral ovariectomy was performed through a midline dorsal section, through which the ovaries were removed and then the incision closed.

Chemical analysis for metabolic parameters

Fasting plasma glucose, HDL, LDL, cholesterol and triglyceride levels were determined using commercially available kits (ERBA diagnostic, Mannheim, Germany). The fasting plasma insulin levels were investigated using ELISA kits (LINCO Research, Missouri, USA). Serum estrogen levels were determined using an EIA kit (Cayman Chemical, Ann Arbor, Michigan, USA). All chemical analyses used to identify metabolic parameters were performed in duplicate in the same assay. The coefficient of variation for the intra- and inter-assays were 6.12% and 10.12% for glucose; 2.35% and 7.16% for HDL; 2.12% and 5.37% for LDL; 2.44% and 5.52% for cholesterol; 7.97% and 13.24% for triglycerides; 4.67% and 10.43% for insulin; and 6.10% and 9.88% for estrogen, respectively.

Table 1
The metabolic parameters in sham and OVX rats receiving either ND or HFD feeding for 4, 8 and 12 weeks.

Parameter	4 weeks				8 weeks				12 weeks			
	NDS	NDO	HFS	HFO	NDS	NDO	HFS	HFO	NDS	NDO	HFS	HFO
Body weight (g)	255.0 ± 4.3	285.8 ± 6.9	292.1 ± 9.6*	356.9 ± 16.8*†‡	275.5 + 6.8	310.0 ± 3.8*	307.3 ± 7.5*	387.1 ± 11.0*†‡	282.5 ± 3.9	334.3 ± 6.8*	328.1 ± 7.8*	418.1 ± 5.9*†‡
Visceral fat (g)	11.0 ± 1.3	9.3 ± 0.8	20.7 ± 1.6*†	22.1 ± 2.2*†	10.6 ± 1.2	14.2 ± 1.0*	25.1 ± 2.3*†	29.2 ± 2.0*†	11.3 ± 0.6	16.3 ± 1.7*	27.7 ± 2.3*†	33.4 ± 1.2*†‡
Uterus (g)	0.4 ± 0.0	0.1 ± 0.0*‡	0.3 ± 0.1	0.1 ± 0.0*‡	0.3 ± 0.0	0.1 ± 0.0*‡	0.4 ± 0.0	0.1 ± 0.0*‡	0.4 ± 0.0	0.1 ± 0.0*‡	0.4 ± 0.0	0.1 ± 0.0*‡
Food intake (g/day)	16.7 ± 1.0	16.1 ± 1.1	17.6 ± 4.4	18.5 ± 1.0	16.6 ± 0.9	15.9 ± 1.1	15.7 ± 0.7	16.1 ± 0.6	15.3 ± 0.7	14.2 ± 1.1	15.2 ± 0.4	15.4 ± 0.5
Glucose (mg %)	128.4 ± 6.7	125.6 ± 8.1	128.1 ± 10.6	128.3 ± 11.4	122.8 ± 7.3	133.6 ± 7.3	133.9 ± 6.8	148.8 ± 7.3*	122.7 ± 5.3	128.4 ± 10.8	127.6 ± 4.1	151.6 ± 6.8*†‡
Cholesterol (mg/dl)	93.2 ± 6.4	104.0 ± 8.6	103.9 ± 9.9	101.1 ± 12.7	107.3 ± 5.0	111.6 ± 4.5	132.1 ± 17.0*	137.2 ± 2.5*†	92.9 ± 5.1	112.1 ± 12.1	137.6 ± 11.5*†	146.4 ± 12.1*†
Triglyceride (mg/dl)	34.0 ± 3.6	32.2 ± 3.5	33.7 ± 3.6	31.6 ± 3.7	47.7 ± 2.6	45.7 ± 4.6	47.8 ± 3.3	46.3 ± 4.8	40.8 ± 3.2	43.8 ± 3.6	43.0 ± 3.3	40.5 ± 6.2
HDL (mg/dl)	5.6 ± 0.32	6.0 ± 0.1	5.6 ± 0.5	5.7 ± 0.4	6.4 ± 0.2	6.6 ± 0.2	6.2 ± 0.2	6.38 ± 0.8	5.7 ± 0.3	5.7 ± 0.2	5.7 ± 0.2	5.8 ± 0.3
LDL (mg/dl)	76.2 ± 3.8	82.7 ± 6.6	75.9 ± 8.5	70.4 ± 8.9	76.3 ± 5.7	87.6 ± 3.6	92.4 ± 5.0*	122.3 ± 2.8*†‡	68.7 ± 5.5	69.0 ± 1.9	113.1 ± 17.3*†	131.1 ± 16.0*†
Insulin (ng/ml)	0.8 ± 0.1	0.8 ± 0.1	0.9 ± 0.2	1.0 ± 0.1	0.9 ± 0.1	1.4 ± 0.2*	1.5 ± 0.2*	1.6 ± 0.2*	0.9 ± 0.1	1.5 ± 0.3*	1.4 ± 1.2*	1.5 ± 0.2*
HOMA index	6.3 ± 1.6	6.1 ± 0.1	7.1 ± 1.4	7.6 ± 1.3	5.6 ± 1.1	11.14 ± 1.70*	12.4 ± 1.9*	12.6 ± 1.5*	7.3 ± 1.8	13.5 ± 2.4*	13.8 ± 2.7*	13.9 ± 2.0*
Serum estrogen (pg/ml)	167.8 ± 39.3	58.7 ± 17.5*‡	151.9 ± 21.2†	63.2 ± 20.6*‡	114.7 ± 12.1	53.29 ± 1.99*‡	117.2 ± 16.9	58.4 ± 3.7*‡	129.4 ± 17.8	63.9 ± 6.5*‡	127.2 ± 7.4†	71.3 ± 6.9*‡
Serum MDA (μM)	3.4 ± 0.6	3.4 ± 0.4	3.5 ± 0.3	3.45 ± 0.33	3.9 ± 0.1	4.19 ± 0.15*	4.1 ± 0.1*	4.8 ± 0.3*†‡	3.39 ± 0.16	4.1 ± 0.2*	4.0 ± 0.1*	4.9 ± 0.2*†‡
Brain MDA (μM)	4.7 ± 0.1	4.6 ± 0.1	4.9 ± 0.1	4.61 ± 0.07	5.7 ± 1.3	8.10 ± 0.13*	7.9 ± 0.1*	9.8 ± 0.4*†‡	5.38 ± 1.19	8.0 ± 0.3*	7.9 ± 0.4*	10.1 ± 0.8*†‡

Data was presented as mean ± SEM. *, $p < 0.05$ compared with NDS, †, $p < 0.05$ compared with NDO, ‡, $p < 0.05$ compared with HFS; n = 5–6/group; NDS: sham ND-fed rats, NDO: ovariectomized ND-fed rats, HFS: sham HFD-fed rats, HFO: ovariectomized HFD-fed rat.

Determination of insulin resistance

Insulin resistance was evaluated using the Homeostasis Model Assessment (HOMA) index (Matthews et al., 1985) and the total area under the curve of the oral glucose tolerance test (OGTT) as described in our previous study (Pratchayasakul et al., 2011b). HOMA was calculated from fasting plasma insulin and fasting plasma glucose concentrations. A higher HOMA index indicated a higher degree of insulin resistance. The HOMA index was determined using the following equation: [(fasting plasma insulin μU/ml) × (fasting plasma glucose mmol/l)] / 22.5.

In addition, the OGTT was investigated at the end of weeks 4, 8 and 12 of the dietary periods. Briefly, the animals were fasted for 12 h before they underwent an OGTT. An OGTT consisted of 2 g/kg body weight glucose feeding by gavage. Blood was collected from a small cut at the tip of the tail immediately before and at 15, 30, 60 and 120 min after glucose feeding. The plasma was utilized for the investigation, and glucose analysis was performed with a commercially available kit (Biotech, Bangkok, Thailand).

Determination of malondialdehyde (MDA) levels

The MDA level was determined by a high performance liquid chromatography method following the protocol used in the previous study (Candan and Tuzmen, 2008).

Extracellular recordings of hippocampal slices for insulin-induced LTD and electrical-induced LTP

Brain slice preparation for extracellular recordings was performed following the guidelines in the previous study (Chattipakorn and McMahon, 2002). Field excitatory postsynaptic potentials (fEPSPs) were recorded according to our previous protocol (Pratchayasakul et al., 2011a,2011b). In the LTD protocol, hippocampal slices were perfused with aCSF for 10 min. as a baseline. After that, the insulin-induced LTD condition was created by perfusion with aCSF plus 500 nM insulin (Humulin R, Eli Lilly, Giessen, Germany) for an additional 10 min, and then the slices were perfused with aCSF for a further 50 min. In the LTP protocol, LTP was induced by delivering high-frequency stimulation (HFS; 4 trains at 100 Hz; 0.5 s duration; 20 s interval). Experiments were performed at least 40 min after HFS. The amount of potentiation was calculated at 40 min after HFS.

Immunoblotting

The subsequent brain homogenates for immunoblotting were prepared as described in our previous study (Pratchayasakul et al., 2011b). Briefly, brain homogenates for immunoblotting were prepared by incubating whole brain slices into aCSF or aCSF plus 500 nM insulin (Humulin R, Eli Lilly, Giessen, Germany) for 5 min. After that, whole brain slices in each conditioned group were homogenized, and used for further immunoblotting. IR protein, Akt/PKB protein, IR tyrosine phosphorylation and Akt/PKB at serine 473 kinases phosphorylation were analyzed by electrophoresis and immunoblotting was carried out with rabbit antibodies for the IR (Santa Cruz Biotechnology, CA, USA; sc-711; 1:1000), Akt/PKB (Cell Signaling Technology, MA, USA; #9272; 1:1000), IR at tyrosine (Santa Cruz Biotechnology, CA, USA; sc-25103-R; 1:1000) and Akt/PKB at serine 473 (Cell Signaling Technology, MA, USA; #9271; 1:1000), respectively. All blots were incubated with a horseradish peroxidase conjugated anti-rabbit secondary antibody (1:2000, Cell Signaling Technology, MA, USA). The protein bands were developed with Amersham hyperfilm ECL (GE Healthcare, Buckinghamshire, UK).

Brain mitochondrial function

After decapitation, the brain tissue was transferred into 10 ml of ice-cold MSE-nagarse solution and homogenized at 600 rpm/min

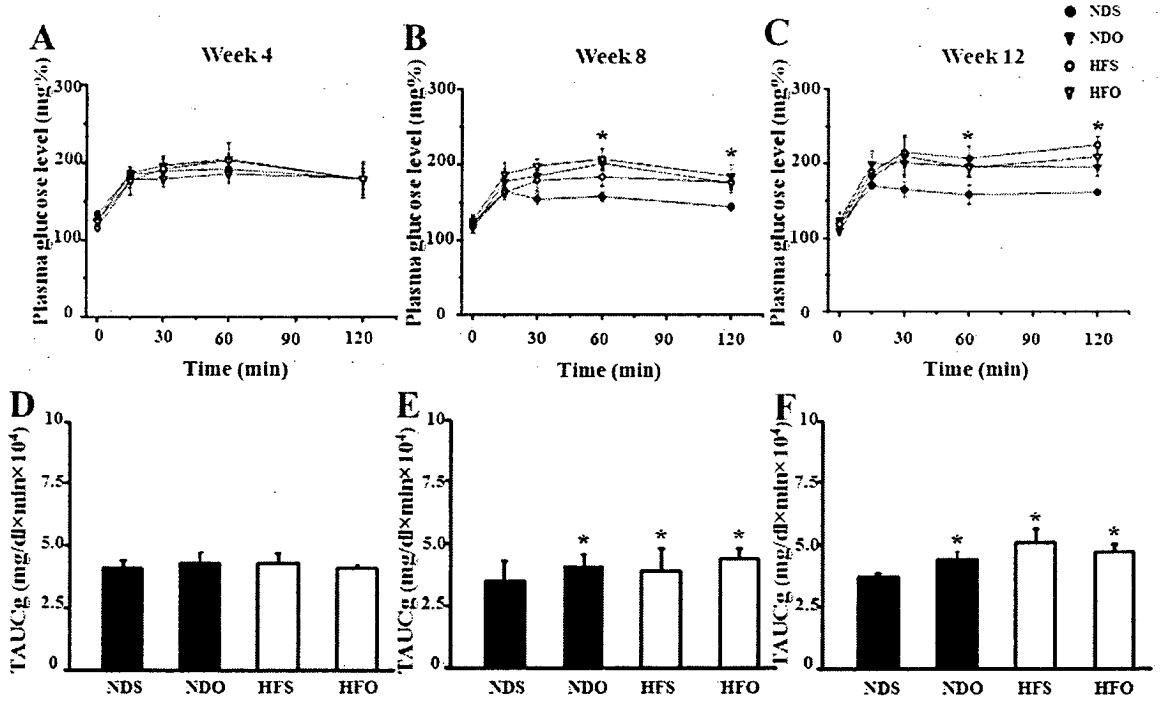


Fig. 1. Glucose response during oral glucose tolerance test from NDS, NDO, HFS and HFO at 4 weeks (A), 8 weeks (B) and 12 weeks (C); and total area under the curve of plasma glucose during an oral glucose tolerance test (TAUCg) from NDS, NDO, HFS and HFO at 4 weeks (D), 8 weeks (E) and 12 weeks (F); *, $p < 0.05$ compared with NDS; n = 5–6/group.

using a homogenizer. The subsequent brain mitochondrial isolation was prepared as described in our previous study (Pipatpiboon et al., 2012). Brain mitochondrial function was determined using a brain mitochondrial reactive oxygen species (ROS) assay, a brain mitochondrial membrane potential ($\Delta\Psi m$) assay and a brain mitochondrial swelling assay. The details of brain mitochondrial function were previously described (Pipatpiboon et al., 2012).

Golgi impregnation and analysis

Since increased dendritic spine density has been reported to be related to LTP expression (Bramham, 2008; Hill and Zito, 2013), we therefore aimed to investigate the dendritic spine density in our experiment. After decapitation, brains were removed and rinsed with double distilled water, and they were then processed for Golgi staining using a commercially available kit (FD Neurotechnologies kit, PK 401, Ellicott City, USA). The details of dendritic spine density analysis were previously described (Sripetchwandee et al., 2014). Briefly, two segments from a pyramidal cell in the CA1 area of the hippocampus were randomly measured. This was the same area for fEPSP recording in our extracellular recordings of hippocampal slices for insulin-induced LTD and electrical-induced LTP. Both segments were located on the tertiary apical dendrites and were viewed through an inverted microscope (IX-81, Olympus, Tokyo, Japan). Three neuronal cells from each brain slice were selected for quantitative analysis (3 slices/animals, n 5–6 animals/group). The number of spines was counted using a hand counter, and the dendritic lengths were measured using Xcellence imaging software (Olympus, Tokyo, Japan).

Morris water maze test (MWM)

In this study, the protocol of MWM was modified from a previous study (Vorhees and Williams, 2006). This experiment determined learning and memory ability with two different types of MWM, acquisition test (hidden platform) and probe trial test (removal of the platform from the water pool) as described in our previous study (Pintana et al., 2012). In the acquisition test, rats were trained to navigate a route to the platform in 4 trials/day for 5 days, with an inter-trial interval of 15 s. For each trial, rats were given 120 s to find the platform, and the time taken to reach the platform was recorded. In the probe trial test, the platform was removed, and the time spent in the target quadrant was recorded. After testing was completed, times taken to reach the platform, times spent in the target quadrant, and swim speeds were calculated using Smart 3.0 software (Panlab, Harvard Apparatus, Barcelona, Spain). In addition, the open-field test was developed to determine the locomotor activity, and was modified from the method used by Arakawa (Arakawa, 2005). The open field consisted of a black platform with a 75 cm × 75 cm floor and 40-cm walls. The box floor was drawn with white lines (6 mm) to form 25 equal squares. The animals were placed into the box and observed for 2 min. The numbers of lines which the animals crossed were counted as a representation of locomotor activity.

Statistical methods

Data was presented as mean ± SEM. All statistical analyses were performed using the program SPSS (version 17; SPSS, Chicago, Ill., USA). The significance of the difference in all parameters was calculated using a two-way ANOVA (diet X surgery) followed by post-hoc Fisher's protected least significant difference (LSD) test. A two-way ANOVA with repeated measurements was used to compare the training trials of the MWM test. For the main effects, the effect sizes were calculated using Eta-squared, η^2. For all comparisons, a value of $p < 0.05$ was considered to be statistically significant.

Results

A High-fat diet aggravated the impairment of peripheral insulin sensitivity under estrogen-deprived conditions

Initial animal body weight, plasma glucose and plasma insulin levels showed no significant difference between all groups. The effects of the ovariectomy were confirmed by determining uterine weight and serum estrogen levels at the end of 4, 8 and 12-weeks of the dietary periods. The ovariectomy resulted in a decrease in uterine weight and serum estrogen levels in both the ND and HF rats (for uterine weight: $F(1,52) = 203.44$, $p < 0.001$, $\eta^2 = 0.69$ at 4 weeks; $F(1,45) = 210.87$, $p < 0.001$, $\eta^2 = 0.29$ at 8 weeks; $F(1,49) = 205.56$, $p < 0.001$, $\eta^2 = 0.74$ at 12 weeks; for estrogen: $F(1,31) = 40.28$, $p < 0.001$, $\eta^2 = 0.47$ at 4 weeks; $F(1,24) = 34.68$, $p < 0.001$, $\eta^2 = 0.61$ at 8 weeks; $F(1,27) = 35.92$, $p < 0.001$, $\eta^2 = 0.56$ at 12 weeks; Table 1).

At the end of week four, sham-operated HF-fed rats (HFS) and ovariectomized HF-fed rats (HFO) had significantly increased body weight and visceral fat compared to sham ND-fed rats (NDS) and ovariectomized ND-fed rats (NDO) ($F(1,14) = 20.64$, $p < 0.001$, $\eta^2 = 0.65$ for body weight; $F(1,49) = 41.34$, $p < 0.001$, $\eta^2 = 0.67$ for visceral fat; Table 1). However, the levels of glucose, cholesterol, triglyceride, HDL, LDL, insulin, HOMA index and the total area under the glucose curve (TAUCg) from the OGTT showed no significant difference between groups (Table 1 and Figs. 1A, D).

By weeks 8 and 12, the NDO, HFS and HFO rats had developed obesity, indicated by increased body weight and visceral fat (for body

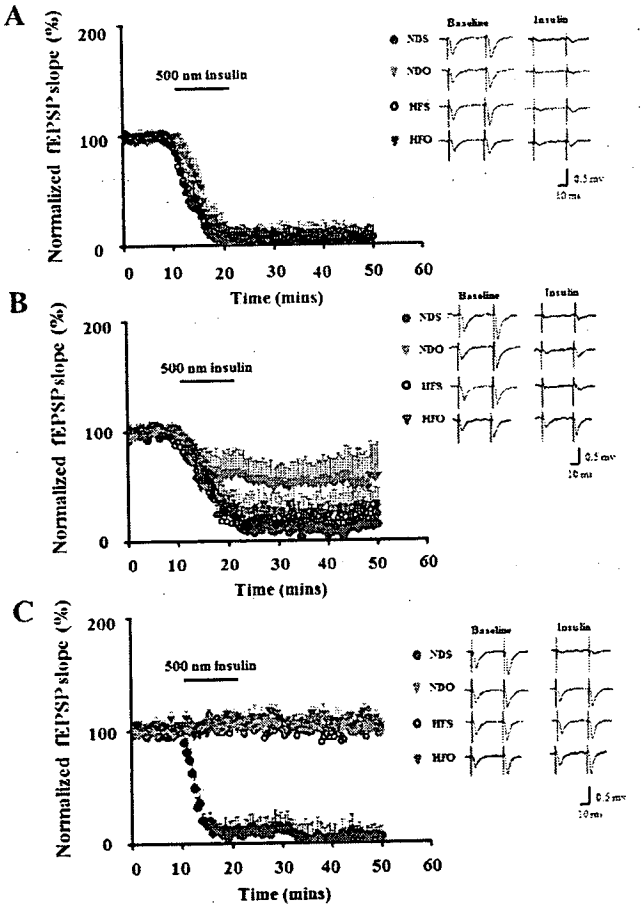


Fig. 2. The degree of insulin-mediated LTD observed from hippocampal slices of NDS, NDO, HFS and HFO at 4 weeks (A), 8 weeks (B) and 12 weeks (C); (n = 5–7 independent slices, n = 6 animals/group).

weight: $F(1,51) = 53.51$, $p < 0.001$, $\eta^2 = 0.65$ at 8 weeks; $F(1,51) = 123.72$, $p < 0.001$, $\eta^2 = 0.61$ at 12 weeks; for visceral fat: $F(1,43) = 48.04$, $p < 0.001$, $\eta^2 = 0.63$ at 8 weeks; $F(1,46) = 111.45$, $p < 0.001$, $\eta^2 = 0.65$ at 12 weeks; Table 1), and the impairment of peripheral insulin sensitivity, demonstrated by an increase in insulin level, HOMA index and TAUCg, when compared with the NDS rats (for insulin: $F(1,34) = 4.38$, $p = 0.044$, $\eta^2 = 0.19$ at 8 weeks; $F(1,93) = 3.95$, $p = 0.047$, $\eta^2 = 0.13$ at 12 weeks; for HOMA: $F(1,32) = 5.84$, $p = 0.022$, $\eta^2 = 0.26$ at 8 weeks; $F(1,35) = 4.15$, $p = 0.048$, $\eta^2 = 0.12$ at 12 weeks; for TAUCg: $F(1,16) = 5.11$, $p = 0.038$, $\eta^2 = 0.17$ at 8 weeks; $F(1,29) = 17.14$, $p = 0.001$, $\eta^2 = 0.54$ at 12 weeks; Table 1 and Figs. 1B, C, E, F). In addition, plasma LDL and cholesterol levels of the HFS and HFO rats showed a significant increase when compared to those of the NDS rats (for LDL: $F(1,15) = 25.81$, $p < 0.001$, $\eta^2 = 0.72$ at 8 weeks; $F(1,23) = 13.72$, $p = 0.001$, $\eta^2 = 0.41$ at 12 weeks; for cholesterol: $F(1,29) = 9.50$, $p = 0.004$, $\eta^2 = 0.37$ at 8 weeks; $F(1,35) = 8.47$, $p = 0.006$, $\eta^2 = 0.20$ at 12 weeks; Table 1). Interestingly, these impaired metabolic parameters were highest in the HFO rats ($p < 0.05$; Table 1). These findings at weeks 8 and 12 suggest that either estrogen deprivation alone or a high-fat diet alone impaired peripheral insulin sensitivity, and that high-fat diet aggravated the severity of that impairment under conditions of estrogen-deprivation.

A high-fat diet accelerated the impairment of brain insulin sensitivity under conditions of estrogen-deprivation

At week four, the degree of insulin-induced LTD detected from brain slices of the NDS, NDO, HFS and HFO rats showed no statistically significant difference between the groups (Fig. 2A). At week eight, the degree of insulin-induced LTD was significantly reduced in HFO rats compared to that of the NDS, NDO and HFS rats ($F(1,19) = 6.42$, $p = 0.020$, $\eta^2 = 0.34$, Fig. 2B). At week 12, insulin-induced LTD was diminished in the NDO, HFS and HFO rats ($F(1,19) = 63.48$, $p < 0.001$, $\eta^2 = 0.91$, Fig. 2C).

In addition to insulin-induced LTD, brain insulin signaling was determined. At the end of weeks 4, 8 and 12, the expression of IR and Akt/PKB proteins showed no statistically significant difference between the groups (Figs. 3A–C, 4A–C). At week four, the levels of tyrosine phosphorylation of IR and Akt/PKB phosphorylation at the serine 473 site were also not significantly different (Figs. 3D, 4D). However, at week 8 the levels of tyrosine phosphorylation of IR (pIR) and Akt/PKB phosphorylation at the serine 473 site (Akt-ser) were significantly decreased in the HFO rats, when compared with those of the NDS, NDO and HFS rats ($F(1,13) = 4.87$, $p = 0.041$, $\eta^2 = 0.58$ for pIR; $F(1,8) = 5.71$, $p = 0.044$, $\eta^2 = 0.11$ for Akt-ser; Figs. 3E, 4E). At week 12, the levels of tyrosine phosphorylation of IR and Akt/PKB phosphorylation at the serine 473 site of the NDO, HFS and HFO rats were significantly reduced compared with those of the NDS rats ($F(1,39) = 4.11$, $p = 0.048$, $\eta^2 = 0.48$ for pIR; $F(1,23) = 8.42$, $p = 0.010$, $\eta^2 = 0.60$ for Akt-ser; Figs. 3F, 4F). These findings suggest that either estrogen deprivation alone or a high-fat diet alone impaired brain insulin sensitivity, and that a high-fat diet accelerated that impairment under estrogen-deprived conditions.

A high-fat diet accelerated the impairment of brain mitochondrial function under estrogen-deprived condition

Brain mitochondria play an important role in the regulation of Ca^{2+}, synaptic plasticity and neuronal survival (Mattson et al., 2008). Previous studies demonstrated that mitochondrial dysfunction affected learning and memory in several models including streptozotocin (STZ)-induced diabetic rats (Ye et al., 2011), old-age female rats (Platano et al., 2008) and HFD-fed rats (Pintana et al., 2012). Therefore, this study investigated the effects of a high-fat diet on brain mitochondrial function under conditions of estrogen deprivation. We found that brain mitochondrial function was not significantly different between groups at week four (Figs. 5A, D, G). At week eight, brain mitochondrial dysfunction occurred in the HFO rats as indicated by increased brain mitochondrial ROS production, brain mitochondrial membrane depolarization and brain mitochondrial swelling, when compared with the NDS rats ($F(1,9) = 5.24$, $p = 0.041$, $\eta^2 = 0.55$ for mitochondrial ROS production; $F(1,13) = 4.79$, $p = 0.046$, $\eta^2 = 0.22$ for mitochondrial membrane depolarization; $F(1,32) = 4.92$, $p = 0.041$, $\eta^2 = 0.29$ for mitochondrial swelling; Figs. 5B, E, H). At week 12, brain mitochondrial dysfunction was observed in the NDO, HFS and HFO rats ($F(1,16) = 5.24$, $p =$

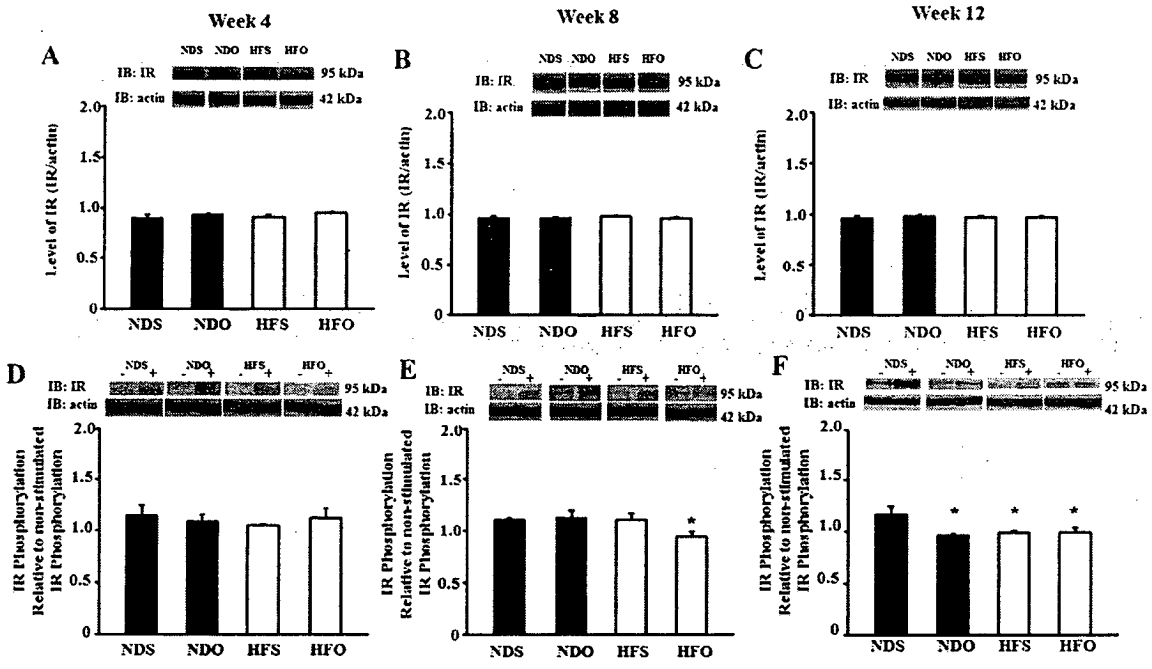


Fig. 3. Representative blots of IR protein in brain slices harvested from the NDS, NDO, HFS and HFO rats at 4 weeks (A), 8 weeks (B) and 12 weeks (C). Representative blots of IR tyrosine phosphorylation in brain slices harvested from NDS, NDO, HFS and HFO rats at 4 weeks (D), 8 weeks (E) and 12 weeks (F); *, $p < 0.05$ compared with NDS; n = 5–6/group; −, no insulin stimulation; +, insulin stimulation.

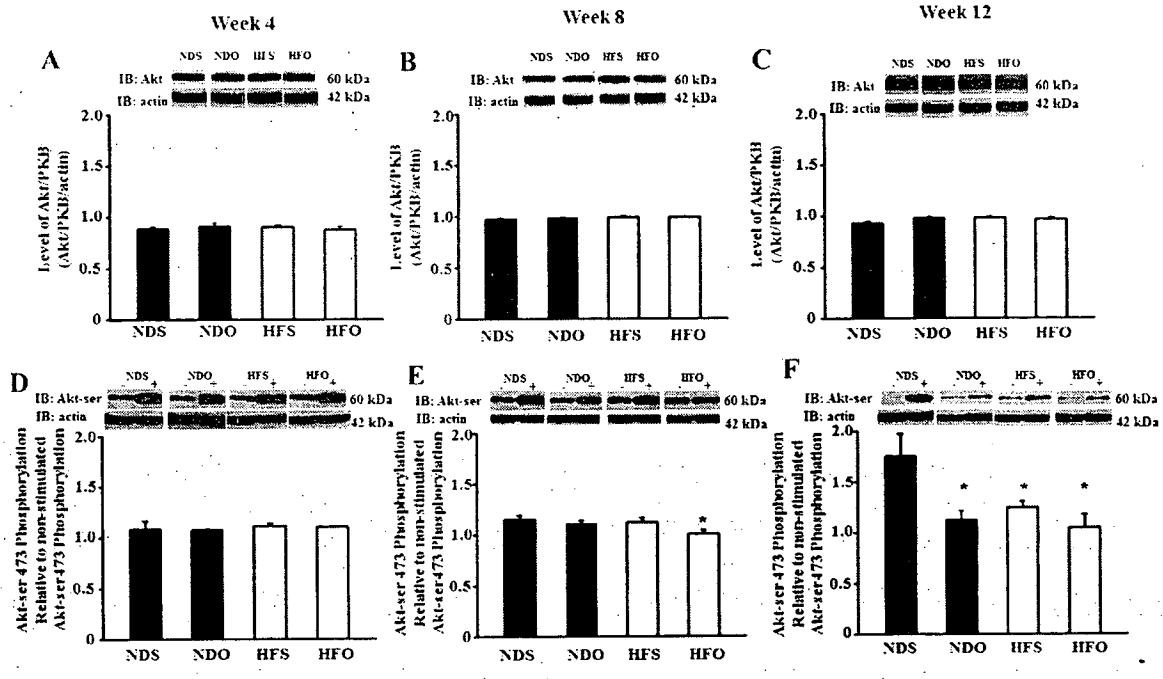


Fig. 4. Representative blots of protein level of Akt/PKB in brain slices harvested from the NDS, NDO, HFS and HFO rats at 4 weeks (A), 8 weeks (B) and 12 weeks (C). Representative blots of Akt/PKB phosphorylation at the serine 473 site in brain slices harvested from NDS, NDO, HFS and HFO rats at 4 weeks (D), 8 weeks (E) and 12 weeks (F); *, $p < 0.05$ compared with NDS; n = 5–6/group; −,no insulin stimulation; +, insulin stimulation.

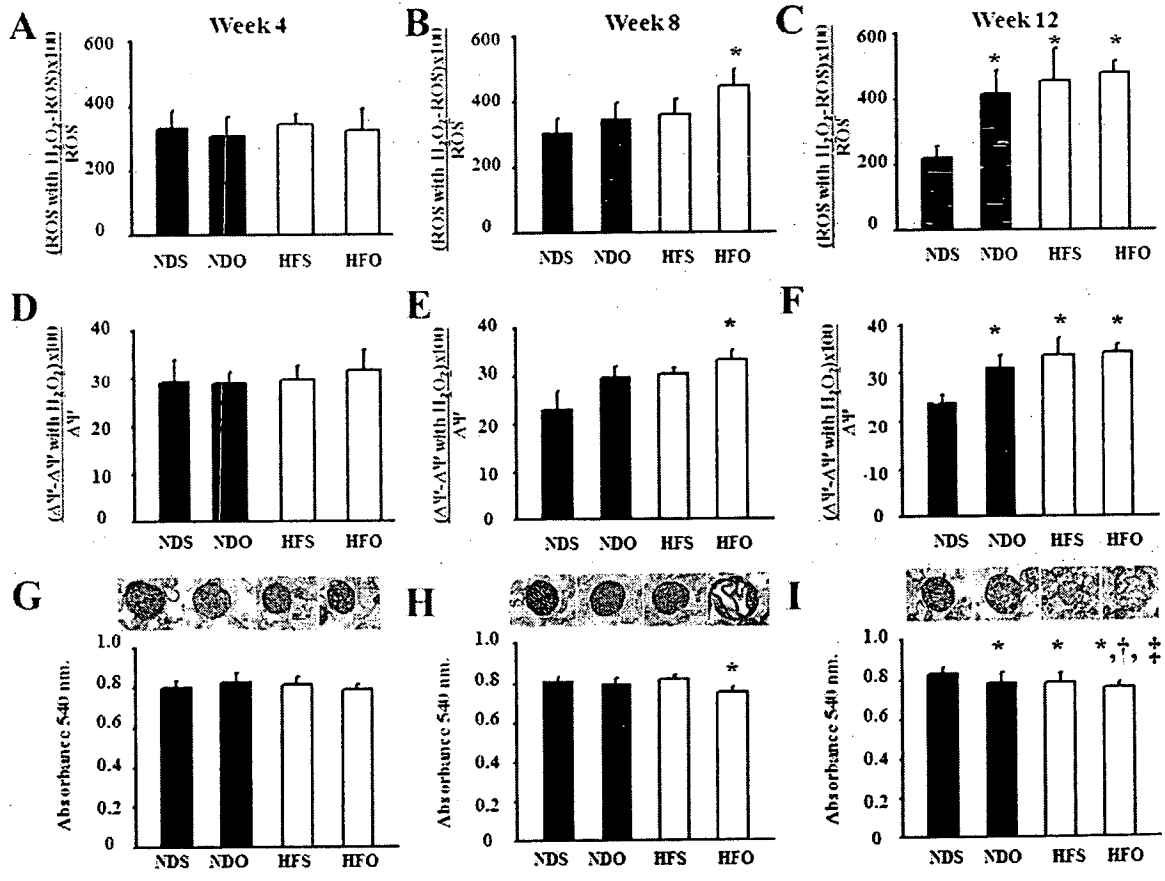


Fig. 5. Brain mitochondrial ROS production from the NDS, NDO, HFS and HFO rats at 4 weeks (A), 8 weeks (B) and 12 weeks (C); Brain mitochondrial membrane potential change ($\Delta\psi_m$) from the NDS, NDO, HFS and HFO rats at 4 weeks (D), 8 weeks (E) and 12 weeks (F); Brain mitochondrial swelling and transmission electron microscopy (original magnification ×25,000) shows the ultrastructure of brain mitochondria from the NDS, NDO, HFS and HFO rats at 4 weeks (G), 8 weeks (H) and 12 weeks (I); *, $p < 0.05$ compared with NDS, †, $p < 0.05$ compared with NDO, ‡, $p < 0.05$ compared with HFS; n = 5–6/group.

0.036, $\eta^2 = 0.36$ for mitochondrial ROS production; $F(1,27) = 7.51$, $p = 0.021$, $\eta^2 = 0.21$ for mitochondrial membrane depolarization; $F(1,26) = 13.94$, $p = 0.001$, $\eta^2 = 0.42$ for mitochondrial swelling; Figs. 5C, F, I). In addition, the degree of brain mitochondrial swelling was greatest in the HFO rats ($p < 0.05$; Fig. 5I). Also this disruption in brain mitochondrial morphology, indicated by unfolding and swelling, was observed earlier (at week eight) in the HFO rats, and later at week 12 in the NDO and HFS rats (Figs. 5H, I). These findings suggest that either estrogen deprivation alone or a high-fat diet alone caused the impairment of brain mitochondrial function, and that a high-fat diet accelerated that impairment under estrogen-deprived conditions.

A high-fat diet aggravated an increase in serum and brain oxidative stress under conditions of estrogen-deprivation

In addition to brain mitochondrial dysfunction, serum and brain oxidative stress levels were investigated. At week 4, serum and brain MDA levels were not significantly different between groups. However, at weeks 8 and 12, serum and brain MDA levels in the NDO, HFS and HFO rats were significantly increased, when compared with NDS rats (for serum MDA: $F(1,26) = 10.54$, $p = 0.003$, $\eta^2 = 0.63$ at 8 weeks; $F(1,28) = 24.54$, $p < 0.001$, $\eta^2 = 0.48$ at 12 weeks; for brain MDA: $F(1,14) = 7.84$, $p = 0.021$, $\eta^2 = 0.50$ at 8 weeks; $F(1,14) = 10.78$, $p = 0.005$, $\eta^2 = 0.60$ at 12 weeks; Table 1). Interestingly, the serum and brain MDA levels in the HFO rats were significantly higher than that of the NDO and HFS rats ($p < 0.05$; Table 1). These results suggest that either estrogen deprivation alone or a high-fat diet alone leads to increased serum and brain oxidative stress, and that a high-fat diet aggravated the severity of oxidative stress under estrogen-deprived conditions.

A high-fat diet aggravated the impairment of hippocampal synaptic plasticity under conditions of estrogen-deprivation

Several studies have demonstrated that the impairment of hippocampal synaptic plasticity was influenced by oxidative stress (Massaad and Klann, 2011; Ye, 2013). Therefore, hippocampal synaptic plasticity, including electrical-induced LTP as well as the dendritic spine density, was determined. At week four, the degree of electrical-mediated LTP, which was calculated using hippocampal slices of the NDS, NDO, HFS and HFO rats, was not significantly different (Fig. 6A). In addition, the number of dendritic spines in the CA1 hippocampus was not significantly different between groups (Fig. 7A).

At weeks 8 and 12, electrical-induced LTP of the NDO, HFS and HFO rats was significantly decreased, when compared with that of NDS rats ($F(1,11) = 22.70$, $p = 0.001$, $\eta^2 = 0.52$ at 8 weeks; $F(1,17) = 14.90$, $p = 0.001$, $\eta^2 = 0.44$ at 12 weeks; Figs. 6B, C). In addition, the electrical-induced LTP of the HFO rats was significantly attenuated, when compared with that of the NDO and HFS rats ($p < 0.05$; Figs. 6B, C). The density of dendritic spines in the CA1 hippocampus of the NDO, HFS and HFO rats was significantly decreased, when compared with that of the NDS rats ($F(1,12) = 15.60$, $p = 0.002$, $\eta^2 = 0.78$ at 8 weeks; $F(1,18) = 27.09$, $p < 0.001$, $\eta^2 = 0.85$ at 12 weeks; Figs. 7B, C). Interestingly, the number of dendritic spines in the HFO rats was the lowest among all groups ($p < 0.05$; Figs. 7B, C). These findings suggest that either estrogen deprivation alone or a high-fat diet alone impairs the hippocampal synaptic plasticity, and that a high-fat diet aggravates that impairment under conditions of estrogen-deprivation.

A high-fat diet accelerated the impairment of cognitive function under conditions of estrogen-deprivation

Before the MWM test at each time period, the locomotor activity of all groups was determined using the open-field test. The number of lines that the rats crossed during the test was not significantly different between all groups. This finding indicates that the locomotor activity of all groups before the cognitive test was not significantly different.

The time to reach the platform in the acquisition test from the first to the fifth day of training in all experimental groups significantly decreased ($F(4,27) = 23.87$, $p < 0.001$, $\eta^2 = 0.36$ at 4 weeks, $F(4,20) = 17.88$, $p < 0.001$, $\eta^2 = 0.27$ at 8 weeks, $F(4,22) = 19.08$, $p < 0.001$, $\eta^2 = 0.49$ at 12 weeks; Figs. 8A,B,C). However, the learning and memory tests were not significantly different between groups at week 4 (Figs. 8A, D). At week 8, the mean time to reach the platform during the acquisition test of the HFO rats was significantly increased, when compared with that of the NDS, NDO and HFS rats ($F(1,22) = 6.08$, $p = 0.022$, $\eta^2 = 0.29$; Fig. 8B). In addition, the mean time spent in the target quadrant during the probe test of the HFO rats was significantly decreased, when compared with that of the NDS, NDO and HFS rats ($F(1,78) = 3.97$, $p = 0.046$, $\eta^2 = 0.29$; Fig. 8E).

At week 12, decreased learning and memory behaviors of the NDO, HFS and HFO rats were observed (Figs. 8C, F), as indicated by the increased mean time to reach the platform during the acquisition test ($F(1,24) = 7.56$, $p = 0.036$, $\eta^2 = 0.23$; Fig. 8C), and the decreased mean time spent in the target quadrant during the probe test ($F(1,24) = 4.73$, $p = 0.040$, $\eta^2 = 0.26$; Fig. 8F). In addition, the swim speed of each rat was recorded, and there were no significant differences in the swim speed between all groups (24.71 ± 1.89, 23.71 ± 1.61, 23.04 ± 2.20 and 25.83 ± 1.20 cm/s, in NDS, NDO, HFS and HFO, respectively). These findings confirmed that the impairment of cognitive function was due to spatial memory deficit, instead of the differences in weight and fat content of the animals. All of these findings indicate that either estrogen deprivation alone or a high-fat diet alone impairs the learning and memory behaviors, and that a high-fat diet

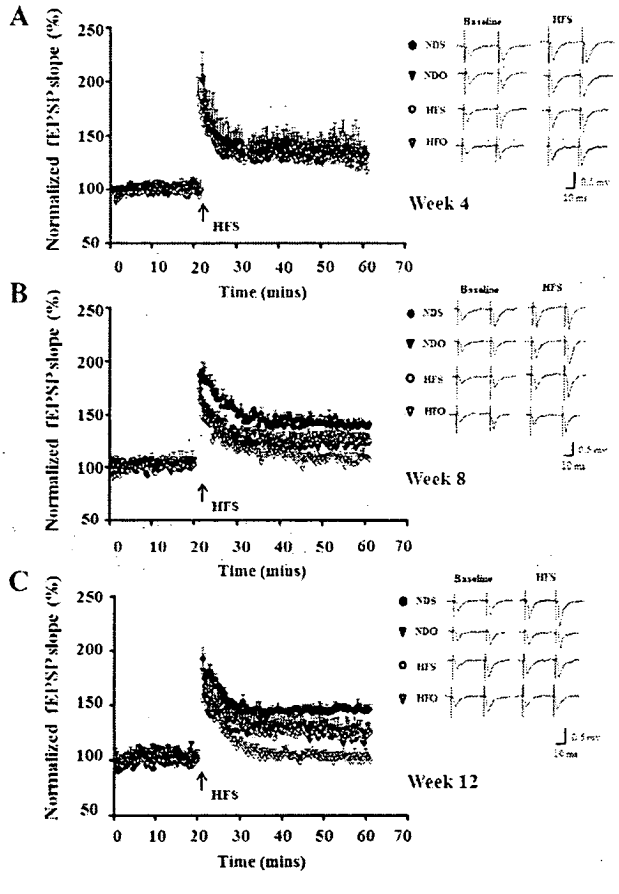


Fig. 6. The degree of electrical-mediated LTP observed from hippocampal slices of NDS, NDO, HFS and HFO at 4 weeks (A), 8 weeks (B) and 12 weeks (C); (n = 5–7 independent slices, n = 6 animals/group).

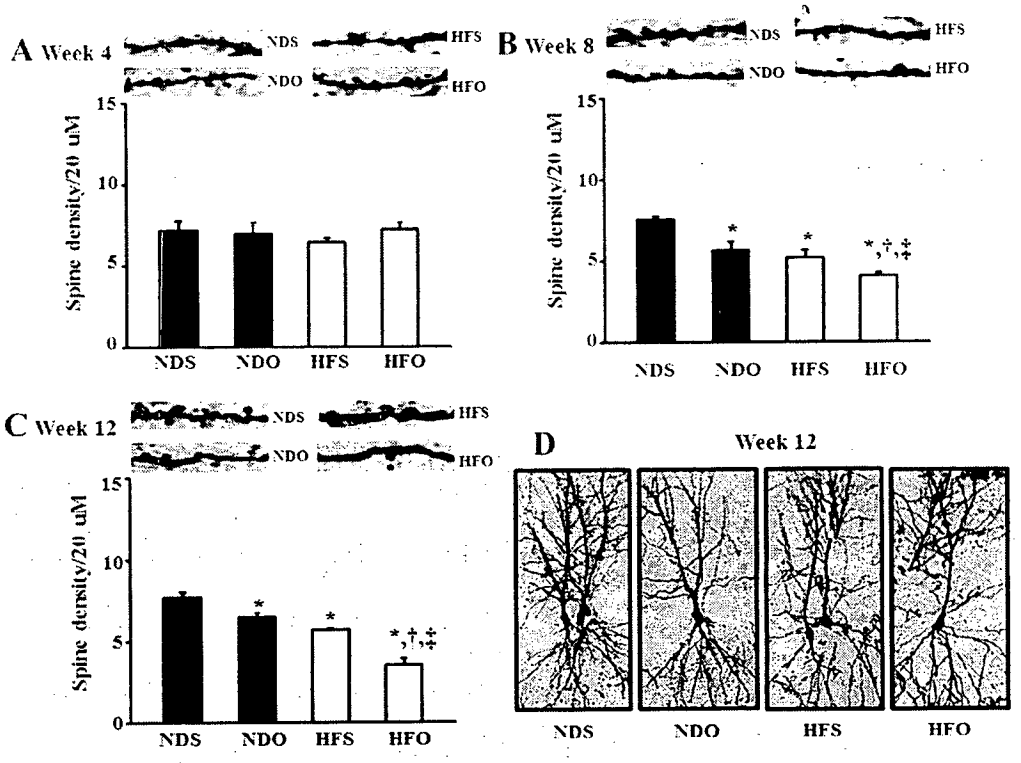


Fig. 7. The number of dendritic spines on tertiary dendrites in apical dendrite from the NDS, NDO, HFS and HFO rats at 4 weeks (A), 8 weeks (B) and 12 weeks (C); a picture of a representative neuron from 12 weeks of NDO, HFS and HFO rats (D) *, $p < 0.05$ compared with NDS, †, $p < 0.05$ compared with NDO, ‡, $p < 0.05$ compared with HFS; n = 5–6/group.

accelerates the cognitive impairment under conditions of estrogen-deprivation.

Discussion

The major findings of this study are as follows: 1) impaired peripheral insulin sensitivity was initially observed at week 8 in the NDO, HFS, and HFO rats; 2) the impairment of brain insulin sensitivity, indicated by the reduction of insulin-induced LTD, and brain insulin signaling, as well as brain mitochondrial dysfunction occurred earlier (at week 8) in the HFO rats, and was found later at week 12 in the NDO, HFS and HFO rats; 3) the occurrence of oxidative stress and hippocampal synaptic dysfunction was initially observed at week 8 in the NDO, HFS and HFO rats; 4) the impaired cognitive function developed earlier (at week

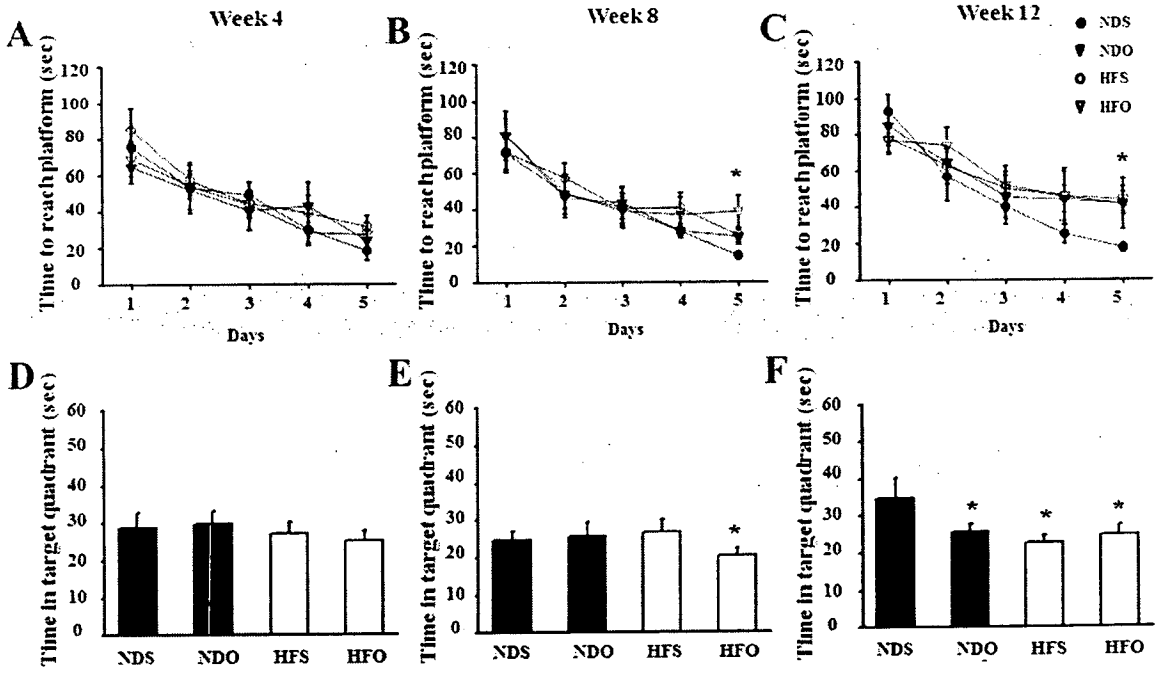


Fig. 8. Time to reach platform in acquisition test from the NDS, NDO, HFS and HFO rats at 4 weeks (A), 8 weeks (B) and 12 weeks (C); Time spent in target quadrant in probe test from the NDS, NDO, HFS and HFO rats at 4 weeks (D), 8 weeks (E) and 12 weeks (F); *, $p < 0.05$ compared with NDS; n = 5–6/group.

8) in the HFO group, and was found later at week 12 in the NDO and HFS groups; 5) either estrogen deprivation alone or a high-fat diet alone caused impaired peripheral insulin sensitivity, reduced brain insulin sensitivity, brain mitochondrial dysfunction, hippocampal synaptic dysfunction and cognitive impairment; 6) a high-fat diet significantly accelerated and aggravated the severity of these deleterious effects under conditions of estrogen-deprivation.

Previous studies demonstrated that either a high-fat diet alone or estrogen deprivation alone could impair peripheral insulin sensitivity (Funaki, 2009; Mauvais-Jarvis et al., 2013; Pratchayasakul et al., 2011b). Our previous studies (Pipatpiboon et al., 2012; Pratchayasakul et al., 2011b) and the present study confirmed that obesity induced by HF consumption impaired peripheral insulin sensitivity, as indicated by increased body weight, visceral fat, plasma glucose level, plasma insulin level, HOMA index, and the total area under the curve (TAUCg). In addition, it has been shown that estrogen deprivation alone also caused obesity, leading to the development of peripheral insulin resistance (Alonso et al., 2006; Babaei et al., 2010). Consistent with those studies, this study showed that 8 weeks after a bilateral ovariectomy, rats had both increased body weight and visceral fat, leading to reduced peripheral insulin sensitivity. Interestingly, the severity of impaired peripheral insulin sensitivity in rats on a high-fat diet and estrogen deprived rats was significantly greater than rats with a high-fat diet alone or with estrogen deprivation alone. These findings suggest that a high-fat diet aggravates the severity of peripheral insulin resistance in estrogen-deprived rats. On consideration of these findings, it is therefore possible that a high-fat diet on top of estrogen deprivation could lead to the development of Type II diabetes, as indicated in this study by the increased plasma glucose levels found in rats on both a high-fat diet and with estrogen-deprivation.

Interestingly, our results demonstrated that peripheral insulin resistance occurred earlier (at week 8), whereas the impairment of brain insulin sensitivity and brain mitochondrial function developed later (at week 12) in both the estrogen-deprived group and the high-fat diet group. However, the high-fat diet with estrogen-deprived rats developed the worst peripheral insulin resistance, and had brain insulin resistance and brain mitochondrial dysfunction occurring simultaneously with the occurrence of peripheral insulin resistance. Thus, we demonstrated for the first time that a high-fat diet in rats accelerated the development of brain insulin resistance under conditions of estrogen-deprivation. It has been shown that estrogen deprivation alone can cause an obese-insulin resistant condition (Babaei et al., 2010; Barros and Gustafsson, 2011). Although several studies demonstrated that impaired insulin sensitivity was caused by several mechanisms, increased oxidative stress has been shown to play a major role in this undesirable effect (Boden, 1997; Evans et al., 2002; Faraj et al., 2004; Smith and Minson, 2012). Moreover, brain insulin resistance is also known to be strongly associated with brain mitochondrial dysfunction (Boden, 1997; Pintana et al., 2012; Pipatpiboon et al., 2012; Pratchayasakul et al., 2011b). Furthermore, it has been shown that mitochondrial dysfunction affected the activation of several serine kinase pathways, leading to defective insulin signal transduction (Rhee, 2006; Saini, 2010) and brain insulin resistance (Pipatpiboon et al., 2012). In the present study, the findings that a high-fat diet in rats accelerated the development of brain insulin resistance under estrogen-deprived conditions could be due to the fact that rats under the combined high-fat diet with estrogen deprivation had the severest degree of oxidative stress, peripheral insulin resistance and brain mitochondrial dysfunction, thus leading to the early development of brain insulin resistance. Our findings emphasized the very important role of oxidative stress caused by either a high-fat diet or estrogen deprivation, which could lead to the reduction of peripheral and brain insulin sensitivity, as observed in the present study.

It has been shown that increased oxidative stress plays an important role in neurodegenerative diseases, including Alzheimer's disease, Parkinson's disease (Finkel and Holbrook, 2000) and dementia in aging (Krieglstein et al., 2000). These pathological conditions have been identified by increased neuronal apoptosis and impaired hippocampal synaptic plasticity, as indicated by decreased LTP amplitude and a reduction in dendritic spine density (Avila-Costa et al., 1999; Rivas-Arancibia et al., 2010). In this study, we have demonstrated that either estrogen deprivation alone or a high-fat diet alone impaired the hippocampal synaptic plasticity, as indicated by decreased LTP and decreases in the density of apical dendrite spines of the CA1 hippocampus. A high-fat diet aggravated those impairments in the estrogen-deprived rats. Although it has been shown that either a high-fat diet alone or estrogen deprivation alone could lead to increased oxidative stress levels in the brain leading to the impairment of hippocampal synaptic plasticity, here we demonstrated for the first time that a high-fat diet significantly aggravated that impairment in rats under an estrogen-deprived condition.

Previous studies demonstrated that rats fed with a HF with high glucose for eight months demonstrated impaired spatial learning ability, evidenced by a decreased dendritic spine density and reduced LTP at the Schaffer-CA1 synapse (Karimi et al., 2013; Stranahan et al., 2008). In addition, our previous study showed that a 12-week HF consumption in male rats caused cognitive impairment via increased brain MDA levels and mitochondrial ROS production, as well as impaired brain insulin sensitivity (Pintana et al., 2012). Also, ovariectomized rats showed obvious spatial learning and memory deficits in the MWM test with a significant loss of neurons and impaired synaptic function in the hippocampus (Qu et al., 2013; Roseman et al., 2012). In this study it has been demonstrated for the first time that a high-fat diet accelerated the development of cognitive impairment in rats under an estrogen-deprived condition. The possible explanation of the worsening cognitive impairment in rats on a high-fat diet under conditions of estrogen-deprivation could be due to the drastically increased peripheral insulin resistance and oxidative stress level in those rats, leading to brain mitochondrial dysfunction, brain insulin receptor dysfunction and reduced hippocampal synaptic plasticity.

In conclusion, this study demonstrated that either a high-fat diet alone or estrogen deprivation alone caused impaired peripheral insulin sensitivity, the reduction of brain insulin sensitivity, brain mitochondrial dysfunction, hippocampal synaptic dysfunction and cognitive impairment. Also, a high-fat diet significantly accelerated and aggravated those deleterious effects under conditions of estrogen-deprivation.

Limitation

One limitation of the present study was the lack of investigation into the effects of HF on brain function in non-obese rats. Although previous studies demonstrated the effects of obesity on cognitive decline (Gerges et al., 2003; Winocur et al., 2005), there is a report demonstrating that diet-induced cognitive impairment could precede weight gain and obesity (Davidson et al., 2013). This issue needs further investigation in the future.

Acknowledgments

This work was supported by Thailand Research Fund TRF-BRG5780016 (SC), TRF-TRG5680018 (WP), TRF-TRG 5780002 (SK), TRG58(JS), National Research Council of Thailand (SC), a NSTDA Research Chair Grant from the National Science and Technology Development Agency (NC) and Chiang Mai University Excellent Center Award (NC). The authors would like to thank Ms. Juntira Sanit for her technical assistance throughout the project.

References

Alonso, A., Fernandez, R., Moreno, M., Ordonez, P., Gonzalez-Pardo, H., Conejo, N.M., Diaz, F., Gonzalez, C., 2006. Positive effects of 17beta-estradiol on insulin sensitivity in aged ovariectomized female rats. J. Gerontol. A Biol. Sci. Med. Sci. 61, 419–426.

Arakawa, H., 2005. Age dependent effects of space limitation and social tension on open-field behavior in male rats. Physiol. Behav. 84, 429–436.

Avila-Costa, M.R., Colin-Barenque, L., Fortoul, T.I., Machado-Salas, P., Espinosa-Villanueva, J., Rugerio-Vargas, C., Rivas-Arancibia, S., 1999. Memory deterioration in an oxidative stress model and its correlation with cytological changes on rat hippocampus CA1. Neurosci. Lett. 270, 107–109.
Babaei, P., Mehdizadeh, R., Ansar, M.M., Damirchi, A., 2010. Effects of ovariectomy and estrogen replacement therapy on visceral adipose tissue and serum adiponectin levels in rats. Menopause Int. 16, 100–104.
Barros, R.P., Gustafsson, J.A., 2011. Estrogen receptors and the metabolic network. Cell Metab. 14, 289–299.
Boden, G., 1997. Role of fatty acids in the pathogenesis of insulin resistance and NIDDM. Diabetes 46, 3–10.
Bramham, C.R., 2008. Local protein synthesis, actin dynamics, and LTP consolidation. Curr. Opin. Neurobiol. 18, 524–531.
Candan, N., Tuzmen, N., 2008. Very rapid quantification of malondialdehyde (MDA) in rat brain exposed to lead, aluminium and phenolic antioxidants by high-performance liquid chromatography-fluorescence detection. Neurotoxicology 29, 708–713.
Chattipakorn, S.C., McMahon, L.L., 2002. Pharmacological characterization of glycine-gated chloride currents recorded in rat hippocampal slices. J. Neurophysiol. 87, 1515–1525.
Daniel, J.M., Fader, A.J., Spencer, A.L., Dohanich, G.P., 1997. Estrogen enhances performance of female rats during acquisition of a radial arm maze. Horm. Behav. 32, 217–225.
Davidson, T.L., Hargrave, S.L., Swithers, S.E., Sample, C.H., Fu, X., Kinzig, K.P., Zheng, W., 2013. Inter-relationships among diet, obesity and hippocampal-dependent cognitive function. Neuroscience 253, 110–122.
Evans, J.L., Goldfine, I.D., Maddux, B.A., Grodsky, G.M., 2002. Oxidative stress and stress-activated signaling pathways: a unifying hypothesis of type 2 diabetes. Endocr. Rev. 23, 599–622.
Evsen, M.S., Ozler, A., Gocmez, C., Varol, S., Tunc, S.Y., Akil, E., Uzar, E., Kaplan, I., 2013. Effects of estrogen, estrogen/progesteron combination and genistein treatments on oxidant/antioxidant status in the brain of ovariectomized rats. Eur. Rev. Med. Pharmacol. Sci. 17, 1869–1873.
Faraj, M., Lu, H.L., Cianflone, K., 2004. Diabetes, lipids, and adipocyte secretagogues. Biochem. Cell Biol. 82, 170–190.
Finkel, T., Holbrook, N.J., 2000. Oxidants, oxidative stress and the biology of ageing. Nature 408, 239–247.
Funaki, M., 2009. Saturated fatty acids and insulin resistance. J. Med. Investig. 56, 88–92.
Gerges, N.Z., Aleisa, A.M., Alkadhi, K.A., 2003. Impaired long-term potentiation in obese zucker rats: possible involvement of presynaptic mechanism. Neuroscience 120, 535–539.
Henderson, V.W., 2008. Cognitive changes after menopause: influence of estrogen. Clin. Obstet. Gynecol. 51, 618–626.
Hill, T.C., Zito, K., 2013. LTP-induced long-term stabilization of individual nascent dendritic spines. J. Neurosci. 33, 678–686.
Karimi, S.A., Salehi, I., Komaki, A., Sarihi, A., Zarei, M., Shahidi, S., 2013. Effect of high-fat diet and antioxidants on hippocampal long-term potentiation in rats: an in vivo study. Brain Res. 1539, 1–6.
Krieglstein, K., Richter, S., Farkas, L., Schuster, N., Dunker, N., Oppenheim, R.W., Unsicker, K., 2000. Reduction of endogenous transforming growth factors beta prevents ontogenetic neuron death. Nat. Neurosci. 3, 1085–1090.
Luine, V.N., Richards, S.T., Wu, V.Y., Beck, K.D., 1998. Estradiol enhances learning and memory in a spatial memory task and effects levels of monoaminergic neurotransmitters. Horm. Behav. 34, 149–162.
Massaad, C.A., Klann, E., 2011. Reactive oxygen species in the regulation of synaptic plasticity and memory. Antioxid. Redox Signal. 14, 2013–2054.
Matsuzawa-Nagata, N., Takamura, T., Ando, H., Nakamura, S., Kurita, S., Misu, H., Ota, T., Yokoyama, M., Honda, M., Miyamoto, K., Kaneko, S., 2008. Increased oxidative stress precedes the onset of high-fat diet-induced insulin resistance and obesity. Metabolism 57, 1071–1077.
Matthews, D.R., Hosker, J.P., Rudenski, A.S., Naylor, B.A., Treacher, D.F., Turner, R.C., 1985. Homeostasis model assessment: insulin resistance and beta-cell function from fasting plasma glucose and insulin concentrations in man. Diabetologia 28, 412–419.
Mattson, M.P., Gleichmann, M., Cheng, A., 2008. Mitochondria in neuroplasticity and neurological disorders. Neuron 60, 748–766.
Mauvais-Jarvis, F., Clegg, D.J., Hevener, A.L., 2013. The role of estrogens in control of energy balance and glucose homeostasis. Endocr. Rev. 34, 309–338.
Pintana, H., Apaijai, N., Pratchayasakul, W., Chattipakorn, N., Chattipakorn, S.C., 2012. Effects of metformin on learning and memory behaviors and brain mitochondrial functions in high fat diet induced insulin resistant rats. Life Sci. 91, 409–414.
Pipatpiboon, N., Pratchayasakul, W., Chattipakorn, N., Chattipakorn, S.C., 2012. PPARgamma agonist improves neuronal insulin receptor function in hippocampus and brain mitochondria function in rats with insulin resistance induced by long term high-fat diets. Endocrinology 153, 329–338.
Pipatpiboon, N., Pintana, H., Pratchayasakul, W., Chattipakorn, N., Chattipakorn, S.C., 2013. DPP4-inhibitor improves neuronal insulin receptor function, brain mitochondrial function and cognitive function in rats with insulin resistance induced by high-fat diet consumption. Eur. J. Neurosci. 37, 839–849.
Platano, D., Fattoretti, P., Balietti, M., Giorgetti, B., Casoli, T., Di Stefano, G., Bertoni-Freddari, C., Aicardi, G., 2008. Synaptic remodeling in hippocampal CA1 region of aged rats correlates with better memory performance in passive avoidance test. Rejuvenation Res. 11, 341–348.
Pratchayasakul, W., Chattipakorn, N., Chattipakorn, S.C., 2011a. Effects of estrogen in preventing neuronal insulin resistance in hippocampus of obese rats are different between genders. Life Sci. 89, 702–707.
Pratchayasakul, W., Kerdphoo, S., Petsophonsakul, P., Pongchaidecha, A., Chattipakorn, N., Chattipakorn, S.C., 2011b. Effects of high-fat diet on insulin receptor function in rat hippocampus and the level of neuronal corticosterone. Life Sci. 88, 619–627.
Qu, N., Wang, L., Liu, Z.C., Tian, Q., Zhang, Q., 2013. Oestrogen receptor alpha agonist improved long-term ovariectomy-induced spatial cognition deficit in young rats. Int. J. Neuropsychopharmacol. 16, 1071–1082.
Rhee, S.G., 2006. Cell signaling. H2O2, a necessary evil for cell signaling. Science 312, 1882–1883.
Rivas-Arancibia, S., Guevara-Guzman, R., Lopez-Vidal, Y., Rodriguez-Martinez, E., Zanardo-Gomes, M., Angoa-Perez, M., Raisman-Vozari, R., 2010. Oxidative stress caused by ozone exposure induces loss of brain repair in the hippocampus of adult rats. Toxicol. Sci. 113, 187–197.
Roseman, A.S., McGregor, C., Thornton, J.E., 2012. Estradiol attenuates the cognitive deficits in the novel object recognition task induced by sub-chronic phencyclidine in ovariectomized rats. Behav. Brain Res. 233, 105–112.
Saini, V., 2010. Molecular mechanisms of insulin resistance in type 2 diabetes mellitus July 15. World J. Diabetes 1, 68–75.
Sherwin, B.B., 2005. Estrogen and memory in women: how can we reconcile the findings? Horm. Behav. 47, 371–375.
Smith, M.M., Minson, C.T., 2012. Obesity and adipokines: effects on sympathetic overactivity. J. Physiol. 590, 1787–1801.
Sripetchwandee, J., Pipatpiboon, N., Pratchayasakul, W., Chattipakorn, N., Chattipakorn, S.C., 2014. DPP-4 inhibitor and PPARgamma agonist restore the loss of CA1 dendritic spines in obese insulin-resistant rats. Arch. Med. Res. 45, 547–552.
Stranahan, A.M., Norman, E.D., Lee, K., Cutler, R.G., Telljohann, R.S., Egan, J.M., Mattson, M.P., 2008. Diet-induced insulin resistance impairs hippocampal synaptic plasticity and cognition in middle-aged rats. Hippocampus 18, 1085–1088.
Vorhees, C.V., Williams, M.T., 2006. Morris water maze: procedures for assessing spatial and related forms of learning and memory. Nat. Protoc. 1, 848–858.
Winocur, G., Greenwood, C.E., Piroli, G.G., Grillo, C.A., Reznikov, L.R., Reagan, L.P., McEwen, B.S., 2005. Memory impairment in obese Zucker rats: an investigation of cognitive function in an animal model of insulin resistance and obesity. Behav. Neurosci. 119, 1389–1395.
Ye, J., 2013. Mechanisms of insulin resistance in obesity. Front. Med. 7, 14–24.
Ye, L., Wang, F., Yang, R.H., 2011. Diabetes impairs learning performance and affects the mitochondrial function of hippocampal pyramidal neurons. Brain Res. 1411, 57–64.

เอกสารแนบหมายเลข 47

PLOS | ONE

RESEARCH ARTICLE

Heart Rate Variability as an Alternative Indicator for Identifying Cardiac Iron Status in Non-Transfusion Dependent Thalassemia Patients

Karn Wijarnpreecha[1,2,3], Natthaphat Siri-Angkul[1,2,3], Krekwit Shinlapawittayatorn[1,2,3], Pimlak Charoenkwan[3,4], Suchaya Silvilairat[3,4], Chate Siwasomboon[5], Pannee Visarutratna[5], Somdet Srichairatanakool[6], Adisak Tantiworawit[7], Arintaya Phrommintikul[7], Siriporn C. Chattipakorn[1,3,8], Nipon Chattipakorn[1,2,3]*

1 Cardiac Electrophysiology Research and Training Center, Faculty of Medicine, Chiang Mai University, Chiang Mai, Thailand, **2** Cardiac Electrophysiology Unit, Department of Physiology, Faculty of Medicine, Chiang Mai University, Chiang Mai, Thailand, **3** Center of Excellence in Cardiac Electrophysiology, Chiang Mai University, Chiang Mai, Thailand, **4** Department of Pediatrics, Faculty of Medicine, Chiang Mai University, Chiang Mai, Thailand, **5** Department of Radiology, Faculty of Medicine, Chiang Mai University, Chiang Mai, Thailand, **6** Department of Biochemistry, Faculty of Medicine, Chiang Mai University, Chiang Mai, Thailand, **7** Department of Internal Medicine, Faculty of Medicine, Chiang Mai University, Chiang Mai, Thailand, **8** Department of Oral Biology and Diagnostic Sciences, Faculty of Dentistry, Chiang Mai University, Chiang Mai, Thailand

* nchattip@gmail.com

CrossMark
click for updates

OPEN ACCESS

Citation: Wijarnpreecha K, Siri-Angkul N, Shinlapawittayatorn K, Charoenkwan P, Silvilairat S, Siwasomboon C, et al. (2015) Heart Rate Variability as an Alternative Indicator for Identifying Cardiac Iron Status in Non-Transfusion Dependent Thalassemia Patients. PLoS ONE 10(6): e0130837. doi:10.1371/journal.pone.0130837

Academic Editor: Jonghan Kim, Northeastern University, UNITED STATES

Received: March 5, 2015

Accepted: May 26, 2015

Published: June 17, 2015

Copyright: © 2015 Wijarnpreecha et al. This is an open access article distributed under the terms of the Creative Commons Attribution License, which permits unrestricted use, distribution, and reproduction in any medium, provided the original author and source are credited.

Data Availability Statement: All relevant data are within the paper and its Supporting Information files.

Funding: A Research Chair Grant from the National Science and Technology Development Agency (NC), Faculty of Medicine Endowment Fund (PC and NC), Thailand Research Fund BRG5780016 (SCC) and RSA5780040 (AP) and the Chiang Mai University Center of Excellence Award (NC). The funders had no role in study design, data collection and analysis, decision to publish, or preparation of the manuscript.

Abstract

Background

Iron-overload cardiomyopathy is a major cause of death in thalassemia patients due to the lack of an early detection strategy. Although cardiac magnetic resonance (CMR) T2* is used for early detection of cardiac iron accumulation, its availability is limited. Heart rate variability (HRV) has been used to evaluate cardiac autonomic function and found to be depressed in thalassemia. However, its direct correlation with cardiac iron accumulation has never been investigated. We investigated whether HRV can be used as an alternative indicator for early identification of cardiac iron deposition in thalassemia patients.

Methods

Ninety-nine non-transfusion dependent thalassemia patients (23.00 (17.00, 32.75) years, 35 male) were enrolled. The correlation between HRV recorded using 24-hour Holter monitoring and non-transferrin bound iron (NTBI), hemoglobin (Hb), serum ferritin, LV ejection fraction (LVEF), and CMR-T2* were determined.

Results

The median NTBI value was 3.15 (1.11, 6.59) μM. Both time and frequency domains of HRV showed a significant correlation with the NTBI level, supporting HRV as a marker of

Competing Interests: The authors have declared that no competing interests exist.

iron overload. Moreover, the LF/HF ratio showed a significant correlation with CMR-T2* with the receiver operating characteristic (ROC) curve of 0.684±0.063, suggesting that it could represent the cardiac iron deposit in thalassemia patients. HRV was also significantly correlated with serum ferritin and Hb.

Conclusions

This novel finding regarding the correlation between HRV and CMR-T2* indicates that HRV could be a potential marker in identifying early cardiac iron deposition prior to the development of LV dysfunction, and may be used as an alternative to CMR-T2* for screening cardiac iron status in thalassemia patients.

Introduction

Thalassemia intermedia are mild forms of thalassemia and known as non-transfusion dependent thalassemia (NTDT) [1, 2]. Anemia in NTDT is typically not as severe as thalassemia major or transfusion dependent thalassemia (TDT). However, heart failure from iron overload cardiomyopathy is still the most common cause of death in NTDT patients despite the effectiveness of iron chelating agents [3, 4]. Iron-overload in NTDT patients is caused by an increased gastrointestinal iron absorption secondary to chronic anemia, ineffective erythropoiesis, and hepcidin deficiency [3–9]. The increased iron absorption could lead to the accumulation of iron at a rate of 2–5 grams per year depending on the degree of bone marrow expansion and peripheral hemolysis [7, 10]. Eventually, NTDT patients develop iron overload leading to serious complications as seen in the TDT patients, complication including end-organ damage due to iron overload, bone changes and hypercoagulability [7, 8, 10]. Currently, not only the prevention of iron overload, but early detection of iron overload cardiomyopathy is also an important strategy to prevent cardiac failure in NTDT patients.

It has been shown that iron overload cardiomyopathy can be reversible only if early intensive chelation therapy has been initiated [11–13]. Over the past decades, several biochemical and clinical parameters as well as radiological investigations have been used to determine the cardiac iron status. Serum ferritin has been widely used for decades to represent the iron status in the body due to its strong correlation with liver iron concentration [12, 14]. However, it is not just specific to the iron-overload condition [12, 15, 16], and low levels of serum ferritin do not necessarily represent a low risk of iron overload cardiomyopathy [17]. Non-transferrin-bound iron (NTBI), a low molecular weight and free-form iron, can be detected in plasma when serum transferrin is fully saturated [18, 19]. This form of iron can cause cardiovascular injury and cardiac cell apoptosis by its reduction and oxidation of free iron [3, 5, 18, 20–27]. Several studies demonstrated that NTBI levels can be used as an index to indicate iron-overload conditions and also have a significant correlation with the vital organ damage in TDT [28–31] and NTDT [32, 33] patients. As a result, NTBI can be one of the best biochemical parameters that represent cardiac iron status. However, their use is limited due to the cost, and it is not available in all research centers. Although the cardiac magnetic resonance (CMR) T2* is currently used as a gold standard for early detection of iron overload cardiomyopathy [5, 17, 34], its use is currently limited due to its cost and availability worldwide. According to this limitation, CMR T2* might not be the best practical strategy for early detection of iron overload cardiomyopathy or screening the cardiac iron status in thalassemia, especially for those in developing countries. Other available tests, such as conventional electrocardiogram,

endomyocardial and liver biopsy, and echocardiography are not shown to be helpful for early detection of iron overload cardiomyopathy [12, 35–37]. In contrast, growing evidence suggests that heart rate variability (HRV), an easily accessible diagnostic parametric, reliable, low-cost and non-invasive test can represent cardiac autonomic function, and could be an important practical assessment strategy for early detection of iron overload cardiomyopathy in thalassemia patients [12, 38, 39].

For decades, HRV has been used to evaluate cardiac autonomic function in patients with heart disease, including post-myocardial infarction [40–42], heart failure, and also TDT patients who are prone to have iron overload cardiomyopathy and increased risk of heart failure [38, 40, 43–45]. Although previous studies demonstrated the depressed HRV status in thalassemia, there is no study showing the correlation between HRV and CMR T2* in NTDT patients. In this study, we sought to determine whether HRV can be used as an alternative indicator for early detection of the cardiac iron status in the thalassemia patients. The hypotheses were tested that HRV has a strong correlation with the NTBI and also CMR T2*. In this cross-sectional study, HRV was determined in NTDT patients, and the relationship between HRV and biochemical parameters, clinical parameters, echocardiographic findings, and CMR T2* values were evaluated.

Materials and Methods

Study protocol

The study protocol was approved by the Institutional Ethics Committee of the Faculty of Medicine, Chiang Mai University, Chiang Mai, Thailand. NTDT patients enrolled in this study were defined as having thalassemia and receiving no more than seven RBC transfusions per year in the last five years, with age ranged between 10–50 years, and did not have any infectious diseases or acute illnesses during the investigation. Exclusion criteria included patients with a contraindication to MRI, and clinical evidence of other secondary causes of pulmonary hypertension, including human immunodeficiency virus infection, hepatitis virus infection, collagen vascular diseases, cirrhosis, chronic obstructive airway diseases and acquired heart disease associated with pulmonary hypertension. All patients were treated at Chiang Mai University Hospital during September 2013 to May 2014. All patients and their parents in the case of minorities gave written informed consent.

Patient charts were reviewed for thalassemia diagnosis and genotypes, transfusion history, history of splenectomy, details of drugs history, and comorbidities. The body weight, height and liver size were recorded in each patient. Laboratory profiles (Mean Hb and serum ferritin in the last 12 months, hematocrit (Hct), maximum ferritin in the past 5 years, plasma NTBI, labile plasma iron (LPI)), echocardiography, 24-h Holter ECG recording for HRV analysis, CMR T2* were collected and analyzed at the time of entry. The correlation between HRV and NTBI, hemoglobin (Hb), serum ferritin, LV ejection fraction (LVEF), CMR T2* were determined.

Heart rate variability measurement

The SEER Light Holter system (GE Healthcare, Milwaukee, WI, USA) was used. An ECG was recorded continuously for 24 h. The computer software MARS software version 7, GE Healthcare, Milwaukee, WI, USA was used to scan for rhythm disturbance and to detect and label each QRS complex. Excessive noise and artifacts were noted, and ectopy was quantified. The time-domain analyses included average heart rate, average R-R intervals (NN), standard deviation of the R-R intervals over a 24-h period (SDNN), standard deviation of all 5-min mean R-R intervals (SDANN), average standard deviation of all 5-min R-R intervals (ASDNN), the percentage of R-R intervals with more than 50-ms variation (pNN50), and the square root of

mean squared differences of successive R-R intervals (rMSSD). The frequency-domain analyses were done with the same analytical software using Fast-Fourier transform analysis. The obtained frequency-domain indices were the total power (0–0.4 Hz), high-frequency power (HF, 0.15–0.4 Hz) spectral density, low-frequency power (LF, 0.04–0.15 Hz) spectral density, and very-low-frequency power (0.003–0.04 Hz) spectral density. Total power expresses the magnitude of the entire HRV, whereas HF power reflects the parasympathetic tone, and LF power indicates the sympathovagal interactions[40]. These power spectral densities were expressed in absolute units (ms^2).

The designated physician who operated and fitted the Holter monitor to the patients was blinded to the patients' information. The subjects were fitted with the Holter monitor after blood sample collection at the Holter unit of the Faculty of Medicine, Chiang Mai University. In the present study, none of the included patients took medications such as beta-blockers, calcium channel blockers, statins, and ACE-inhibitors which could affect the HRV.

Laboratory profiles

Mean Hb and serum ferritin in the last 12 months, hematocrit (Hct), maximum ferritin in the past 5 years, plasma NTBI, labile plasma iron (LPI) were determined in each patient at the date of entry.

Measurement of hematological parameters

Complete blood counts were performed using an automated hematological analyzer (Beckman Coulter A^C.T 5diff, Coulter Corp., Miami, FL, USA).

Measurement of ferritin

The Roche Cobas E601 (Germany) Immunology Analyzer was used to determine serum ferritin using a sandwich principle. In the first incubation, a plasma sample of 10 μL, a biotinylated monoclonal ferritin-specific antibody, and a monoclonal ferritin-specific antibody labeled with a ruthenium complex formed a sandwich complex. In the second incubation, after addition of streptavidin-coated microparticles, the complex became bound to the solid phase via the interaction of biotin and streptavidin. The reaction mixture was aspirated into the measuring cell where the micro particles were magnetically captured onto the surface of the electrode. The unbound substance was then removed with ProCell/ProCell M. The application of a voltage to the electrode then induced chemiluminescent emission which was measured by a photomultiplier. Results were determined via a calibration curve which was specifically generated by a 2-point calibration and a master curve provided via the reagent barcode [46, 47].

Quantification of plasma NTBI

Plasma NTBI was determined as described in the previous study [48]. First, a small volume of aluminium chloride solution (a final concentration of 200 μM) was added to 450-μL plasma and incubated at room temperature for 1 hr. Then, 50 μL of 800-mM nitril-otriacetic acid (NTA) (a final concentration of 80 mM) solution at pH 7.0 was added and the mixture was incubated for 30 minutes at room temperature to produce a ferric-nitrilotriacetate complex, Fe^{3+}-$(NTA)_2$. Then, the Fe^{3+}-$(NTA)_2$ was separated from plasma proteins by spinning plasma mixture through a membrane filter (30-kDa cut-off, polysulfone type, 0.5-mL capacity) at 12,000 *g*, 15°C for 45 min. The ultrafiltrate was injected into a non-metallic 50-μL loop and analyzed with the high performance liquid chromatography (HPLC) technique. HPLC requirements were composed of a glass analytical column (ChromSep-ODSI, 100 x 3.0 mm, 5 μm)

and a mobile-phase solvent (3 mM CP22 in 19% acetronitrile buffered with 5 mM MOPS pH 7.0). Having been isocratically eluted with the mobile-phase solvent at a flow rate of 1.0 mL/min, NTBI as Fe^{3+}-(NTA)2 was fractionated on the column, then immediately on-column derivatized with CP22 to form a Fe^{3+}-$(CP22)_3$ complex. The resulting orange-colored Fe^{3+}--$(CP22)_3$ product was on-line detected at 450 nm with the SpecMonitor 2300 flow-cell detector (LDC Milton-Roy Inc., FL, USA). The NTBI peak height was integrated and recorded for further determination of NTBI concentration from the calibration curve. A calibration curve was produced by plotting the obtained peak height values on the *y*-axis against iron concentration on the *x*-axis. An equation of linear regression line was used to calculate the plasma NTBI concentration.

Measurement of LPI concentration

In principle, redox-active LPI converts dihydrorhodamine (DHR) to oxidized fluorescent rhodamine (R), leading to an increase in fluorescence intensity (FI) [21]. A plasma sample of 20 μL was incubated with/without 5 mmol/L DFP at 37°C for 30 min and DHR solution containing ascorbic acid was then added (180 μL). Kinetic spectrofluorometry (λex 485 nm, λem 538 nm) was performed immediately for 40 min at 37°C with a reading every 2 min. The increasing FI was followed and the slope of the FI was plotted against the reaction time between 15–40 minutes. A calibration curve was created from a standard ferrous ammonium sulfate (FAS) solution (0–20 μmol/L). The difference in the rate of DHR oxidation represents a component of the redox active LPI in plasma. The LPI concentration was calculated from the calibration curve relating to the difference in the slope with/without DFP versus the standard iron concentration [49].

Echocardiographic studies

The standard two dimensional and Doppler trans-thoracic echocardiography was performed at rest in all enrolled patients with Philips iE33 (Philips Healthcare, Bothell, WA, USA). Left ventricular end-diastolic dimension (LVEDD) and left ventricular end-systolic dimension (LVESD) were measured, and left ventricular ejection fraction (LVEF), stroke volume, cardiac output, and fractional shortening (FS) were determined based on the calculation of LV volumes by the method of discs, following the recommendations by the American Society of Echocardiography (ASE), and using apical two- and four- chamber views to measure cardiac function [50, 51].

Impaired systolic LV dysfunction (LVEF < 55% or LVFS < 35%) was also determined in NTDT patients[51]. Diastolic function was evaluated from mitral inflow velocities (E-wave, A wave, E/A ratio) and deceleration time (DT) using pulsed wave (PW) Doppler in the apical four-chamber view. PW tissue-Doppler velocities were acquired at end-expiration, in the apical four-chamber view, with the sample positioned at the lateral mitral annulus, measuring early diastolic (E') and late diastolic (A') velocities and calculating the E/E' ratio. Diastolic dysfunction was defined by E/A ratio, DT and E/E' according to the current guideline [52].

Magnetic resonance imaging

Magnetic resonance acquisition was performed using a 1.5T MR scanner (GE, HDxt, Milwaukee, WI, USA), using an 8-channel body array. For the measurements of myocardial iron overload, we used a T2* gradient—echo multi-echo sequence (flip angle 25 degree, matrix: 192 x 128 pixels, field of view 38 x 28.5 cm, bandwidth 125 kHz, slice thickness 10.0 mm, number of excitations 1, view per segment 4, repetition time 18.5 ms). A single mid ventricular short-axis

view of the left ventricle was acquired at eight echo times (TEs) (1.7 ms, which increased in 2.0–2.1 ms increments) in a single end-expiratory breath-hold.

Cardiac magnetic resonance (CMR) T2* analysis was performed on a workstation (Advantage Window 4.6, GE healthcare) using commercial analysis software (StarMap 4.0, GE Healthcare). According to the previous study, the 95% confidence interval of normal CMR T2* value (>20ms) was assessed [17, 53]. The values 14–20 ms were regarded as mild iron overload, values between 10 and 14 ms were regarded as moderate iron overload, and a T2* less than 10 ms was regarded as severe iron overload [17].

Statistical analysis

Numerical data are presented as median (25th, 75th percentile) due to the skewed distribution of numerical data. Differences between splenectomized and non-splenectomized NTDT patients were performed using the parametric independent student T-test. CMR T2* was regarded as the gold standard diagnostic technique. The correlations between HRV and laboratory profiles, echocardiographic parameters, CMR T2* were determined using the Spearman's rank correlation. A *P* value of less than 0.05 was considered statistically significant. Statistical analysis was performed with the use of SPSS version 13.0 for Windows (SPSS Inc., Chicago, IL, USA). The receiver operative characteristic (ROC) curve was analyzed, and the binary logistic regression analysis, forward likelihood method, was also applied to determine the association between CMR T2* and HRV.

Results

One hundred patients were enrolled in this study. One patient was excluded since this patient refused the MRI investigation. Clinical and biochemical characteristics, echocardiographic parameters, CMR T2* values, and HRV of NTDT patients (n = 99) were summarized in Table 1. NTDT patients in this study consisted of 62 beta-thalassemia and 37 Hb H diseases (71 had never had a blood transfusion, 12 had blood transfusion only once in the last 12 months, and 16 had blood transfusion < 7 times in the last 12 months). A total of 35 patients (35%) had a splenectomy before the evaluation. Forty-two patients (42%) were receiving iron chelating drugs (24 deferiprone, 3 desferrioxamine, 2 deferaxirox, and 13 combined iron chelating agents).

In this study, the median CMR T2* was 43.95 (39.68, 48.75) ms which indicated that the NTDT patients have preserved CMR T2* values (T2* > 20 ms, n = 98). The comparison of HRV between the splenectomized (n = 35) and non-splenectomized (n = 64) group was shown in the supplementary table (S1 Table). Time-domain (SDNN and SDANN) HRV parameters were significantly lower in the splenectomized group (107.00 (81.00, 137.00) vs 122.00 (99.75, 151.00) and 96.00 (69.00, 116.00) vs 115.50 (88.25, 138.75), $P = 0.008$ and 0.002, respectively). Moreover, the number of blood transfusions and serum ferritin in the last 12 months, maximum ferritin in the past 5 years, NTBI, and LPI were also significantly higher in the splenectomized group.

The correlations analysis between time and frequency domains of HRV and clinical and biochemical parameters was presented in Table 2. All time-domain (SDNN, SDANN, ASDNN and rMSSD), and frequency-domain (LF and HF) HRV parameters showed a significant correlation with mean Hb, mean serum ferritin levels in the last 12 months, maximum ferritin in the past 5 years, and the number of blood transfusion in the last 12 months. Moreover, both time-domain (SDNN and SDANN) and frequency-domain (LF/HF ratio) HRV parameters were also showed a strong correlation with the NTBI. However, none of the HRV parameters showed any correlation with echocardiographic parameters or LPI levels (data not shown).

Table 1. Demographic, clinical, biochemical characteristics, echocardiographic measurement, cardiac magnetic resonance (CMR) T2*, time-domain and frequency-domain HRV parameters of non-transfusion dependent thalassemia (NTDT) patients (n = 99).

Parameters	Median (25th, 75th percentile)
Age (years)	23.00 (17.00, 32.75)
Gender	
Male (n (%))	35 (35.4%)
Female (n (%))	64 (64.6%)
Splenectomy (%)	35 (35.4%)
Number of blood transfusions in last 12 months	0.00 (0.00, 1.00)
Mean hemoglobin in last 12 months (g/dL)	7.80 (7.10, 8.78)
Hematocrit (%)	25.10 (22.00, 28.80)
MCV	64.90 (59.50, 71.10)
Mean ferritin in last 12 months (ng/dL)	673.50 (318.00, 1009.25)
Maximum ferritin in the past 5 years (ng/dL)	849.00 (396.00, 1925.00)
NTBI (μM)	3.15 (1.11, 6.59)
LPI (μM)	1.12 (0.01, 1.93)
Echocardiographic values	
LVEDD (mm)	4.90 (4.50, 5.30)
LVESD (mm)	3.10 (2.88, 3.40)
LVEF (%)	65.80 (61.79, 70.10)
FS (%)	36.20 (32.75, 39.50)
CMR T2* (ms)	43.95 (39.68, 48.75)
HRV-Time domain	
SDNN (ms)	114.00 (95.00, 142.00)
SDANN (ms)	105.00 (86.00, 130.00)
ASDNN (ms)	43.00 (37.00, 56.00)
rMSSD (ms)	25.00 (18.00, 35.00)
HRV-Frequency domain	
LF (ms2)	14.98 (11.54, 18.35)
HF (ms2)	11.17 (7.66, 16.60)
LF/HF ratio	1.39 (1.16, 1.61)

NTBI, non-transferrin-bound iron; LPI, labile plasma iron; SDNN, standard deviation of all normal sinus R-R intervals in the entire 24-h recording; SDANN, standard deviation of all averaged normal sinus R-R intervals for all 5-min segment in the 24-h recordings; ASDNN, average of the standard deviations of all R-R intervals for all 5-min segments in the 24-h recordings; rMSSD, root mean square of the mean of the squared difference of two consecutive R-R intervals; LF, low frequency power; HF, high frequency power; LF/HF ratio, ratio of power in low/high frequency.

doi:10.1371/journal.pone.0130837.t001

Since the echocardiographic data demonstrated that the enrolled patients did not have any abnormal LV function whereas the NTBI level was detected, these findings suggested that the patients were in an early stage of iron overload without any functional abnormality or impaired systolic or diastolic function. Moreover, a significant correlation between HRV parameters and CMR T2* was demonstrated in which the LF/HF ratio showed a significant correlation with CMR T2* values (R = -0.227, P = 0.026).

NTBI, non-transferrin-bound iron; SDNN, standard deviation of all normal sinus R-R intervals in the entire 24-h recording; SDANN, standard deviation of all averaged normal sinus R-R intervals for all 5-min segment in the 24-h recordings; ASDNN, average of the standard

Table 2. The correlations between HRV parameters and other clinical parameters in non-transfusion dependent thalassemia (NTDT) patients.

Spearman's rho	Mean hemoglobin in last 12 months	Mean ferritin in last 12 months	Maximum ferritin in the past 5 years	NTBI	Number of blood transfusions in last 12 months
HRV-Time domain					
SDNN (ms)	0.387‡	-0.338‡	-0.484‡	-0.224*	-0.314†
SDANN (ms)	0.345‡	-0.332‡	-0.482‡	-0.221*	-0.326‡
ASDNN (ms)	0.462‡	-0.364‡	-0.505‡	-0.138	-0.259†
rMSSD (ms)	0.330‡	-0.324‡	-0.445‡	-0.187	-0.237*
HRV-Frequency domain					
LF (ms2)	0.487‡	-0.341‡	-0.474‡	-0.093	-0.230*
HF (ms2)	0.408‡	-0.334‡	-0.448‡	-0.169	-0.221*
LF/HF ratio	-0.045	0.152	0.196	0.204*	0.094

*$P < 0.05$.

†$P < 0.01$.

‡$P < 0.001$

doi:10.1371/journal.pone.0130837.t002

deviations of all R-R intervals for all 5-min segments in the 24-h recordings; rMSSD, root mean square of the mean of the squared difference of two consecutive R-R intervals; LF, low frequency power; HF, high frequency power; LF/HF ratio, ratio of power in low/high frequency.

From the correlations analysis between CMR T2* and HRV, and clinical parameters, only LF/HF and mean Hb in last 12 months were correlated with CMR T2* values. The binary logistic regression analysis was performed to determine the correlations of CMR T2* and HRV and other clinical parameters. Using the multivariate forward likelihood method with adjustments

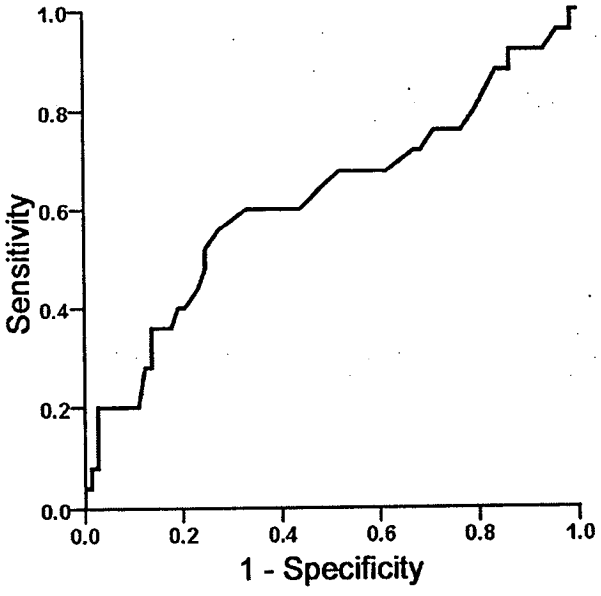


Fig 1. Receiver operating characteristic (ROC) curve of the HRV for the prediction of myocardial iron deposition determined by CMR T2*.

doi:10.1371/journal.pone.0130837.g001

for age, sex, splenectomy, and iron chelating drug use, we found that only the LF/HF (odds ratio 8.710, 95% CI 2.324–32.649, $P = 0.001$), but not the mean Hb in the last 12 months significantly correlated with CMR T2*. Since there is only one NTDT patient in this study that had CMR T2* <20 ms, we could not use the same cut point to determine cardiac iron overload as shown previously in TDT patients [17]. Therefore, the lowest quartile CMR T2* value (40 ms) of our study population was used as the cut point to determine cardiac iron overload in NTDT patients. The predicted area under the ROC curve of mean Hb level in last 12 months was 0.618±0.071 (95%CI: 0.478–0.757; $P = 0.08$). However, the predicted area under the ROC curve of LF/HF was 0.684±0.063 (95%CI: 0.561–0.807; $P = 0.006$) (Fig 1).

Discussion

The major findings in this study are that the time-domain and frequency-domain of HRV parameters showed a significant correlation with the NTBI, mean Hb, serum ferritin, number of blood transfusions, and CMR T2*.

HRV assessment is a technique that measures the beat-to-beat variability in the R-R intervals, which can imply the cardiac autonomic regulation. The decreased time-domain parameters or increased LF/HF ratio indicates there is a cardiac sympathovagal imbalance which is generally known as "depressed HRV" [40, 54]. Depressed HRV has been demonstrated in both thalassemic mice and thalassemia patients, and has been shown to be associated with cardiac autonomic dysfunction and can lead to the early detection of iron overload cardiomyopathy [12, 38, 55, 56]. Despite those reports, there is no clinical study that directly investigates the relationship between HRV and NTBI and CMR T2* to elucidate the potential of HRV as the alternative assessment of cardiac iron status.

Growing evidence from studies on thalassemic mice suggests that they had high NTBI levels and also had depressed HRV compared to the wild-type mice [12, 57, 58]. In the present study, it has been demonstrated for the first time the significantly correlations between HRV parameters and the NTBI, mean Hb, ferritin and number of blood transfusions in the last 12 months, and maximum ferritin in the past 5 years of NTDT patients. These findings emphasize the potential role of HRV as an indicator of iron status under iron overload condition.

It has been proposed that HRV may be used to indicate cardiac iron accumulation. Available data in animal studies supported this possibility by demonstrating that HRV showed a correlation with iron accumulation in the heart [12, 58]. Despite reports in animal studies, the direct correlation between HRV and CMR T2* together with NTBI has never been investigated in a clinical study. Although there is one small clinical study with 34 TDT patients which showed no correlation between HRV and serum ferritin, and NTBI [39], the study itself was too small to find a statistically significant correlation. As demonstrated in the present study, the correlation between HRV and CMR T2* and NTBI suggested the possibility that HRV might be an alternative indicator of both body iron status and cardiac iron status under iron overload conditions. This study also demonstrated for the first time that only LF/HF was significantly correlated with CMR T2* values as determined by the binary logistic regression analysis. ROC curve analysis also demonstrated that only LF/HF was significantly correlated with CMR T2* values. These findings suggested that LF/HF could be the best clinical parameters to predict CMR T2* values for early detection of cardiac iron overload in NTDT patients. Moreover, it has been shown that cardiac autonomic dysfunction develops before myocardial contractility dysfunction or cardiac iron loading in TDT patients [41]. Therefore, CMR T2* and echocardiography, which cannot evaluate cardiac autonomic function, still have limitations when compared to the HRV.

In splenectomized patients, it has been shown that they had significantly higher serum ferritin, transferrin saturation, and desferrioxamine-induced urinary iron excretion (DFU) when

compared to the non-splenectomized patients [59]. In the present study, it was found that the NTBI, LPI, and maximum ferritin in the past 5 years were also significantly higher in the splenectomized group. These findings strongly indicated that the spleen plays an important role in iron regulation [59]. The free form of NTBI both in plasma (LPI) and intracellular (labile cellular iron, LCI) has been shown to produce reactive oxygen species (ROS) via Haber-Weiss and Fenton reaction, leading to cardiovascular injury from lipid peroxidation, damage to cellular proteins, nucleic acids, mitochondria, and cellular organelles, and also cardiac cell apoptosis [3, 5, 6, 18, 20–22, 24, 25, 27, 60, 61]. It has been shown that the oxidative stress from many pathological conditions including iron overload can lead to sympathovagal disturbance and significantly depressed HRV [58, 62–70]. This study demonstrated for the first time that the splenectomized NTDT group had a significantly lower time-domain (SDNN and SDANN) HRV compared to the non-splenectomized group. Therefore, it could be suggested that splenectomized patients have higher NTBI and LPI levels leading to oxidative stress-mediated cardiac autonomic dysfunction, thus resulting in depressed HRV as observed in this study.

Study Limitation

One limitation of this study was the lack of a healthy control group or an additional group with a disease associated with cardiac iron overload, such as hereditary hemochromatosis. Although the inclusion of this latter group would allow us to differentiate whether the effects on HRV are specifically from iron overload, or from a combination of iron overload and anemia, hereditary hemochromatosis is extremely rare in our population, therefore the addition of this group is not possible for this study.

Since most of the severity of cardiac iron overload of NTDT patients in this study were out with the traditional MRI cut-off for significant cardiac iron overload (CMR T2* > 20), we could not divide NTDT patients by a CMR T2* severity assessment. This study performed a cross-sectional study and could not take into account the morbidity and mortality prediction in this group of patients. Moreover, there was a significant female sex bias and the population was predominantly young adults. Both sex and age can influence HRV substantially and may limit the generalizability of the findings. Future prospective studies with long-term follow-up and larger sample are needed for this purpose.

Conclusion

Early detection of iron overload cardiomyopathy to initiate early chelation therapy in thalassemia patients is a strategy to prevent cardiac complications and decrease the mortality rate. The findings of this study regarding the correlation between HRV and NTBI levels, and CMR T2* indicate that HRV could be a potential marker in identifying body free iron status as well as cardiac iron status in NTDT patients.

Supporting Information

S1 Table. Comparison of HRV indices in non-transfusion dependent thalassemia (NTDT) patients according to splenectomy.
(DOC)

Author Contributions

Conceived and designed the experiments: PC NC. Performed the experiments: KW NS KS PC S. Silvilairat CS PV S. Srichairatanakool AT AP SCC NC. Analyzed the data: KW NS KS PC S. Silvilairat CS PV S. Srichairatanakool AT AP SCC NC. Contributed reagents/materials/analysis

tools: PC S. Silvilairat CS PV S. Srichairatanakool AT AP SCC NC. Wrote the paper: KW.NS KS PC CS AP SCC NC.

References

1. Taher A, Vichinsky E, Musallam K, Cappellini MD, Viprakasit V. In: Weatherall D, editor. Guidelines for the Management of Non Transfusion Dependent Thalassaemia (NTDT). Nicosia, Cyprus2013. PMID: 24672826
2. Weatherall DJ. The definition and epidemiology of non-transfusion-dependent thalassemia. Blood reviews. 2012; 26 Suppl 1:S3–6. doi: 10.1016/S0268-960X(12)70003-6 PMID: 22631040
3. Kremastinos DT, Farmakis D, Aessopos A, Hahalis G, Hamodraka E, Tsiapras D, et al. Beta-thalassemia cardiomyopathy: history, present considerations, and future perspectives. Circulation Heart failure. 2010; 3(3):451–8. doi: 10.1161/CIRCHEARTFAILURE.109.913863 PMID: 20484195
4. Maakaron JE, Cappellini MD, Taher AT. An update on thalassemia intermedia. Le Journal medical libanais The Lebanese medical journal. 2013; 61(3):175–82. PMID: 24422369
5. Gujja P, Rosing DR, Tripodi DJ, Shizukuda Y. Iron overload cardiomyopathy: better understanding of an increasing disorder. Journal of the American College of Cardiology. 2010; 56(13):1001–12. doi: 10.1016/j.jacc.2010.03.083 PMID: 20846597
6. Murphy CJ, Oudit GY. Iron-overload cardiomyopathy: pathophysiology, diagnosis, and treatment. Journal of cardiac failure. 2010; 16(11):888–900. doi: 10.1016/j.cardfail.2010.05.009 PMID: 21055653
7. Origa R, Galanello R, Ganz T, Giagu N, Maccioni L, Faa G, et al. Liver iron concentrations and urinary hepcidin in beta-thalassemia. Haematologica. 2007; 92(5):583–8. PMID: 17488680
8. Taher A, El Rassi F, Isma'eel H, Koussa S, Inati A, Cappellini MD. Correlation of liver iron concentration determined by R2 magnetic resonance imaging with serum ferritin in patients with thalassemia intermedia. Haematologica. 2008; 93(10):1584–6. doi: 10.3324/haematol.13098 PMID: 18728025
9. Wijampreecha K, Kumfu S, Chattipakorn SC, Chattipakorn N. Cardiomyopathy Associated with Iron Overload: How Does Iron Enter Myocytes and What are the Implications for Pharmacological Therapy? Hemoglobin. 2015; 39(1):9–17. doi: 10.3109/03630269.2014.987869 PMID: 25572185
10. Pippard MJ, Callender ST, Warner GT, Weatherall DJ. Iron absorption and loading in beta-thalassaemia intermedia. Lancet. 1979; 2(8147):819–21. PMID: 90918
11. Davis BA, Porter JB. Long-term outcome of continuous 24-hour deferoxamine infusion via indwelling intravenous catheters in high-risk beta-thalassemia. Blood. 2000; 95(4):1229–36. PMID: 10666195
12. Koonrungsesomboon N, Chattipakorn SC, Fucharoen S, Chattipakorn N. Early detection of cardiac involvement in thalassemia: From bench to bedside perspective. World journal of cardiology. 2013; 5 (8):270–9. doi: 10.4330/wjc.v5.i8.270 PMID: 24009816
13. Tanner MA, Galanello R, Dessi C, Smith GC, Westwood MA, Agus A, et al. Combined chelation therapy in thalassemia major for the treatment of severe myocardial siderosis with left ventricular dysfunction. Journal of cardiovascular magnetic resonance: official journal of the Society for Cardiovascular Magnetic Resonance. 2008; 10:12.
14. Olivieri NF, Brittenham GM, Matsui D, Berkovitch M, Blendis LM, Cameron RG, et al. Iron-chelation therapy with oral deferiprone in patients with thalassemia major. The New England journal of medicine. 1995; 332(14):918–22. PMID: 7877649
15. Orino K, Lehman L, Tsuji Y, Ayaki H, Torti SV, Torti FM. Ferritin and the response to oxidative stress. The Biochemical journal. 2001; 357(Pt 1):241–7. PMID: 11415455
16. Piperno A. Classification and diagnosis of iron overload. Haematologica. 1998; 83(5):447–55. PMID: 9658731
17. Anderson LJ, Holden S, Davis B, Prescott E, Charrier CC, Bunce NH, et al. Cardiovascular T2-star (T2*) magnetic resonance for the early diagnosis of myocardial iron overload. European heart journal. 2001; 22(23):2171–9. PMID: 11913479
18. Brissot P, Ropert M, Le Lan C, Loreal O. Non-transferrin bound iron: a key role in iron overload and iron toxicity. Biochimica et biophysica acta. 2012; 1820(3):403–10. doi: 10.1016/j.bbagen.2011.07.014 PMID: 21855608
19. Maas RP, Voets PJ, de Swart L, Swinkels DW. [Non-transferrin-bound iron: a promising biomarker in iron overload disorders]. Nederlands tijdschrift voor geneeskunde. 2013; 157(49):A6258. PMID: 24299624
20. Emerit J, Beaumont C, Trivin F. Iron metabolism, free radicals, and oxidative injury. Biomedicine & pharmacotherapy = Biomedecine & pharmacotherapie. 2001; 55(6):333–9.

21. Esposito BP, Breuer W, Sirankapracha P, Pootrakul P, Hershko C, Cabantchik ZI. Labile plasma iron in iron overload: redox activity and susceptibility to chelation. Blood. 2003; 102(7):2670–7. PMID: 12805056

22. Hershko C, Link G, Cabantchik I. Pathophysiology of iron overload. Annals of the New York Academy of Sciences. 1998; 850:191–201. PMID: 9668540

23. Horwitz LD, Rosenthal EA. Iron-mediated cardiovascular injury. Vascular medicine. 1999; 4(2):93–9. PMID: 10406456

24. Lekawanvijit S, Chattipakorn N. Iron overload thalassemic cardiomyopathy: iron status assessment and mechanisms of mechanical and electrical disturbance due to iron toxicity. The Canadian journal of cardiology. 2009; 25(4):213–8. PMID: 19340344

25. Papanikolaou G, Pantopoulos K. Iron metabolism and toxicity. Toxicology and applied pharmacology. 2005; 202(2):199–211. PMID: 15629195

26. Shander A, Cappellini MD, Goodnough LT. Iron overload and toxicity: the hidden risk of multiple blood transfusions. Vox sanguinis. 2009; 97(3):185–97. doi: 10.1111/j.1423-0410.2009.01207.x PMID: 19663936

27. Wood JC, Enriquez C, Ghugre N, Otto-Duessel M, Aguilar M, Nelson MD, et al. Physiology and pathophysiology of iron cardiomyopathy in thalassemia. Annals of the New York Academy of Sciences. 2005; 1054:386–95. PMID: 16339687

28. al-Refaie FN, Wickens DG, Wonke B, Kontoghiorghes GJ, Hoffbrand AV. Serum non-transferrin-bound iron in beta-thalassaemia major patients treated with desferrioxamine and L1. British journal of haematology. 1992; 82(2):431–6. PMID: 1419825

29. Cabantchik ZI, Breuer W, Zanninelli G, Cianciulli P. LPI-labile plasma iron in iron overload. Best practice & research Clinical haematology. 2005; 18(2):277–87.

30. Piga A, Longo F, Duca L, Roggero S, Vinciguerra T, Calabrese R, et al. High nontransferrin bound iron levels and heart disease in thalassemia major. American journal of hematology. 2009; 84(1):29–33. doi: 10.1002/ajh.21317 PMID: 19006228

31. Porter JB, Garbowski M. The pathophysiology of transfusional iron overload. Hematology/oncology clinics of North America. 2014; 28(4):683–701, vi. doi: 10.1016/j.hoc.2014.04.003 PMID: 25064708

32. Domenica Cappellini M, Tavazzi D, Duca L, Marelli S, Fiorelli G. Non-transferrin-bound iron, iron-related oxidative stress and lipid peroxidation in beta-thalassemia intermedia. Transfusion science. 2000; 23(3):245–6. PMID: 11099903

33. Taher A, Musallam KM, El Rassi F, Duca L, Inati A, Koussa S, et al. Levels of non-transferrin-bound iron as an index of iron overload in patients with thalassaemia intermedia. British journal of haematology. 2009; 146(5):569–72. doi: 10.1111/j.1365-2141.2009.07810.x PMID: 19604239

34. Borgna-Pignatti C, Meloni A, Guerrini G, Gulino L, Filosa A, Ruffo GB, et al. Myocardial iron overload in thalassaemia major. How early to check? British journal of haematology. 2014; 164(4):579–85. doi: 10.1111/bjh.12643 PMID: 24460526

35. Berdoukas V, Dakin C, Freema A, Fraser I, Aessopos A, Bohane T. Lack of correlation between iron overload cardiac dysfunction and needle liver biopsy iron concentration. Haematologica. 2005; 90 (5):685–6. PMID: 15921384

36. Cavallaro L, Meo A, Busa G, Coglitore A, Sergi G, Satullo G, et al. [Arrhythmia in thalassemia major: evaluation of iron chelating therapy by dynamic ECG]. Minerva cardioangiologica. 1993; 41(7–8):297–301. PMID: 8139777

37. Fitchett DH, Coltart DJ, Littler WA, Leyland MJ, Trueman T, Gozzard DI, et al. Cardiac involvement in secondary haemochromatosis: a catheter biopsy study and analysis of myocardium. Cardiovascular research. 1980; 14(12):719–24. PMID: 7260965

38. Alp A, Ozdogan O, Guloglu CC, Turker M, Atabay B. Heart rate variability in beta-thalassaemia major with or without cardiac siderosis. Cardiology in the young. 2014; 24(2):263–7. doi: 10.1017/S1047951113000036 PMID: 23402458

39. Rutjanaprom W, Kanlop N, Charoenkwan P, Sittiwangkul R, Srichairatanakool S, Tantiworawit A, et al. Heart rate variability in beta-thalassemia patients. European journal of haematology. 2009; 83(5):483–9. doi: 10.1111/j.1600-0609.2009.01314.x PMID: 19594617

40. Heart rate variability. Standards of measurement, physiological interpretation, and clinical use. Task Force of the European Society of Cardiology and the North American Society of Pacing and Electrophysiology. European heart journal. 1996; 17(3):354–81. PMID: 8737210

41. Harris PR, Sommargren CE, Stein PK, Fung GL, Drew BJ. Heart rate variability measurement and clinical depression in acute coronary syndrome patients: narrative review of recent literature. Neuropsychiatric disease and treatment. 2014; 10:1335–47. doi: 10.2147/NDT.S57523 PMID: 25071372

42. La Rovere MT, Pinna GD, Hohnloser SH, Marcus FI, Mortara A, Nohara R, et al. Baroreflex sensitivity and heart rate variability in the identification of patients at risk for life-threatening arrhythmias: implications for clinical trials. Circulation. 2001; 103(16):2072–7. PMID: 11319197

43. Franzoni F, Galetta F, Di Muro C, Buti G, Pentimone F, Santoro G. Heart rate variability and ventricular late potentials in beta-thalassemia major. Haematologica. 2004; 89(2):233–4. PMID: 15003899

44. Gurses D, Ulger Z, Levent E, Aydinok Y, Ozyurek AR. Time domain heart rate variability analysis in patients with thalassaemia major. Acta cardiologica. 2005; 60(5):477–81. PMID: 16261777

45. Nolan J, Batin PD, Andrews R, Lindsay SJ, Brooksby P, Mullen M, et al. Prospective study of heart rate variability and mortality in chronic heart failure: results of the United Kingdom heart failure evaluation and assessment of risk trial (UK-heart). Circulation. 1998; 98(15):1510–6. PMID: 9769304

46. Blackmore S, Hamilton M, Lee A, Worwood M, Brierley M, Heath A, et al. Automated immunoassay methods for ferritin: recovery studies to assess traceability to an international standard. Clinical chemistry and laboratory medicine: CCLM / FESCC. 2008; 46(10):1450–7.

47. Kaltwasser JP. [Indication for serum ferritin determination]. Deutsche medizinische Wochenschrift. 1980; 105(10):319–21. PMID: 7363762

48. Singh S, Hider RC, Porter JB. A direct method for quantification of non-transferrin-bound iron. Analytical biochemistry. 1990; 186(2):320–3. PMID: 2363505

49. Chansiw N, Pangjit K, Phisalaphong C, Porter JB, Evans P, Fucharoen S, et al. Effect of a novel oral active iron chelator: 1-(N-acetyl-6-aminohexyl)-3-hydroxy-2-methylpyridin-4-one (CM1) in iron-overloaded and non-overloaded mice. Asian Pacific journal of tropical medicine. 2014; 7S1:S155–61. doi: 10.1016/S1995-7645(14)60223-6 PMID: 25312112

50. Schiller NB, Shah PM, Crawford M, DeMaria A, Devereux R, Feigenbaum H, et al. Recommendations for quantitation of the left ventricle by two-dimensional echocardiography. American Society of Echocardiography Committee on Standards, Subcommittee on Quantitation of Two-Dimensional Echocardiograms. Journal of the American Society of Echocardiography: official publication of the American Society of Echocardiography. 1989; 2(5):358–67.

51. Aessopos A, Farmakis D, Deftereos S, Tsironi M, Tassiopoulos S, Moyssakis I, et al. Thalassemia heart disease: a comparative evaluation of thalassemia major and thalassemia intermedia. Chest. 2005; 127(5):1523–30. PMID: 15888823

52. Nagueh SF, Appleton CP, Gillebert TC, Marino PN, Oh JK, Smiseth OA, et al. Recommendations for the evaluation of left ventricular diastolic function by echocardiography. European journal of echocardiography: the journal of the Working Group on Echocardiography of the European Society of Cardiology. 2009; 10(2):165–93.

53. Shabanian R, Heidari-Bateni G, Kocharian A, Mashayekhi M, Hosseinzadeh S, Kiani A, et al. Augmentation of left atrial contractile function: a herald of iron overload in patients with beta thalassemia major. Pediatric cardiology. 2010; 31(5):680–8. doi: 10.1007/s00246-010-9693-x PMID: 20383704

54. Malliani A. Heart rate variability: from bench to bedside. European journal of internal medicine. 2005; 16(1):12–20. PMID: 15733815

55. Kardelen F, Tezcan G, Akcurin G, Ertug H, Yesilipek A. Heart rate variability in patients with thalassemia major. Pediatric cardiology. 2008; 29(5):935–9. doi: 10.1007/s00246-008-9240-1 PMID: 18551333

56. Yetimakman AF, Oztarhan K, Aydogan G. Comparison of tissue Doppler imaging with MRI t2* and 24-hour rhythm holter heart rate variability for diagnosing early cardiac impairment in thalassemia major patients. Pediatric hematology and oncology. 2014; 31(7):597–606. doi: 10.3109/08880018.2014.891681 PMID: 24684386

57. Incharoen T, Thephinlap C, Srichairatanakool S, Chattipakorn S, Winichagoon P, Fucharoen S, et al. Heart rate variability in beta-thalassemic mice. International journal of cardiology. 2007; 121(2):203–4. PMID: 17113168

58. Kumfu S, Chattipakorn S, Chinda K, Fucharoen S, Chattipakorn N. T-type calcium channel blockade improves survival and cardiovascular function in thalassemic mice. European journal of haematology. 2012; 88(6):535–48. doi: 10.1111/j.1600-0609.2012.01779.x PMID: 22404220

59. Fiorelli G, Fargion S, Piperno A, Battafarano N, Cappellini MD. Iron metabolism in thalassemia intermedia. Haematologica. 1990; 75 Suppl 5:89–95. PMID: 2086386

60. Bartfay WJ, Bartfay E. Iron-overload cardiomyopathy: evidence for a free radical—mediated mechanism of injury and dysfunction in a murine model. Biol Res Nurs. 2000; 2(1):49–59. PMID: 11232511

61. Gao X, Campian JL, Qian M, Sun XF, Eaton JW. Mitochondrial DNA damage in iron overload. The Journal of biological chemistry. 2009; 284(8):4767–75. doi: 10.1074/jbc.M806235200 PMID: 19095657

62. Apaijai N, Pintana H, Chattipakorn SC, Chattipakorn N. Cardioprotective effects of metformin and vildagliptin in adult rats with insulin resistance induced by a high-fat diet. Endocrinology. 2012; 153(8):3878–85. doi: 10.1210/en.2012-1262 PMID: 22621958

63. Apaijai N, Pintana H, Chattipakorn SC, Chattipakorn N. Effects of vildagliptin versus sitagliptin, on cardiac function, heart rate variability and mitochondrial function in obese insulin-resistant rats. British journal of pharmacology. 2013; 169(5):1048–57. doi: 10.1111/bph.12176 PMID: 23488656

64. Campos C, Casali KR, Baraldi D, Conzatti A, Araujo AS, Khaper N, et al. Efficacy of a low dose of estrogen on antioxidant defenses and heart rate variability. Oxidative medicine and cellular longevity. 2014; 2014:218749. doi: 10.1155/2014/218749 PMID: 24738017

65. Chuang HC, Hsueh TW, Chang CC, Hwang JS, Chuang KJ, Yan YH, et al. Nickel-regulated heart rate variability: the roles of oxidative stress and inflammation. Toxicology and applied pharmacology. 2013; 266(2):298–306. doi: 10.1016/j.taap.2012.11.006 PMID: 23164665

66. Lee MS, Eum KD, Fang SC, Rodrigues EG, Modest GA, Christiani DC. Oxidative stress and systemic inflammation as modifiers of cardiac autonomic responses to particulate air pollution. International journal of cardiology. 2014; 176(1):166–70. doi: 10.1016/j.ijcard.2014.07.012 PMID: 25074558

67. Malfitano C, Barboza C, Mostarda C, da Palma R, Dos Santos C, Rodrigues B, et al. Diabetic hyperglycemia attenuates sympathetic dysfunction and oxidative stress after myocardial infarction in rats. Cardiovascular diabetology. 2014; 13(1):131.

68. Pavithran P, Nandeesha H, Sathiyapriya V, Bobby Z, Madanmohan T. Short-term heart variability and oxidative stress in newly diagnosed essential hypertension. Clinical and experimental hypertension. 2008; 30(7):486–96. doi: 10.1080/10641960802251875 PMID: 18855253

69. Supakul L, Pintana H, Apaijai N, Chattipakorn S, Shinlapawittayatorn K, Chattipakorn N. Protective effects of garlic extract on cardiac function, heart rate variability, and cardiac mitochondria in obese insulin-resistant rats. European journal of nutrition. 2014; 53(3):919–28. doi: 10.1007/s00394-013-0595-6 PMID: 24142245

70. Thiyagarajan R, Pal P, Pal GK, Subramanian SK, Bobby Z, Das AK, et al. Cardiovagal modulation, oxidative stress, and cardiovascular risk factors in prehypertensive subjects: cross-sectional study. American journal of hypertension. 2013; 26(7):850–7. doi: 10.1093/ajh/hpt025 PMID: 23466463

เอกสารแนบหมายเลข 48

Research Paper

Dipeptidyl peptidase-4 inhibitor improves cardiac function by attenuating adverse cardiac remodelling in rats with chronic myocardial infarction

Tharnwimol Inthachai[1,2], Suree Lekawanvijit[1,3], Sirinart Kumfu[1,2], Nattayaporn Apaijai[1,2], Wanpitak Pongkan[1,2], Siriporn C. Chattipakorn[1,4] and Nipon Chattipakorn[1,2]

[1]*Cardiac Electrophysiology Research and Training Center, Faculty of Medicine, Chiang Mai University, Chiang Mai, Thailand*
[2]*Cardiac Electrophysiology Unit, Department of Physiology, Faculty of Medicine, Chiang Mai University, Chiang Mai, Thailand*
[3]*Department of Pathology, Faculty of Medicine, Chiang Mai University, Chiang Mai, Thailand*
[4]*Department of Oral Biology and Diagnostic Science, Faculty of Dentistry, Chiang Mai University, Chiang Mai, Thailand*

New Findings

- **What is the central question of this study?**
  Although cardioprotective effects of dipeptidyl peptidase-4 (DPP-4) inhibitors have been demonstrated, their cardiac effects in chronic myocardial infarction (MI) are unclear. We determined the effects of a DPP-4 inhibitor on cardiac function and remodelling in rats with chronic MI.
- **What is the main finding and its importance?**
  We demonstrated, for the first time, that DPP-4 inhibitor, but not metformin, exerted similar efficacy in improving cardiac function and attenuating cardiac fibrosis compared with enalapril in rats with chronic MI. These findings reveal benefits additional to the glycaemic control by the DPP-4 inhibitor in chronic MI, and it might become the new drug of choice for MI in patients with diabetes mellitus.

Adverse cardiac remodelling after myocardial infarction (MI) leads to progressive heart failure. Dipeptidyl peptidase-4 (DPP-4) inhibitors are new antidiabetic drugs that exert cardioprotection. However, their role in cardiac function and remodelling in chronic MI is unclear. We hypothesized that the DPP-4 inhibitor vildagliptin reduces adverse cardiac remodelling and improves cardiac function in rats with chronic MI. These effects were also compared with enalapril and metformin. Male Wistar rats ($n = 36$) with chronic MI induced by ligation of the left anterior descending coronary artery were divided into six groups to receive vehicle, vildagliptin (3 mg kg^{-1} day^{-1}), metformin (30 mg kg^{-1} day^{-1}), enalapril (10 mg kg^{-1} day^{-1}), combined metformin and enalapril or combined vildagliptin and enalapril for 8 weeks. At the end of the study, plasma malondialdehyde (MDA), heart rate variability (HRV), left ventricular (LV) function, pathological and biochemical studies of cardiac remodelling were investigated. Our study demonstrated that rats with chronic MI had increased oxidative stress levels, depressed HRV, adverse cardiac remodelling, indicated by cardiac fibrosis, and LV dysfunction. Treatment with vildagliptin or enalapril significantly decreased oxidative stress, attenuated cardiac fibrosis and improved HRV and LV function. We conclude that vildagliptin exerts similar cardioprotective effects to enalapril in attenuating oxidative stress and cardiac fibrosis and improving cardiac function in rats with chronic MI. Metformin does not provide these benefits in this model. Moreover, addition of either metformin

Experimental Physiology

© 2015 The Authors. Experimental Physiology © 2015 The Physiological Society
DOI: 10.1113/EP085108

or vildagliptin to enalapril does not provide additional benefit in attenuating cardiac remodelling or improving LV function compared with enalapril alone.

(Resubmitted 28 January 2015; accepted after revision 27 March 2015; first published online 30 March 2014)
Corresponding author N. Chattipakorn: Cardiac Electrophysiology Research and Training Center, Faculty of Medicine, Chiang Mai University, Chiang Mai 52000, Thailand. Email: nchattip@gmail.com

Introduction

Heart failure is the most common complication and the major cause of morbidity and mortality in survivors of myocardial infarction (MI; Minicucci *et al.* 2011). Post-MI cardiac structural changes, the so-called 'cardiac remodelling', which comprises cardiac hypertrophy, interstitial fibrosis, progressive wall thinning and ventricular chamber dilatation (Sutton *et al.* 2000; Gajarsa *et al.* 2011), contribute to progressive cardiac dysfunction and heart failure. These processes are associated with persistent activation of neurohormonal systems, such as the sympathetic nervous system and renin–angiotensin–aldosterone system, and increased oxidative stress. Generally, post-MI cardiac remodelling begins rapidly, usually within the first few hours, and continues to progress for weeks to months (Cohn *et al.* 2000). Patients with major cardiac remodelling are at high risk of heart failure progression and sudden cardiac death after MI (Cohn *et al.* 2000; Bunch *et al.* 2007). Thus, a reversal in cardiac remodelling is potentially a key therapeutic strategy in these patients to prevent sudden cardiac death and to slow the progression of heart failure. An angiotensin-converting enzyme inhibitor, such as enalapril, has been shown to exert cardioprotective effects in MI (Wang *et al.* 2004; Ocaranza *et al.* 2006).

Growing evidence demonstrates that several anti-diabetic drugs exert cardioprotective effects in addition to their glycaemia-controlling effect (Apaijai *et al.* 2012; Myat *et al.* 2014), including a first-line antidiabetic drug, metformin (Tahrani *et al.* 2007; Scarpello *et al.* 2008), and a new class of antidiabetic drug, gliptin (Plutzky, 2011; Hocher *et al.* 2012). Previous studies demonstrated that both metformin and vildagliptin exerted beneficial effects on cardiac autonomic regulation and cardiac function by attenuating the cardiac sympathovagal imbalance and improving cardiac contractile function in obese, insulin-resistant models (Apaijai *et al.* 2012). In a cardiac ischemia–reperfusion model, it has been shown that metformin and vildagliptin also improved cardiac function impaired by ischemia–reperfusion injury (Apaijai *et al.* 2014). Moreover, both metformin and gliptin, which have been used to treat patients with type 2 diabetes, have been demonstrated to decrease cardiac remodelling and improve left ventricular (LV) function in both animal (Liu *et al.* 2010; Yin *et al.* 2011; Takahashi *et al.* 2013) and clinical studies in non-diabetic and diabetic patients with MI (Sokos *et al.* 2006; Hausenloy *et al.* 2008; Lexis *et al.* 2014). However, comparison between these two drugs of the cardiac effects in chronic MI and investigation of the potential additional cardioprotective effects of using either metformin or gliptin in combination with an angiotensin-converting enzyme inhibitor, a conventional pharmacological treatment of chronic MI, have not been carried out.

In the present study, we determined the effects of metformin and vildagliptin on cardiac remodelling in rats with chronic MI induced by ligation ligation of the left anterior descending (LAD) coronary artery. Our hypotheses were as follows: (i) metformin and vildagliptin decrease oxidative stress and cardiac remodelling and improve heart rate variability (HRV) and LV function in rats with chronic MI; and (ii) a combination of either metformin or vildagliptin with enalapril exerts synergistic effects on cardioprotection in rats with chronic MI.

Methods

Ethical approval

All of the experiment procedures were conducted in accordance with an approved protocol from the Institution Animal Care and Use Committee at the Faculty of Medicine, Chiang Mai University, Chiang Mai, Thailand, and complied with the ARRIVE guidelines.

Animal preparation

Male Wistar rats weighing 400–450 g were obtained from the National Animal Center, Salaya Campus, Mahidol University, Thailand. All animals were fed with normal rat chow and *ad libitum* water and housed in a temperature-controlled environment with a 12 h–12 h light–dark cycle. All rats had MI induced by LAD coronary artery ligation, as previously described (Lekawanvijit *et al.* 2012). Briefly, animals were intubated and mechanically ventilated with 2% isoflurane in oxygen at a flow of 1.0 l min^{-1}. After the animal was deeply anaesthetized, a left-side thoracotomy was performed, and the LAD branch of the left coronary artery was exposed and ligated ~4 mm from its origin. Subsequently, positive pressure was applied to the lungs via the ventilator before closing the chest wall. Three days after LAD coronary artery ligation, all rats were

© 2015 The Authors. Experimental Physiology © 2015 The Physiological Society

randomly divided into six groups to receive one of the following treatments for 8 weeks by intragastric gavage: vehicle (normal saline); enalapril (10 mg kg^{-1}; Berlin Pharmaceutical Industry, Bangkok, Thailand); metformin (15 mg kg^{-1}, twice a day; Glucophage; Merck Serono, Bangkok, Thailand); vildagliptin (3 mg kg^{-1}, once a day; Galvus; Novartis, Bangkok, Thailand); combined metformin and enalapril; or combined vildagliptin and enalapril (n = 5–7 per group). Heart rate variability was assessed and blood samples were collected at baseline and at the end of treatment. Echocardiography was performed at baseline, at 4 weeks post-MI and at the end of treatment. At the end of treatment, all rats were anaesthetized as described below (see subsection entitled '*Measurement of LV pressure*') and LV function was assessed using an intraventricular pressure-recording system via the pressure catheter (Scisense, London, Ontario, Canada). The heart was removed to determine the infarct size and cardiac remodelling, including cardiomyocyte hypertrophy and cardiac fibrosis. Heart tissue was also used for Western blot analysis.

Determination of plasma MDA level

Plasma MDA levels were measured by HPLC-based assay (Thermo Scientific, Bangkok, Thailand; Apaijai *et al.* 2012). Plasma MDA was mixed with phosphoric acid (H_3PO_4) and thiobarbituric acid (TBA) to create TBA reactive substance. The plasma TBA reactive substance concentration was reported as the MDA equivalent concentration from a standard curve of the HPLC-based assay (Mateos *et al.* 2005).

Analysis of HRV

Heart rate variability was used to determine the cardiac sympathovagal balance (Incharoen *et al.* 2007; Apaijai *et al.* 2012). The lead II ECG was recorded in all rats using Powerlab (AD Instruments, Sydney, NSW, Australia). Data of R–R interval variability from the ECG were analysed using the MATLAB program (Incharoen *et al.* 2007; Apaijai *et al.* 2013). In the present study, the frequency domain method was used to represent the HRV (Apaijai *et al.* 2012; Supakul *et al.* 2014). The frequency domain has three major oscillatory components, namely the high-frequency (HF; 0.6–3 Hz) band, representing cardiac parasympathetic activity, the low-frequency (LF; 0.2–0.6 Hz) band, representing cardiac sympathetic and parasympathetic activity, and the very low-frequency (VLF; below 0.2 Hz) band. The LF/HF ratio was used to indicate cardiac sympathovagal balance (Apaijai *et al.* 2012). A reduction in HRV or increase in the LF/HF ratio represents cardiac sympathovagal imbalance.

Echocardiography

M-Mode echocardiography (HP/Agilent Philips Sonos 4500; Agilent Technologies, Santa Clara, CA, USA) was used to determine LV posterior wall diameter during diastole (LVPWd), interventricular septum during diastole (IVSd), LV internal diameter during diastole (LVIDd), LV posterior wall diameter during systole (LVPWs), interventricular septum during systole (IVSs) and LV internal diameter during systole (LVIds). The percentage of fractional shortening (%FS) was calculated to indicate LV systolic performance by using the following equation: %FS = [(LVIDd − LVIds)/LVIDd] × 100 (McDonald, 1976).

Measurement of LV pressure

Rats were anaesthetized using zoletil (50 mg kg^{-1}; Virbac, Laboratories, Carros, France) and xylazine (0.15 mg kg^{-1}; Laboratory Carlier, SA, Barcelona, Spain) via I.M. injection (Apaijai *et al.* 2012; Supakul *et al.* 2014). The rats were ventilated with room air via a tracheostomy tube. The right carotid artery was identified and cannulated with a pressure catheter (Scisense) to measure LV pressure for 20 min (Supakul *et al.* 2014). Parameters including heart rate, end-systolic pressure (ESP), end-diastolic pressure (EDP), maximal (dP/dt_{max}) and minimal rate of change of pressure (dP/dt_{min}) were analysed using the Labscribe analytical software program (iWorx System Inc., Dover, NH, USA) (Apaijai *et al.* 2012; Chinda *et al.* 2012).

Assessment of myocardial infarct size

Tissue harvesting was performed at the end of the LV pressure assessment while animals were still under deep anaesthesia. The left ventricle was divided horizontally into three sections. Mid-LV cross-sections were stained with Picrosirius Red and scanned for infarct size analysis. Assessment was performed in animals with transmural infarction where the full thickness of the LV wall from the endocardium to epicardium was replaced by fibrotic scar tissue (Goldman *et al.* 1995). Infarct size was reported as an average of the proportions of LV endocardial and epicardial circumferences occupied by the infarct as previously described (Goldman *et al.* 1995).

Determination of cardiac remodelling

Mid-LV cross-sections were stained with Haematoxylin and Eosin and scanned with an Aperio ScanScope (Aperio Technologies, Inc., Vista, CA, USA). Fifty LV cardiomyocytes with equal-sized nuclei were randomly selected for analysis of cellular cross-sectional area using Aperio ImageScope version 11.1.2.760 (Lekawanvijit *et al.*

© 2015 The Authors. Experimental Physiology © 2015 The Physiological Society

Table 1. Effects of pharmacological interventions on metabolic parameters and organ weight index

Metabolic parameter/organ weight index	Groups						
	MI + V	MI + E	MI + M	MI + Vil	MI + M&E	MI + Vil&E	Significance
BW (g)	491 ± 14	497 ± 18	490 ± 15	505 ± 15	500 ± 20	494 ± 8	n.s.
Food intake (g)	22 ± 2	21 ± 2	23 ± 1	22 ± 2	21 ± 1	22 ± 2	n.s.
LV/BW (g kg^{-1})	2.13 ± 0.27	1.88 ± 0.32	2.13 ± 0.14	1.98 ± 0.06	1.92 ± 0.26	2.06 ± 0.19	n.s.
RV/BW (g kg^{-1})	0.49 ± 0.10	0.42 ± 0.09	0.45 ± 0.03	0.41 ± 0.05	0.40 ± 0.04	0.38 ± 0.04	n.s.
Atrium/BW (g kg^{-1})	0.35 ± 0.03	0.31 ± 0.08	0.30 ± 0.07	0.30 ± 0.09	0.31 ± 0.08	0.28 ± 0.06	n.s.
Lung/BW (g kg^{-1})	3.61 ± 0.62	3.32 ± 0.63	3.70 ± 0.48	3.14 ± 0.17	3.07 ± 0.22	3.46 ± 0.22	n.s.
Infarct size (%)	36 ± 3	36 ± 5	37 ± 4	37 ± 4	31 ± 4	29 ± 3	n.s.

One-way ANOVA; BW, $F = 0.549$, $P = 0.738$; LV/BW, $F = 1.374$, $P = 0.262$; RV/BW, $F = 1.066$, $P = 0.399$; atrium/BW, $F = 0.690$, $P = 0.635$; lung weight/BW, $F = 1.681$, $P = 0.170$; and infarct size, $F = 0.558$, $P = 0.731$. Abbreviations: BW, body weight; E, enalapril; LV, left ventricular weight; M, metformin; M&E, metformin and enalapril; MI, myocardial infarction; n.s., non-significant; RV, right ventricular weight; V, vehicle; Vil, vildagliptin; Vil&E, vildagliptin and enalapril.

Table 2. Effects of pharmacological interventions on LV function in rats with chronic MI

Left ventricular pressure parameters	Groups					
	MI + V	MI + E	MI + M	MI + Vil	MI + M&E	MI + Vil&E
HR (beats min^{-1})	270 ± 48	273 ± 51	253 ± 50	240 ± 27	257 ± 19	260 ± 65
ESP (mmHg)	87 ± 10	138 ± 17*	94 ± 18†	116 ± 30†*	128 ± 23*	126 ± 24*
EDP (mmHg)	32 ± 7	15 ± 4*	31 ± 7†	23 ± 7*	18 ± 5*	19 ± 4*
dP/dt_{max} (mmHg s^{-1})	6837 ± 830	25,279 ± 383*	9376 ± 2019†	17,097 ± 5973†*	24,916 ± 2113*	24,113 ± 6053*
dP/dt_{min} (mmHg s^{-1})	−4280 ± 268	−8221 ± 956*	−4461 ± 657†	−8842 ± 1549*	−9338 ± 1529*	−10,161 ± 1554*

*$P < 0.05$ *versus* MI + V at 8 weeks post-MI; †$P < 0.05$ *versus* MI + E at 8 weeks post-MI. One-way ANOVA; HR, $F = 0.422$, $P = 0.830$; ESP, $F = 5.456$, $P = 0.001$; EDP, $F = 6.176$, $P = 0.001$; dP/dt_{max}, $F = 6.491$, $P = 0.000$; and dP/dt_{min}, $F = 5.767$, $P = 0.001$. Abbreviations: dP/dt_{max}, maximal pressure; dP/dt_{min}, minimal pressure; E, enalapril; EDP, end-diastolic pressure; ESP, end-systolic pressure; HR, heart rate; M, metformin; M&E, combined metformin and enalapril; MI, myocardial infarction; V, vehicle; Vil, vildagliptin; Vil&E, combined vildagliptin and enalapril.

2012). Measurements from each animal were averaged and data expressed as the mean ± SEM for each group. For determination of cardiac fibrosis, cardiac sections stained with Picrosirius Red were scanned with the Aperio ScanScope. The proportional area of matrix deposition in the peri-infarct and non-infarcted areas were analysed separately using the positive pixel count v9 algorithm for Picrosirius Red stain intensity (Lekawanvijit *et al.* 2012).

Western blot analysis

At the end of the study, heart tissues were collected, quickly frozen in liquid nitrogen and stored at −80°C until utilization as described previously (Kumphune *et al.* 2011). Heart tissue was homogenized with 1 ml of tissue lysis buffer, subsequently homogenized at 4°C and incubated on ice for 30 min, followed by centrifugation at 15493g for 10 min at 4°C, after which the supernatant was collected as 100 μl aliquots. Equal amounts (34 μg) of the total protein were mixed with the loading buffer (1 mg ml^{-1}; 10% mercaptoethanol, 0.05% Bromophenol Blue, 75 mM Tris–HCl, pH 6.8, 2% SDS and 10% glycerol), boiled for 5 min and loaded onto a 10% gradient SDS-polyacrylamide gel. Then, the protein was transferred to a nitrocellulose membrane in the presence of the glycine–methanol transfer buffer (20 mM Tris base, 0.15 M glycine and 20% methanol) in a transfer system (Bio-Rad, Hercules, CA, USA). The nitrocellulose membrane was blocked with 5% skimmed milk in 1× TBS-T buffer (20 mM Tris–HCl, pH 7.6, 137 mM NaCl and 0.05% Tween-20) for 1 h at room temperature. The membrane was subsequently exposed to anti-Bax (Santa Cruz Biotechnology, Santa Cruz, CA, USA), anti-Bcl-2, anti-active caspase-3, anti-phosphorylated connexin (Cx) 43, anti-transforming growth factor-β (TGF-β), anti-phosphorylated p38 (p-p38) and p38 mitogen-activated protein kinase (MAPK), and anti-phosphorylated p44/42 (p-p44/42) and p44/42 MAPK (Cell Signaling Technology, Danvers, MA, USA) overnight at 4°C. The signals were developed by

© 2015 The Authors. Experimental Physiology © 2015 The Physiological Society

incubating with enhanced chemiluminescence reagent and subjected to autoradiography.

Statistical analysis

All data were expressed as mean values ± SEM. Two-way ANOVA with repeated measures followed by a least significant difference (LSD) *post hoc* test was used to determine variables measured repeatedly at multiple time points, including %FS, LF/HF ratio and plasma MDA. One-way ANOVA followed by an LSD *post hoc* test was used to determine variables measured at a single time point. A value of $P < 0.05$ was considered statistically significant.

Results

Metabolic parameters and organ weight index in rats with chronic MI among various treatment groups

At 8 weeks post-MI, the effects of pharmacological interventions on the body weight (BW), food intake and LV/BW, lung/BW, right ventricle/BW and atrium/BW ratios are shown in Table 1. Our results demonstrated

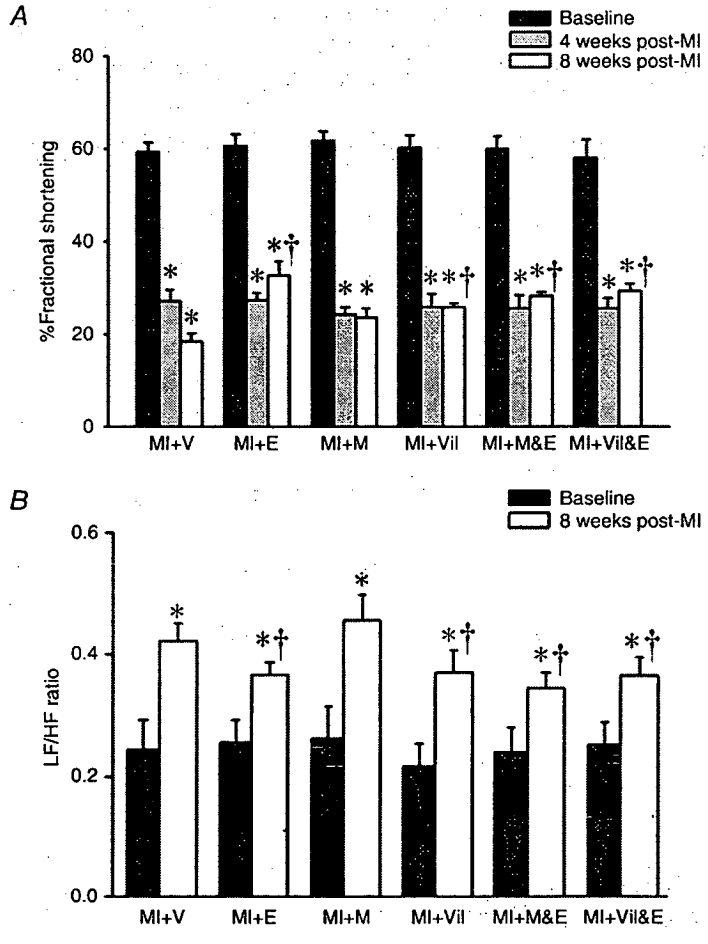


Figure 1. Effects of pharmacological interventions on percentage of fractional shortening (%FS) and low-frequency/high-frequency (LF/HF) ratio in rats with chronic myocardial infarction (MI)
n = 5–7 per group. *A*, all pharmacological interventions, except metformin (MI + M group), improved %FS at 8 weeks post-MI. *B*, all pharmacological interventions, except MI + M, decreased the LF/HF ratio at 8 weeks post-MI. Two-way ANOVA; %FS, time course effect (F = 426.608, P = 0.000), treatment effect (F = 2.634, P = 0.044, and time course and treatment effects (F = 2.888, P = 0.005); and LF/HF ratio, time course effect (F = 113.640, P = 0.000), treatment effect (F = 3.098, P = 0.002), and time course and treatment effects (F = 3.670, P = 0.011). Abbreviations: M, metformin; M&E, combined metformin and enalapril; E, enalapril; V, vehicle; Vil, vildagliptin; Vil&E, combined vildagliptin and enalapril. *$P < 0.05$ *versus* baseline of the same group, †$P < 0.05$ *versus* MI + V group at 8 weeks post-MI.

© 2015 The Authors. Experimental Physiology © 2015 The Physiological Society

that these parameters were not significantly different among different treatment groups compared with the vehicle-treated group.

Infarct size in rats with chronic MI among various treatment groups

Ligation of the LAD coronary artery resulted in an infarct size of 36 ± 3, 36 ± 5, 37 ± 4, 37 ± 4, 31 ± 4 and 29 ± 3% in the vehicle group (MI + V), enalapril-treated group (MI + E), metformin-treated group (MI + M), vildagliptin-treated group (MI + Vil), combined metformin- and vildagliptin-treated group (MI + M&E) and combined vildagliptin- and enalapril-treated group (MI + Vil&E), respectively. There was no significant difference in the infarct size among different treatment groups (Table 1). These results indicated the similar degree of infarct size induced by LAD coronary artery occlusion in all treatment groups.

Left ventricular function in rats with chronic MI among various treatment groups

At 4 weeks post-MI, %FS was decreased in all groups of rats with chronic MI. All pharmacological treatments in the present study did not significantly improve %FS when compared with the MI + V group after 4 weeks of treatment (Fig. 1*A*). However, %FS was significantly improved after 8 weeks of treatment in MI + E, MI + Vil, MI + M&E and MI + Vil&E groups, but not in the MI + M group. Moreover, rats in the MI + E group had a significantly higher %FS than those in the MI + Vil group. No significant difference was observed when comparing the %FS of the MI + E group with the MI + M&E and MI + Vil&E groups (Fig. 1*A*).

Results from the LV pressure study showed that all treatment groups, except MI + M, showed a significant increase in ESP and dP/dt_{max} and a significant decrease in EDP and dP/dt_{min} after 8 weeks of treatment compared with the MI + V group (Table 2). In addition, the MI + E group had significantly higher ESP and dP/dt_{max} than the MI + Vil group, while no difference was observed when compared with the MI + M&E and MI + Vil&E groups (Table 2). There was no significant difference of EDP and dP/dt_{min} among the MI + E, MI + Vil, MI + M&E and MI + Vil&E groups.

Heart rate variability in rats with chronic MI among various treatment groups

At baseline, the LF/HF ratio was not different among different treatment groups (Fig. 1*B*). At 8 weeks post-MI, all groups had an increased LF/HF ratio when compared with the baseline. However, all treatment groups, except the MI + M group, showed a significant reduction in the LF/HF ratio when compared with the MI + V group. There

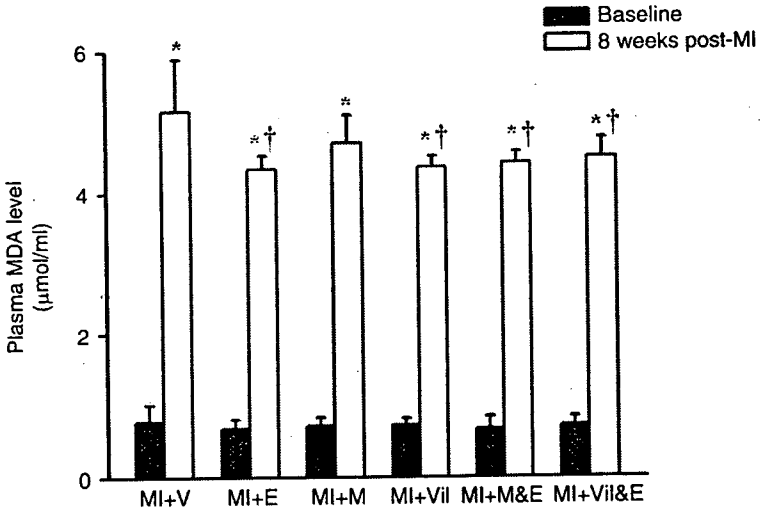


Figure 2. Effects of pharmacological interventions on plasma malondialdehyde (MDA) concentration in rats with chronic MI
n = 5–7 per group. All pharmacological interventions, except metformin (MI + M group), decreased plasma MDA concentration at 8 weeks post-MI. *$P < 0.05$ *versus* baseline of the same group, †$P < 0.05$ *versus* MI + V at 8 weeks post-MI. Two-way ANOVA; time course effect ($F = 4209.660$, $P = 0.000$), treatment effect ($F = 3.996$, $P = 0.007$), and time course and treatment effects ($F = 3.347$, $P = 0.016$). Abbreviations are as for Fig. 1.

© 2015 The Authors. Experimental Physiology © 2015 The Physiological Society

was no significant difference in HRV among the MI + E, MI + Vil, MI + M&E and MI + Vil&E groups.

Oxidative stress in rats with chronic MI among various treatment groups

At baseline, plasma MDA concentrations were not significantly different among different treatment groups (Fig. 2). At 8 weeks post-MI, all groups had increased plasma MDA levels compared with the baseline. However, rats in the MI + E, MI + Vil, MI + M&E and MI + Vil&E groups had significantly lower plasma MDA levels compared with the MI + V group. There was no significant difference in the plasma MDA among the MI + E, MI + Vil, MI + M&E and MI + Vil&E groups. The plasma MDA concentration in the MI + M group was not different from the MI + V group.

Cardiac remodelling among various treatment groups

At 8 weeks post-MI, cardiac fibrosis in the peri-infarct area was not significantly different among different treatment groups (Fig. 3*B*). Interestingly, a significant reduction in cardiac fibrosis in the non-infarcted area was observed in the MI + E, MI + Vil, MI + M&E and MI + Vil&E groups, but not in the MI + M group, when compared with the MI + V group (Fig. 3*A*). Our results also demonstrated that cardiomyocyte cross-sectional area

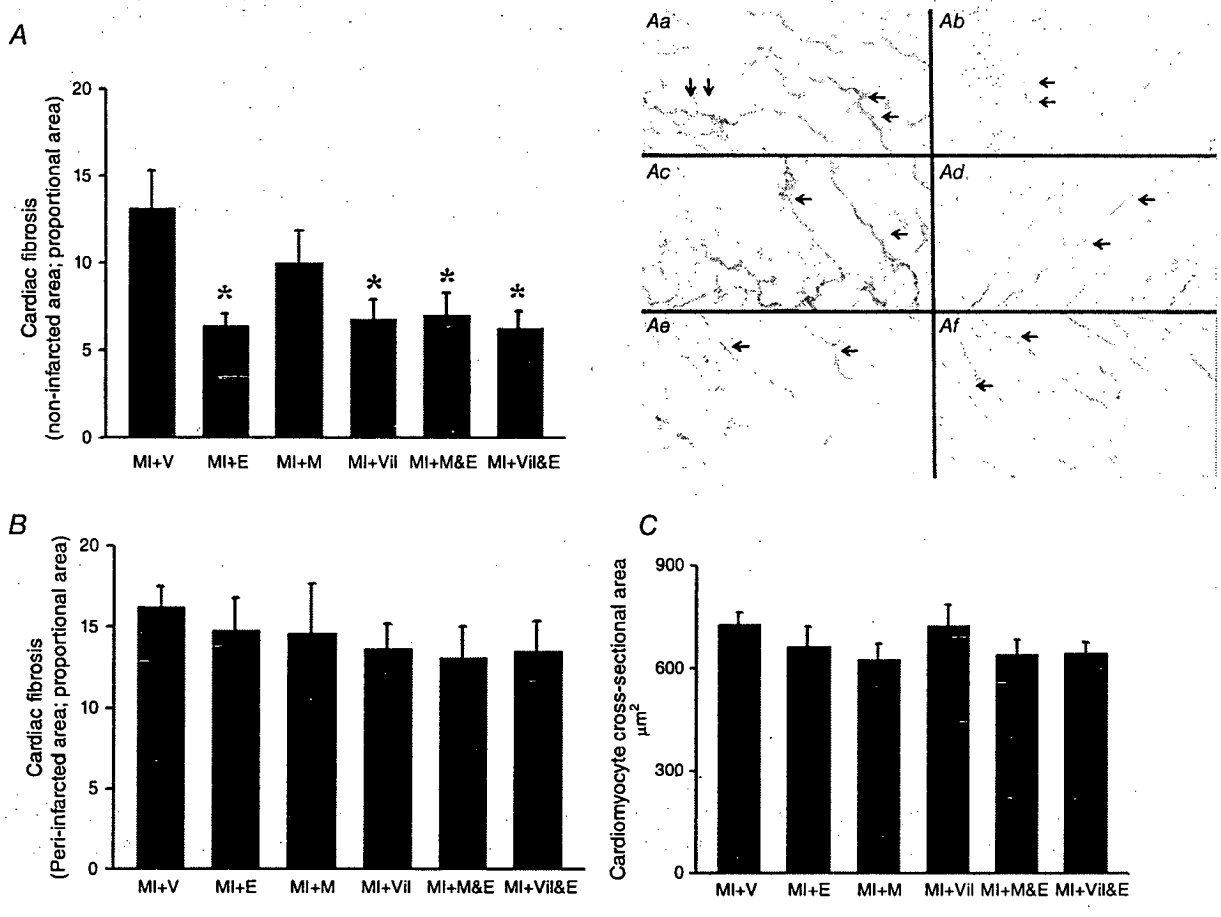


Figure 3. Effects of pharmacological interventions on cardiac fibrosis in the non-infarct area (*A*), peri-infarct area (*B*) and cardiomyocyte cross-sectional area (*C*) in rats with chronic MI
n = 5–7 per group. *A* (right panel) demonstrates fibrosis stained in red (arrows) in the non-infarcted zone of the heart in the following treatments: MI + V (*Aa*), MI + E (*Ab*), MI + M (*Ac*), MI + Vil (*Ad*), MI + M&E (*Ae*) and MI + Vil&E (*Af*). Picrosirius Red staining, ×20 objective, Aperio ImageScope. All pharmacological interventions, except metformin (MI + M), attenuated cardiac fibrosis in the non-infarcted area. $^*P < 0.05$ *versus* MI + V group. One-way ANOVA: cardiac fibrosis in non-infarcted zone ($F = 3.680$, $P = 0.011$), peri-infarct area ($F = 0.381$, $P = 0.858$) and cardiomyocyte cross-sectional area ($F = 0.954$, $P = 0.461$). Abbreviations are as for Fig. 1.

© 2015 The Authors. Experimental Physiology © 2015 The Physiological Society

was not significantly different among different treatment groups compared with the MI + V group (Fig. 3*C*).

Protein expression in rats with chronic MI among various treatment groups

Western blot analysis showed a decreased Bax/Bcl-2 ratio in the MI + E, MI + M&E and MI + Vil&E groups, but not in the MI + M and MI + Vil groups, compared with the MI + V group (Fig. 4). In all drug treatment groups, the p-p44/42 protein expression was significantly decreased, compared with the MI + V group (Fig. 5). However, no significant difference in p-p44/42 protein expression was found among these drug-treated groups. The expression levels of active caspase-3, TGF-β, p-p38 and p-connexin 43 (serine368 residue) were also not significantly different among all groups (Fig. 6).

Discussion

The major findings of the present study in the setting of chronic MI are as follows. Rats with chronic MI induced by ligation of the LAD coronary artery developed a cardiac sympathovagal imbalance (i.e. depressed HRV), increased oxidative stress level, cardiac fibrosis and LV dysfunction. Treatment with enalapril and vildagliptin, but not metformin, improved HRV, reduced oxidative stress, attenuated cardiac fibrosis and improved LV function.

In the present study, rats with chronic MI developed cardiac sympathovagal imbalance at 8 weeks post-MI as indicated by an increased LF/HF ratio. Our finding is consistent with previous clinical studies that demonstrated increased sympathetic and decreased parasympathetic activity in patients with chronic MI (Chattipakorn *et al.* 2007; Oliveira *et al.* 2013). Moreover, the depressed HRV has been shown to be associated with increased oxidative stress level (Pavithran *et al.* 2008). Our findings suggested that increased plasma MDA concentration in rats with chronic MI could be linked to the increased LF/HF ratio we observed. In the present study, we demonstrated that both enalapril and vildagliptin, but not metformin, could reduce the oxidative stress level and improve HRV in rats with chronic MI to a similar degree, suggesting a strong association between the reduced oxidative stress level and improved cardiac autonomic balance in these conditions. It has been shown that the increased sympathetic activity in chronic MI could be aggravated in stress conditions, and that this increase in sympatho-excitation in turn could significantly impact the progression of heart failure (Triposkiadis *et al.* 2009; Kishi, 2012). It is also possible that the drugs could affect various elements of the cardiac nervous system and that the potential cardioprotective effects of this pharmacological therapy could be related to their effects on cardiac-related neurons rather than direct effects on cardiomyocytes. Future study is needed

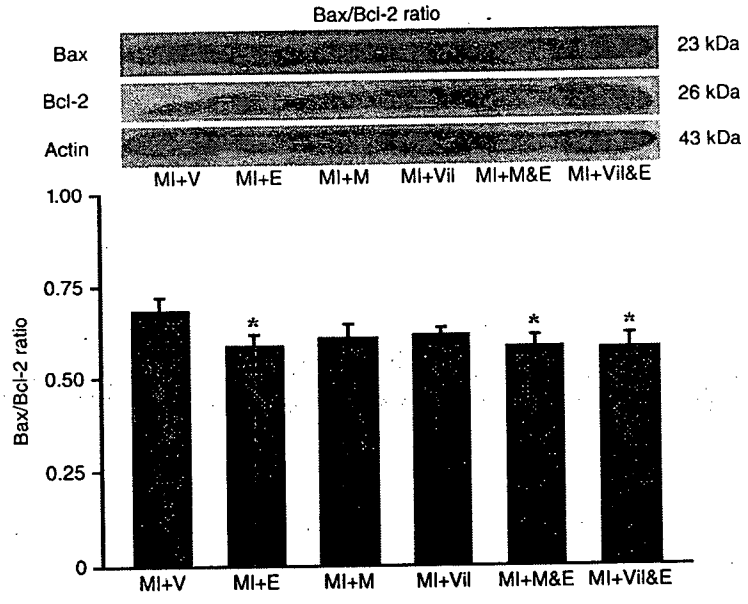


Figure 4. Effects of pharmacological interventions on Bax/Bcl-2 ratio in rats with chronic MI
$n = 5$–7 per group. Enalapril treatment (MI + E, MI + E&M and MI + E&Vil groups) significantly decreased the Bax/Bcl-2 ratio. *$P < 0.05$ *versus* MI + V group. One-way ANOVA ($F = 2.825$, $P = 0.038$). Abbreviations are as for Fig. 1.

© 2015 The Authors. Experimental Physiology © 2015 The Physiological Society

to test this hypothesis. The fact that these drugs could improve cardiac sympathovagal balance and decrease oxidative stress may also provide a long-term benefit on the progression of heart failure in this chronic MI model.

In rats with chronic MI, cardiac systolic and diastolic dysfunction is commonly found (Bauersachs *et al.* 2001; Izutani *et al.* 2002). Given that the infarct size in our rats with chronic MI was not different among different treatment groups, the improved LV function observed with both enalapril and vildagliptin, but not metformin, treatment could contribute to the improved cardiac remodelling by these drugs. In a pressure overload-induced heart failure model, vildagliptin was shown to decrease cardiac interstitial fibrosis and increase %FS and survival rate (Takahashi *et al.* 2013). In the present study, vildagliptin reduced cardiac fibrosis significantly, consistent with a previous report in a different model. However, the effect of vildagliptin on LV function has been inconsistently reported. In a study by Yin *et al.* (2011), vildagliptin given at 3 weeks after LAD coronary artery ligation provided no protective effects on cardiac function and remodelling in this long-term chronic MI model. This could be due to the late administration of the drug after MI onset. Post-MI, it has been shown that ventricular remodelling can continue for weeks in a subacute stage to months in a chronic stage of remodelling (Gajarsa *et al.* 2011). Therefore, in the study by Yin *et al.* (2011) it is possible that the remodelling process was already completed at the time vildagliptin was administered, leading to failed protection against cardiac dysfunction and adverse remodelling. Unlike the study by Yin *et al.* (2011), the treatment was started on the third day after ligation of the LAD coronary artery in the present study, when the remodelling process was still in an acute stage, thus exerting the cardioprotection in our rats with chronic MI. These findings suggest that early administration of vildagliptin may attenuate adverse cardiac remodelling in the chronic MI model.

Previous studies demonstrated that increased cardiac fibrosis can lead to diastolic dysfunction (Moreo *et al.* 2009; Konstam *et al.* 2011). Interestingly, we found that treatment with vildagliptin, but not metformin, could decrease cardiac fibrosis, similar to that found in the enalapril group in rats with chronic MI; therefore, the improvement in cardiac fibrosis by enalapril and vildagliptin observed in this study could be responsible for the improved LV function. Moreover, oxidative stress and cardiac sympathovagal imbalance have been demonstrated to be associated with cardiac dysfunction (Ferrara *et al.* 2002; Grieve *et al.* 2003). This notion is supported by our findings that both enalapril and vildagliptin, but not metformin, attenuated these impairments and might play an important role in improved LV function in the rats with chronic MI observed in our study.

In addition to fibrosis and oxidative stress, increased cellular apoptosis has also been shown to be involved in LV dysfunction (Sam *et al.* 2000; Grieve *et al.* 2003). Bax and Bcl-2 are proteins involved in the apoptotic

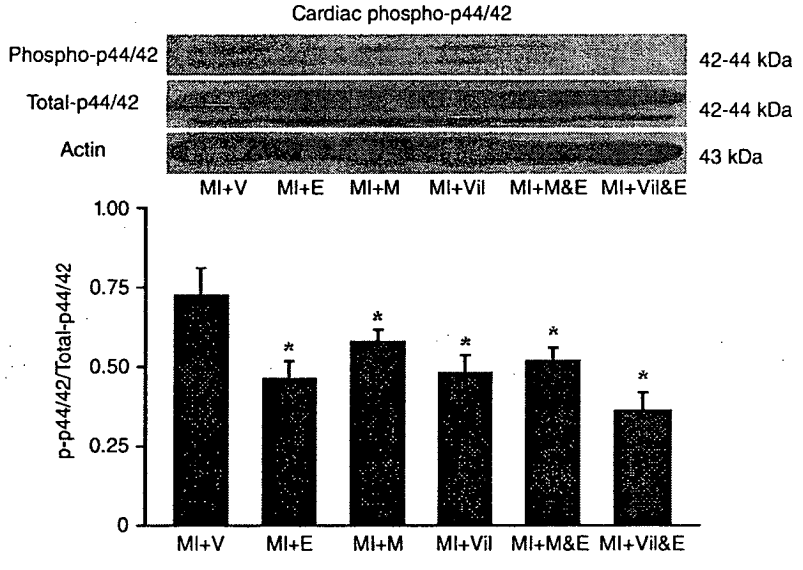


Figure 5. Effects of pharmacological interventions on the levels of phosphorylated p44/42 (p-p44/42) per total p-44/42 in rats with chronic MI
$n = 5$–7 per group. All pharmacological treatments significantly decreased p-p44/42 protein expression. $^*P < 0.05$ *versus* MI + V group. One-way ANOVA ($F = 4.065$, $P = 0.008$). Abbreviations are as for Fig. 1.

© 2015 The Authors. Experimental Physiology © 2015 The Physiological Society

process (Krijnen *et al.* 2002). The activation of Bax leads to its translocation into the mitochondria, which triggers mitochondrial membrane permeability, resulting in the release of cytochrome *c* and activation of caspase-9 and -3, leading to apoptotic cell death (Crow *et al.* 2004). Previous studies have demonstrated that an increased Bax/Bcl-2 ratio indicates increased apoptosis (Yang *et al.* 2001). In the present study, only enalapril, but neither metformin nor vildagliptin, could decrease the Bax/Bcl-2 ratio, suggesting that only enalapril exerted an anti-apoptotic effect in chronic MI.

In chronic MI, the inflammatory process also plays an important role in cardiac remodelling (Nian *et al.* 2004; Anzai, 2013). Transforming growth factor-β, which is a pro-inflammatory and profibrotic cytokine, has been shown to be involved in cardiac remodelling (Dobaczewski *et al.* 2011). Both phospho-p38 and phospho-p44/42 MAPKs, which are downstream signalling mediators of TGF-β, have been reported to be involved in fibroblast proliferation and extracellular matrix deposition (Bujak *et al.* 2007). In the present study, both vildagliptin and enalapril significantly decreased phospho-p44/42 MAPK expression, which could be responsible for decreased cardiac fibrosis in the non-infarcted area in hearts of rats with chronic MI. In this regard, although metformin decreased phospho-p44/42 MAPK protein expression, it did not exert cardioprotection. This could be due to the fact that metformin did not exert an antioxidative effect and did not attenuate cardiac sympathovagal imbalance as the other two drugs did. These findings suggest that the antioxidative effect might play a crucial role in preventing adverse cardiac

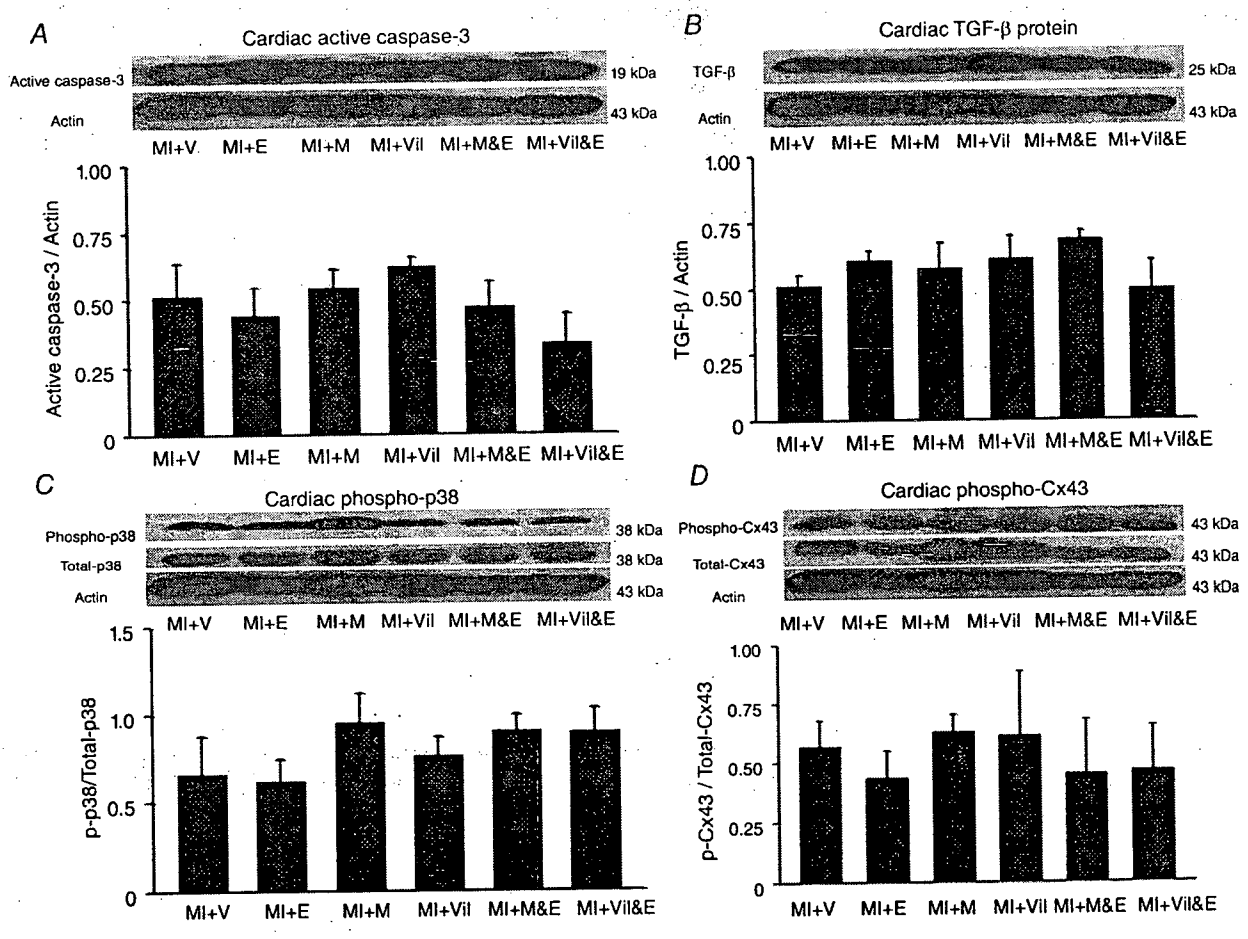


Figure 6. Effects of pharmacological interventions on the levels of active caspase-3 (*A*), transforming growth factor-β (TGF-β; *B*), phosphorylated p38 (p-p38; *C*) and phosphorylated connexin 43 (p-Cx43; *D*) at serine483 residue in rats with chronic MI
n = 5–7 per group. There was no significant difference among different treatment groups. One-way ANOVA; active caspase-3 ($F = 0.809$, $P = 0.552$), TGF-β ($F = 0.849$, $P = 0.528$), p-p38 ($F = 1.211$, $P = 0.334$) and p-Cx43 ($F = 0.206$, $P = 0.957$). Abbreviations are as for Fig. 1.

© 2015 The Authors. Experimental Physiology © 2015 The Physiological Society

remodelling and cardiac dysfunction. However, several studies have demonstrated beneficial effects of metformin in a chronic MI model with a higher dose and longer duration than those used in our study (Yin *et al.* 2011; Cittadini *et al.* 2012). In addition, a previous study showed that administration of metformin at the same dose used in our study could improve diastolic function in rats with insulin resistance (Apaijai *et al.* 2012). The cardioprotective benefit of metformin in this model could be due to the fact that metformin is an antidiabetic drug that exerts its beneficial effects on the cardiovascular system through its reduction of insulin resistance. Thus, metformin could be more beneficial in patients with diabetes or insulin-resistant conditions than in normal subjects with MI. Nevertheless, further investigation is needed to verify the effect of metformin on cardiac function in non-diabetic and diabetic subjects with superimposed chronic MI.

Although enalapril and vildalgliptin attenuated oxidative stress, cardiac sympathovagal imbalance, cardiac fibrosis and cardiac dysfunction, in combination vildagliptin and enalapril did not have a synergistic effect on cardioprotection. This could be due to the fact that enalapril exerted maximal effects on the reduction of oxidative stress and phospho-p44/42 expression compared with vildagliptin alone. Interestingly, vildagliptin, which is an antidiabetic drug, could decrease cardiac fibrosis to a similar extent to enalapril, which is a first-line drug for treatment of chronic MI. This finding suggests that a DPP-4 inhibitor may be the drug of choice for patients with chronic MI who have insulin resistance or type 2 diabetes. Further investigation is needed to warrant its clinical application.

In conclusion, we demonstrated that rats with chronic MI induced by ligation of the LAD coronary artery developed a cardiac sympathovagal imbalance, increased oxidative stress, cardiac fibrosis and cardiac contractile dysfunction. In addition, vildagliptin, but not metformin, attenuated these impairments by improving HRV, reducing oxidative stress and cardiac fibrosis, and improving LV function to a similar extent to that observed with enalapril treatment, suggesting cardioprotective benefits of vildagliptin in addition to its glycaemic control in this chronic MI model.

References

Anzai T (2013). Post-infarction inflammation and left ventricular remodeling: a double-edged sword. *Circ J* **77**, 580–587.

Apaijai N, Chinda K, Palee S, Chattipakorn S & Chattipakorn N (2014). Combined vildagliptin and metformin exert better cardioprotection than monotherapy against ischemia-reperfusion injury in obese-insulin resistant rats. *PLoS ONE* **9**, e102374.

Apaijai N, Pintana H, Chattipakorn SC & Chattipakorn N (2012). Cardioprotective effects of metformin and vildagliptin in adult rats with insulin resistance induced by a high-fat diet. *Endocrinology* **153**, 3878–3885.

Apaijai N, Pintana H, Chattipakorn SC & Chattipakorn N (2013). Effects of vildagliptin versus sitagliptin, on cardiac function, heart rate variability and mitochondrial function in obese insulin-resistant rats. *Br J Pharmacol* **169**, 1048–1057.

Bauersachs J, Galuppo P, Fraccarollo D, Christ M & Ertl G (2001). Improvement of left ventricular remodeling and function by hydroxymethylglutaryl coenzyme A reductase inhibition with cerivastatin in rats with heart failure after myocardial infarction. *Circulation* **104**, 982–985.

Bujak M & Frangogiannis NG (2007). The role of TGF-β signaling in myocardial infarction and cardiac remodeling. *Cardiovasc Res* **74**, 184–195.

Bunch TJ, Hohnloser SH & Gersh BJ (2007). Mechanisms of sudden cardiac death in myocardial infarction survivors: insights from the randomized trials of implantable cardioverter-defibrillators. *Circulation* **115**, 2451–2457.

Chattipakorn N, Incharoen T, Kanlop N & Chattipakorn S (2007). Heart rate variability in myocardial infarction and heart failure. *Int J Cardiol* **120**, 289–296.

Chinda K, Chattipakorn S & Chattipakorn N (2012). Cardioprotective effects of incretin during ischaemia-reperfusion. *Diab Vasc Dis Res* **9**, 256–269.

Cittadini A, Napoli R, Monti MG, Rea D, Longobardi S, Netti PA, Walser M, Sama M, Aimaretti G, Isgaard J & Sacca L (2012). Metformin prevents the development of chronic heart failure in the SHHF rat model. *Diabetes* **61**, 944–953.

Cohn JN, Ferrari R & Sharpe N, on behalf of an International Forum on Cardiac Remodeling (2000). Cardiac remodeling—concepts and clinical implications: a consensus paper from an international forum on cardiac remodeling. *J Am Coll Cardiol* **35**, 569–582.

Crow MT, Mani K, Nam YJ & Kitsis RN (2004). The mitochondrial death pathway and cardiac myocyte apoptosis. *Circ Res* **95**, 957–970.

Dobaczewski M, Chen W & Frangogiannis NG (2011). Transforming growth factor (TGF)-β signaling in cardiac remodeling. *J Mol Cell Cardiol* **51**, 600–606.

Ferrara R, Mastrorilli F, Pasanisi G, Censi S, D'aiello N, Fucili A, Valgimigli M & Ferrari R (2002). Neurohormonal modulation in chronic heart failure. *Eur Heart J* **Supplement D 4**, D3–D11.

Gajarsa JJ & Kloner RA (2011). Left ventricular remodeling in the post-infarction heart: a review of cellular, molecular mechanisms, and therapeutic modalities. *Heart Fail Rev* **16**, 13–21.

Goldman S & Raya TE (1995). Rat infarct model of myocardial infarction and heart failure. *J Card Fail* **1**, 169–177.

Grieve DJ & Shah AM (2003). Oxidative stress in heart failure. More than just damage. *Eur Heart J* **24**, 2161–2163.

Hausenloy DJ & Yellon DM (2008). GLP-1 therapy: beyond glucose control. *Circ Heart Fail* **1**, 147–149.

Hocher B, Reichetzeder C & Alter ML (2012). Renal and cardiac effects of DPP4 inhibitors – from preclinical development to clinical research. *Kidney Blood Press Res* **36**, 65–84.

© 2015 The Authors. Experimental Physiology © 2015 The Physiological Society

Incharoen T, Thephinlap C, Srichairatanakool S, Chattipakorn S, Winichagoon P, Fucharoen S, Vadolas J & Chattipakorn N (2007). Heart rate variability in β-thalassemic mice. *Int J Cardiol* **121**, 203–204.

Izutani S, Yoshiyama M, Omura T, Yoshida K, Nakamura Y, Kim S, Takeuchi K & Yoshikawa J (2002). Nipradilol can prevent left ventricular systolic and diastolic dysfunction after myocardial infarction in rats. *Circ J* **66**, 289–293.

Kishi T (2012). Heart failure as an autonomic nervous system dysfunction. *J Cardiol* **59**, 117–122.

Konstam MA, Kramer DG, Patel AR, Maron MS & Udelson JE (2011). Left ventricular remodeling in heart failure: current concepts in clinical significance and assessment. *JACC Cardiovasc Imaging* **4**, 98–108.

Krijnen PA, Nijmeijer R, Meijer CJ, Visser CA, Hack CE & Niessen HW (2002). Apoptosis in myocardial ischaemia and infarction. *J Clin Pathol* **55**, 801–811.

Kumphune S, Bassi R, Jacquet S, Sicard P, Clark JE, Verma S, Avkiran M, O'Keefe SJ & Marber MS (2011). A chemical genetic approach reveals that p38α MAPK activation by diphosphorylation aggravates myocardial infarction and is prevented by the direct binding of SB203580. *J Biol Chem* **285**, 2968–2975.

Lekawanvijit S, Kompa AR, Manabe M, Wang BH, Langham RG, Nishijima F, Kelly DJ & Krum H (2012). Chronic kidney disease-induced cardiac fibrosis is ameliorated by reducing circulating levels of a non-dialysable uremic toxin, indoxyl sulfate. *PLoS ONE* **7**, e41281.

Lekawanvijit S, Kompa AR, Zhang Y, Wang BH, Kelly DJ & Krum H (2012). Myocardial infarction impairs renal function, induces renal interstitial fibrosis, and increases renal KIM-1 expression: implications for cardiorenal syndrome. *Am J Physiol Heart Circ Physiol* **302**, H1884–H1893.

Lexis CP, Wieringa WG, Hiemstra B, vanDeursen VM, Lipsic E, vander Harst P, vanVeldhuisen DJ & vander Horst IC (2014). Chronic metformin treatment is associated with reduced myocardial infarct size in diabetic patients with ST-segment elevation myocardial infarction. *Cardiovasc Drugs Ther* **28**, 163–171.

Liu Q, Anderson C, Broyde A, Polizzi C, Fernandez R, Baron A & Parkes DG (2010). Glucagon-like peptide-1 and the exenatide analogue AC3174 improve cardiac function, cardiac remodeling, and survival in rats with chronic heart failure. *Cardiovasc Diabetol* **9**, 76.

McDonald IG (1976). Echocardiographic assessment of left ventricular function in aortic valve disease. *Circulation* **53**, 860–864.

Mateos R, Lecumberri E, Ramos S, Goya L & Bravo L (2005). Determination of malondialdehyde (MDA) by high-performance liquid chromatography in serum and liver as a biomarker for oxidative stress. Application to a rat model for hypercholesterolemia and evaluation of the effect of diets rich in phenolic antioxidants from fruits. *J Chromatogr B Analyt Technol Biomed Life Sci* **827**, 76–82.

Minicucci MF, Azevedo PS, Polegato BF, Paiva SA & Zornoff LA (2011). Heart failure after myocardial infarction: clinical implications and treatment. *Clin Cardiol* **34**, 410–414.

Moreo A, Ambrosio G, DeChiara B, Pu M, Tran T, Mauri F & Raman SV (2009). Influence of myocardial fibrosis on left ventricular diastolic function: noninvasive assessment by cardiac magnetic resonance and echo. *Circ Cardiovasc Imaging* **2**, 437–443.

Myat A, Redwood SR, Gersh BJ, Yellon DM & Marber MS (2014). Diabetes, incretin hormones and cardioprotection. *Heart* **100**, 1550–1561.

Nian M, Lee P, Khaper N & Liu P (2004). Inflammatory cytokines and postmyocardial infarction remodeling. *Circ Res* **94**, 1543–1553.

Ocaranza MP, Godoy I, Jalil JE, Varas M, Collantes P, Pinto M, Roman M, Ramirez C, Copaja M, Diaz-Araya G, Castro P & Lavandero S (2006). Enalapril attenuates downregulation of angiotensin-converting enzyme 2 in the late phase of ventricular dysfunction in myocardial infarcted rat. *Hypertension* **48**, 572–578.

Oliveira NL, Ribeiro F, Alves AJ, Teixeira M, Miranda F & Oliveira J (2013). Heart rate variability in myocardial infarction patients: effects of exercise training. *Rev Port Cardiol* **32**, 687–700.

Pavithran P, Nandeesha H, Sathiyapriya V, Bobby Z & Madanmohan T (2008). Short-term heart variability and oxidative stress in newly diagnosed essential hypertension. *Clin Exp Hypertens* **30**, 486–496.

Plutzky J (2011). The incretin axis in cardiovascular disease. *Circulation* **124**, 2285–2289.

Sam F, Sawyer DB, Chang DL, Eberli FR, Ngoy S, Jain M, Amin J, Apstein CS & Colucci WS (2000). Progressive left ventricular remodeling and apoptosis late after myocardial infarction in mouse heart. *Am J Physiol Heart Circ Physiol* **279**, H422–H428.

Scarpello JH & Howlett HC (2008). Metformin therapy and clinical uses. *Diab Vasc Dis Res* **5**, 157–167.

Sokos GG, Nikolaidis LA, Mankad S, Elahi D & Shannon RP (2006). Glucagon-like peptide-1 infusion improves left ventricular ejection fraction and functional status in patients with chronic heart failure. *J Card Fail* **12**, 694–699.

Supakul L, Pintana H, Apaijai N, Chattipakorn S, Shinlapawittayatorn K & Chattipakorn N (2014). Protective effects of garlic extract on cardiac function, heart rate variability, and cardiac mitochondria in obese insulin-resistant rats. *Eur J Nutr* **53**, 919–928.

Sutton MG & Sharpe N (2000). Left ventricular remodeling after myocardial infarction: pathophysiology and therapy. *Circulation* **101**, 2981–2988.

Tahrani AA, Varughese GI, Scarpello JH & Hanna FW (2007). Metformin, heart failure, and lactic acidosis: is metformin absolutely contraindicated? *BMJ* **335**, 508–512.

Takahashi A, Asakura M, Ito S, Min KD, Shindo K, Yan Y, Liao Y, Yamazaki S, Sanada S, Asano Y, Ishibashi-Ueda H, Takashima S, Minamino T, Asanuma H, Mochizuki N & Kitakaze M (2013). Dipeptidyl-peptidase IV inhibition improves pathophysiology of heart failure and increases survival rate in pressure-overloaded mice. *Am J Physiol Heart Circ Physiol* **304**, H1361–H1369.

Triposkiadis F, Karayannis G, Giamouzis G, Skoularigis J, Louridas G & Butler J (2009). The sympathetic nervous system in heart failure physiology, pathophysiology, and clinical implications. *J Am Coll Cardiol* **54**, 1747–1762.

© 2015 The Authors. Experimental Physiology © 2015 The Physiological Society

Wang J, Guo X & Dhalla NS (2004). Modification of myosin protein and gene expression in failing hearts due to myocardial infarction by enalapril or losartan. *Biochim Biophys Acta* **1690**, 177–184.

Yang B, Johnson TS, Thomas GL, Watson PF, Wagner B, Skill NJ, Haylor JL & El Nahas AM (2001). Expression of apoptosis-related genes and proteins in experimental chronic renal scarring. *J Am Soc Nephrol* **12**, 275–288.

Yin M, Silljé HH, Meissner M, vanGilst WH & deBoer RA (2011). Early and late effects of the DPP-4 inhibitor vildagliptin in a rat model of post-myocardial infarction heart failure. *Cardiovasc Diabetol* **10**, 85.

Yin M, vander Horst IC, vanMelle JP, Qian C, vanGilst WH, Sillje HH & deBoer RA (2011). Metformin improves cardiac function in a nondiabetic rat model of post-MI heart failure. *Am J Physiol Heart Circ Physiol* **301**, H459–H468.

Additional information

Competing interests

None declared.

Author contributions

T.I., S.L., S.K., N.P. and W.P.: data collection, analysis, interpretation, drafting the work and final approval of the manuscript. S.C.C. and N.C.: study concept and design, data analysis and interpretation, drafting the work and final approval of the manuscript. All persons designated as authors qualify for authorship, and all those who qualify for authorship are listed.

Funding

This work was supported by the NSTDA Research Chair Grant from the National Science and Technology Development Agency (N.C.), Thailand Research Fund RTA5580006 (N.C.), BRG5780016 (S.C.C.), MRG5680079 (S.L.) and TRG5780002 (S.K.) and Chiang Mai University Center of Excellence Award (N.C.).

Acknowledgements

Vildagliptin was kindly provided by Novartis (Thailand).

© 2015 The Authors. Experimental Physiology © 2015 The Physiological Society

เอกสารแนบหมายเลข 49

AGE (2015) 37: 28
DOI 10.1007/s11357-015-9766-0

Obese-insulin resistance accelerates and aggravates cardiometabolic disorders and cardiac mitochondrial dysfunction in estrogen-deprived female rats

Sivaporn Sivasinprasasn · Piangkwan Sa-nguanmoo · Wasana Pratchayasakul · Sirinart Kumfu · Siriporn C. Chattipakorn · Nipon Chattipakorn

Received: 2 January 2015 / Accepted: 9 March 2015 / Published online: 20 March 2015
© American Aging Association 2015

Abstract Women have a lower incidence of cardiovascular diseases (CVD) than men at a similar age but have an increased incidence of CVD and metabolic syndrome after menopause, indicating the possible protective effects of estrogen on cardiometabolic function. Although obesity is known to increase CVD risks, its impact on the heart on estrogen deprivation is still inconclusive. We investigated the effects of obese-insulin resistance on cardiometabolic function in estrogen-deprived ovariectomized rats. Adult female ovariectomized (O) or sham (S)-operated rats randomly received either normal diet (ND, 19.77 % fat) or high-fat diet (HF, 57.60 % fat) (n=6/group) for 12 weeks. The heart rate variability (HRV), left ventricular (LV) performance, cardiac autonomic balance, cardiac mitochondrial function, metabolic parameters, oxidative stress, and apoptotic markers were determined at 4, 8, and 12 weeks. Insulin resistance developed at week 8 in NDO, HFS, and HFO rats as indicated by increased plasma insulin and HOMA index. However, only HFO rats had elevated plasma cholesterol level at week 8, whereas HFS rats had showed elevation at week 12. In addition, only HFO rats had depressed HRV, impaired LV performance indicated by decreased fractional shortening (%FS) and cardiac mitochondrial dysfunction indicated by increased mitochondrial ROS level, mitochondrial depolarization and swelling, as early as week 8, whereas other groups exhibited them at week 12. Either estrogen deprivation or obesity alone may impair metabolic parameters, cardiac autonomic balance, and LV and mitochondrial function. However, an obese insulin-resistant condition further accelerated and aggravated the development of these cardiometabolic impairments in estrogen-deprived rats.

Keywords Obesity · Insulin resistance · Estrogen deprivation · Mitochondria · Cardiometabolic function

S. Sivasinprasasn · P. Sa-nguanmoo · W. Pratchayasakul · S. Kumfu · S. C. Chattipakorn · N. Chattipakorn
Cardiac Electrophysiology Research and Training Center, Faculty of Medicine, Chiang Mai University, Chiang Mai 50200, Thailand

S. Sivasinprasasn
School of Health Science, Mae Fah Luang University, Chiang Rai 57100, Thailand

S. Sivasinprasasn · P. Sa-nguanmoo · W. Pratchayasakul · S. Kumfu · N. Chattipakorn
Cardiac Electrophysiology Unit, Department of Physiology, Faculty of Medicine, Chiang Mai University, Chiang Mai 50200, Thailand

S. C. Chattipakorn
Department of Oral Biology and Diagnostic Science, Faculty of Dentistry, Chiang Mai University, Chiang Mai 50200, Thailand
e-mail: nchattip@gmail.com

S. Sivasinprasasn · P. Sa-nguanmoo · W. Pratchayasakul · S. Kumfu · S. C. Chattipakorn · N. Chattipakorn (✉)
Center of Excellence in Cardiac Electrophysiology Research, Chiang Mai University, Chiang Mai 50200, Thailand
e-mail: nchattip@gmail.com

Introduction

Cardiovascular disease (CVD) has been the major cause of death for several decades and is expected to remain so

until 2030 (Mathers and Loncar 2006). It has been shown that women have a lower incidence of CVD than men at a similar age, but the incidence increases after the onset of menopause (Vitale et al. 2009). A bilateral ovariectomy (OVX) in women has also been shown to be associated with increased mortality from CVDs (Rivera et al. 2009), which may be due to the fact that estrogen is essentially involved in the regulation of cardiac function. It has been shown that a cardiac sympathovagal imbalance is commonly found in postmenopausal women, and estrogen replacement helps improve this cardiac autonomic dysfunction (Yang et al. 2013). Estrogen deficiency has been shown to reduce myocardium contractile response to calcium and beta-adrenergic receptor stimulation indicating contractile dysfunction of the heart (Ribeiro et al. 2013). Depletion of endogenous estrogen also causes endothelial dysfunction indicated by decreased endothelial relaxation and increased endothelial contraction of arterioles via reactive oxidative species augmentation and vascular nitric oxide reduction (Wang et al. 2014). These increase in cases of oxidative stress and endothelial dysfunction after estrogen deprivation could induce arterial stiffness, inflammation, arthrosclerosis, and plaque rupture leading to tissue ischemia and infarction (Higashi et al. 2009).

Obese-insulin resistance is considered an important risk factor for CVDs due to its negative impact on glucose and lipid metabolism, blood clotting factors, arterial wall health, left ventricular (LV) mass, and blood pressure regulation (Ginsberg 2000). Accumulated adipocytes in obesity caused an increase in adipocytokines and a decrease in adiponectin levels resulting in inflammation, thrombosis, and association with coronary artery disease and myocardial ischemia (Karmazyn et al. 2008). Ovariectomized rats also exhibited an altered plasma lipid profile and increased fat deposition in liver, muscle, and heart (Leite et al. 2009). Since menopause is associated with adverse effects on platelet function and systolic blood pressure (Bonithon-Kopp et al. 1990), combined conditions of estrogen deprivation and obese-insulin resistance would be expected to aggravate the deleterious effects of either one on the heart. Clinical evidence also shows that postmenopausal women have an increased prevalence of metabolic syndrome which is also another risk factor for CVD (Carr 2003).

Although the adverse impact of estrogen deprivation and metabolic syndromes is interrelated and both conditions are known to be associated with the development of cardiac dysfunction, the mechanisms involved as well as the onsets of metabolic and cardiac disorders following estrogen deprivation are still not well-understood. In addition to cardiac performance, the changes in cardiac mitochondrial function such as ROS production, mitochondrial membrane potential, and mitochondrial swelling at the different time points after estrogen deprivation, along with obese-insulin resistance, are also unknown. Therefore, in this study, the influences of female sex hormone deprivation and obese-insulin resistance on metabolic status, cardiac autonomic regulation, LV contractile function, and cardiac mitochondrial function, as well as the underlying mechanisms, have been investigated at several time points to clarify their effects on the progression of cardiometabolic dysfunction. We tested the hypothesis that the obese-insulin resistant condition accelerates and aggravates the development of metabolic disorders, cardiac autonomic imbalance, and cardiac mitochondrial dysfunction in estrogen-deprived female rats.

Methods

Animals

Female Wistar rats (weighing 200–220 g, n=72) were obtained from the National Animal Center (Salaya campus, Mahidol University, Bangkok, Thailand). The rats were housed in a temperature-controlled room (25 °C) with a 12/12-h dark/light cycle setting. All experimental procedures were approved by the Institutional Animal Care and Use Committee at the Faculty of Medicine, Chiang Mai University, in compliance with NIH guidelines.

Experimental protocol

Rats were randomized into a sham (S)-operated group and a bilateral ovariectomized (OVX) group. One week after surgery, rats from both groups were divided into two further groups, one to be fed on a normal diet (ND, contain 19.77 % energy from fat) and the second on a high-fat diet (HF, contain 59.28 % energy from fat) (Pratchayasakul et al. 2011). This gave a total of four experimental groups (n=18/group) including (a) normal diet-fed sham-operated rats (NDS), (b) high-fat diet-fed sham-operated rats (HFS), (c) normal diet-fed

ovariectomized rats (NDO), and (d) high-fat diet-fed ovariectomized rats (HFO). In each of these four experimental groups, rats were fed with their prescribed diet and subdivided to be terminated at the three different times of 4, 8, and 12 weeks (n=6 for each time course). Body weight and food intake were recorded throughout the experiment. At the end of each assigned time course in each experimental group, blood samples were collected from tail vein for determinations of metabolic parameters and estrogen levels. Oral glucose tolerance testing (OGTT), heart rate variability (HRV) for cardiac autonomic balance, and echocardiography were carried out at each time course. At the end of the study protocol, rats were anesthetized with isoflurane via inhalation and terminated by decapitation. The hearts were rapidly removed and homogenized for cardiac mitochondrial function and biochemical studies.

Surgical procedure of ovariectomy

Rats were anesthetized with xylazine (0.15 ml/kg) and zolitil (50 mg/kg) via intraperitoneal injection and ventilated with room air (Pratchayasakul et al. 2014). The bilateral ovariectomy procedure was performed as described previously (Pratchayasakul et al. 2014). After hair shaving and skin cleaning, a midline dorsal skin incision between the inferior crest of the rib cage and superior base of the thigh was made to access the abdominal pelvic cavity. The uterine tube and ovary were identified. Both ovaries were completely removed, and uterine horns were returned into the pelvic cavity. Then, the abdominal wall was sutured, and the incision was closed. After the operation, rats were individually housed in a clear box with dry bedding for 1 week before being divided into the normal diet or high-fat diet-fed groups.

Metabolic function and estrogen level determinations

Fasting plasma insulin levels were detected using a sandwich enzyme-linked immunosorbent assay (ELISA) kit (Millipore, MI, USA). Fasting plasma glucose, cholesterol, and triglyceride (TG) concentrations were determined by colorimetric assay using a commercially available kit (Biotech, Bangkok, Thailand). Degrees of insulin resistance were assessed using homeostasis model assessment (HOMA) which uses the fasting plasma insulin level and fasting plasma glucose concentration its calculation (Pratchayasakul et al. 2014). Plasma estrogen concentration was measured by using a competitive enzyme immunoassay (EIA) kit (Cayman Chemical Company, MI, USA).

HRV test

HRV is a noninvasive assessment of cardiac autonomic function (Chattipakorn et al. 2007). Electrocardiograms (ECG), lead II, were recorded from each rat using a signal transducer (PowerLab 4/25 T, ADInstrument) and operated through the Chart 5.0 program for 20 min. ECG data were analyzed using a frequency-domain method using the MATLAB program. A high-frequency (HF) component (ranging between 0.15–0.40 Hz) is considered to be a marker of parasympathetic tone while low-frequency (LF) component (ranging between 0.04–0.15 Hz) is considered to be a marker of parasympathetic and sympathetic tone (Chattipakorn et al. 2007). Cardiac sympathetic/parasympathetic balance was reported as a LF/HF ratio. Increased LF/HF ratio indicates imbalanced cardiac autonomic regulation (i.e. depressed HRV) (Apaijai et al. 2013; Chattipakorn et al. 2007).

Echocardiography

Echocardiography was used to noninvasively assess the LV function. Animals were lightly anesthetized with 2 % isoflurane with oxygen (2 l/min) via inhalation. The echocardiography probe (S12, Hewlett Packard) which was connected to an echocardiograph (SONOS4500, Philips) was placed on the chest and moved enabling collection of the data along the long and short axes of the heart. Signals from M-mode echocardiography at the level of the papillary muscles were recorded to determine left ventricular internal diameter at the end of diastole (LVIDd) and left ventricular internal diameter at the end of the systole (LVIDs) (Semaming et al. 2014). Fractional shortening (FS) was calculated to estimate contractile function using the formula: FS% = [(LVIDd − LVIDs) / LVIDd] × 100 (Overbeek et al. 2006).

Cardiac mitochondrial function study

For cardiac mitochondrial function study, the mitochondrial ROS production, mitochondrial membrane potential changes, and mitochondrial swelling were determined using the method as described previously

(Apaijai et al. 2013; Palee et al. 2011). In brief, in each rat, the heart was removed at the end of the study and chopped into small pieces on an ice-cold plate. Then, cardiac tissues were homogenized and centrifuged to isolate cardiac mitochondria. Cardiac mitochondrial ROS production was measured by staining cardiac mitochondria with dichlorohydrofluoresce in diacetate (DCFDA) dye for 25 min, after which a fluorescent microplate reader (Model and brand) was used to detect the ROS level using the excitation wavelength of 485 nm and emission wavelength at 530 nm (Palee et al. 2011; Apaijai et al. 2013). For mitochondrial membrane potential change, the dye 5,5′,6,6′-tetrachloro-1,1′,3,3′-tetraethylbenzimidazolcarbocyanine iodide (JC-1) was used. The green fluorescent (JC-1 monomer) was excited at the wavelength of 485 nm and the emission detected at 590 nm while the red fluorescent (JC-1 aggregates) was excited at the wavelength of 485 nm and the emission detected at 530 nm. A decreased red/green fluorescence intensity ratio indicates depolarization of the mitochondrial membrane (Chinda et al. 2014). Isolated mitochondria were also measured for the change in the absorbance using a spectrophotometer at 540 nm for 30 min to identify any cardiac mitochondrial swelling. Decreased absorbance in a mitochondrial suspension indicates mitochondrial swelling (Chinda et al. 2014). Cardiac mitochondrial morphology was also studied using a transmission electron microscope (TEM; JEM-1200 EX II, JEOL Ltd., Japan).

Determination of oxidative stress

Malondialdehyde (MDA) concentrations in cardiac tissues and serum were measured by a high performance liquid chromatography (HPLC) system (Thermo Scientific, Bangkok, Thailand) as described previously (Apaijai et al. 2014). Serum and protein from cardiac tissues were mixed with 10 % trichloroacetic acid (TCA) containing BHT then heated at 90 °C for 30 min and cooled down to room temperature. The mixture was centrifuged, and the supernatant was mixed with 0.44 M H_3PO_4 and 0.6 % thiobabituric acid (TBA) solution to generate thiobarbituric acid reactive substances (TBARS). The solution was filtered through a syringe filter (polysulfone type membrane, pore size 0.45 μm, Whatman International, Maidstone, UK) and analyzed with the HPLC system. Data were analyzed with BDS software (BarSpec Ltd., Rehovot, Israel), and plasma TBARS concentration was determined directly from a standard curve generated from a standard reagent for MDA at different concentrations (0–10 μM) and reported as MDA equivalent concentration (Apaijai et al. 2013).

Cardiac expression of Bax and Bcl-2

Western blot analysis was used for protein expression of Bax and Bcl-2 as described previously (Chinda et al. 2014). Briefly, rat myocardial tissues were homogenized in a lysis buffer (containing 1 % Nonidet P-40, 0.5 % sodium deoxycholate, and 0.1 % sodium dodecyl sulfate (SDS) in 1× PBS) in order to extract protein. Then, the homogenate was centrifuged at 13,000 rpm for 10 min. Total protein (50–80 mg) was mixed with the loading buffer (consists of 5 % mercaptoethanol, 0.05 % bromophenol blue, 75 nM Tris-HCl, 2 % SDS, and 10 % glycerol with pH 6.8) in 1-mg/ml proportion, and the mixture was boiled for 5 min and loaded into 10 % gradient SDS-polyacrylamide gel. After that, proteins were transferred to a polyvinyldene difluoride (PVDF) membrane with the presence of a glycine/methanol transfer buffer (containing 20-mM Tris base, 0.15-M glycine, and 20 % methanol) in a transfer system (Bio-Rad). PVDF membranes were incubated in 5 % skim milk in 1× TBS-T buffer (containing 20-mM Tris-HCl (pH 7.6), 137-nM NaCl, and 0.05 % Tween-20) for 1 h at room temperature then exposed to anti-Bax, anti-Bcl-2 (Cell Signaling Technology, Danvers, MA, USA) and anti-actin (Sigma-Aldrich, St. Louis, MO, USA) for 12 h. Bound antibody was detected by horseradish peroxidase conjugated with anti-rabbit or anti-mouse IgG. Enhanced chemiluminescence (ECL) detection reagents were administered to visualize peroxidase reaction products.

Statistical analysis

The data for each experiment were presented as mean± SE. For all comparisons, the significance of the difference between the mean was calculated by SPSS program (SPSS version 16, SPSS Inc.) using one-way ANOVA followed by post hoc, LSD test. P value less than 0.05 ($P<0.05$) was considered statistically significant.

Results

High-fat diet consumption accelerated and aggravated adverse changes of metabolic profiles and oxidative stress in estrogen-deprived rats

In week 4, both estradiol levels and uterus weight showed significant decrease in both NDO and HFO groups indicating endogenous estrogen-deprived conditions from the removal of ovaries. Ingestion of a high-fat diet for 4 weeks markedly increased body weight in HFO rats when compared with NDS, NDO, and HFS rats (Table 1). Visceral fat deposition significantly increased in both HFS and HFO rats; however, the amount of daily food intake was not significantly different between the groups during the 4 weeks (Table 1). No significant differences between groups were found for the metabolic parameters and serum and cardiac MDA at this time-course.

At week 8, peripheral insulin resistance had developed in NDO, HFS, and HFO rats as demonstrated by a significant increase of insulin level and HOMA index in these groups (Table 2). However, only HFO rats showed a markedly increased level of plasma glucose and total cholesterol compared with NDS and NDO rats. Moreover, HFO rats also had higher levels of visceral fat, body weight, and total cholesterol than HFS rats, indicating the early development with worse impairment of the metabolic parameters in the HFO group at this time-course (Table 2).

At week 12, similar to results seen in week 8, the HFO rats still demonstrated the worst metabolic impairment as indicated by an increase of the body weight, visceral fat, plasma glucose, and plasma cholesterol when compared with the other groups at this time-course (Table 3).

Consistent with the metabolic parameters, the serum MDA level was also increased only in HFO rats beginning at week 8 (Table 2). However, it was not until week 12 that the plasma MDA was elevated in NDO and HFS rats (Table 3). The serum MDA in HFO rats was found to be the highest compared to NDO and HFS groups at this time-course (Table 3). Regarding cardiac MDA level, there was no significant difference between all groups during week 4 and week 8, but they were elevated in NDO, HFS, and HFO groups only at week 12 (Table 3).

Obese-insulin resistance due to high-fat diet consumption accelerated LV contractile dysfunction and cardiac sympathovagal imbalance in estrogen-deprived rats

For cardiac function, although both fractional shortening (%FS) and ejection fraction (%EF) were not

Table 1 Metabolic parameters investigated at 4 weeks after ovariectomy

Parameters	Normal diet		High-fat diet	
	Sham	OVX	Sham	OVX
Body weight (g)	266.66±9.18	285.83±6.88	284.16±6.37	327.00±4.35*†‡
Visceral fat (g)	11.83±1.21	10.12±0.90	19.58±1.32*†	20.51±1.65*†
Uterus weight (g)	0.33±0.02	0.10±0.00*‡	0.36±0.05†	0.10±0.01*‡
Glucose (mg%)	119.30±6.43	120.39±8.75	121.18±7.01	122.84±8.80
Cholesterol (mg%)	96.62±6.04	103.03±7.35	103.89±9.90	105.82±13.35
Triglyceride (mg%)	37.76±3.62	32.54±3.90	38.23±3.80	32.10±3.44
Insulin (ng/ml)	0.82±0.07	0.82±0.05	0.87±0.12	0.97±0.09
HOMA index	5.71±0.25	6.53±0.55	6.54±1.70	7.10±1.36
Estradiol level (pg/ml)	139.26±34.87	43.32±10.64*‡	132.29±26.12†	49.85±19.25*‡
Serum MDA (μmol/ml)	3.45±0.61	3.62±0.40	3.53±0.34	3.60±0.32
Cardiac MDA (μmol/ml)	2.27±0.20	1.92±0.77	2.19±0.07	2.31±0.37
Food intake (g/day)	16.65±0.98	16.10±1.13	17.57±0.43	17.60±0.30

Values are mean±SE for six rats per group

OVX ovariectomized, *HOMA* homeostasis model assessment, *MDA* malondialdehyde

*$P<0.05$ vs. NDS, †$P<0.05$ vs. NDO, ‡$P<0.05$ vs. HFS

Table 2 Metabolic parameters investigated at 8 weeks after ovariectomy

Parameters	Normal diet		High-fat diet	
	Sham	OVX	Sham	OVX
Body weight (g)	275.0±5.52	306.42±3.57*	313.7±8.22*	378.57±8.5*†‡
Visceral fat (g)	11.34±1.24	15.36±1.24*	24.11±1.48*†	30.34±1.49*†‡
Uterus weight (g)	0.37±0.02	0.09±0.00*‡	0.39±0.01†	0.09±0.00*‡
Glucose (mg%)	125.74±7.29	126.09±4.82	130.02±5.90	149.70±8.47*†
Cholesterol (mg%)	101.63±4.46	106.42±2.69	105.50±4.95	138.96±3.30*†‡
Triglyceride (mg%)	41.99±5.73	36.39±0.22	35.61±2.50	34.49±2.35
Insulin (ng/ml)	1.01±0.12	1.59±0.18*	1.52±0.18*	1.55±0.12*
HOMA index	6.48±0.94	11.75±1.88*	12.05±1.42*	13.30±1.43*
Oestradiol level (pg/ml)	117.66±10.11	50.76±2.21*‡	117.44±16.78†	59.61±2.62*‡
Serum MDA (μmol/ml)	3.47±0.16	4.00±0.22	4.04±0.19	4.67±0.27*†‡
Cardiac MDA (μmol/ml)	1.36±0.84	1.37±0.55	1.90±0.28	1.97±0.74
Food intake (g/day)	15.71±1.14	15.20±1.14	16.19±0.74	16.55±0.65

Values are mean±SE for six rats per group

OVX ovariectomized, *HOMA* homeostasis model assessment, *MDA* malondialdehyde

*$P<0.05$ vs. NDS, †$P<0.05$ vs. NDO, ‡$P<0.05$ vs. HFS

significantly different between all groups in week 4, HFO rats were the first group to exhibit significant reduction in both %FS (Fig. 1a) and %EF (Fig. 1b) beginning at week 8. LV dysfunction in the NDO and HFS rats was not observed until week 12 (Fig. 1a, b).

For cardiac autonomic function, there was no significant alteration in cardiac autonomic balance among all groups in week 4 (Fig. 1c). However, in week 8, only HFO rats developed depressed HRV as indicated by a significant increase in the LF/HF

Table 3 Metabolic parameters investigated at 12 weeks after ovariectomy

Parameters	Normal diet		High-fat diet	
	Sham	OVX	Sham	OVX
Body weight (g)	284.28±3.68	336.87±4.81*	342.22±4.93*	419.50±4.56*†‡
Visceral fat (g)	12.20±0.51	16.26±1.13*‡	31.14±1.62*†	35.20±0.94*†‡
Uterus weight (g)	0.39±0.02	0.10±0.00*‡	0.45±0.03†	0.10±0.00*‡
Glucose (mg%)	124.27±5.79	130.67±7.84	135.03±5.60	160.84±5.93 *†‡
Cholesterol (mg%)	88.72±5.84	106.74±10.06	125.63±13.5*†	156.75±11.8*†‡
Triglyceride (mg%)	31.60±3.25	32.47±2.10	31.70±3.01	31.58±3.07
Insulin (ng/ml)	0.87±0.14	1.57±0.27*	1.57±0.25*	1.58±0.11*
HOMA index	5.21±0.40	11.74±2.01*	11.92±2.27*	12.90±1.91*
Estradiol level (pg/ml)	127.65±20.95	62.37±7.23*‡	129.37±8.16†	74.37±7.11*‡
Serum MDA (μmol/ml)	3.52±0.16	4.31±0.14*	3.99±0.12*	4.80±0.16*†‡
Cardiac MDA (μmol/ml)	5.76±0.96	13.41±1.50*	12.09±2.35*	11.69±2.01*
Food intake (gram/day)	13.21±0.97	14.29±0.77	15.91±0.50*	16.30±0.58*

Values are mean±SE for six rats per group

OVX ovariectomized, *HOMA* homeostasis model assessment, *MDA* malondialdehyde

*$P<0.05$ vs. NDS, †$P<0.05$ vs. NDO, ‡$P<0.05$ vs. HFS

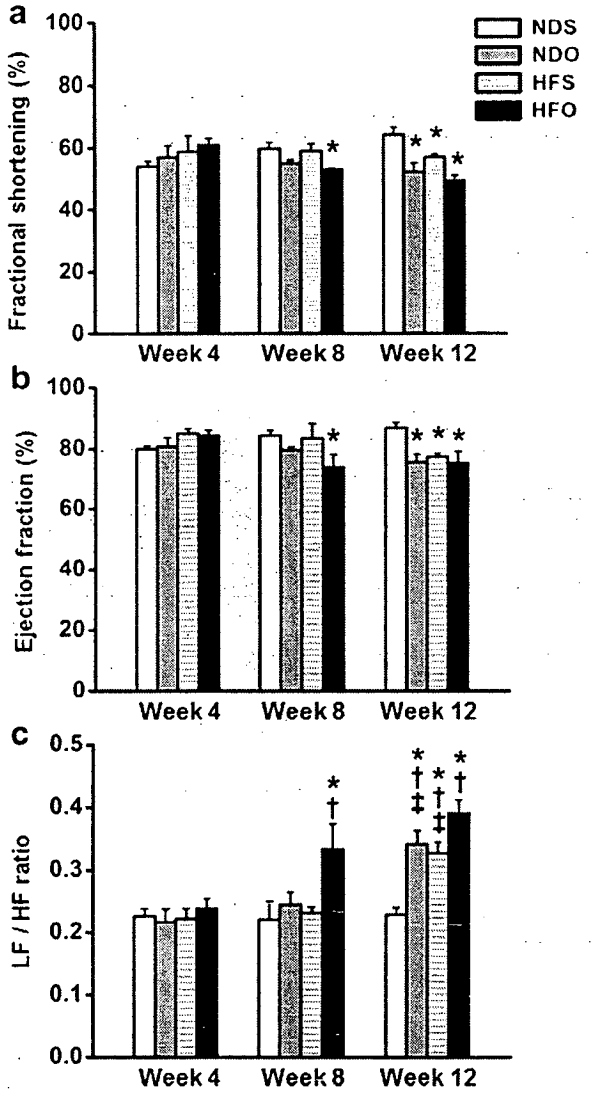


Fig. 1 Effects of obese-insulin resistance on left ventricular function and HRV in estrogen-deprived rats. High-fat fed ovariectomized rats (HFO) early exhibited impaired fractional shortening (FS) (**a**) and ejection fraction (%EF) (**b**) at 8 weeks while normal-diet fed ovariectomized rats (NDO) and high-fat fed sham-operated rats (HFS) were affected at 12 weeks (**c**). LF/HF ratio firstly increased in HFO at 8 weeks then in NDO and HFS at 12 weeks. Values are mean±SE for six rats per group. *$P<0.05$ vs. normal-diet fed sham-operated rats (NDS) in the same week, †$P<0.05$ vs. its 4-week data and ‡$P<0.05$ vs. its 8-week data

ratio (Fig. 1c), suggesting that cardiac autonomic imbalance was firstly initiated in this group at this time-course. In week 12, rats in NDO, HFS, and HFO groups had an increased LF/HF ratio when compared with the NDS group (Fig. 1c). Moreover, the LF/HF ratio in week 12 of HFO rats exhibited a greater increased LF/HF ratio when compared to that in week 4 and week 8 (Fig. 1c), indicating the progressive impairment of cardiac sympathovagal balance over time in HFO rats.

Obese-insulin resistance due to high-fat diet consumption decreased anti-apoptotic protein and accelerated cardiac mitochondrial impairment in estrogen-deprived rats

In the heart, the expressions of Bax and Bcl-2 showed no significant difference among all groups at week 4 (Fig. 2a, b). In week 8, the Bax level was also not different in all groups. It was not until week 12 that the level of Bax expression was increased in NDO, HFS, and HFO groups (Fig. 2a). In contrast, beginning at week 8, the Bcl-2 level was found to decrease only in the HFO rats, and it continued to decrease in week 12 (Fig. 2b). The Bcl-2 level in NDO and HFS was not altered at any time-course. Moreover, a reduced Bax/Bcl-2 ratio was found in NDO, HFS, and HFO groups in week 12 (Fig. 2c).

Cardiac mitochondrial ROS production, mitochondrial membrane potential change, and mitochondrial swelling showed no difference between all groups during week 4 (Fig. 3). In week 8, cardiac mitochondrial dysfunction was found only in HFO rats as indicated by significantly increased ROS levels, decreased $\Delta\Psi$ (indicating mitochondrial depolarization), and cardiac mitochondrial swelling (Fig. 3a–c). It was not until week 12 that NDO and HFS rats developed cardiac mitochondrial dysfunction (Fig. 3).

Discussion

The major findings from the present study clearly demonstrated that obese-insulin resistance induced by high-fat diet consumption not only aggravated the impairments of metabolic function but also accelerated the development of cardiac autonomic imbalance, LV dysfunction, oxidative stress, and cardiac mitochondrial dysfunction, when a rat was under estrogen-deprived conditions. A summary of these findings is showed in Table 4.

Chronic high-fat diet consumption is a common factor that contributes to the development of obesity and induces several subsequent clinical diseases such as insulin resistance, diabetes mellitus, and cardiovascular disease (Marinou et al. 2010). In HFO rats, increasing of body weight and visceral fat was accelerated as well as

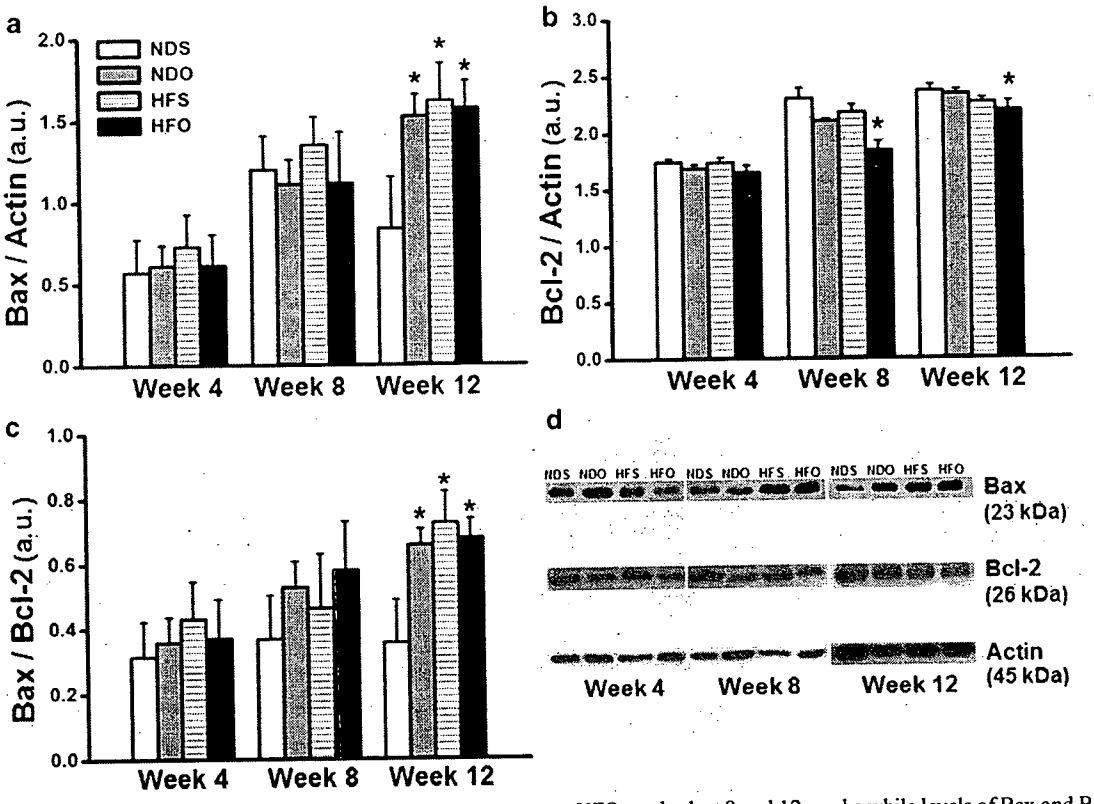


Fig. 2 Effects of obese-insulin resistance on cardiac cellular apoptosis in estrogen-deprived rats. Bax expression (**a**), Bcl-2 expression (**b**), Bax/Bcl-2 ratio (**c**), and representative bands of Bax, Bcl-2, and actin from blotting analysis (**d**). Bcl-2 level was reduced in HFO rats both at 8 and 12 weeks while levels of Bax and Bax/Bcl-2 ratio were increased in HFO, NDO, and HFS at 12 weeks. Values are mean±SE for six rats per group. *$P<0.05$ vs. NDS in the same time period

hyperglycemia and dyslipidemia which were aggravated compared with NDO rats, suggesting the negative effect of obese-insulin resistance on metabolic status in OVX rats. It has been shown that excessive fat accumulation increased oxidative stress, induced mitochondrial impairment, and has been implicated with insulin resistance (Apaijai et al. 2013). Higher levels of MDA and mitochondrial ROS found in HFO rats, compared with NDO and HFS rats, could be essentially contributed to not only the acceleration but also the aggravation of the metabolic disturbance observed in these rats.

The present study has also demonstrated the early development of impaired cardiac autonomic balance (i.e. depressed HRV) in HFO rats. It is well-known that impaired cardiac autonomic balance is associated with increased sympathetic activity and oxidative stress (Apaijai et al. 2013). It has been shown that increased oxidative stress, which was indicated by increased MDA and ROS levels, was an important factor that affected HRV since increased ROS level could cause sympathetic overactivity via inactivation of nitric oxide (Ye et al. 2006). Cardiac sympathovagal disturbance was also previously reported to occur in ovariectomized female rats and was restored by estrogen therapy to reduce oxidative stress, suggesting the considerable impact of oxidative stress on HRV (Campos et al. 2014). In the present study, it was found that the early development of oxidative stress in HFO rats could be responsible for the early development of impaired HRV in these rats, indicating that either obese-insulin resistance or estrogen deprivation could accelerate and aggravate the oxidative stress status when both conditions were combined, leading to early impairment of the HRV as seen in this study. Moreover, although either obese-insulin resistance or estrogen deprivation alone could impair cardiac autonomic balance, we demonstrated that there was earlier development of depressed HRV in the obese-insulin resistant with estrogen-deprived (HFO) rats. These findings indicate that obese-insulin resistance

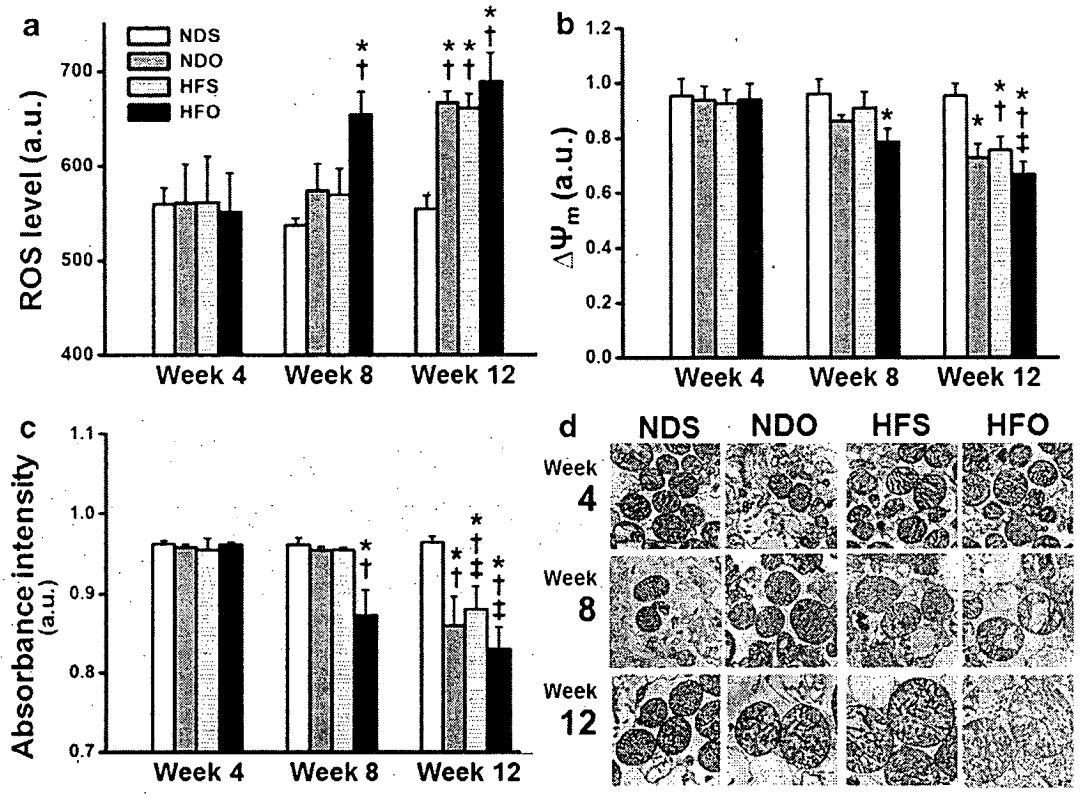


Fig. 3 Effects of obese-insulin resistance on cardiac mitochondrial function in estrogen-deprived rats. Cardiac mitochondrial ROS level (**a**), cardiac mitochondrial membrane potential change (**b**), cardiac mitochondrial swelling (**c**), and transmission electron micrographs illustrate cardiac mitochondria from rats at 4, 8, and 12 weeks in each group (**d**). Cardiac mitochondrial impairment was found earlier (week 8) in HFO rats and later (week 12) in NDO and HFS rats. Values are mean±SE for six rats per group. *$P<0.05$ vs. NDS in the same week, †$P<0.05$ vs. its 4-week data and ‡$P<0.05$ vs. its 8-week data

accelerated the development of HRV impairment in estrogen-deprived rats.

Cardiac function is the most important parameter that has been shown to be affected by either obese-insulin resistance or estrogen deprivation. It was suggested that obesity-associated regression of cardiac performance was mediated through myocardial metabolic change by increased myocardial fatty acid uptake and oxygen consumption (Peterson et al. 2004). Besides the metabolic pathway, impaired cardiac mitochondrial function including increased cardiac mitochondrial ROS production, mitochondrial membrane depolarization, and mitochondrial swelling has been shown to cause cellular apoptosis

Table 4 Summary of cardiometabolic impairment of the experiment groups

Impairment	8 week				12 week			
	NDS	NDO	HFS	HFO	NDS	NDO	HFS	HFO
Metabolic disturbance		✓	✓	✓✓		✓	✓	✓✓
LV contractile dysfunction				✓		✓	✓	✓
Cardiac autonomic imbalance				✓		✓	✓	✓
Oxidative stress				✓		✓	✓	✓✓
Cardiac mitochondrial impairment				✓		✓	✓	✓

(Chinda et al. 2014). In the present study, although either estrogen deprivatio (NDO) or obese-insulin resistance (HFS) alone could cause LV contractile dysfunction, this deleterious effect was accelerated in HFO rats when compared with NDO and HFS rats. These findings suggested that obese-insulin resistant conditions accelerated the development of this LV impairment. Moreover, the development of cardiac mitochondrial dysfunction was also observed earlier in HFO rats, suggesting that the impairment of cardiac mitochondrial function could be responsible for LV dysfunction. Moreover, reduced cardioprotection and higher apoptosis levels indicated by reduced Bcl-2 level together with increased Bax levels as demonstrated in this study support the important role of cardiac mitochondrial function as a vital mechanism underlying this cardiac contractile impairment.

In conclusion, our findings demonstrated that either the loss of endogenous estrogen by ovariectomy alone (Vogel et al. 2013) or obese-insulin resistance alone (Apaijai et al. 2013) could abrogate cardiometabolic protection that therefore result in cardiometabolic disorders. However, when obese insulin-resistant conditions were added to estrogen-deprived conditions, it not only aggravated the development of metabolic disturbance but also accelerated this deleterious effect as well as contributed to the development of LV dysfunction and cardiac sympathovagal imbalance. The underlying mechanisms could be due to the increased oxidative stress and the deterioration of cardiac mitochondrial function as demonstrated in the present study (Table 4). Therefore, our findings clearly demonstrated that obese-insulin resistance caused by high-fat diet consumption accelerated the development of cardiac and metabolic dysfunction through oxidative stress generation and mitochondrial dysfunction in estrogen-deprived female rats. The available treatment for estrogen deprivation with obese-insulin resistance, in addition to postmenopausal hormone therapy, may include antidiabetic or blood-glucose control agents in order to improve the impaired metabolic status. Our team had previously reported that an oral-antidiabetic drug, dipeptidyl peptidase-4 inhibitor, not only improves plasma insulin and cholesterol profiles but also helps decrease cardiac oxidative stress and mitochondrial dysfunction (Apaijai et al. 2013). Future studies are needed to investigate the roles of estrogen replacement therapy as well as the dipeptidyl peptidase-4 inhibitor in this study model.

Acknowledgments This work was supported by a NSTDA Research Chair Grant from the National Science and Technology Development Agency (NC), the Thailand Research Fund RTA5580006 (NC), BRG5780016 (SC), TRG5680018 (WP), TRG5780002 (SK), Faculty of Medicine Endowment Fund (WP), and the Chiang Mai University Center of Excellence Award (NC).

Conflict of interest None

References

Apaijai N, Pintana H, Chattipakorn SC, Chattipakorn N (2013) Effects of vildagliptin versus sitagliptin, on cardiac function, heart rate variability and mitochondrial function in obese insulin-resistant rats. Br J Pharmacol 169:1048–1057

Apaijai N, Chinda K, Palee S, Chattipakorn S, Chattipakorn N (2014) Combined vildagliptin and metformin exert better cardioprotection than monotherapy against ischemia-reperfusion injury in obese-insulin resistant rats. PLoS One 9:e102374

Bonithon-Kopp C, Scarabin PY, Darne B, Malmejac A, Guize L (1990) Menopause-related changes in lipoproteins and some other cardiovascular risk factors. Int J Epidemiol 19:42–48

Campos C, Casali KR, Baraldi D, Conzatti A, Araujo AS, Khaper N, Llesuy S, Rigatto K, Bello-Klein A (2014) Efficacy of a low dose of estrogen on antioxidant defenses and heart rate variability. Oxid Med Cell Longev 2014:218749

Carr MC (2003) The emergence of the metabolic syndrome with menopause. J Clin Endocrinol Metab 88:2404–2411

Chattipakorn N, Incharoen T, Kanlop N, Chattipakorn S (2007) Heart rate variability in myocardial infarction and heart failure. Int J Cardiol 120:289–296

Chinda K, Sanit J, Chattipakorn S, Chattipakorn N (2014) Dipeptidyl peptidase-4 inhibitor reduces infarct size and preserves cardiac function via mitochondrial protection in ischaemia-reperfusion rat heart. Diab Vasc Dis Res 11:75–83

Ginsberg HN (2000) Insulin resistance and cardiovascular disease. J Clin Invest 106:453–458

Higashi Y, Noma K, Yoshizumi M, Kihara Y (2009) Endothelial function and oxidative stress in cardiovascular diseases. Circ J 73:411–418

Karmazyn M, Purdham DM, Rajapurohitam V, Zeidan A (2008) Signalling mechanisms underlying the metabolic and other effects of adipokines on the heart. Cardiovasc Res 79:279–286

Leite RD, Prestes J, Bernardes CF, Shiguemoto GE, Pereira GB, Duarte JO, Domingos MM, Baldissera V, de Andrade Perez SE (2009) Effects of ovariectomy and resistance training on lipid content in skeletal muscle, liver, and heart; fat depots; and lipid profile. Appl Physiol Nutr Metab 34:1079–1086

Marinou K, Tousoulis D, Antonopoulos AS, Stefanadi E, Stefanadis C (2010) Obesity and cardiovascular disease: from pathophysiology to risk stratification. Int J Cardiol 138:3–8

Mathers CD, Loncar D (2006) Projections of global mortality and burden of disease from 2002 to 2030. PLoS Med 3:e442

Overbeek LI, Kapusta L, Peer PG, de Korte CL, Thijssen JM, Daniels O (2006) New reference values for echocardiographic dimensions of healthy Dutch children. Eur J Echocardiogr 7:113–121

Palee S, Weerateerangkul P, Surinkeaw S, Chattipakorn S, Chattipakorn N (2011) Effect of rosiglitazone on cardiac electrophysiology, infarct size and mitochondrial function in ischaemia and reperfusion of swine and rat heart. Exp Physiol 96:778–789

Peterson LR, Waggoner AD, Schechtman KB, Meyer T, Gropler RJ, Barzilai B, Davila-Roman VG (2004) Alterations in left ventricular structure and function in young healthy obese women: assessment by echocardiography and tissue Doppler imaging. J Am Coll Cardiol 43:1399–1404

Pratchayasakul W, Chattipakorn N, Chattipakorn SC (2011) Effects of estrogen in preventing neuronal insulin resistance in hippocampus of obese rats are different between genders. Life Sci 89:702–707

Pratchayasakul W, Chattipakorn N, Chattipakorn SC (2014) Estrogen restores brain insulin sensitivity in ovariectomized non-obese rats, but not in ovariectomized obese rats. Metabolism 63:851–859

Ribeiro RF Jr, Potratz FF, Pavan BM, Forechi L, Lima FL, Fiorim J, Fernandes AA, Vassallo DV, Stefanon I (2013) Carvedilol prevents ovariectomy-induced myocardial contractile dysfunction in female rat. PLoS One 8:e53226

Rivera CM, Grossardt BR, Rhodes DJ, Brown RD Jr, Roger VL, Melton LJ III, Rocca WA (2009) Increased cardiovascular mortality after early bilateral oophorectomy. Menopause 16: 15–23

Semaming Y, Kumfu S, Pannangpetch P, Chattipakorn SC, Chattipakorn N (2014) Protocatechuic acid exerts a cardioprotective effect in type 1 diabetic rats. J Endocrinol 223:13–23

Vitale C, Mendelsohn ME, Rosano GM (2009) Gender differences in the cardiovascular effect of sex hormones. Nat Rev Cardiol 6:532–542

Vogel H, Mirhashemi F, Liehl B, Taugner F, Kluth O, Kluge R, Joost HG, Schurmann A (2013) Estrogen deficiency aggravates insulin resistance and induces beta-cell loss and diabetes in female New Zealand obese mice. Horm Metab Res 45: 430–435

Wang D, Wang C, Wu X, Zheng W, Sandberg K, Ji H, Welch WJ, Wilcox CS (2014) Endothelial dysfunction and enhanced contractility in microvessels from ovariectomized rats: roles of oxidative stress and perivascular adipose tissue. Hypertension 63:1063–1069

Yang SG, Mlcek M, Kittnar O (2013) Estrogen can modulate menopausal women's heart rate variability. Physiol Res 62(Suppl 1):S165–S171

Ye S, Zhong H, Yanamadala S, Campese VM (2006) Oxidative stress mediates the stimulation of sympathetic nerve activity in the phenol renal injury model of hypertension. Hypertension 48:309–315

เอกสารแนบหมายเลข 50

PLOS | ONE

RESEARCH ARTICLE

Chronic Testosterone Replacement Exerts Cardioprotection against Cardiac Ischemia-Reperfusion Injury by Attenuating Mitochondrial Dysfunction in Testosterone-Deprived Rats

Wanpitak Pongkan[1,2,4], **Siriporn C. Chattipakorn**[1,3,4], **Nipon Chattipakorn**[1,2,4]*

1 Cardiac Electrophysiology Research and Training Center, Faculty of Medicine, Chiang Mai University, Chiang Mai, Thailand, 2 Cardiac Electrophysiology unit, Department of Physiology, Faculty of Medicine, Chiang Mai University, Chiang Mai, Thailand, 3 Department of Oral Biology and Diagnostic Sciences, Faculty of Dentistry, Chiang Mai University, Chiang Mai, Thailand, 4 Center of Excellence in Cardiac Electrophysiology Research, Chiang Mai University, Chiang Mai, Thailand

* nchattip@gmail.com

CrossMark
click for updates

OPEN ACCESS

Citation: Pongkan W, Chattipakorn SC, Chattipakorn N (2015) Chronic Testosterone Replacement Exerts Cardioprotection against Cardiac Ischemia-Reperfusion Injury by Attenuating Mitochondrial Dysfunction in Testosterone-Deprived Rats. PLoS ONE 10(3): e0122503. doi:10.1371/journal.pone.0122503

Academic Editor: John Calvert, Emory University, UNITED STATES

Received: December 3, 2014

Accepted: February 18, 2015

Published: March 30, 2015

Copyright: © 2015 Pongkan et al. This is an open access article distributed under the terms of the Creative Commons Attribution License, which permits unrestricted use, distribution, and reproduction in any medium, provided the original author and source are credited.

Data Availability Statement: All relevant data are within the paper.

Funding: This work was supported by a NSTDA Research Chair Grant from the National Science and Technology Development Agency (NC), grants from the Thailand Research Fund RTA5580006 (NC) and BRG5780016 (SC), the Royal Golden Jubilee PhD program (NC and WP), Faculty of Medicine Endowment Fund (NC), and the Chiang Mai University Center of Excellence Award (NC). The funders had no role in study design, data collection

Abstract

Background

Although testosterone deficiency is associated with increased risks of heart disease, the benefits of testosterone therapy are controversial. Moreover, current understanding on the cardiac effect of testosterone during cardiac ischemia-reperfusion (I/R) periods is unclear. We tested the hypothesis that testosterone replacement attenuates the impairment of left ventricular (LV) function and heart rate variability (HRV), and reduces the infarct size and arrhythmias caused by I/R injury in orchiectomized (ORX) rats.

Methodology

ORX or sham-operated male Wistar rats (n = 24) were randomly divided and received either testosterone (2 mg/kg, subcutaneously administered) or the vehicle for 8 weeks. The ejection fraction (EF) and HRV were determined at baseline and the 4th and 8th week. I/R was performed by left anterior descending coronary artery ligation for 30 minutes, followed by a 120-minute reperfusion. LV pressure, arrhythmia scores, infarct size and cardiac mitochondrial function were determined.

Results

Prior to I/R, EF and HRV were impaired in the ORX group, but were restored in the testosterone-treated group. During I/R, arrhythmia scores and the infarct size were greater, and cardiac mitochondrial function was impaired, whereas the time to 1st VT/VF onset and the LV end-systolic pressure were decreased in the ORX group when compared to the sham

and analysis, decision to publish, or preparation of the manuscript.

Competing Interests: The authors have declared that no competing interests exist.

group. Testosterone replacement attenuated the impairment of these parameters in ORX rats during I/R injury, but did not show any benefit or adverse effect in non-ORX rats.

Conclusions

Testosterone replacement restores cardiac function and autonomic regulation, and exerts cardioprotective effects during the I/R period via mitochondrial protection in ORX rats.

Introduction

Androgen deficiency commonly occurs in middle aged to older men and sometimes includes younger men with underlying hypothalamopituitary or testicular disorders [1]. It is also known that testosterone deficiency is a risk factor for cardiovascular diseases (CVD) and coronary artery diseases (CAD) [2–4]. Previous studies have shown that there is a correlation between men with testosterone deficiency or low serum testosterone and an increased prevalence and risk of CVD and CAD [4–6], thus suggesting there may be a possible role for testosterone replacement therapy as a potential therapeutic strategy to prevent CVD in those groups of patients [7–9].

Although physiological testosterone replacement is an inexpensive and well-tolerated therapy, it does require careful monitoring [10]. Recent studies suggested a beneficial effect of physiological testosterone replacement therapy on lipid profiles [11] and ischemic insults of the heart [12, 13]. In hearts subjected to ischemia-reperfusion (I/R) injury, previous *in vitro* and *ex vivo* studies reported that testosterone exerts a cardioprotective effect through androgen receptors [1, 12–16]. Despite these reports, the roles of testosterone replacement therapy are still controversial since inconsistent reports exist regarding the effects of testosterone on the heart which had undergone I/R injury [17, 18]. Furthermore, information regarding the roles of testosterone deficiency/replacement in the I/R hearts were obtained from studies using *ex vivo* models [12, 19–21], making it difficult to translate these findings into the clinical setting.

In the present study, the effect of testosterone replacement was investigated on the left ventricular function, cardiac autonomic regulation being determined by the heart rate variability (HRV), cardiac arrhythmias, myocardial infarct size, cardiac mitochondrial function and the underlying mechanism in the I/R hearts of testosterone-deprived rats using an *in vivo* study model. We tested the hypothesis that testosterone-deprived rats develop left ventricular (LV) dysfunction and depressed HRV, and also that testosterone replacement attenuates the impairment of LV function and HRV, reduces cardiac arrhythmias and myocardial infarction size and attenuates cardiac mitochondrial dysfunction and apoptosis caused by I/R injury.

Materials and Methods

Animal preparation

All experiments were approved by the Institutional Animal Care and Use Committee of the Faculty of Medicine, Chiang Mai University, Chiang Mai, Thailand. Adult male Wistar rats weighing 300–350 grams were obtained from the National Laboratory Animal Center, Mahidol University, Bangkok, Thailand. All animals were housed in a climate controlled room (22–25°C with a 12-hour light/dark cycle) and fed on a normal diet of standard pelletized rat food and water *ad libitum*.

Orchiectomy procedure

Rats were anesthetized and maintained using Isoflurane 2–3% in a dorsal recumbent position, and the skin of the scrotal area was shaved and scrubbed by sterile technique. An orchiectomy was performed using the scrotal approach technique [22]. A small incision was made at the tip of the scrotum, and the tunica vaginalis was incised and the testis, vas deferens and the spermatic blood vessels were exposed. Then, the blood vessels and vas deferens were ligated using absorbable sutures. The testis and epididymal fat pad was removed using the open technique. When the bleeding stopped, the remaining tissues were returned into the sac and the procedure repeated on the opposite testis. The skin incision was closed with a non-absorbable suture. Rats were monitored carefully to prevent any chewing of sutures and other complications. An analgesic drug and antibiotics were injected subcutaneously for 3 days after the operation.

Surgical procedure of myocardial I/R

Rats were anesthetized by intramuscular injection of Zolitil (ZolazepamTiletamine) 50 mg/kg combined with Xylazine 3 mg/kg [23]. Then, tracheotomies were performed via a ventral midline incision. Rats were ventilated via the tracheotomy with room air from a positive pressure ventilator (Harvard Apparatus, Massachusetts, USA) to maintain PCO_2, PO_2, and pH parameters under physiological conditions. A Lead II electrocardiogram (ECG) (PowerLab 4/25 T, AD Instrument) was monitored throughout the study. The right carotid artery was canulated with a pressure conductance catheter (Scisense Instrument, Ontario, Canada) to measure the left ventricular pressure during the I/R period. A left-side thoracotomy at the fourth intercostal space was performed and the heart was exposed. The heart was allowed to stabilize for 15 minutes and then the left anterior descending coronary artery (LAD) was ligated at approximately 2 mm from its origin by a 5–0 silk suture with an atraumatic surgical needle threaded through a small stainless steel snare for the coronary artery occlusion [23]. Ischemia was confirmed by an ST elevation on the ECG and regional pallor of myocardial tissues of the ischemic area. I/R injury was induced by 30 minutes of ischemia, followed by 120 minutes of reperfusion.

Experimental protocol

Rats were randomly divided into 2 groups (n = 16/group); a sham operated group and an orchiectomized (ORX) group. One week after orchiectomy, rats in each group were divided into two subgroups (n = 8/group) to be treated with either castor oil (control) or testosterone (2 mg/kg, subcutaneous injection) daily for 8 weeks. HRV and echocardiograms were carried out 3 times throughout the entire experiment; before the orchiectomy, then 4 and 8 weeks after the testosterone treatment. At the end of testosterone treatment (week 8), all rats underwent cardiac I/R, and cardiac function and arrhythmia parameters were determined in all groups. At the end of the experiment, the heart was removed to determine myocardial infarction size, cardiac mitochondrial function and a western blot analysis was carried out for assessment of apoptosis and gap junction protein.

Heart rate variability (HRV) determination

Prior to the I/R study, the HRV was used to investigate cardiac autonomic regulation. The electrocardiogram (ECG) was recorded for 20 minutes in each rat using the PowerLab system (PowerLab 4/25T, AD instrument) with chart 5.0. Data from the ECG recording was analyzed using the MATLAB program [24]. Power spectra of RR interval variability were obtained by the Fast Fourier Transform (FFT) algorithm and the three major oscillatory components including high frequency (HF), low frequency (LF) and very low frequency (VLF) were

determined. Parasympathetic activity was regarded as HF (0.6–0.3 Hz). Association of sympathetic and parasympathetic activity was regarded as LF (0.2–0.6 Hz). To minimize the effect of changes in total power on the LF and HF components, LF and HF were expressed as normalized units (LFnu and HFnu) by dividing LF or HF by the total power minus VLF. The LF/HF ratio was considered as an index of cardiac sympathovagal tone balance [25, 26]. An increased LF/HF ratio indicates a cardiac sympathovagal imbalance [27].

Cardiac function determination

Prior to the I/R protocol, left ventricular function was assessed using an echocardiograph (SONOS4500, Philips). The chest area was shaved and rats were stabilized in a supine position. The probe was gently placed on the chest and moved to enable the collecting of data along the short and long axes of the heart. Signals from M-mode echocardiography at the level of the papillary muscles were recorded. Parameters obtained from the echocardiogram including left ventricular internal dimensions during systole (LVIDs) and diastole (LVIDd), and left ventricular posterior wall thickness during systole (LVPWs) and diastole (LVPWd) were recorded. Fractional shortening (FS) was calculated using the formula: %FS = (LVIDd—LVIDs) x 100 / LVIDd.

At the end of the experiment, left ventricular pressure during I/R injury was evaluated using an intravascular pressure catheter. The right carotid artery was canulated and the pressure in the LV chamber was recorded using a LabScribe2 program (iWorx Systems Inc., Dover, NH, USA) [23, 28]. Heart rate (HR), left ventricular end-systolic pressure (LVESP) and left ventricular end-diastolic pressure (LVEDP) were assessed prior to the occlusion of the LAD, at the end of ischemic period and at the end of reperfusion period.

Arrhythmia determination during the I/R period

The ECG (Lead II) was monitored throughout the I/R period using PowerLab 4/25 (AD Instruments, Inc., Colorado Springs, CO, USA). The occurrence of arrhythmia was characterized using the Lambeth Conventions [29] and arrhythmia scores were determined based on the following criteria [30]: *score 0* = premature ventricular contractions (PVCs) < 50 beats; *score 1* = PVC between 50 and 499 beats; *score 2* = PVC > 500 beats and/or one episode of spontaneously reverting ventricular tachycardia or ventricular fibrillation (VT/ VF); *score 3* = more than one episode of spontaneously reverting VT/VF (<1 min of total combined duration); *score 4* = 1–2 min of total combined VT/VF and *score 5* = >2 min of VT/VF. The VT/VF incidence and the time to first VT/VF onset were also determined.

Infarct size determination

At the end of the experiment, the heart was removed from the body and the LAD was occluded again at the same site as previously during the ischemic period. The heart was mounted on the modified Langendorff apparatus via the aorta and irrigated with normal saline to wash out any blood from the chambers and vessels [23]. Evans blue (0.5%) was retrogradely infused through the aortic root. The area which was not infused and stained by Evan blue was defined as the area at risk (AAR). The heart was cut horizontally from the apex to the occluding site into 7–8 slices [23] and these were immersed and incubated in 37°C Triphenyltetrazolium chloride (TTC) for 12 minutes to distinguish the infarct tissues (white area) from the viable myocardium (red area). The area which demonstrated neither blue nor red was defined as the infarct site. The area measurements were performed with Image tool software version 3.0 [23].

Cardiac mitochondrial function study

At the end of the experiment, cardiac mitochondria were isolated from non-ischemic and ischemic areas of the ventricles, and protein concentration was determined as previously described [23, 31]. Cardiac mitochondrial functions were determined by measuring the mitochondrial reactive oxygen species (ROS) production, mitochondrial membrane potential change ($\Delta\Psi m$) and mitochondrial swelling [23, 28].

Measurement of cardiac mitochondrial ROS production

Mitochondrial ROS production was determined by using Dichlorohydro-fluorescein diacetate dye (DCFDA) [32, 33]. The DCFDA diffused through the mitochondrial membrane and is deacetylated by intracellular esterases to a non-fluorescent compound which was later oxidized by ROS into dichlorofluorescein (DCF). DCF was a highly fluorescent compound which could be detected by fluorescence spectroscopy with maximum excitation. Increasing of DCF indicated the increasing of ROS production. Fluorescent intensity of the DCF was measured with an excitation wavelength at 485 nm and an emission wavelength at 530 nm by a fluorescent microplate reader and represented as arbitrary units (a.u.) of fluorescent intensity [23, 34].

Measurement of cardiac mitochondrial membrane potential change ($\Delta\Psi m$)

Mitochondrial membrane potential change was determined by using the dye 5,5′,6,6′-tetrachloro-1,1′,3,3′-tetraethylbenzimidazolcarbocyanine iodide (JC-1) and was determined as fluorescence intensity by using a fluorescent microplate reader [23, 34]. The JC-1 monomer (green fluorescence) and aggregate (red fluorescence) forms were excited at the same wavelength of 485 nm, whereas the emission of the JC-1 monomer and aggregate forms were detected at wavelength 590 nm and 530 nm, respectively. The change in mitochondrial membrane potential was calculated from the ratio of red to green fluorescence (red/green fluorescence intensity ratio). A decrease in the red/green fluorescence intensity ratio indicates mitochondrial membrane depolarization [23, 34].

Measurement of cardiac mitochondrial swelling

The isolated mitochondrial suspension was used to determine mitochondrial swelling using a microplate reader (Synergy HT, Bio Tek, **Winooski**, Vermont, USA) to measure the change in the absorbance of the mitochondrial suspension at 540 nm (A540). Cardiac mitochondrial swelling was indicated by a decrease in the absorbance by the mitochondrial suspension [23, 34]. Transmission electron microscopy (TEM) was also used to determine the morphology of isolated cardiac mitochondria from both non-ischemic (remote) and ischemic areas [23].

Western blot analysis

Heart tissues were collected from ischemic and non-ischemic (remote) areas, quickly frozen in liquid nitrogen and stored at −80°C until used [23]. Myocardial protein extract was prepared by a homogenization of nitrogen-frozen heart tissues in a lysis buffer (containing 1% Nonidet P-40, 0.5% sodium deoxycholate, 0.1% sodium dodecyl sulfate (SDS) in 1×PBS), and subsequently homogenized at 4°C, and then centrifuged at 13000 round/minute for 10 minutes and defined as total protein. The total protein was mixed with loading buffer [10% mercaptoethanol, 0.05% bromophenol blue, 75 mM Tris-HCl, pH 6.8, 2% sodium dodecyl sulphate (SDS) and 10% glycerol] and heated at 95°C for 10 min. Then, the protein samples were subjected to 10% or 15% SDS polyacrylamide gel electrophoresis (SDS-PAGE) and transferred to

polyvinylidene difluoride membranes using a semi-dry transfer system (Trans-Blot SD; Bio-Rad, Hercules, CA, USA). The membranes were blocked with 5% non-fat skimmed milk in TBST (20 mM Tris-HCl, pH 7.6, 137 mM NaCl and 0.1% Tween-20) for 1 hour. The membranes were subsequently exposed to anti-Bax (Santa Cruz Biotechnology, Santa Cruz, CA, USA), anti-Bcl-2 (Cell Signaling Technology, Danvers, MA, USA), anti-total Connexin 43 (Santa Cruz Biotechnology, Santa Cruz, CA, USA), anti-Connexin 43 phosphorylated at S368 (Cell Signaling Technology, Danvers, MA, USA), or β-actin (Santa Cruz Biotechnology, Santa Cruz, CA, USA), overnight at 4°C. On the next day, the membranes were washed and incubated with horseradish peroxidase–conjugated secondary antibody (Cell Signaling Technology, Danvers, MA, USA) for 1 hour at room temperature. The signals were developed by incubating with an enhanced chemiluminescense reagent and subjected to autoradiography. The immunoblot films were scanned and the band density was analyzed using ImageJ analysis (NIH image).

Statistical analysis

Data were expressed as mean ± SEM. Statistical comparison within groups was analyzed with a one-way ANOVA with a post-hoc LSD test, whereas statistical comparison between groups was analyzed using a Student's *t*-test. A Chi-squared test was performed to compare the VT/VF incidence among groups. All statistical analysis was performed using SPSS version 10.0. The statistical significance was accepted at the level of a p-value less than 0.05.

Results

Testosterone replacement improved both cardiac function and HRV in ORX rats

In ORX rats, serum testosterone was markedly decreased when compared with the sham rats (Table 1). Beginning at 4 weeks after ORX, the impairment of both cardiac function and cardiac autonomic balance (i.e. LF/HF ratio) was demonstrated. The echocardiogram showed that the fractional shortening (FS) and the ejection fraction (EF) were decreased significantly, whereas the LF/HF ratio was markedly increased, when compared with the sham group (Fig 1). Testosterone replacement significantly improved the cardiac function by increasing the FS (Fig 1(A)) and EF (Fig 1(B)), and improved cardiac sympathovagal balance by decreasing the LF/HF ratio (Fig 1(C)) in ORX rats.

Testosterone improved left ventricular pressure during I/R injury in ORX rats

The changes in the left ventricular pressure at different time points are shown in Table 2. At baseline, the LVESP was significantly lower in ORX rats compared to the sham rats, whereas the heart rate and LVEDP showed no difference between the groups. However, testosterone

Table 1. Summary of blood serum testosterone concentration at week 8.

Parameters	SV	OV	ST	OT
Blood serum testosterone (ng/ml)	3.4 ± 0.25	0.03 ± 0.01 *	4.3 ± 0.21 †	3.6 ± 0.24 †

SV = Sham+Vehicle, OV = ORX+Vehicle, ST = Sham+Testosterone, OT = ORX+Testosterone.

*p <0.05 vs. SV group

†p <0.05 vs. OV group.

doi:10.1371/journal.pone.0122503.t001

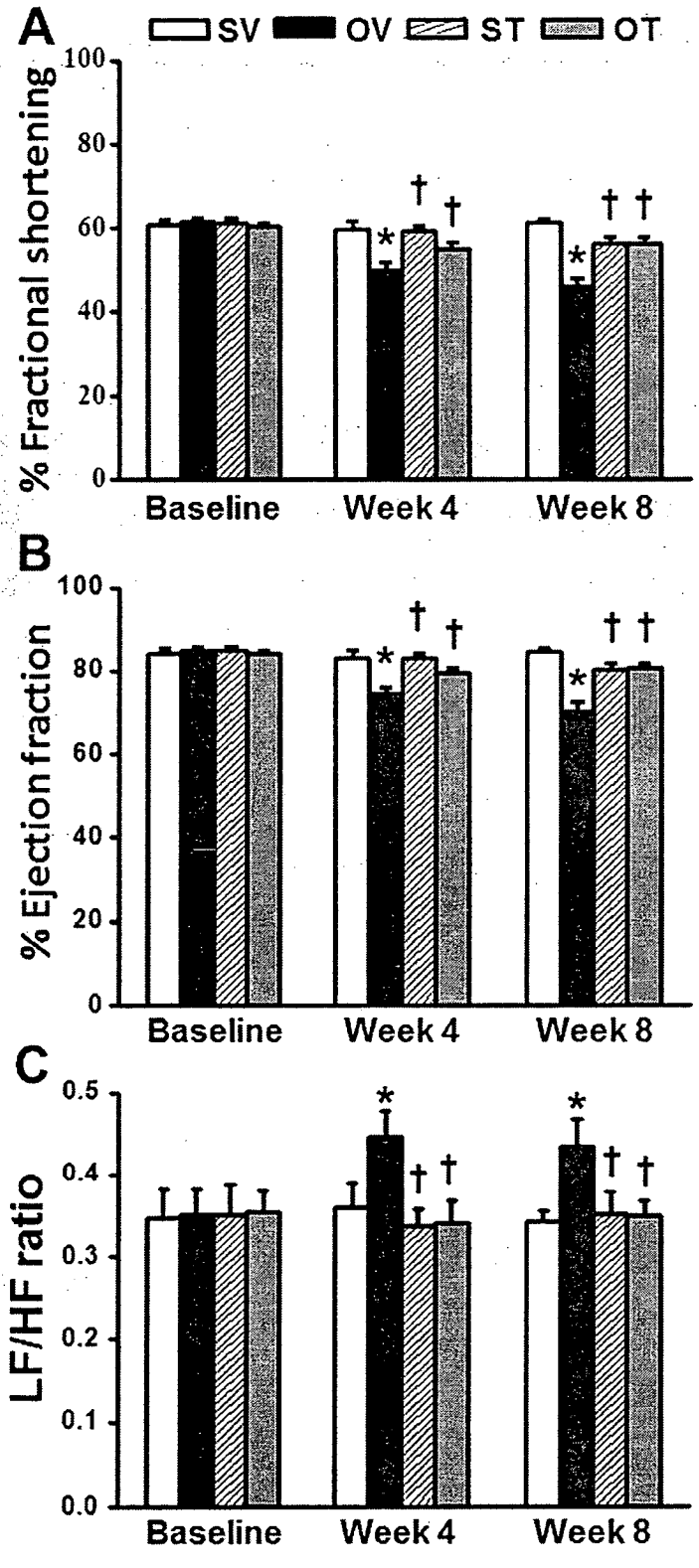

A
SV
OV
ST
OT
% Fractional shortening
100
80
60
40
20
0
Baseline
Week 4
Week 8
B
% Ejection fraction
100
80
60
40
20
0
Baseline
Week 4
Week 8
C
LF/HF ratio
0.5
0.4
0.3
0.2
0.1
0.0
Baseline
Week 4
Week 8

Fig 1. Effect of testosterone replacement on fractional shortening (FS), ejection fraction (EF) and heart rate variability (represent as Low frequency/High frequency ratio: LF/HF ratio) prior I/R injury. (A, B) Testosterone replacement restored the FS and EF at week 4 and 8, when compared with OV group. (C) Testosterone replacement reduced LF/HF ratio at week 4 and 8, when compared with OV group. *p < 0.05 vs. SV group, †p < 0.05 vs. OV group. SV = Sham+Vehicle, OV = ORX+Vehicle, ST = Sham +Testosterone, OT = ORX+Testosterone.

doi:10.1371/journal.pone.0122503.g001

replacement in ORX rats helped to restore the LVESP to the same level as in the sham rats (Table 2). During the I/R injury (i.e. at the end of ischemia and end of reperfusion), both ORX and sham rats that were given testosterone replacement had higher LVESP than the vehicle-treated ORX rats.

Testosterone decreased cardiac arrhythmias during I/R injury in ORX rats

During I/R, the VT/VF incidence showed no difference among all groups (Fig 2(A)). However, in ORX rats, the arrhythmia score was significantly greater, whereas the time to the first VT/VF onset was significantly lower, when compared with the sham group, indicating the high susceptibility to arrhythmias. Interestingly, testosterone replacement markedly attenuated cardiac arrhythmias during I/R by prolonging the time to the 1st VT/VF onset (Fig 2(B)) and reducing the arrhythmia score (Fig 2(C)). Consistent with this finding, the western blot analysis of connexin 43 showed that the phosphorylated connexin 43 per total connexin 43 ratio (P-Connexin 43/T-Connexin 43 ratio) was significantly decreased in ORX rats treated with a vehicle, whereas testosterone replacement significantly increased P-Connexin 43/T-Connexin 43 ratios back to the level of that in the sham group (Fig 2D).

Testosterone reduced the infarct size in I/R heart of ORX rats

The area at risk (AAR) was not significantly different in all groups. However, the infarct size of ORX rats was significantly greater compared with the sham group (Fig 3A). ORX rats with testosterone replacement had smaller infarct size than in the vehicle-treated ORX rats, accounting for approximately 36% reduction in infarct size (Fig 3A).

Western blot analysis showed that anti-apoptotic protein Bcl-2 expression in the heart of ORX rats treated with vehicle was significantly decreased compared with the sham group, whereas the pro-apoptotic protein Bax expression was markedly increased (Fig 3B and 3C),

Table 2. Effects of Testosterone on heart rate and left ventricular pressure during I/R injury.

Parameter	Baseline				End of ischemia				End of reperfusion			
	SV	OV	ST	OT	SV	OV	ST	OT	SV	OV	ST	OT
HR	230.9 ±17	236.8±8	227.4 ±15	209.8±10	233.7 ±23.9	234.1 ±13.2	221.1 ±17.7	199.8 ±9.0	257.5 ±24.9	255.1 ±14.5	240.3 ±17.5	225.7 ±16.8
LVESP	113.1 ±6.4	94.6 ±4.1*	111.8 ±3†	113.4 ±3.5†	88.1±9.0	69.5±7.7	92.1 ±6.5†	92.4 ±10.2†	105.7 ±5.3	88.9±5.3	109.9 ±5.2†	113.4±5†
LVEDP	16.7 ±2.2	19.8 ±2.2	16.8 ±0.7	24.7±8.9	23.5±3.6	25.3±3.1	20±5.9	22.1±8.8	20.4±2.8	26.3 ±2.4*	21±8.1†	21.0 ±8.1†

SV = Sham+Vehicle, OV = ORX+Vehicle, ST = Sham+Testosterone, OT = ORX+Testosterone. HR = heart rate; LVESP = left ventricular end-systolic pressure; LVEDP = left ventricular end-diastolic pressure.

*p < 0.05 vs. SV group

†p < 0.05 vs. OV group.

doi:10.1371/journal.pone.0122503.t002

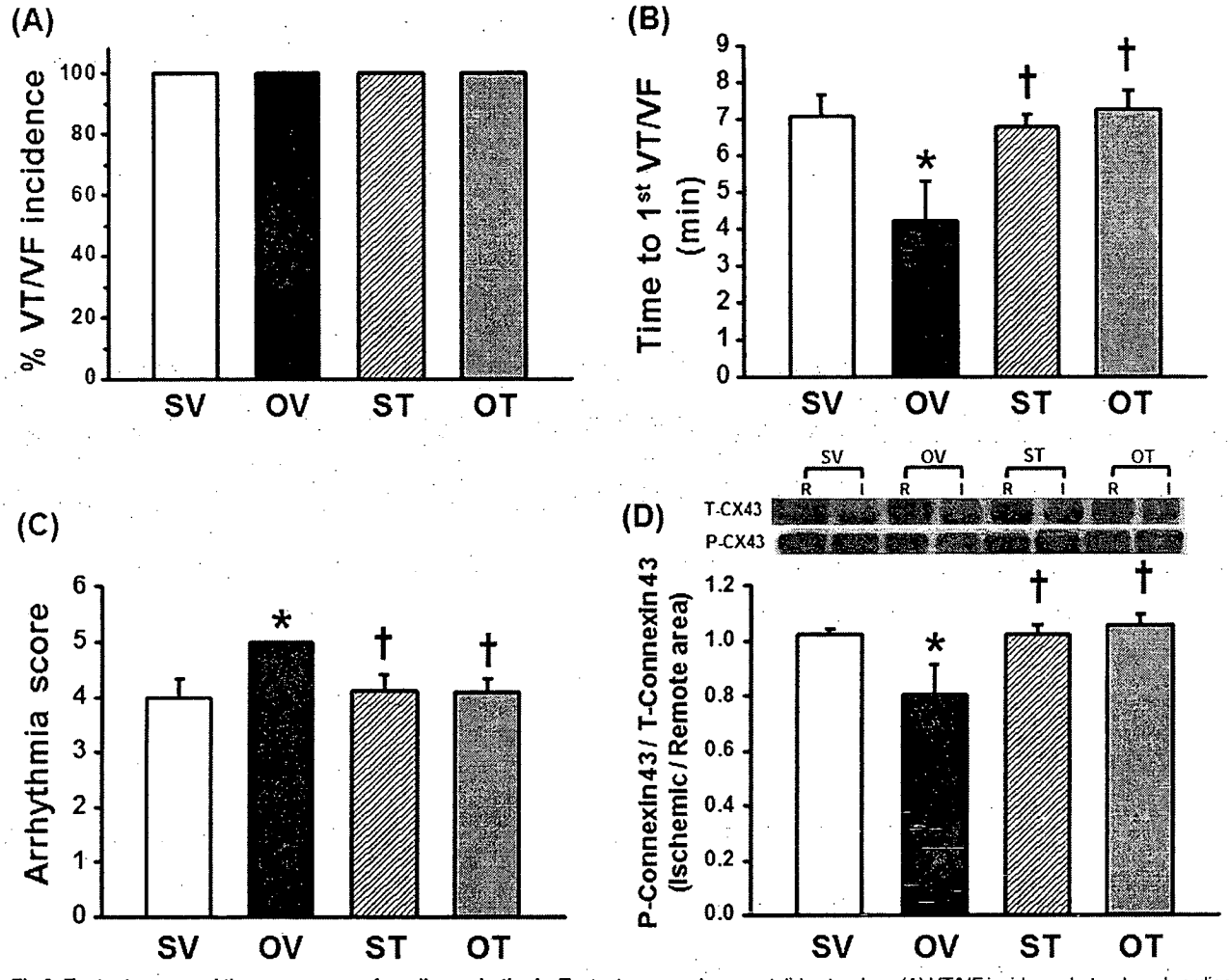


Fig 2. Testosterone and the occurrence of cardiac arrhythmia. Testosterone replacement did not reduce (A) VT/VF incidence but reduced cardiac arrhythmia by increasing (B) Time to 1st VT/VF incidence and decreasing (C) arrhythmia score, compared to ORX group. (D) Testosterone increased P-Connexin 43/T-Connexin 43 ratio compared to OV group. *p < 0.05 vs. SV group, †p < 0.05 vs. OV group. SV = Sham+Vehicle, OV = ORX+Vehicle, ST = Sham+Testosterone, OT = ORX+Testosterone. VT = Ventricular tachycardia, VF = Ventricular fibrillation, R = Remote area, I = Ischemic area, CX43 = Connexin 43

doi:10.1371/journal.pone.0122503.g002

compared with the sham group. Consistently, the Bax/Bcl-2 ratio in the ORX rats treated with vehicle was also increased (Fig 3D). ORX rats with testosterone replacement had increased Bcl-2 expression, decreased Bax expression and decreased Bax/Bcl-2 ratio, compared to the vehicle-treated ORX rats (Fig 3B–3D).

Testosterone attenuated cardiac mitochondrial dysfunction in ORX rats with cardiac I/R injury

Cardiac mitochondria taken from the ischemic myocardium in ORX rats demonstrated increased mitochondrial ROS production (Fig 4A), increased mitochondrial swelling which was indicated by the decrease in absorbance (Fig 4B) and increased mitochondrial depolarization which was indicated by the decrease of the red/green fluorescent intensity ratio (Fig 4C),

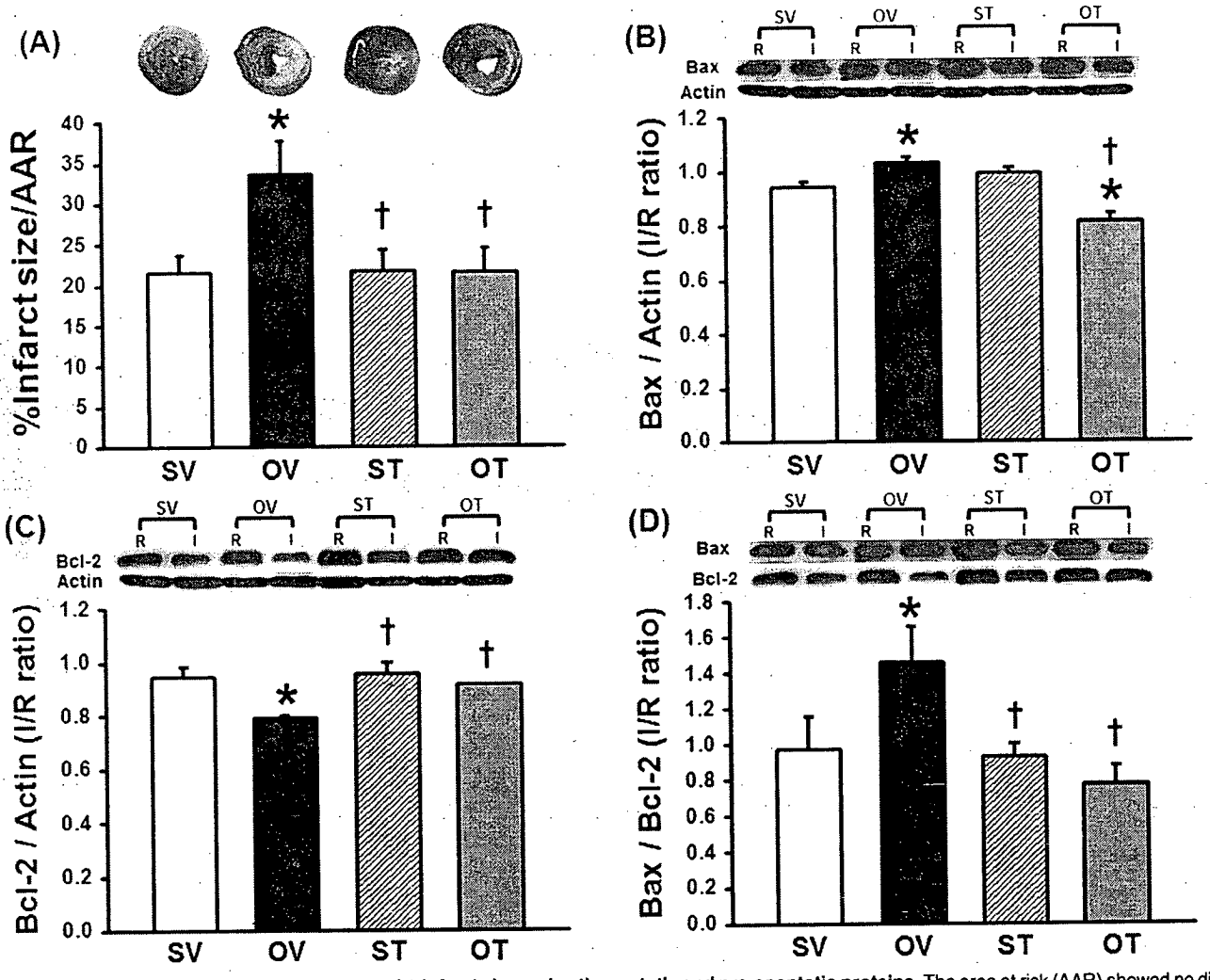


Fig 3. Effect of testosterone replacement on the infarct size and anti-apoptotic and pro-apoptotic proteins. The area at risk (AAR) showed no different among all groups. (A) Testosterone replacement reduced the infarct size by 36%, compared to the OV group. Testosterone attenuated apoptotic process as indicated by (B) increased anti-apoptotic Bcl-2, (C) decreased pro-apoptotic Bax expression, and (D) reduced Bax/Bcl-2 ratio, compared to the OV group. *$p < 0.05$ vs. SV group, †$p < 0.05$ vs. OV group. SV = Sham+Vehicle, OV = ORX+Vehicle, ST = Sham+Testosterone, OT = ORX+Testosterone, R = Remote area, I = Ischemic area

doi:10.1371/journal.pone.0122503.g003

compared to the non-ischemic area. However, testosterone replacement in ORX rats attenuated cardiac mitochondrial dysfunction in the ischemic myocardium which was indicated by a reduction in mitochondrial ROS production (Fig 4A), decreased cardiac mitochondrial swelling (Fig 4B) and reduced cardiac mitochondrial depolarization (Fig 4C). Representative pictures of cardiac mitochondria taken from the transmission electron microscope (TEM) are shown in Fig 4D. Mitochondrial swelling, which is indicated by abnormal morphology together with the loss of cristae of the cardiac mitochondrion in the ischemic area, was observed in the ORX rats treated with the vehicle. In ORX rats with testosterone replacement, cardiac mitochondrial swelling was observed to be markedly reduced in the ischemic myocardium.

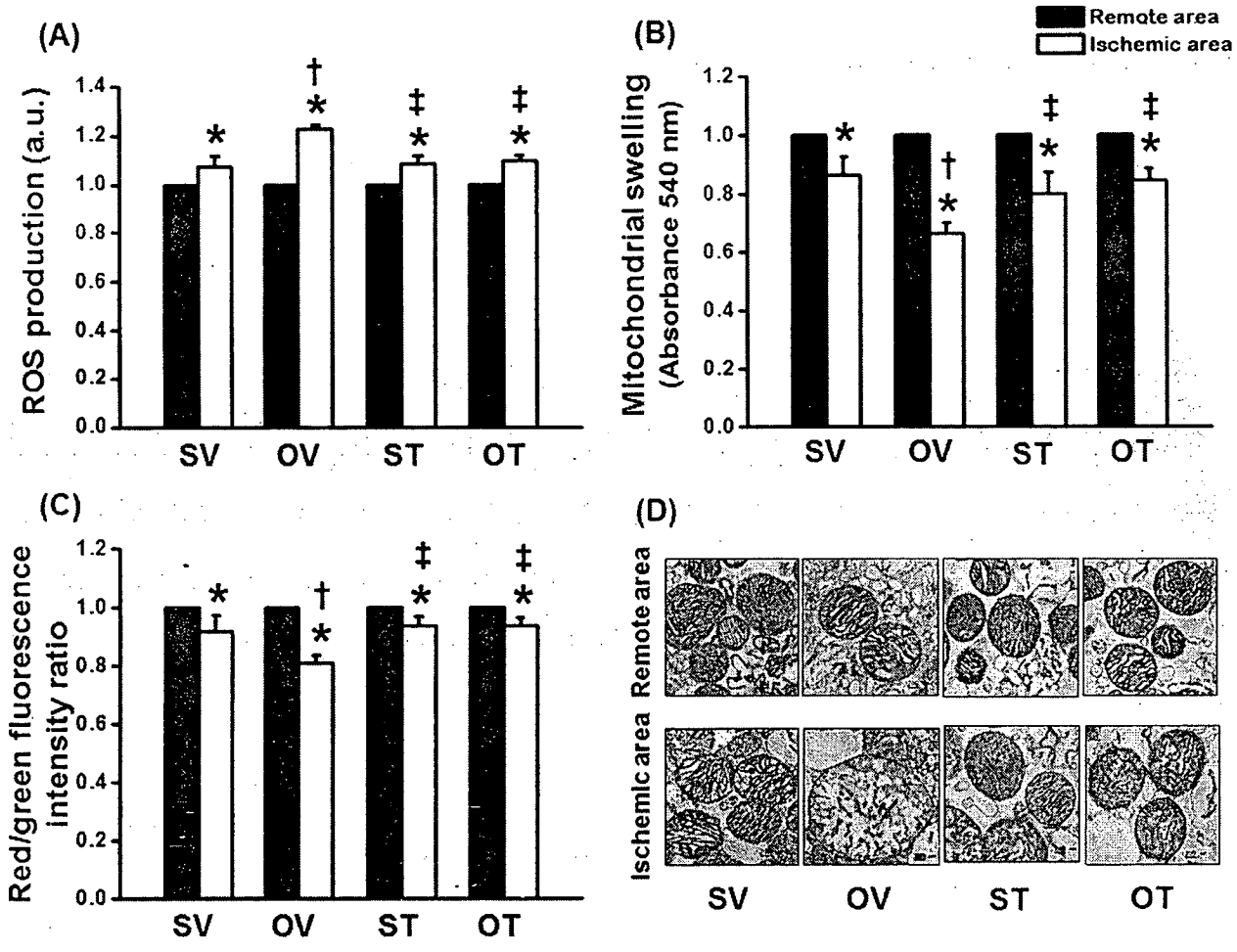


Fig 4. Effect of testosterone on cardiac mitochondria after ischemic-reperfusion period. Testosterone improved cardiac mitochondrial function by showing (A) reduced reactive oxygen species (ROS) production, (B) attenuated mitochondrial swelling and (C) attenuated mitochondrial membrane depolarization in ischemic area. (D) Testosterone also attenuated the deterioration of cardiac mitochondrial morphology. *$p < 0.05$ vs. Remote area, †$p < 0.05$ vs. SV group, ‡$p < 0.05$ vs. OV group. SV = Sham+Vehicle, OV = ORX+Vehicle, ST = Sham+Testosterone, OT = ORX+Testosterone

doi:10.1371/journal.pone.0122503.g004

Discussion

In this study, the cardioprotective effects of testosterone in testosterone-deprived rats heart with I/R injury were demonstrated. The major findings of this study are as follows. Prior to I/R injury, testosterone replacement provided cardioprotective effects in testosterone-deprived rats as indicated by (1) improved cardiac functions by markedly preserved %EF and %FS, and (2) attenuated cardiac sympathovagal imbalance by a markedly decreased LF/HF ratio. During the I/R period, testosterone replacement in ORX rats exerted the beneficial effects as indicated by (1) improved left ventricular pressure; (2) markedly decreased infarct size; (3) reduced fatal cardiac arrhythmias by increased time to 1st VT/VF onset and reduced arrhythmia scores; and (4) attenuated cardiac mitochondrial dysfunction caused by I/R injury by reducing ROS production, cardiac mitochondrial swelling and mitochondria membrane depolarization.

In ORX rats, our results emphasized the importance of the physiological level of testosterone by demonstrating the adverse effects of testosterone deprivation on the left ventricular

function and cardiac sympathovagal regulation. In this study, decreasing of FS and EF were observed starting at week 4 after orchiectomy, whereas testosterone replacement clearly demonstrated cardioprotective effects by improving the left ventricular function in the testosterone-treated group. This finding is consistent with the previous studies which also indicated that cardiac muscle is one of the target organs of testosterone hormone, which plays a beneficial role on cardiac function by improving cardiac contractility and improved calcium regulation [35, 36]. In addition to impaired left ventricular function in ORX rats, testosterone deprivation also significantly affected the cardiac autonomic tone balance as shown by an increased LF/HF ratio (i.e. so-called depressed HRV) in ORX rats. We found that depressed HRV was initially observed in week 4 after ORX, whereas testosterone replacement could restore the HRV in the testosterone-treated group. This result is consistent with a previous clinical report in men with stable coronary artery disease (CAD) which demonstrated that a high level of blood testosterone was associated with reduced sympathovagal imbalance [37]. Since depressed HRV is known to be associated with increased oxidative stress [38, 39] and that testosterone deprivation has been shown to affect the antioxidant defense system in the left ventricle (LV) [40] and associated with the increased oxidative stress [41, 42], testosterone replacement could play a crucial role in the protection of cardiac sympathovagal imbalance by reducing the oxidative stress and the enhancing of the antioxidant defense system. This hypothesis is supported by the findings of this study that ORX rats had increased cardiac mitochondrial ROS production, and testosterone attenuated ROS level.

During the I/R period, the results clearly demonstrated that ORX rats treated with testosterone had a higher LVESP than in the untreated group, indicating that testosterone plays a beneficial role in the post-ischemic functional recovery. This finding is consistent with previous reports using ORX rats with I/R and myocardial infarction models which demonstrated that chronic testosterone replacement (physiological and supraphysiological dose) confers cardioprotection by maintaining intracellular calcium homeostasis [21, 43]. However, inconsistent reports exist which showed that acute administration of testosterone at a physiological level could depress the recovery of myocardial function during I/R injury by inducing hypertrophic response in the heart via androgen receptors, resulting in an increase of ventricular stiffness [19]. These discrepancies in findings regarding the role of testosterone on the cardiac function during I/R could be due to differences in the experimental model. Nevertheless, the findings of this study demonstrated for the first time in *in vivo* that chronic administration of testosterone improved left ventricular function during I/R.

During I/R injury, this study clearly demonstrated that ORX rats were susceptible to arrhythmias as indicated by a shorter interval of time to 1st VT/VF onset and higher arrhythmia scores than those in the control group, while testosterone replacement in ORX rats had a longer time to 1st VT/VF onset and lower arrhythmia scores. This finding is consistent with a previous study in rats which demonstrated that the physiological dose of testosterone (2 mg/kg) combined with adrenergic stimulation could reduce reperfusion arrhythmias during I/R injury by reducing the incidence of a premature ventricular beat [12]. It is possible that the mechanism that testosterone attenuated cardiac arrhythmias during I/R injury was involved with connexin 43 phosphorylation. It has been shown that the phosphorylation of connexin 43 at serine 368 residue plays an essential role in preserving cell to cell communication through gap junctions in the myocardium, and that decreased connexin 43 phosphorylation could facilitate arrhythmias [23, 31, 44]. This study demonstrated that testosterone-deprived rats had decreased connexin 43 phosphorylation, and that testosterone treatment increased the phosphorylation of connexin 43, resulting in increased cell to cell communication, and fatal arrhythmias were attenuated during the I/R period.

The myocardial infarct size has been shown to be associated with the severity of left ventricular dysfunction as well as mortality rate [23, 31, 45, 46]. Since myocardial infarction plays an essential role in cardiac dysfunction, reduction in the infarct size would be of great benefit regarding contractility. In this study, it was demonstrated that testosterone replacement in ORX rats reduced the infarct size caused by I/R injury by 36% when compared to the untreated group. This finding is consistent with previous studies that testosterone could significantly reduce the infarct size in the hearts subjected to I/R injury [12, 43]. The mechanism responsible for infarct size reduction in the testosterone-treated ORX rats could be due to the reduced apoptosis and the reduction of cardiac mitochondrial dysfunction. In this study, it was found that testosterone attenuated myocardial apoptosis by increasing anti-apoptotic (Bcl-2) proteins and reducing pro-apoptotic (Bax) proteins.

Moreover, cardiac mitochondrial dysfunction, as indicated by increased mitochondrial ROS production, mitochondrial depolarization and mitochondrial swelling, was prominent in the ischemic myocardium of ORX rats subjected to I/R injury, and these dysfunctions were attenuated by the testosterone replacement. Mitochondria are known to play an essential role in the cell survival especially in cardiomyocytes [47]. During an I/R period, the oxidative phosphorylation rate at the inner mitochondrial membrane is reduced, leading to a decrease in the energy production and causing a rapid increase in ROS production [48]. When the accumulation of ROS is high enough to reach a critical threshold level [49], it triggers the opening of the mitochondrial permeability transition pores (mPTP) or the inner membrane anion channels (IMAC), resulting in the collapse of the mitochondrial membrane potential which is known as mitochondrial membrane depolarization [49–51]. Moreover, the prolonged opening of mPTP could lead to bi-directional diffusion of low molecular weight molecules across the inner mitochondrial membrane. Since high molecular weight molecules (i.e. proteins) remain in the matrix, this leads to an increase in the matrix osmotic pressure and resulting in mitochondrial swelling and/or mitochondrial membrane rupture. This will cause the release of cytochrome c and other proapoptotic proteins, leading to apoptotic cell death [52, 53]. Since testosterone has been shown to reduce ROS generation [42] and suppress oxidative stress [54], it is possible that this anti-oxidative effect of testosterone could be responsible for its cardioprotection in this study. This hypothesis is supported by our findings that testosterone attenuates cardiac mitochondrial ROS levels and reduced mitochondrial dysfunction during I/R injury. These beneficial effects of testosterone replacement in ORX rats could also play an important role in decreasing the cellular apoptotic process, infarct size and cardiac arrhythmias as well as improving LV function during I/R injury.

Conclusions

Testosterone replacement exerts cardioprotective effects by improving left ventricular function and cardiac sympathovagal balance impaired by testosterone deprivation in ORX rats. Chronic testosterone replacement also ameliorates left ventricular dysfunction, and reduces the infarct size and cardiac arrhythmias impaired by I/R injury under testosterone-deprived conditions. The mechanisms responsible for these beneficial effects of testosterone could be due to its ability to attenuate cardiac mitochondrial dysfunction and cardiomyocyte apoptosis. These findings provide important information regarding the cardioprotective benefits of testosterone in testosterone-deprived subjects with and without I/R injury. Future clinical studies are needed to determine its clinical usefulness in patients with acute myocardial infarction.

Acknowledgments

The authors would like to thank Dr. Kroekkiat Chinda and Dr. Siripong Palee for their technical assistance on animal surgery, and Dr. Sirinart Kumfu, Dr. Jirapas Sripetchwandee, Ms. Sivaporn Sivasinprasasn, Ms. Nattayaporn Apaijai and Ms. Jantira Sanit for their technical assistance on Western blot and mitochondrial analysis.

Author Contributions

Conceived and designed the experiments: WP SC NC. Performed the experiments: WP SC NC. Analyzed the data: WP SC NC. Contributed reagents/materials/analysis tools: WP SC NC. Wrote the paper: WP SC NC.

References

1. Yeap BB. Androgens and cardiovascular disease. Curr Opin Endocrinol Diabetes Obes. 2010; 17 (3):269–76. doi: 10.1097/MED.0b013e3283383031 PMID: 20186051
2. Traish AM, Kypreos KE. Testosterone and cardiovascular disease: an old idea with modern clinical implications. Atherosclerosis. 2011; 214(2):244–8. doi: 10.1016/j.atherosclerosis.2010.08.078 PMID: 20869058
3. Haring R, Volzke H, Steveling A, Krebs A, Felix SB, Schofl C, et al. Low serum testosterone levels are associated with increased risk of mortality in a population-based cohort of men aged 20–79. Eur Heart J. 2010; 31(12):1494–501. doi: 10.1093/eurheartj/ehq009 PMID: 20164245
4. Kelly DM, Jones TH. Testosterone: a vascular hormone in health and disease. J Endocrinol. 2013; 217 (3):R47–71. doi: 10.1530/JOE-12-0582 PMID: 23549841
5. Yildirir A, Kabakci G, Can I, Erbas B. Men with coronary artery disease have lower levels of androgens than men with normal coronary angiograms. Eur Heart J. 2001; 22(7):612–3. PMID: 11259151
6. Wu FC, von Eckardstein A. Androgens and coronary artery disease. Endocr Rev. 2003; 24(2):183–217. PMID: 12700179
7. Corona G, Vignozzi L, Sforza A, Maggi M. Risks and benefits of late onset hypogonadism treatment: an expert opinion. World J Mens Health. 2013; 31(2):103–25. doi: 10.5534/wjmh.2013.31.2.103 PMID: 24044106
8. Saad F. Androgen therapy in men with testosterone deficiency: can testosterone reduce the risk of cardiovascular disease? Diabetes Metab Res Rev. 2012; 28 Suppl 2:52–9. doi: 10.1002/dmrr.2354 PMID: 23280867
9. Weiss EP, Villareal DT, Ehsani AA, Fontana L, Holloszy JO. Dehydroepiandrosterone replacement therapy in older adults improves indices of arterial stiffness. Aging cell. 2012; 11(5):876–84. doi: 10.1111/j.1474-9726.2012.00852.x PMID: 22712469
10. Wang C, Nieschlag E, Swerdloff R, Behre HM, Hellstrom WJ, Gooren LJ, et al. Investigation, treatment and monitoring of late-onset hypogonadism in males: ISA, ISSAM, EAU, EAA and ASA recommendations. Eur J Endocrinol. 2008; 159(5):507–14. doi: 10.1530/EJE-08-0601 PMID: 18955511
11. Uyanik BS, Ari Z, Gumus B, Yigitoglu MR, Arslan T. Beneficial effects of testosterone undecanoate on the lipoprotein profiles in healthy elderly men. A placebo controlled study. Jpn Heart J. 1997; 38(1):73–82. PMID: 9186283
12. Tsang S, Wu S, Liu J, Wong TM. Testosterone protects rat hearts against ischaemic insults by enhancing the effects of alpha(1)-adrenoceptor stimulation. Br J Pharmacol. 2008; 153(4):693–709. PMID: 18157169
13. Borst SE, Quindry JC, Yarrow JF, Conover CF, Powers SK. Testosterone administration induces protection against global myocardial ischemia. Horm Metab Res. 2009; 42(2):122–9. doi: 10.1055/s-0029-1241843 PMID: 19862668
14. Bell JR, Mellor KM, Wollermann AC, Delbridge LM. Cardiac ischaemic stress: cardiomyocyte Ca(2), sex and sex steroids. Clin Exp Pharmacol Physiol. 2011; 38(10):717–23. doi: 10.1111/j.1440-1681.2011.05567.x PMID: 21722161
15. Sanada S, Komuro I, Kitakaze M. Pathophysiology of myocardial reperfusion injury: preconditioning, postconditioning, and translational aspects of protective measures. Am J Physiol Heart Circ Physiol. 2011; 301(5):H1723–41. doi: 10.1152/ajpheart.00553.2011 PMID: 21856909
16. Tsang S, Liu J, Wong TM. Testosterone and cardioprotection against myocardial ischemia. Cardiovasc Hematol Disord Drug Targets. 2007; 7(2):119–25. PMID: 17584046

17. Wang M, Wang Y, Abarbanell A, Tan J, Weil B, Herrmann J, et al. Both endogenous and exogenous testosterone decrease myocardial STAT3 activation and SOCS3 expression after acute ischemia and reperfusion. Surgery. 2009; 146(2):138–44. doi: 10.1016/j.surg.2009.03.035 PMID: 19628067

18. Huang C, Gu H, Zhang W, Herrmann JL, Wang M. Testosterone-down-regulated Akt pathway during cardiac ischemia/reperfusion: a mechanism involving BAD, Bcl-2 and FOXO3a. J Surg Res. 2010; 164 (1):e1–11. doi: 10.1016/j.jss.2010.07.041 PMID: 20850791

19. Crisostomo PR, Wang M, Wairiuko GM, Morrell ED, Meldrum DR. Brief exposure to exogenous testosterone increases death signaling and adversely affects myocardial function after ischemia. Am J Physiol Regul Integr Comp Physiol. 2006; 290(5):R1168–74. PMID: 16439666

20. Nam UH WM, Crisostomo PR, Markel TA, Lahm T, Meldrum KK, Lillemoe KD, et al. The effect of chronic exogenous androgen on myocardial function following acute ischemia-reperfusion in hosts with different baseline levels of sex steroids. J Surg Res. 2007(142:):113–8. PMID: 17597161

21. Borst SE, Quindry JC, Yarrow JF, Conover CF, Powers SK. Testosterone administration induces protection against global myocardial ischemia. Horm Metab Res. 2010; 42(2):122–9. doi: 10.1055/s-0029-1241843 PMID: 19862668

22. Foley PL. Common Surgical Procedures in Rodents. In: RJDaS M.A., editor. Laboratory Animal Medicine and Management. Office of Animal Research Education and Compliance, University of Virginia, Charlottesville, VA, USA: International Veterinary Information Service, Ithaca NY (www.ivis.org); 2005.

23. Chinda K, Sanit J, Chattipakorn S, Chattipakorn N. Dipeptidyl peptidase-4 inhibitor reduces infarct size and preserves cardiac function via mitochondrial protection in ischaemia-reperfusion rat heart. Diab Vasc Dis Res. 2014; 11(2):75–83. doi: 10.1177/1479164113516134 PMID: 24357666

24. Glos M, Romberg D, Fietze I, Penzel T. Heart rate and systolic blood pressure variability before and during obstructive sleep apnea episodes. Conf Proc IEEE Eng Med Biol Soc. 2007; 2007:263–6. PMID: 18001940

25. Lima AH, Forjaz CL, Silva GQ, Meneses AL, Silva AJ, Ritti-Dias RM. Acute effect of resistance exercise intensity in cardiac autonomic modulation after exercise. Arq Bras Cardiol. 2011; 96(6):498–503. PMID: 21503389

26. Latchman PL, Mathur M, Bartels MN, Axtell RS, De Meersman RE. Impaired autonomic function in normotensive obese children. Clin Auton Res. 2011; 21(5):319–23. doi: 10.1007/s10286-011-0116-8 PMID: 21318460

27. Apaijai N, Chinda K, Palee S, Chattipakorn S, Chattipakorn N. Combined vildagliptin and metformin exert better cardioprotection than monotherapy against ischemia-reperfusion injury in obese-insulin resistant rats. PloS one. 2014; 9(7):e102374. doi: 10.1371/journal.pone.0102374 PMID: 25036861

28. Surinkaew S, Kumphune S, Chattipakorn S, Chattipakorn N. Inhibition of p38 MAPK during ischemia, but not reperfusion, effectively attenuates fatal arrhythmia in ischemia/reperfusion heart. J Cardiovasc Pharmacol. 2013; 61(2):133–41. doi: 10.1097/FJC.0b013e318279b7b1 PMID: 23107875

29. Curtis MJ, Hancox JC, Farkas A, Wainwright CL, Stables CL, Saint DA, et al. The Lambeth Conventions (II): guidelines for the study of animal and human ventricular and supraventricular arrhythmias. Pharmacol Ther. 2013; 139(2):213–48. doi: 10.1016/j.pharmthera.2013.04.008 PMID: 23588158

30. Curtis MJ, Walker MJ. Quantification of arrhythmias using scoring systems: an examination of seven scores in an in vivo model of regional myocardial ischaemia. Cardiovasc Res. 1988; 22(9):656–65. PMID: 3242835

31. Palee S, Weerateerangkul P, Chinda K, Chattipakorn SC, Chattipakorn N. Mechanisms responsible for beneficial and adverse effects of rosiglitazone in a rat model of acute cardiac ischaemia-reperfusion. Exp Physiol. 2013; 98(5):1028–37. doi: 10.1113/expphysiol.2012.070433 PMID: 23291914

32. Chin LK, Yu JQ, Fu Y, Yu T, Liu AQ, Luo KQ. Production of reactive oxygen species in endothelial cells under different pulsatile shear stresses and glucose concentrations. Lab Chip. 2011; 11(11):1856–63. doi: 10.1039/c0lc00651c PMID: 21373653

33. Wang J, Wang Y, Wong C. Oestrogen-related receptor alpha inverse agonist XCT-790 arrests A549 lung cancer cell population growth by inducing mitochondrial reactive oxygen species production. Cell Prolif. 2010; 43(2):103–13. doi: 10.1111/j.1365-2184.2009.00659.x PMID: 20447055

34. Sripetchwandee J, Kenknight SB, Sanit J, Chattipakorn S, Chattipakorn N. Blockade of mitochondrial calcium uniporter prevents cardiac mitochondrial dysfunction caused by iron overload. Acta Physiol (Oxf). 2013.

35. Curl CL, Delbridge LM, Canny BJ, Wendt IR. Testosterone modulates cardiomyocyte Ca(2+) handling and contractile function. Physiol Res. 2009; 58(2):293–7. PMID: 18380535

36. Witayavanitkul N, Woranush W, Bupha-Intr T, Wattanapermpool J. Testosterone regulates cardiac contractile activation by modulating SERCA but not NCX activity. Am J Physiol Heart Circ Physiol. 2013; 304(3):H465–H72. doi: 10.1152/ajpheart.00555.2012 PMID: 23203968

37. Wranicz JK, Rosiak M, Cygankiewicz I, Kula P, Kula K, Zareba W. Sex steroids and heart rate variability in patients after myocardial infarction. Ann Noninvasive Electrocardiol. 2004; 9(2):156–61. PMID: 15084213

38. Brook RD, Rajagopalan S, Pope CA, Brook JR, Bhatnagar A, Diez-Roux AV, et al. Particulate matter air pollution and cardiovascular disease: An update to the scientific statement from the American Heart Association. Circulation. 2010; 121(21):2331–78. doi: 10.1161/CIR.0b013e3181dbece1 PMID: 20458016

39. Chahine T, Baccarelli A, Litonjua A, Wright RO, Suh H, Gold DR, et al. Particulate air pollution, oxidative stress genes, and heart rate variability in an elderly cohort. Environ Health Perspect. 2007; 115 (11):1617–22. PMID: 18007994

40. Klapcinska B, Jagsz S, Sadowska-Krepa E, Gorski J, Kempa K, Langfort J. Effects of castration and testosterone replacement on the antioxidant defense system in rat left ventricle. J Physiol Sci. 2008; 58 (3):173–7. doi: 10.2170/physiolsci.RP002208 PMID: 18445310

41. Chen H, Cangello D, Benson S, Folmer J, Zhu H, Trush MA, et al. Age-related increase in mitochondrial superoxide generation in the testosterone-producing cells of Brown Norway rat testes: relationship to reduced steroidogenic function? Exp Gerontol. 2001; 36(8):1361–73. PMID: 11602210

42. Hwang TI, Liao TL, Lin JF, Lin YC, Lee SY, Lai YC, et al. Low-dose testosterone treatment decreases oxidative damage in TM3 Leydig cells. Asian J Androl. 2011; 13(3):432–7. doi: 10.1038/aja.2010.159 PMID: 21297653

43. Chen Y, Fu L, Han Y, Teng Y, Sun J, Xie R, et al. Testosterone replacement therapy promotes angiogenesis after acute myocardial infarction by enhancing expression of cytokines HIF-1a, SDF-1a and VEGF. Eur J Pharmacol. 2012; 684(1–3):116–24. doi: 10.1016/j.ejphar.2012.03.048 PMID: 22724132

44. Lampe PD, TenBroek EM, Burt JM, Kurata WE, Johnson RG, Lau AF. Phosphorylation of connexin43 on serine368 by protein kinase C regulates gap junctional communication. J Cell Biol. 2000; 149 (7):1503–12. PMID: 10871288

45. Hasche ET, Fernandes C, Freedman SB, Jeremy RW. Relation between ischemia time, infarct size, and left ventricular function in humans. Circulation. 1995; 92(4):710–9. PMID: 7641348

46. Miller TD, Christian TF, Hopfenspirger MR, Hodge DO, Gersh BJ, Gibbons RJ. Infarct size after acute myocardial infarction measured by quantitative tomographic 99mTc sestamibi imaging predicts subsequent mortality. Circulation. 1995; 92(3):334–41. PMID: 7634446

47. Halestrap AP, Doran E, Gillespie JP, O'Toole A. Mitochondria and cell death. Biochem Soc Trans. 2000; 28(2):170–7. PMID: 10816121

48. Niizuma K, Endo H, Chan PH. Oxidative stress and mitochondrial dysfunction as determinants of ischemic neuronal death and survival. J Neurochem. 2009; 109 Suppl 1:133–8. doi: 10.1111/j.1471-4159.2009.05897.x PMID: 19393019

49. Aon MA, Cortassa S, Marban E, O'Rourke B. Synchronized whole cell oscillations in mitochondrial metabolism triggered by a local release of reactive oxygen species in cardiac myocytes. J Biol Chem. 2003; 278(45):44735–44. PMID: 12930841

50. Hausenloy DJ, Duchen MR, Yellon DM. Inhibiting mitochondrial permeability transition pore opening at reperfusion protects against ischaemia-reperfusion injury. Cardiovasc Res. 2003; 60(3):617–25. PMID: 14659807

51. Thummasorn S, Kumfu S, Chattipakorn S, Chattipakorn N. Granulocyte-colony stimulating factor attenuates mitochondrial dysfunction induced by oxidative stress in cardiac mitochondria. Mitochondrion. 2011; 11(3):457–66. doi: 10.1016/j.mito.2011.01.008 PMID: 21292035

52. Crompton M. The mitochondrial permeability transition pore and its role in cell death. Biochem J. 1999; 341 (Pt 2):233–49.

53. Halestrap AP, Pasdois P. The role of the mitochondrial permeability transition pore in heart disease. Biochim Biophys Acta. 2009; 1787(11):1402–15. doi: 10.1016/j.bbabio.2008.12.017 PMID: 19168026

54. Marin DP, Bolin AP, dos Santos Rde C, Curi R, Otton R. Testosterone suppresses oxidative stress in human neutrophils. Cell Biochem Funct. 2010; 28(5):394–402. doi: 10.1002/cbf.1669 PMID: 20589735

เอกสารแนบหมายเลข 51

HEMOGLOBIN

http://informahealthcare.com/hem
ISSN: 0363-0269 (print), 1532-432X (electronic)

Hemoglobin, Early Online: 1–9
© 2015 Informa Healthcare USA, Inc. DOI: 10.3109/03630269.2014.987869

informa
healthcare

REVIEW ARTICLE

Cardiomyopathy Associated with Iron Overload: How Does Iron Enter Myocytes and What are the Implications for Pharmacological Therapy?

Karn Wijarnpreecha[1,2]*, Sirinart Kumfu[1,2]*, Siriporn C. Chattipakorn[1,2,3], and Nipon Chattipakorn[1,2]

[1]*Cardiac Electrophysiology Research and Training Center, Faculty of Medicine, Chiang Mai University, Chiang Mai, Thailand,*
[2]*Cardiac Electrophysiology Unit, Department of Physiology, Faculty of Medicine, Chiang Mai University, Chiang Mai, Thailand, and*
[3]*Center of Excellence in Cardiac Electrophysiology Research, Chiang Mai University, Chiang Mai, Thailand*

Abstract

Iron overload cardiomyopathy is one of the most common causes of death in thalassemia patients. Although new iron chelating agents have been developed, the mortality rate from heart failure remains elevated as a result of iron overload. This could be due to the fact that our understanding of the underlying mechanism of iron uptake into cardiomyocytes is still unclear, thus impeding the discovery and refinement of more effective therapy for thalassemia therapeutic strategies in thalassemic iron overload cardiomyopathy. Growing evidence indicates that multiple routes of iron entry into cardiomyocytes exist under iron overload conditions. These include both L-type (LTCC) and T-type (TTCC) calcium channels, divalent metal transporter 1 (DMT1) and transferrin receptors (TfRs). In this review, the routes of iron uptake into cardiomyocytes under iron overload conditions are presented. Evidence from pharmacological interventions in support or against the possible route of iron entry of each portal in cardiomyocytes are also comprehensively summarized and discussed.

Keywords

Calcium channel, cardiomyopathy, iron overload, iron uptake, thalassemia

History

Received 30 April 2014
Revised 9 July 2014
Accepted 14 July 2014
Published online 9 January 2015

Hemoglobin Downloaded from informahealthcare.com by Chiang Mai University on 01/26/15
For personal use only.

Introduction

Iron is an essential element in the human body. Most of the iron in the body is used in hemoglobin (Hb) synthesis (1). Moreover, iron is also used to produce myoglobin, cytochrome P450 (CYP450) and is involved in the electron transport chain in cellular respiration (1). The ability of iron to act as an electron donor and an acceptor can cause cell injury through production of reactive oxygen species (ROS) (2–4). Since the human body does not have a mechanism for iron excretion, iron overload conditions due to either hereditary hemochromatosis (primary) or regular blood transfusions in thalassemia, as well as other abnormal Hb diseases (secondary), can result in excess iron uptake and chronic deposition in peripheral tissues (liver, spleen, bone marrow, heart, β cells of the pancreas, pituitary and central nervous system and vascular smooth muscle) (1).

Although the most commonly employed treatments such as regular blood transfusions and iron chelation can improve survival in β-thalassemia major (β-TM) patients, iron overload cardiomyopathy is still the most common cause of death in these patients (5,6). Therefore, improving our understanding of the mechanisms underlying iron uptake into the heart under systemic iron overload conditions may improve the likelihood that therapy will be improved and thereby lead to improved survival. Currently, the underlying mechanism of iron uptake into the heart in iron overload conditions is not fully understood (7).

Conventionally, under the physiological condition, the uptake of ferrous iron (Fe^{2+}) into cells is achieved by the divalent metal transporter 1 (DMT1) (8,9). Another conventional route of iron entry into cells is via the transferrin receptor (TfR). Transferrin (Tf) binds to ferric iron (Fe^{3+}) with extremely high affinity called holo-transferrin (HoloTf) (10,11). Then, HoloTf binds to cell surface TfR and forms the TfR/Tf complex that is internalized through TfR-mediated endocytosis (10,11). However, growing evidence demonstrated that the calcium channels, both L-type (LTCC) and T-type (TTCC), could be the main routes of iron uptake into the heart under iron overload conditions (12–17). Studies in the past decade have shown that TfR and DMT1 are also key portals for uptake of iron into the heart under iron overload conditions, however, their role has never been investigated in a clinical setting (12,13,18). Although there are several new proposed therapeutic agents that may be beneficial in iron overload conditions, lack of clinical evidence is currently the limitation for their use in thalassemia patients (5,6,19,20). Currently, one of the most interesting agents is the calcium channel blocker. In this study, the routes of iron uptake into cardiomyocytes under iron overload conditions will be reviewed. Evidence from pharmacological interventions in

*KW and SK contributed equally in this study.

Address correspondence to Professor Nipon Chattipakorn, Cardiac Electrophysiology Research and Training Center, Faculty of Medicine, Chiang Mai University, 110 Intrawaroros Road, Chiang Mai 50200, Thailand. Tel: +66-53-945-329. Fax: +66-53-945-368. E-mail: nchattip@gmail.com

RIGHTSLINK

support or against the possible routes of iron entry of each portal in cardiomyocytes are also comprehensively summarized and discussed. From this overview the limitations of the treatments, the results and arguments of many studies about the route of iron uptake into the heart under iron overload conditions in the past decade are also presented, and can thus inform further preclinical and clinical studies.

Pathophysiology of iron overload cardiomyopathy

Thalassemic patients are prone to have iron overload as a result of regular blood transfusions (secondary iron overload or transfusional siderosis) (5,19,20). Increased intestinal iron absorption from ineffective erythropoiesis is only a minor cause (5,19,20). Once serum Tf (protein bound iron in plasma) has a saturation of over 45.0%, non transferrin bound iron (NTBI) will appear, and this form of iron can induce cardiovascular injury (21). The rate of NTBI uptake into cardiomyocytes is greater than Tf bound iron under iron overload conditions (22). Unfortunately, the uptake of NTBI is not regulated by a normal negative-feedback mechanism in the same way as Tf bound iron (21,23). Although the source of NTBI is still unknown, the free form of NTBI, both in plasma [labile plasma iron (LPI)] and intracellular [labile cellular iron (LCI) or labile iron pool (LIP)] can cause cardiovascular injury from the properties of reduction and oxidation of iron (2–5,19,21,24–28). These properties of NTBI can produce reactive oxygen species (ROS) (Haber-Weiss and Fenton reaction) leading to lipid peroxidation that causes cardiac cell apoptosis and interstitial fibrosis (2–5,19,21,24–28). Furthermore, high ROS production can also damage cellular proteins, DNA and other cellular organelles such as lysosomes and mitochondria (26,29). Previous studies suggested that mitochondrial dysfunction could be responsible for cardiac failure resulting from chronic iron overload (30,31). It has been shown that chronic iron overload can cause cumulative iron-mediated damage to mitochondrial DNA, thus impaired synthesis and function of mitochondrial respiratory chain subunits and leading to the loss of respiratory capacity and cardiac dysfunction (30,31). Furthermore, the increase in ROS production can cause ROS concentrations to reach the threshold level, which can trigger the opening of the inner membrane anion channel and mitochondrial permeability transition pore (32,33). This results in mitochondrial depolarization and mitochondrial swelling, leading to the release of cytochrome c, activation of caspase pathways, and cell death by necrosis and/or apoptosis (32,33). Moreover, the excess iron levels can slow calcium ion (Ca^{2+}) current inactivation which leads to an increase in the Ca^{2+} influx. These processes can be aggravated and impair diastolic function (restrictive cardiomyopathy) in early stages of the disease. If iron levels still increase, the Ca^{2+} entry into the heart will decrease due to the Fe^{2+} competition and eventually cause systolic dysfunction (dilated cardiomyopathy) (20). The summarized results of pathophysiology of iron overload cardiomyopathy are shown in Figure 1.

Despite the clear mechanism of iron-mediated cardiovascular injury, the exact theory of channel uptake of iron into cardiomyocytes under iron overload condition is still controversial (7). Although the major form of iron entry into cardiomyocytes under iron overload is Fe^{2+}, evidences exist that Fe^{3+} can be accessed in relatively low levels (34–36). To understand the mechanism of iron overload cardiomyopathy, many researchers have studied channel expressions and roles of uptake of iron in iron overload conditions. However, results remain controversial and need to be confirmed. From these data, new therapeutic strategies may be developed to decrease iron uptake into the heart and may improve survival of thalassemia patients in the future.

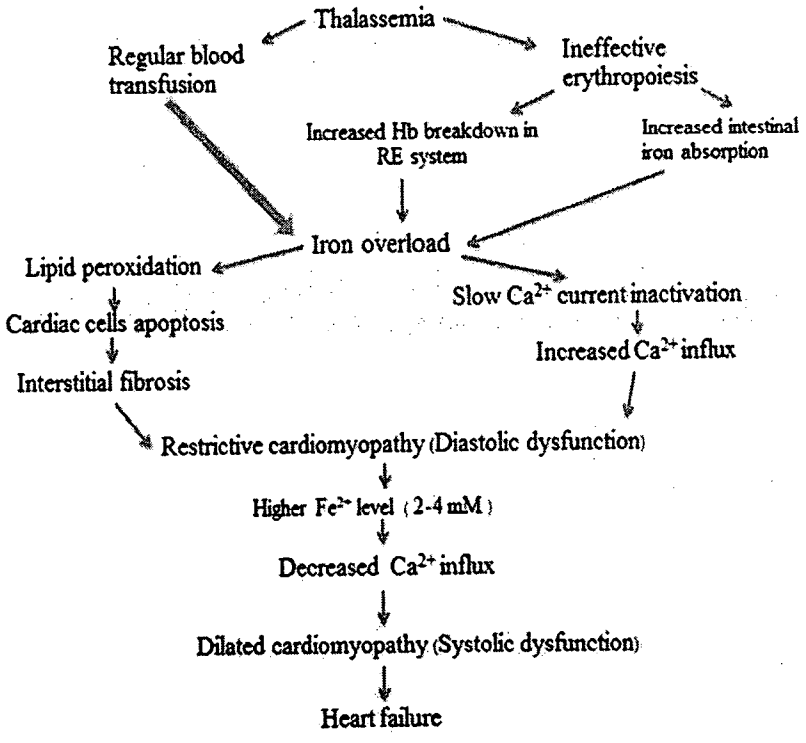


Figure 1. Pathophysiology of iron overload cardiomyopathy in thalassemia.

Hemoglobin Downloaded from informahealthcare.com by Chiang Mai University on 01/26/15
For personal use only.

RIGHTSLINK

Hemoglobin Downloaded from informahealthcare.com by Chiang Mai University on 01/26/15
For personal use only.

DOI: 10.3109/03630269.2014.987869

The expression of channels involved in iron uptake into cardiomyocytes under iron overload condition

In the past decade, several studies have carried out investigations of the expression of various portals as possible routes of iron entry into cardiomyocytes under iron overload conditions to evaluate the relationship of iron status and channels expression at both mRNA and protein levels. Four main channels reported to be involved in iron uptake into cardiomyocytes include TfRs, DMT1, LTCC and TTCC.

The expression of TfR mRNA and protein under iron overload conditions was not consistent as shown in Table 1. The variation of TfR mRNA and protein expression might be due to various factors including the difference in the model of experiments, the dose and route of iron administration and the duration of iron loading in each study. The conclusion of the channel involved in iron uptake from the data of mRNA and protein expression cannot be confidently predicted due to the variation in the data. The evidence has shown that Fe^{2+} is the main form of iron entering into cardiomyocytes under iron overload conditions (21,23). Therefore, TfR that binds to iron in Fe^{3+} form is not a main route of iron uptake under iron overload conditions (37). In the DMT1 study (Table 2), most of the evidence is concordant which suggest post transcriptional expression (decreased protein expression) in the rat heart under iron overload conditions although DMT1 uptake of iron is in Fe^{2+} form (37). Therefore, it can be concluded that DMT1 is not the main channel responsible for iron uptake into the heart. The possible main channels that are responsible for the uptake of iron into the heart might be LTCC that is unchanged in mRNA expression (Table 3), and TTCC that increased mRNA expression under iron overload conditions (Table 4). However, further studies are needed to prove the protein expression to support the important role of the iron uptake of these two channels.

The summary of mRNA and protein expression of each channel is shown in Table 5. Most reports in the past decade studied the mRNA and protein expression of TfR and DMT1 in iron overload conditions. There is only one study from Kumfu *et al.* (12) that represented mRNA expression of both LTCC and TTCC under iron overload conditions. Although Oudit *et al.* (16) stated the LTCC currents are not decreased in iron overload, this experiment did not evaluate mRNA or protein expression directly. Nevertheless, their report supports the point that LTCC has an important role in iron uptake under iron overload condition.

Evidence that supports or denies channels involved in iron uptake into cardiomyocytes under iron overload conditions

In most recent studies, the experiments are focused on changing iron levels after administering blocking agents to target specific channels to understand the relationship of iron levels in cardiomyocytes and the role of each channel in iron uptake. From the above section, TfR (uptake of Fe^{3+}) and DMT1 (decreased protein expression) may not be the main channels involved in iron uptake under iron overload conditions. Most of the studies focused on the LTCC that was thought to be the major pathway of iron uptake leading to iron overload cardiomyopathy (16). This channel is the only

Table 1. Evidence to support transferrin receptor expression in the heart under iron overload condition.

Bound Fe species	Model	Intervention	Identification techniques	TfR mRNA Expression Under Iron Overload			TfR Protein Expression Under Iron Overload			Refs.
				Increased	Decreased	Not changed	Increased	Decreased	Not changed	
Fe^{3+}	*In vitro* Cultured neonatal SD rat cardiomyocytes	Loaded FAC (5–80 μg/mL) for 3 days	Northern blot	×	✓	×	×	×	×	(47)
Fe^{3+}	Cultured neonatal SD rat cardiomyocytes	Loaded FAC (20 μg/mL) for 72 hours	RT-PCR and Western blot	×	×	✓	×	✓	×	(48)
Fe^{3+}	*In vivo* Male SD rats	Fed 2.5% carbonyl iron diet for 6 weeks	RT-PCR	×	✓	×	×	×	×	(40)
Fe^{3+}	Male Wistar rats	Injected iron dextran (200 mg/kg/week) IP for 4 weeks	Western blot	×	×	×		×	×	(49)
Fe^{3+}	C57BL/6 mice aged 10–12 weeks	Fed diet with 2% carbonyl iron for 6 weeks	Q-RT-PCR and microarray	×	✓	×	×	×	×	(50)
Fe^{3+}	Newly weaned male SD rats (21 days old)	Fed diet with iron 18.916 ppm for 3 weeks	Western blot	×	×	×	×	×	✓	(45)
Fe^{3+}	Male SD rats (21 days old)	Fed diet with 2.5% carbonyl iron for 6 weeks	Northern and Western blot	×	✓	×	×	✓	×	(51)

SD: Sprague-Dawley rat; FAC: ferric ammonium citrate; RT-PCR: reverse-transcription polymerase chain reaction; Q-RT-PCR: quantitative reverse-transcription polymerase chain reaction.

RIGHTSLINK

Hemoglobin Downloaded from informahealthcare.com by Chiang Mai University on 01/26/15
For personal use only.

Table 2. Evidence to support divalent metal transporter 1 expression in the heart under iron overload condition.

Bound Fe species	Model	Intervention	Identification techniques	DMT1 mRNA Expression Under Iron Overload			DMT1 Protein Expression Under Iron Overload			Refs.
				Increased	Decreased	Not changed	Increased	Decreased	Not changed	
Fe^{2+}	*In vitro* Cultured neonatal SD rat cardiomyocytes	Loaded FAC (20 μg/mL) for 72 hours	RT-PCR	×	×	✓	×	×	×	(48)
Fe^{2+}	*In vivo* Male SD rats	Fed 2.5% carbonyl iron diet for 6 weeks	RT-PCR and Western blot	×	×	✓	×	✓	×	(40)
Fe^{2+}	Male Wistar rats	Injected iron dextran (200 mg/kg/week) IP for 4 weeks	Western blot	×	×	×	×	✓	×	(49)
Fe^{2+}	Male SD rats	Fed high iron diet for 6 weeks	RT-PCR and Western blot	×	×	✓	×	✓	×	(52)
Fe^{2+}	Newly weaned male SD rats (21 days old)	Fed diet with iron 18.916 ppm for 3 weeks	RT-PCR and Western blot	×	×	✓	×	×	✓	(45)
Fe^{2+}	Specific pathogen-free male ICR mice	Fed 120 mg/Fe/kg for 4 weeks	RT-PCR	×	×	✓	×	×	×	(53)

SD: Sprague-Dawley rat; FAC: ferric ammonium citrate; RT-PCR: reverse-transcription polymerase chain reaction; ICR: imprinting control region.

Table 3. Evidence supports L-type calcium channel expression in the heart under iron overload condition.

Bound Fe species	Model	Intervention	Identification techniques	LTCC mRNA Expression Under Iron Overload			LTCC Protein Expression Under Iron Overload			Refs.
				Increased	Decreased	Not Changed	Increased	Decreased	Not changed	
Fe^{2+}	*In vivo* Adult C57/BL6 het. mice	Fed FE diet (0.2% ferrocene w/w) 120 days	RT-PCR	×	×	✓	×	×	×	(12)

het.: heterozygous (thalassemic) mice; RT-PCR: reverse transcription polymerase chain reaction.

Table 4. Evidence to support T-type calcium channel expression in the heart under iron overload condition.

Bound Fe species	Model	Intervention	Identification techniques	TTCC mRNA Expression Under Iron Overload			TTCC Protein Expression Under Iron Overload			Refs.
				Increased	Decreased	Not changed	Increased	Decreased	Not changed	
Fe^{2+}	*In vivo* Adult C57/BL6 het. mice	Fed FE diet (0.2% ferrocene w/w) 120 days	RT-PCR	✓	×	×	×	×	×	(12)

het.: heterozygous (thalassemic) mice; RT-PCR: reverse transcription polymerase chain reaction.

RIGHTSLINK

Table 5. Summary of channel expression for iron uptake into cardiomyocytes under iron overload condition.

		mRNA Expression Under Iron Overload; Refs.			Protein Expression Under Iron Overload; Refs.		
Channels	Bound Fe Species	Increased	Decreased	Not Changed	Increased	Decreased	Not Changed
TfR	Fe^{3+}	–	(40, 47, 51, 50)	(48)	(49)	(51)	(48, 45)
DMT1	Fe^{2+}	–	–	(45, 40, 48, 52, 53)	–	(40, 49, 52)	(45)
LTCC	Fe^{2+}	–	–	(12)	–	–	–
TTCC	Fe^{2+}	(12)	–	–	–	–	–

TfR: Transferrin receptor; DMT1: divalent metal transporter 1; LTCC: L-type calcium channel; TTCC: T-type calcium channel.

Table 6. Evidence in support/against transferrin receptor as the route of iron uptake into cardiomyocytes under iron overload conditions.

Model	Intervention	Result	Interpretation	Ref.
In vitro Cultured mice cardiomiyocytes (WT, het.; DH)	Anti-TfR1 Ab 5, 10 μg/mL + Fe^{2+} 285.6 μM for 48 hours	Anti-TfR1 Ab did not prevent iron uptake into cardiomyocytes	TfR1 is not the pathway of iron uptake into cultured cardiomyocytes	(13)

WT: wild type; het.: heterozygous (thalassemic) mice; DH: double heterozygous mice Hb E (*HBB*: c.79G>A).

Hemoglobin Downloaded from informahealthcare.com by Chiang Mai University on 01/26/15
For personal use only.

channel proven by clinical studies (38,39) to improve cardiac function and decrease iron levels in patients with the iron overload conditions. Recently, results from Kumfu *et al.* (12,13) and Lopin *et al.* (14) proposed the possibility that TTCC could also be one of the major pathways involved in iron uptake into the heart.

The reports that support the hypothesis that TfR is not a major pathway for iron uptake under iron overload conditions are shown in Table 6. Regarding published reports on DMT1 (Table 7), the *in vitro* study from Kumfu *et al.* (13) is consistent with the Ke *et al.* (40) report, which demonstrated that decreased DMT1 expression was observed under iron overload conditions, suggesting that DMT1 might not be a portal of iron entry in cardiomyocytes. However, *in vivo* studies from Kumfu *et al.* (12) and Davis *et al.* (41) support DMT1 as the route of iron uptake in the heart under iron overload conditions. The inconsistent findings might be due to the different model of experiments, dosage and route of iron administration, and the duration of iron loading in each study. Future experiments in an *in vivo* model and additional clinical studies are needed to clarify the potentially important role of this channel.

The other main channels that have recently been shown to play an important role in iron uptake are calcium channels, both LTCC and TTCC. The summary of evidence that supports or opposes the involvement of LTCC and TTCC in iron uptake into cardiomyocytes under iron overload condition are shown in Table 8 and Table 9, respectively. The LTCC was first explored to investigate if it is the channel that takes up iron under iron overload conditions by Tsushima *et al.* (17). Since then, there has been much evidence to support the roles of LTCC as a portal of iron entry into the heart from many studies both *in vivo* and from clinical models. However, published findings do not consistently support the role of LTCC. The evidence against LTCC being the channel that takes up iron was reported by Parkes *et al.* (35) and Kumfu *et al.* (13). They found that the LTCC blocker cannot decrease cellular iron levels in cultured cardiomyocytes under iron overload conditions. However, both experiments used *in vitro* models that differ from the models supporting LTCC. This could be because the cultured neonatal rat cardiomyocytes have smaller L-type calcium currents and high rates of myocyte death that decreases LTCC blocker potential in decreasing iron levels, and misinterprets the role of the LTCC iron uptake (16). The different models of *in vitro* and *in vivo* studies produce different results from each study (Table 8).

The other possible main channel involving iron uptake in the heart is the TTCC. Until now, there are only three pieces of evidence regarding TTCC, and it all supports the hypothesis that Fe^{2+} can enter into cardiomyocytes through this channel under iron overload conditions (Table 9). Under physiological condition, TTCC expression normally disappears in the myocardium after birth (42,43). However, it can reappear in the heart under some pathological conditions including myocardial infarction, heart failure, and iron overload cardiomyopathy (42,43). Recently, Kumfu *et al.* (12,13) demonstrated that the TTCC gene was reexpressed in the heart of thalassemic mice, and was also upregulated under iron overload conditions. Moreover, treatment with the TTCC blocker, efonidipine, significantly reduced the cardiac iron uptake both in cultured cardiomyocytes and *in vivo* models under iron overload conditions, thus improving cardiac functions (12,13). These findings suggested that TTCC could play an important role on cardiac iron uptake under iron overload conditions (12,13). Recently, using a patch clamp recording technique, Lopin *et al.* (14) reported that Fe^{2+} can inhibit Ca^{2+} currents, and that Fe^{2+} could enter cardiomyocytes through TTCC under iron overload conditions. However, further studies both in clinical and *in vivo* settings are needed to confirm the role of these channels and their potential use in preventing iron overload cardiomyopathy.

Besides Fe^{2+}, Fe^{3+} can enter into cardiomyocytes under iron overload conditions but in relatively lower levels (35,36). Kumfu *et al.* (34) reported the experimental findings about Fe^{3+} not being taken up by LTCC, TTCC, DMT1, or TfR. The true mechanism of Fe^{3+} uptake is still questionable, but

RIGHTSLINK

Hemoglobin Downloaded from informahealthcare.com by Chiang Mai University on 01/26/15
For personal use only.

Table 7. Evidence in support/against divalent metal transporter 1 as the route of iron uptake into cardiomyocytes under iron overload conditions.

Model	Intervention	Result	Interpretation	Refs.
In vitro Cultured mice cardiomiyocytes (WT, het.; DH)	Added ebselen 12.5, 25 μM for 60 min. + Fe^{2+} 285.6 μM for 48 hours	Ebselen (DMT1 blocker) did not prevent iron uptake into cardiomyocytes	DMT1 is not the pathway of iron uptake into cultured cardiomyocytes	(13)
In vivo B6D2F1 mice (5–8 weeks old)	Gave 10 mg iron dextran IP/mouse/day + ebselen 25 mg/kg/PO/mouse/day	Ebselen (DMT1 blocker) decreased iron concentrations in heart tissue	DMT1 is the route of iron uptake into cardiomyocytes	(41)
Adult C57/BL6 WT, het. mice	Fed FE diet (0.2% ferrocene w/w)/120 days; gave ebselen (5 mg/kg) IP daily for last 30 days	Ebselen (DMT1 blocker) improved function, decreased cardiac iron levels	DMT1 is the route of iron entry into iron overloaded thalassemic hearts	(12)

WT: wild type; het.: heterozygous (thalassemic) mice; DH: double heterozygous mice with Hb E (*HBB*: c.79G > A); DMT1: divalent metal transporter 1; IP: intraperitoneal injection; PO: per oral.

Table 8. Evidence in support/against L-type calcium channel as the route of iron uptake into cardiomyocytes under iron overload conditions.

Model	Intervention	Result	Interpretation	Refs.
In vitro Cultured mice cardiomyocytes (WT, het., DH)	Verapamil (0–80 μM) + Fe^{2+} 285.6 μM for 48 hours	Verapamil did not prevent iron uptake into cardiomyocytes	LTCC is not the pathway of iron uptake into cultured cardiomyocytes	(13)
Cultured neonatal rat cardiomyocytes	Added FAC (13.75% iron by weight) for 3–5 days, then gave LTCC blockers (nifedipine, verapamil, diltiazem)	LTCC blockers did not inhibit Fe^{2+}, Fe^{3+} into iron-loaded cells; nifedipine increased Fe^{2+}, Fe^{3+} uptake into cardiomyocytes	LTCC is not the route of iron uptake into cultured cardiomyocytes	(35)
Ex vivo Isolated perfusion SD rat hearts	Perfused with 100 nm/L of $^{59}Fe^{2+}$ and $^{59}Fe^{3+}$ for 15 min. Added nifedipine (10 μmol/L), Bay K 8644 (100 nmol/L) and isoproterenol (100 nmol/L)	LTCC blockers (nifedipine) increased $^{59}Fe^{2+}$ uptake; LTCC agonists (Bay K 8644 and isoproterenol) increased $^{59}Fe^{2+}$ uptake into cardiomyocytes	Myocardial Fe^{2+} iron uptake occurs via LTCC	(17)
In vivo Adult C57/BL6 WT, het. Mice	Fed FE diet (0.2% ferrocene w/w) for 120 days. Gave verapamil (10 mg/kg) IP twice daily, nifedipine (5 mg/kg) IP daily for last 30 days	Verapamil and nifedipine improved cardiac function, decreased cardiac iron levels	LTCC is the route of iron entry into iron overloaded thalassemic hearts	(12)
Male B6D2F1 mice (3–5 weeks old)	Gave 20 mg iron dextran IP/mouse/day + amlodipine 2.5 mg in 200 mL water PO/mouse/day for 4 weeks	Amlodipine decreased iron uptake into the heart	LTCC is the route of iron uptake into cardiomyocytes	(54)
Male B6D2F1 mice and male mice (FVB/n strain) with cardiac-specific over-expression of LVDCC	Gave amlodipine or verapamil 0.1 mg/mL (10 mg/kg/day) then administered iron dextran 1.25 mg/25 g body weight/day IP for 12 weeks (iron-loading protocol)/16 weeks (survival studies	Amlopidine and verapamil decreased cardiac iron levels. Iron-overloaded transgenic mice increased myocardial iron levels	Cardiac LVDCCs are key transporters of iron into cardiomyocytes	(15)
Male C57/BL6 12-week-old mice	Gave iron dextran (1 g/kg) IP once a week + propranolol (40 mg/kg/day) via drinking water for 8 weeks	Blocking of LTCC by propranolol improved cardiac function	LTCC blocker is useful in iron-overloaded mice	(55)
8-week-old HJV KO mice	Gave verapamil 0.2 mg/mL via drinking water	Verapamil decreased cardiac iron levels in verapamil-treated groups	LTCC is the route of iron uptake into cardiomyocytes	(56)
Clinical 15 β-TM patients	Gave iron chelators + amlodipine 5 mg/day for 12 months	Heart MRI T2* increased significantly at 6 and 12 months and reduced serum ferritin in 12 months	LTCC blocker decreased cardiac iron levels assessed by MRI T2*	(38)
Case report 81-year-old man with heart failure and macrocytic anemia	DFO + verapamil (120 mg/day) for 18 months	Serum ferritin 1000 ng/mL and improved cardiac function	LTCC blocker + DFO may be effective in IOC at its early stage	(39)

WT: wild type; het.: heterozygous (thalassemic) mice; DH: double heterozygous mice with Hb E (*HBB*: c.79G > A);SD: Sprague-Dawley mice; FAC: ferric ammonium citrate; LTCC: L-type calcium channel; IP: intraperitoneal injection; LVDCC: L-type voltage dependent calcium channel; HJV KO: hemojuvelin knockout mice; β-TM: β-thal major; MRI T2*: magnetic resonance imaging T2*; IOC: iron overload cardiomopathy.

RIGHTSLINK

Table 9. Evidence in support/against T-type calcium channel as route of iron uptake into cardiomyocytes under iron overload condition.

Model	Intervention	Result	Interpretation	Refs.
In vitro Cultured mice cardiomiyocytes (WT, het.; DH)	Efonidipine (0–20 mM) + Fe^{2+} 285.6 mM for 48 hours	Efonidipine (TTCC blocker) prevented iron uptake into cardiomyocytes	Iron uptake in cultured thalassemic cardiomyocytes mainly mediated by TTCC	(13)
Transfected HEK293 cells with $Ca_V3.1$ channels	Patch-clamp experiments evaluated $^{59}Fe^{2+}$ uptake through cells, with or without NNC 55-0395 (selective TTCC inhibitor)	$Ca_V3.1$ channels (TTCC) can uptake Fe^{2+} into cells	TTCC is the pathway of iron entry under iron overload conditions	(14)
In vivo Adult C57/BL6 WT, het. mice	Fed FE diet (0.2% ferrocene w/w) for 120 days; gave efonidipidine (4 mg/kg) IP daily for last 30 days	Efonidipine (TTCC blocker) improved cardiac function, decreased cardiac iron levels	TTCC is the route of iron entry into iron overloaded thalassemic hearts	(12)

WT: wild type; het.: heterozygous (thalassemic) mice; DH: double heterozygous mice with Hb E (*HBB*: c.79G > A); IP: intraperitoneal injection; TTCC: T-type calcium channel.

Hemoglobin Downloaded from informahealthcare.com by Chiang Mai University on 01/26/15
For personal use only.

the possible pathway may be by Fe^{3+} binding with a chaperone protein or through an iron-enclosed vesicle system facilitating entry into cardiomyocytes (34–36). Future studies regarding the pathway of Fe^{3+} uptake into cardiomyocytes may help develop new treatments for preventing iron overload cardiomyopathy in thalassemia.

The role of zinc transporter in iron uptake into the heart under iron overload conditions

In addition to the aforementioned four channels, recent studies reported the expression of Zip14 (Slc39a14) and Zip8 (Slc39a8), the ZIP family of metal-iron transporters, in the heart under iron overload conditions. Although Zip14 has been shown to involve iron uptake in liver cells (44,45), currently there is no evidence that Zip14 can cause the uptake of iron into cardiomyocytes. However, it has been shown that the expression of Zip8 mRNA levels was increased in thalassemic mice heart tissues compared with wild-type mice controls (13). However, no evidence was found that zinc transporters can cause the uptake of iron into the heart directly under iron overload conditions. Currently, Zip14 and Zip8, the zinc transporters, are not included as channels involved in iron uptake into cardiomyocytes. Further investigation regarding iron uptake into the heart by this route is still needed.

Pharmacological intervention of channels that allow the uptake of iron into cardiomyocytes

Most of the studies focused on pharmacological interventions using LTCC and TTCC blockers both *in vitro* and *in vivo* models by assessing iron levels in the heart or cardiomyocytes after the administration of blockers of each channel (Table 8, Table 9). Recently, a report by Kumfu *et al.* (12) showed that LTCC, TTCC and DMT1 blockers reduced iron uptake into the heart but only DMT1 and TTCC blockers improved survival rates. However, these data were debated by Das *et al.* (7) that administration of an LTCC blocker by intraperitoneal injection can lead to acute hypotension and death so the survival rate cannot be improved. However, a study by Oudit *et al.* (15) reported that the administration of LTCC blocker in drinking water can improve survival, decrease hypotension and arrhythmia. The other reason put forward by Das *et al.* (7) was that efonidipine (a TTCC blocker) is not the selective TTCC blocker, since it can also block LTCC (7). Nevertheless, the beneficial effects obtained from the non selective TTCC blocker was still greater than the LTCC blocker alone, suggesting the important role of TTCC in iron entry into the heart (12). Further experiments regarding the role of selective TTCC blockers in cases of iron overload are needed to prove this experimental finding. Recently, Lopin *et al.* (14) studied selective TTCC blockers and proved that TTCC can take up iron into cardiomyocytes under iron overload conditions. Even though there is much evidence from *in vitro* and *in vivo* studies to support the blocking of DMT1, LTCC and TTCC leading to a decrease in iron levels in rat cardiomyocytes and thus improving survival rates, only the LTCC blocker has supporting evidence from clinical studies showing the improved cardiac function and decreased iron levels in the heart evaluated by magnetic resonance imaging T2* (MRI T2*) (38,39). However, larger and longer cohort studies are needed to verify these findings since there were no differences in the iron levels in the heart and serum ferritin between the amlodipine and non amlodipine treated groups after a 1 year follow-up. Moreover, this study did not determine the effect of LTCC blockers on the improvement of cardiac function (38). In a human report, Mainous *et al.* (46) found an association between the use of calcium channel blockers (CCBs) and lower serum ferritin levels in individuals with hypertension. However, this study is not the iron overload model. A case report from Sugishita *et al.* (39) is the only clinical study that reported that verapamil with deferoxamine (DFO) can improve cardiac function in early stages of iron overload cardiomyopathy. Future larger randomized clinical controlled trials are needed to evaluate this further.

Proposed mechanism for non transferrin bound iron uptake into heart under iron overload conditions

From the current available evidence, it can be proposed that the NTBI uptake mechanisms in the heart under iron overload conditions are mainly via LTCC, TTCC and DMT1 as shown in Figure 2. Treatment with iron chelator [DFO, deferiprone (DFP), deferasirox (DFX)], LTCCs blocker (verapamil, nifedipine, amlodipine), TTCC blocker (efonidipine) and DMT1 blocker (ebselen) could decrease iron uptake into the heart and improve cardiac dysfunction under iron overload

RIGHTSLINK

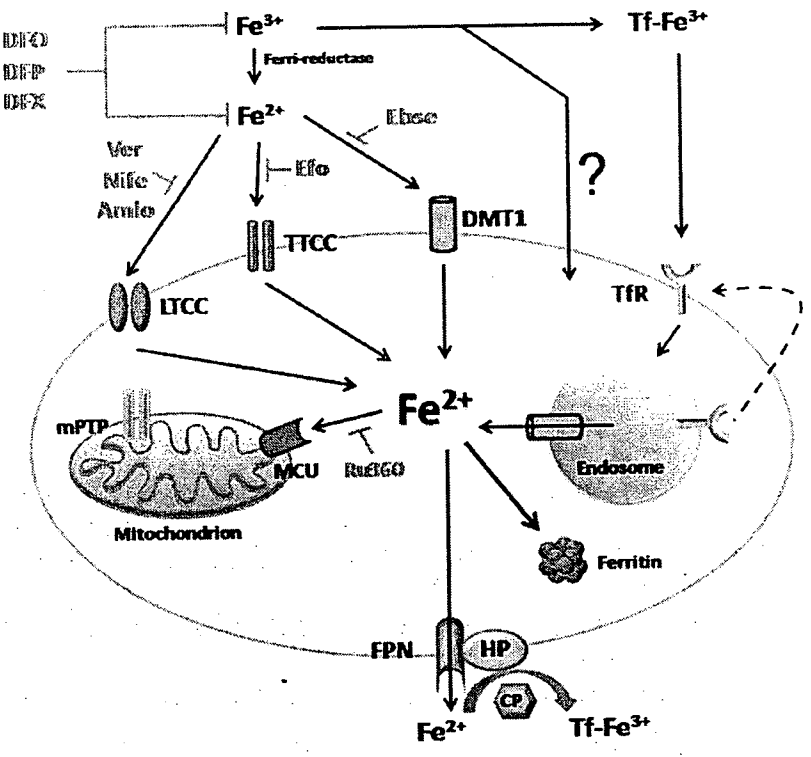


Figure 2. Proposed mechanism for NTBI uptake into the heart under iron overload conditions. TTCC: T-type calcium channel; LTCC: L-type calcium channel; DMT1: divalent metal transporter1; Tf: transferrin; TfR: transferrin receptor; mPTP: mitochondrial permeability transition pore; MCU: mitochondrial calcium uniporter; CP: ceruloplasmin; HP: hephaestin; FPN: ferroportin; DFO: deferoxamine; DFP: deferiprone; DFX: deferasirox; Ver: LTCC blocker verapamil; Nife: nifedipine; Amlo: amlodipine; Efo: TTCC blocker efonidipine; Ebse: DMT1 blocker ebselen. The (T) symbol means inhibition effects.

conditions. Treatment with mitochondrial calcium uniporter (MCU) blocker (Ru360) could improve cardiac mitochondrial dysfunction caused by iron overload. All of these findings suggested that TTCC, LTCC and DMT1 play important roles in iron uptake in the heart and MCU mainly plays a role in iron uptake into cardiac mitochondria under iron overload conditions (Figure 2). Future clinical studies are needed to validate the clinical significance for their use in iron overload patients.

Conclusions

Iron overload cardiomyopathy is a serious condition and one of the most common causes of death in thalassemic patients despite the development of new iron chelating drugs. Understanding the routes of iron entry may beneficially influence the development of new therapeutic treatments for thalassemia and iron overload disorders. Although the mechanism of iron uptake is still not completely understood, the possible pathway of iron uptake is the calcium channels, whether LTCC or TTCC, that can take up Fe^{2+}, a form of NTBI entry into the heart, under iron overload conditions. Further clinical studies are needed to confirm the role of these channels and also to study the pharmacological interventions of these channels in thalassemia patients.

Declaration of interest

This study was supported by grants from the Thailand Research Fund RTA5580006 (to NC), BRG5780016 (to SCC), TRG5780002 (to SK) and the Chiang Mai University Excellence Center Award, Chiang Mai, Thailand (to NC). The authors report no conflicts of interest. The authors alone are responsible for the content and writing of this article.

References

1. Andrews NC. Disorders of iron metabolism. N Engl J Med. 1999; 341(26):1986–1995.
2. Emerit J, Beaumont C, Trivin F. Iron metabolism, free radicals, and oxidative injury. Biomed Pharmacother. 2001;55(6):333–339.
3. Esposito BP, Breuer W, Sirankapracha P, *et al.* Labile plasma iron in iron overload: Redox activity and susceptibility to chelation. Blood. 2003;10(7):2670–2677.
4. Papanikolaou G, Pantopoulos K. Iron metabolism and toxicity. Toxicol Appl Pharmacol. 2005;202(2):199–211.
5. Kremastinos DT, Farmakis D, Aessopos A, *et al.* β-Thalassemia cardiomyopathy: History, present considerations, and future perspectives. Circ Heart Fail. 2013;3(3):451–458.
6. Pennell DJ, Udelson JE, Arai AE, *et al.* Cardiovascular function and treatment in β-thalassemia major: A consensus statement from the American Heart Association. Circulation. 2013; 128(3):281–308.
7. Das SK, Oudit GY. Voltage-gated Ca2+ channels as key mediators of iron-transport and iron-overload cardiomyopathy: L-type vs. T-type Ca+ channels. Eur J Haematol. 2012;88(6):476–477.
8. Fleming MD, Romano MA, Su MA, *et al.* Nramp2 is mutated in the anemic Belgrade (b) rat: Evidence of a role for Nramp2 in endosomal iron transport. Proc Natl Acad Sci USA. 1998; 95(3):1148–1153.
9. Gunshin H, Mackenzie B, Berger UV, *et al.* Cloning and characterization of a mammalian proton-coupled metal-ion transporter. Nature. 1997;38(6641):482–488.
10. Aisen P. Transferrin receptor 1. Int J Biochem Cell Biol. 2004; 36(11):2137–2143.
11. Roy CN, Blemings KP, Deck KM, *et al.* Increased IRP1 and IRP2 RNA binding activity accompanies a reduction of the labile iron pool in HFE-expressing cells. J Cell Physiol. 2002;190(2):218–226.
12. Kumfu S, Chattipakorn S, Chinda K, *et al.* T-type calcium channel blockade improves survival and cardiovascular function in thalassemic mice. Eur J Haematol. 2012;88(6):535–548.
13. Kumfu S, Chattipakorn S, Srichairatanakool S, *et al.* T-type calcium channel as a portal of iron uptake into cardiomyocytes of β-thalassemic mice. Eur J Haematol. 2011;86(2):156–166.
14. Lopin KV, Gray IP, Obejero-Paz CA, *et al.* Fe^{2+} block and permeation of CaV3.1 (α1G) T-type calcium channels: Candidate

Hemoglobin Downloaded from informahealthcare.com by Chiang Mai University on 01/26/15
For personal use only.

RIGHTSLINK

Hemoglobin Downloaded from informahealthcare.com by Chiang Mai University on 01/26/15
For personal use only.

mechanism for non-transferrin-mediated Fe^{2+} influx. Mol Pharmacol. 2012;82(6):1194–1204.
15. Oudit GY, Sun H, Trivieri MG, *et al.* L-type Ca2+ channels provide a major pathway for iron entry into cardiomyocytes in iron-overload cardiomyopathy. Nat Med. 2003;9(9):1187–1194.
16. Oudit GY, Trivieri MG, Khaper N, *et al.* Role of L-type Ca2+ channels in iron transport and iron-overload cardiomyopathy. J Mol Med. 2006;84(5):349–364.
17. Tsushima RG, Wickenden AD, Bouchard RA, *et al.* Modulation of iron uptake in heart by L-type Ca2+ channel modifiers: possible implications in iron overload. Circ Res. 1999;84(11):1302–1309.
18. Anderson LJ, Westwood MA, Holden S, *et al.* Myocardial iron clearance during reversal of siderotic cardiomyopathy with intravenous desferrioxamine: A prospective study using T2* cardiovascular magnetic resonance. Br J Haematol. 2004;127(3):348–355.
19. Gujja P, Rosing DR, Tripodi DJ, *et al.* Iron overload cardiomyopathy: Better understanding of an increasing disorder. J Am Coll Cardiol. 2010;56(13):1001–1012.
20. Murphy CJ, Oudit GY. Iron-overload cardiomyopathy: Pathophysiology, diagnosis, and treatment. J Card Fail. 2010; 16(11):888–900.
21. Brissot P, Ropert M, Le Lan C, *et al.* Non-transferrin bound iron: A key role in iron overload and iron toxicity. Biochim Biophys Acta. 2012;1820(3):403–410.
22. Link G, Pinson A, Hershko C. Heart cells in culture: A model of myocardial iron overload and chelation. J Lab Clin Med. 1985; 106(2):147–153.
23. Randell EW, Parkes JG, Olivieri NF, *et al.* Uptake of non-transferrin-bound iron by both reductive and nonreductive processes is modulated by intracellular iron. J Biol Chem. 1994; 269(23):16046–16053.
24. Hershko C, Link G, Cabantchik I. Pathophysiology of iron overload. Ann N Y Acad Sci. 1998;850:191–201.
25. Horwitz LD, Rosenthal EA. Iron-mediated cardiovascular injury. Vasc Med. 1999;4(2):93–99.
26. Lekawanvijit S, Chattipakorn N. Iron overload thalassemic cardiomyopathy: Iron status assessment and mechanisms of mechanical and electrical disturbance due to iron toxicity. Can J Cardiol. 2009; 25(4):213–218.
27. Shander A, Cappellini MD, Goodnough LT. Iron overload and toxicity: The hidden risk of multiple blood transfusions. Vox Sang. 2009;97(3):185–197.
28. Wood JC, Enriquez C, Ghugre N, *et al.* Physiology and pathophysiology of iron cardiomyopathy in thalassemia. Ann N Y Acad Sci. 2005;1054:386–395.
29. Bartfay WJ, Bartfay E. Iron-overload cardiomyopathy: Evidence for a free radical — mediated mechanism of injury and dysfunction in a murine model. Biol Res Nurs. 2000;2(1):49–59.
30. Gao X, Campian JL, Qian M, *et al.* Mitochondrial DNA damage in iron overload. J Biol Chem. 2009;284(8):4767–4775.
31. Gao X, Qian M, Campian JL, *et al.* Mitochondrial dysfunction may explain the cardiomyopathy of chronic iron overload. Free Radic Biol Med. 2010;49(3):401–407.
32. Zorov DB, Juhaszova M, Sollott SJ. Mitochondrial ROS-induced ROS release: An update and review. Biochim Biophys Acta. 2006; 1757(5–6):509–517.
33. Thunmasorn S, Kumfu S, Chattipakorn S, *et al.* Granulocyte-colony stimulating factor attenuates mitochondrial dysfunction induced by oxidative stress in cardiac mitochondria. Mitochondrion. 2011;11(3):457–466.
34. Kumfu S, Chattipakorn S, Fucharoen S, *et al.* Ferric iron uptake into cardiomyocytes of β-thalassemic mice is not through calcium channels. Drug Chem Toxicol. 2013;36(3):329–334.
35. Parkes JG, Olivieri NF, Templeton DM. Characterization of Fe2+ and Fe3+ transport by iron-loaded cardiac myocytes. Toxicology. 1997;117(2–3):141–151.
36. Shvartsman M, Kikkeri R, Shanzer A, *et al.* Non-transferrin-bound iron reaches mitochondria by a chelator-inaccessible mechanism: Biological and clinical implications. Am J Physiol Cell Physiol. 2007;293(4):C1383–C1394.
37. Hentze MW, Muckenthaler MU, Andrews NC. Balancing acts: Molecular control of mammalian iron metabolism. Cell. 2004; 117(3):285–297.
38. Fernandes JL, Sampaio EF, Fertrin K, *et al.* Amlodipine reduces cardiac iron overload in patients with thalassemia major: A pilot trial. Am J Med. 2013;126(9):834–837.
39. Sugishita K, Asakawa M, Usui S, *et al.* A case of iron overload cardiomyopathy: Beneficial effects of iron chelating agent and calcium channel blocker on left ventricular dysfunction. Int Heart J. 2009;50(6):829–838.
40. Ke Y, Chen YY, Chang YZ, *et al.* Post-transcriptional expression of DMT1 in the heart of rat. J Cell Physiol. 2003;196(1):124–130.
41. Davis MT, Bartfay WJ. Ebselen decreases oxygen free radical production and iron concentrations in the hearts of chronically iron-overloaded mice. Biol Res Nurs. 2004;6(1):37–45.
42. Huang B, Qin D, Deng L, *et al.* Reexpression of T-type Ca2+ channel gene and current in post-infarction remodeled rat left ventricle. Cardiovasc Res. 2000;46(3):442–449.
43. Martinez ML, Heredia MP, Delgado C. Expression of T-type Ca^{2+} channels in ventricular cells from hypertrophied rat hearts. J Mol Cell Cardiol. 1999;31(9):1617–1625.
44. Liuzzi JP, Aydemir F, Nam H, *et al.* Zip14 (Slc39a14) mediates non-transferrin-bound iron uptake into cells. Proc Natl Acad Sci USA. 2006;103(37):13612–13617.
45. Nam H, Wang CY, Zhang L, *et al.* ZIP14 and DMT1 in the liver, pancreas, and heart are differentially regulated by iron deficiency and overload: Implications for tissue iron uptake in iron-related disorders. Haematologica. 2013;98(7):1049–1057.
46. Mainous AG III, Weinberg ED, Diaz VA, *et al.* Calcium channel blocker use and serum ferritin in adults with hypertension. Biometals. 2012;25(3):563–568.
47. Parkes JG, Liu Y, Sirna JB, *et al.* Changes in gene expression with iron loading and chelation in cardiac myocytes and non-myocytic fibroblasts. J Mol Cell Cardiol. 2000;32(2):233–246.
48. Liu Y, Parkes JG, Templeton DM. Differential accumulation of non-transferrin-bound iron by cardiac myocytes and fibroblasts. J Mol Cell Cardiol. 2003;35(5):505–514.
49. Zhao N, Sun Z, Mao Y, *et al.* Myocardial iron metabolism in the regulation of cardiovascular diseases in rats. Cell Physiol Biochem. 2010;25(6):587–594.
50. Rodriguez A, Hilvo M, Kytomaki L, *et al.* Effects of iron loading on muscle: Genome-wide mRNA expression profiling in the mouse. BMC Genomics. 2007;8:379.
51. Qian ZM, Chang YZ, Leung G, *et al.* Expression of ferroportin1, hephaestin and ceruloplasmin in rat heart. Biochim Biophys Acta. 2007;1772(5):527–532.
52. Chen YY, Xia Q, Qian ZM. [Developmental expression and regulation of divalent metal transporter 1 in rat heart]. Zhejiang Da Xue Xue Bao Yi Xue Ban. 2003;32(2):131–136.
53. Kim DW, Kim KY, Choi BS, *et al.* Regulation of metal transporters by dietary iron, and the relationship between body iron levels and cadmium uptake. Arch Toxicol. 2007;81(5):327–334.
54. Crowe S, Bartfay WJ. Amlodipine decreases iron uptake and oxygen free radical production in the heart of chronically iron overloaded mice. Biol Res Nurs. 2002;3(4):189–197.
55. Musumeci M, Maccari S, Sestili P, *et al.* The C57BL/6 genetic background confers cardioprotection in iron-overloaded mice. Blood Transfus. 2013;11(1):88–93.
56. Otto-Duessel M, Brewer C, Wood JC. Interdependence of cardiac iron and calcium in a murine model of iron overload. Transl Res. 2011;157(2):92–99.

RIGHTSLINK

เอกสารแนบหมายเลข 52

Review

Current evidence of temozolomide and bevacizumab in treatment of gliomas

Danop Nanegrungsunk[1,2], Wimrak Onchan[3], Nipon Chattipakorn[2,4], Siriporn C. Chattipakorn[2,5]

[1]Department of Anesthesiology, Faculty of Medicine, Chiang Mai University, Thailand, [2]Neurophysiology Unit, Cardiac Electrophysiology Research and Training Center, Faculty of Medicine, Chiang Mai University, Thailand, [3]Division of Therapeutic Radiology and Oncology, Department of Radiology, Faculty of Medicine, Chiang Mai University, Thailand, [4]Department of Physiology, Faculty of Medicine, Chiang Mai University, Thailand, [5]Department of Oral Biology and Diagnostic Science, Faculty of Dentistry, Chiang Mai University, Thailand

Objective: This review article summarizes *in vitro*, *in vivo*, and clinical evidence pertaining to temozolomide (TMZ) and bevacizumab (BEV) efficacy and mechanism of action in gliomas.
Methods: Relevant publications published before June 2013 in PubMed database were reviewed.
Results: Temozolomide and BEV are current chemotherapeutic agents treating patients with high-grade glioma, including glioblastoma. *In vitro* and *in vivo* studies have proposed discordant cell death pathways for TMZ as either apoptosis or autophagy using different experimental setting details or cell lines. In addition, BEV may cause cell death through hypoxia-induced autophagy or unspecific indirect effects on cancer cells. The complexity of cancer cells in glioma has contributed to their resistance of both chemotherapies. In clinical trials, overall survival duration in glioma patients with recurrence (8–9 months) is lower than that in newly diagnosed patients (12–15 months).
Conclusion: Our collected data support the addition of radiotherapy, BEV, and other targeted agents to TMZ treatment, indicating prolonged survival duration in newly diagnosed patients. However, the optimal regimen for treating high-grade glioma cannot be concluded without more clinical trials.

Keywords: Glioma, Temozolomide, Bevacizumab, Apoptosis, Autophagy

Introduction

Glioma refers to the following glial cell-derived brain cancers: ependymoma, astrocytoma, oligodendroglioma, or mixed glioma (oligoastrocytoma). According to World Health Organization (WHO), gliomas are classified into four grades.[1–3] Grade I and II gliomas represent non-invasive low-grade tumors, such as atrocytoma (WHO grade II), pilocytic astrocytoma (WHO grade I), oligodendroglioma (WHO grade II), ependymoma (WHO grade II), and mixed oligoastrocytoma (WHO grade II). The high-grade gliomas are WHO grade III and IV gliomas, including anaplastic (malignant) astrocytoma (WHO grade III), glioblastoma multiforme (WHO grade IV), neuroepithelial tumors of uncertain origin (WHO grade IV), and anaplastic (malignant) oligodendroglioma (WHO grade III). Grade III gliomas exhibit nuclear atypia and mitotic activity of cancer cells. In addition to these grade III features, the presence of microvascular proliferation or necrosis of tumor found in grade IV glioma[1,3,4] usually leads to a worse prognosis and exhibits more aggressiveness.[1–3]

Glioblastoma or glioblastoma multiforme, classified as a high-grade glioma, is the most common and lethal primary malignant glioma.[5] The clinical hallmarks of glioblastoma are its aggressive growth and high recurrence rates after an optimal treatment of surgery and chemoradiation. With the current standard of care, patients with glioblastoma only have a median survival of 12–15 months after the first initial diagnosis.[6]

The current standard therapy for glioblastoma is surgical removal of tumor together with radiotherapy and/or chemotherapy.[7–10] Supportive treatment aims toward relieving undesired symptoms and improving neurological function. Palliative treatment usually focuses on improving the quality of the remaining life and achieving a longer survival time.

Surgery for glioblastoma

Maximally feasible resection of glioblastoma is the most critical aspect of treatment.[11] The maximal removal of tumors has several beneficial effects

Correspondence to: Siriporn C. Chattipakorn, Neurophysiology Unit, Cardiac Electrophysiology Research and Training Center, Faculty of Medicine, Chiang Mai University, Chiang Mai 50200, Thailand; Department of Oral Biology and Diagnostic Science, Faculty of Dentistry, Chiang Mai University, Chiang Mai 50200, Thailand. Email: scchattipakorn@gmail.com; siriporn.c@cmu.ac.th

© W. S. Maney & Son Ltd 2015
DOI 10.1179/1743132814Y.0000000423

including: histo-pathological diagnosis, relief of neurological defects from compressive tumor mass, and extending the survival time.[12] Unfortunately, after total tumor removal, glioblastoma may later develop recurrent tumors either adjacent to the original site[13] or at more distant lesions in either one of both hemispheres.[5,14] Therefore, adjunctive therapies, including radiation and/or chemotherapy, have been applied after surgery to slow down and/or to suppress the recurrence of glioblastoma.[10]

Radiotherapy for glioblastoma

For the past three decades, radiotherapy has been the standard treatment following glioblastoma surgery, and this combination can significantly increase patient survival times.[9,10] A randomized clinical trial among 303 patients with anaplastic glioma demonstrated that patients receiving surgery with radiation had nearly double the median survival time of patients receiving surgery without radiation.[15] In addition, previous studies showed that the total radiation dose of 60 Gy was optimal for high-grade glioma treatment.[16,17] However, another study indicated that whole brain radiotherapy for multifocal glioblastoma did not result in additional clinical benefits over targeted three-dimensional conformal radiotherapy.[18] Moreover, radiation therapy for brain cancer may lead to complications such as radiation brain necrosis and cognitive decline. These complications depend on several factors including: dosage of radiation therapy, tumor severity, the combination of radiation with chemotherapy, patient age, and health status.[19]

Chemotherapy for glioblastoma

Chemotherapy is used to abolish proliferating cancer cells and has become a primary regimen treatment. The most common chemotherapeutic agents for glioblastoma are temozolomide and bevacizumab.

In March 2005, the U.S. Food and Drug Administration approved temozolomide (TMZ) concomitantly with radiotherapy for treatment of adults with newly diagnosed glioblastoma as well as using TMZ alone for maintenance treatment. In a large multicenter randomized clinical trial of 573 glioblastoma patients, the combined radiation/TMZ treatment group had a greater median survival of 2.5 months when compared with survival of patients receiving the standard radiation alone (14.6 [95% CI, 13.2–16.8] vs 12.1 months, respectively [95% CI, 11.2–13.0]).[6,20] In addition to this clinically meaningful and statistically significant survival benefit, TMZ presented minimal toxicity[20] and could also induce a radio-sensitizing property in tumor cells.[21]

In May 2009, the U.S. Food and Drug Administration approved bevacizumab (BEV), an anti-angiogenic agent, to treat patients with the recurrent glioblastoma based on radiographic response.[22–24] However, a previous study did not show a significant benefit of treatment with BEV alone compared with combined BEV and irinotecan (topoisomerase I inhibitor) in recurrent glioblastoma patients.[24] Whereas, a phase II study demonstrated that a regimen of combined daily TMZ and biweekly BEV had little adverse effects,[25] the median survival duration of glioblastoma patients treated with either TMZ or BEV alone or combined TMZ and BEV was approximately 9 months.[24–26] These findings suggest that the combination of TMZ and BEV to treat glioblastoma might not be clinically beneficial.

Several studies showed that the overall survival times of glioblastoma patients with chemotherapy were quite short.[6,23,27–33] The reasons behind the lower efficacy of chemotherapy for glioblastoma may be due to several complicating factors of glioblastoma itself; for example, (1) glioblastoma cells have been shown to resist chemotherapy[27,34,35]; (2) chemotherapeutic agents have limited capacity to cross blood brain barrier[36]; and (3) the normal brain has limited tolerance to chemotherapeutic agents.[36]

Although several chemotherapeutic agents can be found in the current pharmaceutical market, TMZ and BEV have been commonly used for glioblastoma therapy. To understand the effectiveness and underlying mechanism of both drugs on glioblastoma treatment, this review has summarized reports on glioblastoma treated with TMZ and BEV from *in vitro* studies and *in vivo* studies, as well as clinical trials. Furthermore, the underlying mechanisms of either TMZ or BEV added to other targeted agents to treat glioblastoma have been summarized.

Search Strategy and Selection Criteria for This Review

Relevant publications in the PubMed database published before June 2013 were identified by using search terms 'glioma,' 'glioblastoma,' 'brain tumor,' 'cell death pathway,' 'apoptosis,' 'autophagy,' 'senescence,' 'temozolomide,' and 'bevacizumab.' Only articles published in English were reviewed.

Evidence of Chemotherapy for Gliomas/ Glioblastomas Treated with Either Temozolomide or Bevacizumab

Temozolomide

TMZ is an alkylating agent that delivers a methyl group to purine bases of DNA to form O^6-methylguanine (O^6MeG), which acts as cytotoxic lesion initiating cell death. O^6MeG causes several DNA changes in the subsequent replication cycle and leads to cell cycle arrest in the G2/M phase, as demonstrated in glioblastoma cell lines.[37] However, one of the major problems of TMZ in glioblastoma treatment is the resistance of glioma cells, since

O^6MeG can be removed by methylguanine methyltransferase (MGMT) protein or can be ineffective in mismatch repair (MMR)-deficient tumors. Glioblastoma with MGMT[38] or with MMR deficiency[39] is classified as glioblastoma resistant to TMZ. Because specific underlying cell death mechanisms from TMZ are complex and unable to be concluded, we summarized all the current postulated mechanisms to clarify the TMZ-induced death mechanisms.

In vitro *studies of TMZ in glioblastoma therapy*

Several *in vitro* studies have shown that TMZ can damage glioblastoma cells via several different mechanisms, including apoptosis,[40–42] autophagy,[43,44] and a complex process between apoptosis, autophagy, and senescence[45] (Table 1).

TMZ has been shown to mainly induce apoptotic signals from O^6MeG, which is the lesion responsible for apoptosis induction.[40–42] A study from Hirose and colleagues demonstrated that the subsequent inability to replicate DNA of glioma cells can lead to a p53-associated apoptotic cell death.[40] Moreover, Roos and colleagues exhibited that the apoptotic cell death mechanism of TMZ, which originated from O^6MeG, requires apoptotic signaling from different sources, including Fas/CD95/Apo-1 receptors in p53 non-mutated glioma and mitochondria in p53-mutated glioma.[41] In addition, Jiang and colleagues proposed that anti-tumor effects of TMZ on glioma cells occurred through the ROS-dependent SIRT1 signaling pathway.[42] Hence, in *in vitro* glioma cell lines, TMZ-induced apoptosis is thought to be the main mechanism to abolish glioblastoma, but apoptotic signal induction and specific molecular pathway have not been identified.

TMZ-induced autophagy is another putative mechanism of TMZ action on cancer cells. It has been proposed that autophagy could lead to either cancer cell survival or cell death, depending on several factors.[43,44] Kanzawa *et al.* demonstrated that after application with TMZ and 3-methyladenine, an early stage autophagy inhibitor, the autophagy process was blocked and the anti-tumor effect of TMZ was suppressed.[44] On the other hand, after application with TMZ and bafilomycin A1, a specific late-stage autophagy inhibitor, the cytotoxicity of TMZ for malignant gliomas was enhanced by consequently inducing apoptosis.[44] This study demonstrated that the application of late-stage autophagy inhibitor could increase the therapeutic efficacy of TMZ in glioma cell death and TMZ would induce autophagy rather than apoptosis.[44]

The anti-tumor effects of TMZ can be complicated. Knizhnik and colleagues demonstrated in glioma cells that TMZ can induce cell death via a complex process between apoptosis, autophagy, and senescence.[45] Senescence is a state when viable cells stop synthesizing DNA with the unknown endpoint of either survival or death.[45] They demonstrated that TMZ-induced cell death could be divided into two pathways: the apoptosis alone (via caspase pathway) and the autophagy followed by a cellular senescence.[45] They further demonstrated that these two pathways were determined by multiple factors such as time courses of TMZ exposure and ataxia-telangiectasia mutated protein (ATM), i.e., a protein involved in regulating either autophagy or apoptosis.[45] The autophagy pathway inhibited the opposed apoptosis pathway, and then progressed cells to senescence.[45] Thus, it could be assumed that autophagy might be a survival mechanism chosen by gliomas to undergo senescence rather than an immediate death as apoptosis when therapeutic dose of TMZ were used.[45] Knizhnik and colleagues also found that autophagy, senescence, and apoptosis of glioma cells occurred at 72, 96, and 120 hours after TMZ exposure, respectively.[45] These time-dependent mechanisms of TMZ-induced cell death might explain the different cell death mechanisms reported previously in different studies since they measured TMZ-induced cell death at different time courses.[40–42]

From all *in vitro* studies, the reasons of discordant cell death mechanism are due to different duration of TMZ exposure,[45] ATM,[45] different TMZ concentration, and different experimented cell lines. As a result of TMZ-induced autophagy, it is possible that the high recurrent rate in glioblastoma patients and the unsatisfactory clinical survival rate might not only be due to the resistant mechanisms of tumors such as MGMT and deficiency of MMR but also due to the autophagy helping the tumor to survive as it plays a protective role to opposing the apoptosis pathway. Moreover, an additional treatment with an autophagy inhibitor may enhance the beneficial therapeutic effects of TMZ for patients with glioblastoma.

In vivo *studies of TMZ in glioblastoma therapy*

The *in vivo* studies of TMZ are summarized in Table 2. A meta-analysis from Hirst and colleagues found a variability in TMZ sensitivity between different tumor models.[46] These findings reflect either the degree of differentiation of the tumor or the resistance to TMZ through a variety of mechanisms,[47] including MGMT expression. Moreover, Mathieu and colleagues demonstrated that TMZ could act as an anti-angiogenic compound in glioblastoma cells of a mouse model.[48] They found that the combination of TMZ and BEV increased the survival of glioma-bearing mice; when compared with each single drug therapy.[48] Therefore, the genomic analysis of drug resistance/sensitivity as well as the combination of additional agents with TMZ may give

Table 1 ***In vitro*** **studies of temozolomide treatment on glioma cells**

Cell lines	Concentration of TMZ/exposure time	Major findings	Interpretation	Reference
U87 glioma cells (p53-wild-type or p53-deficient); LN-Z308 cells	TMZ 100 μM/3 hours	TMZ-induced G_2-M arrest and led to cell apoptosis through p53 effects, $p21^{Waf1/Cip1}$, and/or other p53-regulated proteins.	TMZ-induced apoptosis in glioma cells.	Hirose *et al.*[40]
Six malignant glioma cell lines (U373-MG, T98G, U251-MG, GB-1, U87-MG, and A172)	TMZ 100 μM/72 hours	Clinically achievable dose (100 μM) of TMZ-induced autophagy, not apoptosis. Application of an autophagy inhibitor (e.g., bafilomycin A1) augmented the action of TMZ.	Clinical dose of TMZ-induced autophagy, not apoptosis.	Kanzawa *et al.*[44]
Malignant glioma cells: p53 non-mutated glioma cells and p53-mutated glioma cells	Various concentration/N/A	The apoptotic signal originated from O^6-methylguanine (O^6MeG) required Fas/CD95/Apo-1 receptor activation in p53 non-mutated glioma cells. In p53-mutated glioma, O^6MeG triggered mitochondrial apoptotic pathway. Sensitivity to TMZ depended on methylguanine methyltransferase (MGMT), p53, proliferation rate and DSB repair.	TMZ-induced cells apoptosis.	Roos *et al.*[41]
Hs683, U87, T98G human GBM cell lines and U373 GBM cells	TMZ 100 μM/72 hours	TMZ decreased the expression of proangiogenic factor, a capillary network formation and an overall growth of endothelial cells	TMZ impaired the growth of GBM cells.	Mathieu *et al.*[48]
Isolated endotheliums from gliomas and non-tumor specimens; and glioma cell line U87MG, U251	TMZ 100 μM/72 hours or 7 days	TMZ demonstrated cytotoxicity to glioma cell lines, but did not affect the viability or proliferation rate of endothelial cells, which led to tumor angiogenesis.	TMZ had no apparent effect to endothelium, but it has toxicity to glioma cell lines.	Virrey *et al.*[68]
TMZ-sensitive U251 cells, TMZ-resistant (UTMZ); primary and TMZ-resistant GBM xenograft lines	TMZ 500 μM/48 hours	Resistance to TMZ-induced apoptosis was caused by a mitochondrial adaptive response to TMZ genotoxic stress with a major contribution from cytochrome *c* oxidase.	Mitochondrial adaptive response caused a resistance to TMZ-induced apoptosis.	Oliva *et al.*[69]
U-118 GBM cell line	250, 500 μM/48 hours	In TMZ-treated GBM cells, only 250 μM TMZ caused cell death via both apoptosis and autophagy pathway. Autophagy, indicated by the expression of the autophagy-associated protein, reduced the percentage of cells underwent apoptosis.	TMZ-induced apoptosis and autophagy. Apoptosis pathway can be counteracted by autophagy.	Carmo *et al.*[43]
TMZ-sensitive and TMZ-resistant glioma cells, and TMZ-resistant GBM xenograft lines (xenolines)	300 μM/72 hours	TMZ-resistant cells showed a disturbed redox system, a lowered mitochondrial ROS production, and resistance to the oxidative stress, compared to parent cells.	TMZ resistance was caused by disturbed mitochondrial function and redox system.	Oliva *et al.*[70]
Grade IV glioma cell lines SHG44 and U251 cells were treated with TMZ	100 μM/72 hours	TMZ, inducing G(2)/M cell cycle arrest, inhibited cell proliferation and induced apoptosis with concentration-dependence via ROS-dependent SIRT1 signaling pathway.	TMZ-induced apoptosis via ROS pathway.	Jiang *et al.*[42]
LN-229 and U87MG glioma cell lines	≤100 μM/N/A	O^6MeG triggered autophagy, senescence, and apoptosis, each in a specific time-dependence. Autophagy was a survival mechanism and attenuated the level of apoptosis.	TMZ can induce cell apoptosis, autophagy, and senescence.	Knizhnik *et al.*[45]

N/A: not available; GBM: glioblastoma multiforme; TMZ: temozolomide.

Table 2 ***In vivo*** **studies of temozolomide treatment on glioma**

Subject	Agent regimen	Major findings	Interpretation	Reference
Orthotopic xenografts of human Hs683 and U373 GBM cells in nude mice	TMZ 40 mg/kg intravenous three times a week for 3–5 consecutive weeks	TMZ acts as an anti-angiogenic compound. Combination of BEV with TMZ increased the survival of glioma-bearing mice in comparison to either BEV or TMZ alone	TMZ showed anti-angiogenesis property.	Mathieu *et al.*[48]
Intracranial glioma mouse model by implantation U87MG glioma cells	TMZ 3 mg/kg via gavage (for 7 days) every 2 weeks until approximately 60 days	TMZ did not demonstrate significant change of microvascular density.	TMZ had no apparent anti-angiogenesis effect.	Virrey *et al.*[68]
Systematic review and meta-analysis: from 60 publications in glioma models (2443 animals)	N/A	TMZ prolonged survival by a factor of 1.88 (95% CI 1.74–2.03). TMZ reduced tumor volume by 50.4% (41.8–58.9) compared with untreated controls. There were heterogeneity among studies and a bias.	TMZ improved survival time in animal models	Hirst *et al.*[46]

BEV: bevaczumab; N/A: not available; GBM: glioblastoma multiforme; TMZ: temozolomide.

Table 3 Clinical trial of temozolomide in patients with glioma

Study type	No. of patients/ histology of tumor	Dosage regimen (temozolomide in mg/m^2/day)	Response rate			Progression-free survival		Overall survival	Reference
			CR (%)	PR (%)	SD (%)	PFS at 6, 12 months (%)	Median (months)	Median (months)	
RCT	195/(AA + GB)	150–200 for 5 days [q4wk]	N/A	N/A	N/A	30.1, 12.0	3.3	8.6	Wick *et al.*[38]
RCT	112/ReGB	150 or 200 for 5 days [q4wk]	0	5.4	40.2	21, N/A	N/A	N/A	Yung *et al.*[71]
Clinical trial	162/ReHGG	150 or 200 for 5 days [q4wk]	8	27	27	46, 24	5.4	13.6	Yung *et al.*[56]
Clinical trial	138/ReHGG	150 or 200 for 5 days [q4wk]	1	7	45	18, N/A	2.1	5.4	Brada *et al.*[32]
Clinical trial	103/ReHGG	150 initially then 200 for 5 days [q4wk]	CR + PR = 11		47	22, N/A	4.2	5.8	Bower *et al.*[67]
Clinical trial	91/ReGBM	150 or 200 for 5 days [q4wk] (>3 cycles) then TMZ 50 o.d.	N/A	N/A	N/A	23.9, N/A	1.8–3.7	N/A	Perry *et al.*[72]
Controlled trial	46/GB	150–200 for 5 days [q4wk]	CR + PR = 23.9		56.5	N/A	16	26.4	Sanson *et al.*[73]
Clinical trial	41/ReHGG	150 for 5 days [q4wk]	7.5	15	42.5	48.5, 34.7	5.6	9.3	Brandes *et al.*[26]
Clinical trial	29/ReAA	150 or 200 for 5 days [q4wk] (>3 cycles) then TMZ o.d.	N/A	N/A	N/A	35.7, N/A	N/A	N/A	Perry *et al.*[72]

AA: anaplastic astrocytoma; CR: complete response; GB: glioblastoma; HGG: high-grade glioma; N/A: not available; o.d.: once daily; OS: overall survival; PFS: progression-free survival; PR: partial response; q4wk: every 4 weeks; RCT: randomized controlled trial; Re: recurrent; SD: stable disease.

insights into the future development of better chemotherapy regimen for glioblastomas.[48]

The clinical studies of TMZ in glioblastoma therapy

Chemotherapy regimen of TMZ alone is still a clinically acceptable treatment of high-grade glioblastoma. To focus on the effect of TMZ on glioblastoma, we gathered several clinical studies in which only TMZ was prescribed to both newly diagnosed glioma patients and those with recurrence (Table 3). From both patient groups, the results such as median survival time tended to vary among studies, but almost all of the large clinical trials showed median survival times between 8.6 and 13.6 months after TMZ treatment [15,36].

Bevacizumab

BEV is a humanized monoclonal antibody against vascular endothelial growth factor-A (VEGF-A). It prevents the activation of the VEGF receptor and the subsequent signaling cascades involved in tumor angiogenesis.

In vitro studies of BEV in glioblastoma therapy

Evidence regarding the effects of BEV from *in vitro* study is summarized in Table 4. As an only *in vitro* study, von Baumgarten and colleagues found that BEV failed to inhibit glioma cell proliferation.[49]

In vivo studies of BEV in glioblastoma therapy

Many *in vivo* studies (as summarized in Table 5) indicated that BEV reduced tumor blood supply,[48–50] induced starvation,[49] and displayed direct anti-tumoral effects[49,51] such as hypoxia-induced autophagy.[52] However, Keunen and colleagues found that BEV application resulted in an increase in tumor invasion into adjacent normal brain tissue.[50]

In the administration of clinical doses (5–25 mg/kg) of BEV into a mouse model of glioma, the regression of glioma cells could occur independently from vascular regression, suggesting that high doses of BEV had indirect anti-cancer cell properties.[49] In addition, Hu and colleagues found that the direct anti-tumoral mechanism of BEV was hypoxia-induced autophagy, which was proposed as a cytoprotective adaptive response.[52] Their data showed that there was an increase of glioblastoma cell death if those cells had been treated with additional autophagy inhibitor to BEV.[52] Although BEV-induced autophagy might possibly lead to the resistance of cancer cells to BEV therapy, i.e., the cytoprotection of cancer following BEV treatment, BEV treatment still gave a longer survival time in mice bearing orthotopic gliomas/glioblastomas.[49,53] Thus, despite the current *in vivo* evidences support the benefit of BEV in prolonged survival time and enhanced regression of glioma/glioblastoma cells, the actual efficacy in inducing cancer cell death and decreasing invasiveness are questioned.

Clinical studies of BEV in glioblastoma treatment

Several chemotherapy-based clinical trials of a BEV regimen were conducted in recurrent high-grade glioma patients (Table 6). Four of these studies found the survival time following BEV therapy ranged from 6.4 to 9.2 months.[23,24,54,55] The mean survival time of BEV therapy alone was less than that of TMZ therapy alone (9.2 vs 13.6 months, respectively).[24,56]

Combined chemotherapy with temozolomide or bevacizumab along with other agents may be the most effective glioblastoma treatment

Table 7 summarized reports on efficacy of combined chemotherapy of either TMZ or BEV and other agents and their mechanisms to induce glioblastoma cell death.

TMZ-induced cell death pathways have recently been shown to occur through apoptosis, autophagy, and senescence in *in vitro* experiments. After additional agents were combined with TMZ as noted in Table 7, glioma cell death pathways have become more complex. In addition to previously proposed mechanisms (i.e., apoptosis, autophagy, and senescence), mitotic catastrophe was also postulated as a combined chemotherapy mechanism of action.[57–60] These multiple mechanisms emphasize the complexity of the O^6MeG in combination with agents acting at another different specific point of the cell death pathway.

BEV-induced cell death pathways have been studied mainly *in vivo* due to its anti-angiogenic effect. Those studies suggested that the possible mechanisms of BEV-induced cell death are through autophagy caused by hypoxia and unspecific indirect effects to cancer cells (Table 7). However, results from autophagy have also been reported as a cytoprotective adaptive response, leading to promotion of tumor resistance in some studies.[50,52] After combined BEV with other

Table 4 ***In vitro*** **studies of bevacizumab treatment in glioma cells**

Subject	Concentration of BEV/exposure time	Major findings	Interpretation	Reference
The human glioblastoma cell line U87MG	BEV 5-1000 ng/ml/48 hours	There was no effect of BEV on glioma cell proliferation.	BEV did not inhibit glioma cell proliferation.	von Baumgarten *et al.*[49]

BEV: bevacizumab; GBM: glioblastoma multiforme.

Table 5 ***In vivo*** **studies of bevacizumab to glioma**

Subject	Agent regimen	Major findings	Interpretation	Reference
Orthotopic xenografts of human Hs683 GBM cells are injected into brains of mice	BEV 10 mg/kg intravenous and/or TMZ 40 mg/kg oral three times a week for three consecutive weeks	TMZ impaired angiogenesis. Combining BEV with TMZ increased the survival of glioma-bearing mice in comparison to each compound administered alone.	BEV provided anti-angiogenic effect, and TMZ also impaired angiogenesis.	Mathieu *et al.*[48]
Orthotopic of U87 malignant glioma cells in mouse model	BEV 0.5, 5, and 25 mg/kg intra-peritoneal every 2 days for 12 days	High dose (25 mg/kg) of BEV had direct anti-cancer properties *in vivo*. Medium (5 mg/kg) and high (25 mg/kg) doses decreased tumor growth and prolonged survival.	BEV had direct anti-cancer properties *in vivo*.	von Baumgarten *et al.*[49]
Sixteen patients with recurrent GBMs	BEV 10 mg/kg intravenous biweekly	BEV-induced relative tumor hypoxia (T2' decrease) and affected energy homeostasis in recurrent GBM. BEV impaired oxidative energy metabolism and vascular function, and showed direct anti-tumoral effects in recurrent glioblastoma patients.	BEV showed direct anti-tumoral effects in recurrent glioblastoma patients.	Hattingen *et al.*[51]
Human GBM-derived spheroids are transplanted in nude rats	BEV N/A dose intravenous weekly for 3 weeks	BEV decreased mitochondria number and vascular supply, intratumoral blood flow, but a 68% increase in infiltrating tumor cells in the brain parenchyma.	BEV reduced tumor blood supply and vessel density, but increased cell invasion into normal brain.	Keunen *et al.*[50]
U87MG and T98G glioma xenografts.	BEV and/or chloroquine N/A dose	Autophagy inhibitors disrupted hypoxia-induced glioblastoma autophagy, then induced cell death by apoptosis. Combined therapy (BEV + chloroquine) inhibited tumor growth in a prolonged and significant effect. With BEV alone, hypoxia-induced tumor cell autophagy was a cytoprotective adaptive response, thus promoting treatment resistance.	BEV led to hypoxia-induced tumor autophagy (cytoprotective adaptation). Adding autophagy inhibitor to BEV showed a significant therapeutic benefit.	Hu *et al.*[52]
Mice bearing orthotopic U87 malignant glioma cells	BEV 10 mg/kg intra-peritoneal twice a week and/or sunitinib 50 mg/kg oral gavage (Monday–Friday) until 2, 4, and 6 weeks	BEV significantly prolonged survival compared with the control or sunitinib alone. Combination of BEV with sunitinib improved survival compared to BEV alone.	BEV significantly prolonged survival of transplanted mice and anti-angiogenic phase compared with sunitinib alone.	Piao *et al.*[53]
GBM (U87) cells, injected to mice skin.	BEV 10 mg/kg intra-peritoneal every 3 days	CAIX knockdown and BEV treatment acted in reducing xenograft growth rate synergistically in the glioblastoma cell line U87	BEV and knockdown CAIX reduced growth rate of glioblastoma cells synergistically.	McIntyre *et al.*[74]
Mice baring xenograft: BRG2 or BEG3 cells are injected into caudate or subcutaneous layer.	BEV 10 mg/kg intra-peritoneal twice weekly	β1 antibody attenuated growth of BRG xenograft tumors and increased tumor cell apoptosis. Beta1 integrin targeting potentiated anti-angiogenic therapy and inhibited the growth of BEV-resistant GBM.	Beta1 integrin targeting increased tumor cell apoptosis and enhanced BEV action.	Carbonell *et al.*[75]
GBM cells (U87-MG or U118-MG) are implanted into either BALB/c SCID or athymic nude mice.	BEV 2.5 mg/kg/dose intra-peritoneal every 3 days and/or DCA 50 mg/kg/dose oral gavage twice daily	DCA, an agent targeting tumor metabolism, reversed the hypoxic adaptation to BEV and enhanced its anti-tumor effects in mouse xenografts. BEV and DCA together dramatically blocked tumor growth compared to either drug alone.	DCA reversed BEV-induced hypoxic adaptation and enhanced BEV's anti-tumor effect.	Kumar *et al.*[76]

BEV: bevacizumab; CAIX: carbonic anhydrase IX; DCS: dichloroacetate; GBM: glioblastoma multiforme; N/A: not available; TMZ: temozolomide.

Table 6 Clinical trials of bevacizumab to patients with recurrent high-grade glioma patients

Study type	No. of patients/ histology of glioma	Regimen	Response rate CR (%)	PR (%)	SD (%)	Progression-free survival PFS-6, 12 months (%)	Median (months)	Overall survival Median (months)	Reference
RCT	85/GB	BEV 10 mg/kg biweekly	1.2	27.2	N/A	42.6, N/A	4.2	9.2	Friedman *et al.*[24]
Cohort	50/GB	BEV 15 mg/kg biweekly	0	N/A	N/A	25, N/A	27	6.4	Raizer *et al.*[54]
Retrospective cohort	50/GB	BEV 10 mg/kg biweekly	0	42	0	42, 22	1	8.5	Chamberlain and Johnston[55]
Cohort	48/GB	BEV 10 mg/kg biweekly	2	33	20	29, N/A	4	7.75	Kreisl *et al.*[23]

BEV: bevacizumab; CR: complete response; GB: glioblastoma; N/A: not available; OS: overall survival; PFS: progression-free survival; PR: partial response; RCT: randomized controlled trial; SD: stable disease.

agents such as autophagy inhibitors, the glioma cell death was increased and was noticed as apoptosis.[52] Thus, to increase the BEV-induced cell death effect, an addition of targeting agents (e.g., chloroquine) would augment the death of glioma/glioblastoma cells.

By the implication of the pharmacologic principle with the *in vitro* and *in vivo* results in Table 7, multimodal cancer chemotherapy, not only single agent like TMZ or BEV, should provide a higher efficacy in damaging cancer cells than a single agent due to the fact that each of different drugs would give different targeting responses, and the sum of additive outcomes would be largely magnified.

Clinical studies in newly diagnosed or recurrent glioma patients with the combined chemotherapy of either temozolomide or bevacizumab with other agents

Clinical studies demonstrated the benefits of combined multiple chemotherapies in glioblastoma, but with some inconsistent results. In current standard care, patients with glioblastoma generally have median survival times of 12–15 months.[6] We summarized these

Table 7 Postulated mechanisms of temozolomide, bevacizumab, and/or other agents in glioma cells (*in vitro*/*in vivo* studies)

Agent	Study type	Ameliorate cell death	Suggested mechanism	Reference
Temozolomide (TMZ)	*In vitro*	Yes	Apoptosis	40–43,45
Temozolomide (TMZ)	*In vitro*	May not	Autophagy	43–45
Temozolomide (TMZ)	*In vitro*	May not	Senescence	45,77
TMZ + radiation	*In vitro*	Yes, additive	Autophagy	78–81
TMZ + benzylguanine	*In vitro*	Yes	Autophagy	82
TMZ + tamoxifen or hypericin	*In vitro*	Yes	Apoptosis	83
TMZ + adeno-associated virus vectors encoding recombinant secreted TRAIL (S-TRAIL) and neural stem cell-S-TRAIL	*In vitro*	Yes	N/A	84
TMZ + resveratrol (Rsv)	*In vitro*	Yes	Mitotic catastrophe	58–60
TMZ + valproic acid	*In vitro*	Yes	Apoptosis autophagy	85
TMZ + GSH inhibitor	*In vitro*	Maybe	N/A	86
TMZ + CHk 1 kinase inhibitor	*In vitro*	Yes	Mitotic catastrophe	57
Bevacizumab (BEV)	*In vivo*	May not	Decreased blood supply Increased cell invasion	50
Bevacizumab (BEV)	*In vitro, in vivo*	May not, but can be cytoprotective adaptive response	Hypoxic induced autophagy	52
Bevacizumab (BEV)	*In vivo*	Yes, prolong survival	Decrease vascularity	53
BEV high dose	*In vivo*	Yes, prolong survival	Indirect anti-cancer cell	49
BEV + autophagy inhibitor, e.g., chloroquine	*In vivo*	Yes	Apoptosis	52
BEV + Beta1 integrin targeting	*In vivo*	Yes	N/A	75
TMZ + BEV	*In vivo*	Yes, increase survival	Apoptosis Autophagy Anti-angiogenesis	48
BEV + dichloroacetate (targeting tumor metabolism)	*In vivo*	Yes	Reverse hypoxic adaptation	76

N/A: not applicable.

Table 8 Summary of clinical trials pertaining to temozolomide and bevacizumab in treatment of newly diagnosed high-grade glioma patients

Study type	No. of patients/ histology of tumor	Dosage regimen	Response rate			Progression-free survival		Overall survival	Reference
			CR (%)	PR (%)	SD (%)	PFS at 6 and 12 months (%)	Median (months)	Median (months)	
Temozolomide alone									
RCT	195/(AA + GB)	TMZ 150–200 for 5 days [q4wk]	N/A	N/A	N/A	30.1, 12.0	3.3	8.6	Wick *et al.*[38]
Controlled trial	46/GB	TMZ 150–200 for 5 days [q4wk]	CR + PR = 23.9		56.5	N/A	16	26.4	Sanson *et al.*[73]
Radiotherapy alone									
RCT	286/GB	RT 60 Gy	N/A	N/A	N/A	36.4, 9.1	5.0	12.1	Stupp *et al.*[20]
RCT	178/(AA + GB)	RT 60 Gy	N/A	N/A	N/A	N/A	4.7	9.6	Wick *et al.*[38]
RCT	53/GB	RT (60 Gy in 30 fractions)	N/A	N/A	N/A	44.9, 7.74	5.2	7.7	Athanassiou *et al.*[87]
RCT	35/GB	RT 60 Gy	N/A	N/A	N/A	N/A	6	15	Kocher *et al.*[88]
Prospective cohort	25/GB	RT 60 Gy	N/A	N/A	N/A	N/A	N/A	9.3	Niyazi *et al.*[89]
Temozolomide plus radiotherapy									
RCT	463/GB	Concomitant TMZ 75 o.d. [for6wk] with RT 2 Gy 5 days/week [for6wk]; then TMZ 150–200 for 5 days [q4wk]	N/A	N/A	N/A	53.3, 40.8	6.2	16.7	Chinot *et al.*[90]
RCT	311/GB	Concomitant TMZ 75 o.d. [for6wk] with RT 2 Gy 5 days/week [for6wk]; then TMZ 150–200 for 5 days [q4wk]	N/A	N/A	N/A	77.5, 42.8	7.3	16.1	Gilbert *et al.*[62]
RCT	287/GB	Concomitant TMZ 75 o.d. [for6wk] with RT 2 Gy 5 days/week [for6wk]; then TMZ 150–200 for 5 days [q4wk]	N/A	N/A	N/A	53.9, 26.9	6.9	14.6	Stupp *et al.*[20]
RCT	57/GB	TMZ 75 o.d. + RT (60 Gy in 30 fractions) then followed by six cycles of TMZ 150 mg/m^2/day [q4wk]	N/A	N/A	N/A	67.1, 36.6	10.8	13.4	Athanassiou *et al.*[87]
RCT	43/GB	TMZ 50 o.d. + RT 60 Gy	NA	NA	NA	46	5.0	15.1	Clarke *et al.*[27]
RCT	30/GB	TMZ 75 o.d. + RT 60 Gy	N/A	N/A	N/A	N/A	7	17	Kocher *et al.*[88]
Clinical trial	160/GB	TMZ 50–75 + RT 60 Gy	N/A	N/A	N/A	59, 31	6	16	Combs *et al.*[91]
Clinical trial	110/GB	TMZ 75 [for 6 weeks] + RT 60 Gy; then TMZ 150–200 for 5 days [q4wk]	NA	NA	NA	NA	7.6	21.1	Lai *et al.*[66]
Clinical trial	103/GB	TMZ 150 or 200 for 5 days [q4wk] + RT 60 Gy	27	45	N/A	75.7, 32.7	10	18	Joo *et al.*[92]
Clinical trial	68/GB	TMZ 75 + RT (60 Gy in 30 fractions) then followed by six cycles of TMZ 150 [q4wk]	N/A	N/A	N/A	N/A	6.6	11.6	Gunjur *et al.*[93]
Clinical trial	22/GB	TMZ 150 or 200 for 5 days [q4wk] + RT 30 Gy	N/A	N/A	N/A	45, N/A	5.5	9.4	Muni *et al.*[94]
Retro cohort	215/GB	TMZ + RT	N/A	N/A	N/A	N/A	5.8	14.3	Lam and Chambers[95]
Cohort	78/GB	TMZ 75 + RT 40 Gy; then TMZ 150–200 for 5 days [q4wk]	N/A	N/A	N/A	N/A, 20	6	12.4	Minniti *et al.*[96]
Cohort	75/HGG	TMZ 150 initially then 200 for 5 days [q4wk] + RT 60 Gy	N/A	N/A	41	N/A	N/A	N/A	Newlands *et al.*[97]
Retro cohort	33/HGG (AA 21 + AO 21)	TMZ 75 + RT (60 Gy in 30 fractions) then followed by six cycles of TMZ 150 [q4wk]	CR + PR = 61		82	N/A, 74	N/A	N/A	Kim *et al.*[98]
Prospective cohort	18/GB	TMZ 75 per day + RT 60 Gy	N/A	N/A	N/A	N/A	N/A	6.4	Niyazi *et al.*[89]
Matched cohort	17/GB	TMZ 150 or 200 for 5 days [q4wk] + RT 30 Gy	N/A	N/A	N/A	N/A	6.3	15	Sampson *et al.*[99]

Table 8 Continued

Study type	No. of patients/ histology of tumor	Dosage regimen	Response rate			Progression-free survival		Overall survival	Reference
			CR (%)	PR (%)	SD (%)	PFS at 6 and 12 months (%)	Median (months)	Median (months)	
Temozolomide plus radiotherapy plus bevacizumab or other agents									
RCT	458/GB	TMZ 75 + RT 60 Gy + BEV	N/A	N/A	N/A	79.9, 24.0	10.6	16.8	Chinot *et al.*[61]
RCT	309/GB	TMZ 75 + RT 60 Gy + BEV	N/A	N/A	N/A	52.8, 31.1	10.7	15.7	Gilbert *et al.*[62]
Clinical trial	125/GB	TMZ 75 + RT 60 Gy + BEV	N/A	N/A	N/A	87.2, 63.1	13.8	N/A	Vredenburgh *et al.*[100]
Clinical trial	75/GB	TMZ + RT + BEV + irinotecan	NA	NA	NA	N/A, 62.7	14.2	21.2	Vredenburgh *et al.*[100]
Clinical trial	70/GB	TMZ 75 for 5 days [q4wk] + RT 60 Gy + BEV 10 mg/kg [q2wk]	NA	NA	NA	NA	13.6	19.6	Lai *et al.*[66]
Clinical trial	51/GB	TMZ 75 for 5 days [q4wk] + RT 60 Gy + BEV 10 mg/kg [q2wk]	NA	NA	NA	85.1, 51	13	23	Narayana *et al.*[31]
Retro cohort	44/HGG	TMZ 75 + RT 60 Gy + carmustine wafers	N/A	N/A	59	63, 35	7.0	12.7	Bock *et al.*[101]
Matched cohort	18/GB	TMZ 150 or 200 for 5 days [q4wk] + RT 30 Gy + epidermal growth factor receptor variant III	N/A	N/A	N/A	67, N/A	14.2	26	Sampson *et al.*[99]
Temozolomide plus bevacizumab and/or other agents; without radiation									
RCT	42/GB	TMZ 150 for 7 days [q2wk] 2 cycles; then 13-cis-retinoic acid 100 mg/m^2 day 1–21 [q4wk]	NA	NA	NA	56	6.6	17.1	Clarke *et al.*[27]
Clinical trial	41/GB	TMZ 150–200 for 5 days [q4wk] + BEV 10 mg/kg [q2wk]	N/A	24.4	68.3	N/A	5.2	11.7	Lou *et al.*[30]
Clinical trial	35/(GB + Re GB)	Pre-targeting locoregional radioimmunotherapy + TMZ 200 for 5 days [q4wk]	N/A	N/A	N/A	N/A	10	25	Bartolomei *et al.*[102]
Retrospective cohort	247/GB	TMZ 150–200 for 5 days [q4wk] + Cis-retinoic acid 100 mg/m^2 [1–21 days, q4wk]	N/A	N/A	15	NR	N/A	15.1	Pitz *et al.*[103]
Clinical trial	68/GB	TMZ 150–200 for 5 days [q4wk] + BVZ 10 mg/kg [q2wk] + everolimus 10 mg after 4 weeks	N/A	N/A	N/A	N/A	11.3	13.9	Hainsworth *et al.*[104]

AA: anaplastic astrocytoma; AO: anaplastic oligodendroglioma; BEV: bevacizumab (usually 10 mg/kg, otherwise specified); CR: complete response; GB: glioblastoma; HGG: high-grade glioma; N/A: not available; o.d.: once daily; OS: overall survival; PFS: progression-free survival; PR: partial response; q2wk: every 2 weeks; q4wk: every 4 weeks; for6wk: for 6 weeks; RCT: randomized controlled trial; Re: recurrent; RT: radiation therapy (usually in total dose of 60 Gy) except that specified; SD: stable disease; TMZ: temozolomide (in unit of mg/m^2/day). The objective response is measured according to WHO criteria: complete response: complete disappearance of all detectable lesions as determined by two observations not less than 4 weeks apart; partial response: ≥50% reduction in the sum of the products of the two largest perpendicular diameters of all measurable lesions, determined by two observations not less than 4 weeks apart; progressive disease: ≥25% increase in any measurable lesion or the appearance of a new lesion; no change: <50% reduction in total tumor volume or a <25% increase in any measurable lesion.

Table 9 Summary of clinical trials pertaining to temozolomide and bevacizumab in treatment of recurrent glioma patients

Study type	No. of patients/histology of glioma	Regimen	Response rate			Progression-free survival	Overall survival		Reference
			CR (%)	PR (%)	SD (%)	PFS-6, 12 (%)	Median (months)	Median (months)	
Temozolomide alone									
RCT	112/GB	TMZ 150 or 200 for 5 days [q4wk]	0	5.4	40.2	21, 8	N/A	N/A	Yung *et al.*[71]
Clinical trial	162/HGG	TMZ 150 or 200 for 5 days [q4wk]	8	27	27	46, N/A	N/A	13.6	Yung *et al.*[56]
Clinical trial	138/HGG	TMZ 150 or 200 for 5 days [q4wk]	1	7	45	18, N/A	2.1	5.4	Brada *et al.*[32]
Clinical trial	103/HGG	TMZ 150 initially then 200 for 5 days [q4wk]	CR + PR = 11		47	22, N/A	4.2	5.8	Bower *et al.*[67]
Clinical trial	91/GB	TMZ 150 or 200 for 5 days [q4wk] (>3 cycles) then TMZ 50 o.d.	N/A	N/A	N/A	23.9, N/A	9.3	N/A	Perry *et al.*[72]
Clinical trial	41/HGG	TMZ 150 for 5 days [q4wk]	7.5	15	42.5	48.5, 34.7	5.6	9.3	Brandes *et al.*[26]
Clinical trial	29/AA	TMZ 150 or 200 for 5 days [q4wk] (>3 cycles) then TMZ 50 o.d.	N/A	N/A	N/A	35.7, 60.7	14.6	N/A	Perry *et al.*[72]
Bevacizumab alone									
RCT	85/GB	BEV	1.2	27.2	N/A	42.6, N/A	4.2	9.2	Friedman *et al.*[24]
RCT	50/GB	BEV	N/A	N/A	N/A	18, N/A	3	N/A	Taal *et al.*[65]
Cohort	50/GB	BEV 15 mg/kg	0	N/A	N/A	25, N/A	27	6.4	Raizer *et al.*[54]
Retrospective cohort	50/GB	BEV	0	42	0	42, 22	1	8.5	Chamberlain and Johnston[55]
Cohort	48/GB	BEV	2	33	20	29, N/A	4	7.75	Kreisl *et al.*[23]
Temozolomide plus irinotecan									
Clinical trial	18/GB	TMZ 200 for 5 days + irinotecan 125 on 6th, 13th, and 20th day then TMZ 200 for 5 + irinotecan 350 mg/m^2 on day 6	11.1	16.7	55.6	39, N/A	5.5	N/A	Gruber[105]
Clinical trial	14/AG	TMZ 200 for 5 days + irinotecan 125 on 6th, 13th, and 20th day then TMZ 200 for 5 + irinotecan 350 mg/m^2 on day 6	21.4	14.3	64.3	71, N/A	7.25	N/A	Gruber and Buster[105]
Bevacizumab plus irinotecan,[1] temozolomide, and/or other agents									
RCT	82/GB	BEV + irinotecan	N/A	N/A	N/A	50.3, N/A	5.6	8.7	Friedman *et al.*[24]
Controlled trial	13/GB	BEV + etoposide (50 mg/m^2)	0	0	40	0, N/A	1	3.2	Reardon *et al.*[106]
Controlled trial	10/GB	BEV + TMZ (50 mg/m^2/day daily)	0	0	62	7.7, N/A	2	4.75	Reardon *et al.*[106]
Clinical trial	40/GB	BEV + carboplatin + irinotecan	N/A	N/A	N/A	46.5, N/A	N/A	8.3	Reardon *et al.*[107]
Clinical trial	32/GB	BEV + TMZ (50 mg/m^2/day daily)	N/A	N/A	N/A	18.8, N/A	3.95	9.25	Desjardins *et al.*[25]
Clinical trial	17/HGG	BEV + irinotecan	0	19	48	N/A	N/A	N/A	Chen *et al.*[108]
Clinical trial	27/HGG	BEV + irinotecan	14.8	14.8	44.4	40, N/A	5.5	7	Poulsen *et al.*[109]
Cohort	37/GB	BEV + irinotecan or carboplatin	N/A	N/A	N/A	N/A	5	9	Narayana *et al.*[110]
Cohort	35/GB	BEV 10 and 15 mg/kg + irinotecan various regimen	N/A	N/A	N/A	46, N/A	6	10.5	Vredenburgh *et al.*[111]
Cohort	35/GB	BEV + irinotecan	N/A	57	43	46, N/A	6	10.5	Vredenburgh *et al.*[112]
Cohort	33/AG	BEV + irinotecan	9.1	51.5	33.3	55, N/A	6.9	15	Desjardins *et al.*[63]
Cohort	17/GB	BEV 5 mg/kg + irinotecan	10.5	36.8	10.5	25, N/A	4.2	7	Bokstein *et al.*[113]
Cohort	13/GB	BEV 5 and 10 mg/kg + irinotecan	0	77	23	N/A	6	6.75	Ali *et al.*[114]

Table 9 Continued

Study type	No. of patients/histology of glioma	Regimen	Response rate			Progression-free survival		Overall survival	Reference
			CR (%)	PR (%)	SD (%)	PFS-6, 12 (%)	Median (months)	Median (months)	
Retrospective cohort	12/GB	BEV + irinotecan	0	44	41	46, N/A	3.8	7.1	Kang *et al.*[115]
Retro cohort	37/GB	BEV + irinotecan	5.4	62.2	16.2	63.7, N/A	7.6	11.5	Zuniga *et al.*[116]
	14/AG		14.3	64.3	14.3	78.6, N/A	13.4	N/A	
Retrospective cohort	25/AO	BEV + irinotecan	20	52	16	42, N/A	4.6	N/A	Taillibert *et al.*[117]
Cohort	23/GB	BEV + irinotecan	4.3	56.5	34.4	30, N/A	4.6	9.23	Vredenburgh *et al.*[111]
	9/AG		0	66.7	33.3	56, N/A	6.9	N/A	
	Total 32		3.1	59.4	34.4	38, N/A	5.3	N/A	
Bevacizumab plus non-specific chemotherapy (NSC)									
RCT	54/GB	BEV + fotemustine 75 mg/m^2	4	48	37	42.6, N/A	5.2	9.1	Soffietti *et al.*[64]
RCT	44/GB	BEV + lomustine 90 mg/m^2	N/A	N/A	N/A	41, N/A	4	N/A	Taal *et al.*[65]
retrospective cohort	55/HGG	BEV + NSC[2]	2.3	31.8	29.5	39, N/A	5.5	8.2	Norden *et al.*[118]
Retrospective cohort	54/HGG	BEV + NSC[3]	0	28	56	33, N/A	4.1	N/A	Quant *et al.*[119]
Cohort	44/GB	BEV + NSC[4]	NA	NA	NA	41, N/A	4.25	9.0	Nghiemphu *et al.*[120]

[1]Irinotecan (125 mg/m^2 every 2 weeks for patients not on enzyme-inducing antiepileptic drugs [EIAEDs] and 340 mg/m^2 every 2 weeks for patients on EIAEDs.
[2]Non-specific chemotherapies include irinotecan (125 mg/m^2 every 2 weeks for patients not on enzyme-inducing antiepileptic drugs [EIAEDs] and 340 mg/m^2 every 2 weeks for patients on EIAEDs), carboplatin (AUC of 5–6), carmustine (200 mg/m^2 every 6 weeks), and temozolomide (150–200 mg/m^2 for 5 days every 4 weeks).
[3]As the bevacizumab-containing regimen, the additional chemotherapies include irinotecan, lomustine, carmustine, carmustine, erlotinib, or etoposide.
[4]Most patients, 31 of 44, received concurrent irinotecan, eight patients received carboplatin, three patients received lomustine, and two patients received etoposide. Twenty-seven of these patients also continued on with bevacizumab at progression, in combination with other chemotherapeutic agents.
AA: anaplastic astrocytoma; AG: anaplastic glioma; BEV: bevacizumab (usually 10 mg/kg, otherwise specified); CR: complete response; GB: glioblastoma; HGG: high-grade glioma; N/A: not available; OS: overall survival; PFS: progression-free survival; PR: partial response; RCT: randomized controlled trial; SD: stable disease; TMZ: temozolomide (in unit of mg/m^2/day).
The objective response is measured according to WHO criteria: complete response: complete disappearance of all detectable lesions as determined by two observations not less than 4 weeks apart; partial response: ≥ 50% reduction in the sum of the products of the two largest perpendicular diameters of all measurable lesions, determined by two observations not less than 4 weeks apart; progressive disease: ≥ 25% increase in any measurable lesion or the appearance of a new lesion; no change: <50% reduction in total tumor volume or a <25% increase in any measurable lesion.

Table 10 Comparative table of the chosen strongest clinical evidence up to 2013

Agent(s) of treatment	Median survival duration (months)	Study type [Reference]
Newly diagnosed glioma patients		
Temozolomide	8.6*	RCT[38]
Radiation	12.6*	RCT[20]
Temozolomide + radiation	14.6*	RCT[20]
Temozolomide + radiation + bevacizumab	16.8*	RCT[61]
Temozolomide + bevacizumab	11.7	Clinical trial[30]
Recurrent glioma patients		
Temozolomide	13.6*	Clinical trial[56]
Bevacizumab	9.2	RCT[24]
Bevacizumab + temozolomide	9.2	Clinical trial[25]
Bevacizumab + irinotecan	8.7	RCT[24]

*The study contained number of sample size more than 100 people in a particular group.
RCT: randomized control trial.

results in two comparative clinical outcome tables, including newly diagnosed glioma (Table 8) and recurrent glioma (Table 9). In addition, we summarized the strongest evidence from both tables (Tables 8 and 9) into one overall comparative table (Table 10).

Newly diagnosed glioma patients

From clinical trials of several treatment regimens in newly diagnosed glioma patients (Table 8), treatment of new cases of high-grade gliomas by TMZ alone resulted in median survival duration of 8.6 months, compared to 12.6 months on radiation alone.[20,38] Due to the randomized control trial of Stupp *et al.*, which demonstrated significantly greater survival in combined radiation with TMZ (14.6 months) than that of radiotherapy alone (12.1 months),[20] the treatment of chemoradiation in newly diagnosed glioma patients has been globally accepted as the current standard of care.

In recent phase III trials, the addition of BEV to radiotherapy–TMZ treatment did not statistically improve survival duration in newly diagnosed glioblastomas.[61,62] However, it has been shown to improve 6-month-progression-free survival and maintain the quality of life in these patients.[61]

Recurrent glioma patients

The recurrent glioma clinical trials using different therapeutic regimens are summarized in Table 9. Recent studies suggest that the combination of bevacizumab and nitrosoureas, including fortemustine or lomustine, have not yet shown significant improvement of survival in recurrent high-grade gliomas, when compared to BEV alone.[25,63–65] Overall survival duration in glioma patients with recurrence is lower than that in newly diagnosed patients. Most of the trials reported a median survival duration of 5–9 months following optimal chemotherapy.[20,30,66]

Determining the most effective regimen for recurrent glioblastoma patients was not possible due to the inconsistency of results (Table 9). For instance, according to the high-grade glioma patients treated with TMZ alone, Yung and colleagues demonstrated the distinct survival duration of 13.6 months,[56] while other large multicenter phase II trials revealed 5.4–5.8 months.[32,67] The possible causes of inconsistent results might be the lack of randomization, and differences between initial doses and site locations. Thus, further randomized controlled trials are required to determine the best treatment in recurrent gliomas.

Comparison of overall survival between current chemotherapeutic regimens

In Table 10, from the overall collected data, the best treatment regimen could not be definitively concluded especially in studies of recurrent high-grade glioma patients, where inadequate sample sizes and non-randomized study designs occurred. However, in patients with a newly diagnosed high-grade phenotype, who routinely receive TMZ, we conclude the following: (1) the addition of radiotherapy to TMZ is strongly beneficial, (2) the addition of BEV to TMZ seems to be beneficial, or (3) the addition of both radiotherapy and BEV to TMZ seems to give the longest survival duration.

Conclusion

Temozolomide and bevacizumab are current chemotherapeutic agents treating patients with high-grade glioma, including glioblastoma. At this time, it can be concluded that TMZ can be mainly and effectively used in newly diagnosed glioblastoma patients, while either TMZ or BEV can be effectively used in the treatment of glioblastoma patients with recurrence. However, it is still premature to assume which chemotherapeutic agents are the best for the treatment of recurrent glioblastoma, comparing between TMZ and BEV, since more strong clinical evidence is still needed. The cancer cell death mechanisms of TMZ, an alkylating agent, are possible through apoptosis and autophagy, whereas the mechanisms of BEV, an anti-angiogenesis agent, are through autophagy caused by hypoxia and unspecific indirect effect to cancer cells. However, the complexity of cancer cells in glioma has

contributed to its resistance to or less efficacy of both chemotherapy therapies. Although additional agents have been applied to both chemotherapies in some studies and have revealed some benefits with alternating cancer cell death pathways, further studies in every aspect, including genomic studies, drug mechanism studies, drug resistance/sensitivity studies, and studies of combination of additional alternatively acting agents are still necessary for longer survival outcomes and better quality of remaining life for patients.

Disclaimer Statements

Contributors All authors have contributed to the work and agreed with the presented findings.

Funding This study was supported by Thailand Research Fund TRF-BRG57 (SC), TRF-RTA5580006 (NC), Faculty of Medicine Chiang Mai University Endowment Fund (NC), National Research Council of Thailand (SC), and Chiang Mai University Excellent Center Award (NC).

Conflicts of interest The authors declare that there are no conflicts of interest.

Ethics approval Not applicable.

References

1 Thurnher MM. 2007 World Health Organization classification of tumours of the central nervous system. Cancer Imag. 2009;9(Spec No A):S1–3.
2 Bruce JN Harris JE, Kennedy B. Staging of brain cancers. Available from: http://emedicine.medscape.com, 2013.
3 Louis DN, Ohgaki H, Wiestler OD, Cavenee WK, Burger PC, Jouvet A, *et al.* The 2007 WHO classification of tumours of the central nervous system. Acta Neuropathol. 2007;114:97–109.
4 Gonzales M. The 2000 World Health Organization classification of tumours of the nervous system. J Clin Neurosci. 2001;8:1–3.
5 Dunn GP, Rinne ML, Wykosky J, Genovese G, Quayle SN, Dunn IF, *et al.* Emerging insights into the molecular and cellular basis of glioblastoma. Genes Dev. 2012;26:756–84.
6 Stupp R, Hegi ME, Mason WP, van den Bent MJ, Taphoorn MJ, Janzer RC, *et al.* Effects of radiotherapy with concomitant and adjuvant temozolomide versus radiotherapy alone on survival in glioblastoma in a randomised phase III study: 5-year analysis of the EORTC-NCIC trial. Lancet Oncol. 2009;10:459–66.
7 Minniti G, Muni R, Lanzetta G, Marchetti P, Enrici RM. Chemotherapy for glioblastoma: current treatment and future perspectives for cytotoxic and targeted agents. Anticancer Res. 2009;29:5171–84.
8 Grossman SA, Batara JF. Current management of glioblastoma multiforme. Semin Oncol. 2004;31:635–44.
9 Brandes AA. State-of-the-art treatment of high-grade brain tumors. Semin Oncol. 2003;30:4–9.
10 Reardon DA, Wen PY. Therapeutic advances in the treatment of glioblastoma: rationale and potential role of targeted agents. Oncologist. 2006;11:152–64.
11 Lacroix M, Abi-Said D, Fourney DR, Gokaslan ZL, Shi W, DeMonte F, *et al.* A multivariate analysis of 416 patients with glioblastoma multiforme: prognosis, extent of resection, and survival. J Neurosurg. 2001;95:190–8.
12 Sanai N, Berger MS. Glioma extent of resection and its impact on patient outcome. Neurosurgery. 2008;62:753–64; discussion 264–6.
13 Hochberg FH, Pruitt A. Assumptions in the radiotherapy of glioblastoma. Neurology. 1980;30:907–11.
14 Parsa AT, Wachhorst S, Lamborn KR, Prados MD, McDermott MW, Berger MS, *et al.* Prognostic significance of intracranial dissemination of glioblastoma multiforme in adults. J Neurosurg. 2005;102:622–8.
15 Walker MD, Alexander E Jr, Hunt WE, MacCarty CS, Mahaley MS Jr, Mealey J Jr *et al.* Evaluation of BCNU and/or radiotherapy in the treatment of anaplastic gliomas. A cooperative clinical trial. J Neurosurg. 1978;49:333–43.
16 Fulton DS, Urtasun RC, Scott-Brown I, Johnson ES, Mielke B, Curry B, *et al.* Increasing radiation dose intensity using hyperfractionation in patients with malignant glioma. Final report of a prospective phase I-II dose response study. J Neurooncol. 1992;14:63–72.
17 Wick W, Hartmann C, Engel C, Stoffels M, Felsberg J, Stockhammer F, *et al.* NOA-04 randomized phase III trial of sequential radiochemotherapy of anaplastic glioma with procarbazine, lomustine, and vincristine or temozolomide. J Clin Oncol. 2009;27:5874–80.
18 Showalter TN, Andrel J, Andrews DW, Curran WJ Jr, Daskalakis C, Werner-Wasik M. Multifocal glioblastoma multiforme: prognostic factors and patterns of progression. Int J Radiat Oncol Biol Phys. 2007;69:820–4.
19 Lawrence YR, Li XA, el Naqa I, Hahn CA, Marks LB, Merchant TE, *et al.* Radiation dose-volume effects in the brain. Int J Radiat Oncol Biol Phys. 2010;76:S20–7.
20 Stupp R, Mason WP, van den Bent MJ, Weller M, Fisher B, Taphoorn MJ, *et al.* Radiotherapy plus concomitant and adjuvant temozolomide for glioblastoma. N Engl J Med. 2005;352:987–96.
21 Chamberlain MC, Glantz MJ, Chalmers L, Van Horn A, Sloan AE. Early necrosis following concurrent Temodar and radiotherapy in patients with glioblastoma. J Neurooncol. 2007;82:81–3.
22 Johnson DR, Leeper HE, Uhm JH. Glioblastoma survival in the United States improved after food and drug administration approval of bevacizumab: a population-based analysis. Cancer. 2013;119:3489–95.
23 Kreisl TN, Kim L, Moore K, Duic P, Royce C, Stroud I, *et al.* Phase II trial of single-agent bevacizumab followed by bevacizumab plus irinotecan at tumor progression in recurrent glioblastoma. J Clin Oncol. 2009;27:740–5.
24 Friedman HS, Prados MD, Wen PY, Mikkelsen T, Schiff D, Abrey LE, *et al.* Bevacizumab alone and in combination with irinotecan in recurrent glioblastoma. J Clin Oncol. 2009;27:4733–40.
25 Desjardins A, Reardon DA, Coan A, Marcello J, Herndon JE II, Bailey L, *et al.* Bevacizumab and daily temozolomide for recurrent glioblastoma. Cancer. 2012;118:1302–12.
26 Brandes AA, Ermani M, Basso U, Amistà P, Berti F, Scienza R, *et al.* Temozolomide as a second-line systemic regimen in recurrent high-grade glioma: a phase II study. Ann Oncol. 2001;12:255–7.
27 Clarke JL, Iwamoto FM, Sul J, Panageas K, Lassman AB, DeAngelis LM, *et al.* Randomized phase II trial of chemoradiotherapy followed by either dose-dense or metronomic temozolomide for newly diagnosed glioblastoma. J Clin Oncol. 2009;27:3861–7.
28 Groves MD, Puduvalli VK, Hess KR, Jaeckle KA, Peterson P, Yung WK, *et al.* Phase II trial of temozolomide plus the matrix metalloproteinase inhibitor, marimastat, in recurrent and progressive glioblastoma multiforme. J Clin Oncol. 2002;20:1383–8.
29 Levin VA, Phuphanich S, Yung WK, Forsyth PA, Maestro RD, Perry JR, *et al.* Randomized, double-blind, placebo-controlled trial of marimastat in glioblastoma multiforme patients following surgery and irradiation. J Neurooncol. 2006;78:295–302.
30 Lou E, Peters KB, Sumrall AL, Desjardins A, Reardon DA, Lipp ES, *et al.* Phase II trial of upfront bevacizumab and temozolomide for unresectable or multifocal glioblastoma. Cancer Med. 2013;2:185–95.
31 Narayana A, Gruber D, Kunnakkat S, Golfinos JG, Parker E, Raza S, *et al.* A clinical trial of bevacizumab, temozolomide, and radiation for newly diagnosed glioblastoma. J Neurosurg. 2012;116:341–5.
32 Brada M, Hoang-Xuan K, Rampling R, Dietrich PY, Dirix LY, Macdonald D, *et al.* Multicenter phase II trial of temozolomide in patients with glioblastoma multiforme at first relapse. Ann Oncol. 2001;12:259–66.
33 Friday BB, Anderson SK, Buckner J, Yu C, Giannini C, Geoffroy F, *et al.* Phase II trial of vorinostat in combination

with bortezomib in recurrent glioblastoma: a north central cancer treatment group study. Neuro Oncol. 2012;14:215–21.
34 Hegi ME, Diserens AC, Gorlia T, Hamou MF, de Tribolet N, Weller M, *et al.* MGMT gene silencing and benefit from temozolomide in glioblastoma. N Engl J Med. 2005;352:997–1003.
35 Li S, Jiang T, Li G, Wang Z. Impact of p53 status to response of temozolomide in low MGMT expression glioblastomas: preliminary results. Neurol Res. 2008;30:567–70.
36 Lawson HC, Sampath P, Bohan E, Park MC, Hussain N, Olivi A, *et al.* Interstitial chemotherapy for malignant gliomas: the Johns Hopkins experience. J Neurooncol. 2007;83:61–70.
37 Kanzawa T, Bedwell J, Kondo Y, Kondo S, Germano IM. Inhibition of DNA repair for sensitizing resistant glioma cells to temozolomide. J Neurosurg. 2003;99:1047–52.
38 Wick W, Platten M, Meisner C, Felsberg J, Tabatabai G, Simon M, *et al.* Temozolomide chemotherapy alone versus radiotherapy alone for malignant astrocytoma in the elderly: the NOA-08 randomised, phase 3 trial. Lancet Oncol. 2012;13:707–15.
39 Zhang J, Stevens MF, Bradshaw TD. Temozolomide: mechanisms of action, repair and resistance. Curr Mol Pharmacol. 2012;5:102–14.
40 Hirose Y, Berger MS, Pieper RO. p53 effects both the duration of G2/M arrest and the fate of temozolomide-treated human glioblastoma cells. Cancer Res. 2001;61:1957–63.
41 Roos WP, Batista LF, Naumann SC, Wick W, Weller M, Menck CF, *et al.* Apoptosis in malignant glioma cells triggered by the temozolomide-induced DNA lesion O^6-methylguanine. Oncogene. 2007;26:186–97.
42 Jiang Y, Sun Y, Yuan Y: [Mechanism of temozolomide-induced anti-tumor effects on glioblastoma cells in vitro is via ROS-dependent SIRT1 signaling pathway]. Zhonghua zhong liu za zhi. 2012;34:734–8.
43 Carmo A, Carvalheiro H, Crespo I, Nunes I, Lopes MC. Effect of temozolomide on the U-118 glioma cell line. Oncol Lett. 2011;2:1165–70.
44 Kanzawa T, Germano IM, Komata T, Ito H, Kondo Y, Kondo S. Role of autophagy in temozolomide-induced cytotoxicity for malignant glioma cells. Cell Death Differ. 2004;11:448–57.
45 Knizhnik AV, Roos WP, Nikolova T, Quiros S, Tomaszowski KH, Christmann M, *et al.* Survival and death strategies in glioma cells: autophagy, senescence and apoptosis triggered by a single type of temozolomide-induced DNA damage. PLoS One. 2013;8:e55665.
46 Hirst TC, Vesterinen HM, Sena ES, Egan KJ, Macleod MR, Whittle IR. Systematic review and meta-analysis of temozolomide in animal models of glioma: was clinical efficacy predicted? Br J Cancer. 2013;108:64–71.
47 Zhang J, Stevens MF, Laughton CA, Madhusudan S, Bradshaw TD. Acquired resistance to temozolomide in glioma cell lines: molecular mechanisms and potential translational applications. Oncology. 2010;78:103–14.
48 Mathieu V, De Nève N, Le Mercier M, Dewelle J, Gaussin JF, Dehoux M, *et al.* Combining bevacizumab with temozolomide increases the antitumor efficacy of temozolomide in a human glioblastoma orthotopic xenograft model. Neoplasia. 2008;10:1383–92.
49 von Baumgarten L, Brucker D, Tirniceru A, Kienast Y, Grau S, Burgold S, *et al.* Bevacizumab has differential and dose-dependent effects on glioma blood vessels and tumor cells. Clin Cancer Res. 2011;17:6192–205.
50 Keunen O, Johansson M, Oudin A, Sanzey M, Rahim SA, Fack F, *et al.* Anti-VEGF treatment reduces blood supply and increases tumor cell invasion in glioblastoma. Proc Natl Acad Sci USA. 2011;108:3749–54.
51 Hattingen E, Jurcoane A, Bähr O, Rieger J, Magerkurth J, Anti S, *et al.* Bevacizumab impairs oxidative energy metabolism and shows antitumoral effects in recurrent glioblastomas: a 31P/1H MRSI and quantitative magnetic resonance imaging study. Neuro Oncol. 2011;13:1349–63.
52 Hu YL, DeLay M, Jahangiri A, Molinaro AM, Rose SD, Carbonell WS, *et al.* Hypoxia-induced autophagy promotes tumor cell survival and adaptation to anti-angiogenic treatment in glioblastoma. Cancer Res. 2012;72:1773–83.
53 Piao Y, Liang J, Holmes L, Zurita AJ, Henry V, Heymach JV, *et al.* Glioblastoma resistance to anti-VEGF therapy is associated with myeloid cell infiltration, stem cell accumulation, and a mesenchymal phenotype. Neuro Oncol. 2012;14:1379–92.
54 Raizer JJ, Grimm S, Chamberlain MC, Nicholas MK, Chandler JP, Muro K, *et al.* A phase 2 trial of single-agent bevacizumab given in an every-3-week schedule for patients with recurrent high-grade gliomas. Cancer. 2010;116:5297–305.
55 Chamberlain MC, Johnston SK. Salvage therapy with single agent bevacizumab for recurrent glioblastoma. J Neurooncol. 2010;96:259–69.
56 Yung WK, Prados MD, Yaya-Tur R, Rosenfeld SS, Brada M, Friedman HS, *et al.* Multicenter phase II trial of temozolomide in patients with anaplastic astrocytoma or anaplastic oligoastrocytoma at first relapse. J Clin Oncol. 1999;17:2762–71.
57 Hirose Y, Berger MS, Pieper RO. Abrogation of the Chk1-mediated G(2) checkpoint pathway potentiates temozolomide-induced toxicity in a p53-independent manner in human glioblastoma cells. Cancer Res. 2001;61:5843–9.
58 Yuan Y, Xue X, Guo RB, Sun XL, Hu G. Resveratrol enhances the antitumor effects of temozolomide in glioblastoma via ROS-dependent AMPK-TSC-mTOR signaling pathway. CNS Neurosci Ther. 2012;18:536–46.
59 Filippi-Chiela EC, Thomé MP, Bueno e Silva MM, Pelegrini AL, Ledur PF, Garicochea B, *et al.* Resveratrol abrogates the temozolomide-induced G2 arrest leading to mitotic catastrophe and reinforces the temozolomide-induced senescence in glioma cells. BMC Cancer. 2013;13:147.
60 Lin CJ, Lee CC, Shih YL, Lin TY, Wang SH, Lin YF, *et al.* Resveratrol enhances the therapeutic effect of temozolomide against malignant glioma in vitro and in vivo by inhibiting autophagy. Free Radic Biol Med. 2012;52:377–91.
61 Chinot OL, Wick W, Mason W, Henriksson R, Saran F, Nishikawa R, *et al.* Bevacizumab plus radiotherapy-temozolomide for newly diagnosed glioblastoma. N Engl J Med. 2014;370:709–22.
62 Gilbert MR, Dignam JJ, Armstrong TS, Wefel JS, Blumenthal DT, Vogelbaum MA, *et al.* A randomized trial of bevacizumab for newly diagnosed glioblastoma. N Engl J Med. 2014;370:699–708.
63 Desjardins A, Reardon DA, Herndon JE II, Marcello J, Quinn JA, Rich JN, *et al.* Bevacizumab plus irinotecan in recurrent WHO grade 3 malignant gliomas. Clin Cancer Res. 2008;14:7068–73.
64 Soffietti R, Trevisan E, Bertero L, Cassoni P, Morra I, Fabrini MG, *et al.* Bevacizumab and fotemustine for recurrent glioblastoma: a phase II study of AINO (Italian Association of Neuro-Oncology). J Neurooncol. 2014;116:533–41.
65 Taal W, Oosterkamp HM, Walenkamp AME, *et al.* A randomized phase II study of bevacizumab versus bevacizumab plus lomustine versus lomustine single agent in recurrent glioblastoma: the Dutch BELOB study. American Society of clinical oncology (ASCO) Annual Meeting, Chicago, IL, USA J.Clin Oncol 31, 2013 (suppl; abstr 2001).
66 Lai A, Tran A, Nghiemphu PL, Pope WB, Solis OE, Selch M, *et al.* Phase II study of bevacizumab plus temozolomide during and after radiation therapy for patients with newly diagnosed glioblastoma multiforme. J Clin Oncol. 2011;29:142–8.
67 Bower M, Newlands ES, Bleehen NM, Brada M, Begent RJ, Calvert H, *et al.* Multicentre CRC phase II trial of temozolomide in recurrent or progressive high-grade glioma. Cancer Chemother Pharmacol. 1997;40:484–8.
68 Virrey JJ, Golden EB, Sivakumar W, Wang W, Pen L, Schönthal AH, *et al.* Glioma-associated endothelial cells are chemoresistant to temozolomide. J Neurooncol. 2009;95:13–22.
69 Oliva CR, Nozell SE, Diers A, McClugage SG III, Sarkaria JN, Markert JM, *et al.* Acquisition of temozolomide chemoresistance in gliomas leads to remodeling of mitochondrial electron transport chain. J Biol Chem. 2010;285:39759–67.
70 Oliva CR, Moellering DR, Gillespie GY, Griguer CE. Acquisition of chemoresistance in gliomas is associated with increased mitochondrial coupling and decreased ROS production. PLoS One. 2011;6:e24665.
71 Yung WK, Albright RE, Olson J, Fredericks R, Fink K, Prados MD, *et al.* A phase II study of temozolomide vs. procarbazine in patients with glioblastoma multiforme at first relapse. Br J Cancer. 2000;83:588–93.
72 Perry JR, Bélanger K, Mason WP, Fulton D, Kavan P, Easaw J, *et al.* Phase II trial of continuous dose-intense temozolomide in recurrent malignant glioma: RESCUE study. J Clin Oncol. 2010;28:2051–7.

73 Sanson M, Cartalat-Carel S, Taillibert S, Napolitano M, Djafari L, Cougnard J, *et al.* Initial chemotherapy in gliomatosis cerebri. Neurology. 2004;63:270–5.

74 McIntyre A, Patiar S, Wigfield S, Li JL, Ledaki I, Turley H, *et al.* Carbonic anhydrase IX promotes tumor growth and necrosis in vivo and inhibition enhances anti-VEGF therapy. Clin Cancer Res. 2012;18:3100–11.

75 Carbonell WS, DeLay M, Jahangiri A, Park CC, Aghi MK. beta1 Integrin targeting potentiates antiangiogenic therapy and inhibits the growth of bevacizumab-resistant glioblastoma. Cancer Res. 2013;73:3145–54.

76 Kumar K, Wigfield S, Gee HE, Devlin CM, Singleton D, Li JL, *et al.* Dichloroacetate reverses the hypoxic adaptation to bevacizumab and enhances its antitumor effects in mouse xenografts. J Mol Med. 2013;91:749–58.

77 Günther W, Pawlak E, Damasceno R, Arnold H, Terzis AJ. Temozolomide induces apoptosis and senescence in glioma cells cultured as multicellular spheroids. Br J Cancer. 2003;88:463–9.

78 Palumbo S, Pirtoli L, Tini P, Cevenini G, Calderaro F, Toscano M, *et al.* Different involvement of autophagy in human malignant glioma cell lines undergoing irradiation and temozolomide combined treatments. J Cell Biochem. 2012;113:2308–18.

79 Barazzuol L, Jena R, Burnet NG, Jeynes JC, Merchant MJ, Kirkby KJ, *et al.* In vitro evaluation of combined temozolomide and radiotherapy using X rays and high-linear energy transfer radiation for glioblastoma. Radiat Res. 2012;177:651–62.

80 Ito H, Daido S, Kanzawa T, Kondo S, Kondo Y. Radiation-induced autophagy is associated with LC3 and its inhibition sensitizes malignant glioma cells. Int J Oncol. 2005;26:1401–10.

81 Lomonaco SL, Finniss S, Xiang C, Decarvalho A, Umansky F, Kalkanis SN, *et al.* The induction of autophagy by gamma-radiation contributes to the radioresistance of glioma stem cells. Int J Cancer. 2009;125:717–22.

82 Kanzawa T, Germano IM, Kondo Y, Ito H, Kyo S, Kondo S. Inhibition of telomerase activity in malignant glioma cells correlates with their sensitivity to temozolomide. Br J Cancer. 2003;89:922–9.

83 Gupta V, Su YS, Wang W, Kardosh A, Liebes LF, Hofman FM, *et al.* Enhancement of glioblastoma cell killing by combination treatment with temozolomide and tamoxifen or hypericin. Neurosurg Focus. 2006;20:E20.

84 Hingtgen S, Ren X, Terwilliger E, Classon M, Weissleder R, Shah K. Targeting multiple pathways in gliomas with stem cell and viral delivered S-TRAIL and Temozolomide. Mol Cancer Ther. 2008;7:3575–85.

85 Ryu CH, Yoon WS, Park KY, Kim SM, Lim JY, Woo JS, *et al.* Valproic acid downregulates the expression of MGMT and sensitizes temozolomide-resistant glioma cells. J Biomed Biotechnol. 2012;2012:987495.

86 Kohsaka S, Takahashi K, Wang L, Tanino M, Kimura T, Nishihara H, *et al.* Inhibition of GSH synthesis potentiates temozolomide-induced bystander effect in glioblastoma. Cancer Lett. 2013;331:68–75.

87 Athanassiou H, Synodinou M, Maragoudakis E, Paraskevaidis M, Verigos C, Misailidou D, *et al.* Randomized phase II study of temozolomide and radiotherapy compared with radiotherapy alone in newly diagnosed glioblastoma multiforme. J Clin Oncol. 2005;23:2372–7.

88 Kocher M, Frommolt P, Borberg SK, Rühl U, Steingräber M, Niewald M, *et al.* Randomized study of postoperative radiotherapy and simultaneous temozolomide without adjuvant chemotherapy for glioblastoma. Strahlenther Onkol. 2008;184:572–9.

89 Niyazi M, Schwarz SB, Suchorska B, Belka C. Radiotherapy with and without temozolomide in elderly patients with glioblastoma. Strahlenther Onkol. 2012;188:154–9.

90 Chinot OL, de La Motte Rouge T, Moore N, Zeaiter A, Das A, Phillips H, *et al.* AVAglio: phase 3 trial of bevacizumab plus temozolomide and radiotherapy in newly diagnosed glioblastoma multiforme. Adv Ther. 2011;28:334–40.

91 Combs SE, Wagner J, Bischof M, Welzel T, Edler L, Rausch R, *et al.* Radiochemotherapy in patients with primary glioblastoma comparing two temozolomide dose regimens. Int J Radiat Oncol Biol Phys. 2008;71:999–1005.

92 Joo JD, Chang JH, Kim JH, Hong YK, Kim YH, Kim CY. Temozolomide during and after radiotherapy for newly diagnosed glioblastomas: a prospective multicenter study of Korean patients. J Korean Neurosurg Soc. 2012;52:92–7.

93 Gunjur A, Bressel M, Ryan G. The addition of temozolomide does not change the pattern of progression of glioblastoma multiforme post-radiotherapy. J Med Imaging Radiat Oncol. 2012;56:567–73.

94 Muni R, Minniti G, Lanzetta G, Caporello P, Frati A, Enrici MM, *et al.* Short-term radiotherapy followed by adjuvant chemotherapy in poor-prognosis patients with glioblastoma. Tumori. 2010;96:60–4.

95 Lam N, Chambers CR. Temozolomide plus radiotherapy for glioblastoma in a Canadian province: efficacy versus effectiveness and the impact of O^6-methylguanine-DNA-methyltransferase promoter methylation. J Oncol Pharm Pract. 2012;18:229–38.

96 Minniti G, Lanzetta G, Scaringi C, Caporello P, Salvati M, Arcella A, *et al.* Phase II study of short-course radiotherapy plus concomitant and adjuvant temozolomide in elderly patients with glioblastoma. Int J Radiat Oncol Biol Phys. 2012;83:93–9.

97 Newlands ES, O'Reilly SM, Glaser MG, Bower M, Evans H, Brock C, *et al.* The Charing Cross Hospital experience with temozolomide in patients with gliomas. Eur J Cancer. 1996;32A:2236–41.

98 Kim YH, Park CK, Cho WH, Kim IA, Moon S, Choe G, *et al.* Temozolomide during and after radiation therapy for WHO grade III gliomas: preliminary report of a prospective multicenter study. J Neurooncol. 2011;103:503–12.

99 Sampson JH, Heimberger AB, Archer GE, Aldape KD, Friedman AH, Friedman HS, *et al.* Immunologic escape after prolonged progression-free survival with epidermal growth factor receptor variant III peptide vaccination in patients with newly diagnosed glioblastoma. J Clin Oncol. 2010;28:4722–9.

100 Vredenburgh JJ, Desjardins A, Reardon DA, Peters KB, Herndon JE II, Marcello J, *et al.* The addition of bevacizumab to standard radiation therapy and temozolomide followed by bevacizumab, temozolomide, and irinotecan for newly diagnosed glioblastoma. Clin Cancer Res. 2011;17:4119–24.

101 Bock HC, Puchner MJ, Lohmann F, Schütze M, Koll S, Ketter R, *et al.* First-line treatment of malignant glioma with carmustine implants followed by concomitant radiochemotherapy: a multicenter experience. Neurosurg Rev. 2010;33:441–9.

102 Bartolomei M, Mazzetta C, Handkiewicz-Junak D, Bodei L, Rocca P, Grana C, *et al.* Combined treatment of glioblastoma patients with locoregional pre-targeted 90Y-biotin radioimmunotherapy and temozolomide. Q J Nucl Med Mol Imaging. 2004;48:220–8.

103 Pitz MW, Lipson M, Hosseini B, Lambert P, Guilbert K, Lister D, *et al.* Extended adjuvant temozolomide with cis-retinoic acid for adult glioblastoma. Curr Oncol. 2012;19:308–14.

104 Hainsworth JD, Shih KC, Shepard GC, Tillinghast GW, Brinker BT, Spigel DR. Phase II study of concurrent radiation therapy, temozolomide, and bevacizumab followed by bevacizumab/everolimus as first-line treatment for patients with glioblastoma. Clin Adv Hematol Oncol. 2012;10:240–6.

105 Gruber ML, Buster WP. Temozolomide in combination with irinotecan for treatment of recurrent malignant glioma. Am J Clin Oncol. 2004;27:33–8.

106 Reardon DA, Desjardins A, Peters K, Gururangan S, Sampson J, Rich JN, *et al.* Phase II study of metronomic chemotherapy with bevacizumab for recurrent glioblastoma after progression on bevacizumab therapy. J Neurooncol. 2011;103:371–9.

107 Reardon DA, Desjardins A, Peters KB, Gururangan S, Sampson JH, McLendon RE, *et al.* Phase II study of carboplatin, irinotecan, and bevacizumab for bevacizumab naive, recurrent glioblastoma. J Neurooncol. 2012;107:155–64.

108 Chen W, Delaloye S, Silverman DH, Geist C, Czernin J, Sayre J, *et al.* Predicting treatment response of malignant gliomas to bevacizumab and irinotecan by imaging proliferation with [18F] fluorothymidine positron emission tomography: a pilot study. J Clin Oncol. 2007;25:4714–21.

109 Poulsen HS, Grunnet K, Sorensen M, Olsen P, Hasselbalch B, Nelausen K, *et al.* Bevacizumab plus irinotecan in the treatment patients with progressive recurrent malignant brain tumours. Acta Oncol. 2009;48:52–8.

110 Narayana A, Kelly P, Golfinos J, Parker E, Johnson G, Knopp E, *et al.* Antiangiogenic therapy using bevacizumab in

recurrent high-grade glioma: impact on local control and patient survival. J Neurosurg. 2009;110:173–80.
111 Vredenburgh JJ, Desjardins A, Herndon JE II, Marcello J, Reardon DA, Quinn JA, *et al.* Bevacizumab plus irinotecan in recurrent glioblastoma multiforme. J Clin Oncol. 2007;25:4722–9.
112 Vredenburgh JJ, Desjardins A, Herndon JE II, Dowell JM, Reardon DA, Quinn JA, *et al.* Phase II trial of bevacizumab and irinotecan in recurrent malignant glioma. Clin Cancer Res. 2007;13:1253–9.
113 Bokstein F, Shpigel S, Blumenthal DT. Treatment with bevacizumab and irinotecan for recurrent high-grade glial tumors. Cancer. 2008;112:2267–73.
114 Ali SA, McHayleh WM, Ahmad A, Sehgal R, Braffet M, Rahman M, *et al.* Bevacizumab and irinotecan therapy in glioblastoma multiforme: a series of 13 cases. J Neurosurg. 2008;109:268–72.
115 Kang TY, Jin T, Elinzano H, Peereboom D. Irinotecan and bevacizumab in progressive primary brain tumors, an evaluation of efficacy and safety. J Neurooncol. 2008;89:113–8.
116 Zuniga RM, Torcuator R, Jain R, Anderson J, Doyle T, Ellika S, *et al.* Efficacy, safety and patterns of response and recurrence in patients with recurrent high-grade gliomas treated with bevacizumab plus irinotecan. J Neurooncol. 2009;91:329–36.
117 Taillibert S, Vincent LA, Granger B, Marie Y, Carpentier C, Guillevin R, *et al.* Bevacizumab and irinotecan for recurrent oligodendroglial tumors. Neurology. 2009;72:1601–6.
118 Norden AD, Young GS, Setayesh K, Muzikansky A, Klufas R, Ross GL, *et al.* Bevacizumab for recurrent malignant gliomas: efficacy, toxicity, and patterns of recurrence. Neurology. 2008;70:779–87.
119 Quant EC, Norden AD, Drappatz J, Muzikansky A, Doherty L, Lafrankie D, *et al.* Role of a second chemotherapy in recurrent malignant glioma patients who progress on bevacizumab. Neuro Oncol. 2009;11:550–5.
120 Nghiemphu PL, Liu W, Lee Y, Than T, Graham C, Lai A, *et al.* Bevacizumab and chemotherapy for recurrent glioblastoma: a single-institution experience. Neurology. 2009;72:1217–22.

เอกสารแนบหมายเลข 53

Hindawi Publishing Corporation
Evidence-Based Complementary and Alternative Medicine
Volume 2015, Article ID 593902, 11 pages
http://dx.doi.org/10.1155/2015/593902

Hindawi

Review Article

Pharmacological Properties of Protocatechuic Acid and Its Potential Roles as Complementary Medicine

Yoswaris Semaming,[1,2] Patchareewan Pannengpetch,[3] Siriporn C. Chattipakorn,[2,4,5] and Nipon Chattipakorn[2,5,6]

[1] *Veterinary Technology Program, Faculty of Technology, Udon Thani Rajabhat University, Udon Thani 41000, Thailand*
[2] *Cardiac Electrophysiology Research and Training Center, Faculty of Medicine, Chiang Mai University, Chiang Mai 50200, Thailand*
[3] *Department of Pharmacology, Faculty of Medicine, Khon Kaen University, Khon Kaen 40002, Thailand*
[4] *Department of Oral Biology and Diagnostic Science, Faculty of Dentistry, Chiang Mai University, Chiang Mai 50200, Thailand*
[5] *Center of Excellence in Cardiac Electrophysiology Research, Chiang Mai University, Chiang Mai 50200, Thailand*
[6] *Cardiac Electrophysiology Unit, Department of Physiology, Faculty of Medicine, Chiang Mai University, Chiang Mai 50200, Thailand*

Correspondence should be addressed to Nipon Chattipakorn; nchattip@gmail.com

Received 25 November 2014; Accepted 19 January 2015

Academic Editor: Sonia Piacente

Copyright © 2015 Yoswaris Semaming et al. This is an open access article distributed under the Creative Commons Attribution License, which permits unrestricted use, distribution, and reproduction in any medium, provided the original work is properly cited.

This paper reviews the reported pharmacological properties of protocatechuic acid (PCA, 3,4-dihydroxy benzoic acid), a type of phenolic acid found in many food plants such as olives and white grapes. PCA is a major metabolite of anthocyanin. The pharmacological actions of PCA have been shown to include strong *in vitro* and *in vivo* antioxidant activity. In *in vivo* experiments using rats and mice, PCA has been shown to exert anti-inflammatory as well as antihyperglycemic and antiapoptotic activities. Furthermore, PCA has been shown to inhibit chemical carcinogenesis and exert proapoptotic and antiproliferative effects in different cancerous tissues. Moreover, *in vitro* studies have shown PCA to have antimicrobial activities and also to exert synergistic interaction with some antibiotics against resistant pathogens. This review aims to comprehensively summarize the pharmacological properties of PCA reported to date with an emphasis on its biological properties and mechanisms of action which could be therapeutically useful in a clinical setting.

1. Introduction

Protocatechuic acid (PCA, 3,4-dihydroxybenzoic acid) is a phenolic compound found in many food plants such as *Olea europaea* (olives), *Hibiscus sabdariffa* (roselle), *Eucommia ulmoides* (du-zhong), *Citrus microcarpa* Bunge (calamondin), and *Vitis vinifera* (white wine grapes) [1–3]. PCA content varies considerably depending on the type of food.

Recently, several investigations have shown that PCA is a major metabolite of complex polyphenols, especially anthocyanins [4, 5]. Anthocyanins have been shown to affect a variety of physiological activities which are of great benefit to health, including a reduced risk of cardiovascular diseases. This particular beneficial effect is partly due to the anti-inflammatory properties [6–8], antioxidant and free radical scavenging activities [9–12], peroxidation inhibition [13], and estrogenic/antiestrogenic activity [14] of PCA. PCA is of particular nutritional interest since it is a main anthocyanin metabolite that can reach tissues in amounts which can exert biological effects on health [15]. *In vivo* studies demonstrated that male balb/cA mice which were fed a standard diet supplemented with PCA for 12 weeks showed increased PCA levels in plasma and tissues such as brain, heart, liver, and kidney [16]. Moreover, PCA itself has been shown to possess antioxidant properties as well as having other potential health benefits such as anti-inflammatory effects.

The aim of this review is to comprehensively summarize the pharmacological properties of PCA reported to date including antioxidant, anti-inflammatory, antihyperglycemia, antiapoptosis/proapoptosis, and antimicrobial activities, with an emphasis on the biological properties and mechanisms of action which could be potentially useful in a clinical setting.

Table 1: Summary of *in vitro* studies of antioxidant activities of PCA.

Model	Method	PCA concentration	Major finding	Interpretation	Reference
Biochemical assay	(i) TBAR assay (ii) H_2O_2 assay (iii) DPPH assay	0.05 and 0.10 mg/mL	(i) PCA increased % inhibition of lipid peroxidation (ii) PCA increased % scavenging of H_2O_2 (iii) PCA increased % scavenging of DPPH	PCA exerted antioxidant activity	[22]
J774 A.1 macrophages	J774 A.1 macrophages	3 and 25 mol/L	(i) PCA decreased oxidation of LDL (ii) PCA inhibited O_2 and H_2O_2 production (iii) PCA increased GSH content (iv) PCA restored GR and GPx activities (v) PCA restored the γ-GCS mRNA, GR, and GPx expression	PCA had an antioxidant activity via activation of mRNA transcription of GSH-related enzymes	[23]
J774 A.1 macrophages	Direct PCA application to cells	25 μM	(i) PCA increased GSH, GPx, and GR expression (ii) PCA increased Nrf2 expression and activation (iii) PCA increased JNK mRNA level	PCA increased macrophage endogenous antioxidants via JNK-mediated Nrf2 activation	[24]
Human neuronal cell line	H_2O_2-induced oxidative stress	25, 50, and 100 μM	(i) PCA inhibited ROS formation at cytosolic level (ii) PCA inhibited apoptotic events (iii) PCA improved mitochondrial function (iv) PCA decreased DNA fragmentation	PCA reduced apoptosis via ROS reduction, improved mitochondrial function, and inhibited DNA fragmentation	[25]
PC12 cells	H_2O_2-induced oxidative damage	50, 100, 150, and 200 μM	(i) PCA increased cell viability (ii) PCA decreased % LDH release	PCA prevented H_2O_2-induced cell death	[26]
BNLCL2 cells	H_2O_2-induced oxidative damage	1, 5, 10, 20, and 100 μg/mL	(i) PCA affected DPPH scavenging activity (ii) PCA inhibited liposome peroxidation (iii) PCA reduced intracellular ROS level	PCA had a radical scavenging activity and antioxidant property	[27]

2. Antioxidant Activity of PCA

Oxidative stress plays a key role in the pathogenesis of degenerative diseases such as cardiovascular diseases, diabetes mellitus, neurodegenerative diseases, cancer, and aging [17–21]. Mounting evidence from both *in vitro* and *in vivo* studies demonstrates that PCA exerts potent antioxidative effects. In *in vitro* studies, as summarized in Table 1, PCA was shown to have free radical scavenging and antioxidant activities by decreasing lipid peroxidation and increasing the scavenging of hydrogen peroxide (H_2O_2) and diphenylpicrylhydrazyl (DPPH) [22]. In J77A.1 macrophage, PCA decreased oxidized low-density lipoprotein levels (LDL), inhibited superoxide ($O_2^{\bullet}$) and H_2O_2 production, and also restored glutathione (GSH) related enzymes via c-Jun N-terminal kinase (JNK) mediated nuclear factor (erythroid-derived 2) like 2 (Nrf2) activation [23, 24]. PCA also reduced reactive oxygen species (ROS) induced apoptosis by improving mitochondrial function, inhibiting DNA fragmentation in H_2O_2-induced oxidative stress in human neuronal cells [25], preventing lactate dehydrogenase (LDH) release in H_2O_2-induced oxidative stress in PC12 cells [26], and inhibiting intracellular ROS level in BNLCL2 cells [27].

Consistent with *in vitro* reports, *in vivo* studies (as summarized in Table 2) also demonstrated that PCA treatment decreased oxidative stress by promoting endogenous antioxidant enzymes in aging rats and also reduced H_2O_2-induced oxidative damage in aging mice, thus indicating that PCA could prevent oxidative damage in aging animals [26, 28]. PCA also decreased advance glycation end products (AGEs) and ROS production in D-galactose-induced ROS and AGEs formation in mice [29]. In streptozotocin (STZ) induced diabetic rats, PCA was also found to decrease ROS formation in liver, heart, kidney, and brain by restoring endogenous antioxidant enzyme activities [3, 30]. All of these findings indicated that the PCA possess potential antioxidant activity, suggesting that it could be used as a complementary medication to prevent oxidative damage in various degenerative diseases.

Table 2: Summary of *in vivo* studies of antioxidant activities of PCA.

Model	Method	PCA dose/ route/ duration	Major finding	Interpretation	Reference
Sprague-Dawley rat	STZ-induced TIDM (50 mg/kg, ip)	50, 100 mg/kg, po	(i) PCA decreased plasma MDA (ii) PCA decreased cardiac MDA (iii) PCA decreased mitochondrial ROS production	PCA deceased oxidative stress in TIDM rats	[30]
Sprague-Dawley rat	H_2O_2-induced oxidative damage in young and age rats	5 mg/kg/day for 7 days (ip)	(i) PCA improved scores during the passive avoidance testing (ii) PCA decreased MDA in brain of aged rat (iii) PCA increased GSH-PX activity	PCA promoted endogenous antioxidant enzymatic activities and inhibited ROS generation	[26]
Mice	D-galactose-induced ROS and AGEs	0.5%, 1%, or 2% in diet for 8 weeks	(i) PCA decreased ROS and protein carbonyl content (ii) PCA retained GSH content (iii) PCA decreased CML, pentosidine, sorbitol, fructose, and methylglycoxal level in brain	PCA had antiglycative and antioxidant activity by retaining GSH	[29]
Mice	Young and aged	5 and 10 mg/kg (ip) for 7 days	In aged rats (i) PCA elevated splenic weight (ii) PCA increased the activities of GSH-PX (iii) PCA increased catalase (CAT) activity (iv) PCA decreased malondialdehyde (MDA) level	PCA was a potential antiageing agent by promoting endogenous antioxidant enzymatic activities	[28]
Mice	STZ-induced DM (50 mg/kg/iv)	1%, 2%, and 4% in diet for 8 weeks	(i) PCA at all concentrations decreased cardiac and renal MDA level (ii) PCA at 2% and 4% increased cardiac and renal GSH level (iii) PCA at 2% and 4% decreased cardiac and renal GSSG formation (iv) PCA at 2% and 4% increased GPX and catalase activity in cardiac and renal tissues	PCA had an antioxidative effect through the restoration of endogenous antioxidants	[3]

3. Anti-Inflammatory Activity of PCA

The inflammatory process is regulated by coordinated activation of both pro- and anti-inflammatory mediators in tissue cells (such as fibroblasts, endothelial cells, tissue macrophages, and mast cells) and also by the recruitment of leucocytes [31, 32]. Prolonged activation of proinflammatory mediators causes tissue injury and organ dysfunction. As a consequence, chronic inflammation plays a critical role in the pathophysiology of major chronic diseases including obesity, cardiovascular disease, diabetes mellitus, Alzheimer's disease, and many types of cancer [33, 34]. The mediators, including nitric oxide (NO), lipid mediators, cytokines/chemokines, adhesion molecules, and matrix metalloproteinases (MMPs), are involved in the initiation, maintenance, and resolution of the inflammatory process [35, 36].

A summary of *in vitro* studies regarding the effects of PCA on the inflammatory process is shown in Table 3. PCA was shown to suppress tumor necrosis factor alpha (TNF-α), interleukin- (IL-) 1β, inducible nitric oxide synthase (iNOS), and cyclooxygenase 2 (COX-2) expression via the regulation of the nuclear factor kappa-light-chain-enhancer of activated B cells (NF-kB) and mitogen-activated protein kinase (MAPK) activation in lipopolysaccharide- (LPS-) induced RAW 264.7 cell damage [37]. Moreover, PCA also suppressed vascular cell adhesion protein 1 (VCAM-1) and intercellular adhesion molecule 1 (ICAM-1) mRNA expression in TNF-α-induced cellular damage [38] and inhibited monocyte infiltration [39].

Consistent with *in vitro* reports, animal studies (Table 4) demonstrated that PCA strongly inhibited inflammation by inhibiting carrageenan-induced inflammation in mice by decreasing TNF-α, IL-1β, and prostaglandin E2 (PGE_2) levels, suppressed iNOS and COX-2 expression in apolipoprotein E (ApoE) deficient mice [37], prevented LPS-induced sepsis in mice via decreased NO levels and suppressed IL-10 [40], reduced VCAM-1 and ICAM-1 [38], and inhibited monocyte/macrophage infiltration in mice [39]. Moreover, PCA also prevented coagulation and inflammation in STZ-induced diabetic rats by inhibiting the plasma levels of the plasminogen activator inhibitor 1 (PAI-1), antithrombin III (AT-III), protein C, C-reactive protein (CRP), and von Willebrand factor (vWF) and reduced IL-6, TNF-α, and monocyte chemoattractant protein-1 (MCP-1) levels in the heart and kidneys [3]. These findings suggest that the anti-inflammatory effects of PCA might be beneficial in various chronic degenerative diseases in which the inflammatory process plays an important part in the pathogenesis.

4. Antihyperglycemic Activity of PCA

Maintenance of glucose homeostasis by strict hormonal control is of the utmost importance to human physiology

Table 3: Summary of *in vitro* studies of anti-inflammatory activities of PCA.

Model	Method	PCA concentration	Major finding	Interpretation	Reference
RAW 264.7 cells	Lipopolysaccharide-(LPS-) induced cellular damage	1, 2, 5, and 25 μM	(i) PCA decreased TNF-α and IL-1β (ii) PCA decreased NO and PGE_2 (iii) PCA inhibited iNOS and COX-2 expression (iv) PCA inhibited IkB-α degradation (v) PCA inhibited NF-kB phosphorylation (vi) PCA inhibited p38, ERK, and JNK	PCA had anti-inflammatory effects by regulating NF-kB and MAPK activation	[37]
Mouse aortic endothelial cell (MAEC)	TNF-α-induced cellular damage	0.05, 0.5, 5.0, 10, 20, and 40 μmol/L	(i) PCA inhibited adhesion of HL-60 cells to MAECs (ii) PCA suppressed VCAM-1 and ICAM-1 mRNA expression (iii) PCA reduced NF-kB activation	PCA had an anti-inflammatory effect by inhibiting monocyte adhesion molecules	[38]
Cell culture	Isolated peripheral blood monocytes (PBMs) from ApoE-deficient mice	0.125, 0.25, and 0.5 μmol/L	(i) PCA decreased CCR2 protein and mRNA expression (ii) PCA inhibited mouse PBMs migration	PCA exerted antiatherogenic properties by inhibiting monocyte infiltration	[39]

Table 4: Summary of *in vivo* studies of anti-inflammatory activities of PCA.

Model	Method	PCA dose/ route/ duration	Major finding	Interpretation	Reference
Mice	Carrageenan-induced inflammation in BALB/c mice	5 and 25 mg/kg, po (24 h)	(i) PCA reduced exudate (ii) PCA decreased protein content (iii) PCA reduced leukocyte number (iv) PCA inhibited TNF-α, IL-1β, and PGE_2 level (v) PCA inhibited COX-2 and NF-kB expression	PCA exerted anti-inflammatory effects by inhibiting NF-kB activation.	[37]
Mice	ApoE-deficient mice	0.033% (w/w) of diet for 20 weeks	(i) PCA reduced sinus plague area (ii) PCA decreased cholesterol accumulation in aortas (iii) PCA reduced VCAM-1 and ICAM-1 expression in aortas (iv) PCA reduced NF-kB binding activity (v) PCA reduced plasma-soluble VCAM-1 and ICAM-1 levels	PCA exerted antiatherosclerosis effects by inhibiting adhesion molecules and reducing NF-kB activation	[38]
Mice	Thioglycollate-induced peritonitis in ApoE-deficient mice	25 mg/kg (po) for 11 days	(i) PCA decreased CCR2 protein and mRNA expression in PBMs of ApoE-deficient mice (ii) PCA reduced macrophage infiltration into the abdominal cavity	PCA exerted antiatherogenic properties by inhibiting monocyte/macrophage infiltration	[39]
Mice	LPS-induced sepsis (20 mg/kg, ip)	50 mg/kg (ip) single dose	(i) PCA reduced lethality (ii) PCA suppressed TNF-α and IL-10 (iii) PCA decreased plasma ALT levels (iv) PCA decreased plasma nitrite/nitrate levels (v) PCA decreased hepatic MDA levels	PCA exerted sepsis prevention properties by inhibiting inflammatory cytokines and antioxidant activity	[40]
Mice	STZ-induced DM (50 mg/kg/iv)	1%, 2%, and 4% in diet for 8 weeks	(i) PCA lowered plasma PAI-1 levels (ii) PCA increased plasma AP-III levels (iii) PCA increased plasma protein C levels (iv) PCA lowered plasma CRP levels (v) PCA decreased plasma von Willebrand factor (vi) PCA reduced IL-6, TNF-α, and MCP-1 levels in heart and kidney	PCA exerted anticoagulatory and anti-inflammatory effects by lowering inflammatory cytokines	[3]

Table 5: Summary of *in vitro* study of antihyperglycemic activities of PCA.

Model	Model/method	PCA concentration	Major finding	Interpretation	Reference
Human omental adipocytes and murine adipocyte 3T3-L1 cells	oxLDL-induced insulin resistance	100 μM	(i) PCA increased glucose uptake (ii) PCA increased GLUT4 translocation (iii) PCA increased PPARγ activity (iv) PCA increased adiponectin	PCA exerted an insulin-like activity in adipocytes by increasing PPARγ activation	[45]

Table 6: Summary of *in vivo* studies of antihyperglycemic activities of PCA.

Model	Model/method	PCA dose/ route/ duration	Major finding	Interpretation	Reference
Sprague-Dawley rat	STZ-induced T1DM (50 mg/kg, ip)	50, 100 mg/kg (po)	(i) PCA decreased FBG (ii) PCA decreased HbA_{1c}	PCA exerted hypoglycemic effects in T1DM	[30]
Mice	STZ-induced DM (50 mg/kg, iv)	1%, 2%, and 4% in diet for 8 weeks	(i) PCA lowered plasma glucose levels (ii) PCA increased insulin levels (iii) PCA decreased TG and TC content in plasma, heart, and liver	PCA attenuated diabetic conditions by lowering plasma glucose, increasing insulin, and lowering triglyceride levels	[3]
Sprague-Dawley rat	STZ-induced DM (40 mg/kg, ip)	50, 100, 200 mg/kg/day (po) for 45 days	(i) PCA decreased plasma glucose levels (ii) PCA decreased HbA_{1c} levels (iii) PCA increased plasma insulin levels (iv) PCA increased hexokinase activity and increased glycogen content in liver (v) PCA decreased activity of glucose 6-phosphatase and fructose 1,6-bisphosphatase in liver (vi) PCA reduced adipose tissue of DM pancreas and normalized pancreatic islets	PCA exerted antihyperglycemic effects by restoring carbohydrate metabolic enzyme activity and increasing plasma insulin levels	[46]
Mice	STZ-induced DM (50 mg/kg, iv)	2% and 4% in diet for 12 weeks	(i) Content of PCA increased in plasma, brain, heart, liver, and kidney (ii) PCA decreased water intake and food intake (iii) PCA increased body weight (iv) PCA decreased urine volume (v) PCA reduced plasma glucose levels (vi) PCA increased plasma insulin levels (vii) PCA decreased plasma BUN level (viii) PCA increased creatinine clearance rate (ix) PCA decreased HbA_{IC} level (x) PCA decreased urine glycated albumin (xi) PCA reduced renal production of CML, pentosidine, sorbitol, and fructose (xii) PCA decreased brain content of CML, pentosidine, fructose, and sorbitol (xiii) PCA decreased urinary albumin (xiv) PCA reduced level of fibronectin, type-IV collagen, and TGF-β in renal tissue (xv) PCA reduced renal activity and expression of AR and SDH (xvi) PCA increased renal activity and expression of GLI (xvii) PCA decreased renal activity and mRNA expression of PKC-α and PKC-β (xviii) PCA decreased RAGE mRNA expression	PCA had an antihyperglycemic, antiglycative and renoprotective effects via increasing plasma insulin, reducing plasma glucose, reducing renal level of glycation end products, fibronectin, TGF-β, and repressing renal activity and expression of AR, SDH, GLI, PKC-α, PPAR-γ, restoring PPAR-γ, and suppressing RAGE	[16]

Table 7: Summary of *in vitro* studies of antiapoptotic activities of PCA in noncancer cells.

Model	Model/method	PCA concentration	Major finding	Interpretation	Reference
HUVECs and Jurkat cells	TNF-α-induced cell death	50, 100 μM and 1 nM	(i) PCA inhibited TNF-α-induced HUVECs and Jurkat cells death (ii) PCA increased NF-kB activation (iii) PCA increased degradation of IkB	PCA exerted cell-protective effects via increased IkB degradation and subsequent NF-kB activation	[49]
PC12 cells	MPP^+-induced mitochondrial dysfunction and apoptotic cell death	0.3, 0.6, and 1.2 mM	(i) PCA reduced the number of cell death (ii) PCA at 0.6 and 1.2 mM decreased percentage of depolarized cell, reduced ROS formation, and increased GSH content (iii) PCA at 0.6 and 1.2 mM decreased caspase-3 activity and increased Bcl-2 protein	PCA exerted antiapoptotic activities via attenuated changes of mitochondrial membrane permeability and decreased oxidative stress damage	[50]
Isolated NSCs of embryonic rat	Direct PCA application to cells	0.006, 0.03, 0.06, and 0.12 mM	(i) PCA at 0.03, 0.06, and 0.12 mM increased cellular viability (ii) PCA reduced nuclear fragmentation (iii) PCA reduced the levels of apoptosis (iv) PCA decreased endogenous ROS level (v) PCA decreased caspase-3 activity	PCA inhibited cell apoptosis via suppression of the caspase cascade	[51]
PC12 cells	H_2O_2-induced apoptosis	0.006, 0.03, 0.06, and 0.12 mM	(i) PCA (over 0.3 mM) increased cellular viability (ii) PCA reduced LDH leakage (iii) PCA reduced apoptotic sub-G1 population	PCA promoted cell viability and inhibited apoptotic cell death	[52]
PC12 cells	MPP^+-induced apoptotic cell death	0.33, 0.65, and 1.30 mM	(i) PCA reduced cell death in a dose-dependent manner (ii) PCA treatment exhibited normal cellular morphology and normal mitochondria (iii) PCA increased tyrosine hydroxylase expression (iv) PCA reduced oligomeric α-synuclein (v) PCA increased monomeric α-synuclein	PCA had neuroprotective effects via reducing cell death and inhibiting oligomerization of α-synuclein	[53]
Rat primary hepatocytes	t-BHP (1.5 mM) induced oxidative damage	0.02, 0.05, and 0.10 mg/mL	(i) PCA 0.05 and 0.10 mg/mL decreased LDH, ALT, and MDA (ii) PCA prevented mitochondrial depolarization (iii) PCA increased scavenging activity on DPPH	PCA had a cell-protective effect via its antioxidant and scavenging activity	[54]

[41, 42]. Failure of the control of glucose levels, with defects in both insulin action and insulin secretion, can result in a metabolic syndrome which is a multisymptom disorder of energy homeostasis [43]. It has been demonstrated that peroxisome proliferator-activated receptor gamma (PPARγ) is one of several targets of insulin activity, which regulates the expression and activity of key players in the maintenance of glucose transport machinery efficiency, such as glucose transporter (GLUT) 4 and adiponectin [44, 45]. In *in vitro* studies, as summarized in Table 5, PCA has been shown to exert an insulin-like activity in oxidized LDL-induced insulin resistance in adipocytes via increased PPARγ activation [45]. Similarly, *in vivo* studies (Table 6) also demonstrated that PCA decreased blood glucose levels in STZ-induced diabetes via restored carbohydrate metabolic enzyme activity, increased plasma insulin level, and normalized the activity of pancreatic islets [3, 30, 46]. These findings suggest that PCA provides antihyperglycemic effects in addition to its reported antioxidant and anti-inflammatory effects.

5. Antiapoptosis versus Proapoptotic Activity of PCA

Polyphenols have been shown to improve cell survival and protect against cytotoxicity by inhibiting apoptosis [18]. However, they can also induce apoptosis and prevent tumor growth [47, 48]. These opposite effects are mainly due to its effects on the controlling of the cell redox state. Evidence from *in vitro* studies (Table 7) revealed that PCA has cell-protective effects via increased IkB degradation and subsequent NF-kB activation in TNF-α-induced cell death [49], attenuated changes of the mitochondrial membrane

Table 8: Summary of *in vitro* studies of proapoptotic activity of PCA in cancer cells.

Model	Model/method	PCA concentration	Major finding	Interpretation	Reference
HL-60 leukemia cells	Direct PCA application to cells	0.2, 0.5, 1, and 2 mM	(i) PCA increased DNA fragmentation (ii) PCA declined hyperphosphorylated RB level (iii) PCA reduced Bcl-2 protein expression (iv) PCA increased Bax protein expression	PCA had an antiproliferative effect via induced RB phosphorylation and degradation and Bcl-2 protein suppression in cancer cells	[55]
Human gastric adenocarcinoma (AGS) cells	Direct PCA application to cells	0.5, 1.0, 2.0, 4.0, 6.0, 8.0, and 9.0 mM	(i) PCA increased apoptotic bodies formation (ii) PCA increased p-JNK expression (iii) PCA increased p-p53 expression (iv) PCA increased phosphorylation of ATF-2 at $Thr^{69/71}$ and c-Jun at Ser^{73} (v) PCA increased Fas expression (vi) PCA increased FasL expression (vii) PCA decreased Bcl-2 expression (viii) PCA increased Bax expression	PCA induced apoptosis via JNK/p38 MAPK pathway, activated Fas/FasL pathway, increased translocation of Bax, and reduced Bcl-2 in cancer cells	[56]
HepG2 hepatocellular carcinoma cells	Direct PCA application to cells	0, 3, 10, 30, 100, and 300 μmol/L	(i) PCA decreased viability of HepG2 hepatocellular carcinoma (ii) PCA increased JNK and p53 expression	PCA induced cell death via activating JNK and p38 MAPK pathways in cancer cells	[57]
Human breast, lung, liver, cervix, and prostate cancer cells	Direct PCA application to cells	1, 2, 4, and 8 μmol/L	(i) PCA decreased viability (ii) PCA enhanced DNA fragmentation (iii) PCA decreased MMP (iv) PCA lowered Na^+-K^+-ATPase activity (v) PCA increased caspase-3 activity (vi) PCA increased caspase-8 activity (vii) PCA decreased ICAM-1 level (viii) PCA at 2, 4, and 8 μmol/L decreased VEGF level (ix) PCA suppressed IL-6 and IL-8 levels	PCA had anticancer properties via increased apoptosis or suppressed invasion and metastasis cancer cells	[58]

permeability, decreased oxidative stress damage and increased Bcl-2 levels in 1-methyl-4-phenylpyridinium- (MPP^+-) induced apoptotic cell death [50], decreased caspase-3 activity in isolated neuronal stem cells (NSCs) [51], and reduced LDH leakage in H_2O_2-induced apoptosis [52]. In MPP^+-induced cell death, PCA treatment resulted in a return to normal cellular morphology and normal mitochondria [53]. Moreover, PCA has been shown to have cell-protective effects via antioxidant and scavenging activities [54].

Unlike the cells described in Table 7, evidence from cancer cell studies (Table 8) demonstrated that PCA can induce apoptosis and prevent the growth of tumor cells via causing reduced Bcl-2 protein, increased Bax protein expression in human leukemia (HL-60) cells [55], via activated JNK/p38 MAPK pathways and Fas/FasL pathways, increased translocation of Bax, and reduced Bcl-2 levels in human gastric adenocarcinoma cells [56] and via induced JNK and p38 MAPK pathways in HepG2 hepatocellular carcinoma cells [57]. Moreover, PCA also demonstrated anticancer properties by causing apoptosis or suppressing invasion and metastasis in human breast, lung, liver, cervix and prostate cancer cells [58]. Consistently, an *in vivo* study (Table 9) also demonstrated that PCA inhibited *N*-nitrosomethylbenzylamine (NMBA) induced esophageal tumorigenesis by its inhibitory effects on genes associated with inflammation in rats [59].

6. Antimicrobial Activity of PCA

In vitro studies (Table 10) demonstrated that PCA has an antimicrobial effect against gram positive and negative bacteria and fungi [60, 61]. PCA also prevented contamination of meat by *Campylobacter* and aerobes, by decreasing lipid oxidation [62]. PCA exerted its antibacterial effects due to its ability to inhibit bacterial growth and increase the synergistic effects of antibiotics hence reducing the possibility of resistance to drugs [63]. These antimicrobial activities of PCA have been proposed as promising applications in both health protection and food preservation in order to avoid food-borne illnesses [62, 64].

Table 9: Summary of *in vivo* studies of proapoptotic activity of PCA.

Model	Method	PCA dose/ route/ duration	Major finding	Interpretation	Reference
Rat	NMBA-induced esophageal cancer in rats	PCA 0.05% in diet for 15, 25, and 35 weeks	(i) PCA reduced area of hyperplasia began at week 25 (ii) PCA reduced COX-2, iNOS, soluble epoxide hydrolase (she), and pentraxin-3 (PTX3) mRNA expression levels	PCA prevented esophageal tumorigenesis, by inhibitory effects on genes associated with inflammation	[59]

Table 10: Summary of *in vitro* studies of antimicrobial activity of PCA.

Model	Method	PCA concentration	Major finding	Interpretation	Reference
Campylobacter spp	Antimicrobial activity testing	(i) 10 mg/mL (ii) 5, 10 mg/100 g beef	(i) PCA inhibited growth and susceptible and antibiotic-resistant *Campylobacter species* (ii) PCA inhibited growth of aerobes in beef samples (iii) PCA decreased lipid oxidation levels in ground beef	(i) PCA could preserve foods to prevent contamination by *Campylobacter* and aerobes, via decreased lipid oxidation	[62]
Pseudomonas aeruginosa	Antimicrobial susceptibility testing	2,000 μg/mL	(i) PCA inhibited growth of *Pseudomonas aeruginosa* (ii) PCA plus sulfamethoxazole increased synergistic mode of inhibition of *P. aeruginosa*	(i) PCA had an antibacterial effect by inhibiting bacterial growth and increasing the synergistic effects on antibiotics to reduced drug resistance	[63]
Bacteria and fungi	Antimicrobial activity testing	1.22–625 μg/mL	(i) PCA prevented 80% of the growth of organisms	(i) PCA had an antimicrobial effect against gram positive and negative bacteria and against fungi	[60]
Helicobacter pylori	Antimicrobial susceptibility testing	8–64 mg/L	(i) PCA inhibited growth of *H. pylori* (ii) PCA reduced drug-resistant *H. pylori* (iii) PCA at (32–40 mg/L) reduced urease activity of *H. pylori* to 40%	(i) PCA had growth prevention effects on *H. pylori*	[61]

7. Conclusion

Growing evidence suggests the significant biological potential of PCA through the modulation of cellular signals involved in the control of oxidative stress and inflammation. Moreover, its antiapoptotic effects in normal cells and proapoptotic effects in cancer cells suggest definite benefits as a potential chemotherapeutic agent. However, much evidence of such properties has been collected from cellular and animal studies, while clinical studies are still lacking. Future clinical studies are needed to warrant the clinical usefulness of the PCA.

Conflict of Interests

The authors declare that there is no conflict of interests regarding the publication of this paper.

Acknowledgments

This work was supported by the Thailand Research Fund RTA5580006 (NC) and BRG5780016 (SC), Chiang Mai University Center of Excellence Award (NC), Udon Thani Rajabhat University Fund (YS), and a NSTDA Research Chair Grant from the National Science and Technology Development Agency (NC).

References

[1] W.-L. Lin, Y.-J. Hsieh, F.-P. Chou, C.-J. Wang, M.-T. Cheng, and T.-H. Tseng, "Hibiscus protocatechuic acid inhibits lipopolysaccharide-induced rat hepatic damage," *Archives of Toxicology*, vol. 77, no. 1, pp. 42–47, 2003.

[2] L. A. Pacheco-Palencia, S. Mertens-Talcott, and S. T. Talcott, "Chemical composition, antioxidant properties, and thermal

stability of a phytochemical enriched oil from Açai (*Euterpe oleracea* Mart.)," *Journal of Agricultural and Food Chemistry*, vol. 56, no. 12, pp. 4631–4636, 2008.

[3] P. Li, X. Q. Wang, H. Z. Wang, and Y. N. Wu, "High performance liquid chromatographic determination of phenolic acids in fruits and vegetables," *Biomedical and Environmental Sciences*, vol. 6, no. 4, pp. 389–398, 1993.

[4] P. Vitaglione, G. Donnarumma, A. Napolitano et al., "Protocatechuic acid is the major human metabolite of cyanidin-glucosides," *Journal of Nutrition*, vol. 137, no. 9, pp. 2043–2048, 2007.

[5] R. C. Pimpao, T. Dew, M. E. Figueira et al., "Urinary metabolite profiling identifies novel colonic metabolites and conjugates of phenolics in healthy volunteers," *Molecular Nutrition & Food Research*, vol. 58, no. 7, pp. 1414–1425, 2014.

[6] J. González-Gallego, M. V. García-Mediavilla, S. Sánchez-Campos, and M. J. Tuñó, "Fruit polyphenols, immunity and inflammation," *British Journal of Nutrition*, vol. 104, supplement 3, pp. S15–S27, 2010.

[7] R. Landberg, Q. Sun, E. B. Rimm et al., "Selected dietary flavonoids are associated with markers of inflammation and endothelial dysfunction in U.S. women," *The Journal of Nutrition*, vol. 141, no. 4, pp. 618–625, 2011.

[8] A. E. Rotelli, T. Guardia, A. O. Juárez, N. E. de la Rocha, and L. E. Pelzer, "Comparative study of flavonoids in experimental models of inflammation," *Pharmacological Research*, vol. 48, no. 6, pp. 601–606, 2003.

[9] M. Garcia-Alonso, A.-M. Minihane, G. Rimbach, J. C. Rivas-Gonzalo, and S. de Pascual-Teresa, "Red wine anthocyanins are rapidly absorbed in humans and affect monocyte chemoattractant protein 1 levels and antioxidant capacity of plasma," *The Journal of Nutritional Biochemistry*, vol. 20, no. 7, pp. 521–529, 2009.

[10] H. Wang, M. G. Nair, G. M. Strasburg et al., "Antioxidant and antiinflammatory activities of anthocyanins and their aglycon, cyanidin, from tart cherries," *Journal of Natural Products*, vol. 62, no. 2, pp. 294–296, 1999.

[11] M. P. Kähkönen and M. Heinonen, "Antioxidant activity of anthocyanins and their aglycons," *Journal of Agricultural and Food Chemistry*, vol. 51, no. 3, pp. 628–633, 2003.

[12] H. Matsumoto, Y. Nakamura, M. Hirayama, Y. Yoshiki, and K. Okubo, "Antioxidant activity of black currant anthocyanin aglycons and their glycosides measured by chemiluminescence in a neutral pH region and in human plasma," *Journal of Agricultural and Food Chemistry*, vol. 50, no. 18, pp. 5034–5037, 2002.

[13] T. Tsuda, K. Shiga, K. Ohshima, S. Kawakishi, and T. Osawa, "Inhibition of lipid peroxidation and the active oxygen radical scavenging effect of anthocyanin pigments isolated from *Phaseolus vulgaris* L," *Biochemical Pharmacology*, vol. 52, no. 7, pp. 1033–1039, 1996.

[14] A. Cassidy, S. de Pascual Teresa, and G. Rimbach, "Molecular mechanisms by which dietary isoflavones potentially prevent atherosclerosis," *Expert Reviews in Molecular Medicine*, vol. 5, no. 24, pp. 1–15, 2003.

[15] C. D. Kay, P. A. Kroon, and A. Cassidy, "The bioactivity of dietary anthocyanins is likely to be mediated by their degradation products," *Molecular Nutrition and Food Research*, vol. 53, supplement 1, pp. S92–S101, 2009.

[16] C.-Y. Lin, S.-J. Tsai, C.-S. Huang, and M.-C. Yin, "Antiglycative effects of protocatechuic acid in the kidneys of diabetic mice," *Journal of Agricultural and Food Chemistry*, vol. 59, no. 9, pp. 5117–5124, 2011.

[17] M. B. Moura, L. S. dos Santos, and B. van Houten, "Mitochondrial dysfunction in neurodegenerative diseases and cancer," *Environmental and Molecular Mutagenesis*, vol. 51, no. 5, pp. 391–405, 2010.

[18] B. L. Queen and T. O. Tollefsbol, "Polyphenols and aging," *Current Aging Science*, vol. 3, no. 1, pp. 34–42, 2010.

[19] D. A. Patten, M. Germain, M. A. Kelly, and R. S. Slack, "Reactive oxygen species: stuck in the middle of neurodegeneration," *Journal of Alzheimer's Disease*, vol. 20, no. 2, pp. S357–S367, 2010.

[20] H. Kaneto, N. Katakami, M. Matsuhisa, and T.-A. Matsuoka, "Role of reactive oxygen species in the progression of type 2 diabetes and atherosclerosis," *Mediators of Inflammation*, vol. 2010, Article ID 453892, 11 pages, 2010.

[21] D. A. Patten, M. Germain, M. A. Kelly, and R. S. Slack, "Reactive oxygen species: stuck in the middle of neurodegeneration," *Journal of Alzheimer's Disease*, vol. 20, supplement 2, pp. S357–S367, 2010.

[22] Z. Sroka and W. Cisowski, "Hydrogen peroxide scavenging, antioxidant and anti-radical activity of some phenolic acids," *Food and Chemical Toxicology*, vol. 41, no. 6, pp. 753–758, 2003.

[23] R. Masella, R. Varì, M. D'Archivio et al., "Extra virgin olive oil biophenols inhibit cell-mediated oxidation of LDL by increasing the mRNA transcription of glutathione-related enzymes," *Journal of Nutrition*, vol. 134, no. 4, pp. 785–791, 2004.

[24] R. Varì, M. D'Archivio, C. Filesi et al., "Protocatechuic acid induces antioxidant/detoxifying enzyme expression through JNK-mediated Nrf2 activation in murine macrophages," *Journal of Nutritional Biochemistry*, vol. 22, no. 5, pp. 409–417, 2011.

[25] A. Tarozzi, F. Morroni, S. Hrelia et al., "Neuroprotective effects of anthocyanins and their in vivo metabolites in SH-SY5Y cells," *Neuroscience Letters*, vol. 424, no. 1, pp. 36–40, 2007.

[26] G.-F. Shi, L.-J. An, B. Jiang, S. Guan, and Y.-M. Bao, "*Alpinia* protocatechuic acid protects against oxidative damage in vitro and reduces oxidative stress in vivo," *Neuroscience Letters*, vol. 403, no. 3, pp. 206–210, 2006.

[27] T.-H. Chou, H.-Y. Ding, R.-J. Lin, J.-Y. Liang, and C.-H. Liang, "Inhibition of melanogenesis and oxidation by protocatechuic acid from *Origanum vulgare* (Oregano)," *Journal of Natural Products*, vol. 73, no. 11, pp. 1767–1774, 2010.

[28] X. Zhang, G.-F. Shi, X.-Z. Liu, L.-J. An, and S. Guan, "Antiageing effects of protocatechuic acid from *Alpinia* on spleen and liver antioxidative system of senescent mice," *Cell Biochemistry and Function*, vol. 29, no. 4, pp. 342–347, 2011.

[29] S.-J. Tsai and M.-C. Yin, "Anti-glycative and anti-inflammatory effects of protocatechuic acid in brain of mice treated by d-galactose," *Food and Chemical Toxicology*, vol. 50, no. 9, pp. 3198–3205, 2012.

[30] Y. Semaming, S. Kumfu, P. Pannangpetch, S. C. Chattipakorn, and N. Chattipakorn, "Protocatechuic acid exerts a cardioprotective effect in type 1 diabetic rats," *Journal of Endocrinology*, vol. 223, no. 1, pp. 13–23, 2014.

[31] C. A. Feghali and T. M. Wright, "Cytokines in acute and chronic inflammation," *Frontiers in Bioscience*, vol. 2, pp. d12–d26, 1997.

[32] T. Lawrence and D. W. Gilroy, "Chronic inflammation: a failure of resolution?" *International Journal of Experimental Pathology*, vol. 88, no. 2, pp. 85–94, 2007.

[33] M. I. Fonseca, S.-H. Chu, A. M. Berci et al., "Contribution of complement activation pathways to neuropathology differs among mouse models of Alzheimer's disease," *Journal of Neuroinflammation*, vol. 8, no. 1, article 4, 2011.

[34] R. Medzhitov, "Inflammation 2010: new adventures of an old flame," *Cell*, vol. 140, no. 6, pp. 771–776, 2010.

[35] A. M. Manicone and J. K. McGuire, "Matrix metalloproteinases as modulators of inflammation," *Seminars in Cell and Developmental Biology*, vol. 19, no. 1, pp. 34–41, 2008.

[36] T. Lawrence and C. Fong, "The resolution of inflammation: anti-inflammatory roles for NF-κB," *The International Journal of Biochemistry & Cell Biology*, vol. 42, no. 4, pp. 519–523, 2010.

[37] S.-W. Min, S.-N. Ryu, and D.-H. Kim, "Anti-inflammatory effects of black rice, cyanidin-3-O-β-d-glycoside, and its metabolites, cyanidin and protocatechuic acid," *International Immunopharmacology*, vol. 10, no. 8, pp. 959–966, 2010.

[38] D. Wang, X. Wei, X. Yan, T. Jin, and W. Ling, "Protocatechuic acid, a metabolite of anthocyanins, inhibits monocyte adhesion and reduces atherosclerosis in apolipoprotein E-deficient mice," *Journal of Agricultural and Food Chemistry*, vol. 58, no. 24, pp. 12722–12728, 2010.

[39] D. Wang, T. Zou, Y. Yang, X. Yan, and W. Ling, "Cyanidin-3-O-β-glucoside with the aid of its metabolite protocatechuic acid, reduces monocyte infiltration in apolipoprotein E-deficient mice," *Biochemical Pharmacology*, vol. 82, no. 7, pp. 713–719, 2011.

[40] J.-J. Yan, J.-S. Jung, Y.-J. Hong et al., "Protective effect of protocatechuic acid isopropyl ester against murine models of sepsis: inhibition of TNF-alpha and nitric oxide production and augmentation of IL-10," *Biological and Pharmaceutical Bulletin*, vol. 27, no. 12, pp. 2024–2027, 2004.

[41] E. D. Rosen and B. M. Spiegelman, "Adipocytes as regulators of energy balance and glucose homeostasis," *Nature*, vol. 444, no. 7121, pp. 847–853, 2006.

[42] E. Selvin, M. W. Steffes, H. Zhu et al., "Glycated hemoglobin, diabetes, and cardiovascular risk in nondiabetic adults," *The New England Journal of Medicine*, vol. 362, no. 9, pp. 800–811, 2010.

[43] D. M. Nathan, P. A. Cleary, J.-Y. C. Backlund et al., "Intensive diabetes treatment and cardiovascular disease in patients with type 1 diabetes," *The New England Journal of Medicine*, vol. 353, no. 25, pp. 2643–2653, 2005.

[44] J. R. Jones, C. Barrick, K.-A. Kim et al., "Deletion of PPARγ in adipose tissues of mice protects against high fat diet-induced obesity and insulin resistance," *Proceedings of the National Academy of Sciences of the United States of America*, vol. 102, no. 17, pp. 6207–6212, 2005.

[45] B. Scazzocchio, R. Varì, C. Filesi et al., "Cyanidin-3-O-β-glucoside and protocatechuic acid exert insulin-like effects by upregulating PPARγ activity in human omental adipocytes," *Diabetes*, vol. 60, no. 9, pp. 2234–2244, 2011.

[46] R. Harini and K. V. Pugalendi, "Antihyperglycemic effect of protocatechuic acid on streptozotocin-diabetic rats," *Journal of Basic and Clinical Physiology and Pharmacology*, vol. 21, no. 1, pp. 79–91, 2010.

[47] M. D'Archivio, C. Santangelo, B. Scazzocchio et al., "Modulatory effects of polyphenols on apoptosis induction: relevance for cancer prevention," *International Journal of Molecular Sciences*, vol. 9, no. 3, pp. 213–228, 2008.

[48] C. Giovannini, B. Scazzocchio, R. Varì, C. Santangelo, M. D'Archivio, and R. Masella, "Apoptosis in cancer and atherosclerosis: polyphenol activities," *Annali dell'Istituto Superiore di Sanita*, vol. 43, no. 4, pp. 406–416, 2007.

[49] J. Zhou-Stache, R. Buettner, G. Artmann, C. Mittermayer, and A. K. Bosserhoff, "Inhibition of TNF-α induced cell death in human umbilical vein endothelial cells and Jurkat cells by protocatechuic acid," *Medical and Biological Engineering and Computing*, vol. 40, no. 6, pp. 698–703, 2002.

[50] S. Guan, B. Jiang, Y. M. Bao, and L. J. An, "Protocatechuic acid suppresses MPP^+-induced mitochondrial dysfunction and apoptotic cell death in PC12 cells," *Food and Chemical Toxicology*, vol. 44, no. 10, pp. 1659–1666, 2006.

[51] S. Guan, D. Ge, T.-Q. Liu, X.-H. Ma, and Z.-F. Cui, "Protocatechuic acid promotes cell proliferation and reduces basal apoptosis in cultured neural stem cells," *Toxicology in Vitro*, vol. 23, no. 2, pp. 201–208, 2009.

[52] S. Guan, Y.-M. Bao, B. Jiang, and L.-J. An, "Protective effect of protocatechuic acid from *Alpinia oxyphylla* on hydrogen peroxide-induced oxidative PC12 cell death," *European Journal of Pharmacology*, vol. 538, no. 1–3, pp. 73–79, 2006.

[53] H.-N. Zhang, C.-N. An, M. Xu, D.-A. Guo, M. Li, and X.-P. Pu, "Protocatechuic acid inhibits rat pheochromocytoma cell damage induced by a dopaminergic neurotoxin," *Biological and Pharmaceutical Bulletin*, vol. 32, no. 11, pp. 1866–1869, 2009.

[54] T.-H. Tseng, C.-J. Wang, F.-S. Kao, and H.-Y. Chu, "Hibiscus protocatechuic acid protects against oxidative damage induced by tert-butylhydroperoxide in rat primary hepatocytes," *Chemico-Biological Interactions*, vol. 101, no. 2, pp. 137–148, 1996.

[55] T.-H. Tseng, T.-W. Kao, C.-Y. Chu, F.-P. Chou, W.-L. Lin, and C.-J. Wang, "Induction of apoptosis by *Hibiscus protocatechuic* acid in human leukemia cells via reduction of retinoblastoma (RB) phosphorylation and Bcl-2 expression," *Biochemical Pharmacology*, vol. 60, no. 3, pp. 307–315, 2000.

[56] H.-H. Lin, J.-H. Chen, C.-C. Huang, and C.-J. Wang, "Apoptotic effect of 3,4-dihydroxybenzoic acid on human gastric carcinoma cells involving JNK/p38 MAPK signaling activation," *International Journal of Cancer*, vol. 120, no. 11, pp. 2306–2316, 2007.

[57] E. C. H. Yip, A. S. L. Chan, H. Pang, Y. K. Tam, and Y. H. Wong, "Protocatechuic acid induces cell death in HepG2 hepatocellular carcinoma cells through a c-Jun N-terminal kinase-dependent mechanism," *Cell Biology and Toxicology*, vol. 22, no. 4, pp. 293–302, 2006.

[58] M.-C. Yin, C.-C. Lin, H.-C. Wu, S.-M. Tsao, and C.-K. Hsu, "Apoptotic effects of protocatechuic acid in human breast, lung, liver, cervix, and prostate cancer cells: potential mechanisms of action," *Journal of Agricultural and Food Chemistry*, vol. 57, no. 14, pp. 6468–6473, 2009.

[59] D. S. Peiffer, N. P. Zimmerman, L.-S. Wang et al., "Chemoprevention of esophageal cancer with black raspberries, their component anthocyanins, and a major anthocyanin metabolite, protocatechuic acid," *Cancer Prevention Research*, vol. 7, no. 6, pp. 574–584, 2014.

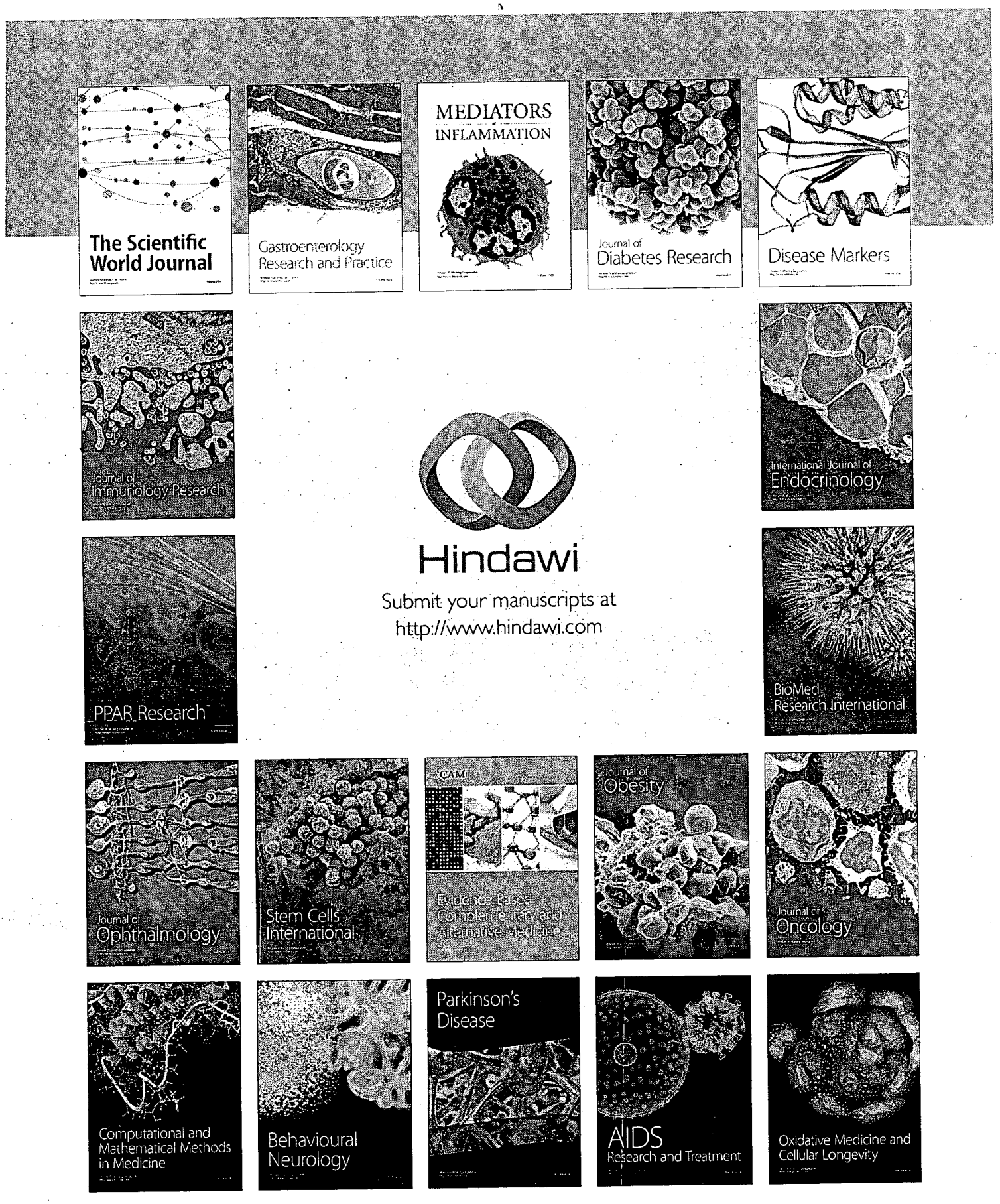
[60] V. Kuete, F. Nana, B. Ngameni, A. T. Mbaveng, F. Keumedjio, and B. T. Ngadjui, "Antimicrobial activity of the crude extract, fractions and compounds from stem bark of *Ficus ovata* (Moraceae)," *Journal of Ethnopharmacology*, vol. 124, no. 3, pp. 556–561, 2009.

[61] W. H. Liu, C. C. Hsu, and M. C. Yin, "In vitro anti-Helicobacter pylori activity of diallyl sulphides and protocatechuic acid," *Phytotherapy Research*, vol. 22, no. 1, pp. 53–57, 2008.

[62] M.-C. Yin and C.-Y. Chao, "Anti-Campylobacter, anti-aerobic, and anti-oxidative effects of roselle calyx extract and protocatechuic acid in ground beef," *International Journal of Food Microbiology*, vol. 127, no. 1-2, pp. 73–77, 2008.

[63] P. Jayaraman, M. K. Sakharkar, C. S. Lim, T. H. Tang, and K. R. Sakharkar, "Activity and interactions of antibiotic and phytochemical combinations against pseudomonas aeruginosa in vitro," *International Journal of Biological Sciences*, vol. 6, no. 6, pp. 556–568, 2010.

[64] C.-Y. Chao and M.-C. Yin, "Antibacterial effects of roselle calyx extracts and protocatechuic acid in ground beef and apple juice," *Foodborne Pathogens and Disease*, vol. 6, no. 2, pp. 201–206, 2009.


The Scientific World Journal
Gastroenterology Research and Practice
MEDIATORS INFLAMMATION
Journal of Diabetes Research
Disease Markers
Journal of Immunology Research
International Journal of Endocrinology
Hindawi
Submit your manuscripts at
http://www.hindawi.com
PPAR Research
BioMed Research International
Journal of Ophthalmology
Stem Cells International
eCAM
Evidence-Based Complementary and Alternative Medicine
Journal of Obesity
Journal of Oncology
Computational and Mathematical Methods in Medicine
Behavioural Neurology
Parkinson's Disease
AIDS Research and Treatment
Oxidative Medicine and Cellular Longevity

เอกสารแนบหมายเลข 54

Pharmaceutical Biology

http://informahealthcare.com/phb
ISSN 1388-0209 print/ISSN 1744-5116 online
Editor-in-Chief: John M. Pezzuto
Pharm Biol, Early Online: 1–11
© 2015 Informa Healthcare USA, Inc. DOI: 10.3109/13880209.2015.1014569

informa
healthcare

ORIGINAL ARTICLE

Inhibition of p38 MAPK activation protects cardiac mitochondria from ischemia/reperfusion injury

Sarawut Kumphune[1,2], Sirirat Surinkaew[1], Siriporn C. Chattipakorn[1,3,4], and Nipon Chattipakorn[1,4,5]

[1]*Cardiac Electrophysiology Research and Training Center, Faculty of Medicine, Chiang Mai University, Chiang Mai, Thailand,* [2]*Department of Medical Technology, Faculty of Allied Health Sciences, Naresuan University, Phitsanulok, Thailand,* [3]*Faculty of Dentistry, Chiang Mai University, Chiang Mai, Thailand,* [4]*Center of Excellence in Cardiac Electrophysiology, Chiang Mai University, Chiang Mai, Thailand, and* [5]*Cardiac Electrophysiology Unit, Department of Physiology, Faculty of Medicine, Chiang Mai University, Chiang Mai, Thailand*

Abstract

Context: Cardiac cell death and fatal arrhythmias during myocardial ischemia/reperfusion (I/R) can be reduced by p38 MAPK inhibition. However, the effects of p38 MAPK inhibition on cardiac mitochondria have not been investigated.

Objective: We tested the hypothesis that p38 MAPK inhibition at different times during I/R protects cardiac mitochondrial functions.

Materials and methods: Adult Wistar rats were subjected to 30 min of left anterior descending coronary artery (LAD) occlusion, followed by 120 min of reperfusion. A 2 mg/kg bolus infusion of p38 MAPK inhibitor, SB203580, was given before or during ischemia, or at reperfusion. Mitochondrial function and ultrastructure were assessed and Western blots were performed.

Results: Administration of SB203580 at any time point of I/R significantly attenuated the mitochondrial ultrastructure change, mitochondrial swelling, by increasing the absorbance at 540 nm (I/R control 0.42 ± 0.03; pretreatment 0.58 ± 0.04; during ischemia 0.49 ± 0.02; at reperfusion 0.51 ± 0.02, $p < 0.05$), similar to reactive oxygen species (ROS) generation (I/R control 1300 ± 48; pretreatment 1150 ± 30; during ischemia 1000 ± 50; at reperfusion 1050 ± 55, $p < 0.05$). Only SB203580 given before or during ischemia attenuated mitochondrial membrane depolarization (I/R control 0.78 ± 0.04; pretreatment 1.02 ± 0.03; during ischemia 1.05 ± 0.12, $p < 0.05$). In addition, pre-treatment of SB203580 significantly reduced the phosphorylation of p53, CREB, Bax, cytochrome c, and cleaved caspase 3.

Discussion and conclusion: The results from this study showed for the first time that p38 MAPK inhibition protects mitochondria from I/R injury.

Keywords

Apoptotic regulatory signaling, mitochondrial functions, SB203580

History

Received 25 May 2014
Revised 17 January 2015
Accepted 29 January 2015
Published online 16 April 2015

Pharmaceutical Biology Downloaded from informahealthcare.com by JHU John Hopkins University on 07/03/15
For personal use only.

Introduction

Acute myocardial infarction has been a serious health burden in most countries around the world for many decades (World Health Organization [WHO], 2008). Although myocardial reperfusion has been shown to be an effective way of myocardial salvage, reperfusion itself has been known to cause cellular injury (Gottlieb et al., 1994). One of the major underlying cellular mechanisms following myocardial ischemia/reperfusion (I/R) injury has been shown to be cardiac mitochondrial dysfunction. For example, I/R injury has been shown to cause cardiac mitochondrial swelling, increased cardiac mitochondrial reactive oxygen species (ROS) production, and cardiac mitochondrial membrane depolarization (Baines, 2009). Cardiac mitochondrial dysfunction following I/R injury is known to trigger cellular necro-apoptosis (Gottlieb, 2011).

Correspondence: Nipon Chattipakorn, Cardiac Electrophysiology Research and Training Center, Faculty of Medicine, Chiang Mai University, Chiang Mai 50200, Thailand. Tel: +66 53 945329. Fax: +66 53 945368. E-mail: nchattip@gmail.com

Previous studies demonstrated that the activation of the 38 kDa mitogen which activates protein kinase (p38 MAPK) during myocardial ischemia aggravates lethal cellular injury, particularly during I/R injury (Bogoyevitch et al., 1996; Clark et al., 2007; Kumphune et al., 2012). The pharmacological catalytic site inhibitor SB203580 has been shown to prevent p38 MAPK activation, and has beneficial effects on the heart, including reduced cardiomyocyte death and infarct size as well as attenuation of left ventricular function impairment in the myocardial I/R model (Barancik et al., 2000; Clark et al., 2007; Kumphune et al., 2010; Surinkaew et al., 2013). Recently, we reported the cardioprotective effects of SB203580 administered at different time courses of I/R injury models, and demonstrated that SB203580 given at each time course could reduce the infarct size even when given at the reperfusion onset (Surinkaew et al., 2013). Interestingly, SB203580 not only reduced the infarct size but also decreased I/R-induced arrhythmias. The anti-arrhythmic effect of SB203580 was clearly seen only when the drug was given prior to reperfusion. These findings indicated the importance of the timing of drug administration on the therapeutic

RIGHTSLINK

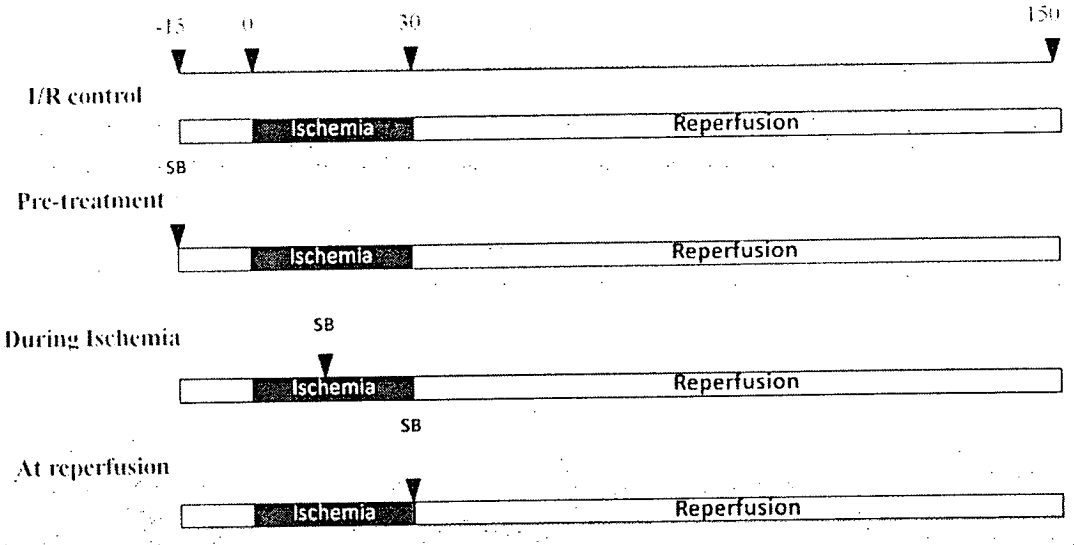


Figure 1. Study protocol for experimental groups and timing of SB203580 (SB) or normal saline solution (NSS) administration.

outcomes. Since cardiac mitochondria have been shown to play an important role in arrhythmogenesis and infarct size during I/R, it is proposed that the beneficial effect of p38 MAPK inhibitor in infarct size reduction and arrhythmias could possibly be due to its effect on the cardiac mitochondria. However, this hypothesis has never been investigated.

In addition, it has been known that the activation of p38 MAPK could activate several downstream signaling molecules such as p53 (Perfettini et al., 2005; Singhal et al., 2002; Thornton & Rincon, 2009), cAMP response element-binding protein (CREB) (Arnould et al., 2002; Lochner et al., 2009). These signaling molecules play an important role in controlling the cellular necro-apoptotic regulatory molecules such as Bax, Bcl2, caspase 3, and cytochrome c, possibly via the mitochondrial apoptotic pathway (Krijnen et al., 2002; Lundberg & Szweda, 2004; Murphy et al., 2000; Saikumar et al., 1998). However, the effects of SB203580 on these signaling markers, in terms of linkage between cardiac mitochondrial dysfunction and cell death, have not been intensively investigated. Therefore, in the present study, we determined the effects of p38 MAPK inhibitor, SB203580, given at different times during the I/R cycle on cardiac mitochondrial function, including mitochondrial swelling, mitochondrial ROS production, mitochondrial membrane potential changes ($\Delta\Psi_m$), as well as cardiac mitochondrial ultrastructure, in an *in vivo* I/R rat model. Moreover, the signaling cascades involved in cardiac mitochondrial protection downstream to p38 MAPK activation including p53 and CREB as well as the necro-apoptotic regulatory molecules including Bax, Bcl2, caspase 3, and cytochrome c were also determined.

Materials and methods

Animal model

Adult male Wistar rats weighing 350–400 g were obtained from the National Animal Center, Salaya Campus, Mahidol University, Bangkok, Thailand. All animals were housed in a room maintained under constant environmental conditions (temperature 22–25 °C and a constant 12 h light/dark cycle) and received a standard rat diet and water *ad libitum*. All animal experiments were approved by the Institutional Animal Care and Use Committees, and conformed to the Guide for the Care and Use of Animals of the Faculty of Medicine, Chiang Mai University, Chiang Mai, Thailand.

Ischemia and reperfusion protocol

Myocardial ischemia/reperfusion (I/R) was induced by the left anterior descending coronary artery (LAD) ligation for 30 min, followed by reperfusion for 120 min as described previously (Lv et al., 2008). An ischemic heart was confirmed by the change in the myocardial tissue color and ST elevation on the electrocardiogram that was recorded throughout the experiment. The left femoral vein was cannulated for administration of either 2 mg/kg SB203580HCl (Tocris, Ellisville, MO) (Ward et al., 2001) or normal saline as a vehicle at 0.33 ml/min for 3 min (Lv et al., 2008). In the treatment groups, rats were divided into three treatment groups to receive one of the following; SB203580 at 15 min before LAD occlusion (pretreatment group), SB203580 at 15 min after the onset of ischemia (during ischemia group), or SB203580 at the onset of reperfusion (reperfusion group) (Figure 1). At the end of the reperfusion period, the heart was excised and washed in cold saline solution. The whole ventricular tissue was homogenized for mitochondrial study or Western blot analysis.

Mitochondrial isolation

Mitochondria were freshly isolated from myocardial tissue by differential centrifugation as describe previously (Thummasorn et al., 2011). Briefly, ventricular tissues were homogenized in ice-cold isolated buffer (300 mM sucrose, 0.2 mM EGTA, 5 mM TES, pH 7.2) and centrifuged at 800 × *g*, 4 °C for 5 min. Then, the supernatants were collected and re-centrifuged at 8800 × *g*, 4 °C for 5 min. The mitochondrial pellet was washed by resuspending in ice-cold isolation buffer and re-centrifuged at 8800 × *g*, 4 °C for 5 min.

Pharmaceutical Biology Downloaded from informahealthcare.com by JHU John Hopkins University on 07/03/13
For personal use only.

RIGHTSLINK

Pharmaceutical Biology Downloaded from informahealthcare.com by JHU John Hopkins University on 07/03/15
For personal use only.

The isolated mitochondrial and cytosolic fraction was subjected to Western blot analysis using rabbit polyclonal antibody against VDAC1/Porin – Mitochondrial loading control (Abcam, Cambridge, MA).

The mitochondrial protein concentration was determined by the bicinchoninic acid (BCA) method, using bovine serum albumin (BSA) as a standard. A similar concentration of isolated cardiac mitochondria at 0.4 mg/ml was used to examine mitochondrial swelling, mitochondrial ROS production, and alteration of mitochondrial membrane potential ($\Delta\Psi_m$).

Determination of mitochondrial swelling

To determine the sensitivity to membrane permeability transition (mPT), the mitochondrial swelling was measured. The isolated cardiac mitochondria were re-suspended in respiration buffer consisting of 100 mM KCl, 50 mM sucrose, 10 mM HEPES, and 5 mM KH_2PO_4. The permeability transition-induced swelling of mitochondria was measured by rapid loss of the absorbance at λ 540 nm by the spectrophotometric method. The isolated cardiac mitochondria (0.4 mg/ml) were incubated with 1.5 ml of respiration buffer, and then the decrease in the absorbance was measured for 30 min at room temperature. The data were represented in arbitrary units of absorbance. The decreased absorbance indicated mitochondrial swelling (Thummasorn et al., 2011).

Determination of mitochondrial ROS production

The mitochondrial ROS production was assessed by measuring the intensity of the fluorescent signal of fluorescent 2′,7′-dichlorohydrofluorescein (DCF), which was converted from non-fluorescent 2′,7′-dichlorofluorescein-diacetate (DCFH-DA) in the presence of ROS (Li et al., 2001). Isolated cardiac mitochondria (0.4 mg/ml) were incubated with 2 μM DCFH-DA for 30 min at room temperature. The fluorescence intensity was determined by a fluorescence microplate ready with the excitation at λ 485 nm and emission at λ 530 nm. The ROS level was expressed in arbitrary units of fluorescence intensity of DCF. The increased fluorescent intensity indicated increased ROS production (Thummasorn et al., 2011).

Determination of mitochondrial membrane potential changes

To test the hypothesis that treatment by SB203580 can protect the loss of $\Delta\Psi_m$, the JC1 dye was used to measure $\Delta\Psi_m$ of cardiac mitochondria function. The JC-1 or 5,5′,6,6′-tetrachloro-1,1′,3,3′-tetraethylbenzimidazolcarbocyanine iodide is a lipophilic cationic dye that is capable of entering the mitochondrial membrane. The monomeric form of JC-1 produces a green fluorescence. Increasing the mitochondrial membrane potential changes ($\Delta\Psi_m$) caused aggregation of the dye, which appeared as red fluorescein. Alteration of $\Delta\Psi_m$ causes changes in the red:green ratio. Isolated cardiac mitochondria (0.4 mg/ml) were incubated with 5 μM JC-1 at 37 °C for 30 min. The fluorescence intensity for monomeric green fluorescein was determined by a fluorescence microplate reader with the excitation at λ 485 nm and emission at λ 530 nm, while the aggregate red fluorescein was determined by fluorescence microplate reader with the excitation at λ 485 nm and emission at λ 590 nm. The ratio of red to green fluorescence intensity ratio was determined. The decreased red to green fluorescent intensity ratio indicated mitochondrial membrane depolarization (Thummasorn et al., 2011).

Identification of cardiac mitochondrial ultrastructure

The mitochondrial pellet was fixed in 2.5% glutaraldehyde at 4 °C overnight. Then, the pellet was rinsed in 0.1 M phosphate buffer (PO_4) for 15 min twice and post-fixed in 1% cacodylate-buffer osmium tetroxide for 2 h at room temperature. The mitochondrial pellet was rinsed in 0.1 M phosphate buffer (PO_4) 5 min twice and was dehydrated in a graded series of ethanol, 50% ethanol for 5 min twice, 70% ethanol for 5 min twice, 85% ethanol for 5 min twice, 95% ethanol for 5 min twice, and 100% ethanol for 5 min twice. After that, the pellet was infiltrated with propylene oxide (PO) for 10 min twice, followed by the cocktail between resin and PO in a 1:2 ratio for 30 min, resin and PO in a 1:1 ratio for 60 min and resin overnight, respectively. On the next day, the pellet was embedded in EM-bed 812 resin (Thummasorn et al., 2011). Ultrathin sections were cut with diamond knife, placed in copper grids, and stained with uranyl acetate and lead citrate. The cardiac mitochondria were identified with a transmission electron microscope (TEM) (Thummasorn et al., 2011).

Western blot analysis

The heart tissue was homogenated in extraction buffer (20 mmol/L Tris HCl, 1 mmol/L Na_3VO_4, 5 mmol/L NaF). The heart protein was collected and subjected to 10% or 15% SDS-polyacrylamide gel electrophoresis then transferred to polyvinylidene difluoride membranes, which were blocked for 2 h with 5% non-fat milk in Tris-buffered saline (pH 7.4) containing 0.1% Triton X-100. The membranes were probed overnight at 4 °C with the appropriate primary antibody as follows: total-p38, phospho-p38, and phospho-HSP27 (Cell Signaling Technology, Danvers, MA), total-p53, phospho-p53, total-CREB, phospho-CREB, Bax, Bcl2, Cytochrome c, caspase-3 (Santa Cruz Biotechnology, Inc, Santa Cruz, CA). After washing and exposure to horseradish peroxidase-conjugated secondary antibody for 1 h at room temperature, antibody–antigen complexes were visualized by enhanced chemiluminescence assay. Bands corresponding to the protein of interest appeared as dark regions on the developed film. The film images of the Western blots were scanned and were analyzed using Image J (NIH image, National Institutes of Health, Bethesda, MD) analysis software (Tanno et al., 2003). For quantitation of the proteins of interest, phosphorylated proteins were normalized to total protein expression.

Statistical analysis

All data were expressed as mean ± SEM. Statistical analysis was performed with one-way analysis of variance (ANOVA) and *post-hoc* analysis with LSD. All procedures were performed with an SPSS statistical program (Version 15.0, SPSS Inc., Chicago, IL). A p-values < 0.05 was accepted as statistically significant.

RIGHTSLINK

Results

p38 MAPK inhibition by SB203580 attenuated cardiac mitochondrial dysfunction following I/R injury

Isolated cardiac mitochondria used in this study were subjected to Western blot analysis against Anti-VDAC1/porin protein to ensure that the isolated protein contain mitochondria. The results showed that VDAC1/porin protein was detected in isolated mitochondrial fraction, but not in cytosolic fraction (Figure 2A). The myocardial I/R injury caused cardiac mitochondrial swelling by decreased absorbance at 540 nm, increased mitochondrial ROS production, and mitochondrial membrane depolarization (Figure 2). Although administration of SB203580 at any time point of I/R protocol significantly attenuated cardiac mitochondrial swelling (Figure 2B), pretreatment of SB203580 was found to be the most effective timing to prevent cardiac mitochondrial swelling (pretreatment 0.58 ± 0.04 versus I/R control 0.42 ± 0.03, $p < 0.05$), compared with drug treatment during ischemia (during ischemia 0.49 ± 0.02 versus I/R control 0.42 ± 0.03, $p < 0.05$) or at the onset of reperfusion (at reperfusion 0.51 ± 0.02 versus I/R control 0.42 ± 0.03, $p < 0.05$) (Figure 2B). Administration of SB203580 also significantly reduced ROS production in cardiac mitochondria caused by I/R injury in all groups, compared with the I/R control group (I/R control 1300 ± 48; pretreatment 1150 ± 30; during ischemia 1000 ± 50; at reperfusion 1050 ± 55, $p < 0.05$) (Figure 2C). For cardiac mitochondrial membrane potential alteration, we found that administration of SB203580 prior to ischemia or during ischemia significantly prevented the change of mitochondrial membrane potential caused by I/R injury, when compared with the I/R control group (I/R control 0.78 ± 0.04; pretreatment 1.02 ± 0.03; during ischemia 1.05 ± 0.12) (Figure 2D). However, SB203580 administered at the onset of reperfusion failed to prevent mitochondrial depolarization (I/R control 0.78 ± 0.04; at reperfusion 0.71 ± 0.05) (Figure 2D).

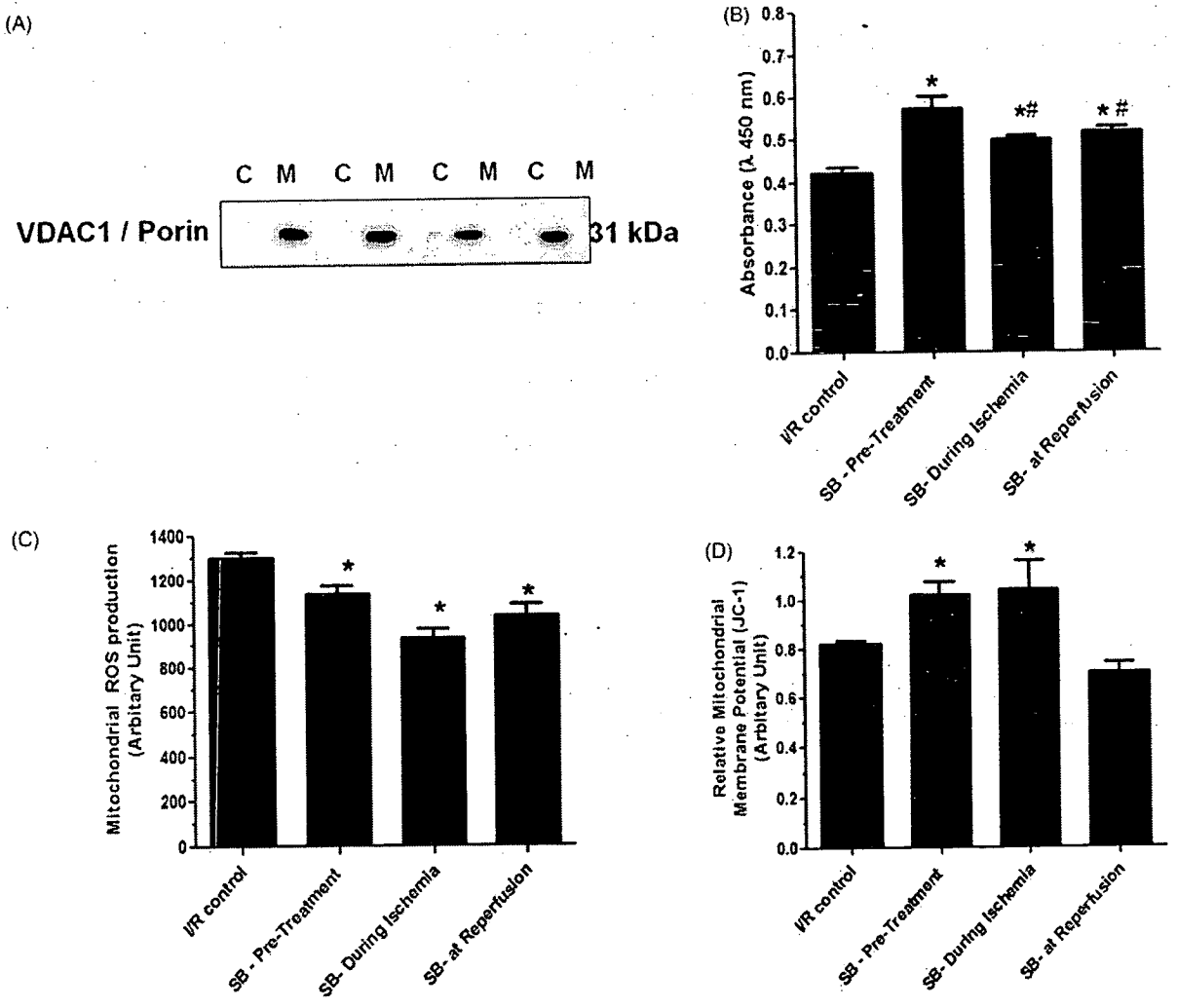


Figure 2. Effects of SB203580 on cardiac mitochondrial function. (A) Western blot analysis using antibody against mitochondrial VDAC1/Porin in cytoplasmic fraction (C), and mitochondrial fraction (M) of isolated cardiac mitochondria. (B) Mitochondrial swelling, (C) mitochondrial ROS production, (D) mitochondrial membrane potential change, when SB203580 was administered before, during ischemia, or at the onset of reperfusion in ischemia/reperfusion rats ($n = 4$–7 animals/group). *$p < 0.05$ versus the vehicle group, #$p < 0.05$ versus the pretreatment group.

RIGHTSLINK

Pharmaceutical Biology Downloaded from informahealthcare.com by JHU John Hopkins University on 07/03/15
For personal use only.

Pharmaceutical Biology Downloaded from informahealthcare.com by JHU John Hopkins University on 07/03/15
For personal use only.

Inhibition of p38 MAPK protected I/R-induced cardiac mitochondrial ultrastructure disruption

Our results demonstrated that I/R injury not only caused cardiac mitochondrial dysfunction but also distorted the cardiac mitochondrial ultrastructure by increasing matrix space and disorganization of the cristae (Figure 3A). Administration of SB203580 at any time points could preserve the cardiac mitochondrial ultrastructure from the disruption caused by I/R injury (Figure 3B and C). Interestingly, administration of SB203580 prior to ischemia gave the most effective treatment to protect I/R induced-cardiac mitochondria ultrastructure rupture (Figure 3D), when compared with the groups received SB203580 during ischemia or at the onset of reperfusion.

p38 MAPK inhibitor, SB203580, protected cardiac mitochondria by attenuation of apoptotic regulatory molecules activation

Myocardial I/R has been shown to cause activation of p38 MAPK and its activities by phosphorylation of downstream signaling molecules HSP27 (Larsen et al., 1997). The administration of the p38 MAPK inhibitor SB203580, prior to or during ischemia, significantly reduced p38 MAPK phosphorylation as well as its activity to phosphorylate the downstream substrate HSP27 (Figure 4A–C). However, SB203580 given at the onset of reperfusion did not reduce the p38 MAPK phosphorylation as well as the level of phosphorylated HSP27 (Figure 4A–C). Moreover, we found that pretreatment of SB203580 inhibited the phosphorylation of p53 and CREB, while SB203580 given during ischemia failed to inhibit the activation of these two downstream molecules (Figure 4A, D, and E). However, SB203580 given at the onset of reperfusion inhibited the phosphorylation of p53 and CREB (Figure 4A, D, and E). Since mitochondrial dysfunction is the key determination for cell death, especially the necro-apoptosis in I/R injury (Gottlieb, 2011), the effects of SB203580 on apoptotic regulatory molecules such as Bax, Bcl2, caspase 3, and cytochrome c were also determined. Our results showed that administration of SB203580 at every time point reduced the level of cleaved caspase 3 (Figure 5A and

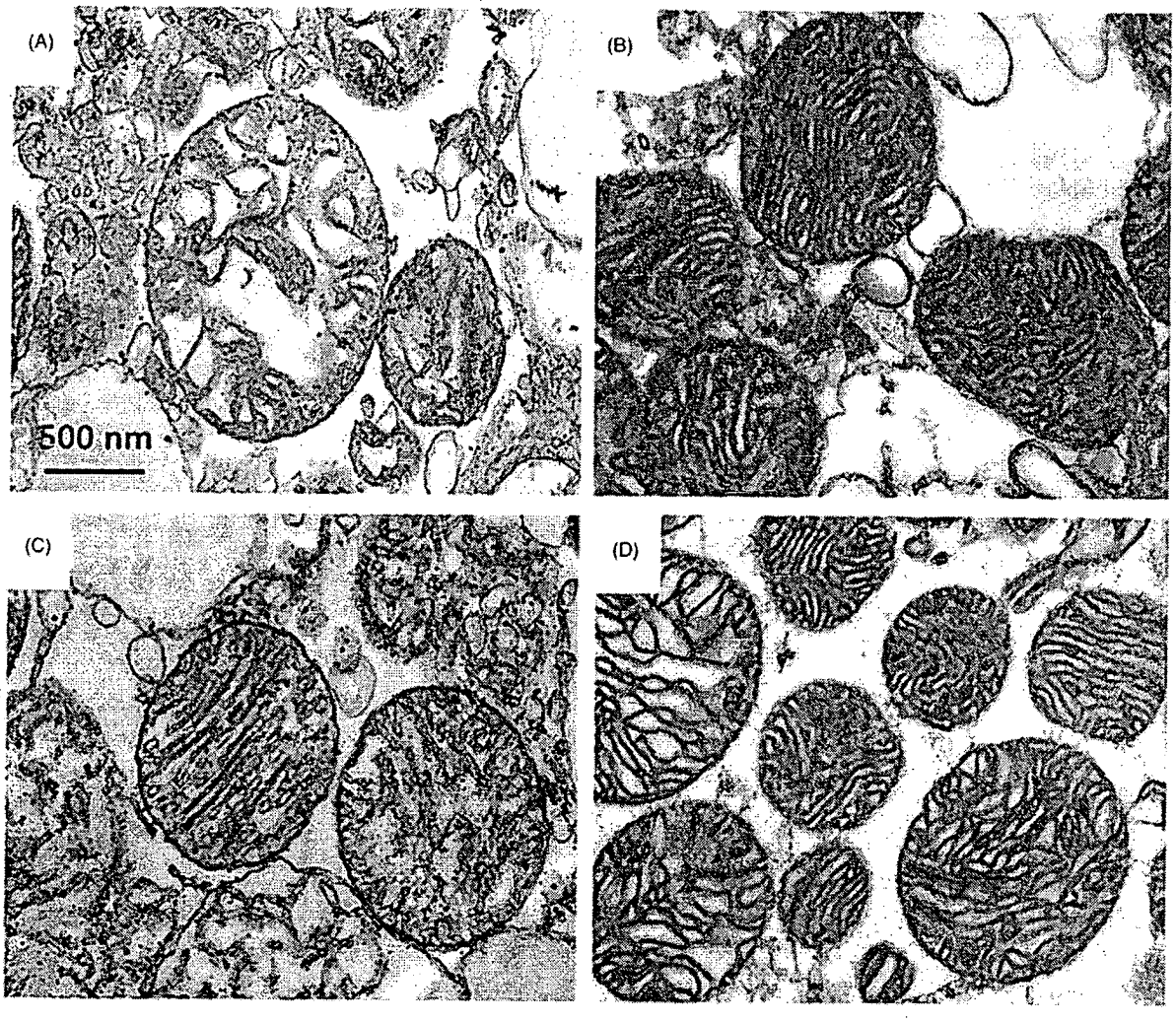


Figure 3. Effects of SB203580 on cardiac mitochondrial ultrastructure. Cardiac mitochondria were isolated from rats subjected to myocardial ischemia/reperfusion injury (A) in the presence of SB203580 before (B), during ischemia (C), or at the onset of reperfusion (D). The mitochondrial pellet was embedded in EM-bed 812 resin. Ultrathin sections were cut and stained with uranyl acetate and lead citrate. $^{*}p < 0.05$ versus the vehicle group ($n = 4$–5 animals/group).

RIGHTSLINK

Pharmaceutical Biology Downloaded from informahealthcare.com by JHU John Hopkins University on 07/03/15
For personal use only.

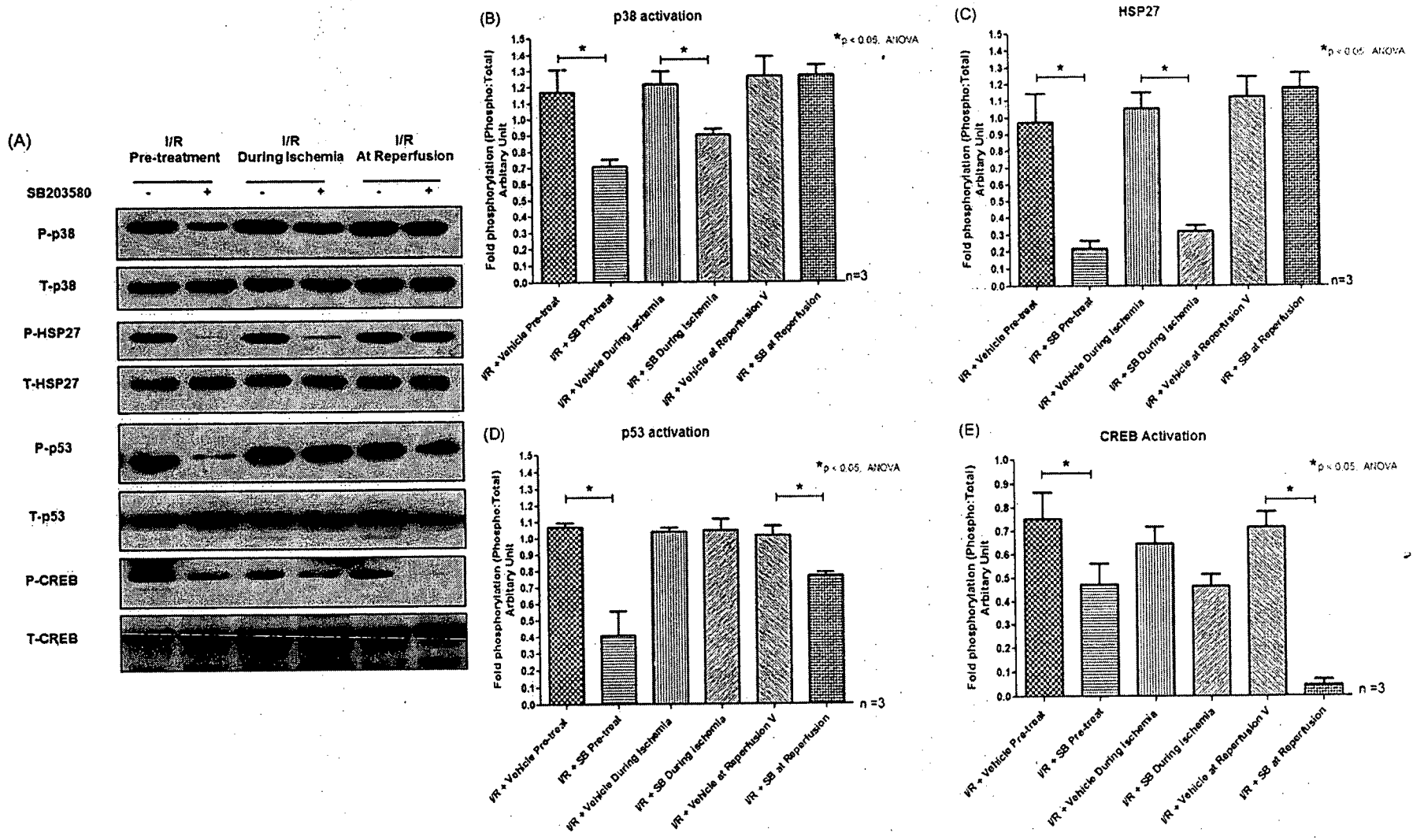


Figure 4. (A) Effects of SB203580 on p38 MAPK activation and downstream substrates, HSP27, p53, and CREB. The heart homogenates were collected and subjected to Western blot analysis to detect the activation of interested proteins. (B–E) The quantitation of fold phosphorylation of p38 MAPK activation and downstream substrates, HSP27, p53, and CREB by Western blot analysis ($n = 3$ animals/group). *$p < 0.05$ versus the vehicle group.

RIGHTSLINK

Pharmaceutical Biology Downloaded from informahealthcare.com by JHU John Hopkins University on 07/03/15
For personal use only.

DOI: 10.3109/13880209.2015.1014569

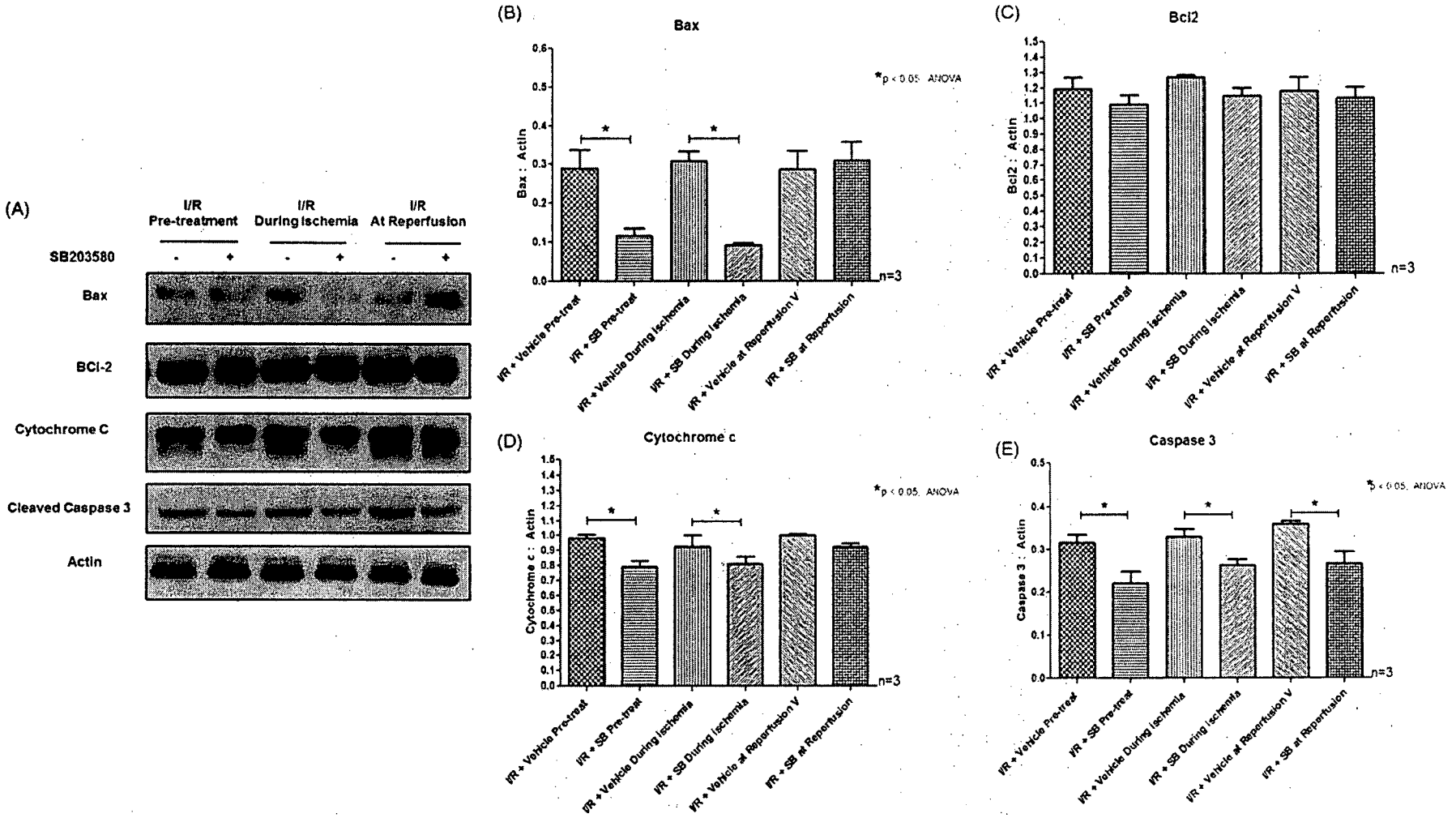


Figure 5. (A) Effects of SB203580 on apoptotic regulatory proteins. The heart homogenates were collected and subjected to Western blot analysis to detect the expression of Bax, Bcl2, Cytochrome c, and cleaved caspase-3. (B–E) The quantitation of protein expression of Bax, Bcl2, Cytochrome c, and cleaved caspase-3 by Western blot analysis ($n = 3$ animals/group). *$p < 0.05$ versus the vehicle group.

RIGHTSLINK

E), although SB203580 given prior to or during ischemia, but not at the onset of reperfusion, significantly decreased Bax expression and cytochrome c level (Figure 5A and D), without any changes in levels of Bcl2 expression (Figure 5A–C).

Discussion

Cardiac mitochondrial dysfunction is known as a key mechanism involved in I/R injury and cardiac cell death (Baines, 2009; Baines et al., 2007; Berkich et al., 2003; Di Lisa et al., 2007; Halrestrap et al., 2004; Jennings & Ganote, 1976). The excessive formation of ROS during I/R injury has been shown to induce the prolonged-opening of mitochondria permeability transition pore (MPTP), thus dissipating the proton electrochemical gradient or $\Delta\Psi_m$, consequently causing ATP insufficiency, leading to further ROS generation and the loss of intact cardiac mitochondrial ultrastructure, which finally resulted in cardiac mitochondrial swelling and rupture (Vaseva et al., 2012). This process is known to trigger the apoptotic program due to the leakage of pro-apoptotic molecules from ruptured mitochondria (Green & Reed, 1998). Therefore, prevention or attenuation of the degree of cardiac mitochondrial dysfunction caused by I/R injury is one of the most promising clinical targets.

In the present study, we demonstrated for the first time the protective effect of p38 MAPK inhibitor, SB203580, on cardiac mitochondrial function in the heart underwent I/R injury, and provided molecular mechanistic insights of cardiac mitochondrial protection by p38 MAPK inhibiting necro-apoptosis regulatory cascades. The major findings of this study were that in the heart that underwent I/R injury, administration of SB203580 before or during ischemia attenuated cardiac mitochondrial dysfunction caused by I/R as indicated by preventing mitochondrial swelling, reducing mitochondrial ROS generation, and attenuating mitochondrial membrane potential depolarization. However, giving SB203580 at the onset of reperfusion failed to prevent the loss of mitochondrial membrane potential, in which cardiac mitochondrial depolarization plays an important role in arrhythmogenesis (O'Rouke, 2000). These findings could provide the mechanistic explanation of our previous report, which demonstrated from our previous study that the infarct size reduction was found at all-time points of SB203580 treatment, but treatment of SB203580 before or during ischemia, but not at reperfusion, decreased the incidence of ventricular tachycardia/ventricular fibrillation (VT/VF) incidence (Surinkaew et al., 2013). Although SB203580 showed a protective effect on cardiac mitochondrial swelling, ROS production, and mitochondrial membrane potential depolarization, the mitochondrial respiration was not performed and was considered a limitation of this study.

In response to I/R stress, p53 protein has been known to be activated and accumulated in the mitochondrial matrix, induced ROS generation and subsequently caused transient mitochondrial outer membrane permeabilization (MOMP), resulting in the release of cytochrome c, which subsequently cause apoptosis by activation of caspase 3 (Vaseva et al., 2012). Therefore, p53 activation in I/R is considered as a key molecule to trigger and regulate mitochondrial cellular necro-apoptosis (Krijnen et al., 2002). It is important to note that p53 could be phosphorylated by p38 MAPK (Bulavin et al., 1999; Perfettini et al., 2005; Thornton & Rincon, 2009), and mediated cell death (Singhal et al., 2002), suggesting that the significant linkage of p38 MAPK and p53 regulates mitochondrial apoptotic pathway. In the present study, administration of p38 MAPK inhibitor prior to LAD ligation significantly reduced p53 phosphorylation as well as significantly decreased Bax expression, cytochrome c, and the level of cleaved caspase 3. These molecular findings may explain the effect of p38 MAPK inhibition prior to the ischemic period significantly attenuated I/R-induced cardiac mitochondrial dysfunction and also decreased apoptotic cascade activation. This suggested that the treatment of p38 MAPK inhibitor before an ischemic insult is the effective timing of treatment in terms of cardiac mitochondrial protection and reduction of apoptotic signaling activation. Similar to the report from Kimura et al. (2006) that pretreatment of p38 MAPK inhibitor prior to myocardial ischemia could inhibit mitochondrial morphological damage. However, this study lacked information regarding mitochondrial function. Despite these facts, clinical application is limited since most acute myocardial infarction patients already have coronary occlusion prior to their arriving at the hospital. Therefore, administration of p38 MAPK inhibitor during myocardial ischemia or in reperfusion period would be more appropriate in an actual clinical setting.

Inhibition of p38 MAPK during ischemia or at the onset of reperfusion also provided cardioprotective benefits, but at a lower degree of protection compared to the pre-treatment. Administration of SB203580 during ischemia reduced p38 MAPK activity without affecting the downstream molecules p53. Since p53 has been shown to be rapidly phosphorylated within 5 min after onset of ischemia (Kim et al., 2013), therefore, administration of SB203580 15 min after the onset of ischemia was not early enough to inhibit p38 MAPK induced p53 phosphorylation. However, giving SB203580 during ischemia reduced the expression of pro-apoptotic protein Bax, cleaved caspase 3, which could attenuate cell death. Therefore, giving SB203580 late after the onset of ischemia may not be capable of deactivating p53 molecules that have been rapidly phosphorylated in the ischemic episode, but could inhibit the signaling cascade that sufficiently attenuates mitochondrial damage and cell death.

Although administration of SB203580 at the onset of reperfusion could not protect mitochondria membrane depolarization, it was still sufficient to attenuate cardiac mitochondrial swelling, ROS production, and mitochondrial structure, although to a lesser extent when compared with giving SB203580 before or during ischemia. Administration of SB203580 at the onset of reperfusion failed to reduce p38 MAPK activity on HSP27, but decreased the phosphorylation of p53 and CREB. These findings suggest that p53 and CREB are downstream molecules of p38 MAPK that were not activated via HSP27, or could possibly be regulated by other unidentified signaling pathways that could be affected by SB203580. Furthermore, SB203580 given at reperfusion could only reduce cleaved caspase 3 levels without any change in the Bax, Bcl2, and cytochrome c. The reduction of cleaved caspase 3 level could sufficiently attenuate the

Pharmaceutical Biology Downloaded from informahealthcare.com by JHU John Hopkins University on 07/03/13
For personal use only.

RIGHTSLINK

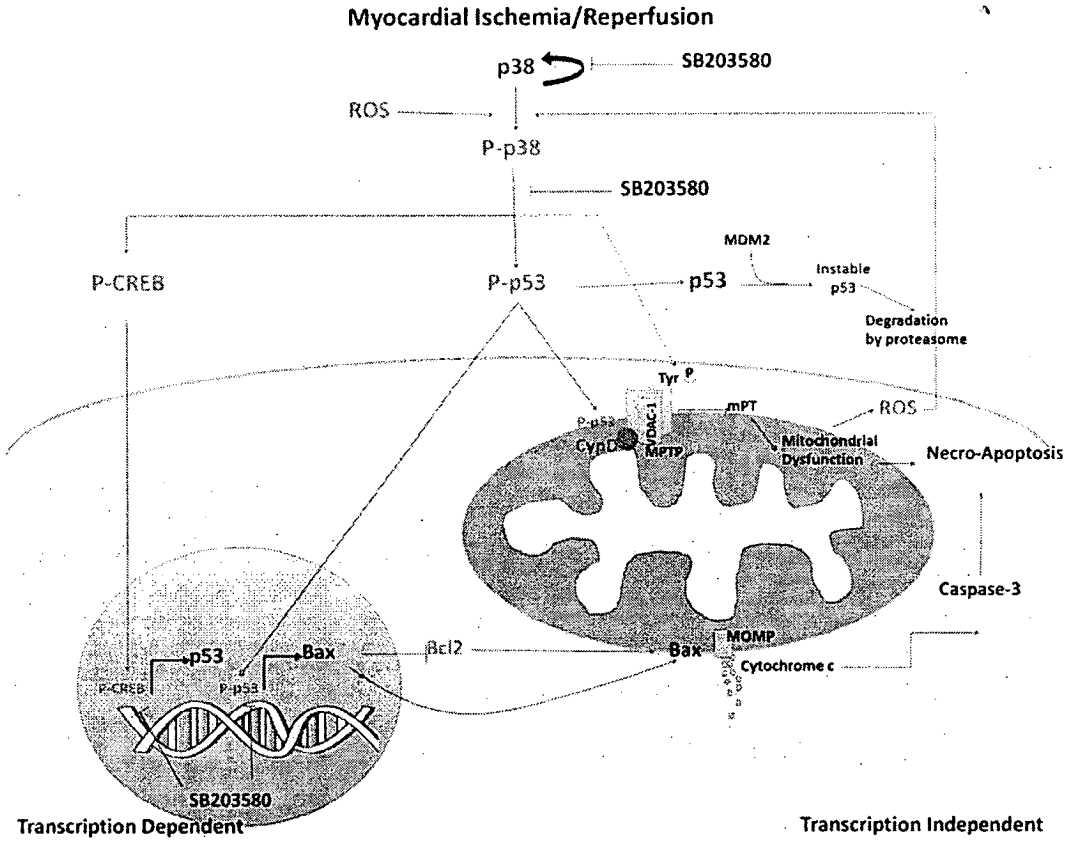


Figure 6. The proposed mechanistic pathway of I/R-activated p38 MAPK and downstream activation involving mitochondrial trigger cell death. Myocardial I/R injury caused p38 MAPK activation, which consequently activated p53 phosphorylation. Phosphorylated p53 stabilized and accumulated in mitochondrial matrix during I/R injury and mediated MPTP opening. Activation of p53 also activated proapoptotic Bax protein, which regulated cytochrome c release, and activation of caspase 3 (transcription independent manner). p38 MAPK also phosphorylated CREB, which in turn regulated p53 gene transcription. Inhibition of p38 MAPK by SB203580 reduced p53 phosphorylation, CREB phosphorylation, and thus protected cardiac mitochondria from I/R injury and cell death.

apoptotic pathway, which is consistent with the results from our previous report that SB203580 given at the onset of reperfusion also reduced the infarct size (Surinkaew et al., 2013).

Inhibition of p38 MAPK by SB203580 reduced the p53 activation and Bax expression level, which may in turn attenuate the release of cytochrome c level to trigger the activity of caspase 3 mediated apoptosis (Hsu et al., 2007; Perfettini et al., 2005; Son et al., 2009). The impairment of mitochondrial activity has been found to activate cAMP-responsive element-binding protein (CREB) phosphorylation at Ser133 (Arnould et al., 2002), which in turn activated p53 in a transcriptional dependent manner (Figure 6). Down regulation of p53 could also affect the p53-mediated mitochondrial dysfunction and apoptosis. Therefore, inhibition of CREB phosphorylation could target a p53 regulation. It has been shown that, during ischemia, CREB is activated as a downstream event of p38 MAPK activation (Lochner et al., 2009), in which its phosphorylation could be inhibited by SB203580. On the contrary, we found that the protein expression level of p53 was not changed, suggesting a transcriptional-independent mechanism. This could be due to the study protocol that aimed to study the acute effects of the p38 MAPK inhibitor. The duration of inhibitor treatment as well as duration of I/R protocol may not be sufficient to initiate the transcriptional processes of p53. In this study, administration of SB203580 inhibited p53 phosphorylation and subsequently influenced Bax expression, resulting in decreased mitochondrial membrane permeability, cytochrome c, and caspase 3 levels (Figure 6). The limitation of this study was that our results provided limited mechanistic insights of SB203580 on cardiac mitochondria, since the protein levels of apoptotic factors, e.g., Bax, Bck-2, and Cytochrome c as well as p53 and CREB were performed in homogenated whole heart tissue. This may not sufficiently provide the information regarding the translocation of these apoptotic factors from cytoplasm to mitochondria. In addition, phosphorylation of the voltage-dependent anion channel (VDAC) -1, which is a porin protein involved in mitochondrial regulator of cell survival (Baines et al., 2007; Cesura et al., 2003; McEnery et al., 1992; Premkumar & Simantov, 2002), facilitates other protein binding in MPTP and mediates mitochondrial damage. Schwertz et al. (2007) reported that VDAC-1 was a downstream substrate of p38 MAPK during I/R injury. Inhibition of p38 MAPK by PD169316 has been shown to significantly reduce the phosphorylation of VDAC-1, and reduce cardiac cell injury. However, the effects of SB203580 on VDAC-1 phosphorylation in cardiac mitochondria from myocardial I/R model will need to be further investigated.

Pharmaceutical Biology Downloaded from informahealthcare.com by JHU John Hopkins University on 07/03/15
For personal use only.

RIGHTSLINK

Conclusions

In summary, this is the first report demonstrating that p38 MAPK inhibition by SB203580 reduced cardiac mitochondrial dysfunction caused by I/R injury through the attenuation of the mitochondrial apoptotic pathway. Moreover, our data suggests that the therapeutic potential of SB203580 in protecting cardiac mitochondria from I/R injury provides more clinical benefit when given prior to reperfusion.

Declaration of interest

The authors report that they have no conflicts of interest. This study was supported by grants from the Thailand Research Fund MRG5480017 (SK), the Royal Golden Jubilee Ph.D. Program (SS, NC), Thailand Research Fund RTA5580006 (NC), BRG5780016 (SC), the Chiang Mai University Center of Excellence Award (NC) and a NSTDA Research Chair Grant from the National Science and Technology Development Agency (NC).

References

Arnould T, Vankoningsloo S, Renard P, et al. (2002). CREB activation induced by mitochondrial dysfunction is a new signaling pathway that impairs cell proliferation. *EMBO J* 21:53–63.

Baines CP. (2009). The mitochondrial permeability transition pore and ischemia–reperfusion injury. *Basic Res Cardiol* 104:181–8.

Baines CP, Kaiser RA, Sheiko T, et al. (2007). Voltage-dependent anion channels are dispensable for mitochondrial-dependent cell death. *Nat Cell Biol* 9:550–5.

Barancik M, Htun P, Strohm C, et al. (2000). Inhibition of the cardiac p38-MAPK pathway by SB203580 delays ischemic cell death. *J Cardiovasc Pharmacol* 35:474–83.

Berkich DA, Salama G, Lanoue KF. (2003). Mitochondrial membrane potentials in ischemic hearts. *Arch Biochem Biophys* 420:279–86.

Bogoyevitch MA, Gillespie BJ, Ketterman AJ, et al. (1996). Stimulation of the stress-activated mitogen-activated protein kinase subfamilies in perfused heart. p38/RK mitogen-activated protein kinases and c-Jun N-terminal kinases are activated by ischemia/reperfusion. *Circ Res* 79: 162–73.

Bulavin DV, Saito S, Hollander MC, et al. (1999). Phosphorylation of human p53 by p38 kinase coordinates N-terminal phosphorylation and apoptosis in response to UV radiation. *EMBO J* 18:6845–54.

Cesura AM, Pinard E, Schubenel A, et al. (2003). The voltage-dependent anion channel is the target for a new class of inhibitors of the mitochondrial permeability transition pore. *J Biol Chem* 278: 49812–18.

Clark JR, Sarafraz N, Marber MS. (2007). Potential of p38-MAPK inhibitors in the treatment of ischaemic heart disease. *Pharmacol Ther* 116:192–206.

Di Lisa F, Canton M, Memabo R, et al. (2007). Mitochondria and cardioprotection. *Heart Fail Rev* 12:249–60.

Gottlieb RA. (2011). Cell death pathways in acute ischemia/reperfusion injury. *J Cardiovasc Pharmacol Ther* 16:233–8.

Gottlieb RA, Burleson KO, Kloner RA, et al. (1994). Reperfusion injury induces apoptosis in rabbit cardiomyocytes. *J Clin Invest* 94:1621–8.

Green DR, Reed JC. (1998). Mitochondria and apoptosis. *Science* 281: 1309–12.

Halrestrap AP, Clarke SJ, Javadov SA. (2004). Mitochondrial permeability transition pore opening during myocardial reperfusion – A target for cardioprotection. *Cardiovasc Res* 61:372–85.

Hsu MJ, Hsu CY, Chem BC, et al. (2007). Apoptosis signal-regulating kinase 1 in amyloid beta peptide-induced cerebral endothelial cell apoptosis. *J Neurosci* 27:5719–29.

Jennings RB, Ganote CE. (1976). Mitochondrial structure and function in acute myocardial ischemic injury. *Circ Res* 38:I80–91.

Kim YA, Kim MY, Yu HY, et al. (2013). Gadd45beta is transcriptionally activated by p53 via p38alpha-mediated phosphorylation during myocardial ischemic injury. *J Mol Med (Berl)* 91:1303–13.

Kimura H, Shintani-ishida K, Nakajima M, et al. (2006). Ischemic preconditioning or p38 MAP kinase inhibition attenuates myocardial TNF alpha production and mitochondria damage in brief myocardial ischemia. *Life Sci* 78:1901–10.

Krijnen PA, Nijmeijer R, Meijer CJ, et al. (2002). Apoptosis in myocardial ischaemia and infarction. *J Clin Pathol* 55:801–11.

Kumphune S, Bassi R, Jacquet S, et al. (2010). A chemical genetic approach reveals that p38alpha MAPK activation by diphosphorylation aggravates myocardial infarction and is prevented by the direct binding of SB203580. *J Biol Chem* 285:2968–75.

Kumphune S, Chattipakorn S, Chattipakorn N. (2012). Role of p38 inhibition in cardiac ischemia/reperfusion injury. *Eur J Clin Pharmacol* 68:513–24.

Larsen JK, Yamboliev IA, Weber LA, Gerthoffer WT. (1997). Phosphorylation of the 27-kDa heat shock protein via p38 MAP kinase and MAPKAP kinase in smooth muscle. *Am J Physiol* 273: L930–40.

Li L, Tao JJ, Davaille J, et al. (2001). 15-Deoxy-delta 12,14-prostaglandin J2 induces apoptosis of human hepatic myofibroblasts. A pathway involving oxidative stress independently of peroxisome-proliferator-activated receptors. *J Biol Chem* 276:38152–8.

Lochner A, Marais E, Genade S, et al. (2009). Protection of the ischaemic heart: Investigations into the phenomenon of ischaemic preconditioning. *Cardiovasc J Afr* 20:43–51.

Lundberg KC, Szweda LI. (2004). Initiation of mitochondrial-mediated apoptosis during cardiac reperfusion. *Arch Biochem Biophys* 432: 50–7.

Lv X, Wan J, Yang J, et al. (2008). Cytochrome P450 omega-hydroxylase inhibition reduces cardiomyocyte apoptosis via activation of ERK1/2 signaling in rat myocardial ischemia–reperfusion. *Eur J Pharmacol* 596:118–26.

Mcenery MW, Snowman AM, Trifiletti RR, Snyder SH. (1992). Isolation of the mitochondrial benzodiazepine receptor: Association with the voltage-dependent anion channel and the adenine nucleotide carrier. *Proc Natl Acad Sci USA* 89:3170–4.

Murphy KM, Ranganathan V, Farnsworth ML, et al. (2000). Bcl-2 inhibits Bax translocation from cytosol to mitochondria during drug-induced apoptosis of human tumor cells. *Cell Death Differ* 7:102–11.

O'Rouke B. (2000). Pathophysiological and protective roles of mitochondrial ion channels. *J Physiol* 529:23–36.

Perfettini JL, Castedo M, Nardacci R, et al. (2005). Essential role of p53 phosphorylation by p38 MAPK in apoptosis induction by the HIV-1 envelope. *J Exp Med* 201:279–89.

Premkumar A, Simantov R. (2002). Mitochondrial voltage-dependent anion channel is involved in dopamine-induced apoptosis. *J Neurochem* 82:345–52.

Saikumar P, Dong Z, Weinberg JM, Vemkatachalam MA. (1998). Mechanisms of cell death in hypoxia/reoxygenation injury. *Oncogene* 17:3341–9.

Schwertz H, Carter JM, Abdudureheman M, et al. (2007). Myocardial ischemia/reperfusion causes VDAC phosphorylation which is reduced by cardioprotection with a p38 MAP kinase inhibitor. *Proteomics* 7: 4579–88.

Singhal PC, Bhaskaran M, Patel J, et al. (2002). Role of p38 mitogen-activated protein kinase phosphorylation and Fas-Fas ligand interaction in morphine-induced macrophage apoptosis. *J Immunol* 168: 4025–33.

Son KN, Pugazhenthi S, Lipton HL. (2009). Activation of tumor suppressor protein p53 is required for Theiler's murine encephalomyelitis virus-induced apoptosis in M1-D macrophages. *J Virol* 83: 10770–7.

Surinkaew S, Kumphune S, Chattipakorn S, Chattipakorn N. (2013). Inhibition of p38 MAPK during ischemia, but not reperfusion, effectively attenuates fatal arrhythmia in ischemia/reperfusion heart. *J Cardiovasc Pharmacol* 61:133–41.

Tanno M, Bassi R, Gorog DA, et al. (2003). Diverse mechanisms of myocardial p38 mitogen-activated protein kinase activation: Evidence for MKK-independent activation by a TAB1-associated mechanism contributing to injury during myocardial ischemia. *Circ Res* 93: 254–61.

Thornton TM, Rincon M. (2009). Non-classical p38 map kinase functions: Cell cycle checkpoints and survival. *Int J Biol Sci* 5:44–51.

Pharmaceutical Biology Downloaded from informahealthcare.com by JHU John Hopkins University on 07/03/15
For personal use only.

RIGHTSLINK

Thummasorn S, Kumfu S, Chattipakorn S, Chattipakorn N. (2011). Granulocyte-colony stimulating factor attenuates mitochondrial dysfunction induced by oxidative stress in cardiac mitochondria. *Mitochondrion* 11:457–66.

Vaseva AV, Marchenko ND, Ji K, et al. (2012). p53 Opens the mitochondrial permeability transition pore to trigger necrosis. *Cell* 149:1536–48.

Ward KW, Proksch JW, Azzaranot LM, et al. (2001). Preclinical pharmacokinetics of SB-203580, a potent inhibitor of p38 mitogen-activated protein kinase. *Xenobiotica* 31:783–97.

World Health Organization. (2008). World Heath Statistics 2008 [Online]. Available from: http://www.who.int/entity/whosis/whostat/EN_WHS08_Full.pdf [last accessed 19 Apr 2014].

Pharmaceutical Biology Downloaded from Informahealthcare.com by JHU John Hopkins University on 07/03/15
For personal use only.

RIGHTSLINK

เอกสารแนบหมายเลข 55

Cardiovasc Drugs Ther (2014) 28:549–562
DOI 10.1007/s10557-014-6553-6

REVIEW ARTICLE

Roles of Obese-Insulin Resistance and Anti-Diabetic Drugs on the Heart with Ischemia-Reperfusion Injury

Nattayaporn Apaijai · Siriporn C. Chattipakorn · Nipon Chattipakorn

Published online: 5 October 2014
© Springer Science+Business Media New York 2014

Abstract The incidence of obesity with insulin resistance is increasing worldwide. This condition is also known as a risk factor of coronary artery disease and associated with increased arrhythmias, impaired left ventricular function, and increased infarct size during cardiac ischemia-reperfusion (I/R) injury. The proposed mechanisms are due to impaired glucose utilization and pro-survival signaling molecules, and increased inflammatory cytokines, which have been demonstrated in the I/R hearts in various models of obese-insulin resistance. However, the cardiac effects of diets in the I/R heart are still unsettled since several studies reported that high-caloric diet consumption might protect the heart from I/R injury. Although several therapeutic strategies such as anti-diabetic drugs, natural compounds as well as treadmill exercise have been proposed to exert cardioprotection in the I/R heart in obese-insulin resistant animals, some interventions including ischemic post-conditioning failed to protect the heart from I/R injury. In this comprehensive review, reports from both genetic deletion and dietary-induced obese-insulin resistant animal models regarding the effects of obese-insulin resistance on metabolic parameters, cardiac function, infarct size, and molecular mechanisms under I/R injury are summarized. Moreover, the effects of anti-diabetic drugs and other pharmacological interventions on these parameters in an obese-insulin resistant model under I/R injury are also comprehensively summarized and discussed.

Keywords Obesity · Left ventricular function · Infarct size · Ischemia-reperfusion injury · Insulin resistance

Introduction

Obese-insulin resistance is a condition which can result from a high-caloric diet intake and impairment of energy balance [1, 2]. In basic research, the genetic deletion model and dietary-induced obesity have been widely used to demonstrate the characteristics of insulin resistance including weight gain and hyperinsulinemia with euglycemia [3–6]. It has been shown that obesity and insulin resistance increase the risk of ischemic heart disease [7]. In myocardial ischemia due to coronary artery occlusion, reperfusion therapy is an essential treatment to increase blood flow to the ischemic area. Although reperfusion increases the blood flow to the myocardium, it also generates serious oxidative stress which activates the cellular apoptotic pathway to induce myocardial cell death [8]. Since an obese-insulin resistant condition has been demonstrated to increase oxidative stress and is associated with increased coronary artery disease [5, 8, 9], ischemia-reperfusion (I/R) processes occurring under this condition could therefore provoke a greater oxidative stress production [10]. Moreover, this condition is known to relate to inflammatory cytokine accumulation, increased cell apoptosis, and decreased glucose utilization, leading to cardiac dysfunction and marked cell apoptosis [8, 11, 12].

Growing evidence indicates that improving pro-survival signaling and reducing inflammatory cytokines may exert cardioprotective effects in obese-insulin resistant models [13–16]. Currently, there is a growing number of reports available on the roles of obese-insulin resistance in the I/R

N. Apaijai · S. C. Chattipakorn · N. Chattipakorn
Cardiac Electrophysiology Research and Training Center, Faculty of Medicine, Chiang Mai University, Chiang Mai 50200, Thailand

N. Apaijai · N. Chattipakorn (✉)
Cardiac Electrophysiology Unit, Department of Physiology, Faculty of Medicine, Chiang Mai University, Chiang Mai 50200, Thailand
e-mail: nchattip@gmail.com

S. C. Chattipakorn
Department of Oral Biology and Diagnostic Sciences, Faculty of Dentistry, Chiang Mai University, Chiang Mai 50200, Thailand

heart [13–35]. However, inconsistent reports exist. Interestingly, despite the fact that pharmacological interventions given prior to I/R exerted cardioprotection [13–22, 32, 33], several pharmacological interventions as well as ischemic post-conditioning have been shown to fail to protect the heart when given after I/R injury [23, 27], thus indicating the importance of the timing of intervention. In this review, reports from both genetic deletion and various dietary-induced obese-insulin resistant animal models regarding the effects of obese-insulin resistance on metabolic parameters, cardiac function, infarct size, and molecular mechanisms under I/R injury are summarized. Moreover, the effects of anti-diabetic drugs and other pharmacological interventions on these parameters in an obese-insulin resistant model under I/R injury are also comprehensively presented and discussed. We used the electronic database PubMed as the source of selected articles published in English. Twenty-three pre-clinical studies were obtained using obesity, insulin resistance, and cardiac ischemia-reperfusion injury as keywords, and sixteen clinical trials were obtained using obesity, insulin resistance, and myocardial infarction as keywords.

Obese-Insulin Resistant Models and Changes in Metabolic Parameters

Growing evidence reported that obesity is associated with glucose intolerance and dyslipidemia [4]. Both genetic deletion and diet-induced obesity are widely used to replicate characteristics of metabolic syndrome in humans [6, 18, 20, 23, 25, 27, 30–33]. According to the International Diabetes Federation (IDF), the metabolic syndrome is defined as a person having central obesity (a waist circumference≥94 cm for men, and≥80 cm for women) plus any two of the following four factors including raised triglyceride level (≥150 mg/dL), reduced HDL cholesterol level (<40 mg/dL in males, and <50 mg/dL in females), raised blood pressure (systolic BP≥ 130 mmHg, Diastolic BP≥85 mmHg), and raised fasting plasma glucose levels (≥100 mg/dL). Genetic deletion models including Zucker obese rats and *ob/ob* mice are leptin receptor mutant animals which have been used in many reports. Zucker obese rats develop obese-insulin resistance which is characterized by increased body weight and hyperinsulinemia, but the plasma glucose level was still normal. However, Zucker diabetic fatty rats (ZDF) rats have an obese-insulin resistant condition similar to that in Zucker obese rats, but their plasma glucose level is high. The *ob/ob* mice and KK-A(y) mice develop obese-insulin resistance, however their blood glucose level was also increased [14, 18, 23, 31].

In addition to genetic deletion models of obese-insulin resistance, diet-induced obesity has also been commonly used for insulin resistant models to represent the human lifestyle. Either high-fat or high-carbohydrate food is usually chosen to induce obese-insulin resistance. Previous studies demonstrated that a high-fat diet (HFD) could increase body weight, plasma insulin, leptin, and cholesterol levels [13, 22, 33, 34], indicating the development of obese-insulin resistance. Insulin sensitivity is also impaired in HFD-fed rats as indicated by increased blood glucose levels during an oral-glucose tolerance test (OGTT) [22]. Thakker and colleagues demonstrated that the homeostatic model assessment (HOMA-IR) was also increased in HFD-fed rats, indicating insulin resistance [34]. The obese-insulin resistant condition was also observed in high-carbohydrate, high-fat high-carbohydrate as well as western diet fed animals [10, 21, 24–26, 28, 29]. Interestingly, Huisamen and colleagues reported that rats fed with diet-induced obesity (DIO) which contained 33 % condensed milk could induce hyperphagia, thus leading to obesity and insulin resistance, decreased plasma glucagon like peptide-1 (GLP-1), with unchanged plasma glucose level in these animals [15, 19]. The summary of these animal models of obese-insulin resistance with their metabolic parameter changes is shown in Table 1.

Effects of Obese-Insulin Resistance on the Heart Subject to I/R Injury

Obese-insulin resistance is known as a risk factor of ischemic heart disease [36, 37]. Although myocardial reperfusion is an important therapeutic approach in this setting, reperfusion itself could lead to an increase of oxidative stress and inflammatory responses [38, 39]. Previous studies investigated the effects of obese-insulin resistance as well as pharmacological interventions on the heart undergoing ischemia-reperfusion (I/R) injury [10, 13–22, 29, 31–33].

During I/R, left ventricular (LV) function is generally impaired. Sidell and colleagues showed that the percent recovery of LV developed pressure (LVDP) and the rate pressure produce were greatly reduced in Zucker obese rats compared to lean rats, suggesting worsening LV dysfunction [32]. In a diet-induced obesity (DIO) model, DIO-fed rats including high-caloric diet-fed rats, obesogenic diet-fed rats, and HFD-fed rats had increased LV dysfunction compared to the control during reperfusion in an ex vivo setting [15, 19, 21, 22, 25, 35]. Consistent with those ex vivo reports, in an in vivo study, DIO diet has been shown to cause worsening of LV dysfunction in obese pigs after I/R injury [26].

However, inconsistent reports exist. Ghaboura and colleagues reported that rats fed with HFD which contained 33 % fat for 4 weeks had similar LV dysfunction to that in normal diet fed rats in an ex vivo setting of I/R injury [13]. Moreover, Lekli and colleagues reported that the degree of LV dysfunction in Zucker obese rats during I/R was similar to that in lean rats. [20]. Interestingly, Donner and colleagues showed a cardioprotective effect of a high-carbohydrate diet; they

Table 1 Summary of the effects of obesity in various animal models on metabolic parameters prior to I/R injury

Model	Diet/ Duration	Major findings	Interpretation	Ref.
Genetic deletion models				
Zucker obese rats	Standard chow diet	- Increased plasma insulin and triglyceride levels - Plasma glucose level unchanged.	Zucker obese rats developed insulin resistance.	[27]
Zucker obese rats	Standard chow diet	Increased body weight, plasma insulin, and plasma glucose levels	Zucker obese rats developed obese-insulin resistance with hyperglycemia.	[20]
Zucker fatty rats	Standard chow diet	- Increased body weight, plasma free fatty acid, and triglyceride levels. - Plasma glucose level unchanged.	Zucker fatty rats developed obesity.	[32]
ob/ob mice	Standard chow diet	Increased body weight, blood glucose, insulin, and total cholesterol levels.	*ob/ob* mice developed obese-insulin resistance and hypercholesterolemia.	[18, 23, 31]
KK-A(y) mice	Standard chow diet	Increased body weight, plasma glucose, insulin, total cholesterol, triglyceride levels, and increased HOMA-IR	KK-A(y) mice developed obese-insulin resistance and hyperglycemia.	[14]
HFD				
HFD-fed rats	Diet containing 35 % fat, 4 weeks	Increased body weight, plasma insulin, triglyceride, and leptin levels	HFD-fed rats developed obese-insulin resistance.	[13]
HFD-fed rats	Diet containing 45 % fat, 6 weeks	Increased body weight, blood glucose, serum insulin, and FFA levels	HFD-fed rats developed obese-insulin resistance, hyperglycemia	[22]
HFD-fed rats	Diet containing 45 % kcal from fat, 12 weeks	- Increased body weight, plasma insulin, leptin, cholesterol levels - Blood glucose and triglyceride levels unchanged.	HFD-fed rats developed obese-insulin resistance.	[33]
HFD-fed rats	Diet containing 42 % kcal from fat, 24 weeks	Increased body weight, plasma insulin, glucose, and HOMA-IR levels	HFD-fed rats developed obese-insulin resistance, and hyperglycemia.	[34]
High-carbohydrate diet				
High-carbohydrate fed rats	Diet containing 82 % carbohydrate, 32 weeks	Increased body weight, triglyceride, and leptin levels.	High-carbohydrate fed rats developed obesity.	[24]
High-carbohydrate fed mice	Diet containing 66 % carbohydrate, 11–12 weeks	Increased body weight, plasma insulin, and leptin levels.	High-carbohydrate fed mice developed obese-insulin resistance.	[29]
High-fructose fed rats	Diet containing 66 % fructose, 4 weeks	Increased body weight, and plasma insulin levels.	High-fructose fed rats developed obese-insulin resistance.	[28]
DIO				
DIO-fed rats	Diet containing 65 % carbohydrate, 16 weeks	Increased body weight, visceral fat, plasma insulin, and free fatty acid	DIO-fed rats developed obese-insulin resistance.	[25]
DIO -fed rats	Diet containing 60 % carbohydrate, 16 weeks	Increased body weight, intraperitoneal fat, serum glucose, insulin, and angiotensin II levels	DIO-fed rats developed obese-insulin resistance and hyperglycemia.	[19]
DIO -fed rats	Diet containing 60 % carbohydrate, 16 weeks	- Increased body weight, intraperitoneal fat, plasma insulin levels - Reduced plasma GLP-1 level-Blood glucose was unchanged.	DIO-fed rats developed obese-insulin resistance.	[15]
DIO -fed rats	Diet containing 65 % carbohydrate, 16 weeks	- Increased body weight, visceral fat, serum insulin, leptin, triglyceride, HOMA-IR levels - Reduced serum high-density lipoprotein	DIO-fed rats developed obese-insulin resistance.	[21]
DIO -fed pigs	Diet containing 25 % coconut oil and 20 % high-fructose corn syrup, 7 months	Increased body weight, blood pressure, insulin, glucose, triglyceride, cholesterol, and area under the curve for glucose during intravenous glucose tolerance test	DIO-fed rats developed obese-insulin resistance and hyperglycemia.	[26]
DIO -fed rats	Diet containing 45 % fructose and 40 % fat, 4 weeks	Increased body weight	DIO-fed rats developed obesity.	[10]

**HFD* high-fat diet, *FFA* free fatty acid, *HOMA-IR* homeostasis model assessment for insulin resistance, *DIO* diet induced obesity

**DIO* diet-induced obesity, *GLP-1* glucagon like peptide-1, *HOMA-IR* homeostasis model assessment for insulin resistance

found that a high-carbohydrate diet improved LV function in rats after I/R injury [24]. These discrepancies among the different diet-induced obese-insulin resistant models could be partly attributed to the fact that the fat compositions in the diet used to feed the animals as well as the duration were not consistent. In genetic deletion models with I/R, the effects of obese-insulin resistance on the LV function are still unclear. However, inconsistent findings could be due to the different ages of animal used in those studies. A summary of reports on the effects of obese-insulin resistance on the LV function during I/R is shown in Table 2.

In addition to LV dysfunction, myocardial infarction is commonly observed after I/R injury. Several genetic deletion models of obesity including *ob/ob* mice and KK-A(y) mice demonstrated an increased infarct size after I/R injury compared with the wild-type (WT) mice [14, 23, 31]. The infarct size was also increased in diet-induced obese rats in an ex vivo setting with I/R [25, 35]. However, inconsistent findings exist in which some studies reported that the infarct size was not changed in Zucker obese rats as well as in diet induced obese-insulin resistant animals after I/R in both the in vivo and ex vivo setting compared with the control group [20, 27, 29, 33]. In addition, rats fed with high-carbohydrate [24] or high-fructose diet [28] have been shown to have smaller infarct size in an in vivo setting of I/R injury compared to normal diet group. A summary of reports on the effects of obese-insulin resistance on the infarct size during I/R is shown in Table 2.

Previous studies demonstrated that the mechanisms responsible for the impairment of LV function and increased infarct size involve an impairment of glucose utilization [20, 32], increased inflammatory response [14, 22], impaired insulin signaling [19] and reperfusion injury salvage kinase (RISK) signaling [35]. In obesity with I/R injury, TNF-α which is a pro-inflammatory cytokine has been shown to increase [14, 22]. It activates TNF-α receptors which then activate other key molecules which are responsible for causing insulin resistance [40]. In addition, TNF-α also activates IκB kinase (IKK), causing the phosphorylation of IκBα, leading to nuclear translocation of NF-κB and promoting inflammatory cytokines gene expression, thus resulting in an accumulation of inflammation [40]. Moreover, TNF-α activates JNK pathway which is a stress signal, thus promoting a phosphorylation of insulin receptor substrate-1 (IRS-1) at the serine residue [41, 42]. Under normal conditions, IRS-1 is usually phosphorylated at the tyrosine residue to promote normal insulin signaling and maintain normal glucose utilization [43, 44]. Under the insulin resistant condition, serine phosphorylation can cause a reduction in Akt-phosphorylation [15, 19, 35], leading to a reduction of the glucose transporter-4 (GLUT-4) membrane translocation. Evidences demonstrated that GLUT-4 was reduced in obese-insulin resistant rats with or without I/R injury [20, 32]. Further studies are needed to elucidate the possible synergistic effect of I/R on GLUT-4 reduction in obese-insulin resistant subjects. Furthermore, Akt is also involved in the RISK pathway. The RISK pathway consists of Akt and ERK signaling which are the pro-survival kinases, which can promote cardioprotection during I/R injury [8]. In the obese-insulin resistant condition, ERK1/2 and Akt phosphorylation are decreased [15, 19, 35]. Moreover, a phosphorylation of eNOS (downstream of Akt) is also reduced [19, 35]. These effects can activate pro-apoptotic signaling and mitochondrial permeability transition pore (mPTP) opening, leading to cell apoptosis and LV dysfunction in obese-insulin resistant animals [30]. However, there is a study which demonstrated that during I/R high-carbohydrate diet induced obese-insulin resistant rats had increased Akt, GSK3β, and eNOS phosphorylation [24], indicating cardioprotection in these high carbohydrate-fed rats. A summary of reports regarding the proposed mechanisms for obese-insulin resistance on the cardiac function and infarct size during I/R periods is shown in Table 2. All of these findings suggest that genetic deletion or diet-induced obese-insulin resistance can greatly impair cardiac function and increase infarct size through an excessive release of inflammatory cytokines, an impairment of insulin signaling, a reduction of glucose utilization, and an inhibition of the RISK pathway during I/R injury (Fig. 1). Additionally, the heart requires adenosine triphosphate (ATP) to maintain normal cardiac function. ATP is generated from both free fatty acid (FFA) and carbohydrate. Under physiological conditions, FFA from both the plasma and the intracellular triacylglycerol storage are the major oxidative source (70 %) in the heart, with a lesser contribution from carbohydrate [45]. However, it has been shown that the heart is able to change the major source of energy supply from FFA to carbohydrate under stress conditions. For example, during ischemia oxygen supply is disrupted, and carbohydrate oxidation becomes a major source of ATP production in the heart [46] This process is known as metabolic flexibility. In the heart, metabolic flexibility is its ability to alter fuel oxidation to fuel availability [47]. Under insulin resistant conditions, an impairment of insulin signaling occurs, followed by reduced glucose uptake and reduced ability of the heart to use glucose as a substrate for ATP production [48]. Thus, a large amount of FFA is delivered to the heart, and it has been implicated in the accumulation of intracellular lipids. However, excess FFA can increase intracellular oxidative stress [47, 49]. Since insulin-resistant heart have difficulties in using glucose as a substrate for energy production, myocardial ischemia in the insulin resistant heart could lead to ATP depletion, along with severe oxidative stress generated after ischemia and reperfusion. These factors can result in left ventricular dysfunction and increased myocardial infarct size in obese-insulin resistant rats, when compared with normal rats.

Table 2 Summary of the effects of obese-insulin resistance on LV function, infarct size, and molecular mechanism in the I/R heart

Models	I/R protocol (Ischemia/reperfusion duration)	Major findings			Interpretation	Ref.
		LV function	Infarct size	Molecular mechanism		
Genetic deletion models						
Zucker obese rats	*ex vivo* Global ischemia (30-min/120-min)	↔	↔	Reduced GLUT-4 expression compared with WT	Although Zucker obese rats and normal rats had similar degree of LV dysfunction and infarct size, Zucker obese rats had reduced glucose utilization compared to lean rats	[20]
Zucker fatty rats	*ex vivo* Low-flow ischemia (32-min/32-min)	↓	N/A	Reduced GLUT-4 expression	LV dysfunction was worsening in Zucker rats, compared to lean rats through reduced glucose utilization	[32]
Zucker obese rats	*in vivo* Left coronary artery (LCA) ligation (25-min/120-min)	N/A	↔	N/A	Zucker obese rats and normal rats had similar degree of infarct size during I/R injury.	[27]
ob/ob mice	*in vivo* Coronary artery ligation (30-min/24-h)	N/A	↑	N/A	*ob/ob* mice had larger infarct size than wild-type mice.	[23, 31]
KK-A(*y*) mice	*in vivo* LCA ligation (40-min/72-h)	N/A	↑	- Increased neutrophil and macrophage infiltration - Increased TNFα, MIP-2, MCP-1, and KC	KK-A(*y*) mice had larger infarct size than normal rats due to an increasing of the inflammatory responses.	[14]
HFD						
HFD-fed rats	*ex vivo* Global ischemia (25-min/30-min)	↔	N/A	Phosphorylation of Akt and ERK were not changed	HFD-fed rats had similar degree of LV dysfunction, and HFD did not impair survival pathway in I/R heart compared to normal diet-fed rats.	[13]
HFD-fed rats	*ex vivo* Global ischemia(20-min/30-min)	↓	N/A	Reduced HSP 72 expression and increased serum TNFα	LV dysfunction was worsening in HFD-fed rats compared to normal diet-fed rats.	[22]
HFD-fed rats	*in vivo* Left coronary artery ligation (25-min/120-min)	N/A	↔	N/A	HFD rats and normal diet-fed rats had similar degree of infarct size during I/R injury.	[33]
High-carbohydrate diet						
High-carbohydrate fed rats	*ex vivo* Global ischemia (25-min/60-min)	↑	↓	Increased Akt, GSK3β, membrane eNOS phosphorylation	High-carbohydrate diet improved LV function and reduced infarct size via improved RISK signaling during I/R compared to normal diet fed rats.	[24]
High-carbohydrate fed mice	*ex vivo*Global ischemia (35-min/45-min)	N/A	↔	N/A	High-carbohydrate fed rats and normal diet-fed rats had similar degree of infarct size during I/R injury.	[29]
High-fructose fed rats	*in vivo* Left coronary artery ligation (30-min/4-h)	N/A	↓	N/A	High-fructose fed rats had smaller infarct size than normal diet-fed rats.	[28]
DIO						
DIO-fed rats	*ex vivo* LAD ligation (40-min/120-min)	↓	↑	N/A	LV function was worsening and infarct size was larger in DIO-fed rats compared to normal diet-fed rats.	[25]
DIO-fed rats	*ex vivo* LAD ligation (35-min/60-min)	↓	N/A	Reduced insulin-induced Akt, eNOS, and IRS-1 phosphorylation	LV function was worsening in DIO-fed rats compared to normal diet-fed rats due to an impairment of insulin signaling pathway.	[19]
DIO-fed rats	*ex vivo* Low-flow ischemia (45-min/30-min)	↓	N/A	Reduced PKB/Akt^{ser473} and ERK42/44 phosphorylation	LV function was worsening in DIO-fed rats compared to normal diet-fed rats due to an impairment of survival pathway e.g. Akt and ERK	[15]
DIO-fed rats	*ex vivo* LAD ligation (40-min/2-h)	↓	N/A	N/A	LV function was worsening in DIO-fed rats compared to normal diet-fed rats.	[21]
DIO-fed pigs	*in vivo* LAD ligation (45-min/120-min)	↓	N/A	N/A	LV function was worsening in DIO-fed pigs compared to normal diet-fed pig.	[26]

Table 2 (continued)

Models	I/R protocol (Ischemia/reperfusion duration)	Major findings			Interpretation	Ref.
		LV function	Infarct size	Molecular mechanism		
DIO-fed rats	*ex vivo* Coronary artery ligation (40-min/30-min)	↓	↑	Reduced Akt and eNOS phosphorylation	LV function was worsening and infarct size was larger in DIO-fed rats compared to normal diet-fed rats due to an impairment of RISK pathway.	[35]

**LCA* left coronary ligation, *LVDP* left ventricular developed pressure, *LV* left ventricle, *N/A* not assessed

**HFD* high-fat diet, *LVDP* left ventricular developed pressure, *LV* left ventricle, *RISK* reperfusion injury salvage kinase, *N/A* not assessment

**LAD* left anterior descending coronary artery, *DIO* diet induced obesity, *LV* left ventricle, *RISK* reperfusion injury salvage kinase, *N/A* not assessment

**DIO* diet- induced obesity, *LAD* left anterior descending coronary artery, *N/A* not assessment, *LV* left ventricle

Effects of Anti-Diabetic Drugs on LV Function and Infarct Size in Obese-Insulin Resistance with I/R

During I/R periods, cardiac function is markedly impaired in obese-insulin resistant animals. Although anti-diabetic drugs that effectively improve insulin sensitivity have been shown to reduce insulin resistance in various animal models [14,15, 32,] data regarding their effects on LV function during I/R are still limited since there are only a few studies investigating this issue. Several studies have shown that both insulin and PPAR-δ agonists given prior to I/R injury improved LV function in obese-insulin resistant rats in both in vivo and ex vivo settings [16, 17, 32]. Furthermore, Cardenas and colleagues reported that insulin could reduce the incidence of ventricular tachycardia in diet-induced obese-insulin resistant rats during I/R in an ex vivo setting [17]. However, unlike insulin and

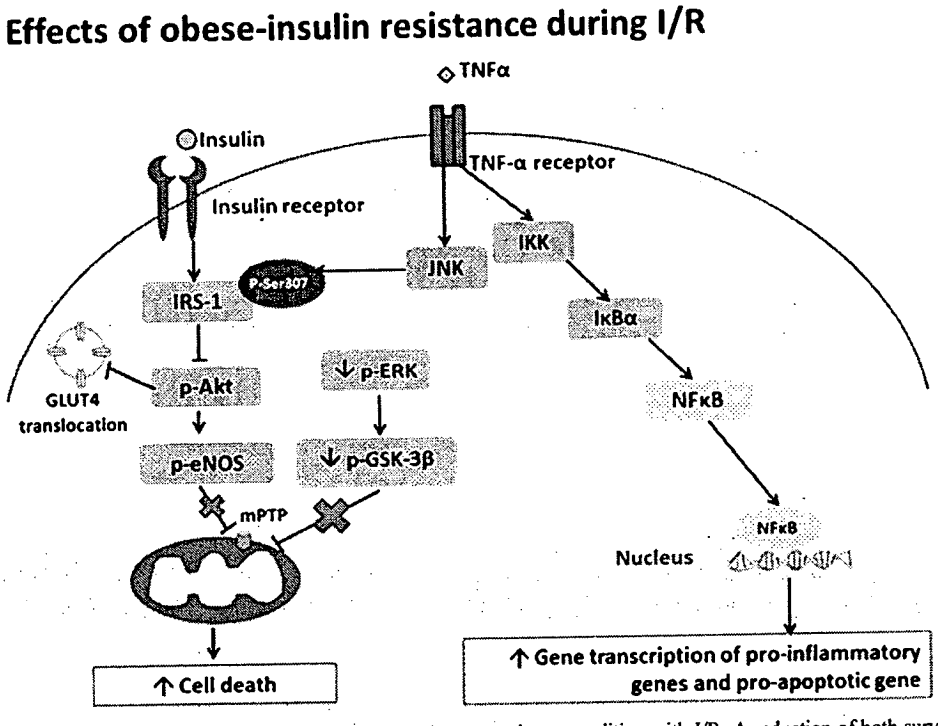


Fig. 1 Effects of obese-insulin resistance on the heart subject to I/R. During I/R injury, inflammatory cytokines such as TNF-α are increased in obese-insulin resistance, and could induce pro-inflammatory and pro-apoptotic gene transcription, and impair insulin signaling and RISK pathway. Moreover, TNF- α activates JNK which impairs insulin signaling by phosphorylating IRS-1 on serine 307 residue and inhibiting Akt phosphorylation, leading to inhibition of GLUT-4 translocation. In addition, a reduction of ERK phosphorylation was observed in obese-insulin resistant condition with I/R. A reduction of both survival kinases causes mPTP opening, resulting in LV dysfunction and increased infarct size in obese-insulin resistant rats. TNF-α; tumor necrosis factor-alpha, IKK; the I kappa B kinase, NFκB; nuclear factor kappa-light-chain-enhancer of activated B cells, IRS-1; insulin receptor substrate-1, GLUT-4; glucose transporter-4, mPTP; mitochondrial permeability transition pore, eNOS; endothelial nitric oxide synthase

Table 3 Effects of anti-diabetic drugs on LV function, infarct size, and molecular mechanism in obese-insulin resistance animal models with cardiac I/R

Model	I/R protocol (Ischemia/ reperfusion duration)	Drug/ Dose/ Route	Major findings			Interpretation	Ref.
			LV function	Infarct size	Molecular mechanism		
Genetic deletion models							
Zucker obese rats	*in vivo* LAD ligation (30-min/4-h)	PPAR-δ agonist, 10 mg/kg/day, PO, 7 days prior to I/R	↑	↓	-Reduced serum IL-6, IL-8, apoptotic myocytes, caspase-3 activity, Bax, and Bid expression - Increased Bcl-2, PDK2, and Akt expression	PPAR-δ agonist improved LV function and reduced infarct size via reduced inflammation, apoptosis, and increased pro-survival signaling in Zucker obese rats compared to Zucker obese rats treated with vehicle.	[16]
Zucker fatty rats	*ex vivo* Low-flow ischemia (32-min/32-min)	Rosiglitazone, 3 mg/kg/day, PO, 7 days prior to I/R	↑	N/A	Prevented the greater loss of ATP and restored GLUT4 expression	Rosiglitazone improved LV function via improved glucose utilization in Zucker fatty rats compared to Zucker fatty rats treated with vehicle.	[32]
KK-A(*y*) mice	*in vivo* Left coronary artery ligation (25-min/120-min)	Pioglitazone, 25 mg/kg/day, IP, 14 days prior to I/R	N/A	↓	Reduced neutrophil and macrophage infiltration, MCP-1, KC, TNFα, and MMP-9	Pioglitazone reduced infarct size via reduced inflammation in KK-A(*y*) mice compared to KK-A(*y*) mice treated with vehicle.	[14]
HFD							
HFD-fed rats	*in vivo* Left coronary artery ligation (25-min/120-min)	AMPK activator (A769662), 6 mg/kg, IP, 30 min prior to I/R	N/A	↓	Increased $AMPK^{Thr172}$ and eNOS phosphorylation, and myocardial nitrite and nitrate levels	AMPK activator reduced infarct size via improved AMPK activation and vascular endothelial function in HFD rats compared with control HFD rats.	[33]
DIO							
DIO-fed rats	*ex vivo* Low-flow ischemia (45-min/30-min)	DPP-4 inhibitor (PFK275-055), 10 mg/kg day, PO, 4 weeks prior to I/R	↔	↓	Increased PKB/Akt^{scr473} and ERK 42/44 phosphorylation	DPP-4 inhibitor did not improve LV function but reduced infarct size in DIO rats compared to DIO-fed rats treated with vehicle. The beneficial effect could be due to DPP-4 improved cardiac signaling including Akt and ERK	[15]
DIO-fed rats	*ex vivo* Global ischemia (25-min/15-min)	Insulin, 50 μU/ml, bolus prior to I/R	↑	N/A	N/A	Insulin improved LV function and reduced arrhythmia in DIO rats compared with control rats.	[17]

**LAD* left anterior descending coronary artery, *HFD* high-fat diet, PPAR-δ; peroxisome proliferator-activated receptor delta, *PO* per oral, *IP* intraperitoneal, *I/R* ischemia reperfusion, *AMPK* AMP-activated protein kinase, *LV* left ventricle, *LVDP* left ventricular developed pressure, *IL* interleukin, *GLUT* glucose transporter, *eNOS* endothelial nitric oxide synthase, *AMPK* AMP-activated protein kinase, *MCP* monocyte chemoattractant protein, *KC* keratinocyte chemoattractant, *MMP-9* matrix metallopeptidase-9, *TNFα* tumor necrosis factor alpha, *N/A* not assessment

**DIO* diet induced obesity, *DPP-4* dipeptidyl peptidase-4, *PO* per oral, I/R; ischemia/reperfusion, *N/A* not assessment, *LV* left ventricle

PPAR-δ agonist, chronic treatment with DPP-4 inhibitors has failed to improve LV function which was impaired in diet-induced obese-insulin resistant rats after I/R [15]. A summary of reports on the effects of anti-diabetic drugs on LV function during I/R in obese-insulin resistant models is shown in Table 3.

Although the effect of obese-insulin resistance on myocardial infarct size (as discussed earlier) remains controversial [14, 20, 23, 27, 29, 31, 33, 35], anti-diabetic drugs have been shown consistently to reduce the infarct size during I/R in obese-insulin resistant animals [14, 15, 32]. In genetic deletion models, Honda and colleagues reported that chronic pioglitazone treatment reduced the infarct size in a KK-A(y) mice with I/R [14]. In diet-induced obese-insulin resistant rat models, chronic DPP-4 inhibitor treatment reduced the infarct size after I/R in an ex vivo setting [15]. Moreover, AMPK activator also reduced the infarct size by 33 % [33] in an in vivo setting of I/R. A summary of reports regarding the effects of anti-diabetic drugs on the infarct size in I/R hearts of obese-insulin resistant models are shown in Table 3.

Mechanisms by which anti-diabetic drugs protected the obese-insulin resistant heart from I/R injury including improved LV function and reduced infarct size have been investigated (Table 3). The cardioprotective effects of these drugs involve insulin signaling, RISK signaling, an energy homeostasis signaling (AMPK), and inflammatory responses. For insulin signaling, the PPAR-δ agonist rosiglitazone has been shown to reduce serum glucose levels, infarct size, improve LV function in an I/R setting by increasing GLUT-4 expression and reduce ATP loss during I/R, suggesting that rosiglitazone protected the heart against I/R by improved glucose utilization in obese-insulin resistant rats [32]. For RISK signaling, chronic DPP-4 inhibitor treatment has been shown to protect the heart from I/R injury via an activation of the PKB/Akt and ERK signaling, which are key proteins of pro-survival signaling [15]. Phosphorylation of Akt and ERK has been shown to inhibit mPTP opening in the mitochondria during the reperfusion period [11, 12]. During ischemia, mPTP remains closed and will be opened once the myocardium is reperfused [50]. Opening of the mPTP causes a release of cytochrome *c* which activates a caspase cascade, leading to cell death [51]. DPP-4 inhibition has been shown to reduce cell death through an improved pro-survival signaling in obese-insulin resistant animals.

Five Adenosine monophosphate-activated protein kinase (AMPK) is known to play a part in regulating cellular energy homeostasis [33, 52]. During I/R, energy depletion was observed and disrupted cellular energy homeostasis. Metformin is an anti-diabetic drug which reduces ATP depletion during I/R by activating AMPK signaling and has been shown to protect the heart during I/R injury [53]. Song and colleagues reported that AMPK activation increased phosphorylation of $AMPK^{thr172}$ and eNOS, and exerted cardioprotection after I/R injury in HFD induced obese-insulin resistant rats [33].

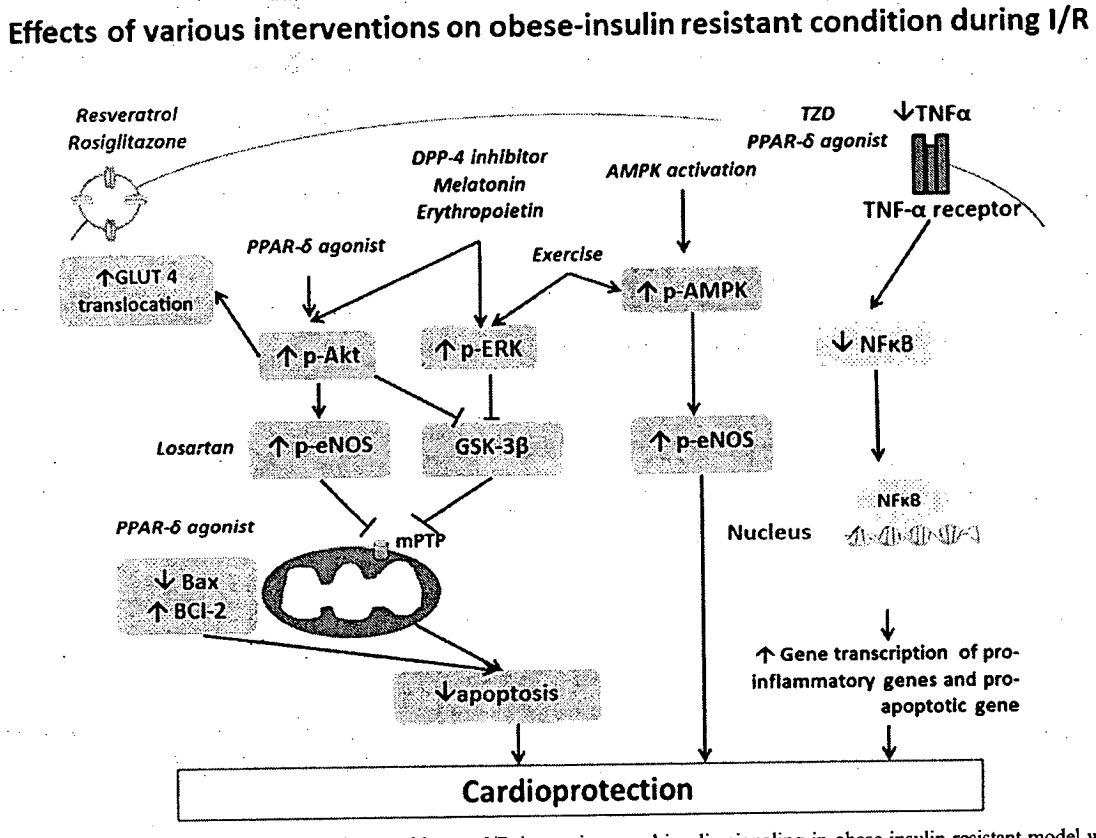


Fig. 2 Effects of various interventions on the heart subject to I/R in obese-insulin resistant models. Pre-treatment with DPP-4 inhibitors, melatonin, erythropoietin, PPAR-δ agonist, resveratrol, losartan, and TZD has been shown to exert cardioprotection in obese-insulin resistant condition. TZD and PPAR-δ agonists protect the heart against I/R by reducing pro-inflammatory and pro-apoptotic gene transcription. Furthermore, PPAR-δ agonists, DPP-4 inhibitors, melatonin, erythropoietin, and exercise improve LV function and decrease infarct size by increased pro-survival signaling (Akt and ERK) which could prevent mPTP opening and inhibit apoptotic pathways. Moreover, resveratrol and rosiglitazone improved insulin signaling in obese-insulin resistant model with I/R by increasing GLUT-4 translocation. Exercise and AMPK activation prevent LV dysfunction through an activation of AMPK. DPP-4; dipeptidyl-peptidase-4, TZD; thiazolidinedione, PPAR-δ; peroxisome proliferator activated delta, TNF-α; tumor necrosis factor-alpha, NFκB; nuclear factor kappa-light-chain-enhancer of activated B cells, eNOS; endothelial nitric oxide synthase, AMPK; 5' adenosine monophosphate-activated protein kinase, mPTP; mitochondrial permeability transition pore, GLUT-4; glucose transporter-4, LV; left ventricle

Author's personal copy

In addition to insulin and RISK and AMPK signaling, inflammatory responses are important mechanisms responsible for LV dysfunction and myocardial infarction during cardiac I/R injury. PPAR-δ agonists have been shown to exert cardioprotective effects during I/R injury by reducing inflammatory cytokines [14, 16]. Furthermore, Yue and colleagues demonstrated that PPAR-δ agonists could reduce apoptotic signaling including caspase-3 activity and Bax expression, and increase phosphorylation of pro-survival proteins such as Bcl-2 and Akt [16], suggesting that cardioprotective effects of PPAR-δ agonists could be due to an anti-inflammatory as well as an anti-apoptotic property of this drug. Table 3 summarizes the reports regarding the involved mechanisms of anti-diabetic drugs responsible for cardioprotection during I/R in obese-insulin resistant animal models. The proposed mechanisms of the cardioprotection of those anti-diabetic drugs are also illustrated in Fig. 2.

Effects of Other Interventions on LV Function and Infarct Size in Obese-Insulin Resistance with I/R Heart

In addition to anti-diabetic drugs, several treatment strategies have been used to attenuate cardiac dysfunction during I/R in various models of obese-insulin resistance. These reports include the effects of resveratrol, geranylgeranylacetone (GGA), erythropoietin, and melatonin on LV function during I/R, which demonstrated that they improved LV function in both in vivo and ex vivo settings [13, 20–22]. In addition, chronic treatment with resveratrol also reduced arrhythmias during I/R [17, 20]. Although losartan (an angiotensin II receptor antagonist drug used to treat hypertension) had no effect on metabolic parameters, it increased the percentage of recovery of aortic output and total work in diet-induced obese rats during I/R in an ex vivo setting [19]. Thus, the effects of these interventions on LV function may not be solely depending on their effects on improved metabolic parameters. However, cyclosporin A, an mPTP blocker, given at the end of coronary artery occlusion failed to improve LV function which was impaired during I/R [15, 27]. In addition, Liu and colleagues evaluated the effects of dietary modification on LV function, and reported that high-fat low-carbohydrate diet given as a dietary modification impaired LV function in an ex vivo setting of I/R compared with low-fat control diet [10]. A summary of these reports is shown in Table 4.

In addition to LV function, the effects of other interventions besides anti-diabetic drugs on infarct size in the hearts of obese-insulin resistant models during I/R have been investigated. Treatment with erythropoietin, resveratrol, melatonin, N,N,N-trimethylspingosine, and losartan has been shown to significantly decrease infarct size due to I/R in obese-insulin resistant rats [13, 18, 19, 21]. Pons and colleagues reported that treadmill exercise for 4 weeks also reduced infarct size in *ob/ob* mice subject to I/R injury [31]. In contrast, the role of ischemic post-conditioning on infarct size in obese-insulin resistant models is still controversial since it has been shown to reduce the infarct size in an ex vivo setting [29], whereas no benefit was found in the in vivo setting [23]. Moreover, cyclosporin A given at the end of coronary artery occlusion failed to reduce the infarct size in Zucker obese rats [27]. These findings suggest that the timing of pharmacological interventions and exercise during I/R periods may influence the change in infarct size caused by I/R in obese-insulin resistant animals. A summary of these reports is shown in Table 4.

Similar to the cardioprotective mechanisms of anti-diabetic drugs, the mechanisms responsible for the cardioprotection of these interventions and exercise has been proposed to involve improved glucose utilization [20], improved survival signaling [13, 21, 31], and reduced cellular apoptosis [13]. Lekli and colleagues reported that resveratrol exerts cardioprotection via improved glucose utilization by increasing GLUT-4 expression in obese-insulin resistant rats with cardiac I/R [20]. For survival signaling, melatonin, erythropoietin, and losartan have been shown to increase Akt, ERK, and eNOS phosphorylation which are pro-survival signals involved in the RISK pathway [19, 21, 31]. In addition, erythropoietin also reduces apoptotic nuclei, and is believed to have an infarct-limiting effect in HFD-induced obese insulin resistant rats with I/R [13]. Furthermore, Pons and colleagues demonstrated that phosphorylation of AMPK also increased in *ob/ob* mice treated with treadmill exercise prior to I/R injury, suggesting that exercise could reduce infarct size by improved cellular energy homeostasis [31].

During I/R injury, p38 mitogen-activated protein kinase (p38 MAPK) and Heat Shock protein (HSP 72) have been shown to be involved in cellular stress responses [54]. Nduhirabandi and colleagues demonstrated that treatment with melatonin for 16 weeks prior to I/R injury could reduce p38 MAPK phosphorylation compared to their control in DIO-fed rats, suggesting that melatonin protected the I/R heart via reduced cellular stress response [21]. Several studies have shown that HSP72 overexpression exerts cardioprotection by inhibiting activation of caspase-9 and caspase-3 which are apoptosis markers [55, 56]. Ooie and colleagues reported that geranylgeranylacetone (GGA) could increase HSP72 expression in HFD-fed rats with I/R injury [22], leading to reduced cell apoptosis after I/R. However, ischemic post-conditioning failed to protect the heart against I/R injury since it had no effects on any survival

Table 4 Effects of other pharmacological interventions on LV function, infarct size, and molecular mechanism in obese-insulin resistance animal models with cardiac I/R

Model	I/R protocol (Ischemia/ reperfusion duration)	Drug/ Dose/ Route	Major findings			Interpretation	Ref.
			LV function	Infarct size	Molecular mechanism		
Genetic deletion models							
Zucker obese rats	*ex vivo* Global ischemia (30-min/120-min)	Resveratrol, 5 mg/kg/day, PO, 14 days prior to I/R	↑	↓	Increased GLUT-4 expression	Resveratrol improved LV function, reduced arrhythmia, and infarct size via improved glucose utilization in Zucker obese rats compared to vehicle treated Zucker obese rats.	[20]
Zucker obese rats	*in vivo* Left coronary artery ligation (25-min/120-min)	Cyclosporin A, 5 mg/kg, IV, at the end of occlusion	↔	↔	N/A	Cyclosporin A did not improve LV and did not reduce infarct size in Zucker obese rats compared to vehicle treated Zucker obese rats.	[27]
ob/ob mice	*in vivo* Left coronary artery ligation (30-min/24-h)	N,N,N-trimethylsphinggosine (TMS), 0.025 mg/kg, IV, at the onset of occlusion	N/A	↓	N/A	TMS reduced infarct size in *ob/ob* mice compared to vehicle treated *ob/ob* mice	[18]
ob/ob mice	*in vivo* Coronary artery ligation (30-min/24-h)	Ischemic post-conditioning	N/A	↔	Post-conditioning had no effects on Akt and ERK1/2 phosphorylation	Ischemic post-conditioning could not protect the heart from I/R injury in *ob/ob* mice.	[23]
ob/ob mice	*in vivo* Coronary artery ligation (30-min/24-h)	Treadmill exercise, 5 days/ week, 4 weeks prior to I/R	N/A	↓	Increased Akt, p70S6K, ERK, and AMPK phosphorylaiton	Treadmill exercise reduced infarct size via improved survival signaling and reduced apoptosis in *ob/ob* mice compared to vehicle treated *ob/ob* mice.	[31]
HFD							
HFD-fed rats	*ex vivo* Global ischemia (25-min/30-min)	Erythropoietin, 1,000 IU/Kg, bolus, at the onset of reperfusion	↑	↓	- Increased Akt, ERK, MEK1/2, and Raf phosphorylation - Reduced apoptotic nuclei	Erythropoietin improved LV function and reduced infarct size via improved glucose utilization in HFD rats	[13]
HFD-fed rats	*ex vivo* Global ischemia (20-min/30-min)	GGA, 200 mg/kg, PO, 24-h prior to I/R	↑	N/A	Increased HSP72 expression	GGA improved LV function via increased HSP72 expression in HFD rats.	[22]
High-carbohydrate diet							
High-carbohydrate fed rats	*ex vivo* Global ischemia (35-min/45-min)	Ischemic post-conditioning, 10secI/R, 6 cycles	N/A	↓	N/A	Ischemic post-conditioning reduced infarct size in high-carbohydrate fed rats.	[29]
DIO							
DIO-fed rats	*ex vivo* LAD ligation (35-min/60-min)	Losartan, 10 mg/kg/day, PO, 7 dyas prior to I/R	↑	↓	Increased insulin-induced eNOS^{ser1177} phosphorylation	Losartan improved LV function and reduced infarct size via improved vascular endothelial function in DIO rats.	[19]
DIO-fed rats	*ex vivo* LAD ligation (40-min/2-h)	Melatonin, 4 mg/kg, PO, 16 weeks prior to I/R	↑	↓	- Increased PKB/Akt^{ser473} and ERK 42/44 and reduced p38 MAPK phosphorylation	Melatonin improved LV function and reduced infarct size via improved RISK, and reduced stress pathway in DIO rats.	[21]
DIO-fed rats	*ex vivo* Low-flow ischemia (60-min/60-min)	High-fat low-carbohydrate diet (diet modification), 2 weeks prior to I/R	↓	N/A	- Decreased SOD, glutathione peroxidase, nuclear respiratory factor 1, and mitochondrial transcription factor A	Changing from high-carbohydrate to low-carbohydrate diet caused worsening LV dysfunction due to a reduction of anti-oxidant enzymes and mitochondrial biogenesis in high-fat fed DIO rats.	[10]

**IV* intravenous, *LVDP* left ventricular developed pressure, *VF* ventricular fibrillation, *N/A* not assessment, *LV* left ventricle, *GLUT* glucose transporter

**PO* per oral, *I/R* ischemia/reperfusion, *LVDP* left ventricular developed pressure, *N/A* not assessment, *LV* left ventricle, *HFD* high-fat diet, *DIO* diet induced obesity, *HSP* heat shock protein, *eNOS* endothelial nitric oxide synthase, *SOD* superoxide dismutase

Table 5 Effects of obesity during myocardial infarction in clinical studies

Model	Number	Major findings	Interpretation	Ref.
Obese patients	158,546	- Increased ischemic heart disease hospitalization	Obesity increased risk of hospitalization for ischemic heart disease.	[57]
Obese patients with STEMI	451	- E/A ratio were lower in the obese group. - BMI was independently associated with E/A. - Ejection fraction, wall motion score index, and myocardial S velocities were comparable among normal weight, overweight, and obese groups.	Obesity impaired diastolic function in patient with STEMI	[59]
Obese patients with coronary artery disease	7,479	- HbA1c was increased and associated with increasing risk of cardiovascular adverse outcomes and all-cause mortality including nonfatal myocardial infarction.	Obesity increased risk of myocardial infarction.	[58]
Obese patients with non-ST elevation acute coronary syndrome	6,560	- The highest waist circumference group had a higher risk of cardiovascular death, myocardial infarction, or recurrent ischemia.	Central obesity increased risk of cardiovascular death and myocardial infarction.	[60]
Obese patients with ST-segment elevation acute myocardial infarction	3,734	- The highest mortality rate was observed in the highest waist hip ratio and low BMI groups.	Central obesity increased mortality rate.	[61]
Obese patients with chronic heart failure	979	- Obese patients had a higher rate of pump failure death. - Sudden death rate was not different between lean and obese patients.	Obesity increased risk of pump failure death but not sudden death.	[62]
Obese patients with acute myocardial infarction	6,676	- Increasing waist to hip ratio increased mortality rate	Central obesity increased mortality rate.	[63]
Obese patients with post-acute myocardial infarction	6,632	- All-cause mortality was not different between obese and non-obese patients.	Obesity did not increase all-cause mortality.	[64]
Obese patients after myocardial infarction and LV dysfunction	1,231	- All-cause mortality and sudden cardiac death were lower in obese patient	Obesity reduced mortality and sudden cardiac death.	[65]
Obese patients with myocardial infarction	89	- Increasing BMI was associated with decreased morbidity and mortality compared with normal-weight patients.	Obesity reduced morbidity and mortality.	[67]
Obese patients with myocardial infarction	22,576	- Infarct size was smaller in obese patients than normal body weight patients.	Obesity reduced infarct size.	[66]

protein signaling [23]. Moreover, diet modification from DIO to high-fat low-carbohydrate diet significantly impaired LV function by reducing antioxidants including superoxide dismutase (SOD), and impairing mitochondrial function by reduced mitochondrial biogenesis markers [10]. The summary of these reports is shown in Table 4.

Table 6 Effects of various interventions on obesity during myocardial infarction in clinical studies

Model	Number	Treatment	Major findings	Interpretation	Ref.
Obese patients with acute coronary syndrome	7,427	Percutaneous intervention, 5-years follow-up	- Obese patients had a higher rate of target vessel revascularization and early stent thrombosis.	Obesity increased stent thrombosis after percutaneous intervention.	[72]
Obese patients with ST segment elevation acute myocardial infarction	3,076	Percutaneous intervention	- Final thrombolysis in myocardial infarction flow grade not different between normal and obese groups.	Obesity did not increased adverse cardiac effects.	[71]
Obese patients with multi-vessel coronary artery disease	607	Sirolimus-eluting stents in the arterial revascularization therapies, 1-year follow-up	- Incidence of death, myocardial infarction, and repeated revascularization not different between normal and obese patients.	Obesity did not increase adverse cardiac effects.	[70]
Obese patients with coronary artery disease	1,314	Coronary artery bypass graft surgery and lovastatin, 40–80 mg/day, 4–5 years follow-up	- Aggressive statin treatment reduced death, non-fatal myocardial infarction, stroke, CABG surgery, or angioplasty compared with placebo group.	Lovastatin may be protective against obesity-related acceleration of coronary heart disease.	[74]
Obese patients with myocardial infarction	31	Physical training, 12 weeks	- Reduced blood insulin and glucose level compared with baseline	Physical training improved insulin resistance in obese patients with myocardial infarction.	[73]

Effects of Obesity and Myocardial Infarction in Clinical Studies

The association between obesity, insulin resistance and myocardial infarction has been shown in previous clinical studies. Joshy and colleagues reported that the number of hospitalizations from ischemic heart disease and risk of myocardial infarction were greater in obese patients than normal patients [57, 58]. In obese patients with MI, diastolic dysfunction was observed and was associated with an increased body mass index (BMI) [59]. Furthermore, obese patients with acute myocardial infarction and chronic heart failure have a higher mortality rate than normal patients [60–63]. However, the effect of obesity during myocardial infarction is still controversial. Wu and colleagues reported that the mortality rate was not different between obese and normal patients [64]. Moreover, several studies have shown that mortality rate and infarct size were lower in obese than normal patients [65–67]. The obesity paradox is a complex phenomenon, which may occur in heart failure patients who have a higher BMI or waist circumference. Several studies have demonstrated that these patients have a better chance of survival, with better prognosis when compared with the normal-weight heart failure patient [68, 69]. However, the mechanism responsible for the beneficial effects of the obesity paradox on the heart with myocardial infarction is still unclear, and those studies are limited in numbers, and the sample size in those studies is small. Additionally, there is only one study investigating the effect of obesity on infarct size in obese patients. Reports regarding the effects of obesity in myocardial infarction patients are summarized in Table 5.

A growing list of reports concerns the effects of obesity on various treatments in myocardial infarction patients. Although obesity does not increase adverse cardiac effects and mortality rate [70, 71], Sarno and colleagues demonstrated that early stent thrombosis was observed in obese patients with myocardial infarction after treatment with percutaneous intervention [72]. On the other hand, several studies tested the effects of pharmacological interventions and exercise in obese patients with myocardial infarction, and found that aggressive treatment with lovastatin protected the heart against acceleration of coronary heart disease, and physical training could reduce insulin resistance in obese patients [73, 74]. Although data regarding the effects of obesity on the heart and mortality rate during myocardial infarction are still limited, treatment with lovastatin and physical training could be beneficial in obese-insulin resistant patients. Reports regarding the effects of various interventions on obesity in myocardial infarction in myocardial infarct patients are summarized in Table 6.

Conclusions

Growing evidence suggests that obese-insulin resistance may aggravate cardiac dysfunction during I/R injury. This has been proposed to be due to the impairment of insulin signaling and pro-survival signaling, and increased inflammation under obese-insulin resistant condition. Anti-diabetic drugs DPP-4 inhibitors and TZD, as well as other pharmacological interventions including angiotensin II receptor antagonists, resveratrol, AMPK activation, erythropoietin, GGA, insulin, and exercise have been shown to protect the heart from I/R injury in obese-insulin resistant models, in which the protective effects however were observed only when treatments were given prior to I/R. These cardioprotective effects have been proposed to occur via increased pro-survival kinases, improved glucose utilization, and reduced inflammation.

Acknowledgment This work was supported by the Thailand Research Fund Royal Golden Jubilee PhD Program (NC and NA), the Thailand Research Fund RTA5580006 (NC), BRG5780016 (SC), and the Chiang Mai University Excellent Center Award (NC).

Conflict of Interest The authors declare that they have no conflict of interest.

References

1. Jequier E. Obesity. Impairment of energy intake or of energy expenditure. Ann Endocrinol (Paris). 1995;56(2):87–92.
2. Pratchayasakul W, Kerdphoo S, Petsophonsakul P, Pongchaidecha A, Chattipakorn N, Chattipakorn SC. Effects of high-fat diet on insulin receptor function in rat hippocampus and the level of neuronal corticosterone. Life Sci. 2011;88(13–14):619–27.
3. Beck B. Neuropeptide Y, in normal eating and in genetic and dietary-induced obesity. Philos Trans R Soc Lond B Biol Sci. 2006;361(1471):1159–85.
4. DeFronzo RA, Ferrannini E. Insulin resistance. A multifaceted syndrome responsible for NIDDM, obesity, hypertension, dyslipidemia, and atherosclerotic cardiovascular disease. Diabetes Care. 1991;14(3):173–94.
5. Matsuzawa-Nagata N, Takamura T, Ando H, Nakamura S, Kurita S, Misu H, et al. Increased oxidative stress precedes the onset of high-fat diet-induced insulin resistance and obesity. Metabolism. 2008;57(8):1071–7.
6. West DB, York B. Dietary fat, genetic predisposition, and obesity: lessons from animal models. Am J Clin Nutr. 1998;67(3 Suppl):505S–12.
7. Fujita H, Kang M, Eren M, Gleaves LA, Vaughan DE, Kume T. Foxc2 is a common mediator of insulin and transforming growth factor beta signaling to regulate plasminogen activator inhibitor type I gene expression. Circ Res. 2006;98(5):626–34.
8. Hausenloy DJ, Yellon DM. Reperfusion injury salvage kinase signalling: taking a RISK for cardioprotection. Heart Fail Rev. 2007;12(3–4):217–34.
9. Carillon J, Romain C, Bardy G, Fouret G, Feillet-Coudray C, Gaillet S, et al. Cafeteria diet induces obesity and insulin resistance associated with oxidative stress but not with inflammation: improvement by dietary supplementation with a melon superoxide dismutase. Free Radic Biol Med. 2013;65C:254–61.

10. Liu J, Lloyd SG. High-fat, low-carbohydrate diet alters myocardial oxidative stress and impairs recovery of cardiac function after ischemia and reperfusion in obese rats. Nutr Res. 2013;33(4):311–21.
11. Miura T, Tanno M. Mitochondria and GSK-3beta in cardioprotection against ischemia/reperfusion injury. Cardiovasc Drugs Ther. 2010;24(3):255–63.
12. Miura T, Tanno M. The mPTP and its regulatory proteins: final common targets of signalling pathways for protection against necrosis. Cardiovasc Res. 2012;94(2):181–9.
13. Ghaboura N, Tamareille S, Ducluzeau PH, Grimaud L, Loufrani L, Croue A, et al. Diabetes mellitus abrogates erythropoietin-induced cardioprotection against ischemic-reperfusion injury by alteration of the RISK/GSK-3beta signaling. Basic Res Cardiol. 2011;106(1):147–62.
14. Honda T, Kaikita K, Tsujita K, Hayasaki T, Matsukawa M, Fuchigami S, et al. Pioglitazone, a peroxisome proliferator-activated receptor-gamma agonist, attenuates myocardial ischemia-reperfusion injury in mice with metabolic disorders. J Mol Cell Cardiol. 2008;44(5):915–26.
15. Huisamen B, Genis A, Marais E, Lochner A. Pre-treatment with a DPP-4 inhibitor is infarct sparing in hearts from obese, pre-diabetic rats. Cardiovasc Drugs Ther. 2011;25(1):13–20.
16. Yue TL, Nerurkar SS, Bao W, Jucker BM, Sarov-Blat L, Steplewski K, et al. In vivo activation of peroxisome proliferator-activated receptor-delta protects the heart from ischemia/reperfusion injury in Zucker fatty rats. J Pharmacol Exp Ther. 2008;325(2):466–74.
17. Cardenas G, Torres JC, Zamora J, Banos G. Isolated heart function during ischemia and reperfusion in sucrose- fed rats: effect of insulin infusion. Cardiovasc Pathol. 2005;14(5):256–64.
18. Gundewar S, Calvert JW, Elrod JW, Lefer DJ. Cytoprotective effects of N, N, N-trimethylsphingosine during ischemia- reperfusion injury are lost in the setting of obesity and diabetes. Am J Physiol Heart Circ Physiol. 2007;293(4):H2462–71.
19. Huisamen B, Perel SJ, Friedrich SO, Salie R, Strijdom H, Lochner A. ANG II type I receptor antagonism improved nitric oxide production and enhanced eNOS and PKB/Akt expression in hearts from a rat model of insulin resistance. Mol Cell Biochem. 2011;349(1–2):21–31.
20. Lekli I, Szabo G, Juhasz B, Das S, Das M, Varga E, et al. Protective mechanisms of resveratrol against ischemia-reperfusion-induced damage in hearts obtained from Zucker obese rats: the role of GLUT-4 and endothelin. Am J Physiol Heart Circ Physiol. 2008;294(2):H859–66.
21. Nduhirabandi F, Du Toit EF, Blackhurst D, Marais D, Lochner A. Chronic melatonin consumption prevents obesity-related metabolic abnormalities and protects the heart against myocardial ischemia and reperfusion injury in a prediabetic model of diet-induced obesity. J Pineal Res. 2011;50(2):171–82.
22. Ooie T, Kajimoto M, Takahashi N, Shinohara T, Taniguchi Y, Kouno H, et al. Effects of insulin resistance on geranylgeranylacetone-induced expression of heat shock protein 72 and cardioprotection in high-fat diet rats. Life Sci. 2005;77(8):869–81.
23. Bouhidel O, Pons S, Souktani R, Zini R, Berdeaux A, Ghaleb B. Myocardial ischemic postconditioning against ischemia-reperfusion is impaired in ob/ob mice. Am J Physiol Heart Circ Physiol. 2008;295(4):H1580–6.
24. Donner D, Headrick JP, Peart JN, du Toit EF. Obesity improves myocardial ischaemic tolerance and RISK signalling in insulin-insensitive rats. Dis Model Mech. 2013;6(2):457–66.
25. du Toit EF, Nabben M, Lochner A. A potential role for angiotensin II in obesity induced cardiac hypertrophy and ischaemic/reperfusion injury. Basic Res Cardiol. 2005;100(4):346–54.
26. Huang JV, Lu L, Ye S, Bergman BC, Sparagna GC, Sarraf M, et al. Impaired contractile recovery after low-flow myocardial ischemia in a porcine model of metabolic syndrome. Am J Physiol Heart Circ Physiol. 2013;304(6):H861–73.
27. Huhn R, Heinen A, Hollmann MW, Schlack W, Preckel B, Weber NC. Cyclosporine a administered during reperfusion fails to restore cardioprotection in prediabetic Zucker obese rats in vivo. Nutr Metab Cardiovasc Dis. 2010;20(10):706–12.
28. Jordan JE, Simandle SA, Tulbert CD, Busija DW, Miller AW. Fructose-fed rats are protected against ischemia/reperfusion injury. J Pharmacol Exp Ther. 2003;307(3):1007–11.
29. Lacerda L, Opie LH, Lecour S. Influence of tumour necrosis factor alpha on the outcome of ischaemic postconditioning in the presence of obesity and diabetes. Exp Diabetes Res. 2012;2012:502654.
30. Lacerda L, Somers S, Opie LH, Lecour S. Ischaemic postconditioning protects against reperfusion injury via the SAFE pathway. Cardiovasc Res. 2009;84(2):201–8.
31. Pons S, Martin V, Portal L, Zini R, Morin D, Berdeaux A, et al. Regular treadmill exercise restores cardioprotective signaling pathways in obese mice independently from improvement in associated co-morbidities. J Mol Cell Cardiol. 2013;54:82–9.
32. Sidell RJ, Cole MA, Draper NJ, Desrois M, Buckingham RE, Clarke K. Thiazolidinedione treatment normalizes insulin resistance and ischemic injury in the Zucker fatty rat heart. Diabetes. 2002;51(4):1110–7.
33. Song T, Lv LY, Xu J, Tian ZY, Cui WY, Wang QS, et al. Diet-induced obesity suppresses sevoflurane preconditioning against myocardial ischemia-reperfusion injury: role of AMP-activated protein kinase pathway. Exp Biol Med (Maywood). 2011;236(12):1427–36.
34. Thakker GD, Frangogiannis NG, Zymek PT, Sharma S, Raya JL, Barger PM, et al. Increased myocardial susceptibility to repetitive ischemia with high-fat diet-induced obesity. Obesity (Silver Spring). 2008;16(12):2593–600.
35. Wensley I, Salaveria K, Bulmer AC, Donner DG, Du Toit EF. Myocardial structure, function, and ischaemic tolerance in a rodent model of obesity with insulin resistance. Exp Physiol. 2013;98(11):1552–64.
36. Lew EA, Garfinkel L. Variations in mortality by weight among 750, 000 men and women. J Chronic Dis. 1979;32(8):563–76.
37. Eckel RH. Obesity and heart disease: a statement for healthcare professionals from the nutrition committee, American heart association. Circ. 1997;96(9):3248–50.
38. Yellon DM, Hausenloy DJ. Myocardial reperfusion injury. N Engl J Med. 2007;357(11):1121–35.
39. Hausenloy DJ, Yellon DM. Myocardial ischemia-reperfusion injury: a neglected therapeutic target. J Clin Invest. 2013;123(1):92–100.
40. Shoelson SE, Lee J, Goldfine AB. Inflammation and insulin resistance. J Clin Invest. 2006;116(7):1793–801.
41. Aguirre V, Uchida T, Yenush L, Davis R, White MF. The c-Jun NH(2)-terminal kinase promotes insulin resistance during association with insulin receptor substrate-1 and phosphorylation of Ser(307). J Biol Chem. 2000;275(12):9047–54.
42. Cai D, Yuan M, Frantz DF, Melendez PA, Hansen L, Lee J, et al. Local and systemic insulin resistance resulting from hepatic activation of IKK-beta and NF-kappaB. Nat Med. 2005;11(2):183–90.
43. De Fea K, Roth RA. Modulation of insulin receptor substrate-1 tyrosine phosphorylation and function by mitogen-activated protein kinase. J Biol Chem. 1997;272(50):31400–6.
44. Gual P, Le Marchand-Brustel Y, Tanti JF. Positive and negative regulation of insulin signaling through IRS-1 phosphorylation. Biochimie. 2005;87(1):99–109.
45. Stanley WC, Lopaschuk GD, Hall JL, McCormack JG. Regulation of myocardial carbohydrate metabolism under normal and ischaemic conditions. Potential for pharmacological interventions. Cardiovasc Res. 1997;33(2):243–57.
46. van den Brom CE, Bulte CS, Loer SA, Bouwman RA, Boer C. Diabetes, perioperative ischaemia and volatile anaesthetics: consequences of derangements in myocardial substrate metabolism. Cardiovasc Diabetol. 2013;12:42.
47. Galgani JE, Moro C, Ravussin E. Metabolic flexibility and insulin resistance. Am J Physiol Endocrinol Metab. 2008;295(5):E1009–17.

48. Deng JY, Huang JP, Lu LS, Hung LM. Impairment of cardiac insulin signaling and myocardial contractile performance in high-cholesterol/fructose-fed rats. Am J Physiol Heart Circ Physiol. 2007;293(2):H978–87.
49. Carley AN, Severson DL. Fatty acid metabolism is enhanced in type 2 diabetic hearts. Biochim Biophys Acta. 2005;1734(2):112–26.
50. Bopassa JC, Michel P, Gateau-Roesch O, Ovize M, Ferrera R. Low-pressure reperfusion alters mitochondrial permeability transition. Am J Physiol Heart Circ Physiol. 2005;288(6):H2750–5.
51. Sarti P, Silver RB, Paroli L, Nikonorov I, Blanck TJ. Permeability of rat heart myocytes to cytochrome c. Cell Mol Life Sci. 1999;56(11–12):1061–9.
52. Hardie DG, Ross FA, Hawley SA. AMPK: a nutrient and energy sensor that maintains energy homeostasis. Nat Rev Mol Cell Biol. 2012;13(4):251–62.
53. Solskov L, Lofgren B, Kristiansen SB, Jessen N, Pold R, Nielsen TT, et al. Metformin induces cardioprotection against ischaemia/reperfusion injury in the rat heart 24 hours after administration. Basic Clin Pharmacol Toxicol. 2008;103(1):82–7.
54. Tanno M, Bassi R, Gorog DA, Saurin AT, Jiang J, Heads RJ, et al. Diverse mechanisms of myocardial p38 mitogen-activated protein kinase activation: evidence for MKK-independent activation by a TAB1-associated mechanism contributing to injury during myocardial ischemia. Circ Res. 2003;93(3):254–61.
55. Quindry JC, Hamilton KL, French JP, Lee Y, Murlasits Z, Tumer N, et al. Exercise-induced HSP-72 elevation and cardioprotection against infarct and apoptosis. J Appl Physiol (1985). 2007;103(3):1056–62.
56. Ravagnan L, Gurbuxani S, Susin SA, Maisse C, Daugas E, Zamzami N, et al. Heat-shock protein 70 antagonizes apoptosis-inducing factor. Nat Cell Biol. 2001;3(9):839–43.
57. Joshy G, Korda RJ, Attia J, Liu B, Bauman AE, Banks E. Body mass index and incident hospitalisation for cardiovascular disease in 158 546 participants from the 45 and Up study. Int J Obes (Lond). 2014;38(6):848–56.
58. Andersson C, van Gaal L, Caterson ID, Weeke P, James WP, Coutinho W, et al. Relationship between HbA1c levels and risk of cardiovascular adverse outcomes and all-cause mortality in overweight and obese cardiovascular high-risk women and men with type 2 diabetes. Diabetologia. 2012;55(9):2348–55.
59. Poyraz F, Turfan M, Kocaman SA, Yazici HU, Sen N, Tulmac M, et al. Effect of overweight and obesity on the left ventricular systolic and diastolic functions in patients with acute myocardial infarction. Clin Invest Med. 2012;35(4):E229–36.
60. Kadakia MB, Fox CS, Scirica BM, Murphy SA, Bonaca MP, Morrow DA. Central obesity and cardiovascular outcomes in patients with acute coronary syndrome: observations from the MERLIN-TIMI 36 trial. Heart. 2011;97(21):1782–7.
61. Lee SH, Park JS, Kim W, Shin DG, Kim YJ, Kim DS, et al. Impact of body mass index and waist-to-hip ratio on clinical outcomes in patients with ST-segment elevation acute myocardial infarction (from the Korean acute myocardial infarction registry). Am J Cardiol. 2008;102(8):957–65.
62. Gastelurrutia P, Pascual-Figal D, Vazquez R, Cygankiewicz I, Shamagian LG, Puig T, et al. Obesity paradox and risk of sudden death in heart failure results from the MUerte subita en insuficiencia cardiaca (MUSIC) study. Am Heart J. 2011;161(1):158–64.
63. Kragelund C, Hassager C, Hildebrandt P, Torp-Pedersen C, Kober L. Impact of obesity on long-term prognosis following acute myocardial infarction. Int J Cardiol. 2005;98(1):123–31.
64. Wu AH, Pitt B, Anker SD, Vincent J, Mujib M, Ahmed A. Association of obesity and survival in systolic heart failure after acute myocardial infarction: potential confounding by age. Eur J Heart Fail. 2010;12(6):566–73.
65. Choy B, Hansen E, Moss AJ, McNitt S, Zareba W, Goldenberg I. Relation of body mass index to sudden cardiac death and the benefit of implantable cardioverter-defibrillator in patients with left ventricular dysfunction after healing of myocardial infarction. Am J Cardiol. 2010;105(5):581–6.
66. Pingitore A, Di Bella G, Lombardi M, Iervasi G, Strata E, Aquaro GD, et al. The obesity paradox and myocardial infarct size. J Cardiovasc Med (Hagerstown). 2007;8(9):713–7.
67. Uretsky S, Messerli FH, Bangalore S, Champion A, Cooper-Dehoff RM, Zhou Q, et al. Obesity paradox in patients with hypertension and coronary artery disease. Am J Med. 2007;120(10):863–70.
68. Horwich TB, Fonarow GC, Hamilton MA, MacLellan WR, Woo MA, Tillisch JH. The relationship between obesity and mortality in patients with heart failure. J Am Coll Cardiol. 2001;38(3):789–95.
69. Lavie CJ, Alpert MA, Arena R, Mehra MR, Milani RV, Ventura HO. Impact of obesity and the obesity paradox on prevalence and prognosis in heart failure. JACC Heart Fail. 2013;1(2):93–102.
70. Khattab AA, Daemen J, Richardt G, Rioux P, Amann FW, Levy R, et al. Impact of body mass index on the one- year clinical outcome of patients undergoing multivessel revascularization with sirolimus-eluting stents (from the arterial revascularization therapies study part II). Am J Cardiol. 2008;101(11):1550–9.
71. Kosuge M, Kimura K, Kojima S, Sakamoto T, Ishihara M, Asada Y, et al. Impact of body mass index on in- hospital outcomes after percutaneous coronary intervention for ST segment elevation acute myocardial infarction. Circ J. 2008;72(4):521–5.
72. Sarno G, Raber L, Onuma Y, Garg S, Brugaletta S, van Domburg RT, et al. Impact of body mass index on the five-year outcome of patients having percutaneous coronary interventions with drug-eluting stents. Am J Cardiol. 2011;108(2):195–201.
73. Stochmal A, Jasiak-Tyrkalska B, Stochmal E, Huszno B, Kawecka-Jaszcz K. The influence of physical training on metabolic indices in men with myocardial infarction and impaired glucose tolerance. Przegl Lek. 2007;64(6):410–5.
74. Wee CC, Girotra S, Weinstein AR, Mittleman MA, Mukamal KJ. The relationship between obesity and atherosclerotic progression and prognosis among patients with coronary artery bypass grafts the effect of aggressive statin therapy. J Am Coll Cardiol. 2008;52(8):620–5.

เอกสารแนบหมายเลข 56

NRC Research Press

ARTICLE

Garlic extract attenuates brain mitochondrial dysfunction and cognitive deficit in obese-insulin resistant rats

Hiranya Pintana, Jirapas Sripetchwandee, Luerat Supakul, Nattayaporn Apaijai, Nipon Chattipakorn, and Siriporn Chattipakorn

Appl. Physiol. Nutr. Metab. Downloaded from www.nrcresearchpress.com by Université de Montréal on 11/20/14
For personal use only.

Abstract: Oxidative stress in the obese-insulin resistant condition has been shown to affect cognitive as well as brain mitochondrial functions. Garlic extract has exerted a potent antioxidant effect. However, the effects of garlic extract on the brain of obese-insulin resistant rats have never been investigated. We hypothesized that garlic extract improves cognitive function and brain mitochondrial function in obese-insulin resistant rats induced by long-term high-fat diet (HFD) consumption. Male Wistar rats were fed either normal diet or HFD for 16 weeks (n = 24/group). At week 12, rats in each dietary group received either vehicle or garlic extract (250 and 500 mg·kg^{-1}·day^{-1}) for 28 days. Learning and memory behaviors, metabolic parameters, and brain mitochondrial function were determined at the end of treatment. HFD led to increased body weight, visceral fat, plasma insulin, cholesterol, and malondialdehyde (MDA) levels, indicating the development of insulin resistance. Furthermore, HFD rats had cognitive deficit and brain mitochondrial dysfunction. HFD rats treated with both doses of garlic extract had decreased body weight, visceral fat, plasma cholesterol, and MDA levels. Garlic extract also improved cognitive function and brain mitochondrial function, which were impaired in obese-insulin resistant rats caused by HFD consumption.

Key words: brain, learning and memory, antioxidant, high-fat diet, metabolic syndrome.

Résumé : Le stress oxydatif en condition d'insulinorésistance chez les obèses affecte selon des études les fonctions cognitives et les mitochondries cérébrales. L'extrait d'ail présente de puissantes propriétés antioxydantes. Toutefois, il n'y a pas d'études traitant des effets de l'extrait d'ail sur le cerveau de rats obèses insulinorésistants. L'hypothèse est la suivante : l'extrait d'ail améliore les fonctions cognitives et les fonctions des mitochondries cérébrales de rats obèses insulinorésistants à la suite de la consommation à long terme d'aliments riches en gras. On alimente durant 16 semaines (n = 24/groupe) des rats mâles Wistar au moyen d'un régime normal ou riche en gras (« HFD »). À la 12^{e} semaine, les rats de chaque groupe reçoivent durant 28 jours soit le véhicule soit l'extrait d'ail (250 et 500 mg·kg^{-1}·jour^{-1}). À la fin du traitement, on évalue les comportements en matière d'apprentissage et de mémoire, les variables métaboliques et les fonctions des mitochondries cérébrales. Les rats du groupe HFD présentent une plus grande masse corporelle, plus de gras abdominal, d'insuline plasmatique, de cholestérol et de malonaldéhyde (« MDA »), ce qui témoigne du développement de l'insulinorésistance. En outre, les rats HFD présentent un déficit cognitif et une dysfonction des mitochondries cérébrales. Les rats HFD ayant reçu les deux doses de l'extrait d'ail présentent une diminution de la masse corporelle, du gras viscéral, du cholestérol plasmatique et de MDA. L'extrait d'ail améliore chez des rats obèses insulinorésistants les fonctions cognitives et les fonctions des mitochondries cérébrales détériorées par un régime HFD. [Traduit par le Rédaction]

Mots-clés : cerveau, apprentissage et mémoire, antioxydant, régime riche en gras, syndrome métabolique.

Introduction

Insulin resistance is a pathological condition in which target tissues have insufficient ability to respond to optimal plasma insulin concentration (Guo and Tabrizchi 2006), and plays an important role in the development of type 2 diabetes mellitus (T2DM) (Petersen and Shulman 2006; Orgel and Mittelman 2013). Growing evidence revealed the positive correlation between cognitive impairment and T2DM (Gispen and Biessels 2000; Stranahan et al. 2008; Plastino et al. 2010). Our previous studies showed that long-term high-fat diet (HFD) consumption not only induced peripheral insulin resistance, but also caused brain insulin resistance (Pratchayasakul et al. 2011; Pintana et al. 2012; Pipatpiboon et al. 2013). Several studies also demonstrated that brain insulin resistance induced by an HFD was related to cognitive decline (Steen et al. 2005; Wada et al. 2005; de la Monte 2013). Furthermore, our recent studies demonstrated that the cognitive deficit following long-term HFD consumption was due to the impairment of brain mitochondrial function (Pintana et al. 2012; Pintana et al. 2013; Pipatpiboon et al. 2013).

Garlic (*Allium sativum*) has been widely used as a spice as well as an alternative medicine in many countries (Hasani-Ranjbar et al. 2010; Li et al. 2013). Although there are several components in garlic extract, including allylmethy, diallyl, diallydisulfide, and diallytrisulfide (Gupta and Porter 2001), allicin has been shown to potentially exert biological and therapeutic effects (Ali et al. 2000; Ashafaq et al. 2012). Several studies showed that garlic extract has multiple pharmacological effects such as anti-microbial effects

Received 3 July 2014. Accepted 17 August 2014.

H. Pintana,* J. Sripetchwandee,* L. Supakul, N. Apaijai, and N. Chattipakorn. Neurophysiology Unit, Cardiac Electrophysiology Research and Training Center, Faculty of Medicine, Chiang Mai University, Chiang Mai, Thailand.
S. Chattipakorn. Neurophysiology Unit, Cardiac Electrophysiology Research and Training Center, Faculty of Medicine, Chiang Mai University, Chiang Mai, Thailand; Department of Oral Biology and Diagnostic Science, Faculty of Dentistry, Chiang Mai University, Chiang Mai, Thailand.
Corresponding author: Siriporn Chattipakorn (e-mail: siriporn.c@cmu.ac.th).
*These authors contributed equally in the manuscript.

Appl. Physiol. Nutr. Metab. Downloaded from www.nrcresearchpress.com by Universite de Montreal on 11/20/14
For personal use only.

(Weber et al. 1992; Karuppiah and Rajaram 2012; Houshmand et al. 2013), anti-inflammation (Kim S.R. et al. 2013), as well as antioxidant (Dairam et al. 2008; Brunetti et al. 2009). Moreover, recent studies showed the therapeutic effects of garlic as indicated by anti-hyperlipidemia and anti-thrombosis (Ali et al. 1990; Pedraza-Chaverri et al. 2000; Hasani-Ranjbar et al. 2010). Furthermore, garlic provided cardioprotective effects including anti-arrthymias and improved defibrillation efficacy (Isensee et al. 1993; Sungnoon et al. 2008). In the brain, numerous studies showed that garlic extract prevented cognitive decline under pathological conditions such as Alzheimer's disease and cerebral ischemia (Chauhan and Sandoval 2007; Javed et al. 2011; Ashafaq et al. 2012). However, the protective effect of garlic extract in the brain of obese-insulin resistant rats induced by long-term HFD consumption has never been investigated.

In the present study, we determined the therapeutic effects of garlic extract in the brain of obese-insulin resistant rats caused by long-term HFD consumption. We hypothesized that the administration of garlic extract could attenuate peripheral insulin resistance, cognitive dysfunction, as well as brain mitochondrial dysfunction in obese-insulin resistant rats caused by long-term HFD consumption.

Experimental procedures

Animal preparation

Adult male Wistar rats weighing 180–200 g (n = 48) were obtained from the National Animal Center, Salaya Campus, Mahidol University, Thailand. All experiments were performed in accordance with an approved protocol from the Faculty of Medicine, Chiang Mai University Institutional Animal Care and Use Committee, in compliance with National Institutes of Health guidelines. Rats were housed in a room under constant environmental conditions (22–25 °C and 12-h light/12-h dark cycle). Rats were randomly divided into 2 groups to receive either a normal-diet (ND) or an HFD (n = 24/group) for 16 weeks. In the ND group, rats were fed with standard laboratory chow containing 19.77% energy from fat. In the HFD group, rats were fed with diet containing 59.28% energy from fat (Pintana et al. 2012, 2013; Pipatpiboon et al. 2012). At week 12, rats in each group were subsequently divided into 3 subgroups to receive normal saline as a vehicle or 250 mg·kg^{-1}·day^{-1} garlic extract or 500 mg·kg^{-1}·day^{-1} garlic extract (n = 8/subgroup) for 28 days by intragastric gavage feeding. Garlic extract solution was prepared from the commercial garlic extract powder capsules (Immunitop, Bangkok, Thailand) and dissolved in deionized water (2 mL·kg^{-1} of body weight). Each capsule contained 370 mg of garlic extract, which has 3500 μg of allicin. Food intake was recorded every day, whereas the body weight was recorded weekly. Blood samples were collected at week 12 (prior to garlic extract administration) and at the end of garlic treatment. Morris Water Maze (MWM) task was used to determine learning and memory behaviors in each animal, which was performed at the end of the garlic treatment. Then, rats were deeply anesthetized (an intraperitoneal injection of 80 mg·kg^{-1} thiopental) and were decapitated. The brain was rapidly removed and used for the determination of brain mitochondrial function and brain malondialdehyde (MDA) levels.

Determination of plasma glucose, cholesterol, and insulin levels

Plasma glucose and total cholesterol levels were determined by a colorimetric assay using a commercial kit (Biotech, Bangkok, Thailand). Plasma insulin levels were measured using a sandwich ELISA kit (Linco Research, St. Charles, Mo., USA). Homeostasis Model Assessment (HOMA), a mathematical model describing the degree of insulin resistance, was used to determine insulin resistance, and a higher HOMA index represents a higher degree of insulin resistance (Apaijai et al. 2012; Pintana et al. 2012; Pipatpiboon et al. 2012).

Determination of brain and plasma MDA levels

Brain and plasma MDA levels were determined using the HPLC-based analysis as previously described (Pintana et al. 2012). In brief, brain tissues were homogenized using a phosphate buffer with pH 2.8. Plasma and homogenated brain tissues were mixed with H_3PO_4 and thiobarbituric acid (TBA) to produce TBA reactive substances (TBARs). Plasma and brain TBARs concentrations were calculated directly from a standard curve and reported as the MDA equivalent concentrations (μmol·L^{-1}).

Brain mitochondrial isolation and the determination of brain mitochondrial function

Brain mitochondrial isolation was prepared as previously described (Pipatpiboon et al. 2013; Sripetchwandee et al. 2013). Briefly, rats were deeply anesthetized with thiopental (80 mg·kg^{-1}, intraperitoneal injection) and brains were immediately removed into ice-cold MSE solution (containing 225 mmol·L^{-1} mannitol, 75 mmol·L^{-1} sucrose, 1 mmol·L^{-1} EGTA, 5 mmol·L^{-1} HEPES, and 1 mg·mL^{-1} BSA, pH 7.4). Each brain was further transferred into 5 mL of cold MSE-nagarse solution. After that, brain tissue was homogenized and centrifuged to collect brain mitochondrial pellets. Brain mitochondrial pellets were collected and dissolved in a cold respiration buffer (containing 150 mmol·L^{-1} KCl, 5 mmol·L^{-1} HEPES, 5 mmol·L^{-1} $K_2HPO_4 \cdot 3H_2O$, 2 mmol·L^{-1} L-glutamate, and 5 mmol·L^{-1} pyruvate sodium salt). Protein concentration was determined by the bicinchoninic acid assay (Walker 1994). In the present study, brain mitochondrial function was determined by measuring the brain mitochondrial reactive oxygen species (ROS) production, mitochondrial membrane potential changes, and mitochondrial swelling. Brain mitochondrial morphology was also determined using the transmission electron microscope (Pipatpiboon et al. 2013; Sripetchwandee et al. 2013).

Determination of brain mitochondrial ROS production

Brain mitochondrial ROS production was determined by using dichlorohydro-fluorescein diacetate (DCFDA) dyes, and was measured by using a fluorescent microplate reader (Pipatpiboon et al. 2013; Sripetchwandee et al. 2013). Isolated brain mitochondria were incubated with 2 μmol·L^{-1} DCFDA at 25 °C for 20 min. The excitation and emission wavelength of dichlorohydro-fluorescein (DCF) fluorescence was 485 and 530 nm, respectively. The ROS level was shown as arbitrary units of fluorescence intensity of DCF.

Determination of brain mitochondrial membrane potential changes ($\Delta\Psi_m$)

Brain mitochondrial membrane potential changes ($\Delta\Psi_m$) were measured using the 5,5′,6,6′-tetrachloro-1,1′,3,3′-tetraethylbenzimidazolcarbocyanine iodide (JC-1) dye. Isolated brain mitochondria were stained with JC-1 (5 μmol·L^{-1}) at 37 °C for 15 min (Pipatpiboon et al. 2013; Sripetchwandee et al. 2013). JC-1 monomer form (green fluorescence) was excited at the wavelength of 485 nm and emitted at the wavelength of 530 nm, whereas the JC-1 aggregated form (red fluorescence) was excited at the wavelength of 485 nm and emitted at the wavelength of 590 nm. The fluorescent intensity was detected by a fluorescent microplate reader. The change in mitochondrial membrane potential was calculated as the red/green fluorescent intensity ratio, and the brain mitochondrial depolarization was indicated by a decreased red/green fluorescent intensity ratio (Pipatpiboon et al. 2013; Sripetchwandee et al. 2013).

Determination of brain mitochondrial swelling

Brain mitochondrial swelling was determined by the detection of the absorbance in the mitochondrial suspension using a microplate reader. A decreased absorbance of the brain mitochondrial

Appl. Physiol. Nutr. Metab. Downloaded from www.nrcresearchpress.com by Université de Montréal on 11/20/14
For personal use only.

suspension indicated brain mitochondrial swelling (Pipatpiboon et al. 2013; Sripetchwandee et al. 2013). Transmission electron microscope (TEM) was also used to visualize the brain mitochondrial morphology (Sripetchwandee et al. 2013).

MWM task

MWM was determined as described previously (Vorhees and Williams 2006; Pipatpiboon et al. 2013). The experimental protocol was divided into 2 phases including an acquisition test and a probe test. In the acquisition test, rats were put in a water pool with 4 different starting points per day for 5 consecutive days. In this protocol, rats were placed in a randomized starting point. The time was recorded immediately after the rat was placed into the water pool until it found a submerged platform. Spending time in this phase was reported as time to reach the platform. Then, the rat was placed in the other 3 starting points. The probe test was performed on the sixth day in each rat. In this phase, the platform was removed and each rat was placed into the water pool with their head facing towards water. The time was recorded immediately after placing the rat into the water pool and stopped after 90 s of recording. Spending time in this phase was reported as the time spent in the target quadrant.

Statistical analysis

All data were expressed as means ± SE. Data were processed using SPSS for Windows (version 16; SPSS Inc., Chicago, Ill., USA). One-way ANOVA followed by the least square difference post hoc test was used to determine the difference between groups. Data from brain mitochondrial function were analyzed using the nonparametric Kruskal–Wallis *H*, followed by the Mann–Whitney *U* test. Data from the MWM test were performed using the 2-way ANOVA, followed by Fisher's post hoc analysis. *P* value <0.05 was considered statistically significant.

Ethics

All experiments were approved by the Institutional Animal Care and Use Committees of the Faculty of Medicine, Chiang Mai University, Chiang Mai, Thailand (permit no. 01/2557).

Results

Effects of HFD consumption and garlic treatments on metabolic parameters

After 12 weeks of dietary feeding, rats in the HFD group had a significant increase in body weight, visceral fat, and plasma total cholesterol level, compared with the ND group (Table 1). An increased plasma insulin level and HOMA index in HFD-fed rats indicated an insulin-resistant condition (Table 1). Moreover, rats in the HFD group developed plasma oxidative stress as indicated by an increased plasma MDA level and brain oxidative stress as indicated by an increase in brain MDA level (Table 1).

HFD rats treated with either 250 (HF250) or 500 (HF500) mg·kg^{-1}·day^{-1} of garlic extract had decreased visceral fat, plasma total cholesterol, insulin levels, and HOMA index, whereas the body weight in both groups (HF250 and HF500) was not different from that in HFD rats treated with vehicle (Table 2). Furthermore, HFD rats treated with garlic extract also had reduced plasma MDA levels as well as brain MDA levels (Table 2). However, no differences were found on any metabolic parameters between ND rats treated with vehicle and garlic extract (Table 2).

HFD consumption led to the impairment of learning and memory, and garlic extract treatment restored this impairment in obese-insulin resistant rats

HFD impaired learning and memory behaviors as indicated by an increase in both the time to reach the platform and the time spent in the target quadrant, compared with the ND group ($P < 0.05$, Fig. 1A and 1B, respectively). Nevertheless, an impaired learning and memory following HFD consumption was significantly attenuated by 250 and 500 mg·kg^{-1}·day^{-1} of garlic extract administration (Fig. 1). In the ND-fed rats, garlic extract of both concentrations (250 and 500 mg·kg^{-1}·day^{-1}) did not alter learning and memory behaviors since the time to reach the platform and the time spent in the target quadrant were not different from the vehicle-treated ND-fed rats (Fig. 1).

Table 1. Effects of long-term high-fat diet consumption on metabolic parameters.

	Week 12	
Metabolic parameters	ND	HFD
Body weight (g)	419±90	538.75±10.87*
Food intake (g)	24.76±1.56	25.2±0.18
Plasma insulin (ng·mL^{-1})	1.96±0.06	3.55±1.22*
Plasma glucose (mg·dL^{-1})	149.35±8.71	150.44±7.72
HOMA index	18.76±4.33	27.55±2.59*
Plasma total cholesterol (mg·dL^{-1})	75.83±1.68	112.33±5.6*

*$P < 0.05$ vs. ND. HFD, high-fat diet fed rats; HOMA, Homeostasis Model Assessment; ND, normal-diet fed rats.

HFD consumption impaired brain mitochondrial function, and garlic extract attenuated this impairment in brain mitochondria of obese-insulin resistant rats

HFD significantly impaired brain mitochondrial function as indicated by increased brain mitochondrial ROS production, brain mitochondrial depolarization, and brain mitochondrial swelling (Fig. 2). The electron microscope also revealed that the brain mitochondrial morphology in HFD-fed rats was markedly changed as indicated by the loss of folded cristae, compared with that in ND-fed rats (Fig. 2D).

In HFD rats treated with garlic extract, brain mitochondrial ROS level was decreased (Fig. 2A), mitochondrial depolarization was attenuated (Fig. 2B), and brain mitochondrial swelling was also reduced (Fig. 2C), compared with vehicle-treated HFD-fed rats. The TEM study demonstrated that garlic extract treatment preserved the brain mitochondrial morphology as shown by vivid folded cristae, compared with the HFD rats treated with vehicle (Fig. 2D). However, brain mitochondrial function was not different between ND-fed rats treated with vehicle and garlic extract (Fig. 2).

Discussion

The major findings from the present study are as follows: (*i*) HFD consumption led to peripheral insulin resistance, oxidative stress, brain mitochondrial dysfunction, and learning and memory deficit; and (*ii*) garlic extract attenuated peripheral insulin resistance and oxidative stress, and improved brain mitochondrial function and learning and memory behaviors in obese-insulin resistant rats caused by long-term HFD consumption.

Consistent with recent reports, chronic HFD consumption in the present study led to the development of oxidative stress as well as insulin resistance as indicated by an increased plasma insulin level and a HOMA index, together with increased body weight, visceral fat, plasma total cholesterol, and MDA levels (Craft 2005; Apaijai et al. 2012; Anderson et al. 2013; Pipatpiboon et al. 2013). Previous studies also demonstrated that HFD could cause learning and memory impairment (Davidson et al. 2013; Valladolid-Acebes et al. 2013). Consistent with these reports, HFD-induced cognitive impairment was observed in our study as indicated by an increase in the time to reach the platform and a decrease in the time spent in the target quadrant in MWM tasks in the present study.

HFD is known to induce free radicals generation (Charradi et al. 2013; Li and Periwal 2013). Excessive free radicals have been shown to induce cellular lipid peroxidation, leading to the production of cytotoxic aldehyde products including 4-hydroxylnonenal and MDA (Tsukamoto 1993; Kim do Y. et al. 2013). Oxidative stress has been shown to play an important role in cognitive impairment

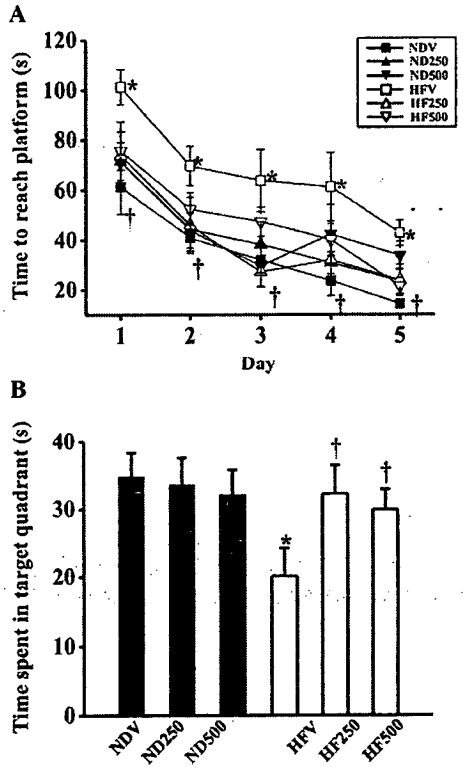
Appl. Physiol. Nutr. Metab. Downloaded from www.nrcresearchpress.com by Université de Montréal on 11/20/14
For personal use only.

Table 2. Effects of 250 mg·kg^{-1} and 500 mg·kg^{-1} of garlic extract on metabolic parameters in normal and high-fat diet fed rats.

Metabolic parameters	NDV	ND250	ND500	HFV	HF250	HF500
Body weight (g)	450±10	457±13.2	479±12.9	564.3±14.5*	561.1±14.9*	575±21.7*
Food intake (g)	22.6±0.7	21.4±1	21.1±0.8	22.4±0.5	22.0±1.7	23±0.4
Visceral fat (g)	29.4±4.6	21.5±1.6	22.7±1.5	64.5±4.5*	52.2±3*,†	52.6±3.2*,†
Plasma insulin (ng·mL^{-1})	1.8±0.3	1.7±0.9	1.7±0.3	3.7±0.4*	1.6±0.1†	1.9±0.5†
Plasma glucose (mg·dL^{-1})	150.7±6.5	142.1±8.5	141.9±9	154.1±14.1	147.4±7.7	143.8±11.7
HOMA index	15.9±0.3	13.7±5.0	15.4±3.1	26.4±1.6*	13.9±1.5†	15.8±3.1†
Plasma total cholesterol (mg·dL^{-1})	80.9±8.4	81.3±11	77.3±4.3	158±10*	85.3±6.5†	84±8.6†
Plasma MDA (μmol·L^{-1})	1.9±0.07	1.83±0.05	1.95±0.11	7±0.1*	1.72±0.05†	1.81±0.07†
Brain MDA (μmol·L^{-1}·mg protein^{-1})	1.04±0.2	0.9±0.07	0.84±0.1	2.21±0.26*	0.83±0.1†	0.72±0.1†

*$P < 0.05$ vs. NDV; †$P < 0.05$ vs. HFV. HF250, high-fat diet fed rats treated with 250 mg·kg^{-1}·day^{-1} of garlic extract; HF500, high-fat diet fed rats treated with 500 mg·kg^{-1}·day^{-1} of garlic extract; HFV, high-fat diet fed rats treated with vehicle; HOMA, Homeostasis Model Assessment; MDA, malondialdehyde; ND250, normal-diet fed rats treated with 250 mg·kg^{-1}·day^{-1} of garlic extract; ND500, normal-diet fed rats treated with 500 mg·kg^{-1}·day^{-1} of garlic extract; NDV, normal-diet fed rats treated with vehicle.

Fig. 1. Effects of long-term high-fat diet consumption and garlic extract on learning and memory behavior including the time to reach the platform (A) and the time spent in the target quadrant (B). *, $P < 0.05$ vs. normal diet groups; †, $P < 0.05$ vs. rats treated with vehicle (HFV). HF250, high-fat diet fed group treated with 250 mg·kg^{-1}·day^{-1} of garlic extract; HF500, high-fat diet fed group treated with 500 mg·kg^{-1}·day^{-1} of garlic extract; HFD, high-fat diet fed group treated with vehicle; ND250, normal-diet fed group treated with 250 mg·kg^{-1}·day^{-1} of garlic extract; ND500, normal-diet fed group treated with 500 mg·kg^{-1}·day^{-1} of garlic extract; NDV, normal-diet fed group treated with vehicle.

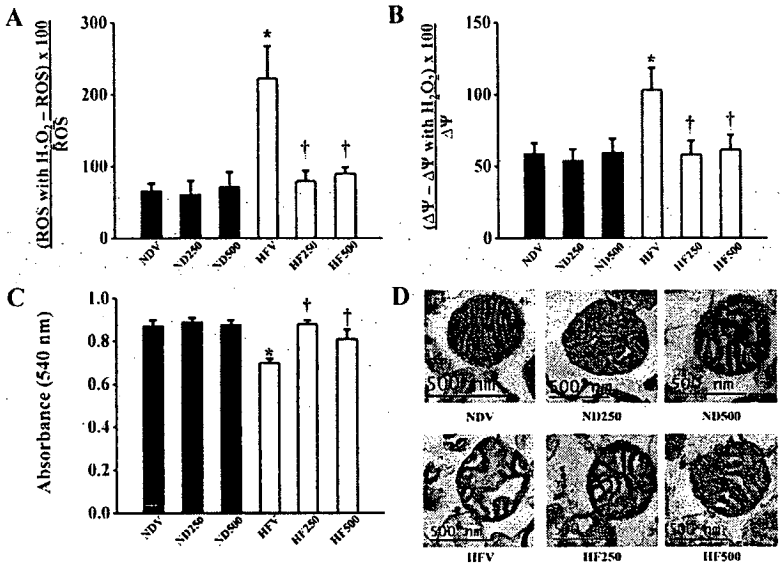


(Serrano and Klann 2004; Alzoubi et al. 2013). Since the brain is a highly vulnerable organ to oxidative stress (Jikumaru and Inoue 2013), a pathological oxidative stress condition could induce brain dysfunction, leading to the impairment of learning and memory. In the present study, we found that HFD consumption for 12 weeks increased plasma MDA levels and brain MDA levels, indicating an increased brain oxidative stress following HFD consumption, and thus could be responsible for learning and memory deficit in these obese-insulin resistant rats.

Mitochondria are important organelles in cells since they are the cellular energy production sources (Darley-Usmar 2004). In mitochondria, ROS are produced and used for mitochondrial oxidative phosphorylation (Smeitink et al. 2001; Chen et al. 2003). However, excessive ROS could lead to mitochondrial dysfunction and cellular apoptosis (Desagher and Martinou 2000; Galluzzi et al. 2012). Recent studies demonstrated that brain mitochondrial dysfunction caused brain dysfunctions, particularly in memory decline (Ye et al. 2011; Pipatpiboon et al. 2013). Consistent with our previous studies (Pintana et al. 2012, 2013; Pipatpiboon et al. 2012, 2013), long-term HFD consumption induced brain mitochondrial dysfunction as indicated by an increased brain mitochondrial ROS production, brain mitochondrial depolarization, as well as mitochondrial swelling, and consequently resulted in learning and memory deficit. Moreover, supporting evidence demonstrated that mitochondria are the primary targets for oxidative damage (Lin and Beal 2006; Bonnard et al. 2008). Therefore, HFD-induced oxidative stress in obese-insulin resistant rats, which was observed in our present study, could be responsible for brain mitochondrial dysfunction (Ortiz Mdel et al. 2013).

In the present study, garlic extract (250 and 500 mg·kg^{-1}·day^{-1}) was demonstrated to attenuate the changes in metabolic parameters of HFD-fed rats by decreasing visceral fat, plasma total cholesterol level, plasma insulin level, and HOMA index, suggesting that garlic treatments improved insulin sensitivity. These findings are consistent with previous studies reporting this beneficial effect of garlic extract. Moreover, previous studies also showed that garlic supplement decreased oxidative stress by modulating lipid peroxidation (Saravanan and Prakash 2004; Perez-De La Cruz et al. 2006). In the present study, the decreased plasma MDA level and brain MDA level in HFD-fed rats treated with garlic supplements suggested the anti-oxidative effect of garlic. In addition, the MWM results showed that garlic extract could improve learning and memory, which was impaired in HFD-fed rats. Since insulin resistance and oxidative stress are associated with cognitive decline, our findings suggested that improved learning and memory behaviors in HFD rats treated with garlic extract could be due to its ability to attenuate peripheral insulin resistance and oxidative stress condition. (Padiya et al. 2011; K et al. 2013). Our previous studies clearly demonstrated that feeding rats with HFD for 8 weeks caused peripheral insulin resistance by increasing insulin level without changing the plasma glucose, and that the brain insulin signaling at this period was still intact, indicating peripheral insulin resistance without brain insulin resistance (Pratchayasakul et al. 2011). However, our previous studies also demonstrated clearly that 12-week HFD consumption significantly caused both peripheral insulin resistance (as indicated by hyperinsulinemia

Fig. 2. Effects of long-term high-fat diet consumption and garlic extract on brain mitochondrial function, including brain mitochondrial reactive oxygen species (ROS) production (A), brain mitochondrial membrane potential changes (B), brain mitochondrial swelling (C), and representative electron micrographs of brain mitochondria from different groups (D). Mitochondrial morphological changes representing damaged mitochondria or swollen mitochondria could be characterized by the unfolding cristae, outer membrane collapse, and the enlargement of mitochondrial matrix. *, $P < 0.05$ vs. normal diet groups; †, $P < 0.05$ vs. rats treated with vehicle (HFV). HF250, high-fat diet fed group treated with 250 mg·kg^{-1}·day^{-1} of garlic extract; HF500, high-fat diet fed group treated with 500 mg·kg^{-1}·day^{-1} of garlic extract; HFD, high-fat diet fed group treated with vehicle; ND250, normal-diet fed group treated with 250 mg·kg^{-1}·day^{-1} of garlic extract; ND500, normal-diet fed group treated with 500 mg·kg^{-1}·day^{-1} of garlic extract; NDV, normal-diet fed group treated with vehicle.



with euglycemia) and impaired brain insulin signaling as indicated by decreased phosphorylation of insulin receptor, insulin receptor substrate-1, and Akt-ser 473, indicating brain insulin resistance (Pratchayasakul et al. 2011; Pipatpiboon et al. 2012; Pipatpiboon et al. 2013). This model of brain insulin resistance because of a 12-week HFD consumption has been well established. Therefore, the model of overt brain insulin resistance is available, and peripheral insulin resistance occurred first (i.e., at 8 weeks), followed by brain insulin resistance (at 12 weeks), in the 12-week HFD consumption model that was used in this study. In the present study, although the beneficial effects of garlic in the brain for cognitive improvement could be due to its alleviation of brain insulin resistance, our study limitation is that brain insulin signaling was not determined.

In addition, the therapeutic effects of garlic treatment in the brain as demonstrated in the present study could be due to the direct effect of allicin, a major component in garlic supplement, since it has been shown previously that allicin could freely pass through the phospholipids bilayers structure of the blood brain barrier (Rabinkov et al. 1998; Miron et al. 2000; Li et al. 2012; Zhu et al. 2012).

Previous studies demonstrated that garlic attenuated mitochondrial dysfunction in several organs including the brain (Perez-De La Cruz et al. 2006; Atif et al. 2009). We further demonstrated that under obese-insulin resistant condition, an impairment of brain mitochondrial function could be restored by garlic extract treatment as indicated by brain mitochondrial ROS reduction, prevention of brain mitochondrial depolarization, and the attenuation of brain mitochondrial swelling. These improvements could also be responsible for the improvement of cognitive function in obese-insulin resistant rats.

Conclusion

Long-term HFD consumption resulted in the development of peripheral insulin resistance, increased oxidative stress, brain mitochondrial dysfunction, and learning and memory deficit. Garlic extract improved peripheral insulin resistance and decreased circulation and brain oxidative stress, resulting in the improvement of brain mitochondrial function and cognitive function in obese-insulin resistant rats.

Study limitation

Although the present study showed the beneficial effects of garlic supplement on brain functions, the level of active components or allicin in either plasma or brain level was not investigated. Improved insulin sensitivity could also be due to an increased energy expenditures. However, indirect calorimetry was not determined in the present study. Future studies are needed to investigate the involvement of garlic extract treatment and energy expenditure in improving insulin sensitivity and brain function. In addition, the involved mechanisms of garlic extract on the respiratory substrates on each complex of the respiratory chain are needed to be investigated in the future.

Conflict of interest statement

The authors declare that they have no conflicts of interest.

Acknowledgements

This work was supported by grants from the Thailand Research Fund TRF-BRG5780016 (S.C.), TRF-RTA5580006 (N.C.), Faculty of Medicine Chiang Mai University Endowment Fund (N.C.), National Research Council of Thailand (S.C.), Thailand Research Fund through the Royal Golden Jubilee Program (PHD/0248/2552: J.S. and S.C.; PHD/0025/2555: H.P. and S.C.), and Chiang Mai University Excellent Center Award (N.C.).

References

Ali, M., Thomson, M., Alnaqeeb, M.A., Al-Hassan, J.M., Khater, S.H., and Gomes, S.A. 1990. Antithrombotic activity of garlic: its inhibition of the synthesis of thromboxane-B_2 during infusion of arachidonic acid and collagen in

Appl. Physiol. Nutr. Metab. Downloaded from www.nrcresearchpress.com by Université de Montréal on 11/20/14
For personal use only.

Appl. Physiol. Nutr. Metab. Downloaded from www.nrcresearchpress.com by Université de Montréal on 11/20/14
For personal use only.

rabbits. Prostaglandins Leukot. Essent. Fatty Acids, 41: 95–99. doi:10.1016/0952-3278(90)90060-X. PMID:2274570.

Ali, M., Al-Qattan, K.K., Al-Enezi, F., Khanafer, R.M.A., and Mustafa, T. 2000. Effect of allicin from garlic powder on serum lipids and blood pressure in rats fed with a high cholesterol diet. Prostaglandins Leukot. Essent. Fatty Acids, 62: 253–259. doi:10.1054/plef.2000.0152. PMID:10882191.

Alzoubi, K.H., Khabour, O.F., Salah, H.A., and Hasan, Z. 2013. Vitamin E prevents high-fat high-carbohydrates diet-induced memory impairment: the role of oxidative stress. Physiol. Behav. 119: 72–78. doi:10.1016/j.physbeh.2013.06.011. PMID:23769690.

Anderson, R.A., Qin, B., Canini, F., Poulet, L., and Roussel, A.M. 2013. Cinnamon counteracts the negative effects of a high fat/high fructose diet on behavior, brain insulin signaling and Alzheimer-associated changes. PLoS One, 8: e83243. doi:10.1371/journal.pone.0083243. PMID:24349472.

Apaijai, N., Pintana, H., Chattipakorn, S.C., and Chattipakorn, N. 2012. Cardioprotective effects of metformin and vildagliptin in adult rats with insulin resistance induced by a high-fat diet. Endocrinology, 153: 3878–3885. doi:10.1210/en.2012-1262. PMID:22621958.

Ashafaq, M., Khan, M.M., Shadab Raza, S., Ahmad, A., Khuwaja, G., Javed, H., et al. 2012. S-allyl cysteine mitigates oxidative damage and improves neurologic deficit in a rat model of focal cerebral ischemia. Nutr. Res. 32: 133–143. doi:10.1016/j.nutres.2011.12.014. PMID:22348462.

Atif, F., Yousuf, S., and Agrawal, S.K. 2009. S-allyl L-cysteine diminishes cerebral ischemia-induced mitochondrial dysfunctions in hippocampus. Brain Res. 1265: 128–137. doi:10.1016/j.brainres.2008.12.077. PMID:19401183.

Bonnard, C., Durand, A., Peyrol, S., Chanseaume, E., Chauvin, M.A., Morio, B., et al. 2008. Mitochondrial dysfunction results from oxidative stress in the skeletal muscle of diet-induced insulin-resistant mice. J. Clin. Invest. 118: 789–800. PMID:18188455.

Brunetti, L., Menghini, L., Orlando, G., Recinella, L., Leone, S., Epifano, F., et al. 2009. Antioxidant effects of garlic in young and aged rat brain in vitro. J. Med. Food, 12: 1166–1169. doi:10.1089/jmf.2008.0176. PMID:19857085.

Charradi, K., Elkahoui, S., Limam, F., and Aouani, E. 2013. High-fat diet induced an oxidative stress in white adipose tissue and disturbed plasma transition metals in rat: prevention by grape seed and skin extract. J. Physiol. Sci. 63: 445–455. doi:10.1007/s12576-013-0283-6. PMID:24158847.

Chauhan, N.B., and Sandoval, J. 2007. Amelioration of early cognitive deficits by aged garlic extract in Alzheimer's transgenic mice. Phytother. Res. 21: 629–640. doi:10.1002/ptr.2122. PMID:17380553.

Chen, Q., Vazquez, E.J., Moghaddas, S., Hoppel, C.L., and Lesnefsky, E.J. 2003. Production of reactive oxygen species by mitochondria: central role of complex III. J. Biol. Chem. 278: 36027–36031. doi:10.1074/jbc.M304854200. PMID:12840017.

Craft, S. 2005. Insulin resistance syndrome and Alzheimer's disease: age- and obesity-related effects on memory, amyloid, and inflammation. Neurobiol. Aging, 26(Suppl 1): 65–69. PMID:16266773.

Dairam, A., Fogel, R., Daya, S., and Limson, J.L. 2008. Antioxidant and iron-binding properties of curcumin, capsaicin, and S-allylcysteine reduce oxidative stress in rat brain homogenate. J. Agric. Food Chem. 56: 3350–3356. doi:10.1021/jf0734931. PMID:18422331.

Darley-Usmar, V. 2004. The powerhouse takes control of the cell: the role of mitochondria in signal transduction. Free Radical Biol. Med. 37: 753–754. doi:10.1016/j.freeradbiomed.2004.05.026. PMID:15304251.

Davidson, T.L., Hargrave, S.L., Swithers, S.E., Sample, C.H., Fu, X., Kinzig, K.P., and Zheng, W. 2013. Inter-relationships among diet, obesity and hippocampal-dependent cognitive function. Neuroscience, 253: 110–122. doi:10.1016/j.neuroscience.2013.08.044. PMID:23999121.

de la Monte, S.M. 2013. Intranasal insulin therapy for cognitive impairment and neurodegeneration: current state of the art. Expert Opin. Drug Deliv. 10: 1699–1709. doi:10.1517/17425247.2013.856877. PMID:24215447.

Desagher, S., and Martinou, J.C. 2000. Mitochondria as the central control point of apoptosis. Trends Cell Biol. 10: 369–377. doi:10.1016/S0962-8924(00)01803-1. PMID:10932094.

Galluzzi, L., Kepp, O., Trojel-Hansen, C., and Kroemer, G. 2012. Mitochondrial control of cellular life, stress, and death. Circ. Res. 111: 1198–1207. doi:10.1161/CIRCRESAHA.112.268946. PMID:23065343.

Gispen, W.H., and Biessels, G.J. 2000. Cognition and synaptic plasticity in diabetes mellitus. Trends Neurosci. 23: 542–549. doi:10.1016/S0166-2236(00)01656-8. PMID:11074263.

Guo, L., and Tabrizchi, R. 2006. Peroxisome proliferator-activated receptor gamma as a drug target in the pathogenesis of insulin resistance. Pharmacol. Ther. 111: 145–173. doi:10.1016/j.pharmthera.2005.10.009. PMID:16305809.

Gupta, N., and Porter, T.D. 2001. Garlic and garlic-derived compounds inhibit human squalene monooxygenase. J. Nutr. 131: 1662–1667. PMID:11385050.

Hasani-Ranjbar, S., Nayebi, N., Moradi, L., Mehri, A., Larijani, B., and Abdollahi, M. 2010. The efficacy and safety of herbal medicines used in the treatment of hyperlipidemia; a systematic review. Curr. Pharm. Des. 16: 2935–2947. doi:10.2174/138161210793176464. PMID:20858178.

Houshmand, B., Mahjour, F., and Dianat, O. 2013. Antibacterial effect of different concentrations of garlic (*Allium sativum*) extract on dental plaque bacteria. Indian J. Dent. Res. 24: 71–75. doi:10.4103/0970-9290.114957. PMID:23852236.

Isensee, H., Rietz, B., and Jacob, R. 1993. Cardioprotective actions of garlic (*Allium sativum*). Arzneimittelforschung, 43: 94–98. PMID:8457243.

Javed, H., Khan, M.M., Khan, A., Vaibhav, K., Ahmad, A., Khuwaja, G., et al. 2011. S-allyl cysteine attenuates oxidative stress associated cognitive impairment and neurodegeneration in mouse model of streptozotocin-induced experimental dementia of Alzheimer's type. Brain Res. 1389: 133–142. doi:10.1016/j.brainres.2011.02.072. PMID:21376020.

Jikumaru, M., and Inoue, M. 2013. Pathophysiology of oxystress-induced tissue damage in cerebrovascular disease. Brain Nerve, 65: 871–878. PMID:23832989.

Sivaraman, K., Senthilkumar, G.P., Sankar, P., and Bobby, Z. 2013. Attenuation of oxidative stress, inflammation and insulin resistance by allium sativum in fructose-fed male rats. J. Clin. Diagn. Res. 7: 1860–1862. PMID:24179882.

Karuppiah, P., and Rajaram, S. 2012. Antibacterial effect of *Allium sativum* cloves and *Zingiber officinale* rhizomes against multiple-drug resistant clinical pathogens. Asian Pac. J. Trop. Biomed. 2: 597–601. doi:10.1016/S2221-1691(12)60104-X. PMID:23569978.

Kim, do Y., Kim, J., Ham, H.J., and Choue, R. 2013. Effects of d-alpha-tocopherol supplements on lipid metabolism in a high-fat diet-fed animal model. Nutr. Res. Pract. 7: 481–487. doi:10.4162/nrp.2013.7.6.481. PMID:24353834.

Kim, S.R., Jung, Y.R., An, H.J., Kim, D.H., Jang, E.J., Choi, Y.J., et al. 2013. Anti-wrinkle and anti-inflammatory effects of active garlic components and the inhibition of MMPs via NF-kappaB signaling. PLoS One, 8: e73877. doi:10.1371/journal.pone.0073877. PMID:24066081.

Li, L., Sun, T., Tian, J., Yang, K., Yi, K., and Zhang, P. 2013. Garlic in clinical practice: an evidence-based overview. Crit. Rev. Food Sci. Nutr. 53: 670–681. doi:10.1080/10408398.2010.537000. PMID:23638928.

Li, X.H., Li, C.Y., Lu, J.M., Tian, R.B., and Wei, J. 2012. Allicin ameliorates cognitive deficits ageing-induced learning and memory deficits through enhancing of Nrf2 antioxidant signaling pathways. Neurosci. Lett. 514: 46–50. doi:10.1016/j.neulet.2012.02.054. PMID:22390900.

Li, Y., and Periwal, V. 2013. Synergy in free radical generation is blunted by high-fat diet induced alterations in skeletal muscle mitochondrial metabolism. Biophys. J, 104: 1127–1141. doi:10.1016/j.bpj.2013.01.025. PMID:PMC3870805.

Lin, M.T., and Beal, M.F. 2006. Mitochondrial dysfunction and oxidative stress in neurodegenerative diseases. Nature, 443: 787–795. doi:10.1038/nature05292. PMID:17051205.

Miron, T., Rabinkov, A., Mirelman, D., Wilchek, M., and Weiner, L. 2000. The mode of action of allicin: its ready permeability through phospholipid membranes may contribute to its biological activity. Biochim. Biophys. Acta, 1463: 20–30. doi:10.1016/S0005-2736(99)00174-1. PMID:10631291.

Orgel, E., and Mittelman, S.D. 2013. The links between insulin resistance, diabetes, and cancer. Curr. Diab. Rep. 13: 213–222. doi:10.1007/s11892-012-0356-6. PMID:23271574.

Ortiz, M.C., Lores-Arnaiz, S., Albertoni Borghese, M.F., Balonga, S., Lavagna, A., Filipuzzi, A.L., et al. 2013. Mitochondrial dysfunction in brain cortex mitochondria of STZ-diabetic rats: Effect of L-Arginine. Neurochem. Res. 38: 2570–2580. doi:10.1007/s11064-013-1172-3. PMID:24190597.

Padiya, R., Khatua, T.N., Bagul, P.K., Kuncha, M., and Banerjee, S.K. 2011. Garlic improves insulin sensitivity and associated metabolic syndromes in fructose fed rats. Nutr. Metab. (Lond.), 8: 53. doi:10.1186/1743-7075-8-53.

Pedraza-Chaverri, J., Medina-Campos, O.N., Granados-Silvestre, M.A., Maldonado, P.D., Olivares-Corichi, I.M., and Hernandez-Pando, R. 2000. Garlic ameliorates hyperlipidemia in chronic aminonucleoside nephrosis. Mol. Cell Biochem. 211: 69–77. doi:10.1023/A:1007106632313. PMID:11055549.

Perez-De La Cruz, V., Gonzalez-Cortes, C., Pedraza-Chaverri, J., Maldonado, P.D., Andres-Martinez, L., and Santamaria, A. 2006. Protective effect of S-allylcysteine on 3-nitropropionic acid-induced lipid peroxidation and mitochondrial dysfunction in rat brain synaptosomes. Brain Res. Bull. 68: 379–383. doi:10.1016/j.brainresbull.2005.09.013. PMID:16377446.

Petersen, K.F., and Shulman, G.I. 2006. Etiology of insulin resistance. Am. J. Med. 119: S10–S16. doi:10.1016/j.amjmed.2006.01.009. PMID:16563942.

Pintana, H., Apaijai, N., Pratchayasakul, W., Chattipakorn, N., and Chattipakorn, S.C. 2012. Effects of metformin on learning and memory behaviors and brain mitochondrial functions in high fat diet induced insulin resistant rats. Life Sci. 91: 409–414. doi:10.1016/j.lfs.2012.08.017. PMID:22925597.

Pintana, H., Apaijai, N., Chattipakorn, N., and Chattipakorn, S.C. 2013. DPP-4 inhibitors improve cognition and brain mitochondrial function of insulin-resistant rats. J. Endocrinol. 218: 1–11. doi:10.1530/JOE-12-0521. PMID:23591914.

Pipatpiboon, N., Pratchayasakul, W., Chattipakorn, N., and Chattipakorn, S.C. 2012. PPARgamma agonist improves neuronal insulin receptor function in hippocampus and brain mitochondria function in rats with insulin resistance induced by long term high-fat diets. Endocrinology, 153: 329–338. doi:10.1210/en.2011-1502. PMID:22109891.

Pipatpiboon, N., Pintana, H., Pratchayasakul, W., Chattipakorn, N., and Chattipakorn, S.C. 2013. DPP4-inhibitor improves neuronal insulin receptor function, brain mitochondrial function and cognitive function in rats with insulin resistance induced by high-fat diet consumption. Eur. J. Neurosci. 37: 839–849. doi:10.1111/ejn.12088. PMID:23240760.

Plastino, M., Fava, A., Pirritano, D., Cotronei, P., Sacco, N., Sperli, T., et al. 2010. Effects of insulinic therapy on cognitive impairment in patients with Alzheimer disease and diabetes mellitus type-2. J. Neurol. Sci. 288: 112–116. doi:10.1016/j.jns.2009.09.022. PMID:19836029.

Pratchayasakul, W., Kerdphoo, S., Petsophonsakul, P., Pongchaidecha, A., Chattipakorn, N., and Chattipakorn, S.C. 2011. Effects of high-fat diet on

insulin receptor function in rat hippocampus and the level of neuronal corticosterone. Life Sci. **88**: 619–627. doi:10.1016/j.lfs.2011.02.003. PMID:21315737.

Rabinkov, A., Miron, T., Konstantinovski, L., Wilchek, M., Mirelman, D., and Weiner, L. 1998. The mode of action of allicin: trapping of radicals and interaction with thiol containing proteins. Biochim. Biophys. Acta, **1379**: 233–244. doi:10.1016/S0304-4165(97)00104-9. PMID:9528659.

Saravanan, G., and Prakash, J. 2004. Effect of garlic (*Allium sativum*) on lipid peroxidation in experimental myocardial infarction in rats. J. Ethnopharmacol. **94**: 155–158. doi:10.1016/j.jep.2004.04.029. PMID:15261977.

Serrano, F., and Klann, E. 2004. Reactive oxygen species and synaptic plasticity in the aging hippocampus. Ageing Res. Rev. **3**: 431–443. doi:10.1016/j.arr.2004.05.002. PMID:15541710.

Smeitink, J., van den Heuvel, L., and DiMauro, S. 2001. The genetics and pathology of oxidative phosphorylation. Nat. Rev. Genet. **2**: 342–352. doi:10.1038/35072063. PMID:11331900.

Sripetchwandee, J., Sanit, J., Chattipakorn, N., and Chattipakorn, S.C. 2013. Mitochondrial calcium uniporter blocker effectively prevents brain mitochondrial dysfunction caused by iron overload. Life Sci. **92**: 298–304. doi:10.1016/j.lfs.2013.01.004. PMID:23333832.

Steen, E., Terry, B.M., Rivera, E.J., Cannon, J.L., Neely, T.R., Tavares, R., et al. 2005. Impaired insulin and insulin-like growth factor expression and signaling mechanisms in Alzheimer's disease–is this type 3 diabetes? J. Alzheimers Dis. **7**: 63–80. PMID:15750215.

Stranahan, A.M., Norman, E.D., Lee, K., Cutler, R.G., Telljohann, R.S., Egan, J.M., and Mattson, M.P. 2008. Diet-induced insulin resistance impairs hippocampal synaptic plasticity and cognition in middle-aged rats. Hippocampus, **18**: 1085–1088. doi:10.1002/hipo.20470. PMID:18651634.

Sungnoon, R., Shinlapawittayatorn, K., Chattipakorn, S.C., and Chattipakorn, N. 2008. Effects of garlic on defibrillation efficacy. Int. J. Cardiol. **126**: 143–144. doi:10.1016/j.ijcard.2007.01.083. PMID:17434624.

Tsukamoto, H. 1993. Oxidative stress, antioxidants, and alcoholic liver fibrogenesis. Alcohol, **10**: 465–467. doi:10.1016/0741-8329(93)90066-W. PMID:8123201.

Valladolid-Acebes, I., Fole, A., Martín, M., Morales, L., Victoria Cano, M., Ruiz-Gayo, M., and Olmo, N.D. 2013. Spatial memory impairment and changes in hippocampal morphology are triggered by high-fat diets in adolescent mice. Is there a role of leptin? Neurobiol. Learn. Mem. **106**: 18–25. doi:10.1016/j.nlm.2013.06.012.

Vorhees, C.V., and Williams, M.T. 2006. Morris water maze: procedures for assessing spatial and related forms of learning and memory. Nat. Protoc. **1**: 848–858. doi:10.1038/nprot.2006.116. PMID:17406317.

Wada, A., Yokoo, H., Yanagita, T., and Kobayashi, H. 2005. New twist on neuronal insulin receptor signaling in health, disease, and therapeutics. J. Pharmacol. Sci. **99**: 128–143. doi:10.1254/jphs.CRJ05006X. PMID:16210778.

Walker, J.M. 1994. The bicinchoninic acid (BCA) assay for protein quantitation. Methods Mol. Biol. **32**: 5–8. PMID:7951748.

Weber, N.D., Andersen, D.O., North, J.A., Murray, B.K., Lawson, L.D., and Hughes, B.G. 1992. In vitro virucidal effects of *Allium sativum* (garlic) extract and compounds. Planta. Med. **58**: 417–423. doi:10.1055/s-2006-961504. PMID:1470664.

Ye, L., Wang, F., and Yang, R.H. 2011. Diabetes impairs learning performance and affects the mitochondrial function of hippocampal pyramidal neurons. Brain Res. **1411**: 57–64. doi:10.1016/j.brainres.2011.07.011. PMID:21798520.

Zhu, J.W., Chen, T., Guan, J., Liu, W.B., and Liu, J. 2012. Neuroprotective effects of allicin on spinal cord ischemia-reperfusion injury via improvement of mitochondrial function in rabbits. Neurochem. Int. **61**: 640–648. doi:10.1016/j.neuint.2012.06.021. PMID:22750272.

Appl. Physiol. Nutr. Metab. Downloaded from www.nrcresearchpress.com by Université de Montréal on 11/20/14
For personal use only.

เอกสารแนบหมายเลข 57

ELSEVIER

CrossMark

Archives of Medical Research

Archives of Medical Research 45 (2014) 547–552

ORIGINAL ARTICLE

DPP-4 Inhibitor and PPARγ Agonist Restore the Loss of CA1 Dendritic Spines in Obese Insulin-resistant Rats

Jirapas Sripetchwandee,[a,b] Noppamas Pipatpiboon,[a,b] Wasana Pratchayasakul,[a,b] Nipon Chattipakorn,[a,b] and Siriporn C. Chattipakorn[a,c]

[a]*Neurophysiology Unit, Cardiac Electrophysiology Research and Training Center, Faculty of Medicine,* [b]*Cardiac Electrophysiology Unit, Department of Physiology, Faculty of Medicine,* [c]*Department of Oral Biology and Diagnostic Sciences, Faculty of Dentistry, Chiang Mai University, Chiang Mai, Thailand*

Received for publication May 4, 2014; accepted September 12, 2014 (ARCMED-D-14-0250).

Background and Aims. Obesity induced by high-fat diet (HFD) impaired brain insulin receptor function, caused cognitive decline as well as reduced dendritic spine density. Previous studies suggested that dipeptidyl peptidase IV (DPP-4) inhibitor and peroxisome proliferator-activated receptor-gamma (PPARγ) agonist exerted the neuroprotective effects in obese insulin-resistant rats. However, the effects of these drugs on dendritic spines in obese insulin-resistant rats have not yet been investigated. In the present study, we determined the effects of DPP-4 inhibitor and PPARγ agonist on dendritic spines density of obese insulin-resistant rats caused by HFD.

Methods. Male Wistar Rats were divided into two groups. Animals in each group were fed with normal diet (ND) or HFD for 12 weeks. After then, rats in each group were subdivided into three subgroups to receive either vehicle or vildagliptin (3 mg/kg/day) or pioglitazone (10 mg/kg/day) for 3–4 weeks. At the end of the experiment, the metabolic parameters and density of dendritic spines in CA1 hippocampus were determined.

Results. We found that HFD-fed rats caused peripheral insulin resistance as well as the reduction of the density of dendritic spines in CA1 hippocampus. Treatment with both DPP-4 inhibitor and PPARγ agonist in HFD-fed rats improved insulin sensitivity as well as increased the number of dendritic spines in CA1 hippocampus. Moreover, both drugs have equally improved this deterioration.

Conclusion. Our findings indicate that DPP-4 inhibitor and PPARγ agonist restored the reduction of dendritic spines caused by HFD, suggesting the beneficial roles of DPP-4 inhibitors and PPARγ agonists in neurodegenerative disorders. © 2014 IMSS. Published by Elsevier Inc.

Key Words: Vildagliptin, Pioglitazone, Dendritic spines, High-fat diet, Insulin resistance.

Introduction

Insulin resistance is the pathological condition characterized by hyperinsulinemia with euglycemia. It has been known that insulin resistance is correlated with cognitive decline (1). Our previous studies demonstrated that 12-week high-fat diet (HFD) consumption caused not only peripheral insulin resistance but also brain insulin resistance (2–4). Moreover, HFD contributed to the deleterious effects in the brain including impaired brain insulin receptor function, decreased brain mitochondrial function as well as learning and memory decline (4).

Hippocampus plays an important role in the learning and memory process (5,6). The synaptic communication in the CNS during learning and memory process depends on dendritic spines morphology, size and number (7). Previous studies showed that the reduction of dendritic spines was associated with cognitive decline, suggesting the positive correlation of density of dendritic spines and the cognitive

Address reprint requests to: Siriporn C. Chattipakorn, DDS, PhD, Neurophysiology Unit, Cardiac Electrophysiology Research and Training Center, Faculty of Medicine, Chiang Mai University, Department of Oral Biology and Diagnostic Science, Faculty of Dentistry, Chiang Mai University, Chiang Mai, 50200, Thailand; Phone: 011-66-53-944-451; FAX: 011-66-53-222-844; E-mail: scchattipakorn@gmail.com or siriporn.c@cmu.ac.th

0188-4409/$ - see front matter. Copyright © 2014 IMSS. Published by Elsevier Inc.
http://dx.doi.org/10.1016/j.arcmed.2014.09.002

function (8–10). In addition, previous study suggested that high-calorie intake reduced dendritic spines density, leading to impaired cognitive function (11).

It has been known that antidiabetic drugs including DPP-4 inhibitors or PPARγ agonists provided the beneficial effects in the central nervous system (CNS). For example: a) DPP-4 inhibitor increased brain GLP-1 levels and decreased beta amyloid precursor protein (APP) as well as attenuated amyloid β deposit in transgenic mouse model of Alzheimer's disease (AD) (12), b) DPP-4 inhibitor reduced the inflammation in cerebral structure (12), c) PPARγ agonists exerted the neuroprotective effects by decreased brain oxidative stress (13), d) PPARγ agonists facilitated amyloid clearance in murine model of AD (14,15) and e) PPARγ agonists improved learning and memory in both animals and clinical studies (16–18). In addition, recent studies have shown that either DPP-4 inhibitors or PPARγ agonist restored the cognitive impairment induced by HFD consumption (2).

Our previous studies suggest the beneficial effects of either DPP-4 inhibitor or PPARγ agonist on brain insulin resistance by improving brain insulin receptor function as well as brain mitochondrial function (2,19). However, the effect of either DPP-4 inhibitor or PPARγ agonist on dendritic spines density in obese insulin resistant rats induced by HFD has not yet been investigated. In the present study, we determined whether either DPP-4 inhibitor; vildagliptin, or PPARγ agonist; pioglitazone, improves the reduction of dendritic spines density in obese insulin resistant rats induced by HFD. We hypothesized that either vildagliptin or pioglitazone attenuates dendritic spines loss following obese insulin resistant condition.

Materials and Methods

Male Wistar rats weighing 180–200 g (n = 36) obtained from the National Laboratory Animal Center, Salaya Campus, Mahidol University, Thailand were used. All experiments were conducted in accordance with an approved protocol from the Faculty of Medicine, Chiang Mai University Institutional Animal Care and Use Committee, in compliance with NIH guidelines. The animals were divided into two dietary groups (n = 18/group): animals in each group received either a normal diet (ND) with 19.77% total energy from fat or a high-fat diet (HFD) with 59.28% total energy from fat. At the end of the 12-week dietary treatment, a blood sample of each animal was obtained from a tail vein after 5 h of fasting for determination of metabolic parameters.

After 12 weeks of either ND or HFD feeding, animals in each group were equally randomized into three subgroups (n = 6/subgroup) to receive either 3 mg/kg/day of vildagliptin (Novartis Pharma Stein AG, Stein, Switzerland) dissolved in normal saline (2 mL/kg/day) for 21 days or 10 mg/kg/day pioglitazone (Takeda Pharmaceutical Company Limited, Tokyo, Japan) dissolved in normal saline (2 mL/kg/day) for 28 days or a vehicle (normal saline solution of 2 mL/kg/day) for 28 consecutive days. Doses and time courses for drug administration were given according to previous studies (19–22). Blood samples were collected from a tail vein after 5 h of fasting at the end of treatments to determine metabolic parameters. After that, rats were deeply anesthetized and decapitated. Brain in each animal was rapidly removed and used for determining brain dendritic spine density using Golgi staining technique.

Analysis of Plasma Cholesterol, Glucose and Insulin Levels

Plasma glucose and cholesterol concentrations were determined via colorimetric assay using commercial kits (Biotech, Bangkok, Thailand). Plasma insulin level was determined by Sandwich ELISA (LINCO Research, St. Charles, MO) as described in our previous studies (2,3). Homeostasis Model Assessment (HOMA) was used to determine insulin resistance (2,3). A higher level of HOMA index indicates a higher degree of insulin resistance.

Golgi Impregnation and Analysis

After decapitation, the brain was removed and rinsed with double-distilled water and placed in provided solutions from the Rapid Golgi Stain Kit (FD Neurotechnologies Kit, PK 401, Ellicott City, MD). Golgi impregnation was performed as described previously (23,24). For analysis of dendritic spine density, two segments from pyramidal cells in the CA1 hippocampus area were randomly measured with 100–200 μm apart from soma and 20–30 μm in dendritic length. The first segment was located on the secondary basal dendrites and the second segment was located on the tertiary apical dendrites. Six neuronal cells per brain slices were chosen for quantitative analysis (3 slices/animals, n = 6 animals/group). Dendritic spines were viewed by an inverted microscope using a 60x oil-immersion objective lens (IX-81, Olympus, Tokyo, Japan). The number of spines was counted using a hand counter, and the dendritic length was measured using Xcellence imaging software (Olympus). The spine density was expressed as the number of spines/10 μm of dendritic length.

Data Analysis

Data were presented as mean ± SE. Comparisons of the effects of diet and drug treatment on biochemical parameters and dendritic spine density were calculated using two-way ANOVA followed by the LSD post-hoc analysis using SPSS 17.0 (Chicago, IL); $p < 0.05$ was considered as statistically significant.

Table 1. Effect of long-term high-fat diet consumption on metabolic parameters

	Week 12	
Metabolic parameters	**ND**	**HFD**
Body weight (g)	437 ± 7.46	530 ± 12.32[a]
Food intake (g)	22.39 ± 2.44	23.98 ± 1.27
Plasma insulin (ng/mL)	1.77 ± 0.09	3.31 ± 0.26[a]
Plasma glucose (mg/dL)	126.10 ± 8.71	125.31 ± 3.97
HOMA index	13.52 ± 4.27	28.18 ± 3.79[a]
Plasma cholesterol (mg/dL)	202.82 ± 3.34	247.51 ± 2.89[a]

ND, normal diet fed rats; HFD, high-fat diet fed rats; HOMA, Homeostasis Model Assessment.
[a]$p < 0.05$ vs. ND.

Results

Effects of High-fat Diet (HFD) Consumption and Pharmacological Interventions on Metabolic Parameters

Twelve-week HFD-fed rats significantly increased in body weight, visceral fat, plasma cholesterol level, plasma insulin level, and HOMA index compared to 12-week ND-fed rats (Table 1). These findings suggested that HFD consumption induced peripheral insulin resistance.

In ND-fed rats, treatment with either pioglitazone or vildagliptin did not change the metabolic parameters compared to vehicle-treated ND-fed rats (Table 2). In HFD-fed rats, vildagliptin treatment showed a significant reduction in plasma cholesterol level, whereas the other metabolic parameters did not improve compared to HFD-fed rats treated with vehicle (Table 2). Nevertheless, our previous study showed that vildagliptin improved oral glucose tolerance test (OGTT) as well as insulin glucose tolerance test (IGTT), suggesting the beneficial effect of vildagliptin in improving the insulin sensitivity in HFD-fed rats (19). In contrast, administration of pioglitazone in HFD-fed rats attenuated peripheral insulin resistance indicated by decreased plasma cholesterol, plasma glucose, plasma insulin and HOMA index, whereas body weight and visceral fat were increased in pioglitazone-treated HFD-fed rats (Table 2). These findings suggested that pioglitazone also improved insulin sensitivity.

HFD Consumption Decreased Dendritic Spine Density and Treatments with either Vildagliptin or Pioglitazone Increased Dendritic Spines in HFD-fed Rats

HFD consumption significantly decreased the number of dendritic spines on secondary and tertiary dendrites in apical dendrites compared with those of ND-fed rat as shown in Figure 1A. However, the reduction of dendritic spine density following HFD consumption was attenuated by the treatment with either vildagliptin or pioglitazone (Figure 1B).

Treatment with either vildagliptin or pioglitazone in HFD-fed rats restores dendritic spines density to the normal level, whereas both treatments had no effect in the density of dendritic spines of ND-fed rats as shown in Figure 1B. Moreover, the number of dendritic spines in both treatments of HFD-fed rats did not reach the statistical difference. These findings suggest that antidiabetic drugs including PPARγ agonist and DPP-4 inhibitor prevented the loss of dendritic spines caused by HFD.

Discussion

The major findings of the present study are as follows: a) HFD consumption caused peripheral insulin resistance and decreased dendritic spine density in CA1 hippocampus, b) treatment with either DPP-4 inhibitor; vildagliptin or PPARγ agonist; pioglitazone attenuated peripheral insulin resistance and restored the loss of dendritic spines caused by HFD consumption.

Consistent with our previous studies, HFD consumption induced peripheral insulin resistance via increased body weight, visceral fat, plasma cholesterol, plasma insulin levels and HOMA index, whereas plasma glucose level did not change (2–4). In addition, several studies showed

Table 2. Effect of vildagliptin and pioglitazone on body weight, visceral fat, plasma cholesterol, plasma glucose, plasma insulin and HOMA index in rats fed with ND and HFD

Metabolic parameters	**NDV**	**NDVil**	**NDP**	**HFV**	**HFVil**	**HFP**
Body weight (g)	433.32 ± 4.73	437.5 ± 16.52	461.25 ± 5.15	542.5 ± 18.87[a]	548.70 ± 10.07[a]	582.5 ± 13.14[a,b]
Food intake (g)	21.95 ± 3.61	21.11 ± 4.69	22.86 ± 3.47	23.35 ± 2.19	22.78 ± 1.71	24.25 ± 3.48
Visceral fat (g)	36.48 ± 2.34	33.89 ± 1.78	41.16 ± 3.61	52.57 ± 2.91[a]	56.68 ± 2.50[a]	63.78 ± 4.43[a,b]
Plasma cholesterol (mg/dL)	246.73 ± 6.72	216.33 ± 15.09	225.00 ± 10.09	323.91 ± 8.24[a]	234.66 ± 11.74[b]	234.78 ± 9.22[b]
Plasma glucose (mg/dL)	139.96 ± 6.23	125.15 ± 6.56	131.00 ± 4.69	150.05 ± 3.24	129.90 ± 5.42	123.94 ± 7.96[b]
Plasma insulin (ng/mL)	1.53 ± 0.08	1.89 ± 0.21	1.75 ± 0.08	3.92 ± 0.31[a]	3.89 ± 0.29[a]	2.24 ± 0.31[a,b]
HOMA index	11.79 ± 0.28	15.07 ± 0.44	13.59 ± 0.89	31.12 ± 0.56[a]	29.27 ± 1.88[b]	15.42 ± 1.70[b]

ND, normal diet fed rats; HFD, high-fat diet fed rats; NDV, normal diet fed rats treated with vehicle; NDVil, normal diet fed rats treated with vildagliptin; NDP, normal diet fed rats treated with pioglitazone; HFV, high-fat diet fed rats treated with vehicle; HFVil, high-fat diet fed rats treated with vildagliptin; HFP, high-fat diet fed rats treated with pioglitazone; HOMA, Homeostasis Model Assessment; MDA, malondialdehyde.
[a]$p < 0.05$ vs. NDV.
[b]$p < 0.05$ vs. HFV.

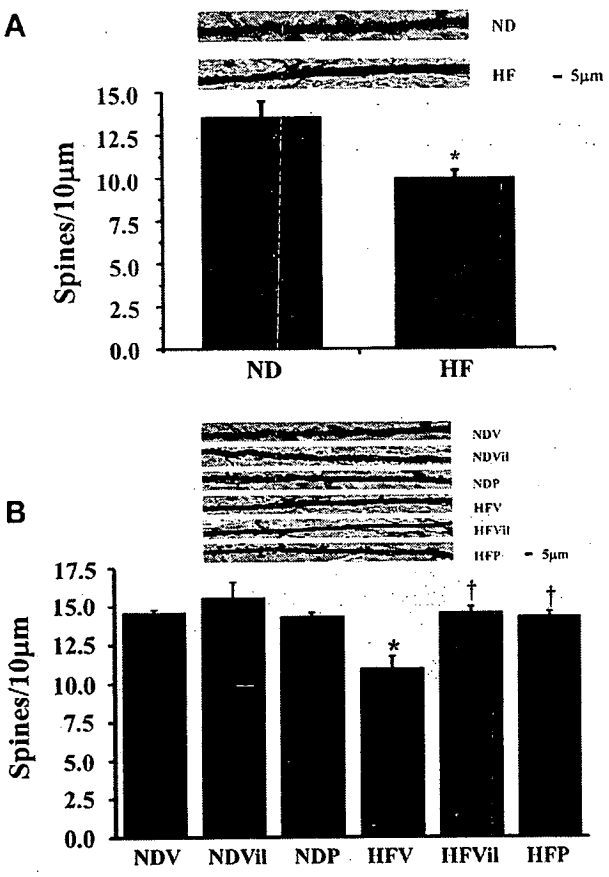


Figure 1. Effects of HFD consumption (A) and treatment with vildagliptin and pioglitazone (B) on dendritic spine density. $^{*}p < 0.05$ vs. NDV, $^{\dagger}p < 0.05$ vs. HFV. NDV, normal diet-fed subgroup treated with vehicle (normal saline); NDVil, normal diet-fed subgroup treated with vildagliptin; NDP, normal diet-fed subgroup treated with pioglitazone; HFV, high-fat diet-fed subgroup treated with vehicle (normal saline); HFVil, high-fat diet-fed subgroup treated with vildagliptin; HFP, high-fat diet-fed subgroup treated with pioglitazone.

that long-term HFD consumption not only induced peripheral insulin resistance but also brain insulin resistance indicated by an impaired brain insulin signaling and function (2–4,19). HFD-induced brain insulin resistance has shown to be associated with the impairment of cognitive function (19,25,26). The reduction of brain insulin sensitivity also demonstrated to be correlated with cognitive decline in neurodegenerative disorders (27–29).

Dendritic spines are dynamic structures representing the underlying mechanisms of learning and memory (7,30,31). A recent study indicated that the loss of dendritic spines density was caused by insulin resistance (32). Moreover, insulin has shown to play a role in dendritic spine formation (33,34). Consistent with those recent studies, the present study showed that HFD-induced insulin resistance also causes the loss of dendritic spines, indicated by the decrease in dendritic spine number. Our previous study demonstrated that HFD-induced brain insulin resistance is responsible for cognitive decline (4,19,35). The present finding and our previous studies suggest that cognitive decline in brain insulin resistant condition may occur via the loss of dendritic spines.

A previous study showed that plasma cholesterol levels could cross blood-brain barrier and reach the brain and consequently increase brain cholesterol level (36). Hypercholesterolemia caused the deleterious effects to the brain such as a) accelerated synaptic loss by decreased synaptophysin levels (37), b) decreased anti-oxidants in the brain (38) and increased inflammatory cytokines in the brain (39,40), c) caused the impairment of electrical-induced long-term potentiation and long-term depression in HFD-fed rats (41), d) impaired learning and memory (39,40), e) reduced brain insulin signaling (42) and f) decreased dendritic spine density in HFD-fed rats (32,34,43). Moreover, recent studies showed that insulin signaling was related to dendritic spine formation in primary cultures of rat hippocampal neurons by activated phosphatidylinositol 3-kinase PI3K/Akt/mammalian target of rapamycin (mTOR) signaling pathways (33). In contrast, the inactivation of PI3K/Akt/mTOR signaling pathway by pharmacological intervention inhibited insulin-increased dendritic spine (33). These findings indicated that insulin signaling plays an important role in the regulation of dendritic spine formation. Furthermore, morphology and size as well as the number of dendritic spines are important for learning and memory processes (7). Our study demonstrated that HFD consumption reduced dendritic spines number in CA1 hippocampus, consistent with a previous study (11). Moreover, our recent studies have shown that HFD consumption impaired brain insulin signaling by decreasing insulin receptor (IR) phosphorylation, insulin receptor substrate-1 (IRS-1) phosphorylation and Akt ser-473 phosphorylation (2,3). These impairments might be the underlying mechanisms in association with the reduction of dendritic spine density, which were found in the present study.

In the present study, vildagliptin reduced plasma cholesterol level, although the other metabolic parameters did not change. This effect could result from the downregulation of genes required for cholesterol synthesis as well as fatty acid oxidation as previously described (44). In the brain we found that vildagliptin treatment attenuated dendritic spine loss following HFD consumption. This might occur via the direct effect of vildagliptin in which improved brain insulin sensitivity as demonstrated by improving IR, IRS-1 and Akt Ser-473 phosphorylation as described in our previous study (19) via GLP-1 activity (45–47). Moreover, because hypercholesterolemia is related to the loss of dendritic spine density (32,34,43) and that HFD-fed rats treated with vildagliptin indicated the decreased plasma cholesterol level, the improved effects in density spine density could be due to this mechanism. These findings suggested that vildagliptin treatment used in the present study could restore dendritic spine density through improving brain insulin signaling and reducing plasma cholesterol level.

Pioglitazone treatment in HFD-fed rats significantly decreased plasma cholesterol levels and improved peripheral insulin sensitivity as indicated by reduced HOMA index, similar to a previous study (48). In brain, pioglitazone administration increased dendritic spine density. It has been shown that pioglitazone could cross the blood-brain barrier (49,50) to provide the protective effects in brain. Recent studies demonstrated that pioglitazone improved insulin sensitivity in skeletal muscle and brain as indicated by the increased phosphorylation of IR, IRS-1, GSK-3β levels as well as PI3K activities (51,52). In our recent study using PPARγ agonist, rosiglitazone, we found that rosiglitazone improved brain insulin sensitivity by increasing brain Akt Ser-473 phosphorylation in HFD-fed rats following rosiglitazone treatment (2). PPARγ agonist increased dendritic spine density possibly through the direct effects of PPAR agonist to improve brain insulin sensitivity or improve peripheral insulin sensitivity or decrease plasma cholesterol level as previously shown in the results.

Our recent studies have already demonstrated that obese insulin-resistant rats had cognitive impairment, particularly deficits in hippocampal-dependent memory as shown by impaired Morris Water Maze test (4,19,35). Moreover, we also demonstrated that DPP-4 inhibitors (both sitagliptin and vildagliptin) improved cognitive function in these obese insulin-resistant rats (19,35). Although we have no data suggesting the therapeutic effects of PPARγ agonists on the cognitive function, a number of studies already indicated that PPARγ agonists attenuated cognitive deficit in both obese animal model and diabetic animal model (16,53,54). All of these findings from previous reports including our own studies and our findings from the present study firmly suggest that both DPP-4 inhibitor and PPARγ agonist could attenuate cognitive impairment in obese insulin-resistant rats through their ability to increase the density of dendritic spines.

From the present study, the protective effects of both vildagliptin and pioglitazone on dendritic spines in CA1 hippocampus in obese insulin-resistant models suggested that antidiabetic drugs exerted beneficial effects in the treatment of cognitive decline in obese insulin-resistant models.

Study Limitations

Although the present study demonstrated the restorative effects of both DPP-4 inhibitor and PPARγ agonist on dendritic spine density in obese insulin-resistant rats, the effect of the combination of both drugs on this parameter was not investigated. Future studies are warranted to determine whether a combined therapy could provide the synergistic effects on the improvement of dendritic spine density as well as the cognitive functions in obese insulin-resistant model.

In conclusion, the present study suggests that both DPP-4 inhibitor and PPARγ agonist restored the reduction of dendritic spines caused by obese insulin-resistant condition. An increment of dendritic spine density could preserve learning and memory function; therefore, DPP-4 inhibitors and PPARγ agonists can be useful drugs ameliorating cognitive impairment in obese insulin-resistant patients.

Acknowledgments

This work was supported by grants from the Thailand Research Fund TRF-BRG5780016 (SC), TRF-RTA5580006 (NC), Faculty of Dentistry, Chiang Mai University (SC), Faculty of Medicine Chiang Mai University Endowment Fund (NC), National Research Council of Thailand (SC), and Chiang Mai University Excellent Center Award (NC).

References

1. Cole AR, Astell A, Green C, et al. Molecular connexions between dementia and diabetes. Neurosci Biobehav Rev 2007;31:1046–1063.
2. Pipatpiboon N, Pratchayasakul W, Chattipakorn N, et al. PPARgamma agonist improves neuronal insulin receptor function in hippocampus and brain mitochondria function in rats with insulin resistance induced by long term high-fat diets. Endocrinology 2012;153:329–338.
3. Pratchayasakul W, Kerdphoo S, Petsophonsakul P, et al. Effects of high-fat diet on insulin receptor function in rat hippocampus and the level of neuronal corticosterone. Life Sci 2011;88:619–627.
4. Pintana H, Apaijai N, Pratchayasakul W, et al. Effects of metformin on learning and memory behaviors and brain mitochondrial functions in high fat diet induced insulin resistant rats. Life Sci 2012;91: 409–414.
5. Kalalian-Moghaddam H, Baluchnejadmojarad T, Roghani M, et al. Hippocampal synaptic plasticity restoration and anti-apoptotic effect underlie berberine improvement of learning and memory in streptozotocin-diabetic rats. Eur J Pharmacol 2012;698:259–266.
6. Chen Y, Yu D, Wei Q, et al. Effect of lead exposure on synaptic structural plasticity in the hippocampus of postnatal Wistar rat. Wei Sheng Yan Jiu 2012;41:394–398.
7. Harms KJ, Dunaevsky A. Dendritic spine plasticity: looking beyond development. Brain Res 2007;1184:65–71.
8. Chen Y, Rex CS, Rice CJ, et al. Correlated memory defects and hippocampal dendritic spine loss after acute stress involve corticotropin-releasing hormone signaling. Proc Natl Acad Sci USA 2010;107: 13123–13128.
9. Grove M, Demyanenko G, Echarri A, et al. ABI2-deficient mice exhibit defective cell migration, aberrant dendritic spine morphogenesis, and deficits in learning and memory. Mol Cell Biol 2004;24: 10905–10922.
10. Ricobaraza A, Cuadrado-Tejedor M, Marco S, et al. Phenylbutyrate rescues dendritic spine loss associated with memory deficits in a mouse model of Alzheimer disease. Hippocampus 2012;22:1040–1050.
11. Stranahan AM, Norman ED, Lee K, et al. Diet-induced insulin resistance impairs hippocampal synaptic plasticity and cognition in middle-aged rats. Hippocampus 2008;18:1085–1088.
12. D'Amico M, Di Filippo C, Marfella R, et al. Long-term inhibition of dipeptidyl peptidase-4 in Alzheimer's prone mice. Exp Gerontol 2010;45:202–207.
13. Gupta R, Gupta LK. Improvement in long term and visuo-spatial memory following chronic pioglitazone in mouse model of Alzheimer's disease. Pharmacol Biochem Behav 2012;102:184–190.
14. Mandrekar-Colucci S, Karlo JC, Landreth GE. Mechanisms underlying the rapid peroxisome proliferator-activated receptor-gamma-mediated amyloid clearance and reversal of cognitive deficits in a murine model of Alzheimer's disease. J Neurosci 2012;32:10117–10128.
15. Inestrosa NC, Godoy JA, Quintanilla RA, et al. Peroxisome proliferator-activated receptor gamma is expressed in hippocampal

neurons and its activation prevents beta-amyloid neurodegeneration: role of Wnt signaling. Exp Cell Res 2005;304:91–104.
16. Jiang LY, Tang SS, Wang XY, et al. PPARgamma agonist pioglitazone reverses memory impairment and biochemical changes in a mouse model of type 2 diabetes mellitus. CNS Neurosci Ther 2012;18:659–666.
17. Wang BW, Hok V, Della-Chiesa A, et al. Rosiglitazone enhances learning, place cell activity, and synaptic plasticity in middle-aged rats. Neurobiol Aging 2012;33:835.e13–835.e30.
18. Cowley TR, O'Sullivan J, Blau C, et al. Rosiglitazone attenuates the age-related changes in astrocytosis and the deficit in LTP. Neurobiol Aging 2012;33:162–175.
19. Pipatpiboon N, Pintana H, Pratchayasakul W, et al. DPP4-inhibitor improves neuronal insulin receptor function, brain mitochondrial function and cognitive function in rats with insulin resistance induced by high-fat diet consumption. Eur J Neurosci 2013;37:839–849.
20. Luo D, Hou X, Hou L, et al. Effect of pioglitazone on altered expression of Abeta metabolism-associated molecules in the brain of fructose-drinking rats, a rodent model of insulin resistance. Eur J Pharmacol 2011;664:14–19.
21. Baraka A, El Ghotny S. Study of the effect of inhibiting galanin in Alzheimer's disease induced in rats. Eur J Pharmacol 2010;641:123–127.
22. Kumar A, Vashist A, Kumar P. Potential role of pioglitazone, caffeic acid and their combination against fatigue syndrome-induced behavioural, biochemical and mitochondrial alterations in mice. Inflammopharmacology 2010;18:241–251.
23. Frankfurt M, Salas-Ramirez K, Friedman E, et al. Cocaine alters dendritic spine density in cortical and subcortical brain regions of the postpartum and virgin female rat. Synapse 2011;65:955–961.
24. Inagaki T, Frankfurt M, Luine V. Estrogen-induced memory enhancements are blocked by acute bisphenol A in adult female rats: role of dendritic spines. Endocrinology 2012;153:3357–3367.
25. Woo J, Shin KO, Park SY, et al. Effects of exercise and diet change on cognition function and synaptic plasticity in high fat diet induced obese rats. Lipids Health Dis 2013;12:144.
26. Pancani T, Anderson KL, Brewer LD, et al. Effect of high-fat diet on metabolic indices, cognition, and neuronal physiology in aging F344 rats. Neurobiol Aging 2013;34:1977–1987.
27. Cholerton B, Baker LD, Craft S. Insulin, cognition, and dementia. Eur J Pharmacol 2013;719:170–179.
28. Steen E, Terry BM, Rivera EJ, et al. Impaired insulin and insulin-like growth factor expression and signaling mechanisms in Alzheimer's disease—is this type 3 diabetes? J Alzheimers Dis 2005;7:63–80.
29. Park S, Kim da S, Kang S, et al. beta-Amyloid-induced cognitive dysfunction impairs glucose homeostasis by increasing insulin resistance and decreasing beta-cell mass in non-diabetic and diabetic rats. Metabolism 2013;62:1749–1760.
30. Sala C, Segal M. Dendritic spines: the locus of structural and functional plasticity. Physiol Rev 2014;94:141–188.
31. Lai KO, Ip NY. Structural plasticity of dendritic spines: the underlying mechanisms and its dysregulation in brain disorders. Biochim Biophys Acta 2013;1832:2257–2263.
32. Stranahan AM, Lee K, Martin B, et al. Voluntary exercise and caloric restriction enhance hippocampal dendritic spine density and BDNF levels in diabetic mice. Hippocampus 2009;19:951–961.
33. Lee CC, Huang CC, Hsu KS. Insulin promotes dendritic spine and synapse formation by the PI3K/Akt/mTOR and Rac1 signaling pathways. Neuropharmacology 2011;61:867–879.
34. Calvo-Ochoa E, Hernandez-Ortega K, Ferrera P, et al. Short-term high-fat-and-fructose feeding produces insulin signaling alterations accompanied by neurite and synaptic reduction and astroglial activation in the rat hippocampus. J Cereb Blood Flow Metab 2014;218:1001–1008.
35. Pintana H, Apaijai N, Chattipakorn N, et al. DPP-4 inhibitors improve cognition and brain mitochondrial function of insulin-resistant rats. J Endocrinol 2013;218:1–11.
36. Bjorkhem I. Crossing the barrier: oxysterols as cholesterol transporters and metabolic modulators in the brain. J Intern Med 2006; 260:493–508.
37. Umeda T, Tomiyama T, Kitajima E, et al. Hypercholesterolemia accelerates intraneuronal accumulation of Abeta oligomers resulting in memory impairment in Alzheimer's disease model mice. Life Sci 2012;91:1169–1176.
38. de Oliveira J, Hort MA, Moreira EL, et al. Positive correlation between elevated plasma cholesterol levels and cognitive impairments in LDL receptor knockout mice: relevance of cortico-cerebral mitochondrial dysfunction and oxidative stress. Neuroscience 2011;197:99–106.
39. Thirumangalakudi L, Prakasam A, Zhang R, et al. High cholesterol-induced neuroinflammation and amyloid precursor protein processing correlate with loss of working memory in mice. J Neurochem 2008;106:475–485.
40. Ullrich C, Pirchl M, Humpel C. Hypercholesterolemia in rats impairs the cholinergic system and leads to memory deficits. Mol Cell Neurosci 2010;45:408–417.
41. Hwang LL, Wang CH, Li TL, et al. Sex differences in high-fat diet-induced obesity, metabolic alterations and learning, and synaptic plasticity deficits in mice. Obesity (Silver Spring) 2008;18:463–469.
42. Taghibiglou C, Bradley CA, Gaertner T, et al. Mechanisms involved in cholesterol-induced neuronal insulin resistance. Neuropharmacology 2009;57:268–276.
43. Valladolid-Acebes I, Fole A, Martin M, et al. Spatial memory impairment and changes in hippocampal morphology are triggered by high-fat diets in adolescent mice. Is there a role of leptin? Neurobiol Learn Mem 2013;106:18–25.
44. Flock G, Baggio LL, Longuet C, et al. Incretin receptors for glucagon-like peptide 1 and glucose-dependent insulinotropic polypeptide are essential for the sustained metabolic actions of vildagliptin in mice. Diabetes 2007;56:3006–3013.
45. Acitores A, Gonzalez N, Sancho V, et al. Cell signalling of glucagon-like peptide-1 action in rat skeletal muscle. J Endocrinol 2004;180: 389–398.
46. Gonzalez N, Acitores A, Sancho V, et al. Effect of GLP-1 on glucose transport and its cell signalling in human myocytes. Regul Pept 2005; 126:203–211.
47. Redondo A, Trigo MV, Acitores A, et al. Cell signalling of the GLP-1 action in rat liver. Mol Cell Endocrinol 2003;204:43–50.
48. Srinivasan K, Viswanad B, Asrat L, et al. Combination of high-fat diet-fed and low-dose streptozotocin-treated rat: a model for type 2 diabetes and pharmacological screening. Pharmacol Res 2005;52:313–320.
49. Grommes C, Karlo JC, Caprariello A, et al. The PPARgamma agonist pioglitazone crosses the blood-brain barrier and reduces tumor growth in a human xenograft model. Cancer Chemother Pharmacol 2013;71:929–936.
50. Swanson CR, Joers V, Bondarenko V, et al. The PPAR-gamma agonist pioglitazone modulates inflammation and induces neuroprotection in parkinsonian monkeys. J Neuroinflammation 2011;8:91.
51. Hayakawa T, Shiraki T, Morimoto T, et al. Pioglitazone improves insulin signaling defects in skeletal muscle from Wistar fatty (fa/fa) rats. Biochem Biophys Res Commun 1996;223:439–444.
52. Ponce-Lopez T, Liy-Salmeron G, Hong E, et al. Lithium, phenserine, memantine and pioglitazone reverse memory deficit and restore phospho-GSK3beta decreased in hippocampus in intracerebroventricular streptozotocin induced memory deficit model. Brain Res 2011;1426:73–85.
53. Pathan AR, Gaikwad AB, Viswanad B, et al. Rosiglitazone attenuates the cognitive deficits induced by high fat diet feeding in rats. Eur J Pharmacol 2008;589:176–179.
54. Sharma B, Singh N. Behavioral and biochemical investigations to explore pharmacological potential of PPAR-gamma agonists in vascular dementia of diabetic rats. Pharmacol Biochem Behav 2011;100:320–329.

เอกสารแนบหมายเลข 58

Journal of Geriatric Cardiology (2014) 11: 151–157
©2014 JGC All rights reserved; www.jgc301.com

Research Article · Open Access ·

Phosphodiesterase-3 inhibitor (cilostazol) attenuates oxidative stress-induced mitochondrial dysfunction in the heart

Siriporn C. Chattipakorn[1,2], Savitree Thummasorn[1], Jantira Sanit[1], Nipon Chattipakorn[1,3]

[1]*Cardiac Electrophysiology Research and Training Center, Department of Physiology, Faculty of Medicine, Chiang Mai University, Chiang Mai 50200, Thailand*

[2]*Faculty of Dentistry, Chiang Mai University, Chiang Mai 50200, Thailand*

[3]*Biomedical Engineering Center, Chiang Mai University, Chiang Mai 50200, Thailand*

Abstract

Background Cilostazol is a type 3 phosphodiesterase inhibitor which has been previously demonstrated to prevent the occurrence of tachyarrhythmia and improve defibrillation efficacy. However, the mechanism for this beneficial effect is still unclear. Since cardiac mitochondria have been shown to play a crucial role in fatal cardiac arrhythmias and that oxidative stress is one of the main contributors to arrhythmia generation, we tested the effects of cilostazol on cardiac mitochondria under severe oxidative stress. **Methods** Mitochondria were isolated from rat hearts and treated with H_2O_2 to induce oxidative stress. Cilostazol, at various concentrations, was used to study its protective effects. Pharmacological interventions, including a mitochondrial permeability transition pore (mPTP) blocker, cyclosporine A (CsA), and an inner membrane anion channel (IMAC) blocker, 4'-chlorodiazepam (CDP), were used to investigate the mechanistic role of cilostazol on cardiac mitochondria. Cardiac mitochondrial reactive oxygen species (ROS) production, mitochondrial membrane potential change and mitochondrial swelling were determined as indicators of cardiac mitochondrial function. **Results** Cilostazol preserved cardiac mitochondrial function when exposed to oxidative stress by preventing mitochondrial depolarization, mitochondrial swelling, and decreasing ROS production. **Conclusions** Our findings suggest that cardioprotective effects of cilostazol reported previously could be due to its prevention of cardiac mitochondrial dysfunction caused by severe oxidative stress.

J Geriatr Cardiol 2014; 11: 151–157. doi: 10.3969/j.issn.1671-5411.2014.02.014

Keywords: Phosphodiesterase-3 inhibitor; Cilostazol; Mitochondria; Heart; Oxidative stress; Membrane potential; Ischemia

1 Introduction

Cilostazol is a selective type-3 phosphodiesterase inhibitor that has been used to treat claudication. Unlike other type-3 phosphodiesterase inhibitors, such as milrinone and vesnarinone which have been shown to increase cyclic adenosine monophosphate (cAMP) levels, arrythmogenisis, and mortality rates in heart failure patients,[1,2] growing evidence suggests that cilostazol could be cardioprotective.[3–14] This could be due to the fact that cilostazol inhibits not only type 3 phosphodiesterase, but also adenosine uptake, thus reducing the cAMP levels.[15,16] Previous studies also demonstrated the cardioprotective effects of cilostazol by preventing the occurrence of fatal arrhythmias in Brugada's syndrome.[17] Our recent study demonstrated that cilostazol could stabilize the cardiac electrophysiology and prevent fatal arrhythmias by increasing the ventricular fibrillation threshold as well as increasing the defibrillation efficacy.[18] Despite these beneficial effects, the definite mechanism of cilostazol in arrhythmia prevention is still unclear.

Cardiac mitochondrial dysfunction has been shown to play an important role in cardiac arrhythmogenesis.[19] It has been shown that depolarization of cardiac mitochondrial membrane potential occurring during various stress conditions, including ischemia-reperfusion, could initiate fatal arrhythmia in the heart.[19] Oxidative stress due to high levels of reactive oxygen species (ROS) produced in the mitochondria during ischemia-reperfusion has been shown to play an important role in triggering the cardiac mitochondrial membrane potential changes.[19,20] Although several drugs and chemical substances have been demonstrated to attenuate mitochondrial dysfunction caused by oxidative

Correspondence to: Nipon Chattipakorn, MD, PhD, Cardiac Electrophysiology Research and Training Center (CERT), Faculty of Medicine, Chiang Mai University, Chiang Mai 50200, Thailand. E-mail: nchattip@gmail.com

Telephone: +66-53-945329 **Fax:** +66-53-945368

Received: January 15, 2014 **Revised:** May 5, 2014

Accepted: May 30, 2014 **Published online:** June 8, 2014

stress;[19,21–23] the role of cilostazol on cardiac mitochondrial function has never been investigated.

In the present study, we tested the hypothesis that cilostazol can prevent cardiac mitochondrial dysfunction caused by H_2O_2-induced severe oxidative stress by attenuating mitochondrial swelling, preventing mitochondrial depolarization, and reducing ROS production in cardiac mitochondria.

2 Methods

2.1 Animal preparation

This study was approved by the Institutional Animal Care and Use Committee at the Faculty of Medicine, Chiang Mai University. Wistar rats (300–350 g) obtained from the National Laboratory Animal Center, Mahidol University, Bangkok, Thailand, were housed in a room with temperature 22–25°C and had a constant 12-h light/dark cycle. All animals received standard pelleted rat diet and water *ad libitum*.

2.2 Isolated cardiac mitochondria preparation

Cardiac mitochondria were isolated based upon the protocol described previously.[20] In brief, each rat was injected intraperitoneally with thiopental (80 mg/kg), and the heart was removed and homogenized in ice-cold buffer containing sucrose 300 mmol/L, N-(tris (hydroxymethyl) methyl)-2-aminoethanesulfonic acid sodium salt (TES) 5 mmol/L, and ethylene glycol tetraacetic acid (EGTA) 0.2 mmol/L, pH 7.2 at 4°C. The homogenate was centrifuged at 800 r/min for 5 min and the supernatant was collected and centrifuged at 8,800 r/min for 5 min. Cardiac mitochondrial pellets were resuspended in an ice-cold buffer and centrifuged again at 8,800 r/min for 5 min. Protein concentration was determined according to the bicinchoninic acid (BCA) assay.[24]

2.3 Experimental protocols

Isolated cardiac mitochondria from rat hearts were used in all study protocols. Identification of cardiac mitochondria was performed using electron microscopy. Application of H_2O_2 at 2 mmol/L with a 5-min incubation time was used to induce oxidative stress in cardiac mitochondria. This concentration and incubation time were chosen as been shown to effectively cause cardiac mitochondrial dysfunction by inducing mitochondrial swelling, increasing mitochondrial ROS production, and depolarizing mitochondrial membrane potential.[20]

In the first protocol, 20-μmol/L cilostazol was applied to cardiac mitochondria at various incubation times (5–20 min) prior to H_2O_2 application. The time in which cilostazol could effectively protect cardiac mitochondrial dysfunction caused by H_2O_2 was chosen for the next protocol. In the second protocol, various concentrations of cilostazol (5–40 μmol/L) were studied with the incubation time obtained from the first protocol. Vehicle-treated mitochondria were used as a control group.

In the third protocol, the protective mechanism of cilostazol on cardiac mitochondria was investigated using a pharmacological intervention approach. Cyclosporine A (CsA) and 4'-chlorodiazepam (CDP) were used for this purpose. CsA is a blocker of the mitochondrial permeability transition pore (mPTP),[20,25] whereas CDP is known to inhibit the opening of the inner membrane anion channel (IMAC).[20] In this protocol, cardiac mitochondria were randomly assigned into 10 treatment groups (n = 8 per group), consisting of the control (vehicle); cilostazol (effective dose of cilostazol obtained from the second protocol); CsA (5 μmol/L); CDP (100 μmol/L); H_2O_2; H_2O_2 with cilostazol; H_2O_2 with CsA; H_2O_2 with CDP; H_2O_2 with cilostazol + CsA; and H_2O_2 with cilostazol + CDP. In each study protocol, cardiac mitochondria in each group were investigated for mitochondrial swelling, mitochondrial ROS production, and mitochondrial membrane potential changes.

2.4 Determination of cardiac mitochondrial swelling, ROS production and membrane potential changes

Cardiac mitochondrial swelling was determined in all groups by measuring the change in the absorbance of the cardiac mitochondrial suspension at 540 nm ($A540$) using a microplate reader.[20,25] Mitochondria (0.4 mg/mL) were incubated in respiration buffer (containing 100 mmol/L KCl, 50 mmol/L sucrose, 10 mmol/L 4-(2-hydroxyethyl)-1-piperazineethanesulfonic acid (HEPES), and 5 mmol/L KH_2PO_4, pH 7.4 at 37°C) with the addition of 10-mmol/L pyruvate/malate. Mitochondrial swelling was indicated by a decrease in the absorbance of the suspension.[20]

ROS production in cardiac mitochondria was determined using dichlorohydro-fluorescein diacetate (DCFDA),[26] and measured by a fluorescent microplate reader.[20] Cardiac mitochondria (0.4 mg/mL) were incubated at 25°C with 2-μmol/L of DCFDA for 20 min. The mitochondrial suspension was gently agitated and incubated at room temperature for measurements. DCFDA passed through the mitochondrial membranes where it was oxidized in the presence of H_2O_2 to DCF (a fluorescent form). Fluorescence was determined at λ_{ex} 485 nm and λ_{em} 530 nm according to the spectral characteristics of DCF. The ROS levels were expressed as arbitrary units of fluorescence intensity of DCF.[20]

Changes in the cardiac mitochondrial membrane potential were determined using the dye 5,5',6,6'-tetrachloro-1,1',3,3'-tetraethylbenzimidazolcarbocyanine iodide (JC-1).[20,27,28] The isolated cardiac mitochondria (2 mg/mL) were stained with JC-1 (310 nmol/L) at 37°C for 30 min. The intensity of fluorescence was determined using a fluorescent microplate reader. JC-1 monomer fluorescence (green) was excited at 485 nm and the emission was detected at 530 nm. JC-1 aggregate fluorescence (red) was excited at 485 nm and the emission fluorescence was recorded at 590 nm. Cardiac mitochondrial depolarization was indicated by a decrease in the red/green fluorescence intensity ratio.[20]

2.5 Statistical analysis

All data were expressed as means ± SE. Comparisons among groups were determined by one-way ANOVA, followed by the Fisher post-hoc test. $P < 0.05$ was considered statistically significant.

3 Results

3.1 Effects of cilostazol on cardiac mitochondrial swelling, ROS production and membrane potential changes

Application of H_2O_2 at 2 mmol/L caused cardiac mitochondrial dysfunction as represented by decreased absorbance indicating mitochondrial swelling (Figure 1A), increased ROS levels (Figure 1B), and a decreased red/green fluorescent ratio indicating mitochondrial membrane depolarization (Figure 1C), in comparison to the control group. When 20-μmol/L cilostazol was applied to cardiac mitochondria, there was no change in absorbance, ROS levels, or mitochondrial membrane potential in cardiac mitochondria at any of the incubation times. However, the application of cilostazol to cardiac mitochondria for 5, 10, and 20 min prior to H_2O_2 application could prevent mitochondrial swelling, decrease ROS levels, and prevent mitochondrial depolarization caused by H_2O_2 (Figure 1). From this

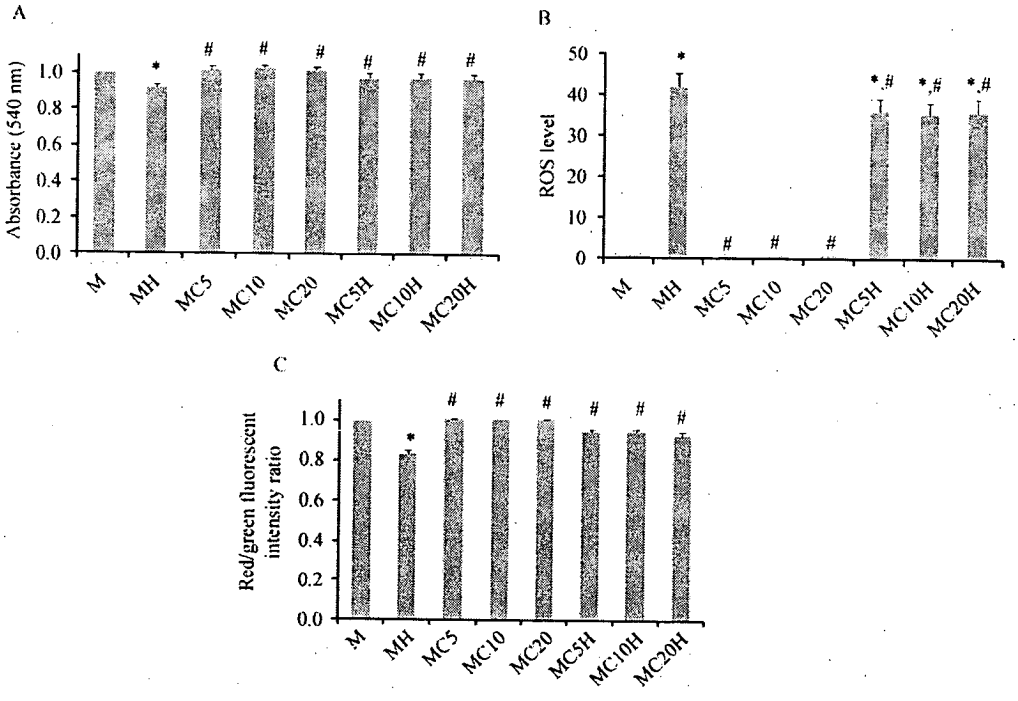


Figure 1. Effects of incubation times of 20-μmol/L cilostazol on cardiac mitochondrial swelling (A), ROS levels (B), and membrane potential change (C) after 4-min H_2O_2 application. Without H_2O_2, cilostazol applied to cardiac mitochondria for 5, 10, and 20 min did not alter the absorbance, ROS levels, or membrane potential of cardiac mitochondria, in comparison with the control group. Application of H_2O_2 to cardiac mitochondria caused marked cardiac mitochondrial swelling, increased ROS levels, and a decreased red/green fluorescent intensity ratio (i.e., mitochondrial depolarization). When cilostazol was applied to cardiac mitochondria for 5, 10 and 20 min prior to H_2O_2 application, it could prevent mitochondrial swelling, decrease ROS levels, and prevent mitochondrial depolarization, in comparison with the H_2O_2 treated group. M: cardiac mitochondria without any treatment; MH: cardiac mitochondria treated with H_2O_2; MC5/MC10/MC20: cardiac mitochondria treated with 20 μmol/L cilostazol for 5, 10, and 20 min without H_2O_2 application, respectively; MC5H/MC10H/MC20H: cardiac mitochondria treated with 20 μmol/L cilostazol for 5, 10, and 20 min prior to H_2O_2 application, respectively. $^*P < 0.05$ *vs.* M group, $^\#P < 0.05$ *vs.* H_2O_2 treated mitochondria. ROS: reactive oxygen species.

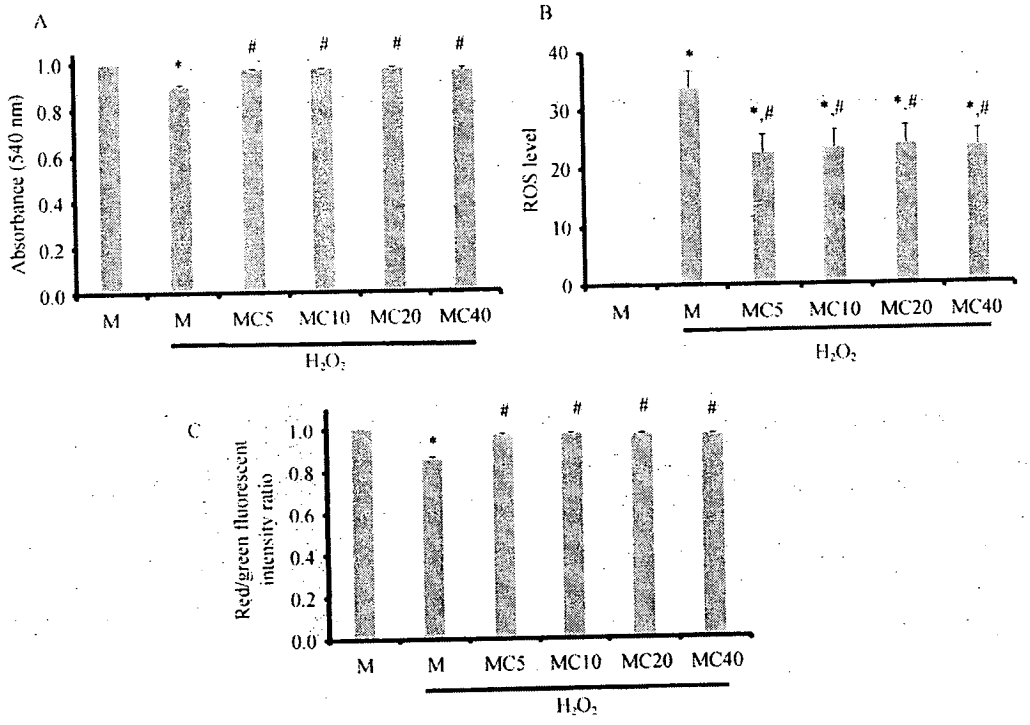


Figure 2. Effects of different concentrations of cilostazol on cardiac mitochondrial swelling (A), ROS levels (B), and membrane potential changes (C) after 4-min H_2O_2 application. Cilostazol at 5, 10, and 20 μmol/L with a 10 min incubation period could effectively prevent cardiac mitochondrial swelling, decrease ROS levels, and prevent mitochondrial membrane depolarization, in comparison with the H_2O_2 treated group. M: cardiac mitochondria without any treatment; MC5/MC10/MC20/MC40: cardiac mitochondria treated with cilostazol at 5, 10, 20, and 40 μmol/L for 5 min, respectively. $^*P < 0.05$ *vs.* M group; $^{\#}P < 0.05$ *vs.* H_2O_2 treated mitochondria. ROS: reactive oxygen species.

protocol, a 10-min incubation time was chosen for cilostazol as the standard period for subsequent protocols in this study.

To investigate the dose-dependent effect of the drug, cilostazol at 5, 10, 20, and 40 μmol/L was tested for its protective effect, and the results are shown in Figure 2. All tested concentrations of cilostazol could significantly prevent mitochondrial swelling caused by H_2O_2 (Figure 2A). Furthermore, all tested concentrations of cilostazol could decrease the ROS levels (Figure 2B) and prevent cardiac mitochondrial depolarization induced by H_2O_2 application (Figure 2C). From this protocol, 5-μmol/L cilostazol was chosen as the standard concentration for subsequent protocols in this study.

3.2 Effects of cilostazol, CsA, and CDP on cardiac mitochondrial swelling, mitochondrial ROS levels and mitochondrial membrane potential changes

The protective effects of cilostazol, CsA and CDP on cardiac mitochondria were tested, and the results are shown in Figure 3. cilostazol, CsA and CDP did not alter the

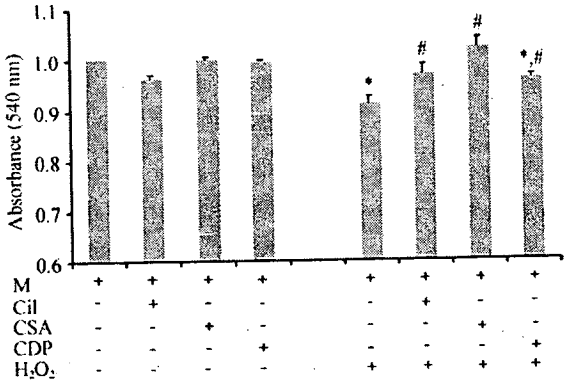


Figure 3. Effects of cilostazol, CsA, and CDP on cardiac mitochondrial swelling. Cardiac mitochondria were pretreated with cilostazol (5 μmol/L, 10 min incubation), CsA, or CDP prior to the administration of H_2O_2. Cilostazol and CsA completely protected cardiac mitochondrial swelling caused by H_2O_2, whereas CDP could only partially protect cardiac mitochondrial swelling. $^*P < 0.05$ *vs.* M (control group), $^{\#}P < 0.05$ *vs.* H_2O_2 treated group. CDP: 4'-chlorodiazepam; Cil: cilostazol; CsA: cyclosporine A; M: cardiac mitochondria without any treatment.

absorbance in cardiac mitochondria. In H_2O_2-treated cardiac mitochondria, the groups that were pretreated with Cilostazol and CsA did not show mitochondrial swelling caused by H_2O_2. Although CDP could attenuate cardiac mitochondrial swelling caused by H_2O_2, it could not restore the absorbance to the baseline level (Figure 3).

For cardiac mitochondrial ROS production, Cilostazol and CDP did not alter the ROS level, whereas CsA caused a slight increase in ROS levels in cardiac mitochondria without H_2O_2 application (Figure 4). In H_2O_2-treated cardiac mitochondria, the groups that were treated with cilostazol, CDP and CsA had decreased ROS levels, compared to the H_2O_2 treated group. However, the amount of ROS reduction was the greatest in the CsA, cilostazol + CDP, and cilostazol + CsA groups.

For cardiac mitochondrial membrane potential changes, cilostazol, CsA and CDP did not alter cardiac mitochondrial membrane potential (Figure 5). While H_2O_2 caused cardiac mitochondrial depolarization, pretreatment with cilostazol, CsA, CDP, cilostazol + CDP, and cilostazol + CsA could prevent cardiac mitochondrial depolarization caused by H_2O_2.

4 Discussion

The major finding of the present study is that cilostazol prevents cardiac mitochondrial dysfunction caused by severe oxidative stress due to H_2O_2 application. The protective

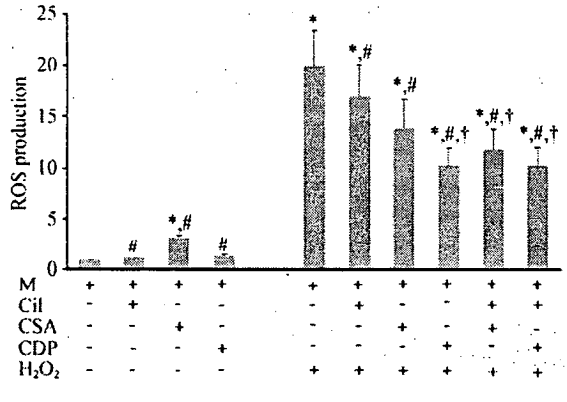


Figure 4. Effects of cilostazol, CsA, and CDP on ROS production in cardiac mitochondria. Without H_2O_2, cilostazol and CDP did not alter the ROS levels, whereas CsA caused a slight increase in ROS levels in cardiac mitochondria. While H_2O_2 caused a marked increase in ROS levels, cilostazol, CsA, and CDP could significantly decrease the ROS levels created by H_2O_2. $^*P < 0.05$ *vs.* M (control group), $^{\#}P < 0.05$ *vs.* H_2O_2 treated group, $^{\dagger}P < 0.05$ *vs.* (CsA + H_2O_2) treated group. CDP: 4'-chlorodiazepam; Cil: cilostazol; CsA: cyclosporine A; M: cardiac mitochondria; ROS: reactive oxygen species.

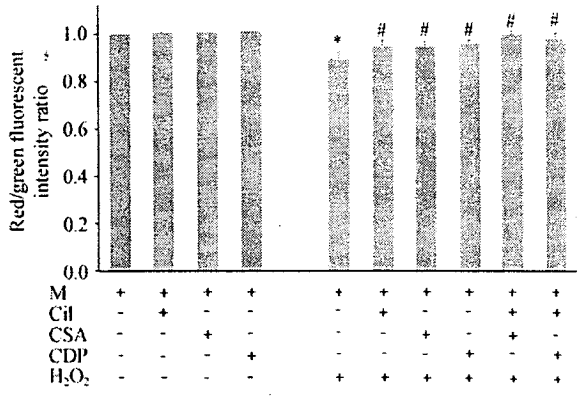


Figure 5. Effects of cilostazol, CsA, and CDP on cardiac mitochondrial membrane potential changes. Without H_2O_2, cilostazol, CsA and CDP did not alter the cardiac mitochondrial membrane potential. While H_2O_2 caused mitochondrial depolarization, cilostazol, CsA and CDP could completely prevent cardiac mitochondrial membrane depolarization caused by H_2O_2. $^*P < 0.05$ *vs.* M (control) group, $^{\#}P < 0.05$ *vs.* H_2O_2 treated group. CDP: 4'-chlorodiazepam; Cil: cilostazol; CsA: cyclosporine A; M: cardiac mitochondria.

effects of cilostazol include prevention of cardiac mitochondrial swelling, decreased mitochondrial ROS production, and prevention of cardiac mitochondrial depolarization due to oxidative stress induced by H_2O_2.

Previous studies demonstrate that cilostazol can have antiarrhythmic effects in both animal models and patients.[18,29] However, its effects on cardiac mitochondria have never been investigated. Since cardiac mitochondrial dysfunction has been shown to be associated with cardiac arrhythmias,[21] it is possible that the antiarrhythmic effect of cilostazol could, in part, be due to its protective effects regarding cardiac mitochondria. We previously demonstrated that oxidative stress in cardiac mitochondria caused by H_2O_2 can cause cardiac mitochondrial dysfunction, and that this model can be used to study the efficacy of drugs for their potential cardioprotective effects.[20] As shown in our study, cilostazol demonstrated its effects in preventing cardiac mitochondrial swelling, decreasing mitochondrial ROS production, and preventing cardiac mitochondrial membrane depolarization due to H_2O_2 application, indicating that this drug can assist in the prevention of cardiac mitochondrial dysfunction caused by severe oxidative stress.

In the present study, the mechanism of cardiac mitochondrial protection by cilostazol was tested using a pharmacological approach. It is known that oxidative stress with increased ROS production can lead to an opening of the mPTP in cardiac mitochondria, resulting in mitochondrial swelling and membrane potential depolarization.[30,31] In our study, when CsA was applied to cardiac mitochondria prior

to H_2O_2 application, it was possible to prevent cardiac mitochondrial swelling, decrease ROS production, and prevent cardiac mitochondrial membrane depolarization. Although cilostazol offers effects that prevent cardiac mitochondrial dysfunction similar to those found with CsA, the reduction of mitochondrial ROS production in the cilostazol-treated group was less than that of the CsA-treated mitochondria. Nevertheless, cilostazol could still prevent mitochondrial depolarization similar to that of the CsA-treated group, suggesting that the effects of cilostazol on ROS reduction were already sufficient to bring the ROS levels down to a level below the critical threshold that causes mitochondrial depolarization.[20] The prevention of cardiac mitochondrial dysfunction including the restoration of mitochondrial membrane potential by cilostazol could be responsible for its previously reported antiarrhythmic effects.[3,18] There are several limitations in the present study. It is well known that the roles of PDE-3 involve both cAMP and cyclic guanosine monophosphate (cGMP), however, it has been demonstrated that PDE-3 is functionally a cAMP-hydrolyzing enzyme.[32] In the present study, we did not determine the effects of cilostazol on cAMP and cGMP. Moreover, it has been shown that PDE-3 inhibitor could exert cardioprotective benefits via its activation of cAMP-dependent protein kinase A (PKA) and potentiating the opening of mitochondrial Ca^{2+}-activated K^+ channels.[33] In the present study, the roles of cilostazol on the PKA and mitochondrial Ca^{2+}-activated K^+ channels were not investigated. Future studies are needed to determine the effects of cilostazol on these signaling cascades.

In conclusion, under oxidative stress, cilostazol prevents cardiac mitochondrial dysfunction by attenuating cardiac mitochondrial swelling, ROS production, and mitochondrial membrane potential changes in cardiac mitochondria. These effects, particularly those regarding the prevention of cardiac mitochondrial depolarization, may explain its previously found antiarrhythmic effect.

5 Acknowledgements

This study is supported by grants from the Thailand Research Fund BRG (SCC), RTA 5580006 (NC), and Chiang Mai University Excellence Center Award (NC).

References

1 Feldman AM, Bristow MR, Parmley WW, *et al.* Effects of vesnarinone on morbidity and mortality in patients with heart failure. Vesnarinone Study Group. *N Engl J Med* 1993; 329: 149–155.

2 Packer M, Carver JR, Rodeheffer RJ, *et al.* Effect of oral milrinone on mortality in severe chronic heart failure. The PROMISE Study Research Group. *N Engl J Med* 1991; 325: 1468–1475.

3 Atarashi H, Endoh Y, Saitoh H, *et al.* Chronotropic effects of cilostazol, a new antithrombotic agent, in patients with bradyarrhythmias. *J Cardiovasc Pharmacol* 1998; 31: 534–539.

4 Cone J, Wang S, Tandon N, *et al.* Comparison of the effects of cilostazol and milrinone on intracellular cAMP levels and cellular function in platelets and cardiac cells. *J Cardiovasc Pharmacol* 1999; 34: 497–504.

5 Feldman AM, McNamara DM. Reevaluating the role of phosphodiesterase inhibitors in the treatment of cardiovascular disease. *Clin Cardiol* 2002; 25: 256–262.

6 Gamssari F, Mahmood H, Ho JS, *et al.* Rapid ventricular tachycardias associated with cilostazol use. *Tex Heart Inst J* 2002; 29: 140–142.

7 Kambayashi J, Liu Y, Sun B, *et al.* Cilostazol as a unique antithrombotic agent. *Curr Pharm Des* 2003; 9: 2289–2302.

8 Kishida M, Watanabe K, Tsuruoka T. [Effects of cilostazol in patients with bradycardiac atrial fibrillation]. *J Cardiol* 2001; 37: 27–33.

9 Kodama-Takahashi K, Kurata A, Ohshima K, *et al.* Effect of cilostazol on the ventricular escape rate and neurohumoral factors in patients with third-degree atrioventricular block. *Chest* 2003; 123: 1161–1169.

10 Toyonaga S, Nakatsu T, Murakami T, *et al.* Effects of cilostazol on heart rate and its variation in patients with atrial fibrillation associated with bradycardia. *J Cardiovasc Pharmacol Ther* 2000; 5: 183–191.

11 Tsuchikane E, Fukuhara A, Kobayashi T, *et al.* Impact of cilostazol on restenosis after percutaneous coronary balloon angioplasty. *Circulation* 1999; 100: 21–26.

12 Tsuchiya T. Role of pharmacotherapy in Brugada syndrome. *Indian Pacing Electrophysiol J* 2004; 4: 26–32.

13 Tsuji T, Ueda H, Nakatsu T, *et al.* Effects of cilostazol on heart rate and its variability in patients with sick sinus syndrome. *Clin Drug Invest* 2001; 21: 605–612.

14 Watanabe K, Ikeda S, Komatsu J, *et al.* Effect of cilostazol on vasomotor reactivity in patients with vasospastic angina pectoris. *Am J Cardiol* 2003; 92: 21–25.

15 Liu Y, Shakur Y, Yoshitake M, *et al.* Cilostazol (Pletal): a dual inhibitor of cyclic nucleotide phosphodiesterase type 3 and adenosine uptake. *Cardiovasc Drug Rev* 2001; 19: 369–386.

16 Wang S, Cone J, Fong M, *et al.* Interplay between inhibition of adenosine uptake and phosphodiesterase type 3 on cardiac function by cilostazol, an agent to treat intermittent claudication. *J Cardiovasc Pharmacol* 2001; 38: 775–783.

17 Tsuchiya T, Ashikaga K, Honda T, *et al.* Prevention of ventricular fibrillation by cilostazol, an oral phosphodiesterase inhibitor, in a patient with Brugada syndrome. *J Cardiovasc Electrophysiol* 2002; 13: 698–701.

18 Kanlop N, Shinlapawittayatorn K, Sungnoon R, *et al.* Cilos-

tazol attenuates ventricular arrhythmia induction and improves defibrillation efficacy in swine. *Can J Physiol Pharmacol* 2010; 88: 422–428.

19 Cortassa S, Aon MA, Winslow RL, O'Rourke B. A mitochondrial oscillator dependent on reactive oxygen species. *Biophys J* 2004; 87: 2060–2073.

20 Thummasorn S, Kumfu S, Chattipakorn S, *et al.* Granulocyte-colony stimulating factor attenuates mitochondrial dysfunction induced by oxidative stress in cardiac mitochondria. *Mitochondrion* 2011; 11: 457–466.

21 Aon MA, Cortassa S, Marban E, *et al.* Synchronized whole cell oscillations in mitochondrial metabolism triggered by a local release of reactive oxygen species in cardiac myocytes. *J Biol Chem* 2003; 278: 44735–44744.

22 Brady NR, Hamacher-Brady A, Westerhoff HV, *et al.* A wave of reactive oxygen species (ROS)-induced ROS release in a sea of excitable mitochondria. *Antioxid Redox Signal* 2006; 8: 1651–1665.

23 Chen Q, Moghaddas S, Hoppel CL, *et al.* Ischemic defects in the electron transport chain increase the production of reactive oxygen species from isolated rat heart mitochondria. *Am J Physiol Cell Physiol* 2008; 294: C460–C466.

24 Walker JM. The bicinchoninic acid (BCA) assay for protein quantitation. *Methods Mol Biol* 1994; 32: 5–8.

25 Ruiz-Meana M, Garcia-Dorado D, Miro-Casas E, *et al.* Mitochondrial Ca^{2+} uptake during simulated ischemia does not affect permeability transition pore opening upon simulated reperfusion. *Cardiovasc Res* 2006; 71: 715–724.

26 Novalija E, Kevin LG, Eells JT, *et al.* Anesthetic preconditioning improves adenosine triphosphate synthesis and reduces reactive oxygen species formation in mitochondria after ischemia by a redox dependent mechanism. *Anesthesiology* 2003; 98: 1155–1163.

27 Di Lisa F, Blank PS, Colonna R, *et al.* Mitochondrial membrane potential in single living adult rat cardiac myocytes exposed to anoxia or metabolic inhibition. *J Physiol* 1995; 486 (Pt 1): 1–13.

28 Tong V, Teng XW, Chang TK, *et al.* Valproic acid II: effects on oxidative stress, mitochondrial membrane potential, and cytotoxicity in glutathione-depleted rat hepatocytes. *Toxicol Sci* 2005; 86: 436–443.

29 Kanlop N, Chattipakorn S, Chattipakorn N. Effects of cilostazol in the heart. *J Cardiovasc Med* (Hagerstown) 2011; 12: 88–95.

30 Petronilli V, Penzo D, Scorrano L, *et al.* The mitochondrial permeability transition, release of cytochrome c and cell death. Correlation with the duration of pore openings *in situ*. *J Biol Chem* 2001; 276: 12030–12034.

31 Zoratti M, Szabo I. The mitochondrial permeability transition. *Biochim Biophys Acta* 1995; 1241: 139–176.

32 Rao YJ, Xi L. Pivotal effects of phosphodiesterase inhibitors on myocyte contractility and viability in normal and ischemic hearts. *Acta Pharmacol Sin* 2009; 30: 1–24.

33 Fukasawa M, Nishida H, Sato T, *et al.* 6-[4-(1-Cyclohexyl-1H-tetrazol-5-yl)butoxy]-3,4-dihydro-2-(1H)quinolinone (cilostazol), a phosphodiesterase type 3 inhibitor, reduces infarct size via activation of mitochondrial Ca^{2+}-activated K^+ channels in rabbit hearts. *J Pharmacol Exp Ther* 2008; 326: 100–104.

เอกสารแนบหมายเลข 59

Vagus nerve stimulation initiated late during ischemia, but not reperfusion, exerts cardioprotection via amelioration of cardiac mitochondrial dysfunction

Krekwit Shinlapawittayatorn, MD, PhD,* Kroekkiat Chinda, DVM,* Siripong Palee, PhD,* Sirirat Surinkaew, PhD,* Sirinart Kumfu, PhD,* Sarawut Kumphune, PhD,* Siriporn Chattipakorn, DDS, PhD,*† Bruce H. KenKnight, PhD,‡ Nipon Chattipakorn, MD, PhD*

*From the *Cardiac Electrophysiology Research and Training Center, Department of Physiology, Faculty of Medicine, †Department of Oral Biology and Diagnostic Science, Faculty of Dentistry, Chiang Mai University, Chiang Mai, Thailand, and ‡Emerging Therapies, Cyberonics Inc, Houston, Texas.*

BACKGROUND We previously reported that vagus nerve stimulation (VNS) applied immediately at the onset of cardiac ischemia provides cardioprotection against cardiac ischemic-reperfusion (I/R) injury.

OBJECTIVE This study aimed to determine whether VNS applied during ischemia or at the onset of reperfusion exerts differential cardioprotection against cardiac I/R injury.

METHODS Twenty-eight swine (25–30 kg) were randomized into 4 groups: Control (sham-operated, no VNS), VNS-ischemia (VNS applied during ischemia), VNS-reperfusion (VNS applied during reperfusion), and VNS-ischemia+atropine (VNS applied during ischemia with 1 mg/kg atropine administration). Ischemia was induced by left anterior descending (LAD) coronary artery occlusion for 60 minutes, followed by 120 minutes of reperfusion. VNS was applied either 30 minutes after LAD coronary artery occlusion or at the onset of reperfusion and continued until the end of reperfusion. Cardiac function, infarct size, myocardial levels of connexin 43, cytochrome *c*, tumor necrosis factor α, and interleukin 4, and cardiac mitochondrial function were determined.

RESULTS VNS applied 30 minutes after LAD coronary artery occlusion, but not at reperfusion, markedly reduced ventricular fibrillation incidence and infarct size (~59%), improved cardiac function; attenuated cardiac mitochondrial reactive oxygen species production, depolarization, swelling, and cytochrome *c* release; and increased the amount of phosphorylated connexin 43 and interleukin 4 as compared with the Control group. These beneficial effects of VNS were abolished by atropine.

CONCLUSION VNS could provide significant cardioprotective effects even when initiated later during ischemia, but was not effective after reperfusion. These findings indicate the importance of timing of VNS initiation and warrant the potential clinical application of VNS in protecting myocardium at risk of I/R injury.

KEYWORDS Vagus nerve stimulation; Ischemic-reperfusion injury; Acetylcholine; Heart; Cardioprotection

ABBREVIATIONS **IL-4** = interleukin 4; **I/R** = ischemic-reperfusion; **LAD** = left anterior descending; **LV** = left ventricular; **MI** = myocardial infarction; **PCI** = percutaneous coronary intervention; **PVC** = premature ventricular contraction; **ROS** = reactive oxygen species; **VF** = ventricular fibrillation; **VNS** = vagus nerve stimulation; **VT** = ventricular tachycardia

(Heart Rhythm 2014;11:2278–2287) © 2014 Heart Rhythm Society. All rights reserved.

Introduction

Acute myocardial infarction (MI) is a major cause of morbidity and mortality worldwide.[1] In patients with MI, timely and effective myocardial reperfusion with either thrombolytic therapy or primary percutaneous coronary intervention (PCI) is the most effective modality for salvaging viable myocardium.[2] However, the process of abruptly restoring blood flow to the ischemic tissues can itself induce further death of the myocardium, a phenomenon known as myocardial ischemic-reperfusion (I/R) injury.[3,4] Although advances in PCI technology, reduced procedure times, and appropriate use of pharmacological agents (antiplatelet and antithrombotic) for maintaining coronary flow have improved outcomes, attenuation of myocardial reperfusion injury remains unresolved.[5]

The autonomic nervous system has been shown to play an important role in the regulation of cardiac function.[6] During acute myocardial I/R injury, cardiac adrenergic receptor activation contributes to cellular dysfunction, which, if

This work was supported in part by the Thailand Research Fund TRF-CHE Research Grant for New Scholar MRG5580125 (to Dr Shinlapawittayatorn), BRG 5780016 (to Dr Chattipakorn), RTA5580006, Chiang Mai University Excellence Center Award (to Dr Chattipakorn), and Cyberonics. Dr Chattipakorn has served as a member of the scientific advisory board of Cyberonics. Dr KenKnight is an employee of Cyberonics. **Address reprint requests and correspondence:** Dr Krekwit Shinlapawittayatorn, Cardiac Electrophysiology Research and Training Center, Department of Physiology, Faculty of Medicine, Chiang Mai University, Chiang Mai 50200, Thailand. E-mail address: kshinlap@gmail.com.

1547-5271/$-see front matter © 2014 Heart Rhythm Society. All rights reserved. http://dx.doi.org/10.1016/j.hrthm.2014.08.001

untreated, promotes degradation of cardiac performance and upregulation of apoptotic signaling in affected cardiac myocytes.[7,8] Over the past decade, chronic, intermittent vagus nerve stimulation (VNS) has been shown to be feasible in humans and exerts cardiprotective effects in both chronic ischemic cardiomyopathy and heart failure.[9–11] Specifically, in ischemic hearts, VNS applied before ischemia has been shown to limit the infarct size and attenuate I/R injury via its nicotinic pathway, independent of heart rate changes.[12] Furthermore, we recently demonstrated that VNS applied immediately at the onset of ischemia markedly reduced the infarct size, improved ventricular function, and caused a dramatic reduction in ventricular tachycardia/ventricular fibrillation (VT/VF) episodes.[13] However, a direct translation of these experimental observations to clinical reality is hampered by the fact that in patients with acute MI, treatment is typically initiated only after the onset of ischemia. In the present study, we hypothesized that VNS applied later after myocardial ischemia but before reperfusion exerts cardioprotective effects against I/R injury. Furthermore, we determined whether VNS applied at the onset of reperfusion exerted differential cardioprotection against I/R injury.

Methods

Detailed methods are available in the Online Supplemental Appendix. Briefly, 28 swine (25–30 kg) were randomized into 4 groups (Figure 1A): Control (sham operated, no VNS), VNS-Ischemia (VNS applied during ischemia), VNS-Reperfusion (VNS applied during reperfusion), and VNS-Ischemia+Atropine (VNS applied during ischemia with 1 mg/kg atropine administration). Ischemia was induced by left anterior descending (LAD) coronary artery occlusion for 60 minutes, followed by 120 minutes of reperfusion. VNS (3.5 mA, 20 Hz, continuously recurring cycles of 21-second ON, 30-second OFF) was applied either 30 minutes after LAD coronary artery occlusion or at the onset of reperfusion and continued until the end of reperfusion. A bipolar pacing lead and anchor lead were placed around the mid-cervical left vagus nerve (Figure 1B). During the ischemic and reperfusion periods, arrhythmia incidence and left ventricular (LV) function were continuously monitored and recorded by using electrocardiography and the pressure-volume loop recording system, as described previously.[13] After 120 minutes of reperfusion, the heart was removed and sectioned for infarct size, cardiac mitochondrial function, and Western blot analysis. Data were presented as mean ± SD. A P value of $<.05$ was considered statistically significant. All experiments were approved by the Institutional Animal Care and Use Committee of the Faculty of Medicine, Chiang Mai University, Chiang Mai, Thailand.

Results

Effect of VNS on the heart rate and electrocardiographic parameters during the I/R period

The electrophysiological effects of VNS were examined in 28 pigs, in which heart rate (HR) and PR interval were measured continuously during the I/R period. In the Control and VNS-Reperfusion groups, HR during the ischemic period increased significantly compared with baseline HR (Figure 2A). When VNS was applied during ischemia, HR was not different from baseline HR. However, in the VNS-Ischemia+Atropine group, HR during ischemic and reperfusion periods increased, suggesting that sympathetic activity might be relatively increased by a muscarinic blockade. Nevertheless, while statistically there was a difference in HR (Figure 2A), it is possible that physiologically there appears

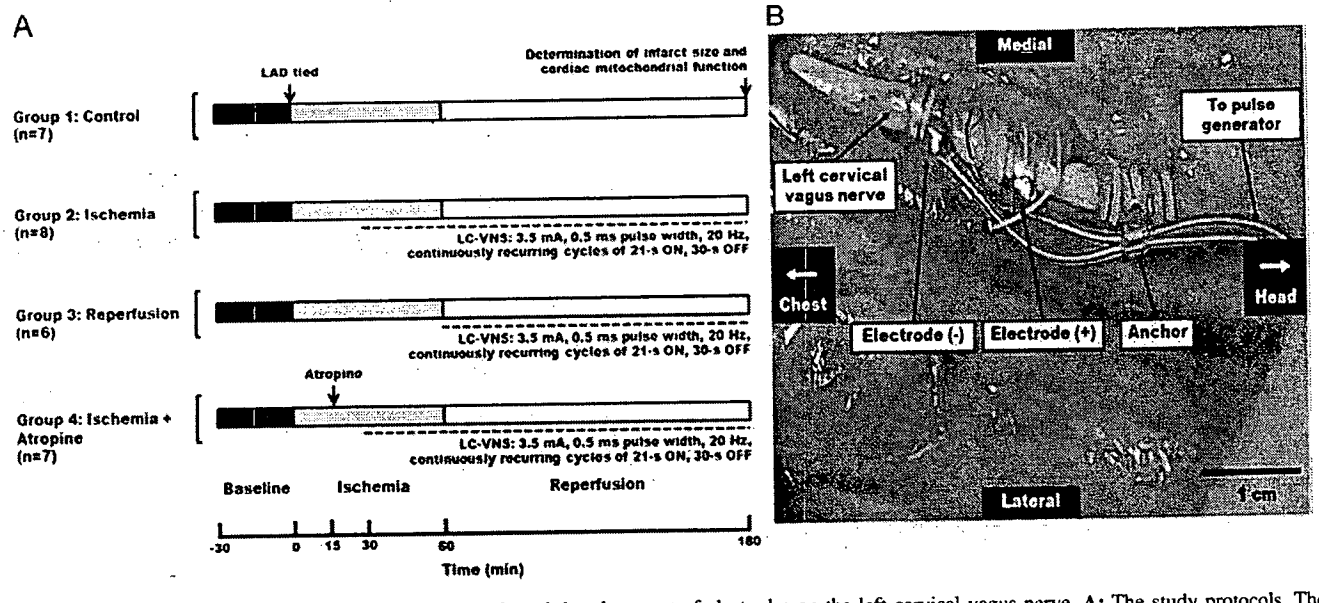


Figure 1 Schematic representation of the study protocols and the placement of electrodes on the left cervical vagus nerve. **A:** The study protocols. The ischemic period (60 minutes) was induced by rapid, complete ligation of the LAD coronary artery. The reperfusion period was 120 minutes. **B:** A bipolar pacing lead and anchor lead were placed around the mid-cervical left vagus nerve. LAD = left anterior descending; LC-VNS = left cervical vagus nerve stimulation.

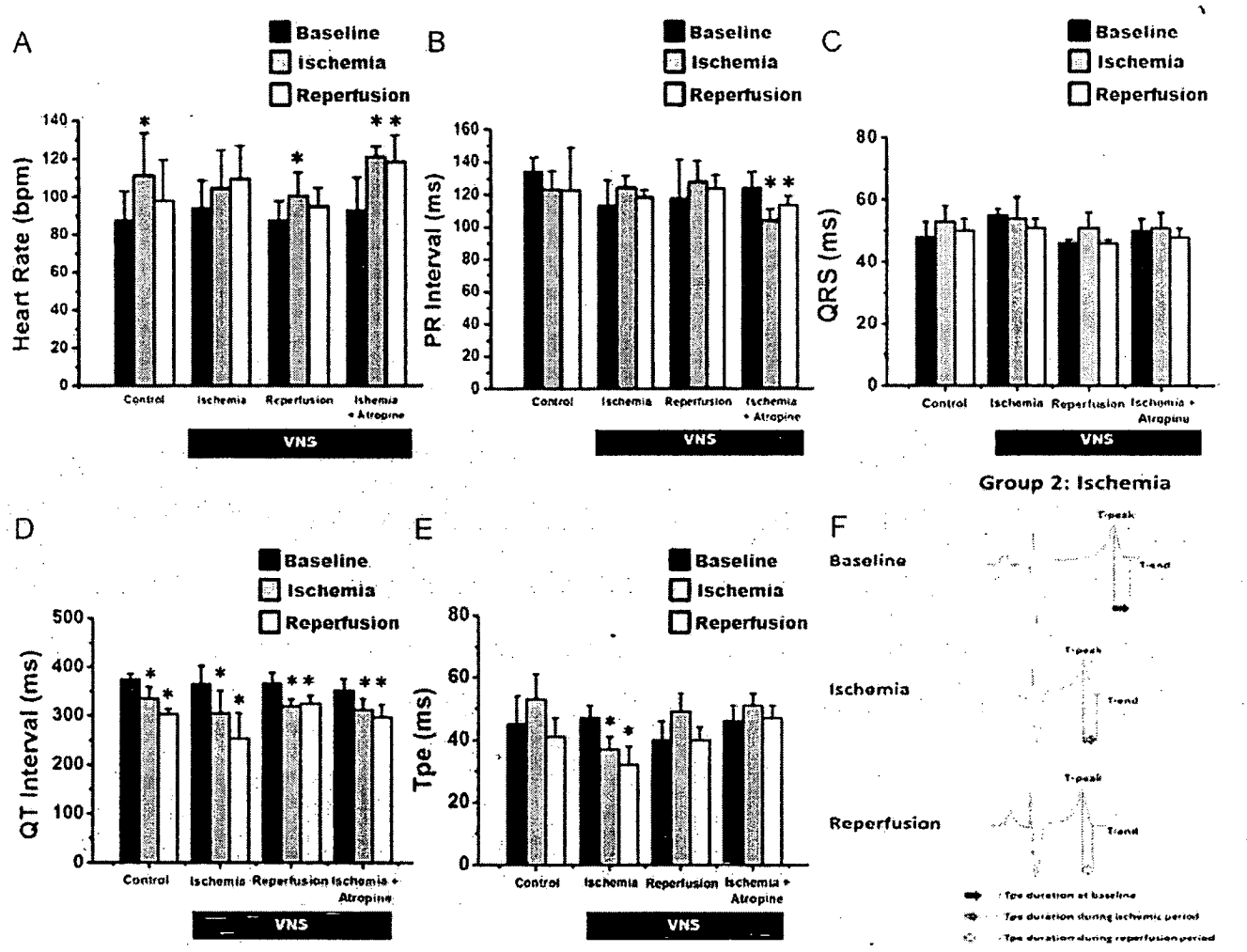


Figure 2 Effect of VNS on the heart rate and electrocardiographic parameters during the ischemic-reperfusion period. **A:** Effect of VNS on the heart rate. **B:** Effect of VNS on the mean PR interval. **C:** Effect of VNS on the mean QRS duration. **D:** Effect of VNS on QT intervals. **E:** Effect of VNS on the Tpe interval. **F:** Representative of the Tpe interval seen in group 2 at baseline and during ischemic and reperfusion periods. Data are presented as mean ± SD. $^{*}P < .05$ vs baseline. Tpe = T-wave peak to end; VNS = vagus nerve stimulation.

to be no difference between groups and conditions. There was no significant difference in the PR interval during the baseline, ischemic, and reperfusion periods among groups (Figure 2B). However, PR intervals during ischemic and reperfusion periods were significantly reduced in the VNS-Ischemia+Atropine group, suggesting a relative sympathetic predominance after the muscarinic blockade. Mean QRS duration during the baseline, ischemic, and reperfusion periods was not different among groups (Figure 2C). QT intervals during ischemia and reperfusion were significantly decreased in all groups (Figure 2D). However, during ischemia and reperfusion, time from T-wave peak to end was significantly decreased only in the VNS-Ischemia group, and this effect was abolished by atropine (Figures 2E and 2F).

VNS applied during ischemia protected the heart against reperfusion arrhythmias by increasing connexin 43 phosphorylation

Figure 3A represents a premature ventricular contraction (PVC)–initiated self-terminating VT in 4 different groups. However, the PVC and VT cycle lengths were not different among groups (Figure 3B). The total number of PVCs was markedly decreased in both VNS-Ischemia and VNS-Reperfusion groups as compared with the Control group (Figure 4A). This effect was abolished by atropine, indicating that VNS reduced the frequency of spontaneous PVCs during ischemic and reperfusion periods through muscarinic receptor activation. Moreover, the total number of VT/VF episodes was significantly reduced in the VNS-Ischemia group, and atropine administration abolished the antiarrhythmic effect of VNS (Figure 4B). However, the time to spontaneous VT/VF onset was not significantly different among groups during ischemic and reperfusion periods (Figure 4C). Figure 4D shows the effect of VNS on connexin 43 phosphorylation. Quantitative densitometric analysis revealed that the levels of connexin 43 phosphorylation at serine 368 residue in the VNS-Ischemia and VNS-Reperfusion groups were significantly increased compared with the Control group (Figure 4D). Interestingly, atropine inhibited the increased connexin 43 phosphorylation in the VNS-Ischemia+Atropine group, suggesting that the level of

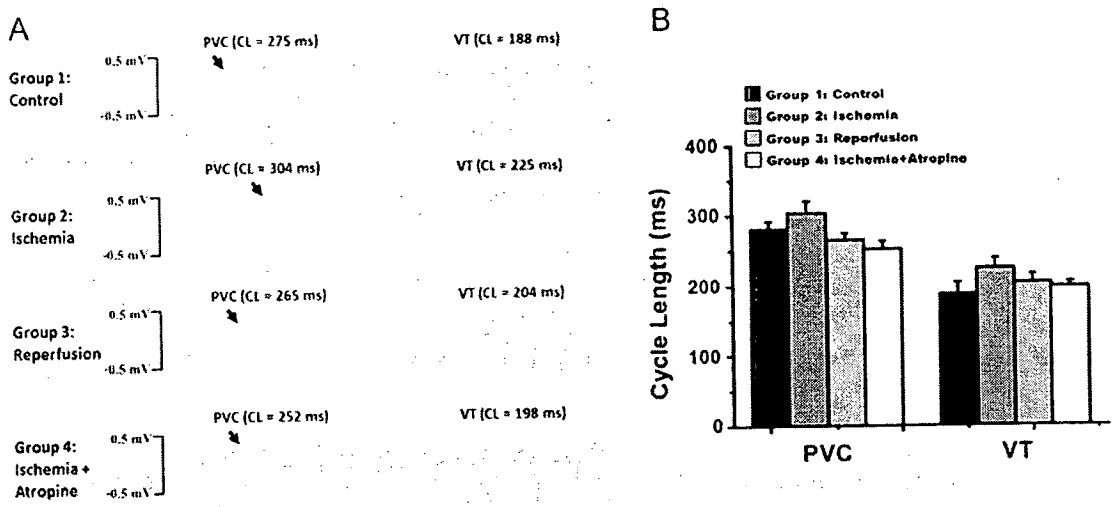


Figure 3 Representative electrocardiographic tracings illustrating PVC-induced ventricular tachycardia and PVC and VT CLs. **A:** A PVC-initiated self-terminating ventricular tachycardia in 4 different groups. **B:** The PVC and VT CLs were not different among groups. Data are presented as mean ± SD. CL = cycle length; PVC = premature ventricular contraction; VT = ventricular tachycardia.

phosphorylated connexin 43 during the acute I/R period was increased by muscarinic receptor activation.

VNS applied during ischemia preserved LV function and reduced infarct size

The effect of VNS on LV contractile function is shown in Table 1. In the Control group, the stroke volume and ejection fraction were significantly decreased and the end-diastolic pressure was significantly increased during the I/R period compared with the baseline period. VNS applied during ischemia, but not at the onset of reperfusion, preserved LV functional performance during ischemia and reperfusion periods. However, the beneficial effect of VNS was completely abolished by the administration of atropine. Figure 5 illustrates the effect of VNS on the infarct size. Myocardial infarct size was expressed as the percentage of the area at risk. The area at risk, expressed as a percentage of the total ventricular mass, was not different between groups (Control 32.8% ± 5%; VNS-Ischemia 33.5% ± 5%; VNS-Reperfusion 34.2% ± 1%; VNS-Ischemia+Atropine 38.9% ± 4%; $P = 0.5$). Interestingly, VNS applied during ischemia, but not at the onset of reperfusion, significantly reduced myocardial infarct size (by a mean of 59%), and this effect was completely abolished by atropine.

VNS applied during ischemia protected cardiac mitochondrial integrity by mitigating cytochrome *c* release

Cardiac mitochondrial dysfunction including increased reactive oxygen species (ROS) production, decreased red/green fluorescent intensity ratio (which indicated mitochondrial membrane depolarization), and decreased absorbance (indicative of mitochondrial swelling) has been shown to participate in myocyte dysfunction and degradation of cardiac contractile performance, arrhythmias, and myocyte apoptosis and infarct size during and after I/R injury. Our results demonstrated that VNS applied during ischemia significantly decreased mitochondrial ROS production (Figure 6A) and prevented mitochondrial membrane depolarization (Figure 6B) and mitochondrial swelling (Figure 6C) in the ischemic myocardium as compared with the ischemic area of the Control group. VNS applied during ischemia, but not at the onset of reperfusion, also significantly decreased the cytochrome *c* release (Figure 6D) as compared with the Control group. Again, these effects were abolished by atropine, suggesting the importance of muscarinic modulation during VNS.

Electron photomicrographs demonstrated that in the ischemic area of the Control group, I/R-induced severe mitochondrial damage was observed, as demonstrated by noted mitochondrial swelling accompanied by a disruption in membrane integrity (Figure 7). VNS applied during ischemia, but not reperfusion, significantly attenuated cardiac mitochondrial swelling after I/R injury, and this effect was abolished by atropine. Moreover, in order to determine the effect of VNS on the inflammatory response, the levels of the anti-inflammatory cytokine interleukin 4 (IL-4) and the pro-inflammatory cytokine tumor necrosis factor α were determined. VNS applied during ischemia significantly increased the anti-inflammatory cytokine IL-4 as compared with the Control group (176.8 ± 34.5 pg/mL vs 84.7 ± 11.4 pg/mL; $P < .05$). The IL-4 levels of both the VNS-Reperfusion and VNS-Ischemia+Atropine groups were not different from those of the Control group (123.8 ± 20.8 pg/mL and 72.2 ± 22.1 pg/mL, respectively; $P = 0.1$). The level of the pro-inflammatory cytokine tumor necrosis factor α in the heart was not different among groups (Control 537.4 ± 52.5 pg/mL; VNS-Ischemia 498.2 ± 45.1 pg/mL; VNS-Reperfusion 529.2 ± 32.6 pg/mL; VNS-Ischemia+Atropine 493.1 ± 73.5 pg/mL; $P = 0.1$).

Discussion

In the present study, we investigated whether VNS applied late during ischemia or at the onset of reperfusion exerted

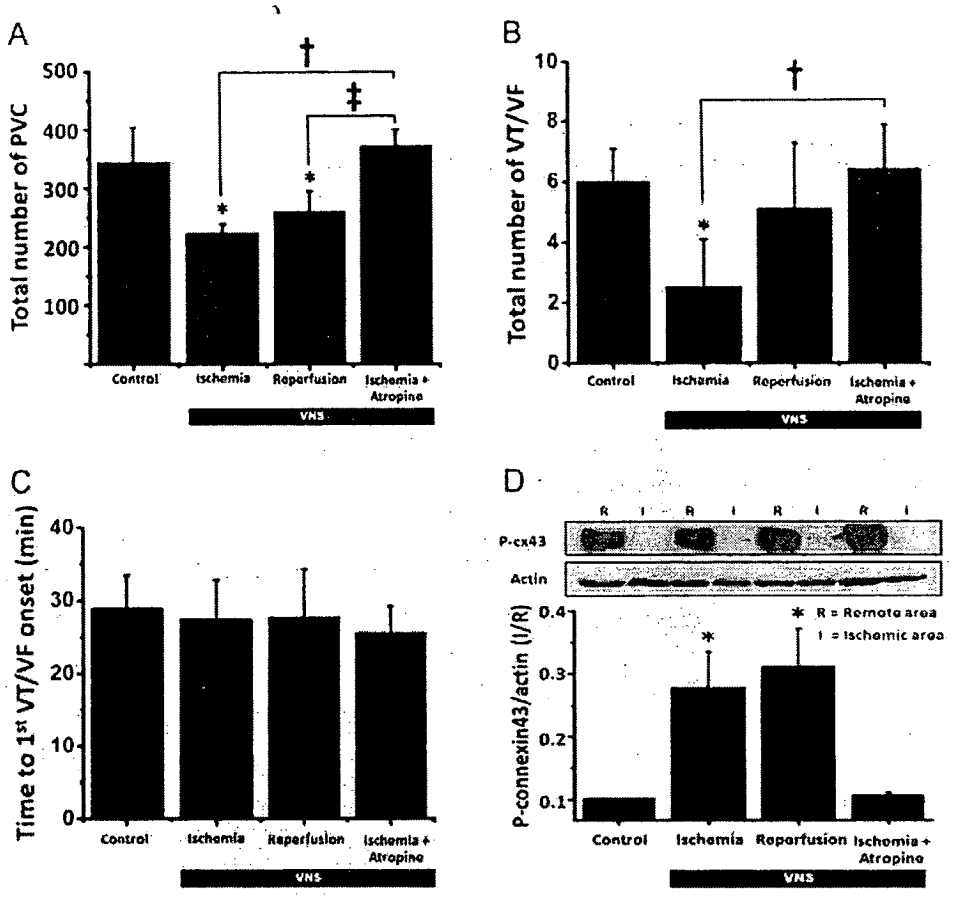


Figure 4 VNS applied during ischemia protected the heart against reperfusion arrhythmias by increasing the phosphorylation of connexin 43. **A:** The total number of PVCs was markedly decreased in both VNS-Ischemia and VNS-Reperfusion groups as compared with the Control group. **B:** The total number of VT/VF episodes was significantly reduced in the VNS-Ischemia group compared with the Control group. **C:** However, the time to VT/VF onset was not significantly different among groups during ischemic-reperfusion periods. **D:** Both VNS-Ischemia and VNS-Reperfusion groups significantly increased the phosphorylation of connexin 43 at serine 368 in the ischemic myocardium as compared with the Control group (n = 4 per group). Data are presented as mean ± SD. $^{*}P < .05$ vs Control group; $^{\dagger}P < .05$ vs VNS-Ischemia+Atropine group; $^{\ddagger}P < .05$ vs VNS-Ischemia+Atropine group. PVC = premature ventricular contraction; VF = ventricular fibrillation; VNS = vagus nerve stimulation; VT = ventricular tachycardia.

differential cardioprotection against I/R injury. The major findings of this study are as follows. VNS applied during ischemia provided cardioprotective effects against I/R injury (1) by preventing reperfusion arrhythmias by increasing the phosphorylation of connexin 43 at the serine 368 residue and reducing time from T-wave peak to end (an indicator of transmural dispersion of repolarization) and (2) by preserving LV function by reducing infarct size and via its action on cardiac mitochondrial integrity through its antiapoptotic and anti-inflammatory effects. However, VNS applied at the onset of reperfusion did not produce cardioprotection against I/R injury, suggesting that timing of VNS initiation with respect to the onset of myocardial ischemia is an important determinant of its therapeutic efficacy. Our results provide novel evidence that VNS applied later during an ischemia episode provides significant cardioprotection and prevents the attenuation of LV function in a large animal model of I/R injury. Moreover, our finding strengthens and extends the mechanistic explanation of previous reports, which indicated that VNS applied before ischemia or at the onset of coronary occlusion exerted cardioprotection and improved LV function during the I/R period.[12–15]

Antiarrhythmogenic effects of VNS during the I/R period

Previous studies demonstrated that VNS exerts antiarrhythmogenic effects during the ischemic period. Zuanetti et al[16] provided the first evidence that some VT could be modulated and reduced by vagal activation. Moreover, an elegant study by Schwartz and colleagues[15] in conscious dogs clearly demonstrated that enhanced vagus nerve activity by means of right cervical VNS prevented spontaneous VT in a model with healed MI, exercise testing, and intermittent ischemia. In the present study, we found that VNS applied later during ischemia, but not at the onset of reperfusion, still significantly decreased the occurrence of PVCs, the number of spontaneous VT/VF episodes, and time from T-wave peak to end. It is well recognized that connexin 43, a major cardiac gap junction in the ventricles, contributes to intercellular communication and electrical coupling.[17,18] Moreover, a marked dephosphorylation of ventricular connexin 43 has been observed during the process of electrical uncoupling induced by ischemia.[19] A recent study by Ando et al[20] demonstrated that VNS applied before ischemia effectively inhibits the loss of the phosphorylated isoform of connexin

Table 1 Effects of VNS and muscarinic receptor blocker on pressure-volume loop–derived functional parameters

	Control			VNS-Ischemia			VNS-Reperfusion			VNS-Ischemia+Atropine		
Parameter	Baseline	Ischemia	Reperfusion	Baseline	Ischemia	Reperfusion	Baseline	Ischemia	Reperfusion	Baseline	Ischemia	Reperfusion
SV (mL)	25 ± 2	9 ± 4*	9 ± 4*	23 ± 4	18 ± 6	20 ± 6	22 ± 2	7 ± 2*	10 ± 2*	23 ± 3	7 ± 2*	6 ± 3*
EF (%)	56 ± 5	27 ± 9*	27 ± 8*	54 ± 9	42 ± 4	43 ± 6	53 ± 8	28 ± 9*	27 ± 4*	55 ± 8	28 ± 6*	24 ± 8*
ESP (mm Hg)	80 ± 11	83 ± 6	81 ± 13	73 ± 7	74 ± 6	81 ± 14	74 ± 14	73 ± 11	79 ± 16	81 ± 11	81 ± 9	82 ± 8
EDP (mm Hg)	9 ± 6	17 ± 7*	20 ± 8*	7 ± 2	8 ± 4	10 ± 1	7 ± 2	16 ± 5*	13 ± 1*	9 ± 5	20 ± 7*	21 ± 7*

Summary of left ventricular functional parameters at baseline, at the end of ischemia, and at the end of reperfusion (n = 6–8 per group). Values are presented as mean ± SD.
EDP = end-diastolic pressure; EF = ejection fraction; ESP = end-systolic pressure; SV = stroke volume; VNS = vagus nerve stimulation.
*$P < .05$ vs baseline.

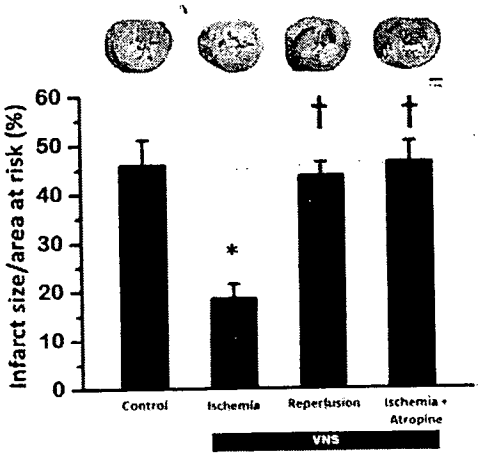


Figure 5 VNS applied during ischemia markedly reduced the infarct size. Myocardial infarct size was expressed as the percentage of the area at risk (AAR). The AAR, expressed as a percentage of the total ventricular mass, were not different among groups (Control 32.8% ± 5%; VNS-Ischemia 33.5% ± 5%; VNS-Reperfusion 34.2% ± 1%; VNS-Ischemia+Atropine 38.9% ± 4%; $P = 0.5$). Interestingly, VNS applied during ischemia significantly reduced myocardial infarct size and this effect was reversed by atropine: Control 45.7% ± 14% (n = 7); VNS-Ischemia 18.6% ± 8% (n = 8); VNS-Reperfusion 43.6% ± 6% (n = 6); VNS-Ischemia+Atropine 46.4% ± 11% (n = 7). The inset shows representative photographs obtained after Evan Blue and triphenyltetrazolium chloride staining. Blue indicates nonthreatened myocardium, red indicates the noninfarcted area within the AAR, and white indicates myocardial infarction. Data are presented as mean ± SD. *$P < .05$ vs Control group; †$P < .05$ vs VNS-Ischemia group. VNS = vagus nerve stimulation.

43 during acute MI. Thus, we hypothesized that VNS applied during ischemia exerts antiarrhythmogenic effects by modulating the level of connexin 43 phosphorylation. It has been shown previously that the phosphorylation of connexin 43 at the serine 368 residue could lead to the prevention of phosphorylation at the other connexin 43 residues, thus maintaining electrical coupling with ventricular myocytes.[19,21] In the present study, we demonstrated that VNS applied during ischemia markedly increased connexin 43 phosphorylation at the serine 368 residue during the I/R period. Therefore, functional preservation of connexin 43 at serine 368 by VNS might play a crucial role in the antiarrhythmogenic effects during the I/R period. In our study, VNS applied at the onset of reperfusion significantly increased the phosphorylation of connexin 43 at the serine 368 residue. However, it could attenuate only the number of PVCs, but not the number of VT/VF episodes, as observed in the VNS-Ischemia group. This observation might be explained by the difference in the structural substrate, such as infarct size, which was larger in the VNS-Reperfusion group and, owing to the wave length theory, influenced the VT/VF incidence.[22–24] Moreover, our findings suggested that during ischemia and reperfusion, VNS mainly improved ventricular repolarization, but not depolarization, since there were no significant differences in QRS intervals (a parameter of depolarization) in all timing of VNS initiation. However, our results showed that VNS increased the phosphorylation of connexin 43. Future cardiac mapping study should be done to assess this discrepancy.

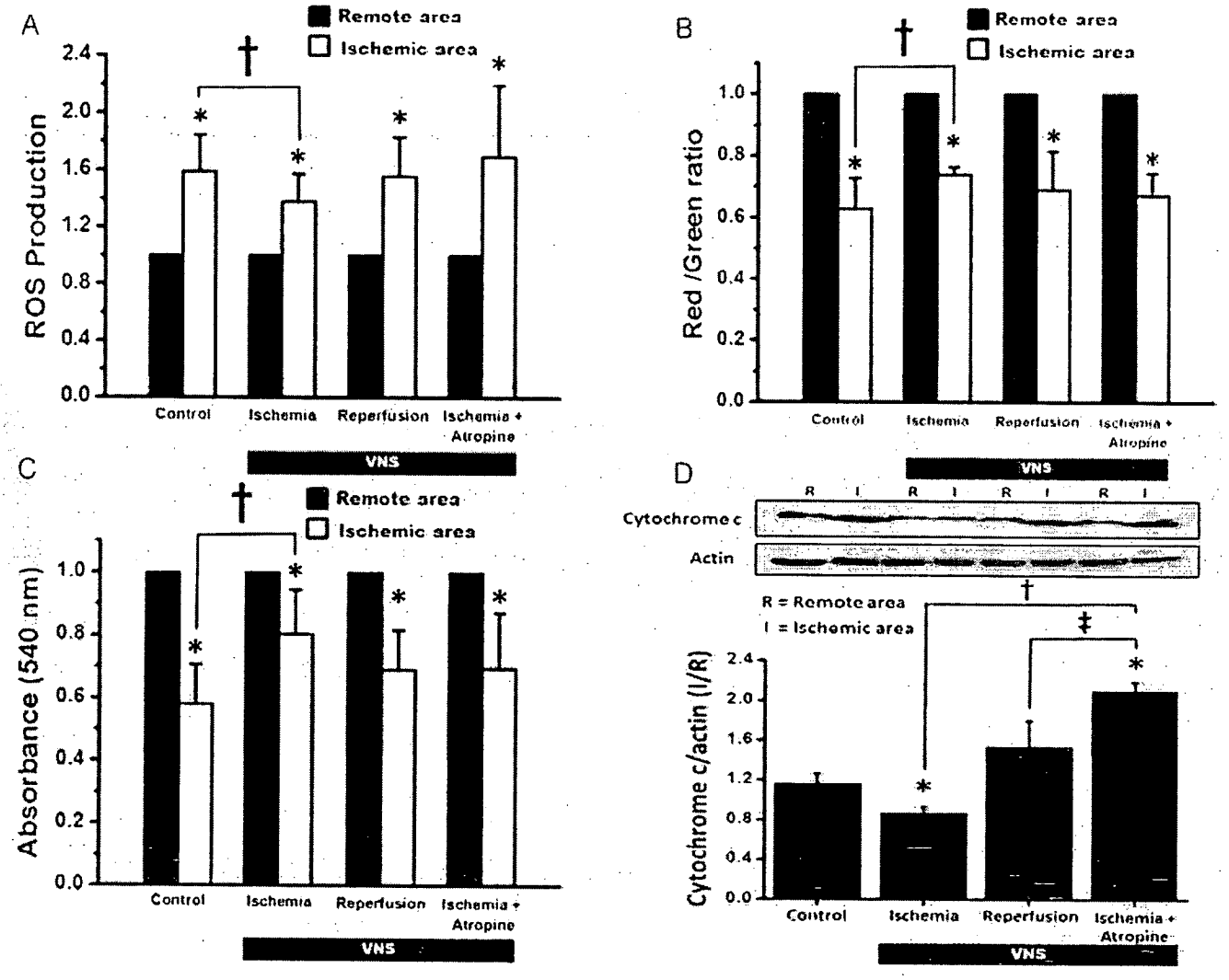


Figure 6 VNS applied during ischemia protected cardiac mitochondrial integrity by mitigating cytochrome *c* release. VNS applied during ischemia significantly decreased mitochondrial ROS production (**A**; n = 4 per group) and prevented mitochondrial membrane depolarization (**B**; n = 4 per group) and mitochondrial swelling (**C**; n = 4 per group) in the ischemic myocardium as compared with the ischemic area of the Control group. VNS applied during ischemia significantly decreased cytochrome *c* release (**D**; n = 4 per group) as compared with the Control group. Again, these effects were abolished by atropine, suggesting the importance of muscarinic modulation during VNS. Data are presented as mean ± SD. $^{*}P < .05$ vs remote area (panels A-C) or vs Control group (panel D); $^{\dagger}P < .05$ vs ischemic area of the Control group (panels A-C) or vs VNS-Ischemia+Atropine group (panel D); $^{\ddagger}P < .05$ vs VNS-Reperfusion group (panel D). ROS = reactive oxygen species; VNS = vagus nerve stimulation.

VNS effects on LV function and infarct size

Our finding that VNS applied during ischemia, but not at the onset of reperfusion, preserved LV functional performance is consistent with previous studies. In rats subjected to global I/R with intact vagal innervation, right cervical VNS–treated LV showed significantly better performance throughout the 120-minute reperfusion period and that VNS exerted a marked anti-infarct effect irrespective of the heart rate as compared with sham stimulation.[25] The preserved LV function provided by VNS might be explained by a reduction in the myocardial infarct size. In the present study in swine, VNS applied during ischemia, but not at the onset of reperfusion, significantly reduced myocardial infarct size by 59%. However, we recently reported that VNS applied immediately at the onset of ischemia dramatically reduced myocardial infarct size by 89%.[13] These findings suggested that timing of VNS initiation with respect to the onset of myocardial ischemia is an important determinant of VNS therapeutic efficacy and that the earlier the VNS is applied, the smaller the infarct size.

Mechanisms responsible for infarct size reduction by VNS

Myocardial I/R injury leads to the activation of cell death programs, including cytochrome *c*–mediated apoptosis and necrosis. Thus, the beneficial effect of VNS in reducing the infarct size suggests that it may have an antiapoptotic effect. In the present study, we found that VNS applied during ischemia, but not at the onset of reperfusion, markedly decreased cytochrome *c* release, suggesting that it may be involved in the suppression of mitochondrial permeability

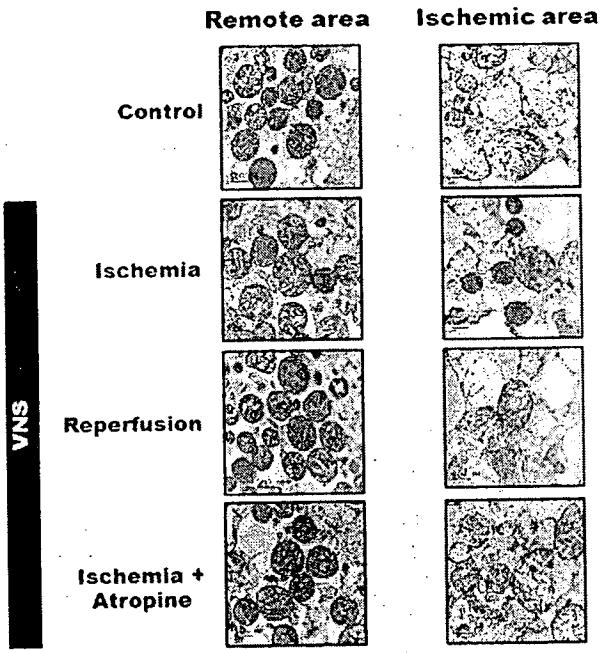


Figure 7 Representative electron photomicrographs of cardiac mitochondrial ultrastructure. In the ischemic area of the Control group, I/R-induced severe mitochondrial damage was observed as indicated by marked cardiac mitochondrial swelling accompanied by a disruption in membrane integrity. However, VNS applied during ischemia, but not reperfusion, significantly protected cardiac mitochondrial swelling after I/R injury, and this effect was abolished by atropine. I/R = ischemic-reperfusion; VNS = vagus nerve stimulation.

transition pore opening that prevented myocardial apoptosis.[25] A previous study in rats demonstrated that VNS prevented downregulation of the antiapoptotic protein Bcl-2 and suppressed cytochrome *c* release and reperfusion-induced opening of mitochondrial permeability transition pore,[25] which is also consistent with our finding. Therefore, the decreased cytochrome *c* release could be responsible for the infarct size reduction observed in this study. Moreover, we have shown that one potential mechanism of the pronounced cardioprotective effect of VNS during the I/R period could be due to its prevention of cardiac mitochondrial dysfunction. Increased ROS production and oscillation of the mitochondrial membrane potential change have been shown to play an important role in the genesis of cardiac arrhythmias and MI.[26] Our data indicate that VNS stabilized cardiac mitochondrial membrane potential by protecting the depolarization of mitochondrial membrane potential. This could lead to the reduction of arrhythmias that occurred during the I/R period in the VNS group. Moreover, mitochondrial ROS reduction and decreased mitochondrial swelling could be responsible for the decreased infarct size in the VNS group. Our findings that these beneficial effects of VNS were abolished by atropine suggest a dominant muscarinic receptor involvement. In addition to its anti-apoptosis, previous studies demonstrated that VNS exerts an anti-inflammatory effect.[12,27,28] Inflammatory processes have been shown to play a critical role in myocardial I/R injury. In the present study, VNS applied during ischemia, but not at the onset of reperfusion, significantly increased the myocardial anti-inflammatory cytokine IL-4. A recent clinical study has shown that serum IL-4 concentrations on admission and immediately after PCI were significantly lower in patients who subsequently developed severe cardiac dysfunction.[29] Another experimental study also reported that IL-4 protects B cells from apoptosis and prevents mitochondrial damage as shown by the maintenance of mitochondrial membrane potential change.[30] Therefore, the anti-inflammatory effect of VNS could also be responsible for the reduction in the infarct size reported in this study. Moreover, our finding suggested that myocardial insult leading to myocardial cell death occurred early during ischemia as shown by a smaller infarct size when VNS was applied immediately at the onset of ischemia[13] or later during ischemia compared to that at the onset of the reperfusion period.

Study limitations

Some limitations of the present study are also important to note. Our study was conducted in anesthetized healthy animals, whereas most victims of cardiac arrest have significant coronary lesions. A majority of the large animal studies on the effects of VNS have been performed in canine models. In contrast to dogs, pigs have no collateralized coronary arteries.[31] Thus, our model might be similar to the patients who have a first coronary event accompanied by fatal ischemia. Furthermore, we did not measure the myocardial interstitial level of acetylcholine at the ischemic area during VNS. However, a previous study demonstrated that electrical stimulation of the vagal efferent during acute MI produced the significant additive release of acetylcholine to the myocardial interstitial space.[32] Therefore, such an additional release of acetylcholine in response to VNS during ischemia would play a critical role in cardioprotection against I/R injury. Moreover, in the present study, there was no significant change in heart rate during VNS, which is contrary to a previous study.[33] This discrepancy may be due to different VNS parameters used in that study and ours. It is known that VNS-induced bradycardia is dependent on stimulation parameters including voltage, current, duration, and frequency. By adjusting the VNS parameters, graded sinus bradycardia could be achieved and strong VNS can produce long pauses and sinus arrest. Nevertheless, a recent study[34] suggested that "low-dose" stimulation with no cardiac synchronization may be equally effective than higher amplitude stimulation coupled to the heart rate, and a heart rate reduction may not necessarily be an ideal surrogate marker of the favorable effects at the ventricular level.[35] In view of the present study, VNS initiating during ischemia may thus offer a novel adjunctive myocardial salvage approach to current percutaneous coronary and pharmacological interventions designed to reduce myocardial reperfusion injury.

Conclusions

We have thus provided compelling evidence that VNS after myocardial ischemia onset provided significant cardioprotection and improved LV function in a large animal model of I/R injury. However, cardioprotection associated with VNS is diminished or absent when VNS was applied at the onset of reperfusion. These findings suggest that timing of VNS initiation with respect to the onset of ischemia is an important determinant of its therapeutic efficacy. The underlying potential mechanisms of such cardioprotection of VNS are associated with its prevention of reperfusion arrhythmias by increasing the phosphorylation of connexin 43 at the serine 368 residue, decreasing time from T-wave peak to end, preserving LV function by reducing infarct size, and protecting cardiac mitochondrial integrity through its anti-apoptotic and anti-inflammatory effects. Thus, these data strongly support the notion that VNS is emerging as a promising therapeutic modality in combination with reperfusion therapy for protecting myocardium at risk of I/R injury due to coronary artery disease.

Appendix

Supplementary data

Supplementary data associated with this article can be found in the online version at http://dx.doi.org/10.1016/j.hrthm.2014.08.001.

References

1. Yasuda S, Shimokawa H. Acute myocardial infarction: the enduring challenge for cardiac protection and survival. Circ J 2009;73:2000–2008.
2. Yellon DM, Hausenloy DJ. Myocardial reperfusion injury. N Engl J Med 2007;357:1121–1135.
3. Entman ML, Smith CW. Postreperfusion inflammation: a model for reaction to injury in cardiovascular disease. Cardiovasc Res 1994;28:1301–1311.
4. Hawkins HK, Entman ML, Zhu JY, Youker KA, Berens K, Dore M, Smith CW. Acute inflammatory reaction after myocardial ischemic injury and reperfusion: development and use of a neutrophil-specific antibody. Am J Pathol 1996;148:1957–1969.
5. Hausenloy DJ, Yellon DM. Myocardial ischemia-reperfusion injury: a neglected therapeutic target. J Clin Invest 2013;123:92–100.
6. Levy MN. Sympathetic-parasympathetic interactions in the heart. Circ Res 1971;29:437–445.
7. Aidonidis I, Brachmann J, Seller H, Demowsky K, Czachurski J, Kubler W. Cardiac sympathetic nervous activity during myocardial ischemia, reperfusion and ventricular fibrillation in the dog-effects of intravenous lidocaine. Cardiology 1992;80:196–204.
8. Baines CP. How and when do myocytes die during ischemia and reperfusion: the late phase. J Cardiovasc Pharmacol Ther 2011;16:239–243.
9. Schwartz PJ, De Ferrari GM, Sanzo A, Landolina M, Rordorf R, Raineri C, Campana C, Revera M, Ajmone-Marsan N, Tavazzi L, Odero A. Long term vagal stimulation in patients with advanced heart failure: first experience in man. Eur J Heart Fail 2008;10:884–891.
10. Hauptman PJ, Schwartz PJ, Gold MR, Borggrefe M, Van Veldhuisen DJ, Starling RC, Mann DL. Rationale and study design of the increase of vagal tone in heart failure study: INOVATE-HF. Am Heart J 2012;163:954–962. e951.
11. Dicarlo L, Libbus I, Amurthur B, Kenknight BH, Anand IS. Autonomic regulation therapy for the improvement of left ventricular function and heart failure symptoms: the ANTHEM-HF study. J Card Fail 2013;19:655–660.
12. Calvillo L, Vanoli E, Andreoli E, Besana A, Omodeo E, Gnecchi M, Zerbi P, Vago G, Busca G, Schwartz PJ. Vagal stimulation, through its nicotinic action, limits infarct size and the inflammatory response to myocardial ischemia and reperfusion. J Cardiovasc Pharmacol 2011;58:500–507.
13. Shinlapawittayatorn K, Chinda K, Palee S, Surinkaew S, Thunsiri K, Weerateerangkul P, Chattipakorn S, Kenknight BH, Chattipakorn N. Low-amplitude left vagus nerve stimulation significantly attenuates ventricular dysfunction and infarct size through prevention of mitochondrial dysfunction during acute ischemia-reperfusion injury. Heart Rhythm 2013;10:1700–1707.
14. Kakinuma Y, Ando M, Kuwabara M, Katare RG, Okudela K, Kobayashi M, Sato T. Acetylcholine from vagal stimulation protects cardiomyocytes against ischemia and hypoxia involving additive non-hypoxic induction of HIF-1alpha. FEBS Lett 2005;579:2111–2118.
15. Vanoli E, De Ferrari GM, Stramba-Badiale M, Hull SS Jr, Foreman RD, Schwartz PJ. Vagal stimulation and prevention of sudden death in conscious dogs with a healed myocardial infarction. Circ Res 1991;68:1471–1481.
16. Zuanetti G, De Ferrari GM, Priori SG, Schwartz PJ. Protective effect of vagal stimulation on reperfusion arrhythmias in cats. Circ Res 1987;61:429–435.
17. Garcia-Dorado D, Rodriguez-Sinovas A, Ruiz-Meana M. Gap junction-mediated spread of cell injury and death during myocardial ischemia-reperfusion. Cardiovasc Res 2004;61:386–401.
18. Severs NJ, Bruce AF, Dupont E, Rothery S. Remodelling of gap junctions and connexin expression in diseased myocardium. Cardiovasc Res 2008;80:9–19.
19. Beardslee MA, Lerner DL, Tadros PN, Laing JG, Beyer EC, Yamada KA, Kleber AG, Schuessler RB, Saffitz JE. Dephosphorylation and intracellular redistribution of ventricular connexin43 during electrical uncoupling induced by ischemia. Circ Res 2000;87:656–662.
20. Ando M, Katare RG, Kakinuma Y, Zhang D, Yamasaki F, Muramoto K, Sato T. Efferent vagal nerve stimulation protects heart against ischemia-induced arrhythmias by preserving connexin43 protein. Circulation 2005;112:164–170.
21. Lampe PD, TenBroek EM, Burt JM, Kurata WE, Johnson RG, Lau AF. Phosphorylation of connexin43 on serine368 by protein kinase C regulates gap junctional communication. J Cell Biol 2000;149:1503–1512.
22. Mines GR. On dynamic equilibrium in the heart. J Physiol 1913;46:349–383.
23. Rensma PL, Allessie MA, Lammers WJ, Bonke FI, Schalij MJ. Length of excitation wave and susceptibility to reentrant atrial arrhythmias in normal conscious dogs. Circ Res 1988;62:395–410.
24. Wiener N, Rosenblueth A. The mathematical formulation of the problem of conduction of impulses in a network of connected excitable elements, specifically in cardiac muscle. Arch Inst Cardiol Mex 1946;16:205–265.
25. Katare RG, Ando M, Kakinuma Y, Arikawa M, Handa T, Yamasaki F, Sato T. Vagal nerve stimulation prevents reperfusion injury through inhibition of opening of mitochondrial permeability transition pore independent of the bradycardiac effect. J Thorac Cardiovasc Surg 2009;137:223–231.
26. Brown DA, O'Rourke B. Cardiac mitochondria and arrhythmias. Cardiovasc Res 2010;88:241–249.
27. Katare RG, Ando M, Kakinuma Y, Arikawa M, Yamasaki F, Sato T. Differential regulation of TNF receptors by vagal nerve stimulation protects heart against acute ischemic injury. J Mol Cell Cardiol 2010;49:234–244.
28. Marrero MB, Bencherif M. Convergence of alpha 7 nicotinic acetylcholine receptor-activated pathways for anti-apoptosis and anti-inflammation: central role for JAK2 activation of STAT3 and NF-kappaB. Brain Res 2009;1256:1–7.
29. Szkodzinski J, Hudzik B, Osuch M, Romanowski W, Szygula-Jurkiewicz B, Polonski L, Zubelewicz-Szkodzinska B. Serum concentrations of interleukin-4 and interferon-gamma in relation to severe left ventricular dysfunction in patients with acute myocardial infarction undergoing percutaneous coronary intervention. Heart Vessels 2011;26:399–407.
30. Lemaire C, Andr au K, Fraisse CS, Adam A, Souvannavong V. IL-4 inhibits apoptosis and prevents mitochondrial damage without inducing the switch to necrosis observed with caspase inhibitors. Cell Death Differ 1999;6:813–820.
31. Maxwell MP, Hearse DJ, Yellon DM. Species variation in the coronary collateral circulation during regional myocardial ischaemia: a critical determinant of the rate of evolution and extent of myocardial infarction. Cardiovasc Res 1987;21:737–746.
32. Kawada T, Yamazaki T, Akiyama T, Sato T, Shishido T, Inagaki M, Takaki H, Sugimachi M, Sunagawa K. Differential acetylcholine release mechanisms in the ischemic and non-ischemic myocardium. J Mol Cell Cardiol 2000;32:405–414.
33. Shen MJ, Shinohara T, Park HW, et al. Continuous low-level vagus nerve stimulation reduces stellate ganglion nerve activity and paroxysmal atrial tachyarrhythmias in ambulatory canines. Circulation 2011;123:2204–2212.
34. Hamann JJ, Ruble SB, Stolen C, Wang M, Gupta RC, Rastogi S, Sabbah HN. Vagus nerve stimulation improves left ventricular function in a canine model of chronic heart failure. Eur J Heart Fail 2013;15:1319–1326.
35. Kong SS, Liu JJ, Hwang TC, Yu XJ, Zhao M, Yuan BX, Lu Y, Kang YM, Wang B, Zang WJ. Optimizing the parameters of vagus nerve stimulation by uniform design in rats with acute myocardial infarction. PLoS One 2012;7:e42799.

CLINICAL PERSPECTIVES

Although advances in percutaneous coronary technology, reduced procedure times, and appropriate use of pharmacological approaches (antiplatelet and antithrombotic) for maintaining coronary flow have improved outcomes, attenuation of myocardial reperfusion injury remains unresolved. Therefore, novel therapeutic strategies are needed to prevent myocardial reperfusion injury and further reduce the infarct size as well as improve left ventricular function and clinical outcomes in patients with acute myocardial infarction. Here, we showed that vagus nerve stimulation (VNS) applied after myocardial ischemia onset, but not at the onset of reperfusion, provided significant cardioprotection against ischemia-reperfusion injury. Furthermore, our findings suggest that timing of VNS initiation with respect to the onset of ischemia is an important determinant of its therapeutic efficacy. The underlying potential mechanisms of such cardioprotection of VNS are associated with its prevention of reperfusion arrhythmias by increasing the phosphorylation of connexin 43 at the serine 368 residue, decreasing time from T-wave peak to end (an indicator of transmural dispersion of repolarization), preserving left ventricular function by reducing infarct size, and protecting cardiac mitochondrial integrity through its antiapoptotic and anti-inflammatory effects. A possible clinical implication is that VNS might be used as an adjunctive myocardial salvage approach to current percutaneous coronary and pharmacological interventions designed to protect myocardium at risk of ischemic-reperfusion injury. However, large, multicenter, randomized controlled clinical trials are still required to determine whether VNS can improve clinical outcomes for the patients affected with myocardial infarction.

เอกสารแนบหมายเลข 60

International Journal of Cardiology 176 (2014) 1030–1032

Contents lists available at ScienceDirect

International Journal of Cardiology

journal homepage: www.elsevier.com/locate/ijcard

Letter to the Editor

Application of vagus nerve stimulation from the onset of ventricular fibrillation to post-shock period improves defibrillation efficacy

Kittiya Thunsiri [a,b], Krekwit Shinlapawittayatorn [b,c,1], Kreokkiat Chinda [b], Siripong Palee [b], Sirirat Surinkaew [b], Siriporn C. Chattipakorn [b,d], Bruce H. KenKnight [e], Nipon Chattipakorn [b,c,*]

[a] Biomedical Engineering Center, Faculty of Engineering, Chiang Mai University, Chiang Mai, Thailand
[b] Cardiac Electrophysiology Research and Training Center, Faculty of Medicine, Chiang Mai University, Chiang Mai, Thailand
[c] Cardiac Electrophysiology Unit, Department of Physiology, Faculty of Medicine, Chiang Mai University, Chiang Mai, Thailand
[d] Department of Oral Biology and Diagnostic Science, Faculty of Dentistry, Chiang Mai University, Chiang Mai, Thailand
[e] Emerging Therapies, Cyberonics Inc, Houston, TX, USA

ARTICLE INFO

Article history:
Received 3 June 2014
Accepted 26 July 2014
Available online 15 August 2014

Keywords:
Defibrillation threshold
Ventricular fibrillation
Vagus nerve stimulation

Sudden cardiac death remains a major unresolved clinical problem worldwide. Many of these deaths result from malignant ventricular arrhythmias, including ventricular fibrillation (VF) [1]. Although the most effective treatment for VF is electrical defibrillation, several studies have suggested the potential for myocardial damage when high-energy shocks were applied during defibrillation [2]. Thus, the improvement of defibrillation efficacy has been extensively studied in an attempt to lower the shock strength required for successful defibrillation including modulation of the autonomic nervous system by vagus nerve stimulation (VNS). Although left cervical (LC) VNS has been used as a therapeutic tool for epilepsy and drug resistant depression, a previous study has shown that VNS applied 8 s before the defibrillation onset could decrease the defibrillation energy [3]. Moreover, a growing number of studies have suggested that increased sympathetic activity [4] and rapid repetitive cardiac electrical activities occurring after defibrillation (post-shock activation) could be responsible for failed defibrillation [5–7]. Therefore, we hypothesized that by applying LC VNS continuously beginning at the VF onset until the post-shock period could improve defibrillation efficacy by decreasing the defibrillation threshold (DFT). The study has been approved by the Institutional Animal Care and Use Committees of the Faculty of Medicine, Chiang Mai University. All animals were cared for according to the *Guide for the Care and Use of Laboratory Animals* published by the US National Institutes of Health (NIH Publication No. 85-23, revised 1996). Thirteen anesthetized pigs (30–35 kg) were used in this study. In each pig, shocking electrodes were placed at the right ventricular (RV) apex and the junction between superior vena cava and right atrium. VF was induced by 60-Hz alternating current delivered from an electrode at the tip of the RV catheter. Defibrillation was attempted with biphasic truncated exponential shocks after 10 s of VF. LC VNS was applied at the onset of VF at 5 Hz and at durations of 10, 15, and 20 s. The DFT was determined at the beginning of the study and after LC VNS by the three reversal up–down protocol. A minimum of 4 min was allowed to elapse between VF episodes. The surface ECG was monitored and recorded throughout the experiments. Pigs were randomly divided into 2 groups. Group 1 ($n = 7$) received 10 mA, 5 Hz VNS at different durations (10, 15 and 20 s). In group 2 ($n = 6$), the effective VNS parameter selected from group 1 was applied in the presence of 3% Mepivacaine for blocking the effect of VNS. For the local nerve block, the LC vagus nerve was caudally covered by the nerve cuff which is the route for the administration of 3% Mepivacaine. Mepivacaine was maintained in the nerve cuff for the entire experiment.

In group 1, VNS (5 Hz) significantly prolonged P–R and R–R intervals (approximately 17 ± 2% change for P–R interval and 18 ± 1% change for R–R interval at all durations) while caused no change in QRS complex and Q–T interval (Table 1). The delivered voltage and energy of the DFT were significantly decreased only at VNS durations of 15 and 20 s (Fig. 1A). In the present study, VNS parameter of 5 Hz with 20 s duration was selected for group 2 study. To verify if improved defibrillation efficacy was from VNS, sodium channel blocker Mepivacaine was used in group 2. Our results showed that VNS significantly prolonged P–R and R–R intervals, and Mepivacaine did not alter the P–R and R–R intervals (Table 1). Moreover, the beneficial effect of VNS on the DFT reduction was abolished when the LC vagus nerve was locally blocked by 3% Mepivacaine (Fig. 1B).

The parasympathetic innervation of the heart is modulated through the vagus nerve. It is known that right VNS can cause bradycardia,

* Corresponding author at: Cardiac Electrophysiology Research and Training Center, Faculty of Medicine, Chiang Mai University, Chiang Mai 50200, Thailand. Tel.: +66 53 945 329; fax: +66 53 945 368.
E-mail address: nchattip@gmail.com (N. Chattipakorn).
[1] These two authors contributed equally to this work.

http://dx.doi.org/10.1016/j.ijcard.2014.07.302
0167-5273/© 2014 Elsevier Ireland Ltd. All rights reserved.

Table 1
ECG parameters at baseline, and during VNS.

Frequency (Hz)	Duration (s)	Condition	P–R interval (ms)	R–R interval (ms)	QRS complex (ms)	Q–T interval (ms)
Group 1						
5	10	**Baseline**	114 ± 28	662 ± 113	33 ± 17	334 ± 40
		Stimulation	133 ± 23*	781 ± 169*	34 ± 16	329 ± 42
	15	**Baseline**	122 ± 37	705 ± 119	36 ± 17	349 ± 46
		Stimulation	140 ± 23*	840 ± 153*	35 ± 15	345 ± 44
	20	**Baseline**	119 ± 40	698 ± 123	39 ± 18	337 ± 52
		Stimulation	142 ± 29*	824 ± 141*	41 ± 18	337 ± 53
Group 2 (with 3% Mepivacaine local block)						
5	20	**Baseline**	93 ± 10	577 ± 96		
		Stimulation	117 ± 16*	716 ± 11*		
		Block	93 ± 15	536 ± 69		

* $P < 0.05$ vs Baseline.

whereas left VNS induces AV block. Although LC VNS was performed in the present study, the prolonged R–R interval was shown when compared with the baseline. Based on the richly parasympathetic nerve innervation throughout all chambers of the swine heart [8], the prolonged R–R interval could be due to the direct transfer of the electrical stimulation to the SA node.

The effective VNS parameters in the present study were 5 Hz with 15 or 20 s which are continuously VNS applied from VF onset until 5 or 10 s after the defibrillation, suggesting that VNS applied long enough to cover the post-shock period significantly increased the defibrillation efficacy as shown in Fig. 1A. The previous studies suggested that rapid cardiac electrical activities occurring after defibrillation (post-shock activation) could be responsible for the failed defibrillation [5–7]. Thus, the DFT reduction might be explained by the cardiac electrophysiological modulation by the VNS which modulated the cardiac electrical activities during the post-shock period. Interestingly, the effect of parasympathetic modulation observed in our present study was also consistent with the previous experiment, which demonstrated that parasympathomimetic drugs not only decreased the DFT but also increased ventricular fibrillation threshold (VFT) [9]. The increased VFT occurs via post-ganglionic efferent fibers which is a direct action of VNS on the ventricle [9]. Furthermore, in the isolated innervated rabbit heart preparation [4], VNS has been shown to increase the VFT, making VF harder to induce. In our experiment we also found that some of our animals failed to develop VF by the same amount of AC current after VNS was applied (unpublished data).

To verify the roles of VNS in improved defibrillation efficacy, Mepivacaine was used for blocking nerve impulses via the vagus nerve. Prior to Mepivacaine application, VNS caused the prolongation of P–R and R–R intervals, and also reduced the DFT. After Mepivacaine was applied, VNS did not make any change on both P–R and R–R intervals and the DFT, compared with the baseline. This finding strongly confirmed that the beneficial effects of VNS on the electrophysiological properties of the heart were modulated through the vagus nerve. However, the major limitation of this study is that the direct electrophysiological parameters such as the action potential duration and the effective refractory period were not measured. Future studies are needed to investigate whether these parameters were modulated by VNS.

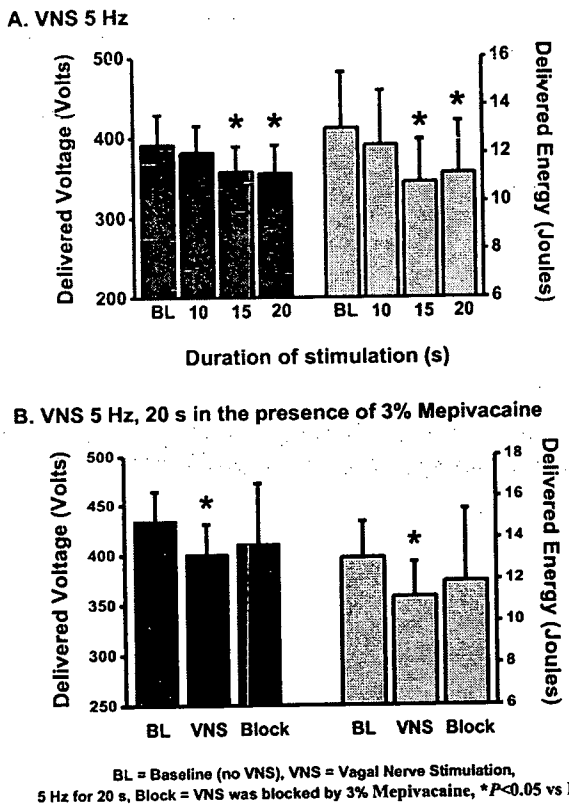


Fig. 1. Effects of VNS frequencies and durations on delivered voltage and delivered energy of DFT.

Funding sources

This study was supported by the Thailand Research Fund TRF-CHE Research Grant for New Scholars MRG5580125 (KS), BRG5780016 (SC), RTA5580006 (NC), and the Chiang Mai University Excellent Center Award (NC).

Conflict of interest

The authors report no relationships that could be construed as a conflict of interest.

References

[1] McRae AT, Chung MK, Asher CR. Arrhythmogenic right ventricular cardiomyopathy: a cause of sudden death in young people. Cleve Clin J Med 2001;68:459–67.
[2] Nakagawa Y, Sato Y, Kojima T, et al. Electrical defibrillation outcome prediction by waveform analysis of ventricular fibrillation in cardiac arrest out of hospital patients. Tokai J Exp Clin Med 2012;37:1–5.
[3] Murakawa Y, Yamashita T, Ajiki K, Hayami N, Omata M, Nagai R. Effect of cervical vagal nerve stimulation on defibrillation energy: a possible adjunct to efficient defibrillation. Jpn Heart J 2003;44:91–100.
[4] Ng GA, Brack KE, Patel VH, Coote JH. Autonomic modulation of electrical restitution, alternans and ventricular fibrillation initiation in the isolated heart. Cardiovasc Res 2007;73:750–60.
[5] Chattipakorn N, Banville I, Gray RA, Ideker RE. Mechanism of ventricular defibrillation for near-defibrillation threshold shocks: a whole-heart optical mapping study in swine. Circulation 2001;104:1313–9.

[6] Chattipakorn N, Fotuhi PC, Ideker RE. Prediction of defibrillation outcome by epicardial activation patterns following shocks near the defibrillation threshold. J Cardiovasc Electrophysiol 2000;11:1014–21.
[7] Chattipakorn N, Fotuhi PC, Ideker RE. Pacing following shocks stronger than the defibrillation threshold: impact on defibrillation outcome. J Cardiovasc Electrophysiol 2000;11:1022–8.
[8] Ulphani JS, Cain JH, Inderyas F, et al. Quantitative analysis of parasympathetic innervation of the porcine heart. Heart Rhythm 2010;7:1113–9.
[9] Morillo CA, Jones DL, Klein GJ. Effects of autonomic manipulation on ventricular fibrillation and internal cardiac defibrillation thresholds in pigs. Pacing Clin Electrophysiol 1996;19:1355–62.

เอกสารแนบหมายเลข 61

223:1 13–23

Protocatechuic acid exerts a cardioprotective effect in type 1 diabetic rats

Yoswaris Semaming[1,2], Sirinart Kumfu[1,3], Patchareewan Pannangpetch[1,2], Siriporn C Chattipakorn[1,4] and Nipon Chattipakorn[1,3]

[1]Cardiac Electrophysiology Research and Training Center, Faculty of Medicine, Chiang Mai University, Chiang Mai 50200, Thailand
[2]Department of Pharmacology, Faculty of Medicine, Khon Kaen University, Khon Kaen 40002, Thailand
[3]Cardiac Electrophysiology Unit, Department of Physiology, Faculty of Medicine and [4]Department of Oral Biology and Diagnostic Sciences, Faculty of Dentistry, Chiang Mai University, Chiang Mai 50200, Thailand

Correspondence should be addressed to N Chattipakorn
Email
nchattip@gmail.com

Abstract

Oxidative stress has been shown to play an important role in the pathogenesis of diabetes-induced cardiac dysfunction. Protocatechuic acid (PCA) is a phenolic compound, a main metabolite of anthocyanin, which has been reported to display various pharmacological properties. We proposed the hypothesis that PCA exerts cardioprotection in type 1 diabetic (T1DM) rats. T1DM was induced in male Sprague–Dawley rats by a single i.p. injection of 50 mg/kg streptozotocin (STZ) and groups of these animals received the following treatments for 12 weeks: i) oral administration of vehicle, ii) oral administration of PCA at a dose of 50 mg/kg per day, iii) oral administration of PCA at a dose of 100 mg/kg per day, iv) s.c. injection of insulin at a dose of 4 U/kg per day, and v) a combination of PCA, 100 mg/kg per day and insulin, 4 U/kg per day. Metabolic parameters, results from echocardiography, and heart rate variability were monitored every 4 weeks, and the HbA1c, cardiac malondialdehyde (MDA), cardiac mitochondrial function, and cardiac BAX/BCL2 expression were evaluated at the end of treatment. PCA, insulin, and combined drug treatments significantly improved metabolic parameters and cardiac function as shown by increased percentage fractional shortening and percentage left ventricular ejection fraction and decreased low-frequency:high-frequency ratio in T1DM rats. Moreover, all treatments significantly decreased plasma HbA1c and cardiac MDA levels, improved cardiac mitochondrial function, and increased BCL2 expression. Our results demonstrated for the first time, to our knowledge, the efficacy of PCA in improving cardiac function and cardiac autonomic balance, preventing cardiac mitochondrial dysfunction, and increasing anti-apoptotic protein in STZ-induced T1DM rats. Thus, PCA possesses a potential cardioprotective effect and could restore cardiac function when combined with insulin treatment. These findings indicated that supplementation with PCA might be helpful for the prevention and alleviation of cardiovascular complications in T1DM.

Key Words
- type 1 diabetes
- oxidative stress
- cardiac mitochondrial dysfunction
- protocatechuic acid

Journal of Endocrinology
(2014) **223**, 13–23

http://joe.endocrinology-journals.org
DOI: 10.1530/JOE-14-0273

© 2014 Society for Endocrinology
Printed in Great Britain

Published by Bioscientifica Ltd.

Journal of Endocrinology

Introduction

Diabetes and cardiac complications have become a public health problem of considerable magnitude. Cardiac dysfunction is the most common serious complication of diabetes mellitus and has become one of the leading causes of the increased mortality in both Type 1 and Type 2 diabetes. A streptozotocin (STZ)-induced type 1 diabetic rat has been used as an animal model for the investigation of pharmacological interventions and also for the study of diabetic complications including diabetes-induced cardiac dysfunction (Krishna *et al.* 2005, Naowaboot *et al.* 2009). Clinically, cardiac dysfunction may occur without major vascular lesions, indicating a primary role for the direct effects of diabetes on cardiomyocytes (Trost & LeWinter 2001, Dyntar *et al.* 2006). These characteristics further result in diabetes-induced cardiac dysfunction through cellular pathological changes, especially increased oxidative stress, mitochondrial dysfunction, and cardiac autonomic neuropathy (An & Rodrigues 2006, Boudina & Abel 2007). Oxidative damage plays an important role in the occurrence and development of cardiac dysfunction in this case (Asbun & Villarreal 2006, Kumar & Sitasawad 2009). Oxidative stress is known to potentially lead to biological damage to macromolecules and activates maladaptive signaling pathways, which may cause cell dysfunction and cell death (Sies 1991).

Protocatechuic acid (PCA, 3,4-dihydroxybenzoic acid), a phenolic compound, is isolated from the dried flowers of *Hibiscus sabdariffa* Linn. It is a main metabolite of complex polyphenols, especially anthocyanins, which are converted to PCA and also abundantly formed and absorbed in the large intestine because of microbial metabolization (Kay *et al.* 2005, Vitaglione *et al.* 2007). Previous reports of both *in vitro* and *in vivo* studies have demonstrated that PCA has anti-carcinogen (Tseng *et al.* 2000, Yip *et al.* 2006, Lin *et al.* 2007, Yin *et al.* 2009), anti-hyperglycemia (Lin *et al.* 2009, 2011, Harini & Pugalendi 2010, Scazzocchio *et al.* 2011), antioxidant (Liu *et al.* 2002, Sroka & Cisowski 2003, Masella *et al.* 2004, Shi *et al.* 2006, Tarozzi *et al.* 2007, Lin *et al.* 2009, Chou *et al.* 2010, Vari *et al.* 2011, Zhang *et al.* 2011), and anti-inflammatory properties (Yan *et al.* 2004, Min *et al.* 2010, Wang *et al.* 2010, 2011). However, no scientific investigation has yet been conducted on the effect of PCA on diabetes-induced cardiac dysfunction, which is also caused by oxidative stress, and thus this investigation was conducted to study the anti-hyperglycemic activity of PCA and the effect of PCA on diabetes-induced cardiac dysfunction and other related metabolic parameters in STZ-induced diabetic rats. We tested the hypothesis that PCA could attenuate cardiac complications by reducing oxidative stress, ameliorating cardiomyocyte apoptosis, and improving the cardiac autonomic balance and cardiac mitochondrial function in STZ-induced diabetic rats.

Materials and methods

Animals

A total of 36 male Sprague–Dawley rats with body weights of 250–280 g were acquired from the National Laboratory Animal Center, Mahidol University, Salaya, Nakornpathom. All experiments complied with the standards for the care and use of experimental animals and were approved by the Faculty of Medicine, Chiang Mai University Institutional Animal Care and Use Committee. After 7 days of acclimatization, diabetes was induced in 30 of the rats by a single i.p. injection of 50 mg/kg body weight of STZ dissolved in 0.1 M citric buffer (pH 4.5). Normal control rats ($n=6$) received injections of citric buffer (vehicle). Ten days after vehicle/STZ injection, only diabetic rats with fasting blood glucose (FBG) over 300 mg/dl were included in the experiments (Jiang *et al.* 2011, Zhao *et al.* 2014). Rats were assigned to one of six groups with six rats in each group and were treated as follows: normal rats treated with vehicle (NMV), diabetic rats treated with vehicle (DMV), diabetic rats treated with insulin at a dose of 4 U/kg (DMI), diabetic rats treated with PCA at a dose of 50 mg/kg (DML), diabetic rats treated with PCA at a dose of 100 mg/kg (DMH) (Harini & Pugalendi 2010), and diabetic rats treated with DMH and insulin at a dose of 4 U/kg (DMHI). All treatments were administered daily for 12 weeks. Fifty percent propylene glycol (vehicle) and PCA (Sigma Chemical Co. Ltd) were administrated orally using gavage feeding, and insulin was injected subcutaneously. The animals were given free access to feed and drinking water. The body weight and food intake were recorded weekly. Echocardiography was performed and heart rate variability (HRV) was measured every 4 weeks and blood sampling from tail vein was performed after fasting for 12 h to measure plasma glucose, insulin, and malondialdehyde (MDA) levels. At the end of a 12-week treatment, animals were deeply anesthetized and then killed; the hearts were collected for investigation of mitochondrial function, MDA, and BAX and BCL2 protein levels, and blood was collected for investigation of HbA1c.

http://joe.endocrinology-journals.org
DOI: 10.1530/JOE-14-0273
© 2014 Society for Endocrinology
Printed in Great Britain
Published by Bioscientifica Ltd.

FBG, plasma insulin, and HbA1c level determination

FBG level was determined using a glucometer (Accu-Chek Advantage II; Roche Diagnostics). Plasma insulin levels were measured by Sandwich ELISA (LINCO Research, Saint Charles, MO, USA; Pratchayasakul *et al.* 2011). Plasma HbA1c was determined based on the competitive turbidimetric inhibition immunoassay (Roche Diagnostics Ltd).

Plasma and cardiac MDA level determination

Plasma and cardiac MDA level was determined using a HPLC-based assay (Thermo scientific, Bangkok, Thailand). Cardiac tissue was homogenized in phosphate buffer, pH 2.8. Plasma and cardiac tissue were mixed with H_3PO_4 and thiobarbituric acid (TBA) to produce TBA-reactive substances (TBARSs). The plasma and cardiac TBARS concentrations were determined from a standard curve and reported as being equivalent to the MDA concentration (Apaijai *et al.* 2013).

Echocardiography

The echocardiographic parameters were measured in each rat using an HP/Agilent Philips Sonos 4500 (Agilent Technologies, Santa Clara, CA, USA). An echocardiography probe was placed in gentle contact with the chest, and images were collected along the parasternal short axis of the heart (Lekawanvijit *et al.* 2012). M-mode echocardiography was performed at the level of the papillary muscles. Percentage fractional shortening (%FS) and percentage left ventricular ejection fraction (%LVEF) were determined.

HRV analysis

The output from electrocardiogram (ECG) lead II was recorded in each rat using the PowerLab (ADInstruments, Sydney, NSW, Australia) and the Chart 5.0 programs (Raher *et al.* 2008). During ECG recording, rats were placed in a restraint and prohibited from movement (Incharoen *et al.* 2007, Raher *et al.* 2008, Kumfu *et al.* 2012). The high-frequency (HF, 0.6–3.0 Hz) component, representing cardiac parasympathetic activity, and low-frequency (LF, 0.2–0.6 Hz) component, representing cardiac sympathetic and parasympathetic activity, were determined using the MATLAB program (Raher *et al.* 2008). The LF:HF ratio was considered to be an indicator of cardiac sympathetic/parasympathetic tone balance (Ohuchi *et al.* 2000). An increased LF:HF ratio (i.e. depressed HRV) indicated a cardiac sympathovagal imbalance (Incharoen *et al.* 2007).

Cardiac mitochondrial function determination

Cardiac mitochondrial isolation was performed as described previously (Thummasorn *et al.* 2011). Cardiac mitochondrial function was assessed by determining production of cardiac mitochondrial reactive oxygen species (ROS), cardiac mitochondrial membrane potential change, and cardiac mitochondrial swelling (Thummasorn *et al.* 2011, Apaijai *et al.* 2012, Chinda *et al.* 2013). The components of the buffers used in the analysis of cardiac mitochondrial function consisted of KCl, sucrose, HEPES, KH_2PO_4, and pyruvate/malate that have no ADP/ATP. The measurements of mitochondrial function in each group were made during State IV respiration.

Cardiac mitochondrial ROS production Cardiac mitochondria were incubated with 2-μM DCFH-DA dye at 25 °C for 20 min. The dye was excited at λ_{ex} 485 nm and detected at λ_{em} 530 nm using a fluorescent microplate reader (BioTek Instruments, Winooski, VT, USA). An increase in the fluorescence intensity indicated increased mitochondrial ROS production (Thummasorn *et al.* 2011, Apaijai *et al.* 2013, Chinda *et al.* 2013).

Cardiac mitochondrial membrane potential changes Cardiac mitochondrial membrane potential changes were determined using 5-μM JC-1 dye as described previously (Thummasorn *et al.* 2011, Apaijai *et al.* 2013). In brief, cardiac mitochondria were incubated with JC-1 at 37 °C for 30 min. JC-1 monomer form (green-fluorescent) was excited at λ_{ex} 485 nm and detected at λ_{em} 590 nm, and JC-1 aggregate form (red-fluorescent) was excited at λ_{ex} 485 nm and detected at λ_{em} 530 nm using a fluorescent microplate reader. A decrease in the red:green fluorescence intensity ratio indicated cardiac mitochondrial membrane depolarization (Thummasorn *et al.* 2011, Apaijai *et al.* 2013, Chinda *et al.* 2013).

Cardiac mitochondrial swelling Cardiac mitochondria were incubated with 1.5-mM respiration buffer containing 100 mM KCl, 10 mM HEPES, and 5 mM KH_2PO_4, and the absorbance was determined using a spectrophotometer as described previously (Thummasorn *et al.* 2011, Apaijai *et al.* 2013). Cardiac mitochondrial swelling was indicated by a decrease in the detected absorbance (Thummasorn *et al.* 2011, Apaijai *et al.* 2013, Chinda *et al.* 2013).

Cardiac mitochondrial morphology Cardiac mitochondria were fixed with 2.5% glutaraldehyde in 0.1-M

http://joe.endocrinology-journals.org
DOI: 10.1530/JOE-14-0273
© 2014 Society for Endocrinology
Printed in Great Britain
Published by Bioscientifica Ltd.

phosphate buffer overnight and post-fixed in 1% cacodylate buffer osmium tetroxide for 2 h, and then dehydrated with a graded ethanol series (Thummasorn *et al.* 2011). Cardiac mitochondria were embedded in Epon-Araldite, cut with a diamond knife, and stained with uranyl acetate and lead acetate (Thummasorn *et al.* 2011). Cardiac mitochondrial morphology was detected using a transmission electron microscope (TEM; Thummasorn *et al.* 2011).

Western blot analysis of BAX and BCL2 protein expression levels

Myocardial protein extracts were prepared by homogenization of nitrogen-frozen myocardial tissues in a 300-ml extraction buffer containing 20-mM Tris–HCl (pH 6.8), 1-mM sodium orthovanadate, 5-mM sodium fluoride, and a protease inhibitor. Total protein concentration was determined using a Bio-Rad protein assay kit (Bio-Rad Laboratories). Samples of 50–80 μg of total protein were mixed with a loading buffer (5% betamercaptoethanol, 0.05% bromophenol blue, 75 mM Tris–HCl (pH 6.8), 2% SDS, and 10% glycerol), and loaded on 10% SDS–acrylamide gels. Proteins were transferred onto PVDF membrane in a glycine/methanol-transfer buffer (Palee *et al.* 2013, Surinkaew *et al.* 2013) in a Wet/Tank blotting system (Bio-Rad Laboratories). Membranes were blocked in 5% skim milk in Tris-buffered saline and Tween (TBST) buffer. Western blot analysis for BAX and BCL2 was performed using myocardial tissues. Membranes were exposed to mouse monoclonal anti-rat Bax and Bcl2 (1:1000 dilution, Santa Cruz Biotechnology). Bound antibody was detected by HRP conjugated with an anti-rabbit IgG (1:2000 dilution, Cell Signaling Technology, Danvers, MA, USA). The membranes were developed using the Amersham ECL Prime Western Blotting Detection Reagent (GE Healthcare, Buckinghamshire, UK) and densitometric analysis was carried out (Surinkaew *et al.* 2013).

Statistical analysis

Metabolic parameters, echocardiography, and HRV data are expressed as mean ± S.D., and others are expressed as mean ± S.E.M. One-way ANOVA followed by the least significant difference (LSD) *post hoc* test was used to test the differences among the groups. $P<0.05$ was considered statistically significant.

Results

Effects of pharmacological interventions on body weight, food intake, FBG, and plasma insulin in diabetic rats

At 10 days after STZ injection, diabetic rats were characterized by body weight loss, polyphagia, hyperglycemia, and insulin deficiency (Tables 1 and 2). Beginning at week 4 of insulin and combined drug treatments in diabetic rats, there were significantly increases in body weight and plasma insulin levels, and decreases in food intake and FBG levels, compared with DMV rats (Tables 3, 4 and 5). Beginning at week 4 for both doses of PCA treatment in diabetic rats, the FBG level significantly decreased when compared with DMV rats, whereas there was no alteration in body weight, food intake, and plasma insulin level in these rats (Tables 3, 4 and 5).

Table 1 Metabolic parameters, echocardiography, and heart rate variability (HRV) in normal and diabetic rats at baseline and 10 days after vehicle/STZ injection. Values are expressed as mean ± S.D.

	Baseline		10 days after vehicle/STZ injection	
Parameters	NM	DM	NM	DM
Metabolic parameters				
Body weight (g)	274±9	274±11	316±9*	261±17†
Food intake (g/day)	20±2	21±2	22±2	24±2†
Fasting blood glucose (mg/dl)	94±3	95±6	100±5	400±36†
Plasma insulin (ng/ml)	1.49±0.37	1.48±0.38	1.39±0.44	0.56±0.25†
Plasma MDA (μmol/ml)	1.05±0.03	1.03±0.03	1.04±0.02	1.04±0.02
Echocardiography				
Fractional shortening (%)	55±3	54±4	55±2	53±3
LV ejection fraction (%)	81±3	82±3	81±2	75±4
HRV				
LF:HF ratio	0.24±0.04	0.24±0.04	0.21±0.04	0.23±0.04

NM, normal rat; DM, diabetic rat; LV ejection fraction, left ventricular ejection; LF:HF ratio, low-frequency:high-frequency ratio. *$P<0.05$ vs baseline and †$P<0.05$ vs NM at 10 days after vehicle injection.

http://joe.endocrinology-journals.org
DOI: 10.1530/JOE-14-0273
© 2014 Society for Endocrinology
Printed in Great Britain
Published by Bioscientifica Ltd.

Journal of Endocrinology

Table 2 Metabolic parameters, echocardiography, and heart rate variability (HRV) at 10 days after vehicle/STZ injection. Values are expressed as mean ± s.d. of five to six rats in each group

Parameters	NMV	DMV	DMI	DML	DMH	DMHI
Metabolic parameters						
Body weight (g)	316±9	261±14*	270±20*	256±12*	250±16*	273±16*
Food intake (g/day)	22±2	24±2*	24±1*	24±2*	25±2*	25±2*
Fasting blood glucose (mg/dl)	100±5	394±33*	400±40*	392±26*	414±48*	407±36*
Plasma insulin (ng/ml)	1.51±0.60	0.67±0.29*	0.55±13*	0.52±0.31*	0.56±0.27*	0.50±0.30*
Plasma MDA (μmol/ml)	1.04±0.02	1.04±0.02	1.03±0.03	1.04±0.02	1.03±0.02	1.03±0.02
Echocardiography						
Fractional shortening (%)	55±2	53±2	55±4	52±4	54±5	52±3
LV ejection fraction (%)	80±2	77±3	76±4	75±4	75±4	74±5
HRV						
LF:HF ratio	0.21±0.04	0.22±0.03	0.22±0.05	0.23±0.03	0.26±0.05	0.23±0.06

NMV, normal rats treated with vehicle; DMV, diabetic rats treated with vehicle; DMI, diabetic rats treated with insulin, 4 U/kg; DML, diabetic rats treated with PCA, 50 mg/kg; DMH, diabetic rats treated with PCA, 100 mg/kg; DMHI, DMH + insulin, 4 U/kg; LV ejection fraction, left ventricular ejection fraction; LF:HF ratio, low-frequency:high-frequency ratio; *$P<0.05$ vs NMV.

Effects of pharmacological interventions on plasma MDA in diabetic rats

At 4 weeks after the STZ injection, plasma MDA levels were significantly increased in DMV rats when compared with NMV rats (Tables 3, 4 and 5). All treatments in diabetic rats significantly decreased the plasma MDA level, compared with DMV rats.

Effects of pharmacological interventions on echocardiography in diabetic rats

During week 4 after the STZ injection, diabetic rats developed cardiac contractile dysfunction that was characterized by significantly decreased %FS and %LVEF when compared with NMV rats (Tables 3, 4 and 5). Moreover, beginning at the fourth week for the insulin group and combined drug group, and in the eighth week after both doses of PCA treatment, a significant increase in the %FS and %LVEF occurred in diabetic rats when compared with DMV rats (Tables 3, 4 and 5). Interestingly, beginning at week 8 of PCA treatment at a dose of 100 mg/kg in diabetic rats, the echocardiography results did not differ from those for DMI rats. During week 12 of the combined drug treatment in diabetic rats, the echocardiography was restored to a normal status, whereas DMI alone could not achieve a similar benefit as %FS and %LVEF were still lower than those in the normal rats.

Effects of pharmacological interventions on HRV in diabetic rats

At 4 weeks after STZ injection, diabetic control rats had a significantly increased LF:HF ratio when compared with NMV rats, indicating a cardiac autonomic imbalance

Table 3 Effects of pharmacological interventions on metabolic parameters, echocardiography, and heart rate variability (HRV) at week 4 of treatment. Values are expressed as mean ± s.d. of five to six rats in each group

Parameters	NMV	DMV	DMI	DML	DMH	DMHI
Metabolic parameters						
Body weight (g)	397±23	237±40*	310±18*,†	234±25*,‡	241±16*,‡	296±30*,†
Food intake (g/day)	23±2	34±2*	29±1*,†	33±2*,‡	33±2*,‡	29±2*,†
Fasting blood glucose (mg/dl)	99±5	431±88*	166±25*,†	316±42*,†,‡	291±58*,†,‡	155±42*,†
Plasma insulin (ng/ml)	1.30±0.29	0.32±0.13*	1.50±0.86†	0.57±0.20*,‡	0.46±0.09*,‡	1.28±0.10†
Plasma MDA (μmol/ml)	1.03±0.08	1.14±0.10*	1.05±0.05†	1.03±0.04†	1.00±0.02†	0.98±0.06†
Echocardiography						
Fractional shortening (%)	58±4	43±3*	55±3†	43±2*,‡	44±2*,‡	56±2†
LV ejection fraction (%)	82±3	68±4*	79±3†	68±2*,‡	69±3*,‡	80±3†
HRV						
LF:HF ratio	0.23±0.08	0.45±0.06*	0.269±0.025†	0.42±0.04*,‡	0.41±0.03*,‡	0.25±0.06†

NMV, normal rats treated with vehicle; DMV, diabetic rats treated with vehicle; DMI, diabetic rats treated with insulin, 4 U/kg; DML, diabetic rats treated with PCA, 50 mg/kg; DMH, diabetic rats treated with PCA, 100 mg/kg; DMHI, DMH + insulin, 4 U/kg; LV ejection fraction, left ventricular ejection fraction; LF:HF ratio, low-frequency:high-frequency ratio. *$P<0.05$ vs NMV, †$P<0.05$ vs DMV, and ‡$P<0.05$ vs DMI.

© 2014 Society for Endocrinology
Printed in Great Britain
Published by Bioscientifica Ltd.

Table 4 Effects of pharmacological interventions on metabolic parameters, echocardiography, and heart rate variability (HRV) at week 8 of treatment. Values are expressed as mean ± s.d. of five to six rats in each group

Parameters	NMV	DMV	DMI	DML	DMH	DMHI
Metabolic parameters						
Body weight (g)	411±46	233±23*	323±32*,†	244±23*,‡	243±17*,‡	319±24*,†
Food intake (g/day)	24±1	36±1*	30±1*,†	34±1*,‡	35±2*,‡	31±2*,†
Fasting blood glucose (mg/dl)	94±6	441±42*	164±42*,†	331±46*,†,‡	270±53*,†,‡	156±31*,†
Plasma insulin (ng/ml)	1.71±1.14	0.43±0.14*	1.49±1.01†	0.42±0.08*,‡	0.46±0.19*,‡	2.01±0.91†
Plasma MDA (μmol/ml)	1.87±0.03	2.09±0.08*	1.88±0.03†	1.90±0.04†	1.89±0.03†	1.88±0.02†
Echocardiography						
Fractional shortening (%)	58±4	33±4*	55±5†	49±1*,†,‡	51±1*,†	55±4†
LV ejection fraction (%)	82±3	55±4*	79±4†	74±1*,†,‡	75±2*,†	80±3†
HRV						
LF:HF ratio	0.23±0.06	0.55±0.06*	0.31±0.10†	0.44±0.06*,†,‡	0.37±0.07*,†	0.30±0.06†

NMV, normal rats treated with vehicle; DMV, diabetic rats treated with vehicle; DMI, diabetic rats treated with insulin, 4 U/kg; DML, diabetic rats treated with PCA, 50 mg/kg; DMH, diabetic rats treated with PCA, 100 mg/kg; DMHI, DMH + insulin, 4 U/kg; LV ejection fraction, left ventricular ejection fraction; LF:HF ratio, low-frequency/high-frequency ratio. *$P<0.05$ vs NMV, †$P<0.05$ vs DMV, and ‡$P<0.05$ vs DMI.

(Table 3). During the fourth week of insulin and of combined drug treatment, and week 8 of both dosages of PCA, there was a significant decrease in the LF:HF ratio in diabetic rats, compared with DMV rats (Tables 3, 4 and 5). Interestingly, beginning at week 8 of PCA treatment at a dose of 100 mg/kg in diabetic rats, the HRV did not differ from that for insulin treatment in diabetic rats.

Effects of pharmacological interventions on plasma HbA1c levels in diabetic rats

At week 12 of treatment, DMV had significantly elevated plasma HbA1c levels when compared with NMV rats. PCA (both doses), insulin, and combined drug treatments in diabetic rats decreased the plasma HbA1c levels, compared with DMV rats (Fig. 1A).

Effects of pharmacological interventions on cardiac MDA levels in diabetic rats

At the end of treatment, cardiac MDA levels were significantly increased in DMV rats, compared with NMV rats (Fig. 1B). PCA (both doses), insulin, and combined drug treatments in diabetic rats significantly decreased cardiac MDA levels, compared with DMV rats. Interestingly, in DMH, the cardiac MDA level decreased similarly to that of to DMI rats.

Effects of pharmacological interventions on cardiac mitochondrial function and morphology in diabetic rats

Cardiac mitochondrial ROS production at the end of treatment was significantly increased in DMV rats,

Table 5 Effects of pharmacological intervention on metabolic parameters, echocardiography, and heart rate variability (HRV) at week 12 of treatment. Values are expressed as mean ± s.d. of five to six rats in each group

Parameters	NMV	DMV	DMI	DML	DMH	DMHI
Metabolic parameters						
Body weight (g)	444±23	225±12*	353±18*,†	243±21*,‡	246±19*,‡	339±23*,†
Food intake (g/day)	24±3	38±3*	33±2*,†	35±2*,‡	34±3*,‡	32±1*,†
Fasting blood glucose (mg/dl)	102±7	541±64*	184±26*,†	312±90*,†,‡	270±58*,†,‡	176±27*,†
Plasma insulin (ng/ml)	1.23±0.21	0.39±0.07*	1.39±0.81†	0.56±0.14*,‡	0.49±0.22*,‡	1.23±0.80†
Plasma MDA (μmol/ml)	2.14±0.02	2.25±0.05*	2.16±0.03†	2.19±0.03*,†	2.19±0.04*,†	2.13±0.02†
Echocardiography						
Fractional shortening (%)	57±3	33±3*	52±3*,†	49±3*,†	48±5*,†	56±3†,‡
LV ejection fraction (%)	82±2	54±5*	75±3*,†	74±3*,†	73±5*,†	80±3†,‡
HRV						
LF:HF ratio	0.24±0.05	0.54±0.13*	0.31±0.04†	0.41±0.06*,†	0.34±0.04*,†	0.29±0.14†

NMV, normal rats treated with vehicle; DMV, diabetic rats treated with vehicle; DMI, diabetic rats treated with insulin, 4 U/kg; DML, diabetic rats treated with PCA, 50 mg/kg; DMH, diabetic rats treated with PCA, 100 mg/kg; DMHI, DMH + insulin, 4 U/kg; LV ejection fraction, left ventricular ejection fraction; LF:HF ratio, low-frequency:high-frequency ratio. *$P<0.05$ vs NMV, †$P<0.05$ vs DMV, and ‡$P<0.05$ vs DMI.

© 2014 Society for Endocrinology
Printed in Great Britain
Published by Bioscientifica Ltd.

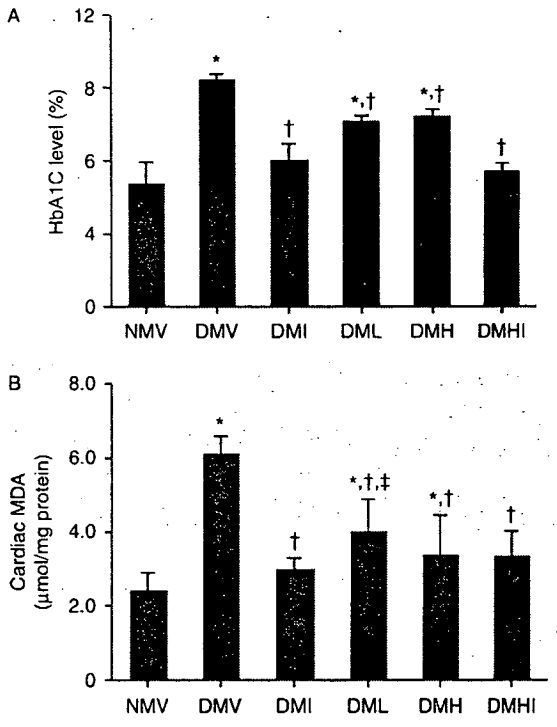


Figure 1
Effects of pharmacological interventions on plasma HbA1c and cardiac MDA levels. At the end of treatments, (A) plasma HbA1c level was increased in DMV rats, all treatments significantly decreased plasma HbA1c levels in diabetic rats. (B) Cardiac MDA level was elevated in DMV rats, and all treatments decreased cardiac MDA level in diabetic rats. Values are expressed as mean ± S.E.M. NMV, normal rats treated with vehicle; DMV, diabetic rats treated with vehicle; DMI, diabetic rats treated with insulin, 4 U/kg; DML, diabetic rats treated with PCA, 50 mg/kg; DMH, diabetic rats treated with PCA, 100 mg/kg; DMHI, DMH + insulin, 4 U/kg. $^{*}P<0.05$ vs NMV, $^{\dagger}P<0.05$ vs DMV, $^{\ddagger}P<0.05$ vs DMI.

compared with NMV rats (Fig. 2A). PCA (both doses), insulin, and combined drug treatments in diabetic rats significantly reduced the mitochondrial ROS levels, compared with DMV rats. For mitochondrial membrane potential change, the red:green fluorescence intensity ratio was significantly decreased in DMV rats, compared with NMV rats, indicating cardiac mitochondrial membrane depolarization. All treatments attenuated mitochondrial depolarization, compared with DMV rats (Fig. 2B). For assessment of cardiac mitochondrial swelling, the absorbance was significantly decreased in the DMV rats, compared with NMV rats, indicating mitochondrial swelling (Fig. 2C). Moreover, PCA (both doses), insulin, and combined drug treatments significantly decreased mitochondrial swelling in diabetic rats, compared with DMV rats (Fig. 2C). The TEM images of cardiac mitochondria from each group are shown in Fig. 2D. Compared with the intact cardiac mitochondria of NMV rats, unfolded cristae were mostly found in DMV rats, indicating mitochondrial swelling. All treatments attenuated mitochondrial swelling, as indicated by decreased unfolded cristae in diabetic rats.

Effects of pharmacological interventions on BAX and BCL2 protein expression in the heart of diabetic rats

At week 12 after treatment, in the DMV rats, although BAX expression was not changed (Fig. 3A), BCL2 expression was significantly decreased compared with NMV rats (Fig. 3B). PCA (both doses), insulin, and combined drug treatments significantly increased BCL2 protein levels in diabetic rats, compared with DMV rats (Fig. 3B and C).

Discussion

This study demonstrated that STZ-induced type 1 diabetic rats were characterized by hyperglycemia, insulin deficiency, body weight loss, polyphagia, increased oxidative damage, depressed HRV, cardiac contractile dysfunction, cardiac mitochondrial dysfunction, and decreased cardiac anti-apoptotic BCL2 protein levels. The insulin and combined drug treatments increased the plasma insulin level, elevated body weight, and reduced food intake. In addition, all treatments in diabetic rats decreased the blood glucose level, reduced oxidative damage, improved HRV, attenuated cardiac dysfunction, prevented cardiac mitochondrial dysfunction, and increased BCL2 protein expression in diabetic rats. Interestingly, PCA at a dose of 100 mg/kg improved HRV and cardiac dysfunction similarly to insulin treatment in diabetic rats. Moreover, diabetic rats treated with combined drugs had echocardiography results restored to a normal status, whereas insulin alone could not achieve this. Insulin and combined drug treatments in diabetic rats also restored HRV.

A previous study demonstrated that PCA administration prevented the increase in plasma glucose and HbA1c levels and the decrease in plasma insulin levels in STZ-induced diabetic rats (Harini & Pugalendi 2010). PCA normalized the activities of gluconeogenic enzymes such as glucose 6-phosphatase and fructose 1,6-bisphosphatase, as well as that of the glycolytic enzyme glucokinase (Harini & Pugalendi 2010). In STZ-induced diabetic mice, dietary supplementation with PCA improved glycemic control and attenuated homeostatic disorders (Lin *et al.* 2009, 2011). Consistent with our findings, PCA treatment alone decreased hyperglycemia, whereas it could not

© 2014 Society for Endocrinology
Printed in Great Britain
Published by Bioscientifica Ltd.

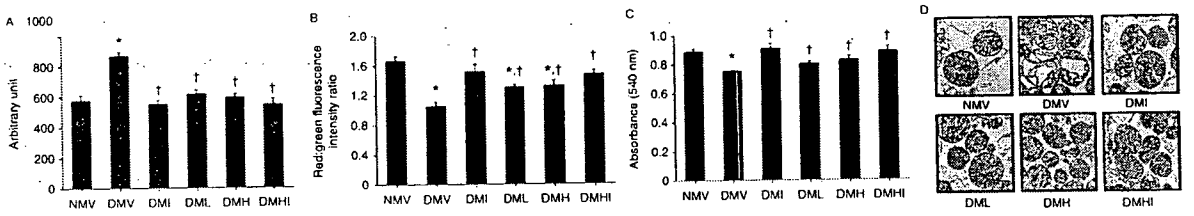


Figure 2
Effects of pharmacological interventions on cardiac mitochondrial function and morphology. (A) Cardiac mitochondrial ROS production was increased in DMV rats; all treatments reduced mitochondrial ROS production in diabetic rats. (B) Cardiac mitochondrial swelling was increased in DMV rats; all treatments prevented mitochondrial swelling in diabetic rats. (C) Cardiac mitochondrial membrane depolarization was increased in DMV rats; all treatments prevented mitochondrial membrane depolarization in diabetic rats. (D) Representative TEM images of mitochondrial morphology. Values are expressed as mean ± S.E.M. NMV, normal rats treated with vehicle; DMV, diabetic rats treated with vehicle; DMI, diabetic rats treated with insulin, 4 U/kg; DML, diabetic rats treated with PCA, 50 mg/kg; DMH, diabetic rats treated with PCA, 100 mg/kg; DMHI, DMH + insulin, 4 U/kg. $^{*}P<0.05$ vs NMV and $^{\dagger}P<0.05$ vs DMV.

increase insulin levels in STZ-induced diabetic rats. As PCA has been shown to exert an insulin-like activity by increasing glucose uptake via enhancing GLUT4 translocation and adiponectin secretion caused by the increased PPARγ activity in adipocytes (Scazzocchio *et al.* 2011), this could be the mechanism responsible for its glycemic effect observed in this study.

The increased ROS generation and impaired antioxidant defenses both contribute to oxidative stress in diabetes. Most of the ROS generated within cells are from mitochondria that were exposed to hyperglycemia (Brownlee 1995, Shen *et al.* 2006). The MDA is an index of oxidative damage. Results from previous studies indicated that plasma and tissue MDA levels are elevated in STZ-induced diabetic rats, and that PCA decreased plasma, renal, and cardiac MDA levels, as well as elevated antioxidant defense in STZ-induced diabetic mice (Lin *et al.* 2009, Naowaboot *et al.* 2009). Consistent with results from our study, diabetic rats treated with PCA had decreased oxidative damage in both plasma and cardiac tissues. PCA also attenuated cardiac mitochondrial ROS production in diabetic rats, especially PCA at a dose of 100 mg/kg, which exhibited a strong potency similar to that of the insulin treatment. Increased ROS has been proposed to amplify hyperglycemia-induced MAPK isoform activation and increase advanced glycation end product (AGE) formation (Brownlee 1995, Koya & King 1998), which could promote cell injury that contributes to the development of cardiac dysfunction in diabetes. HbA1c is one of the AGEs, a form of hemoglobin that is measured primarily to identify the average plasma glucose concentration over prolonged periods of time. Monitoring HbA1c in type 1 diabetic patients may improve the outcomes (Larsen *et al.* 1990). Results from a previous study indicated that PCA decreased plasma HbA1c levels and tissue AGEs in STZ-induced diabetic mice (Lin *et al.* 2011). Consistent with our findings, PCA decreased plasma HbA1c levels in STZ-induced diabetic rats.

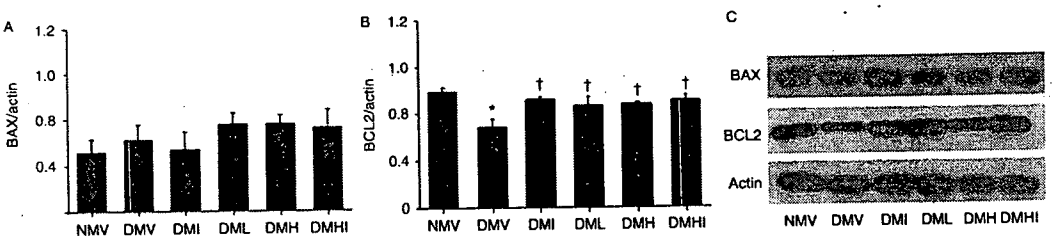


Figure 3
Effects of pharmacological interventions on cardiac BAX and BCL2 levels. (A) Cardiac BAX expression was not different among groups. (B) Cardiac BCL2 expression was decreased in DMV rats; all treatments increased cardiac BCL2 expression in diabetic rats. (C) Representative blot bands for BAX and BCL2 in each group. Values are expressed as mean ± S.E.M. NMV, normal rats treated with vehicle; DMV, diabetic rats treated with vehicle; DMI, diabetic rats treated with insulin, 4 U/kg; DML, diabetic rats treated with PCA, 50 mg/kg; DMH, diabetic rats treated with PCA, 100 mg/kg; DMHI, DMH + insulin, 4 U/kg. $^{*}P<0.05$ vs NMV and $^{\dagger}P<0.05$ vs DMV.

http://joe.endocrinology-journals.org
DOI: 10.1530/JOE-14-0273
© 2014 Society for Endocrinology
Printed in Great Britain
Published by Bioscientifica Ltd.

In human studies, progressive autonomic dysfunction and depressed HRV in diabetic patients indicated cardiac autonomic neuropathy (Malpas & Maling 1990, Kudat *et al.* 2006). The results from an animal study indicated that HRV was depressed in the STZ-induced diabetic rat (Fazan *et al.* 1997). As depressed HRV has been associated with increased oxidative damage, such as increased plasma MDA levels (Pavithran *et al.* 2008), the prevention of depressed HRV in diabetic rats by PCA could be due to its ability to decrease oxidative stress in this study.

Results from previous studies indicated that the cardiac function index including ejection fraction and stroke volume was depressed at 4 weeks following STZ-induced diabetes (Crespo *et al.* 2008, 2011). Consistent with our findings, echocardiography showed a reduction of %FS and %LVEF in diabetic rats in this study. Moreover, mitochondria are known to be the source of energy required for the heart to function properly. The effects of PCA in reducing oxidative stress as well as attenuating cardiac mitochondrial dysfunction could be responsible for improved cardiac function as observed in this study. Supporting this statement is the fact that beginning at 4 weeks for insulin or combined drug treatments and at 8 weeks for both doses of PCA treatment, improved cardiac function was observed in STZ-induced diabetic rats included in our study. It is important to note that despite the fact that PCA improved cardiac function, insulin could provide this improvement faster (by the fourth week of treatment) than PCA (by the eighth week).

Overproduction of ROS in diabetes can activate the mitochondrial pathway, resulting in loss of mitochondrial membrane integrity and release of cytochrome *c*, apoptotic protease-activating factor 1, and other pro-apoptotic factors in the cytoplasm. Maintenance of mitochondrial membrane potential depends on pro-apoptotic (Bax) and anti-apoptotic (Bcl2) members of Bcl2 family, causing or preventing cytochrome *c* release. PCA has been shown to prevent apoptosis by attenuating the change in the mitochondrial membrane permeability, decreasing oxidative damage, and increasing anti-apoptotic BCL2 expression in MPP^+-induced mitochondrial dysfunction and apoptotic cell death in PC12 cells (Guan *et al.* 2006). These findings were consistent with our study demonstrating that PCA improved cardiac mitochondrial function and increased cardiac BCL2 level in diabetic rats.

In summary, in the hearts of STZ-induced diabetic rats, cardiac autonomic imbalance and cardiac dysfunction were developed. PCA, insulin, and combined drug treatments attenuated these adverse effects by attenuating hyperglycemia, oxidative damage, cardiac autonomic imbalance, and cardiac mitochondrial dysfunction, and increasing anti-apoptotic protein. These findings indicated that PCA could exert beneficial effects on the heart in type 1 DM and may be used as a supplement to prevent cardiac complications in diabetic patients.

Declaration of interest

The authors declare that there is no conflict of interest that could be perceived as prejudicing the impartiality of the research reported.

Funding

This work was supported by the Faculty of Medicine Chiang Mai University Endowment Fund (N C), the Thailand Research Fund RTA5580006 (N C) and BRG 57 (S C C), TRG 57 (S K), Chiang Mai University Excellent Center Award (N C), and Udon Thani Rajabhat University Fund (Y S).

References

An D & Rodrigues B 2006 Role of changes in cardiac metabolism in development of diabetic cardiomyopathy. *American Journal of Physiology. Heart and Circulatory Physiology* **291** H1489–H1506. (doi:10.1152/ajpheart.00278.2006)

Apaijai N, Pintana H, Chattipakorn SC & Chattipakorn N 2012 Cardioprotective effects of metformin and vildagliptin in adult rats with insulin resistance induced by a high-fat diet. *Endocrinology* **153** 3878–3885. (doi:10.1210/en.2012-1262)

Apaijai N, Pintana H, Chattipakorn SC & Chattipakorn N 2013 Effects of vildagliptin versus sitagliptin, on cardiac function, heart rate variability and mitochondrial function in obese insulin-resistant rats. *British Journal of Pharmacology* **169** 1048–1057. (doi:10.1111/bph.12176)

Asbun J & Villarreal FJ 2006 The pathogenesis of myocardial fibrosis in the setting of diabetic cardiomyopathy. *Journal of the American College of Cardiology* **47** 693–700. (doi:10.1016/j.jacc.2005.09.050)

Boudina S & Abel ED 2007 Diabetic cardiomyopathy revisited. *Circulation* **115** 3213–3223. (doi:10.1161/CIRCULATIONAHA.106.679597)

Brownlee M 1995 Advanced protein glycosylation in diabetes and aging. *Annual Review of Medicine* **46** 223–234. (doi:10.1146/annurev.med.46.1.223)

Chinda K, Palee S, Surinkaew S, Phornphutkul M, Chattipakorn S & Chattipakorn N 2013 Cardioprotective effect of dipeptidyl peptidase-4 inhibitor during ischemia–reperfusion injury. *International Journal of Cardiology* **167** 451–457. (doi:10.1016/j.ijcard.2012.01.011)

Chou TH, Ding HY, Lin RJ, Liang JY & Liang CH 2010 Inhibition of melanogenesis and oxidation by protocatechuic acid from *Origanum vulgare* (oregano). *Journal of Natural Products* **73** 1767–1774. (doi:10.1021/np100281g)

Crespo MJ, Zalacain J, Dunbar DC, Cruz N & Arocho L 2008 Cardiac oxidative stress is elevated at the onset of dilated cardiomyopathy in streptozotocin-diabetic rats. *Journal of Cardiovascular Pharmacology and Therapeutics* **13** 64–71. (doi:10.1177/1074248407307854)

Crespo MJ, Marrero M, Cruz N, Quidgley J, Creagh O, Torres H & Rivera K 2011 Diabetes alters cardiovascular responses to anaesthetic induction agents in STZ-diabetic rats. *Diabetes & Vascular Disease Research* **8** 299–302. (doi:10.1177/1479164111421035)

Dyntar D, Sergeev P, Klisic J, Ambuhl P, Schaub MC & Donath MY 2006 High glucose alters cardiomyocyte contacts and inhibits myofibrillar formation. *Journal of Clinical Endocrinology and Metabolism* **91** 1961–1967. (doi:10.1210/jc.2005-1904)

© 2014 Society for Endocrinology
Printed in Great Britain
Published by Bioscientifica Ltd.

Fazan R Jr, Ballejo G, Salgado MC, Moraes MF & Salgado HC 1997 Heart rate variability and baroreceptor function in chronic diabetic rats. *Hypertension* **30** 632–635. (doi:10.1161/01.HYP.30.3.632)

Guan S, Jiang B, Bao YM & An LJ 2006 Protocatechuic acid suppresses MPP^+-induced mitochondrial dysfunction and apoptotic cell death in PC12 cells. *Food and Chemical Toxicology* **44** 1659–1666. (doi:10.1016/j.fct.2006.05.004)

Harini R & Pugalendi KV 2010 Antihyperglycemic effect of protocatechuic acid on streptozotocin-diabetic rats. *Journal of Basic and Clinical Physiology and Pharmacology* **21** 79–91. (doi:10.1515/JBCPP.2010.21.1.79)

Incharoen T, Thephinlap C, Srichairatanakool S, Chattipakorn S, Winichagoon P, Fucharoen S, Vadolas J & Chattipakorn N 2007 Heart rate variability in β-thalassemic mice. *International Journal of Cardiology* **121** 203–204. (doi:10.1016/j.ijcard.2006.08.076)

Jiang H, Fang J, Wu B, Yin G, Sun L, Qu J, Barger SW & Wu S 2011 Overexpression of serine racemase in retina and overproduction of D-serine in eyes of streptozotocin-induced diabetic retinopathy. *Journal of Neuroinflammation* **8** 119. (doi:10.1186/1742-2094-8-119)

Kay CD, Mazza GJ & Holub BJ 2005 Anthocyanins exist in the circulation primarily as metabolites in adult men. *Journal of Nutrition* **135** 2582–2588.

Koya D & King GL 1998 Protein kinase C activation and the development of diabetic complications. *Diabetes* **47** 859–866. (doi:10.2337/diabetes.47.6.859)

Krishna KM, Gopal GS, Chalam CR, Madan K, Kumar VK, Prakash GJ & Annapurna A 2005 The influence of sulindac on diabetic cardiomyopathy: a non-invasive evaluation by Doppler echocardiography in streptozotocin-induced diabetic rats. *Vascular Pharmacology* **43** 91–100. (doi:10.1016/j.vph.2005.02.012)

Kudat H, Akkaya V, Sozen AB, Salman S, Demirel S, Ozcan M, Atilgan D, Yilmaz MT & Guven O 2006 Heart rate variability in diabetes patients. *Journal of International Medical Research* **34** 291–296. (doi:10.1177/147323000603400308)

Kumar S & Sitasawad SL 2009 *N*-acetylcysteine prevents glucose/glucose oxidase-induced oxidative stress, mitochondrial damage and apoptosis in H9c2 cells. *Life Sciences* **84** 328–336. (doi:10.1016/j.lfs.2008.12.016)

Kumfu S, Chattipakorn S, Chinda K, Fucharoen S & Chattipakorn N 2012 T-type calcium channel blockade improves survival and cardiovascular function in thalassemic mice. *European Journal of Haematology* **88** 535–548. (doi:10.1111/j.1600-0609.2012.01779.x)

Larsen ML, Horder M & Mogensen EF 1990 Effect of long-term monitoring of glycosylated hemoglobin levels in insulin-dependent diabetes mellitus. *New England Journal of Medicine* **323** 1021–1025. (doi:10.1056/NEJM199010113231503)

Lekawanvijit S, Kompa AR, Zhang Y, Wang BH, Kelly DJ & Krum H 2012 Myocardial infarction impairs renal function, induces renal interstitial fibrosis, and increases renal KIM-1 expression: implications for cardiorenal syndrome. *American Journal of Physiology. Heart and Circulatory Physiology* **302** H1884–H1893. (doi:10.1152/ajpheart.00967.2011)

Lin HH, Chen JH, Huang CC & Wang CJ 2007 Apoptotic effect of 3,4-dihydroxybenzoic acid on human gastric carcinoma cells involving JNK/p38 MAPK signaling activation. *International Journal of Cancer* **120** 2306–2316. (doi:10.1002/ijc.22571)

Lin CY, Huang CS, Huang CY & Yin MC 2009 Anticoagulatory, antiinflammatory, and antioxidative effects of protocatechuic acid in diabetic mice. *Journal of Agricultural and Food Chemistry* **57** 6661–6667. (doi:10.1021/jf9015202)

Lin CY, Tsai SJ, Huang CS & Yin MC 2011 Antiglycative effects of protocatechuic acid in the kidneys of diabetic mice. *Journal of Agricultural and Food Chemistry* **59** 5117–5124. (doi:10.1021/jf200103f)

Liu CL, Wang JM, Chu CY, Cheng MT & Tseng TH 2002 *In vivo* protective effect of protocatechuic acid on tert-butyl hydroperoxide-induced rat hepatotoxicity. *Food and Chemical Toxicology* **40** 635–641. (doi:10.1016/S0278-6915(02)00002-9)

Malpas SC & Maling TJ 1990 Heart-rate variability and cardiac autonomic function in diabetes. *Diabetes* **39** 1177–1181. (doi:10.2337/diab.39.10.1177)

Masella R, Vari R, D'Archivio M, Di Benedetto R, Matarrese P, Malorni W, Scazzocchio B & Giovannini C 2004 Extra virgin olive oil biophenols inhibit cell-mediated oxidation of LDL by increasing the mRNA transcription of glutathione-related enzymes. *Journal of Nutrition* **134** 785–791.

Min SW, Ryu SN & Kim DH 2010 Anti-inflammatory effects of black rice, cyanidin-3-*O*-β-D-glycoside, and its metabolites, cyanidin and protocatechuic acid. *International Immunopharmacology* **10** 959–966. (doi:10.1016/j.intimp.2010.05.009)

Naowaboot J, Pannangpetch P, Kukongviriyapan V, Kukongviriyapan U, Nakmareong S & Itharat A 2009 Mulberry leaf extract restores arterial pressure in streptozotocin-induced chronic diabetic rats. *Nutrition Research* **29** 602–608. (doi:10.1016/j.nutres.2009.06.002)

Ohuchi H, Suzuki H, Yasuda K, Arakaki Y, Echigo S & Kamiya T 2000 Heart rate recovery after exercise and cardiac autonomic nervous activity in children. *Pediatric Research* **47** 329–335. (doi:10.1203/00006450-200003000-00008)

Palee S, Weerateerangkul P, Chinda K, Chattipakorn SC & Chattipakorn N 2013 Mechanisms responsible for beneficial and adverse effects of rosiglitazone in a rat model of acute cardiac ischaemia–reperfusion. *Experimental Physiology* **98** 1028–1037. (doi:10.1113/expphysiol.2012.070433)

Pavithran P, Nandeesha H, Sathiyapriya V, Bobby Z & Madanmohan T 2008 Short-term heart variability and oxidative stress in newly diagnosed essential hypertension. *Clinical and Experimental Hypertension* **30** 486–496. (doi:10.1080/10641960802251875)

Pratchayasakul W, Kerdphoo S, Petsophonsakul P, Pongchaidecha A, Chattipakorn N & Chattipakorn SC 2011 Effects of high-fat diet on insulin receptor function in rat hippocampus and the level of neuronal corticosterone. *Life Sciences* **88** 619–627. (doi:10.1016/j.lfs.2011.02.003)

Raher MJ, Thibault HB, Buys ES, Kuruppu D, Shimizu N, Brownell AL, Blake SL, Rieusset J, Kaneki M, Derumeaux G *et al.* 2008 A short duration of high-fat diet induces insulin resistance and predisposes to adverse left ventricular remodeling after pressure overload. *American Journal of Physiology. Heart and Circulatory Physiology* **295** H2495–H2502. (doi:10.1152/ajpheart.00139.2008)

Scazzocchio B, Vari R, Filesi C, D'Archivio M, Santangelo C, Giovannini C, Iacovelli A, Silecchia G, Li Volti G, Galvano F *et al.* 2011 Cyanidin-3-*O*-β-glucoside and protocatechuic acid exert insulin-like effects by upregulating PPARγ activity in human omental adipocytes. *Diabetes* **60** 2234–2244. (doi:10.2337/db10-1461)

Shen X, Zheng S, Metreveli NS & Epstein PN 2006 Protection of cardiac mitochondria by overexpression of MnSOD reduces diabetic cardiomyopathy. *Diabetes* **55** 798–805. (doi:10.2337/diabetes.55.03.06.db05-1039)

Shi GF, An LJ, Jiang B, Guan S & Bao YM 2006 Alpinia protocatechuic acid protects against oxidative damage *in vitro* and reduces oxidative stress *in vivo*. *Neuroscience Letters* **403** 206–210. (doi:10.1016/j.neulet.2006.02.057)

Sies H 1991 Oxidative stress: from basic research to clinical application. *American Journal of Medicine* **91** 31S–38S. (doi:10.1016/0002-9343(91)90281-2)

Sroka Z & Cisowski W 2003 Hydrogen peroxide scavenging, antioxidant and anti-radical activity of some phenolic acids. *Food and Chemical Toxicology* **41** 753–758. (doi:10.1016/S0278-6915(02)00329-0)

Surinkaew S, Kumphune S, Chattipakorn S & Chattipakorn N 2013 Inhibition of p38 MAPK during ischemia, but not reperfusion, effectively attenuates fatal arrhythmia in ischemia/reperfusion heart. *Journal of Cardiovascular Pharmacology* **61** 133–141. (doi:10.1097/FJC.0b013e318279b7b1)

Tarozzi A, Morroni F, Hrelia S, Angeloni C, Marchesi A, Cantelli-Forti G & Hrelia P 2007 Neuroprotective effects of anthocyanins and their *in vivo*

© 2014 Society for Endocrinology
Printed in Great Britain
Published by Bioscientifica Ltd.
Journal of Endocrinology

metabolites in SH-SY5Y cells. *Neuroscience Letters* **424** 36–40. (doi:10.1016/j.neulet.2007.07.017)

Thummasorn S, Kumfu S, Chattipakorn S & Chattipakorn N 2011 Granulocyte-colony stimulating factor attenuates mitochondrial dysfunction induced by oxidative stress in cardiac mitochondria. *Mitochondrion* **11** 457–466. (doi:10.1016/j.mito.2011.01.008)

Trost S & LeWinter M 2001 Diabetic cardiomyopathy. *Current Treatment Options in Cardiovascular Medicine* **3** 481–492. (doi:10.1007/s11936-001-0022-9)

Tseng TH, Kao TW, Chu CY, Chou FP, Lin WL & Wang CJ 2000 Induction of apoptosis by hibiscus protocatechuic acid in human leukemia cells via reduction of retinoblastoma (RB) phosphorylation and Bcl-2 expression. *Biochemical Pharmacology* **60** 307–315. (doi:10.1016/S0006-2952(00)00322-1)

Vari R, D'Archivio M, Filesi C, Carotenuto S, Scazzocchio B, Santangelo C, Giovannini C & Masella R 2011 Protocatechuic acid induces antioxidant/detoxifying enzyme expression through JNK-mediated Nrf2 activation in murine macrophages. *Journal of Nutritional Biochemistry* **22** 409–417. (doi:10.1016/j.jnutbio.2010.03.008)

Vitaglione P, Donnarumma G, Napolitano A, Galvano F, Gallo A, Scalfi L & Fogliano V 2007 Protocatechuic acid is the major human metabolite of cyanidin-glucosides. *Journal of Nutrition* **137** 2043–2048.

Wang D, Wei X, Yan X, Jin T & Ling W 2010 Protocatechuic acid, a metabolite of anthocyanins, inhibits monocyte adhesion and reduces atherosclerosis in apolipoprotein E-deficient mice. *Journal of Agricultural and Food Chemistry* **58** 12722–12728. (doi:10.1021/jf103427j)

Wang D, Zou T, Yang Y, Yan X & Ling W 2011 Cyanidin-3-O-β-glucoside with the aid of its metabolite protocatechuic acid, reduces monocyte infiltration in apolipoprotein E-deficient mice. *Biochemical Pharmacology* **82** 713–719. (doi:10.1016/j.bcp.2011.04.007)

Yan JJ, Jung JS, Hong YJ, Moon YS, Suh HW, Kim YH, Yun-Choi HS & Song DK 2004 Protective effect of protocatechuic acid isopropyl ester against murine models of sepsis: inhibition of TNF-α and nitric oxide production and augmentation of IL-10. *Biological & Pharmaceutical Bulletin* **27** 2024–2027. (doi:10.1248/bpb.27.2024)

Yin MC, Lin CC, Wu HC, Tsao SM & Hsu CK 2009 Apoptotic effects of protocatechuic acid in human breast, lung, liver, cervix, and prostate cancer cells: potential mechanisms of action. *Journal of Agricultural and Food Chemistry* **57** 6468–6473. (doi:10.1021/jf9004466)

Yip EC, Chan AS, Pang H, Tam YK & Wong YH 2006 Protocatechuic acid induces cell death in HepG2 hepatocellular carcinoma cells through a c-Jun N-terminal kinase-dependent mechanism. *Cell Biology and Toxicology* **22** 293–302. (doi:10.1007/s10565-006-0082-4)

Zhang X, Shi GF, Liu XZ, An LJ & Guan S 2011 Anti-ageing effects of protocatechuic acid from Alpinia on spleen and liver antioxidative system of senescent mice. *Cell Biochemistry and Function* **29** 342–347. (doi:10.1002/cbf.1757)

Zhao SM, Wang YL, Guo CY, Chen JL & Wu YQ 2014 Progressive decay of Ca^{2+} homeostasis in the development of diabetic cardiomyopathy. *Cardiovascular Diabetology* **13** 75. (doi:10.1186/1475-2840-13-75)

Received in final form 17 July 2014
Accepted 28 July 2014
Accepted Preprint published online 29 July 2014

Journal of Endocrinology

© 2014 Society for Endocrinology
Printed in Great Britain
Published by Bioscientifica Ltd.

เอกสารแนบหมายเลข 62

PLOS | ONE

Combined Vildagliptin and Metformin Exert Better Cardioprotection than Monotherapy against Ischemia-Reperfusion Injury in Obese-Insulin Resistant Rats

Nattayaporn Apaijai[1,2], Kroekkiat Chinda[1,2], Siripong Palee[1,5], Siriporn Chattipakorn[1,3], Nipon Chattipakorn[1,2,4]*

1 Cardiac Electrophysiology Research and Training Center, Faculty of Medicine, Chiang Mai University, Chiang Mai, Thailand, 2 Cardiac Electrophysiology Unit, Department of Physiology, Faculty of Medicine, Chiang Mai University, Chiang Mai, Thailand, 3 Department of Oral Biology and Diagnostic Sciences, Faculty of Dentistry, Chiang Mai University, Chiang Mai, Thailand, 4 Biomedical Engineering Center, Chiang Mai University, Chiang Mai, Thailand, 5 School of Medicine, Mae FahLuang University, Chiang Rai, Thailand

Abstract

Background: Obese-insulin resistance caused by long-term high-fat diet (HFD) consumption is associated with left ventricular (LV) dysfunction and increased risk of myocardial infarction. Metformin and vildagliptin have been shown to exert cardioprotective effects. However, the effect of these drugs on the hearts under obese-insulin resistance with ischemia-reperfusion (I/R) injury is unclear. We hypothesized that combined vildagliptin and metformin provide better protective effects against I/R injury than monotherapy in obese-insulin resistant rats.

Methodology: Male Wistar rats were fed either HFD or normal diet. Rats in each diet group were divided into 4 subgroups to receive vildagliptin, metformin, combined vildagliptin and metformin, or saline for 21 days. Ischemia due to left anterior descending artery ligation was allowed for 30-min, followed by 120-min reperfusion. Metabolic parameters, heart rate variability (HRV), LV function, infarct size, mitochondrial function, calcium transient, Bax and Bcl-2, and Connexin 43 (Cx43) were determined. Rats developed insulin resistance after 12 weeks of HFD consumption. Vildagliptin, metformin, and combined drugs improved metabolic parameters, HRV, and LV function. During I/R, all treatments improved LV function, reduced infarct size and Bax, increased Bcl-2, and improved mitochondrial function in HFD rats. However, only combined drugs delayed the time to the first VT/VF onset, reduced arrhythmia score and mortality rate, and increased p-Cx43 in HFD rats.

Conclusion: Although both vildagliptin and metformin improved insulin resistance and attenuate myocardial injury caused by I/R, combined drugs provided better outcomes than single therapy by reducing arrhythmia score and mortality rate.

Citation: Apaijai N, Chinda K, Palee S, Chattipakorn S, Chattipakorn N (2014) Combined Vildagliptin and Metformin Exert Better Cardioprotection than Monotherapy against Ischemia-Reperfusion Injury in Obese-Insulin Resistant Rats. PLoS ONE 9(7): e102374. doi:10.1371/journal.pone.0102374

Editor: Shang-Zhong Xu, University of Hull, United Kingdom

Received February 24, 2014; **Accepted** June 18, 2014; **Published** July 18, 2014

Copyright: © 2014 Apaijai et al. This is an open-access article distributed under the terms of the Creative Commons Attribution License, which permits unrestricted use, distribution, and reproduction in any medium, provided the original author and source are credited.

Funding: This work was supported by the Thailand Research Fund RTA5580006 (NC), BRG (SC), the Thailand Research Fund Royal Golden Jubilee Program (NC and NA), and the Chiang Mai University Excellent Center Award (NC). Vildagliptin was kindly provided by Novartis (Thailand). The funders had no role in study design, data collection and analysis, decision to publish, or preparation of the manuscript.

Competing Interests: This work was supported by the Thailand Research Fund RTA5580006 (NC), BRG (SC), the Thailand Research Fund Royal Golden Jubilee Program (NC and NA), and the Chiang Mai University Excellent Center Award (NC). Vildagliptin was kindly provided by Novartis (Thailand). These funders had no role in study design, data collection and analysis, decision to publish, or preparation of the manuscript. This support also does not alter the authors' adherence to PLOS ONE policies on sharing data and materials.

* Email: nchattip@gmail.com

Introduction

Long-term high-fat diet consumption is known to cause obesity, insulin resistance, and cardiac dysfunction [1], and have been shown to increase the risk of having ischemic heart disease [2]. While revascularization is the goal of myocardial ischemia treatment, reperfusion therapy is known to induce reperfusion injury and lead to greater myocardial damage. This adverse effect has been shown to be even more severe in obese insulin resistance, resulting in increased infarct size and increased myocardial susceptibility to ischemia-reperfusion (I/R) injury [3,4]. I/R injury has been shown to associate with fatal cardiac arrhythmias [5]. Cardiac mitochondrial damage has been implicated as one of the major factors responsible for myocardial cell death from I/R injury [6]. Several lines of evidence showed that increased intracellular and mitochondrial calcium accumulation can trigger cell apoptosis [6,7]. Previous studies also demonstrated that decreased Connexin 43 (Cx43), the principal gap junction protein, is found in acute myocardial infarction [8]. Many studies demonstrated that loss of Cx43expression in the heart could result in a markedly increase in incidence of arrhythmia [9,10].

Several anti-diabetic drugs including dipeptidyl peptidase 4 (DPP-4) inhibitors and metformin have been shown to exert cardioprotective effects in addition to their glycemic control [11,12]. A recent study reported the beneficial effects of combined DPP-4 inhibitor and metformin on metabolic parameters in type 2

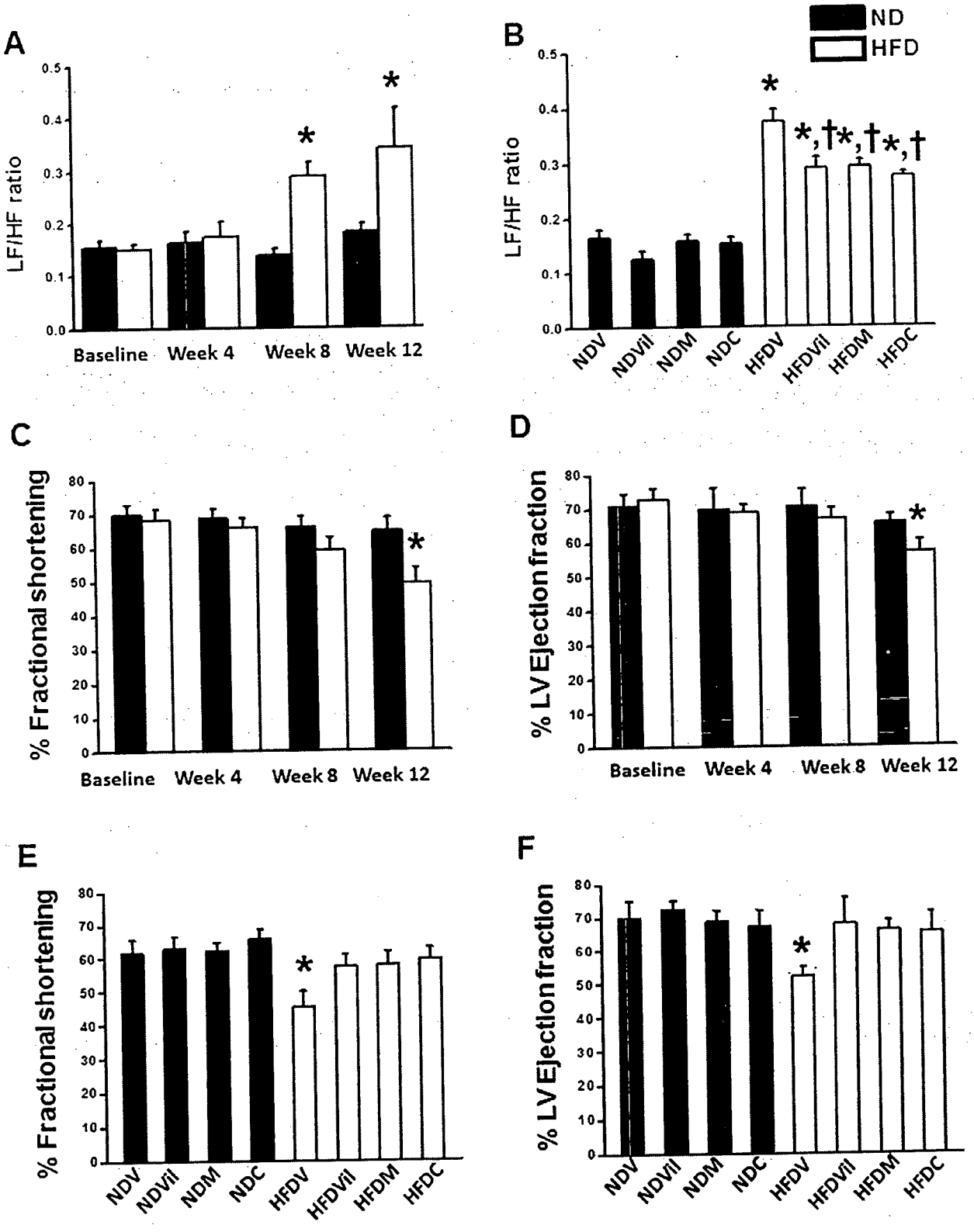


Figure 1. Effects of HFD consumption, vildagliptin, metformin, and combined drugs on HRV and echocardiographic parameters. (A) The LF/HF ratio was increased at week 8th and week 12thof HFD consumption.*$p<0.05$ vs. baseline, n = 11/group. (B) Vildagliptin, metformin, and combined drugs reduced the LF/HF ratio in HFD rats. *$p<0.05$ vs. NDV, $^{\dagger}p<0.05$ vs. HFDV, n = 11/group, (C) %FS was decreased after 12 weeks of HFD

consumption.*p<0.05 vs. ND, n = 11/group. (D) LVEF was decreased after 12 weeks of HFD consumption.*p<0.05 vs. ND, n = 11/group. (E) Vildagliptin, metformin, and combined drugs increased %FS in HFD rats. *p<0.05 vs. HFDV, n = 11/group. (F) Vildagliptin, metformin, and combined drugs increased LVEF in HFD rats. *p<0.05 vs. HFDV, n = 11/group.
doi:10.1371/journal.pone.0102374.g001

diabetic patients [13]. However, the role of these drugs including combined drugs therapy on cardiac function, heart rate variability (HRV), cardiac mitochondrial function, and intracellular calcium regulation during I/R in long-term HFD-induced obese insulin resistant rats have not been investigated.

We have previously reported the protective effects of vildagliptin and metformin on metabolic parameters and LV function in obese-insulin resistant rats [14]. In the present study, we determine the effects of a DPP-4 inhibitor vildagliptin, metformin, and combined drugs on the hearts of obese-insulin resistant rats underwent I/R injury. We hypothesized that vildagliptin and metformin provide cardioprotective effects against I/R injury in obese-insulin resistant rats, and we demonstrate that combined drugs exert better cardioprotection than either single drug regimen.

Materials and Methods

Animals and diet

All experiments in this study were approved by the Faculty of Medicine, Chiang Mai University Institutional Animal Care and Use Committee (Permit No. 29/2555), in compliance with NIH guidelines, and in accordance with the ARRIVE guidelines for reporting experiments involving animals [15]. Male Wistar rats weighing 180–200 g were obtained from the National Animal Center, Salaya Campus, Mahidol University, Bangkok, Thailand. Rats were allowed to acclimate for seven days and housed in 12/12 hour dark/light cycle with controlled temperature (25°C). They were divided into 2 groups to receive either normal diet (ND; a standard laboratory pelleted diet containing 19.8% energy from fat) or high-fat diet (HFD; a diet containing 59.3% energy from fat) [1,16]. Rats were fed with their diet for 15 weeks. At week 12, rats in each dietary group were divided into 4 subgroups to receive vildagliptin 3-mg/kg/day (Galvus, Novartis, Bangkok, Thailand) [14], metformin 30-mg/kg/day (Glucophage, Merkserono, Bangkok, Thailand) [14], combination of vildagliptin and metformin, or vehicle (0.9% normal saline solution in an equal volume) for another 21 days via gavage feeding. Body weight and food intake were recorded weekly, and blood samples were collected from the tail vein at baseline, 12th week, and at the end of treatment (15th week). HRV was determined at baseline, 4th week, 8thweek, 12thweek, and 15thweek (the end of pharmacological interventions).

Metabolic parameters

Plasma glucose, total cholesterol, and triglyceride levels were determined using a commercial colorimetric assay kit (Erba Diagnostics Mannheim GmbH, Mannheim, Germany) [16]. Plasma HDL level was determined using a commercial colorimetric assay kit (Biovision, California, USA) [1], and plasma LDL level was calculated using Friedewald equation [17]. Plasma insulin level was determined using a commercial sandwich ELISA kit (LINCO research, Missouri, USA) [1]. The Homeostasis Model Assesment (HOMA) index was used to assess insulin resistance. Increased HOMA index indicates a higher degree of insulin resistance [18].

Plasma and cardiac malondialdehyde (MDA) level

Plasma and cardiac MDA level was determined using high performance liquid chromatography (HPLC) based assay (Thermo scientific, Bangkok, Thailand) [1]. Plasma was mixed with H_3PO_4 and thiobarbituric acid (TBA) to produce thiobarbituric acid reactive substances (TBARS). Plasma TBARS was determined from a standard curve and reported as equivalent to the MDA concentration [1].

Heart rate variability (HRV)

Lead II electrocardiogram (ECG) was recorded for 20 minutes in conscious rats using PowerLab (AD instruments, Sydney, Australia) with Chart 5.0 program. Power spectra of R-R interval variability were obtained using Fast Fourier Transform (FFT) algorithm [1,19]. High-frequency band (HF; 0.6–3 Hz), Low-frequency band (LF; 0.2–0.6 Hz), and Very low-frequency band (VLF; below 0.2 Hz) were detected and calculated as integrals under the respective part of the power spectral density function. To minimize the effect of changes in total power on the LF and HF bands, LF and HF bands were expressed as normalized units by dividing them with the total power minus VLF [19]. LF/HF ratio was analyzed using analytical program [1]. The LF/HF ratio was considered a measure of cardiac sympathovagal balance. Increased LF/HF ratio indicated depressed HRV [19].

Echocardiography

At baseline, 4thweek, 8thweek, 12thweek, and 15th week (post-treatment), echocardiographic parameters were measured in each rat using a HP/Agilent Philips Sonos 4500 (Agilent technologies, Massachusetts, USA). An echocardiography probe was placed in gentle contact with the chest, and images were collected along the parasternal short axis of the heart [20]. M-mode echocardiography was performed at the level of the papillary muscles. %Fractional shortening (%FS) and left ventricular ejection fraction (LVEF) were determined.

Ischemia-reperfusion injury protocol

At the end of treatment, rats were subject to I/R injury protocol (Figure 1). Rats were anesthetized using Zoletil (50 mg/kg, Virbac Laboratories, Carros, France) and Xylazine (0.15 mg/kg, LaboratoriosCalier, Barcelona, Spain), intramuscularly. Zoletil is a combination of a dissociative anesthetic agent, tiletamine hypochloride, and a tranquilizer, zolazepam hydrochloride. The onset of action is 3–5 minutes by intramuscular route. We checked the depth of anesthesia by testing the absence of eyelid reflex and the tail pinch reflex. To maintain anesthesia, we used xylazine (0.15 mg/kg) which is an $\alpha 2$ adrenergic receptor agonist results in sedation, analgesia, and muscle relaxation and provides a sedative effect within 1–3 hours. Tracheostomy was performed and rats were ventilated with room air from a positive pressure rodent ventilator (CWE, Inc, Ardmore, Pennsylvania, USA). Lead II ECG was recorded throughout the experiment to determine the time to the 1st ventricular tachycardia/ventricular fibrillation (VT/VF) onset, VT/VF incidence, and arrhythmia scores. Arrhythmia score was characterized in accordance with the Lambeth conventions and using a score as described by Curtis and Walker [21]. A left-side thoracotomy was performed at the fourth intercostal space, and the pericardium was incised to expose the

Table 1. Effects of HFD consumption on metabolic parameters at baseline and 12-week after HFD consumption.

Metabolic parameters	Baseline		Week 12	
	ND	HFD	ND	HFD
Body weight (g)	191±2	190±9	480±10*	595±28*,†
Food intake (g/day)	26±1	29±1	29±2	26±2
Plasma insulin (ng/ml)	1.8±0.2	1.7±0.3	1.6±0.5	4.4±0.7*,†
Plasma glucose (mg/dl)	130±9	135±6	131±6	137±8
HOMA index	15±2	14±3	14±4	35±9*,†
Plasma total cholesterol (mg/dl)	41±5	42±4	41±2	53±3*,†
Plasma triglyceride (mg/dl)	70±6	72±8	80±8	87±5
Plasma HDL (mg/dl)	9.6±1	8.3±0.8	10.7±1	7.4±1.7*,†
Plasma LDL (mg/dl)	17.4±1	19.4±0.8	14.3±1.3	28.2±1.7*,†
Plasma MDA (μmol/ml)	2.9±0.2	3.1±0.1	3.3±0.2	6.4±0.1*,†

ND = normal diet, HFD = high-fat diet. *$P<0.05$ vs. Baseline, †$P<0.05$ vs. ND week 12.
doi:10.1371/journal.pone.0102374.t001

heart. Left anterior descending (LAD) coronary artery was identified and ligated at approximately 2 mm distal to its origin [5,22]. The end of a ligature was passed through a small vinyl tube, which is used to occlude the LAD by pulling the thread. ST elevation was used to confirm ischemia. The heart was subject to ischemia for 30 minutes, then the ligature was loosened for the ischemic myocardium to be reperfused for 120 minutes.

Left-ventricular (LV) function

The right carotid artery was identified and the pressure-volume (P-V) catheter (Scisense, Ontario, Canada) was inserted and advanced into the left ventricle to determine the cardiac function during I/R injury. Heart rate (HR), end-systolic pressure (ESP), end-diastolic pressure (EDP), maximum pressure (Pmax), minimum pressure (Pmin), dP/dtmax, dP/dtmin, stroke work (SW), and stroke volume/body weight (SV/BW) were determined prior to I/R injury protocol, at the end of occlusion, and at the end of reperfusion using analytical software program (Labscribe, Dover, New Hampshire, USA).

Infarct size determination

After 150 minutes of I/R period, the heart was excised and mount on the modified Langendorff apparatus via the aorta. Cold saline solution was used to flush out the blood, after which the LAD was re-occluded and 1-ml of 0.5% (w/v) Evans blue dye was injected to define the area at risk. Evans blue dye stained the perfused myocardium, whereas the LAD occlusion area did not stained with Evans blue dye, after which the heart was sliced into pieces with approximately 1-mm thickness for each slice and incubated with 1% buffered 2,3,5-triphenyltetrazolium chloride (TTC) (Sigma-Aldrich, St. Louis, Missouri, USA), followed by placing them in 10% formalin overnight [5,22]. The infarct and remote areas were determined using the image tool software version 3.0. The infarct size was calculated depending on the weight of each slice according to Reiss et al.'s formula [5,11,23].

Determination of cardiac mitochondrial function

For mitochondrial study, mitochondria were obtained from the ischemic myocardium and remote myocardium from fresh hearts. Ischemic area was obtained from left ventricular apex and remote area was obtained from right ventricle. The heart was minced and homogenized in the mitochondrial isolation buffer, pH 7.2, containing 300 mM sucrose, 0.2 mM EGTA, 5 mM TES. Homogenates was centrifuged at 800 g, 4°C for 5 min. The supernatant was collected and centrifuged at 8800 g, 4°C for 5 min. Then, the mitochondrial pellet was resuspended in the mitochondrial isolation buffer and centrifuged at 8800 g, 4°C for 5 min. The mitochondria were collected and the protein concentration was determined by the bicinchoninic acid method [22]. Cardiac mitochondrial function was assessed by determining cardiac mitochondrial reactive oxygen species (ROS) production, cardiac mitochondrial membrane potential change, and cardiac mitochondrial swelling [11,14,24].

Cardiac mitochondrial ROS production. Cardiac mitochondria were incubated with2 μM DCFH-DA dye at 25°C for 20 minutes. The dye was excited at λ_{ex} 485 nm and detected at λ_{em} 530 nm using fluorescent microplate reader (BioTek Instruments, Winooski, Vermont, USA). An increase in the fluorescent intensity indicated an increased mitochondrial ROS production [1,11,24].

Cardiac mitochondrial membrane potential changes. Cardiac mitochondrial membrane potential changes were determined using 5- μM JC-1 dye as described previously [1,24]. In brief, cardiac mitochondria were incubated with JC-1 at 37°C for 30 minutes. JC-1 monomer form (green fluorescent) was excited at λ_{ex} 485 nm and detected at λ_{em} 590 nm, and JC-1 aggregate form (red fluorescent) was excited at λ_{ex} 485 nm and detected at λ_{em} 530 nm using a fluorescent microplate reader. An increase in the red/green fluorescent intensity ratio indicates cardiac mitochondrial membrane depolarization [1,11,24].

Cardiac mitochondrial swelling. Cardiac mitochondria were incubated with 1.5-mM respiration buffer containing 100 mMKCl, 10 mM HEPES, 5 mM KH2PO4, and the absorbance was determined using a spectrophotometer as described previously [1,24]. Cardiac mitochondrial swelling is indicated by a decrease in the detected absorbance [1,11,24].

Cardiac mitochondria morphology. Cardiac mitochondria were fixed with 2.5% glutaraldehyde in a 0.1-M phosphate buffer overnight and post fixed in a 1% cacodylate-buffer osmium tetroxide for 2 hours, then dehydrated with graded series of ethanol [24]. Cardiac mitochondria were embedded in Epon-Araldite, cut with a diamond knife, and stained with uranyl acetate and lead acetate[24]. Cardiac mitochondria morphology were detected using a transmission electron microscope [24].

Table 2. Effects of vildagliptin, metformin, and combination of vildagliptin and metformin on metabolic parameters (n = 11/group).

Parameters	NDV	NDVil	NDM	NDC	HFDV	HFDVil	HFDM	HFDC
Body weight (g)	478±11	454±14	439±12	472±14	608±18*	567±28*	566±7*	586±36*
Visceral fat (g)	22±1	23±2	22±3	22±1	50±4*	42±4*	46±3*	56±5*
Food intake (g/day)	22±1	25±1	22±3	23±2	22±2	25±1	19±2	19±1
Plasma glucose (mg/dl)	135±12	143±12	130±14	139±13	138±9	132±5	134±16	135±11
Plasma insulin (ng/ml)	2.3±0.3	1.7±0.4	2.1±0.4	2.3±0.3	5.4±0.6*	3.1±0.5†	3.8±0.2†	3.3±0.2†
HOMA Index	19±3	18±5	16±4	20±3	32±5*	23±4†	26±2†	22±1†
Plasma total cholesterol (mg/dl)	49±6	44±4	49±2	54±3	63±4*	43±3†	51±2†	42±3†
Plasma triglyceride (mg/dl)	86±5	79±1	85±4	86±2	88±4	80±2	87±4	84±2
Plasma HDL (mg/dl)	12.1±1	10.9±2	11.8±2	10±1	7.6±1*	10.6±2†	10.9±1†	12±2†
Plasma LDL (mg/dl)	19.7±1	17.2±2	20.2±2	20±3	37±1*	20.4±2†	22.7±1†	23.2±1†
Plasma MDA (μmol/ml)	3.6±0.1	3.5±0.1	3.7±0.1	3.1±0.1	6.8±0.1*	6.1±0.2*†	6.3±0.2*†	6.3±0.1*†
Cardiac MDA (μmol/mgprotein)	23.5±3.4	12.8±3.9*	14.5±2.8*	11.8±2.9*	32.7±4.6*	12.8±1.6†	14.2±1.7†	12.5±2.7†

*$P<0.05$ vs. NDV, †$P<0.05$ vs. HFDV.

doi:10.1371/journal.pone.0102374.t002

Western blot analysis

The myocardial tissues for western blot study was obtained from the fresh heart at the end of the I/R protocol. The ischemic myocardium was obtained from the left ventricular apex and intact myocardium was obtained from the right ventricle. Myocardial protein extracts were prepared by a homogenization of nitrogen-frozen myocardial tissues (ischemia and remote area) in a 300- μl extraction buffer containing 20-mMTris-HCl (pH 6.8), 1-mM Sodium orthovanadate, 5-mMSodium fluoride, and protease inhibitor. Total protein concentration was determined using a Bio-Rad protein assay kit (Bio-Rad Laboratories, Hercules, California, USA). Fifty to 80 μg of total protein were mixed with loading buffer (5% betamercaptoethanol, 0.05% bromophenol blue, 75 mMTris-HCl (pH 6.8), 2% SDS and 10% glycerol), and loaded onto the 10% SDS-Acrylamide gels. Proteins were transferred to polyvinylidenedifluoride (PVDF) membrane in a glycine/methanol transferred buffer [5,22] in a Wet/Tank blotting system (Bio-Rad Laboratories, Hercules, California, USA). Membranes were blocked in 5% skim milk in Tris-Buffered Saline and Tween (TBST) buffer. Western blot analysis for Bax, Bcl-2, total Connexin-43, and Connexin43 phosphorylated at Ser368 was done in myocardial tissues. Membranes were exposed to mouse polyclonal anti-rat Bax and Bcl-2 (1:1000 dilution, Santa Cruz Biotechnology, Dallas, Texas, USA), Phospho-Cx43(Ser368), Cx43 (1:1000 dilution, Cell Signaling Technology, Danvers, Massachusetts, USA). Bound antibody was detected by horseradish peroxidase conjugated with anti-rabbit IgG (1:2000 dilution, Cell Signaling Technology, Danvers, Massachusetts, USA). The membranes were developed using the Amersham enhanced chemiluminescence Prime Western Blotting Detection Reagent (GE healthcare, Buckinghamshire, UK) and densitometric analysis was carried out [5].

Ventricular cardiomyocyte isolation

A separated group of thirty-two male Wistar rats was used in the intracellular calcium transient study. Rats were anesthetized by intraperitoneal injection of thiopental (1 ml/kg, Research institute of antibiotics and biotransformation, Prague, Czechoslovakia), and 0.2-ml heparin (LEO pharma, Ballerup, Denmark) was injected into the femoral vein. The heart was excised quickly with decent length of aorta and mounted on the cannula and tied with suture. The blood was washed out with solution 1 (Tyrode's solution and 750 μM $CaCl_2$) then switched to solution 2 (Tyrode's solution and 100 μM ethylene glycol tetraacetic acid (EGTA) for 4 minutes, and switched to solution 3 (Tyrode's solution, 100 μM $CaCl_2$, and 1 mg/ml collagenase (Worthington, Lakewood, New Jersey, USA)) for 10 minutes. The ventricles were cut and triturated in solution 3 at 37°C for 30 minutes, and were then filtered with a nylon mesh. The cells were left to settle down for 10 minutes and solution 3 was removed. Cells were resuspened in solution 4 (Tyrode's solution, 0.5 mM $CaCl_2$, and 1% BSA) for 10 minutes. Cells were resuspened in 10 ml of solution 5 (Tyrode's solution, 1 mM $CaCl_2$) and were ready for calcium transient study [22].

Intracellular calcium transient

The measurement of cardiomyocyte calcium transient was performed using a modified method from Wongchareon*et al.* [25] as described previously [22]. Isolated cardiomyocytes were incubated with 25- μM Fura-2/AM (Sigma Chemical, St. Louis, Massachusetts, USA) in 37°C, 5% CO_2, for 30 minutes. Fura-2 was excited at ultraviolet light wavelength of 340 nm and 387 nm by monochromator from xenon arc lamp controlled by a microfluorometry system (OSP 100-CA, Olympus, Tokyo, Japan). The excitation light was directed into an inverted microscope (IX-

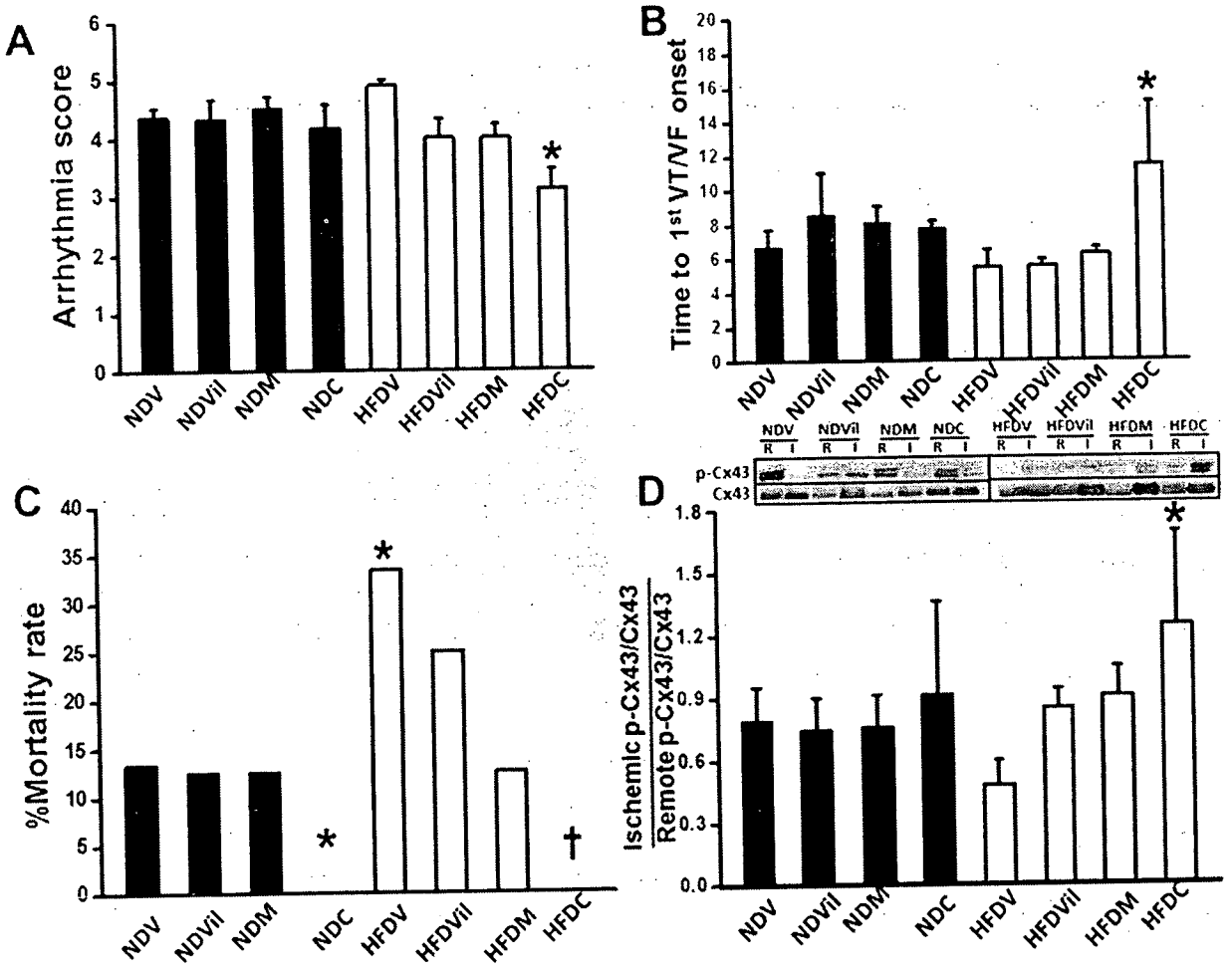


Figure 2. Effects of vildagliptin, metformin, combined drugs on arrhythmia, mortality rate, and phosphorylation of Cx43 level. (A) Combined drugs reduced arrhythmia score in HFD rats.*p<0.05 vs. HFDV, n = 11/group. (B) Combined drugs delayed time to the 1st VT/VF onset in HFD rats. *p<0.05 vs. HFDV, n = 11/group. (C) Mortality rate was higher in HFDV, and combined drugs reduced mortality rate in both ND and HFD rats. *p<0.05 vs. NDV, †p<0.05 vs. HFDV, n = 11/group. (D) Combined drugs increased p-Cx43 in HFD rats. *p<0.05 vs. HFDV, n = 5/group.
doi:10.1371/journal.pone.0102374.g002

70, Olympus, Tokyo, Japan). The emitted fluorescent intensity from Fura-2 was detected at wavelength 500 nm and digitized at 200 Hz. The ratio of fluorescent emission of two wavelengths was recorded as the index of intracellular calcium. The intracellular calcium transient peak amplitude and decay rate were measured during 1-Hz field-stimulation with a 10-ms twice-threshold strength square-pulse wave [22]. After baseline recording, 2-mM hydrogen peroxide (H_2O_2) was applied onto cardiomyocytes to induce oxidative stress (mimicking the ischemic process), after which the ratio of fluorescent emission of two wavelengths was recorded to determine the differences on intracellular calcium transient under oxidative stress condition among cardiomyocytes taken from the hearts of rats treated with vildagliptin, metformin, combined drugs, and vehicle.

Statistical Analysis

Data were expressed as mean ± SEM. One-way ANOVA followed by Fisher's least significant difference post hoc was used to test the different among the group. Mortality rate and VT/VF incidence were analyzed using Chi-square test. Mitochondrial function was analyzed using Kruskal-Wallis H followed by Mann-Whitney U test. $P<0.05$ was considered statistical significant.

Results

Effects of metformin and vildagliptin on metabolic parameters

At baseline, metabolic parameters were not different between ND and HFD group (Table 1). After 12 weeks of HFD consumption, the body weight, plasma insulin, plasma cholesterol, plasma MDA levels and HOMA index were increased in HFD rats, compared with ND rats (Table 1). Vildagliptin, metformin, and combined drugs reduced plasma insulin, plasma total cholesterol, plasma LDL, plasma and cardiac MDA levels and increased plasma HDL level in HFD rats, compared with HFD rats treated with vehicle (HFDV) (Table 2). No difference on these parameters was found between monotherapy and combined drugs.

Table 3. Effects of metformin, vildagliptin, and combination of vildagliptin and metformin on cardiac function before I/R injury (n = 11/group).

Cardiac function	NDV	NDVil	NDM	NDC	HFDV	HFDVil	HFDM	HFDC
Heart rate (bpm)	237±15	199±17	221±12	213±28	241±18	244±11	209±7	230±15
ESP (mmHg)	85±6	83±9	81±3	94±7	68±5*	93±10†	90±10†	91±9†
EDP (mmHg)	10±2	9±3	6±1	9±5	21±6*	8±2†	8±2†	10±1†
Pmax (mmHg)	108±7	87±9	82±11	101±5	93±8	117±15	94±11	114±14
Pmin (mmHg)	11±5	5±3	3±1	8±3	14±4	9±3	8±2	10±2
dP/dtmax (mmHg/s)	10090±1501	9487±442	10189±369	10561±781	8439±393	10081±1945	9077±737	11626±1974
dP/dtmin (mmHg/s)	−6378±1281	−4557±1162	−4119±891	−6205±454	−5388±428	−5226±800	−4714±632	−5761±1292
SW (mmHg/ml)	14653±784	12541±1440	14528±1106	14813±935	13698±1433	14929±1893	13495±1568	15446±1268
SV/BW (ul)	1.06±0.12	1.06±0.13	1.12±0.10	1.16±0.15	0.65±0.05*	1.08±0.14†	1.10±0.09†	1.04±0.2†

*P<0.05 vs. NDV, †P<0.05 vs. HFDV.

doi:10.1371/journal.pone.0102374.t003

Effects of metformin and vildagliptin on HRV

At baseline, the LF/HF ratio was not different between ND and HFD rats (Figure 1A). The LF/HF ratio was increased after 8 weeks of HFD consumption (Figure 1A). After treatment, the LF/HF ratio was not different in ND groups (Figure 1B). Treatments with vildagliptin, metformin, and combined drugs significantly reduced the LF/HF ratio in HFD rats (Figure 1B), indicating an improved cardiac sympathovagal balance in HFD rats.

Effects of metformin and vildagliptin on left ventricular function prior to I/R

At baseline, %FS and LVEF were not different between ND and HFD. We found that %FS and LVEF were decreased after 12 weeks of HFD consumption, compared with ND (Figure 1C–D). After treatment, vildagliptin, metformin, and combined drugs restored %FS and LVEF in HFD rats, compared with HFDV (Figure 1E–F).

Effects of metformin and vildagliptin on arrhythmia score during I/R

Arrhythmia score tended to be higher during I/R in HFDV than NDV rats, but the value did not reach statistical significance (Figure 2A). Only HFD rats treated with combined drugs had reduced arrhythmia score (Figure 2A). The time to 1st VT/VF onset was not different between NDV and HFDV. In ND rats, time to 1st VT/VF onset was not different among different treatment groups. In HFD rats, only combined drugs delayed time to the first VT/VF onset in HFD rats (Figure 2B). We also found that HFDV rats had a higher mortality rate, compared with the NDV group (Figure 2C). The mortality rate was reduced only in ND and HFD rats treated with combined drugs (Figure 2C). We determined the levels of Cx43 phosphorylation in heart tissues since it has been shown to closely associate with arrhythmia during I/R, and found that Cx43 phosphorylation was not different among the different treatments in ND groups (Figure 2D). However, in HFD rats, the phosphorylation of Cx43 was increased only in HFD rats treated with combined drugs (Figure 2D).

Effects of metformin and vildagliptin on left ventricular function during I/R

Baseline LV function data by P-V loop assessment prior to I/R are shown in Table 3. LV function was not different among ND groups prior to I/R injury. ESP, SV/BW were decreased and EDP was increased in HFDV rats, compared with NDV group ($p<0.05$ vs. NDV, Table 3). All treatments increased ESP and SV/BW and reduced EDP in HFD rats ($p<0.05$ vs. HFDV, Table 3).

LV function data at the end of LAD occlusion are shown in Table 4. At the end of LAD occlusion, all treatments increased the dP/dt_{max}, and combined drugs also increased the ESP in ND rats, compared with the NDV group ($p<0.05$ vs. NDV). In HFDV rats, the HR and EDP were increased and the ESP and SV/BW was decreased ($p<0.05$ vs. NDV). All treatments reduced the EDP, and increased the ESP, dP/dt_{max}, and SV/BW in HFD rats ($p<0.05$ vs. HFDV, Table 4).

LV function data at the end of reperfusion are shown in Table 5. At the end of reperfusion, LV function was not different among ND groups. In HFD groups, the ESP and SV/BW was decreased and the EDP was increased in the HFDV group ($p<0.05$ vs. NDV). All treatments reduced the EDP and increased the ESP and SV/BW in HFD rats ($p<0.05$ vs. HFDV, Table 5).

Table 4. Effects of vildagliptin, metformin, and combination of vildagliptin and metformin on cardiac function at the end of Occlusion (n = 11/group).

Cardiac function	NDV	NDVil	NDM	NDC	HFDV	HFDVil	HFDM	HFDC
Heart rate (bpm)	214±11	200±12	227±17	213±12	266±23*	249±14	243±23	242±26
ESP (mmHg)	74±4	82±7	83±20	103±3*	66±7*	90±8†	93±6†	90±7†
EDP (mmHg)	15±4	10±1	11±2	9±2	26±4*	13±2†	12±1†	14±2†
Pmax (mmHg)	95±5	96±9	99±20	105±3	106±11	94±8	102±6	109±10
Pmin (mmHg)	10±4	5±1	6±1	12±2	11±3	9±3	13±2	14±2
dP/dtmax (mmHg/s)	7709±1049	12088±2244*	12245±1716*	13906±2385*	4849±394	11060±2295†	12040±2132†	12565±1091†
dP/dtmin (mmHg/s)	−4002±475	−4077±572	−5724±912	−5252±395	−4411±561	−3982±813	−4005±460	−4038±844
SW (mmHg/ml)	10941±1492	12886±1162	12004±2505	13998±637	10020±1456	10620±1937	9776±1553	10237±2322
SV/BW (μl)	1.28±0.38	1.58±0.19	1.13±0.27	0.89±0.20	0.60±0.04*	0.89±0.16†	0.98±0.10†	0.93±0.08†

*$P<0.05$ vs. NDV, †$P<0.05$ vs. HFDV.

doi:10.1371/journal.pone.0102374.t004

Effects of metformin and vildagliptin on the infarct size

In this study, the area at risk (AAR) was not different among all groups. We found that the infarct size/AAR was increased in the HFDV group, compared with the NDV group (Figure 3A–B). All treatments reduced the infarct size in both ND and HFD rats (Figure 3A–B). The western blot analysis revealed that the Bax expression was not different among groups of ND rats (Figure 3C). However, the Bax expression was increased in the HFDV rats, compared with the NDV group. In HFD rats, vildagliptin and metformin reduced the Bax expression, compared with the HFDV group. Moreover, Bax expression was markedly decreased in HFD rats treated with combined drugs, compared with the HFDV group (Figure 3C). The Bcl-2 expression was not different among ND groups (Figure 3D). The Bcl-2 expression was decreased in the HFDV rats, compared with the NDV group, and all treatments increased Bcl-2 expression in HFD rats (Figure 3D).

Effects of metformin and vildagliptin on cardiac mitochondrial function and morphology

Our data demonstrated that mitochondrial ROS production was increased in the ischemic area of both NDV and HFDV groups, compared to the remote (non-ischemic) area (Figure 4A). Moreover, the ROS level in the ischemic area was also significantly higher in the HFDV rats, compared to the NDV rats. All treatments reduced mitochondrial ROS production in the ischemic area of HFD rats (Figure 4A).For mitochondrial membrane potential change, the red/green fluorescent intensity ratio was decreased in the ischemic area of both NDV and HFDV groups, compared with their remote areas, indicating mitochondrial membrane depolarization (Figure 4B). All treatments could attenuate mitochondrial depolarization (Figure 4B). For mitochondrial swelling assessment, we found that the absorbance was decreased in the ischemic area of both NDV and HFDV groups, compared with their remote areas, indicating mitochondrial swelling (Figure 4C). Moreover, mitochondrial swelling was significantly greater in the HFDV rats, compared to the NDV rats. All treatments increased the absorbance in both ND and HFD rats (Figure 4C).

Representative images of cardiac mitochondria from the transmission electron microscopy showed the unfolded cristae which is an indicator of mitochondrial swelling. Compared to the intact cardiac mitochondria in the remote area of the NDV rat (Figure 4D), we found that unfolded cristae were mostly found in the ischemic area of the NDV (Figure 4E) and HFDV rats (Figure 4J). Moreover, cardiac mitochondria in the remote area of the HFDV rat (Figure 4I) also had unfolded cristae compared to that in the NDV group, indicating mitochondrial swelling. The marked unfolded cristae were found in the ischemic area of

Table 5. Effects of vildagliptin, metformin, and combination of vildagliptin and metformin on cardiac function at the end of Reperfusion (n = 11/group).

Cardiac function	NDV	NDVil	NDM	NDC	HFDV	HFDVil	HFDM	HFDC
Heart rate (bpm)	281±23	248±18	286±63	237±25	343±48	252±30	281±31	264±25
ESP (mmHg)	82±3	82±14	86±30	96±8	65±4*	91±18†	94±6†	97±8†
EDP (mmHg)	9±3	8±2	11±3	9±3	23±1*	9±3†	9±2†	11±1†
Pmax (mmHg)	117±8	126±10	109±19	97±9	102±10	116±17	110±5	123±9
Pmin (mmHg)	7±2	8±2	8±3	9±4	10±2	6±2	10±2	9±2
dP/dtmax (mmHg/s)	9216±553	12625±2759	10536±1899	10593±2807	8285±1089	9732±1806	10855±816	10776±1761
dP/dtmin (mmHg/s)	−6621±657	−6715±1673	−6431±651	−6551±1434	−7858±1440	−8777±850	−7945±1243	−7550±684
SW (mmHg/ml)	11823±2519	13943±846	10847±743	11095±1073	12374±1219	11775±1270	11434±313	10228±414
SV/BW (μl)	1.02±0.28	1.74±0.26	0.92±0.12	1.00±0.13	0.67±0.02*	1.04±0.18†	0.97±0.07†	0.94±0.18†

*$P<0.05$ vs. NDV, †$P<0.05$ vs. HFDV.

doi:10.1371/journal.pone.0102374.t005

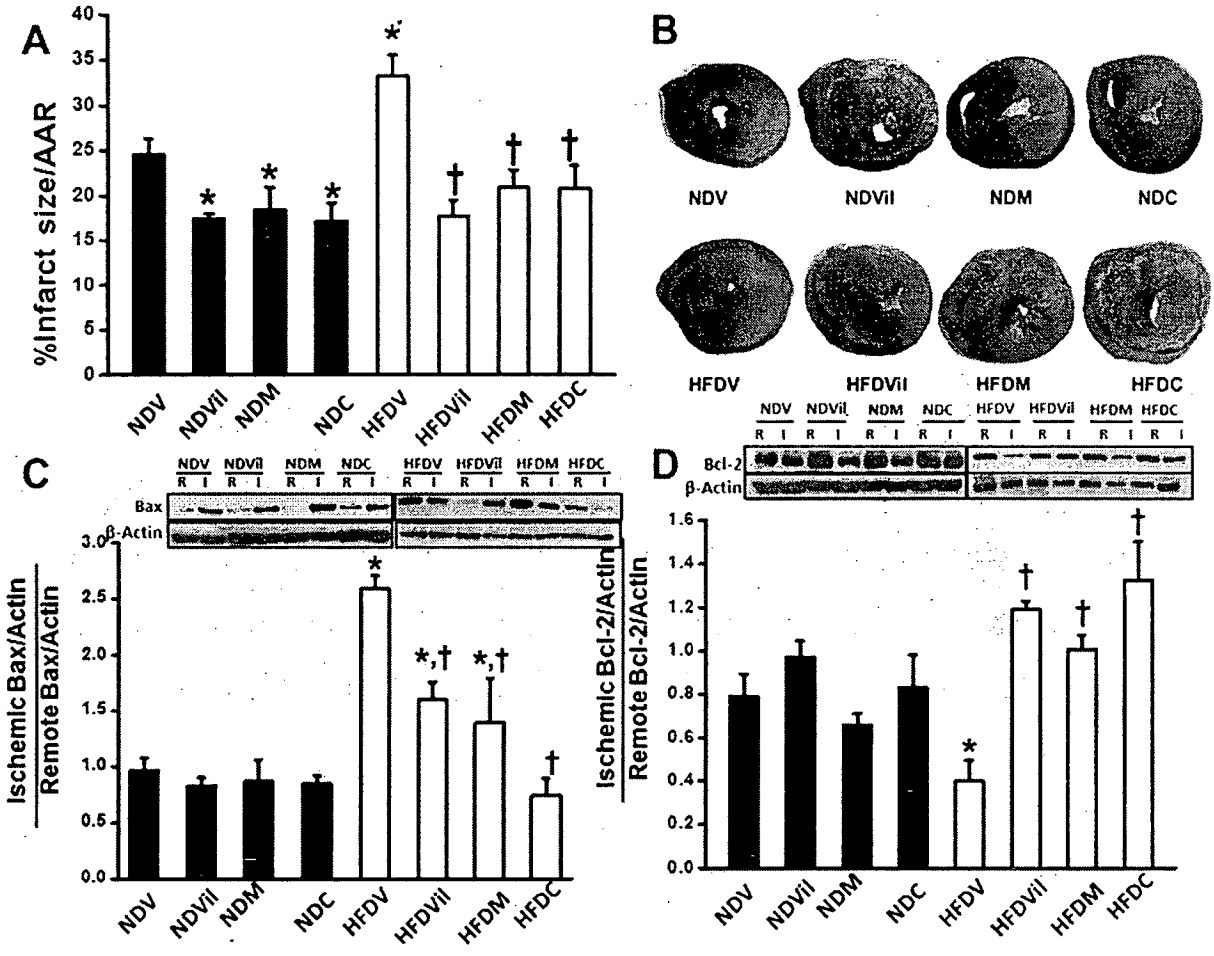


Figure 3. Effects of vildagliptin, metformin, and combined drugs on infarct size, Bax, and Bcl-2 expression. (A) Infarct size was increased in HFDV, and all treatments reduced infarct size in both ND and HFD rats. *p<0.05 vs. NDV, †p<0.01 vs. HFDV, n = 6/group. (B) Representative images showing TTC staining for infarct size determination. (C) Bax expression was increased in HFDV, and all treatments reduced Bax expression in HFD rats. *p<0.05 vs. NDV, †p<0.05 vs. HFDV, n = 5/group. (D) Bcl-2 expression was decreased in HFDV, and all treatments increased Bcl-2 expression in HFD rats. *p<0.05 vs. NDV, †p<0.05 vs. HFDV, n = 5/group.
doi:10.1371/journal.pone.0102374.g003

HFDV. All treatments prevented unfolded cristae in both ND (Figure 4F–H) and HFD rats (Figure 4K–M).

Effects of metformin and vildagliptin on intracellular calcium transient

Our results demonstrated that the intracellular diastolic calcium level was increased in HFDV hearts, compared with the NDV group (Figure 5A). After treated with H_2O_2, intracellular diastolic calcium level was increased in both NDV and HFDV groups, compared with their control. We found that all treatments prevented a change in the intracellular diastolic calcium under oxidative stress condition (Figure 5A).

Calcium transient amplitude was significantly decreased in the HFDV group, compared with the NDV group (Figure 5B). After treated with H_2O_2, calcium transient amplitude was not different from baseline of its own group for both NDV and HFDV rats. However, cardiomyocytes from HFD rats treated with vildagliptin, metformin, and combined drugs had a significant increase in calcium transient amplitude both at baseline and with the presence of H_2O_2 (Figure 5B).

Calcium transient decay rate was significantly decreased in the HFDV cardiomyocytes, compared with the NDV group (Figure 5C). Calcium transient decay rate in the HFDV group was not different from baseline after treated with H_2O_2. All treatments significantly increased calcium decay rate in HFD cardiomyocytes both at baseline and with the presence of H_2O_2 (Figure 5C). Representatives of signals of intracellular calcium transients from cardiomyocytes from each group are shown in Figure 5D.

Discussion

Findings from the present study demonstrated that HFD caused obese-insulin resistance, increased oxidative stress level, depressed HRV, and LV dysfunction. Treatment with vildagliptin, metformin, and combined drugs improved insulin resistance, reduced oxidative stress level, improved HRV, and attenuated LV dysfunction in obese-insulin resistant rats prior to I/R. Under I/R condition, all treatments improved LV dysfunction, reduced the infarct size, prevented cardiac mitochondrial dysfunction, decreased Bax and increased Bcl-2 expression, and reduced cardiac

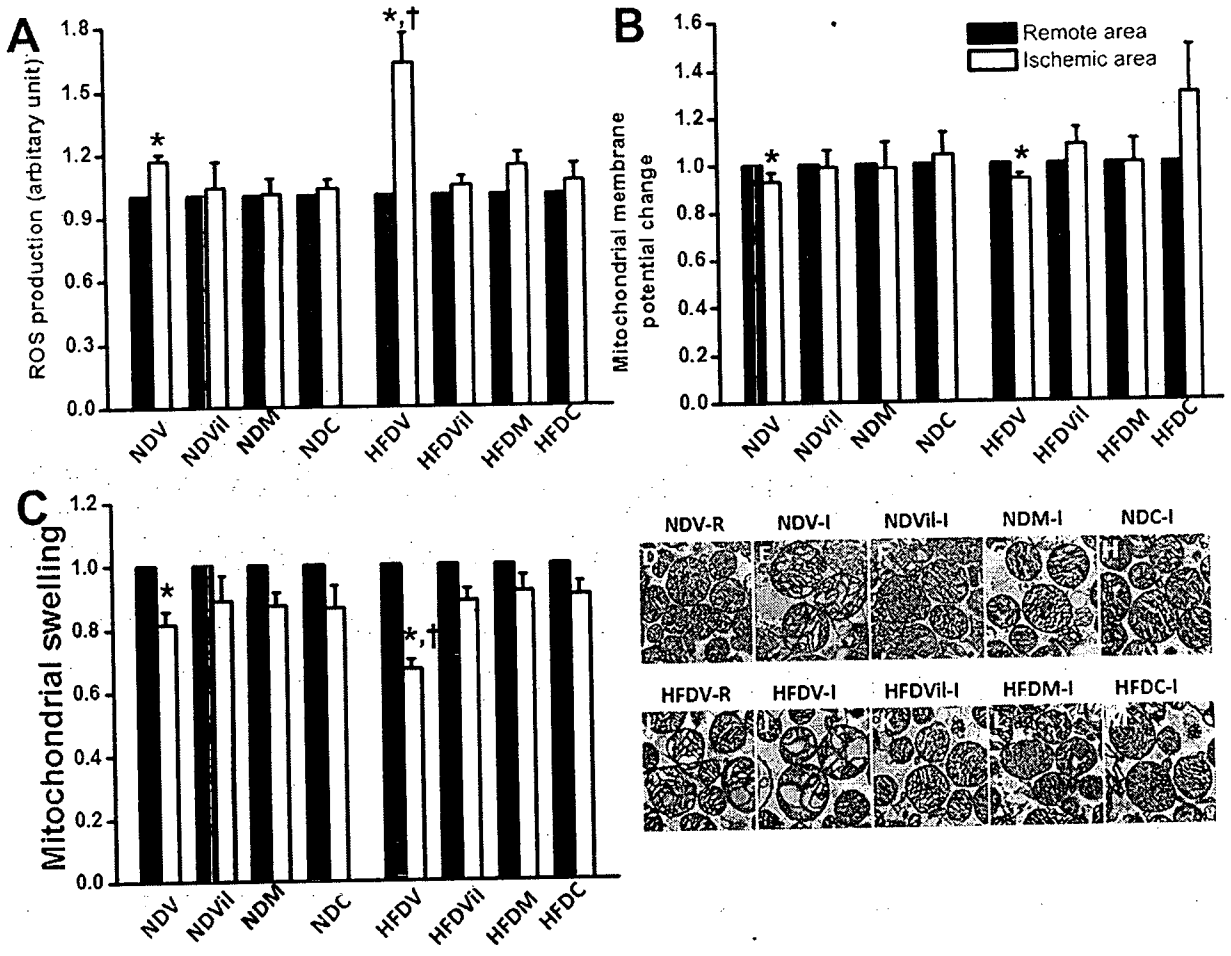


Figure 4. Effects of vildagliptin, metformin, and combined drugs on cardiac mitochondrial function and morphology. (A) Mitochondrial ROS production was increased in ischemic area of NDV and HFDV, Mitochondrial ROS production was higher in HFDV than NDV, and all treatments reduced mitochondrial ROS production. *$p<0.05$ vs. remote area, †$p<0.05$ vs. ischemic area of NDV, n = 5/group. (B) Mitochondrial membrane depolarization was found in ischemia area of NDV and HFDV, all treatment prevented mitochondrial membrane depolarization. *$p<0.05$ vs. remote area of NDV, n = 5/group. (C) An absorbance was decreased in ischemic area of NDV and HFDV. The reduction of absorbance was greater in HFDV than NDV, and all treatments prevented mitochondrial swelling, *$p<0.05$ vs. remote area of NDV, n = 5/group. (D–M) Cardiac mitochondrial morphology

doi:10.1371/journal.pone.0102374.g004

oxidative stress level. Furthermore, all treatments improved intracellular calcium transient regulation in the absence and presence of H_2O_2 in the obese-insulin resistant rats. However, only combined drugs could reduce the arrhythmia score, mortality rate, delayed the time to the 1st VT/VF onset, and increased Cx-43 phosphorylation.

In this study, rats developed insulin resistance after 12 weeks of HFD consumption. This finding is consistent with previous studies in which long-term HFD consumption could induce hyperinsulinemia and increased HOMA index, indicating insulin resistance, as well as oxidative stress after 12 weeks of HFD consumption [1,14,16,26]. Previous studies have shown the beneficial effects of vildagliptin and metformin on metabolic parameters [14,27,28]. Our data showed that vildagliptin and metformin improved insulin resistance and metabolic parameters as well as oxidative stress in obese-insulin resistant rats. Clinical study reported that vildagliptin in addition to metformin reduced fasting plasma insulin level and HOMA-IR in type 2 diabetic patients [13]. Our study showed that all treatment reduced plasma cholesterol levels. However, the levels of cholesterol in this study were lower than that reported in our previous study [14]. Although these differences could be due to different kits and methods used, all drugs could still decrease the cholesterol levels, compared to the control. Moreover, clinical studies as well as studies in diabetic and insulin resistant animal models reported that vildagliptin and metformin could ameliorate oxidative stress levels [14,29,30]. In the present study, rats in all treatment groups had reduced plasma MDA level (prior to I/R) and reduced cardiac MDA level (after I/R), suggesting that vildagliptin and metformin improved insulin resistance and exerted an anti-oxidative stress benefit in obese-insulin resistant rats.

HRV is an indicator of cardiac sympathovagal balance [19]. Previous studies demonstrated that cardiac sympathovagal imbalance was observed in long-term HFD fed rats [14,31]. Consistent with previous studies, we found that the LF/HF ratio was increased after 8 weeks of HFD consumption, indicating cardiac

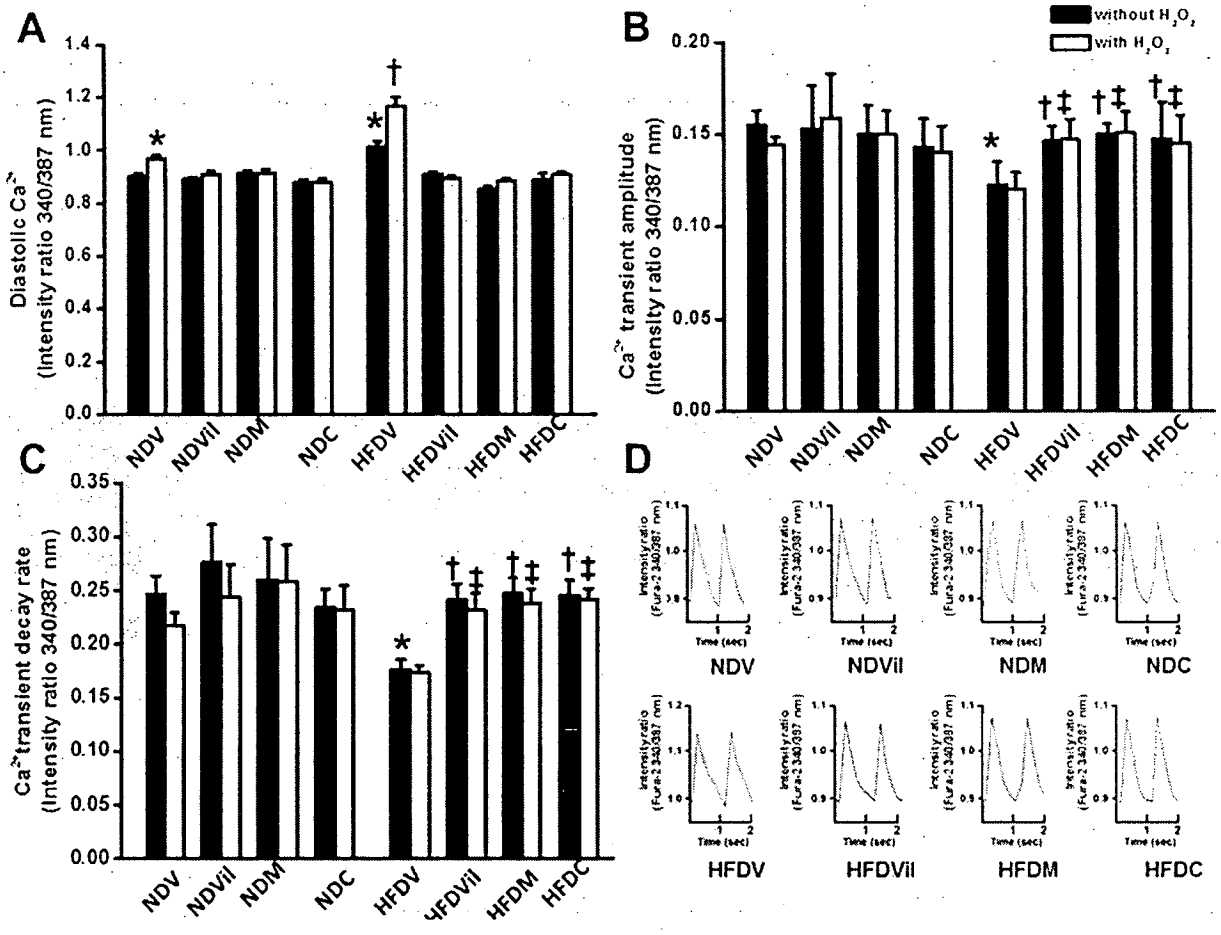


Figure 5. Effects of vildagliptin, metformin, and combined drugs on intracellular calcium regulation. (A) Intracellular diastolic calcium was increased in HFDV. All treatments reduced intracellular diastolic calcium in HFD rats. (B) Calcium transient amplitude was decreased in HFDV. All treatments improved calcium transient amplitude in HFD rats. (C) Calcium transient decay rate was reduced in HFDV. All treatments increased the calcium transient decay rate in HFD rats. (D) Representative calcium transient tracing for calcium transient parameters determination. *$p<0.05$ vs. baseline NDV, †$p<0.01$ vs. baseline HFDV, ‡$p<0.05$ vs. HFDV with H_2O_2 n = 8 cells/group
doi:10.1371/journal.pone.0102374.g005

sympathovagal imbalance. Vildagliptin, metformin, and combined drugs improved the HRV by decreasing LF/HF ratio in obese-insulin resistant rats. Since depressed HRV has been reported to be associated with increased oxidative stress such as an increased MDA level [32], the improved HRV in obese-insulin resistant rats by the drugs found in our study could be due to the reduced oxidative stress caused by these drugs.

Previous studies have shown that long-term HFD consumption caused LV dysfunction [14,31], and that vildagliptin and metformin could improve LV function in obese-insulin resistant rats [14]. Consistent with previous studies, we found that LV ejection fraction and fractional shortening were reduced after 12 weeks of HFD consumption. Vildagliptin and metformin improved the LV ejection fraction and fractional shortening in the present study. Moreover, we also found that these drugs reduced intracellular diastolic calcium, improved intracellular calcium transient amplitude and decay rate in obese-insulin resistant rats. These findings suggested that one of the mechanisms responsible for improved LV function by vildagliptin and metformin could be attributed to their role in the improved intracellular calcium regulation.

In the present study, vildagliptin and metformin reduced the infarct size caused by I/R injury in obese-insulin resistant rats. Chinda and colleagues reported previously that vildagliptin reduced the infarct size in swine hearts with I/R injury [11], and several studies have demonstrated that metformin also reduced the infarct size in both non-diabetic and diabetic animals [33,34,35]. Our results further demonstrated that both vildagliptin and metformin also exerted infarct size reduction benefit in the obese-insulin resistant rat model. The mechanism responsible for this benefit of both drugs could partly due to their anti-apoptotic effects as indicated by reduced Bax and increased Bcl-2 expression. Bax is a pro-apoptotic protein, whereas Bcl-2 is an anti-apoptotic protein, both of which are known to regulate apoptosis during I/R. Furthermore, we demonstrated in the present study that both metformin and vildagliptin could attenuate cardiac mitochondrial dysfunction caused by I/R injury. It has been shown previously that both Bax and Bcl-2 are associated with mitochondrial ROS level [36]. Several studies have shown that metformin improved cardiac mitochondrial function and ultrastructure in insulin resistant rats, diabetic rats, and normal rats with I/R injury [14,37,38]. In the present study, we demonstrated that vildagliptin

and metformin improved cardiac mitochondrial function and ultrastructure in obese-insulin resistant rats. All of these findings suggested that vildagliptin and metformin reduced the infarct sized by attenuating myocardial apoptosis and cardiac mitochondrial dysfunction. The improved cardiac mitochondrial function as well as infarct size reduction could also be responsible for improved LV function during I/R.

Despite the beneficial effects of metformin and vildagliptin as a single therapy in the present study, we found that only vildagliptin and metformin giving as combined therapy reduced fatal arrhythmias as well as delayed time to the first VT/VF onset during I/R in this obses-insulin resistant rats. This antiarrhythmic effect could be due to the fact that only rats treated with combined metformin and vildagliptin had increased Cx43 phosphorylation. Cx 43 is a cardiac gap junction protein, and it has been shown previously that the engraftment of Cx43 expressing cells could protect the heart against the induction of ventricular tachycardia in mice with myocardial infarction model [39]. Cx 43 phosphorylation at serine 368 has been shown to protect against cardiac arrhythmias during I/R [5,40]. Our data suggested that the increased Cx43 phosphorylation by combined metformin and vildagliptin could be a mechanism responsible for arrhythmia reduction and leading to decrease arrhythmic death from I/R in obese-insulin resistant rats.

Conclusions

In conclusion, long-term HFD consumption induced obese-insulin resistance, oxidative stress, cardiac autonomic imbalance, and LV dysfunction. Vildagliptin, metformin, and combined drugs attenuated these adverse effects. Under I/R, these drugs prevented LV dysfunction and reduced infarct size, that was associated with decreased mitochondrial function, improved intracellular calcium regulation, increased anti-apoptotic protein, and reduced pro-apoptotic protein. Only combined metformin and vildagliptin exert better benefits by reduced cardiac arrhythmia score and arrhythmic death during I/R injury in obese-insulin resistant rats by increasing Cx-43 phosphorylation.

Acknowledgments

The authors would like to thank Dr. Wanpitak Pongkan, Ms. Sivaporn Sivasinprasasn and Ms. Piangkwan Sa-nguanmoo for their technical assistance on ventricular cardiomyocyte isolation.

Author Contributions

Conceived and designed the experiments: SC NC. Performed the experiments: NA KC SP. Analyzed the data: NA KC SP SC NC. Contributed reagents/materials/analysis tools: SC NC. Wrote the paper: NA SC NC.

References

1. Apaijai N, Pintana H, Chattipakorn SC, Chattipakorn N (2013) Effects of vildagliptin versus sitagliptin, on cardiac function, heart rate variability and mitochondrial function in obese insulin-resistant rats. Br J Pharmacol 169: 1048–1057.
2. Shibata R, Sato K, Pimentel DR, Takemura Y, Kihara S, et al. (2005) Adiponectin protects against myocardial ischemia-reperfusion injury through AMPK- and COX-2-dependent mechanisms. Nat Med 11: 1096–1103.
3. du Toit EF, Smith W, Muller C, Strijdom H, Stouthammer B, et al. (2008) Myocardial susceptibility to ischemic-reperfusion injury in a prediabetic model of dietary-induced obesity. Am J Physiol Heart Circ Physiol 294: H2336–2343.
4. Wensley I, Salaveria K, Bulmer AC, Donner DG, Du Toit EF (2013) Myocardial Structure, Function, and Ischaemic Tolerance in a Rodent Model of Obesity with Insulin Resistance. Exp Physiol. (in press)
5. Surinkaew S, Kumphune S, Chattipakorn S, Chattipakorn N (2013) Inhibition of p38 MAPK during ischemia, but not reperfusion, effectively attenuates fatal arrhythmia in ischemia/reperfusion heart. J Cardiovasc Pharmacol 61: 133–141.
6. Honda HM, Korge P, Weiss JN (2005) Mitochondria and ischemia/reperfusion injury. Ann N Y Acad Sci 1047: 248–258.
7. Di Lisa F, Bernardi P (2006) Mitochondria and ischemia-reperfusion injury of the heart: fixing a hole. Cardiovasc Res 70: 191–199.
8. Jackson PE, Feng QP, Jones DL (2008) Nitric oxide depresses connexin 43 after myocardial infarction in mice. Acta Physiol (Oxf) 194: 23–33.
9. Danik SB, Rosner G, Lader J, Gutstein DE, Fishman GI, et al. (2008) Electrical remodeling contributes to complex tachyarrhythmias in connexin43-deficient mouse hearts. FASEB J 22: 1204–1212.
10. Poelzing S, Rosenbaum DS (2004) Altered connexin43 expression produces arrhythmia substrate in heart failure. Am J Physiol Heart Circ Physiol 287: H1762–1770.
11. Chinda K, Palee S, Surinkaew S, Phornphutkul M, Chattipakorn S, et al. (2013) Cardioprotective effect of dipeptidyl peptidase-4 inhibitor during ischemia-reperfusion injury. Int J Cardiol 167: 451–457.
12. Whittington HJ, Hall AR, McLaughlin CP, Hausenloy DJ, Yellon DM, et al. (2013) Chronic metformin associated cardioprotection against infarction: not just a glucose lowering phenomenon. Cardiovasc Drugs Ther 27: 5–16.
13. Derosa G, Ragonesi PD, Carbone A, Fogari E, D'Angelo A, et al. (2013) Evaluation of the positive effects on insulin-resistance and beta-cell measurements of vildagliptin in addition to metformin in type 2 diabetic patients. Pharmacol Res 73: 20–26.
14. Apaijai N, Pintana H, Chattipakorn SC, Chattipakorn N (2012) Cardioprotective effects of metformin and vildagliptin in adult rats with insulin resistance induced by a high-fat diet. Endocrinology 153: 3878–3885.
15. Kilkenny C, Browne W, Cuthill IC, Emerson M, Altman DG (2010) Animal research: reporting in vivo experiments: the ARRIVE guidelines. Br J Pharmacol 160: 1577–1579.
16. Pratchayasakul W, Kerdphoo S, Petsophonsakul P, Pongchaidecha A, Chattipakorn N, et al. (2011) Effects of high-fat diet on insulin receptor function in rat hippocampus and the level of neuronal corticosterone. Life Sci 88: 619–627.
17. Friedewald WT, Levy RI, Fredrickson DS (1972) Estimation of the concentration of low-density lipoprotein cholesterol in plasma, without use of the preparative ultracentrifuge. Clin Chem 18: 499–502.
18. Pipatpiboon N, Pratchayasakul W, Chattipakorn N, Chattipakorn SC (2012) PPARgamma agonist improves neuronal insulin receptor function in hippocampus and brain mitochondria function in rats with insulin resistance induced by long term high-fat diets. Endocrinology 153: 329–338.
19. Chattipakorn N, Incharoen T, Kanlop N, Chattipakorn S (2007) Heart rate variability in myocardial infarction and heart failure. Int J Cardiol 120: 289–296.
20. Lekawanvijit S, Kompa AR, Zhang Y, Wang BH, Kelly DJ, et al. (2012) Myocardial infarction impairs renal function, induces renal interstitial fibrosis, and increases renal KIM-1 expression: implications for cardiorenal syndrome. Am J Physiol Heart Circ Physiol 302: H1884–1893.
21. Curtis MJ, Hancox JC, Farkas A, Wainwright CL, Stables CL, et al. (2013) The Lambeth Conventions (II): Guidelines for the study of animal and human ventricular and supraventricular arrhythmias. Pharmacol Ther 139: 213–248.
22. Palee S, Weerateerangkul P, Chinda K, Chattipakorn SC, Chattipakorn N (2013) Mechanisms responsible for beneficial and adverse effects of rosiglitazone in a rat model of acute cardiac ischaemia-reperfusion. Exp Physiol 98: 1028–1037.
23. Riess ML, Rhodes SS, Stowe DF, Aldakkak M, Camara AK (2009) Comparison of cumulative planimetry versus manual dissection to assess experimental infarct size in isolated hearts. J Pharmacol Toxicol Methods 60: 275–280.
24. Thummasorn S, Kumfu S, Chattipakorn S, Chattipakorn N (2011) Granulocyte-colony stimulating factor attenuates mitochondrial dysfunction induced by oxidative stress in cardiac mitochondria. Mitochondrion 11: 457–466.
25. Wongcharoen W, Chen YC, Chen YJ, Chang CM, Yeh HI, et al. (2006) Effects of a Na+/Ca2+ exchanger inhibitor on pulmonary vein electrical activity and ouabain-induced arrhythmogenicity. Cardiovasc Res 70: 497–508.
26. Pintana H, Apaijai N, Pratchayasakul W, Chattipakorn N, Chattipakorn SC (2012) Effects of metformin on learning and memory behaviors and brain mitochondrial functions in high fat diet induced insulin resistant rats. Life Sci 91: 409–414.
27. Mari A, Sallas WM, He YL, Watson C, Ligueros-Saylan M, et al. (2005) Vildagliptin, a dipeptidyl peptidase-IV inhibitor, improves model-assessed beta-cell function in patients with type 2 diabetes. J Clin Endocrinol Metab 90: 4888–4894.
28. Bikman BT, Zheng D, Kane DA, Anderson EJ, Woodlief TL, et al. (2010) Metformin Improves Insulin Signaling in Obese Rats via Reduced IKKbeta Action in a Fiber-Type Specific Manner. J Obes 2010.
29. Esteghamati A, Eskandari D, Mirmiranpour H, Noshad S, Mousavizadeh M, et al. (2013) Effects of metformin on markers of oxidative stress and antioxidant reserve in patients with newly diagnosed type 2 diabetes: a randomized clinical trial. Clin Nutr 32: 179–185.
30. Avila Dde L, Araujo GR, Silva M, Miranda PH, Diniz MF, et al. (2013) Vildagliptin ameliorates oxidative stress and pancreatic beta cell destruction in type 1 diabetic rats. Arch Med Res 44: 194–202.
31. Supakul L, Pintana H, Apaijai N, Chattipakorn S, Shinlapawittayatorn K, et al. (2013) Protective effects of garlic extract on cardiac function, heart rate

variability, and cardiac mitochondria in obese insulin-resistant rats. Eur J Nutr. (in press)
32. Pavithran P, Nandeesha H, Sathiyapriya V, Bobby Z, Madanmohan T (2008) Short-term heart variability and oxidative stress in newly diagnosed essential hypertension. Clin Exp Hypertens 30: 486–496.
33. Bhamra GS, Hausenloy DJ, Davidson SM, Carr RD, Paiva M, et al. (2008) Metformin protects the ischemic heart by the Akt-mediated inhibition of mitochondrial permeability transition pore opening. Basic Res Cardiol 103: 274–284.
34. Gundewar S, Calvert JW, Jha S, Toedt-Pingel I, Ji SY, et al. (2009) Activation of AMP-activated protein kinase by metformin improves left ventricular function and survival in heart failure. Circ Res 104: 403–411.
35. Calvert JW, Gundewar S, Jha S, Greer JJ, Bestermann WH, et al. (2008) Acute metformin therapy confers cardioprotection against myocardial infarction via AMPK-eNOS-mediated signaling. Diabetes 57: 696–705.
36. Zhang Y, Dong Y, Wu X, Lu Y, Xu Z, et al. (2010) The mitochondrial pathway of anesthetic isoflurane-induced apoptosis. J Biol Chem 285: 4025–4037.
37. Barreto-Torres G, Parodi-Rullan R, Javadov S (2012) The Role of PPARalpha in Metformin-Induced Attenuation of Mitochondrial Dysfunction in Acute Cardiac Ischemia/Reperfusion in Rats. Int J Mol Sci 13: 7694–7709.
38. Whittington HJ, Hall AR, McLaughlin CP, Hausenloy DJ, Yellon DM, et al. (2013) Chronic metformin associated cardioprotection against infarction: not just a glucose lowering phenomenon. Cardiovasc Drugs Ther 27: 5–16.
39. Roell W, Lewalter T, Sasse P, Tallini YN, Choi BR, et al. (2007) Engraftment of connexin 43-expressing cells prevents post-infarct arrhythmia. Nature 450: 819–824.
40. Srisakuldee W, Nickel BE, Fandrich RR, Jiang ZS, Kardami E (2006) Administration of FGF-2 to the heart stimulates connexin-43 phosphorylation at protein kinase C target sites. Cell Commun Adhes 13: 13–19.

เอกสารแนบหมายเลข 63

HEMOGLOBIN

http://informahealthcare.com/hem
ISSN: 0363-0269 (print), 1532-432X (electronic)

Hemoglobin, Early Online: 1–9
© 2015 Informa Healthcare USA, Inc. DOI: 10.3109/03630269.2014.987869

informa
healthcare

REVIEW ARTICLE

Cardiomyopathy Associated with Iron Overload: How Does Iron Enter Myocytes and What are the Implications for Pharmacological Therapy?

Karn Wijarnpreecha[1,2]*, Sirinart Kumfu[1,2]*, Siriporn C. Chattipakorn[1,2,3], and Nipon Chattipakorn[1,2]

[1]*Cardiac Electrophysiology Research and Training Center, Faculty of Medicine, Chiang Mai University, Chiang Mai, Thailand,*
[2]*Cardiac Electrophysiology Unit, Department of Physiology, Faculty of Medicine, Chiang Mai University, Chiang Mai, Thailand, and*
[3]*Center of Excellence in Cardiac Electrophysiology Research, Chiang Mai University, Chiang Mai, Thailand*

Abstract

Iron overload cardiomyopathy is one of the most common causes of death in thalassemia patients. Although new iron chelating agents have been developed, the mortality rate from heart failure remains elevated as a result of iron overload. This could be due to the fact that our understanding of the underlying mechanism of iron uptake into cardiomyocytes is still unclear, thus impeding the discovery and refinement of more effective therapy for thalassemia therapeutic strategies in thalassemic iron overload cardiomyopathy. Growing evidence indicates that multiple routes of iron entry into cardiomyocytes exist under iron overload conditions. These include both L-type (LTCC) and T-type (TTCC) calcium channels, divalent metal transporter 1 (DMT1) and transferrin receptors (TfRs). In this review, the routes of iron uptake into cardiomyocytes under iron overload conditions are presented. Evidence from pharmacological interventions in support or against the possible route of iron entry of each portal in cardiomyocytes are also comprehensively summarized and discussed.

Keywords

Calcium channel, cardiomyopathy, iron overload, iron uptake, thalassemia

History

Received 30 April 2014
Revised 9 July 2014
Accepted 14 July 2014
Published online 9 January 2015

Hemoglobin Downloaded from informahealthcare.com by Chiang Mai University on 01/26/15
For personal use only.

Introduction

Iron is an essential element in the human body. Most of the iron in the body is used in hemoglobin (Hb) synthesis (1). Moreover, iron is also used to produce myoglobin, cytochrome P450 (CYP450) and is involved in the electron transport chain in cellular respiration (1). The ability of iron to act as an electron donor and an acceptor can cause cell injury through production of reactive oxygen species (ROS) (2–4). Since the human body does not have a mechanism for iron excretion, iron overload conditions due to either hereditary hemochromatosis (primary) or regular blood transfusions in thalassemia, as well as other abnormal Hb diseases (secondary), can result in excess iron uptake and chronic deposition in peripheral tissues (liver, spleen, bone marrow, heart, β cells of the pancreas, pituitary and central nervous system and vascular smooth muscle) (1).

Although the most commonly employed treatments such as regular blood transfusions and iron chelation can improve survival in β-thalassemia major (β-TM) patients, iron overload cardiomyopathy is still the most common cause of death in these patients (5,6). Therefore, improving our understanding of the mechanisms underlying iron uptake into the heart under systemic iron overload conditions may improve the likelihood that therapy will be improved and thereby lead to improved survival. Currently, the underlying mechanism of iron uptake into the heart in iron overload conditions is not fully understood (7).

Conventionally, under the physiological condition, the uptake of ferrous iron (Fe^{2+}) into cells is achieved by the divalent metal transporter 1 (DMT1) (8,9). Another conventional route of iron entry into cells is via the transferrin receptor (TfR). Transferrin (Tf) binds to ferric iron (Fe^{3+}) with extremely high affinity called holo-transferrin (HoloTf) (10,11). Then, HoloTf binds to cell surface TfR and forms the TfR/Tf complex that is internalized through TfR-mediated endocytosis (10,11). However, growing evidence demonstrated that the calcium channels, both L-type (LTCC) and T-type (TTCC), could be the main routes of iron uptake into the heart under iron overload conditions (12–17). Studies in the past decade have shown that TfR and DMT1 are also key portals for uptake of iron into the heart under iron overload conditions, however, their role has never been investigated in a clinical setting (12,13,18). Although there are several new proposed therapeutic agents that may be beneficial in iron overload conditions, lack of clinical evidence is currently the limitation for their use in thalassemia patients (5,6,19,20). Currently, one of the most interesting agents is the calcium channel blocker. In this study, the routes of iron uptake into cardiomyocytes under iron overload conditions will be reviewed. Evidence from pharmacological interventions in

*KW and SK contributed equally in this study.

Address correspondence to Professor Nipon Chattipakorn, Cardiac Electrophysiology Research and Training Center, Faculty of Medicine, Chiang Mai University, 110 Intrawaroros Road, Chiang Mai 50200, Thailand. Tel: +66-53-945-329. Fax: +66-53-945-368. E-mail: nchattip@gmail.com

RIGHTSLINK

support or against the possible routes of iron entry of each portal in cardiomyocytes are also comprehensively summarized and discussed. From this overview the limitations of the treatments, the results and arguments of many studies about the route of iron uptake into the heart under iron overload conditions in the past decade are also presented, and can thus inform further preclinical and clinical studies.

Pathophysiology of iron overload cardiomyopathy

Thalassemic patients are prone to have iron overload as a result of regular blood transfusions (secondary iron overload or transfusional siderosis) (5,19,20). Increased intestinal iron absorption from ineffective erythropoiesis is only a minor cause (5,19,20). Once serum Tf (protein bound iron in plasma) has a saturation of over 45.0%, non transferrin bound iron (NTBI) will appear, and this form of iron can induce cardiovascular injury (21). The rate of NTBI uptake into cardiomyocytes is greater than Tf bound iron under iron overload conditions (22). Unfortunately, the uptake of NTBI is not regulated by a normal negative-feedback mechanism in the same way as Tf bound iron (21,23). Although the source of NTBI is still unknown, the free form of NTBI, both in plasma [labile plasma iron (LPI)] and intracellular [labile cellular iron (LCI) or labile iron pool (LIP)] can cause cardiovascular injury from the properties of reduction and oxidation of iron (2–5,19,21,24–28). These properties of NTBI can produce reactive oxygen species (ROS) (Haber-Weiss and Fenton reaction) leading to lipid peroxidation that causes cardiac cell apoptosis and interstitial fibrosis (2–5,19,21,24–28). Furthermore, high ROS production can also damage cellular proteins, DNA and other cellular organelles such as lysosomes and mitochondria (26,29). Previous studies suggested that mitochondrial dysfunction could be responsible for cardiac failure resulting from chronic iron overload (30,31). It has been shown that chronic iron overload can cause cumulative iron-mediated damage to mitochondrial DNA, thus impaired synthesis and function of mitochondrial respiratory chain subunits and leading to the loss of respiratory capacity and cardiac dysfunction (30,31). Furthermore, the increase in ROS production can cause ROS concentrations to reach the threshold level, which can trigger the opening of the inner membrane anion channel and mitochondrial permeability transition pore (32,33). This results in mitochondrial depolarization and mitochondrial swelling, leading to the release of cytochrome c, activation of caspase pathways, and cell death by necrosis and/or apoptosis (32,33). Moreover, the excess iron levels can slow calcium ion (Ca^{2+}) current inactivation which leads to an increase in the Ca^{2+} influx. These processes can be aggravated and impair diastolic function (restrictive cardiomyopathy) in early stages of the disease. If iron levels still increase, the Ca^{2+} entry into the heart will decrease due to the Fe^{2+} competition and eventually cause systolic dysfunction (dilated cardiomyopathy) (20). The summarized results of pathophysiology of iron overload cardiomyopathy are shown in Figure 1.

Despite the clear mechanism of iron-mediated cardiovascular injury, the exact theory of channel uptake of iron into cardiomyocytes under iron overload condition is still controversial (7). Although the major form of iron entry into cardiomyocytes under iron overload is Fe^{2+}, evidences exist that Fe^{3+} can be accessed in relatively low levels (34–36). To understand the mechanism of iron overload cardiomyopathy, many researchers have studied channel expressions and roles of uptake of iron in iron overload conditions. However, results remain controversial and need to be confirmed. From these data, new therapeutic strategies may be developed to decrease iron uptake into the heart and may improve survival of thalassemia patients in the future.

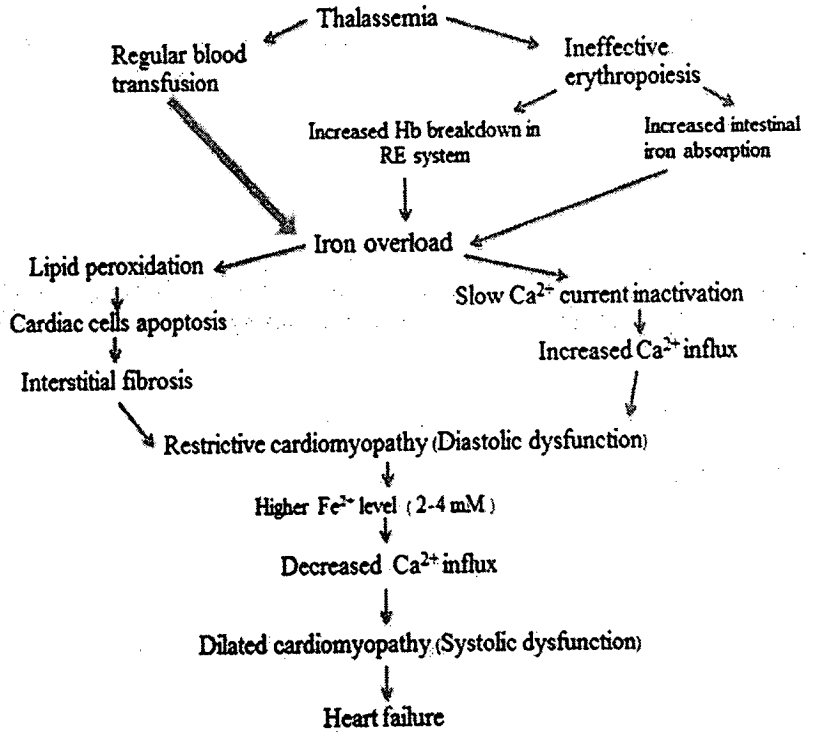


Figure 1. Pathophysiology of iron overload cardiomyopathy in thalassemia.

Hemoglobin Downloaded from informahealthcare.com by Chiang Mai University on 01/26/15
For personal use only.

RIGHTSLINK

Hemoglobin Downloaded from informahealthcare.com by Chiang Mai University on 01/26/15
For personal use only.

DOI: 10.3109/03630269.2014.987869

The expression of channels involved in iron uptake into cardiomyocytes under iron overload condition

In the past decade, several studies have carried out investigations of the expression of various portals as possible routes of iron entry into cardiomyocytes under iron overload conditions to evaluate the relationship of iron status and channels expression at both mRNA and protein levels. Four main channels reported to be involved in iron uptake into cardiomyocytes include TfRs, DMT1, LTCC and TTCC.

The expression of TfR mRNA and protein under iron overload conditions was not consistent as shown in Table 1. The variation of TfR mRNA and protein expression might be due to various factors including the difference in the model of experiments, the dose and route of iron administration and the duration of iron loading in each study. The conclusion of the channel involved in iron uptake from the data of mRNA and protein expression cannot be confidently predicted due to the variation in the data. The evidence has shown that Fe^{2+} is the main form of iron entering into cardiomyocytes under iron overload conditions (21,23). Therefore, TfR that binds to iron in Fe^{3+} form is not a main route of iron uptake under iron overload conditions (37). In the DMT1 study (Table 2), most of the evidence is concordant which suggest post transcriptional expression (decreased protein expression) in the rat heart under iron overload conditions although DMT1 uptake of iron is in Fe^{2+} form (37). Therefore, it can be concluded that DMT1 is not the main channel responsible for iron uptake into the heart. The possible main channels that are responsible for the uptake of iron into the heart might be LTCC that is unchanged in mRNA expression (Table 3), and TTCC that increased mRNA expression under iron overload conditions (Table 4). However, further studies are needed to prove the protein expression to support the important role of the iron uptake of these two channels.

The summary of mRNA and protein expression of each channel is shown in Table 5. Most reports in the past decade studied the mRNA and protein expression of TfR and DMT1 in iron overload conditions. There is only one study from Kumfu *et al.* (12) that represented mRNA expression of both LTCC and TTCC under iron overload conditions. Although Oudit *et al.* (16) stated the LTCC currents are not decreased in iron overload, this experiment did not evaluate mRNA or protein expression directly. Nevertheless, their report supports the point that LTCC has an important role in iron uptake under iron overload condition.

Evidence that supports or denies channels involved in iron uptake into cardiomyocytes under iron overload conditions

In most recent studies, the experiments are focused on changing iron levels after administering blocking agents to target specific channels to understand the relationship of iron levels in cardiomyocytes and the role of each channel in iron uptake. From the above section, TfR (uptake of Fe^{3+}) and DMT1 (decreased protein expression) may not be the main channels involved in iron uptake under iron overload conditions. Most of the studies focused on the LTCC that was thought to be the major pathway of iron uptake leading to iron overload cardiomyopathy (16). This channel is the only

Table 1. Evidence to support transferrin receptor expression in the heart under iron overload condition.

Bound Fe species	Model	Intervention	Identification techniques	TfR mRNA Expression Under Iron Overload			TfR Protein Expression Under Iron Overload			Refs.
				Increased	Decreased	Not changed	Increased	Decreased	Not changed	
Fe^{3+}	*In vitro* Cultured neonatal SD rat cardiomyocytes	Loaded FAC (5–80 μg/mL) for 3 days	Northern blot	X	✓	X	X	X	X	(47)
Fe^{3+}	Cultured neonatal SD rat cardiomyocytes	Loaded FAC (20 μg/mL) for 72 hours	RT-PCR and Western blot	X	X	✓	X	✓	X	(48)
Fe^{3+}	*In vivo* Male SD rats	Fed 2.5% carbonyl iron diet for 6 weeks	RT-PCR	X	✓	X	X	X	X	(40)
Fe^{3+}	Male Wistar rats	Injected iron dextran (200 mg/kg/week) IP for 4 weeks	Western blot	X	X	X		X	X	(49)
Fe^{3+}	C57BL/6 mice aged 10–12 weeks	Fed diet with 2% carbonyl iron for 6 weeks	Q-RT-PCR and microarray	X	✓	X	X	X	X	(50)
Fe^{3+}	Newly weaned male SD rats (21 days old)	Fed diet with iron 18.916 ppm for 3 weeks	Western blot	X	X	X	X	X	✓	(45)
Fe^{3+}	Male SD rats (21 days old)	Fed diet with 2.5% carbonyl iron for 6 weeks	Northern and Western blot	X	✓	X	X	✓	X	(51)

SD: Sprague-Dawley rat; FAC: ferric ammonium citrate; RT-PCR: reverse-transcription polymerase chain reaction; Q-RT-PCR: quantitative reverse-transcription polymerase chain reaction.

RIGHTSLINK

Hemoglobin Downloaded from informahealthcare.com by Chiang Mai University on 01/26/15
For personal use only.

Table 2. Evidence to support divalent metal transporter 1 expression in the heart under iron overload condition.

Bound Fe species	Model	Intervention	Identification techniques	DMT1 mRNA Expression Under Iron Overload			DMT1 Protein Expression Under Iron Overload			Refs.
				Increased	Decreased	Not changed	Increased	Decreased	Not changed	
Fe^{2+}	*In vitro* Cultured neonatal SD rat cardiomyocytes	Loaded FAC (20 μg/mL) for 72 hours	RT-PCR	×	×	✓	×	×	×	(48)
Fe^{2+}	*In vivo* Male SD rats	Fed 2.5% carbonyl iron diet for 6 weeks	RT-PCR and Western blot	×	×	✓	×	✓	×	(40)
Fe^{2+}	Male Wistar rats	Injected iron dextran (200 mg/kg/week) IP for 4 weeks	Western blot	×	×	×	×	✓	×	(49)
Fe^{2+}	Male SD rats	Fed high iron diet for 6 weeks	RT-PCR and Western blot	×	×	✓	×	✓	×	(52)
Fe^{2+}	Newly weaned male SD rats (21 days old)	Fed diet with iron 18.916 ppm for 3 weeks	RT-PCR and Western blot	×	×	✓	×	×	✓	(45)
Fe^{2+}	Specific pathogen-free male ICR mice	Fed 120 mg/Fe/kg for 4 weeks	RT-PCR	×	×	✓	×	×	×	(53)

SD: Sprague-Dawley rat; FAC: ferric ammonium citrate; RT-PCR: reverse-transcription polymerase chain reaction; ICR: imprinting control region.

Table 3. Evidence supports L-type calcium channel expression in the heart under iron overload condition.

Bound Fe species	Model	Intervention	Identification techniques	LTCC mRNA Expression Under Iron Overload			LTCC Protein Expression Under Iron Overload			Refs.
				Increased	Decreased	Not Changed	Increased	Decreased	Not changed	
Fe^{2+}	*In vivo* Adult C57/BL6 het. mice	Fed FE diet (0.2% ferrocene w/w) 120 days	RT-PCR	×	×	✓	×	×	×	(12)

het.: heterozygous (thalassemic) mice; RT-PCR: reverse transcription polymerase chain reaction.

Table 4. Evidence to support T-type calcium channel expression in the heart under iron overload condition.

Bound Fe species	Model	Intervention	Identification techniques	TTCC mRNA Expression Under Iron Overload			TTCC Protein Expression Under Iron Overload			Refs.
				Increased	Decreased	Not changed	Increased	Decreased	Not changed	
Fe^{2+}	*In vivo* Adult C57/BL6 het. mice	Fed FE diet (0.2% ferrocene w/w) 120 days	RT-PCR	✓	×	×	×	×	×	(12)

het.: heterozygous (thalassemic) mice; RT-PCR: reverse transcription polymerase chain reaction.

RIGHTSLINK

Table 5. Summary of channel expression for iron uptake into cardiomyocytes under iron overload condition.

		mRNA Expression Under Iron Overload; Refs.			Protein Expression Under Iron Overload; Refs.		
Channels	Bound Fe Species	Increased	Decreased	Not Changed	Increased	Decreased	Not Changed
TfR	Fe^{3+}	–	(40, 47, 51, 50)	(48)	(49)	(51)	(48, 45)
DMT1	Fe^{2+}	–	–	(45, 40, 48, 52, 53)	–	(40, 49, 52)	(45)
LTCC	Fe^{2+}	–	–	(12)	–	–	–
TTCC	Fe^{2+}	(12)	–	–	–	–	–

TfR: Transferrin receptor; DMT1: divalent metal transporter 1; LTCC: L-type calcium channel; TTCC: T-type calcium channel.

Table 6. Evidence in support/against transferrin receptor as the route of iron uptake into cardiomyocytes under iron overload conditions.

Model	Intervention	Result	Interpretation	Ref.
In vitro Cultured mice cardiomiyocytes (WT, het.; DH)	Anti-TfR1 Ab 5, 10 μg/mL + Fe^{2+} 285.6 μM for 48 hours	Anti-TfR1 Ab did not prevent iron uptake into cardiomyocytes	TfR1 is not the pathway of iron uptake into cultured cardiomyocytes	(13)

WT: wild type; het.: heterozygous (thalassemic) mice; DH: double heterozygous mice Hb E (*HBB*: c.79G>A).

Hemoglobin Downloaded from informahealthcare.com by Chiang Mai University on 01/26/15
For personal use only.

channel proven by clinical studies (38,39) to improve cardiac function and decrease iron levels in patients with the iron overload conditions. Recently, results from Kumfu *et al.* (12,13) and Lopin *et al.* (14) proposed the possibility that TTCC could also be one of the major pathways involved in iron uptake into the heart.

The reports that support the hypothesis that TfR is not a major pathway for iron uptake under iron overload conditions are shown in Table 6. Regarding published reports on DMT1 (Table 7), the *in vitro* study from Kumfu *et al.* (13) is consistent with the Ke *et al.* (40) report, which demonstrated that decreased DMT1 expression was observed under iron overload conditions, suggesting that DMT1 might not be a portal of iron entry in cardiomyocytes. However, *in vivo* studies from Kumfu *et al.* (12) and Davis *et al.* (41) support DMT1 as the route of iron uptake in the heart under iron overload conditions. The inconsistent findings might be due to the different model of experiments, dosage and route of iron administration, and the duration of iron loading in each study. Future experiments in an *in vivo* model and additional clinical studies are needed to clarify the potentially important role of this channel.

The other main channels that have recently been shown to play an important role in iron uptake are calcium channels, both LTCC and TTCC. The summary of evidence that supports or opposes the involvement of LTCC and TTCC in iron uptake into cardiomyocytes under iron overload condition are shown in Table 8 and Table 9, respectively. The LTCC was first explored to investigate if it is the channel that takes up iron under iron overload conditions by Tsushima *et al.* (17). Since then, there has been much evidence to support the roles of LTCC as a portal of iron entry into the heart from many studies both *in vivo* and from clinical models. However, published findings do not consistently support the role of LTCC. The evidence against LTCC being the channel that takes up iron was reported by Parkes *et al.* (35) and Kumfu *et al.* (13). They found that the LTCC blocker cannot decrease cellular iron levels in cultured cardiomyocytes under iron overload conditions. However, both experiments used *in vitro* models that differ from the models supporting LTCC. This could be because the cultured neonatal rat cardiomyocytes have smaller L-type calcium currents and high rates of myocyte death that decreases LTCC blocker potential in decreasing iron levels, and misinterprets the role of the LTCC iron uptake (16). The different models of *in vitro* and *in vivo* studies produce different results from each study (Table 8).

The other possible main channel involving iron uptake in the heart is the TTCC. Until now, there are only three pieces of evidence regarding TTCC, and it all supports the hypothesis that Fe^{2+} can enter into cardiomyocytes through this channel under iron overload conditions (Table 9). Under physiological condition, TTCC expression normally disappears in the myocardium after birth (42,43). However, it can reappear in the heart under some pathological conditions including myocardial infarction, heart failure, and iron overload cardiomyopathy (42,43). Recently, Kumfu *et al.* (12,13) demonstrated that the TTCC gene was reexpressed in the heart of thalassemic mice, and was also upregulated under iron overload conditions. Moreover, treatment with the TTCC blocker, efonidipine, significantly reduced the cardiac iron uptake both in cultured cardiomyocytes and *in vivo* models under iron overload conditions, thus improving cardiac functions (12,13). These findings suggested that TTCC could play an important role on cardiac iron uptake under iron overload conditions (12,13). Recently, using a patch clamp recording technique, Lopin *et al.* (14) reported that Fe^{2+} can inhibit Ca^{2+} currents, and that Fe^{2+} could enter cardiomyocytes through TTCC under iron overload conditions. However, further studies both in clinical and *in vivo* settings are needed to confirm the role of these channels and their potential use in preventing iron overload cardiomyopathy.

Besides Fe^{2+}, Fe^{3+} can enter into cardiomyocytes under iron overload conditions but in relatively lower levels (35,36). Kumfu *et al.* (34) reported the experimental findings about Fe^{3+} not being taken up by LTCC, TTCC, DMT1, or TfR. The true mechanism of Fe^{3+} uptake is still questionable, but

RIGHTSLINK

Hemoglobin Downloaded from informahealthcare.com by Chiang Mai University on 01/26/15
For personal use only.

Table 7. Evidence in support/against divalent metal transporter 1 as the route of iron uptake into cardiomyocytes under iron overload conditions.

Model	Intervention	Result	Interpretation	Refs.
In vitro Cultured mice cardiomiyocytes (WT, het.; DH)	Added ebselen 12.5, 25 μM for 60 min. + Fe^{2+} 285.6 μM for 48 hours	Ebselen (DMT1 blocker) did not prevent iron uptake into cardiomyocytes	DMT1 is not the pathway of iron uptake into cultured cardiomyocytes	(13)
In vivo B6D2F1 mice (5–8 weeks old)	Gave 10 mg iron dextran IP/mouse/day + ebselen 25 mg/kg/PO/mouse/day	Ebselen (DMT1 blocker) decreased iron concentrations in heart tissue	DMT1 is the route of iron uptake into cardiomyocytes	(41)
Adult C57/BL6 WT, het. mice	Fed FE diet (0.2% ferrocene w/w)/120 days; gave ebselen (5 mg/kg) IP daily for last 30 days	Ebselen (DMT1 blocker) improved function, decreased cardiac iron levels	DMT1 is the route of iron entry into iron overloaded thalassemic hearts	(12)

WT: wild type; het.: heterozygous (thalassemic) mice; DH: double heterozygous mice with Hb E (*HBB*: c.79G > A); DMT1: divalent metal transporter 1; IP: intraperitoneal injection; PO: per oral.

Table 8. Evidence in support/against L-type calcium channel as the route of iron uptake into cardiomyocytes under iron overload conditions.

Model	Intervention	Result	Interpretation	Refs.
In vitro Cultured mice cardiomyocytes (WT, het., DH)	Verapamil (0–80 μM) + Fe^{2+} 285.6 μM for 48 hours	Verapamil did not prevent iron uptake into cardiomyocytes	LTCC is not the pathway of iron uptake into cultured cardiomyocytes	(13)
Cultured neonatal rat cardiomyocytes	Added FAC (13.75% iron by weight) for 3–5 days, then gave LTCC blockers (nifedipine, verapamil, diltiazem)	LTCC blockers did not inhibit Fe^{2+}, Fe^{3+} into iron-loaded cells; nifedipine increased Fe^{2+}, Fe^{3+} uptake into cardiomyocytes	LTCC is not the route of iron uptake into cultured cardiomyocytes	(35)
Ex vivo Isolated perfusion SD rat hearts	Perfused with 100 nm/L of $^{59}Fe^{2+}$ and $^{59}Fe^{3+}$ for 15 min. Added nifedipine (10 μmol/L), Bay K 8644 (100 nmol/L) and isoproterenol (100 nmol/L)	LTCC blockers (nifedipine) increased $^{59}Fe^{2+}$ uptake; LTCC agonists (Bay K 8644 and isoproterenol) increased $^{59}Fe^{2+}$ uptake into cardiomyocytes	Myocardial Fe^{2+} iron uptake occurs via LTCC	(17)
In vivo Adult C57/BL6 WT, het. Mice	Fed FE diet (0.2% ferrocene w/w) for 120 days. Gave verapamil (10 mg/kg) IP twice daily, nifedipine (5 mg/kg) IP daily for last 30 days	Verapamil and nifedipine improved cardiac function, decreased cardiac iron levels	LTCC is the route of iron entry into iron overloaded thalassemic hearts	(12)
Male B6D2F1 mice (3–5 weeks old)	Gave 20 mg iron dextran IP/mouse/day + amlodipine 2.5 mg in 200 mL water PO/mouse/day for 4 weeks	Amlodipine decreased iron uptake into the heart	LTCC is the route of iron uptake into cardiomyocytes	(54)
Male B6D2F1 mice and male mice (FVB/n strain) with cardiac-specific over-expression of LVDCC	Gave amlodipine or verapamil 0.1 mg/mL (10 mg/kg/day) then administered iron dextran 1.25 mg/25 g body weight/day IP for 12 weeks (iron-loading protocol)/16 weeks (survival studies	Amlopidine and verapamil decreased cardiac iron levels. Iron-overloaded transgenic mice increased myocardial iron levels	Cardiac LVDCCs are key transporters of iron into cardiomyocytes	(15)
Male C57/BL6 12-week-old mice	Gave iron dextran (1 g/kg) IP once a week + propranolol (40 mg/kg/day) via drinking water for 8 weeks	Blocking of LTCC by propranolol improved cardiac function	LTCC blocker is useful in iron-overloaded mice	(55)
8-week-old HJV KO mice	Gave verapamil 0.2 mg/mL via drinking water	Verapamil decreased cardiac iron levels in verapamil-treated groups	LTCC is the route of iron uptake into cardiomyocytes	(56)
Clinical 15 β-TM patients	Gave iron chelators + amlodipine 5 mg/day for 12 months	Heart MRI T2* increased significantly at 6 and 12 months and reduced serum ferritin in 12 months	LTCC blocker decreased cardiac iron levels assessed by MRI T2*	(38)
Case report 81-year-old man with heart failure and macrocytic anemia	DFO + verapamil (120 mg/day) for 18 months	Serum ferritin 1000 ng/mL and improved cardiac function	LTCC blocker + DFO may be effective in IOC at its early stage	(39)

WT: wild type; het.: heterozygous (thalassemic) mice; DH: double heterozygous mice with Hb E (*HBB*: c.79G > A);SD: Sprague-Dawley mice; FAC: ferric ammonium citrate; LTCC: L-type calcium channel; IP: intraperitoneal injection; LVDCC: L-type voltage dependent calcium channel; HJV KO: hemojuvelin knockout mice; β-TM: β-thal major; MRI T2*: magnetic resonance imaging T2*; IOC: iron overload cardiomopathy.

RIGHTSLINK

Table 9. Evidence in support/against T-type calcium channel as route of iron uptake into cardiomyocytes under iron overload condition.

Model	Intervention	Result	Interpretation	Refs.
In vitro Cultured mice cardiomiyocytes (WT, het.; DH)	Efonidipine (0–20 mM) + Fe^{2+} 285.6 mM for 48 hours	Efonidipine (TTCC blocker) prevented iron uptake into cardiomyocytes	Iron uptake in cultured thalassemic cardiomyocytes mainly mediated by TTCC	(13)
Transfected HEK293 cells with $Ca_V3.1$ channels	Patch-clamp experiments evaluated $^{59}Fe^{2+}$ uptake through cells, with or without NNC 55-0395 (selective TTCC inhibitor)	$Ca_V3.1$ channels (TTCC) can uptake Fe^{2+} into cells	TTCC is the pathway of iron entry under iron overload conditions	(14)
In vivo Adult C57/BL6 WT, het. mice	Fed FE diet (0.2% ferrocene w/w) for 120 days; gave efonidipidine (4 mg/kg) IP daily for last 30 days	Efonidipine (TTCC blocker) improved cardiac function, decreased cardiac iron levels	TTCC is the route of iron entry into iron overloaded thalassemic hearts	(12)

WT: wild type; het.: heterozygous (thalassemic) mice; DH: double heterozygous mice with Hb E (*HBB*: c.79G > A); IP: intraperitoneal injection; TTCC: T-type calcium channel.

Hemoglobin Downloaded from informahealthcare.com by Chiang Mai University on 01/26/15
For personal use only.

the possible pathway may be by Fe^{3+} binding with a chaperone protein or through an iron-enclosed vesicle system facilitating entry into cardiomyocytes (34–36). Future studies regarding the pathway of Fe^{3+} uptake into cardiomyocytes may help develop new treatments for preventing iron overload cardiomyopathy in thalassemia.

The role of zinc transporter in iron uptake into the heart under iron overload conditions

In addition to the aforementioned four channels, recent studies reported the expression of Zip14 (Slc39a14) and Zip8 (Slc39a8), the ZIP family of metal-iron transporters, in the heart under iron overload conditions. Although Zip14 has been shown to involve iron uptake in liver cells (44,45), currently there is no evidence that Zip14 can cause the uptake of iron into cardiomyocytes. However, it has been shown that the expression of Zip8 mRNA levels was increased in thalassemic mice heart tissues compared with wild-type mice controls (13). However, no evidence was found that zinc transporters can cause the uptake of iron into the heart directly under iron overload conditions. Currently, Zip14 and Zip8, the zinc transporters, are not included as channels involved in iron uptake into cardiomyocytes. Further investigation regarding iron uptake into the heart by this route is still needed.

Pharmacological intervention of channels that allow the uptake of iron into cardiomyocytes

Most of the studies focused on pharmacological interventions using LTCC and TTCC blockers both *in vitro* and *in vivo* models by assessing iron levels in the heart or cardiomyocytes after the administration of blockers of each channel (Table 8, Table 9). Recently, a report by Kumfu *et al.* (12) showed that LTCC, TTCC and DMT1 blockers reduced iron uptake into the heart but only DMT1 and TTCC blockers improved survival rates. However, these data were debated by Das *et al.* (7) that administration of an LTCC blocker by intraperitoneal injection can lead to acute hypotension and death so the survival rate cannot be improved. However, a study by Oudit *et al.* (15) reported that the administration of LTCC blocker in drinking water can improve survival, decrease hypotension and arrhythmia. The other reason put forward by Das *et al.* (7) was that efonidipine (a TTCC blocker) is not the selective TTCC blocker, since it can also block LTCC (7). Nevertheless, the beneficial effects obtained from the non selective TTCC blocker was still greater than the LTCC blocker alone, suggesting the important role of TTCC in iron entry into the heart (12). Further experiments regarding the role of selective TTCC blockers in cases of iron overload are needed to prove this experimental finding. Recently, Lopin *et al.* (14) studied selective TTCC blockers and proved that TTCC can take up iron into cardiomyocytes under iron overload conditions. Even though there is much evidence from *in vitro* and *in vivo* studies to support the blocking of DMT1, LTCC and TTCC leading to a decrease in iron levels in rat cardiomyocytes and thus improving survival rates, only the LTCC blocker has supporting evidence from clinical studies showing the improved cardiac function and decreased iron levels in the heart evaluated by magnetic resonance imaging T2* (MRI T2*) (38,39). However, larger and longer cohort studies are needed to verify these findings since there were no differences in the iron levels in the heart and serum ferritin between the amlodipine and non amlodipine treated groups after a 1 year follow-up. Moreover, this study did not determine the effect of LTCC blockers on the improvement of cardiac function (38). In a human report, Mainous *et al.* (46) found an association between the use of calcium channel blockers (CCBs) and lower serum ferritin levels in individuals with hypertension. However, this study is not the iron overload model. A case report from Sugishita *et al.* (39) is the only clinical study that reported that verapamil with deferoxamine (DFO) can improve cardiac function in early stages of iron overload cardiomyopathy. Future larger randomized clinical controlled trials are needed to evaluate this further.

Proposed mechanism for non transferrin bound iron uptake into heart under iron overload conditions

From the current available evidence, it can be proposed that the NTBI uptake mechanisms in the heart under iron overload conditions are mainly via LTCC, TTCC and DMT1 as shown in Figure 2. Treatment with iron chelator [DFO, deferiprone (DFP), deferasirox (DFX)], LTCCs blocker (verapamil, nifedipine, amlodipine), TTCC blocker (efonidipine) and DMT1 blocker (ebselen) could decrease iron uptake into the heart and improve cardiac dysfunction under iron overload

RIGHTSLINK

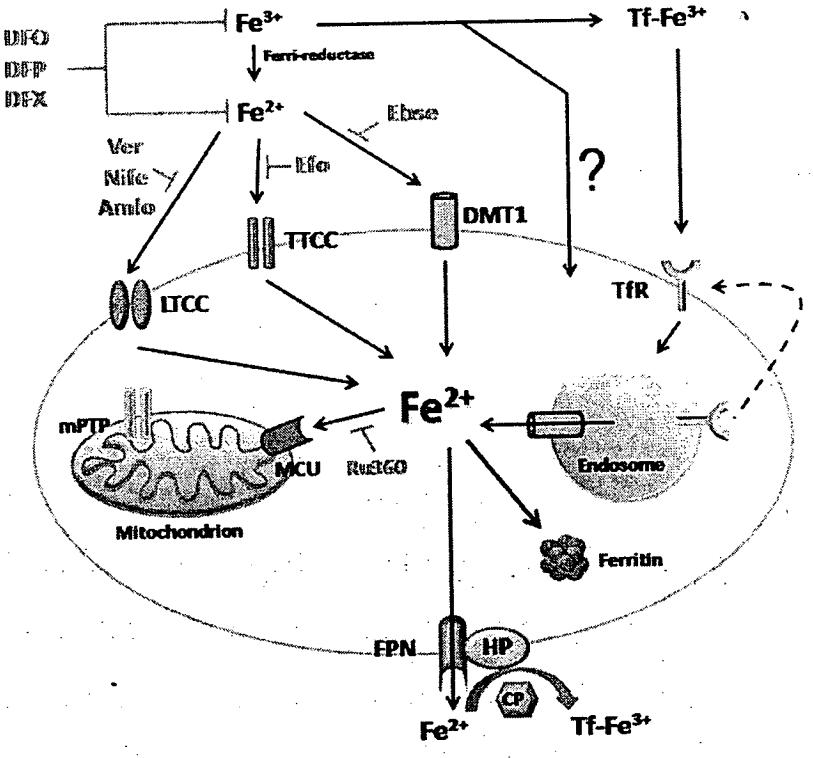


Figure 2. Proposed mechanism for NTBI uptake into the heart under iron overload conditions. TTCC: T-type calcium channel; LTCC: L-type calcium channel; DMT1: divalent metal transporter1; Tf: transferrin; TfR: transferrin receptor; mPTP: mitochondrial permeability transition pore; MCU: mitochondrial calcium uniporter; CP: ceruloplasmin; HP: hephaestin; FPN: ferroportin; DFO: deferoxamine; DFP: deferiprone; DFX: deferasirox; Ver: LTCC blocker verapamil; Nife: nifedipine; Amlo: amlodipine; Efo: TTCC blocker efonidipine; Ebse: DMT1 blocker ebselen. The (T) symbol means inhibition effects.

conditions. Treatment with mitochondrial calcium uniporter (MCU) blocker (Ru360) could improve cardiac mitochondrial dysfunction caused by iron overload. All of these findings suggested that TTCC, LTCC and DMT1 play important roles in iron uptake in the heart and MCU mainly plays a role in iron uptake into cardiac mitochondria under iron overload conditions (Figure 2). Future clinical studies are needed to validate the clinical significance for their use in iron overload patients.

Conclusions

Iron overload cardiomyopathy is a serious condition and one of the most common causes of death in thalassemic patients despite the development of new iron chelating drugs. Understanding the routes of iron entry may beneficially influence the development of new therapeutic treatments for thalassemia and iron overload disorders. Although the mechanism of iron uptake is still not completely understood, the possible pathway of iron uptake is the calcium channels, whether LTCC or TTCC, that can take up Fe^{2+}, a form of NTBI entry into the heart, under iron overload conditions. Further clinical studies are needed to confirm the role of these channels and also to study the pharmacological interventions of these channels in thalassemia patients.

Declaration of interest

This study was supported by grants from the Thailand Research Fund RTA5580006 (to NC), BRG5780016 (to SCC), TRG5780002 (to SK) and the Chiang Mai University Excellence Center Award, Chiang Mai, Thailand (to NC). The authors report no conflicts of interest. The authors alone are responsible for the content and writing of this article.

References

1. Andrews NC. Disorders of iron metabolism. N Engl J Med. 1999; 341(26):1986–1995.
2. Emerit J, Beaumont C, Trivin F. Iron metabolism, free radicals, and oxidative injury. Biomed Pharmacother. 2001;55(6):333–339.
3. Esposito BP, Breuer W, Sirankapracha P, *et al.* Labile plasma iron in iron overload: Redox activity and susceptibility to chelation. Blood. 2003;10(7):2670–2677.
4. Papanikolaou G, Pantopoulos K. Iron metabolism and toxicity. Toxicol Appl Pharmacol. 2005;202(2):199–211.
5. Kremastinos DT, Farmakis D, Aessopos A, *et al.* β-Thalassemia cardiomyopathy: History, present considerations, and future perspectives. Circ Heart Fail. 2013;3(3):451–458.
6. Pennell DJ, Udelson JE, Arai AE, *et al.* Cardiovascular function and treatment in β-thalassemia major: A consensus statement from the American Heart Association. Circulation. 2013; 128(3):281–308.
7. Das SK, Oudit GY. Voltage-gated Ca2+ channels as key mediators of iron-transport and iron-overload cardiomyopathy: L-type vs. T-type Ca+ channels. Eur J Haematol. 2012;88(6):476–477.
8. Fleming MD, Romano MA, Su MA, *et al.* Nramp2 is mutated in the anemic Belgrade (b) rat: Evidence of a role for Nramp2 in endosomal iron transport. Proc Natl Acad Sci USA. 1998; 95(3):1148–1153.
9. Gunshin H, Mackenzie B, Berger UV, *et al.* Cloning and characterization of a mammalian proton-coupled metal-ion transporter. Nature. 1997;38(6641):482–488.
10. Aisen P. Transferrin receptor 1. Int J Biochem Cell Biol. 2004; 36(11):2137–2143.
11. Roy CN, Blemings KP, Deck KM, *et al.* Increased IRP1 and IRP2 RNA binding activity accompanies a reduction of the labile iron pool in HFE-expressing cells. J Cell Physiol. 2002;190(2):218–226.
12. Kumfu S, Chattipakorn S, Chinda K, *et al.* T-type calcium channel blockade improves survival and cardiovascular function in thalassemic mice. Eur J Haematol. 2012;88(6):535–548.
13. Kumfu S, Chattipakorn S, Srichairatanakool S, *et al.* T-type calcium channel as a portal of iron uptake into cardiomyocytes of β-thalassemic mice. Eur J Haematol. 2011;86(2):156–166.
14. Lopin KV, Gray IP, Obejero-Paz CA, *et al.* Fe^{2+} block and permeation of CaV3.1 (α1G) T-type calcium channels: Candidate

Hemoglobin Downloaded from informahealthcare.com by Chiang Mai University on 01/26/15
For personal use only.

RIGHTSLINK

mechanism for non-transferrin-mediated Fe^{2+} influx. Mol Pharmacol. 2012;82(6):1194–1204.
15. Oudit GY, Sun H, Trivieri MG, *et al.* L-type Ca2+ channels provide a major pathway for iron entry into cardiomyocytes in iron-overload cardiomyopathy. Nat Med. 2003;9(9):1187–1194.
16. Oudit GY, Trivieri MG, Khaper N, *et al.* Role of L-type Ca2+ channels in iron transport and iron-overload cardiomyopathy. J Mol Med. 2006;84(5):349–364.
17. Tsushima RG, Wickenden AD, Bouchard RA, *et al.* Modulation of iron uptake in heart by L-type Ca2+ channel modifiers: possible implications in iron overload. Circ Res. 1999;84(11):1302–1309.
18. Anderson LJ, Westwood MA, Holden S, *et al.* Myocardial iron clearance during reversal of siderotic cardiomyopathy with intravenous desferrioxamine: A prospective study using T2* cardiovascular magnetic resonance. Br J Haematol. 2004;127(3):348–355.
19. Gujja P, Rosing DR, Tripodi DJ, *et al.* Iron overload cardiomyopathy: Better understanding of an increasing disorder. J Am Coll Cardiol. 2010;56(13):1001–1012.
20. Murphy CJ, Oudit GY. Iron-overload cardiomyopathy: Pathophysiology, diagnosis, and treatment. J Card Fail. 2010; 16(11):888–900.
21. Brissot P, Ropert M, Le Lan C, *et al.* Non-transferrin bound iron: A key role in iron overload and iron toxicity. Biochim Biophys Acta. 2012;1820(3):403–410.
22. Link G, Pinson A, Hershko C. Heart cells in culture: A model of myocardial iron overload and chelation. J Lab Clin Med. 1985; 106(2):147–153.
23. Randell EW, Parkes JG, Olivieri NF, *et al.* Uptake of non-transferrin-bound iron by both reductive and nonreductive processes is modulated by intracellular iron. J Biol Chem. 1994; 269(23):16046–16053.
24. Hershko C, Link G, Cabantchik I. Pathophysiology of iron overload. Ann N Y Acad Sci. 1998;850:191–201.
25. Horwitz LD, Rosenthal EA. Iron-mediated cardiovascular injury. Vasc Med. 1999;4(2):93–99.
26. Lekawanvijit S, Chattipakorn N. Iron overload thalassemic cardiomyopathy: Iron status assessment and mechanisms of mechanical and electrical disturbance due to iron toxicity. Can J Cardiol. 2009; 25(4):213–218.
27. Shander A, Cappellini MD, Goodnough LT. Iron overload and toxicity: The hidden risk of multiple blood transfusions. Vox Sang. 2009;97(3):185–197.
28. Wood JC, Enriquez C, Ghugre N, *et al.* Physiology and pathophysiology of iron cardiomyopathy in thalassemia. Ann N Y Acad Sci. 2005;1054:386–395.
29. Bartfay WJ, Bartfay E. Iron-overload cardiomyopathy: Evidence for a free radical — mediated mechanism of injury and dysfunction in a murine model. Biol Res Nurs. 2000;2(1):49–59.
30. Gao X, Campian JL, Qian M, *et al.* Mitochondrial DNA damage in iron overload. J Biol Chem. 2009;284(8):4767–4775.
31. Gao X, Qian M, Campian JL, *et al.* Mitochondrial dysfunction may explain the cardiomyopathy of chronic iron overload. Free Radic Biol Med. 2010;49(3):401–407.
32. Zorov DB, Juhaszova M, Sollott SJ. Mitochondrial ROS-induced ROS release: An update and review. Biochim Biophys Acta. 2006; 1757(5–6):509–517.
33. Thummasorn S, Kumfu S, Chattipakorn S, *et al.* Granulocyte-colony stimulating factor attenuates mitochondrial dysfunction induced by oxidative stress in cardiac mitochondria. Mitochondrion. 2011;11(3):457–466.
34. Kumfu S, Chattipakorn S, Fucharoen S, *et al.* Ferric iron uptake into cardiomyocytes of β-thalassemic mice is not through calcium channels. Drug Chem Toxicol. 2013;36(3):329–334.
35. Parkes JG, Olivieri NF, Templeton DM. Characterization of Fe2+ and Fe3+ transport by iron-loaded cardiac myocytes. Toxicology. 1997;117(2–3):141–151.
36. Shvartsman M, Kikkeri R, Shanzer A, *et al.* Non-transferrin-bound iron reaches mitochondria by a chelator-inaccessible mechanism: Biological and clinical implications. Am J Physiol Cell Physiol. 2007;293(4):C1383–C1394.
37. Hentze MW, Muckenthaler MU, Andrews NC. Balancing acts: Molecular control of mammalian iron metabolism. Cell. 2004; 117(3):285–297.
38. Fernandes JL, Sampaio EF, Fertrin K, *et al.* Amlodipine reduces cardiac iron overload in patients with thalassemia major: A pilot trial. Am J Med. 2013;126(9):834–837.
39. Sugishita K, Asakawa M, Usui S, *et al.* A case of iron overload cardiomyopathy: Beneficial effects of iron chelating agent and calcium channel blocker on left ventricular dysfunction. Int Heart J. 2009;50(6):829–838.
40. Ke Y, Chen YY, Chang YZ, *et al.* Post-transcriptional expression of DMT1 in the heart of rat. J Cell Physiol. 2003;196(1):124–130.
41. Davis MT, Bartfay WJ. Ebselen decreases oxygen free radical production and iron concentrations in the hearts of chronically iron-overloaded mice. Biol Res Nurs. 2004;6(1):37–45.
42. Huang B, Qin D, Deng L, *et al.* Reexpression of T-type Ca2+ channel gene and current in post-infarction remodeled rat left ventricle. Cardiovasc Res. 2000;46(3):442–449.
43. Martinez ML, Heredia MP, Delgado C. Expression of T-type Ca^{2+} channels in ventricular cells from hypertrophied rat hearts. J Mol Cell Cardiol. 1999;31(9):1617–1625.
44. Liuzzi JP, Aydemir F, Nam H, *et al.* Zip14 (Slc39a14) mediates non-transferrin-bound iron uptake into cells. Proc Natl Acad Sci USA. 2006;103(37):13612–13617.
45. Nam H, Wang CY, Zhang L, *et al.* ZIP14 and DMT1 in the liver, pancreas, and heart are differentially regulated by iron deficiency and overload: Implications for tissue iron uptake in iron-related disorders. Haematologica. 2013;98(7):1049–1057.
46. Mainous AG III, Weinberg ED, Diaz VA, *et al.* Calcium channel blocker use and serum ferritin in adults with hypertension. Biometals. 2012;25(3):563–568.
47. Parkes JG, Liu Y, Sirna JB, *et al.* Changes in gene expression with iron loading and chelation in cardiac myocytes and non-myocytic fibroblasts. J Mol Cell Cardiol. 2000;32(2):233–246.
48. Liu Y, Parkes JG, Templeton DM. Differential accumulation of non-transferrin-bound iron by cardiac myocytes and fibroblasts. J Mol Cell Cardiol. 2003;35(5):505–514.
49. Zhao N, Sun Z, Mao Y, *et al.* Myocardial iron metabolism in the regulation of cardiovascular diseases in rats. Cell Physiol Biochem. 2010;25(6):587–594.
50. Rodriguez A, Hilvo M, Kytomaki L, *et al.* Effects of iron loading on muscle: Genome-wide mRNA expression profiling in the mouse. BMC Genomics. 2007;8:379.
51. Qian ZM, Chang YZ, Leung G, *et al.* Expression of ferroportin1, hephaestin and ceruloplasmin in rat heart. Biochim Biophys Acta. 2007;1772(5):527–532.
52. Chen YY, Xia Q, Qian ZM. [Developmental expression and regulation of divalent metal transporter 1 in rat heart]. Zhejiang Da Xue Xue Bao Yi Xue Ban. 2003;32(2):131–136.
53. Kim DW, Kim KY, Choi BS, *et al.* Regulation of metal transporters by dietary iron, and the relationship between body iron levels and cadmium uptake. Arch Toxicol. 2007;81(5):327–334.
54. Crowe S, Bartfay WJ. Amlodipine decreases iron uptake and oxygen free radical production in the heart of chronically iron overloaded mice. Biol Res Nurs. 2002;3(4):189–197.
55. Musumeci M, Maccari S, Sestili P, *et al.* The C57BL/6 genetic background confers cardioprotection in iron-overloaded mice. Blood Transfus. 2013;11(1):88–93.
56. Otto-Duessel M, Brewer C, Wood JC. Interdependence of cardiac iron and calcium in a murine model of iron overload. Transl Res. 2011;157(2):92–99.

Hemoglobin Downloaded from informahealthcare.com by Chiang Mai University on 01/26/15
For personal use only.

RIGHTSLINK

เอกสารแนบหมายเลข 64

METABOLISM CLINICAL AND EXPERIMENTAL 63 (2014) 851–859

Available online at www.sciencedirect.com

Metabolism

www.metabolismjournal.com

Estrogen restores brain insulin sensitivity in ovariectomized non-obese rats, but not in ovariectomized obese rats

Wasana Pratchayasakul[a,b], Nipon Chattipakorn[a,b], Siriporn C. Chattipakorn[a,c,*]

[a] Neurophysiology Unit, Cardiac Electrophysiology Research and Training Center, Faculty of Medicine, Chiang Mai University, Chiang Mai, Thailand

[b] Cardiac Electrophysiology Unit, Department of Physiology, Faculty of Medicine, Chiang Mai University, Chiang Mai, Thailand

[c] Department of Oral Biology and Diagnostic Science, Faculty of Dentistry, Chiang Mai University, Chiang Mai, Thailand

ARTICLE INFO

Article history:
Received 29 October 2013
Accepted 17 March 2014

Keywords:
High-fat diet
Ovariectomy
Insulin-induced LTD
Brain insulin signaling

ABSTRACT

Objective. We previously demonstrated that obesity caused the reduction of peripheral and brain insulin sensitivity and that estrogen therapy improved these defects. However, the beneficial effect of estrogen on brain insulin sensitivity and oxidative stress in either ovariectomy alone or ovariectomy with obesity models has not been determined. We hypothesized that ovariectomy alone or ovariectomy with obesity reduces brain insulin sensitivity and increases brain oxidative stress, which are reversed by estrogen treatment.

Materials/Methods. Thirty female rats were assigned as either sham-operated or ovariectomized. After the surgery, each group was fed either a normal diet or high-fat diet for 12 weeks. At week 13, rats in each group received either the vehicle or estradiol for 30 days. At week 16, blood and brain were collected for determining the peripheral and brain insulin sensitivity as well as brain oxidative stress.

Results. We found that ovariectomized rats and high-fat diet fed rats incurred obesity, reduced peripheral and brain insulin sensitivity, and increased brain oxidative stress. Estrogen ameliorated peripheral insulin sensitivity in these rats. However, the beneficial effect of estrogen on brain insulin sensitivity and brain oxidative stress was observed only in ovariectomized normal diet-fed rats, but not in ovariectomized high fat diet-fed rats.

Conclusions. Our results suggested that reduced brain insulin sensitivity and increased brain oxidative stress occurred after either ovariectomy or obesity. However, the reduced brain insulin sensitivity and the increased brain oxidative stress in ovariectomy with obesity could not be ameliorated by estrogen treatment.

© 2014 Elsevier Inc. All rights reserved.

Abbreviations: HFD, high-fat diet; OVX, ovariectomy; sham, sham-operated; HFOE, ovariectomized HFD-fed rats with estradiol administration; HFOV, ovariectomized HFD-fed rats with vehicle treatment; HFSV, sham HFD-fed rats with vehicle treatment; ND, normal diet; NDOE, ovariectomized ND-fed rats with estradiol administration; NDOV, ovariectomized ND-fed rats with vehicle administration; NDSV, sham ND-fed rats with vehicle administration; OVX, ovariectomized; LTD, long term depression; Akt/PKB, serine/threonine protein kinase/protein kinase B; IR, insulin receptor; MDA, malondialdehyde; ROS, reactive oxygen species; TBA, thiobabituric acid solution; TCA, trichloroacetic acid; aCSF, artificial cerebrospinal fluid; BHT, butylated hydroxytoluene.

* *Corresponding author at:* Department of Oral Biology and Diagnostic Science, Faculty of Dentistry, Chiang Mai University, Chiang Mai, Thailand 50200. Tel.: +66 53 944 451; fax: +66 53 222 844.

E-mail addresses: s.chat@chiangmai.ac.th, scchattipakorn@gmail.com (S.C. Chattipakorn).

http://dx.doi.org/10.1016/j.metabol.2014.03.009
0026-0495/© 2014 Elsevier Inc. All rights reserved.

1. Introduction

The loss of ovarian function associated with menopause or ovariectomy (OVX) has been shown to be related to increased oxidative stress levels in several organs [1–3]. It is known that oxidative stress plays a role in the impairment of insulin sensitivity via the inactivation of insulin signaling [4,5]. In addition, several studies showed that OVX caused the reduction of insulin sensitivity, which may progress to peripheral insulin resistance, obesity, and the development of Type II diabetes [6,7]. Several studies showed that estrogen therapy reduced peripheral insulin resistance, indicated by improved insulin sensitivity, reduced obesity, lowered lipid and cholesterol levels and decreased oxidative stress levels [8–11].

Our previous studies have shown that obesity induced by a high-fat diet (HFD) led to not only peripheral insulin resistance, but also brain insulin resistance, indicated by the impairment of insulin-induced long term depression (LTD) [12–14]. We also demonstrated that obesity increased brain oxidative stress, as indicated by increased brain malondialdehyde (MDA) levels and brain mitochondrial reactive oxygen species (ROS) production [12,15]. Furthermore, we previously demonstrated that chronic (30-day) administration of estrogen attenuated the occurrence of obesity-induced brain insulin resistance in female rats with intact ovary [13]. However, the effects of OVX alone on the brain insulin sensitivity and brain oxidative stress, and the effect of estrogen replacement on brain insulin sensitivity and brain oxidative stress in this model have not been investigated. Furthermore, the effects of estrogen administration on peripheral and brain insulin sensitivity as well as brain oxidative stress in the model of OVX combined with obesity induced by HFD have never been determined. In the present study, we tested the hypotheses that 1) OVX alone or OVX combined with obesity leads to reduced peripheral and brain insulin sensitivity and increased brain oxidative stress and 2) estrogen administration ameliorates the peripheral and brain insulin sensitivity as well as decreased brain oxidative stress that occurred following OVX alone or OVX combined with obesity.

2. Materials and methods

2.1. Animal models and experimental protocols

All experiments were conducted in accordance with an approved protocol from the Faculty of Medicine, Chiang Mai University Institutional Animal Care and Use Committee, in compliance with NIH guidelines. Thirty female Wistar rats weighing 180–200 g (~ 6–7 weeks old) were obtained from the National Animal Center, Salaya Campus, Mahidol University, Thailand. All animals were individually housed in a temperature and light-controlled environment (12 h of light and 12 h of dark). Rats were randomly assigned as either sham-operated (sham; S; n = 10) or ovariectomized (OVX; O; n = 20). One week after the OVX surgery, rats were fed either a normal diet (ND; 19.7% E fat) or a high-fat diet (HFD; 59.3 % E fat) for 12 weeks. Animals in the ND group were fed with a standard laboratory pellet diet (Mouse Feed Food No. 082, C.P. Company, Bangkok, Thailand). Animals in the HFD group were fed a diet containing 59.3% total energy from fat, the major composition of fat was saturated fatty acid from lard as described in our previous study [14]. During week 13, rats in each dietary group were divided to receive subcutaneous administration of either vehicle (V; 90% sesame oil + 10% ethanol) or estrogen (E; 50 μg/kg estradiol velerate; Progynon, Schering, Berlin, Germany) for 30 consecutive days, as described in our previous study [13]; rats were still presented either an ND or HFD feeding during the treatment period. Thus, there was a total of six experimental subgroups (n = 5/subgroup) in this study that included sham ND-fed rats with vehicle administration (NDSV), ovariectomized ND-fed rats with vehicle administration (NDOV), ovariectomized ND-fed rats with estradiol administration (NDOE), sham HFD-fed rats with vehicle treatment (HFSV), ovariectomized HFD-fed rats with vehicle treatment (HFOV) and ovariectomized HFD-fed rats with estradiol administration (HFOE). The animals were housed in individual cages with free access to food and water. Body weight and food intake were recorded daily. At the end of the experimental periods (Week 16), animals were deeply anesthetized with isoflurane after fasting for at least five hours and decapitated. Blood samples were collected, the plasma was separated and stored at −80 °C for subsequent biochemical analyses including plasma glucose, total cholesterol, triglyceride, insulin and estrogen assay. Total visceral fat, including peritoneal, periovarian and perirenal fat pads, was removed and weighed. The brain was rapidly removed for electrophysiological and biochemical analyses including insulin-induced LTD, IR and Akt/PKB phosphorylation and MDA level.

2.2. Ovariectomy procedure

Female rats were anesthetized with xylazine (LBS Laboratories, Bangkok, Thailand; 0.15 ml/kg) and Zoletil (Virbac Laboratories, Carros, France; 50 mg/kg). The bilateral ovariectomy was performed through a midline dorsal skin incision. The incision was centered between the bottom of the rib cage and the front of the hind limb. The skin was separated from the underlying muscle. The connections between the uterine tubes and uterine horn inside peritoneal cavity were transected, the ovaries were removed and the incision was closed.

2.3. Chemical analyses for glucose, total cholesterol, triglyceride, insulin and estrogen levels

Fasting plasma glucose, total cholesterol and triglyceride concentrations were determined by colorimetric assay using commercially available kits (Biotech, Bangkok, Thailand). The fasting plasma insulin levels were measured by Sandwich ELISA kits (LINCO Research, Missouri, USA). Serum estrogen levels were measured using an enzyme immunoassay kit (Cayman Chemical, Ann Arbor, Michigan, USA).

2.4. Determination of insulin resistance (HOMA index)

Insulin resistance was assessed by the Homeostasis Model Assessment (HOMA) index [16], as a mathematical model describing the degree of insulin resistance, calculated from the fasting plasma insulin and the fasting plasma glucose concentration. A higher HOMA index indicated a higher degree of insulin resistance.

2.5. Brain slice preparation

At the end of experimental period, the animals were anesthetized with isoflurane after fasting for at least five hours. Brain slice preparation followed our previous study guidelines [17]. After decapitation, the brain was removed and immersed in ice-cold "high sucrose" aCSF containing (mmol/L): NaCl 85; KCl 2.5; $MgSO_4$ 4; $CaCl_2$ 0.5; NaH_2PO_4 1.25; $NaHCO_3$ 25; glucose 25; sucrose 75; kynurenic acid 2; ascorbate 0.5, saturated with 95% O_2/5% CO_2 (pH 7.4). Hippocampal slices were cut using a vibratome (Vibratome, St. Louis, Missouri, USA). Following a 30-min post-slice incubation in high sucrose aCSF, slices were transferred to a standard aCSF solution containing (mmol/L): NaCl 119; KCl 2.5; $CaCl_2$ 2.5; $MgSO_4$ 1.3; NaH_2PO_4 1; $NaHCO_3$ 26; and glucose 10, saturated with 95% O_2/5% CO_2 (pH 7.4) for an additional 30 min, before being used for the extracellular recordings.

2.6. Extracellular recording of hippocampal slices

To investigate insulin-induced long-term depression (LTD), the hippocampal slices were transferred to a submersion recording chamber and continuously perfused at three to four ml/min with standard aCSF warmed to 25–28 °C). Field excitatory postsynaptic potentials (fEPSPs) were evoked by stimulating the Schaffer collateral–commissural pathway with a bipolar tungsten electrode, while recordings were gathered from the stratum radiatum of the hippocampal CA1 region with micropipettes (3 Mohm) filled with 2 mol/L NaCl. The stimulus frequency was 0.033 Hz. The stimulus intensity was adjusted to yield an fEPSP of 0.8–1.0 mV in amplitude. Hippocampal slices were perfused with aCSF (as baseline condition) for ten minutes and then perfused with aCSF plus 500 nmol/L insulin (as insulin stimulation) for ten minutes, after which the hippocampal slices were perfused with aCSF again (wash out) and recorded for the next 30 min. All data were filtered at 3 kHz, digitized at 10 kHz, and stored on a computer using pClamp 9.2 software (Axon Instruments, Foster City, CA, USA). The initial slope of the fEPSPs was measured and plotted versus time using Origin 8.0 software.

2.7. Preparation of brain homogenates for immunoblotting

To examine the alteration of brain insulin-mediated phosphorylation of the IR and Akt/PKB, eight whole brain slices per animal were placed into either aCSF or aCSF plus 500 nmol/L insulin (Humulin R, Eli Lilly, Giessen, Germany) for five minutes. Then, four whole brain slices in each conditioned group were homogenized in 500 μl of ice-cold brain slice lysis buffer [1 mmol/L EDTA, 1 mmol/L EGTA, 1% NP-40, 1% Triton X-100 and supplemented with a protease inhibitor cocktail (Roche complete mini-tablets, Roche Molecular Biochemicals, Indianapolis, Indiana, USA)]. Next, the homogenates were centrifuged at 15,000 *g* for 30 min at 4 °C and the protein concentration was measured from cytosol fraction by using the Bio-Rad DC Protein assay kit (Bio-Rad Laboratories, Hercules, California, USA). These cytosol fractions were then stored at −80 °C for further biochemical analysis of the tyrosine phosphorylation of IR and the serine phosphorylation of Akt/PKB. To determine the level of IR and Akt/PKB protein expression in the brain, another set of four whole brain slices in aCSF was homogenized over ice in non-ionizing lysis buffer containing: 100 mmol/L NaCl, 25 mmol/L EDTA, 10 mmol/L Tris, 1% Triton X-100, 1% NP-40 supplemented with a protease inhibitor cocktail (Roche Molecular Biochemicals).

2.8. Immunoblotting

IR tyrosine phosphorylation and Akt/PKB at serine 473 kinases phosphorylation were electrophoresed and immunoblotted with rabbit antibodies for IR at tyrosine and Akt/PKB at serine 473, respectively. Examination of the level of IR and Akt/PKB protein expression was conducted with homogenates prepared from another set of four whole brain slices. These proteins were resolved by the immunoblot assay conducted with rabbit anti-IR at tyrosine phosphorylation, IR, Akt/PKB at serine 473 kinases phosphorylation and Akt/PKB (Santa Cruz Biotechnology, California, USA). For loading control, immunoblotting for each membrane was incubated with anti-β-actin (1:400; rabbit polyclonal; Sigma, St. Louis, Missouri, USA). All membranes for visualizing the phosphorylation and the protein levels of IR and Akt/PKB expression were incubated with secondary goat anti-rabbit antibody conjugated with horseradish peroxidase (1:8000 in TBST, Bio-Rad Laboratories). The protein bands were visualized on Amersham hyperfilm ECL (GE Healthcare, Buckinghamshire, UK) using Amersham ECL western blotting detection reagents (GE Healthcare). Band intensities were quantified by Scion Image and the results were shown in average signal intensity (arbitrary) units.

2.9. Brain malondialdehyde (MDA) level

Brain malondialdehyde (MDA) level, an indicator of oxidative stress, was determined by a high performance liquid chromatography (HPLC) method [18]. Briefly, the brain homogenates were mixed with 10% trichloroacetic acid (TCA) containing butylated hydroxytoluene (BHT), incubated at 90 °C for 30 min, and centrifuged at 6000 rpm for 10 min. The supernatant was mixed with H_3PO_4 and thiobabituric acid solution (TBA), incubated at 90 °C for 30 min. MDA levels were measured via the absorbance detected at 532 nm by the HPLC system, and were determined directly from the standard curve, and reported as the MDA equivalent concentration.

2.10. Statistical analysis

Data are presented as mean ± SEM. All statistical analyses were performed using the program SPSS (version 16; SPSS, Chicago, Ill., USA). For all comparisons, the significance of the difference between the mean were calculated by a three-way ANOVA and post-hoc analysis with Fisher's test with $p < 0.05$.

3. Results

3.1. Estradiol administration improved peripheral insulin sensitivity in both ovariectomized ND-fed rats and ovariectomized HFD-fed rats

Rats exposed to an HFD for 12 weeks increased body weight and reduced insulin sensitivity as evidenced by increased fasting

Table 1 – Estrogen administration improved the body weight, visceral fat, uterine weight and plasma estrogen level in both ovariectomized rats and HFD-fed rats.

Group	Food intake (g/wk)	Body weight (g)	Visceral fat (g)	Uterine weight (g)	Plasma Estrogen (pg/ml)
NDSV	97.00 ± 2.00	271.00 ± 6.40	14.97 ± 1.04	0.51 ± 0.05	135.20 ± 12.69
NDOV	89.00 ± 6.40	332.00 ± 19.85 †	18.27 ± 1.46	0.14 ± 0.02 †	29.53 ± 8.60 †
NDOE	102.00 ± 4.63	275.00 ± 14.32 ‡	12.86 ± 2.01	0.83 ± 0.18 ‡	226.92 ± 19.23 ‡
HFSV	106.00 ± 5.34	422.00 ± 27.46 *	46.43 ± 3.42 *	0.53 ± 0.07	135.03 ± 16.84
HFOV	103.00 ± 7.18	490.00 ± 33.42 *,†	52.46 ± 6.55 *	0.41 ± 0.08 *	78.63 ± 23.67 †
HFOE	105.00 ± 4.47	350.00 ± 20.98 *,‡	27.75 ± 3.80 *,‡	0.85 ± 0.05 ‡	264.45 ± 22.95 ‡

*$p < 0.05$ compared with normal diet group in the same experimental subgroups, †$p < 0.05$ compared with sham-operated group in the same experimental subgroup, ‡$p < 0.05$ compared with vehicle-treated group in the same experimental subgroup; n = 4–5/group; NDSV = sham ND-fed rats with vehicle administration, NDOV = ovariectomized ND-fed rats with vehicle administration, NDOE = ovariectomized ND-fed rats with estradiol administration, HFSV = sham HFD-fed rats with vehicle treatment, HFOV = ovariectomized HFD-fed rats with vehicle treatment, HFOE = ovariectomized HFD-fed rats with estradiol administration.

plasma total cholesterol, fasting plasma insulin and HOMA index (Table 1, Fig. 1). In addition, ovariectomy (OVX) reduced insulin sensitivity in ND feeding, as evidenced by increased body weight, fasting plasma glucose levels, fasting plasma insulin levels and HOMA index (Table 1, Fig. 1). Interestingly, OVX increased the severity of reduced insulin sensitivity in the obese group as shown by significantly increased plasma total cholesterol, plasma insulin levels and HOMA index, compared with sham HF-fed rats and ovariectomized ND-fed rats (Fig. 1). However, the estrogen therapy for 30 days had significantly positive effects on improving insulin sensitivity in both ovariectomized ND-fed rats and ovariectomized HFD-fed rats, as indicated by decreased body weight, visceral fat, fasting plasma total cholesterol levels, fasting plasma glucose levels, fasting plasma insulin levels and HOMA index (Table 1, Fig. 1). Moreover, we found that the fasting plasma triglyceride was not significantly different between experimental groups (NDSV: 273.80 ± 16.82 mg%; NDOV: 299.00 ± 9.91 mg%; NDOE: 301.40 ± 6.81 mg%; HFSV: 301.80 ± 22.93 mg%; HFOV: 301.40 ± 17.16 mg%; and HFOE : 299.60 ± 7.95 mg %).

Furthermore, we confirmed the effect of OVX by determining uterine weight and serum estrogen levels. We found that OVX resulted in decreased uterine weight and serum estrogen levels in both ND- and HFD-fed rats (Table 1). However, one month of estrogen therapy significantly attenuated these effects, compared to the vehicle-treated ND rats or vehicle-treated HFD rats ($p < 0.05$; Table 1). In addition, our study demonstrated that there was no significant difference of serum estradiol level between both dietary groups; this result was consistent with previous studies [19,20].

3.2. *Estradiol administration prevented the impairment of brain insulin receptor function only in ovariectomized ND-fed rats, but not in ovariectomized HFD-fed rats*

Brain insulin receptor function in hippocampus was determined by insulin-induced LTD. In ND-fed rats, we found that 500 nmol/L insulin applied to hippocampal slices reduced the size of the fEPSP responses or insulin-induced LTD in the sham-operated group. In contrast, insulin-induced LTD was impaired in ovariectomized ND-fed rats. However, one month of estrogen therapy reversed that impairment of insulin-induced LTD in ovariectomized ND-fed rats. In addition, the percentage of insulin-mediated LTD observed from slices of sham ND-fed rats with vehicle administration and ovariectomized ND-fed rats with estrogen administration was not significantly different (n = 8–9 independent slices per group, n = 4–5 animals/group, Fig. 2A). These findings suggest that the OVX alone in non-obese rats can lead to the impairment of brain insulin receptor function, and estrogen therapy could reverse that impairment.

In HFD-fed rats, insulin-induced LTD was impaired following obesity as indicated by the disappearance of insulin-induced LTD in the hippocampus of sham HFD-fed rats (n = 8–9 independent slices per group, n = 4–5 animals/group, Fig. 2B). In addition, OVX impaired insulin-induced LTD to the same percentages as sham HFD-fed rats. Interestingly, estradiol administration did not reverse that impairment effect in ovariectomized HFD-fed rats (Fig. 2B). These findings suggest that either obesity or OVX can lead to the impairment of brain insulin receptor function; however, estrogen therapy could not reverse that impairment in obese rats with OVX.

3.3. *Estradiol administration improved brain insulin signaling only in ovariectomized ND-fed rats, but not in ovariectomized HFD-fed rats*

To investigate mechanisms associated with the beneficial effects of estradiol administration on brain insulin receptor function, we determined whether estradiol improves brain insulin signaling, particularly IR and Akt/PKB signaling in the brain. Our results demonstrated that the level of IR and Akt/PKB proteins was not different in both sham and ovariectomized (OVX) rats receiving either ND or HFD. Furthermore, estradiol administration did not alter IR and Akt/PKB protein expressions in the brain of all treatment groups (Figs. 3A, 4A). However, the levels of tyrosine phosphorylation of IR and Akt/PKB phosphorylation at the serine 473 site were significantly decreased following either obesity or OVX. In ND-fed rats, we found that IR and Akt/PKB phosphorylation were impaired following an OVX (Figs. 3B, 4B). Similar to the insulin-induced LTD data, we found that 30 days of estrogen therapy reversed the impairment of insulin-mediated IR and Akt/PKB phosphorylation (Figs. 3B, 4B). These findings suggest that OVX in non-obese rats can lead to the impairment of brain insulin receptor function possibly via decreased IR and Akt/PKB phosphorylation, and that estrogen therapy could reverse this impairment. In HFD-fed rats, IR and Akt/PKB phosphorylation

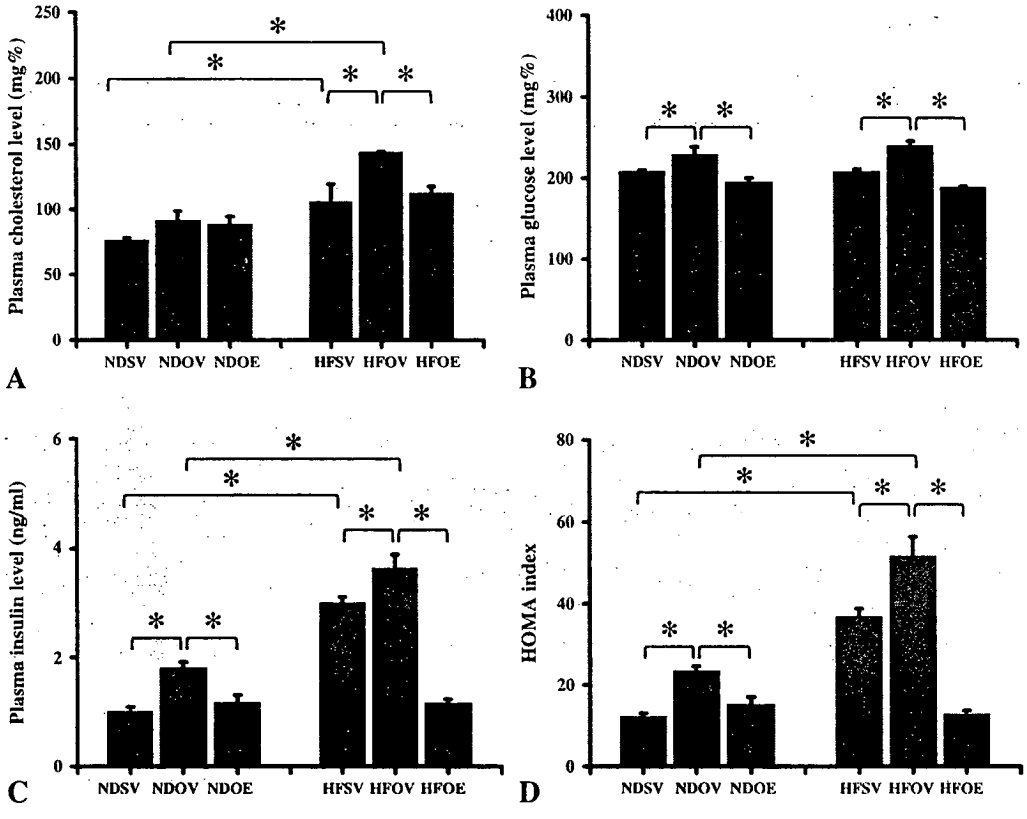


Fig. 1 – Estradiol administration improved peripheral insulin sensitivity in ovariectomized rats. (A) Plasma cholesterol level (mg%), (B) plasma glucose level (mg%), (C) plasma insulin level (ng/ml) and (D) HOMA index from the NDSV, NDOV, NDOE, HFSV, HFOV, and HFOE groups. *$p < 0.05$ compared with the same experimental subgroups; n = 4–5/group; NDSV = sham ND-fed rats with vehicle administration, NDOV = ovariectomized ND-fed rats with vehicle administration, NDOE = ovariectomized ND-fed rats with estradiol administration, HFSV = sham HFD-fed rats with vehicle treatment, HFOV = ovariectomized HFD-fed rats with vehicle treatment, HFOE = ovariectomized HFD-fed rats with estradiol administration.

were impaired following obesity (Figs. 3B, 4B). In addition, the ovariectomized HFD-fed rats had impaired IR and Akt/PKB phosphorylation to the same degree as in the sham HFD-fed rats. Interestingly, estrogen therapy prevented the impairment of IR and Akt/PKB phosphorylation in the sham HFD-fed rats, but not in the ovariectomized HFD-fed rats (Figs. 3B, 4B).

3.4. *The combination of high-fat diet consumption and estrogen deprivation increased the severity of brain oxidative stress levels*

Several studies demonstrated that the oxidative stress plays a role on the impairment of insulin signaling and synaptic plasticity [4,21]. Moreover, either the obesity alone or OVX alone caused the increment of oxidative stress in the brain [15,22]. In the present study, brain oxidative stress was determined by MDA level. We found that brain MDA level significantly increased following either obese induced by HFD or OVX, compared with sham ND-fed rats (Fig. 5). Interestingly, the brain MDA level in ovariectomized HFD-fed rats was significantly higher than the other treatment groups ($p < 0.05$, Fig. 5). This result suggests that the combination of obesity and OVX enhances the severity of oxidative damage in the brain. In addition, one month of estradiol administration significantly decreased the brain MDA level in ovariectomized ND-fed rats, but not in ovariectomized HFD-fed rats ($p < 0.05$, Fig. 5).

4. Discussion

The major findings of the present study are 1) non-obese rats with OVX caused the impairment of peripheral and brain insulin sensitivity as well as increased brain oxidative stress, 2) obese rats induced by HFD consumption with or without OVX also caused the impairment of peripheral and brain insulin sensitivity as well as increased brain oxidative stress, 3) estrogen therapy improved the peripheral insulin sensitivity in non-obese rats with OVX as well as obese rats with and without OVX, and 4) estrogen therapy improved the brain insulin sensitivity and brain oxidative stress only in non-obese rats with OVX, but not in obese rats with OVX.

The present study observed that obese rats without OVX caused the impairment of peripheral and brain insulin sensitivity. The excess saturated fatty acid intake from HFD led to an accumulation of saturated fatty in adipose tissues as indicated by increased visceral fat. In addition to weight gain in the HFD

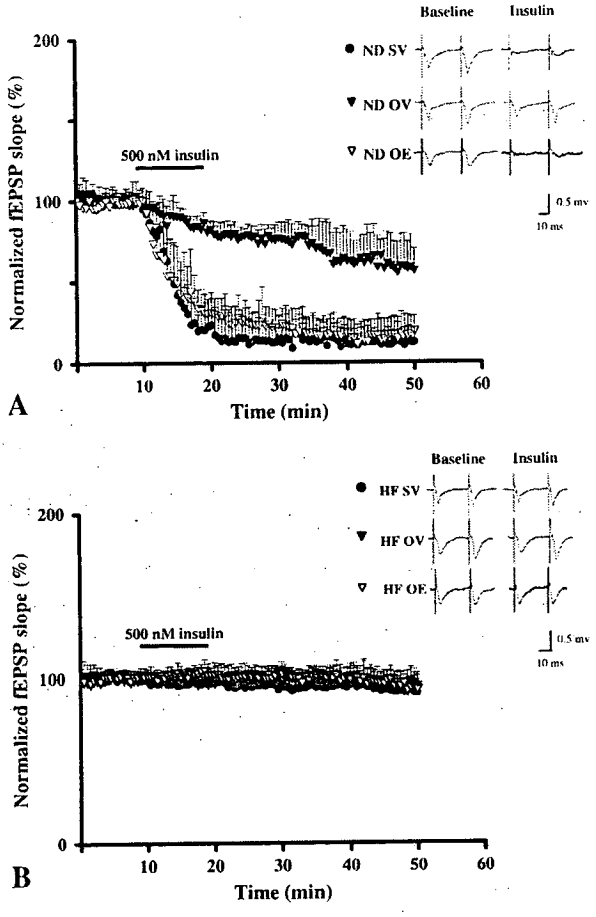


Fig. 2 – Estrogen administration for 30 days significantly improved the impairment of insulin-mediated long term depression in the CA1 hippocampus only in ovariectomized ND-fed rats, but not in ovariectomized HFD-fed rats. (A) A summary of average normalized fEPSPs (fEPSPt/fEPSPo with fEPSPs being points at which fEPSP slopes stabilized) from NDSV, NDOV and NDOE (n = 8–9 independent slices, n = 4–5 animals/group) brain slices; NDSV = sham ND-fed rats with vehicle administration, NDOV = ovariectomized ND-fed rats with vehicle administration, NDOE = ovariectomized ND-fed rats with estradiol administration (B) A summary of average normalized fEPSPs (fEPSPt/fEPSPo with fEPSPs being points at which fEPSP slopes stabilized) from HFSV, HFOV and HFOE (n = 8–9 independent slices, n = 4–5 animals/group) brain slices; HFSV = sham HFD-fed rats with vehicle treatment, HFOV = ovariectomized HFD-fed rats with vehicle treatment, HFOE = ovariectomized HFD-fed rats with estradiol administration.

group, the excess saturated fatty acids from HFD could affect the insulin signaling by stimulating several potential mediators such as diacylglycerol, inflammatory cytokines, immune cells and oxidative stress [23–25] causing the impairment of insulin signaling cascades, thus leading to decreased insulin sensitivity [12,14,23,26]. Several mechanisms have been shown to be responsible for the reduction of insulin sensitivity caused by HFD including lipotoxicity [27], adipocyte derived hormone [28], sympathetic over-activity [29] and increased oxidative stress [23]. Consistent with previous reports, our data emphasized the role of oxidative stress caused by HFD, leading to the reduction of insulin sensitivity as observed in the present study.

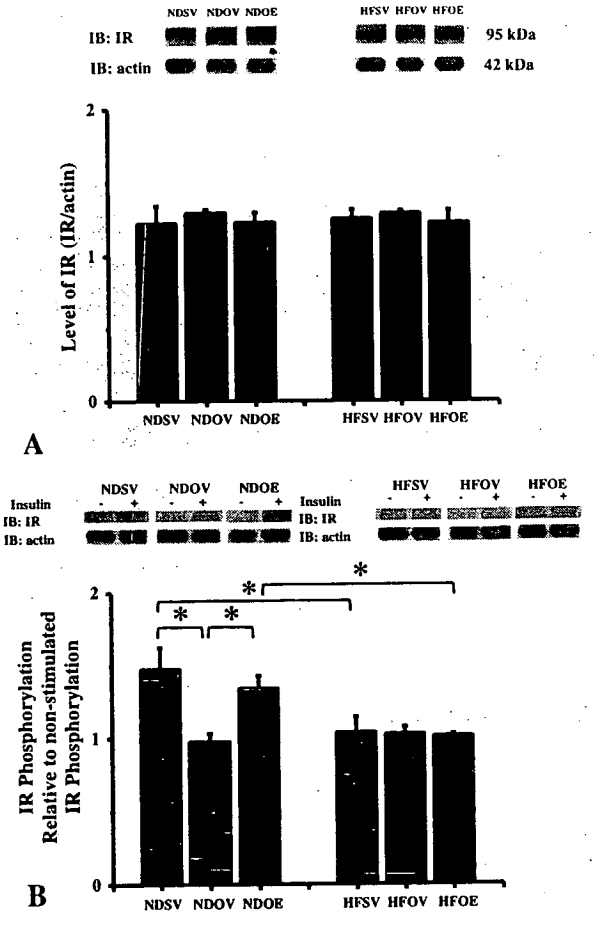


Fig. 3 – Estrogen administration for 30 days significantly improved the impairment of insulin-induced tyrosine phosphorylation of brain IR only in the ovariectomized ND-fed rat, but not in ovariectomized HFD-fed rats. (A) Representative blots of protein level of IR in brain slices harvested from the NDSV, NDOV, NDOE, HFSV, HFOV and HFOE groups. The densitometric quantitation of blots from all groups was not different. (B) Representative blots of IR tyrosine phosphorylation in brain slices harvested from the NDSV, NDOV, NDOE, HFSV, HFOV and HFOE groups. All immunoblotting lanes were loaded with equal amounts of protein (40 μg/lane). *$p < 0.05$ compared with the same experimental subgroups; n = 4–5/group; NDSV = sham ND-fed rats with vehicle administration, NDOV = ovariectomized ND-fed rats with vehicle administration, NDOE = ovariectomized ND-fed rats with estradiol administration, HFSV = sham HFD-fed rats with vehicle treatment, HFOV = ovariectomized HFD-fed rats with vehicle treatment, HFOE = ovariectomized HFD-fed rats with estradiol administration; –, no insulin stimulation; +, insulin stimulation.

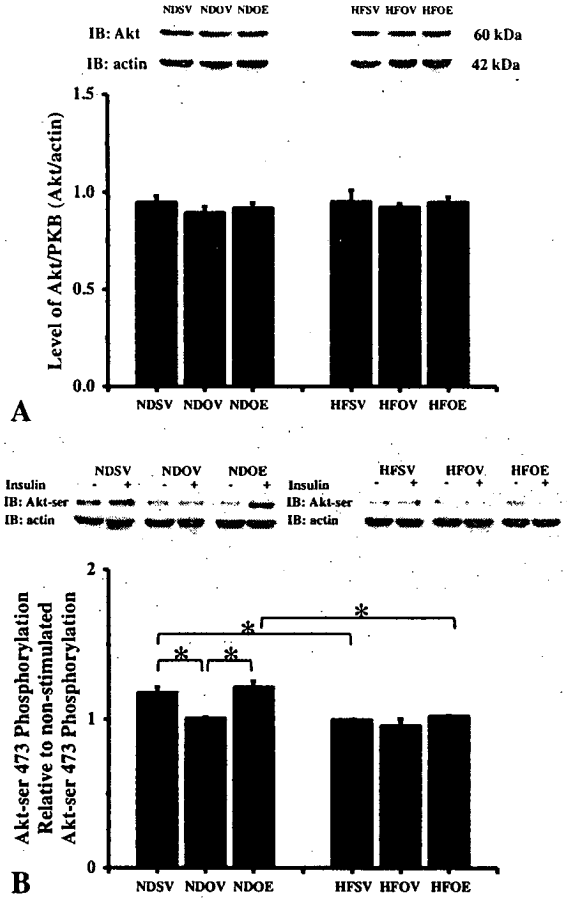


Fig. 4 – Estrogen administration for 30 days significantly improved the impairment of insulin-induced serine phosphorylation of brain Akt/PKB only in the ovariectomized ND-fed rat, but not in ovariectomized HFD-fed rats.
(A) Representative blots of protein level of AKt/PKB in brain slices harvested from the NDSV, NDOV, NDOE, HFSV, HFOV and HFOE groups. The densitometric quantitation of blots from all groups was not different. (B) Representative blots of serine 473 kinase of Akt/PKB phosphorylation in brain slices harvested from the NDSV, NDOV, NDOE, HFSV, HFOV and HFOE groups. All immunoblotting lanes were loaded with equal amounts of protein (40 μg/lane). *p < 0.05 compared with the same experimental subgroups; n = 4–5/group; NDSV = sham ND-fed rats with vehicle administration, NDOV = ovariectomized ND-fed rats with vehicle administration, NDOE = ovariectomized ND-fed rats with estradiol administration, HFSV = sham HFD-fed rats with vehicle treatment, HFOV = ovariectomized HFD-fed rats with vehicle treatment, HFOE = ovariectomized HFD-fed rats with estradiol administration; –, no insulin stimulation; +, insulin stimulation.

We also found that non-obese rats with OVX had impaired peripheral and brain insulin sensitivity. This is consistent with previous studies demonstrating that OVX rats developed obesity, dyslipidemia, impaired glucose tolerance and impaired insulin-mediated glucose uptake [30,31]. Therefore, the impairment of peripheral and brain insulin sensitivity following OVX could be due to increased fat mass, increased plasma lipid profiles, hyperglycemia, elevated inflammatory markers and enhanced oxidative stress in OVX models as shown in the present study and others [32,33]. Our present study demonstrated that obese rats as well as OVX rats did not have hypertriglyceridemia, compared to lean rats. No change in hypertriglyceridemia in our study was similar to other previous studies, in which OVX rats [31,34,35] as well as HFD-fed animals did not develop hypertriglyceridemia [14,36,37]. It has been shown that excessive intake of fat initially leads to an accumulation of triglyceride in liver and adipose tissues. After both liver and adipose tissues are saturated with triglyceride, the hypertriglyceridemia will be observed [36–38]. In addition, the lack of estrogen effect on plasma triglyceride levels has been observed in the present study. These findings are similar with previous studies [31,35].

The reduction of peripheral insulin sensitivity in obese with or without OVX and non-obese rats with OVX could be reversed by estrogen therapy. Our findings confirmed the therapeutic effects of exogenous estrogen on the impairment of peripheral insulin sensitivity induced by OVX as shown in several previous studies [30,31,39]. Moreover, chronic administration of estradiol to OVX HFD-fed mice was recently shown to protect against glucose intolerance and insulin resistance, and to improve insulin signaling in skeletal muscles, when compared with vehicle-treated control mice [40].

Moreover, the present study was the first study to demonstrate that reduced brain insulin sensitivity occurs in the OVX non-obese rats and that estrogen treatment can restore brain insulin sensitivity. The beneficial effect of estrogen in brain may be due to the action of estrogen in improving peripheral insulin sensitivity and directly decreased brain oxidative stress levels as shown in the present study. Furthermore, several studies showed that estrogen may play an important role in moderating brain glucose metabolism via enhanced glucose uptake into the

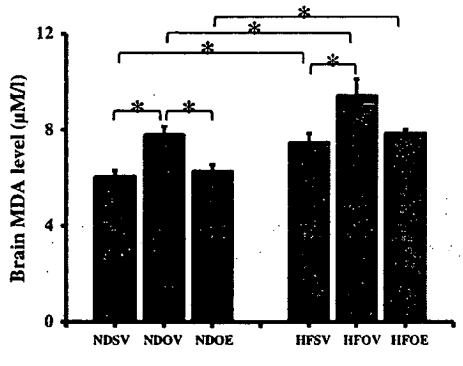


Fig. 5 – The combination of obesity and OVX could accelerate the severity of brain malondialdehyde (MDA) level. *p < 0.05 compared with the same experimental subgroups; n = 4–5/group; NDSV = sham ND-fed rats with vehicle administration, NDOV = ovariectomized ND-fed rats with vehicle administration, NDOE = ovariectomized ND-fed rats with estradiol administration, HFSV = sham HFD-fed rats with vehicle treatment, HFOV = ovariectomized HFD-fed rats with vehicle treatment, HFOE = ovariectomized HFD-fed rats with estradiol administration.

brain and increased ATP generation in neurons [41,42], in which increased brain glucose metabolism may be the other possible mechanism to restore brain insulin sensitivity in OVX models. As the limitation of the present study, this possibility has not been investigated. Therefore, further investigation about this possibility will be required.

In contrast to non-obese rats, the reduction of brain insulin sensitivity in obese rats with OVX could not be restored by estrogen therapy. The possible explanation of these findings was that the combination of obese and OVX aggravates visceral fat accumulation, leading to higher increased peripheral and brain oxidative stress levels as well as other potential mediators in the brain. This possibility is supported by the recent study [43]. Ludgero-Correia and colleagues demonstrated that the combination of obese with OVX model aggravated serum lipotoxicity, adipocyte derived hormone and adipo-cytokine levels [43]. In addition, the reduction of brain insulin sensitivity under the condition of obesity combined with OVX could also occur via the central effects including increased brain pro-inflammation and reduced brain glucose uptake. However, these possibilities were not investigated in the present study. Future study is needed to explore this issue. Therefore, the aggravation of those possible toxicities in the brain of the combined OVX with obesity may be above the efficiency of estrogen therapy.

In summary, the present study demonstrated that non-obese rats with OVX impaired peripheral and brain insulin sensitivity, and increased brain oxidative stress, and estrogen therapy could improve these impairments. Obese female rats induced by HFD with or without OVX also reduced peripheral and brain insulin sensitivity as well as increased brain oxidative stress. However, estrogen therapy improved only peripheral insulin sensitivity, but not brain insulin sensitivity and brain oxidative stress in these obese rats with OVX.

Author contributions

WP: designed the study, performed the experiments, analyzed the data, and wrote the manuscript; NC: designed the study, analyzed the data, and wrote the manuscript; SCC: designed the study, performed the experiments, analyzed the data, and wrote the manuscript.

Funding

This work was supported by the Thailand Research Fund grants: TRF-BRG (SC), TRF-RTA5580006 (NC), TRF-TRG5680018 (WP), Chiang Mai University Young Researcher Fund (WP), Faculty of Medicine Chiang Mai University Endowment Fund (NC), National Research Council of Thailand (SC), and Chiang Mai University Excellent Center Award (NC).

Disclosure statement

The authors declare that there is no conflict of interest that could be perceived as prejudicing the impartiality of the research reported.

REFERENCES

[1] Evsen MS, Ozler A, Gocmez C, et al. Effects of estrogen, estrogen/progesteron combination and genistein treatments on oxidant/antioxidant status in the brain of ovariectomized rats. Eur Rev Med Pharmacol Sci 2013;17(14):1869–73.
[2] Notsu M, Yamaguchi T. Secondary osteoporosis or secondary contributors to bone loss in fracture. Effects of oxidative stress on bone metabolism. Clin Calcium 2013;23(9):1285–92.
[3] Yuan L, Dietrich AK, Nardulli AM. 17beta-estradiol alters oxidative stress response protein expression and oxidative damage in the uterus. Mol Cell Endocrinol 2013;382(1):218–62.
[4] Ye J. Mechanisms of insulin resistance in obesity. Front Med 2013;7(1):14–24.
[5] Aoi W, Naito Y, Yoshikawa T. Role of oxidative stress in impaired insulin signaling associated with exercise-induced muscle damage. Free Radic Biol Med 2013;65:1265–72.
[6] Proudler AJ, Felton CV, Stevenson JC. Ageing and the response of plasma insulin, glucose and c-peptide concentrations to intravenous glucose in postmenopausal women. Clin Sci 1992;83(4):489–94.
[7] Strotmeyer ES, Steenkiste AR, Foley Jr TP, et al. Menstrual cycle differences between women with type 1 diabetes and women without diabetes. Diabetes Care 2003;26(4):1016–21.
[8] Bryzgalova G, Lundholm L, Portwood N, et al. Mechanisms of antidiabetogenic and body weight-lowering effects of estrogen in high-fat diet-fed mice. Am J Physiol Endocrinol Metab 2008;295(4):E904–12.
[9] Godsland IF. Oestrogens and insulin secretion. Diabetologia 2005;48(11):2213–20.
[10] Palin SL, Kumar S, Sturdee DW, et al. HRT in women with diabetes—review of the effects on glucose and lipid metabolism. Diabetes Res Clin Pract 2001;54(2):67–77.
[11] Abbas AM, Elsamanoudy AZ. Effects of 17beta-estradiol and antioxidant administration on oxidative stress and insulin resistance in ovariectomized rats. Can J Physiol Pharmacol 2011;89(7):497–504.
[12] Pipatpiboon N, Pratchayasakul W, Chattipakorn N, et al. PPARγ agonist improves neuronal insulin receptor function in hippocampus and brain mitochondria function in rats with insulin resistance induced by long term high-fat diets. Endocrinology 2012;153(1):329–38.
[13] Pratchayasakul W, Chattipakorn N, Chattipakorn SC. Effects of estrogen in preventing neuronal insulin resistance in hippocampus of obese rats are different between genders. Life Sci 2011;89(19–20):702–7.
[14] Pratchayasakul W, Kerdphoo S, Petsophonsakul P, et al. Effects of high-fat diet on insulin receptor function in rat hippocampus and the level of neuronal corticosterone. Life Sci 2011;88(13–14):619–27.
[15] Pintana H, Apaijai N, Pratchayasakul W, et al. Effects of metformin on learning and memory behaviors and brain mitochondrial functions in high fat diet induced insulin resistant rats. Life Sci 2012;91(11–12):409–14.
[16] Matthews DR, Hosker JP, Rudenski AS, et al. Homeostasis model assessment: insulin resistance and beta-cell function from fasting plasma glucose and insulin concentrations in man. Diabetologia 1985;28(7):412–9.
[17] Chattipakorn SC, McMahon LL. Pharmacological characterization of glycine-gated chloride currents recorded in rat hippocampal slices. J Neurophysiol 2002;87(3):1515–25.
[18] Candan N, Tuzmen N. Very rapid quantification of malondialdehyde (MDA) in rat brain exposed to lead, aluminium and phenolic antioxidants by high-performance liquid chromatography–fluorescence detection. Neurotoxicology 2008;29(4):708–13.

[19] Bendale DS, Karpe PA, Chhabra R, et al. 17-beta oestradiol prevents cardiovascular dysfunction in post-menopausal metabolic syndrome by affecting SIRT1/AMPK/H3 acetylation. Br J Pharmacol 2013;170(4):779–95.
[20] Clinton SK, Li PS, Mulloy AL, et al. The combined effects of dietary fat and estrogen on survival, 7,12-dimethylbenz(a) anthracene-induced breast cancer and prolactin metabolism in rats. J Nutr 1995;125(5):1192–204.
[21] Massaad CA, Klann E. Reactive oxygen species in the regulation of synaptic plasticity and memory. Antioxid Redox Signal 2011;14(10):2013–54.
[22] Yao J, Brinton RD. Estrogen regulation of mitochondrial bioenergetics: implications for prevention of alzheimer's disease. Adv Pharmacol 2012;64:327–71.
[23] Evans JL, Goldfine ID, Maddux BA, et al. Oxidative stress and stress-activated signaling pathways: a unifying hypothesis of type 2 diabetes. Endocr Rev 2002;23(5):599–622.
[24] Funaki M. Saturated fatty acids and insulin resistance. J Med Invest 2009;56(3–4):88–92.
[25] Kennedy A, Martinez K, Chuang CC, et al. Saturated fatty acid-mediated inflammation and insulin resistance in adipose tissue: mechanisms of action and implications. J Nutr 2009;139(1):1–4.
[26] King GL, Loeken MR. Hyperglycemia-induced oxidative stress in diabetic complications. Histochem Cell Biol 2004;122(4):333–8.
[27] Boden G. Role of fatty acids in the pathogenesis of insulin resistance and niddm. Diabetes 1997;46(1):3–10.
[28] Faraj M, Lu HL, Cianflone K. Diabetes, lipids, and adipocyte secretagogues. Biochem Cell Biol 2004;82(1):170–90.
[29] Smith MM, Minson CT. Obesity and adipokines: effects on sympathetic overactivity. J Physiol 2012;590:1787–801.
[30] Alonso A, Fernandez R, Moreno M, et al. Positive effects of 17beta-estradiol on insulin sensitivity in aged ovariectomized female rats. J Gerontol A Biol Sci Med Sci 2006;61(5):419–26.
[31] Babaei P, Mehdizadeh R, Ansar MM, et al. Effects of ovariectomy and estrogen replacement therapy on visceral adipose tissue and serum adiponectin levels in rats. Menopause Int 2010;16(3):100–4.
[32] Barros RP, Gustafsson JA. Estrogen receptors and the metabolic network. Cell Metab 2011;14(3):289–99.
[33] Mauvais-Jarvis F, Clegg DJ, Hevener AL. The role of estrogens in control of energy balance and glucose homeostasis. Endocr Rev 2013;34(3):309–38.
[34] Bruschi F, Meschia M, Soma M, et al. Lipoprotein(a) and other lipids after oophorectomy and estrogen replacement therapy. Obstet Gynecol 1996;88(6):950–4.
[35] Shinoda M, Latour MG, Lavoie JM. Effects of physical training on body composition and organ weights in ovariectomized and hyperestrogenic rats. Int J Obes Relat Metab Disord 2002;26(3):335–43.
[36] Gauthier MS, Favier R, Lavoie JM. Time course of the development of non-alcoholic hepatic steatosis in response to high-fat diet-induced obesity in rats. Br J Nutr 2006;95(2):273–81.
[37] Hwang LL, Wang CH, Li TL, et al. Sex differences in high-fat diet-induced obesity, metabolic alterations and learning, and synaptic plasticity deficits in mice. Obesity 2010;18(3):463–9.
[38] Manco M, Calvani M, Mingrone G. Effects of dietary fatty acids on insulin sensitivity and secretion. Diabetes Obes Metab 2004;6(6):402–13.
[39] Alonso A, Gonzalez-Pardo H, Garrido P, et al. Acute effects of 17 beta-estradiol and genistein on insulin sensitivity and spatial memory in aged ovariectomized female rats. Age 2010;32(4):421–34.
[40] Riant E, Waget A, Cogo H, et al. Estrogens protect against high-fat diet-induced insulin resistance and glucose intolerance in mice. Endocrinology 2009;150(5):2109–17.
[41] Bishop J, Simpkins JW. Estradiol enhances brain glucose uptake in ovariectomized rats. Brain Res Bull 1995;36(3):315–20.
[42] Brinton RD. Estrogen-induced plasticity from cells to circuits: predictions for cognitive function. Trends Pharmacol Sci 2009;30(4):212–22.
[43] Ludgero-Correia Jr A, Aguila MB, Mandarim-de-Lacerda CA, et al. Effects of high-fat diet on plasma lipids, adiposity, and inflammatory markers in ovariectomized c57bl/6 mice. Nutrition 2012;28(3):316–23.

เอกสารแนบหมายเลข 65

Endocrine Research

http://informahealthcare.com/erc
ISSN: 0743-5800 (print), 1532-4206 (electronic)

Endocr Res, 2014; 39(4): 144–151
© 2014 Informa Healthcare USA, Inc. DOI: 10.3109/07435800.2013.879168

informa
healthcare

REVIEW

Possible roles of insulin signaling in osteoblasts

Sakarat N. Pramojanee[1], Mattabhorn Phimphilai[2], Nipon Chattipakorn[3,4], and Siriporn C. Chattipakorn[1,3]

[1]Department of Oral Biology and Diagnostic Science, Faculty of Dentistry, [2]Department of Medicine, Faculty of Medicine, Chiang Mai University, Chiang Mai, Thailand, [3]Neurophysiology Unit, Cardiac Electrophysiology Research and Training Center, Chiang Mai University, Chiang Mai, Thailand, and [4]Biomedical Engineering Center, Chiang Mai University, Chiang Mai, Thailand

Abstract

Insulin and its downstream signaling pathway are indispensable for postnatal bone growth and turnover by having influence on both osteoblast and osteoclast development. Insulin signaling regulates both bone formation by osteoblasts and bone resorption by osteoclasts; however, the regulation occurs mainly through the insulin signaling pathway within osteoblasts. An impairment of osteoblastic insulin signaling leads to an impaired bone quality by affecting osteoblast proliferation, differentiation and survival. The insulin signaling pathway and MAPK and PI3K/Akt pathways play pivotal roles in the differentiation, function and survival of bone cells. Current evidence suggests that osteoblastic insulin signaling not only modulates bone growth and turnover but is also required for energy metabolism. Several mice models with impaired insulin signaling exhibited both bone and metabolic phenotypes, including symptoms of low bone mass, obesity, glucose intolerance and insulin resistance. In this review, we discuss the key findings that suggest a pivotal role of osteoblastic insulin signaling in both bone and energy metabolism.

Keywords

Energy metabolism, insulin receptor, insulin signaling pathway, osteoblasts, undercarboxylated osteocalcin

History

Received 1 September 2013
Revised 22 November 2013
Accepted 16 December 2013
Published online 27 March 2014

Endocr Res Downloaded from informahealthcare.com by Chiang Mai University on 02/09/15
For personal use only.

Introduction

Insulin, a hormone produced by the beta cells of the pancreas, is a potential regulator controlling cell growth and glucose metabolism in all mammals. Since the first discovery of insulin in 1922 by Banting and Best (1), the effects of insulin have been extensively studied. Insulin becomes functional after binding to insulin receptors, which are present in most tissues, including bone and osteoblasts. It is well known that insulin plays an important role in glucose metabolism via increased cellular glucose uptake (2). Insulin not only plays a role in glucose metabolism (2), but also plays important roles in bone tissue by influencing osteoblast proliferation and differentiation, as shown in several *in vitro* studies (3–6). Insulin directly stimulates the proliferation of cultured osteoblastic cells (4,6) and also induces osteoblast differentiation markers, such as osteocalcin (6), collagen (3,5) and alkaline phosphatase (6). Moreover, an *in vivo* study showed that insulin induces increased bone formation to two or three times the initial level when administered locally on mouse calvariae, as indicated by increased osteoid surface area, osteoblast surface area and osteoblast numbers (7). In addition to affecting osteoblasts, insulin influences chondrocyte proliferation and differentiation, as well as metatarsal bone growth (8). These findings suggest that insulin plays important roles in the development of bone and cartilage. Furthermore, the impairment of insulin signaling within osteoblasts has recently been shown to cause abnormal energy metabolism. This review describes details in the roles of insulin signaling within osteoblasts as well as the effects of osteoblast insulin signaling on glucose and energy metabolism.

Correspondence: Siriporn C. Chattipakorn, DDS, PhD, Department of Oral Biology and Diagnostic Science, Faculty of Dentistry, Chiang Mai University, Chiang Mai 50200, Thailand. Tel: +11 66 53 944 451. Fax: +11 66 53 222 844. E-mail: s.chat@chiangmai.ac.th, scchattipakorn@gmail.com

Insulin signaling pathway

The insulin signaling pathway plays roles in the metabolic and mitogenic effects in many cell types including osteoblasts. The main components of the insulin signaling pathway are the insulin receptors and the intracellular signaling pathway, which includes mitogen-activated protein kinases (MAPK) and phosphatidylinositol-3 kinase (PI3K/Akt) (9) as shown in Figure 1. Insulin initiates a diverse array of biological responses when binding to the insulin receptors (IRs) which are tyrosine kinase receptors (10). Once activated, the insulin receptors become autophosphorylated on tyrosine residues and then phosphorylated downstream on insulin receptor substrate (IRS) on its tyrosine residues. The tyrosine phosphorylation of the IRS is the functional form of the insulin signaling cascade, whereas the serine phosphorylation of the IRS is considered a suppressor of insulin signaling (11,12). The IRSs are determined as key mediators in insulin and insulin-like growth factor-1 (IGF-1) signaling. They act as docking proteins between insulin/IGF-1 receptors and intracellular signaling molecules containing c-Src tyrosine kinase (Src) homology 2 (SH2) domains (13). Even though there are four members of the IRS family, IRS1, IRS2, IRS3 and IRS4,

RIGHTSLINK

DOI: 10.3109/07435800.2013.879168

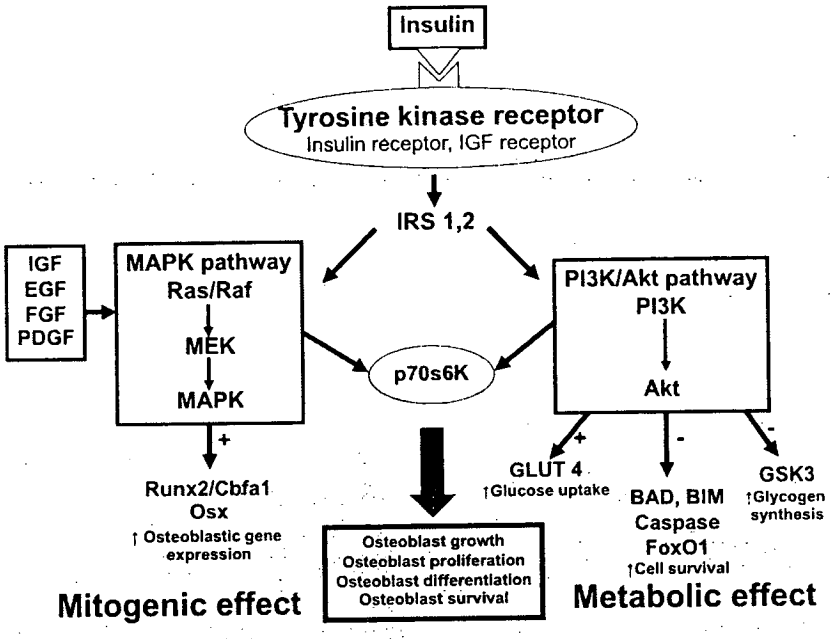


Figure 1. Schematic model illustrating insulin signaling pathway and end of cellular response to osteoblastic insulin signaling. In this model, insulin stimulation results in the activation of the insulin receptor substrate (IRS), followed by an activation of an intracellular MAPK pathway and PI3-K/Akt pathway that is necessary for osteoblast growth, osteoblast differentiation and osteoblast survival.

Endocr Res Downloaded from informahealthcare.com by Chiang Mai University on 02/09/15
For personal use only.

only IRS1 and IRS2 play important roles in bone growth and development through insulin signaling transduction, which can be activated by either insulin or IGF-I (14–16). Following IRS tyrosine phosphorylation, two main downstream intracellular signaling pathways including MAPK (Erk1/2 MAPK) and PI3K become activated (17).

The MAPK pathway is mainly responsible for mitogenic function involving gene expression, but the PI3K pathway plays an important role in metabolic function and cell survival throughout the body (9). The MAPK pathway is activated by Ras–Raf signaling, a family of kinases that respond to several growth factors in the extracellular space, including epidermal growth factor (EGF), fibroblast growth factor (FGF), platelet-derived growth factor (PDGF), insulin-like growth factor (IGF) and insulin (18–20). This pathway principally controls cell growth, proliferation and differentiation (6,19), but has minimal effects on metabolic regulation (18).

The PI3K/Akt pathway controls insulin-mediated metabolic effects through the activity of many downstream mediators, including glucose transporter 4 (GLUT4), protein kinase C (PKC) and glycogen synthase kinase 3 (GSK3) (9,21,22). PI3K is a key molecule regulating insulin function, mainly via the activation of Akt/PKB and PKC cascades. Shepherd (23) has suggested that Akt is the central element modulating insulin action. Activation of Akt induces glycogen synthesis through the inhibition of GSK3 protein synthesis via mTOR and its downstream elements and enhances cell survival through the inhibition of several pro-apoptotic agents including Bad, Forkhead family transcription factors and GSK3 (9,22,24,25). Although the MAPK and PI3K/Akt pathways are involved in different roles in insulin action, both pathways may share a common task in cell growth and differentiation through the activation of p70S6K (26). The diagram of the proposed insulin signaling pathway and the cellular response to insulin signaling is illustrated in Figure 1.

The physiological roles of insulin in bone

Several studies have shown that insulin receptor signaling is indispensible for bone remodeling by regulating both osteoblast and osteoclast function (16,27). Insulin receptors are expressed in both osteoblasts and osteoclasts (27,28). However, it is possible that insulin affects bone turnover mainly through the response of osteoblasts to insulin via insulin signaling within osteoblasts. Previous *in vitro* studies have demonstrated that treatment of osteoblasts with insulin induces phosphorylation of the insulin receptor and its downstream mediators, including IRS-1, Akt, GSK3β, Forkhead box protein (FoxO1) and p70S6K (4,27). These mediators lie in the PI3K/Akt pathway, which is a central regulator in the metabolic and mitogenic actions of insulin on bone in mice (29,30). In addition, the recent *in vitro* study found that FoxO1, a downstream mediator of insulin signaling, acts as a potential regulator in the redox balance by protecting against oxidative stress in osteoblast, suggesting that insulin signaling plays roles in bone formation (31). In accordance with *in vitro* studies, Fulzele et al. (32) demonstrated that mice lacking insulin receptors in their osteoblasts (Ob-ΔIR mice) developed postnatal osteopenia with normal longitudinal bone growth, as determined by the reduction of trabecular number and thickness and an increase in trabecular spaces. The Ob-ΔIR mice, mice lacking insulin receptors in osteoblasts, were generated by crossing osteocalcin-Cre (OC-Cre) transgenic mice (33) with $IR^{flox/flox}$ mice (34). In addition, this mouse model also showed an impairment of osteogenic cell proliferation and differentiation after stimulation with insulin and IGF (32). This evidence indicated the essential roles of insulin signaling within osteoblasts for the differentiation process of osteoblasts and the formation of the bone. In terms of osteoclastogenesis, Ogata et al. (16) demonstrated that the development of osteoclasts in the coculture of hemopoietic cells and osteoblasts depended

RIGHTSLINK

solely on the IRS-1 expression in osteoblasts. The IRS-1-deletion osteoblasts could not produce osteoclast differentiation factors, the RANKL/ODF, which are key regulators of osteoclastogenesis (16). In accordance with the *in vitro* studies, Ferron et al. (27) showed that osteoblast-specific insulin receptor-deficient mice (InsRosb−/− mice) had a reduction of CathepsinK (Ctsk) and T-cell immune regulator 1 (Tcirg1) expression, which are required in the osteoclast bone resorption process. Despite the InsRosb−/− mice model demonstrating a decrease in osteoclast bone resorption, these mice still also had a reduction of bone mass, suggesting a higher extent of bone formation suppression than that of bone resorption. Therefore, all of this evidence indicated that insulin receptor signaling impacts on bone turnover at both bone formation and bone resorption and mainly acts through the insulin signaling pathway within osteoblasts.

Interestingly, the Ob-ΔIR mice exhibited not only skeletal defects as shown by decreased trabecular bone mass but also energy metabolism defects, as shown by an increase in adiposity and insulin resistance (32). These findings suggest that osteoblastic insulin signaling not only exerts effects on bone acquisition but also on energy metabolism. The interaction of osteoblastic insulin signaling and energy metabolism is discussed in a later part of this review article. In contrast to the Ob-ΔIR mice, Irwin et al. (35) demonstrated that bone specific insulin receptor knockout mice (IRKO-L1) exhibit an increase in cortical bone mass and also preserved trabecular bone density. The IRKO-L1 mice are insulin receptor knockout (IRKO) mice that were crossed with transgenic mice expressing the human insulin receptor driven by the Ttr promoter to generate Insr−/−, Ttr-Insr (IRKO-L1) mice. Moreover, unlike the Ob-ΔIR mice and InsRosb−/− mice that exhibited hyperglycemia and insulin resistance (27,32), the IRKO-L1 mice had normal metabolic phenotype parameters (euglycemia) (35) as shown in Table 2. The differences in bone phenotypes between the Ob-ΔIR mice and the IRKO-L1 mice may be due to:

(1) the IRKO-L1 mice having a compensatory response as indicated by an increase in IGF receptor signaling in osteoblasts, in which IGF receptors share the same metabolic pathway for the IR signaling (35)
(2) IRKO-L1 mice having lower levels of advanced glycation end products (AGEs) than Ob-ΔIR mice, possibly influencing bone turnover.

Several *in vitro* studies have revealed the detrimental effects of AGEs on bone cells, including the induction of osteoblast apoptosis (36), the interference with the mineralization of mouse osteoblastic cell lines (37) and also a reduction of osteoclastic activity in cultured mouse unfractionated bone cells (38).

It is known that both insulin and IGF can initiate the insulin signaling pathway, through binding to insulin receptors because both share a similar molecular structure (39). However, IGF has a lower binding affinity to the insulin receptor (39). On the other hand, insulin also can bind to IGF receptors, which are abundantly expressed in osteoblasts (40). Thus, both insulin and IGF could share the same metabolic pathway and have a reciprocal relationship, as illustrated in several previous studies (35,40). Irwin et al. (35) illustrated that insulin receptor knockout mice exhibited normal bone density due to an increase in IGF-1 receptor signaling. Consistent with the previous studies, Fulzele et al. (40) showed that the deletion of IGF-1 receptors in osteoblasts led to an enhancement of insulin signaling by increasing insulin-induced Akt phosphorylation. Those findings suggest that insulin receptors and IGF signaling are compensatory mechanisms to maintain bone mass.

Effects of insulin signaling pathway in bone cells

As mentioned previously, insulin signaling regulates both bone formation by osteoblasts and bone resorption by osteoclasts; however, the regulation occurs mainly through the insulin signaling pathway within osteoblasts. Several *in vitro* and *in vivo* studies have indicated that the insulin signaling pathway components, including insulin receptor (IR), insulin receptor substrate (IRS 1, 2), MAPK and PKB/Akt, are essential for osteoblast proliferation, survival and differentiation (6,14,16,29,32). The proposed mechanism of insulin receptor action following insulin stimulation on the production of cellular mitogenic and metabolic effects is shown in Figure 1.

In contrast to the insulin receptors which are expressed in both osteoblasts and osteoclasts, IRS-1 is expressed only in osteoblasts (16). Despite the fact that IRS-1 is expressed only in osteoblasts, it plays an important role in the regulation of both bone formation and bone resorption leading to the turnover of the bone. IRS-1 modulates osteoblast proliferation and differentiation as illustrated in several *in vitro* studies. Genetic deletion of IRS-1 (IRS−/−) in osteoblasts leads to an impaired osteoblast proliferation and differentiation (16,41), as well as a decrease in osteoblast survival and mineralization (41). The key mechanism leading to these detrimental findings in IRS1−/− osteoblasts were a reduction of tyrosine phosphorylation of IRS-1 and Akt, a downstream mediator of IRS-1 (16,41). IRS-1 also regulates bone resorption by enhancing receptor activators of nuclear factor kappa-B ligand (RANKL), a key regulator of osteoclastogenesis, within the osteoblast (16). Similar to the studies in osteoblasts, IRS (−/−) chondrocytes showed an impairment of chondrocyte proliferation and differentiation, as well as the induction of chondrocyte apoptosis due to a reduction of Akt phosphorylation (42). Because the effects of IRS-1 on osteoblasts, osteoclasts and chondrocytes, the mice with the genetic deletion of IRS-1 (IRS1−/−) have shown a reduction in bone length, indicating retardation in their skeletal growth, and osteopenia due to low bone turnover (16,43,44). In addition, IRS-1 (−/−) mice have delayed bone healing due to the suppression of callus formation. These findings suggest that IRS-1 leads to an anabolic effect on bone during bone turnover due to a higher activation of osteoblast and chondrocyte development than that of osteoclast development. In contrast to IRS-1, IRS-2 is more extensively expressed in osteoclasts than in osteoblasts (14,16). Although IRS-2 has a more pronounced expression in osteoclasts, it also impacts on bone formation rather than bone resorption (14). As shown by Akune et al. (14), osteoblast-IRS-2 deficient animals developed osteopenia due to an impaired osteoblast development but showed enhanced osteoclastogenesis. The cultured IRS-2−/− osteoblasts

Endocr Res Downloaded from informahealthcare.com by Chiang Mai University on 02/09/15
For personal use only.

RIGHTSLINK

DOI: 10.3109/07435800.2013.879168

showed a reduced differentiating capacity and matrix synthesis when compared to wild-type osteoblasts (14). In conclusion, IRS-1 plays a dominant role in skeletal growth and bone turnover, whereas IRS-2 regulates bone formation and does not affect longitudinal bone growth.

IRS-1 and IRS-2 phosphorylation activate two downstream intracellular signal transduction pathways, MAPK and PI3K/Akt, which regulate the expression of multiple important transcriptional factors for osteoblast development. Both MAPK and PI3K/Akt pathways play pivotal roles in bone cell differentiation, function and survival. The MAPK pathway regulates the expression of osteoblast-specific transcriptional factors, such as Runx2/cbfa1 and Osterix (Osx), which are essential for osteoblast development (6,45). Yang et al. (6) illustrated that the activation of MAPK by insulin enhanced Osx expression in human osteoblastic cells. In terms of the PI3K/Akt pathway, this pathway has been shown to be involved in multiple steps of osteoblast development. Kawamura et al. (29) demonstrated that the genetic deletion of Akt1 reduces the expression of Runx 2/cbfa1 but increases osteoblast apoptosis. In addition, Mukherjee and Rotwein (46) demonstrated that the inhibition of Akt activity reduces alkaline phosphatase accumulation, mineralization and longitudinal bone growth, and indicated that Akt signaling is needed for multiple steps of osteoblast differentiation. By using a different mouse model, Liu et al. (47) also demonstrated the role of the PI3K/Akt pathway in osteoblast differentiation and function. A genetic deletion of Pten, a negative regulator of PI3K, led to progressive increase in bone mineral density (BMD) throughout life. This was as a result of an increased bone formation rate, indicating an anabolic effect of PI3K/Akt pathway on bone (47). The PI3K/Akt pathway not only controls osteoblasts, it also controls osteoclast development (29). Kawamura and colleagues showed that Akt deletion mice had a decrease in osteoclast differentiation and survival. However, impaired osteoclast differentiation may partly be contributed to by the decrease of RANKL expression in Akt−/− osteoblasts (29).

As mentioned previously, either insulin-activated MAPK or PI3K/Akt pathways can control the differentiation and function of bone cells. Both studies by Burguera et al. (48) and Yang et al. (6) demonstrated using human osteoblastic cells that insulin regulates osteoblast growth and differentiation through both MAPK and PI3K pathways. Both pathways are required in osteoblast development; hence both pathways may share a convergence point leading to common effects in osteoblast proliferation and differentiation. It is conceivable that p70S6 kinase is this convergence point because this kinase can be activated by either MAPK (49) or PI3K/Akt (50). Grey and associates illustrated that p70S6K acts as a common downstream mediator of the MAPK and PI3K/Akt pathways by regulating osteoblast survival and differentiation (26) (Figure 1). The evidence of the role of insulin receptors and insulin signaling pathways on bone is presented in Tables 1 and 2.

Insulin and osteoblastic insulin signaling contribute to different bone phenotypes in type 1 diabetes and type 2 diabetes

Diabetes mellitus (DM) is a metabolic disease characterized by high blood glucose (hyperglycemia). DM can be classified into four types that include type 1 DM (T1DM), type 2 DM (T2DM), gestational DM and congenital DM. However, both T1DM and T2DM are chronic conditions that cannot be cured. T1DM is characterized by insulin deficiency while T2DM is characterized by insulin resistance leading to hyperinsulinemic condition (51). Several studies have widely demonstrated an increased risk of osteoporosis and

Table 1. Effects of genetic deletion of insulin signaling within osteoblasts.

	Major findings	References
IR−/− osteoblast	↓osteoblast proliferation ↑osteoblast apoptosis ↓osteoblast differentiation ↓ osteoblast marker expression • Run X2 • osteocalcin	Fulzele et al. (32)
IRS-1−/− osteoblast	↓ cell proliferation and differentiation ↓ tyrosine phosphorylation	Ogata et al. (16)
IRS-1−/− osteoblast Coculture with bone marrow cells	↓ RANKL/OPG ratio (marker for osteoclast differentiation) ↓ osteoclast number and activity	Ogata et al. (16)
IRS-1−/− chondrocyte	↓mitogenic activity ↓Akt phosphorylation	Shimoaka et al. (42)
IRS-2−/− osteoblast	↓osteoblast proliferation and differentiation ↓matrix protein gene expression (collagen type I, ALP, osteocalcin) but unchanged osteblastic differentiation gene (Runx2, Lrp5, Id-1) ↑osteoclast differentiation marker • RANKL/OPG ratio • MMP-13	Akune et al. (14)
Deletion of IGF-1R osteoblast	↑insulin receptor signaling Phosphorylation IRS1,2 ERK/Akt	Fulzele et al. (40)
Akt−/− osteoblast	↑ osteoblast apoptosis ↓Runx 2 expression ↓RANKL (osteoclast differentiation marker)	Kawamura et al. (29)
Akt−/− osteoclast	↓osteoclast survival and differentiation	Kawamura et al. (29)

Endocr Res Downloaded from informahealthcare.com by Chiang Mai University on 02/09/15
For personal use only.

RIGHTSLINK

Table 2. Changes of metabolic and skeletal phenotypes in animals with defective insulin signaling within osteoblasts.

Defective insulin signaling component	Metabolic phenotype	Skeletal phenotype	References
Insulin receptor (Ob-ΔIR mice)	Insulin resistance High blood glucose Increased adiposity	Osteopenia Normal skeletal growth	Fulzele et al. (32)
Insulin receptor ($InsR_{osb}$−/−) mice	High blood glucose Reduced serum insulin from a decrease in b-cell mass and proliferation	Osteopenia	Ferron et al. (27)
Insulin receptor (IRKO-L1) mice	Euglycemia	Normal bone density Normal skeletal growth Decreased marrow adiposity	Irwin et al. (35)
(IRS 1−/−) mice	Hyperinsulinemia	Osteopenia Reduced skeletal growth (~20%) Low bone turnover osteopenia in bone	Ogata et al. (16)
(IRS 1−/−) mice	N/A	Reduced skeletal growth Low bone turnover osteopenia in cartilage	Hoshi et al. (43)
(IRS 1−/−) mice	N/A	Impaired bone healing Reduced callus formation	Shimaoka et al. (42)
(IRS 1−/−) mice	Insulin resistance	Retarded skeletal growth	Tamemoto et al. (44)
IRS-2	N/A	Osteopenia in both trabecular and cortical bone Reduced bone formation and increased bone resorption No effect on skeletal growth	Akune et al. (14)
AKT (oteoblast and osteoclast)	N/A	Low bone turnover osteopenia	Kawamura et al. (29)
Pten (negative regulator of PI3-K)	N/A	Progressively increased in BMD throughout life Increased bone formation rate	Liu et al. (47)

fragility leading to fractures in both T1DM and T2DM (49,52,53). However, some different bone phenotypes have been illustrated in both types of DM. While low bone mineral density (BMD) with marked higher risk of fractures was shown in T1DM, a preserved BMD with slight higher risk of fractures was demonstrated in T2DM (49,53,54). The difference of insulin level and insulin responsiveness in both types of DM partially contributed to different skeletal phenotypes exhibited in T1DM and T2DM (4,30,49,53,55–57). Because insulin has anabolic actions on bone, insulin deficiency conditions in T1DM could mean lower bone formation which can lead to low BMD and then increased fracture risk. Several clinical studies have demonstrated that lower BMD and increased osteoporosis resulting from insulin deficiency were developed in T1DM (49,53). Moreover, the mechanism of diabetic-induced bone loss in T1DM was shown to be associated with a reduced bone formation rather than an increased bone resorption (58). McCabe and colleagues (58) demonstrated that the mechanism contributing to bone loss in T1DM results from low bone turnover with a decrement in osteoblast number. Since insulin acts as an anabolic agent on bone, long term administration of insulin in T1DM patients could preserve their bone mass (59).

In contrast to T1DM, T2DM exhibited normal or higher BMD as shown in several clinical studies (56,60). Hyperinsulinemia is thought to be one of the contributing factors for increased bone mass in T2DM (55–57,61). Reid proposed that hyperinsulinemia in insulin resistant conditions can enhance bone formation by increasing osteoblastic activity, as well as inhibiting bone resorption by decreasing osteoclastic activity (62). In addition, several clinical studies clearly demonstrated a positive correlation between insulin and BMD (55,57), suggesting insulin is an important factor in determining bone acquisition. Despite the fact that hyperinsuinemia found in T2DM should lead to anabolic actions on bone, a striking high BMD is rarely observed in this type of DM. Interestingly, increased fracture risk in the bone of T2DM has been clearly evidenced similarly to that found in T1DM (49). One of the possibilities leading to this observed bone phenotypes in T2DM is osteoblastic insulin resistance in T2DM. An impairment of osteoblastic insulin signaling leads to abnormal skeletal phenotypes such as decreased bone mass, increased bone porosity and reduced bone strength as shown in several *in vivo* studies (16,27,29,32). In addition, our recent study showed that osteoblastic insulin signaling is impaired in insulin resistant rats (pre-diabetic condition) resulting in a decrement in osteoblast proliferation and survival leading to increased jaw bone porosity (4). Therefore, both high plasma insulin levels and impaired osteoblastic insulin signaling are important factors contributing to skeletal phenotypes in T2DM.

Osteoblast insulin signaling as a gateway for bone-mediated energy metabolism

It has been recently demonstrated that bone is able to modulate energy metabolism via their secreted molecules, undercarboxylated osteocalcin (27,63). Pertinently, this bone-mediated energy metabolism occurred throughout the insulin signaling pathway within osteoblasts. Osteocalcin is produced and secreted into the extracellular matrix and circulates only via osteoblasts during bone formation (64). It contains three glutamic acid residues that are post-translationally modified by gamma-glutamyl carboxylase. Based on gamma-carboxylation, osteocalcin is classified into two types: (1) a gamma-carboxylated (Gla-OCN) form that has high affinity for calcium hydroxyapatite within bone and (2) an undercarboxylated form (Glu-OCN) that can be released

Endocr Res Downloaded from informahealthcare.com by Chiang Mai University on 02/09/15
For personal use only.

RIGHTSLINK

DOI: 10.3109/07435800.2013.879168

Endocr Res Downloaded from informahealthcare.com by Chiang Mai University on 02/09/15
For personal use only.

easily into the systemic circulation (65). The Glu-OCN influences both insulin secretion and sensitivity as documented by Lee and colleagues using several mice models (63,66). The first model, a genetic deletion of osteocalcin (OC−/−), exhibited a lean physique and several abnormal metabolic phenotypes including high plasma glucose, low insulin and high insulin resistance (63). These metabolic phenotypes in the OC−/− mice resulted from a reduction in pancreatic β-cell mass and serum adiponectin, which caused a decrement in insulin production and insulin sensitivity, respectively (63). The second model, the Esp gene modulating model also confirmed the roles of osteocalcin in energy metabolism. The Esp gene encodes osteotesticular protein tyrosine phosphatase (OST-PTP), which functions by dephosphorylating IR in osteoblasts, leading to a reduction of osteocalcin activity from the osteoblasts (27). The Esp knockout mice (Esp−/−) mice had opposite metabolic findings compared to the OC−/− mice, while bone-specific overexpression of OST-PTP showed the identical metabolic phenotypes as shown in OC−/− mice (63). Finally, the most convincing results were shown by Ferron and colleagues by using recombinant Glu-OCN. They illustrated that the administration of recombinant Glu-OCN improved all metabolic abnormalities in OC−/− mice, as well as in high fat diet (HFD)-induced insulin resistance, in gold thioglucose (GTG)-induced obesity and in diabetic mouse models (66). These findings suggest that the osteoblast-specific secreting molecule, Glu-OCN, plays a role in modulating glucose and energy metabolism (as proposed in Figure 2).

As osteoblast-secreting Glu-OCN functions as a bone-generating hormone to control energy metabolism, this hormone has to be tightly regulated to balance energy expenditure of the body. Insulin and osteoblastic insulin signaling have been shown as regulators of Glu-OCN production and release. Fulzele et al. (32) demonstrated that osteoblast-specific deletion of insulin receptor mice not only exhibited low bone mass, due to decreased osteoblast development and survival, but also exhibited obesity and insulin resistance resulting from low serum Glu-OCN,

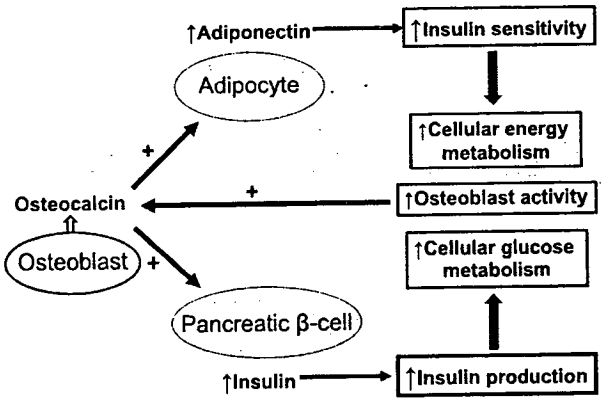


Figure 2. Roles of bone on energy and glucose metabolism through osteocalcin. Osteocalcin, the osteoblast-secreted molecule, enhances both insulin and adiponectin (insulin sensitizing adipokine) expression, leading to enhancement of insulin secretion and insulin sensitivity, respectively. Subsequently, increased cellular glucose and energy metabolism are developed. Furthermore, osteoblast activity is increased as a result, increased osteocalcin production.

indicating an upstream signal of Glu-OCN by the insulin receptors. Simultaneously, Ferron et al. (27) illustrated how those osteoblast-specific insulin receptor-deficient mice led to an impaired glucose tolerance due to a decrease in pancreatic β-cell proliferation and insulin secretion, indicating one role of the osteoblast insulin receptors for regulating whole body glucose metabolism. The underlined mechanism for osteoblasts to regulate glucose metabolism is the feedback loop of insulin signaling and bone resorption. Insulin receptor activation transmitted signals to inhibit FoxO1 and then osteoprotegerin (OPG) within the osteoblasts, which then led to an increase of Tcirg1 expression within osteoclasts that involved acid production during the bone resorption process by osteoclasts. This acidification would change the carboxylated form of osteocalcin (Gla-OCN) which is stored in the extracellular matrix of the bone to the undercarboxylated form (Glu-OCN) that is easily released from the bone. The Glu-OCN that is released into the systemic circulation, directly enhanced insulin production and release from the pancreatic β-cells. This insulin production then perpetuates Glu-OCN production by activating insulin receptors and their downstream signaling pathway. Therefore, insulin receptors and their signaling pathway function as a gateway for communication between bone turnover and energy metabolism in a feedback manner.

Osteocalcin favoring glucose and energy metabolism in human studies

To date, emerging evidence of osteocalcin on metabolic parameters is illustrated in several human studies (67–73). Cross-sectional studies reveal that total osteocalcin is associated with several metabolic parameters, including body mass index (BMI), fat mass, fasting glucose, fasting insulin, HOMA index, metabolic syndrome and development of diabetes (69,70,72,73). Total osteocalcin was shown to associate with lower BMI (70,72), lower fat mass (70), lower fasting glucose and insulin (69,70,72,73), whereas inversely correlate with insulin sensitivity, as shown by the HOMA index (72,73). These findings suggest that osteocalcin is positively associated with insulin sensitivity and energy metabolism in humans. Furthermore, in several cross-sectional studies, total osteocalcin and Glu-OCN have been shown to be associated with the prevalence of metabolic syndrome and diabetes (67,68,72). Interestingly, Ngarmukos and colleagues first proposed using serum osteocalcin as a predictor of type 2 diabetes. They showed that serum osteocalcin level was inversely associated with the future development of type 2 diabetes, suggesting the potential use of serum osteocalcin as a predictor of the incidence of diabetes (71).

Conclusion

Insulin signaling within osteoblasts plays an essential role in both bone and energy metabolism. Osteoblast insulin signaling influences osteoblast proliferation, differentiation and survival as well as osteoclast formation; however, it favors bone formation rather than bone resorption. Osteoblast insulin signaling also regulates insulin, glucose and energy metabolism via enhancing undercarboxylated osteocalcin

RIGHTSLINK

production and release to promote insulin production and insulin sensitivity in a feedback manner. Therefore, a defective mechanism in osteoblast insulin signaling would lead to the impairment of bone quantity and quality, as well as the possibility of contributing to abnormal glucose and energy metabolism.

Declaration of interest

This review was supported by grants from the Thailand Research Fund BRG (S.C.C.), RTA 5580006 (N.C.), Chiang Mai University Excellent Center Award (N.C.), MRG5480270 (M.P.) and the authors thank Dr. M. Kevin O. Carroll for his editorial assistance.

References

1. Banting FG, Best CH. Pancreatic extracts. 1922. J Lab Clin Med 1990;115:254–72.
2. Ituarte EA, Halstead LR, Iida-Klein A, et al. Glucose transport system in UMR-106-01 osteoblastic osteosarcoma cells: regulation by insulin. Calcif Tissue Int 1989;45:27–33.
3. Kream BE, Smith MD, Canalis E, Raisz LG. Characterization of the effect of insulin on collagen synthesis in fetal rat bone. Endocrinology 1985;116:296–302.
4. Pramojanee SN, Phimphilai M, Kumphune S, et al. Decreased jaw bone density and osteoblastic insulin signaling in a model of obesity. J Dent Res 2013;92:560–65.
5. Pun KK, Lau P, Ho PW. The characterization, regulation, and function of insulin receptors on osteoblast-like clonal osteosarcoma cell line. J Bone Miner Res 1989;4:853–62.
6. Yang J, Zhang X, Wang W, Liu J. Insulin stimulates osteoblast proliferation and differentiation through ERK and PI3K in MG-63 cells. Cell Biochem Funct 2010;28:334–41.
7. Cornish J, Callon KE, Reid IR. Insulin increases histomorphometric indices of bone formation in vivo. Calcif Tissue Int 1996;59:492–5.
8. Luo XH, Guo LJ, Yuan LQ, et al. Adiponectin stimulates human osteoblasts proliferation and differentiation via the MAPK signaling pathway. Exp Cell Res 2005;309:99–109.
9. Saltiel AR, Kahn CR. Insulin signalling and the regulation of glucose and lipid metabolism. Nature 2001;414:799–806.
10. White MF, Kahn CR. The insulin signaling system. J Biol Chem 1994;269:1–4.
11. Savage DB, Petersen KF, Shulman GI. Mechanisms of insulin resistance in humans and possible links with inflammation. Hypertension 2005;45:828–33.
12. White MF. IRS proteins and the common path to diabetes. Am J Physiol Endocrinol Metab 2002;283:E413–22.
13. Sesti G, Federici M, Hribal ML, et al. Defects of the insulin receptor substrate (IRS) system in human metabolic disorders. FASEB J 2001;15:2099–111.
14. Akune T, Ogata N, Hoshi K, et al. Insulin receptor substrate-2 maintains predominance of anabolic function over catabolic function of osteoblasts. J Cell Biol 2002;159:147–56.
15. Lee YH, White MF. Insulin receptor substrate proteins and diabetes. Arch Pharm Res 2004;27:361–70.
16. Ogata N, Chikazu D, Kubota N, et al. Insulin receptor substrate-1 in osteoblast is indispensable for maintaining bone turnover. J Clin Invest 2000;105:935–43.
17. Taniguchi CM, Emanuelli B, Kahn CR. Critical nodes in signalling pathways: insights into insulin action. Nature reviews 2006;7: 85–96.
18. Avruch J, Khokhlatchev A, Kyriakis JM, et al. Ras activation of the Raf kinase: tyrosine kinase recruitment of the MAP kinase cascade. Recent Prog Horm Res 2001;56:127–55.
19. Lovicu FJ, McAvoy JW. FGF-induced lens cell proliferation and differentiation is dependent on MAPK (ERK1/2) signalling. Development 2001;128:5075–84.
20. Werner H, Le Roith D. The insulin-like growth factor-I receptor signaling pathways are important for tumorigenesis and inhibition of apoptosis. Crit Rev Oncog 1997;8:71–92.
21. Czech MP, Corvera S. Signaling mechanisms that regulate glucose transport. J Biol Chem 1999;274:1865–8.
22. Shepherd PR, Withers DJ, Siddle K. Phosphoinositide 3-kinase: the key switch mechanism in insulin signalling. Biochem J 1998;333: 471–90.
23. Shepherd PR. Mechanisms regulating phosphoinositide 3-kinase signalling in insulin-sensitive tissues. Acta Physiol Scand 2005; 183:3–12.
24. Bertrand L, Horman S, Beauloye C, Vanoverschelde JL. Insulin signalling in the heart. Cardiovasc Res 2008;79:238–48.
25. Zundel W, Giaccia A. Inhibition of the anti-apoptotic PI(3)K/Akt/Bad pathway by stress. Genes Dev 1998;12:1941–6.
26. Grey A, Chen Q, Xu X, et al. Parallel phosphatidylinositol-3 kinase and p42/44 mitogen-activated protein kinase signaling pathways subserve the mitogenic and antiapoptotic actions of insulin-like growth factor I in osteoblastic cells. Endocrinology 2003;144: 4886–93.
27. Ferron M, Wei J, Yoshizawa T, et al. Insulin signaling in osteoblasts integrates bone remodeling and energy metabolism. Cell 2010;142: 296–308.
28. Thomas DM, Udagawa N, Hards DK, et al. Insulin receptor expression in primary and cultured osteoclast-like cells. Bone 1998; 23:181–6.
29. Kawamura N, Kugimiya F, Oshima Y, et al. Akt1 in osteoblasts and osteoclasts controls bone remodeling. PloS One 2007;2:e1058.
30. Wei J, Karsenty G. Bone as a site of insulin resistance in type 2 diabetes. BioMed Central Proceedings 2012. 74 p.
31. Rached MT, Kode A, Xu L, et al. FoxO1 is a positive regulator of bone formation by favoring protein synthesis and resistance to oxidative stress in osteoblasts. Cell Metab 2010;11:147–60.
32. Fulzele K, Riddle RC, DiGirolamo DJ, et al. Insulin receptor signaling in osteoblasts regulates postnatal bone acquisition and body composition. Cell 2010;142:309–19.
33. Zhang M, Xuan S, Bouxsein ML, et al. Osteoblast-specific knockout of the insulin-like growth factor (IGF) receptor gene reveals an essential role of IGF signaling in bone matrix mineralization. J Biol Chem 2002;277:44005–12.
34. Bruning JC, Michael MD, Winnay JN, et al. A muscle-specific insulin receptor knockout exhibits features of the metabolic syndrome of NIDDM without altering glucose tolerance. Mol Cell 1998;2:559–69.
35. Irwin R, Lin HV, Motyl KJ, McCabe LR. Normal bone density obtained in the absence of insulin receptor expression in bone. Endocrinology 2006;147:5760–7.
36. Alikhani M, Alikhani Z, Boyd C, et al. Advanced glycation end products stimulate osteoblast apoptosis via the MAP kinase and cytosolic apoptotic pathways. Bone 2007;40:345–53.
37. Ogawa N, Yamaguchi T, Yano S, et al. The combination of high glucose and advanced glycation end-products (AGEs) inhibits the mineralization of osteoblastic MC3T3-E1 cells through glucose-induced increase in the receptor for AGEs. Horm Metab Res 2007; 39:871–5.
38. Yamagishi S, Nakamura K, Inoue H. Possible participation of advanced glycation end products in the pathogenesis of osteoporosis in diabetic patients. Med Hypotheses 2005;65: 1013–5.
39. De Meyts P, Whittaker J. Structural biology of insulin and IGF1 receptors: implications for drug design. Nat Rev 2002;1: 769–83.
40. Fulzele K, DiGirolamo DJ, Liu Z, et al. Disruption of the insulin-like growth factor type 1 receptor in osteoblasts enhances insulin signaling and action. J Biol Chem 2007;282:25649–58.
41. Bu YH, He YL, Zhou HD, et al. Insulin receptor substrate 1 regulates the cellular differentiation and the matrix metallopeptidase expression of preosteoblastic cells. J Endocrinol 2010;206: 271–7.
42. Shimoaka T, Kamekura S, Chikuda H, et al. Impairment of bone healing by insulin receptor substrate-1 deficiency. J Biol Chem 2004;279:15314–22.
43. Hoshi K, Ogata N, Shimoaka T, et al. Deficiency of insulin receptor substrate-1 impairs skeletal growth through early closure of epiphyseal cartilage. J Bone Miner Res 2004;19:214–23.
44. Tamemoto H, Kadowaki T, Tobe K, et al. Insulin resistance and growth retardation in mice lacking insulin receptor substrate-1. Nature 1994;372:182–6.

Endocr Res Downloaded from informahealthcare.com by Chiang Mai University on 02/09/15
For personal use only.

RIGHTSLINK

45. Xiao G, Jiang D, Thomas P, et al. MAPK pathways activate and phosphorylate the osteoblast-specific transcription factor, Cbfa1. J Biol Chem 2000;275:4453–9.
46. Mukherjee A, Rotwein P. Akt promotes BMP2-mediated osteoblast differentiation and bone development. J Cell Sci 2009;122:716–26.
47. Liu X, Bruxvoort KJ, Zylstra CR, et al. Lifelong accumulation of bone in mice lacking Pten in osteoblasts. Proc Natl Acad Sci USA 2007;104:2259–64.
48. Burguera B, Brunetto A, Garcia-Ocana A, et al. Leptin increases proliferation of human steosarcoma cells through activation of PI(3)-K and MAPK pathways. Med Sci Monit 2006;12:BR341–9.
49. Vestergaard P. Discrepancies in bone mineral density and fracture risk in patients with type 1 and type 2 diabetes – a meta-analysis. Osteoporos Int 2007;18:427–44.
50. Blume-Jensen P, Hunter T. Oncogenic kinase signalling. Nature 2001;411:355–65.
51. Shanik MH, Xu Y, Skrha J, et al. Insulin resistance and hyperinsulinemia: is hyperinsulinemia the cart or the horse? Diab Care 2008;31:S262–8.
52. Karimifar M, Pasha MA, Salari A, et al. Evaluation of bone loss in diabetic postmenopausal women. J Res Med Sci 2012;17:1033–8.
53. Vestergaard P, Rejnmark L, Mosekilde L. Relative fracture risk in patients with diabetes mellitus, and the impact of insulin and oral antidiabetic medication on relative fracture risk. Diabetologia 2005; 48:1292–9.
54. de L II, van der Klift M, de Laet CE, et al. Bone mineral density and fracture risk in type-2 diabetes mllitus: the Rotterdam Study. Osteoporos Int 2005;16:1713–20.
55. Barrett-Connor E, Kritz-Silverstein D. Does hyperinsulinemia preserve bone? Diabetes Care 1996;19:1388–92.
56. Dennison EM, Syddall HE, Aihie Sayer A, et al. Type 2 diabetes mellitus is associated with increased axial bone density in men and women from the Hertfordshire Cohort Study: evidence for an indirect effect of insulin resistance? Diabetologia 2004;47:1963–8.
57. Stolk RP, Van Daele PL, Pols HA, et al. Hyperinsulinemia and bone mineral density in an elderly population: The Rotterdam Study. Bone 1996;18:545–9.
58. McCabe LR. Understanding the pathology and mechanisms of type I diabetic bone loss. J Cell Biochem 2007;102:1343–57.
59. Campos Pastor MM, Lopez-Ibarra PJ, Escobar-Jimenez F, et al. Intensive insulin therapy and bone mineral density in type 1 diabetes mellitus: a prospective study. Osteoporos Int 2000;11: 455–9.
60. Strotmeyer ES, Cauley JA, Schwartz AV, et al. Diabetes is associated independently of body composition with BMD and bone volume in older white and black men and women: The Health, Aging, and Body Composition Study. J Bone Miner Res 2004;19: 1084–91.
61. Yuksel O, Dokmetas HS, Topcu S, et al. Relationship between bone mineral density and insulin resistance in polycystic ovary syndrome. J Bone Miner Metab 2001;19:257–62.
62. Reid IR. Relationships between fat and bone. Osteoporos Int 2008; 19:595–606.
63. Lee NK, Sowa H, Hinoi E, et al. Endocrine regulation of energy metabolism by the skeleton. Cell 2007;130:456–69.
64. Weinreb M, Shinar D, Rodan GA. Different pattern of alkaline phosphatase, osteopontin, and osteocalcin expression in developing rat bone visualized by in situ hybridization. J Bone Miner Res 1990; 5:831–42.
65. Clemens TL, Karsenty G. The osteoblast: an insulin target cell controlling glucose homeostasis. J Bone Miner Res 2011;26: 677–80.
66. Ferron M, Hinoi E, Karsenty G, Ducy P. Osteocalcin differentially regulates beta cell and adipocyte gene expression and affects the development of metabolic diseases in wild-type mice. Proc Natl Acad Sci USA 2008;105:5266–70.
67. Hwang YC, Jeong IK, Ahn KJ, Chung HY. Circulating osteocalcin level is associated with improved glucose tolerance, insulin secretion and sensitivity independent of the plasma adiponectin level. Osteoporos Int 2012;23: 1337–42.
68. Iki M, Tamaki J, Fujita Y, et al. Serum undercarboxylated osteocalcin levels are inversely associated with glycemic status and insulin resistance in an elderly Japanese male population: Fujiwara-kyo Osteoporosis Risk in Men (FORMEN) Study. Osteoporos Int 2012;23:761–70.
69. Kanazawa I, Yamaguchi T, Yamamoto M, et al. Serum osteocalcin level is associated with glucose metabolism and atherosclerosis parameters in type 2 diabetes mellitus. J Clin Endocrinol Metab 2009;94:45–9.
70. Kanazawa I, Yamaguchi T, Yamauchi M, et al. Serum undercarboxylated osteocalcin was inversely associated with plasma glucose level and fat mass in type 2 diabetes mellitus. Osteoporos Int 2011;22:187–94.
71. Ngarmukos C, Chailurkit LO, Chanprasertyothin S, et al. A reduced serum level of total osteocalcin in men predicts the development of diabetes in a long-term follow-up cohort. Clin Endocrinol 2012;77: 42–6.
72. Saleem U, Mosley Jr TH, Kullo IJ. Serum osteocalcin is associated with measures of insulin resistance, adipokine levels, and the presence of metabolic syndrome. Arterioscler Thromb Vasc Biol 2010;30:1474–8.
73. Yeap BB, Chubb SA, Flicker L, et al. Reduced serum total osteocalcin is associated with metabolic syndrome in older men via waist circumference, hyperglycemia, and triglyceride levels. Eur J Endocrinol 2010;163:265–72.

Endocr Res Downloaded from informahealthcare.com by Chiang Mai University on 12/09/13
For personal use only.

RIGHTSLINK

เอกสารแนบหมายเลข 66

OPEN ACCESS Freely available online

PLOS | ONE

Combined Therapy of Iron Chelator and Antioxidant Completely Restores Brain Dysfunction Induced by Iron Toxicity

Jirapas Sripetchwandee[1], Noppamas Pipatpiboon[1], Nipon Chattipakorn[1]*, Siriporn Chattipakorn[1,2]

1 Neurophysiology Unit, Cardiac Electrophysiology Research and Training Center, Department of Physiology, Faculty of Medicine, Chiang Mai University, Chiang Mai, Thailand, 2 Department of Oral Biology and Diagnostic Science, Faculty of Dentistry, Chiang Mai University, Chiang Mai, Thailand

Abstract

Background: Excessive iron accumulation leads to iron toxicity in the brain; however the underlying mechanism is unclear. We investigated the effects of iron overload induced by high iron-diet consumption on brain mitochondrial function, brain synaptic plasticity and learning and memory. Iron chelator (deferiprone) and antioxidant (n-acetyl cysteine) effects on iron-overload brains were also studied.

Methodology: Male Wistar rats were fed either normal diet or high iron-diet consumption for 12 weeks, after which rats in each diet group were treated with vehicle or deferiprone (50 mg/kg) or n-acetyl cysteine (100 mg/kg) or both for another 4 weeks. High iron-diet consumption caused brain iron accumulation, brain mitochondrial dysfunction, impaired brain synaptic plasticity and cognition, blood-brain-barrier breakdown, and brain apoptosis. Although both iron chelator and antioxidant attenuated these deleterious effects, combined therapy provided more robust results.

Conclusion: In conclusion, this is the first study demonstrating that combined iron chelator and anti-oxidant therapy completely restored brain function impaired by iron overload.

Citation: Sripetchwandee J, Pipatpiboon N, Chattipakorn N, Chattipakorn S (2014) Combined Therapy of Iron Chelator and Antioxidant Completely Restores Brain Dysfunction Induced by Iron Toxicity. PLoS ONE 9(1): e85115. doi:10.1371/journal.pone.0085115

Editor: Efthimios M. C. Skoulakis, Alexander Fleming Biomedical Sciences Research Center, Greece

Received September 28, 2013; **Accepted** December 2, 2013; **Published** January 6, 2014

Copyright: © 2014 Sripetchwandee et al. This is an open-access article distributed under the terms of the Creative Commons Attribution License, which permits unrestricted use, distribution, and reproduction in any medium, provided the original author and source are credited.

Funding: This work was supported by grants from the Thailand Research Fund TRF-BRG (SC), TRF-RTA5580006 (NC), Faculty of Medicine Chiang Mai University Endowment Fund (NC), National Research Council of Thailand (SC), Thailand Research Fund through the Royal Golden Jubilee Program (PHD/0248/2552: JS and SC), and Chiang Mai University Excellent Center Award (NC). The funders had no role in study design, data collection and analysis, decision to publish, or preparation of the manuscript.

Competing Interests: The authors have declared that no competing interests exist.

* E-mail: scchattipakorn@gmail.com

Introduction

Iron acts as an essential element for cellular processes in several organs, including the central nervous system [1]. In the brain, iron is required for brain function such as myelination [2], neurotransmitter synthesis [3], nitric oxide metabolism [4], and other biochemical activities [5]. Although the brain relies on iron availability for many important functions, it is also a highly vulnerable organ to iron-induced oxidative stress. Excessive iron accumulation or iron overload in the brain can be found in a normal aging brain [6], or under the pathologic alterations of iron homeostasis [7]. Iron overload is commonly found in beta-thalassemic patients with regular blood transfusions [8,9]. The major organ dysfunction related to hemosiderosis is principally hepatic cirrhosis and cardiomyopathy [10,11]. However, little is known regarding iron overload due to chronic blood transfusion associated with brain dysfunction. It has been known that the regulation of iron in the brain, particularly in the hippocampus is crucial for learning and memory [12,13]. A previous study in beta-thalassemic patients with iron overload demonstrated the potential role of hemosiderosis on cognitive impairment [14,15]. Although synaptic plasticity is an important process in learning and memory [16], its association with iron overload in the brain is unclear. A recent study also suggested the beneficial role of iron in N-methyl-D-aspartate receptor-dependent stimulation of calcium-induced brain synaptic plasticity [17]. This finding suggested that iron was required for synaptic plasticity. However, the synaptic plasticity under an iron overload condition has rarely been studied. In addition, the underlying mechanism of iron overload onto the brain synaptic plasticity as well as learning and memory has not yet been investigated.

Mitochondria are vital organelles, which produce energy for cells, particularly in the brain [18]. In fact, iron could act as a cofactor in mitochondria for the oxidative phosphorylation process [5]. Excessive iron accumulation could affect brain mitochondrial function resulting in neurodegeneration [19]. Therefore, it is possible that systemic iron overload may cause brain iron accumulation, leading to impaired brain mitochondrial function, brain apoptosis, and eventually the disruption of learning and memory. However, this possibility has not yet been investigated.

Oxidative stress has been proposed as one of the major contributing factors in iron-overload brain [20]. To protect against the deleterious effects of brain iron accumulation, potential strategies are to protect the brain from iron-induced oxidative stress. N-acetyl cysteine (NAC) has been commonly known as an antioxidant agent. Several studies have shown that NAC

attenuated the oxidative stress by reducing reactive oxygen species (ROS) production in the retinal blood vessels and the heart of rat models [21,22].

Besides anti-oxidative strategy, iron chelator has been commonly used to prevent iron-overload induced organ dysfunction [23,24]. The iron chelators, including deferiprone (L1), or deferoxamine (DFO), are widely used to chelate iron overload in thalassemic patients. Several studies have shown that iron chelation prevents the deleterious effects of iron accumulation in the brain during brain injury [25,26], suggesting that iron chelation can be a potential strategy for protection from neurodegenerative disorders during iron overload. However, the effects of either deferiprone, NAC or the combined agents on the brain under iron-overload conditions have not yet been investigated.

In the present study, we investigated whether iron overload induced by long-term high iron diet (HFe) consumption could lead to brain iron accumulation, decreased brain synaptic plasticity, impaired learning and memory as well as brain mitochondrial dysfunction and brain apoptosis. In addition, we determined the effects of antioxidant agent as well as an iron chelator on synaptic plasticity, learning and memory and brain mitochondrial function in HFe-fed rats. We hypothesized the following: 1) Iron overload condition induced by long-term HFe consumption causes plasma oxidative stress, leading to blood brain barrier breakdown, allowing iron to enter and accumulate in the brain, thus leading to brain oxidative stress, 2) Iron overload causes brain mitochondrial dysfunction, brain apoptosis, impaired synaptic plasticity, and learning and memory deficit, 3) Pharmacological interventions with deferiprone and NAC attenuate the iron overload induced brain dysfunctions and 4) Combined therapy of deferiprone and NAC restores brain functions after iron overload induced by long-term HFe consumption.

Materials and Methods

Animal Preparation

All animal studies were approved by the Institutional Animal Care and Use Committee (IACUC) at the Faculty of Medicine, Chiang Mai University (Permit number: 06/2556). Adult male Wistar rats (120–160 g, n = 66) were obtained from the National Laboratory Animal Center, Mahidol University, Bangkok, Thailand. All experiments were conducted in accordance to ARRIVE guidelines. They were housed in a room maintained under constant environmental conditions (temperature 22–25°C and a constant 12-hour light/dark cycle).

Experimental Protocols

The experimental protocols were set to determine the effects of iron overload induced by long-term HFe consumption on peripheral parameters and brain functions, and the effects of pharmacological intervention on iron-overload induced brain dysfunctions.

In the first protocol (Figure 1A), male Wistar rats were randomly divided equally to receive either a normal diet (0.018% Fe/kg of diet, ND) or High iron diet (0.2% Fe/kg of diet, HFe) (n = 12/group). Then, rats in each dietary group were divided into 2 subgroups to receive the assigned diet for either 4 weeks or 8 weeks (n = 6/subgroup). In the second protocol (see figure 1B), male Wistar rats were randomly assigned to receive either ND (n = 18) or HFe diet (n = 24) for 8 weeks. Then, rats in the HFe group were further divided into 4 subgroups (n = 6/subgroup), including 1) HFe treated with saline (HFeV), 2) HFe treated with NAC (HFeNAC), 3) HFe treated with L1 (HFeL1) and 4) HFe treated with L1 combined with NAC (HFeL1+NAC). Rats in the ND group were divided into 3 subgroups, including 1) ND treated with saline (NDV), 2) ND treated with NAC (NDNAC), and 3) ND treated with L1 (NDL1). NDV and HFeV subgroups received 0.9% normal saline solution (NSS) as a vehicle at 2 ml/kg/day. NDNAC and HFeNAC subgroups received NAC 100 mg/kg/day (Sigma-Aldrich, St Louis, MO, USA; dissolved in normal saline 2 ml/kg/day). NDL1 and HFeL1 subgroups received deferiprone (L1) 50 mg/kg/day (Government Pharmaceutical Organization, Bangkok, Thailand; dissolved in normal saline 2 ml/kg/day). HFeL1+NAC subgroup received L1 50 mg/kg/day combined with NAC 100 mg/kg/day (dissolved in normal saline 2 ml/kg/day). Each subgroup received the assigned treatment for 4 consecutive weeks by gavage feeding.

At the end of the experiment, rats were deeply anesthetized (3% isoflurane and intraperitoneal injection of 80 mg/kg thiopental) and decapitated, and the brain excepted cerebellum region was rapidly removed, and separated into 2 halves. The first half was used for brain slices preparation to determine the long-term potentiation (LTP) and western blot analysis. The second half was used for isolated brain mitochondria preparation or stored at −80°C for brain iron and malondialdehyde (MDA) determination. Furthermore, blood samples from tail veins were collected every month of each experiment, and kept in Na-heparin tube for determination of plasma non-transferrin bound iron (NTBI) and MDA levels. The summary of the experimental protocols are shown in figure 1.

Quantification of Plasma Non-transferrin Bound Iron (NTBI)

To determine iron overload condition, plasma NTBI concentration was measured using nitrilotriacetic acid disodium salt (NTA) chelation/HPLC method [27]. Plasma was incubated with 80-mM NTA solution, pH 7.0 for 30 minutes at room temperature to produce Fe^{3+}- $(NTA)_2$ complex and then subsequently separated from plasma proteins via plasma mixture spinning with a membrane filter (Nanostep®, 30-kDa cut off, polysulfone type; Pall life Sciences, Ann Arbor, MI USA). Concentration of Fe^{3+}-$(NTA)_2$ complex representing NTBI in the ultrafiltrate was determined by a non-metallic HPLC system. NTBI concentration was calculated from a calibration curve made with differential iron concentrations of Fe^{3+}- $(NTA)_2$ in 80 mM NTA, pH 7.0 ranging 0–16 μM.

Quantification of Plasma and Brain Malondialdehyde (MDA)

To determine oxidative stress condition, plasma and brain malondialdehyde (MDA) concentrations were measured by the HPLC method [28]. Brain tissues were homogenized in a phosphate buffer pH 2.8. Homogenated brain or plasma was mixed with 10% trichloroacetic acid (TCA) containing butylated hydroxytoluene (BHT) (50 ppm), heated at 90°C for 30 minutes, and then cooled down and consequently centrifuged at 6,000 rpm for 10 minutes. Supernatant was mixed with 0.44 M H_3PO_4 and 0.6% thiobarbituric acid (TBA) solution and then incubated at 90°C for 30 minutes. MDA levels were determined via the absorbance detected at 532 nm by the HPLC system, and were calculated directly from the standard curve, and reported as the MDA equivalent concentration (μM).

Brain Iron Level Assay

Brain iron determination was performed using a method modified from a previous study [29]. A homogenated brain was

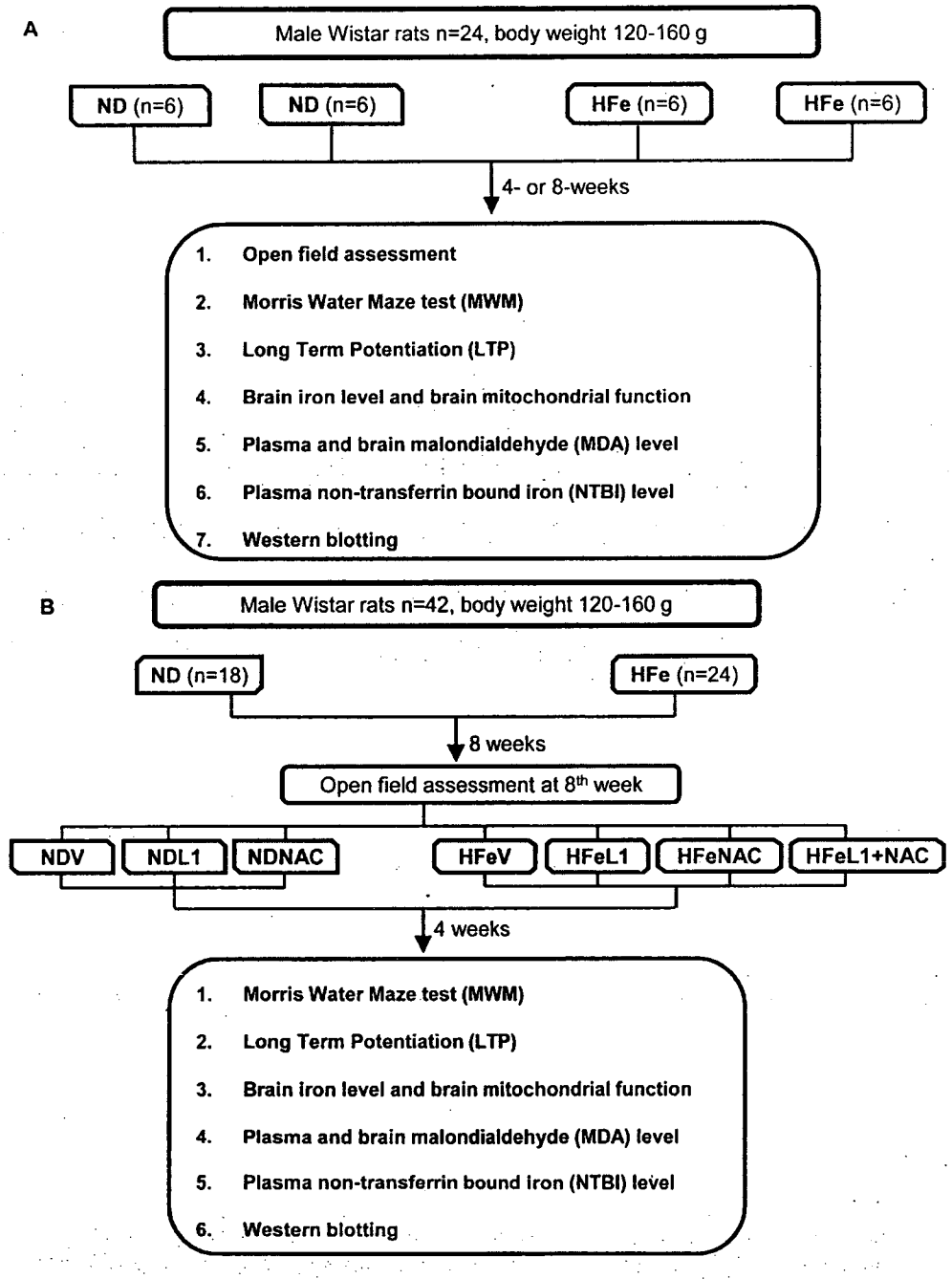


Figure 1. Summarized experimental diagrams. Each panel represented protocol 1 (A) and protocol 2 (B). ND: normal diet fed group; HFe: high iron diet fed group; MDA: malondialdehyde; NTBI: non-transferrin bound iron; V: vehicle; L1: deferiprone; NAC: n-acetyl cysteine.
doi:10.1371/journal.pone.0085115.g001

precipitated in protein precipitated solution (1:1). The mixed solution was heated at 95°C for 1 hour and cooled down to room temperature. The mixed sample was centrifuged at 8,200 *g* for 10 minutes. A supernatant was mixed in chromagen solution (1:1). For blank, a supernatant was mixed with 1.5 mol/l sodium acetate containing 0.1% TGA. The sample was incubated for 30 minutes at room temperature. Absorbance of samples was determined using a microplate reader at 562 nm.

Brain Slices Preparation

Brain slices (400 μm) were prepared using a vibratome (Vibratome Co., Saint Louis, MO) [30]. Briefly, after a 30-minutes post slice incubation in high-sucrose aCSF, the brain slices were transferred to a standard aCSF solution and saturated with 95% O_2/5% CO_2 (pH 7.4) for an additional 30 minutes at room temperature (22–24°C). Brain slices (n = 3 brain slices per animal) were used for extracellular recording.

Extracellular Recording of Brain Slices for Long-term Potentiation (LTP)

Brain slices were transferred to a submersion recording chamber and continuously perfused at 3–4 ml/min with standard artificial cerebrospinal fluid (aCSF) warmed to 28–29°C. Field excitatory postsynaptic potentials (fEPSPs) was evoked by stimulating the Schaffer collateral-commissural pathway with a bipolar tungsten electrode, while the fEPSPs recordings were taken from the stratum radiatum of the hippocampal CA1 region with micropipettes filled with 2 M NaCl. Brain slices were perfused with aCSF and recorded as a baseline condition for 10 minutes. LTP was induced by delivering high-frequency tetani (high-frequency stimulation (HFS); 4 trains at 100 Hz; 0.5 s duration; 20 s interval) at 1.5 times the baseline stimulation intensity. Experiments were performed for at least 50 minutes after HFS. The amount of potentiation was calculated at 30 minutes after tetanus. Data were filtered at 3 kHz, digitized at 10 kHz, and stored in a computer using pClamp 9.2 software (Axon Instruments, CA, USA). The initial slope of the fEPSPs was measured and plotted against time.

Western Blotting

Brain protein were collected as previously described [31]. Briefly, proteins were separated on 10% sodium dodecyl sulfate (SDS)-polyacrylamide gels by sodium dodecyl sulfate-polyacrylamide gels electrophoresis (SDS-PAGE); Bio-Rad Laboratories, Foster City, CA, USA. Then, proteins were transferred to polyvinylidene difluoride (PVDF) membrane. PVDF membranes were blocked with 5% non-fat milk in 1×TBST buffer for 1 hour at room temperature. After that, membranes were subsequently exposed to primary antibodies including anti-Bax (Santa Cruz Biotechnology, Santa Cruz, CA, USA), anti-Bcl-2 (Cell Signaling Technology, Danvers, MA, USA), anti-occludin (Santa Cruz Biotechnology), or actin (Cell Signaling Technology) overnight at room temperature, respectively. All membranes were incubated with a secondary goat anti-rabbit antibody, conjugated with horseradish peroxidase (Cell Signaling Technology, Danvers, MA, USA). Finally, the proteins bands were visualized on Amersham hyperfilm enhanced chemiluminescence (ECL) by the Amersham ECL Western blotting detection reagents system (GE healthcare, Buckinghamshire, UK). Total results were shown as average signal intensity.

Isolation of Brain Mitochondria

Brain mitochondria were isolated using the method described previously [32]. Mitochondrial pellets were collected and dissolved in cold respiration (RES) buffer [33]. The protein concentration was determined according to the Bicinchoninic Acid (BCA) Assay as previously described [34].

Determination of Brain Mitochondrial Swelling

Brain mitochondrial swelling assay was determined by the changes in the absorbance of the mitochondrial suspensions at 540 nm using a microplate reader [35]. Mitochondria (0.533 mg/ml) were incubated in RES buffer. The decreased in absorbance represented brain mitochondrial swelling.

Determination of Pharmacological Interventions on Brain Mitochondrial Membrane Potential Changes ($\Delta\Psi_m$)

Brain mitochondrial membrane potential changes were determined using a fluorescent dye, 5, 5′, 6, 6′-tetrachloro-1, 1′, 3, 3′-tetraethylbenzimidazolcarbocyanine iodide (JC-1) [36]. In this protocol, brain mitochondria (0.552 mg/ml) were stained with JC-1 (310 nM) at 37°C for 15 minutes. The fluorescent intensity was determined using a fluorescent microplate reader. The fluorescence of JC-1 monomer form (green) was excited at 488 nm and the emission was detected at 530 nm. JC-1 aggregate (red) fluorescence was excited at 488 nm and emission fluorescence was detected at 590 nm. Mitochondrial depolarization was indicated by a decreased red/green fluorescent intensity ratio ($\Delta\Psi$m).

Determination of Brain Mitochondrial ROS Production

Brain mitochondrial ROS production was determined using dichlorohydro-fluorescein diacetate (DCFDA) dye [37]. In this protocol, brain mitochondria (0.552 mg/ml) were incubated with 2-μM DCFDA for 20 minutes. Fluorescence was determined at λex 485 nm and λem 530 nm using a fluorescent microplate reader. The ROS level was represented as arbitrary units of fluorescence intensity of dichlorohydro-fluorescein (DCF).

Identification of Brain Mitochondria Using Electron Microscopy

A transmission electron microscope was used to study brain mitochondrial morphology. The preparation of brain mitochondria for electron microscope was done according to the method described previously [32,38]. Briefly, isolated brain mitochondria were fixed overnight in 2.5% glutaraldehyde in 0.1 M cacodylate buffer, pH 7.4 at 4°C. After that, brain mitochondria were postfixed with 1% cacodylate-buffered osmium tetroxide at room temperature for 2 hours. The brain mitochondrial pellets were subsequently dehydrated in a graded series of ethanol and embedded in Epon-Araldite. Ultrathin sections were cut by a diamond knife, then placed on copper grids and stained with uranyl acetate, lead citrate, and observed with a transmission electron microscope.

Open Field Assessment

Open-field assessment was developed to evaluate the anxiety behavior and general locomotors activity in rodents [39,40]. Each animal was placed into the box and allowed to spend 5 minutes to explore the box. The numbers of lines which the animals crossed in the peripheral area of the open-field were counted as activity. This parameter was used to exclude the different locomotors activity among rats.

Morris Water Maze Task (MWM)

MWM was modified from the previous study [41]. The experimental protocol was divided into 2 different phases 1) acquisition test (hidden platform), and 2) probe trial test (removal of the platform from the water pool). In the acquisition test, animals performed 4 different starting points per day for 5 consecutive days. Animals were placed in a randomized starting point with their head turned towards the border of the water pool, the time started recording after placing the animal into the water and stopped recording when the animal found the submerged platform. After that, the animals were placed at the other 3 starting points. All animals performed the probe test on the sixth day. The animals were placed into the water with their head facing towards the water. Time recording starting after placing the animal into the water and the experiment was finished after 90 seconds. Time to reach the platform and time spent in the quadrant which previously contained the platform were recorded.

Data Analysis

The data for each experiment were presented as mean ± standard error of mean. The data were processed using SPSS (Statistical Package for Social Sciences, Chicago, IL, USA) release 16.0 for Windows. For all comparisons, the significance of the difference between the mean was calculated by Two-way ANOVA, followed by Fisher's least significant difference *post hoc* analysis. The data from brain mitochondrial function were analyzed using non-parametric Kruskal-Wallis H followed by the Mann-Whitney U test. $P<0.05$ was considered statistically significant.

Results

Iron Overload Induced by 4- and 8-week High Iron Diet (HFe) Consumption Increased not only Plasma NTBI Levels and Peripheral Oxidative Stress, but also Brain Iron Accumulation and Brain Oxidative Stress

Four- and eight week high iron (HFe)-fed rats had lower body weights than normal diet (ND)-fed rats (Table 1). We found that both 4- and 8-week HFe-fed rats had iron overload as indicated by increased plasma non-transferrin bound iron (NTBI, Table 1). In addition, increased plasma malondialdehyde (MDA) level was observed in HFe-fed rats (Table 1). HFe-fed rats had high levels of brain iron accumulation and brain oxidative stress as indicated by a significant increase in brain iron and brain MDA level (Table 1). In addition, the iron overload condition, increased oxidative stress, level of brain iron deposition and increased brain oxidative stress occurred in a time-dependent manner of HFe consumption (Table 1).

Iron Overload Induced by HFe Led to the Impairment of Learning and Memory and Impaired Brain Synaptic Plasticity

High iron diet consumption for 4- and 8-week had no effect on locomotors activity of those rats as indicated by no significant differences in the number of line crossings in rats between both dietary groups in the open field tests (Fig. 2A). However, the iron overload condition caused significant learning and memory deficit as indicated by increased time to reach target platform and decreased time spent in target quadrant of HFe-fed rats compared to those of ND-fed rats during the Morris Water test ($p<0.05$, Fig. 2B and 2C). We also found that the decreased learning process represented by the increase in time to reach a target platform of HFe-fed rats appeared in a time-dependent manner of HFe consumption (Fig. 2B). However, the decreased memory process as indicated by the decrease in time spent in a target quadrant of HFe-fed rats did not occur in a time-dependent manner of HFe consumption (Fig. 2C).

The long term potentiation (LTP) process in CA1 hippocampus was determined in rats of both dietary groups to study brain synaptic plasticity which is an important process for information storage of memory in the brain [42]. After high frequency stimulation (HFS), brain LTP occurred in ND-fed rats, but was absent in HFe-fed rats (3 independent slices/animals, n = 6 animals/group, Fig. 2D). At the 30-minute period after LTP induction, the increments of LTP magnitude compared to baseline in ND-fed rats were 68.72±6.73% for 4-week and 65.79±6.02% for 8-week HFe consumption. However, the LTP magnitudes among these ND groups did not reach statistical difference.

Brain Mitochondrial Dysfunction in HFe-fed Rats

To investigate brain mitochondrial function, brain mitochondrial reactive oxygen species (ROS) production, brain mitochondrial membrane potential change, and brain mitochondrial swelling were determined in both HFe-fed rats and ND-fed rats. We found increased brain mitochondrial ROS production, increased brain mitochondrial depolarization and brain mitochondrial swelling in HFe-fed rats compared with those of ND-fed rats (Fig. 3). This mitochondrial dysfunction also occurred in a time-dependent manner of HFe consumption (Fig. 3).

HFe Consumption Leads to the Blood-brain Barrier Breakdown and Brain Apoptosis

The expression of occludin, which is the tight junction marker in cerebral endothelial cells was determined to investigate the blood-brain barrier (BBB) breakdown [43,44]. HFe-fed rats had decreased expression of occludin, compared to ND rats (Fig. 4A). Moreover, the expression of occludin in 8-week HFe-fed rats was significantly lower than that in 4-week HFe-fed rats, suggesting that the BBB breakdown induced by iron overload occurred in a time-dependent manner of HFe consumption.

Although HFe consumption had no effect on the expression of anti-apoptotic marker Bcl-2, the expression of apoptotic marker Bax was markedly increased (Figure 4B-4C). The ratio of Bax/Bcl-2 was also significantly increased, compared to those of ND-fed rats (Fig. 4D). Both BBB breakdown and increased apoptotic marker occurred in a time-dependent manner of HFe consumption.

Although either iron chelator deferiprone (L1) or anti-oxidant n-acetyl cysteine (NAC) attenuated the iron overload condition as well as brain dysfunctions, their combined therapy restored those defects induced by iron overload.

Table 1. Effects of 4-, and 8-week high iron diet consumption on body weight, plasma NTBI, plasma MDA, brain MDA and brain iron level in rats.

Parameters	ND4w	HFe4w	ND8w	HFe8w
Body weight (g)	317.00±3.74	260.83±3.75*	395.00±8.37	305.71±10.99*†
Plasma NTBI (μM)	0	2.51±0.118*	0	3.35±0.141*†
Plasma MDA (μM)	6.42±2.58	23.36±1.72*	10.30±3.46	31.31±3.90*†
Brain MDA (μM/mg protein)	0.83±0.04	1.25±0.04*	1.02±0.10	1.50±0.07*†
Brain iron (μM/mg protein)	7.45±0.13	9.62±0.28*	7.55±0.16	12.91±1.27*†

*$p<0.05$ vs. Normal diet-fed rats,
†$p<0.05$ vs. High iron diet-fed rats for 4 weeks. ND; normal diet-fed rats, HFe; high iron diet-fed rats, 4w; 4-week diet consumption, 8w; 8-week diet consumption, NTBI; non-transferrin bound iron, MDA; malondialdehyde.
doi:10.1371/journal.pone.0085115.t001

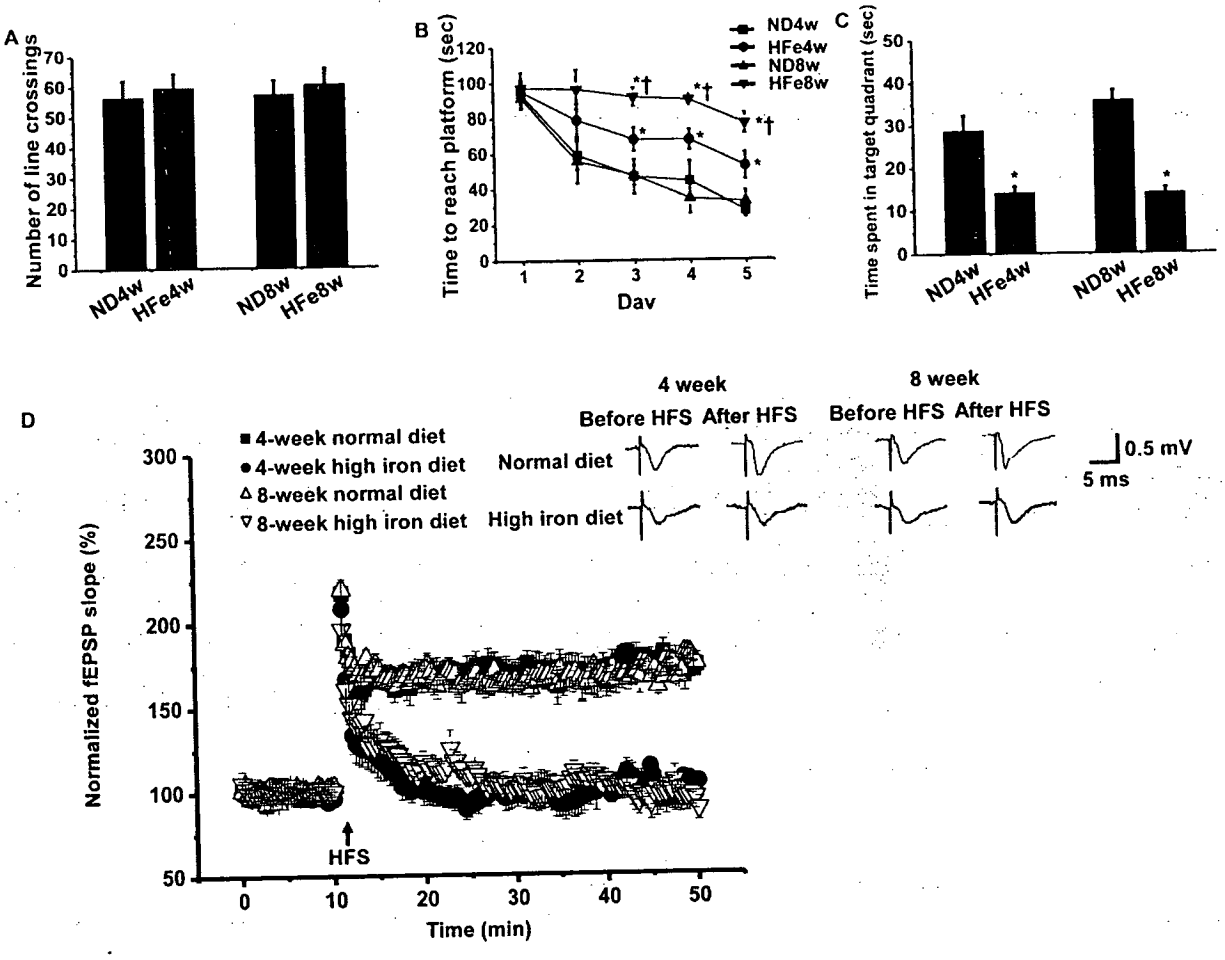


Figure 2. Effects of iron overload on learning and memory behavior. Each panel represented locomotors activity (A) and learning and memory behavior which was indicated by time to reach platform (B) and time spent in target quadrant (C) and brain synaptic plasticity (D). *$P<0.05$ vs. Normal diet groups; †$P<0.05$ vs. HFe4w. ND: normal diet fed groups; HFe: high-iron diet fed groups.
doi:10.1371/journal.pone.0085115.g002

Effects of L1 and NAC on peripheral and brain parameters in iron overload condition. Treatment with either L1 or NAC alone significantly attenuated the adverse effects of iron overload condition in HFe-fed rats as indicated by increased body weight, and decreased plasma NTBI and plasma MDA levels. No differences of these parameters were found between both therapies. However, despite the reduction of plasma NTBI and MDA by either treatment, they did not reach the normal levels as shown in ND-fed rats (Table 2). Similarly, brain MDA level and brain iron level of HFeL1 rats and HFeNAC rats were also significantly decreased, compared to those of HFeV rats, but did not reach the normal levels as shown in the ND group (Table 2). However, the combination of L1 and NAC treatment (HFeL1+NAC) completely restored plasma NTBI, plasma MDA level, brain MDA level and brain iron level in HFe-fed rats to the same levels as shown in ND group ($p<0.05$, Table 2).

L1 and NAC attenuated learning and memory deficit, and the impairment of brain synaptic plasticity following iron overload condition. Although HFe consumption for 12 weeks led to altered peripheral parameters including decreased body weight, increased plasma NTBI and plasma MDA as well as increased brain MDA level and accumulated brain iron level (Table 2), it did not affect the locomotors activity (Fig. 5A).

In the vehicle-treated rats, 12-week HFe consumption required significantly increased time to reach a platform and decreased time spent in a target quadrant, compared to those of ND-fed rats, suggesting the learning and memory deficit following HFe consumption (Fig. 5B and 5C). Neither L1nor NAC treatment alone changed the learning and memory in ND-fed rats (Fig. 5D and 5F). In HFe-fed rats, either L1 or NAC therapy alone significantly improved learning and memory as shown by decreased time to reach a platform, and increased time spent in a target quadrant (Fig. 5E and 5F). In addition, the combined therapy of L1 and NAC completely restored brain functions that were impaired by HFe by improving learning and memory process (Fig. 5E and 5F).

Rats in the 12-week HFe consumption also had impaired brain synaptic plasticity as shown by the absent of an electrical-induced LTP after electrical stimulation (3 independent slices/animals, n = 6 animals/group, Fig. 6A). Moreover, treatment with either L1 or NAC alone did not alter the electrical-induced LTP in ND-fed rats (Fig. 6B). At 30 minutes following the LTP induction, the increment of LTP magnitude compared to baseline in ND-fed rats

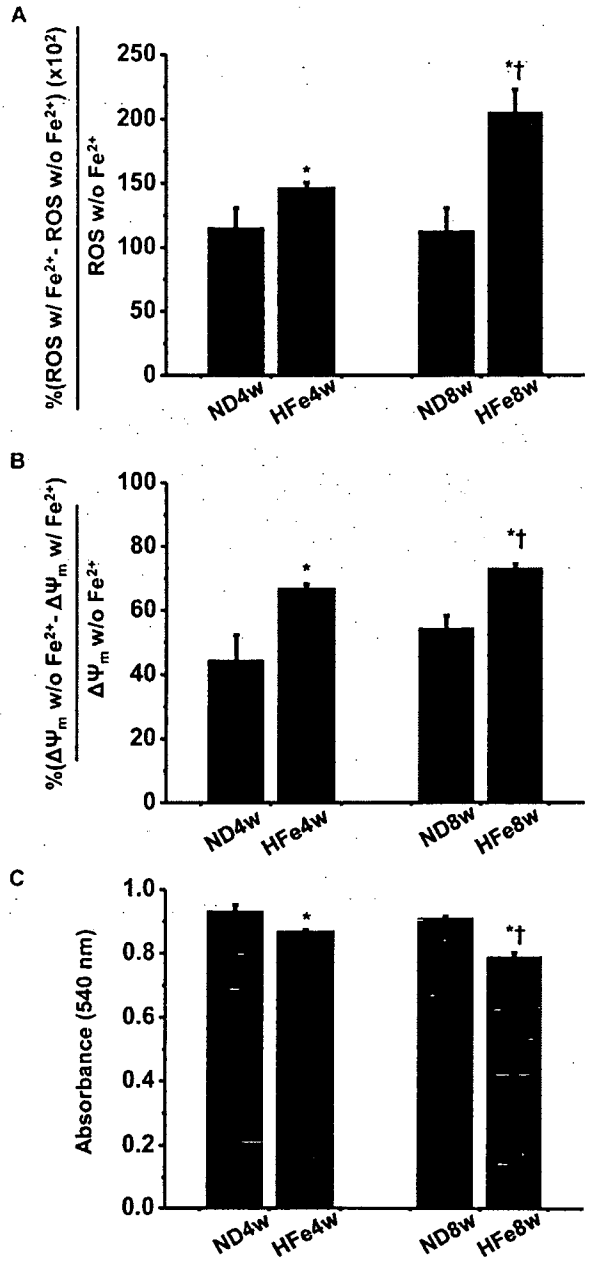


Figure 3. Effects of iron overload on brain mitochondrial function. Each panel represented brain mitochondrial ROS production (A), brain mitochondrial membrane potential changes (B) and brain mitochondrial swelling (C). *$P<0.05$ vs. Normal diet groups; †$P<0.05$ vs. HFe4w. ND: normal diet fed groups; HFe: high-iron diet fed groups.
doi:10.1371/journal.pone.0085115.g003

were 61.68±2.85%, 63.57±13.52% and 66.05±13.52% for NDV, NDL1 and NDNAC, respectively (3 independent slices/animals, n = 6 animals/group). Either L1 or NAC alone significantly attenuated the impaired LTP in HFe-fed rats (Fig. 6C). At 30 minutes following the LTP induction, the increment of LTP magnitude compared to baseline were 39.12±8.81% for HFeL1 and 34.10±3.45% for HFeNAC. The increased LTP magnitude between HFeL1 and HFeNAC groups was significantly increased compared to that of HFe-fed rats treated with vehicle.

In addition, combined treatment of L1 and NAC in HFe-fed rats restored the impairment of brain synaptic plasticity (3 independent slices/animals, n = 6 animals/group, Fig. 6C). At 30 minutes after the LTP induction, the increment of LTP magnitude compared to the baseline in the HFeL1+NAC group was 67.36±10.51%, which was significantly increased compared to that of HFeV rats, HFeL1 rats and HFeNAC rats (Fig. 6C).

L1 or NAC improved brain mitochondrial dysfunction caused by iron overload condition. Twelve week HFe consumption led to brain mitochondrial dysfunction as indicated by increased brain mitochondrial ROS production, brain mitochondrial depolarization, and brain mitochondrial swelling (Fig. 7). HFe-fed rats treated with either L1 or NAC significantly preserved brain mitochondrial function in HFe-fed rats, compared to that of HFe-fed rats treated with vehicle (Fig. 7). Moreover, electron microscopic images revealed that brain mitochondria in HFe-fed rats had altered morphology including unfolded cristae, compared to the normal brain mitochondria, indicating brain mitochondrial swelling (Fig. 7C). Treatment with either L1 or NAC alone in HFe-fed rats attenuated brain mitochondrial dysfunction as shown by decreased mitochondrial ROS level (Fig. 7A), decreased membrane potential change (Fig. 7B), and reduced mitochondrial swelling caused by iron overload (Fig. 7C and 7D). However, the combination of L1 and NAC therapy in HFe-fed rats restored brain mitochondrial function and morphology, compared to that of HFe-fed rats treated with vehicle or treated with either L1 or NAC alone (Fig. 7).

L1 or NAC improved the blood-brain barrier breakdown and brain apoptosis caused by iron overload. Both L1 and NAC administration in HFe-fed rats significantly increased the expression of occludin, compared to that of HFe-fed rats treated with vehicle (Fig. 8A). In addition, either L1 or NAC therapy alone also significantly decreased the expression of Bax, although the expression of Bcl-2 in HFe-fed rats was not altered in any groups compared to the control (Fig. 8B and 8C). The Bax/Bcl-2 ratio was also decreased in the L1 and NAC-treated groups (Fig. 8D).

Interestingly, the combination of L1 and NAC therapy restored the occludin expression in HFe-fed rats, suggesting the prevention of BBB breakdown (Fig. 8A). Furthermore, it also attenuated the expression of apoptosis markers, indicating the protective effects of these combined drugs against brain apoptosis caused by HFe consumption (Fig. 8B and 8D).

Discussion

The major findings of the present study are as follows: 1) Long-term HFe consumption caused iron overload by increasing plasma NTBI and brain iron level, and led to peripheral and brain oxidative stress, 2) HFe induced iron overload was time-dependent of HFe consumption, 3) Iron overload led to learning and memory deficit, abolished brain synaptic plasticity, brain apoptosis, and caused brain mitochondrial dysfunction as indicated by increased brain mitochondrial ROS production, brain mitochondrial depolarization and brain mitochondrial swelling, 4) Brain iron-overload following HFe consumption occurred via the blood-brain barrier breakdown, 5) The pharmacological intervention using either deferiprone or n-acetyl cysteine alone attenuated these deleterious effects of iron overload and 6) The present study is the first study that demonstrated that the combination of deferiprone and n-acetyl cysteine exerted the robust effects by restoring brain function following iron overload.

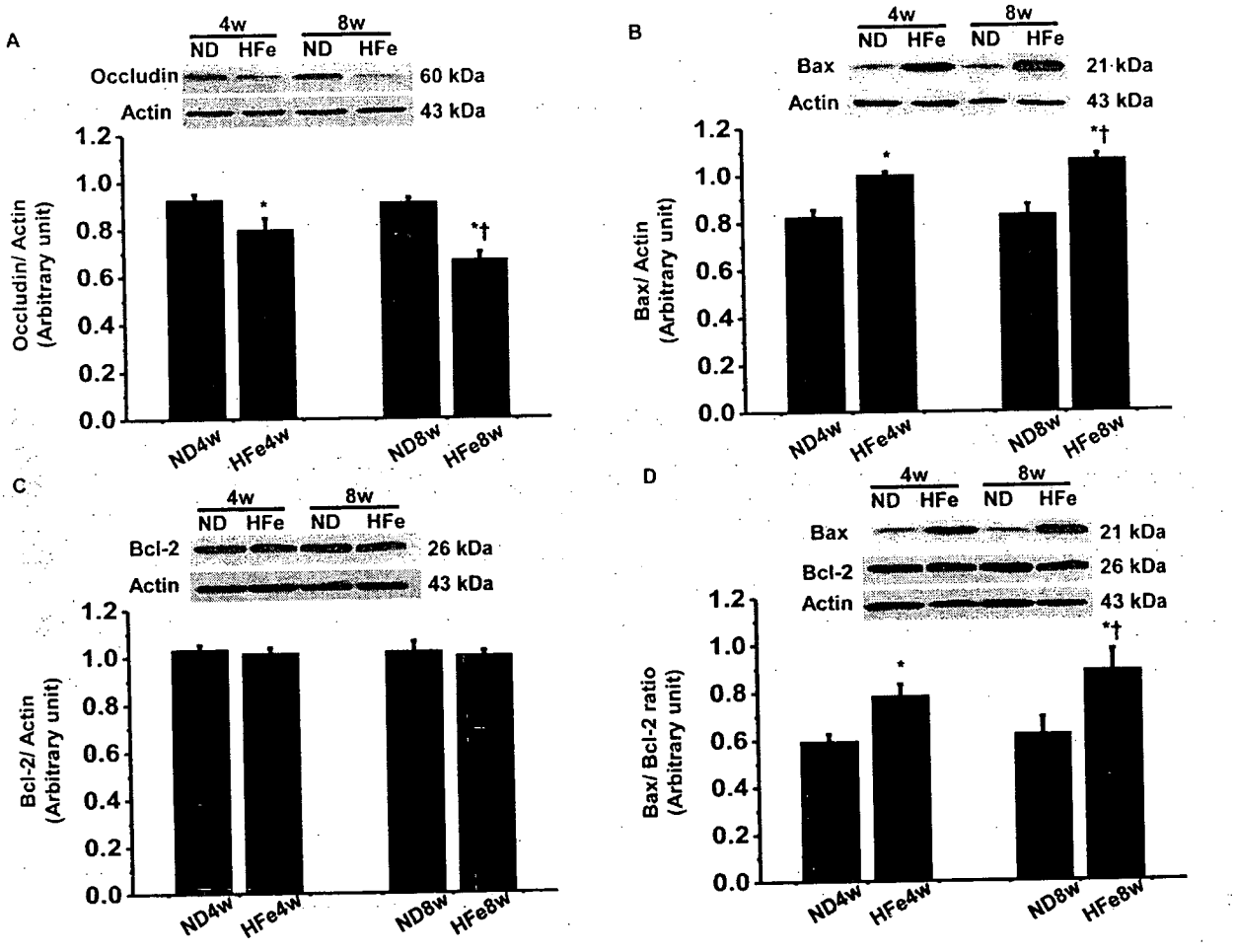


Figure 4. Effects of iron overload on BBB breakdown and apoptosis. Each panel represented the expression of tight junctions protein; occludin (A), apoptotic-protein; Bax (B) and anti-apoptotic protein; Bcl-2 (C) and Bax/Bcl-2 ratio (D). *$P<0.05$ vs. Normal diet groups; †$P<0.05$ vs. HFe4w. ND: normal diet fed groups; HFe: high-iron diet fed groups.
doi:10.1371/journal.pone.0085115.g004

In the present study, chronic HFe consumption induced iron-overload condition as indicated by an increased plasma non-transferrin bound iron (NTBI). The plasma NTBI is known to be catalyzed, resulting in the production of highly toxic free hydroxyl radicals via Fenton reactions [45,46]. These excessive free radicals have been shown to cause cellular lipid peroxidation and increased cytotoxic aldehyde products including 4-hydroxylnonenal (HNE) and malondialdehyde (MDA) [10,47]. Consistent with these reports, we found that in rats fed with HFe increased plasma NTBI were observed with increased plasma MDA. In the present

Table 2. Effects of the pharmacological interventions on body weight, plasma NTBI, plasma MDA, brain MDA and brain iron level in high iron diet-fed rats.

Parameters	NDV	NDL1	NDNAC	HFeV	HFeL1	HFeNAC	HFeL1+NAC
Body weight (g)	433.33±18.56	401.67±37.56	411.67±13.02	325.00±9.92*	358.33±19.26*†	362.5±11.60*†	366.67±11.12*†‡
Plasma NTBI (μM)	0	0	0	3.99±0.51*	0.44±0.19*†	0.54±0.37*†	0
Plasma MDA (μM)	26.01±2.62	26.93±4.47	27.48±3.79	60.76±1.81*	54.75±2.30*†	55.41±2.12*†	31.11±1.6†‡
Brain MDA (μM/mg protein)	0.97±0.12	0.85±0.16	0.73±0.12	1.71±0.05*	1.30±0.15*†	1.25±0.05*†	0.81±0.08†‡
Brain iron (μM/mg protein)	8.30±0.52	7.78±0.367	7.99±0.49	23.59±3.33*	13.29±1.23*†	13.70±1.67*†	8.50±0.37†‡

*$p<0.05$ vs. Normal diet-fed rats,
†$p<0.05$ vs. High iron diet-fed rats treated with vehicle,
‡$p<0.05$ vs. High iron diet-fed rats treated with either L1 or NAC. ND; normal diet-fed rats, HFe; high iron diet-fed rats, V; vehicle, L1; deferiprone, NAC; n-acetyl cysteine, NTBI; non-transferrin bound iron, MDA; malondialdehyde.
doi:10.1371/journal.pone.0085115.t002

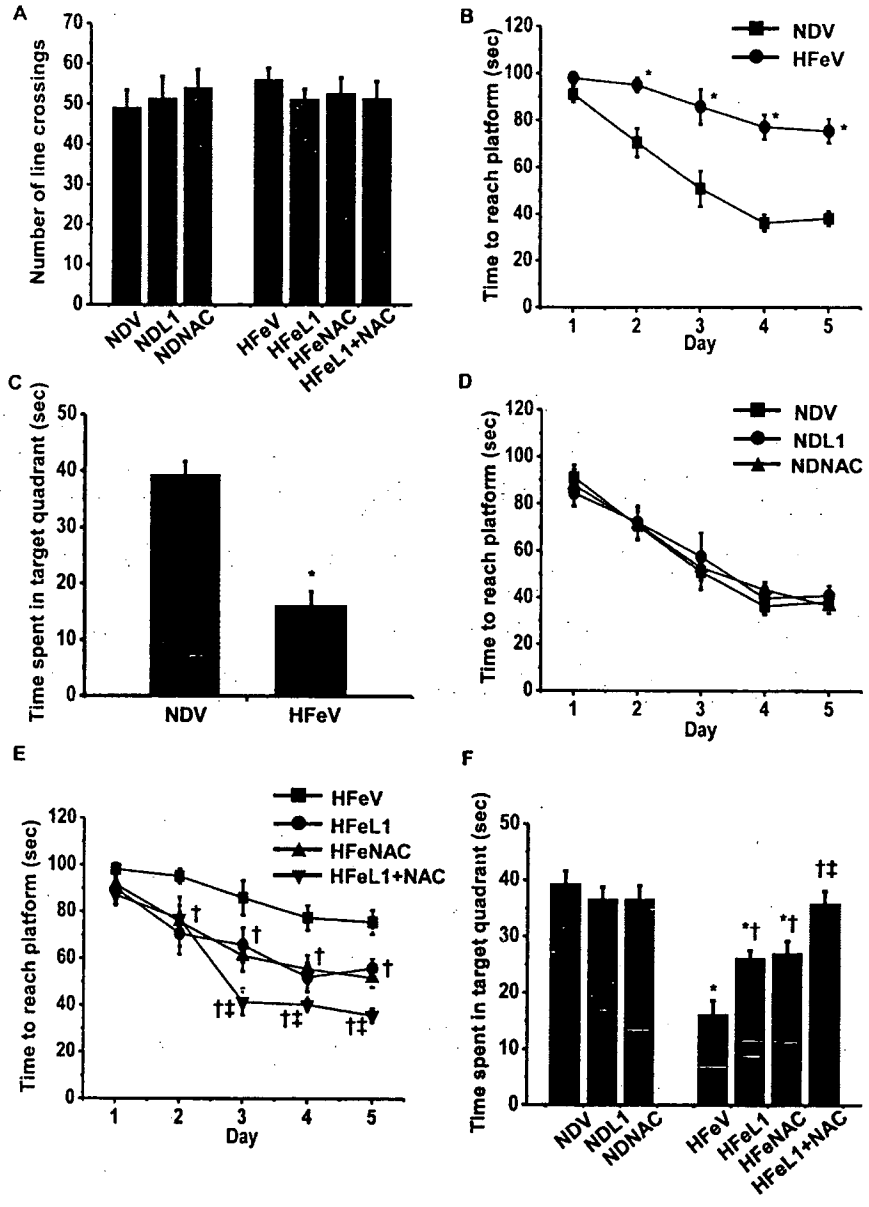


Figure 5. Effects of the pharmacological interventions by deferiprone and n-acetyl cysteine on learning and memory behavior. Each panel represented locomotors activity (A) and learning and memory behavior indicated by time to reach platform (B, D and F) and time spent in target quadrant (C and E). *$P<0.05$ vs. Normal diet treated with vehicle (NDV); †$P<0.05$ vs. HFe treated with vehicle (HFeV); ‡$P<0.05$ vs. HFe treated with either L1 or NAC (HFeL1 or HFeNAC). ND: normal diet fed groups; HFe: high-iron diet fed groups; L1: deferiprone; NAC: n-acetyl cysteine.
doi:10.1371/journal.pone.0085115.g005

study, increased brain iron accumulation in HFe rats was also observed. It is known that plasma iron could not normally pass the intact blood-brain barrier (BBB) since the BBB is a diffusion barrier playing a role in brain defensive mechanism [48]. Under several pathological conditions, the decrease of tight junction protein occludin could be observed, indicating the BBB disruption [43,44]. Won and colleagues demonstrated in a brain injury model that decreased expression of tight junction proteins could be observed, causing an increased BBB permeability, and eventually leading to increased brain iron accumulation [49]. In the present study, increased occludin expression was observed, indicating the BBB disruption and could be responsible for increased brain iron accumulation in HFe rats. In addition, increased brain iron level could also cause further lipid peroxidation in the brain as shown by increased brain MDA level in our study.

Mitochondria are vital organelles since they are the power houses of cells [50]. Although iron is required as a cofactor in the oxidative phosphorylation process in the mitochondria for ATP production, excessive iron could cause severe oxidative stress including ROS and MDA levels, which is harmful to the cells [51–55] and mitochondria [32,51,53,56–58]. As demonstrated in the present study, HFe rats had high levels of brain iron, leading to brain oxidative stress and brain mitochondrial dysfunction as indicated by increased brain mitochondrial ROS production,

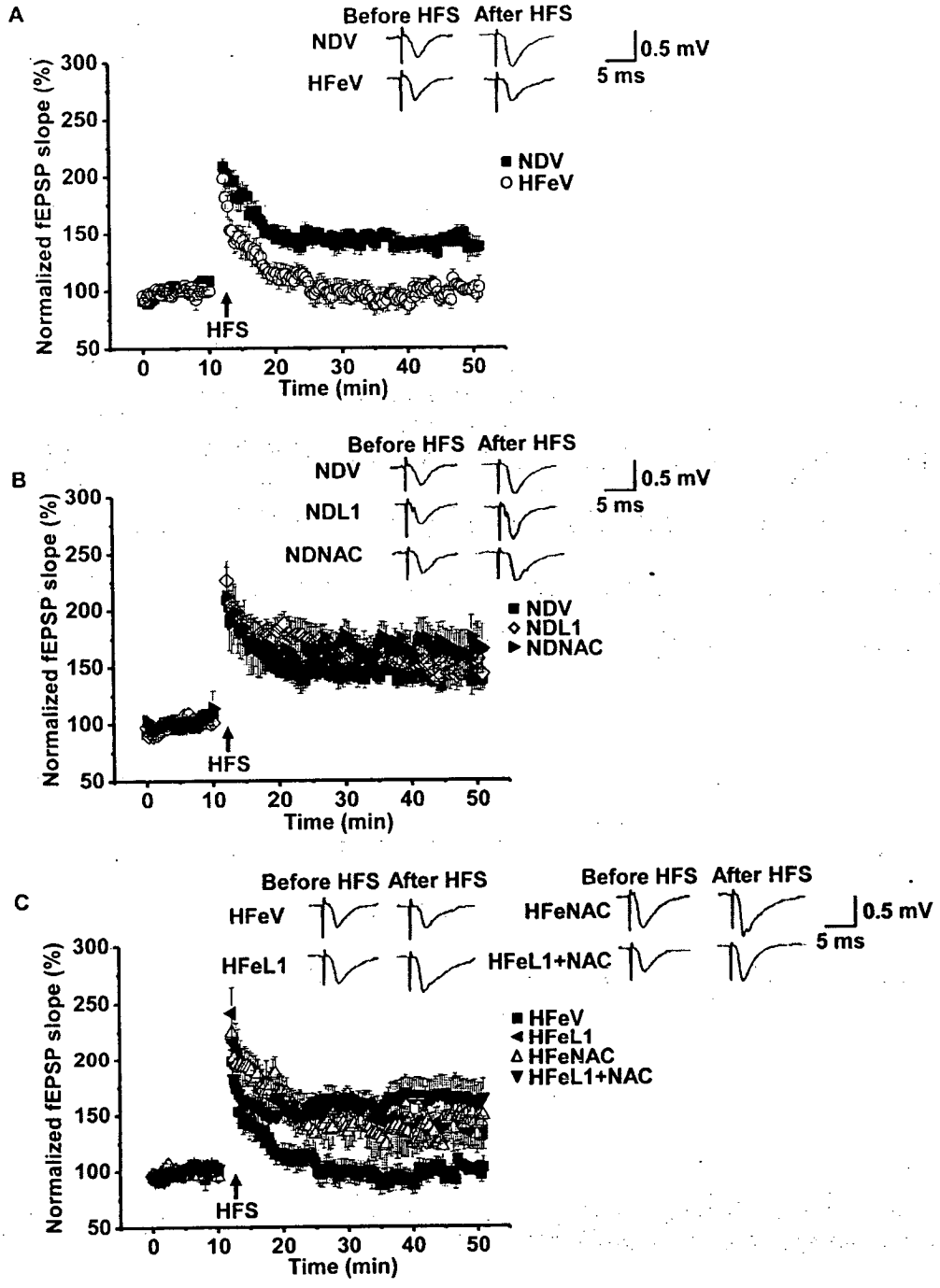


Figure 6. Effects of the pharmacological interventions by deferiprone and n-acetyl cysteine on brain synaptic plasticity. Each panel represented brain synaptic plasticity in NDV vs. HFeV (A), ND groups (B) and HFe groups (C). ND: normal diet fed group; HFe: high iron diet fed group; L1: deferiprone; NAC: n-acetyl cysteine.
doi:10.1371/journal.pone.0085115.g006

brain mitochondrial depolarization and brain mitochondrial swelling. It has been shown that mitochondrial dysfunction is a primary cause of the cellular apoptosis [59–61]. Consistent with these reports, we found that iron overload in the brain increased brain apoptosis as shown by increased expression of Bax and Bax/Bcl-2 ratio without changing the Bcl-2 expression. These findings suggested that iron overload causes brain mitochondrial dysfunction, leading to brain apoptosis.

It has been known that iron overload leading to iron toxicity could be observed in several organs particularly in the brain [10,62–66]. Several studies showed that iron toxicity in the brain caused memory deficit [65–67]. In the present study, chronic HFe

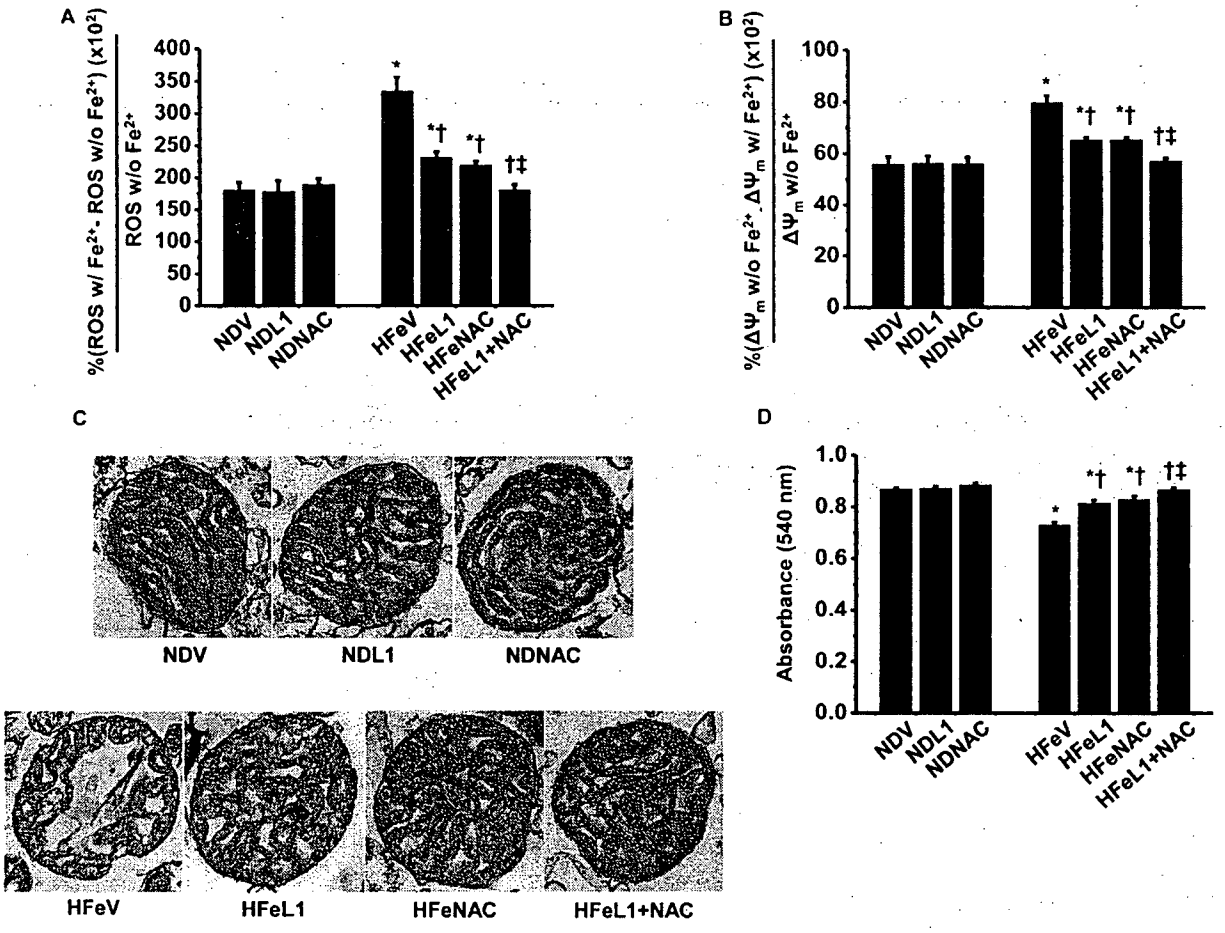


Figure 7. Effects of the pharmacological interventions by deferiprone and n-acetyl cysteine on brain mitochondrial function. Each panel represented brain mitochondrial ROS production (A), brain mitochondrial membrane potential changes (B), brain mitochondrial morphological changes (C) and brain mitochondrial swelling (D). *$P<0.05$ vs. Normal diet treated with vehicle (NDV); †$P<0.05$ vs. HFe treated with vehicle (HFeV); ‡$P<0.05$ vs. HFe treated with either L1 or NAC (HFeL1 or HFeNAC). ND: normal diet fed groups; HFe: high-iron diet fed groups; L1: deferiprone; NAC: n-acetyl cysteine.

doi:10.1371/journal.pone.0085115.g007

consumption induced iron overload also led to learning and memory deficit as shown in the Morris Water Maze test. Consistent with the learning and memory deficit, we also found that the brain synaptic plasticity, the important process of the learning and memory [42,68], was impaired following iron overload condition. These findings indicated that iron overload condition could cause cognitive impairment, and that brain mitochondrial dysfunction would be the primary target responsible for this adverse effect.

Although HFe-fed rats showed the significant reduction of their body weight, compared to ND-fed rats (Table 1), this reduction of body weight in HFe-fed rats did not cause the alteration in muscle activity during Morris water maze test. This is due to the fact that the locomotors activity as well as the time to reach the target platform between ND-fed rats and HFe-fed rats on the 1st and 2nd day of the acquisition test (after iron overload) were not significantly different (Fig. 2A), indicating that the muscle activity for swimming of both groups was similar. Thus, increased time to reach the target platform on the 3rd-5th day of the acquisition test, and decreased time spent in the target quadrant on the 6th day of probe test in HFe-fed rats compared to ND-fed rats during the Morris Water test (as shown in Fig. 2B and 2C) should directly indicate the impairment of learning and memory.

Surprisingly, we noticed that the defective "learning" process, as measured by the acquisition test, brain mitochondrial dysfunction and increased brain apoptotic markers were exhibited in a time-dependent manner of HFe consumption. However, the defective "memory" process, as measured by the probe test and the impairment of brain synaptic plasticity were not exhibited in a time-dependent manner of HFe consumption. These findings suggested that 1) The learning process in the brain required certain amounts of healthy brain mitochondria and healthy neurons to be able to function, and 2) The memory process was associated with the brain synaptic plasticity. Since the brain synaptic plasticity is an essential process of the memory formation [69], our findings indicated that iron overload not only impaired the learning process, but also destroyed the memory process.

Although pharmacological intervention of iron overload has been widely used, the effects of pharmacological interventions on brain dysfunction following iron overload have been rarely investigated. Iron chelators such as deferiprone (L1) and deferoxamine were widely used to attenuate the harmful effects from iron

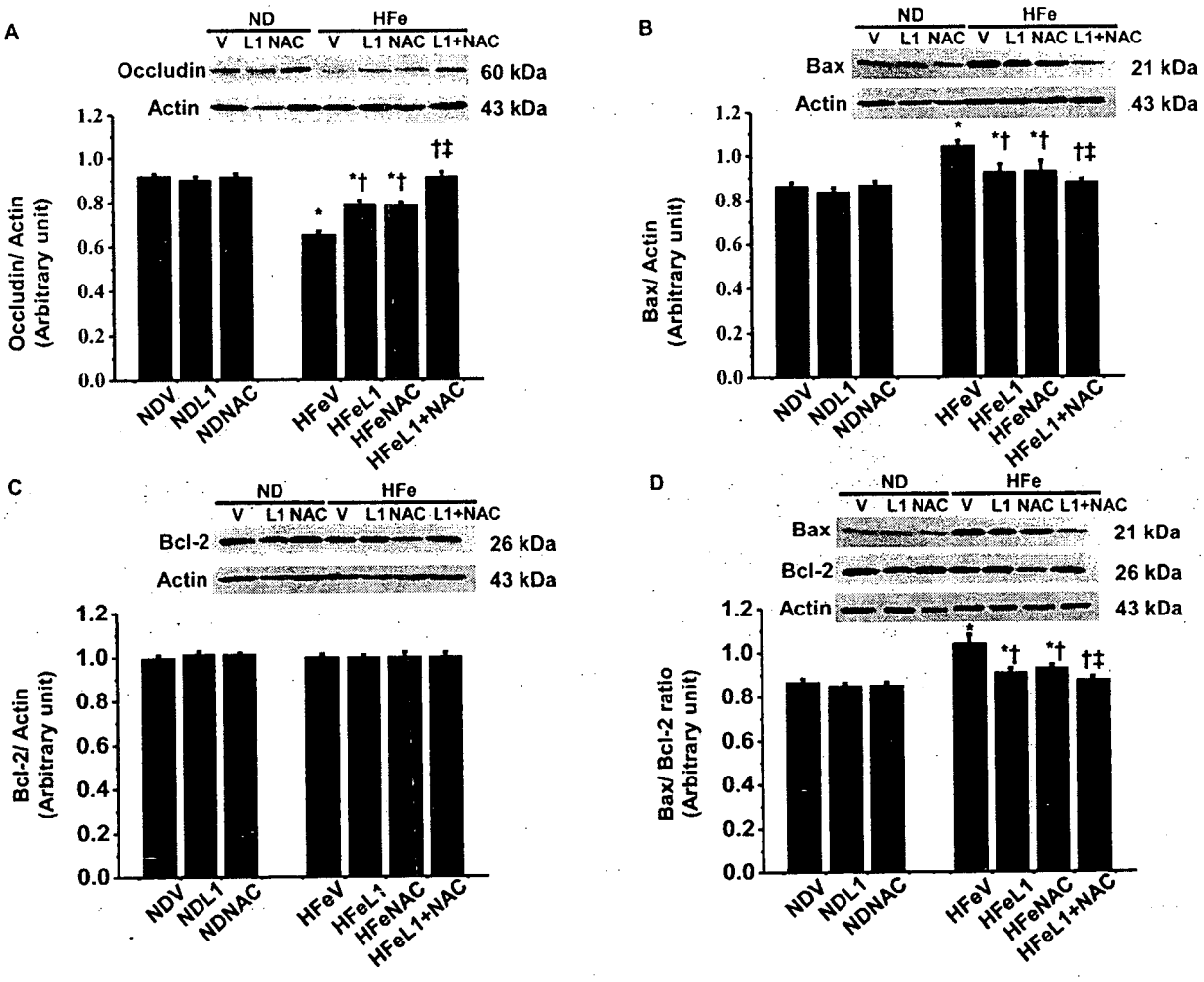


Figure 8. Effects of the pharmacological interventions by deferiprone and n-acetyl cysteine on BBB breakdown and apoptosis. Each panel represented the expression of tight junction protein; occludin (A), apoptotic-protein; Bax (B) and anti-apoptotic protein; Bcl-2 (C) and Bax/Bcl-2 ratio (D). *$P<0.05$ vs. Normal diet treated with vehicle (NDV); †$P<0.05$ vs. HFe treated with vehicle (HFeV); ‡$P<0.05$ vs. HFe treated with either L1 or NAC (HFeL1 or HFeNAC). ND: normal diet fed groups; HFe: high-iron diet fed groups; L1: deferiprone; NAC: n-acetyl cysteine.
doi:10.1371/journal.pone.0085115.g008

overload condition in thalassemic patients [70,71]. However, L1 has an advantage over deferoxamine since it could be orally administered whereas deferoxamine administration needed to be injected. Several studies demonstrated the potential effect of iron chelation therapy in brain injury [25,26]. Those findings implied that iron chelation therapy might be useful in attenuating brain dysfunction induced by iron overload. Consistent with this concept, our study demonstrated that L1 could attenuate brain dysfunction from iron overload.

Since oxidative stress from iron overload was also responsible for brain dysfunction, another potential strategy to protect the brain from iron-overload induced oxidative stress would be an anti-oxidative therapy. N-acetyl cysteine (NAC) has been commonly used as an antioxidant [72]. Several studies suggested the beneficial effect of NAC in oxidative stress by decreasing ROS production [21,22]. In the present study, NAC administration alone in HFe-fed rats could attenuate brain dysfunction in a similar fashion observed with L1 therapy. These findings suggest that both iron chelator and antioxidant agent alone provided the beneficial effects in iron overload induced brain dysfunction. Nevertheless, neither L1 nor NAC treatment alone could completely restore the brain function following iron overload.

Despite the concept that both antioxidant and iron chelation would be essential in treating iron overload, the effects of combination of both agents in treating brain dysfunction due to HFe-induced iron overload have been rarely investigated. We further explored whether the combination of L1 and NAC treatment on brain function following iron overload provided more beneficial effects than the single agent therapy. Interestingly, we demonstrated for the first time that combined therapy of L1 and NAC completely restored brain function impaired by long-term HFe consumption. The possible mechanisms of the combination therapy to recover brain dysfunction induced by iron overload would be due to several beneficial effects provided by each agent. First, combined therapy could decrease iron accumulation via L1, and decrease iron-induced oxidative-stress by NAC as well as L1, which was previously shown to act as an anti-oxidant agent [73]. Second, both L1 and NAC had been shown to have direct effects on the brain since both drugs could pass the blood brain barrier [74,75]. As a result, the combined

therapy could provide dual beneficial effects in both plasma and directly in the brain. As demonstrated for the first time by our study, the combined therapy provided a greater therapeutic benefit by restoring brain function impaired by iron overload. Future clinical studies are needed to confirm the beneficial effects of the combined L1 and NAC observed in the present report. Summarized proposed mechanisms including brain dysfunctions following iron overload, and the effects of pharmacological interventions on attenuating brain dysfunction are illustrated in figure 9.

Conclusions

The present study demonstrated the deleterious effects of iron overload in the brain as presented by learning and memory deficit, inhibition of brain synaptic plasticity, brain mitochondrial dysfunction and brain apoptosis. Iron overload condition led to blood-brain barrier breakdown causing an increased brain iron level and consequently causing brain dysfunction. Pharmacological interventions by either iron chelator; L1 or an antioxidant; NAC attenuated iron overload-induced brain dysfunctions. However, combined L1 and NAC not only attenuated but also restored brain dysfunctions impaired by long-term HFe consump-

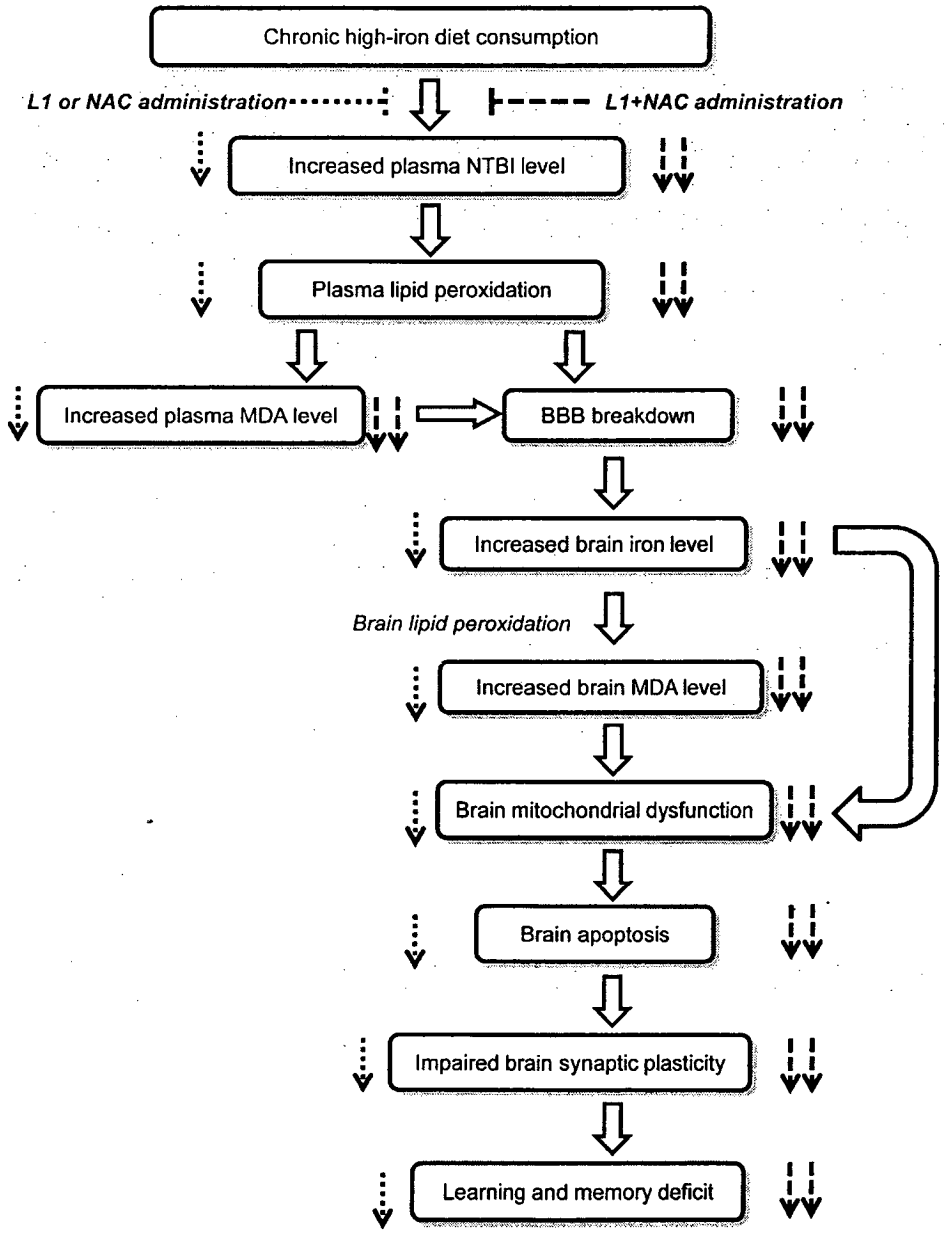


Figure 9. Diagram illustrated the proposed mechanisms. The diagram showed the proposed mechanisms of brain dysfunctions as well as the pharmacological therapy on brain dysfunctions following iron overload. Dotted arrows indicate the effects of either L1 or NAC treatment, dashed arrows indicate the combined L1 and NAC treatment. L1: deferiprone; NAC: n-acetyl cysteine.
doi:10.1371/journal.pone.0085115.g009

tion. The present study is the first study to show that the combined therapy with L1 and NAC provided the greater beneficial effects in improving brain dysfunction caused by iron overload.

Study Limitations

Although our study suggested that brain iron overload led to brain dysfunctions and the pharmacological interventions using L1 and NAC showed the beneficial effects on brain functions, the effects of brain iron overload on the metabolism of other metal ions such as Zn^{2+} and Cu^{2+}, and the effects of combined therapy on brain function under the physiological condition was not investigated in the present study. Moreover, high iron level is known to be associated with the infection and inflammation. Previous studies reported that under iron overload condition, thalassemic patients were susceptible to the microbial infection [76–78]. In addition, previous study showed that iron overload could also lead to systemic inflammation [79–83]. Recent studies showed that systemic inflammation under several pathological conditions could lead to BBB dysfunction as well as microbial infection [82,84–89]. All of these findings suggested that iron overload was associated with infection and inflammation, which could have influenced BBB integrity and led to BBB dysfunction. Future studies are needed to clarify these mechanisms related to BBB dysfunction as well as the BBB permeability under this pathological condition.

Author Contributions

Conceived and designed the experiments: JS NC SC. Performed the experiments: JS NP. Analyzed the data: JS. Contributed reagents/materials/analysis tools: NC SC. Wrote the paper: JS NC SC. Critical review of the article: JS NC SC.

References

1. Hidalgo C, Nunez MT (2007) Calcium, iron and neuronal function. IUBMB Life 59: 280–285.
2. Connor JR, Menzies SL (1996) Relationship of iron to oligodendrocytes and myelination. Glia 17: 83–93.
3. Youdim MB, Green AR (1978) Iron deficiency and neurotransmitter synthesis and function. Proc Nutr Soc 37: 173–179.
4. Weiss G, Werner-Felmayer G, Werner ER, Grunewald K, Wachter H, et al. (1994) Iron regulates nitric oxide synthase activity by controlling nuclear transcription. J Exp Med 180: 969–976.
5. Vatassery GT, DeMaster EG, Lai JC, Smith WE, Quach HT (2004) Iron uncouples oxidative phosphorylation in brain mitochondria isolated from vitamin E-deficient rats. Biochim Biophys Acta 1688: 265–273.
6. McNeill A, Chinnery PF (2011) Neurodegeneration with brain iron accumulation. Handb Clin Neurol 100: 161–172.
7. Benarroch EE (2009) Brain iron homeostasis and neurodegenerative disease. Neurology 72: 1436–1440.
8. Ceci A, Felisi M, De Sanctis V, De Mattia D (2003) Pharmacotherapy of iron overload in thalassaemic patients. Expert Opin Pharmacother 4: 1763–1774.
9. Hershko C (2010) Pathogenesis and management of iron toxicity in thalassemia. Ann N Y Acad Sci 1202: 1–9.
10. Lekawanvijit S, Chattipakorn N (2009) Iron overload thalassemic cardiomyopathy: iron status assessment and mechanisms of mechanical and electrical disturbance due to iron toxicity. Can J Cardiol 25: 213–218.
11. Origa R, Galanello R, Ganz T, Giagu N, Maccioni L, et al. (2007) Liver iron concentrations and urinary hepcidin in beta-thalassemia. Haematologica 92: 583–588.
12. Fretham SJ, Carlson ES, Georgieff MK (2011) The role of iron in learning and memory. Adv Nutr 2: 112–121.
13. Yehuda S, Youdim ME, Mostofsky DI (1986) Brain iron-deficiency causes reduced learning capacity in rats. Pharmacol Biochem Behav 25: 141–144.
14. Monastero R, Monastero G, Ciaccio C, Padovani A, Camarda R (2000) Cognitive deficits in beta-thalassemia major. Acta Neurol Scand 102: 162–168.
15. Armstrong FD (2005) Thalassemia and learning: Neurocognitive functioning in children. Ann N Y Acad Sci 1054: 283–289.
16. Martin SJ, Grimwood PD, Morris RG (2000) Synaptic plasticity and memory: an evaluation of the hypothesis. Annu Rev Neurosci 23: 649–711.
17. Munoz P, Humeres A, Elgueta C, Kirkwood A, Hidalgo C, et al. (2011) Iron mediates N-methyl-D-aspartate receptor-dependent stimulation of calcium-induced pathways and hippocampal synaptic plasticity. J Biol Chem 286: 13382–13392.
18. Yin F, Boveris A, Cadenas E (2012) Mitochondrial energy metabolism and redox signaling in brain aging and neurodegeneration. Antioxid Redox Signal.
19. Reddy PH, Reddy TP (2011) Mitochondria as a Therapeutic Target for Aging and Neurodegenerative Diseases. Curr Alzheimer Res: 393–409.
20. Maaroufi K, Save E, Poucet B, Sakly M, Abdelmelek H, et al. (2011) Oxidative stress and prevention of the adaptive response to chronic iron overload in the brain of young adult rats exposed to a 150 kilohertz electromagnetic field. Neuroscience 186: 39–47.
21. Khanna AK, Xu J, Mehra MR (2011) Antioxidant N-acetyl cysteine reverses cigarette smoke-induced myocardial infarction by inhibiting inflammation and oxidative stress in a rat model. Lab Invest 92: 224–235.
22. Zhu Y, Zhang XL, Zhu BF, Ding YN (2012) Effect of antioxidant N-acetylcysteine on diabetic retinopathy and expression of VEGF and ICAM-1 from retinal blood vessels of diabetic rats. Mol Biol Rep 39: 3727–3735.
23. Cassinerio E, Roghi A, Pedrotti P, Brevi F, Zanaboni L, et al. (2012) Cardiac iron removal and functional cardiac improvement by different iron chelation regimens in thalassemia major patients. Ann Hematol 91: 1443–1449.
24. Miura Y, Matsui Y, Kaneko H, Watanabe M, Tsudo M (2010) Iron chelation therapy with deferasirox results in improvement of liver enzyme level in patients with iron overload-associated liver dysfunction. Case Rep Med 2010: 675060.
25. Boddaert N, Le Quan Sang KH, Rotig A, Leroy-Willig A, Gallet S, et al. (2007) Selective iron chelation in Friedreich ataxia: biologic and clinical implications. Blood 110: 401–408.
26. Hua Y, Keep RF, Hoff JT, Xi G (2008) Deferoxamine therapy for intracerebral hemorrhage. Acta Neurochir Suppl 105: 3–6.
27. Kumfu S, Chattipakorn S, Chinda K, Fucharoen S, Chattipakorn N (2012) T-type calcium channel blockade improves survival and cardiovascular function in thalassemic mice. Eur J Haematol 88: 535–548.
28. Fabian E, Poloskey P, Kosa L, Elmadfa I, Rethy LA (2011) Activities of antioxidant enzymes in relation to oxidative and nitrosative challenges in childhood asthma. J Asthma 48: 351–357.
29. Rebouche CJ, Wilcox CL, Widness JA (2004) Microanalysis of non-heme iron in animal tissues. J Biochem Biophys Methods 58: 239–251.
30. Pipatpiboon N, Pratchayasakul W, Chattipakorn N, Chattipakorn SC (2012) PPARgamma agonist improves neuronal insulin receptor function in hippocampus and brain mitochondria function in rats with insulin resistance induced by long term high-fat diets. Endocrinology 153: 329–338.
31. Pipatpiboon N, Pintana H, Pratchayasakul W, Chattipakorn N, Chattipakorn SC (2013) DPP4-inhibitor improves neuronal insulin receptor function, brain mitochondrial function and cognitive function in rats with insulin resistance induced by high-fat diet consumption. Eur J Neurosci 37: 839–849.
32. Sripetchwandee J, Sanit J, Chattipakorn N, Chattipakorn SC (2013) Mitochondrial calcium uniporter blocker effectively prevents brain mitochondrial dysfunction caused by iron overload. Life Sci 92: 298–304.
33. Kulawiak B, Kudin AP, Szewczyk A, Kunz WS (2008) BK channel openers inhibit ROS production of isolated rat brain mitochondria. Exp Neurol 212: 543–547.
34. Walker JM (1994) The bicinchoninic acid (BCA) assay for protein quantitation. Methods Mol Biol 32: 5–8.
35. Ruiz-Meana M, Garcia-Dorado D, Miro-Casas E, Abellan A, Soler-Soler J (2006) Mitochondrial Ca2+ uptake during simulated ischemia does not affect permeability transition pore opening upon simulated reperfusion. Cardiovasc Res 71: 715–724.
36. Tong V, Teng XW, Chang TK, Abbott FS (2005) Valproic acid II: effects on oxidative stress, mitochondrial membrane potential, and cytotoxicity in glutathione-depleted rat hepatocytes. Toxicol Sci 86: 436–443.
37. Novalija E, Kevin LG, Eells JT, Henry MM, Stowe DF (2003) Anesthetic preconditioning improves adenosine triphosphate synthesis and reduces reactive oxygen species formation in mitochondria after ischemia by a redox dependent mechanism. Anesthesiology 98: 1155–1163.
38. Chelli B, Falleni A, Salvetti F, Gremigni V, Lucacchini A, et al. (2001) Peripheral-type benzodiazepine receptor ligands: mitochondrial permeability transition induction in rat cardiac tissue. Biochem Pharmacol 61: 695–705.
39. Stanford SC (2007) The Open Field Test: reinventing the wheel. J Psychopharmacol 21: 134–135.
40. Denenberg VH (1969) Open-field bheavior in the rat: what does it mean? Ann N Y Acad Sci 159: 852–859.
41. Vorhees CV, Williams MT (2006) Morris water maze: procedures for assessing spatial and related forms of learning and memory. Nat Protoc 1: 848–858.
42. Neves G, Cooke SF, Bliss TV (2008) Synaptic plasticity, memory and the hippocampus: a neural network approach to causality. Nat Rev Neurosci 9: 65–75.
43. Lochhead JJ, McCaffrey G, Quigley CE, Finch J, DeMarco KM, et al. (2010) Oxidative stress increases blood-brain barrier permeability and induces alterations in occludin during hypoxia-reoxygenation. J Cereb Blood Flow Metab 30: 1625–1636.

44. Liu W, Hendren J, Qin XJ, Shen J, Liu KJ (2009) Normobaric hyperoxia attenuates early blood-brain barrier disruption by inhibiting MMP-9-mediated occludin degradation in focal cerebral ischemia. J Neurochem 108: 811–820.
45. Bartfay WJ, Bartfay E (2000) Iron-overload cardiomyopathy: evidence for a free radical–mediated mechanism of injury and dysfunction in a murine model. Biol Res Nurs 2: 49–59.
46. Crichton RR, Wilmet S, Legssyer R, Ward RJ (2002) Molecular and cellular mechanisms of iron homeostasis and toxicity in mammalian cells. J Inorg Biochem 91: 9–18.
47. Janero DR, Burghardt B (1989) Thiobarbituric acid-reactive malondialdehyde formation during superoxide-dependent, iron-catalyzed lipid peroxidation: influence of peroxidation conditions. Lipids 24: 125–131.
48. Ballabh P, Braun A, Nedergaard M (2004) The blood-brain barrier: an overview: structure, regulation, and clinical implications. Neurobiol Dis 16: 1–13.
49. Won SM, Lee JH, Park UJ, Gwag J, Gwag BJ, et al. (2011) Iron mediates endothelial cell damage and blood-brain barrier opening in the hippocampus after transient forebrain ischemia in rats. Exp Mol Med 43: 121–128.
50. Darley-Usmar V (2004) The powerhouse takes control of the cell; the role of mitochondria in signal transduction. Free Radic Biol Med 37: 753–754.
51. Cheng J, Wang F, Yu DF, Wu PF, Chen JG (2011) The cytotoxic mechanism of malondialdehyde and protective effect of carnosine via protein cross-linking/mitochondrial dysfunction/reactive oxygen species/MAPK pathway in neurons. Eur J Pharmacol 650: 184–194.
52. Gao Y, Wang N, Zhang Y, Ma Z, Guan P, et al. (2013) Mechanism of protective effects of Danshen against iron overload-induced injury in mice. J Ethnopharmacol 145: 254–260.
53. Liang LP, Jarrett SG, Patel M (2008) Chelation of mitochondrial iron prevents seizure-induced mitochondrial dysfunction and neuronal injury. J Neurosci 28: 11550–11556.
54. Koppenol WH (2001) The Haber-Weiss cycle–70 years later. Redox Rep 6: 229–234.
55. Valko M, Morris H, Cronin MT (2005) Metals, toxicity and oxidative stress. Curr Med Chem 12: 1161–1208.
56. Kumfu S, Chattipakorn S, Fucharoen S, Chattipakorn N (2012) Mitochondrial calcium uniporter blocker prevents cardiac mitochondrial dysfunction induced by iron overload in thalassemic mice. Biometals 25: 1167–1175.
57. Long J, Liu C, Sun L, Gao H, Liu J (2009) Neuronal mitochondrial toxicity of malondialdehyde: inhibitory effects on respiratory function and enzyme activities in rat brain mitochondria. Neurochem Res 34: 786–794.
58. Sen T, Sen N, Tripathi G, Chatterjee U, Chakrabarti S (2006) Lipid peroxidation associated cardiolipin loss and membrane depolarization in rat brain mitochondria. Neurochem Int 49: 20–27.
59. Green DR, Reed JC (1998) Mitochondria and apoptosis. Science 281: 1309–1312.
60. Vannuvel K, Renard P, Raes M, Arnould T (2013) Functional and morphological impact of ER stress on mitochondria. J Cell Physiol 228: 1802–1818.
61. Desagher S, Martinou JC (2000) Mitochondria as the central control point of apoptosis. Trends Cell Biol 10: 369–377.
62. Anderson GJ (2007) Mechanisms of iron loading and toxicity. Am J Hematol 82: 1128–1131.
63. Ramm GA, Ruddell RG (2005) Hepatotoxicity of iron overload: mechanisms of iron-induced hepatic fibrogenesis. Semin Liver Dis 25: 433–449.
64. Maaroufi K, Had-Aissouni L, Melon C, Sakly M, Abdelmelek H, et al. (2009) Effects of prolonged iron overload and low frequency electromagnetic exposure on spatial learning and memory in the young rat. Neurobiol Learn Mem 92: 345–355.
65. de Lima MN, Polydoro M, Laranja DC, Bonatto F, Bromberg E, et al. (2005) Recognition memory impairment and brain oxidative stress induced by postnatal iron administration. Eur J Neurosci 21: 2521–2528.
66. Perez VP, de Lima MN, da Silva RS, Dornelles AS, Vedana G, et al. (2010) Iron leads to memory impairment that is associated with a decrease in acetylcholinesterase pathways. Curr Neurovasc Res 7: 15–22.
67. de Lima MN, Presti-Torres J, Caldana F, Grazziotin MM, Scalco FS, et al. (2007) Desferoxamine reverses neonatal iron-induced recognition memory impairment in rats. Eur J Pharmacol 570: 111–114.
68. Citri A, Malenka RC (2008) Synaptic plasticity: multiple forms, functions, and mechanisms. Neuropsychopharmacology 33: 18–41.
69. Zagaar M, Dao A, Levine A, Alhaider I, Alkadhi K (2013) Regular Exercise Prevents Sleep Deprivation Associated Impairment of Long-Term Memory and Synaptic Plasticity in The CA1 Area of the Hippocampus. Sleep 36: 751–761.
70. Jamuar SS, Lai AH (2012) Safety and efficacy of iron chelation therapy with deferiprone in patients with transfusion-dependent thalassemia. Ther Adv Hematol 3: 299–307.
71. Jomova K, Valko M (2011) Importance of iron chelation in free radical-induced oxidative stress and human disease. Curr Pharm Des 17: 3460–3473.
72. Reddy PS, Rani GP, Sainath SB, Meena R, Supriya C (2011) Protective effects of N-acetylcysteine against arsenic-induced oxidative stress and reprotoxicity in male mice. J Trace Elem Med Biol 25: 247–253.
73. Hider RC, Roy S, Ma YM, Le Kong X, Preston J (2011) The potential application of iron chelators for the treatment of neurodegenerative diseases. Metallomics 3: 239–249.
74. Fredenburg AM, Sethi RK, Allen DD, Yokel RA (1996) The pharmacokinetics and blood-brain barrier permeation of the chelators 1,2 dimethly-, 1,2 diethyl-, and 1-[ethan-1'ol]-2-methyl-3-hydroxypyridin-4-one in the rat. Toxicology 108: 191–199.
75. Farr SA, Poon HF, Dogrukol-Ak D, Drake J, Banks WA, et al. (2003) The antioxidants alpha-lipoic acid and N-acetylcysteine reverse memory impairment and brain oxidative stress in aged SAMP8 mice. J Neurochem 84: 1173–1183.
76. Kontoghiorghes GJ, Kolnagou A, Skiada A, Petrikkos G (2010) The role of iron and chelators on infections in iron overload and non iron loaded conditions: prospects for the design of new antimicrobial therapies. Hemoglobin 34: 227–239.
77. Spellberg B, Andes D, Perez M, Anglim A, Bonilla H, et al. (2009) Safety and outcomes of open-label deferasirox iron chelation therapy for mucormycosis. Antimicrob Agents Chemother 53: 3122–3125.
78. Zarember KA, Cruz AR, Huang CY, Gallin JI (2009) Antifungal activities of natural and synthetic iron chelators alone and in combination with azole and polyene antibiotics against Aspergillus fumigatus. Antimicrob Agents Chemother 53: 2654–2656.
79. Mehta V, Pei W, Yang G, Li S, Swamy E, et al. (2013) Iron is a sensitive biomarker for inflammation in multiple sclerosis lesions. PLoS One 8: e57573.
80. Urrutia P, Aguirre P, Esparza A, Tapia V, Mena NP, et al. (2013) Inflammation alters the expression of DMT1, FPN1 and hepcidin, and it causes iron accumulation in central nervous system cells. J Neurochem 126: 541–549.
81. Mariani R, Trombini P, Pozzi M, Piperno A (2009) Iron metabolism in thalassemia and sickle cell disease. Mediterr J Hematol Infect Dis 1: e2009006.
82. Weiss N, Miller F, Cazaubon S, Couraud PO (2009) The blood-brain barrier in brain homeostasis and neurological diseases. Biochim Biophys Acta 1788: 842–857.
83. Barluzzi R, Saleppico S, Nocentini A, Boelaert JR, Neglia R, et al. (2002) Iron overload exacerbates experimental meningoencephalitis by Cryptococcus neoformans. J Neuroimmunol 132: 140–146.
84. Ortiz GG, Pacheco-Moises FP, Bitzer-Quintero OK, Ramirez-Anguiano AC, Flores-Alvarado LJ, et al. (2013) Immunology and Oxidative Stress in Multiple Sclerosis: Clinical and Basic Approach. Clin Dev Immunol 2013: 708659.
85. Barichello T, Generoso JS, Silvestre C, Costa CS, Carrodore MM, et al. (2012) Circulating concentrations, cerebral output of the CINC-1 and blood-brain barrier disruption in Wistar rats after pneumococcal meningitis induction. Eur J Clin Microbiol Infect Dis 31: 2005–2009.
86. Combes V, Guillemin GJ, Chan-Ling T, Hunt NH, Grau GE (2012) The crossroads of neuroinflammation in infectious diseases: endothelial cells and astrocytes. Trends Parasitol 28: 311–319.
87. Denes A, Ferenczi S, Kovacs KJ (2011) Systemic inflammatory challenges compromise survival after experimental stroke via augmenting brain inflammation, blood- brain barrier damage and brain oedema independently of infarct size. J Neuroinflammation 8: 164.
88. McColl BW, Rothwell NJ, Allan SM (2008) Systemic inflammation alters the kinetics of cerebrovascular tight junction disruption after experimental stroke in mice. J Neurosci 28: 9451–9462.
89. Frohman EM, Racke MK, Raine CS (2006) Multiple sclerosis–the plaque and its pathogenesis. N Engl J Med 354: 942–955.